JUBILEE VOLUME

Acc.
22.8.88

Cwk-H02900-20-P0244447

AJR

20

American
Journal of
Roentgenology

January 1988

Reliable histological and cytological fine needle aspiration biopsies ...from E-Z-EM

PercuCut™

PercuCut™ Cut-Biopsy Needles from E-Z-EM provide reliable results in virtually all soft-tissue biopsies. Patented, specially designed "keyhole" cutting-edges on the cannula tip precisely core tissue samples. Ultra-thin-wall tubing maximizes sample size while minimizing needle gauge and patient trauma.

Three PercuCut needle designs allow the physician complete flexibility in obtaining a biopsy sample.

Cut-Biopsy Needle—a keyhole cutting-edge cannula with stylet. Includes a unique syringe which creates and maintains negative pressure during the biopsy procedure.

Coaxial Sheath Cut-Biopsy Needle—a three-part sheath/cannula/stylet design for multiple samples through a single puncture. Our unique aspirating syringe system is also included.

Self-Aspirating Cut-Biopsy Needle—a biopsy needle that combines our keyhole-cutting technology with a specially designed self-aspirating diaphragm hub which permits one-hand operation without a syringe.

PercuCut Needles have proven their ability to provide excellent, reliable histological and cytological samples in virtually all soft-tissue biopsies. All use a straight-tracking trocar pointed stylet for precise placement, and are available in gauges and lengths to suit any application.

For additional information on all of the PercuCut products, contact your local representative, or call E-Z-EM toll-free at 1-800-544-4624. In New York call 516-333-8230.

E-Z-EM
More than barium—much more

E-Z-EM®
E-Z-EM, Inc.
7 Portland Avenue
Westbury, N.Y. 11590

Our patented "keyhole" cutting-edge cannula and straight-tracking trocar pointed stylet.

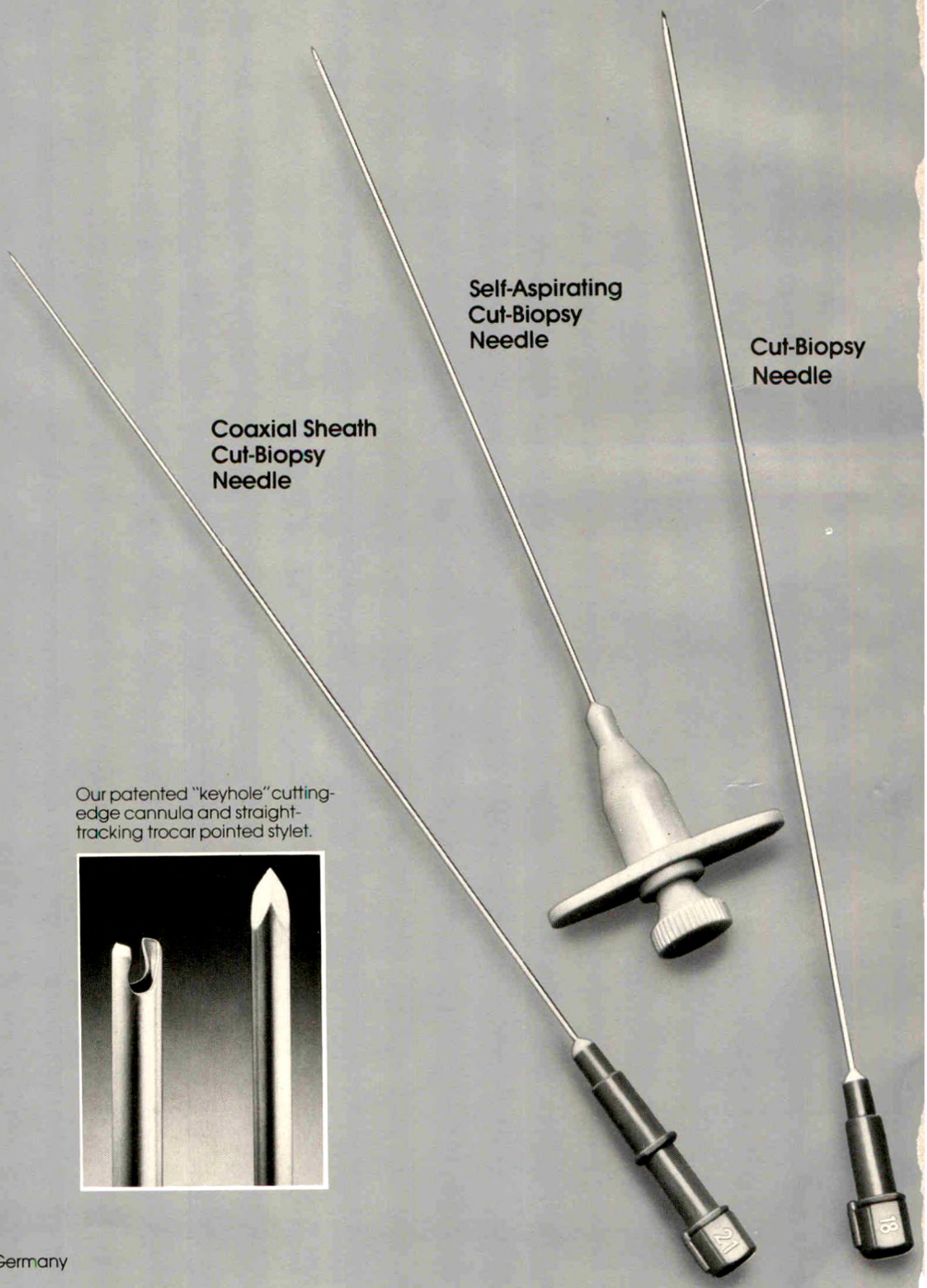

CIRCLE 5 ON READER SERVICE CARD

© 1987 E-Z-EM, Inc.

Manufactured for E-Z-EM by Angiomed® West Germany

Official Journal of the American Roentgen Ray Society

AJR

American Journal of Roentgenology
Diagnostic Imaging and Related Sciences

P 24,447

Editor-In-Chief Robert N. Berk, *San Diego, California*

Editor Emeritus Melvin M. Figley, *Seattle, Washington*

Associate Editor Saskia von Waldenburg Hilton, *San Diego, California*

Consulting Editor Juan M. Taveras, *Boston, Massachusetts*

Statistician Charles C. Berry, *San Diego, California*

Editorial Board

John R. Amberg
William L. Ashburn
Itamar Aviad
Lawrence W. Bassett
Gregory P. Borkowski
William G. Bradley, Jr.
Peter L. Cooperberg
Peter M. Doubilet
N. Reed Dunnick
David K. Edwards
Ronald G. Evens
David S. Feigin
Paul J. Friedman
William R. Hendee
John R. Hesselink
Charles B. Higgins
Melvyn T. Korobkin
Thomas L. Lawson
Bruce L. McClennan
Albert A. Moss
Jeffrey H. Newhouse
Donald L. Resnick
Stewart R. Reuter
Charles R. Rohrmann, Jr.
Peter M. Ronai
Sjef H. J. Ruijs
Stuart S. Sagel
David J. Sartoris
Edward A. Sickles
Barry A. Siegel
David D. Stark
Edward T. Stewart
Eric vanSonnenberg

Editorial Staff: Elizabeth A. Whalen, *publications supervisor*; Linda Wood, Barbara Rose, and Barbara L. Halliburton, *manuscript editors*; Nancy Rydbeck, *office manager*; Elaine Sherman, *administrative assistant*; Geraldine Perillo, *administrative secretary*.

All business correspondence, including display (not classified) advertising, subscriptions, address changes, reprints, and permission requests should be addressed to Williams & Wilkins, 428 East Preston Street, Baltimore, MD 21202. Correspondence regarding editorial matters and classified advertising should be addressed to the editorial office, AJR, 2223 Avenida de la Playa, Suite 200, La Jolla, CA 92037-3218. For manuscript submission, see Guidelines for Authors, next page. Undelivered or damaged copies replaced within 60 days of publication; 90 days for foreign subscribers. Allow 90 days for address changes.
AJR, AMERICAN JOURNAL OF ROENTGENOLOGY (ISSN 0361 803X) is published monthly by American Roentgen Ray Society, 428 E. Preston Street, Baltimore, MD 21202. Annual dues include $50 for journal subscription. Second class postage paid at Baltimore, MD and at additional mailing offices. Postmaster send address changes (Form 3579) to Williams & Wilkins, 428 East Preston St., Baltimore, MD 21202. Subscription rates $100 ($135 foreign); institutions $110 ($145 foreign); in training $25; single copy $16 ($19). Japanese rates include airfreight. Japanese yen price is available from our sole agent USACO Corporation, 13-12, Shimbashi 1-Chome, Minato-Ku, Tokyo 105, Japan, telephone 03-502-6471. Subscriptions in South Korea are available only through our sole agent in Korea: Korea-America Medical Books Co., Ltd. (KAMBOOK) 209 Yun kun-dong, Chongro-ku, Seoul, Korea (telephone: 745-3151; telex: K25211 KAMBC; FAX: 745-3153). All subscriptions to South Korea will be shipped by air freight after January 1, 1988. There is an air freight surcharge of $12.00 over the regular subscription rate for this journal in South Korea to partially compensate for air freight costs. Airmail rates furnished on request. Indexed by *Current Contents* and *Index Medicus*. Copyright © 1987 by American Roentgen Ray Society.
0361-803X/88$2.00

Evac-Q-Kwik® advantages are as clear as the X-ray you get.

Use this checklist to compare other bowel preps:

	EVAC-Q-KWIK	Other Preps
Taste	Pleasant, cherry flavor	
Fluid intake	40 fl oz	
Reconstitution	No	
Enema	No	
Cost	Low	
Adminstration time	6 hours	
Sugar	No	
Alcohol	No	
Sodium content	Low	

Evac-Q-Kwik thoroughly cleans the colon. Patients arrive ready for X-ray. No staff time or extra prepping needed. One take is all—virtually every time. This means better work flow, cost containment and patient comfort.

Everything is in the kit, including easy-to-follow instructions. No mixing, no enemas, no alcohol, no sugar, low sodium… and low cost. Easy to use for better compliance.

Seeing is believing. Give Evac-Q-Kwik a trial.

There's more.

Take advantage of our service materials:
☐ Inservice film for nurses ☐ Multi-language instruction sheets ☐ Radiology work sheets ☐ "What to expect" booklet for patients. Ask your Adria Representative, or drop us a line. Adria Laboratories, Columbus, Ohio 43215.

Evac-Q-Kwik®

Clean colon, clear advantages.

Adria®

Adria Laboratories
Columbus, OH 43215

AJR Guidelines for Authors

Address new and revised manuscripts, correspondence, and classified ads to the Editor:

AJR Editorial Office
2223 Avenida de la Playa, Suite 200
La Jolla, CA 92037-3218 Telephone: (619) 459-2229

Inquiries regarding subscriptions, display advertising, reprints, or permission to republish *AJR* material should be addressed to the publisher:

The Williams & Wilkins Co.
428 E. Preston St.
Baltimore, MD 21202 Telephone: (301) 528-4133

The *AJR* publishes original contributions to the advancement of medical diagnosis and treatment. Submitted manuscripts should not contain previously published material and should not be under consideration for publication elsewhere. Papers dealing with neuroradiology should be addressed to: American Journal of Neuroradiology, Dept. of Radiology, Massachusetts General Hospital, Boston, MA 02114. At the discretion of the *AJR* Editor, *AJNR* articles that are of interest to the general reader may be republished in the *AJR*. Neuroradiologic papers sent to the *AJR* will be forwarded to the Editorial Office of the *AJNR*.

Manuscript decisions are based on peer review. Reviewers receive manuscripts without title pages to ensure an unbiased review. All accepted manuscripts are subject to editing. Statements made in the article, including changes made by the Editor or manuscript editor, are the responsibility of the author and not of the *AJR* or its publisher. Authors will be sent the edited manuscript, galley proof, and proofs of illustrations. If the corresponding author will be unavailable to review galleys, arrangements should be made for a coauthor or colleague to read and return the proof.

General Guidelines for Major Papers

Abstract. Clearly state (in 200 words or less) the purpose, methods, results, and conclusions of the study. Include actual data.

Introduction. Briefly describe the purpose of the investigation, including relevant background information.

Methods. Describe the research plan, the materials (or subjects), and the methods used, in that order. Explain in detail how disease was confirmed and how subjectivity in observations was controlled.

Results. Present results in a clear, logical sequence. If tables are used, do not duplicate tabular data in text, but do describe important trends and points.

Discussion. Describe the limitations of the research plan, materials (or subjects), and methods, considering both the purpose and the outcome of the study. When results differ from those of previous investigators, explain the discrepancy.

AUTHOR'S CHECKLIST

For priority handling, complete the following checklist, sign the copyright form on the reverse side of this page, and include both with the manuscript.

_____ Two copies of the manuscript (the original and a photocopy) and two complete sets of figures are submitted. One copy has been retained by the author.

_____ If appropriate, *AJR* Guidelines for case reports, technical notes, pictorial essays, or letters to the Editor have been followed. (See page A5.)

_____ The manuscript, including references, figure legends, and tables, is typed double-spaced on 8½ × 11 in. (21.6 × 27.9 cm) *nonerasable* paper. Right-hand margins are not justified.

_____ All manuscript pages are numbered consecutively beginning with the abstract. Authors' names do not appear on the manuscript pages.

_____ The manuscript is organized as follows: title page, blind title page (title only), abstract, introduction, methods, results, discussion, acknowledgments, references, tables, figure legends, and figures.

_____ Informed consent has been obtained from patients who participated in clinical investigations. If experiments were performed on animals, authors complied with NIH guidelines for use of laboratory animals.

_____ Use of unfamiliar acronyms and abbrevations is kept to a minimum. When abbreviations are used they are defined at first mention, followed by the abbreviation in parentheses.

_____ Metric measurements are used throughout, or the metric equivalent is given in parentheses.

_____ Names and locations (city and state only) of manufacturers are given for equipment and nongeneric drugs.

Title Page

_____ The following information is given: title of article; names and complete addresses (including zip code) of all authors; current addresses of authors who have moved since study; acknowledgment of grant or other assistance. The corresponding author is clearly identified, and a current address and phone number are given.

_____ Two copies of a blind title page are included giving only the title (without the authors' names) for use in the review process.

Abstract

_____ An abstract of approximately 200 words concisely states the purpose, methods, and results of the study in one paragraph. Actual data are included. Conclusions are stated in a second, summary paragraph.

_____ No abbreviations or reference citations are used.

References

_____ References (not to exceed 35) are typed double-spaced starting on a separate page and are **numbered consecutively in the order in which they appear in the text**.

_____ All references are cited in the text and are enclosed in brackets and typed on line with the text (not superscript).

_____ Unpublished data are not cited in the reference list, but are cited parenthetically in the text, for example, (Smith DJ, personal communication), (Smith DJ, unpublished data). This includes papers submitted, but not yet accepted, for publication.

_____ Inclusive page numbers (e.g., 333–335) are given for all references.

_____ Journal names are abbreviated according to *Index Medicus*.

_____ Style and punctuation of references follow the format illustrated in the following examples (all authors are listed when six or less; when seven or more authors, the first three are listed, followed by "et al."):

Journal article

1. Long RS, Roe EW, Wu EU, et al. Membrane oxygenation: radiographic appearance. *AJR* **1986**;146:1257–1260

Book

2. Smith LW, Cohen AR. *Pathology of tumors*, 6th ed. Baltimore: Williams & Wilkins, **1977**:100–109

Chapter in a book

3. Breon AJ. Serum monitors of bone metastasis. In: Clark SA, ed. *Bone metastases*. Baltimore: Williams & Wilkins, **1983**:165–180

Paper presented at a meeting

4. Lau FS, Kirk AN, Beck RA. MR imaging of the spine. Presented at the annual meeting of the American Roentgen Ray Society, Washington, DC, April 1986

Tables

_____ Each table is typed double-spaced on a separate page without vertical or horizontal rules; each has a short, descriptive title. Tables do not exceed two pages in length and contain at least four lines of data.

_____ Tables are numbered in the order in which they are cited in the text.

_____ Abbreviations are defined in an explanatory note below each table.

_____ Tables are self-explanatory and do not duplicate data given in the text or figures.

_____ All arithmetic (percentages, totals, differences) has been double checked for accuracy, and tabular data agree with data given in the text.

Figures and Legends

_____ Two complete sets of original figures are submitted unmounted in labeled envelopes.

_____ Figures are clean, unscratched, 5 × 7 in. (13 × 18 cm) glossy prints with white borders. A separate print is submitted for each figure *part*.

_____ All figure parts relating to one patient are in one figure.

_____ Each figure is labeled on the back with the figure number and an arrow indicating "top." For black-and-white figures, labeling is done on a gummed label, which is then affixed to the back of the print. *Never* use labels on color figures, but write figure number on the back lightly in pencil. *Never* use ink on front or back of any figures.

_____ Author's names are *not* written on the backs of figures.

_____ Only removable (rub-on) arrows and letters are used on the figures. Symbols are uniform in size and style and are not broken or cracked.

_____ Images are uniform in size and magnification.

_____ Line drawings are done in black ink on a white background. They are professional in quality, and all use the same size type. (Only glossy prints are acceptable.)

_____ Written permission has been obtained for use of all previously published illustrations (and copies of permission letters are included), and an appropriate credit line is given in the legends.

_____ Legends are typed double-spaced, and figure numbers correspond with the order in which the figures are cited in the text.

Transfer of Copyright Agreement, Exclusive Publication Statement, and Conflict of Interest Acknowledgment

Complete copyright to the article entitled: _____

_____

is hereby transferred to the American Roentgen Ray Society (for United States government employees to the extent transferable), effective if and when the article is accepted for publication in the *American Journal of Roentgenology*. In the case of the authors who are officers or employees of the United States government, the American Roentgen Ray Society recognizes that works prepared by officers or employees of the United States government as part of their official government duties are in the public domain.

Authors reserve all proprietary rights other than copyright, such as patent rights and the right to use all or part of this article in future works of their own. The authors retain the right of replication, subject only to crediting the original source of publication and receiving written permission from the publisher.

Authors guarantee that this manuscript contains no matter that is libelous or otherwise unlawful, invades individual privacy, or infringes any proprietary rights.

Authors understand that they will receive no royalty or other compensation from the American Roentgen Ray Society or the publisher.

Authors guarantee that the editor has been or will be informed of any proprietary or commercial interest or conflicts of interest the authors may have that relate directly or indirectly to the subject of this article.

Finally, the authors certify that none of the material in this manuscript has been published previously or is currently under consideration for publication elsewhere.

_____	_____	_____
First author/date	Second author	Third author
_____	_____	_____
Fourth author	Fifth author	Sixth author

This agreement must be signed by all authors in order for the manuscript to be published.

Case Reports

A case report is a brief description of a special case that provides a message that transcends the individual patient.

Format. There is no abstract. The introduction should be a short paragraph giving the general background and the specific interest of the case. No more than one case should be described in detail (similar ones can be mentioned briefly in the discussion). Emphasis should be on the radiologic aspects; clinical information must be limited to that necessary to provide a background for the radiology. The discussion should be succinct and should focus on the specific message and relevance of radiologic methods. A review of the literature is not appropriate.

Length. Maximum of five double-spaced, typewritten pages, including the references but not the title page or figure legends.

References. Maximum of eight.

Figures. Maximum of three or four, unless the text is shortened accordingly. Legends must not repeat the text.

Tables and Acknowledgments. Not appropriate in case reports.

Technical Notes

A technical note is a brief description of a specific technique or procedure, modification of a technique, or equipment of interest to radiologists.

Format. No abstract, headings, or subheadings are required. If headings are used, they should be a combination of "Case Report," "Materials and Methods," "Results," and "Discussion." A brief one-paragraph introduction should be included to give the general background. Discussion should be limited to the specific message, including the uses of the technique or equipment. Literature reviews and lengthy case reports are not appropriate.

Length. Maximum of five double-spaced, typewritten pages, including the references but not the title page or figure legends.

References. Maximum of eight.

Figures. Maximum of two, unless the text is shortened accordingly.

Tables and Acknowledgments. Not appropriate in technical notes.

Pictorial Essays

A pictorial essay is an article that conveys its message through illustrations and their legends. Unlike other *AJR* articles, which are based on original research, pictorial essays serve primarily as teaching tools, like exhibits at a scientific meeting. They are not encyclopedic book chapters. No abstract is necessary.

Length. Maximum of four double-spaced, typewritten pages, including the references but not the title page or figure legends.

References. Maximum of four.

Figures. Maximum of 30 figure *parts*. Number should be as few as necessary to convey the message of the paper.

Tables and Acknowledgments. Not appropriate in pictorial essays.

Letters to the Editor and Replies

Letters to the Editor and Replies should offer objective and constructive criticism of published articles. Letters may also discuss matters of general interest to radiologists.

Format. All letters should be typed double-spaced on nonletterhead paper, with no greeting or salutation. Signature and affiliation should appear at the end of the letter. Titles for letters should be short and pertinent. The title for a reply is simply "Reply."

Length. Maximum of two double-spaced, typewritten pages, including references.

References. Maximum of four.

Figures. Maximum of two.

Tables and Acknowledgments. Not appropriate in Letters to the Editor and Replies.

Opinions, Commentaries, and Perspectives

Opinions, commentaries, and perspectives are special articles dealing with controversial topics or issues of special concern to radiologists.

Format. Include a title page but no abstract. Headings may be used to break up the text.

Length. Maximum of five double-spaced, typewritten pages.

References. Maximum of five.

Tables and Figures. Maximum of four.

Computer Page Articles

Articles published on the computer page deal with practical computer applications to radiology.

Format. Include a title page but no abstract.

Length. Maximum of eight double-spaced, typewritten pages.

References. Maximum of five.

Figures and Tables. Maximum of five. Computer printouts are not acceptable. Figures must be submitted as 5 × 7 in. glossy prints.

All submissions to the *AJR* must be accompanied by a completed copy of the Author's Checklist and the signed Copyright Agreement.

THE RIGHT FILM FOR EVERY SUBJECT FROM KODAK

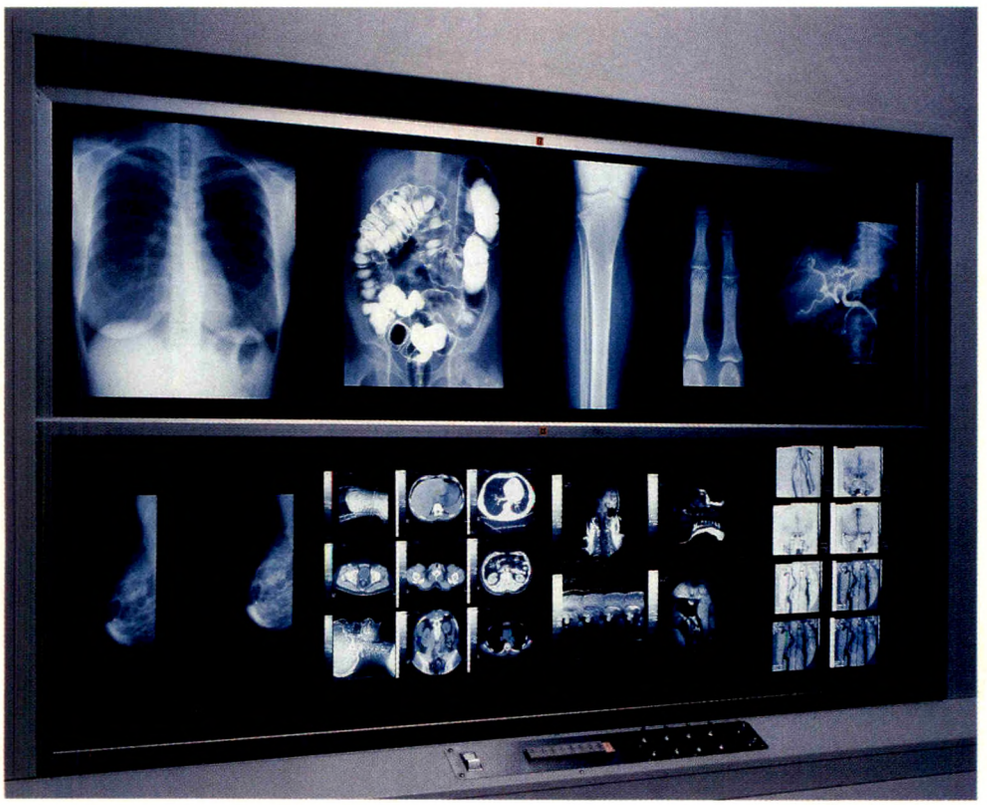

Whatever the procedure, there's always a Kodak film for the job. Always with the quality you've come to expect from Kodak.

There's a Kodak film for every diagnostic imaging modality and procedure—including extremities, mammography, photofluorography, cinefluorography, duplicating and radiation therapy. In fact, there's usually an array of films for each purpose, so there's not only one that's right for the job, but right for the particular subject as well.

They're all there when you need them, each with the consistent quality you expect from any Kodak product. All with the service and support that help make them as cost-effective as they are good. Your Kodak representative has the details.

Kodak
Official Diagnostic Imaging Products Sponsor of the 1988 Olympic Games

The new vision of Kodak

Kodak

© Eastman Kodak Company, 1987

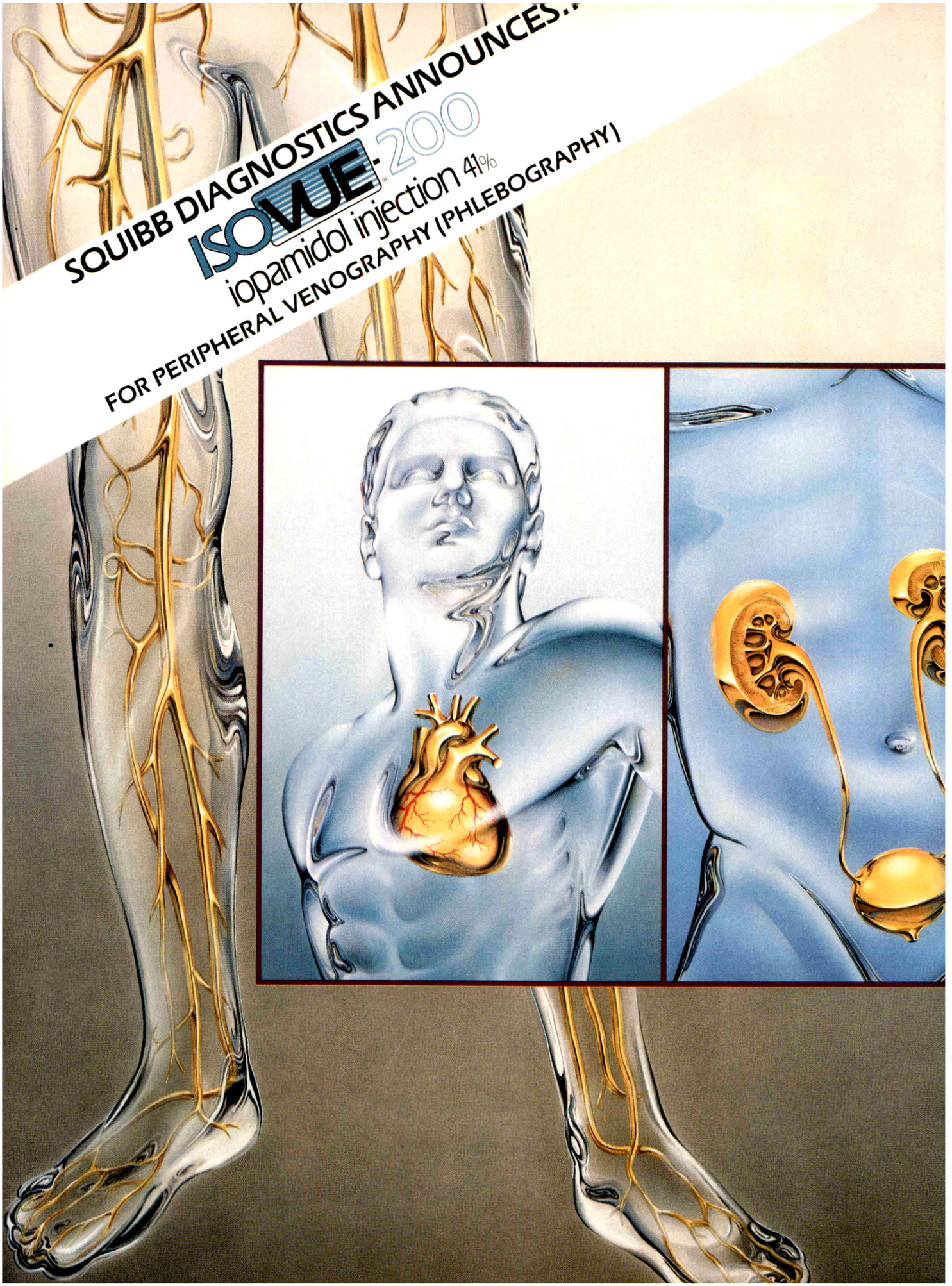
SQUIBB DIAGNOSTICS ANNOUNCES
ISOVUE-200
iopamidol injection 41%
FOR PERIPHERAL VENOGRAPHY (PHLEBOGRAPHY)

In radiologic contrast procedures

ISOVUE® / ISOVUE-M®

iopamidol injection

THE CLEAR CHOICE

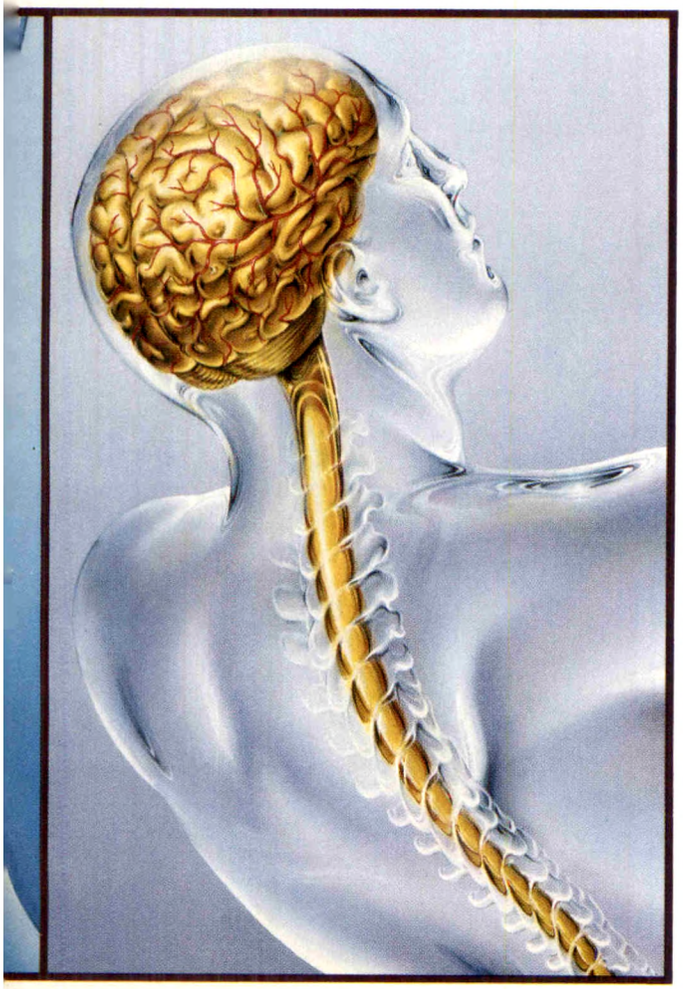

A broad range of indications

Peripheral arteriography
Coronary arteriography and ventriculography
IVP (excretory urography)
Myelography (lumbar, thoracic, cervical, total columnar)
Cerebral arteriography
CT head and body imaging
CT cisternography and ventriculography
Visceral arteriography (selective)
Aortography
IA-DSA
Peripheral venography (phlebography)

The only nonionic contrast agents you need to stock

SQUIBB™ Diagnostics

CIRCLE 14 ON READER SERVICE CARD

Please see brief summary of prescribing information on adjacent pages.

This product is under license from Bracco Industria Chimica, S.p.A. U.S. Patent #4,001,323

© 1988 E.R. Squibb & Sons, Inc., Princeton, NJ

647-508

Issued: January 1988

ISOVUE®-128 (Iopamidol Injection 26%)
ISOVUE®-200 (Iopamidol Injection 41%)
ISOVUE®-300 (Iopamidol Injection 61%)
ISOVUE®-370 (Iopamidol Injection 76%)
ISOVUE-M® 200 (Iopamidol Injection 41%)
ISOVUE-M® 300 (Iopamidol Injection 61%)

INDICATIONS AND USAGE

ISOVUE (Iopamidol Injection) is indicated for intra-arterial digital subtraction angiography (DSA) of the cerebral and abdominal vasculature and for angiography throughout the cardiovascular system, including cerebral and peripheral arteriography, coronary arteriography and ventriculography, selective visceral arteriography and aortography, peripheral venography (phlebography), and intravenous excretory urography and intravenous contrast enhancement of computed tomographic (CECT) head and body imaging.

ISOVUE-M (Iopamidol Injection) is indicated for intrathecal administration in neuroradiology including myelography (lumbar, thoracic, cervical, total columnar), and for contrast enhancement of computed tomographic (CECT) cisternography and ventriculography.

CONTRAINDICATIONS

ISOVUE (Iopamidol Injection)

None.

ISOVUE-M (Iopamidol Injection)

Intrathecal administration of corticosteroids with iopamidol is contraindicated. Because of overdosage considerations, immediate repeat myelography in the event of technical failure is contraindicated (see interval recommendation under DOSAGE AND ADMINISTRATION). Myelography should not be performed in the presence of significant local or systemic infection where bacteremia is likely.

WARNINGS

ISOVUE-M (Iopamidol Injection)

The need for myelographic examination should be carefully evaluated. Iopamidol should be administered with caution in patients with increased intracranial pressure or suspicion of intracranial tumor, abscess or hematoma, those with a history of convulsive disorder, severe cardiovascular disease, chronic alcoholism, or multiple sclerosis, and elderly patients. Particular attention must be given to state of hydration, concentration of medium, dose, and technique used in these patients.

If frankly bloody cerebrospinal fluid is observed, the possible benefits of a myelographic examination should be considered in terms of risk to the patient.

Patients on anticonvulsant medication should be maintained on this therapy.

Direct intracisternal or ventricular administration for standard radiography (without computerized tomographic enhancement) is not recommended. Inadvertent intracranial entry of a large or concentrated bolus of the contrast medium, which increases the risk of neurotoxicity, can be prevented by careful patient management. Also, effort should be directed to avoid rapid dispersion of the medium causing inadvertent rise to intracranial levels (e.g., by active patient movement). If such intracranial entry of the medium occurs, prophylactic anticonvulsant treatment with diazepam or barbiturates orally for 24 to 48 hours should be considered.

Use of medications that may lower the seizure threshold (phenothiazine derivatives, including those used for their antihistaminic properties; tricyclic antidepressants; MAO inhibitors; CNS stimulants; analeptics; antipsychotic agents) should be carefully evaluated. While the contributory role of such medications has not been established, some physicians have discontinued these agents at least 48 hours before and for at least 24 hours following intrathecal use.

Focal and generalized motor seizures have been reported after intrathecal use of water-soluble contrast agents including iopamidol. In several of those cases reported with iopamidol, higher than recommended doses were employed. Therefore *avoid:*

- Deviations from recommended neuroradiologic procedure or patient management.
- Use in patients with a history of epilepsy unless medically justified.
- Overdosage.
- Intracranial entry of a bolus or premature diffusion of a high concentration of the medium.
- Failure to maintain elevation of the head during the procedure, on the stretcher, and in bed.
- Excessive and particularly active patient movement or straining.

ISOVUE (Iopamidol Injection)

Caution must be exercised in patients with severely impaired renal function, those with combined renal and hepatic disease, or anuria particularly when larger doses are administered.

Radiopaque diagnostic contrast agents are potentially hazardous in patients with multiple myeloma or other paraproteinemia, particularly in those with therapeutically resistant anuria. Myeloma occurs most commonly in persons over age 40. Although neither the contrast agent nor dehydration has been proved separately to be the cause of anuria in myelomatous patients, it has been speculated that the combination of both may be causative. The risk in myelomatous patients is not a contraindication; however, special precautions are required.

Contrast media may promote sickling in individuals who are homozygous for sickle cell disease when injected intravenously or intraarterially.

Administration of radiopaque materials to patients known or suspected of having pheochromocytoma should be performed with extreme caution. If, in the opinion of the physician, the possible benefits of such procedures outweigh the considered risks, the procedures may be performed; however, the amount of radiopaque medium injected should be kept to an absolute minimum. The blood pressure should be assessed throughout the procedure and measures for treatment of a hypertensive crisis should be available. These patients should be monitored very closely during contrast-enhanced procedures.

Reports of thyroid storm following the use of iodinated radiopaque diagnostic agents in patients with hyperthyroidism or with an autonomously functioning thyroid nodule suggest that this additional risk be evaluated in such patients before use of any contrast medium.

PRECAUTIONS

General

Diagnostic procedures which involve the use of any radiopaque agent should be carried out under the direction of personnel with the prerequisite training and with a thorough knowledge of the particular procedure to be performed. Appropriate facilities should be available for coping with any complication of the procedure, as well as for emergency treatment of severe reaction to the contrast agent itself. After parenteral administration of a radiopaque agent, competent personnel and emergency facilities should be available for at least 30 to 60 minutes since severe delayed reactions may occur.

Preparatory dehydration is dangerous and may contribute to acute renal failure in patients with advanced vascular disease, diabetic patients, and in susceptible nondiabetic patients (often elderly with preexisting renal disease). *Patients should be well hydrated prior to and following iopamidol administration.*

The possibility of a reaction, including serious, life-threatening, fatal, anaphylactoid or cardiovascular reactions, should always be considered (see ADVERSE REACTIONS). Patients at increased risk include those with a history of a previous reaction to a contrast medium, patients with a known sensitivity to iodine per se, and patients with a known clinical hypersensitivity (bronchial asthma, hay fever, and food allergies). The occurrence of severe idiosyncratic reactions has prompted the use of several pretesting methods. However, pretesting cannot be relied upon to predict severe reactions and may itself be hazardous for the patient. It is suggested that a thorough medical history with emphasis on allergy and hypersensitivity, prior to the injection of any contrast medium, may be more accurate than pretesting in predicting potential adverse reactions. A positive history of allergies or hypersensitivity does not arbitrarily contraindicate the use of a contrast agent where a diagnostic procedure is thought essential, but caution should be exercised. Premedication with antihistamines or corticosteroids to avoid or minimize possible allergic reactions in such patients should be considered (see CONTRAINDICATIONS). Reports indicate that such pretreatment does not prevent serious life-threatening reactions, but may reduce both their incidence and severity.

General anesthesia may be indicated in the performance of some procedures in selected patients; however, a higher incidence of adverse reactions has been reported with radiopaque media in anesthetized patients, which may be attributable to the inability of the patient to identify untoward symptoms, or to the hypotensive effect of anesthesia which can reduce cardiac output and increase the duration of exposure to the contrast agent.

Even though the osmolality of iopamidol is low compared to diatrizoate or iothalamate based ionic agents of comparable iodine concentration, the potential transitory increase in the circulatory osmotic load in patients with congestive heart failure requires caution during injection. These patients should be observed for several hours following the procedure to detect delayed hemodynamic disturbances.

In angiographic procedures, the possibility of dislodging plaques or damaging or perforating the vessel wall should be borne in mind during catheter manipulations and contrast medium injection. Test injections to ensure proper catheter placement are suggested. Following arteriographic procedures, gentle pressure hemostasis is required, followed by observation and immobilization of the limb for several hours to prevent hemorrhage from the site of arterial puncture.

The inhibitory effects of nonionic contrast media on mechanisms of hemostasis have been shown, in vitro, to be less than ionic contrast media at comparable concentrations. For this reason, standard angiographic procedures should always be followed: angiographic catheters should be flushed frequently, and prolonged contact of blood with contrast in syringes and catheters should be avoided.

Selective coronary arteriography should be performed only in selected patients and those in whom the expected benefits outweigh the procedural risk. The inherent risks of angiocardiography in patients with chronic pulmonary emphysema must be weighed against the necessity for performing this procedure. Angiography should be avoided whenever possible in patients with homocystinuria, because of the risk of inducing thrombosis and embolism.

In addition to the general precautions previously described, special care is required when venography is performed in patients with suspected thrombosis, phlebitis, severe ischemic disease, local infection or a totally obstructed venous system.

Extreme caution during injection of contrast media is necessary to avoid extravasation and fluoroscopy is recommended. This is especially important in patients with severe arterial or venous disease.

If nondisposable equipment is used, scrupulous care should be taken to prevent residual contamination with traces of cleansing agents.

Information For Patients

Patients receiving injectable radiopaque diagnostic agents should be instructed to:

1. Inform your physician if you are pregnant.
2. Inform your physician if you are diabetic or if you have multiple myeloma, pheochromocytoma, homozygous sickle cell disease, or known thyroid disorder (see WARNINGS).
3. Inform your physician if you are allergic to any drugs, food, or if you had any reactions to previous injections of substances used for x-ray procedures (see PRECAUTIONS, General).
4. Inform your physician about any other medications you are currently taking, including nonprescription drugs, before you have this procedure.

Drug Interactions

Renal toxicity has been reported in a few patients with liver dysfunction who were given oral cholecystographic agents followed by intravascular contrast agents. Administration of intravascular agents should therefore be postponed in any patient with a known or suspected hepatic or biliary disorder who has recently received a cholecystographic contrast agent.

Other drugs should not be admixed with iopamidol.

Drug/Laboratory Test Interactions

The results of PBI and radioactive iodine uptake studies, which depend on iodine estimations, will not accurately reflect thyroid function for up to 16 days following administration of iodinated contrast media. However, thyroid function tests not depending on iodine estimations, e.g., T3 resin uptake and total or free thyroxine (T4) assays are not affected.

Any test which might be affected by contrast media should be performed prior to administration of the contrast medium.

Laboratory Test Findings

In vitro studies with animal blood showed that many radiopaque contrast agents, including iopamidol, produced a slight depression of plasma coagulation factors including prothrombin time, partial thromboplastin time, and fibrinogen, as well as a slight tendency to cause platelet and/or red blood cell aggregation (see PRECAUTIONS, General).

Transitory changes may occur in red cell and leucocyte counts, serum calcium, serum creatinine, serum glutamic oxalacetic transaminase (SGOT), and uric acid in urine; transient albuminuria may occur.

These findings have not been associated with clinical manifestations.

Carcinogenesis, Mutagenesis, Impairment Of Fertility

In animal reproduction studies performed on rats, intravenously administered iopamidol did not induce adverse effects on fertility or general reproductive performance.

In studies to determine mutagenic activity, iopamidol did not cause any increase in mutation rates.

Pregnancy Category B

No teratogenic effects attributable to iopamidol have been observed in teratology studies performed in animals. There are, however, no adequate and well controlled studies in pregnant women. It is not known whether iopamidol crosses the placental barrier or reaches fetal tissues. However, many injectable contrast agents cross the placental barrier in humans and appear to enter fetal tissues passively. Because animal teratology studies are not always predictive of human response, this drug should be used during pregnancy only if clearly needed.

Radiologic procedures involve a certain risk related to the exposure of the fetus to ionizing radiation.

Labor and Delivery

It is not known whether use of contrast agents during labor or delivery has immediate or delayed adverse effects on the fetus, prolongs the duration of labor or increases the likelihood that forceps delivery or other obstetrical intervention or resuscitation of the newborn will be necessary.

Nursing Mothers

It is not known whether iopamidol is excreted in human milk. However, many injectable contrast agents are excreted unchanged in human milk. Although it has not been established that serious adverse reactions occur in nursing infants, caution should be exercised when intravascular contrast media are administered to nursing women because of potential adverse reactions, and consideration should be given to temporarily discontinuing nursing.

Pediatric Use

Safety and effectiveness in children have not been established.

ADVERSE REACTIONS

ISOVUE (Iopamidol Injection)

Adverse reactions following the use of iopamidol are usually mild to moderate, self-limited, and transient.

In a clinical trial with 100 patients undergoing intra-arterial DSA, adverse reactions possibly attributed to ISOVUE-128 administration were nausea (2%), headache (1%) and vomiting (1%). One patient with preexisting renal impairment and severe bilateral renal vascular disease experienced renal failure, possibly secondary to a subsequent acute episode of congestive heart failure and/or drug administration (see Warnings).

In angiocardiography (597 patients), the adverse reactions with an estimated incidence of one percent or higher are: hot flashes 3.4%; angina pectoris 3.0%; flushing 1.8%; bradycardia 1.3%; hypotension 1.0%; hives 1.0%.

Intravascular injection of contrast media is frequently associated with the sensation of warmth and pain, especially in peripheral arteriography and venography; pain and warmth are less frequent and less severe with ISOVUE (Iopamidol Injection) than with diatrizoate meglumine and diatrizoate sodium injection.

The following table of incidence of reactions is based on clinical studies with ISOVUE in about 1941 patients.

Adverse Reactions

System	Estimated Overall Incidence > 1%	≤ 1%
Cardiovascular	none	tachycardia hypotension hypertension myocardial ischemia circulatory collapse S-T segment depression bigeminy extrasystoles ventricular fibrillation angina pectoris bradycardia transient ischemic attack thrombophlebitis
Nervous	pain (2.8%) burning sensation (1.4%)	vasovagal reaction tingling in arms grimace faintness
Digestive	nausea (1.2%)	vomiting anorexia
Respiratory	none	throat constriction dyspnea pulmonary edema
Skin and Appendages	none	rash urticaria pruritus flushing
Body as a Whole	hot flashes (1.5%)	headache fever chills excessive sweating back spasm
Special Senses	warmth (1.1%)	taste alterations nasal congestion visual disturbances
Urogenital	none	urinary retention

Regardless of the contrast agent employed, the overall estimated incidence of serious adverse reactions is higher with *coronary arteriography* than with other procedures. Cardiac decompensation, serious arrhythmias, or myocardial ischemia or infarction may occur during *coronary arteriography and left ventriculography.* Following coronary and ventricular injections, certain electrocardiographic changes (increased QTc, increased R-R, T-wave amplitude) and certain hemodynamic changes (decreased systolic pressure) occurred less frequently with ISOVUE (Iopamidol Injection) than with diatrizoate meglumine and diatrizoate sodium injection; increased LVEDP occurred less frequently after ventricular iopamidol injections.

In *aortography,* the risks of procedures also include injury to the aorta and neighboring organs, pleural puncture, renal damage including infarction and acute tubular necrosis with oliguria and anuria, accidental selective filling of the right renal artery during the translumbar procedure in the presence of preexisting renal disease, retroperitoneal hemorrhage from the translumbar approach, and spinal cord injury and pathology associated with the syndrome of transverse myelitis.

Adverse effects reported in clinical literature for iopamidol include arrhythmia, arterial spasms, hematuria, periorbital edema, involuntary leg movement, malaise, and triggering of deglutition; some of these may occur as a consequence of the procedure. Other reactions may also occur with the use of any contrast agent as a consequence of the procedural hazard; these include hemorrhage or pseudoaneurysms at the puncture site, brachial plexus palsy following axillary artery injections, chest pain, myocardial infarction, and transient changes in hepatorenal chemistry tests. Arterial thrombosis, displacement of arterial plaques, venous thrombosis, dissection of the coronary vessels and transient sinus arrest are rare complications.

ISOVUE-M (Iopamidol Injection)

The most frequently reported adverse reactions following intrathecal administration of iopamidol are headache, nausea, vomiting and musculoskeletal pain. These reactions usually occur 1 to 10 hours after injection, almost all occurring within 24 hours. They are usually mild to moderate in degree lasting for a few hours and usually disappearing within 24 hours. Rarely, headaches may be severe or persist for days. Headache is often accompanied by nausea and vomiting, and tends to be more frequent and persistent in patients not optimally hydrated.

Backache, neck stiffness, numbness and paresthesias, leg or sciatic-type pain occurred less frequently, often in the form of a transient exacerbation of preexisting symptomatology. Transient alterations in vital signs may occur and their significance must be assessed on an individual basis.

The following table of incidence of reactions is based on clinical studies with ISOVUE-M (Iopamidol Injection) in about 615 patients.

Adverse Reactions

System	Estimated Overall Incidence > 1%	≤ 1%
Body as a Whole	headache (18.1%)	pyrexia muscle weakness hot flashes malaise fatigue weakness
Digestive	nausea (7.3%) vomiting (3.7%)	diarrhea heartburn
Musculoskeletal	back pain (2.3%) leg pain (1.4%) neck pain (1.1%)	leg cramps sciatica cervicobrachial irritation meningeal irritation radicular irritation, lumbosacral other musculoskeletal pain involuntary movement burning sensation
Cardiovascular	hypotension (1.1%)	tachycardia hypertension chest pain

Adverse Reactions (con't)

System	Estimated Overall Incidence > 1%	≤ 1%
Nervous	none	emotional stress dizziness paresthesia confusion hallucinations lightheadedness syncope numbness cold extremities
Urogenital	none	urinary retention
Respiratory	none	dyspnea
Skin and Appendages	none	rash
Miscellaneous	none	injection site pain

Other adverse effects reported in clinical literature for iopamidol include facial neuralgia, tinnitus, and sweating.

Major motor seizures have been reported in the clinical literature and since market introduction in the United States. Early onset of seizures (less than two hours) is indicative of early substantial intracranial entry. Transitory EEG changes occur and usually take the form of slow wave activity.

While not observed in controlled clinical studies with ISOVUE-M (Iopamidol Injection), or reported in clinical literature, the following adverse reactions may occur because they have been reported with other nonionic contrast agents: cardiovascular (arrhythmias); aseptic meningitis syndrome; allergy or idiosyncrasy (chills, pruritus, nasal congestion, Guillain-Barre syndrome); CNS irritation (psycho-organic syndrome: mild and transitory perceptual aberrations such as depersonalization, anxiety, depression, hyperesthesia, disturbances in speech, sight, or hearing, and disorientation; in addition, hyperreflexia or areflexia, hypertonia or flaccidity, restlessness, tremor, echoacousia, echolalia, asterixis or dysphasia have occurred). Profound mental disturbances have rarely been reported (various forms and degrees of aphasia, mental confusion or disorientation); the onset is usually at 8 to 10 hours and lasts for about 24 hours without aftereffects.

However, occasionally they have been manifest as apprehension, agitation, or progressive withdrawal to the point of stupor in several instances. In a few cases, these have been accompanied by transitory hearing loss or other auditory symptoms and visual disturbances (believed subjective or delusional). Persistent cortical loss of vision in association with convulsions, and ventricular block have been reported. Rarely, persistent though transitory weakness in the leg or ocular muscles has been reported. *Peripheral neuropathies* have been rare and transitory. They include sensory and/or motor or nerve root disturbances, myelitis, persistent leg muscle pain or weakness, or sixth nerve palsy, or cauda equina syndrome. Muscle cramps, fasciculation or myoclonia, spinal convulsion, or spasticity are unusual.

General Adverse Reactions To Contrast Media

Reactions known to occur with parenteral administration of iodinated ionic contrast agents (see the listing below) are possible with any nonionic agent. Approximately 95 percent of adverse reactions accompanying the use of other water-soluble intravascularly administered contrast agents are mild to moderate in degree. However, life-threatening reactions and fatalities, mostly of cardiovascular origin, have occurred.

Reported incidences of death from the administration of other iodinated contrast media range from 6.6 per 1 million (0.00066 percent) to 1 in 10,000 patients (0.01 percent). Most deaths occur during injection or 5 to 10 minutes later, the main feature being cardiac arrest with cardiovascular disease as the main aggravating factor. Isolated reports of hypotensive collapse and shock are found in the literature. The incidence of shock is estimated to be 1 out of 20,000 (0.005 percent) patients.

Adverse reactions to injectable contrast media fall into two categories: chemotoxic reactions and idiosyncratic reactions. Chemotoxic reactions result from the physico-chemical properties of the contrast medium, the dose, and the speed of injection. All hemodynamic disturbances and injuries to organs or vessels perfused by the contrast medium are included in this category. Experience with iopamidol suggests there is much less discomfort (e.g., pain and/or warmth) with peripheral arteriography. Fewer changes are noted in ventricular function after ventriculography and coronary arteriography.

Idiosyncratic reactions include all other reactions. They occur more frequently in patients 20 to 40 years old. Idiosyncratic reactions may or may not be dependent on the amount of drug injected, the speed of injection, the mode of injection, and the radiographic procedure. Idiosyncratic reactions are subdivided into minor, intermediate, and severe. The minor reactions are self-limited and of short duration; the severe reactions are life-threatening and treatment is urgent and mandatory.

The reported incidence of adverse reactions to contrast media in patients with a history of allergy is twice that for the general population. Patients with a history of previous reactions to a contrast medium are three times more susceptible than other patients. However, sensitivity to contrast media does not appear to increase with repeated examinations. Most adverse reactions to intravascular contrast agents appear within one to three minutes after the start of injection, but delayed reactions may occur (see PRECAUTIONS, General).

Because measurable plasma levels are attained following the intrathecal administration of iopamidol, adverse reactions reported with the use of intravascular contrast agents are theoretically possible. In addition to the adverse drug reactions reported for iopamidol, the following additional adverse reactions have been reported with the use of other intravascular contrast agents and are possible with the use of any water-soluble iodinated contrast agent:

Cardiovascular: vasodilation, cerebral hematomas, petechiae, hemodynamic disturbances, sinus bradycardia, transient electrocardiographic abnormalities, ventricular fibrillation.

Digestive: nausea, vomiting, severe unilateral or bilateral swelling of the parotid and submaxillary glands.

Nervous: paresthesia, dizziness, convulsions, paralysis, coma.

Respiratory: increased cough, asthma, laryngeal edema, pulmonary edema, bronchospasm, rhinitis, dyspnea.

Skin and Appendages: injection site pain usually due to extravasation and/or erythematous swelling, skin necrosis.

Urogenital: osmotic nephrosis of proximal tubular cells, renal failure, pain.

Special Senses: bilateral ocular irritation; lacrimation; conjunctival chemosis, infection, and conjunctivitis; itching.

The following reactions may also occur: neutropenia, thrombophlebitis, flushing, pallor, weakness, severe retching and choking, wheezing, cramps, tremors, and sneezing.

HOW SUPPLIED

ISOVUE-128: 10 x 50 mL vials; ISOVUE-200: 10 x 50 mL vials and 10 x 100 mL bottles; ISOVUE-300: 10 x 50 mL vials and 10 x 100 mL bottles and 10 x 150 mL bottles; ISOVUE-370: 10 x 50 mL vials and 10 x 100 mL, 10 x 150 mL and 10 x 200 mL bottles; ISOVUE-M 200: 10 x 20 mL vials; ISOVUE-M 300: 10 x 15 mL vials.

STORAGE

ISOVUE® and ISOVUE-M® (iopamidol injection) should be stored at room temperature not exceeding 86° F. Protect from light.

For full prescribing information consult package insert.

J3-702A/J3-652E/J3-653E.

© 1987 E.R. Squibb & Sons, Inc., Princeton, NJ 647-508 Issued: November 1987

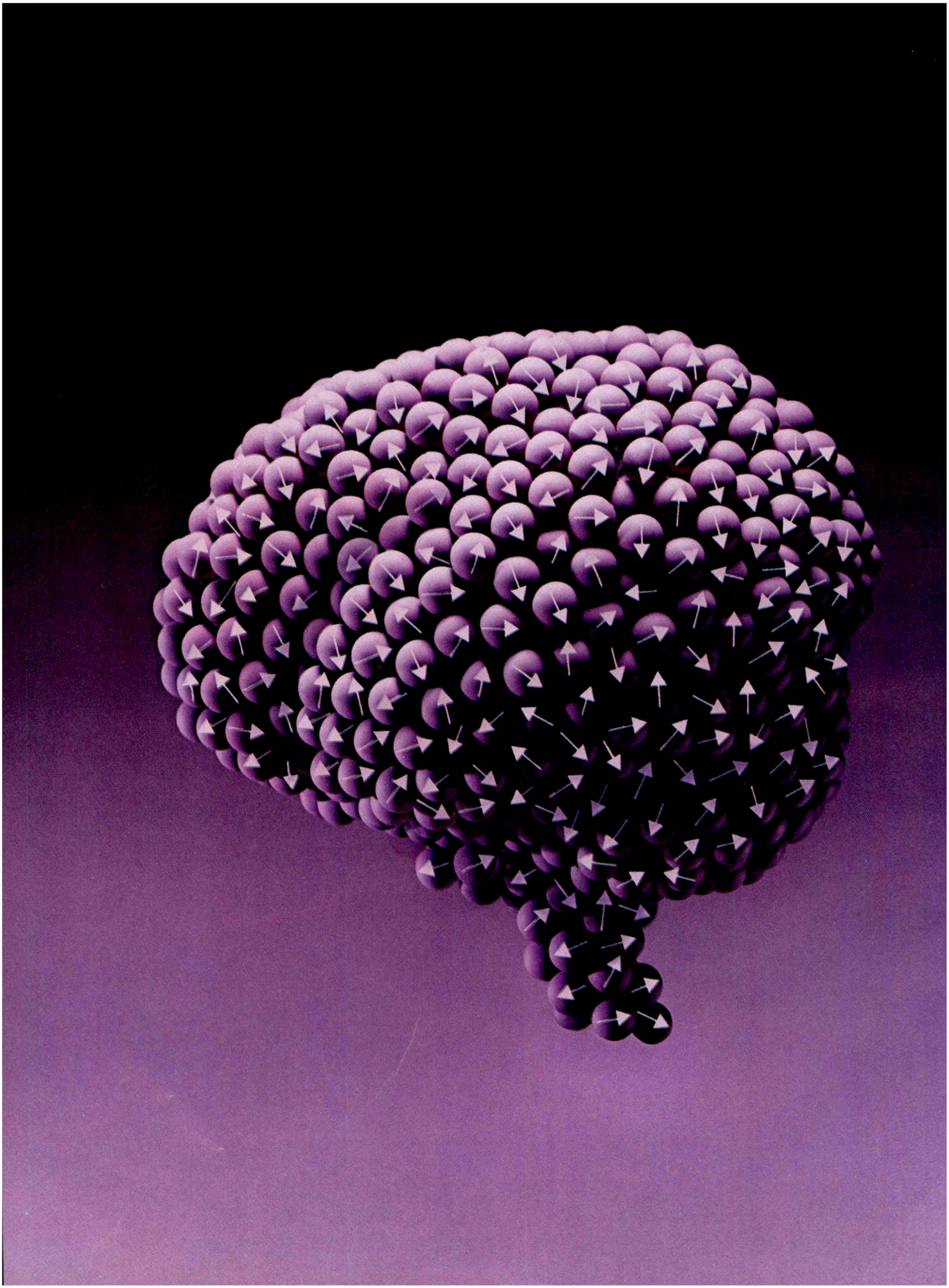

COMING SOONER THAN YOU THINK *MRI*

BEYOND THE IMAGINATION

Imaging that's going to give you the details you've always wanted. Images that help define and differentiate. That's what the researchers at Berlex Imaging have been working on. Our research is dedicated to developing contrast material so you can see as you've never seen before. The results of our research may be here sooner than you think. But it's only the beginning of imaging beyond the imagination from Berlex.

BERLEX IMAGING™

Berlex Imaging
300 Fairfield Road
Wayne, NJ 07470

Yes, I want to be one of the first to know about MRI beyond the imagination.

name

address

city state zip

( ) area code telephone no.

specialty (including subspecialty) ID number

CIRCLE 34 ON READER SERVICE CARD

© 1987, Berlex Laboratories, Inc. All rights reserved.

890-1 890-1.1 Printed in USA September 1987

Need shelf space?

Williams & Wilkins is your source for back issues of this journal in microform.

Free Up 98% Of
Your Shelf Space With
Microform Conversion

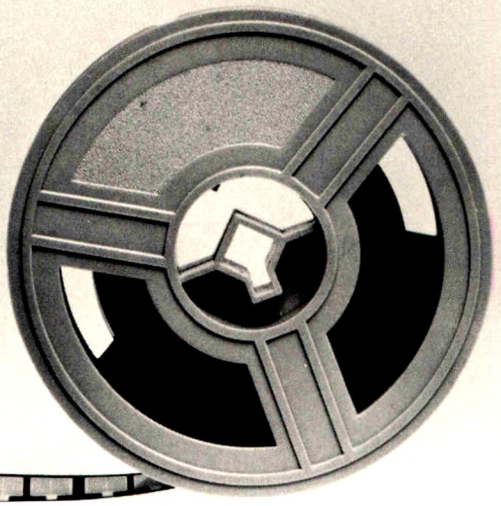

MICROFILM editions are available for this journal direct from the publisher. Many Williams & Wilkins journals as well as those journals distributed by the Publishing Services Division of Waverly Press, Inc. are also available for a single volume year or on a standing order basis.

FOR ORDERING INFORMATION: Write to the address below or call **TOLL-FREE 1-800-638-6423.** In Maryland call **COLLECT** 528-4105.

☐ **Please send me microform back issue ordering information for** _____
Journal Name

Name _____

Title _____

Address _____

City/State/Zip _____

Mail to:

Williams & Wilkins
Microform Sales
Attention: Yvonne Hahn
428 East Preston Street
Baltimore, Maryland 21203

or

266 Fulham Road
London SW10 9EL England

Formats available:
- 16-mm reel
- 35-mm reel
- 16-mm cartridge (3M or Kodak)
- positive or negative film

MICROAD 50567

Sets the tract record for BE prep.

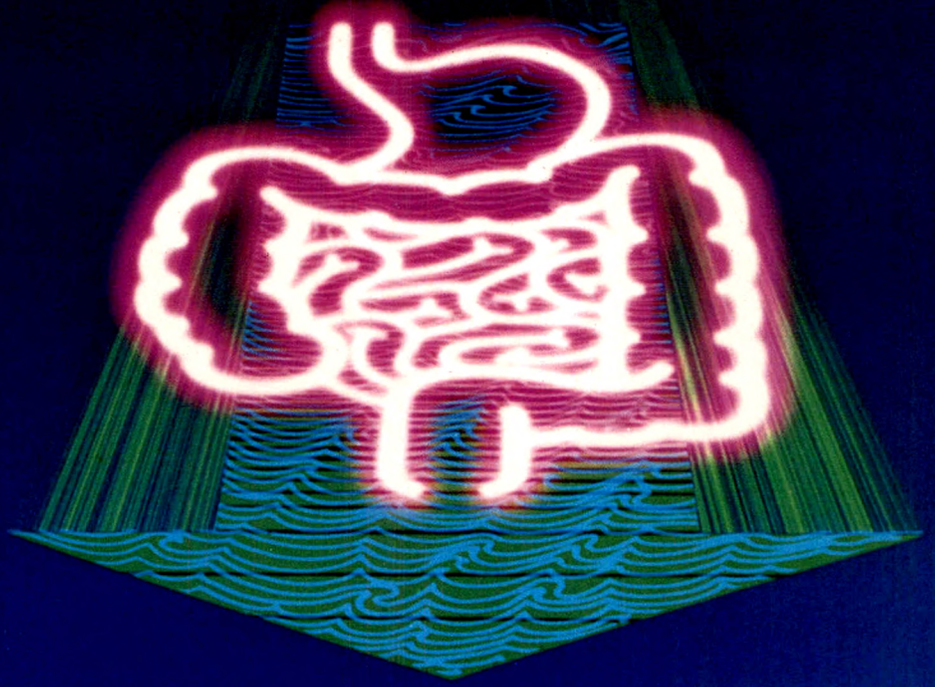

New Lower Price

GoLYTELY®

(PEG Electrolyte for Gastrointestinal Lavage Solution)

Excellent results in 4 hours . . . clinical studies have shown that GoLYTELY is equal in efficacy to a rigorous one- to two-day prep for air-contrast barium studies, particularly if **bisacodyl USP*** is also given to ensure the evacuation of any residual fluid.[1,2]

Patients prefer GoLYTELY because it's a more convenient routine to follow at home and it's usually well tolerated, even by older patients.[3] And since it's premeasured—just make up to volume in its own container with tap water—GoLYTELY guards against incorrect or inadequate usage.

Professionals prefer GoLYTELY because it can keep more patients ambulatory longer. For hospitalized patients, GoLYTELY can reduce length of stay because the prep takes less time.

With a clean bowel, repeat exams are less frequent—a plus under DRGs. Prescribed volumes of GoLYTELY solution can be given without significant change in water or electrolyte balance.

GoLYTELY is generally well tolerated and side effects are transient. Patients with impaired gag reflex who are prone to regurgitation or aspiration should be observed during the administration of GoLYTELY. If obstruction or perforation is suspected, appropriate studies should be performed to rule out these contraindications. GoLYTELY is also contraindicated in patients with gastric retention, toxic colitis, or toxic megacolon.

*Complimentary tablets of bisacodyl, USP, are attached to the patient pamphlet **Bowel Preparation Before Your Barium Enema.** A supply is available to professionals by writing Braintree Laboratories at the address below.

BRIEF SUMMARY: Before prescribing, see package insert or *PDR*.

INDICATIONS AND USAGE: GoLYTELY is indicated for bowel cleansing prior to colonoscopy and barium enema x-ray examination.

CONTRAINDICATIONS: GoLYTELY is contraindicated in patients with gastrointestinal obstruction, gastric retention, bowel perforation, toxic colitis, or toxic megacolon.

WARNINGS: No additional ingredients—eg, flavorings—should be added to the solution. GoLYTELY should be used with caution in patients with severe ulcerative colitis.

PRECAUTIONS: *General:* Patients with impaired gag reflex, unconscious or semiconscious patients, and patients prone to regurgitation or aspiration should be observed during the administration of GoLYTELY, especially if it is administered via nasogastric tube. If a patient experiences severe bloating, distention, or abdominal pain, administration should be slowed or discontinued temporarily until the symptoms abate. If gastrointestinal obstruction or perforation is suspected, appropriate studies should be performed to rule out these conditions before administration of GoLYTELY.

ADVERSE REACTIONS: Nausea, abdominal fullness, and bloating are the most common adverse reactions (occurring in up to 50% of patients) to administration of GoLYTELY. Abdominal cramps, vomiting, and anal irritation occur less frequently. These adverse reactions are transient and subside rapidly. Isolated cases of urticaria, rhinorrhea, and dermatitis —which may represent allergic reactions—have been reported.

CAUTION: Federal law prohibits dispensing without prescription.

STORAGE: Store in sealed container at 59°-86°F When reconstituted, keep solution refrigerated. Use within 48 hours. Discard unused portion.

(NDC 52268-0100-01). Revised 10/1/86

Made by Lyne Laboratories, Stoughton, MA 02072, for BRAINTREE LABORATORIES, INC., P.O. Box 361, Braintree, MA 02184.

References: 1. Ernstoff JJ, et al: *Gastroenterology* 1983; 84:1512-1516. **2.** Girard CM, et al: AJR 1984; 142:1147-1149. **3.** DiPalma JA, et al: *Am J Gastroenterol* 1986; 81:652-655.

CIRCLE 35 ON READER SERVICE CARD

LABORATORIES · INC
Braintree

There are reasons
S.&S. X-RAY ACCESSORIES
are preferred...

PROVEN the best in X-Ray Departments throughout the world

UNEQUALLED in design, construction and—quality

REPUTATION unmatched for RELIABILITY and PERFORMANCE

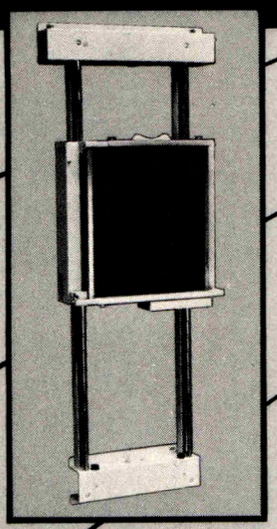

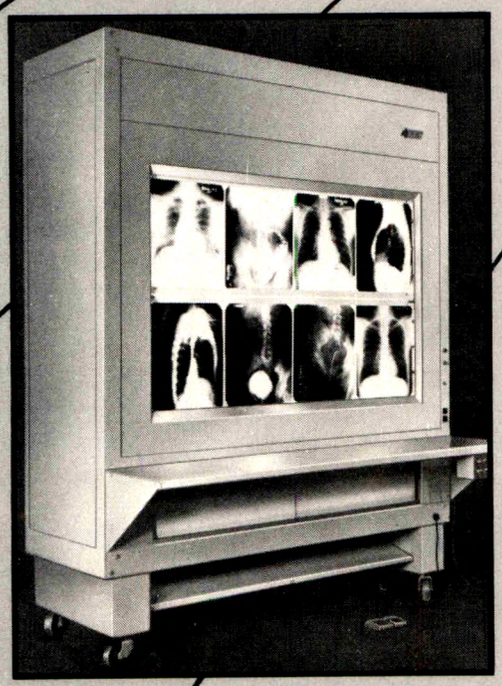

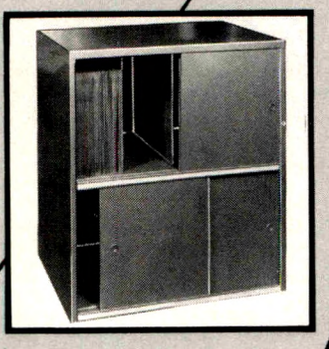

- Motorized Viewers
- Illuminators
- Transfer Cabinets
- File Cabinets
- Protective Panels
- Protective Aprons
- Wall Cassette Holders
- Dryers
- Safelights
- Dark Room Cabinets
- Storage Chests
- Loading Bins
- X-Ray Accessories

For more than 30 years, S. & S. has been meeting Radiologists' needs with a complete line of illuminators and accessories.

Contact S. & S. or your local x-ray dealer for additional information.

MANUFACTURED BY
S. & S. X-RAY PRODUCTS INC.

The Complete Line of X-Ray Accessories
Call Toll Free: 800-221-6634

Telephone: 718-649-8500
1101 LINWOOD STREET, BROOKLYN, NY 11208

CIRCLE 9 ON READER SERVICE CARD

Conray® (iothalamate meglumine injection U.S.P. 60%)

Each milliliter contains 600 mg of iothalamate meglumine, 0.09 mg edetate calcium disodium as a stabilizer and 0.125 mg of monobasic sodium phosphate as a buffer. The solution provides 28.2% (282 mg/mL) organically bound iodine.

Conray®-43 (iothalamate meglumine injection U.S.P. 43%)

Each milliliter contains 430 mg of iothalamate meglumine, 0.110 mg edetate calcium disodium as a stabilizer and 0.115 mg of monobasic sodium phosphate as a buffer. The solution provides 20.2% (202 mg/mL) organically bound iodine.

INDICATIONS AND USAGE

CONRAY is indicated for use in excretory urography, cerebral angiography, peripheral arteriography, venography, arthrography, direct cholangiography, endoscopic retrograde cholangiopancreatography, contrast enhancement of computed tomographic brain images, cranial computerized angiotomography, intravenous digital subtraction angiography and arterial digital subtraction angiography.

CONRAY-43 is indicated for use in lower extremity venography, intravenous infusion urography, contrast enhancement of computed tomographic brain images and arterial digital subtraction angiography.

CONRAY and CONRAY-43 may also be used for enhancement of computed tomographic scans performed for detection and evaluation of lesions in the liver, pancreas, kidneys, abdominal aorta, mediastinum, abdominal cavity and retroperitoneal space. Continuous or multiple scans separated by intervals of 1-3 seconds during the first 30-90 seconds post-injection of the contrast medium (dynamic CT scanning) may provide enhancement of diagnostic significance, and may be of benefit in establishing diagnoses of certain lesions in these sites with greater assurance than is possible with CT alone, and in supplying additional features of the lesions. In other cases, the contrast agent may allow visualization of lesions not seen with CT alone, or may help to define suspicious lesions seen with unenhanced CT. Subsets of patients in whom delayed body CT scans might be helpful have not been identified. Inconsistent results have been reported and abnormal and normal tissues may be isodense during the time frame used for delayed CT scanning. The risks of such indiscriminate use of contrast media are well known and such use is not recommended. At present, consistent results have been documented using dynamic CT techniques only.

CONTRAINDICATIONS

Refer to PRECAUTIONS, General, concerning hypersensitivity. CONRAY and CONRAY-43 should not be used for myelography. Arthrography should not be performed if infection is present in or near the joint. Percutaneous transhepatic cholangiography is contraindicated in patients with coagulation defects and prolonged prothrombin times. Endoscopic retrograde cholangiopancreatography is contraindicated during an acute attack of pancreatitis or during severe clinically evident cholangitis and in patients in whom endoscopy is prohibited.

WARNINGS

Serious or fatal reactions have been associated with the administration of iodine containing radiopaque media. It is of utmost importance to be completely prepared to treat any contrast medium reaction.

Serious neurologic sequelae, including permanent paralysis, have been reported following cerebral arteriography, selective spinal arteriography and arteriography of vessels supplying the spinal cord. The intravascular injection of a contrast medium should never be made following the administration of vasopressors since they strongly potentiate neurologic effects.

In patients with subarachnoid hemorrhage, a rare association between contrast administration and clinical deterioration, including convulsions and death, has been reported. Therefore, administration of intravascular iodinated ionic contrast media in these patients should be undertaken with caution.

A definite risk exists in the use of intravascular contrast agents in patients who are known to have multiple myeloma. In such instances anuria has developed resulting in progressive uremia, renal failure and eventually death. Although neither the contrast agent nor dehydration has separately proved to be the cause of anuria in myeloma, it has been speculated that the combination of both may be causative factors. The risk in myelomatous patients is not a contraindication to the procedure; however, partial dehydration in the preparation of these patients for the examination is not recommended since this may predispose to precipitation of myeloma protein in the renal tubules. No form of therapy, including dialysis, has been successful in reversing the effect. Myeloma, which occurs most commonly in persons over 40, should be considered before instituting intravascular administration of contrast agents.

Administration of radiopaque materials to patients known or suspected to have pheochromocytoma should be performed with extreme caution. If, in the opinion of the physician, the possible benefits of such procedures outweigh the considered risks, the procedures may be performed; however, the amount of radiopaque medium injected should be kept to an absolute minimum. The blood pressure should be assessed throughout the procedure, and measures for treatment of a hypertensive crisis should be available.

Contrast media have been shown to promote the phenomenon of sickling in individuals who are homozygous for sickle cell disease when the material is injected intravenously or intra-arterially.

Convulsions have occurred in patients with primary or metastatic cerebral lesions following the administration of iodine-containing radiopaque media for the contrast enhancement of CT brain images.

In patients with advanced renal disease, iodinated contrast media should be used with caution, and only when the need for the examination dictates, since excretion of the medium may be impaired. Patients with combined renal and hepatic disease, those with severe hypertension or congestive heart failure, and recent renal transplant recipients may present an additional risk.

Renal failure has been reported in patients with liver dysfunction who were given an oral cholecystographic agent followed by an intravascular iodinated radiopaque agent and also in patients with occult renal disease, notably diabetics and hypertensives. In these classes of patients there should be no fluid restriction and every attempt made to maintain normal hydration, prior to contrast medium administration, since dehydration is the single most important factor influencing further renal impairment.

Acute renal failure has been reported in diabetic patients with diabetic nephropathy and in susceptible non-diabetic patients (often elderly with pre-existing renal disease) following the administration of iodinated contrast agents. Therefore, careful consideration of the potential risks should be given before performing this radiographic procedure in these patients.

Caution should be exercised in performing contrast medium studies in patients with endotoxemia and/or those with elevated body temperatures.

Reports of thyroid storm occurring following the intravascular use of iodinated radiopaque agents in patients with hyperthyroidism or with an autonomously functioning thyroid nodule, suggest that this additional risk be evaluated in such patients before use of this drug. Iodine containing contrast agents may alter the results of thyroid function tests which depend on iodine estimation, e.g. PBI and radioactive iodine uptake studies. Such tests, if indicated, should be performed prior to the administration of this preparation.

PRECAUTIONS

General

Diagnostic procedures which involve the use of iodinated intra-vascular contrast agents should be carried out under the direction of personnel skilled and experienced in the particular procedure to be performed. All procedures utilizing contrast media carry a definite risk of producing adverse reactions. While most reactions may be minor, life threatening and fatal reactions may occur without warning. The risk-benefit factor should always be carefully evaluated before such a procedure is undertaken. At all times a fully equipped emergency cart, or equivalent supplies and equipment, and personnel competent in recognizing and treating adverse reactions of all severity, or situations which may arise as a result of the procedure, should be immediately available. If a serious reaction should occur, immediately discontinue administration. Since severe delayed reactions have been known to occur, emergency facilities and competent personnel should be available for at least 30 to 60 minutes after administration. (See ADVERSE REACTIONS).

Preparatory dehydration is dangerous and may contribute to acute renal failure in infants, young children, the elderly, patients with pre-existing renal insufficiency, patients with advanced vascular disease and diabetic patients.

Severe reactions to contrast media often resemble allergic responses. This has prompted the use of several provocative pretesting methods, none of which can be relied on to predict severe reactions. No conclusive relationship between severe reactions and antigen-antibody reactions or other manifestations of allergy has been established. The possibility of an idiosyncratic reaction in patients who have previously received a contrast medium without ill effect should always be considered. Prior to the injection of any contrast medium, the patient should be questioned to obtain a medical history with emphasis on allergy and hypersensitivity. A positive history of bronchial asthma or allergy, including food, a family history of allergy, or a previous reaction or hypersensitivity to a contrast agent may imply a greater than usual risk. Such a history, by suggesting histamine sensitivity and consequently proneness to reactions, may be more accurate than pre-testing in predicting the potential for reaction, although not necessarily the severity or type of reaction in the individual case. A positive history of this type does not arbitrarily contraindicate the use of a contrast agent, when a diagnostic procedure is thought essential, but does call for caution. (See ADVERSE REACTIONS).

Prophylactic therapy including corticosteroids and antihistamines should be considered for patients who present with a strong allergic history, a previous reaction to a contrast medium, or a positive pre-test since in these patients the incidence of reaction is two to three times that of the general population. Adequate doses of corticosteroids should be started early enough prior to contrast medium injection to be effective and should continue through the time of injection and for 24 hours after injection. Antihistamines should be administered within 30 minutes of the contrast medium injection. Recent reports indicate that such pre-treatment does not prevent serious life-threatening reactions, but may reduce both their incidence and severity. A separate syringe should be used for these injections.

General anesthesia may be indicated in the performance of some procedures in young or uncooperative children and in selected adult patients; however, a higher incidence of adverse reactions has been reported in these patients, and may be attributable to the inability of the patient to identify untoward symptoms or to the hypotensive effect of anesthesia which can prolong the circulation time and increase the duration of contact of the contrast agent.

Angiography should be avoided whenever possible in patients with homocystinuria because of the risk of inducing thrombosis and embolism.

Information for Patients: Patients receiving iodinated intra-vascular contrast agents should be instructed to:

1. Inform your physician if you are pregnant.
2. Inform your physician if you are diabetic or if you have multiple myeloma, pheochromocytoma, homozygous sickle cell disease or known thyroid disease. (See WARNINGS).
3. Inform your physician if you are allergic to any drugs, food or if you had any reactions to previous injections of dyes used for x-ray procedures. (See PRECAUTIONS, General).
4. Inform your physician about any other medications you are currently taking including non-prescription drugs.

Carcinogenesis, Mutagenesis, Impairment of Fertility: No long-term animal studies have been performed to evaluate carcinogenic potential. However, animal studies suggest that this drug is not mutagenic and does not affect fertility in males or females.

Pregnancy Category B: Reproduction studies have been performed in mice, rats, and rabbits at doses up to 6.6 times the human dose and have revealed no evidence of impaired fertility or harm to the fetus due to CONRAY. There are however no adequate and well controlled studies in pregnant women. Because animal reproduction studies are not always predictive of human response, this drug should be used during pregnancy only if clearly needed.

Nursing Mothers: Iothalamate salts are excreted unchanged in human milk. Because of the potential for adverse effects in nursing infants, bottle feedings should be substituted for breast feedings for 24 hours following the administration of this drug.

PRECAUTIONS FOR SPECIFIC PROCEDURES:

Excretory Urography

Infants and small children should not have any fluid restrictions prior to excretory urography. Injections of CONRAY and CONRAY-43 represent an osmotic load which, if superimposed on increased serum osmolality due to partial dehydration, may magnify hypertonic dehydration. (See WARNINGS and PRECAUTIONS, General concerning preparatory dehydration).

Brief summary continued on last page of ad.

F R O M M A L L

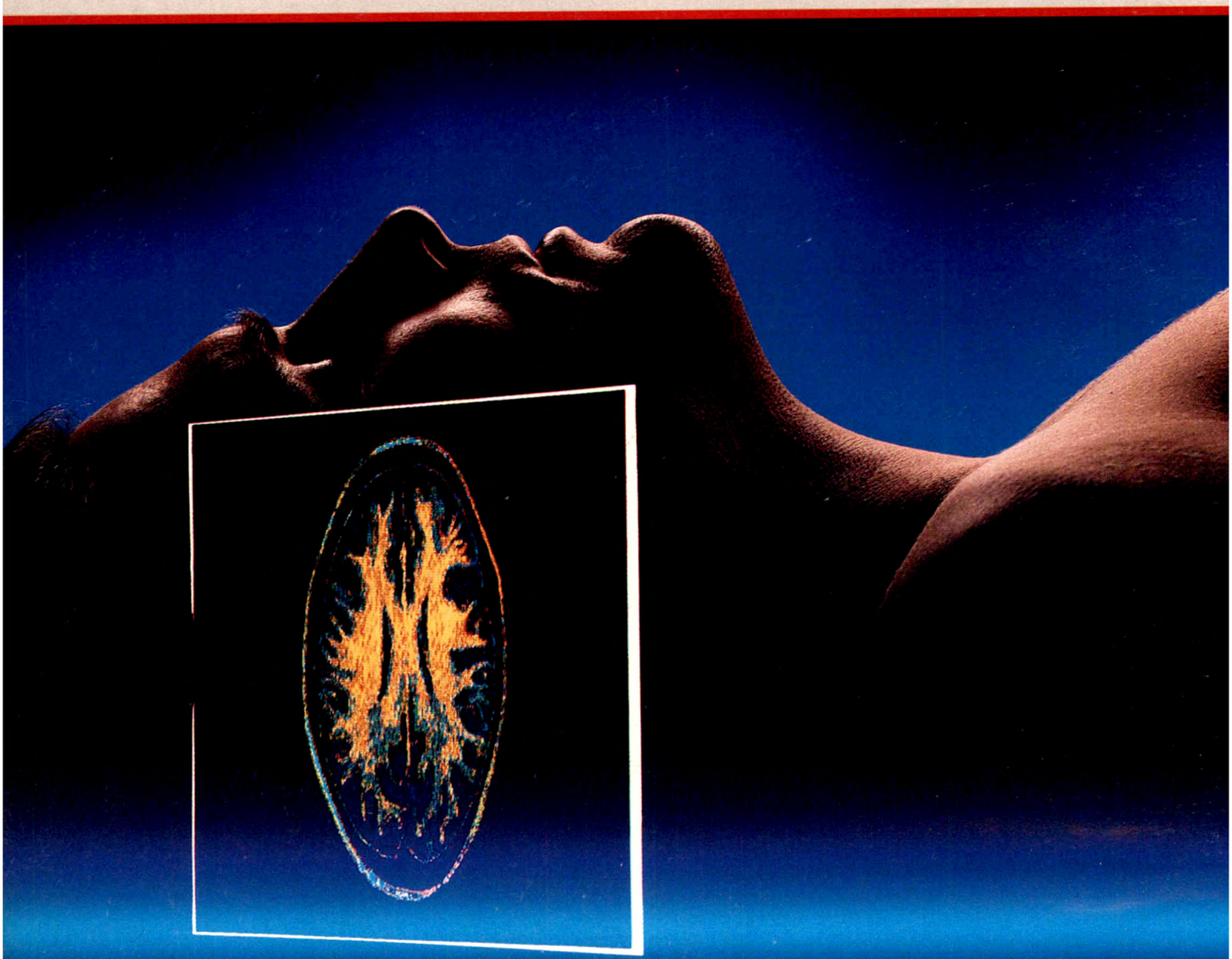

As versatile as they

Conray®-43 (iothalamate meglumine injection U.S.P. 43%): Unique benefits for CT and venography

Conray®-43 provides an ideal iodine concentration for use in lower extremity venography, CT scans, and infusion urography. Conray-43 combines good visualization with low toxicity and excellent patient tolerance. Because of its low viscosity, Conray-43 offers a shorter infusion time for a 200 mL dose versus 150 mL dose of 60% solution. The lower osmolality of Conray-43 compared to a 60% conventional agent may mean less post-procedural phlebitis, with no loss of imaging quality.

For routine CT and lower extremity venography procedures, give your patients the unique benefits of Conray-43—the affordable, well-tolerated alternative.

Please see preceding page and final page of ad for brief summary of prescribing information.

©1987 Mallinckrodt, Inc.

are affordable

Conray® (iothalamate meglumine injection U.S.P. 60%):
A proven performer

Conray® offers you reliable performance, proven in over 15 million procedures in the last five years, ranging from IVPs to enhancement of CT images. Conray provides an iodine content that yields good visualization with low toxicity and good patient tolerance.

The viscosity allows for bolus injection or rapid infusion, where necessary. And the variety of vial and bottle sizes lets you choose the Conray volume and mode of administration you need in your practice.

With this kind of clinical versatility and affordability, it's no surprise that Conray is the #1 brand of conventional iodinated contrast media—the standard by which all others are judged.

MALLINCKRODT®

Changing the look of medicine

Continuation of brief summary for Conray® and Conray®-43

Cerebral Angiography

Cerebral angiography should be performed with special caution in patients with advanced arteriosclerosis, severe hypertension, cardiac decompensation, senility, recent cerebral thrombosis or embolism, and migraine.

Peripheral Arteriography and Venography

Moderate decreases in blood pressure occur frequently with intra-arterial (brachial) injections. This change is usually transient and requires no treatment, however, the blood pressure should be monitored for approximately ten minutes following injection. Special care is required when venography is performed in patients with suspected thrombosis, phlebitis, severe ischemic disease, local infection or a totally obstructed venous system. In the presence of venous stasis, vein irrigation with normal saline should be considered following the procedure. Venography is optimally performed with a more dilute solution such as Conray®-43 (Iothalamate Meglumine Injection USP 43%).

Extreme caution during injection of the contrast agent is necessary to avoid extravasation and fluoroscopy is recommended. This is especially important in patients with severe arterial or venous disease.

Arthrography

During arthrography, strict aseptic technique is required to prevent the introduction of infection. Fluoroscopic control should be used to insure proper introduction of the needle into the synovial space and prevent extracapsular injection. Aspiration of excessive synovial fluid will reduce the pain on injection and prevent the rapid dilution of the contrast agent. It is important that undue pressure not be exerted during the injection.

Direct Cholangiography

In the presence of acute pancreatitis, direct cholangiography, if necessary, should be employed with caution, injecting no more than 5 to 10 mL without undue pressure. Percutaneous transhepatic cholangiography should only be attempted when compatible blood for potential transfusions is in readiness and emergency surgical facilities are available. The patient should be carefully monitored for at least 24 hours to insure prompt detection of bile leakage and hemorrhage. Appropriate pre-medication of the patient is recommended and drugs which are cholespastic, such as morphine, should be avoided. Respiratory movements should be controlled during introduction of the needle.

Endoscopic Retrograde Cholangiopancreatography

Endoscopic retrograde cholangiopancreatography should only be performed by personnel skilled and experienced with the procedure, and careful attention to technique is essential for the success and safety of the procedure. Fluoroscopy is mandatory during injection to prevent over distention of the duct systems.

Contrast Enhancement in Body Computed Tomography

It is advisable to insure that patients are adequately hydrated prior to the contrast enhanced body CT examination. Patient motion, including respiration, can markedly affect image quality, therefore, patient cooperation is essential. The use of an intravascular contrast medium can obscure tumors in patients undergoing CT evaluation of the liver resulting in a false negative diagnosis. Dynamic CT scanning is the procedure of choice for malignant tumor enhancement.

Intravenous Digital Subtraction Angiography

The risks associated with IV DSA are those usually attendent with catheter procedures and include intramural injections, vessel dissection and tissue extravasation. Small test injections of contrast medium made under fluoroscopic observation to insure the catheter tip is properly positioned, and in the case of peripheral placement that the vein is of adequate size, will reduce this potential.

Patient motion, including respiration and swallowing, can result in marked image degradation yielding non-diagnostic studies. Therefore, patient cooperation is essential.

Arterial Digital Subtraction Angiography

The risks associated with arterial DSA are those usually attendent with catheter procedures. Following the procedure, gentle pressure hemostasis is required, followed by observation and immobilization of the limb for several hours to prevent hemorrhage from the site of arterial puncture.

ADVERSE REACTIONS

Adverse reactions to injectable contrast media fall into two categories: chemotoxic reactions and idiosyncratic reactions.

Chemotoxic reactions result from the physio-chemical properties of the contrast media, the dose and speed of injection. All hemodynamic disturbances and injuries to organs or vessels perfused by the contrast medium are included in this category.

Idiosyncratic reactions include all other reactions. They occur more frequently in patients 20 to 40 years old. Idiosyncratic reactions may or may not be dependent on the amount of dose injected, the speed of injection, the mode of injection and the radiographic procedure. Idiosyncratic reactions are subdivided into minor, intermediate and severe. The minor reactions are self-limited and of short duration; the severe reactions are life-threatening and treatment is urgent and mandatory.

Fatalities have been reported following the administration of iodine-containing contrast agents. Based upon clinical literature, the incidence of death is reported to range from one in 10,000 (0.01 percent) to less than one in 100,000 (0.001 percent).

The following adverse reactions have been observed in conjunction with the use of iodine-containing contrast agents.

The most frequent adverse reactions are nausea, vomiting, facial flush and a feeling of body warmth. These are usually of brief duration. Other reactions include the following:

Hypersensitivity reactions: Dermal manifestations of urticaria with or without pruritus, erythema and maculopapular rash. Dry mouth. Sweating. Conjunctival symptoms. Facial, peripheral and angioneurotic edema. Symptoms related to the respiratory system include sneezing, nasal stuffiness, coughing, choking, dyspnea, chest tightness and wheezing, which may be initial manifestations of more severe and infrequent reactions including asthmatic attack, laryngospasm and bronchospasm with or without edema, pulmonary edema, apnea and cyanosis. Rarely, these allergic-type reactions can progress into anaphylaxis with loss of consciousness and coma and severe cardiovascular disturbances.

Cardiovascular reactions: Generalized vasodilation, flushing and venospasm. Occasionally, thrombosis or rarely, thrombophlebitis. Red blood cell clumping and agglutination, crenation and interference in clot formation. Extremely rare cases of disseminated intravascular coagulation resulting in death have been reported. Severe cardiovascular responses include rare cases of hypotensive shock, coronary insufficiency, cardiac arrhythmia, fibrillation and arrest. These severe reactions are usually reversible with prompt and appropriate management; however, fatalities have occurred.

Technique reactions: Extravasation with burning pain, hematomas, ecchymosis and tissue necrosis, paresthesia or numbness, vascular constriction due to injection rate, thrombosis and thrombophlebitis.

Neurological reactions: Spasm, convulsions, aphasia, syncope, paresis, paralysis resulting from spinal cord injury and pathology associated with syndrome of transverse myelitis, visual field losses which are usually transient but may be permanent, coma and death.

Other reactions: Headache, trembling, shaking, chills without fever and light-headedness. Temporary renal shutdown or other nephropathy.

ADVERSE REACTIONS FOR SPECIFIC PROCEDURES:

Cerebral Angiography

The major sources of cerebral arteriographic adverse reactions appear to be related to repeated injections of the contrast material, administration of doses higher than those recommended, the presence of occlusive atherosclerotic vascular disease and the method and technique of injection.

Adverse reactions are normally mild and transient. A feeling of warmth in the face and neck is frequently experienced. Infrequently, a more severe burning discomfort is observed.

Serious neurological reactions that have been associated with cerebral angiography and not listed under the general Adverse Reactions include stroke, amnesia and respiratory difficulties.

Cardiovascular reactions that may occur with some frequency are bradycardia and decrease in systemic blood pressure. The blood pressure change is transient and usually requires no treatment.

Peripheral Arteriography and Venography

Hemorrhage and thrombosis have occurred at the puncture site of the percutaneous injection. Brachial plexus injury has been reported following axillary artery injection. Thrombophlebitis, syncope and very rare cases of gangrene have been reported following venography.

Arthrography

Arthrography may induce joint pain or discomfort which is usually mild and transient but occasionally may be severe and persist for 24 to 48 hours following the procedure. Effusion requiring aspiration may occur in patients with rheumatoid arthritis.

Direct Cholangiography

Adverse reactions may often be attributed to injection pressure or excessive volume of the medium resulting in overdistention of the ducts and producing local pain.

Some of the medium may enter the pancreatic duct which may result in pancreatic irritation. Occasionally, nausea, vomiting, fever, and tachycardia have been observed. Pancholangitis resulting in liver abscess or septicemia has been reported.

In percutaneous transhepatic cholangiography, some discomfort is common, but severe pain is unusual. Complications of the procedure are often serious and have been reported in 4 to 6 percent of patients. These reactions have included bile leakage and biliary peritonitis, gall bladder perforation, internal bleeding (sometimes massive), blood-bile fistula resulting in septicemia involving gram-negative organisms, and tension pneumothorax from inadvertent puncture of the diaphragm or lung. Bile leakage is more likely to occur in patients with obstructions that cause unrelieved high biliary pressure.

Endoscopic Retrograde Cholangiopancreatography

Adverse reactions that have occurred which are attributable to either the ERCP procedure or contrast agent include nausea, vomiting, fever, severe abdominal pain, duodenal wall intravasation, septicemia, pancreatitis and perforation of the common bile duct associated with pathology.

DOSAGE AND ADMINISTRATION

Details on dosage are provided in the Conray and Conray-43 package insert. CONSULT FULL PACKAGE INSERT BEFORE USE.

Rev. August 1987

MALLINCKRODT®

Diagnostic Products Division
Mallinckrodt, Inc.
Post Office Box 5840
St. Louis, MO 63134

CLEAR-Pb®* MOBILE X-RAY BARRIERS
...great performance never looked so good!

A complete family of **CLEAR-Pb** Lead-Plastic Mobile X-Ray Barriers... the most extensive line of its kind ever produced.

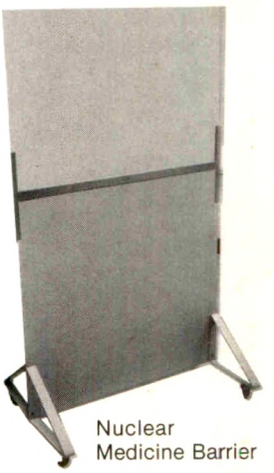

Nuclear Medicine Barrier

CLEAR-Pb Mobile X-Ray Barriers offer you total body protection from secondary radiation in radiology suites, O.R.'s and Special Procedures rooms. You'll also find them in cardiac cath rooms, as well as in mammographic, nuclear medicine and dental suites.
Our lead-impregnated, transparent plastic viewing panels are crystal-clear and shatter-resistant...perfect for mobile unit use. A choice of lead equivalencies and a wide variety of sizes lets you select the correct size to meet the needs of *your* department. Shield one, two or more people the easy way!

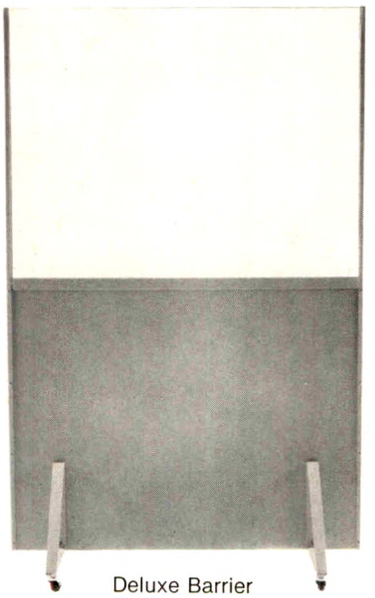

Deluxe Barrier

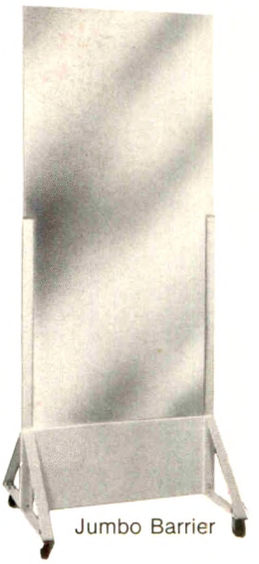

Jumbo Barrier

The Winning Combination: Total-body Shielding and Panoramic Visibility!

The distortion-free clarity and generous size of each CLEAR-Pb viewing panel provides you with exceptional visibility over a wide field of view. Patient and equipment can be seen at a glance, and the large viewing area puts patients at ease, too. No more need to put up with tiny, lead-glass viewing windows. Today's look is attractive, spacious, open, thanks to the versatility of CLEAR-Pb Lead-Plastic.

Need more details?
We have them. Request Bulletin 3225-44

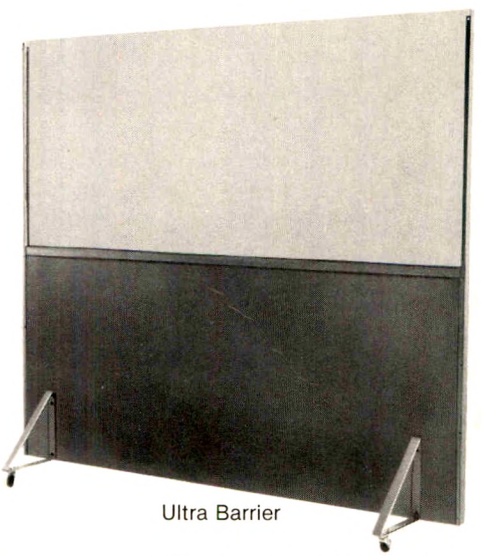

Ultra Barrier

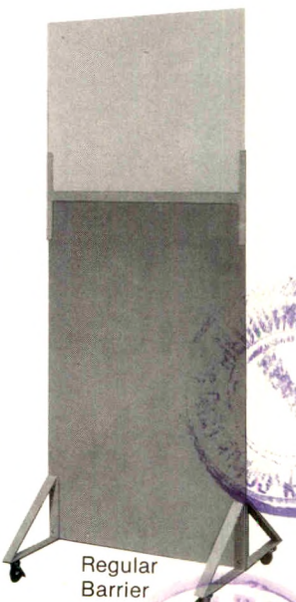

Regular Barrier

NUCLEAR ASSOCIATES

VICTOREEN

A Division of VICTOREEN, INC.
100 VOICE ROAD
CARLE PLACE, NY 11514-1593
(516) 741-6360
A Subsidiary of Sheller-Globe SG

CIRCLE 16 ON READER SERVICE CARD

®VICTOREEN, Inc. *U.S. Patents 4,129,524 and 4,182,821

FOR TOTAL BODY SHIELDING, THE CLEAR CHOICE IS CLEAR-Pb

Very fast. Very versatile. And very hard to top. Toshiba's TCT-600 Whole Body Scanner delivers the superior technology you want at the price you want to pay.
Compare the TCT-600 with competitive models.
SUPERIOR.
AFFORDABLE.
We challenge our competition to surpass this technology: ▲ a unique "shift mechanism" that achieves optimum patient dose utilization ▲ superior spatial resolution capable of detecting small anatomical details of 0.55mm ▲ instantaneous multi-planar reconstruction ▲ unique patient couch lowers to 30cm ▲ total examination study in less than fourteen minutes ▲ breakeven at under three patients per day.
We'll go head to head with the best of our competition on technical leadership, image quality, throughput, lifecost, and total service. We are committed to providing whatever it takes to ensure customer satisfaction. So before you make a decision, ask some tough questions. Call your Toshiba representative today, and ask for "20 questions to ask your CT representative."
HEAD TO HEAD
Toshiba Medical Systems, 2441 Michelle Drive, Tustin, CA 92680 (714) 730-5000, (800) 421-1968
In Touch with Tomorrow
TOSHIBA
GLOBAL IMAGING SPECIALISTS

Get the complete story on the new medical technologies and instrumentation of today...and tomorrow

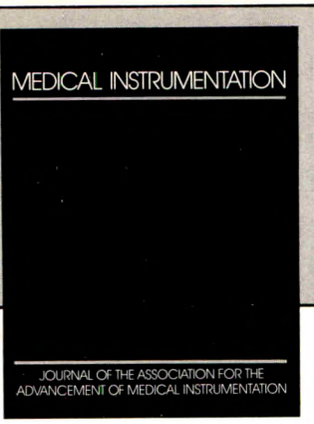

MEDICAL INSTRUMENTATION

The official journal of the Association for the Advancement of Medical Instrumentation

Editor-in-Chief: Charles A. Rawlings, Ph.D., C.C.E.

If you are involved in the design, manufacturing, clinical application, specification, regulation, or administrative facets of medical device technology, make MEDICAL INSTRUMENTATION the first journal you reach for when you want the latest developments, innovations, and advances in this fast-paced field.

Each bimonthly issue alerts you to trends and forecasts in the development, design, regulation, and clinical applications of medical instruments, devices, and systems. Original papers and timely articles help you keep pace with changes in the field that can have great effect on your work...new government standards and codes...new clinical uses...new approaches to enhancing quality, reliability, safety...key technologic breakthroughs ...and more.

Several special issues yearly are carefully planned around a single topic of current interest. Recent and upcoming special issues include —

- Environmental Therapeutic Devices for Infants
- Lasers in Medicine
- Neurologic Instrumentation and Techniques
- Alternative Communication Devices
- Respiratory Equipment

MEDICAL INSTRUMENTATION's coverage spans the disciplines, giving you a well-rounded perspective on trends in many areas — instrumentation for cardiovascular monitoring...clinical engineering...certification...instrumentation in anesthesiology.

Keep pace with technology and subscribe to **MEDICAL INSTRUMENTATION** today! Just clip out the coupon below or call **FREE** 1-800-638-6423 from anywhere in the U.S. (except Alaska), or call **COLLECT** in Maryland at 528-4105.

Williams & Wilkins

GET UP TO 3 YEARS AT THESE LOW RATES!

MEDICAL INSTRUMENTATION

The official journal of the Association for the Advancement of Medical Instrumentation

Keeping pace with the technologies of today... and tomorrow

☐ 3 years ☐ 2 years ☐ 1 year
☐ Individual $60/year
☐ Institution $85/year
☐ In-training $35/year
(Please add $10/year outside U.S.)

☐ Check enclosed ☐ Bill me
☐ VISA ☐ MasterCard ☐ American Express

card # expiration date

signature/PO#

Printed in USA

name

address

city/state/zip

Maryland residents please add 5% sales tax. Subscriptions outside the U.S. must be prepaid, in U.S. dollars only. Please allow up to 8 weeks for delivery of first issue. Surface deliveries outside the U.S. may take up to 16 weeks. Airmail rates available on request.

Mail to:
Williams & Wilkins
P.O. Box 23291
Baltimore, MD 21203

266 Fulham Road
London SW10 9EL England

MIAD 1062 88

In intrathecal imaging:

Because you can't be sure how every patient will react...

Improve the safety profile.

Better patient tolerance, measured subjectively and objectively.[1-5]

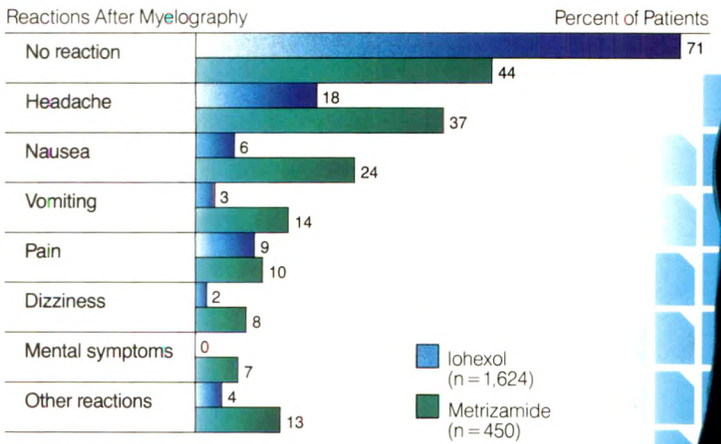

Adapted from Shaw et al.[2] Data on file, Winthrop Pharmaceuticals.[4]
All adverse reactions reported are included and are irrespective of drug relationship. If a patient had more than one type of reaction, each is counted separately under the respective reaction type.

Lower incidence of EEG changes compared with iopamidol or metrizamide.[2,5]

Excellent diagnostic quality.

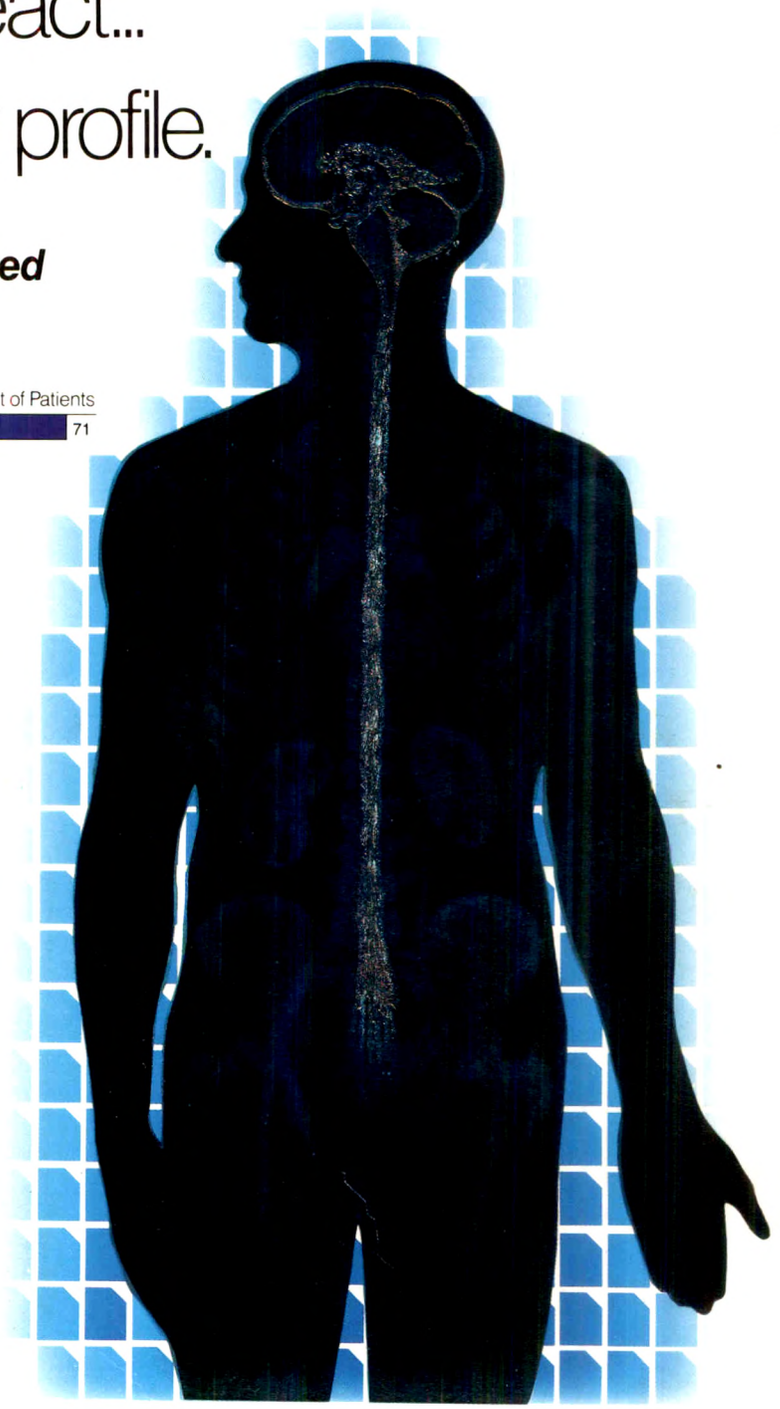

NONIONIC

OMNIPAQUE®

(IOHEXOL)

THE NEW STANDARD IN INTRATHECAL IMAGING.

See next page for important product information concerning contraindications, warnings, adverse reactions, patient selection, and precautionary recommendations.

OMNIPAQUE®
INJECTION (IOHEXOL)
INTRATHECAL

180

240

300

PLEASE CONSULT FULL PRODUCT INFORMATION BEFORE USING. A SUMMARY FOLLOWS:

DESCRIPTION: OMNIPAQUE is a nonionic, water-soluble radiographic contrast medium for intrathecal administration in concentrations of 180, 240, and 300 mgI/mL. Each milliliter of iohexol solution contains 1.21 mg tromethamine and 0.1 mg edetate calcium disodium with the pH adjusted between 6.8 and 7.7 with hydrochloric acid or sodium hydroxide. All solutions are sterilized by autoclaving, are nonpyrogenic, and contain no preservatives, so unused portions should be discarded.

CONTRAINDICATIONS–Intrathecal: OMNIPAQUE should not be administered to patients with a known hypersensitivity to iohexol. Myelography should not be performed in the presence of significant local or systemic infection where bacteremia is likely. Intrathecal administration of corticosteroids with OMNIPAQUE is contraindicated. Because of the possibility of overdosage, immediate repeat myelography in the event of technical failure is contraindicated.

WARNINGS–General: If grossly bloody CSF is encountered, the possible benefits of a myelographic procedure should be considered in terms of the risk to the patient.

Caution is advised in patients with a history of epilepsy, severe cardiovascular disease, chronic alcoholism, or multiple sclerosis.

Elderly patients may present a greater risk following myelography. The need for the procedure in these patients should be evaluated carefully. Special attention must be paid to dose and concentration of the medium used, hydration, and technique used.

Patients who are receiving anticonvulsants should be maintained on this therapy. Should a seizure occur, intravenous diazepam or phenobarbital sodium is recommended. In patients with a history of seizure activity who are not on anticonvulsant therapy, premedication with barbiturates should be considered.

Prophylactic anticonvulsant treatment with barbiturates should be considered in patients with evidence of inadvertent intracranial entry of a large or concentrated bolus of the contrast medium, since there may be an increased risk of seizure in such cases.

Drugs that lower the seizure threshold, especially phenothiazine derivatives, including those used for their antihistamine or antinauseant properties, are not recommended for use with OMNIPAQUE. Others include MAO inhibitors, tricyclic antidepressants, CNS stimulants, and psychoactive drugs described as analeptics, major tranquilizers, or antipsychotic drugs. While the contributory role of these medications has not been established, the use of such drugs should be based on physician evaluation of potential benefits and potential risks. Physicians have discontinued these agents at least 48 hours before and for at least 24 hours postprocedure. Care is required in patient management to prevent inadvertent intracranial entry of a large dose or concentrated bolus of the medium. Also, effort should be directed to avoid rapid dispersion of the medium causing inadvertent rise in intracranial levels (eg, by active patient movement). Direct intracisternal or ventricular administration for standard radiography (not CT) is not recommended.

In most reported cases of major motor seizures with nonionic myelographic media, one or more of the following factors were present. Therefore avoid:

- Deviations from recommended procedure or in myelographic management.
- Use in patients with a history of epilepsy.
- Overdosage.
- Intracranial entry of a bolus or premature diffusion of a high concentration of the medium.
- Medication with neuroleptic drugs or phenothiazine antinauseants.
- Failure to maintain elevation of the head during the procedure, on the stretcher, or in bed.
- Excessive and particularly active patient movement or straining.

PRECAUTIONS–General: Diagnostic procedures that involve the use of radiopaque diagnostic agents should be carried out under the direction of personnel with the prerequisite training and with a thorough knowledge of the particular procedure to be performed. Appropriate facilities should be available for coping with any complication of the procedure, as well as for emergency treatment of reactions to the contrast agent itself. After parenteral administration of a radiopaque agent, competent personnel and emergency facilities should be available, since delayed reactions have been reported (see ADVERSE REACTIONS).

Preparatory dehydration may be dangerous and may contribute to acute renal failure in patients with advanced vascular disease, diabetic patients, and in susceptible nondiabetic patients (often elderly with preexisting renal disease). Dehydration in these patients seems to be enhanced by the osmotic diuretic action of contrast agents. *Patients should be well hydrated prior to and following iohexol administration.*

The possibility of a reaction, including serious, life-threatening, fatal, anaphylactoid, or cardiovascular reactions, should always be considered (see ADVERSE REACTIONS). Therefore, it is of utmost importance that a course of action be carefully planned in advance for the immediate treatment of serious reactions, and that adequate and appropriate facilities and personnel be readily available in case of a severe reaction.

The possibility of an idiosyncratic reaction in susceptible patients should always be considered (see ADVERSE REACTIONS). The susceptible population includes patients with a history of a previous reaction to contrast media, patients with a known sensitivity to iodine per se, and patients with a known clinical hypersensitivity: bronchial asthma, hay fever, and food allergies.

A thorough medical history with emphasis on allergy and hypersensitivity, prior to the injection of any contrast medium, may be more accurate than pretesting in predicting potential adverse reactions.

A positive history of allergy or hypersensitivity does not arbitrarily contraindicate the use of a contrast agent where a diagnostic procedure is thought essential, but caution should be exercised (see ADVERSE REACTIONS). Premedication with antihistamines or corticosteroids, to avoid or minimize possible allergic reactions in such patients, should be considered.

In patients with severe renal insufficiency or failure, compensatory biliary excretion of the drug is anticipated to occur, with a slow clearance into the bile. Patients with hepatorenal insufficiency should not be examined unless the possibility of benefit clearly outweighs the additional risk. Sterile technique must be used with any spinal puncture.

When OMNIPAQUE is to be injected using plastic disposable syringes, the contrast medium should be drawn into the syringe and used immediately. If nondisposable equipment is used, scrupulous care should be taken to prevent residual contamination with traces of cleansing agents. **Parenteral drug products should be inspected and discarded if particulate matter or discoloration is present.**

Repeat Procedures. If in the clinical judgment of the physician sequential or repeat examinations are required, a suitable interval of time between administrations should be observed to allow for normal clearance of the drug from the body.

Information for Patients: When receiving injectable radiopaque diagnostic agents, inform your physician: if you are pregnant; if you are diabetic; if you have multiple myeloma, pheochromocytoma, homozygous sickle cell disease, or known thyroid disorder; if you are allergic to any drugs or food or if you had any reactions to previous injections of dyes used for x-ray procedures; about any other medications you are currently taking, including nonprescription drugs, before you are administered this drug.

Drug Interactions (See WARNINGS–General): In nonelective procedures in patients on the drugs described, consider prophylactic use of anticonvulsants.

Carcinogenesis, Mutagenesis, Impairment of Fertility: No long-term animal studies have been performed to evaluate carcinogenic potential, mutagenesis, or whether OMNIPAQUE can affect fertility in men or women.

Pregnancy Category B: Reproduction studies have been performed in rats and rabbits with up to 100 times the recommended dose. No evidence of impaired fertility or harm to the fetus has been demonstrated due to OMNIPAQUE; there are, however, no studies in pregnant women. Because animal reproduction studies are not always predictive of human response, this drug should be used during pregnancy only if clearly indicated.

Nursing Mothers: It is not known to what extent iohexol is excreted in human milk. However, many injectable contrast agents are excreted unchanged in human milk. Although it has not been established that serious adverse reactions occur in nursing infants, caution should be exercised when intravascular contrast media are administered to nursing women. Bottle feedings may be substituted for breast feedings for 24 hours following administration of OMNIPAQUE.

Pediatric Use: Safety and effectiveness in children have not been established.

ADVERSE REACTIONS–Intrathecal: The most frequently reported adverse reactions with OMNIPAQUE 180, OMNIPAQUE 240, and OMNIPAQUE 300 are headache, mild to moderate pain including backache, neck ache and stiffness, nausea and vomiting. These reactions usually occur 1 to 10 hours after injection, and almost all occur within 24 hours. They are usually mild to moderate in degree, lasting for a few hours and usually disappearing within 24 hours. Rarely, headaches may be severe or persist for days. Headache is often accompanied by nausea and vomiting and tends to be more frequent and persistent in patients not optimally hydrated. Transient alterations in vital signs may occur and their significance must be assessed on an individual basis. Those reactions reported in clinical studies with OMNIPAQUE are listed below in decreasing order of occurrence, based on clinical studies of 1,624 patients.

Headaches: The most frequently occurring adverse reaction following myelography has been headache, with an incidence of approximately 18%. Headaches may be caused either by a direct effect of the contrast medium or by CSF leakage at the dural puncture site. However, in managing the patient, it is considered more important to minimize intracranial entry of contrast medium by postural management than to attempt to control possible CSF leakage (see PATIENT MANAGEMENT).

Pain: Mild to moderate pain including backache, neck ache and stiffness, and neuralgia occurred following injection, with an incidence of about 8%.

Nausea and Vomiting: Nausea was reported with an incidence of about 6%, and vomiting about 3% (see PATIENT MANAGEMENT). Maintaining normal hydration is very important. The use of phenothiazine antinauseants is not recommended (see WARNINGS–General). Reassurance to the patient that the nausea will clear usually is all that is required.

Dizziness: Transient dizziness was reported in about 2% of the patients.

Other Reactions: Other reactions occurring with an individual incidence of less than 0.1% included: feeling of heaviness, hypotension, hypertonia, sensation of heat, sweating, vertigo, loss of appetite, drowsiness, hypertension, photophobia, tinnitus, neuralgia, paresthesia, difficulty in micturition, and neurological changes. All were transient and mild with no clinical sequelae.

General Adverse Reactions to Contrast Media: Physicians should remain alert for the occurrence of adverse effects in addition to those discussed above, particularly the following reactions which have been reported in the literature for other nonionic, water-soluble myelographic media and rarely with iohexol. These have included, but are not limited to, aseptic and bacterial meningitis and CNS and other neurologic disturbances.

An aseptic meningitis syndrome has been reported rarely (less than 0.01%). It was usually preceded by pronounced headaches, nausea, and vomiting. Onset usually occurred about 12 to 18 hours postprocedure. Prominent features were meningismus and fever, sometimes with oculomotor signs and mental confusion. Lumbar puncture revealed a high white cell count and high protein content, often with a low glucose level and absence of organisms. The condition usually started to clear spontaneously about 10 hours after onset, with complete recovery over 2 to 3 days.

Allergy or Idiosyncrasy: Chills, fever, profuse diaphoresis, pruritus, urticaria, nasal congestion, dyspnea, and Guillain-Barré syndrome.

CNS Irritation: Mild and transitory perceptual aberrations, such as hallucinations, depersonalization, amnesia, hostility, amblyopia, diplopia, photophobia, psychosis, insomnia, anxiety, depression, hyperesthesia, visual or auditory or speech disturbances, confusion and disorientation. In addition, malaise, weakness, EEG changes, meningismus, hyperreflexia or areflexia, hypertonia or flaccidity, hemiplegia, paralysis, quadriplegia, restlessness, tremor, echoacousia, echolalia, asterixis, and dysphasia have occurred.

Profound mental disturbances have also rarely been reported: various forms and degrees of aphasia, mental confusion, or disorientation. Onset is usually at 8 to 10 hours and lasts for about 24 hours. Occasionally, they have been manifest as apprehension, agitation, or progressive withdrawal in several instances to the point of somnolence, stupor, and coma. In a few cases, these have been accompanied by transitory hearing loss or other auditory symptoms and visual disturbances (believed subjective or delusional), including unilateral or bilateral loss of vision, which may last for hours. In one case, persistent cortical loss of vision has been reported in association with convulsions. Ventricular block has been reported; amnesia of varying degrees may be present for the reaction event.

Rarely, persistent though transitory weakness in the leg or ocular muscles has been reported. Peripheral neuropathies have been rare and transitory. They include sensory and/or motor or nerve root disturbance, myelitis, persistent leg muscle pain or weakness, 6th nerve palsy, or cauda equina syndrome. Muscle cramps, fasciculation or myoclonia, spinal convulsion, or spasticity are unusual and have responded promptly to a small intravenous dose of diazepam.

In general, the reactions that are known to occur on parenteral administration of iodinated contrast agents are possible with any nonionic agent. Approximately 95% of adverse reactions accompanying the use of water-soluble contrast agents are mild to moderate in degree. However, severe, life-threatening, anaphylactoid, and fatal reactions, mostly of cardiovascular origin, have occurred. Adverse reactions to injectable contrast media fall into two categories: chemotoxic reactions and idiosyncratic reactions.

Chemotoxic reactions result from the physicochemical properties of the contrast medium, the amount of the dose and the speed of injection. All hemodynamic disturbances and injuries to organs or vessels perfused by the contrast medium are included in this category.

Idiosyncratic reactions occur more frequently in patients 20 to 40 years old and may or may not be dependent on the amount of dose injected, the speed of injection, and the radiographic procedure. They are subdivided into minor, intermediate, and severe. The minor reactions are self-limited and of short duration; the severe reactions are life-threatening, and treatment is urgent and mandatory.

The reported incidence of adverse reactions to the contrast medium in patients with a history of allergy is twice that of the general population. Patients with a history of previous reactions to a contrast medium are three times more susceptible than other patients. However, sensitivity to contrast media does not appear to increase with repeated examination.

Most adverse reactions to injectable contrast media appear within 1 to 3 minutes after the start of injection, but delayed reactions may occur.

OVERDOSAGE: Although clinical consequences of overdosage with OMNIPAQUE have not been reported, physicians should be aware that incorrect management of the patient can permit inadvertent early intracranial entry of normal doses of the medium, thereby increasing CNS reactions.

The intracisternal LD_{50} value of OMNIPAQUE (in grams of iodine per kilogram body weight) is greater than 2.0 in mice.

References: 1. Kieffer SA, Binet EF, Davis DO, et al: Lumbar myelography with iohexol and metrizamide: A comparative multicenter prospective study. *Radiology* 1984; 151:665-670. **2.** Shaw DD, Bach-Gansmo T, Dahlstrom K: Iohexol: summary of North American and European clinical trials in adult lumbar, thoracic, and cervical myelography with a new nonionic contrast medium. *Invest Radiol* 1985; 20(suppl 1):44-50. **3.** Latchaw RE, Hirsch WL Jr, Horton JA, et al: Iohexol vs metrizamide: Study of efficacy and morbidity in cervical myelography. *AJNR* 1985; 6:931-933. **4.** Data on file, Winthrop Pharmaceuticals. **5.** Lamb JT: Iohexol vs. iopamidol for myelography. *Invest Radiol* 1985; 20(suppl 1):37-43.

© 1987 WINTHROP PHARMACEUTICALS 71171:3777

Winthrop PHARMACEUTICALS
Winthrop Pharmaceuticals
Division of Sterling Drug Inc.
New York, NY 10016

Volume 150: The Third Jubilee-Anniversary Volume

Robert N. Berk[1]

A jubilee is a 50th anniversary celebration, so this issue of the *AJR*, which starts volume 150, marks the beginning of the third jubilee volume of the Journal. The Journal is 82 years old. It began in 1906 as the *American Quarterly of Radiology* and in 1913 became the *American Journal of Roentgenology* [1].

It is fitting that this special volume be dedicated to Melvin M. Figley, editor emeritus of the Journal. Dr. Figley retired as editor-in-chief in 1985, after a decade of extraordinary leadership. Under his direction, the quality of the *AJR* soared. Because of his unstinting personal dedication and his remarkable talent, the Journal's stature in the medical community increased more than during any other time in the Journal's history.

To mark the jubilee celebration, volume 150 will contain several special features. These include reproduction of selected articles from volumes 1, 50, and 100, along with commentaries on them by current authorities; perspectives, editorials, and opinions on timely topics; special progress-in-radiology articles; and a unique anniversary cover.

Comparison of this issue with the first jubilee volume (volume 50, published in 1943) and the second jubilee volume (volume 100, published in 1967) shows emphatically that enormous strides have been made in the quality and quantity of the Journal's content. Published papers are now more sharply focused, shorter, and more tightly edited. The average length of articles published in volume 150 will be approximately five pages, compared to nine and seven pages in papers published in volumes 50 and 100, respectively. The information provided is more polished. It is more accurate, conclusions are better substantiated by the data provided, and the illustrations are of higher quality.

Publication of the articles is more timely [2]. The average time between submission and acceptance is now 3.8 weeks, compared with 7 to 10 weeks in the past. Now the average time between submission and publication is 5 months (1 month for the editorial decision, 1 month for revision, and 3 months for editing and printing). This is two or three times faster than in the earlier days of the Journal's history.

The quantity of the papers has certainly increased. In volume 150, 250 papers will appear; that is almost triple the number published in volume 50 (90 papers) and nearly double that published in volume 100 (150 papers).

The goal of the Journal, to enrich the general fund of radiologic knowledge, has been achieved in grand style. The radiologic community has a right to be proud of the Journal and to consider it a prized resource for the specialty. This goal could not have been achieved without the dedication of thousands of individuals who have contributed to these 150 volumes. The commitment of the current group of more than 700 manuscript reviewers is acknowledged with special gratitude. These authorities take time from their busy practices, without remuneration or recognition, to give first priority to the detailed evaluation of manuscripts. The quality of the Journal truly rests in their hands.

This 150th volume is a product not only of the current editors, authors, and reviewers, but of all those who have contributed so much to the *AJR* since the first volume was published 82 years ago. In the six issues of this jubilee anniversary volume, we will salute these people on whose shoulders we stand and attempt to consider what the future holds for our dynamic specialty.

REFERENCES

1. Figley MM. *AJR* celebrates 75th anniversary. *AJR* **1981**;136:215
2. Berk RN. *AJR* achieves goal to speed publication. *AJR* **1987**;149:312

[1] Editor-in-Chief, *American Journal of Roentgenology*, 2223 Avenida de la Playa, Ste. 200, La Jolla, CA 92037-3218.

AJR 150:1, January 1988 0361–803X/88/1501–0001 © American Roentgen Ray Society

Dedication to Melvin M. Figley, M.D.

Raymond A. Gagliardi, President, American Roentgen Ray Society[1]

Volume 150 of the *American Journal of Roentgenology*, marking the third jubilee-anniversary volume of the Journal, is dedicated to Editor Emeritus Melvin Morgan Figley of Seattle, WA.

Dr. Figley's contributions to international radiology are very well known. Called to the University of Washington as Chairman of the Department of Radiology in 1958, Dr. Figley built this department into one outstanding for its clinical radiology as well as its teaching and radiologic research. His interest in cardiovascular and pulmonary radiology has made him a leader in this area, and his list of contributions to the medical literature is an impressive and significant one. He has been honored by many radiologic societies and has received the Gold Medal of the Association of University Radiologists (an organization that he served both as founding member and later as President), the Gold Medal of the American College of Radiology, and the Gold Medal of the Radiological Society of North America. After Dr. Figley's retirement as Editor of the *AJR*, the American Roentgen Ray Society created its Distinguished Service Award in order to recognize the unique quality of his service to the ARRS and world radiology in general.

He has served in leadership capacities in almost every important radiologic society in the world. His greatest contributions came in his services to the American Roentgen Ray Society. Dr. Figley served on its Executive Council from 1971 to 1987, serving as Chairman in 1975 and as President of the ARRS from 1983–1984. His most important role, however, was as Editor of the *American Journal of Roentgenology* from 1976 until 1986, retiring after 10 years of devoted service.

It is difficult to quantify his contribution to the *American Journal of Roentgenology*. Dr. Figley took over a journal that was in serious trouble, both scientifically and financially. In a brief period, he reoriented the entire editorial direction, actually changed the name of the journal itself, reorganized its format, and increased its quality so that it is now clearly recognized as one of the foremost radiologic journals. It is no secret that the Executive Council of the ARRS made a determined effort to dissuade Dr. Figley from retiring as Editor of the *AJR*. With characteristic modesty, he believed that it was time for new approaches by younger hands, which he hoped could reinvigorate the Journal he had almost single-handedly rescued from oblivion. Much of the Journal's present stature is a direct result of Dr. Figley's untiring efforts.

His commitment to excellence in all things is well known and is reflected in the reputation he enjoys as one of the great radiologic teachers and scholars of our generation. This commitment to excellence has also shown through in his personal life where he has demonstrated the qualities of loving husband, understanding father, and fast friend.

Dr. Figley has received many honors and awards for his contributions to radiology, but the Executive Council of the ARRS, the Editor and Editorial Staff of the *AJR*, and the Publication Committee of the ARRS believe that he deserves one more personal and specific commendation; in that spirit and with surpassing pride, this volume is dedicated to a great man and a good friend, Dr. Melvin M. Figley.

[1] Department of Radiology, St. Joseph Mercy Hospital, 900 Woodward Ave., Pontiac, MI 48053. Address reprint requests to R. A. Gagliardi.

AJR 150:2, January 1988 0361–803X/88/1501–0002 © American Roentgen Ray Society

Commentary

American Journal of Roentgenology: Historical Reflections

Raymond A. Gagliardi[1]

In 1900 William McKinley was President of the United States, then a nation of 76 million people; Oklahoma, Arizona, and New Mexico were still Territories; the Boer War was raging in South Africa; and Victoria still reigned as queen-empress of the British Empire. Also in 1900, a small group of physicians met to form the "Roentgen Society of the United States."

At that time, only 4 years after word of Roentgen's discovery had stunned the world, roentgenology was in a chaotic state and this small band of physicians, meeting in the office of Heber Robarts of St. Louis, MO, hoped to develop standards for responsible medical use of the promising new rays. The group held its first annual meeting in December 1900 and formally called itself The American Roentgen Ray Society (ARRS) [1, 2]. While fighting to establish radiology as a genuine medical specialty, these pioneers also recognized the need to make new knowledge available to everyone using the rays. There was already a publication owned by Dr. Robarts, *The American X-Ray Journal*, which was succeeded in 1902 by the *Transactions of the American Roentgen Ray Society*. These were annual collections of business meeting minutes, committee reports, and all of the papers that had been presented at Society meetings. As was customary in those times, extemporaneous discussions of the papers were also included. Manufacturers with exhibits at the meeting had the option of placing a small ad in the *Transactions*.

As the Society grew, it became apparent that the *Transactions* could not publish all the new material being developed in various institutions, and so in 1906 the ARRS authorized the establishment of the *American Quarterly of Roentgenology* [3]. Some difficulty, apparently financial, was encountered in the publication of the first volume of the *Quarterly* (October 1906–July 1907) [3], so that the second volume did not appear until December 1909! In the interim, publication of the *Transactions* was resumed. In 1909 the *American Quarterly of Roentgenology* was established as the official organ of the American Roentgen Ray Society, and a new effort was made to broaden its financial base [4]. A subscription price of $5/year was set, and by the following year the Quarterly was both a financial and a scientific success.

The Editors

The first editor of the Quarterly was Preston M. Hickey of Detroit, MI, whose vision included a strong specialty in radiology and a broader scope for the Journal to establish its importance in the scientific world. In 1911, abstracts of radiologic papers from other journals were included, and some years later this abstracts section had become a major feature of the Journal. The Journal prospered, and quarterly publication was no longer adequate to meet the radiologic community's growing needs. Thus in 1913 the Journal began publishing on a monthly basis, and its name was changed to the *American Journal of Roentgenology*.

In 1915, because of the continuously increasing editorial load, the responsibilities for publication and legal ownership were transferred from Dr. Hickey to Paul B. Hoeber, publisher, of New York City. The editorial office remained in Detroit and was expanded.

In 1916, after 10 years of development and devotion, Dr. Hickey submitted his resignation. His last year as editor had been the most prosperous in the history of the Journal and it

Received August 3, 1987; accepted after revision September 9, 1987.
[1] Department of Radiology, St. Joseph Mercy Hospital, 900 Woodward Ave., Pontiac, MI 48053. Address reprint requests to R. A. Gagliardi.

 0361–803X/88/1501–0003 © American Roentgen Ray Society

is difficult now, 82 years later, to fully appreciate his contribution to the development of radiologic education and publications. He began his career as a pathologist and otolaryngologist (with a strong interest in photography), but then turned his attention to radiology when he realized the tremendous possibilities of the new kind of ray. In addition to his work in helping radiology grow and gain recognition, he was constantly working on new approaches to and improvements in the young specialty. It may surprise some readers to learn that in the early days, only posteroanterior and anteroposterior projections were used in radiology and that it was Dr. Hickey who first thought of taking oblique views for better localization of abdominal calcifications, particularly ureteral stones. In those early days radiology was considered a form of photography, and the negative images were printed and read as positive photographs. Dr. Hickey discovered, perhaps by accident, that there was even better definition if the negative images were viewed directly on a viewbox. Except in times of war, the paper print was no longer used. Things we now take for granted required imagination and dedication. The first editor of the Journal, Preston Hickey, supplied these qualities in full measure.

After Dr. Hickey, Dr. James T. Case of Battle Creek, MI, was chosen as editor of the Journal, but shortly after, he was called into the army where he became the senior-ranking radiologist in the American Expeditionary Forces. In July 1918, he resigned and was replaced by Dr. H. M. Imboden of New York. Apparently, during Dr. Case's editorship, much of the work was carried out by Augustus Crane, also of Battle Creek. Dr. Crane was never listed as editor of the Journal, although he apparently was the de facto editor from 1917 to 1918.

During this period, the American Radium Society came into being; it was founded in 1916 by a group of physicians who were using radium and studying its therapeutic applications. Not all of its members were radiologists, but most of the papers read before the Society were published in the *American Journal of Roentgenology*. After agreement in 1922 that the Journal would be designated as the official organ of the American Radium Society, the Executive Council of the ARRS voted to change the name of the Journal to the *American Journal of Roentgenology and Radium Therapy*.

Dr. Imboden concluded his editorship in 1923 and was succeeded by Dr. Arthur Christie of Washington, DC, who promptly began issuing two volumes annually instead of one, practically doubling the amount of material published. Dr. Christie also expanded the abstracts section to include articles of interest to radiologists, although not necessarily about radiologic topics.

Dr. Christie resigned in 1929 and in 1930 Lawrence Reynolds of Detroit became editor, serving 31 years, longer than any other editor of the Journal. At the same time that Dr. Reynolds assumed the editorship, the Society resumed ownership of the Journal and entered into an agreement with the Charles C Thomas Company for publication and distribution [5]. The Journal continued to grow and prosper and had the largest circulation of any of the radiology journals in this country. But there was some criticism of the choice of articles, since Dr. Reynolds accepted 85% of submissions, as compared with a present acceptance rate of 35%. This made for a large backlog of papers and often the time between submission and publication was 12 months or more. In 1956 Dr. Reynolds introduced issues devoted to narrow subjects. Nine issues were on diagnosis, often a single category, and three issues were devoted to radiation therapy. This policy had mixed results. While it would speed up publication of some important articles, another article of equal importance was kept waiting until the appropriate subject issue was published. Nevertheless, the Journal was well regarded and was financially successful. Dr. Reynolds was named president-elect and president of the ARRS in 1948 and 1949, during which time Dr. Merrill C. Sosman was appointed acting editor, but the editorial office remained in Detroit. No manuscripts were sent to Boston, and most of the decisions continued to be made as before. After Dr. Reynolds' death in 1961, he was succeeded by his long-time associate Traian Leucutia, a radiation therapist with considerable experience in both radiology and editorial work. During Dr. Leucutia's tenure, the advent of nuclear technology led to another change in the name of the Journal; it became the *American Journal of Roentgenology, Radium Therapy, and Nuclear Medicine*.

Because of the growing number of pages in each issue, by 1965 the bound seminannual volumes had become thick and unwieldy, and so, for the first time, the Journal published three annual volumes instead of two and the cost of a subscription increased from $15 to $20 per year. At the same time, an agreement was established with the Association of University Radiologists, at that time a fledgling organization, to publish the 10 best papers from its spring meeting. Dr. Leucutia concluded 10 years of distinguished service in 1974 and was succeeded in January 1975 by his associate, Dr. E. Frederick Lang of Detroit, who served as acting editor for 1 year.

In January 1976, after 45 years in Detroit, the editorial office was moved to Seattle, WA, when Dr. Melvin Figley was appointed editor. The office staff was strengthened and associate editors were appointed who shared the review and decision-making responsibilities. For the first time in 70 years, the editors received salaries. The name was changed back to the *American Journal of Roentgenology* (*AJR*). Consideration was given to naming the Journal the *American Journal of Radiology*, but because of the historic association of the Society with the name Roentgen, the original title seemed more appropriate. Mandatory peer review of submissions was introduced, publication was accelerated, and the quality of the illustrations was improved. Within a few years, the Journal had regained its position as one of the world's leading medical journals. Since contributions from the American Radium Society had greatly declined, publications on therapeutic radiology were terminated and the half-century association of the two sponsoring societies was concluded in 1977. In 1985, after 10 years of brilliant service, Dr. Figley retired as editor. This responsibility was assumed by Robert N. Berk, and the editorial office was moved to San Diego, CA.

The Publication Committees

Editor's note: In this section, the editor has added to the author's words in order to highlight the contributions of Dr. Gagliardi himself.

Dr. Raymond A. Gagliardi was elected chairman of the Publication Committee in 1975 and immediately undertook review of the financial structure of the Journal, which had been unchanged for 45 years. After soliciting proposals from several publishers, he worked out a unique agreement with the Williams & Wilkins Company, changing the entire method of reimbursement to the Society [6]. This was immediately beneficial to the Society and eventually to the publisher as the Journal's circulation improved and its income increased. Thanks to Dr. Gagliardi's insight, the association with Williams & Wilkins, which continues to this day, has greatly benefited the American Roentgen Ray Society, rendering it more financially secure than ever before.

In addition to revitalizing the *AJR*, Drs. Figley and Gagliardi, together with the American Society of Neuroradiology, founded a new journal, *The American Journal of Neuroradiology* (*AJNR*). A separate office was established in Boston under the able editorship of Dr. Juan Taveras and a unique publication relationship was set up [7]. All neuroradiologic articles sent to the *AJR* were transferred to the *AJNR* for its disposition with the understanding that published articles of interest to general radiologists would be promptly reprinted from the *AJNR* in the *AJR*. The Seattle office provided redactory services for both journals. The acceptance of this unusual arrangement, which benefits readers of both journals, was directly attributable to the cooperative efforts of Drs. Taveras, David Davis, Gagliardi, and Figley and the Publication Committees of the two Societies. The *AJNR* was an almost immediate success, both scientifically and financially. In 1986, The American Roentgen Ray Society relinguished ownership of the *AJNR* to the American Society of Neuroradiology with the gratifying knowledge that a real service had been done for radiology by helping to launch a journal that in a few short years had become the leading neuroradiologic journal in the world. The cooperative arrangement for joint publication of articles still continues and should serve as a model for other subspecialty journals.

Dr. M. Paul Capp succeeded to the chairmanship of the Publication and Editorial Policy Committees in 1981 and continued the fine relationship with Williams & Wilkins. He oversaw the financial operations of both editorial offices and has maintained the profitability of both Journals. In 1985 he directed the selection of a new editor.

Interesting Highlights

Many interesting anecdotes are associated with the publication of the Journal over the years. In 1974, for example, there were three radiologists in the Soviet Union who subscribed to the Journal. At that time the Soviet government requested permission to make 120 photocopies of the monthly issues in return for a small payment. This request was denied by the Publication Committee and the Executive Council, and in the following year, two of the three subscriptions were cancelled. The single subscription in the USSR continues to this day.

In the early 1950s, when the printer of the Journal was having labor problems, it was not uncommon for two or three issues to appear simultaneously, one on time and the others several months late. In 1976, July arrived before June to the consternation of the horoscopists! Fortunately, the present publisher assiduously respects the calendar, and the Journal consistently is delivered to readers during the first week of its publication month.

Reading the early issues of the Journal is pure delight, and it can be startling to read about a Kathode [sic] or see a reference to the Becquerel rays. There is even a discussion of sales of "burn-proof" X-ray equipment. In 1902, Dr. J. Rudis-Jacinsky of Cedar Rapids, IA, reported on the first involvement of X-rays in a malpractice suit [8]. The allegations against the attending orthopedist were that he had set the fracture poorly, but the serial skiagraphs [sic] showed that this was actually a refracture. At the time, X-ray photographs in judicial actions were not always acceptable. In one verdict the judge ruled, "In an action against a physician for negligence, X-ray photographs are admissible with a proper caution against their being treated as infallible" [9]. An interesting footnote to this story is that an editorial published in 1930 complained that malpractice rates were as high as $32/year, with an extra $14 added on for those using therapy equipment or radium!

An article published in the April 1911 issue of the *American Quarterly of Roentgenology* dealt with the treatment of malignant lesions [10]. In his summary, the author proudly announced, "With regard to dosage, I have thrown out all the apparatus for measuring. I use my brain and my experience." So much for physics!

The Journal also carried momentous science. In 1914, W. D. Coolidge presented his classic paper on the new type of vacuum roentgen ray tube, "A Powerful Roentgen Ray Tube with a Pure Electron Discharge" [11]. The invention of the vacuum X-ray tube was a turning point in radiology, and the original paper in volume 1 of the *AJR* should be read by all radiologists, especially younger radiologists who are interested in knowing about the origins of the field.

In 1930 the *AJR* carried another breakthrough article, by Dr. Stafford Warren, titled "Roentgenologic Study of the Breast" [12]. While there is no reference to radiographic technique, the reproductions are outstanding and are equal to those we make today with far more sophisticated equipment. It is interesting that Dr. Warren used almost the same diagnostic criteria as those in use today.

Early issues of the Journal also dealt with political matters. In an editorial published in 1931 [13], Dr. T. A. Groover questioned whether radiology could survive as a specialty and whether its work would be taken over by other specialties, partly because of the indifference of many hospital administrators to the needs of radiologists. Dr. Groover said, "Whenever radiologists gather together, one is apt to hear

expressions of apprehension as to the future of radiology as a specialty of medicine."

Seen from the perspective of 82 years of the *AJR*, everything is different, yet in some ways nothing has changed. The same concerns held by the leaders of the American Roentgen Ray Society in 1910 are the concerns of the leadership today. Also, successive editors have been concerned about advances in technology that recently have spawned many new journals. However, through all the changes, the *American Journal of Roentgenology* has continued its high standards of educational service to the radiologic community. When someone writes another history of the *AJR*, perhaps in a future anniversary issue, it will surely be reported that the vision of its founders was realized throughout the years and that the *American Journal of Roentgenology* has never failed in its mission and obligation to its readers.

REFERENCES

1. Gagliardi RA. Presidential address. *AJR* **1987**;149:415–417
2. Erskine AW. Organized roentgenology in America. *Radiology* **1945**;45:549–554.
3. Johnston GC. Meeting proceedings. *Am Q Roentgenol* **1906**; 1:73.
4. Brown P. Meeting minutes. *Am Q Roentgenol* **1909**; 2:62
5. Reynolds L. Editorial. *AJR* **1930**;23:74
6. Gagliardi RA. The old order changeth. *AJR* **1979**; 132:146
7. Figley MM, Taveras JM. The *American Journal of Neuroradiology*. *AJNR* **1980**;1:103
8. Rudis-Jacinsky J. Case studies. *Trans ARRS* **1902**;57–65
9. Brown P. Presidential address. *Am Q Roentgenol* **1908**;5:232
10. Rudis-Jacinsky J. Malignant lesions. *Am Q Roentgenol* **1911**;13:68–85
11. Coolidge, WD. A powerful roentgen ray tube with a pure electron discharge. *AJR* **1914**;1:115–124
12. Warren S. Roentgenologic study of the breast. *AJR* **1930**;24:113–124
13. Groover TA. Editorial. *AJR* **1930**;24:190

1988 AMERICAN ROENTGEN RAY SOCIETY MEETING

MAY 8–13, 1988
SAN FRANCISCO HILTON HOTEL
SAN FRANCISCO, CA

See page 201 and February issue for further information.

ROENTGEN EXAMINATIONS FOR HEAD INJURIES

By A. L. GRAY, RICHMOND, VA.

To no exposed part of the human anatomy is traumatism followed by results so uncertain, as to the cranium. Injuries apparently trivial often produce the gravest consequences while the converse is also not infrequently true.

The opinion of the Roentgenologist is more relied upon by the surgeon in cranial examinations than in almost any other of the diagnostic fields of Roentgenology, and the necessity for accuracy in technique and conclusions is plainly evident. The importance of examining the skull after injuries of only moderate severity has so often been impressed by the Roentgen findings that it needs no comment in advocacy thereof. Permit me to say, however, that in infants and very young children the thinness of the cranial vault renders injury to the intracranial structures far more liable than in adults, and the damage often escapes detection until some serious manifestations appear in later life. It seems entirely reasonable to conclude that permanent injury often results from the carelessness of a nurse, who, on her daily trips to the park, having forgotten her charge by reason of the attentions of the ever present suitor, is awakened from her dreams by the cry of the little one who has tumbled from the bench or has pitched head first from its carriage to the pavement beneath. Such injuries as these are usually never reported to the parents, and the abrasion or contusion, if noticeable, is explained in some other plausible way. The convulsions and palses that come on later are called idiopathic or are attributed to birth trauma and the true cause remains forever unknown.

In injuries of greater severity it is very common for the patient to be rendered immediately unconscious, and perhaps, in a few hours the mind clears and the attending physician dismisses the case as one of "concussion of the brain." The real nature of the injury may or may not be revealed later. Unfortunately fracture of the skull usually does not give rise to focal signs that can be detected, and inspection, palpation, and percussion are very imperfect guides. The presence of haematomata is usually a most valuable sign, but may be misleading and often in extensive fractures this sign is entirely wanting. The value of the Roentgen examination should be not alone in ascertaining whether or not a fracture be present, but, in the absence of other determining factors, in enabling the surgeon to decide whether or not an operation is indicated and the site and nature of the operation if it is deemed advisable. If craniotomy be considered unnecessary, the permanent record of the Roentgen plate will be a guide for a future operation, should the subsequent history of the case demand it.

For accuracy in the diagnosis the sharpest possible detail is demanded. Unless this be obtained, a definite exclusion of fracture can not be made. To exclude fracture the plates should show plainly the bone structure, sutures, and fine grooves for the smaller branches of the epi-dural and diploic vessels. In the very young, where the grooves are too faintly marked, the outline of the skull should be sharply cut throughout, and all the sutures clearly visible.

The difficulty of obtaining detail in plates of supposed head fractures is familiar to all of us who are connected with emergency hospitals. The patient is usually not only unable to give intelligent assistance, but oftener than otherwise, resists all efforts to keep his head still. The ingenuity of the operator and his assistants is sorely taxed.

This paper is reprinted from *AJR* **1914**;1:294–297.
***AJR* 150:7–10, January 1988** 0361–803X/88/1501–0007 © American Roentgen Ray Society

It is especially difficult to obtain sharp stereoscopic plates, since the time required in exposures and shifting must be from 2 to 8 seconds, and all the usual braces and weights must be discarded. The motion of respiration and even the cardiac impulses must be overcome.

Of the methods devised for surmounting these obstacles I wish to mention the use of sand bags against the chin or chin and nucha, padded clamps, and a modified lateroprone position with the upper shoulder supported so as to allow free antero-posterior movement of the chest in respiration.

In children it is often possible to make a quick single exposure at the end of expiration, and in adults I have taken advantage of the long pause in the Cheyne-Stokes type of respiration that is not infrequent when the injury is grave.

I have employed recently a very simple and effective method of holding the head still without the use of clamps, weights, or other apparatus that might tend to interfere with the interpretation of the plates. I use two or more lengths of gauze bandage 2½ or 3 inches wide, and loop the middle of one of them around the patient's head, fastening the free ends to some suitable fixed portion of one side of the table. The second bandage is correspondingly placed with the free ends toward the opposite side. The head is thus pulled from two opposite directions and when the tension is sufficient to stop all movement, the free ends of the second bandage are securely tied to the table. If these two are found insufficient without exerting too great force, a third bandage is looped under the chin and fixed at the head of the table. Should the table be so con-

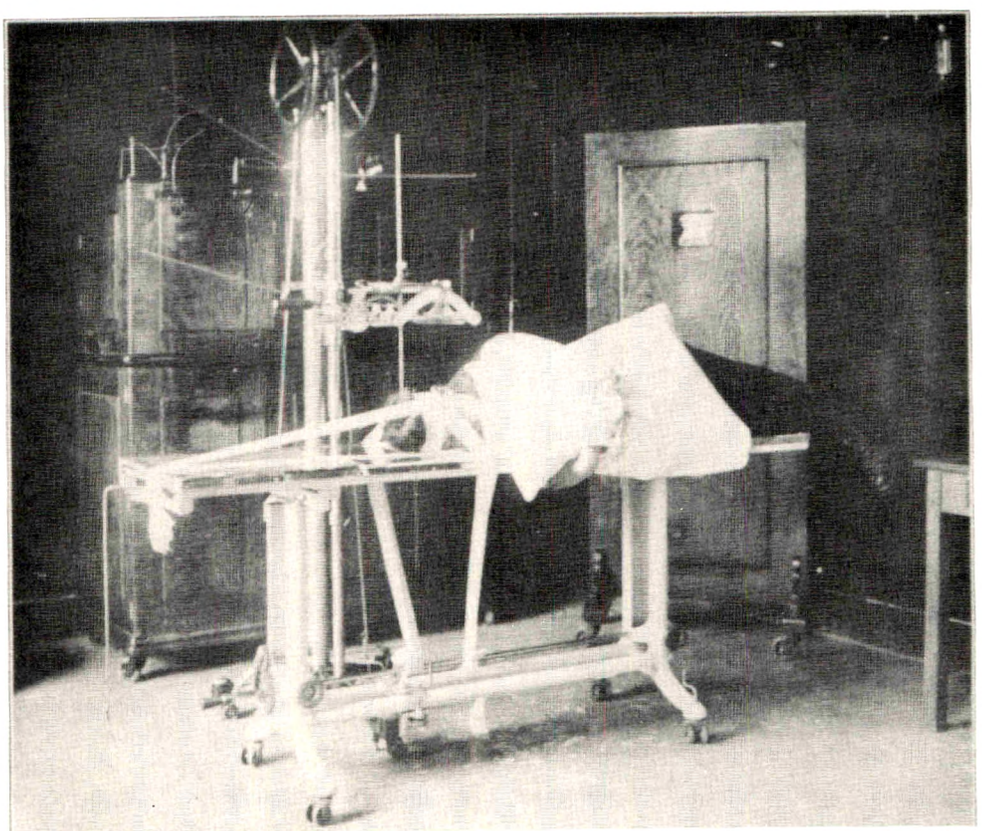

Illustrating Dr. Gray's Method for Stereoscopic Examination of Skull

structed as not to furnish convenient fixed points for the attachment of the bandages, I employ heavy sand bags to which the free ends of the bandages are tied. There is thus afforded support from all sides and perceptible motion is usually entirely abolished. The transparency of the bandages permits the making of head plates unmarred by extraneous objects. In some of my sharpest plates I have given an exposure of as much as ten seconds while the patient's respiration proceeded normally.

Since the extent of a cranial injury can be determined far more accurately by the stereoscope, whenever possible this method should be pursued, but if detail is not practicable it is necessary to make single plates from several directions.

The position of the head for the Roentgen examination is usually suggested by the presence of contusions or other marks of violence, but these are by no means always present. This is often true of fractures about the base where the injury has been produced by indirect violence. The usual bleeding from the ears, nose or eyes is not a constant accompaniment.

By far the greatest amount of information may be obtained from a stereoscopic examination made with the head placed on one side with its mesial plane parallel with the plate. The target should be in a vertical line through the bregma, and the tube should shift transversely with this line as a center and at a distance not greater than 22 inches from the plate. This position not only shows the vault clearly but also admits of a better view of the base. In the absence of guiding factors, an examination thus made will prove most advantageous.

The best position for plates of definite portions of the skull will suggest itself readily to the experienced Roentgenographer. A general rule, however, that may be applied is, attempt not only to throw the part in such a position on the plate that the overlying structures will not confuse the picture, but so place the head and direct the rays that the region sought will stand out as conspicuously as possible.

For a correct interpretation of the plates it is clearly necessary that the Roentgenologist should be thoroughly familiar with the normal grooves and depressions in the skull. The presence of exaggerated Pacchionian depressions has occasionally caused a considerable degree of perplexity in injuries supposed to have been produced by puncturing bodies. The development of the skull and the presence of Wormian bones and the sutures surrounding them should be held in mind especially in the young, lest they lead to a misinterpretation. Perhaps the most difficult fracture of the vault to recognize is one occurring in the groove for the trunk of the middle meningeal artery. If a linear fracture is confined to this groove, it is questionable whether it can be recognized. Diploic veins especially the anterior and posterior temporal often produce very marked thinning of the bones along their courses and may be mistaken for fractures.

In one case in my experience a linear fracture followed the course of an abnormally large diploic vein. Upon operation it was found that the outer table only was involved. It may be generally stated that, if the plate throughout shows no blurring, a fracture line will appear sharply cut and with characteristic angles and irregularities, while a vessel groove or canal shades from its center to the edges and disappears into the adjacent bone.

Having determined the presence and extent of a fracture, the Roentgenologist is frequently called upon by a surgeon for advice as to the course to be pursued by him. The special points to be considered are:

1. The Location. This should be considered both as regards probable damage to vital portions of the intra-cranial contents by the causative injury and also the degree of traumatism entailed by an operation at the site involved. The location should also be considered in relation to extra-cranial structures especially the nasal, pharyngeal,

and auditory cavities in regard to the probability of infection through compound wounds.

2. Shape. Whether linear, circular, stellate or of a jagged and irregular course. These points will, to a great degree, aid in determining probable localized pressure from depressed fragments.

3. Size of the fissure, or the amount of separation of the edges of the fragments, which also gives an idea of the probable damage to the soft tissues as well as the possibility of hernia or excessive scar tissue at the side of the wound.

4. Course, as to the probability of damage to blood vessels, nerves or other important structures.

5. Whether the margins are overlapped or are dodging each other. From consideration of these points we may obtain valuable information in estimating the extent of the fracture, the injury to soft structures and the degree of compression.

6. Age. By reason of the thinness and pliant condition of the skull of an infant, it is probable that a marked degree of accommodation may take place resulting in perfect compensation or complete return to the normal. A blow that would cause a depressed fracture in the adult will often produce an indentation without fracture in the very young child. In such cases, intra-cranial pressure alone may obliterate the depression. The possible interference with cerebral development at the site of the injury, however, should be carefully weighed. The patency of the fontanelles is to be considered in operations for general decompression. Nature's method of relieving the situation may leave less scar tissue and close in the cranial orifice far more perfectly than the most skilful surgeon.

Finally it is very important that the Roentgenologist should follow his patient to the operating table taking with him the plate or an accurate diagram of the conditions. He should, if possible, remain throughout the operation to see that the impressions he has received are also in the mind of the operator.

312 E. Franklin St.

SLIDES

1. Showing detail. Jones. Hematoma.
2. Same. Headon. Fracture Mastoid.
3. Sand bag against chin only. Thompson child. Fracture extensive and dodging.
4. Padded sand bags. Bigger. Fracture Occipital bone.
5. Padded clamps. Malcom. Multiple cracks. Aeroplane case.
6. Shoulder supported. No other fixation. Moorefield.
7. Quick exposure at end of expiration. Nash child, crying. Dent in frontal bone.
8. Interval of Cheyne-Stokes respiration. Hoagland. Extensive gaping fracture of parietal.
9. Illustrating also separation of margins. Sack. Fracture of parieto-temporal region to parieto-occipital suture.
10. Illustrating head held in position.
11. Same showing centering rod over bregma.
12. Radiograph of same head immediately after last photo. (One of stereoscopic pair.)
13. Same case as No. 1. Stereoscopic with head fixed by bandages.
14. Exposure of 8 seconds. One of stereoscopic pair, head fixed by bandages Dr. Clark.

The reader's attention is directed to the Commentary on this article, which starts on page 13 of this issue.

A Tribute to a Pioneer Radiologist: Alfred Leftwich Gray, M.D. (1873–1932)

Craig E. Barnes[1]

Dr. Alfred Gray, the author of "Roentgen Examinations of Head Injury," first published in Volume I of the *AJR* (1914) and now published again in this issue (see p. 7), was a pioneer radiologist who practiced in Richmond, VA, from 1902 to 1932 [1]. He served on the faculty of the University College of Medicine in Richmond as an instructor in anatomy and orthopedic surgery from 1899 to 1901 and as professor of physiology from 1901 and 1913. When the University College merged with the Medical College of Virginia (MCV) in 1913, he was made an associate in roentgenology. In 1916, he became the first professor of roentgenology at MCV, a position that he held until his death 16 years later. He also served as Dean of the medical school from 1913 to 1920.

In 1910, 15 years after the discovery of X-ray, there were a few hundred physicians practicing radiology in the United States. A survey of the members of the American Roentgen Ray Society in that year showed that of those responding, only 27% limited their practice to radiology, while the remainder divided their time between this and another specialty or general practice. Dr. Gray, who began his X-ray work in 1902, had limited his practice to radiology in 1908. His training and background in pathology, anatomy, and physiology made him particularly well suited for this new field. This is evidenced by his success as a radiologist and by his authorship of more than 35 articles about the application of X-ray in diagnosis and therapy.

The subjects of his publications ran the gamut of the diagnostic and therapeutic radiology of his day. Some of his papers focused on clarifying myths and misconceptions about X-rays, and other papers of his concentrated on the proper use of X-rays. His first paper, published in 1903, "X-rays in the Treatment of Superficial Cancer," described the curative action of X-rays, the need for shielding normal tissue, and the importance of directing the radiation only to the cancer. Another paper, written in 1906, documented the first successful application of X-ray therapy in the treatment of bladder cancer. In 1908, he wrote a paper dealing with the value of X-ray in the diagnosis of such conditions as kidney stones, bone diseases, and aneurysms of the aortic arch, in which he discussed the importance of having films interpreted by radiologists rather than by less-qualified physicians. In an article about the diagnosis of chest disease written in the same year, Dr. Gray emerged as one of the first radiologists to advocate the use of radiologic plates rather than fluoroscopy in chest diagnosis. His seminal article, "Roentgen Ray Examination of Head Injury," published in 1914, is reproduced in this issue of the Journal (see p. 7).

When Gray limited his practice to radiology he became part of a small group of physicians who called themselves "radiologists." These pioneers formed the American Roentgen Ray Society and the Radiological Society of North America in an attempt to elevate the use of X-ray for diagnosis and therapy to the status of a medical specialty. Gray's advocacy of this plan is clearly seen in many of his papers and addresses in which he stressed the importance of radiation protection and the value of X-rays in diagnosis; he also pointed out that the true value of the radiologist lay not just in his ability to take X-rays, but rather in his ability to interpret them.

A man of great energy, Dr. Gray served as president of the American Roentgen Ray Society in 1915. In his presidential address to the Society, titled "A Brief Review of the Progress of Roentgenology in the Past Decade," he looked back at the advances in X-ray apparatus, diagnosis, and therapy [2]. The major progress in X-ray machines centered around improvements in generators and X-ray tubes. New generator systems had allowed X-ray operators to control voltage and increase

[1] Department of Radiology, Bowman Gray School of Medicine, Winston-Salem, NC. Address reprint requests to C. E. Barnes, 1181 Edenwood Dr., Winston-Salem, NC 27103.

AJR 150:11–12, January 1988 0361–803X/88/1501–0011 © American Roentgen Ray Society

amperage, thus enabling them to speed up exposures so that they could stop the motion of the heart on chest radiographs, an impossible feat in 1905. In X-ray tubes, the hot cathode was introduced, and this in turn led to greater consistency and reproducibility of the X-ray beam. Progress in diagnosis was at least in part attributed to equipment changes that allowed for speed and uniformity of exposures, thereby making radiographs more useful and avoiding the dangers of fluoroscopy without significant loss of information. Another advance in diagnosis during the same decade was the standard use of contrast media for the detection of gastrointestinal diseases.

Dr. Gray died in 1932 after enduring a long bout of renal cancer. Thus ended the life of a pioneer radiologist to whom all subsequent generations of radiologists owe a debt of gratitude.

ACKNOWLEDGMENT

The assistance of Jaime Tisnado and Frederick J. Spencer are gratefully acknowledged.

REFERENCES

1. Brown P. Alfred Leftwich Gray (1873–1932). *Am J Roentgenol Radium Ther* **1932**;28:679–681
2. Gray AL. A brief review of the progress of roentgenology in the past decade. *Am J Roentgenol* **1915**;2:869–871

Commentary

Neuroimaging and Head Injuries: Where We've Been—Where We're Going

Robert M. Quencer[1]

Had Dr. Alfred Gray known 75 years ago that his article, "Roentgen Examinations for Head Injuries," [1] would be chosen as the focus for a commentary in a jubilee issue of the *AJR*, he might have been surprised, particularly if he had known that it was going to serve as the starting point for discussing advances in the imaging of head trauma. He would have thought it highly improbable that in future years, visualization of the cerebral vasculature would be achieved by direct injection of radiopaque material into the carotid and vertebral arteries, he would have thought it nearly impossible that layered sections of the brain could be visualized by the use of computer manipulation of X-ray data, and he would have thought it in the realm of science fiction that large magnets and RF energies could be used to form an image of the brain based on its hydrogen content. Because of the remarkable technological advances radiologists have witnessed over the past 2 decades, we, probably more than our predecessors, are capable of reflecting on what may be contained in volume 200 of the *AJR*, 25 years from now, when the brain-injured patient is discussed.

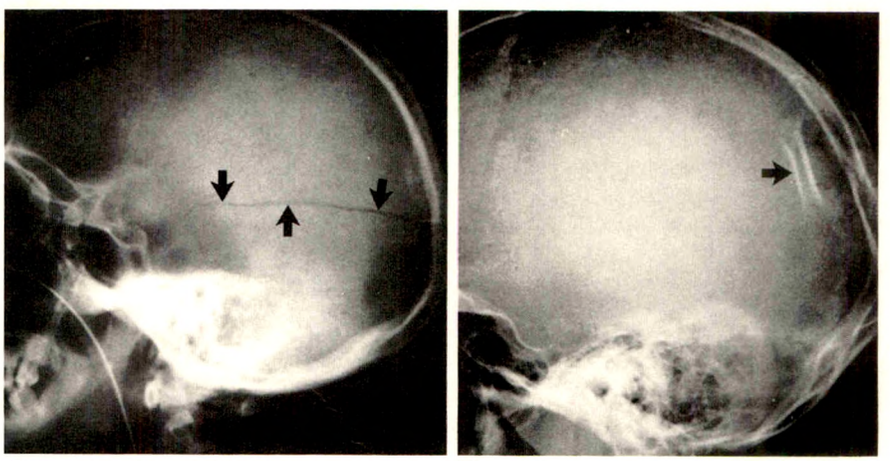

Fig. 1.—Skull films. Lateral films show two major types of fractures, linear (*A*, *arrows*) and depressed (*B*, *arrow*). Fractures should be described in terms of their extent, location, depth of depressed fragment, and relationship to major vessels.

This article is a commentary on the anniversary reprint by Gray, which starts on page 7 of this issue.
Received July 31, 1987; accepted August 24, 1987.
[1] Department of Radiology (R-308), Division of Magnetic Resonance Imaging, University of Miami School of Medicine, P.O. Box 016308, Miami, FL 33101.

AJR **150:13–18, January 1988** 0361–803X/88/1501–0013 © American Roentgen Ray Society

1913

Before we look closely at the present and envision the future, it may be worthwhile to step back in time and examine Gray's article and assess what impact it may have had on the radiologic diagnosis of head trauma. Before 1913, there were only a few reports on skull radiography [2], and published information concerning the radiographic findings in head trauma was scant. Although no radiographs accompanied Gray's report, it is likely that his short article was considered by his peers to be an important contribution to the literature because it dealt with techniques of skull radiography, it reported methods used to diminish patient motion, it described the appearance of skull fractures, and it differentiated these fractures from normal structures.

From the comments in the opening paragraph of his article, it is evident that Gray recognized the fact that skull films address basically the issue of bone injury and do not speak directly to underlying brain damage. It was known that the radiographic signs of injury might be small but the clinical consequences could be great. Problems described by Gray in the interpretation of skull films have been the subject of many published articles over the years, and in fact, those same problems plague today's emergency room radiologists. The difficulty of distinguishing normal anatomic structures such as sutures, diploic veins, and dural vessels from fractures is, as Gray recognized, partly alleviated by good-quality films, but as we know, it is most effectively addressed by an experienced eye. Since head-injured patients should not be heavily sedated, patient motion is handled today with restraints in much the same manner as in 1913. In gravely ill patients, Gray took advantage of the apneic episodes that occurred during Cheyne-Stokes respiration to reduce image degradation due to motion. His recommendation that a fracture be described in terms of its location, shape, size, relationship to blood vessels, and possible depression is still valid today (Fig. 1). This type of information was undoubtedly of value to the attending surgeon, who may have been considering trephination, the common method of decompressing extraaxial hematomas at that time. Of interest, also in 1913, Stewart [3] in the *AJR* and Luckett [4] in the surgical literature independently reported the same patient who had suffered a fracture through the frontal sinus and developed pneumocephalus, an entity that had not been described previously. How in 1913 this ability to radiographically assess head trauma affected patient outcome is not known, since such clinical data were not collected on a large scale.

1943

By the time the 50th volume of the *AJR* was published in 1943, pneumoencephalography and arteriography had already been introduced. Air ventriculography was first described by Dandy [5] in 1918, and his article was reprinted in the *AJR* shortly thereafter [6]. Arising from this seminal work, which incidentally Lindgren [2] believed signaled the birth of neuroradiology, came many reports on pneumoencephalography, but limited use was made of this technique in the acutely head-injured patient. The obvious danger of performing a lumbar puncture and injecting air into the subarachnoid space in the face of a potentially expanding intracerebral mass was well known. The successful radiographic demonstration of the cerebral blood vessels by Moniz in 1927 (cited in [2]) was a medical advance of landmark proportions. However, it was not until the 35th volume of the *AJR* in 1936 that direct injection of contrast material into the carotid arteries was described [7]. It appears, however, that this technique was rarely, if ever, used in head injuries, and skull series remained the primary means of imaging these patients. In fact, as if to emphasize this point, in 1943 an article on skull fractures [8] reiterated some of the same observations concerning skull fractures vs normal structures made by Gray 30 years earlier.

Of interest, in November 1942, on the eve of the 50th volume of the *AJR*, it was shown for the first time that a dye injected into a patient at the time of surgery could be seen to stain cerebral tumors [9]. Six years after this demonstration of blood-brain barrier breakdown, Moore [10] reported the ability to detect brain tumors with the aid of an external counting system after the injection of radioactive diiodoflu-

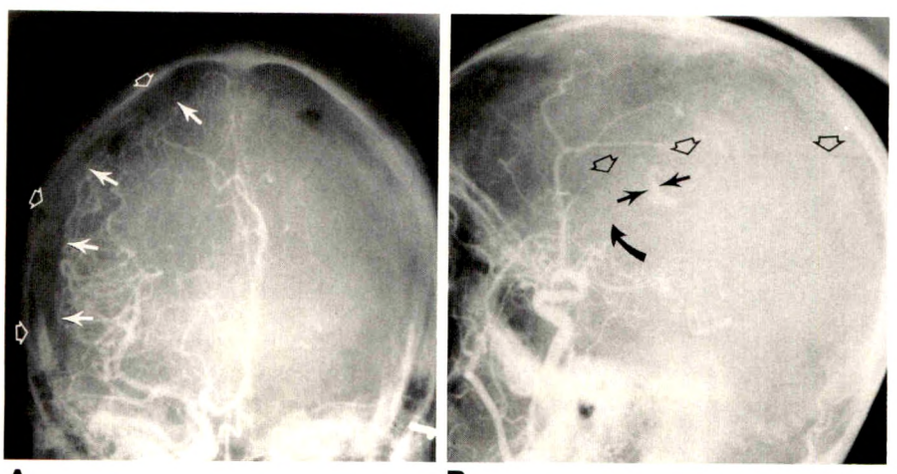

Fig. 2.—Cerebral angiography. Before CT, cerebral angiography was often used in acute head trauma to distinguish extra- from intraaxial hematomas.

***A*, Diagnosis of extraaxial mass (acute subdural hematoma) was made because of separation between brain surface (*solid arrows*) and inner table of skull (*open arrows*).**

***B*, Extravasation of contrast material (*straight solid arrows*) from middle meningeal artery (*curved arrow*) into large epidural hematoma is seen. Fracture line (*open arrows*) extends across meningeal groove, and tracking of contrast material along meningeal groove is noted.**

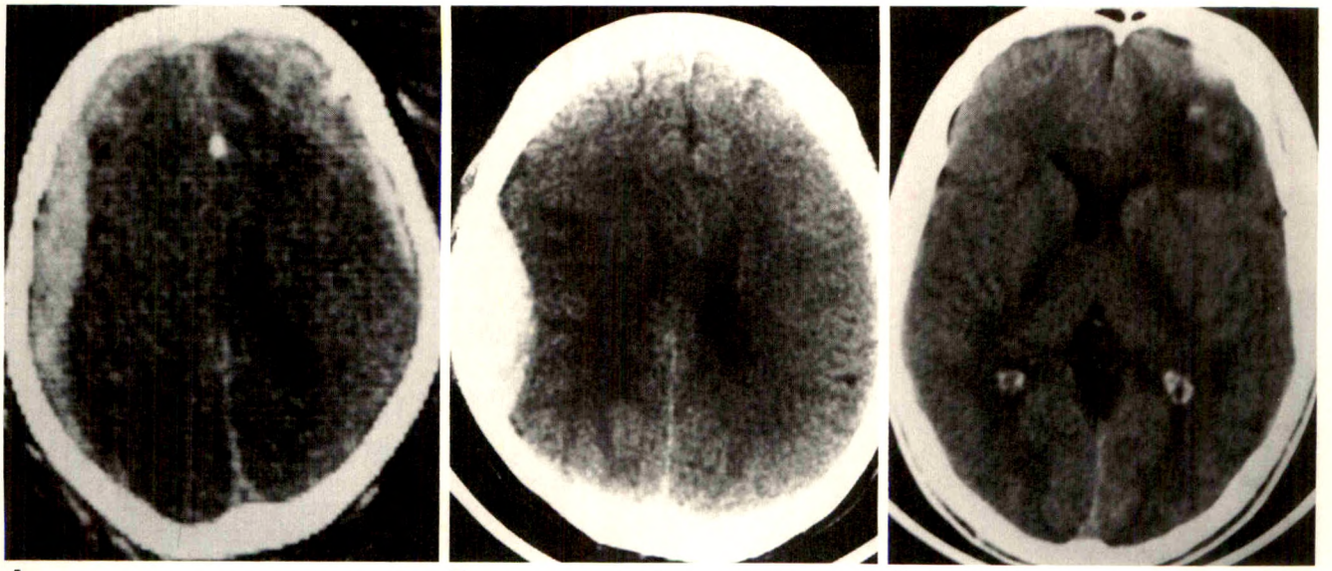

Fig. 3.—CT.

***A* and *B*, First-generation CT scan (*A*) (EMI Mark I) in 1976 clearly shows the presence of left (early CT scans were viewed from superior to inferior) parietal subdural hematoma. Angiography was obviated in such cases. Configuration of the hematoma in *A* is different from biconvex shape of the epidural hematoma seen in *B*, which is from a later-generation scanner (GE 8800).**

***C*, Distinction between extra- and intraaxial hematomas and contusions in left frontal lobe (GE 9800) is rapid and accurate.**

orescein. One of Moore's original 12 cases was in fact suspected preoperatively of having a subdural hematoma, but at surgery a meningioma was found. This problem of distinguishing between different types of convexity lesions continued to be noted in later years. From these roots, radionuclide scanning took hold with the development of newer isotopes and improved methods for detecting the emitted radiation. Uses for radionuclide scanning in head injuries were reported in subsequent years.

1967

In the 100th volume of the *AJR*, published in 1967, fractures and distortions of the newborn skull occurring during delivery were described and illustrated [11]. Again, as in articles published in 1913 and 1943, the necessity of distinguishing fractures from normal structures was stressed.

Just 1 year before the 100th volume of the *AJR*, an article was published showing the appearance of subdural hematomas and their imitators on radionuclide brain scanning with ^{99m}Tc-pertechnetate [12]. This technique was applicable to chronic extraaxial collections such as subdural hematomas, since a membrane that could concentrate the radionuclide had to form before abnormal activity was seen. Flow studies made practical by the development of the gamma camera could show diminished flow to the hemisphere, where a sizeable subdural hematoma was present. Despite this, brain scanning over the years made little impact on the diagnosis and treatment of acute head injuries, because under emergency circumstances, angiography was required. Even in instances of suspected chronic subdural hematomas on radionuclide studies, angiography was often needed for definitive diagnosis.

Although by the mid-1960s the use of selective cerebral angiography had begun, direct carotid artery puncture in the evaluation of acute head trauma was frequently employed. This technique was useful in determining the presence or absence of an intracranial mass and distinguishing intra- from extraaxial collections (Fig. 2). One report [13] indicated that, before the widespread use of cerebral angiography, one-half of all exploratory burr holes for subdural hematomas were negative for clots. While carotid and brachial angiography were important in the treatment of head injuries, two articles published in 1967 showed that a number of entities could masquerade as subdural hematomas [14, 15]. The need to visualize the hematomas themselves rather than infer their presence by vascular displacement was clearly needed. The answer to this problem was just around the corner in the form of CT.

1988

Now, at the time of the publication of the 150th volume of the *AJR*, a number of methods exist for examining head injuries. It was, however, the epic advance in neuroimaging, made possible by the development of CT [16], that had the greatest impact on the evaluation of these patients. With CT, most of the questions left unresolved by skull films and angiography were answered. On an acute basis, intracerebral hematomas were distinguished from edema, and the exact location and size of a hematoma, whether intra- or extraaxial, was determined (Fig. 3). The necessity of empirically perform-

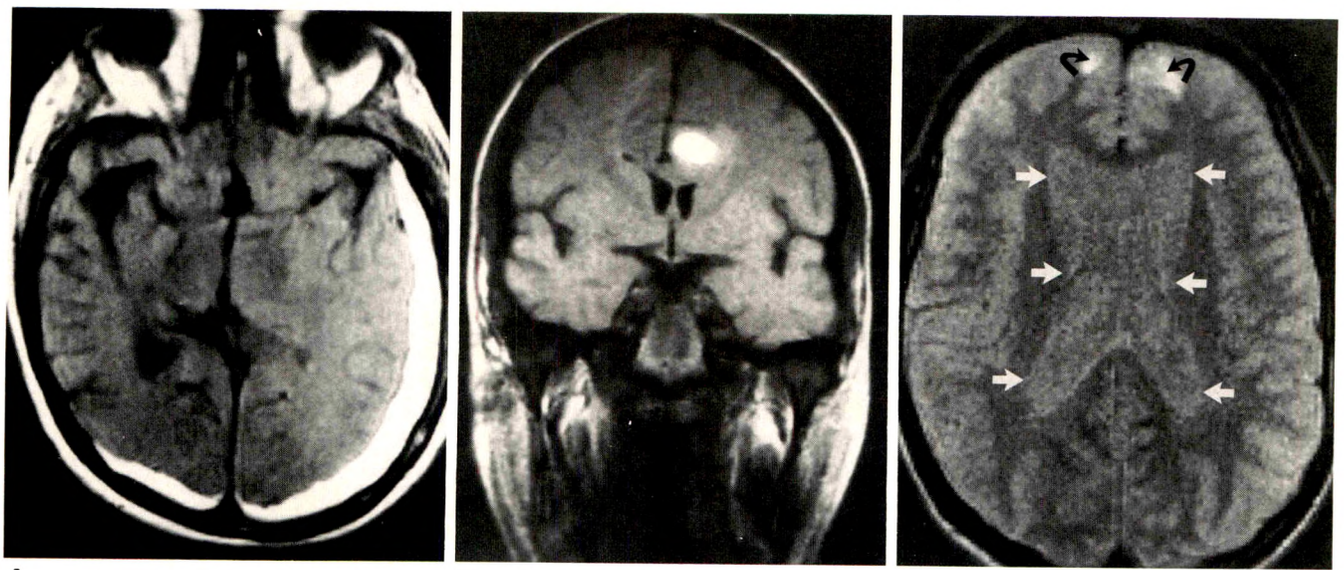

Fig. 4.—MR imaging. MR is not currently used in acute head trauma, but can play a role when there are absent or equivocal findings in subacute or chronic trauma.

A, Hyperintense signal on T1-weighted image with a repetition time (TR) of 850 msec and echo time (TE) of 26 msec (0.5 T, Picker Vista) extends along entire left cerebral convexity and involves right occipital extraaxial space.

B, Hyperintense signal (TR = 1000 msec, TE = 26 msec) in left cingulate gyrus in patient with significant trauma 3 weeks before this study. Both *A* and *B* show shortening of T1 relaxation times consistent with methemoglobin within subacute hematoma. Mass effect caused by hematomas is evident in both cases.

C, Bifrontal hyperintense signal abnormalities (*long arrows*) and hydrocephalus (*short arrows*) are present on T2-weighted image (TR = 2000 msec, TE = 80 msec) in patient who had trauma in remote past. Areas such as these may explain cognitive dysfunction or personality changes and may correlate with areas of abnormal metabolism on positron emission tomography.

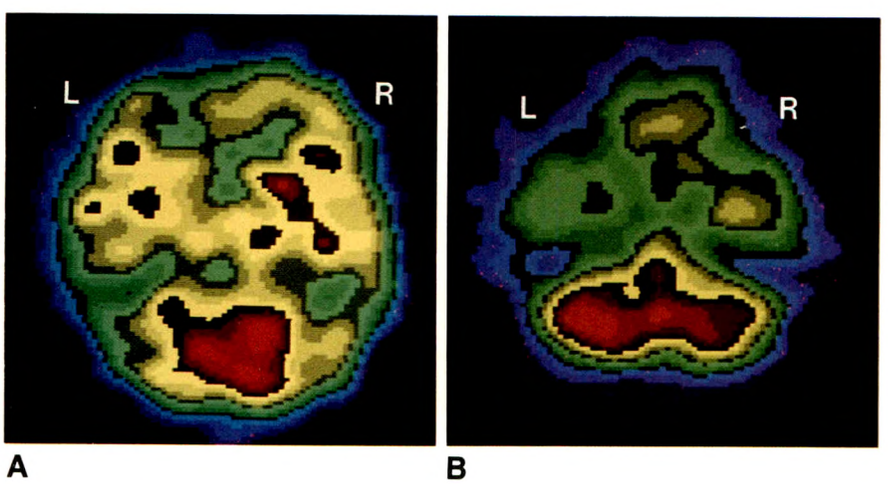

Fig. 5.—Positron emission tomography (PET).

A, PET scan (PETT V Scanner) with F18 fluorodeoxyglucose in patient who had experienced severe frontal head trauma in the distant past. Evidence is seen of decreased glucose utilization in left and right frontal lobes (*green areas*).

B, Lower level. Asymmetry in glucose utilization between left and right inferior temporal lobes, with decreased metabolism on left. Relatively high activity (*red*) in cerebellum reflects generally lowered metabolism in rest of brain.

ing bilateral craniotomies, or worse, performing a craniotomy only to find a diffusely swollen brain (as frequently happened in the pre-CT days), was eliminated. A decade and a half of experience has shown CT to have been the most significant development in medical imaging of the injured brain.

It is reasonable to wonder how such an advance affected the prognosis of patients with acute head injuries. The first attempt to collect data on a significant number of head injuries was begun in 1968 at the Institute of Neurological Sciences in Glasgow, and in 1977 the results of 700 *severe* head injuries from Scotland, The Netherlands, and the United States were published [17]. It appeared that few if any CT scans were obtained because the only radiologic studies mentioned were skull films. The absence or presence of an intracranial hematoma was based on clinical or surgical findings. Six months after their injuries, approximately 50% of the patients had died and 20% had a recovery judged to be "good," although good did not necessarily mean restoration

of normality or a return to work. In the remaining 30%, significant disability remained.

The establishment of a cooperative effort in the United States to collect information on hospitalized patients with *severe* head injuries was reported in 1983 [18] and included the results of CT scanning. It is difficult, however, to determine the effect that CT alone has had on the improved prognosis of severely head-injured patients, because during the acute stages of the injury many of the medical measures now commonly used were not used in the past. Intubation, maintenance of blood pressure and oxygenation, hyperventilation, hyperosmotic diuresis, intracranial pressure monitoring, and CT have all contributed to decreased morbidity and mortality, particularly when this care is delivered by a regional trauma center and/or when the primary admission is to a neurology or neurosurgical unit. CT findings that correlate adversely with prognosis are known and include focal lesions and obliteration of the basal cisterns [19]. Even though CT can demonstrate some of the pathologic conditions, it alone cannot be used as a predictor of patient outcome, and CT is believed, therefore, to be of greater diagnostic than prognostic value [20].

Recent publications have shown the general relationship between the degree of severity of the initial injury and the outcome of survivors [21]. In severe injuries with an initial Glascow Coma Scale (GCS) of 7 or less, the outlook is bleak, and if the patients survive, a residual disability is expected. In moderately severe injuries (GCS of 8–11), estimates are that up to two-thirds of those patients will have a residual disability; in mild injuries (initial GCS of 13–15), a 10% disability can be expected.

During the 1970s and early 1980s, while CT was being refined and new generations of this equipment entered the market, the groundwork was being laid for the eventual emergence of MR as a useful imaging tool. Although the phenomena of nuclear magnetic resonance had been discovered years before, Damadian [22], in a landmark article in *Science*, reported the ability to detect the presence of solid malignant tumors in rats by the measurement of T1 and T2 relaxation times. This discipline was advanced further by Lautebur [23] when he described "zeugmatography," a method for the formation of an MR image. With this technique, spatial information could be derived by noting the response of a sample to an inhomogeneous environment. Four years later in 1977, the first MR images in a human were published, first in a wrist [24] and then in a hand [25].

In three separate articles in 1980, the first brain MR images were published [26–28]. By comparing those early images with the high-quality scans currently available on high-field-strength systems, it is obvious that a quantum leap in medical imaging has occurred in the past half decade. Despite the exquisite anatomic detail MR affords us (Figs. 4A and 4B), it has no defined role in the management of acute head trauma. The answers necessary to care for these patients are more straightforward and far easier to obtain with CT than with MR. It is probable that, in the chronic head injury, MR will play an increasingly significant role by depicting areas of contusion, gliosis, and encephalomalacia that may not be seen on CT (Fig. 4C); as a result, the subtle long-term problems of cognitive dysfunction, learning disabilities, and memory loss may be explained. Positron emission tomography, which portrays the diminished regional metabolism accompanying functional impairments from head injuries (Fig. 5), may, in conjunction with MR, also find a wider use. How this information will translate into patient care remains an area of surgical and neuropsychological speculation.

The Future

In the future, we can expect specialized imaging of the brain that will reflect the important neurophysiological changes that occur in chronically injured brains. Focal changes in sodium and other ions as determined with MR could give additional clues in explaining the presence and type of neurologic dysfunctions in some of these patients. It is also within the realm of possibility that we will one day have the means of detecting and imaging the neurohumoral mediators of brain injury. It is hoped the ability to more successfully manage and treat patients will result from such studies. In addition to these technological advances, future epidemiologic studies could reveal how new therapeutic regimens and imaging techniques affect the long- and short-term outcomes of patients with head injuries of varying severity. The impact of these medical advances would then be clear.

The radiologic evaluation of the head-injured patient has come a long way since the publication of the inaugural issue of the *AJR*. Within a relatively short period of time, imaging techniques that in Dr. Gray's time would have been considered impossible are now routinely used. One can only hope that in the year 2013, when the fourth jubilee issue of the AJR is published, physicians will comment on how crude our techniques were in 1988 and how far medical imaging and treatment have progressed in the past 25 years.

REFERENCES

1. Gray AL. Roentgen examinations for head injuries. *AJR* **1913**;1:294–297
2. Lindgren E. A history of neuroradiology. In: Newton TH, Potts DG, eds. *Radiology of the skull and brain*, vol 1. St. Louis: Mosby, **1971**:1–25
3. Stewart WH. Fracture of the skull with air in the ventricles. *AJR* **1913**;1:83–87
4. Luckett WH. Air in the ventricles of the brain following a fracture of the skull. *Surg Gynecol Obstet* **1913**;17:237–240
5. Dandy WE. Ventriculography following the injection of air into the cerebral ventricles. *Ann Surg* **1918**;68:5–11
6. Dandy WE. Ventriculography following the injection of air into the cerebral ventricles. *AJR* **1919**;6:26–36
7. Loman J, Myerson A. Visualization of the cerebral vessels by direct intracarotid injection of thorum dioxide (Thorotrast). *AJR* **1936**;35:188–193
8. Kenning JC, Harris ID. Some considerations concerning the roentgen diagnosis of skull fracture. *Radiology* **1943**;41:532–537
9. Sorsby A, Wright AD, Elkales A. Vital staining in brain surgery. Preliminary note. *J R Soc Med* **1942**;36:137–140
10. Moore GE. Use of radioactive diiodofluorescein in the diagnosis and localization of brain tumors. *Science* **1948**;107:569–571
11. Chesler CN. The newborn skull: the diagnosis of fracture. *AJR* **1967**;100:92–99
12. Heiser WJ, Quinn JL, Mollihan MV. The crescent pattern of increased radioactivity in brain scanning. *Radiology* **1966**;87:483–488

13. Rosenbluth PR, Arias B, Quartetti EV, Carney AL. Current management of subdural hematoma. *JAMA* **1962**;179:759–762
14. Ferris EJ, Lehrer H, Shapiro J. Pseudo-subdural hematoma. *Radiology* **1967**;88:75–84
15. Lehrer H, DePalma N, Ferris E. Cerebrovascular occlusive disease as a differential diagnosis in subdural hematomas. *Radiology* **1967**;88:85–89
16. Hounsfield GN. Computerized transverse axial scanning. I. Description of the system. *Br J Radiol* **1973**;46:1016–1023
17. Jennett B, Teasdal G, Galbrath S, et al. Severe head injuries in three countries. *J Neurol Neurosurg Psychiatry* **1977**;40:291–298
18. Marshall LF, Becker DP, Bowers SA, et al. The national traumatic coma data bank. *J Neurosurg* **1983**;59:276–284
19. Toutant SM, Klauber MR, Marshall LF, et al. Absent or compressed basal cisterns on first CT scan: ominous predictors of outcome in severe head injury. *J Neurosurg* **1984**;61:691–694
20. Narayan RK, Greenberg RP, Miller JD, et al. Improved confidence of outcome prediction in severe head injury. A comparative analysis of the clinical examination, multimodality evoked potentials, CT scanning and intracranial pressure. *J Neurosurg* **1981**;54:751–762
21. Kraus JF. Epidemiology of head injury. In: Cooper PR, ed. *Head injury*. Baltimore: Williams & Wilkins, **1987**:1–19
22. Damadian R. Tumor detection by nuclear magnetic resonance. *Science* **1971**;171:1151–1153
23. Lautebur PC. Image formation by induced local interactions. Examples employing nuclear magnetic resonance. *Nature* **1973**;242:190–191
24. Hinshaw WS, Bottomley PS, Holland GN. Radiographic thin-section image of the human wrist by nuclear magnetic resonance. *Nature* **1977**;270:722–723
25. Andrew ER, Bottomley PA, Hinshaw WS, Holland GN, Moore WS, Simaroy C. NMR images by the multiple sensitive point method: application to larger biological systems. *Phys Med Biol* **1977**;22:971–974
26. Holland GN, Moore WS, Hawkes RC. Nuclear magnetic resonance tomography of the brain. *J Comput Assist Tomogr* **1980**;4:1–3
27. Holland GN, Hawkes RC, Moore WS. Nuclear magnetic resonance (NMR) tomography of the brain: coronal and sagittal sections. *J Comput Assist Tomogr* **1980**;4:429–433
28. Hawkes RC, Holland GN, Moore WS, Worthington BS. Nuclear magnetic resonance (NMR) tomography of the brain: a preliminary clinical assessment with demonstration of pathology. *J Comput Assist Tomogr* **1980**;4:577–586

Editorial

Threats to the Quality of Peer-Reviewed Radiology Journals: Identification of the Problem and Possible Solutions

Robert N. Berk[1]

The publication of the third jubilee-anniversary volume of the *AJR*, volume 150, coincides with the completion of my second year as editor of the Journal. The work in these 2 years has been interesting and satisfying, but it also has been sobering: sobering because of a growing realization that publication in radiology could and should be substantially more than it is.

Compared with volume 50, which appeared in 1943, or with volume 100, which appeared in 1967, the quality of the Journal has unquestionably improved. Papers are now more sharply focused and more carefully written and edited, and they are published in a more timely fashion. Most authors are to be congratulated for their perspicacity, industry, high standards, and dedication to the goal of the Journal, which is to enrich the general fund of radiologic knowledge. They submit well-polished papers of increasing significance and are largely responsible for the progress made since earlier anniversary volumes of the Journal.

Nonetheless, some authors are also responsible for shallow offerings, duplication, poor scholarship, careless workmanship, and even dishonesty. Other peer-reviewed radiology journals are similarly affected. Submissions of such character, and there are many, threaten the quality of the journals and demean the honor and trust inherent in all scientific publications. This editorial examines these threats and how they erode journal quality, and suggests strategies for remedying the situation.

The infractions that pose the threats are particularly troublesome because they are pervasive. Authors are guilty when they are so driven to publish a large number of papers that they lose sight of the importance of quality. Some apparently feel no shame in having their names associated with careless, trivial, unsound, or unoriginal articles. They recognize that their work is second-rate, but they are willing to have it published if it escapes rejection through some flaw in the review process.

The quality of the journals is threatened when authors submit manuscripts to more than one journal at the same time, when they duplicate previously published reports, or when they purposefully fragment their manuscripts to increase the number of papers that they publish. An author's refusal to postpone writing a paper until a large number of cases is available also impairs quality; it usually means the difference between a classic article and an inconsequential one.

Radiologists who allow their names to be listed as a coauthors when they have made no substantive contribution to the article detract from the integrity of the journals [1]. They make a mockery of authorship [2]. Being a coauthor implies active participation in the research. A coauthor should be able to vouch for the adequacy and accuracy of both the data and the conclusions reached. Merely providing ideas or criticism, supplying funding and administration, or helping to write the manuscript does not constitute coauthorship. Abuse of coau-

[1] Editor-in-Chief, *American Journal of Roentgenology*, 2223 Avenida de la Playa, Ste. 200, La Jolla, CA 92037-3218. Address reprint requests to R. N. Berk.

AJR **150:19–21, January 1988** 0361–803X/88/1501–0019 © American Roentgen Ray Society

thorship is a major reason why in the last decade there has been an exponential increase in the number of authors yet only a linear increase in the number of papers published [3].

Submission of articles that lack good scholarship is an affront to the journals. Such articles reflect a failure to plan a well-organized, properly controlled, prospective analysis of a particular problem. Often these are retrospective reports describing studies that have either a poor experimental design or none at all. The authors of such articles make no effort to eliminate bias or provide controls, and their conclusions are unsubstantiated by the data provided.

Authors who submit poorly written manuscripts for publication show disrespect for the journals. These are muddled papers full of grammatical errors and garbled language. The focus of such papers is inconsistent, and the message is hopelessly blurred. They are written carelessly with no consideration of the guidelines provided for authors by the journals. Such offerings force the editorial office to become a school for remedial English. This slapdash approach to the preparation of manuscripts suggests similar carelessness in the collection of the data, raising suspicions about the authenticity of the research.

Authors further contribute to the problem when they are reluctant to revise their manuscripts in accordance with the suggestions made by the editor. Such arrogant authors view editors as adversaries rather than as partners. Speed rather than quality is their guiding principle. Moreover, when their manuscript is rejected, these authors do not even bother to correct the flaws pointed out to them before submitting the paper to another journal.

The most serious threat to the quality of peer-reviewed radiology journals is, of course, fraud. This is an overt form of deception that involves fabrication, exaggeration, or plagiarism of data in either laboratory or clinical research. Of all the transgressions, fraud is the most visible, the most malignant, and the easiest to define and identify. It is also the least tolerable. A prime example occurred at the University of California, San Diego, where authorities found that certain papers published in radiology journals by a member of the radiology department were based on experiments that were never performed or grossly exaggerated [4, 5].

Editors serve both the author and the reader in their zeal for quality. They are advocates for both parties in the information transfer. The bottom line of their work is to keep poor manuscripts out of print. Therefore, it is the editor's fault if such manuscripts are accepted for publication. Editors are ultimately responsible for what is published. If papers are flawed, the journal is flawed; the editor is accountable.

Extent of the Problem

No data are available that allow an accurate estimate of the extent to which these problems threaten radiology journals. Up to now the acceptance of papers by journals has been based on trust, so there have been no audits to determine if that trust was being abused.

There is no indication that the problems of deceit, poor scholarship, and careless workmanship are more serious in radiology than they are in other medical specialties or that they are worse in the United States than in other countries. Most radiologists are completely honest and respectful in their dealings with the journals. Only a minority contribute to the problems that are the focus of this discussion.

Optimists are confident that fraud is rare, whereas cynics are certain it occurs frequently. Both lack the evidence needed to justify their conclusions. Is the San Diego scandal only the tip of the iceberg? If the renowned pediatric radiologist John Caffey had devised a way to disclose fraud as he did to detect child abuse [6], would there be as much shock at the amount of fraud as there was at the frequency of child abuse?

Even if complete fabrication of data is rare, how often do authors exaggerate the number of experiments performed, the number of cases reviewed, or the extent to which findings are confirmed? How often is the collected information intentionally distorted in order to exaggerate the certainty and importance of the author's conclusions?

The extent to which other, relatively less serious infractions threaten the quality of the journals is easier to assess. It cannot be denied that they are common and pervasive. Some deceptions seem to be accepted as a permissible part of the system. Unoriginal, poorly conceived retrospective studies, insignificant anecdotes, and slipshod manuscripts are received in editorial offices daily. Papers with more authors than cases are common.

Cooper et al. [7] observed that articles with improperly designed protocols or incorrectly interpreted data are the rule in assessments of the efficacy of MR imaging. They evaluated the scientific quality of 56 reports on the efficacy of MR imaging in 10 or more patients in various journals. None were prospective studies. Proof of diagnostic accuracy (the gold standard) was established by surgery or autopsy in only 7%. Forty-eight percent used none of the following terms: sensitivity, specificity, accuracy, false positive, false negative, or predictive value. Twenty-five percent used only one of these terms, 12% used two, and 15% used three. None of the papers contained evidence of blinding of the readers with regard to the diagnosis or the results of other tests.

It is unlikely that these problems are proportionally more common today than they were in the past. Consider that the number of papers published in the United States has increased from 468 in two journals in 1960 to 2861 papers in 16 journals in 1984 [3]. If the improper conduct present in 1960 has burgeoned proportionally, the absolute amount of such behavior must have increased dramatically.

Confronting the Problem

Any conduct that threatens the quality and integrity of radiology journals is unacceptable. Poor scholarship and shoddy workmanship are to be condemned; outright fraud is intolerable. Perfect behavior is an unrealistic goal, but these problems are sapping the vitality of the journals, wasting the time of their readers, and, most importantly, slowing the growth and threatening the integrity of the specialty.

The problem must be attacked at many levels. Renewed emphasis must be placed on quality rather than on quantity.

An author with a curriculum vitae that bulges with trivial and unoriginal articles must be chastised rather than rewarded, criticized rather than congratulated, and looked at with suspicion rather than assumed to be highly productive. Academic institutions must continue to deal harshly with authors convicted of fraud. As in the past, this usually means total derailment of their careers.

To increase the quality of published papers, radiology department chairmen, medical school deans, and chairmen of academic promotions committees must be more suspicious of faculty members who publish a large number of papers each year. Questions must be raised more often: Are the articles substantive? Were the data collected honestly? Was the author intimately involved with the work? These authorities must accelerate their efforts to base academic promotions on the quality of publications rather than solely on quantity. They must let candidates for promotion know that eyebrows will be raised if they have too many publications. The tenet "publish or perish" must be rewritten "publish worthwhile articles or perish."

One way to achieve this goal would be to adopt Angell's idea [8] of limiting the number of publications that can be considered for academic promotion or grant funding. Under her plan, promotion committees and granting agencies would appraise only the candidate's three best publications in any 1 year, or perhaps the five best publications in any 5 years. Other publications would not be listed.

Department chairmen should supervise the publications of their faculty more closely and develop more realistic standards of productivity. They should do more to encourage the planning and performance of carefully designed prospective studies about important issues. They should devise a means to identify the type and degree of participation of every author listed on papers published by the faculty.

Young investigators should be given formal instruction in using statistics, planning research projects, collecting and interpreting data, and preparing manuscripts. Experienced people should be made available to serve as consultants, and they should be used frequently. When necessary, editorial assistants should be employed to help write manuscripts.

Editors and manuscript reviewers must redouble their dedication to the elimination of trivial, unsound, and/or unoriginal articles from their journals. They should raise their standards of scholarship, rejecting more papers that lack originality; that are based on improperly designed, retrospective, or poorly controlled investigations; that have insufficient numbers of cases; or that suffer from slipshod manuscript preparation.

Editors should agree to establish a policy whereby every radiology journal audits a certain percentage of accepted papers, selected at random. Like a tax audit, authors would be required to submit the raw data (experiment data books, clinical records, and radiographic images) that form the basis of their articles, and these would be studied by the editor or his surrogate to determine the article's validity. In addition, the editor would have the right to review the raw data of any submitted article without the risk of impugning the author's reputation.

When rejected articles are submitted for publication in a second journal, editors should share the comments of the initial reviewers (Siegelman SS, personal communication). This would require authors to revise their papers according to the suggestions of the original reviewers before resubmitting their papers to another journal, thus preventing the ideas in the first review from being wasted. This is not to say that the second editorial decision should be biased by the first reviews. The second editor should use new reviewers and make a separate decision about the suitability of the manuscript for publication.

Conclusion

Threats to the quality and integrity of radiology journals must be kept in proper perspective. The emphasis on deception, poor scholarship, and careless workmanship given here must not cause anyone to lose sight of the fact that most authors are honest, respectful, and sincere in their dealings with journals. The majority are dedicated to doing the most substantive research they can and to writing the best articles possible. Readers can rest assured that when the fourth-jubilee anniversary volume of the *AJR*, volume 200, is published in 2013, it will be even more informative than volume 150, published this year.

The situation is no worse in radiology than in any other medical specialty, but it is significant enough to lower the quality of radiology journals, to slow their growth, and to threaten their integrity. The problems will not disappear and are likely to get worse unless there is a concerted effort by authors, editors, and others to confront them openly.

Radiologists must insist on high standards. They must be absolutely honest in their dealings with the journals and have an uncompromising regard for ethical principles. The demand for high quality must be unremitting. Then, and only then, will the threats to the quality of radiology journals be mitigated. Then, and only then, will publications in radiology be all that they can and should be.

REFERENCES

1. Chew FS. Coauthorship in radiology journals. *AJR* **1988**;150:23–26
2. Huth EJ, Irresponsible authorship and wasteful publication. *Ann Intern Med* **1986**;104:257–259
3. Chew FS. The scientific literature in diagnostic radiology for American readers: a survey and analysis of journals, papers, and authors. *AJR* **1986**;147:1055–1061
4. Marshall E. San Diego's tough stand on research fraud. *Science* **1986**;234:534–535
5. Friedman PJ. Fraud in radiologic research. *AJR* **1988**;150:27–30
6. Caffey J. Multiple fractures in the long bones of infants suffering chronic subdural hematomas. *AJR* **1946**;56:163–173
7. Cooper LS, Chalmers TC, McNally M. Magnetic resonance imaging: poor quality of published evaluations of diagnostic precision. *Clin Res* **1985**;33:597A
8. Angell M. Publish or perish: a proposal. *Ann Intern Med* **1986**;104:261–262

P24,447

Book Review

Nuclear Medicine Annual 1987. Edited by Leonard M. Freeman and Heidi S. Weissmann. New York: Raven, 364 pp., 1987. $80

Each chapter in this yearly publication is a separate, unrelated article pertaining to the general field of nuclear medicine. The authors are from departments of nuclear medicine in major teaching hospitals.

Each article is comprehensive, with thorough coverage of its subject and extensive references. New and timely topics are discussed in each *Annual*, and each book also includes an evaluation of a much used technique, including paragraphs on the uses of modifications of the basic procedure, study of new isotopes being tried or others on the horizon, and an objective evaluation of the results. In this regard, the 1987 issue has lengthy articles on diuretic renography, adrenal scintigraphy, and isotopic evaluation of the lower urinary tract in children.

Other chapters each year discuss the advantages and disadvantages of a new technique or a new piece of equipment. In this volume, single-photon emission CT (SPECT) is evaluated. The authors of this chapter discuss the experiences they had after the introduction of a SPECT camera in their department. Studies performed on the SPECT device are compared with those that involved use of a conventional camera. The discussion includes what should be looked for when considering the purchase of a SPECT imaging device.

The lead article in the 1987 volume is a detailed, all-encompassing treatise on the problems and changes of aging, especially situations in which these changes can be documented by using isotopes. This includes coverage of what occurs in numerous body systems as a person grows older.

Some topics could be upgraded almost yearly. Myocardial infarction is one of these timely subjects. This year, detection and quantitation of myocardial infarction are covered completely, including modes of diagnosis, discussion of risk of infarction, isotopes used now, research on future isotopes, studies performed during the treatment phase, modes of treatment, complications, and, finally, how to tell when a patient is ready to be discharged.

The printing, paper, and reproductions are of excellent quality, as they have been over the many years that the *Annual* has been published. The publication is small, compact, and easily carried, but it has one inherent minor limitation. Complex imaging sequences with comparisons are sometimes necessarily placed back to back; consequently, the reader must turn pages to appreciate the total picture.

I recommend the 1987 *Annual* to students who are interested in a total evaluation of any one of the topics discussed and to any practicing physician, radiology resident, or staff radiologist who wants more detailed information about when and why certain tests should be ordered, what their limitations are, and what new studies are being evaluated. Because no single volume of this series includes all topics, I further recommend that previous as well as future volumes be read and saved together near the viewbox for ready reference when a question about nuclear medicine arises.

James A. Usselman
Scripps Clinic
La Jolla, CA 92037

Perspective

Coauthorship in Radiology Journals

Felix S. Chew[1]

Diagnostic radiology journals are publishing an increasing number of articles with many authors (Fig. 1). The number of authors per article is also increasing, and this increase in authors has been far more rapid than the increase in articles [1] (Fig. 2). As radiology journals do not limit the number of authors per article, the rapid increase in authors reflects the individual and aggregate behavior of their contributors. Also, since first authorship is limited by the number of articles, it is coauthorship that has increased most rapidly. (The "first author" of a paper is defined here as the author listed first, regardless of the total number of authors; a "coauthor" is any subsequently listed author.) Coauthorship complicates the proper crediting of work to researchers, creates problems in the indexing and retrieval of papers, and may affect the actual performance of research. Collaborative research and concomitant multiple authorship have some legitimacy and advantage both in allowing the rapid aggregation of data from separate sources and in bringing together researchers from different disciplines; some studies might not be feasible otherwise. However, such strategies appear to refocus research activities rather than increase them [1]. Instances of fraudulent coauthorship in the recent medical literature, including radiology, have been described [2, 3].

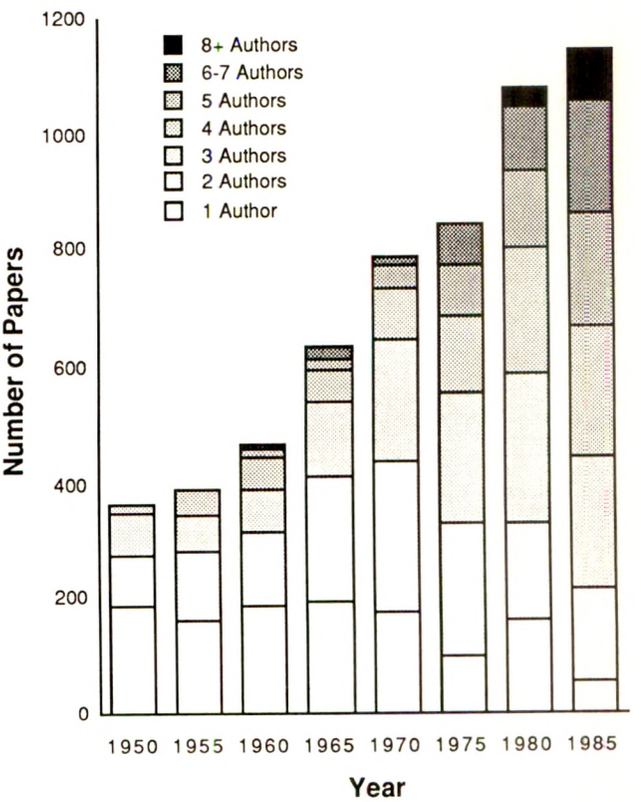

Fig. 1.—Stacked column graph shows the increasing numbers and proportions of multiauthored articles published in *AJR* and *Radiology* (combined data adapted from [1]).

Pervasiveness of Coauthorship

The frequency of coauthorship in radiology journals was examined by searching MEDLARS (National Library of Medicine, Bethesda, MD) for the publications of an arbitrary sample of diagnostic radiology researchers. The sample, consisting

Received July 14, 1987; accepted after revision August 24, 1987.
[1] Department of Radiology, State University of New York Health Science Center at Syracuse, 750 E. Adams St., Syracuse, NY 13210.

of 136 authors who published in the July 1982 issue of the *AJR*, was intended to be representative of the clinical diagnostic radiology research community. The MEDLARS search located the articles of all individuals in the sample that were published between 1980 and 1985 in diagnostic radiology journals.

The number of coauthorships accumulated by many was impressive, ranging from none to 82 in the 6-year period studied (median = 6, mean = 11.9) (Table 1). The total number of articles published ranged from 1 to 87 (median = 10, mean = 16.4). Such rapid and sustained rates of publication virtually ensure that the time spent on each publication by the most prolific coauthors is small. Preparation and revision of major manuscripts for publication in the sciences require an average of about 82 hr of time by the authors, excluding the actual research [4].

The researchers with the most coauthorships have articles with more coauthors. The 5% of researchers with the most coauthorships had an average of 6.2 authors per paper in 1985; 70% of their papers had five or more authors. These 5% also had a higher proportion of articles with more authors as well as more authors per article than the average for all articles published the same year in the *AJR* and *Radiology* [1]. In contrast to this, the 10% of the researchers with medial numbers of coauthorships had an average of 3.8 authors per article; only 29% of their articles had five or more authors.

Coauthorship is a simple means of inflating a bibliography without necessarily increasing productivity. This does not imply that coauthorship is necessarily inappropriate or without value; on the contrary, it is now the usual situation in scientific publication. For example, in 1985, 95% of the papers published by *Radiology* and the *AJR* had coauthors [1]. Nonetheless, to prevent abuses of the system, researchers should consider the level of participation that merits coauthorship. One view is that all authors, including coauthors, should have had sufficient involvement with the work and the article reporting it to be able to defend its method, results, and conclusions without reservation [5, 6]. To accept coauthorship under other circumstances seems at best foolish and at worst esurient and dishonest.

Although multiple authorship appears well entrenched in the radiologic literature, only a few highly prolific authors account for most of the coauthorships: 15% of researchers account for 53% of coauthorships. By their example, these few may set *de facto* standards and goals for the specialty. Prolificacy in publication is a common pathway to promotion and prominence in the profession.

Pressure to Publish

It is self-evident that there must be considerable incentive to publish and to publish frequently. Since most articles emanate from academic medical centers [1], the pressures to publish must originate there. It seems likely that quantitative expectations for research productivity in promotion and grant proceedings are to blame, at least in part, for the publish-or-perish syndrome [2–8]. A specific numeric criterion may appear explicitly on documents of appointment. For example, in one university department, the goal for each faculty member was "to be involved in three publications annually in refereed journals," two of which could be coauthored. Scientists, particularly medical scientists with public funding, have a positive obligation to publish their work. Some incentive is healthy, but even the most reasonable expectations may spawn excess.

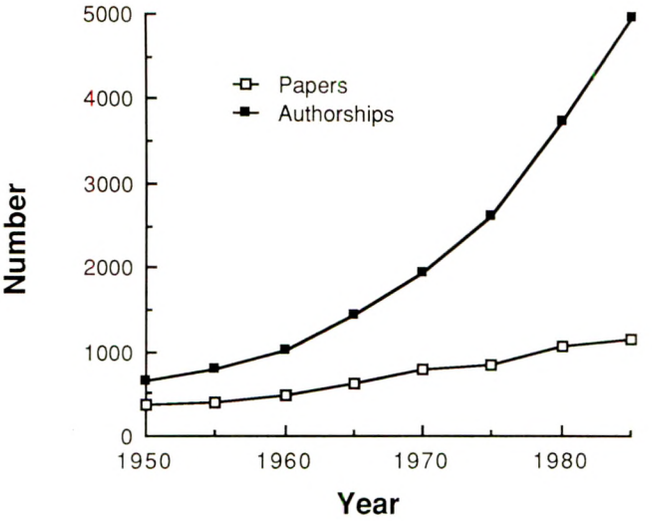

Fig. 2.—Line graph shows exponential increase in authorships with linear increase in published articles in *AJR* and *Radiology* (combined data adapted from [1]).

The medical literature takes little notice of multiple authorship. Full lists of authors are isolated to title pages, and such lists are truncated in the tables of contents and bibliographies of journals and by indexing services, sometimes to a single author. The identities of coauthors are lost to all but those with the actual journal pages. If coauthorship becomes more difficult and less acceptable as a means of building a bibliography, a more insidious abuse becomes attractive: wasteful publication.

Wasteful Publication

Wasteful publication may take two forms [5]. "Divided publication" is the publication of a single piece of research in installments of "least publishable units" [7]. "Repetitive publication" multiplies the publications possible from essentially the same content and is accomplished by submission to multiple journals or by adding small successive bits of data and then republishing. In both abuses, results and conclusions are strewn across the literature separated by journal and time. This strategy is self-defeating in a situation in which everyone wants to publish, but only a few want to read [9]. In addition to the obvious problem a reader has in collecting all of these together, the resources of scientific publication are wasted [5]. Assuming that the research was worthwhile to begin with, only the last of any such string of articles (the one with *all* the information) would be necessary to a reader. Since only 9% of the papers published in radiology journals

TABLE 1: Distribution of the Number of Coauthorships Accumulated by 136 Diagnostic Radiology Researchers, 1980–1985

No. of Coauthorships	No. of Researchers	Cumulative %	
		Of Researchers	Of Coauthorships
0	4	2.9	0.0
1	32	26.5	2.0
2	14	36.8	3.7
3	3	39.0	4.2
4	7	44.1	6.0
5	7	49.3	8.1
6	6	53.7	10.3
7	1	54.4	10.8
8	9	61.0	15.2
9	2	62.5	16.3
10	2	64.0	17.5
11	1	64.7	18.2
12	4	67.6	21.2
13	4	70.6	24.4
14	2	72.1	26.1
15	2	73.5	27.9
16	3	75.7	30.9
17	5	79.4	36.1
20	2	80.9	38.6
21	1	81.6	39.9
22	1	82.4	41.2
23	1	83.1	42.6
24	1	83.8	44.1
26	2	85.3	47.3
27	1	86.0	49.0
28	2	87.5	52.4
29	1	88.2	54.2
30	3	90.4	59.8
32	1	91.2	61.7
33	1	91.9	63.8
37	2	93.4	68.3
40	1	94.1	70.8
44	1	94.9	73.5
48	1	95.6	76.4
51	1	96.3	79.6
58	1	97.1	83.1
60	1	97.8	86.8
63	1	98.5	90.7
69	1	99.3	95.0
82	1	100.0	100.0

Note.—A total of 1625 coauthorships were accumulated by 136 researchers.

TABLE 2: Distribution of the Proportion of Coauthorships Relative to All Authorships for 136 Diagnostic Radiology Researchers, 1980–1985

% of Coauthorships	No. of Researchers	Cumulative % of Researchers
100	50	36.8
≥90	13	46.3
≥80	14	56.6
≥70	13	66.2
≥60	13	75.7
≥50	10	83.1
≥40	6	87.5
≥30	9	94.1
≥20	3	96.3
≥10	1	97.1
≥0	4	100.0

Note.—Data for 136 researchers have been aggregated into intervals of 10%.

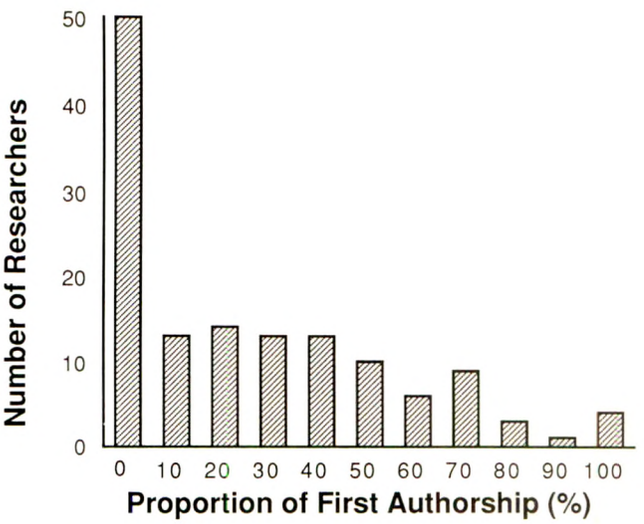

Fig. 3.—Histogram for 136 researchers of the percentage of first-authored articles relative to total papers published in diagnostic radiology journals over 6 years (1980–1985).

account for 49% of all citations to radiology literature [10], there is a considerable level of noise for the amount of signal.

The net advantage of accumulating large numbers of coauthorships is unclear. By distinguishing coauthorships from first authorships for individuals in the sample of researchers studied, the percentage of all authorships that were coauthorships was found to range from 0 to 100% (median = 83%, mean = 76%) (Table 2). Fifty researchers (36.8%) had only coauthorships, and four (3%) had only first authorships (Fig. 3). The average ratio of coauthorships to first authorships was 2.7. Bibliographies bloated with coauthored items are cumbersome and may discourage detailed analysis of the articles, losing those of quality and significance amidst the distracters. In a very real and practical sense, coauthorships can be both irrelevant and detrimental.

Remedies

Scientists are remembered for their best, most important works. A sensible approach to evaluating a researcher's work might rely on his defense of a few self-selected, first-authored papers [6, 8]. In view of the length of time required to initiate, complete, and publish research (as well as the time frame for promotions in most academic settings), a limit of three to five articles may be appropriate. According to Angell [8], this might (1) improve the quality of medical research by allowing more ambitious but time-consuming studies, (2) improve the accuracy and precision of the promotion and grant-funding processes by allowing fuller evaluation of the quality of a researcher's work, and (3) eliminate some of the "fluff" from the scientific literature [8]. Discounting bibliographies inflated with coauthorships is already universally practiced by appointment

and promotion committees (Berk RN, personal communication), but explicit notice of such action is often lacking.

Although journals may impose limitations on coauthorship, editors and reviewers may become more alert to attempts at divided or repetitive publication, and departments and academic institutions may create review mechanisms and establish more appropriate expectations, no system that preserves the academic freedom necessary to good scientific work can always stop a determined, unethical author [11]. The ultimate imperative for ethical behavior rests with the individual. To preserve academic freedom, the research community must be self-policing. The issue is not moot, for the future direction of radiology as a discipline depends on sound research and scholarship.

ACKNOWLEDGMENT

The computer bibliographic searches were performed by Jackie Mardikian, State University of New York Health Science Center Library, Syracuse.

REFERENCES

1. Chew FS. The scientific literature in diagnostic radiology for American readers: a survey and analysis of journals, papers, and authors. *AJR* **1986**;147:1055–1061
2. Marshall E. San Diego's tough stand on research fraud. *Science* **1986**;234:534–535
3. Petersdorf RG. The pathogenesis of fraud in medical science. *Ann Intern Med* **1986**;104:252–254
4. King DW, McDonald DD, Roderer NK. *Scientific journals in the United States: their production, use, and economics.* Stroudsburg, PA: Hutchinson Ross, **1981**
5. Huth EJ. Irresponsible authorship and wasteful publication. *Ann Intern Med* **1986**;104:257–259
6. Relman AS. Lessons from the Darsee affair (editorial). *N Engl J Med* **1983**;308:1415–1417
7. Broad WJ. The publishing game: getting more for less. *Science* **1981**;211:1137–1139
8. Angell M. Publish or perish: a proposal. *Ann Intern Med* **1986**;104: 261–262
9. Price DJD. Ethics of scientific publication. *Science* **1964**;144:655–657
10. Chew FS, Relyea-Chew A. How research becomes knowledge in radiology: an analysis of citations to published papers. *AJR* **1988**;150:31–37
11. Putman CE. The responsibilities of authorship (editorial). *Invest Radiol* **1987**;22:95

Perspective

Fraud in Radiologic Research

Paul J. Friedman[1]

Research fraud is nothing new. Altering data to fit hypotheses has a long, largely unrecognized history. Modern analyses have shown that respectable figures from the archives of science, such as Galileo, Mendel, and Newton, improved their results by various manipulations that do not meet contemporary standards of accurate reporting. Wholesale invention of data also has occurred in the remote as well as the recent past. Broad and Wade [1] detail these and a host of other examples of the failure of science to live up to its ideals of truth and objectivity. One's reaction on reading about these major and minor cases of misrepresentation or fraud is to think, "It can't happen here." But indeed it has happened in radiology, just as it has in other biomedical fields. The following case report concerns a person who is well known in radiology, but I have chosen to call him "Dr. A" in order to emphasize the general aspects of the problem rather than focus on issues specific to this case.

Case Report

Dr. A graduated from medical school in 1974 and came to the University of California, San Diego (UCSD), where he was a resident in medicine for the next 3 years. From 1977 to 1979 he was a research fellow in cardiology and nuclear medicine. After the first year his primary supervisor went on leave, and he pursued his research more or less independently. He then took a 2-year clinical fellowship in cardiology, continuing his laboratory and clinical research with only nominal supervision. Because he was a successful "self-starter," he was allowed to pursue whatever projects interested him. He spent the last 6 months as a junior cardiology faculty member doing research and teaching in cardiac radiology. In 1981, Dr. A joined the department of radiology as a junior faculty member in the cardiovascular section, whose chief also went on leave a year later, leaving Dr. A to teach cardiac radiology, supervise fellows in the cardiovascular training program, and manage the radiology laboratory. The cardiovascular radiology chief decided not to return, and another recent fellow was put in charge of the division while Dr. A began his residency in radiology. Dr. A continued to do research and publish articles throughout his residency, supervising fellows and residents in the laboratory and preparing research and training grant applications.

In anticipation of his completing his residency, Dr. A was proposed for a regular faculty appointment in Radiology, and plans were made for him to become chief of cardiac radiology. However, 3 months before the appointment was to take place, a senior faculty member in the department of radiology prepared to write a letter of recommendation for the appointment by reading several recent papers. He noticed peculiarities in data tables in two publications. Both studies had the same mean and standard deviation but had different numbers of animals. Neither paper acknowledged that the results had been published elsewhere, nor could such duplication have occurred with any measurable mathematical probability. The chairman of radiology was notified and investigated the matter further. When he found other irregularities he alerted the Dean's office that there was a question about the validity of some of Dr. A's work.

Dr A was asked directly if there had been some kind of error. Initially he said that he would look over the original data and explain. He then reported that he could not locate any of the data, resigned his residency position in radiology, withdrew the already-approved research and training grants, and refused to communicate further with anyone from the University. A formal investigation was promptly instituted by the Dean to determine whether fraudulent research had been published. The investigation followed previously established guidelines for responding to charges of unethical practice.

[1] School of Medicine, M-002, University of California, San Diego, La Jolla, CA 92093. Address reprint requests to P. J. Friedman.

AJR 150:27–30, January 1988 0361–803X/88/1501–0027 © American Roentgen Ray Society

A multidisciplinary faculty committee including representatives from both cardiology and radiology reviewed recent publications, interviewed several of Dr. A's research fellows, technicians, and colleagues, and reported to the Dean that there was clearcut evidence of research fraud in three submitted manuscripts, two of which had been published. The news media had been informed of the investigation by unknown persons, but reporters agreed to wait for the committee's conclusions before announcing the scandal. The committee informed the relevant granting agencies when the investigation was started, and reported its findings at the conclusion.

Dr. A was offered an opportunity to retract these and any other papers that could not, in retrospect, be documented. The attorney who represented Dr. A proposed that a statement be sent to the journals concerning certain of Dr. A's papers. This statement did not acknowledge the existence of fictitious data or conclusions, nor would Dr. A (under his lawyer's guidance) meet with the faculty committee or admit any wrongdoing. The committee found this unacceptable and sent a letter of retraction to the journal that had published the two fraudulent papers.

The job was not finished, however. With every one of Dr. A's papers potentially tainted, readers would be unsure of which results could be trusted, and coauthors' bibliographies would be ruined. Journals, news reporters, coauthors, and committee members all questioned the rest of Dr. A's bibliography. In response, the Dean formed a new committee to deal with this question and to make general recommendations on actions that the institution could take to prevent future occurrences.

Fifteen months later, the committee had finished reading all 147 papers in Dr. A's bibliography, had written twice to all his coauthors for additional information, had interviewed several key supervisors and coworkers, and had formulated conclusions about the validity of each paper and the factors contributing to Dr. A's unethical activities. The committee then made a series of recommendations on measures that could be taken by the institution and its faculty to reduce the likelihood of future research fraud. Dr. A's papers were classified as either valid, fraudulent (with documentary or testimonial evidence that research was not done as reported), or questionable (lacking either firm evidence of fraud or informed support by the coauthors). Of 147 manuscripts reviewed (137 of which had been published already), 79 were considered valid, 55 questionable, and 13 fraudulent. All the journals, granting agencies, and coauthors were informed of the conclusions about each paper. The press published several rounds of articles and comments, including a report in *Science*, "San Diego's Tough Stand on Research Fraud" [2]. Dr. A, his academic career in radiology and cardiology abruptly terminated, was tracked down by reporters and was asked to leave at least one hospital position because of the adverse local publicity.

Comment

In what way was UCSD "tough"? Instead of presuming that these purported works of scholarship were "innocent until proven guilty," the University took the position that the results of scientific investigation must be proved, and sometimes proved again, in the face of challenge [3]. The burden is always on the investigator, not the challenger, to prove a point. Therefore, the coauthors were challenged to present proof that work had been done, that data had been collected as described, and that statistical analysis had been performed, with results as reported. Since Dr. A's contributions could no longer be trusted, it was necessary to obtain coauthors' assurances that they either had possession of original data or had personally observed its collection and verified its analysis, and had personal knowledge that the published report accurately reflected the procedures and results of the studies. It seemed a reasonable approach to find at least one coauthor for each step in the research-to-publication process to vouch for its validity.

Coauthors who had actually collected data themselves (typically research fellows or residents) usually had retained possession of it, or could testify to the authenticity of the experiments. In one instance, coauthors had assumed that all the reported experiments had been performed, but had only witnessed half of them. Independent laboratory records showed that only half the experiments could have been carried out. In other papers, statistical tests were reported that no one else had performed or checked, or methods were modified to appear more accurate or significant. In recent papers, whole series of experiments were reported that had not been done and probably would have been technically impossible to accomplish with the numbers of animals and success rates reported. The coauthors either had not seen the manuscripts, had not signed copyright releases, or had allowed their names to be used despite minimal participation in the study, such as reading the manuscript, discussing the research protocol, or doing related experiments for another paper.

"Publish or perish" has long been the maxim governing survival in a research university. Clearly, Dr. A was a victim of this pressure to publish, but still it is hard to absolve him of personal responsibility for his actions. His peers coped with this pressure in different ways, although his predecessors in cardiology and radiology had set a standard of great productivity. Some coauthors had agreed to share responsibility for Dr. A's research publications simply to expand a curriculum vitae. Others were unsure of the ethics of receiving credit for work that they had not even seen, but lacked the self-confidence to raise the issue with senior faculty members.

The members of the committee were surprised at the extent to which Dr. A's coauthors passively accepted the events that followed. Not one wrote to the journals themselves asking for a retraction of papers whose validity they now had reason to doubt, and none showed any interest in repeating experiments or statistical analyses to prove whether the original research was valid. Perhaps the level of denial should not have been surprising in view of their previous acceptance of Dr. A's work at face value.

Radiologists seemed ignorant of the fact that Dr. A was not held in high esteem by members of the department of medicine. Considering itself fortunate to have such a productive person eager to contribute to its training and research,

the radiology faculty did not look closely at what others thought about Dr. A. No one noticed the degree to which his research and training had been performed without effective supervision.

Recommendations and Conclusion

Recommendations to the Faculty

Several recommendations were made by the committee to the school and to the scientific journals that support research communication. These ideas were tempered, however, by a recognition that research fraud is one of the risks of the individualistic research enterprise that has produced so many good researchers and results. Placing restrictions on individual initiative will do more damage than good. Having unrealistic expectations of journal reviewers will not achieve more critical or penetrating reviews. The following are some of the final recommendations made by the UCSD faculty committee to the faculty. (1) Peer review of faculty should focus on the quality, not the quantity, of published work. (2) Work in which one does not have a significant role should not be counted. Collaboration in research should continue to be encouraged, but coauthors should take more responsibility for reviewing submitted and final manuscripts. Coauthorship should reflect scientific involvement and imply responsibility for the work reported. (3) Each department should develop guidelines for the supervision of research trainees, including written evaluation, standards for research laboratory supervision, and a policy on publication. The investigator's responsibility for the preservation of raw research data should be communicated and exemplified. (4) Research supervisors should recognize a responsibility to review the experimental procedures, data analyses, and manuscripts of those working in their laboratories. (5) New faculty and trainees should be clearly informed of the expectations of the laboratory, the department, and the university in their performance. Realistic standards of research productivity should be encouraged. (6) Faculty and trainees should be informed of the policy on unethical research practices. It should be considered an academic obligation for them to inform responsible superiors if they have reservations about the integrity of the work of another.

Recommendations to Journals

Professional journals also have a responsibility to take actions to minimize fraud. The response of journals to notification that certain of Dr. A's papers were fraudulent and others were suspicious (since no one could vouch for them adequately) was mixed. Some published the requested statements; others, on the advice of their attorneys, avoided publishing any statement that might discredit an individual scientist for fear of libel. Many did not acknowledge the correspondence that had been sent to them.

The UCSD faculty committee had specific recommendations for journal editors: (1) All journals should require the signed approval of final manuscripts by all coauthors. (2) Peer review of manuscripts submitted to journals should be carried out with more care, especially with regard to statistical evaluations. (3) Journals should not be so insistent on publishing short papers, since this encourages fragmentation and republication of data.

Public Acknowledgment of Fraud

What is the responsibility of the institution to communicate these events and conclusions to the public? No one enjoys having one's mistakes probed by the press. It may be difficult to get colleagues to speak frankly if confidentiality is not guaranteed. Unproved allegations, if published, could be very damaging to a scientist's career, regardless of the outcome. Dr. A's loss of a job as a result of investigative reporting was a punishment not anticipated by the review committee. There are fears that granting agencies will take a negative attitude toward the whole institution in response to reported investigations of fraud.

These fears and concerns must be balanced by other considerations. Supervision of the expenditures of grant funds carries with it a responsibility to keep the granting agency informed of violations of ethical or scientific standards. The public also deserves to know if its trust has been abused. Covering up problems and errors eventually will arouse public suspicion and affect its support for the entire research community. Although many scientists do not acknowledge it, their privileged position is part of a contract with society that must be maintained with honesty and openness; there must also be a willingness to discuss and deal with problems.

Accordingly, an organization must act with sensitivity and courage in responding to charges of research fraud. The preliminary investigations should be carried out confidentially and carefully to avoid damaging the reputations of innocent individuals, but decisions should not be left to the discretion of a single individual, especially not to one with a vested interest in "keeping the lid on." It is inappropriate to inform public or external agencies of all inquiries into charges of unethical research, but when a formal investigation is initiated, concerned granting agencies and journals should be notified. The National Institutes of Health require notification even prior to the decision to undertake an investigation in cases with allegations of very serious misconduct, including criminal violations, or of significant health hazards.

The press may learn about such an investigation through informants or by reading National Institutes of Health documents under the Freedom of Information Act. In any case, however, the press should be officially informed by the institution at the end of the process if any fraudulent activity has been discovered. If the press solicits information during an investigation, a promise of frank disclosure at the conclusion should ward off premature negative publicity and allow for a balanced and well-prepared presentation of facts and recommendations. Even if an individual has made serious mistakes in behavior, an institution—be it a school or a profession—can salvage its integrity by dealing with the problem in a serious and thorough manner and by respecting the public's right to know the facts.

Conclusion

It is an unfortunate part of a competitive system that some individuals or groups will not abide by the rules that govern

the majority. One should be careful of individual rights in dealing with these cases and not overreact, but neither should one ignore unethical behavior. When problems arise, investigation and correction should be based on peer group action. At all times, researchers should be aware that they are role models.

REFERENCES

1. Broad W, Wade N. *Betrayers of the truth*. New York: Simon & Schuster, **1982**
2. Marshall E. San Diego's tough stand on research fraud. *Science* **1986**;234:534–535
3. Engler R, Covell J, Friedman P, Peters R, Kitcher P. Misrepresentation and responsibility in medical research. *N Engl J Med* (in press)

American Roentgen Ray Society
Residents' Award Papers, 1988

The ARRS announces competition for the 1988 President's Award and two Executive Council Awards for the best papers concerning the clinical application of the radiologic sciences.

Awards

The winner of the President's Award will receive a certificate and a $1000 prize. The winners of the two Executive Council Awards will each be given a certificate and a prize of $500. The winners will be announced on March 15, 1988. Winning papers will be presented at the ARRS annual meeting at the San Francisco Hilton Hotel, San Francisco, CA, May 7–12, 1988. Winning papers will be submitted for early publication in the *American Journal of Roentgenology*. All other papers will be returned to the authors.

Regulations

Eligibility is limited to residents or fellows in radiology who have not yet completed 4 years of approved training in a radiologic discipline. A letter from the resident's department chairman attesting to this status must accompany the manuscript. The resident must be the sole or senior author and be responsible for all or most of the project.

Submitted manuscripts must not exceed 5000 words and have no more than 10 illustrations. Four copies of the manuscript and illustrations are required.

Deadline for submissions is January 29, 1988. Send papers to:

B. G. Brogdon, M.D.
Chairman, Committee on Education & Research
American Roentgen Ray Society
Department of Radiology
University of South Alabama Medical Center
2451 Fillingim Street
Mobile, AL 36617

How Research Becomes Knowledge in Radiology: An Analysis of Citations to Published Papers

Felix S. Chew[1]
Annemarie Relyea-Chew[2]

The process by which research becomes generally disseminated knowledge in radiology was studied by an analysis of reference citations. A citation is the event that occurs when one paper is listed as a reference by another paper. Analysis of the citations received by 30 diagnostic radiology journals in 1985 showed that five journals received 73% of the citations. Approximately half of the citations were made to papers over 5 years old. Analysis of the citations received by the 1977 issues of eight journals over a 9-year period showed a rapid rise in the number of citations received, a peak in the third year after publication, and a slow, exponential decline. Analysis of citations to a group of individual papers showed that 10% of the papers received nearly 50% of the citations.

This information suggests that citations to the radiology literature are concentrated among a handful of papers in a few journals. The citation activities of individual journals reflect in part their editorial policies. Parameters of citation activity may be relevant to selecting journals for subscription, reading, or publication. The radiology literature has lasting relevance and receives citations for many years. Advancement of the science of radiology follows the lead of a very few works; the most frequently cited papers concern practical techniques and procedures.

Scientific papers published in peer-reviewed radiology journals are records of research. Some information from this research is incorporated into radiology's common body of knowledge; other information is lost, shown to be invalid, or becomes obsolete. As new papers are published, old ones tend to lose their currency and disappear beneath the constant stream of new information. By analyzing the citations to papers published in radiology journals, we seek to describe the way in which this occurs. Our particular focus will be on the literature's longevity and the proportion of useful papers.

Materials and Methods

Papers published in radiology journals as well as the radiology journals themselves were studied by an analysis of reference citations. A citation is the event that occurs when one paper (the cited paper) is listed as a reference by another paper (the citing paper) [1]. If all citations to all papers published in a particular journal are aggregated, then the citation activity of the journal itself can be studied. The annual *Journal Citation Reports* (*JCR*) volumes of the *Science Citation Index* (*SCI*) [2–11] list data of this kind. One can look up a specific paper and find out which papers have cited it in the period of time covered by the particular index volume; one can also look up a specific journal and find out which journals have cited it and the number of times they did so. For this study, we analyzed three sets of citation data: contemporaneous citations made in 1985 to a large group of diagnostic radiology journals (with a detailed examination of a smaller group of core journals), citations made to the 1977 issues of a small group of core journals over a 9-year period, and citations made to a sample of individual papers.

Received August 7, 1987; accepted after revision September 30, 1987.

[1] Department of Radiology, State University of New York, Health Science Center at Syracuse, 750 E. Adams St., Syracuse, NY 13210. Address reprint requests to F. S. Chew.

[2] College of Law, Syracuse University, Syracuse, NY 13210.

AJR 150:31–37, January 1988
0361–803X/88/1501–0031
© American Roentgen Ray Society

Contemporaneous Citations to Journals

Citation data concerning all 30 journals of diagnostic radiology indexed by the *SCI* were obtained from the 1986 *JCR* volume [2]. There are many more extant diagnostic radiology periodicals, but these evidently received too few citations for *SCI* coverage. No attempt was made to examine journals that published a few radiology papers but whose editorial emphasis was elsewhere. The data studied included the total number of citations received in 1985 by all issues of the journals, the number of citable source items published in 1984, the impact factor, and the cited half-life.

Source items are usually papers. However, depending on the discretion of the indexer, editorials and signed letters may sometimes be counted, especially if they include references. Abstracts of papers published in other journals, society announcements, meeting programs and abstracts, book reviews, and the like would not usually be considered as source items.

The impact factor is a ratio between the number of citations a journal receives and the number of source items it publishes. A journal's impact factor for 1985 is the number of citations received in 1985 to items published in 1983 and 1984, divided by the total number of source items published by that journal in 1983 and 1984. A difference in citation rates between two journals may simply reflect a difference in the number of source items published. The impact factor is a method of correcting for the size of a journal, allowing comparison of large and small journals [12]. A high impact factor indicates that the journal contains source items of immediate and relatively high utility to subsequent publications. A low impact factor will result if the source items are cited infrequently during the 2 years after publication, regardless of how frequently they may be cited subsequently.

The term "cited half-life" refers to the amount of time that passes between the publication of the cited paper and the publication of the citing papers. The cited half-life of a journal, then, is the number of journal publication years (going back from the current year) that account for 50% of the total citations received by the cited journal in the current year [12], or more simply, the median age of the cited papers. For example, if the cited half-life for a journal in 1985 were 5.0 years, then half of the citations received by that journal in 1985 would have been made to issues published in 1980 or later, and half would have been made to issues published before 1980. A journal with a long cited half-life receives many citations to papers in older issues.

A small group of eight core journals was studied in greater detail: *Radiology*, the *American Journal of Roentgenology* (*AJR*), *Journal of Nuclear Medicine*, *British Journal of Radiology*, *Investigative Radiology*, *Clinical Radiology*, *Neuroradiology*, and *ROFO: Fortschritte auf dem Gebiete der Rontgenstrahlen und der Nuklearmedizin*. These journals were among those that had been identified as dominating the citation activity of the entire radiology literature [13]. For these journals, the number of citations received in 1985 to all current and previous issues was tabulated by the year of the journal issue cited in order to profile the age of currently cited papers.

Citations to Journals Over Time

Citation data from 1977 to 1985 for the eight core journals previously listed were available (no citation data were available for any journal for the year 1976 [11]). The numbers of citations made to the 1977 issues of each of these journals in each of the years from 1977 to 1985 were obtained from the appropriate *JCR* volumes [2–10].

Citations to Individual Papers

An arbitrary sample of papers was assembled by using all 119 of the scientific papers published in the January, February, and March 1980 issues of the *AJR*, a major journal of clinical diagnostic radiology. The computerized data base of the *SCI*, SCISEARCH (Institute for Scientific Information, Philadelphia, PA), was searched by remote computer terminal for the total number of citations received by each of these papers in the period from January 1981 to February 1986.

Results

Contemporaneous Citations to Journals

In aggregate, the 30 diagnostic radiology journals indexed by the *SCI* received 64,420 citations in 1985 and published 4129 source items in 1984 (Table 1). Citation activity was concentrated among a few journals. The five journals that received the most citations accounted for 73% of all citations and 44% of the source items. For individual journals, the number of citations received in 1985 ranged from 20,212 to 24, with a mean of 2147 and a median of 686; the number of source items published in 1984 ranged from 647 to 24, with a mean of 138 and a median of 96.

The impact factors ranged from 4.3 to 0.3, with a mean of 1.2 and a median of 1.1 (Table 1).

The cited half-lives ranged from 8.5 to 1.8 years, with a mean of 5.1 years and a median of 5.2 years (Table 1). Approximately half the citations received were made to papers that were over 5 years old.

The number of citations received by the core journals as a group in 1985 was spread widely over many previous years' issues (Table 2), with a peak centered over the 1983 issues (Fig. 1). Citations received in 1985 to journals 10 or more years old made up 26.2% of the total citations. Combined data are presented in Table 2, but in the distribution of current citations over previous issues, there was very little variation among the individual journals.

Citations to Journals Over Time

Citations to the 1977 issues of the core journals rose rapidly with time, peaked in the second and third years after publication, and then gradually declined (Fig. 2). Table 3 presents combined data, but there was little variation in this pattern among the individual journals. The decline with time (4 or more years after publication) in the number of citations received fitted an exponential function ($r = .99$):

$$y = 1.35 \times 10^{-0.046x}$$

where y is the number of citations received in 1 year (normalized to the maximum ever received in a single year), and x is the number of years after publication.

Citations to Individual Papers

Citation activity for individual papers was concentrated among a small percentage of papers. In the period studied from 1981 to 1986, the 119 papers in the sample received a total of 1208 citations. The mean number of citations received was 10.2, with a median of 5 (Table 4). The 12 papers cited

TABLE 1: Citation Activity for 30 Diagnostic Radiology Journals[a]

Journal Title	Citations Received in 1985 (%)[b]	Source Items in 1984 (%)[c]	Impact Factor[d]	Cited Half-Life[e]
Radiology	20,212 (31.4)	647 (15.7)	3.7	5.6
AJR	13,229 (20.5)	499 (12.1)	2.8	5.7
J Nucl Med	6,781 (10.5)	193 (4.7)	4.3	5.4
Br J Radiol	3,721 (5.8)	205 (5.0)	1.2	8.5
J Comput Assist Tomogr	3,292 (5.1)	267 (6.5)	1.8	4.1
ROFO	1,627 (2.5)	313 (7.6)	0.8	4.6
Invest Radiol	1,592 (2.5)	158 (3.8)	1.2	6.0
AJNR	1,547 (2.4)	163 (3.9)	2.0	2.7
Neuroradiology	1,511 (2.3)	94 (2.3)	1.3	6.3
Clin Radiol	1,481 (2.3)	102 (2.5)	1.2	6.7
JCU	1,215 (1.9)	122 (3.0)	1.2	4.8
Acta Radiol Diagn	1,078 (1.7)	92 (2.3)	0.9	6.9
Radiol Clin North Am	992 (1.5)	59 (1.4)	1.8	5.8
Semin Nucl Med	926 (1.4)	40 (1.0)	1.5	5.7
Clin Nucl Med	707 (1.1)	211 (5.1)	0.5	4.3
J Ultrasound Med	666 (1.0)	121 (2.9)	1.9	1.8
Gastrointest Radiol	612 (1.0)	74 (1.8)	0.8	5.3
Pediatr Radiol	523 (0.8)	106 (2.6)	0.9	4.5
Semin Roentgenol	447 (0.7)	31 (0.8)	1.0	6.9
Radiologe	411 (0.6)	98 (2.4)	0.5	5.0
Skeletal Radiol	370 (0.6)	42 (1.0)	0.4	4.5
J Can Assoc Radiol	340 (0.5)	107 (2.6)	0.3	6.4
Urol Radiol	313 (0.5)	38 (0.9)	1.1	3.6
Diagn Imag Clin Med	216 (0.3)	53 (1.3)	0.9	
Eur J Radiol	198 (0.3)	78 (1.9)	1.1	3.5
CT J Comput Tomogr	159 (0.2)	56 (1.4)	0.5	3.8
J Nucl Med Allied Sci	101 (0.2)	43 (1.0)	0.4	4.3
Comput Radiol	65 (0.1)	59 (1.4)	0.3	
CRC Crit Rev Diagn Imag	64 (0.1)	24 (0.6)	0.3	
Med Ultrasound	24 (0.0)	34 (0.8)	0.3	
Totals[f]	64,420 (100.0)	4,129 (100.0)		
Mean	2,147 (3.3)	138 (3.3)	1.2	5.1
Median	686 (1.1)	96 (2.3)	1.1	5.2

[a] Adapted from Garfield [2]. Listed in order of decreasing total number of citations received in 1985.

[b] Total citations received during 1985 to all years of journal.

[c] Source items include papers and sometimes other citable material, such as letters, editorials, or commentaries.

[d] Impact factor is a ratio of citations received to source items published: citations received in 1985 to items published in 1983 and 1984, divided by the total source items in 1983 and 1984. The impact factor provides a method of correcting for the size of a journal, allowing comparison of large and small journals.

[e] The number of journal publication years going back from the current year that account for 50% of the total citations received by the cited journal in the current year. Cited half-life reflects the age of the cited journal issues.

[f] Percentages do not add up to precisely 100% because of rounding.

TABLE 2: Citations Received by Core Radiology Journals[a] in 1985: Distribution by Year of the Cited Journals

Year of Journals	Citations Received in 1985	
	Number	Percent[b]
1985	787	1.6
1984	4,676	9.3
1983	6,251	12.5
1982	5,335	10.6
1981	4,485	8.9
1980	4,306	8.6
1979	3,508	7.0
1978	3,091	6.2
1977	2,567	5.1
1976	2,025	4.0
Earlier	13,123	26.2
Totals	50,154	100.0

[a] Combined data for the following journals: *Radiology*, *AJR*, *J Nucl Med*, *Br J Radiol*, *Invest Radiol*, *Clin Radiol*, *Neuroradiology*, and *ROFO*.

most frequently (10% of the 119 papers) received a total of 599 citations (49.6% of all citations); the 62 papers least frequently cited (52% of the 119 papers) received a total of 129 citations (10.7% of all citations) (Fig. 3).

Discussion

A literature survey is an integral part of the preparation of a scientific manuscript, but authors generally do not attempt to include an exhaustive bibliography. In many circumstances, the literature is too voluminous for full utilization, so authors select a few key references sufficient to document statements, provide context, and guide further reading. A particular author's choice of which specific papers to cite may have less to do with the intrinsic quality of the cited paper than with other factors, such as familiarity and propinquity [1]. For example, authors would be less likely to cite papers that are difficult to find or that are published in foreign languages.

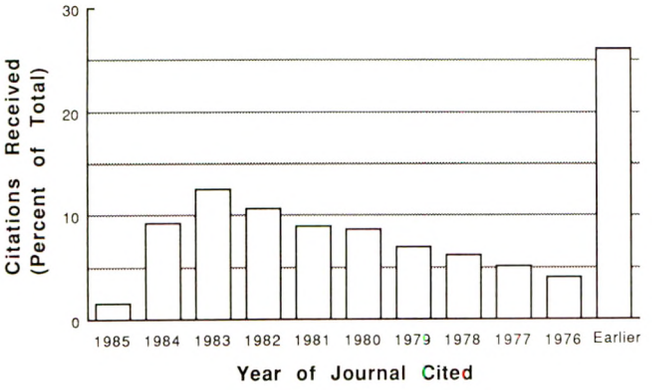

Fig. 1.—Citations received in 1985 by core diagnostic radiology journals (*Radiology*, *AJR*, *J Nucl Med*, *Br J Radiol*, *Invest Radiol*, *Clin Radiol*, *Neuroradiology*, *ROFO*). Graph shows distribution of citations with respect to the year of the journal issues cited.

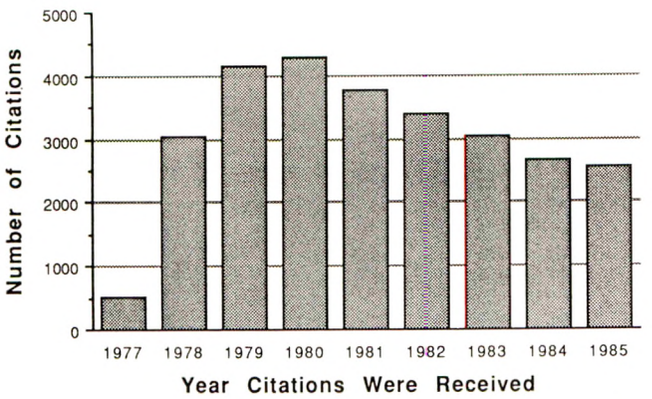

Fig. 2.—Citations received by the 1977 issues of eight diagnostic radiology journals (*Radiology*, *AJR*, *J Nucl Med*, *Br J Radiol*, *Invest Radiol*, *Clin Radiol*, *Neuroradiology*, *ROFO*). Graph shows number of citations received each year from 1977 to 1985. Decrease in citations from 1980 to 1985 is exponential.

Contemporaneous Citations to Journals

Medical journals have many functions. In addition to providing readers with current awareness of new developments in research, journals also perform educational and archival functions and, through peer review, a quality-control function as well. Because original publication in peer-reviewed journals is integral to professional advancement and recognition in academic settings, journals also serve as public logbooks of authors' achievements. These functions are often at cross-purposes; for example, a preliminary report of a new research protocol may be important for current awareness but unsuitable for archiving. The final report of a large series of cases may be important to archive, but if preliminary results have already been published, it may be unsuitable for providing current awareness. Thus differences in the citation activities of various journals may reflect in part an editorial emphasis on different journal functions.

The concentration of citations among only a few of the journals has been observed previously [13] and is a well-established bibliometric principle [1, 14]. Some journals, including *AJR*, impose a limit on the number of references allowed. Because diagnostic radiology journals tend to cite themselves more often than they cite each other [13], such limitations applied systematically may affect citation activity, generally tending to decrease citations [15].

TABLE 3: Citations Received Each Year by the 1977 Issues of Core Radiology Journals[a] from 1977 to 1985

Year CItations Were Received	Years After Publication	Number of Citations Received for Year
1977	0	516
1978	1	3051
1979	2	4145
1980	3	4291
1981	4	3774
1982	5	3410
1983	6	3052
1984	7	2675
1985	8	2567

[a] Combined data for the following journals: *Radiology*, *AJR*, *J Nucl Med*, *Br J Radiol*, *Invest Radiol*, *Clin Radiol*, *Neuroradiology*, and *ROFO*.

TABLE 4: Citations Received Between January 1981 and February 1986 by a Sample of 119 Papers Published in AJR[a]

No. of Citations	No. of Papers (%)[b]	Cumulative %	
		Of Papers	Of Citations
110	1 (0.8)	0.8	9.1
74	2 (1.7)	2.5	21.4
57	1 (0.8)	3.4	26.1
48	2 (1.7)	5.0	34.0
41	1 (0.8)	5.8	37.4
35	1 (0.8)	6.7	40.3
34	2 (1.7)	8.4	45.9
25	1 (0.8)	9.2	48.0
19	3 (2.5)	11.8	52.7
18	1 (0.8)	12.6	54.2
17	3 (2.5)	15.1	58.4
16	2 (1.7)	16.8	61.1
15	3 (2.5)	19.3	64.8
13	2 (1.7)	21.0	67.0
12	3 (2.5)	23.5	69.9
11	5 (4.2)	27.7	74.5
10	2 (1.7)	29.4	76.2
9	3 (2.5)	31.9	78.4
8	4 (3.4)	35.3	81.0
7	10 (8.4)	43.7	86.8
6	5 (4.2)	47.9	89.3
5	8 (6.7)	54.6	92.6
4	4 (3.4)	58.0	94.0
3	14 (11.8)	69.7	97.4
2	8 (6.7)	76.5	98.8
1	15 (12.6)	89.1	100.0
0	13 (10.9)	100.0	100.0

[a] Papers were published in the January, February, and March 1980 issues of *AJR*.

[b] Percentages do not add up to precisely 100% because of rounding.

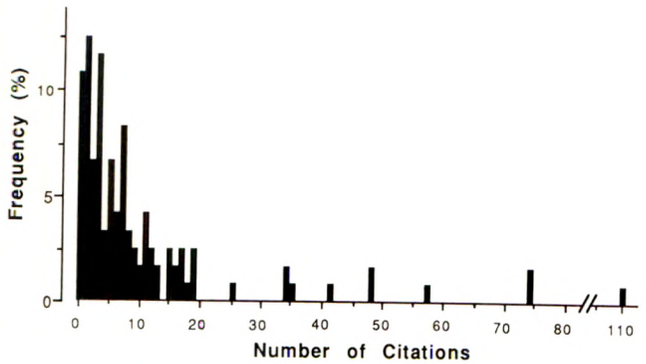

Fig. 3.—Citations received between January 1981 and February 1986 by a sample of 119 papers published in *AJR* in the first quarter of 1980. Vertical axis shows the percentage of the 119 papers that received the number of citations indicated along horizontal axis. There is a sharply peaked distribution that is skewed to the right.

The impact factor is calculated from the number of citations received by papers in a journal in the 2 years after publication divided by the number of source items published during the same period. A low impact factor may reflect little emphasis on current awareness, publication of many educational papers that might not be cited immediately or often, a research field with relatively low activity, or simply obscurity. One journal that, to a certain extent, combines all of these elements is *CRC Critical Reviews in Diagnostic Imaging*. With an impact factor of 0.3 and a small circulation, this journal publishes detailed, scholarly critiques of a few highly select items from the published literature, months to years after the subject paper was originally published. Another example is *Skeletal Radiology*, with a impact factor of 0.4. In addition to publishing major papers in a mature research area, *Skeletal Radiology* publishes many educational "test" cases for the readership to exercise its diagnostic acumen; these are actually case reports that are unlikely to be cited immediately or often. A high impact factor often indicates that the journal emphasizes current awareness in an active research field or that it is preeminent in its field. Examples of this type of journal are the *Journal of Nuclear Medicine* and *Radiology*, which have factors of 4.3 and 3.7, respectively.

New journals will have a short cited half-life. *The Journal of Ultrasound in Medicine*, for example, with a cited half-life of only 1.8 years, was first published in 1982, and the *American Journal of Neuroradiology*, with a cited half-life of 2.7 years, was first published in 1980. A short cited half-life may also reflect an editorial policy that emphasizes current awareness. Journals that cater to a rapidly moving research field should also have short cited half-lives, but such journals also tend to be relatively new. A long cited half-life may reflect either emphasis on archival literature or a slowly evolving, mature research field. Very long publication lags in the journals that publish the citing papers will also lengthen the cited half-life. The *British Journal of Radiology*, with the longest cited half-life among the journals studied (8.5 years), is cited by itself more frequently than by any other journal [13], but its lag time between submission and publication is not unusually long. However, it appears to favor archival literature and also publishes a relatively high proportion of papers in the slowly evolving, mature research fields of radiation hazards and protection, radiotherapy, radiobiology, and physics as applied to radiology. This content is unique among clinical diagnostic radiology journals and may account for the long cited half-life.

Because of the American origin of the *SCI* and the dominance of English-language publications in science and medicine, there is a tendency to underestimate the citation activity of journals that publish in other languages. This is likely the case with ROFO, which publishes mostly in German and which may have many of its non–English-language citations uncounted.

A library with limited resources may consider citation activity, among other factors, a relevant criterion in selecting journals for subscription [12, 14].

Citations to Journals Over Time

The distribution (among previous years of issue) of citation counts received by journals in 1985 (Fig. 1) and those received over time by journals published in 1977 (Fig. 2) both indicate that the older literature continues to be cited for many years, albeit in ever-declining numbers. Extrapolation of the decline in citations received by journals published in 1977 suggests that if 100 citations are received during the third year after publication, then 28 citations should be received during the 15th year after publication, and 10 citations should be received during the 25th year after publication. Clearly, some papers in the radiology literature have lasting relevance.

Citations to Individual Papers

The key feature of the distribution of citations among the sample of 119 individual papers is that 10% of the papers accounted for 50% of the citations. If this distribution of citations among individual papers is generalized to the five radiology journals that were cited most frequently (Table 1), it can be estimated that 2.2% of the papers account for 25% of the citations to all 30 diagnostic radiology journals indexed by the *SCI*, and 9.2% of the papers account for 49% of the citations. These distributions suggest that a few papers in a few journals dominate citations in the entire field. As a corollary, most papers are cited infrequently or not at all. Research in radiology follows the lead of a very few works.

The quality of a scientific paper depends on intrinsic features such as the originality and clarity of its hypothesis, the elegance and appropriateness of its methods, and the erudition and creativity of its discussion. The importance and usefulness of a paper is extrinsic and depends on its context: the relationship of the research to past and future work. Context may be defined by citations. Citations made by the paper identify relevant previous work and knowledge; citations to the paper identify the trail of subsequent research. The time required to initiate, complete, and publish research results in a lag between publication and citation. As the research front moves forward and away, the citations generally decline. Work that is obscure or inapplicable to further

research, even though valid, may receive no citations. Work that is flawed usually will not be cited. A well-known work that has become commonly accepted knowledge may be cited frequently, but as the knowledge is taught and retaught, occasionally the primary source may become obliterated and as a consequence receive no further citations [16]. Some papers may receive many citations regularly for many years, but this is exceptional [17].

It is a general observation in science that papers describing techniques, so-called "blue-collar" science, are usually cited more often than papers proposing theories or reporting experiments [18]. This study supports that observation; the most frequently cited papers all concerned description, application, comparison, or validation of imaging techniques or interventional procedures.

Citation counts have been suggested (and used) as measures of scientific productivity for individual researchers. This represents an extension of the use of journals as public logbooks of authors' achievements. Some controversies concerning this practice have been reviewed [1, 15]. In such an application, rather than dealing with hundreds of citations distributed among dozens of papers, one is likely to be counting a few citations to a few papers. Generalizations that are valid with large samples may not be valid in individual cases. Citations measure in a general way the usefulness of published papers to subsequent papers [1].

Selecting references for a paper is a prerogative of authors; the precise reasons why authors cite particular papers in specific instances are unclear. Proposed reasons for making specific citations range from the serious to the frivolous; they include identifying methods or equipment, providing background reading, giving credit for related work, paying homage to pioneers, and deliberately attempting to manipulate citation frequencies [15]. According to Garfield [1], concerted, deliberate attempts to manipulate citation frequency are rare and should be patently obvious. Self-citation (an author citing his own work) and citation of the work of coauthors is relatively common, but often it reflects continuing work in a specific area of interest or a narrow field of expertise. High rates of citation may indicate a useful or provocative paper in a field of wide interest; low rates of citation may simply indicate a narrow field and cannot be construed as prima facie evidence of a poor-quality paper. The gross numbers of citations may be affected by the time course of sampling the citations, the journal of publication of both cited and citing papers, and the type of paper (description of technique, case report, and so on). It must also be realized that citation rates are different for different fields of research and that citations are not necessarily specific indicators of validity or accuracy.

Discriminating Among Journals

Readers of radiology literature are faced with an exponentially increasing volume of material [13]. For example, *Radiology* and the *AJR* together published 392 papers in 1955 and 1148 papers in 1985, but the number of diagnostic radiology journals extant increased fourfold in the same period [13]. To keep up, readers must be more and more selective in their reading. If a reader is able to select the few papers in the literature that will receive the bulk of the citations and is content with reading the least amount of literature, that reader would need to read fewer than 85 papers per year (those 85 will account for 25% of citations received). The difficulty, of course, occurs in selecting which papers to read (the 85 papers, in this example, would be 2.2% of the literature). One selection criterion might be by journal: the journals that receive the most citations and that have the highest impact factors are most likely to publish papers that will be frequently cited.

Contributors to the literature are faced with an exponentially increasing number of diagnostic radiology journals as potential outlets for their work [13]. Most strive to publish in journals that will reach a specific audience and give their work the greatest visibility. We would suggest that the number of citations received by a journal, its impact factor, and its cited half-life are useful factors to consider when choosing a journal in which to publish.

Obsolescence Anxiety

The scientific process is orderly but time-consuming. The amount of time that passes between the inception of the research and publication of the paper describing its results and conclusions raises the possibility of obsolescence before publication. In a rapidly evolving field like diagnostic radiology, in which simultaneous discovery is commonplace because of the uniformity of research materials and methods, this possibility assumes considerable significance. Some journals have responded by attempting to decrease the interval of time between submission and publication of a manuscript [19–20].

One unfortunate consequence of obsolescence anxiety is the publication of tenuous preliminary or premature findings. In the context of rapid dissemination of current research information, presentation of work in progress at scientific meetings has become increasingly popular. Many such presentations never reach peer-reviewed publication [15]. In selecting items for perusal, readers should be more concerned with factors such as the pertinence of the paper to current needs and the intrinsic quality of the work, rather than with mere currency of publication [15]. Rushing research or ending it prematurely is no shortcut in the scientific process. The duration of the actual research is brief compared with the time required for publication, and a well-crafted paper has considerable longevity.

ACKNOWLEDGMENTS

Data from the *Journal Citation Reports*® of the *Science Citation Index*® and from *SCISEARCH* (copyright 1977–1986 by the Institute for Scientific Information®, Philadelphia, PA) were used with permission. The computer searches were performed by James A. Capodagli, SUNY Health Science Center Library, Syracuse, NY.

REFERENCES

1. Garfield E. *Citation indexing: its theory and application in science, technology, and humanities.* New York: Wiley, **1979**

2. Garfield E, ed. *SCI journal citation reports. A bibliometric analysis of science journals in the ISI data base. Science citation index 1985 annual, vol. 18.* Philadelphia: ISI Press, **1986**
3. Garfield E, ed. *SCI journal citation reports. A bibliometric analysis of science journals in the ISI data base. Science citation index 1984 annual, vol. 15.* Philadelphia: ISI Press, **1985**
4. Garfield E, ed. *SCI journal citation reports. A bibliometric analysis of science journals in the ISI data base. Science citation index 1983 annual, vol. 15.* Philadelphia: ISI Press, **1984**
5. Garfield E, ed. *SCI journal citation reports. A bibliometric analysis of science journals in the ISI data base. Science citation index 1982 annual, vol. 14.* Philadelphia: ISI Press, **1983**
6. Garfield E, ed. *SCI journal citation reports. A bibliometric analysis of science journals in the ISI data base. Science citation index 1981 annual, vol. 14.* Philadelphia: ISI Press, **1982**
7. Garfield E, ed. *SCI journal citation reports.. A bibliometric analysis of science journals in the ISI data base. Science citation index 1980 annual, vol. 14.* Philadelphia: ISI Press, **1981**
8. Garfield E, ed. *SCI journal citation reports. A bibliometric analysis of science journals in the ISI data base. Science citation index 1979 annual, vol. 14.* Philadelphia: ISI Press, **1980**
9. Garfield E, ed. *SCI journal citation reports. A bibliometric analysis of science journals in the ISI data base. Science citation index 1978 annual, vol. 13.* Philadelphia: ISI Press, **1979**
10. Garfield E, ed. *SCI journal citation reports. A bibliometric analysis of science journals in the ISI data base. Science citation index 1977 annual, vol. 13.* Philadelphia: ISI Press, **1978**
11. Garfield E, ed. *SCI journal citation reports. A bibliometric analysis of science journals in the ISI data base. Science citation index 1976 annual, vol. 13.* Philadelphia: ISI Press, **1977**
12. Garfield E. Citation analysis as a tool in journal evaluation. *Science* **1972**;178:471–479
13. Chew FS. The scientific literature in diagnostic radiology for American readers: a survey and analysis of journals, papers, and authors. *AJR* **1986**;147:1055–1061
14. Kronick DA. *The literature of the life sciences: reading, writing, research.* Philadelphia; ISI Press, **1985**
15. Cronin B. *The citation process: the role and significance of citations in scientific communication.* London: Taylor Graham, **1984**
16. Garfield E. The "obliteration phenomenon" in science . . . and the advantage of being obliterated. *Essays of an information scientist*, vol 2. Philadelphia: ISI Press, **1978**:396–398
17. Chew FS. *AJR*: the 50 most frequently cited papers in the past 50 years. *AJR* (in press)
18. Garfield E. The 300 most-cited authors, 1961–1976, including coauthors. 3A. Their most cited papers. Introduction and journal analysis. *Essays of an information scientist*, vol 3. Philadelphia: ISI Press, **1979**:689–700
19. Figley MM. Publication in radiology: challenges to tradition. *Radiology* **1985**;157:633–636
20. Berk RN. *AJR* achieves goal to speed publication. *AJR* **1987**;149:312

Book Review

Introductory Physics of Nuclear Medicine, 3rd ed. By Ramesh Chandra. Philadelphia: Lea & Febiger, 233 pp., 1987. $18.50

This book is designed to be used by residents and technicians in nuclear medicine. This edition has been expanded from previous versions to include information on emission tomography; at the same time, the earlier material on rectilinear scanners has been reduced. It appears that the author's main goal is to provide a terse text for the teaching of physics as related to nuclear medicine. The book is compact, and it does cover the major topics of importance to current practice. However, I was not altogether satisfied with the amount of detail on some topics, and I question if the text is adequate for a modern course in the physics of nuclear medicine.

The material is organized into 16 chapters, three appendixes, and a special section on suggested reading for more information. This last section is particularly important because of the lack of detail in several sections of this book. In fact, it might have been better if the author had expanded the reference section to ensure that the reader is directed to an adequate range of reference material.

The first chapter is a review of basic principles of atomic physics. Chapter 2 continues the review into nuclear physics and the areas of nuclear structure and decay processes. Chapter 3 introduces the various decay laws and the concepts of half-life and the statistics of nuclear decay. Chapter 4 discusses the production of radionuclides, including nuclear reactions and generator systems. Radiopharmaceuticals are discussed in chapter 5, with good coverage of many of the products used in clinical nuclear medicine. Chapter 6 covers the interaction of radiation with matter and includes discussions of basic interactions, range, stopping power, linear transfer of energy, and the normal interactions of photons with matter. Chapter 7 presents radiation dosimetry with more detail than normally is seen in introductory texts. Detection of radiation is covered in chapter 8, with discussions on gas-filled, scintillation, and semiconductor detectors. Chapter 10 is the first of two chapters dealing with imaging systems and simple probe units. This chapter also includes information on bone-density scanners, a topic not found in many such books. The second chapter on imaging systems, chapter 11, focuses on area detectors (e.g., scintillation cameras) and on interfacing such systems with computers. Chapter 12 covers quality assurance and basic system testing. Chapter 13 is devoted to the topic of contrast detection in the final image. Emission tomography is covered in chapter 14, and biological effects of radiation are discussed in chapter 15. Finally, chapter 16 covers radiation safety. The appendixes include material on characteristics of some common radionuclides, tables of CGS (centimeter-gram-second) and SI (International System) units, and exponential tables.

Overall, the range and organization of the material is well thought out. The number of figures is the minimum needed, and the figures are simple and of high quality. Some of the material is covered in detail with supporting examples, such as the information on half-life and common radiopharmaceuticals. However, most of the material is presented rather superficially and without much detail. This is acceptable for a text for an introductory course, but even for that purpose important points are not covered. To be more specific, the discussions on Compton scattering do not include the scattering equations nor do they provide good examples of the distribution of scattered events from the patient and the impact on imaging. The new material on emission tomography is simplistic and does not provide adequate preparation for understanding the options and problems encountered in the use of emission tomography. This lack of detail is, in my opinion, a major drawback to this book. As part of a course on the physics of nuclear medicine, this text would be useful, and it does have the advantage of being compact and relatively inexpensive. However, it is not adequate by itself, and supplementary material would be needed.

Thomas K. Lewellen
University Hospital, University of Washington
Seattle, WA 98195

Perspective

Future Advances and Directions in Imaging Research

Walter L. Robb[1]

The theme of this paper is not taken from a researcher or a radiologist, but from an individual who unintentionally turned out to be a good prophet of technology: the poet T. S. Eliot. In his poem "The Rock," he asked, "how is our wisdom lost in knowledge . . . How is our knowledge lost in information?" A later commentator, the information scientist John R. Pierce, added, "How is our information lost in data?" [1]. Today technology is offering us new and exciting ways to invert that process and more effectively extract information from data, knowledge from information, and, perhaps, wisdom from knowledge.

Physical methods of sensing continue to advance and offer major challenges. For example, in CT technology we still face the photon limitations of the Coolidge tube and the need for a monochromatic source of X-rays. Synchrotron radiation offers a possible solution, but this introduces a new set of challenges: finding a way to reduce an electron accelerator to perhaps 1 ft (30 cm) in diameter while increasing the energy so that a useful percentage of the photons are in the diagnostic imaging range. There are many more such challenges. In this paper, however, I will focus not on generating data, but on using it: turning it into information, and turning the information into knowledge.

Advances in electronic hardware and software are making it possible to turn data into information. The electronics revolution steadily increases the density of integrated circuits and decreases their cost. New software helps make possible integrated circuits that are custom-designed for specific tasks. The merging of improvements in software and hardware is generating changes that may lead to improvements in medical imaging. I will concentrate on three opportunities.

Digital Signal Processing

Digital signal processing and transmission are widely used in aerospace systems. Digital TV is just a matter of time. Those well-funded applications outside of medicine will make it possible to apply the new technology in radiology.

The information content of a complex CT slice is 3 million bits. That of a chest radiograph is more than 24 million bits per image, or, after compression to remove redundant information, 10 million bits per image. Increasing the capacity of information channels on a telephone line and moving these millions of bits rapidly cause the cost to rise sharply.

Display is also an issue. Viewing a TV monitor, even a 512-line, high-resolution monitor, does not provide as wide a dynamic range as viewing an X-ray shadowgraph. New flat-panel displays, now under development for aerospace applications, may be the answer. Introducing them in a cost-driven environment will be difficult, but I believe these problems will be eventually solved and that the solutions will result in fast, reliable, inexpensive systems that ensure a consistent level of image quality and reproducibility.

Digital techniques will make possible vision systems that automatically detect features or objects. This has been done for a long time in such applications as automated blood-cell counting and analysis of images consisting of only a few hundred pixels [2]. For automatic detection of more compli-

Received August 21, 1987; accepted after revision September 23, 1987.
This article is based on a talk given at the conference, "The Impact of New Imaging Technology on Health Care, Research, and Teaching," San Francisco, CA, October 1986.
[1] GE Research and Development Center, P.O. Box 8, Schenectady, NY 12301. Address reprint requests to W. L. Robb.

 0361–803X/88/1501–0039 © American Roentgen Ray Society

cated features in more complicated images, however, progress has been slow. These challenges are a lot more demanding than audio or even video signal processing. After all, the telephone company or TV station that filters a few details out of its message or picture will not be sued for malpractice. In addition, the system of the human eye and brain is very good at many important image-processing jobs that are difficult for machines, such as edge-detection, filtering out noise, and comparing "before" and "after" images.

Again, the defense community is pushing the frontiers. At the GE Research and Development Center, we are tackling the problem of identifying airplanes on the ground from a reconnaissance satellite or aircraft [3]. A typical airport scene has about 4 million pixels. Our ultimate goal is to be able to pick out and identify the airplanes in about 1 sec. By current methods on a minicomputer, it takes 1 day or more to analyze such a picture. One of the most promising ways to decrease this time sharply is through the use of highly parallel processors. Such machines are only in the early developmental stage today [4]. However, 12 years ago, a microprocessor-based array processor as used in CT was also at an early stage.

Visual scene analysis requires new software. For the airport images, the plane taking the picture might be coming in at an angle. So a general solid model of the target object needs to be constructed off-line before the mission starts, since such a model demands much computer time and memory. Then, on-line, the profile that the camera might be expected to see at that angle is generated. This model-based approach is relevant to medical problems, because location of an organ or abnormality within the body also involves looking from different angles and getting different profiles.

Computer-Aided Design and Engineering

Research started outside medical imaging studies might also have a big impact in computer-aided design and engineering for radiology. Until recently, the resolution in three-dimensional (3D) computer graphics was too low for medical imaging. Images that accurately reproduced the data looked blocky and jagged. Those images that smoothed out the data lost detail, and they looked fuzzy and out of focus.

New algorithms now give pictures of the surface that use all the information and that are also smooth, sharply focused, and realistically shaded [5]. We have made accurate and realistic-looking images of the skull (Fig. 1) and abdomen (Fig. 2), using data derived from 20–100 contiguous CT scans. The density can be selected to give images at different depths. In the abdomen, for example, the viewer can look at intestine, muscle, bone, or everything at once.

We have also made images of the head from the data in 50 contiguous slices. We have imaged the arteries through the use of flow contrast rather than density; MR imaging is accurate in visualizing flow. The images were made by using a new algorithm to determine surface shape. The result is realistic and uses all the original data.

One of these 3D pictures typically requires up to 50 CT slices, each with a resolution of 256 × 256, for a total of 6 megabytes of data. The image can be generated on a GE CT 9800 with the array processor of a CT scanner (the current top-of-the-line model) in about 10 min. Once generated, the image can be used to produce a typical study—that is, a rotated or otherwise manipulated image—in only 4 sec.

In the future, a custom-designed accelerator board implementing image algorithms possibly may be used (1) to move or rotate the image with a joystick in real time or (2) to move a simplified version of the image until the desired view is obtained and then to fill in the details.

The technique has been used so far on about 100 patients. In one instance, surgery was performed to make a 90° change in the direction of a patient's spine. The surgeon later said that he could not have performed the surgery successfully without the 3D imaging capability.

The medical applications of these methods may move beyond computer graphics into computer-aided engineering. In industry, for example, it is now possible to subject a new design for an automobile bumper to a simulated 5 mi/hr (8.1 km/hr) collision, by using the computer model of the part and computer-aided engineering software. This kind of 3D engineering analysis and display might be used to depict, for example, the strain on a spine or the blood flow or derived wall motion of a heart.

Artificial Intelligence

Artificial intelligence might be defined as the use of computers to do jobs that require recognizable intelligence when done by a person. Some of its medical applications are well known. We now have several projects in artificial intelligence called "expert systems": computer software that captures the methods and knowledge used by a human expert in one particular domain. The first expert systems were developed by computer scientists who sat down with the experts, listened to them explain their methods, and then programmed those methods into the software. That was too slow and expensive. Today's approaches use an expert-system "shell" built by the computer scientists, into which the expertise can be fitted easily.

For one of these systems, the expert, without the aid of a computer scientist, can build an expert system on the shell [6, 7]. Its applications include designing gas turbines, designing plastic molds, and even evaluating credit risks. It works by a rule-based approach. The expert's methods are expressed in a series of "if-then" rules. The rules are then hooked together logically in the form of a tree, over which the computer can lead the user to get to the root of the problem. These rule-based systems today involve several hundred or even a few thousand rules, expressed in thousands or tens of thousands of lines of software code. They are typically run on a workstation or on one of the more powerful personal computers. The real issue, however, is not length of program or power of the computer; it is the development of more powerful methods of representing and manipulating knowledge.

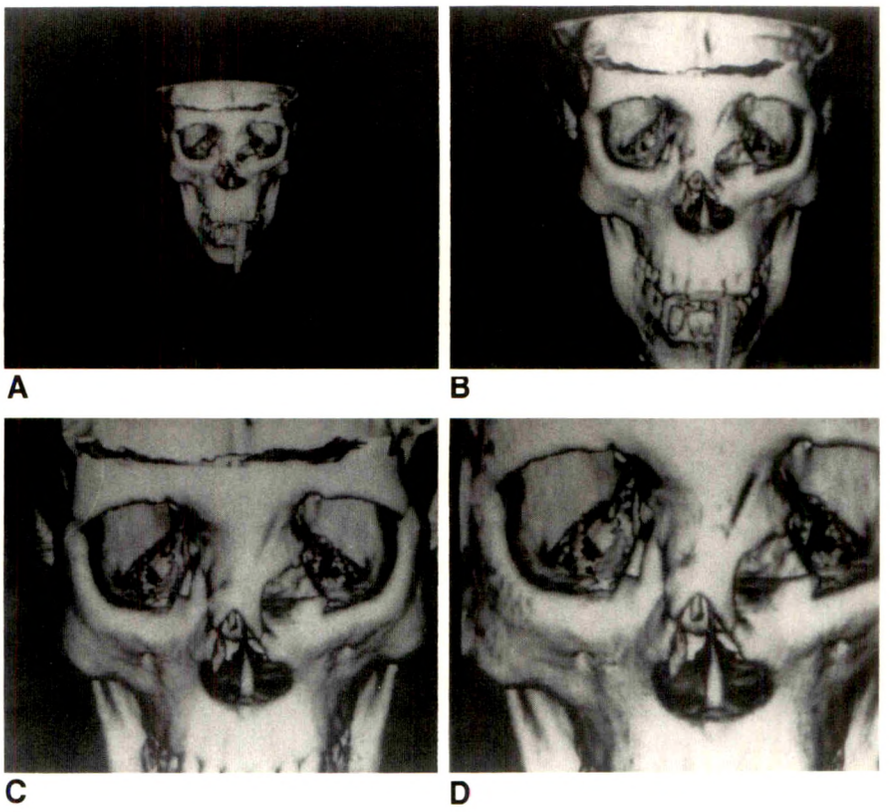

Fig. 1.—93-slice CT study of head, showing skull at four magnifications (*A–D*). (CT data from Milwaukee Medical College; three-dimensional image made at GE Research & Development Center.)

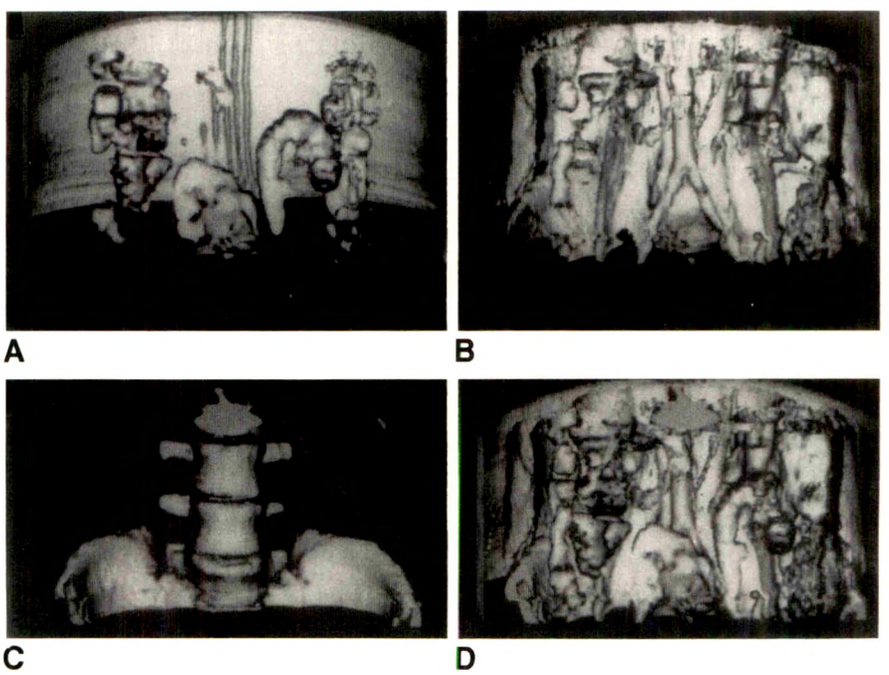

Fig. 2.—30-slice CT study of abdomen, showing (*A*) anterior abdominal structures; (*B*) deeper structures around aortic bifurcation; (*C*) bone; and (*D*) composite picture of *A*, *B*, and *C*.

One way is to use some methods that humans use, such as making decisions based on incomplete information or drawing on analogies. We have research under way in these areas. We are also moving beyond the rule-based approach. Many human experts do not only know what to do, but also why to do it: they have mental models of what is really going on. Certainly this is true in medicine. We are now doing research on that model-based approach, and we are developing model-based systems for the control of communication satellites and high-performance aircraft.

I do not want to oversell artificial intelligence. For a long time, expert systems will remain only moderately intelligent assistants, rather than true experts. Some really difficult problems, such as using a radiograph to help diagnose illness, will be among the last conquered by an expert system, long after one has become the world's chess champion. But for a wide range of less demanding tasks, such as controlling darkroom quality, expert systems will help humans perform beyond their level of immediate knowledge.

Conclusion

Consideration of future advances and directions of research must take into account both the continuing advance of physical methods of sensing and better ways of making use of the data that have been sensed. In the past, medical diagnostics has piggybacked on physics, and it will continue to do so. Increasingly, however, it will also piggyback on the sciences of information and automation. I have sketched out some opportunities in the fields of digital signal processing, computer-aided imaging and analysis, and artificial intelligence. I do not present them as a substitute for human talents but as amplifiers of human talents. They are means of turning data into information and turning information into knowledge. However, the human still must take the final creative step and generate wisdom. I'm fully convinced that humans will always stay one step ahead of their machines.

REFERENCES

1. Inose H, Pierce JR. *Information technology and civilization*. New York: Freeman & Co., **1984**:ix
2. Fountain T. *Processor arrays*. New York: Academic Press, **1987**
3. Thomson DW, Mundy JL. Three-dimensional model matching. *Proc intl conf robotics and automation*. **1987**;1:208–219
4. Hillis WD. *The connection machine*. Cambridge, MA: Massachusetts Institute of Technology, **1987**
5. Cline HE, Lorensen WE, Ludke S. High-resolution 3D reconstruction of CT images of the head (report 86CRD160). Schenectady, NY: GE Research & Development Center, September **1986**
6. Sweet LM. Artificial intelligence research at General Electric. *AI Mag* **1985**;Fall:220–223
7. Dietz PW. GEN-X: an environment for building rule-based expert systems (report 86CRD041). Schenectady, NY: GE Research & Development Center, March **1986**

Perspective

Horizons in Gallstone Therapy—1988

Eric vanSonnenberg[1,2] and Alan F. Hofmann[2]

The National Cooperative Gallstone Study in 1981 [1] estimated that 20 million people in the United States have gallstone disease. A careful prospective study recently confirmed a similar frequency in Italy [2]. The enormity of the problem is evidenced by the well over $1 billion annual cost of treatment in the United States. The bulk of the expense is accounted for largely by the 500,000–600,000 cholecystectomies performed annually [1, 3]. Gallstone-related pancreatitis and choledocholithiasis contribute to this substantial cost. The protean manifestations of gallstone disease account for its being one of the most common causes of hospitalization for surgical procedures [4].

A host of therapeutic alternatives to cholecystectomy is becoming available. These developments for gallstone disease likely will parallel the precedent set with kidney stones, the treatment of which has been revolutionized. Extracorporeal shock-wave lithotripsy (ESWL) and percutaneous contact dissolution with solvents, supplemented with oral medication to prevent recurrence, herald a new horizon in the management of gallstones. This paper highlights the current status of these new developments and targets fertile areas for future research. Integration of these techniques with traditional cholecystectomy is addressed.

Extracorporeal Shock-Wave Lithotripsy

The success of ESWL for renal calculi made it natural to extend the technology to the treatment of gallstones. The original clinical work was done in Munich, Germany, by Sauerbruch et al. [5]. Brendel, in association with the Dornier Company, was a pioneer in the field of shock-wave therapy [5]. These investigators modified a renal lithotriptor, enabling its use for the treatment of gallstones. Sonography was coupled to the extant machine; this permitted accurate localization of the gallbladder, the typically nonopaque gallstones, and the fragments resulting from ESWL. Methods for positioning the patient were altered to expose the right upper quadrant, and focusing of the shock waves was improved to enhance fragmentation of the gallstones.

Currently, more than 300 patients have undergone ESWL for gallstones in Germany. Success, defined as the eventual absence of stones and fragments as delineated by sonography, has been achieved in more than 80% of patients (Sauerbruch T, Paumgartner G, personal communication). In virtually all of the other patients, the stones were fragmented and reduced in size. Complications have been few. Mild to moderate pancreatitis was the most significant and developed in two patients. Biliary colic has been the preponderant side effect; it has occurred in approximately one-third of patients. As a result, outpatient analgesics have been required after ESWL for these patients. The need for adjunctive procedures with ESWL has been decidedly uncommon; the use of endoscopic papillotomy has been rare [5, 6].

A drawback to this form of treatment is the relatively stringent criteria for selection of patients, which have ensured the excellent success and safety to date. Presently, ESWL is

Received July 23, 1987; accepted after revision August 25, 1987.
The work of AFH was supported in part by grants DK 21506 and 32130 from the U.S. National Institutes of Health and by a grant-in-aid from the Falk Foundation, e.V., West Germany.
[1] Department of Radiology, University of California, San Diego, Medical Center, 225 Dickinson St., San Diego, CA 92103. Address reprint requests to E. vanSonnenberg.
[2] Department of Medicine, University of California, San Diego, Medical Center, San Diego, CA 92103.

applied to 25–30% of patients with gallstones who are referred for therapy. In the Munich study [5, 6], eligibility for treatment was defined as follows: (1) symptoms of gallstone disease, (2) stones less than 2.5 cm in diameter, (3) fewer than four stones, (4) absence of a calcific nidus or peripheral calcific rim, and (5) visualization of the gallbladder on oral cholecystogram (implying patency of the cystic duct). Patency was considered essential to permit fragments to pass. Only patients who were healthy enough to undergo cholecystectomy were accepted into the study.

A combination of chenodeoxycholic (Chenodiol) and ursodeoxycholic acids was used before and after ESWL [5, 6]. These drugs render bile unsaturated in cholesterol and should promote dissolution of the fragments. In addition, the drugs are likely to induce choleresis. A trial comparing ESWL alone with ESWL plus adjunctive ursodeoxycholic acid will be conducted in a number of institutions in the United States over the next year. Many issues related to ESWL have been highlighted in two recent commentaries [7, 8].

Percutaneous Techniques

Contact Dissolution

Transcatheter infusion of cholesterol solvents has been effective for contact dissolution of gallstones. Catheters are placed into the gallbladder by using fluoroscopy, sonography, or a combination (rarely with CT) of guidance techniques. The modified Seldinger technique using a coaxial system is preferred for insertion of the catheter. The transhepatic route is recommended and may be essential to prevent leakage of bile [9].

At present, methyl-*tert*-butyl ether (MTBE), an analog of diethyl ether, is the agent of choice for dissolving cholesterol gallstones [9–11]. MTBE is far more effective for cholesterol stones than monooctanoin (Moctanin), the previously preferred agent. A Mayo Clinic study [9] showed dissolution of stones exposed to MTBE, whenever calcium was not a major component of the stone. Potential side effects of MTBE include sedation, transient pain, hemolysis, foul odor, and damage to certain types of catheters and occlusion balloons [9, 11]. The balloons are used to block flow of MTBE from the gallbladder or common bile duct into the duodenum; this reduces the likelihood of side effects. MTBE is not yet approved for marketing.

Other solvents are being tested for the dissolution of noncholesterol stones [12], such as calcium salts of bilirubin and other anions and proteins. At present, dissolution is applicable for cholesterol calculi only, the major type of gallstones in developed countries. Both injection by hand and dedicated pump systems for delivery of solvent have been used [9–12]. Improved mixing of solvent and prevention of leakage by control of intraluminal pressure appear to be advantages of a recently developed computer-controlled pump [12].

Dissolution via solvents is effective for cholesterol stones, whatever the number and size of the stones; this is an advantage compared with ESWL, for which number and size have been restrictions. The time required for dissolution can be lengthy (3–25 hr); this is the main limitation of percutaneous contact dissolution [9–11]. High-speed delivery systems most likely would shorten the duration of contact dissolution to 1–2 days, inclusively. Widespread use of percutaneous contact dissolution will require improved techniques for delivery of solvents.

Mechanical Removal

Several methods are effective for mechanical removal of gallstones from the gallbladder. A percutaneous cholecystostomy tract created with a catheter can be dilated after the tract has matured [13, 14]. This permits insertion of baskets and contact lithotriptors [15] for fragmentation and removal of stones. Mechanical extraction of fragments has been used in conjunction with dissolution, when dissolution has reduced the size of the stones but not eliminated the residua. Surgical cholecystostomy combined with subsequent removal of stones via a basket is another alternative [16]. Attempts at percutaneous ablation of the gallbladder have not yet proved applicable to humans [17–19].

Oral Agents

Two bile acids have been effective for dissolution of cholesterol gallstones: chenodeoxycholic acid and its congener, ursodeoxycholic acid [1, 20–22]. Chenodeoxycholic acid (cheno) was introduced first, but use of it has decreased because of its adverse effects. Diarrhea is the side effect that most frequently interrupts therapy. Liver function tests become mildly abnormal in 15–20% of patients, and severe dysfunction (albeit reversible) occurs in 3% of patients [1, 20].

Ursodeoxycholic acid (urso) presently is undergoing evaluation in the United States. Its use is more widespread in Europe. Studies have shown comparable effectiveness of urso and cheno for cholesterol stones; however, urso is more attractive because of its lower dosage to achieve dissolution and the lack of side effects [20]. Urso is the more expensive of the two drugs. A combination of the two agents has been used before and after both ESWL and percutaneous contact dissolution to eliminate residual concretions after primary treatment [6, 11]. A combination of the two agents may be superior to either agent alone.

Both cheno and urso are slow-acting if used as primary therapy; 6 months to 2 years may be required for effective dissolution. Another drawback is that resistant stones (about 40%) cannot always be identified in advance. Stones recur in 50% of successfully treated patients if the drugs are discontinued. Current evidence suggests that optimal use of these agents is to prevent recurrence of stones after primary therapy by ESWL or dissolution.

Options for Ductal Stones

The aforementioned techniques have been used for common duct and intrahepatic stones, albeit much less frequently than for gallstones [5, 10]. With ESWL, bile duct stones

preferably are localized by fluoroscopy rather than by sonography. To permit visualization of the stones, either the duct must be opacified (by percutaneous or endoscopic catheters), or the calculi must be calcified. Preliminary data suggest that these stones may be fragmented [5, 9, 23–25], but adjunctive endoscopic techniques may be required for removal of the fragments.

Percutaneous transhepatic, T-tube, and endoscopic catheters have been used for dissolution of stones in the bile ducts by MTBE and monooctanoin [10, 26, 27]. Disadvantages of MTBE depend on whether it passes into the duodenum; if so, systemic absorption, duodenitis, and sedation may ensue. Occlusion balloons have been used to block the flow of MTBE into the intestine. Both intra- and extrahepatic stones have been dissolved effectively. Dissolution may be combined with the use of a basket to achieve complete removal of stones. Common duct stones that form years after cholecystectomy frequently calcify; hence they are amenable to partial dissolution only (i.e., the noncalcified portions). Pulverization and laser pyrolysis are being explored for the treatment of ductal stones.

TABLE 1: Selection Criteria for ESWL and Percutaneous Contact Dissolution with Solvents for Treatment of Gallstones

Criteria	ESWL	Percutaneous Contact Dissolution with Solvents
Symptoms	Yes	Yes
Stone size	<2.5 cm	Unlimited
Number of stones	Fewer than four	Unlimited
Stone composition	Cholesterol, pigmented, ± calcified	Cholesterol only
Bilirubinate stones	Yes	No
Calcified stones		
Nidus	No	No
Rim	±	No
Patent cystic duct	Necessary	Desirable
Functioning gallbladder	Necessary	Desirable
Overall applicability	20–30% of patients	75–80% of patients
Risk; adverse effects	Low; biliary colic	Low; bile peritonitis
Patient acceptability	High	High

Note.—ESWL = extracorporeal shock-wave lithotripsy.

Unresolved Issues

Many issues are unresolved. Perhaps the primary one is whether screening should be used to detect asymptomatic gallstones in healthy patients. If calculi are found, is treatment justified to reduce the eventual morbidity of gallstone disease and to reduce the staggering costs? With established symptomatic disease, the fundamental questions are the age and medical status at which nonsurgical options are advisable for patients. The likelihood of recurrence of stones vs the feasibility and cost of long-term oral medications or repeat ESWL or percutaneous procedures is the key issue for healthy, relatively young patients who have gallstones.

Selection of patients for ESWL vs contact dissolution is yet to be determined. Table 1 summarizes current advantages and disadvantages of each. Whether dissolution and ESWL should be used in conjunction with each other to both broaden the indications and shorten the duration of each needs to be addressed.

Whether the effects of making a patient stone-free diminish the likelihood of chronic cholecystitis and carcinoma of the gallbladder will have an impact on the role of surgery. These questions must be answered vis a vis cholecystectomy, which completely eliminates the risk of cholecystitis and carcinoma. The 0.7–2.5% risk of mortality with cholecystectomy also must be considered [27, 28]; the lower figure is more representative of large series. However, elderly, critically ill patients who have acute cholecystitis are more likely to have a higher mortality rate; they therefore stand to benefit most from nonsurgical options.

What will be the role of cholecystectomy if the alternative techniques are effective treatment for a large number of patients with gallstones? Continuing indications for de novo operation would appear to include (1) acute cholecystitis, (2) hydrops/empyema/abscess in a good candidate for surgery, (3) porcelain gallbladder, and (4) densely calcified stones. Failure of the nonsurgical techniques or severe complications also should prompt cholecystectomy.

Conclusion

Although the future treatment of gallstones is uncertain, change is imminent. Balancing the exploding technological advances with standard cholecystectomy is a pragmatic long-range issue. Immediate questions focus on broadening the applicability of ESWL and contact dissolution and on minimizing risks, side effects, and duration of therapy. The interplay of oral medication and mechanical removal of gallstones in the broad scheme will require extensive trials and experience. Change is certain; for the new treatments, how, when, and to whom are all unresolved issues.

ACKNOWLEDGMENT

Our appreciation to Peggy Clark for preparation of the manuscript.

REFERENCES

1. Schoenfield LJ, Lachin JM, Baum RA, et al. Chenodiol (chenodeoxycholic acid) for dissolution of gallstones: the national cooperative gallstone study. *Ann Intern Med* **1981**;95(3):257–282
2. Rose Group for the Epidemiology and Prevention of Cholelithiasis (GREPCO). Prevalence of gallstone disease in an Italian adult female population. *Am J Epidemiol* **1984**;119:796–805
3. Ranofsky AL. Surgical operations in short-stay hospitals: United States 1975. Hyattsville, MD: National Center for Health Statistics, **1978** (Vital and health statistics, series 13, no. 34, DHEW, publication number PHS 78-1785)
4. Luft HS, Bunker JP, Enthoven AC. Should operations be regionalized? The empirical relation between surgical volume and mortality. *N Engl J Med* **1979**;301:1364–1369
5. Sauerbruch T, Delius M, Paumgartner G, et al. Fragmentation of gallstones by extracorporeal shock waves. *N Engl J Med* **1986**;314:818–822
6. Sackmann M, Delius M, Sauerbruch T, et al. Extracorporeal shock wave

lithotripsy of gallbladder stones: results of 101 treatments. Presented at the Digestive Disease Week and the annual meeting of The American Gastroenterological Association, Chicago, May **1987**
7. Ferrucci JT. Biliary lithotripsy: what will the issues be? *AJR* **1987**;149: 227–231
8. Burhenne HJ. The promise of extracorporeal shock-wave lithotripsy for the treatment of gallstones. *AJR* **1987**;149:233–235
9. May GR, Thistle JL. Percutaneous cholecystostomy for gallstone dissolution by methyl-tert-butyl ether. Presented at the scientific assembly and annual meeting of the Radiological Society of North America, Chicago, Nov. **1986**
10. Allen MJ, Borody TJ, Bugliosi TF, May GR, LaRusso NF, Thistle JL. Rapid dissolution of gallstones by methyl-tert-butyl ether. *N Engl J Med* **1985**;312:217–220
11. vanSonnenberg E, Hofmann AF, Neoptolemus J, Wittich GR, Princenthal RA, Willson SW. Gallstone dissolution with methyl-tert-butyl ether via percutaneous cholecystostomy: success and caveats. *AJR* **1986**; 146:865–867
12. Zakko SF, Hofmann AF, Schteingart C, vanSonnenberg E, Wheeler HO. Microprocessor assisted solvent transfer (MAST) system for infusion of methyl-tert-butyl ether (MTBE) or other gallstone (gs) solvents into the gallbladder (gb). *Gastroenterology* **1987**;92(5)[Pt. II]:1794
13. Kerlan RK Jr, LaBerge JM, Ring EJ. Percutaneous cholecystolithotomy: preliminary experience. *Radiology* **1985**;157:653–656
14. vanSonnenberg E, Wittich GR, Casola G, et al. Diagnostic and therapeutic percutaneous gallbladder procedures. *Radiology* **1986**;160:23–26
15. Burhenne HJ. Electrohydrolytic fragmentation of retained common duct stones. *Radiology* **1975**;117:721–722
16. Burhenne HJ. Interventional cholelithotomy as an alternative to cholecystectomy with or without the surgeon? *Invest Radiol* **1986**;21:594–595
17. Remley KB, Cubberley DA, Watanabe AS, Nelson JA, Colby TV. Systemic absorption of gallbladder sclerosing agents in the rabbit: a preliminary study. *Invest Radiol* **1986**;21:396–399
18. Getrajadman GI, O'Toole K, Laffey KJ, Martin EC. Cystic duct occlusion and transcatheter sclerosis of the gallbladder in the rabbit. *Invest Radiol* **1986**;21:400–403
19. Salomonowitz E, Frick MP, Simmons RL, et al. Obliteration of the gallbladder without formal cholecystectomy. *Arch Surg* **1984**;119:725–729
20. Roda E, Bazzoli F, Morselli M, et al. Ursodeoxycholic acid vs chenodeoxycholic acid as cholesterol gallstone-dissolving agents: a comparative randomized study. *Hepatology* **1982**;2:804–810
21. Bachrach WH, Hofmann AF. Ursodeoxycholic acid in the treatment of cholesterol cholelithiasis. Part II. *Dig Dis Sci* **1982**;27(9):833–856
22. Ward A, Dodgen RW, Heel RC, Speight TM, Avery GS. Ursodeoxycholic acid: a review of its pharmacological properties and therapeutic efficacy. *Drugs* **1984**;27:95–131
23. Becker CD, Fache JS, Gibney RG, Stoller JL, Burhenne HJ. Case report. Treatment of retained cystic duct stones using extracorporeal shockwave lithotripsy. *AJR* **1987**;148:1121–1122
24. Gelfand DW, McCullough DL, Myers RT, D'Sousa VJ, Leinbach LB, Faust KB. Case report. Choledocholithiasis: successful treatment with extracorporeal lithotripsy. *AJR* **1987**;148:1114–1116
25. Teplick SK, Pavlides CA, Goodman LR, Babayan VK. In vitro dissolution of gallstones: comparison of monooctanoin, sodium dehydrocholate, heparin, and saline. *AJR* **1982**;138:271–273
26. Butch RJ, MacCarty RL, Mueller PR, et al. Monooctanoin perfusion treatment of intrahepatic calculi. *Radiology* **1984**;153:375–377
27. Meyer KA, Capos NJ, Mittelpunkt AI. Personal experience with 1,261 cases of acute and chronic cholecystitis and cholelithiasis. *Surgery* **1967**;61(5):661–668
28. Huber DF, Martin EW Jr, Cooperman M. Cholecystectomy in elderly patients. *Am J Surg* **1983**;146:719–721

Progress in Radiology

Penile Angiography: The Last Angiographic Frontier

Joseph J. Bookstein[1]

A unique combination of scientific disinterest, misinformation, therapeutic nihilism, and social taboos has long relegated male impotence to the realm of folk medicine. Within the past few years, however, these primitive influences have begun to yield, and impotence has become increasingly recognized as a legitimate field of medical investigation. A major impetus for the scientific investigation of penile erection was provided by the recent discovery of the erectogenicity of intracavernosal smooth-muscle relaxants [1, 2]. That one discovery led to dramatic changes in concepts of the physiology of erection; proof of the existence and mechanism of venoocclusion; methods for diagnosing and quantitating venoocclusive insufficiency; recognition of the high frequency of venogenic impotence; improved methods of arterial imaging; and a practical pharmacotherapeutic method.

The fundamental circulatory nature of penile erection implies a major role for angiography in the investigation of erectile function and dysfunction. Indications exist for both diagnostic and therapeutic angiographic procedures in both the arterial and venous beds. Conventional angiographic methods have proved insufficient, however, and new equipment and techniques were needed for adequate evaluation. Fortunately, an array of sophisticated diagnostic and therapeutic angiographic techniques, developed through experience with other organ systems, was now available for use in the study of impotence. With angiography as their forte, radiologists can extend their interests beyond clinical investigations to include all aspects of erectile morphology and physiology. Radiologists should embrace the opportunity to become involved in this exciting and rapidly progressing field, for indeed it may represent the last angiographic frontier.

Altered Physiologic Concepts

Until 1980, penile erection was attributed primarily to increased corpora cavernosal arterial flow, with secondary engorgement of cavernosal sinusoids [1]. The discovery of the erectogenic effects of intracavernosal (but not intraarterial) injection of papaverine [2] and other smooth-muscle relaxants [3] has shifted the emphasis to relaxation of smooth muscle in the walls of the cavernosal sinusoids as the initiating process of cavernosal erection. As sinusoidal muscle tone diminishes and the sinusoids begin to distend with blood, the small peripheral venous tributaries become compressed between the peripheral sinusoids and the unyielding peripheral tunica albuginea (Fig. 1) [4, 5]. Thus activation of the venoocclusive mechanism is an intrinsic sequela of cavernosal muscular relaxation.

The mediators of sinusoidal muscular relaxation are poorly understood. Acetylcholine, released by parasympathetic nerve terminals, has long been considered a mediator [6], but evidence is controversial and other agents, including vasoactive intestinal polypeptide, probably also play a role [7]. A substance released by the endothelium, termed endothelium-derived relaxing factor (EDRF) is required for acetycholine-induced relaxation [8–10]. This substance may be a key factor in impotence, and will probably be the object of intensive investigation in the near future.

With the onset of sinusoidal muscular relaxation, resistance to arterial flow is inherently reduced (Fig. 1), and arterial flow increases markedly until cavernosal pressure approaches systolic. Augmented arterial flow seems to be required for rapid erection, although it is now apparent that erection can

Received August 11, 1987; accepted after revision September 9, 1987.
[1] Department of Radiology, University of California, San Diego, Medical Center, 225 W. Dickinson St., San Diego, CA 92103. Address reprint requests to J. J. Bookstein.

AJR 150:47–54, January 1988 0361–803X/88/1501–0047 © American Roentgen Ray Society

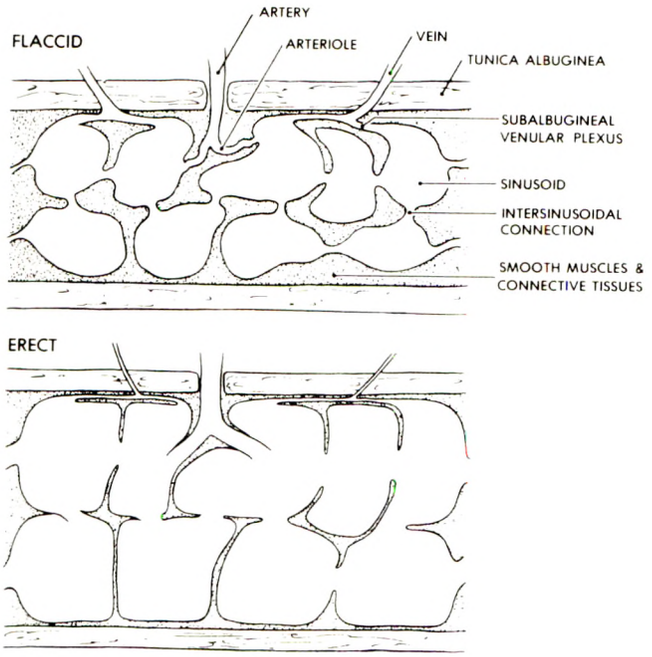

Fig. 1.—Cavernosal smooth-muscle relaxation as single unifying event of penile erection. (Reprinted with permission from Fournier et al. [4].)

***Top*, In flaccid state, sinusoidal vascular space and arterial inflow are limited by wall tonus. Venous outflow is unimpeded.**

***Bottom*, After neurostimulation or intracavernosal papaverine injection, sinusoidal smooth muscle relaxes and distended sinusoids compress and obstruct peripheral venules against tunica albuginea. Simultaneously, resistance to arterial flow decreases until cavernosal pressures approach systolic pressures.**

eventually be achieved with arterial flow rates as low as 2–6 ml/min [11], if the venoocclusive mechanism is fully competent.

After orgasm, sinusoidal muscular tone increases, presumably because of alpha adrenergic sympathetic discharge. The sinusoids shrink, releasing the venoocclusive mechanism and simultaneously increasing resistance to arterial inflow.

Causes of Impotence

In 1910, Steckel, who was a student of Freud's, stated that 90% of all impotence was psychogenic [12]. This maxim persisted into the 1970s, when objective tests such as nocturnal penile tumescence and Doppler examinations began to suggest a high frequency of organic disease. It now appears that an organic basis can be recognized in more than 50% of impotent patients, and that vasculogenic impotence is the most frequent organic cause. In our series to date of 110 relatively unselected impotent patients, vasculogenic impotence was found in 72 (65%): impotence was venogenic in 28 (25%), arteriogenic in 19 (17%), and combined venogenic and arteriogenic in 25 (23%).

The diagnostic criteria for venogenic impotence vary considerably among institutions. We reserve the term for patients with cavernosal leak exceeding 45 ml/min after intracavernosal injection of a full muscle-relaxant dose of papaverine-phentolamine mix (see following section). Persistent leakage implies an organic basis for the insufficiency, although the pathophysiology still is not well understood. Our diagnostic criteria for arteriogenic impotence require the obstruction to be bilateral and hemodynamically significant.

Trauma is a frequent cause of vasculogenic impotence [13]. Of 11 such patients in our series, 10 had arteriogenic or venogenic impotence, either alone or in combination. Of nine diabetics, five had vasculogenic impotence.

Indications for Investigation

A history of absent nocturnal erections suggests an organic cause for impotence. Otherwise, history and physical examination, as well as ordinary laboratory tests, usually play a limited role. Determination of the cause of impotence requires increasingly sophisticated diagnosis in keeping with the specificity of any planned therapy. For example, if papaverine injections are planned, specific diagnosis is hardly required. On the other hand, arterial revascularization or venoablative therapy require highly specific and accurate angiographic diagnosis.

After establishing the absence of normal nocturnal erections by history or a snap-gauge test, a variety of screening tests may be performed before proceeding to angiography. We and others [14] have found it useful to give patients an intracavernosal injection of a small dose (15–30 mg) of papaverine mixed with 0.25–0.5 mg of phentolamine mesylate (Regitine, Ciba, Edison, NJ). When erection fails to occur within an hour, either in the office or at an arranged sexual situation, we have found venogenic impotence (alone or in combination) to be present in 75% of patients. A normal response to papaverine excludes venogenic impotence but does not completely exclude arteriogenic impotence.

The ratio of penile-to-arm blood pressure is termed the penile-brachial index (PBI). The normal index is greater than 0.75. An index of 0.61–0.74 is usually considered indeterminate, and a value of less than 0.60 indicates arterial obstruction. In our experience and that of others [15], the PBI is only moderately accurate. In 48 cases, we have found a sensitivity and specificity of about 70% (Bookstein, unpublished data).

The Rigiscan (Dacomed, Minneapolis, MN) is an automated device that measures both nocturnal tumescence and rigidity at the base and tip of the penis [16]. In our experience, the results are reasonably reliable in recognizing organic impotence, but do not distinguish arteriogenic from venogenic causes.

Evaluation of the cavernosal artery with duplex scanning before and after the intracavernosal injection of papaverine has been recommended by Lue et al. [17]. Inadequate increase of caliber and flow velocity of the cavernosal artery between the two observations suggest arterial insufficiency.

Although the yield is small, routine endocrine screening for serum levels of testosterone, prolactin, follicle-stimulating hormone, and luteinizing hormone [18], and various tests for penile neurologic function, probably are also warranted.

The reliability of these screening tests has not yet been proved through careful comparison with angiography, and sometimes we proceed directly to angiography without intermediary screening.

Performance of Angiography

Invasive vascular procedures (arteriography, cavernosometry, and cavernosography) constitute the gold standard for diagnosis of vasculogenic impotence. These angiographic methods include (1) outpatient performance on a single occasion under mild sedation; (2) the use of selective magnification arteriography; (3) the intracavernosal injection of 60 mg papaverine admixed with 1 mg phentolamine; (4) the use of nonionic contrast agents for arteriography and dilute contrast for cavernosography; and (5) quantitation of venoocclusive insufficiency [11, 19].

Cavernosometry refers to a method of determining cavernosal pressure response to standardized rates and volumes of fluid infusion in order to define the presence and degree of venous leak. We developed the pharmacologic maintenance-erectile-flow method to quantitate venoocclusive insufficiency in terms of milliliters per minute. The method is performed by determining the rate of infusion required to maintain an intracavernosal pressure equal to, or greater than, systolic pressure.

Cavernosography refers to radiographic demonstration of the corpora cavernosa and their venous effluents after intracavernosal injection of (dilute) contrast agent. In impotence it serves primarily to define persistent routes of venous egress, but it is not reliable in determining the presence or magnitude of abnormal corporal leak.

Penile angiography requires full relaxation of the smooth muscle of the corpus cavernosum by the use of drugs. This simultaneously augments arterial flow and activates venoocclusion. In our experience, both nonvasodilated arteriography or cavernosography and cavernosometry without pharmacologic activation of the venoocclusive mechanism are unreliable. The dose of 60 mg papaverine mixed with 1 mg phentolamine seems to be at least as effective as any other agent(s), and greater doses seem to have no further effect. Importantly, papaverine is thought to act independently of EDRF [10].

Detailed consideration of technical aspects of performance of angiographic procedures is beyond the scope of this review, and interested readers may refer to previous publications [11, 19, 20].

Priapism is an occasional sequela of intracavernosal papaverine-phentolamine injection. Detumescence should be induced after 4 hr of erection by using cavernosal aspiration via a 19-gauge needle and intracavernosal injection of one or two doses of 10–15 μg of epinephrine.

The Normal Arteriogram

Satisfactory angiographic evaluation of arteriogenic impotence requires precise demonstration of the penile arterial supply from the aortic bifurcation to the tip of the penis (Fig. 2). Neglecting a portion of this vascular tree can lead to errors in diagnosis and therapy. For example, transluminal angioplasty of a proximal stenosis of a pudendal artery is frequently contraindicated by the demonstration of severe distal occlusive disease. In addition, patent cavernosal branches should be shown to arise from any artery intended for recanalization. Magnification techniques are often necessary for adequate definition of these small branches (Figs. 3 and 4).

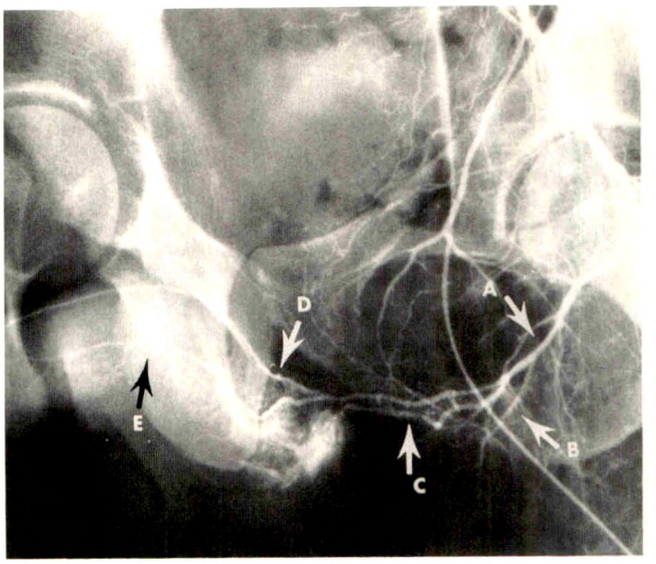

Fig. 2.—Normal selective left pudendal arteriogram in right posterior oblique projection performed 5 min after intracavernosal injection of papaverine-phentolamine. 31-year-old man with impotence caused by diabetes (same case as that shown in Fig. 5).

A = internal pudendal artery; B = scrotal branch; C = artery to bulb of the corpus spongiosum; D = dorsal penile artery; E = cavernosal artery, with stain of corpus cavernosum.

The major arterial supply of the penis is derived from the anterior division of each internal iliac artery via the internal pudendal artery. Typically, each internal pudendal artery then gives rise to three major branches: an artery to the bulb of the corpus spongiosum, an artery to the corpus cavernosum, and the dorsal penile artery, which passes to the glans (Fig. 2). Points of clinical significance include the following. (1) The dorsal penile arteries usually supply perforators to the mid-distal corpus cavernosum. For this reason, bypass into a proximally occluded dorsal penile artery will usually improve flow to the corpora cavernosa. (2) Anatomic variants are the rule and include the origin of both cavernosal arteries from one side, hypoplasia or absence of one dorsal penile artery, and supplemental internal pudendal arteries. Because of the frequency of variants, nonvisualization of a cavernosal artery on one side does not necessarily indicate obstruction of that artery, but rather that it may arise from the contralateral side or a supplemental pudendal artery. (3) Abundant potential collateral routes exist in the penis that become functional in the presence of organic obstruction. Observing the presence or absence of such collaterals is helpful in evaluating the hemodynamic significance of arterial stenoses.

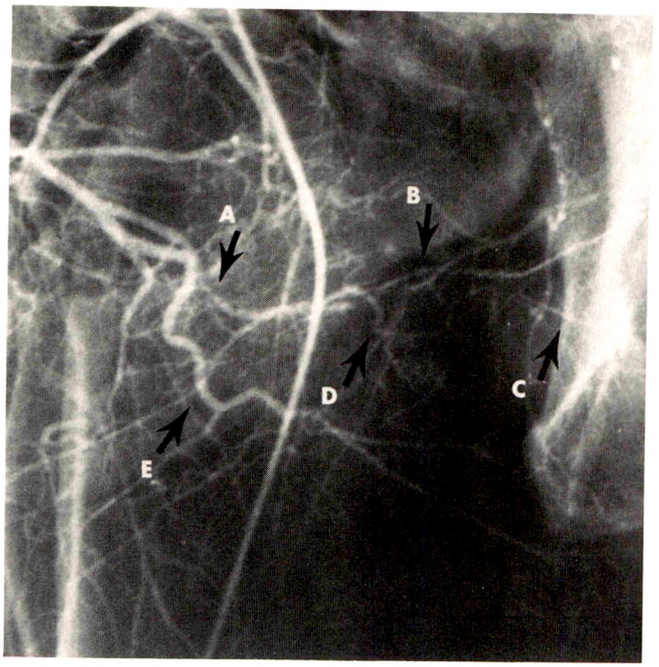

Fig. 3.—Posttraumatic arteriogenic impotence. 42-year-old truck driver with repeated perineal injury caused by bouncing motion due to poor suspension in patient's truck. Selective magnification arteriography was necessary for adequate demonstration. (Abnormalities were similar on patient's other side.)

A = severe focal narrowing of right penile artery; B = marked narrowing of proximal dorsal penile artery; C = sparse reconstitution of proximally occluded cavernosal artery filling by collateral; D = artery to bulb of corpus spongiosum; E = scrotal artery.

Cavernosometry and cavernosography showed a normal venoocclusive mechanism. Patient underwent a unilateral inferior epigastric-to-dorsal penile artery bypass and was able to develop fully rigid erections. However, after 2 months, the anastomosis avulsed during intercourse and impotence recurred. A repeat arteriogram showed occlusion at distal anastomosis.

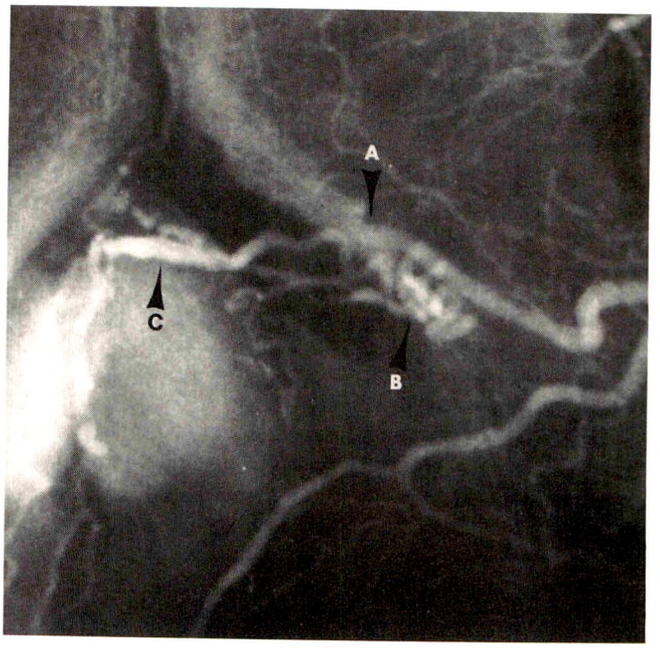

Fig. 4.—Arteriogenic impotence requiring selective magnification studies for demonstration. This 62-year-old man had been impotent for 24 months. Both cavernosal arteries arose originally from left side. A patent dorsal penile artery was present on right.

A = obstruction of penile artery; B = collaterals filling cavernosal artery; C = reconstituted cavernosal trunk that supplies two distal arteries.

Because of normal pulsations of dorsal penile artery and a normal penile-brachial index, arteriogenic impotence had not been strongly suspected. Inadequacy of collateral arterial flow to corpora cavernosa was supported by observation of a poorly pulsatile pressure wave during cavernosometry.

The Abnormal Arteriogram

While arterial obstruction may be observed at any level, a strong predilection exists for involvement of the distal internal pudendal artery or proximal portions of the penile branches (Figs. 3 and 4). A prerequisite for arteriogenic impotence seems to be bilaterally significant obstruction. Thus unilateral revascularization may restore potency [21]. There also exists a remarkable tendency for bilateral symmetry; disease that is unilateral and hemodynamically significant is rare. For these two reasons the selective arteriogram may be limited to the initial side if at least one normal ipsilateral cavernosal and dorsal penile artery are visualized, and if there is no evidence of collateral flow to suggest contralateral disease.

Normal Cavernosometry and Cavernosography

In normal subjects studied without intracavernosal injection of papaverine, intracavernosal infusion of 100 ml of dilute contrast medium at the rate of 2 ml/sec raised intracavernosal pressures to only about 45 mm Hg [22]. Cavernosograms showed flow into all penile veins and erectile structures: the deep dorsal penile vein, the crural perforators, the glans and spongiosa, superficial penile veins, and the external pudendals. Such studies did not allow reliable diagnosis of venoocclusive insufficiency, quantitation of venous leak, or identification of the sites of abnormal venous leak.

When cavernosometry and cavernosography were repeated after intracavernosal injection of papaverine-phentolamine, pressure in normal subjects always rose above 100 mm Hg, and angiograms showed little opacification of any penile venous system (Fig. 5).

Normal values for the pharmacologic maintenance-erectile-flow method are only 2–12 ml/min [11].

Cavernosal Studies in Venogenic Impotence

The pressure response to intracavernosal infusion is subnormal in patients with abnormal venous leak. The rate of leakage, as quantified by the pharmacologic maintenance-erectile-flow method, can be greater than 180 ml/min. Leakage of up to 20 ml/min seems to be of little clinical significance. Leakage of 25–45 ml/min may be significant in the presence of some compromise in arterial flow. Leakage of more than

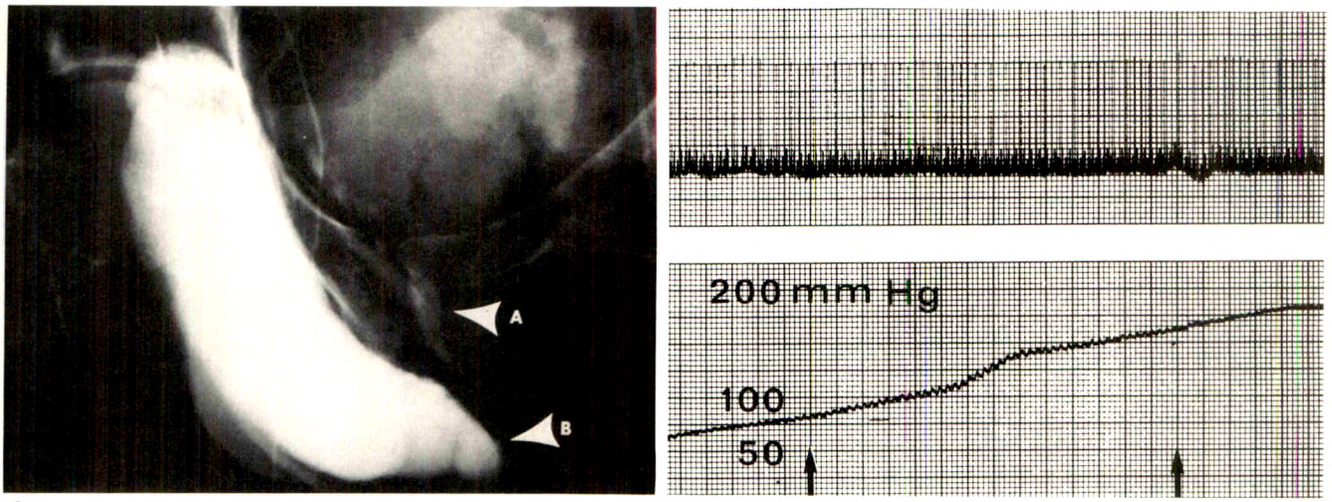

Fig. 5.—Normal cavernosogram in 31-year-old diabetic with impotence and hypertension (same patient as that shown in Fig. 2). 20 min after intracaversonal injection of papaverine-phentolamine, infusion of diluted contrast medium at rate of 12 ml/min enabled patient to maintain an erection with cavernosal pressures of 180 mm Hg.

***A*, Cavernosography shows almost no venous drainage. A = minimal opacification of preprostatic plexus; B = left crura without visualized crural perforators.**

***B*, Infusion was begun at rate of 45 ml/min and was gradually decreased as pressure rose. After about 120 sec, pressure was maintained at 180 mm Hg by an infusion at 12 ml/min. During infusion, pulsatility of pressure pulse becomes apparent as pressure rises between about 80 mm Hg (*left arrow*) and 170 mm Hg (*right arrow*), suggesting systolic and diastolic intracavernosal artery pressures of this amount.**

45 ml/min seems to cause impotence regardless of the status of the arterial supply.

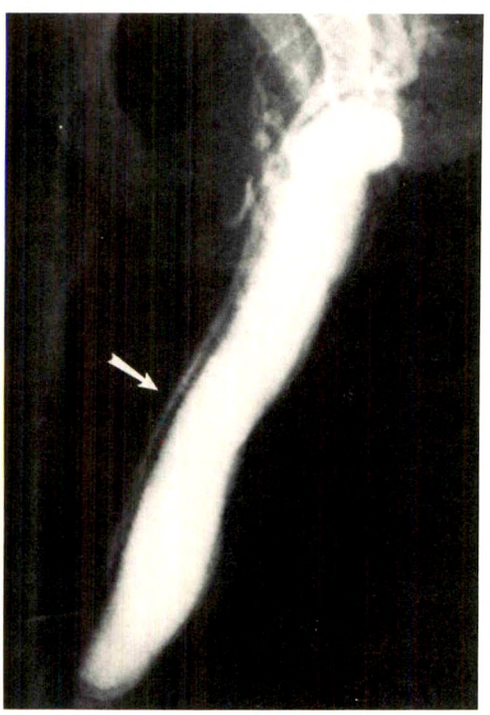

Fig. 6.—Venoocclusive insufficiency, primarily via deep dorsal penile vein (*arrow*). 62-year-old man with arteriogenic and venogenic impotence. Despite bilateral pudendal arterial obstruction shown by arteriography, patient regained sexual function after percutaneous transcatheter occlusion of dorsal penile and pudendal veins.

Identification of the site of leakage is important in planning venoablative therapy (see following section). Abnormal venous leakage most frequently occurs via the deep dorsal penile vein (Fig. 6) and/or the crural perforators into the pudendal veins (Fig. 7). Drainage also can occur predominantly via the corpus sponiosum or via superficial veins on the dorsal or ventral aspects of the penis into the external pudendal veins.

Therapy

The role of radiology is best understood in the light of currently available therapeutic options. Over the past decade, implantation of semirigid or inflatable penile prostheses has become an accepted form of therapy. The level of satisfaction experienced by the patient and his partner is difficult to evaluate, but satisfaction rates seem to vary from about 50% to nearly 100% [23, 24]. Three to 8 percent of prostheses eventually require removal [24, 25], usually because of infection, and the overall complication rates vary from about 7 to 15%.

Many centers now offer therapeutic programs that involve self-administration of papaverine into the corpora cavernosa. Zorgniotti and Lefleur [26] report good responses in over 80% of patients. Papaverine is effective in a wide variety of conditions, including venogenic, arteriogenic, and neurogenic impotence. Our experience suggests that cavernosal fibrosis may develop after a time, and that some patients become refractory to treatment. Other smooth-muscle relaxants such as prostaglandin E_2 require further evaluation and may prove to be more effective.

For arteriogenic impotence, a variety of revascularization

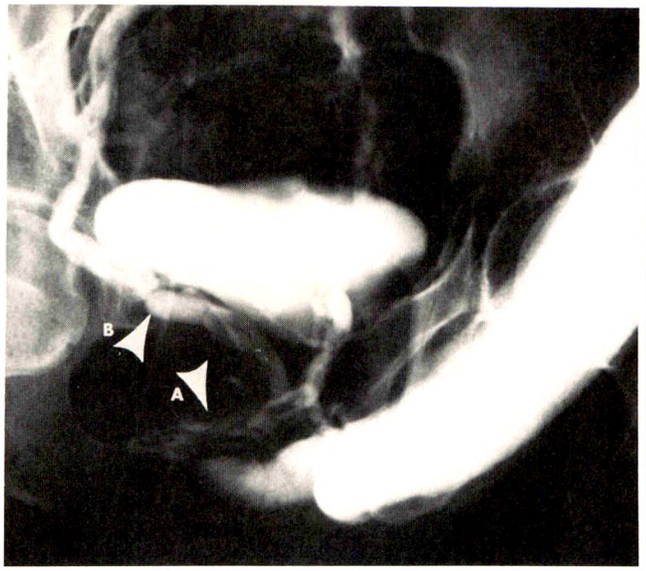

A

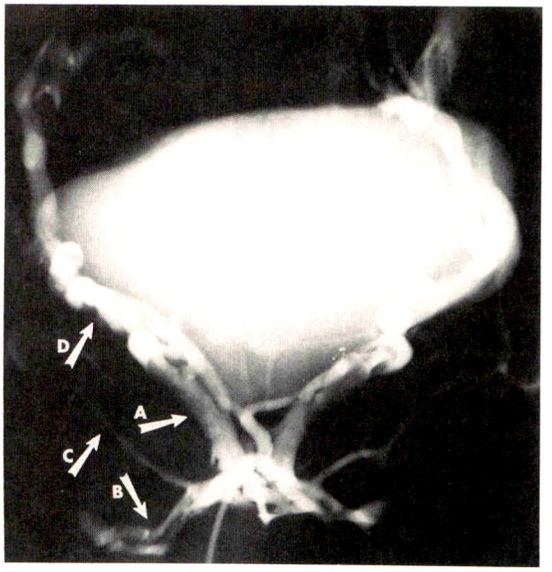

B

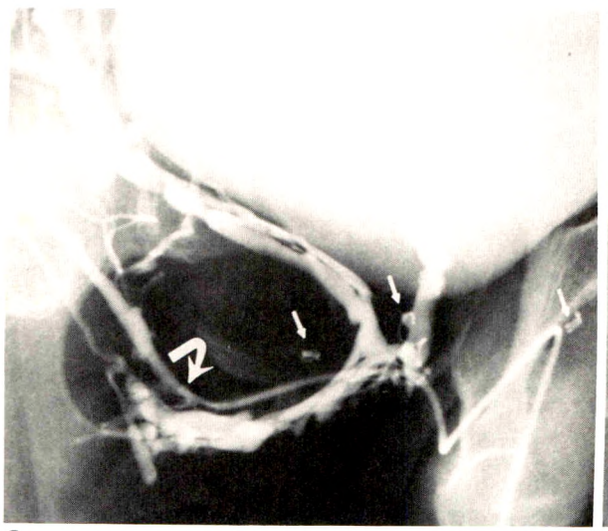

C

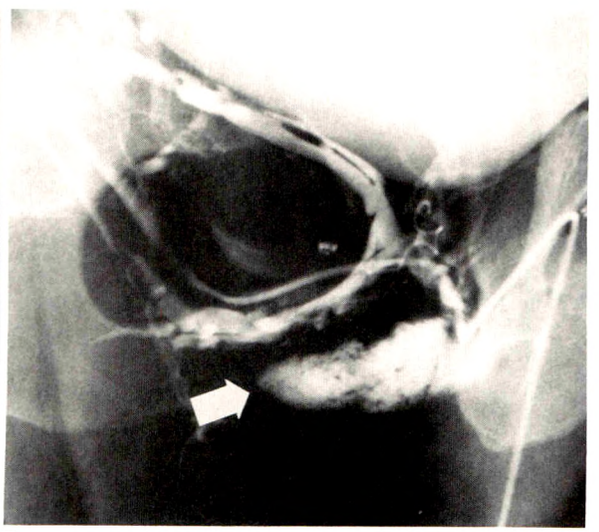

D

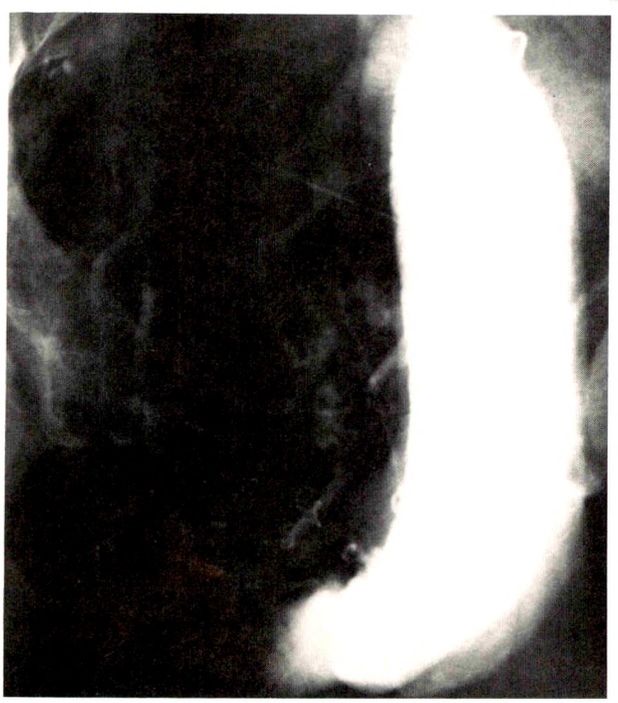

E

Fig. 7.—Venoocclusive insufficiency, primarily via crural perforators. 31-year-old man with an 8-year history of impotence. Cavernosometry showed leak of 60 ml/min at pressure of 150 mm Hg.

A, Cavernosogram shows leakage primarily via crural perforators into pudendal vein (*arrowhead* A) and then via preprostatic plexus into vesical veins (*arrowhead* B). Note absence of appreciable opacification in region of deep dorsal penile vein (compare with Fig. 6).

B, Direct venogram after percutaneous puncture of deep dorsal penile vein. A = preprostatic plexus, B = pudendal veins, C = obturator vein, D = vesical vein.

C, Incidental to transcatheter venoocclusion, selective venography of a pudendal vena comitans (in oblique projection) shows no reflux into crura (*curved arrow* indicates tip of catheter). Several coils have already been placed (*straight arrows*).

D, During same injection as that shown in *C*, a Valsalva maneuver was performed showing reflux via crural perforators (only barely visible) into right crus (*arrow*). Sclerosant was injected into these and other perforators.

E, 1 week later, multiple coils are seen in penile veins. (In no case has a coil migrated.) Cavernosography no longer shows opacification of preprostatic plexus, and all pudendal veins that received emboli or sclerosant are occluded. 1 week after this study, patient began to note improved erections and has since partially regained sexual potency.

procedures may be employed including internal iliac bypass, the Michal procedure (epigastric-cavernosal anastomosis) [27–29], inferior epigastric-dorsal penile arterial anastomoses [30], and arterialization of the deep dorsal penile vein [31, 32]. Results after revascularization of the internal iliac artery are mixed [21, 33]. Many failures probably reflect missed diagnosis of associated venous leak or distal arterial disease. Obstruction of the internal pudendal or penile arteries often can be treated by anastomosis into the dorsal penile artery, with favorable results in 40% [34]. Results after arterialization of the dorsal penile vein have been more encouraging [31, 32]. Direct arterial anastomoses into the corpus cavernosum almost always fail and are no longer recommended [27–29].

An increasing number of anecdotal reports describe favorable responses after transluminal angioplasty of one or both common or internal iliac arteries [35–38]. The technical problems of more distal angioplasty have also been partially overcome [39], and the primary problem seems to be careful selection of patients. Suitable candidates should have short stenoses or occlusions, bilaterally significant disease, patent distal arteries, and an adequate venoocclusive mechanism.

Ligation of the deep dorsal vein and some of the circumflex tributaries has been reported to improve sexual function in 40–70% of patients [40, 41]. Our experience with cavernosography, however, shows that a significant portion of the leakage in most patients with venogenic impotence occurs via crural perforators [11], where surgical ligation has not yet been feasible.

After pilot animal studies (Bookstein et al., unpublished data), we have performed transcatheter venoablation in nine patients to date, using coils, Gelfoam, and sclerosants. These patients all had severe venous leak that was unresponsive to intracavernosal injection of papaverine (Fig. 7). The resultant venous occlusion seemed to be extensive and permanent. Eight of the nine patients developed improved nocturnal erections and improved pharmacologic maintenance erectile flow. After treatment, sexual performance was rated as normal in one, as markedly improved in three, as slightly improved in four, and as unimproved in one.

Conclusions

The study of impotence offers opportunities for radiologists to become involved in an important new field of investigation. Radiologic participation will be most meaningful if radiologists develop interdisciplinary interests beyond imaging to include full understanding of all aspects of penile morphology and physiology. A critical mass of scientific expertise has been recruited to the subject, and continuing fundamental advances in diagnosis, therapy, and prevention are occurring at a rapid rate.

REFERENCES

1. Conti G, L'érection du pénis humain et ses bases morphologique vascularies. *Acta Anat* **1952**;14:17–62
2. Virag R. Intracavernous injection of papaverine for erectile failure. *Lancet* **1982**;2:938
3. Brindley GS. Cavernosal alpha-blockade: a new technique for investigating and treating erectile impotence. *Br J Psychiatry* **1984**;143:332–337
4. Fournier GR, Juenemann KP, Lue TF, Tanagho EA. Mechanisms of venous occlusion during canine penile erection: an anatomic demonstration. *J Urol* **1987**;137:163–167
5. Lue TF, Takamura T, Umraiya M, Schmidt RA, Tanagho EA. Hemodynamics of erection in the monkey. *J Urol* **1983**;130:1237–1241
6. Benson GS, McConnell J, Lipshultz LI. Neuromorphology and neuropharmacology of the human penis. An in vitro study. *J Clin Invest* **1980**;65:506–513
7. Ottesen B, Wagner G, Virag R, Fahrenkrug J. Penile erection: possible role for vasoactive intestinal polypeptide as a neurotransmitter. *Br Med J* **1984**;288:9–14
8. Vanhoutte PM, Rubanyi GM, Millar VM, Houson DS. Modulation of vascular smooth muscle contraction by the endothelium. *Ann Rev Physiol* **1986**;48:307–320
9. Palmer RMJ, Ferrige AG, Moncada S. Nitric oxide release accounts for the biological activity of endothelium-derived relaxing factor. *Nature* **1987**;327:524–526
10. Peach MJ, Singer HA, Loeb AL. Mechanisms of endothelium-dependent vascular smooth muscle relaxation. *Biochem Pharmacol* **1985**;34:1867–1874
11. Bookstein JJ. Cavernosal venoocclusive insufficiency in male impotence: evaluation of degree and location. *Radiology* **1987**;164:175–178
12. Morley JE. Impotence. *Am J Med* **1986**;80:897–905
13. Lurie AL, Bookstein JJ, Kessler WO. The angiography of post-traumatic impotence. *J Urol* (in press)
14. Abber JC, Lue TF, Orvis BO, McClure RD, Williams RD. Diagnostic tests for impotence: a comparison of papaverine injection with the penile-brachial index and nocturnal penile tumescence monitoring. *J Urol* **1986**;135:923–925
15. Condra M, Morales A, Surridge DH, Owen JA, Marshall P, Fenemore J. The unreliability of nocturnal penile tumescence recording as an outcome measurement in the treatment of organic impotence. *J Urol* **1986**;135:280–282
16. Bradley WE. New techniques in evaluation of impotence. *Urology* **1987**;29:383–388
17. Lue TF, Hricak H, Marich KW, Tanagho EA. Vasculogenic impotence evaluated by high-resolution ultrasonography and pulsed Doppler spectrum analysis. *Radiology* **1985**;155:777–781
18. Maatman TJ, Montague DK. Routine endocrine screening in impotence. *Urology* **1986**;27:499–502
19. Bookstein JJ, Valji K, Parsons L, Kessler W. Pharmacoarteriography in the evaluation of impotence. *J Urol* **1987**;137:333–337
20. Bookstein JJ, Lang E. Penile magnification pharmacoarteriography: details of intrapenile arterial anatomy. *AJR* **1987**;148:883–888
21. Flanigan DP, Sobinsky KR, Schuler JJ, Buchbinder D, Borozan PG, Meyer JP. Internal iliac artery revascularization in the treatment of vasculogenic impotence. *Arch Surg* **1985**;120:271–274
22. Bookstein JJ, Valji K, Parsons L, Kessler W. Penile pharmacocavernosography and cavernosometry in the evaluation of impotence. *J Urol* **1987**;137:772–776
23. Stewart TD. Penile prostheses: a psychiatric perspective. *Adv Psychosom Med* **1986**;15:211–225
24. Moul JW, McLeod DG. Experience with the AMS 600 malleable penile prosthesis. *J Urol* **1986**;135:929–931
25. Thomalla JV, Thompson ST, Rowland RG, Mulcahy JJ. Infectious complications of penile prosthetic implants. *J Urol* **1987**;138:65–67
26. Zorgniotti AW, Lefleur RS. Auto-injection of the corpus cavernosum with a vasoactive drug combination for vasculogenic impotence. *J Urol* **1985**;133:39–41
27. Hawatmeh IS, Houttuin E, Gregory JG, Blair OM, Purcell MH. The diagnosis and surgical management of vasculogenic impotence. *J Urol* **1982**;127:910–914
28. Zorgniotti AW, Rossi G, Padula G, Makovsky RD. Diagnosis and therapy of vasculogenic impotence. *J Urol* **1980**;123:674–676
29. Metz P, Frimodt-Moller C. Epigastrico-cavernous anastomosis in the treatment of arteriogenic impotence. *Scand J Urol Nephrol* **1983**;17:271–275
30. McDougall WS, Jeffery RF. Microscopic penile revascularization. *J Urol* **1983**;129:517–521
31. Bennett AH, Rivard DJ, Blanc RP, Moran M. Reconstructive surgery for vasculogenic impotence. *J Urol* **1986**;136:599–601
32. Balko A, Malhotra CM, Wincze JP, et al. Deep-penile-vein arterialization

for arterial and venous impotence. *Arch Surg* **1986**;121:774–777
33. Dewar ML, Blundell PE, Lidstone D, Herba MJ, Chiu RC-J. Effects of abdominal aneurysmectomy, aortoiliac bypass grafting and angioplasty on male sexual potency: a prospective study. *Can J Surg* **1985**;28:154–157
34. Sharlip ID, Bennett AH, Lewis RW. American experience with arterial and venous procedures for impotence. Presented at the annual meeting of the American Urologic Association, Anaheim, CA, May **1987**
35. Castaneda-Zuniga WR, Smith A, Kaye K, et al. Transluminal angioplasty for treatment of vasculogenic impotence. *AJR* **1982**;139:371–373
36. Van Unnik JG, Marsman JWP. Impotence due to the external iliac steal syndrome treated by percutaneous transluminal angioplasty. *J Urol* **1984**;131:544–545
37. Becker GJ, Rowe DM, Holden RW, Dalsing MC, Bendick PJ. Percutaneous transluminal angioplasty for vasculogenic impotence. *Indiana Med* **1986**;79:256–262
38. Angelini P, Fighali S. Early experience with balloon angioplasty of internal iliac arteries for vasculogenic impotence. *Cathet Cardiovasc Diagn* **1987**;13:107–110
39. Bookstein JJ. New technique in impotence shows hope. *Urol Times* **1987**;14:1
40. Wespes E, Schulman CC. Venous leakage: surgical treatment of a curable cause of impotence. *J Urol* **1985**;133:796–798
41. Lewis RW, Puyau FA, Bell DP. Another surgical approach for vasculogenic impotence. *J Urol* **1986**;136:1210–1212

Clinical Evaluation of a Medical Image Management System for Chest Images

Ronald L. Arenson[1]
Sridhar B. Seshadri
Harold L. Kundel
Debra DeSimone
Frans Van der Voorde
Warren B. Gefter
David M. Epstein
Wallace T. Miller
Judith M. Aronchick
Michael B. Simson
Paul N. Lanken
Satjeet Khalsa
Inna Brikman
Michael Davey
Nancy Brisbon

The clinical efficacy and physicians' assessment of a medical image management system (MIMS) for chest images that involved the medical intensive care unit (MICU) and the radiology department were evaluated. A token-passing fiber-optic network was implemented to connect display stations in the MICU and in the chest reading area in the radiology department with a laser film digitizer and an archiving system. To study the clinical efficacy of this sytem, blocks of 8 weeks during which portable chest images were digitized and immediately made available in the MICU were alternated with blocks of 8 weeks during which film images only were available. Approximately 3000 portable chest examinations were tracked; patients were entered into the study at a rate of 65 per month. Data on time intervals associated with the examination process were collected from MICU physicians, radiologists, radiographers, and film librarians. The time from the completion of an examination to the time an action was taken that was based on radiographic findings showed significant reductions during the digital periods for certain actions. For example, the time to begin drug therapy decreased from a mean of 4.7 hr when films were viewed to a mean of 3.3 hr when digital images were viewed.

In conclusion, if prompt action by the MICU physician improves a patient's outcome, a positive effect on patient care will result from the immediate availability of radiographic images.

Traditional systems for generating, handling, transporting, and archiving diagnostic images have had a head start in the competition with the medical image management systems (MIMS) that are being developed today. MIMS, often referred to as picture archiving and communication systems (PACS), are being designed to replace film and file rooms with digital storage and retrieval. As described previously [1], these systems potentially could speed medical images to physicians and other health-care professionals, greatly reduce space taken up by archives, reduce operating costs for film libraries, and improve the quality of radiologists' work. In the context of this paper, "film" is taken to mean the conventional radiographic film, "digital image" is the digital representation of the film, and "image" is either the film or its digital representation.

Decades of development spent on fine tuning conventional equipment and methods for handling radiographic images have resulted in a series of products with which the users are thoroughly familiar. The rates of transmission needed to equal a film-librarian carrying a heavy folder of films are difficult to surpass by affordable present-day electronic technology [2]. The design of an electronic user-interface with a MIMS that begins to rival the simplicity of a stack of films and several viewboxes on the wall must be sophisticated. A MIMS must provide harmonious operation, combining both technological sophistication and ease of use. A new and effective effort to standardize equipment and communication techniques is a prerequisite to success. An unprecedented level of involvement by users is required in this development to ensure that the systems adequately satisfy present and future needs. Continuous testing of prototypes for adequacy and effectiveness in the users' environment is the key to success.

Received July 13, 1987; accepted after revision September 23, 1987.

This work was supported in part by grant no. HL 33332 from the National Heart, Lung, and Blood Institute, U. S. Public Health Service.

[1] Department of Radiology, Hospital of the University of Pennsylvania, 3400 Spruce St., Philadelphia, PA 19104. Address reprint requests to R. L. Arenson.

AJR 150:55–59, January 1988
0361–803X/88/1501–0055
© American Roentgen Ray Society

We describe the prototype MIMS in operation at the Hospital of the University of Pennsylvania and present the results of a pilot clinical program involving the medical intensive care unit (MICU). The overall goal of our MICU project was to determine the effect that a MIMS has on care of patients in a setting in which rapid access to radiographic information may have a direct impact on a patient's outcome.

Materials and Methods

Hardware

The design of the six-node MIMS used in our department began in early 1981 and has evolved substantially since [3–7]. The six nodes include the image-acquisition station, the image-archival station, the high-resolution viewing station, the medium-resolution viewing station, and the network-research station. Work is underway to develop software for a VIEW-2000 display station from Virtual Imaging (Sunnyvale, CA). Figure 1 is a schematic of the topology of the network.

After the MICU films are processed, a Du Pont (Wilmington, DE) Film DRS-1 Laser Scanner is used to generate a digital representation of the image on the film (see Fig. 2). The size of the pixel matrix produced by the scanner is 1684 × 2048 (horizontal × vertical). However, this matrix is subsampled at the scanner to generate a 1024 × 1024 image file. The depth of each pixel is 12 bits (4096 discrete levels of gray). The digitized image is transmitted over a fiber-optic token-passing ring manufactured by Proteon Associates (Boston, MA). The network transports images and concomitant information from node to node at a signaling rate of 10 megabits/sec.

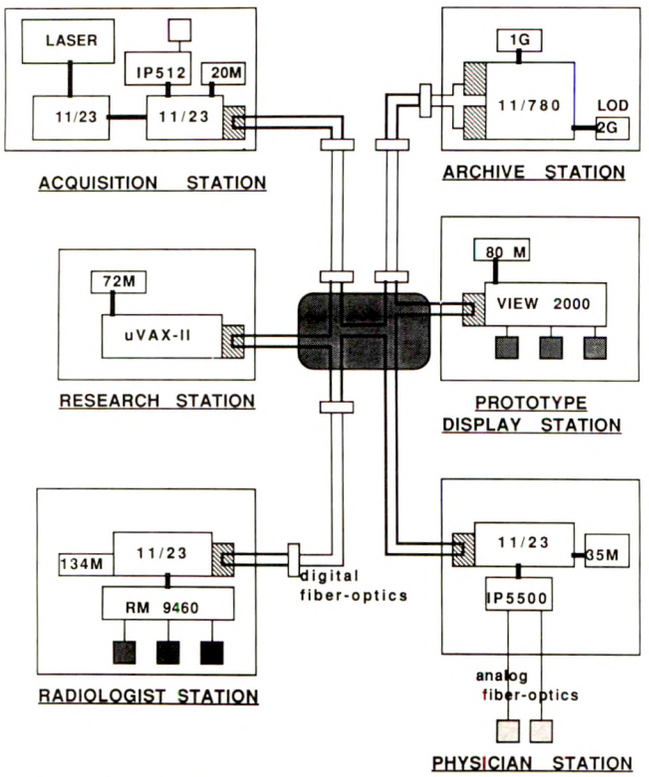

Fig. 1.—Topology of present prototype medical image management system. The VIEW-2000 display station will be operational soon. See text for details on equipment.

Images are archived on a VAX-11/780 from Digital Equipment Corp. (Maynard, MA). Two 456-megabyte Winchester disks are used to archive the 200 most current images and the system's software. Images are archived continuously to a Laser Optical Disk manufactured by Perceptics (Knoxville, TN).

The medium-resolution physician's station, located in the MICU, is centered around a Gould DeAnza (San Jose, CA) IP 5500 Image Processor with two display channels, each of which are 512 × 512 pixels by 8 bits deep (Fig. 3). The physician communicates with the system by using the auxiliary keypad of a standard VT-100 keyboard. The details of the design of the keypad have been described elsewhere [8]. The zoom feature permits the display of any selected quarter of the image at the full (1024 × 1024) resolution available in the image file.

A high-resolution radiologist's station centered around a Ramtek 9460 (Santa Clara, CA) is also available. This system has three memory channels with spatial resolutions of 1280 × 1024 (Fig. 4). The software packages for the medium- and high-resolution systems have essentially identical front-end structures because it is important that a physician be able to use both systems with minimal difficulty.

Software

Currently, three packages are running on the network. Two packages, which are similar from the user's perspective, operate on the physician's station and the radiologist's station. A third package runs on the acquisition station for input of images and demographic data. The three programs interact heavily with the networking software to enable the movement of data around the ring. All software at the applications level was designed and implemented in-house. The design of this software, from the user's point of view, has been described in detail elsewhere [8–10].

The software for the physician's and radiologist's stations presents an alphabetic list of the current patients in the MICU. Choosing a patient's name brings up a list of the available images for that patient. Once a particular image is selected, it is displayed on the first image-display monitor, which is designated the reference monitor. Associated demographic information appears on the VT-100 terminal screen. The user now can manipulate the image by using the auxiliary keypad. The available functions are pan/scroll, pseudozoom, true zoom, modified window/level, nonlinear contrast transforms, and gray-level reversal. The user can, with a single keystroke, call up the "next image." The selection of the next image is based on rules built into the system [8, 10]. The automated sequencing of images is appealing to physicians who prefer minimal interaction with the system when selecting a view. The sequence is standardized and therefore becomes routine and expected. For example, the transfer of images from the archive to the physician's station is expedited by a prefetch algorithm that moves images that will most likely be called up. This substantially reduces the waiting time between request and display of an image.

The MICU Experiment

The research project described here involved the transmission of digital images generated from portable chest radiographs taken in the MICU. The purpose was to determine the efficacy of a MIMS in comparison with that of a traditional film-based system.

To realize these goals, we planned three chronologically sequential, but somewhat interwoven, phases. The first phase was the installation of the digital image/data transmission network between the film-acquisition area, the chest-reading area, the MICU reading area, and the image archive. The second was the design and development of

Fig. 2.—Image acquisition station where films from medical intensive care unit are digitized immediately after processing.

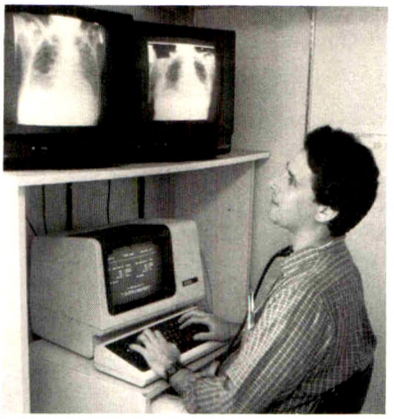

Fig. 3.—Display station, located in conference room of medical intensive care unit, presents full images at 512 × 512 pixels or a quadrant of the image at 1024 × 1024 pixels.

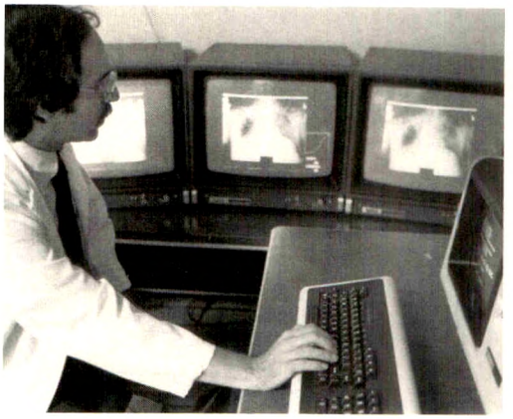

Fig. 4.—Radiologist's station, located in chest reading area, provides 1024 × 1024 pixel images.

simple, yet powerful, software to move and manipulate the images. Rule-based design was incorporated wherever possible, and the software was tested on personnel in the radiology department and MICU. The third phase was the evaluation period. Once all the involved groups became familiar with the system, we began evaluating the efficacy of the operation from two perspectives: clinical and technological. Test intervals of 8 weeks during which the digital system was available were alternated with 8 weeks during which only film images were available. Performance during these intervals was compared.

Each time a clinical situation led to a request for a portable chest image, the staff members involved in the study were asked to record four types of data: binary decisions (yes, no), rating-scale data, confidence levels, and time intervals. We split the data-acquisition forms into as many subcategories as possible to allow us to see the microstructure of the data. However, for presentation purposes, the data appear in a coalesced form.

A similar analysis was made on the data acquired from the film and digital periods. Typical examples of our analyses follow. In addition, in-depth ministudies are being conducted to compare various aspects of viewing films and digital images. From these studies, we expect to generate valuable information concerning the design of workstations and networks.

Logistics of Data Collection

In previous publications [8, 10], flow charts have been used to show the sequence of events from the time an examination is requested to the time action is taken in the MICU. The flow charts also indicated the radiology department's substantial contribution to the decision-making process of the MICU physician. The sequence of events from the request for an examination to the action taken in the MICU was logged by the participating staff members at the time each event occurred. A research coordinator, acting as the liaison between the medical staff and the research group, monitored the process and ensured the integrity of the data. Data were collected at five points in the chain.

The process was triggered when the MICU physician (usually the intern or resident) requested a radiologic examination. The time and clinical reason for the examination were given on the consultation request. The examination was performed, and the radiographer recorded the times the study was begun and completed on the radiographer's form.

The film librarian received the film and placed it on the multiviewer along with previous films for comparison. During the digital period, the films were digitized before they were put on the multiviewer. The number and availability (or nonavailability) of previous examinations were recorded on the librarian's form. In the digital period, information about the digitization process also was acquired on this form. The radiologist then read the film(s) and recorded the findings and the time of interpretation on the radiologist's form. The film librarian then entered the radiologist's preliminary report into the system so that the MICU physicians had access to an interpretation that accompanied the image.

Whenever action taken in the MICU was based on information derived from radiographs, the MICU physicians were asked to fill out an action form. This form recorded information about the action taken, associated times, and methods of communication between the MICU and the radiology department.

Data Bases

Primarily, two data bases are associated with the MIMS. The image data base tracks the MICU patients and their images. The statistical data base uses in-house software for data entry. Modification and display are done with the Datatrieve and ALL-IN-1 packages from Digital Equipment Corp. (Maynard, MA), and analysis is performed with the Statistical Package for the Social Sciences (SPSS) provided by SPSS Inc. (Chicago, IL).

Results

The study was structured with alternating periods of film and digital images. We have completed 6 months of the conventional film system and 6 months during which digital images also were available in the MICU. Approximately 3000 portable chest examinations were tracked; patients were entered into the study at a rate of 65 per month. The populations of patients during the film and digital periods were well matched with respect to age and sex, reasons for requests

for examination, interpretations of examinations, and actions taken.

In the tables, the digital period is split into film and digital because the physicians had the choice to view images digitally, on film, or both. Table 1 shows the various means by which the radiologist communicated information about the images of MICU patients to the appropriate physicians. In the film period, approximately 40% of the time the physicians visited the radiology department to (1) see the images, and/or (2) obtain direct consultations with the radiologists, and/or (3) read the preliminary interpretation attached to the images hanging on the multiviewers in the department. A radiologist conducted a daily conference (Monday through Friday) in the MICU with the clinicians to discuss the interpretations of current films. During the film period, this daily conference was used as a means of communication between the radiologist and the MICU physician approximately 36% of the time. However, when digital images were used, the transmitted preliminary report was used more frequently.

Table 2 details the reductions, categorized by reasons examinations were requested, in the interval between completion of the examination and actions taken in the MICU when digital images were used. The differences are significant ($p < .05$).

Table 3 shows the same interval, from completion of examination to actions taken, but categorized by actions taken by MICU physicians. Again, significant reductions occurred in the time from completion of examination to actions taken when digital images were viewed.

TABLE 1: Modes of Communication Between Physicians and Radiologists

Mode	Film Periods	Digital Periods	
		Digital	Film
No answer	5.2	13.3	3.4
Radiology department	39.9	0.6	30.9
MICU/radiology conference	36.2	1.6	24.5
Telephone	2.3	1.1	1.9
Preliminary report/console	16.3	16.5	6.0

Note.—Numbers are percentages. MICU = medical intensive care unit.

TABLE 2: Hours Between Completion of Examination and Action Taken Categorized According to Reasons for Examination

Reason Why Examination Was Requested	Film Periods	Digital Periods	
		Digital	Film
Lines/devices	4.1 ± 2.9	3.0 ± 2.2	4.3 ± 3.0
Pulmonary	4.4 ± 2.9	3.2 ± 2.1	5.0 ± 2.9
Cardiac	4.6 ± 2.8	3.1 ± 2.1	4.3 ± 2.9
Pleural	3.2 ± 2.9	2.3 ± 1.8	2.5 ± 2.7
Other	4.8 ± 2.9	3.4 ± 2.1	5.1 ± 2.9
All requests combined	4.3 ± 2.9	3.1 ± 2.1	4.4 ± 3.0

Note.—All numbers are means ± standard deviations. Intervals greater than 10 hr were excluded. Decreases in times for digital periods were significant ($p < .05$).

TABLE 3: Hours Between Completion of Examination and Action Taken Categorized According to Actions Taken in the MICU

Action Taken	Film Periods	Digital Periods	
		Digital	Film
None–No significant change	4.4 ± 2.9	3.1 ± 2.2	4.5 ± 3.0
Drug therapy	4.7 ± 2.8	3.3 ± 2.1	4.3 ± 3.0
Additional procedures	4.3 ± 2.8	2.3 ± 1.6	4.4 ± 3.1
Lines/devices	2.3 ± 2.4	2.2 ± 1.5	2.5 ± 2.5
Pleural intervention	3.6 ± 3.2	2.3 ± 1.9	2.5 ± 2.3
Other	3.7 ± 2.9	2.3 ± 1.6	3.1 ± 2.5
All actions combined	4.3 ± 2.9	3.0 ± 2.1	4.1 ± 3.0

Note.—All numbers are means ± standard deviations. Intervals greater than 10 hr were excluded. Decreases in times for digital periods were significant ($p < .05$). MICU = medical intensive care unit.

Discussion

When digital images were used, the MICU physicians relied more heavily on the transmitted preliminary report than on direct consultation with the radiologist (Table 1). Also, when digital images were viewed, a higher percentage of the MICU physicians indicated that they did not communicate with a radiologist. Whenever available, the preliminary report was presented along with the digital images. However, occasionally the images were viewed before the radiologist's interpretation was given.

Any system that reduces the referring physician's reliance on the radiologist's interpretation may be criticized. This article does not resolve the debate over what the radiologist's interpretation contributes to the patient's care in those cases in which the referring physician has a perceived need to see the images directly. Clearly, such systems for transmitting images will make it more practical for referring physicians themselves to view images. Dependence on the radiologist's interpretation probably will correlate well with the quality of the radiologist's consultations. Some radiology departments may wish to prevent the transmission of images until after the interpretation has been made. This study concentrated on the impact of the availability of digital images on the timeliness of actions taken by the MICU physicians.

Whether the statistically significant reductions in time between examination and actions taken have a substantial impact on a patient's outcome is not yet known. Certainly an argument can be made that repositioning central venous lines or detecting pneumothoraces hours earlier may be important.

In Tables 2 and 3, time intervals that exceeded 10 hr were excluded in both the film and digital periods because these intervals were considered "outliers" that artificially obscured the results.

Throughout the digital period, the research coordinator collected comments and suggestions from the clinicians and radiologists on the quality of the images, the user-friendliness of the display console, and physicians' acceptance of the system. The MICU physicians appreciated the opportunity to see the images and obtain the reports from the computer earlier in the day, much before the daily conference. The

system was used every day during rounds with the attending physicians and interns of the MICU, enhancing discussions about patients' care and serving as an excellent teaching tool. The system also was helpful during the weekends and evenings, decreasing the need to visit the radiology department. The effectiveness of the system was especially evident when MICU physicians, while viewing digital images, discovered a pneumothorax in a patient whose condition had begun to deteriorate suddenly.

Another advantage was that, by using the expert rule-based system described earlier, the physicians automatically are presented with previous images. This is important if using these additional studies really make a difference in a patient's outcome. The physicians found it convenient to be able to view and make comparisons with chest films taken at admission, for example, after the patient had been in the MICU for several days.

Two frequent complaints were the time required to retrieve images from the archive and the amount of manipulation required to achieve the desired appearance of the image. A few physicians thought that the quality and resolution were not sufficient to detect small pneumothoraces or discern early infiltrates.

With regard to spatial resolution, although the image is acquired at a 200-μm resolution, resulting in a matrix 1684 $\times$ 2048 pixels by 12 bits, we have presented only 512 $\times$ 512 images on the MICU display. Because the MIMS was designed to operate in a review/comparison mode, we thought that it was sufficient to transmit and store a 1024 $\times$ 1024 matrix obtained by subsampling the image. As described earlier, the entire image can be viewed in a matrix 512 $\times$ 512, or any arbitrary quarter can be viewed at the full stored resolution. One reason for selection of the 512 $\times$ 512 display was to test the hypothesis that a lower resolution system would be sufficient for review and comparison purposes if the true-zoom feature was provided [8]. The equipment for a high-resolution system costs considerably more, and the time required to transmit a 1684 $\times$ 2048 image between nodes is approximately 90 sec, which is four times as long as our present transmission time, and which we thought was prohibitively long.

Now that the clinical evaluation of this medium-resolution system has been completed, we will introduce a high-resolution display station for comparison in the MICU.

Although the physician's display console has been made relatively user-friendly with the specially designed keyboard described earlier, the physicans required a long time to become comfortable with the use of a computer display. Approximately 4 weeks elapsed before they used the system without the encouragement of the research coordinator. Our experience in this project strongly supports the use of rule-based systems to simplify the display sequences and settings so that minimal interaction is needed between the physicians and the system.

The prototype MIMS described here has all the basic components of a full-fledged MIMS. Rapid expansion of the MIMS is expected in the coming year, including teleradiology for remote facilities. Additional investigation will concentrate on spatial- and contrast-resolution requirements, data compression, ACR/NEMA (American College of Radiology/National Equipment Manufacturers' Assoc.) interface, DECRad (Digital Equipment Corporation Radiology Information System) interface [11], and analysis of cost-effectiveness.

Our clinical experience has shown that such a system can hasten transmission of information to health-care providers so that actions can be taken earlier. As further information becomes available, we intend to evaluate the impact of the MIMS on the length of stay both in the MICU and in the hospital.

ACKNOWLEDGMENTS

We acknowledge the technical support of E. I. Du Pont de Nemours and Philips Medical Systems. We also thank Steve J. Strommer and John D. Kahler of the Radiology Media Services Section for their excellent reproduction of the graphics in this paper.

REFERENCES

1. Cox GC, Templeton AW, Dwyer SJ. Digital image management: networking, display, and archiving. *Radiol Clin North Am* **1986**;24:37–54
2. Cox GC, Templeton AW, Anderson WH, Cook LT, Hensley RS, Dwyer SJ. Estimating digital information throughput rates for radiology networks: a model. *Invest Radiol* **1986**;21:162–166
3. Arenson RL, London JW, Morton DE. Fiber optic communication system for medical images. In: *Proceedings of first international conference and workshop on PACS for medical applications* (cat. no. THOO90-1). Newport Beach, CA: SPIE, **1982**:74–79
4. Arenson RL, London JW, Morton DE. Fiber optic network with image storage and display systems. In: *Proceedings of seventh conference on computer applications in radiology*. Reston, VA: American College of Radiology, **1982**:545–561
5. Arenson RL, Morton DE, London JW. Early experience with fiber optic picture archival and communication system for medical images. In: *Proceedings of the SPIE second international conference on PACS for medical applications (PACS II)*. Newport Beach, CA: SPIE, **1983**:116–121
6. Arenson RL, Bergey P, Brikman I, Kundel H, Morton D, Waxler G. Evaluation of a high-resolution film digitizer. In: *Proceedings of the eighth conference on computers in radiology*. Reston, VA: American College of Radiology, **1984**
7. Bergey P, Arenson RL, Brikman I, Kundel H, Morton D, Waxler G. A linear systems approach to medical image capture and display (cat. no. 84CH204709). *IEEE Computer Society 1984, Joint International Symposium and Exhibition*. Arlington, VA: IEEE Computer Society, **1984**:4–7
8. Van der Voorde F, Arenson RL, Kundel H, et al. Development of a physician friendly digital image display console. In: *SPIE Medicine XIV/PACS-IV*. Newport Beach, CA: SPIE, **1986**;626:541–548.
9. Seshadri S, Arenson RL, Van der Voorde F, Khalsa S, Kundel H, Brikman I. Design of a medical image management system: a practical cost-effective approach. In: *Proceedings SCAMC-10*. Washington, DC: SCAMC, **1986**:288–295
10. Seshadri S, Arenson RL, Khalsa S, Brikman I, Van der Voorde F. Prototype PACS at the University of Pennsylvania: software design considerations. Proceedings of Medical Imaging (Conf 767). Newport Beach, CA: SPIE, **1987**:793–800
11. Arenson RL, Seshadri S, Stevens F. The overlapping domains and interface between radiology information management system and medical image management system (PACS). In: *Proceedings of Computer Assisted Radiology. Berlin: Springer-Verlag,* **1987**:855–865

Videotape Review

RSNA Today, Vol. 1, No. 3. Oak Brook, IL: The Radiological Society of North America, 1987. $75

This tape consists of four reviews: "High-Speed Intravascular Drill-Assisted Angioplasty"; "Imaging of Stroke"; The magna cum laude scientific exhibit of the RSNA meeting of 1986, "Dual-Energy-Scanned-Projection Digital Radiography of the Chest"; and a report by the American College of Radiology on nonionic contrast media. These four topics are presented in a 55-min videotape. Three are interviews; the fourth is the presentation of an exhibit by the author.

"High-Speed Intravascular Drill-Assisted Angioplasty" is an early report of a new technology that is undergoing initial clinical evaluation. Although the place of this procedure in radiologic practice is not defined, the approach does show some promise. "Imaging of Stroke" is a round-table discussion by three neuroradiologists. Their suggestions on the use of contrast material and available imaging techniques for stroke patients are well done. The scientific exhibit refers to 5 years of experience in using dual-energy scanned projection digital radiography of the chest. It is an excellent presentation of an exciting new imaging technique. The practical applications of this technology for the demonstration of soft-tissue masses, analysis of calcium within a mass, and evaluation of osteoporosis are covered concisely and clearly. The final presentation is a report by Harry Fisher from the American College of Radiology on the use of the new low-osmolality contrast media. The advantages and disadvantages of these agents are reviewed. Because these agents are so expensive, indications for restricted use in high-risk patients are suggested.

The use of videotapes is an efficient, rapid means for the dispersal of important information. The presentations on this tape are particularly effective. It will be particularly valuable to radiology residents and to radiologists in active practice who want to keep up with the latest developments in radiology. Advertisements are included on the tapes. This is not mentioned as a criticism; medical journals also use advertisements to defray costs.

Jack I. Eisenman
King/Drew Medical Center
Los Angeles, CA 90059

CT Densitometry of Pulmonary Nodules in a Frozen Human Thorax

Jung-Gi Im[1,2]
Gordon Gamsu[1]
Deborah Gordon[1]
Mark G. Stein[1]
W. Richard Webb[1]
Christopher E. Cann[1]
Loren T. Niklason[3]

The influence of (1) calcium concentration, (2) exposure technique, (3) reconstruction algorithm, (4) nodule size, and (5) nodule location on the CT attenuation values (CT density) of pulmonary nodules was examined in a frozen human thorax. Nodules with calcium concentrations of 0–310 mg/ml and diameters of either 0.95 or 1.59 cm were inserted into a frozen, unembalmed human thorax. The nodules were placed either at the lung apex or 4 cm below the tracheal carina. Each nodule was scanned on a GE CT 9800 scanner; five different exposure techniques were used. The slice thickness was uniformly 1.5 mm. As expected, increasing the kilovoltage caused a significant decrease in CT nodule density in all nodules with calcium concentrations greater than 80 mg/ml. The inverse relationship between kilovoltage and nodule density was exaggerated with increasing calcium concentration. A high-resolution (bone) algorithm gave a significantly higher CT number than did a smoothed (standard) algorithm, regardless of nodule size and location, but this difference could be attributed almost entirely to the edge-enhancement effect of the bone algorithm. The CT density of the larger nodules was significantly higher than that of the smaller nodules at calcium concentrations greater than 65 mg/ml for both standard and bone algorithms. Densities were significantly higher in the mid lung than in the apex with a standard algorithm, but this was not the case with a bone algorithm. The GE CT 9800 scanner had a linear response between CT density and increasing calcium concentration within the confines of a human thorax. A high-resolution (bone) reconstruction algorithm has higher spatial resolution but does show an edge-enhancing effect not found with the smoothed algorithm.

Two major variables in CT densitometry for pulmonary nodules are the kilo electron voltage of the X-ray beam and the reconstruction algorithm used; these two parameters should be standardized, with a high kilovoltage and high-resolution algorithm favored on the GE CT 9800 scanner.

CT densitometry of pulmonary nodules is based on the assumption that the presence of calcification in pulmonary nodules is a strong indicator of benignity [1]. CT can detect more accurately lower concentrations of calcium in lung nodules than can chest radiographs or conventional tomograms [2]. Since the initial studies by Siegelman et al. [3] in which benign nodules were differentiated from malignant nodules by using the Pfizer AS&E scanner and a threshold value of 164 H, other studies have shown variable reproducibility of this result [4, 5]. These variations have been attributed to scanner-related factors as well as to subject-related factors, including the size of the patient, the intrathoracic position of the nodule, and the presence of surrounding organs within the plane of scanning [6–10]. The effects of those factors on CT nodule densitometry have been studied previously only in artificial phantoms that simulate the human thorax. Although the newer CT scanners are better equipped to perform quantitative nodule densitometry, their capabilities within the thorax have not been tested. Using a GE CT 9800 scanner, we evaluated the effects of calcium concentration, exposure technique, reconstruction algorithm, nodule size, and nodule location on the CT attenuation values (CT density) of nodules in a frozen human thorax.

Received June 24, 1987; accepted after revision September 23, 1987.

This work was supported in part by a grant from Seoul National University Hospital.

[1]Department of Radiology, Box 0628, University of California, San Francisco, San Francisco, CA 94143. Address reprint requests to G. Gamsu.

[2]Present address: Department of Radiology, School of Medicine, Seoul National University, 28 Yeongun-Dong Chongro-ku, Seoul 110, Korea.

[3]Department of Radiology, Hospitals and Clinics of the University of Alabama, Birmingham, AL 35233.

AJR 150:61–66, January 1988
0361–803X/88/1501–0061
© American Roentgen Ray Society

Materials and Methods

A frozen, unembalmed human thorax, prepared according to the method described by Littleton et al. [11] and Niklason et al. [12], was used to approximate a realistic radiation environment as closely as possible. The thorax was bivalved along a coronal plane, and hemispheric excavations (1 and 1.5 cm in diameter) were cut in the frozen lung surface without compressing adjacent lung tissue. When the two halves of the thorax were brought together, the two hemispheric excavations produced a spherical hole of the same diameter (Fig. 1). Nodules were prepared by mixing calcium hydroxide powder, $Ca(OH)_2$, in molten paraffin and setting them in hemispheric molds. Two hemispheres were opposed to make a nodule. Nodules with seven different calcium concentrations (0, 37.7, 65.4, 89.5, 143, 214, 310 mg/ml) and two different diameters (0.95 and 1.59 cm) were inserted into the appropriate lung cavities for CT scanning.

The influence of the nodule's position on CT density was studied by scanning the 0.95-cm nodules at a level 3 cm above the aortic arch and 4 cm below the tracheal carina. The influence of the size of the nodule on CT density was studied by scanning the 0.95- and 1.59-cm nodules in the mid-lung field. Each nodule, regardless of its size or position, was scanned with five different exposure techniques: (1) 140 kVp/210 mAs; (2) 120 kVp/300 mAs; (3) 80 kVp/720 mAs; (4) 120 kVp/420 mAs; and (5) 120 kVp/510 mAs. The first three techniques produce similar photon fluxes. Slice thickness was 1.5 mm, and a 47.5-cm (large) calibration file was used to include the whole phantom. The scanner was a GE CT 9800 that was precisely calibrated monthly. The GE CT 9800 scanner software used was version "QC." Each image was reconstructed with both a smoothed (standard) algorithm and a high-resolution (bone) algorithm. With the smoothed algorithm, image reconstruction was done with a 34.5-cm field of view and a 512 × 512 matrix, giving a pixel size of 0.67 mm. When the high-resolution algorithm was used, images were constructed on a 320 × 320 matrix with a 0.67-mm pixel (21.25-cm field of view) for comparison with the standard reconstruction and with a 0.25-mm pixel (8.0-cm field of view) to obtain maximal resolution.

The central scan from each nodule was selected for analysis. The pixel map of each slice was printed out. The CT density of each nodule was calculated as the mean of the highest contiguous pixels that constituted 10% of the nodule's surface area. The margin of the nodule was defined by those pixels with a CT number that was more than −530 H (the median value between lung density and the density of a nodule that does not contain calcium).

The statistical analysis employed were two- and three-way between subject analysis of variance. Specific comparisons were performed by using the Tukey A test.

Results

Many of the variables demonstrated significant interactions. However, for convenience, each variable is described separately.

Calcium Concentration

The effect of calcium concentration on CT density was significant ($p < .0001$). Increasing nodule calcium concentration resulted in a linear increase in CT density, regardless of exposure technique, reconstruction algorithm, nodule size, or nodule location (Fig. 2). Theoretically, this relationship is not truly linear, because the paraffin concentration decreases with increasing $Ca(OH)_2$. However, at 140 kVp, the rise in the CT number of large nodules (in the mid lung) that is due to this effect is from −100 to −75 H or 25 H. In total, the CT number rises from −100 to 838 H for 0–310 mg/ml calcium, so the 25-H change due to this effect represents an error of 2.5% in the slope of the calcium vs CT number line. The deviation from linearity is even less (about 0.5%). Representative values of CT number as a function of calcium concentration for the three kilovoltages are given in Table 1.

Exposure Technique

The CT number of all nodules containing calcium increased with decreasing kilovoltage, as anticipated. Because the nodules were made with paraffin as a base, the CT number of

Fig. 1.—CT scan of frozen cadaveric thorax in prone position. 1.59-cm nodule is placed in excavated portion of lung. Notice bivalved thorax sectioned horizontally.

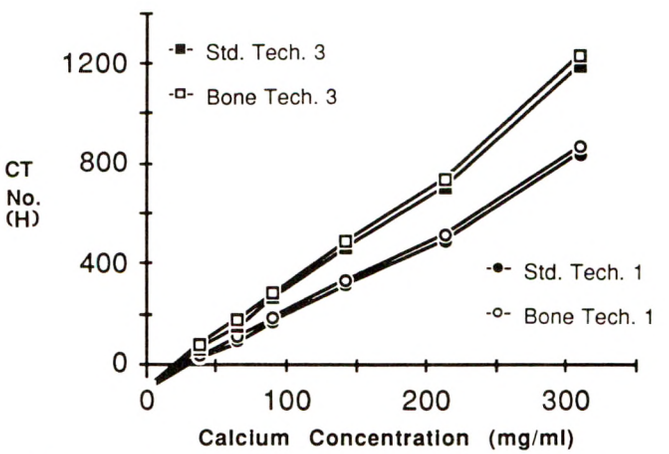

Fig. 2.—Graph of CT density vs calcium concentration using 1.59-cm nodule in mid lung.

Different exposure techniques and reconstruction algorithms give statistically different results. CT density increases linearly with increasing calcium concentrations for both technique 1 (140 kVp/210 mAs) and technique 3 (80 kVp/720 mAs). Density difference between two techniques increases with increasing calcium concentration. CT number with bone algorithm is higher than standard algorithm for both exposure techniques.

TABLE 1: CT Density (H) of Large Nodules in Mid Lung at Three Kilovoltage Levels

Calcium Concentration (mg/ml)	140 kVp/210 mAs		120 kVp/300 mAs		80 kVp/720 mAs	
	Standard (Mean ± SD)	Bone (Mean ± SD)	Standard (Mean ± SD)	Bone (Mean ± SD)	Standard (Mean ± SD)	Bone (Mean ± SD)
0	−100 ± 2	−84 ± 17	−98 ± 14	−80 ± 14	−112 ± 2	−97 ± 15
37.7	26 ± 4	34 ± 14	36 ± 2	43 ± 16	62 ± 2	78 ± 18
65.4	92 ± 4	115 ± 14	103 ± 4	126 ± 13	149 ± 5	181 ± 19
89.5	168 ± 9	184 ± 14	190 ± 14	207 ± 24	265 ± 15	279 ± 24
143	317 ± 14	337 ± 21	345 ± 19	362 ± 28	464 ± 24	489 ± 34
214	491 ± 6	518 ± 16	530 ± 8	560 ± 19	704 ± 8	741 ± 23
310	838 ± 34	868 ± 52	900 ± 35	935 ± 55	1188 ± 50	1230 ± 76

Note.—SD = standard deviation.

the 0 mg/ml nodule decreased with decreasing kilovoltage. This effect is due to the lower effective atomic number of paraffin as compared with water (approximately 5.5 vs 7.4) and simulates the effect of a nodule containing fat. However, the CT number decreased only about 12 H as kilovoltage changed from 140 to 80 kVp, a small value compared with the increase found in the calcium-containing nodules, and did not statistically improve the correlation between nodule calcium concentration and CT number. Table 1 gives the results of CT number vs nodule calcium for the three kilovoltage values tested. We could find no difference in CT number for the three different exposure settings (300, 420, 510 mAs) when kilovoltage was held constant at 120.

Reconstruction Algorithm

The high-resolution (bone) reconstruction algorithm showed a significantly higher nodule density than did the standard algorithm at all calcium concentrations for all exposure techniques, for both nodule sizes, and at both locations ($p < .05$). The CT density measured with the bone algorithm was 8–54 H higher than that measured with the standard algorithm.

Figure 3 illustrates the density across the nodule for both reconstruction algorithms. The bone algorithm shows a higher mean CT density. However, in the center of the nodule, the bone algorithm shows a higher CT number of only 3 H. The edge-enhancing effect for the bone algorithm is about 25 H (or approximately 3%) at a mean CT density of 130 H. For the standard algorithm, the mean density is less and there is no edge-enhancing effect.

The difference in density measured with the two algorithms increased significantly with increasing calcium concentration, except for the small nodule in the mid lung. For the large nodule in the mid lung, the CT density difference between the two algorithms at 0 mg/ml calcium concentration was 16 H and progressively increased to 36 H at a calcium concentration of 310 mg/ml (Fig. 2).

Nodule Position

Nodule CT densities in the mid lung were significantly higher than those at the lung apex when reconstructed with the standard algorithm ($F[1, 360] = 7.568$, $p < .01$) (Fig. 4). However, the differences were only 10–23 H and were not systematic. The bone algorithm likewise showed small density differences, with the density in the mid lung generally being higher than that at the apex. These differences in density were not statistically significant, and they decreased with increasing calcium concentrations for both reconstruction algorithms.

With the standard algorithm, the nodule with a calcium concentration of 37.7 mg/ml was 23 H higher in the mid lung than at the apex. The nodule with a concentration of 214 mg/ml showed only a 10-H difference between the two sites. Similarly, with the bone algorithm, the positional differences were only 4–30 H.

Nodule Size

A significant difference was seen between the CT densities of the small and large nodules for both the standard algorithm ($F[1, 1176] = 684.3$, $p < .0001$) (Fig. 5) and bone algorithm

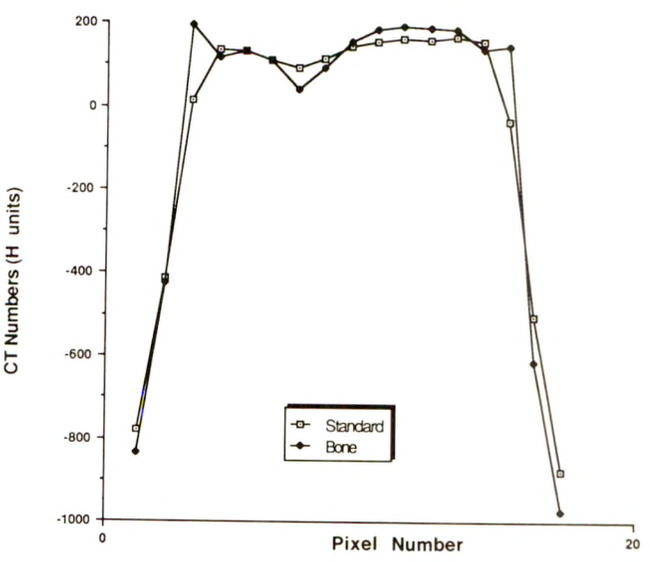

Fig. 3.—CT density plots across 0.95-cm nodule with an 89.5-mg/ml calcium concentration scanned at lung apex by using 120 kVp/300 mAs (pixel size, 0.67 mm).

Mean density of bone algorithm is higher than that of standard algorithm. CT numbers at edge of nodule are higher and transition to lung density is steeper with bone algorithm.

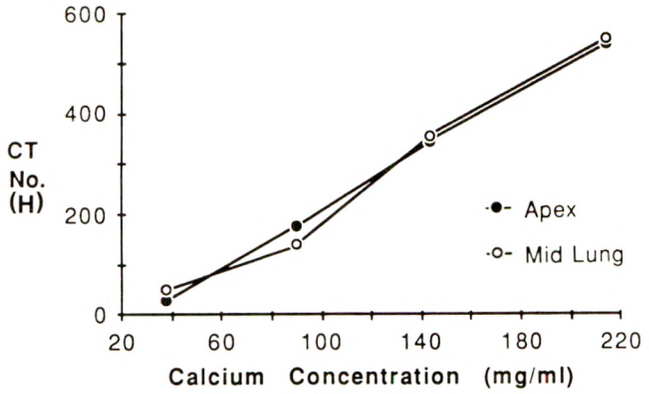

Fig. 4.—Graph of CT density vs calcium concentration using 0.95-cm nodule reconstructed with standard algorithm. Density of nodule in mid lung is higher than when at apex, except calcium concentration of 89.5 mg/ml (thought to be a rogue point).

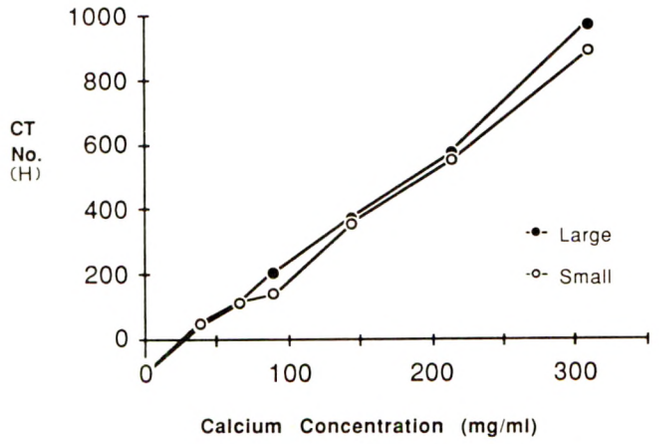

Fig. 5.—Graph of CT density vs calcium concentration for 1.59-cm (large) and 0.95-cm (small) nodules in mid lung reconstructed with standard algorithm. Density of large nodule is statistically higher than that of small nodule when calcium concentration is greater than 65.4 mg/ml.

($F[1, 1176] = 169.4$, $p < .0001$). The larger nodule had a significantly higher CT density than the smaller nodule when it contained a calcium concentration greater than 89.5 mg/ml ($p < .05$). The difference in the CT density of the two nodules increased steadily with increasing calcium concentration greater than 89.5 mg/ml. The two nodules remained significantly different for both reconstruction algorithms ($p < .0001$). For instance, with the standard algorithm, the density of the large nodule was only 1 H higher than that of the small nodule at a calcium concentration of 65.4 mg/ml, whereas at a concentration of 310 mg/ml, the density of the large nodule was 86 H higher than that of the small one.

Pixel Size

The difference in density between the two pixel sizes (0.25 and 0.67 mm, reconstructed with the bone algorithm) ranged from 0 to 3 H with the small nodules in the mid lung, which was not statistically significant. A similar result was obtained with the large nodules in the mid lung and with the small nodules at the lung apex.

Discussion

More than half (54%) of all resected solitary pulmonary nodules are benign granulomas [13]. An invasive diagnostic workup such as needle aspiration or exploratory thoracotomy could be avoided if there were sound criteria for establishing benignity by using a noninvasive method. It has been shown that CT nodule densitometry can be used to make this determination [3, 14–16]. However, scanner-related as well as subject-related sources of CT density variability have made it difficult to establish specific CT criteria for benignity. Nevertheless, CT nodule densitometry is used clinically in many centers, although its use has not become standard practice [14].

X-ray attenuation in the CT energy range is a combination of Compton scatter and photoelectric absorption [17]. As calcium concentration increases, both the mass density and the photoelectric absorption within the nodule increase, resulting in a linear increase in the attenuation values. Zerhouni et al. [8] found that the GE 8800 scanner did not show system linearity. The nonlinearity was attributed to positional variations in CT attenuation. We have shown that the GE CT 9800 scanner has an excellent linear response of CT density with increasing calcium concentration, regardless of nodule position, size, or the technique used.

Of the scanner-related factors that would vary the CT density of nodules, kilovoltage showed the most pronounced effect on CT density. As kilovoltage decreases, both Compton scatter and photoelectric absorption increase, resulting in an increase in CT density values [18]. The inverse relationship between kilovoltage and CT density is augmented by increasing calcium concentrations, producing the diverging plots seen in Figure 2. This calcium-concentration–related divergence in CT density, when the kilovoltage changes, is attributed to the cubic relationship between photoelectric effect and the atomic number of calcium.

Scanning an object with CT initially provides X-ray intensity measurements, known as raw data. From these raw data the CT numbers are derived as the "processed data" and are depicted pictorially after the reconstruction process [19]. Current CT scanners use a filtered-back projection method of image reconstruction [20].

The convolution filter of all current CT scanners is optimized for best visualization of the object of interest. Convolution of more adjacent projections improves the signal-to-noise ratio and thus the contrast resolution in a large region of interest, but this can only occur at the expense of spatial resolution. With smoothed algorithms, the convolution extends to more adjacent projections than it does with high-resolution algorithms. The net effect of smoothed algorithms is higher contrast but lower spatial resolution; the reverse is true with high-resolution (e.g., bone) algorithms [19].

When density differences are small, such as in nodules within a tissue phantom, a measurable CT density difference

between algorithms is not found. However, with lung nodules surrounded by air, the mean density and the density distribution within the nodule vary with the reconstruction algorithm [3].

With a high-resolution algorithm, the CT density at the edge of a pulmonary nodule could be overestimated, while the CT values of the surrounding lung would be underestimated. This "overshoot-undershoot" artifact is known to produce a variation equal to approximately 9% of the difference in the density between the adjacent tissues at the edge of a lung mass [21]. We found that there was approximately a 2–3% overshoot at the edge of nodules that contain high concentrations of calcium. With a Pfizer AS&E scanner, CT density increased as the diameter of an object in air decreased, when a high-resolution reconstruction algorithm was used [8]. However, with a smoothed algorithm, the CT density increased as the diameter of the object increased. The discrepancy between the two algorithms can be attributed to an overshoot effect with high-resolution algorithms that is augmented as the size of the object decreases. In the present study, the GE CT 9800 scanner showed higher CT density with the larger nodule for both the smoothed algorithm and the high-resolution algorithm. We can conclude that the edge-overshoot effect of the high-resolution algorithm on the GE CT 9800 scanner has been diminished to such an extent that nodule densitometry will be markedly improved. Our results also showed that density was 10–40 H higher with the high-resolution algorithm than with the smoothed algorithm, regardless of calcium concentration, nodule size, or nodule location. This difference is attributable mainly to the inherent characteristics of the high-resolution algorithm, including less volume averaging at the edges owing to reduced convolution of neighboring projections (Kernel effect) [19] and some edge enhancement (overshoot) [8]. Since the 10% highest contiguous pixels were selected for the mean CT density, an algorithm with higher spatial resolution will better define small, high-density objects, effectively raising the CT density of any inhomogeneous structure. In addition, the greater amount of noise (pixel standard deviation) in the high-resolution image increased the mean CT number of the highest 10% pixels by 6 H with the exposure techniques we used.

CT numbers of the mid-lung nodules are higher than those of the apex nodules because of a beam-hardening effect [22]. The chest wall at the lung apex contains thicker bones and muscles than does the mid lung, causing an increased beam-hardening effect at the lung apex. This results in a lowering of the attenuation valve of apex nodules. Moderate positional variations in the CT density of a reference phantom, similar to those found in the present study, were found by de Geer et al. [10].

The specific results in this study and the specific CT numbers are only applicable to the GE CT 9800 scanner. The general principles apply to many scanners. However, the differences that exist between types of scanners are significant enough that these data still cannot be generalized.

The major variability in CT pulmonary nodule densitometry occurs because of changes in kilovoltage and reconstruction algorithms. Both of these factors are readily standardized for any given scanner model. Cross-calibration between scanners is feasible for quantitative CT [23]. In this study, the measured CT density as a function of calcium concentration was more linear at the high kilovoltage than at the low kilovoltage, possibly because of reduced statistical noise in the data, thus favoring the use of high kilovoltage for accurate calcium measurement. On the other hand, the low kilovoltage gave better sensitivity for low concentrations of calcium, and thus the choice of kilovoltage will be dictated by the choice between sensitivity and accuracy. The high-resolution algorithm as used in this study leads to no penalty in quantitative results, at least for nodules as small as 1 cm in diameter, and may provide better sensitivity to calcium in nodules that are inhomogeneous.

The variability caused by other scanner-related technical factors and positional differences may be statistically significant but probably is not enough to be clinically important. Research still must be done to determine which calcium concentration within a pulmonary nodule indicates that malignancy is unlikely and then to find the corresponding CT number for diagnostic use. The minimal detectable and quantifiable amount of calcium within a pulmonary nodule is about 10 mg/ml [17], almost four times less than the least amount used in the present studies. Sufficient calcium to produce visible density on thin-section CT is considerably more than 40 mg/ml and has a CT number above 200 H [15]. Those pulmonary nodules with a representative CT number below 200 H, and that are not overtly calcified on CT, remain a problem. The ability to discriminate between benign and malignant nodules on the basis of CT numbers below 200 H should not be related to variations in scanner performance.

At present, we advocate nodule densitometry by using high kilovoltage and amperage, a high-resolution reconstruction algorithm, and 1- to 1.5-mm-thick sections. Nodules that are well circumscribed, less than 2 cm in diameter, and overtly calcified, or that have a representative CT number of over 150 H (approximately 70 mg/ml of calcium), are followed with the presumption that they are benign. The nodules measuring between 150 and 200 H should be given special attention.

REFERENCES

1. O'Keefe ME, Good CA, McDonald JR. Calcification in solitary nodules of the lung. *AJR* **1957**;77:1023–1033
2. Muhm JR, Brown LR, Crowe JK. Use of computed tomography in the detection of pulmonary nodules. *May Clin Proc* **1977**;52:345–348
3. Siegelman SS, Zerhouni EA, Leo FP, Khouri NF, Stitik FP. CT of solitary pulmonary nodule. *AJR* **1980**;135:1–13
4. Freundlich IM, Horsley WW, Udall C. Evaluation of pulmonary masses by CT number: a modification of the Siegelman method. Presented at the annual meeting of the Radiological Society of North America, Chicago, IL, November **1981**
5. Godwin JD, Speckman JM, Fram EK, et al. Distinguishing benign from malignant pulmonary nodules by computed tomography. *Radiology* **1982**;144:349–351
6. Levi C, Gray JE, McCullough EC, Hattery RR. The unreliability of CT numbers as absolute values. *AJR* **1982**;139:443–447
7. McCullough EC, Morin RL. CT-number variability in thoracic geometry. *AJR* **1983**;141:135–140
8. Zerhouni EA, Spivey JF, Morgan RH, Leo FP, Stitik FP, Siegelman SS.

Factors influencing quantitative CT measurements of solitary pulmonary nodules. *J Comput Assist Tomogr* **1982**;6:1075–1087
9. Godwin JD, Fram EK, Cann CE, Gamsu G. CT densitometry of pulmonary nodules: a phantom study. *J Comput Assist Tomogr* **1982**;6:254–258
10. de Geer G, Gamsu G, Cann C, Webb WR. Evaluation of a chest phantom for CT nodule densitometry. *AJR* **1986**;147:21–25
11. Littleton JT, Brogdon BG, Durizch ML, Callahan WP. Human chest phantom. *Radiology* **1982**;145:829–831
12. Niklason LT, Hickey NM, Chakraborty DP, et al. Simulated pulmonary nodules: detection with dual-energy digital versus conventional radiography. *Radiology* **1986**;160:589–593
13. Siegelman SS, Stitik FP, Summer WR. *Management of the patient with a localized pulmonary lesion.* New York: Grune & Stratton, **1979**:339–358
14. Zerhouni EA, Stitik FP, Siegelman SS, et al. CT of the pulmonary nodule: a cooperative study. *Radiology* **1986**;160:319–327
15. Proto AV, Thomas SR. Pulmonary nodules studied by computed tomography. *Radiology* **1985**;156:149–153
16. Zerhouni EA, Boukadoum M, Siddiky MA, et al. A standard phantom for quantitative CT analysis of pulmonary nodules. *Radiology* **1983**;149:767–773
17. Cann CE, Gamsu G, Birnberg FA, Webb WR. Quantification of calcium in solitary pulmonary nodules using single- and dual-energy CT. *Radiology* **1982**;145:493–496
18. Meredith WJ, Massey JB. *Fundamental physics of radiology,* 2nd ed. Baltimore: Williams & Wilkins, **1972**:76–77
19. Joseph PM, Hilal SK, Schulz RA, Kelcz F. Clinical and experimental investigation of a smoothed CT reconstruction algorithm. *Radiology* **1980**;134:507–516
20. Brooks RA, DiChiro G. Theory of image reconstruction in computed tomography. *Radiology* **1975**;117:561–572
21. Bracewell RN. *The Fourier transform and its application.* New York: McGraw-Hill, **1978**:210–211
22. Rao SP, Alfidi RJ. The environmental density artifact: a beam hardening effect in computed tomography. *Radiology* **1981**;141:223–227
23. Cann CE. Quantitative CT applications: comparison of current scanners. *Radiology* **1987**;162:257–261

Obstructive Sleep Apnea Syndrome: Preoperative Radiologic Evaluation

Todd Hegstrom[1,2]
Lawrence L. Emmons[1]
Eric Hoddes[3]
Timothy Kennedy[3]
Kent Christopher[3]
Timothy Collins[3]
Bryan Spofford[3]

The purpose of this study was to determine whether lateral radiographs of the pharynx and fluoroscopy of the lateral pharynx in the sleeping patient could be used as predictors of surgical success in patients undergoing soft-palate surgery for obstructive sleep apnea. A total of 12 patients had surgery after radiologic evaluation. There were six surgical successes and six failures. No successes occurred in patients with a soft-palate length of less than 46 mm, nor were there any successes among patients whose initial point of obstruction on fluoroscopy was inferior to the level of the soft palate. There was one surgical failure among patients in whom fluoroscopy showed upper airway obstruction beginning at the level of the soft palate during sleep.

Results suggest that a patient is most likely to benefit from soft-palate resection if the soft palate is long—we conservatively suggest greater than 40 mm—and if sleep fluoroscopy of the lateral pharynx shows airway obstruction beginning at the level of the soft palate.

In obstructive sleep apnea, the patient experiences a mechanical airway obstruction caused by partial or total collapse of upper airway structures during sleep [1]. Obstructive sleep apnea can result in pulmonary hypertension, cor pulmonale, and sudden death. Palatopharyngoplasty, which involves a partial resection of pharyngeal and palatal soft tissue, is the most commonly used surgical treatment for obstructive sleep apnea [2, 3].

Unscreened patients with obstructive sleep apnea show measurable improvement after palatopharyngoplasty in approximately 50% of cases [4]. Radiographic and fluoroscopic imaging techniques have been used in an attempt to predict which patients are most likely to benefit from surgical intervention [5–7]. CT has been used to show airway narrowing [8, 9], but correlation with surgical results has not been reported.

This study was conducted to determine whether preoperative lateral radiographs of the pharynx and fluoroscopy of the lateral pharynx in the sleeping patient (somnofluoroscopy) could be used together to predict which patients are most likely to have a successful outcome after palatopharyngoplasty.

Materials and Methods

Twelve patients who had documented obstructive sleep apnea and who subsequently underwent palatopharyngoplasty were evaluated. The diagnosis of obstructive sleep apnea syndrome was made after all-night polysomnography in which respiration, nasal and oral airflow, and oxyhemoglobin saturation were measured while the patient was sleeping. Apnea and hypopnea were defined as complete or partial cessation of airflow at the nose and mouth lasting more than 10 sec. A diagnosis of obstructive sleep apnea was made if the patient exhibited clinical symptoms (e.g., snoring and excessive daytime sleepiness) and had more than five episodes of obstructive apnea or hypopnea per hour of sleep.

Lateral radiographs of the pharynx and fluoroscopy of the pharynx during sleep were attempted in all 12 patients. The radiographs were performed according to standardized

Received June 26, 1987; accepted after revision September 16, 1987.

[1] Department of Radiology, AMI/Presbyterian Denver Medical Center, 1719 E. 19th Ave., Denver, CO 80218. Address reprint requests to L. L. Emmons.

[2] Present address: Diagnostic Radiology Associates, Methodist Hospital, 3615 19th St., Lubbock, TX 79408.

[3] Institute of Transtracheal Oxygen Therapy, AMI/Denver Presbyterian Medical Center, 1719 E. 19th Ave., Denver, CO 80219.

AJR 150:67–69, January 1988
0361–803X/88/1501–0067
© American Roentgen Ray Society

techniques described by Riley and others [5, 6]. The radiographs were obtained in the left lateral position with a film-tube distance of 60 in. (150 cm) and with the patient seated. In some cases, the patient was given a swallow of barium before the radiograph to better define the margins of the soft palate. The soft-palate length was the only measurement made in this study; it was measured in millimeters from the most posterior aspect of the hard palate (the posterior nasal spine) to the tip of the soft palate (Fig. 1).

A portable C-arm fluoroscopic unit was used to perform somnofluoroscopy. Patients were placed in the supine position on a padded fluoroscopic table, and the fluoroscopic unit was positioned so that the field of view included the most posterior aspect of the hard palate, the soft palate in its entirety, and the hyoid bone. This field of view was obtainable in all patients. A videocassette recorder was used to record fluoroscopy. All of the somnofluoroscopic studies were scheduled for late afternoon to increase the likelihood that the patient would be able to fall asleep.

After the patient was positioned, the room lights were dimmed and the patient was allowed to fall asleep. The procedure was monitored by a radiologic technologist who summoned the radiologist at the onset of sleep, noisy breathing, or snoring. No sedatives were used to help induce sleep. Nine of the 12 patients were able to sleep during the examination despite the novel surroundings and the need to remain supine throughout the study. By listening to the sounds of the patient's respiration, the radiologist could time the fluoroscopy to coincide with periods of apnea. Fluoroscopy time was held to under 5 min in all cases and most typically to less than 3 min.

A radiologist documented the level of obstruction seen on the videotape of the somnofluoroscopy and classified it into one of three categories (Fig. 2): obstruction at the soft-palate level only (type 1); obstruction at the level of the soft palate initially, followed by closure of the more distal airway (type 2); or airway collapse distal to the soft palate or simultaneous total airway closure (type 3).

The patients in the study were tested again with all-night polysomnography after surgery. Patients were considered a surgical success if the number of apneas plus hypopneas per hour of sleep was reduced by 50% or more as compared with their initial sleep study, or if the total number of apneas plus hypopneas fell to within normal limits (i.e., five or less per hour of sleep).

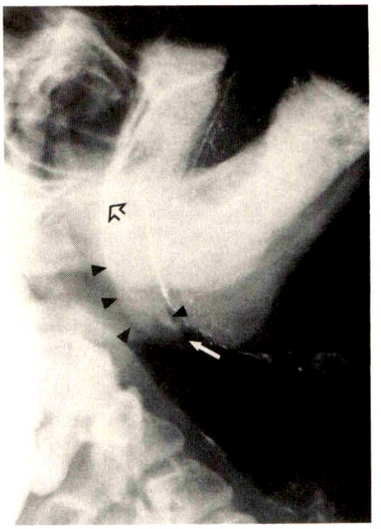

Fig. 1.—Lateral radiograph of pharynx shows measurement of soft-palate length. *Open arrow* indicates posterior tip of hard palate. *White arrow* indicates tip of soft palate. *Arrowheads* outline margins of soft palate.

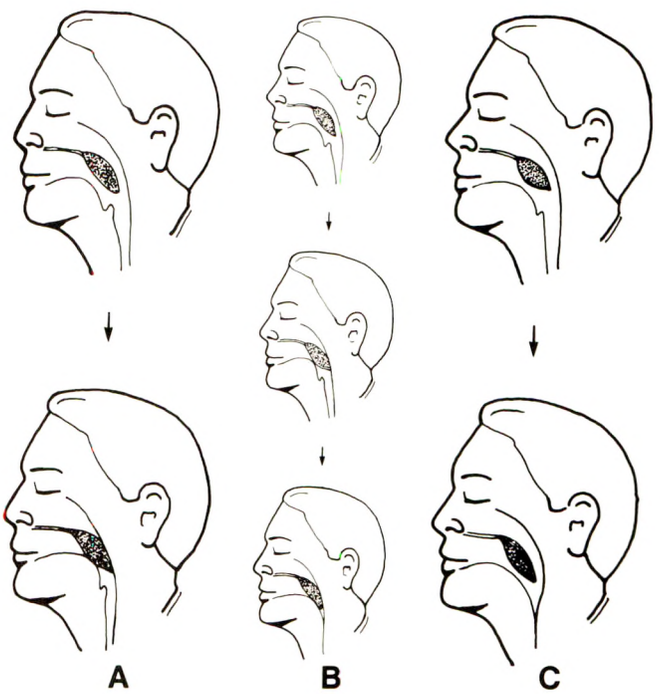

Fig. 2.—*A*, Type-1 airway obstruction. Obstruction occurs at level of soft palate only during somnofluoroscopy.
***B*, Type-2 airway obstruction. Obstruction occurs initially at level of soft palate followed by closure of more distal airway.**
***C*, Type-3 airway obstruction. Obstruction initially occurs distal to soft palate. Airway at soft palate level may close or remain open.**

Results

A total of 12 patients with documented obstructive sleep apnea underwent palatopharyngoplasty and follow-up sleep evaluations. Six of these 12 patients were surgical failures and showed little or no improvement in the numbers of nocturnal apneas and hypopneas. Six patients were surgical successes.

There were no successes in patients with a soft-palate length of less than 46 mm, and there were no successes in patients with a type-3 obstruction on somnofluoroscopy. All six successes had soft palates measuring 46 mm or more in length and a type-1 or type-2 obstruction. One patient who had a soft palate measuring 50 mm in length and a type-1 obstruction on somnofluoroscopy was a surgical failure.

Because of scheduling restrictions, only one attempt was made at somnofluoroscopy. Three patients were unable to fall asleep during the examination. One of these three patients had a soft-palate length of 66 mm and was a surgical success. The two other patients had palate lengths of 34 and 36 mm, respectively, and were surgical failures. These patients have been included in this report because they underwent the basic screening test of soft-palate length measurement.

Discussion

Palatopharyngoplasty results in objective improvement in approximately 50% of patients with documented obstructive

sleep apnea who otherwise have not been screened [4]. The purpose of this retrospective study was to evaluate a method of preoperative screening by using two easily observed variables: soft-palate length and site of initial airway obstruction.

Riley et al. [5] have analyzed the lateral radiograph of the pharynx in patients with obstructive sleep apnea. In one publication, they compared measurements of the soft-palate length, the width of the posterior airway space (posterior pharynx to base of tongue), and the position of the hyoid bone in patients with obstructive sleep apnea and in control subjects. They found that among patients without clinically evident mandibular abnormality, the soft-palate length was significantly longer in obstructive sleep apnea patients than in control subjects (mean, 47 vs 37 mm). The width of the posterior airway space was similar in both obstructive sleep apnea patients and control subjects. The position of the hyoid bone with respect to the mandible was considered to be normal in half of the patients and lower than normal in the other half. No correlation between soft-palate length and surgical success was available.

In a subsequent study, Riley and coworkers [6] described six patients who underwent palatopharyngoplasty for obstructive sleep apnea, four of whom did not improve after surgery. In these four patients, the hyoid bone was abnormally low, suggesting an anatomic abnormality at the base of the tongue, leading to airway obstruction inferior to the level of the soft palate and possibly independent of the soft tissues that would be removed at palatopharyngoplasty. No mention was made of soft-palate length in this study.

The studies by Riley and coworkers [5, 6] suggest that a long soft palate is associated with obstructive sleep apnea and that palatopharyngoplasty failure may be related to closure of the airway inferior to the level of the soft palate in some patients.

Katsantonis and Walsh [7] evaluated the use of fluoroscopy of the lateral pharynx during sleep for selecting candidates for palatopharyngoplasty. They studied 26 consecutive patients with documented obstructive sleep apnea who underwent palatopharyngoplasty. They characterized the level of initial and final obstruction as being either above or below a line drawn through the middle of the C2 vertebral body. Patients with an initial point of obstruction above this line had good surgical results in 10 (67%) of 15 cases. Only one of 11 patients with initial obstruction below C2 improved with surgery. Whether or not the airway collapsed distally after initial obstruction above C2 was found not to be significant.

Airway obstruction generally occurs over a broad area, and determination of the exact point of initial airway obstruction with respect to C2 is often uncertain and variable for a given patient. The location of initial obstruction with respect to the soft palate is much easier to observe and is more consistent. It also seems less artificial, since the surgical resection includes the soft palate. Therefore, this is the landmark that we chose to use.

On the basis of our early findings, we would propose that the initial radiologic screening procedure in patients with obstructive sleep apnea should be a lateral radiograph of the pharynx. We would conservatively suggest that patients having soft palates of 40 mm or less in length are not likely to benefit from palate surgery. This value was chosen because of the small population studied, the variability in the measurement process, and the necessity to be conservative until more data are available. If the soft palate is longer than 40 mm, somnofluoroscopy should be performed to evaluate the location of the obstructive process. Patients with type-1 or type-2 obstructions are likely to benefit from palatoplasty, whereas those with type-3 obstructions are unlikely to improve. The decision to proceed with surgery should be based on soft-palate length alone if somnofluoroscopy is not successful.

This study involved a small number of patients, and the findings obviously represent a preliminary correlation of surgical and radiologic results. Although further study is necessary, we believe that the probability for successful palatopharyngoplasty procedures for obstructive sleep apnea would improve with the radiologic approach that we describe.

REFERENCES

1. Strohl KP, Cherniack NS, Gothe B. Physiologic basis of therapy for sleep apnea. *Am Rev Respir Dis* **1986**;134:791–802
2. Fujita S, Conway W, Zorick F, Roth T. Surgical correction of anatomic abnormalities in obstructive sleep apnea syndrome: uvulopalatopharyngoplasty. *Otolaryngol Head Neck Surg* **1981**;89:923–934
3. Kimmelman CP, Levine SB, Shore ET, Millman RP. Uvulopalatopharyngoplasty: a comparison of two techniques. *Laryngoscope* **1985**;95:1488–1490
4. Simmons FB, Guilleminault C, Miles LE. The palatopharyngoplasty operation for snoring and sleep apnea: an interim report. *Otolaryngol Head Neck Surg* **1984**;92:375–380
5. Riley R, Guilleminault C, Herran J, Powell N. Cephalometric analysis and flow-volume loops in obstructive sleep apnea patients. *Sleep* **1983**;6:303–311
6. Guilleminault C, Riley R, Powell N. Obstructive sleep apnea and abnormal cephalometric measurements: implications for treatment. *Chest* **1984**;86:793–794
7. Katsantonis GP, Walsh JK. Somnofluoroscopy: its role in the selection of candidates for uvulopalatopharyngoplasty. *Otolaryngol Head Neck Surg* **1986**;94:56–60
8. Ell SR, Jolles H, Galvin JR. Cine CT demonstration of nonfixed upper airway obstruction. *AJR* **1986**;146:669–677
9. Suratt PM, Dee P, Atkinson RL, Armstrong P, Wilhoit SC. Fluoroscopic and computed tomographic features of pharyngeal airway in obstructive sleep apnea. *Am Rev Respir Dis* **1983**;127:487–492

Chest Imaging Update

American Roentgen Ray Society Annual Meeting Friday Symposium

May 13, 1988, San Francisco Hilton and Tower, San Francisco, CA

Computed Tomography	Moderator: Stewart Sagel
8:00 a.m.	Overview (*Sagel*)
8:10 a.m.	Focal lung disease (*Zerhouni*)
8:35 a.m.	Diffuse lung disease (*Müller*)
9:00 a.m.	Staging of bronchogenic carcinoma (*Pugatch*)
Interventional Radiography	
9:25 a.m.	Intrathoracic drainage procedures (*Westcott*)
9:45 a.m.	Percutaneous biopsy of central lesions (*Weisbrod*)
10:05 a.m.	Coffee break
Digital Imaging	Moderator: Carl Ravin
10:25 a.m.	Overview (*Ravin*)
10:35 a.m.	Digital angiography (*Barth*)
10:55 a.m.	Digital radiography (*MacMahon*)
Magnetic Resonance Imaging	Moderator: Gordon Gamsu
11:15 a.m.	Overview (*Gamsu*)
11:25 a.m.	Intrathoracic vascular lesions (*Webb*)
11:50 a.m.	Applications of MRI of the thorax (*McLoud*)

Postbiopsy Pneumothorax: Estimating the Risk by Chest Radiography and Pulmonary Function Tests

George D. Fish[1]
John H. Stanley[1, 2]
K. Scott Miller[3]
Stephen I. Schabel[1]
Susan E. Sutherland[4]

Pulmonary function tests and chest radiographs of 160 patients who had had percutaneous needle biopsy of lung lesions were reviewed to determine the value of these examinations in estimating the risk of postbiopsy pneumothorax. Chest radiographs were evaluated subjectively for changes of obstructive and restrictive airway disease and for size and depth of lesion. Pulmonary function tests, consisting of simple spirometry (forced vital capacity, percentage of predicted forced vital capacity, forced expiratory volume in 1 sec, percentage of predicted forced expiratory volume in 1 sec, and [forced expiratory in 1 sec/forced vital capacity] × 100), and the pulmonologist's interpretation were evaluated. Pneumothorax developed in 46% (31/67) of patients who had obstructive airway disease according to the results of pulmonary function tests and in 42% (34/81) of those who had obstructive airway disease according to changes on chest radiographs, compared with 19% (10/53) and 25% (17/67) of those who had normal pulmonary function tests and chest radiographs, respectively. Pneumothorax developed in 46% (23/50) of patients who had findings of obstructive airway disease on both pulmonary function tests and on chest radiographs, compared with 7% (2/28) of patients who were classified as normal by both criteria. None of the patients who had normal pulmonary function tests required placement of a chest tube, whereas 19% (13/67) of those who had obstructive airway disease required chest tubes. Decreasing size of lesion and increasing depth of lesion were associated with a significant increase in the risk of pneumothorax.

We conclude that the results of chest radiographs and pulmonary function tests are useful parameters for estimating the risk of postbiopsy pneumothorax.

Radiographically guided percutaneous needle biopsy of lung lesions is an accepted, safe, and reliable means of obtaining pulmonary tissue for pathologic examination. Several authors [1–3] have shown greater than 90% accuracy in the diagnosis of malignant disease, and the accuracy of diagnosis of benign disease exceeds 80%.

Significant complications from the procedure are rare, except for the development of pneumothorax, which occurs in 13–40% of cases [1–10]. Previous reports have associated numerous factors with the development of pneumothorax. These included size of biopsy needle, number of needle passes, cooperation of the patient, size and depth of lesion, and age and sex of the patient [1, 4, 5, 9, 10]. In addition, obstructive airway disease (diagnosed by evaluation of chest radiograph) has been associated with a higher rate of pneumothorax [9, 10].

We retrospectively reviewed the pulmonary function tests and chest radiographs of 160 patients who had undergone percutaneous needle biopsy of lung lesions to determine if the results of these procedures could enhance our ability to estimate a patient's risk for the development of pneumothorax after biopsy.

Materials and Methods

The medical records of 458 patients who had had percutaneous lung biopsy at our institution between 1980 and 1985 were reviewed. All patients who had had pulmonary

Received July 13, 1987; accepted after revision September 4, 1987.

[1] Department of Radiology, Medical University of South Carolina, 171 Ashley Ave., Charleston, SC 29425-0720. Address reprint requests to S. I. Schabel.

[2] Present address: Delaney Radiology, 2212 Delaney Ave., Wilmington, NC 28403.

[3] Department of Medicine, Medical University of South Carolina, Charleston, SC 29425.

[4] Department of Biometry, Medical University of South Carolina, Charleston, SC 29425.

AJR 150:71–74, January 1988
0361–803X/88/1501–0071
© American Roentgen Ray Society

function testing within 1 year of their percutaneous needle biopsies were included in the study group. We included those tested more than 1 year before biopsy only if their tests were interpreted to show severe obstructive or severe restrictive airway disease. Patients tested more than 1 year after biopsy were included only if they had normal pulmonary functions. Age was not a criteria for inclusion in the study.

Pulmonary function tests included forced expiratory volume in 1 sec, percentage of predicted forced expiratory volume in 1 sec, forced vital capacity, percentage of predicted forced vital capacity, and (forced expiratory volume in 1 sec/forced vital capacity) × 100. The results were reviewed and interpreted by using established criteria: Obstructive disease was defined as either forced expiratory volume in 1 sec or forced vital capacity less than 70% of predicted, with forced expiratory volume in 1 sec/forced vital capacity less than 70%. Restrictive disease was defined as forced vital capacity less than 70% of predicted, with forced expiratory volume in 1 sec/forced vital capacity greater than 70%. Findings were considered normal if all parameters were ≥70% of predicted values.

Posteroanterior and left lateral chest radiographs made within 1 week before percutaneous needle biopsy were reviewed independently by three radiologists who had no knowledge of the results of pulmonary function tests or of which patients had sustained a pneumothorax. Patients were placed into one of three groups according to the following subjective criteria: (1) obstructive lung disease, defined as evidence of hyperinflation (i.e., increased retrosternal air space, flattened hemidiaphragms and paucity of vascular markings) or bullae; (2) restrictive disease, defined as decreased lung volume with increased interstitial markings; and (3) normal, defined as no evidence of obstructive or restrictive airway disease. Classification depended on agreement of two of three radiologists.

Size and depth of lesion from the chest wall and number of needle passes were recorded also. Frontal expiratory chest radiographs obtained immediately after biopsy and all chest radiographs obtained over the next 48 hr after biopsy were reviewed for the presence of pneumothorax.

Biopsies were performed and supervised by a staff radiologist and by numerous residents in radiology who had variable levels of experience. A 22-gauge Chiba needle was used as previously described [2].

Results

The study group included 129 men and 31 women (age range, 21–84 years; mean, 61). One hundred five patients had uncomplicated biopsies, whereas pneumothorax developed in 55 (34%). Of those with pneumothorax, 17 (11% of total population) required placement of a chest tube because of progressive shortness of breath and/or enlarging pneumothorax. All pneumothoraces resolved without further complication.

Size of lesion ranged from 0.6 to 12 cm (average, 3.1 cm); lesions were slightly smaller in patients who had pneumothorax ($p < .05$). Depth ranged from 1 to 10 cm; lesions were significantly deeper in patients who had pneumothorax ($p < .01$) (Table 1).

No significant differences were found between groups for age, sex, or the number of needle passes (Tables 1 and 2).

Decreased forced expiratory volume in 1 sec and (forced expiratory volume in 1 sec/forced vital capacity) × 100 were associated with an increased frequency of pneumothorax,

TABLE 1: Risk Factors for Pneumothorax

Parameter	No Pneumothorax	Pneumothorax	*p* Value
Lesion depth (cm)	3.3 ± 0.23	4.3 ± 0.34	.01
Lesion size (cm)	3.4 ± 0.20	2.7 ± 0.20	.05
Number of needle passes	1.7 ± 0.07	1.6 ± 0.10	NS
Age (years)	60.2 ± 1.02	62.2 ± 1.38	NS
Men (%)	80	82	NS
FEV_1 (l/sec)	2.2 ± 0.08	1.8 ± 0.10	.01
FVC (l)	3.1 ± 0.09	2.9 ± 0.14	NS
$FEV_1/FVC \times 100$	71.3 ± 1.21	64.3 ± 1.97	.001

Note.—*p* values are from analysis of variance. All values are means ± standard errors. NS = not significant; FEV_1 = forced expiratory volume in 1 sec; FVC = forced vital capacity; FEV_1/FVC = forced expiratory volume in 1 sec/forced vital capacity.

TABLE 2: Number of Patients Requiring One, Two, or Three Needle Passes

Number of Needle Passes	Number of Patients Without Pneumothorax (%)	Number of Patients with Pneumothorax (%)
1	46 (44)	28 (51)
2	51 (49)	23 (42)
3	8 (8)	4 (7)

Note.—$\chi^2 = 0.755$; $p = .6856$.

whereas forced vital capacity was not a significant predictor (Table 1). Fifty-two of 67 patients who had obstructive airway disease as shown by pulmonary function tests were classified correctly by findings on chest radiographs. Twenty-nine diagnoses of obstructive airway disease that were based on chest radiographs were false-positive. Use of chest radiographs to assess patients for the presence of obstructive airway disease was not significantly associated with the frequency of pneumothorax (Table 3).

Patients who had obstructive airway disease according to the results of pulmonary function tests experienced a twofold increase in the frequency of pneumothorax (46%) vs those whose results were normal (19%) (Table 3). Patients who had restrictive airway disease were at increased risk as well (35%). However, the number of patients who had restrictive airway disease according to findings on radiographs alone or findings on both radiographs and pulmonary function tests was too small for meaningful analysis (Table 3). When the radiologist and pulmonologist agreed in their interpretations, the trend was striking. Pneumothorax developed in only 7% (2/28) of normal subjects vs 46% (23/50) of patients who had obstructive airway disease. No significant difference was noted between these two populations with respect to the number of needle passes or size or depth of lesion (Table 4).

Thirteen of those who had obstructive airway disease (by pulmonary function tests) and pneumothorax required placement of a chest tube, as did three of those who had restrictive

TABLE 3: Frequency of Pneumothorax According to Results of Chest Radiographs and Pulmonary Function Tests

Procedure	Interpretation			*p* Value
	Percent Normal	Percent Obstructive Airway Disease	Percent Restrictive Airway Disease	
Chest radiograph	25 (17/67)	42 (34/81)	33 (4/12)	NS
Pulmonary function tests	19 (10/53)	46 (31/67)	35 (14/40)	.01
Both	7 (2/28)	46 (23/50)	40 (2/5)	.001

Note.—*p* values are from chi-square analysis. "Both" indicates that interpretation of the chest radiograph and pulmonary function tests were identical. Numbers in parentheses indicate number of patients in whom pneumothorax developed divided by number of patients in that diagnostic category.

TABLE 4: Number of Needle Passes and Depth and Size of Lesion in Patients With or Without Obstructive Airway Disease as Shown by Both Chest Radiographs and Pulmonary Function Tests

Parameter	Findings	
	Normal	Obstructive Airway Disease
Number of needle passes	1.8 ± 0.14	1.7 ± 0.10
Depth of lesion (cm)	3.1 ± 0.44	3.7 ± 0.37
Size of lesion (cm)	3.3 ± 0.32	3.1 ± 0.28

Note.—All values are means ± standard error. Analysis of variance showed no significant differences between normal findings and findings of obstructive airway disease for any of these three parameters.

disease. Only one patient with normal pulmonary function tests required a chest tube, and he had obvious bullae on chest radiograph.

Discussion

One of the many variables thought to predispose a patient to postbiopsy pneumothorax is the presence of obstructive airway disease. Poe et al. [10] showed this association by using lung volumes determined from chest radiographs by the method of Barnhard et al. [11]. They found a twofold increase in the prevalence of pneumothorax in patients who had more than 120% predicted total lung capacity. Sinner's series [9] of more than 2000 patients showed a near threefold increase in pneumothorax among patients thought to have moderate to marked chronic obstructive pulmonary disease on the basis of chest radiographs alone.

Our results indicate that the results of pulmonary function tests aid in assessing a patient's risk for postbiopsy pneumothorax. We now advise patients who have obstructive lung disease (by pulmonary function tests) that they have a greater than 45% chance of developing pneumothorax, with a 20% chance of requiring a chest tube [12]. Patients with normal pulmonary function tests are told that they have a 20% risk of pneumothorax, with little likelihood of requiring placement of a chest tube unless chest radiographs show bullae.

As previously shown, smaller, deeper lesions increase the risk of pneumothorax [9]. Such lesions are more difficult to biopsy and thus require greater cooperation by the patient. In addition, deep lesions may require crossing more than one pleural surface. The lack of association between the number of needle passes and the risk of pneumothorax is difficult to explain. Poe et al. [10] showed similar results, whereas others [4, 5, 9] have shown a clear correlation.

A poor correlation between interpretations of chest radiographs and frequency of pneumothorax likely reflects our subjective approach to assessment for obstructive airway disease. We chose this approach because of its simplicity and because it is likely the approach used in daily practice by most radiologists. When pulmonary function tests are used as the gold standard, our sensitivity (70%) compares favorably with results obtained by using more objective criteria [13]. However, our false-positive rate (36%) was high, which indicates the inaccuracy of interpretations of routine chest radiographs for assessing obstructive airway disease as compared with previously described objective criteria [10, 13].

Our study group included 35% of the total number of patients who had had percutaneous lung biopsies at our institution between 1980 and 1985. Obviously, only those who had had pulmonary function tests could be included. Most patients who undergo pulmonary function testing do so because of clinical suspicion of airway disease or as a preoperative evaluation before pulmonary resection. Consequently, most of those excluded in our study probably were considered clinically normal, and, in fact, the pneumothorax rate for the patients not included was 26%. If these patients had undergone pulmonary function tests, they most likely would have been part of our "normal" group.

Pulmonary function tests (i.e., simple spirometry) are useful in assessment of the risk of pneumothorax due to percutaneous needle biopsy of lung lesions. We do not propose that they be obtained to determined which patients should or should not undergo needle biopsy. Rather, the results of these tests can help us to inform our patients better and be better prepared ourselves for handling a potential pneumothorax. The decision as to whether a patient should undergo needle biopsy should not depend on the risk for developing pneumothorax but instead on the clinical assessment of whether the patient can withstand one if it does occur. The increased risk (greater than twofold in patients with obstructive airway disease) does not preclude percutaneous needle biopsy. Most pneumothoraces resolve spontaneously, and the remainder are easily treated with small-bore chest tubes. Patients who have both normal pulmonary function tests and normal chest radiographs can be reassured that they are at low risk for pneumothorax and probably will not require a chest tube.

REFERENCES

1. Khouri NF, Stitik FP, Erozan YS, et al. Transthoracic needle aspiration biopsy of benign and malignant lung lesions. *AJR* **1985**;144:281–288
2. Stanley JH, Fish GD, Andriole JG, et al. Lung lesions: cytologic diagnosis

by fine needle biopsy. *Radiology* **1987**;162:389–391
3. Westcott JL. Direct percutaneous needle aspiration of localized pulmonary lesions: results in 422 patients. *Radiology* **1980**;137:31–35
4. Johnsrude IS, Silverman JF, Weaver MD, McConnell RW. Rapid cytology to decrease pneumothorax incidence after percutaneous biopsy. *AJR* **1985**;144:793–794
5. Stevens JM, Jackman RJ. Outpatient needle biopsy of the lung: its safety and utility. *Radiology* **1984**;151:301–304
6. Jereb M. The usefulness of needle biopsy in chest lesions of different sizes and locations. *Radiology* **1980**;134:13–15
7. Herman PF, Hessel SJ. The diagnostic accuracy and complications of closed lung biopsies. *Radiology* **1977**;125:11–14
8. Lalli AF, McCormack LJ, Zelch M, Reich NE, Belovich D. Aspiration biopsies of chest lesions. *Radiology* **1978**;127:35–40
9. Sinner WN. Complications of percutaneous transthoracic needle aspiration biopsy. *Acta Radiol [Diagn]* (Berl) **1976**;17:813–828
10. Poe RH, Kallay MC, Wicks CM, Odoroff CL. Predicting risk of pneumothorax in needle biopsy of the lung. *Chest* **1984**;85:232–235
11. Barnhard HJ, Pierce JA, Joyce JW, Bates JH. Roentgenographic determination of total lung capacity. *Am J Med* **1960**;28:51–60
12. Perlmutt LM, Braun SD, Newman GE, et al. Transthoracic needle aspiration: use of a small chest tube to treat pneumothorax. *AJR* **1987**;148:849–851
13. Reich SB, Weinshelbaum A, Yee J. Correlation of radiographic measurements and pulmonary function tests in chronic obstructive airway disease. *AJR* **1985**;144:695–699

Now Available
(Limited Quantities)

1987 American Roentgen Ray Society Categorical Course Syllabus
Gastrointestinal Radiology
Editor: Gary G. Ghahremani, M.D.

Contains 161 pages of textbook-quality information and illustrations reviewing recent advances and current concepts in gastrointestinal radiology. Written by leading authorities in the field.

Send $25 per copy, along with name and address, to:

American College of Radiology
Publications Division
P.O. Box 2348
Merrifield, VA 22116-2348

(Price includes shipping/handling charges at book rate. Indicate if first-class delivery requested and add $5 per copy.)

Mediastinal Cysts: Diagnosis by CT and Needle Aspiration

Janet E. Kuhlman[1]
Elliot K. Fishman[1]
Ko Pen Wang[2]
Elias A. Zerhouni[1]
Stanley S. Siegelman[1]

Five patients with bronchogenic or enteric cysts were diagnosed by using a combination of CT and transbronchial or transesophageal needle aspiration. Serous or mucoid fluid was successfully aspirated in each case. Cultures of the fluid were negative for pathogens, and cytologic examinations showed no malignancy. Mediastinoscopy and thoracotomy were avoided in all patients, including one symptomatic patient whose symptoms resolved after needle aspiration.

CT with transbronchial or transesophageal needle aspiration represents a practical alternative to surgery in the evaluation of congenital mediastinal cysts.

Congenital mediastinal cysts encompass a spectrum of bronchopulmonary malformations that includes bronchogenic cysts, esophageal duplications, and neurenteric cysts. All of these entities probably share a common embryogenesis as a result of anomalous budding from the primitive foregut and early tracheobronchial tree [1].

In the adult, congenital mediastinal cysts represent approximately 10% of all mediastinal masses [2]. Because they are benign, these lesions pose a particular challenge to the radiologist and clinician to diagnose and manage them noninvasively. Mediastinal cysts often are detected incidentally on routine chest radiograph or barium swallow in otherwise asymptomatic individuals [2]. In some cases, symptoms or a change in the appearance of the lesion may suggest malignancy and require a more definite evaluation. Because radiologic evaluation in the past frequently has been inconclusive, many adults with benign mediastinal cysts have required mediastinoscopy or thoracotomy.

Our approach to the suspected mediastinal cyst has changed as a result of the experience gained with five patients diagnosed by using a combination of CT and transbronchial or transesophageal needle aspiration.

Materials and Methods

The study group consisted of five patients ranging in age from 26 to 77 years. Each had been referred for further CT evaluation of a mediastinal mass (one patient was previously described in a case report [3]). Three patients were asymptomatic, but either because of the appearance of the lesion or a change in its size, further evaluation was deemed necessary. Two patients were symptomatic and required definitive diagnosis or treatment. Symptoms requiring further investigation included dysphagia and anorexia (both in one patient [3]) and myasthenia gravis (one patient).

CT scans were obtained with either a Siemens DR-3 scanner (5 sec, 450 mAs, 120 kVp, and 8-mm collimation) or an AS&E scanner (10 sec, 200 mAs, 125 kVp, and 8-mm collimation). A presumptive diagnosis of benign mediastinal cyst was based on the following CT findings: (1) a smooth, oval, or tubular mass with well-defined margins and no evidence of a thick or irregular wall; (2) homogeneous CT attenuation, usually but not invariably in the range of water density (0–20 H); (3) no vascular enhancement; (4) no infiltration of adjacent mediastinal structures; and (5) characteristic location in the paratracheal, carinal, subcarinal, or paraesophageal region.

Received August 3, 1987; accepted after revision September 23, 1987.

[1] The Russell H. Morgan Department of Radiology and Radiological Sciences, The Johns Hopkins Medical Institutions, Baltimore, MD 21205. Address reprint requests to E. K. Fishman, Dept. of Radiology, Johns Hopkins Hospital, 600 N. Wolfe St., Baltimore, MD 21205.

[2] Division of Pulmonary Medicine, The Johns Hopkins Medical Institutions, Baltimore, MD 21205.

AJR 150:75–78, January 1988
0361–803X/88/1501–0078
© American Roentgen Ray Society

On the basis of CT findings suggesting the diagnostic possibility of a bronchogenic or enteric cyst, either a transbronchial or transesophageal needle aspiration is performed for diagnosis. The technique of transbronchial or transesophageal needle aspiration has been described previously [4]. The aspiration equipment includes a commercially available 120-cm, polyethylene sheath with an attached 18- to 22-gauge, 12-mm beveled needle (Mill-Rose Co., Mentor, OH) (Fig. 1). After premedication with intramuscular meperidine and atropine, the patient receives topical anesthesia with 2% xylocaine of the oropharynx and nasopharynx. A flexible bronchoscope or endoscope is introduced to the appropriate level based on the CT findings. Next, the polyethylene sheath with attached needle and inner stylet is passed through the endoscope until the needle tip projects beyond the lumen of the scope. The stylet is retracted, the needle is passed into the lesion, and a syringe is applied to a proximal port for aspiration and drainage. One case required use of a rigid bronchoscope. Aspirated cyst fluid was cultured for pathogens and sent for cytopathologic analysis.

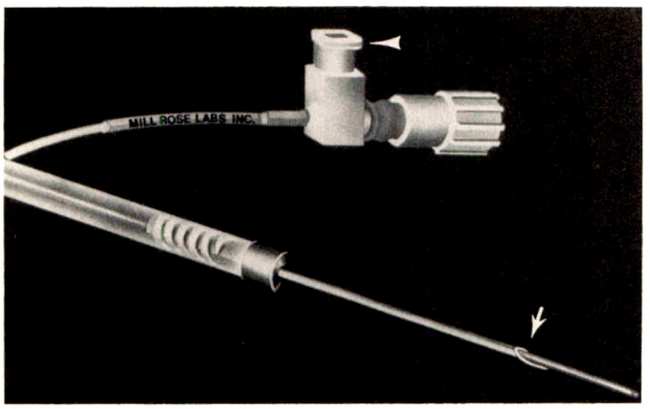

Fig. 1.—Transbronchial needle aspiration. Needle aspiration equipment includes a polyethylene sheath with proximal aspiration side port (*arrowhead*) and attached 18- to 22-gauge needle with inner stylet (*arrow*).

Results

A combination of CT and transbronchial or transesophageal needle aspiration was used to confirm the presence of a cystic mediastinal lesion in all five patients (Figs. 2 and 3). The mediastinal cysts ranged in size from 2.5 × 3 to 3 × 7 cm and were located in the right paratracheal region (two cases), carinal or subcarinal region (two cases), and paraesophageal area (one case). CT attenuations of the lesions ranged from water density to near soft-tissue density. Clear yellow fluid was obtained in four patients, and brown turbid fluid was obtained in one patient. Amounts aspirated ranged from 6 to 70 ml. Cultures of the fluid were negative for pathogens, and cytologic examinations showed no malignant cells. The procedures were tolerated well; no infections or hemorrhagic complications occurred.

Immediate follow-up CT scans (four cases) or chest radiographs (one case) showed a decrease in the size of the mediastinal cyst in each case. The change in the size of the lesion varied with the amount of fluid aspirated. Subsequent serial follow-up CT scans were available in two patients. One patient in whom a large amount of fluid had been drained (Fig. 2) showed no reaccumulation of fluid on repeat CT examinations at 3 and 6 months. A second patient in whom a small amount of fluid had been removed for diagnostic purposes showed a stable lesion with no change in its size from preaspiration CT scans 1½ months later.

Surgery was avoided in three asymptomatic patients. In one symptomatic patient with a mediastinal cyst, the symptoms resolved after needle aspiration; no relapse had occurred 1 year later. One patient with severe myasthenia gravis had a mediastinal cyst diagnosed, excluding the possibility of thymoma or malignancy without resorting to surgery.

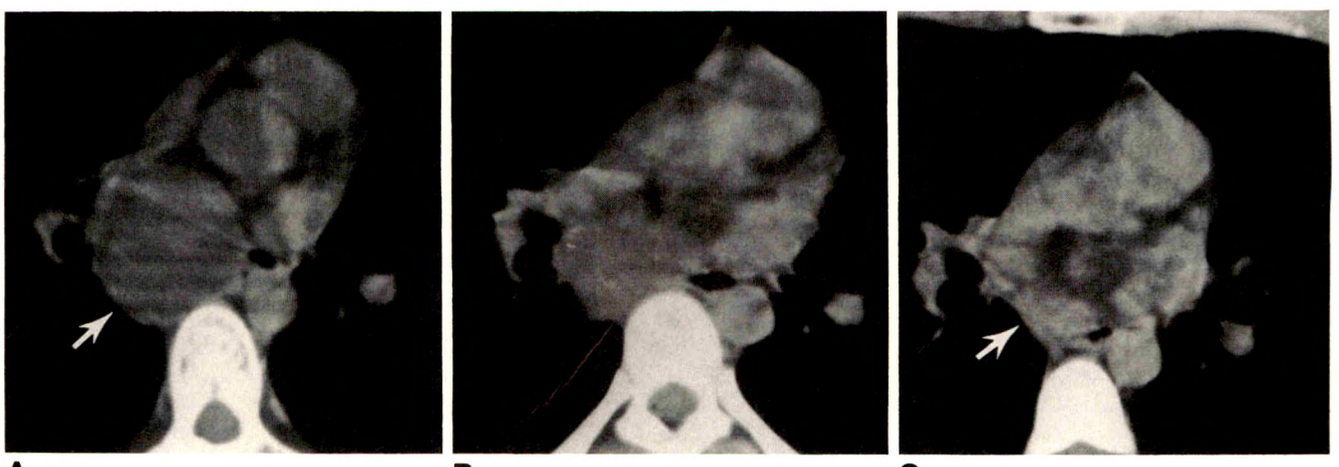

Fig. 2.—26-year-old man with large subcarinal mass.

***A*, CT scans show a 6 × 6 cm fluid-filled cyst (*arrow*) with homogeneous CT attenuation measuring 10–20 H. Mediastinal cyst splays carina and displaces bronchus intermedius laterally.**

***B*, CT scan immediately after transbronchial needle aspiration of 70 ml of fluid. Cyst now measures 3 × 2 cm.**

***C*, Follow-up CT scan 6 months later shows no reaccumulation of fluid but only a soft-tissue remnant (*arrow*).**

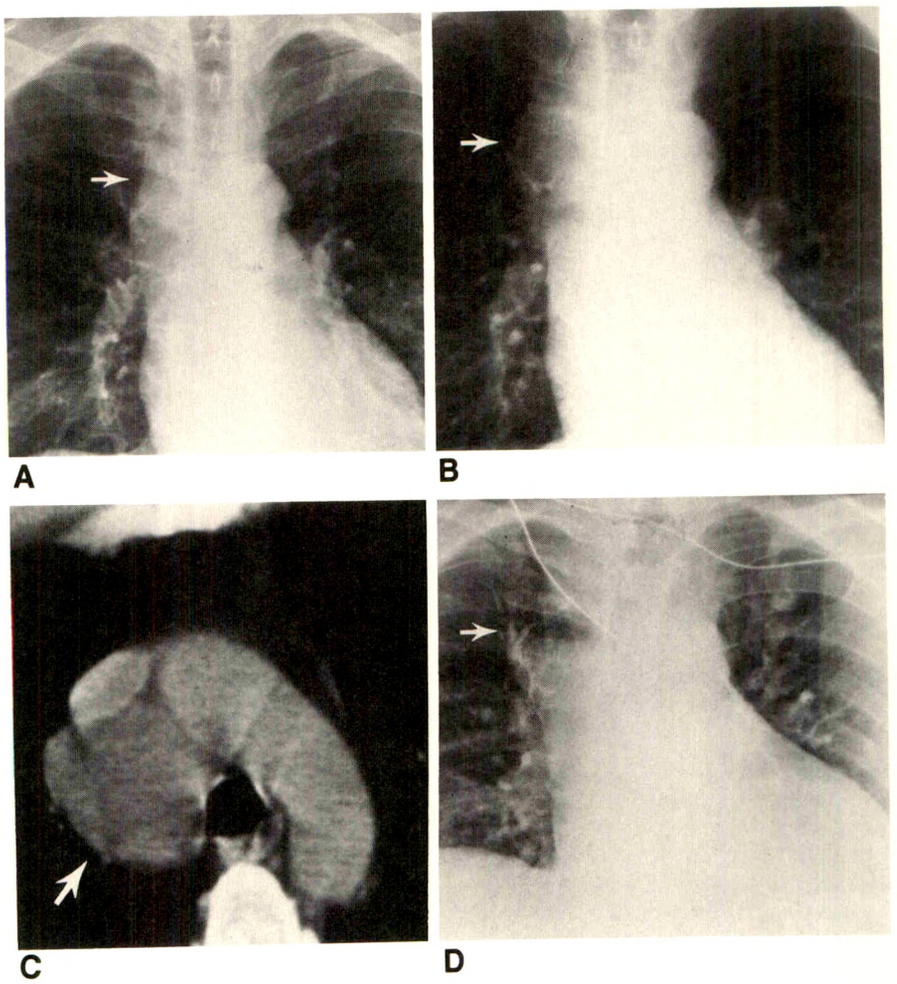

Fig. 3.—Asymptomatic 51-year-old man with enlarging right paratracheal mass.

***A* and *B*, Chest radiographs obtained in 1982 (*A*) and in 1985 (*B*) show that mass (*arrows*) has increased in size.**

***C*, CT scan shows 4 × 5 cm oval, right paratracheal lesion (*arrow*) with homogeneous CT attenuation and a density slightly less than that of soft-tissue. Findings are suggestive of bronchogenic cyst.**

***D*, Follow-up chest radiograph immediately after transbronchial aspiration of 45 ml of fluid shows air-fluid level appearing in cyst (*arrow*).**

Discussion

In the adult, congenital mediastinal cysts often present as asymptomatic mediastinal masses. When signs and symptoms occur, they may include dysphagia, weight loss, anorexia, wheezing, nonproductive cough, or recurrent pneumonitis [2, 5–7], findings often suggestive of underlying malignancy. Mediastinal cysts can also enlarge in size over time [5].

The traditional approach to mediastinal cysts, especially those that have atypical features or that are symptomatic, has been mediastinoscopy or surgical excision for definitive diagnosis [7]. CT with transbronchial or transesophageal needle aspiration represents an alternative, nonsurgical approach to treating these patients. It also can obviate more expensive and invasive mediastinoscopy or thoracotomy, both of which are associated with higher morbidity and require general anesthesia.

Transbronchial needle aspiration in the mediastinum was first used for mediastinal staging of lung cancer; the technique was developed because of a need to reach lymph node groups not readily accessible by mediastinoscopy, notably the subcarinal and retrotracheal areas [4]. Subsequently, the technique has been used to evaluate a variety of mediastinal masses including tumors, abscesses, and now mediastinal cysts. Because of their typical locations in the paratracheal, subcarinal, and paraesophageal regions, mediastinal cysts of congenital origin are ideal candidates for this approach, either transbronchially or transesophageally.

Although mediastinal cysts have been reached percutaneously with transthoracic needles [8], the intimate association of most mediastinal cysts with the tracheobronchial tree and esophagus allows for a shorter approach and needle passage with the endoscopic technique. The distance traversed is smaller and vascular structures are more easily avoided. Mediastinal cysts located deep within the mediastinum near the subcarinal region and around the esophagus are more difficult to reach percutaneously; with the endoscopic approach, they are still relatively accessible.

CT plays an important complementary role in this nonsurgical approach to mediastinal cysts. CT confirms the presence of a mediastinal mass and often can provide a strong presumptive diagnosis of benign mediastinal cyst. If the patient is asymptomatic, and characteristic CT features of a fluid-filled cyst are seen, conservative management with follow-up CT examinations to confirm stability in size is one option.

However, if the patient is symptomatic, if the lesion has changed in size, or if an underlying malignancy is suspected on clinical grounds, further evaluation is usually required. Surgery still may be avoided by combining CT with transbronchial needle aspiration. The absence of malignant cells or pathogens from aspirated fluid, although not providing a definitive pathologic diagnosis of mediastinal cyst, does provide substantiating evidence that there is a benign cystic lesion that can be followed conservatively.

CT documents the nonvascular nature of the lesion, its size, and its anatomic relationship to other mediastinal structures, including the tracheobronchial tree and great vessels, before needle aspiration. By identifying these important relationships, the radiologist can safely guide the endoscopist to the target. CT is also helpful for follow-up, both immediately after the procedure (to document decrease in size of the cyst and to check for potential complications) and for long-term follow-up. Further study will be required to determine whether aspirated mediastinal cysts eventually reaccumulate fluid and whether long-term symptomatic relief can be achieved by using this technique.

Finally, none of our five patients had mediastinal cysts with CT attenuations greater than that of soft-tissue density. High-density mediastinal cysts have been reported with CT coefficients as high as 120 H [9]. It is not known whether the gelatinous or highly mucoid contents of these cysts can be aspirated by using this technique.

REFERENCES

1. Heithoff KB, Shashikant MS, Williams HJ, et al. Bronchopulmonary foregut malformations—a unifying etiological concept. *AJR* **1976**;126:45–55
2. Kirwan WO, Walbaum PR, McCormack RM. Cystic intrathoracic derivatives of the foregut and their complications. *Thorax* **1973**;28:424–428
3. Kuhlman JE, Fishman EK, Siegelman SS, Wang KP. Esophageal duplication cyst: CT diagnosis and transesophageal needle aspiration. *AJR* **1985**;145:531–532
4. Scatarige JC, Wang KP, Siegelman SS. Transbronchial needle aspiration biopsy of the mediastinum. In: Siegelman SS, ed. *Contemporary issues in computed tomography*, Vol. 4. *Computed tomography of the chest*. New York: Churchill Livingstone, **1984**:59–79
5. Whitaker JA, Deffenbaugh LD, Cooke AR. Esophageal duplication cyst. *Am J Gastroenterol* **1980**;73:329–332
6. Hocking M, Yound DC. Duplications of the alimentary tract. *Br J Surg* **1981**;68:92–96
7. Sirivella S, Ford WB, Zikria EA. Foregut cysts of the mediastinum: results in 20 consecutive surgically treated cases. *J Thorac Cardiovasc Surg* **1985**;90:776–782
8. Fitch SJ, Tonkin ID, Tonkin AK. Imaging of foregut duplication cysts. *RadioGraphics* **1986**;6:189–201
9. Mendelson DS, Rose JS, Efremidis SC, Kirschner PA, Cohen BA. Bronchogenic cysts with high CT numbers. *AJR* **1983**;140:463–465

MR Imaging of the Transverse Sinus of the Pericardium

Jung-Gi Im[1,2]
Alan Rosen[3]
W. Richard Webb[1]
Gordon Gamsu[1]

On MR images of the chest, a low-signal-intensity band is often seen between the ascending aorta and left atrium in the transverse plane, and between the right pulmonary artery and left atrium in the coronal and sagittal planes. CT and MR of cadavers, with injection of contrast media into the pericardial space, confirmed that this structure was the transverse sinus of the pericardium. Retrospective review of MR studies in 45 patients without evidence of pericardial disease showed the transverse sinus of the pericardium in 80% (32/40) of transverse ECG-gated images, 78% (7/9) of sagittal ECG-gated images, and 67% (14/21) of coronal ECG-gated images. Nongated studies showed the sinus infrequently.

Knowledge of the three-dimensional anatomy of the transverse sinus of the pericardium and of its typical MR appearance should allow its recognition and preclude misinterpretation.

The transverse sinus of the pericardium lies behind the ascending aorta and main pulmonary artery and extends transversely between the right and left pericardial spaces (Fig. 1) [1–4]. The CT appearance of the transverse sinus has recently been described in patients with pericardial effusions [5]. On MR of subjects without pericardial disease, we have noticed a low-signal-intensity structure in this location, which can mimic an anomalous vessel, left coronary artery, aortic dissection, or enlarged mediastinal lymph nodes. CT and MR in cadavers, before and after introduction of contrast media into the pericardial space, confirmed that this structure is the transverse sinus of the pericardium. We illustrate the MR, multiplanar sectional anatomy of the transverse sinus in cadavers and in patients without pericardial disease.

Materials and Methods

Cadaver Studies

Two fresh unembalmed cadavers were chosen from preliminary CT scans of six cadavers. One cadaver was selected because it had an apparently normal pericardium and the other because of the presence of a pericardial effusion.

A GE 9800 scanner was used for the CT scans, with contiguous slice thicknesses of 10 and 1.5 mm (120 kVp, 120 mA, 3 sec). Coronal and sagittal images were reformatted from the 1.5-mm scan data. Each cadaver was scanned both before and after introduction of a contrast agent into the pericardium. As a CT contrast agent, 200 ml of 3% solution of Angiovist 282 (diatrizoate meglumine) was injected after the CT-guided introduction of a 4.8-French catheter into the preaortic superior pericardial recess.

MR images were obtained with a Diasonics MT/S imaging system operating at 0.35 T with a proton-resonance frequency of 15 mHz. A multislice spin-echo technique was used, with heavy T1 weighting (repetition time [TR] of 0.25 or 0.5 sec, echo time [TE] of 30 msec) and four averages. Pixel size was 1.7 mm. Slice thickness was approximately 7 mm with a 3-mm interslice gap. Transverse, coronal, and sagittal images were obtained both before and after contrast injection. Also, the cadavers were scanned both before and after introduction of 300

Received August 5, 1987; accepted after revision September 25, 1987.

This work was supported in part by a grant from the Seoul National University Hospital.

[1] Department of Radiology, Box 0628, University of California, San Francisco, School of Medicine, San Francisco, CA 94143-0628. Address reprint requests to W. R. Webb.

[2] Present address: Department of Radiology, School of Medicine, Seoul National University, 28 Yeongun-Dong Chongro-Ku, Seoul, 110 Korea.

[3] Department of Anatomy, University of California, San Francisco, School of Medicine, San Francisco, CA 94143-0628.

***AJR* 150:79–84, January 1988**
0361–803X/88/1501–0079
© American Roentgen Ray Society

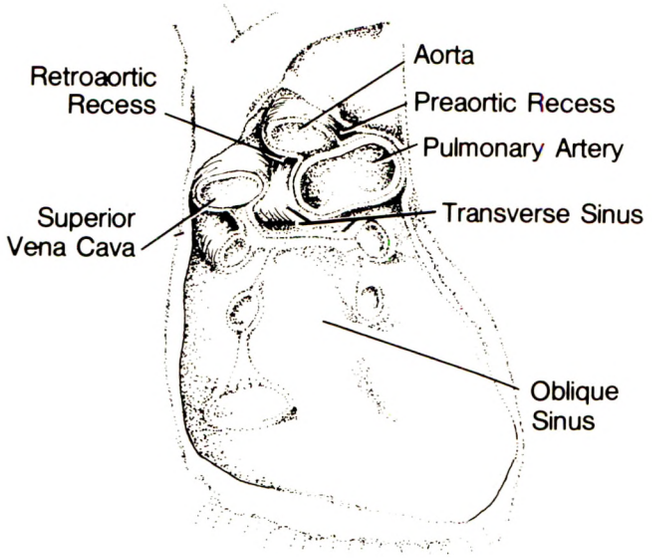

Fig. 1.—Retrocardiac pericardial space, viewed from the front. Transverse sinus, under right pulmonary artery, separates it from left atrium. To the right of midline, transverse sinus extends cephalad, anterior to right pulmonary artery, and behind aorta, to communicate with retroaortic superior pericardial recess and pericardial space anterior to superior vena cava. To the left, transverse sinus passes behind main pulmonary artery and communicates with left pericardial space. (Adapted from Netter [1] and modified from McMurdo et al. [2]. © Copyright 1978. CIBA-GEIGY Corporation. Reproduced with permission from THE CIBA COLLECTION OF MEDICAL ILLUSTRATIONS by Frank H. Netter, MD. All rights reserved.)

ml of water into the pericardium. Before the injection of water, the contrast agent that had been introduced for CT was removed.

Patient Studies

The study group consisted of two normal volunteers and 43 patients who had undergone MR imaging of the chest. Ages ranged from 13 to 76 years (mean, 45 years). None had evidence of a pericardial effusion clinically or on MR images. Forty-two subjects had ECG-gated images, and 16 of these had both gated and nongated images. The remaining three subjects had nongated images only. Slice thickness was 7 mm with a 3-mm interslice gap. On ECG-gated images, the TR was determined by heart rate and ranged from 0.75 to 1.1 sec. First-echo images with a TE value of 30 msec were obtained in 39 subjects. In the remaining six subjects, both first-echo (30 msec) and second-echo (60 msec) images were obtained. During each imaging sequence, five or 10 adjacent slices were acquired with two (27 subjects) or four (18 subjects) averages. Forty-eight studies (42 subjects) were performed in the transverse plane (40 ECG-gated, eight nongated). Nongated transverse studies were done with a TR value of 2.0 sec. Thirteen subjects were imaged in the sagittal plane (nine ECG-gated, four nongated). The nongated sagittal images were obtained with a TR value of 1.0 or 1.5 sec. Thirty-three studies (19 subjects) were performed in the coronal plane (21 ECG gated, 12 nongated). The nongated coronal images were obtained with a TR value of 2.0 sec.

All images were analyzed to determine the presence and appearance of the transverse sinus of the pericardium at various locations and in the different imaging planes.

Results

The transverse sinus connects the right and left pericardial spaces behind the proximal ascending aorta and main pulmonary artery. Although the transverse sinus was not visible in its entirety in any patient, it was seen as such in the cadaver with the pericardial effusion. For descriptive purposes, the sinus will be described sequentially as it appears in the sagittal, transverse, and coronal planes.

Sagittal Plane

The anatomy of the transverse sinus is most easily understood in the sagittal plane. On ECG-gated MR in the sagittal plane, seven of nine patients showed segments of the transverse sinus (Table 1).

In or near the midline, a horizontal or slightly oblique segment of the transverse sinus lies under the right pulmonary artery, separating the artery from the left atrium (Fig. 2A). We called this the infrapulmonary segment of the transverse sinus. Although it was well seen in the cadavers, probably because of some collapse of the adjacent vascular structures, it was rarely visible in the patients studied with MR (Fig. 3).

From the anterior infrapulmonary segment, the transverse sinus extends superiorly and inferiorly, behind the ascending aorta (Figs. 2 and 3); this part of the transverse sinus we named the retroaortic segment. The superior extension of the retroaortic segment separates the aorta from the right pulmonary artery. To the right of the midline, the superior extension of the retroaortic segment communicates with the superior pericardial recess (Fig. 3A) and the right pericardial space. The inferior extension of the retroaortic segment extends anteriorly and inferiorly for 1–2 cm into the triangular space between the ascending aorta and left atrium. This inferior extension is the largest and most frequently seen segment of the transverse sinus when imaged in the sagittal plane.

In or near the midline, an additional extension of the transverse sinus arises from the posterior aspect of the infrapulmonary segment. This extension courses superiorly, posterior to the right pulmonary artery; thus it is named the retropulmonary segment.

To the left of the midline, only the infrapulmonary segment is visible, lying between the main pulmonary artery and left atrium (Figs. 2B and 3C). Depending on the orientation of the pulmonary artery, the infrapulmonary segment is often ori-

TABLE 1: Sensitivity of MR Imaging in Showing Transverse Sinus of Pericardium

Imaging Mode	No. of Sinuses Shown/No. of Studies	Sensitivity (%)
Transverse		
Nongated	4/8	50
ECG-gated	32/40	80
Sagittal		
Nongated	2/4	50
ECG-gated	7/9	78
Coronal		
Nongated	3/12	25
ECG-gated	14/21	67

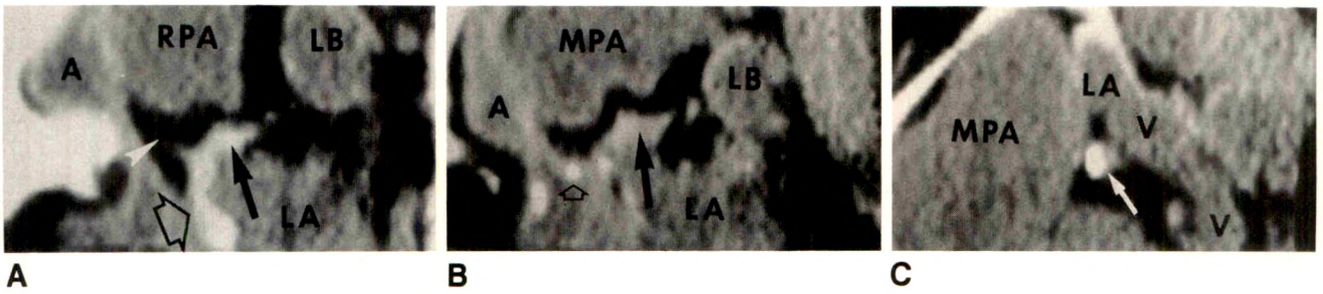

Fig. 2.—Sagittal reformations of thin-section CT in cadaver, after contrast injection into pericardium.

A, Near midline, infrapulmonary segment of transverse sinus (*black arrow*) is located between right pulmonary artery (RPA) and left atrium (LA). Superior (*arrowhead*) and inferior (*open arrow*) extensions of retroaortic segment are also opacified. Inferior extension is largest. Retropulmonary segment is not visible. Aorta (A) is partially collapsed. Left main bronchus (LB) is filled with aspirated material.

B, 2 cm to left of midline. Only infrapulmonary segment (*black arrow*) of transverse sinus is visible, lying between main pulmonary artery (MPA) and left atrium (LA). Note emerging, partially calcified, left coronary artery (*open arrow*). Aorta (A) and left main bronchus (LB) were also identified.

C, 3 cm to left of midline, transverse sinus caps left atrial appendage (LA) and communicates anteriorly with left pericardial space. Atrial appendage separates left coronary artery (*white arrow*) from transverse sinus. Main pulmonary artery (MPA) and pulmonary veins (V) are also shown.

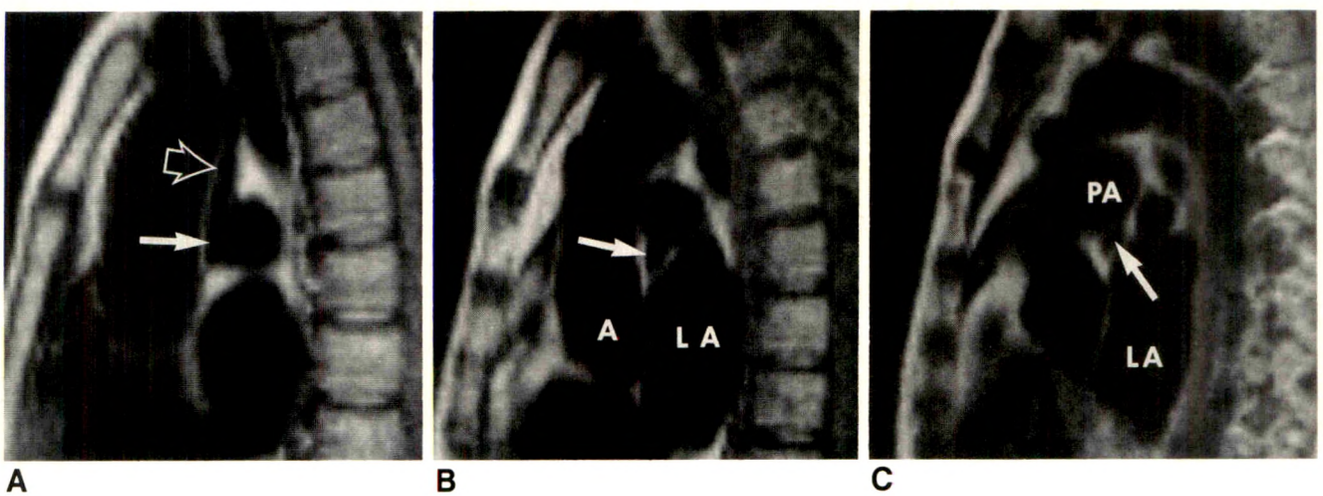

Fig. 3.—ECG-gated sagittal MR image of a normal subject.

A, 1 cm to right of midline, retroaortic, superior pericardial recess (*open arrow*) is continuous with superior extension of retroaortic segment of transverse sinus (*solid arrow*). This appearance mimics aortic dissection.

B, In midline, inferior extension of retroaortic segment of transverse sinus is visible as a typically triangular low-intensity area (*arrow*) between ascending aorta (A) and left atrium (LA) and under right pulmonary artery. The infrapulmonary segment is not visible.

C, 1 cm to left of midline, infrapulmonary segment (*arrow*) lies under main pulmonary artery (PA) and anterior and superior to left atrium (LA). Left coronary artery is not clearly distinguishable from transverse sinus.

ented obliquely and directed anteriorly and inferiorly, parallel to the wall of the pulmonary artery. Farther to the left, the infrapulmonary segment caps the left atrial appendage. This segment is conical and communicates with the left pericardial space (Fig. 2C).

In the sagittal plane, the left coronary artery arises anteriorly to the inferior extension of the retroaortic segment (Fig. 2B). Farther to the left, it is located within the fat anterior to the infrapulmonary segment, and passes anteriorly to the left atrial appendage (Fig. 2C). The left coronary artery is sometimes visible as a round signal void on MR in patients and is not always distinguishable from the infrapulmonary segment (Fig. 3C).

Transverse Plane

On transverse MR of patients, segments of the transverse sinus were visible in 32 (80%) of 40 with ECG-gated scans (Table 1). Most frequently seen were the inferior extension of the retroaortic segment (29 subjects, 73%), the superior extension of the retroaortic segments (8 subjects, 20%), and the retropulmonary segment (5 subjects, 13%) (Fig. 4).

The inferior extension of the retroaortic segment was an oblique band of low signal intensity posterior to the ascending aortic, at the level of the superior left atrium (Figs. 4B, 4C, and 5C). The superior extension of the retroaortic segment connects to the retroaortic portion of the superior pericardial

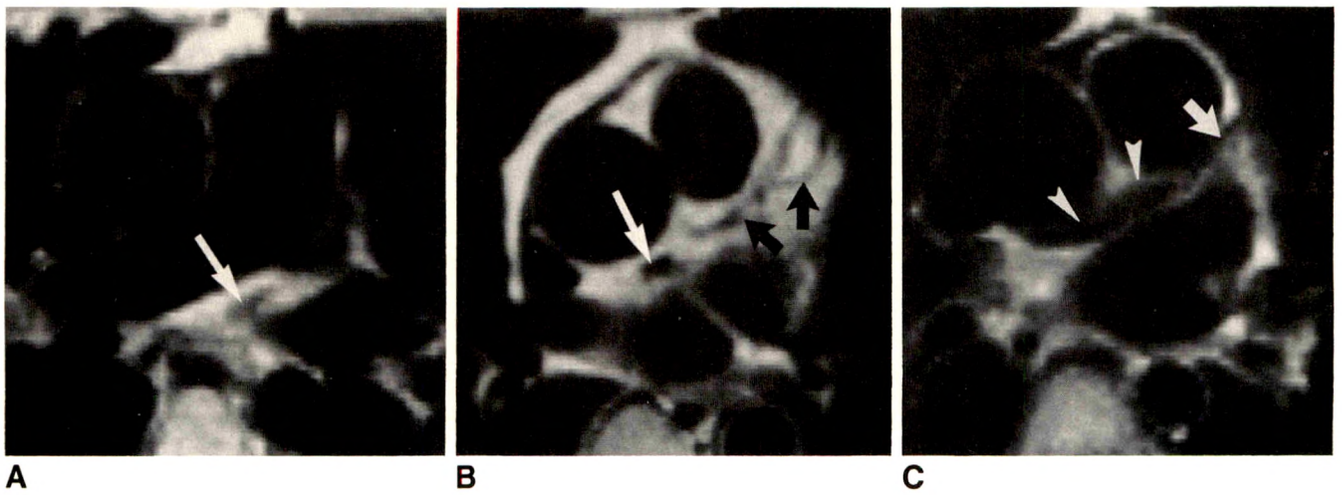

Fig. 4.—ECG-gated transverse MR imaging of three different subjects at different levels.

A, A bandlike area of low signal intensity (*arrow*) within subcarinal fat posterior to right pulmonary artery represents retropulmonary segment of transverse sinus. Relatively high signal intensity compared with that of vessels is due to partial-volume averaging. Its characteristic location and shape should allow its differentiation from lymph node.

B, Signal void (*white arrow*) between aorta and top of left atrium represents inferior extension of retroaortic segment of transverse sinus. Note that branching left coronary artery is located further anteriorly and to the left (*black arrows*).

C, Broad, bandlike, very-low-signal-intensity structure (*arrowheads*) represents inferior extension of retroaortic segment (behind aorta) and infrapulmonary segment, lying behind main pulmonary artery. Also note anterior descending branch of left coronary artery (*arrow*).

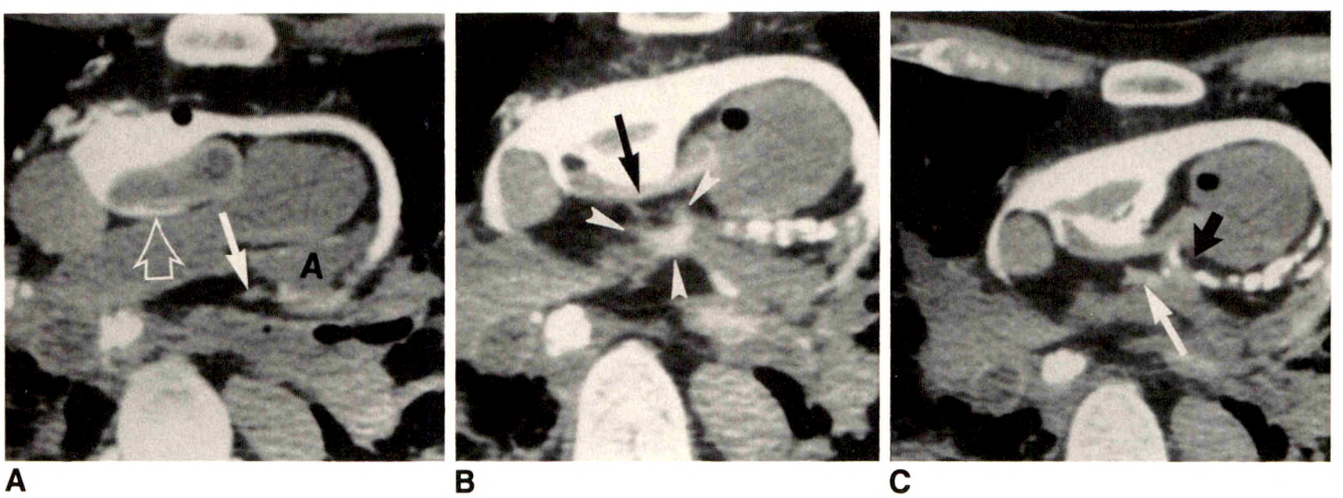

Fig. 5.—Thin-section CT scans of cadaver shown in Fig. 2, after contrast injection.

A, Scan at level of right pulmonary artery shows superior extension of retroaortic segment (*open arrow*). The retropulmonary segment (*solid arrow*) is located medial to left atrial appendage (A) and posterior to right pulmonary artery. Note calcified subcarinal lymph node. Bronchi are filled with aspirated material.

B, 7.5 mm below *A*. Infrapulmonary segment of transverse sinus (*arrowheads*) lies parallel to scan plane. Ascending aorta (*arrow*) is collapsed. Calcified left coronary artery is lateral to transverse sinus.
left coronary artery is lateral to transverse sinus.
arrow).

recess. This segment was a crescent area of low signal intensity between the aorta and right pulmonary artery (Fig. 5A). The retropulmonary segment was a thin, curvilinear band along the posterior wall of the right pulmonary artery (Fig. 4A). The infrapulmonary segment was occasionally seen behind the main pulmonary artery, appearing continuous medially with the inferior retroaortic segment (Figs. 4C and 5B). The left coronary artery lies anteriorly and to the left of the retroaortic segment and infrapulmonary segment, and the left coronary artery is easily distinguishable from the transverse sinus in this plane (Fig. 5).

Coronal Plane

The infrapulmonary segment was visible as a horizontal, linear, low-intensity band between the right pulmonary artery

and left atrium in 14 (67%) of 21 subjects with ECG-gated MR (Table 1; Figs. 4, 6, and 7). In some cases, volume averaging of the inferior extension of the retroaortic segment with the aorta or left atrium caused it to appear as an ill-defined broad area of low signal intensity just posterior to the aorta (Fig. 7). In the coronal plane, the left coronary artery was visible to the left and inferior to the infrapulmonary segment (Fig. 7). Laterally, the left atrial appendage separated the transverse sinus and left coronary artery.

MR Signal Intensity

In cadavers, the signal intensity of the transverse sinus was similar to the supernatant from the separated blood within the heart and great vessels: lower than muscle, but higher than aerated lung. Fluid aspirated from the pericardium of the cadavers was serous. On MR of subjects, the intensity was low, similar to aerated dependent lung (Figs. 2, 3, and 6). A slight increase in signal intensity was seen on second-echo images. However, even on the second-echo images of scans gated to end diastole, which show intense signal within cardiac chambers and great vessels, signal from the sinus remained low, allowing clear differentiation.

Discussion

The extensions of the pericardium that envelope the great vessels form two tubes. Anterosuperiorly, the aorta and pulmonary artery are enclosed in one tube; while posteriorly, the superior and inferior vena cavae and the pulmonary veins are enclosed in a second tube [3, 6]. The passage or connection between these two pericardial tubes is the transverse pericardial sinus [3]. On the right side, the transverse sinus communicates with the right pericardial space anterior to the superior vena cava; on the left side, it merges freely with the pericardial space lateral to the left atrial appendage (Fig. 1).

The transverse sinus of the pericardium has received little attention in the radiologic literature. One report describes the CT appearance of this structure in a patient with a pericardial effusion and in a few normal subjects [5]. Because CT has limited contrast resolution and viewing planes, the sinus is not readily displayed on routine CT scans. MR has both better contrast resolution and multidirectional imaging capability, and, thus, often it shows segments of the transverse sinus. These can be misinterpreted, because of their low signal intensity, as mediastinal vessels. The proposed imaging of the proximal coronary arteries with MR requires differentiation of the artery from the transverse sinus, and this can be difficult in some instances.

Between the ascending aorta and left atrium there is a triangular fatty space containing the inferior extension of the retroaortic segment [4]. This portion of the transverse sinus is the most frequently seen on both sagittal and transaxial MR images (Figs. 3 and 4). However, it is oriented almost vertically and its visualization in the coronal plane is infrequent because of partial-volume averaging. On coronal MR views, the infrapulmonary segment is most frequently seen. The superior extension of the retroaortic segment can be misinterpreted as the second lumen of an aortic dissection, especially in the sagittal plane (Fig. 3A). A similar problem can occur with the superior pericardial recess [2, 7]. Continuity of the retroaortic segment with the superior pericardial recess and its visualization at a site only 1–2 cm to the right of the mid-sagittal plane help in its identification. The retropulmonary segment usually appears as a thin, curvilinear structure adjacent to the posterior wall of the right pulmonary artery [4, 5, 8]. However, it can appear on MR as a thick band that may mimic a subcarinal lymph node (Fig. 2C). Persistent low signal intensity on T2-weighted images indicates pericardial fluid rather than a lymph node [9].

The left coronary artery lies anterior to the transverse sinus, but in the sagittal plane, their differentiation may be difficult except at the level of the left atrial appendage, where the appendage separates the transverse sinus above from the left coronary artery anteriorly and inferiorly. In the transverse and coronal planes, the left coronary artery is distinguishable from the transverse sinus, being lateral and anterior or inferior to the retroaortic segment or infrapulmonary segment.

Normally the pericardial sac is lubricated by 20–25 ml of serous fluid [10, 11]. On MR in cadavers, the signal intensity

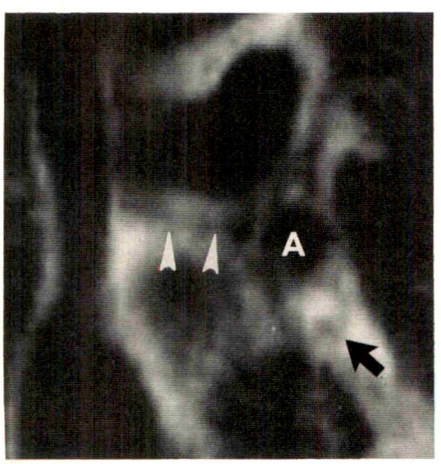

6

Fig. 6.—ECG-gated coronal MR. Infrapulmonary segment portion of transverse sinus appears as a linear area of low signal intensity (*arrowheads*) between right pulmonary artery above and left atrium below. Note left atrial appendage (A) and left coronary artery (*arrow*).

Fig. 7.—Coronal reformatted CT image of cadaver in Fig. 2 after contrast injection. At level of right pulmonary artery (R), relationship of infrapulmonary segment (*solid arrow*) and inferior extension of retroaortic segment (*open arrows*) is visible. Infrapulmonary segment communicates with left pericardium, above left atrial appendage (AA). Calcified left coronary artery (*white arrowheads*) lies lateral and inferior to infrapulmonary segment and atrial appendage. Calcified lymph node is superior to right pulmonary artery (R).

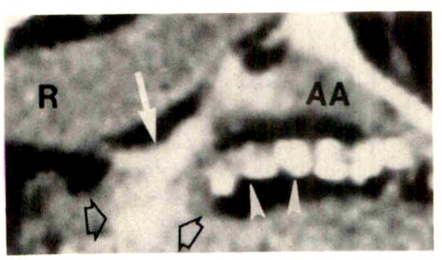

7

of pericardial fluid was similar to that of serum (blood supernatant) within the cardiac chambers and great vessels. However, on MR in subjects, the pericardial fluid appears almost as a signal void, with an intensity near to that of aerated lung, at all pulse sequences and echoes and throughout the cardiac cycle.

Sechtem et al. [12, 13] suggested cardiac motion as a cause of the low signal intensity of normal pericardial fluid. Higher signal intensity of stationary fluid shown in our cadaveric MR images and the higher signal intensity of pericardial effusion shown on MR images of patients with pericardial adhesions [13] support the contention of motion-induced signal loss of pericardial fluid. Fluid within the pericardial sac moves in nonlaminar patterns caused by cardiac pulsation. These flow patterns should have an accelerated flow component [12] as well as spatial velocity variation [11] within the imaged plane, and both factors will lead to signal loss by spin-phase change phenomena [14, 15] on both first- and second-echo images. However, the low protein content of physiologic pericardial fluid (one-third to one-fourth that of blood) [16] may also contribute to the low signal intensity [9]. The slight increase in signal intensity on most of the second-echo images with a TR value of more than 1.0 sec., compared with intensity on first-echo images, is probably due to the combined effects of an overall increase in signal noise, even-echo rephasing [17], and the long T2-value of fluid [18].

REFERENCES

1. Netter F. Heart. In: Yonkman F, ed. *The CIBA collection of medical illustrations*, vol. 5. Rochester, NY: CIBA, **1978**:5
2. McMurdo KK, Webb WR, von Schulthess GK, Gamsu G. MR of the superior pericardial recesses. *AJR* **1985**;145:985–988
3. Williams PL, Warwick R. *Gray's anatomy*, 36th ed. Philadelphia: Saunders, **1980**:634–643
4. Han MC, Kim C-W. *Sectional human anatomy: correlated with CT and MR*. Seoul: Ilchokak; Tokyo: Igaku-Shoin, **1986**:87–90.
5. Levy-Ravetch M, Auh YH, Rubenstein WA, Whalen JP, Kazam E. CT of the pericardial recesses. *AJR* **1985**;144:707–714
6. Healey JE, Gibbon JH. Intrapericardial anatomy in relation to pneumonectomy for pulmonary carcinoma. *Thorac Cardiovasc Surg* **1950**;19:864–873
7. Aronberg DJ, Peterson RR, Glazer HS, Sagel SS. The superior sinus of the pericardium: CT appearance. *Radiology* **1984**;153:489–492
8. Chasen MH, McCarthy MJ, Gilliland JD, Floyd JL. Concepts in CT of the thorax. *RadioGraphics* **1986**;6:793–832
9. Webb WR. MR of the hila and mediastinum. *Cardiovasc Intervent Radiol* **1986**;8:306–313
10. Moncada R, Baker M, Salinas M, et al. Diagnostic role of CT in pericardial heart disease: congenital defects, thickening, neoplasms and effusions. *Am Heart J* **1982**;103:263–282
11. Gibson AT, Segal MB. A study on the composition of pericardial fluid, with special reference to the probable mechanism of fluid formation. *J Physiol (Lond)* **1978**;277:367–377
12. Sechtem U, Tscholakoff D, Higgins CB. MR of the normal pericardium. *AJR* **1986**;147:239–244
13. Sechtem U, Tscholakoff D, Higgins CB. MR of the abnormal pericardium. *AJR* **1986**;147:245–252
14. von Schulthess GK, Higgins CB. Blood flow imaging with MR: spin-phase phenomena. *Radiology* **1985**;157:687–695
15. von Schulthess GK, Fisher M, Crooks LE, Higgins CB. Gated MR imaging of the heart: intracardiac signals in patients and healthy subjects. *Radiology* **1985**;156:125–132
16. Pujadas G. *Coronary angiography*. New York: McGraw-Hill, **1980**:64–65
17. Bradley WG, Valuch V. NMR even echo rephasing in slow laminar flow. *J Comput Assist Tomogr* **1984**;8:594–598
18. Stark DD, Higgins CB, Lanzer P, et al. MR of the pericardium: normal and pathologic findings. *Radiology* **1984**;150:469–474

Technical Note

The Left Ventricular Echogenic Focus: A Normal Finding

David W. Levy[1] and Marshall C. Mintz

Sonography is frequently used to delineate fetal cardiac anatomy. During routine examinations an echogenic focus within the left ventricle is frequently seen. This structure appears near the papillary muscle and moves with the mitral leaflets throughout the cardiac cycle. In order to determine the prevalance and significance of this finding, we prospectively recorded its presence or absence in 118 consecutive examinations. This finding occurs too frequently to represent a pathologic lesion, and it is most likely a normal developmental structure related to the mitral apparatus. Awareness of this finding should prevent misinterpretation.

Materials and Methods

Visualization of a left ventricular echogenic focus (LVEF) was prospectively sought in 118 consecutive second- and third-trimester fetal sonographic examinations in which a four-chamber view of the heart was obtained. If possible, a long-axis view of the fetal heart was also obtained. No cases were scanned for presumed cardiac anomalies. Sonograms were obtained on commercially available equipment (General Electric, Milwaukee, WI; Diasonics, Milipas, CA) using both 3.5- and 5.0-MHz linear-array and sector transducers.

Results

A small LVEF in the region of the papillary muscle and/or chordae tendineae was present in 24 (20%) of the 118 cases studied (Figs. 1 and 2). The LVEF was seen in 12 (22%) of 55 cases scanned between 14 and 24.9 weeks of gestation and 12 (19%) of 63 cases scanned from 25 weeks to term. The LVEF always moved in unison with the valve leaflets and was seen on four-chamber views as well as long-axis views

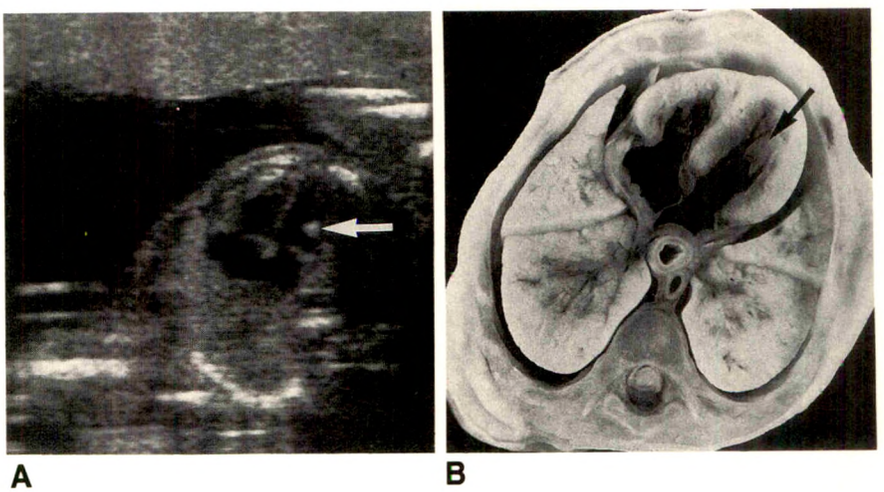

A B

Fig. 1.—*A*, Sonogram of 21.5-week fetus showing four-chamber view of heart. Left ventricular echogenic focus is seen (*arrow*).

***B*, Anatomic section corresponding to 1A showing that papillary muscle (*arrow*) is in same location as echogenic focus. (Reprinted with permission from Isaacson G, et al. [1], p. 65.)**

Received June 26, 1987; accepted after revision August 14, 1987.

[1] Both authors: Department of Radiology, Hospital of the University of Pennsylvania, 3400 Spruce St., Philadelphia, PA 19104. Address reprint requests to M. C. Mintz.

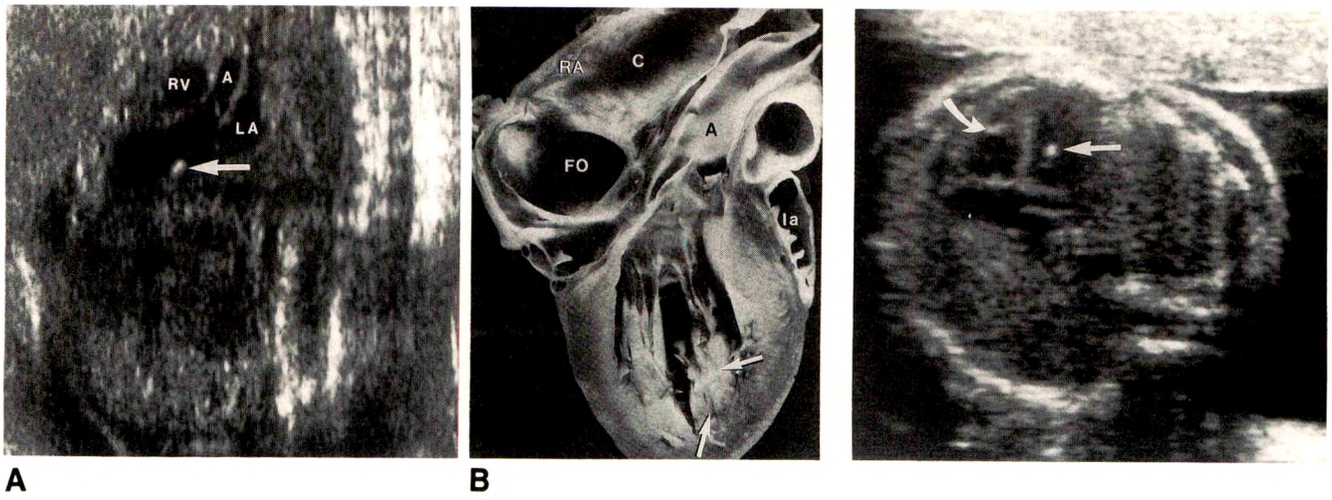

Fig. 2.—*A*, Sonogram of 23-week fetus illustrating long-axis view of left ventricle. Left ventricular echogenic focus is identified (*arrow*). RV = right ventricle; LA = left atrium; A = aorta.

***B*, Anatomic section corresponding to *A* showing that echogenic focus is in same location as papillary muscle (*arrows*). RA = right atrium; C = inferior vena cava; A = aorta; FO = valve forming wall of fossa ovalis; la = left atrial appendage. (Reprinted with permission from Isaacson et al. [1], p. 171.)**

Fig. 3.—Sonogram of 24-week fetus showing four-chamber view of heart. Left (*straight arrow*) and right (*curved arrow*) ventricular echogenic foci are seen.

of the left ventricle. An analogous echogenic structure within the right ventricle was seen in 2 (1.7%) of the 118 patients (Fig. 3). All cases had a normal cardiac rate and rhythm.

Discussion

The atrioventricular valves arise primarily from the endocardial cushions, while the left and right ventricular cavities develop by means of excavation of their myocardial walls. The resulting papillary muscles and chordae tendineae are products of variable degrees of ventricular wall excavation [2]. The larger size of the left ventricular papillary muscle may explain why it is more frequently visualized than is the right ventricular papillary muscle. The variable detection of the LVEF between patients may be related to individual variations in myocardial excavation.

Although sonographic evaluation of fetal cardiac anatomy has been described, the echogenic focus has not been previously described in reports that would have mentioned the focus if it had been recognized [3–5]. Although the true nature of the LVEF in the live, beating fetal or neonatal heart has not been proven, its high prevalence indicates a benign etiology, and its location suggests that it is related to the developing papillary muscle and/or chordae tendineae. When seen, this structure should be recognized as normal and not confused with a disease process. However, if an arrhythmia or fetal hydrops is seen in association with a larger echogenic focus in a different position within the heart, other causes such as a rhabdomyoma or teratoma should be considered [6].

REFERENCES

1. Isaacson G, Mintz MC, Crelin ES. *Atlas of fetal sectional anatomy*. New York: Springer-Verlag, **1986**:65, 171
2. Pallie W. Embryology of the human arterial system (arteriogenesis). In: Schwartz CJ, Werthersen NT, Wolf S, eds. *Structure and function of the circulation*. New York: Plenum Press, **1980**:47–48
3. Axel L. Real-time sonography of fetal cardiac anatomy. *AJR* **1983**; 141:283–288
4. Jeffrey RB, Laing FC. High-resolution real-time sonography of fetal cardiovascular anatomy. *J Ultrasound Med* **1982**;1:249–251
5. Jeanty P, Romero R, Hobbins JC. Vascular anatomy of the fetus. *J Ultrasound Med* **1984**;3:113–122
6. Dennis MA, Appareti K, Manco-Johnson ML, Clewell W, Wiggins J. The echocardiographic diagnosis of multiple fetal cardiac tumors. *J Ultrasound Med* **1985**;4:327–329

MR Imaging of the Aorta After Surgery for Aortic Dissection

Richard D. White[1,2]
Daniel J. Ullyot[3]
Charles B. Higgins[2]

MR imaging is known to be an effective technique for the noninvasive diagnosis of thoracic aortic disease, but it has not been used to monitor the appearance of the aorta or the fate of the false lumen after surgery for aortic dissection. This study describes our initial experience with postsurgical MR imaging of aortic dissection (nine type A and two type B) to evaluate prognostically important features, including the status of residual false lumen. The most notable findings were (1) aneurysmal dilatation beyond the interposed graft (11/11 cases), (2) residual intimal flap (10/11 cases) with at least partial patency of the false lumen (10/10 cases), and (3) origin of a visceral vessel from the false lumen in persistently dissected abdominal aorta (6/9 cases). Evaluation of residual false lumen by double-spin-echo-intensity and phase-display techniques showed evidence of slow blood flow with variable amounts of thrombus in eight of 10 cases. Differentiation between signal within the false lumen due to slow flow and signal due to thrombus was facilitated by phase display.

MR imaging can be used for noninvasive monitoring of the aorta after surgical repair of aortic dissection. Since the false lumen usually remains patent after surgical repair, such follow-up of its status seems necessary for identifying potential complications of the original dissection and/or the therapy.

Despite apparently successful therapy for aortic dissection [1, 2], early and long-term consequences of the original aortic dissection are recognized. Patients with surgically repaired aortic dissection remain at considerable risk, primarily from recurrence or progression of dissection or from aneurysm formation, all of which may cause aortic rupture [2, 3]. While persistent patency of the false lumen is common in aortic dissections postoperatively and appears to be often essential for perfusion of vital organs [4, 5], complete thrombosis of the false lumen may provide a natural buttress against further dissection or rupture and thus may result in a better prognosis, at least in patients with medically treated dissection [6]. Consequently, there may be clinical value in following the status of both the false lumen and the aortic diameter in aortic dissections after surgical repair.

Aortography [4] and CT [5] have been used successfully for monitoring aortic dissections after surgical repair, but optimal contrast enhancement may limit their reliability in assessing the false lumen, especially when it is partially or completely thrombosed or has minimal inflow of blood from the true lumen [7].

MR imaging is a useful technique for presurgical evaluation of either a type A dissection (i.e., one involving the ascending segment of the thoracic aorta) or a type B dissection (i.e., one involving the descending thoracic segment distal to the left subclavian artery) [8–10], but little data have been reported about the role of MR in evaluating patients after surgical repair [9]. The present study reports our initial experience with the use of MR imaging after surgery to assess prognostically important features of aortic dissections, and it shows the potential of the recently developed phase-display technique [8, 11, 12] for evaluating the status of the false lumen.

Received July 1, 1987; accepted after revision September 24, 1987.

[1] Department of Radiology, C-309, Box 0628, University of California, San Francisco, 3rd and Parnassus Aves., San Francisco, CA 94143. Address reprint requests to C. B. Higgins.

[2] Present address: Radiology, Georgetown University Hospital, 3800 Reservoir Rd., NW, Washington, DC 20007.

[3] Department of Surgery, University of California, San Francisco, 3rd and Parnassus Aves., San Francisco, CA 94143.

AJR 150:87–92, January 1988
0361–803X/88/1501–0087
© American Roentgen Ray Society

Subjects and Methods

Subjects

From December 1, 1983, to February 25, 1987, 11 patients (age range, 30–80 years; mean, 62 years; gender, 73% men) underwent MR imaging for the postsurgical follow-up evaluation of aortic dissection. This group consisted of nine type A dissections and two type B dissections that previously had been treated surgically. Two patients were included in an earlier study from our institution [9]. The period between surgery and MR examination was variable (range, 2 months–16 years; mean, 58 months). Seven cases of type A dissection, including one that had been limited at first to the proximal ascending aorta, were treated with replacement of the ascending aorta alone. Another type A case was treated by replacement of the ascending aorta and grafting to the left coronary artery. The remaining case of type A dissection, which was limited to the ascending aorta and arch, was treated with an ascending aortic graft, a right coronary artery bypass graft, and an aortic valve prosthesis. Both type B dissections were treated by replacing the proximal descending aorta with a graft.

MR Instrument and Technique

Transaxial spin-echo images were obtained on a superconducting MR system (Diasonics MT/S, San Francisco, CA) operating at 0.35 T, which previously has been discussed in detail [9]. The corresponding hydrogen resonant frequency was 15 MHz.

The 3 year period during which patients were studied represented an evolution in the MR technique used for evaluating aortic dissections. Initially, the MR examinations were performed by using a nongated, double–spin-echo technique (repetition times (TRs) = 1.5 and 2.0 sec; echo times (TEs) = 28 and 56 msec; slice thickness = 7 mm with a 3-mm interslice gap) for imaging both the thoracic and abdominal portions of the aorta (two patients) [9]. Subsequent patients were examined by using an ECG-gated (TR = heart rate), single–spin-echo technique (TE = 30 msec) (eight patients) or double–spin-echo technique (TEs = 30 and 60 msec) (one patient) in the thorax (slice thickness = 10 or 11 mm). A nongated (TR = 1.0 sec), single–spin-echo technique (two patients) or nongated (TR = 2.0 sec), double–spin-echo technique (seven patients) was then used in the abdomen (slice thickness = 10 or 11 mm); the abdominal aorta was not imaged in the two type A cases in which the descending thoracic aorta was spared.

The phase-display technique became available during the course of this study and was used to generate phase-display images in the final seven patients (six type A and one type B dissections). These images reflect phase shift of magnetization vectors, occurring for tissues moving (e.g., blood) relative to the magnetization vectors of surrounding stationary structures (e.g., vertebrae) during the time of application of an asymmetric magnetic gradient [11, 12]. Consequently, a voxel-by-voxel display of regions of blood flow, based on velocity-dependent phase shift of blood protons, can be produced.

Image Interpretation

Although oblique sagittal or coronal images were also available in several patients, only the sequential images from the transaxial plane were used because of their proven value for both visualization of all components of aortic dissection [5, 7, 9, 10] and measurement of aortic diameter [13, 14]. Use of transaxial images also limited the contribution of in-plane flow effect to signal within the false lumen. In addition, to avoid contributions by diastolic pseudogating and wash-in effect, the images analyzed represented systole and were not the initial level in a series. These standard-intensity and phase-display images were interpreted by two of the authors who only had knowledge of the patient's clinical history, including the type of dissection and the surgical history.

For each patient, the aorta was characterized according to (1) presence and extent of residual intimal flap, and presence and extent of false lumen, (2) aneurysmal dilatation of the aorta distal to the graft, and (3) characteristics of blood flow and the presence or absence of thrombus within the false lumen. This analysis was made for the ascending, arch, and descending segments of the thoracic aorta and in the abdominal portion of the aorta; the criteria for these three characteristics of postsurgical aortic dissections are described in the following sections.

The definitive sign of dissection of the aorta on MR images is the presence of an intimal flap (8–10]. Description of the extent of false lumen was based on the detection of this finding on standard-intensity images.

In the aforementioned segments, overall aortic diameter was measured from standard-intensity images, and the determination of the presence or absence of aneurysmal dilatation was based on previously established limits for the thoracic [13] and abdominal portions [14] of the aorta. The limits for each segment were as follows: ascending thoracic, ≥4.0 cm; arch, ≥3.9 cm; descending thoracic, ≥2.9 cm; and abdominal portion, ≥3.0 cm.

The appearance of signal within residual false lumen on standard-intensity and phase-display images provided the basis for determining both the blood flow pattern and the presence or absence of thrombus in each dissected aortic segment. Rapidly flowing blood within the false lumen was characterized by evidence of signal void on standard intensity images and evidence of phase shift on phase-display images (i.e., blacker or whiter shades relative to uniform background gray shade of an immobile structure) [11, 12]. On the other hand, when signal was present within the false lumen, the presence of slow blood flow and/or thrombus had to be considered. Slow blood flow was then identified by the detection of (1) evidence of even-echo rephasing on standard double-spin-echo intensity images (i.e., marked increase in absolute and relative signal intensity from first-echo to second-echo image) [15] and (2) evidence of phase shift on phase-display images. In contrast, identification of thrombus as the cause of signal within the false lumen was based on the fact that neither even-echo rephasing nor phase shift was detected in the regions with such signal.

Results

The anatomic findings from MR evaluation of the cases of surgically repaired aortic dissection included aneurysmal dilatation of a segment of the thoracic aorta distal to the site of grafting in all 11 patients (Fig. 1). For the type A cases, such dilatation was most common in the arch (8/9 = 89%). The abdominal portion of the aorta (imaged in nine cases, but not in the two type A cases in which the descending thoracic segment was spared) was infrequently found to be aneurysmal (3/9 = 33%). In addition, evidence of intimal flap and false lumen distal to the graft was noted in 10 (91%) of 11 patients. In six (67%) of the nine cases with evidence of intimal flap involving the abdominal aorta, the false lumen was identified as being the source of blood supply to one or more abdominal visceral vessels. The left renal artery was the vessel that most frequently originated from the false lumen (5/6 = 83%).

For MR analysis of the status of the false lumen (i.e., rapid or slow blood flow and presence or absence of thrombus), slow blood flow was differentiated from thrombus by the

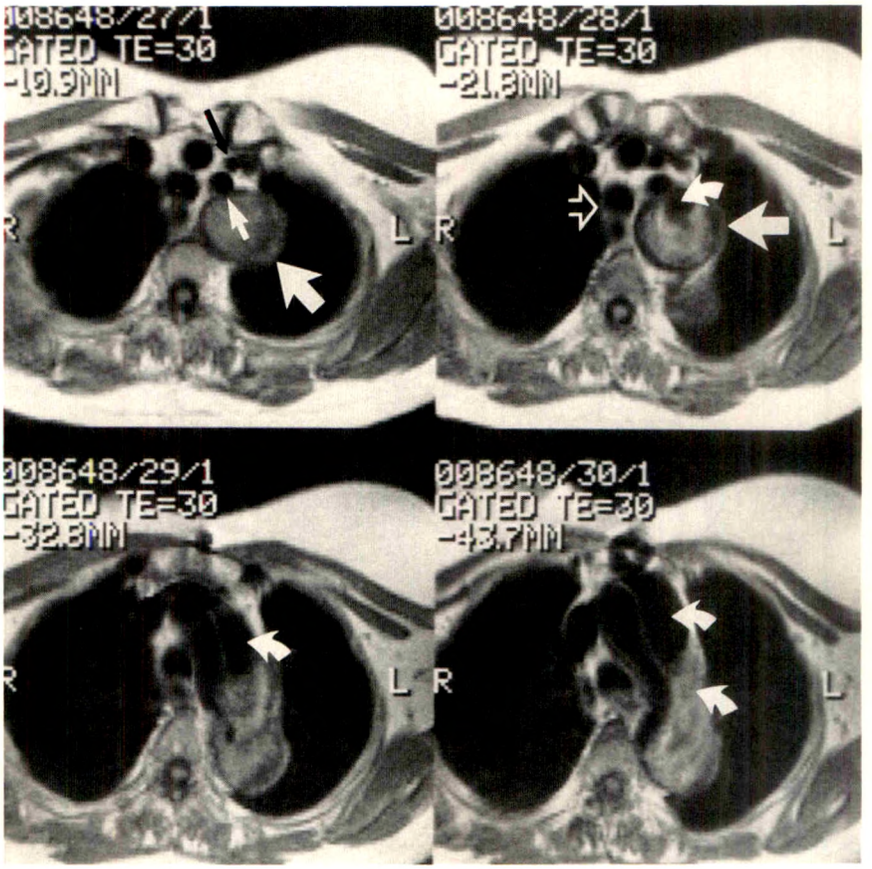

Fig. 1.—Postoperative type A dissection with aneurysmal dilatation of aortic arch.

Four sequential transaxial images (upper left, most cranial; lower right, most caudal) show a focal aneurysmal dilatation (*large white arrows*) extending cranially from superior aspect of aortic arch. Aneurysm arises from residual false lumen (*white curved arrows*) delineated by intimal flap. Both aneurysm and false lumen contain abnormal signal due to slow blood flow and/or thrombus. In addition, aneurysm displaces left common carotid artery (*small black arrow*) and left subclavian artery (*small white arrow*) anteriorly and trachea (*open arrow*) to the right.

presence or absence, respectively, of evidence of even-echo rephasing on the standard double–spin-echo intensity images and phase shift on the phase-display images. In all seven patients with both types of MR images, evidence of even-echo rephasing and evidence of phase shift were either simultaneously present or absent. However, it was difficult to distinguish confidently between regions of slow blood flow and those of thrombus by using the criteria for intensity images alone; this task was made considerably easier by using phase-display images (Fig. 2).

Ultimately, this analysis of the status of the false lumen indicated that there was at least partial patency of the false lumen (i.e., indicated by evidence of rapid or slow blood flow) in all 10 patients with evidence of residual intimal flap. Evidence of rapidly flowing blood within the false lumen was common (9/10 = 90%), especially in the ascending thoracic

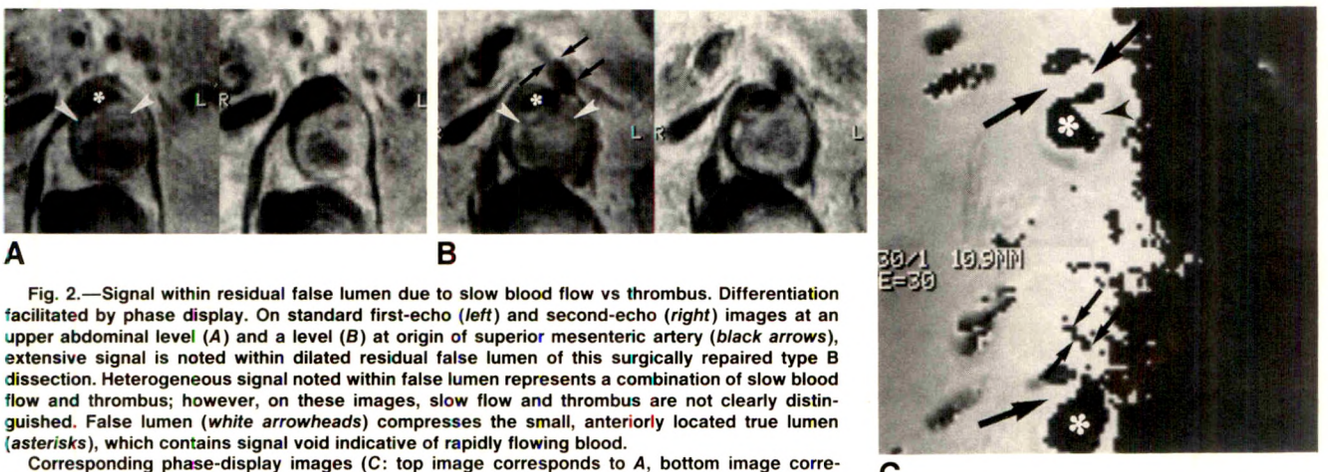

Fig. 2.—Signal within residual false lumen due to slow blood flow vs thrombus. Differentiation facilitated by phase display. On standard first-echo (*left*) and second-echo (*right*) images at an upper abdominal level (*A*) and a level (*B*) at origin of superior mesenteric artery (*black arrows*), extensive signal is noted within dilated residual false lumen of this surgically repaired type B dissection. Heterogeneous signal noted within false lumen represents a combination of slow blood flow and thrombus; however, on these images, slow flow and thrombus are not clearly distinguished. False lumen (*white arrowheads*) compresses the small, anteriorly located true lumen (*asterisks*), which contains signal void indicative of rapidly flowing blood.

Corresponding phase-display images (*C*: top image corresponds to *A*, bottom image corresponds to *B*) clearly show extent of both slow flow (*asterisks*) and thrombus (*arrowhead*) within residual false lumen. Intimal flap (*large black arrows*) appears thick, probably because of adherent thrombus on side of false lumen. Blood flow from false lumen into superior mesenteric artery (*small black arrows*) is also depicted.

segment (6/8 = 75%). Furthermore, slow blood flow within one or more segments of false lumen frequently was found (8/10 = 80%), always in association with variable amounts of thrombus (Fig. 3). The descending thoracic segment and abdominal portion of the aorta showed equally the greatest frequency of slow blood flow within the false lumen (both 5/9 = 56%); the greatest frequency of thrombus was found in the abdominal aorta (6/9 = 67%).

Discussion

Currently, more than 70% of patients with aortic dissection recover if treated medically or surgically [1, 2]. Originally, surgical therapy was aimed at both the resection of the entry site of the dissected segment and obliteration of the false lumen [16]. A 1979 report [2] shows, however, that neither a late mortality rate nor the frequency of repeated surgery are influenced by surgical resection of the intimal tear and that patency of the false lumen is not associated with worsened late clinical status or the increased need for another operation. Indeed, several follow-up aortographic [4] and CT [5] studies of aortic dissection after surgical repair have shown that the false lumen remains patent in most patients despite attempted obliteration. In these cases, communication between the true lumen and the false lumen through reentry sites appears to be the mechanism for both persistent patency of the false lumen and perfusion of vital organs (e.g., the left kidney). If the vital organs are not dependent on the false lumen for their blood supply, complete thrombosis of the false lumen may influence prognosis favorably [6]. Because there is a tendency for the false lumen to continue to undergo changes, including alterations in its overall size and the degree of thrombosis [17, 18], the prognosis also may fluctuate with time.

Aneurysmal dilatation of the dissected aorta is also frequently noted after surgical repair [5, 7] and in chronic dissections that are being treated medically [17, 18]. Because of its propensity to lead to aortic rupture, aneurysmal dilatation suggests an unfavorable prognosis.

The value of MR imaging in the evaluation of nonsurgically treated aortic dissections has been described [8–10]. Cumulative experience suggests that MR may be as effective as CT in evaluating dissections, sharing with it the advantages of the transaxial imaging approach for delineating the intimal flap and false lumen [7] and for assessing aortic diameter [13, 14]; the additional advantage of MR is that it avoids the need for contrast administration. In addition, straight or oblique

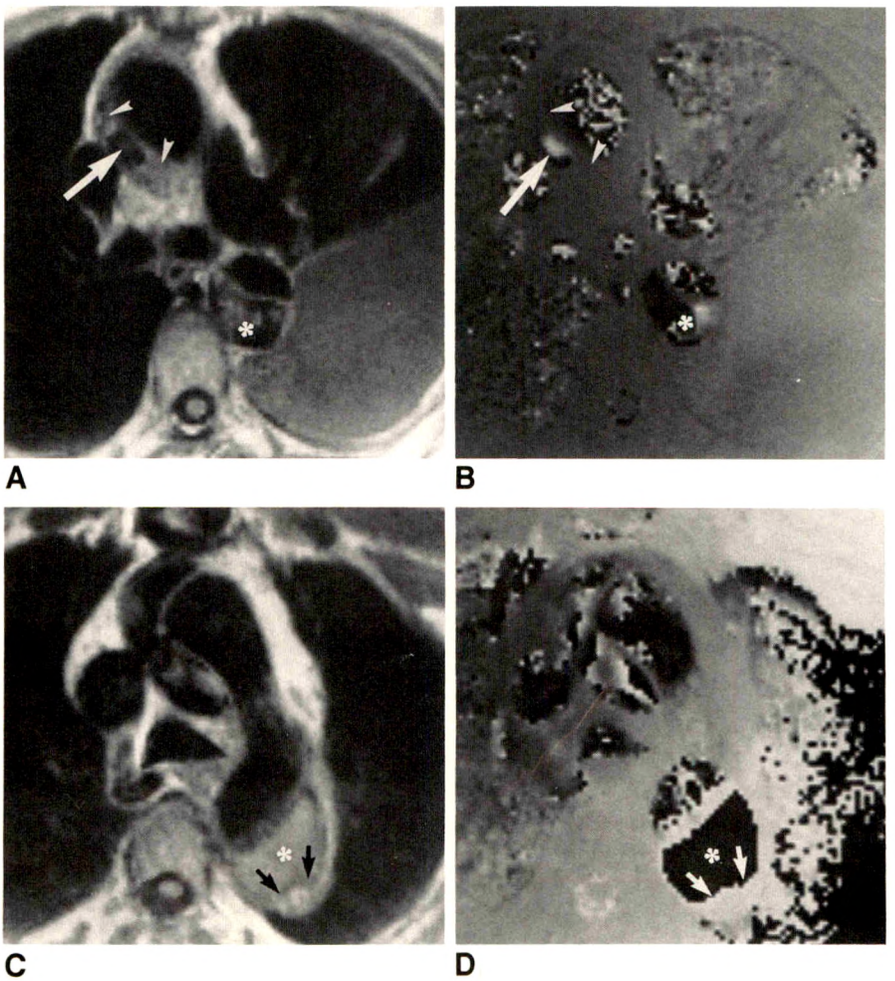

Fig. 3.—Typical appearances of slow blood flow in combination with thrombus within residual false lumen after surgical repair of a type A dissection. Images are shown for two patients with surgically repaired type A dissections with abnormal signal within residual false lumen, which is due to both slow flow and thrombus. Standard first-echo intensity images are accompanied by corresponding phase-display images (second-echo images were not obtained).

***A* and *B*, In ascending segment of thoracic aorta, residual dissection above graft is noted on intensity image. Extent of slow blood flow (*large arrows*) and extent of thrombus (*arrowheads*) are clearly delineated within false lumen on phase-display image. Intimal flap appears immobile (shade matching that of immobile structures, such as vertebra and large left pleural effusion) and thickened by adherent thrombus. In a similar manner, signal within false lumen in descending segment (*asterisks*) can be identified by phase display as being entirely due to slow blood flow (shade contrasts sharply with that of immobile structures).**

***C* and *D*, In descending segment of thoracic aorta, signal filling of false lumen on intensity image might be easily attributed to either complete thrombosis or slow flow. Phase-display image clearly shows presence of extensive slow blood flow (*asterisks*) and a small amount of thrombus (*small arrows*), with shades contrasting and matching, respectively, those of immobile structures (e.g., intimal flap and chest wall).**

sagittal or coronal imaging of the aorta may be performed directly with MR for further anatomic description of disease, whereas this information can be obtained only indirectly with CT by computed reconstruction.

The present study reports our initial experience with the use of MR for the postsurgical follow-up evaluation of dissections of the aorta. Several anatomic features of postoperative aortic dissection that have been discussed previously [4, 5] are reinforced by the MR findings in this study. They include the high frequency of (1) patency of the residual false lumen, (2) aneurysmal dilatation of the aorta distal to the graft, (3) slow blood flow and thrombus within the false lumen, and (4) origin of visceral vessels to vital organs (e.g., the left renal artery) from the false lumen in the dissected abdominal aorta. The observation that the abdominal aorta with residual dissection is characterized by thrombus within the false lumen in the absence of aneurysmal dilatation apparently has not been described previously, and its pathophysiologic and prognostic significance is unclear. Unfortunately, these observations must be recognized as somewhat speculative since no gold standard (e.g., additional imaging results or surgical or postmortem findings) was available in this study.

The differentiation between aortic dissection with slow blood flow and/or thrombus within its false lumen on the one hand and aneurysm with adherent mural thrombus on the other is now a well-recognized limitation of both aortography and CT [7]. This distinction is important at the time of the initial evaluation for suspected thoracic aortic disease and in the postoperative follow-up evaluation of aortic dissections, during which the confirmation of the presence or absence of recurrence or progression of dissection, of aneurysmal dilatation of the aorta, or of thrombus within the false lumen may be sought [2, 3, 6].

MR imaging relies on the same general guidelines described for CT [7] for the differentiation between aortic dissection with complete thrombosis of the false lumen and aneurysm with adherent thrombus based on the diameter and shape of the involved aortic segment and its patent lumen. On the other hand, possibly MR is superior to CT for documenting the presence of at least minimal blood flow within a false lumen, thereby improving the accuracy in identifying dissection and restricting the occasions in which these two forms of the aortic disease might be confused.

The distinction between causes of flow-related signal enhancement of blood (e.g., wash-in artifacts, even-echo rephasing, diastolic pseudogating, and in-plane flow) and intravascular thrombus by MR has typically depended on the identification of the pattern of change in abnormal intravascular signal intensity on standard-intensity images with prolonged TEs [15]. These changes are related not only to the blood-flow velocity and direction and the thrombotic-material character but also to the specific MR pulse sequence and MR system used. Although the presence and absence of even-echo rephasing [15] may be used effectively for differentiating slow blood flow from thrombus, respectively, region-of-interest analysis for this phenomenon can become tedious and visual assessment can become problematic [11]. Like slowly flowing blood, thrombus may produce variable signal intensity on standard spin-echo images, depending on the age of the thrombotic material [19, 20]. Therefore, in a clinical setting it may be difficult to distinguish confidently between slowly flowing blood and thrombus by using standard-intensity images alone.

In this study, we used the recently developed phase-display technique [11, 12] to facilitate this often difficult differentiation between signal within the false lumen due to slow flow and that due to thrombus. Using a version of the phase-display technique for semiquantitative analysis of in-plane flow, Dinsmore et al. [8] evaluated the blood-flow patterns within the true and false lumina before surgery in a patient with a type A dissection. The phase-shift information needed for phase-display is derived from conventional spin-echo pulse sequences with no additional reconstruction software and at little or no additional machine or patient time. This information can be used to generate on a voxel-by-voxel basis a sensitive map of moving protons in flowing blood that appear quite different from that of regions of stationary protons in thrombus of any age [11, 12]. The phase-display technique generally provides clear-cut and easily interpreted images, reflecting the distribution of both slow blood flow and thrombus in regions of unidentified signal noted within the false lumen on standard-intensity images, and it may obviate more lengthy examinations for the acquisition of later spin-echo images.

Phase shift is not restricted to blood-flow motion; anything that is moving during the application of the gradients (e.g., the patient, the heart, the chest wall, or mobile polypoid thrombus) may produce observable phase shift. This can result in failure to correctly identify an intravascular lesion, because such a phase shift might be misinterpreted as flowing blood. Furthermore, because of the cyclic nature of the phase-shift representation, a specific phase shift (i.e., 360°) can be displayed as the same shade of gray as an adjacent immobile structure. This can result in incorrectly identifying an intravascular lesion when, in fact, flowing blood is present. In addition, technical factors (e.g., inhomogeneity in the static magnetic field, magnetic susceptibility in chronic hemorrhage/thrombus) may alter local phase progression, which then may be misinterpreted as phase shift due to motion.

Unfortunately, the superiority of phase-shift analysis over the analysis of even-echo rephasing for the differentiation between slow blood flow and thrombus has not been definitively proved by this or any previous study [11]. A large comparison study with separate blinded interpretations of standard double–spin-echo intensity images and corresponding phase-display images is needed to accomplish this purpose, as well as to further elucidate the problems and pitfalls associated with the phase-display technique.

REFERENCES

1. Wheat MW Jr. Treatment of dissecting aneurysms of the aorta: current status. *Prog Cardiovasc Dis* **1973**;16:87–101
2. Miller DC, Stinson EB, Oyer PE, et al. The operative treatment of aortic dissection: experience with 125 patients over a sixteen-year period. *J Thorac Cardiovasc Surg* **1979**;78:365–382
3. Cabrol C, Pavie A, Mesnildrey P, et al. Long-term results with total replacement of the ascending aorta and reimplantation of the coronary arteries. *J Thorac Cardiovasc Surg* **1986**;91:17–25

4. Guthanar DF, Miller DC, Silverman JF, Stinson EB, Wexler L. Fate of the false lumen following surgical repair of aortic dissections: an angiographic study. *Radiology* **1979**;133:1–8
5. Mathieu D, Keita K, Loisance D, Cachera JP, Rousseau M, Vasile N. Postoperative CT follow-up of aortic dissection. *J Comput Assist Tomogr* **1986**;10:216–218
6. Dinsmore RE, Willerson JT, Buckley MJ. Dissecting aneurysm of the aorta: aortographic features affecting prognosis. *Radiology* **1972**;105:567–572
7. White RD, Lipton MJ, Higgins CB, et al. Noninvasive evaluation of suspected thoracic aortic disease by contrast-enhanced computed tomography. *Am J Cardiol* **1986**;57:282–290
8. Dinsmore RE, Wedeen VJ, Miller SW, et al. MRI of dissection of the aorta: recognition of the intimal tear and differential flow velocities. *AJR* **1986**;146:1286–1288
9. Amparo EG, Higgins CB, Hricak H, Sollitto R. Aortic dissection: magnetic resonance imaging. *Radiology* **1985**;155:399–406
10. Goldman AP, Kotler MN, Scanlon MH, Ostrum B, Parameswaran R, Parry WR. The complementary role of magnetic resonance imaging, Doppler echocardiography, and computed tomography in the diagnosis of dissecting thoracic aneurysms. *Am Heart J* **1986**;111:970–981
11. von Schulthess GK, Augustiny N. Calculation of T2 values versus phase imaging for the distinction between flow and thrombus in MR imaging. *Radiology* **1987**;164:549–554
12. White EM, Edelman RR, Wedeen VJ, Brady TJ. Intravascular signal in MR imaging: use of phase display for differentiation of blood-flow signal from intraluminal disease. *Radiology* **1986**;161:245–249
13. Sommerhoff BA, Sechtem UP, Schiller MB, Lipton MJ, Higgins CB. MRI of the thoracic aorta in Marfan patients. *J Comput Assist Tomogr* **1987**;11:633–639
14. Amparo EG, Hoddick WK, Hricak H, et al. Comparison of magnetic resonance imaging and ultrasonography in the evaluation of abdominal aortic aneurysms. *Radiology* **1985**;154:451–456
15. von Schulthess GK, Higgins CB. Blood flow imaging with MR: spin-phase phenomena. *Radiology* **1985**;157:687–695
16. DeBakey ME, Cooley DA, Creech O Jr. Surgical considerations of dissecting aneurysm of the aorta.*Ann Surg* **1955**;142:586–612
17. Yamaguchi T, Naito H, Ohta M, et al. False lumens in type III aortic dissections progress: CT study. *Radiology* **1985**;156:757–760
18. Ambos MA, Rothberg M, Lefleur RS, Weiner S, McCauley DI. Unsuspected aortic dissection: the chronic "healed" dissections. *AJR* **1979**;132:221–225
19. Rapoport S, Sostman HD, Pope C, Camputaro C, Holcomb W, Gore JC. Venous clots: evaluation with MR imaging. *Radiology* **1987**;162:527–530
20. Erdman WA, Weinreb JC, Cohen JM, Buja LM, Chaney C, Peshock RM. Venous thrombosis: clinical and experimental MR imaging. *Radiology* **1986**;161:233–238

Thrombosis of the Splanchnic Veins: CT Diagnosis

Robert L. Vogelzang[1]
Richard M. Gore[1]
Sara L. Anschuetz[1]
Andres T. Blei[2]

Fourteen patients had mesenteric, portal, or splenic venous thrombosis that was diagnosed primarily by contrast-enhanced CT. The group included five patients with coagulopathy, three with pancreatic carcinoma, two with cirrhosis and portal hypertension, one with pancreatitis, and one with hepatocellular carcinoma. In two patients, no etiology was determined. In all cases, CT easily identified low-density venous thrombosis, which frequently involved more than one vein. In four patients, all three splanchnic veins were involved; five patients had occlusion of two veins. In five patients, only one vein was involved. Additional CT findings included ascites, collateral veins, hepatomegaly, and splenomegaly. No venous wall enhancement was found. CT also was helpful in defining the cause of thrombosis in six of 14 patients. Mesenteric edema and/or bowel wall thickening was not identified. None of the patients had classic clinical evidence of splanchnic venous occlusion, and none died primarily of that disease. The major morbidity suffered by these patients stemmed from complications of splanchnic venous occlusion, and nine patients ultimately required sclerotherapy, splenectomy, and portal decompression.

We conclude that CT is useful in the diagnosis of splanchnic venous thrombosis. Our experience suggests that mesenteric, splenic, and/or portal venous thrombosis may occur more commonly than has been previously thought and that the disease in many cases is not life threatening.

The diagnosis of splanchnic venous thrombosis is difficult because of the protean clinical manifestations and diverse causes of this disorder. Prompt detection is important because portal and mesenteric venous thrombosis accounts for between 5% and 15% of all cases of mesenteric vascular ischemia, and an estimated mortality rate of 20% [1, 2]. The definitive, nonsurgical diagnosis of portal, splenic, and superior mesenteric venous thrombosis traditionally has been established by arterial portography, splenoportography, and/or transhepatic portography [3–5]. These, however, are invasive, costly, and time-consuming procedures that usually are performed only when there is significant clinical suspicion of venous thrombosis. There are scattered case reports and small series in the literature that suggest that cross-sectional imaging techniques also may be useful in the diagnosis of mesenteric and portal venous thrombosis [6–9]. In this paper, we discuss our experience with contrast-enhanced CT in the study of 14 patients with splanchnic venous thrombosis.

Subjects and Methods

The clinical records of all patients in whom CT studies first established the diagnosis of portal, splenic, and/or superior mesenteric venous thrombosis and who were seen at Northwestern Memorial Hospital from March 1984 through May 1986 were reviewed. The group included 11 men and three women ranging in age from 21 to 72 years. The causes of the venous thrombosis included coagulopathy resulting from protein C deficiency, oral contraceptive use, excessive factor VIII administration, or sepsis (five patients); pancreatic

Received July 20, 1987; accepted after revision September 17, 1987.

[1] Department of Radiology, Northwestern University Medical School and Northwestern Memorial Hospital, Olson Pav., 710 N. Fairbanks Ct., Chicago, IL 60611. Address reprint requests to R. L. Vogelzang at Northwestern Memorial Hospital.

[2] Department of Medicine, Northwestern University Medical School and Northwestern Memorial Hospital, Chicago, IL 60611.

AJR 150:93–96, January 1988
0361–803X/88/1501–0093
© American Roentgen Ray Society

carcinoma (three patients); cirrhosis and portal hypertension (two patients); pancreatitis (one patient); and hepatocellular carcinoma (one patient). The underlying cause was established by surgery in five patients, by laboratory data (mainly coagulation abnormalities) in three patients, by percutaneous biopsy in three patients, and by clinical history in one patient. In two patients, the cause could not be determined, despite an extensive clinical and laboratory evaluation.

CT scans were performed on a General Electric CT/9800 unit using a scan time of 2 sec with contiguous 10-mm sections through the abdomen. Additional 5-mm sections often were obtained through the region of interest. All scans were performed after the administration of oral and IV contrast material. IV contrast material was administered as a bolus of 50 ml of 60% contrast (Conray 325, Mallinckrodt, St. Louis, MO) followed by a rapid infusion of 300 ml of 30% contrast (Conray 30, Mallinckrodt). Precontrast scans were not obtained. In six patients, the CT diagnosis of venous occlusion was confirmed by angiographic procedures when arterial portography or splenoportography showed occlusion or filling defects within the involved vessels. Three had the diagnosis documented surgically by direct inspection, and one patient with hepatocellular carcinoma had CT biopsy of tumor within the portal vein. In four others, CT findings, laboratory data, and clinical course alone were considered sufficiently characteristic to establish the diagnosis.

Two authors reviewed the CT findings. The CT scans were evaluated for the presence and location of venous thrombosis, the presence of collateral venous channels, splenomegaly, hepatomegaly, and ascites. The intensity of venous wall enhancement was also noted and was compared with the walls of other nonthrombosed veins, such as the vena cava. Scans also were reviewed for their ability to show the cause of venous thrombosis and other associated abnormalities.

Results

A summary of the CT findings in all groups of patients is contained in Table 1. Overall comparison of findings in the various groups showed virtually no differences in the spectrum of CT findings associated with venous thrombosis. Low-density thrombus was identified within the involved veins in all 14 patients. Involvement of multiple veins was common and was seen in nine patients (Fig. 1). Four patients had three thrombosed veins, and five had two veins involved (three with mesenteric and splenic thrombosis, one with mesenteric and portal thrombosis, and one with splenic and portal thrombosis). The three splanchnic veins were involved with similar frequency, and collateral vessels also were commonly seen (12 patients) (Fig. 2). Splenomegaly was present in seven (50%) of the 14 patients, while ascites and hepatomegaly were present in four and two patients, respectively.

In six patients the cause of venous occlusion was correctly determined by CT, including all four with tumor (Figs. 3 and 4) and two others with either cirrhosis or pancreatitis.

In the evaluation of wall enhancement, the thinness of the involved vein wall precluded the use of numeric determination of the attenuation coefficient of the wall, but careful visual comparison of the intensity of wall enhancement between involved and uninvolved veins indicated no differences; in all cases we found no venous wall enhancement (Figs. 1B, 2, and 3B).

Discussion

Splanchnic venous thrombosis is an uncommon disorder caused by a variety of different conditions including cirrhosis, pancreatitis, neoplasm, coagulopathy, sepsis, splenectomy, and other abdominal surgery [1, 2, 10, 11]. Clinically, the patients may have either acute or chronic abdominal pain, fever, leukocytosis, hematochezia, or ileus or bowel infarction, but they also may be relatively asymptomatic. The diagnosis of this disorder has been difficult and traditionally has relied on angiography [3–5].

Recent reports have documented the utility of CT in diagnosing this condition and have emphasized the basic findings

TABLE 1: CT Findings in Splanchnic Venous Thrombosis

CT Findings	Cause of Thrombosis						
	Coagulopathy	Pancreatic Carcinoma	Cirrhosis and Portal Hypertension	Pancreatitis	HCC	Unknown	Total
Total No. of patients	5	3	2	1	1	2	14
Clot visualized	5	3	2	1	1	2	14
Veins involved (according to CT results)							
Splenic	4	2	1	1	0	0	8
SMV	5	2	1	0	1	2	11
Portal	4	1	1	0	1	1	8
Number of veins involved							
1 vein	0	2	1	1	0	1	5
2 veins	2	0	1	0	1	1	5
3 veins	3	1	0	0	0	0	4
Accentuated enhancement of venous wall	0	0	0	0	0	0	0
Collateral veins present	4	3	2	1	1	1	12
Cause determined by CT	0	3	1	1	1	0	6
Splenomegaly	3	0	2	1	0	1	7
Hepatomegaly	1	0	1	0	0	0	2
Ascites	3	0	1	0	0	0	4

Note.—HCC = hepatocellular carcinoma; SMV = superior mesenteric vein.

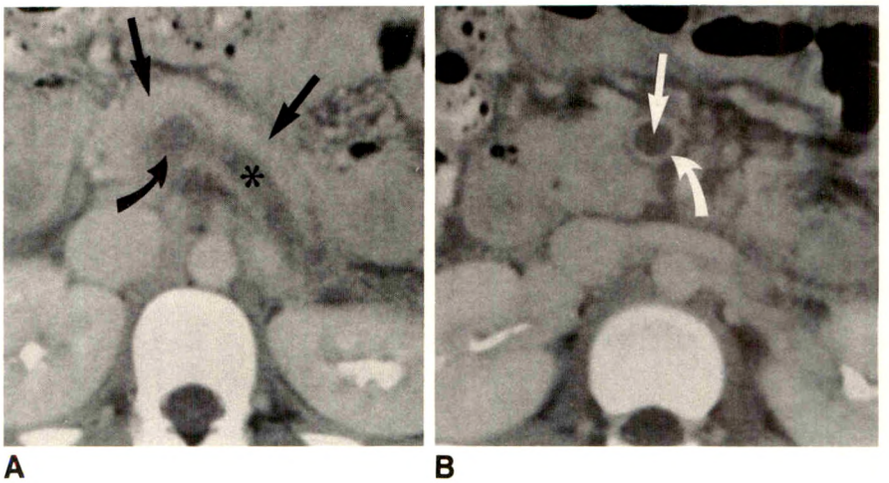

Fig. 1.—CT scans show extensive mesenteric venous thrombosis as a result of excessive factor VIII administration after splenectomy.

A, Scan at level of pancreas (*straight arrows*) shows low-density thrombus within splenic vein (*asterisk*) and superior mesenteric vein (*curved arrow*).

B, Scan at a lower level shows characteristic appearance of venous thrombosis. Note low-attenuation central filling defect (*straight arrow*) with venous wall (*curved arrow*) showing enhancement similar to that in other large abdominal veins.

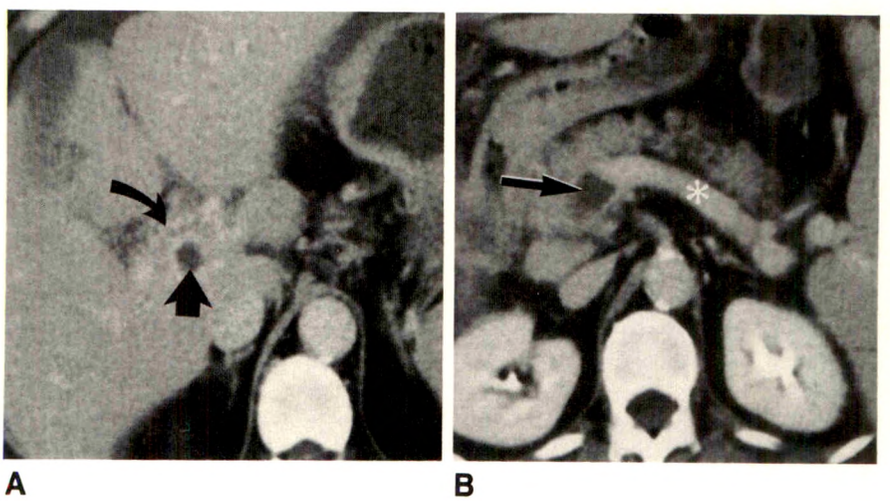

Fig. 2.—CT scans show portal and superior mesenteric venous thrombosis caused by diverticulitis and sepsis.

A, Low-density thrombus within main portal vein (*short straight arrow*). Note periportal collateral veins (*curved arrow*).

B, Scan at level of mesenteric confluence. Splenic vein (*asterisk*). Low-density thrombus extends into superior mesenteric vein (*arrow*).

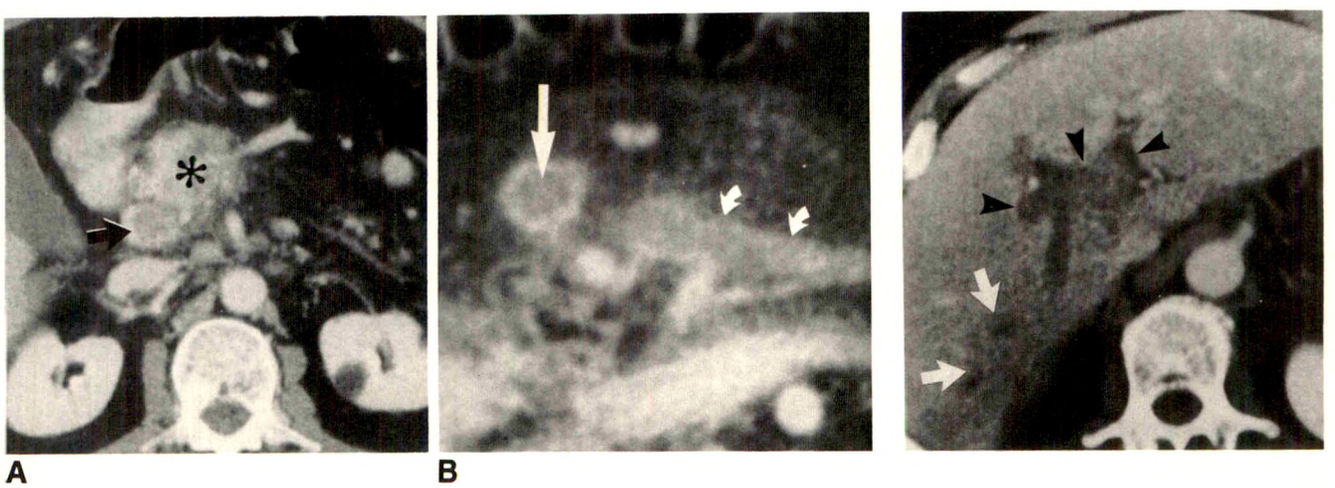

Fig. 3.—CT scans show pancreatic carcinoma.

A, Scan at level of pancreatic head shows irregular mass (*asterisk*) with superior mesenteric venous clot (*arrow*).

B, Magnified view of scan through mesentery shows low-density thrombus within superior mesenteric vein (*large straight arrow*) as well as thrombus extending into a branch (*small curved arrows*). Wall enhancement is accentuated by contrast with adjacent mesenteric fat but is no greater than in other vessels.

Fig. 4.—CT scan shows hepatocellular carcinoma with tumor thrombus within portal vein. Small, irregular, low-density mass in right lobe (*white arrows*). Branching central low-attenuation tumor thrombus (*black arrowheads*) fills central portal vein.

of low-attenuation intraluminal clot sharply outlined by a venous wall that is perceived as being of increased density [6–9, 12, 13]. Other signs include enlargement of the affected vein, bowel wall thickening, and mesenteric edema in cases of superior mesenteric venous occlusion with infarction or impending infarction [14–16]. Occasionally, the presence of venous collaterals also has been noted [15, 17].

Our findings in this relatively diverse group of patients parallel and amplify the experience of others (with a few exceptions). The frequency of multiple vein involvement was higher in our study than in most studies reported in the literature, although one group [17] indicated that 11 of their 17 patients had "other contiguous veins" involved; these authors did not specify which veins were involved or how many. Additionally, our findings show that the venous wall contrast enhancement seen in splanchnic venous thrombosis is in fact normal and is not an indication of increased proliferation of vasa vasorum or hyperemia, as others have suggested [17]. The visual perception of increased wall enhancement is related to contrast between the low-density thrombus and the wall; the finding is more marked when the vessel is surrounded by mesenteric fat (Fig. 3B) than when it is surrounded by other enhanced structures such as pancreatic parenchyma (Fig. 2B).

None of our patients showed evidence of bowel wall thickening or mesenteric edema, which has been associated with either frank superior mesenteric venous infarction or severe ischemia related to venous occlusion [14–16]. None of the 11 patients who had superior mesenteric venous thrombosis had significant abdominal pain, but rather they usually had vague localizing signs and symptoms and, except for three who died of malignancy, the patients are still alive. Seven of the 11, however, experienced significant morbidity related to mesenteric and/or portal occlusion, such as recurrent variceal bleeding or ascites, that required sclerotherapy or surgical portal decompression. This discrepancy between our clinical experience and that of others was also noted by Rosen et al. [6] and is probably due to the fact that CT scanning of the abdomen is now frequently performed in many clinical situations in which mesenteric venous thrombosis may be an incidental secondary finding. In addition, the widespread use of fast scanners with excellent spatial and contrast resolution makes the detection of such thrombi easier and more likely. There is, however, good evidence that mesenteric venous thrombosis can occur without severe clinical sequelae. Johnson and Baggenstoss [10] correlated intestinal infarction with the degree of mesenteric occlusion and showed that in cases in which only the superior mesenteric vein and its larger tributaries were thrombosed, intestinal infarction was uncommon. When small veins (vasa rectae and venous arcades) were involved, infarction inevitably occurred.

Splenic vein thrombosis, on the other hand, is never considered a life-threatening condition, but it can cause hypersplenism and isolated gastric varices [18]. Three of our patients had splenic vein occlusion, two with isolated splenic vein thrombosis and one in combination with portal occlusion. In this group there was some morbidity (one patient with hypersplenism required splenectomy), but overall the condition itself was quite benign.

In conclusion, CT was capable of defining splanchnic venous thrombosis; however, we did not directly compare the efficacy of CT with that of angiography and therefore did not determine the sensitivity of CT.

REFERENCES

1. Grendell JH, Ockner RK. Mesenteric venous thrombosis. *AJR* **1982**;82:358–372
2. Naitove A, Weisman RE. Primary mesenteric venous thrombosis. *Ann Surg* **1965**;161:516–523
3. Clemett AR, Chang J. The radiologic diagnosis of spontaneous mesenteric venous thrombosis. *Am J Gastroenterol* **1975**;63:209–215
4. Tey PH, Sprayregen S, Ahmed A, Chan KF. Mesenteric vein thrombosis: angiography in two cases. *AJR* **1981**;136:809–811
5. Clark RA, Gallant TE. Acute mesenteric ischemia; angiographic spectrum. *AJR* **1984**;142:555–562
6. Rosen A, Korobkin M, Silverman PM, Dunnick NR, Kelvin FM. Mesenteric vein thrombosis: CT identification. *AJR* **1984**;143:83–85
7. Vigo M, De Faveri D, Biondetti PR, Bendetti L. CT demonstration of portal and superior mesenteric vein thrombosis in hepatocellular carcinoma. *J Comput Assist Tomogr* **1980**;4:627–629
8. Miller VE, Berland LL. Pulsed Doppler duplex sonography and CT of portal vein thrombosis. *AJR* **1985**;145:73–76
9. Merritt CRB. Ultrasonographic demonstration of portal vein thrombosis. *Radiology* **1979**;133:425–427
10. Johnson CC, Baggenstoss AH. Mesenteric vascular occlusion: study of 99 cases of occlusion of veins. *Mayo Clin Proc* **1949**;24:628–636
11. North JP, Wollenman OJ. Venous mesenteric occlusion in course of migratory thrombophlebitis. *Surg Gynecol Obstet* **1952**;95:665–671
12. Vujic I, Rogers CI, Leveen HH. Computed tomographic detection of portal and superior mesenteric vein thrombosis in hepatocellular carcinoma. *J Comput Assist Tomogr* **1980**;4:627–629
13. Kneeland JB, Auh YH, Zirinsky K, Rubenstein W, Kazam E. MR, CT, and ultrasonographic demonstration of splenic vein thrombosis. *J Comput Assist Tomogr* **1984**;8:1199–1200
14. Nichols DM. Computed tomography in acute mesenteric vein thrombosis. *J Comput Assist Tomogr* **1984**;8:171–172
15. Mathieu D, Vasile N, Grenier P. Portal thrombosis: dynamic CT features and course. *Radiology* **1985**;154:737–741
16. Matos C, Van Gansbeke D, Zalcman M, et al. Mesenteric vein thrombosis: early CT and US diagnosis and conservative management. *Gastrointest Radiol* **1986**;11:322–325
17. Subramanyam BR, Balthazar EM, Lefleur RS, Horii SC, Hulnick DH. Portal venous thrombosis: correlative analysis of sonography, CT, and angiography. *Am J Gastroenterol* **1984**;79:773–776
18. Glynn MJ. Isolated splenic vein thrombosis. *Arch Surg* **1986**;121:723–725

Barrett's Esophagus: Diagnosis by Double-Contrast Esophagography

Alison M. Gilchrist[1, 2]
Marc S. Levine[1]
Robert F. Carr[3]
Scott H. Saul[3]
David A. Katzka[4]
Hans Herlinger[1]
Igor Laufer[1]

A blinded, retrospective study was performed to determine the role of double-contrast esophagography in diagnosing Barrett's esophagus. The study group consisted of 200 patients who had double-contrast esophagrams and endoscopy because of severe reflux symptoms. The radiographs were reviewed by two gastrointestinal radiologists who had no knowledge of the endoscopic findings. Patients were classified as being at high risk for Barrett's esophagus if the radiographs revealed a high stricture or ulcer or a reticular mucosal pattern; at moderate risk if the radiographs revealed a distal peptic stricture and/or reflux esophagitis; and at low risk if none of the aforementioned findings were present. When these radiologic criteria were used, 10 patients (5%) were thought to be at high risk, 73 (37%) at moderate risk, and 117 (58%) at low risk for Barrett's esophagus. Endoscopic correlation revealed biopsy-proved Barrett's mucosa in nine (90%) of 10 patients at high risk, in 12 (16%) of 73 at moderate risk, and in only one (1%) of 117 at low risk for Barrett's esophagus. Thus, endoscopy is clearly indicated for patients in the high-risk group. Because of the lower prevalence of Barrett's esophagus in the moderate-risk group, clinical judgment should be used in deciding when to perform endoscopy in these patients. However, most patients were in the low-risk group, and the prevalence of Barrett's esophagus was so low in this group that endoscopy does not appear to be warranted.

Thus, the major value of double-contrast esophagography is its ability to separate patients into high-, moderate-, and low-risk groups for Barrett's esophagus to determine the relative need for endoscopy and biopsy.

Barrett's esophagus is a well-recognized condition in which there is progressive columnar metaplasia of the distal esophagus caused by long-standing gastroesophageal reflux and reflux esophagitis [1–5]. It is unclear why some patients with reflux esophagitis develop Barrett's esophagus and others do not. Nevertheless, Barrett's esophagus is considered a premalignant condition and is associated with a significantly increased risk of developing adenocarcinoma [6–15]. As a result, periodic endoscopic surveillance has been advocated for early detection of cancer in these patients [6–15].

The classic radiologic features of Barrett's esophagus are a high esophageal stricture or ulcer associated with a hiatal hernia and/or gastroesophageal reflux [1, 16–18]. However, recent studies have found that strictures are actually more common in the distal esophagus and that the majority of cases do not fit the classic description of a high stricture or ulcer [19–21]. A reticular mucosal pattern has also been described as a highly specific sign of Barrett's esophagus on double-contrast esophagography [22], but this finding is only present in a minority of cases [18, 20–23] and its specificity has been questioned [18, 24]. Other, more common findings in Barrett's esophagus, such as gastroesophageal reflux, hiatal hernias, and reflux esophagitis, are nonspecific since they can be present in patients with uncomplicated reflux disease. Thus, radiographic findings that are relatively specific for Barrett's esophagus are not sensitive, and those that are sensitive are not specific. Many investigators therefore believe that esophagography has limited

Received July 27, 1987; accepted after revision September 9, 1987.

[1] Department of Radiology, Hospital of the University of Pennsylvania, 3400 Spruce St., Philadelphia, PA 19104. Address reprint requests to M. S. Levine.

[2] Present address: Department of Radiology, Royal Victoria Hospital, Grosvenor Rd., Belfast, Northern Ireland.

[3] Department of Pathology, Hospital of the University of Pennsylvania, Philadelphia, PA 19104.

[4] Department of Internal Medicine, Hospital of the University of Pennsylvania, Philadelphia, PA 19104.

AJR 150:97–102, January 1988
0361–803X/88/1501–0097
© American Roentgen Ray Society

value as a screening examination for Barrett's esophagus and that endoscopy and biopsy are required to diagnose this condition.

Many previous studies of Barrett's esophagus have included a retrospective analysis of the radiographic findings to determine the frequency of various abnormalities in this condition. To determine whether radiologic criteria can be used to quantitate the risk of Barrett's esophagus and, thus, to determine the relative need for endoscopic biopsies in these patients, we performed a blinded review of double-contrast esophagrams in 200 patients with reflux symptoms who underwent radiologic and endoscopic examinations.

Materials and Methods

Records of upper gastrointestinal endoscopic examinations performed at our hospital between 1980 and 1986 were reviewed randomly until 300 patients were identified who had had endoscopy because of severe reflux-related symptoms. Radiology files subsequently were reviewed until 200 patients were identified who had had double-contrast esophagrams within 2 months of the endoscopic examination. Those 200 patients form the basis for this study. Ninety-one were men, and 109 were women. The average age was 49.3 years (range, 19–82 years). Twelve patients had undergone previous antireflux operations, most frequently a Nissen fundoplication. All of the esophagrams were performed as biphasic examinations with upright double-contrast and prone single-contrast views of the esophagus, as described by Laufer [25]. The average interval between the radiologic and endoscopic examinations was about 4 weeks.

The radiographs from those 200 esophagrams were reviewed jointly by two gastrointestinal radiologists who had no knowledge of the endoscopic findings. The films were assessed first to determine the quality of the double-contrast examination. The study was graded as excellent if esophageal distension was adequate, with a thin layer of high-density barium producing a smooth, uniform mucosal coating throughout the esophagus. The study was graded as poor if esophageal distension was inadequate or if the mucosal surface was obscured by a thick layer of barium, undissolved effervescent agent, debris, or other artifacts. Studies of intermediate quality were graded as good or fair.

The radiographs were evaluated for the presence or absence of a sliding hiatal hernia, reflux esophagitis, a mid- or distal esophageal stricture or ulcer, reticular mucosal pattern, and/or features of malignancy. After the radiographs had been blindly evaluated and the patients classified as being at high, moderate, or low risk for Barrett's esophagus, the original radiographic reports were then reviewed to determine whether spontaneous gastroesophageal reflux or abnormal motility had been present during the fluoroscopic examination.

The radiologic criteria for diagnosing reflux esophagitis included ulceration, irregularity or nodularity of the mucosa, and/or thickening of the longitudinal folds (i.e., folds greater than 3 mm in width). Esophagitis was graded radiographically as mild if slight nodularity of the mucosa and/or fold-thickening were present, moderate if significant nodularity, fold-thickening, and/or superficial ulceration were present, and severe if a markedly irregular mucosa, grossly thickened folds, and/or extensive ulceration were observed. High esophageal or mid-esophageal strictures were defined as those 5 cm or more above the gastroesophageal junction; distal (i.e., peptic) strictures were those below this level. Strictures were classified as mild if they were greater than 2 cm in maximal diameter, moderate if 1–2 cm in diameter, and severe if less than 1 cm in diameter. Other radiographic features of the stricture, such as its symmetry and margins, also were evaluated to determine whether it had a benign or malignant appearance.

Each of the 200 patients was then classified as being at high, moderate, or low risk for Barrett's esophagus on the basis of the following radiologic criteria. The patient was considered to be at high risk if the radiographs revealed a high esophageal stricture or ulcer or a reticular mucosal pattern, since these findings are thought to be highly suggestive of this condition [1, 16–18, 22]. As reported previously, a reticular mucosal pattern was characterized radiographically by innumerable, tiny, barium-filled grooves or crevices on the mucosal surface of the esophagus, often resembling the "areae gastricae" seen on double-contrast studies of the stomach [22]. The patient was considered to be at moderate risk if the radiographs revealed a distal stricture and/or reflux esophagitis, since previous studies have shown that about 45% of patients with peptic strictures [26] and 10% with reflux esophagitis [8, 12, 15, 27] have Barrett's mucosa. Finally, the patient was considered to be at low risk if none of the aforementioned findings were present.

The radiographic findings were then correlated with the endoscopic findings. All endoscopic examinations were performed with a GIF-K Olympus endoscope (Olympus, New Hyde Park, NY). The endoscopy reports were reviewed to determine whether there was endoscopic evidence of reflux esophagitis, strictures, or other abnormalities. When present, esophagitis and strictures were graded as mild, moderate, or severe on the basis of the endoscopic description. In addition, esophageal biopsy specimens were available for review by an experienced gastrointestinal pathologist in 66 cases. Barrett's esophagus was diagnosed in 21 of those cases, as defined histologically by Paull et al. [28]. The diagnostic criteria for Barrett's esophagus included (1) the presence of columnar epithelium in biopsies 2 cm or more above the gastroesophageal junction or 2 cm or more above a manometrically identified lower esophageal sphincter in the presence of a hiatal hernia; (2) the presence of intestinal metaplasia in biopsies from any part of the esophagus; and (3) the presence of junctional epithelium in biopsies of tissue from the distal esophagus (taken an unknown distance from the gastroesophageal junction) when biopsies from a second endoscopic examination several months earlier or later fulfilled either of the first two criteria for Barrett's esophagus. In one other patient in whom endoscopic biopsies were not obtained, a presumptive diagnosis of Barrett's esophagus was made because of the endoscopic finding of velvety, pinkish-red tongues of mucosa extending more than 2 cm above the gastroesophageal junction. In the remaining 133 patients who had no endoscopic biopsies, no evidence of Barrett's esophagus was observed endoscopically. Some cases of Barrett's esophagus could conceivably have been missed in this group, since biopsies were not obtained. However, previous studies have shown that endoscopy has a sensitivity of greater than 90% in diagnosing Barrett's esophagus, solely on the basis of the endoscopic appearance [29, 30].

Results

Radiographic Findings

The quality of the double-contrast examination was graded as excellent in 83 patients (42%), as good in 69 (34%), as fair in 41 (20%), and as poor in seven (4%). Sixty-one patients had radiologic evidence of reflux esophagitis; 24 of those patients also had strictures. Twenty-two other patients had strictures without active esophagitis. The remaining 117 patients had no evidence of esophagitis or strictures. The radiographic findings are summarized in Table 1.

TABLE 1: Radiographic Findings in 200 Patients with Reflux Symptoms

Finding	No. of Patients (%)
Hiatal hernia	83 (41.5)
Gastroesophageal reflux	73 (36.5)
Reflux esophagitis	61 (30.5)
Nodular mucosa	46 (23.0)
Ulceration	27 (13.5)
Thickened folds	23 (11.5)
Stricture	46 (23.0)
Mid	9 (4.5)
Distal	37 (18.5)
Abnormal motility	25 (12.5)
Reticular mucosal pattern	4 (2.0)

Correlation of Radiographic and Endoscopic Findings

The overall radiologic sensitivity in diagnosing reflux esophagitis was 52% (53/102) for all grades of esophagitis, 71% (32/45) for moderate or severe esophagitis, and 85% (17/20) for severe esophagitis (Table 2). At the same time, the radiologic specificity in diagnosing reflux esophagitis was 92% (90/98). Endoscopy detected only 43% (20/46) of all radiographically diagnosed strictures (Table 3). At the same time, endoscopy failed to detect a single stricture not seen on esophagography.

Radiographic Assessment of Barrett's Esophagus

Ten patients (5%) were thought to be at high risk for Barrett's esophagus on esophagography because of a high stricture in nine (Figs. 1A and 1B) and a high ulcer in one. Four of those patients had a reticular mucosal pattern adjacent to the distal aspect of the stricture (Fig. 1B). Endoscopy and biopsy confirmed the presence of Barrett's esophagus in nine of those 10 cases (90%). The remaining patient with a high stricture and reticular mucosal pattern had biopsy-proved squamous-cell carcinoma. Seventy-three other patients (37%) were thought to be at moderate risk for Barrett's esophagus: in 15, because of a stricture in the distal esophagus without esophagitis (Fig. 2); in 35, because of reflux esophagitis without a stricture (Fig. 3); and in 23, because of reflux esophagitis as well as a distal stricture. Endoscopic biopsies confirmed the presence of Barrett's esophagus in 12 (16%) of those 73 cases. The remaining 117 patients (58%) were thought to be at low risk for Barrett's esophagus because of the absence of esophagitis or strictures on esophagography. Although endoscopy revealed esophagitis in 49 of those 117 cases, 46 were mild or moderate and only three were severe. Endoscopic biopsies revealed Barrett's esophagus in one of those three patients with severe reflux esophagitis. In that patient, however, the double-contrast esophagram was thought to be of only fair quality because of a thick layer of barium that obscured mucosal detail in the distal esophagus. In the other 116 patients, no endoscopic evidence of Barrett's mucosa was found.

TABLE 2: Correlation of Radiographic and Endoscopic Findings in Diagnosing Reflux Esophagitis

Findings on Esophagography	Findings on Endoscopy			
	None	Mild	Moderate	Severe
None	90	36	10	3
Mild	4	19	9	7
Moderate	4	2	6	0
Severe	0	0	0	10

TABLE 3: Correlation of Radiographic and Endoscopic Findings in Diagnosing Strictures

Findings on Esophagography	Findings on Endoscopy			
	None	Mild	Moderate	Severe
None	154	0	0	0
Mild	10	6	0	0
Moderate	15	1	7	0
Severe	1	0	0	6

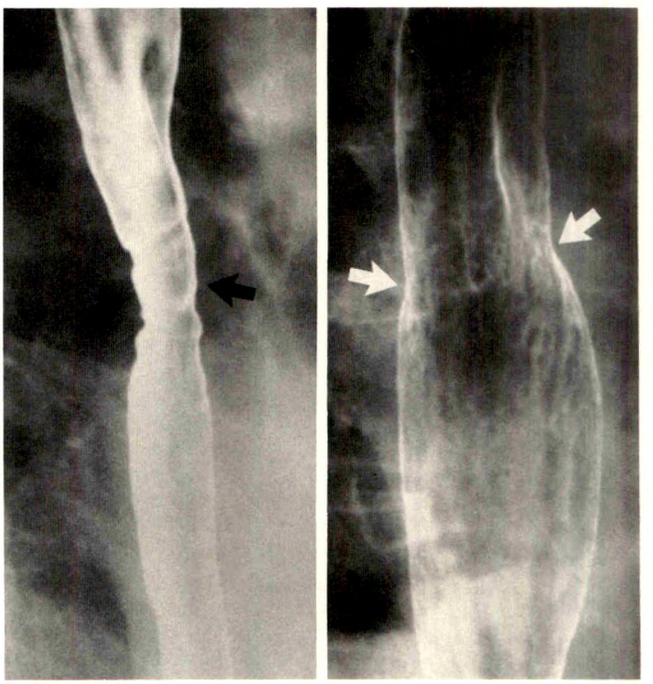

A B

Fig. 1.—*A* and *B*, Double-contrast esophagrams show mid-esophageal strictures (*arrows*) in two patients classified as being at high risk for Barrett's esophagus. Also note reticular mucosal pattern adjacent to relatively early stricture (*arrows*) in patient in *B*. Both patients had endoscopically proved Barrett's esophagus.

If a positive diagnosis of Barrett's esophagus is made in all patients who are at high or moderate risk for this condition on esophagography, our overall radiologic sensitivity is 95% (21/22), but our specificity is only 65% (116/178). If these

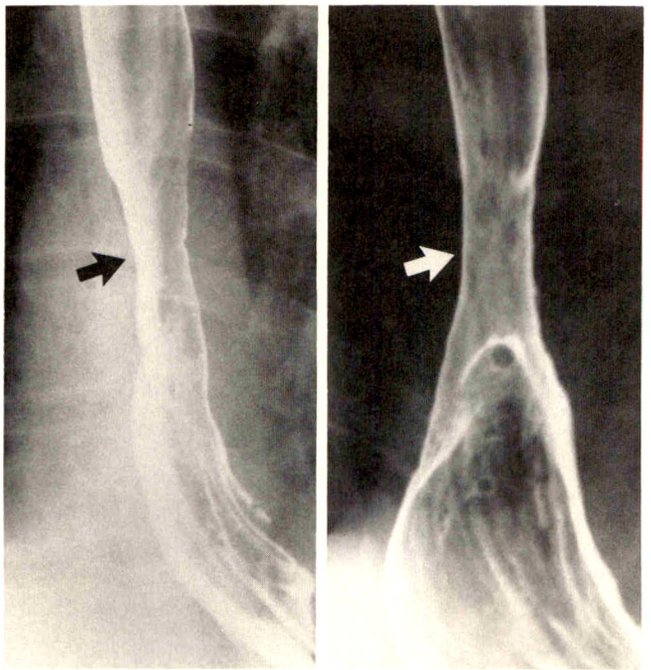

A B

Fig. 2.—*A* and *B*, Double-contrast esophagrams show smooth peptic strictures (*arrows*) in distal esophagus without active esophagitis in two patients classified as being at moderate risk for Barrett's esophagus. Endoscopy confirmed presence of stricture in both patients, but endoscopic biopsies revealed Barrett's mucosa only in patient in *A*.

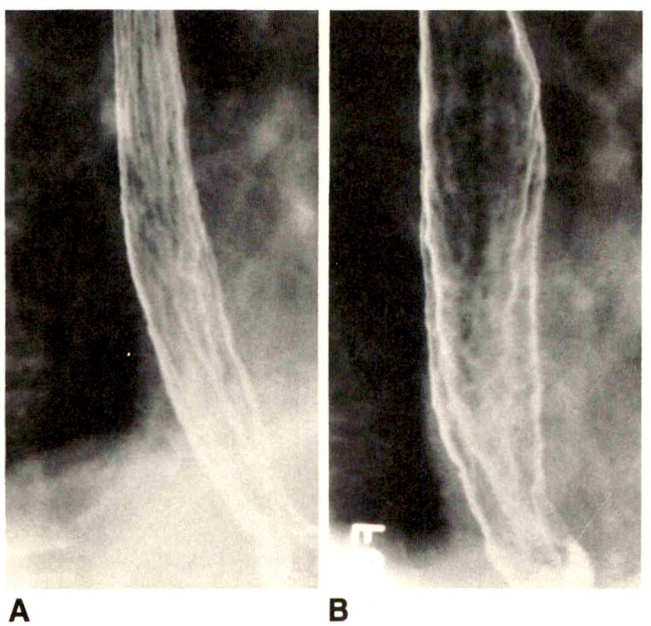

A B

Fig. 3.—*A* and *B*, Double-contrast esophagrams show reflux esophagitis with nodular, irregular mucosa and thickened folds in distal third of esophagus in two patients classified as being at moderate risk for Barrett's esophagus. Endoscopy confirmed presence of reflux esophagitis in both patients, but endoscopic biopsies revealed Barrett's mucosa only in patient in *A*.

criteria are used, the positive predictive value of the radiologic examination is only 25% (21/83), but the negative predictive value is 99% (116/117). If, however, Barrett's esophagus is only diagnosed in patients who are at high risk for this condition on esophagography, our specificity increases to 99% (177/178), but our sensitivity decreases to 41% (9/22).

Radiographic Assessment of Adenocarcinoma

Four patients who were at high risk for Barrett's esophagus because of a high esophageal stricture had additional radiographic findings suspicious for a superimposed adenocarcinoma. In all four cases, asymmetry of the stricture and/or nodularity or irregularity of the adjacent mucosa were observed. The presence of malignancy was confirmed endoscopically in only one of these cases. However, this case proved to be a squamous-cell carcinoma rather than an adenocarcinoma in Barrett's esophagus. The patient had a superficial spreading lesion that was mistaken radiographically for the reticular pattern of Barrett's mucosa.

Seven other patients who were at moderate risk for Barrett's esophagus on esophagography had additional radiographic findings that were considered equivocal for a superimposed malignancy. Only one of those seven patients had histologically proved adenocarcinoma arising in Barrett's mucosa. The latter patient had an irregular stricture in the distal esophagus. An associated adenocarcinoma was suspected because of asymmetry, overhanging margins, and ulceration within the stricture.

Discussion

Barrett's esophagus is a well-recognized condition in which the normal squamous epithelium in the esophagus has been replaced by a columnar epithelial lining owing to chronic reflux esophagitis [1–5]. Recent data suggest that this condition is more common than has previously been recognized. In various studies, the prevalence of Barrett's esophagus in patients with reflux esophagitis has ranged from 8% to 20%, with an overall prevalance of about 10% [8, 12, 15, 27]. In our study, Barrett's esophagus was detected in 11% of patients (22/200) who underwent endoscopy for reflux-related symptoms. However, this figure may be skewed in favor of Barrett's esophagus, since all of our patients had reflux symptoms severe enough to warrant both radiologic and endoscopic examinations.

Barrett's esophagus is important because it is a premalignant condition in which the risk of developing adenocarcinoma is perhaps 30–40 times greater than it is in the general population [31, 32]. It is widely believed that adenocarcinoma evolves through a sequence of progressively severe epithelial dysplasia, carcinoma-in-situ, and invasive carcinoma in preexisting areas of columnar metaplasia. In recent studies, the prevalence of adenocarcinoma in patients with Barrett's esophagus has ranged from 2.4% to 46.5%, with an overall prevalence of about 15% [6, 8, 12, 15, 33–35]. Prevalence data may exaggerate the risk of cancer [31, 32], since most

patients with Barrett's esophagus do not seek medical attention until complications such as ulcers, strictures, or malignancy develop. Nevertheless, many investigators advocate periodic endoscopic surveillance with biopsy and cytology at 6-month or yearly intervals for early detection of cancer in Barrett's esophagus [6–15].

The classic radiologic features of Barrett's esophagus consist of a high esophageal stricture or ulcer, often associated with a sliding hiatal hernia and gastroesophageal reflux [1, 16–18]. Although these findings should be highly suggestive of Barrett's esophagus, they are found in only 28–48% of patients with this condition [18–22]. A reticular mucosal pattern also has been described as a relatively specific sign of Barrett's esophagus on double-contrast esophagography, particularly if located adjacent to a stricture [22]. However, this finding has been observed in only 5–30% of patients with Barrett's esophagus [18, 20–24]. Similarly, in our study, a high stricture or ulcer or a reticular mucosal pattern were present on double-contrast esophagography in only nine (41%) of 22 patients with this condition. Thus, esophagography is an inadequate screening examination for Barrett's esophagus when the diagnosis is restricted to patients who have the classic radiologic features of this condition.

Because Barrett's esophagus develops as the sequela of long-standing reflux esophagitis, it is not surprising that these patients often have radiologic evidence of hiatal hernias, gastroesophageal reflux, reflux esophagitis, and peptic strictures [17–23]. However, these radiologic findings may occur without associated Barrett's metaplasia. As a result, inclusion of these findings as criteria for Barrett's esophagus increases the sensitivity of the radiologic examination but decreases its specificity, so that many patients would be referred unnecessarily for endoscopy and biopsy [23]. Thus, esophagography is thought to have limited value in diagnosing this condition.

In our study, however, patients were classified radiographically as being at high, moderate, or low risk for Barrett's esophagus. Ninety percent of patients (9/10) who were thought to be at high risk for Barrett's esophagus because of a high stricture or ulcer or reticular mucosal pattern had pathologically proved Barrett's mucosa (Fig. 1). However, only 5% of all patients in the study group were placed in this category. A much larger group of patients (37%) were thought to be at moderate risk for Barrett's esophagus because of reflux esophagitis and/or distal peptic strictures (Figs. 2 and 3). Only 16% (12/73) in this category had Barrett's mucosa. However, the majority of patients (58%) were thought to be at low risk for Barrett's esophagus because of the absence of esophagitis or strictures. Only one of 117 patients (less than 1%) in this category had Barrett's esophagus on endoscopy. This patient had a suboptimal double-contrast examination because pooling of barium in the distal esophagus obscured mucosal detail. Because the predictive value of a negative esophagram (i.e., patients who were at low risk radiographically for Barrett's esophagus) was greater than 99%, our experience suggests that unnecessary endoscopy could be avoided in patients who have no evidence of esophagitis or strictures on double-contrast examinations.

Because endoscopy is a considerably more expensive procedure than double-contrast radiography, significant financial savings could result from screening these patients with esophagography rather than with esophagoscopy. At our hospital, the fee for a double-contrast esophagram is $135, whereas the fee for esophagoscopy is between $425 and $550, depending on the number of biopsies taken. In our study, the total cost of performing radiologic examinations on 200 patients with reflux symptoms was $27,000. Because esophagoscopy was required for 83 patients who were at moderate or high risk for Barrett's esophagus on barium studies, the additional cost for performing endoscopy on these patients was about $40,000, and the total cost was about $67,000. In contrast, the cost for performing esophagoscopy on these 200 patients was about $100,000. Thus, the cost for performing double-contrast esophagography as a screening examination with follow-up esophagoscopy in selected cases is about one-third less than that of performing endoscopy as the initial examination in these patients. On a national scale, the economic implications are enormous.

It has been documented previously that endoscopy is more sensitive than double-contrast esophagography in detecting reflux esophagitis [36–39]. However, most false-negative radiologic examinations occur in patients who have mild or moderate esophagitis, whereas severe esophagitis is rarely missed on esophagography [36–39]. In our study, the overall radiologic sensitivity in diagnosing reflux esophagitis was only 53%, but most cases of reflux esophagitis missed radiographically were mild, and only one patient whose esophagitis was missed on esophagography had Barrett's esophagus. Thus, our study suggests that esophagitis severe enough to cause Barrett's esophagus almost always can be detected on technically adequate double-contrast examinations.

Other patients with Barrett's esophagus may have peptic strictures without esophagitis [26]. Although severe peptic strictures are readily detected on both radiologic and endoscopic examinations, low-grade strictures actually may be easier to diagnose on esophagography [40]. In our study, 63% of mild or moderate radiologic strictures were missed on endoscopy, but no endoscopic strictures were missed on esophagography.

In summary, we believe that patients should be classified radiographically into high-, moderate-, and low-risk groups for Barrett's esophagus on double-contrast esophagography. Patients who are at high risk for Barrett's esophagus because of a high stricture or ulcer or a reticular mucosal pattern almost always have this condition, so that endoscopy and biopsy should be performed for a definitive diagnosis. A larger group of patients are at moderate risk for Barrett's esophagus because of reflux esophagitis or peptic strictures, so that clinical judgment should be used regarding the decision for endoscopy in this group based on the severity of reflux symptoms, age, and overall health of the patient. However, the majority of patients have no evidence of esophagitis or strictures, and the risk of Barrett's esophagus is so low in this group that endoscopy does not appear to be warranted. Thus, the major value of double-contrast esophagography is its ability to separate patients into high-, moderate-, and low-

risk groups for Barrett's esophagus to determine the relative need for endoscopy and biopsy in these patients.

REFERENCES

1. Burgess JN, Payne WS, Andersen HA, Weiland LH, Carlson HC. Barrett esophagus: the columnar-epithelial-lined lower esophagus. *Mayo Clin Proc* **1971**;46:728–734
2. Mangla JC. Barrett's esophagus: an old entity rediscovered. *J Clin Gastroenterol* **1981**;3:347–356
3. Bozymski EM, Herlihy KJ, Orlando RC. Barrett's esophagus. *Ann Intern Med* **1982**;97:103–107
4. Sjogren RW, Johnson LF. Barrett's esophagus: a review. *Am J Med* **1983**;74:313–321
5. Spechler SJ, Goyal RK. Barrett's esophagus. *N Engl J Med* **1986**; 315:362–371
6. Hawe A, Payne WS, Weiland LH, Fontana RS. Adenocarcinoma in the columnar epithelial lined lower (Barrett) oesophagus. *Thorax* **1973**;18: 511–514
7. Belladonna JA, Hajdu SI, Bains MS, Winawer SJ. Adenocarcinoma in situ of Barrett's esophagus diagnosed by endoscopic cytology. *N Engl J Med* **1974**;291:895–896
8. Naef AP, Savary M, Ozzello L. Columnar-lined lower esophagus: an acquired lesion with malignant predisposition. *J Thorac Cardiovasc Surg* **1975**;70:826–835
9. Poleynard GD, Marty AT, Birbaum WB, Nelson LE, O'Reilly RR. Adenocarcinoma in the columnar-lined (Barrett) esophagus. *Arch Surg* **1977**;112:997–1000
10. Berenson MM, Riddell RH, Skinner DB, Freston JW. Malignant transformation of esophageal columnar epithelium. *Cancer* **1978**;41:554–561
11. Haggitt RC, Tryzelaar J, Ellis FH, Colcher H. Adenocarcinoma complicating columnar epithelium-lined (Barrett's) esophagus. *Am J Clin Pathol* **1978**;70:1–5
12. Starnes VA, Adkins RB, Ballinger JF, Sawyers JL. Barrett's esophagus: a surgical entity. *Arch Surg* **1984**;119:563–567
13. Harle IA, Finley RJ, Belsheim M. Management of adenocarcinoma in a columnar-lined esophagus. *Ann Thorac Surg* **1985**;40:330–336
14. Sanfey H, Hamilton SR, Smith RRL, Cameron JL. Carcinoma arising in Barrett's esophagus. *Surg Gynecol Obstet* **1985**;161:570–574
15. Sarr MG, Hamilton SR, Marrone GC, Cameron JL. Barrett's esophagus: its prevalence and association with adenocarcinoma in patients with symptoms of gastroesophageal reflux. *Am J Surg* **1985**;149:187–192
16. Missakian MM, Carlson HC, Andersen HA. The roentgenologic features of the columnar epithelial-lined lower esophagus. *AJR* **1967**;99:212–217
17. Robbins AH, Hermos JA, Schimmel EM, Friedlander DM, Messian RA. The columnar-lined esophagus: analysis of 26 cases. *Radiology* **1977**;123: 1–7
18. Chen YM, Gelfand DW, Ott DJ, Wu WC. Barrett esophagus as an extension of severe esophagitis: analysis of radiologic signs in 29 cases. *AJR* **1985**;145:275–281
19. Robbins AH, Vincent ME, Saini M, Schimmel EM. Revised radiologic concepts of the Barrett esophagus. *Gastrointest Radiol* **1978**;3:377–381
20. Shapir J, DuBrow R, Frank P. Barrett oesophagus: analysis of 19 cases. *Br J Radiol* **1985**;58:491–493
21. Agha FP. Radiologic diagnosis of Barrett's esophagus: critical analysis of 65 cases. *Gastrointest Radiol* **1986**;11:123–130
22. Levine MS, Kressel HY, Caroline DF, Laufer I, Herlinger H, Thompson JJ. Barrett esophagus: reticular pattern of the mucosa. *Radiology* **1983**;147:663–667
23. Chernin MM, Amberg JR, Kogan FJ, Morgan TR, Sampliner RE. Efficacy of radiologic studies in the detection of Barrett's esophagus. *AJR* **1986**;147:257–260
24. Vincent ME, Robbins AH, Spechler SJ, Schwartz R, Doos WG, Schimmel EM. The reticular pattern as a radiographic sign of the Barrett esophagus: an assessment. *Radiology* **1984**;153:333–335
25. Laufer I. *Double-contrast gastrointestinal radiology*. Philadelphia: Saunders, **1979**:79–80
26. Spechler SJ, Sperber H, Doos WG, Schimmel EM. The prevalence of Barrett's esophagus in patients with chronic peptic esophageal strictures. *Dig Dis Sci* **1983**;28:769–774
27. Burbige EJ, Radigan JJ. Characteristics of the columnar-cell lined (Barrett's) esophagus. *Gastrointest Endosc* **1979**;25:133–136
28. Paull A, Trier JS, Dalton MD, Camp RC, Loeb P, Goyal RK. The histologic spectrum of Barrett's esophagus. *New Engl J Med* **1976**;295:476–480
29. Winters C, Spurling TJ, Chobanian SJ, et al. Barrett's esophagus: a prevalent, occult complication of gastroesophageal reflux disease. *Gastroenterology* **1987**;92:118–124
30. Katzka D, Plotkin A, Saul S, et al. A controlled study of toluidine blue staining in patients with Barrett's metaplasia of the esophagus (abstr). *Gastroenterology* **1986**;90:1485
31. Spechler SJ, Robbins AH, Rubins HB, et al. Adenocarcinoma and Barrett's esophagus: an overrated risk? *Gastroenterology* **1984**;87:927–933
32. Cameron AJ, Ott BJ, Payne WS. The incidence of adenocarcinoma in columnar-lined (Barrett's) esophagus. *N Engl J Med* **1985**;313:857–859
33. Radigan LR, Glover JL, Shipley FE, Shoemaker RE. Barrett esophagus. *Arch Surg* **1977**;112:486–491
34. Skinner DB, Walther BC, Riddell RH, Schmidt H, Iascone C, DeMeester TR. Barrett's esophagus: comparison of benign and malignant cases. *Ann Surg* **1983**;198:554–565
35. Levine MS, Caroline D, Thompson JJ, Kressel HY, Laufer I, Herlinger H. Adenocarcinoma of the esophagus: relationship to Barrett mucosa. *Radiology* **1984**;150:305–309
36. Ott DJ, Gelfand DW, Wu WC. Reflux esophagitis: radiographic and endoscopic correlation. *Radiology* **1979**;130:583–588
37. Koehler RE, Weyman PJ, Oakley HF. Single- and double-contrast techniques in esophagitis. *AJR* **1980**;135:15–19
38. Ott DJ, Wu WC, Gelfand DW. Reflux esophagitis revisited: prospective analysis of radiologic accuracy. *Gastrointest Radiol* **1981**;6:1–7
39. Creteur V, Thoeni RF, Federle MP, et al. The role of single and double-contrast radiography in the diagnosis of reflux esophagitis. *Radiology* **1983**;147:71–75
40. Ott DJ, Chen YM, Wu WC, Gelfand DW. Endoscopic sensitivity in the detection of esophageal strictures. *J Clin Gastroenterol* **1985**;7:121–125

Case Report

Electrical Injury in the Esophagus

Michael E. Flisak[1] and Scott Berman

Esophageal strictures are nonspecific abnormalities for which numerous possible causes exist. Traumatic strictures most frequently result from caustic ingestion. This report describes an additional unusual cause of an esophageal stricture—electrical injury—that has not been reported previously.

Case Report

A 34-year-old male cocaine abuser was admitted complaining of odynophagia after a suicide attempt. During an attempted self-electrocution, the patient swallowed the cut end of an electrical cord and then plugged the other end into a wall socket.

A Gastrografin swallow (Squibb, Princeton, NJ) was performed before endoscopy to rule out perforation (Fig. 1A). This revealed mucosal irregularity along the lateral esophageal wall at the level of C7–T1. There was no extravasation of contrast material. Endoscopy revealed charred and inflamed mucosa on the lateral and anterior esophageal walls distal to the cricopharyngeus.

Treatment during hospitalization consisted of gastrostomy tube placement, stenting of the injured site, and parenteral administration of steroids and antibiotics. The patient was discharged after 2 weeks in satisfactory condition with the tube in place.

Four weeks after discharge from the hospital, the patient complained of worsening dysphagia. An esophagram showed a weblike stricture at the site of previous injury (Fig. 1B). Repeated attempts at dilatation of this area failed to provide symptomatic relief. Resection

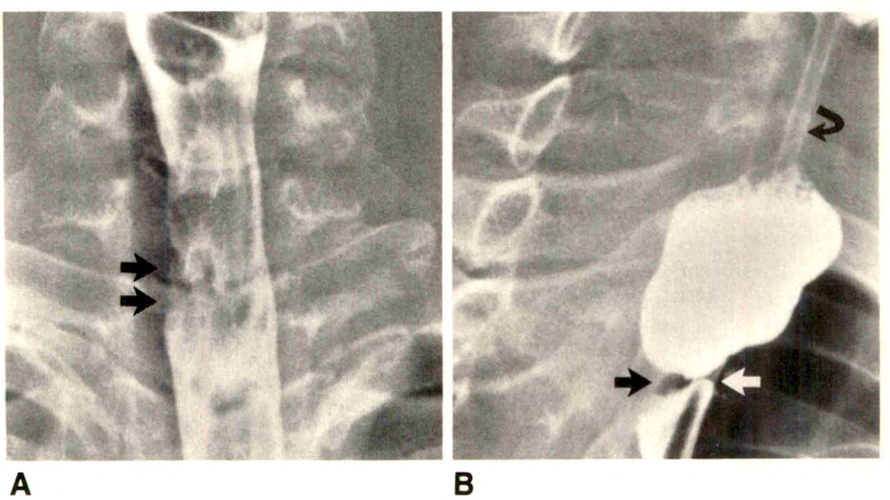

Fig. 1.—*A*, Gastrografin esophagram at time of admission, anteroposterior view. Eccentric area of irregular narrowing along right lateral esophageal wall is seen at level of C7–T1 (*arrows*).

***B*, Follow-up barium esophagram. Short, weblike stricture has formed at site of esophageal injury (*straight arrows*). Feeding tube is in place (*curved arrow*).**

Received July 15, 1987; accepted after revision August 18, 1987.

[1] Both authors: Department of Radiology, Loyola University Medical Center, Foster G. McGaw Hospital, 2160 S. First Ave., Maywood, IL 60153. Address reprint requests to M. E. Flisak.

of the stricture with primary end-to-end anastomosis was successful, and the patient has been asymptomatic over a 3-month follow-up period.

Discussion

An esophageal stricture is a nonspecific radiographic or endoscopic finding. Most commonly, it represents a fibrotic area that arises in response to an inflammatory or neoplastic stimulus. Although most are of benign etiology, neoplastic causes must also be considered, especially when the stricture is atypical in appearance.

In most cases, a carefully taken history will elicit the probable cause of the stricture. Occasionally, endoscopy and biopsy are indicated, especially to differentiate an unusual stricture from a neoplastic lesion [1].

A single previous case of electrical injury to the esophagus has been reported as a complication of esophageal temperature monitoring during general anesthesia [2, 3]. In this case, however, radiographic studies were not done, and esophageal stricture did not occur. Electrodes have been developed for transesophageal atrial pacing. In animal studies, pill electrodes can cause esophageal mucosal injury when current levels greater than 75 mA are applied over a relatively short time span (i.e., less than 30 min) [4]. To our knowledge, there are no reports of esophageal injury due to their use in humans. In our case, the current was applied for only a fraction of a second, but the current level was probably between 15 and 20 A.

REFERENCES

1. Margulis AR, Burhenne HJ, eds. *Alimentary tract radiology*. St. Louis: Mosby, **1983**:579–582.
2. Parlar EO. Electrical surgical burn at the site of an esophageal temperature probe. *Anesthesiology* **1984**;61(1):93–95
3. Weiss FR. Technique of avoiding esophageal burns. *Anesthesiology* **1985**;62(3):370
4. Jenkins JM, Dick M, Collins S, O'Neill W, Campbell RM. Use of the pill electrode for transesophageal atrial pacing. *PACE* July **1985**;8(4):512–527

Case Report

Enteroliths in a Continent Ileostomy

Emily R. Fox,[1] Taylor Chung, and Igor Laufer

During the past 20 years, much progress has been made in creating ileostomies that function well in patients who have had a panproctocolectomy. In 1967, Kock [1] designed an internal ileal reservoir with a nipple valve to maintain continence in these patients. The Kock pouch reservoir can be emptied easily by means of intermittent intubation [1]. In an extensive review of 479 patients, Goldman and Rombeau [2] found that 80% maintained continence. A major complication associated with the pouch ileostomy is bacterial overgrowth and stasis, a condition that is clinically characterized by increased output, cramping, and nausea and vomiting. In our patient, the formation of enteroliths was complicated by recurrent episodes of stasis and bacterial overgrowth. Surgical removal of the concretions was necessary before the patient's symptoms resolved.

Case Report

A 39-year-old woman had severe pancolitis from ulcerative colitis for which she underwent a total colectomy and Kock pouch ileostomy in 1978. At the time of her admission, she had a 3-month history of diarrhea (with increased output) and abdominal cramps, and a weight loss of approximately 20 lb. (9 kg). These symptoms were attributed to a bacterial overgrowth in the pouch reservoir, but only transient relief was obtained when metronidazole was given. When the medication was discontinued, the symptoms promptly recurred.

Abdominal radiographs taken over a 6-year period from time of surgical formation of the continent ileostomy revealed the slow development of calcifications in the pelvis that gradually had increased in size and number (Fig. 1A). A barium study showed residual fluid and multiple freely mobile enteroliths of varying size and configuration (Fig. 1B).

Endoscopy revealed an erythematous, exudative, boggy mucosa with a friable surface. Enteroliths were observed, and a fragment was removed. Infrared spectroscopy showed the fragment to be composed of calcium hydroxyapatite salts and proteinaceous material.

The patient continued to have abdominal discomfort and increased ileostomy output despite repeated courses of metronidazole therapy. Surgical exploration of the Kock pouch revealed approximately 15 enteroliths ranging in size from 5 to 12 mm, many intimately associated with embedded mural sutures (Fig. 1C).

Since the surgical removal of the enteroliths 10 months ago, the patient has remained continent and asymptomatic.

Discussion

Enteroliths may be divided into two categories—primary and secondary—depending on their site of formation. Primary enteroliths form within the bowel lumen proper, whereas secondary enteroliths (such as gallstones) are formed outside the gastrointestinal tract and erode into the bowel lumen. Primary enterolith formation requires stasis (usually from a degree of obstruction) and the alkaline milieu of the succus entericus, which is composed of calcium phosphate, carbonate, and oxalate salts [3]. The concretions may be purely calcific precipitates of the succus entericus, or formation may be initiated by nidi, such as ingested vegetable fiber or other foreign bodies. Our case is an example of enterolith formation induced by undigested vegetable matter and nonabsorbable suture material. We postulate that the patient's continent stoma and small-caliber intubation catheter provided a functional stenosis, allowing dietary fiber residue and suture material to accumulate and slowly calcify, forming pouch enteroliths.

Received July 13, 1987; accepted after revision August 25, 1987.

[1] All authors: Department of Radiology, Hospital of the University of Pennsylvania, 3400 Spruce St., Philadelphia, PA 19104. Address reprint requests to I. Laufer.

AJR 150:105–106, January 1988 0361–803X/88/1501–0105 © American Roentgen Ray Society

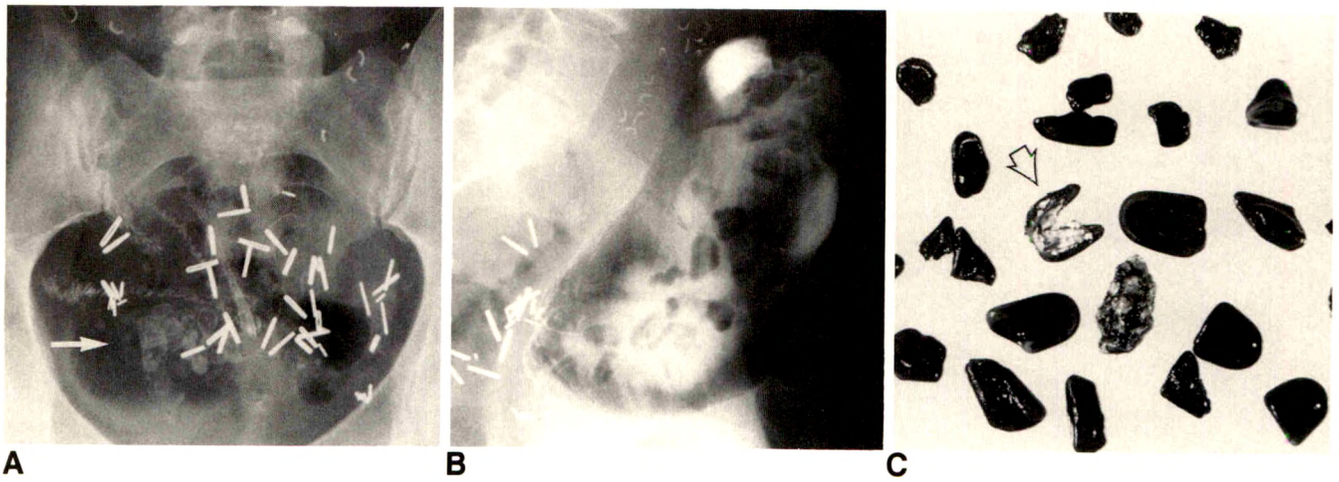

Fig. 1.—*A*, Enterolith formation. Plain abdominal radiograph shows radiopaque enteroliths (*arrow*). Surgical clips from ileal surgery and clips from a hysterectomy are evident.
***B*, Barium study of Kock pouch. Lateral abdominal view shows multiple freely mobile filling defects within continent ileostomy reservoir.**
***C*, Surgically removed enteroliths vary in size and shape. A sectioned enterolith (*arrow*) reveals a central nidus of vegetable matter.**

Beart et al. [4] have suggested that patients with Kock pouches should avoid high-residue diets since high-residue foods have a tendency to block drainage catheters. No cases of catheter obstruction or bezoar formation have been described in a Kock pouch. However, when persistent food residue or foreign bodies remain in the appropriate chemical milieu for a prolonged period, enterolith formation is not unusual.

Despite repeated courses of antibiotic therapy in this patient, symptomatic relief was not obtained until after surgical removal of the enteroliths. Therefore, a critical mass of enteroliths presumably had an irritative effect on the pouch mucosa and contributed to the obstruction of the drainage catheter, propagating stasis and bacterial overgrowth. Radiographic evaluation of the continent ileostomy by ileostomal barium enema has been described to evaluate architectural derangements of the pouch [5, 6]. In our case, the barium study was essential for localization and characterization of the calcific densities seen on the plain films. In retrospect, the patient had enteroliths 6 years before her recurrent bouts of bacterial overgrowth. The combination of early recognition of enterolith formation by careful scrutiny of plain films and barium studies, dietary restraints, and the use of larger intubation catheters may prevent the symptomatic complications of pouch enterolith formation.

REFERENCES

1. Kock NG. Intra-abdominal "reservoir" in patients with permanent ileostomies. Preliminary observations on a procedure resulting in fecal "continence" in five ileostomy patients. *Arch Surg* **1969**;99:223–230
2. Goldman SL, Rombeau JL. The continent ileostomy: a collective review. *Dis Colon Rectum* **1978**;21:594–599
3. Grettve S. Contributions to knowledge of primary true concrements in small bowel. *Acta Chir Scand* **1947**;387–410
4. Beart RW, Beahrs OH, Kelly KA, Dozois RR, Wolf SA. The continent ileostomy: a viable alternative. *Mayo Clin Proc* **1979**;54:643–645
5. Montagne JP, Kressel HY, Moss AA, Schrock TR. Radiologic evaluation of the continent (Kock) ileostomy. *Radiology* **1978**;127:325–329
6. Stephens DH, Mantell BE, Kelly KA. Radiology of the continent ileostomy. *AJR* **1979**;132:717–721

CT of the Liver: A Survey of Prevailing Methods for Administration of Contrast Material

Robert K. Zeman[1]
Lynn A. Clements[1]
Paul M. Silverman[1]
David M. Paushter[1,2]
Brian Garra[1]
Mark H. Jaffe[1]
Letitia R. Clark[1]

The members of the Society of Body Computed Tomography were surveyed to determine the most frequently used method of administering contrast material in CT studies of the liver. The respondents represented CT departments performing liver examinations in 22 institutions. No department relied solely on noncontrast scans. In 12 (54%) of 22 institutions, only contrast-enhanced scans were performed. The preferred dose for enhancement was 150 ml of 60% contrast material. Eight (36%) of the 22 respondents obtained images during the administration of a bolus of contrast material, whereas nine (41%) obtained images during the administration of a sustained drip infusion given after a loading bolus. Follow-up in 1987 revealed that two departments had switched to obtaining images during the administration of a bolus.

The availability of CT power injectors and refinements in the rapid-scanning capabilities of CT scanners have increased the popularity of obtaining images of the liver during the administration of a bolus of contrast material. Despite this, in many departments, contrast material is still administered via drip infusion in CT studies of the liver.

Various protocols for administration of contrast material have been used to provide enhancement for CT examination of the liver. Methods of administration include injection of a bolus, injection of a bolus followed by drip infusion, and drip infusion. The contrast material may be delivered by a gravity-fed IV drip, injected by hand, or injected mechanically. Recent investigations [1–6] have suggested that dynamic enhancement (i.e., rapid scanning with progressive movement of the table during injection of a bolus of contrast material) is superior to other procedures for enhancement. To assess the spectrum of techniques actually used to administer contrast material, we surveyed the members of the Society of Computed Body Tomography.

Materials and Methods

A 14-question survey on methods of administering contrast material in CT studies of the liver was sent to the 40 members of the Society of Computed Body Tomography. The Society had 37 members in academic departments and three in private practice at the time of the survey. Two questions subsequently were omitted from the tabulations because they gave superfluous information. A section for narrative comments was included also.

Four members did not perform liver studies routinely and therefore did not fill out the questionnaire. Ten replied that another member of the Society within their department would respond on their behalf. Two questionnaires were not completed, so a total of 24 members replied to the survey. Among these 24, two duplicate responses from the same institution were deleted. The data reported represent the methods used in 21 academic departments and one private practice. The data were tabulated in 1986. A successful follow-up telephone call was made in 1987 to all but two of the facilities that had responded originally.

Results

Although no institution represented in the Society relied on noncontrast scans only, in five institutions, enhanced scans were performed only if a suspicious finding

Received August 4, 1987; accepted after revision September 23, 1987

[1] Department of Radiology, Georgetown University Hospital, 3800 Reservoir Rd., N.W., Washington, DC 20007. Address reprint requests to R. K. Zeman.

[2] Present address: Department of Radiology, Cleveland Clinic Foundation, 9500 Euclid Ave., Cleveland, OH 44106.

AJR 150:107–109, January 1988
0361–803X/88/1501–0107
© American Roentgen Ray Society

was identified on the unenhanced images. In three departments, both noncontrast and contrast-enhanced scans were always performed. The majority of respondents (12/22) performed contrast-enhanced scans only. The narrative answers and follow-up telephone calls revealed that three institutions added noncontrast scans to their usual contrast-only protocol when hypervascular metastases were suspected.

The actual scanning methods used in the institutions varied greatly. In 17 of 22 departments, scans were performed either during administration of a bolus of contrast material (8/22) or during a drip infusion given after a loading bolus (9/22). Two reasons were cited for using the infusion method: (1) it did not require a physician in the CT suite during scanning and (2) it allowed the contrast injection to be prolonged so that the entire liver could be imaged. Only four of the respondents thought that a drip infusion of contrast material (without a loading bolus) would give adequately high levels of circulating contrast material. In one department, scans were performed immediately after a bolus of contrast material had been injected. At the time of the 1987 follow-up, two departments that previously had used a drip infusion were switching to administration via a bolus.

The narrative responses reflected variability in the definition of "dynamic." Ten respondents indicated that dynamic implied obtaining sections as fast as possible in a preprogrammed sequence with any given CT instrument, regardless of the method of delivery of contrst material. Eight respondents, however, noted that dynamic also implied that sections should be obtained during administration of a bolus of contrast material. Four respondents suggested that, irrespective of whether the CT scanner was set in a dynamic mode, only scans obtained within 2–3 min after arrival of contrast material in the liver should be considered dynamic, because extravascular equilibration would occur after 2–3 min. Of the nine respondents who obtained images during a drip infusion given after a loading bolus of contrast material, two actually set their machines in the dynamic mode for obtaining images.

The rate and method of delivering contrast material varied greatly. At the time of the original survey, a hand-injected contrast bolus was being used in 12 institutions. In six departments a machine injector was being used. At the time of the 1987 follow-up, bolus injection by hand had been replaced by injection by a machine in three institutions. A significant minority (9/22) of the respondents stated that they had not actually determined the rate at which contrast material was injected. Among the 13 departments in which the rate had been determined, 1 ml/sec was used in six. Three departments used an injection rate of 2 ml/sec or greater. Two institutions used 0.5 ml/sec, and two others used intermediate rates of injection.

The total amount of contrast material used by the majority (11/19) of respondents was 150 ml. All but four respondents used 60% urographic contrast material; one used 42%, one used 50%, and two used some other concentration. One respondent used ethiodized oil emulsion-13 (EOE-13). Another routinely used delayed (4 hr) scanning for dedicated liver examinations. Three additional respondents stated in the 1987 follow-up that delayed scanning was a useful adjunct but was performed only occasionally.

The delay between the initiation of contrast administration and the initiation of scanning was highly variable, from 0 to 60 sec. The most frequently reported delay before scanning was 21–45 sec (7/18). Only six of the 22 respondents complained that limitations in the heat capacity of the tube hampered their ability to scan the liver dynamically. Eight of the responding institutions had instruments capable of performing 12 to 16 sections without waiting for cooling of the tube. In all but two of the remaining departments, more than 16 sections could be done. Ten respondents stated that under some circumstances the liver could not be covered in a single dynamic sequence. Six of the 10 completed the examination of the liver nondynamically during recirculation of the contrast material.

The 22 institutions surveyed had a total of 44 CT scanners. These included GE 9800 (15), GE 8800 (10), Siemens DR series (nine), Picker 600 or 1200 (five), and other scanners (five). Four sites added the "Quick" package to their GE 9800 in 1987.

Discussion

The survey results revealed a wide variability in methods used to administer contrast material. Achieving high levels of circulating contrast during imaging was considered important by 17 of the 22 respondents. Although the literature [2, 3] states that high levels are achieved best by injection of a bolus, in 41% of the surveyed institutions contrast material was administered as a loading bolus followed by a drip infusion. Although this technique does result in high levels of circulating contrast material, prolonging the time of injection by using infusion carries the risk that imaging will be completed after extracellular equilibration has occurred. This extracellular equilibration is a significant cause of reduced lesion conspicuity [6].

More than 50% of the departments preferred a dose of 150 ml of 60% contrast material. Only two institutions specified using a lower concentration of contrast material. The question of which rate of administration is optimal remains unresolved. Nine respondents had not determined the actual rate of administration. In six institutions, 1 ml/sec was used. The relative merits of specific rates of injection have not been discussed yet in the literature. In only six of the responding departments was a power injector being used at the time of the original survey, but this number had increased to nine by 1987 because of the availability of dedicated CT injectors.

Three respondents performed unenhanced scans when hypervascular metastatic lesions were suspected. Enhancement via a bolus of contrast material may obscure lesions such as those due to metastatic renal cell carcinoma or carcinoid [7]. Although delayed (4 hr) scanning also may be useful in these patients, only four respondents specifically mentioned ever using this valuable technique [8, 9].

Finally, the narrative answers suggested a variable definition of dynamic scanning. The consensus was that two parameters must be defined for dynamic CT of the liver: (1) the timing of the scan sequence and (2) the timing and method of contrast administration. Completion of approximately 12 to

16 sections, each 1 cm thick, within 2 to 3 min takes greatest advantage of peak levels of intravascular contrast. Some recent CT units can achieve this rate of exposure without using a preprogrammed dynamic mode (i.e., single scans with deferred reconstruction). Administration of a bolus of contrast material within this 2- to 3-min interval results in the most favorable pharmacokinetics for the detection of liver lesions [1–6]. The survey data suggested that pragmatic constraints, such as not being able to scan through the entire liver during the injection of a bolus, has prevented universal acceptance of this method. The narrative answers to the survey and the 1987 follow-up suggest that the popularity of scanning during a sustained infusion will decrease as the rapid-scanning capabilities of CT instruments improve.

ACKNOWLEDGMENTS

The authors thank the members of the Society of Computed Body Tomography for their candid comments and Krystine M. Williams for assistance in preparing this manuscript.

REFERENCES

1. Young SW, Turner RJ, Castellino RA. A strategy for the contrast enhancement of malignant tumors using dynamic computed tomography and intrasvascular pharmacokinetics. *Radiology* **1980**;137:137–147
2. Foley WD, Berland LL, Lawson TL, Smith DF, Thorsen MK. Contrast enhancement technique for dynamic hepatic computed tomographic scanning. *Radiology* **1983**;147:797–803
3. Berland LL, Lawson TL, Foley WD, Melrose BL, Chintapalli KN, Taylor AJ. Comparison of pre- and postcontrast CT in hepatic massas. *AJR* **1982**;138:853–858
4. Freeny PC, Marks WM. Patterns of contrast enhancement of benign and malignant hepatic neoplasms during bolus dynamic and delayed CT. *Radiology* **1986**;160:613–618
5. Alpern MB, Lawson TL, Foley WD, et al. Focal hepatic masses and fatty infiltration detected by enhanced dynamic CT. *Radiology* **1986**;158:45–49
6. Paushter DM, Zeman RK, Schiebler ML, Choyke PL, Jaffe MH, Clark LR. Comparison of intravenous contrast enhancement techniques in the CT evaluation of hepatic metastases (abstr 278). *Radiology* **1985**;157(P):115
7. Bressler EL, Alpein MB, Glazer GM, Francis IR, Ensinger WD. Hypervascular hepatic metastases: CT evaluation. *Radiology* **1987**;162:49–51
8. Phillips VM, Erwin BC, Bernardino ME. Delayed iodine scanning of the liver: promising CT technique. *J Comput Assist Tomogr* **1985**;9:415–416
9. Perkerson RB Jr, Erwin BC, Baumgartner BR, et al. CT densities in delayed iodine hepatic scanning. *Radiology* **1985**;155:445–446

Book Review

Trauma Imaging in the Thorax and Abdomen. By Alexander Rosenberger, Olga B. Adler, and Rosalind H. Troupin. Chicago: Year Book Medical, 155 pp. 1987. $42

This text on imaging of the thorax and abdomen after trauma represents a collaborative effort between workers at Rambam Medical Center in Haifa, Israel, and the Hospital of the University of Pennsylvania. Much of the illustrative matieral is derived from imaging studies of victims of combat in Lebanon.

The text reviews trauma imaging from a brief historical perspective first and then considers the biomechanics of blunt and penetrating injury. Each subsequent chapter concerns imaging and is divided along anatomic lines (e.g., chest wall and diaphragm, pleural space, lung parenchyma, mediastinum). In addition to imaging, each chapter briefly reviews the relevant anatomy, pathophysiology, and clinical considerations pertinent to the anatomic region under discussion.

The text is generally well written, concise, and easy to read and comprehend. The illustrations tend to be somewhat small and are variable in quality, but they usually convey the message of the text. The references concluding each section, although limited in number, are usually both pertinent and up-to-date.

Although the work purports to cover many imaging techniques for trauma to the chest and abdomen, the coverage of angiographic pathology, sonography, nuclear medicine techniques, and interventional techniques in trauma is limited. Perhaps this is due to the increasing emphasis on CT imaging in trauma. In particular, the section on abdominal visceral trauma is, for the most part, a recapitulation of the techniques and experience described by Federle and coworkers at San Francisco General Hospital. Because of the book's short length, the number of illustrations is limited to classic examples of major pathologic changes; many entities are described rather than illustrated.

The text does succeed in covering a lot of material in a crisp, succinct fashion and does a particularly good job of handling some of the major controversies in the field, such as CT vs peritoneal lavage in abdominal trauma, CT in mediastinal trauma, and CT vs radionuclide imaging in the evaluation of splenic injury. Although the authors do offer their opinions on these subjects, they do not offer much hard data from their own experiences to support those opinions.

I would recommend this text to radiology residents who are interested in the subject and to nonradiologists who deal with traumatized patients, since it is an easy-to-comprehend overview of imaging in thoracicoabdominal trauma. However, its limited scope and length are not adequate for radiologists who seek in-depth coverage of this emerging radiologic discipline. The recent text by Toombs and Sandler, *Computed Tomography in Trauma*, and the second edition of *Computed Tomography in the Evaluation of Trauma* by Federle and Brant-Zawadski, although limited to consideration of CT in trauma, offer more detailed discussions and more illustrations.

Stuart E. Mirvis
University of Maryland Medical System
Baltimore, MD 21201

Hepatic Perivascular Lymphedema: CT Appearance

D. Bradley Koslin[1]
Robert J. Stanley[1]
Lincoln L. Berland[1]
Myung S. Shin[1]
Stephen C. Dalton[1,2]

The CT appearance of dilated hepatic lymphatics in liver transplant recipients has been described recently. We have observed similar findings of presumed hepatic lymphatic dilatation and perivascular lymphedema in 20 patients seen over an 8-month period, none of whom had received a liver transplant. Review of these patients' records showed that 18 (90%) of 20 had underlying disease processes that could have caused dilated lymphatics as a result of either increased lymph flow or lymphatic obstruction. We have grouped these processes into three etiologic categories: (1) posttraumatic hepatic lymphatic obstruction, (2) obstruction caused by malignant lymphadenopathy, and (3) congestive hepatomegaly caused by cardiac decompensation.

The appearance of hepatic lymphatic dilatation and surrounding lymphedema needs to be recognized so that lymphatic dilatation is not mistaken for dilated intrahepatic bile ducts.

In a recent report [1], the CT appearance of dilated hepatic lymphatics and related lymphedema in liver transplant recipients was described. The dilatation of the lymphatics was shown to be due to lymphatic stasis caused by the interruption of lymphatic vessels during the transplant surgery. The lymphatic stasis was histologically documented in a pig model, and dilated periportal lymphatics were present in biopsies of two transplanted livers. We have observed a similar appearance of presumed lymphatic dilatation and associated lymphedema in 20 patients, none of whom had received a liver transplant. We present these cases and speculate on the cause of this appearance.

Materials and Methods

During an 8-month period from January to August 1987, 20 patients examined with CT for a variety of clinical indications were found to have prominent hypodense perivascular zones very similar to those seen in patients with transplanted livers. The clinical indications for CT evaluation were varied and consisted of evaluation of blunt trauma (five), abdominal pain (four), fever of unknown origin (one), suspected abscess (two), retroperitoneal hematoma (one), possible liver abnormality (three), and staging of malignant neoplasm (four). All patients were studied with incremental dynamic scanning both during and after a 2-min IV injection of iodinated contrast medium (30–42 g of iodine) [2]. Either a GE 9800 or a Philips TX60 was used, and contiguous 1-cm-thick slices were obtained. Two patients also were scanned before IV contrast administration. Three patients had follow-up scans. The first patient's follow-up study was performed after a 10-day interval. The second patient's follow-up was performed after a 5-week interval. The third had two follow-up studies performed 7 and 17 weeks after the first scan. An analysis of the CT studies and the patients' hospital records was undertaken to determine possible reasons for the similar CT appearance in the 20 cases.

Results

Review of the patients' records showed that 18 of them had underlying disease processes that could cause lymphatic dilatation due to either increased lymph flow

Received August 3, 1987; accepted after revision September 4, 1987.

[1] Department of Radiology, University of Alabama Hospital, 619 S. 19th St., Birmingham, AL 35233. Address reprint requests to D. B. Koslin.

[2] Present address: Chatham Radiologists, P.A., 9 Medical Arts Ctr., Savannah, GA 31405.

AJR 150:111–113, January 1988
0361–803X/88/1501–0111
© American Roentgen Ray Society

or lymphatic obstruction. Three etiologic categories were identified: (1) posttraumatic hepatic lymphatic obstruction, (2) obstruction caused by malignant lymphadenopathy, and (3) congestive hepatomegaly caused by cardiac decompensation.

Category 1

Four patients had sustained blunt abdominal trauma. One had a periportal hematoma, the second and third developed intrahepatic hematomas associated with intraperitoneal hemorrhage, and the fourth sustained a compression fracture of the 12th thoracic vertebral body with an associated large retrocrural hematoma. All four had abnormal hypodense periportal zones, and the second and fourth patients also had hypodense zones encircling the intrahepatic inferior vena cava (Fig. 1). Follow-up scans on the first and fourth patients at 10 days and 35 days, respectively, showed complete resolution of the hematomas and hypodense perivascular zones.

Category 2

Two of the 20 patients had malignant neoplasms. One patient had hepatic metastases and periportal lymphadenopathy. The other patient had extensive retroperitoneal lymphadenopathy most prominent in the area of the cisterna chyli and the proximal thoracic duct (Fig. 2). This patient had three separate CT examinations. On the first two studies, which were separated by a period of 7 weeks, prominent hypodense zones were seen surrounding the portal venous system, with little intervening change in the size of the retroperitoneal lymphadenopathy. The third scan performed 10 weeks after the second showed development of a hypodense zone surrounding the intrahepatic portion of the inferior vena cava, as well as a slight decrease in the size but not the extent of the retroperitoneal lymphadenopathy.

Category 3

Twelve patients were found to have cardiomegaly and clinical evidence consistent with cardiac decompensation. Six patients had bilateral pleural effusions. Four of the patients also had ascites. All 12 had intrahepatic perivascular hypodense zones (Fig. 3), and three of them had hypodense zones surrounding the hepatic veins.

Other Patients

One patient with prominent hypodense perivascular zones had two separate disease processes, either of which might have caused the finding. The patient had congestive heart failure with cardiomegaly, ascites, and gallbladder-wall thickening on the CT examination. The other possible cause of the hypodense perivascular zones was periportal lymphadenopathy, which subsequently was proved to be benign reactive hyperplasia.

In the other two patients, hypodense zones surrounded the portal venous system and the intrahepatic segment of the vena cava. However, in neither patient was there an apparent explanation for these zones. The first patient had a history of ischemic heart disease and borderline cardiomegaly but no indications of congestive heart failure or of an elevated central venous pressure. The other patient had sustained blunt abdominal trauma but had no abdominal visceral injuries or hematomas.

Discussion

The origin of the hepatic lymph is threefold. Most lymph is derived from the liver sinusoids, a lesser portion is derived from the bile ducts, and a small amount is derived from the hepatic artery [3].

The sinusoids are separated from the liver cells by the perisinusoidal space of Disse. The wall of the sinusoids is highly permeable to plasma proteins and therefore no colloidosmotic pressure gradient exists. In the absence of this gradient, the fluid movement across the wall of the sinusoids is directly influenced by hydrostatic pressure changes. With any rise of venous pressure (e.g., during congestive heart failure), fluid formation in the hepatic interstitial compartment is enhanced and hepatic lymph flow is increased [3].

Lymphatic vessels have been found adjacent to epithelial

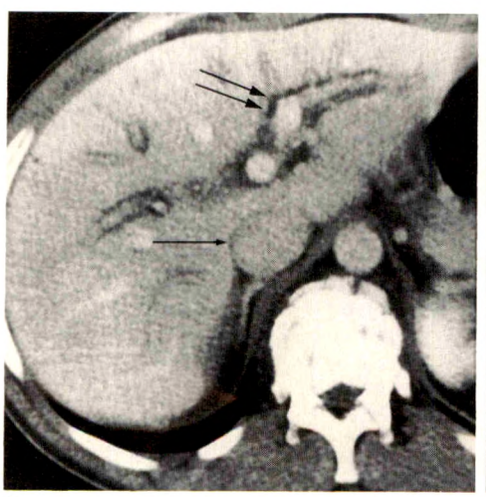

1

2

Fig. 1.—CT scan in a 31-year-old man with a compression fracture of the 12th thoracic vertebra shows hypodense periportal zones (*double arrows*) and hypodense zone surrounding inferior vena cava (*single arrow*). An associated hematoma was seen more clearly at slightly lower levels. On a follow-up scan obtained 35 days later, hypodense perivascular zones and hematoma had resolved.

Fig. 2.—CT scan in a 51-year-old man with metastatic adenocarcinoma shows hypodense periportal (*double arrows*) and pericaval (*single arrow*) zones. Periportal lymphadenopathy was present at lower levels.

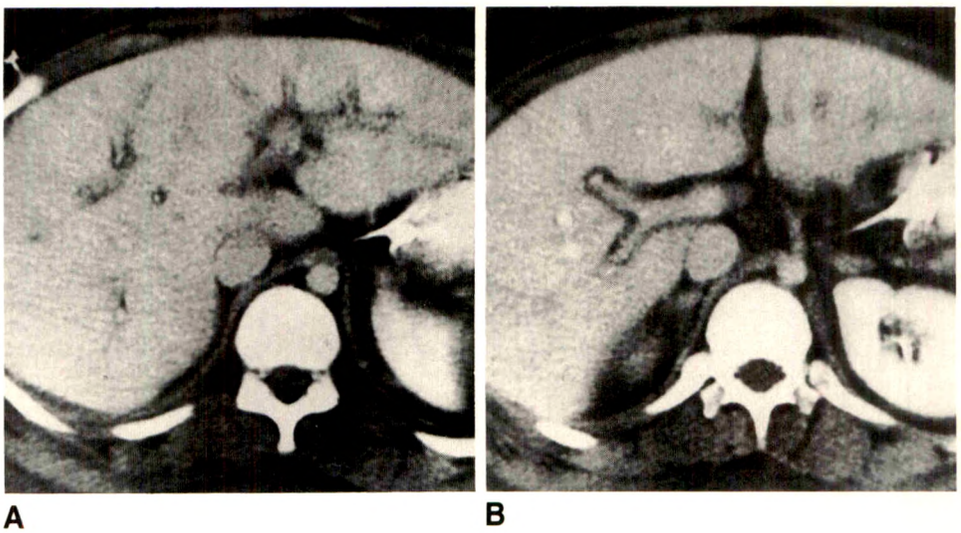

A B

Fig. 3.—*A* and *B*, CT scans in a 19-year-old woman with congestive heart failure show hypodense periportal zones. Pertinent CT findings on other slices were cardiomegaly, pleural effusions, and gallbladder wall edema.

cells in the bile-duct walls. It has been postulated that there is simple passage of bile constituents into these lymphatics [3]. Experimental ligation of the common bile duct has increased lymph flow up to three times its normal value [3]. Capillaries within the portal tract are supplied by the hepatic artery. An increased capillary pressure or a decreased colloidosmotic pressure of the blood plasma results in augmented filtration and the production of a greater amount of protein-poor interstitial fluid, which is then drained by the lymph channels [3].

Microscopically demonstrable lymphatics are seen in the connective tissue that surrounds the portal and hepatic venules, hepatic arterioles, and bile ductules [3]. Only when there is increased lymph production or lymphatic obstruction will intrahepatic lymphatics become visible radiographically or at laparoscopy [3]. More than 80% of the hepatic lymph is drained by collecting vessels along the portal vein and bile duct. These collecting vessels eventually drain into the cisterna chyli. The remaining lymph drainage occurs along the hepatic veins either directly into the thoracic duct or into retrosternal lymphatics, which follow the internal mammary vessels and drain into the great veins in the root of the neck [3].

Thus, there are anatomic and physiologic bases for several causes of dilated hepatic lymphatics in addition to that reported in liver transplant recipients [1]. In our first category (patients who sustained blunt abdominal trauma), all patients had intraabdominal hematomas. From the foregoing description, it can be seen that all these hematomas were located in sites that could lead to compression and thus obstruction of the hepatic lymphatic system. The lymphatic dilatation and associated lymphedema reversed in two patients whose hematomas resolved.

A second cause of extrinsic compression resulting in lymphatic dilatation is the presence of high abdominal lymphadenopathy. This was present in two patients with malignant neoplasms. Benign causes of lymphadenopathy (e.g., granulomatous disorders) could also cause lymphatic dilatation that would be detectable by CT. Lymphatic dilatation may be reversible in this group as well.

The third cause of lymphatic dilatation in our group of patients was cardiac decompensation. Cardiac decompensation causes increased venous pressure, which in turn increases lymph flow. This increase can cause dilatation of the lymphatics. Although no follow-up scans were obtained in these patients, it is reasonable to assume that their lymph dilatation is reversible if the elevated venous pressures can be corrected. This study did not determine a level of elevated central venous pressure above which evidence of lymphatic dilatation might be seen. However, the six patients in this group all had chronic congestive heart failure.

Occasionally, lymphatic dilatation and lymphedema may be seen in patients in whom a cause is not readily identifiable. This occurred in two cases in this series.

The possibility that the appearance we observed is actually perivascular edema rather than lymphedema seems unlikely for two reasons. First, the CT appearance is similar to that reported in CT studies of liver transplant recipients [1]. In that report, two patients had liver biopsies that showed dilated periportal lymphatics. Lymphedema was histologically proved in the animal model discussed in this report. Second, some patients who have portal hypertension, hypoproteinemia, and edema caused by liver disease or those who have Budd-Chiari syndrome probably will have perivascular edema. However, we have not seen hypodense perivascular zones in CT scans of a patient with either of these histories nor, to our knowledge, has such a finding been reported by others.

The identification of the appearance of dilated hepatic lymphatics and surrounding lymphedema is important, so that it is not mistaken for the CT appearance of dilated intrahepatic bile ducts, which ventrally parallel but do not surround the intrahepatic portal venous system. This CT finding of apparent lymphatic dilatation is not rare; in fact, we saw 20 such cases over an 8-month period, during which time we performed over 2500 CT body scans. Awareness of its appearance and causes should increase its recognition.

REFERENCES

1. Marincek B, Barbier PA, Becker CD, Mettler D, Ruchti C. CT appearance of impaired lymphatic drainage in liver transplants. *AJR* **1986**;147: 519–523
2. Foley WD, Berland LL, Lawson TL, Smith DF, Thorsen MK. Contrast enhancement technique for dynamic hepatic computed tomographic scanning. Radiology 1983;147:797–803
3. Deimer EE. Lymphatic anatomy. In: Herlinger H, Lunderquist A, Wallace S, eds. *Clinical radiology of the liver*. New York: Dekker, **1983**:55–63

Categorical Course in Breast Imaging

American Roentgen Ray Society 88th Annual Meeting

May 8–12, 1988, San Francisco Hilton and Tower, San Francisco, CA

Program Chairman: *Stephen A. Feig, Philadelphia, PA*; (215) 928-7253

Sunday, May 8	
9:00–9:10 a.m.	Welcome from the President (*Gagliardi*)
9:10–9:15 a.m.	Introduction (*Feig*)
9:15–10:00 a.m.	Xeromammography: principles, equipment, technique, quality control (*Sickles*)
10:30–11:30 a.m.	Screen-film mammography: principles, equipment, technique, quality control (*Feig*)
11:30 a.m.–Noon	American College of Radiology Mammography Accreditation Program (*McLelland*)
Break	
1:30–2:15 p.m.	Breast masses: differential diagnosis (*Adler*)
2:15–3:00 p.m.	Breast calcifications: differential diagnosis (*Rebner*)
Break	
3:30–4:10 p.m.	Mammography of the treated breast (*Paulus*)
4:10–4:50 p.m.	Practical solutions to common mammographic problems (*Sickles*)
4:50–5:30 p.m.	Prebiopsy localization of nonpalpable breast lesions (*Kopans*)
Monday, May 9	
1:30–2:10 p.m.	Mammographic-pathologic correlation (*Troupin*)
2:10–2:50 p.m.	Breast ultrasound: equipment, technique, interpretation, accuracy (*Bassett*)
2:50–3:30 p.m.	Fine needle aspiration biopsy, ductography, pneumocystography (*Logan*)
Break	
4:00–4:45 p.m.	Panel: Diagnostic problem cases (Moderator: *Feig*; members: *Bassett*, *Kopans*, *Rebner*, *Troupin*)
4:45–5:30 p.m.	Panel: Subtle signs of carcinoma (Moderator: *Feig*; members: *Adler*, *Logan*, *McLelland*, *Moskowitz*, *Sickles*)
Tuesday, May 10	
4:00–4:45 p.m.	Issues in breast cancer screening (*Moskowitz*)
4:45–5:15 p.m.	How to establish a low-cost community screening program (*McLelland*)
5:15–5:30 p.m.	Discussion
Wednesday, May 11	
4:00–4:30 p.m.	Wording the mammography report (*Feig*)
4:30–5:15 p.m.	Medicolegal aspects of mammography (*Brenner*)
5:15–5:30 p.m.	Discussion
Thursday, May 12	
4:00–4:30 p.m.	Transillumination lightscanning (*D'Orsi*)
4:30–5:00 p.m.	Breast MR (*Alcorn*)
5:00–5:30 p.m.	Digital mammography (*Merritt*)
5:30–5:35 p.m.	Concluding remarks (*Feig*)

Pyogenic Liver Abscess:
Contrast-Enhanced MR Imaging in Rats

Ralph Weissleder[1]
Sanjay Saini[1]
David D. Stark[1]
Guillermo Elizondo[1]
Carolyn Compton[2]
Jack Wittenberg[1]
Joseph T. Ferrucci, Jr.[1]

MR imaging was used to evaluate experimentally induced pyogenic liver abscesses in an animal model. Rats were examined before and after IV administration of either gadolinium-diethylenetriaminepentaacetic acid (Gd-DTPA), ferrite particles, or both contrast agents together. Pyogenic liver abscesses appeared hypointense on T1-weighted images and hyperintense on T2-weighted images. Bolus administration of Gd-DTPA using a fast spin-echo sequence with repetition time of 250 msec and echo time of 20 msec (SE 250/20) showed transient selective enhancement of normal hepatic tissue and increased lesion conspicuity, quantitatively assessed by the contrast-to-noise ratio, which increased from −35.7 to −59.0. Delayed leakage of Gd-DTPA into the abscess center partially obscured small lesions at 30–60 min. Ferrite particles reduced the signal intensity of normal liver, and the abscess then appeared homogenously hyperintense. Applying the SE 500/32 sequence, the contrast-to-noise ratio increased from −1.2 to +74.0. Coordinated administration of both contrast agents showed a further increase in contrast to +94.0, with a hyperintense abscess rim surrounded by hypointense liver.

Gd-DTPA increases abscess–liver contrast by rim enhancement of the abscess wall, and ferrite increases the abscess–liver contrast by selectively decreasing the signal intensity of surrounding normal liver. As a result of increased contrast-to-noise ratio, both contrast agents, alone or in combination, increase the conspicuity of hepatic abscesses.

Pyogenic liver abscesses (PLAs) most commonly occur in older patients with cancer, biliary disease, and bacteremia [1–3]. Symptoms and signs of PLA are often nonspecific, delaying diagnosis and treatments that are known to improve prognosis [2–5]. The mortality rate of undrained abscesses has been reported to be 100% [6], and without the use of tomographic imaging studies, 50% of PLAs have been correctly diagnosed only at autopsy [1, 2, 7, 8].

The MR appearance of PLA in humans has not yet been reported. To evaluate the potential of MR imaging and the diagnostic efficacy of contrast-enhancement techniques, we conducted a laboratory study using a well-defined animal model of hepatic abscess.

Materials and Methods

Animal Model

The technique developed by Weinstein and others [9, 10] was used to induce pyogenic liver abscesses in Sprague-Dawley rats. Briefly, a bacterial inoculum of colonic contents was anaerobically filtered and directly injected into the liver of 12 Sprague Dawley rats (500 g). Two animals died within 12 hr after inoculation and were excluded from the study. The 10 surviving animals were imaged 5–7 days after surgery. Bacteriologic examination of the inoculum revealed a polymicrobic growth of *Escherichia coli*, enterococci, *Staphylococcus aureus*, and an abundant mixed anaerobic bacteria. This mixture was identical to that described in human liver abscesses [6].

Received July 1, 1987; accepted after revision September 4, 1987.

S. Saini was supported in part by the Research and Education Fund of the Radiological Society of North America. D. D. Stark was supported by the American Cancer Society (JFRA-163 and PDT-326).

[1] Department of Radiology, Massachusetts General Hospital and Harvard Medical School, Boston, MA 02114. Address reprint requests to D. D. Stark, Dept. of Radiology, Massachusetts General Hospital, Fruit St., Boston, MA 02114.

[2] Department of Pathology, Massachusetts General Hospital and Harvard Medical School, Boston, MA 02114.

***AJR* 150:115–120, January 1988**
0361–803X/88/1501–0120
© American Roentgen Ray Society

Pathology

After imaging was completed, all livers were removed intact at autopsy. After 2 days of fixation in formalin, the livers were examined grossly and then sliced in 2–3 mm sections to detect foci of abscess formation. Histologic specimens were routinely stained with hematoxylin-eosin. Additional Masson trichrome stains for collagen and Prussian blue stain for iron were performed on two specimens.

MR Contrast Agents

Anesthesized animals were restrained with adhesive tape, and before imaging was started, a heparin-flushed IV line was placed in the tail vein. Gadolinium–diethylenetriaminepentaacetic acid (Gd-DTPA) (Berlex, Cedar Knolls, NJ) and polymer-coated ferrite particles (Advanced Magnetics Inc., Cambridge, MA) were injected via the tail vein without removing the animal from the imager. Gd-DTPA was used in seven animals at a concentration of 0.2 mmol/kg. Forty minutes after Gd-DTPA injection and imaging, ferrite at a dose of 0.05 mmol/kg was injected (Gd-Fe double-contrast technique), and additional images were obtained. In three other animals, ferrite particles at a concentration of 0.05 mmol Fe/kg were administered first. Ten minutes after completion of imaging, Gd-DTPA was injected (Fe-Gd double-contrast technique), and additional images were obtained.

MR Imaging

MR imaging was performed on a 0.6-T (25.1-MHz) Technicare magnet described in detail previously [11, 12]. Coronal and transverse multislice images were obtained with a slice thickness of 4 mm and a 192 × 256 matrix. When a head coil with a field of view (FOV) of 21 cm was used, pixel dimensions were 1.1 × 0.8 mm; when the FOV was 26 cm, pixel size was 1.3 × 1 mm.

Pulse sequences included precontrast T1-weighted spin echo (SE) pulse sequence with a repetition time (TR) of 250 msec and an echo time (TE) of 20 msec (SE 250/20), an SE 500/32 sequence, and a T2-weighted, SE 1500/60 sequence. After administration of contrast agents, only optimized pulse sequences (highest contrast-to-noise ratio) were used for each contrast agent [13]. Immediately after injection of Gd-DTPA, SE 250/20 images were obtained (two acquisitions, 1.6-min scan time). Subsequent serial imaging was performed at 10 and 30 min after injection by using the SE 250/20 pulse sequence with six acquisitions (4.8-min scan time). Ferrite-enhanced MR imaging was performed 10 min after administration of the contrast agent by using an SE 500/32 sequence with six acquisitions (9.6-min scan time).

Image Analysis

Identical operator-defined regions of interest (ROI) were used to measure the signal intensity (SI) of liver, abscess wall, abscess center, and paraspinous muscle. Image noise was measured by using a large ROI ventral to the animal, offset in the phase-encoding direction [14]. This ROI provided a measure of image noise that included ghost noise. Contrast between the abscess and the liver (C/N) was calculated as the signal intensity difference normalized to the standard deviation of noise (N) according to the formula C/N = (SI abscess − SI liver)/SI noise. C/N is an effective parameter for quantitating MR-pulse-sequence performance, and the absolute magnitude of C/N, designated as |±C/N|, correlates with lesion detectability [12, 14]. Negative C/N values indicate relatively hypointense (dark) abnormalities, and positive C/N values indicate relatively hyperintense (bright) abnormalities. For the comparison of different pulse sequences performed, C/N ratios were normalized to reflect a standard scanning time of 9.6 min, except for the rapid 1.5-min scan [14]. Normalization was performed by using the formula $C/N_{9.6\ min} = (C/N) \times \sqrt{9.6/\text{scan time}}$.

Results

Pathology

On gross examination, murine livers were sectioned transversely at 2- to 3-mm intervals. A solitary intraparenchymal abscess cavity was readily identified in each specimen. Abscesses ranged in size from 2 to 15 mm in greatest dimension. On histologic examination, PLAs appeared as well-circumscribed defects with three grossly identifiable zones: a central zone of liquefactive necrosis surrounded by a collar of coagulation necrosis and a peripheral rim of granulation tissue (Fig. 1). At this early stage of abscess formation, no true fibrosis (such as that found in more chronic lesions) was present yet. Hepatic parenchyma surrounding the abscesses showed moderate sinusoidal dilatation indicative of hepatic edema. Uptake of ferrite particles by macrophages in the abscess cavity or abscess wall might be expected; however, this was not seen histologically.

Precontrast Images

When the SE 250/20 pulse sequence was used, PLAs were easily detectable in nine of the 10 animals (Fig. 2A). One abscess, measuring 2 × 2 mm, was identified only in retrospect. PLAs typically appeared markedly hypointense to liver with an abscess–liver C/N of −35.7. Lesion detectability correlated closely with the quantitative C/N values. The size of the lesions measured by MR corresponded closely with correlative pathologic measurements.

When the SE 500/32 pulse sequence was used, nine of the 10 PLAs were detected. The small abscess (2 × 2 mm) was not identified. PLAs appeared slightly hypo- or isointense relative to liver (C/N = −1.2) (Fig. 2B).

Nine PLAs were detected on T2-weighted SE 1500/60 images. The 2-mm lesion was not visible even in retrospect. The abscesses were hyperintense (C/N = +7.1) (Fig. 2C). Typically the lesions appeared larger than on corresponding T1-weighted images and than by autopsy measurements.

Gd-DTPA

After the bolus administration of Gd-DTPA, all seven PLAs studied (ranging in size from 3 to 15 mm) were correctly identified by using the 1.6-min, 250/20 scan technique (Fig. 3). Indeed, both qualitatively and quantitatively, the Gd-DTPA–enhanced fast-scan technique was superior to more lengthy noncontrast scans. Detectability improved because the contrast agent selectively enhanced specific morphologic features within the lesion itself. The abscess rim consisting of granulation tissue became sharply defined and showed maximal C/N (−59.0) relative to the abscess center. High-contrast, abrupt transitions between liver, abscess, rim, and abscess

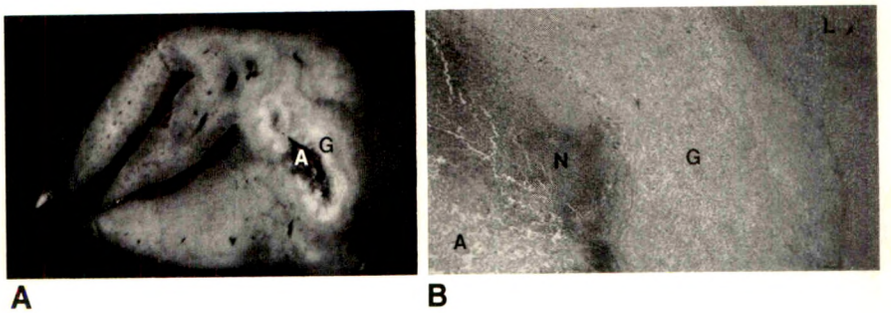

Fig. 1.—Pyogenic liver abscess.
A, Gross specimen of experimental model of pyogenic liver abscess. MR images of this animal are shown in Figs. 4A and 4B. Lesion measures 15 mm in greatest diameter and consists of a central, partially liquefied necrotic center (A), surrounded by friable white necrotic tissue. Granulation tissue (G) separates abscess from hepatic parenchyma. (×2.6)
B, Histology. Central cavity (A) has undergone liquefactive necrosis. Irregular rim of coagulative necrosis (N) with cords of nonviable hepatic parenchyma is seen at inner margin of abscess wall. At abscess periphery, a zone of acutely inflamed granulation tissue (G) forms border between necrotic tissue and surrounding liver (L).

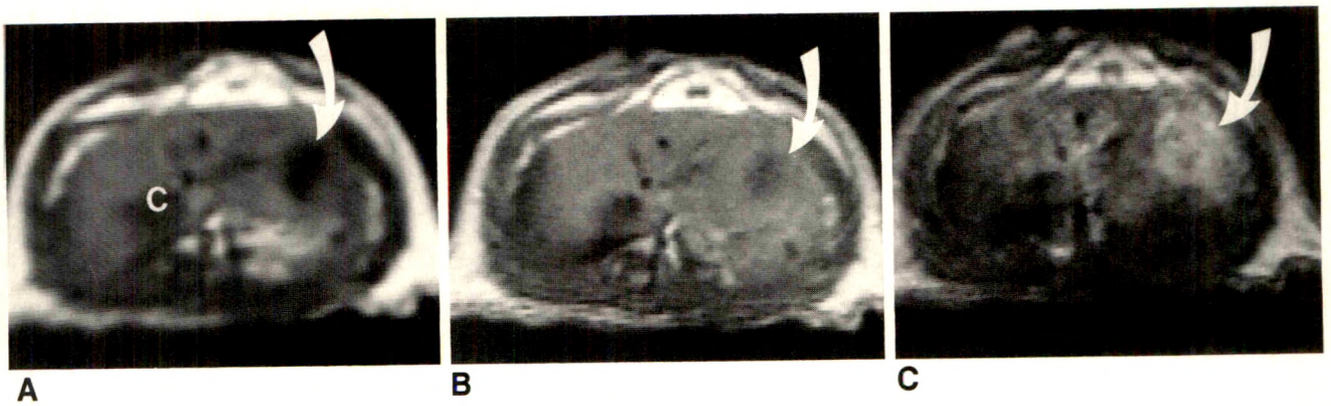

Fig. 2.—Unenhanced MR image of a 2 × 4 mm pyogenic liver abscess.
A, T1-weighted, SE 250/20 image shows abscess cavity (2 × 4 mm) as a hypointense region (*arrow*). C = inferior vena cava.
B, Mixed T1-weighted and T2-weighted SE 500/32 image. Abscess (*arrow*) is still visible but more isointense relative to liver than on *A*.
C, T2-weighted SE 1500/60 image. Abscess (*arrow*) appears hyperintense relative to liver, and lesion appears larger (4 × 6 mm) than in *A*.

Fig. 3.—Serial images (SE 250/20) after the administration of Gd-DTPA (0.2 mmol/kg).
A, Preinjection control image. *Curved arrow* = abscess.
B, 1½ min after administration of Gd-DTPA, liver signal intensity increases, and abscess periphery enhances as a hyperintense rim around hypointense abscess cavity.
C, After 30 min, abscess cavity slowly increases in signal intensity because of Gd-DTPA fill-in.

center maximized lesion conspicuity. Lesion size appeared unchanged compared with that of the lesions shown on SE 250/20 precontrast images.

The abscess center initially enhanced to a lesser degree than normal liver tissue but gradually increased in signal intensity as GD-DTPA leaked into the necrotic central cavity from the adjacent hypervascular rim [15]. As a result, lesion-center-to-liver C/N declined from −35.7 to −12.4 during the first 30-60 min after contrast administration.

Ferrite Particles

Ferrite-enhanced MR imaging improved lesion conspicuity; all three PLAs, including the 2 × 2 mm lesion, were easily

detected (Figs. 4 and 5). After administration of ferrite particles, the liver signal intensity decreased 86%, whereas the signal intensity of the abscess did not change significantly (6.7 ± 3.7%). The abscess was clearly delineated as a relatively hyperintense lesion without rim enhancement. Ferrite-enhanced lesion–liver C/N was greater (+74) than any C/N for Gd-DTPA. Lesion size was identical to that measured before the administration of ferrite.

Double-Contrast Technique

All 10 PLAs were correctly identified after the administration of both contrast agents. Qualitatively as well as quantitatively it did not matter which contrast agent was given first, as PLAs appeared as hyperintense lesions in contrast to the low hepatic signal intensity (Fig. 6). Lesion–liver C/N increased maximally (+94) achieving a greater C/N than with either contrast agent alone. The double-contrast technique exploits the Gd-DTPA–induced increase in signal of the abscess rim, contrasting it to the ferrite-induced decreased signal from normal liver.

Discussion

Unenhanced T1-weighted and T2-weighted MR images show no specific morphologic features that can be used to distinguish intrahepatic abscesses from metastases. PLAs tended to be larger on T2-weighted images than on corresponding T1-weighted images, and our histologic data show that this difference is due to edema of intact liver tissue adjacent to the abscess rim. Similar MR findings have been observed in patients with amebic liver abscesses [16]. Although the presence of hepatic edema is of interest in making diagnoses and monitoring therapy, it is most likely that similar, although less extensive, patterns of edema can be seen in association with malignant lesions.

MR imaging with Gd-DTPA is optimized by using heavily T1-weighted pulse sequences because of its predominant T1-shortening effect on perfused tissue [15, 17, 18]. As a non-targeted, water-soluble, ionic contrast agent, Gd-DTPA shows pharmacokinetics and biodistribution characteristics similar to iodinated contrast agents [19, 20]. PLAs typically show a rim of enhancement at the margin of the abscess cavity because of an increased capillary permeability for Gd-DTPA as well as an increase in local distribution volume [17, 21]. Rim enhancement after administration of Gd-DTPA has also been reported to occur in tumors [22–24]. Gd-DTPA also diffuses into the abscess cavity, increasing its signal intensity on delayed T1-weighted images. This fill-in time is slow because the necrotic abscess cavity is devoid of vessels. Typically, the 30- to 60-min delay in central enhancement is considerably longer than the 5- to 10-min delay in central

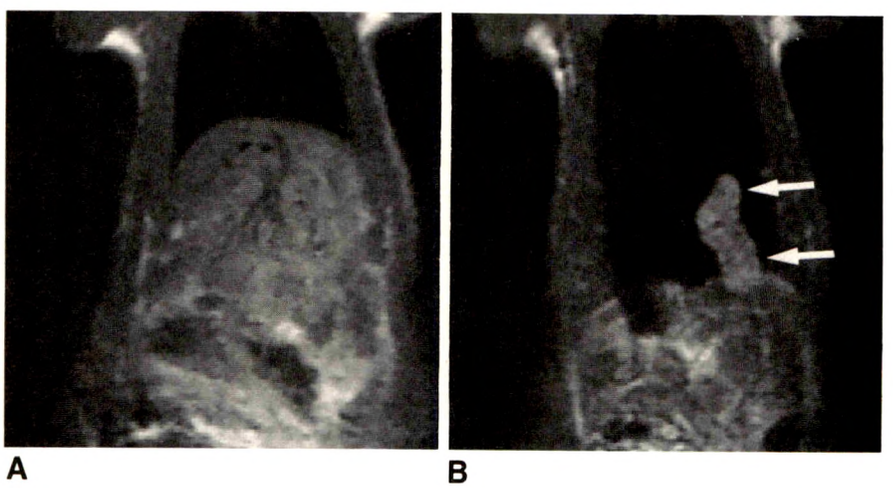

Fig. 4.—Ferrite-enhanced MR images of pyogenic liver abscess (0.05 mmol ferrite particles/kg). Same specimen as Fig. 1A.

***A*, Abscess appears isointense to liver on coronal precontrast SE 500/32 image.**

***B*, Abscess becomes clearly detectable after administration of ferrite (*arrows*).**

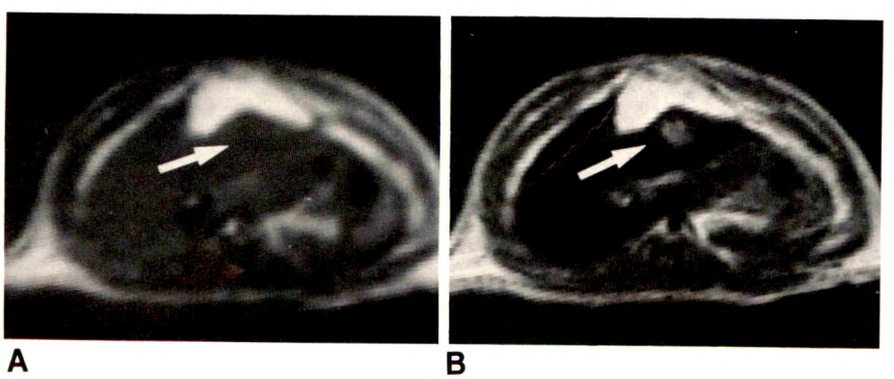

Fig. 5.—Ferrite-enhanced MR images of microabscess (0.05 mmol ferrite particles/kg).

***A*, In this animal, precontrast image (SE 250/20) barely identifies abscess as a hypointense lesion (*arrow*).**

***B*, After administration of ferrites, microabscess (2 × 2 mm) becomes readily visible (*arrow*).**

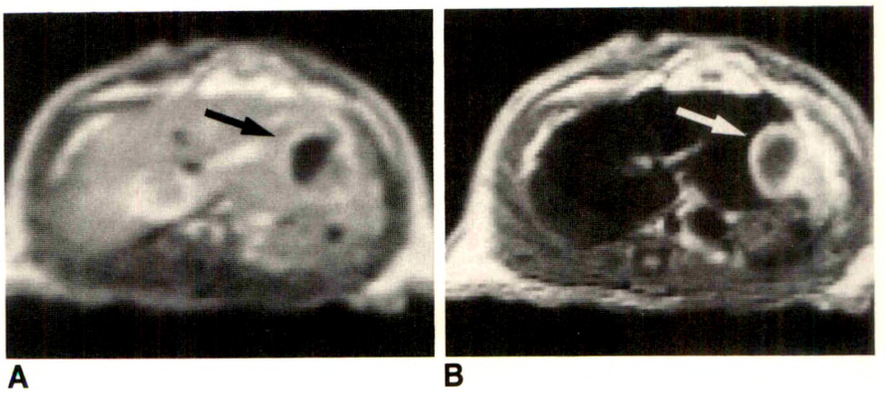

Fig. 6.—Double-contrast technique.
***A*, After Gd-DTPA is injected, abscess appears hypointense relative to liver showing the typical ring enhancement (*arrow*). Same animal as in Fig. 2.**
***B*, After administration of ferrites, abscess appears as a prominent, ringlike intrahepatic lesion (*arrow*). Contrast achieved with combined use of both contrast agents is greater than with either agent alone.**

enhancement reported for hypovascular, nonnecrotic tumors of comparable size [13]. Fill-in time in tumors varies among histologically diverse lesions, depending on lesion vascularity [15, 24–26]. Sequential Gd-DTPA–enhanced MR imaging may provide helpful information in the differential diagnosis of hemangiomas [25, 26], tumors [15, 26], and abscesses. However, some necrotic liver tumors probably will show the same pattern of edema and contrast enhancement as PLAs. Our results suggest that Gd-DTPA will increase conspicuity of small abscesses (65% increase in abscess–liver C/N), and that clinical data will remain essential for differential diagnosis.

MR imaging with ferrite is most effective in conjunction with slightly T2-weighted pulse sequences, as ferrites predominantly act to shorten T2. Most importantly, the biodistribution of IV ferrite particles is selective. Particles are rapidly phagocytosed by macrophages of the reticuloendothelial system, reducing the T2 relaxation time and image signal intensity of normal liver, spleen, and bone marrow [27]. PLAs become more easily detectable as hyperintense lesions relative to surrounding hypointense liver. This selective enhancement is attributable to the exclusion of ferrite particles from the abscess cavity. Unlike Gd-DTPA, ferrite particles are too large to undergo diffusion into the abscess cavity. Our data show that ferrite is effective for improving conspicuity of small PLAs (107% increase in abscess–liver C/N). Unfortunately, ferrite shows no potential for aiding in the differential diagnosis of inflammatory and neoplastic lesions because of the nonspecific exclusion by masses not containing reticuloendothelial cells.

Both Gd-DTPA and ferrite, used together in our double-contrast technique, show the same biodistribution and kinetics as when used alone. MR imaging is optimized by using pulse sequences with mixed T1- and T2-dependencies [13]. Because Gd-DTPA is a nonspecific interstitial contrast agent, it enhances liver, the abscess rim, and later the abscess center, whereas ferrite decreases the signal intensity of surrounding edematous and uninvolved liver. Lesion conspicuity is maximized by coordinated use of both contrast agents because their effects are complementary and additive (163% increase in abscess–liver C/N).

MR contrast agents are able to increase abscess–liver C/N and thus increase the conspicuity of small lesions. MR contrast agents may be particularly useful in early detection of miliary abscesses in immunosuppressed patients [4] and micrometastases in cancer patients [28]. Pharmacologic techniques and imaging methods developed in appropriate animal models accurately predict efficacy in clinical use. Preliminary data also suggest that Gd-DTPA is safe when administered as a bolus [24–26] and that IV ferrites do not cause any harmful effects [29].

REFERENCES

1. Heymann AD. Clinical aspects of grave pyogenic abscesses of liver. *Surg Gynecol Obstet* **1979;**149:209–213
2. Rubin RH, Swartz MN, Malt R. Hepatic abscess: changes in clinical, bacteriologic and therapeutic aspects. *Am J Med* **1974**;57:601–610
3. Ribaudo JM, Ochsner A. Intrahepatic abscesses: amebic and pyogenic. *Am J Surg* **1973**;125:567–574
4. Callen PW, Filly RA, Marcus FS. Ultrasonography and computed tomography in the evaluation of hepatic microabscesses in the immunosuppressed patient. *Radiology* **1980**;136:433–434
5. Johnson RD, Mueller PR, Ferrucci JT Jr, et al. Percutaneous drainage of pyogenic liver abscesses. *AJR* **1985**;144:463–467
6. Balasegaram M. Management of hepatic abscess. *Curr Probl Surg* **1981**;18:284–340
7. Altemeier WA III, Schowengerdt CG, Whiteley DH. Abscesses of the liver: surgical considerations. *Arch Surg* **1970**;101:258–265
8. Schraibman IG. Non-parasitic liver abscess. *Br J Surg* **1974**;61:709–712
9. Weinstein WM, Onderdonk AB, Bartlett JG, et al. Experimental intra-abdominal abscesses in rats: development of an experimental model. *Infect Immun* **1975**;10:1250–1255
10. Onderdonk AB, Weinstein WM, Sullivan NM, et al. Experimental intra-abdominal abscesses in rats: quantitative bacteriology of infected animals. *Infect Immun* **1974**;10:1256–1259
11. Kneeland JB, Knowles RJR, Cahill PT. Magnetic resonance imaging systems: optimization in clinical use. *Radiology* **1984**;153:473–478
12. Stark DD, Felder R, Wittenberg J, et al. Magnetic resonance imaging of cavernous hemangioma of the liver: tissue-specific characterization. *AJR* **1985**;145:213–220
13. Weissleder R, Saini S, Stark D, et al. Double contrast MR imaging of liver cancer. *Mag Reson Imag* **1987**;5[S1]:135–136
14. Stark DD, Wittenberg J, Middleton MS, Ferrucci JT. Liver metastases: detection by phase-contrast MR imaging. *Radiology* **1986**;158:327–332
15. Saini S, Stark DD, Brady TJ, Wittenberg J, Ferrucci JT Jr. Dynamic spin-echo MRI of liver cancer using gadolinium-DTPA: animal investigation. *AJR* **1986**;147:357–362
16. Elizondo G, Weissleder R, Stark DD, et al. Amebic liver abscesses: diagnosis and treatment evaluation by MRI. *Radiology* **1987**;165:795–800
17. Runge VM, Clanton JA, Price AC, et al. Evaluation of contrast-enhanced MR imaging in a brain-abscess model. *AJNR* **1985**;6:139–147

18. Wolf GL, Joseph PM, Goldstein EJ. Optimal pulsing sequences for MR contrast agents. *AJR* **1986**;147:367–371
19. Halvorsen RA, Korobkin M, Foster WL, Silverman PM, Thompson WM. The variable CT appearance of hepatic abscesses. *AJR* **1984**;141:941–946
20. Thompson WM, Stude RA, McDonald MI, et al. Computed tomographic evaluation of an experimental model for pyogenic liver abscess. *Invest Radiol* **1985**;20:152–158
21. Grossman RI, Wolf G, Biery D, et al. Gadolinium enhanced nuclear magnetic resonance images of experimental brain abscesses. *J Comput Assist Tomogr* **1984**;8:204–207
22. Heywang SH, Hahn D, Schmidt H, et al. MR imaging of the breast using gadolinium-DTPA. *J Comput Assist Tomogr* **1986**;10:199–204
23. Revel D, Brasch R, Paajanen H, et al. Gd-DTPA: contrast enhancement and tissue differentiation in MR imaging of experimental breast carcinoma. *Radiology* **1986**;158:319–323
24. Hamm B, Wolf KJ, Felix R. Conventional and rapid MR imaging of the liver with Gd-DTPA. *Radiology* **1987**;164:313–320
25. Mano I, Yoshida H, Nakabayashi K, et al. Fast spin echo imaging with suspended respiration: gadolinium enhanced MR imaging of liver tumors. *JCAT* **1987**;11:73–80
26. Ohtomo K, Itai Y, Yoshikawa K, et al. Hepatic tumors: dynamic MR imaging. *Radiology* **1987**;163:27–31
27. Saini S, Stark DD, Hahn PF, Wittenberg J, Brady TJ, Ferrucci JT Jr. Ferrite particles: a superparamagnetic MR contrast agent for the reticuloendothelial system. *Radiology* **1987**;162:211–216
28. Foster JH, Lundy J. Liver metastasis. *Curr Probl Surg* **1981**;18:160–202
29. Bacon B, Stark DD, Park CH, et al. Ferrite particles: a new MRI contrast agent. Lack of acute or chronic hepatotoxicity following intravenous administration. *J Lab Clin Med* **1987**;110:164–171

Case Report

Splenic Lymphangiomatosis: CT Diagnosis

Frank Pistoia[1] and Stuart K. Markowitz

Lymphangiomas are benign congenital malformations of the lymphatic system usually affecting the neck and axilla [1]. Involvement of the visceral organs is less common [2]. Splenic involvement is quite rare; approximately 90 cases have been reported [3]. We report a case of splenic lymphangiomatosis in which the CT appearance suggested the correct diagnosis.

Case Report

A 43-year-old woman presented with left upper quadrant abdominal pain, malaise, and weakness. Physical examination disclosed only a tender, nodular mass in the left upper quadrant. Laboratory examination included a normal hemogram and platelet count and normal renal and liver function tests.

Sonography showed splenomegaly due to multiple hypoechoic lesions of the spleen. CT showed an enlarged spleen with multiple discrete low-attenuation foci that did not enhance after administration of IV contrast material (Fig. 1A). The lesions measured approximately 15–20 H, and several had small marginal linear calcifications. A splenectomy was performed. Gross examination revealed subcapsular and intrasplenic cysts (Fig. 1B). The histologic diagnosis was lymphangiomatosis.

Discussion

Lymphangiomas are benign malformations composed of endothelial-lined cysts containing lymph and were first described by Rodenber in 1828 [4]. They are classified as one of three types—either capillary, cavernous, or cystic—de-

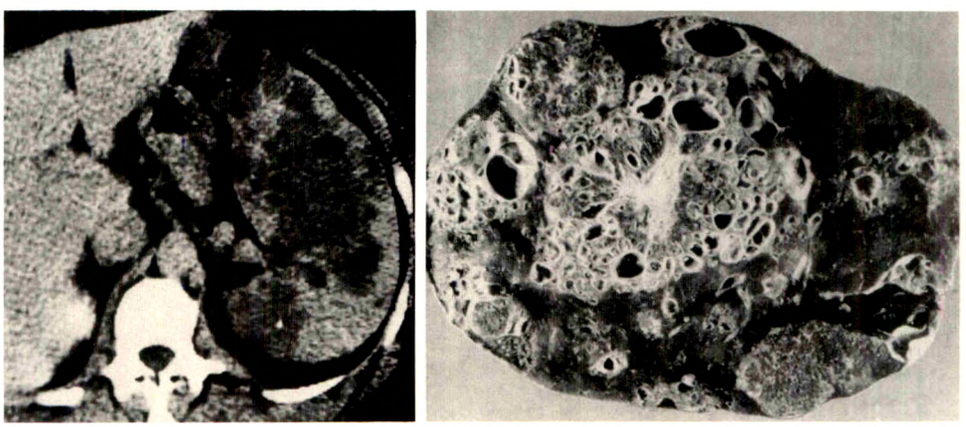

A B

Fig. 1.—*A*, CT scan after administration of contrast material shows low-density, nonenhancing cystic areas within an enlarged spleen. Calcification is noted in posterior aspect of spleen.
***B*, Cut surface of spleen shows multiple cysts of varying sizes.**

Received July 24, 1987; accepted after revision August 25, 1987.
[1] Both authors: Department of Radiology, Hartford Hospital, 80 Seymour St., Hartford, CT 06115. Address reprint requests to F. Pistoia.

pending on the size of the lymphatic channels [5]. Lymphangiomas are commonly found in the neck and axilla (cystic hygroma) and less commonly in the mediastinum, retroperitoneum, and extremities [4]. Although visceral involvement is uncommon, lymphangiomas have been described in the liver, spleen, kidney, colon, and penis [5]. Splenic involvement is rare, with approximately 90 cases reported [3].

Plain film evaluation may disclose splenomegaly, curvilinear calcifications in cyst walls, and mass effect on adjacent viscera [5]. Radionuclide scans show splenomegaly with multiple focal defects [6]. Sonography shows hypoechoic spaces within the spleen. Internal echoes may be noted. These depend on the size of the lesions, the presence of septations, and proteinaceous debris [5]. Angiographic findings include well-defined avascular lesions scattered throughout the spleen with absence of neovascularity, arteriovenous shunting, and venous pooling. A characteristic "Swiss-cheese" appearance has been described [7]. CT shows low-density (15–33 H), nonenhancing, sharply marginated, thin-walled lesions [3].

The differential diagnosis of multifocal splenic disease is extensive and includes lymphoma, infarction, septic emboli, metastases (melanoma, breast, ovary, and lung), and splenic cysts. Determination of the cystic nature of the lesions is extremely helpful and narrows the differential diagnosis considerably. The clinical classification of splenic cysts by Pearl and Nassar [8] is useful; the three categories are (1) parasitic cysts (*Taenia echinococcus*), (2) primary cysts with true cellular lining, such as those that are endothelial-lined (hemangioma, lymphangioma) and those that are epithelial-lined (dermoid, epidermoid, transitional cell lined); and (3) secondary or traumatic cysts without a true cellular lining.

The presence of thin-walled, well-defined, nonenhancing splenic cysts, which contains mural calcifications, may suggest the diagnosis of lymphangiomatosis.

ACKNOWLEDGMENT

We thank Christine M. Volzo for her secretarial assistance.

REFERENCES

1. Bill AH, Sumner DS. A unified concept of lymphangioma and cystic hygroma. *Surg Gynecol Obstet* **1965**;120:79–86
2. Peradotto F, Zanetti PP, Obialero M, et al. Lymphangioma of the spleen. Remarks on two observed cases. *Minerva Med* **1986**;75:2295–2300
3. Pyatt RS, Williams ED, Clark M, Gaskins R. CT diagnosis of splenic cystic lymphangiomatosis. *J Comput Assist Tomogr* **1981**;5(3):446–448
4. Avigad S, Jaffe R, Frand M, Yakov I, Yaacov R. Lymphangiomatosis with splenic involvement. *JAMA* **1976**;236:2315–2317
5. Rao BK, AuBuchon J, Lieberman LM, Polcyn RE. Cystic lymphangiomatosis of the spleen: a radiologic-pathologic correlation. *Radiology* **1981**;141:781–782
6. Novetsky GJ, Epstein AJ. Cystic lymphangiomatosis: an unusual cause of splenic scintigraphic defects. *Clin Nucl Med* **1982**;7:416–417
7. Tuttle RJ, Minielly JA. Splenic cystic lymphangiomatosis: an unusual cause of massive splenomegaly. *Radiology* **1978**;126:47–48
8. Pearl GS, Nassar VH. Cystic lymphangioma of the spleen. *South Med J* **1979**;72:667–669

Gallbladder and Bile Duct Abnormalities in AIDS: Sonographic Findings in Eight Patients

Allan J. Romano[1]
Eric vanSonnenberg[1,2]
Giovanna Casola[1]
Barbara B. Gosink[1]
Cynthia E. Withers[1,3]
J. Allen McCutchan[2]
George R. Leopold[1]

Gallbladder and biliary tract abnormalities were observed on sonography in eight patients with AIDS. The studies were obtained to evaluate right upper quadrant pain (two patients), tenderness (three patients), and abnormal liver function tests (eight patients). The two major sonographic findings were gallbladder wall thickening (eight patients), which often was marked, and bile duct dilatation (two patients). Gallbladder wall thickness varied from 4 to 15 mm and was greater than 1 cm in four patients. Follow-up sonograms in five patients showed increasing wall thickness in four and decreasing thickness in one, but these findings did not correlate well with the clinical status of the patient. Pericholecystic fluid was shown in three cases. None of the patients had gallstones. Common bile duct dilatation varied from 12 to 15 mm; no specific cause for dilatation was found by cholangiography. *Mycobacterium avium intracellulare* was recovered from the gallbladder in one patient, and *Cryptosporidium* was recovered from the duodenum in two patients.

AIDS should be considered in the differential diagnosis of gallbladder wall thickening or bile duct dilatation in the appropriate clinical setting. These findings may indicate opportunistic infection of the biliary tract. A disparity may exist between the mild symptoms and signs (or lack of symptoms and signs) related to the gallbladder and bile ducts and the sometimes marked sonographic abnormalities.

Sporadic reports initially described bile duct dilatation and gallbladder wall thickening in 10 patients with AIDS [1–8]. A recent report emphasized the similarity of bile duct findings to sclerosing cholangitis and papillary stenosis [9]. Over the past 2 years, we have encountered eight patients with AIDS who had abnormal gallbladders and/or common ducts on sonography. Their clinical courses were variable and not always in accord with the sonographic findings. An association with opportunistic infections is suggested but unproved. We report our observations and summarize the previous reports.

Materials and Methods

Twenty-five patients with proved AIDS had sonography because of right upper quadrant abdominal pain over a 2-year period. The sonograms were normal with respect to the gallbladder and biliary tree in 17. The remaining eight had abnormal sonograms and form the basis of this study. All eight patients were homosexual men ranging in age from 23 to 40 years. Five of the eight had follow-up sonograms, for a total of 17 studies. Three patients had CT scans, and one each had percutaneous transhepatic cholangiography and ERCP. All patients had elevated liver function tests at the time of the initial abnormal sonogram. SGOT values ranged from 25 to 2550 IU/l (normal, 7–45 IU/l); SGPT was between 10 and 511 IU/l (normal, 0–45 IU/l); alkaline phosphatase varied from 111 to 1080 (normal, 30–130 IU/l); and bilirubin levels reached as high as 3.6 mg/dl (range, 0.7–3.6 mg/dl; normal, 0.2–1.0 mg/dl).

Three patients had cryptosporidiosis of the gastrointestinal tract. In two of these, duodenal aspirates were positive for *Cryptosporidium*, and all three had *Cryptosporidium* recovered from stool specimens. Four patients had Kaposi sarcoma (none in the gallbladder or liver), and two had disseminated *Mycobacterium avium intracellulare*. Two patients had rectal

Received June 24, 1987; accepted after revision September 16, 1987.

[1]Department of Radiology, University of California Medical Center, 225 Dickinson St., H-756, San Diego, CA 92103. Address reprint requests to E. vanSonnenberg.

[2]Department of Medicine, University of California Medical Center, San Diego, CA 92103.

[3]Present address: Department of Radiology, Mount Sinai Hospital, Toronto, Ontario, M5G 1X5, Canada.

AJR 150:123–127, January 1988
0361–803X/88/1501–0123
© American Roentgen Ray Society

herpes, and two others were chronic carriers of hepatitis B virus. One patient each had active hepatitis B infection, cytomegalovirus colitis, *Entamoeba histolytica* infection, and stool culture positive for *Clostridium difficile*, *Candida enteritis*, giardiasis, or *Salmonella* gastroenteritis. Three of the eight patients died from complications of AIDS. One autopsy was performed. A second patient underwent exploratory laparotomy and cholecystectomy.

Results

Sonograms showed thickening of the gallbladder wall in all eight patients, measuring between 4 and 15 mm (normal ≤3 mm) (Table I). The average wall thickness was 9.4 mm. The gallbladder walls were echogenic in five patients, hypoechoic in one patient, and had normal echogenicity in two patients (Fig. 1). The gallbladder was enlarged in one patient, measuring 11 cm in length. Pericholecystic fluid was present in three patients. None of the patients had gallstones. Sonograms were repeated in five patients, three of whom had previously normal gallbladder walls that became thickened, measuring 9 mm in one patient and 11 mm in two. The patient whose gallbladder wall had increased to 9 mm subsequently returned to normal (2 mm) in 4 days (Fig. 2). The largest increase in thickness was 9 mm, occurring in two patients (from 2 to 11 mm in one patient and from 6 to 15 mm in another). One patient who had a mildly thickened gallbladder wall showed no change on a follow-up sonogram.

The liver function tests correlated poorly with the results of follow-up sonograms. In the four patients in whom the gallbladder wall had increased in thickness, results of the biochemical tests improved (one patient), worsened (two patients), or remained unchanged (one patient). The liver function tests improved in the patient whose gallbladder wall was stable at 4 mm. Liver function level remained mildly elevated and unchanged in the patient whose thickened gallbladder wall returned to normal.

Sonography showed that two patients had progressive common duct dilatation. In one patient, the diameter of the common duct increased from 5 to 12 mm. In the other patient, the common duct increased from 11 to 15 mm on a follow-

TABLE 1: Sonographic Biliary Findings in Patients with AIDS

Patient No.	Symptoms and Signs	Gallbladder Wall Thickness[a] (mm)		Common Duct Size[b] (mm)		Course of Liver Function Tests	Clinical Course
		Initial	Follow-up	Initial	Follow-up		
1	Diarrhea, fever, vomiting, weight loss	<3	11	<5	12	Improved	Died
2	Right upper quadrant tenderness, diarrhea, fever, weight loss, weakness	4	4	11	15	Improved	Died
3	Diarrhea, fever, weight loss, malaise	12	ND	<5	ND	ND	Died
4	Abdominal tenderness, fever, vomiting, diarrhea, lethargy	2	11	4	4	Worsened	No change
5	Acute right upper quadrant pain, fever, chills, nausea, vomiting	2	9	4	ND	No change	Improved
6	Right upper quadrant pain, nausea, vomiting	6	15	4	ND	Worsened	Cholecystectomy
7	Right upper quadrant tenderness, diarrhea, shortness of breath	7	ND	3	ND	No change	Improved
8	Nausea, vomiting, diarrhea, lethargy	6	ND	<5	ND	ND	No change

Note.—ND = not done.

[a] Normal ≤3 mm.

[b] Normal <6 mm.

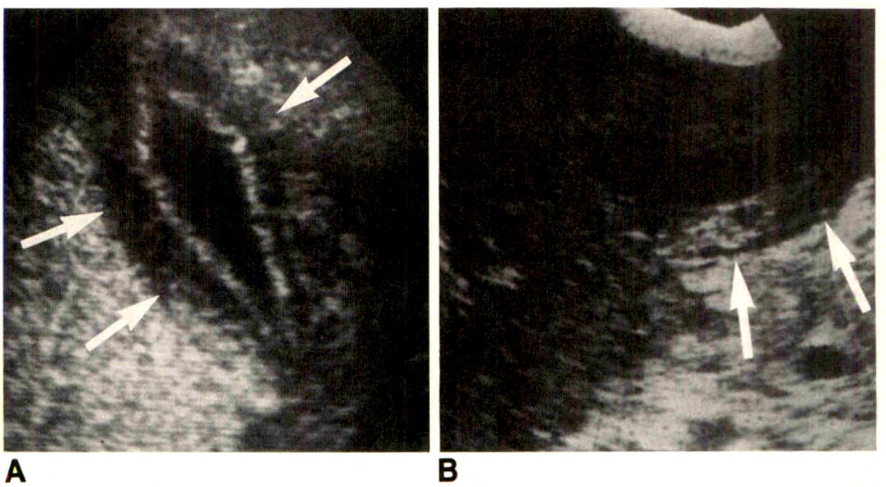

Fig. 1.—*A–D*, Sonograms showing marked gallbladder wall thickening (*arrows*) in four different patients. Gallbladder wall measures 11 mm in both *A* and *B* and 9 mm in both *C* and *D*. Note variable hypo- and hyperechogenicity and pericholecystic fluid.

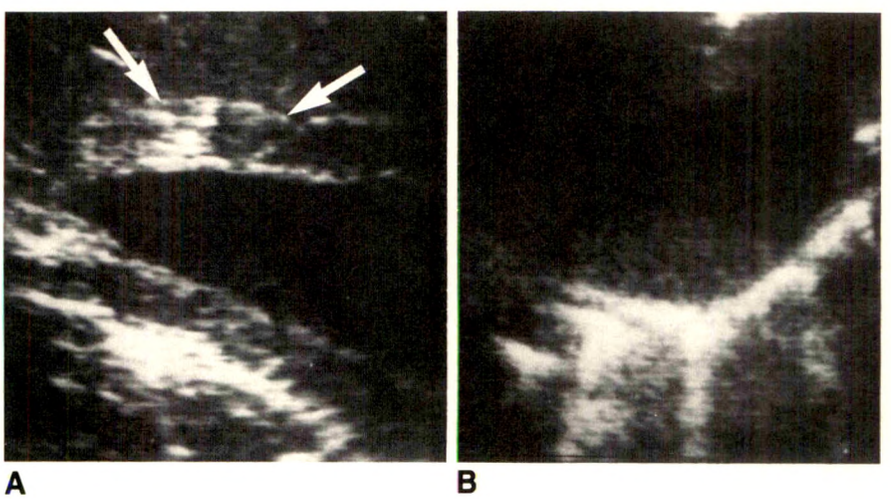

Fig. 2.—*A* and *B*, Poor correlation between gallbladder wall thickness and clinical parameters. Initial sonogram (not shown) revealed normal gallbladder wall thickness.

***A*, 4 days later, repeat scan showed a thickened gallbladder wall (9 mm) (*arrows*), although there were no signs of cholecystitis and liver function tests remained unchanged.**

***B*, A follow-up scan 3 days later revealed a sludge-filled gallbladder with normal wall thickness.**

up scan. No specific cause for obstruction was visualized by transhepatic cholangiography or ERCP in these patients. Both studies showed mild narrowing of the distal common bile duct caused by ampullary inflammation (Fig. 3). Contrast material flowed into the duodenum in each patient. Thickened duodenal and proximal jejunal mucosal folds, characteristic of nonspecific inflammation, were noted on the upper gastrointestinal series in one patient. In both patients, duodenal

aspirates obtained at endoscopy were positive for *Cryptosporidium*. One of the patients with common duct dilatation also had pancreatic duct dilatation (4 mm).

In all three patients who had CT scans, the gallbladder wall thickening was confirmed; the wall enhanced with IV contrast material (Fig. 4). Two of these patients also had pericholecystic fluid collections that were evident on the sonograms. Marked periportal adenopathy was not seen.

One patient underwent laparotomy. The wall of the gallbladder was thickened and chronically inflamed. Histologic stains of the gallbladder were positive for acid-fast bacilli contained within histiocytes, consistent with the diagnosis of *Mycobacterium avium intracellulare*. Postmortem findings in another patient showed a normal gallbladder, although the wall had measured 12 mm on sonography.

Discussion

Data from our patients and from previous reports suggest that biliary tract abnormalities occur in patients with AIDS [1–10]. Gallbladder wall thickening is the most frequently noted finding; the other major finding is either extra- or intrahepatic bile duct dilatation or both. The cause of these abnormalities is unknown, although in some of these patients opportunistic organisms have been found in the gallbladder or in the bile. *Cryptosporidium* and cytomegalovirus have been noted most frequently, and *Mycobacterium avium intracellulare*, *Candida albicans*, and *Klebsiella pneumoniae* occur sporadically [1–9]. Most of these patients had proved gastrointestinal cryptosporidiosis.

Follow-up sonograms in our patients showed changes in the gallbladder wall thickness that did not necessarily correlate with the clinical status of the patients or the results of biochemical tests. Despite the marked gallbladder wall thickening in most of the patients, in only one patient was there sufficient clinical suspicion of cholecystitis to require cholecystectomy. Rapid changes in the gallbladder wall size suggest that edema accounts for much of the observed wall thickness.

Sonographic evidence of thickening of the gallbladder wall

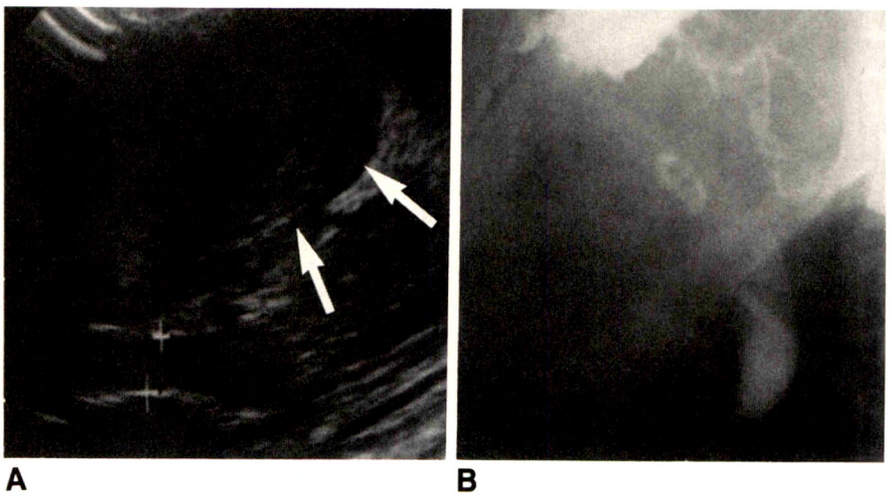

Fig. 3.—*A* and *B*, Gallbladder and bile duct abnormalities in AIDS patient with right upper quadrant pain.

***A*, Sonogram shows a common duct that measures 11 mm (*between cursors*) and that is associated with marked thickening of the gallbladder wall (*arrows*) and pericholecystic fluid.**

***B*, Transhepatic cholangiogram shows a dilated common bile duct with smooth distal narrowing. There is extravasation of contrast material in the liver.**

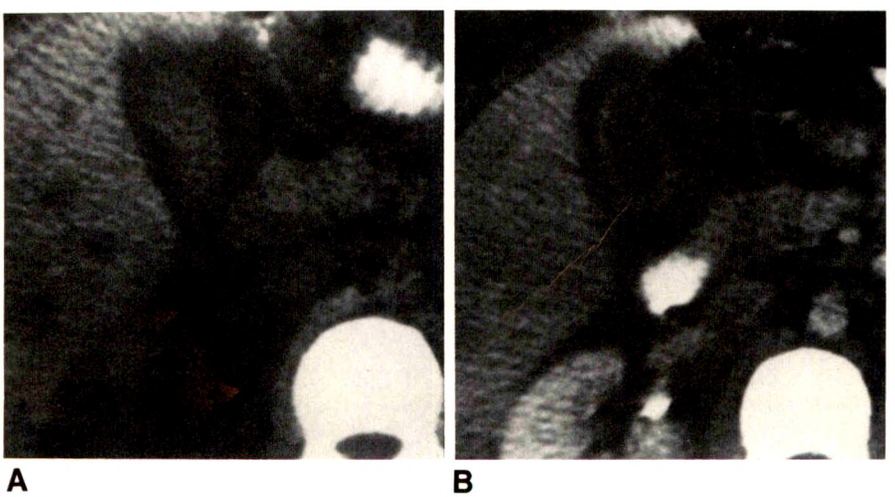

Fig. 4.—Precontrast (*A*) and postcontrast (*B*) CT scans show a thick-walled gallbladder with wall enhancement.

is known to occur with acute and chronic cholecystitis, ascites, hypoproteinemia, hepatitis, congestive heart failure, elevated portal venous pressures, multiple myeloma, and renal disease [11–18]. However, the sonographic findings in our patients could not be clearly attributed to any of these factors. Marked abdominal adenopathy is encountered frequently in those patients with AIDS who have Kaposi sarcoma, non-Hodgkin lymphoma, and *Mycobacterium avium intracellulare* [18]. Regional lymphatic obstruction by nodes also is proposed as a cause of gallbladder wall thickening [19]. Although the cause remains uncertain, AIDS should be included in the differential diagnosis of gallbladder wall thickening in the appropriate clinical setting.

The pathogenesis of bile duct dilatation is most likely related to opportunistic infection and inflammation, caused most frequently by *Cryptosporidium* [20–24]. Edema of the papilla appears to result in bile duct dilatation. Passive pancreatic duct dilatation also was observed in one of our patients; this too suggests that papillary inflammation causes partial obstruction of both ducts. Dolmatch et al. [9] found endoscopic biopsies of the ampulla to be positive for opportunistic organisms in several patients in their series who experienced the severe changes associated with cholangitis.

Current evidence [1–10] points to involvement of the gallbladder and biliary ducts in some patients with AIDS. Further studies are needed to determine whether biliary or systemic factors are responsible and what type of organisms are involved. Lastly, the clinical relevance of gallbladder and bile duct abnormalities remains to be defined.

ACKNOWLEDGMENT

Our appreciation to Peggy Clark for preparation of the manuscript.

REFERENCES

1. Guarda LA, Stein SA, Cleary KA, Ordonez NG. Human cryptosporidiosis in the acquired immune deficiency syndrome. *Arch Pathol Lab Med* **1983**;107:562–566
2. Blumberg RS, Kelsey P, Perrone T, Dickersin R, Laquaglia M, Ferrucci J. Cytomegalovirus and *Cryptosporidium*: associated acalculous gangrenous cholecystitis. *Am J Med* **1984**;76:1118–1123
3. Pitlik SD, Fainstein V, Garza D, et al. Human cryptosporidiosis: spectrum of disease. *Arch Intern Med* **1983**;143:2269–2275
4. Costel EE, Wheeler AP, Gregg CR. *Campylobacter fetus* ssp fetus cholecystitis and relapsing bacteremia in a patient with acquired immunodeficiency syndrome. *South Med J* **1984**;77:928–929
5. Kavin H, Jonas RB, Chowdhury L, Kabins S. Acalculous cholecystitis and cytomegalovirus infection in the acquired immunodeficiency syndrome. *Ann Intern Med* **1986**;104:53–54
6. Burt AD, Scott G, Schiach CR, Isles CG. Acquired immunodeficiency syndrome in a patient with no known risk factors: a pathologic study. *J Clin Pathol* **1984**;37:471–474
7. Gross TL, Wheat J, Bartlett M, O'Connor KW. AIDS and multiple system involvement with *Cryptosporidium*. *Am J Gastroenterol* **1986**;81:456–458
8. Cockerill FR, Hurley DV, Malagelada JR, et al. Polymicrobial cholangitis and Kaposi's sarcoma in blood product transfusion-related acquired immunodeficiency syndrome. *Am J Med* **1986**;80:1237–1241
9. Dolmatch BL, Laing FC, Federle MP, Jeffrey RB, Cello J. AIDS-related cholangitis: radiographic findings in nine patients. *Radiology* **1987**; 163:313–316
10. Pitlik SD, Fainstein V, Rios A, Guarda L, Mansell PW, Hersh EM. Cryptosporidial cholecystitis (letter). *N Engl J Med* **1983**;308:967
11. Shaler WJ, Leopold GR, Scheible FW. Sonography of the thickened gallbladder wall: a nonspecific finding. *AJR* **1981**;136:337–339
12. Fiske CE, Laing FC, Brown TW. Ultrasonographic evidence of gallbladder wall thickening in association with hypoalbuminemia. *Radiology* **1980**;135:713–716
13. Ralls PW, Quinn MF, Juttner HU, Halls JM, Boswell WD. Gallbladder wall thickening: Patients without intrinsic gallbladder disease. *AJR* **1981**; 137:65–68
14. Jeffrey RB, Nyberg DA, Bottles K, et al. Abdominal CT in acquired immunodeficiency syndrome. *AJR* **1986**;146:7–13
15. Carroll BA. Gallbladder wall thickening secondary to focal lymphatic obstruction. *J Ultrasound Med* **1983**;2:89–91
16. Vincent ME, Robbins AH. *Mycobacterium avium-intracellulare* complex enteritis: pseudo-Whipple disease in AIDS. *AJR* **1985**;144:921–922
17. Berk RN, Wall SD, McArdle CB, et al. Cryptosporidiosis of the stomach and small intestine in patients with AIDS. *AJR* **1984**;143:549–554
18. Kotler DP, Gaetz HP, Lang M, Klein EB, Holt PR. Enteropathy associated with the acquired immunodeficiency syndrome. *Ann Intern Med* **1984**;101:421–428
19. Weinstein L, Edelstein SM, Madara JL, et al. Intestinal cryptosporidiosis complicated by disseminated cytomegalovirus infection. *Gastroenterology* **1981**;81:584–591
20. Current WL, Reese NC, Ernst JV, Bailey WS, Heyman MB, Weinstein WM. Human cryptosporidiosis in immunocompetent and immunodeficient persons. *New Engl J Med* **1983**;308:1252–1257
21. Soave R, Danner RL, Honig CL, et al. Cryptosporidiosis in homosexual men. *Ann Intern Med* **1984**;100:504–511
22. Kovatch RM, White JD. Cryptosporidiosis in two juvenile rhesus monkeys. *Vet Pathol* **1972**;9:426–440
23. Acosta JM, Nardi GL. Papillitis: inflammatory disease of the ampulla of vater. *Arch Surg* **1966**;92:354–361
24. Teixidor HS, Honig CL, Norsoph E, Albert S, Mouradian JA, Whalen JP. Cytomegalovirus infection of the alimentary canal: radiologic findings with pathologic correlation. *Radiology* **1987**;163:317–323

Books Received

Receipt of books is acknowledged as a courtesy to the sender. Books considered of sufficient interest are reviewed as space permits. If the book has been reviewed in the *AJR*, the date of its review is given in parenthesis.

Diagnostic Radiology 1987. Edited by Alexander R. Margulis and Charles A. Gooding. St. Louis: Mosby, 564 pp., 1987. $85 (10/87)

Operative Ultrasound of the Liver and Biliary Ducts. By Henri Bismuth and Deenis Castaing. New York: Springer-Verlag, 89 pp., 1987. $39 (10/87)

A Diagnostic Approach to Chest Diseases. Differential Diagnoses Based on Roentgenographic Patterns, 3rd ed. By Glen A. Lillington. Baltimore: Williams & Wilkins, 530 pp., 1987. $86 (10/87)

Contrast Media in Pediatric Radiology. Workshop Berlin, August 22–24, 1985. Edited by H. J. Kaufmann. New York: Karger, 119 pp., 1987. $40 (10/87)

Biological Effects and Health Implications of Radiofrequency Radiation. By Sol M. Michaelson and James C. Lin. New York: Plenum, 675 pp., 1987. $79.50 (10/87)

Diagnostic Imaging of the Chest. By Paul R. Goddard. New York: Churchill Livingstone, 173 pp., 1987. $83 (10/87)

Diagnostic Imaging in Neurological Disease. By Ivan Moseley. New York: Churchill Livingstone, 283 pp., 1987. $98 (10/87)

Radionuclides in Nephrology. Edited by A. Bischof-Delaloye and M. D. Blaufox. (vol. 56 of Contributions to Nephrology, series edited by G. M. Berlyne and S. Giovannetti.) New York: Karger, 278 pp., 1987. $149.50 (10/87)

Practical Guide to Quality Assurance in Medical Imaging. By B. M. Moores, E. T. Henshaw, S. A. Watkinson, and B. J. Pearcy. New York: Wiley, 131 pp., 1987. $34.95 (10/87)

Physics and Engineering of Medical Imaging. Edited by Riccardo Guzzardi. The Netherlands: Kluwer, 996 pp., 1987. $210 (11/87)

Handbook of Gastrointestinal Imaging. Edited by R. Kristina Gedgaudas-McClees. New York: Churchill Livingstone, 274 pp., 1987. $49 (11/87)

Elements of Digital Radiology. A Professional Handbook and Guide. By H. K. Huang. Englewood Cliffs, NJ: Prentice Hall, 370 pp., 1987. $59.95 (11/87)

A Multimodality Approach to Breast Imaging. By Saar Porrath. Rockville, MD: Aspen, 333 pp., 1986. (11/87)

Noninvasive Imaging of Cardiac Metabolism. Single Photon Scintigraphy, Positron Emission Tomography and Nuclear Magnetic Resonance. Edited by E. E. van der Wall. Boston: Nijhoff, 311 pp., 1987. $105.50 (11/87)

The Clinical Recognition of Congenital Heart Disease, 3rd ed. By Joseph K. Perloff. Philadelphia: Saunders, 720 pp., 1986. $95 (11/87)

Diagnostic and Interventional Catheterization in Congenital Heart Disease. By James E. Lock, John F. Keane, and Kenneth E. Fellows. The Netherlands: Kluwer, 189 pp., 1987. $55 (11/87)

Investigational Techniques in Oncology. Edited by Norman M. Bleehen. New York: Springer-Verlag, 222 pp., 1987. $79 (11/87)

Computer Tomographic Imaging and Anatomic Correlation of the Human Brain. By C. Plets, A. L. Baert, G. L. Nijs, and G. Wilms. Boston: Nijhoff, 111 pp., 1987. $71.50 (12/87)

Gamuts in Radiology. By Benjamin Felson and Maurice M. Reeder. Cincinnati: Audiovisual Radiology, 925 pp., 1987. $95 (12/87)

Ultrasonography of the Neck. By Jean-Noel Bruneton. New York: Springer-Verlag, 118 pp., 1987. $65.50 (12/87)

Exercises in Radiological Diagnosis. By Pankaj Joshi and Cecilia Freed. Boston: Butterworth, 151 pp., 1987. $27.95 (12/87)

Diagnostic Imaging of Child Abuse. By Paul K. Kleinman. Baltimore: Williams & Wilkins, 297 pp., 1987. $55.95 (12/87)

Ultrasonic Diagnosis of Cerebrovascular Disease, 2nd ed. Edited by M. P. Spencer. The Netherlands: Kluwer, 306 pp., 1987. $79.50 (12/87)

Breast Cancer Detection. Mammography and Other Methods in Breast Imaging, 2nd ed. Edited by Lawrence W. Bassett and Richard H. Gold. Orlando: Grune & Stratton, 204 pp., 1987. $59 (12/87)

The Clinician's Guide to Diagnostic Imaging. Cost-Effective Pathways. By Zachary D. Grossman, Felix S. Chew, David A. Ellis, and Stephen C. Brigham. New York: Raven, 287 pp., 1987. $21.50 (12/87)

Radiopharmaceuticals in Nuclear Medicine Practice. By Richard J. Kowalsky and J. Randolph Perry. Norwalk, CT: Appleton & Lange, 500 pp., 1987. $95 (12/87)

Manual for Radiology Article Filing Program. By Robert Livingston, 1987. Purchase directly from the author at 2908 E. Republican, Seattle, WA 98112. $20 (software) (12/87)

RSNA Today, Vol. 1, No. 2. Oak Brook, IL: The Radiological Society of North America, 1987. $75 (videotape) (12/87)

Esophageal Motility Testing. By Donald O. Castell, Joel E. Richter, and Christine Boag Dalton. New York: Elsevier, 212 pp., 1987. $45

Cerebral Visual Disturbance in Infantile Encephalopathy. By Onno van Nieuwenhuizen. Boston: Nijhoff, 204 pp., 1987. $64

Cancers of the Head and Neck. Edited by Charlotte Jacobs. Boston: Nijhoff, 294 pp., 1987. $102.50

Adjuvant Therapy of Cancer V. Edited by Sydney E. Salmon. Orlando, FL: Grune & Stratton, 806 pp., 1987.

Asbestos and Other Natural Mineral Fibres. Geneva: World Health Organization, 194 pp., 1987. $9.60

Guides to Clinical Aspiration Biopsy. Retroperitoneum and Intestine. By Kenneth C. Suen. New York: Igaku-Shoin, 214 pp., 1987. $43.50

Technical Note

Choledocholithiasis: Percutaneous Pulverization with a High-Speed Rotational Catheter

Mark H. Wholey[1] and Sanford Smoot

We report the application of a new experimental device in which mechanical lithotripsy has been performed within the common bile duct through the existing T-tube tract. Pulverization and fragmentation of large retained stones within the common duct may be possible by means of a high-speed rotational Kensey dynamic angioplasty catheter.

Technique

The Kensey dynamic angioplasty catheter (Theratec Inc., Miami, FL) is an experimental device designed for recanalizing the totally obstructed arterial vessel (Fig. 1). The initial prototype uses an 8-French catheter that incorporates a high-speed rotational cable with a distal cam that achieves a speed approaching 90,000 rpm. An

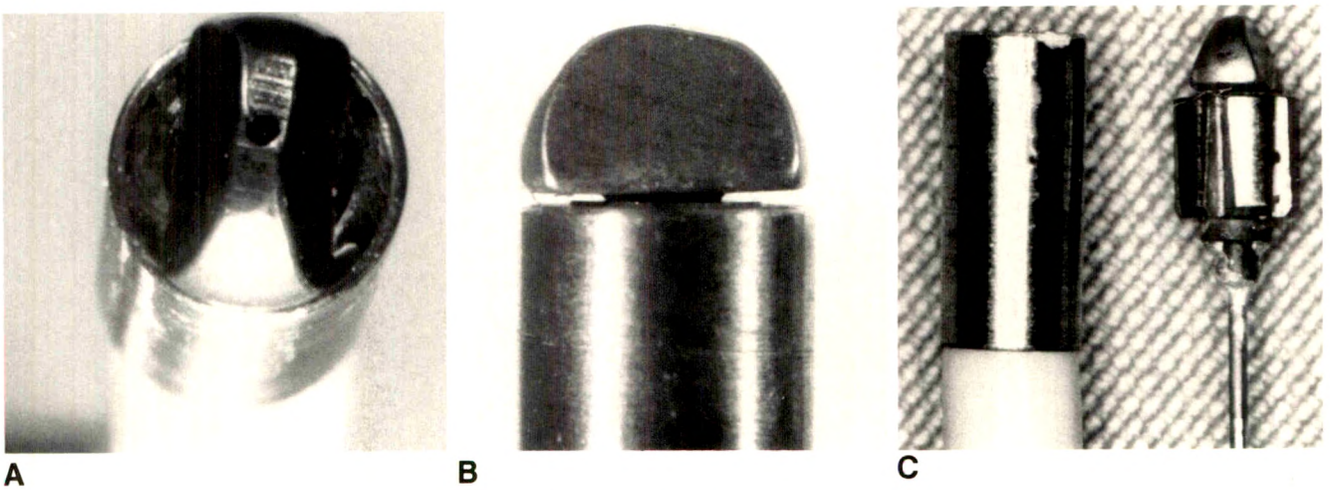

Fig. 1.—*A*, Distal tip of Kensey catheter. Cam is shown with distal end hole for infusate.
***B*, Longitudinal view of distal aspect of catheter and distal cam.**
***C*, Disassembled catheter. 8-French catheter and stainless steel metallic cable and rotational cam are shown.**

Received August 3, 1987; accepted after revision September 9, 1987.

[1] Both authors: Department of Radiological Sciences and Diagnostic Imaging, Shadyside Hospital and the University of Pittsburgh, Pittsburgh, PA 15232. Address reprint requests to M. H. Wholey, Dept. of Radiological Sciences and Diagnostic Imaging, Shadyside Hospital, 5230 Centre Ave., Pittsburgh, PA 15232.

AJR **150:129–130, January 1988** 0361–803X/88/1501–0129 © American Roentgen Ray Society

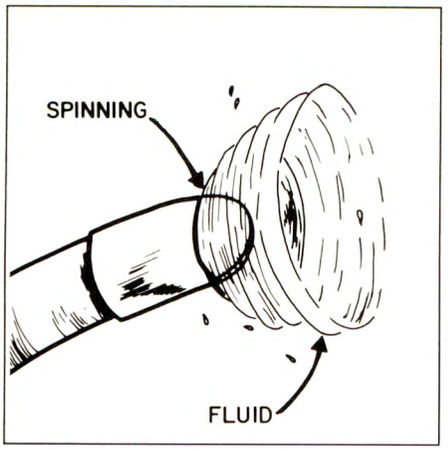

Fig. 2.—Diagram of Kensey catheter. For angioplasty, urokinase is added to infusate; however, for pure opacification, a mixture of saline and contrast material can be used.

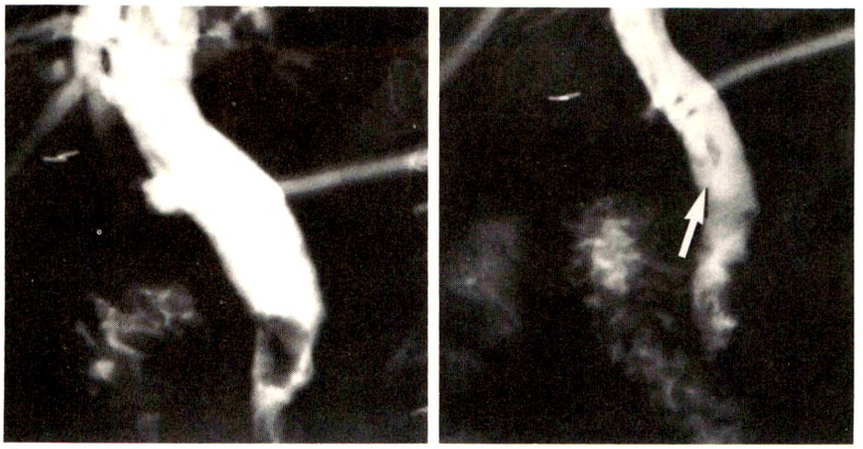

Fig. 3.—*A*, T-tube cholangiogram in anteroposterior projection showing 2-cm stone at distal aspect of common duct.

B, After application of Kensey catheter, there is essentially complete pulverization of stone. Residual fragments are visible (*arrow*). Follow-up cholangiogram 24 hr later was normal.

infusate of physiologic saline is combined with contrast material at an injection flow rate of approximately 30 ml/min through a modified Medrad Mark IV injector (Medrad Inc., Pittsburgh, PA). The infusate combined with the rotational cam within a cylinder creates a vortex (Fig. 2), and the stones are drawn to the center of the vortex where the high-speed rotational tip pulverizes the stones.

Initially, the Kensey catheter was used in vitro on calcium carbonate stones within a fluid-filled cylinder. After only minimal application, portions of the stone were pulverized into tiny fragments. The higher the rotational speed of the cam was, the greater the degree of pulverization was. Experimentally, with the cam rotational speeds at 150,000 rpm, pulverization resulted in particulate matter as small as 5–10 μm.

Our clinical experience is based on the application of the Kensey catheter in a 70-year-old woman who was referred 5 weeks after cholecystectomy for removal of a 2-cm retained common bile duct calculus (Fig. 3A). Prior attempts to extract the stone through the existing T-tube tract by conventional methods were unsuccessful. Several other smaller stones that were present in the common duct had been retrieved successfully by conventional basket technique. The single retained large stone, however, required additional measures, and the application of the Kensey dynamic catheter was recommended. Written permission by the Food and Drug Administration was given for this single application and as an addition to the existing protocol. After administration of 5 mg of IV diazepam followed by 50 μg of fentanyl, the existing T-tube was exchanged for a 10-French intraaortic balloon sheath. The intraaortic balloon sheath followed the appropriate positioning of the guidewire adjacent to the stone in the distal duct. The Kensey catheter was then passed through the sheath to the distal common duct, allowing the tip to protrude only 5 mm beyond the protection of the sheath. The dynamic angioplasty catheter was then rotated at speeds of 90,000 rpm. During the mechanical lithotripsy, fragmentation of the stone occurred rapidly. The larger fragments were simply retrieved with the Dormia basket, while the smaller pulverized particles were flushed with saline either through the existing T-tube tract or into the duodenum. The cholangiogram taken after the procedure revealed only a few tiny residual fragments and a minimal degree of periampullary edema (Fig. 3B). A 10-French catheter, however, was easily passed through the ampulla, showing satisfactory patency. On the next day there were no residual stones, and significant debris and resolution of the periampullary edema had occurred. The time for the procedure was approximately 30 min, and the procedure was tolerated satisfactorily by the patient. There were no postprocedure complications.

Discussion

The concept of mechanically crushing or fragmenting residual common duct stones is not new. Dormia baskets were used in this capacity by Burhenne in 1975 [1, 2]. In 1984, Lear and Ring [3] described electrohydraulic fragmentation of retained common duct stones through an existing T tube. In 1985, Bean and Daughtry [4] used experiences from ultrasonic lithotripsy in the pelvocalyceal structures of the kidneys to apply a mechanical-fragmentation procedure to the biliary tree.

During the application of the Kensey catheter within the biliary tree, we noted that the fluid being injected through the tip performs two functions. (1) A vortex is established around the catheter tip. (2) This vortex creates a vacuum within the center to which the material is drawn. The cam at the distal aspect of the catheter has been carefully designed to pulverize the calcific atheromatous material frequently present in occlusive arterial disease. The cam has also been designed to avoid damage to the adjacent normal viscoelastic tissues. When the cam is positioned within the common bile duct and protected by the sheath, its basic design should work the same way. At present, the catheter used is approximately 3 mm in external diameter (8 French). Current studies are using catheters with smaller dimensions, including 5- and 3-French catheters.

In certain patients with large retained biliary calculi for which existing methods of removal have been unsuccessful, the application of the Kensey device to pulverize the retained stones may be an additional tool for nonsurgical intervention.

REFERENCES

1. Burhenne HJ. Electrohydraulic fragmentation of retained common duct stones. *Radiology* **1975**;117:721–722
2. Burhenne HJ. Percutaneous extraction of retained biliary tract stones: 661 patients. *AJR* **1980**;134:888–898
3. Lear JL, Ring EA. Percutaneous transhepatic electrohydraulic lithotripsy. *Radiology* **1984**;150:589–590
4. Bean WJ, Daughtry JD. Ultrasonic lithotripsy of retained common bile duct stones. *AJR* **1985**;144:1275–1276

Antegrade Transluminal Dilatation of Benign Ureteral Strictures:
Long-Term Results

Erich K. Lang[1]
Lawrence W. Glorioso III

The long-term results (follow-up of 15 months or longer) of antegrade transluminal dilatation of 127 benign ureteral strictures are assessed and analyzed. The overall success rate is 50%. When lesions were classified according to age of the stricture, status of vascular supply, and other etiologic factors contributing to formation, the following findings were evident: transluminal dilatation was successful in 30 (91%) of 33 patients with fresh strictures in whom there was no evidence of compromised vascular supply; in 23 (53%) of 43 similar strictures older than 3 months; in 3 (25%) of 12 with fresh strictures with evidence of vascular compromise; and in 7 (18%) of 39 with similar older strictures. Regardless of age of stricture and other etiologic factors, transluminal dilatation was successful in 53 (70%) of 76 patients with strictures without evidence of ischemic compromise but was successful in only 10 (20%) of 51 with strictures with evidence of devitalization.

These findings emphasize the importance of considering both the age and vascular supply of a stricture and adjacent ureter when making the decision about treatment by antegrade transluminal dilatation.

Retrograde bougie dilatation is a time-honored nonsurgical method for management of benign ureteral strictures [1]. Because many ureteral strictures were not amenable to retrograde catheterization and hence to dilatation via this route, techniques for an antegrade approach were needed. Percutaneous nephrostomy provides ready antegrade access [2, 3]. Transluminal dilatation can be carried out by using a balloon catheter or tapered coaxial Teflon dilators [4, 5]. The goal is to correct permanently or at least to substantially reduce an existing urodynamically significant stricture. Today, antegrade transluminal dilatation has become the procedure of choice for the treatment of benign ureteral strictures [2, 4, 6–9]. This technique spares the patient extensive surgical procedures and the inconvenience and risks of either a chronic indwelling stent or a permanent percutaneous nephrostomy [2, 4, 6]. Management by chronic indwelling stent is reserved for strictures associated with malignant disease [3]. Treatment by percutaneous nephrostomy is advocated only as a temporary measure to preserve renal function.

This communication reports the long-term results of transluminal dilatation of benign ureteral strictures and attempts to identify the factors that jeopardize success.

Received April 22, 1987; accepted after revision September 9, 1987.

[1] Both authors: Department of Radiology, Louisiana State University Medical Center, 1542 Tulane Ave., New Orleans, LA 70112. Address reprint requests to E. K. Lang.

AJR 150:131–134, January 1988
0361–803X/88/1501-0131
© American Roentgen Ray Society

Materials and Methods

From May 1978 to February 1985, 152 percutaneous transluminal dilatations of benign ureteral strictures were performed in 149 patients via an antegrade route. Twenty-two patients, three of whom had strictures involving both ureters, were lost to follow-up. This study is based on the remaining 127 strictures in 127 patients who were followed for at least 15 months. Forty-five strictures were less than 3 months old, and 82 were older.

Selection of Patients

Only patients with urodynamically significant but benign strictures were included in this study. The diagnosis of stricture (1) of the ureter, (2) of the ureteropelvic junction, or (3) at a ureteroileostomy or ureteroneocystostomy site was established in all 127 patients by antegrade pyelogram and/or antegrade ureterogram.

The urodynamic significance of the lesion was established in 102 patients by computerized radionuclide urogram, in 12 patients solely by the Whitaker test, and in another 13 by criteria derived from a combination of the two techniques [10]. IV urograms were available in 112 patients, and Lasex washout urograms were available in eight others.

A number of factors contributing to the formation of strictures were identified. These included neoplastic disease, primary or iatrogenic trauma, intrinsic or adjacent inflammatory disease, and, in particular, compromise of the vascular supply of the ureter [1].

Sixty patients had underlying malignant disease; however, the possibility of a malignant cause for the stricture was eliminated by brush biopsy (if the lesion involved the uroepithelium) or by guided thin-needle biopsy of periureteric tissues (if retroperitoneal or pelvic neoplasms were suspected of involving the ureter by contiguous extension) [11]. Although 17 of these 60 patients either have since died of neoplastic disease or now show recurrence, cytopathologic examination at the time of transluminal dilatation determined the strictures to be fibrotic.

In 22 patients, the histologic diagnosis of a devitalized segment of the ureter was established on the surgical resection specimen. Radiologic findings and an injury mechanism predisposing to devitalization suggested avascular necrosis as cause for the stricture in another 29 patients.

The results of transluminal dilatation were judged on both a short-term basis (within 3 months after the procedure) and a long-term basis (3 months or more). The morphologic effect of transluminal dilatation was assessed in all patients by antegrade ureterograms performed immediately after dilatation and/or 2 days after removal of the indwelling stent catheter. The computed radionuclide urogram was accepted as gold standard for detecting deterioration of renal function and thus for indicating recurrence or perseverance of a urodynamically significant stricture. Serial follow-up radionuclide urograms were performed on the first or second day after removal of the ureteral stent, then at monthly intervals for 3 months and at 6-month intervals thereafter. Whitaker tests were performed 2 days after removal of the stent catheter in 46 patients in whom the computed radionuclide urogram and antegrade urogram could not establish unequivocably the perseverance of a urodynamically significant stricture [10].

Technique

Detailed etiologic, morphologic, and topographic information about the stricture was gathered before deciding on the type of treatment. In 54 patients, retrograde ureterograms were added to the antegrade study to better define the length of the stricture and its distal margins.

Entry into the renal collecting system and passage of the guidewire (Meditech, Watertown, MA) across the ureteral stricture followed established techniques [2, 4, 6, 9]. Thereafter, a balloon catheter was introduced and seated across the lesion. To prevent recoil and dislodgment when the balloon was inflated, the guidewire was always coiled in either the bladder or the ileal loop. In some patients, the guidewire was passed through the stoma of the ureteroileostomy to stabilize the balloon.

The length of the balloon had been determined on the preceding diagnostic study. The balloon needed to extend to either side of the stricture by a margin of at least 0.5 cm. Balloons either 4 or 6 mm in diameter were favored for ureteric strictures, those 6–10 mm were used for ureteropelvic junction strictures, and those 8–10 mm were used for strictures occurring at a ureteroileostomy site.

From 1978 through 1981, low-pressure balloons (Meditech) were used; thereafter, high-pressure (reinforced-polyethylene) balloons (Cook, Bloomington, IN) generally were used. With one exception (a 1.43-mm coronary balloon catheter, USCI, Bard, Billerica, MA), 7-French balloon catheters were deployed in all patients.

Low-pressure balloons always were distended manually by using a 1- to 5-ml syringe. A mixture of contrast medium diluted with water at a 1:4 ratio was used for distending the balloon and offered good visualization and only minimally increased viscosity. Pressure delivered by pressure injector (14–20 lb) was used for distension of most high-pressure balloons.

The balloon was distended repeatedly for 30–60 sec until the disappearance of the "waist" that indicates the presence of a stricture. Lack of reformation of a waist configuration (when the balloon was deflated) was the accepted criterion for complete and successful dissolution of the stricture [2].

After successful dilatation, a ureteral stent was placed across the stricture. Strictures without historical inference suggesting devitalization were intubated for 3 weeks. All strictures presumed to be caused by devitalization were intubated for 6 weeks. Strictures at the ureteropelvic junction attendant to dismembered pyeloplasty were intubated for 6–8 weeks.

Initially, the largest stent that could be fitted comfortably, 7- or 8-French, was seated. Thereafter, at weekly intervals, stents were exchanged for progressively larger ones until a 9- or 10-French stent had been seated. This was done to reduce the ill effects of cicatricial restricturing. To facilitate exchange, we used externalized stents in more than 90% (115) of our patients. During the early phases of this study through 1981, polyethylene stents were favored, later polyurethane stents were used (Cook). After removal of the ureteral stent, a nephrostomy tube was placed into the kidney pelvis for 48 hr as a safeguard against temporary obstruction by ureteral edema [12].

Bougie dilatation with a tapered vanAndel catheter (Cook) or tapered coaxial Teflon dilators (Single Step dilator, Cook) were preferred for strictures located at the ureteropelvic junction and at ureteroneocystostomy sites in patients with kidney transplants [5, 13]. To establish a straight line for the transfer of force when bougie-dilating ureteropelvic junction strictures, we chose entry via the superior calyceal group [2, 9].

After bougie dilatation of strictures in ureters that were cadaveric transplants, externalized stents were maintained for a maximum of 7 days and then internalized [2]. This precaution was deemed necessary to prevent infection in immunosuppressed patients.

At times, guidewires introduced via an antegrade approach were retrieved from an ileal conduit or the female urethra. (Control of both the cephalad and caudal ends of the guidewire permitted forceful bougie dilatation in either direction.)

Results

Regardless of etiology, 30 (91%) of 33 strictures that were treated within 3 months after causative noxious injury and that had no evidence of compromised vascular supply were treated successfully by antegrade transluminal dilatation (Table 1). Conversely, only 23 (53%) of 43 similar strictures that had been treated after a delay of more than 3 months were treated successfully by transluminal dilatation (Table 1).

Moreover, the rate of early failure (3 months or less) was higher in patients in whom transluminal dilatation was at-

TABLE 1: Results of Transluminal Dilatation of Ureteral Strictures

Age of Stricture: Etiologic Factor	Strictures Without Vascular Compromise			Strictures with Vascular Compromise		
	Total No. Dilatations	Early Failures	Late Failures	Total No. Dilatations	Early Failures	Late Failures
<3 months:						
Nonneoplastic	29	1	2	8	5	1
Neoplastic[a]	4	0	0	4	3	0
>3 months:						
Nonneoplastic	18	2	3	12	7	1
Neoplastic[a]	25	10	5	27	20	4

[a] Benign strictures occurring in patients with underlying neoplastic disease, often as a consequence of treatment of neoplasm.

tempted on older strictures; 1 (3%) in 33 with fresh strictures, 12 (28%) in 43 with old strictures (Table 1). The late-failure rate (3 months or later) for fresh strictures without evidence of vascular compromise was 6% (2/33); for similar older strictures, this rate was 19% (8/43) (Table 1).

Irrespective of age of stricture and other etiologic factors, transluminal dilatation failed in 23 (30%) of 76 strictures without evidence of vascular compromise, but in 41 (80%) of 51 strictures with evidence of devitalization (Table 1). In the latter group, 35 were termed early failures and 19 of these represented procedural failures (i.e., failure to place the balloon across the lesion, attain full distension of the balloon, or produce an acceptable lumen after bougi dilatation). Conversely, in the group of 76 patients in whom strictures with an apparently intact vascular supply had been dilated, there were only three procedural failures.

In the presence of devitalization, the success rate with fresh strictures was 25% (3/12); with similar older strictures, this rate was 18% (7/39 patients) (Table 1).

The frequency of vascular compromise of the adjacent ureter or stricture was higher in patients with underlying neoplastic disease (31 [52%] of 60 patients) than in patients with nonneoplastic etiologies (20 [30%] of 67 patients) (Table 1). The rate of early failure of transluminal dilatation is higher for strictures with neoplastic etiologies than for those with other etiologies. Early failures occurred in 20 (74%) of 27 of such older strictures complicated by vascular compromise (Table 1). Sixteen of these were procedural failures.

Strictures with evidence of compromised vascular supply attendant to radiation therapy of underlying neoplastic disease were consistently refractory to management by transluminal dilatation. Eight of nine such patients were procedural failures. In the remaining patient, temporary reprieve was gained for 4½ months, but ultimately a long stricture refractory to further transluminal dilatation redeveloped.

In 16 patients, a second attempt at transluminal dilatation of a recurrent stricture has been carried out; in three, a third dilatation has been attempted. Of these, only one case of an older stricture without compromised vascular supply or neoplastic etiology has been successful so far. Four others have not yet been followed for the obligatory 15-month period after the second or third attempt at transluminal dilatation, so success or failure has not been determined.

Complications were rare and minor. The ureter was perforated in 11 patients while an attempt was being made to pass the guidewire. In 10, stents ultimately were placed across the stricture, which ensured adequate treatment of the perforation. The last patient was treated by percutaneous nephrostomy drainage. There were no sequelae in these 11 patients. In another 34 patients, a reduced renal-plasma flow rate was noted on computed radionuclide urograms on the day of removal of an indwelling stent and after treatment by transluminal dilatation. IV urograms, however, correctly suggested the diagnosis of mucosal edema, which subsided in all patients within 3 days under treatment by percutaneous nephrostomy.

Discussion

Percutaneous transluminal dilatation of ureteral strictures was successful in 50% of our patients followed for at least 15 months. This is comparable to other reported results for similar techniques [4, 6, 8, 14].

An analysis of our data revealed that two factors had profound influence on results: the age of and vascular-supply status of the stricture and adjacent segments of the ureter.

The influence of the age of a stricture on response to percutaneous transluminal dilatation has been widely recognized [2, 4, 6, 8, 9, 14]. Although predilection of refractory strictures at the ureterovesical or ureterocolonic junction has raised the question of vascular compromise, this lead has not been pursued [4, 8, 14].

In our series, percutaneous transluminal dilatation was effective in 91% of patients with fresh strictures without evidence of vascular compromise and in 53% of similar older strictures, but in only 25% of fresh strictures with vascular compromise and 18% of similar older strictures. These statistics stress the influence of these two factors on treatment results.

Chronicity appears to have a profound impact on the pathologic makeup of such strictures. It increases the procedural failure rate of transluminal dilatation.

No procedural failures occurred when 33 fresh strictures without ischemia were being dilated; however, in 43 similar older strictures, three procedural failures occurred. Similarly,

in 12 patients with fresh strictures compromised by ischemia there were three procedural failures, whereas in 39 similar older strictures we encountered 16 procedural failures. The increased procedural-failure rate reflects the technical problems encountered when a stricture becomes more dense and fibrotic with age.

Ischemia is the most adverse factor influencing the ability to dilate such strictures and attain salutary long-term results. A number of factors predispose to ischemic changes of the stricture or adjacent ureter. Chronicity (age) in itself may set the stage for ischemic damage. A dense, fibrotic stricture compresses vessels and thereby reduces flow rate. Decreased oxygenation causes fibrosis and therefore the formation of a dense stricture. Thus, a vicious cycle is established. Moreover, the damage caused by dilatation of the stricture is repaired by deposition of fibroblasts and then subject to the same vicious cycle.

Certain injury mechanisms are particularly prone to cause devitalization [13, 15]. Such injury mechanisms include surgical procedures designed to remove periureteric lymphatics (Wertheim hysterectomy), radiation therapy, chemotherapy, inflammatory conditions prone to cause end-arteritis obliterans (tuberculosis), nearby passage of a high-velocity projectile causing thrombosis of end arteries, chronic rejection in kidney transplants, or impaction of a calculus for a prolonged period of time. In fact, unrecognized devitalization may be a prominent factor in the formation of many strictures of the female pelvic ureter. The fragile nature of the vascular supply of the pelvic portion of the female ureter predisposes it to this complication.

To reduce the impact of inevitable restricturing by cicatricial repair, we advocate placement of successively larger ureteral stents (7- to 10-French) over 3–6 weeks. Fibrocytic healing is completed within 3 weeks, and the lumen through the cicatricially-altered ureter is established by the size of the indwelling stent. Although contraction of scar tissue may occur at a later date, the pathophysiologic impact of this late process is less pronounced. Despite the reservation expressed by other investigators that large stents may cause ureteral ischemia and thence stricture, we have not observed any adverse effect of larger vs smaller stents [4].

The mere presence of neoplastic disease did not influence the curability of benign ureteral strictures by antegrade transluminal dilatation. For example, no failures of antegrade transluminal dilatation occurred among four fresh ureteral strictures in patients with a history of underlying neoplastic disease. However, the diagnosis of strictures in patients with neoplastic disease was often delayed. In patients with underlying neoplastic disease, 87% (52/60) of strictures were older strictures. Moreover, 52% (31/60) of such strictures also manifested ischemic compromise. It is therefore not surprising that 12 procedural and ultimately 24 failures occurred in 27 older strictures with ischemic compromise in patients with underlying neoplastic disease.

Meticulous follow-up by computed radionuclide urography is the key to early recognition of deteriorating renal function that may indicate restricturing. Then antegrade ureterograms and/or Whitaker tests can be performed to confirm recurrence of the stricture and institute corrective measures such as repeated antegrade transluminal dilatation or surgery.

Admittedly, surgical resection of ureteral segments with compromised vascular supply and reanastomosis of only viable and well-perfused segments result in a higher cure rate for ureteral strictures [16–18]. However, in many instances, the vascular supply of long segments of both ureters is compromised, and such salvage procedures as transureteroureterostomy, Boari flaps, and bowel interposition devised to bridge noncompromised to noncompromised tissues become exceedingly difficult (if not impossible) [16–18].

On the basis of our experience, transluminal dilatation is the procedure of choice for fresh strictures with seemingly intact vascular supply. Surgery may be preferable in the management of strictures with impaired vascular supply because the culprit tissue initiating the vicious cycle is removed. Nonetheless, an attempt at antegrade transluminal dilatation of even older or ischemically compromised strictures may be justified. Some such strictures respond to this relatively noninvasive and inexpensive procedure; for the other patients, surgery is neither significantly delayed nor compromised. Moreover, some of the procedural failures in our early experience may prove amenable to antegrade transluminal dilatation with the now-used high-pressure balloons.

REFERENCES

1. Witherington R, Shalor WC. Treatment of postoperative ureteral stricture by catheter dilatation: a forgotten procedure. *Urology* **1980**;16:592–595
2. Lang EK. Percutaneous nephrostomy. Presented at the annual meeting of the American Roentgen Ray Society, Boston, MA, April **1985** (categorical course, pp. 91–98)
3. Lang EK, Price ET. Redefinitions of indications for percutaneous nephrostomy. *Radiology* **1983**;147:419–426
4. Banner MP, Pollack HM. Dilatation of ureteral stenosis: techniques and experience in 44 patients. *AJR* **1984**;143:793–798
5. Cardella JF, Hunter DW, Castaneda-Zunida WR, Young AT, Amplatz K. Coaxial cancer dilator (technical note). *Radiology* **1985**;157:820
6. Reimer DE, Oswalt GC Jr. Iatrogenic ureteral obstruction treated with balloon dilatation. *J Urol* **1981**;126:689–690
7. Kadir S, White RI Jr, Engle R. Balloon dilatation of a ureteropelvic junction obstruction. *Radiology* **1982**;143:263–264
8. Dixon GD, Morre JD, Stockton R. Successful dilatation of ureteroileal anastomotic stenosis using Gruntzig catheter. *Urology* **1982**;19:555–558
9. Lang EK. Antegrade ureteral stenting for dehiscence, strictures, and fistulae. *AJR* **1984**;143:795–801
10. Whitaker RJ. Percutaneous upper urinary tract dynamics in equivocal obstruction. *Urol Radiol* **1981**;2:187–189
11. Lang EK, Alexander R, Barnett T, Palomar J, Hamway S. Brush biopsy of the pyelocalyceal lesions via a percutaneous translumbar approach. *Radiology* **1978**;129:623–627
12. Lavine RS, Pollack HM, Banner MP. Transient ureteral obstruction after ureteral stenting. *AJR* **1982**;138:323–327
13. Gianello P. Ischemic necrosis of the allograft ureter. *Transplant Proc* **1984**;16(5):1301–1303
14. Johnson CD, Oke EJ, Dunnick NR, et al. Percutaneous balloon dilatation in ureteral strictures. *AJR* **1987**;148:181–184
15. Spirnak JP, Persky L, Resnick MI. Management of civilian ureteral gunshot wounds, a review of 8 patients. *J Urol* **1985**;134:733–736
16. Young JD Jr. Ureteroureterostomy and transureteroureterostomy. In: Glenn JF, ed. *Urologic surgery*. Philadelphia: Lippincott, **1983**:427–434
17. Politano VA. Ureteroplasty and ureteral replacement. In: Glenn JF, ed. *Urologic surgery*. Philadelphia: Lippincott, **1983**:439–446
18. Boyarsky S. Ureteral strictures, fistulas and trauma. In: Glenn JF, ed. *Urologic surgery*. Philadelphia: Lippincott, **1983**:447–455

Stage IB Cervical Carcinoma: Comparison of Clinical, MR, and Pathologic Staging

Deborah Rubens[1]
John R. Thornbury[1]
Cynthia Angel[2]
Mark H. Stoler[3]
Stan L. Weiss[1]
Robert M. Lerner[1]
Jackson Beecham[2]

In patients with stage IB cervical carcinoma (carcinoma confined to the cervix), accurate staging is essential in order to determine the best treatment strategy—that is, whether to use surgery alone or surgery in combination with pre- or postsurgical radiation therapy. Currently, decisions regarding the management of patients are made on the basis of clinical staging that has an error rate of 34–39% (when surgical staging is used as the standard). To investigate the value of MR in staging patients with IB cervical cancer, we performed prospective MR examinations in 27 patients who had cervical carcinoma. Of these, 10 were clinically staged as having IB cervical carcinoma and underwent radical hysterectomy, providing specimens for pathologic correlation. In six of these 10 patients, the extent of disease had been underestimated during clinical examination under anesthesia. These six patients would have received radiation therapy before surgery had the MR information been used at the treatment-planning stage.

MR imaging correlated better with surgical pathology than did clinical examination under anesthesia in determining the location and extent of tumor. MR imaging should be used in conjunction with clinical staging to determine appropriate therapy in patients with stage IB cervical carcinoma.

In patients with stage IB cervical carcinoma, the selection of optimal therapy depends on precise assessment of the extent of disease before surgery. Appropriate International Federation of Gynecology and Obstetrics (FIGO) staging is required to distinguish IB carcinoma (confined to the cervix) from more advanced stages of disease (beyond the cervix to the upper two-thirds of the vagina [IIA], the parametrium [IIB], the lower one-third of the vagina [IIIA], the pelvic sidewall or ureter [IIIB], or the bladder, rectum, or distant sites [IV]). In addition, precise clinical assessment of tumor volume is necessary, as patients with large exophytic IB lesions or barrel-shaped cervices will receive presurgical radiation therapy followed by extrafascial hysterectomy, while more localized IB lesions are treated by radical hysterectomy. Previous studies have shown errors of 34–39% in clinical staging (when surgical staging is used as the standard) [1], while CT has an accuracy rate of only 50% in distinguishing IB from IIB lesions [1, 2] and cannot distinguish the primary lesion within the cervix at all. We evaluated the role of MR in determining the extent of tumor within the cervix and in accurately staging the disease.

Materials and Methods

Between April 1985 and April 1987, 27 patients with carcinoma of the uterine cervix were evaluated with 1.5-T MR. Fourteen of these patients were staged as having IB lesions after examination under anesthesia. Of this subset, four patients were thought clinically to have bulky disease and were treated with radiation therapy before hysterectomy. The remaining 10 patients, who ranged in age from 27 to 76 years, underwent radical hysterectomy, providing specimens for pathologic correlation. These 10 patients, all of whom had primary, untreated cervical carcinoma, were prospectively evaluated with MR and clinical examination (including examination under anesthesia as well as cystoscopy and sigmoidoscopy). CT was

Received July 13, 1987; accepted after revision September 17, 1987.

This work was supported in part by grant #1 ROI HS05427-01 from the National Center for Health Services Research and Health Care Technology Assessment.

[1] Department of Radiology, University of Rochester Medical Center, 601 Elmwood Ave., P.O. Box 694, Rochester, NY 14642. Address reprint requests to D. Rubens.

[2] Department of Obstetrics and Gynecology, University of Rochester Medical Center, Rochester, NY 14642.

[3] Department of Pathology and Laboratory Medicine, University of Rochester Medical Center, Rochester, NY 14642.

AJR 150:135–138, January 1988
0361–803X/88/1501–0135
© American Roentgen Ray Society

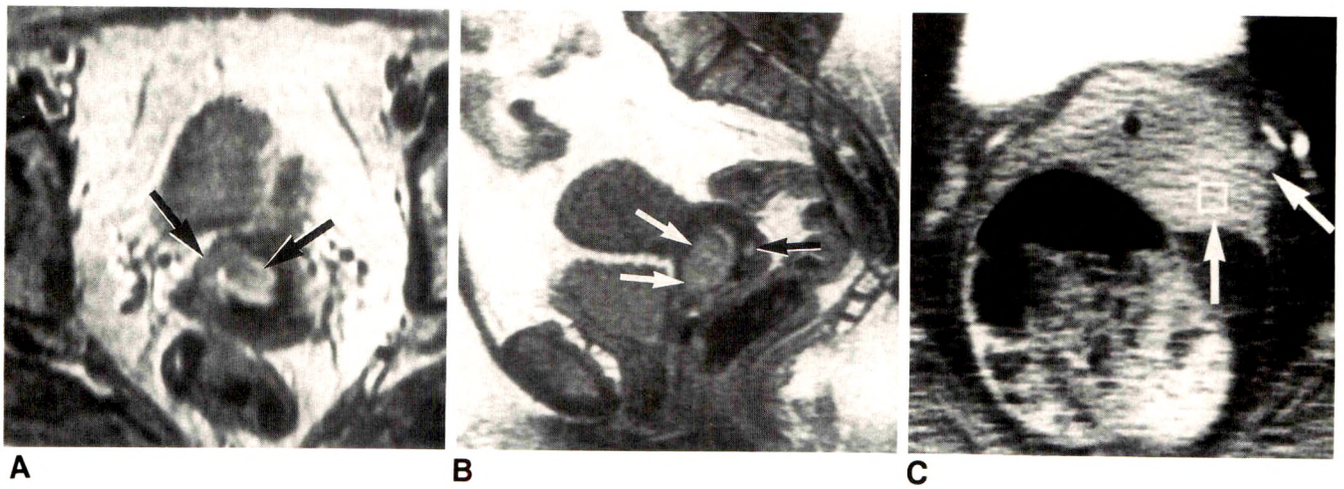

Fig. 1.—CT and MR images.
***A*, Axial MR image (TR = 2000 msec, TE = 40 msec) shows a high-signal lesion (*arrows*) extending along entire right and anterior portion of cervix.**
***B*, Sagittal view shows craniocaudal tumor extent with bulk of tumor mass in anterior lip (*white arrows*), as well as a small focus posteriorly (*black arrow*). MR predicts deep primary tumor extending into stroma.**
***C*, CT image shows soft-tissue bulk on left with mild thickening of proximal left uterosacral ligament (*arrows*).**

performed in seven of 10 patients. The three evaluations were performed within a 2-week period. Treatment choices were determined solely on the basis of the clinical examination.

All patients were examined under anesthesia by the gynecologic surgeon to determine the appropriate clinical FIGO stage. The cervix and vagina were visually inspected for superficial evidence of the extent of tumor. Biopsies were not routinely performed since patients were usually referred only after a biopsy had confirmed the diagnosis of invasive carcinoma. However, if vaginal lesions were identified that would change the clinical stage, these were biopsied at the time of examination under anesthesia. Bimanual palpation was performed to assess the bulk of the cervix and to estimate the tumor volume. The parametria, uterosacral ligaments, and pelvic sidewalls were palpated to assess tumor extension. The rectum was examined manually and sigmoidoscopically to check for tumor extension. Cystoscopy was also performed to detect bladder involvement.

CT imaging was performed in seven of the 10 patients with a General Electric 8800 CT scanner; oral, IV, and rectal contrast materials were used. Oral contrast material consisted of 1000 ml of E-Z-Cat (E-Z-M, Whitby, Ont., Canada) given 30 min before the examination. Rectal contrast material was provided by a 500-ml Gastrografin enema (Squibb, Princeton, NJ) given on the CT table as imaging began. A vaginal tampon was inserted for air contrast, and IV contrast material was administered as a 50-ml bolus of a 60% iodine solution at the beginning of the scan; a second 50-ml bolus was given at the level of the cervix. Slice thickness was 1 cm from the mid abdomen to the cervix; 0.5-cm targeted slices were used through the cervix. CT staging was performed by using the criteria of Walsh and Goplerud [1] and Vick et al. [3]. Stage I cervical carcinoma is confined to the cervix. Stage IIB disease has irregular cervical borders, a parametrial mass, or prominent parametrial soft-tissue strands. Stage IIIB disease exhibits sidewall extension or hydronephrosis. CT examinations were interpreted prospectively without knowledge of clinical or MR results.

MR examinations were performed in all 10 patients by using a 1.5-T General Electric Signa system. Pulse sequences included a sagittal series through the uterus (5-mm-thick slices with no gaps, repetition time [TR] of 2000 msec, echo time [TE] of 40 or 80 msec) and an axial series (1-cm-thick slices with no gaps, TR of 2000 msec, TE of 40 or 80 msec) from the base of the cervix to the aortic bifurcation. A third axial partial-saturation sequence was originally used (TR of 600 msec, TE of 25 msec, 1-cm-thick slices with no gaps) through the cervix and uterus. Recently this sequence has been replaced by a fat-suppression sequence. All sequences were performed on a 128 × 256 matrix with two excitations (one average). MR imaging time averaged 45 min.

Tumor on MR (Figs. 1A and 1B) was identified as high signal intensity replacing the normal low-signal-intensity cervical stroma. Staging criteria were those used for CT (above) plus the inclusion of stages IIA (tumor in the upper two-thirds of the vagina) and IIIA (tumor in the lower one-third of the vagina). All MR studies were interpreted prospectively without knowledge of the results of CT or clinical examination.

Assessments of the extent of tumor were prospectively drawn on axial and sagittal diagrams for each clinical, MR, CT, and pathologic examination. The imaging and clinical examinations were then compared with the pathologic findings. Parametrial extension and lymph node involvement were also evaluated. Estimates of lesion size (in centimeters) were given for clinical and MR examinations and were then compared with pathologic measurements. Agreement within 1 cm in each plane was considered a concordant result. A mismatch of more than 1 cm in one or more planes was classified as a discordant result. In all cases the prospective, blinded initial assessments were used to determine the accuracy of each method as measured against the pathologic findings.

Results

MR and clinical staging both agreed with pathologic staging and assigned all 10 patients to stage IB. Of the seven patients who had CT examinations, four were correctly staged as IB and three were overstaged as IIB. CT therefore provided no useful staging information as compared with either clinical or MR evaluations. Examination under anesthesia, CT, MR imaging, and frozen-section examination all failed to detect

microscopic tumor invasion of 1-cm-diameter pelvic lymph nodes in one patient. Pelvic lymph node involvement does not change the FIGO stage; however, it does alter the patient's prognosis and sometimes the therapy. In the remaining patients, there was no evidence of nodal involvement on presurgical examinations or in the hysterectomy specimens.

In evaluating the extent of primary tumor within the cervix, clinical staging was correct in only three of 10 patients; the extent was underestimated in six and overestimated in one. MR was correct in nine of 10 patients and underestimated the tumor in one patient. CT was unable to identify the primary tumor at all (Fig. 1C) and therefore contributed nothing to treatment decisions regarding stage IB lesions. Cervical tumor was identified on the T2-weighted MR images as a high-signal-intensity lesion as compared with the normally low-signal-intensity cervical stroma (Figs. 1A and 1B). The high-signal regions on the MR images corresponded exactly to invasive carcinoma pathologically. In the one case in which MR underestimated the extent of primary tumor, only a small zone of high signal was seen on the posterior cervical lip (Fig. 2). Surgical pathology showed a plaquelike lesion covering the entire portio of the cervix with a maximum invasion of 3–5 mm on the posterior lip. In addition to the primary lesions, three of the 10 patients had foci of carcinoma in situ that could not be detected by MR.

The outcome in each case was related directly to the estimate of the extent of disease made in clinical staging. All six patients in whom the extent of disease was underestimated clinically required postsurgical radiation therapy. In five of these six patients, the tumor volume was markedly underestimated by clinical examination, whereas MR showed that 50–90% of the cervix had been replaced by tumor. The remaining patient had a 2-cm lesion on the anterior lip, replacing 20% of the cervix. At examination under anesthesia, the lesion was thought to be smaller and confined to the endocervical canal, whereas MR showed that it extended through the cervical stroma, correctly predicting the transmural tumor involvement seen histologically (Figs. 3A and 3B).

Discussion

In our comparison of clinical examination and MR in the FIGO staging of stage IB carcinoma of the cervix, both methods correlated exactly with the surgical staging. The 34–39% error rate for clinical staging reported in the literature [1] includes all stages of cervical carcinoma and does not discriminate particularly between stage IB and stage II disease. When stages I and II are considered separately, 20–22% of patients with stage I carcinoma and 39–44% of patients with stage II disease were understaged clinically [4, 5]. In addition, our sample size is small, and we lack pathologic specimens for any clinical stage II disease.

In assessing the extent of disease within the cervix, MR most closely approximated the pathologic findings in the hysterectomy specimens, with correct estimates in nine of 10 patients, whereas clinical examination was correct in only three of 10 patients. Accurate presurgical estimates of the extent and location of tumor are required to make appropriate decisions regarding patient management. Presurgical radiation therapy is used in patients with barrel-shaped cervices or large exophytic lesions.

At our institution postsurgical radiation therapy of IB lesions is performed if positive lymph nodes or transmural invasion are present, if tumor margins in the hysterectomy specimen are inadequate, or if a majority of the cervix has been replaced by tumor. There is a 15–20% frequency of major bowel complications (including fistula, obstruction, perforation, and stricture) when radiation therapy is performed after radical

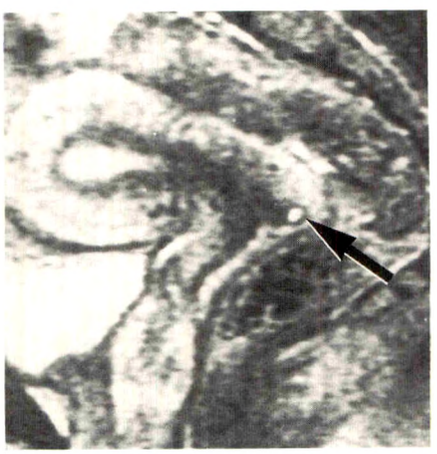

Fig. 2.—Sagittal T2-weighted image (TR = 2000 msec, TE = 80 msec) shows a large cervix with only a small zone of increased signal on posterior lip (*arrow*). Clinical estimate of disease was 50% replacement. Pathologic examination revealed a superficial lesion with a 3–5 mm depth of invasion (maximal on posterior lip).

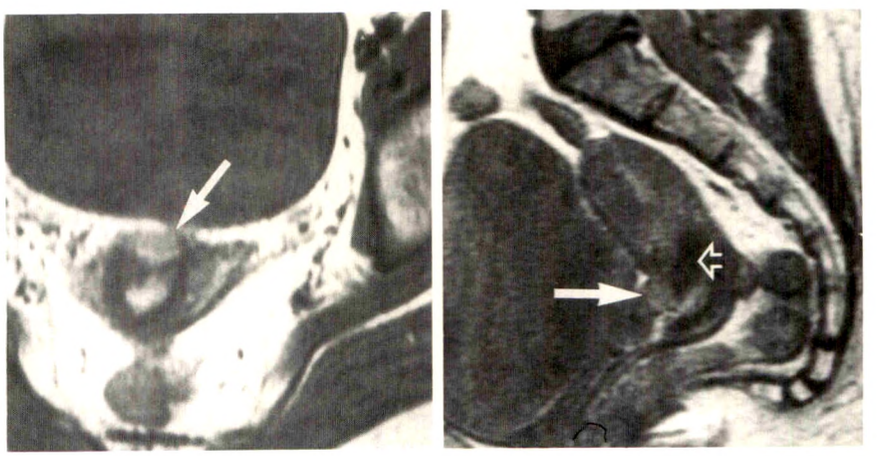

A B

Fig. 3.—*A*, Axial image through cervix (TR = 2000 msec, TE = 40 msec) shows a focus of increased signal anteriorly (*arrow*). Note transmural extent of lesion. Clinically this tumor was thought to be confined to the endocervix.

B, Sagittal view (TR = 2000 msec, TE = 40 msec) shows tumor location (*solid arrow*) as well as replacement of normal low-signal-intensity cervical stroma (*open arrow*). Fat plane between cervix and bladder is preserved.

hysterectomy, as compared with a 7.5% frequency when therapy is performed before surgery [6]. With surgery alone, the frequency of complications is 1%, while with radiation alone, the frequency is 3.5% [6]. Clearly, the choice and timing of radiation therapy are important to ensure that the patient will receive optimal care.

During our investigation of the accuracy of MR, decisions regarding the use of surgery and radiation therapy were made by the gynecologic surgeon on the basis of clinical staging alone. MR during this period was considered investigational in nature. Of 10 patients, the extent of primary cervical disease was underestimated clinically in six. These six patients all required postsurgical radiation therapy. Had the MR findings been available at the treatment-planning stage, these six patients would have received radiation therapy before surgery and would have had an extrafascial hysterectomy rather than a radical hysterectomy.

A pitfall for MR is that it underestimated the extent of disease in very superficial lesions and did not detect foci of carcinoma in situ. These MR findings correlate well with those reported in the literature for low- and high-field-strength machines [7, 8]. In these instances, examination under anesthesia complemented MR in detecting superficial and in situ lesions. MR also failed to detect microscopic invasion of normal-sized pelvic lymph nodes. However, neither clinical examination, CT, nor frozen-section examination detected the microscopic tumor in this patient.

In conclusion, MR correlated better with surgical pathology than did either clinical examination or CT in determining the extent of primary tumor. MR was equal to examination under anesthesia in staging patients, and both were superior to CT, which overstaged three of seven patients. MR was equal to clinical evaluation and CT in assessing pelvic adenopathy. In assessing stage IB cervical carcinoma, MR provides valuable information for treatment planning that cannot be obtained with clinical staging alone.

ACKNOWLEDGMENTS

The authors thank Elizabeth Pender for editorial assistance and manuscript preparation.

REFERENCES

1. Walsh JW, Goplerud DR. Prospective comparison between clinical and CT staging in primary cervical carcinoma. *AJR* **1981**;137:997–1003
2. Whitley NO, Brenner DE, Francis A, et al. Computed tomographic evaluation of carcinoma of the cervix. *Radiology* **1982**;142:439–446
3. Vick CW, Walsh JW, Wheelock JB, Brewer WH. CT of the normal and abnormal parametria in cervical cancer. *AJR* **1984**;143:597–603
4. van Nagell JR Jr, Roddick HW Jr, Lowin DM. The staging of cervical cancer: inevitable discrepancies between clinical staging and pathologic findings. *Am J Obstet Gynecol* **1971**;100:973–978
5. Averette HE, Dudan RC, Ford JH Jr. Exploratory celiotomy for surgical staging of cervical cancer. *Am J Obstet Gynecol* **1972**;113:1090–1096
6. Perez CA, DiSaia PJ, Knapp RC, Young RC. Gynecologic tumors. In: DeVita VT Jr, Hellman S, Rosenberg SA, eds. *Cancer: principles and practice of oncology*, vol. 1, 2nd ed. Philadelphia: Lippincott, **1985**:1013–1081
7. Togashi K, Nishimura K, Itoh K, et al. Uterine cervical cancer: assessment with high-field MR imaging. *Radiology* **1986**;160:431–435
8. Worthington JL, Balfe DM, Lee JKT, et al. Uterine neoplasms: MR imaging. *Radiology* **1986**;159:725–730

Endometrial Abnormalities:
Evaluation with Transvaginal Sonography

Ellen B. Mendelson[1]
Marcela Bohm-Velez
Neal Joseph
Harvey L. Neiman

The value of transvaginal sonography in detecting gynecologic disease currently is being defined. To evaluate transvaginal depiction of the endometrium, transvaginal sonograms were compared with conventional transabdominal scans in 29 patients whose sonograms revealed endometrial abnormalities. The two techniques were compared for image quality and ability to provide unique diagnostic information. Sonographic findings included fluid collections (16), thickened and/or echogenic endometria (10), endometrial irregularities (two), and echogenic foci (two). Clinical diagnoses included early intrauterine pregnancies (five), pseudogestational sacs of ectopic pregnancy (one), intrauterine contraceptive devices (two), endometrial carcinoma (one), and intrauterine synechiae with amenorrhea (Asherman syndrome) (two). In most cases (77%), diagnostic information was obtainable by either transabdominal or transvaginal sonograms, although in 23% transvaginal scanning provided unique diagnostic information not available with the transabdominal technique. In no case did transabdominal sonography contribute diagnostic information not provided transvaginally. The quality of the transvaginal image was judged to be better than that of the transabdominal image in 63% of cases; image quality was the same in 33% of cases and worse in 3% of cases.

The results show that transvaginal sonography is often superior to transabdominal scanning in the evaluation of endometrial abnormalities. Transvaginal sonography may be the preferred technique in these cases.

Transvaginal sonography is a new endosonographic technique in which high-frequency transducers are placed in the vaginal vault to image pelvic structures directly. Preliminary reports support the usefulness of this technique [1]. Transvaginal imaging of the ovaries, particularly in cases of infertility, is useful to assess follicular growth and to guide aspiration of follicular contents for in vitro fertilization [2–4]. To determine the value of transvaginal sonography in detecting diseases of the endometrium, we compared the transvaginal and transabdominal sonograms in 29 patients with endometrial abnormalities.

Materials and Methods

During the past 15 months, we examined nearly 300 patients by using both transvaginal scanning and conventional abdominal sonography. The scans of 29 of these patients whose sonograms showed abnormal endometrial findings were included in this study. Twenty-eight patients were premenopausal, ranging in age from 17 to 38 years; one 60-year-old woman was postmenopausal. Sonographic examinations were included if abnormalities were present on either transvaginal or transabdominal scans. Many findings could be identified with either technique.

Clinical indications for sonography included bleeding, abdominal pain, palpation of a pelvic mass, infertility, and location of an intrauterine contraceptive device. Standard full-bladder transabdominal scans and transvaginal scans were performed in all cases.

Transabdominal sonography was performed first by using either Acuson, Philips, Diasonics, or General Electric scanners. A variety of linear and sector scanners ranging in frequency from 3 to 5 MHz was used. With the patient's bladder full, the uterus was scanned

Received May 14, 1987; accepted after revision September 23, 1987.

[1] All authors: Department of Radiology, West Penn Hospital, 4800 Friendship Ave., Pittsburgh, PA 15224. Address reprint requests to E. B. Mendelson.

AJR 150:139–142, January 1988
0361–803X/88/1501–0139
© American Roentgen Ray Society

longitudinally and transversely. The patients were then asked to void, and transvaginal sonograms were obtained. A Philips 5-MHz, 13-mm (diameter), forward-looking, mechanical-sector transducer was used with a Philips SDR 1500 unit. It has a sector angle of 90°, and its point of maximum focus is 5 cm (range, 2.5–7 cm). The length of the probe is 19.5 cm, and the length of the handle is 10.2 cm. The widest diameter of the probe footprint is 2.8 cm. The probe was placed inside a condom that contained coupling gel. Additional gel was placed on the covered probe.

The advantages of having the transducer closer to the pelvic viscera were explained to each patient. If the patient preferred, she inserted the probe into the vagina herself. Most frequently, however, the transducer was placed by the radiologist or technologist. Depth of probe insertion was dependent on the length of the vagina in individual cases. When there was appropriate insertion, the uterine fundus was frequently the first structure to come into view, which was helpful for orientation. Multiple sections through the uterus were recorded in coronal and sagittal planes.

Four radiologists separately evaluated each study, comparing the transabdominal scans with the transvaginal scans in each case. Two authors had knowledge of the patients' clinical circumstances and had monitored the studies at the time they were performed. The other two authors had no clinical information and had not seen the sonograms earlier. Transvaginal and conventional transabdominal techniques were compared in random sequence, depending on the order in which films were pulled from the jackets. In judgments of image quality, at least three of the four radiologists had to agree in each case. In most cases, agreement was unanimous.

All of the sonographic findings were categorized and tabulated (Table 1). For each group of sonographic findings, transvaginal images were graded as better than, equal to, or worse than transabdominal images in terms of image quality, a composite sonographic characteristic including resolution, contrast, and anatomic delineation. If the sonographic appearance permitted a specific diagnosis from several diagnostic possibilities, the transvaginal and transabdominal images were then compared to determine if either provided unique diagnostic information. Diagnoses were confirmed surgically, when possible, by definitive sonographic findings or by a combination of clinical findings and sonographic correlation.

Results

Thirty endometrial abnormalities were identified in the 29 women studied. The sonographic findings were classified as follows: (1) hypoechoic and anechoic collections, (2) increased endometrial echogenicity and thickness, (3) serpiginous irregularities, and (4) echogenic shadowing foci.

Sixteen (53%) of the sonographic findings represented fluid within the endometrial cavity. These fluid collections ranged in diameter from 0.3 to 1.5 cm. In 12 (75%) of these 16 collections, the transvaginal scans had better image quality than did the transabdominal studies; in the other four (25%), the image quality was equal. In no instance did the transabdominal technique provide better image quality.

Transvaginal scanning gave diagnostic information not obtained by using the transabdominal technique in seven (44%) of the 16 cases. In five cases, the transvaginal approach showed yolk sacs (four cases) or fetal poles (one case) within these fluid collections that were not seen by transabdominal scanning (Fig. 1). The transvaginal findings established these fluid collections as small gestational sacs. In the other two cases, fluid collections not imaged by standard transabdominal technique were identified transvaginally. One of these fluid collections was a pseudogestational sac in a patient with an adnexal mass that was an ectopic pregnancy. The other fluid collection, which was not clinically significant, was most likely related to the periovulatory phase of the patient's menstrual cycle.

Increased endometrial echogenicity and thickness were seen in nine premenopausal women suspected of having ectopic pregnancies. Six of these patients, whose serum beta human chorionic gonadotropin assays were positive, had surgically proved ectopic pregnancies, and the endometrial thickening probably represented decidual reaction. In three patients, endometrial thickening was present without other clinical evidence for ectopic pregnancy, and the sonographic findings were nonspecific, possibly related to menstrual phase. The tenth patient was postmenopausal and presented with pelvic pain. Sonographic findings included a polypoid echogenic mass and fluid within the endometrial cavity (Fig. 2), representing, respectively, endometrial carcinoma and entrapped fluid. Each of these sonographic findings was placed into a separate category. In four (40%) of these ten patients, the endometrium was visualized better on the transvaginal scans. In six patients (60%), the image quality was the same

TABLE 1: Comparison of Sonographic Findings[a]

Sonographic Findings	Total No. of Findings (%)	Image Quality			Clinical Correlation (no. of patients)
		TA Better (%)	TV Better (%)	TA and TV Equal (%)	
Hypoechoic and anechoic collections	16 (53)	0	12 (75)	4 (25)	Gestational sacs (5), pseudogestational sacs (1), periovulatory nonspecific collections (10)
Increased endometrial echogenicity and thickness	10 (33)	0	4 (40)	6 (60)	Ectopic pregnancy (6), normal menstrual cycle (3), endometrial carcinoma (1)
Serpiginous irregularities	2 (7)	0	2 (100)	0	Intrauterine synechiae (2)
Echogenic shadowing foci	2 (7)	1 (50)	1 (50)	0	Contraceptive devices (2)
Total number of findings (%)	30 (100)	1 (3)	19 (63)	10 (33)	

[a] Note.—29 patients with endometrial diseases had both transvaginal (TV) and transabdominal (TA) sonograms. One patient had two abnormal findings, so the total number of findings is 30.

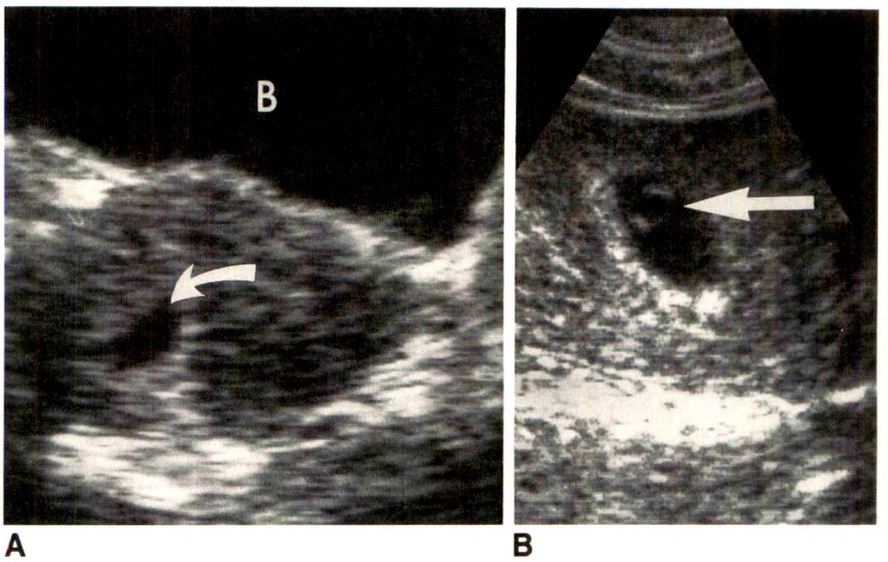

Fig. 1.—16-year-old girl with a clinical diagnosis of ectopic pregnancy.

***A*, Transabdominal sonogram shows a small endometrial fluid collection (*arrow*) with no internal echoes. No distinct echogenic foci could be seen on multiple views. Full bladder (B).**

***B*, Transvaginal coronal projection reveals yolk sac (*arrow*) within fluid collection establishing an intrauterine pregnancy.**

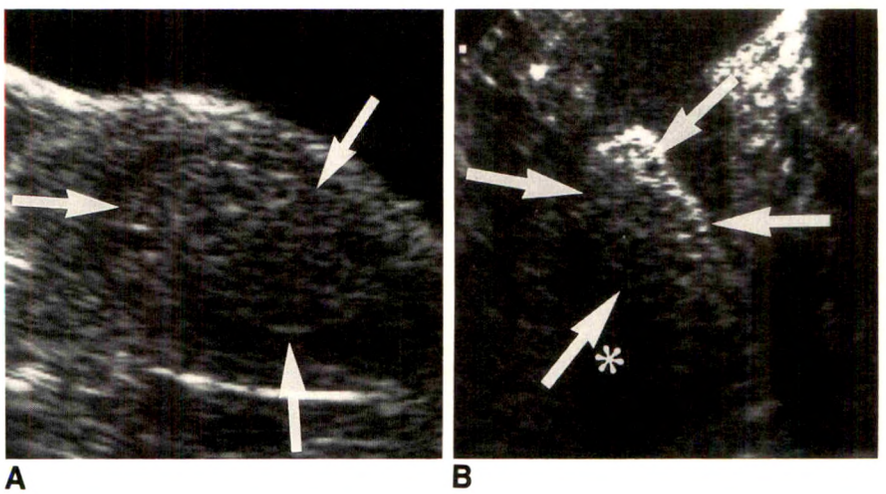

Fig. 2.—Endometrial carcinoma in a 60-year-old woman with pelvic pain.

***A*, Transabdominal longitudinal sonogram shows echogenic mass (*arrows*) surrounded by fluid within endometrium.**

***B*, Transvaginal sagittal sonogram shows mass to be polypoid (*arrows*) and separates mass from myometrium. Fluid collection (*asterisk*) is more obvious than on transabdominal sonography.**

with both transabdominal and transvaginal techniques. In none of these cases did either scanning technique provide unique diagnostic information.

Serpiginous echogenic endometrial irregularities surrounding multiple cystic areas were seen in two infertile patients with the clinical diagnosis of Asherman syndrome, a postcurettage or postinflammatory condition marked by intrauterine synechiae, amenorrhea, and infertility. In one patient, the findings on hysterosalpingography correlated with the sonographic appearance (Fig. 3). In both cases, the images obtained transvaginally were of better quality, although both techniques yielded the same diagnostic information.

Echogenic shadowing foci were seen in the endometria of two asymptomatic patients in whom location of intrauterine contraceptive devices was of concern. In one case, the quality of the image was better in the abdominal scan. The larger field of view in the standard full-bladder transabdominal sonogram allowed us to identify the intrauterine device. In the other case, echogenicity and shadowing were better shown transvaginally. However, the findings were identified with both techniques.

Of the 30 endometrial sonographic findings studied, transvaginal image quality was better than that provided by standard technique in 19 (63%), and in 10 (33%) the image quality was the same. In seven (23%) of the sonographic findings, the transvaginal technique contributed unique diagnostic information not available by transabdominal scanning. In no case did the full-bladder technique provide unique diagnostic information that was not obtainable transvaginally.

Discussion

The ability of sonography to detect subtle changes in the endometrium makes it the diagnostic technique of choice. Endometrial findings that can be detected sonographically have been well described [5–7]. These include intrauterine fluid collections, thickened endometria, and echogenic foci that may cause acoustic shadowing [8–11].

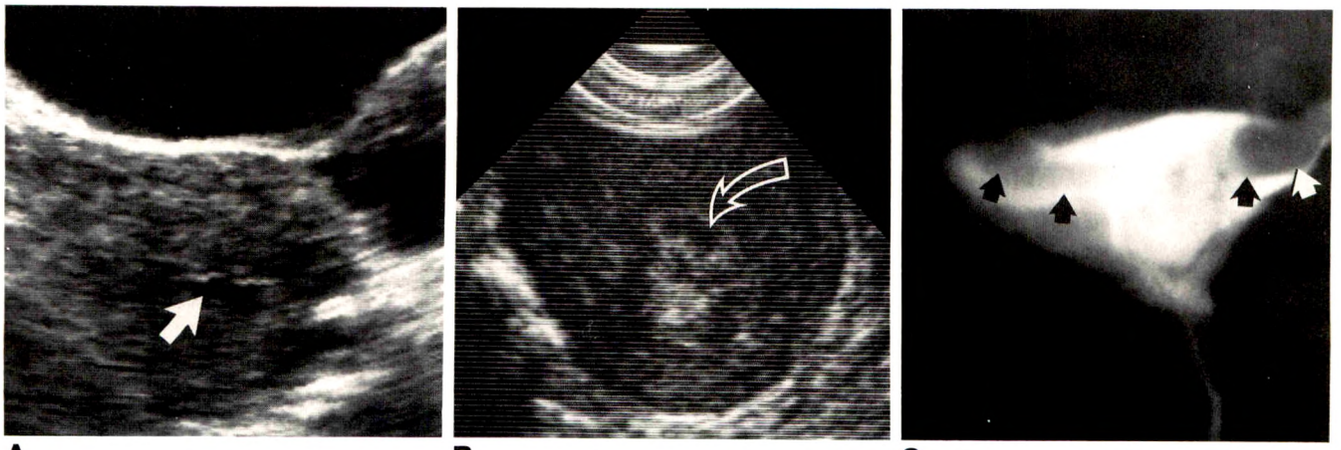

Fig. 3.—30-year-old infertility patient with history of multiple dilatation and curettage procedures.
***A*, Transabdominal transverse scan suggests tiny cystic structures within echogenic endometrium (*arrow*).**
***B*, Transvaginal scan better characterizes irregular echogenic structures with cystic components (*arrow*).**
***C*, Hysterosalpingogram shows irregular filling defects (*arrows*) in fundus of uterus consistent with synechiae (Asherman syndrome).**

While transvaginal scanning provided notably better image quality in most cases, it yielded diagnostic information not available by transabdominal scanning in only seven (23%) of the 30 findings; in all of these cases, the patients had endometrial fluid collections. In five of the seven cases, additional diagnostic information was of clinical significance. Transvaginal visualization of a yolk sac or fetal pole within the fluid collection, not identified by transabdominal sonography, established the existence of an early intrauterine gestational sac. A yolk sac could be seen at least 1 week earlier with the transvaginal technique than with the transabdominal technique.

Transvaginal scanning depicts the endometrial-myometrial interface more clearly than does the full-bladder transabdominal technique. In a postmenopausal patient with an endometrial polypoid mass due to carcinoma, the myometrium was clearly separable from the endometrium, and there was no suggestion of invasion. In the two patients with intrauterine contraceptive devices, transvaginal scanning helped to confirm their positions within the endometrium. Ability to visualize the interface between endometrium and myometrium has clinical applicability when perforation or embedding of these devices is suspected.

The proximity of the transvaginal probe to the endometrium accounts for higher resolution (with greater anatomic detail and better tissue textural differentiation) than that afforded by transabdominal probes of the same frequency. Transvaginal sonography's limited field of view is a drawback in patients with extensive adnexal lesions but is not a consideration when the endometrium is of concern. In our study, there was no situation in which transabdominal scanning was able to provide significant information not revealed by transvaginal scanning. Transvaginal sonography, however, supplied additional information, permitting a diagnosis to be made in 23% of the patients; this was particularly important in excluding ectopic pregnancies. These preliminary findings suggest that the transvaginal approach may be the technique of choice in evaluating the endometrium for suspected abnormalities.

REFERENCES

1. Mendelson EB, Bohm-Velez M, Joseph N, Neiman HL. Gynecologic imaging: comparison of transabdominal and transvaginal sonography. *Radiology* (in press)
2. Feichtinger W, Kemeter P. Transvaginal sector scan sonography for needle guided transvaginal follicle aspiration and other applications in gynecologic routine and research. *Fertil Steril* **1986**;45:722–725
3. Schwimer S, Lebovic J. Transvaginal pelvic ultrasonography: accuracy in follicle and cyst size determination. *J Ultrasound Med* **1985**;4:61–63
4. Dellenbach P, Nissand I, Moreau L, Feger B, Plumere C, Gerlinger P. Transvaginal sonographically controlled follicle puncture for oocyte retrieval. *Fertil Steril* **1985**;44:656–662
5. Fleischer A, Kalemeris G, Machin J, Entman S, James AE Jr. Sonographic depiction of normal and abnormal endometrium with histopathologic correlation. *J Ultrasound Med* **1986**;5:445–452
6. Fleischer A, Kalemeris G, Entman S. Sonographic depiction of the endometrium during normal cycles. *Ultrasound Med Biol* **1986**;12:271–277
7. Fleischer A, Pittaway D, Beard L, et al. Sonographic depiction of endometrial changes occurring with ovulation induction. *J Ultrasound Med* **1984**;3:341–346
8. Breckenridge J, Kurtz A, Ritchie W, Macht E Jr. Postmenopausal uterine fluid collection: indicator of carcinoma. *AJR* **1982**;139:529–534
9. Brandt T, Levy E, Grant T, Marut E, Leland J. Endometrial echo and its significance in female fertility. *Radiology* **1985**;157:225–229
10. Laing FC, Filly R, Marks W, Brown T. Ultrasonic demonstration of endometrial fluid collections unassociated with pregnancy. *Radiology* **1980**;137:471–474
11. Callen P, DeMartini W, Filly R. The central uterine cavity echo: a useful anatomic sign in the ultrasonographic evaluation of the female pelvis. *Radiology* **1979**;131:187–190

Case Report

Carcinoid of the Kidney: Radiologic Findings

Dave K. McKeown,[1] Gia-Khanh Nguyen,[2] Brian Rudrick[2], and Mary Ann Johnson[1]

Primary carcinoid tumor of the kidney is an extremely rare lesion. Only 10 cases have been reported in the literature [1–7]. This report describes a case with radiologic findings.

Case Report

A 33-year-old man was referred to the University of Alberta Hospitals for investigation of painless hematuria associated with a right renal mass. Repeat sonography confirmed a hyperechoic mass centered at the renal sinus with anterolateral extension into the upper pole of the right kidney. The mass was incompletely marginated by a thin, anechoic rim (Fig. 1A). Angiography showed that the mass was relatively hypovascular, supplied by a small superior right renal artery (Fig.1B). Selective right main renal artery opacification revealed displacement of vascular branches, infundibula, and calices by the mass in a manner simulating the appearance of a renal cyst (Fig. 1C).

A right radical nephrectomy was performed. Examination of the specimen showed a 5-cm-diameter multilobulated mass separated from the renal capsule by a thin rim of compressed renal parenchyma. Microscopically, the neoplasm was a primary renal carcinoid tumor with foci of anaplastic small cell carcinoma. The patient was well with no evidence of metastatic disease 3 years after surgery.

Discussion

Carcinoid tumor in the kidney presents little difficulty in histologic diagnosis despite its rare location. Its histogenesis, however, is not as readily understood, as the neuroendocrine cells are not normally detected in kidney or renal pelvis.

Radiologically, primary renal carcinoid tumor is an addition to the list of rare causes for a renal mass. Since the first recognized case in 1966 [1], 10 cases of primary renal carcinoid tumor have been reported. Three of these cases arose within teratoid malformations of the kidney [2, 3] and presumably had radiologic features atypical for a renal cell carcinoma. Another case was found during histologic reassessment of a misdiagnosed renal cell carcinoma for which gross and radiologic features were not provided [4].

Of the remaining six cases, all were described as moderate- to large-sized tumors ranging from 7 to 30 cm in greatest dimension [1, 3–7]. Five were reported to be predominantly solid; one was cystic [5], with tumor in soft polypoid projections from the cyst wall. Both central [6] and peripheral [3] calcification was described, and tumor margination by a fibrous capsule was frequently noted [3, 4, 6, 7]. Excretory urography was performed in four cases. The excretory urogram was interpreted as normal in one instance [1], as unilateral nonexcretion in another [7], and as mild caliceal or renal pelvis dilatation in the other two [4, 6]. Angiographic findings in a single case showed peripheral hypovascularity around an essentially avascular mass [6]. No descriptions of sonographic or CT findings have been reported previously.

The partial pseudoencapsulation in our case is interesting, as are the sonographically hyperechoic texture and angiographically hypovascular nature of the tumor, which are features also shown in a second example of renal carcinoid seen

Received June 22, 1987; accepted after revision August 18, 1987.

[1] Department of Radiology and Diagnostic Imaging, W. C. Mackenzie Health Sciences Centre, 8440 114th St., Edmonton, Alberta T6G 2B7, Canada. Address reprint requests to D. K. McKeown.

[2] Department of Laboratory Medicine, W. C. Mackenzie Health Sciences Centre, Edmonton, Alberta T6G 2B7, Canada.

AJR **150:143–144, January 1988** 0361–803X/88/1501–0143 © American Roentgen Ray Society

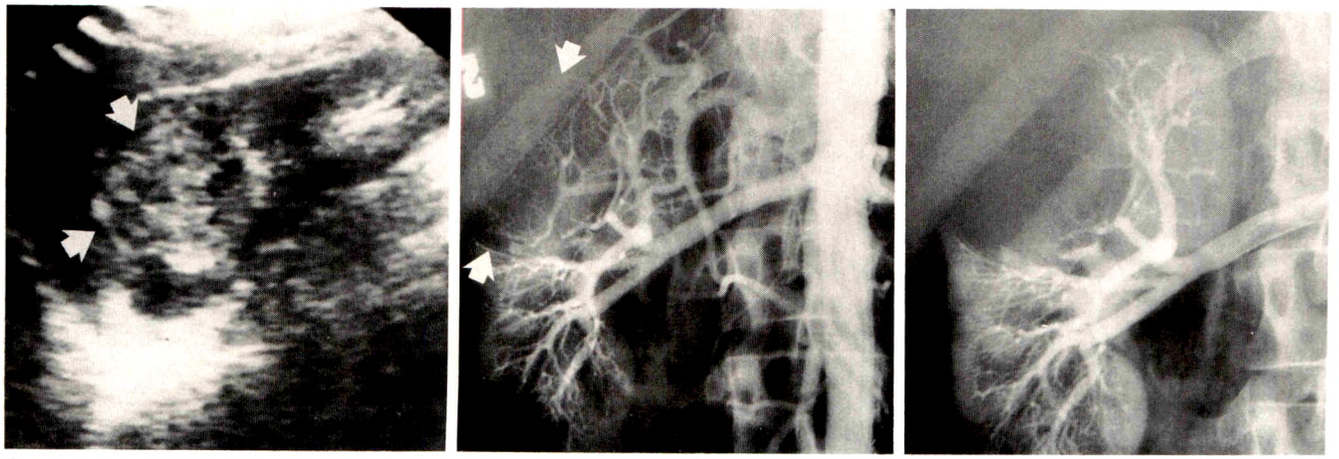

Fig. 1.—*A*, Longitudinal sonogram shows round hyperechoic mass (*arrows*) incompletely marginated by thin, anechoic rim.
***B*, Angiogram shows tumor to be hypovascular (*arrows*).**
***C*, Selective angiogram shows tumor displacing branches of main right renal artery. Appearance simulates a cyst.**

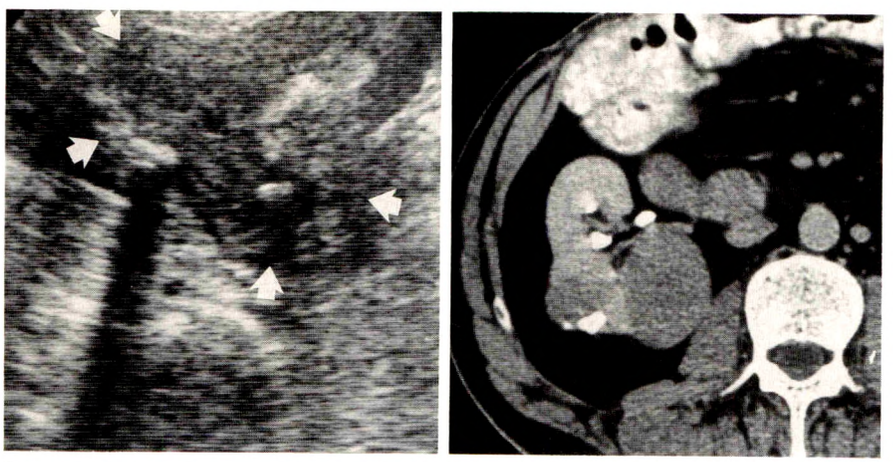

Fig. 2.—*A*, Transverse sonogram of right kidney in right anterior oblique position shows hyperechoic mass and shadowing from calcification (*arrows*).
***B*, Contrast-enhanced CT scan at similar level. Bilobed tumor enhances minimally and contains foci of globular calcification.**

recently at the University of Alberta Hospitals (Fig. 2A). This additional carcinoid was a bilobed tumor arising from the renal pelvis. It contained peripheral foci of globular calcification (Fig. 2B).

All of these radiographic features have been observed in renal cell carcinoma, the major differential diagnosis. Subramanyam and Bosniak [8] noted that in renal cell carcinoma a pseudocapsule of compressed parenchyma and fibrous tissue often is present. Also, renal cell carcinoma could have an echogenicity less than, more than, or similar to that of normal renal parenchyma, with increased echogenicity often but not always corresponding to increased vascularity. Further, renal cell carcinoma, while classically hypervascular, is necrotic, and thus is angiographically hypovascular or "avascular" in about 5% of cases. Finally, radiologically detectable calcification is present in 10–20% of cases of renal cell carcinoma. Thus, while it is evident that the few reported renal carcinoids share some radiographic features with renal cell carcinoma, it is hoped that more cases of carcinoid of the kidney will be studied by imaging techniques to further define the radiologic characteristics of these neoplasms.

ACKNOWLEDGMENT

The authors thank J Bruce Beckwith (Seattle, WA) for his valued opinion.

REFERENCES

1. Resnick ME, Unterberger H, McLoughlin PT. Renal carcinoid producing the carcinoid syndrome. *Med Times* **1966**;94:895–896
2. Fetissof F, Benatre A, Dubois MP, Lanson Y, Arbeille-Brassart B, Jobard P. Carcinoid tumor occurring in a teratoid malformation of the kidney. An immunohistochemical study. *Cancer* **1984**;54:2305–2308
3. Petersen RO. Kidney. In: Petersen RO, ed. *Urologic pathology*. Philadelphia: Lippincott, **1986**:1–179
4. Zak FG, Jindrak K, Capozzi K. Carcinoidal tumor of the kidney. *Ultrastruct Pathol* **1983**;4:51–59
5. Toker C. Carcinoidal renal tumor. *J Urol* **1974**;111:10–11
6. Stahl RE, Sidhu GS. Primary carcinoid of the kidney. Light and electron microscopic study. *Cancer* **1979**;44:1345–1349
7. McDonald EC, Mukai K, Burke BA, Sibley RK. Primary carcinoid tumor of the kidney; a light and electron microscopic, and immunohistochemical study. *J Urol* **1983**;130:333–335
8. Subramanyam BR, Bosniak MA. Renal parenchymal and capsular tumors in adults. In: Taveras JM, Ferrucci JT, eds. *Radiology diagnosis–imaging–intervention*, vol 4. Philadelphia: Lippincott, **1986**:1–15

Case Report

Renal Stone Ileus

Duke K. Bahn,[1] Richard K. J. Brown,[1] Alan A. Reidinger,[1] Peter A. Duhamel,[2] Ker-Yen Shei,[1] Haribabu Gontina,[3] and Robert M. Brenner[3]

Renoalimentary fistulae are rare and most often are caused by malignant disease. Simple and spontaneous fistulae do occur but are unusual. We report a case of renoduodenal fistula, associated with a staghorn calculus that passed through the fistula and caused a small bowel obstruction.

Case Report

An 88-year-old woman presented with typical signs and symptoms of small bowel obstruction. Previous medical history included a cholecystectomy and a known staghorn calculus in the right kidney. In 1984 the patient fell, injuring her right flank. A draining sinus developed that persisted until 3 months before she was admitted to the hospital.

An earlier plain abdominal radiograph had revealed a large staghorn calculus in the right kidney (Fig. 1A). However, an abdominal film at the time of admission showed only a small calculus in the kidney (Fig. 1B). A larger fragment of the stone was evident in the lower abdomen. Dilatation of the small bowel was present, suggesting an early small bowel obstruction. A CT scan showed that the calculus was located within the lumen of the distal ileum.

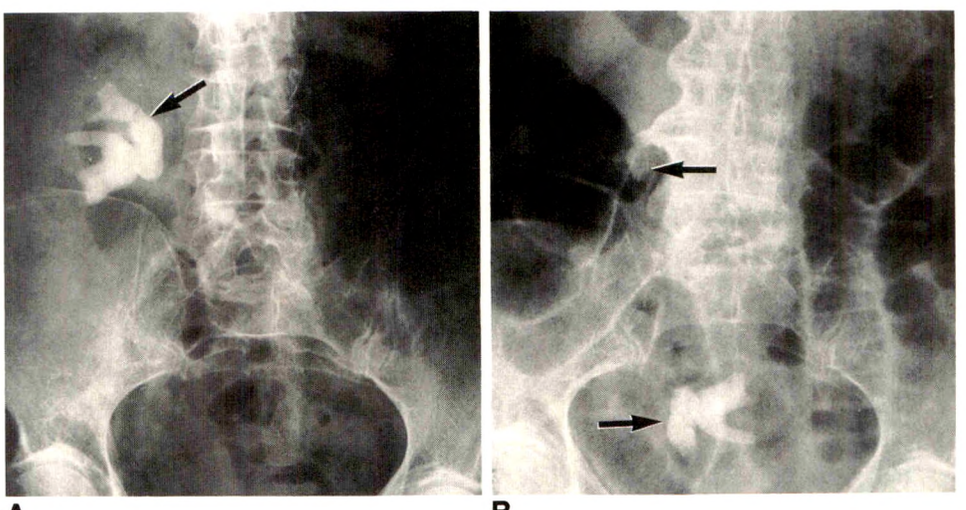

Fig. 1.—*A*, Plain abdominal radiograph made before admission shows staghorn calculus in right kidney. Calculus is fragmented in its upper portion (*arrow*).

***B*, Plain film at time of admission shows an early small bowel obstruction. Notice that small portion of calculus remained in kidney and main portion of calculus is now in lower abdomen (*arrows*).**

Received July 10, 1987; accepted after revision August 25, 1987.

[1] Department of Radiology, Crittenton Hospital, 1101 W. University, Rochester, MI 48063. Address reprint requests to D. K. Bahn.
[2] Department of Surgery, Crittenton Hospital, 1101 W. University, Rochester, MI 48063.
[3] Department of Urology, Crittenton Hospital, 1101 W. University, Rochester, MI 48063.

 0361–803X/88/1501–0145 © American Roentgen Ray Society

At surgery, the diagnosis of renal stone ileus was confirmed and the renoduodenal fistula was identified. The staghorn calculus was removed from the distal ileal loop. Because the patient was a poor surgical risk, the fistulous tract was not repaired. The patient had an uneventful postsurgical course.

Discussion

There have been no previous reports of small bowel obstruction resulting from a renal stone passed through a renoduodenal fistula (i.e., renal stone ileus). We believe that the cause of the fistula in this case was trauma with subsequent chronic nonspecific inflammation.

Renoalimentary fistulae are rare and usually are caused by malignant disease [1, 2]. However, chronic inflammation including tuberculosis and hydatid disease have all been cited as causes [1, 3, 4]. Recently, there have been a few case reports of renoduodenal fistulae as complications of percutaneous nephrolithotomy [5]. Jones [6] reported a case of mechanical duodenal obstruction caused by a calculus that passed through a fistula between the right renal pelvis and the duodenum. Renocolic fistulae are probably the most common form of renoalimentary fistulae [3].

Although renal stone ileus is rare, it should be considered in cases of small bowel obstruction in which there is an abdominal calculus with an unusual shape and location.

REFERENCES

1. McEwan A. Pyelo-duodenal fistula. *Br J Urol* **1948**;40:350–353
2. Goodwin WE, Winter CC, Turner RD. Fistula between bowel and urinary tract. *J Urol* **1969**;84:95–105
3. Arthur GW, Morris DG. Reno-alimentary fistula. *Br J Surg* **1966**;53:396–402
4. Boggs JE, Blundon KE, Davis DM. Pyelo-duodenal fistula. *J Urol* **1961**;86:199–204
5. Culkin DJ, Wheelers JS, Canning JR. Nephro-duodenal fistula. *J Urol* **1985**;134:528–530
6. Jones GRM. Renal calculus ileum. *J Can Assoc Radiol* **1983**;34:51–52

Paleoradiology

Three-Dimensional CT Reconstructions of an Ancient Human Egyptian Mummy

Myron Marx[1] and Sue H. D'Auria[2]

Between 1983 and 1987, 15 wrapped human Egyptian mummies were studied with both CT and conventional film/screen radiography in a collaborative project between the Department of Radiology, Brigham and Women's Hospital, Boston, MA, and the Museum of Fine Arts, Boston. Preliminary results from this project have been reported previously [1]. We recently took the digitized CT data from the examination of the mummy Tabes, Songstress of Amun, and created three-dimensional images. This data manipulation resulted in realistic images of the surface of the mummy, who was wrapped not only in hundreds of yards of linen but in an opaque and artfully painted cartonnage (an inner coffin made of linen and plaster, which is similar in consistency to papier-mâché). These images represent not only a technological tour de force but give vivid meaning to the concept of imaging.

The mummies of Tabes, Songstress of Amun, and her husband, Nes-Ptah, the Barber of Amun, were given to the Museum of Fine Arts, Boston, by a private collector in 1872. Tabes, who died in her early thirties, has one of the most beautifully and sensitively painted cartonnages in the museum's collection (Fig. 1). From the artistic style represented on her cartonnage, from cartonnage inscriptions, and from her method of mummification, it is estimated that she died circa 950 B.C. (early Dynasty XXII). Tabes and her husband, who died in his sixties, lived in ancient Thebes, which is near modern Luxor, Egypt.

The process of mummification was primarily a process of desiccation shaped by complex religious beliefs. The goal was to preserve the corpse in as lifelike an appearance as possible. Although axial CT images provided a great deal of information of anatomic and Egyptologic interest, it did not reveal that which was of most importance to the ancient

Fig. 1.—Photograph of cartonnage of Tabes.

Received August 13, 1987; accepted after revision September 9, 1987.
[1] Department of Radiology, Pacific Presbyterian Medical Center, P. O. Box 7999, San Francisco, CA 94120. Address reprint requests to M. Marx.
[2] Department of Egyptian and Near Eastern Art, Museum of Fine Arts, Boston, 465 Huntington Ave., Boston, MA 02115.

AJR 150:147–149, January 1988 0361–803X/88/1501-0147 © American Roentgen Ray Society

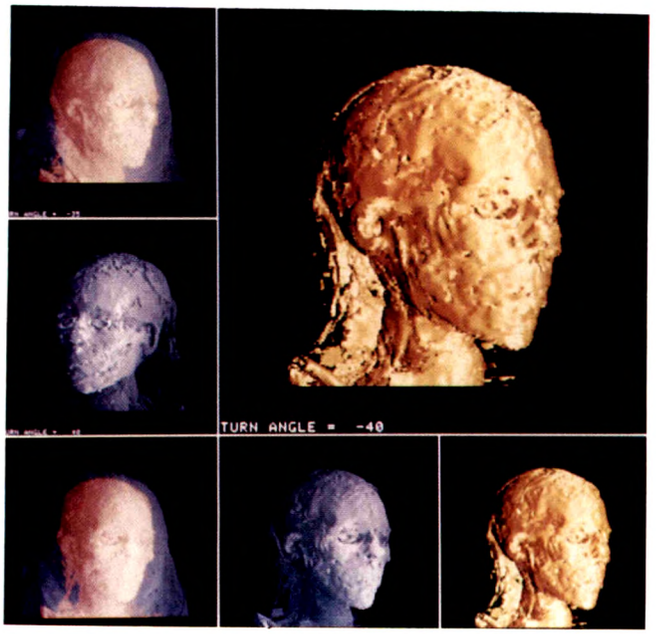

Fig. 2.—Contour images of head of Tabes. Large image in *upper right-hand corner* and images *center and right on bottom* and *center left* show contours of surface or skin of head and neck in blue or gold light. *Upper and lower left* images show surface contouring of linen wrappings, made blue and transparent, with skin-contour images of head, in yellow, seen underneath. Note single, loosely applied band of linen wrapping on the right at ear, face, and neck levels.

Egyptians, namely, how the mummy looked. It did not show how successful the art of the embalmer was and how his efforts had weathered the millennia.

Technique

The CT examination was performed on a Siemens Somatom DRH. Multiple, 2-mm-thick, axial sections of the head and neck were obtained at 2-mm intervals, and multiple, 4-mm-thick, axial sections of the chest, abdomen, and pelvis were obtained at 4-mm intervals. Scanning parameters were 125 kV, 40 mAs, and 5-sec scan time. Three-dimensional reconstructions were obtained at CEMAX, Inc., Santa Clara, CA, using a CEMAX 1500X system.

Discussion

Although three-dimensional contours of bones and internal structures were generated, the most intriguing images were those of the surface of the mummy. Images of the head show a curious bulge in the ventral aspect of the mid and caudal regions of the neck due to the uneven application of subcutaneous packing materials (Figs. 2 and 3). The eyes of Tabes were untreated and are shrunken. Because this resulted in an appearance that was not lifelike, preparers of mummies of this and later periods occasionally removed the orbital contents and replaced them with wax. Magical amulets were then placed over the orbits to restore sight to the artificial eyes. A defect in the soft tissues of the nose is seen and is

Fig. 3.—Contour image of surface of head of Tabes, in yellow, and of linen wrappings, in light blue. Front portion of linen wrappings about face of mummy have been removed so that face can be seen.

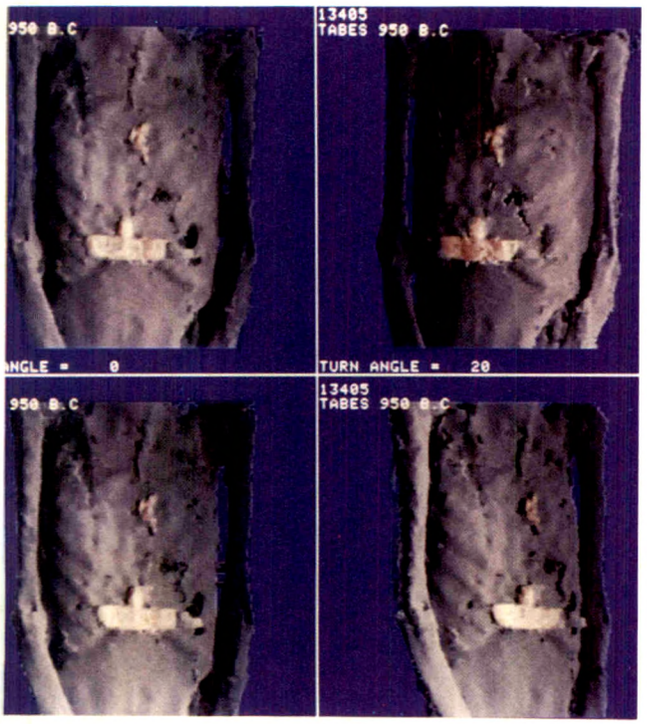

Fig. 4.—Frontal and shallow oblique contour images of chest and upper abdomen of Tabes. Metallic amulet, heart scarab, and winged figure are seen in yellow, whereas body of Tabes is seen in gray. Amulet and winged figure are metallic, probably gold. Round heart scarab seen immediately above winged figure is made of stone. Note many defects and cracks on surface of mummy as well as details of ribs, umbilicus, and nipples. Left nipple is in its anatomic position; right nipple appears displaced laterally near anterior axillary line.

due to this portion of the face being wedged against the inner surface of the cartonnage. The ears are clearly identified, as is hair matted with resin.

Images of the chest and upper abdomen show details of a metal amulet placed on the sternum, a heart scarab (a beetle-shaped amulet prescribed by the *Egyptian Book of the Dead* to ensure safe passage of the deceased through the trial of judgment and into the afterlife) placed over the region of the xiphoid, and, immediately beneath it, a winged metallic amulet (Fig. 4). The ribs are clearly seen, as is the umbilicus. Multiple defects in the mummy's skin are noted, the largest being immediately to the left of the scarab and winged amulet. The embalmer's large incision in the left anterolateral aspect of the abdomen extends into the left anterior hemipelvis and was not closed, contrary to custom.

Three-dimensional images from axial CT data is a further advance in the nondestructive and noninvasive evaluation of Egyptian mummies, offering a different and perhaps more appropriate perspective of these objects. Surface details were apparent that were not appreciated on axial images. The use of medical-imaging technology in nontraditional fields represents an opportunity for the exchange of ideas between historically isolated disciplines and allows the radiologist to make contributions to the understanding of our world and origins.

REFERENCES

1. Marx M, D'Auria SH. CT examination of eleven Egyptian mummies. *RadioGraphics* **1986**;6:321–330

Book Reviews

Bones and Joints. 170 Radiological Exercises for Students and Practitioners. By Michael Runge. New York: Springer-Verlag, 168 pp., 1987.

This soft-cover text, which is about 5 in. (12.7 cm) long and translated from the French, is a self-evaluation book made up of 170 quiz cases on diseases of bones and joints. No text or clinical histories accompany the illustrations. The answers are provided in the second part of the book, along with line drawings that reproduce the radiographs that served as the quiz cases.

The answers have a brief, almost telegraphic text in some places, whereas in others the radiographic abnormalities are ennumerated with either limited or no discussion of the specific entity. Therefore, the answers primarily serve to point out the radiographic abnormalities and the diagnoses drawn from those observations. Because this little book is designed to test the reader's diagnostic accuracy and not to provide instruction, it will be useful to residents who have some background knowledge in musculoskeletal diseases, but it has little to offer a resident in the first 6 months of training. Because it is not a text that evaluates at any length the entities radiographically displayed, it has limited instructional value. With the exception of two or three images, the illustrations are of good quality, and, since the text in the answers is so short, little has been lost in the translation. However, some of the terms used, such as "osteoarthritis includes infectious involvement of a joint," could be confusing. This might explain why Fig. 123, which looks like a long-standing infection, has been diagnosed as "talotibial osteoarthritis."

It takes a few hours to go through the cases, which cover mainly tumors, arthropathies, and infections. The major shortcoming of the book is that it is unlikely to be used more than twice because there is so little to learn from the text. Residents who were shown this book liked the interrogative aspect of it but were ambivalent about making a purchase, especially because they did not know its exact price. The syllabi of the American College of Radiology, which are likely significantly more expensive, do a far more comprehensive job of evaluating and instructing.

For a nominal price, this text could find a place in radiology libraries looking to expand their self-evaluation material to serve, even if only a couple of times, each succeeding generation of residents.

Murali Sundaram
St. Louis University Medical Center
St. Louis, MO 63104

Pocket Guide to Pediatric Fractures. By John A. Ogden. Baltimore: Williams & Wilkins, 245 pp., 1987. $25.50

It would take a high degree of teaching skill to produce both an outstanding, in-depth, original, lengthy work on a topic and an outstanding, pocket-sized distillation of the key practical elements of the same subject. John Ogden's *Skeletal Injury in the Child* (Philadelphia: Lea & Febiger, 1982) achieves the first goal, but his *Pocket Guide to Pediatric Fractures* does not quite succeed in the second task.

The book does fit into a large pocket, does begin with an effective summary of general principles, and does illustrate selected fractures almost flawlessly with fine radiographic reproductions and interpretative line drawings (the last executed by Richard Remington). Indeed, the reproductions show a metaphyseal fragment in the example of type I [sic] epiphyseolysis (Fig. 13) in the section on growth mechanism injuries. Brief discussions follow on neonatal fractures, myelodysplasia, osteogenesis imperfecta, head injury, stress fractures, and child abuse. Finally, sequential highlight discussions deal with fractures at individual sites, including the spine, and give recommended treatment and possible complications. Relevant references appear with each chapter.

Although Ogden does pack a wealth of pertinent information into each brief "chapter" (usually two pages), I am uneasy with the omission of material that would make the work even more useful. For example, the discussion of child abuse is skimpy; distinction is not made between anterior and posterior shoulder dislocation, and so-called Sever disease is retained as a full-fledged entity.

Nonetheless, this little book is potentially highly useful as a *vade mecum* for radiologists, both as a quick source of images and data and as a repository of classic references. It reflects the experience of an important teacher of pediatric orthopedics, and I recommend it.

Alan E. Oestreich
Children's Hospital Medical Center
Cincinnati OH 45229-28997

Pictorial Essay

Cross-Sectional Imaging of the Capsular Mechanism of the Glenohumeral Joint

Michael B. Zlatkin,[1] Ann G. Bjorkengren, Victoria Gylys-Morin, Donald Resnick, and David J. Sartoris

Because of its anatomic structure, the glenohumeral joint (GHJ) is one of the most mobile joints in the body. As such it is one of the more unstable and most frequently dislocated articulations. Bankart [1] was the first to stress that lesions of the glenoid labrum are the principal pathogenic factor in recurrent anterior GHJ dislocations. Later investigators, however, disputed the predominant role of the glenoid labrum [2, 3], and the concept of the capsular mechanism of the shoulder was developed [2, 3]. Lesions of the anterior capsular mechanism are now believed to be the most significant factor predisposing to recurrent anterior GHJ instability [2–4].

Although the anatomy of the capsular mechanism is complex, detailed knowledge of it is required to correctly interpret imaging studies of this region. The purpose of our study was to use CT, MR, and correlative anatomic sections to further define the cross-sectional appearance of both the normal and abnormal capsular mechanism of the GHJ.

Materials and Methods

The study was divided into two parts. The first portion of the study was a detailed analysis of the anatomic structures of the capsular mechanism using 11 cadaveric shoulders. CT was performed in seven specimens after the injection of approximately 12 ml of air. All CT examinations were performed on a Technicare 2060 HR scanner in the axial plane with slice thickness of 5 mm and slice interval of 3 mm. MR scans were performed in four specimens after injection of 12 ml of gadolinium-DTPA dimeglumine (Schering, Berlin) in two specimens, and 0.9% saline in two others. Images were obtained using a 1.5-T superconducting system and a standard 13.5-cm circular surface coil (General Electric, Milwaukee, WI) with the shoulder placed in a prone position on the coil in order to maximize visualization of the anterior structures. Imaging techniques included spin-echo (SE) pulse sequences, either 600/20 (repetition time [TR] msec/echo time [TE] msec) for those specimens injected with gadolinium or 2000/20, 70 for those specimens injected with saline. The section thickness was 5 mm with a 2.5-mm intersection gap. A data acquisition matrix of 256 × 256 was used with a field of view of 12 cm or 16 cm and two signal acquisitions. MR imaging was performed in both the coronal and axial planes in all specimens. Anatomic sections were then prepared with the use of a band saw. The specimens were all sectioned at 5-mm intervals in the axial plane, and serial photographs of each section were taken for later study. Two specimens were dissected from a posterior approach for demonstration of the gross anatomy of this region.

In the second portion of the study, five shoulder specimens were fixed in an apparatus modeled after that described by Oveson and Sojbjerg [5]. This immobilized the glenoid region of the scapula and the thorax. The arm was then subjected to stress in abduction and external rotation. After considerable force was exerted, a sudden laxity was obtained in three of the specimens and these shoulders could then be subjected to recurrent subluxations. CT air arthrography was performed in all specimens and MR arthrography with gadolinium was performed in two. Imaging parameters were identical to those described previously, and all specimens were then sectioned in the axial plane to verify the pathologic lesions shown.

Received July 1, 1987; accepted after revision September 9, 1987.
This work was supported in part by Veterans Administration grant #SA306.
[1] All authors: Department of Radiology, Veterans Administration Medical Center and the University of California Medical Center, San Diego, CA 92103. Address reprint requests to D. Resnick, Dept. of Radiology, VA Medical Center, 3350 LA Jolla Village Dr., San Diego, CA 92161.

AJR 150:151–158, January 1988 0361–803X/88/1501–0151 © American Roentgen Ray Society

Results

Normal Findings

The anterior capsular mechanism consists of the synovial membrane, the capsule and glenohumeral ligaments, the glenoid labrum, the subscapularis bursa and related recesses, and the subscapularis muscle and tendon [2] (Fig. 1). This mechanism functions as a barrier against anterior displacement of the humeral head in external rotation. The glenohumeral ligaments are thickened areas of the anterior capsule and act to reinforce it. They course from the glenoid to the lesser tuberosity of the humerus and consist of the superior, middle, and inferior ligaments. Between the superior and middle glenohumeral ligaments is the opening for the superior subscapularis bursa.

In order to facilitate an understanding of the cross-sectional anatomy, we identified four specific levels (Fig. 2). The first level is the superior portion of the glenoid fossa. The tendon of the long head of the biceps originates at this level in common with the superior glenoid labrum. The complex consisting of the superior aspect of the anterior capsule and superior glenohumeral ligament are seen coursing medially (Figs. 3A–D).

The superior subscapularis bursa is identified at the second level (Fig. 4). This bursa is formed by the synovial membrane of the anterior capsule, and it communicates with the joint between the superior and middle glenohumeral ligaments (Figs. 1 and 2). It is present in up to 90% of people [2]. The bursa extends along the superior tendinous border of the subscapularis muscle medially toward the inferior surface of the coracoid process. Its base is also attached to the anterior surface of the subscapularis tendon for a variable extent and extends over a similar area between the capsule and posterior surface of the tendon (Figs. 4E and 4F). In the superior aspect of the bursa, folds of capsular tissue can be seen and should not be mistaken for pathologic structures (Figs. 4A and 4B). Another structure that is identified in the superior aspect of the bursa is the inferior portion of the superior glenohumeral ligament (Figs. 4C and 4D).

At level 3, the mid-glenoid level, one can best assess the capsular insertion, which can be of three types [6] (Fig. 5). In type 1, the capsule inserts near the glenoid labrum (Figs. 6A and 6B). In types 2 or 3, a more medial insertion along the scapular neck is present (Figs. 6C and 6D). This may form a recess underneath the subscapularis muscle. At level 3, the middle glenohumeral ligament may be identified as a structure distinct from the capsule when outlined by air or contrast material (Figs. 7A and 7B). It also may be depicted as a thickened structure posterior to the subscapularis tendon and capsule (Figs. 7C and 7D).

Level 4 is at the inferior portion of the glenoid cavity. Diffuse thickening of the complex consisting of the anteroinferior aspect of the capsule and the inferior glenohumeral ligament is seen in this region. The capsule at this level inserts directly into the labrum (Fig. 8).

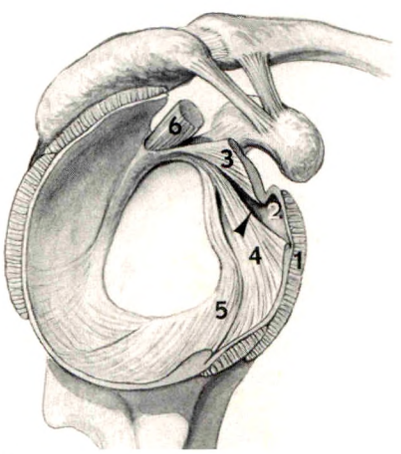

A

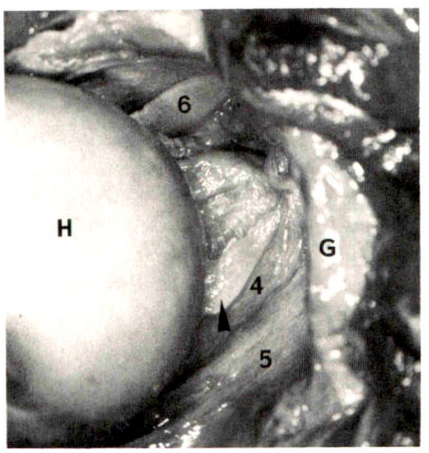

B

Fig. 1.—*A*, Diagram of capsular mechanism. Subscapularis muscle (1) is anterior. Fibrous capsule (2) and superior (3), middle (4), and inferior (5) glenohumeral ligaments are also shown. Opening for superior subscapularis bursa is between superior and middle ligaments (*arrowhead*). Origin of long head of biceps in supraglenoid region is also seen (6).

***B*, Shoulder specimen dissected from posterior aspect. Capsule and glenohumeral ligaments (4 and 5) as well as opening into superior subscapularis bursa (*arrowhead*) are identified. Superiorly, biceps tendon is seen (6). (H = humeral head, G = glenoid).**

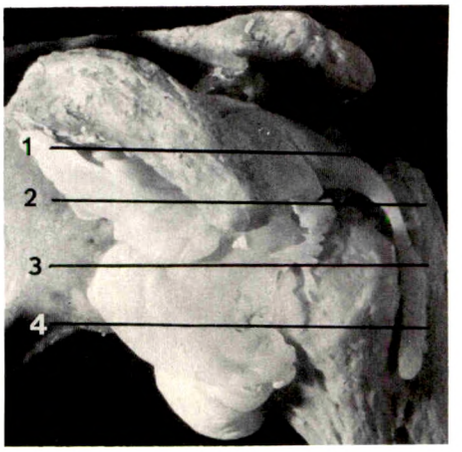

Fig. 2.—Shoulder specimen (injected with methyl methacrylate to simulate normal distended joint) depicting four anatomic levels (1–4) discussed in the text.

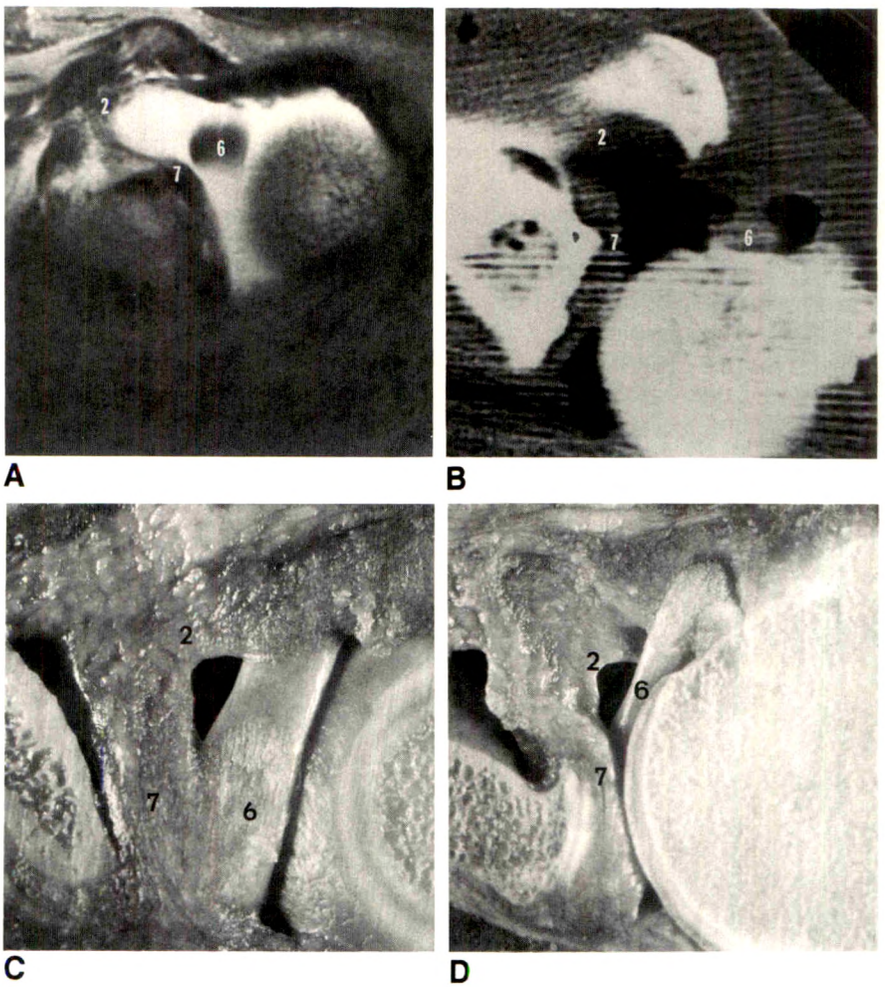

Fig. 3.—Level 1. MR scan after injection with saline (*A*), CT scan after injection with air (*B*), and corresponding anatomic sections (*C* and *D*) illustrate anatomy of level 1. Biceps tendon (6) and superior labrum (7) can be identified. Superior aspect of capsule (2) and superior glenohumeral ligament are seen coursing together more medially.

With MR, images obtained in the coronal plane allow excellent visualization of the superior and inferior portions of the labrum (Fig. 9A). One can also easily visualize other structures of the anterior capsular mechanism (Figs. 9B and 9C).

Abnormal Findings

We obtained satisfactory images in three of the five specimens in which we attempted to create recurrent anterior dislocations or subluxations. In one specimen a CT scan showed a large anterior pouch (Fig. 10). An MR scan in another specimen injected with gadolinium showed abnormal signal and configuration of the glenoid labrum. The injected gadolinium was seen extending through a capsular tear beneath the subscapularis muscle (Fig. 11A). The corresponding anatomic sections revealed a labral and capsular tear (Fig. 11B). An MR scan in a second specimen also injected with gadolinium revealed an area of high signal in the anterior labrum (Fig. 12A). The corresponding anatomic section showed an undisplaced labral tear (Fig. 12B).

Discussion

Detailed knowledge of the anatomy of the capsular mechanism is required if cross-sectional images obtained with CT or MR are to be interpreted correctly.

We believe that considering the cross-sectional anatomy at four distinct levels facilitates comprehension of the normal structures and allows recognition of abnormal findings. Because considerable variability may exist in the arrangement of the capsular structures [2, 7], we have presented only the most common arrangements.

The results of our study indicate that CT arthrography allows identification of the vast majority of relevant anatomic structures of the anterior capsular mechanism. These results are in general agreement with those emphasized by Rafii et al. [8], although these investigators did not use imaging-anatomic correlation. Furthermore, our results suggest that MR imaging after the injection of either gadolinium DTPA or saline can also elegantly depict the important structures of the anterior capsular mechanism of the GHJ.

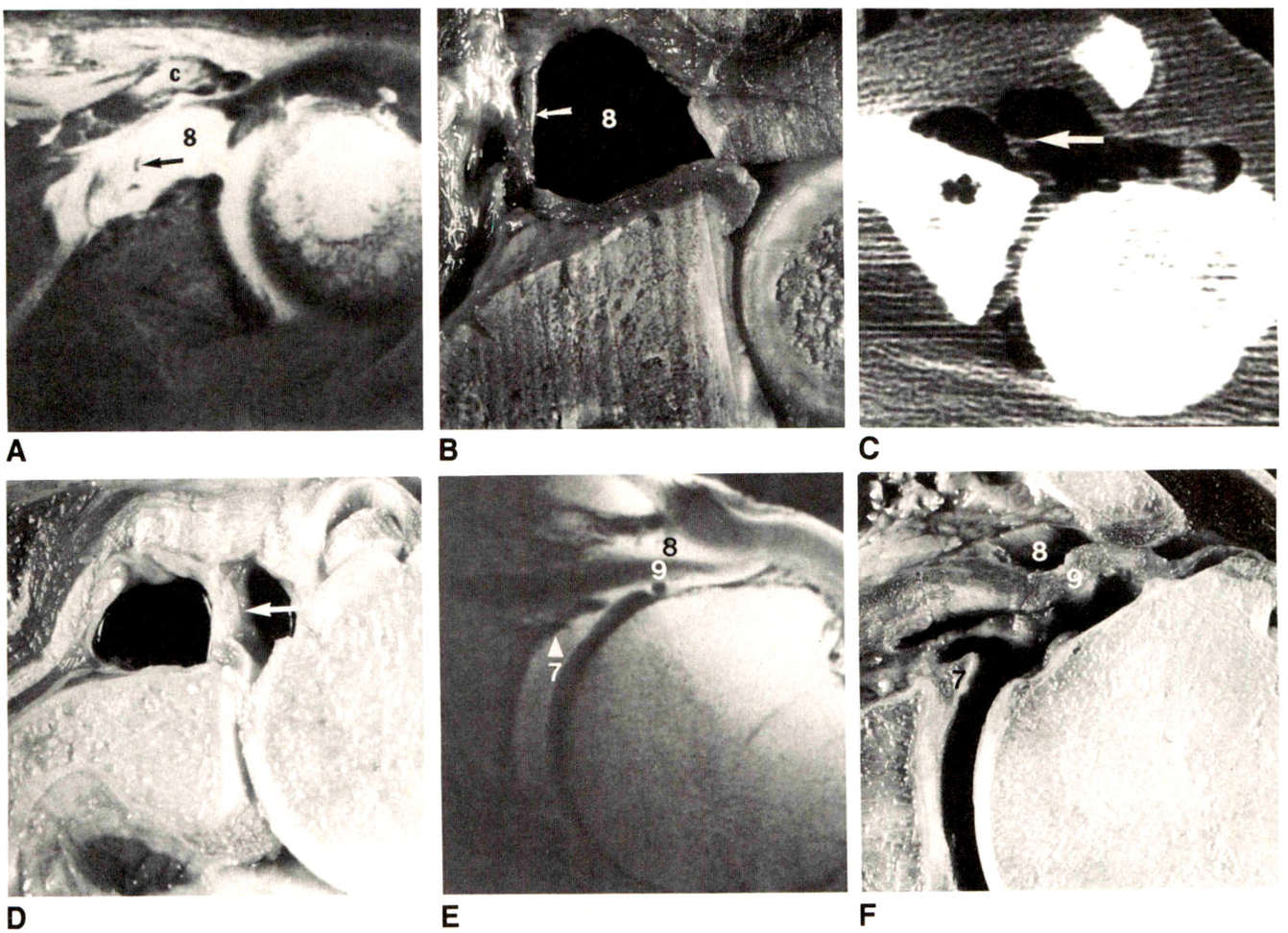

Fig. 4.—Level 2. *A* and *B*, MR scans after injection with saline and corresponding anatomic section. Superior subscapularis (8) bursa is seen. Prominence of this bursa may be a predisposing factor in recurrent anterior dislocations. Within superior aspect of bursa, folds of capsular tissue may normally be identified. They appear as structures of decreased signal on MR scans (*arrows*). 4c = coracoid process.

C and *D*, Another structure that can be identified in superior aspect of bursa is inferior portion of superior glenohumeral ligament, seen as a soft-tissue band on CT scan (*C*) and corresponding anatomic section (*D*) (*arrows*).

E and *F*, Slightly more inferiorly, MR scan after injection with gadolinium (*E*) and corresponding anatomic section (*F*) show superior subscapularis bursa (8) extending over anterior aspect of subscapularis tendon (9). Note also anterior glenoid labrum (7 and *arrowhead*).

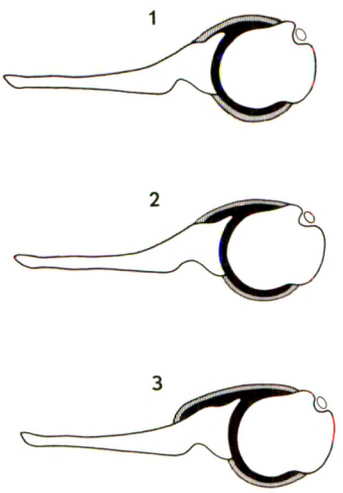

Fig. 5.—Diagram illustrating three types of anterior capsule insertions. Type 1 inserts in or near labrum; types 2 and 3 insert more medially along scapular neck. A type-3 capsule is also thought to be a predisposing factor in recurrent glenohumeral dislocations.

The spectrum of abnormalities that have been observed clinically and experimentally in association with recurrent anterior GHJ subluxations or dislocations include Hill-Sachs lesions, capsule and labral tears and detachments, formation of a large anterior pouch, and laxity of the subscapularis muscle and tendon [2, 5, 7, 9]. As most of the shoulder specimens in our study were derived from patients of advanced age, while most recurrent dislocations occur in younger patients, the lesions we produced experimentally may not correspond completely to those seen in the clinical setting. These lesions do, however, help to confirm the utility of CT arthrography in showing abnormal lesions of the capsular mechanism. On the basis of our findings, considerable potential also exists for MR imaging in the evaluation of patients with shoulder instability. Whether intraarticular injection will be required in such patients is not yet clear, and further investigation in this area is required.

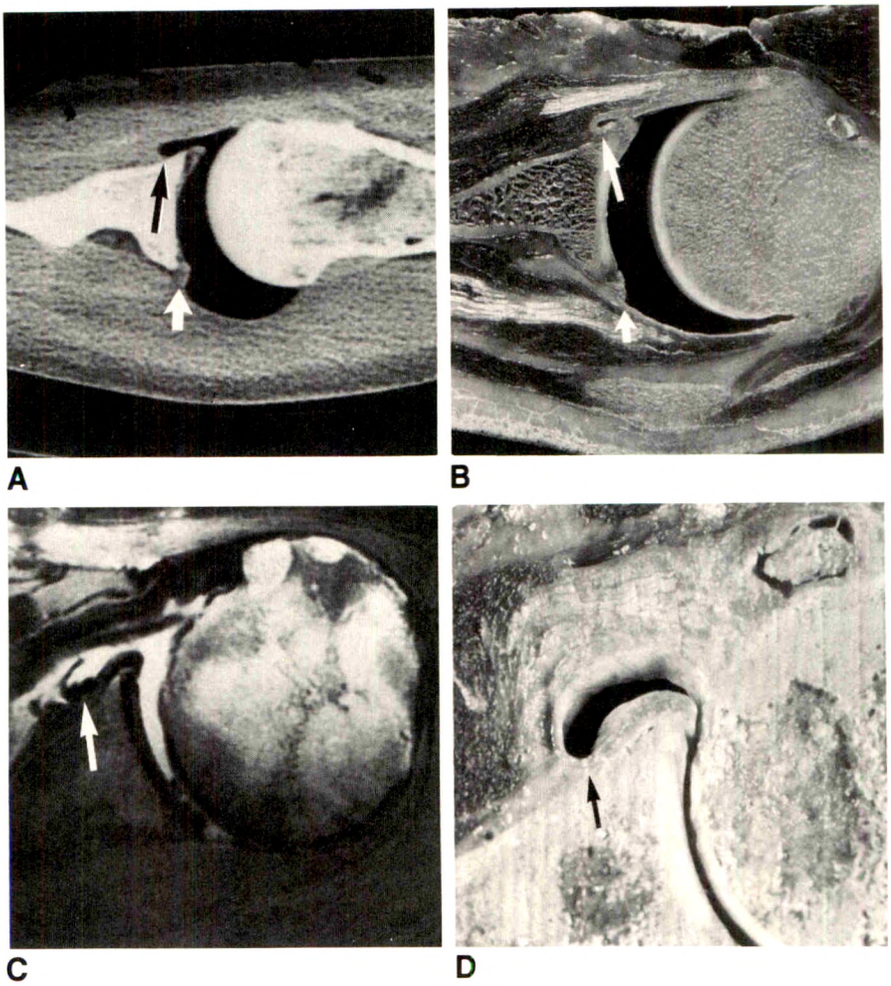

Fig. 6.—Level 3. Capsular insertion.

***A* and *B*, CT scan (*A*) and anatomic section (*B*) show a type-1 capsular insertion (*long arrows*). Posterior capsule always inserts directly into labrum (*short arrows*).**

***C* and *D*, A broader insertion (*arrows*) along scapula is seen in this MR scan (*C*) and anatomic section (*D*). (Foci of high signal in humeral head in this cadaver were thought to be related to metastatic disease. Images in Figs. 8B, 9A, and 9B were obtained from this same specimen.)**

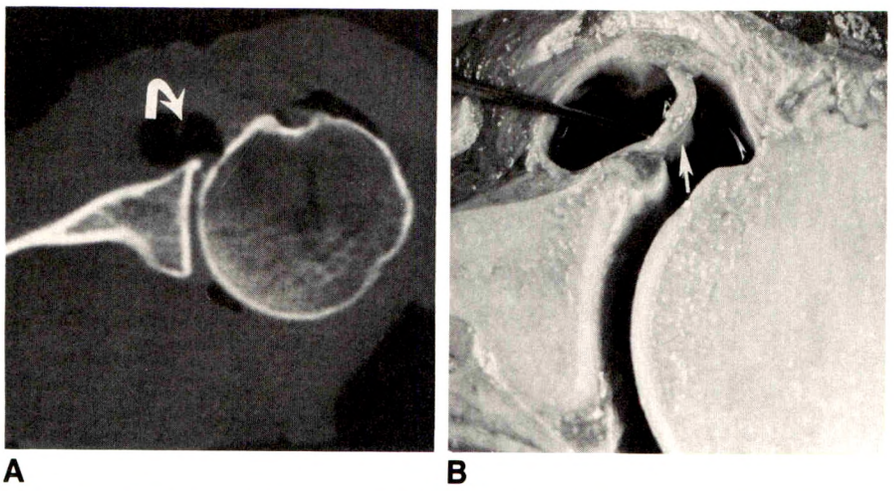

A B

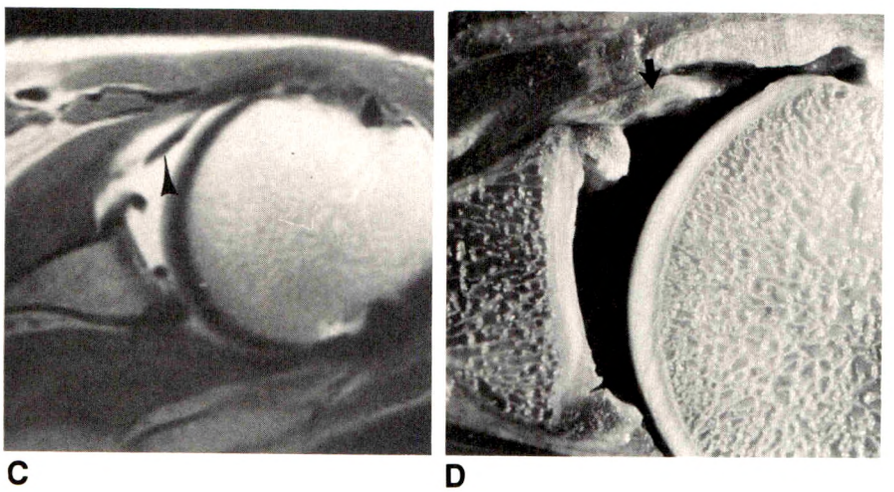

C D

Fig. 7.—Level 3. Middle glenohumeral ligament.

A and *D*, Middle glenohumeral ligament may be identified as a separate structure from the capsule in this region and is outlined by air on this CT scan (*A*, *curved arrow*) and anatomic section (*B*, *arrow*). It may also be identified as a thick structure posterior to subscapularis tendon and capsule, as is shown in another MR scan (*C*, *arrowhead*) and anatomic section (*D*, *arrow*).

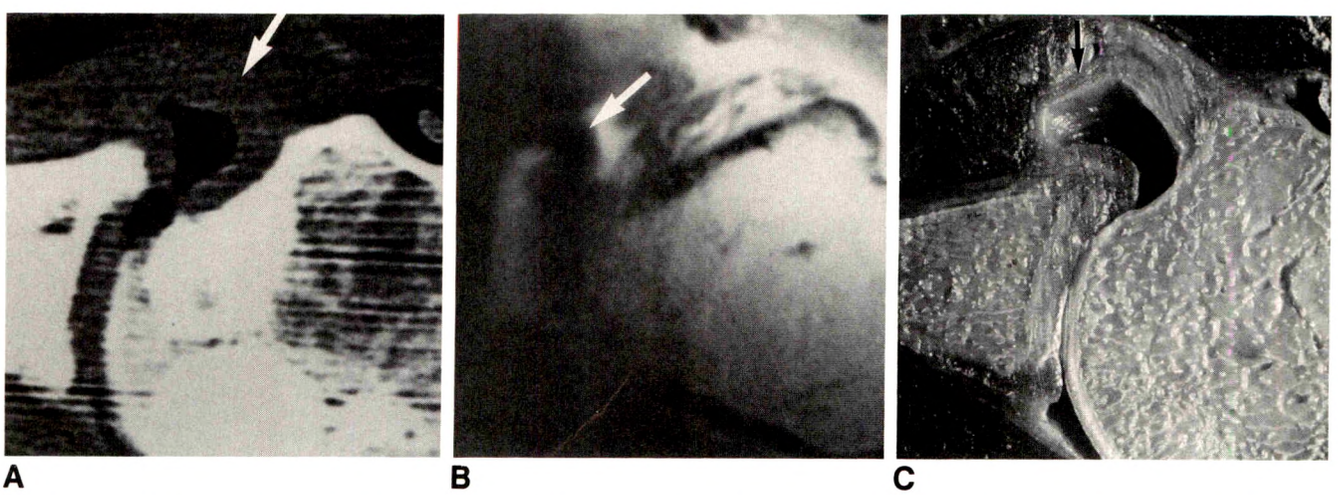

A B C

Fig. 8.—Level 4. CT scan (*A*) and accompanying MR image (*B*) after injection with gadolinium and corresponding anatomic section (*C* illustrate the complex of the anteroinferior aspect of capsule and inferior glenohumeral ligament (*arrows*). Capsule at this level will always insert directly into labrum. *B* is from same specimen as Fig. 6.

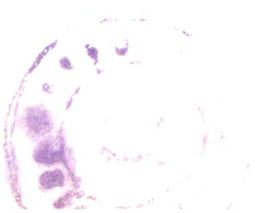

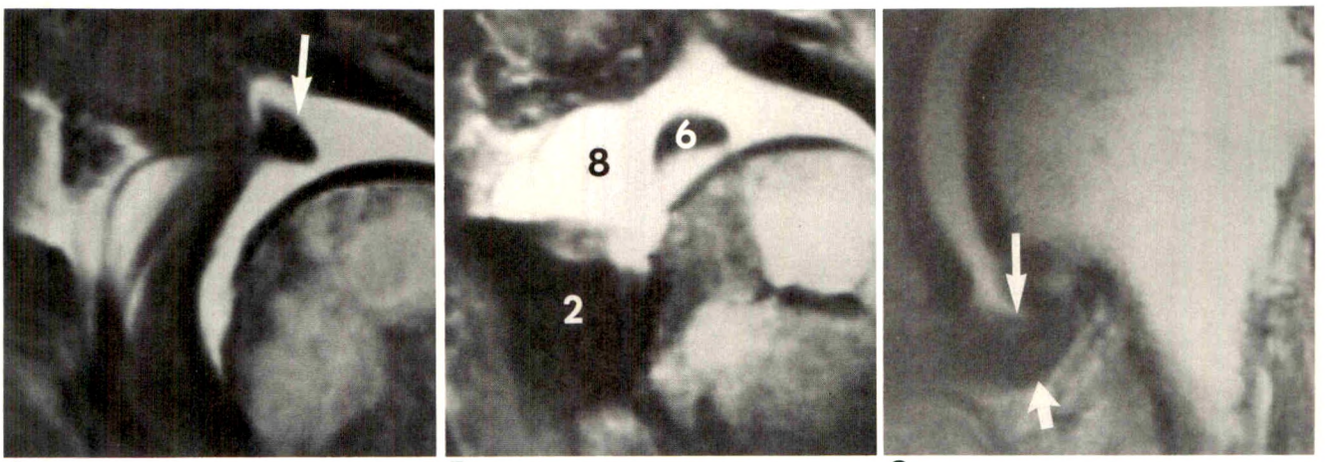

Fig. 9.—Coronal MR scans after injection with saline (*A* and *B*) and gadolinium (*C*). *A* and *B* are from same specimen as Fig. 6. Superior labrum (*arrow*) is well seen in *A*. At a level more anterior in *B*, one can see anterior fibrous capsule (2), biceps tendon (6), and superior subscapularis bursa (8). In *C*, axillary pouch (*long arrow*) and anteroinferior capsule (*short arrow*) are evident.

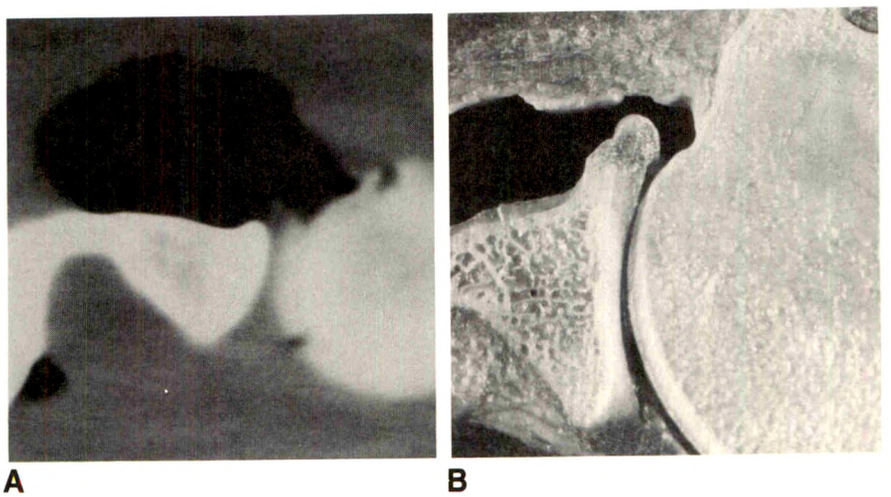

Fig. 10.—Capsular abnormality: anterior pouch.

A and *B*, CT scan and corresponding anatomic section show a large anterior pouch.

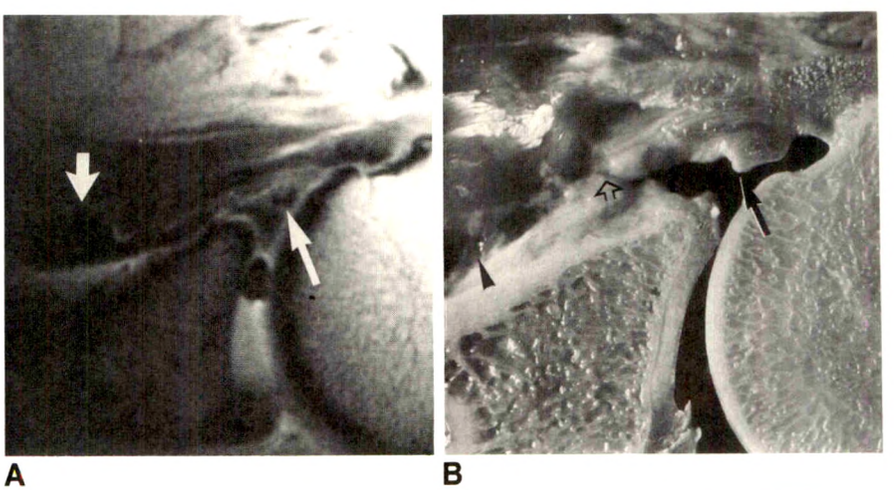

Fig. 11.—Capsular abnormality: labral and capsular tear.

A, MR scan in a specimen injected with gadolinium shows increased signal intensity in region of glenoid labrum (*long arrow*). Contrast material and air are seen extending beneath subscapularis muscle, which is separated from scapula (*short arrow*).

B, Corresponding anatomic section shows labral tear (*closed arrow*), capsular tear (*open arrow*), and detached subscapularis (*arrowhead*).

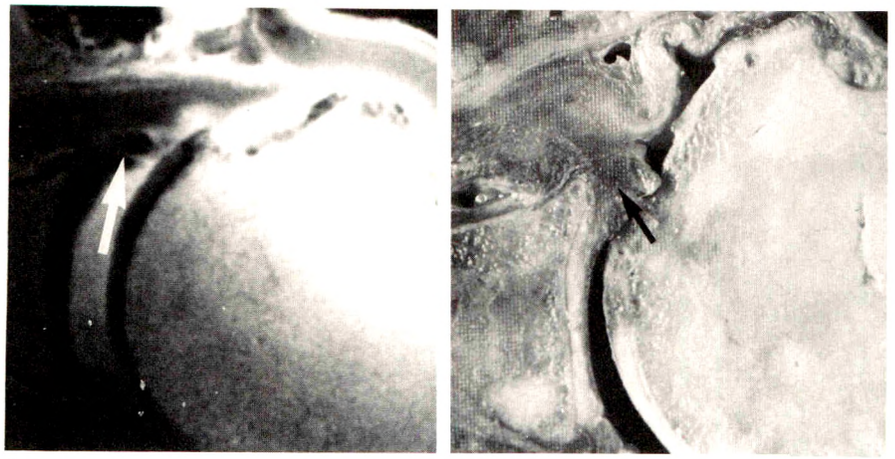

Fig. 12.—Small labral tear.

***A*, MR image after injection with gadolinium reveals a linear area of high signal intensity in anterior labrum (*arrow*).**

***B*, Anatomic section at same level shows an undisplaced labral tear (*arrow*).**

REFERENCES

1. Bankart ASB. The pathology and treatment of recurrent dislocation of the shoulder joint. *Br J Surg* **1938**;26:23–29
2. Moseley HF, Overgaard B. The anterior capsular mechanism in recurrent anterior dislocation of shoulder. Morphological and clinical studies with special references to the glenoid labrum and the gleno-humeral ligaments. *J Bone Joint Surg [Br]* **1962**;44-B:913–927
3. Townley CO. The capsular mechanism in recurrent dislocation of the shoulder. *J Bone Joint Surg [Am]* **1956**;38-A:1–12
4. Turkel SJ, Panio MW, Marshal JL, Girgis FG. Stabilizing mechanisms preventing anterior dislocation of the gleno-humeral joint. *J Bone Joint Surg [Am]* **1981**;63-A:1208–1217
5. Ovesen J, Sojbjerg JO. Lesions in different types of anterior glenohumeral joint dislocation: an experimental study. *Arch Orthop Trauma Surg* **1986**;105:216–218
6. Kummel BM. Spectrum of lesions of the anterior capsular mechanism of the shoulder. *Am J Sports Med* **1979**;7:111–120
7. Rothman RH, Marvel JP, Heppenstall RB. Anatomic consideration in glenohumeral joint. *Orthop Clin North Am* **1975**;6:341–352
8. Rafii M, Firooznia H, Golimbu C, Minkoff J, Bonamo J. CT arthrography of capsular structures of the shoulder. *AJR* **1986**;146:361–367
9. Rafii M, Firooznia H, Bonamo JJ, Minkoff J, Golimbu C. Athlete shoulder injuries: CT arthrographic findings. *Radiology* **1987**;162:559–564

Case Report

Posttrauma Intracapsular Bone Fragments: Association with Meniscal Tears

John Richmond[1] and Robert C. Sarno[2]

Pathognomonic findings of meniscal tear on plain knee radiographs have not been described. However, bone fragments (ossicles) within menisci have been described and in some instances have been thought to be evidence of meniscal injury [1, 2]. A patient presented after an injury with intracapsular bone ossification in the posterior medial knee joint on a plain film radiograph. At arthroscopy, the density represented a bony avulsion of the posterior intercondylar area at the insertion of the posterior horn of the medial meniscus and was accompanied by a longitudinal tear of the posterior medial meniscus. Three additional patients presented with similar findings. The plain film finding of an ossification in the posterior medial joint in a patient with past knee trauma may suggest posterior longitudinal meniscal tear.

Case Report

A 33-year-old man sustained a twist injury to the right knee with subsequent episodic swelling and popping. Arthroscopy performed at an outside institution 18 months after the injury was reportedly normal. Three years after the injury, because of persistent symptoms, the patient was referred to the New England Medical Center for evaluation. Anteroposterior and lateral radiographs of the right knee revealed an elliptical bony density projecting into the region of the posterior medial meniscus (Fig. 1). Arthroscopic examination revealed a longitudinal tear of the posterior horn of the medial meniscus and an avulsed portion of bone from the posterior intercondylar area. After arthroscopic excision of the unstable meniscal fragment and bone, the patient was asymptomatic.

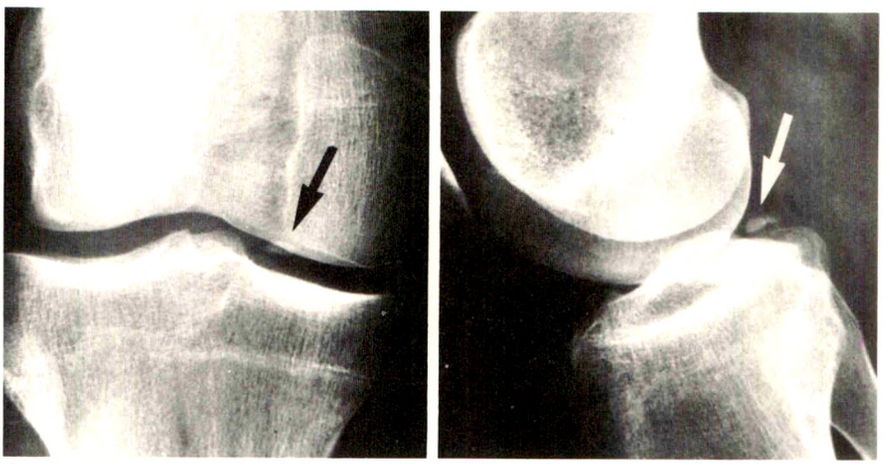

Fig. 1.—Anteroposterior (*A*) and lateral (*B*) radiographs of the knee show elliptical bony density in posterior medial joint space in area of posterior horn of meniscus.

Received August 10, 1987; accepted after revision September 9, 1987.

[1] Department of Orthopedics, Tufts University and New England Medical Center Hospitals, 750 Washington St., Boston, MA 02111.

[2] Department of Radiology, Tufts University and New England Medical Center Hospitals, Boston, MA 02111. Address reprint requests to R. C. Sarno, Dept. of Radiology, Box 127, New England Medical Center Hospitals, 750 Washington St., Boston, MA 02111.

AJR **150:159–160, January 1988** 0361–803X/88/1501–0159 © American Roentgen Ray Society

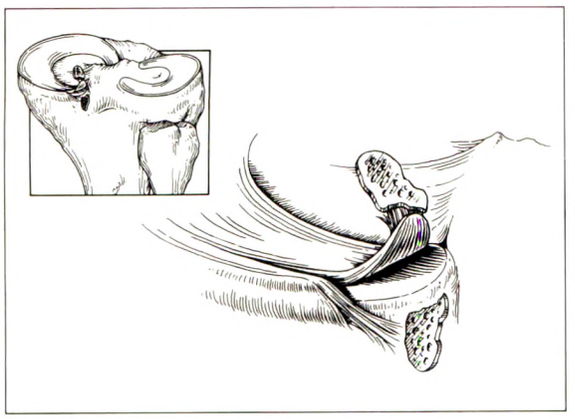

2

3

Fig. 2.—*Insert*, Posterior view of tibial surface of the knee shows site of bone avulsion from posterior intercondylar region of tibia at attachment of meniscal tibial ligament. *Larger image*, Focal view of posterior attachment of medial meniscus. Tibial bone fragment is seen projecting into joint space and remains attached to meniscus by portions of posterior ligament.

Fig. 3.—Tunnel view of the knee shows a sharply marginated linear density (*arrow*) projected just medial to medial tibial spine, which on lateral view was in posterior joint space.

Discussion

Although rare, the presence of ossicles within the menisci of the knee in humans has been reported [3, 4]. Whether they represent vestigial structures [3, 5, 6] that occur in totally asymptomatic patients or whether they develop as a result of trauma with accompanying metaplastic, heterotopic ossification [1, 2] has been a controversial issue. There are reports of meniscal calcifications surrounded by normal menisci [7], giving support to the belief that these meniscal ossifications are developmental, vestigial structures. Other reports of these ossifications describe them as occurring after knee injury [1, 2, 8]. Symeonides and Ionnides [8] reported three such cases in which the ossicles were associated with pain and the patients experienced relief of symptoms after the excision of the bone-containing portion of the meniscus. That report indicated that the ossification within the menisci is posttraumatic and clinically significant.

We examined a patient with previous knee trauma in whom a calcification was present in the posterior medial joint space of the knee on plain film radiographs. At arthroscopy, the bony fragment was seen to have arisen as an avulsion from the posterior intercondylar area of the tibia at the site of insertion of the posterior horn of the medial meniscus (Fig. 2). In addition, the patient had an accompanying longitudinal tear of the posterior horn of that meniscus. After we had seen this patient, three additional patients presented with posttrauma knee pain and similar plain film findings. Arthroscopy showed all three to have longitudinal tears of the posterior horn of the medial meniscus and a bony fragment in the joint arising from the point of insertion of the posterior horn of that medial meniscus. None of the patients had arthrograms. In the three patients examined 18 months or more after the initial injury, the bony fragment was somewhat elliptical and appeared well corticated with a convex posterior margin and flattened inferior surface. In one case in which the bone fragment was identified on plain film and at arthroscopy immediately after the injury (Fig. 3), the bone fragment appeared noncorticated and had sharp margins without evidence of the rounding that was evident in the other cases.

In this case (and in the three additional cases described above), plain films showed a bone fragment in the region of the posterior medial meniscus with meniscal injury. These findings also suggest a likely origin of the meniscal ossicle, which previously was thought to occur in patients with posttrauma knee pain [5]: instead, the fragment may arise as an avulsion of the posterior intercondylar area and not as heterotopic bone formation within the medial meniscus, as had been postulated previously [1]. In the posttrauma patient, the occurrence of a bony density in the area of the posterior limb of the medial meniscus should raise the possibility of an associated longitudinal tear of that meniscus.

REFERENCES

1. Burrows HJ. Two cases of ossification in the internal semilunar cartilage. *Br J Surg* **1934**;21:404–410
2. Mariani PP, Puddu G. Meniscal ossicle. A case report. *Am J Sports Med* **1981**;9(6):392–393
3. Rosen IE. Unusual intrameniscal lunulae. Three case reports. *J Bone Joint Surg [Am]* **1958**;40-A:925–928
4. Conforty B, Lotem M. Ossicles in human menisci: report of two cases. *Clin Orthop* **1979**;144:272–275
5. Pedersen HE. The ossicles of the semilunar cartilages of rodents. *Anat Rec* **1949**;105:1–9
6. Glass RS, Barnes MB, Kells DU, et al. Ossicles of knee menisci. Report of seven cases. *Clin Orthop* **1975**;3:163–171
7. Watson-Jones R, Roberts RE. Calcification, decalcification and ossification. *Br J Surg* **1934**;31:461–499
8. Symeonides PP, Ionnides G. Ossicles of knee menisci. Report of three cases. *J Bone Joint Surg [Am]* **1972**;54-A (6):1288–1292

Case Report

Osteosclerotic Sarcoidosis

Ibrahim F. Abdelwahab[1] and Alex Norman

This case is presented because of the infrequency of osteosclerotic sarcoidosis and because osteosclerotic lesions can easily be confused with metastatic bone cancer or lymphoma.

Case Report

A 52-year-old black man was admitted to the Beth Israel Medical Center in January, 1983, because of weight loss, abdominal pain, and generalized weakness that had persisted since September 1982. Urinary tract problems included nocturia, urgency, frequency, and dribbling. A maculopapular rash had developed over the patient's extremities and back 4 months before his hospitalization.

Palpable nodes were present in the left supraclavicular fossa; the liver was tender and nodular and was enlarged 6.0 cm below the costal margin; the spleen was also enlarged.

The laboratory studies showed an increased alkaline phosphatase of 523 units, a total protein of 8.2 mg, and a globulin of 4.4 mg. The cholesterol level was 159 mg/dl. The hemoglobin was 13.1 g, and

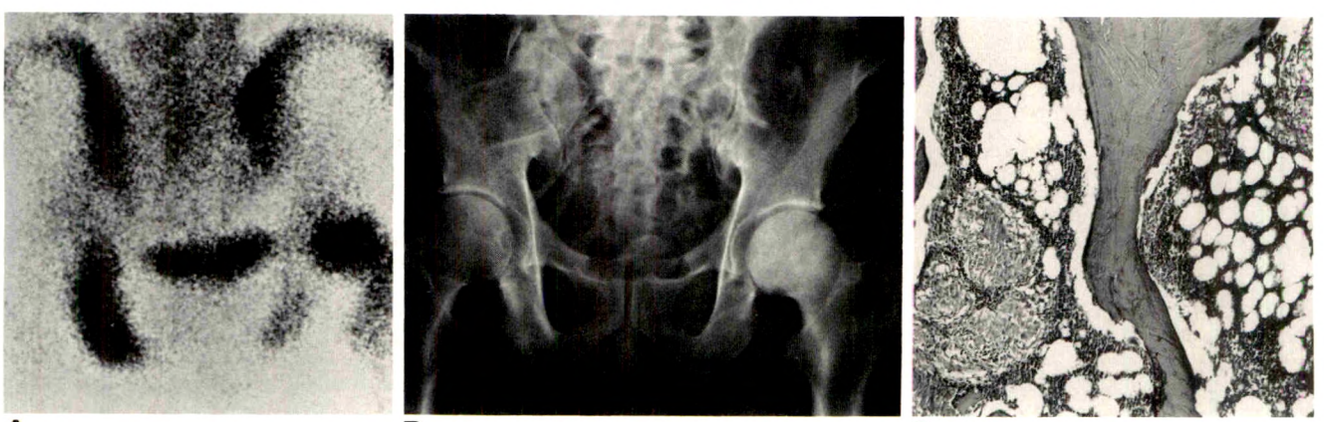

Fig. 1.—*A*, Scintigram shows radionuclide uptake in left femoral head and neck as well as in right ischium.
***B*, Radiograph shows sclerosis of left femoral head and neck and right ischium.**
***C*, Photomicrograph from a trocar biopsy of femoral head shows noncaseating sarcoid granulomata in marrow spaces with surrounding reactive bone consisting of irregular cement lines with minimal osteoblastic and osteoclastic activity. Granulomata consist of epithelioid cells, Langhans giant cells, and lymphocytes (×120).**

Received February 26, 1987; accepted after revision August 14, 1987.
[1] Both authors: Departments of Radiology, Hospital for Joint Diseases Orthopaedic Institute, New York, NY 10003 and New York University Medical Center, New York, NY 10016. Address reprint requests to A. Norman, Dept. of Radiology, Hospital for Joint Diseases Orthopaedic Institute, 301 E. 17th St., New York, NY 10003.

the WBC count was 5200 with a normal differential. The sedimentation rate was elevated (45 mm/hr).

An IV urogram showed an impacted stone in the proximal end of the right ureter that caused an obstructive hydronephrosis. The right kidney was displaced downward by the liver.

Radionuclide scintigraphy with ^{99m}Tc pyrophosphate showed avid uptake in the left hip, in the right ischium, and at the base of the skull (Fig. 1A). A ^{99m}Tc sulphur-colloid scan confirmed that the liver and spleen were enlarged.

A radiographic survey of the skeleton defined multifocal sclerotic lesions in the left femoral head and neck, in the right ischium, and at the base of the sphenoid bone (Fig. 1B). A clinical diagnosis of metastatic bone cancer was made, and this prompted a biopsy of the left femoral head.

The histopathologic features included noncaseating granulomata in the marrow consisting of epithelioid cells, Langhans giant cells, and lymphocytes diagnostic of sarcoid. Reactive sclerosis was present (Fig. 1C). A biopsy of a left supraclavicular node showed histopathology that was identical to the changes in the bone. The patient was treated with corticosteroids, and his condition had improved by the time he left the hospital.

Discussion

Sarcoidosis of bone is a well-documented condition [1, 2]. When the skeleton is involved, it typically affects the bones of the hands and feet. Atypical sites of involvement are the pelvis, spine, ribs, long bones, and skull [2–9]. Classically, the lesions are radiolucent with a pattern of cystic and coarsely reticulated bone [4–10]. The lesions may progress to destroy the bone and infiltrate the soft tissues. Characteristically, there is no evidence of joint involvement or periosteal reaction [3, 5–9].

In an exceptional case of sarcoidosis, osteoblastic lesions are noted. These lesions usually involve the axial skeleton (skull, spine, pelvis, and ribs) or long tubular bones (femur). Compared with the involvement of the small tubular bones, only a few cases of osteosclerotic sarcoidosis have been reported [3, 6–9].

Patients with sarcoidosis of the hands and feet are usually asymptomatic; in contrast, sarcoid affecting the spine is often painful. The radiographic appearance of the axial lesions is unusual for an infectious process; the disk space is unaffected and there is no paraspinal mass.

Rodman et al. [2] described the first antemortem case of vertebral sarcoidosis. A large lytic lesion surrounded by a thin sclerotic margin was noted in the 11th thoracic vertebral body. It was clinically diagnosed as tuberculous spondylitis. However, the biopsy disclosed a noncaseating sarcoid granuloma. Similar cases have been reported in the lower thoracic and lumbar spine [4].

Our case of osteosclerotic sarcoidosis is significant for several reasons. First, this 52-year-old man is the oldest reported patient to have osteoblastic changes (typically, patients range in age from 23 to 36 years). Second, this patient has osteoblastic lesions involving not only the femur and pelvis but also the base of the skull, which is indeed an unusual location for sarcoid. The fact that this patient was black, however, was consistent with the characteristics of other patients with osteosclerotic sarcoidosis. In fact, of the six patients reported in the literature [3, 6–9], only one was white.

Clinically, 80–90% of cases with bone involvement have associated lung, mediastinal, and/or supraclavicular nodal disease. Skin sarcoidosis occurs in almost every patient with bone lesions [1]. Pulmonary and/or mediastinal sarcoid often coexists with skeletal foci in the hands and feet. This is not true for the osteosclerotic type; the bony changes in osteosclerotic sarcoidosis can appear years after the lung disease is arrested [3, 6–9].

The predilection of osteosclerotic sarcoidosis for unusual sites in the skeleton is striking. Of the six cases reported [3, 6–9], the pelvis was affected in all six; the femur, spine, skull, and ribs in three; and the clavicle in one.

Although sclerosing sarcoidosis is a rare disease, it still should be considered in the differential diagnosis of dense bone lesions (e.g., osteoblastic metastatic bone cancer, lymphoma, Paget disease, systemic mastocytosis, osteopetrosis, and less often a fungal or *Brucella* spondylitis) [3]. Rohatgi [10] speculated that the magnitude of the disease could influence the prognosis. Therefore, he suggested that the simplest and most sensitive way to assess skeletal involvement is to use ^{99m}Tc diphosphonate bone scintigraphy and that the most effective way to detect the extent of pulmonary and extrapulmonary involvement is to use ^{67}Ga scans [10].

REFERENCES

1. Mayrock RL, Bertrand P, Morrison CE. Manifestations of sarcoidosis. *Am J Med* **1963**;35:67–89
2. Rodman T, Funderburk EE Jr, Myerson RM. Sarcoidosis with vertebral involvement. *Ann Intern Med* **1959**;50:213–218
3. Young DA, Laman ML. Radiodense skeletal lesions in Boeck's sarcoid. *Am J Roentgenol Rad Ther Nucl Med* **1972**;114:553–558
4. Goobar JE, Gilmer WS Jr, Carroll DS, et al. Vertebral sarcoidosis. *JAMA* **1961**;178:1162–1163
5. Teirstein AS, Wolf BS, Siltzbach LE. Sarcoidosis of the skull. *N Engl J Med* **1961**;265:65–68
6. Bonakdapour A, Levy W, Aegerter EE. Osteosclerotic changes in sarcoidosis. *Am J Roentgenol Rad Ther Nucl Med* **1971**;113:646–649
7. Lin SR, Levy W, Go EB, et al. Unusual osteosclerotic changes in sarcoidosis, simulating osteoblastic metastases. *Radiology* **1974**;106:311–312
8. Weston M, Duffy P. Osteosclerosis in sarcoidosis. *Aust Radiol* **1975**;19:191–193
9. Marcove R, Rooney R, Weis LD. Osteosclerotic lesions in sarcoidosis—report of a case. *Clin Orthop* **1977**;129:248–250
10. Rohatgi PK. Radioisotope scanning in osseous sarcoidosis. *AJR* **1980**;134:189–191

MR Imaging of Chiari II Malformation

Taher El Gammal[1]
Edward K. Mark[2]
Betty S. Brooks[1]

High-field-strength MR imaging was performed in one patient with Chiari III and 19 patients with Chiari II malformations. The MR features were compared with descriptions in the literature and correlated with previously described surgical and postmortem findings and with the results of previous radiologic investigations in this group of patients. Several new observations were apparent from the MR examinations. In 75% of the 20 cases, the underdeveloped tentorium with a wide incisura allowed inferior displacement of the medial posterior cerebrum, which appeared closely applied to a flattened aspect of the superior cerebellum. Previously reported CT descriptions of "pseudotumor of the tentorium" and "towering cerebellum" may be more related to the technique of the radiologic examination than to true upward herniation of the cerebellum. Elongation of the mesencephalon with increase in the mamillopontine distance was present in the majority of our cases and has not been previously emphasized. Some patients had atypical changes or appeared to be borderline cases between the Chiari I and Chiari II categories of malformation, and MR provided considerable diagnostic assistance in these cases.

The noninvasive, in vivo evaluation of MR contributed a great deal to our further understanding of this congenital Chiari malformation.

We report our experience with 19 cases of Chiari II and one of Chiari III malformation examined with high-field-strength MR imaging. Information obtained in the past has relied on autopsy material, surgical observations, and investigative radiologic procedures such as air studies, CT, myelography, and CT myelography. MR provides a new viewpoint with in vivo, detailed anatomic images that can be correlated with the knowledge from previous methods of study of this interesting developmental malformation.

Subjects and Methods

Twenty patients 1 day to 25 years old and including one stillborn infant were evaluated. There were eight males and 12 females. Every patient had hydrocephalus and all had myelomeningocele, except one with an encephalocele at the craniovertebral junction (Chiari III) and diastematomyelia in the lumbar region. All but two had had shunts placed before the MR study. In five, MR was performed at the time of initial diagnosis of Chiari II. In the other 15, MR was performed during follow-up outpatient visits to the Neurosurgery Clinic.

MR examinations were performed with a General Electric 1.5-T Signa system. Limited T1-weighted sagittal series-only studies were performed with a repetition time (TR) of 800 and echo time (TE) of 25 msec, four excitations, 24-cm field of view, and 256 × 256 matrix. For infants younger than 3 months old, a TR of 1000 msec was used. The slice thickness was 3 mm with 1-mm interval interslice spacing in all patients except one, for whom 5-mm-thick slices were used. Three patients also had MR studies of the spine, cervical in two and lumbar in one. In three patients a complete cranial MR study was performed, which included a coronal and transaxial spin-echo pulse sequence series with TR = 2000 msec and TE = 25, 50 or TE = 25, 65 msec. Sedation was given in all cases, most often with IV Seconal at a dose of 2 ml/kg.

This article appears in the November/December 1987 issue of *AJNR* and the January 1988 issue of *AJR*.

Received February 12, 1987; accepted after revision May 4, 1987.

Presented at the annual meeting of the American Society of Neuroradiology, San Diego, January 1987.

[1] Department of Radiology, Section of Neuroradiology, Medical College of Georgia, 1120 15th St., Augusta, GA 30912. Address reprint requests to T. El Gammal.

[2] Department of Surgery, Section of Neurosurgery, Medical College of Georgia, Augusta, GA 30912.

***AJR* 150:163–170, January 1988**
0361–803X/88/1501–0163
© American Roentgen Ray Society

Results

Craniovertebral Junction, Cervical Spinal Canal, and Cervical Cord

Caudal displacement of cerebellar tissue was present in every case. The inferior tip of the vermis was located between the C2–C3 level in the majority of cases. In 10 patients (50%), herniated vermis could be clearly delineated as being separate from the cerebellar tonsils. Tonsillar herniation without evidence of vermian ectopia was noted in one patient.

Medullary herniation with resultant kinking or "spur" at the cervicomedullary junction was found in 15 of 19 patients and could not be evaluated in one patient with a very large head because the image included only the uppermost cervical region.

Hydromyelia was demonstrated by cranial MR in three cases; in one patient cranial and spinal MR failed to reveal a hydromyelia after surgical drainage.

Brainstem, Aqueduct, and Fourth Ventricle

Stretching and inferior displacement of the aqueduct and fourth ventricle was demonstrated in 15 patients. In five of these, the fourth ventricle was significantly dilated with massive dilatation in one. Aqueductal stenosis was found in eight cases.

Elongation and inferior displacement of the brainstem was noted in 15 of 20 patients. The pons appeared flattened in all of these patients. A concave clivus with a wide prepontine subarachnoid space was associated with eight of the 15 (Figs. 1–3). In one, the pons was noted pressing against a straight clivus.

In four other patients a normal brainstem was found. The last case was intermediate between the patients with normal brainstem and those with definite elongation and caudal displacement (Fig. 4), with mild changes of a slightly stretched aqueduct and fourth ventricle and minimal flattening of the pons.

Relationship of the Tentorium and Superior Surface of the Cerebellum

In 15 of 20 patients MR revealed a definitely flattened appearance of the superior aspect of the cerebellum. The superior surface of the vermis was close to the level of the foramen magnum in three. In four of these 15 patients a notably vertical orientation of the straight sinus was evident, consistent with a wide tentorial incisura (Figs. 1B and 3). The medial posterior cerebrum could be seen in close relation to the flattened superior cerebellum in the majority of these 15 patients.

In two patients with complete cranial MR studies the ventricular trigones were noted to be close together near the midline, again indicative of inferior displacement of the cerebral hemispheres in relation to the tentorium and flattened superior cerebellum.

Mesencephalon, Mamillopontine Distance, and Third Ventricle

In 12 patients, pointing or "beaking" of the quadrigeminal plate consequent to fusion of the colliculi was seen. There was vertical elongation of the mesencephalon with increase in the mamillopontine distance in 10 cases. Measurement of the mamillopontine distance varied between 1.3 and 3.0 cm as a computer-corrected actual patient size measurement. Normal values in adult patients do not exceed 1.2 cm [1]. In

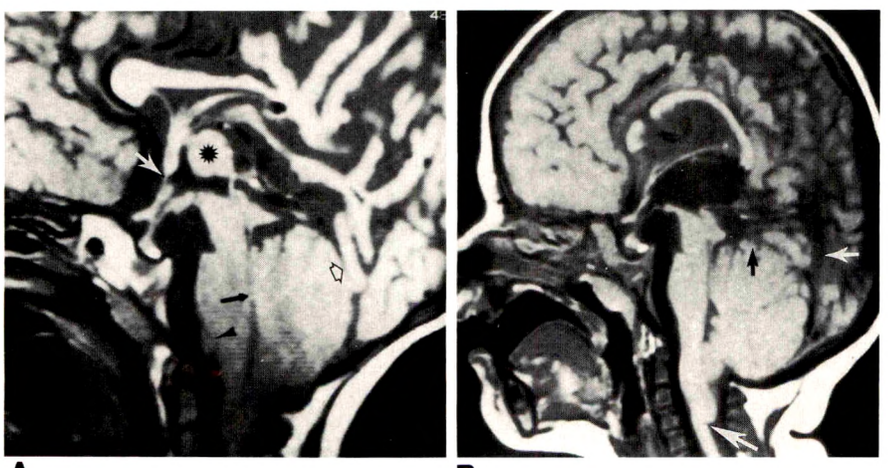

A **B**

Fig. 1.—Advanced changes of Chiari II malformation in two patients with long-term shunting.

***A*, Aqueduct and fourth ventricle are stretched (*solid black arrow*); there is a large massa intermedia (*asterisk*) and pseudodiverticulum of lamina terminalis (*white arrow*). Note flattened pons away from concave clivus and pointed quadrigeminal plate. Apparent lobulation of lower pons (*black arrowhead*) is produced by encircling of brainstem by cerebellar hemisphere. Note increase in mamillopontine distance. Atrophic posterior parietal lobe is herniated through wide tentorium (*open arrow*), and superior aspect of cerebellum appears flat. Aqueduct is incompletely seen and may be blocked.**

***B*, Stretching of brainstem with elongation of mesencephalon with increase in mamillopontine distance. Again, flat pons is situated at some distance from concave clivus. The massa intermedia is absent, and diverticula are in relation to hypothalamus and lamina terminalis. Defect in anterior corpus callosum is from shunt procedure. There is also a pointed quadrigeminal plate and aqueduct stenosis. Note kink between medulla oblongata and upper cervical cord (*large white arrow*). Superior surface of vermis is flattened (*black arrow*) with herniation of medial posterior hemisphere through tentorium. Straight sinus is vertical (*small white arrow*). Aqueduct is probably obstructed in its midportion.**

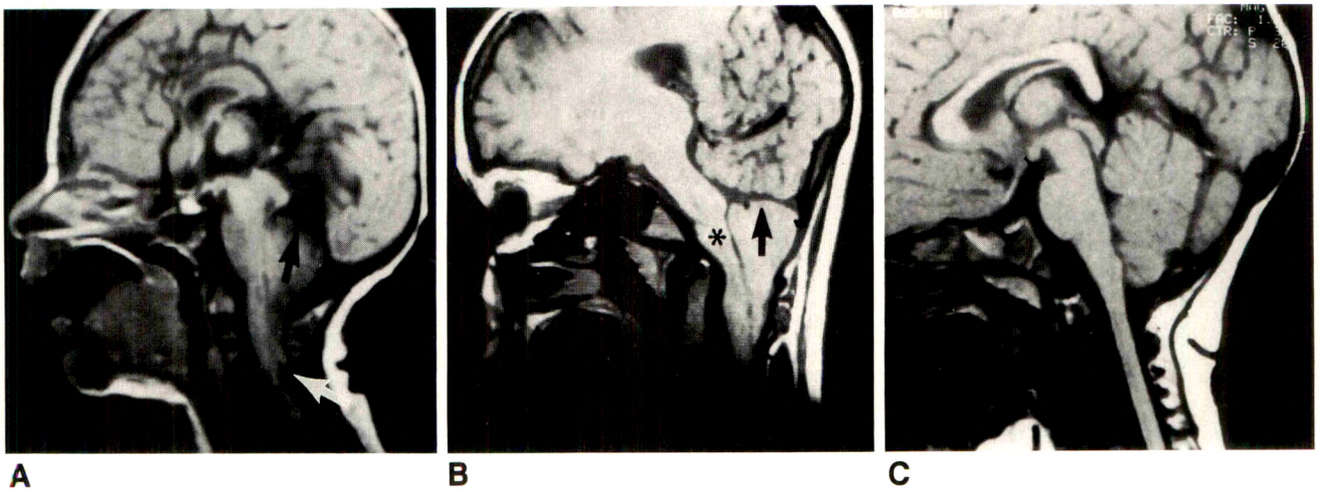

Fig. 2.—*A* and *B*, Two patients with severe inferior location of cerebellum.

A, Significant inferior location of cerebellum and flattened superior cerebellum (*black arrow*). Kink between medulla oblongata and spinal cord is indicated (*white arrow*).

B, Severe inferior displacement of cerebellum. Superior cerebellum is flat (*arrow*) and is seen just above foramen magnum with adjacent herniated cerebrum. Pons is flat (*asterisk*), lying just above odontoid. There is severe stretching of mesencephalon with marked increase in mamillopontine distance.

C, Normal study in 8-month-old child shows normal mamillopontine distance (*black line*). Note normal appearance of pointed superior vermis.

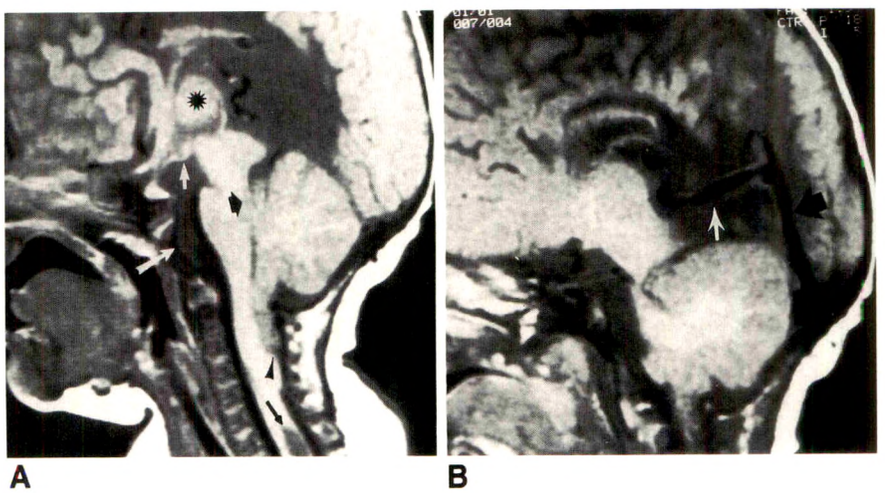

Fig. 3.—Chiari II malformation with hydromyelia in 10-year-old girl.

A, Large massa intermedia (*asterisk*), low stretched fourth ventricle (*short black arrow*), hydromyelia (*long black arrow*), and herniated cerebellar vermis (*arrowhead*). There is diverticulum of third ventricle in relation to mamillary body (*short white arrow*). Clivus is concave (*long white arrow*), with considerable distance separating it from flattened pons. Quadrigeminal plate is pointed. Extremely attenuated corpus callosum as well as atrophy of posterior cerebrum resulting in large subarachnoid space above apex of tentorium may be from pressure atrophy from previous hydrocephalus.

B, Note vertical, posteriorly placed straight sinus (*black arrow*) and long vein of Galen (*white arrow*).

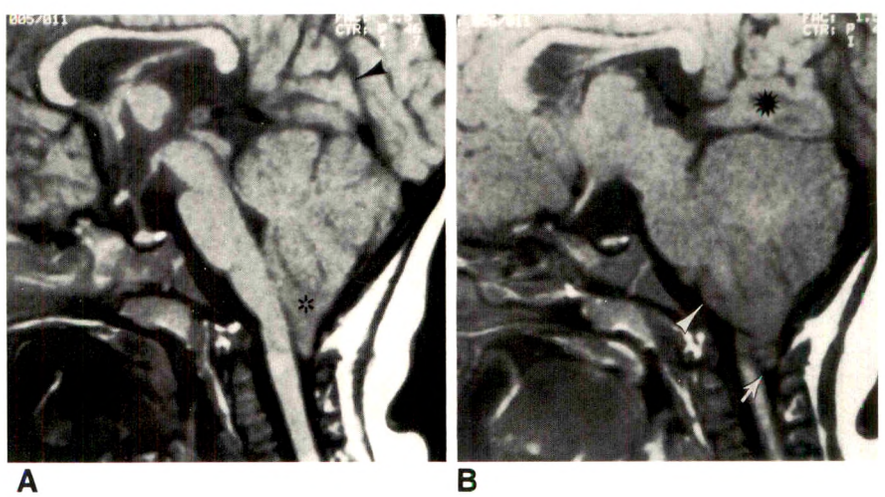

Fig. 4.—1-year-old girl with milder changes of Chiari II malformation. Fourth ventricle and aqueduct are only slightly stretched. Cerebellar ectopia includes both inferior vermis and tonsil (*asterisk*, *A*; *arrow*, *B*). Tentorial opening is wide and there is vertical orientation at line of attachment along straight sinus that was shown in contiguous section (*arrowhead*, *A*). Herniation of medial temporoparietal cerebrum (*asterisk*, *B*) through wide tentorium above flattened superior vermis of cerebellum. Belly of pons appears relatively flattened. In *B*, anterior portion of cerebellum encircles brainstem (*arrowhead*).

two patients, the mamillopontine distance was diminished. The reduction was severe in one of these, in whom there was marked distension of the supratentorial ventricles owing to hydrocephalus. In this patient the mamillary body was seen nearly touching the pons. In the other patient, the brainstem and midline ventricles appeared normal.

Diverticula and pseudodiverticula of the third ventricle were noted in 10 patients. In five, the pseudodiverticula with accessory massa intermedia were seen in relation to the lamina terminalis. In two patients, the diverticula arose from the floor of the hypothalamus, and in three, there were diverticula present in relation to both the hypothalamus and the lamina terminalis.

A large (greater than 1 cm actual patient measurement) massa intermedia was found in 11 patients. An accessory massa intermedia close to but separate from the lamina terminalis was noted in two patients. One of our cases also showed complete obliteration of the third ventricle, most likely as a result of inflammatory changes occurring after chronic shunting.

Discussion

A detailed description of the morbid findings in a full-term infant with spina bifida, craniolacunae, herniation of cerebellar vermis, elongated brainstem, and fourth ventricle through the foramen magnum was first published by Clealand [2] in 1883. In 1891, Chiari [3] reported the morbid findings in infants with varying degrees of hindbrain deformity, and he classified them into three types (I, II, and III). In 1894, Arnold [4] reported one infant with fourth ventricular and cerebellar herniation. Contributions and observations of numerous authors over the years have resulted in the elaboration of many of the neuroanatomic features now regarded as part of the Arnold-Chiari [5–7] or Chiari II [8] malformation.

The radiologic features and evaluations of Chiari II using air studies and polytomography have been reported [8–12], and subsequently water-soluble contrast media have been used to delineate the midline ventricles [13, 14]. Recently, Naidich et al. [15–18] described the CT features of Chiari II with surgical and pathologic correlation.

Currently, high-field-strength MR affords the opportunity for noninvasive evaluation of all the distinctive features of this congenital malformation.

Cervical Spinal Canal and Hydromyelia

Inferior displacement of stretched brainstem with kink between the medulla oblongata and the spinal cord associated with vermian herniation constitute the most important pathologic features of Chiari II malformation [6, 7]. These abnormalities below the foramen magnum have been shown radiologically with oily contrast media [9], by air studies [8, 19], and more recently with water-soluble contrast material in combination with both conventional tomography and CT [18].

With MR, the typical findings of cerebellar vermian herniation and spinomedullary kink or spur in the upper cervical region were found in 15 of 20 patients (Figs. 1, 2A, and 2B) and hydromyelia was demonstrated by cranial MR in three (15%) of 20 cases in our series (Fig. 3). The frequency of hydromyelia in pathologic reports has varied between 20–83% [6, 7] (Table 1). The frequency in our series may be falsely low because sagittal MR in the majority of patients only included the upper cervical spinal canal. Hydromyelia is most frequently demonstrated in the lower cervical and dorsal regions [6] and therefore may have been missed in 17 of our cases. In six of 26 cases reported by Cameron [6], narrowing of the distended central canal in the upper cervical region was found. In two patients who had water-soluble contrast media examinations, this same finding was seen (Figs. 5 and 6). Since the majority of patients (18 of 20) were studied after shunting, collapse of the hydromyelic cavity after shunting may also have contributed to a falsely low frequency in this series. Hall et al. [20] provided some insight into the importance of shunting in Chiari II patients in a report of five cases with severe progressive spasticity. Three patients had definite improvement after shunting of the lateral ventricles. This was postulated to be from collapse of the hydromyelia, which they demonstrated with Pantopaque studies. For the patient in Figure 5, a severe progressive spasticity showed similar, very significant clinical improvement after drainage of the hydromyelia to the cervical subarachnoid space.

Cerebellum and Tentorium

In 35% of a series of cases examined postmortem by Peach [7], upward herniation of the cerebellum was described. Radiologically, Zimmerman et al. [21] reported the CT appear-

TABLE 1: Comparison Between Current MR Findings of Chiari II Malformations and Previous Postmortem Studies

Finding	% of Cases (No.)		
	Present series (n = 20)	Cameron [6] (n = 26)	Peach [7] (n = 20)
Elongation of brainstem and low medulla; stretched aqueduct and fourth ventricle	75 (15/20)	96	90
Kinking of medulla on spinal cord	79 (15/19)	Noted	55
Caudal cerebellum	100 (20/20)	96	90
Hydromyelia	15 (3/20)	83	20
Beaking of quadrigeminal plate	60 (12/20)	Noted	75
Large massa intermedia	55 (11/20)	63	90
Large fourth ventricle	25 (5/20)	Not noted	25

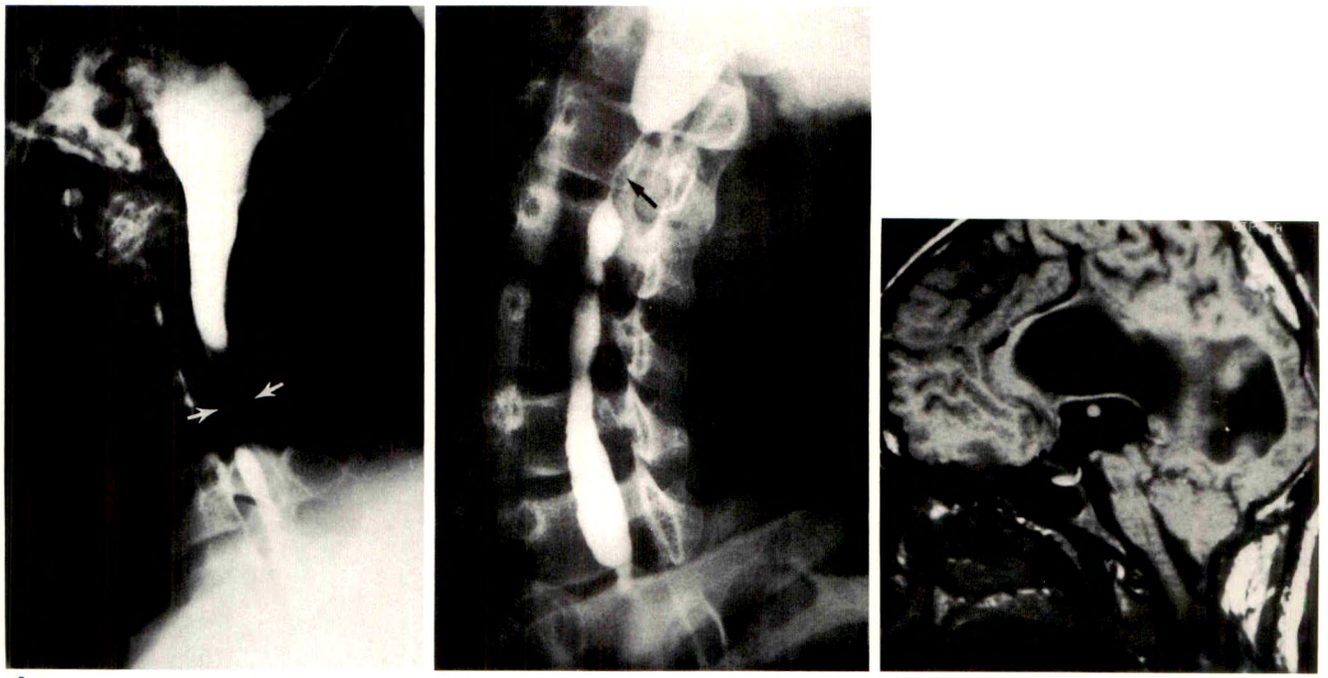

Fig. 5.—17-year-old boy with hydromyelia shown by intraventricular metrizamide.

A and *B*, Lateral (*A*) and oblique (*B*) radiographs after intraventricular metrizamide show hydromyelia with narrowed segment in upper cervical region (*arrow*, *B*). Dilated fourth ventricle merges imperceptibly into hydromyelia. Poor filling of hydromyelia behind body of C3 may be from adhesions (*arrows*, *A*).

C, Stretching of brainstem and aqueduct, and dilated fourth ventricle. Superior vermis is flat. Mamillopontine distance is increased and pons appears flat. Caudally displaced parietal lobe rests on top of flattened vermis. MR was performed after shunting of syrinx to subarachnoid space, which is why fourth ventricle appears smaller than in *A* and *B*.

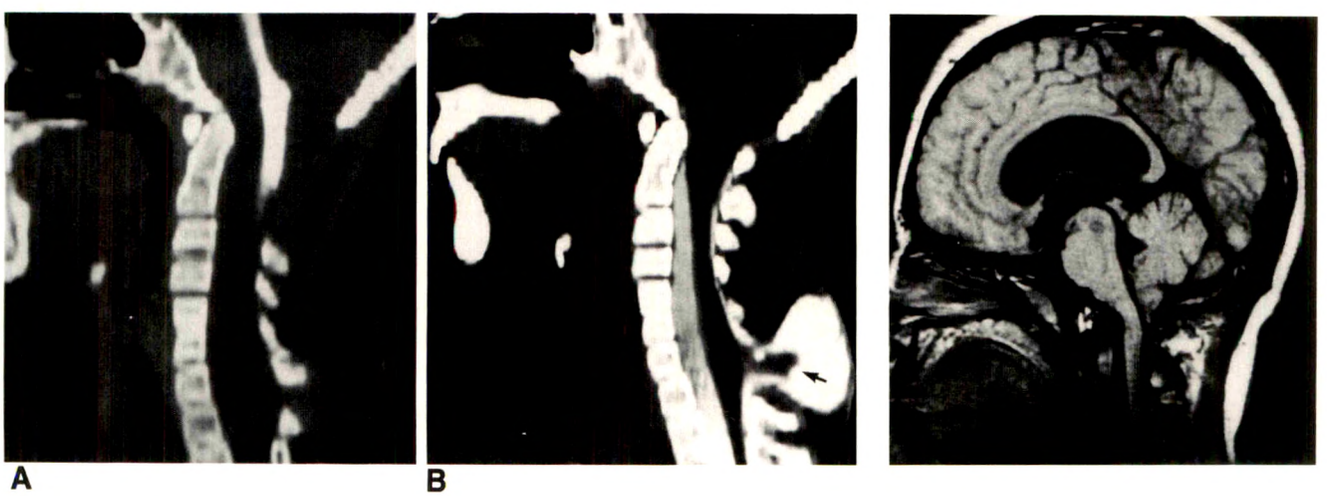

Fig. 6.—Chiari II malformation with stenosis between fourth ventricle and hydromyelia.

A, Sagittal reformatted CT ventriculogram shows low fourth ventricle, which does not appear to communicate with hydromyelia in cervical cord. There is meningomyelocele at cervicothoracic junction (*asterisk*).

B, Sagittal reformatted CT myelocisternogram shows expanded hydromyelic cord extending into meningomyelocele (*arrow*). Cerebellar ectopia is evident at craniovertebral junction. Transaxial IV-enhanced CT section just above meningomyelocele (not shown) revealed hydromyelia that did not communicate with fourth ventricle probably because of narrowing of its upper part.

Fig. 7.—Chiari I malformation. Midsagittal MR shows pointed, inferiorly displaced tonsil; angulation between medulla oblongata and cervical spinal cord; expanded trumpeted upper medulla; and rounded belly of the pons. Mamillopontine distance is reduced, partly because of hydrocephalus.

ance of "pseudotumor of the tentorium" in meningomyelocele patients, and Naidich et al. [16] later used the term "towering cerebellum," which was attributed to upward herniation from the inability of the small posterior fossa in Chiari II patients to accommodate posterior fossa contents. However, in 15 (75%) of our 20 cases examined by MR, the intracranial cerebellum appeared small, and the medial posterior cerebrum was clearly seen below the level of the straight sinus adjacent to the midline above the superior aspect of the cerebellar vermis, which had a flat appearance (Figs. 1, 2, 4, and 5C). We noted a fairly normal triangular configuration of the superior cerebellar vermis in three other cases, and in two patients there was an intermediate appearance between the normal and the horizontal or flattened shape seen in the other 15.

In two patients, the intracranial cerebellum did appear large with a high position of the vermis. In both patients, the attachment of the tentorium was normal in position with a normal forward inclination and orientation of the straight sinus. There was elongation and caudal displacement of the fourth ventricle in both. The cerebellar tonsils and inferior vermis were caudally displaced in one patient, and in the other, only the tonsils were positioned below the foramen magnum.

An abnormal vertical orientation of the straight sinus was found in four of our 20 patients, and in three of these the apex of the tentorium was also high (Figs. 1B and 3B). This correlates with the observation made by McCoy et al. [8] that the falcotentorial junction may be located in an unusually high position in the midline, although the underdeveloped tentorial leaflets then extend inferiorly and laterally in an abnormally low position. This results in a very large tentorial incisura. In our three patients in whom transaxial MR was performed, the medial aspects of the posterior cerebral hemispheres were observed close to the midline, and the ventricular trigones appeared to approach one another. In midsagittal and parasagittal sections close to the midline, the medial posterior cerebrum was demonstrated below the falcotentorial junction in apposition to the flattened surface of the cerebellum (Figs. 1, 2B, 4, and 5C). MR observations are consistent with the concept, therefore, that upward herniation of the cerebellum will be seen less often in Chiari II as the severity of the degree of the tentorial hypoplasia increases, and in fact, there is downward displacement of the medial posterior cerebrum adjacent to the midline.

Transaxial CT studies with standard 20° angulation to the canthomeatal plane may produce a "pseudotumor of the tentorium" appearance because inferior posterior fossa sections at the level of the low tentorial hiatus will demonstrate a component of the cerebellum that appears relatively large in comparison with the small amount of the inferiorly located posterior cerebral hemispheres. In normal patients, posterior sections at these levels include only the cerebellum. Coronal sections were not obtained in most of our cases; however, it is expected they would have confirmed our observations in the sagittal projection and may possibly have added other information as well.

A wide subarachnoid cistern above the cerebellum has been noted on CT studies [17]. This may occur consequent to parenchymal loss in the medial posterior aspects of the cerebral hemispheres owing to pressure atrophy from hydrocephalus in some patients (Figs. 1A and 3). Peach [7] made pathologic observations of brain-tissue loss involving inferior and posterior portions of the cerebral hemispheres in some of his patients, and this has also been demonstrated radiologically on air studies [10].

Pons and the Concave Clivus

A flattened pons, noted in 15 of our 20 patients, was found to be associated with concavity of the clivus in eight. MR demonstrated that the concavity involved the basioccipital portion while the basisphenoid remained straight (Figs. 1, 3, and 5C), consistent with previous observations by Yu and Deck [22], who suggested that this could be caused by pressure effect of the pons against the clivus. However, polytome air studies in some patients have shown that the pons may be situated a considerable distance from the concave clivus [12, 23]. This observation as well as the MR studies both mitigate against the theory of pressure effect on the clivus by the pons.

Fourth Ventricle and the Aqueduct

In five of 20 cases in this series, dilatation of the inferiorly displaced fourth ventricle was noted. This has been reported from autopsy material [7, 24] and has been shown on air studies [11, 12].

A double-humped appearance of the inferiorly displaced fourth ventricle in Chiari II has also been demonstrated by air studies [8, 9, 11, 12] and attributed to bulging of the inferior vermis [8]. This double-humped appearance was not seen in any of our cases studied with MR.

CT without the use of water-soluble contrast media has not provided adequate delineation of the aqueduct, and this represents a clear-cut advantage of the direct sagittal imaging capability of MR. MR sections 3 mm or less in thickness should be used for consistent and proper delineation of the aqueduct. Nonvisualization is then highly suggestive of aqueduct obstruction. MR may not depict physiologic obstruction, however. Intraventricular contrast studies with air movement from the third ventricle to a low fourth ventricle was noted in apparent aqueduct obstruction [9, 10, 12]. In older children, chronic inflammatory changes after shunting may also result in structural blockage of the aqueduct, contributing to an increased occurrence of aqueduct obstruction with the age of the patient and with shunting.

Mesencephalon and Third Ventricle

Beaking of the quadrigeminal plate, first reported by Clealand [2] in 1883, represents a characteristic morphologic finding in Chiari II patients [6, 7]. Elongation of the mesencephalon, however, has not been stressed in the previous pathologic or radiologic literature and was clearly shown by MR in 50% of the cases in our series. This was confirmed by measurement of the mamillopontine distance, and the values found were well above the normal adult range [1] (Fig. 2C), with measurements of up to 3.0 cm.

TABLE 2: Hindbrain Abnormalities in Chiari I and II Malformations

Feature	Chiari I	Chiari II
Mamillopontine distance	Reduced	Increased
Beaked quadrigeminal plate	No	Yes
Junction between spinal cord and medulla	May show angulation	Kinking or "spur"
Pons	Round	Flat
Medulla oblongata	"Trumpet-shaped" with increased antero-posterior diameter at medullopontine junction	Stretched and low
Cerebellar ectopia	Tonsils	Vermis ± tonsils

The large massa intermedia is a well-known feature associated with Chiari II [6, 7], and other specific morphologic changes seen in the third ventricle have included accessory massa intermedia, diverticula, and pseudodiverticula [9–12, 25]. The pseudodiverticula caused by accessory massa intermedia close to the lamina terminalis have been seen infrequently by air studies in normal patients [26]. A hypothalamic, slitlike recess of the third ventricle was reported in normal cases [27]. These observations are difficult to make with cranial CT, but are clearly outlined with MR (Figs. 1 and 3).

Intermediate Cases

In all of our cases, myelomeningocele was present. In a 1957 review of the literature, Cameron [6] found no report of a myelomeningocele without an associated Chiari II malformation. His postmortem examination of 26 patients with myelomeningocele included two cases with a normal brain and craniovertebral junction, one patient with features of Chiari I malformation, and one atypical case with slight elongation of the brainstem and fourth ventricle but no cerebellar ectopia. A case of myelomeningocele with normal appearance of the midline ventricles has also been illustrated on air studies [9]. On the other hand, classical anatomic features of Chiari II malformation involving cranium and cervical spinal canal have been reported without a myelomeningocele [28, 29]. There is, therefore, a spectrum of changes in hindbrain malformations and myelomeningoceles. In our series, there were five atypical cases. The brainstem appeared nearly normal in four. In one patient, stretching and inferior displacement of the brainstem and fourth ventricle was present, with tonsillar herniation as the only cerebellar ectopia. Included in our series is a case of Chiari III that also had lumbar diastematomyelia. Diastematomyelia of the cervical cord has been demonstrated with water-soluble contrast studies in Chiari II malformations [18].

The most useful features in the distinction of the Chiari I anomaly, illustrated in Figure 7 (El Gammal T, unpublished data), from the Chiari II malformation are summarized in Table 2. MR reveals the relationship of the soft tissues and osseous structures without the artifacts of postmortem examination. MR now provides, noninvasively and with the proper delineation of brainstem, cerebellum, and spinal canal, the best imaging method in the evaluation of borderline cases.

REFERENCES

1. El Gammal T, Allen MB Jr, Brooks BS, Mark EK. MR evaluation of hydrocephalus. *AJNR* **1987**;8:591–597
2. Clealand J. Contribution to study of spina bifida encephalocele and anencephalus. *J Anat* **1883**;17:257–291
3. Chiari H. Uber Veranderungen des Kleinhirns Infolge von Hydrocephalie des Grosshirns. *Dtsch Med Wochenschr* **1891**;17:1172–1175
4. Arnold J. Myelocyste transposition von gewebskeimen and Symbodie. *Beitr Pathol* **1894**;16:1–28
5. Schwalbe E, Gredig M. Uber entwicklungsstorungen des Kleinhirns, hirhstamms und halsmarks bei spina bifida. *Beitr Pathol* **1907**;40:132–194
6. Cameron AH. The Arnold-Chiari and other neuroanatomical malformations associated with spina bifida. *J Pathol* **1957**;73:195–211
7. Peach B. Arnold-Chiari malformation anatomic features of 20 cases. *Arch Neurol* **1965**;12:613–621
8. McCoy WT, Simpson DA, Carter RF. Cerebral malformations complicating spina bifida: radiological studies. *Clin Radiol* **1967**;18:176–182
9. El Gammal T. Extra-ventricular (communicating) hydrocephalus: some observations on midline ventricles. *AJR* **1969**;106:308–328
10. El Gammal T. Follow-up air studies on patients with ventrifculoatrial (V-A) shunts reference to the value of polytomography. *AJR* **1973**;118:155–162
11. El Gammal T, Allen MB Jr, Lott T. Computer assisted tomography and pneumoencephalography in non-tumorous hydrocephalus in infants and children. *J Comput Assist Tomogr* **1977**;1(2):204–210
12. El Gammal T, Allen MB Jr. *An atlas of polytome pneumography*, vol 4. Springfield, IL: Thomas, **1977**:175–195
13. Fitz CR, Harwood-Nash DC, Chuang S, et al. Metrizamide ventriculography and computed tomography in infants and children. *Neuroradiology* **1978**;16:6–9
14. Yamada H, Nakamura S, Tanaka Y, et al. Ventriculography and cisternography with water-soluble contrast media in infants with myelomeningocele. *Radiology* **1982**;143:75–83
15. Naidich TP, Pudlowski RM, Naidich JB. Computed tomographic signs of the Chiari II malformation. I. Skull and dural partitions. *Radiology* **1980**;134:65–71
16. Naidich TP, Pudlowski RM, Naidich JB. Computed tomographic signs of the Chiari II malformation: II. Midbrain and cerebellum. *Radiology* **1980**;134:391–398
17. Naidich TP, Pudlowski RM, Naidich JB. Computed tomographic signs of the Chiari II malformation: III. Ventricles and cisterns. *Radiology* **1980**;134:657–663
18. Naidich TP, McLone DG, Fulling KH. The Chiari II malformation: IV. The hindbrain deformity. *Neuroradiology* **1983**;25:179–197
19. Hemmy DC, Millar EA, Haughton V. Gas myelography in the management of spinal cord disorders in children. *Neuroradiology* **1978**;16:85–86
20. Hall PV, Campbell RL, Kalsbeck JE. Meningomyelocele and progressive hydromyelia: progressive paresis in myelodysplasia. *J Neurosurg* **1975**;43:457–463
21. Zimmerman RD, Breckbill D, Dennis MW, et al. Cranial CT findings in patients with meningomyelocele. *AJR* **1979**;132:623–629
22. Yu HC, Deck MDF. The clivus deformity of Arnold-Chiari malformation. *Radiology* **1971**;101:613–615
23. El Gammal T, Brooks BS. Radiologic evaluation of the craniovertebral

junction. In: Taveras JM, Ferrucci JT, eds. *Radiology: diagnosis/imaging/intervention*, vol 3, chapt 70. Philadelphia: Lippincott, **1986**:1–15

24. Peach B. Cystic prolongation of the fourth ventricle: anomaly associated with the Arnold-Chiari malformation. *Arch Neurol* **1964**;11:609–612
25. Gooding CA, Carter A, Hoare RD. New ventriculographic aspects of Arnold-Chiari malformation. *Radiology* **1967**;89:626–632
26. El Gammal T, Allen MB Jr. *An atlas of polytome pneumography*, vol 4. Springfield, IL: Thomas, **1977**:136–138
27. Sutton D Jr. Radiological assessment of normal aqueduct and 4th ventricle. *Br J Radiol* **1950**;23:208–218
28. Peach B. Arnold-Chiari malformation with normal spine. *Arch Neurol* **1964**;10:497–501
29. Swanson HS, Fincher EF. Arnold-Chiari malformation without bony anomalies. *J Neurosurg* **1949**;6:314–319

Variable Appearances of Subacute Intracranial Hematomas on High-Field Spin-Echo MR

John M. Gomori[1,2]
Robert I. Grossman[1]
David B. Hackney[1]
Herbert I. Goldberg[1]
Robert A. Zimmerman[1]
Larissa T. Bilaniuk[1]

Subacute intracranial hematomas have variable appearances on high-field MR images. They are hyperintense on T1-weighted images owing to methemoglobin, but have variable intensities on T2-weighted images. Observation of the different high-field spin-echo MR intensity patterns of five subacute hematomas suggests that further subcategorization into different methemoglobin states may be possible. In particular, undiluted intracellular methemoglobin is hyperintense on T1-weighted images and markedly hypointense on T2-weighted images, undiluted free methemoglobin should be hyperintense on T1-weighted images and isointense or slightly hypointense on T2-weighted images, and dilute free methemoglobin is hyperintense on both T1- and T2-weighted images. However, it appears that certain regions of subacute hematomas may be difficult to differentiate, by intensity patterns alone, from melanotic melanomas or fat.

We believe that, despite some limitations, MR is useful in dividing subacute intracranial hematomas into their respective methemoglobin states, and also that further subcategorization is possible.

Early experience with MR imaging of intracranial hematomas at 1.5 T has revealed three characteristic signal-intensity patterns [1]:

1. Acute hematomas (<1 week old) are isointense to gray matter on T1-weighted images and markedly hypointense on T2-weighted images. This is ascribed to a selective T2 proton relaxation enhancement (relaxation time shortening) by intracellular deoxyhemoglobin.

2. Subacute hematomas (about 1 week to <1 month old) are initially hyperintense at the hematoma periphery on T1-weighted images. The hyperintensity on T1-weighted images proceeds to fill the whole hematoma and eventually (by 2 weeks) becomes observable on T2-weighted images as well. This is attributed to the formation of intracellular methemoglobin, which is paramagnetic, and to subsequent cell lysis and watery dilution by resorption of the resultant free methemoglobin.

3. In subacute and chronic hematomas, the adjacent brain parenchyma is slightly hypointense on T1-weighted images and markedly hypointense on T2-weighted images. This is because hemosiderin deposits produce a selective T2 relaxation enhancement.

We report our observations on the previously unappreciated variability of the high-field MR intensities of subacute hematomas and discuss the underlying relaxation mechanisms and relevant differential diagnoses.

Subjects and Methods

Over a period of 1 year, we observed five patients with subacute intracranial hematomas from various causes. All hematomas were diagnosed and staged by clinical and CT findings. Two were confirmed surgically and pathologically. MR imaging was performed on a GE 1.5-T superconducting unit. Spin-echo pulse sequences were obtained with 5-mm-thick slices, two excitations, and 256 × 128 acquisition matrixes. T1-weighted images were obtained with

This article appears in the November/December 1987 issue of *AJNR* and the January 1988 issue of *AJR*.

Received October 27, 1986; accepted after revision May 21, 1987.

[1] Department of Radiology, Hospital of the University of Pennsylvania, 3400 Spruce St., Philadelphia, PA 19104. Address reprint requests to R. I. Grossman.

[2] Permanent address: Department of Radiology, Hadassah Hospital, P.O. Box 12000, Jerusalem, Israel 91120.

***AJR* 150:171–178, January 1988**
0361–803X/88/1501–0171
© American Roentgen Ray Society

TABLE 1: MR Intensities of Subacute Hematomas

Case No.	Type of Subacute Hematoma	Age of Hematoma	CT Density	Image Intensity Relative to Gray Matter		
				T1-Weighted	Proton-Density-Weighted	T2-Weighted
1	Spontaneous (normal angiography)	5 days	Increased	Increased	Unchanged	Decreased
2	Small AVM (surgically confirmed)	12 days	Unchanged	Increased	Increased	Increased
			Unchanged	Increased	Slightly increased	Unchanged
3	Traumatic	6 days	Increased	Increased	Unchanged	Decreased
			Decreased	Slightly increased	Increased	Increased
4	Hypertensive	9 days	Increased	Increased	Unchanged	Decreased
5	Traumatic, subdural (surgically confirmed)	7 days	Decreased	Increased	Increased	Increased
			Unchanged	Increased	Unchanged	Decreased

Note.—AVM = arteriovenous malformation.

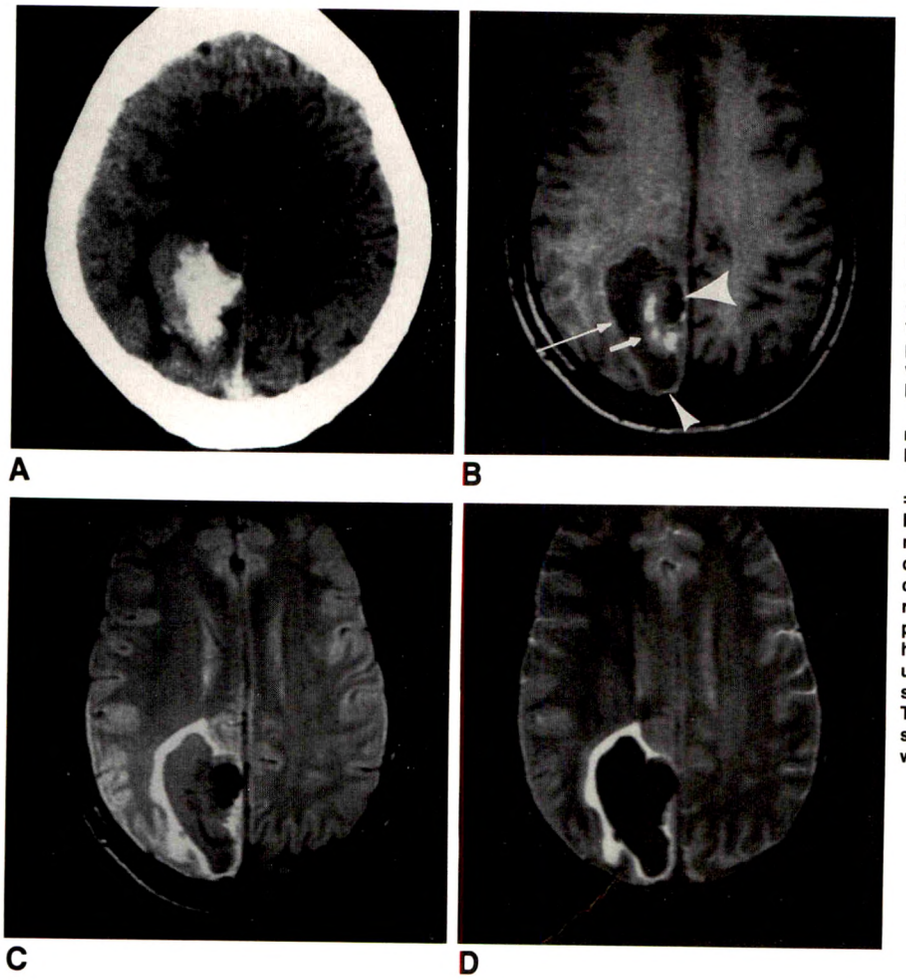

Fig. 1.—Case 1: 5-day-old multicompartmented spontaneous hematoma (normal angiography).

***A*, Unenhanced CT scan (4 days after hemorrhage) shows hyperdense hematoma medially with isodense portion laterally.**

***B*, T1-weighted image, TR = 600 msec, TE = 25 msec. Large lateral segment of hematoma (*long arrow*), slightly hypointense to gray matter, represents intracellular deoxyhemoglobin. Medial to it (*short arrow*) is hyperintense region representing intracellular methemoglobin; medial to this (*large arrowhead*) is small collection of intracellular deoxyhemoglobin more hypointense than lateral segment. Note thin rim of hyperintensity (*small arrowhead*) surrounding whole hematoma representing intracellular methemoglobin.**

***C*, Proton-density-weighted image, TR = 2500 msec, TE = 30 msec. Regions of hyperintensity have become slightly hypointense.**

***D*, T2-weighted image, TR = 2500 msec, TE = 80 msec. All regions have become markedly hypointense. Lateral and medial segments correspond to intracellular deoxyhemoglobin. Medial segment has higher deoxyhemoglobin concentration and higher hematocrit. Hyperintense regions on T1-weighted image are isointense on proton-density-weighted image and markedly hypointense on T2-weighted image because of undiluted intracellular methemoglobin. Note that subcutaneous and diploic fat is hyperintense on T1-weighted image, isointense on proton-density-weighted image, and hypointense on T2-weighted image.**

a repetition time (TR) of 400–800 msec and echo time (TE) of 20–25 msec. Proton-density-weighted images were obtained with a TR of 1500–2500 msec and TE of 20–35 msec. T2-weighted images were obtained with a TR of 1500–2500 msec and TE as a second echo of 40–120 msec.

Results

All subacute hematomas had regions of hyperintensity on T1-weighted images (Table 1 and Figs. 1–5). On proton-density-weighted images these regions were either isointense

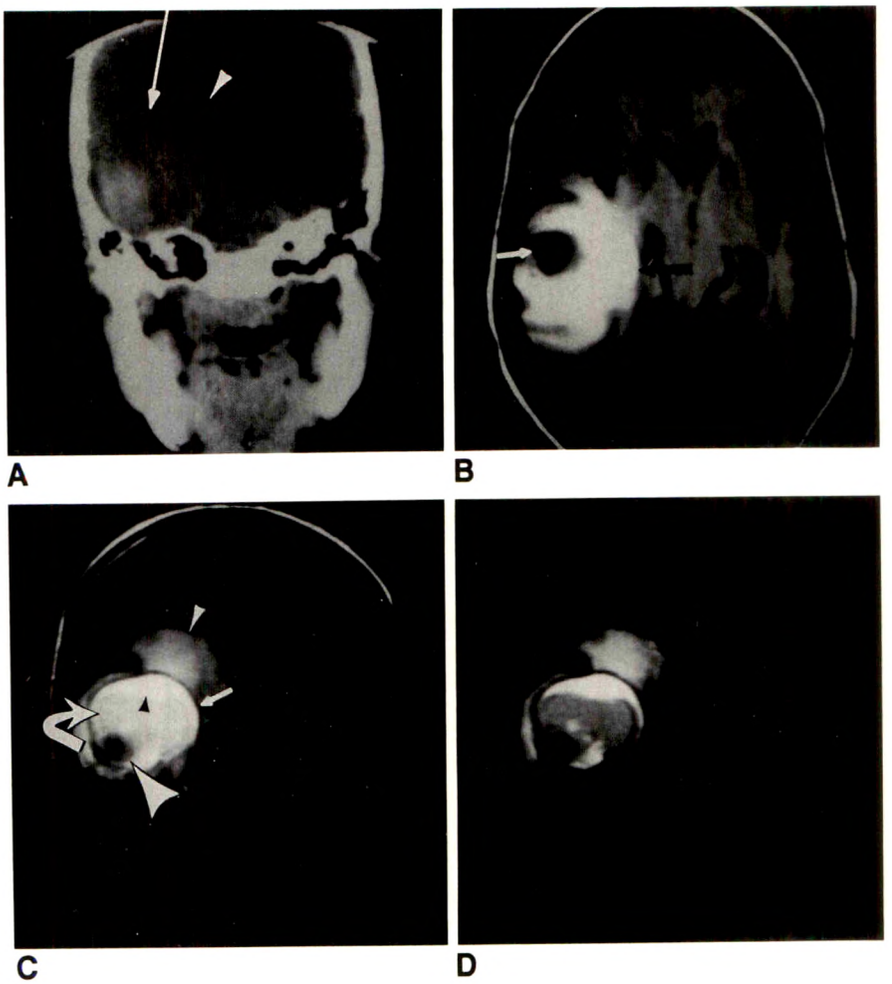

Fig. 2.—Case 2: concentric 12-day-old and 2-day-old hematomas caused by small vascular malformation (surgically confirmed).

***A*, Enhanced coronal CT scan shows acute hyperdense right temporal hematoma surrounded by isodense subacute hematoma. Subtle thin ring of enhancement surrounds hematoma (*arrow*) and hypodensity of edema is seen superomedially (*arrowhead*).**

***B*, T1-weighted image, TR = 800 msec, TE = 20 msec. Central acute hematoma (*white arrow*) consisting of intracellular deoxyhemoglobin is slightly hypointense to gray matter. Surrounding subacute hematoma is markedly hyperintense (*black arrow*).**

***C*, Proton-density-weighted image, TR = 1500 msec, TE = 20 msec. Central acute hematoma (*large white arrowhead*) has remained mildly hypointense to cortex. Surrounding subacute hematoma now shows mildly hyperintense inner region (*curved arrow*) representing dilute intracellular methemoglobin and markedly hyperintense outer region (*black arrowhead*) representing free methemoglobin. Thin peripheral ring of parenchymal hypointensity (*straight arrow*) corresponds to hemosiderin deposition. Surrounding edema (*small white arrowhead*) has become hyperintense.**

***D*, T2-weighted image, TR = 1500 msec, TE = 40 msec. Acute hematoma has become more hypointense. Inner region of subacute hematoma has become isointense to gray matter, while outer region remains markedly hyperintense. Hemosiderin ring appears more hypointense and wider. Surrounding edema remains hyperintense. Acute central hematoma is composed of intracellular deoxyhemoglobin. Outer region of subacute hematoma corresponds to free dilute methemoglobin. Inner region of subacute hematoma corresponds to dilute intracellular methemoglobin.**

or hyperintense. On T2-weighted images, the regions that were isointense on the proton-density images were variably hypointense (Figs. 1 and 3–5), and the regions that were hyperintense on the proton-density-weighted images were variably hyperintense (Figs. 2, 3, and 5). One subacute hematoma (Fig. 1) was only 5 days old, indicating that the hyperintensity on T1-weighted images may appear as early as 5 days.

Discussion

The mechanism for the selective T2 relaxation enhancement of intracellular deoxyhemoglobin, intracellular methemoglobin, and of hemosiderin deposits is the dephasing of water molecules diffusing across field gradients owing to the heterogeneity in the distribution (intracellular or intralysosomal) of the paramagnetic substance (Fe^{2+} with four unpaired electrons for deoxyhemoglobin and Fe^{3+} with five unpaired electrons for methemoglobin, ferritin, and hemosiderin) [2]. In the absence of unpaired electrons, the protons of water molecules relax (realign with the magnetic field) via fluctuations in their local magnetic field caused by the motion of adjacent protons. The presence of unpaired electrons (for example, five unpaired electrons per methemoglobin molecule) creates fluctuations 1000 times larger owing to the electrons' larger magnetic moment. These larger fluctuations enhance the relaxation of protons. This is called the proton-electron dipolar-dipolar proton relaxation enhancement. The hyperintensity of T1-weighted images of subacute and chronic hematomas was ascribed to the proton-electron dipolar-dipolar proton relaxation enhancement of methemoglobin. This interaction drops off extremely rapidly with distance; the water proton must approach within 3Å of the unpaired electron for the interaction to occur. Unlike methemoglobin, the unpaired electrons of deoxyhemoglobin, ferritin, and hemosiderin are inaccessible to water protons for the dipolar-dipolar interaction. Intracellular methemoglobin, which has both relaxation mechanisms, causes significant T1- and T2-relaxation-time shortening. Cell lysis and the dilution of the liberated methemoglobin by resorption leads to a decrease in the T1 and T2 relaxation enhancement of the proton-electron dipolar-dipolar mechanism, and the cessation of the selective T2 relaxation enhancement caused by the intracellular (heterogeneously distributed) methemoglobin.

Heterogeneity in the distribution of any paramagnetic substance (for example, intracellular deoxyhemoglobin or methemoglobin) results in heterogeneity of magnetic susceptibility, which produces field gradients when an external magnetic field is applied. On spin-echo MR, diffusion of water protons

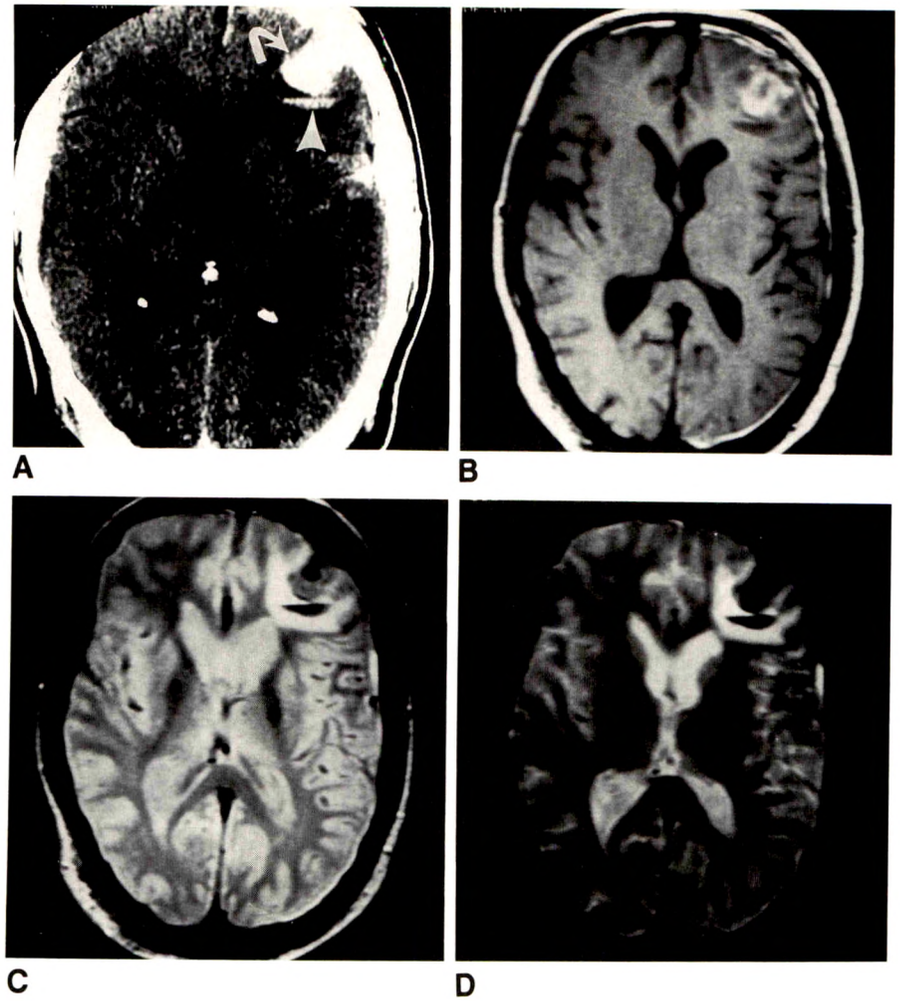

Fig. 3.—Case 3: traumatic 6-day-old hematoma.

***A*, Axial unenhanced CT scan (2 days after trauma) shows hyperdense left frontal hematoma (*arrow*). Posterior to it is hematoma region with fluid-fluid level (*arrowhead*) consisting of hypodense supernatant and hyperdense dependent layer. There is also a left temporal contusion.**

***B*, Axial T1-weighted image, TR = 800 msec, TE = 25 msec. Hematoma has hyperintense periphery and isointense center. In fluid-fluid layer supernatant is slightly hyperintense and dependent layer is isointense to gray matter.**

***C*, Proton-density-weighted image, TR = 2500 msec, TE = 35 msec. Hematoma center is hypointense to gray matter and periphery is isointense. Supernatant is markedly hyperintense and dependent layer is hypointense.**

***D*, T2-weighted image, TR = 2500 msec, TE = 70 msec. Hematoma center is quite hypointense, representing intracellular deoxyhemoglobin. Periphery is hypointense, representing intracellular methemoglobin. Supernatant is very hyperintense, representing very dilute-free methemoglobin, and dependent layer is markedly hypointense, representing intracellular deoxyhemoglobin.**

across these magnetic field gradients causes selective T2 relaxation enhancement, which increases as the square of the heterogeneity of the magnetic susceptibility and as the square of the magnetic field strength [1, 2]. It also increases with lengthening of the interecho interval [2]. The proton-electron dipolar-dipolar relaxation enhancement is not dependent on heterogeneity of magnetic susceptibility. It is unaffected by interecho interval and minimally affected by field strength or red cell lysis.

Recently, we studied the in vitro MR relaxation times of blood and their variations with field strength, oxidation state, and cell integrity [2]. That study confirmed the hypothesis of selective T2 relaxation enhancement for intracellular deoxyhemoglobin and methemoglobin and of proton-electron dipolar-dipolar proton relaxation enhancement for methemoglobin. The study also confirmed that the selective T2 relaxation enhancement of intracellular deoxyhemoglobin and of intracellular methemoglobin increases as the square of the magnetic field strength and as the square of the heterogeneity of magnetic susceptibility. The selective T2 relaxation enhancement also increased with prolongation of the interecho interval and was not present after cell lysis. The study demonstrated that the proton-electron dipolar-dipolar relaxation enhancement of methemoglobin was unaffected by field strength, the length of the interecho interval, or cell integrity.

The variable intensities of subacute hematomas on proton-density-weighted images are from differences in dilution. The variable intensities on the T2-weighted images are from both differences in dilution and variations in the selective T2 relaxation enhancement. The variability in the T2 relaxation enhancement is primarily caused by different degrees of cell lysis, resulting in a variable amount of selective T2 proton relaxation enhancement by the intracellular methemoglobin [2]. Cell lysis is more effective in decreasing the selective T2 relaxation enhancement of intracellular methemoglobin than is simple dilution because the methemoglobin released from the lysed cells increases the extracellular magnetic susceptibility. Thus, cell lysis decreases the differences in the magnetic susceptibility between the inside and the outside of the remaining intact RBCs containing methemoglobin. This decrease in the heterogeneity of magnetic susceptibility causes a marked decrease in the selective T2 relaxation enhancement, because the T2 relaxation enhancement is proportional to the square of the variation (heterogeneity) of the magnetic susceptibility [1, 2]. However, a change in the concentration of RBCs containing methemoglobin by dilution with a nonparamagnetic fluid such as plasma causes mild changes in the heterogeneity of magnetic susceptibility until the hematocrit exceeds 90% or is under 10% [1]. Therefore, dilution without lysis of intracellular methemoglobin does not greatly influence the selective T2 relaxation enhancement until it is under a hematocrit of 10%.

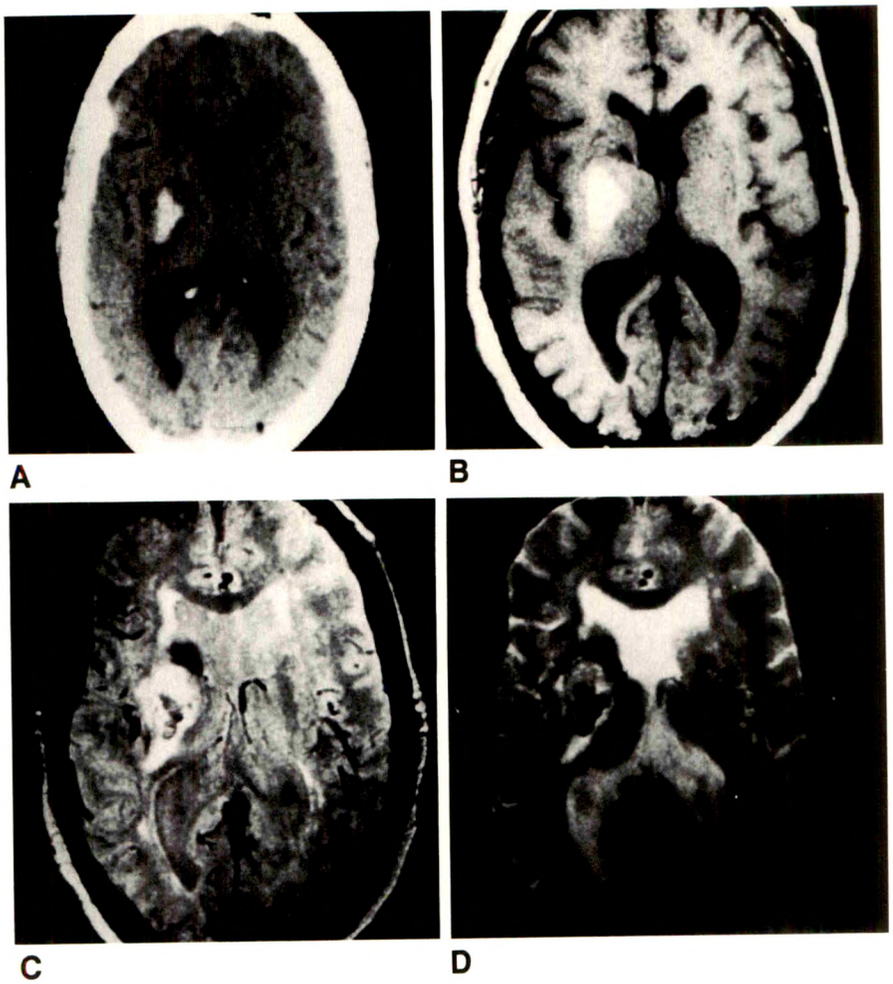

Fig. 4.—Case 4: 9-day-old hypertensive right basal ganglia hematoma in patient who apparently had a previous right caudate hemorrhage.

***A*, Unenhanced CT scan 6 days after hemorrhage shows hyperdense right basal ganglia hematoma.**

***B*, T1-weighted image, TR = 600 msec, TE = 25 msec, shows hyperintense hematoma.**

***C*, Slightly T2-weighted image, TR = 2500 msec, TE = 40 msec. Hematoma is hyperintense in periphery and isointense in center. Caudate is hypointense.**

***D*, T2-weighted image, TR = 2500 msec, TE = 80 msec. Hematoma has become more hypointense, representing intracellular methemoglobin. Caudate is quite hypointense, probably representing hemosiderin deposits of previous caudate hemorrhage.**

Intracellular methemoglobin has a powerful selective T2 relaxation enhancement in addition to its proton-electron dipolar-dipolar relaxation enhancement [2]. The proton density of intracellular methemoglobin or deoxyhemoglobin (hematocrit of 90% after plasma resorption) is similar to that of gray matter [1]. Therefore, purely intracellular methemoglobin is hyperintense on T1-weighted images, isointense or proton-density-weighted images, and quite hypointense on T2-weighted images (Fig. 1).

Panhyperintensity (on all spin-echo sequences) (Fig. 2) is a frequent finding in subacute and chronic hematomas. It is from the proton-electron dipolar-dipolar proton relaxation enhancement of dilute free methemoglobin. This relaxation causes a mild shortening of the T1 and T2 relaxation times, and the diluteness of the solution is responsible for a high proton density. The TRs used in spin-echo MR imaging are much longer than the TEs and usually are not much longer than the T1 relaxation times. The TEs are usually shorter than the T2 relaxation times. Therefore, the T1 shortening and high proton-density effects of dilute methemoglobin will dominate the spin-echo intensity pattern, resulting in panhyperintensity. Free, unbound Fe^{3+} ions also cause proton-electron dipolar-dipolar proton relaxation enhancement [2] and may also play a role in the panhyperintensity of dilute chronic hematomas.

Hyperintensity on T1-weighted images and isointensity on both proton-density- and T2-weighted images indicate a short T1 relaxation time and normal proton density and T2 relaxation time; that is, a proton-electron dipolar-dipolar proton relaxation enhancement without selective T2 proton relaxation enhancement or dilution. Free undiluted methemoglobin should have these properties.

If the hematocrit of intracellular methemoglobin is reduced by dilution without cell lysis (dilute intracellular methemoglobin) then the proton density will be elevated. The decrease in the proton-electron dipolar-dipolar relaxation enhancement is "compensated" by the increase in proton density until there is a great degree of dilution. The decrease in the selective T2 relaxation enhancement will only be evident if the hematocrit is drastically reduced (<10%) [1]. Therefore, the elevation of the proton density will be the most noticeable effect; that is, the T1-weighted image will remain hyperintense, the proton-density and T2-weighted images will become more intense (depending on the degree of dilution), but the T2-weighted image will still be significantly hypointense to the proton-density-weighted image (Fig. 2).

Intermediate states may exist. The intensity patterns of these states will vary between the patterns of the individual components. A combination of intracellular methemoglobin and deoxyhemoglobin will be variably hyperintense on T1-weighted images. The proton-density- and T2-weighted images will not be affected because the proton densities and the T2 relaxation times are similar for intracellular methemoglobin and intracellular deoxyhemoglobin. Similarly, different

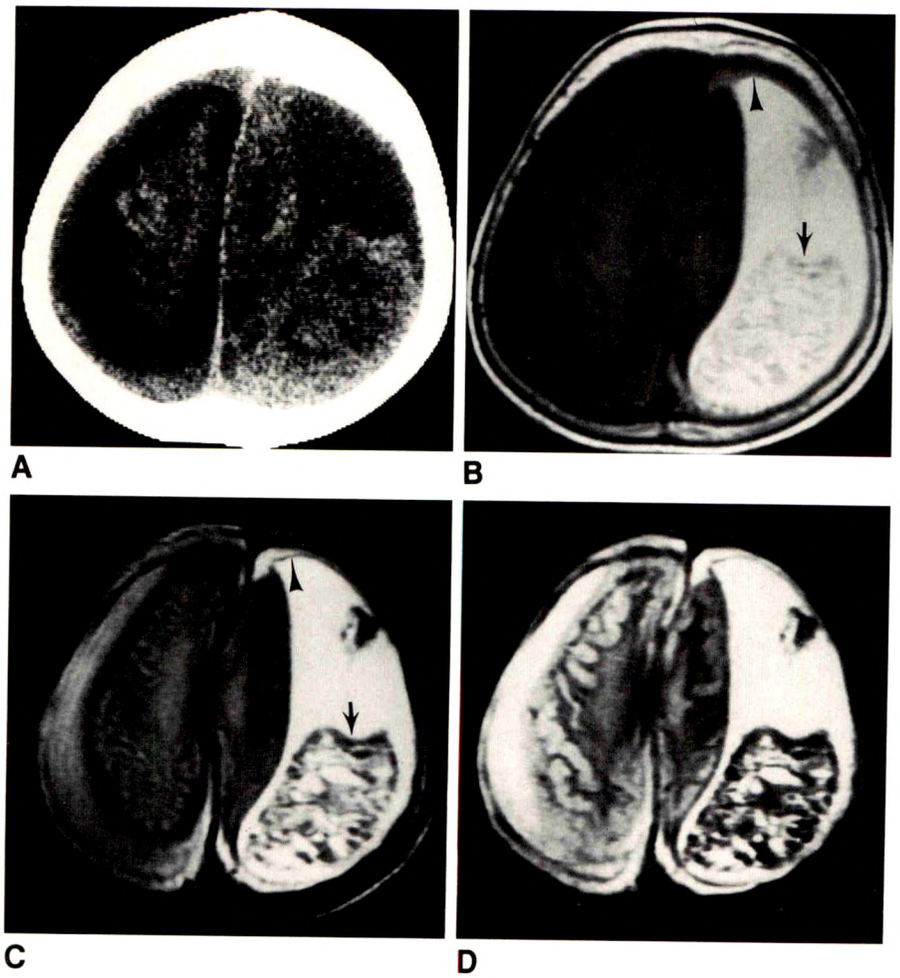

Fig. 5.—Case 5: subacute left subdural hematoma (surgically confirmed) of uncertain age in 3-year-old patient with seizure disorder and recurrent head trauma.

***A*, Unenhanced CT scan shows left subdural hematoma with slightly hypodense supernatant and isodense dependent portion. Small chronic subdural hygroma is on right.**

***B*, T1-weighted image, TR = 600 msec, TE = 20 msec, 7 days after CT study. Supernatant of left subdural hematoma is hyperintense and dependent portion (*arrow*) is less hyperintense with multiple pools of hyperintensity in it. There is small similar region superiorly (*arrowhead*). Right subdural hygroma is isointense.**

***C*, Proton-density-weighted image, TR = 2500 msec, TE = 30 msec. Supernatant remains hyperintense, and dependent (*arrow*) and superior (*arrowhead*) regions are now isointense with multiple pools of hyperintensity. Right subdural hygroma is slightly hyperintense.**

***D*, T2-weighted image, TR = 2500 msec, TE = 80 msec. Supernatant (free dilute methemoglobin) remains very hyperintense. Dependent and superior regions are hypointense (intracellular methemoglobin) with pools of hyperintensity (free dilute methemoglobin). These regions represent areas of clot lysis. Right subdural hygroma is now hyperintense.**

degrees of lysis of intracellular methemoglobin will result in variable T2-weighted image hypointensities because of the change in selective T2 proton relaxation enhancement caused by the variable decreases in the heterogeneity of the magnetic susceptibility. The T1-weighted and proton-density-weighted images will be relatively unaffected because both intracellular and undiluted free methemoglobin have similar proton-electron dipolar-dipolar proton relaxation enhancement and proton density. Various degrees of free methemoglobin dilution will cause the T1-weighted image to vary from hyperintensity to hypointensity, the proton-density-weighted image to vary from isointensity to hyperintensity and then back to isointensity, and the T2-weighted image to vary from isointensity to hyperintensity. As the free methemoglobin is diluted it loses its proton-electron dipolar-dipolar enhancement and its proton density increases to that of CSF. CSF has such long T1 and T2 relaxation times that on conventional spin-echo MR images with TRs less than 3000 msec it will be hypointense on T1-weighted images, mildly hypointense or isointense on proton-density-weighted images, and hyperintense on T2-weighted images. Of course other combinations may occur as well; for example, undiluted free deoxyhemoglobin and free methemoglobin. In this case there will be variable hyperintensity on T1-weighted images with isointensity on proton-density- and T2-weighted images.

Figure 6 illustrates the four possible methemoglobin states and Table 2 presents the functional relationships between the methemoglobin states and the resultant relaxation enhancements and proton density. In Table 2, the (Hct)(100 − Hct) factor is the heterogeneity factor [1]. The 1/T2* on gradient-echo MR is proportional to the field gradient across the cell membrane and the 1/T2 of spin-echo MR is proportional to the square of the field gradient. The gradient across the cell membrane is proportional to the difference in magnetic susceptibility across the cell membrane and to the field strength. The fractions in the equations result from the fact that methemoglobin has five and deoxyhemoglobin has four unpaired electrons per iron atom, and that the magnetic susceptibility is proportional to the number of unpaired electrons. Table 3 presents the patterns of the relative relaxation times and proton densities occurring in the various types of regions associated with subacute intracranial hematomas. Of course, mixtures will have patterns intermediate to their individual components.

A report by Di Chiro et al. [3] demonstrated the evolution of intracranial hemorrhage in a monkey on high-resolution MR imaging at 0.5 T. Their images (interpreted in light of the importance of susceptibility heterogeneity) at days 2–3 were characteristic of intracellular deoxyhemoglobin; days 4–8, of intracellular methemoglobin; and days 5–15, of dilute free

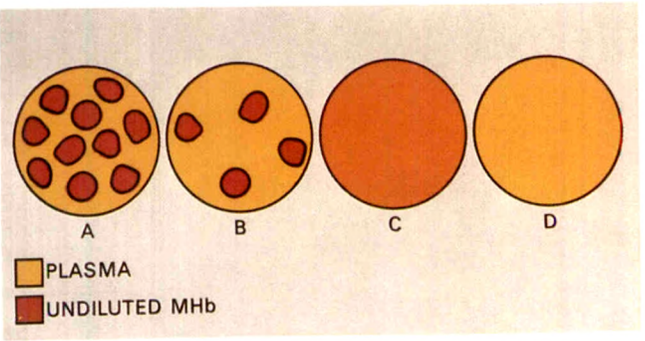

Fig. 6.—Four possible methemoglobin (MHb) states are combinations of methemoglobin and plasma. *Plasma*: no magnetic susceptibility; no dipolar-dipolar relaxation enhancement; high proton density. *Methemoglobin*: high magnetic susceptibility; has dipolar-dipolar relaxation enhancement; if undiluted, has average proton density.

***A*, Undiluted intracellular methemoglobin: has magnetic susceptibility heterogeneity (T2 shortening); has dipolar-dipolar relaxation enhancement (T1 shortening); has average proton density.**

***B*, Dilute intracellular methemoglobin: has some magnetic susceptibility heterogeneity; has some dipolar-dipolar relaxation enhancement; has high proton density.**

***C*, Undiluted free methemoglobin: has no magnetic susceptibility heterogeneity; has dipolar-dipolar relaxation enhancement; has average proton density.**

***D*, Dilute free methemoglobin: has no magnetic susceptibility heterogeneity; has some dipolar-dipolar relaxation enhancement; has high proton density.**

TABLE 2: Functional Relationships Between Hemoglobin States, Relaxation Rates, and Proton Density

$$\text{T2 PRE} \propto (\text{Hct})(100 - \text{Hct})\,[\,(\text{MHb}) + 24/35\,(\text{Hb}) - \text{MHb} - 24/35\ \text{Hb}]^2\text{Bo}^2$$

$$\text{T2* PRE} \propto (\text{Hct})(100 - \text{Hct})\,[\,(\text{Mhb}) + 24/35\,(\text{Hb}) - \text{MHb} - 24/35\ \text{Hb}]^2\text{Bo}$$

$$\text{PEDD PRE} \propto (\text{MHb}) + \text{MHb}$$

$$\text{PD}_w - \text{PD}_h \propto (\text{MHb}) + (\text{Hb}) + (\text{HbO}_2) + \text{MHb} + \text{Hb} + \text{HbO}_2$$

Note.—$\propto$ = approximately equal to; T2 PRE = 1/T2 on spin-echo MR owing to susceptibility heterogeneity; T2* PRE = 1/T2* on gradient-echo MR owing to susceptibility heterogeneity; PEDD PRE = 1/T1 and 1/T2 owing to proton-electron dipolar-dipolar proton relaxation enhancement; Hct = hematocrit; circled MHb = intracellular methemoglobin; MHb = extracellular (free) methemoglobin; circled Hb = intracellular deoxyhemoglobin; Hb = extracellular (free) deoxyhemoglobin; circled HbO_2 = intracellular oxyhemoglobin; HbO_2 = extracellular oxyhemoglobin; PD_w = proton density of pure water; PD_h = proton density of the subacute hematoma; Bo = strength of magnetic field. Magnetic susceptibility is proportional to n (n+2), where n = the number of unpaired electrons; hence, the fraction 24/35 for 4 and 5 unpaired electrons (decxyhemoglobin and methemoglobin, respectively).

methemoglobin, as well as of hemosiderin at 2 months.

Melanin is a free-radical trap and can chelate paramagnetic metal ions. The unpaired electrons of the free radicals and of the chelated metal ions and probably of associated methemoglobin are the source of melanin's paramagnetism [4, 5]. The major paramagnetic effect of significance to spin-echo MR imaging is the proton-electron dipolar-dipolar interaction [6]. In deeply pigmented melanomas without gross pathologic evidence of hemorrhage this interaction can cause sufficient proton relaxation enhancement to mimic methemoglobin's hyperintensity on T1-weighted images (Fig. 7). However, melanotic melanomas are not as hyperintense on T2-weighted images as free dilute methemoglobin is nor as hypointense as undiluted intracellular methemoglobin. Thus, melanotic melanomas may be difficult to distinguish from certain regions of subacute hematomas. Fat is hyperintense on T1-weighted images, isointense on proton-density images, and hypointense on T2-weighted images at high field strengths (1.5 T) (Fig. 1). It may also be difficult to differentiate it from regions of subacute hematomas or from melanotic melanomas. However, associated MR and clinical findings usually allow the differentiation of melanotic melanoma, fat, and subacute hematomas.

Rapid imaging by gradient echoes rather than by spin echoes has recently been introduced. Its sensitivity to T2* allows the effects of susceptibility heterogeneity to be detected at much lower field strengths [7, 8], at the cost of lower signal to noise and increased sensitivity to field gradients because of the magnet and the macroscopic susceptibility heterogeneity and chemical shifts. Although subacute hematomas have not yet been carefully studied by gradient-echo techniques, they should have characteristics similar to those observed on high-field spin-echo MR. One additional effect seen on gradient-echo techniques can be confusing. It is the peripheral hypointensity caused by the border between macroscopic regions of different susceptibilities, for example, dense calcium–soft tissue; air–soft tissue; fat–water; and deoxyhemoglobin, methemoglobin, or hemosiderin and soft tissue. These must be differentiated from marginal hemosiderin deposits around hemorrhagic lesions. Marginal hemosiderin deposits have both T2* shortening and T2 shortening on spin-echo images because of both macroscopic and microscopic susceptibility heterogeneity.

Our current clinical MR observations and previous in vitro models indicate that further subcategorization of subacute hematomas is possible on the basis of T1-, proton-density-, and T2-weighted images. However, melanotic melanomas and fat may be difficult to differentiate, by intensity patterns alone, from certain regions of subacute hematomas.

REFERENCES

1. Gomori JM, Grossman RI, Goldberg HI, Zimmerman RA, Bilaniuk LT. Intracranial hematomas: imaging by high-field MR. *Radiology* **1985**;157:87–93
2. Gomori JM, Grossman RI. Mechanisms responsible for the MR appearance and evolution of intracranial hemorrhage. Presented at the annual meeting of the Radiological Society of North America, Chicago, December **1986**

TABLE 3: Relative Relaxation Times and Proton Densities in Regions Associated with Subacute Intracranial Hematomas

Region	Relaxation Time or Proton Density		
	T1-Weighted	Proton-Density-Weighted	T2-Weighted
Dilute intracellular methemoglobin[a]	Decreased	Increased	Decreased
Dilute (free) lysate (free) methemoglobin[a]	Decreased	Increased	Unchanged or increased
Undiluted intracellular methemoglobin[a]	Decreased	Unchanged	Decreased
Undiluted (free) lysate (free) methemoglobin[a]	Decreased	Unchanged	Unchanged
Dilute intracellular deoxyhemoglobin	Unchanged or increased	Increased	Decreased
Dilute intracellular and lysate (free) oxyhemoglobin; lysate (free) deoxyhemoglobin; or any dilute protein solution, edema, tumor, or CSF	Unchanged or increased	Increased	Unchanged or increased
Intracellular deoxyhemoglobin or hemosiderin	Unchanged	Unchanged	Decreased
Gray matter (standard) or undiluted (free) lysate (free) deoxyhemoglobin or oxyhemoglobin, or undiluted intracellular oxyhemoglobin	Unchanged	Unchanged	Unchanged
Hemosiderin deposits ± calcifications	Unchanged	Decreased	Decreased
Very dense calcifications, dura, or flow void	Unchanged	Decreased	Unchanged

[a] Can be mimicked by fat or melanin.

Note.—Undiluted = concentration equivalent to hematocrit of 90%.

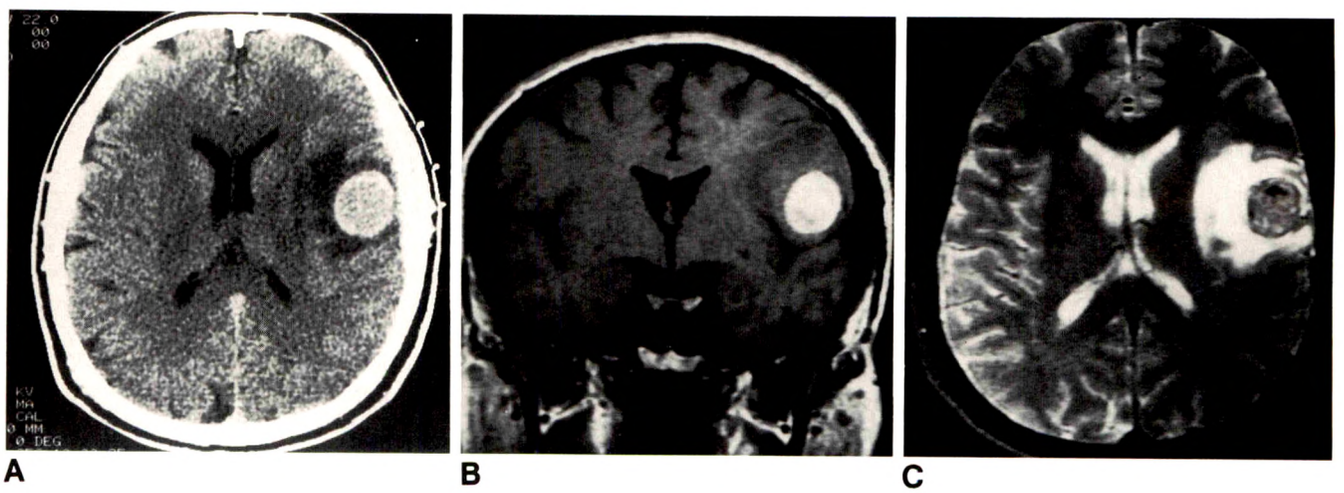

Fig. 7.—Nonhemorrhagic (pathologically proved) melanotic melanoma metastasis.

***A*, Unenhanced CT scan shows high-absorption left frontal mass surrounded by low-absorption regions (edema).**

***B*, T1-weighted image, TR = 600 msec, TE = 20 msec. Tumor is hyperintense because of proton-electron dipolar-dipolar proton relaxation enhancement of melanin.**

***C*, T2-weighted image, TR = 2500 msec, TE = 80 msec. Tumor is mostly isointense with some regions of hypointensity. There is no peripheral hemosiderin ring. Surrounding edema is hyperintense.**

3. Di Chiro G, Brooks RA, Girton ME, et al. Sequential MR studies of intracerebral hematomas in monkeys. *AJNR* **1986**;7:193–199
4. Symons MCR, Rideout J, Worthington BS, Thomas DB, Young IR. Possible relaxation mechanisms for protons in melanomas. Presented at the annual meeting of the Society of Magnetic Resonance in Medicine, August **1985**
5. Enochs WS, Bennet HF, Brown RD, Koenig SH, Swartz HM. Proton relaxation rates in synthetic melanin solutions: implications for mechanisms of enhanced relaxation in melanin-containing tissues. Presented at the annual meeting of the Society of Magnetic Resonance in Medicine, Montreal, August **1986**
6. Gomori JM, Grossman RI, Shields JA. Augsburger JJ, Joseph PM, DeSimeone D. Choroidal melanomas: correlation of NMR spectroscopy and MR imaging. *Radiology* **1986**;158:443–445
7. Edelman RR, Johnson K, Buxton R, et al. MR of hemorrhage: a new approach. *AJNR* **1986**;7:751–756
8. Bydder GM, Steiner RE, Young IR. Low-field MR imaging of intracerebral hemorrhage. Presented at the annual meeting of the Radiological Society of North America, Chicago, December **1986**

MR of Neuronal Migration Anomalies

A. James Barkovich[1,2]
Sylvester H. Chuang[3]
David Norman[2]

Migration anomalies are congenital malformations caused by insults to migrating neuroblasts during the third to fifth gestational months. Included in this group are agyria, pachygyria, polymicrogyria, unilateral megalencephaly, schizencephaly, and gray matter heterotopias. Patients who have these conditions present clinically with developmental delay and seizures, and abnormal motor skills are noted in the more severely affected infants. To determine the utility of MR as a method for imaging in these patients, we used MR to evaluate 13 patients who had the full spectrum of migration anomalies. MR was more sensitive than CT in detecting these anomalies because of its better contrast between gray and white matter. We found that MR was particularly more sensitive in detecting schizencephaly, where recognizing the presence of gray matter lining the cleft is critical to distinguishing that disease from porencephaly, and in detecting polymicrogyria, where critical details of cortical architecture are obscured on CT by the overlying bone. Multiplanar capabilities were also found to be essential, since narrow clefts may not be detected when the imaging plane is parallel to the cleft.

MR should be the primary imaging method for infants who have seizures or developmental delay.

Abnormalities of cell migration are characterized by ectopic location of neurons in the cerebral cortex. This broad group of anomalies includes agyria, pachygyria, polymicrogyria, schizencephaly, unilateral megalencephaly, and gray matter heterotopias. All these entities have been characterized pathologically and in vivo by sonography and CT. MR is an imaging technique uniquely suited to study these anomalies because of its exceptional differentiation between gray and white matter and its high-resolution multiplanar display of anatomy.

In a review of 537 MR studies in the pediatric age group, we identified 13 patients with migration anomalies. We review the salient features of these anomalies and their MR appearance. The relationship of the pathologic anatomy to theories of pathogenesis is emphasized.

Subjects and Methods

Thirteen patients with migration anomalies were scanned, including two with lissencephaly, four with schizencephaly, two with unilateral megalencephaly, two with isolated polymicrogyria, and three with isolated gray matter heterotopias. The four patients with schizencephaly also had foci of polymicrogyria. One of the patients with unilateral megalencephaly had foci of ectopic gray matter. The patients' ages ranged from 4 months to 21 years, with a mean of 6.6 years and a median age of 3.5 years. The mean age is skewed by two patients with schizencephaly who were 17 and 21 years old. The patients were referred for imaging because of seizures, mental retardation, developmental delay, or enlarging head size (see Table 1).

Ten patients were examined on a 1.5-T GE Signa unit. Three patients were examined on a 0.35-T Diasonics MT/S scanner. Slice thickness was 5 mm with a 2.5-mm interslice gap. Spin echo (SE) images were obtained with a TR of 2000 msec and TE of 35–40 msec and 70–80 msec in the transverse and coronal planes and a TR of 600 msec and TE of 25 msec

This article appears in the November/December 1987 issue of *AJNR* and the January 1988 issue of *AJR*.

Received March 13, 1987; accepted June 1, 1987.

The views expressed in this article are those of the authors and do not reflect the official policy or position of the Department of the Army, Department of Defense, or the U.S. Government.

Presented in part at the annual meeting of the American Society of Neuroradiology, New York, May 1987.

[1] Department of Radiology, Letterman Army Medical Center, Presidio of San Francisco, CA 94129-6700. Address reprint requests to Technical Publications Editor HSHH-ZCT.

[2] Department of Radiology, Neuroradiology Section, University of California School of Medicine, San Francisco, CA 94143.

[3] Department of Radiology, Neuroradiology Section, Hospital for Sick Children, Toronto, Ontario M5G 1X8, Canada.

***AJR* 150:179–187, January 1988**
0361–803X/88/1501–0179
© American Roentgen Ray Society

TABLE 1: Summary of Patient Data

Patient	Age	Presenting Symptoms[a]	MR Diagnosis
1	4 mo	S	Lissencephaly
2	4 y	S, DD	Lissencephaly
3	8 y	DD	Polymicrogyria
4	2 y	S, DD	Polymicrogyria
5	12 mo	S, DD	Schizencephaly (bilateral vertical clefts: one narrow, one wide); polymicrogyria in and adjacent to clefts
6	7 mo	S, DD	Schizencephaly (bilateral horizontal clefts: both narrow); polymicrogyria and pachygyria in adjacent brain
7	17 y	S, DD	Schizencephaly (unilateral horizontal wide cleft); polymicrogyria in and adjacent to cleft; ectopic gray matter
8	21 y	S	Schizencephaly (unilateral vertical cleft with fused lips)
9	2 y	S, DD, H	Unilateral megalencephaly
10	8 y	S, DD	Unilateral megalencephaly
11	7 y	S	Heterotopic gray matter
12	2 y	S	Heterotopic gray matter
13	3 y	S	Heterotopic gray matter

[a] Abbreviations: S = seizures; DD = developmental delay; H = hemiplegia.

in the axial, coronal, or sagittal plane, as indicated. The results of these studies are included in the Discussion section.

Pathologic confirmation was not obtained. Migration anomalies were diagnosed from the characteristic gross morphology of the affected brains, which has been established from pathologic and CT experience.

Discussion

The phenomenon of neuronal migration has been known since the turn of the century [1]. The neurons that constitute the mammalian brain are generated in proliferative zones situated along the ventricular surface of the developing brain [1–4]. At the end of the second gestational month, the neurons migrate from their site of origin along radially aligned glial cells to relatively distant final positions [3, 4] (Figs. 1 and 2). At this point they differentiate further, grow axons and dendrites, and develop synaptic contacts with other neurons [4].

The final position of the neurons within the cortex varies inversely with the time of cell origin. Those cells generated earlier migrate to the deeper cortical layers relatively quickly (3–4 days). The cells generated later end their migration in the more superficial cortex; this migration takes place over several weeks. The major cell migration activity lasts about 2 months, beginning in the eighth fetal week and ending at about week 16 [4, 5]. Smaller waves of cell migration continue up to week 25. Any insult to the brain during this period results in a migration anomaly.

The normal human cerebral cortex is six-layered, the sizes of the layers varying with the location. There is a marginal layer (I), external granular layer (II), external pyramidal layer (III), internal granular layer (IV), internal pyramidal layer (V), and fusiform layer (VI) (Fig. 3). The common underlying feature

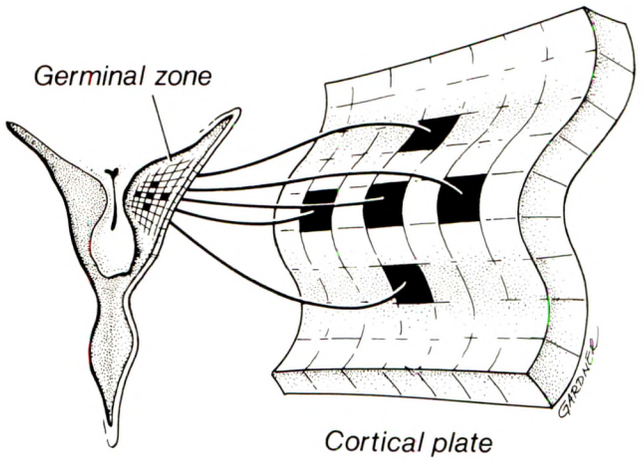

Fig. 1.—Schematic drawing shows relationship of the germinal matrix in wall of lateral ventricle to the developing cortical plate. There is a one-to-one correspondence between the site of cell proliferation within the germinal zone and its eventual destination within the cortical plate. Corresponding regions are connected by radial glial cells that span entire thickness of hemisphere. Neurons migrate along these radial cells, eventually arriving at predestined locations on the enlarged, convoluted cortical surface. (Adapted from [4].)

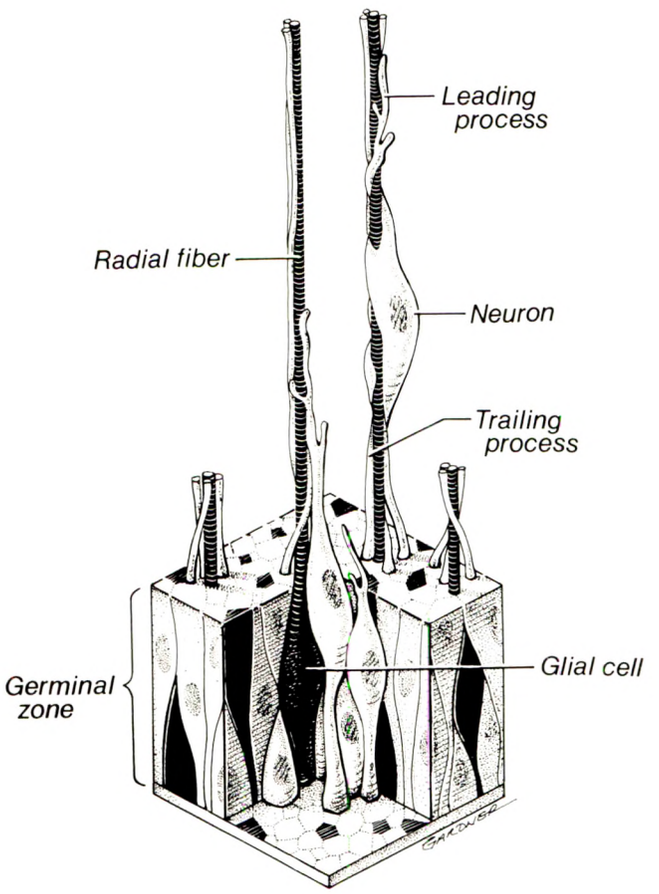

Fig. 2.—Illustration of relationship of migrating neurons to fibers of the radial glial cells. Migrating neuron is seen ascending the glial fiber (radial fiber) led by multiple pseudopodia. Any damage to radial glial fiber will presumably cause an arrest of cell migration at that point. (Adapted from [4].)

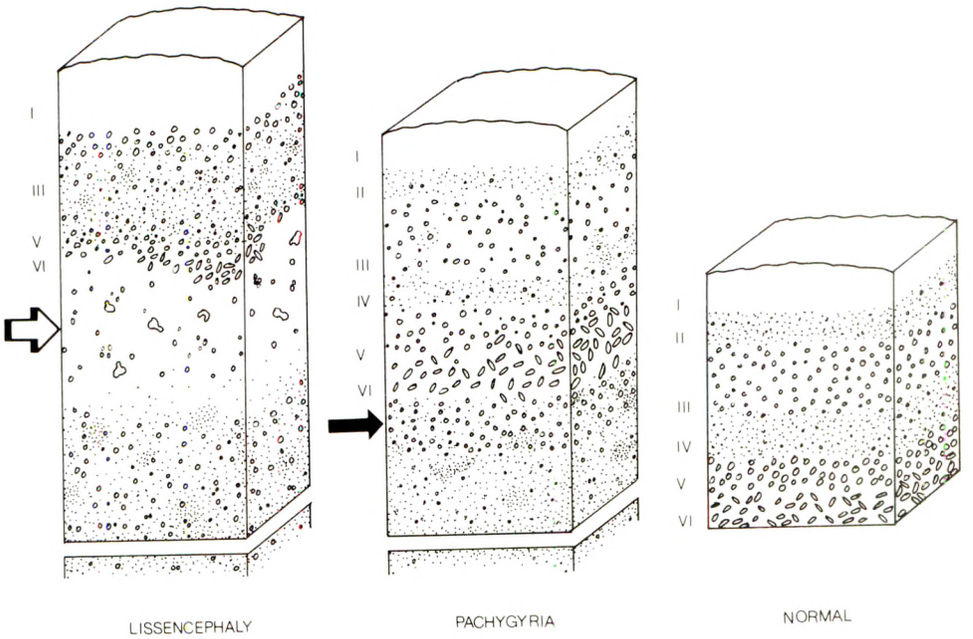

Fig. 3.—Cortical architecture in agyric (labeled lissencephaly) and pachygyric regions of brain as compared with normal cortical architecture. In agyric cortex there is a large cell-sparse layer (*open arrow*) that separates a disorganized cortex (outer cellular layer) from a thick layer of ectopic neurons located medially. Pachygyric cortex is more organized into normal cortical layers and cell-sparse layer (*closed arrow*) is thinner and populated by more cells. In general, there is a thinner layer of heterotopic neurons in the pachygyric cortex. (Adapted from [11].)

of the migration anomalies is an abnormal location of neurons both within and outside of the cortex. In general the cortex is thickened by a large, disorganized layer of neurons whose migration has been prematurely halted. The subcortical layer of white matter is thinned because organization of the neurons, which subsequently stimulates axonal growth, has not occurred [1–4].

It was generally believed that migration anomalies were sporadic events that occurred secondary to environmental insults during the first two trimesters. There is now increasing evidence of a genetic transmission or at least a genetic susceptibility to many of these anomalies [5–10]. Thus, the expression of an insult (vascular, infectious, teratogenic, etc.) is influenced both by the stage of brain development and the underlying genetic susceptibility of the fetus.

Agyria/Pachygyria (Lissencephaly)

The term agyria refers to an absence of cortical gyri. In fact, most "agyric" brains have at least small areas of gyral formation [1, 2]. These areas of broad, flat, shallow gyri are referred to as areas of pachygyria. The term lissencephaly ("smooth brain") is sometimes used as a synonym for agyria and at other times as a more general term encompassing the agyria/pachygyria complex. We shall use the term in the latter sense.

Pathologically, both agyric and pachygyric regions of brain have a so-called four-layered cortex, composed of a molecular layer, an outer cellular layer, a cell-sparse layer, and an inner cellular layer. The cell-sparse zone is believed to be an area of laminar necrosis occurring secondary to metabolic insult of the brain during the period of neuronal migration. Neuronal migration through this region is thereafter impaired; moreover, degeneration occurs in neurons that have already migrated but have their axonal and dendritic connections interrupted within the layer of necrosis [11]. The cortex remains thick because it encompasses the radial columns of migrating cells that are arrested in mid-migration. The subcortical white matter is thin because the organization phase during which axonal and dendritic connections are established is markedly diminished (Fig. 4).

Dobyns and associates [9, 10, 12] have recently described this entity as a series of "syndromes with lissencephaly." They describe three separate classes based on gross pathologic features that they attempt to correlate with specific clinical syndromes. The clinical and CT findings in these classes have been thoroughly discussed [9, 10, 12]. Van Allen and Clarren [13] and Alvarez et al. [14] have disputed these classifications, demonstrating similar clinical manifestations in children whose brains had quite dissimilar gross morphology, although all the brains were within the lissencephaly spectrum. Moreover, Alvarez has suggested that the clinical syndrome may be related more to cytoarchitectonic abnormalities of the brainstem than to cortical anomalies [14]. It is clear that the understanding of these anomalies is at a very early stage.

In the case that we imaged, MR exquisitely demonstrated the abnormal cytoarchitecture. The normal ratio of gray to white matter is reversed (Fig. 5). Within the thickened cortex can be seen a circumferential band of high intensity on the T2-weighted images, which is thicker and more prominent in the parietooccipital region. This is believed to represent the cell-sparse layer that is known to have diminished numbers of neurons and myelinated fibers and increased glial tissue [11, 15, 16], and presumably therefore it has an increased water content. The gray and white matter are otherwise of normal intensity. Coronal images show the temporal lobes to be less affected, as is commonly seen pathologically. In the sagittal plane, a small brainstem is seen, reflecting the lack of development of the corticospinal tracts.

The pattern of brain involvement with the more severely

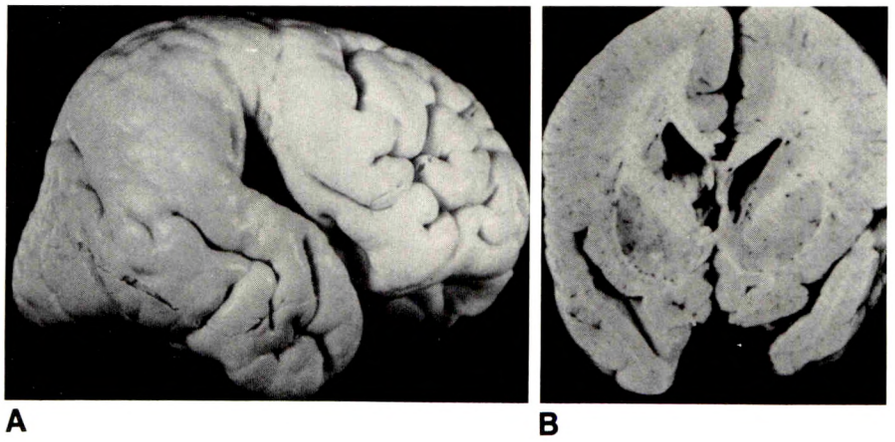

Fig. 4.—Lateral view (*A*) and coronal section (*B*) demonstrate characteristic features of lissencephaly. There is pachygyria in frontal and temporal regions with an agyric cortex in posterior temporoparietal watershed area. This distribution suggests a vascular component in the etiology of the malformation. There is thickening of the cortex due to arrested neuronal migration with corresponding reduction of white matter. (Reprinted with permission from [2].)

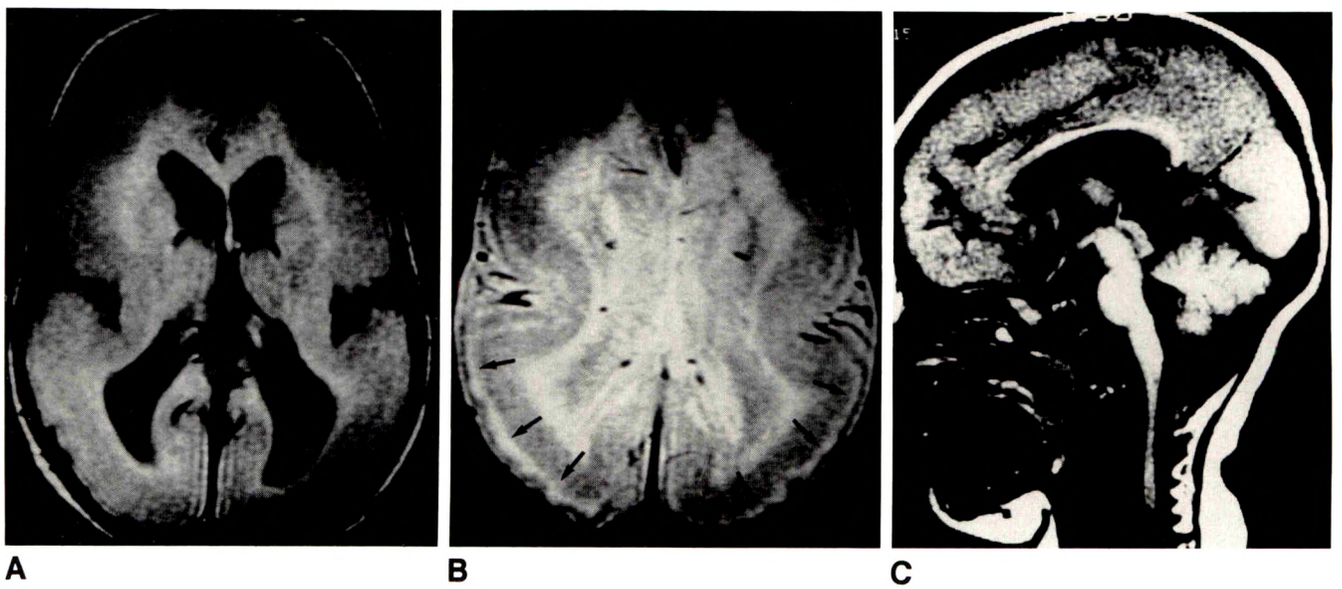

Fig. 5.—Patient 1. *A*, SE 2000/35. Axial image demonstrates thickening of gray matter and thinning of white matter in this patient who has lissencephaly. There is pachygyria in frontal lobes with agyria in temporoparietooccipital region that suggests a vascular etiology as explained in the text.

***B*, SE 2000/70. Axial image again demonstrates a thickened cortex. An irregular rim of high intensity in outer cortex (*arrows*) probably represents an area of laminar necrosis, the cell-sparse layer.**

***C*, SE 600/25. Sagittal image shows a thin corpus callosum and narrow brainstem. These are secondary to a lack of development of association and corticospinal tracts.**

affected (agyric) regions in the posterior parietal watershed area and the less severely affected pachygyric regions more frontally would seem to support the hypothesis by Stewart et al. [11] of a vascular component in the etiology of our particular cases of lissencephaly. Stewart theorizes that the cell-sparse layer is a region of laminar necrosis impeding the migration of neuroblasts. In the watershed area, the ischemia and therefore the area of laminar necrosis is most severe, hence the barrier to migration is most severe. Indeed, we saw increased thickness of the cell-sparse layer in this region on MR. In view of this evidence and the strong evidence for genetic etiologic factors as well [7–10, 12], it is likely that a complex combination of genetic susceptibility and in utero insult is involved in the development of this entity.

Polymicrogyria

Polymicrogyria (PMG) is an anomaly characterized by excessive cerebral convolutions, increased cortical thickness, and abnormal cortical histology. It is a relatively common malformation, reported in one study [17] in 5% of 500 consecutive autopsies of patients that had mental deficiencies. It is frequently found at autopsy in patients with other congenital cerebral anomalies such as schizencephaly or the Chiari II malformation. The location is commonly in the insular area, invoking the possibility of a vascular etiology [18].

Histologically, one sees a four-layered cortex composed of a marginal layer, an outer cellular layer, a cell-sparse layer, and an inner cellular layer. The outer cellular layer is laminated

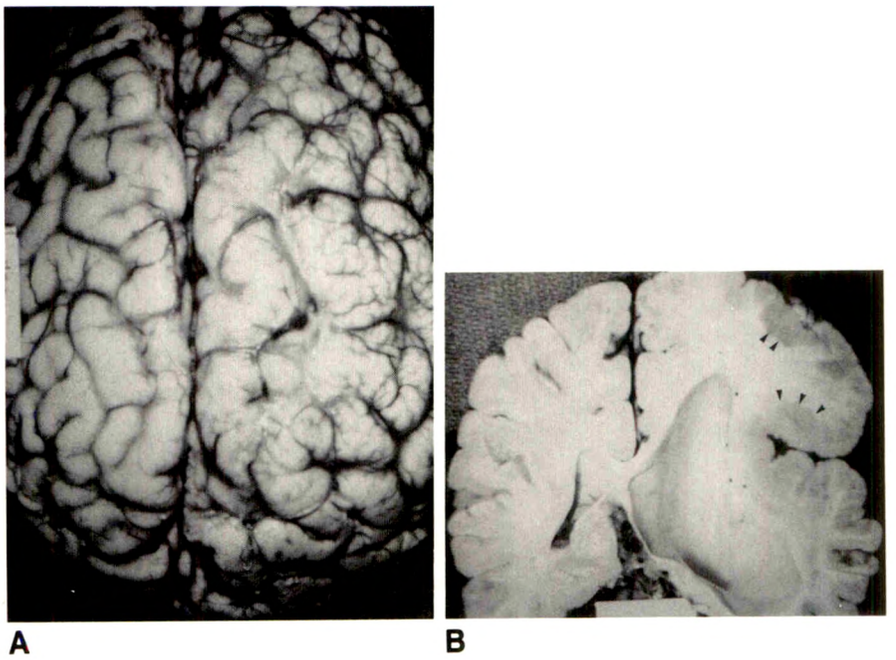

Fig. 6.—Superior view (*A*) and coronal section (*B*) demonstrate polymicrogyria in a patient who has unilateral megalencephaly. There are an increased number of closely set, miniature, shallow gyri over the cortical surface. In some places, because of fusion of adjacent gyri, sulci are shallow or absent and cortical surface becomes paradoxically smooth.

***B*, Cut section reveals a thickened cortex with a flattened inner cortical border (*arrowheads*). Also notice marked overgrowth of left hemisphere with enlargement of ipsilateral lateral ventricle. These findings are characteristic of unilateral megalencephaly. (Courtesy of Dr. Richard Davis, Neuropathology Section, University of California, San Francisco.)**

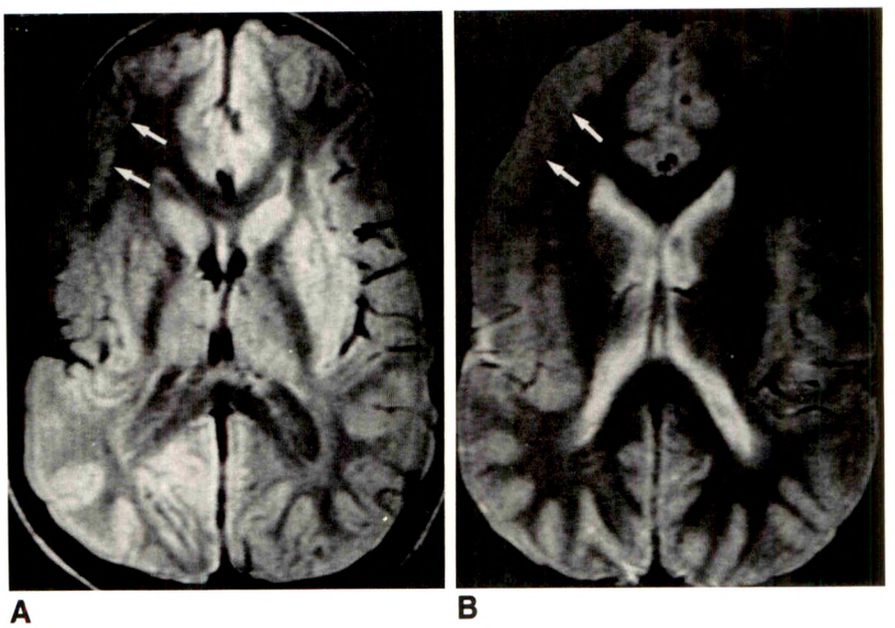

Fig. 7.—Patient 3. *A*, SE 2000/35 and *B*, SE 2000/70. Axial images reveal thickening of right posterior frontal cortex (*arrows*). No gyri are seen in this region; instead, there is a paradoxically smooth cortex as was seen in all cases of polymicrogyria. Normal fingerlike extensions of white matter (compare the left side) are absent.

with sublayers corresponding to and contiguous with layers II, III, and IV of the normal cortex, while the inner cellular layer is contiguous with and architecturally similar to layer VI. It is uncertain whether the insult causing the laminar necrosis of layer V occurs during or after the completion of cell migration [18, 19]. In either event, the resulting gross pathologic picture is of multiple small, shallow convolutions on the brain surface. In the topographic center of the lesion, the convolutional folding of the deep cortical layers are often so exaggerated that the surface of the brain becomes paradoxically smooth [18] (Fig. 6).

CT findings of PMG have not been described, possibly because the overlying calvarium causes beam hardening that makes detailed evaluation of the cortex difficult. Moreover, pathologic proof is difficult to obtain and the CT appearance is not so distinctive as, for example, schizencephaly, to allow confident diagnosis on the CT findings alone. In our cases, although not pathologically proved, we saw many of the gross pathologic characteristics of PMG (Fig. 7), which included a thickening of the cortex with absence of detectable gyri within the region. Moreover, the underlying white matter appeared somewhat diminished, and we saw characteristic involvement

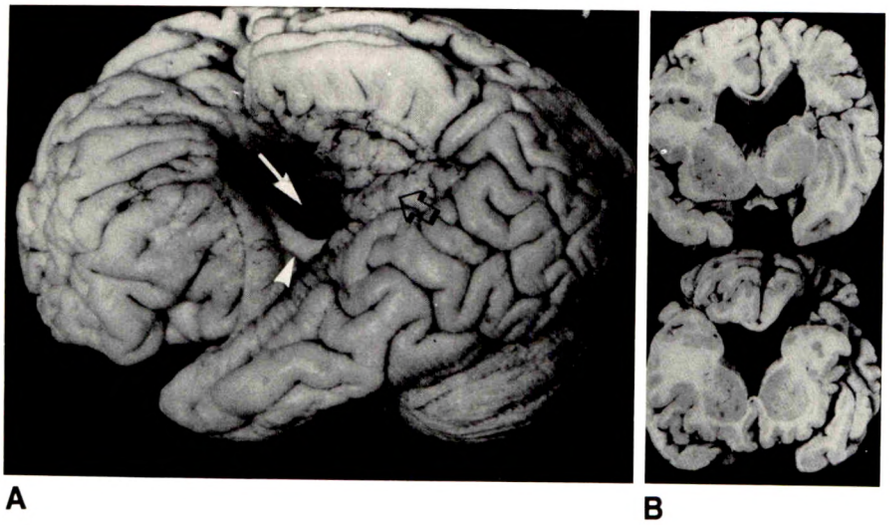

Fig. 8.—Schizencephaly. *A*, Holohemispheric cleft can be seen in left cerebral hemisphere. Cleft has choroid plexus in its floor (*closed arrow*) and ependyma lining the wall (*arrowhead*). There is surrounding polymicrogyria (*open arrow*).

B, Coronal sections show bilateral clefts lined by gray matter. Septum pellucidum is absent. (Reprinted with permission from [2].)

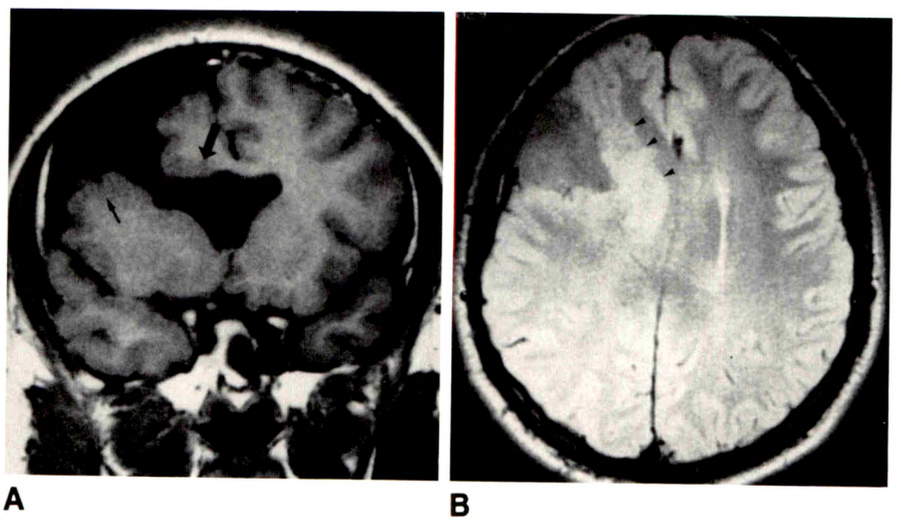

Fig. 9.—Patient 8. *A*, Coronal SE 600/20 and *B*, axial SE 2000/35 images reveal a large unilateral holohemispheric cleft lined by cortex. Cortex is thickened along cleft (*arrowheads*) and adjacent gyri are abnormal (*small arrow*). Ectopic gray matter lines frontal horn (*large arrow*). This patient was 17 years old when scanned, presenting with mild developmental delay and seizures.

of the opercular region [18]. The fact that no zone of long T2 is seen corresponding to a cell-sparse layer may be explained by the fact that this layer is smaller and less "sparse" in PMG than in the agyric cortex; more neurons and axons are present, and therefore little change in signal intensity would be expected.

In three of our cases, the PMG was associated with schizencephaly. In these patients, PMG was manifested as areas of abnormal gyri and thickened cortex lining the hemispheric clefts and in the cortex immediately adjacent to the clefts. In two patients, the PMG was isolated; the posterior frontal region was involved in one and the posterior temporal region in the other.

Schizencephaly

The term schizencephaly was introduced by Yakovlev and Wadsworth [20, 21] in 1946 to describe bilateral, nearly symmetrical, full-thickness clefts within the cerebral hemispheres. Pathologically, these clefts are characterized by an infolding of cortical gray matter along the cleft (Fig. 8) with a fusion of the pial lining of the brain and the ependyma of the ventricle forming a characteristic "pial-ependymal seam." Moreover, gray matter heterotopias and areas of polymicrogyria are found within and near the cleft. The lips of the defects may be separated or fused.

The most widely accepted theory for the pathogenesis of this anomaly is that a segmental failure occurs in the formation of a portion of the germinal matrix or in the migration of the primitive neuroblasts contained therein [20, 22, 23]. Alternative theories include (1) destruction of the previously formed hemisphere sometime before the sixth gestational month [24] and (2) a spectrum of encephaloclastic disorders, ranging from hydranencephaly to porencephaly to schizencephaly [25–27].

Clinically, the patients demonstrate a broad range of neurologic disability that may be related to the amount of brain tissue involved [23, 28]. Clinical features include microce-

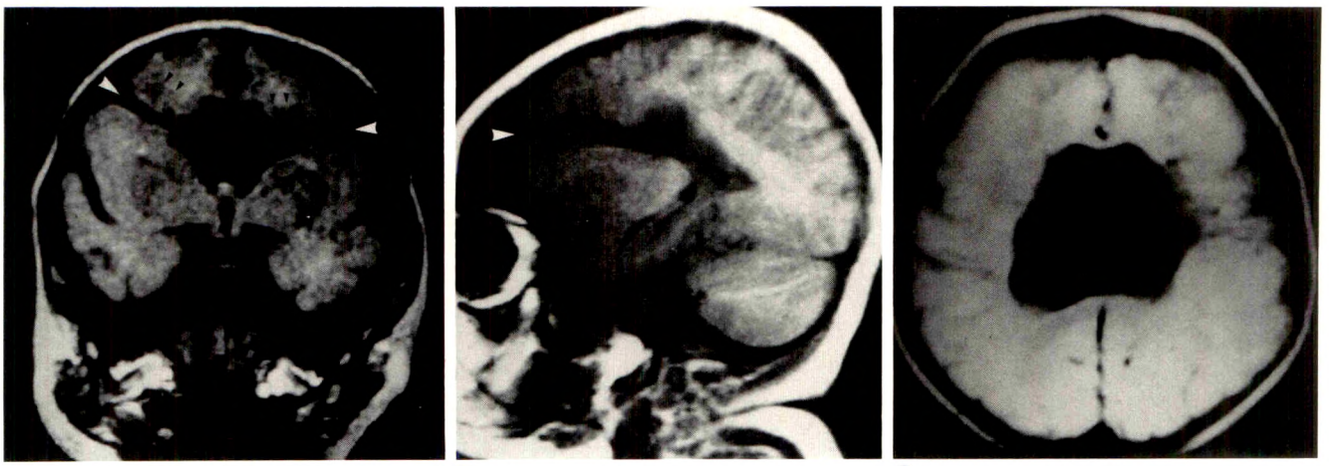

A B C

Fig. 10.—Patient 6. *A*, Coronal SE 1500/40, *B*, sagittal SE 500/30, and *C*, axial SE 2000/30 images demonstrate bilateral, cortex-lined holohemispheric clefts (*white arrowheads*) diagnostic of schizencephaly. Cortex is thickened within clefts (*A*, *black arrowheads*), compatible with polymicrogyria that is usually seen within and near the clefts pathologically. Septum pellucidum is absent, a frequent finding in schizencephaly. Significantly, the narrow, horizontally oriented clefts are not seen on axial image (*C*). These images emphasize that imaging in at least two planes is necessary for proper evaluation of congenital anomalies.

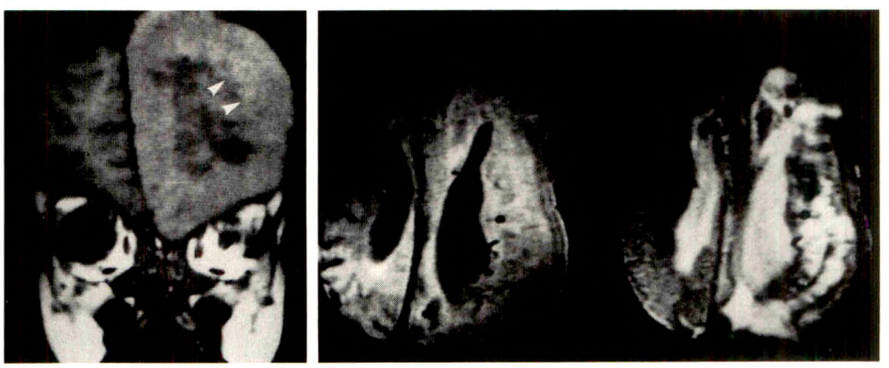

A B

Fig. 11.—Patient 9. *A*, Coronal SE 600/25 and *B*, axial SE 2000/35-70. There is marked overgrowth of left hemisphere with shift of interhemispheric fissure, falx, and superior sagittal sinus to the right. Cortex is markedly thickened (*arrowheads*). White matter is of abnormally low intensity on T1-weighted image (*A*) and high intensity on T2-weighted image (*B*), suggesting decreased myelination and increased water content. *B* shows enlargement of ipsilateral lateral ventricle, characteristic of this anomaly.

phaly, retardation, abnormal motor function, and seizures. Miller et al. [23] report three patients with schizencephaly who have survived into their twenties and thirties, demonstrating only mild neurologic deficits. Both of our patients with unilateral clefts presented near the end of their second decade with mild clinical symptoms, one with seizures and the other with seizures and mild retardation, further supporting this observation. Both patients with bilateral clefts presented in their first year of life with severe developmental delay and seizures.

Our cases of schizencephaly have in common holohemispheric clefts in the region of the pre- and postcentral gyri, which are characteristic of both the pathologic and CT appearance of this entity. Moreover, the finding of continuity of the gray matter from the cortex through the cleft to the subependymal region of the lateral ventricle is clearly shown (Fig. 9). The abnormal gyral pattern surrounding the clefts is consistent with the known pathologic finding of PMG in this region [21]. These findings are crucial in differentiating schizencephaly from porencephaly and other destructive anomalies. This differentiation is of practical importance in terms of genetic counseling, since when a child has a disorder of cell migration 5–20% of subsequent siblings may have brain anomalies [9, 10, 23]. Although there continues to be debate in the literature as to the existence of unilateral schizencephaly [26], our cases clearly show continuity of the gray matter through the cleft into the ventricle. The fact that Yakovlev's initial description included only bilateral cases, therefore, does not exclude unilateral cases from the category but most probably reflects the small size of his original sample. Perhaps the relatively mild symptomatology of the unilateral variant has kept most of these cases from the pathologist's table. If these clefts are indeed due to focal destruction of the germinal matrix, unilateral clefts should be as common or more common than bilateral clefts, and the multiplanar imaging capability and gray/white contrast resolution of MR should allow more unilateral clefts to be found.

The fact that the narrow clefts are identified in only one imaging plane and missed in another is important. These lesions will be overlooked in a significant number of cases if

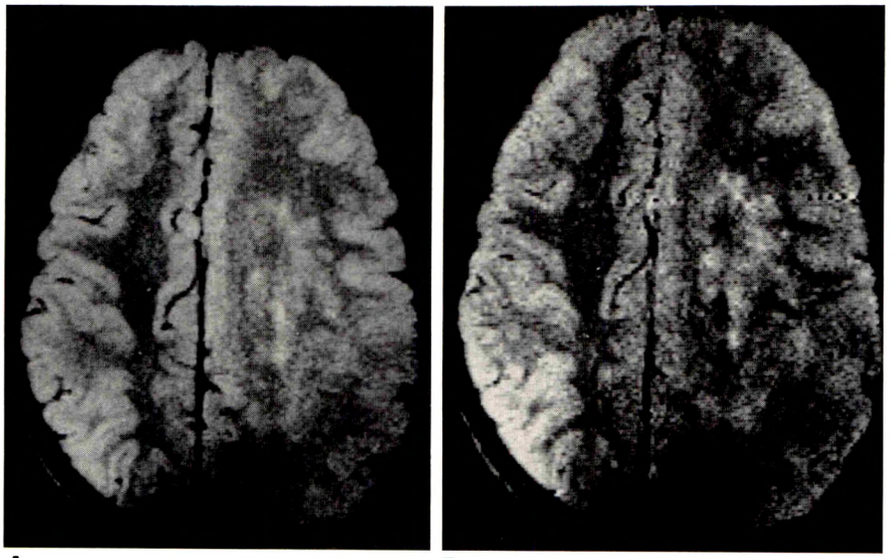

A B

Fig. 12.—Patient 11. Axial SE 2000/30-60 images reveal foci that are isointense with gray matter lying within centrum semiovale. This is characteristic of ectopic gray matter—collections of neurons that have been arrested during migration through the cortex.

imaging is performed in only one plane. In our patient who had bilateral narrow clefts with a horizontal orientation, the abnormality would have been missed entirely or misdiagnosed had the coronal sequences not been obtained (Fig. 10). Similarly, the vertically oriented narrow clefts in the left hemispheres of our first and fourth patients would have been missed had only coronal images been obtained. We believe that imaging of the pediatric patient with early onset of seizures and developmental delay should be performed using 5-mm slice thickness in at least two planes in order to avert such mistakes.

Unilateral Megalencephaly

Unilateral megalencephaly is a rare anomaly of the brain characterized by the early onset of intractable seizures, hemiplegia, and severe developmental delay. There is marked overgrowth of part or all of a cerebral hemisphere with defects in cell migration in the affected areas. The severity ranges from mild lobar enlargement to marked enlargement and architectural distortion of the entire cerebral and cerebellar hemispheres and the ipsilateral brainstem. This anomaly is not associated with corporal hemihypertrophy [29, 30].

Pathologically, severe cases of this anomaly demonstrate areas of lissencephaly and polymicrogyria with a thickened cortex and disorganization of cortical layers without alignment into distinct laminae. Ectopic gray matter is scattered throughout the hemisphere. Mild cases are more focal, often roughly lobar in distribution. Sulcal enlargement is seen and there are foci of PMG (see Fig. 6). Microscopically, in mild cases the architectural distortion of the cortex is less severe and the deeper cortical layers are more severely affected [31].

The MR findings in this anomaly are quite characteristic (Fig. 11). Although enlargement of all or part of a hemisphere can be seen associated with corporal hemihypertrophy or a hemispheric mass lesion, only unilateral megalencephaly is associated with a distorted, thickened cortex and ipsilateral ventricular dilation. The long T1 and long T2 of the ipsilateral centrum semiovale have been noted to correlate with the low density seen in this region on CT, probably representing decreased myelination and increased water content as compared with normal white matter. The perimeter of high-signal intensity in the deep cortex on the T2-weighted images in our first case corresponds with a similar rim of high intensity in our case of lissencephaly, which represents, we believe, gliosis in the cell-sparse layer. Our second case of unilateral megalencephaly, which was less severe and more localized to the temporal lobe, did not show this perimeter of high intensity, perhaps reflecting a less severe anomaly of migration, as in our case of PMG. Moreover, the less extensive case showed less cortical thickening, a more distinct corticomedullary junction, and more distinct foci of heterotopic gray matter in the centrum semiovale.

The recommended therapy for unilateral megalencephaly is surgical resection of the involved lobe or hemisphere [32]. The increased sensitivity of MR in localizing the involved segments should prove quite valuable for surgical planning so that as much viable brain as possible can be preserved.

Heterotopic Gray Matter

Heterotopic gray matter consists of collections of neurons in abnormal locations, which are thought to result from arrest of radial migration of the neuroblasts. Although it is not uncommon to see ectopic single neurons in newborn infants, these aberrations usually disappear within the first few months of life either by regression or by completion of their migration, and they are not considered true heterotopias. True heterotopic nodules vary widely in size and location, appearing anywhere from the subependymal zone to the cortex [1]. They may be isolated anomalies or may be associated with other CNS derangements such as the Chiari II

malformation or PMG. The major clinical symptom is seizures.

The key to recognizing heterotopias is in the use of imaging sequences in which the signal intensity of gray matter is distinct from that of white matter, and section thickness is 5 mm to minimize partial-volume effects. With these parameters, even small heterotopias are easily recognized as foci isointense with gray matter but positioned in the corona radiata or subependymal region (Fig. 12). They are much more readily identified on MR than on CT. The increased sensitivity with MR should enable us to arrive at improved clinical correlation with clinical defects and heterotopias.

Summary

The anomalies of cell migration are readily identified with MR, which is in general more sensitive and more specific than CT. Recognition depends on awareness of the characteristic appearance of the entities and use of the proper imaging technique. Images should be obtained in at least two planes, using a 5-mm slice thickness and both T1- and T2-weighted imaging sequences. The degree to which migration has been impaired is related to the thickness of the cell-sparse layer, which may be visualized on T2-weighted images. Recognition is important for planning proper treatment and for genetic counseling.

REFERENCES

1. Larroche J-C. Malformations of the nervous system. In: Adams JH, Corsellis JAN, Duchen LW, eds. *Greenfield's neuropathology*. New York: Wiley, **1984**:411–421
2. Ludwin SK, Malamud N. Pathology of congenital anomalies of the brain. In: Newton TH, Potts DG, eds. *Radiology of the skull and brain*, vol. 3. *Anatomy and pathology*. St. Louis: Mosby, **1977**:2979–3015
3. Lemire RJ, Loeser JD, Leech RW, Alvord EC. *Normal and abnormal development of the human nervous system*. Hagerstown, MD: Harper & Row, **1985**:231–259
4. Rakic P. Neuronal migration and contact guidance in the primate telencephalon. *Postgrad Med J [Suppl 1]* **1978**;54:25–37
5. Garcia CA, Dunn D, Trevor R. The lissencephaly (agyria) syndrome in siblings. *Arch Neurol* **1978**;35:608–611
6. Jones KL, Gilbert EF, Kaveggia EG, Opitz JM. The Miller-Dieker syndrome. *Pediatrics* **1980**;66:277–281
7. Pagon RA, Clarren SK, Milam DF Jr, Hendrickson AE. Autosomal recessive eye and brain anomalies: Warburg syndrome. *J Pediatr* **1983**;102:542–546
8. Whitley CB, Thompson TR, Mastri AR, Gorlin RJ. Warburg syndrome: lethal neurodysplasia with autosomal recessive inheritance. *J Pediatr* **1983**;102:547–551
9. Dobyns WB, Stratton RF, Greenberg F. Syndromes with lissencephaly. I: Miller-Dieker and Norman-Roberts syndromes and isolated lissencephaly. *Am J Med Genet* **1984**;18:509–526
10. Dobyns WB, Kirkpatrick JB, Hittner HM, Roberts RM, Kretzer FL. Syndromes with lissencephaly. II: Walker-Warburg and cerebro-oculo-muscular syndromes and a new syndrome with type II lissencephaly. *Am J Med Genet* **1985**;22:157–195
11. Stewart RM, Richman DP, Caviness VS Jr. Lissencephaly and pachygyria. An architectonic and topographical analysis. *Acta Neuropathol (Berl)* **1975**;31:1–12
12. Dobyns WB, McCluggage CW. Computed tomographic appearance of lissencephaly syndromes. *AJNR* **1985**;6:545–550
13. Van Allen M, Clarren SK. A spectrum of gyral anomalies in Miller-Dieker (lissencephaly) syndrome. *J Pediatr* **1983**;102:559–564
14. Alvarez LA, Yamamoto T, Wong B, Resnick TJ, Llena JF, Moshé SL. Miller-Dieker syndrome: a disorder affecting specific pathways of neuronal migration. *Neurology* **1986**;36:489–493
15. Jellinger K, Rett A. Agyria-pachygyria (lissencephaly syndrome). *Neuropaediatrie* **1976**;7:66–91
16. Williams RS, Swisher CN, Jennings M, Ambler M, Caviness VS Jr. Cerebro-ocular dysgenesis (Walker-Warburg syndrome): neuropathologic and etiologic analysis. *Neurology* **1984**;34:1531–1541
17. Crome L, Stern J. *The pathology of mental retardation*. London: Churchill, **1967**
18. Richman DP, Stewart RM, Caviness VS Jr. Cerebral microgyria in a 27-week fetus: an architectonic and topographic analysis. *J Neuropathol Exp Neurol* **1974**;33:374–384
19. Dvořák K, Feit J. Migration of neuroblasts through partial necrosis of the cerebral cortex in newborn rats—contribution to the problems of morphological development and developmental period of cerebral microgyria. *Acta Neuropathol (Berl)* **1977**;38:203–212
20. Yakovlev PI, Wadsworth RC. Schizencephalies. A study of the congenital clefts in the cerebral mantle. I. Clefts with fused lips. *J Neuropathol Exp Neurol* **1946**;5:116–130
21. Yakovlev PI, Wadsworth RC. Schizencephalies. A study of the congenital clefts in the cerebral mantle. II. Clefts with hydrocephalus and lips separated. *J Neuropathol Exp Neurol* **1946**;5:169–206
22. Zimmerman RA, Bilaniuk LT, Grossman RI. Computed tomography in migratory disorders of human brain development. *Neuroradiology* **1983**;25:257–263
23. Miller GM, Stears JC, Guggenheim MA, Wilkening GN. Schizencephaly: a clinical and CT study. *Neurology* **1984**;34:997–1001
24. Dekaban A. Large defects in cerebral hemispheres associated with cortical dysgenesis. *J Neuropathol Exp Neurol* **1965**;24:512–530
25. Robinson RG. Agenesis and anomalies of other brain structures. In: Vinken PJ, Bruyn GW, eds. *Handbook of clinical neurology*, vol. 30. *Congenital malformations of the brain and skull. Part I*. Amsterdam: North Holland Publishing Co, **1977**:338–347
26. Raybaud C. Destructive lesions of the brain. *Neuroradiology* **1983**;25:265–291
27. Klingensmith WC III, Cioffi-Ragan DT. Schizencephaly: diagnosis and progression in utero. *Radiology* **1986**;159:617–618
28. Volpe JJ. In: Schaffer AJ, ed. *Major problems in clinical pediatrics*, vol. XXII. Philadelphia: Saunders, **1981**
29. Fitz CR, Harwood-Nash DC, Boldt DW. The radiographic features of unilateral megalencephaly. *Neuroradiology* **1978**;15:145–148
30. Townsend JJ, Nielsen SL, Malamud N. Unilateral megalencephaly: hamartoma or neoplasm? *Neurology* **1975**;25:448–453
31. Manz HJ, Phillips TM, Rowden G, McCullough DC. Unilateral megalencephaly, cerebral cortical dysplasia, neuronal hypertrophy, and heterotopia: cytomorphometric, fluorometric cytochemical, and biochemical analyses. *Acta Neuropathol (Berl)* **1979**;45:97–103
32. King M, Stephenson JBP, Ziervogel M, Doyle D, Galbraith S. Hemimegalencephaly—a case for hemispherectomy? *Neuropediatrics* **1985**;16:46–55

Book Review

The Radiologic Clinics of North America. Imaging in Ophthalmology, Part II. Guest editor: Mahmood F. Mafee. Philadelphia: Saunders, July 1987; 25:667–865. $22.95; by subscription, 6 issues annually for $85

"Tomography of the Orbit," "Orbital Venography," "Ocular Foreign Body Localization," and "Plain View of the Orbits" were some of the articles in the April 1982 issue of *The Radiologic Clinics of North America*, a volume that addressed radiology of the orbit. Comparison of that text with the July 1987 issue shows dramatically the rapid and revolutionary changes that have developed in radiology during the past 15 years. The only shared topics of discussion are dacryocystography and orbital surgery.

An examination of Part II markes it easy to understand why two parts are necessary to cover orbital imaging. Part II is not just a general overview of imaging and ophthalmology in 1987; rather, it includes many specific topics and will serve as an excellent resource for those who are interested in visualizing the orbital contents and parasellar area. These entities, poorly discussed in previous texts that addressed the orbit, are covered thoroughly in this volume. This is not simply a collection of images; it has more text than pictures. For example, an entire chapter, albeit a short one, on persistent hyperplastic primary vitreous discusses the embryology and pathology of this ocular abnormality. This chapter is followed by a discussion of colobomas of the optic nerve and the morning glory anomaly. A section on CT of ocular motility disorders is included also, as is a discussion of disease entities involving the lacrimal gland and lacrimal fossa.

Mahmood F. Mafee is the editor of this issue, and special note should be taken of the extensive contributions he has made to the articles. He is author or coauthor of approximately half of the contents, and these bear his stamp of excellence. Many of these chapters are drawn from his previous publications, but the material has been expanded and updated.

The quality of the images is maintained at a high level throughout this volume, with rare exceptions. Images usually have appropriate arrows and excellent legends. I was pleased by the amount of associated clinical information that accompanies case examples. I also enjoyed chapters written from a neurologic and neurosurgical point of view that discuss the role of imaging in neuroophthalmology and the neurosurgeon's perspective on the approach to parasellar and optic nerve lesions.

Overall, this excellent text offers information that would appeal to a broad spectrum of the radiologic community. For those who do not subscribe to *The Radiologic Clinics of North America*, the May and July 1987 issues are worth purchasing separately; they certainly will be referred to many times. I urge residents and junior attending physicians who have received this publication to refer to the April 1972 issue for an interesting contrast.

Charles M. Citrin
Washington Imaging Center
Chevy Chase, MD 20815

Cerebral Necrosis After Radiotherapy and/or Intraarterial Chemotherapy for Brain Tumors:

PET and Neuropathologic Studies

Giovanni Di Chiro[1]
Edward Oldfield[2]
Donald C. Wright[2]
Domenic De Michele[1]
David A. Katz[3]
Nicholas J. Patronas[1]
John L. Doppman[4]
Steven M. Larson[5]
Masanori Ito[6]
Conrad V. Kufta[2]

Cerebral necrosis after radiotherapy for brain tumors is being recognized as a problem more common than previously estimated. Distinction between this iatrogenic complication and tumor recurrence cannot be made by either CT or MR imaging. By using positron emission tomography (PET) with ^{18}F-deoxyglucose (FDG) we were able to reach a diagnosis of radiation necrosis, later verified, in 10 of 95 patients referred for the purpose of differentiating tumor recurrence from necrosis. The critical PET-FDG feature was focal hypometabolism in the area of necrosis, which contrasted with the hypermetabolism associated with the residual/recurrent tumor.

In addition, four cases of cerebral necrosis after supraophthalmic, intraarterial chemotherapy (BCNU) were studied with the PET-FDG method. The area of chemotherapy damage was also characterized by marked hypometabolism. Histology revealed both similarities and differences between radio- and chemonecrosis.

This article appears in the November/December 1987 issue of *AJNR* and the January 1988 issue of *AJR*.

Received April 14, 1987; accepted after revision June 24, 1987.

Presented in part at the annual meeting of the American Society of Neuroradiology, New Orleans, February 1985.

[1] Neuroimaging Section, National Institute of Neurological and Communicative Disorders and Stroke, Bldg. 10, Rm. 1C-451, National Institutes of Health, Bethesda, MD 20892. Address reprint requests to G. Di Chiro.

[2] Surgical Neurology Branch, National Institute of Neurological and Communicative Disorders and Stroke, National Institutes of Health, Bethesda, MD 20892.

[3] Office of the Clinical Director, National Institute of Neurological and Communicative Disorders and Stroke, National Institutes of Health, Bethesda, MD 20892.

[4] Department of Diagnostic Radiology, The Clinical Center, National Institutes of Health, Bethesda, MD 20892.

[5] Department of Nuclear Medicine, The Clinical Center, National Institutes of Health, Bethesda, MD 20892.

[6] Laboratory of Cerebral Metabolism, National Institute of Mental Health, National Institutes of Health, Bethesda, MD 20892.

***AJR* 150:189–197, January 1988**
0361–803X/88/1501–0189

Radiotherapy and, to a lesser degree, chemotherapy are useful, or relatively useful, treatment tools for malignant primary brain tumors [1]. In both therapeutic methods, selective, high-dosage delivery to the tumoral tissue is the obvious strategy for enhancing their efficacy. However, attempts at improving the survival results by "selectivity-enhancing" variations and adjunctions to the conventional radiotherapy and by superselective intracarotid chemotherapy have not been successful [2, 3]. The main limitation is damage to the normal cerebral tissue, a complication still poorly understood despite extensive research efforts reflected in an enormous, almost unmanageable literature. Unresolved remain critical issues such as dosimetry threshold and chronologic development of this iatrogenic lesion, as well as the additive or potentiating effects of radio- and chemotherapy on each other [4, 5].

A fundamental hindrance to a better knowledge of the brain lesions that may follow radio- and/or chemotherapy is the lack of a readily available method to diagnose and follow these complications. For instance, CT [6] and MR imaging [7] have proved essentially useless for differentiating between radiation necrosis and recurrent or residual brain tumor. Even neuropathologic examinations of biopsy material may be inconclusive, with limited sampling being the main diagnostic difficulty. In addition, neuropathology provides only static information and is not suitable for sequential assessment. Only positron emission tomography (PET) with ^{18}F-deoxyglucose (FDG) offers reliable pathophysiologic and diagnostic data in this area [8–11]. Such PET-FDG technology is not, however, available to most practitioners, or even to many investigators involved in the management of patients with brain tumors. In this report we present our results with PET-FDG in cases of cerebral necrosis after radiation and/or intraarterial chemotherapy. It is hoped that the proffered evidence will convince more investigators to adopt and use this valuable research and diagnostic technique. Wider use of PET-FDG is imperative if we wish to reach a more complete understanding of the serious complications related to our therapeutic efforts.

Materials and Methods

The PET studies were carried out with the Neuro-PET [12], a scanner with a full width at half maximum resolution of 6.5 mm (slice thickness, 1.1 cm; pixel size, 2 mm). The patient data are summarized in Tables 1 and 2. The studies include 10 cases of radiation-induced cerebral necrosis (cases 1–10, Table 1), with eight patients treated by conventional radiotherapy and two with a combination of conventional and interstitial radiotherapy. No chemotherapy was used before the PET-FDG study in five of these cases, whereas various types of adjunctive chemotherapy with both IV and intrathecal drug administration were given to the other five patients. In five of the 10 patients, the tumor diagnosis was glioma, while in three cases the neoplasm was metastatic (thyroid carcinoma, Ewing sarcoma, malignant mela-

TABLE 1: Summary of Patients with Postradiation Necrosis

Case No.	Age	Gender	Original Diagnosis/ Original Surgery	Radiation Therapy (Gy)	IV/Intrathecal (IT) Chemotherapy	CT	MR	Time from RT to PET (months)	Survival (months)
1	M	43	Bifrontal glioblastoma multiforme/yes	E: 63	IV: spiromustine, AZQ	+	+	48	After RT: 72[a] After PET: 24
2	M	35	R frontal astrocytoma anaplastic features	E: 57.6	IV: vincristine	+	NP	30	Lost to follow-up
3	M	39	R frontal atypical oligodendroglioma/yes	E: 57.6	Not administered	+	NP	67	After RT: 78 After PET: 11
4	M	70	L temporoparietal glioblastoma multiforme/yes	E: 45 I: 120	Not administered	+	NP	10	After RT: 11 After PET: 1
5	F	40	R frontoparietal astrocytoma anaplastic features/yes	E: 40 I: 200	Not administered	+	NP	14	After RT: 26 After PET: 12
6	F	3	R parietal metastases/yes	E: 61.2	Not administered	+	NP	12	After RT: 60[a] After PET: 48
7	F	20	R frontal and temporoparietal metastases/yes	E: 58	IV: vincristine, adriamycin, cytoxan; IT: methotrexate, ArA C	+	+	12	After RT: 57 After PET: 45
8	M	68	L frontal, R parietal metastases/no	E: 45	IV: CCNU	+	NP	48	After RT: 108
9	M	47	Bifrontal presumptive glioma/no	E: 60	IV:CCNU	+	NP	48	After RT: 84 After PET: 36
10	F	10	Diffuse central nervous system leukemia/no	E: 48	IT: methotrexate IV: ArA C	+	+	72	After RT: 73 After PET: 1

Note.—In all patients, PET findings were cold, and the post-PET pathologic diagnosis was necrosis. RT = radiation therapy; PET = positron emission tomography; R = right; L = left; E = external beam; I = intrathecal; + = positive; NP = not performed.
[a] This patient died.

TABLE 2: Summary of Patients with Postchemotherapy Necrosis

Case No.	Age	Gender	Original Diagnosis/ Original Surgery	Radiation Therapy (Gy)	Intraarterial BCNU (No. of Courses)	Other Chemotherapy	CT	MR	PET Appearance	Time from BCNU to PET (months)	Post-PET Pathologic Diagnosis	Survival (months)
11	44	F	L temporoparietal glioblastoma multiforme/yes	No	220–325 mg (two)	No	+	NP	Cold	2	Necrosis	After BCNU: 5[a] After PET: 3
12	16	M	L temporoparietal glioblastoma multiforme/yes	No	80 mg (two)	IV CCNU	+	+	Mixed	2.5	Necrosis + glioblastoma multiforme	After BCNU: 15[a] After PET: 12.5
13	34	F	R parietal glioblastoma multiforme/yes	50	220 mg (four)	No	+	+	Cold	23	Necrosis	After BCNU: 42 After PET: 19
14	17	F	L temporoparietal glioblastoma multiforme/yes	60	402 mg (four)	No	+	+	Mixed	6	Necrosis, presumed residual glioma	After BCNU: 44 After PET: 38

Note.—PET = positron emission tomography; BCNU = 1,3-bis 2-chloroethyl-1-nitrosourea; L = left; R = right; + = positive; NP = not performed.
[a] This patient died.

noma). In one patient, glioma had been suspected and had been treated without histologic confirmation, and in one case radiation and intrathecal chemotherapy had been instituted for CNS leukemia.

Of some interest is the fact that the 10 cases of postradiation necrosis were recognized in a population of 95 patients referred for a PET-FDG study to differentiate tumor recurrence from necrosis. In the remaining 85 cases, PET-FDG supported the diagnosis of tumor (hypermetabolic focus) and was later verified at surgery and/or autopsy.

Table 2 includes four patients (cases 11–14, all gliomas) studied by PET-FDG after treatment by supraophthalmic, intracarotid infusion of BCNU (1, 3-bis 2-chloroethyl-1-nitrosourea) alone (two cases), or BCNU before (one case) or after (one case) radiotherapy. While no residual or recurrent tumor was encountered in the 10 cases of postradiation necrosis listed in Table 1, two of the four cases of necrosis after intraarterial chemotherapy showed residual tumor (Table 2). In these two patients, the location of the tumor was quite distinct from the areas of necrosis, perhaps reflecting the selectivity of BCNU delivery caused by drug streaming [13, 14]. CT with IV administration of contrast medium was carried out in all of the 14 cases, and MR imaging was performed in six patients. The MR studies did not include administration of Gd-DTPA or other enhancing media. Post-PET neuropathologic verification of necrosis was obtained in all 14 patients, by biopsy in 12 cases and by autopsy in two. In the two cases with residual tumor (Table 2), biopsy verification of the neoplasm was obtained in one.

Finally, in two patients who are not included in Tables 1 and 2, both extensive radiation necrosis and residual and/or recurrent glioma were present. These two patients, in whom tumor as well as necrosis were verified at surgery, are discussed to demonstrate how PET-FDG allows us to recognize discrete tumoral foci within vast areas of necrosis.

All available pathologic material was reviewed by a neuropathologist. The malignant glial tumors were classified according to the scheme described by Burger and Vogel [15], as opposed to the Kernohan system.

Results

In PET-FDG studies, regions of cerebral necrosis are characterized by a reduced glucose utilization rate (Fig. 1). The metabolic values (mg glucose/100 g/min) of the necrotic areas are expressed in FDG activity ratios, comparing uptake in the suspected necrotic areas with activity in an adjacent region and in a corresponding region in the opposite hemisphere when no bilateral extension is evident (Table 3).

The FDG activity ratios of the necrotic areas were consistently low (Table 3), with mean ratios of 0.54 (postradiation) and 0.34 (postchemotherapy), and individual ratios as low as 0.28 (postradiation) and zero (postchemotherapy). In contrast,

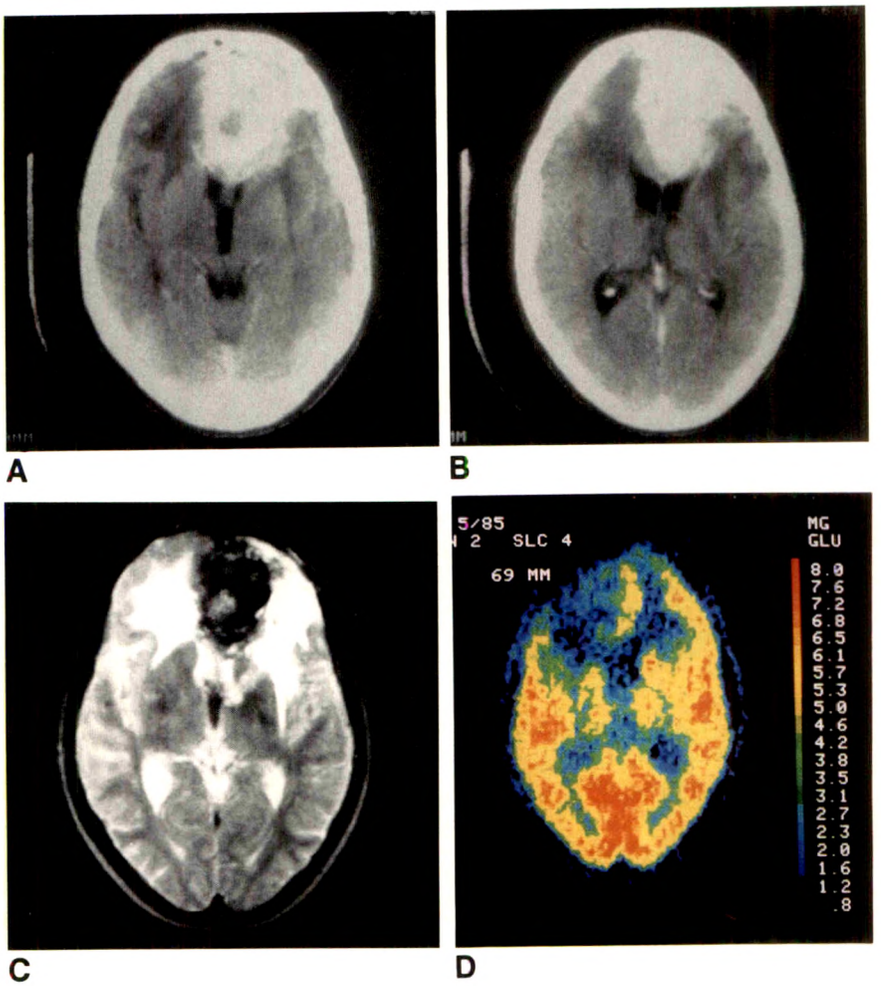

Fig. 1.—Case 1: radiation necrosis.

***A* and *B*, Postcontrast axial CT scans show marked, bifrontal enhancement surrounded by hypodense halo. Lesion is larger on left.**

***C*, MR image (TR = 2500 msec, TE = 120 msec). Mixed-intensity signal from area corresponding to CT enhancement and high-intensity signal from surrounding edema.**

***D*, PET-FDG image at corresponding level. Marked hypometabolism in both prefrontal areas, larger on left. Note selective sparing of interhemispheric gray matter, which is displaced toward right. Color scale indicates range of metabolic values (in mg glucose/100 g/min). (On PET scan only, right side of patient is on right side of image.**

TABLE 3: ^{18}F-Deoxyglucose Positron Emission Tomographic Metabolic Values in Postradiation and Postchemotherapy Necrotic Lesions

Group: Case No.	Ratio of Lesion to:	
	Adjacent Brain	Corresponding, Contralateral Region
Postradiation necrosis:		
1	0.47	0.78
2	0.70	0.68
3	0.50	0.67
4	0.64	0.62
5	0.28	0.18
6	0.64	0.65
7	0.42	0.40
8	0.66	0.53
9	0.54	0.50
10	0.52	0.49
Mean value	0.54	0.55
Postchemotherapy necrosis:		
11	0.61	0.52
12	0[a]	0
13	0.50	0.34
14	0.26[a]	0.19
Mean value	0.34	0.26

[a] The low values in the necrotic areas contrast with the high ratios (tumor/nontumoral areas) of the residual recurrent neoplasms (ratio of 2.50 for case 12 and 2.84 for case 14).

the ratios of the two residual, recurrent tumors (cases 12 and 14) compared with nontumoral (but not necrotic or obviously edematous) areas were high, 2.50 and 2.84, respectively.

As indicated, in some necrotic areas the metabolic activity was reduced to zero (Fig. 2), reflecting total tissue destruction. In some cases, hypometabolism in necrotic areas could not be differentiated from reduced glucose consumption connected with edematous infiltration, although it appeared that metabolism was somewhat higher in edematous than in necrotic brain. On PET-FDG scans of the postradiation cases, the necrosis was mostly confined to the white matter with sparing of the gray matter (Fig. 1). This pattern, characteristic of radiation necrosis [2, 6, 16], was confirmed at autopsy. Deep gray matter was involved, however, in cases of postintraarterial chemotherapy necrosis. This may have been caused by streaming of the BCNU from the middle cerebral into the lenticulostriate arteries, leading to a selective chemoconcentration and consequent selective damage to the basal ganglia.

In two of our cases with brain injury after selective intraarterial chemotherapy, the limits of the total necrosis are clearly outlined in a background of hemispheric hypometabolism. The area most profoundly affected obviously corresponds to the distribution territory of known perforating arteries (Fig. 2). In other cases, only the diffuse hypometabolic changes involving the entire BCNU-injected hemisphere are demonstrated, without evidence of focality. To explain the diffuse hemispheric hypometabolism, one might invoke, as a causative factor, drug streaming in the distal arterial tree causing widely distributed, discrete areas of tissue damage [14]. These multifocal, scattered areas of injury will appear on the relatively low-resolution PET images as confluent, homogeneous regions of hypometabolism. Another explanation for the widespread hypometabolism of the affected hemisphere may be deafferentation. This phenomenon, which is related to damage of deep structures connected by centrifugal pathways with the cortex [17], may also explain the so-called crossed cerebellar diaschisis (Fig. 3). This is characterized by marked hypometabolism in the cerebellar hemisphere contralateral to the cerebral hemisphere where the primary lesion is located, and may be related either to the original tumor or to the posttherapeutic necrotic lesion [18]. Bilateral, postradiation lesions are often asymmetric (Fig. 4), reflecting the radiation field distribution.

Again and again, in these patients, CT was inadequate to differentiate tumoral from necrotic areas (Figs. 1, 2, and 4). In this respect, we found the MR studies even less informative than CT (Figs. 1 and 2).

Our cases of postradiation necrosis were recognized 10–72 months (mean, 33.1) after the termination of the irradiation. This is in agreement with many previous reports [2, 6, 19, 20]. On the other hand, cerebral necrosis after intraarterial chemotherapy occurred much earlier, at 2–23 months (mean, 8.4 months). This may be because of the concentrated manner of chemotherapeutic administration, which contrasts with the usually fractionated delivery of irradiation over time.

Histopathologically, chemotherapy-induced necrosis resembles the more familiar postradiation tissue damage, with white-matter demyelination, focal coagulation necrosis, reactive gliosis, petechial hemorrhages, and prominent vasculopathic changes. The latter involve particularly small arteries and arterioles and include thickened walls, endothelial proliferation, fibrinoid necrosis, and occlusion alternating with irregular dilatation of the vascular lumen [21]. Notably absent, however, in the postchemotherapy vasculopathy are media and adventitial hyalinization and thin-walled teleangiectasias, two changes rather characteristic of the postradiation pathologic syndrome. In the absence of clinical information, these angiopathic differences are the only features that may assist the neuropathologist in the difficult differential diagnosis between chemotherapy and radiation damage. Finally, the gray matter is affected more often in the chemotherapy lesions than in the radiation damage. This gray matter involvement, however, is partly factitious, related to the selective distribution of the chemotherapeutic compound. In Figures 5 and 6, representative histopathologic patterns of postradiation and postchemotherapy necrosis are illustrated.

Discussion

Suppressed glucose utilization is one of the metabolic alterations that occur after radiation [22, 23]. In a previous study [24], we used the ^{14}C-deoxyglucose autoradiographic method to learn whether radiation administered to rat brain, in a dose below that known to result in any histologic change, may nevertheless affect the brain's local rates of glucose utilization. Measurements were made 4 days and 4 weeks

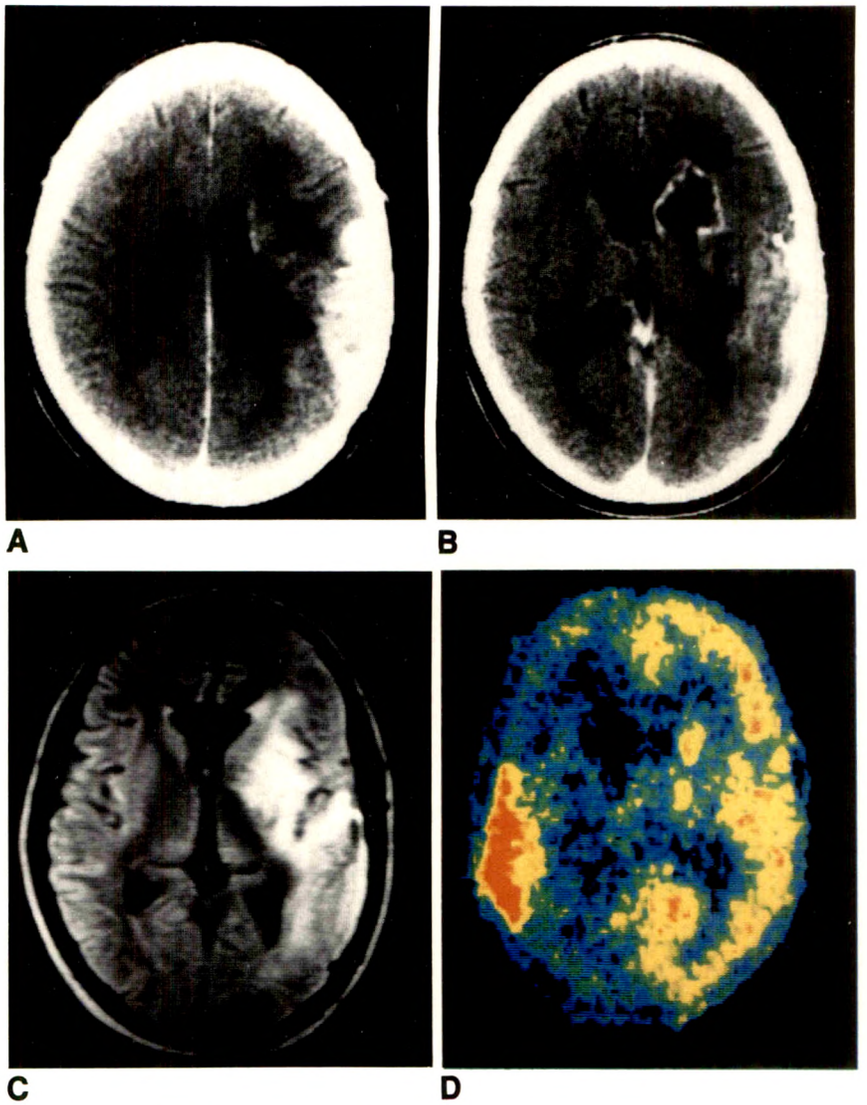

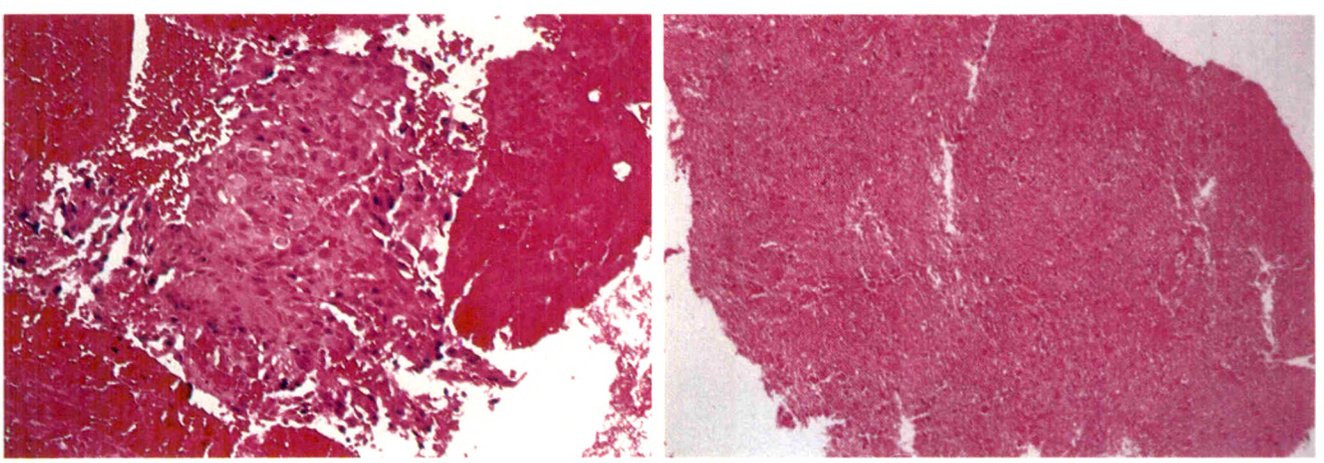

Fig. 2.—Case 12: glioblastoma plus chemotherapy-induced necrosis.

***A*, Postcontrast axial CT scan shows enhancing, superficial, left parietal glioblastoma.**

***B*, Lower level. Markedly hypodense area, sharply outlined by enhancing rim, is seen in left caudate and lenticular nuclei region. This area corresponds to total necrosis caused by intraarterial chemotherapy.**

***C*, 0.5-T MR scan (TR = 2000 msec, TE = 40 msec) through approximate level of *B* shows intense signal in tumoral as well as necrotic areas.**

***D*, PET-FDG scan at approximate level of *B* and *C*. Tumor is markedly hypermetabolic (*red*, *yellow*) contrasting with ametabolic necrotic center (*black*) and hypometabolic hemispheric background (*green*, *blue*). (On PET scan only, right side of patient is on right side of image.)**

***E*, Histology of tumor obtained by stereotactic biopsy reveals glioblastoma.**

***F*, Histology of stereotactic biopsy specimen shows necrotic white matter.**

after exposure of groups of rats to 15 Gy. Rates of glucose utilization in gray- and white-matter structures in both groups were compared with rates in sham-irradiated controls. Statistically significant, lower rates were found in 16 structures 4 days after radiation and in 25 structures 4 weeks after radiation exposure. A weighted average rate for the brain as a whole was 15% below that of the controls for both irradiated groups. In Figure 7, representative ^{14}C-deoxyglucose autoradiographic sections of a control brain and of 4-day and 4-week-postradiation rat brains are illustrated.

Early on in our PET-FDG study of brain tumors we realized that radiation was associated with depressed glucose utilization of the cerebrum as well as of the tumors. We learned to avoid obtaining PET-FDG scans during and soon after radiotherapy in order not to be misled by spuriously low values in the tumoral areas. We also demonstrated that PET-FDG could be used to advantage to differentiate between tumor recurrence from radiation necrosis [8–10]. These findings have been confirmed by other investigators [11]. This report includes our more recent experience with PET-FDG in postradiation necrosis as well as our studies in postintraarterial chemotherapy necrosis. We emphasize that CT and MR scans are essentially useless in the differentiation of tumor vs necrosis. Also, we stress that we have not yet been confronted with a false-positive or a false-negative PET-FDG diagnosis of radiation necrosis. For instance, even when the necrotic changes are overwhelmingly extensive, as in two patients in our series, if a tumoral focus is present, the PET-FDG method will recognize it (Fig. 8). Obviously, diffuse cellular infiltration (paucicellular tumoral spread) may well be beyond the resolving capability of the PET-FDG method.

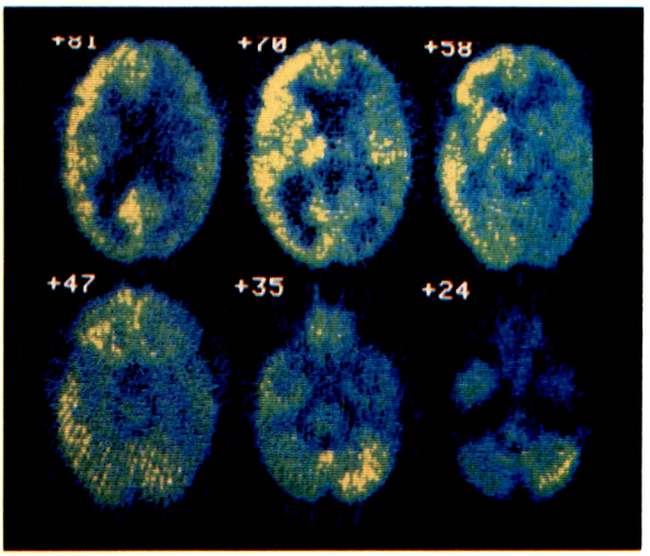

Fig. 3.—Case 13: chemotherapy-induced necrosis. PET-FDG scans show diffuse hypometabolism of entire right cerebral hemisphere (*green*, *blue*). Note that cortex of right cerebellar hemisphere is normometabolic (*yellow*), while left cerebellum is hypometabolic (scans 35 and 24); this phenomenon is referred to as "crossed cerebellar diaschisis." (Right side of patient is on right side of image.)

The dual evidence that radiation affects glucose metabolism and that PET-FDG measures the cerebral glucose metabolic rates and its variations makes this method ideally suited to detect, study, and follow up cerebral radiation damage. In fact, considering the essentially unanimous consensus that neither CT nor MR allows us to reach a diagnosis of radiation necrosis, it is obvious that PET-FDG is one of the few research/diagnostic tools for advancing our knowledge of this iatrogenic complication. Although the amount of information on postchemotherapy necrosis is scanty, we may argue in favor of adopting the PET-FDG technique also for evaluation of this other treatment-related lesion. The similarities between postradiation and postchemotherapy necrosis are probably not surprising [21, 25]. Necrosis, after all, represents a final and common stage for a variety of pathologic processes. The differences in the damage by the two treatment methods perhaps depend on the usually different chronology of the therapeutic regimens, intraarterial therapy being delivered in a shorter time span than radiation is.

In conclusion, PET-FDG is the best diagnostic test currently available for the recognition of cerebral necrosis after radiation and/or chemotherapy and for differentiating necrosis from residual/recurrent tumor. The heuristic importance of the PET-FDG method cannot be overemphasized. The possibility of frequent follow-up studies may allow us to reach a better understanding of the threshold for permanent damage, as well as to sequentially assess the development of necrosis.

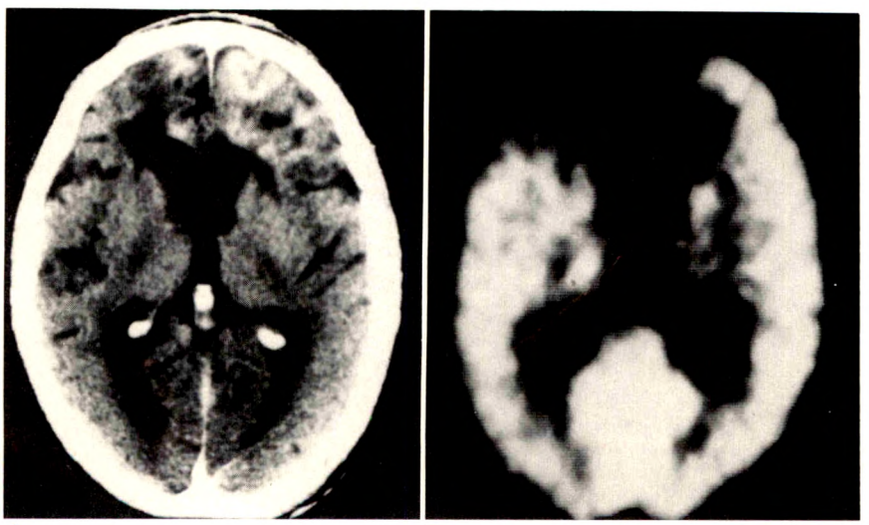

Fig. 4.—Case 8: radiation necrosis.
***A*, Postcontrast axial CT scan shows diffuse changes in both prefrontal areas.**
***B*, PET-FDG scan. Profound hypometabolism in areas corresponding to CT enhancement. Necrotic lesion is larger on left, reflecting radiation field distribution.**

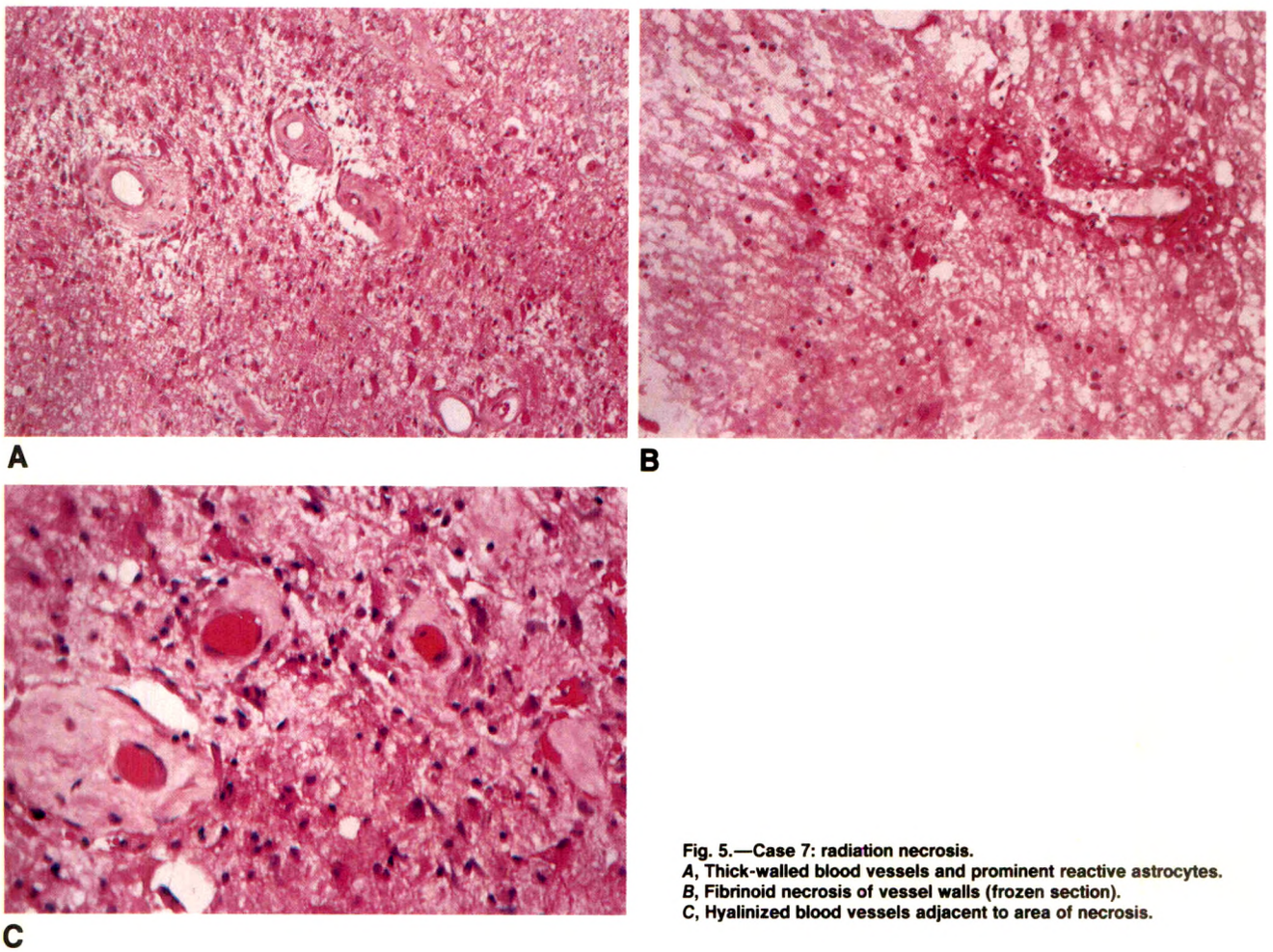

Fig. 5.—Case 7: radiation necrosis.
***A*, Thick-walled blood vessels and prominent reactive astrocytes.**
***B*, Fibrinoid necrosis of vessel walls (frozen section).**
***C*, Hyalinized blood vessels adjacent to area of necrosis.**

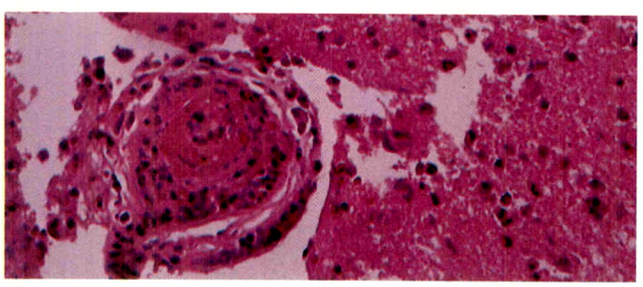

Fig. 6.—Case 14: Chemotherapy necrosis. Note necrotizing vasculitis with transmural inflammation and thrombosis.

REFERENCES

1. Walker MD, Green SB, Byar DP, et al. Randomized comparisons of radiotherapy and nitrosoureas for the treatment of malignant glioma after surgery. *N Engl J Med* **1980**;303:1323–1329
2. Leibel SA, Sheline GE. Radiation therapy for neoplasms of the brain. *J Neurosurg* **1987**;66:1–22
3. Foo SH, Choi IS, Berenstein A, et al. Supraophthalmic intracarotid infusion of BCNU for malignant glioma. *Neurology* **1986**;36:1437–1444
4. Pratt RA, Di Chiro G, Weed JC Jr. Cerebral necrosis following irradiation and chemotherapy for metastatic choriocarcinoma. *Surg Neurol* **1977**;7:117–120
5. Wilson WB, Perez GM, Kleinschmidt-Demasters BK. Sudden onset of blindness in patients treated with oral CCNU and low-dose cranial irradiation. *Cancer* **1987**;59:901–907
6. Martins AN, Johnston JS, Henry JM, Henry JM, Stoffel TJ, Di Chiro G. Delayed necrosis of the brain. *J Neurosurg* **1977**;47:336–345
7. Dooms GC, Hecht S, Brant-Zawadzki M, Berthiaume Y, Norman D, Newton TH. Brain radiation lesions: MR imaging. *Radiology* **1986**;158:149–155
8. Di Chiro G, DeLaPaz RL, Brooks RA, et al. Glucose utilization of cerebral gliomas measured by [^{18}F] fluorodeoxyglucose and positron emission tomography. *Neurology* **1982**;32:1323–1329
9. Patronas NJ, Di Chiro G, Brooks RA, et al. Progress: [^{18}F] fluorodeoxyglucose and positron emission tomography in the evaluation of radiation necrosis of the brain. *Radiology* **1982**;144:885–889
10. Di Chiro G, Patronas NJ, Oldfield EH, Wright DC, Katz DA. PET, CT, and NMR of cerebral necrosis following radiotherapy or intra-arterial chemotherapy for cerebral tumors. *AJNR* **1985**;6:473–474
11. Doyle WK, Budinger TF, Valk PE, Levin VA, Gutlin PH. Differentiation of cerebral radiation necrosis from tumor recurrence by F-18-FDg and Rb-82 positron emission tomography. *J Comput Assist Tomogr* **1987**;11:563–570
12. Di Chiro G, Brooks RA, Bairamian D, et al. Diagnostic and prognostic value of positron emission tomography using [^{18}F] fluorodeoxyglucose in brain tumors. In: Reivich M, Alavi A, eds. *Positron emission tomography*. New York: Liss, **1985**:291–309
13. Lutz RJ, Dedrick RL, Boretos JW, Oldfield EH, Blacklock B, Doppman JL. Mixing studies during intracarotid artery infusions in an in vitro model. *J Neurosurg* **1986**;64:277–283

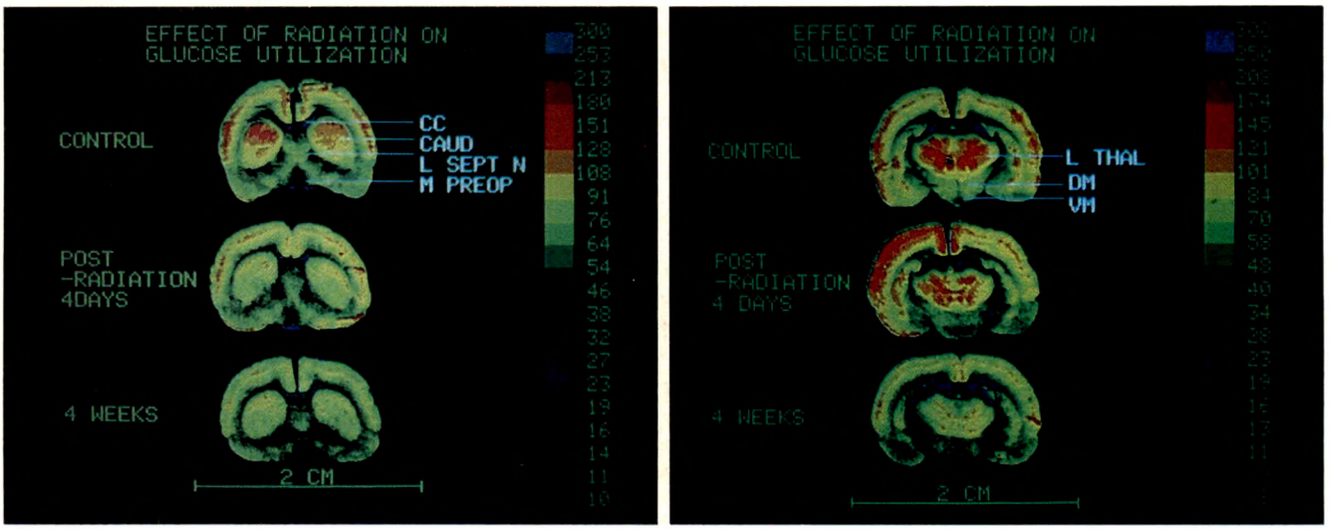

A B

Fig. 7.—^{14}C-deoxyglucose autoradiographs from rat brains (control and 4 days and 4 weeks after irradiation). Bar at right indicates range of rates of glucose utilization (μmol/100 g/min) spanned by each color. Each of the autoradiographs shows three structures displaying rates significantly reduced after irradiation, as compared with those structures in controls. CC = corpus callosum; CAUD = caudate nucleus; L SEPT N = lateral septal nucleus; M PREOP = medial preoptic area; L THAL = lateral thalamic nucleus; DM = dorsomedial nucleus; VM = ventromedial nucleus. Even visually, cerebral metabolic rates in irradiated rats is reduced compared with controls, particularly at 4 weeks after radiation (less red and light yellow, more greenish hue). (Right side of rat is on right side of image.)

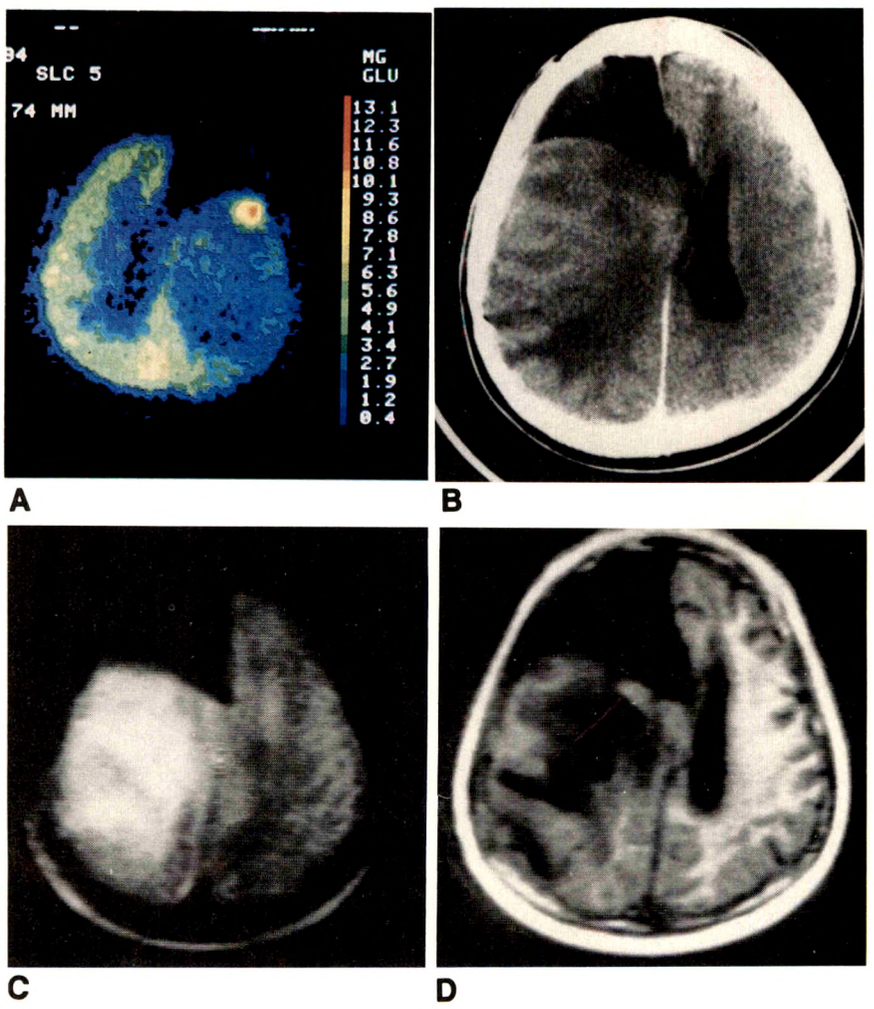

A B C D

Fig. 8.—Recurrent glioblastoma plus necrosis and edema.

A, PET-FDG scan. Note discrete focus of intense hypermetabolism in right frontal region, behind wedgelike defect caused by previous surgery. Vast areas of hypometabolism (blue) are seen in ipsilateral as well as contralateral hemispheres. These changes are from radiation plus IV chemotherapy injury. Color scale indicates range of metabolic values in mg glucose/100 g/min. (On PET scan only, right side of patient is on right side of image.) Tumor recurrence was not identified on either postcontrast CT scan (*B*) or spin-echo (*C*) or inversion-recovery (*D*) MR images.

14. Blacklock JB, Wright DC, Dedrick RL, et al. Drug streaming during intra-arterial chemotherapy. *J Neurosurg* **1986**;64:284–291
15. Burger PC, Vogel FS. *Surgical pathology of the nervous system and its coverings*, 2d ed. New York: Wiley, **1982**:226–265
16. Davis RL, Robertson DM. *Textbook of neuropathology*. Baltimore: Williams & Wilkins, **1985**:454
17. DeLaPaz RL, Patronas NJ, Brooks RA, et al. Positron emission tomographic study of suppression of gray-matter glucose utilization by brain tumors. *AJNR* **1983**;4:826–829
18. Patronas NJ, Di Chiro G, Smith BH, et al. Depressed cerebellar glucose metabolism in supratentorial tumors. *Brain Res* **1984**;291:93–101
19. Haymaker W, Ibrahim MAM, Miquel J, Call N. Delayed radiation effects in the brains of monkeys exposed to X- and γ-rays. *J Neuropathol Exp Neurol* **1968**;27:50–79
20. Rubinstein LJ. Tumors of the central nervous system. In: *Atlas of tumor pathology*, 2d series, fasc 6. Washington, DC: Armed Forces Institute of Pathology, **1972**:349–360
21. Kleinschmidt-DeMasters BK. Intracarotid BCNU leukoencephalopathy. *Cancer* **1986**;57:1276–1280
22. Hickman J, Ashwell G. Effect of irradiation by X-ray upon anaerobic glycolysis in spleen homogenates. *J Biol Chem* **1953**;205:651–659
23. Parkinson JD, Irving CC. Effect of irradiation on glycolysis of rat liver. *Radiat Res* **1956**;5:589–590
24. Ito M, Patronas NJ, Di Chiro G, Mansi L, Kennedy C. Effect of moderate level X-radiation to brain on cerebral glucose utilization. *J Comput Assist Tomogr* **1986**;10(4):584–588
25. Burger PC, Kamenar E, Schold SC, Fay JW, Phillips GL, Herzig GP. Encephalomyelopathy following high-dose BCNU therapy. *Cancer* **1981**;48:1318–1327

FORTHCOMING ARTICLES

SPECIAL ARTICLES FOR JUBILEE ANNIVERSARY VOLUME

***AJR*: the 50 most frequently cited papers in the past 50 years.** *Chew FS*

Anniversary reprint. Mono-osteitic Paget's disease as a clinical entity: roentgenologic observations in nine cases. *Groh JA*

Review Article. Paget disease of bone: current status and a look back to 1943 and earlier. *Resnick D*

CONTRAST MATERIAL

Perspective. Pretreatment with corticosteroids to prevent reactions to IV contrast material: overview and implications. *Lasser RC*

CARDIOPULMONARY RADIOLOGY

Perspective. Lung cancer: update on staging classifications. *Friedman PJ*

Small-cell bronchogenic carcinoma: CT evaluation. *Pearlberg JL, Sandler MA, Lewis JW Jr, Beute GH, Alpern MB*

Asbestos-related pleural disease and asbestosis: a comparison of CT and chest radiography. *Friedman AC, Fiel SB, Fisher MS, Radecki PD, Lev-Toaff AS, Caroline DF*

GASTROINTESTINAL RADIOLOGY

Gastrointestinal inflammation after bone marrow transplantation: graft-versus-host disease or opportunistic infection? *Jones B, Kramer SS, Saral R, et al.*

MR imaging of portal venous thrombosis: correlation with CT and sonography. *Zirinsky K, Markisz JA, Rubenstein WA, et al.*

Case report. Hepatic venoocclusive disease after bone marrow transplantation: diagnosis with duplex sonography. *Kriegshauser JS, Charboneau JW, Letendre L*

Heterotopic gastric mucosa in the duodenum: radiographic findings. *Agha FP, Ghahremani GG, Tsang T-K, Victor TA*

Management of chronic intestinal obstruction: value of percutaneous gastrostomy tube placement. *Picus D, Marx MV, Weyman PJ*

Case report. Infarcted Meckel diverticulum detected by CT. *Russ PD, Friefeld GD, Nauck CJ, Wilmouth RJ*

CT carcinoma of the Colon: detection and preoperative staging by CT. *Balthazar EJ, Megibow AJ, Hulnick D, Naidich DP*

GENITOURINARY AND OBSTETRIC RADIOLOGY

Extracorporeal shock-wave lithotripsy: Prevalence of renal stones 3 to 21 months after treatment. *Miles SG, Kaude JV, Newman RC, Thomas WC, Williams CM*

Extracorporeal shock-wave lithotripsy: long-term complications. *Williams CM, Kaude JV, Newman RC, Peterson JC, Thomas WC*

Commentary. Extracorporeal shock-wave lithotripsy: slam-bang effects, silent side effects. *Mulley AG Jr, Carlson KJ*

Renal transplant dysfunction: MR evaluation. *Winsett MZ, Amparo EG, Fawcett HD, et al.*

Case report. Renal embolization for hematuria: coordination with cystoscopy. *Swartz DA, McLellan GL, Mitchum D, Vines F*

Balloon catheter dilatation of urethral strictures. *Mohammed SH, Wirima J*

MUSCULOSKELETAL RADIOLOGY

Meniscal and ganglion cysts of the knee: MR evaluation. *Burk DL Jr, Dalinka MK, Kanal E, et al.*

Complications of knee ligament reconstruction: plain film analysis. *Manaster BJ, Remley K, Newman AP, Mann FA*

Shoulder impingement syndrome: MR findings in 53 shoulders. *Seeger LL, Gold RH, Bassett LW, Ellman H*

Case report. MR imaging of hemophilic pseudotumors. *Wilson DA, Prince JR*

Case report. MR imaging of Mafucci syndrome. *Unger EC, Kessler HB, Kowalyshyn MJ, Lackman RD, Morea GT*

Case report. Polychondritis affecting the laryngeal cartilages: CT findings. *Casselman JW, Lemahieu SF, Peene P, Stoffels G*

PEDIATRICS AND FETAL RADIOLOGY

Scoliosis examinations: organ dose and image quality with rare-earth screen-film systems. *Fearon T, Vucich J, Butler P, et al.*

MR imaging of Ebstein anomaly: results in four cases. *Link KM, Herrera MA, D'Souza VJ, Formanek AG*

Radiographic evaluation of the chest in infant cardiac allotransplantation. *Toomey FB, Bailey LL, Dang BWR, et al.*

Case report. Food allergy presenting as obstruction in an infant. *McIlhenny J, Sutphen JL, Block CA*

Technical note. The use of midazolam for premedication of infants and children. *Diament MJ, Stanley P*

Case report. Third-trimester fetal sonography: meconium simulating a presacral mass. *Moreland SI, Cohen MI, Leopold GR, Gosink BB*

NEURORADIOLOGY

Temporomandibular joint: MR imaging of internal derangements and postoperative changes. *Schellhas KP, Wilkes CH, Fritts HM, Omlie MR, Heithoff KB, Jahn JA*

Syringomyelia as a consequence of compressive extramedullary lesions: postoperative clinical and radiological manifestations. *Castillo M, Quencer RM, Green BA, Montalvo BM*

Comparison of MR and CT myelography in imaging the cervical and thoracic spine. *Karnaze MG, Gado MH, Sartor KJ, Hodges FJ III*

Treatment of vertebral arteriovenous fistulas. *Halbach VV, Higashida RT, Hieshima GB*

Tolosa-Hunt syndrome revisited: not necessarily a diagnosis of exclusion. *Kwan ESK, Wolpert SM, Hedges TR IV, Laucella M*

VASCULAR RADIOLOGY

Pictorial essay. Color-flow Doppler imaging of carotid artery abnormalities. *Middleton WD, Foley WD, Lawson TL*

Greenfield filter: percutaneous placement in 50 patients. *Denny DF Jr, Dorfman GS, Cronan JJ, Greenwood LH, Morse SS, Yoselevitz M*

The collapsed inferior vena cava: CT evidence of hypovolemia. *Jeffrey RB Jr, Federle MP*

Case report. Splenic artery pseudoaneurysms causing lower gastrointestinal hemorrhage. *Walker TG, Geller SC, Waltman AC*

Pictorial essay. The popliteal artery and its branches: embryologic basis of normal and variant anatomy. *Mauro MA, Jaques PF, Moore M*

Technical Note

Simple Radiation Protection Device for CT

Kedar Chintapalli,[1] William Wentworth,[2] and Charles R. Wilson[1]

We constructed a retractable radiation protection shield for use in the CT scanning room. The shield is placed between the patient and the radiologist while the radiologist injects the contrast medium for CT studies. In this report we describe the construction of this radiation protection shield and its usefulness in decreasing the radiation exposure to radiology personnel.

We constructed a rectangular metal frame 20 × 3.5 in. (50 × 8.8 cm) using two pieces of aluminum box-tubing (50 × 2 cm, each) and two 4-cm-long steel spacers with ¼-in (0.6-cm) holes for ¼-in. bolts. All the supplies used are available in hardware stores. A double-jointed metal arm (Ritter, Rochester, NY) and a lead rubber shield (0.25-mm lead equivalent) (Wolf X-Ray Corp., West Hempstead, NY) were purchased. The lead rubber shield (18 × 24 in. or 45 × 60 cm) is draped over the lower horizontal rod of the rectangular metal frame to give 0.5-mm lead equivalent. This is suspended from the ceiling support of a dental lamp by a double-jointed metal arm

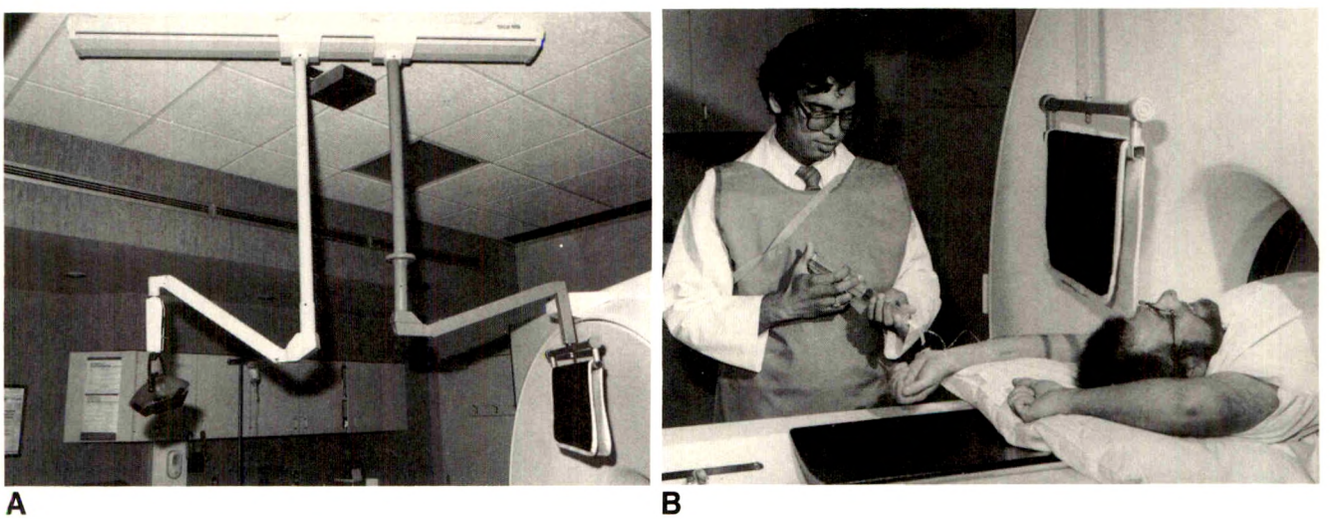

A B

Fig. 1.—*A*, Radiation protection device uses double-jointed metal arm suspended from ceiling support of dental lamp. *B*, Protection shield in place between gantry and radiologist.

Received June 22, 1987; accepted after revision August 18, 1987.

[1] Department of Radiology, The Medical College of Wisconsin and Veterans Administration Medical Center, Milwaukee, WI 53226. Address reprint requests to K. Chintapalli, Department of Radiology, VA Medical Center, Milwaukee, WI 53226.

[2] Department of Biomedical Engineering, Veterans Administration Medical Center, Milwaukee, WI 53226.

AJR 150:199–200, January 1988 0361–803X/88/1501–0199 © American Roentgen Ray Society

as shown in Figure 1A. The dental lamp (Ritter) is used for additional illumination for starting IV lines. Most of our CT studies were done by an incremental dynamic-scan technique with rapid injection of contrast material during the early part of the scanning.

During the dynamic CT studies, a radiologist is present to inject the contrast media. Although the radiologist stays at least 1 ft (30 cm) from the gantry, on occasion one may have to look at the gantry to check for inadvertent local infiltration of the contrast material or to check the patient for any contrast reaction. In doing so, the radiologist looks at the source of radiation (the rotating X-ray tube). To avoid supplying individual leaded eyeglasses and neck shields to our personnel (which are costly, especially when several radiologists are involved), we constructed this retractable radiation protection shield. We used this shield routinely during hand injections of contrast material during the last year (Fig. 1B).

Using an ionization-chamber survey instrument (Victoreen, Panoramic mode 470A, Cleveland, OH), radiation measurements were obtained in the integrated mode. The survey instrument had been calibrated by placing the unit in a known radiation field produced by a cesium-137 source. The energy response of the chamber varies less than ±5% for phantom energies from 44 to 662 keV. The radiation exposure at 1-ft distance from the gantry without the shield during scanning was 0.25 mR/scan (6.5×10^{-8} C/kg per scan). The location of the chamber was approximately the location of the radiologist's head while performing IV injection. When the protection shield was in place, the radiation exposure was reduced to less than 0.02 mR/scan (0.5×10^{-8} C/kg per scan). These measurements were obtained on a GE 8800 CT scanner with 120 kVp, mAs of 614 for a 10-mm-thick head scan and mAs of 960 for a 5-mm-thick abdominal scan. A lead rubber shield of 0.5-mm lead equivalent is expected to reduce the radiation exposure to less than one-tenth of the incidental dose [1]. The acceptable dose to the eye is less than 100 mR/week. In a busy CT section, a radiologist may be exposed to 50% of the acceptable dose, not including the exposure that may be received during fluoroscopic procedures. Use of the protection shield significantly reduces the dose.

Thus, the retractable radiation protection shield is helpful in preventing radiation to the thyroid gland and the lens of the eyes. We used the ceiling support of the existing dental light. When a dental light is not present, a new ceiling support can be constructed to suspend the retractable shield. The simple device can be easily constructed.

REFERENCES

1. National Council on Radiation Protection and Measurements (NCRP). Structural shielding design and evaluation for medical use of X-rays and gamma rays of energies up to 10 MeV (report no. 49). Washington, DC:NCRP, Sept. 15, **1976**

Invitation to the 1988 American Roentgen Ray Society Meeting in San Francisco, CA, May 8–13, 1988

I am pleased to extend an invitation to all radiologists to attend the 88th annual meeting of the American Roentgen Ray Society in San Francisco, CA, May 8–13, 1988. In keeping with the ARRS tradition, outstanding scientific and social programs will be provided.

The excitement of a meeting set in the center of San Francisco requires no further description. The opportunity for busy radiologists to attend a major national meeting while enjoying such an environment is ideal.

The scientific program, instructional courses, and categorical course are certain to be interesting and informative (see Table 1 for schedule).

Scientific Program

Two hundred scientific papers have been selected from a record submission of 650 abstracts. Scientific sessions will be devoted to all major body systems, angiography, interventional techniques, sonography, and mammography. Special emphasis has been placed on discussion of newer developments.

The innovative and extremely well-received Friday morning minisymposium is entitled "Chest Imaging Update, 1988." Theresa McLoud and Gordon Gamsu have assembled an outstanding faculty for what I am sure will be a very stimulating program.

Instructional Courses

Joseph Ferrucci, Chairman of the Instructional Course Committee, has put together 60 instructional courses. Faculty members have been drawn from across the entire country, with emphasis on luminaries from the West Coast. A superlative educational experience is anticipated, and advance registration is recommended.

Categorical Course

An extraordinary categorical course on breast imaging has been fashioned by Stephen Feig. The course covers equipment, principles of diagnosis, biopsy techniques, screening, and all the important aspects of breast imaging. This course is certain to be popular, and advance registration is advised.

Scientific Exhibits

The 220 scientific exhibits coordinated by John Madewell will cover the entire breadth of the field of diagnostic radiology. The technical exhibits will be displayed in the same area as the scientific exhibits to enhance the interaction of the attendees with our technical exhibitors.

TABLE 1: Summary of 1988 American Roentgen Ray Society Meeting

Sunday May 8	Monday May 9	Tuesday May 10	Wednesday May 11	Thursday May 12	Friday May 13
	8–9:30 Instructional courses	8–9:30 Instructional courses	8–9:30 Instructional courses	8–9:30 Instructional courses	8–10 Symposium: chest imaging update
9–noon Categorical course: breast imaging	10–10:30 Opening ceremonies				
	10:30–12:30 Scientific programs	10–12:30 Scientific programs	10–12:30 Awards session/ Caldwell lecture	10–12:30 Scientific programs	10:30–12:30 Symposium: chest imaging update
1:30–3 Categorical course: breast imaging	1:30–3:30 Categorical course: breast imaging	1:30–3:30 Scientific programs	1:30–3:30 Scientific programs	1:30–3:30 Scientific programs	
3:30–5:30 Categorical course: Breast imaging	4–5:30 Instructional courses and categorical course: breast imaging	4–5:30 Instructional courses and categorical course: breast imaging	4–5:30 Instructional courses and categorical course: breast imaging	4–5:30 Instructional courses and categorical course: breast imaging	

Caldwell Lecture

Donald L. Resnick of the University of California at San Diego has accepted an invitation to present the Caldwell Lecture for 1988. His lecture, "Common Disorders of Synovial Joints: Pathogenesis, Imaging Abnormalities, and Complications," promises to be a highlight of the meeting.

Social Events

San Francisco offers an unlimited number of diversions, and George Janetos, Chairman of the Local Arrangements Committee, has engaged Tours West to plan a variety of outstanding tours. The annual golf and tennis tournaments for attendees and their companions are scheduled for Monday. The traditional cocktail party given by the Society in the exhibit area for all registrants will be Tuesday evening and will provide a convenient meeting place before an evening on the town.

This promises to be a truly outstanding event in exceptional surroundings. I hope you will be able to accept our invitation. Plan now to attend.

Lee F. Rogers
President-Elect, ARRS

Forthcoming ARRS Meeting Information

Details of the American Roentgen Ray Society Meeting in San Francisco, CA, May 8–13, 1988, will appear in the **February** and **March** 1988 issues of the *AJR*. The complete scientific program, abstracts of the instructional programs, information about social events, and hotel and travel forms will be published in the Journal.

See pages 70 and 114 of this issue for more information concerning the meeting.

Review of Current Literature

Initials and addresses of corresponding authors are provided in parentheses for each article so that the reader can obtain reprints directly. Abstracts are printed verbatim from each journal.

CLINICAL LITERATURE

The New England Journal of Medicine

Pretreatment with corticosteroids to alleviate reactions to intravenous contrast material. Lasser EC, Berry CC, Talner LB, et al. (ECL, Dept. of Radiology, M-032, UCSD, La Jolla, CA 92093). *N Engl J Med* 317:845–849, Oct. 1987

The x-ray contrast mediums used over the past three decades have been salts of iodinated acids administered in highly hypertonic concentrations. We conducted a multiinstitutional randomized study of the protective effects of pretreatment with corticosteroids against reactions to intravenous contrast material. We gave 6763 patients two doses of oral corticosteroids (methylprednisolone, 32 mg) approximately 12 hours and 2 hours before challenge with contrast material, one dose of oral prednisolone approximately 2 hours before challenge, or placebo in the same dosages. The two-dose corticosteroid regimen, but not the one-dose regimen, significantly reduced the incidence of reactions of all types ($P < 0.05$) except a category of reactions dominated by hives, for which the reduction approached significance ($P = 0.055$).

In recent years, several relatively expensive monomeric nonionic iodinated compounds having approximately half the osmolality of the corresponding ionic compounds and a lower reaction rate have become available. With our two-dose corticosteroid regimen, the incidence of reactions necessitating therapy in patients receiving the ionic medium approximated that reported in an unblinded nonrandomized study of patients receiving a newer intravenous nonionic medium without corticosteroid pretreatment.

We conclude that the much less expensive ionic medium, if administered with corticosteroid pretreatment, may serve as a reasonable alternative to intravenous nonionic medium, without loss of safety.

A prospective study of ultrasonography in the diagnosis of appendicitis. Puylaert JBCM, Rutgers PH, Lalisang RI, et al. (JBCMP, Radiological Dept., Westeinde Hospital, Lijnbaan 32, 2512 VA The Hague, Netherlands). *N Engl J Med* 317:666–669, Sept. 1987

The diagnosis of appendicitis is frequently difficult. We studied prospectively the diagnostic accuracy and clinical impact of abdominal ultrasonography in 111 consecutive patients thought to have appendicitis. Ultrasonography was performed with small high-resolution, linear-array transducers, with the abdomen compressed to displace or compress bowel and fat.

Among 52 patients later shown in surgery to have appendicitis, ultrasonography was unequivocally positive in 39 (sensitivity, 75 percent). Of 31 patients in whom appendicitis was definitely excluded, none had a positive ultrasound examination (specificity, 100 percent). The sensitivity in those with a perforated appendix (28.5 percent) was much lower than in those with acute nonperforating appendicitis (80.5 percent) or appendiceal mass (89 percent), but the low sensitivity did not influence clinical management, since the need for surgery in patients with a perforated appendix was clinically obvious.

Ultrasonography resulted in changes in the proposed management in 29 of the 111 patients (26 percent). It also led to the correct diagnosis in the 16 patients who were found to have a disease other than appendicitis.

We conclude that ultrasonography is a useful aid in the diagnosis of appendicitis.

Bone sarcomas linked to radiotherapy and chemotherapy in children. Tucker MA, D'Angio GJ, Boice JD Jr, et al. (MAT, Environmental Epidemiology Branch, National Cancer Institute, Landow Bldg., Rm. 3C39, Bethesda, MD 20892). *N Engl J Med* 317:588–593, Sept. 1987

We estimated the risk of subsequent bone cancer among 9170 patients who had survived two or more years after the diagnosis of a cancer in childhood.

As compared with the general population, the patients had a relative risk of 133 (95 percent confidence interval, 98 to 176) and a mean (±SE) 20-year cumulative risk of 2.8 ± 0.7 percent. Detailed data on treatment were obtained on 64 patients in whom bone cancer developed after childhood cancer. As compared with 209 matched controls who had survived cancer in childhood but who did not have bone cancer later, patients who had had radiation therapy had a 2.7-fold risk (95 percent confidence interval, 1.0 to 7.7) and a sharp dose–response gradient reaching a 40-fold risk after doses to the bone of more than 6000 rad. The relative dose–response effect among patients who had been treated for retinoblastoma resembled that among patients with all other types of initial tumors, although the cumulative risk of bone cancer in the retinoblastoma group was higher. Similar numbers of patients were treated with orthovoltage and megavoltage; the patterns of risk among categories of doses did not differ according to the type of voltage. After adjustment for radiation therapy, treatment with alkylating agents was also linked to bone cancer (relative risk, 4.7; 95 percent confidence interval, 1.0 to 22.3), with the risk increasing as cumulative drug exposure rose.

We conclude that both radiotherapy and chemotherapy with alkylating agents for childhood cancer increase the subsequent risk of bone cancer.

Cancer

The effect of the respiratory cycle on mediastinal and lung dimensions in Hodgkin's disease: implications for radiotherapy gated to respiration. Willett CG, Linggood RM, Stracher MA, et al. (CGW, Dept. of Radiation Medicine, Cox Bldg., Massachusetts General Hospital, Blossom St., Boston, MA 02114). *Cancer* 60:1232–1237, Sept. 1987

Changes in mediastinal and lung dimensions during respiration were studied to assess the potential of radiotherapy gated to respiration to minimize normal tissue irradiation. Twelve patients with mediastinal Hodgkin's disease were assessed using chest radiographs and thoracic computed tomography (CT) scans both during quiet breathing and at maximum inspiration in the standing, supine, and prone positions. A simple measure of the bulk of mediastinal disease, the ratio of the width of mediastinal mass to thoracic diameter, was determined from posteroanterior (PA) chest radiographs. The volumes of mediastinum, irradiated and protected lung if anteroposterior (AP) and PA mantle fields were used were determined from sequential thoracic CT scans and three-dimensional treatment planning and compared at quiet breathing and deep inspiration. The mediastinal width to thoracic diameter ratio decreased from quiet breathing to deep inspiration an average of 3%, 9%, and 11% for the standing, supine, and prone positions, respectively. Lung volumes as measured from the thoracic CT scans showed that on average, 8% more lung was protected at deep inspiration than at quiet breathing, independent of treatment position. The maximum increase in the percentage of protected lung from quiet breathing to deep inspiration was seen in patients with extensive mediastinal adenopathy suggesting that radiotherapy gated to respiration may be most advantageous in the subset of patients.

Reprinted by permission from the American Cancer Society.

A new approach to chemoembolization therapy for hepatoma using ethiodized oil, cisplatin, and gelatin sponge. Sasaki Y, Imaoka S, Kasugai H, et al. (YS, Dept. of Surgery, The Center for Adult Diseases, Osaka, 1-3-3 Nakamichi Higashinari-ku Osaka, 537, Japan). *Cancer* 60:1194–1203, Sept. 1987

This article reports on a new approach to hepatic arterial chemoembolization therapy using ethiodized oil (Lipiodol, Ultra Fluide), cisplatin, and gelatin sponge (Gelfoam, Upjohn, Kalamazoo, MI) for hepatocellular carcinoma (HCC). The anticancer effects of this therapy on 20 patients who underwent subsequent hepatic resection were evaluated mainly by histologic examination. All main tumors were reduced in size following this therapy. It is notable that in 65% of the patients the tumor size was reduced to less than 50% of that before therapy. All the values of serum α-fetoprotein (AFP) in the patients who exhibited pretreatment levels exceeding 100 ng/ml dropped by more than 50%, and in 55% of them it fell below 20 ng/ml. The concentration of platinum in the tumor tissue was significantly higher than that in the nontumorous tissue. In 15 of 20 patients (75%), the main nodules were completely necrotic. Thirteen of the patients had daughter nodules and/or small intrahepatic metastases (Group A); nine had tumor emboli in the portal (hepatic) vein (Group B); 17 had intracapsular invasions (Group C); and ten had extracapsular invasions (Group D). The ratios of patients with completely necrotic cancer cells in Group A were nine of 13 (69%); in Group B, seven of nine (78%); in Group C, 11/17 (65%); and in Group D, four of 10 (40%). In eight of the 20 patients (40%) no viable cancer cells were recognized at any foci. Lesions other than those with extracapsular invasion could be considerably eliminated with this form of therapy. It is expected that this method will become the therapy of choice not only for palliative treatment but also for preoperative treatment.

Reprinted by permission from the American Cancer Society.

Gianturco expandable wire stents in the treatment of superior vena cava syndrome recurring after maximum-tolerance radiation. Rosch J, Bedell JE, Putnam J, Antonovic R, Uchida B (JR, L-340, 3181 S. W. Sam Jackson Park Rd., Portland, OR 97201). *Cancer* 60:1243–1246, Sept. 1987

Two patients with superior vena cava syndrome (SVCS) recurring after maximum-tolerance radiation were treated by placing a Gianturco expandable wire stent (GEWS) into the obstructed superior vena cava. The SVCS symptoms rapidly disappeared and good short-term (6 months) palliation was achieved. GEWS placement is a promising therapeutic alternative for palliation of SVCS symptoms when other therapeutic modes cannot be used or are not effective.

Reprinted by permission from the American Cancer Society.

Chest

CT of the lung parenchyma and the pulmonary function test. Sider L, Dennis L, Smith LJ, Dunn MM (LS, 710 North Fairbanks Ct., NMH, Chicago, IL 60611). *Chest* 92:406–410, 1987

Computed tomography (CT) views of the lung parenchyma were compared with the corresponding pulmonary function tests (PFTs) in 39 patients. Scans were assigned a quantitative degree of involvement based on previously described CT findings. CT was fairly successful in confirming a normal appearance of the lungs in patients with normal PFTs (ten cases). CT was accurate in detecting the presence of a chronic interstitial pattern in patients with restrictive defects on PFTs (15 cases). CT was generally less successful in both the detection and quantitation in patients with PFT criteria of chronic obstructive lung disease (14 cases).

Circulation

The transstenotic pressure gradient trend as a predictor of acute complications after percutaneous transluminal coronary angioplasty. Redd DCB, Roubin GS, Leimgruber PP, Abi-Mansour P, Douglas JS Jr, King SB III (GSR, Interventional Cardiovascular Medicine, Emory University Hospital, Ste. F-606, 1364 Clifton Rd. N.E., Atlanta, GA 30322). *Circulation* 76(4):792–801. 1987

The transstenotic pressure gradient recorded during coronary angioplasty (PTCA) reflects the dynamic relationship that exists between coronary blood flow and the effective cross-sectional area of the arterial lumen. An apparent relationship between the dynamic behavior of the pressure gradient and subsequent acute vessel closure was observed in our catheterization laboratory. We therefore examined the usefulness of the pressure gradient trend in predicting acute complications after 463 attempted PTCA procedures. Two pressure gradient trend patterns were identified: (1) a rising trend pattern identified by an increasing pressure gradient in the interval after deflation of the angioplasty, and (2) a stable trend pattern identified by a constant or decreasing pressure gradient. The incidence of acute vessel closure (17% vs 4%, $p = .0001$), emergency CABG (5.6% versus 1%, $p<.05$), and myocardial infarction (13% versus 2%, $p<.0001$) after the PTCA procedure was significantly higher among patients with rising trend patterns when compared with patients with stable trend patterns. Multivariate analysis identified independent predictors for an acute closure event as a rising trend pattern ($p<.001$), post-PTCA gradient ($p<.05$), and post-PTCA percent diameter stenosis ($p<.02$). Independent predictors for emergency coronary artery bypass grafting and myocardial infarction were post-PTCA gradient ($p<.001$) and a rising trend pattern (odds ratio = 2.91, $p<.001$), respectively. The dynamic behavior of the gradient trend provides additional useful information about the results of dilatation. This information is available before completion of dilatation and may assist in clinical decision making by identifying those patients who may be at risk for developing acute complications in the post-PTCA period.

Gastroenterology

Normal venous circulation of the gastroesophageal junction: a route to understanding varices. Vianna A, Hayes PC, Moscoso G, et al. (R. Williams, Liver Unit, King's College Hospital, Denmark Hill, London SE5 9RS, United Kingdom). *Gastroenterology* 93:876–889, 1987.

A study into the normal anatomy of the venous circulation of the gastroesophageal junction was undertaken using three complementary techniques (radiology, corrosion casting, and morphometry). Four distinct zones of venous drainage were defined as follows: (a) gastric zone, characterized by a longitudinal venous distribution; (b) palisade zone, composed of parallel vessels arranged in groups, lying mainly within the lamina propria; (c) perforating zone, characterized by "treble clef" shaped veins, which collect and channel blood into extrinsic veins; and (d) truncal zone, composed of four or five deep lying descending veins. This venous system appeared to be mainly distributed within the esophageal mucosal folds. The anatomic pattern suggests that venous flow is bidirectional at the palisade zone, which acts as a high-resistance watershed region between the portal and azygos systems. In patients with portal hypertension this normal vascular system has to accommodate greatly increased venous flow, and the anatomy as demonstrated here offers insight into variceal development.

Reprinted with permission by the American Gastroenterological Association.

Digestive Diseases and Sciences

Radiographic evaluation of esophagus immediately after pneumatic dilatation for achalasia. Ott DJ, Richter JE, Wu WC, Chen YM, Castell DO, Gelfand DW (DJO, Dept. of Radiology, Bowman Gray School of Medicine, Winston-Salem, NC 27103). *Dig Dis Sci* 32(9):962–967, Sept. 1987

Forty-one (98%) of 42 patients with achalasia of the esophagus had pneumatic dilatation performed successfully using the Brown-McHardy dilator. One to four dilatations (mean, 1.9) were done on each patient with inflation pressures of 8–15 psi (mean, 11.1 psi). Immediately after the procedure, all patients were examined radiographically by injection of contrast material into the lower esophagus through a nasoesophageal tube. Two immediate and two delayed perforations occurred. Six intramural hematomas were noted, five of which resolved spontaneously. The luminal diameter at the esophagogastric junction increased from a mean of 4.2 mm before dilatation to 7.5 mm following treatment. Four patients with previous Heller myotomy were dilated without complications. Perforation was more common in patients with a minimal change in the esophagogastric diameter. Thirty-five patients (85%) improved symptomatically within several days following pneumatic dilatation. Excluding patients with perforation, the postdilatation appearance of the lower esophagus poorly correlated with clinical response.

Pancreatic abscess and infected pancreatic necrosis: different local septic complications in acute pancreatitis. Bittner R, Block S, Büchler M, Beger HG (HGB, Dept. of General Surgery, University of Ulm, Steinhövelstr. 9, D-7900 Ulm, Federal Republic of Germany). *Dig Dis Sci* 32(10):1082–1087, Oct. 1987

Local septic complications in acute pancreatitis need to be exactly characterized and defined in order to develop improved concepts for their prevention, early diagnosis, and therapy. While up to now all local septic complications have been termed abscesses, the present study for the first time delineates the morphologic, clinical, and laboratory criteria needed to distinguish between two separate clinical entities: the infected necrosis (IN) and the pancreatic abscess (PA). IN is defined as a diffuse bacterial inflammation of necrotic pancreatic and peripancreatic tissue, but without any significant pus collections. On the other hand, the morphologic substrate of PA is a localized collection of pus surrounded by a more or less distinct capsula. IN becomes clinically evident during the early phase of acute pancreatitis (AP). The patients with IN present both the signs of sepsis and the laboratory findings of AP. Thus in these patients the most fulminant course of AP is observed; 51.8% and 35.7% of them have pulmonary or renal insufficiency, respectively. The mortality of the patients with IN is high and amounts to 32.1%. Pancreatic abscess, on the other hand, does not develop before the fifth week after onset of symptoms and after subsidence of the acute phase of pancreatitis. In these patients laboratory signs of AP-like amylasemia, hypocalcemia, hyperglycemia, and rise of LDH are rarely observed. Corresponding to the lack of pathophysiologic effects of AP per se, pulmonary and renal insufficiencies occur in only 33.3% and 16.7%, respectively, and mortality in these patients is 22.2%. While an abscess may readily be identified by computed tomography, the differentiation between IN and non-IN can be very difficult. The prognostic significance, however, makes this distinction absolutely necessary. According to our experience, surgical debridement is the procedure of choice for patients with IN.

The Journal of Urology

Renal lesions in tuberous sclerosis. Stillwell TJ, Gomez MR, Kelalis PP (PPK, Dept. of Urology, Mayo Clinic, 200 First St. S. W., Rochester, MN 55905). *J Urol* 138:477–481 Sept. 1987

The renal lesion classically associated with tuberous sclerosis is angiomyolipoma. Renal cysts are less frequent, occurring alone or in conjunction with angiomyolipomas. We reviewed the records of 274 patients with tuberous sclerosis registered at our clinic. Of 95 patients evaluated for renal lesions 51 (54 per cent) had positive findings: 45 had angiomyolipomas, 17 had renal cysts and 11 had both lesions. These lesions usually are multiple and bilateral, and are diagnosed most effectively with computerized tomography or ultrasound. Surgery (10 kidneys) was done for life-threatening hemorrhage or suspected malignant lesions.

British Journal of Urology

Effects of vesicoureteric reflux on renal growth and function as measured by GFR, plasma creatinine and urinary concentrating ability: an experimental study in the minipig. Ransley PG, Risdon RA, Godley ML (PGR, Institute of Child Health, London, United Kingdom). *Br J Urol* 60:193–204, 1987

The influence of vesicoureteric reflux (VUR) on renal growth and function measured by glomerular filtration rate (GFR), plasma creatinine concentration and urinary concentrating ability has been examined in a simple one-kidney model in the growing minipig over a period of approximately 5 months. Animals with reflux in association with low voiding pressures and normal bladder function (n = 6), as well as those with raised voiding pressures and abnormal bladder function (n = 5), were investigated together with appropriate non-refluxing controls (n = 12). Urinary infection and renal scarring were avoided since these factors may affect kidney function and growth independently.

Statistical tests of difference failed to demonstrate any effect of VUR on ^{51}Cr EDTA GFR or renal growth even in the presence of elevated voiding pressures and abnormal detrusor function. However, a significant association between VUR and reduced urinary concentrating ability was shown.

Pediatrics

Idiopathic cerebral arterial infarction with paucity of symptoms in the full-term neonate. Roodhooft AM, Parizel PM, Van Acker KJ, Deprettere AJR, Van Reempts PJ (AMR, Dept. of Pediatrics, University of Antwerp, Universiteitsplein, 1, B-2610 Wilrijk, Belgium). *Pediatrics* 80(3):381–385, Sept. 1987

Two full-term neonates, one with convulsions and intermittent generalized hypotonia and one with poor sucking, temperature instability, and lethargy, are reported. CT scan findings suggested cerebral arterial infarction. Arteriography revealed occlusion of the middle cerebral artery, unilaterally in the first and bilaterally in the second patient. The evolution of the infarct could be followed on serial CT scans. No predisposing factors during pregnancy or delivery were found, and serious neurologic deficits developed in both children.

These cases demonstrate that, even in full-term neonates with discrete or moderate neurologic symptoms and born after normal pregnancy and delivery, the possibility of vasooclusive brain infarction should be considered. The diagnosis is suggested by imaging techniques, of which CT scanning seems to have the greatest value at present. This technique also permits the follow-up of the lesions. The prognosis for neurologic development appears to be variable: minor neurologic deficits as well as unexplained spastic hemiplegia in older children may be the consequence of inapparent cerebral arterial infarction in the neonatal period.

Reprinted by permission of *PEDIATRICS* ©1987.

The Journal of Pediatrics

Management of Chiari II complications in infants with myelomeningocele. Charney EB, Rorke LB, Sutton LN, Schut L (EBC, The Children's Hospital of Philadelphia, 34th St. and Civic Center Blvd., Philadelphia, PA 19104). *J Pediatr* 111:364–371, Sept. 1987

Vocal cord paralysis with inspiratory stridor during infancy is a well-recognized complication of the Arnold-Chiari malformation associated with myelomeningocele. Management of these symptoms, however, remains controversial. The outcome in 19 infants with symptoms managed by us during 1978–1984 was therefore reviewed. Ten infants had stridor alone at presentation (clinical grade 1), four infants also had apnea (grade 2), and five infants also had associated cyanotic spells and dysphagia (grade 3). Of 14 ventricular shunt revisions performed, seven were associated with resolution: in five of eight infants with grade 1, two of four with grade 2, and none of two with grade 3 symptoms. Of the 10 posterior fossa decompressions performed, two were associated with clinical resolution: in one of four infants with grade 1, one of two with grade 2, and none of four with grade 3 symptoms. Mortality over 6 months following onset of symptoms was absent among infants with grade 1, one with grade 2, and three with grade 3 symptoms. We propose that differences in outcome among the three groups of infants reflect differences in pathologic processes within the brain stem. We speculate that infants with grade 2 or 3 symptoms have more extensive brain stem damage, such as hemorrhage, infarction, and necrosis. Use of our classification system may be helpful in further studies on intervention modalities in these infants.

RADIOLOGY SUBSPECIALTY JOURNALS

The Journal of Nuclear Medicine

Single-dose captopril scintigraphy in the diagnosis of renovascular hypertension. Sfakianakis GN, Bourgoignie JJ, Jaffe D, Kyriakides G, Perez-Stable E, Duncan RC (GNS, Nuclear Medicine Lab., D-57, University of Miami School of Medicine, P. O. Box 016960, Miami FL 33136). *J Nucl Med* 28(9):1383–1392, Sept. 1987

Renal scintigraphy with [^{99m}Tc]diethylenetriaminepentaacetic acid (DTPA) and/or sodium-iodine-131-o-iodohippurate (HIP) was performed before and after an oral dose of captopril (50 mg) in 18 patients with renovascular hypertension (RVH) due to renal artery stenosis (RAS) and 18 controls. In every patient with RVH, captopril induced, enhanced or sustained abnormal findings on HIP scintigraphy depending on the degree of RAS. With DTPA scintigraphy, renal function decreased after captopril in ten kidneys with RVH-related RAS and adequate baseline renal function, but this phenomenon was not evident in 11 kidneys with RVH and poor renal function. Captopril did not influence HIP or DTPA studies of kidneys with patent renal arteries (patients after successful renal angioplasty, patients with essential hypertension, contralateral kidneys of patients with unilateral RVH) or ipsilateral kidneys with mild and subcritical (<60%) RAS in patients without hypertension and/or normal renal vein renin activity. When HIP and DTPA scintigraphy were compared in the same patients, HIP demonstrated greater sensitivity and specificity than DTPA, particularly in patients with poor renal function. HIP scintigraphy before and after a single dose of captopril may provide a rapid sensitive and minimally invasive test for screening patients with hypertension.

JOURNAL OF THORACIC IMAGING

Radiologic investigation of thoracic metastases from unknown primary sites. Marglin SI, Mortimer J. Castellino RA (SIM, Dept. of Radiology, SB-05, University Hospital, Seattle, WA 98195). *J Thorac Imag* 2(4):38–43, 1987

When a patient presents with thoracic metastases from a tumor whose site of origin is not apparent from the initial history, physical examination, and routine laboratory studies, there is a considerable likelihood that the individual will be subjected to an extensive and frequently unrewarding series of radiologic examinations. An analysis of the "behavior" of so-called tumors of unknown origin suggests that these tumors metastasize to distant sites with a frequency that is different from the more common tumors, that is to say, those whose primary site is readily apparent. While compulsive testing should unquestionably be eschewed, certain radiologic tests are still appropriate. These studies should be supplemented, when necessary, by newer pathologic studies, primarily those that involve the rapidly developing field of immunocytochemistry.

Journal of Ultrasound in Medicine

Intraoperative imaging of the biliary tree: sonography vs. operative cholangiography. Buckley AR, Scudamore CH, Becker CD, Cooperberg PL (PLC, Dept. of Radiology, Vancouver General Hospital, 855 W. 12th Ave., Vancouver, B.C. V5Z 1M9, Canada). *J Ultrasound Med* 6(10):589–595, Oct. 1987

The accepted technique for diagnosing choledocholithiasis at the time of cholecystectomy is operative cholangiography. Reports in the surgical literature suggest that intraoperative ultrasound can replace operative cholangiography in the accurate detection of common duct stones. This prospective study was performed jointly by radiologists and surgeons together in the operating room. Twenty-one patients underwent intraoperative ultrasonography and operative cholangiography at the time of cholecystectomy. In the 16 cases in which both studies were adequate, there were 11 in which no stones were seen on either, three in which stones were seen on both; and two in which stones were diagnosed by sonography alone. In one of these latter cases, the stones were confirmed, making the cholangiogram falsely negative. In the other case, no stones were found so we presume that sonography was falsely positive. Although this technique can be accurate and useful, it is technically demanding, even for an experienced sonologist. We feel that this technique is likely to be of benefit only to the surgeon with considerable ultrasound training, expertise, and motivation.

Reprinted with permission by the American Institute of Ultrasound in Medicine.

Letters

Bone Densitometry

As a developer of both single- and dual-photon absorptiometry (SPA and DPA) and X-ray absorptiometry, I have opposed densitometry for mass screening [1], particularly appendicular SPA, because its diagnostic sensitivity is less than half that of axial densitometry. The 95% confidence limit in predicting axial bone density from SPA values is more than 25%. Values for normal older women average only about 16% higher than those of women with osteoporotic crush fractures, and these two groups have a 10-fold difference of relative risk. Hall [2], Hall et al. [3], and others [4] have (1) underestimated diagnostic sensitivity of axial densitometry and overemphasized the limitations of screenings, (2) confused screening with medically indicated diagnosis, and (3) underestimated the importance of monitoring therapy, even estrogen therapy.

Critics undervalue early diagnosis because their estimates of diagnostic sensitivity are usually (1) outdated, particularly for hip fracture, and (2) derived from patients who are 20 years older than the target perimenopausal group. For women at age 50 years old, the specificity of spinal and femoral DPA for spinal and femoral fractures is about 85% and 97%, respectively, at 90% sensitivity. It is true that measurements of the density of the radius, and even the spine, are not predictive of hip fracture. However, our data and those of several other research groups show an exquisite diagnostic sensitivity for densitometry of the proximal femur. The densities of patients who have hip fractures average 1.5 SD below the densities of age-matched controls and about 4 SD below those of young normal subjects [5]. Measurement of the density of the proximal femur in relation to hip fracture is one of the most sensitive diagnostic tests available in radiology today. Femoral density is four times as sensitive as radial density (which is no better than conventional risk factors such as age and body weight). About 80–90% of the variance in bone strength, and in fracture risk, is associated with density at fracture sites. Hence, axial densitometry gives comparable sensitivity compared with mammography but does not result in costly, painful, and unnecessary biopsies in 70% false-positive cases. Moreover, unlike the case with mammography, identification of patients at high risk is easy. Only 20% of asymptomatic women, ages 50–59 years, are osteopenic (<20% low) in the spine, whereas more than 60% of referred patients are osteopenic [6].

Novices have confused screening (asymptomatic women) with early diagnostic testing (patients with clear medical indications). This confusion inhibits reimbursement for the axial measurements that leading specialists in bone disease consider essential [7]. SPA screening in a minority (<10%) of the more than 1000 facilities that use densitometry has inhibited insurers from reimbursing for axial densitometry, and, as I predicted earlier [1], brought all densitometry into some disrepute.

Critics of densitometry often claim that the test does not have sufficient precision to monitor the various new and effective therapies that stabilize or increase the density of axial bone. This is based on the assumptions that a normal slow rate of loss (1%/year) occurs in osteoporosis and that there are slow if any increases in bone with therapy. These assumptions apply chiefly to the peripheral skeleton. The axial skeleton, however, shows large decreases with disease and large increases with therapy (2–5%/year). Such changes are readily detectable by axial densitometry and, in conjunction with clinical chemistries, provide a basis for clinical decision making. Even estrogens cannot be given without monitoring; long-term bone loss occurs in at least 30% of patients who are treated with these hormones [8, 9].

Axial densitometry in symptomatic patients is not only justifiable but also ethically and legally prudent. Diagnostic and monitoring applications were endorsed by leading clinicians at the recent National Institutes of Health/National Osteoporosis Foundation conference on osteoporosis (February 1987) and are recommended in the practice guidelines of the American Rheumatism Association and by the Society of Nuclear Medicine and the American College of Nuclear Physicians. Unknowledgeable critics of nonscreening densitometry do a disservice (1) to the more than 5 million patients who either have medical problems affecting bone or are undergoing therapies that affect bone and (2) to the 1000 hospitals that treat metabolic bone disease.

Richard M. Mazess
University of Wisconsin and
LUNAR Radiation Corp.
Madison, WI 53713

REFERENCES

1. Mazess RB, Cameron JR. Densitometry of appendicular bone in osteoporosis. *JAMA* **1985**;254(14):1906
2. Hall FM. Bone-mineral screening for osteoporosis. *AJR* **1987**;149:120–122
3. Hall FM, Davis MA, Baran DT. Bone mineral screening for osteoporosis. *N Engl J Med* **1987**;316(4):212–214
4. Cummings SR, Black D. Should perimenopausal women be screened for osteoporosis? *Am Coll Physicians* **1986**;104:817–823
5. Mazess RB, Barden H, Ettinger M, Schultz E. Bone density of the radius, spine and proximal femur in osteoporosis. *J Bone Min Res* (in press)
6. Ettinger M, Mazess RB, Barden H. Insensitivity of peripheral measurement to spinal osteopenia. *J Bone Min Res* **1986**;1:273
7. Riggs BL, Melton LF III. Involutional osteoporosis. *N Engl J Med* **1986**;314:1676–1686
8. Ettinger B, Genant HK, Cann CE. Postmenopausal bone loss is prevented by treatment with low-dosage estrogen with calcium. *Ann Intern Med* **1987**;106(1):40–45
9. Quigley MET, Martin PL, Burnier AM, Brooks P. Estrogen therapy arrests bone loss in elderly women. *Am J Obstet Gynecol* **1987**;156:1516–1521

Reply

Correspondence with Dr. Mazess is always an interesting experience [1], although not one I recommend for everyone. As usual I am overwhelmed with data in support of "medically indicated" bone densitometry and, more specifically, densitometry performed by the method of DPA. Unfortunately, the literature on these subjects is a quagmire of conflicting data and opinion. I should point out also that "physicians should be more skeptical of claims for the superiority of an approach over its competitors when the claims come from persons who would profit monetarily by its adoption" [2].

I am pleased that Dr. Mazess discourages bone mineral screening for osteoporosis. However, many physicians, owners of diagnostic clinics, and even patients, do not share this opinion. Third-party payers legitimately are concerned about the potentially almost limitless demand for this examination if reimbursement is offered.

Dr. Mazess would perform bone densitometry for "medical indications" only, but even this restriction is subject to wide interpretation. Many advocates of bone densitometry recommend that screening examinations be limited to perimenopausal women who are at increased risk for osteoporosis because of family history, medications, body habitus, diet, life-style, etc. [3]. Unfortunately, regardless of these factors, in older women, the risk of osteoporosis developing is close to 100%. The average postmenopausal woman loses 35% of her cortical bone and 50% of her trabecular bone during her lifetime, and if she lives to age 90, she will have an approximately one-third chance of having a hip fracture [3, 4].

I do not think that the solution to the problem of osteoporosis lies in early diagnosis by bone densitometry: Mere knowledge of age and sex permits bone density of the spine or femoral neck to be predicted with an SD of only about 10% [3]. Nor does the answer lie in treatment, which is almost nonexistent. Rather, the solution to the problem of osteoporosis lies in prevention, and, at the present time, the only effective and practical preventive therapy is treatment with estrogen. The real debate on osteoporosis concerns whether postmenopausal women routinely should be treated with estrogen. This treatment not only will reduce bone loss but also, perhaps more importantly, may reduce coronary heart disease [5, 6].

Bone mineral screening is an extraordinarily important research tool. However, it should not be used as a screening examination. I am delighted that Dr. Mazess and I can agree, at least nominally, on this.

Ferris M. Hall
Beth Israel Hospital
Boston, MA 02215

REFERENCES

1. Mazess RB, Genant HK. Bone mineral content in early-postmenopausal and postmenopausal osteoporotic women. *Radiology* **1987**;165:289–290
2. Petitti DB. Competing technologies: implications for the costs and complexity of medical care. *N Engl J Med* **1986**;315:1480–1483
3. Riggs BL, Melton LJ III. Involutional osteoporosis. *N Engl J Med* **1986**;314:1676–1686
4. National Institutes of Health. Concensus conference: osteoporosis. *JAMA* **1984**;252:799–802
5. Hilner BE, Hollenberg JP, Pauker SG. Postmenopausal estrogens in the prevention of osteoporosis: benefit virtually without risk if cardiovascular effects are considered. *Am J Med* **1986**;80:1115–1127
6. MacDonald PC. Estrogen plus progestin in postmenopausal women: act II. *N Engl J Med* **1986**;315:959–961

Risk Management for the Radiologist

In his article on risk management for the radiologist [1], Dr. Smith says that in a malpractice case a radiographic report that states simply "normal chest" is more likely to leave a jury with an impression of haste than a detailed verbose report that lists various structures as normal and certain possible abnormalities as absent. He may be correct, but he presents no evidence for his opinion. I hope that despite his warning radiologists will keep their reports concise. To get into the habit of dictating lengthy reports is to risk burying important findings amid the irrelevant. Moreover, excessive verbiage takes the radiologist extra time to dictate, the transcriber extra time to type, and the clinician extra time to read—if the clinician bothers. True, word processors and other computer-based devices can put out repetitive verbiage with little effort from the radiologist and transcriber. However, generating a report of the kind recommended by Dr. Smith by pushing a button or dictating the word "normal" smacks to me of dishonesty.

I think that the interests of patients, clinicians, and radiologists all are served best by following the advice of Strunk and White to omit needless words.

David M. Jackson
Milton Medical Center
Milton, MA 02186

REFERENCE

1. Smith JP. Risk management for the radiologist. *AJR* **1987**;149:641–643

Reply

Clarity is the hallmark of a good report. What is clear to a fellow physician, however, may be cryptic to the reader who does not have medical training. Our reports are evaluated not only by physicians but also by a variety of laypersons. Peer-review organizations, medical quality assurance committees, private health care insurers, patients, and attorneys may view as essential the words physicians deem needless. I think we can place the needs of our patients and their physicians first, satisfy lay readers, and not bury the important findings among the irrelevant. To accommodate lay readers, I suggest we broaden the scope of the narrative section of our reports; to uphold our commitment to our patients and their physicians, I suggest we apply Dr. Jackson's thoughtful advice and omit needless words.

Justin P. Smith
University Hospital, University of Washington
Seattle, WA 98195

Wall Street Entrepreneurs

I read with interest the article by Dr. Berlin in the September issue of AJR [1]. Dr. Berlin expresses pertinent concerns about the role of venture capital in the development of imaging centers. He is concerned also by radiologists' potential loss of control of their financial and clinical independence. Although not expressed, it appears to be implied that the blame is on the venture capitalists who are always ready to make a fast dollar.

Although I agree with the gist of the essay, I suggest that the reason that venture capitalists have invested in the field is the lack of pertinent training of radiologists by the academic institutions. Although I have not done a comparative study of every radiologic program in the United States, I am familiar with the curricula offered by a few of the best known institutions. None of them offers any mandatory training in business administration, and the matter is not mentioned at any point in the written or oral boards of the American College of Radiology.

The only financial background of newly trained radiologists has been their attempts to balance the meager $10,000 to $25,000 per year on which they have survived during their medical education. I am convinced that any person with an M.B.A. would laugh at the idea that such training is anywhere near what is necessary to operate a multimillion dollar investment.

If we want radiologists to maintain financial independence, the technique is not to fight the venture capitalists but to outsmart them. Indeed radiologists have all the advantages mentioned in Dr. Berlin's essay, but until they have the faintest idea about the business administration involved, they will be unable to understand the deals that are offered, let alone make such deals by themselves.

At a time when residency requirements have been expanded a full 33% (4 years instead of 3) to allow young radiologists to cope better with the current situation, it is urgent that the business aspect of the practice of radiology be included in the training. Doing so would prevent the unfortunate trend that probably is happening in most institutions: The new fourth year is just more of the previous 3 years, with little emphasis on new techniques and their repercussions on the radiologist's practice.

Let us not blame the other guys, and let us be critical of how we prepare the new generations of radiologists. How we act will determine whether radiologists maintain a certain independence or surrender it to better adapted species.

Philippe Jeanty
Vanderbilt University
Nashville, TN 37232

REFERENCE

1. Berlin L. Wall Street entrepreneurs and imaging centers: an insidious threat to radiology. *AJR* **1987**;149:638–640

Reply

My editorial on Wall Street entrepreneurs was directed to radiologists, not venture capitalists. If anyone is to "blame" for permitting the development of a situation that could have a major adverse impact on the financial future of the radiologic profession, it is our colleagues themselves. Through disinterest and apathy, they have created a business vacuum with regards to the purchase and operation of highly expensive technological equipment; the venture capitalists merely step in to fill the existing vacuum.

Although I have no doubt that Dr. Jeanty is correct in his statement that most teaching programs fail to instruct radiology residents adequately in the "business" of radiology, and although I furthermore agree that academic institutions should bolster their programs in this area, nevertheless I would not be as quick as Dr. Jeanty is to criticize these training institutions for the failure of many of today's radiologists to possess enough business sense to operate an office that contains radiologic equipment. Motivation and desire to be one's own boss and to run one's own professional enterprise must be generated from within; they cannot be taught or instilled by a professor. Radiologists who readily permit and, in fact, even encourage a nonradiologist entrepreneur to do what they themselves should do is guilty not so much of lack of knowledge but of complacency. Radiologists who are motivated to acquire practical information on the business of radiology can seek advice from lawyers, accountants, bankers, or business consultants. Local medical societies and local, state, and national radiologic organizations schedule a multitude of programs and seminars on the business aspects of medicine, including, but not limited to, the acquisition and operation of medical imaging centers.

Radiologists who find themselves at both the professional and the financial disposal of venture capitalists who are not radiologists are deluding themselves if they blame their predicament on these businessmen or on radiology training programs. The real fault lies with radiologists themselves, for failing to seek from the many available sources the financial tools they must have to survive and thrive as proud members of a distinguished profession.

Leonard Berlin
Rush North Shore Medical Center
Skokie, IL 60076

Yawning: An Early Manifestation of Vasovagal Reflex

Yawning is defined as "the involuntary act of opening the mouth widely, accompanied by deep inspiration, and frequently stretching of the arms, shoulders, and chest to assist in the inspiratory act followed by relaxation of the muscles involved, usually performed when sleepy or bored" [1]. All my life I have been acutely aware of the yawns of those about me (e.g., audiences I lecture, fraternizers at cocktail parties, my wife). It is this cognizance that led to my recognition of yawning as an early sign of a vasovagal reflex or reaction. Noxious stimuli (e.g., needle sticks, contrast media, release of histamine, rectal distension, fear, and other somatic events) can cause the vagal brainstem nuclei to discharge impulses that lead to acetylcholine-mediated effects on the arterioles and the sinoartrial node, resulting in hypotension and bradycardia. The potential seriousness of these reactions is well documented in the medical literature, particularly for patients who have underlying coronary and cerebral vascular disease [2]. Many signs and symptoms of vasovagal reflex and reaction have been reported: apprehension, restlessness, dizziness, faintness, intestinal cramping, nausea, salivation, sweating, palpitation, dyspnea, syncope, and unconsciousness [3]. I have noticed that in most of the vasovagal reflexes or reactions I encounter, yawning is the first manifestation.

According to definition, yawning is caused by sleepiness or boredom, but I do not think that patients who are undergoing needle sticks, angiography, or barium enemas are ever bored, and their premedication probably does not make them sleepy. Premedication may put them to sleep, but there is no middle ground. So, if a patient begins yawning during a barium enema or a breast localization, place the patient supine, measure the pulse and blood pressure, elevate the patient's legs or place the patient in the Trendelenburg position, open the IV lines, and have the atropine ready. If measures to expand fluid volume are not successful (and beware of patients who are in heart failure), 0.6–0.8 mg of IV atropine usually will reverse the reaction [4].

Thomas G. Cronin, Jr.
St. Francis Hospital
Evanston, IL 60202

REFERENCES

1. *Blakinston's Gould medical dictionary*, 4th ed. New York: McGraw-Hill, **1979**:1491
2. Newton TH, Potts DG, eds. *Radiology of the skull and brain*, vol. 2, book 1: *Angiography*. St. Louis: Mosby, **1974**:1034
3. Andrews EJ. The vagus reaction as a possible cause of severe complications of radiologic procedures. *Radiology* **1976**;121:1–4
4. Kadir S. *Diagnostic angiography*. Philadelphia: Saunders, **1976**:688–689

Meeting News

Society for Magnetic Resonance Imaging Meeting in San Antonio: Notes and Comments

The 5th annual meeting of the Society for Magnetic Resonance Imaging (SMRI) was held in San Antonio, TX, February 27–March 4, 1987. More than 500 participants enjoyed beautiful weather and Texan hospitality with a distinct Mexican flavor. The first 2 days of the meeting were devoted to an educational program organized by W. G. Bradley, President-Elect of the SMRI. Routine clinical applications in the brain and spine were reviewed in detail. Technical developments in body imaging, fast-scanning techniques, contrast agents, spectroscopy, and socioeconomic issues also were addressed by a faculty of 31 well-known researchers who had been selected because of their skill as teachers. The educational program was complemented by an evening tutorial program that consisted of informal clinical case-review sessions organized by J. Weinreb. Attendees were able to show their own interesting or difficult clinical cases and discuss artifacts and other practical issues.

The scientific sessions opened Monday morning with an address by the SMRI president, G. D. Fullerton. Each morning and afternoon session of the 3-day scientific program began with a symposium of invited speakers who reviewed clinical neuroradiology, vascular imaging and flow measurement, artifacts in body imaging, contrast agents, and clinical applications of both spectroscopy and body MR imaging.

Scientific presentations included 215 oral abstracts and 21 posters. The program and abstracts have been published as a special issue of *Magnetic Resonance Imaging* (Vol. 5, Suppl. 1, 1987). The following remarks represent the opinion of a single reviewer and are a representative selection of a few scientific sessions.

Clinical Neuroimaging

Several European groups presented their experience with Gd-DTPA–enhanced MR imaging of the brain. Semmler et al. correlated MR findings with stereotactic biopsies and confirmed that enhancing areas represent regions of tumor. Markl et al. combined fast low-angle shot (FLASH) imaging and fast imaging with steady progression (FISP) with Gd-DTPA enhancement in evaluation of the orbit. This technique shortened the examination time and produced patterns of contrast enhancement similar to those seen with iodine-enhanced CT; meningiomas showed the greatest contrast enhancement. Young et al. studied brain hemorrhage by using susceptibility mapping techniques and found effects in the range of 0.4–1 ppm. Regions of infarction showed no changes in susceptibility when hemorrhage was absent. Measurements from 40 tumors showed susceptibility effects in one-third of cases.

Studies of spinal imaging by means of 1.0- and 1.5-T systems and gradient-echo techniques were reported by several groups. Kanal et al. found improved visualization of the cervical spine when T2-weighted, limited flip-angle gradient-echo scans were used as opposed to more time-consuming, motion-sensitive, T2-weighted spin echoes. Bellon et al. achieved T2 weighting with scan times of 4 min by using the hybrid fast-scan technique. Unger et al. showed that images obtained at 1.5 T were more sensitive than CT scans for detecting tumor involvement of vertebral bodies and in delineating intraspinal extension of tumor and spinal block. Although the field of view of MR imaging is limited when compared with that of bone scintigraphy, MR imaging may be more sensitive for detecting metastatic involvement of vertebral bone marrow when clinical findings localize the pathologic changes to a given region. Dreisbach et al. found good correlation between findings by MR imaging and post-traumatic changes such as cystic myelopathy and myelomalacia. In evaluations of patients with acute spinal trauma, Bennett et al. found that MR imaging was useful for detection of ligamentous injuries, disk protrusions, and epidural hemorrhage. Compression fractures and fragments protruding into the canal could be seen, and hemorrhage or transsection

of the cord were visualized easily at 1.5 T. Fractures of the vertebral body and posterior elements were, however, seen better on CT scans than on MR images.

Vascular Imaging and Flow Measurement

Nishimura et al. reviewed first-generation subtractive methods for projection angiography, including subtraction of images gated diastole-systole, subtraction of images rephased by using gradient nulling from conventional spin-echo images, and subtractive images based on time-of-flight effects by varying the region excited with a 180° inversion pulse. Newer methods that use a sequence of excitation pulses in conjunction with flow-encoding gradients to produce a net excitation of flowing blood only, with static material driven back to equilibrium, were described by the Stanford electrical engineering group. Dumoulin et al. emphasized that MR angiography can be performed in a variety of ways. Their work emphasized use of a short repetition time (30 msec) and multiple excitations to remove artifacts caused by variations in blood velocity during the cardiac cycle. Firmin et al. described their studies of using a gradient-echo even-echo rephasing technique to image the heart by using short- and long-axis views. This technique allowed display of a range of flow velocities and accelerations and was applied to quantitative measurement of flow in and around the cardiac chambers. Cine loop images with color encoding of flow showed temporal variations in flow patterns related to normal opening and closing of cardiac valves. Several groups reported that cine gradient-echo images (also known as rapid, small flip-angle MR imaging or cine MR imaging) were useful in evaluating aortic insufficiency, mitral insufficiency, and pathologic or therapeutic cardiac shunts. As laminar blood flow showed a uniform high signal intensity, low-intensity valve leaflets were seen readily, and thickening due to myxomatous degeneration or other changes was shown. Turbulent flow appeared as a signal void, and regurgitation jets due to valvular incompetence could be seen reliably. Pflugfelder et al. quantitated regurgitant fractions by using a modified Simpson method and found excellent correlation with echocardiography and angiography.

Haacke et al. described studies in which they used the gradient rephasing subtraction technique of MR angiography to image pulmonary vessels as small as 1 mm in diameter. Use of this technique produced a uniform high signal intensity of flowing blood that resulted in the unambiguous identification of airways and absence of the usual spin-echo flow void. A method to improve the reliability of the flow void, eliminating intravascular signal irregularities and ghosting from vessels, was described by Ehman et al. In this procedure, known as the FLAK technique, additional gradients and RF pulses applied outside the multislice imaging volume were used to saturate in-flowing spins.

Motion Artifacts

After the scientific symposium dedicated to motion artifacts in body imaging, Wood et al. presented a theoretical analysis of the interaction between periodic motion and Fourier imaging. Bellon and Haacke described a variety of artifacts related to motion and defects in the scanning process. The results of studies on fast scanning as a method for decreasing the effects of motion were presented by several groups. Holland et al. emphasized the need for short echo delays to achieve adequate signal-to-noise and contrast-to-noise ratios when partial-saturation, rapid imaging techniques are used. Split-phase encoding and asymmetric sampling methods that allow ultrashort TE sequences were described. Wehrli et al. reviewed phase relationships and the effect of residual transverse magnetization in which short-TR gradient-echo techniques (GRASS—gradient-refocused acquisition in steady state) result in steady-state magnetization that contributes significantly to image contrast. In a works-in-progress session, Frahm described the effects that spoiling or refocusing residual transverse magnetization (eliminating or establishing steady-state transverse coherence) has on image contrast.

With the current emphasis on high-field imaging and fast, multislice scanning techniques, the primary safety concern is RF heating of body tissues. Shellock et al. reported a study in which they had used a 1.5-T system and a quadrature excitation coil to deliver specified whole-body specific absorption rates (SAR) and performed thermography of the entire body by using a high-resolution system to detect local regions of increased heating (hot spots). The results confirmed the absence of excessive temperature elevations or abnormal distributions of temperatures in association with high-field imaging and showed the efficiency of blood flow as a thermal regulatory mechanism.

Contrast Agents

Clinical applications of Gd-DTPA were described by many groups. Scientific sessions that focused on research developments emphasized laboratory studies of tissue-specific agents. Engelstad et al. compared Fe-HBED and Fe-EHPG, two iron complexes that cause tissue-specific enhancement of functioning hepatobiliary tissue. Enterohepatic circulation was minimal, and Fe-HBED showed a small advantage in efficacy. Hardy and Henkelman, as well as Majumdar and Gore, presented theoretical models and experimental data and elucidated the mechanism of T2 relaxation caused by superparamagnetic iron oxide (ferrite) particles used experimentally for liver imaging. Selective T2 relaxation, distinct from the mechanism of relaxation associated with paramagnetic substances, has been attributed to diffusion of protons in heterogeneous magnetic-field gradients induced by the heterogeneous tissue distribution of iron oxide particles. The safety of superparamagnetic iron oxides was emphasized by Stark et al., who reported development of a nontoxic, biodegradable formulation. Weissleder et al. described use of superparamagnetic iron oxide in the detection of focal splenic lesions, and Carvlin et al. reported studies of its use in imaging renal vascular perfusion.

In the works-in-progress sessions, Engelstad et al. described a unique approach to the two major problems of spectroscopy: spatial localization and signal-to-noise ratio.

Pharmacologic localization of tumor tissue was achieved by eliminating signal from surrounding normal liver via the T2 relaxation effects of IV administered superparamagnetic particles.

Schaefer et al. described use of the paramagnetic contrast agent manganese-gluconate in contrast-enhanced cardiac imaging in dogs. T2 relaxation enhancement was detected by using conventional (TE = 60 msec) gated cardiac images. The results showed that normally perfused myocardium had a shorter T2 than hypoperfused ischemic zones. Pflugfelder et al. reported studies on a new tetraphosphonate chelate of manganese that showed tissue specificity and caused prolonged enhancement (20–40 min) of normally perfused myocardium.

Many investigators emphasized the need for an oral contrast agent to mark the lumen of the gastrointestinal tract. Kornmesser et al. presented the initial clinical experience with Gd-DTPA formulated as an oral contrast agent. They administered 0.01 mmol Gd-DTPA/kg in mannitol and showed substantial, relatively uniform increases in signal intensity of small bowel, which could be distinguished then from retroperitoneal structures.

Spectroscopy

Ross et al. reported studies in which they used phosphorus-31 MR spectroscopy to monitor cerebral energy metabolism in patients with hepatic encephalopathy. Spectra from the frontal lobes of the brain showed no alteration in intracerebral pH but showed a significant reduction in intracerebral inorganic phosphate (Pi) in patients who had encephalopathy. Ross et al. also described spatially localized phosphorous spectra from the liver acquired by using a three-dimensional phase-depth method. Spectra from the liver clearly could be distinguished from spectra localized to superficial muscle. Tissue volumes were sufficiently small (8 ml) to allow volume-selective mapping of metabolites. Semmler et al. reported a study in which they used a clinical 1.5-T imaging system to obtain phosphorous spectra with a resolution of 0.5 ppm from superficial bone and neuroectodermal tumors. Follow-up studies after chemotherapy showed increases in PCr/Pi and increases in the sum of PCr + Pi. Alterations of these metabolic indexes were observed as early as 24 hr after start of chemotherapy. Several groups reported on investigations of spatially localized in vivo phosphorus spectroscopy of the heart. Bottomley et al. used DRESS with complementary proton surface-coil images to localize spectra from ischemic anterior myocardium in patients who had documented acute infarction. Significant reductions in PCr/Pi and elevated Pi/beta–adenosine triphosphatase were observed. In the works-in-progress sessions, Barany et al. described high-resolution proton spectroscopy of live human tissues. A 1.5-T clinical imaging system was used. Spectra of the brain and liver were analyzed, and meticulous assignments were made to major resonances, such as fatty acid, and minor resonances, such as carnitene, aspartate, glutamine, other amino acids, and nucleotides.

Body Imaging

Diverse anatomic regions and pathologic conditions were reviewed in the scientific sessions. Dietrich et al. compared CT, MR imaging, and sonography in the evaluation of abdominal masses in children. Coronal MR imaging was particularly effective because of its large field of view that included the entire abdomen and pelvis of small patients; CT was limited by the normal absence of fatty-tissue planes in children. Spritzer et al. described application of high-field MR imaging to the detection of parathyroid tumors. The overall accuracy was 90%, which is competitive with established sonographic and scintigraphic techniques. Rapoport et al. described advantages of MR imaging to visualize the brachial plexus. Many groups successfully have used MR imaging to diagnose avascular necrosis in the hip and elsewhere. Mitchell et al. described the pathognomonic "double line" sign that represents the interface between live and dead bone at the periphery of lesions of arteriovenous malformation. Knee arthrography, performed by using fast-imaging techniques was the subject of work-in-progress reports by Froelich and Haggar and by Tyrrel and Gluckert. Both groups exploited the short TR of GRASS and FLASH techniques to perform three-dimensional imaging of the normal and abnormal knee. Because both normal knees and those with meniscal tears showed inherently high tissue contrast, excellent diagnostic results were achieved.

In summary, the SMRI achieved its goal to provide practicing physicians with a detailed guide for establishing clinical indications, insight into laboratory research, and a rational basis for evaluating new technology. Scientists in basic research shared their technical developments in fast imaging, vascular imaging, spectroscopy, and development of contrast agents. We all eagerly await the 6th annual meeting of the SMRI in Boston, February 27–March 2, 1988.

David D. Stark
Massachusetts General Hospital
Boston, MA 02114

News

Selected Topics in Nuclear Radiology—1988

The Dept. of Radiology, University of California, San Diego, School of Medicine, will present Selected Topics in Nuclear Radiology—1988, Jan. 25–28, at the Hotel del Coronado, Coronado (San Diego), CA. The course is intended to acquaint participants with the latest techniques of clinical nuclear imaging. Indications for and details of performing these procedures will be stressed. Possible pitfalls in interpretation, cost-effectiveness relative to other diagnostic methods, and instrumentation needed will be discussed also. A voluntary computer-aided self-assessment program will be available for extra CME credit. Program director: W. L. Ashburn. Guest faculty: B. D. Collier, Jr., I. G. Mena, A. D. Waxman, Ian Brown, John Pike, A. H. Maurer, H. N. Wellman, Randy White. Category 1 credit: 18.75 hr. Fee: physicians, $375; physicians in training and technologists, $275. Information: Dawne Ryals, Ryals & Associates, P.O. Box 920113, Norcross, GA 30092-0113; (404) 641-9773.

Diagnostic Ultrasound at Thomas Jefferson University Hospital

The Division of Diagnostic Ultrasound, Dept. of Radiology, Thomas Jefferson University Hospital, is sponsoring the following courses: Physics and Instrumentation, Jan. 4–8; Cross-Sectional Anatomy, Jan. 11–15; Abdomen, Jan. 18–22; Obstetrics and Gynecology, Jan. 25–29; and Endorectal/Genitourinary Ultrasound, Feb. 26–27. Program director: Barry Goldberg. Category 1 credits will be awarded. Fee: Endorectal/Genitourinary Ultrasound, $450; all others, $575 each. Information: Judith Superior, Education Coordinator, Thomas Jefferson University Hospital, Philadelphia, PA 19107; (215) 928-8533. *Editor's note: Incorrect dates were given for the following seminars in the December 1986* AJR: *Physics and Instrumentation, Cross-Sectional Anatomy, and Abdomen.*

Neuroradiology Seminar

The Dept. of Radiology, Florida Hospital Medical Center, is sponsoring Neuroradiology Seminar, Feb. 21, in Orlando, FL. This 1-day review course will cover "bread and butter" neuroradiology, with special emphasis on CT and MR. The seminar will be directed to diagnostic radiologists and to practicing clinicians in neurology, neurosurgery, and orthopedic surgery. Internists and general surgeons, residents, fellows, nurses, and technologists also will benefit from the practical approach to common neurologic diseases. Faculty: R. Lukin and R. G. Ramsey. Category 1 credits: 7 hr; CEU contact hours: 7. Fee: before Jan. 29, physicians, $125; residents, fellows, nurses, technologists, others, $50; after Jan. 29, $150 and $75, respectively. Information: Rick Mace, Executive Director, Florida Heart Institute, 500 E. Rollins, Ste. 101, Orlando, FL 32803; (305) 897-1575.

UCSD Imaging and Intervention Conference

The 7th annual UCSD Imaging and Intervention Conference will be presented by the Dept. of Radiology, University of California, San Diego, School of Medicine, Feb. 21–24, at the San Diego Marriott (formerly the Hotel Inter-Continental), San Diego, CA. The course will present topics that are current for radiologists in 1988. Practical aspects of imaging and intervention will be highlighted. Program directors: Giovanna Casola, G. R. Leopold, and Eric vanSonnenberg. Guest faculty: Peggy Fritzsche, Thomas Lawson, and Robert Vogelzang. Category 1 credit: 25 hr. Fee: physicians, $400; physicians-in-training and technologists, $275. Information: Dawne Ryals, Ryals & Associates, P.O. Box 920113, Norcross, GA 30092-0113; (404) 641-9773.

Aspen Abdominal, Genitourinary, and Interventional Radiology Seminar

The School of Medicine in New Orleans, Louisiana State University Medical Center, will present the Aspen Abdominal, Genitourinary, and Interventional Radiology Seminar, Feb. 28–March 2, at The Inn, Aspen, CO. The seminar will focus on advances in imaging techniques for the abdomen and genitourinary tract and on advances in techniques of abdominal interventional radiology. A minisymposium on the newest techniques in oncologic genitourinary and abdominal assessment and staging will be presented also. The course has been approved for Category 1 credit. Program coordinator: E. K. Lang. Fee: physicians, $345; students, $295. Information, LSU Continuing Education, 1542 Tulane Ave., New Orleans, LA 70112.

Practical Radiology 1988

The Dept. of Radiology, University of British Columbia, is sponsoring their 6th annual postgraduate course, Practical Radiology 1988, Feb. 28–March 4, at the Whistler ski resort near Vancouver, B. C. Guest faculty: Peter Cockshott, Giles Stevenson, W. J. Dodds, Edward Stewart, R. M. Gore, T. C. McLoud, Albert Moss, James Nelson, Charles Rohrmann, and William Thompson. Category 1 credit: 21 hr. Fee: physicians, $350 (U. S.) or $450 (Canadian); residents and fellows, $225 (U. S.) or $300 (Canadian). Information: H. J. Burhenne,

M.D., Dept. of Radiology, University of British Columbia, 10th Ave. and Heather St., Vancouver, B. C. Canada V5Z 1M9; (604) 875-4355.

Neuroradiology Update/MR Imaging

The Dept. of Radiology, University of California, San Diego, School of Medicine, will present the following course: Neuroradiology Update, March 7–10; Magnetic Resonance Imaging, March 7–11; and MRI for Technologists, March 8–11; at the Hotel del Coronado, Coronado (San Diego), CA. The course is designed for physicians and allied health personnel. It will highlight the physical basis of MR imaging and clinical applications. A description of MR systems and discussion of the fundamentals of imaging contrast will provide participants with a basic understanding of MR imaging. Program director: J. R. Hesselink; associate director, R. F. Mattrey. Guest faculty: W. G. Bradley, Jr., M. N. Brant-Zawadzki, R. C. Brasch, Michele Cain, K. R. Davis, C. B. Higgins, and G. H. Mink. Category 1 credit: up to 28 hr. Fee: combined course: physicians, $425, residents and technologists, $325; neuroradiology course: $350/$250; MR imaging course: $400/$250. Information: Dawne Ryals, Ryals & Associates, P. O. Box 920113, Norcross, GA 30092-0113; (404) 641-9773.

Skeletal Radiology at the Pointe—1988

The Dept. of Diagnostic Radiology, Allegheny General Hospital, will present the 5th annual course on skeletal radiology, March 19–24, at the Pointe Resort, Phoenix, AZ. The course will cover a variety of topics, including bone and soft-tissue tumors and the multidisciplinary approach to their management, osteoporosis, skeletal-dermatologic problems, foot and ankle radiology, bone biopsy, lumbar facet block, musculoskeletal trauma without fracture or dislocation, spinal stability, skeletal MR imaging, shoulder cross-sectional imaging, and metabolic bone disease. Guest faculty: J. M. Destouet, J. M. Harrelson, J. P. Lawson, R. A. McLeod, M. J. Pitt, and D. J. Sartoris. Fee: practicing physicians, $450; residents, fellows, and retirees, $250. Category 1 credit: 20 hr. Information: Sandra Johnston, Dept. of Continuing Education, Allegheny General Hospital, 320 E. North Ave., Pittsburgh, PA 15212-9986; (412) 359-4952.

Thoracic Imaging '88

The Society of Thoracic Radiology will present Thoracic Imaging '88, March 27–31, at the Willard Inter-Continental, Washington, DC. The course has two parts. The scientific sessions will be devoted to the development of new knowledge and hypotheses. The postgraduate course is designed to expand and refine the diagnostic abilities of participants by providing up-to-the-minute reviews and analyses of image characteristics of a wide spectrum of diseases and by describing the best available methods for arriving at a correct diagnosis. Program director: E. N. C. Milne. Category 1 credit: 32 hr. Fee: physicians, $425; residents, fellows, and technologists, $275. Information: Dawne Ryals, Ryals & Associates, P.O. Box 920113, Norcross, GA 30092-0113; (404) 641-9773.

Real-Time Ultrasound in Obstetrics and Gynecology

The Dept. of Radiology and the Office of Continuing Medical Education, The University of Michigan Medical School, will sponsor Real-Time Ultrasound in Obstetrics and Gynecology, April 18–20, at the Towsley Center, The University of Michigan, Ann Arbor, MI. The course is intended for those who have little or no previous experience with real-time sonography and who either have or are contemplating acquisition of a real-time sonographic unit for their practice. Morning lectures will emphasize a broad range of basic and advanced obstetric and gynecologic topics. For the afternoon sessions, course registrants will be divided into groups of five according to skill level for hands-on scanning of selected patients. Enrollment is limited to 30 registrants. Category 1 credit: 20 hr. Information: Gayle Fox, Office of Continuing Medical Education, Towsley Center, Box 0201, The University of Michigan Medical School, Ann Arbor, MI 48109-0201; (313) 763-1400.

Oncologic Imaging Update Course

The Dept. of Radiology and the Office of Continuing Medical Education, University of Florida, will sponsor the 1st annual Oncologic Imaging Update Course, April 29–May 1, at Amelia Island Plantation, Amelia Island, FL. This weekend program will provide a comprehensive update and practical approach to imaging in oncology. Recent advances in multi-modality imaging and the impact on rational diagnosis, staging, and management will be stressed. Course directors: P. R. Ros and J. L. Williams. Guest faculty: M. Viamonte. Category 1 credit: 17 hr. Fee: physicians, $250; residents, $200 (letter required). Information: Office of Continuing Medical Education, Box J-233, JHM Health Center, Gainesville, FL 32610; (904) 392-3143 or 392-3183.

CT, MR Imaging, and Radiologic Technologist Program

The Dept. of Radiology and the Office of Continuing Medical Education, The University of Michigan Medical School, are sponsoring a course entitled Computed Tomography and Magnetic Resonance Imaging and Radiologic Technologist Program. The course will be held May 4–6 at the Towsley Center of The University of Michigan, Ann Arbor, MI. It will review current techniques and applications of body CT and present the most up-to-date information on MR imaging, including uses in the CNS. A series of didactic lectures will be interspersed with workshops. A day-long program specifically for technologists will be presented May 6. It will include lectures and hands-on demonstrations. Category 1 credit: 22.5 hr. Information: Betty Phillips, Office of Continuing Medical Education, Towsley Center, Box 0201, The University of Michigan Medical School, Ann Arbor, MI 48109-0201; (313) 763-1400.

Practical Radiology Review Course

The Dept. of Radiology of the University of Cincinnati College of Medicine will present the New Revised Practical Radiology Review Course, May 16–20. Radiation physics and nuclear medicine will be included. The course is open to radiologists and radiology residents. Category 1 credits: approval pending. Fee: $350. Information: Dr. H. B. Spitz, Dept. of Radiology, University Hospital, 234 Goodman St., M.L. 742, Cincinnati, OH 45267.

Copenhagen Symposium on Detection of Breast Cancer

The 4th International Copenhagen Symposium on Detection of Breast Cancer will be held at Gentofte Hospital, The County Hospital of Copenhagen, University of Copenhagen, Aug. 24–26. Information:

Chief of Radiology, dr. med. Sam Brünner, KAS Gentofte, Roentgenafdelingen, DK-2900 Hellerup, Denmark; or Chief of Radiology, lecturer Bent Langfeldt, Roentgenafdelingen, Aarhus Amtssygehus, DK-8000 Aarhus, Denmark.

Conference on Dose, Time, and Fractionation in Radiation Oncology

The 3rd International Conference on Dose, Time, and Fractionation in Radiation Oncology will be held Sept. 14–17 at the Inn on the Park, Madison, WI. The topic of the conference will be Prediction of Response in Radiation Therapy: The Physical, Biological, and Analytical Basis. The conference is a joint presentation by the American Association of Physicists in Medicine and the University of Wisconsin, Dept. of Human Oncology. Information: Bhudatt Paliwal, Ph.D., Conference Chairman, Dept. of Human Oncology and Medical Physics, University of Wisconsin, 600 Highland Ave., K4/B 100, Madison, WI 53792; (608) 263-8500.

Northern California Radiological Society Officers

The Northern California Radiological Society has elected the following officers for the period June 1987 through May 1988: president, John McGahan; president-elect, Michael Norton; secretary-treasurer, Mark Schneider; program director, Jeff Janes.

The American Board of Radiology Examinations

Written examinations for the American Board of Radiology (ABR) are scheduled for Oct. 6–7, 1988, and Oct. 5–6, 1989. Oral examinations will be held at the Executive West Hotel in Louisville, KY, on May 23–27, 1988, and June 5–9, 1989. The ABR will accept applications for admission to the examinations after July 1, but not later than Sept. 30, in the year *preceding* the year in which the examination is to be taken. For application forms and further information: Office of the Secretary, The American Board of Radiology, 300 Park, Ste. 440, Birmingham, MI 48009.

Correction: Palm Beach Magnetic Resonance Imaging Update

A correction should be made in the Sept. 1987 issue of *AJR* concerning the Palm Beach Magnetic Resonance Imaging Update. The name of the hotel is the *Palm Hotel*.

Meeting and Course Review

For the reader's convenience, a summary of upcoming meetings and courses is provided. Detailed listings are given in the *AJR* issue given in parentheses.

Visiting Fellowships in MR Imaging, times arranged, San Diego, CA (Aug)
Preceptorships in Imaging and Interventional Radiology, 1987–1988, times arranged, San Diego, CA (Dec)
Delaware Valley Magnetic Resonance Imaging Society Monthly Meetings, continuing through May 1988, Philadelphia (Dec)
Congress of the Indian Radiological and Imaging Association, Jan. 14–16, Coimbatore, India (June)
Advanced Seminars in Diagnostic Imaging, Jan. 14–17, Laguna Niguel, CA (Nov)
The Society of Gastrointestinal Radiologists Meeting and Postgraduate Course, Jan. 16–20, Nassau, Bahamas (July)
Chest Imaging, Jan. 18–21, Coronado, CA (Nov)
Duplex Imaging, Jan. 21–23, San Diego, CA (Oct)
Armed Forces Institute of Pathology Courses: AFIP Neuroradiology Review Course, Jan. 23–24, Bethesda, MD; **AFIP Neuropathology Course,** begins Jan. 25, Bethesda, MD (Nov)
Los Angeles Radiological Society Midwinter Conference, Jan. 29–31, Los Angeles (Nov)
Neuroimaging Update, 1988, Jan. 31–Feb. 5, Paradise Island, Bahamas (Nov)
Uroradiology '88, Feb. 1–4, Orlando, FL (Nov)
Breast Imaging 1988, Feb. 1–5, St. Thomas, U.S. Virgin Islands (Sept)
Los Angeles Radiological Society Post Conference Seminar, Feb. 2–6, Kaanapali, Maui, HI (Nov)
International Congress on Interventional Radiology in Cardio-Vascular Diseases, Feb. 3–5, Toulouse, France (Sept)
Thermography in Neuromusculoskeletal Disorders, Feb. 6–7 and April 16–17, New York (Dec)
Intermountain Imaging Conference, Feb. 6–13, Steamboat Springs, CO (Nov)
12th Annual Big Sky Radiology Conference, Feb. 7–12, Great Falls, MT (Sept)
Vascular Imaging and Interventional Radiology at Snowbird, Feb. 7–12, Snowbird, UT (Nov)
Uroradiology Course, Feb. 10–11, Bethesda, MD (Nov)
Practical Aspects of Diagnostic Radiology/Medical Imaging, Feb. 13–19, Snowmass Village, CO (Dec)
Sun Valley Imaging, Feb. 13–20, Sun Valley, ID (Nov)
Diagnostic Radiology and Nuclear Medicine, Feb. 14–21, St. Thomas, U.S. Virgin Islands (Oct)
Palm Beach Magnetic Resonance Imaging Update, Feb. 15–17, West Palm Beach, FL (Sept, amended this issue)
Winter Imaging Seminar, Feb. 15–19, Cancun, Mexico (Dec)
Computed Body Tomography 1988—The Cutting Edge, Feb. 18–21, Orlando, FL (Nov)
Radiology in Seville, Feb. 20–27, Seville, Spain (Oct)
Vail Winter Imaging Seminar IV, Feb. 21–28, Vail, CO (Dec)
Comprehensive Update: Neuroradiology, Body Imaging, and Mammography, Feb. 22–27, Acapulco, Mexico (Nov)
Vascular Imaging and Interventional Radiology at Park City, Feb. 28–March 4, Park City, UT (Nov)
National Conference on Breast Cancer, Feb. 29–March 4, Los Angeles (Nov)
Annual Skeletal Symposium, Feb. 29–March 4, Sun Valley, ID (Dec)
Annual Course of the Society of Computed Body Tomography, Feb. 29–March 4, Monterey, CA (Dec)
The George Simon Award, deadline for receipt of papers, March 1 (Dec)
Doppler Ultrasound in the Canadian Rockies, March 4, Banff Springs Hotel (Dec)
Masters Diagnostic Radiology Conference, March 6–11, Maui, HI (Oct)
The Lyon Conference: Computer Science and Life, March 10–12, Lyon, France (Nov)
Diagnostic Imaging Down Under, March 12–27, Auckland, New Zealand; Sydney and Melbourne, Australia (Oct)
Imaging Living Brain Chemistry, March 17–18, Baltimore, MD (Dec)
Pediatric Radiology 1988, March 17–19, Philadelphia (Sept)
Ultrasound at Vail, March 19–25, Vail, CO (Nov)
International Diagnostic Course: Skeletal Radiology, March 19–26, Davos, Switzerland (Dec)
Society of Cardiovascular & Interventional Radiology Meeting, March 21–24, Orlando, FL (Nov)

The Society of Thoracic Radiology—Annual Postgraduate Course, March 27–31, Washington, DC (July)
International London Course in Whole Body Computed Tomography, March 27–31, Perthshire, Scotland (Nov)
Neuroradiology at Vail, March 28–April 1, Vail, CO (Dec)
National Council on Radiation Protection and Measurements Annual Meeting, March 30–31, Washington, DC (Dec)
Spanish Radiology Seminar, April 3–8, Miami Beach, FL (Oct)
Southern California Chapter of the American Association of Physicists in Medicine Spring Seminar, April 20–22, Las Vegas, NV (Dec)
International Symposium of the Planning of Radiological Departments, April 20–23, Florence, Italy (Sept)
Practical Interventional Radiology April 25–28, Boston, MA (Oct)
Imaging the CNS, April 25–29, Tucson, AZ (Nov)
Radiology Review Course, May 1–6, Miami, FL (Dec)
Fleischner Society Symposium on Chest Disease, May 16–18, Montreal, Quebec (Dec)
International Workshop for the Study of Vascular Anomalies, June 20–22, Hamburg, Germany (Nov)
European Congress of NMR in Medicine and Biology, June 23–25, Berlin, Germany (Oct)
Bowman Gray Abdominal Radiology Fellowship, begins July 1, Winston-Salem, NC (Nov)
International Symposium on Magnetic Resonance Imaging, Dec. 14–16, New Dehli, India (Oct)

AJR carries announcements of courses, symposia, and meetings of interest to its readers if received a minimum of 5 months before the event. There is no charge; receipt of items by the *AJR* Editorial Office is not acknowledged. Submit items for publication typed double spaced. Provide title, date, location, brief description, sponsor, course directors, fees, category I credit, and address and telephone number for additional information. Faculty from the host institution will not be listed. Guest faculty names will appear **only** if initials are provided. Mail news items to *AJR* Editorial Office, 2223 Avenida de la Playa, Suite 200, La Jolla, CA 92037-3218.

American Roentgen Ray Society:
Officers, Committees, and Meeting Information

Officers

President: Raymond A. Gagliardi
President-elect: Lee F. Rogers
1st Vice-president: Gerald D. Dodd
2nd Vice-president: Rosalind H. Troupin
Secretary: Glen W. Hartman
Treasurer: Ronald G. Evens

Executive Council: E. Gedgaudas, J. F. Wiot, L. F. Rogers, R. A. Gagliardi, R. G. Evens, R. N. Berk, F. L. Angell, J. E. Madewell, M. P. Capp, G. W. Hartman, B. G. Brogdon, R. H. Troupin, G. R. Leopold, G. D. Dodd, A. K. Poznanski, A. E. James, Jr., J. T. Ferrucci, Jr., T. C. Beneventano, E. J. Ferris, J. A. Kirkpatrick, Jr., chairman

Committees 1987–1988

Editorial Policy: S. S. Sagel, W. J. Casarella, C. A. Rohrman, Jr., N. C. Whitley, S. V. Hilton, J. M. Taveras, R. N. Berk, M. P. Capp, chairman

Education and Research: C. E. Putman, A. R. Margulis, B. J. Hillman, R. A. McLeod, B. G. Brogdon, chairman

Finance and Budget: B. P. Wood, L. R. James, A. K. Poznanski, A. E. James, Jr., F. L. Angell, chairman

Nominating: A. K. Poznanski, E. Gedgaudas, G. H. Ghahremani

Publications: W. J. Casarella, S. S. Sagel, N. C. Whitley, C. A. Rohrmann, Jr., M. P. Capp, chairman

Membership: E. J. Ferris, G. R., Leopold, A. K. Poznanski, A. E. James, Jr., chairman

Representatives to Other Organizations

American Board of Radiology: E. C. Klatte, L. F. Rogers, T. C. Beneventano

American College of Radiology: L. F. Rogers, G. A. Kling, R. A. Gagliardi, J. M. Dennis, E. J. Ferris, J. E. Madewell

American Medical Association House of Delegates: S. F. Ochsner, K. L. Krabbenhoft, alternate

American National Standards Institute: M. Haskin

National Council on Radiation Protection and Measurements: E. L. Saenger, H. L. Friedell

Meeting Arrangements

Annual Meetings: May 8–13, 1988, Hilton, San Francisco; May 7–13, 1989, Hilton, New Orleans; May 13–18, 1990, Sheraton Washington, Washington, DC

Annual Meeting Committee: H. C. Carlson, G. P. Janetos, E. K. Lang, R. R. Lukin, T. C. Beneventano, chairman

Instruction Courses: R. A. McLeod, associate chairman, J. T. Ferrucci, Jr., chairman

Scientific Program: R. J. Alfidi, A. E. Robinson, J. H. Thrall, M. P. Banner, J. J. Gisvold, T. C. McLoud, E. Buonocore, R. M. Gore, J. J. Kaye, L. F. Rogers, chairman

Scientific Exhibits: K. H. Vydareny, A. V. Proto, S. M. Goldman, J. E. Madewell, chairman

ARRS Membership

An application form is printed on pages 219–220 in this issue of the Journal. For consideration at the 1988 ARRS meeting, send completed forms before February 1, 1988, to Paul Fullagar, administrative director, American Roentgen Ray Society, 1891 Preston White Dr., Reston, VA 22091. Active members are graduates of an approved medical school or hold an advanced degree in an allied science. They must practice radiology or work in an associated science in the United States or Canada and be certified by the American Board of Radiology or the Royal College of Physicians of Canada or otherwise adequately document training and credentials. Corresponding members are foreign radiologists or scientists who are active in radiology or an allied science. Members-in-training are residents or fellows in radiology or postgraduate students in an allied science. Additional application forms can be obtained from the ARRS offices in Reston, VA.

Business Office

Paul Fullagar, administrative director, American Roentgen Ray Society, 1891 Preston White Dr., Reston, VA 22091; (703) 648-8900

Invitation to Membership in the American Roentgen Ray Society

During the American Roentgen Ray Society's (ARRS) 1985 meeting in Boston, society members approved several fundamental changes in the membership application process and created a new category of membership: members-in-training. Also, active members are no longer required to document contributions to radiology by way of teaching or scientific publications.

Active Membership

Candidates for active membership must be graduates of an approved medical school or hold an advanced degree in one of the physical, chemical, or biological sciences. Each must be board certified and active in the practice of radiology or one of its branches in the United States or Canada. Applicants must be endorsed by two members of the ARRS, not necessarily residents of the same community.

Members-in-Training

The new members-in-training membership category is reserved for physicians in a radiology residency or a postresidency program approved by the Radiology Residency Review Committee of the American Council of Graduate Education and for postgraduate students in allied sciences. The status is limited to a maximum of 5 years, starting with the entrance date into the radiology residency. In the fifth or last year, members-in-training are eligible for transfer to active membership.

Corresponding Members

Corresponding members shall be physicians and/or scientists residing in foreign countries who are active in the science of radiology or allied sciences and who are in good ethical standing in the respective countries. They shall pay dues, but shall not have the privilege of voting nor of holding elective office. They may be members of special committees.

Dues and Initiation Fees

A new schedule of fees and dues has been established. Initiation fee for active members is $50. There is no initiation fee for members-in-training. Annual dues for active and corresponding members are $125, payable on January 1 of each year. The dues payment includes a 1-year subscription to the *American Journal of Roentgenology* (*AJR*) and waiver of the annual meeting registration fee. Dues for members-in-training are $25 and include a year's subscription to the *AJR* and waiver of meeting fees. *AJR* subscription rates for domestic nonmembers will be $100 for 1988. The resident subscription rate will remain $25 for residents who do not elect to become members-in-training. Nonmember residents will have a $25 meeting registration fee.

A membership application form is on the following pages. Applications for active membership should be received by February 1 for action during the annual meeting in May. Members-in-training will be eligible for membership upon receipt and processing of the completed application form and dues.

Initiation fees and dues should not accompany the application, but are payable after election upon notice by the secretary. In-training applicants should submit their dues with their applications.

The American Roentgen Ray Society continues to be a vital force in providing an educational forum for the radiologic community. As it embarks on a program of a broader base of membership, we cordially welcome all those who are eligible. Thus, I urge you to complete the application and forward it to Paul Fullagar, Administrative Director, ARRS, 1891 Preston White Dr., Reston, VA 22091

Glen W. Hartman
Secretary

American Roentgen Ray Society Membership Application

Date _____ Category (check one) ☐ Active ☐ Corresponding ☐ In-Training

Name (in full) _____ Age _____

Address & zip code _____ Date of birth _____

_____ Birthplace _____

Education	Institution	Years	Degree/Type
Undergraduate:			
Graduate: (medical school, graduate school, etc.):			
Postgraduate: (internship, residency, fellowship, etc.):			

Licensed to practice _____ (type) in _____ (state, province, etc.)

Active and corresponding membership applicants, complete this section and top of reverse side. In-training applicants, turn to middle of reverse side.

Practice limited to radiology or one of its branches for _____ years, since (date) _____

Present appointments: Academic _____

Hospitals _____

Membership in scientific societies: _____

Offices or committee memberships in scientific societies: _____

Government service (military, civilian): _____

Credentials

I hereby certify that I was issued a certificate of qualification in _____

by the _____
(The American Board of Radiology, the Royal College of Canada, or some other medical specialty organization)

(continued)

Other credentials: _____

Signature _____

We, active members in good standing of the American Roentgen Ray Society and personally acquainted with the applicant, do recommend him/her for Active Membership in the society. **Two references are required.**

Name (print/type) _____ _____

Address _____ _____

_____ _____

Signature _____ _____

In-training applicants must complete this section.

Credentials

I certify that I am serving as a resident/fellow in _____

at _____ Date program begins (began) is _____
(institution)

_____. It ends _____. I understand that the in-training membership is limited to a maximum of 5 years and in my last year I may transfer to active membership.

Signed _____

Program director or department chairman (name and address) _____

_____

Training director's certification

I certify that this applicant is a trainee at the institution named above and qualifies for enrollment as a member-in-training of the American Roentgen Ray Society.

Name (print) _____ Signature _____

Address _____

General Information

Candidates for Active Membership

1. An active member must be a graduate of an approved medical school or hold an advanced degree in one of the physical, chemical, or biological sciences and be certified by the American Board of Radiology or the Royal College of Physicians of Canada, or document training and credentials that are adequate to qualify for membership. Active members shall actively practice radiology or one of its branches in the United States or Canada. Such members are eligible to participate in all activities of the society, including membership on committees, and have full voting privileges.
2. Application must be on an official form, signed by the applicant and at least two active members of the American Roentgen Ray Society, in good standing, who endorse the applicant.
3. Initiation fee is $50.
4. Annual dues are $125, payable on January 1 of each year. Of this amount, $50 is for a 1-year subscription to the *American Journal of Roentgenology*, beginning with the July issue for the year following election to membership.
5. Application must be received by February 1 for action during the 1988 meeting.

Candidates for In-Training Membership

1. In-training members must be serving in a radiology residency or a postresidency fellowship program approved by the Radiology Residency Review Committee of the American Council of Graduate Medical Education or be a postgraduate student in an allied science. Training status must be verified by the program director. In-training members cannot hold offices in the society or vote.
2. Application must be on an official form and signed by the applicant and by the applicant's training or residency program director.
3. In-training status is limited to a maximum of 5 years starting with the entrance date into the radiology residency. In the fifth year, each in-training member will receive an application for transfer to active membership from the society secretary. Those who do not apply for transfer to active membership shall be dropped from membership at the end of the fifth year or last year.
4. There is no initiation fee. Annual dues are $25. Membership includes a subscription to the *American Journal of Roentgenology* and admission to the annual meeting without registration fees.
5. Membership applications will be acted on when received.

All Applicants

1. Do not remit initiation fee or dues until requested by the secretary (except for in-training applicants, who should submit dues with applications).
2. Send completed forms to: Paul Fullagar
   Administrative Director
   American Roentgen Ray Society
   1891 Preston White Dr.
   Reston, VA 22091

Classified Advertisements

Positions Available

ISRAEL, DIAGNOSTIC RADIOLOGY. Opportunities for 3–4 week or longer working vacations in a number of Israeli medical centers, on a volunteer basis. Positions varied, arrangements flexible. For information contact: Jonathan H. Fish, M.D., 1844 San Miguel Dr., #302, Walnut Creek, CA 94596; (415) 947-0560. 8xa

NEURORADIOLOGY OPENINGS—The Dept. of Radiology, Ottawa General Hospital, University of Ottawa, requires a Chief of the Neuroradiology Service and an additional neuroradiologist. This is a newly built university teaching hospital of 530 beds, with an extremely well equipped modern X-ray dept. There is a Philips Angiodiagnost on which approximately 500 cerebral angiograms are performed annually, 2 CAT scanners (EMI brain scanner, about to be replaced, and a GE 9800 body scanner), and a 1.5-T Siemens MRI unit. In addition, there is a unique opportunity for working in the field of NMR spectroscopy with the MR Spectroscopy Unit of the National Research Council of Canada, which has an international reputation. Candidates should be experienced in all aspects of neuroradiology, preferably including interventional neuroradiology. Previous experience in MRI preferable, but not essential. Income is based on a fee-for-service arrangement. In accordance with Canadian Immigration requirements, priority will be given to Canadian citizens and permanent residents of Canada. Applications should be sent to Director, Dept. of Radiology, Ottawa General Hospital, 501 Smyth Rd., Ottawa, Ontario, Canada K1H 8L6; (613) 737-8511. 1a

ANGIOGRAPHY/INTERVENTIONAL RADIOLOGIST—Board-certified radiologist with fellowship training in angiography/interventional radiology for position beginning July 1, 1988. Angiography/Interventional Radiology is an advanced, active section with state-of-the-art equipment and emphasis on interventional procedures. 612-bed teaching hospital. Radiology group is an academically-oriented private practice. Send inquiries to Harvey L. Neiman, M.D., Chairman, Dept. of Radiology, The Western Pennsylvania Hospital, 4800 Friendship Ave., Pittsburgh, PA 15224. 11–1a

AGGRESSIVE DIAGNOSTIC RADIOLOGY GROUP is in need of new associate approximately January to July 1989. Must be board certified to become partner. Would prefer multitalented background including interventional radiology, nuclear medicine, ultrasound, CT, and MRI experience. Ability to speak Spanish helpful but not required. Our group covers 4 hospitals including regional trauma center and 2 offices. Located in The Sparkling City by the Sea. Kindly send CV to Donald R. Brieger, M.D., or R.P. Chepey, M.D., 2481 Morgan, P.O. Box 5608, Corpus Christi, TX 78405. 11–2a

SEEKING BOARD-CERTIFIED RADIOLOGIST for a 40-bed health-care facility in Haily, ID. Billing service available. Progressive medical community. Located just 10 mi from Sun Valley, ID. For further information contact David Farnes, Administrator, Blaine County Medical Center, P.O. Box 927, Haily, ID 83333; (208) 788-2222. 1–2a

NEW YORK CITY SUBURBAN PRACTICE seeks board-certified radiologist, part-time. Hands-on ultrasound skills essential. Solid imaging knowledge. Personality counts. Grow to full-time. CV to Box 18, Meacham Station, Elmont, NY 11003. 1–2a

BC/BE GENERAL DIAGNOSTIC RADIOLOGY ASSOCIATE needed for 130-bed acute-care hospital practice. Proficiency in all modalities except MRI required. Locum tenens assistance desired until a permanent associate is obtained. Send CV and 3 references with initial letter of inquiry to Office Manager, P.O. Box 5046, Rancho Mirage, CA 92210. 12-1ap

RADIOLOGIST TO SHARE PRACTICE with 1 other in an 81-physician group practice clinic. Successful applicant will be board certified or eligible and have expertise in CT, ultrasound, and mammography. The clinic is located in north central Illinois. Chicago and Milwaukee are within 2-hr drives. Send CV in confidence to Richard A. Mueller, Director Human Resources, Rockford Clinic, 2300 N. Rockton Ave., Rockford, IL 61103. Equal opportunity employer m/f/h. 1ap

CT AND ULTRASONOGRAPHY—We are seeking a board-certified radiologist with fellowship training in CT and ultrasonography to join a thriving section in a busy University Hospital. The individual should have a proven background in teaching, research, and patient care. The section includes state-of-the-art CT scanners and ultrasound equipment. Currently, there are 4 full-time faculty and 2 fellows in the section. Stony Brook is located on the highly desirable North Shore of Long Island, with convenient access to New York City. The medical center provides the benefits of academic practice in a suburban setting. Please send CV to Jeffrey R. Crass, M.D., Associate Professor, Dept. of Radiology, Health Sciences Center, Level 4, Room 147, State University of New York at Stony Brook, Stony Brook, NY 11794-8460. SUNY Stony Brook is an affirmative action/equal opportunity educator and employer. 1a

NEW ENGLAND MEDICAL CENTER–TUFTS UNIVERSITY SCHOOL OF MEDICINE is seeking a radiologist in the General Radiology Section. The candidate should have expertise in bone radiology and a desire to participate in all modalities of bone and joint imaging including contrast arthrography. The candidate should also have an interest in orthopedic radiology. The hospital is a 469-bed (112 pediatric) hospital and the principal teaching affiliate of Tufts University School of Medicine. The candidate should be eligible for a faculty position at the medical school. Please direct inquiries and CV to Robert C. Sarno, M.D., Dept. of Radiology, New England Medical Center Hospitals, 750 Washington St., Boston, MA 02111. 1–2ap

DIAGNOSTIC RADIOLOGIST—Board-certified radiologist with training in MRI and neuroradiology needed for 5-radiologist group in suburban NJ, 15 mi from New York City. Practice includes 400-bed hospital and 3 private offices including CT and 2 MRI units. Expertise in MRI and general diagnostic radiology essential. Position leading to partnership. Please send CV to R.F. Mattern, M.D., 116 Park St., Montclair, NJ 07042. 1a

THE DEPT. OF RADIOLOGY, UNIVERSITY HEALTH CENTER OF PITTSBURGH, is seeking staff radiologists with interest, training, or experience in chest, skeletal, and/or general radiology. Positions are available at the Assistant or Associate Professor level and include opportunities in research and teaching. Please forward CV to Richard E. Latchaw, M.D., Interim Chairman, Dept. of Radiology, 3508 Fifth Ave., Pittsburgh, PA 15213. 1a

BAYLOR COLLEGE OF MEDICINE, DEPT. OF RADIOLOGY, is seeking a diagnostic radiologist for the position of Director of Radiologic Education. The physician will be responsible for supervising training of 28 residents and 4 postdoctoral fellows in the 8 affiliated hospitals with some 5000 beds. Clinical responsibilities will be tailored to provide sufficient time for teaching and research. Applicants must be certified by the American Board of Radiology and have demonstrated academic leadership. Appointment level will be Associate Professor or Full Professor, according to credentials. Salary is negotiable. Submit CV and 3 references to James E. Harrell, M.D., Professor and Chairman, Dept. of Radiology, Baylor College of Medicine, One Baylor Plaza, Houston, TX 77030. Baylor College of Medicine is an equal opportunity/affirmative action employer. 1–2a

THERE IS AN UNEXPECTED OPENING FOR A NEURORADIOLOGIST beginning immediately at the University of Massachusetts Medical Center, a 355-bed teaching hospital located about 35 mi west of Boston. The university hospital is a general hospital that includes busy neurosurgical and neurologic services and a neuroradiology residency program. All current aspects of clinical neuroradiology, and head and neck radiology including MRI, CT, angiography, myelography, polytomography, and plain film diagnosis are done at the institution. The radiology dept. is modern and well equipped with 2 GE CT scanners (8800 and 9800), as well as a GE 1.5-T MRI scanner and a second 2.0-T research unit. For further information please contact Edward H. Smith, M.D., Professor and Chairman, Dept. of Radiology, University of Massachusetts Medical Center, 55 Lake Ave. N., Worcester, MA 01655; (617) 856-3252. The University of Massachusetts Medical Center is an equal opportunity/affirmative action employer. 1ap

DIRECTOR OF RADIOLOGY—A 200-bed specialty hospital that is affiliated with a prestigious medical school is seeking a board-certified radiologist to direct the activities of our Radiology and Nuclear Medicine Dept. This position requires an individual with strong clinical and teaching skills, as well as demonstrated administrative ability. Compensation includes a base salary commensurate with experience and ability, private practice billing plan, and a comprehensive benefits program. This is an excellent opportunity for a highly qualified radiologist to join the staff of a well-respected, progressive, and innovative institution located on Manhattan's upper East Side. Qualified candidates should reply in confidence to Administration Office, Chairman of The Search Committee, The Hospital for Special Surgery, 535 E. 70th St., New York, NY 10021. 1–2a

THE DEPT. OF RADIOLOGY, VIRGINIA COMMONWEALTH UNIVERSITY/MEDICAL COLLEGE OF VIRGINIA, Richmond, VA, seeks qualified individuals for faculty positions in diagnostic radiology. Must be ABR-certified or eligible. Academic rank and salary commensurate with experience. Submit CV to P.R.S. Kishore, M.D., Chairman, Dept. of Radiology, Medical College of Virginia, Box 470, Richmond, VA 23298-0470. MCV is an equal opportunity/affirmative action employer. Women and minorities are encouraged to apply. 1&3a

DIAGNOSTIC RADIOLOGIST—Busy 3-man group covering hospital and multimodality outpatient imaging center is seeking a board-certified radiologist. CT, ultrasound, MRI, nuclear medicine, and angiography skills required. Fellowship training and interest in neuroradiology a plus. Generous salary and liberal benefits leading to early partnership. Send CV to Diagnostic Radiology Consultants, 7703 Picardy Ave., Baton Rouge, LA 70809. 1–3a

BOARD-CERTIFIED RADIOLOGIST—Expanding multi-state, midwestern group, practicing in hospitals, clinics, and imaging centers, seeks board-certified radiologist. Progressive individuals with general diagnostic and MRI background preferred. Excellent benefit program. Send CV to Guy Syvertsen, M.D., Senior Vice-President, Reich, Seidelmann & Janicki, 36080 Bainbridge Rd., Solon, OH 44139. 1a

NUCLEAR MEDICINE PHYSICIAN—The University of Washington's Dept. of Radiology has an opening for an academically oriented radiologist in the area of nuclear medicine. Responsibilities include instructing medical students and residents and conducting research. Applicant must possess board certification or eligibility. Send letter and resume to Albert A. Moss, M.D., Dept. of Radiology, SB-05, University of Washington, Seattle, WA 98195. The University of Washington is an equal opportunity employer. 1a

ACADEMIC RADIOLOGIC IMAGING—University of Arkansas for Medical Sciences Imaging Division is seeking an academically oriented radiologist with primary interest in body CT, body MRI, and ultrasound (including obstetric). The imaging program is active and progressive, offering an opportunity for integration of these areas in an atmosphere of excellent facilities and equipment. The position involves teaching, research, and clinical activities at the Assistant or Associate Professor level. Please apply to Charles M. Boyd, M.D., Imaging Division, Dept. of Radiology, University of Arkansas for Medical Science, 4301 W. Markham (Slot 581), Little Rock, AR 72205. 1a

BC/BE DIAGNOSTIC RADIOLOGIST sought for large multispecialty group providing care for staff model BC/BS affiliated HMO as well as FFS practice. Strong consideration given to candidate with angio-interventional and MRI experience. Excellent salary and benefit package. Extensive support system and modern facility located in Columbia, MD, near the cultural advantages and medical schools of the Baltimore-Washington, DC, area. Please direct inquiries and CV to Patuxent Medical Group, Inc., Columbia-FreeState Health System, 2 Knoll North Dr., Columbia, MD 21045, Attn: Human Resources Dept. 1a

UNIVERSITY OF WASHINGTON, DEPT. OF RADIOLOGY seeks Assistant/Associate Professor specializing in basic or applied research in MRI imaging/spectroscopy. Candidate should be PhD with ongoing, independent research program in MRI-related field. Special interest in phosphorous spectroscopy, paramagnetic contrast media, or image acquisition/display would be appropriate. Position will be in Imaging Research Laboratory. Available in-house equipment includes 2-T animal and 1.5-T clinical imaging/spectroscopy systems. Chemistry, X-ray, PET, and physiology faculties and facilities located in discrete geographic area. Expanded spectroscopy capabilities are planned, and nearby chemistry/physics equipment can be used for high-field work. The successful candidate will be expected to continue development of an independent research program, to collaborate where possible with existing laboratory projects, and to participate in departmental teaching programs where appropriate. Resume and 3 references should be sent to Albert A. Moss, M.D., Dept. of Radiology, SB-05, Seattle, WA 98195. The University of Washington is an equal opportunity employer. 1a

PULMONARY RADIOLOGIST—The UCLA School of Medicine has a full-time tenure-track faculty position available in the General Diagnostic Division, Dept. of Radiological Sciences. Academic level of appointment to be determined. Must be eligible for California licensure. Provide CV, a statement of background and interests in academic radiology, and a listing of 5 references. Reply to Richard Gold, M.D., Chief of General Diagnosis, Dept. of Radiological Sciences, UCLA School of Medicine, Los Angeles, CA 90024. The University of California is an equal opportunity/affirmative action employer and encourages applications from members of minority groups and women. 1a

NEURORADIOLOGIST—Opening for experienced neuroradiologist with fellowship training to join partnership of 4 radiologists in outpatient office and 200-bed general hospital. MR experience essential. Currently considering MRI addition to be operational in 12 mo. Practice is in Coeur d' Alene, ID. Beautiful recreational, fishing, and hunting facilities. Excellent opportunity for university-trained radiologist seeking full, private-practice partnership situation. Send letters of inquiry with CV to Richard Hehn, M.D., Radiology Associates of North Idaho, 1104 Ironwood Dr., Coeur d' Alene, ID 83814. 1a

BC/BE DIAGNOSTIC RADIOLOGIST—Immediate opportunity to work with group covering hospital, private practice, and HMO. All modalities present. Southeast Florida location. Florida license necessary. J. Schneider, M.D., 1131 No. 35th Ave., Hollywood, FL 33021. 1ap

CT/ULTRASOUND IMAGER—The University of Washington's Dept. of Radiology has an opening for an academically oriented radiologist in the area of CT/ultrasound imaging. This position will also involve interventional radiology including biopsies and abscess drainage. Responsibilities include instructing medical students and residents and conducting research. Applicant must possess board certification in radiology plus 1-yr related fellowship or clinical experience in radiology post-residency. Send letter and resume to Albert A. Moss, M.D., Dept. of Radiology, SB-05, Seattle, WA 98195. The University of Washington is an equal opportunity employer. 1a

PULMONARY RADIOLOGIST—The University of Washington's Dept. of Radiology has an opening for an academically oriented radiologist in the area of pulmonary imaging. This position will also involve interventional radiology including biopsies and abscess drainage, as well as MRI, CT, and ultrasound. Responsibilities include instructing medical students and residents and conducting research. Applicant must possess board certification in radiology plus 1-yr related fellowship or clinical experience in radiology postresidency. Send letter and resume to Albert A. Moss, M.D., Dept. of Radiology, SB-05, Seattle, WA 98195. The University of Washington is an equal opportunity employer. 1a

MAINE RADIOLOGISTS—Two positions available due to retirement. Requires fellowship training in either noninvasive imaging or invasive procedures including angiography. Join a progressive group and affiliate with excellent medical center. State-of-the-art equipment. Competitive salary and benefit package. Enjoy college town lifestyle in Maine's beautiful lake region. For further information send CV to New England Health Search, 63 Forest Ave., Orono, ME 04473, or call (207) 866-5680 or (207) 866-5685. 1a

DIAGNOSTIC RADIOLOGIST—Excellent opportunity for a board-eligible or a board-certified radiologist to join a group practice in the New Orleans area. The candidate must have training and interest in all areas of diagnostic radiology. Experience in MRI desired. Please submit CV to Martin A. Belanger, M.D., W. Esplanade Ave., Ste. 206, Kenner, LA 70065; (504) 464-0811. 1–3ap

BOARD-CERTIFIED DIAGNOSTIC RADIOLOGIST to join 2-man group in a progressive 100-bed community hospital in the Seacoast area of New Hampshire. Practice includes CT, MRI, ultrasound, mammography, interventional radiology, and R&F. Those candidates having several years of post-residency training and work experience in private practice are preferred. Approximately 32,000 examinations are done per yr. A candidate with broad experience in all diagnostic imaging modalities is required. Send CV to G. Eric Geslien, M.D., Box 790, Exeter, NH 03833. 1ap

RADIOLOGIST—A board-certified/board-eligible radiologist with experience is needed to join the staff of the Alaska Native Medical Center, a 170-bed referral facility for a state-wide system of Indian Health Service hospitals and clinics. Practice stimulating and challenging radiology in a relaxed and casual atmosphere. State-of-the-art in-house CT, sonography, and mammography. Send CV to W. M. Cox, M.D., P.O. Box 10-7741, Anchorage, AK 99510-7741. EOE. 9–2a

DIAGNOSTIC RADIOLOGIST—University Hospital of Jacksonville/University of Florida is seeking an additional staff radiologist for a full-time faculty position. Special interest training or expertise is preferable in interventional, MR, pulmonary, or skeletal imaging. Salary and fringe benefits are excellent. An academic appointment will be at the assistant or associate professor level depending on the qualification of the applicant. Application recruiting deadline is Jan. 15, 1988. Anticipated starting date July 1, 1988. Send CV and references to H. Martin Northup, M.D., Chairman, Search Committee, University Hospital, 655 W. Eighth St., Jacksonville, FL 32209. AA/EOE. 12–1a

PEDIATRIC RADIOLOGIST—Children's Hospital Medical Center of Akron has a position available immediately for a pediatric radiologist. Applicant must be board-certified or board-eligible in diagnostic radiology. Additional training in CT, ultrasound, nuclear medicine, and MRI is desirable. Send CV to Lionel W. Young, M.D., Professor and Chairman, Northeastern Ohio Universities, College of Medicine, C/O Children's Hospital Medical Center of Akron, 281 Locust St., Akron, OH 44308. 12–5a

THE UNIVERSITY OF SOUTH FLORIDA, DEPT. OF RADIOLOGY, is recruiting additional radiology faculty for the Moffitt Cancer Center and Research Institute. We are seeking general academic radiologists with subspecialty expertise in nuclear, musculoskeletal, chest, abdominal, or interventional radiology. Fellowship or equivalent experience is desirable; subspecialty interest should encompass all imaging modalities including MRI. The positions involve clinical service, teaching, and research. Salary and academic rank based on qualifications. Send CV to Robert Clark, M.D., Dept. of Radiology, Moffitt Cancer Center, P.O. Box 280179, Tampa, FL 33682-0179. 12–2ap

VASCULAR/INTERVENTIONAL OPENING for third vascular and interventional radiologist in subspecialized 22-man private practice in 1200-bed fully-equipped teaching hospital. Must have fellowship training and experience with all aspects of vascular and interventional radiology. Write to A.D. Sears, M.D., Chairman, Dept. of Radiology, Baylor University Medical Center, 3500 Gaston, Dallas, TX 75246. 12–3a

BOARD-CERTIFIED OR -ELIGIBLE DIAGNOSTIC RADIOLOGIST to be part of a 3-person imaging-center staff and outpatient specialty clinic in Tacoma, WA. The radiology staff of this specialty center is associated with the larger radiology dept. in hospitals operated by Group Health Cooperative of Puget Sound in Seattle and Redmond, WA. The practice consists of responsibility in ultrasound, nuclear medicine, GI fluoroscopy, mammography, outpatient CT, and diagnostic X-ray. For further details please contact Director of Medical Staff Personnel, Group Health Cooperative of Puget Sound, 521 Wall St., Seattle, WA 98121; (206) 448-6550. 12–3a

BC/DIAGNOSTIC RADIOLOGIST—Special training in MR and/or ultrasound required. Busy hospital and office practice in Washington D.C. suburbs. Early partnership. Available July 1, 1988. Reply Box B62, *AJR* (see address this section). 12–2a

BOARD-CERTIFIED DIAGNOSTIC RADIOLOGIST—university trained with experience in CT, nuclear medicine, ultrasound, and mammography for free-standing imaging center in major city in the Southwest. State-of-the-art equipment with MR planned. No call. Salary leading to partnership. Send CV to Box B72, *AJR* (see address this section). 12–1a

RADIOLOGIST—Excellent opportunity. Seeking board-certified radiologist, preferably with cross-sectional imaging expertise, to join a large, private-practice group covering 3 hospitals and a newly built Diagnostic Center in eastern North Carolina. Excellent benefits and salary. Two years to partnership. Reply Box B64, *AJR* (see address this section). 12–1a

DIAGNOSTIC RADIOLOGIST to work with a group covering both hospital and private practice. CT, ultrasound, and angiography. 1 hr from Boston. Please reply to Box B66, *AJR* (see address this section). 12–1ap

BOARD-CERTIFIED RADIOLOGIST needed immediately to work in Ft. Lauderdale area hospital and private office in Boca-Raton. Current practice includes CT, nuclear medicine, ultrasound, interventional mammography, and pediatrics. Competitive starting salary with partnership in 3 yr. Should have Florida license. Contact David Wagner, Administrator; (305) 344-9990. 12–2a

DIAGNOSTIC RADIOLOGIST, SAN DIEGO AREA—Established 3-person radiology group has immediate opening for a board-certified radiologist with experience in nuclear medicine, mammography, angiography, ultrasound, CT, MRI, and some interventional radiology. Busy hospital and clinic practice. Salary leading to partnership. California license required. Reply with CV to Thomas G. Brault, M.D., Paradise Valley Radiology Medical Group, 2400 E. Fourth St., National City, CA 92050; (619) 470-4190. 12–1ap

CHAIRPERSON, DEPT. OF DIAGNOSTIC RADIOLOGY AND NUCLEAR MEDICINE—Rush-Presbyterian–St. Luke's Medical Center in Chicago invites applications for the position of chairperson of the Dept. of Diagnostic Radiology and Nuclear Medicine. Applicants must be certified by the American Board of Radiology and have substantial academic and administrative credentials. Please send inquiries and CV to Charles M. D'Angelo, M.D., Dept. of Neurological Surgery, Rush-Presbyterian–St. Luke's Medical Center, 1725 W. Harrison St., Chicago, IL 60612. Rush University is an equal opportunity/affirmative action employer. 12–1a

NEW ENGLAND—Two positions for BC/BE diagnostic radiologists with interest and expertise in ultrasound, CT, and mammography to join current, 4-member, office-practice radiology dept. of large, rapidly expanding, multispecialty, prepaid, and FFS practice. Positions available Jan. 1988 and July 1988. Competitive compensation and benefits. Send CV to Ivan R. Green, M.D., Chairman, Dept. of Radiology, Fallon Clinic, 630 Plantation St., Worcester, MA 01605. 12–2a

SEEKING A SECOND, FULL-TIME, TENURED-LINE, ACADEMIC NEURORADIOLOGIST with an opportunity to participate in a developing world-class MRI facility at the University of Kentucky. Busy neuroradiology division with 1536 total neuro procedures (596 angiograms and 940 myelograms), 7346 neuro CT scans, and 1172 neuro MRI scans last yr, including 378 head ultrasounds and intraoperative neuro ultrasound. Excellent equipment with 3 fourth-generation CT scanners, new (6-mo-old) neuroangiographic suite with full imaging capability including state-of-the-art DSA, 2 myelographic suites, 0.15-T resistive MRI (second unit, a 1.5-T superconductive MRI, to be installed early spring 1988), and potential for significant participation in MRI spectroscopic unit already in place (4.7-T Bruker unit). A world-class MRI facility will be built in 2–3 yr with excellent opportunity for spectroscopic research. The University is very strong in neurosciences with excellent neurology and neurosurgery departments, and an Aging Research Center with emphasis on Alzheimer research. Exceptional academic opportunities with excellent academic salary. For details write (include CV) or call C. Lee, M.D. (member ASNR), (606) 233-6155; or H.D. Rosenbaum, M.D. (Chairman of Diagnostic Radiology), (606) 233-8088: Dept. of Radiology, University of Kentucky Medical Center, Lexington, KY 40536. 12–3a

NORTHWEST OPPORTUNITY—Board-certified diagnostic radiologist to join group of 4 at busy 160-bed hospital and private-office practice. Minimum requirements include competence in angiography, CT, and ultrasound. Some limited interventional skills are desirable. Prefer university-trained applicant with imaging fellowship. Excellent benefits and early partnership. Community of 60,000 located on the Columbia River in the beautiful Pacific Northwest 1 hr from Portland, OR. Send CV and inquiries to Michael L. Hanslits, M.D., Longview Radiologists, 1020 11th Ave., Longview, WA 98632. 12–1a

DIAGNOSTIC RADIOLOGIST to join expanding private radiology group in Tampa Bay area. All modalities including MRI and SPECT. Board certification or additional training in nuclear medicine desirable. Send CV to Box B74, *AJR* (see address this section). 12–2a

RADIOLOGIST—Opening for board-certified or board-eligible diagnostic radiologist in large private practice with 3 hospitals and 3 outpatient facilities. Fellowship or practice experience preferred. Requires all aspects of diagnostic radiology including angiography/interventional and MRI. Metropolitan Northeast close to Philadelphia, Princeton, and New York City. Full- or part-time. Send CV with references. Reply Box B78, *AJR* (see address this section). 12–1a

BOARD-CERTIFIED DIAGNOSTIC RADIOLOGIST with subspecialty in cross-sectional imaging (CT/ultrasound) to join established 7-man group at 500-bed, acute-care, medical-school–affiliated hospital in New York City. Well-equipped modern dept. with all imaging modalities (MRI in summer of 1989), plus nearby private office. Minimum of 1-yr fellowship in cross-sectional imaging (CT/ultrasound) required. Postfellowship experience in cross-sectional imaging at a university center would be desirable. Reply Box B85, *AJR* (see address this section). 12xa

NEURORADIOLOGIST, DENVER, CO—Western Radiologists, P.C., a group of 10-diagnostic radiologists engaged in a predominantly hospital-based practice, is seeking an additional member on or about July 1, 1988. The new member should have fellowship training and/or additional experience beyond the residency level in neuroradiology, MRI, and angiography. The group provides diagnostic radiology services for Saint Joseph Hospital, a 565-bed tertiary care teaching hospital, a clinic, and 2 offices. The radiology dept. within the hospital includes state-of-the-art equipment in all imaging modalities. Salary, benefits, vacation time, and time to partnership are all competitive for the Rocky Mountain region. Additional information is available upon request. Interested parties should send their CV to Kim I. McMillin, M.D., Dept. of Diagnostic Imaging, Saint Joseph Hospital, 1835 Franklin St., Denver, CO 80218. 12–2a

ULTRASOUND/CT/MRI—Opportunity for board-certified radiologist specializing in ultrasound, body CT, and body MRI to pursue academic career at The New York Hospital–Cornell Medical Center. Dept. provides state-of-the-art equipment, including Acuson ultrasound, GE 9800 CT, and GE Signa 1.5-T MR. Wide variety of ultrasound examinations include abdominal, Doppler, OB-GYN, small parts, and neonatal head. Prefer candidate with prior fellowship in sectional imaging or ultrasound. Responsibilities include clinical practice, teaching, and research. Please send CV to Elias Kazam, M.D., Dept. of Radiology, The New York Hospital–Cornell Medical Center, 525 E. 68th St., New York, NY 10021. 12–1a

INTERVENTIONAL RADIOLOGIST WANTED—Radiology Associates of Albuquerque, P.A., an 11-physician organization serving 3 major metropolitan hospital facilities, has an opening for an interventional radiologist. Fellowship training or equivalent postgraduate experience is required. CT and ultrasound interpretation also necessary. MRI experience a plus, but not mandatory. Practice is located in Albuquerque, NM. Climate and facilities are outstanding. Qualified applicants may apply by sending CV and references to Radiology Associates of Albuquerque, P.A., 4001 Indian School Rd., NE, Ste. 300, Albuquerque, NM 87110. Attn: Medical Director. 12–1a

CHEST RADIOLOGIST—The Dept. of Radiology of St. Luke's–Roosevelt Hospital Center in New York City is seeking a radiologist with special experience and/or training in thoracic imaging. A strong interest in clinical teaching and research, as well as in patient care, is required. Academic rank will depend on qualifications and experience. The dept. offers excellent facilities and remuneration. The hospital is a 1315-bed, voluntary university hospital of Columbia University College of Physicians & Surgeons. Send inquiries with a CV to Ronald C. Ablow, M.D., Dept. of Radiology, SLRHC, Amsterdam Ave. & 114th St., New York, NY 10025. An equal opportunity employer. 12–1a

GENERAL DIAGNOSTIC RADIOLOGIST WITH INTEREST IN CHEST RADIOLOGY—Diagnostic radiologist with training or experience in MRI. Two positions available on Jan. 1, 1988, to complete staffing for the new VA Medical Center in Minneapolis, MN. Dept. includes MRI, CT, cyclotron with PET scanner, interventional vascular suite, neuroradiology suite, mammography, plus more. Affiliated with the University of Minnesota with non–tenure-tract appointment available at appropriate level. Research and teaching opportunities available. Board certification mandatory for both positions. One-yr fellowship training or equivalent experience in chest radiology and MRI desirable. Send letters of inquiry with CV to Donovan B. Reinke, M.D., Chief of Diagnostic Radiology Service—114, VA Medical Center, 54th St. and 48th Ave. S., Minneapolis, MN 55417. EOE. 12–2a

DIAGNOSTIC RADIOLOGIST—Immediate opening for a board-certified radiologist. Practice includes CT, ultrasound, and myelography. Competitive salary, may lead to full partnership. Ample vacation and meeting time. Please include CV with letter of inquiry. Reply to Box 81, *AJR* (see address this section). 12–1a

MRI RADIOLOGIST—The Dept. of Radiology of St. Luke's–Roosevelt Hospital Center in New York City is seeking a radiologist with experience beyond fellowship in body MRI. A strong interest in clinical teaching and research, as well as in patient care, is required. Academic rank depends on qualifications. The hospital is a 1315-bed, voluntary university hospital of Columbia University College of Physicians & Surgeons. Send inquiries with a CV to Ronald C. Ablow, M.D., Dept. of Radiology, SLRHC, Amsterdam Ave. & 114th St., New York, NY 10025. An equal opportunity employer. 12–1a

DIAGNOSTIC RADIOLOGIST—The Dept. of Radiology of St. Luke's–Roosevelt Hospital Center in New York City is seeking a general radiologist with expertise in CT and ultrasound. The hospital is a 1315-bed, voluntary university hospital of Columbia University College of Physicians & Surgeons. Academic rank depends on qualifications and expertise. Excellent facilities and remuneration. Please send inquiries with a CV to Ronald C. Ablow, M.D., Dept. of Radiology, SLRHC, Amsterdam Ave. & 114th St., New York, NY 10025. An equal opportunity employer. 12–1a

BONE RADIOLOGIST—The Dept. of Radiology of St. Luke's–Roosevelt Hospital Center in New York City is seeking a radiologist with special experience and/or training in skeletal radiology. A strong interest in clinical teaching and research, as well as in patient care, is required. Academic rank depends on qualifications and experience. Excellent facilities and remuneration. The hospital is a 1315-bed, voluntary university hospital of Columbia University College of Physicians & Surgeons, New York City. Please send inquiries with a CV to Ronald C. Ablow, M.D., Dept. of Radiology, SLRHC, Amsterdam Ave. & 114th St., New York, NY 10025. An equal opportunity employer. 12–1a

BC/BE DIAGNOSTIC RADIOLOGIST—Busy hospital and office practice. *All* D.R. skills necessary. Florida license, amicable, and nonsmoker. Stimulating practice and great beach-area lifestyle. Seeking right person for established 6-member practice. Send CV and photo to J.G. Arterburn, M.D., C/O R.A. Castillo, M.D., and Assoc., P.A., 1609 Pasadena Ave. S., St. Petersburg, FL 33707. 11–1ap

FULL-TIME, PART-TIME, OR LOCUM TENENS (LEADING TO PERMANENT) office/hospital-based position in south Texas urban community. Board certification, friendly attitude, good training, motivation, and Texas license required. General radiology practice with fluoroscopy, mammography, nuclear medicine, sonography, CT, and limited MRI. Comfortable hours and remuneration with potential to expand. Reply Box W60, *AJR* (see address this section). 11xa

THOMAS JEFFERSON UNIVERSITY HOSPITAL—Two academically-oriented staff radiologists are sought for positions in a dynamic Dept. of Radiology, now in a rebuilding phase. (1) General diagnostic radiologist. This individual will cover a broad spectrum of diagnostic areas including chest, bone, GI, GU, and breast imaging. One or more of these areas can be emphasized according to individual interests. (2) Ultrasound radiologist. This individual will join one of the largest and most active ultrasound divisions in the world and will participate in the full range of diagnostic and interventional ultrasound studies. Some general diagnostic responsibilities also may be included. Candidates should be board certified or eligible and have interests in clinical radiology, teaching, and research. Please send CV to Robert Steiner, M.D., Co-Director, General Diagnostic Division; Barry Goldberg, M.D., Director, Division of Ultrasound; or David Levin, M.D, Chairman, Dept. of Radiology, Thomas Jefferson University Hospital, Philadelphia, PA 19107. Thomas Jefferson University Hospital is an Equal Opportunity/Affirmative Action Employer. 11–2a

INTERVENTIONAL RADIOLOGIST—Position available at the University of Rochester Medical Center Strong Memorial Hospital, a 750-bed tertiary care facility. An appointment as assistant professor or higher is available at a level appropriate to experience. One-yr fellowship training or equivalent experience is required. Research and teaching opportunities are available in a strong academic dept. with state-of-the-art equipment. Send letters of inquiry to Robert E. O'Mara, M.D., Acting Chairman, Diagnostic Radiology, Box 648, University of Rochester Medical Center, Rochester, NY 14642. EO/AA/M-F employer. 11–1a

VASCULAR/INTERVENTIONAL RADIOLOGISTS—University hospital offers full-time staff position at assistant to associate professor level for vascular/interventional radiologist. Vascular MRI and research opportunities included. Please contact Klemens H. Barth, M.D., Director, Division of Vascular/Interventional Radiology, Georgetown University Hospital, 3800 Reservoir Rd., N.W., Washington, DC 20007; (202) 625-2891. Affirmative action/equal opportunity employer. 11–2a

DIAGNOSTIC RADIOLOGIST BC/BE to join 8-member group in this growing practice and community. Position allows participation in all modalities including MRI. Contact Edward J. Chesna, M.D., 703 N. East St., Bloomington, IL 61701; (309) 829-9473. 11–1a

DIAGNOSTIC RADIOLOGIST, university trained, to join established group of 4 in a beautiful town in northern IL. A 432-bed community hospital with major teaching affiliation with University of Illinois College of Medicine at Rockford. Growing practice, state-of-the-art in all modalities including MRI. Fellowship a plus but not essential. Position available ASAP. Please send CV to W.J. Marx, M.D., P.O. Box 4205, Rockford, IL 61110. 11–1a

GENERAL DIAGNOSTIC RADIOLOGIST AND A BODY CT/ULTRASOUND RADIOLOGIST with an opportunity to participate in a developing world-class MRI facility. The University of Kentucky Medical Center is seeking an additional staff member who will have virtually full-time responsibilities in body cross-sectional radiology. Excellent equipment, including 3 fourth-generation CT scanners. The position also includes a potential for significant participation in the clinical and research activities of a superb, markedly expanded MRI and spectroscopy facility. We are also seeking an additional radiologist with duties in conventional diagnostic procedures. Both positions have exceptional academic opportunities with remuneration far above average for University hospitals. For details call (606) 233-8088 or write (include CV) to H.D. Rosenbaum, M.D., Chairman of Diagnostic Radiology, University of Kentucky Medical Center, Lexington, KY 40536. 11–4a

LARGE (28 RADIOLOGISTS), GROWING, WELL-DIVERSIFIED GROUP IN COLUMBUS, OH seeks an additional radiologist, well-trained in general diagnostic radiology, with additional training in nuclear medicine. Position leads to full partnership without buy-in expense. Send CV to Patrick Cain, M.D., 4040 Longhill Rd., Columbus, OH 43220. 11–1a

FULL-TIME JUNIOR FACULTY POSITION IN NEURORADIOLOGY SECTION for person with primary interest and expertise in surgical (interventional) neuroradiology, and secondary interest in general neuroradiology. Must have completed 2-yr fellowship in neuroradiology. Position covers both UUMC and VAMC on rotational basis with 3 other full-time neuroradiologists. Individual would become Director of Surgical Neuroradiology with specific charge to develop in-house and intermountain area outreach program in interventional neuroangiography. Deadline is Dec. 1, 1987. Applications submitted after the deadline may be considered if no qualified candidates have applied by the deadline. AA/EOE employer. Please reply to University of Utah, Neuroradiology Section, Salt Lake City, UT 84112. 11–1a

FULL-TIME ORTHOPEDIC RADIOLOGIST to join an active orthopedic radiology service; expected to help optimize clinical-care delivery, assist in teaching residents, and help develop a more active orthopedic-interventional and MRI service. Entry rank as assistant professor, tenure track. Time partitioning of 55% orthopedic radiology, 20% chest and breast imaging, and 25% academic time. Must have completed an orthopedic radiology fellowship or have worked 2 yr primarily as an orthopedic radiologist. American Board of Radiology certification required. Deadline is Dec. 1, 1987. Applications submitted after the deadline may be considered if no qualified candidates have applied by the deadline. AA/EOE employer. Please reply to University of Utah, Dept. of Radiology, Salt Lake City, UT 84112. 11–1a

BOARD-CERTIFIED DIAGNOSTIC RADIOLOGIST to join multispecialty private corporation with a well-equipped X-ray area, dedicated mammography, nuclear medicine, high-resolution real-time ultrasound, and whole-body CAT scanner. Send CV and reply to Administrator, Johnson Clinic, P.C., P.O. Box 315, Rugby, ND 58368. 12–1a

THE UNIVERSITY OF ARIZONA, DEPT. OF RADIOLOGY is recruiting a Section Head of Thoracic Radiology and abdominal imaging radiologist for the University Medical Center and a General Radiologist for the VA Medical Center. Candidates should be trained in appropriate imaging modalities and invasive techniques, and interested in teaching and research. Income and academic rank are negotiable. The University of Arizona is an affirmative action/equal opportunity employer. Contact Bruce J. Hillman, M.D., Vice-Chairman, Dept. of Radiology, University of Arizona Health Sciences Center, Tucson, AZ 85724; (602) 626-7368. 9–2a

GENERAL RADIOLOGIST—Progressive 15-member group needs additional radiologist for hospital and office-based practice that serves part of a southwestern community with approximately one-half million population. Position requires board certification. Training and/or experience in mammography, CT, ultrasound, and nuclear medicine is also needed. Contact Tulsa Radiology Associates, Inc., P.O. Box 4939, Tulsa, OK 74159. 11–1a

DIAGNOSTIC RADIOLOGIST—Excellent opportunity for a board-eligible or board-certified radiologist to join a 9-member group in New Orleans, LA. The candidate must have training and an interest in all areas of diagnostic radiology. Experience in MRI required. Please submit CV to Harold R. Neitzschman, M.D., 4400 General Meyer Ave., Ste. 211, New Orleans, LA 70131; (504) 368-5074. 11–1ap

BOARD-CERTIFIED DIAGNOSTIC RADIOLOGIST to join multispecialty private corporation with a well-equipped X-ray area, dedicated mammography, nuclear medicine, high-resolution real-time ultrasound, and whole-body CAT scanner. Send CV and reply to Administrator, Johnson Clinic, P.C., P.O. Box 315, Rugby, ND 58368. 12–1a

FORT MORGAN, NORTHEAST COLORADO COMMUNITY serving 25,000, seeks BC radiologist for hospital-based solo practice. Nuclear medicine, ultrasound, mammography, and angiography. Generous practice assistance. Contact PROSEARCH, 305 NE 102nd Ave., Portland, OR 97220; (503) 256-2070. 11–2a

PRIVATE GROUP SEEKS BOARD-CERTIFIED/ELIGIBLE RADIOLOGIST—Excellent salary and benefits. Near Chicago. Reply with CV to Box A36, *AJR* (see address this section). 11–1a

Positions Desired

RADIOLOGIST, ABR-certified seeks full-time or regular part-time position (i.e., every other month or similar arrangement). Prefer town of less than 100,000. Experienced in all modalities except MRI. Available January 1988. Reply Box A44, *AJR* (see address this section). 11–1b

Fellowships and Residencies

FELLOWSHIP, DEPT. OF RADIOLOGY—Cedars-Sinai Medical Center, a 1201-bed, acute-care, research, and teaching hospital affiliated with the UCLA School of Medicine, has an opening for a 1-yr fellowship with emphasis on CT, ultrasound, MRI, and mammography available July 1, 1988; 18 radiologists associated in practice in dept. with 135 personnel. There are 104,880 inpatient and 9120 outpatient radiologic exams per yr. Applicant must have completed an approved residency in diagnostic radiology, must be board eligible/certified, and have a California state medical license by July 1, 1988. Send CV to N. Zheutlin, M.D., Dept. of Radiology, Cedars-Sinai Medical Center, 8700 Beverly Blvd., Los Angeles, CA 90048. 12–2cp

INTERVENTIONAL/ANGIOGRAPHY/ADVANCED BODY IMAGING FELLOWSHIP IN SAN FRANCISCO AREA—Available July 1, 1988. One-yr fellowship program at 350-bed Stanford University–affiliated hospital and 2 private hospitals. Extensive clinical experience involving all aspects of interventional vascular and nonvascular procedures. Fellow will also participate in MRI scanning and CT scanning including 3-dimensional reconstruction capability. Send inquiries and CV to Ira Fink, M.D., Valley Radiologists Medical Group, Inc., P.O. Box 2F, San Jose, CA 95109. 1–3c

SPECIAL PROCEDURES/IMAGING FELLOWSHIP—St. Mary Medical Center has 2 positions available with combined training in special procedures and imaging beginning July 1, 1988. Special procedures include angiography, angioplasty, embolization, biopsy, drainages, and interventional renal and hepatic procedures. Imaging equipment includes a GE 9800 CT scanner, Signa 1.5-T MRI, and Acuson ultrasound. The staff consists of university-trained subspecialty radiologists. Contact Gregory T. Vanley, M.D., Dept. of Radiology and Medical Imaging, St. Mary Medical Center, 1050 Linden Ave., Long Beach, CA 90801. 1c

ADVANCED IMAGING FELLOWSHIP—A position is now available for a board-certified or board-eligible radiologist in a University of Rochester teaching-hospital complex. The fellowship emphasizes in-depth exposure to CT, ultrasound, and MRI integrated with invasive procedure exposure. Additional positions will be available in January 1988. Please respond to Steven G. Herbert, M.D., Director, Fellowship Program, Diagnostic Radiology Dept., The Genesee Hospital, 224 Alexander St., Rochester, NY 14607. 1–2c

FELLOWSHIPS IN (1) ULTRASOUND/CT/MRI, (2) CARDIOVASCULAR/INTERVENTIONAL, (3) NEURORADIOLOGY/ENT, (4) CARDIOPULMONARY—The Dept. of Radiology at Thomas Jefferson University Hospital offers these 4 subspecialty fellowships each yr. We have a very large and extensively equipped ultrasound division that offers training in all phases of ultrasound including cardiac, vascular, and obstetric. The dept. also has 3 modern CT scanners and a GE 1.5-T MRI unit. The Cardiovascular/Interventional Division is currently being renovated and will house state-of-the-art angiography equipment with DSA. This division performs a full range of both vascular and nonvascular interventional procedures. Neuroradiology is housed in a brand new Neurosciences Imaging Center containing all imaging modalities in a single comprehensive facility. For information and applications to these 4 programs, contact Barry B. Goldberg, M.D. (Ultrasound/CT/MRI); Geoffrey Gardiner, Jr., M.D. (Cardiovascular/Interventional); Carlos Gonzalez, M.D. (Neuroradiology); or Robert Steiner, M.D. (Cardiopulmonary) at the Dept. of Radiology, Thomas Jefferson University Hospital, Philadelphia, PA 19107. 1c

DEPT. OF RADIOLOGY, UNIVERSITY OF ROCHESTER MEDICAL CENTER—One-year fellowship positions available July 1, 1988, or July 1, 1989. Positions include neuroradiology, cardiovascular/angiography, ultrasound/CT/MRI, and pediatric radiology. Requirements include board eligibility or certification in diagnostic radiology and an accredited radiology residency. Candidates must be licensed or eligible to obtain a license to practice medicine in the state of New York. Apply by Dec. 1 of the year before the fellowship starting date. Contact Beverly P. Wood, M.D., Box 648, University of Rochester Medical Center, Rochester, NY 14642. University of Rochester is an affirmative action, equal opportunity employer. 10–3c

IMAGING FELLOWSHIP—Two positions are available for training in body imaging (CT, MRI, and ultrasound). This active university-based program combines excellent facilities and extensive modern equipment with clinical material to provide broad, clinical training. There are opportunities for research in any of these areas if desired. Please apply to Charles M. Boyd, M.D., Imaging Division, Dept. of Radiology, University of Arkansas for Medical Science, 4301 W. Markham (Slot 581), Little Rock, AR 72205. 1c

THE DEPT. OF RADIOLOGY AT THE UNIVERSITY OF COLORADO HEALTH SCIENCES CENTER offers fellowships annually in angiography/interventional, body imaging (ultrasound, CT, and MRI), chest, MRI, neuroradiology, nuclear medicine, and pediatric radiology. With the appointment of Michael L. Manco-Johnson, M.D., as Chairman, the dept. has received a generous commitment of additional state-of-the-art equipment and new faculty. Interested candidates should write for applications to Residency and Fellowship Programs, Dept. of Radiology, Box A030, University of Colorado Health Sciences Center, 4200 E. 9th Ave., Denver, CO 80262. Please indicate which fellowship(s) interest you. Applicants should be board eligible in diagnostic radiology, and foreign medical graduates must have passed the American Medical Qualification Examination prepared by ECFMG. UCHSC is an AA/EOE employer. 1c

MUSCULOSKELETAL RADIOLOGY FELLOWSHIP—The Dept. of Radiology, Georgetown University Hospital announces a new 1-yr fellowship starting July 1, 1988, in musculoskeletal radiology. Equipment includes a 1.5-T Siemens MR, a Varian 4.7-T spectral imager for animal research, 2 GE 9800 Quick CT scanners, and Acuson and ATL ultrasound units. Equipment in nuclear medicine includes 4 single-headed SPECT tomographic cameras, the revolutionary Triad tomographic camera, and a dual-photon densitometer. Full research and clinical experience opportunities in MRI, CT, MSK tumors, rheumatologic disorders, sports medicine, and trauma are program highlights, as well as a strong affiliation with the National Institutes of Health. Send CV to Martha C. Nelson, M.D., Division Director, Musculoskeletal Radiology, Georgetown University Hospital, 3800 Reservoir Rd., N.W., Washington, DC 20007. 12–2cp

INTERVENTIONAL RADIOLOGY FELLOWSHIP—The Rush-Presbyterian–St. Luke's Medical Center is now offering a 1-yr fellowship position beginning July 1, 1988, in interventional radiology. This 750-bed teaching hospital offers extensive experience in all aspects of vascular and nonvascular procedures with a primary emphasis on patient care and clinical research. Send inquiries to Terence Matalon, M.D., Rush-Presbyterian–St. Luke's Medical Center, Dept. of Radiology, 1753 W. Congress Pkwy., Chicago, IL 60612. 11–2c

CARDIOVASCULAR-INTERVENTIONAL RADIOLOGY FELLOWSHIP—Available July 1, 1988. One-year fellowship program at a 750-bed teaching hospital. Extensive clinical experience involving all aspects of cardiovascular imaging, interventional vascular and nonvascular procedures, and availability for clinical or animal research. Send CV and inquiries to Oscar H. Gutierrez, M.D., Dept. of Radiology, Box 648, University of Rochester Medical Center, Rochester, NY 14642. EO/AA/M-F employer. 10–3c

IMAGING FELLOWSHIP offered by the University Hospital of Jacksonville/University of Florida College of Medicine beginning July 1, 1988. The University Hospital is a 489-bed, acute-care hospital providing resident and fellowship training in most of the major medical disciplines including diagnostic radiology. The fellowship will include rotations in CT, ultrasound, and MR designed to provide qualified individuals with additional specialized training and responsibility. Facilities are state-of-the-art with major additions in each area within the past 2 yr. Applicants must be board eligible or board certified in diagnostic radiology and should forward a CV with 3 letters of recommendations to Frederick Vines, M.D., University Hospital, Dept. of Radiology, 655 W. 8th St., Jacksonville, FL 32209; (904) 350-6624. 12–1c

Tutorials/Courses

AUSTRALIA-NEW ZEALAND—IMAGING DOWN UNDER, MARCH 12–27, 1988. International faculty. Auckland, New Zealand, March 13–14; Sydney, Australia, March 18–20; and Melbourne, Australia, March 25–26. Information: Medical Seminars, 21915 Roscoe Blvd., Ste. 222, Canoga Park, CA 91304; (818) 719-7380. 9–2d

Other

FOR LEASE—Fully equipped, operating radiology office in medical building situated in the Princeton, NJ, area. Great opportunity. Reply to P.O. Box 191, Kingston, NJ 08528. 1e

AJR Classified Advertisements Information

Box Responses and Address for Ad Placement

Write Box _____, AJR, Suite 200, 2223 Avenida de la Playa, La Jolla, CA 92037; (619) 459-2229.

How to Place an Ad

AJR accepts classified advertising for Positions Available, Positions Desired, Fellowships and Residencies, and Tutorials/Courses. Ads are accepted by mail or telephone. Institutions should supply purchase orders.

Rates: $6.00/line with a $30 minimum charge. Box service is $10 additional for each month the ad appears. There are discounts for multiple insertions: 10% for 2–3 insertions; 20% for 4 or more. To estimate lines, count all words and divide by 5.5.

Billing: Ads may be prepaid or invoices will be sent after the ad appears.

Deadlines. 6 weeks prior to issue date. For specific deadlines telephone the AJR editorial office.

Estimating Ad Charges

Line charge: divide total words by 5.5 and multiply by $6.00 . . . . $ _____

Multiple insertions? If so, multiply by number . . . . . × _____

Subtotal . . . . . $

Box response requested? If so, multiply number of months by $10.00 . . . . . + _____

Subtotal . . . . . $

Discount applies to two or more insertions. Subtract 10% if ad appears 2–3 months, 20% if 4 months or more . . . . . – _____

Approximate advertising charge . . . . . $

MAKE YOUR PRACTICE THRIVE

in today's complex health care environment

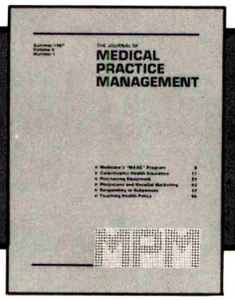

The Journal of MEDICAL PRACTICE MANAGEMENT *Quarterly*

Editor: **Marcel Frenkel, MD, MBA**

■ *Find out what today's issues mean for you and your practice*

Now more than ever, the practice of medicine is changing. You've seen the emergence of HMOs, IPAs, and PPOs...you've felt the impact of DRGs... increased competition...and more. Despite the advent of these alternate delivery systems, most experts firmly believe that private practice is here to stay.

Now there's an intelligent, convenient way to make sure you're getting the important information on trends and issues in health care that will influence your practice of medicine this year... and five years down the road. And for far less than any consultant's hourly fee. With **THE JOURNAL OF MEDICAL PRACTICE MANAGEMENT.**

■ *Timely articles help you make far-sighted decisions*

Featuring articles ranging from the *Financing of Long-Term Care* to *Joint Ventures in Medical Services* to *Medical Practice Where HMOs Dominate,* **THE JOURNAL OF MEDICAL PRACTICE MANAGEMENT** helps you pinpoint what management pitfalls to avoid, what economic forecasts to trust, which markets are targeted for growth, and so much more. In every quarterly issue you'll find departments covering: **health care policy • marketing and organizational structure • taxation, legislation and legal affairs • office management and computerization • manpower and education.**

You'll also find pertinent features like the **Washington Report,** telling you what's brewing in the nation's capital that affects you...**Briefs,** covering statistics, management, hospitals and taxation with timely, concise reports...**Abstracts** of health care management literature...plus **profiles** of for-profit and not-for-profit health care delivery systems.

■ *Founded by a physician for physicians*

Headed by founder and editor Marcel Frenkel, MD, MBA, **THE JOURNAL OF MEDICAL PRACTICE MANAGEMENT** is the only journal of its kind edited by a physician for physicians. Its multidisciplinary editorial board is made up of experts from the fields of public and private management, health care administration, economics, marketing, medical-legal affairs, and others. They are carefully chosen for their extensive knowledge of the management aspects of practicing medicine.

No-risk offer

You've invested a lot of time, money, and hard work to get where you are today. If you'd like to see your practice thrive in today's complex health care environment... give **THE JOURNAL OF MEDICAL PRACTICE MANAGEMENT** a try.

Just return the attached coupon, or call TOLL-FREE 1-800-638-6423, from anywhere in the U.S. except Alaska. In Maryland, call 528-4105 collect. If ever disappointed in your issues of **THE JOURNAL OF MEDICAL PRACTICE MANAGEMENT,** you may cancel your subscription for a full refund on unmailed issues...no questions asked.

☐ **YES!** I want to make the right decisions for my future. Please enter my subscription to THE JOURNAL OF MEDICAL PRACTICE MANAGEMENT *(quarterly)*

☐ Individual $49/year ☐ Institution $65/year
Add $10 outside the U.S.

☐ Check enclosed ☐ Bill me
☐ MasterCard ☐ American Express ☐ VISA

Card # _____ Exp. date _____

Signature/P.O. # _____

Name _____

Address _____

City/State/Zip _____

Maryland residents add 5% sales tax. Subscriptions outside the U.S. must be prepaid. All subscriptions must be paid in U.S. dollars. Please allow 8 weeks for delivery of your first issue, up to 16 weeks for surface delivery outside the U.S. Airmail rates available on request.

Williams & Wilkins
P.O. Box 23291 ☐ Baltimore, Maryland 21203
266 Fulham Road ☐ London SW10 9EL England

MPMAD 50632

UNIVERSITY OF MIAMI

School of Medicine

Department of Radiology is recruiting faculty for the UM/Jackson Memorial Medical Center, a 1300 bed tertiary referral center. Positions available to meet expanding clinical and academic programs in:

THORACIC IMAGING
ABDOMINAL IMAGING
MUSCULOSKELETAL IMAGING
NEURORADIOLOGY
NUCLEAR MEDICINE

Candidates must be board certified or eligible, with fellowship training or equivalent experience. Rank and salary commensurate with qualifications.

Send C.V. to: C.A. Poole, M.D.
Professor and Chairman
Department of Radiology (R-130)
University of Miami School of Medicine
P.O. Box 016960
Miami, Florida 33101

AN AFFIRMATIVE ACTION/EQUAL OPPORTUNITY EMPLOYER

Assignment Saudi Arabia

The **King Faisal Specialist Hospital and Research Centre** in Riyadh, Saudi Arabia offers exceptional opportunities for experienced and qualified Radiologists. The Hospital, a 500-bed specialty referral complex with a large outpatient clinic, is the Kingdom's premier hospital dedicated to providing high quality health care to the citizens of Saudi Arabia.

The following positions are available:

INVASIVE RADIOLOGIST

RADIOLOGIST
(With comprehensive Gastro experience)

RADIOLOGIST
(With experience in Nuclear Radiology)

To be considered for this opportunity, physicians must be board certified, and have current U.S., Canadian or U.K. license to practice and 3 years hospital experience. Academic affiliation is preferred.

For further information and/or to apply, please call our toll-free number (800) 251-2561 or send a detailed curriculum vitae to: **HCA International Company, P.O. Box 550, Dept AJR-188, Nashville, TN 37202.** HCA is an Equal Opportunity Employer.

HCA International Company

Help us to serve you better.....

USE YOUR ZIP CODE

Remember, your zip code provides faster, more direct delivery of your journals. Use it on all correspondence, too.

Discover Montefiore

Henry and Lucy Moses Division
• NEURORADIOLOGIST

Academic position immediately available at the Assistant Professor or Associate Professor level in the Neuroradiology Division of the Department of Radiology. Candidate should have successfully completed an accredited Diagnostic Radiology Residency Program and/or a 2 year Neuroradiology Fellowship Program. BE/BC required. Facilities include two 3rd generation CT Scanners and a mobile Magnetic Resonance Imaging Unit. Plans are being finalized for both a state-of-the-art Magnetic Resonance Imaging Unit and a new Neuroangiography Suite. Interested candidate should send CV to: **George Lantos, Director of Neuroradiology, Department of Radiology, Montefiore Medical Center, 111 East 210 Street, Bronx, New York 10467.**

Montefiore
MEDICAL CENTER
An Equal Opportunity Employer M/F

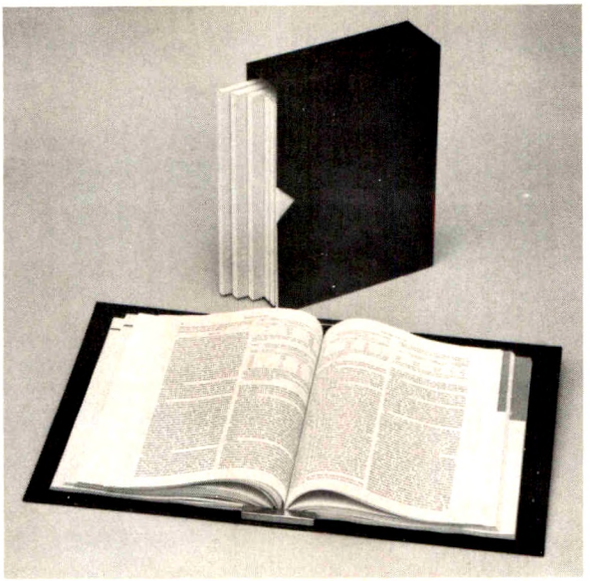

Protect your copies of

AJR: AMERICAN JOURNAL OF ROENTGENOLOGY

with Jesse Jones Binders or Files

Keep your journals clean, orderly, and readily accessible with Jesse Jones Binders or Files. Two Binders or two box style Files are all you need to accommodate a full year's worth of issues. Both Binders and Files are handsomely made with rich black leatherette covers and gold leaf embossed lettering.

Jesse Jones Binders open flat for easy reading and reference and are economically priced at only $9.95 each; 3 for $27.95, or 6 for $52.95 postpaid. The rugged, compact box Files are only $7.95 each; 3 for $21.95, or 6 for $39.95. Add $1.00/unit postage and handling. (Outside the U.S. add $2.50/unit.)

For charge orders call toll free 1-800-972-5858. ($15.00 minimum).

Free gold transfer slips included for indexing volume and year.

Please allow four to five weeks for delivery.

TO: Jesse Jones Industries
499 E. Erie Avenue, DEPT. AJR
Philadelphia, PA 19134

I enclose my check or money order for $_____
(PA residents add 6% sales tax)

Send me ____ ☐ Files ☐ Binders for my journals

Name

Address (will not ship to P.O. Box)

City/State/Zip

Satisfaction guaranteed.

INDEX TO ADVERTISERS

Adria Laboratories A2

Berlex Imaging A12, A13

Braintree Laboratories A15

Eastman Kodak A6, A7

E-Z-EM Company . . . . . Cover 2

FUJI . . . . . Cover 3

HCA International A27

Mallinckrodt, Inc. A17, A18, A19, A20

Montefiore Medical Center A27

Nuclear Associates A21

Osler Institute A14

E. R. Squibb & Sons, Inc. A8, A9, A10, A11

S & S X-Ray A16

Toshiba Medical Systems A22, A23

Winthrop Laboratories A25, A26, A29, A30

University of Miami A27

We try to present an accurate index. Occasionally this may not be possible because of a last-minute change or an omission.

NEW INDICATION

In contrast-enhanced CT... improve the safety profile.

Fewer adverse reactions than with traditional ionics, including reactions that may delay or interrupt procedures.[1-4]

Tolerated "far better than conventional contrast media."[2]

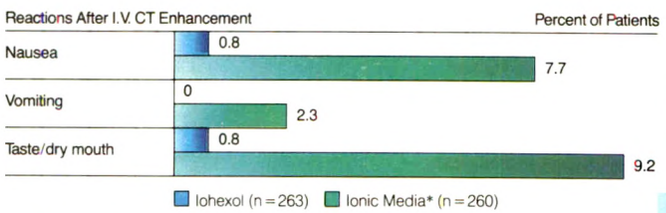

— In 263 CT patients, *no* reports of tachycardia, bradycardia, palpitations, or respiratory difficulties.[1†]

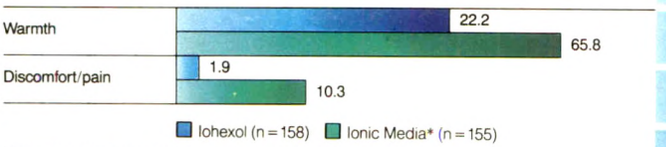

* Metrizoate or ioglicate, comparable concentration and volume per injection.
Adapted from Skalpe.[1]

Lower toxicity.

- Particularly important in enhanced cranial CT.
- An important advantage when the blood-brain barrier may already be disrupted.[1,5]

Now in special convenience/ economy packaging for enhanced CT.

Since adverse reactions can occur with nonionic media, similar precautions to those recommended for ionic media should be utilized for treatment of severe or potentially fatal reactions.

Physicians should remain alert to possible adverse effects that have occurred with other nonionic water-soluble media.

†In a more general patient population, such reactions occur in less than 1 percent.

See next page for important product information concerning contraindications, warnings, adverse reactions, patient selection, and prescribing and precautionary recommendations.

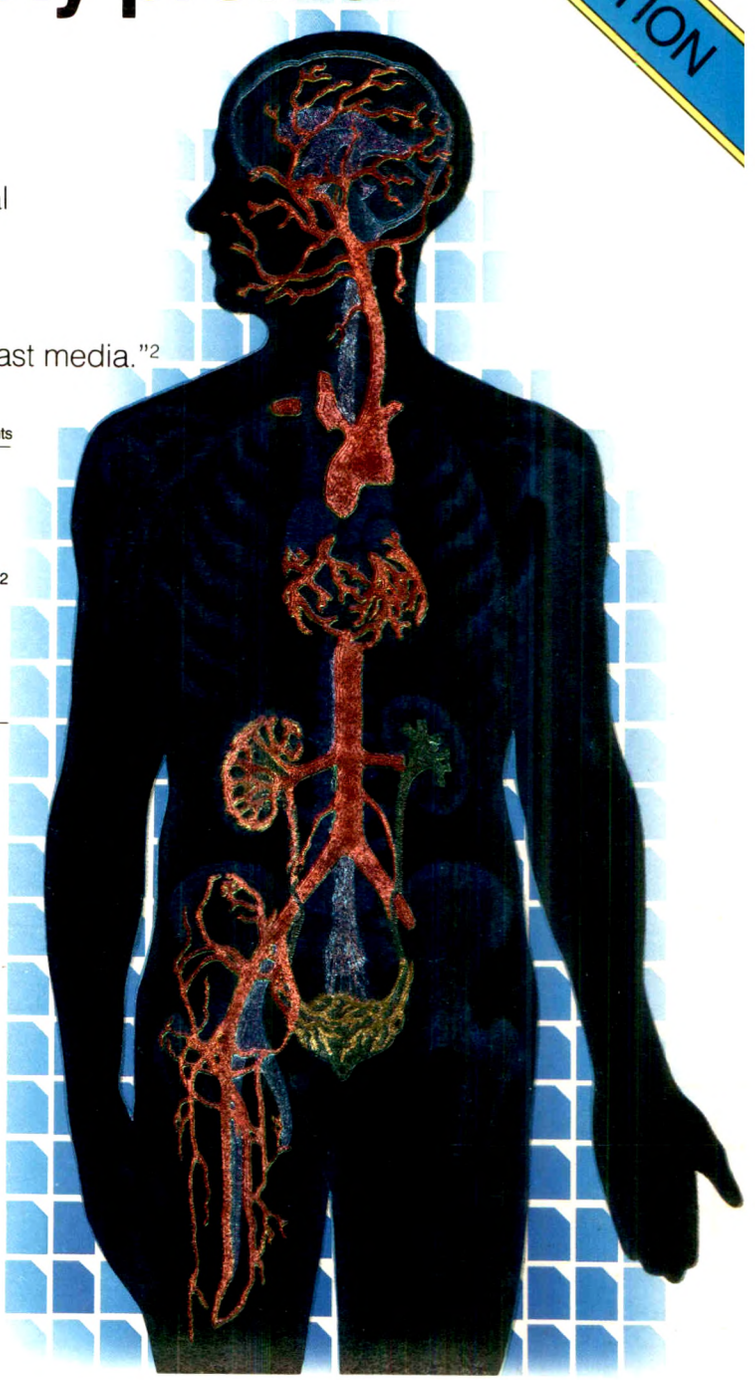

NONIONIC

OMNIPAQUE®

(IOHEXOL)

THE NEW STANDARD IN CONTRAST-ENHANCED IMAGING.

OMNIPAQUE®
INJECTION (IOHEXOL)
INTRAVASCULAR

240

300

350

PLEASE CONSULT FULL PRODUCT INFORMATION BEFORE USING.
A SUMMARY FOLLOWS:

DESCRIPTION: OMNIPAQUE is a nonionic, water-soluble radiographic contrast medium for intravascular administration and is provided in iodine concentrations of 240, 300, and 350 mgI/mL. Each milliliter of iohexol solution contains 1.21 mg tromethamine and 0.1 mg edetate calcium disodium with the pH adjusted between 6.8 and 7.7 with hydrochloric acid or sodium hydroxide, but it contains no preservatives.

CONTRAINDICATIONS: OMNIPAQUE should not be administered to patients with a known hypersensitivity to iohexol.

WARNINGS: OMNIPAQUE should be used with extreme care in patients with: severely impaired renal and/or hepatic function; severe thyrotoxicosis, hyperthyroidism, or an autonomously functioning thyroid nodule; diabetes with a serum creatinine level above 3 mg/dL. Not recommended for use in patients with anuria.

Patients with known or suspected pheochromocytoma should receive a minimum of contrast medium if benefit of the exam is judged to outweigh risk; blood pressure should be monitored throughout the procedure, and measures for the treatment of hypertensive crisis should be readily available.

Contrast agents are potentially hazardous in patients with multiple myeloma or other paraproteinemia, particularly those with therapeutically resistant anuria. The combination of contrast agent and dehydration may precipitate myeloma protein in the renal tubules. No form of therapy, including dialysis, has been successful in reversing the effect. Myeloma, which occurs most commonly in persons over age 40, should be considered before instituting intravascular administration of contrast agents.

PRECAUTIONS: Diagnostic procedures that involve the use of radiopaque diagnostic agents should be carried out under the direction of personnel with the prerequisite training and with a thorough knowledge of the particular procedure to be performed. Appropriate facilities should be available for coping with any complication of the procedure, as well as for emergency treatment of severe reactions to the contrast agent itself. Competent personnel and emergency facilities should be available for at least 30 to 60 minutes postprocedure. The possibility of serious, life-threatening, fatal, anaphylactoid, or cardiovascular reactions should always be considered (see ADVERSE REACTIONS). It is of utmost importance that a course of action be carefully planned in advance for immediate treatment of serious reactions. Preparatory dehydration is dangerous and may contribute to acute renal failure in patients with advanced vascular disease, diabetic patients, and in susceptible nondiabetic patients (often elderly with preexisting renal disease). *Patients should be well hydrated prior to and following iohexol administration.* Careful consideration to the potential risk of acute renal failure should be given before performing excretory urography in diabetic patients with diabetic nephropathy and in susceptible nondiabetic patients (often elderly with preexisting renal disease). Immediately following surgery, excretory urography should be used with caution in renal transplant recipients. The possibility of an idiosyncratic reaction in susceptible patients should always be considered (see ADVERSE REACTIONS). The susceptible population includes patients with a history of a previous reaction to contrast media, patients with a known sensitivity to iodine per se, and patients with a known clinical hypersensitivity: bronchial asthma, hay fever, and food allergies. A thorough medical history with emphasis on allergy and hypersensitivity, prior to the injection of any contrast media, may be more accurate than pretesting in predicting potential adverse reactions.

A positive history of allergies or hypersensitivity does not arbitrarily contraindicate the use of a contrast agent where a diagnostic procedure is thought essential, but caution should be exercised (see ADVERSE REACTIONS). Premedication with antihistamines or corticosteroids to avoid or minimize possible allergic reactions in such patients should be considered. Recent reports indicate that such pretreatment does not prevent serious, life-threatening reactions but may reduce both their incidence and severity.

Even though the osmolality of OMNIPAQUE is low compared to diatrizoate- or iothalamate-based ionic agents of comparable iodine concentration, the potential transitory increase in circulatory osmotic load in patients with congestive heart failure requires caution during injection. These patients should be observed for several hours following the procedure to detect delayed hemodynamic disturbances.

Angiography should be avoided whenever possible in patients with homocystinuria, because of the risk of inducing thrombosis and embolism.

In angiographic procedures, the possibility of dislodging plaques or damaging or perforating the vessel wall should be borne in mind during the catheter manipulations and contrast medium injection. Test injections to ensure proper catheter placement are recommended.

Selective coronary arteriography should be performed only in those patients in whom the expected benefits outweigh the potential risk. The inherent risks of angiocardiography in patients with chronic pulmonary emphysema must be weighed against the necessity for performing this procedure.

When OMNIPAQUE is to be injected using plastic disposable syringes, the contrast medium should be drawn into the syringe and used immediately.

The inhibitory effects of nonionic contrast media on mechanisms of hemostasis have been shown, in vitro, to be less than those of ionic contrast media at comparable concentrations. For this reason, standard angiographic procedures should always be followed: angiographic catheters should be flushed frequently, and prolonged contact of blood with contrast media in syringes and catheters should be avoided.

If nondisposable equipment is used, scrupulous care should be taken to prevent residual contamination with traces of cleansing agents.

Drug/Laboratory Test Interaction: If iodine-containing isotopes are to be administered for the diagnosis of thyroid disease, the iodine-binding capacity of thyroid tissue may be reduced for up to 2 weeks after contrast medium administration. Thyroid function tests which do not depend on iodine estimation, eg, T_3 resin uptake or direct thyroxine assays, are not affected.

Carcinogenesis, Mutagenesis, Impairment of Fertility: No long-term animal studies have been performed to evaluate carcinogenic potential, mutagenesis, or whether OMNIPAQUE can affect fertility in men or women.

Pregnancy Category B: Reproduction studies have been performed in rats and rabbits with up to 100 times the recommended human dose. No evidence of impaired fertility or harm to the fetus has been demonstrated due to OMNIPAQUE. There are, however, no studies in pregnant women. Because animal reproduction studies are not always predictive of human response, this drug should be used during pregnancy only if clearly needed.

Nursing Mothers: It is not known to what extent iohexol is excreted in human milk. However, many injectable contrast agents are excreted unchanged in human milk. Although it has not been established that serious adverse reactions occur in nursing infants, caution should be exercised when intravascular contrast media are administered to nursing women. Bottle feedings may be substituted for breast feedings for 24 hours following administration of OMNIPAQUE.

Pediatric Use: Safety and effectiveness in children have not been established.

ADVERSE REACTIONS: Usually mild to moderate in severity. However, serious, life-threatening, and fatal reactions, mostly of cardiovascular origin, have been associated with the administration of iodine-containing contrast media including OMNIPAQUE. The injection of contrast media is frequently associated with the sensation of warmth and pain, especially in peripheral angiography; pain and warmth are less frequent and less severe with OMNIPAQUE than with many contrast media.

Cardiovascular System: Arrhythmias including PVCs and PACs (3%), angina/chest pain (2%), and hypotension (1%). Others including cardiac failure, asystole, bradycardia, tachycardia, and vasovagal reaction were reported with an individual incidence of less than 0.8%. In controlled clinical trials involving 900 patients, one fatality occurred. A cause-and-effect relationship between this death and iohexol has not been established.

Nervous System: Pain (6%), photomas (3%), headache (2%), and metallic taste (0.8%). Others including anxiety, blurred vision, dizziness, fever, motor and speech dysfunction, convulsion, lightheadedness, paresthesia, somnolence, vertigo, stiff neck, hemiparesis, and nystagmus were reported, with an individual incidence of less than 0.3%.

Respiratory System: Dyspnea and laryngitis, with an individual incidence of 0.1%.

Gastrointestinal System: Nausea (2%) and vomiting (0.5%). Others including diarrhea, dyspepsia, and dry mouth were reported, with an individual incidence of 0.1%.

Skin and Appendages: Urticaria (0.3%) and purpura (0.1%).

General Adverse Reactions to Contrast Media: The following reactions have been reported after administration of other intravascular iodinated contrast media. *Reactions due to technique:* hematomas and ecchymoses. *Hemodynamic reactions:* vein cramp and thrombophlebitis following intravenous injection. *Cardiovascular reactions:* rare cases of cardiac arrhythmias, reflex tachycardia, chest pain, cyanosis, hypertension, hypotension, peripheral vasodilatation, shock, and cardiac arrest. *Renal reactions:* occasionally, transient proteinuria; rarely, oliguria or anuria. *Allergic reactions:* asthmatic attacks, nasal and conjunctival symptoms, dermal reactions such as urticaria with or without pruritus, as well as pleomorphic rashes, sneezing, and lacrimation; rarely, anaphylactic reactions. Rare fatalities have occurred due to these or unknown causes. *Signs and symptoms related to the respiratory system:* pulmonary or laryngeal edema, bronchospasm, dyspnea; or *to the nervous system:* restlessness, tremors, convulsions. *Other reactions:* flushing, pain, warmth, metallic taste, nausea, vomiting, anxiety, headache, confusion, pallor, weakness, sweating, localized areas of edema (especially facial cramps), neutropenia, and dizziness. Rarely, immediate or delayed rigors can occur, sometimes accompanied by hyperpyrexia. Infrequently, "iodism" (salivary gland swelling) from organic iodinated compounds appears 2 days after exposure and subsides by the sixth day.

In general, the reactions that are known to occur upon parenteral administration of iodinated contrast agents are possible with any nonionic agent. Approximately 95% of adverse reactions accompanying the use of water-soluble intravascularly administered contrast agents are mild to moderate in degree. However, severe, life-threatening anaphylactoid reactions, mostly of cardiovascular origin, have occurred.

Reported incidences of death range from 6.6 per 1 million (0.00066%) to 1 in 10,000 (0.01%). Most deaths occur during injection or 5 to 10 minutes later, the main feature being cardiac arrest, with cardiovascular disease as the main aggravating factor. Isolated reports of hypotensive collapse and shock are found in the literature. The incidence of shock is estimated to be 1 out of 10,000 (0.005%) patients.

Adverse reactions to injectable contrast media fall into two categories: chemotoxic reactions and idiosyncratic reactions.

Chemotoxic reactions result from the physicochemical properties of the contrast media, the amount of dose injected, and the speed of injection. All hemodynamic disturbances and injuries to organs or vessels perfused by the contrast medium are included in this category.

Idiosyncratic reactions include all other reactions. They occur more frequently in patients 20 to 40 years old. Idiosyncratic reactions may or may not be dependent on the amount of dose injected, the speed of injection and the radiographic procedure. Idiosyncratic reactions are subdivided into minor, intermediate, and severe. The minor reactions are self-limited and of short duration; the severe reactions are life-threatening and treatment is urgent and mandatory.

The reported incidence of adverse reactions to contrast media in patients with a history of allergy is twice that in the general population. Patients with a history of previous reactions to a contrast medium are three times more susceptible than other patients. However, sensitivity to contrast media does not appear to increase with repeated examinations.

Most adverse reactions to injectable contrast media appear within 1 to 3 minutes after the start of injection, but delayed reactions may occur.

Regardless of the contrast agent employed, the overall estimated incidence of serious adverse reactions is higher with angiocardiography than with other procedures. Cardiac decompensation, serious arrhythmias, angina pectoris, or myocardial ischemia or infarction may occur during angiocardiography and left ventriculography. Electrocardiographic and hemodynamic abnormalities occur less frequently with OMNIPAQUE than with diatrizoate meglumine and diatrizoate sodium injection.

References: 1. Skalpe IO: Enhancement with water-soluble contrast media in computed tomography of the brain and abdomen. *Acta Radiol* 1983; suppl 366, pp 72-75. **2.** Holtås S, Cronqvist S, Renaa T: Contrast enhanced brain CT: Comparison between iohexol and metrizoate. *Invest Radiol* 1985; 20(suppl 1):62-64. **3.** Tschakert H: Tolerability of iohexol and ioglicate for intravenous contrast enhancement in cerebral computed tomography. *Acta Radiol* 1983; suppl 366, pp 76-77. **4.** Skalpe IO, Østensen HM: Contrast media in abdominal computed tomography: A double-blind clinical trial comparing a non-ionic (iohexol) and an ionic (metrizoate) contrast medium. *Acta Radiol* 1983; suppl 366, p 80. **5.** Dawson P: Chemotoxicity of contrast media and clinical adverse effects: a review. *Invest Radiol* 1985; 20(suppl 1):84-91.

© 1987 WINTHROP PHARMACEUTICALS 71386/3801

Winthrop PHARMACEUTICALS
Winthrop Pharmaceuticals
Division of Sterling Drug Inc.
New York, NY 10016

We did it.

Fuji Presents Today's Alternative

Easy to use control panel features digital temperature display, ready and replenishment lights and one-touch power.

The **FPM4200** 90 second, cold-water, X-ray film processor.

Fuji has applied today's technology to *reduce cost, improve performance,* and manufacture the "*next generation*" of 90 second, high capacity processors. The first alternative was the Fuji FPM4000. A hard act to follow right? Wrong. Fuji has put all of the reliability and performance you have come to expect from Fuji into the FPM4200, **TODAY'S ALTERNATIVE.**

We haven't cut corners, we just did what we do best when it comes to the radiological environment—we turn our best ideas into the best products.

- 90 second, cold-water processing
- High capacity, 280 sheets of 14x17 per hour
- Film activated, automatic standby
- Waist-high film delivery
- Digital temperature display
- Extremely quiet operation
- Superior water efficiency

Get the full details about the FPM4200 from your Fuji sales representative, or call toll free 1-(800)-431-1850 In CT (203) 353-0300.

CIRCLE 7 ON READER SERVICE CARD

FUJI I&I *Imaging & Information*

FUJI MEDICAL SYSTEMS U.S.A., INC.
90 Viaduct Road, Stamford, CT 06907

AJR THIRD-JUBILEE VOLUME

1 **Volume 150: the third jubilee-anniversary volume.** *Berk RN*

2 **Dedication to Melvin M. Figley, M.D.** *Gagliardi RA*

SPECIAL ARTICLE

3 **Commentary. *American Journal of Roentgenology*: historical reflections.** *Gagliardi RA*

PROGRESS IN RADIOLOGY

7 **Reprint from volume 1, 1914. Roentgen examinations for head injuries.** *Gray AL*

11 **A tribute to a pioneer radiologist: Alfred Leftwich Gray, M.D. (1873–1932).** *Barnes CE*

13 **Commentary. Neuroimaging and head injuries: where we've been—where we're going.** *Quencer RM*

RADIOLOGY JOURNALS

19 **Editorial. Threats to the quality of peer-reviewed radiology journals: identification of the problem and possible solutions.** *Berk RN*

23 **Perspective. Coauthorship in radiology journals.** *Chew FS*

27 **Perspective. Fraud in radiologic research.** *Friedman PJ*

31 **How research becomes knowledge in radiology: an analysis of citations to published papers.** *Chew FS, Relyea-Chew A*

FUTURE DIRECTIONS OF RADIOLOGY

39 **Perspective. Future advances and directions in imaging research.** *Robb WL*

43 **Perspective. Horizons in gallstone therapy—1988.** *vanSonnenberg E, Hofmann AF*

47 **Progress in Radiology. Penile angiography—the last angiographic frontier.** *Bookstein JJ*

55 **Clinical evaluation of a medical image management system for chest images.** *Arenson RL, Seshadri SB, Kundel HL, et al.*

CARDIOPULMONARY RADIOLOGY

61 **CT densitometry of pulmonary nodules in a frozen human thorax.** *Im J-G, Gamsu G, Gordon D, et al.*

67 **Obstructive sleep apnea syndrome: preoperative radiologic evaluation.** *Hegstrom T, Emmons LL, Hoddes E, et al.*

71 **Postbiopsy pneumothorax: estimating the risk by chest radiography and pulmonary function tests.** *Fish GD, Stanley JH, Miller KS, Schabel SI, Sutherland SE*

75 **Mediastinal cysts: diagnosis by CT and needle aspiration.** *Kuhlman JE, Fishman EK, Wang KP, Zerhouni EA, Siegelman SS*

79 **MR imaging of the transverse sinus of the pericardium.** *Im J-G, Rosen A, Webb WR, Gamsu G*

85 **Technical note. The left ventricular echogenic focus: a normal finding.** *Levy DW, Mintz MC*

VASCULAR RADIOLOGY

87 **MR imaging of the aorta after surgery for aortic dissection.** *White RD, Ullyot DJ, Higgins CB*

93 **Thrombosis of the splanchnic veins: CT diagnosis.** *Vogelzang RL, Gore RM, Anschuetz SL, Blei AT*

GASTROINTESTINAL RADIOLOGY

97 **Barrett's esophagus: diagnosis by double-contrast esophagography.** *Gilchrist AM, Levine MS, Carr RF, et al.*

103 **Case report. Electrical injury in the esophagus.** *Flisak ME, Berman S*

105 **Case report. Enteroliths in a continent ileostomy.** *Fox ER, Chung T, Laufer I*

107 **CT of the liver: a survey of prevailing methods for administration of contrast material.** *Zeman RK, Clements LA, Silverman PM, et al.*

111 **Hepatic perivascular lymphedema—CT appearance.** *Koslin DB, Stanley RJ, Berland LL, Shin MS, Dalton SC*

115 **Pyogenic liver abscess: contrast-enhanced MR imaging in rats.** *Weissleder R, Saini S, Stark DD, et al.*

121 **Case report. Splenic lymphangiomatosis: CT diagnosis.** *Pistoia F, Markowitz SK*

123 **Gallbladder and bile duct abnormalities in AIDS: sonographic findings in eight patients.** *Romano AJ, vanSonnenberg E, Casola G, et al.*

129 **Technical note. Choledocholithiasis: percutaneous pulverization with a high-speed rotational catheter.** *Wholey MH, Smoot S*

GENITOURINARY RADIOLOGY

131 **Antegrade transluminal dilatation of benign ureteral strictures: long-term results.** *Lang EK, Glorioso LW III*

135 **Stage IB cervical carcinoma: comparison of clinical, MR, and pathologic staging.** *Rubens D, Thornbury JR, Angel C, et al.*

139 **Endometrial abnormalities: evaluation with transvaginal sonography.** *Mendelson EB, Bohm-Velez M, Joseph N, Neiman HL*

143 **Case report. Carcinoid of the kidney: radiologic findings.** *McKeown DK, Nguyen G-K, Rudrick B, Johnson MA*

145 **Case report. Renal stone ileus.** *Bahn DK, Brown RKJ, Reidinger AA, et al.*

PALEORADIOLOGY

147 **Three-dimensional CT reconstructions of an ancient human Egyptian mummy.** *Marx M, D'Auria SH*

MUSCULOSKELETAL RADIOLOGY

151 **Pictorial essay. Cross-sectional imaging of the capsular mechanism of the glenohumeral joint.** *Zlatkin MB, Bjorkengren AG, Gylys-Morin V, Resnick D, Sartoris DJ*

159 **Case report. Posttrauma intracapsular bone fragments: association with meniscal tears.** *Richmond J, Sarno RC*

161 **Case report. Osteosclerotic sarcoidosis.** *Abdelwahab IF, Norman A*

NEURORADIOLOGY

163 **MR imaging of Chiari II malformation.** *El Gammal T, Mark EK, Brooks BS*

171 **Variable appearances of subacute intracranial hematomas on high-field spin-echo MR.** *Gomori JM, Grossman RI, Hackney DB, Goldberg HI, Zimmerman RA, Bilaniuk LT*

179 **MR of neuronal migration anomalies.** *Barkovich AJ, Chuang SH, Norman D*

189 **Cerebral necrosis after radiotherapy and/or intraarterial chemotherapy for brain tumors: PET and neuropathologic studies.** *Di Chiro G, Oldfield E, Wright DC, et al.*

RADIATION PROTECTION

199 **Technical note. Simple radiation protection device for CT.** *Chintapalli K, Wentworth W, Wilson CR*

OTHER

30 **ARRS 1988 Residents' award paper**

128 **Books received**

198 **Forthcoming articles**

201 **Invitation to the 1988 ARRS meeting.** *Rogers L*

217 **American Roentgen Ray Society information**

218 **ARRS membership invitation and application**

Book reviews 22, 38, 110, 150, 188

Videotape review 60

203 **Review of current literature**

207 **Letters**

210 **Meeting news. Society for Magnetic Resonance Imaging Meeting in San Antonio: notes and comments.** *Stark DD*

213 **News**

221 **Classified advertisements**

A3 **Guidelines for authors**

JUBILEE VOLUME

Lee.
22.8.88

AJR

American
Journal of
Roentgenology

February 1988
This issue: ARRS Meeting Section

A NEW ADDITION TO THE BEST-SELLING FAMILY OF BARIUM PRODUCTS

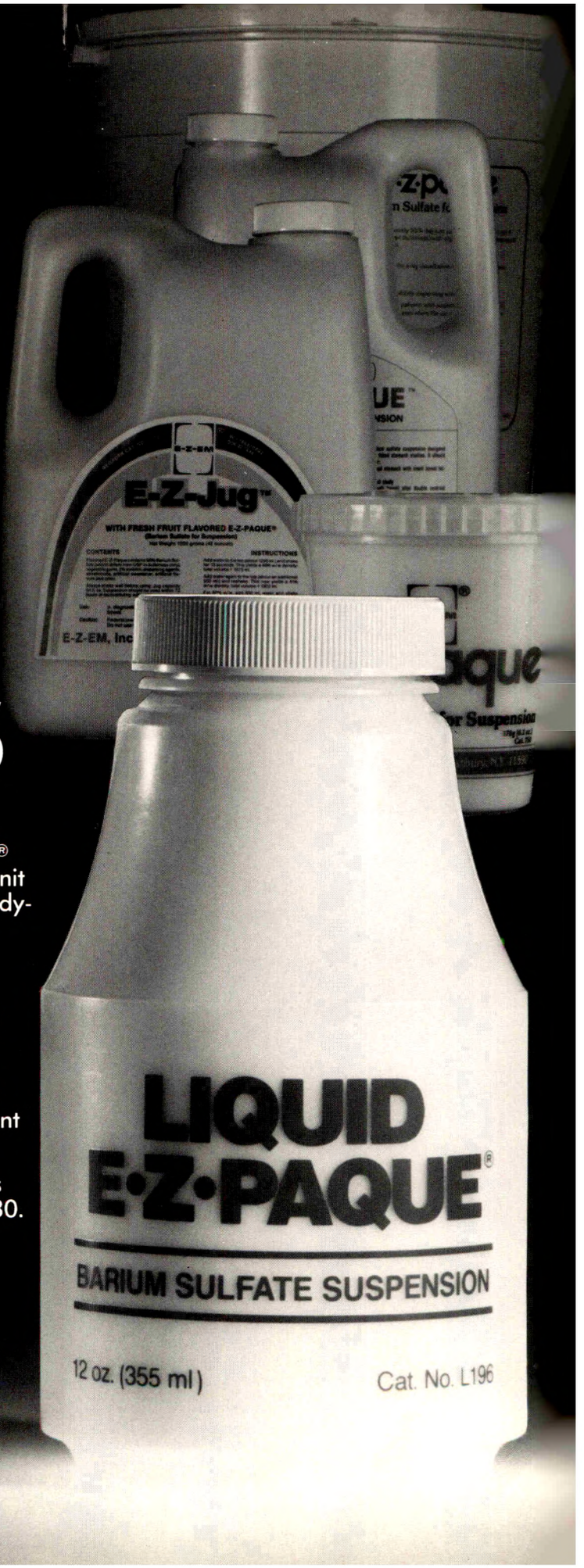

E-Z-EM introduces a new product to the E-Z-Paque® line of barium suspensions—Liquid E-Z-Paque® in unit dose bottles. This new packaging combines the ready-to-use convenience and consistency of a prepared suspension with the time-saving advantages of disposable, single-use bottles.

Improved Liquid E-Z-Paque in unit dose bottles is a multi-purpose, 60% w/v barium sulfate suspension which provides excellent results when used in small bowel and filled stomach studies. And, of course, it has a pleasant fruit flavor that gives excellent patient acceptance.

Ask your E-Z-EM dealer for a free sample, or call us at 1-800-645-3052. In New York, call 516-333-8230.

Cat. No. L196
24 bottles per case

E-Z-EM®
E-Z-EM, Inc.
7 Portland Ave.
Westbury, NY 11590

CIRCLE 30 ON READER SERVICE CARD

© E-Z-EM, Inc., 1987

Official Journal of the American Roentgen Ray Society

AJR

American Journal of Roentgenology
Diagnostic Imaging and Related Sciences

Editor-In-Chief Robert N. Berk, *San Diego, California*

Editor Emeritus Melvin M. Figley, *Seattle, Washington*

Associate Editor Saskia von Waldenburg Hilton, *San Diego, California*

Consulting Editor Juan M. Taveras, *Boston, Massachusetts*

Statistician Charles C. Berry, *San Diego, California*

Editorial Board

John R. Amberg
William L. Ashburn
Itamar Aviad
Lawrence W. Bassett
Gregory P. Borkowski
William G. Bradley, Jr.
Peter L. Cooperberg
Peter M. Doubilet
N. Reed Dunnick
David K. Edwards
Ronald G. Evens
David S. Feigin
Paul J. Friedman
William R. Hendee
John R. Hesselink
Charles B. Higgins
Melvyn T. Korobkin
Thomas L. Lawson
Bruce L. McClennan
Albert A. Moss
Jeffrey H. Newhouse
Donald L. Resnick
Stewart R. Reuter
Charles R. Rohrmann, Jr.
Peter M. Ronai
Sjef H. J. Ruijs
Stuart S. Sagel
David J. Sartoris
Edward A. Sickles
Barry A. Siegel
David D. Stark
Edward T. Stewart
Eric vanSonnenberg

Editorial Staff: Elizabeth A. Whalen, *publications supervisor*; Linda Wood, Barbara Rose, and Barbara L. Halliburton, *manuscript editors*; Nancy Rydbeck, *office manager*; Elaine Sherman, *administrative assistant*; Geraldine Perillo, *administrative secretary*.

All business correspondence, including display (not classified) advertising, subscriptions, address changes, reprints, and permission requests should be addressed to Williams & Wilkins, 428 East Preston Street, Baltimore, MD 21202. Correspondence regarding editorial matters and classified advertising should be addressed to the editorial office, AJR, 2223 Avenida de la Playa, Suite 200, La Jolla, CA 92037-3218. For manuscript submission, see Guidelines for Authors, next page. Undelivered or damaged copies replaced within 60 days of publication; 90 days for foreign subscribers. Allow 90 days for address changes.
AJR, AMERICAN JOURNAL OF ROENTGENOLOGY (ISSN 0361 803X) is published monthly by American Roentgen Ray Society, 428 E. Preston Street, Baltimore, MD 21202. Annual dues include $50 for journal subscription. Second class postage paid at Baltimore, MD and at additional mailing offices. Postmaster send address changes (Form 3579) to Williams & Wilkins, 428 East Preston St., Baltimore, MD 21202. Subscription rates $100 ($135 foreign); institutions $110 ($145 foreign); in training $25; single copy $16 ($19). Japanese rates include airfreight. Japanese yen price is available from our sole agent USACO Corporation, 13-12, Shimbashi 1-Chome, Minato-Ku, Tokyo 105, Japan, telephone 03-502-6471. Subscriptions in South Korea are available only through our sole agent in Korea: Korea-America Medical Books Co., Ltd. (KAMBOOK) 209 Yun kun-dong, Chongro-ku, Seoul, Korea (telephone: 745-3151; telex: K25211 KAMBC; FAX: 745-3153). All subscriptions to South Korea will be shipped by air freight after January 1, 1988. There is an air freight surcharge of $12.00 over the regular subscription rate for this journal in South Korea to partially compensate for air freight costs. Airmail rates furnished on request. Indexed by *Current Contents* and *Index Medicus*. Copyright © 1987 by American Roentgen Ray Society. 0361-803X/88$2.00

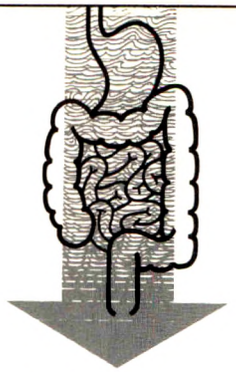

We introduced the 4-hour prep.

Now patients prefer it and professionals prescribe it more. That's why we're the leaders.

GoLYTELY®

PEG-3350 and Electrolytes for Oral Solution

The leading 4-hour routine that reduces prep time, length of hospital stay, and frequency of repeat exams. Convenient, cost-effective GoLYTELY..."the one that comes in a bottle."

BRIEF SUMMARY: Before prescribing, see package insert or PDR.

INDICATIONS AND USAGE: GoLYTELY is indicated for bowel cleansing prior to colonoscopy and barium enema x-ray examination.

CONTRAINDICATIONS: GoLYTELY is contraindicated in patients with gastrointestinal obstruction, gastric retention, bowel perforation, toxic colitis, or toxic megacolon.

WARNINGS: No additional ingredients—eg, flavorings—should be added to the solution. GoLYTELY should be used with caution in patients with severe ulcerative colitis.

PRECAUTIONS: General: Patients with impaired gag reflex, unconscious or semiconscious patients, and patients prone to regurgitation or aspiration should be observed during the administration of GoLYTELY, especially if it is administered via nasogastric tube. If a patient experiences severe bloating, distention, or abdominal pain, administration should be slowed or discontinued temporarily until the symptoms abate. If gastrointestinal obstruction or perforation is suspected, appropriate studies should be performed to rule out these conditions before administration of GoLYTELY.

© 1988 Braintree Laboratories, Inc TRE-1030

CIRCLE 35 ON READER SERVICE CARD

ADVERSE REACTIONS: Nausea, abdominal fullness, and bloating are the most common adverse reactions (occurring in up to 50% of patients) to administration of GoLYTELY. Abdominal cramps, vomiting, and anal irritation occur less frequently. These adverse reactions are transient and subside rapidly. Isolated cases of urticaria, rhinorrhea, and dermatitis—which may represent allergic reactions—have been reported.

CAUTION: Federal law prohibits dispensing without prescription.

STORAGE: Store in sealed container at 59°-86°F. When reconstituted, keep solution refrigerated. Use within 48 hours. Discard unused portion.
(NDC 52268-0100-01)

Made by Lyne Laboratories, Stoughton, MA 02072, for BRAINTREE LABORATORIES, INC., P.O. Box 361, Braintree, MA 02184.

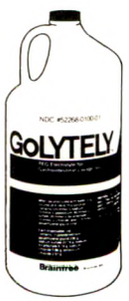

LABORATORIES · INC
Braintree

AJR Guidelines for Authors

Address new and revised manuscripts, correspondence, and classified ads to the Editor:

AJR Editorial Office
2223 Avenida de la Playa, Suite 200
La Jolla, CA 92037-3218 Telephone: (619) 459-2229

Inquiries regarding subscriptions, display advertising, reprints, or permission to republish *AJR* material should be addressed to the publisher:

The Williams & Wilkins Co.
428 E. Preston St.
Baltimore, MD 21202 Telephone: (301) 528-4133

The *AJR* publishes original contributions to the advancement of medical diagnosis and treatment. Submitted manuscripts should not contain previously published material and should not be under consideration for publication elsewhere. Papers dealing with neuroradiology should be addressed to: American Journal of Neuroradiology, Dept. of Radiology, Massachusetts General Hospital, Boston, MA 02114. At the discretion of the *AJR* Editor, *AJNR* articles that are of interest to the general reader may be republished in the *AJR*. Neuroradiologic papers sent to the *AJR* will be forwarded to the Editorial Office of the *AJNR*.

Manuscript decisions are based on peer review. Reviewers receive manuscripts without title pages to ensure an unbiased review. All accepted manuscripts are subject to editing. Statements made in the article, including changes made by the Editor or manuscript editor, are the responsibility of the author and not of the *AJR* or its publisher. Authors will be sent the edited manuscript, galley proof, and proofs of illustrations. If the corresponding author will be unavailable to review galleys, arrangements should be made for a coauthor or colleague to read and return the proof.

General Guidelines for Major Papers

Abstract. Clearly state (in 200 words or less) the purpose, methods, results, and conclusions of the study. Include actual data.

Introduction. Briefly describe the purpose of the investigation, including relevant background information.

Methods. Describe the research plan, the materials (or subjects), and the methods used, in that order. Explain in detail how disease was confirmed and how subjectivity in observations was controlled.

Results. Present results in a clear, logical sequence. If tables are used, do not duplicate tabular data in text, but do describe important trends and points.

Discussion. Describe the limitations of the research plan, materials (or subjects), and methods, considering both the purpose and the outcome of the study. When results differ from those of previous investigators, explain the discrepancy.

AUTHOR'S CHECKLIST

For priority handling, complete the following checklist, sign the copyright form on the reverse side of this page, and include both with the manuscript.

_____ Two copies of the manuscript (the original and a photocopy) and two complete sets of figures are submitted. One copy has been retained by the author.

_____ If appropriate, *AJR* Guidelines for case reports, technical notes, pictorial essays, or letters to the Editor have been followed. (See page A5.)

_____ The manuscript, including references, figure legends, and tables, is typed double-spaced on 8½ × 11 in. (21.6 × 27.9 cm) *nonerasable* paper. Right-hand margins are not justified.

_____ All manuscript pages are numbered consecutively beginning with the abstract. Authors' names do not appear on the manuscript pages.

_____ The manuscript is organized as follows: title page, blind title page (title only), abstract, introduction, methods, results, discussion, acknowledgments, references, tables, figure legends, and figures.

_____ Informed consent has been obtained from patients who participated in clinical investigations. If experiments were performed on animals, authors complied with NIH guidelines for use of laboratory animals.

_____ Use of unfamiliar acronyms and abbrevations is kept to a minimum. When abbreviations are used they are defined at first mention, followed by the abbreviation in parentheses.

_____ Metric measurements are used throughout, or the metric equivalent is given in parentheses.

_____ Names and locations (city and state only) of manufacturers are given for equipment and nongeneric drugs.

Title Page

_____ The following information is given: title of article; names and complete addresses (including zip code) of all authors; current addresses of authors who have moved since study; acknowledgment of grant or other assistance. The corresponding author is clearly identified, and a current address and phone number are given.

_____ Two copies of a blind title page are included giving only the title (without the authors' names) for use in the review process.

Abstract

_____ An abstract of approximately 200 words concisely states the purpose, methods, and results of the study in one paragraph. Actual data are included. Conclusions are stated in a second, summary paragraph.

_____ No abbreviations or reference citations are used.

References

_____ References (not to exceed 35) are typed double-spaced starting on a separate page and are **numbered consecutively in the order in which they appear in the text**.

_____ All references are cited in the text and are enclosed in brackets and typed on line with the text (not superscript).

_____ Unpublished data are not cited in the reference list, but are cited parenthetically in the text, for example, (Smith DJ, personal communication), (Smith DJ, unpublished data). This includes papers submitted, but not yet accepted, for publication.

_____ Inclusive page numbers (e.g., 333–335) are given for all references.

_____ Journal names are abbreviated according to *Index Medicus*.

_____ Style and punctuation of references follow the format illustrated in the following examples (all authors are listed when six or less; when seven or more authors, the first three are listed, followed by "et al."):

Journal article

1. Long RS, Roe EW, Wu EU, et al. Membrane oxygenation: radiographic appearance. *AJR* **1986**;146:1257–1260

Book

2. Smith LW, Cohen AR. *Pathology of tumors*, 6th ed. Baltimore: Williams & Wilkins, **1977**:100–109

Chapter in a book

3. Breon AJ. Serum monitors of bone metastasis. In: Clark SA, ed. *Bone metastases*. Baltimore: Williams & Wilkins, **1983**:165–180

Paper presented at a meeting

4. Lau FS, Kirk AN, Beck RA. MR imaging of the spine. Presented at the annual meeting of the American Roentgen Ray Society, Washington, DC, April 1986

Tables

_____ Each table is typed double-spaced on a separate page without vertical or horizontal rules; each has a short, descriptive title. Tables do not exceed two pages in length and contain at least four lines of data.

_____ Tables are numbered in the order in which they are cited in the text.

_____ Abbreviations are defined in an explanatory note below each table.

_____ Tables are self-explanatory and do not duplicate data given in the text or figures.

_____ All arithmetic (percentages, totals, differences) has been double checked for accuracy, and tabular data agree with data given in the text.

Figures and Legends

_____ Two complete sets of original figures are submitted unmounted in labeled envelopes.

_____ Figures are clean, unscratched, 5 × 7 in. (13 × 18 cm) glossy prints with **white borders.** A separate print is submitted for each figure *part*.

_____ All figure parts relating to one patient are in one figure.

_____ Each figure is labeled on the back with the figure number and an arrow indicating "top." For black-and-white figures, labeling is done on a gummed label, which is then affixed to the back of the print. *Never* use labels on color figures, but write figure number on the back lightly in pencil. *Never* use ink on front or back of any figures.

_____ Author's names are *not* written on the backs of figures.

_____ Only removable (rub-on) arrows and letters are used on the figures. Symbols are uniform in size and style and are not broken or cracked.

_____ Images are uniform in size and magnification.

_____ Line drawings are done in black ink on a white background. They are professional in quality, and all use the same size type. (Only glossy prints are acceptable.)

_____ Written permission has been obtained for use of all previously published illustrations (and copies of permission letters are included), and an appropriate credit line is given in the legends.

_____ Legends are typed double-spaced, and figure numbers correspond with the order in which the figures are cited in the text.

Transfer of Copyright Agreement, Exclusive Publication Statement, and Conflict of Interest Acknowledgment

Complete copyright to the article entitled: _____

_____

is hereby transferred to the American Roentgen Ray Society (for United States government employees to the extent transferable), effective if and when the article is accepted for publication in the *American Journal of Roentgenology*. In the case of the authors who are officers or employees of the United States government, the American Roentgen Ray Society recognizes that works prepared by officers or employees of the United States government as part of their official government duties are in the public domain.

Authors reserve all proprietary rights other than copyright, such as patent rights and the right to use all or part of this article in future works of their own. The authors retain the right of replication, subject only to crediting the original source of publication and receiving written permission from the publisher.

Authors guarantee that this manuscript contains no matter that is libelous or otherwise unlawful, invades individual privacy, or infringes any proprietary rights.

Authors understand that they will receive no royalty or other compensation from the American Roentgen Ray Society or the publisher.

Authors guarantee that the editor has been or will be informed of any proprietary or commercial interest or conflicts of interest the authors may have that relate directly or indirectly to the subject of this article.

Finally, the authors certify that none of the material in this manuscript has been published previously or is currently under consideration for publication elsewhere.

_____	_____	_____
First author/date	Second author	Third author
_____	_____	_____
Fourth author	Fifth author	Sixth author

This agreement must be signed by all authors in order for the manuscript to be published.

Case Reports

A case report is a brief description of a special case that provides a message that transcends the individual patient.

Format. There is no abstract. The introduction should be a short paragraph giving the general background and the specific interest of the case. No more than one case should be described in detail (similar ones can be mentioned briefly in the discussion). Emphasis should be on the radiologic aspects; clinical information must be limited to that necessary to provide a background for the radiology. The discussion should be succinct and should focus on the specific message and relevance of radiologic methods. A review of the literature is not appropriate.

Length. Maximum of five double-spaced, typewritten pages, including the references but not the title page or figure legends.

References. Maximum of eight.

Figures. Maximum of three or four, unless the text is shortened accordingly. Legends must not repeat the text.

Tables and Acknowledgments. Not appropriate in case reports.

Technical Notes

A technical note is a brief description of a specific technique or procedure, modification of a technique, or equipment of interest to radiologists.

Format. No abstract, headings, or subheadings are required. If headings are used, they should be a combination of "Case Report," "Materials and Methods," "Results," and "Discussion." A brief one-paragraph introduction should be included to give the general background. Discussion should be limited to the specific message, including the uses of the technique or equipment. Literature reviews and lengthy case reports are not appropriate.

Length. Maximum of five double-spaced, typewritten pages, including the references but not the title page or figure legends.

References. Maximum of eight.

Figures. Maximum of two, unless the text is shortened accordingly.

Tables and Acknowledgments. Not appropriate in technical notes.

Pictorial Essays

A pictorial essay is an article that conveys its message through illustrations and their legends. Unlike other *AJR* articles, which are based on original research, pictorial essays serve primarily as teaching tools, like exhibits at a scientific meeting. They are not encyclopedic book chapters. No abstract is necessary.

Length. Maximum of four double-spaced, typewritten pages, including the references but not the title page or figure legends.

References. Maximum of four.

Figures. Maximum of 30 figure *parts*. Number should be as few as necessary to convey the message of the paper.

Tables and Acknowledgments. Not appropriate in pictorial essays.

Letters to the Editor and Replies

Letters to the Editor and Replies should offer objective and constructive criticism of published articles. Letters may also discuss matters of general interest to radiologists.

Format. All letters should be typed double-spaced on nonletterhead paper, with no greeting or salutation. Signature and affiliation should appear at the end of the letter. Titles for letters should be short and pertinent. The title for a reply is simply "Reply."

Length. Maximum of two double-spaced, typewritten pages, including references.

References. Maximum of four.

Figures. Maximum of two.

Tables and Acknowledgments. Not appropriate in Letters to the Editor and Replies.

Opinions, Commentaries, and Perspectives

Opinions, commentaries, and perspectives are special articles dealing with controversial topics or issues of special concern to radiologists.

Format. Include a title page but no abstract. Headings may be used to break up the text.

Length. Maximum of five double-spaced, typewritten pages.

References. Maximum of five.

Tables and Figures. Maximum of four.

Computer Page Articles

Articles published on the computer page deal with practical computer applications to radiology.

Format. Include a title page but no abstract.

Length. Maximum of eight double-spaced, typewritten pages.

References. Maximum of five.

Figures and Tables. Maximum of five. Computer printouts are not acceptable. Figures must be submitted as 5 × 7 in. glossy prints.

All submissions to the *AJR* must be accompanied by a completed copy of the Author's Checklist and the signed Copyright Agreement.

A SHARPER PORTRAIT FROM KODAK

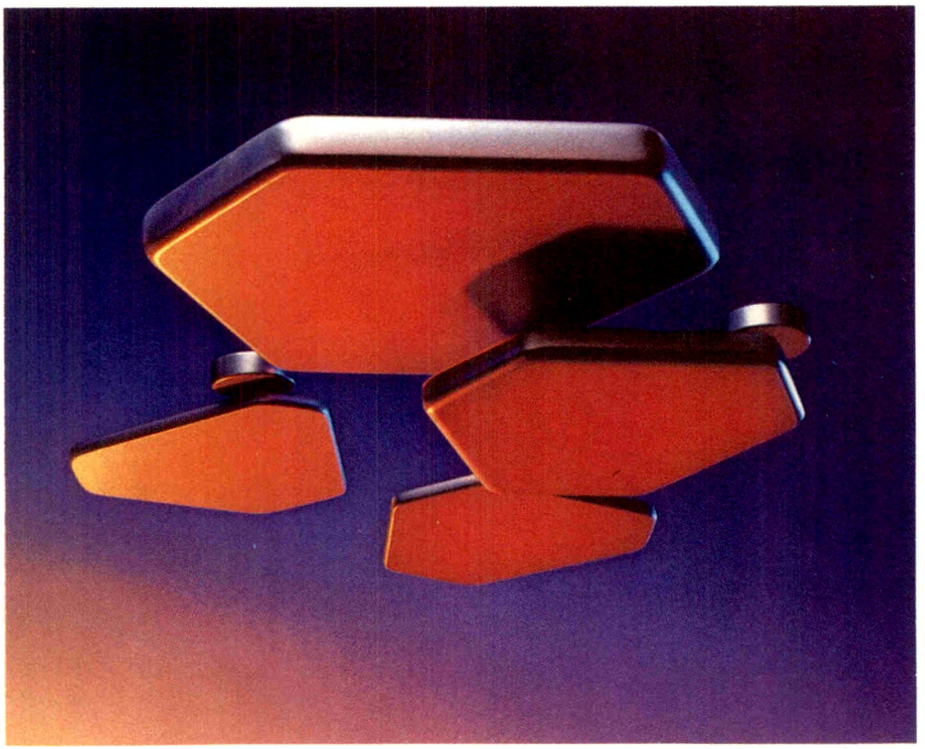

Exclusive Kodak T-Grain emulsions give Kodak T-Mat films extra sharpness that can only mean more detailed "portraits" for better diagnoses. See the difference on your viewbox.

Kodak T-Mat films. The only x-ray films in the world with the sharpness of T-Grain emulsions. A sharpness your Kodak representative can show you, on your own viewbox, in a side-by-side comparison with your present film. It's sharpness you can see, plus all the benefits of rare-earth imaging, including the exposure-reducing speed. At no increase in cost, with even more processing latitude.

And now there is Kodak CFT film, an extremely fine-grain film for cinefluorography with T-Grain emulsion. For a demonstration of the sharpness difference T-Mat films can make, talk to your Kodak representative.

Kodak
Official Diagnostic Imaging Products Sponsor of the 1988 Olympic Games

The new vision of Kodak

Kodak

©Eastman Kodak Company, 1987

Increase your expertise in evaluating CNS lesions

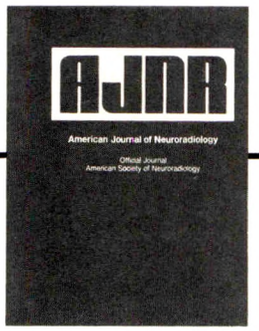

AJNR
American Journal of Neuroradiology

Editor: **Juan M. Taveras, MD,** Harvard Medical School; MGH

Outstanding clinical papers on every aspect of CNS imaging, including spinal diagnosis...informed coverage of head and neck radiology...clear, readable CTs, angiographs, MR imaging and ultrasound studies. These are the features you demand of a quality professional journal. You'll find them in every issue of **AJNR: American Journal of Neuroradiology.**

As you are called upon to perform and interpret more and more sophisticated diagnostic tests — from myelography to CT to newborn ultrasound studies — you need a comprehensive, reliable journal that can keep you abreast of all the latest developments. Each bimonthly issue of **AJNR** brings you timely, clinically pertinent information, as well as important clinical research presented with an eye toward immediate practical application.

Here are just a few of the many excellent articles from the September/October 1987 issue.

Giant Cavernous Aneurysm Associated with Trigeminal Artery: Treatment by Detachable Balloon. *Higashida RT, Halbach VV, Mehringer CM, Hieshima GB*

Intraoperative Digital Subtraction Neuroangiography: A Diagnostic and Therapeutic Tool. *Hieshima GB, Reicher MA, Higashida RT, et al.*

Dose Administration of Gadolinium-DTPA in MR Imaging of Intracranial Tumors. *Niendorf HP, Laniado M, Semmler W, Schörner W, Felix R*

MR and CT Evaluation of Intracranial Sarcoidosis. *Hayes WS, Sherman JL, Stern BJ, Citrin CM, Pulaski PD*

The Role of MR Imaging in Evaluating Metastatic Spinal Disease. *Smoker WRK, Godersky JC, Knutzon RK, Keyes WD, Norman D, Bergman W*

If you can benefit from articles like these, then you should be a regular reader of **AJNR.** Use the attached coupon to subscribe today.

Bimonthly
Personal $110/yr **Institutions** $130/yr
In-training $65/yr *(add $20.00 outside the US)*

ORDER FREE BY PHONE. Just call 1-800-638-6423 from anywhere in the US except AK. Maryland residents, call 528-4105 *collect.*

Williams & Wilkins
P.O. Box 23291 Baltimore, Maryland 21203
266 Fulham Road London SW10 9EL England

Subscribe to AJNR for 3 years and SAVE

Avoid future rate increases and ensure uninterrupted service by placing a multi-year subscription at current rates.

☐ New subscription ☐ Renewal
☐ 3 yrs ☐ 2 yrs ☐ 1 yr
☐ **Personal** $110 ☐ **Institutions** $130 ☐ **In-training** $65
(add $20.00 outside the US)

☐ Also send me the **1988 Bound Volume** at $65.00 ($70.00 outside the US). $2.00 discount for orders placed before October 31, 1988, and for prepaid orders. I understand that the bound volume is *in addition to* my regular subscription and is available only to subscribers. (To be shipped in early 1989. Sorry, bound volumes for years prior to 1988 are not available.) *All bound volume orders must be received by December 31, 1988.*

☐ Check enclosed ☐ Bill me
☐ VISA ☐ MasterCard ☐ American Express

card # exp.

signature/P.O. #

Name

Address

City/State/Zip

MD residents, please add 5% sales tax. Subscription orders from outside the US must be prepaid in US dollars only.

Residents, Fellows, Interns, and Students: when applying for the in-training rate, available for 3 years, please specify name of institution and training status. Rates valid through October 31, 1988.

Please allow 8 weeks for order processing and delivery of your first issue. Surface mail delivery to countries outside the US may take up to 16 weeks. Airmail rates available upon request.

Williams & Wilkins
P.O. Box 23291
Baltimore, Maryland 21203

266 Fulham Road
London SW10 9EL
England

printed in USA

AJNRAD 1030 88

Conray® (iothalamate meglumine injection U.S.P. 60%)

Each milliliter contains 600 mg of iothalamate meglumine, 0.09 mg edetate calcium disodium as a stabilizer and 0.125 mg of monobasic sodium phosphate as a buffer. The solution provides 28.2% (282 mg/mL) organically bound iodine.

Conray®-43 (iothalamate meglumine injection U.S.P. 43%)

Each milliliter contains 430 mg of iothalamate meglumine, 0.110 mg edetate calcium disodium as a stabilizer and 0.115 mg of monobasic sodium phosphate as a buffer. The solution provides 20.2% (202 mg/mL) organically bound iodine.

INDICATIONS AND USAGE

CONRAY is indicated for use in excretory urography, cerebral angiography, peripheral arteriography, venography, arthrography, direct cholangiography, endoscopic retrograde cholangiopancreatography, contrast enhancement of computed tomographic brain images, cranial computerized angiotomography, intravenous digital subtraction angiography and arterial digital subtraction angiography.

CONRAY-43 is indicated for use in lower extremity venography, intravenous infusion urography, contrast enhancement of computed tomographic brain images and arterial digital subtraction angiography.

CONRAY and CONRAY-43 may also be used for enhancement of computed tomographic scans performed for detection and evaluation of lesions in the liver, pancreas, kidneys, abdominal aorta, mediastinum, abdominal cavity and retroperitoneal space. Continuous or multiple scans separated by intervals of 1-3 seconds during the first 30-90 seconds post-injection of the contrast medium (dynamic CT scanning) may provide enhancement of diagnostic significance, and may be of benefit in establishing diagnoses of certain lesions in these sites with greater assurance than is possible with CT alone, and in supplying additional features of the lesions. In other cases, the contrast agent may allow visualization of lesions not seen with CT alone, or may help to define suspicious lesions seen with unenhanced CT. Subsets of patients in whom delayed body CT scans might be helpful have not been identified. Inconsistent results have been reported and abnormal and normal tissues may be isodense during the time frame used for delayed CT scanning. The risks of such indiscriminate use of contrast media are well known and such use is not recommended. At present, consistent results have been documented using dynamic CT techniques only.

CONTRAINDICATIONS

Refer to PRECAUTIONS, General, concerning hypersensitivity. CONRAY and CONRAY-43 should not be used for myelography. Arthrography should not be performed if infection is present in or near the joint. Percutaneous transhepatic cholangiography is contraindicated in patients with coagulation defects and prolonged prothrombin times. Endoscopic retrograde cholangiopancreatography is contraindicated during an acute attack of pancreatitis or during severe clinically evident cholangitis and in patients in whom endoscopy is prohibited.

WARNINGS

Serious or fatal reactions have been associated with the administration of iodine containing radiopaque media. It is of utmost importance to be completely prepared to treat any contrast medium reaction.

Serious neurologic sequelae, including permanent paralysis, have been reported following cerebral arteriography, selective spinal arteriography and arteriography of vessels supplying the spinal cord. The intravascular injection of a contrast medium should never be made following the administration of vasopressors since they strongly potentiate neurologic effects.

In patients with subarachnoid hemorrhage, a rare association between contrast administration and clinical deterioration, including convulsions and death, has been reported. Therefore, administration of intravascular iodinated ionic contrast media in these patients should be undertaken with caution.

A definite risk exists in the use of intravascular contrast agents in patients who are known to have multiple myeloma. In such instances anuria has developed resulting in progressive uremia, renal failure and eventually death. Although neither the contrast agent nor dehydration has separately proved to be the cause of anuria in myeloma, it has been speculated that the combination of both may be causative factors. The risk in myelomatous patients is not a contraindication to the procedure; however, partial dehydration in the preparation of these patients for the examination is not recommended since this may predispose to precipitation of myeloma protein in the renal tubules. No form of therapy, including dialysis, has been successful in reversing the effect. Myeloma, which occurs most commonly in persons over 40, should be considered before instituting intravascular administration of contrast agents.

Administration of radiopaque materials to patients known or suspected to have pheochromocytoma should be performed with extreme caution. If, in the opinion of the physician, the possible benefits of such procedures outweigh the considered risks, the procedures may be performed; however, the amount of radiopaque medium injected should be kept to an absolute minimum. The blood pressure should be assessed throughout the procedure, and measures for treatment of a hypertensive crisis should be available.

Contrast media have been shown to promote the phenomenon of sickling in individuals who are homozygous for sickle cell disease when the material is injected intravenously or intra-arterially.

Convulsions have occurred in patients with primary or metastatic cerebral lesions following the administration of iodine-containing radiopaque media for the contrast enhancement of CT brain images.

In patients with advanced renal disease, iodinated contrast media should be used with caution, and only when the need for the examination dictates, since excretion of the medium may be impaired. Patients with combined renal and hepatic disease, those with severe hypertension or congestive heart failure, and recent renal transplant recipients may present an additional risk.

Renal failure has been reported in patients with liver dysfunction who were given an oral cholecystographic agent followed by an intravascular iodinated radiopaque agent and also in patients with occult renal disease, notably diabetics and hypertensives. In these classes of patients there should be no fluid restriction and every attempt made to maintain normal hydration, prior to contrast medium administration, since dehydration is the single most important factor influencing further renal impairment.

Acute renal failure has been reported in diabetic patients with diabetic nephropathy and in susceptible non-diabetic patients (often elderly with pre-existing renal disease) following the administration of iodinated contrast agents. Therefore, careful consideration of the potential risks should be given before performing this radiographic procedure in these patients.

Caution should be exercised in performing contrast medium studies in patients with endotoxemia and/or those with elevated body temperatures.

Reports of thyroid storm occurring following the intravascular use of iodinated radiopaque agents in patients with hyperthyroidism or with an autonomously functioning thyroid nodule, suggest that this additional risk be evaluated in such patients before use of this drug. Iodine containing contrast agents may alter the results of thyroid function tests which depend on iodine estimation, e.g. PBI and radioactive iodine uptake studies. Such tests, if indicated, should be performed prior to the administration of this preparation.

PRECAUTIONS

General

Diagnostic procedures which involve the use of iodinated intra-vascular contrast agents should be carried out under the direction of personnel skilled and experienced in the particular procedure to be performed. All procedures utilizing contrast media carry a definite risk of producing adverse reactions. While most reactions may be minor, life threatening and fatal reactions may occur without warning. The risk-benefit factor should always be carefully evaluated before such a procedure is undertaken. At all times a fully equipped emergency cart, or equivalent supplies and equipment, and personnel competent in recognizing and treating adverse reactions of all severity, or situations which may arise as a result of the procedure, should be immediately available. If a serious reaction should occur, immediately discontinue administration. Since severe delayed reactions have been known to occur, emergency facilities and competent personnel should be available for at least 30 to 60 minutes after administration. (See ADVERSE REACTIONS).

Preparatory dehydration is dangerous and may contribute to acute renal failure in infants, young children, the elderly, patients with pre-existing renal insufficiency, patients with advanced vascular disease and diabetic patients.

Severe reactions to contrast media often resemble allergic responses. This has prompted the use of several provocative pretesting methods, none of which can be relied on to predict severe reactions. No conclusive relationship between severe reactions and antigen-antibody reactions or other manifestations of allergy has been established. The possibility of an idiosyncratic reaction in patients who have previously received a contrast medium without ill effect should always be considered. Prior to the injection of any contrast medium, the patient should be questioned to obtain a medical history with emphasis on allergy and hypersensitivity. A positive history of bronchial asthma or allergy, including food, a family history of allergy, or a previous reaction or hypersensitivity to a contrast agent may imply a greater than usual risk. Such a history, by suggesting histamine sensitivity and consequently proneness to reactions, may be more accurate than pre-testing in predicting the potential for reaction, although not necessarily the severity or type of reaction in the individual case. A positive history of this type does not arbitrarily contraindicate the use of a contrast agent, when a diagnostic procedure is thought essential, but does call for caution. (See ADVERSE REACTIONS).

Prophylactic therapy including corticosteroids and antihistamines should be considered for patients who present with a strong allergic history, a previous reaction to a contrast medium, or a positive pre-test since in these patients the incidence of reaction is two to three times that of the general population. Adequate doses of corticosteroids should be started early enough prior to contrast medium injection to be effective and should continue through the time of injection and for 24 hours after injection. Antihistamines should be administered within 30 minutes of the contrast medium injection. Recent reports indicate that such pre-treatment does not prevent serious life-threatening reactions, but may reduce both their incidence and severity. A separate syringe should be used for these injections.

General anesthesia may be indicated in the performance of some procedures in young or uncooperative children and in selected adult patients; however, a higher incidence of adverse reactions has been reported in these patients, and may be attributable to the inability of the patient to identify untoward symptoms or to the hypotensive effect of anesthesia which can prolong the circulation time and increase the duration of contact of the contrast agent.

Angiography should be avoided whenever possible in patients with homocystinuria because of the risk of inducing thrombosis and embolism.

Information for Patients: Patients receiving iodinated intra-vascular contrast agents should be instructed to:

1. Inform your physician if you are pregnant.
2. Inform your physician if you are diabetic or if you have multiple myeloma, pheochromocytoma, homozygous sickle cell disease or known thyroid disease. (See WARNINGS).
3. Inform your physician if you are allergic to any drugs, food or if you had any reactions to previous injections of dyes used for x-ray procedures. (See PRECAUTIONS, General).
4. Inform your physician about any other medications you are currently taking including non-prescription drugs.

Carcinogenesis. Mutagenesis, Impairment of Fertility: No long-term animal studies have been performed to evaluate carcinogenic potential. However, animal studies suggest that this drug is not mutagenic and does not affect fertility in males or females.

Pregnancy Category B: Reproduction studies have been performed in mice, rats, and rabbits at doses up to 6.6 times the human dose and have revealed no evidence of impaired fertility or harm to the fetus due to CONRAY. There are however no adequate and well controlled studies in pregnant women. Because animal reproduction studies are not always predictive of human response, this drug should be used during pregnancy only if clearly needed.

Nursing Mothers: Iothalamate salts are excreted unchanged in human milk. Because of the potential for adverse effects in nursing infants, bottle feedings should be substituted for breast feedings for 24 hours following the administration of this drug.

PRECAUTIONS FOR SPECIFIC PROCEDURES:

Excretory Urography

Infants and small children should not have any fluid restrictions prior to excretory urography. Injections of CONRAY and CONRAY-43 represent an osmotic load which, if superimposed on increased serum osmolality due to partial dehydration, may magnify hypertonic dehydration. (See WARNINGS and PRECAUTIONS, General concerning preparatory dehydration).

Brief summary continued on last page of ad.

F R O M M A L L

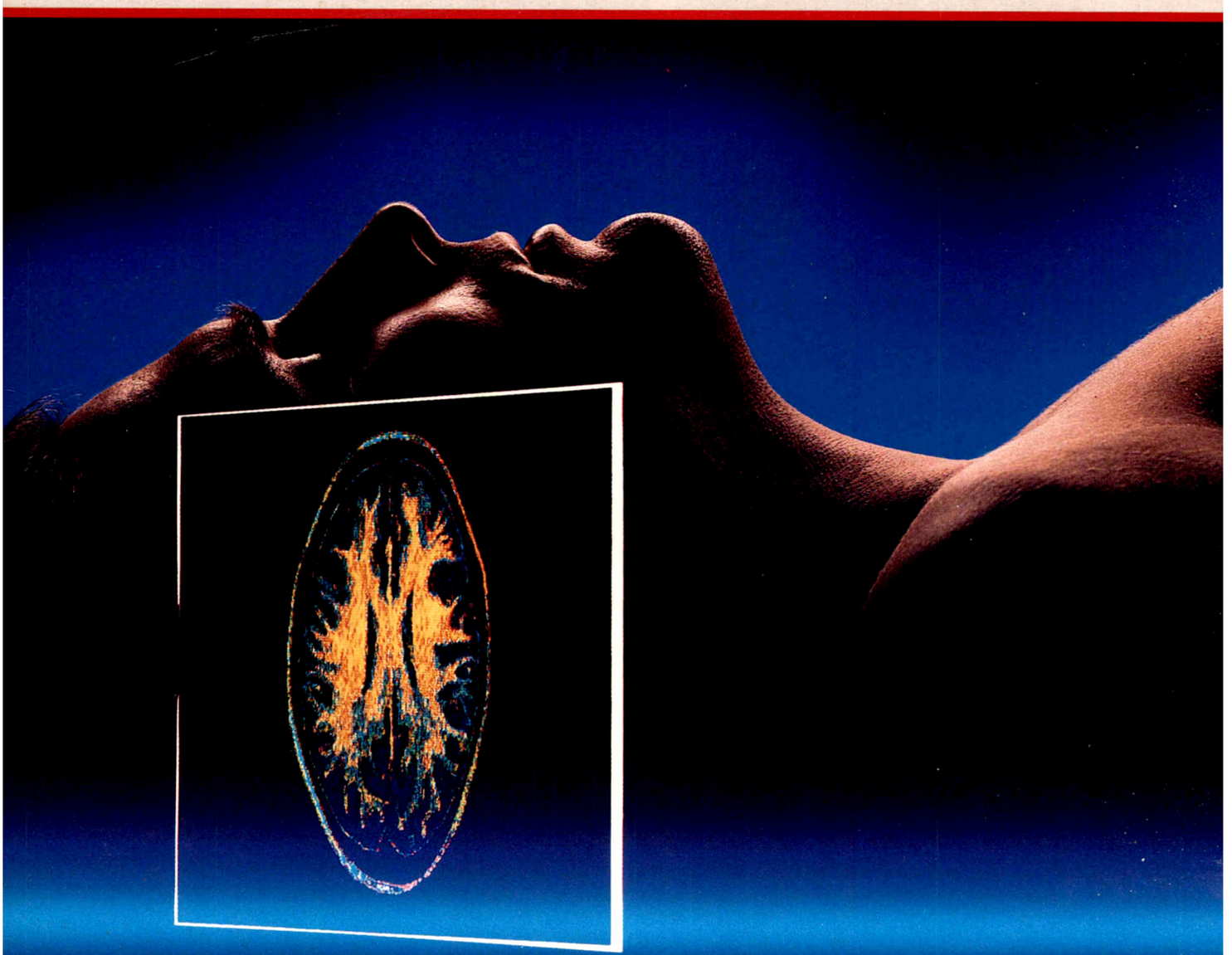

As versatile as they

Conray®-43 (iothalamate meglumine injection U.S.P. 43%): Unique benefits for CT and venography

Conray®-43 provides an ideal iodine concentration for use in lower extremity venography, CT scans, and infusion urography. Conray-43 combines good visualization with low toxicity and excellent patient tolerance. Because of its low viscosity, Conray-43 offers a shorter infusion time for a 200 mL dose versus 150 mL dose of 60% solution. The lower osmolality of Conray-43 compared to a 60% conventional agent may mean less post-procedural phlebitis, with no loss of imaging quality.

For routine CT and lower extremity venography procedures, give your patients the unique benefits of Conray-43—the affordable, well-tolerated alternative.

[redacted]

I N C K R O D T

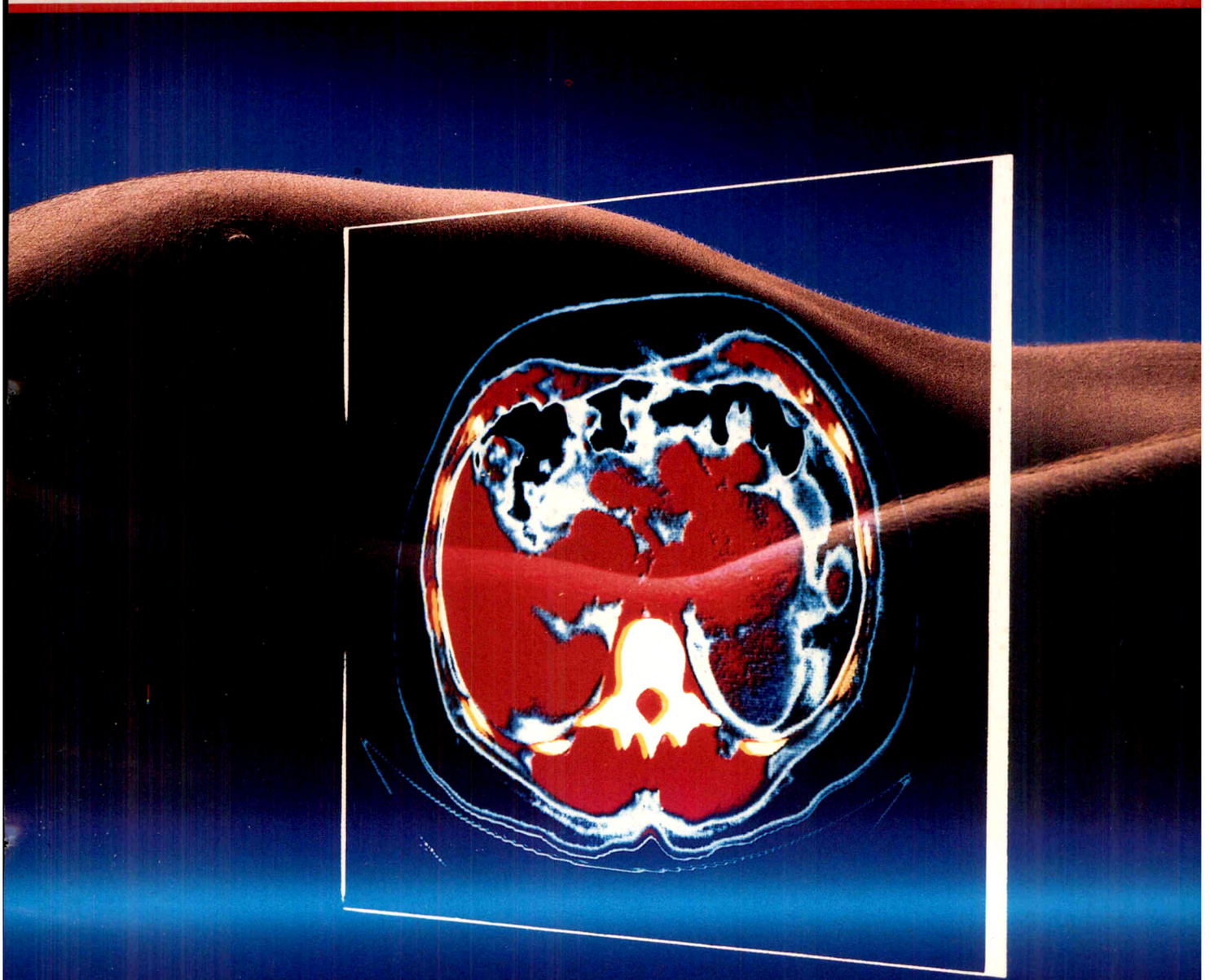

are affordable

Conray® (iothalamate meglumine injection U.S.P. 60%): A proven performer

Conray® offers you reliable performance, proven in over 15 million procedures in the last five years, ranging from IVPs to enhancement of CT images. Conray provides an iodine content that yields good visualization with low toxicity and good patient tolerance.

The viscosity allows for bolus injection or rapid infusion, where necessary. And the variety of vial and bottle sizes lets you choose the Conray volume and mode of administration you need in your practice.

With this kind of clinical versatility and affordability, it's no surprise that Conray is the #1 brand of conventional iodinated contrast media—the standard by which all others are judged.

MALLINCKRODT®

Changing the look of medicine

Continuation of brief summary for Conray® and Conray®-43

Cerebral Angiography

Cerebral angiography should be performed with special caution in patients with advanced arteriosclerosis, severe hypertension, cardiac decompensation, senility, recent cerebral thrombosis or embolism, and migraine.

Peripheral Arteriography and Venography

Moderate decreases in blood pressure occur frequently with intra-arterial (brachial) injections. This change is usually transient and requires no treatment, however, the blood pressure should be monitored for approximately ten minutes following injection. Special care is required when venography is performed in patients with suspected thrombosis, phlebitis, severe ischemic disease, local infection or a totally obstructed venous system. In the presence of venous stasis, vein irrigation with normal saline should be considered following the procedure. Venography is optimally performed with a more dilute solution such as Conray®-43 (Iothalamate Meglumine Injection USP 43%).

Extreme caution during injection of the contrast agent is necessary to avoid extravasation and fluoroscopy is recommended. This is especially important in patients with severe arterial or venous disease.

Arthrography

During arthrography, strict aseptic technique is required to prevent the introduction of infection. Fluoroscopic control should be used to insure proper introduction of the needle into the synovial space and prevent extracapsular injection. Aspiration of excessive synovial fluid will reduce the pain on injection and prevent the rapid dilution of the contrast agent. It is important that undue pressure not be exerted during the injection.

Direct Cholangiography

In the presence of acute pancreatitis, direct cholangiography, if necessary, should be employed with caution, injecting no more than 5 to 10 mL without undue pressure. Percutaneous transhepatic cholangiography should only be attempted when compatible blood for potential transfusions is in readiness and emergency surgical facilities are available. The patient should be carefully monitored for at least 24 hours to insure prompt detection of bile leakage and hemorrhage. Appropriate pre-medication of the patient is recommended and drugs which are cholespastic, such as morphine, should be avoided. Respiratory movements should be controlled during introduction of the needle.

Endoscopic Retrograde Cholangiopancreatography

Endoscopic retrograde cholangiopancreatography should only be performed by personnel skilled and experienced with the procedure, and careful attention to technique is essential for the success and safety of the procedure. Fluoroscopy is mandatory during injection to prevent over distention of the duct systems.

Contrast Enhancement in Body Computed Tomography

It is advisable to insure that patients are adequately hydrated prior to the contrast enhanced body CT examination. Patient motion, including respiration, can markedly affect image quality, therefore, patient cooperation is essential. The use of an intravascular contrast medium can obscure tumors in patients undergoing CT evaluation of the liver resulting in a false negative diagnosis. Dynamic CT scanning is the procedure of choice for malignant tumor enhancement.

Intravenous Digital Subtraction Angiography

The risks associated with IV DSA are those usually attendent with catheter procedures and include intramural injections, vessel dissection and tissue extravasation. Small test injections of contrast medium made under fluoroscopic observation to insure the catheter tip is properly positioned, and in the case of peripheral placement that the vein is of adequate size, will reduce this potential.

Patient motion, including respiration and swallowing, can result in marked image degradation yielding non-diagnostic studies. Therefore, patient cooperation is essential.

Arterial Digital Subtraction Angiography

The risks associated with arterial DSA are those usually attendent with catheter procedures. Following the procedure, gentle pressure hemostasis is required, followed by observation and immobilization of the limb for several hours to prevent hemorrhage from the site of arterial puncture.

ADVERSE REACTIONS

Adverse reactions to injectable contrast media fall into two categories: chemotoxic reactions and idiosyncratic reactions.

Chemotoxic reactions result from the physio-chemical properties of the contrast media, the dose and speed of injection. All hemodynamic disturbances and injuries to organs or vessels perfused by the contrast medium are included in this category.

Idiosyncratic reactions include all other reactions. They occur more frequently in patients 20 to 40 years old. Idiosyncratic reactions may or may not be dependent on the amount of dose injected, the speed of injection, the mode of injection and the radiographic procedure. Idiosyncratic reactions are subdivided into minor, intermediate and severe. The minor reactions are self-limited and of short duration; the severe reactions are life-threatening and treatment is urgent and mandatory.

Fatalities have been reported following the administration of iodine-containing contrast agents. Based upon clinical literature, the incidence of death is reported to range from one in 10,000 (0.01 percent) to less than one in 100,000 (0.001 percent).

The following adverse reactions have been observed in conjunction with the use of iodine-containing contrast agents.

The most frequent adverse reactions are nausea, vomiting, facial flush and a feeling of body warmth. These are usually of brief duration. Other reactions include the following:

Hypersensitivity reactions: Dermal manifestations of urticaria with or without pruritus, erythema and maculopapular rash. Dry mouth. Sweating. Conjunctival symptoms. Facial, peripheral and angioneurotic edema. Symptoms related to the respiratory system include sneezing, nasal stuffiness, coughing, choking, dyspnea, chest tightness and wheezing, which may be initial manifestations of more severe and infrequent reactions including asthmatic attack, laryngospasm and bronchospasm with or without edema, pulmonary edema, apnea and cyanosis. Rarely, these allergic-type reactions can progress into anaphylaxis with loss of consciousness and coma and severe cardiovascular disturbances.

Cardiovascular reactions: Generalized vasodilation, flushing and venospasm. Occasionally, thrombosis or rarely, thrombophlebitis. Red blood cell clumping and agglutination, crenation and interference in clot formation. Extremely rare cases of disseminated intravascular coagulation resulting in death have been reported. Severe cardiovascular responses include rare cases of hypotensive shock, coronary insufficiency, cardiac arrhythmia, fibrillation and arrest. These severe reactions are usually reversible with prompt and appropriate management; however, fatalities have occurred.

Technique reactions: Extravasation with burning pain, hematomas, ecchymosis and tissue necrosis, paresthesia or numbness, vascular constriction due to injection rate, thrombosis and thrombophlebitis.

Neurological reactions: Spasm, convulsions, aphasia, syncope, paresis, paralysis resulting from spinal cord injury and pathology associated with syndrome of transverse myelitis, visual field losses which are usually transient but may be permanent, coma and death.

Other reactions: Headache, trembling, shaking, chills without fever and light-headedness. Temporary renal shutdown or other nephropathy.

ADVERSE REACTIONS FOR SPECIFIC PROCEDURES:

Cerebral Angiography

The major sources of cerebral arteriographic adverse reactions appear to be related to repeated injections of the contrast material, administration of doses higher than those recommended, the presence of occlusive atherosclerotic vascular disease and the method and technique of injection.

Adverse reactions are normally mild and transient. A feeling of warmth in the face and neck is frequently experienced. Infrequently, a more severe burning discomfort is observed.

Serious neurological reactions that have been associated with cerebral angiography and not listed under the general Adverse Reactions include stroke, amnesia and respiratory difficulties.

Cardiovascular reactions that may occur with some frequency are bradycardia and decrease in systemic blood pressure. The blood pressure change is transient and usually requires no treatment.

Peripheral Arteriography and Venography

Hemorrhage and thrombosis have occurred at the puncture site of the percutaneous injection. Brachial plexus injury has been reported following axillary artery injection. Thrombophlebitis, syncope and very rare cases of gangrene have been reported following venography.

Arthrography

Arthrography may induce joint pain or discomfort which is usually mild and transient but occasionally may be severe and persist for 24 to 48 hours following the procedure. Effusion requiring aspiration may occur in patients with rheumatoid arthritis.

Direct Cholangiography

Adverse reactions may often be attributed to injection pressure or excessive volume of the medium resulting in overdistention of the ducts and producing local pain.

Some of the medium may enter the pancreatic duct which may result in pancreatic irritation. Occasionally, nausea, vomiting, fever, and tachycardia have been observed. Pancholangitis resulting in liver abscess or septicemia has been reported.

In percutaneous transhepatic cholangiography, some discomfort is common, but severe pain is unusual. Complications of the procedure are often serious and have been reported in 4 to 6 percent of patients. These reactions have included bile leakage and biliary peritonitis, gall bladder perforation, internal bleeding (sometimes massive), blood-bile fistula resulting in septicemia involving gram-negative organisms, and tension pneumothorax from inadvertent puncture of the diaphragm or lung. Bile leakage is more likely to occur in patients with obstructions that cause unrelieved high biliary pressure.

Endoscopic Retrograde Cholangiopancreatography

Adverse reactions that have occurred which are attributable to either the ERCP procedure or contrast agent include nausea, vomiting, fever, severe abdominal pain, duodenal wall intravasation, septicemia, pancreatitis and perforation of the common bile duct associated with pathology.

DOSAGE AND ADMINISTRATION

Details on dosage are provided in the Conray and Conray-43 package insert. CONSULT FULL PACKAGE INSERT BEFORE USE.

Rev. August 1987

MALLINCKRODT®

Diagnostic Products Division
Mallinckrodt, Inc.
Post Office Box 5840
St. Louis, MO 63134

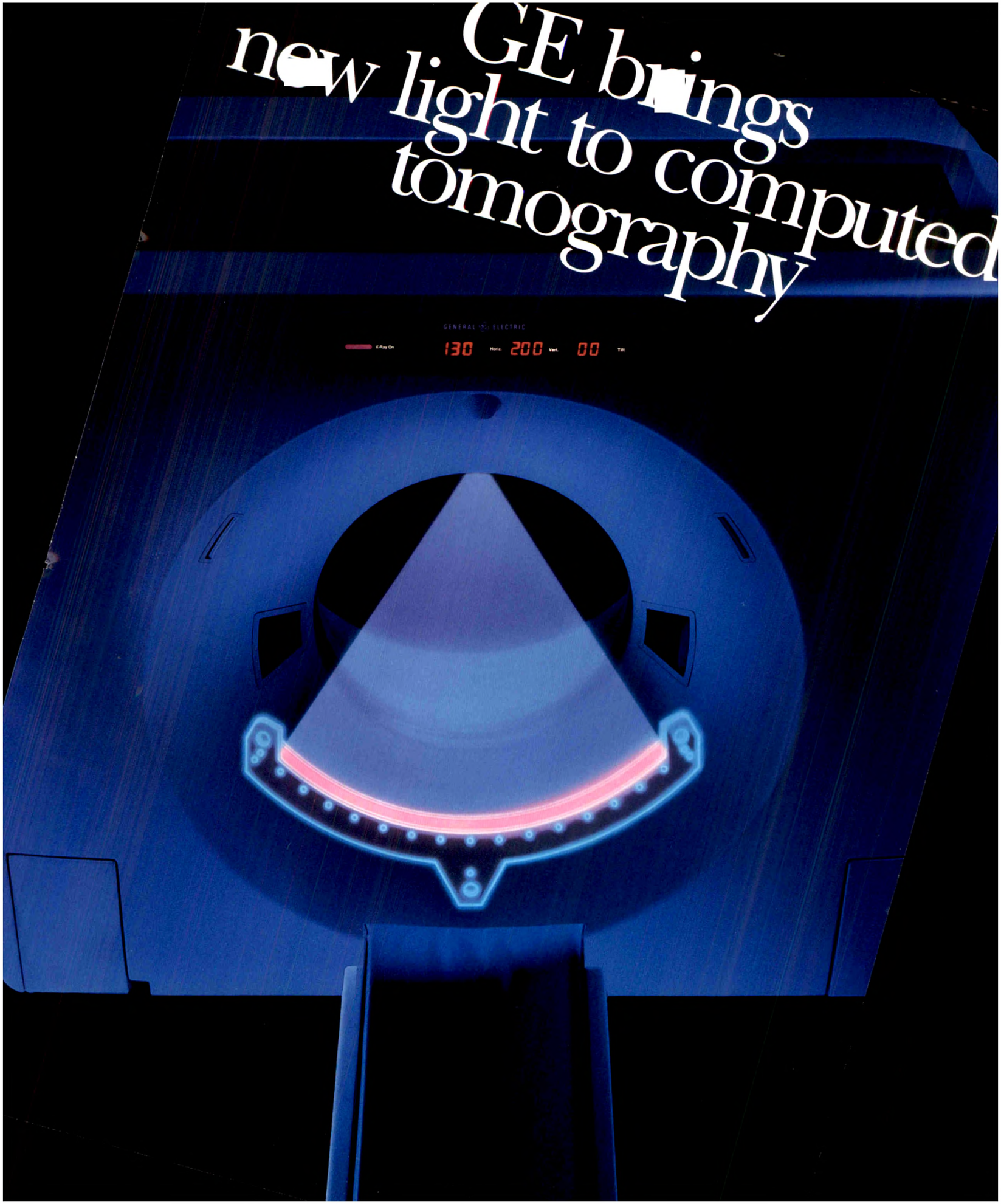
GE brings
new light to computed
tomography
GENERAL ELECTRIC
X-Ray On
130
Horiz.
200
Vert.
00
Tilt

HiLight

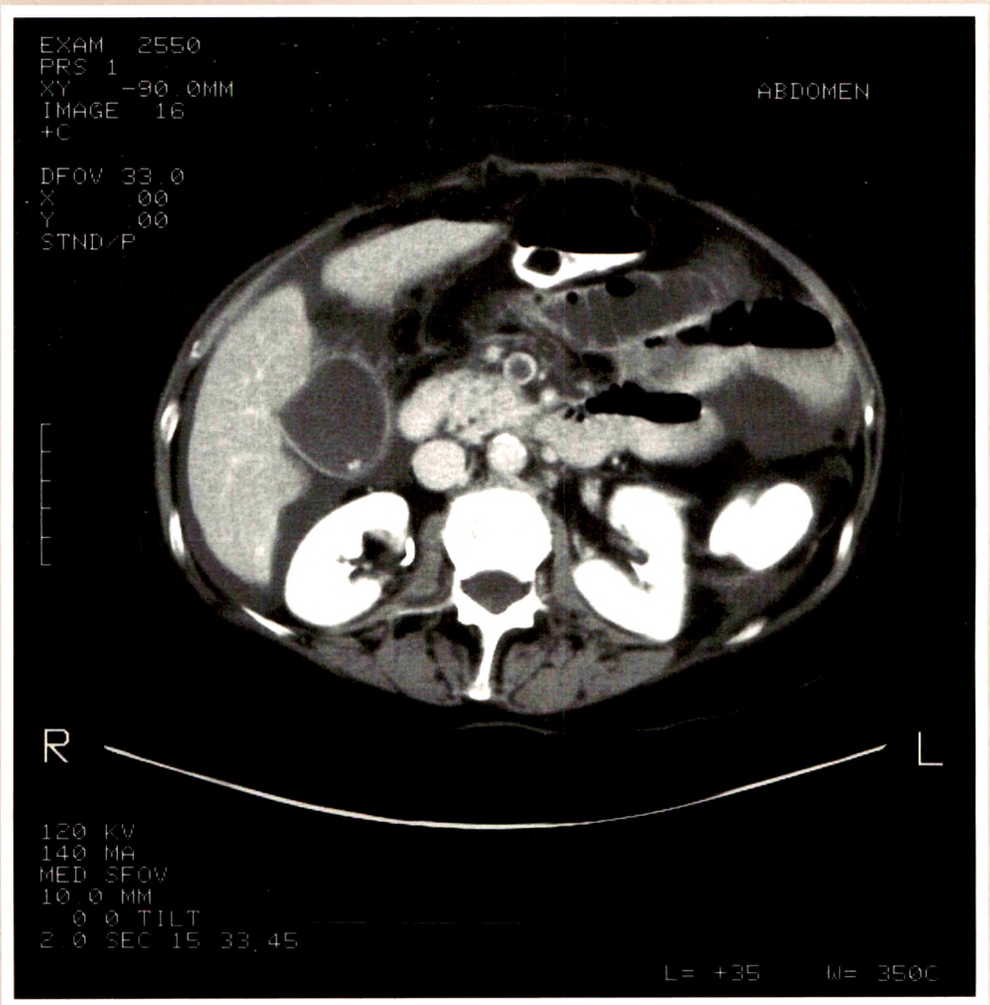

A 2 second, 10 mm scan of the mid-abdomen demonstrates excellent visualization of the periaortic structures. Note the fine detail seen in the bowel wall.

The new CT 9800 HiLight Detector

A revolutionary new detector material from the scientists at GE is producing CT images of extraordinary quality.

With efficiency and sensitivity far beyond that of other detectors, HiLight brings even greater spatial resolution and low contrast detectability to the CT 9800™ Quick system.

In a standard 2 second scan, for example, spatial resolution measures 0.65 mm. In the high resolution mode—0.35 mm. Low contrast detectability is equally impressive—2.5 mm at 0.25% contrast (≤4 rads).

As a result, clinical images are remarkable—even by GE standards. Improved definition between grey and white matter in head studies. Superior detection of liver lesions, periaortic structures and mesenteric vasculature. Clear presentation of the smallest details of anatomy and pathology in studies of the spine, chest, inner ear and orbits.

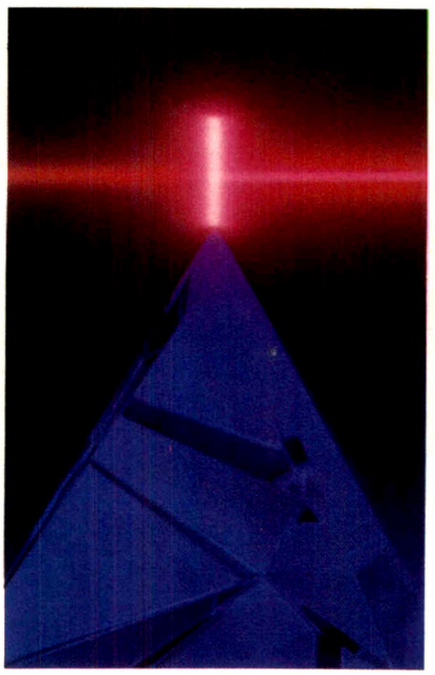

No tradeoffs

Perhaps the most significant aspect of imaging with the CT 9800 Quick/HiLight system is that there are no compromises. In any study you can combine fast scan times with low dose levels and still get superior images.

Which means better pediatric studies. More comprehensive dynamic scanning. More efficient throughput with fewer tube cooling delays.

Dose for dose, scan time for scan time, there is no better image quality available to you in CT today.

Still the standard

CT 9800 Quick continues to be the system by which all others are measured in computed tomography. Its standard features have always been exceptional. Routine 2-second scanning. Ability to scan, reconstruct, display and film slices in less than 16 seconds. Real-time ScoutView,™ dynamic scanning, Arrange™ reformatting and a host of other features that enhance both the clinical effectiveness and efficiency of your CT department.

And now, with the HiLight Detector, we've raised our image quality standards even higher—so you can continue to provide the ultimate in CT imaging to your patients.

The CT 9800 Quick system with the HiLight Detector. An extraordinary combination from GE.

For more information, call GE Medical Systems toll free:

(800) 624-5692.

CIRCLE 3 ON READER SERVICE CARD

GE Medical Systems

How five typical hospitals increased their x-ray departments' operating efficiency by 20%

CURIX and the AGFA-Rhombus are registered trademarks of Agfa-Gevaert, Leverkusen/Antwerp. © 1987 Agfa-Gevaert Rex

CIRCLE 12 ON READER SERVICE CARD

The results are in. With CURIX® "Capacity" Film Center, efficiency goes up...costs go down!

Time savings per exam	↑ Average 20%	See Pg. 4
Time spent with patient	↑ Increased	See Pg. 5
Equipment reliability	↑ 99% uptime	See Pg. 6
Productivity	↑ Increased	See Pg. 7
Personnel costs	↓ Save $111,000	See Pg.
Repeat/waste films	↓ Reduced	See Pg.

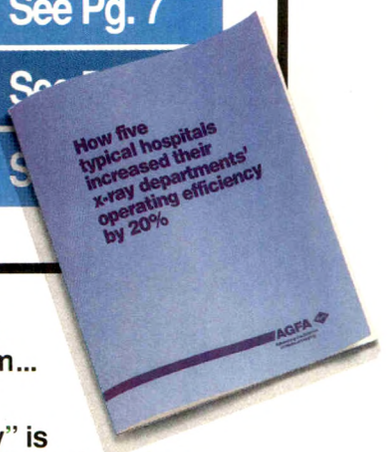

We studied 5 hospitals before and after installation of the CURIX® "Capacity" Film Center - AGFA's automated, daylight, cassette loading, unloading and processing system - and the results are impressive

We also studied 2 hospitals that have been using the CURIX® "Capacity" for over a year, and one of them saved over $111,000 (salaries and benefits) by reassigning 4 personnel as a result of increased productivity.

What does a 20% reduction in total procedure/processing time mean to your radiology department?

- **Decrease total patient time per procedure**, permits additional examinations to be made, or additional patients to be examined.
- **Decrease processing time**, because techniologists are no longer loading and unloading cassettes, waiting for darkroom technicians, walking long distances to and from the darkroom.
- **Increased technologist's time with patient** provides better patient care.
- **Improves staff morale.**
- **Decrease repeat rate, waste of film... and time.**
- **CURIX "Capacity" is always on-the-job...and on-time with an average up-time of over 99%, it won't let you down.**

CURIX "Capacity" is easy to use...all it takes is 15 seconds to unload, reload, and return the cassette to the technologist. And, its only a few steps away from the examination room. Its integrated processor delivers film ready for viewing in only 90 seconds.

This new study proves the tangible benefits of AGFA's advanced daylight film handling system. Request your copy today!

CURIX "Capacity" Film Center...
the shortest route from examination room to viewbox.

For additional information, contact:

Marketing Department
Agfa-Gevaert Rex
A division of Agfa-Gevaert, Inc.
100 Challenger Road
Ridgefield Park, NJ 07660
(201) 641-9566

AGFA Agfa

Advancing the Science of Medical Imaging

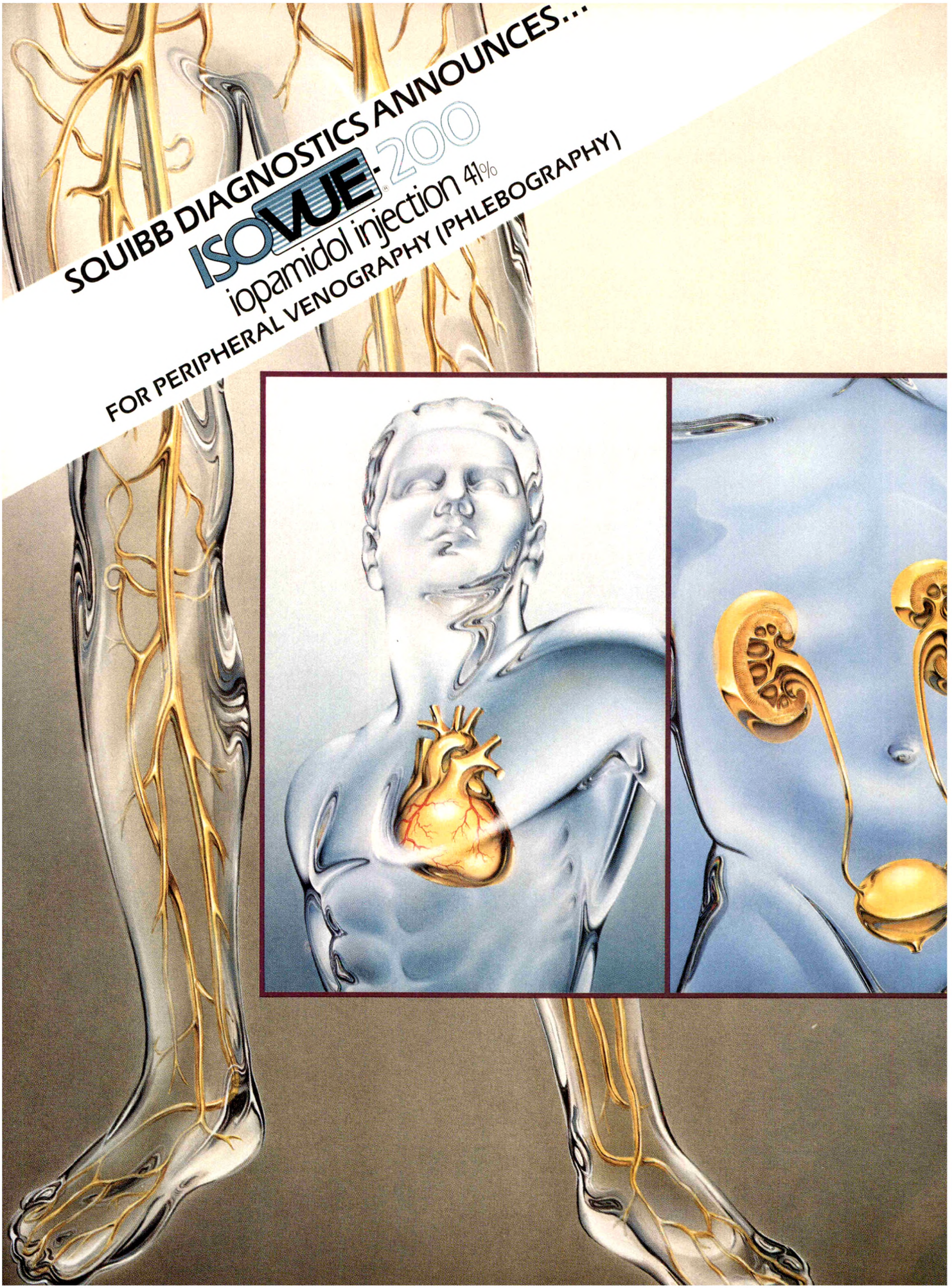
SQUIBB DIAGNOSTICS ANNOUNCES...
ISOVUE®-200
iopamidol injection 41%
FOR PERIPHERAL VENOGRAPHY (PHLEBOGRAPHY)

In radiologic contrast procedures

ISOVUE® / ISOVUE-M®

iopamidol injection

THE CLEAR CHOICE

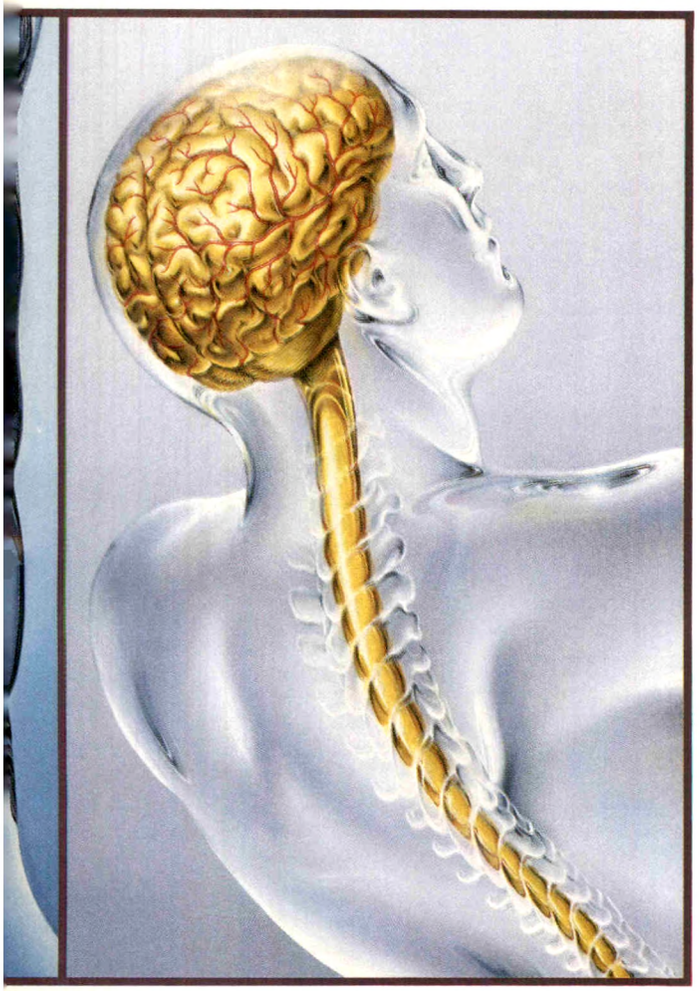

A broad range of indications

Peripheral arteriography
Coronary arteriography and ventriculography
IVP (excretory urography)
Myelography (lumbar, thoracic, cervical, total columnar)
Cerebral arteriography
CT head and body imaging
CT cisternography and ventriculography
Visceral arteriography (selective)
Aortography
IA-DSA
Peripheral venography (phlebography)

The only nonionic contrast agents you need to stock

SQUIBB™ Diagnostics

CIRCLE 14 ON READER SERVICE CARD

Please see brief summary of prescribing information on adjacent pages.

This product is under license from Bracco Industria Chimica, S.p.A. U.S. Patent #4,001,323

© 1988 E.R. Squibb & Sons, Inc., Princeton, NJ

647-508

Issued: January 1988

ISOVUE®-128 (Iopamidol Injection 26%)
ISOVUE®-200 (Iopamidol Injection 41%)
ISOVUE®-300 (Iopamidol Injection 61%)
ISOVUE®-370 (Iopamidol Injection 76%)
ISOVUE-M® 200 (Iopamidol Injection 41%)
ISOVUE-M® 300 (Iopamidol Injection 61%)

INDICATIONS AND USAGE

ISOVUE (Iopamidol Injection) is indicated for intra-arterial digital subtraction angiography (DSA) of the cerebral and abdominal vasculature and for angiography throughout the cardiovascular system, including cerebral and peripheral arteriography, coronary arteriography and ventriculography, selective visceral arteriography and aortography, peripheral venography (phlebography), and intravenous excretory urography and intravenous contrast enhancement of computed tomographic (CECT) head and body imaging.

ISOVUE-M (Iopamidol Injection) is indicated for intrathecal administration in neuroradiology including myelography (lumbar, thoracic, cervical, total columnar), and for contrast enhancement of computed tomographic (CECT) cisternography and ventriculography.

CONTRAINDICATIONS

ISOVUE (Iopamidol Injection)

None.

ISOVUE-M (Iopamidol Injection)

Intrathecal administration of corticosteroids with iopamidol is contraindicated. Because of overdosage considerations, immediate repeat myelography in the event of technical failure is contraindicated (see interval recommendation under DOSAGE AND ADMINISTRATION). Myelography should not be performed in the presence of significant local or systemic infection where bacteremia is likely.

WARNINGS

ISOVUE-M (Iopamidol Injection)

The need for myelographic examination should be carefully evaluated. Iopamidol should be administered with caution in patients with increased intracranial pressure or suspicion of intracranial tumor, abscess or hematoma, those with a history of convulsive disorder, severe cardiovascular disease, chronic alcoholism, or multiple sclerosis, and elderly patients. Particular attention must be given to state of hydration, concentration of medium, dose, and technique used in these patients.

If frankly bloody cerebrospinal fluid is observed, the possible benefits of a myelographic examination should be considered in terms of risk to the patient.

Patients on anticonvulsant medication should be maintained on this therapy.

Direct intracisternal or ventricular administration for standard radiography (without computerized tomographic enhancement) is not recommended. Inadvertent intracranial entry of a large or concentrated bolus of the contrast medium, which increases the risk of neurotoxicity, can be prevented by careful patient management. Also, effort should be directed to avoid rapid dispersion of the medium causing inadvertent rise to intracranial levels (e.g., by active patient movement). If such intracranial entry of the medium occurs, prophylactic anticonvulsant treatment with diazepam or barbiturates orally for 24 to 48 hours should be considered.

Use of medications that may lower the seizure threshold (phenothiazine derivatives, including those used for their antihistaminic properties; tricyclic antidepressants; MAO inhibitors; CNS stimulants; analeptics; antipsychotic agents) should be carefully evaluated. While the contributory role of such medications has not been established, some physicians have discontinued these agents at least 48 hours before and for at least 24 hours following intrathecal use.

Focal and generalized motor seizures have been reported after intrathecal use of water-soluble contrast agents including iopamidol. In several of those cases reported with iopamidol, higher than recommended doses were employed. Therefore *avoid:*

- Deviations from recommended neuroradiologic procedure or patient management.
- Use in patients with a history of epilepsy unless medically justified.
- Overdosage.
- Intracranial entry of a bolus or premature diffusion of a high concentration of the medium.
- Failure to maintain elevation of the head during the procedure, on the stretcher, and in bed.
- Excessive and particularly active patient movement or straining.

ISOVUE (Iopamidol Injection)

Caution must be exercised in patients with severely impaired renal function, those with combined renal and hepatic disease, or anuria particularly when larger doses are administered.

Radiopaque diagnostic contrast agents are potentially hazardous in patients with multiple myeloma or other paraproteinemia, particularly in those with therapeutically resistant anuria. Myeloma occurs most commonly in persons over age 40. Although neither the contrast agent nor dehydration has been proved separately to be the cause of anuria in myelomatous patients, it has been speculated that the combination of both may be causative. The risk in myelomatous patients is not a contraindication; however, special precautions are required.

Contrast media may promote sickling in individuals who are homozygous for sickle cell disease when injected intravenously or intraarterially.

Administration of radiopaque materials to patients known or suspected of having pheochromocytoma should be performed with extreme caution. If, in the opinion of the physician, the possible benefits of such procedures outweigh the considered risks, the procedures may be performed; however, the amount of radiopaque medium injected should be kept to an absolute minimum. The blood pressure should be assessed throughout the procedure and measures for treatment of a hypertensive crisis should be available. These patients should be monitored very closely during contrast-enhanced procedures.

Reports of thyroid storm following the use of iodinated radiopaque diagnostic agents in patients with hyperthyroidism or with an autonomously functioning thyroid nodule suggest that this additional risk be evaluated in such patients before use of any contrast medium.

PRECAUTIONS

General

Diagnostic procedures which involve the use of any radiopaque agent should be carried out under the direction of personnel with the prerequisite training and with a thorough knowledge of the particular procedure to be performed. Appropriate facilities should be available for coping with any complication of the procedure, as well as for emergency treatment of severe reaction to the contrast agent itself. After parenteral administration of a radiopaque agent, competent personnel and emergency facilities should be available for at least 30 to 60 minutes since severe delayed reactions may occur.

Preparatory dehydration is dangerous and may contribute to acute renal failure in patients with advanced vascular disease, diabetic patients, and in susceptible nondiabetic patients (often elderly with preexisting renal disease). *Patients should be well hydrated prior to and following iopamidol administration.*

The possibility of a reaction, including serious, life-threatening, fatal, anaphylactoid or cardiovascular reactions, should always be considered (see ADVERSE REACTIONS). Patients at increased risk include those with a history of a previous reaction to a contrast medium, patients with a known sensitivity to iodine per se, and patients with a known clinical hypersensitivity (bronchial asthma, hay fever, and food allergies). The occurrence of severe idiosyncratic reactions has prompted the use of several pretesting methods. However, pretesting cannot be relied upon to predict severe reactions and may itself be hazardous for the patient. It is suggested that a thorough medical history with emphasis on allergy and hypersensitivity, prior to the injection of any contrast medium, may be more accurate than pretesting in predicting potential adverse reactions. A positive history of allergies or hypersensitivity does not arbitrarily contraindicate the use of a contrast agent where a diagnostic procedure is thought essential, but caution should be exercised. Premedication with antihistamines or corticosteroids to avoid or minimize possible allergic reactions in such patients should be considered (see CONTRAINDICATIONS). Reports indicate that such pretreatment does not prevent serious life-threatening reactions, but may reduce both their incidence and severity.

General anesthesia may be indicated in the performance of some procedures in selected patients; however, a higher incidence of adverse reactions has been reported with radiopaque media in anesthetized patients, which may be attributable to the inability of the patient to identify untoward symptoms, or to the hypotensive effect of anesthesia which can reduce cardiac output and increase the duration of exposure to the contrast agent.

Even though the osmolality of iopamidol is low compared to diatrizoate or iothalamate based ionic agents of comparable iodine concentration, the potential transitory increase in the circulatory osmotic load in patients with congestive heart failure requires caution during injection. These patients should be observed for several hours following the procedure to detect delayed hemodynamic disturbances.

In angiographic procedures, the possibility of dislodging plaques or damaging or perforating the vessel wall should be borne in mind during catheter manipulations and contrast medium injection. Test injections to ensure proper catheter placement are suggested. Following arteriographic procedures, gentle pressure hemostasis is required, followed by observation and immobilization of the limb for several hours to prevent hemorrhage from the site of arterial puncture.

The inhibitory effects of nonionic contrast media on mechanisms of hemostasis have been shown, in vitro, to be less than ionic contrast media at comparable concentrations. For this reason, standard angiographic procedures should always be followed: angiographic catheters should be flushed frequently, and prolonged contact of blood with contrast in syringes and catheters should be avoided.

Selective coronary arteriography should be performed only in selected patients and those in whom the expected benefits outweigh the procedural risk. The inherent risks of angiocardiography in patients with chronic pulmonary emphysema must be weighed against the necessity for performing this procedure. Angiography should be avoided whenever possible in patients with homocystinuria, because of the risk of inducing thrombosis and embolism.

In addition to the general precautions previously described, special care is required when venography is performed in patients with suspected thrombosis, phlebitis, severe ischemic disease, local infection or a totally obstructed venous system.

Extreme caution during injection of contrast media is necessary to avoid extravasation and fluoroscopy is recommended. This is especially important in patients with severe arterial or venous disease.

If nondisposable equipment is used, scrupulous care should be taken to prevent residual contamination with traces of cleansing agents.

Information For Patients

Patients receiving injectable radiopaque diagnostic agents should be instructed to:

1. Inform your physician if you are pregnant.
2. Inform your physician if you are diabetic or if you have multiple myeloma, pheochromocytoma, homozygous sickle cell disease, or known thyroid disorder (see WARNINGS).
3. Inform your physician if you are allergic to any drugs, food, or if you had any reactions to previous injections of substances used for x-ray procedures (see PRECAUTIONS, General).
4. Inform your physician about any other medications you are currently taking, including nonprescription drugs, before you have this procedure.

Drug Interactions

Renal toxicity has been reported in a few patients with liver dysfunction who were given oral cholecystographic agents followed by intravascular contrast agents. Administration of intravascular agents should therefore be postponed in any patient with a known or suspected hepatic or biliary disorder who has recently received a cholecystographic contrast agent.

Other drugs should not be admixed with iopamidol.

Drug/Laboratory Test Interactions

The results of PBI and radioactive iodine uptake studies, which depend on iodine estimations, will not accurately reflect thyroid function for up to 16 days following administration of iodinated contrast media. However, thyroid function tests not depending on iodine estimations, e.g., T3 resin uptake and total or free thyroxine (T4) assays are not affected.

Any test which might be affected by contrast media should be performed prior to administration of the contrast medium.

Laboratory Test Findings

In vitro studies with animal blood showed that many radiopaque contrast agents, including iopamidol, produced a slight depression of plasma coagulation factors including prothrombin time, partial thromboplastin time, and fibrinogen, as well as a slight tendency to cause platelet and/or red blood cell aggregation (see PRECAUTIONS, General).

Transitory changes may occur in red cell and leucocyte counts, serum calcium, serum creatinine, serum glutamic oxalacetic transaminase (SGOT), and uric acid in urine; transient albuminuria may occur.

These findings have not been associated with clinical manifestations.

Carcinogenesis, Mutagenesis, Impairment Of Fertility

In animal reproduction studies performed on rats, intravenously administered iopamidol did not induce adverse effects on fertility or general reproductive performance.

In studies to determine mutagenic activity, iopamidol did not cause any increase in mutation rates.

Pregnancy Category B

No teratogenic effects attributable to iopamidol have been observed in teratology studies performed in animals. There are, however, no adequate and well controlled studies in pregnant women. It is not known whether iopamidol crosses the placental barrier or reaches fetal tissues. However, many injectable contrast agents cross the placental barrier in humans and appear to enter fetal tissues passively. Because animal teratology studies are not always predictive of human response, this drug should be used during pregnancy only if clearly needed.

Radiologic procedures involve a certain risk related to the exposure of the fetus to ionizing radiation.

Labor and Delivery

It is not known whether use of contrast agents during labor or delivery has immediate or delayed adverse effects on the fetus, prolongs the duration of labor or increases the likelihood that forceps delivery or other obstetrical intervention or resuscitation of the newborn will be necessary.

Nursing Mothers

It is not known whether iopamidol is excreted in human milk. However, many injectable contrast agents are excreted unchanged in human milk. Although it has not been established that serious adverse reactions occur in nursing infants, caution should be exercised when intravascular contrast media are administered to nursing women because of potential adverse reactions, and consideration should be given to temporarily discontinuing nursing.

Pediatric Use

Safety and effectiveness in children have not been established.

ADVERSE REACTIONS

ISOVUE (Iopamidol Injection)

Adverse reactions following the use of iopamidol are usually mild to moderate, self-limited, and transient.

In a clinical trial with 100 patients undergoing intra-arterial DSA, adverse reactions possibly attributed to ISOVUE-128 administration were nausea (2%), headache (1%) and vomiting (1%). One patient with preexisting renal impairment and severe bilateral renal vascular disease experienced renal failure, possibly secondary to a subsequent acute episode of congestive heart failure and/or drug administration (see Warnings).

In angiocardiography (597 patients), the adverse reactions with an estimated incidence of one percent or higher are: hot flashes 3.4%; angina pectoris 3.0%; flushing 1.8%; bradycardia 1.3%; hypotension 1.0%; hives 1.0%.

Intravascular injection of contrast media is frequently associated with the sensation of warmth and pain, especially in peripheral arteriography and venography; pain and warmth are less frequent and less severe with ISOVUE (Iopamidol Injection) than with diatrizoate meglumine and diatrizoate sodium injection.

The following table of incidence of reactions is based on clinical studies with ISOVUE in about 1941 patients.

Adverse Reactions

System	Estimated Overall Incidence > 1%	≤ 1%
Cardiovascular	none	tachycardia hypotension hypertension myocardial ischemia circulatory collapse S-T segment depression bigeminy extrasystoles ventricular fibrillation angina pectoris bradycardia transient ischemic attack thrombophlebitis
Nervous	pain (2.8%) burning sensation (1.4%)	vasovagal reaction tingling in arms grimace faintness
Digestive	nausea (1.2%)	vomiting anorexia
Respiratory	none	throat constriction dyspnea pulmonary edema
Skin and Appendages	none	rash urticaria pruritus flushing
Body as a Whole	hot flashes (1.5%)	headache fever chills excessive sweating back spasm
Special Senses	warmth (1.1%)	taste alterations nasal congestion visual disturbances
Urogenital	none	urinary retention

Regardless of the contrast agent employed, the overall estimated incidence of serious adverse reactions is higher with *coronary arteriography* than with other procedures. Cardiac decompensation, serious arrhythmias, or myocardial ischemia or infarction may occur during *coronary arteriography and left ventriculography.* Following coronary and ventricular injections, certain electrocardiographic changes (increased QTc, increased R-R, T-wave amplitude) and certain hemodynamic changes (decreased systolic pressure) occurred less frequently with ISOVUE (Iopamidol Injection) than with diatrizoate meglumine and diatrizoate sodium injection; increased LVEDP occurred less frequently after ventricular iopamidol injections.

In *aortography,* the risks of procedures also include injury to the aorta and neighboring organs, pleural puncture, renal damage including infarction and acute tubular necrosis with oliguria and anuria, accidental selective filling of the right renal artery during the translumbar procedure in the presence of preexisting renal disease, retroperitoneal hemorrhage from the translumbar approach, and spinal cord injury and pathology associated with the syndrome of transverse myelitis.

Adverse effects reported in clinical literature for iopamidol include arrhythmia, arterial spasms, hematuria, periorbital edema, involuntary leg movement, malaise, and triggering of deglutition; some of these may occur as a consequence of the procedure. Other reactions may also occur with the use of any contrast agent as a consequence of the procedural hazard; these include hemorrhage or pseudoaneurysms at the puncture site, brachial plexus palsy following axillary artery injections, chest pain, myocardial infarction, and transient changes in hepatorenal chemistry tests. Arterial thrombosis, displacement of arterial plaques, venous thrombosis, dissection of the coronary vessels and transient sinus arrest are rare complications.

ISOVUE-M (Iopamidol Injection)

The most frequently reported adverse reactions following intrathecal administration of iopamidol are headache, nausea, vomiting and musculoskeletal pain. These reactions usually occur 1 to 10 hours after injection, almost all occurring within 24 hours. They are usually mild to moderate in degree lasting for a few hours and usually disappearing within 24 hours. Rarely, headaches may be severe or persist for days. Headache is often accompanied by nausea and vomiting, and tends to be more frequent and persistent in patients not optimally hydrated.

Backache, neck stiffness, numbness and paresthesias, leg or sciatic-type pain occurred less frequently, often in the form of a transient exacerbation of preexisting symptomatology. Transient alterations in vital signs may occur and their significance must be assessed on an individual basis.

The following table of incidence of reactions is based on clinical studies with ISOVUE-M (Iopamidol Injection) in about 615 patients.

Adverse Reactions

System	Estimated Overall Incidence > 1%	≤ 1%
Body as a Whole	headache (18.1%)	pyrexia muscle weakness hot flashes malaise fatigue weakness
Digestive	nausea (7.3%) vomiting (3.7%)	diarrhea heartburn
Musculoskeletal	back pain (2.3%) leg pain (1.4%) neck pain (1.1%)	leg cramps sciatica cervicobrachial irritation meningeal irritation radicular irritation, lumbosacral other musculoskeletal pain involuntary movement burning sensation
Cardiovascular	hypotension (1.1%)	tachycardia hypertension chest pain

Adverse Reactions (con't)

System	Estimated Overall Incidence > 1%	≤ 1%
Nervous	none	emotional stress dizziness paresthesia confusion hallucinations lightheadedness syncope numbness cold extremities
Urogenital	none	urinary retention
Respiratory	none	dyspnea
Skin and Appendages	none	rash
Miscellaneous	none	injection site pain

Other adverse effects reported in clinical literature for iopamidol include facial neuralgia, tinnitus, and sweating.

Major motor seizures have been reported in the clinical literature and since market introduction in the United States. Early onset of seizures (less than two hours) is indicative of early substantial intracranial entry. Transitory EEG changes occur and usually take the form of slow wave activity.

While not observed in controlled clinical studies with ISOVUE-M (Iopamidol Injection), or reported in clinical literature, the following adverse reactions may occur because they have been reported with other nonionic contrast agents: cardiovascular (arrhythmias); aseptic meningitis syndrome; allergy or idiosyncrasy (chills, pruritus, nasal congestion, Guillain-Barre syndrome); CNS irritation (psycho-organic syndrome: mild and transitory perceptual aberrations such as depersonalization, anxiety, depression, hyperesthesia, disturbances in speech, sight, or hearing, and disorientation; in addition, hyperreflexia or areflexia, hypertonia or flaccidity, restlessness, tremor, echoacousia, echolalia, asterixis or dysphasia have occurred). Profound mental disturbances have rarely been reported (various forms and degrees of aphasia, mental confusion or disorientation); the onset is usually at 8 to 10 hours and lasts for about 24 hours without aftereffects.

However, occasionally they have been manifest as apprehension, agitation, or progressive withdrawal to the point of stupor in several instances. In a few cases, these have been accompanied by transitory hearing loss or other auditory symptoms and visual disturbances (believed subjective or delusional). Persistent cortical loss of vision in association with convulsions, and ventricular block have been reported. Rarely, persistent though transitory weakness in the leg or ocular muscles has been reported. *Peripheral neuropathies* have been rare and transitory. They include sensory and/or motor or nerve root disturbances, myelitis, persistent leg muscle pain or weakness, or sixth nerve palsy, or cauda equina syndrome. Muscle cramps, fasciculation or myoclonia, spinal convulsion, or spasticity are unusual.

General Adverse Reactions To Contrast Media

Reactions known to occur with parenteral administration of iodinated ionic contrast agents (see the listing below) are possible with any nonionic agent. Approximately 95 percent of adverse reactions accompanying the use of other water-soluble intravascularly administered contrast agents are mild to moderate in degree. However, life-threatening reactions and fatalities, mostly of cardiovascular origin, have occurred.

Reported incidences of death from the administration of other iodinated contrast media range from 6.6 per 1 million (0.00066 percent) to 1 in 10,000 patients (0.01 percent). Most deaths occur during injection or 5 to 10 minutes later, the main feature being cardiac arrest with cardiovascular disease as the main aggravating factor. Isolated reports of hypotensive collapse and shock are found in the literature. The incidence of shock is estimated to be 1 out of 20,000 (0.005 percent) patients.

Adverse reactions to injectable contrast media fall into two categories: chemotoxic reactions and idiosyncratic reactions. Chemotoxic reactions result from the physico-chemical properties of the contrast medium, the dose, and the speed of injection. All hemodynamic disturbances and injuries to organs or vessels perfused by the contrast medium are included in this category. Experience with iopamidol suggests there is much less discomfort (e.g., pain and/or warmth) with peripheral arteriography. Fewer changes are noted in ventricular function after ventriculography and coronary arteriography.

Idiosyncratic reactions include all other reactions. They occur more frequently in patients 20 to 40 years old. Idiosyncratic reactions may or may not be dependent on the amount of drug injected, the speed of injection, the mode of injection, and the radiographic procedure. Idiosyncratic reactions are subdivided into minor, intermediate, and severe. The minor reactions are self-limited and of short duration; the severe reactions are life-threatening and treatment is urgent and mandatory.

The reported incidence of adverse reactions to contrast media in patients with a history of allergy is twice that for the general population. Patients with a history of previous reactions to a contrast medium are three times more susceptible than other patients. However, sensitivity to contrast media does not appear to increase with repeated examinations. Most adverse reactions to intravascular contrast agents appear within one to three minutes after the start of injection, but delayed reactions may occur (see PRECAUTIONS, General).

Because measurable plasma levels are attained following the intrathecal administration of iopamidol, adverse reactions reported with the use of intravascular contrast agents are theoretically possible. In addition to the adverse drug reactions reported for iopamidol, the following additional adverse reactions have been reported with the use of other intravascular contrast agents and are possible with the use of any water-soluble iodinated contrast agent:

Cardiovascular: vasodilation, cerebral hematomas, petechiae, hemodynamic disturbances, sinus bradycardia, transient electrocardiographic abnormalities, ventricular fibrillation.

Digestive: nausea, vomiting, severe unilateral or bilateral swelling of the parotid and submaxillary glands.

Nervous: paresthesia, dizziness, convulsions, paralysis, coma.

Respiratory: increased cough, asthma, laryngeal edema, pulmonary edema, bronchospasm, rhinitis, dyspnea.

Skin and Appendages: injection site pain usually due to extravasation and/or erythematous swelling, skin necrosis.

Urogenital: osmotic nephrosis of proximal tubular cells, renal failure, pain.

Special Senses: bilateral ocular irritation; lacrimation; conjunctival chemosis, infection, and conjunctivitis; itching.

The following reactions may also occur: neutropenia, thrombophlebitis, flushing, pallor, weakness, severe retching and choking, wheezing, cramps, tremors, and sneezing.

HOW SUPPLIED

ISOVUE-128: 10 x 50 mL vials; ISOVUE-200: 10 x 50 mL vials and 10 x 100 mL bottles; ISOVUE-300: 10 x 50 mL vials and 10 x 100 mL bottles and 10 x 150 mL bottles; ISOVUE-370: 10 x 50 mL vials and 10 x 100 mL, 10 x 150 mL and 10 x 200 mL bottles; ISOVUE-M 200: 10 x 20 mL vials; ISOVUE-M 300: 10 x 15 mL vials.

STORAGE

ISOVUE® and ISOVUE-M® (iopamidol injection) should be stored at room temperature not exceeding 86° F. Protect from light.

For full prescribing information consult package insert.

J3-702A/J3-652E/J3-653E

© 1987 E.R. Squibb & Sons, Inc., Princeton, NJ 647-508 Issued: November 1987

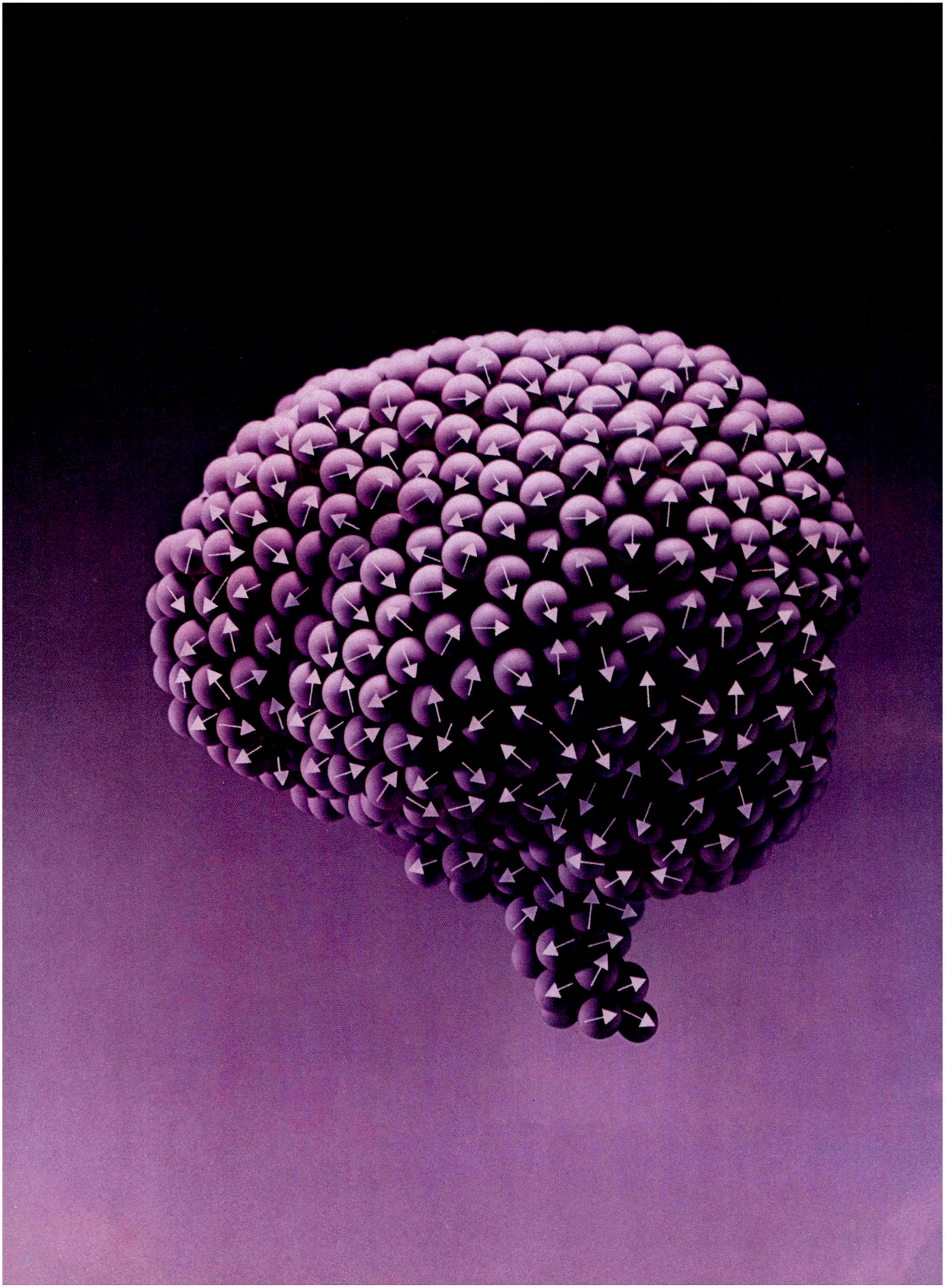

COMING SOONER THAN YOU THINK *MRI*

BEYOND THE IMAGINATION

Imaging that's going to give you the details you've always wanted. Images that help define and differentiate. That's what the researchers at Berlex Imaging have been working on. Our research is dedicated to developing contrast material so you can see as you've never seen before. The results of our research may be here sooner than you think. But it's only the beginning of imaging beyond the imagination from Berlex.

BERLEX IMAGING™

Berlex Imaging
300 Fairfield Road
Wayne, NJ 07470

AJR 2/88

Yes, I want to be one of the first to know about MRI beyond the imagination.

name

address

city state zip

( ) area code telephone no.

specialty (including subspecialty) ID number

CIRCLE 34 ON READER SERVICE CARD

Printed in USA September 1987

Introducing A Sensitive, Well-balanced Approach

The Konica Monarch Mammography System

Minimizes Patient Exposure

Konica Monarch Mammography System provides a balanced approach to mammography by combining optimal image quality, with the benefits of lower dose levels and minimal patient exposure.

Film/Screen Characteristics Ideally Suited for Mammography

Konica Monarch Mammography System is an effective imaging system for the diagnosis of soft tissue masses and calcifications. For screening, Type CM film also has the potential to demonstrate non-palpable lesions.

Konica CM film is compatible with most screen/cassette mammography systems.

Type CM Film

Konica CM orthochromatic film has excellent low density contrast for visualization of calcifications, along with increased soft tissue visibility. Type CM film employs Konica's (HMG) High Ortho Mono-Dispersed Grain Technology.

Advanced HMG Technology uses fine grains, which are more condensed and uniform, and designed to provide optimal imaging for mammography. With Type CM film, you not only see superior resolution and contrast, you're provided with more diagnostic information without having to sacrifice speed.

The Monarch Screen

The Monarch System uses a single rare-earth intensifying screen which incorporates green emitting phosphors and is designed for radiographic examinations where high resolution is required.

In addition to its anti-static characteristics, the textured screen surface also aids in the expulsion of trapped air between the screen and film, resulting in intimate contact for maximum image sharpness.

The Monarch Cassette

The Monarch cassette maintains the film in close and uniform contact with the intensifying screen. The cassettes are designed to allow closer positioning of the film to the chest wall for maximum anatomical diagnosis.

Konica Monarch™

Mammography System

Konica®

411 Newark Pompton Tpke., Wayne, NJ 07470 •
(201) 633-1500

CIRCLE 18 ON READER SERVICE CARD

CIRCLE 17 ON READER SERVICE CARD

The NEW Ackrad H/S Catheter Set for Hysterosalpingography

Now: Easier on the Patient . . . Better for the Physician

The unique small sizes (5 and 7F) of the flexible balloon-bearing catheter provide previously unavailable freedom from trauma for the patient. A placement sheath and inflation syringe are included in the set for a rapid and efficient procedure.

Sample furnished on request.

ACKRAD LABORATORIES, Inc.
70 Jackson Drive, P.O. Box 1085, Cranford, NJ 07016
(201) 276-6390

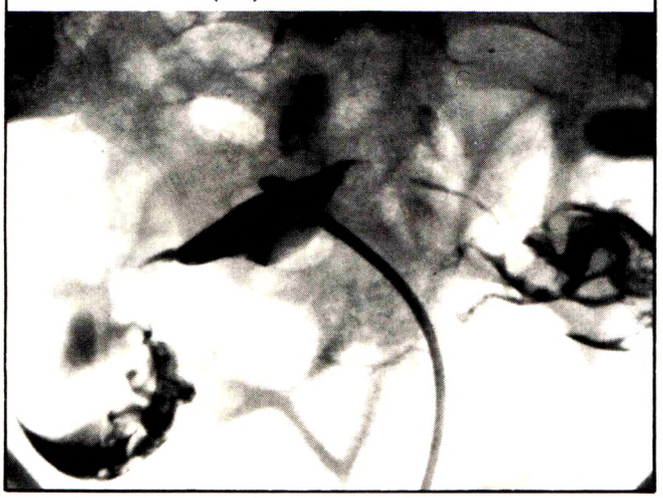

UNIVERSITY OF MIAMI

School of Medicine

Department of Radiology is recruiting faculty for the UM/Jackson Memorial Medical Center, a 1300 bed tertiary referral center. Positions available to meet expanding clinical and academic programs in:

THORACIC IMAGING
ABDOMINAL IMAGING
MUSCULOSKELETAL IMAGING
NEURORADIOLOGY
NUCLEAR MEDICINE

Candidates must be board certified or eligible, with fellowship training or equivalent experience. Rank and salary commensurate with qualifications.

Send C.V. to: C.A. Poole, M.D.
Professor and Chairman
Department of Radiology (R-130)
University of Miami School of Medicine
P.O. Box 016960
Miami, Florida 33101

AN AFFIRMATIVE ACTION/EQUAL OPPORTUNITY EMPLOYER

for prompt subscription service...

attach label here

Please use this coupon and attach a *recent* label in the space provided when writing to us about:

- change of address
- renewal
- questions regarding your subscription

Please use the space below to indicate your *new* address.

Name of Journal_____

Name_____

Address_____

City/State/Zip_____

THE WILLIAMS & WILKINS COMPANY

428 East Preston Street/Baltimore, Maryland 21202

NEW INDICATION

In contrast-enhanced CT... improve the safety profile.

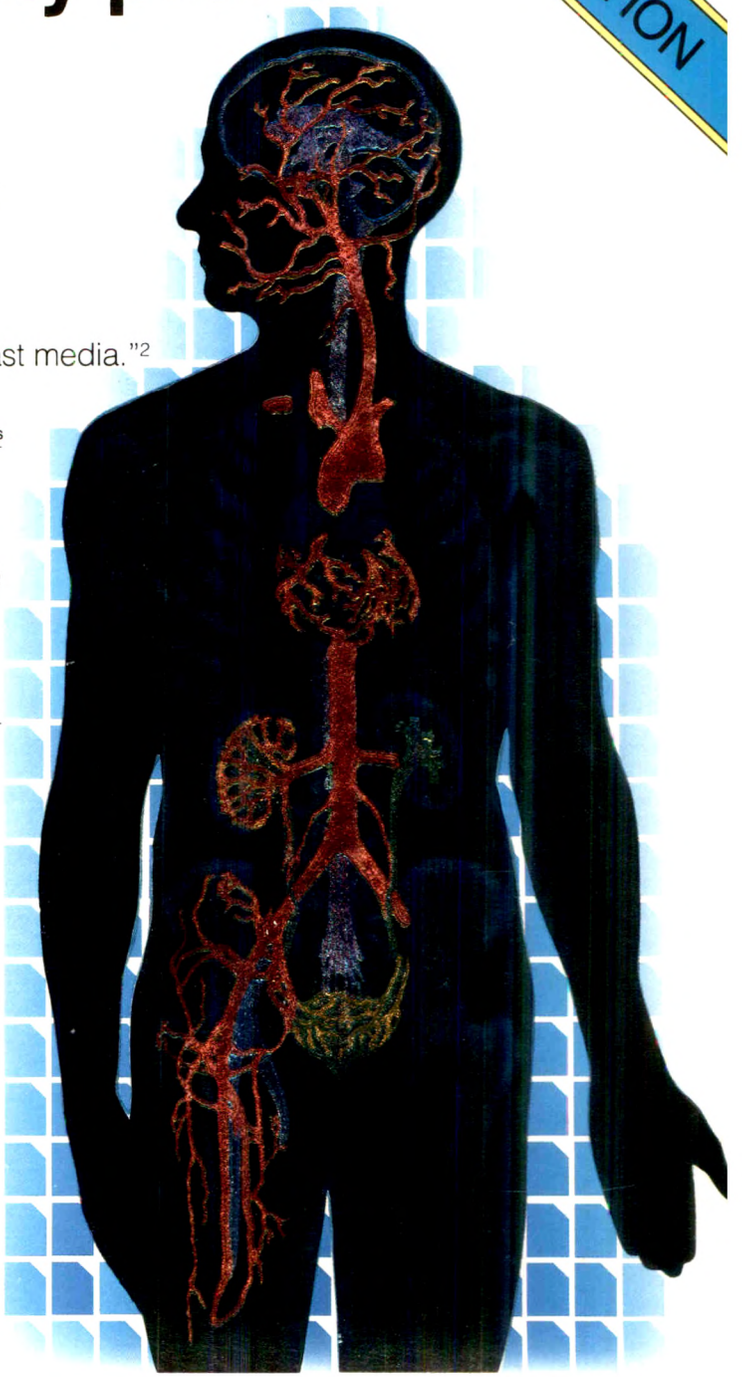

Fewer adverse reactions than with traditional ionics, including reactions that may delay or interrupt procedures.[1-4]

Tolerated "far better than conventional contrast media."[2]

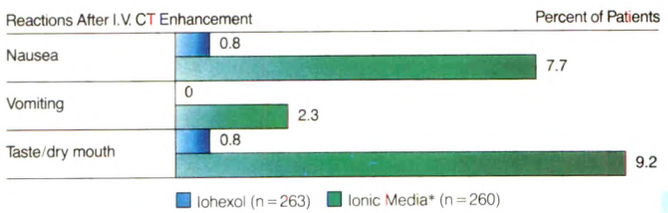

— In 263 CT patients, *no* reports of tachycardia, bradycardia, palpitations, or respiratory difficulties.[†]

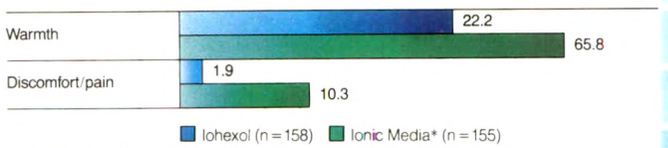

* Metrizoate or ioglicate; comparable concentration and volume per injection
Adapted from Skalpe[1]

Lower toxicity.

- — Particularly important in enhanced cranial CT.
- — An important advantage when the blood-brain barrier may already be disrupted.[1,5]

Now in special convenience/ economy packaging for enhanced CT.

Since adverse reactions can occur with nonionic media, similar precautions to those recommended for ionic media should be utilized for treatment of severe or potentially fatal reactions.

Physicians should remain alert to possible adverse effects that have occurred with other nonionic water-soluble media.

[†]In a more general patient population, such reactions occur in less than 1 percent.

See next page for important product information concerning contraindications, warnings, adverse reactions, patient selection, and prescribing and precautionary recommendations.

NONIONIC

OMNIPAQUE®

(IOHEXOL)

THE NEW STANDARD IN CONTRAST-ENHANCED IMAGING.

OMNIPAQUE®
INJECTION (IOHEXOL)
INTRAVASCULAR

240

300

350

PLEASE CONSULT FULL PRODUCT INFORMATION BEFORE USING.
A SUMMARY FOLLOWS:

DESCRIPTION: OMNIPAQUE is a nonionic, water-soluble radiographic contrast medium for intravascular administration and is provided in iodine concentrations of 240, 300, and 350 mgI/mL. Each milliliter of iohexol solution contains 1.21 mg tromethamine and 0.1 mg edetate calcium disodium with the pH adjusted between 6.8 and 7.7 with hydrochloric acid or sodium hydroxide, but it contains no preservatives.

CONTRAINDICATIONS: OMNIPAQUE should not be administered to patients with a known hypersensitivity to iohexol.

WARNINGS: OMNIPAQUE should be used with extreme care in patients with: severely impaired renal and/or hepatic function; severe thyrotoxicosis, hyperthyroidism, or an autonomously functioning thyroid nodule; diabetes with a serum creatinine level above 3 mg/dL. Not recommended for use in patients with anuria.

Patients with known or suspected pheochromocytoma should receive a minimum of contrast medium if benefit of the exam is judged to outweigh risk; blood pressure should be monitored throughout the procedure, and measures for the treatment of hypertensive crisis should be readily available.

Contrast agents are potentially hazardous in patients with multiple myeloma or other paraproteinemia, particularly those with therapeutically resistant anuria. The combination of contrast agent and dehydration may precipitate myeloma protein in the renal tubules. No form of therapy, including dialysis, has been successful in reversing the effect. Myeloma, which occurs most commonly in persons over age 40, should be considered before instituting intravascular administration of contrast agents.

PRECAUTIONS: Diagnostic procedures that involve the use of radiopaque diagnostic agents should be carried out under the direction of personnel with the prerequisite training and with a thorough knowledge of the particular procedure to be performed. Appropriate facilities should be available for coping with any complication of the procedure, as well as for emergency treatment of severe reactions to the contrast agent itself. Competent personnel and emergency facilities should be available for at least 30 to 60 minutes postprocedure. The possibility of serious, life-threatening, fatal, anaphylactoid, or cardiovascular reactions should always be considered (see ADVERSE REACTIONS). It is of utmost importance that a course of action be carefully planned in advance for immediate treatment of serious reactions. Preparatory dehydration is dangerous and may contribute to acute renal failure in patients with advanced vascular disease, diabetic patients, and in susceptible nondiabetic patients (often elderly with preexisting renal disease). *Patients should be well hydrated prior to and following iohexol administration.* Careful consideration to the potential risk of acute renal failure should be given before performing excretory urography in diabetic patients with diabetic nephropathy and in susceptible nondiabetic patients (often elderly with preexisting renal disease). Immediately following surgery, excretory urography should be used with caution in renal transplant recipients. The possibility of an idiosyncratic reaction in susceptible patients should always be considered (see ADVERSE REACTIONS). The susceptible population includes patients with a history of a previous reaction to contrast media, patients with a known sensitivity to iodine per se, and patients with a known clinical hypersensitivity: bronchial asthma, hay fever, and food allergies. A thorough medical history with emphasis on allergy and hypersensitivity, prior to the injection of any contrast media, may be more accurate than pretesting in predicting potential adverse reactions.

A positive history of allergies or hypersensitivity does not arbitrarily contraindicate the use of a contrast agent where a diagnostic procedure is thought essential, but caution should be exercised (see ADVERSE REACTIONS). Premedication with antihistamines or corticosteroids to avoid or minimize possible allergic reactions in such patients should be considered. Recent reports indicate that such pretreatment does not prevent serious, life-threatening reactions but may reduce both their incidence and severity.

Even though the osmolality of OMNIPAQUE is low compared to diatrizoate- or iothalamate-based ionic agents of comparable iodine concentration, the potential transitory increase in circulatory osmotic load in patients with congestive heart failure requires caution during injection. These patients should be observed for several hours following the procedure to detect delayed hemodynamic disturbances.

Angiography should be avoided whenever possible in patients with homocystinuria, because of the risk of inducing thrombosis and embolism.

In angiographic procedures, the possibility of dislodging plaques or damaging or perforating the vessel wall should be borne in mind during the catheter manipulations and contrast medium injection. Test injections to ensure proper catheter placement are recommended.

Selective coronary arteriography should be performed only in those patients in whom the expected benefits outweigh the potential risk. The inherent risks of angiocardiography in patients with chronic pulmonary emphysema must be weighed against the necessity for performing this procedure.

When OMNIPAQUE is to be injected using plastic disposable syringes, the contrast medium should be drawn into the syringe and used immediately.

The inhibitory effects of nonionic contrast media on mechanisms of hemostasis have been shown, in vitro, to be less than those of ionic contrast media at comparable concentrations. For this reason, standard angiographic procedures should always be followed: angiographic catheters should be flushed frequently, and prolonged contact of blood with contrast media in syringes and catheters should be avoided.

If nondisposable equipment is used, scrupulous care should be taken to prevent residual contamination with traces of cleansing agents.

Drug/Laboratory Test Interaction: If iodine-containing isotopes are to be administered for the diagnosis of thyroid disease, the iodine-binding capacity of thyroid tissue may be reduced for up to 2 weeks after contrast medium administration. Thyroid function tests which do not depend on iodine estimation, eg, T_3 resin uptake or direct thyroxine assays, are not affected.

Carcinogenesis, Mutagenesis, Impairment of Fertility: No long-term animal studies have been performed to evaluate carcinogenic potential, mutagenesis, or whether OMNIPAQUE can affect fertility in men or women.

Pregnancy Category B: Reproduction studies have been performed in rats and rabbits with up to 100 times the recommended human dose. No evidence of impaired fertility or harm to the fetus has been demonstrated due to OMNIPAQUE. There are, however, no studies in pregnant women. Because animal reproduction studies are not always predictive of human response, this drug should be used during pregnancy only if clearly needed.

Nursing Mothers: It is not known to what extent iohexol is excreted in human milk. However, many injectable contrast agents are excreted unchanged in human milk. Although it has not been established that serious adverse reactions occur in nursing infants, caution should be exercised when intravascular contrast media are administered to nursing women. Bottle feedings may be substituted for breast feedings for 24 hours following administration of OMNIPAQUE.

Pediatric Use: Safety and effectiveness in children have not been established.

ADVERSE REACTIONS: Usually mild to moderate in severity. However, serious, life-threatening, and fatal reactions, mostly of cardiovascular origin, have been associated with the administration of iodine-containing contrast media including OMNIPAQUE. The injection of contrast media is frequently associated with the sensation of warmth and pain, especially in peripheral angiography; pain and warmth are less frequent and less severe with OMNIPAQUE than with many contrast media.

Cardiovascular System: Arrhythmias including PVCs and PACs (3%), angina/chest pain (2%), and hypotension (1%). Others including cardiac failure, asystole, bradycardia, tachycardia, and vasovagal reaction were reported with an individual incidence of less than 0.8%. In controlled clinical trials involving 900 patients, one fatality occurred. A cause-and-effect relationship between this death and iohexol has not been established.

Nervous System: Pain (6%), photomas (3%), headache (2%), and metallic taste (0.8%). Others including anxiety, blurred vision, dizziness, fever, motor and speech dysfunction, convulsion, lightheadedness, paresthesia, somnolence, vertigo, stiff neck, hemiparesis, and nystagmus were reported, with an individual incidence of less than 0.3%.

Respiratory System: Dyspnea and laryngitis, with an individual incidence of 0.1%.

Gastrointestinal System: Nausea (2%) and vomiting (0.5%). Others including diarrhea, dyspepsia, and dry mouth were reported, with an individual incidence of 0.1%.

Skin and Appendages: Urticaria (0.3%) and purpura (0.1%).

General Adverse Reactions to Contrast Media: The following reactions have been reported after administration of other intravascular iodinated contrast media. *Reactions due to technique:* hematomas and ecchymoses. *Hemodynamic reactions:* vein cramp and thrombophlebitis following intravenous injection. *Cardiovascular reactions:* rare cases of cardiac arrhythmias, reflex tachycardia, chest pain, cyanosis, hypertension, hypotension, peripheral vasodilatation, shock, and cardiac arrest. *Renal reactions:* occasionally, transient proteinuria; rarely, oliguria or anuria. *Allergic reactions:* asthmatic attacks, nasal and conjunctival symptoms, dermal reactions such as urticaria with or without pruritus, as well as pleomorphic rashes, sneezing, and lacrimation; rarely, anaphylactic reactions. Rare fatalities have occurred due to these or unknown causes. *Signs and symptoms related to the respiratory system:* pulmonary or laryngeal edema, bronchospasm, dyspnea; or *to the nervous system:* restlessness, tremors, convulsions. *Other reactions:* flushing, pain, warmth, metallic taste, nausea, vomiting, anxiety, headache, confusion, pallor, weakness, sweating, localized areas of edema (especially facial cramps), neutropenia, and dizziness. Rarely, immediate or delayed rigors can occur, sometimes accompanied by hyperpyrexia. Infrequently, "iodism" (salivary gland swelling) from organic iodinated compounds appears 2 days after exposure and subsides by the sixth day.

In general, the reactions that are known to occur upon parenteral administration of iodinated contrast agents are possible with any nonionic agent. Approximately 95% of adverse reactions accompanying the use of water-soluble intravascularly administered contrast agents are mild to moderate in degree. However, severe, life-threatening anaphylactoid reactions, mostly of cardiovascular origin, have occurred.

Reported incidences of death range from 6.6 per 1 million (0.00066%) to 1 in 10,000 (0.01%). Most deaths occur during injection or 5 to 10 minutes later, the main feature being cardiac arrest, with cardiovascular disease as the main aggravating factor. Isolated reports of hypotensive collapse and shock are found in the literature. The incidence of shock is estimated to be 1 out of 10,000 (0.005%) patients.

Adverse reactions to injectable contrast media fall into two categories: chemotoxic reactions and idiosyncratic reactions.

Chemotoxic reactions result from the physicochemical properties of the contrast media, the amount of dose injected, and the speed of injection. All hemodynamic disturbances and injuries to organs or vessels perfused by the contrast medium are included in this category.

Idiosyncratic reactions include all other reactions. They occur more frequently in patients 20 to 40 years old. Idiosyncratic reactions may or may not be dependent on the amount of dose injected, the speed of injection and the radiographic procedure. Idiosyncratic reactions are subdivided into minor, intermediate, and severe. The minor reactions are self-limited and of short duration; the severe reactions are life-threatening and treatment is urgent and mandatory.

The reported incidence of adverse reactions to contrast media in patients with a history of allergy is twice that in the general population. Patients with a history of previous reactions to a contrast medium are three times more susceptible than other patients. However, sensitivity to contrast media does not appear to increase with repeated examinations.

Most adverse reactions to injectable contrast media appear within 1 to 3 minutes after the start of injection, but delayed reactions may occur.

Regardless of the contrast agent employed, the overall estimated incidence of serious adverse reactions is higher with angiocardiography than with other procedures. Cardiac decompensation, serious arrhythmias, angina pectoris, or myocardial ischemia or infarction may occur during angiocardiography and left ventriculography. Electrocardiographic and hemodynamic abnormalities occur less frequently with OMNIPAQUE than with diatrizoate meglumine and diatrizoate sodium injection.

References: 1. Skalpe IO: Enhancement with water-soluble contrast media in computed tomography of the brain and abdomen. *Acta Radiol* 1983; suppl 366, pp 72-75. **2.** Holtås S, Cronqvist S, Renaa T: Contrast enhanced brain CT: Comparison between iohexol and metrizoate. *Invest Radiol* 1985; 20(suppl 1):62-64. **3.** Tschakert H: Tolerability of iohexol and ioglicate for intravenous contrast enhancement in cerebral computed tomography. *Acta Radiol* 1983; suppl 366, pp 76-77. **4.** Skalpe IO, Östensen HM: Contrast media in abdominal computed tomography: A double-blind clinical trial comparing a non-ionic (iohexol) and an ionic (metrizoate) contrast medium. *Acta Radiol* 1983; suppl 366, p 80. **5.** Dawson P: Chemotoxicity of contrast media and clinical adverse effects: a review. *Invest Radiol* 1985; 20(suppl 1):84-91.

© 1987 WINTHROP PHARMACEUTICALS 71386/3801

Winthrop PHARMACEUTICALS
Winthrop Pharmaceuticals
Division of Sterling Drug Inc.
New York, NY 10016

Evac-Q-Kwik® advantages are as clear as the X-ray you get.

Use this checklist to compare other bowel preps:

	EVAC-Q-KWIK	Other Preps
Taste	Pleasant, cherry flavor	
Fluid intake	40 fl oz	
Reconstitution	No	
Enema	No	
Cost	Low	
Adminstration time	6 hours	
Sugar	No	
Alcohol	No	
Sodium content	Low	

Evac-Q-Kwik thoroughly cleans the colon. Patients arrive ready for X-ray. No staff time or extra prepping needed. One take is all—virtually every time. This means better work flow, cost containment and patient comfort.

Everything is in the kit, including easy-to-follow instructions. No mixing, no enemas, no alcohol, no sugar, low sodium… and low cost. Easy to use for better compliance.

Seeing is believing. Give Evac-Q-Kwik a trial.

There's more.

Take advantage of our service materials:
☐ Inservice film for nurses ☐ Multi-language instruction sheets ☐ Radiology work sheets ☐ "What to expect" booklet for patients. Ask your Adria Representative, or drop us a line. Adria Laboratories, Columbus, Ohio 43215.

Evac-Q-Kwik®

Clean colon, clear advantages.

Adria®

Adria Laboratories
Columbus, OH 43215

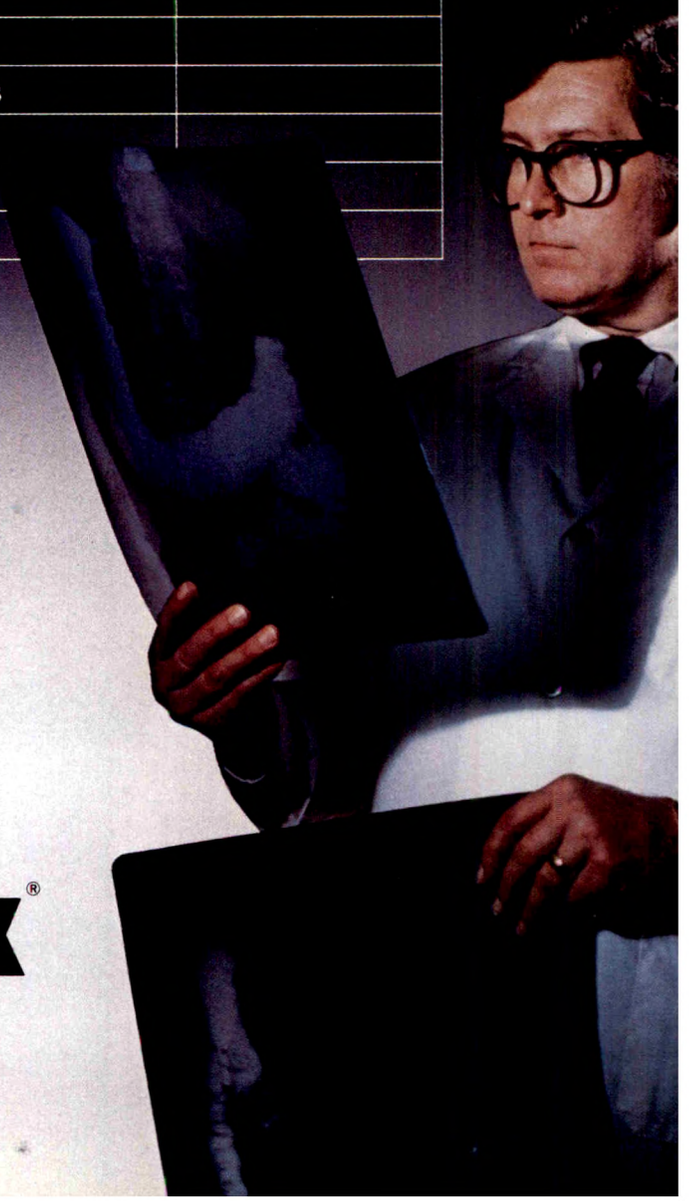

NEW MAMMOGRAPHIC QA PHANTOM*

For Evaluating the Overall Imaging Performance of a Mammographic System

- Intended as an integral part of a complete mammography QA program: evaluates x-ray generator, screen-film combination and film processor.
- Contains test objects that simulate two mammographic indications of breast cancer: "punctuate calcifications and soft tissue fibrillar extensions in adipose tissue."
- Includes 5-step air wedge to gauge for image contrast.

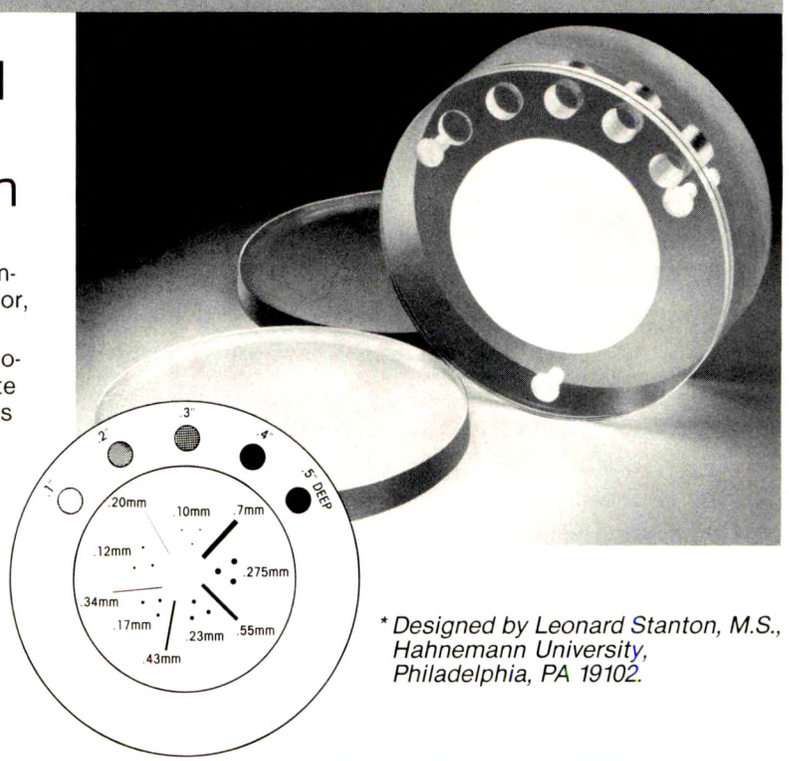

76-001-4 Mammographic Phantom . . . $495.00

Write, or phone 516-741-6360 today!
For more details,
request bulletin 400M-44

** Designed by Leonard Stanton, M.S., Hahnemann University, Philadelphia, PA 19102.*

Federal Agency *Recommends* . . . PLUS
Joint Commission on Accreditation of Hospitals *Requires* . . .

HOSPITALS MUST MONITOR DOSES FROM DIAGNOSTIC RADIOLOGY PROCEDURES!

RAD-CHECK® PLUS X-Ray Exposure Meter

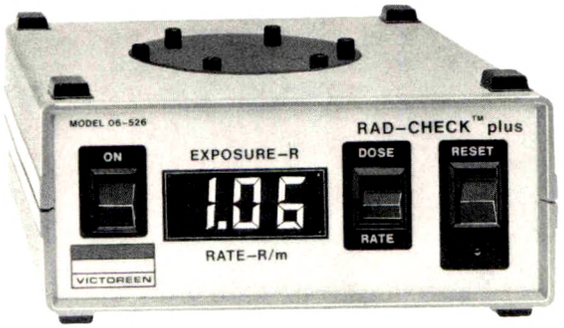

Will Perform This Function Plus Many Others!

APPLICATIONS . . .

- Entrance skin exposure measurements (ESE).
- Fluoroscopy exposure measurements.
- Beam quality - half-value layer (HVL).

ADVANTAGES . . .

- Fast, easy to use: Battery operation and built-in detector eliminate set-up time. Place RAD-CHECK PLUS on x-ray table, collimate, shoot, and read the result!
- Dual range: Dose up to 2 R; dose rate up to 20 R/min.

For more information, request bulletin 356M-44

NUCLEAR ASSOCIATES

VICTOREEN

A Division of VICTOREEN, INC.
100 VOICE ROAD
CARLE PLACE, NY 11514-1593
(516) 741-6360
A Subsidiary of Sheller-Globe SG

*Victoreen, Inc.

CIRCLE 16 ON READER SERVICE CARD

ELEMA-SCHONANDER

The NEW GENERATION PUCK® CM System‡ brings increased versatility, accuracy, safety and operational ease to full-size serial angiography.

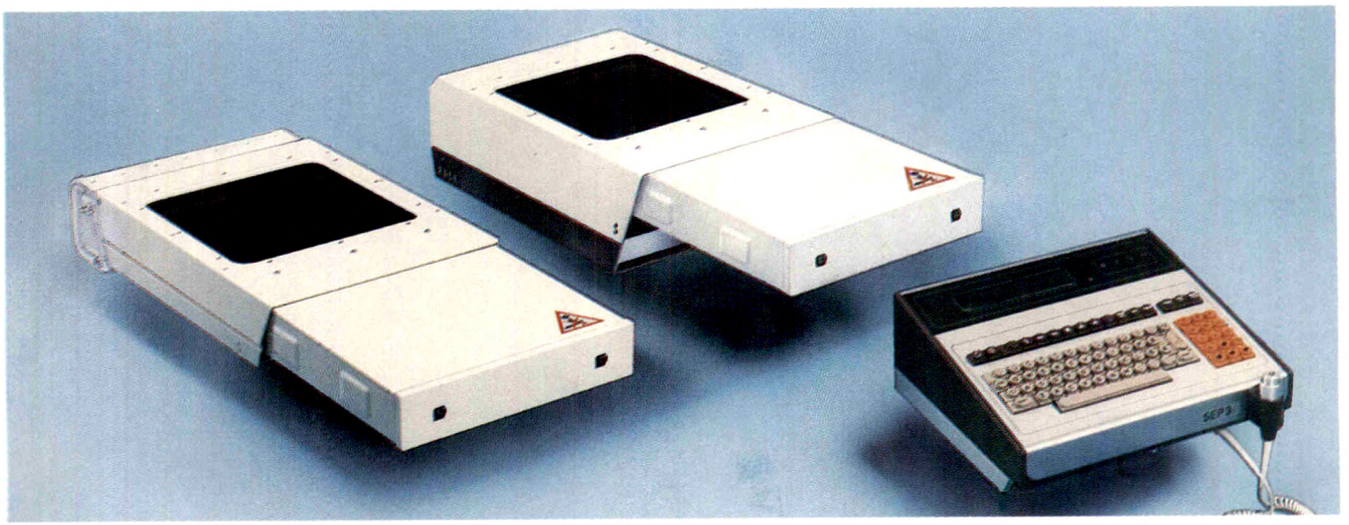

PUCK CM changer, PUCK C changer and SEP-3 program control with keyboard for film marking, programming and program selection

PUCK CM features:

- **Multi-directional**—the same loading magazine and receiving cassette in all positions
- **Light and compact**—only 4-1/2″ thick, thanks to innovative receiving cassette design
- **Extended exposure time**—e.g. 100ms at 4 exp/sec
- **New SEP-3 Program Control** for maximum ease of operation
- **SEP-3 keyboard-operated alphanumeric film marking**—up to 100 characters for comprehensive examination data
- **Electronic shaft encoder control** of internal filmchanger functions

‡ The PUCK CM System consists of: PUCK CM changer for use on multidirectional examination units, as well as in most other applications. PUCK C changer for a.p. and lateral projections including installation in R&F tables. SEP-3 program control.

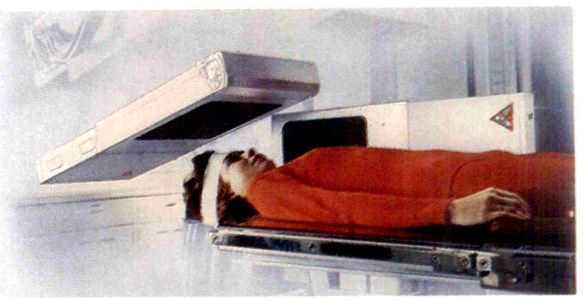

PUCK CM and PUCK C changers in biplane configuration

For further information please contact

elema-schonander

Elema-Schonander, Inc.
2360 N. Palmer Drive, P.O.Box 94517
Schaumburg, IL 60173-3887
Telephone (312) 397-5900

CIRCLE 14 ON READER SERVICE CARD

87218

Keyboard-originated alphanumeric film-marking (reproduced 1/2 actual size)

S&S STATE-OF-THE-ART MAMMOGRAPHIC EQUIPMENT

Mammography Illuminator Ideal for Mammographs

Unmatched illumination excellence plus versatile applications make this series THE state-of-the-art equipment for viewing

8x10 (18x24cm) or 10x12 (24x30cm) mammographs.

A single intensity uniform light source provides brighter illumination per panel. The low leakage trigger start ballast delivers constant "instant-on."

S&S state-of-the-art features include a continuous gravity grip; 1-piece plexiglas viewing panel per tier; and on/off rocker switches to control individual panels. Optional film actuated switches are available.

Maximum flexibility is offered. 1-6 bank widths in single or 2-tier models can be either surface or recess mounted. Also, 2-tier mounting brackets allow fixed angulation for even more versatility. Each tier is constructed of 1-piece heavy-duty steel for longevity.

NY State, phone:
718/ 649-8500

Elsewhere, phone:
800/221-6634

Mammography Moving Grid Bucky System

Far superior to stationary grid techniques, the S&S Moving Grid Bucky has been specifically designed for simple conversion of existing non-bucky equipment —at a fraction of the cost of a totally new mammography unit.

This state-of-the-art add-on system eliminates grid lines, greatly improves contrast

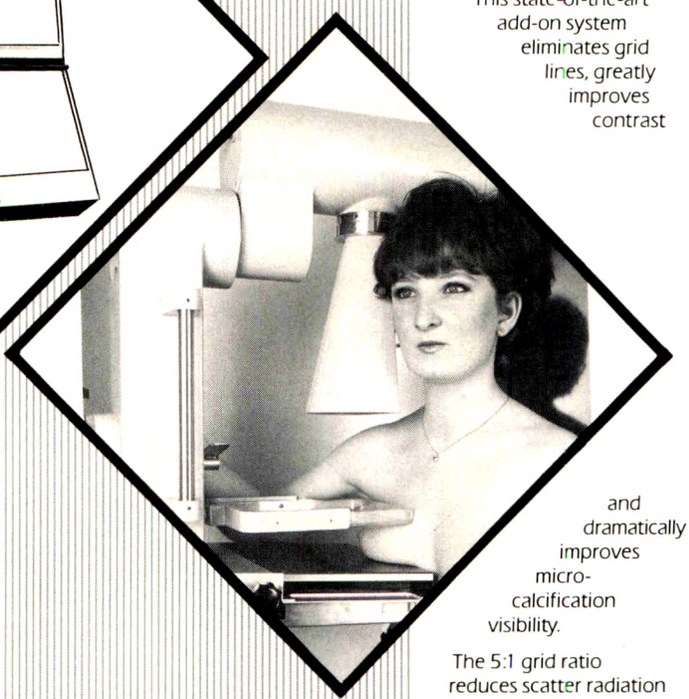

and dramatically improves micro-calcification visibility.

The 5:1 grid ratio reduces scatter radiation up to 70%, and lowest possible dose rates are ensured by carbon fibre grid and cover construction.

Adaption of the S&S bucky to the film plateau of existing mammography equipment is accomplished with 2 adjustable side clamps (supplied).

Model MB12 is available for use with 18x24cm film. Model MB24 serves 24x30cm film.

***New Vertifile Systems specifically designed to store mammographs are also available.**

S&S X-RAY PRODUCTS, INC.
1101 Linwood Street
Brooklyn, NY 11208

CIRCLE 9 ON READER SERVICE CARD

THE LOW OSMOLALITY ISSUE, IN A NUTSHELL

LOW

Iohexol-350
844 mOsm/kg H_2O

LOWER

Iopamidol-370
796 mOsm/kg H_2O

F R O M M A L L

LOWEST

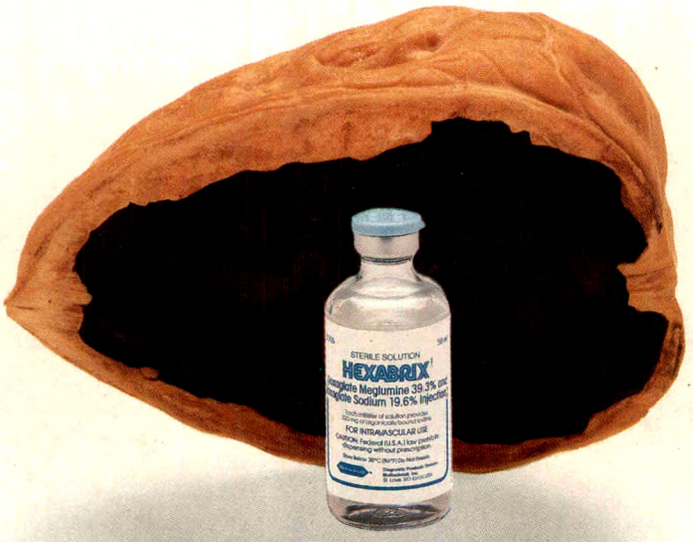

600 mOsm/kg H_2O

The distinct advantages of the Hexabrix profile

When you compare the three newer low-osmolality agents, Hexabrix not only has the lowest osmolality (per mg iodine), but it also offers other important advantages.

Less heat and pain

In studies comparing Hexabrix with iohexol-350 and iopamidol-370 for peripheral arteriography, Hexabrix patients experienced less pain and heat during abdominal aortography than those patients receiving the other agents, taken as a group.[1,2]

Less risk of clotting *in vitro*

Hexabrix has been shown to be a stronger inhibitor of red blood cell clotting *in vitro* than iohexol or iopamidol.[3,4]

Lowest viscosity

At 37°C, Hexabrix (7.5 cps) is less viscous than iopamidol-370 (9.4 cps) or iohexol-350 (10.4 cps).

HEXABRIX†

(ioxaglate meglumine 39.3%/
ioxaglate sodium 19.6% injection)

Changing the look of medicine.

Please see following page for references and brief summary of prescribing information.

INCKRODT

HEXABRIX† (ioxaglate meglumine 39.3%/ioxaglate sodium 19.6% injection)

HEXABRIX®

Each milliliter of HEXABRIX contains 393 mg of ioxaglate meglumine, 196 mg of ioxaglate sodium and 0.10 mg edetate calcium disodium as a stabilizer. The solution contains 3.48 mg (0.15 mEq) sodium in each milliliter and provides 32% (320 mg/mL) organically bound iodine.

CONTRAINDICATIONS

HEXABRIX is contraindicated for use in myelography. Refer to PRECAUTIONS concerning hypersensitivity. Hysterosalpingography should not be performed during the menstrual period, in pregnant patients, in patients with known infection in any portion of the genital tract, or in patients in whom cervical conization or curettage has been performed within 30 days. Arthrography should not be performed if infection is present in or near the joint.

WARNINGS

Serious or fatal reactions have been associated with the administration of iodine containing radiopaque media. It is of utmost importance to be completely prepared to treat any contrast medium reaction.

As with any contrast medium, serious neurologic sequelae, including permanent paralysis, can occur following cerebral arteriography, selective spinal arteriography and arteriography of vessels supplying the spinal cord. The injection of a contrast medium should never be made following the administration of vasopressors, since they strongly potentiate neurologic effects.

In patients with subarachnoid hemorrhage, a rare association between contrast administration and clinical deterioration, including convulsions and death, has been reported. Therefore, administration of intravascular iodinated contrast media in these patients should be undertaken with caution.

A definite risk exists in the use of intravascular contrast agents in patients who are known to have multiple myeloma. In such instances anuria has developed, resulting in progressive uremia, renal failure and eventually death. Although neither the contrast agent nor dehydration has separately proved to be the cause of anuria in myeloma, it has been speculated that the combination of both may be a causative factor. The risk in myelomatous patients is not a contraindication to the procedure; however, partial dehydration in the preparation of these patients for the examination is not recommended since this may predispose to precipitation of myeloma protein in the renal tubules. No form of therapy, including dialysis, has been successful in reversing the effect. Myeloma, which occurs most commonly in persons over 40, should be considered before instituting intravascular administration of contrast agents.

Administration of radiopaque materials to patients known or suspected to have pheochromocytoma should be performed with extreme caution. If, in the opinion of the physician, the possible benefits of such procedures outweigh the considered risks, the procedures may be performed; however, the amount of radiopaque medium injected should be kept to an absolute minimum. The blood pressure should be assessed throughout the procedure, and measures for treatment of a hypertensive crisis should be available.

Since intravascular administration of contrast media may promote sickling in individuals who are homozygous for sickle cell disease, fluid restriction is not advised.

In patients with advanced renal disease, iodinated contrast media should be used with caution and only when the need for the examination dictates, since excretion of the medium may be impaired. Patients with combined renal and hepatic disease, those with severe hypertension or congestive heart failure and recent renal transplant recipients present an additional risk.

Renal failure has been reported in patients with liver dysfunction who were given an oral cholecystographic agent followed by an intravascular iodinated radiopaque agent and also in patients with occult renal disease, notably diabetics and hypertensives. In these classes of patients there should be no fluid restriction and every attempt made to maintain normal hydration prior to contrast medium injection, since dehydration is the single most important factor influencing further renal impairment.

Caution should be exercised in performing contrast medium studies in patients with endotoxemia and/or those with elevated body temperatures.

Reports of thyroid storm occurring following the intravascular use of iodinated radiopaque agents in patients with hyperthyroidism or with an autonomously functioning thyroid nodule, suggest that this additional risk be evaluated before use of this drug. Iodine-containing contrast agents may alter the results of thyroid function tests which depend on iodine estimation, e.g., PBI, and may also affect results of radioactive iodine uptake studies. Such tests, if indicated, should be performed prior to the administration of this preparation.

PRECAUTIONS

Diagnostic procedures which involve the use of iodinated intravascular contrast agents should be carried out under the direction of personnel skilled and experienced in the particular procedure to be performed. All procedures utilizing contrast media carry a definite risk of producing adverse reactions. While most reactions are minor, life-threatening and fatal reactions may occur without warning, and this risk must be weighed against the benefit of the procedure. A fully equipped emergency cart, or equivalent supplies and equipment, and personnel competent in recognizing and treating adverse reactions of all types should always be available. If a serious reaction should occur, immediately discontinue administration. Since severe delayed reactions have been known to occur, emergency facilities and competent personnel should be available for at least 30 to 60 minutes after administration. (See ADVERSE REACTIONS.)

Preparatory dehydration is dangerous and may contribute to acute renal failure in infants, young children, the elderly, patients with pre-existing renal insufficiency, patients with multiple myeloma, patients with advanced vascular disease and diabetic patients.

Acute renal failure has been reported in diabetic patients with diabetic nephropathy and in susceptible non-diabetic patients (often elderly with pre-existing renal disease) following the administration of iodinated contrast agents. Therefore, careful consideration of the potential risks should be given before performing this radiographic procedure in these patients.

Severe reactions to contrast media often resemble allergic responses. This has prompted the use of several provocative pretesting methods, none of which can be relied on to predict severe reactions. No conclusive relationship between severe reactions and antigen-antibody reactions or other manifestations of allergy has been established. The possibility of an idiosyncratic reaction in patients who have previously received a contrast medium without ill effect should always be considered. Prior to the injection of any contrast medium, the patient should be questioned to obtain a medical history with emphasis on allergy and hypersensitivity. A positive history of bronchial asthma or allergy (including food), a family history of allergy, or a previous reaction or hypersensitivity to a contrast agent may imply a greater than usual risk. Such a history may be more accurate than pre-testing in predicting the potential for reaction although not necessarily the severity or type of reaction in the individual case. A positive history of this type does not arbitrarily contraindicate the use of a contrast agent when a diagnostic procedure is thought essential, but does call for caution. (See ADVERSE REACTIONS.)

Prophylactic therapy including corticosteroids and antihistamines should be considered for patients who present with a strong allergic history, a previous reaction to a contrast medium, or a positive pre-test since in these patients the incidence of reaction is two to three times that of the general population. Adequate doses of corticosteroids should be started early enough prior to contrast medium injection to be effective and should continue through the time of injection and for 24 hours after injection. Antihistamines should be administered within 30 minutes of the contrast medium injection. Recent reports indicate that such pre-treatment does not prevent serious life-threatening reactions, but may reduce both their incidence and severity. A separate syringe should be used for these injections.

General anesthesia may be indicated in the performance of some procedures in selected patients; however, a higher incidence of adverse reactions has been reported in these patients, and may be attributable to the inability of the patient to identify untoward symptoms or to the hypotensive effect of anesthesia which can prolong the circulation time and increase the duration of contact of the contrast agent.

Angiography should be avoided whenever possible in patients with homocystinuria because of the risk of inducing thrombosis and embolism.

PRECAUTIONS FOR SPECIFIC PROCEDURES

Pediatric Angiocardiography: It is advisable to monitor for ECG and vital signs changes throughout the procedure.

When large individual doses are administered, sufficient time should be allowed for any observed changes to return to or near baseline prior to making the next injection.

Caution should be used when making right heart injections in patients with pulmonary hypertension or incipient heart failure, since this may lead to increased right side pressures with subsequent bradycardia and systemic hypotension. Patients with pulmonary disease present additional risks.

Caution is advised in cyanotic infants since apnea, bradycardia, other arrhythmias and a tendency to acidosis are more likely to occur.

Since infants are more likely to respond with convulsions than are adults, the amount of total dosage is of particular importance. Repeated injections are hazardous in infants weighing less than 7 kg, particularly when these infants have pre-existing compromised right heart function or obliterated pulmonary vascular beds.

Selective Coronary Arteriography with or without left ventriculography: During the administration of large doses of HEXABRIX, continuous monitoring of vital signs is desirable. Caution is advised in the administration of large volumes to patients with incipient heart failure because of the possibility of aggravating the pre-existing condition. Hypotension should be corrected promptly since it may result in serious arrhythmias.

Special care regarding dosage should be observed in patients with right ventricular failure, pulmonary hypertension, or stenotic pulmonary vascular beds because of hemodynamic changes which may occur after injection into the right heart outflow tract.

Peripheral Arteriography: Moderate decreases in blood pressure occur frequently with intra-arterial (brachial) injections. This change is usually transient and requires no treatment; however, the blood pressure should be monitored for approximately ten minutes following injection.

Extreme caution during injection of the contrast agent is necessary to avoid extravasation and fluoroscopy is recommended. This is especially important in patients with severe arterial disease.

Cerebral Angiography: Cerebral angiography should be performed with special caution in patients with advanced arteriosclerosis, severe hypertension, cardiac decompensation, senility, recent cerebral thrombosis or embolism, and migraine.

Intra-Arterial Digital Subtraction Angiography: The risks associated with IA-DSA are those usually attendant with catheter procedures. Following the procedure, gentle pressure hemostasis is required, followed by observation and immobilization of the limb for several hours to prevent hemorrhage from the site of arterial puncture.

Patient motion, including respiration and swallowing, can result in misregistration leading to image degradation and non-diagnostic studies.

Intravenous Digital Subtraction Angiography: The risks associated with IV-DSA include those usually attendant with catheter procedures and include intramural injections, vessel dissection and tissue extravasation. The potential risk is reduced when small test injections of contrast medium are made under fluoroscopic observation to insure that the catheter tip is properly positioned and, in the case of peripheral placement, that the vein is of adequate size.

Patient motion, including respiration and swallowing, can result in misregistration leading to image degradation and non-diagnostic studies.

Peripheral Venography: Special care is required when venography is performed in patients with suspected thrombosis, phlebitis, severe ischemic disease, local infection or a totally obstructed venous system.

Extreme caution during injection of contrast media is necessary to avoid extravasation and fluoroscopy is recommended. This is especially important in patients with severe arterial or venous disease.

Excretory Urography: Infants and small children should not have any fluid restrictions prior to excretory urography. (See WARNINGS and PRECAUTIONS concerning preparatory dehydration.)

Contrast Enhancement in Body Computed Tomography: Patient cooperation is essential since patient motion, including respiration, can markedly affect image quality. The use of an intravascular contrast medium can obscure tumors in patients undergoing CT evaluation of the liver, resulting in a false negative diagnosis. Dynamic CT scanning is the procedure of choice for malignant tumor enhancement.

Arthrography: Strict aseptic technique is required to prevent the introduction of infection. Fluoroscopic control should be used to insure proper introduction of the needle into the synovial space and prevent extracapsular injection. Aspiration of excessive synovial fluid will reduce the pain on injection and prevent the dilution of the contrast agent. It is important that undue pressure not be exerted during the injection.

Hysterosalpingography: Caution should be exercised in patients suspected of having cervical or tubal carcinoma to avoid possible spread of the lesion by the procedure. Delayed onset of pain and fever (1-2 days) may be indicative of pelvic infection.

Carcinogenesis, Mutagenesis, Impairment of Fertility: No long-term animal studies have been performed to evaluate carcinogenic potential. However, animal studies suggest that this drug is not mutagenic and does not affect fertility in males or females.

Pregnancy Category B: Reproduction studies have been performed in rats and rabbits at doses up to two times the maximum adult human dose and have revealed no evidence of impaired fertility or harm to the fetus due to HEXABRIX. There are, however, no adequate and well controlled studies in pregnant women. Because animal reproduction studies are not always predictive of human response, this drug should be used during pregnancy only if clearly needed.

Nursing Mothers: Ioxaglate salts are excreted unchanged in human milk. Because of the potential for adverse effects in nursing infants, bottle feedings should be substituted for breast feedings for 24 hours following the administration of this drug.

Pediatric Use: Safety and effectiveness in children has been established in pediatric angiocardiography and intravenous excretory urography. Data have not been submitted to support the safety and effectiveness of HEXABRIX in any other indication. (Precautions for specific procedures receive comment under that procedure.)

ADVERSE REACTIONS

Adverse reactions to injectable contrast media fall into two categories: chemotoxic reactions and idiosyncratic reactions.

Chemotoxic reactions result from the physiochemical properties of the contrast media, the dose and the speed of injection. All hemodynamic disturbances and injuries to organs or vessels perfused by the contrast medium are included in this category.

Idiosyncratic reactions include all other reactions. They occur more frequently in patients 20 to 40 years old. Idiosyncratic reactions may or may not be dependent on the dose injected, the speed of injection, the mode of injection and the radiographic procedure. Idiosyncratic reactions are subdivided into minor, intermediate and severe. The minor reactions are self-limited and of short duration; the severe reactions are life-threatening and treatment is urgent and mandatory.

NOTE: Not all of the following adverse reactions have been reported with HEXABRIX. Because HEXABRIX is an iodinated intravascular contrast agent, all of the side effects and toxicity associated with agents of this class are theoretically possible, and this should be borne in mind when HEXABRIX is administered.

Severe, life-threatening anaphylactoid reactions, mostly of cardiovascular origin, have occurred following the administration of HEXABRIX as well as other iodine-containing contrast agents. Most deaths occur during injection or 5 to 10 minutes later, the main feature being cardiac arrest with cardiovascular disease as the main aggravating factor. Isolated reports of hypotensive collapse and shock are found in the literature. Based upon clinical literature, reported deaths from the administration of conventional iodinated contrast agents range from 6.6 per 1 million (0.00066 percent) to 1 in 10,000 patients (0.01 percent).

Regardless of the contrast agent employed, the overall estimated incidence of serious adverse reactions is higher with coronary arteriography than with other procedures. Cardiac decompensation, serious arrhythmias, or myocardial ischemia or infarction may occur during coronary arteriography and left ventriculography.

The most frequent adverse reactions are nausea, vomiting, facial flush and a feeling of body warmth. These are usually of brief duration. In double-blind clinical trials, HEXABRIX produced less discomfort upon injection (pain and heat) when compared to various other contrast agents. Other reactions include the following:

Hypersensitivity reactions: Dermal manifestations of urticaria with or without pruritus, erythema and maculopapular rash. Dry mouth. Sweating. Conjunctival symptoms. Facial, peripheral and angioneurotic edema. Symptoms related to the respiratory system include sneezing, nasal stuffiness, coughing, choking, dyspnea, chest tightness and wheezing, which may be initial manifestations of more severe and infrequent reactions including asthmatic attack, laryngospasm and bronchospasm with or without edema, pulmonary edema, apnea and cyanosis. Rarely, these allergic-type reactions can progress into anaphylaxis with loss of consciousness, coma, severe cardiovascular disturbances, and death.

Cardiovascular reactions: Generalized vasodilation, flushing and venospasm. Occasionally thrombosis or, rarely, thrombophlebitis. Extremely rare cases of disseminated intravascular coagulation resulting in death have been reported. Severe cardiovascular responses include rare cases of hypotensive shock, coronary insufficiency, cardiac arrhythmia, fibrillation and arrest. These severe reactions are usually reversible with prompt and appropriate management; however, fatalities have occurred.

Technique reactions: Extravasation with burning pain, hematomas, ecchymosis and tissue necrosis, vascular constriction due to injection rate, thrombosis and thrombophlebitis.

Neurological reactions: Spasm, convulsions, aphasia, syncope, paresis, paralysis resulting from spinal cord injury and pathology associated with the syndrome of transverse myelitis, visual field losses which are usually transient but may be permanent, coma and death.

Other reactions: Headache, trembling, shaking, chills without fever, hyperthermia and lightheadedness. Temporary renal shutdown or other nephropathy.

Pediatric angiocardiography has been complicated by intramural injection with marked adverse effects on cardiac function.

During selective coronary arteriography with or without left ventriculography, patients may have clinically insignificant ECG changes. The following adverse effects have occurred in conjunction with the administration of iodinated intravascular contrast agents for this procedure: hypotension, shock, anginal pain, myocardial infarction, cardiac arrhythmias (bradycardia, ventricular tachycardia, ventricular fibrillation) and cardiac arrest. Fatalities have been reported. Complications to the procedure include dissection of coronary arteries, dislodgement of atheromatous plaques, perforation, hemorrhage and thrombosis.

Following peripheral arteriography, hemorrhage and thrombosis have occurred at the puncture site of the percutaneous injection. Brachial plexus injury has been reported following axillary artery injection.

The major causes of cerebral arteriographic adverse reactions appear to be repeated injections of the contrast material, administration of doses higher than those recommended, the presence of occlusive atherosclerotic vascular disease and the method and technique of injection. Adverse reactions are normally mild and transient. A feeling of warmth in the face and neck is frequently experienced. Infrequently, a more severe burning discomfort is observed. Transient visual hallucinations have been reported. Serious neurological reactions that have been associated with cerebral angiography and not listed under Adverse Reactions include stroke, amnesia and respiratory difficulties. Visual field defects with anopsia and reversible neurological deficit lasting from 24 hours to 48 hours have been reported. Confusion, disorientation with hallucination, and absence of vision sometimes lasting for one week have also been reported. Cardiovascular reactions that may occur with some frequency are bradycardia and either an increase or decrease in systemic blood pressure. The blood pressure change is transient and usually requires no treatment. Arthrography may induce joint pain or discomfort which is usually mild and transient but occasionally may be severe and persist for 24 to 48 hours following the procedure. Effusion requiring aspiration may occur in patients with rheumatoid arthritis. Fever and pain, cramping and tenderness of the abdomen have been reported following hysterosalpingography.

OVERDOSAGE

Overdosages may occur. The adverse effects of overdosage are life-threatening and affect mainly the pulmonary and cardiovascular systems. The symptoms may include cyanosis, bradycardia, acidosis, pulmonary hemorrhage, convulsions, coma and cardiac arrest. Treatment of an overdose is directed toward the support of all vital functions and prompt institution of symptomatic therapy.

Ioxaglate salts are dialyzable.

The intravenous LD_{50} values of HEXABRIX (in grams of iodine/kilogram body weight) were 11.2 g/kg in mice, >8 g/kg in rats, >6.4 g/kg in rabbits and >10.2 g/kg in dogs.

DOSAGE AND ADMINISTRATION

Details on dosage are provided in the package insert. *CONSULT FULL PACKAGE INSERT BEFORE USE.*

Rev. Jan. 1987

References

1. Schwarten D: Data on file, Mallinckrodt.

2. Murphy WA: Data on file, Mallinckrodt.

3. Mosier LD, Joist JH, et al: In vitro effects of ionic and nonionic contrast media on coagulation, platelet function and fibrinolysis. Presented at the 73rd Meeting of The Radiological Society of North America, Chicago, IL, Nov 30, 1987.

4. Engelhart JA, Smith D, Bull BS, et al: Aspirated blood and low-osmolality contrast agents: An embolic hazard? Presented at the 73rd Meeting of The Radiological Society of North America, Chicago, IL, Dec 1, 1987.

MALLINCKRODT®

Changing the look of medicine.

Diagnostic Products Division
Mallinckrodt, Inc.
Post Office Box 5840
St. Louis, MO 63134

For orders, medical and/or professional assistance call (800) 325-3688 TOLL FREE

©1987 Mallinckrodt, Inc. MLK 5882 †Licensed by Guerbet, S.A. Registered U.S. Patent and Trademark Office. MI22248

AJR: The 50 Most Frequently Cited Papers in the Past 50 Years

Felix S. Chew[1]

Radiology is a practical, technology-based specialty of medicine. Since its inception in 1895 with Röntgen's discovery of X-rays, the growth and development of radiology have paralleled the rise of Western medicine. To the extent that radiology has permitted a better understanding of normal and pathologic gross anatomy and, in many instances normal and abnormal physiology in living patients, its contributions have pervaded and transformed all of medicine. Research in radiology not only looks to improve the mundane tasks of interpreting the shadows and diagnosing disease but also seeks new knowledge in medicine for its own sake, not necessarily by using only radiologic means. The trail of progress can be followed in the scientific literature. In this paper, some of the most influential articles published in *AJR. American Journal of Roentgenology* in the past 50 years are listed and examined from current and historical perspectives. This undertaking helps provide an appreciation for the dynamics of radiologic knowledge and gives context to daily clinical practice.

The 50 Most Frequently Cited Papers Published in the *AJR*

The 50 articles published in the *AJR* that have been cited most frequently in the literature in the years from 1955 to 1986 were identified by searching the computerized data base of the *Science Citation Index*® (Institute for Scientific Information, Philadelphia, PA). This data base did not cover the years before 1955 at the time of the search, and the resulting selection therefore is biased in favor of more recent articles and excludes many older articles of unquestioned importance and influence. Using frequency of citation as the selection criterion also favors selection of more recent articles because of the continual growth in the size of the literature (more articles mean more citations). A citation is the event that occurs when one scientific article (the citing article) uses another (the cited article) as a reference. The *Science Citation Index*® is an ordered listing of cited articles published in scientific journals. The cited articles are listed with their citing articles. A citation indicates that the cited article had relevance to the research reported in the citing article and suggests a close link in the subject material. Citation behavior on the part of authors has been studied inconclusively many times [1]. It seems best to think of it as a phenomenon of the marketplace in which many diverse reasons exist for citing specific articles at particular times. Some of these reasons appear to be idiosyncratic; others relate to the quality and perceived significance of the cited articles [1]. By looking at current citations, it is possible to identify articles published in the past that have influenced current research.

The 50 articles published by *AJR* that received the most citations from 1955 to 1986 are listed in Table 1. The dates of publication range from 1939 to 1982 (Fig. 1). Grant support of some type, either for the research itself or for at least one of the researchers, was mentioned by the authors of 15 of the 50 articles. Twenty-three articles were presented at scientific meetings before they were published.

Received September 1, 1987; accepted after revision October 19, 1987.

[1] Department of Radiology, State University of New York, Health Science Center at Syracuse, 750 E. Adams St., Syracuse, NY 13210. Address reprint requests to F. S. Chew.

AJR 150:227–233, February 1988
0361–803X/88/1502–0227
© American Roentgen Ray Society

TABLE 1: The 50 Papers Published in the *American Journal of Roentgenology* That Were Cited Most Frequently in the Years 1955–1986

1. Collins VP, Loeffler RK, Tivey H. Observations on growth rates of human tumors. *Am J Roentgenol Radium Ther Nucl Med* **1956**;76:988–1000
2. Bydder GM, Steiner RE, Young IR, Hall AS, Thomas DJ, Marshall J. Pallis CA, Legg NJ. Clinical NMR imaging of the brain: 140 cases. *AJR* **1982**;139:215–236
3. Peters MV, Middlemiss KCH. A study of Hodgkin's disease treated by irradiation. *Am J Roentgenol Radium Ther Nucl Med* **1958**;79:114–121
4. Stanley RJ, Sagel SS, Levitt RG. Computed tomography of the body: early trends in application and accuracy of the method. *AJR* **1976**;127:53–67
5. Peters MV. A study of survivals in Hodgkin's disease treated radiologically. *Am J Roentgenol Radium Ther* **1950**;63:299–311
6. Gianturco, C, Anderson JH, Wallace S. Mechanical devices for arterial occlusion. *Am J Roentgenol Radium Ther Nucl Med* **1975**;124:428–435
7. Sheedy PF, Stephens DH, Hattery RR, Muhm JR, Hartman GW. Computed tomography of the body: initial clinical trial with the EMI prototype. *AJR* **1976**;127:23–51
8. Bloom HJG, Wallace ENK, Henk JM. The treatment and prognosis of medulloblastoma in children: a study of 82 verified cases. *Am J Roentgenol Radium Ther Nucl Med* **1969**;105:43–62
9. Vezina JL, Sutton TJ. Prolactin-secreting pituitary microadenomas: roentgenologic diagnosis. *Am J Roentgenol Radium Ther Nucl Med* **1974**;120:46–54
10. Lasser EC, Farr RS, Fujimagari T, Tripp WN. The significance of protein binding of contrast media in roentgen diagnosis. *Am J Roentgenol Radium Ther Nucl Med* **1962**;87:338–360
11. Meaney TF, Weinstein MA, Buonocore E, Pavlicek W, Borkowski GP, Gallagher JH, Sufka B, MacIntyre WJ. Digital subtraction angiography of the human cardiovascular system. *AJR* **1980**;135:1153–1160
12. Robb GP, Steinberg I. Visualization of the chambers of the heart, the pulmonary circulation, and the great blood vessels in man: a practical method. *Am J Roentgenol Radium Ther* **1939**;41:1–17
13. DiChiro G, Nelson KB. The volume of the sella turcica. *Am J Roentgenol Radium Ther Nucl Med* **1962**;87:989–1008
14. Haaga JR, Alfidi RJ, Havrilla TR, Cooperman AM, Seidelmann FE, Reich NE, Weinstein AJ, Meaney TF. CT detection and aspiration of abdominal abscesses. *AJR* **1977**;128:465–474
15. Grüntzig A, Kumpe DA. Technique of percutaneous transluminal angioplasty with the Grüntzig balloon catheter. *AJR* **1979**;132:547–552
16. Mountain CF, Carr DT, Anderson WAD. A system for the clinical staging of lung cancer. *Am J Roentgenol Radium Ther Nucl Med* **1974**;120:130–138
17. Stephens DH, Sheedy PF, Hattery RR, MacCarty RL. Computed tomography of the liver. *AJR* **1977**;128:579–590
18. Hampton AO, Castleman B. Correlation of postmortem chest teleroentgenograms with autopsy findings: with special reference to pulmonary embolism and infarction. *Am J Roentgenol Radium Ther* **1940**;43:305–326
19. Hicks SP. Developmental malformations produced by radiation: a timetable of their development. *Am J Roentgenol Radium Ther Nucl Med* **1953**;69:272–293
20. Crummy AB, Strother CM, Sackett JF, Ergun DL, Shaw CG, Kruger RA, Mistretta CA, Turnipseed WD, Lieberman RP, Myerowitz PD, Ruzicka FF. Computerized fluoroscopy: digital subtraction for intravenous angiocardiography and arteriography. *AJR* **1980**;135:1131–1140
21. Stone RS. Neutron therapy and specific ionization. *Am J Roentgenol Radium Ther* **1948**;59:771–785
22. Gerzof SG, Robbins AH, Birkett DH, Johnson WC, Pugatch RD, Vincent ME. Percutaneous catheter drainage of abdominal abscesses guided by ultrasound and computed tomography. *AJR* **1979**;133:1–8
23. Caffey J. Multiple fractures in the long bones of infants suffering from chronic subdural hematoma. *Am J Roentgenol Radium Ther* **1946**;56:163–173
24. Ingold JA, Reed GB, Kaplan HS, Bagshaw MA. Radiation hepatitis. *Am J Roentgenol Radium Ther Nucl Med* **1965**;93:200–208
25. Gray LH. Radiobiologic basis of oxygen as a modifying factor in radiation therapy. *Am J Roentgenol Radium Ther Nucl Med* **1961**;85:803–815
26. Schatzki R, Gary JE. Dysphagia due to a diaphragm-like localized narrowing in the distal esophagus ("lower esophageal ring"). *Am J Roentgenol Radium Ther Nucl Med* **1953**;70:911–922
27. Merriam GR Jr, Focht EF. A clinical study of radiation cataracts and the relationship to dose. *Am J Roentgenol Radium Ther Nucl Med* **1957**;77:759–785
28. Weissmann HS, Frank MS, Bernstein LH, Freeman LM. Rapid and accurate diagnosis of acute cholecystitis with ^{99m}Tc-HIDA cholescintigraphy. *AJR* **1979**;132:523–528
29. Shehadi WH. Adverse reactions to intravascularly administered contrast media: a comprehensive study based on a prospective survey. *Am J Roentgenol Radium Ther Nucl Med* **1975**;124:145–152
30. Alfidi RJ, Haaga JR, Havrilla TR, Pepe RG, Cook SA. Computed tomography of the liver. *AJR* **1976**;127:69–74
31. Burhenne HJ. Nonoperative retained biliary tract stone extraction: a new roentgenologic technique. *Am J Roentgenol Radium Ther Nucl Med* **1973**;117:388–399
32. Snow JH Jr, Goldstein HM, Wallace S. Comparison of scintigraphy, sonography, and computed tomography in the evaluation of hepatic neoplasms. *AJR* **1979**;132:915–918
33. Sagerman RH, Cassady JR, Tretter P, Ellsworth RM. Radiation induced neoplasia following external beam therapy for children with retinoblastoma. *Am J Roentgenol Radium Ther Nucl Med* **1969**;105:529–535
34. Wallace S, Gianturco C, Anderson JH, Goldstein HM, Davis LJ, Bree RL. Therapeutic vascular occlusion utilizing steel coil technique: clinical applications. *AJR* **1976**;127:381–387
35. Korobkin M, White EA, Kressel HY, Moss AA, Montagne JP. Computed tomography in the diagnosis of adrenal disease. *AJR* **1979**;132:231–238
36. O'Connor JF, Neuhauser EBD. Total body opacification in conventional and high dose intravenous urography in infancy. *Am J Roentgenol Radium Ther Nucl Med* **1963**;90:63–71
37. Tow DE, Wagner HN Jr, Lopez-Majno V, Smith EM, Migita T. Validity of measuring regional pulmonary arterial blood flow with macroaggregates of human serum albumin. *Am J Roentgenol Radium Ther Nucl Med* **1966**;96:664–676
38. Molnar W, Stockum AE. Relief of obstructive jaundice through percutaneous transhepatic catheter—a new therapeutic method. *Am J Roentgenol Radium Ther Nucl Med* **1974**;122:356–367
39. Wolfe JN. Breast patterns as an index of risk for developing breast cancer. *AJR* **1976**;126:1130–1139
40. Welin S, Youker J, Spratt JS Jr, Linnell F, Spjut HJ, Johnson RE, Ackerman LV. The rates and patterns of growth of 375 tumors of the large intestine and rectum observed serially by double contrast enema study (Malmö technique). *Am J Roentgenol Radium Ther Nucl Med* **1963**;90:673–687
41. Davis KR, Taveras JM, New PFJ, Schnur JA, Roberson GH. Cerebral infarction diagnosis by computerized tomography: analysis and evaluation of findings. *Am J Roentgenol Radium Ther Nucl Med* **1975**;124:643–660
42. Stables DP, Ginsberg NJ, Johnson ML. Percutaneous nephrostomy: a series and review of the literature. *AJR* **1978**;130:75–82

TABLE 1: The 50 Papers Published in the *American Journal of Roentgenology* That Were Cited Most Frequently in the Years 1955–1986 (continued)

43. Taveras JM. Multiple progressive intracranial arterial occlusions: a syndrome of children and young adults. *Am J Roentgenol Radium Ther Nucl Med* **1969**;106:235–268
44. Schaner EG, Chang AE, Doppman JL, Conkle DM, Flye MW, Rosenberg SA. Comparison of computed and conventional whole lung tomography in detecting pulmonary nodules: a prospective radiologic-pathologic study. *AJR* **1978**;131:51–54
45. Lukes RJ. Relationship of histologic features to clinical stages in Hodgkin's disease. *Am J Roentgenol Radium Ther Nucl Med* **1963**;90:944–955
46. Batson OV. The vertebral vein system. *Am J Roentgenol Radium Ther Nucl Med* **1957**;78:195–212
47. Crade M, Taylor KJW, Rosenberg AT, de Graaff CS, Minihan P. Surgical and pathological correlation of cholecystosonography and cholecystography. *AJR* **1978**;131:227–229
48. Dunbar JD, Molnar W, Beman FF, Marable SA. Compression of the celiac trunk and abdominal angina: preliminary report of 15 cases. *Am J Roentgenol Radium Ther Nucl Med* **1965**;95:731–744
49. Silverman FN. The roentgen manifestations of unrecognized skeletal trauma in infants. *Am J Roentgenol Radium Ther Nucl Med* **1953**;69:413–427
50. Ferrucci JT Jr, Wittenberg J, Mueller PR, Simeone JF, Harbin WP, Kirkpatrick RH, Taft PD. Diagnosis of abdominal malignancy by radiologic fine-needle aspiration biopsy. *AJR* **1980**;134:323–330

Note.—Founded in 1906 as the *American Quarterly of Roentgenology*, the following titles for the journal have been in subsequent use: *American Journal of Roentgenology* (vol. 1–9, 1913–1922), *American Journal of Roentgenology and Radium Therapy* (vol. 10–67, 1923–1952), *American Journal of Roentgenology, Radium Therapy and Nuclear Medicine* (vol. 68–125, 1952–1975), and *AJR. American Journal of Roentgenology* (vol. 126–present, 1976–present). Papers are listed in order of decreasing frequency of citation.

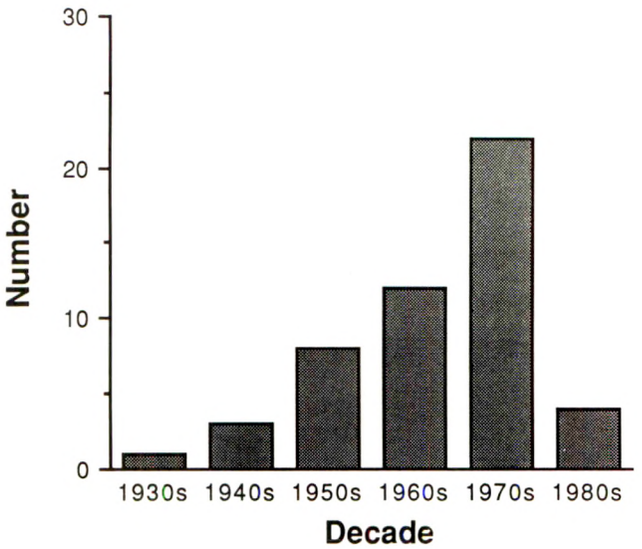

Fig. 1.—Distribution of the 50 most frequently cited papers by publication date.

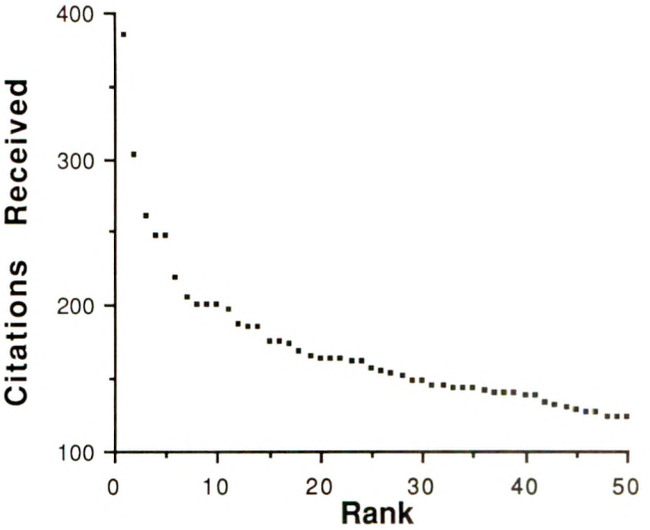

Fig. 2.—Distribution of total citations received among the 50 most frequently cited papers.

The national affiliations of the first authors were the United States in 42, United Kingdom or Canada in three each, and Switzerland or Sweden in one each. The number of citations received from 1955 to 1986 by the individual articles in the group ranged from 123 to 385 (average, 170) (Fig. 2).

Structure of Radiologic Science

The structure of radiologic science as it is applied in response to a problem in imaging and diagnosis can be described as follows. First, a technical advance occurs; this advance makes possible or practical a new method of imaging or intervention. Once the validity of the method has been established, a base of knowledge is developed to guide interpretation of the findings and scope of application. Finally, the mature technique can be used in the general pursuit of new medical knowledge. Most articles in radiologic journals fall along this progression, but with increasing frequency, the basic and engineering research that makes the technical advance possible is published outside the radiologic literature. A less frequent and more erratic event in scientific progress is the establishment of a theoretical basis, or paradigm [2], that provides the context for the orderly process just described.

Cardiac Angiography

Robb and Steinberg [3] published a description of their technique of cardiac angiography in 1939 (Fig. 3A). The

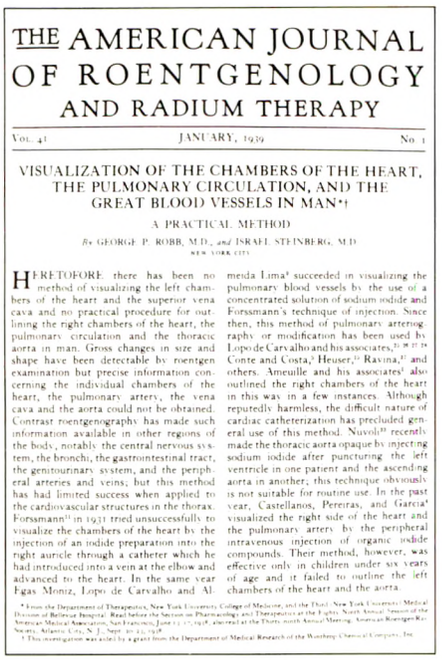

THE AMERICAN JOURNAL OF ROENTGENOLOGY AND RADIUM THERAPY

VOL. 41 JANUARY, 1939 NO. 1

VISUALIZATION OF THE CHAMBERS OF THE HEART, THE PULMONARY CIRCULATION, AND THE GREAT BLOOD VESSELS IN MAN*†

A PRACTICAL METHOD

By GEORGE P. ROBB, M.D., and ISRAEL STEINBERG, M.D.

NEW YORK CITY

A

THE AMERICAN JOURNAL OF ROENTGENOLOGY AND RADIUM THERAPY

VOL. 43 MARCH, 1940 NO. 3

CORRELATION OF POSTMORTEM CHEST TELEROENTGENOGRAMS WITH AUTOPSY FINDINGS

WITH SPECIAL REFERENCE TO PULMONARY EMBOLISM AND INFARCTION*

By AUBREY O. HAMPTON and BENJAMIN CASTLEMAN

B

MULTIPLE FRACTURES IN THE LONG BONES OF INFANTS SUFFERING FROM CHRONIC SUBDURAL HEMATOMA*

By JOHN CAFFEY, M.D.

NEW YORK CITY

C

OBSERVATIONS ON GROWTH RATES OF HUMAN TUMORS*

By VINCENT P. COLLINS, M.D., R. KENNETH LOEFFLER, M.D., and HAROLD TIVEY, M.D.

HOUSTON, TEXAS

D

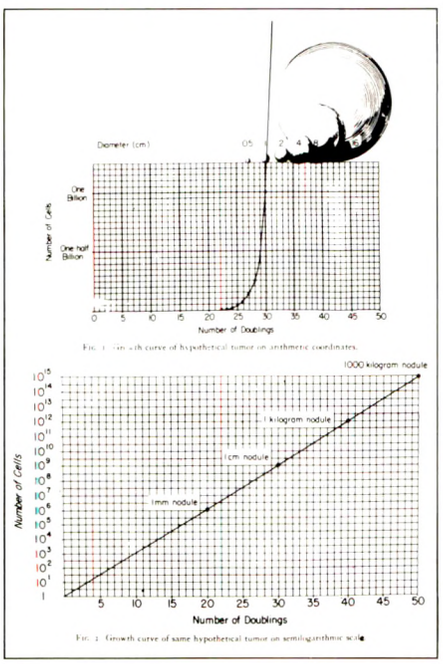

E

Fig. 3.—Samples of the most frequently cited articles published in AJR.

***A*, Cardiac angiography technique of Robb and Steinberg [3].**

***B*, Radiologic-pathologic correlations of pulmonary infarction by Hampton and Castleman [6].**

***C*, Caffey's description of the battered child [7].**

***D* and *E*, Conceptualization of cancer growth rates by Collins, Loeffler, and Tivey [8].**

method consisted of percutaneous placement of a large-bore (12-gauge) needle in the basilic or cephalic vein, rapid injection by hand of radiopaque solution (70% diodrast [3,5-diiodo-4-pyridone-N-acetic acid and diethanolamine]), and carefully timed filming of the subject's chest. Their method provided "information regarding the anatomy and the physiology of the normal and diseased cardiovascular system heretofore unobtainable . . . [opening] a new field for the study of the anatomy and physiology of the circulation." After numerous successful and unsuccessful attempts at improving the method of injection or filming, the method of Robb and Steinberg ultimately was superseded by catheter cineangiocardiography. A resurgence of interest in their work occurred with the advent of IV digital subtraction angiography. In this technique, the large-bore needle is replaced by a plastic catheter, diodrast is replaced by a more dilute and less toxic contrast medium, and the chest films are replaced by computerized fluoroscopy. Citations to the article by Robb and Steinberg virtually had

stopped by 1969, but in the early 1980s, citations started again and rose in parallel with citations to the descriptions of the technique of IV digital subtraction angiography. (The article detailing Seldinger's technique for catheter replacement of the needle in percutaneous angiography, published in *Acta Radiologica* in 1953 [4], is the most frequently cited article ever published in a radiologic journal [5]. *AJR* republished Seldinger's article in 1983, on the 30th anniversary of its original publication.)

Hampton's Hump

Hampton and Castleman [6] published in 1940 the classic work on radiologic-pathologic correlation of pulmonary infarction (Fig. 3B). At postmortem examination, they suspended cadavers vertically with ropes under the arms and a leather harness (canvas was insufficiently sturdy) around the neck and obtained posteroanterior and lateral chest films from a 7-ft. (2.13-m) distance. Subsequently, the lungs and airways were removed intact, inflated with a formalin fixative instilled by gravity, and allowed to fix for 1 week submerged in a bucket of additional fixative. Then, the lung was sectioned, and the radiologist and the pathologist attempted to correlate the findings. Although a detailed enough description of this method was provided so that the article might be considered a "technique article," it continued on with a radiologic-pathologic study of pulmonary infarction. The authors described the gross and microscopic pathologic changes and their evolution with time, parenthetically including the results of some animal work. They described and correlated the radiologic findings, including an explanation of "a convex, slightly irregular 'hump'-shaped shadow," which has become known as Hampton's hump. Further correlation of the radiologic and pathologic findings with clinical findings established the lack of reliable diagnostic clinical signs or symptoms and emphasized that the prevalence of fatal pulmonary infarction was higher than generally appreciated, especially in nonsurgical and noncardiac patients. It had been held previously that pulmonary embolism occurred almost exclusively in cardiac and postsurgical patients. Hampton and Castleman concluded that "an accurate diagnosis of pulmonary infarction is very important because unless proper treatment is carried out the patient may have a fatal embolus." Although angiography and radionuclide scanning have improved the ability to diagnose pulmonary embolism and pulmonary infarction, it remains a perplexing clinical and radiologic problem. The article by Hampton and Castleman continues to receive citations every year.

Pathologic and anatomic verification of the shadows seen on films is fundamental to advancement of the cognitive aspect of radiology. By having the interpretation of images firmly secured in anatomy, pathology, and physiology, radiologists avoid the unchecked flight of diagnostic fancy.

The Battered Child

In 1946 Caffey [7] reported six cases of infants with convulsions and chronic subdural hematomas who also had multiple unexplained long-bone fractures of different ages, for which history of trauma was denied by parents (Fig. 3C). On the basis of radiologic appearances, Caffey then eliminated various potential causes for the fractures and settled on trauma as the proximal cause. The lack of radiologic signs of preexisting general or localized skeletal disease that would predispose to pathologic fracture was key to this conclusion. Although Caffey did not define all of the particulars of the battered child syndrome, or even mention the phrase, his contribution was the conceptual link between the chronic head trauma and the unexplained injuries of the extremities. His conclusion left a clear direction for the researchers who followed: "The injuries which caused the fractures in the long bones of these patients were either not observed or were denied when observed. The motive for denial has not been established." Caffey's article has been cited an average of 6.2 times every year for the past quarter century, including six times in 1986, 40 years after its publication.

The Collins Rule

Collins and coworkers at Baylor University published their "Observations on Growth Rates of Human Tumors" in 1956 [8]; this article has become the most frequently cited article every published in *AJR* (Figs. 3D and 3E). Making the basic assumption that cancer begins with a single malignant cell that divides at a fixed rate, they described the growth of human tumors as a doubling process. This theoretical construct was applied to observations of the growth of pulmonary metastases and of Wilms tumors and led to the derivation of a new intellectual framework for thinking about the diagnosis and management of cancer. If the rate of doubling remained constant, then the gain in tumor volume would increase at an exponential rate, explaining how "cancer cells could increase at a steady rate for a large period of time and then, without change in rate, appear to burgeon in sudden growth." The conceptualization of Collins et al. indicated that clinical diagnosis is a late event in the natural course of cancer and exposed the inadequacy of then-existing clinical concepts of early diagnosis. As a corollary to their analysis of doubling rates of Wilms tumors, they suggested that before a cure could be claimed, follow-up of patients treated for Wilms tumors was necessary for a length of time equal to the age of the patient at diagnosis plus 9 months. This has become known as the Collins rule and still retains its validity and clinical usefulness. Of wider import was the concept that different tumors required different lengths of follow-up. The article by Collins et al. has been cited steadily since publication, including 10 citations in 1986.

Body CT and MR Imaging

The first clinical application of CT was to the brain, where physiologic motion did not interfere with the long scan time of several minutes per slice. CT scanners with apertures large enough for the whole body appeared in 1974, but scan times were still too long to avoid blurring from respiration and peristalsis. In October 1975, prototypes of an EMI general-

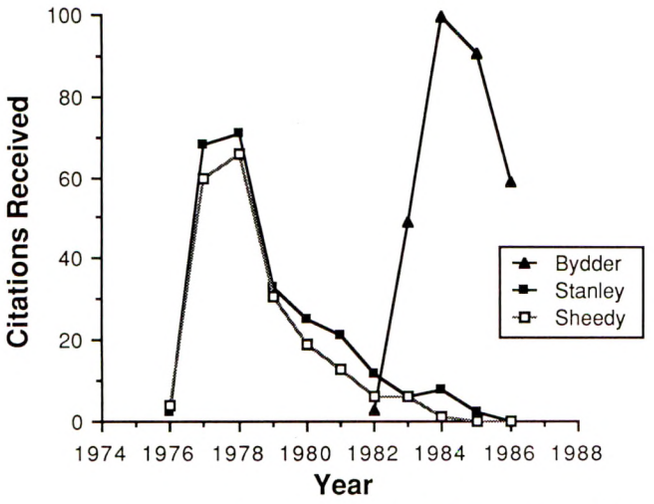

Fig. 4.—Year-by-year citations to papers describing the first clinical trials of new imaging devices: body CT (Stanley et al. [9] and Sheedy et al. [10]) and MR imaging of the brain (Bydder et al. [13]). Vertical axis shows number of citations received by papers in the individual years indicated on horizontal axis.

purpose CT scanner with a 20-sec scan time were set up at the Mallinckrodt Institute of Radiology (St. Louis, MO) and the Mayo Clinic (Rochester, MN) for clinical trials. The articles by Stanley et al. [9] and Sheedy et al. [10] described the results of those trials. Preliminary reports had been published a few months earlier in *Radiology*, after scientific presentations to packed houses at the annual meeting of the Radiological Society of North America in November 1975. Both groups confirmed the diagnostic potential of CT of the abdomen and chest and indicated many areas for further investigation. Written by pioneers in a rapidly expanding field, these articles received an immediate rush of citations as access to CT scanners improved and further research was published. As publications on the use of CT progressed beyond describing incremental technical advances and establishing the validity of various applications, the articles by Stanley et al. and Sheedy et al. became less relevant and citations slowed and stopped (Fig. 4). The assimilation of CT into the clinical practice of radiology occurred in parallel with the publication of research articles concerning CT (Fig. 5), illustrating the interplay in radiology between equipment and research. (Hounsfield's original description of the system of "computerized transverse axial scanning (tomography)," published in the *British Journal of Radiology* in 1973 [11], is the second most frequently cited article ever published in a radiologic journal [12].)

The description of the first clinical trials of MR imaging of the brain was published by Bydder and coworkers at Hammersmith Hospital (London) in 1982 [13]. The pattern of citations to this article appears to be the same as that of the two articles on body CT: a rapid rise followed by a rapid decline. Both the growth of the literature on MR imaging and the dissemination of the equipment have been slower than with CT [14] (Fig. 5).

Conclusions

Radiology advances in many ways, reflecting the diversity of the specialty. Although technical advances have been spectacular and have received the greatest share of attention in the literature, their ultimate significance lies in the way the tools of imaging are applied in the practice of medicine.

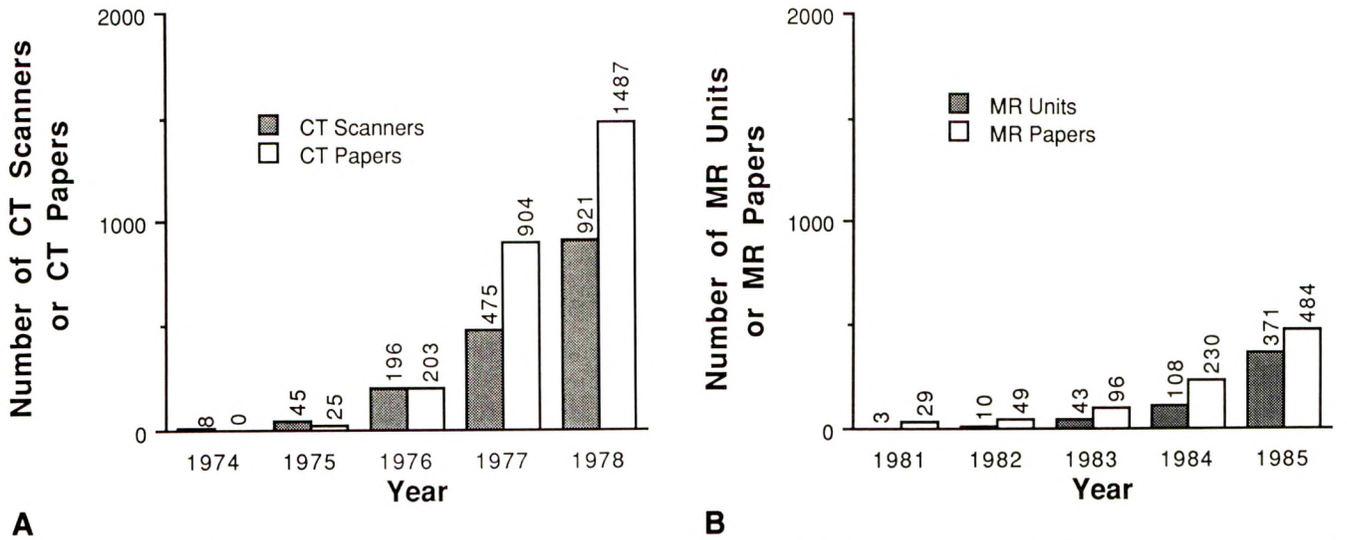

Fig. 5.—Year-by-year publication of papers mentioning new imaging devices in their titles, abstracts, or indexing terms (from a search of MEDLARS that included all journals of medicine and science indexed by the National Library of Medicine, Bethesda, MD) compared with dissemination of the devices themselves [14].

***A*, Cumulative number of installed CT scanners compared with yearly publication of papers concerning CT.**

***B*, Cumulative number of installed MR imagers (units) compared with yearly publication of papers on MR imaging.**

Imaging is one means of acquiring information about patients. With information comes diagnostic precision, and with diagnostic precision comes specific therapy. Imaging is a critical aspect in the modern practice of virtually all fields of medicine, and it has been pivotal in many nonradiologic advances in both diagnosis and management of disease.

Of wider and more enduring significance, perhaps, is the contribution of radiology to the basic understanding of human biology and medicine. Technical advances in radiology may contribute in serendipitous ways. For example, beyond the technical accomplishment of visualization of the interior of the central circulation by simple radiography and the immediate clinical implications of that development, Robb and Steinberg [3] showed the relative safety of the sudden introduction of a huge bolus of foreign matter (contrast material) into the human vasculature and thus launched the angiographic era. Hampton and Castleman [6] used radiology as a tool to study the natural history of a specific disease process, Caffey [7] used radiology to uncover a previously unrecognized syndrome of pathologic social behavior that has implications beyond medicine, and Collins et al. [8] used radiology to make a fundamental observation about tumor biology. The full measure of the contributions of two of radiology's newest tools, CT and MR, has not yet been realized.

ACKNOWLEDGMENTS

The computer searches for citation data were performed by the Institute for Scientific Information®, Philadelphia, PA, under contract. The MEDLARS searches were performed by Jackie Mardikian, SUNY Health Science Center Library, Syracuse, NY. I thank Robert H. Sagerman, Division of Radiation Oncology, and John G. McAfee, Division of Radiological Sciences, SUNY Health Science Center, Syracuse, NY, for their helpful insights.

REFERENCES

1. Cronin B. *The citation process: the role and significance of citations in scientific communication.* London: Taylor Graham, **1984**
2. Kuhn TS. *The structure of scientific revolutions,* 2nd ed., enlarged. Chicago: Univ. of Chicago Press, **1970**
3. Robb GP, Steinberg I. Visualization of the chambers of the heart, the pulmonary circulation, and the great blood vessels in man: a practical method. *Am J Roentgenol Radium Ther* **1939**;41:1–17
4. Seldinger SI. Catheter replacement of the needle in percutaneous arteriography. *Acta Radiol* **1953**;39:368–376
5. Garfield E. The articles most cited in 1961–1982. 2. Another 100 Citation Classics highlight the technology of science. *Curr Contents* **1984**;(29):3–12
6. Hampton AO, Castleman B. Correlation of postmortem chest teleroentgenograms with autopsy findings: with special reference to pulmonary embolism and infarction. *Am J Roentgenol Radium Ther* **1940**;43:305–326
7. Caffey J. Multiple fractures in the long bones of infants suffering from chronic subdural hematoma. *Am J Roentgenol Radium Ther* **1946**;56:163–173
8. Collins VP, Loeffler RK, Tivey H. Observations on growth rates of human tumors. *Am J Roentgenol Radium Ther Nucl Med* **1956**;76:988–1000
9. Stanley RJ, Sagel SS, Levitt RG. Computed tomography of the body: early trends in application and accuracy of the method. *AJR* **1976**;127:53–67
10. Sheedy PF, Stephens DH, Hattery RR, Muhm JR, Hartman GW. Computed tomography of the body: initial clinical trial with the EMI prototype. *AJR* **1976**;127:23–51
11. Hounsfield GN. Computerized transverse axial scanning (tomography). 1. Description of system. *Br J Radiol* **1973**;46:1016–1022
12. Garfield E. The articles most cited in 1961–1982. 10. Another 100 Citation Classics cap the millenary. *Curr Contents* **1986**;(16):3–14
13. Bydder GM, Steiner RE, Young IR, et al. Clinical NMR imaging of the brain: 140 cases. *AJR* **1982**;139:215–236
14. Steinberg EP. The status of MRI in 1986: rates of adoption in the United States and worldwide. AJR **1986**;147:453–455

Book Review

Radiologic-Pathologic Correlation of Musculoskeletal Lesions. by Terry M. Hudson. Baltimore: Williams & Wilkins, 670 pp. 1987. $134.50

This book is intended for all physicians who are interested in musculoskeletal lesions: orthopedic surgeons, radiotherapists, oncologists, radiologists, and pathologists. Its emphasis is the pathologic basis for radiographic images. The extensive material is derived from the author's close association with William F. Enneking, who had a busy referral practice for many years and cared for patients with a wide variety of musculoskeletal diseases.

The gamut of musculoskeletal lesions is covered: benign and malignant bone-forming tumors, benign and malignant cartilage tumors, giant cell tumors, noninfectious granulomas, bone cysts, notochordal remnant tumors, benign fibrous and fibroosseous lesions, malignant fibrous tumors, tumors arising from marrow elements, tibial tumors of unknown origin, tumors arising from vessels, secondary malignant tumors, infections of bones, miscellaneous disorders (Paget disease, bone infarct, some other focal bone lesions), and soft-tissue tumors and related lesions.

Each chapter is written concisely; brief introductory comments are followed by an expansion of the underlying gross and microscopic pathologic changes that dictate the radiologic appearance. The spectrum of radiographic imaging techniques is then presented for each disease: plain radiography, plain tomography, bone scintigraphy, angiography, CT, and, to a lesser extent, MR. A relatively short list includes the major references for the subject of each chapter. The list is followed by beautiful radiologically-pathologically correlated images of the various disease entities.

The textbook is well illustrated. The author typically begins by presenting a classic plain radiograph of the disease under discussion. Where appropriate, nuclear medicine scans, angiograms, CT scans, or MR images are included. Specimen radiography is used liberally. Pathologic support for the radiographic diagnosis is provided by pictures of gross specimens, macroscopic sections, and histologic fields.

A number of the plain radiographs are too light, probably reflecting photographic technique rather than underpenetrated original radiographs. In addition, a number of the images, particularly radiographic images, are displayed in an unusually small format; dimensions of some of these images on the printed page are 2 × 5, 3 × 5, or 4 × 5 cm. This is particularly distracting when the adjacent page has a moderate amount of unused space. The advantage of this format, of course, is to restrict the size of the book, with obvious savings in production costs. I think, however, that this format detracts from the quality of the image and that some potentially valuable information is lost because of this compromise.

The author sometimes uses an excessive amount of labeling in small images, particularly in the case of macroscopic and histologic sections. In addition, he frequently uses two lower-case letters to refer to a single area on an illustration, and the reason for his selection of specific letters is not always apparent. For example, when referring to "pre-existing normal trabeculae," the author uses the label "nb." I think this labeling detracts from the image and makes the legend of the illustration cumbersome.

The author does an excellent job of presenting a logical method of evaluating musculoskeletal lesions. The emphasis is on bone tumors and tumorlike conditions. The exquisite illustrations of pathologic changes enable the physician to acquire a better appreciation for why a radiographic image assumes a particular configuration. Clearly, this is the definitive book dealing with the important concept of radiologic-pathologic correlation of musculoskeletal lesions. This book should be available in the library of all radiology residency programs. I wholeheartedly recommend this book to any physician who is interested in musculoskeletal tumors.

Richard P. Moser, Jr.
Armed Forces Institute of Pathology
Washington, DC 20306-6000

AUGUST, 1943

MONO-OSTEITIC PAGET'S DISEASE AS A CLINICAL ENTITY

ROENTGENOLOGIC OBSERVATIONS IN NINE CASES

By J. A. GROH, M.D.
Department of Roentgenology, Lutheran Hospital
CLEVELAND, OHIO

OUT of a chaos of chronic deforming osteodystrophies, osteomalacias, and osteosarcomas, Sir James Paget selected a certain type of osteitis deformans to clarify this vast group of deforming bone diseases. His classical description was the first step toward a better understanding of the disease which now bears his name. Paget dealt only with the generalized deforming osteitis, even though there were occasional case reports of singular bone lesions of the same type, which appeared not to fall into his group of osteitis deformans.

A typical example quoted by contraverts of mono-osteitic Paget's disease is a case report by Benno Schmidt, in 1874, of a pharmacist, aged fifty-six, with a saber-shin deformity which was thought at first to be a bone sarcoma and which extended to the opposite tibia and femur three years later.

In 1883 Bowlby reported a case of a cab driver with osteitis deformans of the tibia and progressive bowing for over thirty years. There was no extension of the process to other bones of the skeleton. The patient died from an injury to his head.

After the roentgen ray began to be employed, the problem became more complicated. Indistinct single bone lesions could be seen in the spine where biopsies were impossible. Discussions of such cases filled the literature. The affected vertebrae appeared denser on the roentgenogram, and therefore such terms as "vertebrae noire" or "ivory vertebrae" were used, even though they expressed no disease entity but only an anatomic-pathologic description. Although Schmorl reported a biopsied case of a single bone lesion in a tibia as early as 1905, other mono-osteitic cases were still labelled "hereditary lues," "parakanzer," "localized osteomalacia," and "osteomalacia chronica deformans hypertrophica."

I would like to quote Hallermann for his complete and concise definition of osteitis deformans:

> Paget's disease is a specific, mild disease, without known etiology, which involves one or more bones and parts of bones, characterized by a constant structural change, bone resorption, and regeneration within the bone involved, leading to a secondary medullary fibrosis.

In 1931, Schmorl published all his available data on this subject. He gave a detailed pathologic picture, especially in the gross specimen. His descriptive term "mosaic structure" has done much to differentiate this disease from other similar bone diseases. Schmorl accepted the mono-osteitic form of Paget's disease as an entity, as did Hurwitz and Carr in 1913, but he did not agree that it is a rare finding as stated by these authors. Schmorl, in his observations of 4,603 spines, found the single lesion more frequently than the polyosteitic form. He also stated its most frequent site to be the spinal column. Our observations have been in accordance with his findings, even to the extent of demonstrating two distinct types of Paget's disease in a vertebral body. We found the single bone lesion much more frequently than the polyosteitic form. (Five of our 9 mono-osteitic cases have been seen in this office during three years, and in the same interval only 2 polyosteitic cases were observed.) In 6 of our cases the spine was the most frequent site of involvement (66 per cent).

REPORT OF CASES

CASE 1. T. M., male, aged fifty-five, was first

This paper is reprinted verbatim from *AJR* 1943;50:230–243.

seen on December 18, 1931, with a history of a fall in June, 1931, and pain on shoulder abduction of five days' duration. Previous roentgen and physical examinations were negative. Although light treatments and aspirin gave no relief, his symptoms subsided under diathermy. There were no complaints referable to his legs.

He returned in July, 1933, complaining of calluses on his feet. At that time he had marked bilateral hallux valgus and relaxed arches, and note was made of a thickening of the left tibia. On August 14, 1933, he returned for a check-up before operation for correction of the hallux valgus and relaxed arches. Full length films of the left tibia and fibula showed a disrupted coarse, dense trabeculation of the medulla, thickening of the cortex, and anterior bowing of the shaft. The other tibia was normal. Skull, spine, pelvis, chest and extremities were roentgenographed and no areas of involvement found. This patient had never complained of his leg, and the deformity was an incidental finding. He dated the bowing back sixteen years and attributed it to constant trauma at the rolling mill in which he was employed (Fig. 1).

The urine and blood pictures were normal. The blood Wassermann reaction was negative. The blood calcium was 12.4 mg. per 100 cc., blood phosphorus 3.9 mg. per 100 cc., and serum phosphatase 8.8 units (Roberts).

He was seen again in October, 1934, having no complaints referable to the left leg. Roentgen examination of the skull, pelvis, spine and extremities was again negative. The lesion in the left tibia showed no change. The transverse radiant lines in the anterior cortex, representing so-called "umbau" zones of Looser, were found to be the same in number as on previous examination.

CASE II. J. S., male, aged forty-four, was first seen on December 1, 1930, complaining of nasal polypi, which were removed. On November 23, 1931, he returned complaining of low back pain of two days' duration. After a roentgen examination which revealed a localized pathologic process in the second lumbar vertebra (Fig. 2 and 3), he was admitted to the hospital.

There was no history of trauma. The pain had appeared suddenly and was severe enough to keep him awake at night. It was spasmodic in character, at just about the level of the iliac crests. It was associated with every spinal motion, was always localized, and did not radiate. When motionless there was no pain. The patient

FIG. 1. Case I. Anteroposterior and lateral views of the left tibia and fibula showing the typical structural changes of osteitis deformans in the tibia. Note "umbau" zones in the anterior cortex.

had no other complaints. In 1918 he had pneumonia and an unexplained edema of both legs, without fever, pain, phlebitis, or cardiac symptoms. A left varicocele was removed twenty-six years previously. He had fractured his right tibia in 1923 and his right wrist in 1929. The family history was negative.

Palpation of the spine revealed slight prominence of the second lumbar vertebra with tenderness on pressure. There was muscle spasm, hyperesthesia, and pain associated with every spine motion. The left sacrospinalis muscle group was larger and more prominent than the right. Neurologic and other physical examination was negative; laboratory findings were normal.

Roentgen examination showed an increased density of the second lumbar vertebra involving all of its processes. The body projected anteriorly and posteriorly beyond the normal spinal curvature. Its outline was not as sharp as its neighbors, and trabeculations were widely spaced and coarser than normal. The cortex was thicker than normal, encroaching on the medullary portion of the body. Other bones and skull showed no abnormal roentgen findings.

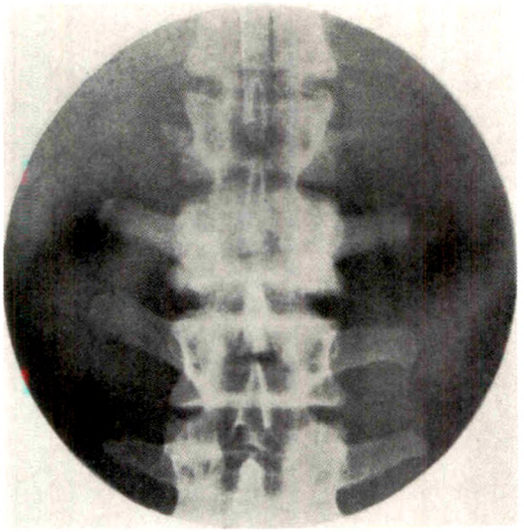

FIG. 2. Case II. Anteroposterior view of the lumbar spine localized over the second lumbar body. Thia centrum is enlarged in all diameters, showing o decisive increase in density, especially confined te the inferior and superior articulating plates. Thers is some rarefaction in the body of the centrum. Trabeculations are coarse, running roughly parallel in a vertical direction. Lamina and processes are involved by the same process.

The patient refused to wear a brace. He signed a release and left the hospital before any specific treatment could be advised.

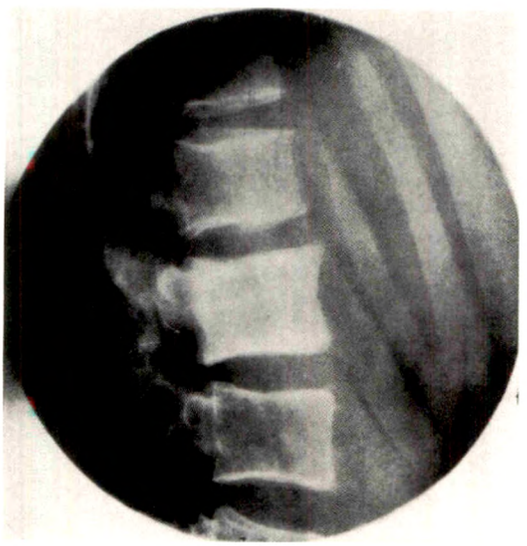

FIG. 3. Case II. Lateral view of the same case as in Figure 2, emphasizing the cortical thickening.

He returned on September 17, 1931, and again on November 25, 1933, presenting the same roentgen findings as before (Fig. 4). The skin over the second lumbar vertebra was reddened, but there was no definite tenderness. There was still spasm and hyperesthesia with motion. The neurologic examination at this time showed decreased sensation to touch and temperature over areas supplied by the first, second, and third lumbar vertebral segments, with increased spontaneous pain over these areas. There was no motor involvement. The reflexes were physiologic. The white blood count was 12,300, with a normal differential count.

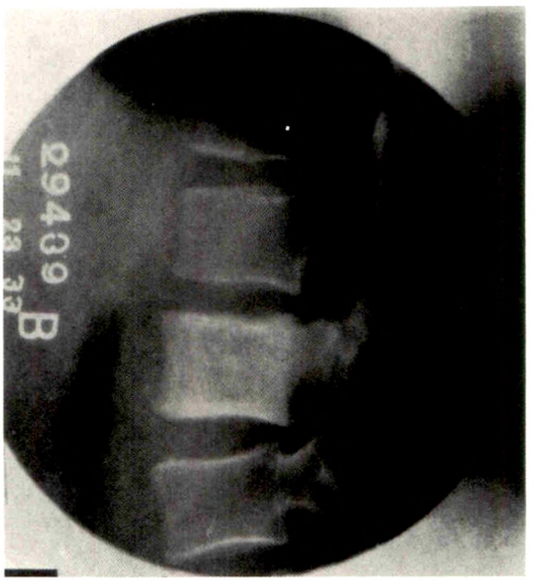

FIG. 4. Case II. Lateral view of the second lumbar vertebra in 1933 showing no change in its appearance over a period of two years.

Hemoglobin was 100 per cent. The smear was normal. The Wassermann and Kline reactions were 1 plus. Serum calcium was 9.5 mg. per 100 cc., serum phosphorus 3.9 mg. per 100 cc., and serum phosphatase 4.7 Roberts units.

The man was unable to work. He had become irritable and stated that his pain was the cause of this condition. He returned to the roentgen department on February 4, 1935. The second lumbar vertebra showed no roentgenographic change since the first examination in 1931. The skull, pelvis, other vertebrae, spine, and both tibiae were again normal.

On February 2, 1938, the patient was examined elsewhere for a low back pain, and

roentgenograms were taken of the lower spine. These came to my attention, and I recognized the patient's name and the appearance of the second lumbar body. There was no change since the earliest examination seven years before (Fig. 5 and 6).

CASE III. B. T., male, aged fifty-five, was seen in November, 1927. He complained of extreme backache over the lower lumbar region of eleven months' duration, loss of appetite, a tired feeling, and incontinence of urine. The family history was negative. His past history revealed an uncomplicated typhoid fever in early life.

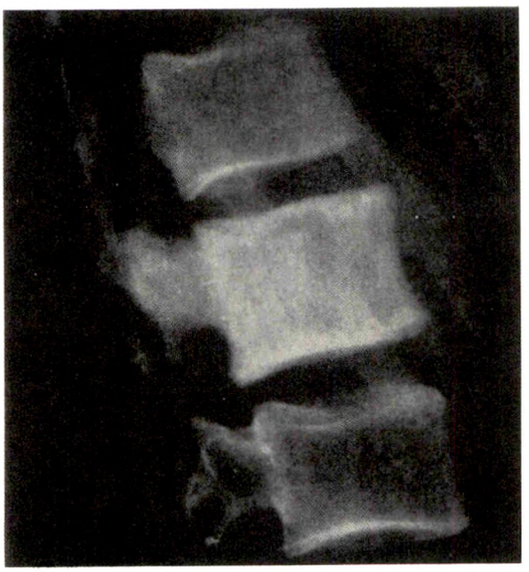

FIG. 5. Case II. A check-up view in 1938, showing no change in the appearance of the second lumbar body.

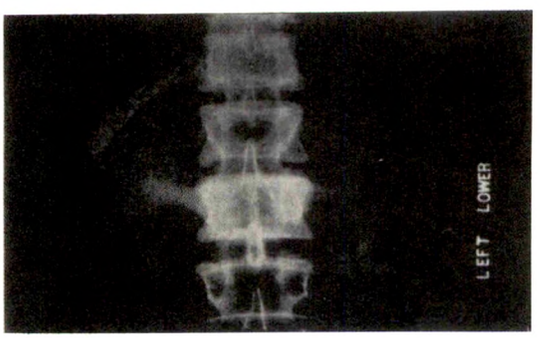

FIG. 6. Case II. Lateral view check-up in 1938. No change of structure since 1931.

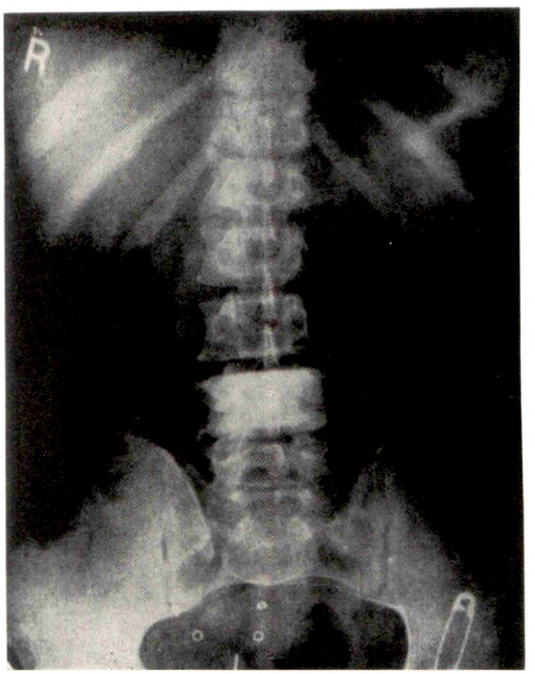

FIG. 7. Case III. Anteroposterior view of lower half of the spine including the sacrum showing the dense irregular, enlarged fourth lumbar body. Its trabeculations cannot be made out. The density is of an even character in comparison to the blotchy type of increased density seen in metastatic carcinoma.

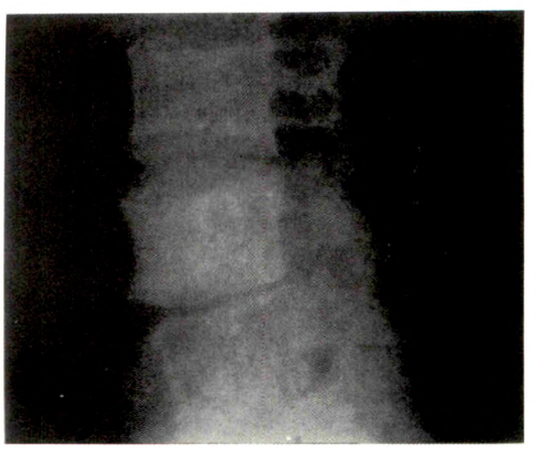

FIG. 8. Case III. Lateral view.

Physical examination revealed a well developed, well nourished male, not acutely ill, with a flaccid paraplegia of the lower limbs. He presented the picture of cardiac decompensation, although little could be elicited by chest

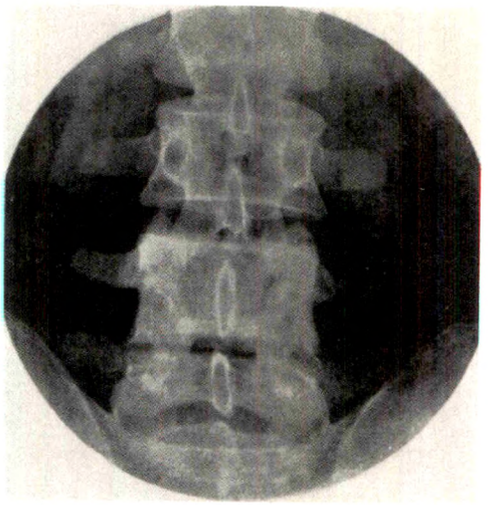

FIG. 9. Case IV. Anteroposterior view of the mid-lumbar section showing the same typical findings in the fourth lumbar as in the previous case. The cortical calcification and thickening are not as pronounced as in the other cases.

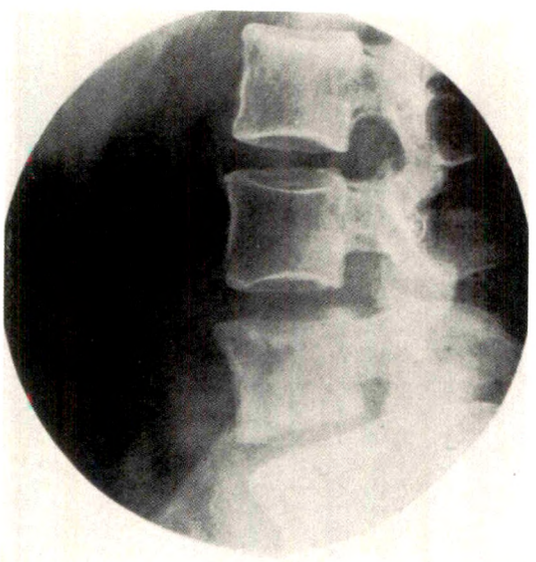

FIG. 10. Case IV. Lateral view of the fourth lumbar vertebra in the same case as in Figure 9.

examination. There was edema of the lower limbs, penis and scrotum. The prostate was enlarged. There were no palpable glandular enlargements. His temperature was normal.

Albumin was present in the urine. Roentgenograms of the lumbar spine showed a dense, irregularly outlined, nodular change in the fourth lumbar vertebra. The body projected forward and laterally beyond the normal spinal curvature and was so dense that no trabeculations were visible. The intervertebral spaces were well maintained. The lamina showed definite involvement by the same sclerosing process (Fig. 7 and 8). The patient returned about two months later for roentgen examination of the entire skeletal system. Skull, pelvis, other vertebrae and the long bones showed no abnormality. The lesion in the fourth lumbar vertebra appeared the same as previously. The patient's illness became rapidly worse, and he died shortly afterward. An autopsy was not obtained.

CASE IV. A. L., male, aged fifty-seven, complained of "indigestion" and upper right quadrant pain, coming in severe attacks beginning in July, 1936. His past history was irrelevant. There were no other systemic disturbances. The physical examination revealed nothing significant.

A cholecystogram showed stones and a poorly functioning gallbladder, and revealed that the fourth lumbar vertebra was considerably increased in density in comparison with the neighboring bodies. Trabeculation was pronounced, mainly cortical, and the trabeculae appeared to be parallel. The cortex of the body was denser than usual. The lateral diameter was increased, and the body projected slightly beyond the normal anterior and posterior curvatures of the lumbar spine.

The blood Wassermann reaction was negative, blood calcium was 11.1 mg. per 100 cc., blood phosphorus 3.0 mg. per 100 cc., and the serum phosphatase was 12.15 Roberts units. The blood smear was normal. The patient specifically denied any vague back pain or discomfort. A checkup of the entire skeletal system on January 21, 1938, showed no other bone involvement, and the appearance of the fourth lumbar body had not changed at all. The blood calcium was elevated to 12.4 mg. per 100 cc. and the blood phosphorus was 3.65 mg. per 100 cc. at the time of the last visit (Fig. 9 and 10).

CASE V. J. C., male, aged fifty-two, had a fall on July 23, 1936. Roentgenograms were taken elsewhere and the eleventh and twelfth ribs found to be fractured. On these films it was noted that the third lumbar vertebra was considerably larger and denser than its neighboring bodies. The trabeculations were coarse and seemed to run in parallel vertical lines. The in-

creased density was mainly due to a dense cortical thickening. It was referred to as "ivory-like" in density. Possible diagnoses suggested were metastatic malignancy from a prostatic carcinoma, Paget's disease, hemangioma of the vertebra. No other bones were roentgenographed to check for multiple lesions.

The patient's family physician found no abnormality or change from the normal on thorough physical examination. The patient worked every day and was watched over a year and a half, showing no indications of metastases. The case was brought to my attention, and I repeated the roentgen examination of the lumbar spine. I was unable to show any change in the appearance of the lumbar body as compared with the first films. The entire skeletal system was roentgenographed and found to be negative. The patient was well in all respects and did not complain of any pain. When questioned about his back he attributed a low backache to his work. He had lost no weight over a period of years (Fig. 11 and 12).

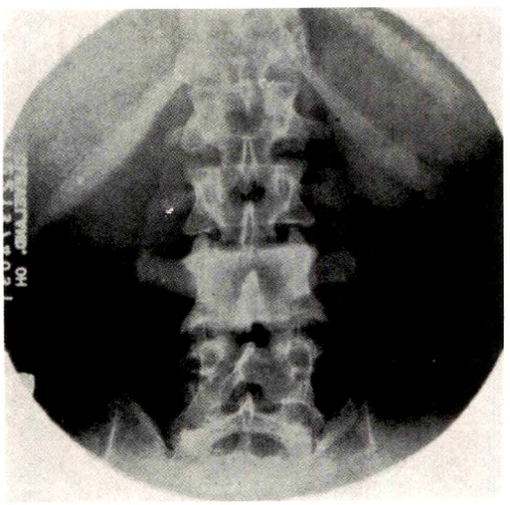

Fig. 11. Case v. Anteroposterior view of the lumbar spine showing the typical structural changes of osteitis deformans in the third lumbar vertebra as seen in previous cases.

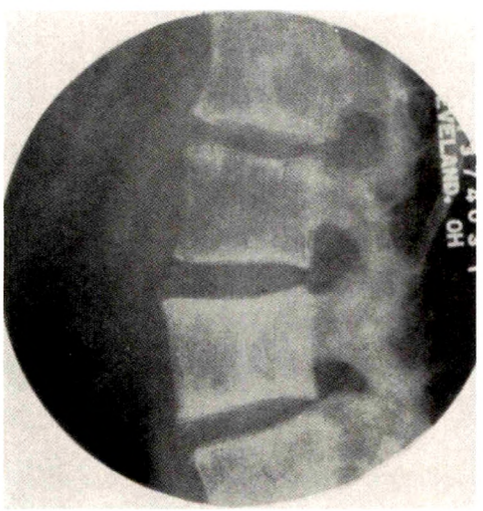

Fig. 12. Case v. Lateral view of the lumbar spine.

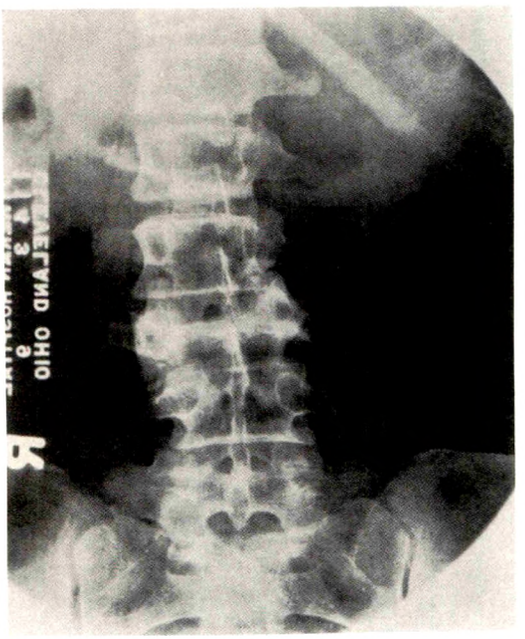

Fig. 13. Case vi. Collapsed fourth lumbar with resulting scoliosis and rotation of spine. The collapse is all central. Note the recognizable Paget structure in remaining portion of body which has not collapsed. Note sixth lumbar bodies.

The blood Wassermann reaction was negative, blood calcium was 9.2 mg. per 100 cc., blood phosphorus was 3.65 mg. per 100 cc. The serum phosphatase was higher in this case than in any of the previous ones and reached a level of 14.6 Roberts units.

Case vi. Y. L., female, aged fifty-one, was seen in November, 1935, complaining of a low backache with pain radiating into the lower limbs and tingling of the toes, exaggerated on exertion. The backache was of twenty-five years' duration.

When she had first noted this backache a diagnosis of "floating kidney" was made. In

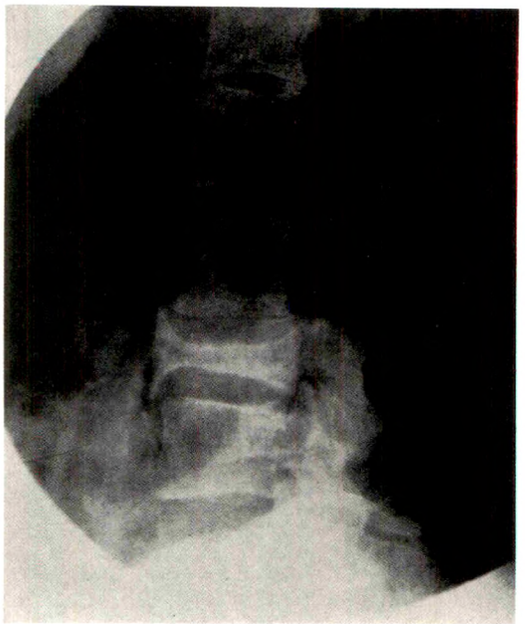

FIG. 14. Case VI. Lateral view.

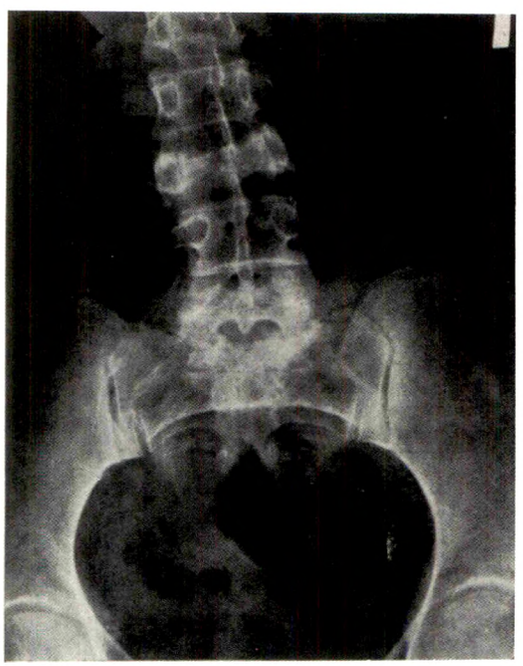

FIG. 15. Case VI. Anteroposterior view of same patient obtained from New York Clinic taken in 1926. In comparison the collapse is not as marked, and the resultant shifting of the upper lumbar spine as severe as at present. Paget changes are more obvious then because the body has not completely collapsed.

1926, her first roentgen examination (Fig. 15) suggested an "old injury to the fourth lumbar body." Other diagnoses at varying later dates were "hemangioma," "giant cell tumor," and in 1935 "old epiphysitis" and another "diseased vertebrae."

Films taken on these dates showed practically no change in the appearance of the fourth lumbar body. Roentgenograms of the entire skeleton were negative. The last films of the lower spine showed the same disease process as in the previous examination, i.e., a sclerosing cortical lesion with rarefaction and structural changes typical of Paget's disease. The body was collapsing due to softening, resulting in a lateral shifting of the spine. Nerve root compression was probably responsible for the present complaints (Fig. 13 and 14).

Physical examination revealed only marked lordosis and right lateral scoliosis of the lumbar spine with localized tenderness over the lower lumbar segments. The reflexes were normal. The blood calcium was 12.74 mg. per 100 cc., blood phosphorus was 4 mg. per 100 cc., serum phosphatase was 13.3 Roberts units. Smears and routine blood studies were normal, and the Kline reaction negative.

CASE VII. M. M., female, aged sixty-three, complained of a limp and pain in the left hip. This limp started about twelve years previously with occasional pain in the left hip, later on becoming more steady but no more severe. About three to four months prior to admission there was a "definite change for the worse." The pain became more intense, and the limp was more pronounced. There was progressive shortening of the left leg. The history was otherwise irrelevant.

There was no loss of weight or appetite. Physical examination showed distortion of the pelvis with tilting to the right and apparent shortening of the left lower limb, with a compensating lumbar scoliosis. Roentgen examination of the entire skeleton showed normal bone structure throughout except in the left pelvis, defined sharply by the left sacroiliac joint posteriorly and the symphysis pubis anteriorly. The left innominate bone showed typical coarse changes about the acetabulum, obliterating all detailed structure. The entire bone was larger than the right. It bulged medially in the midsection about the acetabulum, suggesting a softening of the bone and compensating new bone formation.

The routine blood examination was negative, as was the Kline reaction. The blood calcium was 12.53 mg. per 100 cc., blood phosphorus 3.816 mg. per 100 cc., serum phosphatase 13.1 Roberts units (Fig. 16 and 17).

CASE VIII. W. N., male, aged fifty-one, was seen in March, 1939, with the complaint of sharp pain in the low back of one week's duration, following a fall on his back. There were no other complaints. He had complained of low backache for over ten years and had undergone several physical examinations during these years. The diagnosis was "hysteria," and later, on repeated examinations "sciatica," "subacute infection of the lumbosacral joints," "arthritis," and still later, in 1935, "an early destructive lesion, osteitis of the third lumbar body." Physical examination at this time revealed only rather generalized tenderness over the lumbar spine with some lumbar spasm (Fig. 20).

Roentgen examination of the entire skeleton showed normal bone structure throughout except for the third lumbar body which showed a slight increase in size as compared with the neighboring bodies. There was a rarefaction of the internal structure with coarse parallel trabeculations and typical mosaic structure. There was practically no cortical change as contrasted to the other cases of Paget's disease. Comparison of recent films with others taken elsewhere presented no change in appearance in the third lumbar body since 1931 (Fig. 18 and 19).

The first lumbar body was the site of a recent compression fracture. The patient was admitted to the hospital for a spica cast. Blood examination was negative, the Kline reaction was negative. The blood calcium was 11.8 mg. per 100 cc., blood phosphorus 2.1 mg. per 100 cc., serum phosphatase 14.1 units (Roberts).

Another examination in November, 1939, showed no demonstrable change of the third lumbar body. The compressed vertebrae healed normally.

CASE IX. A. S., male, aged thirty-five, complained of persistent dull pain in the right hip following a fall. A few days after the injury a diagnosis was made of sarcoma of the right ilium on the basis of roentgen examination elsewhere (Fig. 21).

The left pelvis was normal. The right pelvis was decidedly increased in density throughout, this change being most marked about the acetabulum. There was typical mosaic pattern,

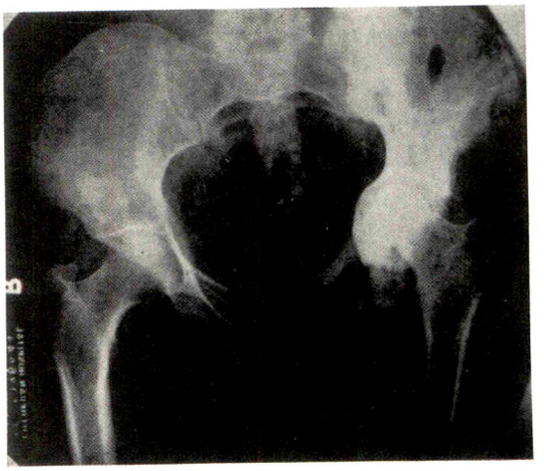

FIG. 16. Case VII. Obvious Paget type bone changes in the left innominate bone, confined to this bone sharply at sacroiliac joint and symphysis. Note bulging of acetabulum medially due to softening of bone.

and trabeculation as seen in Paget's disease. There was no medial bulging of the right pelvis, but the right acetabulum lay at a slightly higher

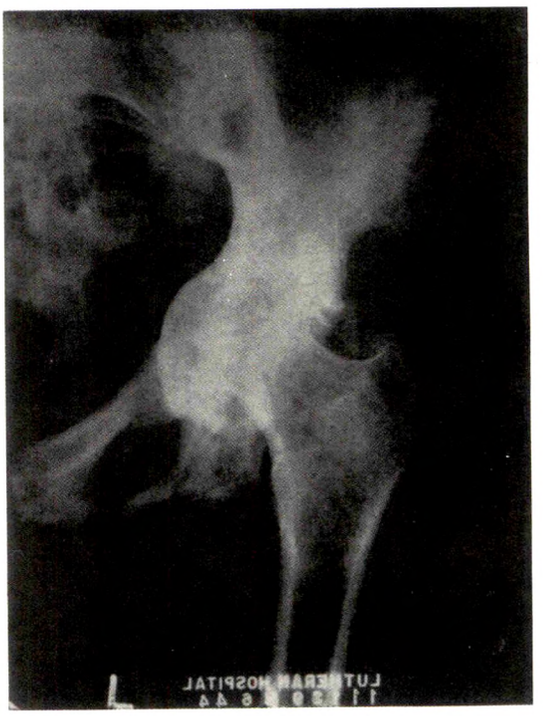

FIG. 17. Case VII. Overexposed close-up view, localized, of same pelvis as in Figure 16, to bring out structural changes.

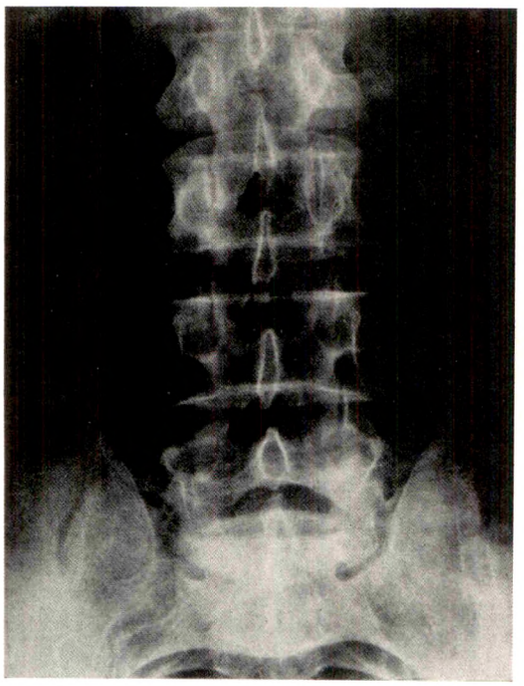

FIG. 18. Case VIII. Earliest Paget change in third lumbar body but typical especially in the lower lateral quadrants with resultant bulging (compare with previous cases). Rearrangement of trabeculae and dense stippling. Note mosaic structure, which is better demonstrable now before cortex becomes too dense. This is a typical fibrous type of Paget's disease.

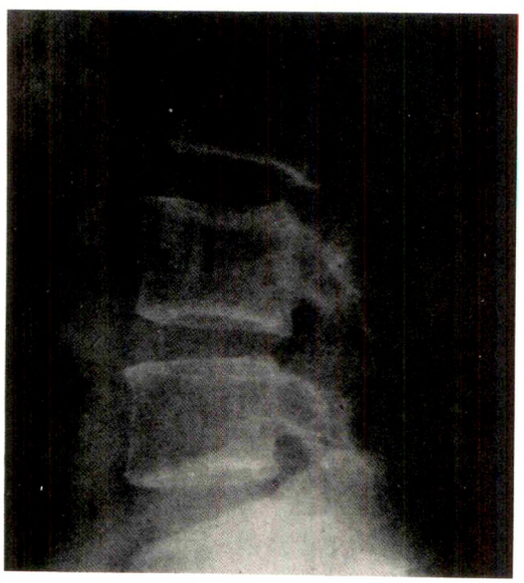

FIG. 19. Case VIII. Lateral view of same case as in Figure 18. There is very little change since 1933, if compared with Figure 20.

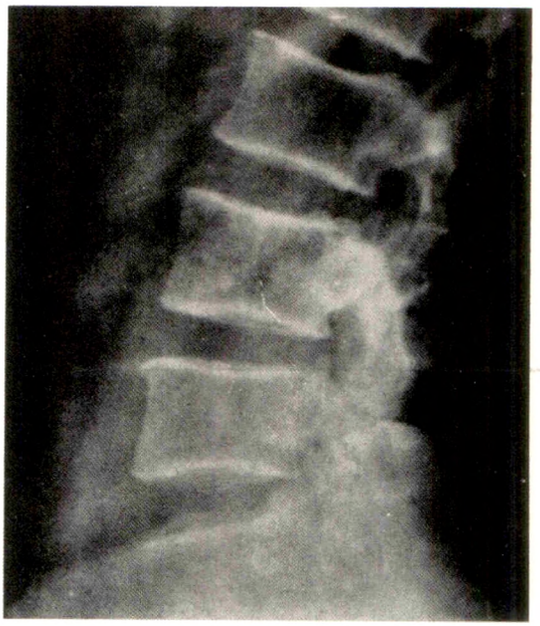

Fig. 20. Case VIII. A lateral view taken in 1933 in Chicago of same case as Figure 19. The lacework of trabeculae is not as obvious then, but the changes in the arches and posterior articulating processes are shown better.

level and was deeper partly because of marked cortical proliferation about the acetabular ridge.

Physical examination was negative. Subsequent films taken of the entire skeleton showed

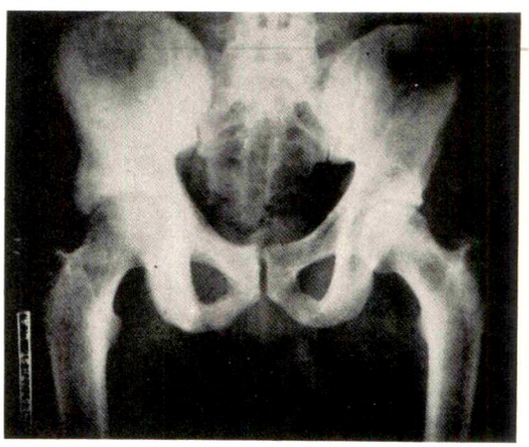

FIG. 21. Case IX. Typical Paget changes observed in the right innominate bone, confined sharply by the sacroiliac joint and the symphysis. The bone is larger, coarser, and denser, with proliferative changes about the acetabulum. Note that there is as yet no medial bulging of the acetabulum, as seen in Case VII.

no other bone involvement. The spine, skull and long bones were negative. The Kline reaction was negative. Routine blood counts and smear were negative. The blood calcium and phosphorus were reported as "normal"; serum phosphatase was 13.6 mg. per 100 cc.

DISCUSSION OF MONO-OSTEITIC PAGET'S DISEASE

As to the etiology of Paget's disease there are still divided ideas. I am inclined to agree with investigators who believe this disease to be a slow infectious process within a bone. There are numerous cases which present a clinical picture of infection: local redness, swelling, and increased surface body heat over the bone affected. There is pain and tenderness. There is periosteal reaction to a possible low grade infection. Malignant changes are seen occasionally. If we can establish a definite entity of a mono-osteitic form of Paget's disease we must look for our etiologic factor locally and not generally as was previously thought. There is no concrete proof that the parathyroids are the cause of the trouble. Calcium and phosphorus levels are normal in Paget's disease.

The lesion must be infectious in nature and may be arrested in its progress as soon as the entire bone is involved. During the early active infection, metastatic foci may be set up in other bones.

The usual arterial calcification present in all cases of Paget's disease seems to be a contributary factor rather than primary. The decreased local blood supply may interfere with a local immunity in a bone against a low grade infection.

Today we accept osteitis deformans as a disease entity, separate from osteitis fibrosa cystica, though ten years ago such men as Assmann thought there was a common etiologic factor for both diseases and that each was a different manifestation of the same disease. Hallermann distinguished between these two diseases in 1929. Schmorl also proved two distinct entities in his reports.

The next problem concerns the delimitations of the disease. Is mono-osteitic Paget's disease a distinct entity or should it be considered an early manifestation of the generalized disease? No discussions have appeared in the English literature since Schmorl published his work. The lapse of discussion since 1931 may be construed as an acceptance of mono-osteitic Paget's disease as a definite entity.

We agree with the earliest authors that when they described doubtful bone lesions and deformities of long bones, no one could state with certainty the extent of the disease in the entire skeleton. Their conclusions were uncertain. There is no doubt that the disease is mainly a roentgenological problem, and because of that fact, our conceptions have become more definite and conclusive. Today the roentgen ray offers a method for study not only of the nature of the disease but also of the extent of the lesion. Is it mono-osteitic or poly-osteitic? We have had cases under observation long enough to be convinced that Paget's disease can occur in one bone only and never become generalized.

As Newton stated fifteen years ago, the lesion is entirely a roentgenological problem in its non-clinical form and no biopsy is necessary. In 1933, Jaffe wrote:

> A critical analysis of the reported clinical cases of the monostatic group shows, however, that only a small number properly belong to this group, for included among reported cases are instances of other local bone diseases, which have been improperly classified, especially localized forms of fibrocystic disease, lues, and forms of bone tumors.

The disease is so definite and regular in the change it produces in the bones involved that to the experienced eye it is recognizable and can be differentiated from the changes in the bones seen in osteitis fibrosa cystica, angioma, osteomalacia, osteomyelitis, lues, and osteoplastic metastatic new growth.

Improved roentgenologic technique in demonstrating bone detail is responsible for our being able to recognize two different types of bone changes in mono-osteitic Paget's disease of the spine.

Schmorl has described the two different Paget types in his voluminous work on pathology of the spine. He has found that part of a vertebral body may be involved early in the disease, but that soon the entire body, with its processes and often its spurs, if any are present, will be uniformly involved. It has also been observed that the lesion extends into the neighboring body through hypertrophic spurs if they form a complete bridge across the intervertebral space.

in the lower extremities bow because they are softened and weight bearing. The innominate bone is definitely denser, enlarged, and bows inward and upward. The acetabulum becomes deeper and rides higher, resulting in a limp. In the vertebrae one type shows a dense cortical frame which has developed because of a fusion of the thick outer layer of trabeculae. The trabeculae in the center of the body become fewer in number, forming a coarse lacework. This type of Paget's disease even-

TABLE I

SUMMARY OF CASES

	Case	Sex	Age	Part Involved	Duration of Symptoms	Type of Complaint	Serum Phosphatase Level*
I	T. M.	M	55	Left tibia	None	Bowing of leg	8.8 mg.
II	J. S.	M	44	Second lumbar	Two days	Short stabs of pain localized in low back	4.7
III	B. T.	M	55	Fourth lumbar	Ten months	Localized backache	Not done
IV	A. L.	M	57	Fourth lumbar	None	None (accidental finding)	12.15
V	J. C.	M	52	Third lumbar	None	None (accidental finding)	14.6
VI	Y. L.	F	51	Fourth lumbar	Twenty-five years	Early: low backache; late: sharp radiating pain legs	13.3
VII	M. M.	F	63	Left innominatum	Twelve years	Little pain in hip, mainly limping	13.1
VIII	W. N.	M	51	Third lumbar	Ten days	Low backache	14.1
IX	A. S.	M	35	Right innominatum	Six days	Dull hip pain following fall six days previously	13.6

* Morrell-Roberts units

It has been said that the term "osteitis deformans" does not apply to the disease in the spinal column. We find affected vertebral bodies to be definitely deformed. The body involved by Paget's disease is enlarged and its trabeculae are coarse, dense, and interlacing, giving us the familiar mosaic structure (the term first employed by Schmorl). There is also a change in shape: a narrowing of the sagittal diameter or thickness.

The disease is characterized by a constant "umbau" (tearing down and building up) of new bone. Trabeculae are fewer, coarser, thicker, and surprisingly softer. The cortical tissue becomes heavier, thicker and denser in structure, probably with some periosteal bone deposit. Long bones

tually collapses under the pressure; the degree of collapse varies. In some cases there is only a decreased sagittal thickness and an enlargement of the body in other diameters. In one of our cases there was at first slight and later complete collapse with a resultant slipping of the body above.

In the other type of Paget's disease, there is more generalized involvement of the vertebral body. The entire body is extremely dense throughout. Its trabecular structure is thickened and coarse; there is no specific dense frame around a hollow body. The segment is enlarged uniformly in all dimensions. The appearance is that of an "ivory vertebra," and there is a problem in differentiating it from similar forms as seen in marble bones, osteoscle-

rotic anemias, leukemia, malignant lymphogranuloma, myeloma (infrequently osteoplastic), osteoplastic metastatic lesions from carcinoma of prostate or breast, and lues. This vertebra withstands a weight bearing pressure and does not collapse.

The non-collapsing type of osteitis deformans is usually without pain or other symptoms, whereas the collapsing type is definitely painful, probably because of compression of the body so minute that it is sometimes not demonstrable roentgenographically. Later symptoms are referable to the further mechanical effects resulting from nerve root compression.

The cases presented show blood chemistry changes similar to those observed by Gutman and Kasabach. The serum calcium and serum phosphorus are within normal levels. The important change is in the serum phosphase activity which is elevated in all polyosteitic cases whereas there may be no or only slight elevation in mono-osteitic cases. The highest value reached in our series of cases was 14.6 units (Morrell and Roberts), which is considerably less than the 59.5 to 130.3 units (Bodansky method), reached in the advanced polyosteitic cases reported by Gutman and Kasabach. There is therefore a direct relationship between the measurable serum phosphatase activity and the extent of bone involvement in the skeleton.

Usually the single bone lesions are found accidentally during roentgen examinations for irrelevant abdominal complaints or during examinations after injury. If the lesion is not located in the spinal column, where it may be symptomless, deformities of the pelvis or long bones give the chief complaints. Spinal lesions are usually spoken of as "non-clinical" because of the absence of clinical findings. Two of our cases gave severe symptoms of nerve root compression localized over the involved spinal area, whereas 3 cases gave no symptoms referable to the findings in the spine.

The lesion is never "generalized," but polyosteitic or mono-osteitic from the onset, and develops rather rapidly in any bone once it shows any sign of involvement. I have observed a femur in a polyosteitic form of Paget's disease which presented such an extreme involvement and bowing over a period of a year and a half that the leg was one and a half inches shorter than in the previous examination, when it showed only some cortical thickening below the lesser trochanter. This contradicts our former concept of Paget's disease as a slowly progressive lesion. Once the whole bone is involved, the lesion reaches an arrested stage and remains so for any number of years. There may be years of slow progressive bone changes due to compression, or even sarcomatous change may develop.

Generally speaking, one can say that Paget's disease does not occur below the age of forty years, but one of the cases presented here is that of a patient only thirty-five years old. Schmorl encountered no instance before the age of forty in 4,603 routine spinal dissections which undoubtedly held many symptomless cases. There must be many cases of mono-osteitic disease in a non-clinical form which do not come under observation until later ages, during examination for some irrelevant trouble.

SUMMARY

1. Nine cases of localized Paget's disease (mono-osteitic) have been presented; the histories, follow-up examinations, and long observation seem to prove that mono-osteitic Paget's disease does not become polyosteitic.

2. Paget's disease is either polyosteitic or mono-osteitic.

3. Mono-osteitic Paget's disease is a distinct entity, not an early stage of a polyosteitic disease, and, though often unrecognized, a more common form than the polyosteitic type.

4. The mono-osteitic form may be of two basic types: (a) a fibrotic, rarefying structural change with softening of bone resulting in deformities, or (b) a sclerotic osteoplastic new bone formation mainly of cortical or periosteal source.

5. Once the disease develops it progresses

rapidly until the affected bone is completely involved and then there is no further recognizable progress.

6. The lesion is most often seen in the lumbar bodies and is essentially a roentgenologic problem in diagnosis, since this is the only means of recognizing it.

7. The blood phosphatase activity is indicative of the amount of bone involvement.*

REFERENCES

1. ASSMANN, H. Klinische Röntgendiagnostik der inneren Erkrankungen. Aufl. III, p. 778.
2. BACHMANN. Ein Beitrag zur Ostitis deformans Paget. *Röntgenpraxis*, 1933, *5*, 161–170.
3. BÁRSONY, T., AND SCHULHOF, O. Der Elfenbeinwirbel. *Fortschr. a. d. Geb. d. Röntgenstrahlen*, 1930, *42*, 597–609.
4. BODANSKY, A., and JAFFE, H. L. Phosphatase studies. III. Serum phosphatase in diseases of the bone; interpretation and significance. *Arch. Int. Med.*, 1934, *54*, 88–110.
5. BOWLBY, A. J. Two cases of curvature of the femur, one due to osteitis deformans, the other to an injury followed by chronic inflammation. *Tr. Path. Soc.*, London, 1883, *34*, 192.
6. BREITLÄNDER. Zentrales osteoplastisches Sarkom eines Wirbels im Röntgenbilde. *Fortschr. a. d. Geb. d. Röntgenstrahlen*, 1926, *34*, 523–525.
7. CONE, S. M. Pathology of osteitis deformans, Paget's disease. *J. Bone & Joint Surg.*, 1922, *4*, 751.
8. GUTMAN, A. B., and KASABACH, H. Paget's disease (osteitis deformans); analysis of 116 cases. *Am. J. M. Sc.*, 1936, *191*, 361–380.
9. HALLERMANN, W. Zur Kenntnis der Ostitis deformans Paget der Wirbelsäule. *Fortschr. a. d. Geb. d. Röntgenstrahlen*, 1929, *40*, 999–1017.
10. HULTÉN, O. Ein Fall von "Elfenbeinwirbel" bei Lymphogranulomatose. *Acta radiol.*, 1927, *8*, 245–251.
11. HURWITZ, S. H. Osteitis deformans (Paget) involving a single bone; report of case. *Am. J. M. Sc.*, 1914, *147*, 855.
12. HURWITZ, S. H., and CARR, G. L. On the mono-osteitic form of Paget's disease of bone. AM. J. ROENTGENOL., 1914–1915, *2*, 755–761.
13. JAFFE, H. L. Paget's disease of bone. *Arch. Path.*, 1933, *15*, 83–131.
14. KASABACH, H. H., and DYKE, C. G. Osteoporosis circumscripta of the skull as a form of osteitis deformans. AM. J. ROENTGENOL. & RAD. THERAPY, 1932, *28*, 192–203.
15. KATHOLICKY. Discussion. *Wien. klin. Wchnschr.*, 1905, *18*, 648.
16. KAY, H. D., SIMPSON, S. L., and RIDDOCH, G. Osteitis deformans. *Arch. Int. Med.*, 1924, *53*, 208.
17. KIENBÖCK, R. Ueber die sogenannte "Ostitis fibrosa (Osteodystrophia fibrosa"). *Fortschr. a. d. Geb. d. Röntgenstrahlen*, 1930, *41*, 34–38.
18. LOOSER, E. Ueber Ostitis deformans und mit ihr Angeblich und Wirklich verwandte Knochenerkrankungen. *Schweiz. med. Wchnschr.*, 1926, *56*, 598–603.
19. MEYER-BORSTEL, H. Ueber die Stellung der Recklinghausenschen zur Pagetschen Knochenerkrankung. *Fortschr. a. d. Geb. d. Röntgenstrahlen*, 1930, *42*, 493–500.
20. MOORE, S. Observations on osteitis deformans. AM. J. ROENTGENOL. & RAD. THERAPY, 1923, *10*, 507–518.
21. NEWTON, F. C. The mono-osteitic type of Paget's disease of bone (osteitis deformans); report of three cases. *Arch. Surg.*, 1924, *8*, 24.
22. PAGET, J. On a form of chronic inflammation of bones. *Med. Chir. Tr.*, 1877, *60*, 37–64.
23. PAGET, J. Additional cases of osteitis deformans. *Med. Chir. Tr.*, 1882, *65*, 225–236.
24. ROBERTS, W. M. Variations in phosphatase activity of blood in disease. *Brit. J. Exper. Path.*, 1930, *11*, 90–95.
25. SCHMIDT, B. Ein Fall von Ostitis deformans. *Arch. d. Heilk.*, 1874, *15*, 81.
26. SCHMIEDEN, V. Beitrag zur Kenntnis der Osteomalacia chronica deformans hypertrophica (Paget). *Deutsche Ztschr. f. Chir.*, 1903, *70*, 207.
27. SCHMORL, G. Ueber Ostitis deformans Paget. *Virchow's Arch. f. path. Anat.*, 1932, *283*, 694–751.
28. SCHMORL, G. Zur Kenntnis der Ostitis deformans Paget. *Fortschr. a. d. Geb. d. Röntgenstrahlen*, 1931, *43*, 202–207.
29. SCHMORL, G. Die gesunde und kranke Wirbelsäule im Röntgenbild. *Fortschr. a. d. Geb. d. Röntgenstrahlen*, Ergänzungsband 43. G. Thieme, Leipzig, 1932.

* Since the evidence of this paper has been compiled, 3 more cases of mono-osteitic Paget's disease have come to my attention. Two of these cases, both of which were localized to the right tibia, were in a mother and her son. The mother was over sixty years of age and the son was forty-two. The mother had complained for over twenty-five years of a painless bowing of the right lower leg which had become painful the last half year. The son complained of no pain, but had noticed a similar bowing in his right lower leg during the past five years. The rest of the skeleton was negative in each patient. These cases are of interest because of the apparent familial nature of the disease in this instance. It should be of interest to investigate this phase of osteitis deformans further.

The third case is a biopsied one. It is the only case which was subjected to a biopsy, and therefore was proved by pathologic section.

30. Stegmann, R. Discussion. *Wien. klin. Wchnschr.*, 1905, *18*, 619.
31. Sutherland, C. G. Differentiation of osteitis deformans and osteoplastic metastatic carcinoma. *Radiology*, 1928, *10*, 150–152.
32. Van Hazel, W., and Andrews, E. Osteitis deformans. *Surg., Gynec. & Obst.*, 1927, *45*, 54–61.
33. Windholz, F. Zur Röntgensymptomatologie der Ostitis deformans Paget (periostale Knochenneubildung). *Fortschr. a. d. Geb. d. Röntgenstrahlen*, 1932, *46*, 188–193.
34. Szerny. Case of localized osteomalacia. *Wien. med. Wchnschr.*, 1873, *39*.
35. Töpfer, D. Ueber ein infiltrierend wachsendes Hämangiom der Haut und multiple Kapillaraktasien der Haut und inneren Organe; zur Kenntnis der Wirbelangiome. *Frankfurt. Ztschr. f. Path.*, 1928, *36*, 337–345.
36. Sicard, J. A., Belot, J., Coste, and Gastaud. Aspects radiographique du cancer vertébral. *J. de radiol. et d'électrol.*, 1925, *9*, 353–382.

Editor's Note

Dr. Jean Adolph Groh, the author of the preceding article, was born in 1901 in Frankfurt, Germany. He came to the United States when he was 20 years old. Unable to speak English, he took English lessons at 25¢ per lesson until he had mastered the language. Dr. Groh entered Muskingum College, New Concord, OH, in 1925, and was accepted at the School of Medicine at Western Reserve University, Cleveland, in 1928. After graduating, Dr. Groh spent 1 year in the Department of Surgery at University Hospitals of Cleveland and then studied for the next 3 years as a resident in Radiology at the same institution.

At the end of his residency, Dr. Groh became the first physician radiologist at Lutheran Hospital in Cleveland. He became head of the Radiology Department there in 1935 and stayed in that position until 1967, when he retired with full honors. In recognition of the esteem that his colleagues had for him, the Board of Trustees at Lutheran Hospital instituted a "Dutch" Groh award, which was given to a staff member at selected intervals. Dr. Groh died in 1968.

Dr. Groh's article on Paget disease reproduced here was originally published in volume 50 of the *AJR* in 1943.

The reader's attention is directed to the Commentary on this article, which appears on the following page.

Review Article

Paget Disease of Bone: Current Status and a Look Back to 1943 and Earlier

Donald Resnick[1]

Paget disease of bone (osteitis deformans) is a condition of unknown cause that affects approximately 3–4% of the population over the age of 40 years [1, 2]. Its name is a tribute to Sir James Paget, an astute clinician whose original description of the disease in 1877 [3] serves as a model to those of us who strive to write with clarity and precision. In that description, Paget presented a detailed report of one patient whom he had observed for approximately 20 years, as well as a brief summary of several other individuals with the same disorder. Although other reports preceded his, Paget's account is recognized as a lesson in accurate and lucid writing, and the disorder is now called Paget disease.

During the 110 years that have elapsed since Paget's landmark article, the disease has been the subject of intense interest, speculation, and investigation. It now is known that Paget disease shows certain geographic and racial characteristics: It is especially common among inhabitants of Great Britain, Australia, and certain areas of continental Europe; it is relatively frequent in the United States but rare in Japan and China. Paget disease predominates in middle-aged and elderly individuals, although reports document its occasional occurrence in young adults [4]. It affects men more often than it affects women, and the age of onset may be slightly lower in men than in women [5]. Familial history of the disease has been identified in some instances, with reports indicating that several members of a family in various generations and identical twins may be affected [6]. Although variable in its clinical manifestations, Paget disease is asymptomatic in most instances. The disorder is characterized by excessive and abnormal remodeling of bone. It passes through active and quiescent phases leading to a combination of osseous resorption and apposition that produce a distinctive pathologic and radiographic appearance in which irregular bone fragments have a thickened and disorganized trabecular (mosaic) pattern (Fig. 1).

A reprint of the report by Groh [7], which appeared in the *AJR* 45 years ago, precedes this paper and underscores the interest that radiologists have had in Paget disease. In Groh's report, he describes nine patients, seven men and two women between the ages of 35 and 63 years, with "localized" involvement of the spine (six patients), innominate bone (two patients), or tibia (one patient). He further comments on the causes and natural history of the disease and the value of the radiographic and laboratory examination in studying its course; in the form of an addendum, Groh notes three other cases in which monostotic involvement was observed. The article is interesting reading and shows the modern radiologist what was known or believed about Paget disease more than 4 decades ago. The information in this paper provides an appraisal of Groh's report and a summary of current concepts of the disease. These are supplemented with quotes derived from the original descriptions of Paget, many of them more than 100 years old, which will emphasize the fact that accurate scientific writing will long be valued.

This article is a commentary on the preceding anniversary reprint by Groh.
Received July 30, 1987; accepted after revision August 28, 1987.
This work was supported in part by VA grant SA306.
[1] Department of Radiology, Veterans Administration Medical Center, 3350 La Jolla Village Dr., San Diego, CA 92161.

 0361–803X/88/1502–0249 © American Roentgen Ray Society

> It is often said or implied that, in our profession, a man cannot be both practical and scientific; science and practice seem to some people to be incompatible. Each man, they say, must devote himself to the one or the other. The like of this has long been said, and it is sheer nonsense.
>
> Sir James Paget (1894) [8]

Etiology

> "With regard to the nature of the process . . . only three things could produce so great an increase in the size of a bone, namely, new growth (tumor), hypertrophy, and chronic inflammation. The first of these may be at once set aside as out of the question, nor is the second much more probable than the first. . . . of the three causes chronic inflammation alone remains."
>
> Sir James Paget (1877), quoting Mr. Butlin [8]

Despite the scrutiny to which Paget disease has been subjected, there still is no consensus about its cause. It has been suggested that Paget disease is an inflammatory, hereditary, neoplastic, vascular, traumatic, endocrinologic, or immunologic disorder [2]. Until recently, the evidence supporting any specific cause has been either nonexistent or inconstant and easily refuted [9]. For example, reports of familial aggregation of cases and of increased prevalence among certain ethnic groups have lead some investigators to argue that an autosomal dominant pattern of inheritance is present, whereas other investigators have emphasized the fundamental role that parathyroid hormone plays in the development of Paget disease. An inflammatory cause has been championed by numerous investigators, including Paget. Indeed, Groh [7], at the outset of his discussion, states in no uncertain terms that the pagetic lesion must be infectious in nature, citing clinical manifestations consistent with infection (such as redness, swelling, and a localized increase in heat) that repeatedly have been described.

In agreement with Paget's original hypothesis and with Groh's strong belief, the theory that the cause is infectious, specifically a viral illness, has gained support by observations in a number of recently published articles [10]. Active pagetic bone is characterized by the presence of giant osteoclasts containing large numbers of nuclei. In 1974, Rebel et al. [11] identified, by ultrastructural examination, organized groups of microcylinders within the nuclei and the cytoplasm of the osteoclasts in areas of bone affected with Paget disease. These intranuclear inclusion bodies, the presence of which have been corroborated in subsequent investigations [12–14], are not observed in osteoblasts or osteocytes in pagetic bone or in osseous tissue derived from patients with a variety of other skeletal disorders, even those characterized by osteoclastic proliferation [2]. The inclusions, however, are not entirely specific for pagetic bone, having been identified within giant cell tumors in patients with [15, 16] or without [17, 18] Paget disease. Ultrastructural characteristics of the pagetic osteoclasts led to the hypothesis that the inclusions have a viral nature. Similar cellular characteristics are observed in disorders produced by certain viruses, specifically subacute sclerosing panencephalitis related to a *Paramyxovirus* of the measles group [19]. Additional morphologic evidence for a viral cause of the intranuclear inclusions has included (1) the dense fibrillar material associated with some of the inclusions is similar to that found in the nuclei of virus-infected cells; (2) filament bundles and spindle-shaped structures enclosed in double membranes observed in the cytoplasm of some osteoclasts are considered an indirect cellular response to viral attacks; and (3) the presence of enormous osteoclasts in pagetic bone is compatible with abnormalities of in vitro measles virus infection [20]. Certain immunologic data have reinforced this viral hypothesis [13, 21], and significant and sustained viral antibody titers against the measles virus have been detected in a few patients with Paget disease. Although the cause of the disease still is not entirely clear, all of the experimental evidence cited above would appear to support the concept that Paget disease is a slowly developing viral infection of osteoclasts.

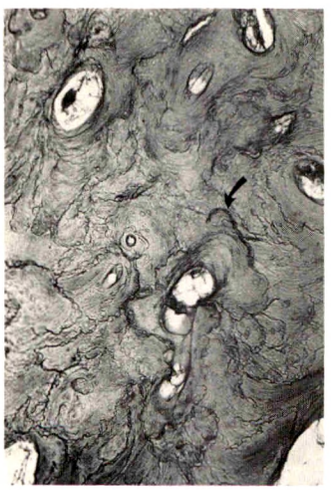

Fig. 1.—Histologic abnormalities of Paget disease: mosaic pattern. Note presence of cement lines (*arrow*) joining areas of lamellar bone.

Skeletal Distribution and Extent

> The most frequent seats of the osteitis have been . . . the tibiae, femora, clavicles, spine and vault of the skull . . . . The skull became gradually larger, so that nearly every year, for many years, his hat and the helmet that he wore as a member of a Yeomanry Corps needed to be enlarged . . . The length of the spine thus seemed lessened, and from a height of six feet one inch, he sank to about five feet nine inches. . . .
>
> Sir James Paget (1877, 1889) [8]

The predilection of Paget disease to affect the axial skeleton is well documented. Particularly characteristic is the involvement of the innominate bone (20–75% of cases), sacrum (30–60%), spine (30–75%), and skull (25–65%). Additionally, the proximal long bones, particularly the femur (25–35% of cases), are commonly affected. A preference for the lower extremities and a tendency for right-sided alterations are other emphasized features of the distribution of Paget disease. The central distribution corresponds to that of hematopoietic red marrow, so that the locations of Paget disease are similar to those of skeletal metastases; however, the relative frequency of tibial involvement and infrequency of rib involvement are features of Paget disease not shared by osseous metastases [2].

Although these general characteristics of Paget disease are well accepted, accurate assessment of the precise distribution of the disease is difficult owing to the facts that osseous lesions are commonly asymptomatic and that a true delineation of the extent and sites of involvement requires an imaging survey of the entire skeleton. Although Paget disease is polyostotic in most cases, it may be initially or totally monostotic in 10–35% of cases. In Groh's description of nine patients with monostotic abnormalities [7], radiographic surveys of classic target areas of the disease were used to verify the absence of involvement at other skeletal sites. At present, the assessment of the extent of skeletal disease might be accomplished better with bone scintigraphy (Fig. 2). As would be expected, areas of osseous disease are depicted as sites either of increased uptake of bone-seeking radiopharmaceutical agents or, in appropriate locations, of marrow replacement [22–25]. The immediate accumulation of radionuclide reflects an increased blood flow to bone, which may explain false-positive brain scintiscans in patients with calvarial Paget disease [26]. Scintigraphic abnormalities may precede radiographic changes, underscoring the greater sensitivity of radionuclide vs radiologic examinations. Furthermore, scintigraphy can document the extent of the initial, osteolytic phase of Paget disease [27], during which increased radionuclide activity may be particularly prominent at the advancing edge of bone lysis, corresponding to sites of intense vascularity, osteoclastosis, and new bone formation [28]. Serial bone scintigraphs may provide objective evidence of the effects of various therapeutic agents (see later discussion).

As noted by Groh [7], monostotic Paget disease appears to predominate in the axial skeleton, although any portion of the skeleton may represent the sole site of involvement. Although Paget disease confined to one bone or a portion of one bone may be more difficult to diagnose, characteristic radiographic findings generally are observed, allowing accurate differentiation from other conditions. In the tubular bones, a predilection for the epiphyseal area, an advancing wedge of radiolucency (Fig. 3), periosteal apposition of new bone leading to widening of the osseous surface, and deformity and fracture are characteristic, although not invariable, features of Paget disease. Rarely, narrowing or contraction of the involved bone is seen [29]. Diaphyseal changes without epiphyseal abnormality (Fig. 4) are extremely unusual but may be observed, particularly in the tibia [30, 31]. Furthermore, in the tibia, the proximal extent of disease may be located not in the epiphysis but in the anterior tibial tubercle (Fig. 5) [32].

Monostotic involvement of the spine, as was evident in six of the nine patients reported by Groh [7], is not difficult to diagnose when typical radiographic features, including the picture-frame vertebral body, are observed (Fig. 6). Groh's description of a second pattern of vertebral involvement, in which more generalized abnormality leads to an ivory vertebral body, is an important observation that may alert the modern radiologist that Paget disease of the spine can simulate lymphoma or skeletal metastases. Further, as illustrated in Groh's article, collapse of an affected vertebral body may complicate accurate diagnosis unless pagetic changes in the remaining portions of the vertebra are identified.

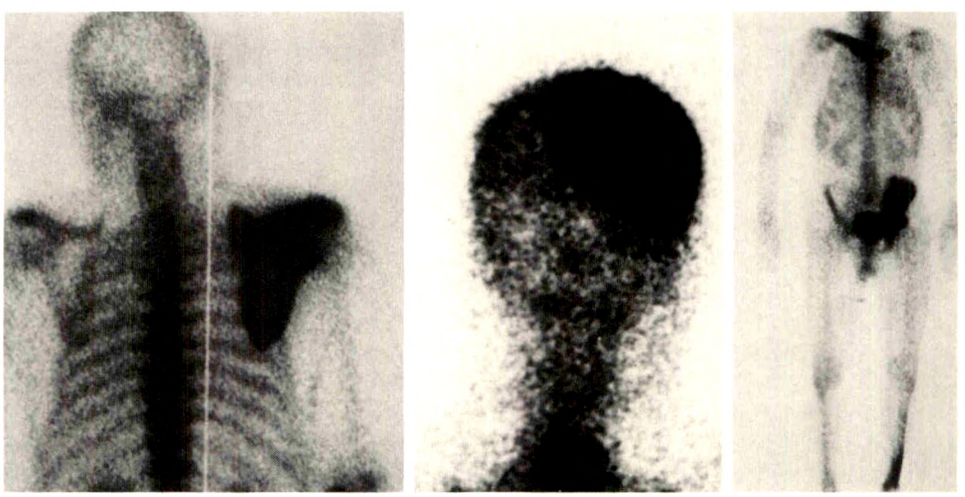

Fig. 2.—Scintigraphy shows extent of skeletal involvement. Intense uptake of bone-seeking radiopharmaceutical agent occurs in each case.
***A*, Scapula.**
***B*, Cranial vault.**
***C*, Clavicle, innominate bone, and tibia.**

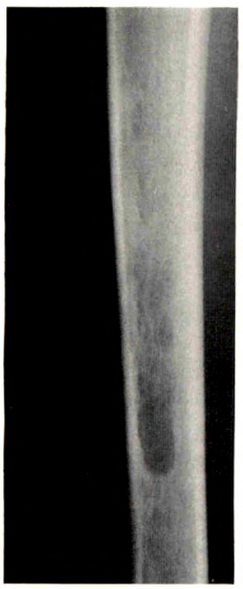

3

4

A

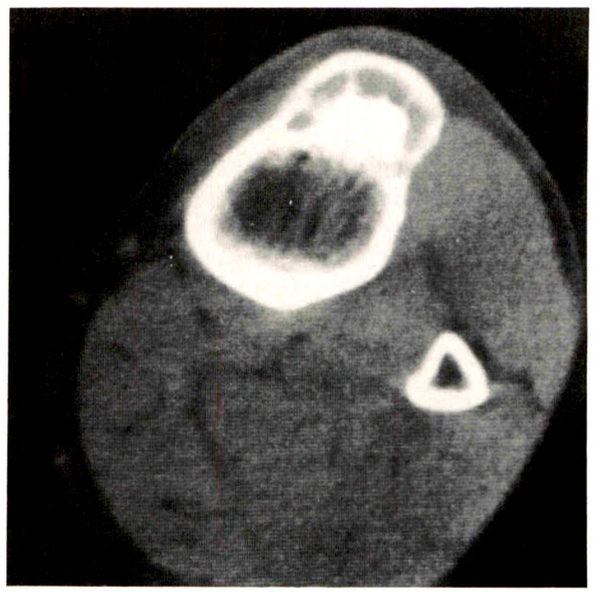

B

Fig. 3.—Osteolytic phase: tubular bone. Radiolucent wedge in diaphysis is well-defined.

Fig. 4.—Diaphyseal involvement of radius. Involvement of this segment of bone without epiphyseal involvement is distinctly unusual.

Fig. 5.—Involvement of the anterior tibial tubercle.

A, Lateral radiograph reveals osteolytic focus of Paget disease extending shaftward from region of tibial tuberosity.

B, Transaxial CT confirms the intracortical location of process.

(Courtesy of H. Rodriguez, Santa Barbara, CA.)

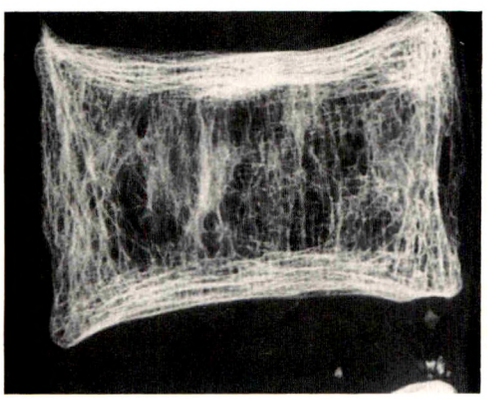

A

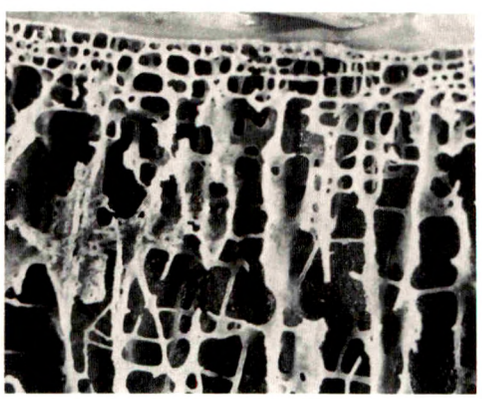

B

Fig. 6.—Picture-frame vertebral body in Paget disease.

A and *B*, Radiograph (*A*) and photograph (*B*) of a macerated vertebral body show condensation of trabeculae at periphery of vertebral body that is characteristic of disease process.

Natural History and Effect of Therapy

The primary event in Paget disease is intense focal bone resorption that is followed by disorderly bone formation, although the coupling of bone resorption and formation in this disease shows considerable variation from one patient to another and, indeed, from one involved skeletal region to another or from one period of time to another in a single individual [33]. The resulting aberrations in normal bone remodeling may lead to variable radiographic appearances, depending on the relative contributions of osseous resorption and apposition within the periosteal and endosteal cortical envelopes [34]. An increased or decreased external bone contour and a narrowed or enlarged marrow cavity may be observed, in sharp contrast to the bone expansion that was long regarded as a universal feature of the disease.

Paget disease generally is considered a relentlessly progressive disorder resulting in the conversion of normal uninvolved bone to abnormal bone, and, ultimately, in involvement of the entire bone. This concept was supported by Groh [7], who indicated the variability in the rate of disease progression.

Numerous investigations have confirmed that variation exists in the rate of conversion of normal to pagetic bone, although, in opposition to Groh's belief that rapid progression might be encountered, most studies have documented a slow, gradual extension of disease. The rate of progression in Paget disease generally has been estimated to be between 7 and 16 mm per year [10, 33, 35, 36]. This relatively slow rate of conversion of normal to diseased bone, combined with the three-dimensional nature of the process, accounts for the common reporting of "unchanged" disease extent on serial radiographs and also explains, in part, the popularity of scintigraphy as an effective method of monitoring the extent (and activity) of the disease.

The absence of any reference to the treatment of Paget disease in Groh's report is understandable, because effective therapeutic agents in this disease have been available only since the 1950s. One such agent is calcitonin, a potent inhibitor of bone resorption, which can lead to relief of pain for patients with Paget disease within weeks of its administration and to a reduction in serum levels of alkaline phosphatase and urinary levels of hydroxyproline. Although the rate of extension of the disease in pagetic patients being treated with calcitonin has been reported to be unchanged when compared with that rate in untreated patients [33], radiographic improvement in the appearance of the pagetic bone during such treatment has been recognized by numerous investigators; such improvement is evident in both cortical and trabecular bone, especially during the osteolytic phases of the disease [37–40]. After the therapy is stopped, a period of rapid bone resorption, even greater than that typical of untreated Paget disease, has been observed [37].

A second agent used in the therapy of Paget disease is disodium etidronate (EHDP), a diphosphonate. Diphosphonates inhibit bone resorption and mineralization by binding to the hydroxyapatite crystals and inhibiting their growth and dissolution [2]. Although, again, an unchanged rate of pro-

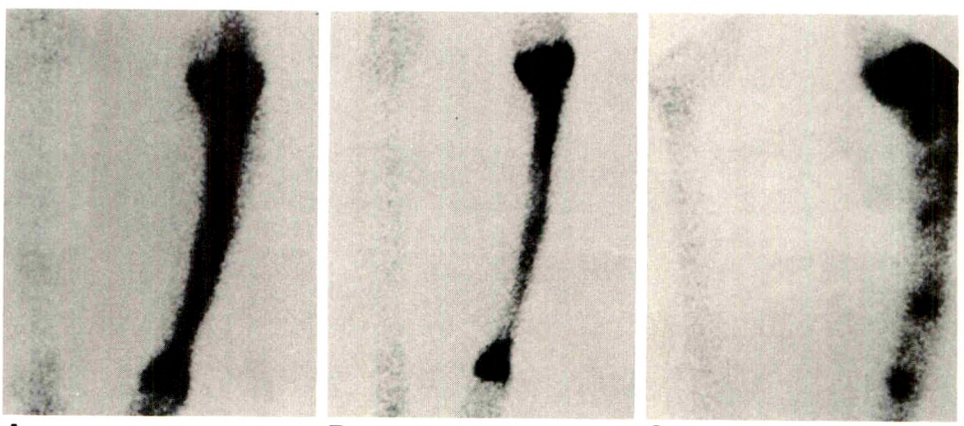

Fig. 7.—Scintigraphic assessment of osseous response to treatment.

***A–C*, Bone scans obtained 1 year apart show (*A*) initial intense accumulation of the radionuclide in tibia with partial resolution (*B* and *C*) over 2-year period during treatment with thyrocalcitonin. Residual activity in *C* corresponded in position to sites of insufficiency fractures.**

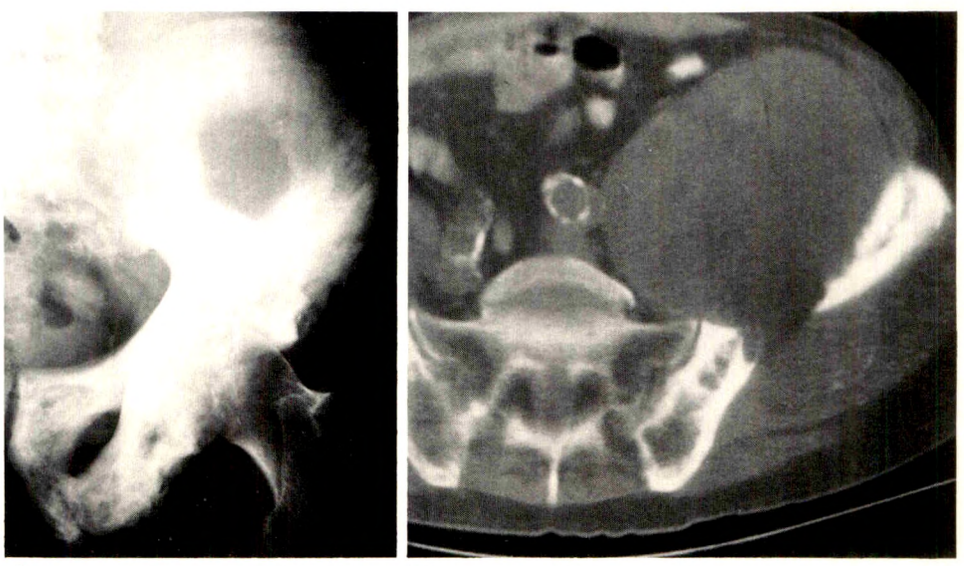

Fig. 8.—Sarcomatous transformation of Paget disease in innominate bone.

***A* and *B*, Radiograph (*A*) and CT scan (*B*) show osteolytic lesion in pagetic ilium with large soft-tissue mass. (Courtesy of P. Kaplan, Omaha, NE.)**

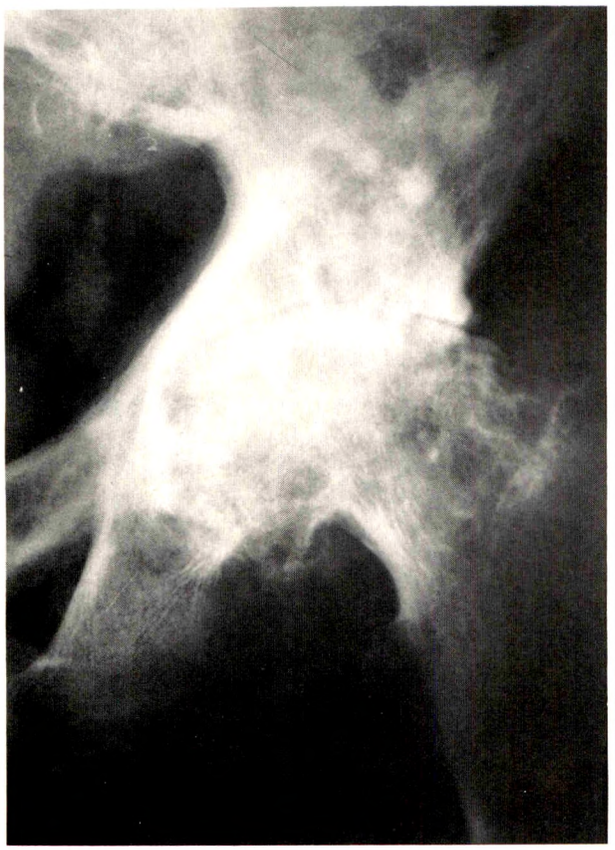

9

Fig. 9.—Osteoarthritis of hip in Paget disease. Joint space narrowing involving superior and axial portions of hip is evident. Pagetic changes are observed in ilium.

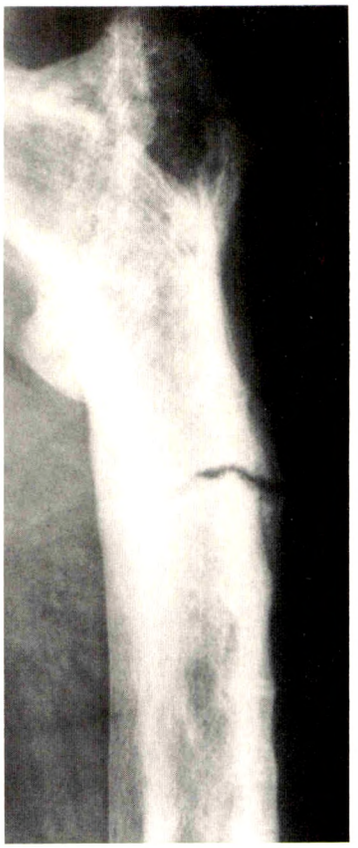

10

Fig. 10.—Fractures in Paget disease. Numerous insufficiency fractures are evident in lateral cortex of femur, and one extends medially, partially across bone. (Courtesy of G. Greenway, Dallas, TX.)

gression of Paget disease during EHDP therapy has been observed in some patients [33], in most patients with the disease, such therapy results in a decrease in skeletal pain, a reduction in serum alkaline phosphatase and urinary hydroxyproline levels, and (based on evaluation of material derived from bone biopsies) a conversion of pagetic bone to a more normal tissue [41–45]. However, a number of reports have indicated an increased frequency of fractures in patients with Paget disease who have been treated with EHDP [46, 47], a complication that may relate to drug dosage and to the occurrence of osteomalacia [47, 48]. Other diphosphonates have been suggested as therapeutic alternatives to EHDP [49] and one, 3-amino-1-hydroxypropilidene-1, 1-diphosphonate (ADP), has been reported to significantly decrease the rate of disease progression [33].

Mithramycin is an antibiotic with cytotoxic activity that has been used successfully in the treatment of Paget disease, leading to a decrease in bone pain and an improvement in laboratory parameters of disease activity [2]. Assessment of the skeletal disease by radiographic and scintigraphic techniques during therapy also has indicated a return to a more normal situation [50], although radiologic change is less frequent and dramatic after the use of mithramycin than after calcitonin treatment. Owing to its significant toxicity, mithramycin administration is best reserved for cases of Paget disease that are resistant to other forms of treatment [51].

Although radiographic improvement may be observed in the appearance of skeletal involvement in Paget disease during treatment with any of the aforementioned therapeutic agents, the changes usually are subtle and dependent on the stage of the disease at the time of the treatment; also, these changes include a conversion of osteolytic lesions to osteosclerotic ones, consolidation of the layered new bone, reappearance of a cortex of uniform density, restoration of corticomedullary differentiation, widening of the medullary canal, thinning of the cortex, a reduction in the external volume of the bone, and a return to normal osseous shape [2]. In monitoring the response of pagetic bone to any of these therapeutic agents, scintigraphy can show a distinct decrease in radionuclide accumulation in diseased areas as a marker of a beneficial therapeutic response (Fig. 7) [52, 53]. On scintigraphy, recurrence of the disease is typically accompanied by a rise in activity in one or more bones or by spread of disease into an adjacent normal bone. When these changes are present, they precede biochemical indicators of recurrent disease.

Complications

> . . . As he was riding and suddenly raised his arm the bone broke near the shoulder . . . and I amputated the arm at the shoulder joint.

> In three out of the five well-marked cases that I have seen or read-of cancer appeared late in life . . . suggesting careful inquiry.
>
> Sir James Paget (1877) [8]

The musculoskeletal complications of Paget disease include osseous deformities, fractures, neoplasms, soft-tissue masses, osteomyelitis, extramedullary hematopoiesis, crystal deposition (monosodium urate, hydroxyapatite and, possibly, calcium pyrophosphate dihydrate), neurologic abnormalities, and degenerative joint disease. Of these, Groh [7] provided examples of deformity of the tibia (leading to anterior bowing of the bone) and innominate bone (producing acetabular protrusion and joint-space diminution in the hip) and commented on nerve-root compression related to vertebral involvement. Spinal stenosis as a complication of Paget disease of the vertebral column has been confirmed subsequently in a number of investigations, especially those in which CT has been used to evaluate the extent of bone involvement [54–57]. Compression of the spinal cord can be due to expansion of bone from the pagetic process, collapse with hemorrhage, deformity, vascular compromise, or neoplastic degeneration; additional neurologic dysfunction in Paget disease may be related to changes in the base of the skull. Cauda equina compression in this disease has also been attributed to ossification of extradural fat [58], and the sciatic nerve may be compressed either in external rotation between an enlarged ischium and lesser trochanter of the femur or in internal rotation between the ilium and piriformis [59].

Neoplastic involvement in Paget disease includes sarcomatous degeneration, giant cell tumor, and superimposition of another tumorous condition, such as metastatic disease, plasma cell myeloma, and lymphoma. Of these, sarcomatous transformation was first recognized by Paget in some of his original five patients. Its reported frequency has varied: In patients with widespread skeletal involvement, sarcomatous degeneration may occur in as many as 5–10%; with less extensive skeletal disease, this complication may be apparent in fewer than 1% of patients [60]. At present, it is generally believed that approximately 1% of patients with Paget disease develop malignant changes [2, 61, 62], although higher rates, on the order of 5%, are still suggested [63]. Sarcomatous degeneration usually is observed in patients who are 55–80 years old; it is slightly more common in men than in women, associated with pain and swelling, typically unifocal, and most commonly evident in the femur, innominate bone (Fig. 8), and humerus. Also, sarcomatous degeneration is apparent in areas of pagetic involvement. Although sarcomas in Paget disease vary widely in their cellularity and cytologic details, they appear to arise from the substratum of fibrous tissue in the pagetic bone. Predominance of certain cells most commonly leads to a diagnosis of osteosarcoma (50–60%) or fibrosarcoma (20–25%), although diagnoses such as chondrosarcoma (10%) and, rarely, sarcoma of myeloid and mesenchymal elements may be entertained. Osteolysis is the dominant radiographic characteristic of the sarcoma.

Giant cell tumors in Paget disease are almost always confined to the skull or the facial bones, with rare involvement of other skeletal sites [64, 65]. Patients with this neoplasm are generally elderly and have polyostotic Paget disease. Metastatic disease and Paget disease also may coexist [66], although the precise relationship between the two conditions is not clear.

Of the articular complications of Paget disease, osteoarthritis—especially in the hip (Fig. 9) and knee—is best known [67–69]. The precise pathogenesis of the joint changes has been debated, although some investigators have supported the concept that a disturbance in endochondral ossification is important [70]. Hypervascularity and rapid turnover in pagetic subchondral bone may lead to accelerated endochondral bone formation, which occurs at the expense of the articular cartilage. Superimposed on this interference with dynamics at the chondroosseous junction are mechanical abnormalities in and around the articulation.

Finally, insufficiency (stress) fractures and acute complete fractures may complicate Paget disease [71, 72]. These are most commonly observed in the bones of the lower extremity, particularly the femur (Fig. 10) and the tibia. As the risk of sarcoma is substantial in cases of complete fracture in Paget disease, biopsy is recommended whenever such a fracture develops [2].

REFERENCES

1. Schmorl G. Ueber Ostitis deformans Paget. *Virchows Arch [A]* **1932**;283:694–751
2. Hamdy RC. *Paget's disease of bone: assessment and management*. New York: Praeger, **1981**
3. Paget J. On a form of chronic inflammation of bones (osteitis deformans). *Med Chir Tr* **1877**;60:37
4. Barry HC. *Paget's disease of bone*. Edinburgh: E&S Livingstone, **1969**:16
5. Ziegler R, Holz G, Rotzler B, Minne H. Paget's disease of bone in West Germany. Prevalence and distribution. *Clin Orthop* **1985**;194:199–204
6. Montagu MFA. Paget's disease (osteitis deformans) and heredity. *Am J Hum Genet* **1949**;1:94–112
7. Groh JA. Mono-osteitic Paget's disease as a clinical entity. Roentgenologic observations in nine cases. *Am J Roentgenol* **1943**;50:230–243 (reprinted *AJR* **1988**;150:235–248)
8. Paget S. *Memoirs and letters of Sir James Paget*, 5th Impression. London: Longmans, Green, **1901**
9. Resnick D, Niwayama G. Paget's disease. In: Resnick D, Niwayama G, eds. *Diagnosis of bone and joint disorders*. Philadelphia: Saunders, **1981**:1721–1754
10. Mirra JM. Pathogenesis of Paget's disease based on viral etiology. *Clin Orthop* **1987**;217:162–170
11. Rebel A, Malkani K, Basle M, Bregeon C. Osteoclast ultrastructure in Paget's disease. *Calcif Tissue Res* **1976**;20:187–199
12. Mills BG, Singer FR. Nuclear inclusions in Paget's disease of bone. *Science* **1976**;194:201–202
13. Mills BG, Singer FR, Weiner LP, Suffin S, Stabile E, Holst P. Evidence for both respiratory syncytial virus and measles virus antigens in the osteoclasts of patients with Paget's disease of bone. *Clin Orthop* **1984**;183:303–311
14. Rebel A, Basle M, Pouplard A, Kouyoumdjian S, Filmon R, Lepatezour A. Viral antigens in osteoclasts from Paget's disease of bone. *Lancet* **1980**;2:344–346
15. Mirra JM, Bauer H, Grant TT. Giant cell tumor with viral-like intranuclear inclusions associated with Paget's disease. *Clin Orthop* **1981**;158:243–251
16. Mirra JM, Gold RH. Case Report 186. *Skeletal Radiol* **1982**;8:67–70
17. Schajowicz F, Ubios AM, Araujo ES, Cabrini RL. Virus-like intranuclear inclusions in giant cell tumor of bone. *Clin Orthop* **1985**;201:247–250
18. Fornasier VL, Flores L, Hastings D, Sharp T. Virus-like filamentous intranuclear inclusions in giant cell tumor, not associated with Paget's disease of bone. A case report. *J Bone Joint Surg [Am]* **1985**;67-A:333–336

19. Rame CS, Powers TM, Kinuko S. Acute multiple sclerosis. Confirmation of "paramyxovirus like" intranuclear inclusions. *Arch Neurol* **1974**;30: 39–46
20. Rebel A, Basle M, Pouplard A, Malkani K, Filmon R, Lepatezour A. Toward a viral etiology for Paget's disease of bone. *Metab Bone Dis Relat Res* **1981**;3:235–238
21. Singer FR, Mills BG. Evidence for a viral etiology of Paget's disease of bone. *Clin Orthop* **1983**;178:245–251
22. Lentle BC, Russell AS, Hesip PG, Percy JS. The scintigraphic findings in Paget's disease of bone. *Clin Radiol* **1966**;27:129–135
23. Khairi MRA, Wellman HN, Robb JA, Johnston CC. Paget's disease of bone (osteitis deformans). Symptomatic lesions and bone scan. *Ann Intern Med* **1973**;79:348–351
24. Miller SW, Castronovo FP, Pendergrass IIP, Potsaid MB. Technetium-99m labeled diphosphonate bone scanning in Paget's disease. *Am J Roentgenol Radium Ther Nucl Med* **1974**;121:177–183
25. Fletcher JW, Butler RL, Henry RE, Solaric-George E, Donati RM. Bone marrow scanning in Paget's disease. *J Nucl Med* **1973**;14:928–930
26. Andrews JT. Osteoporosis circumscripta cranii: its importance in brain scintiscanning. *Australas Radiol* **1976**;20:273–280
27. Velienga CJLR, Pauwels EKJ, Bijvoet OLM. Some characteristics of local scintigraphic and radiologic patterns of Paget's disease of bone (osteitis deformans). *Diagn Imag Clin Med* **1985**;54:273–281
28. Dionne D, Tallefer R, Lebland R, Chartrand R. Osteoporosis circumscripta cranii: a cause for "doughnut" sign on cerebral and bone scans. *Clin Nucl Med* **1983**;8:377
29. Lander PH, Hadjipavlou AG. Paget's disease with contraction of long bones. *Radiology* **1986**;159:471–472
30. Schubert F, Siddle KJ, Harper JS. Diaphyseal Paget's disease: an unusual finding in the tibia. *Clin Radiol* **1984**;35:71–74
31. Schlesinger A, Naimark A, Lee VW. Diaphyseal presentation of Paget's disease in long bones. *Radiology* **1983**;147:83–84
32. Moser RP, Vinh TN, Ros PR, Smirniotopoulos JA, Madewell JE, Berrey BH. Paget's disease of the anterior tibial tubercle. *Radiology* **1987**;164:211–214
33. Maldague B, Malghem J. Dynamic radiologic patterns of Paget's disease of bone. *Clin Orthop* **1987**;217:126–151
34. Lander PH, Hadjipavlou AG. A dynamic classification of Paget's disease. *J Bone Joint Surg [Br]* **1986**;68-B:431–438
35. Zadek RE, Milgram JW. Progression of Paget's disease in the tibia. A case report. *J Bone Joint Surg [Am]* **1976**;58-A:876–878
36. Maldague B, Malghem J. Radiological aspects of Paget's disease of bone. *Acta Orthop Belg* **1974**;40:425–453
37. Doyle FH, Banks LM, Pennock JM. Radiologic observations on bone resorption in Paget's disease. *Arthritis Rheum* **1980**;23:1205–1214
38. Hamilton CR Jr. Effects of synthetic salmon calcitonin in patients with Paget's disease in bone. *Am J Med* **1974**;56:315–322
39. Mallette LE. An unusual morphologic evolution of Paget's disease of bone. *Arthritis Rheum* **1981**;24:1544
40. White MP, Daniels EH, Murphy WA. Osteolytic Paget's bone disease in a young man. Rapid healing with human calcitonin therapy. *Am J Med* **1985**;78:326–332
41. Johnston CC Jr, Khairi MRA, Meunier RJ. Use of etidronate (EHDP) in Paget's disease of bone. *Arthritis Rheum* **1980**;23:1172–1176
42. Siris ES, Canfield RE, Jacobs TP, Baquiran DC. Long term therapy of Paget's disease of bone with EHDP. *Arthritis Rheum* **1980**;23:1177–1184
43. Russell RG, Smith R, Preston C, Walton RJ, Woods CG. Diphosphonates in Paget's disease. *Lancet* **1974**;1:894–898
44. Hosking D, Bijvoet OL. Combined diphosphonate and calcitonin therapy for Paget's disease of bone. *Calcif Tissue Res* **1976**;21[Suppl]:321–326
45. Smith R, Russell RG, Bishop M. Diphosphonates and Paget's disease of bone. *Lancet* **1971**;1:945–947
46. Canfield R, Rosner W, Skinner J, et al. Diphosphonate therapy of Paget's disease of bone. *Clin Endocrinol Metab* **1977**;44:96–106
47. Johnston CC Jr, Altman RD, Canfield RE, Finerman GAM, Tauber JD, Elbert ML. Review of fracture experience during treatment of Paget's disease of bone with etidronate disodium (EHDP). *Clin Orthop* **1981**;172:186–194
48. Boyce BF, Smith L, Fogelman I, Johnston E, Ralston S, Boyle IT. Focal osteomalacia due to low-dose diphosphonate therapy in Paget's disease. *Lancet* **1984**;1:821–824
49. Douglas DL, Duckworth T, Kanis JA, et al. Biochemical and clinical responses to dichloromethylene diphosphonate (Cl_{2MDP}) in Paget's disease of bone. *Arthritis Rheum* **1980**;23:1185–1192
50. Ryan WG, Schwartz. Mithramycin treatment of Paget's disease of bone: exploration of combined mithramycin-EHDP therapy. *Arthritis Rheum* **1980**;23:1155–1161
51. Frame B, Marel GM. Paget's disease: a review of current knowledge. *Radiology* **1981**;141:21–24
52. Vallenga CJLR, Pauwels EKJ, Bijvoet OLM, Hosking DJ, Frigink WB. Bone scintigraphy in Paget's disease treated with combined calcitonin and diphosphonate (EHDP). *Metab Bone Dis Relat Res* **1982**;4:103–112
53. Lee JY. Bone scintigraphy in evaluation of Didronel therapy in Paget's disease. *Clin Nucl Med* **1981**;6:356–358
54. Altman RD. Musculoskeletal complications of Paget's disease of bone. *Arthritis Rheum* **1980**;23:1121–1127
55. Weise GM. Lumbar spinal canal stenosis in Paget's disease. *Spine* **1983**;8:192–198
56. Smidek HH. Neurologic and neurosurgical sequelae of Paget's disease of bone. *Clin Orthop* **1977**;127:70–77
57. Zlatkin MB, Lander PH, Hadjipavlou AG, Levine JS. Paget's disease of the spine: CT with clinical correlation. *Radiology* **1986**;160:155–159
58. Clarke PRR, Williams HI. Ossification in extradural fat in Paget's disease of the spine. *Br J Surg* **1975**;62:571–572
60. Price CHG, Goldie W. Paget's sarcoma of bone. *J Bone Joint Surg [Br]* **1969**;51-B:205–224
61. Wick MP, McLeod RA, Siegal GP, Greditzar HG III, Unni KK. Sarcomas of bone complicating osteitis deformans (Paget's disease). Fifty years experience. *Am J Surg Pathol* **1981**;5:47–59
62. Greditzer HG III, McLeod RA, Unni KK, Beabout JW. Bone sarcomas in Paget's disease. *Radiology* **1983**;146:327–333
63. Schajowicz F, Santini Araujo E, Berenstein M. Sarcomas complicating Paget's disease of bone. A clinicopathological study of 62 cases. *J Bone Joint Surg [Br]* **1983**;65-B:299–307
64. Bonakdarpour A, Harwick R, Pickering J. Case Report 34. *Skeletal Radiol* **1977**;2:52–55
65. Francis R, Lewis E. CT demonstration of giant cell tumor complicating Paget's disease. *J Comput Assist Tomogr* **1983**;7:917–918
66. Roberts JA. Paget's disease and metastatic carcinoma. A case report. *J Bone Joint Surg [Br]* **1986**;68-B:22–23
67. Machtey I, Rodman GP, Benedek TG. Paget's disease of the hip joint. *Am J Med Sci* **1966**;251:524–531
68. Giraham J, Harris WH. Paget's disease involving the hip joint. *J Bone Joint Surg [Br]* **1971**;53-B:650–659
69. Roper BA. Paget's disease involving the hip joint. A classification. *Clin Orthop* **1971**;80:33–38
70. Goldman AB, Bullough P, Kammermans S, Ambos M. Osteitis deformans of the hip joint. *AJR* **1977**;128:601–606
71. Barry HC. Orthopedic aspect of Paget's disease of bone. *Arthritis Rheum* **1981**;23:1128–1130
72. Stevens J. Orthopedic aspects of Paget's disease. *Metab Bone Dis Relat Res* **1981**;3:271–278

Perspective

Pretreatment with Corticosteroids to Prevent Reactions to IV Contrast Material: Overview and Implications

Elliott C. Lasser[1]

A recent report [1] describing the protection against contrast material reactions produced by corticosteroid pretreatment brings into focus a number of issues of interest to radiologists. In a blinded, randomized study carried out in several different institutions, a comparison was made between a two-dose regimen of oral corticosteroids (32 mg of methylprednisolone—Medrol, Upjohn, Kalamazoo, MI) given approximately 12 hr and 2 hr before administration of contrast material, a single-dose regimen of corticosteroids (32 mg) given approximately 2 hr before contrast administration, and corresponding placebo regimens. It was reported that corticosteroids given 12–24 hr before IV ionic contrast administration can provide protection against systemic ionic contrast material toxicity such that the frequency of reactions requiring immediate therapy is not greater than that reported for individuals receiving nonionic contrast media without pretreatment. The single-dose regimen and the placebo did not afford this protection.

Three points deserve special emphasis concerning corticosteroid protection: (1) The protection, as gauged by the decrease in reaction rates of pretreated patients in comparison with those of control subjects, ranged from 23% to 86% (Table 1), depending on the category of reactions under evaluation and the presence or absence of risk factors (defined as a history of a previous reaction and/or a history of any kind of allergy). Patients in the low-risk group uniquely failed to gain any protection in a category of reactions dominated by urticaria but did gain protection in all other categories (Table 1). Complete protection against reactions to contrast material was not accomplished, nor has complete protection ever been reported with any pretreatment. (2) Corticosteroids administered in a single dose approximately 2 hr before contrast administration provided no protection. (3) When comparisons were made in "patients necessitating some form of immediate therapy in the judgment of the attendant physician," the two-dose corticosteroid regimen given 12 and 2 hr before ionic contrast administration appeared to lower the reaction rate to that reported in a large group of patients receiving nonionic media without pretreatment [2].

In designing the study, the investigators originally intended to compare the protective effects of corticosteroids administered over 2–3 days (to correspond with empirical practice) with a regimen of both corticosteroids and antihistamines, and with a regimen of antihistamines alone. In recruiting institutional participation, it soon became apparent that practical logistic considerations would limit the number and duration of tested regimens. Attention was thus focused on those regimens that were thought most likely to produce clear-cut information. The fact that the two-dose regimen provided protection in all but one of the 15 reaction categories examined (Table 1) does not mean that this is an optimal regimen or that additional protection might not be gained by the inclusion of antihistamines and/or beta-adrenergic agonists. However, corticosteroids given in a logistically feasible dose schedule can be safely administered to patients receiving IV ionic contrast media with the expectation that the number of reactions of sufficient severity to necessitate therapy will not differ appreciably from that occurring in patients receiving IV nonionic contrast media.

All of the above, of course, has no bearing on the indications

This work was supported in part by a grant (CA-32856) from the National Cancer Institute.

[1] Department of Radiology, M-032, University of California, San Diego, School of Medicine, La Jolla, CA 92093. Address reprint requests to E. C. Lasser.

AJR 150:257–259, February 1988 0361–803X/88/1502–0257 © American Roentgen Ray Society

TABLE 1: Difference in Reaction Rates Between Patients Treated with Two Doses of Medrol[a] and Patients Treated with Either One Dose of Medrol or a Placebo

Reaction Category[c]	Percentage Difference[b]		
	All Patients	Low-Risk Patients[d]	High-Risk Patients[e]
All reactions	↓31	↓29	↓37
Grade I reactions	↓33	↓43	↓31
Grade II reactions	↓23	↑1	↓45
Grade III reactions	↓62	↓86	↓34
Reactions requiring therapy	↓42	↓35	↓37

Note.—All data in this table are from Lasser et al. [1].

[a] Medrol is produced by Upjohn, Kalamazoo, MI.

[b] ↓ indicates that the reaction rate was lower by this percentage in two-dose patients; ↑ indicates that the reaction rate was higher in two-dose patients.

[c] "All reactions" refers to the total number of reactions in all categories (including grades I–III). Grade I reactions are characterized by a single episode of emesis, nausea, sneezing, and vertigo; grade II reactions include hives, emesis occurring more than one time, and fever or chills (or both); grade III reactions include clinical "shock," bronchospasm, laryngospasm or edema, loss of consciousness, convulsions, a fall in blood pressure, an increase in blood pressure, cardiac arrhythmia, angina, angioedema, or pulmonary edema. "Reactions requiring therapy" were those reactions that necessitated some form of immediate treatment in the judgment of the attendant radiologist.

[d] Low-risk patients had neither a history of adverse reaction to contrast material nor any history of allergy.

[e] High-risk patients include those with a previous adverse reaction to contrast material and/or a history of allergy of any kind.

for using low-osmolar contrast media in specific arterial injections. Here, pain and the chemotoxic (rather than the systemic) effects of the various contrast media become paramount considerations. As of this writing, I am unaware of any data pertaining to the effects of corticosteroids in these situations.

Does all of this suggest that all adult patients (only adults have been studied) receiving ionic contrast media might benefit from corticosteroid pretreatment? Should radiologists consider using corticosteroid pretreatment on a routine basis? Clearly, this is an issue that each radiologist or institution must decide individually. According to the data in the multiinstitutional study [1], corticosteroids would decrease the frequency of reactions of all kinds by at least 20%. Is this a reasonable trade-off for whatever logistic problems and additional expense may arise when corticosteroids are given some hours before contrast administration? What *is* the minimum advance time necessary to achieve protection? Although the multiinstitutional study compared corticosteroid administration 12 and 2 hr before contrast administration with corticosteroid administration 2 hr before contrast administration, is it feasible that a single dose administered at least 6 hr before contrast administration would provide protection?

One can only guess at these answers. My own opinion, based on the pertinent literature [3–7], is that it might be possible to gain protection with only one injection of corticosteroids given several hours (e.g., 6 hr) before contrast administration. For radiologists who wish to consider the option of universal pretreatment, a potential logistic strategy might be as follows: (1) For high-risk patients, use a three-dose, 3-day pretreatment regimen whenever time permits (32 mg of oral methylprednisolone or the equivalent given daily, the last dose 2 hr before contrast administration). (2) For all other patients, when logistics permit, use a two-dose, 2-day pretreatment regimen (32 mg approximately 12 hr before contrast administration and then 32 mg 2 hr before the procedure). (3) For patients in whom prolonged pretreatment is impossible use a single pretreatment 6 hr before the procedure when logistics permit. (4) When no advance pretreatment regimen is logistically feasible and an emergency diagnostic procedure is required, high-risk patients can be immediately pretreated with other drugs (i.e., antihistamines and/or beta-adrenergic agonists [8, 9]), and/or one of the low-osmolar contrast media can be used. No corticosteroids are used in this circumstance. Patients not identifiable as high risk can be injected with either a low-osmolar or a high-osmolar contrast agent.

What are the adverse effects, if any, of corticosteroids alone, and what are the contraindications to their use? In the multiinstitutional study, no effects could be identified in the 4272 patients receiving corticosteroids that differed from those occurring in the 2491 patients receiving placebos. A number of mild and nonspecific reactions occurred equally in both groups. These included vertigo, nausea, emesis, and rash [1]. To our knowledge, there are no other reports of a series of patients receiving corticosteroids in this low dosage. There are a number of reports of patients experiencing anaphylactic reactions to injections of hydrocortisone, but reactions to oral corticosteroids have only rarely been reported [10–12].

Patients might be considered for exclusion from corticosteroid pretreatment in several circumstances. Prudence might dictate that patients with active tuberculosis, systemic fungal infections, or a history of peptic ulcer or diverticulitis within the past year should be excluded from routine pretreatment. Although there are no data to indicate that corticosteroids in the low dosage suggested for routine pretreatment would created problems, there are no data to the contrary. If these individuals have risk factors for systemic contrast reactions, consideration can be given to the use of antihistamines, beta-adrenergic agonists, and/or low-osmolar contrast media.

Finally, several experimental and clinical reports [13–15] indicate that corticosteroids can diminish the intensity of the extravascular accumulation of technetium-99m compounds and of contrast media, and thus might diminish the sensitivity of these compounds in imaging bone and brain under certain circumstances (e.g., tumors, abscesses, trauma). Whether sufficient diagnostic compromise will occur within the corticosteroid pretreatment regimens suggested, however, remains to be established.

REFERENCES

1. Lasser EC, Berry CC, Talner LB, et al. Pretreatment with corticosteroids to alleviate reactions to intravenous contrast material. *N Engl J Med* **1987**;317:845–849
2. Schrott KM, Behrends B, Clauss W, Kaurman J, Lehnert J. Iohexol in der Ausscheidungsurographie: Ergebnisse des Drug-monitoring. *Fortschr Med* **1986**;104:153–156
3. Ellul-Micallef R, Fenech FF. Intravenous prednisolone in chronic bronchial

asthma. *Thorax* **1975**;30:312–315
4. Talbot S, Atkins PC, Zweiman B. In vivo effects of corticosteroids on human allergic responses. I. Effects of systemic administrations of steroids. *Ann Allergy* **1987**;58:363–365
5. Littenberg B, Gluck EH. A controlled trial of methylprednisolone in the emergency treatment of acute asthma. *N Engl J Med* **1986**;314:150–152
6. Schleimer RP, MacGlashan DW Jr, Gillespie E, Lichtenstein LM. Inhibition of basophil histamine release by anti-inflammatory steroids. II. Studies on the mechanism of action. *J Immunol* **1982**;129:1631–1636
7. Morris HG. Mechanisms of action and therapeutic role of corticosteroids in asthma. *J Allergy Clin Immunol* **1985**;75:1–13
8. Greenberger PA, Patterson R, Tapio CM. Prophylaxis against repeated radiocontrast media reactions in 857 cases: adverse experience with cimetidine and safety of β-adrenergic antagonists. *Arch Intern Med* **1985**;145:2197–2200
9. Zweiman B, Mishkin MM, Hildreth EA. An approach to the performance of contrast studies in contrast material–reactive persons. *Ann Intern Med* **1975**;83:159–162
10. Chan CS, Brown IG, Oliver WA, Zimmerman PV. Hydrocortisone-induced anaphylaxis. *Med J Aust* **1984**;141:444–446
11. Krunis NG. Untoward reactions to corticosteroids: intolerance to hydrocortisone. *Ann Allergy* **1976**;36:203–206
12. Mendelson LN, Meltzer EO, Hamburger RN. Anaphylaxis-like reactions to corticosteroid therapy. *J Allergy Clin Immunol* **1974**;54:125–131
13. Crocker EF, Zimmerman RA, Phelps ME, Kuhl DE. The effect of steroids on the extravascular distribution of radiographic contrast material and technetium pertechnetate in brain tumors as determined by computed tomography. *Radiology* **1976**;119:471–474
14. Scott SM, Manaster BJ, Alazraki N, Wooten WW, Murphy K. Technetium-99m imaging of bone trauma: reduced sensitivity caused by hydrocortisone in rabbits. *AJR* **1987**;148:1175–1178
15. Enzmann DR, Britt RH, Placone RC Jr, Obana W, Lyons B, Yeager AS. The effect of short-term corticosteroid treatment on the CT appearance of experimental brain abscesses. *Radiology* **1982**;145:79–84

Chest Imaging Update

American Roentgen Ray Society 88th Annual Meeting, Friday Symposium

May 13, 1988, San Francisco Hilton and Tower, San Francisco, CA

Computed Tomography	Moderator: Stewart Sagel
8:00 a.m.	Overview (*Sagel*)
8:10 a.m.	Focal lung disease (*Zerhouni*)
8:35 a.m.	Diffuse lung disease (*Müller*)
9:00 a.m.	Staging of bronchogenic carcinoma (*Pugatch*)
Interventional Radiography	
9:25 a.m.	Intrathoracic drainage procedures (*Westcott*)
9:45 a.m.	Percutaneous biopsy of central lesions (*Weisbrod*)
10:05 a.m.	Coffee break
Digital Imaging	Moderator: Carl Ravin
10:25 a.m.	Overview (*Ravin*)
10:35 a.m.	Digital angiography (*Barth*)
10:55 a.m.	Digital radiography (*MacMahon*)
Magnetic Resonance Imaging	Moderator: Gordon Gamsu
11:15 a.m.	Overview (*Gamsu*)
11:25 a.m.	Intrathoracic vascular lesions (*Webb*)
11:50 a.m.	Applications of MRI of the thorax (*McLoud*)

Perspective

Lung Cancer: Update on Staging Classifications

Paul J. Friedman[1]

The staging of bronchogenic carcinoma is an important step in the selection of appropriate treatment [1]. Formal staging follows the TNM system, adopted by the International Union Against Cancer and first published in 1974 in the *AJR* [2]. The classification for lung cancer [3] has been improved recently, as reported by Mountain in 1986 [4] (Table 1). Few articles in the radiologic literature to date have made use of the new classification, so this review is intended for radiological clinicians and investigators.

The American Thoracic Society (ATS) improvements on the American Joint Committee (AJC) lymph node classification were reported by Tisi et al. [5] and first applied in a clinical study by Friedman et al. [6]. Since then, several workers have used the original ATS classification, citing its advantages for precise description of nodal involvement [7–9]. The changes in the TNM classification and studies on other node groups in the thorax [10] have required additions to the ATS system, which will be presented here (Table 2).

The stage is determined by (1) the size and location of the primary tumor; (2) the presence of regional (hilar) or mediastinal lymph node involvement; (3) invasion of the pleura, chest wall, or mediastinum; or (4) metastatic spread outside the thorax (Table 1). Staging is the joint responsibility of surgeons, endoscopists, pathologists, and radiologists. The current role of imaging in lung cancer staging is vital and well summarized in the literature [11–15]. Mediastinoscopy plays a pivotal role in detecting or confirming mediastinal metastasis, but description of the method and its results is beyond the scope of this review [1, 12].

Subsequent management of lung cancer is based on several factors in addition to stage; these include the tumor histology; the growth of node metastases through the node capsule; the presence of malignant cells in pleural effusion; and the age, condition, and attitude of the patient. The stage of the tumor most directly correlates with *resectability*; this refers to the technical possibility of removing all malignant tissue with one surgical procedure. The *operability* of a tumor is also affected by the stage and by the other factors listed. Evaluation of operability is based on a judgment about whether survival will be significantly improved after surgery (modified by the expected perioperative morbidity and mortality) as compared with survival with conservative treatment. This is different from another common usage of *operability*, in which it means the general or cardiorespiratory capacity of the patient to withstand surgery.

The new staging scheme [4] is oriented toward eligibility of patients for surgical or other therapy. There is now a distinction between local invasion (T3) and nonresectable spread (T4); similarly, spread to lymph nodes that can be removed (N2) is distinguished from those that cannot be removed surgically (N3). The supraclavicular and scalene nodes have been changed from distant metastases to N3 nodes because they are accessible to regional (radiation) therapy. Stage IIIa denotes patients with a poor prognosis but technically resectable local invasion. Stage IIIb covers patients with nonresectable spread in the thorax. Stage IV patients require systemic therapy for distant spread [3].

Received September 11, 1987; accepted after revision October 27, 1987.

[1] Department of Radiology, University of California, San Diego, Medical Center, H-756, 225 Dickinson St., San Diego, CA 92103. Address reprint requests to P. J. Friedman.

This work was supported in part by the University of California, San Diego, Radiology Research and Education Foundation.

AJR **150:261–264, February 1988** 0361–803X/88/1502–0261 © American Roentgen Ray Society

TABLE 1: The New AJC Classification of Lung Cancer

Stage		Description
TNM CLASSIFICATION		
Primary tumor (T)		
TX		Tumor proved by the presence of malignant cells in bronchopulmonary secretions but not visualized by radiography or bronchoscopy, or any tumor that cannot be assessed as in a retreatment staging
T0		No evidence of primary tumor
TIS		Carcinoma in situ
T1		A tumor that is 3 cm or less in greatest diameter, surrounded by lung or visceral pleura and without evidence of invasion proximal to a lobar bronchus at bronchoscopy (except for superficial endobronchial tumors, which may extend proximal to the main bronchus and still be called T1)
T2		A tumor that is more than 3 cm in greatest diameter, or a tumor of any size that either invades the visceral pleura or has associated atelectasis or obstructive pneumonitis extending to the hilar region. At bronchoscopy, the proximal extent of demonstrable tumor must be within a lobar bronchus or at least 2 cm distal to the carina. Any associated atelectasis or obstructive pneumonitis must involve less than an entire lung.
T3		A tumor of any size with direct extension into the chest wall (including superior sulcus tumors), diaphragm, or the mediastinal pleura or pericardium without involving the heart, great vessels, trachea, esosphagus, or vertebral body; or a tumor in the main bronchus within 2 cm of the carina without involving the carina
T4		A tumor of any size with invasion of the mediastinum involving heart, great vessels, trachea, esophagus, vertebral body, or carina; or presence of malignant pleural effusion (cytologically positive)
Nodal involvement (N)		
N0		No demonstrable metastasis to regional lymph nodes
N1		Metastasis to lymph nodes in the peribronchial region, the ipsilateral hilar region, or both, including direct extension
N2		Metastasis to ipsilateral mediastinal lymph nodes and subcarinal lymph nodes
N3		Metastasis to contralateral mediastinal or hilar lymph nodes, ipsilateral or contralateral scalene, or supraclavicular nodes
Distant metastasis (M)		
M0		No (known) distant metastasis
M1		Distant metastasis present—specify site(s)
STAGE GROUPING		
Occult carcinoma	TX N0 M0	An occult carcinoma with bronchopulmonary secretions containing malignant cells but without other evidence of the primary tumor or evidence of metastasis
Stage 0	TIS N0 M0	Carcinoma in situ
Stage I	T1 N0 M0 T2 N0 M0	A tumor that can be classified T1 or T2 without any nodal or distant metastasis
Stage II	T1 N1 M0 T2 N1 M0	A tumor classified as T1 or T2 with metastasis to the lymph nodes in the peribronchial region and/or ipsilateral hilar region only
Stage IIIa	T3 N0 M0 T3 N1 M0 T1–3 N2 M0	A tumor more extensive than T2 but without invasion of a vital structure, or any tumor up to T3 with metastasis to ipsilateral mediastinal or subcarinal lymph nodes
Stage IIIb	Any T N3 M0 T4 Any N M0	A tumor with invasion of vital mediastinal structures or metastasis to nonresectable nodes, but without spread beyond the thorax
Stage IV	Any T Any N M1	A tumor with metastatic spread beyond the thorax and its regional lymph nodes (i.e., beyond scalene or supraclavicular nodes)

Note. — Classifications and descriptions from Mountain et al. [4]. AJC = American Joint Committee; TNM = tumor-nodal involvement-metastasis.

Lymph Node Classification

The ATS Committee on Lung Cancer considered the idea that the original TNM staging system classified lymph nodes too superficially to provide valid data on the efficacy of different treatments [5]. The categories were N0 (no nodal metastasis), N1 (hilar or regional node involvement), and N2 (mediastinal metastasis). The new classification added N3 to provide the useful distinction between resectable and nonresectable mediastinal nodes, but it did not help separate "hilar" from "mediastinal" nodes. The anatomic definition of the hilum of the lung is a plane through the junction of the lung root and mediastinum, which is not at all the working definition of the hilum that radiologists or surgeons use. The hilar nodes are described as intrapulmonary, outside the mediastinal pleura [2, 3], but the surgeon may find this an elusive definition because the position of a particular node with respect to the mediastinal pleura depends on how forcefully the lung is retracted.

The solution was to relate nodes to fixed anatomic structures or boundaries, such as the bronchi, aortic arch, or azygos vein, and to avoid use of the term "hilar." In deciding the stage in the TNM system with the help of the ATS classification of node regions, a compromise must be made to decide whether 10R and 10L nodes are N1 or N2 (there is no problem if the tumor is contralateral; they are then clearly

TABLE 2: Classification of Lymph Node Locations

Region	Name	Description
1 (R & L)	Supraclavicular	Supraclavicular or scalene nodes (N3)
2 (R & L)	Upper paratracheal	Nodes to the right or left of the midline of the trachea above the level of the aortic arch (N2 if ipsilateral to tumor)
4 (R & L)	Lower paratracheal	Nodes to the right or left of the midline of the trachea from the level of the aortic arch to the top of the azygos vein (R) or the level of the carina (L) (N2 if ipsilateral to tumor)
5	Aortopulmonary	Nodes on the left side of the mediastinum: in the aortopulmonic window lateral to the ligamentum arteriosum, lateral to the aortic arch, or lateral to the pulmonary artery as far as the first left upper lobe branch (N2 for left-sided tumor)
6	Anterior	Nodes anterior to the ascending aorta or the brachiocephalic, left subclavian, and left common carotid arteries (N2 if clearly ipsilateral, otherwise N3)
7	Subcarinal	Nodes caudal to the tracheal carina, but originating within 2 cm (to exclude nodes in regions 8–9 or 11) (always N2)
8 (R & L)	Paraesophageal	Nodes adjacent to the esophagus, right or left of the midline of the esophagus, below region 7 (at least 3 cm below the level of the carina) plus nodes in the right or left pulmonary ligament (included in region 8 because of radiologic inability to distinguish) (N2 if ipsilateral to tumor)
10R	Tracheobronchial	Nodes to the right side of the midline of the trachea from the level of the top of the azygos vein and along the right main bronchus as far as the right upper lobe branch (N1 if ipsilateral, N3 if contralateral to tumor; see text for reason)
10L	Peribronchial	Nodes to the left side of the midline of trachea and along the left main bronchus from the carina to the left upper lobe branch (N2 if ipsilateral to tumor)
11 (R & L)	Intrapulmonary	Nodes along right or left lobar or segmental bronchi, distal to regions 7 and 10 (N1 if ipsilateral, N3 if contralateral)
14 (R & L)	Diaphragmatic	Nodes adjacent to the diaphragm at the cardiophrenic angle (anterior) or near the phrenic nerve (middle); include posterior diaphragmatic nodes in region 8 (N2 if ipsilateral to tumor)

[a] American Thoracic Society Classification [5], revised by author.

N3). Since there are no region-specific data on survival after surgery, which is one of the long-range goals of the ATS classification, the decision is somewhat arbitrary. In view of the differences in ease of direct examination and resection of the node region, adjacent bronchus, and next proximal node region (4R and 4L) on the two sides, I recommend that 10R nodes be classified as N1 (hilar) and 10L nodes as N2 (mediastinal).

Since the ATS publication, the importance of considering superior diaphragmatic nodes in lung cancer has been shown [10]. Accordingly, new numbers have been assigned to these regions (14R and 14L), beyond the numbers previously assigned by the AJC, and they are classified as mediastinal. A small simplification in the paraesophageal and pulmonary ligament node regions has been suggested for the benefit of radiologists: Since these cannot be distinguished by imaging (in the absence of pneumothorax), regions 8 and 9 should be combined as region 8. A change prompted by the new TNM classification [4] is inclusion of the scalene and supraclavicular lymph nodes as regions 1R and 1L. These are no longer classified as extrathoracic metastases (M1), but as N3 nodes, hence they now must be listed as separate node regions (Table 2).

Management

Most radiologists and many thoracic surgeons [16] believe that negative results on CT or MR can reliably eliminate the need for mediastinoscopic biopsy. If mediastinoscopy is not a locally accepted preoperative routine, however, then little is gained by a negative CT scan: The patient would not be "spared" an unnecessary mediastinoscopy, because mediastinoscopy would not have been done. If, however, the scan shows enlarged nodes (N2 or N3) or frank mediastinal invasion (T3 or T4) [17], then a directed biopsy can be performed, which may avoid attempted surgery of an inoperable or

nonresectable lesion. Enlarged nodes cannot be assumed to be the site of metastases and therefore be used to preclude surgery without biopsy.

The low frequency of mediastinal metastasis with radiographic T1 N0 lesions implies that CT would not be cost-effective in such patients. Our experience and that of others [6, 18] suggests that CT may still be useful for 3-cm lesions. We recommend 2 cm as the maximum size of a peripheral primary tumor that can be taken directly to thoracotomy, without CT or mediastinoscopy.

Is detection of hilar metastases of value? N1 metastases clearly affect prognosis and, therefore, operability, but in the absence of any satisfactory nonsurgical therapy, spread to the hilum does not preclude definitive resection. Therefore, the emphasis for radiologists should be on detection of mediastinal (N2–N3) nodal involvement; plain film evidence of insilateral hilar enlargement (N1) should be followed by more careful presurgical evaluation of the mediastinum, rather than by hilar tomography or biopsy.

Ideally, an institution will have locally accepted and consistent criteria for surgery. Staging by noninvasive sizing of lymph nodes is an expensive exercise unless clinical management is responsive to diagnostic findings. Application of the improved TNM and ATS staging systems will allow more uniform description of cases among institutions and increase the possibility of developing clinical records that will be useful in evaluating different modes of therapy. The CT studies to date add up to hundreds of cases with mediastinal metastases, but surgical management in response to the diagnostic information has been variable, so that the efficacy of careful staging in terms of outcomes for patients will not be known for years.

Summary

The AJC for Cancer Staging has improved the TNM system for lung cancer by breaking up the large category of advanced disease into several groups with different treatment implications. Radiologists should be familiar with this system so that they can direct the imaging part of the workup efficiently. The ATS classification of regional lymph nodes [5] also has been updated both to take into account the growing recognition of superior diaphragmatic nodes in lung cancer [10] and to change the supraclavicular lymph nodes from distant metastases to thoracic nodes (in keeping with the revised TNM system [2]). Use of this classification helps radiologists record accurately which nodes are involved and also prompts the film reader to examine all parts of the mediastinum carefully and systematically. The use of CT for staging lung cancer is well established, but its appropriate use and limitations should be recognized [11–16]. The usefulness of MR in special cases is now well described [17, 19, 20], but the hoped-for tissue specificity for tumor has not been realized. Imaging techniques have a primary role in screening for spread of disease, but confirmation by tissue biopsy is a required step in correct management.

REFERENCES

1. Paulson DL, Urschel HC. Selectivity in the surgical treatment of bronchogenic carcinoma. *J Thorac Cardiovasc Surg* **1971**;62:554–562
2. Mountain CF, Carr DT, Anderson WAD. A system for the clinical staging of lung cancer. *AJR* **1974**;120:130–138
3. Task Force on Lung Cancer (chairperson, Mountain CF). *System for staging of lung cancer 1979*. Chicago, IL: American Joint Committee for Cancer Staging and End-Results Reporting, **1979**
4. Mountain CF. A new international staging system for lung cancer. *Chest* **1986**;89:225S–233S
5. Tisi GM, Friedman PJ, Peters RM, et al. Clinical staging of primary lung cancer. Official statement of the American Thoracic Society. *Am Rev Resp Dis* **1983**;127:659–664
6. Friedman PJ, Feigin DS, Liston SE, et al. Sensitivity of radiography, computed tomography and gallium scanning to metastasis of lung carcinoma. *Cancer* **1984**;54:1300–1306
7. Quint LE, Glazer GM, Orringer MB, Francis IR, Bookstein FL. Mediastinal lymph node detection and sizing at CT and autopsy. *AJR* **1986**;147:469–472
8. Glazer GM, Gross BH, Quint LE, Francis IR, Bookstein FL, Orringer MB. Normal mediastinal lymph nodes: number and size according to American Thoracic Society mapping. *AJR* **1985**;144:261–265
9. Glazer HS, Aronberg DJ, Sagel SS, Friedman PJ. CT demonstration of calcified mediastinal lymph nodes: a guide to the new ATS classification. *AJR* **1986**;147:17–25
10. Aronberg DJ, Peterson RR, Glazer HS, Sagel SS. Superior diaphragmatic lymph nodes: CT assessment. *J Comput Assist Tomogr* **1986**;10:937–941
11. Heitzman ER. The role of computed tomography in the diagnosis and management of lung cancer. An overview. *Chest* **1986**;89[Suppl]:237S–241S.
12. Unruh H, Chiu RC. Mediastinal assessment for staging and treatment of carcinoma of the lung. *Ann Thorac Surg* **1986**;41:224–229
13. Filderman AE, Shaw C, Matthay RA. Lung cancer. Part II. Staging and therapy. *Invest Radiol* **1986**;21:173–185
14. Zerhouni EA, Stitik FP. Controversies in computed tomography of the thorax. The pulmonary nodule—lung cancer staging. *Radiol Clin North Am* **1985**;23:407–426
15. Ferguson MK, MacMahon H, Little AG, Golomb HM, Hoffman PC, Skinner DB. Regional accuracy of computed tomography of the mediastinum in staging of lung cancer. *J Thorac Cardiovasc Surg* **1986**;91:498–504
16. Epstein DM, Stephenson LW, Gefter WB, van der Voorde F, Aronchick JM, Miller WT. Value of CT in the preoperative assessment of lung cancer: a survey of thoracic surgeons. *Radiology* **1986**;161:423–427
17. Martini N, Heelan R, Westcott J, et al. Comparative merits of conventional, computed tomographic, and magnetic resonance imaging in assessing mediastinal involvement in surgically confirmed lung carcinoma. *J Thorac Cardiovasc Surg* **1985**;90:639–648
18. Heavey LR, Glazer GM, Gross BH, Francis IR, Orringer MB. The role of CT in staging radiographic $T_1N_0M_0$ lung cancer. *AJR* **1986**;146:285–290
19. Musset D, Grenier P, Carette MF, et al. Primary lung cancer staging: prospective comparative study of MR imaging with CT. *Radiology* **1986**;160:607–611
20. Webb WR, Jensen BG, Sollitto R, et al. Bronchogenic carcinoma: staging with MR compared with staging with CT and surgery. *Radiology* **1985**;156:117–124

Small-Cell Bronchogenic Carcinoma: CT Evaluation

Jay L. Pearlberg[1]
Michael A. Sandler[1]
Joseph W. Lewis, Jr.[2]
Gordon H. Beute[1]
Michael B. Alpern[1]

CT examinations in 37 patients with proved small-cell bronchogenic carcinoma studied before treatment were reviewed. The distribution of lymphadenopathy in the mediastinal compartments designated by the American Thoracic Society was assessed. The frequency of lymph node enlargement was right hilum (43%), left hilum (49%), one or both hila (84%), right upper paratracheal (32%), right lower paratracheal (54%), right tracheobronchial (65%), left upper paratracheal (14%), left lower paratracheal (38%), left peribronchial (35%), paraesophageal (14%), anterior mediastinum (24%), and subcarinal (65%). We also assessed the frequency of additional findings including pleural effusion (38%), pericardial thickening (38%), displacement or narrowing of either the tracheobronchial tree (68%) or major vessels (68%), and hepatic masses (24%). Mediastinal involvement was present in 92% of cases, as compared with 13% reported in a large series based on conventional radiography.

These data show the spectrum of intrathoracic CT findings in proved, untreated cases of small-cell bronchogenic carcinoma.

Numerous articles have been written about the importance and accuracy of CT in evaluating non–small-cell bronchogenic carcinoma [1]. However, previous imaging evaluations of patients with small-cell carcinoma are problematic for several reasons. First, the largest series antedate CT and thus are limited in their accuracy in evaluating the hilum and mediastinum [2, 3]. Second, the more recent papers that discuss CT evaluation use differing classifications of hilar/mediastinal adenopathy and therefore are difficult to compare [4–9]. Finally, reevaluation of the role of radiotherapy and surgery in the treatment of small-cell carcinoma demands a degree of detail that is not provided in most of these recent studies [9–12].

We reviewed CT examinations of the thorax in 37 patients with recently diagnosed small-cell carcinoma. We classified hilar/mediastinal adenopathy according to the staging system of the American Thoracic Society (ATS) for non–small-cell lung cancer and, in this paper, present the spectrum of our intrathoracic findings.

Materials and Methods

Thirty-seven patients with biopsy-proved small-cell bronchogenic carcinoma (including small-cell undifferentiated and oat-cell carcinoma) were evaluated with thoracic CT between 1983 and 1986. All cases were untreated at the time of CT examination. The 37 patients included 21 men and 16 women, ranging in age from 52 to 81 years (average, 67 years). The interval between diagnosis and CT examination ranged from 0 to 44 days (average, 10.6 days).

Thirty-six examinations were conducted with a Picker 1200SX (Picker International, Highland Heights, OH) or a GE CT/T 9800 scanner (General Electric Systems, Milwaukee, WI). One was performed at another institution on a Technicare Delta 2060 scanner (Technicare, Cleveland, OH). All but one of the examinations were begun with bolus IV administration of 100–150 ml meglamine diatrizoate (Angiovist 28%). Rapid scanning extended first from the most caudal part of the hila to the apices for optimal differentiation of hilar vessels from lymph

Received August 17, 1987; accepted after revision October 19, 1987.

Presented at the annual meeting of the American Roentgen Ray Society, Miami Beach, FL, April 1987.

[1] Department of Radiology, Henry Ford Hospital, 2799 W. Grand Blvd., Detroit, MI 48202. Address reprint requests to J. L. Pearlberg.

[2] Department of Surgery, Henry Ford Hospital, 2799 W. Grand Blvd., Detroit, MI 48202.

AJR 150:265–268, February 1988
0361–803X/88/1502–0265
© American Roentgen Ray Society

nodes and then from below the hila through the lung bases at 1-cm intervals. In all but three cases, examination continued into the upper abdomen to include the adrenal glands. Hard copies of the CT scans were obtained at both mediastinal and lung settings.

All CT examinations were reviewed for the following findings: (1) lymphadenopathy (defined as having a short-axis size of >1 cm in the hilum/mediastinum [13] and of ≥6 mm in the superior diaphragmatic and retrocrural areas [14]); (2) displacement or narrowing of either the tracheobronchial tree or major vessels; (3) major (e.g., at least lobar) atelectasis; (4) parenchymal masses not contiguous with hilar/mediastinal mass; (5) pleural effusion; (6) pericardial thickening (defined as >1–2 mm except anterior to the right ventricle, where 3- to 4-mm thickness may be normal [15]); (7) hepatic metastases (areas of low attenuation that did not appear to be cysts in portions of liver included in the study); and (8) adrenal enlargement (thickness >1 cm).

Location of enlarged lymph nodes was by stations defined by the ATS [16]. The frequency of lymphadenopathy in each station, the most common combination of stations involved, and the frequency of other intrathoracic findings were calculated.

Although all patients had biopsy-proved small-cell carcinoma, histologic confirmation was not available for all enlarged lymph nodes (or other abnormalities) in each patient. It is therefore possible that, for example, lymph nodes enlarged by reactive hyperplasia were interpreted as neoplastic.

Results

The distribution of lymph node enlargement is presented in Table 1. Only three patients presented without hilar or mediastinal adenopathy; two had isolated pulmonary nodules and one had a pleura-based mass. Thirty-four patients (92%) presented with mediastinal or mediastinal and hilar lymphadenopathy. Mediastinal adenopathy was present in all of these cases, but was the only site of lymphadenopathy in three (8%). One or both hila were involved in 31 patients (84%), but in no case was hilar adenopathy present without mediastinal involvement. Unilateral adenopathy (involving just one side of the hilum/mediastinum) was present in only five (15%). In 34 patients with hilar/mediastinal adenopathy, the average number of stations (12 total) involved was 5.2 and ranged from two to 11. The stations most commonly involved were subcarinal (station 7) and right tracheobronchial (station 10R) with 24 cases (65%) each. Those least commonly involved were the left upper paratracheal (station 2L) and paraesophageal (station 8) with five patients (14%) each.

Table 2 lists the frequency of other intrathoracic findings. Displacement or narrowing of the tracheobronchial tree (68%) or major vessels (68%) were the most common of these findings; collateral vasculature in association with narrowing of major vessels suggesting the presence of superior vena cava syndrome was seen in three cases. The frequency of pleural effusion and pulmonary nodules is noted in the table, but with the exception of the three cases in which peripheral masses were the sole significant finding, there was no pathologic proof that these represented metastases; no additional biopsies were performed on these lesions since the diagnosis had been established. Table 2 also lists the frequencies of adrenal and hepatic abnormalities since our routine examination for bronchogenic carcinoma includes the upper abdomen through the level of both adrenal glands. However, these findings were not confirmed histologically.

TABLE 1: Distribution of Lymph Node Enlargement in 37 Patients with Proved Small-Cell Bronchogenic Carcinoma

Station	Location	% of Patients
2R	Right upper paratracheal nodes	32
2L	Left upper paratracheal nodes	14
4R	Right lower paratracheal nodes	54
4L	Left lower paratracheal nodes	38
5	Aortopulmonary nodes	51
6	Anterior mediastinal nodes	24
7	Subcarinal nodes	65
8	Paraesophageal nodes	14
10R	Right tracheobronchial nodes	65
10L	Left peribronchial nodes	35
11R	Right hilar nodes	43
11L	Left hilar nodes	49

Discussion

Different staging systems for small-cell carcinoma have been proposed [9–12, 17]. The American Joint Commission Tumor–Nodal Involvement–Metastasis (TNM) [18] staging system is widely used to stage non–small-cell lung cancer. However, TNM staging for small-cell carcinoma fell into disfavor as the prognosis of these patients, who usually were treated by chemotherapy with or without radiotherapy, did not show a close relationship to the TNM stage [9–12]. The two-stage system adopted by the Veterans Administration Lung Cancer Study Group (VAL) [19] was then widely

TABLE 2: Frequency of Extramediastinal/Hilar Findings on CT in 37 Patients with Proved Small-Cell Bronchogenic Carcinoma

CT Findings	No. of Patients (%)
Displacement/narrowing of tracheobronchial tree	25 (68)
Displacement/narrowing of major vessels	25 (68)
With collateral vessels	3 (8)
Major atelectasis	11 (30)
Noncontiguous parenchymal mass	15 (41)
Single	8 (22)
Multiple	7 (19)
Pleural effusions	
Right and/or left	14 (38)
Right	9 (24)
Left	7 (19)
Unilateral	12 (32)
Bilateral	2 (5)
Pericardial thickening	14 (38)
Adrenal enlargement	
Right and/or left	3 (9)[a]
Right	2 (6)
Left	2 (6)
Hepatic masses	9 (26)[a]
Retrocrural adenopathy	2 (5)
Superior diaphragmatic nodes	4 (11)

[a] Upper abdomen was not included on CT examination of three patients.

adopted [10]. This system divides patients into two groups, those with limited disease and those with extensive disease. Limited disease indicates tumor confined to one hemithorax and regional lymphatics that could be included in a radiotherapy portal. Extensive disease indicates a more widespread process [11, 20]. This system divides patients with small-cell carcinoma into two groups with different treatment options (limited disease may be considered for radiotherapy), response rates, and survival times [11, 21, 22].

In recent years there has been a trend toward intensive chemotherapy regimens, aggressive treatment combining chemotherapy and radiotherapy, and a reevaluation of the role of surgery [9, 12, 21]. Several reports have suggested that subsets of patients with extensive disease (according to the VAL classification) may respond to treatment as well as patients with limited disease do [10–12]. These factors have underlined the need for a more detailed system of evaluation than the VAL two-stage system provides [9–12].

The American Joint Committee for Cancer Staging and End Results Reporting has recommended that the TNM classification now be used to describe the extent of disease in small-cell cancer [17]. However, in 1981, the American Thoracic Society suggested a modified form of the TNM staging system for lung cancer [16]. The ATS system has the following advantages: (1) It provides specific anatomic definitions for each nodal station. This facilitates the correlation of studies performed at different centers using the ATS system. (2) The anatomic boundaries of the nodal stations are structures easily identified on CT scans. (3) It allows easy correlation of these nodal stations with anatomic structures defined at mediastinoscopy [16]. Glazer et al. [3] have shown that CT can be used with this system to map normal mediastinal lymph node groups. Friedman et al. [23] used this system to evaluate 45 patients with bronchogenic carcinoma, two of whom had small-cell carcinoma.

Review of the radiologic literature describing intrathoracic small-cell carcinoma reveals several major limitations. The first applies to all studies employing conventional radiographs that generally antedated CT. Conventional radiologic evaluation of the mediastinum is inaccurate [2], and therefore the results are of no value. For example, a compilation of results from several such studies in a current, prominent oncology text [22] reports that mediastinal adenopathy was present in only 14% of 252 cases. A similar compilation in Fraser and Pare's textbook on chest radiology [24] described the presence of mediastinal mass or widening in 13% of 114 cases. This compares with our findings, based on CT, of mediastinal adenopathy in 92% of our 37 cases.

The second limitation applies to techniques used in several studies based on CT [4, 5, 7]. The use of a second-generation scanner with a prolonged (20-sec) scan time [4] or the lack of routine administration of IV contrast material to evaluate the hilum and mediastinum [5, 7] limit the reliability of such examinations.

The final limitation applies to studies performed both with [4–9] and without [18, 24] CT. The lack of a standardized reporting system for hilar/mediastinal findings or even of anatomic definition of nodal stations prevents comparison of these studies. Perhaps the work most comparable to ours is that of Whitley et al. [7] who examined 33 patients with CT before treatment. Nodal involvement was reported in terms of (1) hilum alone (4/33 = 12%) and (2) mediastinum alone (25/33 = 76%) without further anatomic definition. In our series, no patient had hilar adenopathy without mediastinal adenopathy, and only 14% (5/37) had mediastinal adenopathy without hilar adenopathy.

Comparison between this and previous studies can be made for findings outside the mediastinum and hilum. The frequency of pleural effusions (38% vs 40%), pericardial thickening (38% vs 37%), and tracheobronchial compression (68% vs 73%) was remarkably similar in our series and that of Whitley et al. [7]. It is unclear why the frequency of pleural effusion was so much lower in the series of Lewis et al. [5] (0/19) and those compiled by Fraser and Pare [24] (5.3% = 6/114). Lewis et al. [5] found no cases of pericardial thickening, but their criteria for determining the presence of such thickening is not stated.

The frequency of major (lobar/lung) atelectasis in our series was 30%. This is slightly higher than the figure of 22% for lobar or lung atelectasis/pneumonia in 368 cases studied by Mountain [12].

We found noncontiguous parenchymal masses in 41% of our patients. This is a higher frequency than the 19% found in 392 patients studied by Cohen and Mathews [25] with conventional techniques.

The ATS system is clearly applicable to the CT examination of patients with small-cell carcinoma. It is helpful to radiologists because it clearly defines the boundaries of named lymph node stations, to surgeons because the reports are in a form that is consistent with their view at mediastinoscopy, to pulmonologists/oncologists because it provides a precise definition of the extent of disease, and to all those involved because it suggests a uniform reporting system that allows series from different institutions to be adequately compared.

The further development of aggressive treatment for small-cell carcinoma with the use of chemotherapy, radiotherapy, and surgery significantly depends on radiologic input to clearly and definitively outline the precise extent of disease for both therapeutic and prognostic considerations. Thoracic CT in conjunction with the ATS staging system should be of great value.

ACKNOWLEDGMENT

We thank Kym Ross for secretarial assistance.

REFERENCES

1. Pugatch RD, Faling LJ, Daly BD. CT in evaluation of the mediastinum of patients with bronchogenic carcinoma. In: Siegelman SS, ed. *Computed tomography of the chest*, New York: Churchill Livingstone, **1984**:21–36
2. Mintzer R, Malave SR, Neiman HL, Michaelis LL, Vanecko RM, Sanders JH. Computed vs conventional tomography in evaluation of primary and secondary pulmonary neoplasms. *Radiology* **1979**;132:659–663
3. Glazer GM, Francis IR, Gebarski K, Samuels BI, Sorenson KW. Dynamic

incremental computed tomography in evaluation of the pulmonary hila. *J Comput Assist Tomogr* **1983**;7:59–64
4. Harper PG, Houang M, Spiro SG, Geddes D, Hodson M, Souhami RL. Computerized axial tomography in the pretreatment assessment of small-cell carcinoma of the bronchus. *Cancer* **1981**;47:1775–1780
5. Lewis E, Bernardino ME, Valdivieso M, Farha P, Barnes PA, Thomas JL. Computed tomography and routine chest radiography in oat cell carcinoma of the lung. *J Comput Assist Tomogr* **1982**;6:739–745
6. Griffin CA, Lu C, Fishman EK, et al. The role of computed tomography of the chest in the management of small-cell lung cancer. *J Clin Oncol* **1984**;2:1359–1365
7. Whitley NO, Fuks JZ, McCrea ES, et al. Computed tomography of the chest in small cell lung cancer: potential new prognostic signs. *AJR* **1984**;141:885–892
8. Boijsen M, Svennson G, Tylen U. Repeated computed tomography during treatment of small cell carcinoma of the lung. *Acta Radiol [Diagn]* (Stockh) **1985**;26:245–250
9. Norlund JD, Byhardt RW, Foley WD, Unger GF, Cox JD. Computed tomography in the staging of small cell lung cancer: implications for combined modality therapy. *Int J Radiat Oncol Biol Phys* **1985**;11:1081–1084
10. Ihde DC, Hansen HH. Staging procedures and prognostic factors in small cell carcinoma of the lung. In: Greco FA, Oldham RK, Bunn PA Jr eds. *Small cell lung cancer*. New York: Grune & Stratton, **1981**:261–283
11. Ihde DC, Makuch RW, Carney DN, et al. Prognostic implications of stage of disease and sites of metastases in patients with small cell carcinoma of the lung treated with intensive combination chemotherapy. *Am Rev Respir Dis* **1981**;123:500–507
12. Mountain CF. Clinical biology of small cell carcinoma: relationship to surgical therapy. *Semin Oncol* **1978**;5:272–279
13. Glazer GM, Gross BH, Quint LE, Francis IR, Bookstein FL, Orringer MB. Normal mediastinal lymph nodes: number and size. *AJR* **1985**;144:261–265
14. Aronberg DJ, Peterson RR, Glazer HS, Sagel SS. Superior diaphragmatic lymph nodes: CT assessment. *J Comput Assist Tomogr* **1986**;10:937–941
15. Moncada R, Baker M, Salinas M, et al. Diagnostic role of computed tomography in pericardial heart disease: congenital defects, thickening, neoplasms, and effusions. *Am Heart J* **1982**;103:263–282
16. Tisi GM, Friedman PF, Peters RM, et al. Clinical staging of primary lung cancer. *Am Rev Respir Dis* **1983**;127:659–664
17. American Joint Committee for cancer staging and end results reporting. *Staging of lung cancer 1979*. Chicago, IL: Task Force on Lung Cancer, **1979**
18. Mountain CF, Carr DT, Anderson WAD. A system for the clinical staging of lung cancer. *AJR* **1974**;120:130–138
19. Zelen M, Keynote address on biostatistics and data retrieval. *Cancer Chemother Rep* (Part 3) **1973**;4:31–42
20. Hyde L, Yee J, Wilson R, Patno ME. Cell type and the natural history of lung cancer. *JAMA* **1965**;193:52–54
21. Hansen HH, Dombernowsky P, Hirsch FR. Staging procedures and prognostic features in small cell anaplastic bronchogenic carcinoma. *Semin Oncol* **1978**;5:280–287
22. Minna JD, Higgins GA, Glatstein EJ. Cancer of the lung. In: DeVita VT Jr, Hellman S, Rosenberg SA, ed. *Cancer: principles and practices of oncology*, 2nd ed. Philadelphia: Lippincott, **1985**:507–597
23. Friedman PJ, Feigin DS, Liston SE, et al. Sensitivity of chest radiography, computed tomography, and gallium scanning to metastasis of lung carcinoma. *Cancer* **1984**;54:1300–1306
24. Fraser RG, Pare JAP. *Diagnosis of disease of the chest*, 2nd ed. Philadelphia: Saunders, **1978**:1011
25. Cohen MH, Matthews MJ. Small cell bronchogenic carcinoma: a distinct clinicopathologic entity. *Semin Oncol* **1978**;5:234–243

Asbestos-Related Pleural Disease and Asbestosis: A Comparison of CT and Chest Radiography

Arnold C. Friedman[1]
Stanley B. Fiel[2]
Mary S. Fisher[1]
Paul D. Radecki[1]
Anna S. Lev-Toaff[1]
Dina F. Caroline[1]

High-resolution CT (HRCT) has the ability to demonstrate both asbestos-related pleural disease and parenchymal abnormalities consistent with asbestosis. The role of CT in the diagnosis of asbestosis can be defined by comparing it with radiography. We evaluated 60 men who had a history of occupational exposure to asbestos and whose outside chest radiographs were considered abnormal. Chest radiographs (inside films) and HRCT were performed in all patients at our institution and were interpreted independently by experienced radiologists. Outside film results were compiled from the submitted reports. The final conclusion regarding the interpretation of the radiologic examinations was determined by consensus when disagreements existed. Positive predictive values (the likelihood that a positive report is correct) for pleural disease were: outside films 56%, inside films 79%, HRCT 100%. The positive predictive values for parenchymal disease were: outside films 51%, inside films 83%, HRCT 100%.

The addition of HRCT to chest radiography is most useful in eliminating false-positive diagnoses of asbestos-related pleural disease caused by subpleural fat and false-positive diagnoses of parenchymal asbestosis in patients with extensive plaques or emphysema obscuring lung detail. The interpretation of chest radiographs in patients exposed to asbestos is often extremely difficult and subjective, and we recommend that positive findings (except calcified plaques) be confirmed with HRCT.

The ability of CT to reliably differentiate subpleural fat from asbestos-related pleural disease is well known [1, 2]. Two recent studies have documented the characteristic HRCT findings in parenchymal asbestosis [3, 4]. The exact role of HRCT vs chest radiography in the clinical evaluation of patients exposed to asbestos has not been extensively assessed. We report the results of a prospective study of the relative efficacy of chest radiography and HRCT in evaluating patients with suspected asbestos-related disease.

Materials and Methods

Sixty men (average age, 58 years) suspected of having an occupational lung disease made up the study group. Fifty-five patients were referred because of a history of occupational asbestos exposure of at least 1-year duration and outside chest films interpreted as showing asbestos-related pleural disease with or without parenchymal asbestosis. The remaining five all had a similar history of occupational asbestos exposure and were referred because of outside films showing pleural disease and suspected mesothelioma (two), interstitial lung disease with a history of either exposure to chlorine gas (one) or occupational asthma (one), and interstitial lung disease with suspected lung cancer (one).

Chest films were obtained at our institution (inside films) in all cases and consisted of posteroanterior, lateral, and oblique views in 50 patients and posteroanterior and lateral views in the remaining 10.

HRCT was performed in all patients with either a Siemens DR3 or a GE 9800. With the Siemens, a 2-mm scan thickness was used at 30-mm intervals from apex to left atrium, followed by 12-mm intervals to the diaphragm; other parameters were a 7-sec scan time, 720 projections, and a strong edge-enhancement algorithm. With the GE, a 1.5-mm scan

Received July 24, 1987; accepted after revision October 19, 1987.

[1] Department of Diagnostic Imaging, Temple University Hospital, Broad and Ontario Sts., Philadelphia, PA 19140. Address reprint requests to A. C. Friedman.

[2] Division of Pulmonary Medicine, Temple University Hospital, Philadelphia, PA 19140.

AJR 150:269–275, February 1988
0361–803X/88/1502–0269
© American Roentgen Ray Society

thickness was used with a 2-sec scan time, 360 projections, and a bone algorithm. The initial 40 patients were scanned supine with prone repositioning when the lower lungs were partially obscured by gravity-dependent density. The last 20 were scanned in the prone position only, since it became apparent that the latter technique always significantly improved posterior lower lung detail because of less respiratory motion and anterior shift of dependent density.

Outside film results were compiled from the reports submitted with the films. None of the outside interpreters were B-readers (physicians certified by the National Institute of Occupational Safety and Health as expert in the interpretation of chest radiographs of patients exposed to dusts); 75% were pulmonary physicians, and 25% were either radiologists or occupational medicine physicians. Outside films were interpreted as showing asbestos-related pleural disease in 57 patients and as positive for interstitial fibrosis (asbestosis) in 38 patients. Inside films were all blindly interpreted and were scored (according to International Labour Office criteria) by an experienced chest radiologist B-reader. The CT scans were all blindly interpreted by one of the authors who was experienced in chest CT. All cases with disagreements between outside film, inside film, and/or HRCT interpretations were resolved by consensus of the aforementioned radiologists assisted by a pulmonary physician B-reader, and a final radiologic diagnosis was reached. HRCT was not considered infallible in this process (avoiding artificial designation of HRCT as the gold standard), since all radiologic data were evaluated side by side as in routine clinical consultation. Agreement as to the likely radiologic diagnosis and the cause for the diagnostic errors was reached in all but one case (inside films were subtly positive for interstitial disease, while the HRCT was normal). The final radiologic diagnosis was the same as the diagnoses made with outside film, inside film, and HRCT when there was agreement, but when there was disagreement, it was the consensus diagnosis.

Inside films were considered positive for interstitial disease when they scored 1/1 or higher. Similarly, we considered our HRCT findings to be positive only when they were judged unequivocally to be abnormal. There is evidence that 1/0 is found too often on the radiographs of patients who have not been exposed to asbestos (especially smokers) to be a useful discriminator [5, 6]. The profusion score is less important in this clinical context than is the qualitative judgment as to whether interstitial disease compatible with asbestosis is present [6].

Interstitial disease was diagnosed on HRCT when one or more of the following were present: nondependent lines or dense bands not representing vessels extending to the pleural surface (usually, but not always, in the region of a plaque); subpleural curvilinear densities and/or honeycombing, most prominent in the posterior lower lobes [3, 4, 7–11]. These findings are most often found in the posterior lower lobes and correspond to the distribution of abnormalities at pathologic examination [12]. The lines and dense bands extending to the pleural surface most likely represent fibrotic, thickened interlobular septa [4, 12]. The subpleural curvilinear densities seem to represent peribronchiolar fibrosis and alveolar collapse with fibrosis [3]. They are characteristic of parenchymal asbestosis but may be seen in other interstitial diseases.

Alterations in normal density gradients, inhomogeneity of density, and parenchymal distortion were considered nonspecific since they are present in patients with chronic obstructive pulmonary disease [13]. Questionable findings (corresponding to 1/0 or 0/1) were considered negative.

Unfortunately, no pathologic confirmation of diagnosis was obtained in this series, but the above radiologic criteria have been established by previous pathologic correlation [3, 7–10]. HRCT findings described in usual interstitial pneumonia (fibrosing alveolitis) can be transposed to parenchymal asbestosis because the chief pathologic distinction between the former and the latter is the histologic demonstration of asbestos bodies and/or fibers in the latter [3, 12, 14].

The final diagnosis of asbestos-related pleural disease was primarily based on the final radiologic diagnosis. The final diagnosis of parenchymal asbestosis was based on the following criteria: (1) evidence of occupational exposure to asbestos based on the patient's work history and/or the presence of radiologic pleural disease; (2) bilateral late inspiratory or paninspiratory basal crepitations; (3) relevant lung function abnormalities; (4) bilateral basal interstitial fibrosis as the final radiologic diagnosis; and (5) rigorous exclusion of simulative disease and its causes. If at least numbers 1, 4, and 5 were present, a diagnosis of parenchymal asbestosis was reached. In the absence of 4, a combination of 1, 2, 3, and 5 were considered sufficient [6, 14–16]. Note that the diagnosis of parenchymal asbestosis almost always depends primarily on a radiologic appearance compatible with interstitial fibrosis, and measurable impairment of lung function or physical disability need not be present [6, 14].

Radiologic studies were considered true or false positive or true or false negative for pleural disease and parenchymal disease separately. This assignment was based on agreement or disagreement of the blinded interpretation with the final diagnoses, which were all "clinical" since there was no pathologic material.

Results

Thirteen patients (22%) had a final diagnosis of asbestos-related pleural disease without parenchymal involvement, and two patients (3%) had a final diagnosis of parenchymal asbestosis without pleural disease. Nineteen patients (32%) had a final diagnosis of both asbestos-related pleural disease and parenchymal asbestosis. Six of the 21 patients with parenchymal asbestosis had restrictive pulmonary functions (four of the six had crepitations); five of 21 had obstructive changes only; and in 10 patients pulmonary function tests were normal. Of the 15 patients with parenchymal asbestosis and no restrictive pulmonary functions, eight had crepitations. The remaining seven had both inside film and HRCT diagnoses of interstitial fibrosis. Twenty-four patients (40%) had no evidence of asbestos-related pleural disease or interstitial lung disease, and two patients (3%) had other interstitial lung diseases (sarcoid and coal-worker's pneumoconiosis). Thirty-one of the 52 patients with a history of cigarette smoking had clinical evidence of obstructive airways disease.

Inside films were interpreted as showing asbestos-related pleural disease in 38 patients (16 had calcified pleural plaques, all true positive) and as showing parenchymal asbestosis in 23 patients. Four patients who were thought to have parenchymal asbestosis on inside films had a profusion score higher than 1/1. One of these was false positive.

HRCT showed asbestos-related pleural disease in 31 patients (18 with calcification) and parenchymal asbestosis in 21 patients.

All 17 false-positive outside film diagnoses of pleural disease for which both inside films and HRCT had true-negative diagnoses were caused by subpleural fat. The eight false-positive diagnoses of asbestos-related pleural disease on both outside and inside films were caused by subpleural fat in seven and intercostal muscle in one (Fig. 1). The 14 false-positive outside film diagnoses of parenchymal asbestosis for

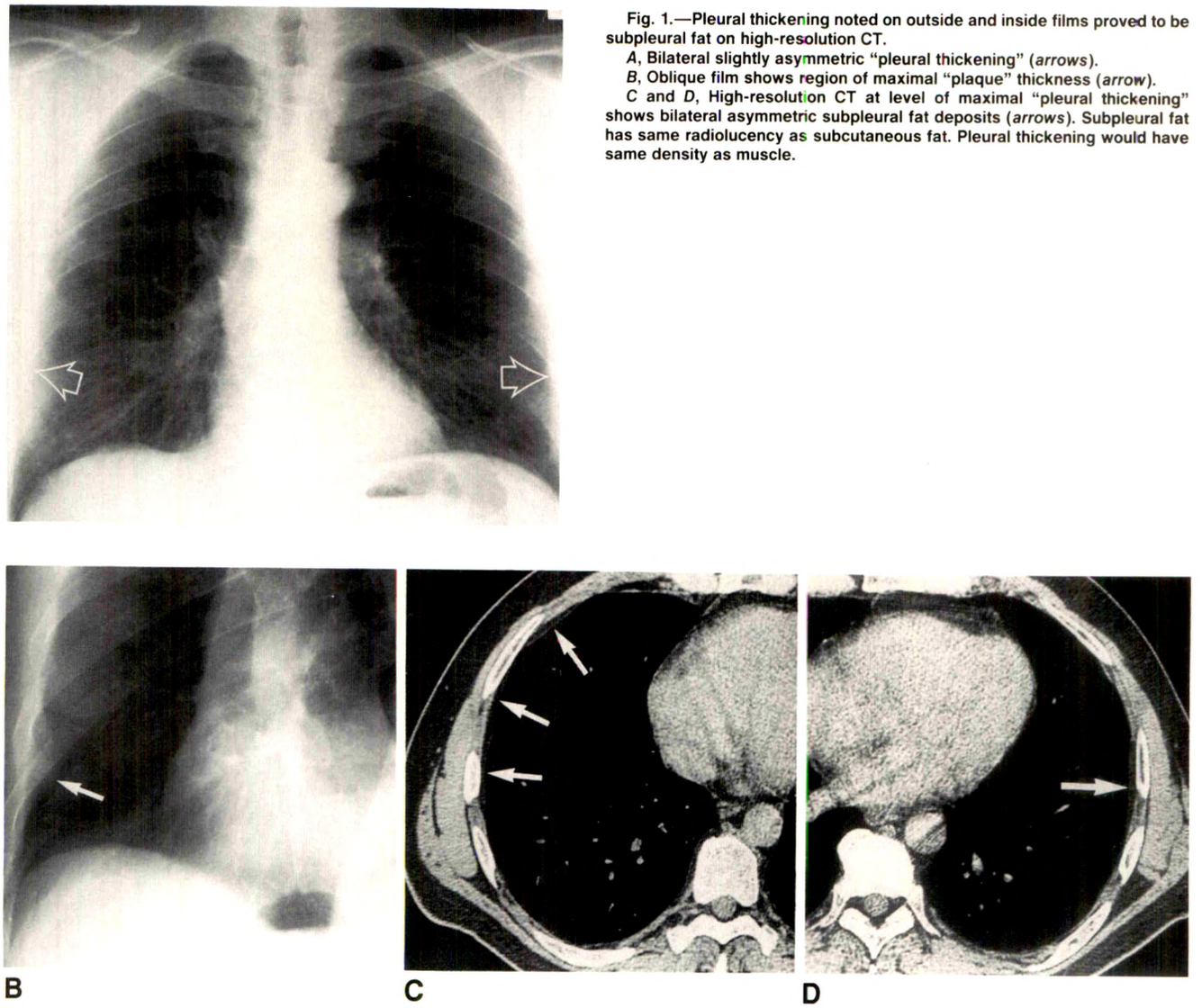

Fig. 1.—Pleural thickening noted on outside and inside films proved to be subpleural fat on high-resolution CT.

***A*, Bilateral slightly asymmetric "pleural thickening" (*arrows*).**

***B*, Oblique film shows region of maximal "plaque" thickness (*arrow*).**

***C* and *D*, High-resolution CT at level of maximal "pleural thickening" shows bilateral asymmetric subpleural fat deposits (*arrows*). Subpleural fat has same radiolucency as subcutaneous fat. Pleural thickening would have same density as muscle.**

which both inside films and HRCT were true-negative were caused by prominent vessels, obscuration of the lung by plaques en face, chronic obstructive pulmonary disease, bronchiectasis, or scarring from surgery or old tuberculosis. The four false-positive diagnoses of parenchymal asbestosis on both outside and inside films were caused by walls of bullae (emphysema) in two (Fig. 2) and focal parenchymal scarring, possibly from previous infection, in two.

There were no false-positive HRCT findings for either pleural or parenchymal disease (in all cases in which HRCT was positive and inside films negative, the chest radiologist agreed that the HRCT was correct).

In only two cases did HRCT depict parenchymal asbestosis not suspected on either outside or inside films. The findings were subtle linear densities adjacent to plaques (Fig. 3). There were two false-negative inside films for pleural disease caused by subtle diaphragmatic plaques (Fig. 4) and one false-negative HRCT scan due to a solitary calcified plaque that was missed because it was in between the slices. There was one case in which outside and inside films were positive for parenchymal asbestosis and HRCT was negative, and consensus could not be reached.

Additional diagnoses made on HRCT that were not made on either outside or inside films were emphysema in seven patients, bronchiectasis in two patients, and benign effusion in one patient thought to have mesothelioma on the basis of outside films. The results including sensitivity, specificity, accuracy, and positive and negative predictive values [17] are summarized in Table 1. Because positive outside films were required for entry into the study, the positive predictive values are the most significant parameter, and a percentage t-test of significance was applied to them. The differences between outside and inside films, outside films and HRCT, and inside films and HRCT for both pleural and parenchymal disease were significant with $p < .05$, $p < .01$, and $p < .025$, respectively.

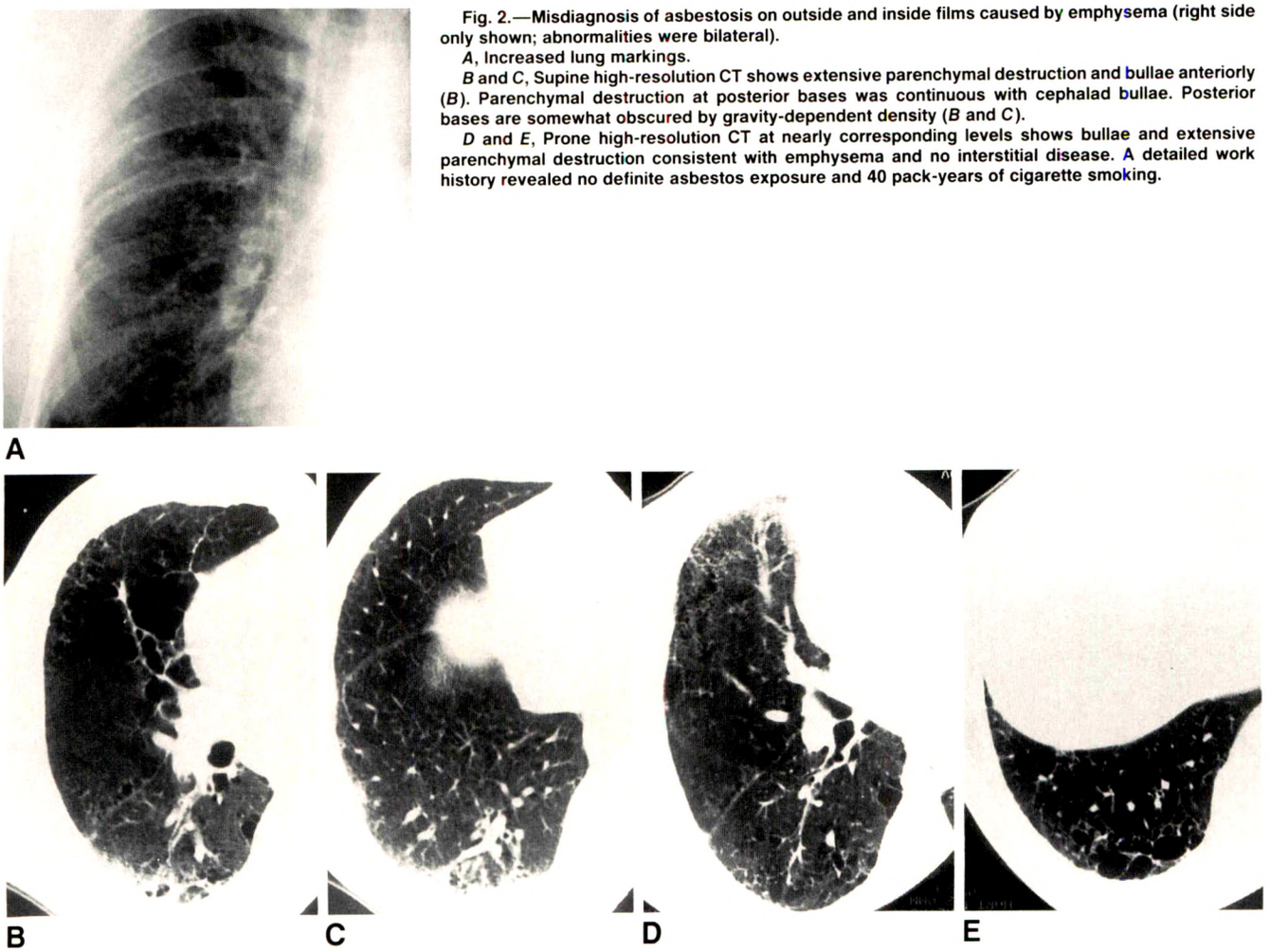

Fig. 2.—Misdiagnosis of asbestosis on outside and inside films caused by emphysema (right side only shown; abnormalities were bilateral).

***A*, Increased lung markings.**

***B* and *C*, Supine high-resolution CT shows extensive parenchymal destruction and bullae anteriorly (*B*). Parenchymal destruction at posterior bases was continuous with cephalad bullae. Posterior bases are somewhat obscured by gravity-dependent density (*B* and *C*).**

***D* and *E*, Prone high-resolution CT at nearly corresponding levels shows bullae and extensive parenchymal destruction consistent with emphysema and no interstitial disease. A detailed work history revealed no definite asbestos exposure and 40 pack-years of cigarette smoking.**

A more confident diagnosis was frequently possible on HRCT as compared with inside films, even when all three studies were tabulated as being in agreement. This was especially true in cases with prominent subpleural fat, nonspecific increased parenchymal markings, or extensive plaques obscuring the lungs. The confidence factor was difficult to quantitate.

Discussion

The specificity of outside films was low, indicating that normal subjects would not be properly identified; the positive predictive values of outside films indicated that a positive diagnosis of pleural or parenchymal disease would be correct in only approximately 50% of patients. Needless anxiety is apt to be created if a patient exposed to asbestos has his or her radiographs interpreted by an inexperienced reader. Because of selection bias, we cannot establish the true frequency of false-negative diagnoses on outside film interpretation, and outside film sensitivity may be artificially high. Similarly, outside film specificity for pleural disease is artificially low because only a few of the final diagnoses were negative.

Chest radiographs interpreted by an expert in evaluating asbestos-related disease (inside films) have high sensitivity, specificity, and negative predictive value. It therefore appears that most normal subjects can be correctly identified at relatively low cost and that most existing lesions will be detected. However, a comparison of outside and inside films and HRCT in a group of exposed patients with negative outside films would best assess negative predictive value, sensitivity, and the screening value of HRCT. Since the positive predictive value for both pleural and parenchymal disease is about 80%, confirmation by HRCT of any abnormalities other than calcified plaques seen on radiographs is recommended. Our results indicate that HRCT will be especially useful in eliminating false-positive diagnoses of noncalcified plaques caused by subpleural fat and prominent intercostal muscles and false-positive diagnoses of parenchymal disease in patients with emphysema or extensive plaques obscuring parenchymal detail. HRCT is not needed merely to confirm the presence of calcified pleural plaques. HRCT is marginally more sensitive than inside films for both pleural and parenchymal disease and does not create additional false-positive findings.

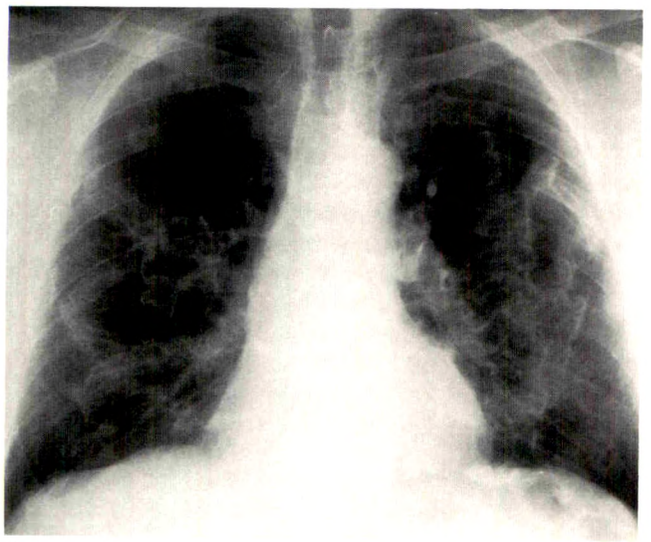

A

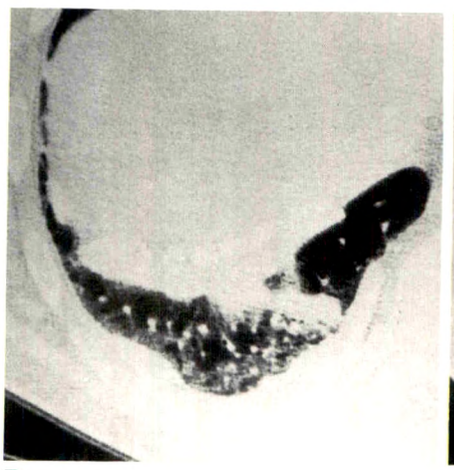

B

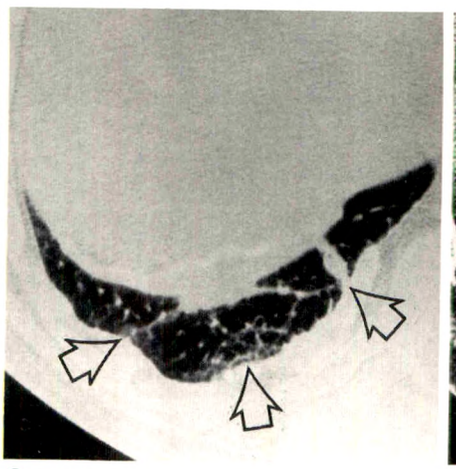

C

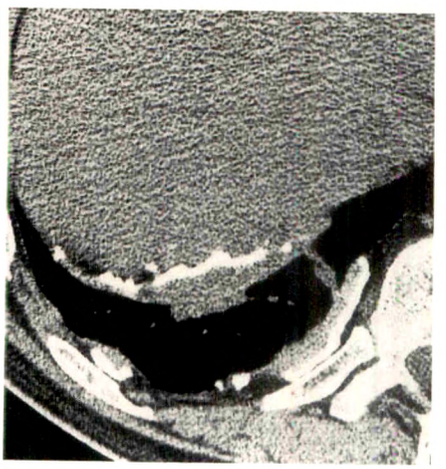

D

Fig. 3.—Parenchymal asbestosis diagnosed by high-resolution CT and missed on inside films with demonstration of the usefulness of prone positioning. Right side only is shown on high-resolution CT; findings on left were similar.

A, Extensive plaques en face obscure underlying parenchyma.

B, Supine high-resolution CT shows posterior lung base obscured by gravity-dependent density.

C, Prone high-resolution CT at same level shows increased lines and bands (*arrows*) especially next to plaques.

D, Corresponding mediastinal windows allow better delineation of calcified plaques.

A

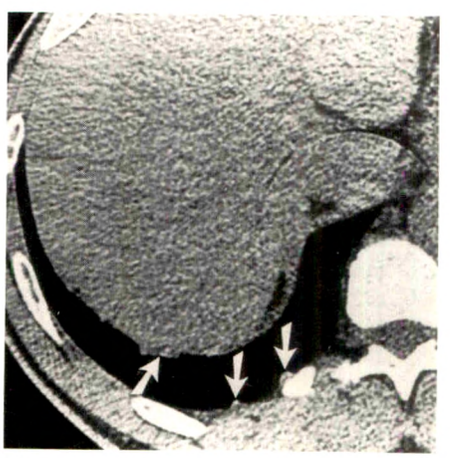

B

Fig. 4.—Subtle diaphragmatic plaques missed on inside films (*A*) but visible on high-resolution CT (*arrows* on *B*).

TABLE 1: Statistical Evaluation of Outside Films, Inside FIlms, and HRCT for Diagnosis of Asbestos-Related Disease

Type of Study	TP	FP	TN	FN	% Sens.	% Spec.	% Acc.	% PPV	% NPV
Pleural Disease									
OSF	32	25	3	0	100	11	58	56	100
ISF	30	8	20	2	94	71	83	79	91
HRCT	31	0	28	1	97	100	98	100	97
Parenchymal Disease									
OSF[a]	19	18	20	2	90	53	66	51	91
ISF[a]	19	4	34	2	90	89	90	83	94
HRCT[b]	21	0	38	0	100	100	100	100	100

Note.—TP = true positive; FP = false positive; TN = true negative; FN = false negative; Sens. = sensitivity = 100 × TP/(TP + FN); Spec. = specificity = 100 × TN/(TN + FP); Acc. = accuracy = 100 × (TP + TN)/(TP + TN + FP + FN); PPV = positive predictive value = 100 × TP/(TP + FP); NPV = negative predictive value = 100 × TN/(TN + FN); OSF = outside films; ISF = inside films; HRCT = high-resolution CT. See Gelfand and Ott [17] for statistical methods.

[a] [1 indeterminate (+)].

[b] [1 indeterminate (−)].

In terms of the patient's management, because there is no effective treatment for asbestos-related pleural disease or asbestosis, the ability of HRCT to pick up subtle disease is not important, except perhaps for purposes of compensation for the worker. More widespread use of HRCT for determining compensation should decrease the frequency of unjust compensation due to false-positive interpretations of radiographs.

Since cigarette smoking is prevalent in this population, the ability of HRCT to differentiate between emphysema, bronchiectasis, and interstitial disease, as well as to delineate their relative extent when they coexist, is often useful [8, 13, 18]. HRCT may be even more useful when it is performed in a nonblinded fashion and targeted to radiographically questionable regions.

Finally, HRCT frequently gives the radiologist increased confidence in the final diagnosis, especially in patients with prominent subpleural fat, nonspecific increased parenchymal markings, or extensive plaques obscuring the underlying lungs (Fig. 5).

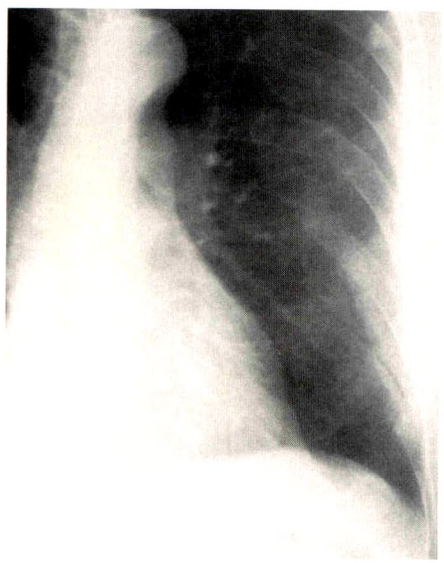

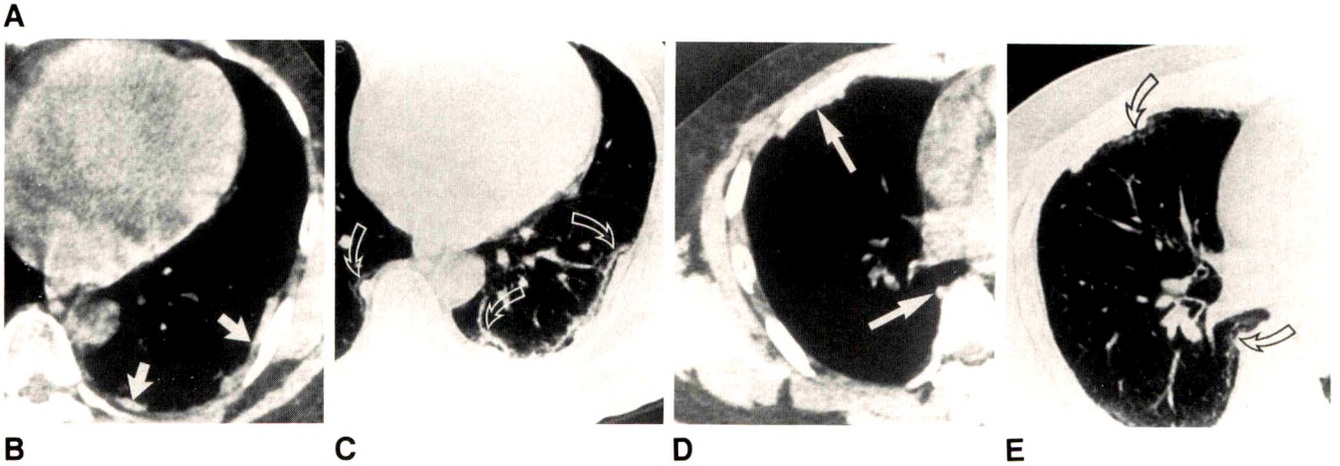

Fig. 5.—Subtle parenchymal asbestosis seen with greater confidence and extent on high-resolution CT than on inside films.

***A*, Obvious plaques on inside films. Left lower lobe interstitial disease was suspected.**

***B* and *C*, Periplaque subpleural curvilinear density (*arrows*) diagnostic of interstitial lung disease. Plaques (*arrows*) are seen better on mediastinal windows (*B*), whereas parenchymal disease is seen better on lung windows (*C*).**

***D* and *E*, Additional (more subtle) interstitial changes adjacent to plaques (*arrows*).**

ACKNOWLEDGMENTS

We are indebted to Martin Black for his helpful suggestions while reviewing this manuscript. We also thank Milne Hewish for illustration preparation. I would like to dedicate this work to the memory of my father, Isidore Friedman, who passed away suddenly and unexpectedly during the preparation of revisions.

REFERENCES

1. Sargent EN, Boswell WD, Ralls PW, Markovitz A. Subpleural fat pads in patients exposed to asbestos: distinction from noncalcified pleural plaques. *Radiology* **1984**;152:273–277
2. Gale ME, Greif WL. Intrafissural fat: CT correlation with chest radiography. *Radiology* **1986**;160:333–336
3. Yoshimura H, Hatakeyama M, Otsuji H, et al. Pulmonary asbestosis: CT study of subpleural curvilinear shadow. *Radiology* **1986**;158:653–658
4. Aberle DR, Ray CS, Gamsu G, Stein MG, Webb WR, Golden J. Characteristics of high-resolution CT of asbestosis. *Radiology* **1986**;161(P):144
5. Epstein DM, Miller WT, Bresnitz EA, Levine MS, Gefter WB. Application of ILO classification to a population without industrial exposure: findings to be differentiated from pneumoconiosis. *AJR* **1984**;142:53–58
6. Weill H. The diagnosis of asbestos-related disease. *Chest* **1987**;91:802–803
7. Bergin CJ, Müller NL. CT of interstitial lung disease: a diagnostic approach. *AJR* **1987**;148:8–15
8. Müller NL, Miller RR, Webb WR, Evans KG, Ostrow DN. Fibrosing alveolitis: CT-pathologic correlation. *Radiology* **1986**;160:585–588
9. Nakata H, Kimoto T, Nakayama T, Kido M, Miyazaki N, Harada S. Diffuse peripheral lung disease: evaluation by high-resolution computed tomography. *Radiology* **1985**;157:181–185
10. Bergin CJ, Müller NL. CT in the diagnosis of interstitial lung disease. *AJR* **1985**;145:505–510
11. Staples CA, Müller NL, Vidal S, Abboud R, Ostrow D, Miller RR. Usual interstitial pneumonia: correlation of CT with clinical, functional, and radiologic findings. *Radiology* **1987**;162:377–381
12. Craighead JE, Abraham JL, Churg A, et al. The pathology of asbestos-associated diseases of the lungs and pleural cavities: diagnostic criteria and proposed grading schema. *Arch Pathol Lab Med* **1982**;108:544–576
13. Bergin CJ, Müller NL, Nichols DA, et al. The diagnosis of emphysema. A computed tomographic-pathologic correlation. *Am Rev Respir Dis* **1986**;133:541–546
14. Murphy RL, Becklake MR, Brooks SM, et al. The diagnosis of nonmalignant disease related to asbestos. *Am Rev Respir Dis* **1986**;134:363–368
15. Parkes WR. *Occupational lung disorders*, 2nd ed. London: Butterworth, **1982**:264
16. Casey KR, Rom WN, Moatamed F. Asbestos-related diseases. *Clin Chest Med* **1981**;2:179–202
17. Gelfand DW, Ott DJ. Methodologic considerations in comparing imaging methods. *AJR* **1985**;144:1117–1121
18. Grenier P, Frantz M, Musset D, Menu Y, Nahum H. Bronchiectasis: assessment by thin-section CT. *Radiology* **1986**;161:95–100

Categorical Course in Breast Imaging

American Roentgen Ray Society 88th Annual Meeting

May 8–12, 1988, San Francisco Hilton and Tower, San Francisco, CA

Program Chairman: *Stephen A. Feig, Philadelphia, PA*; (215) 928-7253

Sunday, May 8	
9:00–9:10 a.m.	Welcome from the President (*Gagliardi*)
9:10–9:15 a.m.	Introduction (*Feig*)
9:15–10:00 a.m.	Xeromammography: principles, equipment, technique, quality control (*Sickles*)
10:30–11:30 a.m.	Screen-film mammography: principles, equipment, technique, quality control (*Feig*)
11:30 a.m.–Noon	American College of Radiology Mammography Accreditation Program (*McLelland*)
Break	
1:30–2:15 p.m.	Breast masses: differential diagnosis (*Adler*)
2:15–3:00 p.m.	Breast calcifications: differential diagnosis (*Rebner*)
Break	
3:30–4:10 p.m.	Mammography of the treated breast (*Paulus*)
4:10–4:50 p.m.	Practical solutions to common mammographic problems (*Sickles*)
4:50–5:30 p.m.	Prebiopsy localization of nonpalpable breast lesions (*Kopans*)
Monday, May 9	
1:30–2:10 p.m.	Mammographic-pathologic correlation (*Troupin*)
2:10–2:50 p.m.	Breast ultrasound: equipment, technique, interpretation, accuracy (*Bassett*)
2:50–3:30 p.m.	Fine needle aspiration biopsy, ductography, pneumocystography (*Logan*)
Break	
4:00–4:45 p.m.	Panel: Diagnostic problem cases (Moderator: *Feig*; members: *Bassett*, *Kopans*, *Rebner*, *Troupin*)
4:45–5:30 p.m.	Panel: Subtle signs of carcinoma (Moderator: *Feig*; members: *Adler*, *Logan*, *McLelland*, *Moskowitz*, *Sickles*)
Tuesday, May 10	
4:00–4:45 p.m.	Issues in breast cancer screening (*Moskowitz*)
4:45–5:15 p.m.	How to establish a low-cost community screening program (*McLelland*)
5:15–5:30 p.m.	Discussion
Wednesday, May 11	
4:00–4:30 p.m.	Wording the mammography report (*Feig*)
4:30–5:15 p.m.	Medicolegal aspects of mammography (*Brenner*)
5:15–5:30 p.m.	Discussion
Thursday, May 12	
4:00–4:30 p.m.	Transillumination lightscanning (*D'Orsi*)
4:30–5:00 p.m.	Breast MR (*Alcorn*)
5:00–5:30 p.m.	Digital mammography (*Merritt*)
5:30–5:35 p.m.	Concluding remarks (*Feig*)

Gastrointestinal Inflammation After Bone Marrow Transplantation:

Graft-Versus-Host Disease or Opportunistic Infection?

Bronwyn Jones[1]
Sandra S. Kramer[1, 4]
Rein Saral[2]
William E. Beschorner[2, 3]
Robert H. Yolken[4]
Timothy R. Townsend[4]
Andrew M. Yeager[4]
Alan Lake[4]
Peter Tutschka[2, 5]
George W. Santos[2]

Gastrointestinal inflammation after allogeneic bone marrow transplantation may be due to acute graft-versus-host disease (GVHD) and/or superinfection with opportunistic organisms. Twenty-eight patients with barium studies suggesting gastrointestinal inflammation after bone marrow transplantation and either acute GVHD, viral infection, or both were studied to characterize the radiographic appearances of each disease and to determine whether acute GVHD could be distinguished from viral superinfection on the basis of radiographic findings. Thirteen patients had minimal or no acute GVHD, with viral infection proved in eight and strongly suspected in four others; the remaining patient was thought to have nonspecific inflammatory bowel disease. Five patients had pure acute GVHD, and 10 patients had viral enteritis superimposed on acute GVHD. Radiographic abnormalities were found in the gastrointestinal tract in both acute GVHD and viral infection and were more extensive than previously reported. Findings were similar in both entities, although gastric abnormalities were not seen in pure acute GVHD but only in viral infection, either alone or together with acute GVHD. Prolonged small bowel barium coating occurred in both viral infection and acute GVHD. Fold thickening evolved into fold effacement with a shaggy contour in two patients with viral infection. Colonic findings in all groups mimicked ulcerative colitis.

Our data indicate that differentiation between acute GVHD and viral enteritis is not possible on the basis of radiographic findings alone. Both entities should be considered when gastrointestinal inflammation occurs after bone marrow transplantation.

Bone marrow transplantation is being performed increasingly for the treatment of leukemia, lymphoma, aplastic anemia, and some metabolic disorders of the hemopoietic system. A significant complication after transplantation is acute graft-versus-host disease (GVHD), which occurs in 50–70% of allogeneic transplants, with a fatal outcome in up to 15% [1–6]. The gastrointestinal tract is one of the major target organs in acute GVHD, with severe mucosal inflammation and profuse secretory diarrhea [7–11]. Usually, gastrointestinal tract involvement parallels that in the skin and can be graded by rectal biopsy [11]; isolated acute GVHD of the bowel is rare [7–10]. Previous reports of the radiographic appearances of gastrointestinal acute GVHD have stressed small bowel involvement with fold thickening or effacement and a characteristic featureless or "ribbon" bowel [12–15].

These severely immunocompromised patients are also at risk for superinfection with opportunistic organisms; for example, infection with enteroviruses such as coxsackie A, adenovirus, or rotavirus can result in rapid clinical deterioration and high mortality [16–23]. We recently encountered five bone marrow transplant patients with enteric viral infection and no evidence of acute GVHD who had abnormalities on barium contrast studies that were indistinguishable from those previously reported in acute GVHD. The barium studies in these five patients and in 23 other consecutive bone marrow transplant patients with abnormal barium studies suggesting acute GVHD, viral enteritis, or both were analyzed to compare the findings in viral superinfection with those of acute GVHD.

Received July 2, 1987; accepted after revision October 7, 1987.

[1] The Russell H. Morgan Department of Radiology and Radiologic Science, The Johns Hopkins Medical Institutions, Baltimore, MD 21205. Address reprint requests to B. Jones, Dept. of Radiology, The Johns Hopkins Hospital, 600 N. Wolfe St., Baltimore, MD 21205.

[2] Department of Oncology, The Johns Hopkins Medical Institutions, Baltimore, MD 21205.

[3] Department of Pathology, The Johns Hopkins Medical Institutions, Baltimore, MD 21205.

[4] Department of Pediatrics, The Johns Hopkins Medical Institutions, Baltimore, MD 21205.

[5] Present address: 1027 University Hospital, 410 W. 10th Ave., Columbus, OH 43210.

AJR 150:277–281, February 1988
0361–803X/88/1502–0277
© American Roentgen Ray Society

Subjects and Methods

Between November 1977 and July 1985, 43 barium contrast studies of the gastrointestinal tract were performed in 28 patients who had received a bone marrow transplant; in all patients the findings suggested inflammation. There were 16 women and 12 men, with an age range of 3–36 years (median, 17.5 years). Reasons for transplantation included acute myeloid leukemia, 11 patients; acute lymphoblastic leukemia, six; aplastic anemia, five; chronic myeloid leukemia, three; and multiple myeloma, acute myelofibrosis, and metachromatic leukodystrophy, one patient each.

Of the 43 contrast studies, there were 41 upper gastrointestinal series with small bowel follow-through and two barium enema examinations. Assessment of the colon was possible in 27 of 41 antegrade studies. In general, because of the extreme debility of the patients, air contrast studies were not performed.

The clinical grade of acute GVHD at the time of the contrast studies was determined by established criteria [24]. Acute GVHD was judged as absent or minimal if the clinical grade was 0 or I and severe if the clinical grade was II or more.

Viral infection was considered confirmed if either an enzyme-linked immunosorbent assay (ELISA) was positive for virus [25] or if vacuolations were present in small bowel or colonic epithelial cells in biopsy or autopsy materials [26]. ELISAs for the detection of rotavirus, adenovirus, coxsackie A and B viruses (multiple serotypes), and *Clostridium difficile* toxin are currently in use at our institution.

Each barium study was analyzed, and the type and distribution of the abnormalities were noted. The radiographs were then reanalyzed to compare the type of radiographic abnormality and the location and extent of disease in acute GVHD, viral infection, and a combination of both entities. There were three groups of patients: in group 1, there were eight patients with proved enteric virus infection and four patients who were clinically thought to have viral infection, none of whom had significant acute GVHD (maximum clinical grade 0 or I); in group 2, there were five patients with acute GVHD and no evidence of superinfection; in group 3, there were 10 patients with both acute GVHD and virus infection. A final patient had nonspecific inflammatory bowel disease with no features to suggest either acute GVHD or enteric viral infection.

Results

Thirteen patients had abnormal studies with minimal or no clinical evidence of acute GVHD. Of these, eight had proved viral infection; in four others, viral infection was strongly suspected on clinical grounds; one patient had nonspecific inflammatory bowel disease. Five patients had moderate-to-severe acute GVHD, and 10 patients had both acute GVHD and viral infection.

None of the patients had radiographic abnormalities in the esophagus.

Gastric abnormalities were present in seven patients and included dilatation, atony with delayed emptying, and retained secretions in six (Figs. 1 and 2), antral deformity in four (Fig. 3), and an unusual coating pattern in five (Fig. 1). In five of the seven patients there was little or no clinical evidence of acute GVHD, and six of the seven were positive for virus: two for adenovirus (one with cytomegalovirus); two for coxsackie virus; and one for rotavirus; one patient had vacuolations on biopsy, consistent with viral infection.

Duodenal abnormalities were present in 17 patients. The entire duodenum was involved in almost all, either with thickening or effacement of mucosal folds or with normal folds replaced by a tubular or shaggy contour (Figs. 2 and 4). Five of the 17 had viral infection without acute GVHD; four patients without acute GVHD were thought on clinical grounds to have viral enteritis; two had acute GVHD and no evidence of virus; and six had both acute GVHD and viral infection. In five patients, the virus involved was coxsackie (in combination with adenovirus in one); in four, adenovirus (in combination with rotavirus in one); in one, atypical rotavirus; and in one, virus unidentified with vacuolated cells at autopsy.

Small intestinal abnormalities were found in all 28 patients and were diffuse in 24; the jejunum was spared in four. Findings included marked fold enlargement, luminal narrowing and separation of loops, or complete effacement of folds (the ribbon bowel) (Figs. 1, 2, 4–6). In two patients with viral infection, fold thickening evolved to a shaggy, featureless appearance with fold effacement on repeat examination 19 and 30 days later, respectively (Fig. 5). In some patients, the ribbon-bowel appearance seemed to be related to luminal distension, and loops of bowel with thickened folds on early radiographs became ribbonlike with more distension. Small bowel transit time was rapid (less than 30 min) in 27 of the 28 patients.

Prolonged mucosal coating was seen in the small bowel in four patients and persisted for more than 24 hr in three patients and for more than 48 hr in another patient (Figs. 1 and 6). These four patients had severe mucosal disease and subsequently passed membranes of sloughed mucosa per rectum. Three of these four patients had viral infection, one with no evidence of acute GVHD, one with grade I acute GVHD, and one with severe acute GVHD; the remaining patient had minimal acute GVHD and was evaluated before the viral assay became available. The viruses involved were adenovirus in two patients and coxsackie virus in one.

Colonic findings were present in 17 patients, shown on barium enema in two and on antegrade studies in 15. Findings included haustral fold enlargement, spasm, ulceration, or loss of haustration, in some cases associated with a granular mucosal pattern similar to that of idiopathic ulcerative colitis (Figs. 1, 2, and 4–6). The findings were diffuse in 12 patients, with a common association being loss of haustration in the left colon and edema and spasm in the right colon. In five patients, the left colon was spared and the right colon was abnormal. The colonic findings occurred in the setting of clinically significant acute GVHD in five patients, viral infection with minimal or no evidence of acute GVHD in eight patients, and both acute GVHD and viral infection in three patients. The other patient had no evidence of acute GVHD and negative viral studies and was thought on clinical grounds to have nonspecific inflammatory bowel disease. The viruses involved were adenovirus in six patients (in association with coxsackie virus in one and rotavirus in one other), coxsackie virus in three, and atypical rotavirus in one.

Discussion

Clinically, the patients could be divided into three categories: those with acute GVHD, those with both acute GVHD and viral infection, and those with viral infection but minimal

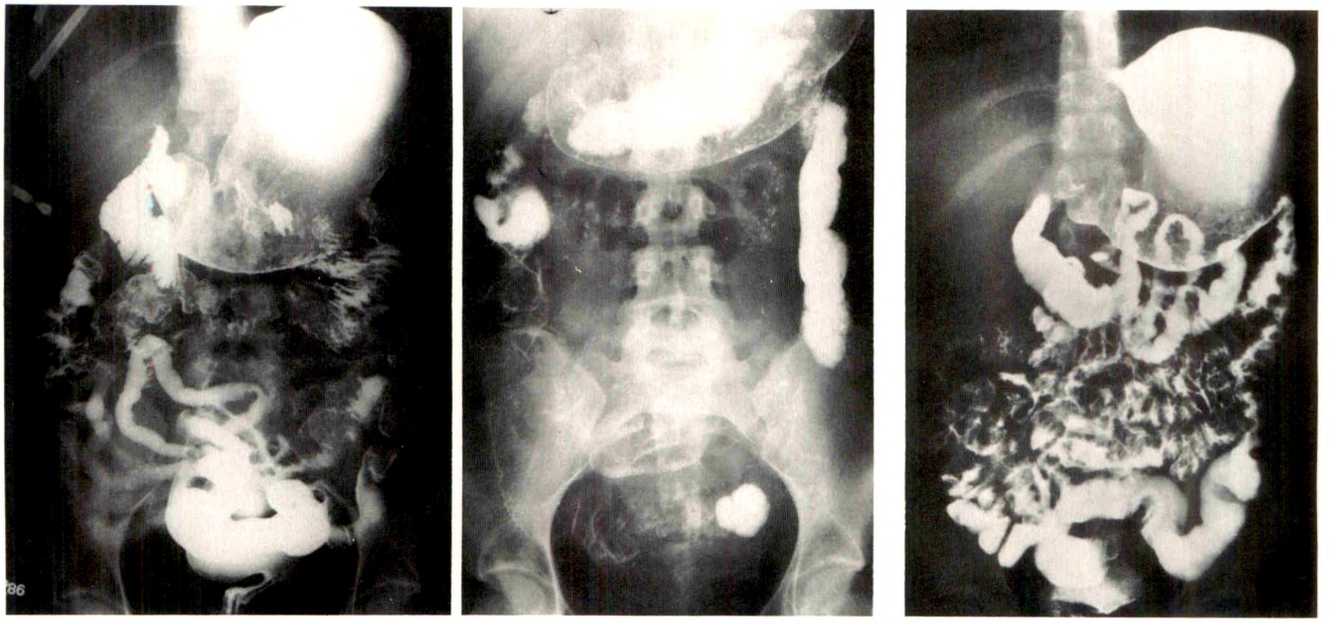

A B

Fig. 1.—A 21-year-old bone marrow transplant patient with grade II acute graft-versus-host disease and adenovirus infection.

A, Small bowel series shows gastric dilatation and atony with an unusual coating pattern. Note thickening of small bowel folds in jejunum and ribbonlike barium in distal ileum. Haustral folds in right colon and transverse colon are enlarged and left colon is ahaustral.

B, Follow-up film made 24 hr later shows persistent gastric atony and unusual coating of stomach and several loops of small bowel in the right lower quadrant.

CT scan obtained on same day showed adherence of barium to mucosa of stomach and small bowel.

Fig. 2.—An 8-year-old girl with no clinical evidence of acute GVHD who clinically was thought to have viral enteritis. A 30-min film obtained 55 days after transplantation shows gastric distension, ribbonlike barium in duodenum and proximal jejunum, and marked thickening of folds in distal jejunum and ileum. Note thickening of haustral folds in colon to mid-descending colon with loss of haustration distally.

Fig. 3.—A 12-year-old boy with grade II acute graft-versus-host disease and a small bowel biopsy showing vacuolations indicative of viral enteritis. Barium studies performed 59 days after transplantation show dilatation of stomach and marked narrowing and deformity of distal gastric antrum and pylorus. There is also mucosal prolapse through the pylorus.

Fig. 4.—A 31-year-old woman with grade II acute graft-versus-host disease and no evidence of viral enteritis. Barium study performed 54 days after transplantation shows thickening of small bowel folds in some segments and a ribbonlike barium pattern in others. Note loss of haustration in distal transverse, descending, and sigmoid colon.

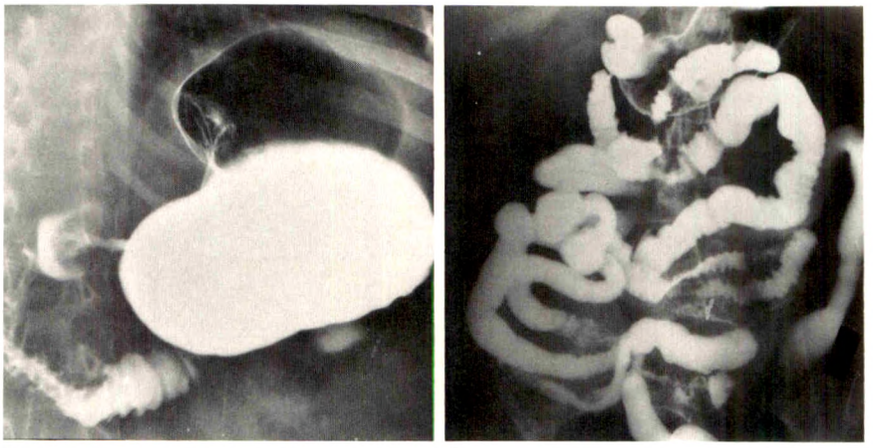

3 4

or no clinical evidence of acute GVHD in other target organs such as the skin and liver. The patients who had no other clinical evidence of acute GVHD may have had subtle, undetected inflammation of the small intestinal epithelium due to acute GVHD as well as viral superinfection. For the sake of discussion, however, these categories are preserved.

The following points emerged from this study: (1) Diffuse gastrointestinal inflammation occurs in both acute GVHD and viral superinfection and involves not only the small intestine but also the stomach, duodenum, and colon. (2) Differentiation between acute GVHD and viral enteritis is not possible on the basis of radiographic findings alone, although gastric involvement and prolonged small bowel coating favor a viral etiology.

The finding of gastric atony is interesting in light of a recent report [18] of cytomegalovirus gastritis in four patients after bone marrow transplantation. Radiographs showed gastric atony in two of these patients; in one case it was associated with marked nodularity. The narrowing and deformity of the

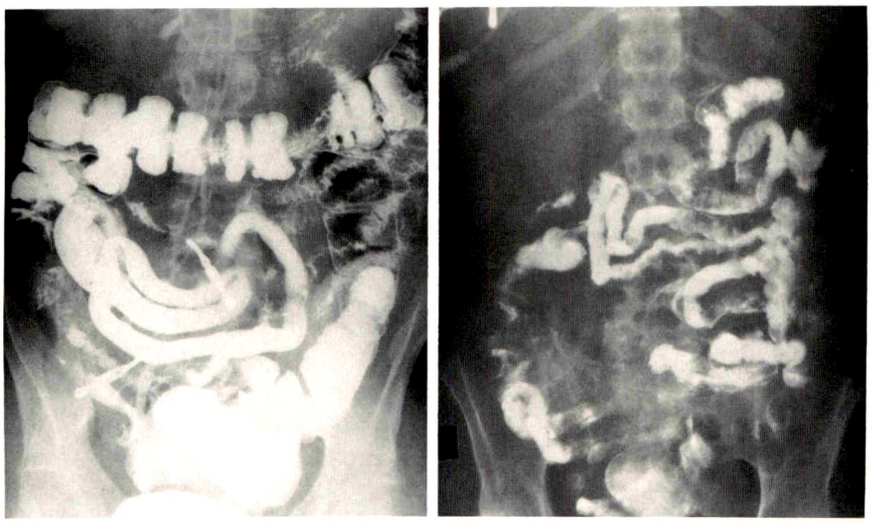

Fig. 5.—A 20-year-old man with no evidence of acute graft-versus-host disease and both rotavirus and adenovirus infection.

A, Small bowel series 41 days after transplantation shows fold thickening in proximal small bowel and ribbonlike barium in distal small bowel. There is spasm in proximal ascending colon.

B, Small bowel series performed 19 days later shows a diffuse, amorphous pattern with almost complete effacement of small bowel folds.

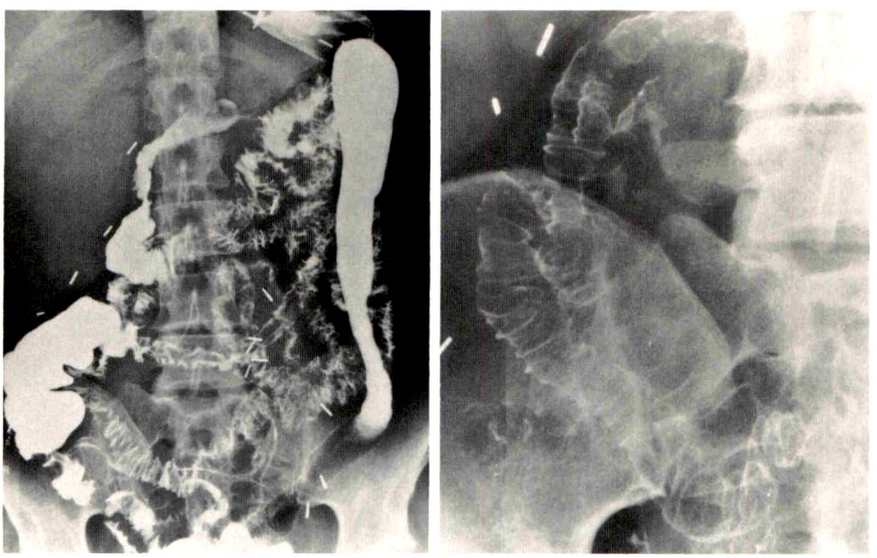

Fig. 6.—A 36-year-old woman with grade I acute graft-versus-host disease and both coxsackie and cytomegalovirus infection.

A, An upper gastrointestinal series done 22 days after transplantation shows diffuse thickening of small bowel folds involving duodenum through ileum. Right colon and transverse colon appear spastic, and left colon is ahaustral.

B, Coned-down film of right lower quadrant 48 hr later shows persistent barium coating of distal small bowel.

antrum, seen in four patients in the present study, can also be seen in other inflammatory diseases such as Crohn disease [27]. Findings were seen in the stomach only in patients who had viral infection (either alone or in combination with acute GVHD), and not in those with pure acute GVHD. However, the number of patients is small; further data are needed before it can be concluded that gastric abnormality can be used as a marker for viral infection.

Prolonged mucosal coating of the stomach and small bowel such as seen here has been observed only in patients who have undergone bone marrow transplantation. Although unusual surface coating has been reported in these patients on CT [28], prolonged coating on barium examinations has not been stressed. What this appearance represents is unknown; the barium may be adherent to mucosa, to submucosa, or to pseudomembranes, or trapped in sloughed mucosa. One patient with persistent coating in the small intestine for over 48 hr died 18 days later; at autopsy the intestinal lumen was filled with pseudomembranes. Pathologic correlation is necessary to clarify the reason for the abnormal coating.

In two patients with viral infection, follow-up examinations (19 and 30 days later, respectively) revealed that fold thickening in the small bowel had evolved to a shaggy, tubular appearance with effacement of folds, an appearance not seen in acute GVHD (Fig. 6). Microscopy in fatal viral enteritis shows severe mucosal damage with widespread ulceration, patchy or diffuse villous atrophy, lymphoid atrophy, and vacuolations in villous epithelial cells [25]; villous shortening and patchy ulceration could result in this amorphous, shaggy appearance. In previous reports of fatal viral enteritis, significant gastrointestinal hemorrhage was a contributing or primary cause of death [20, 21], and in our group of patients, profuse bloody diarrhea was more common in viral infection than in acute GVHD.

Colonic findings in this study were reminiscent of idiopathic inflammatory bowel disease with loss of haustration, spasm, edema, ulceration, or a granular mucosal pattern consistent with mucosal edema or fine ulceration. These findings were similar to those reported recently in cytomegalovirus colitis in AIDS [29–31].

Viral infectious agents included coxsackie virus, adenovirus, rotavirus, atypical rotavirus, and cytomegalovirus, in a few cases combined with other pathogenetic organisms such as *Pseudomonas aeruginosa* or *Clostridium difficile*. Several patients had enteric infection with more than one virus. The relative contribution of each pathogen to the radiographic appearances cannot be determined in the individual patient.

Conclusions

Radiographic findings cannot be used to differentiate acute GVHD from viral enteritis; gastric abnormalities were seen only in viral infection, either alone or combined with acute GVHD. Similarly, the shaggy, amorphous contour of the small intestine in two patients with viral infection was not seen in acute GVHD. Hence, when a bone-marrow-transplant patient develops diarrhea and barium studies show findings suggesting inflammation, both acute GVHD and viral superinfection should be considered. Whereas acute GVHD may improve with intensification of an immunosuppressive regimen, viral enteritis may be worsened.

REFERENCES

1. Slavin RE, Santos GW. The graft versus host reaction in man after bone marrow transplantation: pathology, pathogenesis, clinical features, and implication. *Clin Immunol Immunopathol* **1973**;1:472–498
2. Thomas ED, Storb R, Clift RA, et al. Bone marrow transplantation. *N Engl J Med* **1975**;292:832–843, 895–902
3. Moir DH, Turner JJ, Ma DDF, et al. Autopsy findings in bone marrow transplantation. *Pathology* **1982**;14:197–204
4. Wick MR, Moore SB, Gastineau DA, Hoagland HC. Immunologic, clinical, and pathologic aspects of human graft-versus-host disease. *Mayo Clin Proc* **1983**;58:603–612
5. Beschorner WE. Destruction of the intestinal mucosa after bone marrow transplantation and graft-versus-host disease. *Surv Synth Pathol Res* **1984**;3:264–274
6. Sale GE, McDonald GB, Shulman HM, Thomas ED. Gastrointestinal graft-versus-host disease in man. *Am J Surg Pathol* **1979**;3:291–299
7. McDonald GB, Shulman HM, Sullivan KM, Spencer GD. Intestinal and hepatic complications of human bone transplantation. Part I. *Gastroenterology* **1986**;90:460–477
8. McDonald GB, Shulman HM, Sullivan KM, Spencer GD. Intestinal and hepatic complications of human bone transplantation. Part II. Gastroenterology **1986**;90:770–784
9. Thorning D, Howard JD. Epithelial denudement in the gastrointestinal tracts of two bone marrow transplant recipients. *Hum Pathol* **1986**;17(6):560–566
10. Spencer GD, Shulman HM, Myerson D, Thomas ED, McDonald GB. Diffuse intestinal ulceration after marrow transplantation: a clinicopathologic study of 13 patients. *Hum Pathol* **1986**;17(6):621–633
11. Epstein RJ, McDonald GB, Sale GE, Shulman HM, Thomas ED. The diagnostic accuracy of the rectal biopsy in acute graft-versus-host disease: a prospective study of thirteen patients. *Gastroenterology* **1980**;78:764–771
12. Shimkin PM, DeLellis RA, Carolla RL, Weinstein MA. Graft-versus-host disease. *Radiology* **1972**;102:623–624
13. Rosenberg HK, Serota FT, Koch P, Borden S, August CS. Radiographic features of gastrointestinal graft-versus-host disease. *Radiology* **1981**;138:371–374
14. Fisk JD, Shulman HM, Greening RR, McDonald GB, Sale GE, Thomas ED. Gastrointestinal radiographic features of human graft-versus-host disease. *AJR* **1981**;136:329–336
15. Schimmelpenninck M, Zwaan F. Radiographic features of small intestinal injury in human graft-versus-host disease. *Gastrointest Radiol* **1982**;7:29–33
16. Winston DJ, Gale RP, Meyer DV, Lowell SY. Infectious complications of human bone marrow transplantation. *Medicine* **1979**;58:1–31
17. Zahradnik JM, Spencer MJ, Porter DD. Adenovirus infection in the immunocompromised patient. *Am J Surg* **1980**;68:725–732
18. Strayer DS, Phillips GB, Barker KH, Winokur T, DeSchryver-Kecskemeti K. Gastric cytomegalovirus infection in bone marrow transplant patients. *Cancer* **1981**;48:1478–1483
19. Beschorner WE, Yardley JH, Tutschka PJ, Santos GW. Deficiency of intestinal immunity with graft-versus-host disease in humans. *J Infect Dis* **1981**;144:38–46
20. Yolken RH, Bishop CA, Townsend TR, et al. Infectious gastroenteritis in bone marrow transplant recipients. *N Engl J Med* **1982**;306:1109–1112
21. Townsend TR, Bolyard EA, Yolken RH, et al. Outbreak of coxsackie A1 gastroenteritis: a complication of bone marrow transplantation. *Lancet* **1982**;1:820–823
22. West JC, Armitage JO, Mitros FA, Klassen LW, Corry RJ, Ray T. Cytomegalovirus cecal erosion causing massive hemorrhage in a bone marrow transplant recipient. *World J Surg* **1982**;6:251–255
23. Hochhauser L, Thomaspon G, Somers S. Opportunistic gastritis in graft-versus-host disease. *J Assoc Radiol* **1983**;34:316–318
24. Glucksberg H, Storb R, Fefer A, et al. Clinical manifestations of graft-versus-host disease in human recipients of marrow from HL-A-matched sibling donors. *Transplantation* **1974**;18(4):295–304
25. Trier JS, Schreiber DS, Blacklow NR. The pathology of acute nonbacterial gastroenteritis. In: Yardley JH, Morson BC, Abetts MR, eds. *The gastrointestinal tract. International Academy of Pathology monograph.* Baltimore: Williams & Wilkins, **1977**:36–49
26. Yolken RH. Enzyme-linked immunosorbent assay (ELISA): a practical tool for rapid diagnosis of viruses and other infectious agents. *Yale J Biol Med* **1980**;53:85–92
27. Farman J, Faegenburg D, Dallemand S, Chen CK. Crohn's disease of the stomach. The "ram's horn" sign. *AJR* **1975**;123:242–251
28. Jones B, Fishman EK, Kramer SS, et al. Computed tomography of gastrointestinal inflammation after bone marrow transplantation. *AJR* **1986**;146:691–695
29. Balthazar EJ, Megibow AJ, Fazzini E, Opulencia JF, Engel I. Cytomegalovirus colitis in AIDS: radiographic findings in 11 patients. *Radiology* **1985**;155:585–589
30. Frager DH, Frager JD, Wolf EL, et al. Cytomegalovirus colitis in acquired immune deficiency syndrome: radiologic spectrum. *Gastrointest Radiol* **1986**;11:241–246
31. Teixidor HS, Honig CL, Norsoph E, Albert S, Mouradian JA, Whalen JP. Cytomegalovirus infection of the alimentary canal: radiologic findings with pathologic correlation. *Radiology* **1987**;163:317–323

Book Review

A Practical Approach to Angiography, 2nd edition. By Irwin S. Johnsrude, Donald C. Jackson, and N. Reed Dunnick. Boston: Little, Brown, 565 pp., 1987. $85

The authors of this book have set themselves a most ambitious task, that of discussing in great detail virtually all aspects of modern angiography. Areas covered range from history, equipment, and basic and advanced techniques to the newest developments in interventional angiography. The book includes in-depth discussions of arteriographic and venographic techniques and descriptions of findings in a wide variety of disease states in each of the body parts and organ systems that lend themselves to angiographic investigation. Many of the tricks of the trade that those of us active in the field have learned over the years are described clearly. The authors also discuss such rarely used procedures as lymphangiography and parathyroid angiography. The book even contains a well-written section on what might be called "cerebral angiography for the nonneuroradiologist." An appendix contains valuable miscellaneous information, such as characteristics of contrast agents with reference to the new low-osmolar agents, a table of basic drugs used in angiography, suggested timing of films and volumes of contrast material, charts for estimating degrees of stenosis, and even such esoterica as a formula for the preparation of blue dye for use in lymphangiography.

Illustrations are first-rate, and the many line drawings are helpful in clarifying techniques discussed in the text. The style is readable and concise. I found it somewhat strange that the sections on angioplasty and therapeutic embolization precede the chapters on basic femoral angiography and aortography, but this obviously reflects the authors' interests. Although the book has three contributing authors in addition to the three principal authors, repetition is minimal.

The experienced angiographer will nod in agreement at the many valuable suggestions on various techniques and will appreciate the stands taken on controversial issues. The tyro will find this volume a source for constant referral and rarely will be disappointed when trying to find a solution to a specific problem. I know of no other text that covers this particular material as completely and accurately. In a market in which the supply of angiographic texts seems to be endless, this one quickly, and deservedly, will find its way to the top of the best-sellers' list.

Arnold Chait
The Graduate Hospital
Philadelphia, PA 19146

MR Imaging of Portal Venous Thrombosis: Correlation with CT and Sonography

Kenneth Zirinsky[1]
John A. Markisz
William A. Rubenstein
Patrick T. Cahill
R. James R. Knowles
Yong Ho Auh
Harvey Morrison
Elias Kazam

Fourteen patients with portal venous thrombosis (PVT) diagnosed by CT and/or sonography were studied with MR. Three of the 14 had portal hypertension. The MR findings were compared with those of eight patients with portal hypertension, but without CT or sonographic evidence of PVT. MR imaging showed portal venous thrombosis in all 14 PVT cases. Intraluminal thrombi of less than 5 weeks duration appeared markedly hyperintense relative to liver and muscle on both T1- and T2-weighted images. Older thrombi appeared hyperintense relative to liver and muscle in eight of 11 cases, but only on T2-weighted images. MR showed thrombi in 11% more portal vessels than did CT (MR = 30, CT = 27) and in 28% more vessels than did sonography (MR = 32, sonography = 25). MR also showed 24% more collateral vessels than did CT (MR = 31, CT = 25) and 50% more vessels than did sonography (MR = 33, sonography = 22). Third-echo images (echo time = 96 msec, repetition time = 1500–2150 msec) verified the presence of venous thrombi in 28 (93%) of 30 PVT vessels, and they differentiated flow-related intravascular signal from true thrombi in six (17%) of 36 portal hypertension vessels.

We conclude that MR is a valuable tool for imaging portal vein thrombosis. MR is a good substitute for CT and can be more informative than sonography.

The angiographic, CT, and sonographic diagnoses of portal venous thrombosis (PVT) have been well described [1–6]. IV contrast enhancement, particularly with dynamic rapid-sequence scanning, is essential for the CT diagnosis of PVT [2], whereas pulsed Doppler is a valuable supplement to real-time sonography for diagnosing this condition [5, 6].

With the advent of MR, another noninvasive technique became available for the diagnosis of PVT [7–11]. This report is based on a retrospective study of the MR images in 14 patients who had CT and/or sonographic evidence of PVT. MR is compared with CT and sonography with respect to the ease of visualizing portal vessels, determining the presence of thrombi, and detecting collateral vessels. The MR findings in the PVT group are also compared with those of eight patients who had portal hypertension but had no CT or sonographic evidence of PVT. Finally, the usefulness of third-echo images for identifying portal venous thrombi and for differentiating them from flow-related artifacts is evaluated.

Materials and Methods

The MR studies of 14 consecutive patients with CT and/or sonographic evidence of PVT were reviewed. There were five males and nine females ranging in age from 1.5 to 79 years. Sectional imaging was performed to evaluate fever of unknown origin (four patients), abdominal pain (four patients), jaundice (three cases), ascites (two cases), and hepatosplenomegaly (one patient). Four patients had recent splenectomy for lymphoma, leukemia, myelofibrosis, and trauma; another four patients had liver malignancies (hepatoma in two and metastatic colon carcinoma in two). Five patients had clinical evidence of cirrhosis and portal hypertension, and one patient had echinococcal disease of the liver. In nine of the cases, the diagnosis of PVT was verified with both CT and sonography (Figs. 1–4). In another three cases, PVT

Received November 24, 1986; accepted after revision October 5, 1987.

[1] All authors: Department of Radiology, The New York Hospital–Cornell Medical Center, 525 E. 68th St., New York, NY 10021. Address reprint requests to K. Zirinsky.

AJR 150:283–288, February 1988
0361–803X/88/1502–0283
© American Roentgen Ray Society

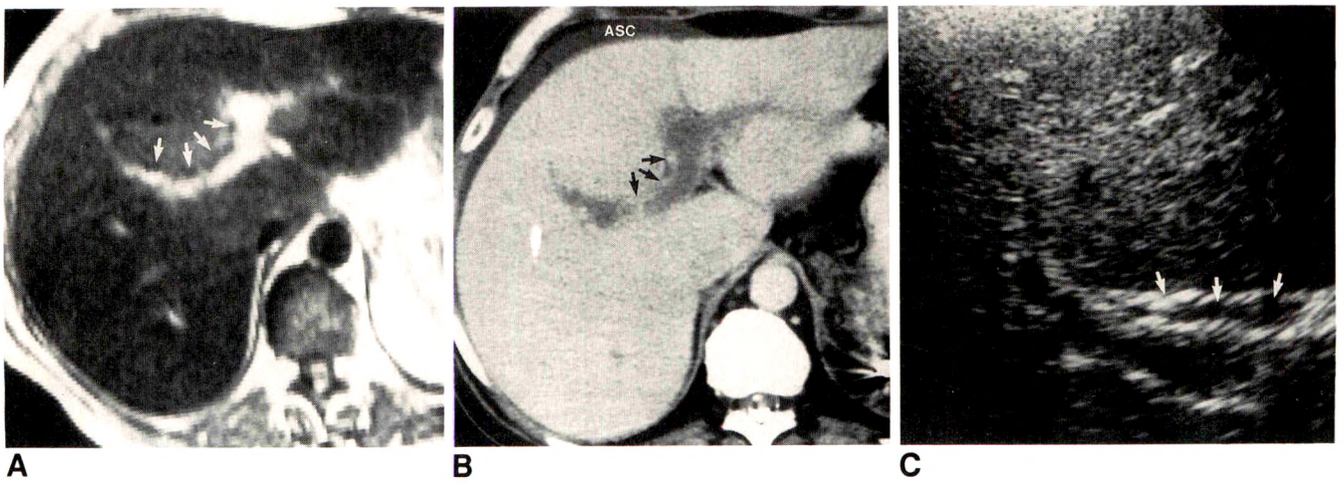

Fig. 1.—Portal venous thrombosis 2 weeks after splenectomy.

A, First-echo MR image (TR = 1600 msec, TE = 32 msec) shows hyperintense thrombus, relative to liver and muscle, in right and left portal veins. Brightness of thrombus increased with second- and third-echo images. A lower transverse section showed hyperintense thrombus in splenic vein. Periportal collaterals (*arrows*). Relatively dark appearance of liver is attributed to iron deposition after multiple blood transfusions for chronic leukemia.

B, CT at approximate level of *A*. A radiolucent thrombus occupies right and left portal veins. Periportal collaterals (*arrows*). Ascites (ASC).

C, Transverse sonogram corresponding to *A* and *B*. Portal vein thrombus is echo free and was diagnosed only when pulsed Doppler showed no portal venous flow. Periportal collaterals (*arrows*).

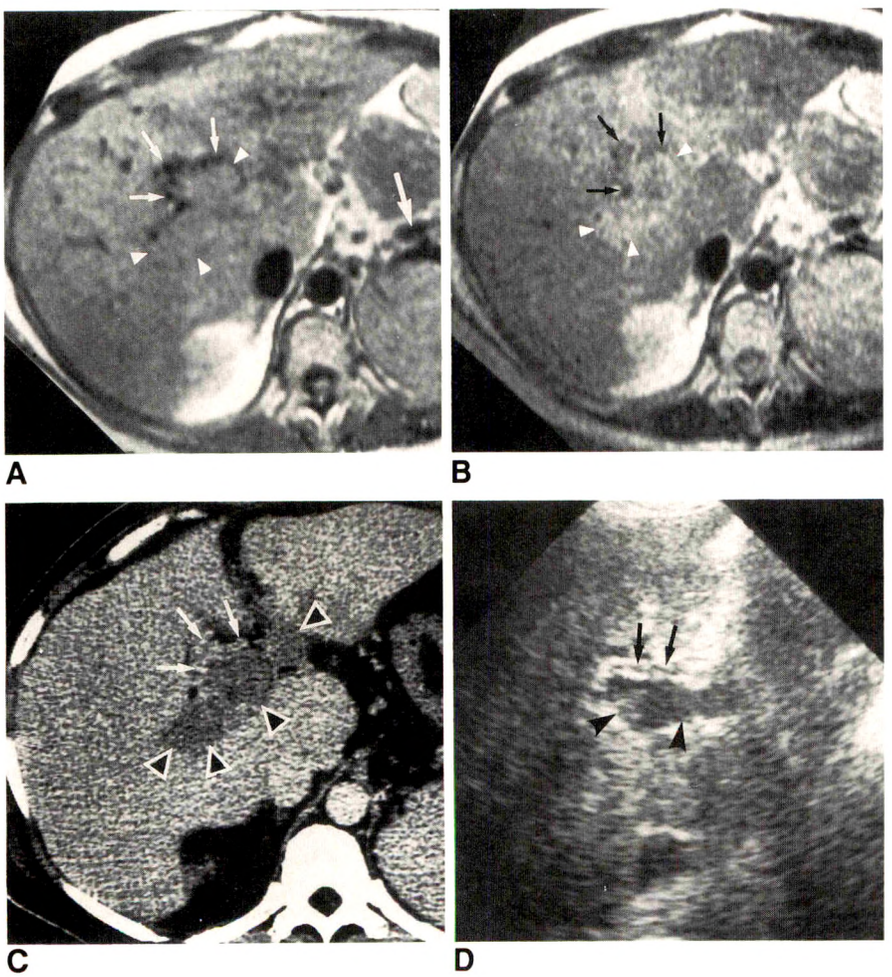

Fig. 2.—Portal venous thrombus at least 5 months old with underlying biopsy-proved cirrhosis.

A, On first-echo MR image (SE 1500/32), expected site of location of portal vein (*arrowheads*) appears isointense with liver. Peripheral collaterals are visible (*small arrows*). Spleen is enlarged. Short gastric collaterals (*large arrow*).

B, On third-echo MR image (SE 1500/96), hyperintensity relative to liver is noted at expected location of thrombosed portal vein (*arrowheads*). Periportal collaterals (*arrows*) are not as well seen as in *A*.

C, On contrast-enhanced CT scan, thrombosed portal vein appears relatively hypodense (*arrowheads*) and is better delineated than in *A* and *B*. Periportal collaterals (*arrows*).

D, Transverse sonogram corresponding to *A*–*C*. Echogenic thrombus is visible within portal vein (*arrowheads*). Periportal collaterals (*arrows*).

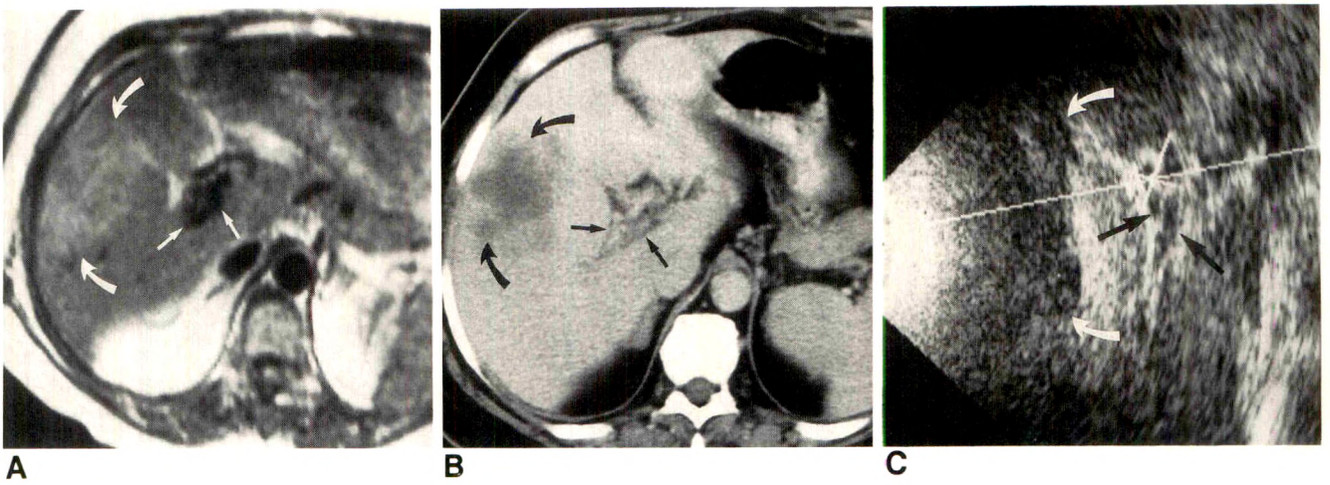

Fig. 3.—Chronic portal vein thrombosis with cavernous transformation.

A, First-echo MR image (SE 1600/32) shows multiple collaterals (*straight arrows*) occupying expected site of location of portal vein and not limited to its peripheral margins (unlike Figs. 2A and 2B). Colon metastasis (*curved arrows*).

B, CT scan corresponding to *A* shows that multiple collaterals (*straight arrows*) have replaced portal vein, which is not visible. Colon metastasis (*curved arrows*).

C, Transverse oblique sonogram slightly above level of *A* and *B*. Multiple collaterals (*straight arrows*) were confirmed by pulsed Doppler tracing, which showed characteristic portal flow. Colon metastasis (*curved arrows*). Image rotated 90° so anatomic features correspond to those in *A* and *B*.

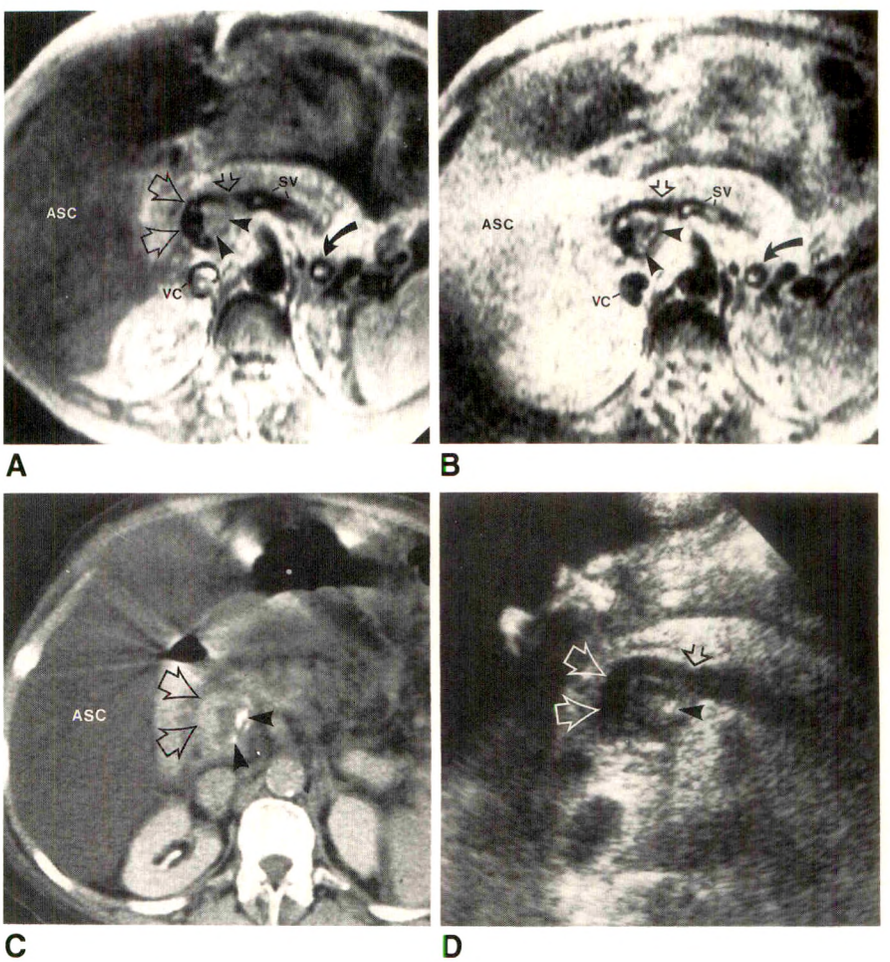

Fig. 4.—Chronic portal and superior mesenteric vein thrombosis with calcified focal thrombus.

A, First-echo MR image (SE 2150/32) shows thrombus (*arrowheads*) within medial two-thirds of portal-superior mesenteric vein junction, with a peripherally patent vascular lumen (*large open arrows*). Thrombus may be present at junction of splenic and superior mesenteric veins (*small open arrow*). Bright signal is noted within vena cava (VC), splenic vein (SV), and in a splenorenal collateral (*curved arrow*). Ascites (ASC).

B, Third-echo MR image (SE 2150/96). Portal venous thrombus (*arrowheads*) is more heterogeneous than in *A* and appears relatively brighter in its anterolateral aspect. Junction of splenic and superior mesenteric veins is now clearly patent (*open arrow*). Slow-flow artifacts have disappeared from vena cava (VC) and have changed in shape and/or location within splenic vein (SV) and in splenorenal collateral (*curved arrow*). Ascites (ASC).

C, CT scan corresponding to *A* and *B* shows calcification (*arrowheads*) in medial portion of portal vein thrombus not seen on MR image. Denser lateral portion of portal vein (*open arrows*) corresponds to patent peripheral portion on MR image. Enlarged portal vein mimics a pancreatic mass on CT. Ascites (ASC).

D, Transverse sonogram corresponding to *A*–*C*. Medial calcification (*arrowhead*) within thrombus casts an acoustic shadow. Patent lateral portion of portal vein (*large open arrows*) and junction with splenic vein (*small open arrow*) are echo free.

had been diagnosed with sonography only. In the remaining two patients, PVT has been verified only by CT.

In the 14 PVT patients, MR imaging was performed with a 0.5-T superconducting magnet (Technicare, Solon, OH). A multislice triple-echo technique was used for the transverse images in 12 patients (repetition time [TR] = 1500–2150 msec; echo time [TE] = 32, 64, and 96 msec). In two patients, only dual echoes were obtained for the transverse images (TE = 32/64 or 64/128 msec). T1-weighted sagittal and coronal multislice, single-echo images were obtained in 10 patients (TR = 500 msec, TE = 32 msec). The slice thickness was 0.75 cm, and the interslice interval was 1.0–1.25 cm. Thrombosis was diagnosed when persistent signal was seen within (or at the expected location of) a vessel on all multiple-echo images (Figs. 1A, 2A, 2B, 4A, and 4B), or when the portal vein was totally replaced by collateral vessels (Fig. 3A). When a portal vessel was devoid of signal on at least one echo, it was considered patent and free of thrombus.

In 11 of the PVT cases, CT scans were performed with GE 8800 or 9800 equipment, using 10-mm collimation and scan times of 10 sec or 2–3 sec, respectively. Consecutive CT sections were obtained through the upper abdomen in deep inspiration (with the patient supine) at intervals of 1.0–1.5 cm. Every patient received IV and oral contrast media. IV glucagon (1 ml) was administered for studies obtained with the slower scanner. In seven cases an IV bolus containing 12–15 g of iodine was given just before scanning, and was followed by continuous infusion of 28 g of iodine (Renografin 60 [diatrizoate meglumine], Squibb, New Brunswick, NJ) as the scans were obtained. In another four cases, dynamic sequential scans were obtained after administering IV boluses of 12–15 g of iodine. Portal venous thrombosis was diagnosed on CT when a focus of decreased attenuation appeared within or at the expected location of a portal vessel (Figs. 1B, 2C, and 4C) or when the vessel was replaced by collaterals (Fig. 3B).

In 12 PVT patients, sonograms were obtained with commercially available real-time equipment by using the highest frequency transducer that provided adequate penetration, usually 3.5 or 5 MHz. With the patient in a left posterior oblique position, transverse images of the confluence of the left and right portal veins, right portal vein bifurcation, and the umbilical portion of the left portal vein were obtained routinely. The main portal vein was also imaged in a longitudinal oblique projection. Transverse and longitudinal imaging of the splenic and superior mesenteric veins, respectively, was also attempted. In six cases, the sonograms were supplemented with duplex pulsed Doppler examination of the portal vessels at frequencies of 3.0 or 5 MHz (Ultramark 8, Advanced Technology Laboratories, Bellevue, WA). The wall filter was set at 50–100 MHz, and sample volume was 1.5–3.0 ml. Time velocity spectra were recorded routinely. Portal venous thrombi were diagnosed by sonography when focal intraluminal echogenicity was identified (Figs. 2D and 4D), when the portal vein was replaced by collaterals (Fig. 3C), or when Doppler signal was absent, even if the vessel was echo free (Fig. 1C). Pulsed Doppler was also used to differentiate portal venous collaterals from hepatic arterial branches and bile ducts.

For each patient with PVT, the MR, CT, and sonographic images were assessed (1) for the extent of venous thrombi; (2) the ease with which the main portal vein, its right and left branches, and its splenic and superior mesenteric tributaries could be delineated; and (3) the presence and location of venous collaterals.

To assess the potential for false-positive diagnoses of venous thrombosis, we compared the MR findings in the PVT group with those in a group of eight patients with portal hypertension (PHT group) in whom there was no evidence of portal venous thrombosis on CT or sonography. The sectional imaging criteria used for diagnosing portal hypertension were cirrhotic liver (nodular contours, enlarged caudate and/or left lobe), splenomegaly, and the presence of portal venous collaterals. Three PVT cases had portal hypertension when the same criteria were used. All eight PHT patients had triple-echo MR studies. Six had CT scans, and five had sonograms showing no portal venous thrombi. The MR, CT, and sonographic studies in the PHT group were performed and analyzed in the same manner as that described for the PVT group.

Results

Portal venous thrombosis was easily diagnosed with MR in all 14 PVT patients (Figs. 1–4). In three patients with post-splenectomy PVT, the thrombi were hyperintense relative to liver and muscle on the first-echo images (relatively T1 weighted) and became even brighter on the more T2-weighted second- and third-echo images (Fig. 1A). Collateral vessels were visible at the periphery of the thrombosed vessels (Fig. 1A). PVT was relatively recent in all three cases (the splenectomies has been performed 1.5–4.5 weeks before MR imaging).

Older thrombi, those approximately 2–18 months old, appeared hyperintense relative to liver and muscle in eight of 11 patients, but only on T2-weighted images (Figs. 2A and 2B). In four PVT cases, collateral vessels were seen at the periphery of the thrombosed veins, suggesting preservation of vascular integrity, even though the vessel may not have been clearly delineated with MR (Figs. 2A and 2B). In another six PVT cases, collateral vessels occupied the entire expected location of the thrombosed vessels and were not limited to its peripheral margins (Fig. 3A). This appearance was most consistent with cavernous transformation of the portal vein. The remaining PVT patient had discrete signal within the extrahepatic portal vein, marginated partially by a peripheral signal-free zone (Figs. 4A and 4B). This finding suggested chronic, retracted thrombus. Calcification in the thrombus was visible in one case with CT and sonography, but not with MR (Figs. 4C and 4D vs Figs. 4A and 4B). In the four patients with liver metastases or hepatoma, the thrombi appeared similar to the other PVT cases on MR, CT, and sonography, without evidence of liver malignancy.

Among the 14 PVT cases, the main portal vein was the most frequent site of thrombosis on MR (13/14 = 93%), followed, in order, by the right portal vein (10/14 = 71%), the left portal vein (8/14 = 57%), the splenic vein (4/14 = 29%), and the superior mesenteric vein (2/14 = 14%). MR helped to visualize 18% more of these portal branches and tributaries than did CT (MR = 46, CT = 39) and 21% more than did sonography (MR = 51, sonography = 42). Similarly, MR showed 11% more of these vessels to be thrombosed than did CT (MR = 30, CT = 27) and 28% more than did sonography (MR = 32, sonography = 25). (Note that the number of features detected by MR changes between correlation with CT and sonography because, although all 14 patients had MR, only 11 patients had CT and 12 patients had sonography. The numbers for MR and CT compare MR and CT features for only the group of 11 patients who had both MR and CT. The numbers for MR and sonography compare only the group of 12 patients who had both MR and sonography.)

Collateral vessels were seen most frequently in the porta

hepatis, along the main portal vein (79% on MR images) and its right and left branches (up to 71% on MR images). They were also visible at the fissure for the ligamentum teres, and in paraumbilical and paraesophageal locations. When these multiple sites were considered together, MR in the PVT group helped to visualize collateral vessels at 24% more sites than CT did (MR = 31, CT = 25) (Figs. 2A and 2C) and at 50% more sites than sonography did (MR = 33, sonography = 22). There was a striking difference in the location of collateral vessels between the PVT and PHT groups. Paraesophageal collaterals were visible on MR images in only 29% (4/14) of the PVT cases but in 75% (6/8) of the PHT cases. However, porta hepatis collaterals, which were visible in 79% (11/14) of the PVT cases, were seen in only 25% (2/8) of the PHT group.

The third-echo image (TE = 96, TR = 1500–2150) was valuable for verifying thrombi that were suspected on the first- and second-echo images. Among 30 thrombosed vessels in the PVT group, maximal intensity relative to muscle was observed on the third-echo images for either part or all of the thrombus in 26 vessels (86%) (Figs. 2A and 2B). In two other vessels (7%), the relative intensity of the thrombus was equal on the second- and third-echo images, exceeding the brightness on the first-echo image. The remaining two vessels (7%) were brightest on the second-echo images. In the PHT group, six (17%) of the 36 vessels became signal free and were diagnosed as unequivocally patent only on the third-echo images. Another 21 vessels (21/36 = 58%) were signal free on the first-echo images and easily diagnosed as patent. The remaining nine vessels (25%) had intraluminal signal surrounded uniformly by a signal-free ring and therefore were diagnosed as patent. In four (11%) of the 36 the peripheral ring was darkest on the third echo, whereas in three (8%) the ring was brightest on the third-echo image. In another two vessels (6%), the ring was darkest on the second echo.

Discussion

The results show that MR is an excellent procedure for imaging the portal venous system. The portal vein, its right and left branches, and its splenic and superior mesenteric tributaries were easier to see with MR than with either CT or sonography. Furthermore, thrombosis of these vessels and associated portal venous collaterals were detected with greater sensitivity by MR than by CT or sonography.

Better results would have been possible with CT had dynamic, rapid-sequence, contrast-enhanced scans been used in every case [2]. Since PVT was not suspected in most of the cases at the time of the initial CT scan, the majority of the studies were obtained in a nondynamic mode. Even with dynamic CT scans, however, proper timing of the scan relative to the bolus injection may be critical for showing thrombi or opacifying collateral vessels [9]. Therefore MR, with the natural signal void provided by rapidly flowing blood, seems preferable to CT for diagnosing PVT.

Similarly, a more favorable comparison of sonography with MR would have been possible if pulsed Doppler [5, 6] had been used routinely to help detect echo-poor thrombus (Fig. 1C). However, the lower sensitivity of sonography in this series was due mainly to the difficulty of visualizing vessels that were obscured by air, omental fat, or a fatty, fibrotic liver. These natural impediments to the sound beam cannot be overcome with Doppler sonography [6].

MR failed to detect calcification within a chronic, retracted thrombus (Fig. 4). This did not preclude MR delineation of the largest portion of the thrombus within the portal vein, but it did interfere with MR visualization of a calcified component of the thrombus in the superior mesenteric vein below the level shown in Fig. 4.

Another potential limitation of MR in the diagnosis of PVT is the slow-flow–enhancement artifact [12], which is more likely to occur in patients with portal hypertension [10]. The increased brightness of this artifact on even echoes is valuable for differentiating it from true intraluminal thrombi [12]. In this regard, the third-echo image was especially useful, because it showed progressively increasing brightness or persistent maximal brightness relative to the first- and second-echo images in most thrombosed vessels (93%). In contrast, a fraction of patent vessels (17%) appeared signal free only on the third-echo image. Although not all patent vessels appeared darkest on the third-echo image, these images nevertheless helped to support the impression of vascular patency by showing changes in the size and location of the intraluminal signal. Sagittal and coronal images helped to confirm suspected flow artifacts in a similar manner. Another valuable sign of vascular patency was the presence of a uniform signal-free ring surrounding an inner bright zone.

In three PVT cases, thrombus that was less than 5 weeks old appeared hyperintense relative to liver and muscle on T1-weighted images and became even brighter on T2-weighted images (Fig. 1A). This observation is in agreement with previous reports on the MR appearance of relatively recent venous thrombi [11, 13]. Histologically, thrombi are completely fibrinized within 2 days after their formation and then undergo variable lysis and organization [11]. It has not been proved, however, that the brightness of the thrombus decreases with time. In one study there was no change in the intensity of thrombi on MR over a 3-week period in an animal model or over a 4-week period in humans [11]. Nevertheless it is tempting to suggest, on the basis of the findings in this study, that thrombi more than 2 months old may lose their relative hyperintensity on T1-weighted images.

Cavernous transformation of the portal vein, which was observed in six of our cases, is defined pathologically as replacement of the portal vein and hepatoduodenal ligament by a spongy network of collateral blood vessels [14]. In a review of 23 autopsies, the obliterated portal vein was still recognizable grossly or microscopically in 13 cases (57%), but there was no trace of it in six cases (26%) [14]. It has been estimated that 1–12 months may be required for cavernous transformation [3, 15]. The appearance of multiple collaterals on MR images, not only at the periphery but also within the expected location of the portal vein lumen, fits the pathologic description of portal cavernoma (Fig. 3). Similar features of this entity have been described on CT and sonography [2–4, 6].

Finally, differences were found in the distribution of collat-

eral vessels between the PVT and PHT groups. In the PHT group, collaterals were seen most frequently in the paraesophageal region. This is consistent with the location of collaterals in previous CT and sonographic reports on patients with portal hypertension [16, 17]. The predominance of porta hepatis collaterals in the PVT group may be a useful indirect sign of the presence of portal venous thrombosis.

MR is a valuable, noninvasive method for diagnosing portal venous thrombosis. It is easier to perform than dynamic CT scanning and can be more informative than sonography, except in the detection of thrombus calcification. The specificity of MR can be improved by using triple-echo imaging to differentiate true thrombi from flow-related artifacts. Thrombi less than 5 weeks old appeared hyperintense relative to liver and muscle on both T1- and T2-weighted images. Older thrombi appeared hyperintense in some patients, but on T2-weighted images only. Portal cavernoma can be diagnosed with MR when multiple collateral vessels occupy the expected location of the portal vein lumen. Collateral vessels in portal vein thrombosis occur most frequently at the porta hepatis, in contrast to the paraesophageal location of most collaterals in portal hypertension.

ACKNOWLEDGMENTS

The authors thank Carmen I. Velazquez, Evelyn Shaw, and Fereshteh Kazam for manuscript preparation.

REFERENCES

1. Subramanyam BR, Balthazar EJ, Lefleur RS, Horii SC, Hulnick DH. Portal venous thrombosis: correlative analysis of sonography, CT, angiography. *Am J Gastroenterol* **1984**;79:773–776
2. Mathieu D, Vasile N, Grenier P. Portal thrombosis: dynamic CT features and course. *Radiology* **1985**;154:737–741
3. Kauzlaric D, Petrovic M, Barmeir E. Sonography of cavernous transformation of the portal vein. *AJR* **1984**;142:383–384
4. Van Gansbeke D, Avni EF, Delcour C, Engelholm L, Struyven J. Sonographic features of portal vein thrombosis. *AJR* **1985**;144:749–752
5. Weltin G, Taylor KJW, Carter AR, Taylor CR. Duplex Doppler: identification of cavernous transformation of the portal vein. *AJR* **1985**;144:999–1001
6. Miller VE, Berland LL. Pulsed Doppler duplex sonography and CT of portal vein thrombosis. *AJR* **1985**;145:73–76
7. Kneeland JB, Auh YH, Zirinsky K, Rubenstein WA, Kazam E. MR, CT, and ultrasonographic demonstration of splenic vein thrombosis. *J Comput Assist Tomogr* **1984**;8:1199–1200
8. Ohtomo K, Itai Y, Furui S, Yoshikawa K, Yashiro N, Iio M. MR imaging of portal vein thrombosis in hepatocellular carcinoma. *J Comput Assist Tomogr* **1985**;9:328–329
9. Hricak H, Amparo E, Fisher MR, Crooks L, Higgins CB. Abdominal venous system: assessment using MR. *Radiology* **1985**;156:415–422
10. Williams DM, Cho KJ, Aisen AM, Eckhauser FE. Portal hypertension evaluated by MR imaging. *Radiology* **1985**;157:703–706
11. Erchman WA, Weinreb JC, Cohen JM, Buja LM, Chaney C, Peshock RM. Venous thrombosis: clinical and experimental MR imaging. *Radiology* **1986**;161:233–238
12. Bradley WG, Waluch V. Blood flow: magnetic resonance imaging. *Radiology* **1985**;154:443–450
13. Macchi PJ, Grossman RI, Gomori J, Goldberg HI, Zimmerman RA, Bilaniuk LT. High field MR imaging of cerebral venous thrombosis. *J Comput Assist Tomogr* **1986**;10:10–15
14. Klemperer P. Cavernomatous transformation of the portal vein: its relation to Banti's disease. *Arch Pathol* **1928**;6:353–362
15. Aldrete JS, Slaughter RL, Han SY. Portal vein thrombosis resulting in portal hypertension in adults. *Am J Gastroenterol* **1976**;65:236–243
16. Ishikawa T, Tsukune Y, Ohyama Y, Fujikawa M, Sakuyama K, Fujii M. Venous abnormalities in portal hypertension demonstrated by CT. *AJR* **1980**;134:271–276
17. Juttner H, Jenney J, Ralls P, Goldstein LI, Reynolds TB. Ultrasound demonstration of portosystemic collaterals in cirrhosis and portal hypertension. *Radiology* **1982**;142:459–463

Case Report

Hepatic Venocclusive Disease After Bone-Marrow Transplantation: Diagnosis with Duplex Sonography

J. Scott Kriegshauser,[1] J. William Charboneau,[1] and Louis Letendre[2]

Venocclusive disease of the liver is a well-known complication of bone-marrow transplantation, especially in patients who have had combined chemotherapy and radiation therapy before transplantation [1–3]. Histopathologic study shows occlusion at the terminal hepatic venules and sublobular veins and centrolobular necrosis. The major hepatic veins are not involved—a finding that distinguishes this entity from the classic Budd-Chiari syndrome. Clinical features include abdominal pain, hepatomegaly, ascites, jaundice, and encephalopathy. We describe a patient who had acute reversal of portal venous flow and visceral edema, which was documented on two duplex sonograms on consecutive days.

Case Report

A 39-year-old woman was referred to our institution for evaluation and treatment of recently discovered idiopathic aplastic anemia. Peripheral blood findings and bone-marrow cellularity fulfilled the criteria for severe aplasia [4]. Before transplantation of allogenic bone marrow, the patient had total lymphoid radiation and four daily doses of cyclophosphamide (40 mg/kg per day) [5]. Three days after transplantation, the patient had mild upper abdominal pain and tenderness. The next day, the pain increased and localized to the right upper quadrant. Serum levels of bilirubin (total, 2.9 mg/dl [normal, <1.1 mg/dl]; direct, 1.8 mg/dl [normal, <0.3 mg/dl]), alkaline phosphatase (502 U/l [normal, 76–196 U/l]), and aspartate aminotransferase (41 U/l [normal, 12–31 U/l]) were elevated. At 5 and 6 days after transplantation, the pain in the right upper quadrant increased, and ascites was evident clinically. The levels of bilirubin, alkaline phosphatase, and aspartate aminotransferase progressively increased. Serum levels of albumin ranged from 2.5 to 3.0 g/dl (normal, 3.5–5.0 g/dl).

A duplex sonographic examination of the abdomen performed on the fifth day after transplantation showed ascites, bilateral pleural effusions, and pronounced thickening of the gallbladder wall, to a diameter of 1.7 cm (Figs. 1A and 1B). Echogenicity within the gallbladder wall was increased, giving it a lamellar appearance. Pulsed Doppler sonography showed hepatopetal flow and patent portal veins (Fig. 1C). Twenty-four hours later, repeat sonographic examination showed an increase in the amount of ascites and increased thickening of the gallbladder wall, to a diameter of approximately 2.3 cm, which obliterated the lumen. Portal venous flow had reversed (Fig. 1D). Direction of flow in the hepatic veins was normal. Loops of small bowel with thickened walls were observed also.

During the following week, the hepatic failure became worse, and the hepatorenal syndrome developed. The patient died 13 days after transplantation. Autopsy revealed acute occlusion of the centrolobular veins, along with massive centrolobular hepatic necrosis and hemorrhagic edema of the gallbladder. The hepatic artery, major hepatic veins, and portal vein were patent. A total of 5.5 l of fluid was found in the peritoneal cavity.

Discussion

The clinical and pathologic features of venocclusive disease in bone-marrow transplantation have been well reviewed [1–3]. Our case illustrates the duplex sonographic findings of acute and fulminant portal venous hypertension. The degree and acuteness of thickening of the gallbladder wall and the overnight reversal of portal venous flow were striking sono-

Received July 24, 1987; accepted after revision October 5, 1987.

[1] Department of Diagnostic Radiology, Mayo Clinic and Mayo Foundation, Rochester, MN 55905. Address reprint requests to J. W. Charboneau, Mayo Clinic, 200 First St. S.W., Rochester, MN 55905.

[2] Division of Hematology and Internal Medicine, Mayo Clinic and Mayo Foundation, Rochester, MN 55905.

AJR 150:289–290, February 1988 0361–803X/88/1502–0289 © American Roentgen Ray Society

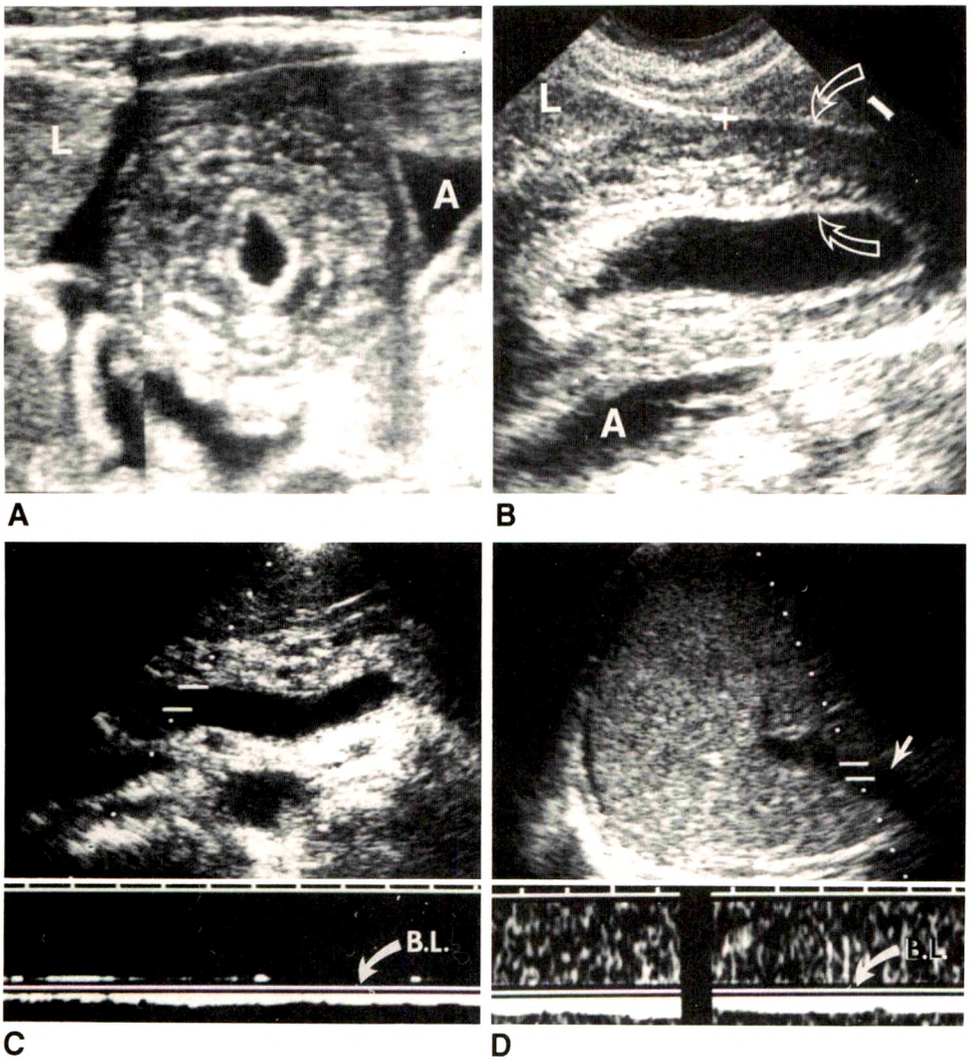

Fig. 1.—Hepatic venocclusive disease after bone-marrow transplantation.

***A* and *B*, Transverse (*A*) and longitudinal (*B*) sonograms show pronounced thickening of gallbladder wall (*arrows* in *B*) and narrow lumen. L = liver; A = ascites.**

***C*, Longitudinal Doppler sonogram of portal vein. Venous waveform projects below zero baseline (B.L. and *arrow*), indicating hepatopetal flow (right to left).**

***D*, Longitudinal Doppler sonogram of portal vein (*straight arrow*) obtained 24 hr after sonogram in *C* shows hepatofugal (left to right) flow. Venous waveform projects below baseline (B.L. and *curved arrow*) as in *C*, but angle made by portal vein and transducer is opposite to that in *C*.**

graphic features that, to our knowledge, have not been reported previously.

The portal venous hypertension in patients who have received bone-marrow transplants develops because of occlusion of the venous outflow, which is probably the result of a direct injury to the hepatic venules and the clogging of the venules with necrotic debris. The combination of chemotherapy and radiation is thought to damage both the venules and the hepatocytes, and further damage to the hepatocytes occurs because of the congestion and hypoxia [3].

Diagnosis based on clinical and laboratory findings can be accurate in identifying these patients [2]. Serial sonographic examinations may aid in the diagnosis and the evaluation of severity. In a patient who has undergone bone-marrow transplantation and in whom clinical findings suggest venocclusive disease, the findings of hepatofugal portal venous flow and pronounced thickening of the gallbladder wall are confirmatory, especially if serial examinations reveal that these developed rapidly. The rapidity of development and the degree of thickening of the gallbladder wall may indicate severity.

REFERENCES

1. McDonald GB, Shulman HM, Sullivan KM, Spencer GD. Intestinal and hepatic complications of human bone marrow transplantation. Part I. *Gastroenterology* **1986**;90:460–477
2. McDonald GB, Sharma P, Matthews DE, Shulman HM, Thomas ED. Venocclusive disease of the liver after bone marrow transplantation: diagnosis, incidence, and predisposing factors. *Hepatology* **1984**;4:116–122
3. McDonald GB, Sharma P, Matthews DE, Shulman HM, Thomas ED. The clinical course of 53 patients with venocclusive disease of the liver after marrow transplantation. *Transplantation* **1985**;39:603–608
4. Camitta BM, Rappeport JM, Parkman R, Nathan DG. Selection of patients for bone marrow transplantation in severe aplastic anemia. *Blood* **1975**;45:355–363
5. Ramsay NK, Kim T, Nesbit ME, et al. Total lymphoid irradiation and cyclophosphamide as preparation for bone marrow transplantation in severe aplastic anemia. *Blood* **1980**;55:344–346

Heterotopic Gastric Mucosa in the Duodenum: Radiographic Findings

Farooq P. Agha[1]
Gary G. Ghahremani[1]
Tat-Kin Tsang[2]
Thomas A. Victor[3]

Heterotopic gastric mucosa in the duodenal bulb was detected by endoscopic examination in 25 adult patients and was confirmed by biopsy in 17 of these patients. The endoscopic findings were correlated with the radiographic features of the lesion on upper gastrointestinal barium studies. On radiographs, this entity usually presented as clusters of 1- to 3-mm plaques raised above the smooth and featureless duodenal mucosa; this was seen in 17 (68%) of 25 patients. A less frequent finding was patches of coarse nodular mucosa with superficial erosions or an ulcer crater (five cases [20%]). The heterotopic gastric mucosa was visible as polypoid masses in two patients and as prominent areae gastricae covering the base of duodenal bulb in another.

The gastric mucosa is unique in its histologic features, its secretory functions, and its propensity to occur at anatomic sites beyond the confines of the stomach. The common locations for heterotopic gastric mucosa (HGM) are the esophagus, Meckel diverticulum, and enteric duplication cysts [1–4]. However, it may be found as ectopic islands located anywhere in the gastrointestinal tract, from the oral cavity to the rectum [5, 6]. Its occurrence also has been noted in the gallbladder or bile ducts [7], as well as in the airways, spinal column, and urinary bladder [1].

The widespread use of upper gastrointestinal endoscopy during the past decade has improved the awareness and detectability of HGM as mucosal plaques covering the duodenal bulb [2, 8]. This entity also has been identified by double-contrast radiography, but experience has been limited [2, 9]. Therefore, we present an analysis of HGM in the duodenal bulb based on a correlative study of the radiologic, endoscopic, and histologic features in 25 cases. The clinical significance of this entity and the spectrum of its radiographic manifestations will be described.

Materials and Methods

Twenty-five adult patients in whom the diagnosis of HGM involving the duodenal bulb was established by endoscopy were included in the study group. The diagnosis was confirmed by biopsy in 17 of the patients. There were nine men and 16 women, ranging in age from 18 to 86 years (mean, 62.4 years). All patients were examined by upper gastrointestinal series using the biphasic technique without glucagon or other pharmacologic agents. Endoscopy was performed 2–10 days after barium examination in all but three patients who had undergone previous endoscopic biopsy.

The main indications for upper gastrointestinal radiography and endoscopy in this group of patients were dyspepsia (eight), epigastric pain (five), anemia or upper gastrointestinal bleeding (four), gastrointestinal symptoms complicating chemotherapy for a variety of malignancies (six), and Crohn disease (two).

Results

The radiographic appearance of HGM in the duodenal bulb was variable. The most common presentation in 17 (68%) of 25 patients was as clusters of 1- to 3-

Received August 10, 1987; accepted after revision October 27, 1987.

Presented at the annual meeting of the American Roentgen Ray Society, Miami Beach, FL, April 1987.

[1] Department of Diagnostic Radiology, Evanston Hospital–McGaw Medical Center of Northwestern University, Evanston, IL 60201. Address reprint requests to G. G. Ghahremani, Dept. of Diagnostic Radiology, Evanston Hospital, 2650 Ridge Ave., Evanston, IL 60201.

[2] Department of Internal Medicine, Evanston Hospital–McGaw Medical Center of Northwestern University, Evanston, IL 60201.

[3] Department of Pathology, Evanston Hospital–McGaw Medical Center of Northwestern University, Evanston, IL 60201.

AJR 150:291–294, February 1988
0361–803X/88/1502–0291
© American Roentgen Ray Society

mm mucosal plaques raised above the background of the flat and featureless mucosa of the duodenal bulb. These minute polypoid lesions usually were located at the base and posterior wall of the duodenal bulb, but sometimes they were scattered randomly throughout the duodenal bulb surface (Figs. 1A and 1B). They were well demarcated from the adjacent normal mucosa. The second type of appearance was coarse nodular mucosa of the duodenal bulb associated with superficial erosions or ulcer craters; this was seen in five (20%) of 25 cases (Figs. 2A, 2B, and 3). In two patients (8%), the HGM presented as a solitary and large sessile polyp in the duodenal bulb (Fig. 4). Another patient had heterotopic gastric mucosa with a prominent areae gastricae pattern covering the base of the duodenal bulb in direct continuity with the mucosa of the stomach. This was a persistent finding in distinction to the transient transpyloric prolapse of the antral mucosa.

Endoscopically, the HGM was limited to the duodenal bulb in all patients. The characteristic appearance was that of multiple clusters of 2- to 3-mm pink-red nodules or a myriad of nodules projecting intraluminally above the smooth, pale-pink duodenal mucosa (Fig. 1C). Occasionally, isolated patches of slightly raised and granular mucosa were observed. This pattern appeared to be different and less prominent than superficial gastric metaplasia owing to postinflammatory changes and regeneration of the mucosa over a healed duodenal ulcer. Furthermore, the presence of HGM could be verified readily during endoscopy by staining with Congo red dye, which caused a black discoloration of the acid-producing mucosal islands [1].

Histopathologic studies were performed on endoscopic biopsies of duodenal mucosa in 17 of the 25 cases. In all instances, there was microscopic identification of gastric epithelial islands with well-formed glands composed of parietal and chief cells, embedded within the otherwise normal duodenal mucosa. Usually, hematoxylin and eosin stain was

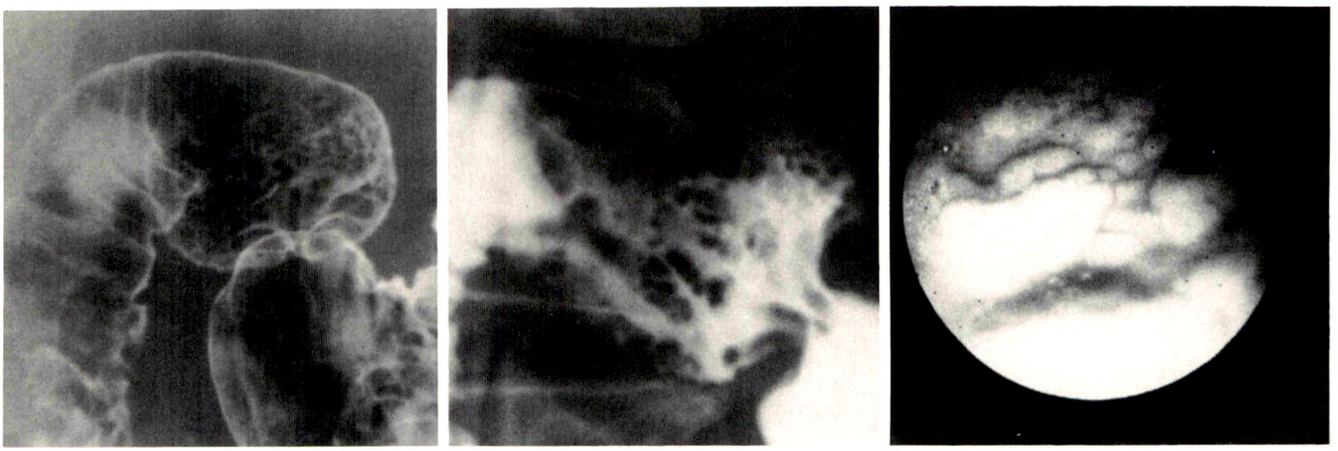

Fig. 1.—Heterotopic gastric mucosa in duodenum of 54-year-old man with dyspeptic symptoms.
***A*, Double-contrast examination of duodenal bulb shows a distinctly nodular surface pattern due to mucosal plaques ranging from 1 to 5 mm in size.**
***B*, Compression spot film also shows a myriad of small polypoid lesions.**
***C*, Endoscopic view of duodenal bulb. Heterotopic gastric mucosa is visible as clusters of red nodules projecting above the otherwise pink mucosa of the duodenum.**

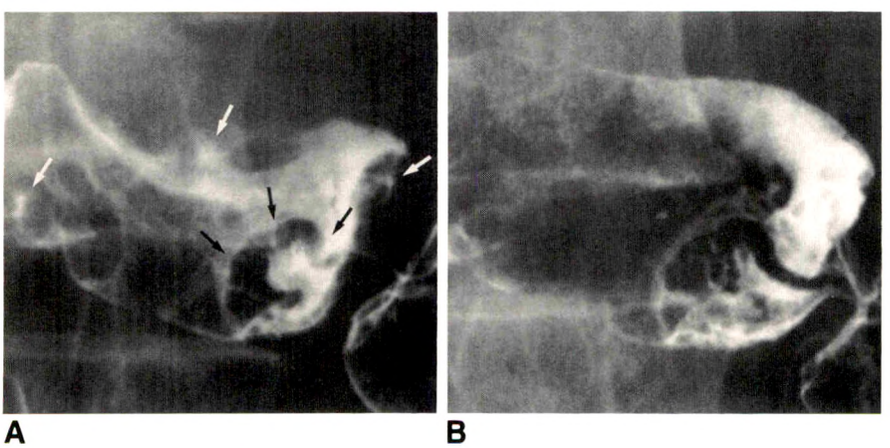

Fig. 2.—Upper gastrointestinal series in 66-year-old man with epigastric pain and anemia.
***A*, Initial study shows a slightly deformed bulb with persistent superficial collections of barium, suggesting erosions (*white arrows*). A large crater is noted in area of raised nodular mucosa (*black arrows*). Endoscopy and biopsy revealed diffuse duodenitis associated with centrally ulcerated patch of heterotopic gastric mucosa.**
***B*, Reexamination 3 months later indicates healing of ulcer and inflammatory changes despite persistence of coarse nodular gastric mucosa covering base and inferior fornix of duodenal bulb. Multiple views showed an unchanged appearance, permitting differentiation from transient transpyloric prolapse of antral mucosa.**

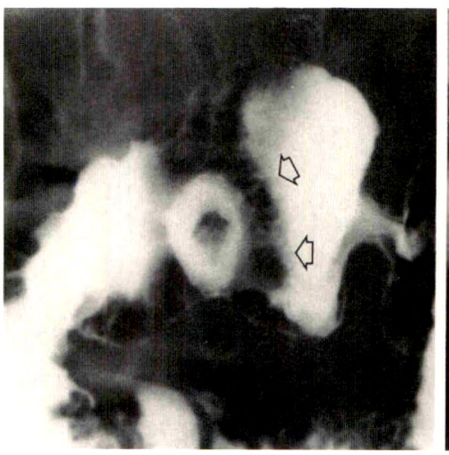

Fig. 3.—Spot film of duodenal bulb in 71-year-old woman with recent episode of upper gastrointestinal hemorrhage. Ulcer crater containing a blood clot and surrounded by a halo of edematous mucosa with a finely reticular surface pattern was detected (*arrows*). Endoscopic biopsies from proximal ulcer margin contained foci of heterotopic gastric mucosa. Ulcer healed after treatment with cimetidine hydrochloride, but heterotopic gastric mucosa became more clearly visible on air-contrast views obtained 2 months later.

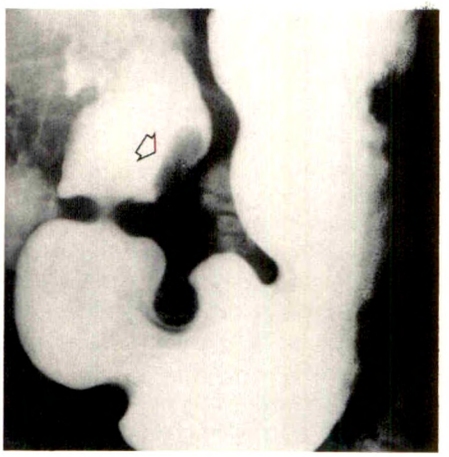

Fig. 4.—Radiograph from upper gastrointestinal series in 70-year-old man with gastritis shows a sessile duodenal polyp (*arrow*). At endoscopy it resembled aberrant pancreas, but biopsies disclosed heterotopic gastric epithelium overlying a polypoid mass of proliferated mucous glands.

3 4

sufficient to establish the diagnosis of HGM. However, several cases required staining with Alcian blue PAS, which resulted in a dark-red coloring of the goblet cells in HGM and permitted its differentiation from the pink duodenal mucosa.

Eight patients had either previous or subsequent upper gastrointestinal series available for comparison; the interval between these studies was from 2 months to 4 years. None showed any significant change in the overall appearance or extent of HGM. In both patients with a duodenal ulcer, the treatment with cimetidine hydrochloride led to complete healing of peptic ulcerations, but the large plaques of HGM remained detectable radiographically (Figs. 2 and 3). The two patients with polypoid masses of HGM underwent endoscopic biopsies but did not have resection of these lesions; they have remained asymptomatic under clinical observation for almost 2 years (Fig. 4).

Discussion

The presence of gastric epithelium in the duodenal bulb was first reported in 1927 by Taylor [10]. He described autopsy findings in two cases in which HGM was macroscopically visible as "small slightly raised patches which showed a peculiar sodden appearance." On the basis of their histopathologic features, he classified HGM into congenital and acquired types. The congenital HGM is composed of well-differentiated gastric mucosa with its normal glandular elements. The acquired lesion represents patchy replacement of the native mucosa by gastric epithelium after inflammatory or peptic processes.

Both congenital and acquired HGM may be found incidentally at autopsy or histopathologic examination of the resected intestine [6, 11, 12]. However, such lesions seldom were diagnosed endoscopically. Spiller et al. [13] found only eight cases of HGM in the duodenal bulb in 900 endoscopic examinations, representing a frequency of 0.9%. Radiographic visualization and diagnosis were also infrequent in the past. In 1973, Cynn and Rickert [14] reported a single case of HGM as a lobulated duodenal polyp 1.5 cm in diameter. Langkemper et al. [2] described the radiologic and endoscopic features of HGM in 22 patients and noted that glucagon-induced hypotonia of the duodenum facilitated the detection on double-contrast upper gastrointestinal examination. We were able to detect HGM without the aid of glucagon or any other pharmacologic agent. The plaques were best seen when the duodenal bulb was distended with gas and coated with barium (Fig. 1A). However, larger aggregates of HGM were detectable on single-contrast radiographs and on compression spot films as well (Fig. 1B).

HGM in the duodenal bulb usually is an incidental finding, whereas its occurrence in Meckel diverticulum manifests clinical symptoms in 57% of cases [3, 4]. Most of our patients presented with dyspepsia, peptic ulcer symptoms, or gastrointestinal bleeding. However, only two (8%) of 25 patients had an ulcer crater within the area covered by HGM. In both instances, treatment with cimetidine led to healing of the ulcers and resolution of clinical symptoms despite the persistence of HGM (Figs. 2 and 3). Two other patients with polypoid duodenal masses covered by HGM had endoscopic evaluation and biopsy of these lesions (Fig. 4), but they have not developed clinical findings. Rarely, obstructive symptoms due to polypoid lesions causing luminal narrowing or intussusception may occur [9]. Blundel et al. [15] have reported a case of biliary obstruction resulting from polypoid HGM at the ampulla of Vater.

HGM in the duodenal bulb usually has a distinct endoscopic appearance, characterized by salmon-red mucosal patches or clusters of nodules raised above the normally pink mucosa of the duodenum (Fig. 1C). The application of 1% Congo red solution as a pH-sensitive stain during endoscopy results in black discoloration of the acid-producing HGM [1]. Nevertheless, endoscopic biopsy and histologic examination are necessary for the accurate diagnosis of HGM and its differentiation from other entities that may cause polypoid or nodular duodenal mucosa. These include hyperplasia of Brunner glands or lymphoid follicles, adenomas, and polyposis syndromes.

The precise cause or pathogenesis of HGM in the duo-

denum has not been ascertained. Most are congenital, whereas others probably are acquired. Development of metaplastic gastric epithelium in the duodenum has been associated with peptic ulcerations, hyperacidity, and alcoholic or uremic duodenitis [8, 10–13]. Dayal and Wolfe [11] have shown that gastrin-producing G-cells are present in HGM of congenital origin occurring within Meckel diverticulum and intestinal duplications but not in acquired metaplasia. However, both kinds of HGM contain the gastric type of mucoid surface cells, which excrete an alkaline juice for cytoprotection against the hydrochloric acid. The same cells selectively accumulate pertechnetate anion (TcO_4^-), thus permitting scintigraphic detection of HGM in Meckel diverticulum and in various other aberrations [3, 4]. Unfortunately, this technique is not suitable for in vivo diagnosis of HGM in duodenal bulb. The reasons include interference by simultaneous radionuclide uptake in the stomach and the fact that only large areas of HGM exceeding 1 cm^2 can be visualized with the gamma camera [3].

REFERENCES

1. Hamilton JW, Thune RG, Morrissey JF. Symptomatic ectopic gastric epithelium of the cervical esophagus: demonstration of acid production with Congo red. *Dig Dis Sci* **1986**;31:337–342
2. Langkemper R, Hock AC, Dekker W, Op den Orth JO. Elevated lesions in the duodenal bulb caused by heterotopic gastric mucosa. *Radiology* **1980**;137:621–624
3. Sfakianakis GN, Conway JJ. Detection of ectopic gastric mucosa in Meckel's diverticulum and in other aberrations by scintigraphy: pathophysiology and 10 year clinical experience. *J Nucl Med* **1981**;22:647–654
4. Sfakianakis GN, Haase GM. Abdominal scintigraphy for ectopic gastric mucosa: retrospective analysis of 143 studies. *AJR* **1982**;138:7–12
5. Picard EJ, Picard JJ, Jorissen J, Jardon M. Heterotopic gastric mucosa in the epiglottis and rectum. *Am J Dig Dis* **1978**;23:217–221
6. Wolf M. Heterotopic gastric epithelium in the rectum: report of three new cases with a review of 87 cases of gastric heterotopia in the alimentary tract. *Am J Clin Pathol* **1971**;55:604–616
7. Kalmen PG, Stone RM, Phillips MJ. Heterotopic gastric tissue of the bile duct. *Surgery* **1981**;81:384–386
8. Shousha S, Spiller RC, Parkins RA. The endoscopically abnormal duodenum in patients with dyspepsia. Biopsy findings in 60 patients. *Histopathology* **1983**;7:23–24
9. McWay P, Dodds WJ, Slota T, Stewart ET, Hogan WJ. Radiographic features of heterotopic gastric mucosa. *AJR* **1982**;139:380–382
10. Taylor AL. The epithelial heterotopia of the alimentary tract. *J Pathol* **1927**;30:415–449
11. Dayal Y, Wolfe HJ. Gastrin-producing cells in ectopic gastric mucosa of developmental and metaplastic origin. *Gastroenterology* **1978**;75:655–660
12. Lessels AM, Martin DF. Heterotopic gastric mucosa in the duodenum. *J Clin Pathol* **1982**;35:591–595
13. Spiller RC, Shousha S, Barnson IG. Heterotopic gastric mucosa in the duodenum. A case report. *Dig Dis Sci* **1982**;27:880–883
14. Cynn WS, Rickert RR. Heterotopic gastric mucosal polyp in the duodenal bulb associated with congenital absence of the gallbladder. *Am J Gastroenterol* **1973**;60:171–177
15. Blundel CR, Kanum CS, Earnest DL. Biliary obstruction by heterotopic gastric mucosa of the ampulla of Vater. *Am J Gastroenterol* **1982**;77:111–114

Chronic Intestinal Obstruction: Value of Percutaneous Gastrostomy Tube Placement

Daniel Picus[1]
Mary Victoria Marx
Philip J. Weyman

Percutaneous gastrostomy tubes were placed in six patients for treatment of nausea and vomiting associated with chronic intestinal obstruction. There were no complications related to the tubes, and in all patient, symptoms were relieved. For the patient, the advantages of gastrostomy over nasogastric drainage include improved comfort, increased mobility, and a decreased risk of pulmonary aspiration.

Percutaneous gastrostomy is a safe procedure and provides excellent palliation for intractable nausea and vomiting in patients with chronic intestinal obstruction.

Percutaneous gastrostomy with radiologic guidance is an effective and safe alternative to both surgical and percutaneous endoscopic gastrostomy [1–3]. The advantages of the percutaneous approach include the use of a local anesthetic, accurate localization of the stomach and overlying organs, and elimination of the need for either an endoscopic or a surgical procedure.

The most common indication for gastrostomy is enteral nutrition (gastric or jejunal) in patients who cannot tolerate oral feeding. Less commonly, gastrostomy tubes are placed for either temporary or long-term decompression of intestinal obstruction [4]. In the past, surgical gastrostomy has been advocated as an alternative to nasogastric suction for the temporary decompression of intestinal ileus after abdominal surgery [5–8]. There have also been several reports of endoscopic and radiologic percutaneous gastrostomy tube placement for long-term palliation in patients with malignant intestinal obstruction [9–12].

We report our experience with percutaneous gastrostomy for long-term intestinal decompression in patients with intractable nausea and vomiting associated with chronic bowel obstruction, either benign or malignant.

Materials and Methods

Between May 1986 and September 1987, we performed percutaneous gastrostomies in 46 patients. In six of these patients, the procedure was performed because of chronic intestinal obstruction.

There were five women and one man ranging in age from 35 to 72 years. The indication for gastrostomy placement in all six patients was intractable nausea and vomiting associated with chronic bowel obstruction. Causes included peritoneal metastases from ovarian carcinoma (two patients), cervical carcinoma (one patient), colon carcinoma (two patients), and chronic relapsing pancreatitis with duodenal obstruction (one patient). The five patients with cancer were terminally ill with widespread carcinomatosis. They had multiple sites of small-bowel obstruction and were not considered candidates for surgical resection.

Coagulation studies were obtained prior to the procedure in all patients. Fluoroscopic guidance was used in five patients, and CT guidance was used in the sixth. All procedures were performed under local anesthesia. An IV analgesic was given when necessary.

The technique used was identical to that used for feeding gastrostomy placement. The stomach is distended with air via a nasogastric tube and is then punctured with an 18-gauge

Received October 1, 1987; accepted after revision October 27, 1987.

[1]All authors: Mallinckrodt Institute of Radiology, Washington University School of Medicine, 510 S. Kingshighway, St. Louis, MO 63110. Address reprint requests to D. Picus.

AJR 150:295–297, February 1988
0361–803X/88/1502–0295
© American Roentgen Ray Society

needle, taking care to avoid overlying bowel. An 0.038-in. (0.097-cm) guidewire (Amplatz extra-stiff wire, Cook, Bloomington, IN) is passed into the stomach, and the tract is sequentially dilated to 18-French by using coaxial dilators (Cook biliary dilators). Care is taken to be certain that the dilators enter, rather than displace, the stomach. Finally, a 20-French Cook peel-away sheath is placed, and a 16- or 18-French Foley balloon catheter (with a 30-ml balloon) is passed through it into the stomach. An end hole is cut in the Foley catheter so it can be passed over the guidewire. The balloon on the Foley catheter is inflated and pulled back against the anterior stomach wall. The catheter is stitched in place and left to gravity drainage. Nasogastric suction is continued overnight, and the nasogastric tube is removed the following day.

Long-term gastrostomy tube management consisted of daily dressing changes with local wound care. Irrigations were rarely needed and were used only when drainage decreased or stopped.

Results

The gastrostomy tubes functioned well in all six patients, eliminating the need for nasogastric suction. All patients had persistent relief of nausea and vomiting after removal of their nasogastric tube. Gravity drainage was used in all cases, and gastric outputs averaged 800–1500 ml/day. Two patients' tubes required intermittent daily irrigation to maintain patency.

No complications occurred. All patients had stable hematocrits after tube placement. One patient died in the hospital 20 days after the procedure as a result of a primary malignancy. The other four patients with malignancies died out of the hospital as a result of their primary disease 27–54 days after tube placement. The sixth patient, who has chronic recurrent pancreatitis, continues to require gastrostomy decompression 4 months after tube placement for chronic duodenal obstruction. Surgical decompression was not performed in this patient in the hope that the duodenal obstruction would subside with resolution of the pancreatitis.

Two patients required modification of the standard technique. The first was a 37-year-old man with long-standing ulcerative colitis and widely metastatic colon cancer. He had had multiple episodes of small-bowel and gastric outlet obstruction caused by peritoneal carcinomatosis and adhesions. A surgical gastrostomy was attempted but was unsuccessful because the stomach could not be dissected free of overlying bowel. A percutaneous gastrostomy tube was placed with CT guidance (Fig. 1). The tract passed through the lateral margin of the left lobe of the liver, as this was the only route available that avoided overlying bowel. Initially, an 8-French catheter was placed. This was exchanged for an 18-French Foley catheter after dilatation of the tract 8 days later.

The second patient had stage IIIB cervical carcinoma that previously had been treated with multiple abdominal surgical procedures and extensive pelvic radiation therapy. CT scan showed multiple peritoneal tumor implants. She presented with severe nausea and vomiting caused by a high-grade small-bowel obstruction. Because of the extensive peritoneal carcinomatosis, as well as bowel adhesions, the only access to the stomach was through the transverse mesocolon (Fig. 2). Initial placement of a 16-French Foley catheter was uneventful.

Neither of these two patients had any difficulty related to the access route used.

Discussion

Long-term nasogastric suction is the traditional treatment for surgically uncorrectable bowel obstruction, either benign or malignant. Nasogastric suction requires the placement of

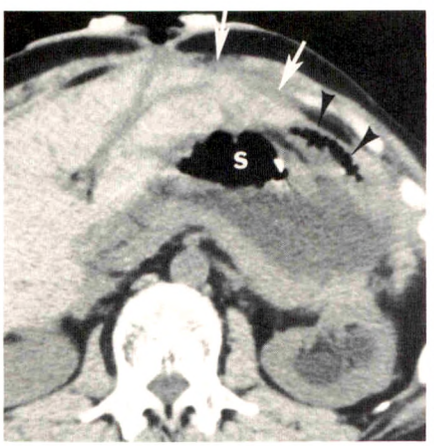

A

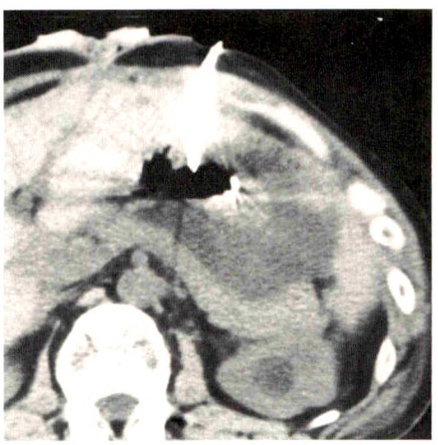

B

Fig. 1.—Patient with small-bowel obstruction due to widely metastatic colon cancer, peritoneal carcinomatosis, and adhesions.

***A*, CT scan shows that only access to stomach (S) is through lateral tip of left lobe of liver (*arrows*). Bowel (*arrowheads*).**

***B*, 8-French gastrostomy tube was successfully placed with CT guidance.**

Fig. 2.—Patient with multiple partial small-bowel obstructions due to extensive peritoneal tumor implants from cervical carcinoma. Serosal surface of transverse colon is involved with tumor. Colon is filled with barium from a previous small-bowel contrast study and is fixed in left upper quadrant. Gastrostomy tube (*solid arrow*) passes through transverse mesocolon. Nasogastric tube (*open arrows*) is used to inflate stomach with air.

a large, stiff tube through the nasopharynx. These tubes are uncomfortable and may result in significant morbidity, including nasal cartilage erosion, otitis media, and aspiration pneumonia. In addition, management of nasogastric tubes usually requires hospitalization, and the patient's mobility is limited because of the requirement for continuous suction.

Gastrostomy is an attractive alternative for bowel decompression. Patients requiring long-term bowel decompression are more comfortable with gastrostomies than with nasogastric tubes. The risk of pulmonary aspiration is lower because no tube passes through the gastroesophageal junction [4, 7, 8]. Other complications associated with nasogastric tubes are also eliminated. Finally, the gastrostomy tube is left to gravity drainage, and patients can be cared for at home or in a hospice setting.

The subset of patients requiring bowel decompression presents several difficulties not seen in patients for whom gastrostomies are placed for enteral nutrition. Both the large and small bowel are frequently involved with tumor. In addition, adhesions are commonly present as a result of previous surgery and/or radiation therapy. Therefore, direct access to the stomach may be limited. In fact, surgical gastrostomy placement was not possible in one of our patients because of extensive adhesions and peritoneal carcinomatosis. Direct CT guidance provided an easy access route through the left lobe of the liver. In another patient, the only approach was through the transverse mesocolon. Tube placement was accomplished without complication. Endoscopically guided gastrostomy in this group of patients may be difficult because overlying bowel cannot be visualized directly as it can with fluoroscopy or CT.

Patients with malignant bowel obstruction often have ascites. We consider massive ascites to be a relative contraindication to percutaneous gastrostomy. Continued ascitic leak at the gastrostomy site may develop and result in difficult local management problems [4]. In fact, we declined percutaneous gastrostomy placement in one patient who had massive ascites associated with multiple sites of small-bowel obstruction caused by metastatic ovarian carcinoma.

In conclusion, we believe that percutaneous gastrostomy is safe and provides excellent, comfortable palliation for intractable nausea and vomiting in patients with chronic intestinal obstruction.

REFERENCES

1. Ho CS, Gray RR, Goldfinger M, Rosen IE, McPherson R. Percutaneous gastrostomy for enteral feeding. *Radiology* **1985**;156:349–351
2. vanSonnenberg E, Wittich GR, Cabrera OA, et al. Percutaneous gastrostomy and gastroenterostomy. 2. Clinical experience. *AJR* **1986**;146:581–586
3. Alzate GD, Coons HG, Elliott J, Carey PH. Percutaneous gastrostomy for jejunal feeding: a new technique. *AJR* **1986**;147:822–825
4. Gauderer MWL, Stellato TA. Gastrostomies: evolution, techniques, indications, and complications. *Curr Probl Surg* **1986**;23:659–719
5. Smith GK, Farris JM. Re-evaluation of temporary gastrostomy as a substitute for nasogastric suction. *Am J Surg* **1961**;102:168–175
6. Grant GN, Elliott DW, Frederick PL. Postoperative decompression by temporary gastrostomy or nasogastric tube: an objective comparison. *Arch Surg* **1962**;85:844–851
7. Ochsner A. The relative merits of temporary gastrostomy and nasogastric suction of the stomach. *Am J Surg* **1977**;133:729–732
8. Kumar SS. Tube gastrostomy: a routine adjunct in major abdominal operations. *Am Surg* **1985**;51:201–203
9. Gemlo B, Rayner AA, Lewis B, et al. Home support of patients with end-stage malignant bowel obstruction using hydration and venting gastrostomy. *Am J Surg* **1986**;152:100–104
10. Stellato TA, Gauderer MWL. Percutaneous endoscopic gastrostomy for gastrointestinal decompression. *Ann Surg* **1987**;205:119–122
11. Wills JS. Percutaneous gastrostomy: applications in gastric carcinoma and gastroplasty stoma dilatation. *AJR* **1986**;147:826–827
12. Malone JM, Koonce T, Larson DM, Freedman RS, Carrasco CHO, Saul PB. Palliation of small bowel obstruction by percutaneous gastrostomy in patients with progressive ovarian carcinoma. *Obstet Gynecol* **1986**;68:431–433

Book Review

Seminars in Interventional Radiology. Pain Control and Neural Blockade in Interventional Radiology. Guest editors: Robert P. Lieberman and Linda J. Miwa. New York: Thieme, September 1987;4(3):135–217. $18; by subscription, 4 issues annually for $56

This issue of *Seminars in Interventional Radiology* is intended for radiologists who perform procedures that are painful in themselves or are intended to relieve pain. Articles written by clinical pharmacists, anesthesiologists, and radiologists are intended, as stated by the authors," to draw from several disciplines a current, comprehensive, and usable review of pain control." Six papers contributed by the College of Pharmacy, University of Nebraska, deal with specific drug categories, including barbiturates, benzodiazepines, narcotics, chloral hydrate, nitrous oxide, ketamine, agonist-antagonist opioids, and droperidol. These articles provide an excellent current source of information on these drugs and include extensive references. The authors have combined well-organized descriptions of mode of action, contraindications, side effects, and drug interactions with discussions of specific dosage schedules. Particularly helpful is the coverage of the newer benzodiazepines that are being used in many departments for radiologic procedures and for which information is lacking in physicians' standard sources on drugs.

Two papers deal specifically with sedation in children. The choices among chloral hydrate; a combination of drugs, such as the "lytic cocktail"; and nitrous oxide analgesia are discussed. Proper emphasis is placed on the need to decide individual cases on the basis of age-related sensitivity, volume of distribution, metabolism, and clearance, rather than to adopt a "routine" prescription. Useful information on these factors in children is provided.

Two papers by anesthesiologists discuss standards of care for monitoring patients during procedures that include the use of sedation. The American Society of Anesthesiologists Committee on Standards of Care has recommended that the patient's oxygenation, ventilation, circulation, and temperature be evaluated regularly at frequent intervals. The authors suggest that "pulse oximetry, EKG, and automated blood pressure monitoring become the norm on every patient in the interventional radiology suite with more invasive monitoring as dictated by the patient's physical status." This prudent recommendation should help interventional radiologists obtain funding for appropriate monitoring equipment.

Rholl, vanBreda, and Katzen of Alexandria, VA, provide a good review of the use of nitrous oxide analgesia in radiologic procedures that is based on their experience with more than 300 cases. Three papers describe specific procedures for regional blocks: percutaneous lumbar sympathectomy, sciatic nerve block, and celiac ganglion block. These detailed descriptions of technique and the accompanying references will be useful to radiologists who wish to undertake these procedures. Tan and Spigos of the University of Illinois have used sciatic block to prevent the discomfort associated with lower extremity angiography. Few angiographers would think that this was necessary in the current era of less irritating, low-osmolality contrast agents. Muehle et al. from the University of California, San Diego, discuss celiac ganglion block and describe a unique anterior approach that they have begun to use successfully.

One area that I think deserves more attention than has been given to it is the use of and choices among local anesthetics. The one paper dealing with these agents, by Landers and Hurlbert, does provide excellent information on the mechanism of allergic reactions and how to deal with the patient who has had an allergic reaction to local anesthetics. However, noticeably missing is a review of available infiltration agents and the rationale for selection of concentration, dosage, and techniques as applied to radiologic procedures.

This issue of *Seminars in Interventional Radiology* is an excellent and much needed source of information for radiologists who use the types of pharmaceuticals discussed in it. I strongly recommend that it be read and kept available as a ready reference.

Kevin G. Ryan
Woodland Clinic Medical Group
Woodland, CA 95695

Case Report

Infarcted Meckel Diverticulum Detected by CT

Paul D. Russ,[1] Geoffrey D. Friefeld,[1] Charles J. Nauck,[2] and Robert J. Wilmouth[3]

A preoperative diagnosis of complicated Meckel diverticulum can be difficult to establish and is not often considered in the adult patient [1]. The clinical manifestations are frequently nonspecific and can mimic other pathologic conditions, such as appendicitis, Crohn disease, and peptic ulcer [1–3]. Various imaging techniques have been used to diagnose Meckel diverticulum, but few cases evaluated by CT have been described [2]. We report an unusual case of an infarcted, twisted Meckel diverticulum that was detected preoperatively by CT.

Case Report

A 59-year-old man had had severe pain in his right lower quadrant, associated with anorexia and watery diarrhea, for 2 days. The abdomen was tender, with rebound and guarding in the right lower quadrant. Bowel sounds were absent. The WBC count was 21,700/mm^3.

CT performed with oral and IV contrast media showed an unopacified sausage-shaped structure (3.0 × 9.8 cm) in the lower midabdomen (Fig. 1A). The mean attenuation coefficient of the mass was 12 H.

On the patient's second day in the hospital, a fever developed, and peritoneal signs worsened. At surgery, an infarcted, unperforated Meckel diverticulum was found arising from the distal ileum. Pathologic examination of the specimen (Fig. 1B) confirmed the presence of a Meckel diverticulum with hemorrhagic necrosis.

Discussion

Meckel diverticulum is the most common congenital anomaly of the gastrointestinal tract; it occurs in approximately 2–3% of the population [2]. Embryologically, it is derived from the unobliterated proximal remnant of the omphalomesenteric duct [1]. Extending as a tubular or saccular outpouching from the antimesenteric border of the ileum, a Meckel diverticulum is located approximately 80–85 cm proximal to the ileocecal valve [2, 4].

Complications of Meckel diverticulum include obstruction, hemorrhage, inflammation, perforation, and herniation [3]. Although the diverticula are lined by ileal mucosa, heterotopic gastric mucosa is found in 15–50% of them, and its presence contributes to ulceration and bleeding [1, 2, 4]. Intestinal obstruction associated with Meckel diverticulum can be caused by volvulus or intussusception. A fibrous cord derived from the distal omphalomesenteric duct can persist and connect the Meckel diverticulum to the umbilicus, predisposing to volvulus. Loops of bowel adjacent to the diverticulum usually are incorporated into a volvulus; an isolated axial volvulus of the Meckel diverticulum only is unusual [1, 2].

Most persons who have Meckel diverticulum remain asymptomatic. The occurrence rate of complicated Meckel diverticulum has been reported to be 15–40% [1, 2, 4], although Soltero and Bill [5] estimated that the lifetime risk is 4%. Symptoms are more frequent during childhood, and the frequency of complications decreases with age [5]. Bleeding and intussusception tend to occur before the affected person is 2 years old. In adults, obstruction and inflammation are relatively more common than hemorrhage [3, 6].

Diagnostic imaging in symptomatic adults who have Meckel diverticulum yields variable results. Plain film findings are usually nonspecific [2]. The routine small-bowel follow-

Received August 4, 1987; accepted after revision September 23, 1987.
[1] Imaging Service, Denver Veterans Administration Medical Center, 1055 Clermont St., Denver, CO 80220. Address reprint requests to P. D. Russ.
[2] Department of Pathology, University of Colorado Health Sciences Center, 4200 E. Ninth Ave., Denver, CO 80262.
[3] Department of Surgery, University of Colorado Health Sciences Center, 4200 E. Ninth Ave., Denver, CO 80262.

AJR 150:299–300, February 1988 0361–803X/88/1502–0299 © American Roentgen Ray Society

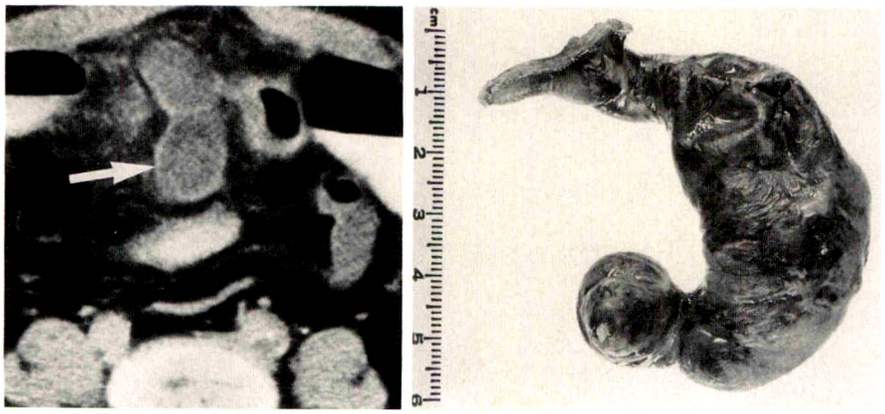

A **B**

Fig. 1.—Meckel diverticulum in 59-year-old man.

***A*, CT scan of lower abdomen shows unopacified water-density mass (*arrow*). Note inflammatory changes in surrounding small-bowel mesentery.**

***B*, Photograph of resected diverticulum made before specimen was sectioned. Exterior surface is covered by hemorrhagic exudate from transmural necrosis and serositis.**

through examination can detect Meckel diverticulum, but it is considered less sensitive than enteroclysis [7, 8]. Pertechnetate radionuclide scintigraphy can accurately diagnose ectopic gastric mucosa in bleeding Meckel diverticulum [6]. Although CT often is used to evaluate patients with abdominal complaints, its role in detecting complicated Meckel diverticulum remains uncertain [2].

Preoperative CT in our patient suggested an inflammatory lesion of the distal small bowel. The differential diagnosis included Crohn disease, interloop abscess, intussusception, and bowel ischemia. A tumor, such as lymphoma, carcinoid, or metastasis, was considered less likely because of the uniform water-density of the lesion. Although attachment by a fibrous cord to the umbilicus was absent, infarction of a twisted Meckel diverticulum was found to be the cause of the patient's abdominal complaints.

REFERENCES

1. Bronen RA, Glick S, Teplick S. Meckel's diverticulum: axial volvulus mimicking emphysematous cholecystitis. *Am J Gastroenterol* **1984**;79:183–185
2. Ghahremani GG. Radiology of Meckel's diverticulum. *CRC Crit Rev Diagn Imaging* **1986**;26:1–43
3. Greenspan L, Abramovitch A, Tomarken J, Cohen Z. Perforation of a Meckel's diverticulum by a foreign body. *Can J Surg* **1983**;26:184–185
4. Dalinka MK, Wunder JF. Meckel's diverticulum and its complications, with emphasis on roentgenologic demonstration. *Radiology* **1973**;106:295–298
5. Soltero MJ, Bill AH. The natural history of Meckel's diverticulum and its relation to incidental removal. *Am J Surg* **1976**;132:168–173
6. Sfakianakis GN, Conway JJ. Detection of ectopic gastric mucosa in Meckel's diverticulum and in other aberrations by scintigraphy. I. Pathophysiology and 10-year clinical experience. *J Nucl Med* **1981**;22:647–654
7. Craig O, Murfitt J. Radiological demonstration of Meckel's diverticulum. *Br J Surg* **1980**;67:881–883
8. Maglinte DT, Elmore MF, Isenberg M, Dolan PA. Meckel diverticulum: radiologic demonstration by enteroclysis. *AJR* **1980**;134:925–932

Carcinoma of the Colon: Detection and Preoperative Staging by CT

Emil J. Balthazar[1]
Alec J. Megibow
Donald Hulnick
David P. Naidich

This report analyzes the detection rate and role of CT in the preoperative evaluation of 90 consecutive, proved cases of colon carcinoma. In this study, the overall detection rate was 84%; however, the rate varied from 68% in unprepared colons to 95% in clean colons that were adequately distended with air. Sensitivity of detection depends mainly on the size of the lesion and the quality of the examination. CT was less sensitive than barium enema in detection, but it had a similar specificity in differentiating neoplastic lesions from inflammatory lesions. On the basis of our criteria of staging, CT evaluation resulted in a sensitivity of 55% for local invasion, 73% for regional nodes, and 79% for liver metastases. Compared with Dukes classification, CT correctly staged 64% of all patients but showed significant variations in staging different groups with lower results in the Dukes A, B, and C patients. CT, however, showed a sensitivity of 81% and a positive predictive value of 100% in detecting Dukes D lesions.

In general, although negative CT findings do not help in staging a colonic tumor, positive findings are highly indicative of neoplastic spread. We believe that this feature justifies the use of CT in the preoperative evaluation of colonic tumors.

CT is used today in the evaluation of patients with known colonic carcinoma as well as for the occasional detection of colonic tumors in patients with nonspecific abdominal complaints. The CT features of colonic carcinoma are generally known [1–3], but the usefulness of CT as a preliminary screening technique, its rate of detection, and its role in preoperative staging remain controversial. Preliminary reports have described staging accuracy rates of 90–100% [1, 2, 4–6]; other investigators, however, have expressed reservations [7, 8] and have shown that only 60% of rectosigmoid lesions [9] and as few as 48% of colorectal lesions [10] can be staged correctly. On the basis of these reports, it has been argued that preoperative local staging of colonic carcinoma is clinically useless, and therefore it is not recommended. Since the number of reported cases is limited, we have described our experience with 90 consecutive patients who had primary carcinoma of the colon. We will attempt to document the CT detection rate, compare detection by CT with detection by barium enema, and evaluate the role of CT in the preoperative staging of these patients.

Materials and Methods

Preoperative CT scans obtained within the past 4 years in 90 consecutive patients with carcinoma of the colon were reviewed retrospectively. In 51 of these patients, the results of barium enema examination also were available for review. The pathologic diagnosis was confirmed in every case, and gross specimens or surgical descriptions with histologic confirmation were available in all patients. This series included 47 men and 43 women ranging in age from 34 to 92 years (mean, 61 years). In most patients, the presence and site of the colonic tumor was known at the time of the CT examination. The tumors were initially diagnosed by CT in 11 patients and were later confirmed by barium enema and/or colonoscopy. There was no control group to allow a determination of false-positive cases.

Received May 18, 1987; accepted after revision October 12, 1987.

[1] All authors: Department of Radiology, New York University Medical Center/Bellevue Hospital, New York, NY 10016. Address reprint requests to E. J. Balthazar, Dept. of Radiology, Bellevue Hospital, 27th St. and 1st Ave., New York, NY 10016.

AJR 150:301–306, February 1988
0361–803X/88/1502–0301
© American Roentgen Ray Society

CT examinations were performed on a GE CT 8800 unit (General Electric Medical Systems, Milwaukee, WI), and standard techniques were used. Unless contrast material was contraindicated, patients received an IV bolus injection of 50 ml diatrozoate 50%, followed by a rapid drip infusion of 300 ml of 30% iodinated contrast material. In eight patients, only nonenhanced images were obtained. All patients received 700–800 ml of 2% diluted barium solution given orally, 50–60 min before scanning. Transaxial images 10 × 10 mm (58 patients) or 10 × 15 mm (32 patients), covering the entire abdomen and pelvis were obtained initially. In addition, in 18 patients repeat CT examinations were done, with 5 × 5 mm sections over the region of interest. Air insufflation of the colon [11, 12] with adequate distension was achieved in 56 patients. No attempt was made to visualize and distend the colonic lumen in the remaining 34 patients.

Colonic tumors were visualized by CT in 76 patients (84%), and CT staging was performed without the knowledge of the pathologic findings. The following three parameters were established and evaluated: (1) local extramural invasion (irregular serrated or spiculated outer contour, tumor mass or strands of soft tissue extending out, and/or streakiness of the pericolic fat); (2) regional nodes (a single adjacent node 1 cm or larger or a cluster of three or more nodes, each less than 1 cm in diameter); (3) distal and/or extensive disease (liver metastases, intraperitoneal and mesenteric tumor, distal retroperitoneal adenopathy, and direct extension into adjacent solid or hollow organs).

Among the 90 cases surveyed, 46 tumors (50%) were located in the rectosigmoid, nine in the descending colon, 11 in the transverse colon, and 24 in the cecum and ascending colon.

Results

Detection

CT detected the colonic tumor in 76 cases but failed to detect it in 14 cases, giving a sensitivity of 84%. The 14 lesions that were missed were evenly distributed throughout the colon and ranged in size from 3 to 6 cm. Three of the undetected tumors belonged to the group of 56 patients examined after colonic air insufflation (5%), while 11 tumors were missed in the group of 34 patients examined without air distension (32% undetected rate). Each tumor had a density that was similar to or slightly higher than that of adjacent muscle and appeared either as a circumferential mass (Fig. 1) (63 patients) or as a discrete focal mass (Fig. 2) (13 cases). The thickness of the tumors varied from 1 to 10 cm, but most were between 2 and 4 cm (mean, 3.4 cm). Most lesions had an uneven, lobulated configuration (Fig. 3), and only four showed perfectly symmetric wall thickening (Fig. 4). The CT density of the tumor was homogeneous in 45 cases (Figs. 3 and 4) and was nonhomogeneous (with patchy areas of low attenuation) in the remaining 31 cases (Fig. 5). CT density did not correlate with histologic type but did correlate with tumor size. The majority of the large lesions (>5 cm in diameter) showed patchy areas of low density.

CT–Barium Enema Correlation

Barium enema examinations were reviewed in 51 patients. All lesions were visualized by barium enema, including those detected by CT and two that were missed by the CT examination. The extent of involvement was better visualized on barium studies, but the thickness of the tumor as well as the presence and degree of exophytic involvement could be established only by CT. In three patients, barium enema examinations showed irregular, thickened mucosal folds and spasticity consistent with a segmental inflammation lesion (Fig. 6). In these cases CT established the correct diagnosis of tumor by showing a typical lobulated and asymmetric soft-tissue mass. In three other instances the CT features resembled diverticulitis and showed only slight symmetric wall thickening and streakiness of the pericolic fat (Fig. 7). In these cases barium studies established the correct diagnosis.

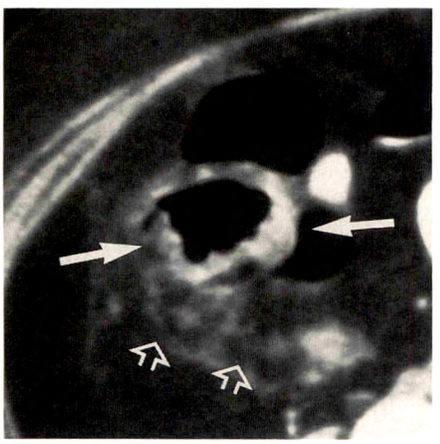

Fig. 1.—CT scan is true positive for local invasion. Cross section of carcinoma of ascending colon (*solid arrows*). Air-filled lumen is irregular, and wall is circumferentially thickened, lobulated, and slightly fuzzy in appearance. Soft-tissue densities are seen in adjacent pericolic fat (*open arrows*). Pathologic examination showed tumor invasion into pericolic fat.

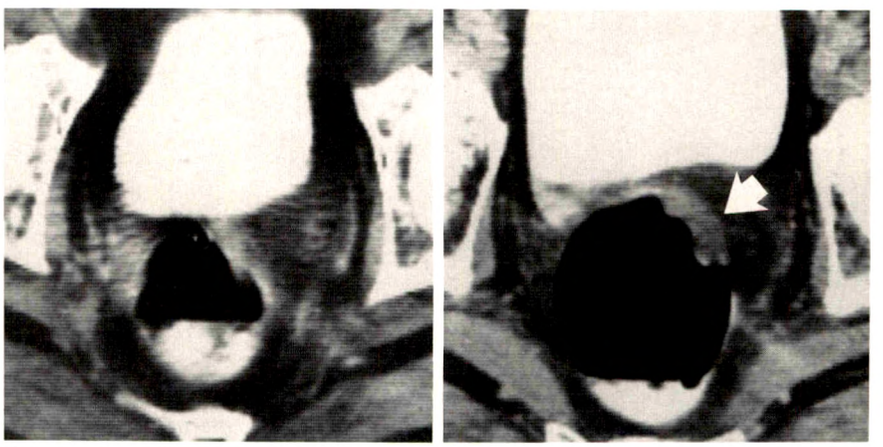

A **B**

Fig. 2.—CT scan is true negative for local invasion and regional adenopathy. Rectal carcinoma visualized only after air insufflation.

***A*, Initially rectum is partially distended and tumor is not well visualized.**

***B*, After air distension, a sharply defined focal lesion of left anterior rectal wall is seen (*arrow*). Pathologic studies showed only muscle invasion and no regional lymphadenopathy.**

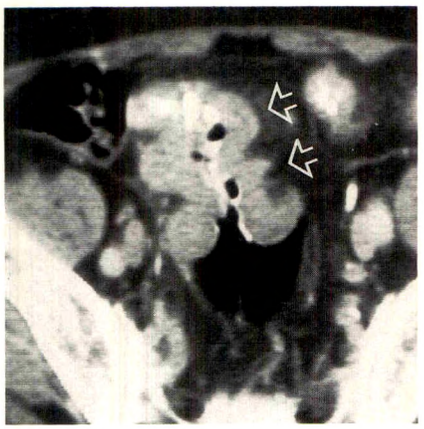

Fig. 3.—CT scan. Longitudinal section of a sigmoid lesion shows narrowed irregular lumen, posterior overhanging edge, and a lobulated asymmetric outer contour (*arrows*). Tumor is infiltrating sigmoid colon circumferentially, has a homogeneous density slightly higher than that of adjacent muscle, and is sharply delineated. Pathologic studies showed tumor invasion into pericolic fat.

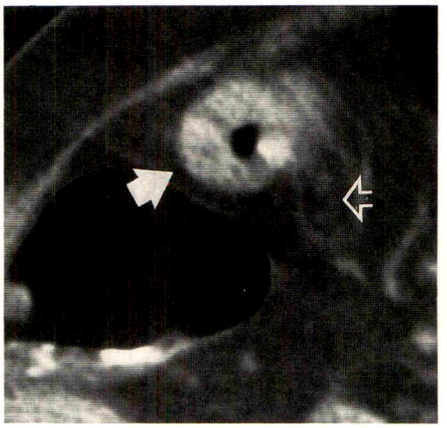

Fig. 4.—CT scan is false negative for invasion and false positive for nodal involvement. Mucinous carcinoma of hepatic flexure presents as symmetric and circumferential wall thickening and severe narrowing of colonic lumen. Tumor has a homogeneous soft-tissue density and a sharply defined outer contour (*solid arrow*). Two small adjacent nodes are seen (*open arrow*). Pathologic studies showed serosal invasion and only reactive nodes.

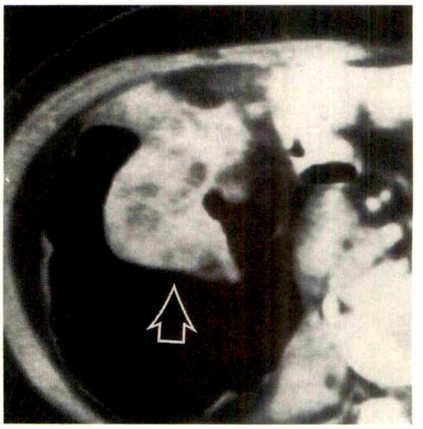

Fig. 5.—Mucinous carcinoma of cecum presenting as large soft-tissue mass of anterior wall with intraluminal and exophytic components (*arrow*). Note lack of homogeneous density with multiple ill-defined patchy areas of low density haphazardly distributed through tumor. Pathologic studies showed tumor extension into fat and positive nodes.

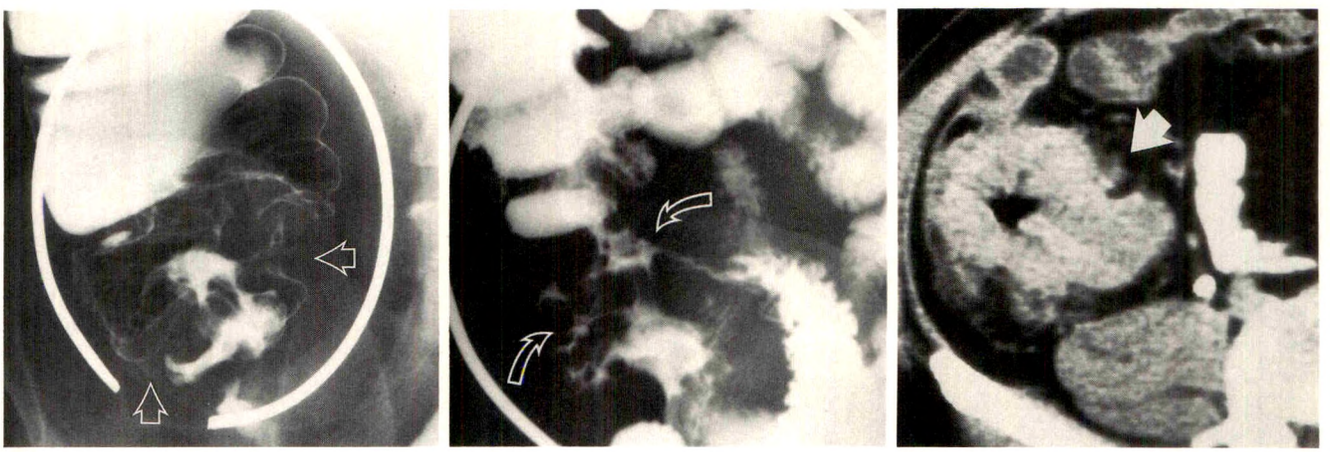

A B C

Fig. 6.—CT scan shows carcinoma of cecum.

A and *B*, Barium enema (*A*) and small-bowel examination (*B*) show irregular, nodular thickening of mucosal folds and spasticity (*arrows*). Cecal inflammatory lesion was initially considered.

C, CT examination reveals a large, circumferential, lobulated soft-tissue mass typical of adenocarcinoma (*arrow*). Pathologic studies revealed tumor extension into fat and positive lymph nodes.

Staging

On the basis of our criteria of staging and after a review of the pathologic findings, the CT evaluation yielded the following results.

Local invasion.—Tumor invasion of serosa and/or pericolic fat was correctly staged by CT in 44 (58%) of the 76 cases. In the group that was incorrectly staged, CT overstaged two cases (6%) and understaged 30 cases (94%). There were 37 true-positive cases (Figs. 1 and 8), two false-positive cases, 30 false-negative cases (Fig. 4), and seven true-negative cases (Fig. 2). CT evaluation resulted in a sensitivity of 55% and a specificity of 77%. While the negative predictive value was 19%, CT exhibited a 95% positive predictive value in determining the existence of local tumor invasion beyond the muscle coat.

Regional nodes.—Nodal involvement was correctly staged by CT in 52 (68%) of 76 cases. In the group that was incorrectly staged, CT overstaged 10 (42%) and understaged 14 (58%) of 24 cases. There were 38 true-positive cases (Figs. 8 and 9), 10 false-positive cases (Fig. 4), 14 false-negative cases, and 14 true-negative cases. CT evaluation

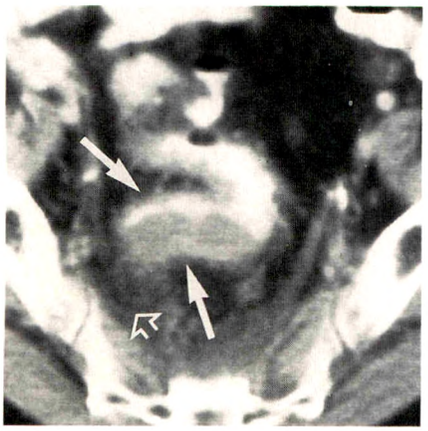

Fig. 7.—CT scan is false negative for invasion and true positive for nodes. On CT, sigmoid carcinoma has features that resemble diverticulitis (*solid arrows*). Note slight thickening of sigmoid wall and some streakiness, with an increase in density of pericolic fat. Cluster of few small nodes is seen posterior to sigmoid colon (*open arrow*). Pathologic examination showed serosal and vascular invasion, and one of nine nodes was positive for tumor.

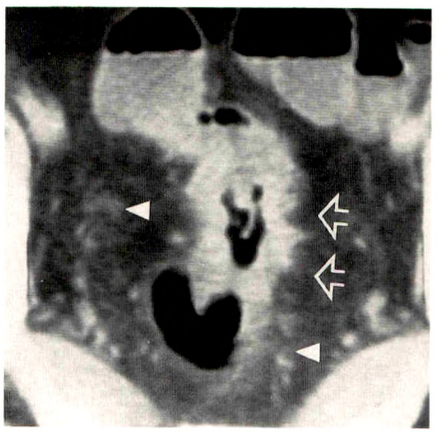

Fig. 8.—CT scan is true positive for local invasion and regional adenopathy. Sigmoid carcinoma shows an irregular serrated outer contour (*open arrows*) and multiple small pericolic soft-tissue densities representing lymph nodes less than 1 cm in diameter (*arrowheads*). Pathologic findings were consistent with pericolic fat infiltration, invasion into lymphatics, and positive regional nodes.

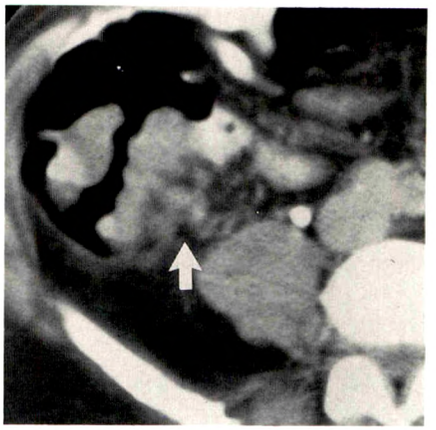

Fig. 9.—CT scan is true positive for regional adenopathy. Carcinoma of right colon appears as a lobulated apple-core lesion with a few large adjacent lymph nodes (*arrow*). Pathologic findings were positive for pericolic fat invasion and regional lymphadenopathy.

yielded a sensitivity of 73% and a specificity of 58%. The positive and negative predictive values were 79% and 50%, respectively.

Distal and/or extensive disease.—Liver metastases were present in 19 patients. CT correctly staged liver metastases in 71 (93%) of 76 cases. Among the five cases that were incorrectly staged, CT overstaged one case and understaged four cases. There were 15 true-positive cases, one false-positive case, four false-negative cases and 56 true-negative cases. The only false-positive case was a small hepatic hemangioma that was interpreted as metastasis. CT evaluation resulted in a sensitivity of 79% and a specificity of 98%. The positive and negative predictive values were 94% and 93%, respectively.

CT correctly staged nine of the 14 cases of tumor invasion of adjacent solid or hollow organs (Fig. 10). Mesenteric and omental metastases and peritoneal seeding were correctly diagnosed in four patients (Fig. 11) but were missed in two. Distal retroperitoneal metastases were detected in three patients. All cases missed on CT were understaged without any false-positive interpretations.

Discussion

Detection

The sensitivity of CT detection depends mainly on the size of the lesion and the quality of the CT examination. In this series the overall detection rate was 84%; however, it varied from 95% when the colonic lumen was distended with air to 68% if no special attempts were made to promote visualization of the colonic lumen (Fig. 2). Most of the tumors that were missed occurred in partially collapsed colons that contained fecal material that interfered with visualization. When optimal visualization is achieved, the CT features of colonic carcinoma are characteristic, leading to a correct diagnosis in most cases. In this series, as expected, CT was less sensitive than barium enema in detecting colonic tumors; however, CT was as accurate as barium enema in differentiating neoplastic from inflammatory colonic lesions. The typical diagnostic features of tumors on CT are short segment of focal or circumferential wall thickening, soft-tissue density that is either homogeneous or that contains patchy areas of low attenuation, narrowed lumen and asymmetric, lobulated configuration (Figs. 1, 3, 5). In only 4% of tumors in this series, the CT features were atypical and were considered compatible with diverticulitis (Fig. 7).

Staging

Analysis of the data reveals that CT correctly staged all three parameters (local invasion, nodal disease, and distant metastases) in only 41% of the evaluated cases (31/76). This lack of correlation is not surprising when comparisons are made between an imaging technique that evaluates gross morphology with a pathologic assessment that is based on histologic examination. Thus, microscopic invasion of serosa, normal-sized nodes partially replaced by tumor, small (<1 cm) peritoneal implants, and liver metastases generally are missed by the CT examination. Since previous reports [9, 10] have shown that the main limitation of CT is in understaging colonic tumors (high rate of false-negative findings), we have applied stringent criteria to staging and have considered 1-cm regional

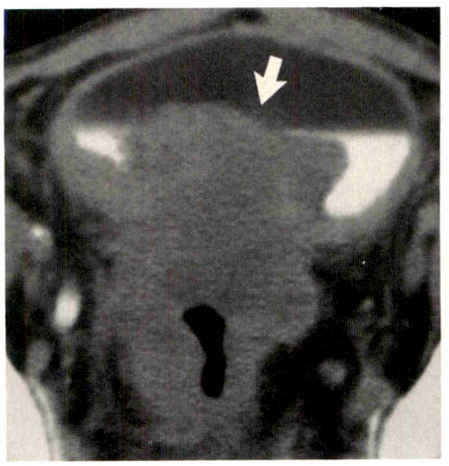

Fig. 10.—CT scan is true positive for adjacent organ invasion. Rectosigmoid carcinoma with invasion into urinary bladder (*arrow*). CT findings were proved at surgery; lesion was considered unresectable.

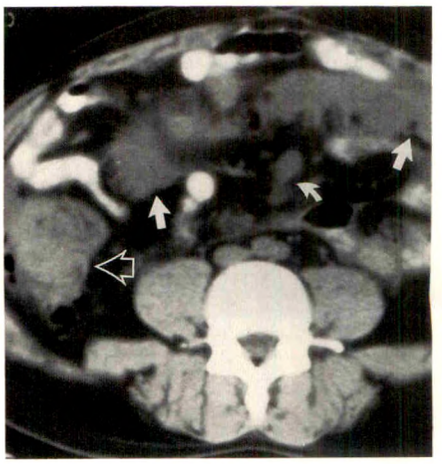

Fig. 11.—CT scan is true positive for peritoneal metastases. Primary cecal carcinoma (*open arrow*) with extensive mesenteric and omental metastases (*solid straight arrows*). Metastatic nodes are seen in mesentery (*solid curved arrow*). CT findings were proved at laparotomy; lesion was considered unresectable.

10 **11**

lymph nodes and clusters of three or more nodes (each <1 cm) positive for metastases. In this series, with one exception, all patients with nodes larger than 1 cm had pathologic evidence of nodal involvement. Our criteria for evaluation of nodal disease significantly increased the accuracy of CT, but did not achieve a sufficiently high sensitivity to be considered clinically useful. In addition, there was no correlation between the number of neoplastic nodes on CT vs pathologic examination and that generally many more positive nodes were found at surgery than on CT. Data obtained from the three parameters evaluated showed a 55% sensitivity for local invasion, 73% for regional nodes, and 79% for liver metastases. Results that should be considered potentially useful in the CT evaluation are the high positive predictive values of 95% for local invasion, 94% for liver metastases, and 100% for peritoneal metastases and invasion of adjacent organs.

Overall Staging: CT vs Dukes Classification

The strengths and weaknesses of CT staging can be better appreciated when the CT results are compared and correlated with a modified Dukes classification: stage A (tumor limited to colonic wall); stage B (spread by direct extension to serosa and/or pericolic fat); stage C (involvement of regional nodes); stage D (involvement of adjacent organs; peritoneal, distal metastases; and/or liver metastases). Analyzed data in this series show that compared with the Dukes classification, CT correctly staged only 64% of all cases. CT staging accuracy, however, showed significant variations among different Dukes categories. It correctly staged four (57%) of seven patients with Dukes A lesions, two (17%) of 12 patients with Dukes B lesions, 17 (68%) of 25 patients with Dukes C tumors, and 26 (81%) of 32 with Dukes D tumors. Most of the inaccuracies (21 cases) occurred in the lower (A, B, and C) Dukes stages, and the best result was the 81% correct staging of Dukes D lesions. In addition, all patients with stage D on CT had pathologically proved Dukes D lesions, leading to a 100% positive predictive value.

Our data regarding the overall sensitivity of local staging of neoplasm of the colon are roughly similar to the recent series by Freeny et al. [10] and Thompson et al. [9]. However, the high sensitivity and high positive predictive value of CT in detecting Dukes D lesions have not been previously emphasized. In this series one-third of our patients had Dukes D lesions, and all eight patients considered unresectable at laparotomy had striking CT changes showing peritoneal metastases and/or local invasion of adjacent organs (Figs. 10 and 11). While inaccuracies in CT staging of Dukes A, B, or C lesions do not affect surgical treatment, detection of Dukes D lesions may lead to changes in surgical planning or preoperative management. Surgical resections may be considered useless or not feasible; limited resections may be done instead of extensive curative procedures; or radiation and/or chemotherapy may be indicated before surgery. For this reason we believe that the preoperative CT evaluation of neoplasms of the colon is useful. In addition, CT is superior to any other single staging technique and can be used to assess the entire peritoneal cavity, retroperitoneum, and solid organs during a single examination. If any imaging technique is considered in the preoperative workup, CT should be regarded as the technique of choice.

On the basis of the data reported in this series, the role of CT in the detection and preoperative staging of carcinoma of the colon can be summarized as follows: (1) The sensitivity of CT to detect colonic carcinoma varies from 68% to 95% and depends on the size of the lesion and quality of examination. Barium enema remains the primary imaging technique to detect neoplasia of the colon. When the radiographic features on barium enema are atypical, CT helps in the preoperative diagnosis. (2) CT has limitations in the overall sensitivity and accuracy of local staging of colon carcinoma. We advocate its use, however, because it has a high sensitivity and a high positive predictive value in detecting advanced (Dukes D) lesions. In these patients, clinically unsuspected CT findings may lead to changes in either the preoperative management or the type of surgical intervention.

ACKNOWLEDGMENT

The authors thank Jane Crafts for manuscript preparation.

REFERENCES

1. Mayes GB, Zornoza J. Computed tomography of colon carcinoma. *AJR* **1980**;135:43–46
2. Thoeni RF, Moss AA, Schnyder P, et al. Detection and staging of primary rectal and rectosigmoid cancer by computed tomography. *Radiology* **1981**;141:135–138
3. Fisher JK. Abnormal colonic wall thickening on computed tomography. *J Comput Assist Tomogr* **1983**;7(1):90–97
4. Dixon AK, Fry IK, Morson BC, et al. Preoperative computed tomography of carcinoma of the rectum. *Br J Radiol* **1981**;54:655–659
5. Zaunbauer W, Haertel M, Fuchs WA, et al. Computed tomography in carcinoma of the rectum. *Gastrointest Radiol* **1981**;6:79–84
6. van Weas PFGM, Koehler PR, Feldberg MAM. Management of rectal carcinoma: impact of computed tomography. *AJR* **1983**;140:1137–1142
7. Grabbe E, Lierse W, Winkler R. The perirectal fascia: morphology and use in staging of rectal carcinoma. *Radiology* **1983**;149:241–246
8. Adalsteinsson B, Glimelius B, Graffman S, et al. Computed tomography in staging rectal carcinoma. *Acta Radiol [Diagn]* (Stockh) **1985**;26:45–50
9. Thompson WM, Halvorsen RA, Foster WL Jr, et al. Preoperative and postoperative CT staging of rectosigmoid carcinoma. *AJR* **1986**;146:703–710
10. Freeny PC, Marks WM, Ryan JA, et al. Colorectal carcinoma evaluation with CT: preoperative staging and detection of postoperative recurrence. *Radiology* **1986**;158:347–353
11. Hamlin DJ, Burgener FA, Sischy B. New technique to stage early rectal carcinoma by computed tomography. *Radiology* **1981**;141:539–540
12. Megibow AJ, Balthazar EJ. Computed tomography of the gastrointestinal tract. St. Louis, MO: Mosby, **1986**:23–31, 279–280

Now Available
(Limited Quantities)

1987 American Roentgen Ray Society Categorical Course Syllabus
Gastrointestinal Radiology
Editor: Gary G. Ghahremani, M.D.

Contains 161 pages of textbook-quality information and illustrations reviewing recent advances and current concepts in gastrointestinal radiology. Written by leading authorities in the field.

Send $25 per copy, along with name and address, to:

American College of Radiology
Publications Division
P.O. Box 2348
Merrifield, VA 22116-2348

(Price includes shipping/handling charges at book rate. Indicate if first-class delivery requested and add $5 per copy.)

Extracorporeal Shock-Wave Lithotripsy: Prevalence of Renal Stones 3–21 Months After Treatment

Steven G. Miles[1]
Juri V. Kaude[1]
Robert C. Newman[2]
William C. Thomas[3]
Clyde M. Williams[1]

One hundred and four (70%) of the first 148 patients who underwent extracorporeal shock-wave lithotripsy (ESWL) at the University of Florida were evaluated for persistent or recurrent renal stone disease. Radiographs obtained 3–21 months after treatment showed that 53 (50%) of 106 treated kidneys were free of stones. In 48 of the 53 kidneys that contained stones, the stones were residual fragments dating from the period immediately after ESWL. New stones had developed in only five kidneys.

The 50% incidence of stone-free kidneys 3–21 months after ESWL is less than the 65–90% rate reported by other institutions in the United States and Europe. After stone removal by ESWL, new stone formation occurs at a rate of 5%, which is much lower than the expected recurrence rate of 37–50%.

Most of the literature on the efficacy of extracorporeal shock-wave lithotripsy (ESWL) is limited to observations made 2–3 months after treatment [1–6]. Only two recent communications report a longer-term follow-up of patients, one after 6 months [7] and the other after more than 1 year [8]. We report an evaluation of 104 patients in whom the presence or absence of renal stones was determined from 3 to 21 months after treatment with ESWL.

Subjects and Methods

During the 4-month period from August 15 to December 18, 1984, 148 patients (170 kidneys) were treated with ESWL for renal stone disease at Shands Hospital of the University of Florida. One hundred fifty-one kidneys received one treatment, 18 received two treatments, and one received three treatments. ESWL was performed with a Dornier HM-3 lithotriptor (Friedrichshafen, W. Germany) applying 200–2800 shocks (average, 1419) at 18–24 kV to the kidney in a single treatment. The treatments were performed by two urologists who had undergone training in ESWL. Most of the patients were treated while under general anesthesia. After the first 50 cases, the usual ventilatory mode was replaced in some cases with high-frequency jet ventilation to reduce kidney movement during respiration [9].

Of the first 148 patients, 104 (106 treated kidneys) were evaluated 3–21 months after ESWL for the presence of remaining or recurrent stones. We personally evaluated 30 of these patients. For the other 74 patients, information about renal stones was obtained from the patients' referring physicians.

Our evaluation employed 14 × 17 in. (35.6 × 43.2 cm) anteroposterior abdominal radiographs and 8 × 10 in. (20.3 × 25.4 cm) oblique radiographs of the treated kidney. Any detectable calcification (1–2 mm or larger) was regarded as a remaining stone fragment. In all patients, radiographs and excretory urograms obtained before and immediately after ESWL were available for comparison.

Results

The 106 treated kidneys (104 patients) were divided into two groups, depending on when the follow-up examinations occurred. Fifty-nine treated kidneys were

Received August 6, 1987; accepted after revision September 29, 1987.

[1] Department of Radiology, University of Florida College of Medicine and Veterans Administration Medical Center, Gainesville, FL. Address reprint requests to C. M. Williams, Chief of Nuclear Medicine (115), Veterans Administration Medical Center, 1601 S. W. Archer Rd., Gainesville, FL 32602.

[2] Department of Surgery, University of Florida College of Medicine and Veterans Administration Medical Center, Gainesville, FL 32602.

[3] Department of Medicine, University of Florida College of Medicine and Veterans Administration Medical Center, Gainesville, FL 32602.

AJR 150:307–309, February 1988
0361–803X/88/1502–0307
© American Roentgen Ray Society

examined 3–12 months after ESWL. Twenty-nine (49%) of these kidneys were free of stones. From 13 to 21 months after ESWL, 24 (51%) of 47 treated kidneys contained no stones. Altogether, 53 (50%) of 106 treated kidneys in 104 patients who were followed radiographically 3–21 months after ESWL, either in our outpatient clinic or by local physicians, were free of stones. Of the remaining 53 kidneys with stones, 48 had residual stones or stone fragments dating from the evaluations immediately after ESWL. In five kidneys (5%), there was new stone formation.

Discussion

In reports of two groups of West German patients, the prevalence of stone-free kidneys 2–3 months after ESWL was 90% and 85%, respectively [1, 2]. However, a lower prevalence of stone-free kidneys has been reported among patients treated in Switzerland and in the United States, ranging from 65% to 77% [3–6]. In the 3–21 month interval after treatment, the prevalence among our patients of stone-free kidneys (50%) was also substantially lower than the 72–84% in recently reported long-term follow-up studies from West Germany [7, 8].

These differences in results cannot be explained by the number of shocks per treatment, since the average number of shocks applied by us (1419) was higher than the 978 to 1382 shocks reported by others [1–2, 5–6]. Although a chemical analysis was not available in all of our patients, it is unlikely that significant differences would exist in composition of radiopaque stones, since most (78–91%) [2, 5] were calcium oxalate/phosphate stones. The size of stones (3–33 mm in our first 100 patients [10]) was also comparable with that reported from other centers in the United States. Most primary stones were smaller than 2 cm, and a few were as large as 3 cm at their greatest diameter.

The relatively small number of evaluated patients could be one explanation for the lower rate of stone-free kidneys in our treated patients. This follow-up study was limited to the group of patients who were treated under the guidelines from the United States Federal Drug Administration (FDA) before this treatment technique was approved for general use on December 19, 1984. We were able to obtain a follow-up in 104 (approximately 70%) of the 148 patients (106 treated kidneys). This compares very favorably both with the results reported by Riehle et al. [6], who were able to evaluate 58% of their patients, and with those recently reported by Zehntner et al. [3], who had a 35% evaluation rate 3 months after ESWL. Possibly our material is biased by a higher return rate of follow-up patients with symptoms. However, such a bias also exists in all follow-up studies without 100% compliance.

Another possible source of error is our acceptance of the reports of referring physicians for 74 of our 104 patients. However, the results of Zehntner et al. [3] (65% stone-free patients 3 months after ESWL) were based entirely on follow-up by the patient's physician.

The examination technique in the 30 patients who returned to our institution for evaluation was important in the detection of remaining stone fragments. In other studies [5, 6], radiographic examinations were performed with only one anteroposterior radiograph, whereas we always obtained an additional, collimated oblique film of the treated kidney. With this different projection of the kidney and with less scattered radiation from a smaller field, small or poorly calcified stones in the kidney are detected more readily. Jensen et al. [11] have shown that an oblique coned-down view adds to the efficacy of stone recognition about as much as tomography does. Stones were detected in 17 (55%) of 31 kidneys examined radiographically by us and in 36 (48%) of 75 kidneys examined by referring physicians.

The fact that our follow-up time was longer than that used by other authors (2 or 3 months) [1, 3, 6] may account for our higher stone detection rate. However, this does not explain the difference between our results and those of long-term follow-up studies recently reported from West Germany [7, 8]. ESWL accomplishes stone fragmentation in 95–99% of patients. Immediately after ESWL, 15–20% of patients are free of stones and 72–76% of kidneys have retained stone fragments [4, 10]. We can conclude from these data that the spontaneous passage of stone fragments may vary greatly.

In five patients, small, poorly calcified deposits (not detectable radiographically) possibly served as the nidi for new stone formation. In two of the five patients with new stone formation, the stones by analysis were 85–90% uric acid. One of these patients had Crohn disease, a disorder known to be accompanied by formation of renal stones. In three patients with recurrent stones, no chemical analysis was performed.

The overall recurrence rate of new stones (five in 106 kidneys, approximately 5%) is considerably less than the expected rate of stone formation of 37–50% in patients with untreated kidney stones [12, 13]. We have no definitive explanation for this low recurrence rate, although, possibly, patients treated with ESWL are more likely to comply with recommendations for large intake of fluids and dietary modification. Also, the difference between our statistics and the usual stone-recurrence rate may relate to the difference in length of follow-up, and, with longer follow-up of ESWL patients, the rate of new stone formation may also be higher. However, Diederichs [8] observed new stones in 35 (3.5%) of 1000 patients 19 months after ESWL; this recurrence rate is even lower than the one observed by us.

Despite a long-term success rate (50%) that is less than that reported by others, ESWL remains the technique of choice for the active treatment of most large kidney stones. During the past 2 years, in combination with percutaneous nephrostomy and continuous removal of stone fragments during ESWL, we have treated larger stones frequently and successfully and also have treated infected stones. To prevent rapid regrowth of struvite stones, all such infected stone material should probably be removed. Surgical nephrolithotomy is now required in only about 1% of patients with kidney stones [3].

REFERENCES

1. Chaussy C, Schmiedt E. Extracorporeal shock wave lithotripsy (ESWL) for kidney stones: an alternative to surgery? *Urol Radiol* **1984**;6:80–87

2. Fuchs G, Miller K, Rossweiler J, Eisenberger F. Extracorporeal shock wave lithotripsy: one-year experience with the Dornier lithotripter. *Eur Urol* **1985**;11:145–149
3. Zehntner C, Ackermann D, Zingg EJ. Die extrakorporale Stosswellenlithotripsie (ESWL): Erfahrungen nach 1000 Behandlungen. *Schweiz Med Wochenschr* **1987**;117:383–390
4. Drach GW, Dretler S, Fair W, et al. Report of the limited United States cooperative study of extracorporeal shock wave lithotripsy. *J Urol* **1986**;135:1127–1133
5. Lingeman JE, Newman D, Hertz JHO, et al. Extracorporeal shock wave lithotripsy: the Methodist Hospital of Indiana experience. *J Urol* **1986**;135:1134–1137
6. Riehle RA, Fair WR, Vaughan ED. Extracorporeal shock wave lithotripsy for upper urinary tract calculi. One year's experience at a single center. *JAMA* **1986**;255:2043–2048
7. Liedl B, Jocham D, Schuster C, Haupt G. Prognosis of residual concretions following ESWL (abstr). *Urol Res* **1987**;15:128
8. Diederichs W. Residual stones after ESWL: a long-term follow up in 1,000 patients (abstr). *Urol Res* **1987**;15:129
9. Boysen PG, Carlson CA, Banner MJ, Gravenstein JS. Ventilation during anesthesia for ESWL. In: Gravenstein JS, Peter K, eds. *Extracorporeal shock wave lithotripsy for renal stone disease. Technical and clinical aspects*. Boston: Butterworth, **1986**:69–75
10. Grantham JR, Millner MR, Kaude JV, Finlayson B, Hunter PT, Newman RC. Renal stone disease treated with extracorporeal shock wave lithotripsy: short-term observations in 100 patients. *Radiology* **1986**;158:203–206
11. Jensen RA, Bollinger B, Skriver E, Finn-Jensen G, McNair P. Radiographic technique of tomography and oblique projections. *Eur J Radiol* **1985**;5:125–126
12. Smith LH. Stone activity. In: Roth PA, Finlayson B, eds. *Stones: clinical management of urolithiasis*. Baltimore, MD: Williams & Wilkins, **1983**:183–186
13. Ljunghall S, Danielson BG, Kallsen R, Fritjofsson A. Prediction of stone recurrence. In: Smith LH, Robertson WG, Finlayson B, eds. *Urolithiasis: clinical and basic research*. New York: Plenum, **1981**:13–16

The reader's attention is directed to the Commentary on this article, which appears on pages 316–318.

Book Review

Gallbladder and Bile Duct Imaging. A Clinical Radiologic Approach. By Robert K. Zeman and Morton I. Burrell. New York: Churchill Livingstone, 799 pp., 1987. $160

This impressive treatise on biliary tract imaging is the product of long-term collaboration by two respected diagnostic radiologists. Their tremendous clinical experience and a critical analysis of the pertinent literature form the foundation of this informative and beautifully illustrated volume.

The 790-page text is arranged logically into 10 separate chapters. The first one describes normal hepatobiliary anatomy and physiology. The second provides an overview of various imaging techniques, but their specific applications are discussed subsequently in the context of the diagnostic approach to individual clinical entities. These are covered in chapters 3 through 9, which address subjects such as acute and chronic biliary tract diseases, cholecystitis and gallstones, diagnosis and management of biliary obstruction, postoperative complications, and hepatobiliary trauma. The final section of the book is devoted to congenital and acquired biliary disorders of children. Each chapter has an extensive bibliography that includes pertinent references from 1970 through 1985.

Unlike the frequently rigid, didactic format of medical textbooks, this monograph has a rather semiformal conversational style mixed with some witty comments. The authors attempt to interact with the reader by presenting questions and answers related to many of the diagnostic dilemmas encountered by practicing radiologists or clinicians. A prescriptive "what-to-do" approach is used to simplify decision making in the diagnosis and management of biliary tract disorders.

This neatly bound and printed book contains 1259 illustrations and 51 tables. The reproduced radiographs, sonograms, and CT scans are of uniformly superb quality, but only a few MR images are included. Multiple examples of both common and rare biliary lesions are shown in an attempt to cover a wide spectrum of presentations. The abundance of illustrated material has led to fragmentation of the text, and many of the figures appear several pages after their actual citation in the text.

Drs. Zeman and Burrell have achieved their goal of producing a most comprehensive and practical source of information about clinical radiology of the gallbladder and bile ducts. This book should appeal to a wide audience of physicians who diagnose or treat biliary disorders. However, it is also highly recommended as a useful addition to the library of all radiology departments.

Gary G. Ghahremani
Evanston Hospital
Evanston, Il 60201

Extracorporeal Shock-Wave Lithotripsy: Long-Term Complications

Clyde M. Williams[1]
Juri V. Kaude[1]
Robert C. Newman[2]
John C. Peterson[3]
William C. Thomas[3]

Of 148 patients who had extracorporeal shock-wave lithotripsy (ESWL) for renal lithiasis in 1984, 21 (14%) returned after 17–21 months for renal function tests (21 patients) and blood pressure determination (20 patients). Quantitative radionuclide renography showed a statistically significant ($p = .048$) decrease in the percentage of effective renal plasma flow (ERPF) to the treated kidney. Two of these patients had developed hypertension requiring treatment but became normotensive when given medication. In the other patients there was a statistically significant increase in both systolic ($p = .0002$) and diastolic ($p = .015$) blood pressures. Information about blood pressure was also obtained from an additional 71 (48%) of the 148 patients; of the total 91 patients (61%) in whom blood pressures were obtained, seven (8%) had developed sufficiently severe hypertension to require treatment beginning within 21 months after ESWL.

Side effects of ESWL for renal lithiasis include hemorrhage, edema, and acute tubular necrosis of the kidney. This form of renal trauma is associated with an immediate decrease in renal function of the treated kidney, and this decrease may be permanent. ESWL is also associated with the onset of hypertension, which may occur immediately or be delayed by several weeks or months. Although the pathogenesis remains unknown, hypertension is an important complication of ESWL in about 8% of patients.

Extracorporeal shock-wave lithotripsy (ESWL) for renal stone disease [1] was first performed at the Shands Hospital of the University of Florida on August 15, 1984, as an experimental clinical procedure. By December 19, 1984, the date on which the United States Federal Drug Administration (FDA) approved the procedure for routine use, we had treated 148 patients. Early in our experience with this new technique, we encountered the abrupt onset of hypertension immediately after ESWL in a patient who also had a perirenal hematoma and a marked decrease in the percentage of effective renal plasma flow (ERPF) to the treated kidney. This experience prompted a prospective study of renal function and morphology immediately after ESWL [2]. Quantitative radionuclide renography disclosed reduced renal function (a decrease in ERPF of more than 5 percentage units) in 10 (30%) of 33 of the treated kidneys, and MR imaging disclosed evidence of renal trauma (edema or hemorrhage) in 24 (63%) of 38 of these treated kidneys. A retrospective review of the medical records of the first 79 patients in this experimental group disclosed that three patients (4%) had developed sustained hypertension immediately after ESWL that required antihypertensive medication [3]. These observations led us to ask four questions: (1) Is a decrease in renal function after ESWL permanent or is it only temporary? (2) Is the hypertension that occurs immediately after ESWL temporary, or will it persist? (3) Because renal trauma may induce hypertension after a delay of weeks or months, what is the long-term prevalence of hypertension? (4) Is there a causal relationship between decreased renal function and hypertension after ESWL?

When permission was obtained from the FDA to perform ESWL on an experimental basis, it was stipulated that all patients should be examined 3 months after

Received August 6, 1987; accepted after revision September 29, 1987.

[1] Department of Radiology, University of Florida College of Medicine and Veterans Administration Medical Center, Gainesville, FL. Address reprint requests to C. M. Williams, Chief of Nuclear Medicine (115), Veterans Administration Medical Center, 1601 S. W. Archer Rd., Gainesville, FL 32602.

[2] Department of Surgery, University of Florida College of Medicine and Veterans Administration Medical Center, Gainesville, FL 32602.

[3] Department of Medicine, University of Florida College of Medicine and Veterans Administration Medical Center, Gainesville, FL 32602.

AJR 150:311–315, February 1988
0361–803X/88/1502–0311
© American Roentgen Ray Society

treatment to determine the efficacy of the procedure and to discover possible complications. Unfortunately, there was poor compliance with this requirement and in the first report of the United States cooperative study [4], 3-month follow-up data were available in only 37% (926/2501) of the patients. For these reasons, we initiated a concerted effort in 1986 to have the first 148 patients treated here under the FDA experimental protocol return to the hospital for evaluation. We report the long-term effects of ESWL on renal function as determined by renography and the prevalence of hypertension occurring after ESWL in this group of patients.

Materials and Methods

A letter was sent to all 148 patients asking them to return to the hospital for an abdominal radiograph, quantitative radionuclide renography, and blood pressure measurement. Of these 148 patients, only 21 (14%) returned for the tests 17–21 months after ESWL. The mean age of these 21 patients was 51 years (range, 28–68 years); nine were women and 12 men. The mean number of shocks per treatment was 1400 (range, 800–2000), and the kilovoltage used ranged from 18 to 24 kV. After these 21 patients had been tested, we were able to obtain follow-up information in an additional 71 patients (48%) either from the referring physicians or from clinical notes made by other physicians at this institution after the ESWL therapy.

Quantitative Radionuclide Renography

We used the comprehensive radionuclide renal function test of Dubovsky et al. [5] and Kontzen et al. [6] in which 300–500 μCi (11.1–18.5 MBq) of ^{131}I-orthoiodohippurate (Hippuran) are administered intravenously 30 min after oral ingestion of 500 ml water. Images were obtained with an Ohio Nuclear Series 100 scintillation camera (Solon, OH) interfaced with an MDS computer (Ann Arbor, MI). Total ERPF was calculated from the formula of Tauxe et al. [7], and the percentage of ERPF for each kidney was obtained from the 1–2 min interval after injection of the radionuclide.

Blood Pressure

Pre-ESWL values were obtained from the medical records in which systolic and diastolic blood pressures were measured in the hospital at 6-hr intervals before ESWL. The average number of measurements was 5.6 (range, 2–15). The mean value of the pre-ESWL blood pressures was compared with post-ESWL follow-up values obtained during the return visit at which time the blood pressure was measured at least three times and the lowest value recorded. An increased systolic blood pressure was considered to be ≥150 mm Hg; an increased diastolic blood pressure, ≥95 mm Hg.

Statistical Analysis

The Student paired t-test and the Pearson correlation were used for the analyses.

Results

Comparison of Renal Function Before and After ESWL

Twenty-one patients had renography after ESWL for comparison with their pretreatment test (Table 1). The total ERPF

TABLE 1: Correlation of Renal Function and Hypertension Before and After ESWL

Age	Gender	Shocks	Effective Renal Plasma Flow (ml/min)							Blood Pressure (mm Hg)					
			Pre-ESWL			Post-ESWL			Change in %	Pre-ESWL		Post-ESWL		Change in Systolic	Change in Diastolic
			Both Kidneys	Treated Kidney	% Treated Kidney	Both Kidneys	Treated Kidney	% Treated Kidney		Systolic	Diastolic	Systolic	Diastolic		
54	F	800	610	340	56	670	340	51	−5	104	73	150	90	+46	+17
33	M	950	685	300	44	655	355	54	+10	106	72	124	78	+18	+6
55	F	2000	515	210	41	525	220	42	+1	126	86	160	94	+34	+8
62	M	1600	510	255	50	510	230	45	−5	145	89	142	80	−3	−9
68	F	1600	160	60	37	95	10	9	−28	122	76	160	100	+38	+24
37	M	1000	765	445	58	690	395	57	−1	112	72	120	80	+8	+8
45	F	800	380	135	35	355	120	33	−2	100	59	112	74	+12	+15
50	F	1600	505	240	48	525	225	43	−5	135	81	160	78	+25	−3
64	F	2000	645	350	54	675	270	40	−14	120	72	156	90	+36	+18
55	F	900	540	270	50	535	290	54	+4	115	85	Normotensive on medication			
39	M	1600	650	265	44	515	230	45	+1	117	75	126	80	+9	+5
63	F	1600	155	70	45	485	225	46	+1	115	79	130	80	+15	+1
39	M	1600	585	315	54	510	215	42	−12	147	94	Normotensive on medication			
59	M	1600	485	295	61	540	340	63	+2	118	83	120	80	+2	−3
64	M	1400	400	170	43	425	150	35	−8	132	82	150	84	+18	+2
35	M	1600	680	340	50	720	355	49	−1	119	83	120	76	+1	−7
48	M	1600	415	260	63	590	220	46	−17	136	82	150	90	+14	+8
28	M	1200	520	265	51	815	385	47	−4	139	74	Not taken after ESWL			
62	M	1100	595	310	52	530	260	49	−3	122	79	130	80	+8	+1
53	M	1000	605	325	54	540	275	51	−3	132	85	130	84	−2	−1
56	F	1700	475	235	49	415	235	56	+7	125	66	140	90	+15	+24
Mean 51		1400	520	260	50	540	255	46		123	78	138	84		
SD ±12		±380	±150	±90	±7	±150	±90	±11		±13	±8	±16	±7		

Note.—ESWL = extracorporeal shock-wave lithotripsy.

to both kidneys increased slightly but not significantly from a mean of 520 ml/min before ESWL to 540 ml/min after ESWL. There was a slight but also insignificant decrease in the ERPF of the treated kidney from a mean of 260 ml/min before ESWL to a mean of 255 ml/min after ESWL. However, the percentage of total ERPF to the treated kidney declined from a mean of 50% before ESWL to a mean of 46% after ESWL, and this decrease was statistically significant ($p = .048$). In addition, the ERPF to the treated kidney decreased by more than 5% in 24% (5/21) of patients.

Comparison of Blood Pressures Before and After ESWL

At the time of post-ESWL renography, blood pressures were recorded in 20 of 21 patients (Table 1). Five patients were taking hydrochlorothiazide before ESWL and recorded no change in medication at the follow-up examination. Two of 20 patients had developed hypertension after ESWL but became normotensive when given medication. The mean systolic blood pressure of the remaining 18 patients increased from 123 mm Hg before ESWL to 138 mm Hg after ESWL, and this increase was statistically significant ($p = .0002$); the mean diastolic blood pressure increased from 78 mm Hg before ESWL to 84 mm Hg after ESWL, and this increase was also statistically significant ($p = .015$). One of these 18 patients was found to have sustained hypertension, and antihypertensive medication was started.

In addition to these 20 patients, we obtained information about blood pressure from the medical records or from the referring physicians in an additional 71 patients. Four (6%) of these 71 patients had developed hypertension after ESWL for which medication was administered, thus yielding an overall prevalence of hypertension in seven (8%) of 91 patients. Of these seven patients, the onset of hypertension requiring treatment was detected immediately after ESWL in three instances, at 6–8 weeks in two instances, and between 6 and 12 months in two instances.

Correlation Between Renal Function Changes and Blood Pressure Changes

A definite trend indicated a correlation between decreasing percentage of ERPF to the treated kidney with increasing systolic and diastolic blood pressure in the 18 patients in whom all measurements were available, but the correlation was not significant in this small series ($p = .12$ for the correlation with systolic blood pressure and $p = .22$ for diastolic blood pressure). However, when we compared the change in the percentage of ERPF to the treated kidney with the absolute blood pressure, we noted a more impressive relationship (Fig. 1). With one exception, all patients with a change in the percentage of ERPF to the treated kidney in the range between −3% and +10% were normotensive. Conversely, with two exceptions, all patients with a change in the percentage of ERPF between −4% and −28% either were hypertensive (systolic ≥ 150 mm Hg and/or diastolic ≥ 95 mm Hg) or had become hypertensive after ESWL and were normotensive when given medication. Although not definitive, these results suggest a long-term correlation between decreased renal function of the treated kidney and hypertension in patients treated with ESWL.

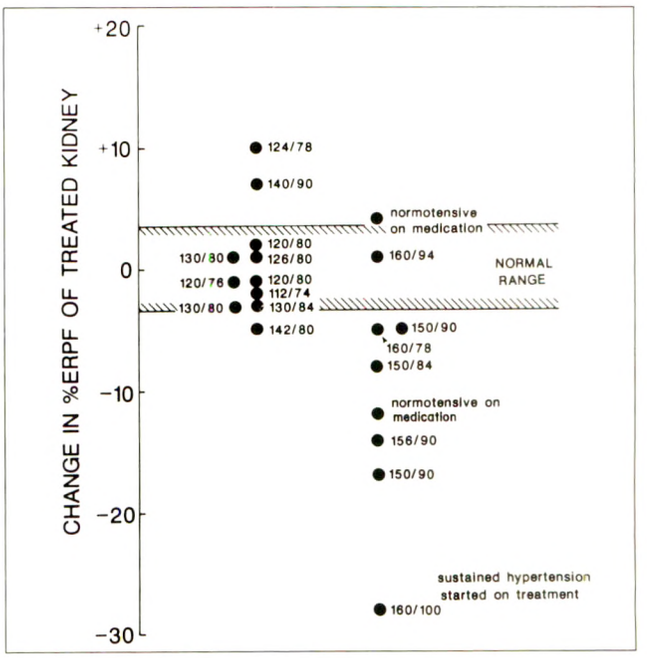

Fig. 1.—Correlation of change in percentage of effective renal plasma flow (ERPF) of treated kidney with blood pressure at 17–21 months after extracorporeal shock-wave lithotripsy (ESWL). Left column shows normotensive patients (systolic blood pressure <150 mm Hg; diastolic blood pressure <95 mm Hg). Right column shows hypertensive patients (systolic blood pressure ≥150 mm Hg and/or diastolic blood pressure ≥95 mm Hg) or patients who had become hypertensive after ESWL and were normotensive on medication.

Discussion

The United States cooperative study of ESWL required a radionuclide renogram before and 3 months after ESWL. The renogram could be performed either with ^{131}I-orthoiodohippuric acid, an agent that is used to measure ERPF, or with ^{99m}Tc-DTPA, which is used to measure glomerular filtration rate (GFR). In either case, the intention was to obtain a quantitative estimate of renal clearance. Because renal clearance of GFR agents is about 20% of renal clearance of ERPF agents, the cooperative study report [4] cited only the change in total renal clearance 3 months after ESWL. Total renal clearances were recorded for 494 patients, of which 241 were decreased, five were unchanged, and 248 were increased. When individual changes were measured, a statistically significant increase of total renal clearance was found. These 3-month post-ESWL results agree well with our 18-month post-ESWL results in which 10 of 21 patients had decreased total ERPF, one of 21 had the same total ERPF, and 10 of 21 had increased total ERPF. Mean total ERPF also increased slightly, but this change did not reach significance.

After unilateral nephrectomy, the remaining kidney may undergo compensatory hypertrophy and an increase in ERPF [8]. Decreased ERPF to a kidney resulting from renal trauma caused by ESWL can probably be compensated for by an increased ERPF to a healthy untreated kidney. For this rea-

son, the measurement of total renal clearance will not detect the presence of an adverse effect of ESWL on a treated kidney unless the untreated kidney is unable to respond. A compensatory increase in ERPF to the untreated healthy kidney may result in an increase in total ERPF to an amount greater than the pre-ESWL value, as was noted in the cooperative study [4] and also in the present report. For this reason the absolute value of the ERPF to the treated kidney, which is obtained by multiplying the percentage of ERPF to the treated kidney by the total ERPF, may not change significantly. The assessment of a change in renal function after ESWL is therefore incomplete without determination of the differential renal function of the treated kidney. Future studies of the acute and long-term effects of ESWL on renal function should always include an analysis of the relative function of the treated kidney.

The normal range of percentage of ERPF to a single kidney in a two-kidney healthy patient is 45–55% [9]. Our range of 35–63% in treated kidneys before ESWL was considerably larger than this, presumably because of the presence of stones and frequently some obstruction. The reproducibility of the percentage of ERPF to a single kidney in a two-kidney patient is ±3% (Dubovsky EV, personal communication). That is, if the percentage of ERPF to a single kidney is 45%, a repeat measurement will be between 42% and 48%. Thus a decrease in the percentage of ERPF to a single kidney from 45% pre-ESWL to 35% post-ESWL would be more than three times the change expected from the error of measurement. In our earlier study of renal function immediately after ESWL [2], we found a significant ($p = .025$) decrease in the percentage of function of the treated kidney when ERPF was measured. We also found that 30% of patients (10/33) had an abnormal decrease in the percentage of ERPF to the treated kidney of more than 5%. These findings have been confirmed by Bomanji et al. [10] who measured GFR in 42 patients immediately after ESWL. They found a significant ($p = .01$) decrease in the percentage function of the treated kidney, and 21% of patients (9/42) had an abnormal decrease in renal function of the treated kidney of 8% or more. When we used either our criterion of abnormality (a decrease of 6% or more) or the criterion of Bomanji et al. (a decrease of 8% or more) [10], we found that 24% of patients had an abnormal decrease in renal function of the treated kidney at 17–21 months. The fact that ESWL may result in a significant decrease in the percentage of ERPF to the treated kidney, both acutely and at 17–21 months, suggests that the decrease in renal function caused by ESWL may be permanent. In none of our 21 patients was there evidence of unrecognized ureteral obstruction as a possible cause of the decreased renal function of the treated kidney.

Peterson and Finlayson [3] reported a 4% (three of 79 patients) frequency of sustained hypertension occurring immediately after ESWL. The data in the present report indicate that sustained hypertension, either occurring immediately after ESWL or developing several months later, may be permanent. The overall frequency of hypertension requiring treatment in our patients was 8% (7/91). This frequency is in close agreement with the recent report of Lingeman and Kulb [11] who found that 24 (8%) of 295 patients required pharmacologic intervention for hypertension that had developed during the 1-year period after ESWL. Beyond the age of about 45 years (in both men and women), systolic blood pressure rises at an average rate of 0.5–1.0 mm Hg/year until the seventh decade [12]. All of the patients with sustained hypertension listed in this report and in the report of Lingeman and Kulb [11] developed hypertension either immediately after ESWL or within 1 year after ESWL, thus exceeding any age-related increase in blood pressure. The combined results of the two series, composed of nearly 400 patients, indicate that clinically significant hypertension arising from renal trauma caused by ESWL is likely to occur in about 8% of patients.

ESWL has been described as a well-engineered, highly selective application of brute force [13]. After a few hundred shocks, macroscopic hematuria caused by intrarenal hemorrhage occurs in virtually all patients [1, 2], and this hemorrhage may be serious in patients who have a tendency to bleed [14, 15]. Although the originators of the procedure recorded a very low frequency (0.6%) of subcapsular hematoma [1], a prospective study with MR imaging revealed a much higher frequency (29%) of subcapsular, perirenal, and/or intraparenchymal hemorrhage [2]. The difference in the rate of occurrence of renal hemorrhage may be attributed to the much less sensitive sonographic technique used by Chaussy et al. [1]. The high frequency of hemorrhage that we documented with MR has been confirmed by three recent studies in which CT [16, 17] and MR [18] were used for evaluation of kidneys treated with ESWL. Experiments with dogs have confirmed that the clinically observed MR and CT abnormalities are caused by renal and subcapsular hemorrhages, frequently associated with small vein thromboses, interstitial edema, and acute tubular necrosis [19–22].

External mechanical trauma is known to result in interstitial edema and extravasation of urine and blood into the interstitial space [23]. These same effects caused by ESWL explain the enlargement of the kidney seen on excretory urography, MR, and CT [2, 16–18, 24], as well as the total and partial parenchymal obstructive patterns seen in renography and the renal edema and hemorrhages seen on MR [2].

We have not yet found the cause of the long-term decrease in the percentage of ERPF to the treated kidney. The partial and total parenchymal obstructive patterns observed by renography immediately after ESWL, and attributed to acute tubular necrosis and edema caused by hemorrhage, were not seen in our patients 17–21 months after ESWL, thus indicating the resolution of these two processes. All but one of 21 patients had a normal excretory phase of the renogram curve of the treated kidney, indicating the absence of mechanical obstruction due to persistent or recurrent stones. The one patient in whom the percentage of ERPF was reduced to a very low value had no stone but a small atrophic kidney. Possibly renal fibrosis, which has been observed in canine kidneys 30 days after ESWL [22], may be responsible for the long-term decrease in the percentage of ERPF to treated kidneys.

Peterson and Finlayson [3] suggested that renal trauma caused by ESWL may cause hypertension as the result of a

perirenal hematoma via the well-known Page kidney effect (trauma → perirenal hemorrhage → fibrosis → compression of renal parenchyma → increased interstitial pressure → decreased renal perfusion → renin release → generation of angiotensin II → hypertension). In a review of 29 cases of Page kidney [25], a history of trauma could be elicited in 78%, and the interval between the trauma and the discovery of hypertension varied widely from 24 hr to 12 years but generally was less than 1 year. Of the seven patients in the present report who developed sustained hypertension after ESWL, three had MR immediately after ESWL and all three of these patients had perirenal or subcapsular hemorrhage. In the immediate post-ESWL period, decreased renal plasma flow may be reasonably attributed to increased interstitial pressure caused by perirenal or intrarenal hemorrhage and the resultant edema. Up to 18 months after ESWL, decreased renal plasma flow may result either from increased interstitial pressure possibly caused by fibrosis due to intrarenal hemorrhage or by fibrosis due to pressure from a perirenal fibrotic process.

Our study of the long-term effects of ESWL on renal function and blood pressure is weakened by the small number of patients and by the absence of any control data, such as the long-term effects on renal function and blood pressure in patients with comparable renal lithiasis treated by other techniques (e.g., percutaneous lithotripsy or surgical lithotomy). Also, the late renal changes and hypertension may not have been due to the trauma of ESWL but to some other process unrelated to renal lithiasis, such as unilateral renal artery stenosis. These alternative explanations can only be adequately addressed by a prospective study with appropriate controls. The observations in this report together with those of Lingeman and Kulb [11] strongly support the need for such a prospective study. Because hypertension induced by renal trauma may be delayed and is often asymptomatic, urologists and other physicians performing ESWL should be alerted to the fact that hypertension is a potentially important complication of the procedure. Our experience shows that blood pressure should be measured periodically for at least 1 year after ESWL.

REFERENCES

1. Chaussy C, Schmiedt E, Joacham D, Brendel W, Forssmann B, Walther V. First clinical experience with extracorporeally induced destruction of kidney stones by shock waves. *J Urol* **1982**;127:417–420
2. Kaude JV, Williams CM, Millner MR, Scott KN, Finlayson B. Renal morphology and function immediately after extracorporeal shock-wave lithotripsy. *AJR* **1985**;145:305–313
3. Peterson JC, Finlayson B. Effects of ESWL on blood pressure. In: Gravenstein J, Peter K, eds. *Extracorporeal shock wave lithotripsy for renal stone disease*. Boston: Butterworth, **1986**:145–150
4. Drach GW, Dretler S, Fair W, et al. Report of the United States cooperative study of extracorporeal shock wave lithotripsy. *J Urol* **1986**;135:1127–1133
5. Dubovsky EV, Logic JR, Diethelm AG, Balch CM, Tauxe WN. Comprehensive evaluation of renal function in the transplanted kidney. *J Nucl Med* **1975**;16:1115–1120
6. Kontzen FN, Tobin M, Dubovsky EV, Tauxe WN. Comprehensive renal function studies: technical aspects. *J Nucl Med Tech* **1977**;5:81–84
7. Tauxe WN, Dubovsky EV, Kidd T, Diaz F, Smith RL. New formulas for the calculation of effective renal plasma flow. *Eur J Nucl Med* **1982**;7:51–54
8. Tauxe WN. Prediction of residual renal function after unilateral nephrectomy. In: Tauxe WN, Dubovsky EV, eds. *Nuclear medicine in clinical urology and nephrology*. Norwalk, CT: Appleton-Century-Crofts, **1985**: 279–285
9. Tauxe WN, Tobin M, Dubovsky EV, Bueschen AJ, Kontzen FN. A macrofunction for computer processing of comprehensive renal function studies. *Eur J Nucl Med* **1980**;5:103–108
10. Bomanji J, Boddy SAM, Britton KE, Nimmon CC, Whitfield HN. Radionuclide evaluation pre- and postextracorporeal shock wave lithotripsy for renal calculi. *J Nucl Med* **1987**;28:1284–1289
11. Lingeman JE, Kulb TB. Hypertension following extracorporeal shock wave lithotripsy (abstr). *J Urol* **1987**;137:142A
12. Dollery CT. Arterial hypertension. In: Beeson PB, McDermott W, Wyngaarden JB, eds. *Cecil textbook of medicine*. Philadelphia: Saunders, **1979**:1199–1223
13. Mulley AG. Shock wave lithotripsy. *N Engl J Med* **1986**;314:845–847
14. Alvarez JA, Gandia VM, Alted EJ, Cantalapiedra JA, Blasco MA, Nunez A. Extracorporeal shock wave lithotripsy in a patient with mild hemophilia (letter to editor). *N Engl J Med* **1986**;315:648
15. Papanicolaou N, Stafford SA, Pfister RC, Althausen AF, Dretler SP. Significant renal hemorrhage following extracorporeal shock wave lithotripsy: imaging and clinical features. *Radiology* **1987**;163:661–664
16. Grote VR, Dohring W, Aeikens B. Computertomographischer und sonographischer Nachweis von renalen und perirenalen Veranderungen nach einer extrakorporalen Stosswellenlithotripsie. *ROFO* **1986**;144:434–439
17. Rubin JI, Arger PH, Pollack HM, et al. Kidney changes after extracorporeal shock wave lithotripsy: CT evaluation. *Radiology* **1987**;162:21–24
18. Baumgartner BR, Dickey KW, Ambrose SS, Walton KN, Nelson RC, Bernardino ME. Kidney changes after extracorporeal shock wave lithotripsy: appearance on MR imaging. *Radiology* **1987**;163:531–534
19. Rath M, Delius M, Enders G, et al. MR appearance of canine kidney exposed to shock waves (abstr). *Radiology* **1985**(P);157:26
20. Brendel W. Effect of shock waves on canine kidneys. In: Gravenstein J, Peter K, eds. *Extracorporeal shock wave lithotripsy for renal stone disease*. Boston: Butterworth, **1986**:141–142
21. Newman RC. Effect of shock waves on canine renal and neurological tissue. In: Gravenstein J, Peter K, eds. *Extracorporeal shock wave lithotripsy for renal stone disease*. Boston: Butterworth, **1986**:143–144
22. Newman RC, Hackett RL, Senior D, Feldman J, Sosnowski J, Finlayson B. Pathologic effects of ESWL on canine renal tissue. *Urology* **1987**;29:194–200
23. Lang EK, Sullivan J, Frentz G. Renal trauma: radiological studies. *Radiology* **1985**;154:1–6
24. Grantham JR, Millner MR, Kaude JV, Finlayson B, Hunter PT, Newman RC. Renal stone disease treated with extracorporeal shock wave lithotripsy: short-term observations in 100 patients. *Radiology* **1986**;158: 203–206
25. Sufrin G. The Page kidney: a correctable form of arterial hypertension. *J Urol* **1975**;113:450–454

The reader's attention is directed to the Commentary on this article, which appears on the following pages.

Commentary

Extracorporeal Shock-Wave Lithotripsy: Slam-Bang Effects, Silent Side Effects?

Albert G. Mulley, Jr.[1], Karen J. Carlson, and Stephen P. Dretler

In February 1984, 4 years after extracorporeal shock-wave lithotripsy (ESWL) was first used in Germany to fragment stones within human kidneys, the ESWL device manufactured by Dornier Systems was brought to the United States. Just 10 months later, on the basis of experience with approximately 2500 treatments at six American hospitals as well as 7000 treatments in Europe, the Food and Drug Administration (FDA) approved the Dornier device. Although the FDA approval stipulated the usual requirements for postmarketing surveillance and reporting of any adverse reactions, the rapid and widespread diffusion of the device and its shock waves was virtually guaranteed when it was described as "an authentic modern miracle" that could be expected both to improve quality and lower costs of care for patients afflicted with kidney stone disease.

Since that pronouncement, nearly 150 Dornier lithotriptors, each with a price tag of approximately two million dollars, have been delivered to American medical centers. With more than 300,000 patients treated worldwide, ESWL has revolutionized the management of "surgical" stone disease. For patients whose persistent pain, obstruction, or urinary infection warrant removal of a stone from the kidney or upper ureter, ESWL is widely considered the treatment of choice.

Ideally, such ready acceptance of a new medical technology would be based on unequivocal scientific evidence of efficacy and safety derived from a randomized controlled trial. But the medical technology supported by such ironclad evidence is the exception rather than the rule, and ESWL is not an exception in this regard. Large series of cases have demonstrated dramatic effectiveness in removing stones that previously required open surgery or percutaneous approaches to the urinary tract; 90% of such stones are removed by extracorporeal lithotripsy. Although immediate adverse effects such as perinephric hematoma and obstruction were reported, in general the short-term complication rates from these early series were impressively low.

But even when "slam-bang" effectiveness and acceptable short-term safety have been shown, the evaluation of a therapeutic technology remains incomplete. In the case of ESWL, two concerns about long-term adverse effects have been repeatedly expressed but remained unresolved. First, no study has determined the effects that small stone fragments remaining after ESWL may have on long-term stone-recurrence rates. Stone fragments are detectable in 10–30% of patients by conventional plain film radiography 3 months after ESWL. Symptomatic recurrences of urolithiasis occur in as many as 50% of patients (including 15% in the first year), so any increase in recurrence rates caused by fragments that remain after ESWL and that serve as nidi for stone formation would offset some of the technique's short-term advantages. Second, ESWL may result in adverse effects on soft tissues adjacent to the stone. Although the force of shock-wave energy is carefully focused on the target stone, the kidney and adjacent soft tissue also are subjected to trauma. Subcapsular, parenchymal, and perinephric hematomas have been detected by imaging after ESWL in 25–75% of cases, substantially higher rates than those reported in earlier studies in which less-sensitive sonographic techniques were used for evaluation. Again, any undiscovered long-term adverse effects on renal function could diminish the net effectiveness of

This work was supported in part by grant number H505604 from the National Center for Health Services Research and Health Care Technology Assessment.

[1] All authors: Massachusetts General Hospital and Harvard Medical School, Boston, MA 02114. Address reprint requests to A. G. Mulley, Jr., General Internal Medicine Unit, Massachusetts General Hospital, Harvard Medical School, Boston, MA 02114.

AJR **150:316–318, February 1988** 0361–803X/88/1502–0316 © American Roentgen Ray Society

ESWL. This is particularly true for the many young patients afflicted with urolithiasis.

It is in this context of the widespread acceptance of ESWL, based primarily on its manifest stone-removal efficacy, that we should view the two reports in this issue from one of the six original ESWL investigating hospitals [1, 2]. Both papers report on attempted long-term follow-up of the original 148 patients treated at Shands Hospital before FDA approval. Miles et al. [1] report that only 52% of treated kidneys were free of stones on abdominal radiographs obtained from 3 to 12 months after treatment; the rest had residual stones or fragments. Although radiographic efficacy is an important element in evaluating the overall effectiveness of ESWL, clinical efficacy—the ability of ESWL to relieve the pain, obstruction, or infection that prompted treatment—is an equally important criterion of effectiveness. Previous studies have shown that the clinical efficacy of ESWL is much greater than its stone-removal efficacy, as stone fragments generally are asymptomatic.

Miles et al. [1] report a rate of new stone formation of 5% at 13–21 months after ESWL, but they do not describe the clinical consequences, if any, of the new stones. Studies of patients treated with other techniques report recurrence rates of 2% up to 2 years after percutaneous ultrasonic lithotripsy and 26% up to 2 years after surgery [3]. Comparison of recurrence rates is difficult among series in which varying techniques are used because of the potential differences in the composition of each study population. The rate of new stone development reported by Miles et al. [1] does seem reassuringly low. However, researchers in future studies need to examine the new-stone rate, the increase in size of existing fragments, and the potential clinical manifestations of such size increases in a larger sample of patients followed for more than 2 years. Future reports should describe clinical consequences as well as radiographic evidence of recurrent stones.

The work of Williams et al. [2] explores the second, potentially more serious concern about the long-term consequences of ESWL. Using quantitative radionuclide renography in a small sample of patients who had undergone ESWL less than 2 years before, the investigators detected a significant decrease in percentage effective renal plasma flow in the treated kidney and significant increases in both systolic and diastolic blood pressure compared with pretreatment measurements. In addition, the rate of development of hypertension requiring treatment was 8% in a larger sample of patients followed for less than 2 years.

Although the report from Williams et al. [2] is provocative, it raises more questions than it answers. How should we respond to the 8% incidence of hypertension? To what extent might it be explained by selective follow-up or differences in measurement techniques in the hospital and ambulatory settings? Despite such potential problems, 8% does seem high in light of previous studies, including that of Blair et al. [4], who found a 4% incidence in previously normotensive patients over 1–12 years, but what is the best basis for comparison? Although no evidence indicates that stone disease per se is associated with an increased risk of hypertension, underlying conditions or complications of urolithiasis may increase the risk of hypertension in some patients. Other stone-removal techniques also jeopardize the kidney and may increase relative risk of hypertension. A higher incidence of hypertension after open surgery or nephrolithotomy has not been detected, but existing data are fragmentary.

The best estimates of the risk of hypertension that can be attributed to ESWL, or other stone-removal techniques, would come from a randomized controlled trial with careful long-term follow-up. In the absence of such a trial, carefully conducted cohort studies including patients treated with alternative approaches could provide reasonable estimates. The findings of the series reported by Williams et al. [2] should stimulate more meaningful, carefully conducted investigations.

While we await results of more definitive studies, the plausibility of a causal relationship between ESWL and hypertension in some patients is worth considering. The findings are consistent with results from other centers. Bomanji et al. [5] have reported a significant decrease in the glomerular filtration rate of the treated kidney of ESWL patients immediately after therapy. Lingeman and Kulb [6] have reported a similar incidence of hypertension requiring pharmacologic treatment after ESWL in a larger series. The short time between ESWL and development of hypertension seems to suggest a causal relationship, especially for the five patients who developed hypertension immediately after or within 2 months after ESWL and less so for those who developed hypertension more than 6 months after treatment. No dose-response relationship has been found between the number of shocks and changes in blood pressure, but the number of patients studied is small.

The biological plausibility of a relationship between ESWL and development of hypertension is a key element in the assessment of causality. A biological model for the production of hypertension due to extrinsic compression of renal parenchyma was established by Page. The mechanism for production of hypertension is not clearly established, but hypertension may be related to increasing interstitial pressure, which causes decreased renal perfusion with compensatory stimulation of renin release. The Page kidney has been a rarely reported cause of hypertension. In most of the reported cases, the interval between trauma to the kidney—the presumed inciting event—and discovery of hypertension was less than 1 year. Thus, the Page kidney mechanism is consistent with the temporal relationship between ESWL and hypertension reported by Williams et al. [2]. Although the size of the perirenal and subcapsular collections in reported cases has been large (usually > 500 ml), smaller hemorrhages may cause sufficient parenchymal compression to stimulate renin release.

Even if decreased renal function and an increased risk of hypertension prove to be long-term side effects of ESWL, lithotripsy will remain an important advance in kidney stone management. When there are clear indications for stone removal, any risks associated with ESWL must be weighed against the significant risks of surgery and percutaneous approaches. However, we must not be so distracted by the slam-bang effects of ESWL that we fail to pay sufficient attention to the quieter, long-term side effects; the risks of

Renal Transplant Dysfunction:
MR Evaluation

Mary Z. Winsett[1]
Eugenio G. Amparo[1]
H. Daniel Fawcett[1]
Rajendra Kumar[1]
Raleigh F. Johnson, Jr.[1]
Deepak G. Bedi[1]
Owen E. Winsett[2]

The results of 45 MR examinations were prospectively compared with the clinical course and biopsy results in 38 renal transplant patients to determine the role of MR in evaluating allograft dysfunction. Twenty-six patients underwent allograft biopsy. In eight patients in whom the biopsy was performed more than 48 hr after MR examination and in 19 patients who did not have a biopsy, the subsequent clinical course was sufficiently diagnostic to determine the specific cause of the transplant dysfunction. Corticomedullary differentiation, graded from 0 to 3, was not helpful in separating rejection (n = 20) from acute tubular necrosis (n = 9), drug toxicity (n = 7), pyelonephritis (n = 2), or normal grafts (n = 7) because of overlap between groups (sensitivity =; 60%, specificity = 60%). In the six patients with two or more MR studies, serial changes in corticomedullary differentiation were not consistent and could not be used to diagnose rejection. When any abnormality of allograft sinus fat, size or shape, or corticomedullary differentiation was considered, the sensitivity for the diagnosis of rejection approached 80%; however, specificity was low (48%).

We conclude that MR imaging is not sufficiently accurate to replace transplant biopsy and therefore has a limited role in the evaluation of transplant dysfunction.

Each year approximately 7500 patients undergo renal transplantation. Because of current surgical and immunosuppressive techniques, in approximately 80% of these patients the kidneys are still functioning 1 year after transplantation [1]. Despite recent advances, however, transplant rejection continues to be a significant problem. Prompt recognition of rejection and treatment are essential if allograft injury is to be minimized.

Preliminary studies have suggested that MR imaging may provide a noninvasive means of diagnosing renal transplant rejection and of distinguishing it from other causes of allograft dysfunction [2–8]. We correlated the MR appearance of transplanted kidneys with the subsequent clinical course and biopsy results in 38 patients to evaluate the ability of MR imaging to differentiate between the various causes of renal transplant dysfunction.

Materials and Methods

Between April 1985 and April 1986, 45 MR examinations were performed in 38 patients who had undergone renal transplantation. Five patients were imaged twice, and one patient was imaged three times. Ten of the transplanted kidneys were from living, related donors, and 28 were from cadaveric donors. Informed consent was obtained from all patients before MR imaging was performed, in accordance with institutional review-board regulations.

Seven patients with normally functioning allografts were examined 4–10 days after transplantation. In all seven, the allografts functioned immediately after transplantation; serum creatinine levels in this group ranged from 1.3 to 1.7 mg/dl at the time of the MR study.

Acute tubular necrosis was diagnosed in nine patients, all of whom had had cadaveric renal transplants. All had anuria or oliguria within 24 hr after transplantation, but none had signs or symptoms of rejection (fever, graft tenderness, or swelling). One patient had two biopsies, one on the day before and one 4 days after the MR examination. All nine had

Received July 20, 1987; accepted after revision October 12, 1987.

This work was supported in part by grants from Cecil and Ida Green and from the Sealy and Smith Foundation.

[1] Department of Radiology G09, University of Texas Medical Branch, Galveston, TX 77550. Address reprint requests to M. Z. Winsett.

[2] Department of Surgery, University of Texas Medical Branch, Galveston, TX 77550.

AJR 150:319–323, February 1988
0361–803X/88/1502–0319
© American Roentgen Ray Society

persistent oliguria at the time of MR examination and showed subsequent improvement in allograft function, as measured by increasing urine output and declining serum creatinine without specific therapy for a rejection episode.

All 20 patients with rejection had biopsies within 0–14 days of the MR examination; 13 of the 20 had biopsies on the same day. In the five patients who had had a biopsy more than 48 hr after MR imaging, the subsequent clinical course determined the diagnosis used for comparison with the MR examination. Seventeen of the 20 underwent MR imaging before biopsy or the start of therapy; the other three underwent MR imaging 1–2 days after biopsy or the start of therapy. The clinical diagnosis of rejection was based on one or more of the following criteria: (1) a significant or sudden decline in renal function; (2) signs or symptoms of graft inflammation (fever, allograft swelling, or tenderness); and (3) response to high-dose steroid therapy. Subsequent biopsies confirmed the clinical diagnosis. The histologic diagnosis of rejection was based on the presence of interstitial and/or perivascular cellular infiltrates, interstitial edema, and complement staining by immunofluorescence.

Seven patients with drug toxicity were imaged 12 days to 2½ years after transplantation. This group included five patients with cyclosporine nephrotoxicity as well as one patient each with tubular injury due to a nonsteroidal antiinflammatory agent and arsenic ingestion. In four patients the diagnosis was made by biopsy, performed within 24 hr of MR examination. Biopsy showed no evidence of rejection (minimal or no cellular infiltrates) and variable degrees of tubular cell injury. In the three patients diagnosed by subsequent clinical course, transplant function showed prompt improvement after decreasing or removing the offending drug.

Both patients with pyelonephritis had positive urine cultures and improved renal function after specific antibiotic therapy. One patient also had a biopsy 3 days after MR examination that showed severe interstitial edema, neutrophilic infiltrates, and microabscess formation that was most pronounced in the renal medulla.

MR imaging was performed with a Technicare superconducting magnet operating at 0.6 T, as described previously [9, 10]. Use of an image matrix of 256 × 128 elements afforded an in-plane spatial resolution of 3.6 × 1.8 mm. Four data acquisitions were averaged per image. In 43 of 45 patients, the multisection, multislice spin-echo (SE) technique was used in the transaxial plane; a body coil was used to obtain 0.8- to 1-cm contiguous slices through the renal transplant and bladder with repetition intervals (TR) of 500–1000 msec and an echo delay (TE) of 32 msec (SE 500–1000/32).

Selected patients underwent coronal (n = 20) and sagittal (n = 4) scans with the same pulse sequences. T2-weighted images (SE 2000/64) were obtained initially (n = 11) but later were discontinued because they failed to provide additional information. The inversion-recovery (IR) technique (IR 2050/32/656) was used in nine cases. In addition to the body coil, an 18-cm receive-only surface coil, was used in the transaxial (n = 6), coronal (n = 7), and sagittal planes (n = 3) with T1-weighted sequences (SE 500–700/32).

The MR examinations were interpreted by three independent observers who had no knowledge of the biopsy or clinical data. When disagreement in interpretation occurred, the interpretation selected by two of three was used. The transplant parameters evaluated included renal size and shape, corticomedullary differentiation (CMD), and presence of renal sinus fat. The studies were also evaluated for hydronephrosis or fluid collections. CMD was graded 0–3 (0 = absent, 1 = faintly visible, 2 = moderately well seen, 3 = clearly defined) (Fig. 1). Measurements of signal intensity were obtained in 43 of 45 patients using operator-defined regions of interest in the cortex and in the adjacent medulla from the body-coil images. (The data from two patients could not be retrieved from computer tapes.) Multiple paired measurements were obtained in each patient (average, five). The mean and standard deviation were calculated for the intensity ratio of cortex to medulla in each group of patients. Statistical analysis of the differences in the mean intensity ratios was performed using the Tukey Studentized range test. Sensitivity (no. of true-positive results/[no. of true-positive results + no. of false-negative results]) and specificity (no. of true-negative results/[no. of true-negative results + no. of false-positive results]) for the diagnosis of rejection were calculated for each of the parameters studied.

Results

Corticomedullary differentiation (CMD), graded from 0 to 3, showed considerable overlap between the groups of patients (Table 1). While all patients with normally functioning transplanted kidneys had CMD judged to be good or excellent, patients with acute tubular necrosis had CMD ranging from 0 to 3, patients with rejection 0–3, drug toxicity 1–3, and pyelonephritis 0–1. If CMD numbers of 2 and 3 are considered normal and 0 and 1 are considered abnormal, the sensitivity of MR for the detection of rejection using CMD alone is 12/20, or 60%, with a specificity of 15/25, or 60%. Visual rating of CMD showed good correlation with intensity-ratio measurements. Intensity ratios of cortex/medulla showed a similar overlap between groups of patients with renal transplant dysfunction (Fig. 2).

Renal sinus fat was judged absent or present (Table 1). Renal sinus fat was more frequently absent in patients with rejection; however, it was also absent in patients with normal kidneys, acute tubular necrosis, drug toxicity, and pyelonephritis. Defining complete absence of renal sinus fat as abnormal, this MR criterion has a sensitivity of 50% for detecting rejection and a specificity of 68%.

When abnormal transplant size or shape, absent renal sinus fat, or diminished CMD are considered together, MR sensitivity and specificity for the diagnosis of rejection are 80% and 48%, respectively, for an overall accuracy of 62.2%.

The six patients who underwent two or more MR examinations illustrate interesting but inconsistent changes in CMD (Fig. 3). Using changes in CMD as the sole criterion, we were able to correctly diagnose rejection in two of five cases, with a false-positive diagnosis in one of two cases with drug toxicity.

Fluid collections frequently were seen by MR imaging; however, most were insignificant postoperative hematomas, typically small collections located posterolateral to the transplanted kidney or in the incision in the anterior abdominal wall (14 patients). Three larger fluid collections were identified. Two patients had mild hydronephrosis detected by MR.

Discussion

Because of the limited availability and expense of MR, its contribution to the workup of renal transplant dysfunction must be carefully scrutinized. As with any new technique, initial enthusiasm regarding its clinical usefulness must subsequently be evaluated [11].

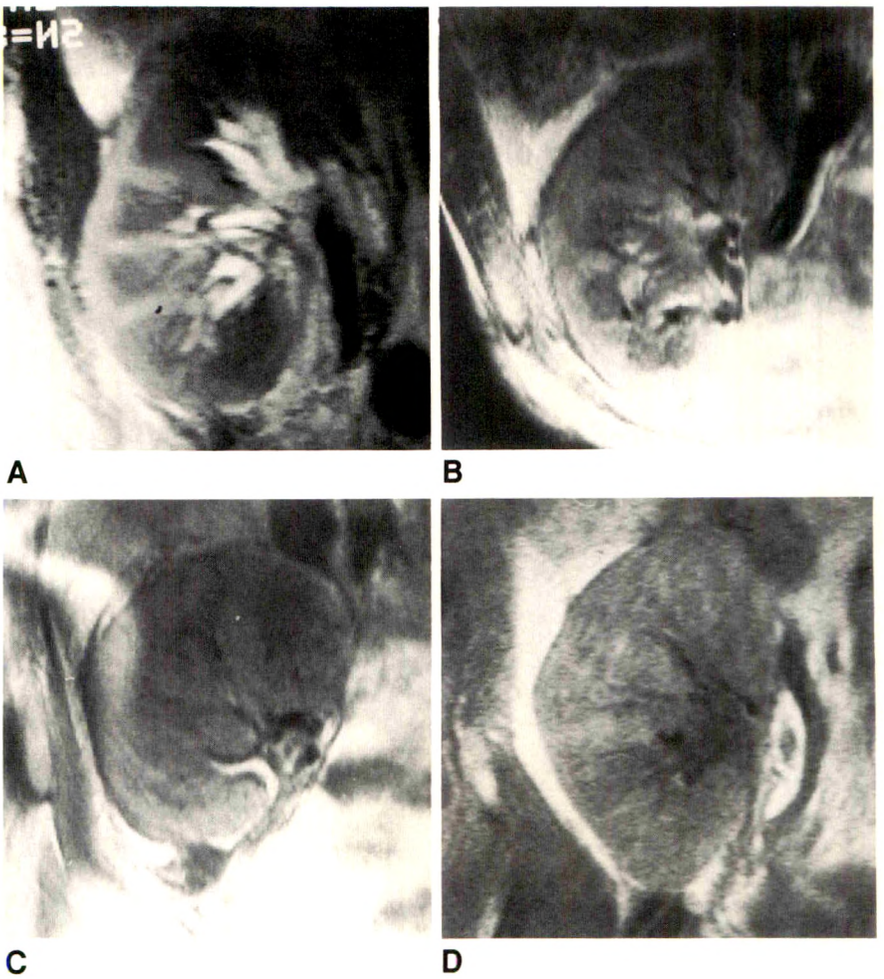

Fig. 1.—Corticomedullary differentiation grades 0–3. All images obtained with surface coils (SE 700/32).

***A*, Corticomedullary differentiation = 3 (excellent) in this normally functioning allograft. Also note abundant renal sinus fat.**

***B*, Corticomedullary differentiation = 2 (good) in an allograft with acute rejection.**

***C*, Corticomedullary differentiation = 1 (faint) in this globular transplant with acute rejection.**

***D*, Corticomedullary differentiation = 0 (absent) in an allograft with acute rejection. Also note absence of renal sinus fat.**

TABLE 1: MR Imaging Criteria for Detecting Renal Transplant Dysfunction

Diagnosis (No. of Patients)	No. of Patients with Diminished CMD[a] (%)	Intensity Ratio: Cortex/Medulla (Mean ± 1 SD)	No. of Patients with Absent Renal Sinus Fat (%)	No. of Patients with Abnormal CMD, Sinus Fat, or Size or Shape[b]
Normal (7)	0 (0)	1.41 ± .17	2 (29)	2 (29)
ATN (9)	5 (56)	1.16 ± .13[c]	3 (33)	6 (67)
Rejection (20)	12 (60)	1.22 ± .14[d]	10 (50)	16 (80)
Drug toxicity (7)	3 (43)	1.24 ± .13	2 (29)	3 (43)
Pyelonephritis (2)	2 (100)	1.14 ± .14	1 (50)	2 (100)

Note.—CMD = corticomedullary differentiation, SD = standard deviation, ATN = acute tubular necrosis.

[a] Diminished CMD was defined as CMD that was subjectively graded as 0 (absent) or 1 (faint).

[b] Abnormal size or shape was defined as a kidney that had increased in size since a previous MR study or a kidney that was globular in shape (i.e., anteroposterior dimension exceeded width). This was observed in six patients (30%) with rejection and was not observed in any patient with another diagnosis.

[c] $p < .01$.

[d] $p < .05$.

Hricak et al. [4] demonstrated a statistically significant lengthening of the calculated T1 value of renal cortex in kidneys with acute rejection, with no significant lengthening of the T1 value of the medulla. Because prolongation of T1 results in decreased signal intensity on T1-weighted images, these changes are also reflected in a change in the intensity ratios between cortex and medulla. Previous investigators have attributed the wide variation in the calculated T1 and T2

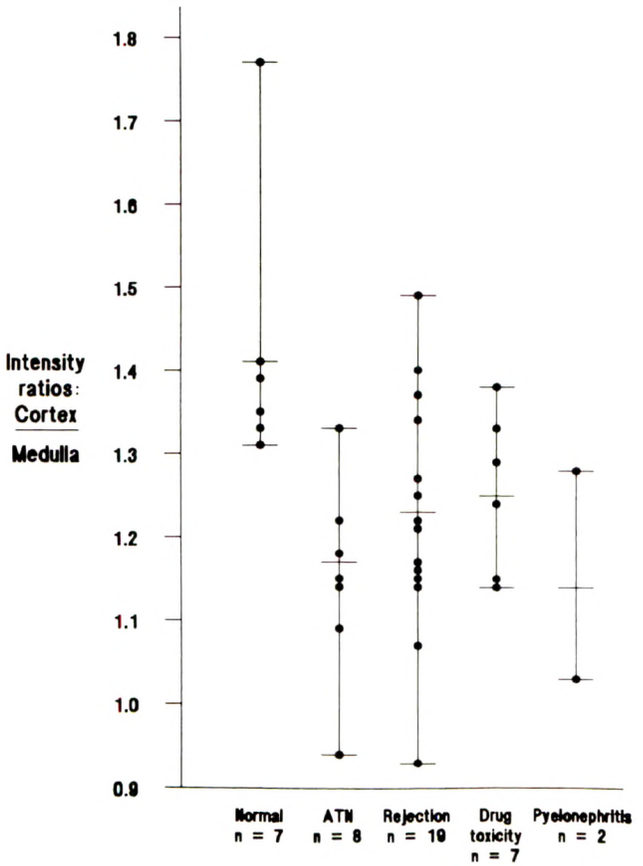

Fig. 2.—Intensity ratios of cortex to medulla.

Upper and lower bars indicate highest and lowest values for each group. Center bar represents mean value. Although normally functioning allografts had higher ratios than did abnormal transplants, some overlap between normal and abnormal groups exist. Considerable overlap is present between groups with transplant dysfunction. ATN = acute tubular necrosis.

Number of points on each line is less than the actual number of patients because of overlapping values. Numbers of patients in the ATN and rejection groups differ from those stated in the text and table, because data for one patient in each group could not be retrieved from computer tapes.

values for cortex and medulla to errors introduced during the calculation of these values [1, 2, 4]. For these reasons, we believe that the actual numeric values are less valuable than are the relative differences in intensity, as measured by intensity ratios of cortex to medulla. Although our use of images with TRs as long as 1000 (usually called mixed or proton-density weighted) do not take full advantage of T1 weighting, studies with other imaging systems, as well as our own experience with native kidneys, have shown this TR to result in increased overall signal without loss of CMD [12]. In a limited number of transplant patients with images obtained using both pulse sequences, CMD on the SE 1000/32 images was judged to be as good as or better than CMD on SE 500/32 images.

In this study, statistically significant differences were seen (1) between the mean intensity ratios (cortex/medulla) for normally functioning transplants and those for transplants with acute tubular necrosis ($p < .01$) and (2) between intensity ratios for normally functioning transplants and those for transplants with rejection ($p < .05$). However, it is of no clinical significance to separate normally functioning kidneys from those that are not functioning normally by any imaging procedure, since this difference is readily apparent through clinical and laboratory assessments. No significant difference was found for the mean intensity ratios of the various causes of renal transplant dysfunction. These data agree with data obtained by Hricak et al. [4] who also found statistically significant differences between percentage corticomedullary contrast and T1 of normal and rejecting allografts.

Other authors [2, 4, 6, 7] have reported the variable MR appearance of kidneys with acute tubular necrosis, ranging from morphologically normal to a marked loss of CMD. No large MR series of patients with acute tubular necrosis has been reported; however, our preliminary data in nine patients combined with the data of others would suggest that MR has a limited role in evaluating patients with early posttransplant dysfunction.

Our study also suggests that it is difficult to use MR to differentiate patients with rejection from those with cyclo-

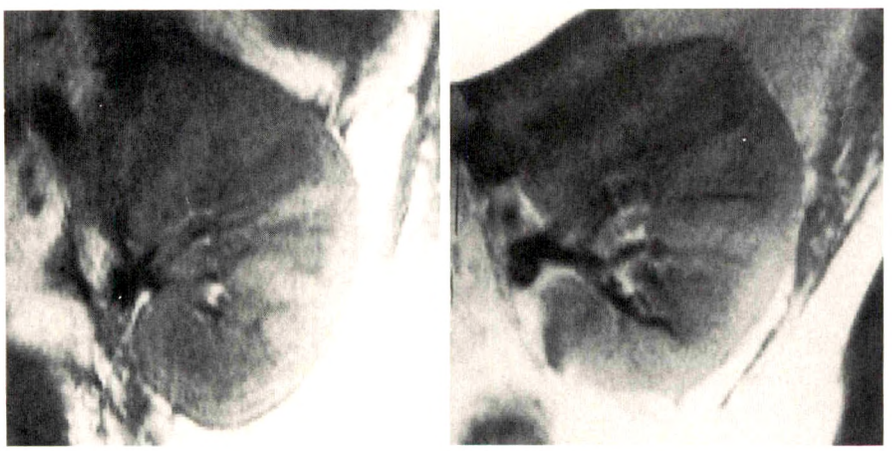

Fig. 3.—Follow-up study shows decrease in corticomedullary differentiation not due to acute rejection.

A, Corticomedullary differentiation = 2 in this allograft with acute rejection. Patient responded to treatment with steroids (SE 700/32).

B, Same patient 9 months later with a second deterioration in function. Corticomedullary differentiation = 1. Patient had cyclosporine nephrotoxicity that responded to decrease of dose (SE 700/32).

sporine nephrotoxicity. Whereas Hricak et al. [4] observed that all five of their patients with cyclosporine nephrotoxicity had excellent CMD, CMD was diminished in three of the seven patients we studied. One explanation for this difference may be the length of time between transplantation and MR examination; the five patients with cyclosporine nephrotoxicity in the study by Hricak et al. [4] were imaged within 14–25 days after transplantation. Our patients were studied from 12 days to 2½ years after transplantation (average, 9½ months). Three patients had been successfully treated in the past for an acute rejection episode. At least two other authors have observed diminished CMD in patients with cyclosporine nephrotoxicity [8, 13]. In neither case did the authors state the time from transplantation to MR imaging.

Hamburger et al. [14] observed that biopsies obtained from normally functioning renal transplants 6 months and 2 years after transplantation showed edema, fibrosis, and cellular infiltrates in 59% and 73%, respectively. These changes were more frequently observed in patients who had had previous rejection episodes, even when the rejection episodes were fully reversible with therapy. The diminished CMD in our patients with drug toxicity may have been related to fibrosis from a previous rejection episode (Fig. 3). We were probably not imaging the isolated effect of drug toxicity on CMD; however, these are variables that cannot be controlled in the clinical setting.

The changes in CMD seen by MR imaging have been attributed to an increase in water content in the interstitium of the kidney, predominantly in the cortex [3, 5]. The biopsy reports in our patients noted moderate-to-severe interstitial edema in 12 of 20 cases of acute cellular rejection. In three patients the amount of interstitital edema was not specifically noted. In five patients with acute rejection, the biopsy showed minimal interstitial edema, despite the presence of severe inflammatory infiltrate. Direct correlation of the amount of edema noted in the biopsy specimens with the degree of diminished CMD was not possible in every case. This may be attributed to several factors: the length of time between the MR examination and the biopsy is one potential weakness of this report. Sampling error from a single biopsy specimen may also be a contributing factor. We propose that the inability of CMD to accurately diagnose rejection may be due to the absence of significant interstitial edema in some patients with acute rejection. In addition, interstitial edema may be seen in patients with other diagnoses. Fibrosis will also prolong T1 and may result in decreased CMD, as may be seen in patients with previous rejection episodes, as well as in normally functioning transplants, because of low-grade, ongoing rejection.

We conclude that, although MR imaging provides excellent visualization of the renal transplant, the appearance of the transplanted kidney is not a specific indicator of the cause of renal transplant dysfunction. The lack of correlation between MR imaging and biopsy or clinical parameters in many patients severely limits its usefulness in the evaluation of patients with renal transplants.

REFERENCES

1. The Canadian Multicentre Transplant Study Group. A randomized clinical trial of cyclosporine in cadaveric renal transplantation. *N Engl J Med* **1983**;309(14):809–815
2. Geisinger MA, Risius B, Jordan ML, Zelch MG, Novick AC, George CR. Magnetic resonance imaging of renal transplants. *AJR* **1984**;143:1229–1234
3. Terrier F, Hricak H, Revel D, et al. Magnetic resonance imaging in the diagnosis of acute renal allograft rejection and its differentiation from acute tubular necrosis (experimental study in the dog). *Invest Radiol* **1985**;20:617–625
4. Hricak H, Terrier F, Demas BE. Renal allografts: evaluation by MR imaging. *Radiology* **1986**;159:435–441
5. Rholl KS, Lee JKT, Ling D, Sicard GA, Griffith RC, Freeman M. Acute renal rejection versus acute tubular necrosis in a canine model: MR evaluation. *Radiology* **1986**;160:113–117
6. Baumgartner BR, Nelson RC, Ball TI, et al. MR imaging of renal transplants. *AJR* **1986**;147:949–953
7. Hricak H, Terrier F, Marotti M, et al. Posttransplant renal rejection: comparison of quantitative scintigraphy, US, and MR imaging. *Radiology* **1987**;162:685–688
8. Steinberg HV, Nelson RC, Murphy FB, et al. Renal allograft rejection: evaluation by Doppler US and MR imaging. *Radiology* **1987**;162:337–342
9. Buonocore E, Borkowski GP, Pavlicek W, Ngo F. NMR imaging of the abdomen: technical considerations. *AJR* **1983**;141:1171–1178
10. Kneeland JB, Knowles RJ, Cahill PT. Magnetic resonance imaging systems: optimization in clinical use. Radiology **1984**;153:473–478
11. Halasz NA. Differential diagnosis of renal transplant rejection: is MR imaging the answer? *AJR* **1986**;147:954–955
12. Hricak H, Crooks L, Sheldon P, Kaufman L. Nuclear magnetic resonance imaging of the kidney. *Radiology* **1983**;146:425–432
13. Lund G, Letourneau JG, Day DL, Crass JR. MRI in organ transplantation. *Radiol Clin North AM* **1987**;25(2):281–288
14. Hamburger J, Crosnier J, BAch JF, Kreis H. *Renal transplantation: theory and practice.* Baltimore, MD; Williams & Wilkins, **1981**

Book Review

General Perspectives. Vol. 1: Advances in Urologic Oncology. Edited by Richard D. Williams. New York: Macmillan, 222 pp., 1987. $37.50

The editor has assembled a distinguished group of contributors from several different disciplines, including urology, oncology, transplantation, and genetics, for this well-produced and informative first volume in the series *Advances in Urologic Oncology*. As stated in the preface, an attempt has been made to give comprehensive reviews of the most promising advances in the diagnosis and treatment of urologic cancer. Reflecting the exciting progress in and increasing complexity of urologic oncology and research on human tumors, particularly during the past decade, the subjects covered range from basic tumor biology to newer methods of diagnosis and methods of treatment, some of which are unproved.

Chapter titles include "Oncogene Expression and Chromosome Rearrangement in Urologic Tumors," "Flow Cytometry in Urologic Cancers," "Tumor Antigens in the Diagnosis, Staging, and Prognosis of Urologic Cancer," "Magnetic Resonance in the Diagnosis and Staging of Urologic Cancer," and "Endourologic Diagnosis and Treatment of Upper Tract Urothelial Tumors." Subsequent chapters include "Photodynamic Techniques in the Treatment of Bladder Cancer," "Hormonal Therapy for Advanced Carcinoma of the Prostate," "Immune Modifiers in Genitourinary Cancers," "Chemotherapy of Disseminated Transitional Cell Carcinoma," and "Diversion Techniques in Urologic Cancer." The general layout is pleasing, and illustrations and figures are well chosen and appropriate in size. One of the strengths of this volume is the coverage of each chosen subject. For example, a reader who has minimal knowledge of tumor genetics can progress through the chapter on this subject and comprehend the details of oncogene expression in the discussed urologic cancers. The chapter on MR imaging is slightly too conservative concerning the role of this technique in tumor staging. Only one of the references listed in this chapter is from 1986. Generally, the references in each chapter are current and include ones published in 1986. This book is of principal interest to urologists, including residents, oncologists, and those radiologists who work with oncologists and need to keep abreast of advances in urologic oncology. The reader cannot fail to be stimulated and to share some of the optimism of the authors.

Noel K. Allan
Loma Linda University Medical Center
Loma Linda, CA 92351

Case Report

Selective Renal Embolization for Hematuria: Coordination with Cystoscopy

Douglas A. Swartz,[1] Garey L. McLellan,[2] Dale Mitchum,[3] and Frederick Vines[2]

A case of selective segmental renal arterial embolization for clinically significant renal hematuria due to sickle cell nephropathy is presented. The patient was heterozygous for the sickle cell trait and had significant anemia caused by the hematuria. The hematuria was refractory to conservative measures. No lesion was identifiable on angiography. The technique by which we identified the bleeding segment in order to coordinate embolization has not been previously reported. The renal segment to be infarcted was selected by cystoscopic observation of the cessation of blood flow from the ipsilateral ureteral orifice during temporary occlusion of the segmental renal branches with a transcatheter angiography balloon. The suspected renal segment was then infarcted by using Gelfoam particles and a single embolization coil. Fourteen months after infarction, the patient remains normotensive and free of hematuria.

Case Report

A 28-year-old woman was hospitalized for painless gross hematuria and anemia. The onset followed the birth of her last child, 13 months before admission. The frequency of hematuria increased; 7 months before admission, hematuria had been occurring daily. An IV pyelogram, abdominal CT, and renal sonogram were normal. Bloody efflux was observed from the right ureteral orifice during cystoscopy. A right retrograde ureterogram was normal.

On admission, the hematocrit was 21%. Hemoglobin electrophoresis showed 67% hemoglobin A and 29% hemoglobin S. Conservative therapy included the infusion of four units of packed red blood cells and hypotonic fluids. When these measures failed, aminocaproic acid (Lederle, Pearl River, NY) was administered without success. An arteriogram was performed, but no lesion was identified. Two more units of packed red blood cells were subsequently required for a symptomatic anemia.

Segmental infarction was necessary because of the continued bleeding and transfusion requirement. After induction of general endotracheal anesthetic, the patient was positioned to allow simultaneous access to the right femoral artery and perineum. The presence of bloody right ureteral efflux was confirmed by cystoscopy. An open-tip, 5-French ureteral catheter (Cook, Inc., Bloomington, IN) was endoscopically placed retrograde into the renal pelvis to allow irrigation of the pyelocaliceal system with saline.

A 6.5-French guiding catheter from a Wholey occlusion coaxial set (Cook, Inc.) was introduced into the right renal artery. Superselective placement of the catheter was facilitated by use of an injectable, steerable guide-wire system (C. R. Bard, Inc., Billerica, MA). The injectable guidewire had an outer diameter of 0.038 in. (0.097 cm) and permitted replacement of the mandril with a steerable, J-tip guidewire (0.016-in. [0.041 cm], outer diameter) [1].

A selective injection reconfirmed normal renal vasculature without the presence of malformations. After positioning the 6.5-French guiding catheter in the selected segmental artery, the 3-French Wholey occlusion balloon catheter was placed through the guiding catheter. The balloon was inflated, and contrast material was injected to confirm occlusion. Immediately after occlusion, 10 ml of saline was gently irrigated through the ureteral catheter until the efflux cleared. The ureteral efflux was then observed for hematuria over a period of 5 min. The sequence of ureteral irrigation and observation was repeated as each of the five segmental renal arteries was serially occluded. Clear right ureteral efflux was observed only when the

Received August 17, 1987; accepted after revision September 16, 1987.
[1] Department of Surgery, Division of Urology, University Hospital, 655 W. 8th St., Jacksonville, FL 32209. Address reprint requests to D. A. Swartz.
[2] Department of Radiology, University Hospital, Jacksonville, FL 32209.
[3] Department of Surgery, University Hospital, Jacksonville, FL 32209.

AJR **150:325–326, February 1988** 0361–803X/88/1502–0325 © American Roentgen Ray Society

single middle segmental artery was occluded. The occlusion was repeated after 30 min to confirm the findings.

Gelfoam particles (Upjohn, Kalamazoo, MI) were embolized into the single middle segmental renal artery. After significantly decreasing renal flow to this segmental artery, an occluding spring embolus (3 mm in diameter, 4 cm long) (Cook, Inc.) was placed in the artery. A pull-back arterial injection confirmed complete occlusion.

After surgery, the patient had transient right flank pain. Her blood pressure remained normal. The hematocrit remained stable, and the urine was clear. A renal scan showed middle segmental infarction and normal perfusion of the remaining parenchyma. Fourteen months after infarction, the patient is normotensive and has had no hematuria.

Discussion

Sickle cell trait occurs in approximately 8% of blacks. Sickle cell hemoglobinopathy accounts for one-third of cases of gross hematuria in blacks [2]. The mechanism is not known but probably involves papillary necrosis due to ischemia caused by red blood cell sickling.

Conservative measures such as hypotonic fluid hydration, sodium bicarbonate, mannitol, and loop diuretics were initially used [3, 4]. Aminocaproic acid, a urokinase inhibitor, has been reported effective in hematuria associated with hemoglobin S [5]. Hematuria can be recurrent and refractory to standard methods of therapy. Nephrectomy is sometimes necessary, despite the risk of development of hematuria in the contralateral kidney [6]. Limited segmental nephrectomy has also been reported as successful after identification of the bleeding segment by open nephroscopy [7].

Whenever possible, conservative surgical management should be attempted. The disease can be bilateral, and patients who have undergone nephrectomy for hematuria may have future bleeds from the remaining kidney [8]. Segmental renal arterial embolization is an ideal surgical alternative because of the reduced morbidity. The problem with applying embolization or segmental resection has been localization of the bleeding renal segment. In most cases of sickle cell nephropathy with gross hematuria, no focal lesion is apparent on the renal arteriogram. Percutaneous nephroscopy and retrograde ureteroscopy could potentially locate the bleeding. Hematuria associated with the routine trauma of nephroscopy and ureteroscopy makes visualization of a bleeding site difficult. Coordination of embolization with nephroscopy or ureteroscopy may also be a problem. This report describes a technique by which the bleeding renal segment can be identified to allow segmental renal embolization. Simultaneous cystoscopic observation of the change in the involved ureter efflux from bloody to clear during temporary occlusion of the segmental renal arteries allows identification of the involved segment.

REFERENCES

1. Sos TA, Cohn DJ, Srur D, Wengrover SI, Saddikni S. A new open-ended guide wire/catheter. *Radiology* **1985**;154:817–818
2. Schaeffer AJ, DelGreco F. Other renal diseases of urologic significance. In: Walsh PC, Grittes RF, Perlmutter AD, Stamey TA, eds. *Cambell's urology*. Philadelphia: Saunders, **1986**:2342–2360
3. Knochel JP. Hematuria in sickle cell trait: the effect of intravenous administration of distilled water, urinary alkalinization, and diuresis. *Arch Intern Med* **1969**;123:160–165
4. Marynick SP, Ramsey EJ, Knochel JP. The effect of bicarbonate and distilled water on sickle cell trait hematuria and in vitro studies on the interaction of osmolality and PH on erythrocyte sickling trait. *J Urol* **1977**;113:793–797
5. Immugul MA, Stevenson T. The use of epsilon-amino caproic acid in the control of hematuria associated with hemoglobinopathies. *J Urol* **1965**;93:100–111
6. Mostofi FK, Vorder Bruegge CF, Diggs LW. Lesions in kidneys removed for unilateral hematuria in sickle cell disease. *Arch Pathol Lab Med* **1957**;63:336–351
7. Douglas LL, Pawaroo J. Conservative surgery for refractory sickle cell hematuria. *J Urol* **1978**;120:385–386
8. Lund HG, Cordonnier JJ, Forbes KA. Gross hematuria in sickle cell disease. *J Urol* **1954**;71:151–158

Balloon Catheter Dilatation of Urethral Strictures

Said H. Mohammed[1]
Jack Wirima[2]

Seven patients with urethral strictures due to different causes were treated by balloon catheter dilatation. The dilatation was performed on an outpatient basis in conjunction with suprapubic voiding cystourethrography and under fluoroscopic control. Only diazepam sedation and topical anesthesia were used. No indwelling catheters were placed in the urethra after the procedure. Six of the seven patients have been followed for 6–26 months, and only two have required redilatations. There have been no complications that required therapy.

The initial success with our technique and that reported by others suggest that balloon catheter dilatation offers a good alternative treatment for urethral strictures to replace bouginage, urethrotomy, and urethroplasty.

Urethral strictures constitute a significant clinical problem that often requires long-term management. Bouginage, urethrotomy, and urethroplasty are the current therapeutic cornerstones. However, the success of these surgical procedures has been limited. They have significant rates of primary failure, with increases in strictures and recurrence of the strictures, as well as a wide range of complications such as bleeding, creation of false passages, incontinence, and perforation of adjacent structures [1–9].

The use of Grüntzig angioplasty catheter and its various modifications in the dilatation of cardiovascular stenoses, biliary tract and gastrointestinal strictures, and ureteral strictures [10–17] has promoted its use in the treatment of urethral strictures [7, 18–20]. We report our experience using balloon catheter dilatation of urethral strictures in seven patients.

Subjects and Methods

Seven men with urethral strictures were treated by balloon catheter dilatation on an outpatient basis. The patients were 16 to 67 years old (mean, 35 years). All the strictures were diagnosed by suprapubic voiding cystourethrography, by using a modification of the technique described by Bryndorf et al. [21]. There were two strictures of the prostatic urethra due to benign prostatic hyperplasia, one traumatic stricture of the membranous urethra, three strictures caused by gonorrhea—two of the bulbous urethra and one of the penile urethra—and one iatrogenic stricture of the bulbous urethra due to prolonged catheterization. Six patients were followed for 6–26 months (mean, 12 months) after the first dilatation. One patient was lost to follow-up.

In our dilatation technique, each patient had a suprapubic voiding cystourethrogram immediately before the dilatation. When the stricture was detected on a spot film, a radiopaque marker was placed at the site, either on the scrotum or penis. The patient was then asked to stop voiding. The contrast medium remaining in the bladder was used for monitoring the progress of the dilatation under intermittent fluoroscopy and for a cystourethrogram at the end of the procedure. The puncture needle was left in the bladder until the end of the dilatation, in case the bladder needed to be refilled with contrast medium. The patient was sedated with diazepam, and a topical anesthesia (2% lidocaine jelly) was instilled into the urethra.

Received July 24, 1987; accepted after revision October 15, 1987.

Presented in part at the meeting of the Danish Society for Diagnostic Radiology, Copenhagen, Denmark, November 1986, and at the European Congress of Radiology, Lisbon, Portugal, June 1987.

[1] Department of Radiology, Kamuzu Central Hospital, Lilongwe, Malawi, and Department of Radiology, Glostrup Hospital, Copenhagen, University Denmark, Copenhagen, Denmark. Address reprint requests to S. H. Mohammed, Dept. of Radiology, Glostrup Hospital, University of Copenhagen, DK-2600 Glostrup, Denmark.

[2] Department of Medicine, Kamuzu Central Hospital, Lilongwe, Malawi.

AJR **150:327–330, February 1988**
0361–803X/88/1502-0327
© American Roentgen Ray Society

With the patient in a steep oblique position, a 0.035-in. (0.09-cm), J-shaped guidewire was passed through the urethra into the bladder. If attempts to do this failed, a 5-French straight angiographic catheter was passed over the guidewire, and the two were negotiated together through the stricture into the bladder. If these attempts also failed, the patient was asked to void, and during the voiding, the catheter and guidewire were passed quickly into the bladder. This was necessary in two patients. Once the guidewire was coiled in the bladder, the angiographic catheter was exchanged for an Olbert balloon catheter. Catheters with balloons that were 4–9 mm in diameter were used. The size of the balloon selected was approximately equal to the combined width of the urethra at and distal to the stenosis. All maneuvers with the guidewire and catheters were performed under fluoroscopic control to avoid the creation of false passages. Once the balloon of the catheter straddled the stricture, it was inflated manually with water-soluble contrast medium for 3–5 min, with intervals of 2–3 min between inflations, until the balloon's waist disappeared. The average number of dilatations during each session was three. In two patients who had long, tight strictures, two balloons of different sizes were used—first a 4-mm balloon and then a 6-mm balloon. After two or three dilatations, the balloon catheter was removed. With the guidewire still in place, the patient was asked to void under fluoroscopy in order to assess the caliber of the urethra proximal to the stenoses and at the narrowed site.

If the prestenotic dilatation was significantly reduced from its caliber before dilatation and if the width of the urethra at the site of the stricture approximated that of the urethra immediately proximal and distal to it, the guidewire was removed (Figs. 1C and 2D). The cystourethrogram was documented on a spot film, and the procedure was terminated. If, on the other hand, the voiding cystourethrography under fluoroscopy did not show an adequate increase in the diameter of the urethra at the site of the stenosis, the balloon catheter was reintroduced into the urethra and the dilatation was repeated until a satisfactory lumen of the stricture was achieved. The puncture needle was then removed from the bladder.

The patients remained in the radiology department until the effects of the sedation subsided. When a patient left the department, he was advised to drink profusely for the next 2 weeks and to start every micturition by clamping the glans penis with his fingers for a few moments in order to dilate the urethra, before passing urine ("autobouginage" or "hydraulic dilatation" [6]). No indwelling catheters were used, so that the risks of infection and restricturing were reduced. Dilatation of the external sphincter was avoided in cases in which the stenoses were close to the external sphincter.

Results

Six of the seven patients were followed for 6–26 months (mean, 12 months). One patient with a 2.5-cm-long bulbous stricture with two false passages (each 2 cm long) had two redilatations within 26 months. The first redilatation was after 6 months and the second after 9 months. The stricture was due to gonorrhea. The patient with a postcatheterization stenosis was redilated once after 15 months, during 26 months of observation. Four patients, two of whom had benign prostatic hypertrophy, were followed for 6–9 months. None of these four have required redilatation.

The only complications were slight leakage of the contrast medium at the puncture site in the bladder and mild hematuria immediately after the dilatation and for the next 24 hr. No complication required therapy. In two of the seven patients, the balloon ruptured during the procedure. Both balloons were inflated manually, as were the others, and we do not have any explanation for the ruptures. The patient with the long, tight bulbous stricture had to be dilated initially in three stages (first with a 5-French angiographic catheter, then with a 4-mm Olbert balloon catheter, and finally with a 6-mm Olbert balloon catheter) before satisfactory relief of the stricture was achieved.

The patients reported a stinging sensation during catheterization but no pain during dilatation. All those followed reported improvement of the urinary stream, which was also apparent during the final cystourethrogram. Patients also reported significant reduction of the frequency of micturition during the follow-up period.

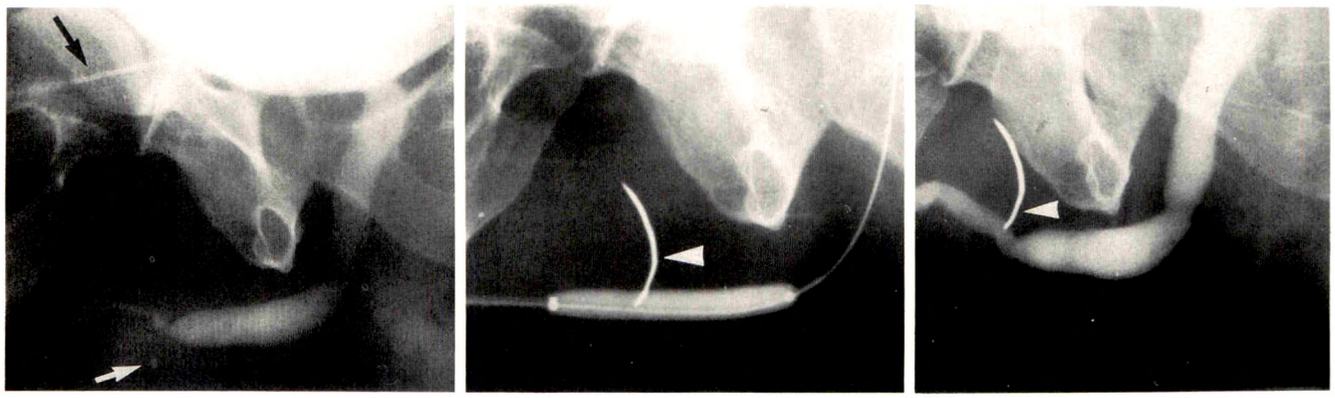

Fig. 1.—Urethral stricture in 57-year-old man treated by balloon dilatation.

***A*, Predilatation suprapubic voiding cystourethrogram showing short bulbous stricture. Puncture needle in bladder (*black arrow*). A stone in an old false passage (*white arrow*).**

***B*, Inflated Olbert balloon catheter in place. Skin marker at the site of the stricture (*arrowhead*).**

***C*, Postdilatation suprapubic voiding cystourethrogram showing lumen of satisfactory width. *Arrowhead* shows skin marker.**

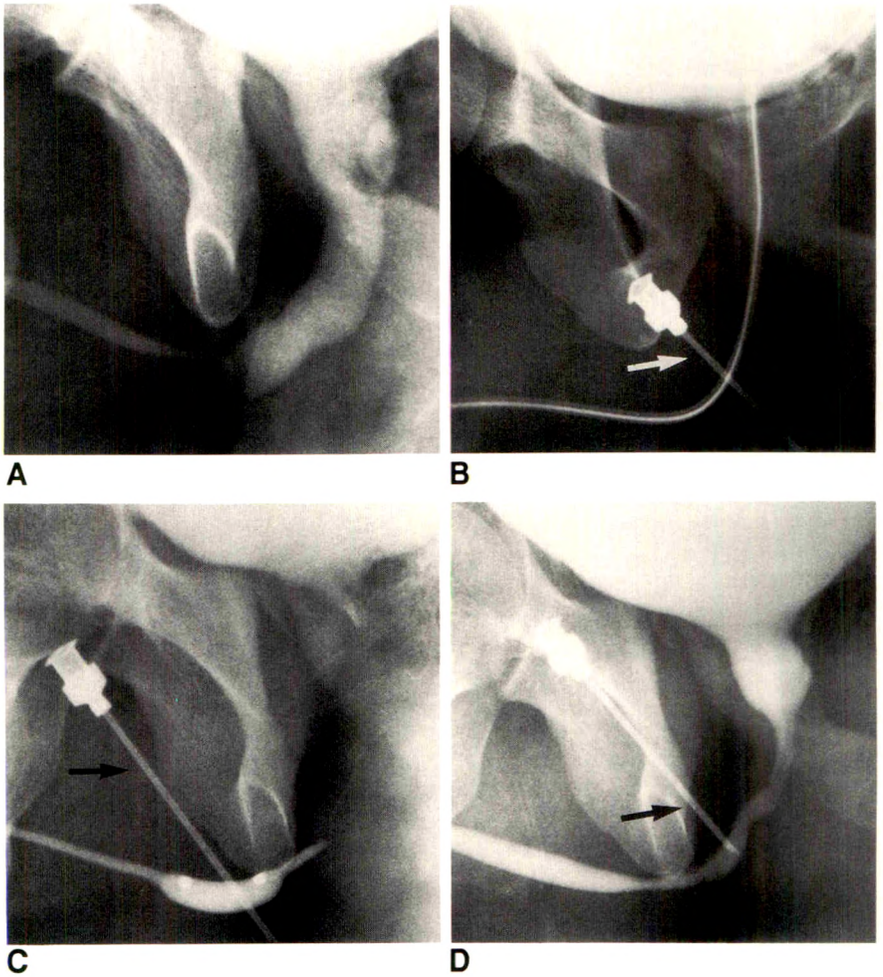

Fig. 2.—Urethral stricture in 18-year-old man treated by balloon dilatation. *Arrows* show skin marker at site of stricture.

***A*, Predilatation suprapubic voiding cystourethrogram showing tight bulbous stricture. Note markedly widened posterior urethra.**

***B*, 5-French angiographic catheter has been passed over a guidewire, through stricture into bladder.**

***C*, After angiographic catheter has been removed, Olbert balloon catheter can be negotiated through stricture and then inflated.**

***D*, Postdilatation suprapubic micturition cystourethrogram showing lumen of satisfactory width and posterior urethra of normal width.**

Discussion

Although antibiotic therapy has significantly reduced the frequency of postinflammatory urethral strictures, this condition continues to pose a common clinical problem. The frequency of urethral strictures due to other causes (such as prolonged catherization of sedentary patients, prostatic hypertrophy with urethral obstruction, and trauma) has increased.

Conventional dilatation techniques for urethral strictures are associated with a high recurrence rate and often with progressive narrowing of the stricture due to scar tissue [3, 4, 6–9]. They are also associated with complications of varying severity, including mild bleeding, creation of false passages, impotence, incontinence, and rupture of the rectum and other neighboring organs. They require repeated hospitalizations because of the high recurrence rates, reported to be 20–50% [2, 4–6, 9].

Balloon dilatation techniques in the cardiovascular system, gastrointestinal and biliary tracts, and upper urinary tract have been effective and economical, and they have had few serious complications [11–18]. Initial reports on balloon dilatation of urethral strictures have shown similar benefits [7, 18–20]. Burhenne et al. [19] and Russinovitch et al. [7] have also raised the possibility of the patient dilating the stricture himself, especially in cases of stricture due to benign prostatic hypertrophy. The concentric, radial forces associated with the expanding balloon cause less trauma to the urethral and periurethral tissues than do the combined radial and longitudinal shearing forces of bouginage and repeated urethral resections [7, 15, 19, 20].

The results of our preliminary experience with seven patients suggest that balloon catheter dilatation is a reliable alternative for treatment of urethral strictures. Not one of our patients required redilatation within the first 3 months after the first dilatation (the period in which 11–43% of reported recurrences occurred after urethrotomy [1, 4, 6]). The two patients that did need redilatation had strictures that were over 2 cm long and had been dilated repeatedly with bougies for several years. These are precisely the patients that have early recurrences after urethrotomies [1, 3, 5, 6].

Our technique of performing the dilatation under fluoroscopic control and in conjunction with suprapubic voiding cystourethrography permits precise detection of the entire

length of the stricture, control of the passage of the guidewire, and accurate placement of the balloon across the stricture. It has obvious advantages over endoscopic balloon dilatation in which the view is limited to one end of the stricture. Retrograde catheterization was possible in all of our patients. The use of a suprapubic puncture of the bladder provides an alternative route for antegrade catheterization, should it be necessary [18]. It also minimizes the risk of infection inherent in repeated retrograde cystourethrograms [22].

ACKNOWLEDGMENTS

We thank Pia Juhl and Beerith Bruhn for typing the manuscript and Jytte Lauritzen and Helle Bardrum for photographic assistance.

REFERENCES

1. Desmond AD, Evans CM, Jameson RM, Woolfenden KA, Gibbon NOK. Critical evaluation of direct vision urethrotomy by urine flow measurement. *Br J Urol* **1981**;53:630–633
2. Godwin RJ. Urethral stone formation following urethroplasty. *Br J Radiol* **1977**;50:113–115
3. Hansen RI, Guldberg O, Møller I. Internal urethrotomy with the Sachse urethrotome. *Scand J Urol Nephrol* **1981**;15:189–191
4. Hjortrup A, Sørensen C, Sanders S, Moesgaard F, Kirkegaard P. Strictures of the male urethra treated by the Otis method. *J Urol* **1983**;130:903–904
5. Holm-Nielsen A, Schultz A, Møller-Pedersen V. Direct vision internal urethrotomy. A critical review of 365 operations. *Br J Urol* **1984**;56:308–312
6. Lipsky H, Hubmer G. Direct vision urethrotomy in the management of urethral strictures. *Br J Urol* **1977**;49:725–728
7. Russinovitch NAE, Lloyd LK, Griggs WP, Jander HP. Balloon dilatation of urethral strictures. *Urol Radiol* **1980**;2:33–37
8. Sachse H. Zur Behandlung der Harnröhrstriktur: die transurethrale Schlitzung unter Sicht mit scharfern Schnitt. *Fortschr Med* **1974**;92:12–15
9. Schmiedt E. Ergebnisse der operativen Harnröhre Chirurgie. *Munch Med Wochenschr* **1973**;115:33–36
10. Grüntzig A. Die perkutane Rekanalisation chronischer arterieller Verschlüsse (Dotter-Prinzip) mit einem neuen doppellumigen Dilatationskatheter. *ROFO* **1976**;124:80–86
11. Dotter CT. Transluminal angioplasty: a long view. *Radiology* **1980**; 135:561–564
12. Burhenne HJ, Morris DC. Biliary stricture dilatation: use of Grüntzig balloon catheter. *J Can Assoc Radiol* **1980**;31:196–197
13. Centola CAP, Jander HP, Russinovich NAE. Balloon dilatation of the papilla of Vater to allow biliary stone passage. *AJR* **1981**;136:613–614
14. Hegedüs V, Ejby Poulsen P. Balloon dilatation of alimentary tract strictures. *Acta Radiol [Diagn]* (Stockh) **1986**;27:681–686
15. Owman T, Lunderquist A. Balloon catheter dilatation of esophageal strictures—a preliminary report. *Gastrointest Radiol* **1982**;7:301–305
16. Renfrew DL, Smith WL, Pringle KC. Per anal balloon dilatation of a post-necrotising enterocolitis stricture of the sigmoid colon. *Pediatr Radiol* **1986**;16:320–321
17. Banner MP, Pollick HM, Ring EJ, Wein AJ. Catheter dilatation of benign ureteral strictures. *Radiology* **1983**;147:427–433
18. Hare WSC, McOmish D, Nunn IN. Percutaneous transvesical antegrade passage of urethral strictures. *Urol Radiol* **1981**;3:107–112
19. Burhenne HJ, Chisholm RJ, Quenville NF. Prostatic hyperplasia: radiological intervention. *Radiology* **1984**;152:655–657
20. Quinn SF, Dyer R, Smathers R, Glass T, Wright E, Roberts C, Burke J, Argenbright J. Balloon dilatation of the prostatic urethra. *Radiology* **1985**;157:57–58
21. Bryndorf J, Rostgaard-Christensen E, Sandø E. Suprapubic micturition cystography with constant filling in children. *Acta Radiol [Diagn]* (Stockh) **1960**;54:204–208
22. Glynn B, Cordon IRS. The risk of infection of the urinary tract as a result of micturating cystourethrography in children. *Ann Radiol* (Paris) **1970**; 13:283

Meniscal and Ganglion Cysts of the Knee: MR Evaluation

D. Lawrence Burk, Jr.[1,2]
Murray K. Dalinka[1]
Emanuel Kanal[3]
Mark L. Schiebler[1,4]
Eve K. Cohen[1,5]
Richard J. Prorok[3]
Warren B. Gefter[1]
Herbert Y. Kressel[1]

Meniscal and ganglion cysts frequently present as palpable masses of the knee but occur at different locations than do popliteal cysts. Meniscal cysts also may be discovered incidentally on studies performed for suspected internal derangement. Sixteen cystic lesions of the knee were evaluated with MR, including 11 meniscal cysts and five ganglion cysts. Scans were performed at 1.5 T by using a transmit/receive extremity coil or a receive-only surface coil. Standard spin-echo imaging, including at least one long-TR/asymmetric-TE sequence, was performed in all cases. In six patients, gradient-echo, reduced flip-angle sequences also were done. All meniscal cysts (but none of the ganglion cysts) were associated with horizontal meniscal tears. Cysts were visualized best on the long-TR/TE images; meniscal tears were seen best on the short-TR/TE and long-TR/short-TE images. Meniscal tears and cysts were also seen well on the fast-scanning sequences. Septations were noted in four meniscal cysts and in four ganglion cysts on the long-TR/TE images. Long-TR/TE images were also useful in showing the relationship between the cyst and joint capsule in three of the ganglion cysts.

MR imaging is an effective, noninvasive method for evaluating cystic lesions of the knee. Meniscal cysts are always associated with underlying horizontal meniscal tears, which can be detected with MR. Ganglion cysts are not associated with meniscal tears, but may have connections to the joint capsule, which can be detected with MR.

Cystic lesions around the knee are a common clinical problem that can be evaluated with a variety of radiographic techniques, including arthrography, sonography, and CT [1, 2]. Popliteal cysts are the most common lesions and characteristically are located at the posterior medial aspect of the knee joint adjacent to the intersection of the medial head of the gastrocnemius muscle and at the distal insertion of the semimembranosus muscle. Popliteal cysts are frequent findings on studies performed for internal derangement of the knee and are easily recognized on MR. Cystic lesions in other locations around the knee are less common and usually represent ganglion or meniscal cysts, although enlarged bursae and synovial herniations can also be encountered. Meniscal cysts characteristically are located at the joint line on the medial or lateral side of the knee and invariably are associated with an underlying horizontal meniscal tear [3]. Ganglion cysts may or may not have a definable connection to the joint and may occur in atypical locations attached to tendon sheaths, within muscle bundles, or adjacent to the tibiofibular joint [4]. The ability of MR to visualize internal derangements of the knee [5] and abnormalities of the surrounding soft tissues [6] makes this technique ideally suited to the evaluation of these cystic lesions.

In this report, we review our experience with MR of meniscal and ganglion cysts to describe their appearance and the features that may be useful in differential diagnosis. The relative value of spin-echo (SE) T1- and T2-weighted sequences are described as well as the use of two different gradient-echo fast-scanning sequences, GRASS (gradient refocused acquisition in the steady state) [7] and PSI (partial saturation interleave) [8].

Received August 3, 1987; accepted after revision September 30, 1987.

[1] Department of Radiology, Hospital of the University of Pennsylvania, Philadelphia, PA 19104.

[2] Present address: Department of Radiology, Thomas Jefferson University Hospital, 1033 Main Bldg., Philadelphia, PA 19107. Address reprint requests to D. L. Burk.

[3] Pittsburgh NMR Institute, Pittsburgh, PA 15213.

[4] Department of Radiology, University of North Carolina, Chapel Hill, NC 27514.

[5] Department of Radiology, The Hospital for Sick Children, Toronto, Ontario M5G 1X8, Canada.

AJR 150:331–336, February 1988
0361–803X/88/1502–0331
© American Roentgen Ray Society

Materials and Methods

Sixteen cystic lesions of the knee were examined with a 1.5-T Signa scanner (General Electric, Milwaukee, WI). A transmit/receive dedicated extremity coil was used in 11 patients, and planar receive-only surface coils were used in the other five patients. SE sequences were performed in at least two different planes in all cases. Sagittal images were obtained in 13 cases, coronal images in 14 cases, and axial images in five cases. Short-TR/TE sequences (600–800/20–25 msec) were used primarily as localizers. At least one long-TR/asymmetric-TE sequence (2000–2500/20 and 80 msec) was obtained in each case. GRASS sequences were obtained in four cases with a TR of 22 msec, a TE of 12 msec, and a flip angle of 30°. PSI sequences were performed in two cases with a TR of 750 msec, a TE of 30 msec, and a flip angle of 20°. The GRASS images were obtained in sequential single-slice acquisitions, and the PSI images were obtained in interleaved multislice acquisitions. Other parameters included a 5-mm slice thickness with 1-mm interslice gaps and 128 × 256 acquisition matrix. The field of view for the spin-echo and PSI sequences varied from 12 to 16 cm. The fields of view for the GRASS sequences were 22.5 cm because of gradient limitations. One or two excitations were used routinely, with one excitation resulting in decreased imaging time and a decreased signal-to-noise ratio.

Fast-scanning sequences were compared with spin-echo sequences obtained in the same plane. The lesions were evaluated for the presence of septations, joint connections, and associated intra-articular disease. Meniscal tears were defined as linear areas of high signal intensity that involved at least one meniscal surface. Surgical correlation was available in 12 cases. Two patients elected to postpone surgery; in two other cases, the cyst ruptured spontaneously, and no surgery was performed. CT scans were available for comparison in two cases. Arthrograms were performed in two patients. No sonograms were performed.

Results

There were 11 meniscal and five ganglion cysts. All five of the ganglion cysts presented as palpable masses. Five meniscal cysts were incidental findings on studies performed for internal derangements, and six presented as palpable masses. Cysts were isointense or hypointense to muscle on short-TR/TE sequences. On the long-TR/short-TE images, all cysts were isointense or slightly hyperintense to muscle. All cysts had high signal intensity on long-TR/TE, PSI, and GRASS sequences and were well circumscribed with smooth walls. Septations were noted on T2-weighted images in four of five ganglion cysts and in four of 11 meniscal cysts. In the two patients with CT scans, the cystic lesions were of low attenuation. Septations in one cyst were identified on the MR image but not on the CT scan.

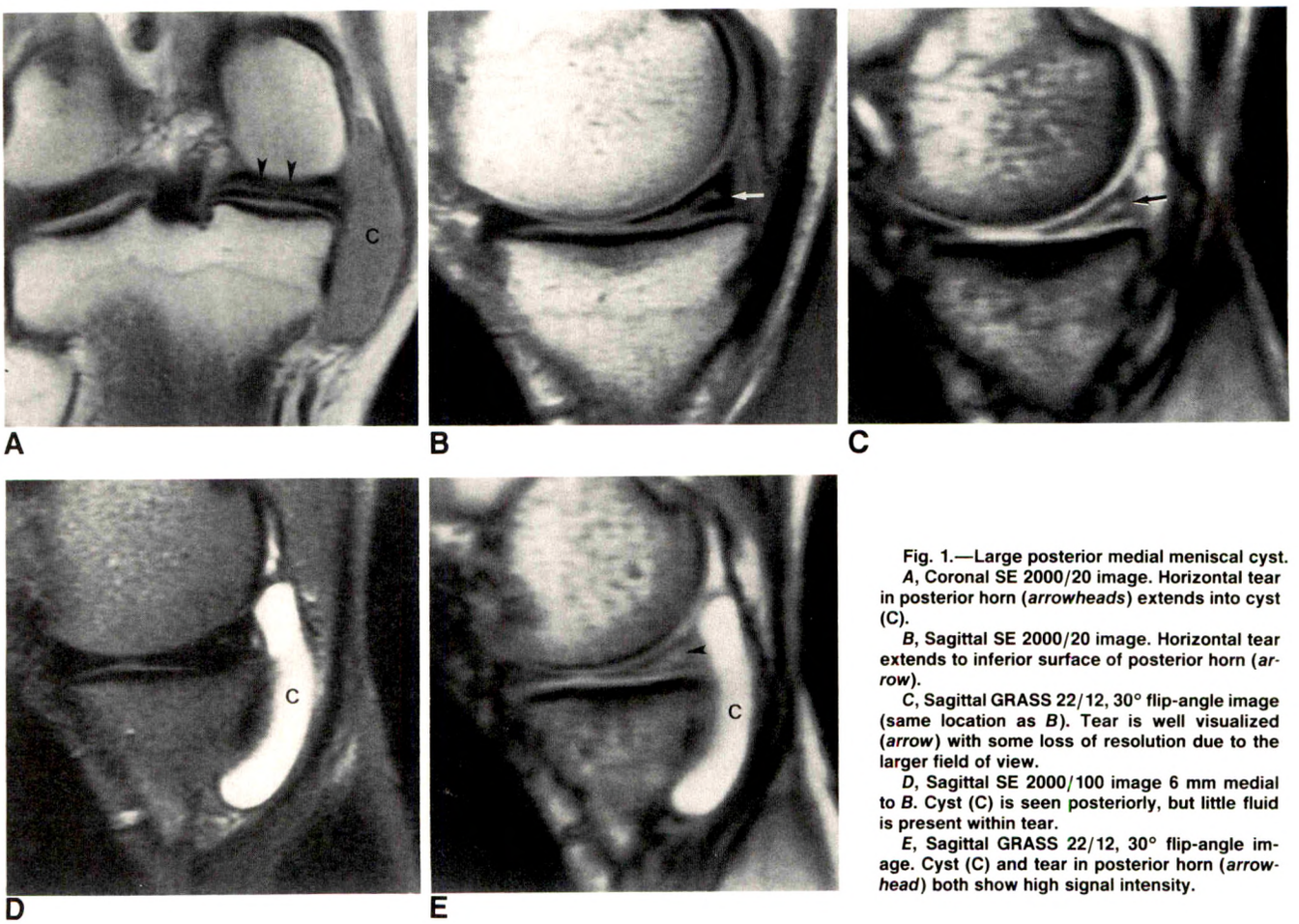

Fig. 1.—Large posterior medial meniscal cyst.
***A*, Coronal SE 2000/20 image. Horizontal tear in posterior horn (*arrowheads*) extends into cyst (C).**
***B*, Sagittal SE 2000/20 image. Horizontal tear extends to inferior surface of posterior horn (*arrow*).**
***C*, Sagittal GRASS 22/12, 30° flip-angle image (same location as *B*). Tear is well visualized (*arrow*) with some loss of resolution due to the larger field of view.**
***D*, Sagittal SE 2000/100 image 6 mm medial to *B*. Cyst (C) is seen posteriorly, but little fluid is present within tear.**
***E*, Sagittal GRASS 22/12, 30° flip-angle image. Cyst (C) and tear in posterior horn (*arrowhead*) both show high signal intensity.**

All 11 meniscal cysts were associated with horizontal or complex meniscal tears extending into the cyst. Arthroscopic confirmation of the tears was available in eight patients. The tears were best visualized on short-TR/TE and long-TR/short-TE images (Fig. 1). The meniscal tears showed high signal intensity equivalent to the cyst on GRASS and PSI images (Fig. 2). In six cases, enough fluid was present within the tears to yield detectable high signal intensity on long-TR/TE images (Fig. 3). There were seven posterior medial cysts, two anterior medial cysts, and two lateral cysts. One of the lateral cysts was associated with a discoid meniscus. The six palpable cysts measured from 2 to 6 cm in diameter. The five incidental cysts measured from 0.5 to 2 cm in diameter. An open surgical biopsy was performed on one of the cysts. In this patient, the relationship of the cyst to the underlying meniscal tear was not seen on the MR study by the operating surgeon. The communication with the joint was discovered during the surgery.

No meniscal tears were detected in the five patients with ganglion cysts. In four patients, the MR findings were confirmed at surgical resection, and the cysts were found to be filled with a viscous, gelatinous material. In one patient, a cyst located superficial to the lateral joint capsule spontaneously ruptured and no surgery was performed. Two patients had intramuscular cysts. One was located in the vastus lateralis muscle and one in the semimembranosus muscle. These cysts were dissected easily from within the muscles at surgery. No definite relationship to the knee joint could be visualized on MR for either of these two lesions. In one of these patients, no connection was shown at arthrography or

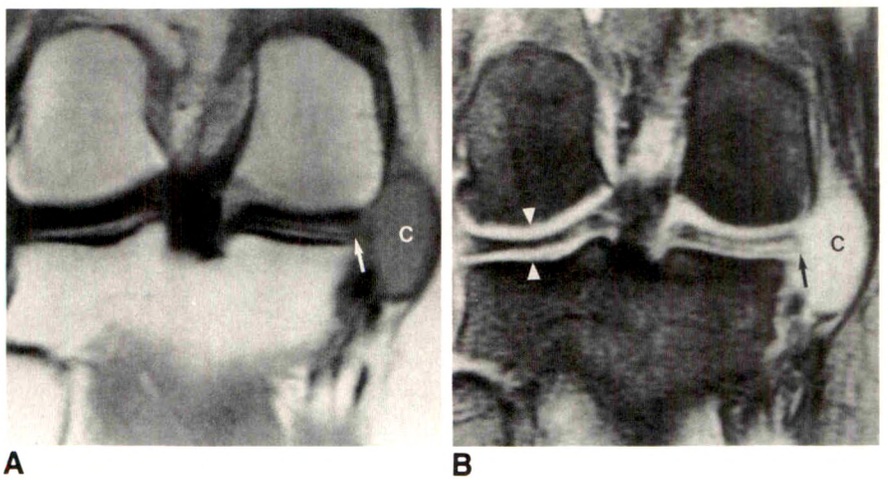

Fig. 2.—Posterior medial meniscal cyst.
***A*, Coronal SE 2000/20 image. Horizontal tear is seen in posterior horn (*arrow*), and cyst (C) has a homogeneous appearance.**
***B*, Coronal GRASS 22/12, 30° flip-angle image. Both tear (*arrow*) and cyst (C) are well visualized with high signal intensity. Hyaline cartilage also has a high signal intensity (*arrowheads*).**

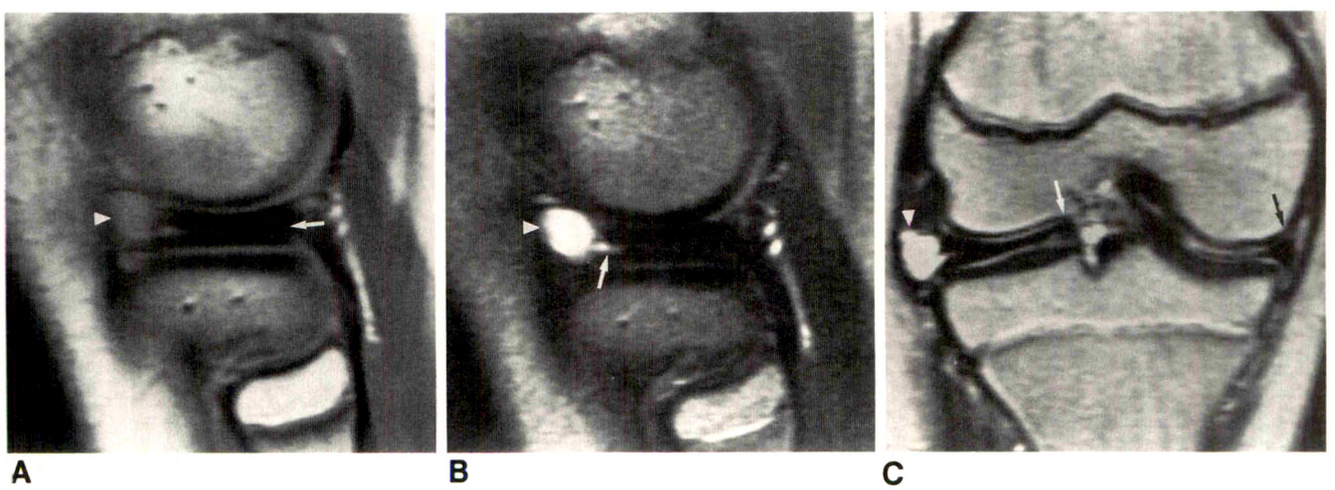

Fig. 3.—Discoid lateral meniscus with horizontal tear and meniscal cyst.
***A*, Sagittal SE 2500/20 image. Horizontal tear extends through entire meniscus (*arrow*), and small cyst is seen anteriorly (*arrowhead*).**
***B*, Sagittal SE 2500/80 image. Fluid within anterior aspect of tear (*arrow*) can be seen extending directly into cyst (*arrowhead*).**
***C*, Coronal SE 2500/80 image. Cyst can be seen deep to lateral capsule (*arrowhead*). Normal medial meniscus (*black arrow*) is much smaller than enlarged lateral meniscus, which extends to intercondylar notch (*white arrow*), covering entire weight-bearing surface of lateral compartment.**

surgery. In the other patient, a fibrous band connecting the cyst to the suprapatellar pouch was noted at surgery but was not detected on MR.

In the other three patients, fluid-filled extensions of the cysts adjacent to the joint capsule could be identified on long-TR/TE images. In one patient with a tibiofibular cyst, who presented with a peroneal nerve palsy, a long connection to the joint capsule was seen (Fig. 4). This relationship was not seen on CT scan or arthrography with delayed films. The connection to the joint capsule could not be visualized definitely at the time of surgery. In another patient with a suprapatellar cyst, the presence of a joint effusion that outlined the suprapatellar pouch was useful in showing the close relationship of the cyst to the joint (Fig. 5). This finding was confirmed at surgery.

Discussion

Meniscal and ganglion cysts of the knee usually present in locations atypical for simple popliteal cysts. Before surgery, it is important to confirm the cystic nature of these lesions, to determine their relationship to the joint, and to evaluate the joint for the presence of associated intraarticular disease. Sonography, CT, and arthrography have been used in the evaluation of cystic lesions of the knee, but each technique has specific limitations. Sonography is excellent for detecting fluid-filled structures but has limited ability to evaluate the relationship of cysts to intraarticular structures. CT can show cysts as well as intraarticular disease [9], but it has limited contrast resolution and may not detect small horizontal meniscal tears [10]. Arthrography can detect cysts that communicate with the joint, but it is a semiinvasive technique and offers little information about noncommunicating cysts [11].

The value of MR in the diagnosis of soft-tissue lesions [12] and knee disease [13] has been well documented. MR is particularly well suited to the evaluation of these cystic lesions of the knee because it can obtain direct multiplanar images with excellent soft-tissue contrast and because it can detect meniscal tears noninvasively without the use of ionizing radiation. These cysts have characteristic appearances on MR that depend on the pulsing sequences used to control image contrast and pathoanatomic considerations specific to the particular lesion.

Pulsing Sequences

Cystic lesions on MR have markedly increased signal intensity on long-TR/TE images and are well circumscribed with

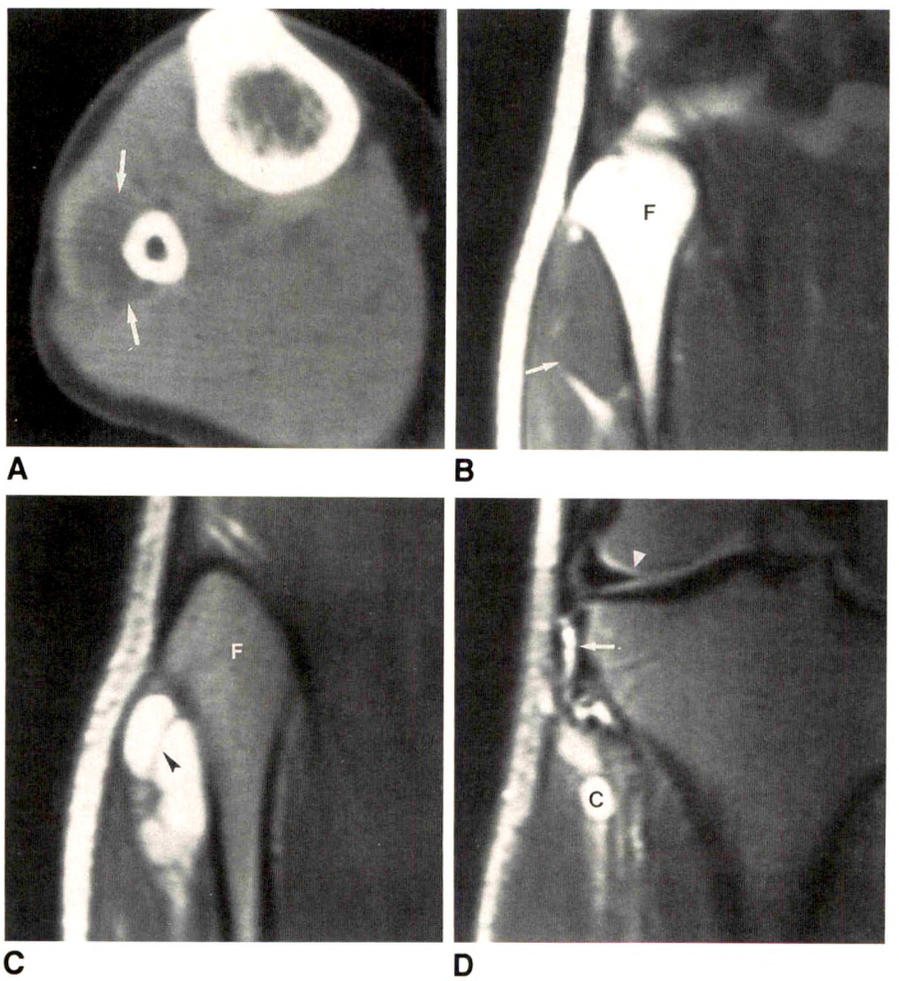

Fig. 4.—Ganglion cyst adjacent to proximal tibiofibular joint, causing peroneal nerve palsy.

***A*, CT scan shows low-attenuation mass lateral to proximal fibula (*arrows*).**

***B*, Coronal SE 600/25 image. Isointense mass (*arrow*) poorly visualized lateral to proximal fibula (F).**

***C*, Coronal SE 2000/50 image. Excellent visualization of well-circumscribed mass with internal septations (*arrowhead*), suggesting diagnosis of a cyst.**

***D*, Coronal SE 2000/75 image. High-signal-intensity connection (*arrow*) visualized between lateral joint capsule and anterior aspect of cyst (C). Normal lateral meniscus (*arrowhead*).**

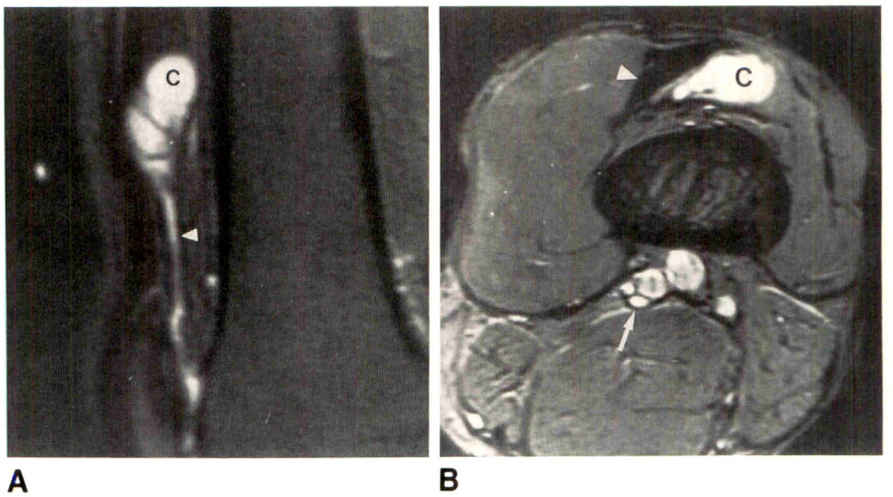

Fig. 5.—Suprapatellar ganglion cyst.
***A*, Sagittal SE 2500/80 image. Small effusion in suprapatellar pouch (*arrowhead*) shows close relationship of septated cyst (C) to joint space.**
***B*, Axial partial saturation interleave 750/30 20° flip-angle image. High-signal-intensity cyst (C) is well visualized posterior lateral to quadriceps tendon (*arrowhead*). Flow enhancement is seen incidentally in popliteal vessels (*arrow*).**

smooth walls. Most meniscal cysts and ganglion cysts are filled with a gelatinous substance and have a high protein concentration. An increase in protein concentration results in relative T1 shortening due to acceleration of relaxation rates of water molecules bound to proteins [14]. This T1-shortening effect accounts for the frequent isointensity of these cystic lesions with surrounding muscle on short-TR/TE sequences. For this reason, meniscal and ganglion cysts may be detected on T1-weighted images only when a visible mass effect on surrounding structures is present. Short-TR/TE images are useful as rapid localizing sequences and in the detection of meniscal tears. The cysts can be seen better on long-TR/short-TE images, which have mixed contrast based on contributions from T1, T2, and proton spin density. Meniscal tears are also seen well on these images. Long-TR/TE images are best for seeing cysts and are also useful for detecting subtle connections to the joint or septations that may not be detectable in other images.

New fast-scanning sequences such as GRASS and PSI offer many of the advantages of long-TR sequences with shorter examination times [15]. Fluid in cysts and meniscal tears can be seen with high signal intensity because of high proton-density and long-T2* values. Relative T2* weighting can be accomplished by using a variety of techniques, but a complete discussion of contrast relationships in fast scanning is beyond the scope of this article. The GRASS and PSI sequences used in the present study provide excellent visualization of cysts and meniscal tears, comparable with that obtained with SE sequences. For comprehensive knee examinations, however, there is limited experience with the use of these fast-scanning techniques in the evaluation of ligamentous, bone marrow, and hyaline cartilage abnormalities [16, 17], and conventional SE techniques remain the gold standard.

Meniscal Cysts

Meniscal cysts are invariably associated with horizontal meniscal tears [18]. Several etiologic theories have been proposed for the development of these cysts, but the dominant theory suggests that synovial fluid is forced out through the underlying tear and accumulates at the meniscocapsular margin to form a cyst [19]. Recurrence of the cysts is common after surgical treatment unless the meniscal tear is addressed [20]. MR demonstration of a tear extending into a meniscal cyst at the joint margin corresponds to the arthrographic visualization of contrast material extending into a club-shaped dilatation at the periphery of a meniscal tear [3]. Complete filling of a large cyst usually does not occur on arthrography because of the gelatinous nature of the cyst fluid.

The largest cysts in this series were located posterior medially, which is consistent with the findings of Smillie [21]. Cysts located posterior to the medial collateral ligament are more apt to penetrate the capsule and expand in an unrestricted fashion. Large cysts of this type may be misdiagnosed clinically as popliteal cysts. On the lateral side, cysts are more likely to be contained within the joint capsule, filling a potential space adjacent to the mid portion of the meniscus between the lateral collateral ligament and the iliotibial band. Meniscal cysts reportedly involve the lateral meniscus more frequently than the medial meniscus, which is the opposite of the findings in the present series. The present small series might be biased by the fact that referring clinicians are more likely to use MR to evaluate patients with large unusual medial cysts, whereas those with the more common small lateral cysts may be sent directly to arthroscopy for treatment of a suspected underlying meniscal tear.

Ganglion Cysts

Ganglion cysts may resemble meniscal cysts in that they present as a mass near the joint, but they are not associated with meniscal tears [22]. These lesions contain a jellylike viscous fluid similar to the material found within meniscal cysts, first described by Hippocrates [23] as having the appearance of "mucoid flesh." Multiple components of ganglia have been described, including a main cyst that may be lobulated and irregular, pseudopodia that extend from the main cyst along fascial planes, and small capsular cysts that communicate with the main cyst and are found within the

substance of the capsule or within the sheath of a tendon [4]. In our cases, no joint communications were identified in the two patients who underwent arthrography, but possible connections to the joint capsule were suggested on MR in three patients. Of course, the lack of dynamic evaluation of the joint spaces on MR does not allow one to see actual movement of fluid from one compartment to the other. Visualization of fluid extensions from the ganglion cysts to the joint capsule may represent visualization of the capsular components of the cyst. Demonstration of the relationship of the cyst to the capsule may be important in differentiating ganglia from other lesions and also in planning surgery, as failure to remove the capsular components of these cysts may lead to recurrence [4].

Ganglion cysts occur in variable locations around the knee, as shown by our five cases. A diagnosis of this benign condition should be considered, even when the mass is located within a muscle bundle. In both cases of intramuscular ganglion, the diagnosis was suggested before surgery by the well-circumscribed, homogeneous appearance on MR. The presence of septations in one of the intramuscular ganglia was considered to be evidence of the cystic nature of the lesion. The tibiofibular cyst and suprapatellar cyst could be distinguished from other lesions by their characteristic anatomic locations and also by the presence of septations. A neural tumor was considered a likely diagnosis in the patient with the tibiofibular cyst who presented with a peroneal nerve palsy, but a cyst was thought to be more likely after the MR examination was done. Nerve compression by a ganglion cyst in this region has been described previously by Sutro [24]. In the suprapatellar cyst, the location adjacent to the suprapatellar pouch was useful in suggesting the appropriate diagnosis. DeSmet and Neff [25] described three cysts in this location that failed to communicate with the joint at arthrography but that were readily diagnosed with CT.

Conclusion

Meniscal and ganglion cysts usually present clinically as palpable masses in locations around the knee that are atypical for popliteal cysts. Meniscal cysts also may be discovered incidentally on studies performed for suspected internal derangement. MR can distinguish between these two types of cystic lesions and can provide valuable information before surgery regarding associated meniscal tears and the relationship of the cysts to the joint. Long-TR/asymmetric-TE, GRASS, or PSI images provide excellent soft-tissue contrast and are valuable in visualizing these lesions.

REFERENCES

1. Hermann G, Yeh H-C, Lehr-Janus C, Berson BL. Diagnosis of popliteal cyst: double-contrast arthrography and sonography. *AJR* **1981**;137: 369–372
2. Lee KR, Cox GG, Neff JR, Arnett GR, Murphey MD. Cystic masses of the knee: arthrographic and CT evaluation. *AJR* **1987**;148:329–334
3. Schuldt DR, Wolfe RD. Clinical and arthrographic findings in meniscal cysts. *Radiology* **1980**;134:49–52
4. McEvedy BV. Simple ganglia. *Br J Surg* **1962**;218:585–594
5. Burk DL Jr, Kanal E, Brunberg JA, Johnstone GF, Swensen HE, Wolf GL. 1.5-T surface coil MRI of the knee. *AJR* **1986**;147:293–300
6. Sundaram M, McGuire MH, Fletcher J, Wolverson MK, Heiberg E, Shields JB. Magnetic resonance imaging of lesions of synovial origin. *Skeletal Radiol* **1986**;15:110–116
7. Wehrli F, Prost JH, Roberts F. The distinguishing properties of gradient-recalled acquisition in the steady state (GRASS). Presented at the annual meeting of the Society for Magnetic Resonance Imaging, San Antonio, TX, February **1987**
8. Campagna NF, Wehrli FW. High-speed imaging with slice-interleaved gradient recalled acquisition. Presented at the annual meeting of the Society for Magnetic Resonance Imaging, San Antonio, TX, February **1987**
9. Manco LG, Lozman J, Coleman ND, Kavanaugh JH, Bilfield BS, Dougherty J. Noninvasive evaluation of knee meniscal tears: preliminary comparison of MR imaging and CT. *Radiology* **1987**;163:727–730
10. Passariello R, Masciocchi C, Zobel BB, DePaulis F, Trecco F. Computed tomography of meniscal cysts of the knee joint. *Eur J Radiol* **1987**;7: 83–86
11. Schwimmer M, Edelstein G, Heiken JP, Gilula LA. Synovial cysts of the knee: CT evaluation. *Radiology* **1985**;154:175–177
12. Totty WG, Murphy WA, Lee JKT. Soft-tissue tumors: MR imaging. *Radiology* **1986**;160:135–141
13. Hartzman S, Reicher MA, Bassett LW, Duckwiler GR, Mandelbaum B, Gold RH. MR imaging of the knee. Part II. Chronic disorders. *Radiology* **1987**;162:553–557
14. Koenig SH, Brown RD. The importance of the motion of water for magnetic resonance imaging. *Invest Radiol* **1985**;20:297–304
15. Wehrli FW. Introduction to fast-scan magnetic resonance. Milwaukee, WI: General Electric Company, **1986**
16. Tyrrell R, Glucker K. Fast 3D imaging of the knee: a comparison with arthroscopy. Presented at the annual meeting of the Society for Magnetic Resonance Imaging, San Antonio, TX, February **1987**
17. Burk DL Jr, Schiebler M, Cohen E, et al. 1.5T multislice interleaved gradient echo MRI of the knee. Presented at the annual meeting of the Society of Magnetic Resonance in Medicine, New York, August **1987**
18. Ferrer-Roca O, Vilalta C. Lesions of the meniscus. Part II. Horizontal cleavages and lateral cysts. *Clin Orthop* **1980**;146:301–307
19. Barrie HJ. The pathogenesis and significance of meniscal cysts. *J Bone Joint Surg [Br]* **1979**;61-B:184–189
20. Becton JL, Young HH. Cysts of semilunar cartilage of the knee. *Arch Surg* **1965**;90:708–712
21. Smillie IS. *Injuries of the knee joint*, 4th ed. Baltimore: Williams & Wilkins, **1971**:94–98
22. Carp L, Stout AP. A study of ganglion. *Surg Gynecol Obstet* **1928**;47: 460–468
23. Hippocrates. In: Withington ET, trans. *Hippocrates; on joints*. London: Heinemann, **1927**; vol. iii: 277
24. Sutro CT. Intraneural ganglion of the common peroneal nerve. *Bull Hosp Joint Dis* **1960**;21:330–331
25. DeSmet AA, Neff JR. Knee arthrography for the preoperative evaluation of juxta-articular masses. *Radiology* **1982**;143:663–666

Knee Ligament Reconstruction:
Plain Film Analysis

B. J. Manaster[1]
Kent Remley[1]
Alan P. Newman[2]
Fred A. Mann[1]

New concepts in knee ligament reconstruction have recently emerged, significantly improving the success of surgical reconstruction of anterior and posterior cruciate ligaments, using high-strength bone–patellar tendon–bone grafts, as well as medial and lateral collateral soft-tissue ligament reconstructions. We reviewed plain radiographs of 50 patients with a total of 72 ligament reconstructions to determine radiographic signs of complications. A major early complication relates to reconstructed ligament positioning. Isometric positioning of the reconstruction is important for all ligaments, but it is most crucial for the femoral portion of the anterior cruciate ligament. Three cases of nonisometric ligament positioning were identified, two anterior cruciate ligaments and one medial collateral ligament. Another early complication is graft fracture, identified in two cases of anterior cruciate ligament reconstruction. Hardware failure did not occur in this series. Late complications include motion of the graft (none in this series) and patellar fracture (one case in this series). Effusions resolved by 4 weeks in 92% of the cases. However, prolonged effusions are usually sterile and should not be mistakenly diagnosed as representing a septic joint if they are an isolated finding. Nonunion of the graft within its osseous tunnel is unusual. Union occurred in 79% of cases by 6 weeks and in 95% of cases by 5 months. Osseous tunnel sclerosis alone is not considered a complication.

We conclude that postoperative plain film radiography is important for assessment of graft and hardware position as well as for the detection of early and late surgical complications.

Ligamentous injuries of the knee continue to be a common occurrence in our increasingly active society. Historically, reconstruction of these ligaments was performed by using only soft tissue, a procedure that required prolonged immobilization of the knee. Radiographic analysis played little or no role in following these repairs because most complications could not be detected on plain films. New surgical concepts for cruciate ligament reconstruction [1] use a higher strength patellar tendon graft, rigidly anchored in the femur and tibia by bone plugs harvested with the patellar tendon graft. This high-strength, rigidly fixed reconstruction allows early mobilization, which requires early and frequent plain films to ensure proper positioning of hardware or the easily visualized graft bone plugs to evaluate possible complications and/or failure. Therefore, the radiologist should be familiar with the normal postoperative appearance of the reconstructed knee as well as with the common complications, so that any deleterious effect of early motion can be detected.

The present study is designed to identify major complications of knee ligament reconstruction that can be detected by plain radiographs. In addition to discussing obvious complications, we identify radiographic features that indicate proper placement of the grafts or hardware in anterior cruciate, posterior cruciate, medial collateral, and lateral collateral ligament reconstructions, because improper graft placement is itself a complication of the surgical procedure. Finally, the natural history of graft incorporation is discussed.

Received July 13, 1987; accepted after revision October 7, 1987.

[1] Department of Radiology, University of Utah School of Medicine, 1A95 Medical Center, Salt Lake City, UT 84132. Address reprint requests to B. J. Manaster.

[2] Department of Orthopedic Surgery, University of Utah School of Medicine, Salt Lake City, UT 84132.

AJR **150:337–342, February 1988**
0361–803X/88/1502–0337
© American Roentgen Ray Society

Subjects and Methods

Two of the authors retrospectively reviewed the plain films of 50 consecutive patients who underwent ligamentous reconstruction of the knee by a specific orthopedic surgeon between 1983 and 1986. The patients (32 men, 18 women) ranged in age from 15 to 38 years. Seventy-two ligament reconstructions were evaluated in these 50 patients: 45 anterior cruciate and eight posterior cruciate ligament reconstructions, and 16 medial collateral ligament and three lateral collateral ligament reconstructions. Plain films of the involved knee were obtained immediately after surgery. Routine projections in patients who underwent reconstruction of the anterior cruciate ligament or posterior cruciate ligament included anteroposterior, lateral, and tunnel (notch) projections. Only anteroposterior and lateral films were obtained for medial or lateral collateral ligament reconstructions. These initial studies were evaluated for graft position (isometric attachment), hardware position, and immediate complications.

After evaluation of ligament-reconstruction position and any immediate complications, evidence of late complications was sought. Sequential comparison studies were routinely obtained at 2 weeks, 6–8 weeks, and 4–6 months. Of the 53 anterior and posterior cruciate ligament reconstructions performed, 44 were followed for at least 6 weeks after surgery, with a mean follow-up of 5.8 months. These follow-up studies were evaluated for bone density, resolution of knee effusion, late complications, and graft failure. The bony portions of the patellar tendon grafts were scrutinized closely for incorporation, change in position, and fracture. Conventional tomography was used in selected cases for further evaluation of suspected abnormalities.

Normal Postoperative Radiographic Appearance

Of the 44 anterior and posterior cruciate ligament reconstructions with adequate follow-up in this study, 42 involved the newer technique of high-strength patellar tendon graft. This reconstruction uses one-third of the patellar tendon, which is harvested with a wedge of bone from both its patellar and tibial insertions to form a bone–patellar tendon–bone composite. The bone plugs harvested with the graft are placed within osseous tunnels drilled in the distal femur and proximal tibia (Fig. 1). The plugs are rigidly fixed. The hardware may be either an interference screw serving to press the bone plug against the side of the drill hole or a staple securing soft tissue attached to the bone plug [2]. The interference screw is placed *beside* the bone graft, and the screws or staples themselves do not represent the site to be evaluated in either anterior or posterior cruciate reconstructions.

Isometry is an important biomechanical principle in knee ligament reconstruction. Isometric points are those points of ligament attachment on the femur and tibia that allow the ligament to maintain a constant length during flexion and extension of the knee [3, 4]. Isometric points may be defined on radiographs (Fig. 2), and placement of grafts or hardware may be assessed for isometry.

The site of interest in the cruciate reconstructions is the opening of the osseous tunnels at the articular surface of the knee. The bone plug portion of the graft may or may not be located at this site, depending on the length of the patellar tendon portion of the graft and the length needed for the reconstruction.

The anterior cruciate ligament extends from the intercondylar eminence of the tibia to the lateral femoral condyle. In general, ligament isometry is dependent on the relative positions of both attachment points. However, for the anterior cruciate ligament (and most knee ligaments), isometry is less sensitive to the site of tibial attachment than to the femoral site. The osseous tunnel through the tibia should generally exit in the region of the anatomic anterior cruciate attachment. Thus, on a lateral film, the tibial osseous tunnel begins distally and anteriorly at the tibial tubercle and courses posteriorly to exit the tibial articular surface immediately anterior to the anterior tibial spine (Fig. 1B). On the anteroposterior or notch views, the tibial osseous tunnel begins on the medial side distally and courses laterally to emerge centrally at the intercondylar eminence on the tibial plateau (Fig. 1A).

If we assume a central (or anatomic) tibial attachment, the isometric point on the lateral femoral condyle for the anterior cruciate ligament lies in close relationship to the anatomic attachment site (Fig. 2) [3–6]. This point can be visualized radiographically on a lateral projection as the intersection of two lines representing the posterior femoral cortex and the intercondylar shelf (Fig. 1B). On the anteroposterior or notch film, the femoral osseous tunnel begins laterally just superior to the lateral femoral condyle and emerges on the superolateral aspect of the intercondylar notch.

The posterior cruciate ligament originates from the posterior aspect

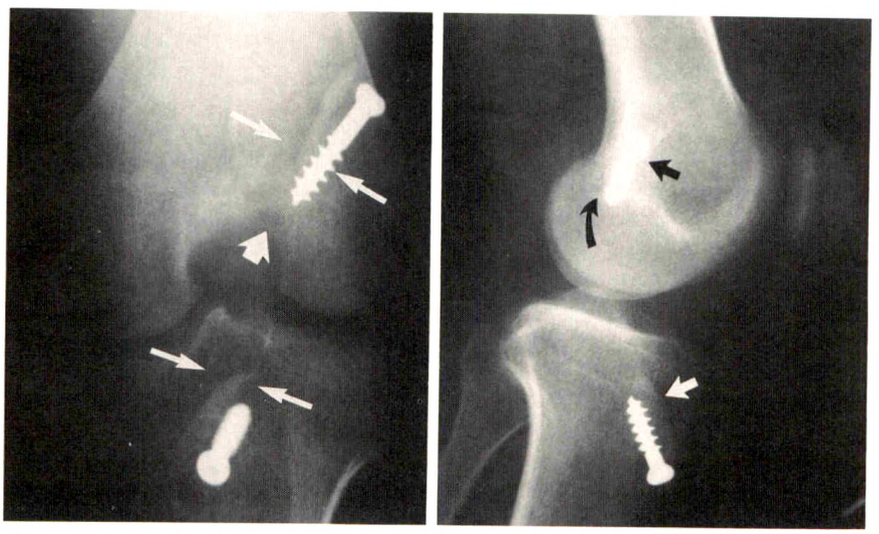

A B

Fig. 1.—Anterior cruciate ligament reconstruction.

***A*, Notch view. Bone plugs are seen within osseous tunnels (*long arrows*), and tunnels emerge on articular surface at isometric sites. Interference screws are located within tunnels and press bone plugs against wall. Also apparent is loss of cortical density on medial wall of lateral femoral condyle (*short arrow*); this surgical widening is called a notch-plasty and serves to improve exposure and avoid impingement of graft within notch.**

***B*, Lateral view shows bone plugs (*straight arrows*) and osseous tunnels to be in normal isometric position (*curved arrow* shows crucial femoral isometric point, at junction of two lines representing posterior femoral cortex and intercondylar shelf).**

of the tibia below the joint line and attaches superiorly to the posterior aspect of the lateral side of the medial femoral condyle. Although the femoral isometric point has not been studied as well, one report suggests that the femoral isometric point occurs at the anterior portion of this femoral attachment site [7]. This location is visualized radiographically as being nearly at the center of the femoral condyle along the line representing the intercondylar shelf on the lateral film (Fig. 2B). Thus, on a lateral film, the femoral osseous tunnel in a posterior cruciate repair courses from an anterior position at its proximal aspect posteriorly to the isometric point as described previously (Fig. 3B). On the anteroposterior film, the proximal aspect of the femoral osseous tunnel is at the medial aspect of the medial femoral condyle and courses distally to enter the intercondylar notch at its junction with the articular surface of the medial femoral condyle (Fig. 3A).

The isometric point for the posterior cruciate ligament on the tibial side is believed to be its anatomic attachment site (Fig. 2). On the lateral film, the osseous tunnel begins distally and anteriorly at the tibial tubercle and courses posteriorly and proximally to emerge from the posterior tibia just below the tibial articular surface (Fig. 3B). On the anteroposterior film, the osseous tunnel begins distally just lateral to the tibial tubercle and courses proximally toward the intercondylar

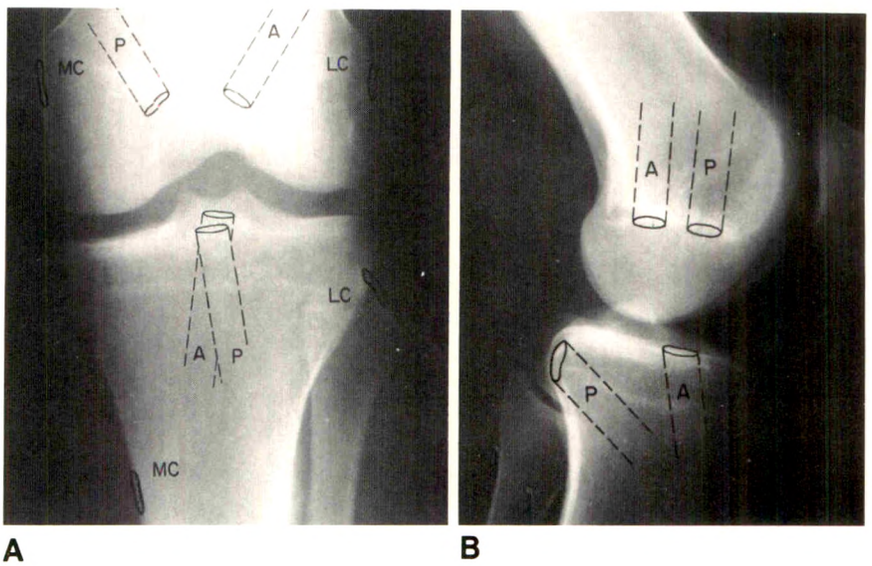

Fig. 2.—Isometric points.

***A*, Anteroposterior film showing ideal sites of femoral and tibial osseous tunnels for anterior (A) and posterior (P) cruciate ligament reconstructions. Isometric points are at tunnel openings on articular surface of knee. Also shown are isometric attachment sites for medial collateral ligaments (MC) and lateral collateral ligaments (LC).**

***B*, Lateral film showing ideal positions of femoral and tibial osseous tunnels for anterior (A) and posterior (P) cruciate ligament reconstructions. See text for precise description of radiographic landmarks for these reconstructions.**

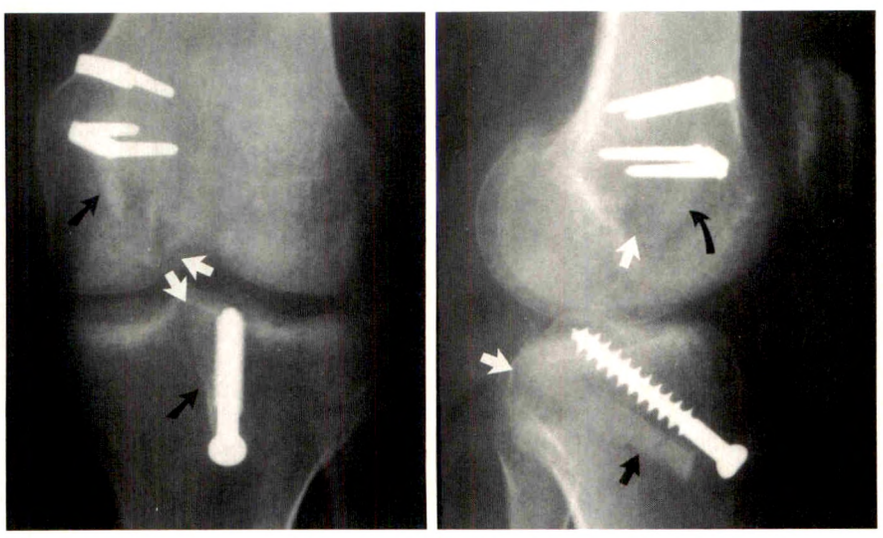

Fig. 3.—Posterior cruciate ligament reconstruction.

***A*, Anteroposterior view. *Black arrows* show bone plugs of bone–patellar tendon–bone graft, and *white arrows* indicate isometric position of osseous tunnels at articular surface. Soft tissues attached to femoral bone plug are secured to femur by staples, rather than by interference screw. Staple position is not important.**

***B*, Lateral view. *Black arrows* show bone plugs, and *white arrows* indicate isometric position of osseous tunnel opening.**

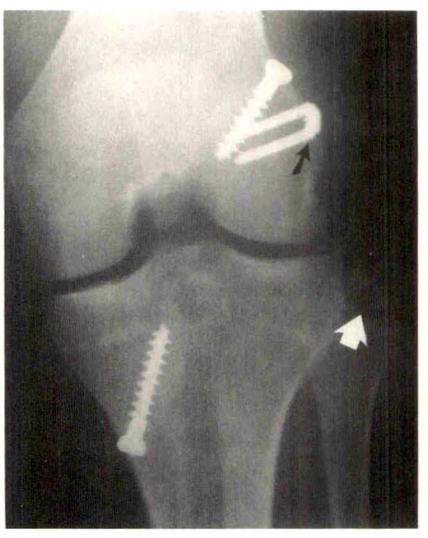

Fig. 4.—Lateral collateral ligament repair, showing staple in normal position just superior to popliteus groove (*black arrow*). Avulsion of fibular styloid process (*white arrow*) frequently occurs, but did not require internal fixation in this case. Anterior cruciate reconstruction is also shown, with screws and bone plugs in normal position.

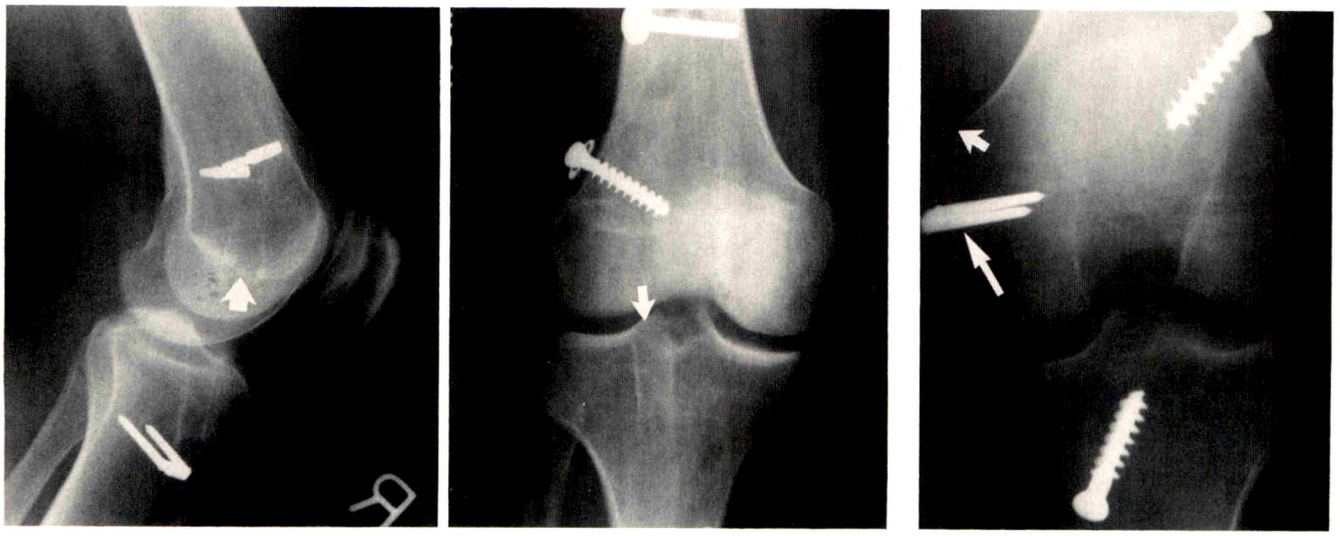

A B

Fig. 5.—Examples of nonisometric reconstruction (from other institutions, included for illustrative purposes but not part of our series).

***A*, Anterior cruciate reconstruction with femoral osseous tunnel (*arrow*) placed anterior to isometric site. Tibial osseous tunnel is in normal position.**

***B*, Previous failed intraarticular anterior cruciate reconstruction with placement of tibial osseous tunnel that is too lateral (*arrow*). After failure, salvage was attempted with prosthetic ligament (proximal and distal screws) and extraarticular augmentation (middle screw).**

Fig. 6.—Medial collateral ligament repair, with nonisometric placement of femoral staple (*long arrow*). This staple should be placed more proximally on femoral condyle, just distal to the adductor tubercle (*short arrow*). A normal anterior cruciate reconstruction is also seen, with interference screws in position.

eminence. In this projection, the tunnel appears to end proximal to the intercondylar eminence, corresponding to the anatomic site of attachment on the tibia posteriorly. (Fig. 3A).

Medial and lateral collateral ligament reconstructions use soft tissues only. Because the presumed isometric attachment sites of the medial collateral ligament correspond to the anatomic femoral and tibial attachments, reconstructions of the medial collateral ligament can easily be evaluated radiographically by the staple placement. On the anteroposterior film, the femoral attachment of the medial collateral ligament is on the medial epicondyle, immediately distal to the adductor tubercle. The tibial attachment is on its medial aspect; it begins at a level corresponding to the distal end of the tibial tubercle and may extend another 2 cm distal to that site (Fig. 2A). The attachments are at the same level on the lateral film, but slightly posterior to the center of the long axes of both the femur and tibia. Staple placement should correspond to these landmarks.

The lateral collateral ligament is shorter than the medial collateral, coursing from the lateral aspect of the lateral femoral condyle distally and slightly posteriorly to insert on the styloid process of the fibular head (Fig. 2A). Like the medial collateral ligament, isometric attachment is at the femoral and fibular anatomic insertion points. On the anteroposterior film, then, staples would be located at the superior aspect of the lateral femoral condyle just superior to the popliteus groove and at the fibular styloid process (Fig. 4). The lateral film would show hardware on the femoral condyle posteriorly (in line with the posterior femoral cortex) and on the fibular head.

Results

The position of the femoral attachment site in the 45 anterior cruciate ligament reconstructions was judged to be isometric in all but two instances. In these two cases, the graft was placed posteriorly. In one case, the radiographic findings correlated well with the clinical findings of nonisometric attachment (increased laxity with knee flexion). Some mild variability was seen in the placement of the tibial osseous tunnel and bone plug, but this did not appear to be significant clinically. Examples of nonisometric graft placement are shown in Figure 5.

Graft placement in all posterior cruciate ligament cases approximated the normal ligament attachment site, the location that currently is considered most satisfactory for reconstructive purposes [7]. Of the 16 medial collateral ligament reconstructions, one repair showed nonisometric placement at the femoral attachment site (Fig. 6). The three lateral collateral ligament repairs all showed isometric placement.

Three complications observed on films obtained immediately after surgery involved fractures. One fracture involved the patella (Fig. 7). A second fracture involved the femoral bone plug itself (Fig. 8). In the third case, holes drilled in the bone plug to assist in pulling the plug through the femoral tunnel acted as a stress concentrator, and the graft fractured at one of these sites. No other immediate complications were found. One case of pseudofracture of the bone graft led to initial misinterpretation (Fig. 9).

Evaluation of the bone density in sequential studies showed osteoporosis of variable severity in 56% of the patients. This finding, as expected, was largely related to the fact that a more severely injured knee frequently requires a longer period in which it is immobilized and does not bear any weight.

Knee effusions were seen on the initial study in all patients undergoing cruciate ligament reconstruction. These usually resolved within 4 weeks, although 8% were found to have effusions in later studies. One patient was clinically and radio-

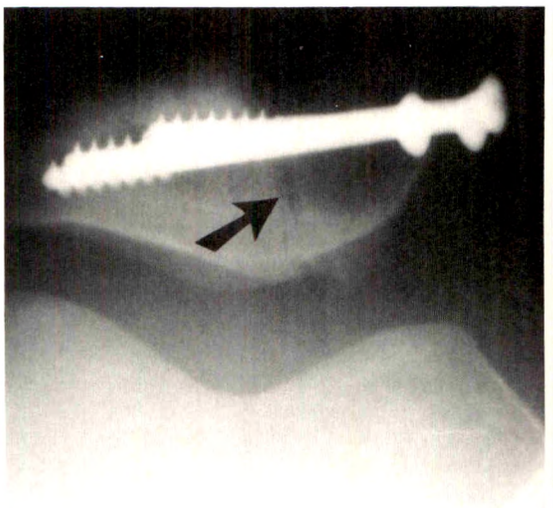

Fig. 7.—Patellar fracture (*arrow*) sustained secondary to harvest of patellar tendon graft. Defect along anterior surface represents donor site.

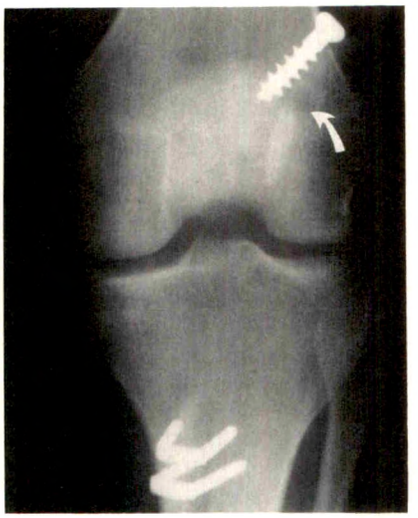

Fig. 8.—Fracture of bone plug (*arrow*) after anterior cruciate ligament reconstruction. Immobilization of knee was required to prevent distal fragment from pulling through osseous tunnel into articular region and causing laxity.

7 8

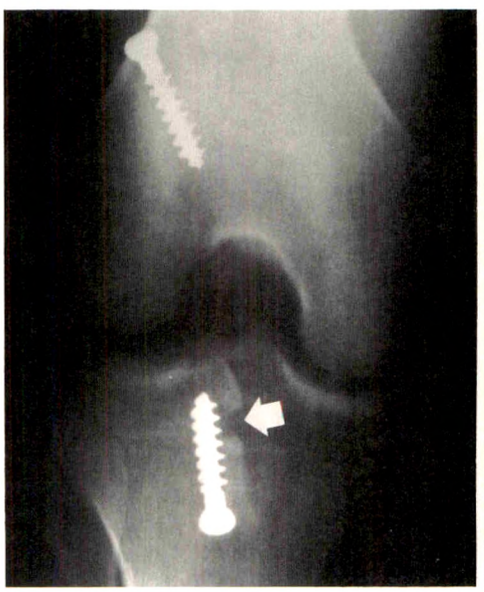

Fig. 9.—"Pseudofracture" of tibial bone plug (*arrow*), which actually is normal growth center in tibial tubercle apophysis of skeletally immature allograft donor.

Fig. 10.—Late follow-up film of anterior cruciate ligament reconstruction shows prominent sclerosis (*arrows*) of both femoral and tibial tunnel margins. Graft incorporation is complete; this appearance is common and is not indicative of complication.

9 10

graphically suspected to have joint sepsis, but cultures of synovial fluid were negative.

Hardware failure (screw or staple breakage or pullout) did not occur in this series. No cases of late graft failure occurred (best detected on either anteroposterior or tunnel view as a relative change in position of the plug). However, in several instances, the inferior pole of the patella was found on the tunnel view to overlie the intercondylar notch, so that there appeared to be bone density within the intercondylar notch and, therefore, graft migration. This confusing appearance is one potential pitfall in interpretation.

Incorporation of the graft was quite variable. In some patients, the graft was not well seen, and assessment of bony union was difficult. Evidence for bony union was seen as early as 3 weeks after cruciate ligament reconstruction with patellar tendon grafts. Of those patients who were followed 6 weeks, 79% showed radiographic signs of incorporation. In those grafts followed at least 5 months, 95% were judged to be incorporated. No significant difference was seen in the rate of bony union between patellar tendon autografts and allografts. There were several cases of a relatively lucent appearance around the graft before incorporation. Sclerosis of the osseous tunnels was also noted in a significant number of cases (Fig. 10).

Discussion

Only one previous report discusses the radiographic appearance of current knee ligament reconstructions [8]. That paper discussed only superficially the appearance of bone–

patellar tendon–bone grafts and restricted its scope to anterior cruciate ligament repairs. The only complication reported was patellar fracture. The present study includes analysis of anterior cruciate, posterior cruciate, medial collateral, and lateral collateral reconstructions. In addition, several important complications are discussed.

Anterior and posterior cruciate ligament reconstruction with rigidly fixed, high-strength graft material theoretically requires placement at isometric points to allow proper function without abnormal stretching or laxity of the ligament during knee motion. Similarly, medial and lateral collateral ligament soft-tissue reconstructions should be isometrically attached. Reconstructions that are not placed isometrically will lead to stretching of the ligament and/or limitation of knee motion (a suboptimal clinical result) and probable failure. Evaluation for isometry is made by plain film analysis. This study identifies radiographic landmarks for isometric points and shows that reconstructions can be evaluated easily for isometric placement. If postoperative films show nonisometric reconstruction, the repair is either revised or protected with immobilization; such repairs require more frequent radiographic follow-up.

Early postoperative knee motion is one of the advantages of the newer ligament reconstructions, but it has the potential complication of early graft failure. Therefore, immediate postoperative films should be evaluated for fracture, especially of the bone plug in anterior or posterior cruciate ligament repairs. Early detection of such graft fractures is vital because a fractured graft may migrate through the tunnel toward the articular surface, resulting in increased laxity of the ligament. If a fracture is detected before such migration occurs, bracing and immobilization may prevent further problems. A pseudofracture may be seen when cadaveric tendon grafts are harvested from skeletally immature donors. The tibial bone plug, harvested from the tibial tubercle apophysis in the immature donor, may show a lucency representing normal lack of fusion of the apophysis and simulate a fracture at this site. In the one case of this finding in our series, knowing that the donor was skeletally immature and obtaining radiographs of the unused remaining half of the donor patellar tendon graft led to the correct interpretation.

When the bone–patellar tendon–bone graft is obtained from the patient, rather than a cadaver, the patella normally has a defect on its anteromedial surface (the bone-plug harvest site). This is seen as a vertical defect on the anteroposterior film or as a groove on the sunrise film. This defect may act as a stress riser and result in patellar fracture.

The relatively common finding of late knee effusions confirms that finding described in another study [8]. Late postoperative knee effusions as an isolated finding are therefore not suggestive of sepsis.

Theoretically, the graft can loosen within the tunnel and with early motion may pull through into the joint. Although such late graft failure was not encountered in this study, it should be evaluated carefully because promptly immobilizing the knee may salvage the procedure.

Our study indicates that graft incorporation can be expected by 5 months (although it often occurs earlier), which is consistent with previous reports [9]. The sclerosis of the osseous tunnels commonly seen on follow-up films may be caused by bone necrosis due to the heat generated during drilling of the tunnel. Another explanation for tunnel sclerosis applies to earlier reconstructions that used only tendinous tissue. Tunnel sclerosis in those cases was thought to represent a tendon "nonunion," that is, fibrous healing to the cortical walls of a sclerotic osseous tunnel. Although composite bone–tendon–bone grafts were used for most reconstructions in this series, occasionally tendinous material extended well into the osseous tunnels, depending on the length of the graft. In these instances, tunnel sclerosis may indicate this same tendon "nonunion" phenomenon. Whatever the explanation, tunnel sclerosis is not a complication.

In summary, new surgical procedures for anterior and posterior cruciate ligament reconstruction have been developed, which are based on use of high-strength graft materials, rigid fixation, and attachment to appropriate isometric points. Isometry is now recognized as important in medial and lateral collateral ligament reconstructions as well. Bone–soft tissue composite grafts used in conjunction with metallic fixation are visualized easily on conventional radiographs. Early motion of the reconstructed knee provides many beneficial effects, but it also carries the potential complication of early failure. Therefore, frequent radiographic studies are needed in these patients to evaluate adequacy of ligament-graft attachment as well as to detect any deleterious effect of early motion.

REFERENCES

1. Noyes FR, Butler DL, Paulos LE, Grood ES. Intraarticular cruciate reconstruction. I. Perspectives on graft strength, vascularization, and immediate motion after replacement. *Clin Orthop* **1983**;172:71–77
2. Kurosaka M, Ardish JT, Yoshiya S. The effect of different surgical methods of graft fixation on mechanical properties and anterior cruciate ligament reconstruction (abstr). *Trans Orthop Res Soc* **1985**;10:80
3. Sidles JA, Garbini JL, Larson RV, Matsen FA. Techniques for characterizing all possible nearly isometric knee ligament insertions (Abstr). *Trans Orthop Res Soc* **1986**;11:411
4. Grood ES, Hefzy MS, Butler DL, Suntay WJ, Siegel MG, Noyes FR. On the placement and the initial tension of anterior cruciate ligament substitutes (Abstr). *Trans Orthop Res Soc* **1983**;8:92
5. Hefzy MS, Grood ES, Noyes FR. ACL intra-articular reconstruction: factors affecting the region of most isometric attachments (abstr). *Trans Orthop Res Soc* **1987**;12:269
6. Sidles JA, Larson RV, Garbini JC, Matsen FA. Ligament length relationships in the moving knee (abstr). *Trans Orthop Res Soc* **1987**;12:269
7. Hefzy MS, Grood ES, Lindenfeld TL. The posterior cruciate ligament: a new look at length patterns (abstr). *Trans Orthop Res Soc* **1986**;11:128
8. Burnstein MI, Ellis BL, Teitge RA, Gross MI, et al. Radiographic features of anterior cruciate ligament reconstruction. *Henry Ford Hosp Med J* **1986**;34:270–274
9. Lambert KL. Vascularized patellar tendon graft with rigid internal fixation for anterior cruciate ligament insufficiency. *Clin Orthop* **1983**;172:85–89

Shoulder Impingement Syndrome:
MR Findings in 53 Shoulders

Leanne L. Seeger[1]
Richard H. Gold[1]
Lawrence W. Bassett[1]
Harvard Ellman[2]

The shoulder impingement syndrome refers to a condition in which the supraspinatus tendon and subacromial bursa are chronically entrapped between the humeral head inferiorly and either the anterior acromion itself, spurs of the anterior acromion or acromioclavicular joint, or the coracoacromial ligament superiorly. As a result, the space for the bursa and tendon is reduced, and repeated trauma to these structures leads to bursitis and rotator cuff injury. Although pain and limitation of motion are common early findings, the diagnosis is often delayed until a complete tear of the rotator cuff has occurred. In an attempt to determine if MR can be used to depict the abnormalities associated with impingement syndrome (subacromial bursitis, supraspinatus tendinitis, and rotator cuff tear), we reviewed 107 MR scans of painful shoulders. Changes consistent with impingement syndrome were found in 53 patients (50%), 32 of whom underwent subsequent arthrography or surgery. MR was found capable of depicting several soft-tissue and bony abnormalities that have been clinically described in impingement syndrome. In regions of inflammation, we found that the supraspinatus tendon and/or the subacromial bursa were compressed by spurs (25 shoulders), capsular hypertrophy of the acromioclavicular joint (six shoulders), and/or a low-lying acromion (14 shoulders). While T1-weighted MR imaging was highly sensitive to abnormalities of the supraspinatus tendon, tendinitis could be differentiated from a small tear of the supraspinatus tendon only with T2-weighted imaging. Large, full-thickness tears, especially if chronic, produced characteristic MR findings on both T1- and T2-weighted images.

We conclude that MR can be used to detect several abnormalities associated with the shoulder impingement syndrome.

Impingement syndrome is a painful condition that most commonly results from entrapment of the supraspinatus tendon between the humeral head and the anterior part of the acromion, coracoacromial ligament, or acromioclavicular joint [1–3]. The tendon of the long head of the biceps muscle may also be compressed [1, 3–5]. The disorder is due most often to repetitive trauma caused by vigorous overhead occupational or athletic endeavors and/or degenerative exostoses [1, 3, 5, 6]. Uncommonly, impingement results from a tumor or other abnormal mass or from the pressure of the coracoid process on the subscapularis tendon. It affects people of all ages from young adults to the elderly. Neer [5] has maintained that 95% of rotator cuff tears result from impingement. He stresses that anatomic variations in the shape and slope of the acromion can lead to a predisposition to impingement syndrome, as can prominence of the acromioclavicular joint [3, 5]. Figure 1 illustrates impingement of the supraspinatus tendon by hypertrophic spurs at the inferior aspect of the acromioclavicular joint.

MR allows detailed imaging of the shoulder [7]. To determine if MR can be used to detect the lesions associated with impingement syndrome, we devised a method of evaluating the syndrome by using MR imaging.

Received September 4, 1987; accepted after revision October 19, 1987.

[1] Department of Radiological Sciences, University of California at Los Angeles School of Medicine, 10833 Le Conte Ave., Los Angeles, CA 90024. Address reprint requests to L. L. Seeger.

[2] Department of Surgery, Division of Orthopedic Surgery, University of California at Los Angeles School of Medicine, Los Angeles, CA 90024.

AJR 150:343–347, February 1988
0361–803X/88/1502–0343
© American Roentgen Ray Society

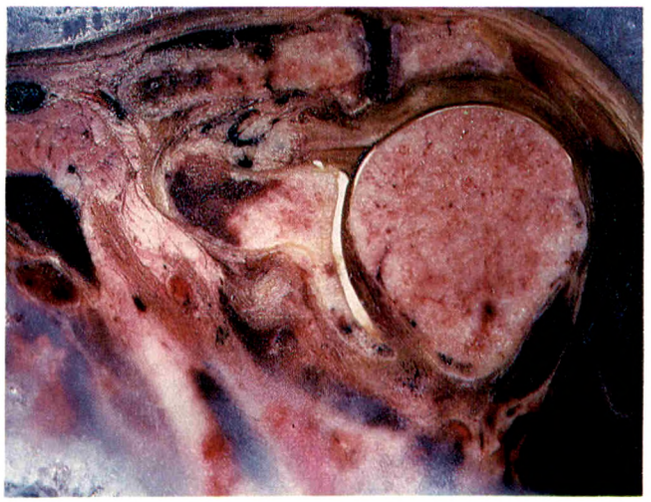

Fig. 1.—Cadaveric cryomicrosection shows depression of supraspinatus tendon by a spur of acromioclavicular joint. Section is oriented obliquely, along long axis of supraspinatus muscle belly.

Materials and Methods

MR scans of 107 shoulders in 96 patients were reviewed. All patients were referred for MR evaluation of a painful shoulder. Patients who had undergone an invasive procedure localized to the shoulder, such as corticosteroid injection or arthrography, within 1 week before scanning were not included.

Scans were performed with a Fonar 0.3-T permanent-magnet system. T1-weighted images were obtained in all patients by using a spin-echo (SE) sequence (echo time [TE] = 28 msec, repetition time [TR] = 300–500 msec). In addition, T2-weighted spin-echo imaging was performed in 46 patients, with a TE of 56–84 msec and a TR of 1500–2000 msec. The decision to add T2-weighted imaging to the protocol was made after data collection was already under way. Images were either 5-mm thick and obtained at 7-mm intervals or were 3-mm thick and obtained at 5-mm intervals. A 256 × 256 matrix was used for imaging and was interpolated to 512 × 512 for display. Pixel size was 0.75 mm^2. A planar surface coil was used for all scans.

The technique for positioning the patient and placement of the surface coil has been described [7]. In that previous study evaluating normal anatomy, we determined that positioning the subject supine with the lower arm across the abdomen (i.e., with the elbow flexed and elevated and the humeral head internally rotated) afforded maximal comfort for normal individuals. Fortuitously, this position produces impingement in susceptible persons [3, 5], thus enhancing the detection of disease.

Images were first acquired in the axial plane, followed by oblique imaging along the long axis of the belly of the supraspinatus muscle [7]. Oblique scanning allowed evaluation of the supraspinatus tendon and muscle in continuity, permitting the localization of regions of abnormal signal intensity and encroachment. Because the supraspinatus tendon is the portion of the rotator cuff that is most vulnerable to trauma in the classic impingement syndrome, evaluation of the tendinous cuff was limited to this structure.

The following soft-tissue structures were evaluated in each case: (1) the subacromial bursa was analyzed for signal intensity, thickness, and anatomic course; (2) the supraspinatus tendon was studied for signal intensity and anatomic course; (3) the musculotendinous junction of the supraspinatus muscle was analyzed for evidence of muscle retraction; and (4) the supraspinatus muscle was analyzed for signal intensity. Other abnormalities indicative of impingement syndrome were also noted, including (1) spurs from the inferior margin of the acromion or acromioclavicular joint, (2) capsular hypertrophy of the acromioclavicular joint, and (3) inferior displacement of the acromion with respect to its articulation with the distal clavicle.

The changes seen on MR were classified into three types, depending on the severity of the abnormalities. Type I, the least severe form of the disorder, implied subacromial bursitis manifested by bursal thickening; the signal intensity of the supraspinatus tendon and muscle remained normal. Type IIa was characterized by abnormally high signal intensity of the supraspinatus tendon, while the supraspinatus muscle remained normal in signal intensity and was without retraction. Type IIb featured a very bright signal within the supraspinatus tendon on T2-weighted images, but the supraspinatus muscle was not retracted; this implied disruption of the cuff, with fluid within the cuff tear. Type III changes included an abnormally high signal intensity from the supraspinatus tendon, as well as retraction of the supraspinatus muscle, indicating complete rupture of the cuff. In cases of type I or II severity, the diagnosis of impingement syndrome was not made unless the subacromial bursa and/or supraspinatus tendon were compressed by overlying structural abnormalities. This was not a requirement of type III disease.

Examples of pertinent normal anatomy are shown in Figure 2. Figures 3–5 represent the different types of impingement syndrome seen on MR.

Results

Using the aforementioned criteria, we identified 53 shoulders in 49 patients whose MR images were consistent with impingement syndrome, with or without complete tear of the rotator cuff. Scans in the remaining 54 patients were either normal or showed other shoulder abnormalities, including isolated labral tear, avascular necrosis of the humeral head, tumor, and infection.

Of the 53 shoulders, six had findings of type I disease (isolated subacromial bursitis) and 29 showed signs of type IIa disease (tendinitis). Lesions implying type IIb or III disease were present in 18 shoulders.

Fourteen of the 35 shoulders with type I and IIa lesions underwent arthrography (eight patients) or arthroscopy (six patients). These examinations yielded small or partial cuff tears in three shoulders with type IIa lesions. The other 11 did not show rotator cuff tears. All 18 complete tears (type IIb or III) were confirmed by either arthrography (12 shoulders) or surgery (six shoulders).

The coracoacromial ligament, a structure that usually is not depicted in MR images of normal shoulders, often was visualized on the oblique images of patients with subacromial bursitis.

Glenohumeral joint effusions, encountered occasionally in patients with type III lesions, were best seen within the dependent (posterior) aspect of the joint on axial images. The fluid manifested low-to-medium signal intensity on T1-weighted images and became bright with T2 weighting. High signal intensity within the supraspinatus tendon on T2-weighted imaging was pathognomonic for a rotator cuff tear (Fig. 6). Fluid was not identified within the subacromial bursa

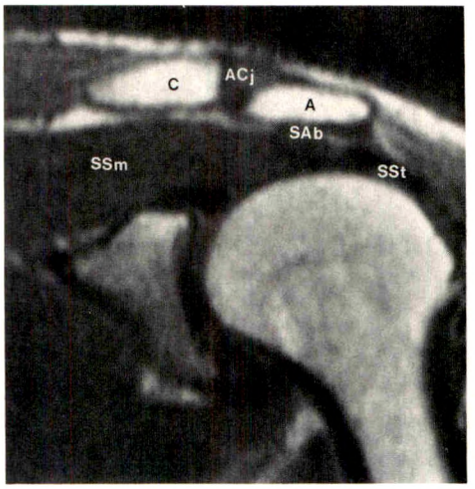

2

Fig. 2.—Oblique SE 500/28 MR image of a normal shoulder. Supraspinatus musculotendinous junction lies inferior to acromion (A) or acromioclavicular joint (ACj). Undersurfaces of acromion and distal clavicle (C) approximate same level, and supraspinatus apparatus courses beneath them in a relatively straight line, without focal depression. Tendon (SSt) of supraspinatus muscle (SSm) is homogeneous and devoid of signal. Subacromial bursa (SAb) is a thin band of high signal intensity.

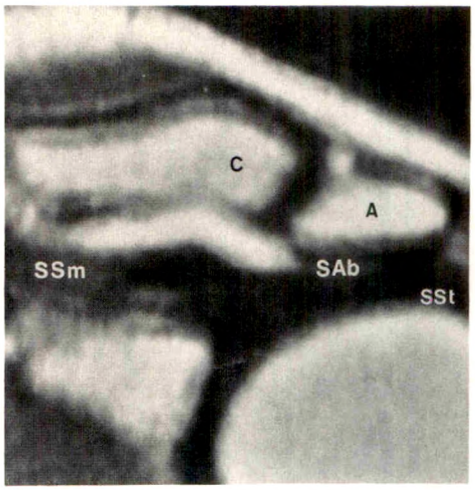

3

Fig. 3.—MR image (SE 500/28) of type I impingement syndrome (subacromial bursitis). SE 500/28 image. Subacromial bursa (SAb) is thickened and compressed by anterior acromion (A), which lies low with respect to distal clavicle (C). Signal intensity of supraspinatus tendon (SSt) is normal. No spurs were present radiographically or at surgery. SSm = supraspinatus muscle.

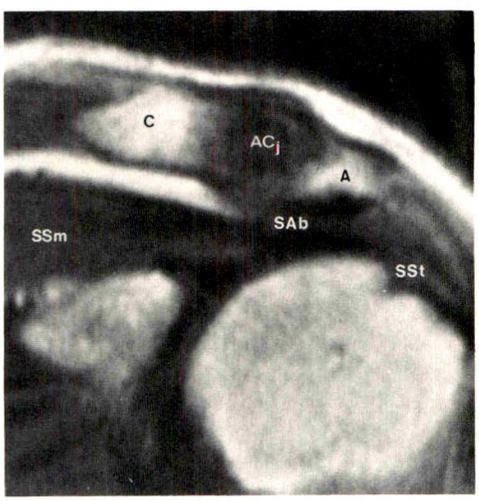

4

Fig. 4.—MR image (SE 500/28) of type IIa impingement syndrome (supraspinatus tendinitis). Medium signal intensity is present within supraspinatus tendon (SSt). Subacromial bursa (SAb) is depressed by hypertrophic acromioclavicular joint (ACj) capsule. Anteroposterior radiograph showed only mild degenerative changes in acromioclavicular joint. A = acromion, C = distal clavicle, SSm = supraspinatus muscle.

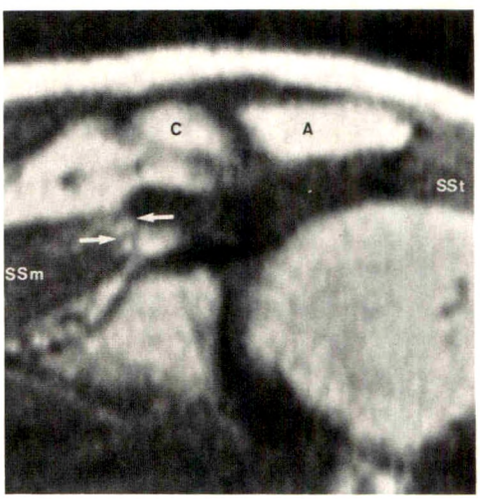

5

Fig. 5.—MR image (SE 500/28) of type III impingement syndrome (complete rotator cuff). SE 500/28 image. Region of supraspinatus tendon (SSt) is replaced by a region of medium signal intensity. Because musculotendinous junction is retracted (*arrows*), this represents a complete rotator cuff tear. A = acromion, C = distal clavicle, SSm = supraspinatus muscle.

of any shoulder, a finding consistent with the extensive surgical experience of one of our authors.

Subacromial or acromioclavicular joint spurs were found in 25 shoulders, and the capsule of the acromioclavicular joint was found to be hypertrophic in six shoulders. The anterior acromion was low-lying with respect to the distal clavicle in 14 shoulders. The subacromial space was completely obliterated in the shoulders of eight patients who had massive, long-standing tears. We assumed that any spurs that might have been present in these shoulders had been worn away by the chronic superior migration of the humeral head.

Small subacromial and acromioclavicular spurs were characterized by foci of signal void. Large spurs frequently contained marrow and were therefore imaged as extensions of bright signal from the parent bone, surrounded by a rim of cortical signal void. Tendons compressed by spurs showed abnormally high signal intensity. The exaggerated thickness of the subacromial bursa often decreased abruptly at the level of the spur, hypertrophic acromioclavicular joint capsule, or low-lying acromion, indicating significant compression (Figs. 3 and 4).

Discussion

We found MR to be an informative, noninvasive means of evaluating impingement syndrome. The impinging structures and entrapped tissues often could be imaged precisely, allowing specific details of the site and extent of bone and soft-tissue disease. Because it permitted differentiation of bursitis, tendinitis, and complete supraspinatus tear, MR could be used for classifying the extent of disease and for therapeutic planning.

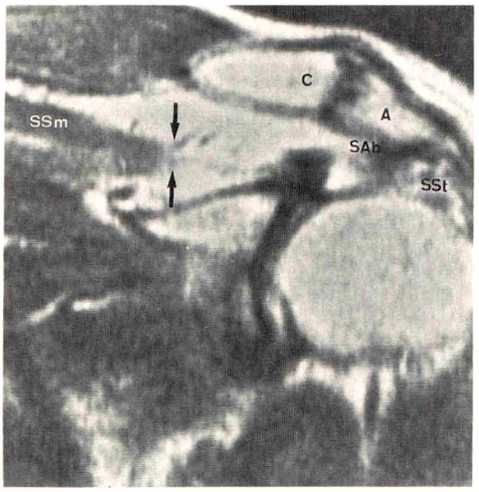

6

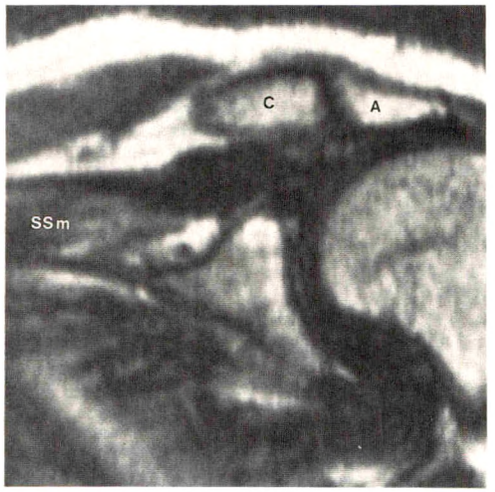

7

Fig. 6.—MR image (SE 2000/84) of type III impingement syndrome (complete rotator cuff tear). High signal intensity is present within supraspinatus tendon (SSt). Musculotendinous junction is retracted (*arrows*). A = acromion, C = distal clavicle, SAb = subacromial bursa, SSm = supraspinatus muscle.

Fig. 7.—MR image (SE 500/28) of type III impingement syndrome (complete rotator cuff tear, chronic). Muscle is retracted. Atrophy is characterized by bright bands of signal within muscle and by its diminished bulk. Signal void at expected site of supraspinatus tendon was found at surgery to represent fluid and a severely degenerated tendon. A = acromion, C = distal clavicle, SSm = supraspinatus muscle.

Neer [5] and Neer and Welsh [8] have described three progressive stages of impingement syndrome as found clinically and at surgery. Stage I consists of edema and hemorrhage and is reversible with conservative therapy. Stage II implies fibrosis and thickening of the subacromial soft tissues, and sometimes a partial tear of the rotator cuff, and is manifested clinically by recurrent pain. Although the management of stage II lesions is controversial, failure of conservative treatment is usually an indication for surgery, most often consisting of division of the coracoacromial ligament and acromioplasty, with or without bursectomy. Stage III represents complete rupture of the rotator cuff and is associated with progressive disability.

Although several clinical tests have been devised to detect impingement syndrome [3, 5, 9], the signs and symptoms are somewhat nonspecific, and the diagnosis is often delayed until the development of a full-thickness tear of the rotator cuff [5]. Similarly, radiology plays little or no role in early diagnosis. Either diagnostic plain radiographic changes are absent, or they occur only late in the course of the disease [2, 5, 10, 11]. Those that occur earliest are sclerosis of the greater tuberosity of the humerus and spurring of the inferior surface of the acromion or acromioclavicular joint. As the disease progresses, radiographs may show the typical bony changes associated with a chronic rotator cuff tear, including an acromiohumeral distance of less than 7 mm [12], superior migration of the humeral head, and a concave depression on the inferior surface of the acromion. However, even in stage III disease, radiographs are often normal. Conversely, irregularity or apparent sclerosis of the greater tuberosity may be a normal variant [6, 10], and spurs of the inferior margin of the acromion or acromioclavicular joint do not necessarily imply associated soft-tissue disease [3].

Arthrography aids little in the early diagnosis of impingement syndrome. Even when performed with conventional tomography or CT, the arthrogram is usually normal in stage I disease and may easily be misconstrued as normal in stage II disease, even in the face of an incomplete or small tear of the rotator cuff [13].

Subacromial bursography has been advocated for the early detection of impingement syndrome, and it may reveal mechanical impingement or difficulty in filling the bursa due to soft-tissue edema and thickening [14, 15]. False-positive results may arise from failure to locate and opacify the bursa, and false-negative results may occur when the arm is not put through an appropriate range of motion. In addition, bursography is invasive and requires manipulation of an already painful joint.

No conclusions can be drawn concerning false-negative MR studies in our series. Patients with normal MR scans were not included in the data analysis, and sufficient follow-up was not available in most of these patients.

In our series, MR failed to delineate three partial tears of the rotator cuff. This may have been due to one or all of the following factors: (1) these three scans were performed early in our experience, before T2-weighted imaging was routinely employed; (2) partial-volume averaging may have masked the small tears; and (3) a low-field-strength system was used for this study. However, failure to detect partial tears such as these has little impact on management, since these patients are usually managed initially without surgery. Moreover, during the treatment of advanced disease, small or partial tears can be identified and repaired at the time of acromioplasty or coracoacromial ligament release. Kneeland et al. [16] identified two partial tears in a recent series evaluating the use of MR imaging in the diagnosis of rotator cuff tears.

MR depicted the extent of muscle retraction in patients with complete rupture of the supraspinatus tendon. Muscular atrophy, also readily apparent, was characterized by bands of bright signal within the muscle belly, indicative of fatty replacement (Fig. 7). Both findings are significant in terms of surgical planning and prognosis.

The thick band of bright signal representing the thickened subacromial bursa did not manifest a central region of lower signal intensity on T1-weighted images. In fact, its appearance was homogeneous and similar to that of subcutaneous fat on both T1- and T2-weighted images. Our hypothesis is that the thickening was due to an increase in fibrofatty tissue caused

by hypertrophied synovium, a structure that may contain abundant adipose tissue and/or edematous areolar tissue [17]. Little or no research has been published on the histology of the subacromial bursa in patients with impingement syndrome, but an abnormal abundance of fibrofatty tissue is found in the subacromial space of these patients at surgery. With time, this tissue becomes less evident, much like the degeneration of the supraspinatus tendon seen with chronic rotator cuff tears as the humeral head migrates superiorly. Unfortunately, chemical-shift imaging was not available for confirmation.

MR images of several of our patients who had normal radiographs showed depression of the thickened subacromial bursa and/or the supraspinatus tendon by the anterior part of the acromion, which often appeared quite large. In all of these patients, the inferior margin of the anterior part of the acromion lay inferior to the undersurface of the distal clavicle, a finding that was not evident on routine anteroposterior radiographs. This substantiates Neer's theory that certain individuals have a predisposition to impingement syndrome by virtue of variations in the size or position of the anterior part of the acromion [5].

Although the linear signal void characterizing the coracoacromial ligament is uncommonly identified on MR scans of normal shoulders, we hypothesize that this structure is made apparent in patients with impingement syndrome by virtue of the surrounding proliferative bursitis.

No attempt was made to evaluate the ability of MR to detect tendinous calcifications. Calcific deposits are often small and lie within inflamed tissue, which already has an abnormal and often inhomogeneous signal intensity.

Striking, mottled foci of low signal intensity were often seen within the marrow of the greater tuberosity of the humerus in shoulders without a rotator cuff tear and with normal radiographs. These were generally seen most clearly on axial images and may indicate significant repetitive trauma to the rotator cuff.

Neer's classification [5] of impingement lesions has not only served to define the extent of impingement syndrome, but it has also greatly assisted in planning its therapy. There is no proof, however, that the anatomic abnormalities described by Neer do represent a sequential progression. Further studies with MR may assist in determining if this is the case, or if Neer's stages of impingement simply represent different, possibly associated abnormalities.

Although the clinical staging system for impingement syndrome has frequently proved useful for managing patients with this disorder, in the absence of a demonstrable lesion many orthopedic surgeons persist in conservative management to the detriment of cuff integrity. There is increasing evidence that timely acromioplasty will retard the progress of rotator cuff deterioration [18]. In some of our patients the detailed soft-tissue anatomy depicted by MR permitted early detection of impingement lesions. It is hoped that the earlier diagnosis of impingement syndrome with MR will facilitate more timely and appropriate treatment, long before the disorder has progressed to its ultimate debilitating and irreversible outcome.

REFERENCES

1. Penny JN, Welsh MB. Shoulder impingement syndromes in athletes and their surgical management. *Am J Sports Med* **1981**;9:11–15
2. Hawkins RJ, Kennedy JC. Impingement syndrome in athletes. *Am J Sports Med* **1980**;8:151–157
3. Neer CS II. Anterior acromioplasty for the chronic impingement syndrome in the shoulder. *J Bone Joint Surg [Am]* **1972**;54-A:41–50
4. Neer CS II, Bigliani LU, Hawkins RJ. Rupture of the long heads of the biceps related to subacromial impingement (abstr). *Orthop Trans* **1977**;1:111
5. Neer CS II. Impingement lesions. *Clin Orthop* **1983**;173:70–77
6. Cone RO III, Resnick D, Danzig L. Shoulder impingement syndrome: radiographic evaluation. *Radiology* **1984**;150:29–33
7. Seeger LL, Ruszkowski JR, Bassett LW, Kay SP, Kahmann RD, Ellman H. MR imaging of the normal shoulder: anatomic correlation. *AJR* **1987**;148:83–91
8. Neer CS II, Welsh RP. The shoulder in sports. *Orthop Clin North Am* **1977**;8:583–591
9. Macnab I, Hastings D. Rotator cuff tendinitis. *Can Med Assoc J* **1968**;99:91–98
10. Hammond G. Complete acromionectomy in the treatment of chronic tendinitis of the shoulder. *J Bone Joint Surg [Am]* **1962**;44-A:494–503
11. Hardy DC, Volger JB III, White RH. The shoulder impingement syndrome: prevalence of radiographic findings and correlation with response to therapy. *AJR* **1986**;147:557–561
12. Ellman H, Hanker G, Bayer M. Repair of the rotator cuff. *J Bone Joint Surg [Am]* **1986**;68-A:1136–1144
13. Preston BJ, Jackson JP. Investigation of shoulder disability by arthrography. *Clin Radiol* **1977**;28:259–266
14. Lie S, Mast WA. Subacromial bursography: technique and clinical application. *Radiology* **1982**;144:626–630
15. Strizak AM, Danzig L, Jackson DW, Greenway G, Resnick D, Staple T. Subacromial bursography. *J Bone Joint Surg [Am]* **1982**;64-A:196–201
16. Kneeland JB, Middleton WD, Carrera GF, et al. MR imaging of the shoulder: diagnosis of rotator cuff tears. *AJR* **1987**;149:333–337
17. Ham AW, Cormack DH. *Histology*, 8th ed. Philadelphia: Lippincott, **1979**:474–477
18. Bigliani LU, Morrison DS, April EW. The morphology of the acromion and its relationship to rotator cuff tears (abstr). *Orthop Trans* **1986**;10:216

Book Review

Radiologic Management of Pelvic Ring Fractures. Systemic Radiographic Diagnosis. By Jeremy W. R. Young and Andrew R. Burgess. Baltimore, MD: Urban & Schwarzenberg, 94 pp., 1987. $39.50

Fractures with or without dislocation of the bony pelvis are a common injury encountered in the patient who has suffered multiple trauma. Pelvic injury is often a major contributor to the fatal outcome of many of these patients, particularly death due to vascular and other soft-tissue injuries. The proper treatment of these patients depends on prompt recognition of fracture patterns and early stabilization of the bone fragments to reduce blood loss and to increase the patient's chance of survival. In 1986 the authors published two papers on the radiographic assessment of pelvic fractures (*Skeletal Radiology* 15:101–109 and *Radiology* 160:445–451). This book is an outgrowth of the authors' early work on the assessment of pelvic injuries and presents their results in an expanded form that would not be possible in the periodic literature.

The book is well organized into nine chapters. The first is a discussion of the goal of the book, which is "to define the whole pelvic ring and to identify specific facture patterns . . . so that the orthopedic surgeon can select the appropriate fixation device and . . . apply the appropriate corrective counterforces." This chapter also contains information about the pool of patients on whom the investigations were based and covers radiographic technique. The second chapter deals with the anatomy and stability of the pelvis. Chapter 3 is an overview of injury force patterns. Chapters 4 through 7 deal with specific fracture patterns that result from lateral compressive forces, anteroposterior forces, vertical shearing and complex mechanisms, and fractures of the pubic rami, respectively. Chapter 8 contains discussions and illustrations of the complications. Chapter 9 provides an integrated summary of the information by means of a table that compares specific injuries due to each particular mechanism and their findings.

Although the authors may not have intended it, this is essentially an atlas on pelvic injury. The text is kept to a minimum and occupies less than 20% of the book. The bulk of the book consists of radiographs of the various injuries. CT images are kept to a minimum and are used only to support the plain-film radiographic findings. All the illustrations are of superb quality.

In summary, this brief, well-illustrated monograph deals with an important subject in a logical, easy-to-follow format. The illustrations are superb, and I find nothing to detract from the book. I recommend it to all radiologists, emergency physicians, and orthopedic surgeons who must deal with pelvic trauma.

Richard H. Daffner
Allegheny General Hospital
Pittsburgh, PA 15212

Case Report

MR Imaging of Hemophilic Pseudotumors

Don A. Wilson[1] and John R. Prince

Pseudotumors are a rare complication of hemophilia occurring in 1–2% of individuals with severe factor VIII or IX deficiency. Masses develop most commonly in the pelvis, thigh, or calf and consist of a slowly expanding, encapsulated coagulum of chronic and acute hemorrhage [1, 2]. The bulk and location of the masses frequently impair mobility. The skin overlying these masses can become necrotic, leading to infection, or the masses can rupture, causing rapid exsanguination [3]. If these pseudotumors are diagnosed early when they are small, they frequently can be managed medically. If, however, they become progressively larger, surgical excision may become the only alternative [3]. Noninvasive imaging of these lesions by CT and sonography has proved useful in diagnosis and in planning treatment [4–6]. MR imaging, because of its ability to characterize blood clots and its multiplanar imaging capability, may be even better suited to these tasks.

Case Report

A 32-year-old man with severe hemophilia (factor VIII less than 1%) had had repeated spontaneous intraarticular bleeding from numerous sites throughout his life. About 10 years earlier, he had noted a nontender mass in the medial aspect of his left thigh. This mass had been expanding slowly over the past 6 months. Physical examination revealed a large, firm mass in the left medial thigh.

A radiograph of the left thigh showed a soft-tissue mass containing small flecks of calcium medial to the proximal shaft of the left femur. There was a mild erosion of the cortex of the proximal femur with associated periostial reaction. MR images through both lower extremities showed at least four sharply circumscribed masses in the adductor muscle group of the left thigh with several smaller adjacent cysts (Fig. 1). Two masses were also seen in the medial aspect of the right upper thigh. All of the masses had a sharply defined rim of very low signal intensity (approaching that of cortical bone) on both T1- and T2-weighted images. On T1-weighted sequences, all of the masses were high in signal intensity but slightly less so than subcutaneous fat (Fig. 1A). On the T2-weighted sequences, the proximal mass in the left thigh and both masses in the right thigh were low in signal intensity; the signal intensity of these masses was similar to that of the adjacent muscle and tendons (Fig. 1B). The two lower masses in the left thigh showed a signal intensity on the T2-weighted sequences that was greater than that of the adjacent muscle but less than that of subcutaneous fat (Fig. 1B). Within the two upper left-sided masses and the lower right-sided mass, the very high signal intensity of multiple irregular circular areas exceeded the signal intensity of subcutaneous fat on T1- and T2-weighted images (Fig. 1). These masses also contained some very low–signal-intensity material with intensities similar to that of cortical bone. The most cephalad mass on the left extended up to the inguinal ligament but did not extend into the pelvis. The superficial femoral vessels could be identified as linear areas of no signal (flow voids) lateral to the masses in the thigh.

The multiple masses in the left thigh were excised surgically, and gross pathologic examination revealed thick-walled cysts filled with old clot and serosanguinous fluid. The walls of the cysts were extremely rigid and firm and were 3–12 mm thick. Microscopic study revealed multiple organizing hematomas (surrounded by a dense, hyalinized, fibrous-tissue capsule) consistent with both recent and old hemorrhage. The pseudotumors seen in the right thigh were treated medically with regular doses of factor VIII and were followed with MR for change in size.

Discussion

The characteristic MR appearance of acute, subacute, and chronic extracranial hematomas has been reported for various

Received August 14, 1987; accepted after revision September 28, 1987.
[1] Both authors: Oklahoma Teaching Hospitals, Magnetic Resonance Center, 940 N.E. 13th St., Oklahoma City, OK 73126.

 0361–803X/88/1502–0349 © American Roentgen Ray Society

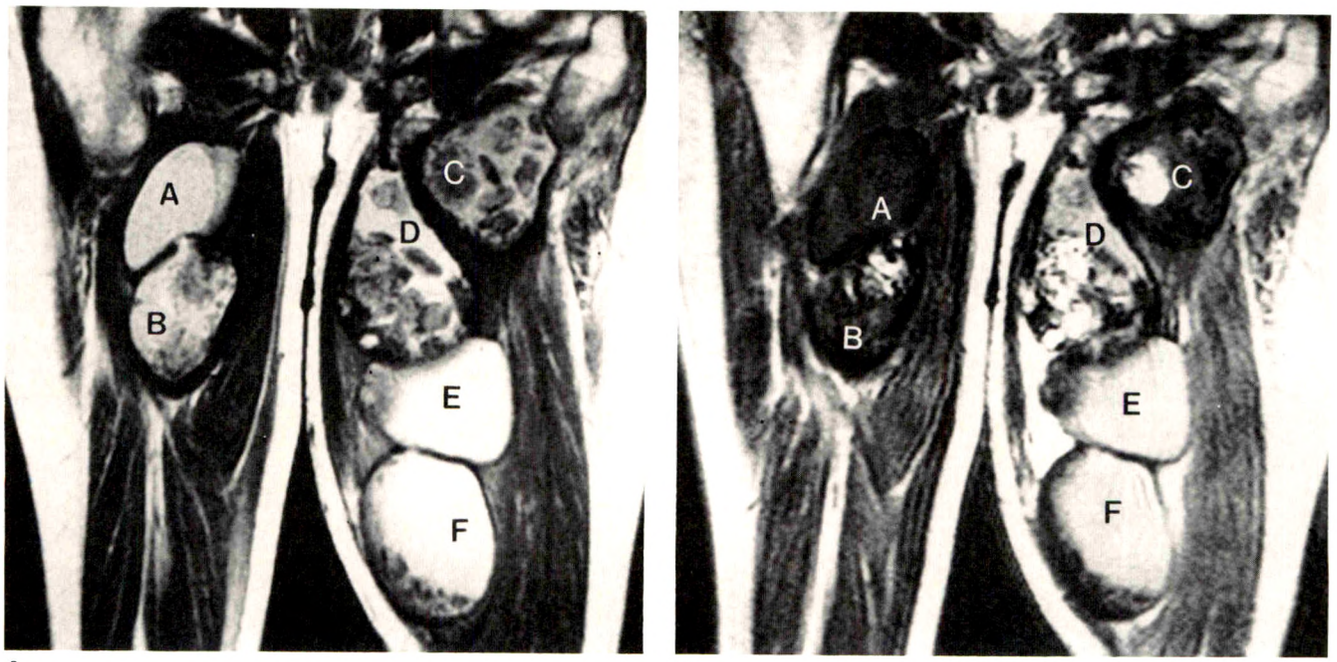

Fig. 1.—*A*, T1-weighted coronal MR image (TR 250 msec, TE 30 msec) of both thighs shows two pseudotumors on right (A, B) and four pseudotumors on left (C–F).

***B*, T2-weighted coronal MR image (TR 2100 msec, TE 100 msec) of both thighs shows a marked reduction in signal intensity of two right (A, B) and upper left (C) pseudotumors, indicating preferential T2 shortening. Many different combinations of signal intensities within these pseudotumors reflect complex processes of acute and chronic hemorrhage and clot organization that occurs in patients with bleeding disorders.**

field strengths [7, 8]. From these studies, it can be predicted that the hypointense rim of these pseudotumors consists of low–signal-intensity fibrous tissue; this was confirmed on microscopic section. When hemosiderin is contained within macrophages in the cyst-wall lining, it is known to have a preferential T2-shortening effect and undoubtedly contributes to the low signal intensity of this structure [8]. All of the pseudotumors contained fluid that was high in signal intensity on T1-weighted images. Fluid with a high signal intensity on T1-weighted images should typically contain intracellular or extracellular methemoglobin. The very low signal intensity of the fluid noted in several of these cysts on T2-weighted images may illustrate the preferential T2 shortening of deoxyhemoglobin and/or the paramagnetic effects of hemosiderin [8]. The small circular areas of high signal intensity on all pulse sequences in the cysts in the upper left thigh and the lower right thigh should represent free methemoglobin within a subacute blood clot. The small areas of low signal intensity on T1-weighted images and high signal intensity on T2-weighted images within the central portion of several of the cysts are most likely produced by serous fluid accumulations within these blood clots. The many different combinations of signal intensities within these pseudotumors reflect the process of remote and recurrent bleeding and clot organization known to occur in patients with bleeding disorders.

The clear definition that MR provided of the number, size, location, and extent of these pseudotumors and their relationship to adjacent vascular structures and bone was helpful to the surgeons who performed the difficult surgical resection. The detection by MR of two previously unknown pseudotumors in the right thigh suggests that this imaging technique may be helpful in screening high-risk patients for the early detection of this condition.

REFERENCES

1. Ahlberg AKM. On the natural history of hemophilic pseudotumor. *J Bone Joint Surg [Am]* **1975**;57-A:1133–1136
2. Jensen PS, Putnam CD. Hemophilic pseudotumor: diagnosis, treatment and complications. *Am J Dis Child* **1975**;129:717–719
3. Gilbert MS. Hemophilic pseudotumor. In: Brinkhous KM, Hemker HC, eds. *Handbook of hemophilia*. Amsterdam: Excerpta Medica, **1975**:435–444
4. Gilford WB, Mintz PD, Blatt PM, Staab EV. CT of hemophilic pseudotumors of the pelvis. *AJR* **1980**;135:167–169
5. Wilson DA, Sexauer CL. Noninvasive evaluation of hemophilic pseudotumor of the pelvis. *Am J Pediatr Hematol Oncol* **1982**;4:95–98
6. Herman G, Yeh H, Gilbert MS. Computed tomography and ultrasonography of the hemophilic pseudotumor and their use in surgical planning. *Skeletal Radiol* **1986**;15:123–128
7. Hahn PF, Saini S, Stark DD, Papanicolaou N, Ferrucci JT. Intraabdominal hematoma: the concentric-ring sign in MR imaging. *AJR* **1987**;148:115–119
8. Rubin JI, Gomori JM, Grossman RI, Gefter WB, Kressel HY. High-field MR imaging of extracranial hematomas. *AJR* **1987**;148:813–817

Case Report

MR Imaging of Maffucci Syndrome

Evan C. Unger,[1] Howard B. Kessler,[1] Michael J. Kowalyshyn,[2] Richard D. Lackman,[3] and G. Tom Morea[4]

Maffucci syndrome consists of a combination of enchondromas and hemangiomas [1]. The most common serious complication of Maffucci syndrome is malignant degeneration of enchondroma to chondrosarcoma, which has been reported in as high as 51% of patients with Maffucci syndrome [2]. In this report, we describe the MR findings in a patient with Maffucci syndrome who presented with chondrosarcoma.

Case Report

A 41-year-old woman with a history of Maffucci syndrome presented with a several-month history of a painful enlarging mass on the posterior left ankle. On physical examination, a mass could be palpated on the posterior aspect of the distal tibia. The most severe cutaneous manifestation was the right hand, which was hypertrophied and deformed with multiple cutaneous bluish masses.

Bone scan showed increased uptake in the right posterior tibia. Radiographic examination revealed an expansile, destructive soft-tissue mass arising from the distal posterior tibia (Fig. 1A). Radiographs of the right hand (Fig. 1A) showed multiple soft-tissue masses with central calcifications and enchondromas.

CT examination of the lower extremities showed expansile lytic lesions arising from the posterior aspect of the distal tibia and the anterior tibia. MR imaging was conducted on a 1.5-T Siemens Magnetom. Spin-echo images were obtained of the lower legs with T1-weighted images (repetition time [TR] = 450 msec; echo time [TE] = 16 msec) in the coronal and sagittal planes and T2-weighted images (TR = 2500 msec, TE = 28 and 70 msec) in the transaxial plane. The T1-weighted images of the legs showed multiple areas of low signal intensity replacing the normal high-signal-intensity fatty marrow (Fig. 1B), findings which corresponded to the radiographically evident enchondromas. On the T1-weighted image, the mass projecting from the posterior surface of the distal left tibia also had low signal intensity, similar to the signal intensity of the presumed enchondromas. On the T2-weighted images (Fig. 1C), the mass had higher signal intensity than the well-defined enchondromas did. In the anterior tibia a smaller, high-signal-intensity, expansile lesion was seen. This anterior lesion was discontinuous with the posterior lesion but had identical signal-intensity characteristics.

MR images of the patient's hand (Fig. 1D) were obtained by using an 18-cm Helmholtz-type surface coil; coronal spin-echo images were obtained with the same parameters as previously described. T2-weighted images showed that the enchondromas in the bones of the patient's right hand had lower signal intensity than did the large mass arising from the posterior left tibia. T2 relaxation values were determined from T2 calculated images. The T2 of bone marrow in the phalanges and tibia, which was noninvolved by enchondroma, measured approximately 40–45 msec. T2 of enchondroma in the phalanges and higher up in the tibia measured 60–65 msec. T2 of the large mass in the posterior tibia and of the anterior tibial lesion measured approximately 103 msec and 115 msec, respectively.

On MR images, two lesions that were observed in the distal tibia appeared discontinuous. Because of this, the surgeon decided to resect the posterior mass and to biopsy the anterior lesion in an attempt to save the limb. On gross examination, the mass had a lobular, shiny, blue cartilaginous appearance with focal cystic change. On histologic examination, both the posterior and anterior tibial masses had an identical appearance. There were focal areas of mature-appearing cartilage that had increased cellularity with >1 nucleus/1 lacunar space and occasional atypical mitoses. Mitotic

Received June 18, 1987; accepted after revision September 23, 1987.

[1] Department of Radiology, Fox Chase Cancer Center, Philadelphia, PA 19111. Address reprint requests to E. C. Unger, Dept. of NMR, Fox Chase Cancer Center, 7701 Burholme Ave., Philadelphia, PA 19111.

[2] Department of Pathology, Fox Chase Cancer Center, Philadelphia, PA 19111.

[3] Department of Orthopedic Oncology, Fox Chase Cancer Center, Philadelphia, PA 19111.

[4] South Jersey Imaging, 55 E. Rte. 70, Marlton, NJ 08053.

 0361–803X/88/1502–0351 © American Roentgen Ray Society

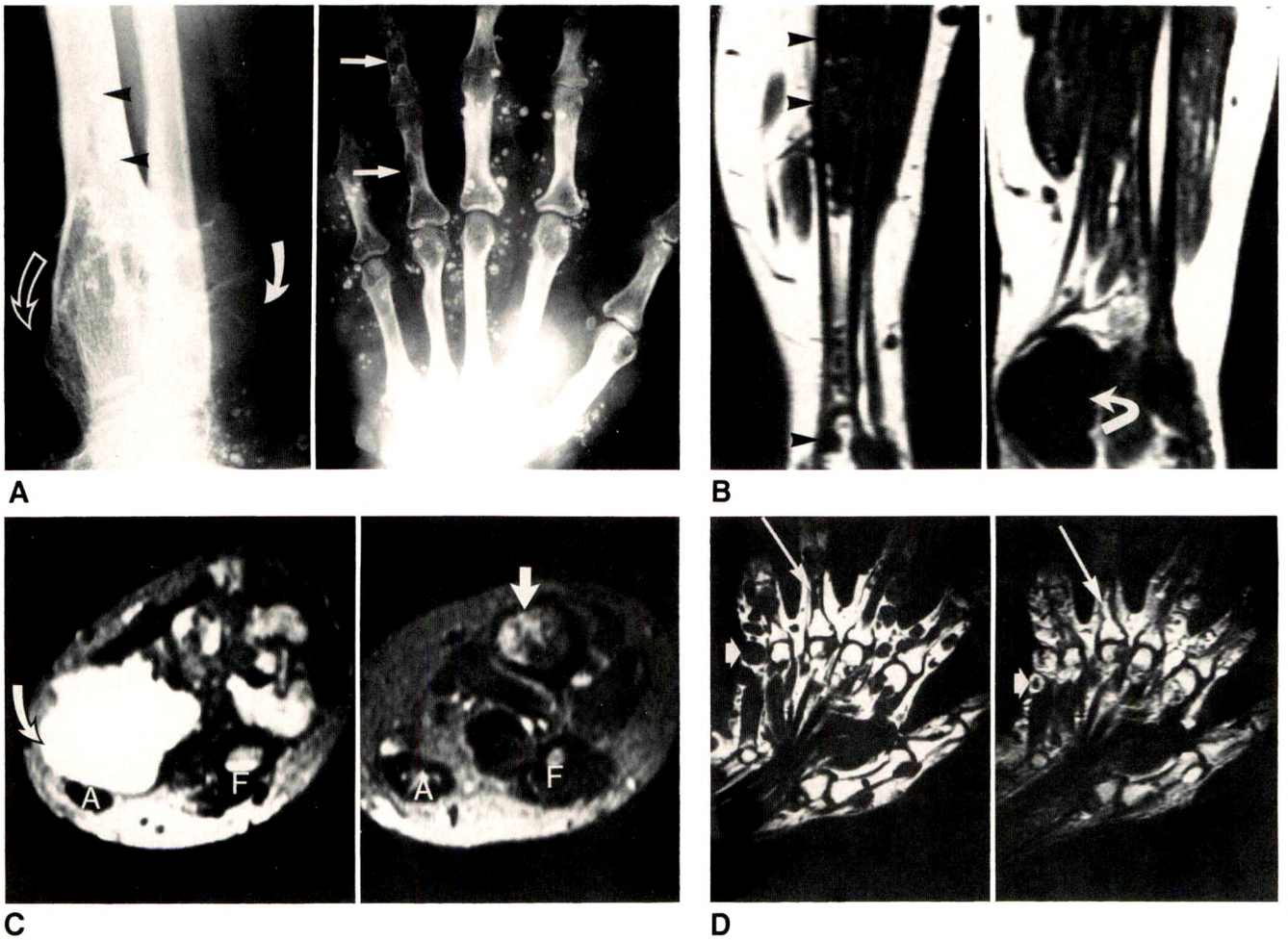

Fig. 1.—40-year-old woman, with Maffucci syndrome and history of cutaneous vascular lesions and hypertrophy of right hand, presented with painful enlarging mass arising from her left ankle.

***A, Left side*: lateral radiograph of left ankle shows mass (*curved solid arrow*) arising from posterior left tibia. There are also a lucent lesion within anterior tibia (*curved open arrow*) and stippled calcification (*arrowheads*) within distal tibial diaphysis. *Right side*: radiograph of right hand shows multiple soft-tissue masses with central calcifications. Enchondromas (*straight arrows*) are seen within bones of hand.**

***B, Left side*: T1-weighted (TR 450 msec/TE 16 msec) coronal MR image shows multiple areas of low signal intensity in fatty marrow of left tibia, corresponding to enchondromas (*arrowheads*). *Right side*: T1-weighted image at a more posterior plane shows soft-tissue mass (*arrow*) arising from posteromedial left tibial metaphysis with signal intensity equal to that of enchondromas.**

***C*, T2-weighted (TR 2500 msec/TE 28 and 70 msec) transaxial images of left tibial metaphysis. *Left side*: image shows high-signal-intensity chondrosarcoma (*curved arrow*) arising from posterior tibia. Anterior high-signal-intensity lesion was biopsied and also proved to be chondrosarcoma. *Right side*: image shows presumably benign enchondroma (*straight arrow*) at a more cephalic scan plane in distal tibia. Enchondroma has lower signal intensity and shorter T2 than chondrosarcoma. A = Achilles tendon, F = fibula.**

***D*, MR images of right hand. *Left side*: T1-weighted (TR 450 msec/TE 16 msec) image shows multiple soft-tissue masses representing cavernous hemangiomas (*short arrow*) that have signal intensity nearly equal to that of muscle. *Right side*: on T2-weighted (TR 2500 msec/TE 28 and 70 msec) image central punctate areas of decreased signal intensity can be seen within cavernous hemangiomas (*short arrow*) corresponding to phleboliths shown on radiographs. Enchondroma (*long arrows*) is nearly isointense to muscle on T1-weighted image and only slightly brighter than marrow on T2-weighted image.**

count of the most cellular areas revealed 10 mitoses/50 high-power fields. These pathologic findings were most consistent with low-grade chondrosarcoma. Because the histologic characteristics of the benign and malignant chondrous lesions were similar, the surgeon decided that the anterior tibial lesion should be followed clinically and that additional surgery should depend on whether the anterior tibial lesion progressed.

Discussion

One-quarter of patients with enchondromatosis and most patients with Maffucci syndrome may eventually develop chondrosarcoma [2]. Distinction between chondrosarcoma and benign enchondroma may be difficult radiographically [3]. Furthermore, there is overlap between the histologic

characteristics of benign enchondromas and those of low-grade chondrosarcoma [4]. In this patient, the T2 of the chondrosarcoma was longer than the T2 of the benign enchondromas. If T2 values can distinguish between chondrosarcoma and benign enchondroma, these values can be used to plan treatment for patients with enchondromatosis. Prolongation of T2 generally reflects elevated water content or increased bulk water [5]. Technical problems in measurement of relaxation values may limit the accuracy of T2 measurements [5]. The measurement of T2, in this case, was derived from only a 2-point data fit by using echo times of 28 and 70 msec; a 3-point data fit would probably be more accurate [5]. Nonetheless, the elevation of T2 in chondrosarcoma of this patient remains an interesting finding that could be useful to help differentiate benign and malignant cartilaginous tissue. In this patient an expansile, painful mass strongly suggested chondrosarcoma. The MR examination was not done for tissue characterization but for anatomic information. The soft-tissue contrast of MR imaging was particularly useful in showing the extent of the lesion and helping make plans for surgery.

Examination of the hand showed the soft-tissue contrast of MR imaging and also allowed comparison of the enchondroma within the phalanges with those in the tibia. We have used MR imaging to examine the hand and forearm of another patient with Maffucci syndrome and found signal-intensity characteristics that are similar to those of the soft-tissue hemangiomas. Low signal was seen on the T1-weighted image that was nearly equal to that of muscle, and high signal was seen on the T2-weighted image similar to that previously described in MR imaging of cavernous hemangioma [6]. The high signal in hemangiomas is probably due to slowly flowing blood and the high proton density of blood [7]. The central low-signal structures corresponded to the radiographically evident phleboliths; the low signal most likely reflects the low proton density and short T2 of phleboliths.

The multiplanar capabilities and soft-tissue contrast of MR imaging are useful for evaluation of musculoskeletal tumors. This case illustrates the utility of MR imaging in the evaluation of Maffucci syndrome. The findings of prolongation of T2 in chondrosarcoma relative to enchondroma suggests that prolongation of T2 may help to distinguish chondrosarcoma from enchondroma.

REFERENCES

1. Maffucci A. Di un caso di enchondroma ed angioma multiplo: contribuzione ell eenesi embrionale dei tumor. *Movimento* **Medico-Chirurgico** **1881**;3:399–412
2. Schwartz HS, Zimmerman NB, Simon MA, Wroble RR, et al. The malignant potential of enchondromatosis. *J Bone Joint Surg [Am]* **1987**;69-A(2): 269–274
3. Mirra JM, Gold RH, Marcove RC. *Bone tumors diagnosis and treatment.* Toronto: Lippincott, **1980**:186–188
4. Spjut HJ. *Tumors of bone and cartilage.* Washington, DC: Armed Forces Institute of Pathology, **1983**:98
5. Bottomley PA, Foster TH, Argersinger RE, Pfeifer LM. A review of normal tissue hydrogen NMR relaxation times and relaxation mechanisms from 1–100 MHz: dependence of tissue type, NMR frequency, temperature, species, excision, and age. *Med Phys* **1984**;11(4):415–448
6. Kaplan PA, Williams SM. Mucocutaneous and peripheral soft-tissue hemangiomas: MR imaging. *Radiology* **1987**;163:163–166
7. George CR, Jacobs G, MacIntyre WJ, et al. Magnetic resonance signal intensity patterns obtained from continuous and pulsatile flow models. *Radiology* **1984**;151:421–428

Book Review

The Running Athlete. Roentgenograms and Remedies. By Helene Pavlov and Joseph S. Torg. Chicago: Year Book Medical, 315 pp., 1987. $55

This tall, extensively illustrated atlas is devoted to the imaging diagnosis of signs and symptoms encountered by professional and amateur runners. Radiographs, arthrograms, nuclear scans, and, occasionally, CT scans or tomograms are presented for each considered entity and are discussed briefly and effectively. These are followed by a short summary of the recommended remedy.

For some less well-known entities, such as subungual exostosis, the discussion is too brief for elucidation for the novice. Other topics are illustrated and discussed effectively, including sesamoid injury, Haglund disease, and osteoid osteoma at several sites. The techniques discussed are well integrated, but relevant sonography and MR imaging are missing.

The book contains many typographical errors, and many "faint lucent lines" are not seen. Otherwise the reproductions are well chosen and printed.

For the topics covered, from toe to spine, this is a valuable book that is pertinent for all radiologists who deal with adults and children who run. Nonetheless, it is incomplete and does not achieve its stated goal; relevant "positional" abnormalities, such as cavus or planus foot, varus or valgus relationships, and even slipped capital femoral epiphysis, are not included.

Alan E. Oestreich
Children's Hospital Medical Center
Cincinnati, OH 45229-2899

Case Report

Polychondritis Affecting the Laryngeal Cartilages: CT Findings

J. W. Casselman,[1] S. F. Lemahieu,[1] P. Peene,[1] and G. Stoffels[2]

Relapsing polychondritis is an inflammatory disease of unknown cause, affecting the ear, nose, respiratory tract, and joint cartilages. An immune reaction against cartilage antigens resulting in cell damage and consequent cartilage destruction is the most widely accepted hypothesis for the cause. The diagnosis is based on both clinical and pathologic findings. Involvement of the upper respiratory tract causes dyspnea, hoarseness, aphonia and airway obstruction due to edema, and collapse of the tracheal and cricoid rings. Only a few cases of relapsing polychondritis studied by CT have been reported [1–2]. We describe a patient who had involvement of the arytenoid as well as the other laryngeal cartilages.

Case Report

A 41-year-old man had a 10-year history of relapsing polychondritis. He initially presented with bilateral auricular chondritis, episcleritis, sternocostal joint arthritis, and an upper respiratory tract infection. His major complaints at that time were hoarseness, dysphagia, fits of coughing, hearing loss, and tenderness over the thyroid cartilage and anterior trachea.

On admission, the patient complained of vertigo, sudden deafness, hoarseness, and dysphagia. Physical examination showed a saddle-nose deformity and deformity of the ear cartilages. Laryngoscopy showed curling and inflammation of the epiglottis, which made good visualization of the glottis difficult. CT showed irregular enlargement of both arytenoid cartilages (Fig. 1A) and to a lesser degree enlargement of the thyroid and cricoid cartilages (Figs. 1A and 1B). The tracheal rings appeared thickened and calcified (Fig. 1C). Calcifications in the pinnae were also shown.

Discussion

The clinical findings of relapsing polychondritis include auricular chondritis, arthropathy, nasal chondritis, ocular inflammation, laryngeal-tracheal tract chondritis, and audiovestibular damage. Cardiovascular and skin involvement are less frequent. Loss of basophilic staining of the cartilage and replacement of destroyed cartilage by fibrous tissue are evident on light microscopy.

CT is a good substitute for laryngotracheograms and conventional tomograms because (1) the cartilage and soft-tissue components are better seen and (2) the instillation of contrast material into the trachea can be avoided.

CT can often be used to confirm the diagnosis by showing (1) involvement of multiple laryngeal cartilages and (2) edema and fibrosis of the soft tissues around these cartilages. Moreover, CT can also show involvement of the cartilages of the ear and nose, two other sites of relapsing polychondritis. The laryngeal changes shown by CT often provide an explanation for symptoms as dysphagia, hoarseness, dyspnea, and respiratory distress. CT findings in chondritis of the cricoid cartilage and epiglottis have been reported before [3, 4].

In this patient, CT showed not only involvement of the cricoid and thyroid cartilages, but also of the arytenoid cartilage. The laryngeal and tracheal cartilages were expanded and calcified rather than destroyed. This can be explained by cartilage hypertrophy, new bone formation in the cartilage, and even formation of nascent cartilage due to a vigorous

Received July 9, 1987; accepted after revision September 23, 1987.
[1] Department of Radiology, University Hospitals K.U. Leuven, Herestraat 49, B-3000 Leuven, Belgium. Address reprint requests to J. W. Casselman.
[2] Department of Otorhinolaryngology, University Hospitals K.U. Leuven, Herestraat 49, B-3000 Leuven, Belgium.

AJR 150:355–356, February 1988 0361–803X/88/1502–0355 © American Roentgen Ray Society

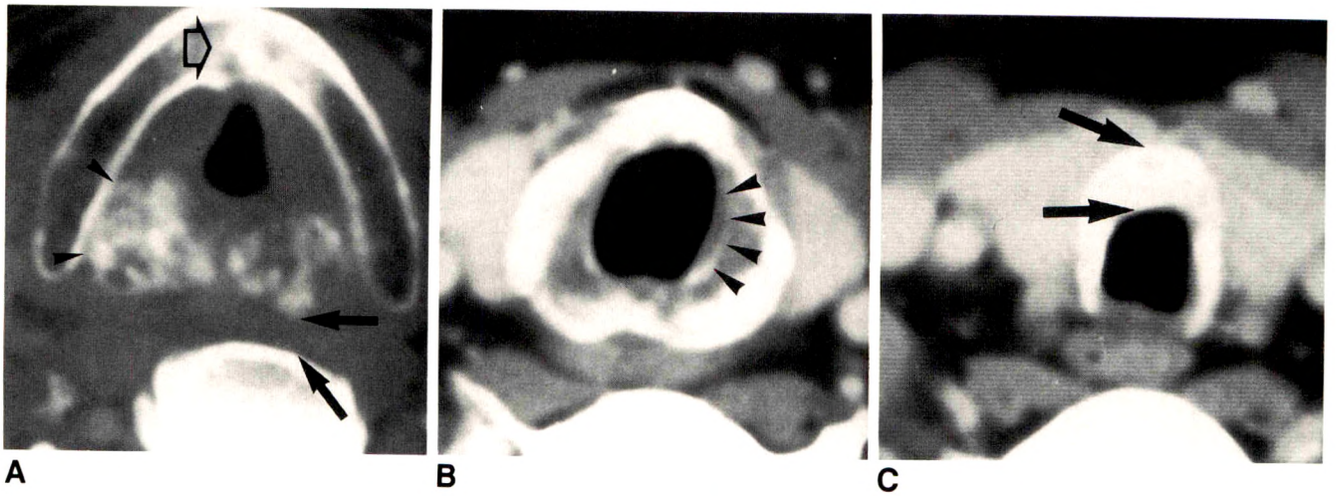

Fig. 1.—*A*, CT scan at level of vocal cords shows both arytenoid cartilages being enlarged and irregular. Right arytenoid cartilage obliterates space between thyroid and arytenoid cartilages and makes contact with thyroid cartilage (*arrowheads*). Arytenoid cartilages nearly touch in midline. Left arytenoid cartilage compresses on hypopharynx (*black arrows*). Anterior portion of thyroid cartilage is also thickened (*open arrow*), and vocal cords are swollen.

***B*, CT scan shows circumferential thickening of cricoid cartilage and edema of mucosa (*arrowheads*).**

***C*, CT scan at level of first tracheal ring shows thickening of tracheal ring, especially anterior part (*black arrows*). There is no significant narrowing of airway lumen at this level.**

reparative response after the dissolution of cartilage [2, 5, 6]. Steroid treatment can also be followed by calcification and ossification of the laryngeal and tracheal cartilages [6]. Abnormal cartilage calcification (perhaps due to chronic inflammation) can occur. Relapsing polychondritis more often involves the trachea than the laryngeal cartilages. Destruction of these tracheal rings or narrowing of the tracheal lumen caused by fibrosis or inflammatory edema may cause respiratory distress [7, 8].

The differential diagnosis in patients with airway narrowing, soft-tissue involvement, and even airway collapse includes Wegener granulomatosis, amyloidosis, other granulomatous disease (sarcoid), and polychondritis. Tracheomalacia due to intubation, tracheobronchopatia osteochondroplastica, tracheal tumors, and saber-sheath trachea also cause narrowing of the airway but can often be differentiated from polychondritis by use of CT. The differential diagnosis of chondritis of multiple laryngeal and tracheal cartilages is limited to relapsing polychondritis and infectious perichondritis.

REFERENCES

1. Mendelson DS, Som PM, Crane R, Cohen BA, Spiera H. Relapsing polychondritis studied by computed tomography. *Radiology* **1985**; 157:489–490
2. Scully RE, Mark EJ, McNeely BU. Case records of the Massachusetts General Hospital, weekly clinicopathological exercises, case 50-1985. *N Engl J Med* **1985**;24:1530–1537
3. McAdam LP, O'Hanalan MA, Bluestone R, Pearson CM. Relapsing polychondritis: prospective study of 23 patients and a review of the literature. *Medicine* **1976**;55:193–215
4. Damiani JM, Levine HL. Relapsing polychondritis—report of ten cases. *Laryngoscope* **1979**;89:929–944
5. Dolan DL, Lemmon GB, Treitelbaum SL. Relapsing polychondritis: analytical literature review and studies on pathogenesis. *Am J Med* **1966**;41: 285–299
6. Johnson TE, Mital N, Rodnan GP, Wilson RJ. Relapsing polychondritis. *Radiology* **1973**;106:313–315
7. Adler D, Bröker HJ, Simmling-Annefeld M. Rezidivierende Polychondritis. Eine Fallbeschreibung unter besonderer Berücksichtigung der Manifestationen im HNO-Bereich. *Laryngol Rhinol Otol* (Stuttg) **1981**;60:187–191
8. Kilman WJ. Narrowing of the airway in relapsing polychondritis. *Radiology* **1978**;126:373–376

Memorial

Edward B. D. Neuhauser, 1908–1987

Edward Blaine Duncan Neuhauser died peacefully in his sleep on September 27, 1987, in his 80th year. After obtaining an M.D. degree from the University of Pennsylvania, he interned at the Pennsylvania Hospital, intending to become an orthopedic surgeon. During residency, however, disenchantment with orthopedic routines set in; the crowning blow was a family of five children, all needing to have their slightly flat feet checked. Seeking more stimulation, he began training in radiology. In 1941, without completing his residency, Dr. Neuhauser became director of radiology at Children's Hospital in Boston. Some of his seniors advised him not to take the position: radiology of children at that time consisted of little more than rickets and pneumonia, and a man of his promise would soon exhaust any ephemeral interest the field might offer. He therefore accepted the position on a 6-month trial basis but, in fact, was Radiologist-in-Chief at that hospital until his retirement 33 years later.

And thus began the phenomenal period of great excitement during which Dr. Neuhauser, in company with Dr. John Caffey at Babies Hospital in New York and a growing band of their associates, established pediatric radiology as a scientific discipline. Some of the subjects clarified by his scientific papers were cystic fibrosis in its many presentations, meconium peritonitis, vascular rings, the radiographic manifestations of leukemia, diaphyseal dysplasia, the etiology of Hirschsprung disease, alimentary duplications, diastematomyelia, Wilms tumors, tricuspid atresia, effects of radiation therapy on bone, atrial septal defect, idiopathic hypercalcemia, hypophosphatasia, neurenteric cysts, total anomalous pulmonary venous drainage, renal tubular ectasia, pulmonary hypertension, the phenomenon of total-body opacification, pulmonary dysmaturity in small prematures, the effects of muscle stress on vertebral growth, Wolman cholesterolosis of the adrenals, injuries to the osseous growth plate, aspiration pneumonitis in childhood, arachnoid cysts in Hurler disease, and the bony manifestations of copper deficiency. His flair for teaching was promptly recognized by medical students, residents, and practicing radiologists, who came from all over the world to spend time in his department.

About 30 years ago, it became evident to Drs. Neuhauser and Caffey and their colleagues in pediatric radiology that this growing body of common interests and knowledge would be furthered by formal organization. In 1958, the first meeting of

the Society for Pediatric Radiology was held; Dr. Neuhauser was the Society's first president. Since 1971, its meetings have been graced by the Neuhauser Lecture. In 1964, he became a founding member of the European Society for Pediatric Radiology.

Dr. Neuhauser was President of the American Roentgen Ray Society in 1959. In his 1952 Caldwell Lecture to that society, entitled "Growth, Differentiation and Disease," he set forth the applications of pediatric radiology to those phenomena. The Mead Johnson Award of the American Academy of Pediatrics was given jointly to him and to Dr. Orvar Swenson for their elucidation of the pathogenesis of Hirschsprung disease. For work in the diagnosis and treatment of Wilms tumor, he shared the Jurzykowski Award in Medical Science with Dr. Sidney Farber and Dr. Robert Gross. He himself lost track of his many other prizes, lectureships, and visiting professorships.

Dr. Neuhauser's major avocation was the Grenfell Mission, begun by Sir Wilfred Grenfell in the 19th century to provide medical care to the people of Labrador and northern Newfoundland. Dr. Neuhauser visited Newfoundland and Labrador frequently, at first giving medical care himself to the scattered inhabitants of that ice-battered coast, later assisting with advice and direction. Because of his knowledge of Arctic medicine, he was sent by the Hudson's Bay Company to inspect its various outposts in 1951. He spent the summer of 1965 as consultant to the government of Denmark, visiting the medical facilities in Greenland and comparing the systems there with those of northern Canada.

To his colleagues, Dr. Neuhauser's most striking attribute was his sparkling brilliance. He was one of the great intuitive diagnosticians. He seemed to have his own systems of perception, unique senses and synapses not possessed by ordinary mortals. He was perfectly prepared to be unorthodox. Sometimes solutions to clinical problems occurred to him in the middle of the night or on awakening, as if his internal computer were busy while the rest of him slept. Another essential characteristic was his ability to run a happy department. His willingness to delegate responsibility, his generous praise, and his genuine interest in his associates' nonmedical activities made being part of his department a joy. He always encouraged his associates to excel in their own ways, not in some fashion decreed from above. Credentials interested him very little; a person's ability and performance, not the weight of his curriculum vitae, earned his respect. A third central trait was his joy in life and in his work. He carried his responsibilities lightly, and this led to a good feeling that was contagious. His boyish enthusiasms caused a fellow department head to call him the world's oldest living child. He embodied the maxim that what one enjoys, one does well. If the radiologic problems of the day began to pall, he discussed gourmet cooking with his residents and students—or Arctic exploration or concepts of tumor growth—until all were refreshed and the work at hand regained its charm.

Dr. Neuhauser retired in 1974, becoming Senior Consultant in Radiology at Children's Hospital and Emeritus Professor of Radiology at Harvard. His summers thereafter were spent in Blue Hill, Maine; his winters were spent in Boston, consulting on obscure radiologic problems, teaching and participating in courses at the Harvard Institute for Learning in Retirement, and pursuing the interests of a lifetime. However, he was unable to alter the central theme of his career, most aptly stated on his gold medal from the Children's Hospital of Philadelphia: "Quippe qui numquam immemor esset puerorum": "he who indeed was never unmindful of children."

Dr. Neuhauser is survived by his widow, the former Gernda von Briesen, two sons, and four grandchildren. He will be remembered by innumerable friends and colleagues as a remarkable physician and a unique human being.

N. Thorne Griscom
Boston, MA 02115

Scoliosis Examinations: Organ Dose and Image Quality with Rare-Earth Screen-Film Systems

Thomas Fearon[1]
James Vucich[2]
Priscilla Butler[3]
William J. McSweeney[1]
George A. Taylor[1]
Bruce M. Markle[1]
Joseph Hoe[1]

We determined the dose to the breast and evaluated the image quality when various high-speed, rare-earth screen-film systems were used in conjunction with breast dose reduction methods in children undergoing scoliosis examinations. In addition, normalized organ dose to the breast, active bone marrow, thyroid, eyes, ovaries, and testes were measured in a pediatric anthropomorphic phantom comparing the anteroposterior and posteroanterior projections. The average measured dose to the breast was 6.9 and 4.0 mrad (10^{-5} Gy), respectively, for nominal 400- and 600-speed, rare-earth screen-film systems used in combination with breast dose reduction methods. The image quality of these systems as evaluated by three radiologists was rated as adequate. The dosimetry results with an anthropomorphic phantom showed that the posteroanterior projection provides approximately a threefold reduction in breast dose as compared with the anteroposterior view. However, the dose to the bone marrow is doubled.

Rare-earth screen-film systems used in combination with simple dose-reduction methods can provide adequate image quality for scoliosis examination while significantly reducing the radiation dose to the breast.

The risk of developing radiation-induced leukemia and breast cancer may be greater in the child [1–2]. Therefore, minimization of radiation exposure to the breast and bone marrow in the treatment and follow-up of scoliosis is of particular concern in pediatric radiology. The increased risk of radiation-induced breast cancer in adolescent girls in addition to the potential for repeated examinations calls attention to the importance of keeping the dose to the breast, as well as to other radiosensitive organs (i.e., bone marrow and thyroid), as low as possible.

Various methods have been used to reduce breast exposure during scoliosis radiography, including high-speed, rare-earth screen-film systems [3–5], breast shields [5–6], posteroanterior instead of anteroposterior projections [4–9], leaded acrylic compensation filters (i.e., "wedge filters") [10–11], and higher kilovoltage [7].

We compared the breast dose for three high-speed, rare-earth screen-film systems in children undergoing scoliosis examinations. The doses were measured for examinations simultaneously employing the following breast dose reduction methods: high-kilovoltage technique; compensating wedge filter; high-speed, rare-earth screen-film systems; and posteroanterior projection. In addition, the image quality of the film systems was evaluated on the basis of anatomic criteria. The organ dose to the breast, active bone marrow, eyes, ovaries, testes, and thyroid was also determined in a pediatric anthropomorphic phantom.

Methods

Clinical Dose Measurements

Clinical dosimetry measurements were carried out by using small, heat-sealed plastic packages, each containing five CaF_2 thermoluminescent dosimeter chips (TLDs). A package

Received August 7, 1987; accepted after revision October 20, 1987.

This work was supported by a grant from the National Cancer Institute (grant number 1 R01CA42421–01) and the Research Foundation of Children's Hospital National Medical Center, Washington, DC.

[1] Departments of Radiology and Child Health and Development, Children's Hospital National Medical Center, George Washington University School of Medicine, Washington, DC 20037. Address reprint requests to T. Fearon, Dept. of Radiology, Children's Hospital National Medical Center, 111 Michigan Ave, N.W., Washington, DC 20010.

[2] Department of Radiology, National Institutes of Health, Bethesda, MD 20892.

[3] Department of Radiology, George Washington University School of Medicine, Washington, DC 20037.

AJR 150:359–362, February 1988
0361–803X/88/1502–0359
© American Roentgen Ray Society

of TLDs was positioned on each patient at the xyphoid. All exposures were performed with a Philips Maximum M-100 generator and Philips Super Rotalix 33/100 X-ray tube (0.6-mm nominal focal spot, 3.0-mm Al half-value layer) under automatic exposure control. The patients were positioned for a posteroanterior projection and the exposures were made at 90 kVp, 183-cm source-image distance (SID), with a 12:1 focused grid and a lead-acrylic compensatory wedge filter (Nuclear Associates, Carle Place, NY). Sixty-nine children (average age, 13 years; range, 6–17 years) undergoing scoliosis examinations participated in the dosimetry measurements. The TLD chips were read out on a thermoluminescent analyzer (Model 2000B Thermoluminescent Analyzer System, Harshaw Chemical Company, Solon, OH), and the TLD output was converted to dose in tissue.

Evaluation of Image Quality

A comparative evaluation of four rare-earth and one calcium tungstate screen-film systems based on the subjective evaluation of anatomic landmarks was carried out for the systems listed in Table 1. All exposures were made with the same Philips system and technique factors as those noted in the dose measurements section above. The automatic exposure control system was adjusted for each screen-film system to produce a net density of 1.20 ± 0.05 for a 15-cm homogeneous lucite phantom.

In 25 children (average age, 13 years), posteroanterior spine films were obtained for each screen-film system evaluated. The test sample of 75 radiographs was chosen from the entire group of films (15 films/system). Radiographs showing gross disease or poor positioning were eliminated. To determine evaluation criteria, three radiologists were asked to delineate those anatomic landmarks present on typical posteroanterior pediatric scoliosis radiographs whose detection is related to the diagnosis of significant radiologic abnormalities; they were then asked to assign a weighted score to each major landmark. The weighting factor reflects the relative diagnostic importance placed on each anatomic landmark by the radiologists. A master list of important landmarks was developed from the individual lists with an average weighted score. The radiologists were then asked to subdivide the major landmarks and assign weighting scores to each. The major anatomic landmarks and associated maximal weighting scores defined by the radiologists were thoracic spine (40%), lumbar spine (40%), iliac crest (15%), ribs (5%), soft tissue (5%), and trabecular patterns (5%). The thoracic and lumbar spine regions were each subdivided with respect to visualization of the pedicles (20%) and vertebral bodies (20%). The radiologists were asked to review and evaluate each radiograph in terms of their subjective visualization of anatomic landmarks. The radiographs were presented in random order under constant viewing conditions. Evaluated parameter scores were used to obtain total percentage scores for each test radiograph, as evaluated by each radiologist. The scores were pooled, and the systems were ranked.

Anthropomorphic Phantom Dose Measurements

An anthropomorphic pediatric phantom (Humanoid System, Carson, CA) representing an average 6-year-old child (height, 120 cm; weight, 20 kg) was used in conjunction with thermoluminescent dosimetry to measure pediatric organ doses for anteroposterior and posteroanterior projections in scoliosis examinations of the spine. The phantom consists of a human skeleton, lungs, and airway. The skeleton is impregnated with tissue-equivalent material (density, 1.002 g/cm^3) and is encased in tissue-equivalent material molded to model an average 6-year-old patient. Lungs are molded of lung-equivalent material (density, 0.433 g/cm^3). The molded phantom is sliced into 20 2.5-cm-thick transaxial sections, each of which contains a matrix of 5-mm holes with 1.5-cm orthogonal spacing. Tissue- and lung-equivalent plugs with internal cavities to accommodate CaF_2 TLD chips are inserted into the grid holes at positions corresponding to organs of interest. The dose to the breast, active bone marrow, eyes, thyroid, ovaries, and testes was measured. The dose to bone marrow was determined from the sum of weighted sampled measurements of 20 bone marrow sites (Table 2). Weighting factors equal to the ratio of the bone marrow at a given site [12] to the total bone marrow of all the sites sampled were assigned to the sampled sites. The thermoluminescent response was converted to dose in tissue by using the calibration factor for each TLD batch and the f-factor; f = 0.92 rad/R (35.7 Gy per kg/C).

TABLE 1: Screen-Film Systems Evaluated

Screen	Film
Dupont: Hi Plus	Dupont: Cronex 4
Kodak: Lanex Regular	Kodak: Ortho H
Kodak: Lanex Regular	Kodak: T-MAT G
Kodak: Lanex Fast	Kodak: T-MAT G
Kodak: Lanex Fast	Kodak: T-MAT H

Results

Table 3 provides breast dose measurements for three rare-earth screen-film systems used under clinical conditions. Table 4 presents anthropomorphic phantom-normalized organ dose measurements for anteroposterior and posteroanterior projections in scoliosis examinations. These phantom measurements clearly demonstrate the advantage in dose reduction to the breast and thyroid for the posteroanterior projec-

TABLE 2: Active Bone Marrow Dose Weighting Factors[a]

Location	Slice (No. of points)	Fraction of Active Bone Marrow[b]	Weighting Factor[c]
Cranium	2 (2)	0.159	0.176
Mandible	6 (1)	0.016	0.018
Scapulae	9 (1)	0.027	0.030
Clavicles	8 (1)	0.009	0.010
Sternum	11 (1)	0.017	0.019
Ribs	11 (1)	0.086	0.098
Cervical spine	6 (1)	0.022	0.024
Thoracic spine	10, 11, 13, 13 (4)	0.089	0.099
Lumbar spine	16 (2)	0.068	0.075
Sacrum	18 (1)	0.055	0.061
Pelvis	18, 19 (4)	0.131	0.145
Femur, tibiae, fibulae, and patella	20 (2)	0.221	0.245
Total		0.900	1.000

[a] Weighting factors are equal to the ratio of bone marrow at a given sample site to total bone marrow of all sites sampled. The dose to the active bone marrow is calculated as a weighted sum of the sampled sites.

[b] Based on a 5-year-old patient described by Christy [12].

[c] The following regions of the skeleton with their associated fraction of active bone marrow are not included in the normalized weighting factor: ankle and foot (0.025), humeri (0.046), ulnae and radii (0.02), wrist and hand bones (0.009).

TABLE 3: Patient Breast Dose from Scoliosis Examinations

System	Age of Patients in Years (Range)	Breast dose[a] mrad (10^{-5} Gy)
Kodak—Lanex Regular/T-MAT G	12.8 ± 2.1 (7–15)	6.9 ± 2.8
Kodak—Lanex Fast/T-MAT G	13.6 ± 2.4 (9–17)	4.0 ± 3.0
Kodak—Lanex Fast/T-MAT H	12.4 ± 2.8 (6–12)	1.8 ± 1.8

[a] Technique: 90 kVp, 183-cm source-image distance, lead acrylic wedge filter, 12:1 grid, automatic exposure control, and posteroanterior projection.

TABLE 4: Normalized Phantom Organ Doses[a]

Organ	Normalized Dose in mrad/R Free-in-Air (0.39 Gy per kg/C)	
	AP Projection	PA Projection
Breast	279 ± 48	94 ± 13
Bone marrow	53 ± 4	110 ± 10
Eyes	4 ± 0.4	2 ± 0.2
Thyroid	526 ± 54	206 ± 22
Ovaries	12.5 ± 2	11.6 ± 1
Testes	4.9 ± 0.3	5.6 ± 0.2

Note.—AP = anteroposterior, PA = posteroanterior.

[a] Table shows normalized organ dose measurements for scoliosis radiography in an anthropomorphic phantom representing an average 6-year-old child.

TABLE 5: Anatomic-Criteria Evaluation of Films of Scoliosis Patients

System	Average Score	Mean Rank	Significant[a] Differences (System Numbers)
1. Hi Plus/Cronex 4	80.2	5	1 > 2, 3, 4, 5
2. Lanex Regular/T-MAT G	74.2	3.7	2 > 4, 5
3. Lanex Fast/T-MAT G	73.3	3.3	3 > 5
4. Lanex Regular/Ortho H	65.8	2	4 > 5
5. Lanex Fast/T-MAT H	49.0	1	—

Note.—Dash indicates that scores from system 5 were lower than on any other system.

[a] Mann-Whitney U Test, $p < .05$.

tion relative to the anteroposterior projection; however, the active bone marrow dose doubles for this projection.

Table 5 presents the results of the anatomic-criteria evaluations of films of scoliosis patients. The average score and mean rank for three radiologist observers are shown.

The raw scores for all of the screen-film systems for each of three observers were analyzed using the Kruskal-Wallis one-way analysis of variance by ranks. At the 95% confidence level, there is no statistical evidence to reject the hypothesis that the scores are from the same population. The Mann-Whitney U test was used to compare the statistical significance of differences in mean scores. Statistically significant differences ($p < .05$) are noted in decreasing order of rank by system number (Table 5).

Discussion

The purpose of this study was to evaluate the effect on image quality of various high-speed, rare-earth screen-film systems while simultaneously employing several methods of breast dose reduction (i.e., posteroanterior projection, high kilovoltage, and compensating wedge filter). Under these conditions, the doses measured at the xyphoid for three rare-earth screen-film systems (Table 3) decreased as a function of the speed of the systems, as expected, and were similar to those found by other investigators who employed the posteroanterior projection as well as various breast dose reduction methods. The doses we found were of relatively low magnitude. On the basis of relative system speed, Dupont Hi Plus/Cronex 4 would deliver a dose to the breast of approximately 15 mrad (10^{-5} Gy).

Table 5 presents the average score of three radiologists that is based on their evaluation of the visualization of anatomic criteria in scoliosis films for each of the screen-film systems considered. The systems were also ranked from 5 (highest) to 1 (lowest) in terms of relative evaluation score. The scores based on the highest-ranked but the slowest-speed system (Hi Plus/Cronex 4, a calcium tungstate screen-film system) was found to be significantly different ($p < .05$) from all of the rare-earth screen-film systems. Scores based on the second- and third-ranked systems (Lanex Regular/T-MAT G and Lanex Fast/T-MAT G, respectively) were not significantly different from each other, but they were significantly different from the two fastest systems (Lanex Regular/Ortho H, nominal 800 speed, and Lanex Fast/T-MAT H, nominal 1200 speed). The average scores for the three highest-ranked systems were within the range rated as adequate according to the evaluation criteria of the radiologist observers in this experiment (i.e., a score ≥72). The radiologists concluded that these systems were adequate for initial as well as follow-up scoliosis examinations. The two fastest systems (mean ranks, 1 and 2) might be considered for follow-up examinations, even though the images are noisy.

Table 4 presents normalized organ dose measurements for scoliosis radiography in an anthropomorphic phantom representing an average 6-year-old child. Clearly, the use of the posteroanterior projection rather than the anteroposterior projection provided approximately a threefold reduction in breast dose. This result is as expected from geometric considerations where the body provides shielding for the breast tissue. Similarly, the thyroid dose is reduced by a factor of approximately 2.5, and the dose to the eye by a factor of two. The dose to the active bone marrow, however, is shown to double for the posteroanterior projection. This finding is similar to that of calculations provided by Rosenstein [13] for a 5-year-old patient. However, Gray et al. [14] indicated that the posteroanterior chest radiograph decreased bone marrow dose relative to the anteroposterior projection. These measurements were performed using an anthropomorphic phantom representing an adult (70-kg man). Beyond the obvious size differences, other problems are associated with estimating an integral volume dose from point measurements at various locations within a phantom: differences in the volume of tissue irradiated, attenuation characteristics of the phan-

toms, and variations in the bone marrow distribution assumed. The distribution of bone marrow is a strong function of age and would, therefore, have a significant influence on the dose delivered to the bone marrow. In a 5-year-old, approximately 20% of the active bone marrow is in the skull, 48% is in the thorax, and the remaining 32% is in the extremities [12]. By the age of 15 years, the major distribution sites have gradually shifted from the skull (10%) and extremities (15%) to the pelvis (19%), vertebrae (28%), and ribs (14%). An expected consequence of this bone marrow redistribution would be a larger dose to the bone marrow in the adult, as compared with that measured in a 6-year-old anthropomorphic phantom for scoliosis examinations. In addition, the shift of bone marrow distribution to the vertebrae is greater than that to the sternum and ribs; therefore, the bone marrow dose for the posteroanterior projection relative to the anteroposterior projection would be expected to be higher in an adolescent patient. The question of which projection provides a lower bone marrow dose remains open; however, we hope to shed some light on this question with future dose measurements to be conducted in an anthropomorphic phantom representing an average 12-year-old patient.

This study shows that the use of the simple dose-reduction techniques can significantly reduce the dose to the breast during routine scoliosis examinations (and, concomitantly, the risk of radiation-induced breast cancer), without loss of important diagnostic information. Gray et al. [5] estimated that dose is reduced 69-fold when these techniques are used instead of more conventional methods. Consider that a patient could receive up to a total of 40 scoliosis radiographs over a period of several years. The use of simple dose-reduction techniques could conceivably result in a dose savings of 10 rad (0.1 Gy) to the breast. This dose level is significant because of the increased risk associated with radiation-induced breast cancer for young women. Boice and Monson [15] estimated the number of excess cases of breast cancer in women who have undergone radiation. For young women (13–20 years old), the estimated risk was 162×10^{-6} for every 1 million women who had received a dose of 1 rad (0.01 Gy). Estimated risk decreased with age: for women 20–29 years old, there were 108×10^{-6} excess cases; for women more than 20 years old, there were 78×10^{-6} excess cases.

Rare-earth screen-film systems can provide adequate image quality in scoliosis examinations (as shown by anatomic-criteria evaluations for initial as well as follow-up studies) while significantly reducing the radiation dose to the radiosensitive breast tissues. The average measured dose to the breast was 4.0 mrad (10^{-5} Gy) for a nominal 600-speed, rare-earth screen-film system in combination with breast dose reduction methods. Faster rare-earth screen-film systems with correspondingly lower dose to the breast may be considered for routine follow-up examinations where secondary causes are no longer in question and decreased image quality is considered acceptable. Anthropomorphic phantom measurements demonstrate a threefold reduction in breast dose by the use of the posteroanterior projection rather than the anteroposterior projection; however, there is a compensating increase in the dose to the active bone marrow.

ACKNOWLEDGMENTS

The authors thank Art Haus and Eastman Kodak Company for supplying the Lanex Fast cassette and T-MAT H film used in this study. They also thank Karen O'Neil for her assistance in providing the radiographs and dosimetry exposures and Debra Janicki for her assistance in typing the manuscript.

REFERENCES

1. Beebe GW, Kato H, Land CE. Studies of the mortality of A-bomb survivors. 6. Mortality and radiation dose, 1950–1974. *Radiat Res* **1978**;75:138–201
2. Boice J, Land C, Shore R, Norman JE, Tokunaga M. Risks of breast cancer following low-dose radiation exposure. *Radiology* **1979**;131:589–597
3. DeSmet AA, Fritz SL, Asher MA. A method for minimizing the radiation exposure from scoliosis radiographs. *J Bone Joint Surg [Am]* **1981**;63-A:156–158
4. Ardran GM, Coates R, Dickson RA, Dixon-Brown A, Harding FM. Assessment of scoliosis in children: low dose radiographic technique. *Br J Radiol* **1980**;53:146–147
5. Gray JE, Hoffman AD, Peterson HA. Reduction of radiation exposure during radiography for scoliosis. *J Bone Joint Surg [Am]* **1983**;65-A:5–12
6. Frank ED, Kuntz JI. A simple method of protecting the breasts during upright lateral radiography for spine deformities. *Radiol Technol* **1983**;55:532–535
7. Drummond D, Ranallo F, Lonstein J, Brooks HL, Cameron J. Radiation hazards in scoliosis management. *Spine* **1983**;8:741–748
8. Rao PS, Gregg EC. A revised estimate of the risk of carcinogenesis from x-rays to scoliosis patients. *Invest Radiol* **1984**;19:58–60
9. Hellstrom G, Irstam L, Nachemson A. Reduction of radiation dose in radiologic examination of patients with scoliosis. *Spine* **1983**;8:28–30
10. Becker J. Adjustable compensating filters for pediatric 72 inch spine radiography. *Radiol Technol* **1979**;51:11–16
11. Gray JE, Stears RT, Frank RT. Shaped, lead-loaded acrylic filters for patient exposure reduction and image quality improvement. *Radiology* **1983**;146:825–828
12. Cristy M. Active bone marrow distribution as a function of age in humans. *Phys Med Biol* **1985**;26:389–400
13. Rosenstein M. *Handbook of selected organ doses for projections common in pediatric radiology*. Washington, DC: HHS Publication (FDA) 79–8079, **1979**
14. Gray JE, Ragozzino MW, Van Lysel MS, Burke TM. Normalized organ doses for various diagnostic radiologic procedures. *AJR* **1981**;137:463–470
15. Boice JD, Monson RR. Breast cancer in women after repeated fluoroscopic examinations of the chest. *J Natl Cancer Inst* **1977**;59:823–832

MR Imaging of Ebstein Anomaly: Results in Four Cases

Kerry M. Link[1]
Marcos A. Herrera
Vincent J. D'Souza
Augustin G. Formanek

We performed ECG-gated MR imaging in four patients (4 months–15 years old), all of whom had a previously diagnosed severe form of Ebstein anomaly of the tricuspid valve. The goal was to study the anatomy of this congenital heart defect with MR imaging. The axial and coronal scans provided the best details. All characteristic abnormalities were seen well: the maintained proximal and faulty distal attachment of the anterior tricuspid leaflet, the absence of both septal and posterior tricuspid leaflets, the size and delineation of the anatomically atrialized chamber of the right ventricle, and the small, compressed trabecular portion with the markedly dilated pumping outflow tract of the right ventricle proper.

Our results suggest that MR may furnish valuable information in patients with Ebstein anomaly when echocardiography is either inconclusive or technically difficult to perform.

Ebstein anomaly (EA) of the tricuspid valve is a rare congenital heart defect found in approximately 0.5–1% of autopsy cases with congenital heart disease [1]. It is characterized by varying degrees of downward displacement or dysplasia of the tricuspid valve and resultant atrialization of a portion of the right ventricle, decreased pumping capacity of the right ventricle proper, and enlargement of the right atrium.

Obtaining a clear anatomic picture with angiocardiography is often difficult because of the markedly enlarged and distorted right side of the heart and because the internal architecture might be obscured by the large amount of contrast medium required for angiographic studies. Therefore cross-sectional echocardiography, which provides a reliable assessment of anatomy and function in EA without requiring invasive investigations [2], is the imaging technique of choice. However, in borderline cases, problems may arise in distinguishing abnormal displacement from lowered septal offsettings of the tricuspid valve in normal persons [3].

MR imaging, which furnishes sectional anatomy in multiple body planes, might yield more detailed information about EA than either echocardiography or angiocardiography. To assess this, we used MR to evaluate four patients with EA.

Materials and Methods

We performed MR studies of the heart in four patients with EA of the tricuspid valve. The patients ranged in age from 4 months to 15 years. Previous diagnosis had been made by either cineangiography or two-dimensional echocardiography. None of the patients had had surgery.

Images were obtained in the body coil of a Picker Vista 1000, resistive, 0.15-T imager (Highland Heights, OH) with a proton-resonance frequency of 6.4 MHz. ECG gating was accomplished by a triggered data-acquisition process in which the R wave initiated a view while the R-R time determined the pulse-repeat time. A software-selective time-delay parameter permitted imaging to begin at a prescribed point in the cardiac cycle.

Spin-echo scans were performed with an echo-delay time of 30–40 msec. Images were

Received August 31, 1987; accepted after revision October 27, 1987.

[1] All authors: Department of Radiology, The Bowman Gray School of Medicine, Wake Forest University, 300 S. Hawthorne Rd., Winston-Salem, NC 27103. Address reprint requests to A. G. Formanek.

AJR 150:363–367, February 1988
0361–803X/88/1502–0363
© American Roentgen Ray Society

acquired with a mutlislice technique in which four to six adjacent 10-mm-thick sections were obtained. Each image used 128 views and four repetitions per view. The pixel size was 2 mm.

All patients had axial and coronal scans. Two patients also had sagittal scans. In the infant, a second set of axial slices was offset by 5 mm with respect to the original imaging level.

The normal anatomy of the right side of the heart as it appears on MR images is as follows: The axial plane provides the best images of the tricuspid valve. Usually one of the sequential images through the entire right ventricle allows good visualization of the anterior and septal leaflets. The attachment of the septal leaflet to the interventricular septum is slightly closer to the heart apex (normal offsetting) than is the attachment of the mitral valve [4] (Fig. 1). Externally, the location of the attachment of the anterior leaflet is marked by the accumulation of fat in the anterior atrioventricular groove or by changes in the thickness of the anterior heart wall (Fig. 2A). These findings pinpoint the location of the right atrioventricular junction. The posterior leaflet of the tricuspid valve typically is not seen on the images. Of the papillary muscles, only the largest anterior one is well visualized, and only in approximately one-third of humans [5]. The second characteristic feature of the right ventricle is the prominent muscular structure, the moderator band, that extends from the ventricular septum to the anterior wall [5] within the trabeculated zone close to the apex (Fig. 1). The shape of the right ventricle changes in the caudocranial direction—the triangular shape of the inflow (inlet) and trabecular zones is replaced by the nearly round, smooth outflow portion (infundibulum) (Figs. 2A and 2B). On the coronal images, the internal anatomy is less clearly depicted because of the oblique orientation of the long axis of the heart, and the components of the tricuspid valve are not commonly visualized. The outflow tract of the right ventricle is clearly visible in its entirety. On the sagittal scans, the tricuspid valve cannot be located because the right ventricle and right atrium are nearly side by side.

Results

In all four of our patients, the axial and coronal images were similar. The markedly dilated right atrium was well defined, and the anatomically atrialized portion of the right ventricle was clearly delineated (Figs. 3 and 4). The wall thickness of the latter is diminished in comparison with that of the right ventricle proper (Fig. 3A). In two patients with a huge atrialized portion medial to the left ventricle, a definite posterior bulge extended to the posterior aspect of the left ventricular free wall or slightly beyond (Fig. 5). In two patients, the atrialized portion occupied the entire width of the right ventricle (Fig. 3); in two, it was located posterior to the large anterior leaflet and extended toward its distal attachment (Fig. 5A). A constant finding was a convex leftward strand, a few millimeters thick, that separated the atrialized portion of the right ventricle from its compressed trabecular portion, including the apex (Figs. 3 and 4).

The infundibulum, well outlined in all patients, was massively dilated. It was situated above the dilated portion of the right ventricle and not above the trabecular portion (Fig. 4). Extreme changes were seen in the size of the infundibulum between diastole and systole (Fig. 6).

The anterior leaflet of the tricuspid valve was well defined in three patients and was proximally attached to the atrioventricular ring (Fig. 3A). In two patients, the entire length of the anterior leaflet, running 2–3 cm parallel to the anterior wall, was visible; laterally, it reached the coarsely trabeculated portion of the right ventricle (Fig. 5). Neither a septal nor a posterior leaflet could be identified in any of the completely imaged hearts.

An atrial-septal defect was diagnosed in the infant; it appeared as a defect in the septum on two adjacent levels and had a sharp, thick margin [6] (Fig. 7A). In three patients, the eustachian valve (a flap valve located in front of the mouth of the inferior vena cava) was identifiable (Fig. 7A).

The left atrium and left ventricle were displaced craniad and laterally and were flattened in the posteroanterior projection. Consequently, the interventricular septum bulged into the left ventricle (Fig. 3).

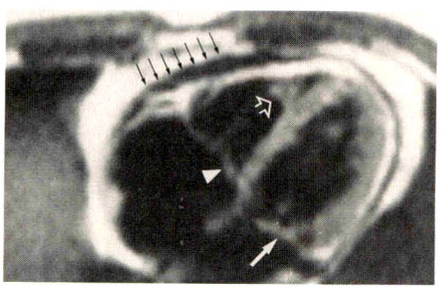

Fig. 1.—Axial scan through midportion of heart shows normal right heart. Septal leaflet of tricuspid valve (*arrowhead*) is closer to cardiac apex than is mitral valve (*solid white arrow*). Moderator band (*open arrow*) is visualized. An incidental finding is thickening of pericardium caused by chronic pericarditis (*black arrows*). Interventricular septum is slightly convex toward right ventricular.

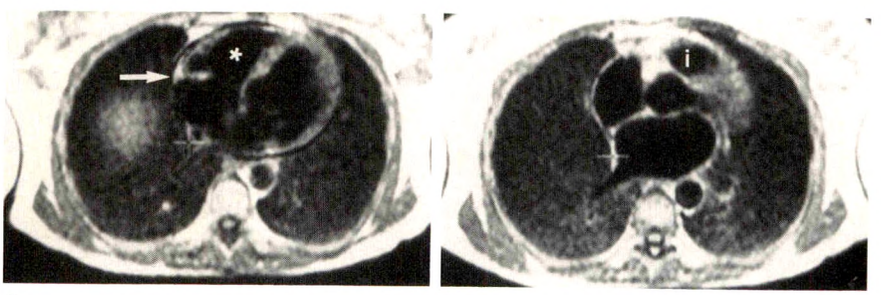

Fig. 2.—Axial scans of a normal heart show differences in shape of right ventricular components. *A*, Triangular inlet and trabecular portions (*asterisk*). *B*, Note oval shape of infundibulum (i). Notice accumulation of fat in right atrioventricular groove (*arrow* in *A*).

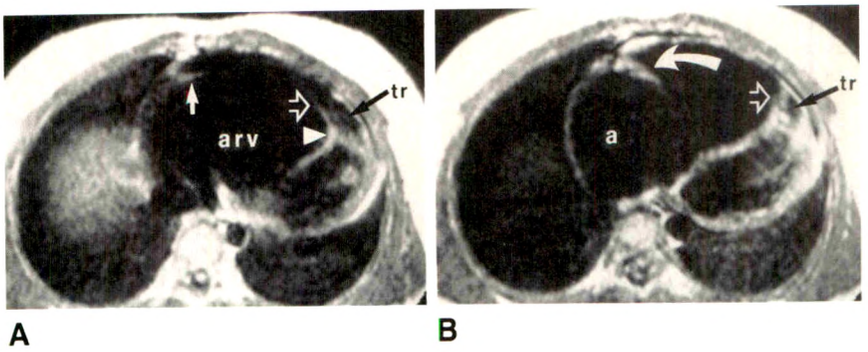

Fig. 3.—Axial scans in 12-year-old boy with Ebstein anomaly show markedly enlarged right atrium (a) and atrialized portion of right ventricle (arv). Proximal attachment of anterior tricuspid leaflet at atrial ventricular junction (*straight white arrow*) and its distal attachment to septum (*arrowhead*) are well seen in *A*. Muscular ridge (*open arrow*) separating compressed trabecular portion (tr and *black arrow*) of right ventricle from atrialized portion is shown on *A* and *B*. Triangular structure (*curved white arrow* in *B*) is adipose tissue between right atrium and dilated right ventricular outflow tract (compare with Fig. 6). Interventricular septum bulges toward left ventricle.

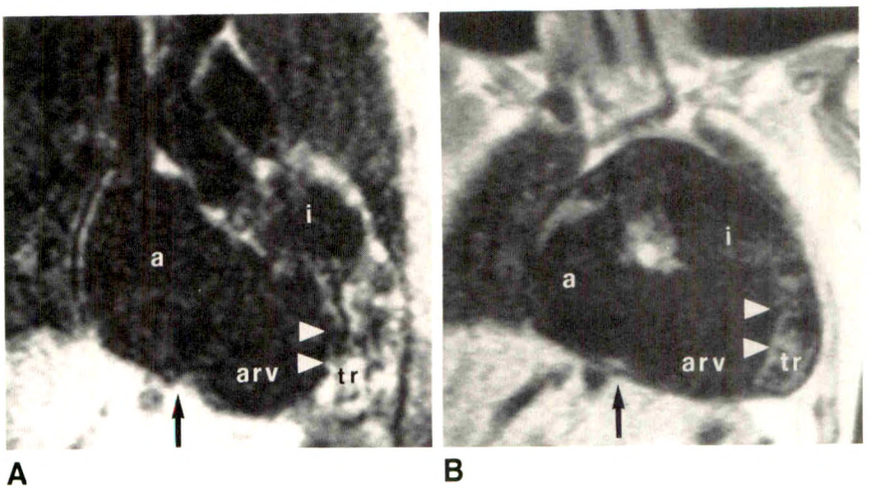

Fig. 4.—Coronal scans in 15-year-old boy (*A*) and in 10-year-old boy (*B*) show four components of right heart in Ebstein anomaly: atria (a), atrialized portion of the right ventricle (arv), compressed trabecular portions (tr), and infundibula (i). *Black arrows* show atrioventricular junction. Atrialized portions of right ventricle are separated from compressed trabecular portions by a leftward convex vertical structure—muscular ridge (*arrowheads*). Notice cranial extension of this muscular ridge. Large infundibula are located above atrialized portions.

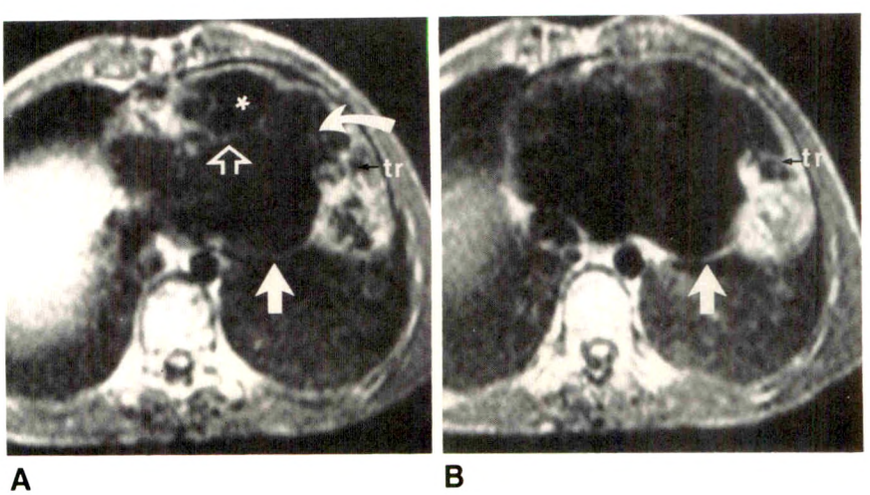

Fig. 5.—Adjacent axial images of patient shown in Fig. 4A. Atrialized portion of right ventricle bulges posteriorly (*solid straight arrows*) and is bordered anteriorly by anterior leaflet of tricuspid valve (*open arrow* in *A*), which courses from atrioventricular junction to its distal insertion—the muscular ridge (*curved arrow*). Recesslike space (*asterisk*) anterior to anterior leaflet is not incorporated into atrialized portion of right ventricle. Small trabecular portion (tr and *black arrows*) is again well shown on both frames.

Discussion

The pathologic findings of EA are as follows: The anterior leaflet of the tricuspid valve always remains medially connected to the right atrioventricular junction [7]. However, in contrast to the normal tricuspid valve, in which the lateral edge of the anterior leaflet is free, in EA this edge is attached variably to the right ventricular wall either by an abnormal anterolateral papillary muscle or by a continuous muscular connection [8]. The septal and posterior leaflets are displaced downward and may be deficient or absent [9].

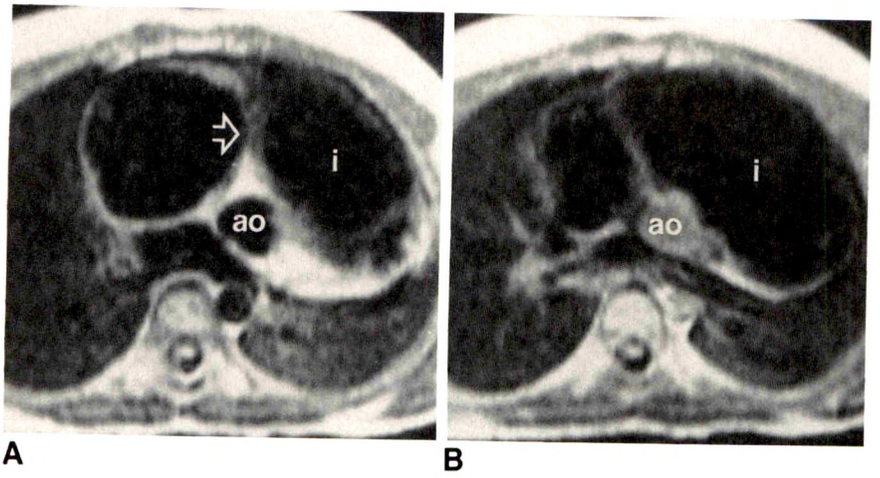

Fig. 6.—Adjacent axial images, *A* in systole and *B* in diastole of patient shown in Fig. 4B. Note large volume changes in right ventricular infundibulum (i). Signals between infundibulum and right atrium (*arrow*) are produced by adipose tissue and not by tricuspid valve. Aorta (ao) is wedged between infundibulum and right atrium.

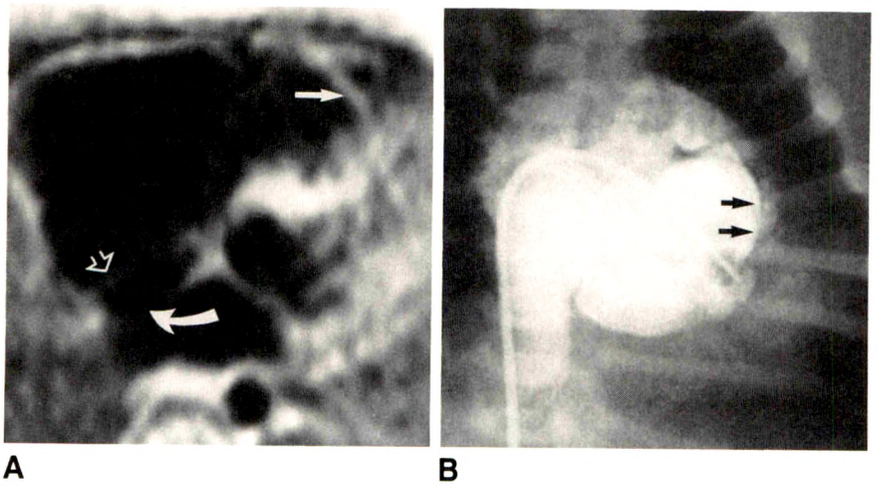

Fig. 7.—*A*, Axial image of an infant shows atrial septal defect (*curved arrow*) and eustachian valve (*open arrow*). Again, boundary (*solid straight arrow*) between atrialized portion and small trabecular portion of right ventricle can be seen.

B, Anteroposterior cineangiogram. Contrast medium is delivered into atrialized portion of right ventricle. Vertical boundary (*arrows*) between atrialized portion and trabeculated portion of right ventricle is well shown and extends to level of infundibulum.

Besides being abnormally inserted, the tricuspid valve is almost always dysplastic; in fact, the dominant feature is dysplasia of the valves rather than displacement [10]. EA can therefore be characterized as a spectrum of features related to the degree of displacement of the proximal leaflet attachments and to the position and structure of their distal attachments [11].

We found no detailed report concerning MR imaging of EA. Brief reference is made to an axial scan showing a distally displaced septal leaflet having a common attachment of its margin with the lateral border of the anterior leaflet; the proximal attachment of the anterior leaflet remained at the right atrioventricular junction [5]. This heart represents a mild form of EA.

Our experience with the more severe form of EA indicates that the MR images closely reflect the pathologic anatomy. The maintained proximal annular attachment of the anterior leaflet was well imaged in three patients (Figs. 3A and 5A). In two patients the diagonally coursing anterior leaflet on the axial images (Fig. 5) corresponds to the sail-like appearance of the leaflet from the anatomic specimen. If the anterior leaflet is not imaged on the axial scans, one may postulate that it is broadly plastered to the anterior wall. The fact that neither the septal nor the posterior leaflets could be traced in any of the four patients is not surprising in view of the pathologic findings in severe forms of EA such as those described above.

In EA, because the orifice of the tricuspid valve does not correspond to the atrioventricular junction, two different compartments result, the anatomically atrialized portion and the hemodynamically effective right ventricle proper. The anatomic atrialization of the right ventricle is well illustrated on both axial and coronal MR images (Figs. 3–5) as the portion of the right ventricle between the atrioventricular annulus and the distal attachment of the abnormal leaflets—the actual tricuspid valve orifice. It involves only the inlet zone of the right ventricle and, no matter how severe the anomaly, the atrialized portion cannot extend beyond the boundaries of the inlet zone because the most distal attachment of the tricuspid valve leaflets is at the abnormal papillary muscles and ridgelike muscular structure at the inlet-trabecular junction [11]. The size of the atrialized portion can vary, however, depending on the severity of the defect.

The lateral delineation of the atrialized portion in our pa-

tients was uniform. On the axial images, it was characterized by a leftward convex strand extending in the anteroposterior direction with broader attachment to the septum (Figs. 3 and 5). On the coronal images, it was a vertical band (several millimeters thick) on the ventricular septum that reached to the infundibulum (Fig. 4). These anatomic features most likely correspond to the ridgelike muscular structure at the inlet-trabecular junction, commonly encompassing the distal faulty attachment of the tricuspid valve apparatus [8, 9, 11].

The angiocardiographic findings (Fig. 7B) attributed to either the laterally displaced anterior leaflet [12] or the displaced tricuspid valve [13] de facto may actually represent the ridgelike or shelflike structure of the inlet-trabecular junction to which the anterior tricuspid leaflet distally is attached; this is seen both in the pathologic specimens and on the MR images.

The second compartment of the right ventricle in EA is composed of the trabecular and outlet zones. However, analysis of the MR images makes it obvious that only the dilated outflow zone is hemodynamically effective. Depending on the heart cycle, this zone displays extreme variations in volume (Fig. 6). On the other hand, the trabecular portion including the apex shows no volume changes at all. Consequently, the pumping component of the right ventricle is confined solely to the infundibulum; its large size and the marked changes in volume reflect this.

The marked dilatation of the right ventricle is well documented on MR images in all three planes. The axial scans show a bulging of the right ventricular wall posteriorly, actually beyond the plane of posterior extension of the left ventricle (Fig. 5). Thus, in severe forms of EA, the posteroinferior border of the heart on a lateral radiograph may be formed by the large right ventricle and not by the left ventricle displaced posteriorly by the right heart.

There is no good explanation for the massive dilatation of the right ventricle in EA; some authors propose that it is an integral component of EA resulting from the deficiency of the right ventricular myocardium [7].

Our results show that MR imaging provides detailed anatomic images of even severe forms of EA and may be valuable whenever there is a need for more information than echocardiography or angiocardiography can provide.

REFERENCES

1. Reinhold-Richter VL. Extreme Ebstein-anomalie. *Zentralbl Allg Pathol* **1984**;129:189–193
2. Radford JD, Graff RF, Neilson GH. Diagnosis and natural history of Ebstein's anomaly. *Br Heart J* **1985**;54:517–522
3. Gussenhoven EJ, Stewart PA, Becker AE, Essed CE, Ligtvoet KM, de Villeneuve VH. "Offsetting" of the septal tricuspid leaflet in normal hearts and in hearts with Ebstein's anomaly: anatomic and echographic correlation. *Am J Cardiol* **1984**;53:172–176
4. Didier D, Higgins CB, Fisher MR, Osaki L, Silverman NH, Cheitlin MD. Congenital heart disease: gated MR imaging in 72 patients. *Radiology* **1986**;158:227–235
5. Markiewicz W, Sechtem U, Higgins CB. Evaluation of the right ventricle by magnetic resonance imaging. *Am Heart J* **1987**;113:8–15
6. Diethelm L, Dery R, Lipton MJ, Higgins CB. Atrial-level shunts: sensitivity and specificity of MR in diagnosis. *Radiology* **1987**;162:181–186
7. Anderson KR, Zuberbuhler JR, Anderson RH, Becker AE, Lie JT. Morphologic spectrum of Ebstein's anomaly of the heart: a review. *Mayo Clin Proc* **1979**;54:174–180
8. Anderson KR, Lie JT. Pathologic anatomy of Ebstein's anomaly of the heart revisited. *Am J Cardiol* **1978**;41:739–745
9. Lev M, Liberthson RR, Joseph RH, et al. The pathologic anatomy of Ebstein's disease. *Arch Pathol* **1970**;90:334–343
10. Becker AE, Decker MJ, Edwards JE. Pathologic spectrum of dysplasia of the tricuspid valve: features in common with Ebstein's malformation. *Arch Pathol* **1971**;91:167–178
11. Zuberbuhler JR, Allwork SP, Anderson RH. The spectrum of Ebstein's anomaly of the tricuspid valve. *J Thorac Cardiovasc Surg* **1979**;77:202–211
12. Deutsch V, Wexler L, Blieden LC, Yahini JH, Neufeld HN. Ebstein's anomaly of tricuspid valve: critical review of roentgenological features and additional angiographic signs. *AJR* **1975**;125:395–411
13. Freedom RM, Culham JAG, Moes CAF. *Angiocardiography of congenital heart disease*. New York: MacMillan, **1984**:111–118

Book Review

Prenatal Ultrasound. A Color Atlas with Anatomic and Pathologic Correlation. By Beverly A. Spirt, Lawrence P. Gordon, and Michael Oliphant. New York: Churchill Livingstone, 148 pp., $70

This book is a color atlas of normal and abnormal fetal developmental anatomy. The book contains two sections. The first traces normal fetal development and correlates sonographic findings with pathologic specimens, radiographs, angiograms, and images from fetoscopy. This "forms a basis for understanding the characteristic sonographic features of the pathologic conditions presented in the second section. At the end of each section selected references, intended for study in greater depth, are provided."

The first section is divided by organ systems into subsections on the spine, fetal skeleton, brain, face, fetal circulation, fetal thorax, abdomen, reproductive system, and placenta. It has virtually no text, but each subsection contains a table of significant developmental milestones for that organ system. The quality of the sonograms is excellent. The pathologic specimens used for correlation are well chosen and clearly depicted and correspond well with the sonograms. The sections on the fetal skeleton and face have some particularly striking images of the gross specimens. The ossified part of the fetal skeleton is stained with alizarin red and the unossified cartilage with alcian blue, corresponding to the sonographically visualized and nonvisualized portions of the fetal skeleton. The fetal angiograms in the subsection on normal fetal circulation are also excellent.

The second section is entitled "Prenatal Pathology." It also is organized into subsections: the CNS, thorax, abdomen, skeleton, placenta, and "Other Entities." Abnormalities of the urinary tract are covered in the subsection on the abdomen. The subsection entitled "Other Entities" includes cystic hygroma, hydrops fetalis, extragonadal teratoma, amnionic band syndrome, two-vessel umbilical cord, and conjoined twins. For each of the major anomalies covered, the sonographic findings of abnormal anatomy are correlated with corresponding gross pathologic findings, plain films, or contrast studies. A concise chart accompanies the description of each major anomaly. Each chart consists of a definition of the abnormality, sonographic criteria for diagnosis, a proposed cause, associated conditions, differential diagnosis, and either classic or recent references. This is an especially useful element of the text. In the second section, as in the first, the quality of the sonograms is excellent, and the correlation of gross pathologic changes with radiographic findings is outstanding.

The authors state that "sonographic imaging . . . demands the integration of embryology, normal developmental anatomy, and pediatric pathology to achieve a logical approach to the fetal sonogram." They have accomplished this in superb fashion. Throughout the book, the correlation of fetal anatomy on sonograms with helpful photographs of gross specimens or radiographic findings is excellent. Many of the illustrations are stunning. I highly recommend this book to sonographers, radiologists, perinatologists, and obstetricians.

Steven K. Sargent
Dartmouth-Hitchcock Medical Center
Hanover, NH 03756

Chest Radiography in Infant Cardiac Allotransplantation

Frances B. Toomey[1]
Leonard L. Bailey[2]
Rose Dang Bui[3]
Mohammad Kanahriyeh[3]
Eugene Petry[3]
Cheryl Mathis[3]
Joyce Johnston[3]
John Mace[3]
Bruce Grill[3]
Marquelle Klooster[3]

Heart transplants were performed in seven infants at Loma Linda University Medical Center from 1985 to 1987. Five of these seven patients survived. In this report, the radiographic appearance of the chest is presented before surgery, immediately after surgery, and during a documented episode of rejection. The most current available chest radiograph is also presented. Acute rejection was confirmed by clinical, echocardiographic, and ECG findings. The only pulmonary infection encountered was mycoplasma pneumonitis. Four patients developed gastrointestinal rotavirus infections and were shown to have dilated proximal small-bowel folds on upper gastrointestinal studies. At the time of this writing, the prognosis for the five surviving infants is good.

We conclude that the radiographs of infants who have received heart transplants show an unusual cardiac contour and slight cardiomegaly. Increasing cardiomegaly can alert one to early rejection. Prominent folds in the small bowel are of uncertain origin and significance, but they may be related to infection resulting from immunosuppression.

From 1985 to 1987, seven infants received cardiac allotransplants at Loma Linda University Medical Center. Five of the seven patients are alive and appear to be developing normally; the oldest is 18 months old. The purpose of this report is to describe the radiographic findings in these five patients.

Materials and Methods

The seven infants who received transplants were between 4 days and 3.5 months old at the time of transplantation. Three were boys and four were girls. Two were born prematurely, and the others were term infants at birth. Five had hypoplastic left heart syndrome. One 2.5-month-old girl suffered from left heart failure caused by atrioventricular canal, diminutive left ventricle, hypoplastic aortic arch, and coarctation. A 3.5-month-old infant had a hypoplastic left heart equivalent, transposition of the great vessels, hypoplastic right heart, hypoplastic aorta, and coarctation. After surgery, all patients received cyclosporine. Prednisone and azathioprine, as well as antithymocyte globulin, were added during rejection episodes.

Since the patients were considered too small to obtain serial muscle biopsy, rejection episodes were evaluated by clinical findings of irritability, anorexia, tachypnea, and tachycardia. Increasing cardiomegaly and pulmonary edema seen on plain anteroposterior chest radiographs, echocardiography showing increased posterior muscle-wall thickness and decreased fiber-shortening fraction, and an additional ECG showing a drop in electrocardiographic voltage and arrhythmias all confirmed the presence of rejection [1]. All patients were followed with serial anteroposterior chest radiographs and routine cultures of sputum and blood. Lung scans were not performed because none were suspected of having pulmonary infarction. Small-bowel series were performed in all five surviving infants. The two infants who died did not have gastrointestinal studies.

Results

The oldest survivor was 18 months old at the time of this writing. Of the two patients who died, one had hypoplastic left heart and died as a result of complica-

Received July 30, 1987; accepted after revision October 20, 1987.

[1] Department of Radiology, Loma Linda University Medical Center, 11234 Anderson St., Loma Linda, CA 92354. Address reprint requests to F. B. Toomey.

[2] Department of Surgery, Loma Linda University Medical Center, Loma Linda, CA 92354.

[3] Department of Pediatrics, Loma Linda University Medical Center, Loma Linda, CA 92354.

AJR 150:369–372, February 1988
0361–803X/88/1502–0369
© American Roentgen Ray Society

tions of a perforated duodenal ulcer on the 13th day after surgery; the other died 4 days after surgery as a result of low cardiac output. There was no evidence of cardiac rejection in either patient. One patient who developed pulmonary infiltrates had positive sputum cultures for *Mycoplasma* on three separate occasions and responded well to antibiotics each time. No other organism was cultured, nor was there any other radiographic evidence of pneumonia. One premature infant died, and the other, living premature infant required respiratory support because she had developed lung scarring before transplantation. Details of these cases have been previously reported [2]. Two patients developed clinical manifestations of recurrent sinusitis, and both had radiographic findings that were consistent with that diagnosis. No organism was cultured, and both patients responded to antibiotics. Four patients had prominent jejunal folds and transient intussusception. Several weeks after the small-bowel series were performed, all four infants with an abnormal mucosal pattern were documented to have rotavirus infections, without a change in the small-bowel pattern. Nine months later, the small-bowel pattern returned almost to normal without a change in the clinical status. Representative examples of the chest radiographs of three of the five surviving patients are presented in Figures 1–3.

Discussion

Previous reports of cardiac transplants have dealt almost exclusively with adults. Weidner et al. [3] noted generalized cardiac dilatation after transplantation. He also described the absence of left ventricular failure patterns during acute rejection and thought an early posttransplant alveolar infiltrate should be interpreted as either pneumonia or infarction. Goldstein et al. [4] indicated that the radiographic appearance of pneumonias occurring after cardiac transplantation was relatively nonspecific as to cause.

Singleton [5], Singleton et al. [6], and Singleton and Colquhoun [7] found that in acute rejection, the heart showed

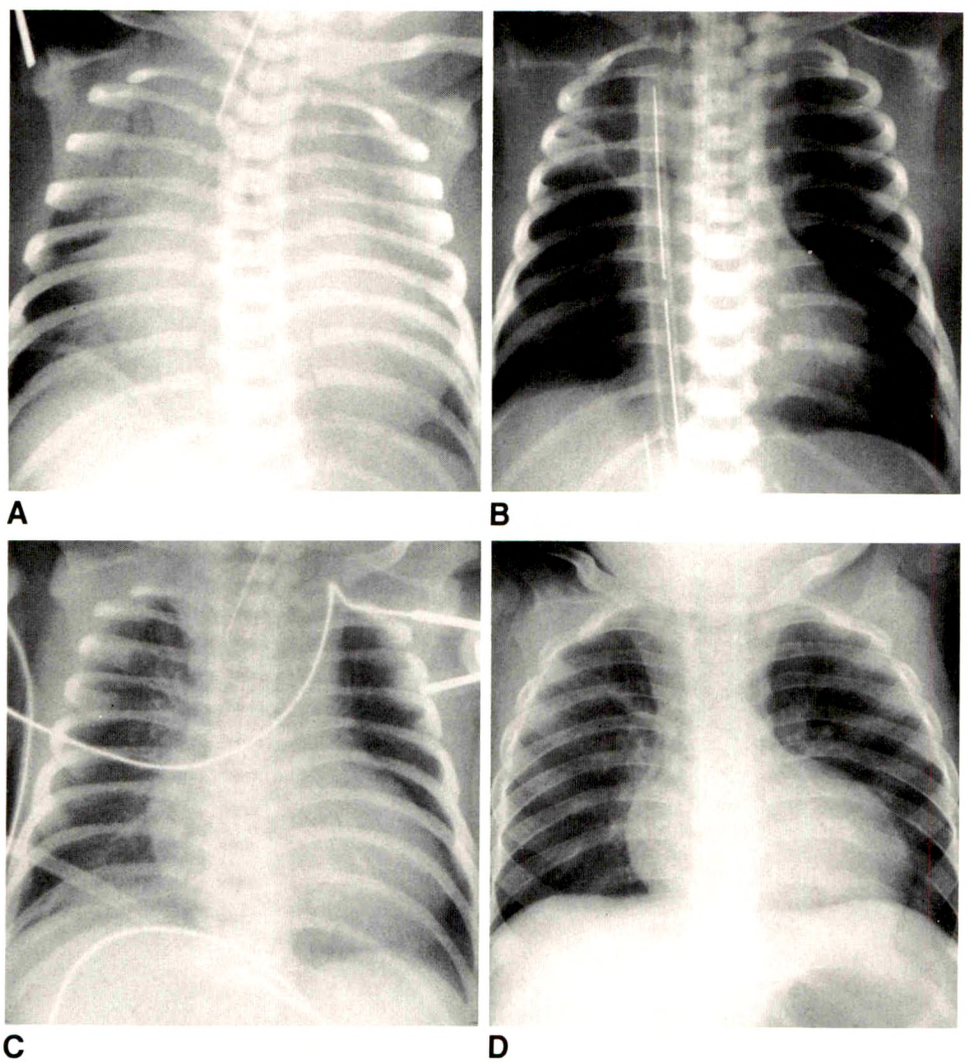

Fig. 1.—*A*, Anteroposterior view of chest in a 4-day-old boy who had hypoplastic left heart. Note that there is cardiomegaly and pulmonary edema before transplantation.

***B*, Anteroposterior view of chest obtained immediately after heart transplantation. Donor heart is normal in size. Minimal left upper lobe atelectasis is present, but lungs are clear otherwise.**

***C*, Anteroposterior view of chest during an episode of acute rejection 1 month after transplantation. Heart is enlarged, and there is minimal pulmonary interstitial edema and right pleural effusion.**

***D*, Anteroposterior and lateral radiograph of chest when patient was 18 months old. Heart is minimally enlarged in its transverse diameter. Right heart border is rounded, and apex points laterally. Superior mediastinum is narrow.**

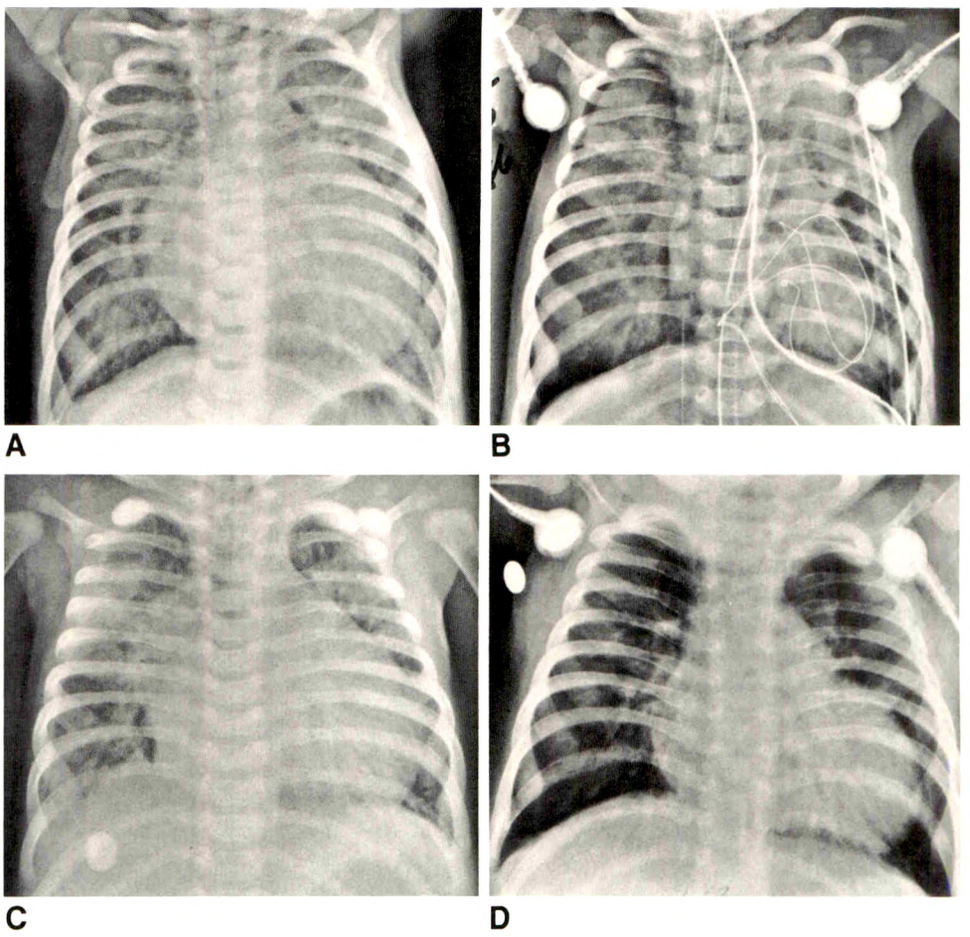

Fig. 2.—*A*, Anteroposterior view of chest in a 3.5-month-old infant who had hypoplastic left heart equivalent (transposition of the great vessels, hypoplastic right heart, hypoplastic aorta, and coarctation). Cardiomegaly and pulmonary venous congestion are present.

B, Chest radiograph obtained after heart transplantation. Donor heart is normal in size. There are bilateral pneumothoraces. Partial left upper lobe atelectasis and pulmonary edema are present.

C, Anteroposterior view of chest obtained during an episode of acute rejection 2 weeks after transplantation. Note cardiomegaly, right pleural effusion, and pulmonary venous congestion.

D, Anteroposterior view of chest at 7 months of age. Heart remains slightly enlarged with a prominent right heart border and apex, clear lung, and narrow superior mediastinum.

increasing dilatation, there were small pleural effusions, and septal lymphatic lines were visible. With chronic rejection, there also was cardiomegaly but minimal or no pulmonary edema. Infections in general, gastrointestinal bleeding, and osteoporosis were also common and apparently were related to immunosuppressive therapy. Silverman et al. [8] described unusual cardiac contours after transplantation and found them to be the result of fitting the dilated atrial portions of the recipient heart with the normal donor heart. Dietz et al. [9] found that the apex of the transplanted heart was rotated laterally, presumably as a result of the surgical procedure.

In the infant, the donor heart has a unique radiographic appearance during the first few days after transplantation (Figs. 1–3). The heart becomes mildly dilated for as yet unknown reasons, although it is speculated that dilatation is related to denervation (Bailey LL, personal communication). Both atria are slightly enlarged, probably because of the large volume of the combined donor and recipient atria [10]. Because most of the thymus has been resected, the superior mediastinum is narrowed. Since the affected hypoplastic aorta was included with the heart in the resection, neither reduction nor enlargement of the aortic shadow is observed.

Increasing cardiomegaly is an early warning sign of rejection and may precede the clinical symptoms by 24 hr (Fig. 3). However, this finding is not present in about half of the episodes. This concurs with the findings of Singleton and Colquhoun [7] and Shirazi et al. [11]. It is particularly important to watch for increasing cardiomegaly in infants since these patients are too small to have serial biopsies for evaluation of rejection.

Bacterial pneumonia or *Mycoplasma pneumonia* should be the first diagnosis when pulmonary opacities appear. Pulmonary infection by opportunistic organisms (e.g., *Pneumocystis carinii*, cytomegalic virus) [12] has not occurred. One patient who had cystomegalic-positive urine cultures did not have pulmonary infiltrates.

The prominent jejunal folds found in three patients are of undetermined origin. Many gastrointestinal problems have been described in adult recipients of heart, renal, and marrow transplants [13, 14]. These have varied from mild diarrhea to fatal perforation. The suggested explanations for gastrointestinal complications have included nonocclusive ischemia, infection, effect of steroid or cyclosporine, and graft-versus-host reaction. The evaluation of our patients is still in progress.

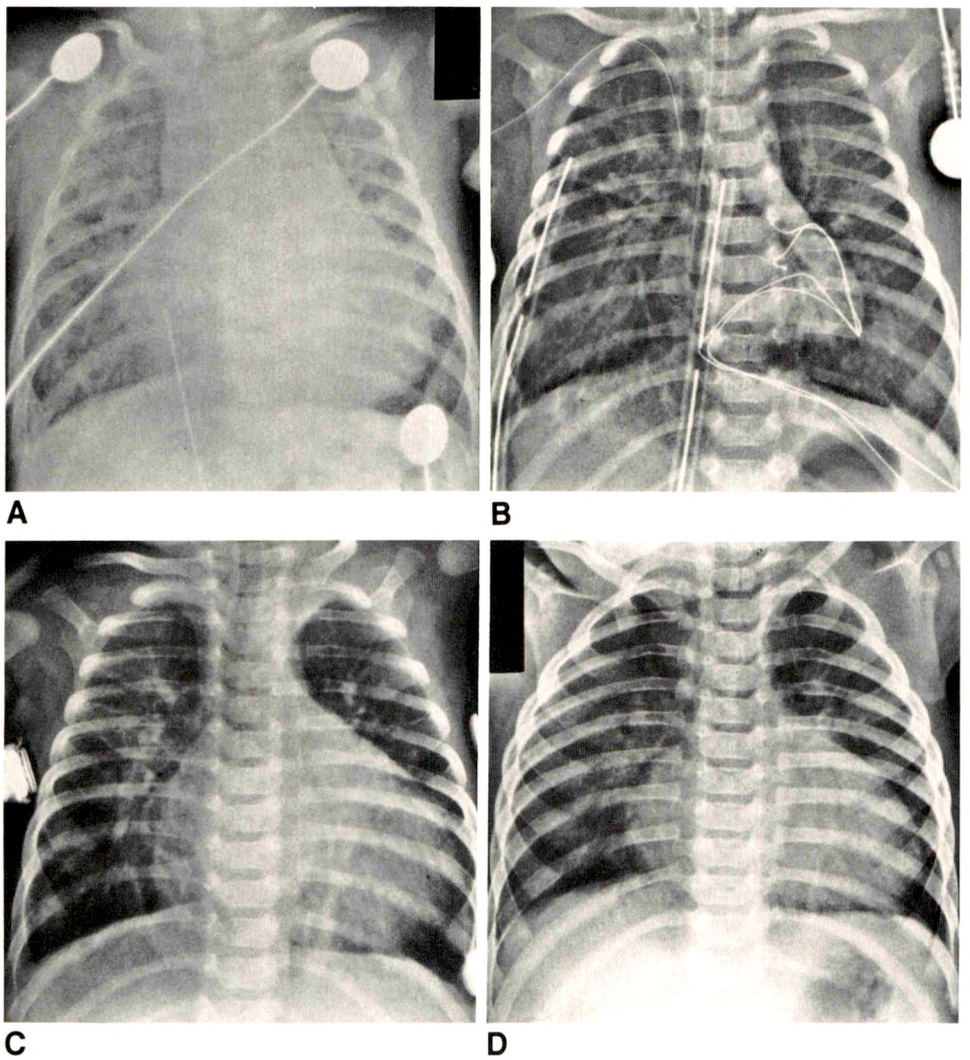

Fig. 3.—*A*, Anteroposterior view of chest in a 2.5-month-old girl who had an atrioventricular canal, diminutive left ventricle, hypoplastic aortic arch, and coarctation. In addition to cardiomegaly and mild pulmonary venous congestion, there are faint linear densities in right upper and middle lobes thought to represent residual scarring from bronchopulmonary dysplasia.

***B*, Anteroposterior view of chest obtained immediately after heart transplantation. Small bilateral pneumothoraces are present, and there is minimal pulmonary edema and right upper lobe collapse.**

***C*, Anteroposterior view of chest obtained 3 weeks after heart transplantation during an episode of rejection. Heart is dilated, and there is septal edema.**

***D*, Recent anteroposterior radiograph of chest shows persistent but decreased cardiomegaly. No septal edema is present, but there are still linear scars in right lung. Superior mediastinum is narrow.**

REFERENCES

1. Bailey LL, Dang Bui R, Nehlsen-Cannarella SL, et al. Surveillance techniques in infant heart transplantation. Presented at the International Symposium on Transplantation, Venice, Italy, March **1987**
2. Bailey LL, Nehlsen-Cannarella SL, Dorosho RW, et al. Cardiac allotransplantation in newborns as therapy for hypoplastic left heart syndrome. *N Engl J Med* **1986**;315:949–951
3. Weidner WAW, Lower RR, Kenys VE, Vanik M. Chest roentgenographic findings in the acute rejection crisis in human cardiac transplants. *Radiology* **1969**;93:1267–1272
4. Goldstein HM, Stinson EB, Castellino RA, et al. Roentgenologic aspects of cardiac transplantation: postoperative pulmonary infections. *AJR* **1971**;11:476–482
5. Singleton EB. Heart transplantation (editorial). *Radiology* **1969**;92:180
6. Singleton EB, Colquhoun J, Harle TS, et al. Radiologic evaluation of cardiac transplantation. *AJR* **1970**;109:1–11
7. Singleton EB, Colquhoun J. Radiologic aspects of cardiac transplantation. *Radiol Clin North Am* **1971**;IX(2):163–174
8. Silverman JF, Griepp RB, Wexler L. Radiographic changes in cardiac contour following cardiac transplantation. *Radiology* **1974**;111:303–306
9. Dietz RR, Patton DD, Copeland JG, McNeill GC. Characteristics of the transplanted heart in the radionuclide ventriculogram. *Heart Transplantation* **1986**;5:113–120
10. Bailey LL, Concepcion W. Shattuch H, Huang L. Method of heart transplantation for treatment of hypoplastic left heart syndrome. *J Thorac Cardiovasc Surg* **1986**;92:1–5
11. Shirazi KK, Amendola MA, Tisnado J, Cho SR, Beachley MC, Lower RR. Radiographic findings in the chest of patients following cardiac transplantation. *Cardiovasc Intervent Radiol* **1983**;6:1–6
12. Wise RH, Myung SS, Gocherman JP, Zoines SL, Rubin E, Nath PH. Pneumonia in bone marrow transplant patients. *AJR* **1984**;143:707–714
13. Puglisi BS, Kauffman HM, Stewart ET, Dodds WJ, Adams MB, Komorowski RA. Colonic perforation in renal transplant patients. *AJR* **1985**;145:555–558
14. Welling RE. Gastrointestinal complications after cardiac surgery. *Arch Surg* **1986**;121:1178–1180

Case Report

Food Allergy Presenting as Obstruction in an Infant

Joan McIlhenny,[1] James L. Sutphen,[2] and Charles A. Block[2]

The radiographic and clinical signs of intestinal obstruction in an infant usually suggest a mechanical or (less commonly) an inflammatory cause. We present a case of food allergy presenting as obstruction in a male infant.

Case Report

A 2-month-old boy was admitted to the pediatric intensive care unit for the acute onset of fever, nonbilious vomiting, abdominal distension, and acidosis (serum bicarbonate 7 mEq/l). His admission height and weight were at the fifth percentile. Physical examination was remarkable for 15% dehydration and a markedly protuberant abdomen. No masses were palpated. At admission there were no eosinophils on peripheral blood smear; however, the WBC count was 16,700 (14 band neutrophils, 30 mature neutrophils, 36 lymphocytes, 10 monocytes, and 10 atypical lymphocytes). Stools were negative for occult blood, and no fecal leukocytes were seen on microscopic examination. The infant had a history of intolerance to milk and soy formulas that was associated with rotavirus infection 3 weeks before the current illness. He had stabilized on Pregestimil (protein hydrolysate, Mead Johnson and Co., Evansville, IN) formula and was gaining weight. A repeat enzyme-linked immunosorbent assay (ELISA) for rotavirus was not performed. A feeding of 4 oz of Isomil (soy formula, Ross Laboratories, Columbus, OH) had been given earlier in the day before the development of his acute illness. At the patient's presentation, plain films of the abdomen revealed marked abdominal distension and a few air-fluid levels (Figs. 1A and 1B). An abdominal sonogram showed multiple dilated, fluid-filled intestinal loops with active peristalsis and no ascites (Fig. 1C). A water-soluble contrast enema showed a normal rectum and multiple extrinsic masses compressing the colon (Figs. 1D and 1E). No intussusception or other obstruction was seen in the colon. The cecum appeared normal, but we were unable to achieve reflux into the terminal ileum. On the upper gastrointestinal examination, barium did not pass beyond the second portion of the duodenum despite prolonged observation in multiple positions (Fig. 1F).

As we could not confidently exclude the possibility of midgut volvulus, a laparotomy was performed. Dilated fluid-filled loops of small bowel were found, and the large bowel was normal. The picture was consistent with an ileus. An intraoperative rectal biopsy was normal with ganglion cells present. Subsequent cultures for bacterial enteric pathogens (*Salmonella*, *Shigella*, *Campylobacter*, *Yersinia*, and *Aeromonas*) were negative. After surgery, allergy scratch tests were positive for milk and soy protein with a 3 × 3 mm wheal for each. Immunoglobulin E was undetectable. Levels of other serum immunoglobulins were normal. Radioallergosorbent tests were not performed. The patient was given 1 g of tofu (soy protein) by mouth, which produced vomiting and guaiac-negative diarrheal stools within 2 hr. A trial feeding of 10 ml of Similac (cow's milk formula, Ross Laboratories) produced irritability and watery stools positive for reducing substances and blood. The infant is currently doing well at 9 months of age on Nutramigen (casein hydrolysate, Mead Johnson and Co.) and strict exclusion of milk and soy products.

Discussion

Radiographic evidence of intestinal obstruction in the first year of life usually indicates a mechanical or physiologic obstruction or an adynamic ileus from adjacent inflammation [1]. The differential diagnosis includes a mechanical obstruction from malrotation with a midgut volvulus, mechanical obstruction from other rare causes (such as a stricture, an internal hernia, or an intussusception caused by a duplication), a physiologic obstruction from Hirschsprung disease, and an adynamic ileus possibly from appendicitis. Infectious gas-

Received July 20, 1987; accepted after revision September 14, 1987.
[1] Department of Radiology, Box 170, University of Virginia Medical Center, Charlottesville, VA 22908. Address reprint requests to J. McIlhenny.
[2] Department of Pediatrics, University of Virginia Medical Center, Charlottesville, VA 22908.

AJR **150:373–375, February 1988** 0361–803X/88/1502–0373 © American Roentgen Ray Society

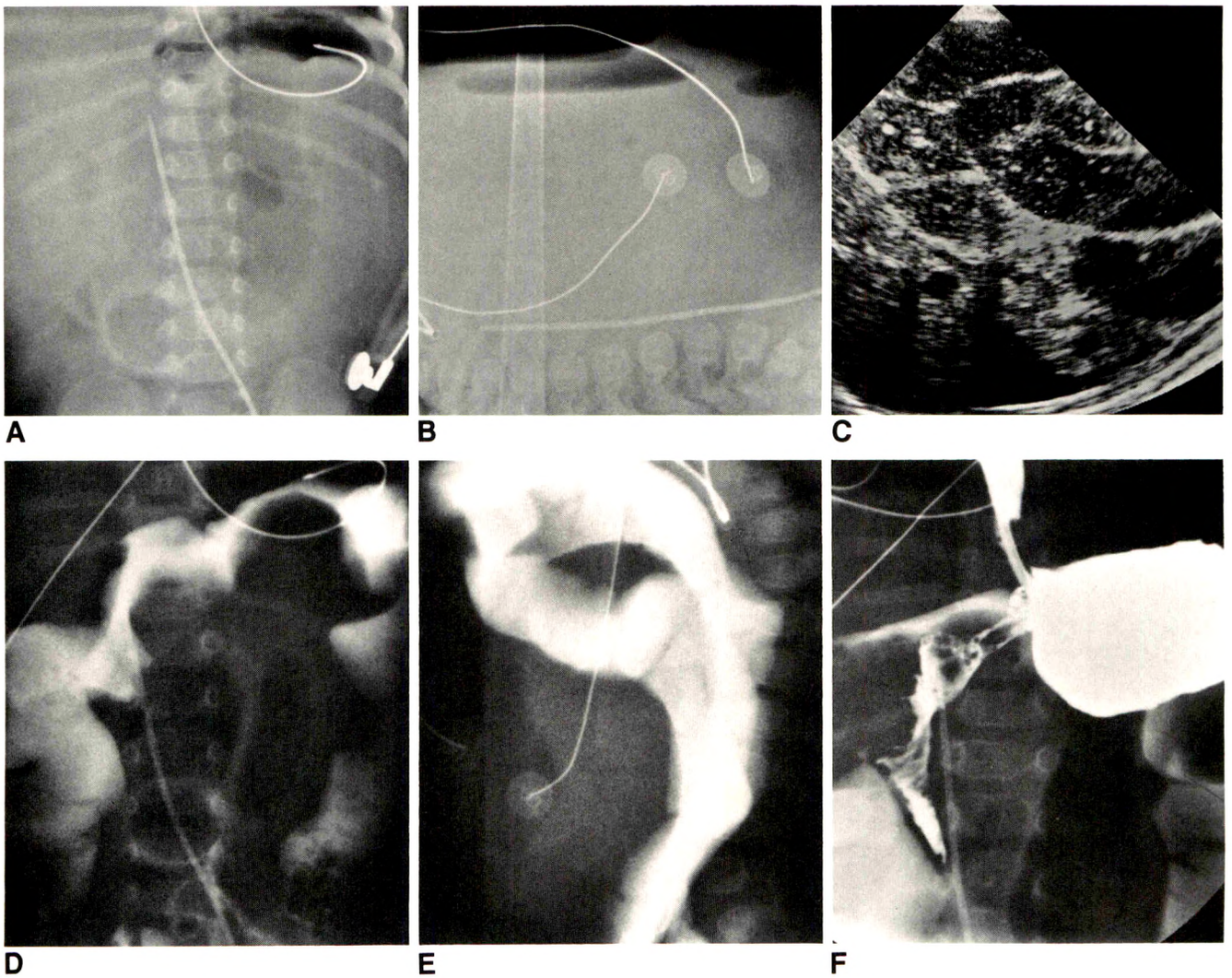

Fig. 1.—*A* and *B*, Radiographs of abdomen showing abdominal distension and several air fluid levels. Umbilical hernia was reducible. *A* is anteroposterior view; *B* is cross-table lateral view.

***C*, Sagittal sonogram showing multiple fluid-filled bowel loops.**

***D* and *E*, Water-soluble enema showing multiple extrinsic masses indenting colon. At surgery, these were found to be dilated loops of small bowel. *D* is anteroposterior view; *E* is lateral view.**

***F*, Anteroposterior view from upper gastrointestinal study shows termination of barium column in proximal duodenum, presumably from compression by dilated bowel loops. Barium also refluxed around nasogastric tube into esophagus. Residual water-soluble contrast material is present in colon.**

troenteritis was considered less likely because of the abrupt onset of the symptoms and their rapidly progressing severity. The active intestinal peristalsis seen with sonography and the paucity of diarrhea led us initially to favor a distal mechanical obstruction. The water-soluble enema excluded colonic causes of obstruction. The upper gastrointestinal series was performed to rule out malrotation with acute volvulus. When barium did not pass beyond the second portion of the duodenum, surgery was performed to exclude the possibility of a midgut volvulus. At surgery, no anatomic abnormalities were found except for distension of the small bowel with fluid.

We postulate that this patient had a massive outpouring of fluid into his small intestine caused by local intestinal anaphylaxis. With a type I reaginic or immediate hypersensitivity response, mast cells are activated and release vasoactive mediators (histamine, prostaglandin D_2, and kinins) and chemotactic factors for macrophages, neutrophils, eosinophils, and platelets. These mast-cell mediators cause increased vascular and mucosal permeability, edema, and smooth-muscle contraction [2].

Two other reports [3, 4] describe infants with a history of formula intolerance, intractable diarrhea, and failure to thrive who were challenged in a hospital setting with oral soy-protein isolate and developed fever, lethargy, hypotension, vomiting, and diarrhea. These children were not diagnostic dilemmas at the time of their challenge tests and did not receive radiologic evaluation. All of these patients had concomitant sensitivity to cow's milk protein (as did our patient) [3, 4]. The validity of using skin tests alone for the detection of food allergies is controversial. In our patient, the response to the

food challenges confirmed the diagnosis of food allergy.

Dietary protein allergy to both cow's milk and soy proteins usually develops before 6 months of age, and reexposure to the offending protein after 1 year of age is often well tolerated. Hence, the allergic response is a self-limited, age-dependent phenomenon, and it is not necessarily a long-term allergy [2]. Radiologists should be aware of this entity in the young infant who presents with obstructive symptoms.

REFERENCES

1. Merten DF. The acute abdomen in childhood. *Curr Probl Diagn Radiol* **1986**;15:335–425
2. Lake A. Food allergy. In: Grand RJ, ed., *Pediatric nutrition: therapy and practice*. Boston: Butterworth, **1987**:615–625
3. Whitington PF, Gibson R. Soy protein intolerance: four patients with concomitant cow's milk intolerance. *Pediatrics* **1977**;59:730–732
4. Minford AMB, McDonald A, Littlewood JM. Food intolerance and food allergy in children: a review of 68 cases. *Arch Dis Child* **1982**;57:742–747

Errata

In the article "Flat Chest in Chronic Bronchopulmonary Dysplasia" by Edwards and Hilton, which appeared in the December 1987 issue of *AJR* (*AJR* **1987**;149:1213–1216), an error was made in the final sentence of the first paragraph of the discussion (page 1215). The sentence should have read "Nevertheless, the statistical difference from unaffected patients is striking ($p < 10^{-6}$), as is the appearance of the lateral chest radiograph in the patients with more severe chest flattening (Fig. 1)." *AJR* regrets this error.

In the article "The Impact of New Imaging Technology on Health Care, Research, and Teaching: An International Symposium" by Figley and Margulis, which appeared in the December 1987 issue of *AJR* (*AJR* **1987**;149:1111–1126), an error was made in the listing of the participants (page 1125). Professor Dado Kovacevich representing Yugoslavia is not deceased. He took the place of Professor Dusko Katunarich, who was his Chief. (Dr. Katunarich was originally to have been one of two representatives of Yugoslavia, but he recently died.)

Book Review

Paediatric Oncology. An Illustrated Introduction. By William R. McWhirter and John P. Masel. Baltimore, MD: Williams & Wilkins and Associates Pty., 316 pp., 1987. $60

The aim of this book, "to provide background information for some of the members of that team who may be involved at some stage with the treatment of childhood cancer," is accomplished in those general terms. This book is an introduction to the practical considerations of pediatric oncology; it is a survey that would benefit generalists among physicians, physician specialists, and associated health professionals. The style is readable, and the book is enhanced by appropriate illustrations—nearly 200 figures of imaging examinations. Most of these are radiographs, but about one-third are special imaging pictures, such as CT scans, sonograms, and scintigrams. Also included are a few clinical photographs, a few MR images, some graphs, scattered tables, and an appendix. The emphasis is on major childhood neoplasms, but many other neoplasms are included, although discussions about them are brief.

Chapter 2, "Investigations in the Management of Cancer," and chapter 3, "Principles of Cancer Treatment," are probably the most appealing and useful chapters for the general readership of *AJR*. However, the chapters on specific diagnoses also are well illustrated, with typical radiographic or other imaging findings that help in showing "the extent of abnormal tissue," and "the effect of the lesion on other tissues and organs." The authors give full credit to diagnostic imaging, to the extent of claiming that sometimes histologic typing from such findings "is quite precise."

Although each chapter is followed by a list of pertinent references, in some instances other significant references are not found in these lists.

Chapter 4, "Psychosocial Aspects of Childhood Cancer," and chapter 13, "The Late Effects of Childhood Cancer," are lagniappes, so to speak, that add to the value of this book. Psychosocial needs are worthy of attention in all of medicine, but especially in children who have cancer. Because the child who survives cancer (overall survival rate of about 50%) has a relatively long time to live, the physician needs to know about the temporary or permanent sequelae.

The book is recommended to general practitioners, pediatricians, radiologists, paramedical professionals who work with children who have cancer, and medical students. It is a good introduction to pediatric oncology, in general, and to diagnostic imaging aspects, in particular.

Lionel W. Young
Children's Hospital, Medical Center of Akron
Akron, OH 44308

Technical Note

The Use of Midazolam for Sedation of Infants and Children

Michael J. Diament[1] and Philip Stanley

Midazolam (Versed, Roche Laboratories, Nutley, NJ), the first water-soluble benzodiazepine, has had widespread acceptance as a parenteral anxiolytic agent and as an anesthetic premedication in both adults and children [1–3]. Over the past year, we have used midazolam in invasive procedures in pediatric patients and have found it to be preferable to diazepam (Valium, Roche Laboratories, Nutley, NJ), which we had previously used.

Materials and Methods

In September 1986, we began using IV midazolam for sedation of patients undergoing invasive procedures. Since February 1987, midazolam has replaced diazepam in our practice. As of August 1987, we had used it in 51 patients who had undergone 56 invasive studies, including angiography, percutaneous drainage, needle biopsy, myelography, arthrography, and sialography. The age range was 5 months–17 years, with an average of 7.6 years.

Our protocol for invasive procedures has been described elsewhere [4]. All patients receiving parenteral medication are attended by a radiology nurse. A pulse oximeter and an automatic device to monitor blood pressure are in place. All the procedures are done in rooms in which full resuscitative equipment is available. We rarely premedicate the patient and prefer to begin IV analgesia and sedation as soon as the patient arrives in the special procedures room. The initial dose of midazolam is 0.1–0.2 mg/kg, up to a maximum of 5 mg for the first aliquot. If the procedure is expected to be painful, (e.g., percutaneous drainage or biopsy), IV meperidine (1.0 mg/kg to a maximum of 25 mg for the first aliquot) is also given. If the degree of sedation or analgesia is inadequate, additional doses are given depending on the patient's response.

After the procedure, the patient is either returned to the hospital ward or, if an outpatient, to the radiology nurses' station. Outpatients are discharged when they are able to take fluids.

Results

All of the procedures in which midazolam was used as an anxiolytic and sedative agent were completed successfully. The time required to achieve adequate sedation varied from 1 min to approximately 30 min. The longer periods were due to our policy of waiting approximately 5 min between supplementary doses of midazolam or meperidine to avoid oversedation. The range of total dose/patient was from 0.20 mg/kg to 1.25 mg/kg. Most patients received less than 0.4 mg/kg. Medication was administered at the same time that the patient was being prepared for the procedure and that scout films were being obtained so that the total time for the examination was not significantly increased, even when longer periods were required for sedation.

Two complications were associated with the use of midazolam. The more serious one occurred in a 14-year-old girl who was undergoing renal transplant angiography for hypertension. Approximately 5 min after the initial injection of meperidine (25 mg) and midazolam (5 mg), her respirations became erratic and the arterial oxygen saturation decreased to approximately 80%. Her condition improved after administration of IV naloxone and oxygen by nasal cannula. There was no evidence of sequelae on follow-up examination. It is uncertain whether the problems were due to meperidine, midazolam, or a combination of the two drugs. Midazolam

Received August 25, 1987; accepted after revision September 28, 1987.

[1] Both authors: Department of Radiology, Childrens Hospital of Los Angeles and the University of Southern California School of Medicine, Los Angeles, CA 90027. Address reprint requests to M. J. Diament, Dept. of Radiology, Childrens Hospital of Los Angeles, 4650 Sunset Blvd., Los Angeles, CA 90027-6089.

AJR **150:377–378, February 1988** 0361–803X/88/1502–0377 © American Roentgen Ray Society

extravasated from a peripheral IV in the foot in a 5-month-old infant, causing erythema around the injection site and a delay in the onset of sedation. The infant did not appear to have pain, and there was no evidence of tissue damage on follow-up examination. The procedure was successfully completed after a new IV line was established.

Discussion

We began to use midazolam because it causes less local irritation with IV injection [5]. In children, the pain is significantly reduced or even eliminated when the drug is injected through small peripheral lines. This is probably due to its water solubility as compared with that of diazepam, which uses propylene glycol as a diluent [1]. With diazepam, we commonly encountered the problem of the patient becoming combative immediately after the injection. This would often take several minutes to resolve. Also, there appears to be lower occurrence of venous complications with midazolam compared with diazepam in most, but not all, reported series [1]. Midazolam can be combined in the same syringe with meperidine or morphine and, unlike diazepam, does not precipitate in standard IV solutions [6].

The half-life of midazolam (1–4 hr) is approximately one-fourth that of diazepam [1]. Most of our examinations require less than 1 hr to perform so that supplementary doses rarely are needed, once effective sedation has been achieved. In all of our outpatient procedures, the patients have been sufficiently awake and alert for discharge from the department within 4 hr after the completion of the study [4]. All of our older patients have reported complete antegrade amnesia after the injection of midazolam.

The dose that we employ is greater than that recommended for invasive diagnostic procedures in the manufacturer's insert [6] but is comparable to that commonly used for anesthetic premedication [1]. An inverse relationship between dose and age has been reported, but considerable individual variation exists [3, 7]. We think that the doses we use are safe as long as the medication is injected over a 1–3 min period and the patient is monitored carefully. Because of the reported experience with the drug and our careful monitoring of patients, we did not think that informed consent for the use of doses higher than those recommended by the manufacturer was necessary.

Midazolam may also be given per rectum [8] or intramuscularly [3]. These routes of administration may be useful either when premedicating a patient or when starting an IV is difficult. However, we prefer to have a line in place in case resuscitative fluids or drugs are required. The oral form of the drug is not available in the United States.

Midazolam has been shown to be an effective anxiolytic agent for a variety of surgical and invasive procedures. Our experience suggests that midazolam is preferable to diazepam for use in children. However, facilities and personnel for resuscitation and careful patient monitoring must be available.

REFERENCES

1. Reves JR, Fragen RJ, Vinik HR, Greenblatt DJ. Midazolam: pharmacology and uses. *Anesthesiology* **1985**;62:310–324
2. Holloway AM, Jordaan DG, Brock-Utne JG. Midazolam for the intravenous induction of anesthesia in children. *Anesth Intensive Care* **1982**;10:340–343
3. Rochette A, Julia JM, Evrard O, Richard C, Julien Y, DuCailer J. Intramuscular premedication with midazolam in infants and children. *Ann Fr Anesth Reanim* **1984**;3:346–350
4. Diament MJ, Bird CR, Stanley P. Outpatient performance of invasive procedures in pediatrics. *Radiology* (in press)
5. Jegarty JE, Dundee JW. Sequelae after the intravenous injection of three benzodiazepines—diazepam, lorazepam and flunitrazepam. *Br Med J* **1977**;2:1384–1385
6. *Physicians desk reference*, 41st ed. Oradell, NJ: Medical Economics Co., **1987**:1684–1686
7. Dundee JW, Halliday NJ, Loughran PG, Harper KW. The influence of age on the onset of anesthesia with midazolam. *Anesthesia* **1985**;40:441–443
8. Saint-Maurice C, Esteve C, Holzer J, et al. Premedication using intrarectal midazolam. Study of effective dosage in pediatric anesthesia. *Ann Fr Anesth Reanim* **1984**;3:181–184

Case Report

Third-Trimester Fetal Sonography: Meconium Simulating a Presacral Mass

Stephen I. Moreland III,[1] Martin I. Cohen,[2] George R. Leopold,[1] and Barbara B. Gosink[1]

Sonography is frequently used in the evaluation of third-trimester pregnancies to determine gestational age or screen for abnormalities that could alter management. Increased resolution has resulted in improved visualization of normal structures, which must be differentiated from pathologic conditions. We report three cases in which rectal meconium simulated a presacral mass.

Case Report

A 32-year-old, gravida 2 para 1 woman was referred for sonographic evaluation late in the third trimester of an uncomplicated pregnancy. Sonograms showed a live, term intrauterine gestation. Sonographic evaluation of the fetus was unremarkable with the exception of a hypoechoic presacral mass measuring 2 × 4.5 cm (Figs. 1A and 1B).

One day later, a 3757-g female neonate was delivered by cesarian section. Physical examination was normal. Sonograms of the neonate before passage of meconium again showed presacral lucency, distinct from the normal uterus. the rectum could not be identified separately from the mass. Digital rectal examination under sonographic observation confirmed that the mass was within the rectal vault. Repeat sonography after passage of meconium showed no evidence of a pelvic mass (Fig. 1C). The neonate did well and was discharged at 5 days of age.

Discussion

We have seen two other cases of rectal meconium (Fig. 2) simulating a presacral mass. Both patients presented late in the third trimester for sonographic evaluation that showed an apparent presacral mass. Healthy, term neonates were born to each patient.

The presacral space is delineated anteriorly by the rectum, posteriorly by the sacrum, inferiorly by the levator ani and coccygeal muscles, superiorly by the peritoneal reflection, and laterally by the ureters and iliac vessels [1]. A review of the literature indicates that a presacral teratoma is the most common cause of a mass in this area in infancy. Differential diagnosis includes imperforate anus, rectal duplication, dermoid tumor, anterior myelomeningocele, lipoma, ependymoma, and sarcoma [2]. Our cases of meconium in the rectal vault simulating a presacral mass indicate another diagnostic possibility in the term fetus and neonate.

The appearance of normal fetal bowel has thus far received little attention in the literature [3, 4]. During the first half of pregnancy, the fetal gut is usually collapsed (except for the stomach), and its echo pattern is difficult to distinguish from those of the abdominal and pelvic viscera. In the middle trimester, small amounts of fluid are commonly visualized in the small bowel and colon of the fetus. Late in pregnancy, the distal portions of the fetal bowel fill with meconium and become visible as hypoechoic tubular structures. This appearance is believed to be responsible for the presacral pseudomass.

These cases illustrate the importance of differentiating normal rectal meconium from abnormal conditions. In the absence of abnormal clinical or physical findings, further evaluation is unnecessary. Clinical evidence of mass or neurologic deficit indicates the need for repeat sonography, preferably

Received July 15, 1987; accepted after revision September 16, 1987.

[1] Department of Radiology, H-756, University of California, San Diego, Medical Center, 225 Dickinson St., San Diego, CA 92103-1990. Address reprint requests to S. I. Moreland III.

[2] Valley Radiologists, Ltd., Phoenix, AZ 85306.

AJR 150:379–380, February 1988 0361–803X/88/1502–0379 © American Roentgen Ray Society

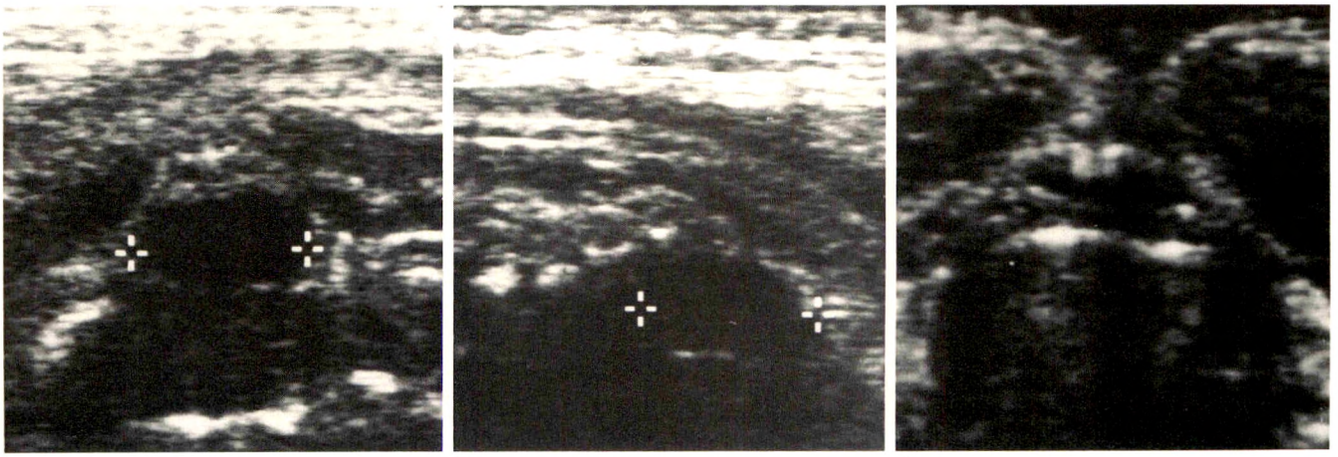

A B C

Fig. 1.—*A* and *B*, Transverse (*A*) and longitudinal (*B*) sonograms of fetal pelvis showing hypoechoic presacral mass (*cursor arrows*).
C, Transverse scan after meconium passage shows disappearance of presacral mass.

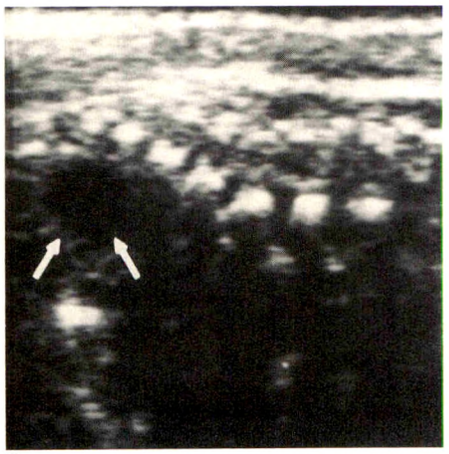

2

Fig. 2.—Sonogram shows another case of meconium simulating pelvic mass (*arrowheads*).

after the passage of meconium, to evaluate for abnormalities of the presacral space.

REFERENCES

1. Gardner E, Gray DJ, O'Rahilly R, Goss CM. *Gray's anatomy*, 4th ed. Philadelphia: Saunders, **1975**:438–506
2. Jewel CT, Miller ID, Ehrlich FE. Rectal duplication: an unusual cause for an abdominal mass. *Surgery* **1973**;74:783–785
3. Nyberg DA, Mack LA, Patton RM, Cyr DR. Fetal bowel, normal sonographic findings. *J Ultrasound Med* **1986**;6:3–6
4. Harris RD, Nyberg DA, Mack LA, Weinberger E. Anorectal atresia: prenatal sonographic diagnosis. *AJR* **1987**;149:395–400

Temporomandibular Joint: MR Imaging of Internal Derangements and Postoperative Changes

Kurt P. Schellhas[1]
Clyde H. Wilkes[2]
Hollis M. Fritts[1]
Mark R. Omlie[3]
Kenneth B. Heithoff[1]
Jeffrey A. Jahn[1]

Nineteen abnormal temporomandibular joints (TMJs) imaged with high-field-strength surface-coil MR are presented to illustrate specific changes associated with disk derangement, trauma, and previous surgery. Cases were selected from a series of 248 TMJ MR studies in 144 patients (9–68 years old, 130 females and 14 males) performed during a 5-month period. Surgical findings were available for correlation in 44 of the 248 joints studied. Increased signal caused by myxoid degeneration within the degenerating meniscus was seen, as were pathologic changes including atrophy, fibrosis, and contracture of masticatory muscles occurring with internal degrangements. Advantages and limitations of MR are discussed with reference to arthrography and videofluoroscopy. High-resolution and partial-flip-angle images of a normal joint are provided for comparison.

In most clinical circumstances, MR is the procedure of choice when examining the TMJ, because it provides contrast resolution of soft-tissue structures superior to that of conventional imaging techniques.

MR is an established technique for diagnosing internal derangements of the temporomandibular joint (TMJ) [1–5]. The lack of ionizing radiation and noninvasive characteristics of MR make it the examination of choice over arthrography in most clinical circumstances. MR provides superior contrast resolution of soft-tissue structures as compared with conventional imaging procedures. Our intention is to present TMJ alterations imaged with a 1.5-T magnet. We report changes observed with trauma and various surgical procedures and describe our early experience with partial-flip-angle imaging techniques.

Materials and Methods

Two hundred forty-eight TMJ MR studies were performed in 144 patients between January 2 and May 30, 1987, with a 1.5-T GE imaging system using an 8.9-cm surface coil. The first 56 joints in the series were imaged with T1-weighted 3-mm-thick contiguous interleaved partial-saturation images that had a repetition time (TR) of 500 msec, echo time (TE) of 20 msec, 256 × 128 matrix with four signal acquisitions, and 12-cm field of view for the closed-mouth series and two acquisitions for the open-mouth sequence. The last 192 joints in the series were studied with contiguous 3-mm-thick sagittal images that had TR = 500 msec, TE = 20 msec, 256 × 256 matrix, and two acquisitions for the closed-mouth series. Open-mouth views were obtained with 3-mm images with a 2-mm gap and two acquisitions. Closed- and open-mouth examinations required 8 min 35 sec and 4 min 18 sec, respectively. Selected cases were examined with the spin-echo technique (TR = 2000 msec, TE = 20/80 msec) if inflammatory disease or joint fluid was suspected. Occasionally, nine contiguous interleaved 3-mm-thick T1-weighted coronal images were obtained through the condyle and pterygoid muscles with TR = 500 msec, TE = 20 msec, 256 × 256 matrix, and one acquisition, mostly to assess suspected bony and muscular disease. Nine sagittal images were obtained through the full width of the condyles after obtaining a short axial localizing sequence (Fig. 1). Most patients (all cases reported) were screened with preliminary submentovertex and open-mouth, jaw-protruded anteroposterior radiographs of the skull base and closed- and open-

This article appears in the November/December 1987 issue of *AJNR* and the February 1988 issue of *AJR*.

Received March 2, 1987; accepted after revision June 22, 1987.

Presented at the annual meeting of the American Society of Head and Neck Radiology, Milwaukee, May 1987.

[1] Center for Diagnostic Imaging, 5775 Wayzata Blvd., Suite 190, St. Louis Park, MN 55416. Address reprint requests to K. P. Schellhas.

[2] Park Place Center, Suite 990, 5775 Wayzata Blvd., St. Louis Park, MN 55416.

[3] 250 Central Ave. N., Wayzata, MN 55391.

***AJR* 150:381–389, February 1988**
0361–803X/88/1502–0381
© American Roentgen Ray Society

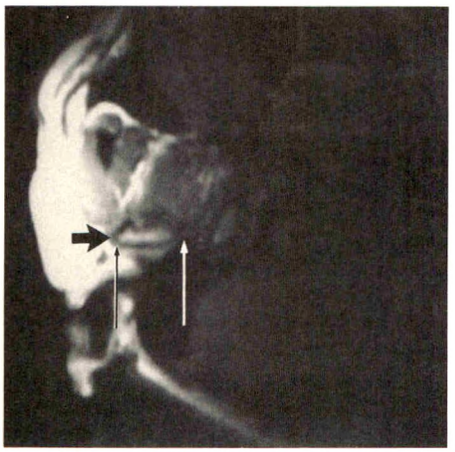

Fig. 1.—T1-weighted axial localizing image (TR = 400 msec, TE = 20 msec, one acquisition, 10 mm thick) prior to sagittal imaging. Patient and condyle (*thick arrow*) are rotated approximately 25° toward vertical surface coil to permit direct sagittal imaging perpendicular to condylar axis. Condylar orientation was predetermined with submentovertex skull radiograph. Imaging is performed from lateral pole of condyle to point beyond medial pole (*thin arrows*) to include lateral pterygoid muscles.

mouth lateral TMJ tomograms. The base view of the skull was used for head positioning relative to the surface coil in an attempt to obtain cephalometrically corrected sagittal MR images. Patients with restricted condylar translation were generally examined in the closed-mouth position only, particularly when significant meniscus displacement and intrinsic derangement was observed. Open-mouth views were obtained when only mild abnormalities were seen on closed-mouth images.

The last 52 joints (29 patients) in the series were studied routinely with a combination of standard T1-weighted closed-mouth and partial-flip-angle techniques or GRASS (gradient recalled acquisition in the steady state), which allowed for rapid sequential scanning of the joint in various stages of opening in as little as 3 sec per image. A technique with TR = 21 msec, TE = 12.5, and flip angle of 30° was used with a 128 × 256 matrix and 16.5-cm field of view. There was no change in patient positioning between standard and partial-flip-angle imaging sequences. A midcondyle location was selected for the single 5-mm-thick image that this technique yields with each imaging sequence. A Burnett TMJ device* was used to regulate the degree of mouth opening. Three to 12 sequential images with 3-mm opening steps were obtained for dynamic viewing of joints. Partial and fully open GRASS images were obtained in conjunction with the standard T1-weighted images in most cases. The average examination time for a bilateral closed-mouth-only examination was about 30 min, while bilateral closed- and open-mouth studies required an average of 50 min. Nine examinations were terminated because of claustrophobia. Six procedures were considered to be technically inadequate for diagnosis owing to patient motion. Nine examinations were inconclusive owing to limitations of spatial resolution and/or unusual anatomy. Arthrography and videofluoroscopy provided conclusive information in five of these nine inconclusive cases. Nine joints (nine patients) were also evaluated with dual-compartment arthrography and videofluoroscopy [6]. To date, surgical results are available in 44 joints from the series.

* Medrad, Inc., Pittsburgh.

Results and Discussion

Normal Joint Anatomy

Normal TMJ anatomy is sharply defined with surface-coil MR (Fig. 2) [2–8]. The normal meniscus is biconcave in appearance and is located between the articular surfaces of the mandibular condyle and temporal bone. The thickest portion of the posterior band of the meniscus is usually centrally situated on top of the condyle in coronal images. A normal meniscus emits a homogeneously low signal. Masticatory muscles and meniscal attachments are demarcated by adjacent fat (Figs. 2 and 3). The superior belly of the lateral pterygoid muscle attaches to the lateral pterygoid plate anteriorly and to the central and medial aspect of the anterior meniscus attachment posteriorly, and asserts traction on the normal meniscus during forward movement (translation) of the condyle. The inferior belly of the lateral pterygoid muscle extends between the inferior aspect of the lateral pterygoid plate and the fovea of the condylar neck and pulls the condyle forward during contraction. The medial pterygoid, the temporalis, and the masseter all function in jaw closure. Abnormalities of muscle function may be directly visualized with dynamic partial-flip-angle techniques [9].

It is important to note that standard T1-weighted open-mouth MR views frequently demonstrate a diminished amplitude of forward condylar translation owing to patient difficulty in maintaining a maximum open-mouth position for the time required for imaging, regardless of the presence or absence of internal derangement. This problem is completely solved with partial-flip-angle techniques, in which images are obtained in as little as 3 sec. T2* characteristics are accentuated with the partial-flip-angle technique used in the study.

Internal Derangements

Abnormalities of meniscus position and morphology are clearly defined with MR (Figs. 3–9). Most internal derangements involve soft-tissue structures, which may be impossible to demonstrate with noninvasive conventional imaging techniques. Anterior displacement of the meniscus is the most common internal derangement affecting the TMJ. With forward meniscus displacement, the posterior attachment (bilaminar zone) is stretched and may exhibit either attenuation or thickening and redundancy (Figs. 5 and 7). Medial or lateral displacement commonly accompanies anterior meniscus displacement and advanced internal derangements. Medial vs lateral meniscus displacement can be determined from sequential sagittal images alone if they cover the full width of the condyle; however, when there is unusual condylar anatomy, coronal images may be applied (Fig. 6). The combination of anterior and medial meniscus displacement is a frequent cause of clinical "closed lock." Thickening and deformity of the meniscus may be observed. Perforations of the meniscus and attachments may be diagnosed (Figs. 7 and 8). Perforation is a common false-positive finding with MR owing to the often attenuated appearance of the stretched bilaminar zone in cases of chronic anterior displacement. Abnormalities of

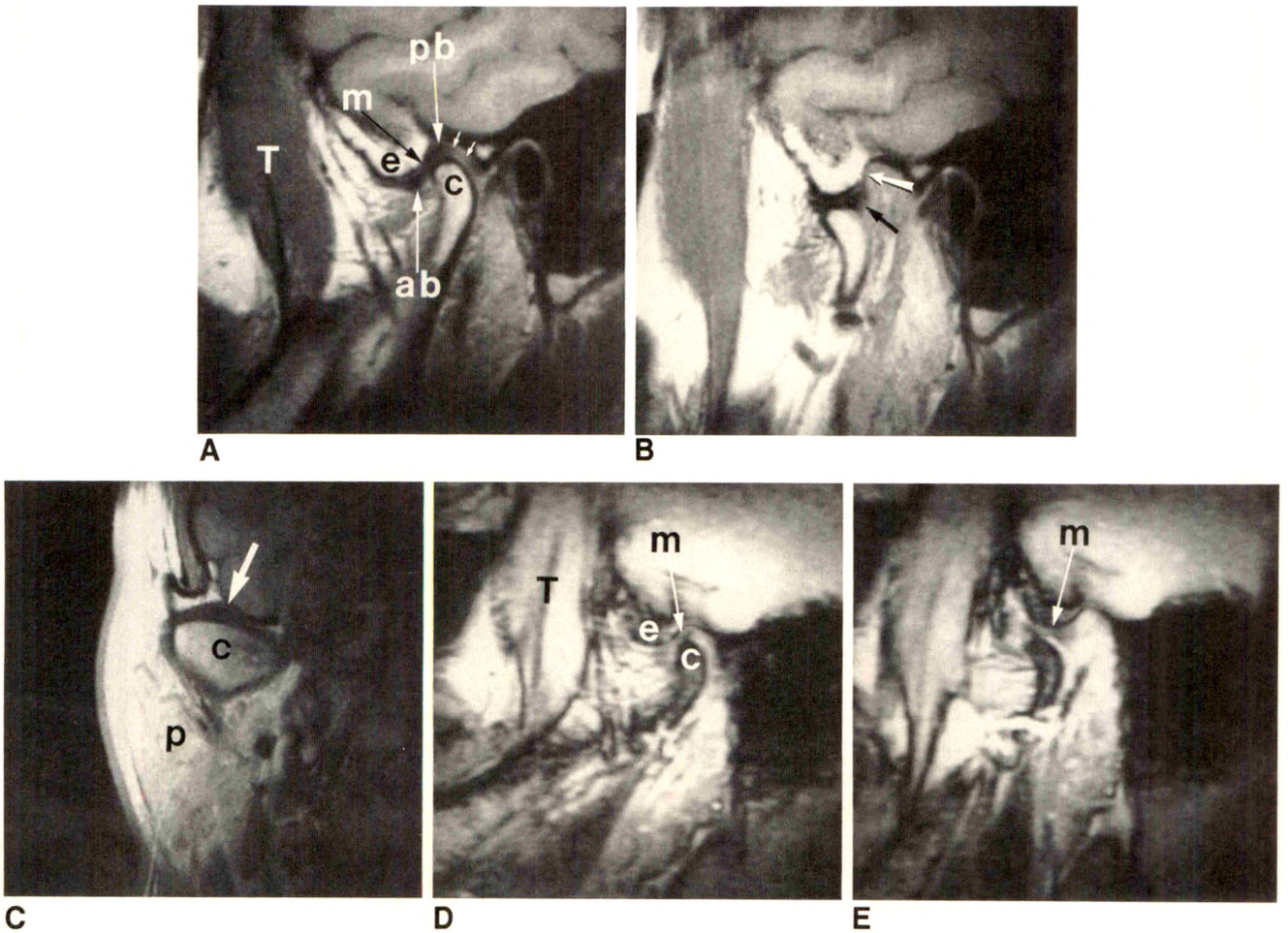

Fig. 2.—Normal temporomandibular joint in closed (*A*) and open (*B*) mouth positions (TR = 500 msec, TE = 20 msec, 256 × 256 matrix, two excitations).

***A*, Meniscus (m) has biconcave appearance and uniform low signal intensity. Posterior band (pb) lies above articular surface of condyle (c). Anterior band (ab) of meniscus lies in front of condyle, proximal to articular eminence (e). Bilaminar zone or posterior meniscus attachment (*arrows*) connects meniscus to temporal bone behind condyle. Temporalis muscle (T) attached onto coronoid process and medial surface of mandible.**

***B*, After translation, condyle lies below eminence. Posterior band of meniscus (*black arrow*) now lies behind condyle. Bilaminar zone (*white arrow*) is redundant owing to limited forward condylar excursion, commonly observed on T1-weighted open-mouth MR images.**

***C*, Coronal image (TR = 500 msec, TE = 20 msec, 256 × 256 matrix, one acquisition) shows normal meniscus (*arrow*) centrally located relative to articular surface of condyle (c). Note adjacent normal parotid gland (p).**

***D* and *E*, Closed (*D*) and open (*E*) mouth partial-flip-angle images (same joint as *A*–*C*) (TR = 21 msec, TE = 12.5 msec, 30° flip angle, 128 × 256 matrix, two acquisitions, 6-sec image, 5 mm thick).**

***D*, Condyle (c) and eminence (e) exhibit diminished signal intensity (compare with *A*) owing to T2* effects. Meniscus (m) and temporalis muscle (T) are defined less sharply than on T1-weighted images.**

***E*, Maximal open-mouth view shows greater degree of forward condylar movement compared with *B*. Meniscus is well defined.**

the lateral pterygoids and other masticatory muscles may be observed primarily or in association with various internal derangements. Fibrosis and contracture of the superior belly of the lateral pterygoid muscle may accompany chronic anterior and medial displacement of the meniscus, particularly when there is rupture or perforation of an attenuated posterior attachment. This finding is also sometimes observed after meniscectomy, with or without prosthetic meniscus implants (Fig. 9). Videofluoroscopy and dynamic partial-flip-angle techniques demonstrate that muscle atrophy frequently accompanies meniscus degeneration and bony deformity.

Intrinsic Histochemical and Structural Meniscus Alterations

Intrinsic histochemical changes within the deranged or degenerating meniscus may be diagnosed in vivo. Myxoid degeneration of meniscus fibrocartilage may result in increased signal intensity within a diseased meniscus, with or without displacement, identical to pathologic changes observed within the knee (Figs. 3, 4, 8, and 10) [10–14]. High-resolution T1-weighted images are needed to diagnose intrinsic meniscus lesions, as these changes may not be apparent on T2-weighted images, in part owing to decreased spatial resolu-

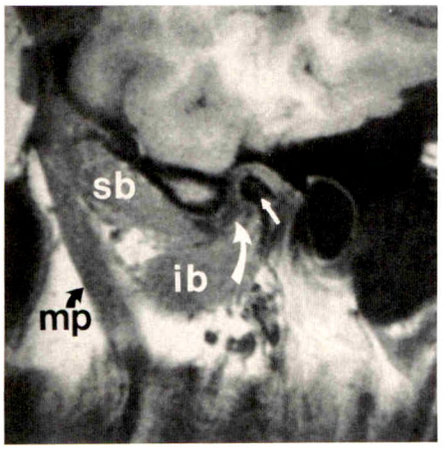

Fig. 3.—Chronic anterior meniscus displacement with normal pterygoid muscles (image through medial pole of condyle), superior belly (sb), and inferior belly (ib) of lateral pterygoid muscle is well defined. Meniscus (*curved arrow*) is anteriorly and medially displaced (medial displacement determined by reviewing sequential lateral to medial images) and shows increased signal (compare with Fig. 2A). Medial pterygoid muscle (mp) lies deep to temporalis muscle. Note diminished signal (*straight arrow*) from hyperostosis in condyle.

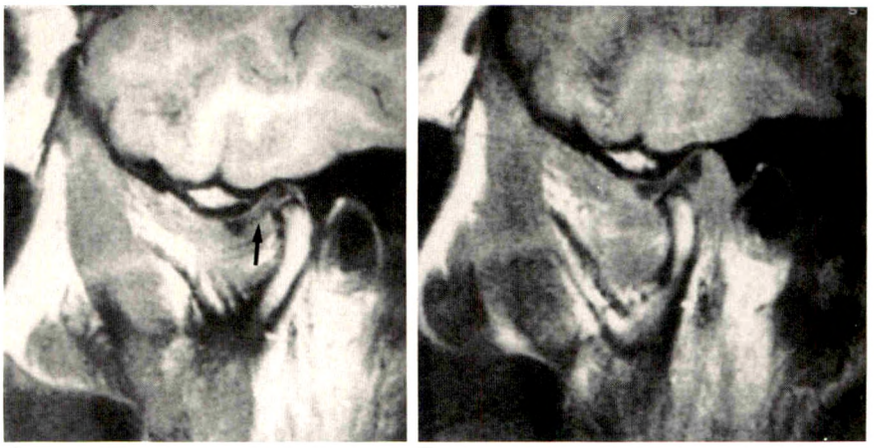

Fig. 4.—Anterior meniscus displacement (*arrow*) with reduction (*B*) in 29-year-old woman with 2-year history of temporomandibular pain and clicking. Note increased meniscus signal (*arrow*).

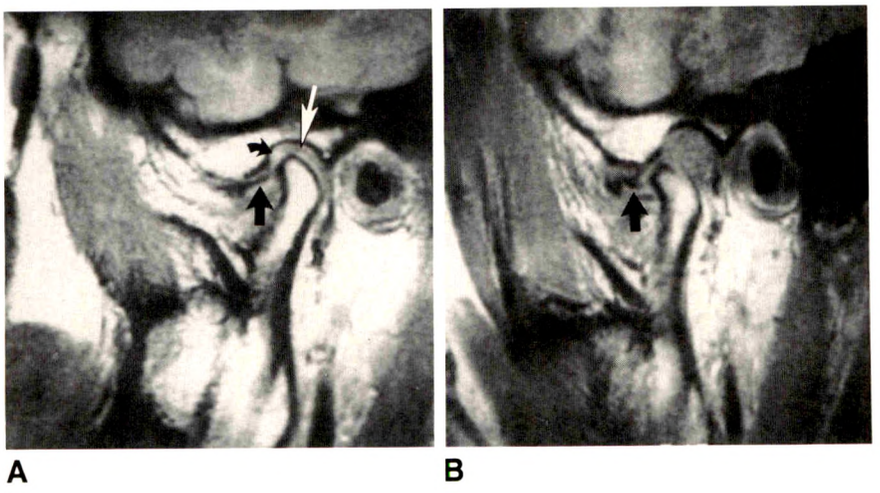

Fig. 5.—Nonreducing chronic meniscus derangement resulting in clinical closed lock.

A, Closed-mouth image shows anterior displacement of meniscus (*straight black arrow*) with stretching of posterior attachment (*white arrow*), which appears attenuated (*curved arrow*) near meniscus attachment (there was no perforation at surgery). Note normal (concentric) condylar positioning within glenoid fossa.

B, Maximal open-mouth view shows nonreduction of thickened and deformed meniscus (*arrow*). Note normal meniscus signal intensity despite chronic displacement and deformity.

tion. With current technology, the normal disk may appear inhomogeneous with 5-mm-thick partial-flip-angle images owing to decreased spatial resolution; therefore, thin-section high-resolution T1-weighted images are recommended for detection of these abnormalities.

Trauma

MR may be used to evaluate the traumatized TMJ for assessment of the severity of injury and surgical planning. Traumatic derangement may result in chronic pain and diminished condylar translation clinically. Muscle spasm, headaches, bony alterations, muscular contracture, and malocclusion are known sequelae of fractures involving the condyle and condylar neck [15]. TMJ hematomas frequently occur with condylar fractures and direct blows to the mandible and commonly result in formation of adhesions (Figs. 11–13). Adhesions are seen as areas of diminished signal intensities on T1-weighted images surrounding or adjacent to the meniscus and condyle, often obliterating the normal fibrofatty tis-

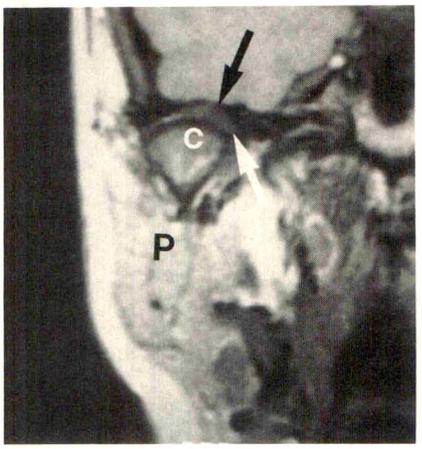

Fig. 6.—Medial displacement of meniscus (3-mm-thick T1-weighted coronal image, obtained with head coil). Posterior band of meniscus (*arrows*) is medially displaced on top of condyle (c). Parotid gland (P) appears normal. Abnormality was detected during head examination performed to evaluate ipsilateral headache and facial pain.

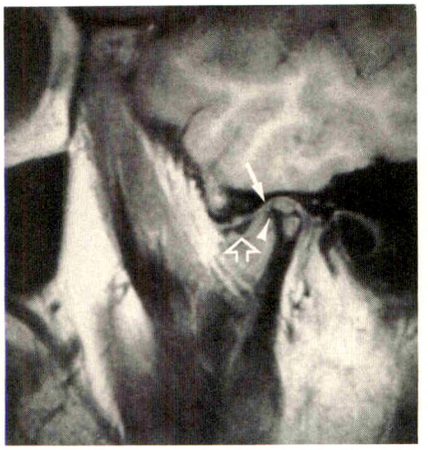

Fig. 7.—Late-stage internal derangement with perforation (surgically proved) of posterior attachment. Meniscus (*open arrow*) is displaced and deformed. Condyle is deformed, and there is an anterior osteophyte (*arrowhead*). Bilaminar zone is attenuated in area of perforation (*solid arrow*).

Fig. 8.—Chronic anterior meniscus displacement (*white arrow*) with increased signal and perforation (surgically proved) of posterior attachment. Anterior attachment (*curved arrow*) is redundant and thickened. Condyle is posteriorly displaced within glenoid fossa and contacts temporal bone posteriorly (*open arrow*) at point of perforation. Small focus of avascular necrosis (*straight black arrow*) is seen in articular surface of condyle.

Fig. 9.—Atrophy and fibrosis of superior belly (*arrows*) of lateral pterygoid muscle after meniscectomy and permanent implant placement. Inferior belly (ib) is normal.

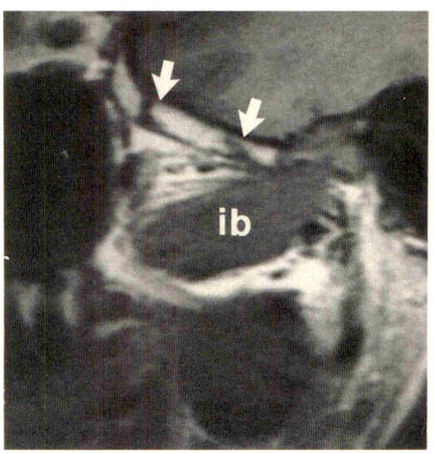

9

Fig. 10.—Increased signal intensity (*straight arrows*) within normally positioned meniscus (*curved arrow*). Note unusually deep glenoid fossa. Clinical symptoms included long-standing headache, facial pain, temporomandibular joint clicking, and episodic locking.

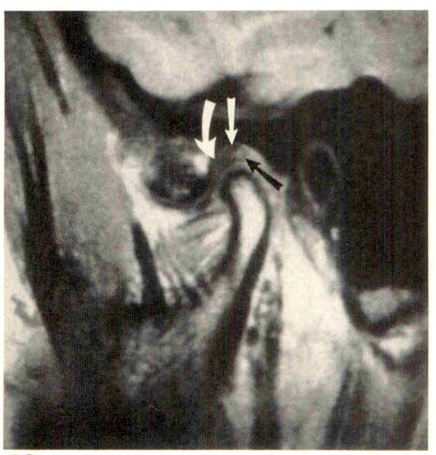

10

sues seen in normal joints [2, 5, 11]. MR is of particular value in the evaluation of late, traumatic sequelae, since soft-tissue structural alterations often cannot be seen with conventional imaging techniques, and arthrography/videofluoroscopy may be difficult to perform when adhesions are present.

Postoperative TMJ

A number of surgical procedures have been described for the correction of internal derangements [15–22]. Simple meniscectomy and meniscus plication procedures are all commonly performed surgical procedures. Condylectomy and reduction osteotomy of the articular eminence (eminectomy) are used less often. A number of different temporary and permanent meniscus implants after disk removal have been and continue to be used. MR permits direct evaluation of the postoperative joint. Limited skull films and conventional lateral tomograms are helpful in conjunction with MR, as it is important to distinguish calcification from hypointense scar tissue. This combination generally clarifies the type and extent of prior joint manipulation. Submentovertex and posteroanterior

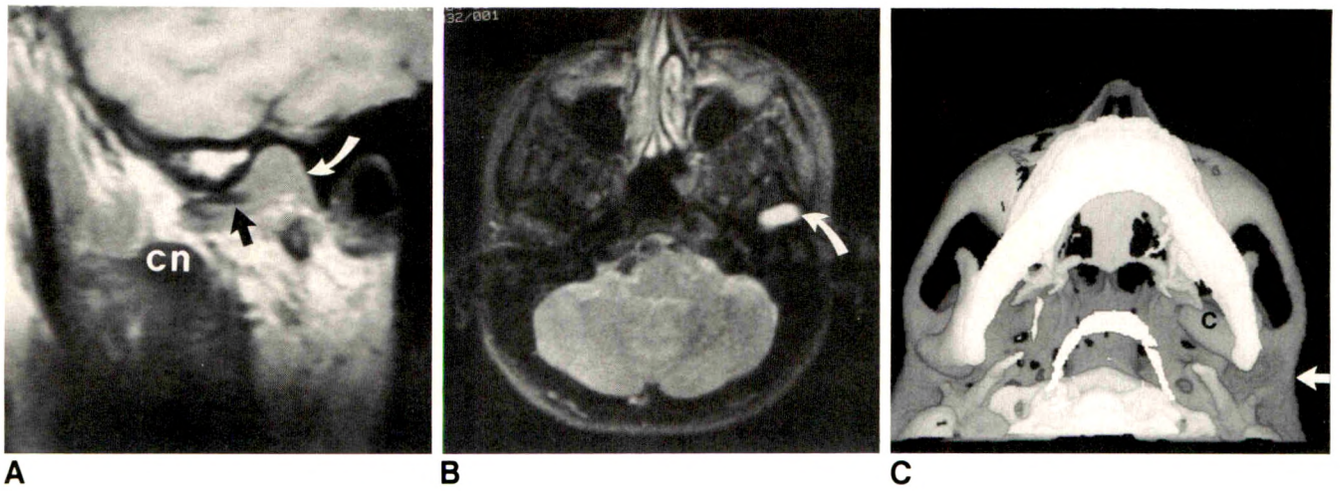

Fig. 11.—Subacute temporomandibular joint trauma.

A, Sagittal closed-mouth image (256 × 128 matrix) shows rotational dislocation of condyle out of glenoid fossa (*white arrow*) owing to condylar neck (cn) fracture. Meniscus (*black arrow*) is anteriorly and medially displaced by lateral pterygoid contracture.

B, Axial spin-echo (TR = 2000 msec, TE = 80 msec) image, 5 mm thick, shows fluid (*arrow*) filling glenoid fossa.

C, 3-D CT scan shows anteromedial displacement of condyle (c) owing to condylar neck fracture. Glenoid fossa (*arrow*) is empty. At surgery, performed to reduce complete closed lock and reposition condyle, adhesions, fluid, and blood breakdown products were found within glenoid fossa above displaced meniscus.

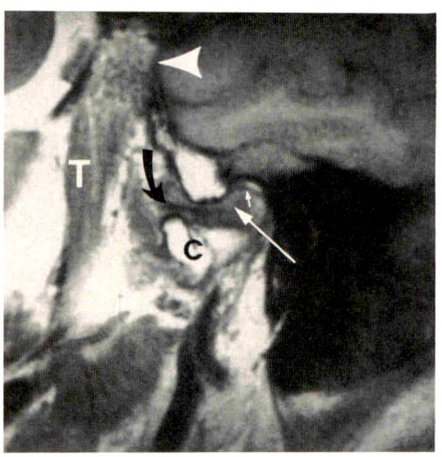

Fig. 12.—Chronic deformity from old intracapsular fracture of condyle (c). Meniscus (*curved arrow*) exhibits normal signal intensity and is normally positioned relative to deformed condyle. Posterior attachment (*short white arrow*) is redundant and separated from meniscus because of large perforation (*long white arrow*) encountered at surgery. Note scarring and fibrosis within medioposterior aspect of temporalis muscle (T) insertion (*arrowhead*).

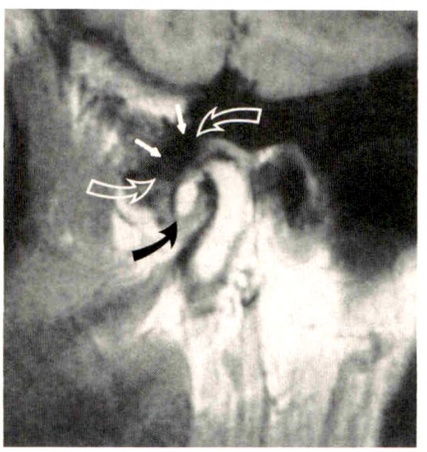

Fig. 13.—Chronic adhesions and dystrophic ossification (*black arrow*) secondary to old trauma. Meniscus (*open arrows*) was found to be totally adherent to temporal bone (*straight arrows*) due to extensive adhesions. Soft-tissue calcification was present throughout joint space.

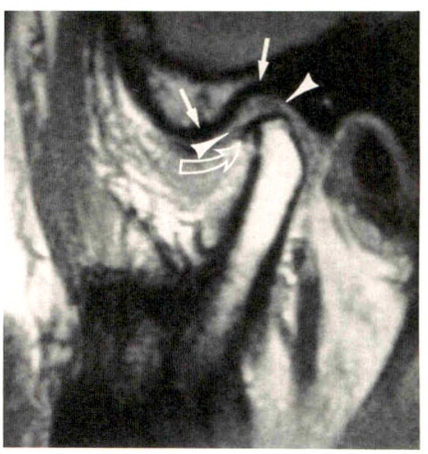

Fig. 14.—Optimal 12-month postmeniscectomy temporomandibular joint. Articular cortex of temporal bone (*straight arrows*) is slightly thickened but retains its normal sigmoid curvature. Articular space (*arrowheads*) is maintained by articular-bearing surface cartilage and fibrofatty tissue on this closed-mouth image. Note prominent attachment from inferior belly of lateral pterygoid muscle (*curved arrow*), shown to be noncalcified on conventional lateral temporomandibular joint tomograms.

open-mouth, jaw-protruded views of the mandible are also helpful, since discrepancies in condylar shape and height may be detected as degenerative remodeling consequences of chronic internal derangements, trauma, and surgical manipulation of the joint.

After meniscectomy, the amputated posterior and anterior meniscal attachments are seen at the margins of the articular space (Figs. 14 and 15). Typically, some remodeling changes result in thickening of the articular surfaces of both the glenoid fossa and condyle, both of which may become slightly flattened. Ideally, the articular space is maintained by bearing surface fibrocartilage. Temporary meniscus implants are commonly used after meniscectomy to prevent the formation of adhesions. Postoperative bony remodeling changes may be

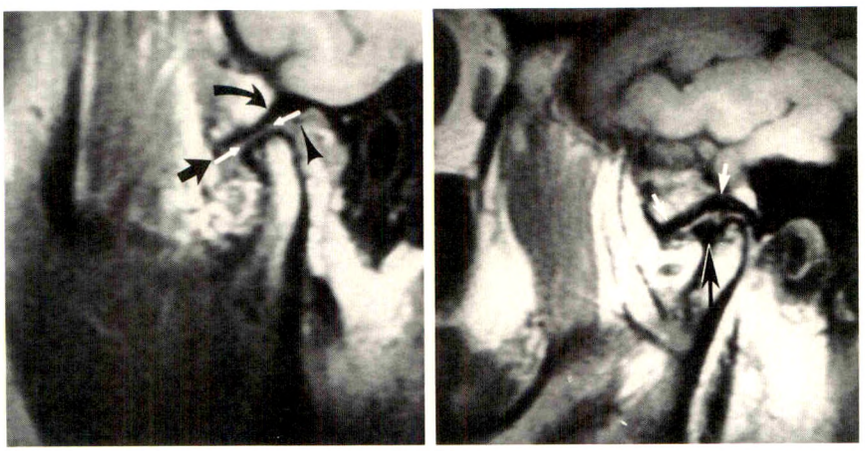

Fig. 15.—Postoperative changes after simple meniscectomy (*A*) and multiple operations including initial permanent prosthesis implantation (*B*).

A, Closed-mouth image shows amputated anterior (*straight black arrow*) and posterior (*arrowhead*) meniscal attachments 42 months after surgery. Joint space (*white arrows*) is present and articular surfaces of condyle and temporal bone (*curved arrow*) are flattened owing to remodeling.

B, Advanced degenerative change 18 months after meniscectomy and permanent implant insertion that subsequently required removal because of joint pain and swelling. Cortex of temporal bone (*white arrows*) is thickened and irregular. Large condylar osteophyte (*black arrow*) is seen anteriorly. Surgery was performed again after imaging for lysis of adhesions.

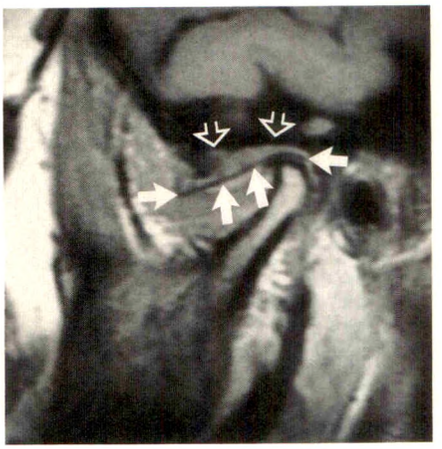

Fig. 16.—Permanent meniscus implant (Proplast) 6 months after insertion. Hypointense prosthesis (*solid arrows*) is sharply demarcated from adjacent tissues. Note postsurgical changes in temporal bone (*open arrows*), where implant is anchored.

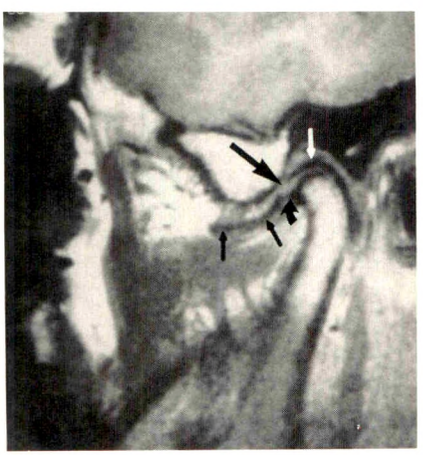

Fig. 17.—Perforation (*long straight arrow*) of permanent Silastic implant (*short straight arrows*) 42 months after insertion. Anterior condylar osteophyte (*curved arrow*) lies beneath perforation. Note absence of destructive skeletal changes with this implant.

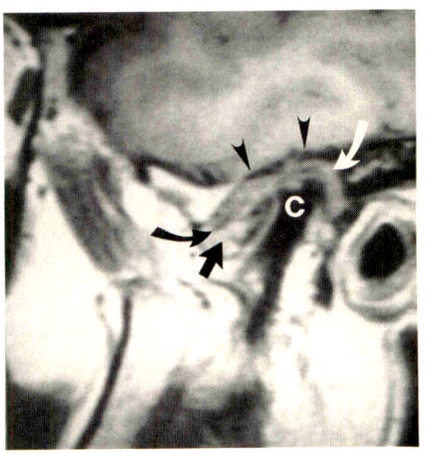

Fig. 18.—Destructive changes associated with permanent meniscus implant (18 months after meniscectomy and Proplast prosthesis insertion). Marked irregularity of condyle (c) is noted with decreased signal intensity interpreted to represent avascular necrosis. Prosthesis (*curved arrows*) is surrounded by highly vascular granulation tissue (*straight arrow*), removed along with prosthesis. Marked irregularity of temporal bone (*arrowheads*) is noted.

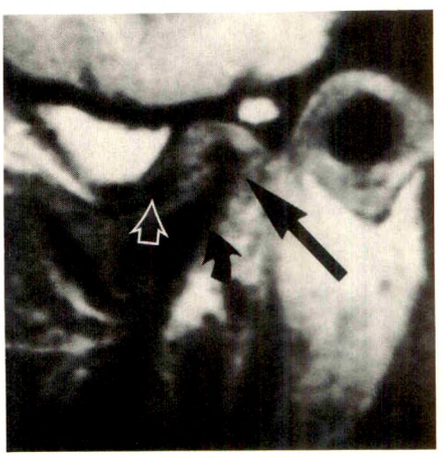

Fig. 19.—Old avascular necrosis and condylar deformity in 31-year-old man with history of bilateral sagittal split mandibular osteotomies and orthognathic manipulation at 25 years of age. Condyle (*straight solid arrow*) and condylar neck (*curved arrow*) are deformed and lack normal signal intensity. Note displaced meniscus (*open arrow*) and condylar malposition within glenoid fossa. (Changes were bilateral.)

distinguished from ordinary osteoarthritis by using conventional tomography alone; however, MR is needed to observe adhesions and other soft-tissue structures within the joint [5, 10, 11]. Relative narrowing of the articular space is often observed without functional disturbance after successful meniscectomy (Fig. 15A). Irregular articular surfaces and adhesions can result from unsuccessful surgery with permanent meniscus implants (Fig. 15B). In this circumstance, the patient may experience pain, crepitus, and limitation of joint motion.

Permanent meniscus prostheses are easily studied with MR (Figs. 16–18). Granulation tissue, joint fluid, and adhesions may be detected. Perforation of an implant can occur (Fig. 17). Destructive changes observed with certain perma-

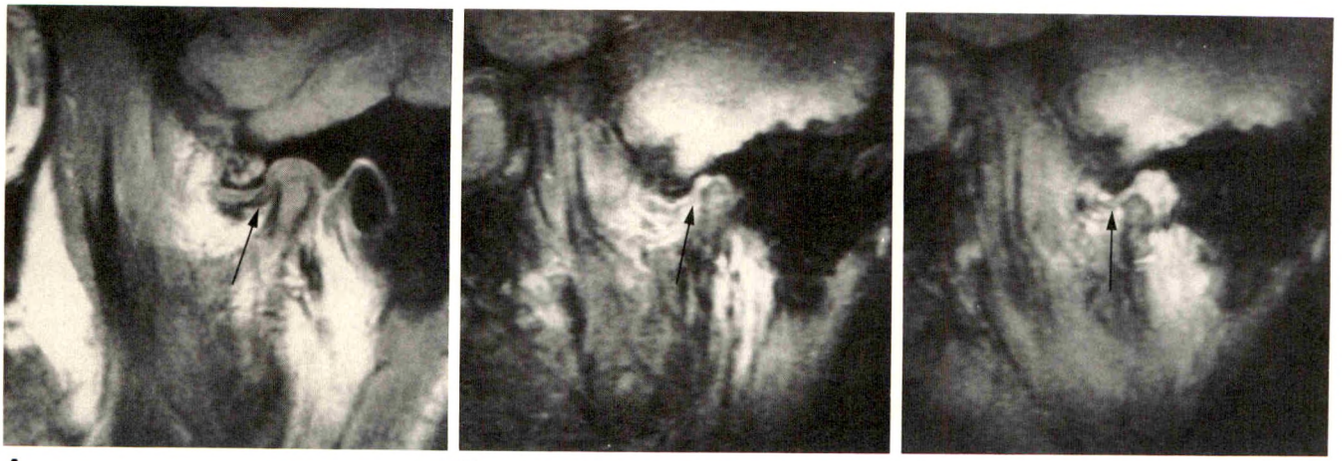

Fig. 20.—Standard T1-weighted (*A*) and 3-sec, partial-flip-angle (*B* and *C*) images show nonreducing meniscus derangement.
***A*, Meniscus (*arrow*) is displaced and deformed.**
***B* and *C*, Closed- (*B*) and maximal open- (*C*) mouth GRASS images (TR = 21 msec, TE = 12.5 msec, 30° flip angle, 256 × 128 matrix, one acquisition, 3 sec) show nonreduction of displaced meniscus (*arrows*).**

nent implants may be assessed, along with physiologic alterations in bony structures (Fig. 18) [23]. Avascular necrosis of the condyle and consequent remodeling changes may follow jaw trauma or orthognathic and surgical manipulation of the TMJ and mandible (Fig. 19). MR signal and morphologic changes are similar to those seen in avascular necrosis of the femoral head [24–26].

Partial-flip-angle imaging techniques permit assessment of joint physiology when sequential dynamic imaging techniques are employed. With GRASS techniques, any number of sequential images can be obtained at incremental degrees of mouth opening in as little time as 3 sec per image (Fig. 20). Partial-flip-angle techniques show immense promise for further investigation into functional derangements of the meniscus and muscles of mastication. Videofluoroscopy of the injected TMJ provides higher spatial resolution of the meniscus; however, this procedure is invasive; requires considerable technique, skill, and expertise on the part of the arthrographer; and does not allow direct observation of jaw musculature.

MR has limitations. Claustrophobia precludes MR imaging of certain patients, while some apprehensive patients may be examined successfully after sedation. Older ferromagnetic dental appliances may cause image degradation, which may on occasion result in inadequate image quality for interpretation. Patient motion may significantly degrade image quality; however, this problem is minimized when patients are properly positioned and secured relative to the surface coil and reminded frequently during the procedure not to move. Partial-flip-angle techniques dramatically reduce image acquisition times and diminish many of the problems related to patient motion, although spatial resolution is sacrificed. With the advent of routine nonorthogonal imaging capability and thin-section three-dimensional volume acquisitions, problems of partial-volume averaging caused by unusual joint orientation will be diminished. Limited skull films including submentovertex and open-mouth, jaw-protruded anteroposterior projections of the skull base and mandible provide useful and important information regarding condylar symmetry and orientation. These data are used during positioning of the patient for an MR examination. When limited skull films and high-quality closed- and open-mouth lateral tomograms are combined with surface-coil MR, patients with advanced meniscus derangements can be evaluated satisfactorily with closed-mouth MR images alone.

We believe that a symptomatic joint exhibiting meniscus displacement, deformity, and intrinsic degeneration is best treated with meniscectomy. In advanced cases, a temporary Silastic implant is inserted into the joint and removed percutaneously after 4 weeks. The temporary implant prevents formation of adhesions in the joint recesses in the early postoperative days. The presence or absence of meniscus reduction relative to the condyle is less important when deformity and intrinsic alterations accompany anterior displacement. Such changes are irreversible and often progress to perforation and subsequent development of osteoarthritis. Meniscectomy performed before perforation both relieves bothersome mechanical symptoms and decreases the likelihood that osteoarthritis will develop.

ACKNOWLEDGMENT

We thank Steven D. Johnson for recent surgical confirmation of the findings in Figure 17.

REFERENCES

1. Katzberg RW, Schenck JF, Roberts D, et al. Magnetic resonance imaging of the temporomandibular joint meniscus. *Oral Surg* **1985**;59:332–335
2. Harms SE, Wilk RM, Wolford LM, et al. The temporomandibular joint: magnetic resonance imaging using surface coils. *Radiology* **1985**;157:133–136
3. Katzberg RW, Bessette RW, Tallents RH, et al. Normal and abnormal

temporomandibular joint: MR imaging with surface coil. *Radiology* **1986**;158:183–189
4. Schellhas KP, Wilkes CH, Heithoff KB, Omlie MR, Block JC. Temporomandibular joint: diagnosis of internal derangements using magnetic resonance imaging. *Minn Med* **1986**;69:516–519
5. Harms SE, Wilk RM. Magnetic resonance imaging of the temporomandibular joint. *Radiographics* **1987**;7(4):521–542
6. Wilkes CH. Arthrography of the temporomandibular joint in patients with the TMJ-pain-dysfunction syndrome. *Minn Med* **1978**;61:645–652
7. Christensen EL, Thompson JR, Hasso AN, Hinshaw DB. Correlative thin section temporomandibular joint anatomy and computed tomography. *Radiographics* **1986**;6(4):703–723
8. Westesson TL. Diagnostic accuracy of double contrast arthrotomography of the temporomandibular joint: correlation with postmortem morphology. *AJNR* **1984**;5:463–468
9. Mills TC, Ortendahl DA, Hylton NM, Crooks LE, Carlson JW, Kaufman L. Partial flip angle MR imaging. *Radiology* **1987**;162:531–539
10. DeBont LGM, Boering G, Liem RSB, et al. Osteoarthritis and internal derangement of the temporomandibular joint: a light microscopic study. *J Oral Maxillofac Surg* **1986**;44:634–643
11. DeBont LGM. Temporomandibular joint articular cartilage structure and function [Doctoral Thesis]. Groningen, The Netherlands: University of Groningen, **1985**
12. Reicher MA, Bassett LW, Gold RH. High-resolution magnetic resonance imaging of the knee joint: pathologic correlations. *AJR* **1985**;145:903–909
13. Reicher MA, Flartzman S, Duckwiler GR, et al. MR imaging of the knee. *Radiology* **1987**;162:547–551
14. Stoller DW, Martin C, Crues JV III, Kaplan L, Mink JH. Meniscal tears: pathological correlation with MR imaging. *Radiology* **1987**;163:731–735
15. Norman JE. Post-traumatic disorders of the jaw joint. *Ann R Coll Surg Engl* **1982**;64:27–36
16. Gallagher DM, Wolford LM. Comparison of Silastic and proplast implants in the temporomandibular joint after condylectomy for osteoarthritis. *J Oral Maxillofac Surg* **1982**;40:627–630
17. Marciani RD, Ziegler RC. Temporomandibular joint surgery: a review of 51 operations. *Oral Surg* **1983**;56:472–476
18. Hall MB. Meniscoplasty of the displaced temporomandibular joint meniscus without violating the inferior joint space. *J Oral Maxillofac Surg* **1984**;42:788–792
19. Oaitis GW Jr, Baker DA. The bilateral eminectomy as definitive treatment. A review of 44 patients. *Int J Oral Surg* **1984**;13:294–298
20. Eriksson L, Westesson PL. Long-term evaluation of meniscectomy of the temporomandibular joint. *J Oral Maxillofac Surg* **1985**;43:263–269
21. Bessette RW, Katzberg RW, Natiella JR, Rose MJ. Diagnosis and reconstruction of the human temporomandibular joint after trauma or internal derangement. *Plast Reconstr Surg* **1985**;75:192–205
22. Sawhney CP. Bony ankylosis of the temporomandibular joint: follow-up of 70 patients treated with arthroplasty and acrylic spacer interposition. *Plast Reconstr Surg* **1986**;77:1–6
23. Lagrotteria L, Scapino R, Granston AS, Felgenhauer D. Patient with lymphadenopathy following temporomandibular joint arthroplasty with proplast. *J Craniomand Pract* **1986**;4(2):172–178
24. Dooms GC, Fisher MR, Hricak H, Richardson M, Crooks LE, Genant HK. Bone marrow imaging: magnetic resonance studies related to age and sex. *Radiology* **1985**;15:429–432
25. Thickman D, Axel L, Kressel HY, et al. Magnetic resonance imaging of avascular necrosis of the femoral head. *Skeletal Radiol* **1986**;15:133–140
26. Markisz JA, Knowles JR, Altchek DW, et al. Segmental patterns of avascular necrosis of the femoral heads: early detection with MR imaging. *Radiology* **1987**;162:717–720

Book Review

Pediatric Neurology and Neuroradiology. Cerebral and Cranial Diseases. By Claus Diebler and Olivier Dulac. New York: Springer-Verlag, 408 pp., 1987. $165

This book covers all the important diseases of the child's brain. The text is deftly written and provides concise and succinct information on all the topics described. Personal observations and references to the literature abound. Blending of the clinical and pathologic aspects of a disease and its imaging counterpart is excellent. The section on neuroimaging consists of CT scans almost exclusively. The scans are of superb quality and lavishly illustrate the various diseases.

This book contains the following chapters: (1) "Cerebral and Cranial Malformation," (2) "Neurocutaneous Syndromes," (3) "Inherited Metabolic Diseases," (4) "Infectious Diseases of the Central Nervous System," (5) "Vascular Disorders," (6) "Intracranial Tumors," (7) "Cranial Trauma," and (8) "Miscellaneous." The table of contents is elaborate.

In my view, the book suffers from two major deficiencies. One is the exclusion of descriptions of diseases of the spinal column and spinal cord. The second is the absence of MR imaging of brain disease (only three MR illustrations are shown). The second problem unfortunately eclipses this otherwise outstanding work. I do not agree with the authors' opinion that "magnetic resonance imaging is very similar to CT imaging." Knowledge of the CT appearance of any brain disease cannot be transposed that easily to its MR appearance.

The book as it stands now should adorn the medical school libraries. Pediatricians, pediatric neurologists, neurosurgeons, and neuroradiologists should find this book especially worthwhile. Trainees in pediatric neurology and neuroradiology should consider it a mandatory reading assignment. The cost of the book is so great that many readers may find it prohibitive.

Mohammad Sarwar
University of Illinois College of Medicine at Chicago
Chicago, IL 60612

Syringomyelia as a Consequence of Compressive Extramedullary Lesions: Postoperative Clinical and Radiological Manifestations

Mauricio Castillo[1]
Robert M. Quencer[1]
Barth A. Green[2]
Berta M. Montalvo[1]

MR imaging was performed to determine the cause of the onset of new neurologic symptoms in five patients who had previously undergone surgical excision of extramedullary masses. Syringomyelia and the absence of recurrent or residual lesions were documented in all cases. Three patients showed long cysts (multiseptated in two and smooth in one) with low signal intensity on both T1- and T2-weighted images. The flow-void phenomenon related to fluid motion in these three cysts, which were enlarging clinically, was responsible for the hypointensity on the T2-weighted images. In two patients the fluid within the lesions behaved similarly to normal nonpulsatile CSF and may have represented syrinx cavities in a state of "arrested growth." Three patients had surgical decompression under real-time intraoperative sonographic control, which showed the presence of intramedullary cyst-fluid pulsations in two cases and the absence of cyst-fluid pulsations in one case. These sonographic observations correlated with the MR findings.

We postulate that these syrinx cavities form as a result both of the effect that the original extramedullary lesion had upon the underlying spinal cord and the subsequent postoperative alterations in the CSF dynamics at the level of prior surgery. Syringomyelia should be considered in patients with recurrent or new symptoms who previously had surgery for extramedullary lesions.

Syringomyelia presenting synchronously with extramedullary tumors has been regarded as rare [1–3], and syringomyelia in patients with prior removal of extramedullary lesions has not been described. Five patients in whom extramedullary lesions had been previously removed were examined by MR imaging. The presence of long syrinx cavities and the absence of residual or recurrent lesions were documented in all cases. Because of this experience, we describe the development of syringomyelia after the removal of extramedullary lesions, and postulate a mechanism for their formation and enlargement.

Subjects and Methods

Five patients ranging in age from 33–61 years (mean, 42 years) were studied. All patients had extramedullary lesions that had been removed 5–24 years previously (mean, 16 years), and all patients were examined on a 0.5- or 1.5-T superconducting MR imaging system. Thin sections (5 mm) in sagittal and axial projections were obtained through the regions of interest. T1-weighted images, TR 500–1000/TE 26–38, and T2-weighted images, TR 1500–2000/TE 80–120, were obtained. Three patients had metrizamide myelography (230 mgI/ml, 10 ml) by lumbar puncture followed by 3-hr delayed CT (GE 9800) using 10-mm slice thickness. One patient had myelocystography (160 mgI/ml, 3 ml). Three patients had surgery, which was monitored with real-time intraoperative sonography using a 7.5-mHz transducer.

This article appears in the November/December 1987 issue of *AJNR* and the February 1988 issue of *AJR*.

Received March 17, 1987; accepted after revision June 3, 1987.

[1] Department of Radiology, Division of Magnetic Resonance Imaging, University of Miami School of Medicine/Jackson Memorial Medical Center, P. O. Box 016308 (R-308), Miami, FL 33101. Address reprint requests to R. M. Quencer.

[2] Department of Neurological Surgery, University of Miami School of Medicine/Jackson Memorial Medical Center, Miami, FL 33101.

***AJR* 150:391–396, February 1988**
0361–803X/88/1502–0391
© American Roentgen Ray Society

Case Reports

Case 1

A 60-year-old woman presented with a 2-year history of bilateral lower extremity weakness and difficulty voiding. Twelve years earlier she had similar symptoms and a T7 meningioma was discovered and removed. Postoperatively, her weakness improved and her voiding difficulty disappeared. On her current examination, increased muscle tone and absent vibratory sense in both lower extremities and urinary incontinence were present. A T1-weighted MR image showed a low signal intensity within a dilated cord (Fig. 1A). This cyst extended from T7 to the conus medullaris and was noted to have irregular borders and internal septations. A T2-weighted image showed the lesion to have similar signal intensity to the adjacent CSF (Fig. 1B). No areas suspicious for tumor recurrence were seen. Metrizamide myelocystography (Fig. 1C) performed at the T12–L1 level clearly showed the multiseptated nature of the lesion (Fig. 1C). Intraoperative spinal sonography confirmed the presence of a large, septated, nonpulsatile cyst (Fig. 1D). The syrinx cavity was shunted into the subarachnoid space, and fluid obtained from the syrinx had an increased protein concentration (65 mg/dl). After surgery, the patient's lower extremity weakness improved; however, bladder control was not regained.

Case 2

Twenty years before her current evaluation, a 61-year-old woman experienced bilateral lower extremity weakness. A T4 meningioma was found and removed, and she recovered completely. Seventeen years later she presented with a new onset of left lower extremity weakness and stiffness of the left foot. Reexploration revealed recurrent meningioma, which was completely removed. The patient improved; however, 1 year later she noted lower extremity weakness, which progressed over the next 2 years. Physical examination showed markedly decreased muscle strength in her left lower extremity and decreased position and vibratory sensation in both lower extremities. Metrizamide myelography showed a block at T11 and delayed metrizamide CT revealed a cord cyst extending from T2 to T11. T1- and T2-weighted MR images showed a low-signal lesion centrally located within an enlarged cord (Fig. 2A). The lesion extended from T1 to T11 and demonstrated some internal areas of increased signal intensity suggesting intracystic septations. No re-

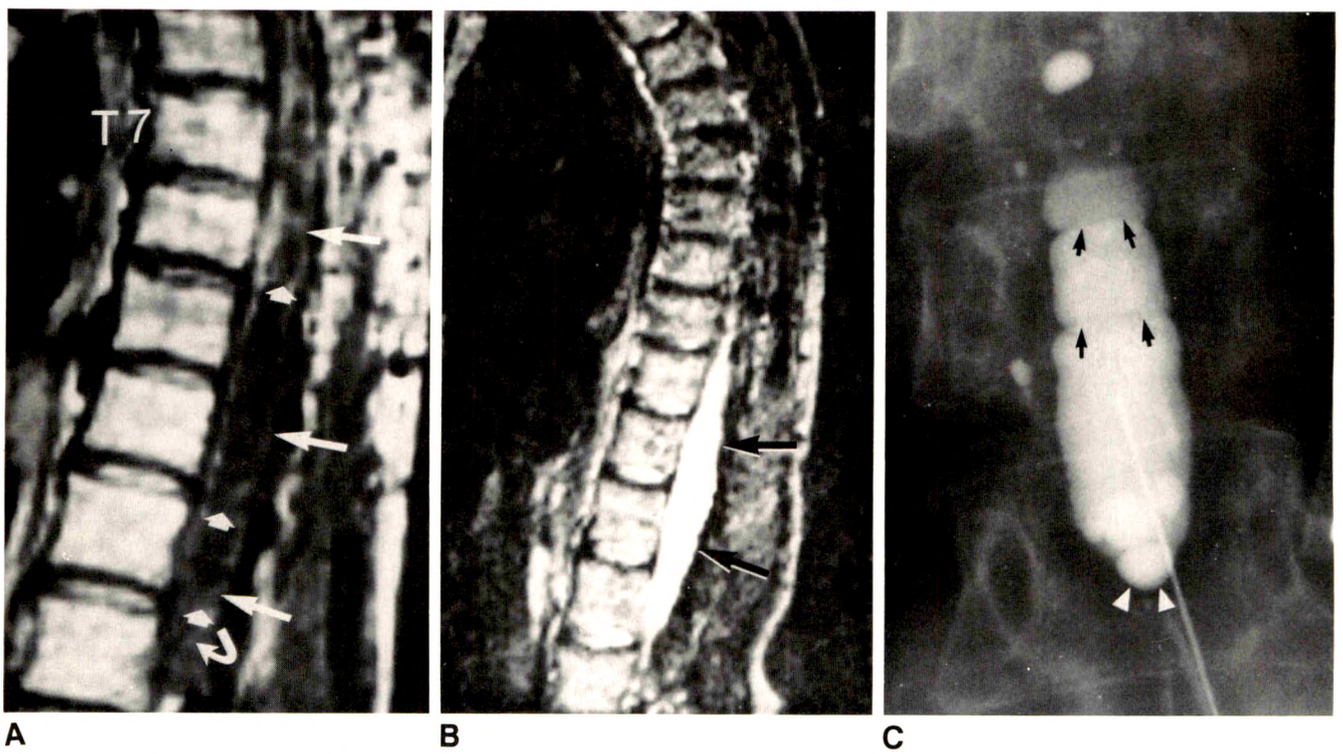

Fig. 1.—Case 1.

***A*, Sagittal T1-weighted 0.5-T MR image (1000/26) at level of lower thoracic and upper lumbar spine. Note intramedullary cyst (*long arrows*) of low signal expanding the cord and extending from level of prior surgery (T7) to conus medullaris (*curved arrow*). Internal septations (*short arrows*) within syrinx are identified.**

***B*, Sagittal T2-weighted MR image (2000/120) with a larger field of view than *A* shows lesion to be of increased signal intensity (*arrows*).**

***C*, Intracystic metrizamide injection (3 ml, 160 mg/ml) shows the multiseptated nature of this intramedullary mass (*arrows*). Note that cyst extends inferiorly to level of conus (*arrowheads*).**

***D*, Sagittal intraoperative spinal sonogram shows cystic nature of intramedullary mass. Lower end of syrinx just above tip of conus is seen, and an intracystic scar is identified (*arrow*). Real-time evaluation showed lack of significant cyst pulsation.**

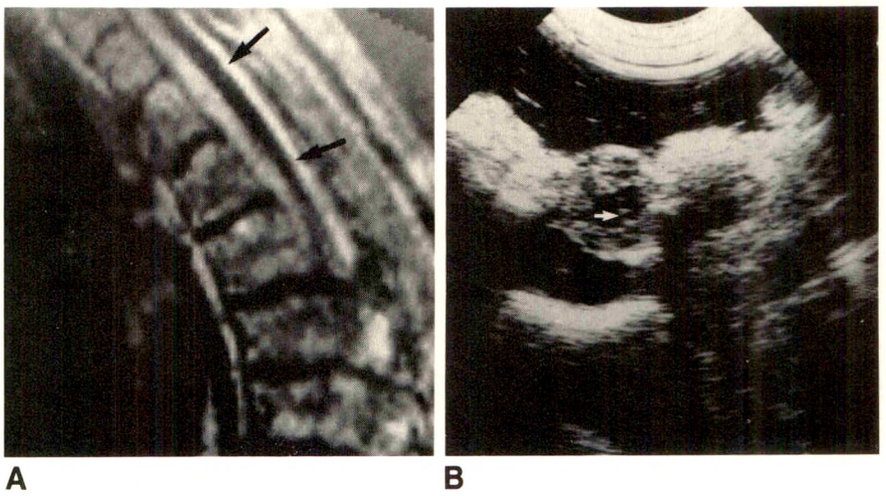

Fig. 2.—Case 2.
***A*, Upper portion of syrinx cavity (*arrows*) is seen on this sagittal T2-weighted 0.5-T MR image (1500/80). The lesion is of low signal intensity and was of similar intensity to that found on T1-weighted image.**
***B*, Transverse intraoperative spinal sonogram at T4 level. A linear area of increased echogenicity (*arrow*) represents intracystic scar. Real-time evaluation showed marked fluid pulsations within cyst.**

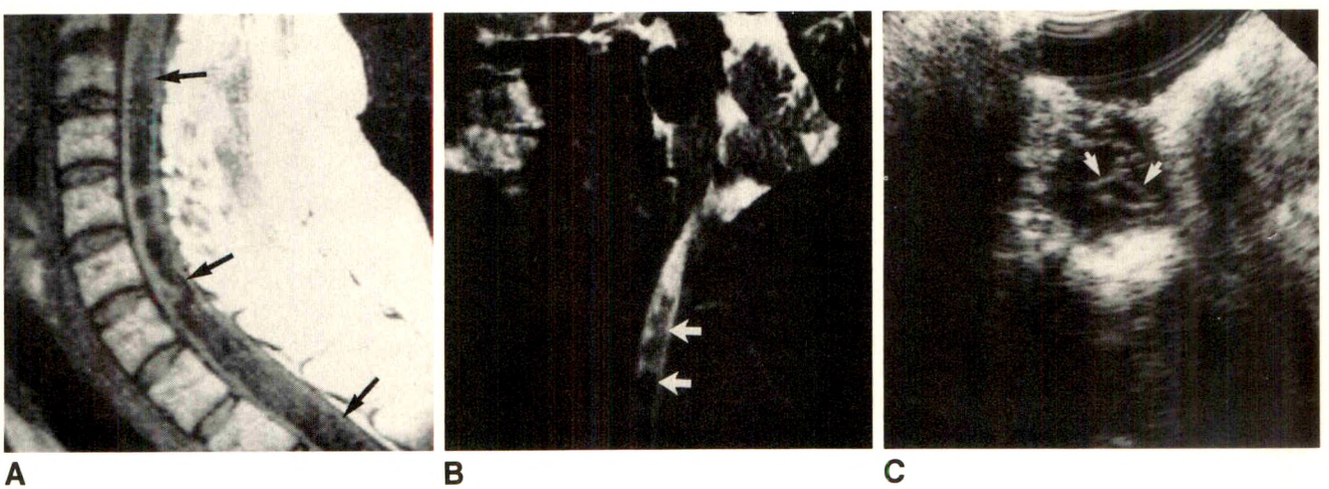

Fig. 3.—Case 3.
***A*, Sagittal T1-weighted 0.5-T MR image (500/38) shows multiseptated syrinx cavity of low signal intensity (*arrows*) extending from upper cervical region to T4.**
***B*, Sagittal T2-weighted MR image (2000/60) of upper cervical spine and head shows low signal intensity of cyst cavity (*arrows*).**
***C*, Transverse intraoperative spinal sonogram at level of C7 confirmed presence of syrinx cavity containing multiple scars (*arrows*). Real-time evaluation revealed cyst pulsations.**

current tumor was seen. Intraoperative spinal sonography (Fig. 2B) confirmed the presence of a multiseptated pulsatile cyst cavity. A syrinx to subarachnoid space shunt was performed. The fluid obtained from the syrinx cavity had an elevated protein (161 mg/dl). Moderate improvement of strength and sensation was noted postoperatively.

Case 3

A 42-year-old man presented with a history of right upper extremity pain, right lower extremity pain and weakness, sphincter dysfunction, and impotence that had progressed over the last 4 years. Twenty-four years earlier he had progressive right-sided weakness and right lower extremity numbness and spasticity. A T4 meningioma was resected. Postoperatively, his symptoms improved. The present physical examination showed increased muscle tone in the right lower extremity, a right Babinski, and areflexia of both upper extremities.

Decreased anal sphincter tone and urinary incontinence were also noted. Metrizamide myelography showed diffuse widening of the cervical spinal cord. On MR, the T1-weighted image showed a low-signal lesion extending from C2 to T4 with irregular borders and multiple areas of increased signal intensity within the lesion (Fig. 3A). The T2-weighted image showed the lesion to be of decreased signal intensity as compared with the adjacent CSF, and multiple septations were seen (Fig. 3B). No residual or recurrent tumor was noted. Intraoperative spinal sonography confirmed the presence of a pulsatile cystic lesion containing multiple scars (Fig. 3C). A syrinx to subarachnoid space shunt was placed. Analysis of the syrinx fluid revealed increased protein content (40 mg/dl). Postoperatively, the patient experienced relief of his symptoms in both upper extremities and regained some sphincter control.

Case 4

A 41-year-old man presented with a 2-year history of paresthesias and progressive weakness of both lower extremities, and wasting of the muscles of the right lower extremity. Twenty years previously he had presented with right-sided intercostal pain and weakness and

numbness of the right foot. A neurilemmoma at the T7–T8 level was resected. Postoperatively, the intercostal pain receded but the symptoms in the right foot persisted. The present physical examination revealed weakness of the entire right lower extremity. On MR, a long, narrow syrinx that was hypointense on T1- and T2-weighted images, and that extended from T1–T6, was identified. This cystic cavity had smooth borders and was centrally located within a nonexpanded spinal cord (Fig. 4). No tumor recurrence was noted. Because the cord was not expanded on MR, no surgery was performed and the patient is being followed clinically.

Case 5

A 33-year-old man was evaluated 5 years earlier for progressive pain and weakness in both upper extremities and the right lower extremity. Physical examination at that time revealed muscle atrophy of the right upper extremities and bilateral Babinski signs. Metrizamide myelography and delayed metrizamide CT showed compression of the spinal cord at C4–C5 by a calcified disk. There was no evidence of metrizamide accumulation within the cord. A diskectomy, anterior decompression, and anterior cervical fusion from C3 to C5 were performed. Postoperatively, the patient experienced remission of his symptoms with the exception of mild pain in the right upper and lower extremities. At present evaluation, the patient complained of interscapular pain radiating to the right upper and lower extremities of 6 months' duration. Sagittal and axial MR was performed and showed a low-signal lesion on the T1-weighted image extending from the level of C1 to C6 (Fig. 5A). The lesion had smooth borders and was centrally located within the spinal cord. The T2-weighted image showed the lesion to be of increased signal intensity, similar to the surrounding CSF (Fig. 5B). Because of the MR findings and the clinically stable symptoms, the patient is being managed conservatively at this time.

Discussion

The most important clinical consideration in patients who have previously been operated on for extramedullary spinal lesions and who present with reappearance or worsening of symptoms is a recurrence of the original lesion. The possibility of secondary syringomyelia must, however, be considered in the differential diagnosis. Syringomyelia coexisting with extramedullary tumors has been reported in only 13 cases [1–3], and to our knowledge, no cases have been described in which syringomyelia was found in patients who had prior removal of extramedullary lesions. We have recently encountered five such patients.

Several mechanisms can be postulated to explain the formation of syringomyelia under conditions that bear some similarities to our cases. Ischemia of the cord with secondary degeneration of the gray matter [4, 5] or filling of an obstructed central canal by CSF that is extrachoroidally produced [3] are two proposed mechanisms. A more recent hypothesis states that long-standing compression of the cord due to the presence of an extramedullary mass may lead to neuroglial damage, which is manifested by enlargement of the extracellular perivascular spaces. The removal of such an extramedullary lesion will not reverse the damage the spinal cord has already sustained nor will the microcystic areas within the cord disappear as a result of the surgery. The formation of multiple subarachnoid adhesions at the level of previous surgery may funnel CSF pulsations toward the area of the damaged cord where microcystic changes have occurred. This situation, in association with focally enlarged Virchow Robin spaces, can lead to the entry of abnormal amounts of CSF into the cord [1]. Over a period of time, the water-hammer effect of these focused CSF pulsations can cause these microcysts to enlarge [1]. This mechanism can explain the formation of long cystic cavities that are either caudal (case 1), rostral (cases 3 and 4), or caudal and rostral (cases 2 and 5) to the initial lesion.

The long symptom-free period experienced by our patients makes it unlikely that large and/or expanding syrinx cavities were present at the time of initial diagnosis. The exact time required for this type of syringomyelia to form and manifest itself is difficult to estimate, but given the proposed theory of formation and propagation, months to years are probably required, similar to that seen in the traumatically injured spinal cord [6]. The pathologic mechanisms that might lead to the formation of this type of syringomyelia are illustrated in Figure 6.

In our cases, MR was able to demonstrate the intramedullary cysts and to suggest their dynamic state. In three of our patients (cases 2, 3, and 4) the T2-weighted images demon-

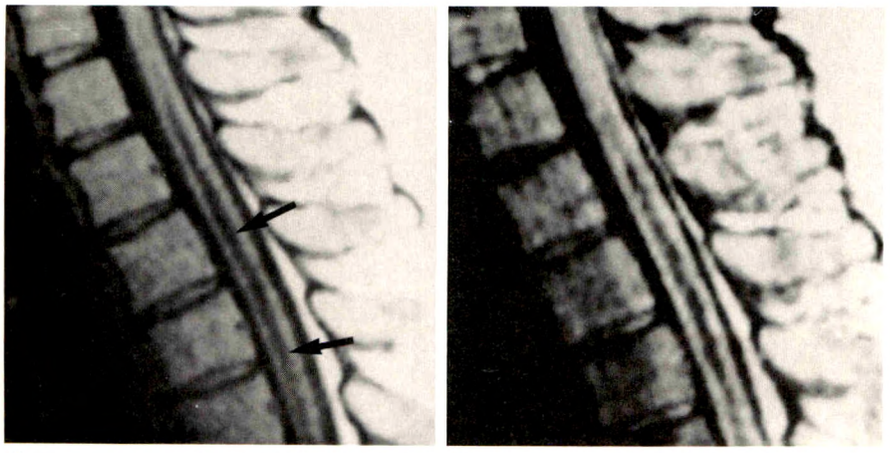

A B

Fig. 4.—Case 4.
***A*, Sagittal T1-weighted 1.5-T MR image (1000/26) shows low-signal central syrinx cavity extending from level of T1 to T6 (*arrows*).**
***B*, Sagittal T2-weighted MR image (2000/80) shows continued low signal intensity within syrinx cavity.**

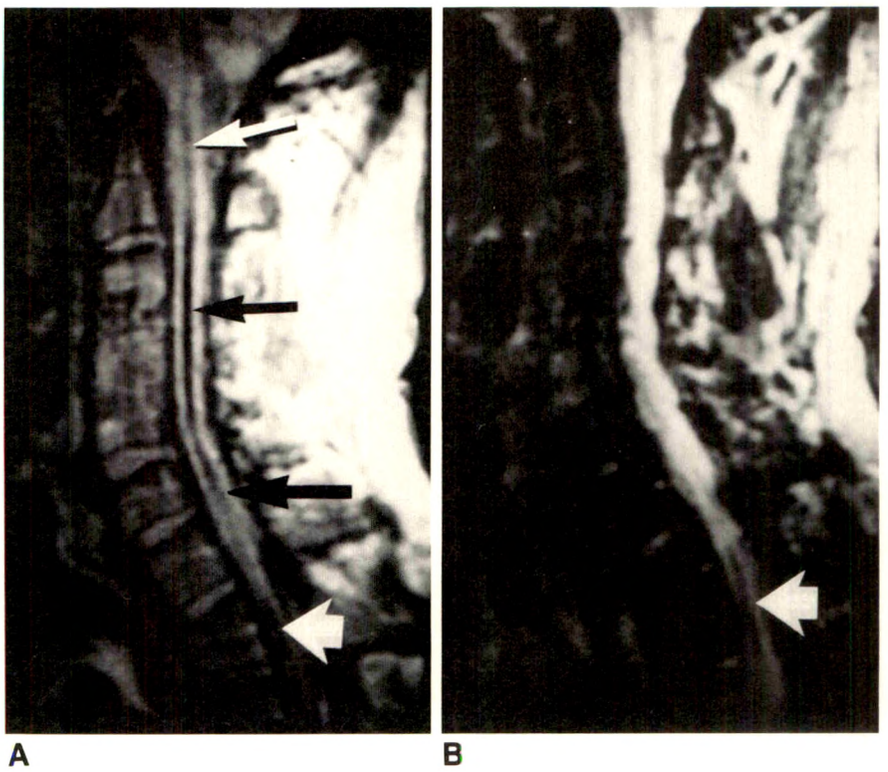

Fig. 5.—Case 5.

***A*, Sagittal T1-weighted 0.5-T MR image (1000/26) of cervical spine shows low signal syrinx cavity extending from C1 to C6 (*thin arrows*) and probably another short intramedullary cyst at the T1–T2 level (*thick arrows* in *A* and *B*). The cord is not dilated.**

***B*, Sagittal T2-weighted MR image (2000/120) shows upper cystic lesion to be of increased signal intensity. Since neither cardiac gating nor extra gradients were used to suppress motion artifacts, we cannot be sure that the hypointensity at T1–T2 does not represent flow artifacts.**

strated long, hypointense syrinx cavities, the appearance of which we believe were secondary to intracystic fluid motion and turbulence. A similar phenomenon has been demonstrated at narrow CSF pathways (foramina of Monro, aqueduct of Sylvius, and foramen of Magendie), where relatively fast pulsatile CSF motion occurs [7, 8]. This flow-void phenomenon is most likely caused by spin phase shifts and time-of-flight effects [9–11]. Although ours is the first study to report a correlation between the CSF motion as suggested by MR and subsequently shown with intraoperative spinal sonography, a recent presentation indicates that pulsatile fluid in cyst cavities can be identified and differentiated from myelomalacia by virtue of its signal augmentation when imaged by gradient echoes [12]. In the three patients who had surgery, fluid analysis from the syrinx cavities revealed increased protein content. Although such chemical changes can play a role in the MR signal characteristics [13], there was no correlation between the protein content and the MR signal in the three patients whose cyst fluid was analyzed. The explanation for this is that the MR signal of such fluid depends far more on its dynamic state (i.e., fluid pulsation and turbulence) than on the composition of the fluid.

The presence of pulsatile and nonpulsatile cystic cavities coexisting has been observed [14]. It may be that where there is an absence of the flow-void phenomenon, restriction of fluid motion by multiple intracystic septations is present. In three of our cases the multiseptated nature of the syrinx cavities was documented by intraoperative spinal sonography (Figs. 1D, 2B, 3C). These intracystic septations represent fibroglial remnants [12] of the spinal cord that probably are segments of neural tissue that were resistant to complete destruction caused by the enlarging syrinx. As these separated compartments develop communications with each other, greater fluid motion may then be allowed, resulting in the flow-void phenomenon within the cyst cavities and promoting their enlargement. Since two of our patients (cases 2 and 3) with multiseptated lesions manifested intrasyrinx flow-void phenomenon, the size of the openings between these cavities may be an important factor in determining the presence or absence of this occurrence. We believe that both multiloculated and uniloculated lesions have a potential for growth that depends on the dynamic state of the fluid in the cyst and the size of the connections between loculations, when they exist. The preoperative identification of these fibroglial remnants is important, because it may indicate to the surgeon the need to lyse the septa in order to create a single cavity suitable for shunt catheter placement. With MR, it is possible that because of the thickness of each slice, septa that appear to be complete may actually be incomplete at surgery.

Given this theory of cord compression and subsequent postoperative syrinx formation, one might think that this situation would be seen more often in patients operated on for chronic compressive extradural lesions, such as a herniated disk. In our limited series, however, we report only one such patient (case 5), leading us to speculate that in extradural lesions, the presence of an intact dura may offer some protection to the spinal cord, which is not present in cases of intradural masses (cases 1–4).

As MR becomes more widespread and is used for the evaluation of patients previously operated on for extramedullary masses, the presence of secondary syringomyelia will become increasingly recognized. In these situations, we suggest that syrinx cavities that are hypointense on T2-weighted

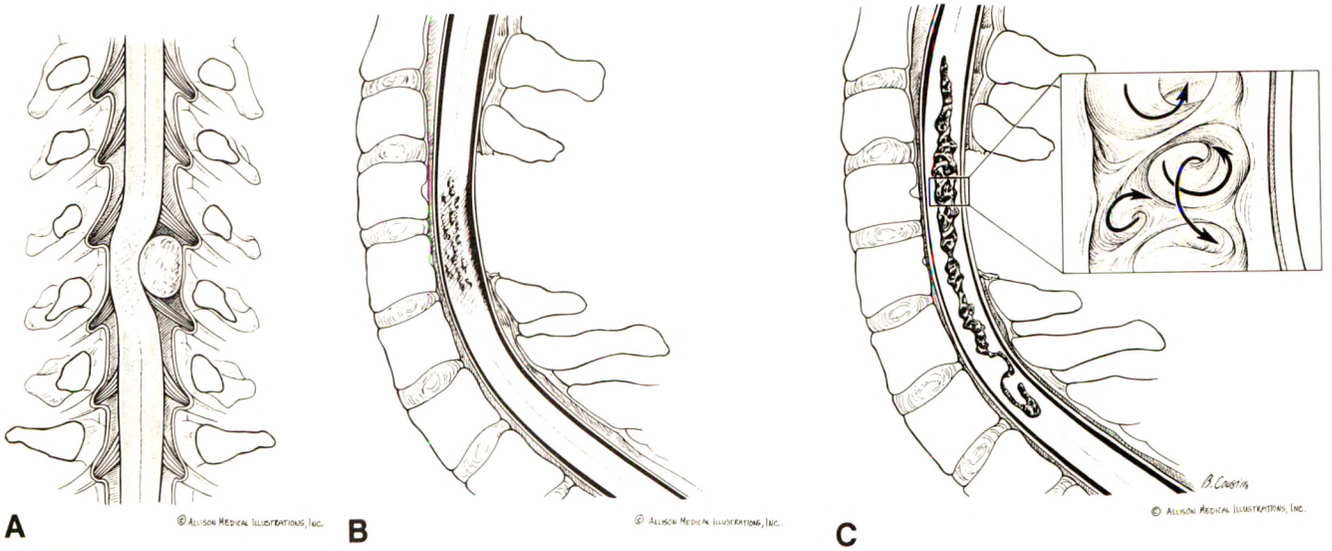

Fig. 6.—Diagrammatic representation of the events that are postulated to lead to the postoperative formation of syringomyelia after the removal of extramedullary lesions.

***A*, Drawing showing a coronal section through cervical spine. Extramedullary mass to left of cord is shown with intramedullary edema and microcystic changes (shaded area) due to long-standing compression of cord.**

***B*, Sagittal view of postoperative cervical spine seen after total extramedullary tumor removal. The cord remains deformed and small cysts are present secondary to coalescence of microcystic changes.**

***C*, Diagram of late postoperative period. The multiple small cysts have joined and formed large, irregular cavities with multiple septations. Multiple adhesions within subarachnoid space, which form at level of prior surgery and may be responsible for directing pulsatile forces to the cord, are not shown in this illustration. The transmitted pulsations can create intracystic flud turbulence (*arrows* in inset), causing expansion of cyst both rostrally and caudally. During periods of active syrinx expansion, this turbulence may manifest as a flow void on T2-weighted images (see text).**

images are more likely to be those that are undergoing active expansion at the time of examination. These are the patients that may benefit most from syrinx decompression (e.g., cases 2 and 3). On the other hand, MR characteristics suggesting the presence of nonpulsatile fluid may represent syrinx cavities that are not undergoing active expansion. In those cases the clinical symptoms and the presence (case 1) or absence of an enlarged cord will determine the therapeutic approach. We do not have an explanation of why, at times, an intramedullary cyst may undergo active expansion both clinically and radiologically and at other times the same cyst may be relatively inactive. In our series, all three patients operated on for syrinx decompression improved clinically. With a nondilated cord, the presence (case 4) or absence (case 5) of an intrasyrinx flow-void phenomenon can give the clinician an indication of possible active syrinx enlargement even when the immediate decision is not to perform surgery. Those patients with flow void might be watched more carefully for signs of clinical deterioration.

In conclusion, we believe MR is the imaging method of choice for the evaluation of patients with new onset neurologic symptoms after the removal of a previous extramedullary mass. Not only can the possibility of recurrent lesion be excluded but the presence of syringomyelia can be documented. Evaluation of the signal intensity from the syrinx when combined with the clinical presentation can supply additional information that may be useful in determining the need for syrinx decompression.

REFERENCES

1. Quencer RM, El Gammal T, Cohen G. Syringomyelia associated with intradural extramedullary masses of the spinal canal. *AJNR* **1986**;7:143–148
2. Barnett HJM, Rewcastle NB. Syringomyelia and tumors of the nervous system. In: Barnett HJM, Foster JB, Hudgson P, eds. *Syringomyelia*. London: Saunders, **1973**:261–301
3. Blaylock RL. Hydrosyringomyelia of the conus medullaris associated with a thoracic meningioma. *J Neurosurg* **1981**;54:833–835
4. Woddward JS, Freeman LW. Ischemia of the spinal cord: an experimental study. *J Neurosurg* **1956**;13:63–72
5. Wilson CB, Bertran V, Norrell HA, Hukuda S. Experimental cervical myelopathy II: acute ischemic myelopathy. *Arch Neurol* **1969**;21:571–589
6. Quencer RM, Green BA, Eismont FJ. Post-traumatic spinal cord cysts: clinical features and characterization with metrizamide computed tomography. *Radiology* **1983**;146:415–423
7. Sherman JL, Citrin CM, Bowen BJ, Gangarosa RE. MR demonstration of cerebrospinal fluid flow by obstructive lesions. *AJNR* **1986**;7:571–579
8. Sherman JL, Citrin CM. Magnetic resonance demonstration of normal CSF flow. *AJNR* **1986**;7:3–6
9. Sherman JL, Citrin CM, Gangarosa RE, Bowen BJ. The MR appearance of CSF flow in patients with ventriculomegaly. *AJNR* **1986**;7:1025–1031
10. Von Schulthess GR, Higgins CB. Blood flow imaging with MR: spin-phase phenomena. *Radiology* **1985**;157:687–695
11. Bradley WG, Waluch VN. Blood flow: magnetic resonance imaging. *Radiology* **1985**;154:443–450
12. Enzmann DR, O'Donohue J, Shuer L, et al. CSF pulsations within nonneoplastic spinal cord cysts. Presented at the 72nd scientific assembly and annual meeting of the Radiological Society of North America, Chicago, December **1986**
13. Yeates A, Brandt-Zawadzki M, Norman D, et al. Nuclear magnetic resonance imaging of syringomyelia. *AJNR* **1983**;4:234–237
14. Sherman JL, Barkovich AJ, Citrin CM. The MR appearance of syringomyelia: new observations. *AJNR* **1986**;7:985–995

Comparison of MR and CT Myelography in Imaging the Cervical and Thoracic Spine

Michael G. Karnaze[1]
Mokhtar H. Gado
Klaus J. Sartor
Fred J. Hodges III

MR imaging and CT myelography were compared in a retrospective study of 38 patients with suspected lesions of the cervical and thoracic spinal canal and cord. Twenty-eight abnormal cases were found, including spondylosis (9), tumors (8), intramedullary cavities (3), arachnoiditis (3), disk-space-centered infection or osteomyelitis (2), nonneoplastic cord swelling (2), and CSF-borne metastasis (1).

MR was equal or superior to CT myelography in depicting cases of cord enlargement, cord compression, and cord atrophy, providing better tissue characterization, no shoulder artifact, and no limitation caused by CSF block. CT myelography was superior to MR in depicting cases of spondylosis and arachnoiditis. It showed superior spatial resolution, which was most pronounced when comparing axial images and hence particularly superior in detecting the lateral extent of disk herniation. Use of surface coils and thin imaging sections is essential for accurate and complete MR evaluation of the cervical and thoracic spine.

CT has been accepted as an effective imaging technique for evaluating the spine. Its use, however, is limited in the cervical and thoracic spine because of the lack of epidural fat in this region. CT myelography performed after intrathecal introduction of water-soluble contrast material improves the contrast sensitivity of CT, but it is invasive and has known side effects [1–7].

Numerous reports have described the potential of MR as a valuable method of imaging the spine, and have compared MR with CT and CT myelography [8–15]. To help determine the role of MR in the evaluation of the cervical and thoracic spine, a comparative study of MR and high-resolution CT myelography was performed.

Materials and Methods

We retrospectively reviewed 38 patients with suspected lesions of the cervical or thoracic spine who underwent both MR and CT myelography. No effort was made to conceal the diagnoses from the reviewers. The patients ranged in age from 1–75 years; 18 were males and 20 were females. In 10 cases no abnormality was found by either imaging technique. The 28 abnormal findings included nine cases of spondylosis, eight neoplasms, three cases of arachnoiditis, three intramedullary cavities, two cases of disk-space infection, two cases of nonneoplastic cord swelling, and one case of CSF-borne metastases. Seventeen cases involved the cervical and 11 involved the thoracic spine.

Surgical or pathologic proof was available in 16 abnormal cases, and clinical and radiographic evidence was available in the remaining 12.

MR was performed with a Siemens Magnetom 0.5-T (initially operating at 0.35 T) or 1.5-T unit. Spin echo (SE) sequences were used yielding three images of the same anatomic level: a T1-weighted image (TR 300 or 500 msec, TE 30 msec), a spin-density-weighted image (TR 1500 or 1800 msec, TE 30 msec), and a T2-weighted image (TR 1500 or 1800 msec, TE 120 msec). A body coil was used in seven cases, a head coil was used in nine cases, and a surface coil was used in 12 cases. Slice thickness was 5 mm for all surface-coil images except one case, in which a 10-mm thickness was used. Ten-millimeter sections were used

This article appears in the November/December 1987 issue of *AJNR* and the February 1988 issue of *AJR*.

Received December 12, 1986; accepted after revision June 9, 1987.

Presented at the annual meeting of the American Roentgen Ray Society, Washington, D.C., April 1986.

[1]All authors: Mallinckrodt Institute of Radiology, 510 S. Kingshighway Blvd., St. Louis, MO 63110. Address reprint requests to M. Gado.

***AJR* 150:397–403, February 1988**
0361–803X/88/1502–0397
© American Roentgen Ray Society

for all head- and body-coil images except one case, in which the head coil and 5-mm sections were used. Sagittal images were obtained in all cases, axial images in 18, and coronal images in five. Images were processed on a 256 × 256 matrix corresponding to 1.2-mm^2 pixel size in all examinations.

CT images were obtained after myelography with water-soluble contrast material on a third-generation scanner*, using 2.0-mm axial scans. Delayed CT scanning 8–24 hr after initial examination was performed in four cases.

In the 38 cases, 43 final *radiologic* diagnoses were made and these were divided into six categories: normal (10), cord swelling (eight), cord atrophy (seven), cord compression (10), extradural lesions without cord compression (five), and arachnoiditis (three). Five of the 28 abnormal cases were included in two different radiologic categories, yielding 33 total abnormal final diagnoses. CT scans and MR images were compared to evaluate the ability of each imaging technique to detect the abnormality and to determine its cause. Reasons for failure or superiority of MR compared with CT myelography were noted.

Results

In the 10 normal cases, MR and CT myelography were equivalent in depicting the normal cord and surrounding CSF space. In the remaining 33 radiologic diagnoses, MR was superior to CT myelography in nine instances, equivalent in 13, and inferior in 11. Results are summarized in Tables 1–4. The remaining five radiologic diagnoses will be discussed separately.

Cord Enlargement

In all eight cases, cord enlargement (Table 1) was detected equally well by MR and CT myelography. However, MR was superior to CT myelography in determining the cause of the abnormality in three cases. In one case of hematomyelia (Fig. 1), CT myelography showed nonspecific cord enlargement while MR showed increased signal of the lesion on the T1- and T2-weighted images. The chemical-shift-imaging technique [16] was employed and showed this to be due to hemorrhage, not to fat. MR was superior in another case of an intramedullary cord cyst at the level of T2, in which MR showed the cavity, which was not seen with delayed CT myelography because of shoulder artifacts. The third case in which MR was superior was one of ependymoma of the cervical cord. CT myelography showed low-density enlargement of the cord. MR showed both the soft-tissue and fluid components of the lesion, confirming that it was a tumor and not a congenital hydromyelia. In no case of cord enlargement was CT myelography superior to MR.

Cord Atrophy

In seven cases of cord atrophy (Table 2) MR was equal to CT myelography in detecting the abnormally small cord in three cases and inferior to CT myelography in four cases. In one of these four cases, MR using surface coil and 5-mm sections showed the atrophic cord but failed to detect a 2-

* Siemens Somatom 2, DR3 or DRH.

TABLE 1: Cord Swelling

Case No.	Age	Gender	Diagnosis	MR Coil	MR (Compared with CT Myelography)
1	75	F	Ependymoma[a]	Surface	Superior
2	52	M	Thoracic cord cyst	Surface	Superior
3	41	M	Cord hemorrhage[a]	Head	Superior
4	16	M	Radiation myelitis	Head	Equivalent
5	41	F	Intradural CSF metastasis	Head	Equivalent
6	35	F	Myelitis[a]	Head	Equivalent
7	2	F	Glioma[a]	Body	Equivalent
8	8	F	Intramedullary tumor	Body	Equivalent

[a] Histologically confirmed.

TABLE 2: Cord Atrophy

Case No.	Age	Gender	Etiology	MR Coil	MR (Compared with CT Myelography)
9	26	M	Cord cavity	Surface	Inferior
10	40	F	Surgery	Surface	Equivalent
11	62	F	Surgery	Surface	Equivalent
12	42	M	Trauma	Head	Equivalent
13	34	F	Unknown	Body	Inferior
14	53	M	Cavity[a]	Body	Inferior
15	38	F	Unknown	Body	Inferior

[a] Histologically confirmed.

TABLE 3: Cord Compression

Case No.	Age	Gender	Diagnosis	MR Coil	MR (Compared with CT Myelography)
16	71	F	Meningioma	Surface	Superior
17	48	M	Herniated cervical disk[a]	Surface	Superior
18	33	M	Herniated cervical disk[a]	Surface	Inferior
19	51	F	Herniated thoracic disk	Surface	Superior
20	39	M	Meningioma[a]	Surface	Superior
21	73	M	Extruded disk fragment	Head	Superior
22	66	M	Cervical subluxation[a]	Head	Inferior
23	41	F	Intradural metastasis	Head	Equivalent
24	44	M	Vertebral osteomyelitis[a]	Body	Equivalent
25	51	M	Schwannoma[a]	Body	Inferior

[a] Histologically confirmed.

TABLE 4: Extradural Lesions Without Cord Compression

Case No.	Age	Gender	Diagnosis	MR Coil	MR (Compared with CT Myelography)
26	66	F	Disk space infection[a]	Surface	Superior
27	39	M	Cervical disk herniation[a]	Surface	Inferior
28	47	M	Cervical bony bars[a]	Head	Inferior
29	52	F	Cervical disk bulge	Head	Equivalent
30	50	M	Cervical bony bars	Body	Equivalent

[a] Histologically confirmed.

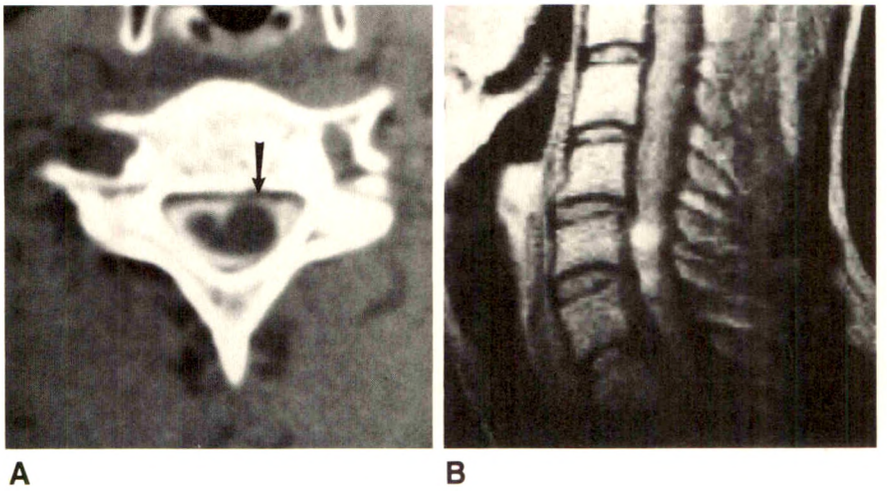

Fig. 1.—Hematomyelia.
A, CT myelogram shows focal nonspecific cord enlargement (*arrow*).
B, Proton-density-weighted MR image shows high signal from hemorrhage. High signal was also present on T1-and T2-weighted images (not shown).

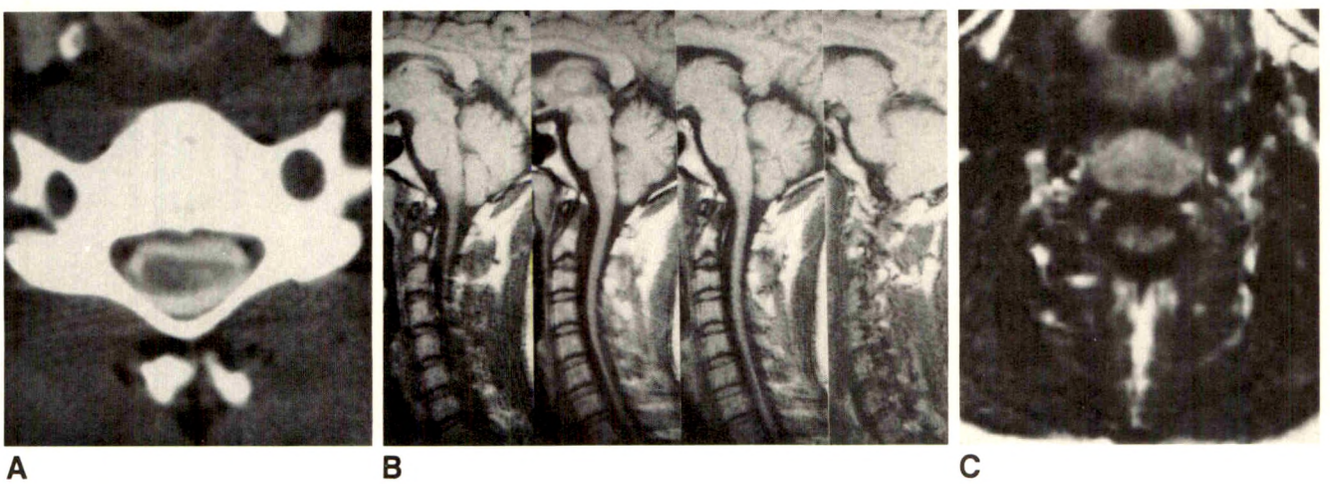

Fig. 2.—Cord atrophy with small cavity.
A, CT myelogram shows atrophic cord and 2-mm contrast-filled cavity in left side of cord.
B, Series of contiguous T1-weighted MR images shows atrophy but fails to demonstrate cavity.
C, Axial T1-weighted MR image shows poor spatial resolution and is much less informative than CT myelogram (see *A*).

mm associated cavity, which was 3 cm in length and was seen on delayed CT scans (Fig. 2). In the other three cases in which MR was inferior, slice thickness was 10 mm and body coil was used, resulting in low spatial resolution. These three cases included a case of atrophy with associated cord arteriovenous malformation, a posttraumatic cavity, and atrophy associated with arachnoiditis. In no case of cord atrophy was MR superior to CT myelography.

Cord Compression

In 10 cases of cord compression (Table 3) MR was superior to CT myelography in five cases, equivalent in two cases, and inferior in three cases. In two of the three cases in which MR was inferior (a cervical intradural schwannoma and a cervical disk herniation), slice thickness was 10 mm and surface coil was not used. In the third case, a herniated cervical disk, CT myelography showed the lateral extent of disk herniation better than MR did, and although surface-coil imaging and 5-mm sections were used, neither axial nor interdigitated images were obtained. Of the five cases in which MR was superior, two cases (a cervical disk herniation and a case of a presumed extruded disk fragment) showed serious degradation of the CT myelography images by shoulder artifacts. In a third case (of presumed thoracic disk herniation), MR allowed better differentiation of the compressed cord, narrowed CSF space, and thoracic disk than CT myelography did (Fig. 3). In the remaining two cases (meningiomas of the thoracic spine), CT myelography showed only the inferior margin of the lesion because of CSF block. No attempts were made to position water-soluble contrast material above the lesion. MR in these two cases showed the upper border and true size of the lesion and its interface with the cord (Fig. 4). In addition, both these lesions demonstrated a low signal intensity on the T2-weighted image, a feature previously reported in intracranial meningiomas [17].

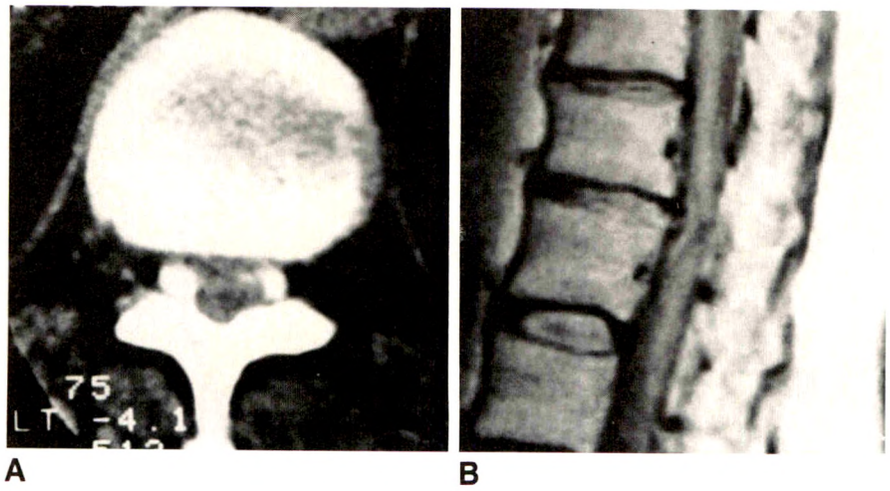

Fig. 3.—Presumed thoracic disk herniation.
A, CT myelogram at level of T11–T12 shows soft-tissue density anterior to cord. Differentiating cord from disk is difficult.
B, Sagittal proton-density-weighted MR image shows cord displaced posteriorly at level of disk space. Cord is well differentiated from disk.

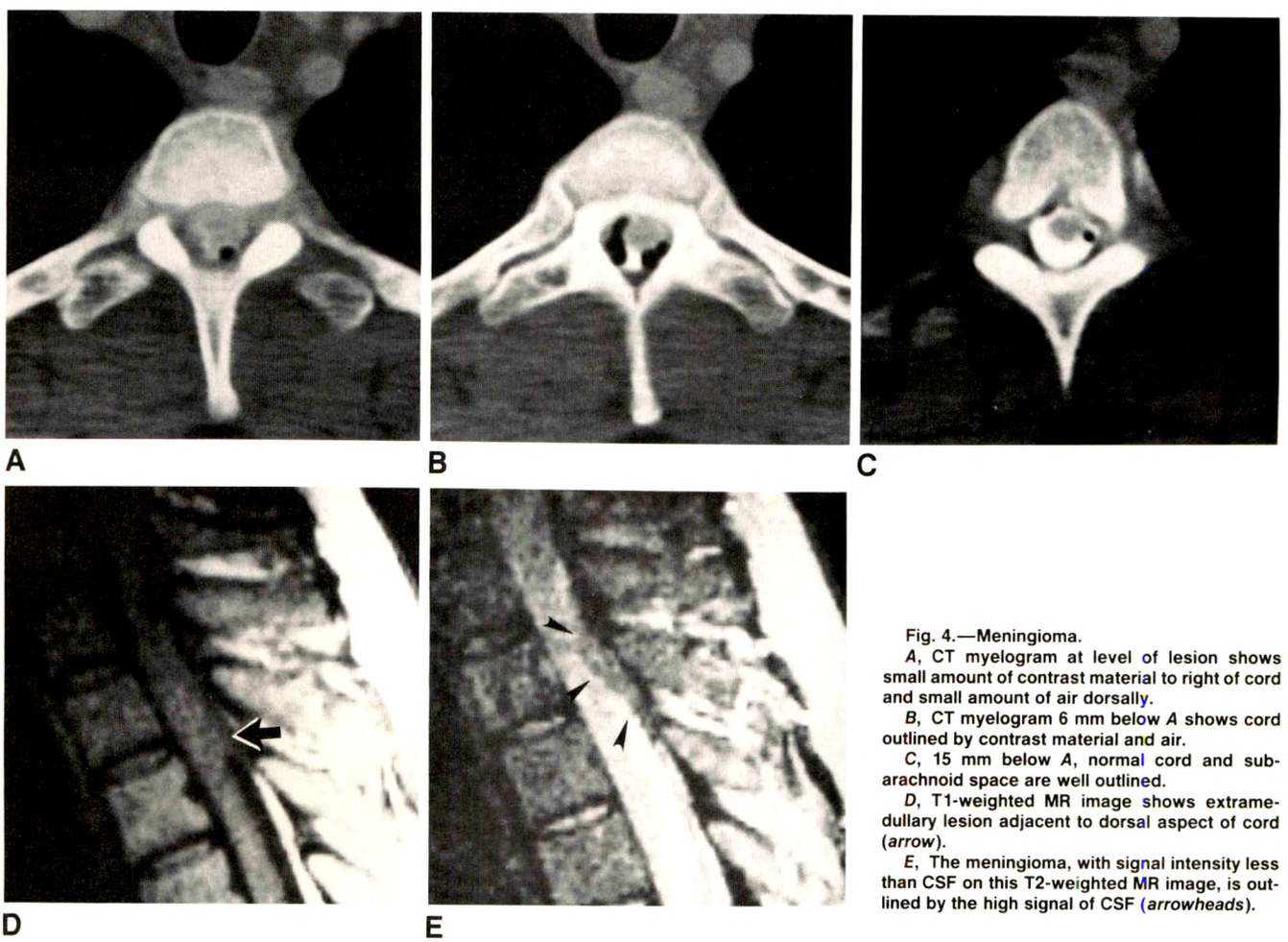

Fig. 4.—Meningioma.
A, CT myelogram at level of lesion shows small amount of contrast material to right of cord and small amount of air dorsally.
B, CT myelogram 6 mm below *A* shows cord outlined by contrast material and air.
C, 15 mm below *A*, normal cord and subarachnoid space are well outlined.
D, T1-weighted MR image shows extramedullary lesion adjacent to dorsal aspect of cord (*arrow*).
E, The meningioma, with signal intensity less than CSF on this T2-weighted MR image, is outlined by the high signal of CSF (*arrowheads*).

Extradural Lesions Without Cord Compression

In five cases of extradural lesions without cord compression (Table 4), MR was superior to CT myelography in one case, equivalent in two cases, and inferior in two cases. MR was superior in a case of disk-space-centered infection by showing decreased signal in the disk space and adjacent vertebral bodies on the T1-weighted images secondary to infection (Fig. 5). Both MR and CT myelography showed the paravertebral mass and the mild extradural encroachment on the anterior aspect of the subarachnoid and epidural spaces. The changes in the vertebral body were not convincing on CT

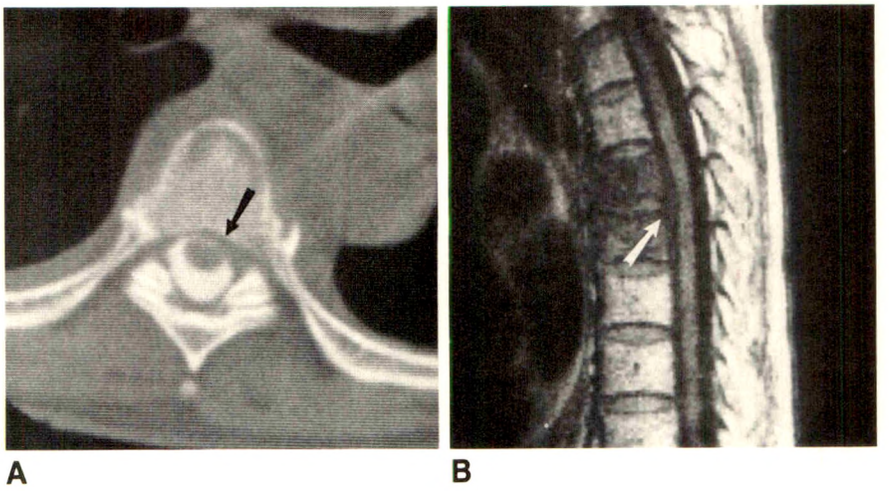

Fig. 5.—Disk-space-centered infection.
A, CT myelogram shows paravertebral mass and extradural soft-tissue density ventral to cord causing narrowing of subarachnoid space (*arrow*). Vertebral body shows mild focal loss of bone density ventrally.
B, Sagittal T1-weighted MR image demonstrates abnormally decreased signal from two adjacent vertebral bodies and some loss of signal from disk space. Extradural extension ventral to cord is also seen (*arrow*).

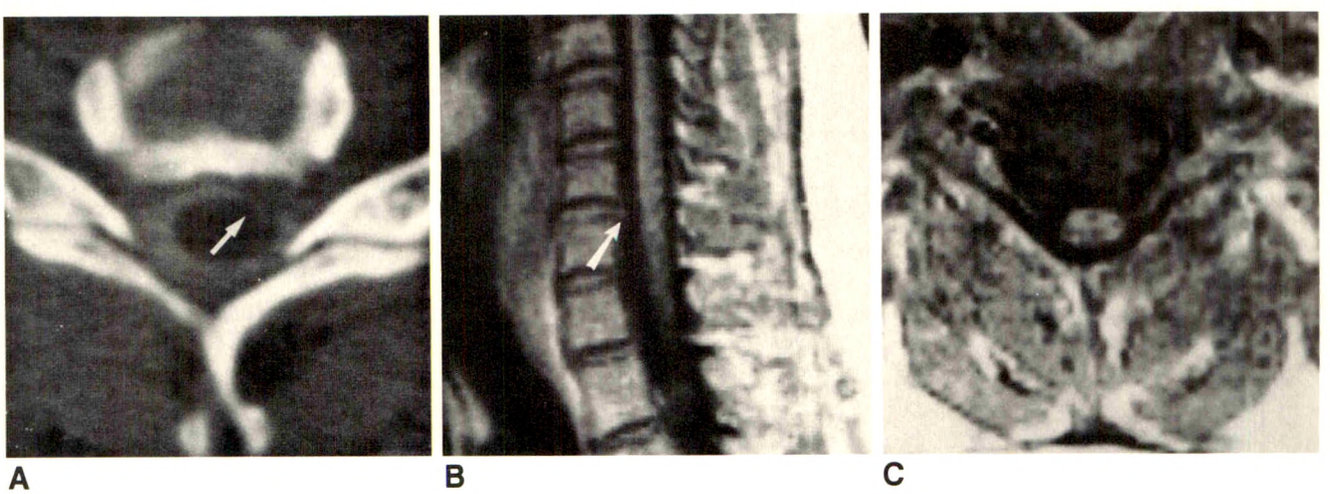

Fig. 6.—Cervical disk herniation.
A, Axial CT myelogram shows soft-tissue density anterior and lateral to cord with narrowing of subarachnoid space (*arrow*).
B, Sagittal T1-weighted MR image shows bulging of C6–C7 disk (*arrow*).
C, Axial T1-weighted MR image fails to show lateral extent of disk as well as CT did.

myelography. On MR, however, the vertebral body changes were clearly demonstrated and the nature of the process was defined as bone-centered. The clinical management was planned accordingly. In one case of osteophytes indenting the subarachnoid space and the intervertebral foramina in the cervical spine, MR was inferior to CT myelography. The case was imaged with a head coil and 10-mm sections. However, in another case in which a surface coil and 5-mm sections were employed, CT myelography was superior to MR because superior spatial resolution allowed CT to show the lateral extent of a cervical disk herniation better than MR did (Fig. 6).

Arachnoiditis

In three cases of arachnoiditis, MR was equivalent to CT myelography in one case and inferior in two cases. In one of the cases in which MR was inferior, MR did provide complementary information by showing no lesion at a site of CSF block on CT myelography. Although MR alone would have missed the diagnosis, lack of abnormal signal from the site of the CSF block indicated arachnoid adhesions and not a mass as the cause of the block on CT myelography. In this case and in one other case, MR did not show arachnoid adhesions or multiple loculated pockets of CSF that were evident on CT myelography.

Coil Selection

The importance of surface-coil imaging in evaluating the cervical and thoracic spine is demonstrated in Table 5. Regardless of the diagnostic category, a surface coil was used in 14 cases, of which MR was superior to CT myelography in seven, equivalent in three, and inferior in four. On the other

TABLE 5: Value of Surface-Coil Imaging

	No. of Cases	Comparison of MR and CT Myelography		
		MR Superior	Equal	MR Inferior
Surface coil	14	7	3	4
Nonsurface coil	19	2	10	7
Total	33	9	13	11

TABLE 6: Advantages of MR over CT Myelography in 11 Cases

Tissue specificity (n = 6)
Hematomyelia
Cervical ependymoma
Thoracic disk herniation
Disk-space-centered infection
Meningioma (n = 2)
Lack of shoulder artifact (n = 3)
Cervical disk herniation
Thoracic cord cavity
Presumed extruded disk fragment
No limitation from CSF block (n = 2)
Meningioma

hand, in the 19 cases in which a surface coil was not used, MR was superior in only two cases, equivalent in 10, and inferior in seven.

Discussion

MR compares favorably with CT myelography in cases of cord swelling and those of cord atrophy and compression if a surface coil and thin sections are used. Advantages of MR include tissue characterization, lack of shoulder artifact, and complete delineation of the lesion in spite of CSF block (Table 6). The contribution of tissue characterization was significant in six of our 33 abnormal diagnoses. Cord hemorrhage (Fig. 1) was characterized by a relative signal increase on both T1- and T2-weighted images. Although fat-containing tumors could have a similar appearance on T1-weighted images, a chemical-shift technique [16] can be used to distinguish the two conditions. Disk-space-centered infection (Fig. 5) was characterized by low signal from the disk space and adjacent vertebral bodies on T1-weighted images, an appearance previously described [18]. In the case of the presumed thoracic disk herniation (Fig. 3), MR differentiated cord, vertebral body, and disk. Because of the lack of difference in density between the cord and disk and the lack of contrast material anteriorly and posteriorly at the level of the lesion, CT myelography did not identify clearly the cord-disk interface. The diagnosis of disk herniation was therefore not made before MR was performed. MR also detected the solid component of a cervical ependymoma by a signal intensity pattern different from parenchyma and CSF. CT myelography could not differentiate a cystic tumor from a syrinx. In two additional cases of thoracic meningioma, the relatively low signal of the lesion on the T2-weighted image suggested the diagnosis, as these signal characteristics have been noted in intracranial meningiomas [17].

Degradation of CT images is common in the lower cervical region and at the cervical thoracic junction. This is caused by the sudden increase in X-ray attenuation at the level of the shoulders. This takes the form of dense, dark streaks across the images [19]. The degradation often results in total loss of the diagnostic image at that level. No such degradation is known in MR, and signal intensity is not attenuated by surrounding tissues. Imaging by MR is far superior than by CT myelography in this region, as was shown in three cases in our series.

Another limitation of CT myelography is seen in cases in which a space-occupying lesion causes block to CSF flow. The contrast material is stopped by the lesion and outlines the lower border of the lesion only. To determine the full extent of the lesion and outline its upper border, contrast material may be introduced by high cervical puncture. Alternatively, the contrast material that has been stopped below the site of the block may be forced to cross the block using a "squeeze" technique [20]. Neither of these techniques was used in our series. High cervical puncture adds to the invasiveness of the procedure. The squeeze technique is reportedly without risk; however, its potential added risk cannot be evaluated until a large series is reported. MR provides complete imaging of the lesion noninvasively.

Although MR was equal or superior to CT myelography in cord enlargement regardless of the coil used, cases of cord compression and atrophy demonstrate the need for surface coils in examining the spine (see Tables 2 and 3). Eight cases of cord compression and atrophy were examined with surface coils. MR was superior to CT myelography in four and equivalent in two. On the other hand, MR was inferior in five and equivalent in three of nine cases with the same diagnoses examined without surface coils.

MR failed in 11 of our cases. However, in eight of these cases the MR technique was suboptimal. The slice thickness was 10 mm and the surface coil was not used early in our experience with the method. There remain three cases in which the proper technique was used. Analysis of these three cases attributed the failure of MR to low spatial resolution, particularly in axial images. For this reason, CT myelography showed to a better advantage a 2-mm cervical cord cavity (Fig. 2). The added high-contrast discrimination caused by entry of contrast material into the cavity enhanced the spatial resolution. For the same reason, the lateral extent of herniated cervical disk was not demonstrated by MR (Fig. 6), and small CSF pockets outlined by arachnoid adhesions were also missed by MR but well shown by CT myelography. However, the absence of abnormal findings on MR in cases of arachnoiditis is not without diagnostic value. Indeed, deformity of the contrast column on myelography and CT myelography may mimic the presence of intradural or extradural lesions. The possibility of such lesions can easily be excluded by the normal appearance on MR images, as shown in one of three cases of arachnoiditis in our series.

The poor quality of axial images as compared with sagittal images on MR limits the usefulness of this technique in

evaluating lateral lesions. Furthermore, sagittal images are difficult to interpret in cases of scoliosis.

Our results suggest that MR can serve as the primary imaging tool in evaluation of the cervical and thoracic spine. If a surface coil is used, MR is equivalent or superior to CT myelography in cases of cord swelling, cord atrophy, and cord compression. CT myelography, however, appears equal or superior to MR in cases of spondylosis and arachnoiditis. It will likely remain so until improved axial images can be generated with MR. Although not addressed in this study, plain CT of the cervical and thoracic spine could perhaps adequately complement MR in showing bony detail and intervertebral foramina, thus significantly decreasing the need for myelography.

Conclusions

MR was equal or superior to CT myelography in our study in categories of cord swelling, cord atrophy, and cord compression. It provided additional information in six of 33 cases because of improved tissue characterization, in three cases because of lack of shoulder artifact, and in two cases with CSF block. CT myelography offers superior spatial resolution, which was important in four cases. CT was equivalent or superior to MR in cases of spondylosis and arachnoiditis. Surface-coil imaging and thin sections are essential if MR is to be used to evaluate the cervical and thoracic spine.

REFERENCES

1. Greitz T, Hindmarsh T. Computer assisted tomography of intracranial CSF circulation using water-soluble contrast medium. *Acta Radiol [Diagn] (Stockh)* **1974**;15:497–507
2. Di Chiro G, Schellinger D. Computed tomography of spinal cord after lumbar intrathecal introduction of metrizamide (computer assisted myelography). *Radiology* **1976**;120:101–104
3. Aubin ML, Vignaud J, Jardin C, Bar D. Computed tomography in 75 clinical cases of syringomyelia. *AJNR* **1981**;2:199–204
4. Dublin AB, McGahan JP, Reid MH. The value of computed tomographic metrizamide myelography in the neuroradiological evaluation of the spine. *Radiology* **1983**;146:79–86
5. Tadmor R, Cacayorin, Kieffer SA. Advantages of supplementary CT in myelography of intraspinal masses. *AJNR* **1983**;4:618–621
6. Landman JA, Hoffman JC Jr, Braun IF, Barrow DL. Value of computed tomographic myelography in the recognition of cervical herniated disk. *AJNR* **1984**;5:391–394
7. Sobel DF, Barkovich AJ, Munderloh SH. Metrizamide myelography and postmyelographic computed tomography: comparative adequacy in the cervical spine. *AJNR* **1984**;5:385–390
8. Bradley WG Jr, Waluch V, Yadley RA, Wycoff RR. Comparison of CT and MR in 400 patients with suspected disease of the brain and cervical spinal cord. *Radiology* **1984**;152:695–702
9. Han JS, Kaufman B, El Yousef JJ, et al. NMR imaging of the spine. *AJNR* **1983**;141:1137–1145
10. Modic MT, Weinstein MA, Pavlicek W, Boumphrey F, Starnes D, Duchesneau PM. Magnetic resonance imaging of the cervical spine: technical and clinical observations. *AJR* **1983**;141:1129–1136, *AJNR* **1984**;5:15–22
11. Norman D, Mills CM, Brant-Zawadzki M, Yeates A, Crooks LE, Kaufman L. Magnetic resonance imaging of the spinal cord and canal: potentials and limitations. *AJR* **1983**;141:1147–1152, *AJNR* **1984**; 5:9–14
12. Hyman RA, Edwards JH, Vacirca JJ, Stein HL. 0.6 T MR imaging of the cervical spine: multislice and multiecho techniques. *AJNR* **1985**;6:229–236
13. Pojunas K, Willliams AL, Daniels DL, Haughton VM. Syringomyelia and hydromyelia: magnetic resonance evaluation. *Radiology* **1984**;153:679–683
14. Lee BCP, Zimmerman RD, Manning JJ, Deck MDF. MR imaging of syringomyelia and hydromyelia. *AJNR* **1985**;6:221–228
15. Modic MT, Pavlicek W, Weinstein MA, et al. Magnetic resonance imaging of intervertebral disk disease. *Radiology* **1984**;152:103–111
16. Dixon WT. Simple proton spectroscopic imaging. *Radiology* **1984**;153:189–194
17. Zimmerman RD, Fleming CA, Saint-Louis LA, Lee BCP, Manning JJ, Deck MDF. Magnetic resonance imaging of meningiomas. *AJNR* **1985**;6:149–157
18. Modic MT, Feiglin DH, Piraino DW, et al. Vertebral osteomyelitis: assessment using MR. *Radiology* **1985**;157:157–166
19. Brooks RA, Di Chiro G. Beam hardening in X-ray reconstructive tomography. *Phys Med Biol* **1976**;21:390–398
20. Kelly WM, Badami P, Dillon W. Epidural block: myelographic evaluation with a single puncture technique using metrizamide. *Radiology* **1984**; 151:417–419

Book Review

Normal Anatomy for Multiplanar Imaging. Vol. 1: Head, Neck, and Spine; Vol. 2: The Trunk and Extremities. By Bharat Raval, Joel W. Yeakley, and John H. Harris, Jr. Baltimore: Williams & Wilkins, 199 pp., 1987. $125

This two-volume atlas correlates line drawings with CT scans and MR images in a side-by-side format. Volume 1 includes chapters portraying the anatomy of the skull, brain, spine, and neck. Volume 2 considers the trunk, pelvis, and extremities. The text is minimal, included to review the technical factors of obtaining CT scans. Essentially no information is included on the technique of MR imaging.

This atlas has many desirable features. It will be valuable as an educational resource for medical students who are being introduced to cross-sectional imaging, as a review for radiology residents who are interpreting CT scans, and as a reference for busy practitioners who want an efficient review of anatomy. Its off-the-shelf value as an anatomic reference should be emphasized also. The deficits of this work are few. Some of the reproductions of the CT scans are too dark; consequently, anatomic features identified in the line drawings are invisible on the scans. The MR images are infrequent, and many are outdated. Some of the reformatted CT images lack the detail necessary for accurate assessment. Scattered typographic errors in the labeling of the line drawings are minor distractions. It must be emphasized, however, that these deficiencies detract minimally from the overall high quality of the line drawings and CT reproductions.

This text will be most valuable for training programs and as a reference. It should be a priority purchase for departmental and office libraries and for the collection of references kept adjacent to CT reading stations.

Charles A. Rohrmann, Jr.
University Hospital, University of Washington
Seattle, WA 98195

Treatment of Vertebral Arteriovenous Fistulas

Van V. Halbach[1]
Randall T. Higashida
Grant B. Hieshima

Twenty patients with vertebral arteriovenous fistulas (eight spontaneous, six traumatic without vertebral artery transection, and six traumatic with vertebral artery transection) were treated by transvascular embolization techniques, resulting in complete fistula closure in all patients. The fistulas were located at C1–C2 in 45%, C2–C3 in 25%, C4–C5 in 15%, C5–C6 in 10%, and C6–C7 in 5%. Trauma was the most common cause: 30% followed knife wounds, 20% followed gunshot injuries, and 10% followed blunt trauma. Eight patients had spontaneous fistulas, two associated with fibromuscular dysplasia. Three patients—all with large, long-standing fistulas—developed neurologic deficits coincident with the abrupt closure of the fistula, which resolved with reestablishment of fistula flow. Two of these patients were treated by staged closure; the other one by gradual closure. In all three cases the result was complete fistula closure without neurologic sequelae. The remaining spontaneous fistulas were all closed by balloon embolization with preservation of the vertebral artery and without deficits. The six patients with traumatic fistulas without transection were cured by balloon embolization, without deficits; in four there was also preservation of vertebral flow. The other six patients had traumatic fistulas with transection and were all cured by balloon embolization with preservation of flow in two. Four patients required bilateral approaches to the fistula to achieve complete fistula closure. The only complication was a mild residual Wallenberg syndrome after occlusion of the posterior inferior cerebellar artery in the treatment of a transection located at C1.

In our opinion, transvascular techniques are the treatment of choice for vertebral arteriovenous fistulas.

Vertebral arteriovenous fistulas are abnormal connections between the extracranial vertebral artery or its branches and neighboring veins. They are uncommon lesions, with only 81 cases reported prior to 1977 [1]. The most common cause of these fistulas is penetrating neck injuries, usually knife wounds or gunshot injuries. Iatrogenic causes include the sequelae of direct puncture of the carotid or vertebral artery for diagnostic angiography [2, 3], inadvertent vertebral damage during the insertion of venous catheters [4, 5], or complications of anterior interbody fusion [6]. Diseases associated with vertebral arteriovenous fistulas include fibromuscular dysplasia [7–9] and neurofibromatosis [10–12]. Blunt trauma in association with cervical spine fracture has been reported as a cause [13, 14]. Many cases are spontaneous [15] and often thought to be congenital. Symptoms often related to the fistula are bruit and neck pain, but brain and spinal cord dysfunction related to steal, venous hypertension, or mechanical compression have also been reported [1, 16]. Traumatic fistulas can present with massive hemorrhage, neurologic deficits, expanding hematomas, pseudoaneurysms, and airway obstruction. Treatments have included proximal ligation, trapping procedures, direct surgical exposure and closure, combined balloon embolization and surgical ligation, and, more recently, embolization with balloons or steel coils [16–20]. Over the past 7 years we have treated 20 vertebral arteriovenous fistulas by transvascular embolization techniques, and we report the results of those treatments.

This article appears in the November/December 1987 issue of *AJNR* and the February 1988 issue of *AJR*.

Received February 18, 1987; accepted after revision June 17, 1987.

[1] All authors: Departments of Radiology and Neurological Surgery, University of California, San Francisco Medical Center, 505 Parnassus Ave., San Francisco, CA 94143. Address reprint requests to V. V. Halbach, Neuroradiology, C-309.

***AJR* 150:405–412, February 1988**
0361–803X/88/1502–0405
© American Roentgen Ray Society

Materials and Methods

Twenty patients with vertebral fistulas were treated by using transarterial embolization. All procedures were performed with local anesthesia and IV sedation to allow continuous neurologic monitoring. The femoral arterial access was used for all diagnostic and therapeutic procedures. A diagnostic angiogram with catheter tip located near the fistula was obtained via the involved vertebral artery, and rapid filming was used to delineate the site of the fistula, presence of arterial narrowing or damage, and draining venous structures. If antegrade flow up the involved vertebral artery above the fistula was not observed, then gentle advancement of a soft-tipped guidewire was attempted to place the diagnostic catheter above the level of the fistula. If successful, an angiogram was obtained with the catheter tip located just above the fistula site. Angiograms of the contralateral vertebral, ipsilateral carotid, thyrocervical, and costocervical arteries were obtained as indicated. If continuity of the artery was maintained (no transection) then a 7.3/5-French coaxial catheter system was placed in the artery with the safest access to the fistula, usually the involved vertebral artery. Systemic anticoagulation with heparin, usually 5000 units bolus and 2500 units/hr in a 70-kg patient, was given unless contraindicated. If the patient had a pseudoaneurysm or expanding hematoma, then anticoagulation was not used. The inner 5-French catheter was removed and a 4/2-French coaxial polyethylene catheter system with a silicone detachable balloon attached to the 2-French catheter was placed through the 7.3-French catheter. The space between the 4- and 7.3-French catheters was perfused with heparinized saline through a sidearm attachment. Injection of contrast material can also be made through this space during balloon placement. The balloon was advanced under fluoroscopic guidance into the fistula and inflated. If in satisfactory position, the balloon was detached by traction or coaxial technique. Attempts were made to preserve vertebral arterial flow if possible.

If vertebral transection was present, an attempt was made to place the catheter system into the distal transected segment via the ipsilateral vertebral artery.

If a vertebral transection was present and the diagnostic catheter could not be advanced into the distal vertebral artery, then a contralateral approach was initially used. The balloon was flow-directed up the contralateral vertebral artery across the junction of the vertebral arteries, down the distal ipsilateral vertebral artery, and to a point above the level of the fistula. If in satisfactory position, the balloon was then detached by gentle traction. The 7.3-French catheter was then placed in the ipsilateral vertebral artery and balloons were positioned in the fistula site and ipsilateral vertebral artery near the site of the fistula. After final detachment, a control angiogram was obtained from all potential collateral sources that could supply the fistula. If the fistula was occluded, the heparin anticoagulation was reversed with IV protamine sulfate (1 mg of protamine sulfate counteracts 100 units of circulating heparin) given slowly over 5 min. Follow-up angiograms were obtained if the patient had symptoms related to the fistula or if the control angiogram demonstrated subtotal occlusion. The patients were followed by the authors at 1-month, 6-month, and yearly intervals after treatment. The follow-up period was 5–72 months (average, 35 months).

The age and gender of each patient, location and cause of the fistula, symptoms, presence of vertebral transection, treatment, and complications are summarized in Table 1.

Results

Nineteen of 20 patients were treated by transarterial balloon embolization. In the other patient (case 12) the orifice of the fistula was too small to permit the balloon to enter the fistula; therefore, a balloon was transiently positioned in the vertebral artery above the fistula and silicone spheres were embolized behind (proximal to) the balloon into the fistula. All 20 patients had complete closure of their fistulas by transvascular treatments.

TABLE 1: Summary of Vertebral Fistulas in Patients Treated with Transvascular Embolization

Case No.	Age	Gender	Site	Cause	Symptoms/Findings	Vertebral Artery Transection/Occlusion	Treatment
1	61	F	R C1	Spontaneous	Bruit	Occlusion	Three balloons
2	23	F	L C1	Spontaneous	Weakness	No	Three balloons
3	29	F	R C4–C5	Spontaneous	Neck pain, radiculopathy	No	One balloon
4	27	M	L C2–C3	Gunshot wound	Hemorrhage	Occlusion	Three balloons
5	24	M	R C1	Gunshot wound	External hemorrhage	Transection/occlusion	Six balloons
6	20	M	L C1	Blunt trauma	Bruit, pain	Transection	Seven balloons
7	20	M	R C5–C6	Spontaneous	Subarachnoid hemorrhage	No	One balloon
8	64	F	L C2–C3	Fibromuscular dysplasia	Bruit, pain	No	One balloon
9	35	M	L C1	Spontaneous	Bruit, pain	No	Two balloons
10	20	M	R C1	Blunt trauma	Bruit	Transection/occlusion	Ten balloons
11	30	M	L C1	Spontaneous	Exercise intolerance	No	Four balloons
12	26	F	L C2–C3	Fibromuscular dysplasia	Pain, bruit, quadriparesis	No	Silastic spheres
13	60	M	R C6–C7	Gunshot wound	Hematoma	No	One balloon
14	61	M	R C4–C5	Stab wound	Bruit	No	One balloon
15	25	M	R C1	Gunshot wound	Bruit	Transection	Six balloons
16	28	M	L C2	Stab wound	External hemorrhage	Transection/occlusion	Five balloons
17	21	M	L C1	Stab wound	External hemorrhage	Transection/occlusion	Three balloons
18	28	M	L C2–C3	Stab wound	External hemorrhage	No	Three balloons
19	26	M	L C4–C5	Stab wound	Pain, hematoma	Occlusion	Two balloons
20	29	M	L C5–C6	Stab wound	Radiculopathy, pain	No	Four balloons

Note.—Treatment resulted in fistula closure in all cases. There was only one complication, occlusion of the posterior inferior cerebellar artery in case 6. R = right; L = left.

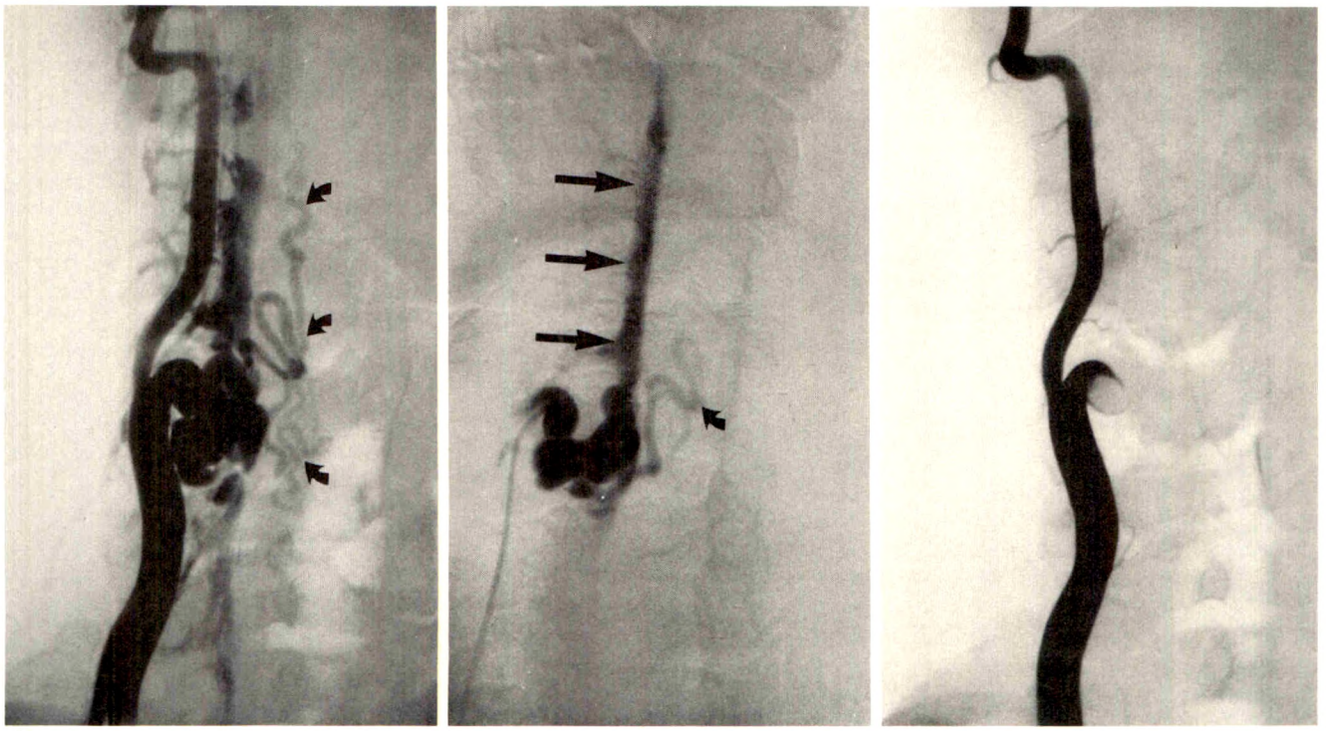

Fig. 1.—Case 7: 20-year-old man with spontaneous vertebral fistula at C5–C6 who presented with massive subarachnoid hemorrhage.
***A*, Anteroposterior view of right vertebral artery injection shows vertebral fistula with venous drainage to epidural venous plexus and medullary veins (*arrows*).**
***B*, Selective radicular artery injection, oblique view, shows site of fistula with venous drainage to epidural venous plexus (*straight arrows*) and medullary veins (*curved arrow*).**
***C*, Selective right vertebral artery injection, anteroposterior view after embolization, shows balloon in fistula with preservation of vertebral flow.**

Spontaneous Fistulas

In spontaneous fistulas the diameter of the involved feeding arteries is often enlarged, presumedly secondary to long-standing fistula flow. Of the eight patients with spontaneous fistulas, three developed reversible neurologic deficits coincident with the abrupt closure of the fistula. With reestablishment of fistula flow the neurologic deficits promptly resolved. Fistula closure was staged in two patients, and in the third the occlusion was gradual over a 2-hr period. None sustained permanent neurologic sequelae.

In all eight patients, transarterial occlusive procedures resulted in complete closure of the fistula and preservation of flow in the involved vertebral artery. Case 7 (Fig. 1) was a 20-year-old man who had subarachnoid hemorrhage secondary to a fistula supplied by a radicular branch of the right vertebral artery with venous drainage to the epidural plexus and medullary veins. A single detachable balloon was positioned at the fistula with complete closure and no further episodes of hemorrhage. Case 1, with a large, high-flow fistula, developed delayed thrombosis in the large vertebral artery weeks after balloon embolization. This event was associated with mild pain, but without neurologic deficit, and was presumed to be secondary to the slow flow in the dilated vessel after closure.

In the two patients with fibromuscular dysplasia, complete closure was achieved without deficits.

Traumatic Fistulas Without Transection

In the six patients with traumatic fistulas without transection, the involved vertebral artery was preserved in four. In the other two patients narrowing and intimal damage in the involved artery prevented preservation of flow. All procedures were performed from the involved vertebral artery and none resulted in neurologic deficits.

Case 14 (Fig. 2) was a 61-year-old man who developed a right vertebral fistula after a penetrating trauma. A single balloon was positioned within the fistula and detached, resulting in complete closure of the fistula.

Traumatic Vertebral Fistulas with Transection

Six patients had complete transection of the vertebral artery. In four patients penetrating injuries were responsible: two knife wounds and two gunshot injuries. In the other two patients, blunt trauma was responsible with severe whiplash in one and fracture of C1 in the other. With complete transection there is retraction of proximal and distal ends of the severed artery away from the site of the injury. There is usually a pseudoaneurysm associated with the fistula. The walls of the pseudoaneurysm are made of clot and offer little structural support unless surrounded by firm structures such as bone or ligaments. Our earliest experience with balloon

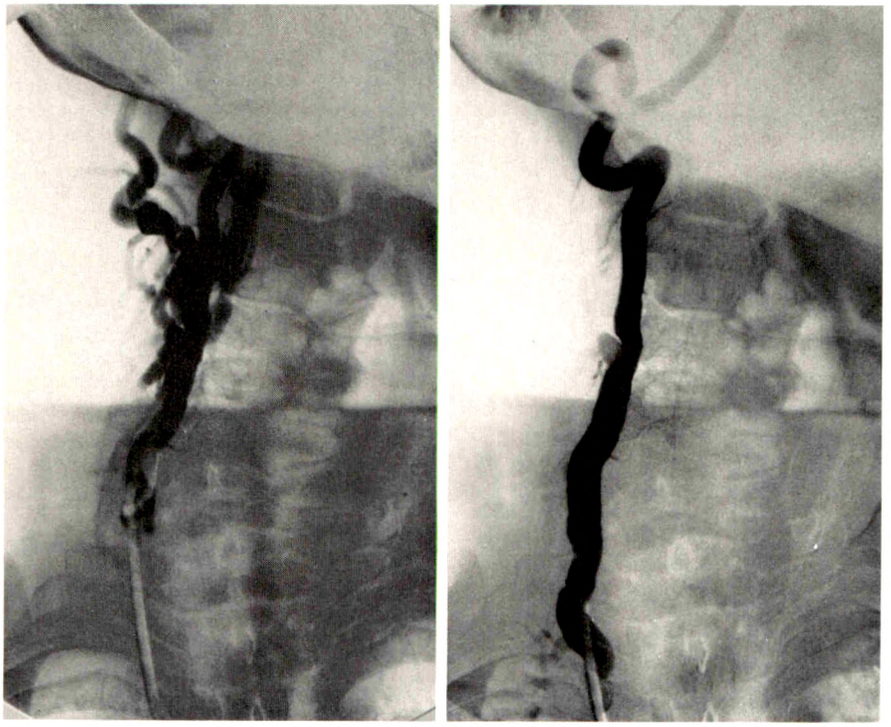

A B

Fig. 2.—Case 14: 61-year-old man with neck injury.

***A*, Right vertebral artery injection, early arterial phase, shows fistula at C4–C5 with drainage to paravertebral veins.**

***B*, Same vessel after embolization. A single balloon has been placed at fistula site with preservation of vertebral artery flow.**

placement within the pseudoaneurysms was that the balloons dissected into the walls of the pseudoaneurysm causing expansion and sometimes mass effect. In case 5 (Fig. 3) there was a vertebral transection with pseudoaneurysm at the level of C1 secondary to a gunshot injury. Several balloons were positioned within the pseudoaneurysm with enlargement of this structure and persistent fistula flow. To achieve closure of the fistula, balloons were positioned in both the proximal and distal severed vertebral artery segments and detached. Because the flow in the distal vertebral is retrograde into the fistula, vertebral artery and fistula occlusion were tolerated in all six patients who required vertebral artery occlusion.

Case 17 (Fig. 4) was a 21-year-old man who developed a left vertebral transection after a knife wound. Injection of the involved vertebral artery showed filling of a pseudoaneurysm at the level of C2. Injection of the contralateral vertebral artery showed retrograde flow down the involved vertebral artery and entry into the same pseudoaneurysm at a higher level. Because of the discontinuity of the severed ends and retrograde flow down the distal left vertebral artery, treatment could not be rendered entirely from the involved side. Therefore, a balloon was flow-directed up the right vertebral artery and then down the distal left vertebral artery. It was detached above the fistula with preservation of flow in the posterior inferior cerebellar artery (PICA). Several more balloons were then detached in the distal left vertebral artery and in the site of the fistula, with complete closure of the fistula without deficits.

Case 10 (Fig. 5) was a 20-year-old man with transection at C1 with pseudoaneurysm formation. The distal vertebral artery could not be reached from an ipsilateral approach. Therefore, a trapping procedure consisting of contralateral followed by ipsilateral occlusion resulted in a complete cure. Note the acute angle between the two vertebral arteries, which required a sharp curve in the 2-French catheter to negotiate this bend. Despite the proximity of the PICA to the fistula site, flow in this vessel was preserved.

The only complication in our series occurred during treatment in case 6, when the PICA origin was occluded. In one of our first cases, previously reported [21], the balloon could not be positioned below the PICA origin because of the proximity to the fistula. Although the patient tolerated test occlusion of the PICA for 20 min, he developed a delayed mild Wallenberg syndrome.

Discussion

The long intraforaminal course and posterior location of the vertebral artery accounts for its rare involvement in penetrating injuries of the neck. Injuries to the short first segment, from its origin to its entry into the foramen transversarium (usually at C6) usually involve other vital structures and have a high morbidity. Most traumatic vertebral fistulas involve the long second portion (intraforaminal), whereas spontaneous fistulas usually involve the third portion (where the artery leaves the foramen of the atlas to where it enters the foramen magnum) [15]. Surgical approaches to these regions have been described but are not without morbidity [22–25]. The earliest attempts at surgical control have involved ligation of the involved vertebral artery [17]. This often has resulted in decreased flow to the fistula but it also could potentiate steal down to the distal vertebral artery and result in cerebral steal

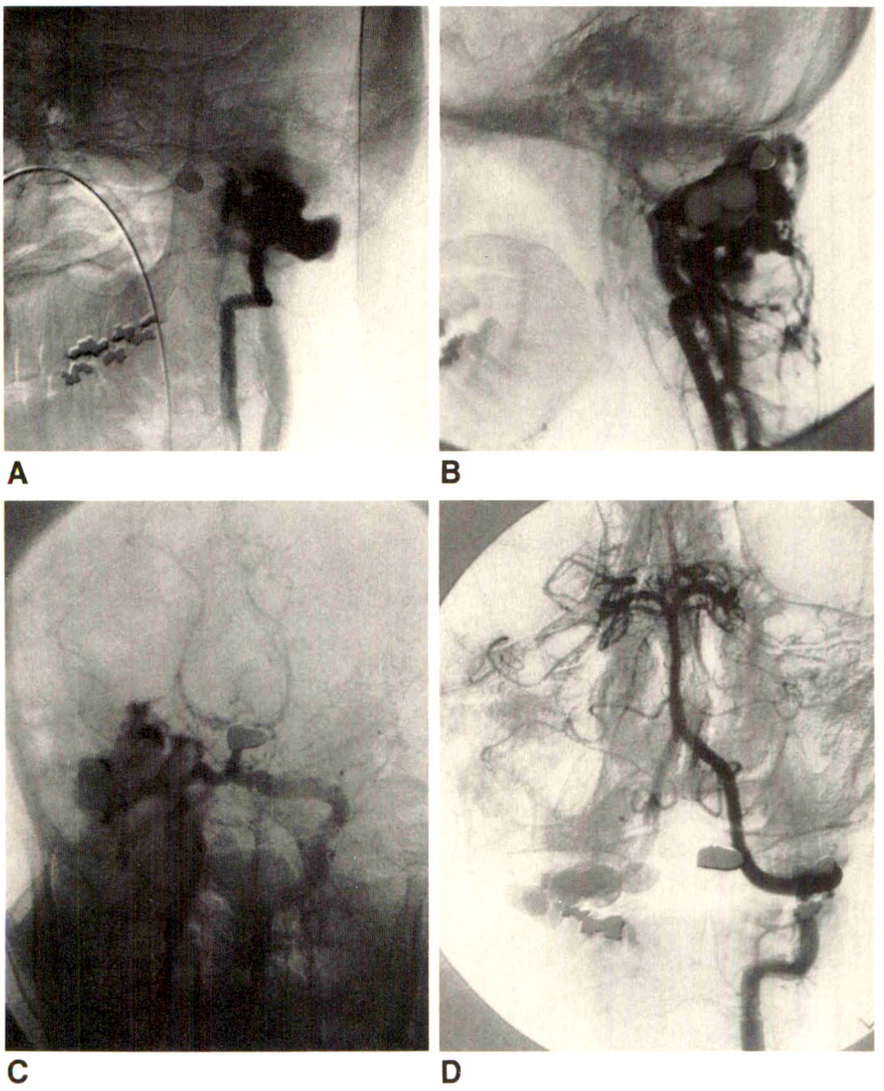

Fig. 3.—Case 5: 24-year-old man.
***A*, Right vertebral artery angiogram, oblique view, shows fistula at C1 with pseudoaneurysm.**
***B*, Same vessel, lateral view, after partial embolization with persistent fistula filling and diversion of venous flow to paravertebral veins.**
***C*, Left vertebral artery injection, Towne projection, with steal down distal right vertebral artery into fistula.**
***D*, Left vertebral artery injection after embolization. Occlusion of fistula with preservation of posterior inferior cerebellar artery.**

symptoms [26, 27]. Trapping procedures with ligation of the vertebral artery on either side of the fistula may be effective; however, collaterals may maintain fistula patency [28]. Surgical exposure of the fistula involving the second portion of the vertebral artery (intraforaminal) can be difficult. The surrounding arterialized Batson plexus can cause extensive hemorrhage during surgical exposure, and damage can occur to surrounding structures such as the phrenic nerve, brachial plexus, and cervical spinal cord [29, 30]. In an attempt to minimize the hemorrhage during surgical exposure, several techniques have been employed, including temporary occlusion of the fistula site with angioplasty catheters [31], intraoperative placement of balloon catheters at the fistula site, and hypotensive anesthesia [30]. Combined surgical and balloon embolization techniques have been used to complete trapping procedures [32–34]. More recently, trapping procedures with detachable balloons and balloon embolization with preservation of vertebral flow have been described [35–37]. Occlusion by spring coils has also been reported [38, 39].

Of the eight spontaneous fistulas in our series, three developed reversible neurologic deficits coincident with the abrupt closure of the fistula. We postulated that the chronically ischemic cerebral vasculature was unable to regulate cerebral blood flow once normal perfusion was reestablished. This has been documented experimentally in animals as well as after surgical resection of large cerebral arteriovenous malformations and is described as normal perfusion-pressure breakthrough [20]. One of our three patients presented with progressive cerebral steal symptoms before treatment, which can signify the cerebral vasculature's loss of normal autoregulation. All three patients had large, long-standing fistulas. In these three patients slow, gradual occlusion in one and staged occlusion in the other two allowed complete fistula closure without the development of permanent neurologic deficits. In addition to the three patients with vertebral fistulas we have also reported the development of normal perfusion-pressure breakthrough during the closure of carotid cavernous fistulas [40]. In all eight patients with spontaneous fistulas in our series, vertebral flow was preserved and complete fistula closure was achieved with transvascular embolization.

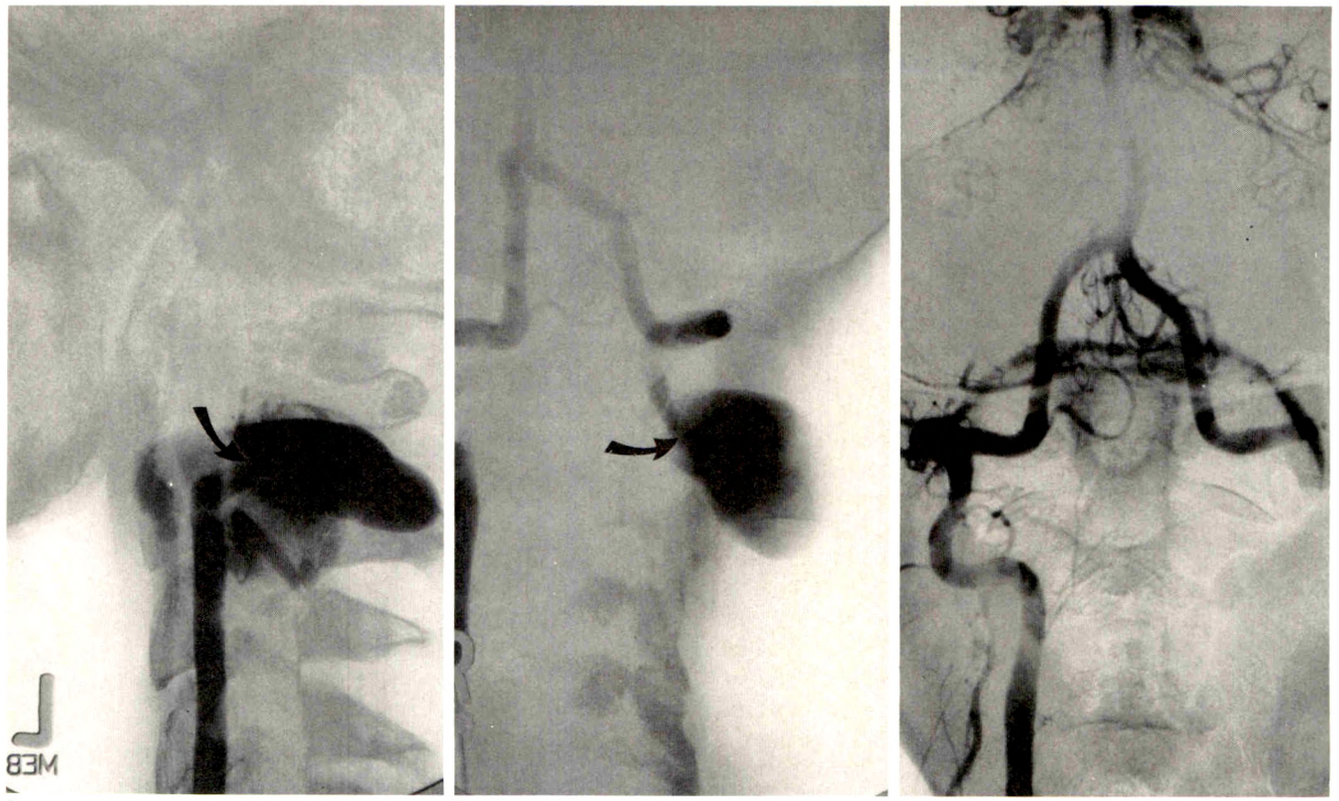

Fig. 4.—Case 17: 21-year-old man with penetrating neck injury.
A, Left vertebral artery injection, lateral view, shows vertebral artery fistula (*arrow*) draining into pseudoaneurysm.
B, Right vertebral artery injection, anteroposterior view, shows retrograde steal down distal left vertebral artery into same pseudoaneurysm (*arrow*). Higher level of entry into pseudoaneurysm is consistent with vertebral transection.
C, Right vertebral artery injection, anteroposterior view, after balloon embolization. Both contralateral and ipsilateral embolization approaches have been used to effect complete fistula closure.

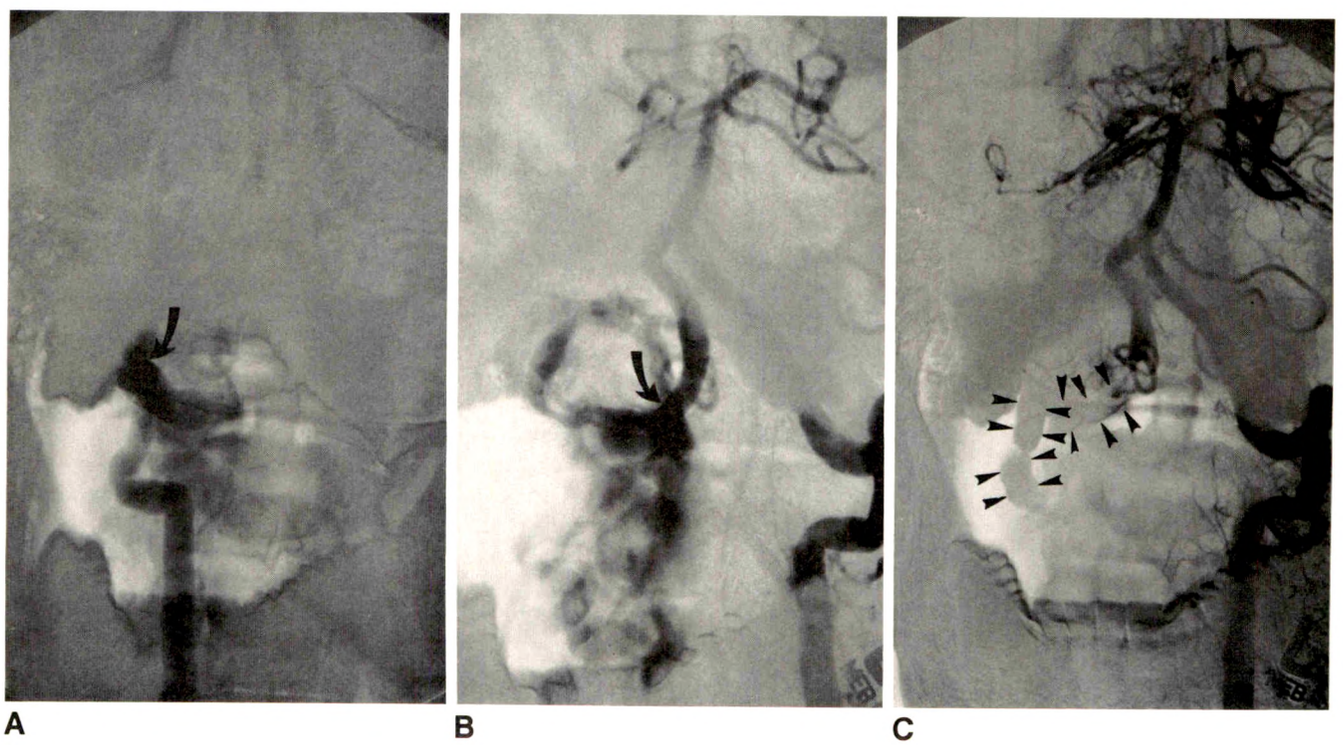

Fig. 5.—Case 10: 20-year-old man with blunt trauma.
A, Right vertebral artery injection, anteroposterior view, shows site of fistula (*arrow*) at C1.
B, Left vertebral artery injection, anteroposterior projection, shows transection (*arrow*) and drainage into pseudoaneurysm.
C, Same vessel, after embolization. By using both contralateral and ipsilateral approaches, balloons (*arrowheads*) have been positioned in both proximal and distal vertebral segments as well as within fistula, resulting in complete cure and preservation of posterior inferior cerebellar artery.

Patients in our series with traumatic fistulas without transection were all treated with transvascular embolization with preservation of flow in four of six involved vertebral arteries.

Vertebral artery transection often presents a diagnostic and therapeutic challenge. Because the cause is often trauma (100% in our series), presentation is generally acute, with external hemorrhage or expanding pseudoaneurysms. The retracted severed ends of the vertebral artery make preservation of flow difficult or impossible. In the six patients in our series with transection, vertebral patency could be preserved only in two. The retracted ends of the vertebral artery and associated pseudoaneurysm often require trapping procedures to achieve fistula closure; these were performed in four patients. Great care must be taken to ensure that the fistula is closed before or coincident with the closure of the vertebral artery. If the proximal vertebral artery is closed before the fistula is obliterated, then increased steal from the distal vertebral artery into the fistula could compromise cerebral circulation. Therefore, in complete vertebral transection where preservation of the artery is not technically possible, the distal vertebral artery should be occluded first. Because of the retraction of the severed ends of the vertebral artery, retrograde flow in the distal vertebral segment, and turbulent flow within the fistula, it is often technically difficult to reach the distal vertebral artery across the fistula site from the ipsilateral approach. It is sometimes necessary to approach the distal vertebral segment from the contralateral vertebral artery to perform a trapping procedure involving the fistula. This maneuver must be undertaken with extreme caution and carries several potential hazards. Occlusion of the contralateral vertebral artery increases the steal from the posterior fossa circulation and may cause neurologic deficits if prolonged. The angle between the two distal vertebral arteries is often acute and negotiation may be difficult. Often, a sharp curve in the distal 2-French catheter is necessary to execute this maneuver. Because of the tortuosity of the distal vertebral arteries, coaxial detachment is impossible. Traction detachment is necessary when the balloon is positioned in the distal vertebral segment above the fistula, and it is important that the final balloon position be below the origin of the PICA. The only complication in our series (in one of our earliest cases) followed occlusion of the PICA, which resulted in the development of a delayed mild Wallenberg syndrome with left face and body hypalgesia and residual clumsiness in the ipsilateral upper extremity.

In addition to the trapping of both the proximal and distal ends of the involved vertebral artery, balloons are placed within the fistula itself to prevent fistula patency from potential collaterals. Both silicone and latex balloons are adequate for occlusion; however, only silicone balloons were used in our series.

In conclusion, transvascular balloon embolization is currently the method of choice in the treatment of vertebral fistulas. In patients with spontaneous or traumatic fistulas without transections, it is often possible to preserve vertebral arterial flow. Patients with long-standing fistulas may be at risk to develop neurologic deficits if abruptly occluded; these can be averted with gradual or staged fistula closure. In patients with transection, a trapping procedure is often necessary to achieve complete fistula closure and can be performed from a transvascular route.

REFERENCES

1. Nagashima C, Iwasaki T, Kawanuma S, Sakaguchi A, Kamisasa A, Suzuki K. Traumatic arteriovenous fistula of the vertebral artery with spinal cord symptoms: case report. *J Neurosurg* **1977**;46:681–687
2. Olson RW, Hillier LB Jr, Svien HJ. Arteriovenous fistula: a complication of vertebral angiography; report of a case. *J Neurosurg* **1963**;20:73
3. Philipsson J, Karnell J. Arteriovenos fistel efter punktion av a. vertebralis for cerebral angiografi. *Opusc Med* (Stockh) **1956**;1:49
4. Colley DP. Vertebral arteriovenous fistula: an unusual complication of Swan-Ganz catheter insertion. *AJNR* **1985**;6(1):103–104
5. Robinson PN, Jewkes DA, Kendall B. Vertebrovertebral arteriovenous fistula: a complication of internal jugular catheterization. *Anaesthesia* **1984**;39(1):46–47
6. Weinberg PE, Flom RA. Traumatic vertebral arteriovenous fistula. *Surg Neurol* **1973**;1:162–167
7. Hieshima GB, Cahan LD, Mehringer CM, Bentson JR. Spontaneous arteriovenous fistulas of cerebral vessels in association with fibromuscular dysplasia. *Neurosurgery* **1986**;18(4):454–458
8. Bahar S, Chiras J, Carpena JP, Meder JF, Bories J. Spontaneous vertebrovertebral arteriovenous fistula associated with fibro-muscular dysplasia: report of two cases. *Neuroradiology* **1984**;26(1):45–49
9. Reddy SV, Karnes WE, Earnest F IV, Sundt TM Jr. Spontaneous arteriovenous fistulas of cerebral vessels in association with fibromuscular dysplasia. *J Neurosurg* **1981**;54(3):399–402
10. Deans WR, Block S, Leibrock L, Berman BM, Skultety FM. Arteriovenous fistula in patients with neurofibromatosis. *Radiology* **1982**;144(1):103–107
11. Parkinson D, Hay R. Neurofibromatosis. *Surg Neurol* **1986**;25(1):109–113
12. Kamiyama K, Endo S, Horie Y, Koshu K, Takaku A. Neurofibromatosis associated with intra- and extracranial aneurysms and extracranial vertebral arteriovenous fistula. *No Shinkei Geka* **1985**;13(8):875–880
13. Hayes P, Gerlock AJ Jr, Cobb CA. Cervical spine trauma: a cause of vertebral artery injury. *J Trauma* **1980**;20(10):904–905
14. Avellanosa AM, Glawauer FE, Oh YS. Traumatic vertebral arteriovenous fistula associated with cervical spine fracture. *J Trauma* **1977**;17:885–888
15. DeBray JM, Bertrand P, Bertrand R, Jeanvoine H. Les fistules arterio-veineuses spontanees de l'artere vertebrale: a propos d'un cas''revue doe la litterature. *Rev Med Interne* **1986**;7(2):133–139
16. Reizine D, Laouiti M, Guimaraens L, Riche MC, Merland JJ. Vertebral arteriovenous fistulas: clinical presentation, angiographical appearance and endovascular treatment—a review of 25 cases. *Ann Radiol* (Paris) **1985**;28(6):425–438
17. Matas R. Traumatisms and traumatic aneurisms of the vertebral artery and their surgical treatment with the report of a cured case. *Ann Surg* **1893**;18:477–521
18. Goodman SJ, Hasso A, Kirkpatrick D. Treatment of vertebrojugular fistula by balloon occlusion: case report. *J Neurosurg* **1975**;43:362–367
19. Debrun G, Legre J, Karbarian M, Tapias PL, Caron JP. Endovascular occlusion of vertebral fistulae by detachable balloon occlusion with conservation of the vertebral blood flow. *Radiology* **1979**;13:141–147
20. Spetzler RF, Wilson CB, Weinstein P, et al. Normal perfusion pressure breakthrough theory. *Clin Neurosurg* **1978**;25:651
21. Miller RE, Hieshima GB, Giannotta SL, Grinnell VS, Mehringer CM, Kerin DS. Acute traumatic vertebral arteriovenous fistula: balloon occlusion with the use of a contralateral approach. *Neurosurgery* **1984**;14(2):225–229
22. Elkin DC, Harris MH. Arteriovenous aneurysm of the vertebral vessels: report of ten cases. *Ann Surg* **1948**;124:934–951
23. Stapleford RG, Gruenberg JC, Wolford DG, Kerchner JB. Vertebral artery injury: case report and review of operative approaches. *Henry Ford Hosp Med J* **1981**;29:148–152
24. Berthelot JL, Andreassian B, Hureau J. Surgical approach to the 3rd segment of the vertebral artery by a paramedian posterior route. *Nouv Presse Med* **1983**;12(22):1423–1425
25. Benhamou AC, George B, Nerland JJ, Bories J, Natali H. Treatment by a direct surgical approach of a false arteriovenous traumatic aneurysm between the vertebral artery and the internal jugular vein at the level of the atlas. *J Chir* (Paris) **1979**;116(11):659–662
26. Chou SN, French LA. Arteriovenous fistula of vertebral vessels in the neck. *J Neurosurg* **1964**;22:77–80
27. Goodman SJ, Hasso A, Kirkpatrick D. Treatment of vertebrojugular fistula by balloon occlusion: case report. *J Neurosurg* **1975**;43:362–367
28. Stecken J, Jan M, Lapierre F, Mbouyou D. Postarteriographic vertebral arteriovenous fistula. *Neurochirurgie* **1983**;29(2):161–165
29. Fairman RM, Grossman RL, Goldberg HL, Kivuls J, Perloff LJ. A new

approach to the treatment of vertebral arteriovenous fistulas. *Surgery* **1984**;95(1):112–115

30. Kornmesser TW, Bergan JJ. Anatomic control of vertebral arteriovenous fistula. *Surgery* **1974**;75:80–86
31. Schumacher M, Arnolds B, Wimmer B, Kauffmann GW, Gilsbach J. Temporary preoperative balloon catheter blockage of a traumatic giant aneurysm and of an a.v. fistula of the vertebral artery. *ROFO* **1985**;143(3):326–330
32. Berguer R, Feldman AJ, Wilner HI, Lazo A. Arteriovenous vertebral fistulae: cure by combination of operation and detachable intravascular balloon. *Ann Surg* **1982**;196(1):65–68
33. Picard L, Marchal JC, Georges B, et al. Radical surgery for a multipedunculated vertebral fistula by a combined sequential endo- and exovascular approach. *Rev Otoneuroophthalmol* **1981**;53(2):167–175
34. Sclafani SJ, Panetta T, Goldstein AS, et al. The management of arterial injuries caused by penetration of zone III of the neck. *J Trauma* **1985**;25(9):871–881
35. Debrun G, Lacour P, Caron JP, Hurth M, Comoy J, Yeravel Y. Detachable balloon and calibrated-leak balloon techniques in the treatment of cerebral vascular lesions. *J Neurosurg* **1978**;49:635–649
36. Hieshima GB, Mehringer CM, Grinnell VS, Hasso AN, Siegel NH, Pribram HF. Emergency occlusive techniques. *Surg Neurol* **1978**;9:293–302
37. Hungerford GD, Perto PL. Detachable balloon treatment of carotid-cavernous and vertebro-vertebral fistulas. *J SC Med Assoc* **1982**;78(9):479–483
38. Roper PR, Guinto FC Jr, Wolma FJ. Posttraumatic vertebral artery aneurysm and arteriovenous fistula: a case report. *Surgery* **1984**;96(3):556–559
39. Kawano Y, Takizawa S, Shibuya H, et al. A successful transcatheter embolization with occluding spring emboli for vertebral arteriovenous fistulas following insertion of Swan-Ganz catheter. *Nippon Ganka Gakkai Zasshi* **1985**;86(3):325–329
40. Halbach VV, Higashida RT, Hieshima GB, Norman D. Normal perfusion breakthrough occurring during treatment of carotid and vertebral fistulas. *AJNR* **1987**;8:751–756

Tolosa-Hunt Syndrome Revisited:
Not Necessarily a Diagnosis of Exclusion

Eddie S. K. Kwan[1]
Samuel M. Wolpert[1]
Thomas R. Hedges III[2]
Michael Laucella[1]

The Tolosa-Hunt syndrome (THS), a steroid-responsive painful ophthalmoplegia secondary to idiopathic granulomatous inflammation, historically has been categorized as a diagnosis of exclusion because of its nonspecific radiologic presentation. Five patients who satisfied the anatomic and clinical criteria of this syndrome underwent high-resolution CT of the orbital apex/cavernous sinus region. Two patients were diagnosed as having orbital apex pseudotumor, two as having cavernous sinus inflammation, and one as having a cavernous sinus epidermoid by the characteristic CT and clinical findings. Follow-up studies while the patients were asymptomatic demonstrated complete resolution of the CT abnormalities in four patients and clinical improvement in all five patients.

Our data suggest that orbital apex pseudotumor and granulomatous inflammation of the cavernous sinus have similar clinical features and should be considered as part of the spectrum of THS. With the advent of high-resolution CT, THS may now be a diagnosis of inclusion. Symptomatic improvement after steroid therapy is an essential but not absolute proof of the syndrome, since lesions such as lymphomas may also respond to steroids. Resolution of the soft-tissue inflammation on CT is an additional criterion for diagnosis.

The hallmark of the Tolosa-Hunt syndrome (THS) is a painful ophthalmoplegia that is steroid responsive. In 1954, Tolosa [1] reported a patient with left orbital pain, ipsilateral progressive visual loss, total left ophthalmoplegia, and hypesthesia over the first division of the trigeminal nerve. Cerebral angiography demonstrated narrowing of the intracavernous segment of the left internal carotid artery; at autopsy, a low-grade nonspecific granulomatous inflammation of the cavernous sinus and adventitia of the carotid artery was identified. In 1961, Hunt et al. [2] reported six cases of remittent unilateral retroorbital pain accompanied by extraocular palsies and occasional supraorbital numbness and blindness; these patients also improved promptly on corticosteroids. Since the radiologic findings of THS in the pre-CT era were often nonspecific and the symptom complex of painful ophthamoplegia could be clinically encountered in patients with other disorders (aneurysms, diabetes mellitus, periarteritis nodosa, parasellar neoplasm/infection, cavernous sinus thrombosis, and carotid cavernous fistula), there has been a strong emphasis in the neurologic and ophthalmologic literature to categorize the THS as a diagnosis of exclusion. With the advent of high-resolution CT, lesions located in the orbital apex, superior orbital fissure, and cavernous sinus region that are directly responsible for the symptoms can now be imaged. As a result, we no longer believe that the THS is a diagnosis of exclusion. While the syndrome is often considered a benign, self-limiting entity, permanent damage to the involved cranial nerves can occur, making prompt diagnosis and steroid therapy mandatory. It is also important that the radiologist be aware of the spectrum of CT findings in this syndrome to obviate surgical exploration. The clinical and radiologic findings in five patients who satisfy the criteria of THS are the subject of this report.

This article appears in the November/December 1987 issue of *AJNR* and the February 1988 issue of *AJR*.

Received February 5, 1987; accepted after revision June 10, 1987.

[1]Department of Radiology, New England Medical Center, 171 Harrison Ave., Boston, MA 02111. Address reprint requests to E. S. K. Kwan.

[2] Section of Neuroophthalmology, New England Medical Center, Boston, MA 02111.

***AJR* 150:413–418, February 1988**
0361–803X/88/1502–0413
© American Roentgen Ray Society

Materials and Methods

Between 1981 and 1986, five patients with THS were evaluated by the neuroophthalmology and neuroradiology sections at our institution. All patients underwent high-resolution 2-mm contrast-enhanced CT* of the orbit and parasellar regions as a part of the diagnostic evaluation of painful ophthalmoplegia. Tissue diagnosis was obtained in one patient. A dramatic response to steroid therapy accompanied either by resolution of the CT abnormality or by long-term follow-up established the diagnosis of THS in the remaining four patients.

Case Reports

Case 1

A 22-year-old white man with a 12-year history of Crohn disease developed bifrontal constant headache accompanied by nausea, numbness of the right upper lip, and diplopia on left lateral and upward gaze 2 weeks before admission. The pain was more severe over his right eye. Physical examination showed normal visual acuity, minimal ptosis of the right upper eyelid, and decreased adduction of the right eye. Pertinent laboratory data included a normal lumbar puncture, sedimentation rate, WBC count, and fasting blood glucose. Antinuclear antibody and rheumatoid factors were negative. The patient underwent high-resolution contrast-enhanced CT through the parasellar region (Fig. 1A).

Since the cause of the diplopia and headache was not clear and the implication of the enlarged right cavenous sinus was not fully appreciated at the time, the headache was treated symptomatically. Over the next 2 weeks, the patient noted increasing horizontal and oblique diplopia. A repeat ophthalmologic examination (now 5 weeks after the onset of symptoms) demonstrated a pupil-sparing third-nerve palsy and a complete fifth-nerve dysfunction. Owing to the patient's age, the lack of bony involvement, and the clinical course, an inflammatory process was considered more likely than malignancy. A therapeutic trial of prednisone was started at 60 mg/day. The patient's headache, ptosis, diplopia, and hypesthesia in the trigeminal distribution responded dramatically within 48 hr, and resolution was complete within 1 week. Follow-up CT demonstrated a normal-appearing right cavernous sinus (Fig. 1B).

Case 2

A healthy 24-year-old white man developed sudden onset of right retrobulbar pain relieved by aspirin 3 weeks before admission. A complete right third nerve palsy was noted over the next several days. A CT brain scan and bilateral carotid angiography at another institution were reported as normal. Since diabetes, parasellar tumor, and posterior communicating artery aneurysms had apparently been excluded, he was started empirically on methyl prednisolone, 24 mg/day to be tapered over a 1-week period. This relieved the headache almost immediately, but the diplopia persisted. Pertinent findings on ophthalmologic examination at our institution included normal visual acuity, ptosis of the right upper eyelid, a poorly reactive dilated right pupil, reduced ocular motility in the direction of all the muscles supplied by the right third nerve, and mild impairment of the motor division of the right fifth nerve. A repeat CT scan of the parasellar region demonstrated a low attenuating mass in the right cavernous sinus (Fig. 2). When steroids were restarted, the patient noted marked improvement of his retrobulbar pain, pupillary functions, and extraocular movements. As the steroids were tapered, there was a mild flare-up of the headache and the ptosis. The working diagnosis was leakage from an epidermoid tumor in the right cavernous sinus with secondary inflammation.

Case 3

A 26-year-old previously healthy black man experienced 2 weeks of generalized fatigue, fever, and night sweats 8 weeks before admission. By 6 weeks before admission, the patient experienced diplopia on left lateral gaze and left retroorbital pain. Pertinent physical findings on admission included visual acuity of 20/25 on the right and 20/60 on the left, a left relative afferent pupillary defect, left lateral rectus dysfunction, hypesthesia over the first division of the left trigeminal nerve, and bilateral inguinal adenopathy. Laboratory studies including lumbar puncture and serology were noncontributory. CT and MR of the brain and parasellar region demonstrated multiple bilateral parenchymal and dural-based lesions (Figs. 3A–3D). The leading differential diagnoses were CNS sarcoidosis and lymphoma. Subsequent chest films and CT scans demonstrated paratracheal, paraaortic, and perihilar adenopathy. A mediastinal lymph-node biopsy showed noncaseating granulomata compatible with sarcoidosis. Visual acuity deteriorated to 20/200 over a 10-day period. The patient was subsequently started on methyl prednisolone, 60 mg every 6 hr, then changed to oral prednisone, 80 mg every morning. Visual acuity on the left transiently improved to 20/30; headache, facial paresthesias, and diplopia all resolved within several days. When the patient prematurely discontinued the prednisone, visual acuity of the left eye deteriorated to 20/400 with the development of a central scotoma. High-dose IV methyl prednisone was therefore administered for a 5-day period followed by oral prednisone. Follow-up CT 8 weeks later demonstrated resolution of all intracranial lesions including the cisternal lesion (Fig. 3E). However, visual acuity on the left side did not improve.

Case 4

A 25-year-old healthy white woman developed diplopia on left lateral gaze several days after an "upper respiratory infection." An orbital CT scan at an outside institution was reported as normal. The deficit remained stable for 1 month until 3 weeks before admission when the patient noted loss of color vision in the left eye and right frontal and left supraorbital headache with radiation to the left occiput. Pertinent findings on ophthalmologic examination at our institution included ptosis and swelling of the left upper lid, minimal proptosis, a left-sided relative afferent pupillary defect, and visual acuity of 20/400 on the left. Extraocular movements of the left eye had decreased in all fields of gaze, especially medially. Laboratory studies including thyroid function tests were normal. CT of the orbit was performed (Figs. 4A and 4B). The clinical diagnosis was orbital apex pseudotumor. The patient was initially treated with prednisone, 100 mg/day, but the lack of response necessitated a change to dexamethasone, 20 mg IV every 6 hr. The diplopia and retroorbital pain subsequently resolved, while the visual acuity in the left eye improved to 20/50 over the next several days. Follow-up CT 1 week later demonstrated a normal orbital apex (Fig. 4C).

Case 5

A 62-year-old black man was initially evaluated at our institution 5 years ago for throbbing temporal/retroorbital headache, proptosis, decreased visual acuity, hypesthesia in the V1 and V2 distributions, and third and sixth cranial nerve palsies all localized on the left side. Extensive evaluation included serology, antinuclear antibody, lupus

* Siemen's Somatom 2 or DR3.

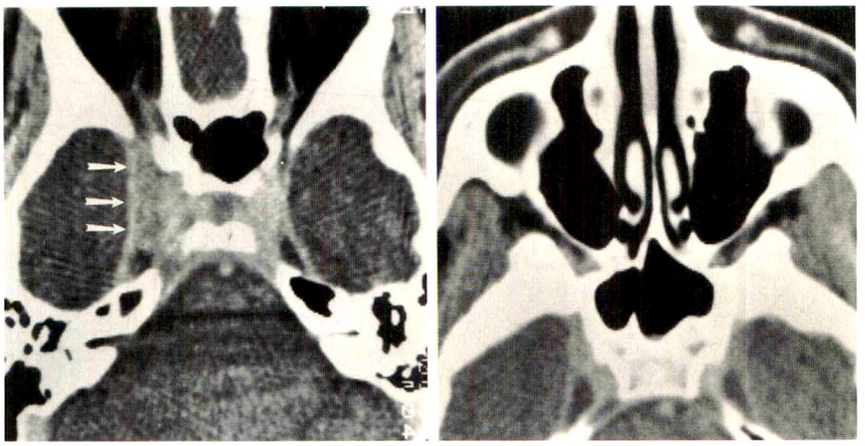

Fig. 1.—Case 1.
A, Axial parasellar CT scan shows asymmetric enlargement of right cavernous sinus (*arrows*) before steroid therapy.
B, Follow-up CT scan 7 months later shows normal-appearing cavernous sinus bilaterally.

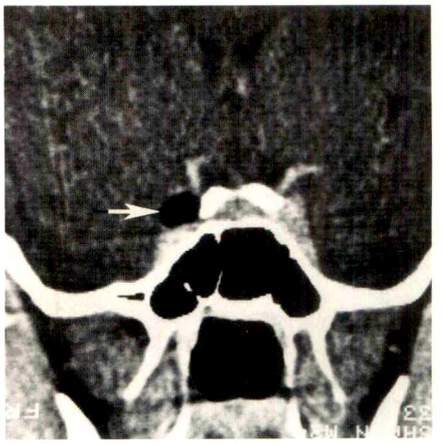

Fig. 2.—Case 2: direct coronal CT scan of parasellar region. Low-density mass within right cavernous sinus (*arrow*) measures −87 H.

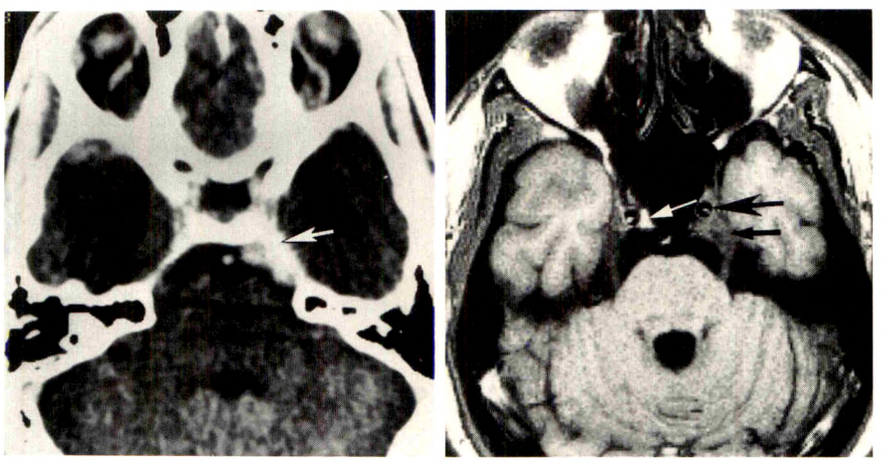

Fig. 3.—Case 3: 26-year-old black man.
A, Axial CT scan shows abnormal enhancement in left prepontine cistern (*arrow*).
B, 3-mm T1-weighted spin-echo image (TR = 600 msec, TE = 17 msec) through same region shows abnormal soft tissue infiltrating posterior cavernous sinus (*small black arrow*), resulting in anterior displacement of left internal carotid artery (*large black arrow*) and effacement of fat within cavernous sinus. Note fat within right cavernous sinus (*white arrow*).
C, Multiple parenchymal enhancing lesions in corpus callosum and left parietal lobe.
D, T2-weighted spin-echo image at same level shows multiple lesions with prolonged T2 in corpus callosum and left centrum semiovale (*arrows*).
E, Cavernous sinuses are now symmetric, and abnormal enhancement in prepontine cistern has resolved after high-dose steroid therapy.

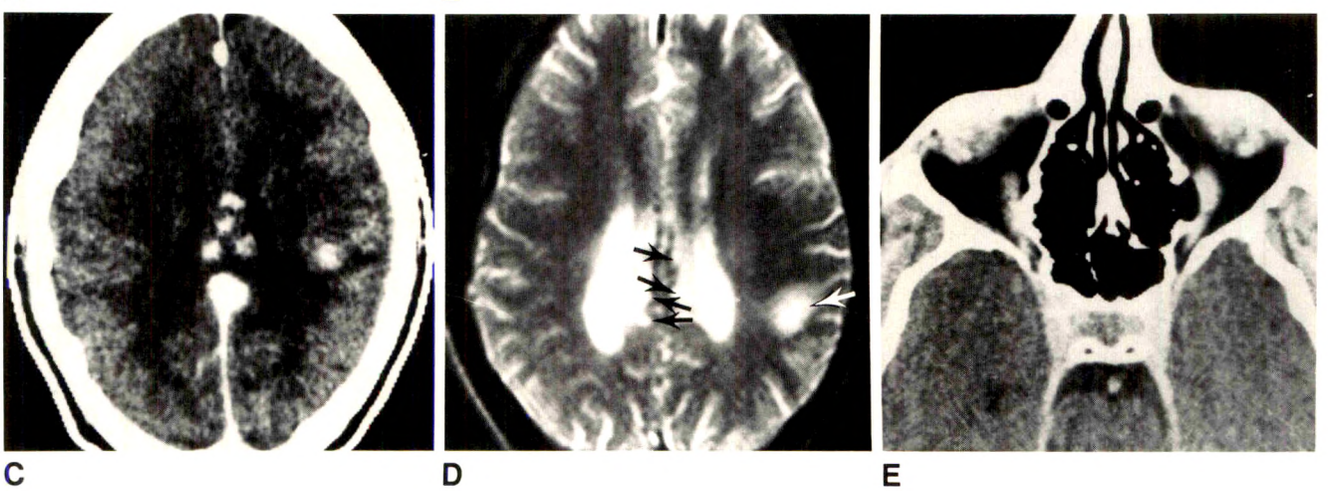

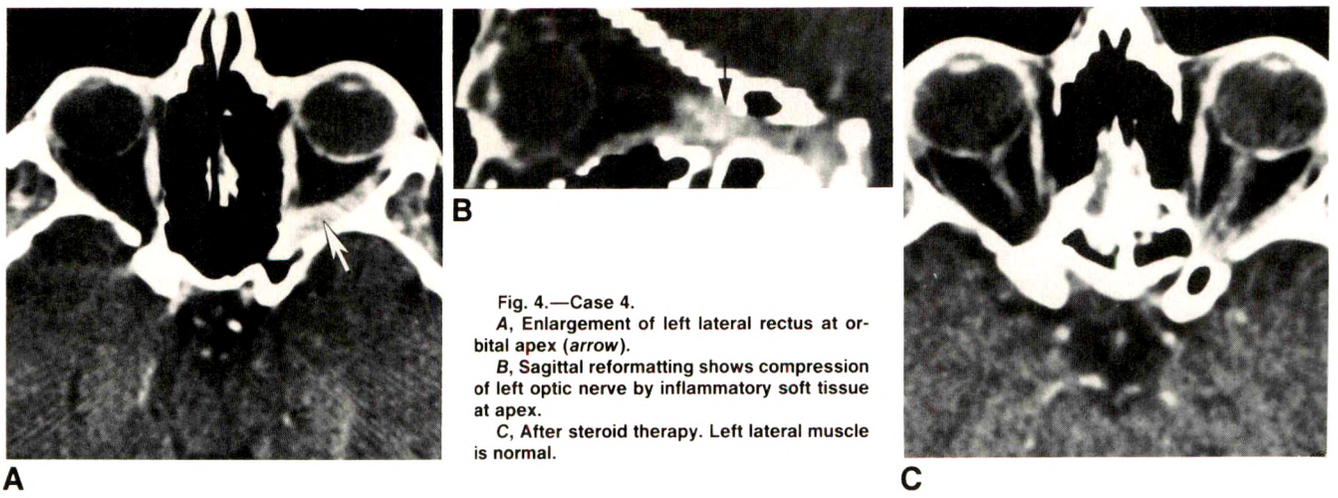

Fig. 4.—Case 4.
A, Enlargement of left lateral rectus at orbital apex (*arrow*).
B, Sagittal reformatting shows compression of left optic nerve by inflammatory soft tissue at apex.
C, After steroid therapy. Left lateral muscle is normal.

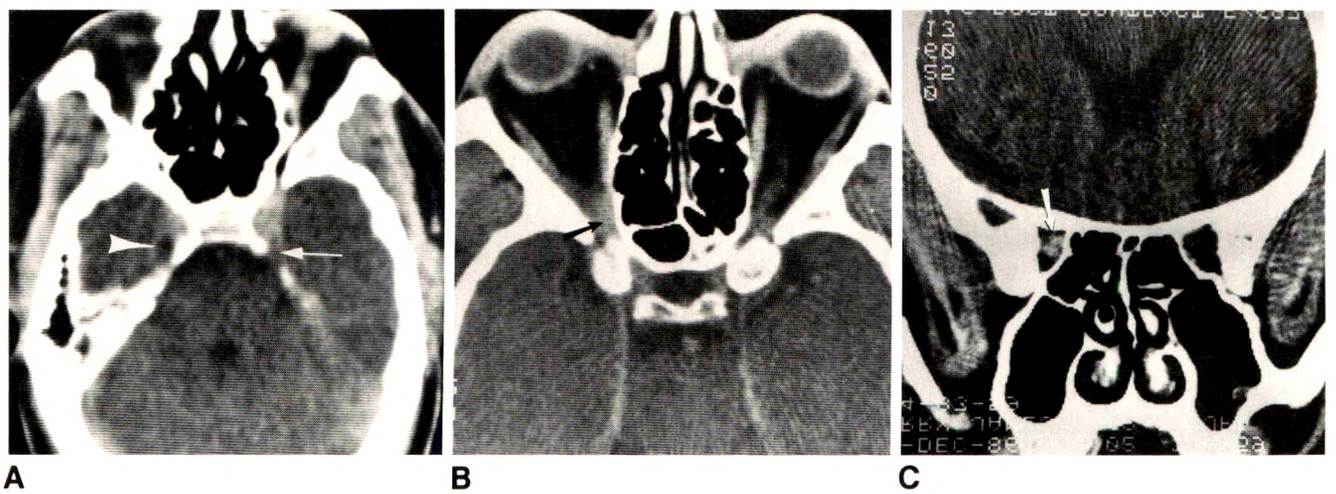

Fig. 5.—Case 5.
A, 4-mm axial CT scan through cavernous sinus shows effacement of left Meckel cave (*arrow*). Note normal Meckel cave (*arrowhead*) on right side of patient.
B, 5 years later. Subtle but definite abnormal soft-tissue mass compresses right orbital apex (*arrows*) on both axial (*B*) and coronal (*C*) views.

erythematosus test, complete blood cell count, fungal and acid-fast bacillus culture of the CSF, cerebral angiography, and temporal artery biopsy; all were negative.

CT of the parasellar region demonstrated partial effacement of the left Meckel cave (Fig. 5A). The major differential diagnoses were occult neoplasm vs idiopathic granulomatous inflammation of the left cavernous sinus. The patient was treated with a tapering dose of oral prednisone starting with 100 mg/day. The headache improved dramatically within 24 hr, while the cranial nerve deficits improved gradually over the next 4 weeks. He remained symptom-free for 5 years until he had a 5-day period of diplopia, retroorbital pain, and decreased visual acuity on the right that prompted his current evaluation. Pertinent findings on ophthalmologic examination included decreased visual acuity to finger counting at 1 m on the right with normal visual acuity on the left, a relative afferent pupillary defect, and third and sixth cranial nerve palsies on the right. CT of the orbit was compatible with apical orbital pseudotumor (Fig. 5B). There was subjective improvement of the diplopia and the retroorbital pain within 48 hr after initiation of oral prednisone of 100 mg/day. The visual acuity returned to 20/25, and there was minimal residual lateral rectus weakness as the steroids were reduced.

Discussion

Painful ophthalmoplegia secondary to idiopathic granulomatous inflammation of the cavernous sinus or the superior orbital fissure that is steroid responsive was given the eponym Tolosa-Hunt syndrome by Smith and Taxdal [3] in 1966 when they reported five cases of painful ophthalmoplegia and confirmed the importance of therapeutic trials of steroids as a diagnostic test. Two strict sets of criteria have to be satisfied before a patient can be given this diagnosis [4]. The first is anatomic, wherein the neurologic deficits have to be directly confined to structures in the cavernous sinus, superior orbital fissure, or orbital apex. These include cranial nerves II, III, IV,

TABLE 1: Summary of Clinical Presentations and Radiologic Findings in Patients with Tolosa-Hunt Syndrome

Case No.	Age	Gender	Associated Systemic Disease	Cranial Nerve Palsies	Decreased Visual Acuity	CT Findings		Residual Deficit
						Before Steroids	After Steroids	
1	22	M	Crohn disease	R III, V complete	No	Enlarged R cavernous sinus	Normal	None
2	24	M	None	R III, V motor	No	Epidermoid in R cavernous sinus	No change	Mild weakness of R superior rectus
3	26	M	Sarcoidosis	L VI, V1	Yes; L 20/60	Enhancement in prepontine cistern, posterior cavernous sinus, and brain	Normal	L visual acuity 20/400
4	25	F	None	L III, IV, VI	Yes; L 20/400	Swelling of L lateral rectus and inflammation at orbital apex	Normal	L visual acuity 20/50
5[a]	57	M	None	L III, VI, V1, V2	Yes; L 20/50	Effacement of Meckel cave	Normal	None
	62	M	—	R III, VI	Yes; R finger counting at 1 m	Increased soft tissue in R orbital apex	Normal	Mild weakness of R lateral rectus

[a] Two episodes 5 years apart.
Note —R = right, L = left.

VI, and V1; parasympathetic pupillodilator fibers of the third nerve; and sympathetic pupilloconstrictor fibers of the pericarotid plexus. Dysfunction of V2 and the motor division of the trigeminal nerve is encountered less often. The second set of criteria relates to the clinical behavior in which "steady" periorbital or retroorbital pain usually precedes but may arise concomitant with the onset of ophthalmoplegia. The symptoms are often relapsing and remitting and can last for days to weeks. Even though the pathologic process is self-limited and spontaneous remissions do occur, a short course of steroids can dramatically relieve the periorbital pain within 24–48 hr, followed by gradual resolution of the cranial nerve dysfunctions. The cause of this syndrome is unknown.

While painful ophthalmoplegia is not an uncommon clinical problem, the THS has been considered a rare clinical entity. Thomas and Yoss [5] reported three cases of THS in a review of 102 patients with parasellar syndrome. An additional four patients satisfied the criteria of this syndrome in an analysis of 1000 cases of paralysis involving cranial nerves III, IV, and VI [6]. In a report by Hasso et al. [7] of 131 patients with cavernous sinus syndrome, idiopathic inflammation of the cavernous sinus was not represented. In the most extensive recent review of this topic by Kline [8] in 1982, the author analyzed 146 patients and emphasized that the THS is categorically a diagnosis of exclusion. Since many disease processes (vascular, neoplastic, or inflammatory) located in the region of the cavenous sinus, superior orbital fissure, and orbital apex can produce a similar pattern of pain and neurologic deficit, the concept of the THS as a diagnosis of exclusion was valid at a time when radiologic evaluation lagged behind clinical understanding. The fact that no consistent or specific abnormality can be identified in the hematologic, bacteriologic, and spinal fluid analyses makes the clinical diagnosis of this group of patients even more elusive.

With the exception of an isolated case report [9], CT has been reported to be essentially normal in the majority of patients with THS [10, 11]. However, erosion of the sella turcica [12], segmental narrowing of the cavernous carotid artery [1, 13, 14], and occlusion of the superior ophthalmic vein in the orbital apex have been described [10, 13, 15, 16]. Since the efficacy of high-resolution CT in the evaluation of the orbital apex [17] and the cavernous sinus regions [18] has been firmly established, we now believe the pathologic processes responsible for the THS can be imaged directly by CT, and this syndrome is now not a diagnosis of exclusion but a diagnosis of inclusion.

The clinical deficits and CT findings in our five patients with six episodes of steroid-responsive painful ophthalmoplegia are summarized in Table 1. Dysfunction of the trigeminal nerve was seen in cases 1–3 and initially in case 5. In each case, CT reliably demonstrated abnormalities in either the cavernous sinus, Meckel cave, or along the course of the cisternal segment of the fifth nerve. Decreased visual acuity as a presenting symptom was observed in cases 3–5. Compression of the optic nerve at the orbital apex by pseudotumor and myositis of the lateral rectus can adequately explain the visual impairment of case 5 (second episode) and case 4. The cause of the decreased visual acuity in case 3 is less obvious. In patients with systemic sarcoidosis, visual impairment most often results from uveitis, retinal detachment, or vitreous hemorrhage [19]. While granulomatous infiltration of sarcoid in the orbital apex and enlargement of the optic nerve have been reported [19–21], they are considered rare phenomena, and were not seen on the scans in case 3. The lack of improvement in visual acuity in this patient after high-dose steroids make retrobulbar neuritis or microscopic infiltration of sarcoid within the optic nerve an unlikely cause of visual impairment, especially in the context that all previously visible CNS lesions resolved on follow-up CT and MR. We speculate that the optic neuropathy in this patient may be secondary to sarcoid angiopathy. Of the five patients in our series, this patient suffered the most severe sequelae, which reemphasizes that, although THS is a self-limiting disease, it can lead to irreversible damage.

CT findings remarkably similar to those in our case 2 have been reported by Kline and Galbraith [9]. Surgical exploration in their case revealed an epidermoid cyst. While we did not have pathologic proof in our case, we believe leakage of the epidermoid contents into the cavernous sinus resulted in an aseptic inflammatory response.

The myositic and orbital apex involvement by pseudotumor [22] in cases 4 and 5 (second episode) represents a different subset of THS—a concept that we believe has not been emphasized in the radiologic literature. The orbital apex, superior orbital fissure, and anterior cavernous sinus are contiguous; granulomatous inflammation in any of the three locations will produce similar symptoms. Granulomatous tissue from orbital pseudotumor and from the cavernous sinus of patients reported by Tolosa [1] and others [23–25] has characteristically demonstrated numerous plasma cells and lymphocytes. Since both subsets of patients respond promptly to steroids, it is both logical and clinically useful to consider orbital apex pseudotumor as part of the spectrum of THS. Clinically, patients with orbital pseudotumor have a higher propensity than do patients with cavernous sinus lesions to present with proptosis, chemosis, and conjunctival injection.

High-resolution CT in patients with THS usually demonstrates soft-tissue infiltration in either the orbital apex or the cavernous sinus with no associated bony destruction on hyperostosis. The contour of the involved cavernous sinus in patients with THS usually has a slightly concave lateral margin in contrast to aneurysm or neuroma, which has a laterally convex margin. The enhancement in THS is less prominent compared with giant cavernous carotid aneurysm or meningioma. THS also can be differentiated from cavernous sinus thrombosis and carotid cavernous fistula by the absence of an enlarged superior ophthalmic vein. The infiltrating mass as a rule resolves after the administration of steroids. Symptomatic improvement following short-term steroids in a patient with painful ophthalmoplegia is an essential clinical feature of THS. The improvement, however, is not absolute proof of the diagnosis, because lymphoma, meningioma, and giant cell tumors have also been reported to respond symptomatically to high-dose steroids initially [5, 26]. Likewise, orbital lymphoma can transiently resolve on CT after steroid therapy.

In conclusion, with the advent of high-resolution CT scanning, abnormal inflammatory soft tissue in both the orbital apex and cavernous sinus directly responsible for painful ophthalmoplegia can now be imaged. As a result, THS can no longer be considered a diagnosis of exclusion. We would like to propose that resolution of soft-tissue inflammation in the orbital apex and cavernous sinus on CT while a patient is asymptomatic and not taking steroids should be an additional clinical criterion of THS. Surgical exploration should rarely be necessary for inflammatory disease in this region unless high-dose steroid therapy fails and there is progressive neurologic deficit and pain.

REFERENCES

1. Tolosa E. Periarteritic lesions of the carotid siphon with the clinical features of a carotid infraclinoid aneurysm. *J Neurol Neurosurg Psychiatry* **1954**;17:300–302
2. Hunt WE, Meagher JN, LeFever HE, Zeman W. Painful ophthalmoplegia. Its relation to indolent inflammation of the cavernous sinus. *Neurology* **1961**;11:56–62
3. Smith JL, Taxdal DSR. Painful ophthalmoplegia. The Tolosa-Hunt syndrome. *Am J Ophthalmol* **1966**;61:1466–1472
4. Hunt WE. Tolosa-Hunt syndrome: one cause of painful ophthalmoplegia. *J Neurosurg* **1976**;44:544–549
5. Thomas JE, Yoss RE. The parasellar syndrome: problems in determining etiology. *Mayo Clin Proc* **1978**;45:617–623
6. Rush JA, Younge BR. Paralysis of cranial nerves III, IV and VI. *Arch Ophthalmol* **1981**;99:76–79
7. Hasso AN, Pop PM, Thompson JR, et al. High resolution thin section computed tomography of the cavernous sinus. *Radiographics* **1982**;2:83–100
8. Kline LB. The Tolosa-Hunt syndrome. *Surv Ophthalmol* **1982**;27:79–95
9. Kline LB, Galbraith JG. Parasellar epidermoid tumor presenting as painful ophthalmoplegia. *J Neurosurg* **1981**;54:113–117
10. Aron-Rosa D, Doyon D, Salamon G, Michotey P. Tolosa-Hunt syndrome. *Ann Ophthalmol* **1978**;10:1161–1168
11. Van Dalen JTW, Bleeker GM. The Tolosa-Hunt syndrome. *Doc Ophthalmol* **1977**;44:167–172
12. Polsky M, Janicki PC, Gunderson CH. Tolosa-Hunt syndrome with sella erosion. *Ann Neurol* **1979**;6:129–131
13. Sondheimer FK, Knapp J. Angiographic findings in the Tolosa-Hunt syndrome: painful ophthalmoplegia. *Radiology* **1973**;106:105–112
14. Kettler HL, Martin JD. Arterial stationary wave phenomenon in Tolosa Hunt syndrome. *Neurology* **1975**;25:765–770
15. Milstein BA, Morretin LB. Report of a case of sphenoid fissure syndrome studied by orbital venography. *Am J Ophthalmol* **1971**;72:600–603
16. Muhletaler CA, Gerlock AJ. Orbital venography in painful ophthalmoplegia (Tolosa-Hunt syndrome). *AJR* **1979**;133:31–34
17. Daniels DL, Pech P, Kay MC, Pojunas K, Williams AL, Haughton VM. Orbital apex: correlative anatomic and CT study. *AJNR* **1985**;6:705–710
18. Kline LB, Acker JD, Post MJD, Vitek JJ. The cavernous sinus: a computed tomographic study. *AJNR* **1981**;2:299–305
19. Beardsley TL, Brown SVL, Sydnor CF, Grimson BS, Klintworth GK. Eleven cases of sarcoidosis of the optic nerve. *Am J Ophthalmol* **1984**;97:62–77
20. Gudeman SK, Selhorst JB, Susac JO, Waybright EA. Sarcoid optic neuropathy. *Neurology* **1982**;32:597–603
21. Dubois PJ, Beardsley T, Klintworth G, et al. Computed tomography of sarcoidosis of the optic nerve. *Neuroradiology* **1983**;24:179–182
22. Nugent RA, Rootman J, Robertson WD, Lapointe JS, Harrison PB. Acute orbital pseudotumors: classification and CT features. *AJNR* **1981**;2:431–436
23. Hallpike JF. Superior orbital fissure syndrome. *J Neurol Neurosurg Psychiatry* **1973**;36:486–490
24. Donin JF, Borit A. Orbital myositis: its relationship to the Tolosa-Hunt syndrome. In: Smith JL, ed. *Neuro-ophthalmology update*. New York City: Masson, **1977**:99–103
25. Levy IS, Wright JE, Lloyd GAS. Orbital and retroorbital pseudotumors. *Mod Probl Ophthalmol* **1975**;14:364–357
26. Fowler TJ, Earl CJ, McAllister VL, McDonald WI. Tolosa-Hunt syndrome. The dangers of an eponym. *Br J Ophthalmol* **1975**;59:149–154

Pictorial Essay

Color-Flow Doppler Imaging of Carotid Artery Abnormalities

William D. Middleton,[1,2] W. Dennis Foley,[1] and Thomas L. Lawson[1]

Recent advances in Doppler imaging techniques have allowed real-time color evaluation of the spatial and temporal flow characteristics in the vessels of the neck. Experience with this new technique is limited; however, initial reports suggest that evaluations of suspected extracranial neurovascular disorders by color-flow Doppler imaging will be more rapid and accurate than evaluations by conventional duplex Doppler [1, 2]. The material presented in this essay was accumulated from routine examinations performed with a color Doppler imaging device during the past 9 months. No attempt has been made to compare color-flow Doppler imaging with conventional duplex Doppler or with angiography.

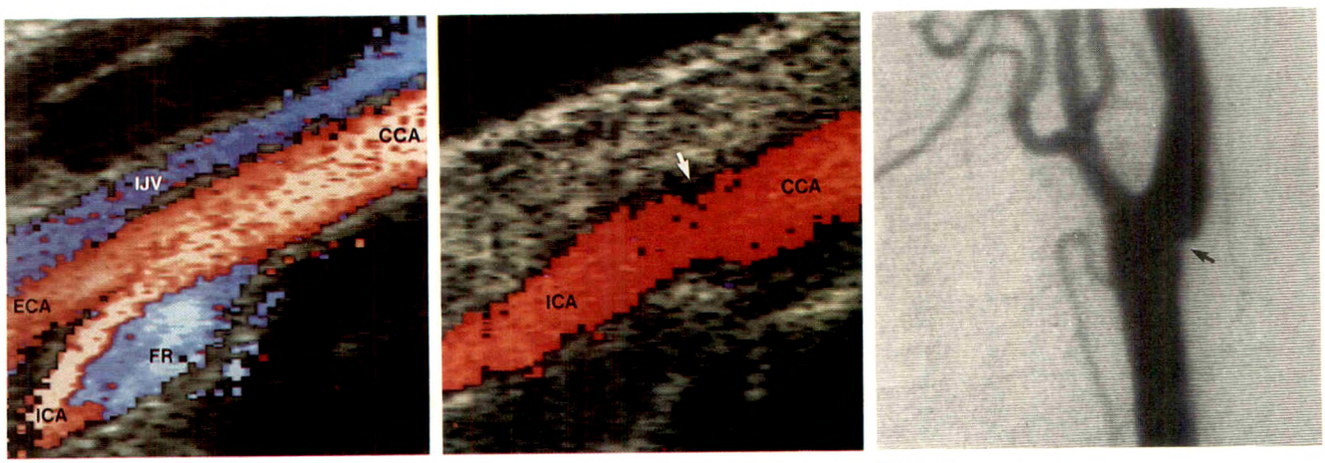

Fig. 1.—Longitudinal sonographic image of a normal carotid bifurcation. Note flow reversal (FR) in carotid bulb opposite origin of external carotid artery (ECA). CCA = common carotid artery; ICA = internal carotid artery; IJV = internal jugular vein.

Fig. 2.—Small plaque without associated flow abnormalities.

***A*, Longitudinal sonographic image shows small homogeneous plaque (*arrow*) at origin of internal carotid artery (ICA), resulting in a 15% stenosis. Peak systolic flow velocity was 60 cm/sec. CCA = common carotid artery.**

***B*, Angiogram confirms small plaque (*arrow*) at origin of internal carotid artery.**

Received August 26, 1987; accepted after revision September 29, 1987.

[1] Department of Radiology, Medical College of Wisconsin, 8700 W. Watertown Plank Rd., Milwaukee, WI 53226.

[2] Present address: Mallinckrodt Institute of Radiology, Washington University School of Medicine, 510 S. Kingshighway Blvd., St. Louis, MO 63110. Address reprint requests to W. D. Middleton.

AJR **150:419–425, February 1988** 0361–803X/88/1502–0419 © American Roentgen Ray Society

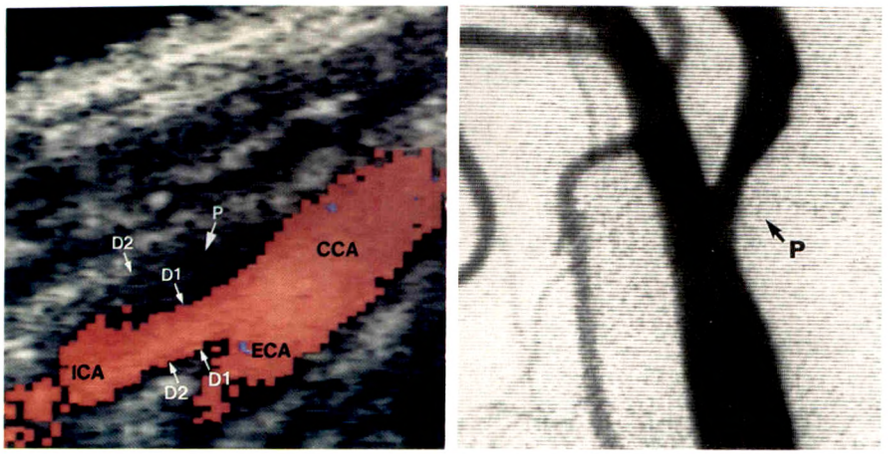

Fig. 3.—Smooth plaque causing no associated flow abnormalities.

A, Longitudinal sonographic image shows smooth homogeneous plaque (P) at origin of internal carotid artery (ICA). Percentage of stenosis can be calculated directly by measuring diameter of flow lumen (D1) and diameter of vessel itself (D2). This plaque narrows lumen by approximately 50%, but causes no associated flow abnormalities; peak systolic flow velocity was 80 cm/sec. Normal flow velocity and inability to differentiate hypoechoic plaque from vessel lumen resulted in a false-negative result on conventional duplex Doppler. ECA = external carotid artery; CCA = common carotid artery.

B, Angiogram confirms smooth plaque (P) at origin of internal carotid artery.

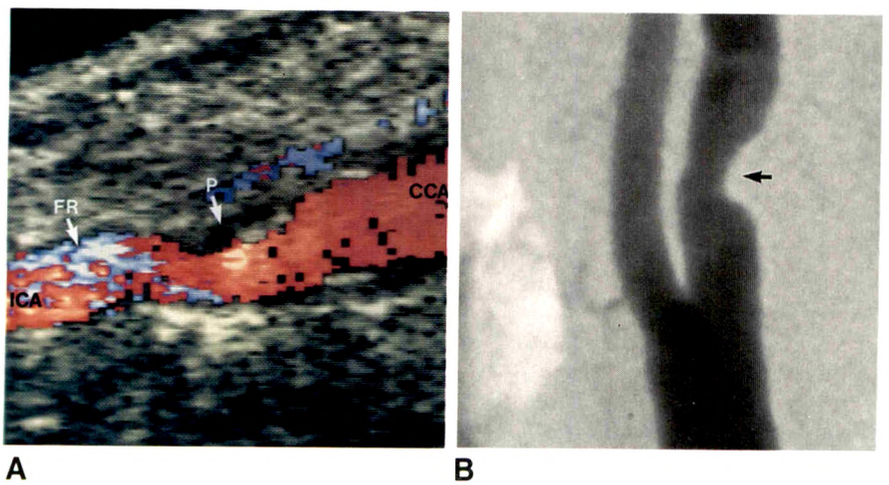

Fig. 4.—Low-grade lesion with associated flow abnormalities.

A, Longitudinal sonographic image shows plaque (P) in internal carotid artery (ICA). Note flow disturbance distal to plaque, manifested as areas of flow reversal (FR) shown in blue. Lumen is narrowed by 45%. Peak systolic flow velocity was 145 cm/sec, which corresponds to a 50–75% stenosis. CCA = common carotid artery.

B, Angiogram confirms focal plaque (*arrow*) in internal carotid artery, causing a 45% stenosis.

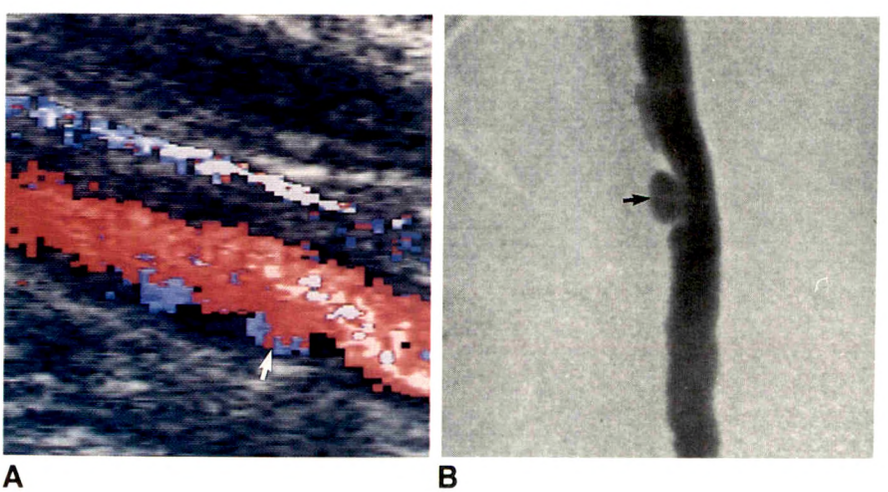

Fig. 5.—Plaque ulceration.

A, Longitudinal sonographic image shows focal ulcer (*arrow*) in common carotid artery. Within ulcer are areas of both antegrade and retrograde flow.

B, Angiogram confirms ulceration (*arrow*) in common carotid artery.

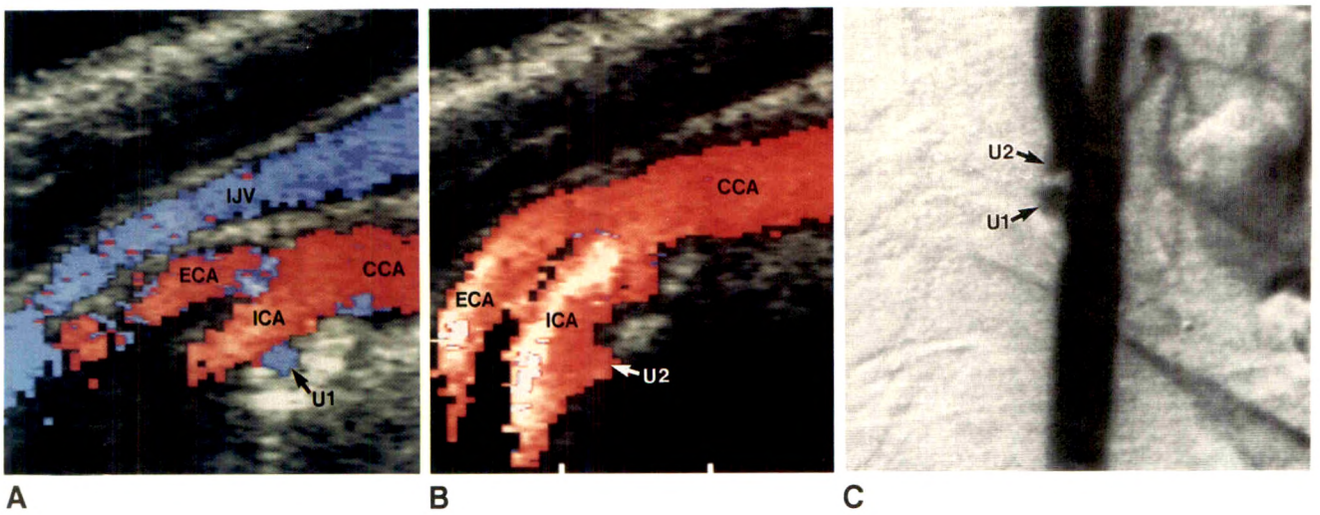

Fig. 6.—Ulceration in internal carotid artery.

A, Longitudinal sonographic image shows proximal ulcer (U1) at origin of internal carotid artery (ICA). Reversed flow in ulceration is seen as blue in this phase of cardiac cycle. ECA = external carotid artery; CCA = common carotid artery; IJV = internal jugular vein.

B, Longitudinal sonographic image shows distal ulceration (U2) in origin of internal carotid artery (ICA). ECA = external carotid artery; CCA = common carotid artery.

C, Angiogram confirms proximal (U1) and distal (U2) ulceration in internal carotid artery.

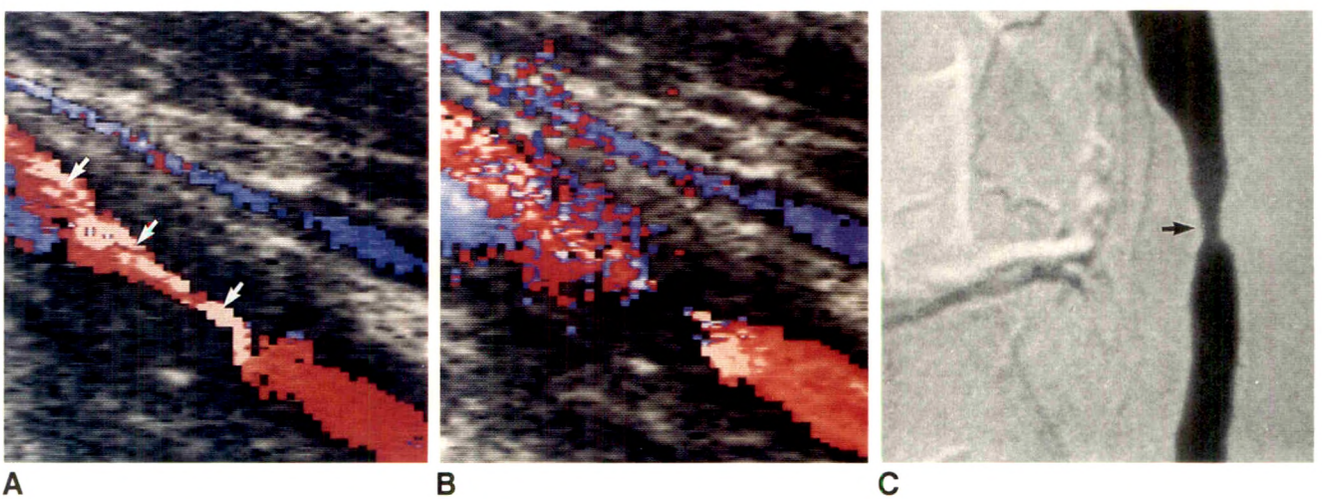

Fig. 7.—High-grade lesion in common carotid artery.

A, Longitudinal sonographic image during late systole shows a high-grade (80%) stenosis of common carotid artery with resultant flow jet (*arrows*) at level of stenosis as well as distally. White coloration of flow jet results from elevated flow velocities at this level. Actual velocity measurements were not obtained in this patient.

B, Longitudinal sonographic image obtained at peak systole shows a bruit. Distortion distal to stenosis results from vibrations within soft tissues caused by turbulent flow.

C, Angiogram confirms high-grade stenosis (*arrow*) in common carotid artery.

Rather, the cases shown were selected as representative examples of abnormalities encountered in our routine clinical practice and are intended to show the spectrum of lesions that one can expect to encounter when using color-flow imaging devices.

Materials and Methods

More than 300 patients were evaluated for suspected extracranial neurovascular disease between September 1986 and June 1987. All examinations were performed with a commercially available color-flow imaging device (QAD 1, Quantum Medical Systems, Issaquah, WA). This unit analyzes the amplitude, phase, and frequency of returning echoes to provide a real-time (18 frames/sec) display showing moving targets in shades of red and blue and stationary targets in gray scale. Color assignment depends on direction of movement (toward or away from the transducer). Color saturation depends on the velocity of the target, with higher velocities being whiter.

The patients were all scanned by using a 7.5-MHz linear-array transducer. Patients were positioned as though they were having a

conventional duplex Doppler examination. In all cases the common carotid, carotid bulb, internal carotid, external carotid, and vertebral arteries were imaged. Point-spectral analysis was performed on areas of flow abnormality identified on the real-time image. If the flow was normal on the real-time image, point-spectral analysis was performed from the area of maximal flow velocity in the vessel. Representative portions of the examination were recorded digitally on videotape.

Results

The flow patern in the normal carotid bifurcation was well shown with color-flow Doppler imaging. A region of peripheral flow reversal was almost invariably present in the carotid bulb opposite the origin of the external carotid artery. This region was at least partially replaced by static blood during diastole. The region of maximal flow velocity in the internal carotid artery was eccentrically positioned opposite the area of flow reversal (Fig. 1). Flow reversal was less frequently present at the origin of the external carotid.

Low-grade lesions (less than 50% stenosis) in the carotid bifurcation were routinely identified by their encroachment on the flow lumen (Figs. 2–4). Percentage of stenosis was generally easy to calculate by directly measuring the flow lumen and then comparing it with the diameter of the vessel itself (Fig. 3). In addition to the classification of low-grade lesions by calculated percentage of stenosis, they also could be divided into those with flow abnormalities (Fig. 4) and those without flow abnormalities (Fig. 3). Plaque ulceration was suggested by the presence of marked plaque irregularity or by visualization of the ulcer crater (Figs. 5 and 6); however, the sensitivity in detecting ulceration has yet to be determined.

Lesions with more than 50% stenosis generally were associated with flow abnormalities including flow jets (Fig. 7), flow reversal (Fig. 8), and occasionally well-defined helical flow patterns (Figs. 9 and 10). Bruits were occasionally seen if tissue vibrations were sufficiently intense (Fig. 7). These flow abnormalities, along with the narrowing of the flow lumen, made high-grade lesions easy to identify. As with low-grade lesions, the percentage of stenosis could be readily calculated

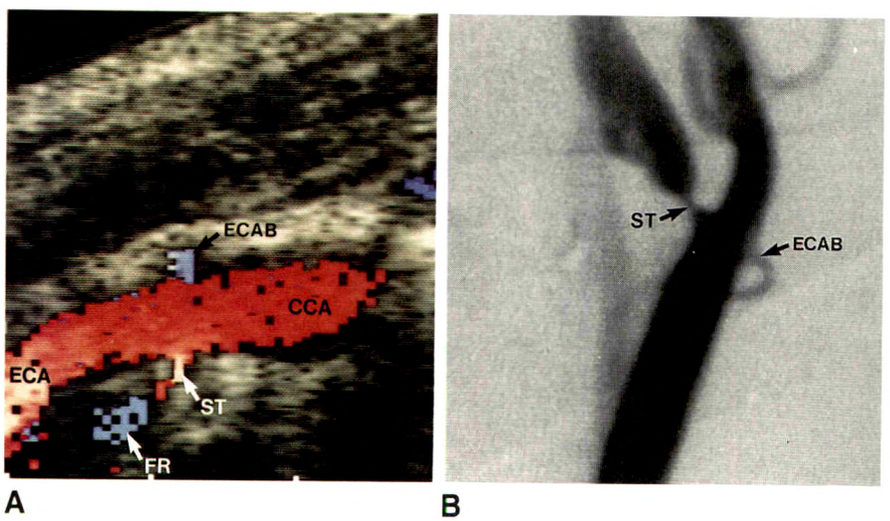

Fig. 8.—High-grade lesion with flow reversal.
A, Longitudinal sonographic image shows high-grade (95%) stenosis (ST) at origin of internal carotid artery resulting in flow reversal (FR) distally. Flow reversal is shown as blue. Peak systolic flow velocity was more than 220 cm/sec and end-diastolic flow velocity was 130 cm/sec, indicating a stenosis of 75–99%. ECA = external carotid artery; CCA = common carotid artery; ECAB = external carotid artery branch.
B, Angiogram confirms high-grade stenosis (ST) at origin of internal carotid artery. ECAB = external carotid artery branch.

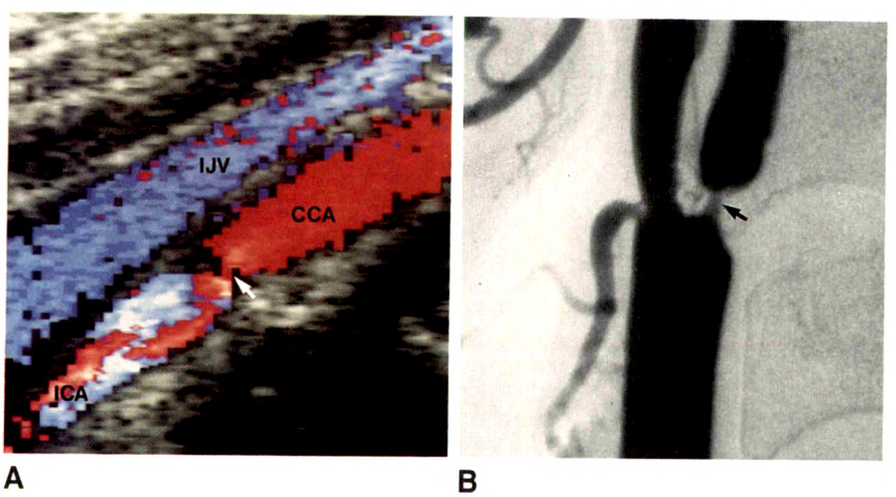

Fig. 9.—High-grade stenosis with associated helical flow pattern.
A, Longitudinal sonographic image shows high-grade (85%) stenosis (*arrow*) with associated helical arrangement of antegrade and retrograde flow in internal carotid artery (ICA). Peak systolic flow velocity was 270 cm/sec, indicating a stenosis of 75–99%. CCA = common carotid artery; IJV = internal jugular vein.
B, Angiogram confirms high-grade stenosis (*arrow*) at origin of internal carotid artery.

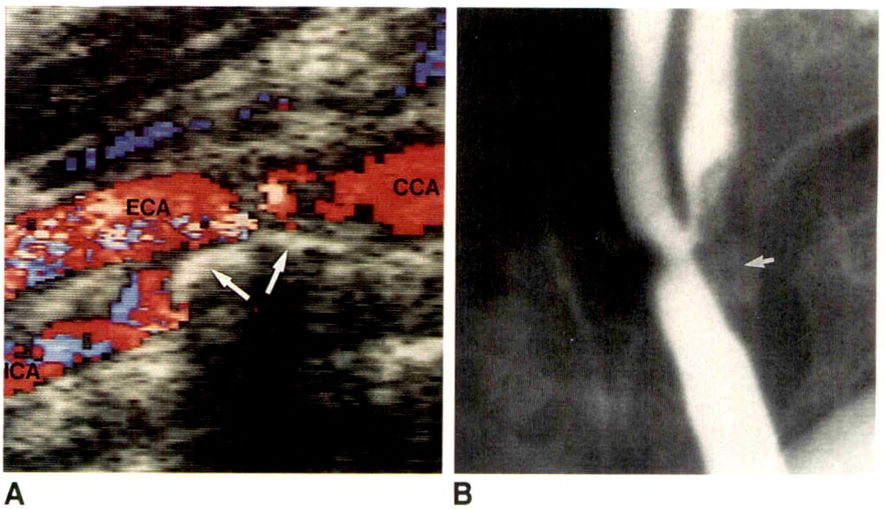

Fig. 10.—High-grade stenosis with associated helical flow pattern.

A, Longitudinal sonographic view of carotid bifurcation shows calcified plaque (*arrows*) at origin of internal carotid artery, with associated helical pattern of forward and reverse flow in internal carotid artery (ICA). Flow disturbances in the external carotid artery (ECA) are due to a plaque at its origin. CCA = common carotid artery.

B, Angiogram confirms a calcified plaque (*arrow*) resulting in high-grade stenosis at origin of internal carotid artery.

directly from the image, without reliance on blood velocity to determine the extent of luminal narrowing.

Complete obstruction of a vessel could be diagnosed when no flow was identified within it (Fig. 11). Obstruction of the internal carotid artery was generally accompanied by "externalization" of the velocity spectral trace of the common carotid artery (Fig. 11B). Because moving targets are portrayed in color and are identified more readily than with conventional

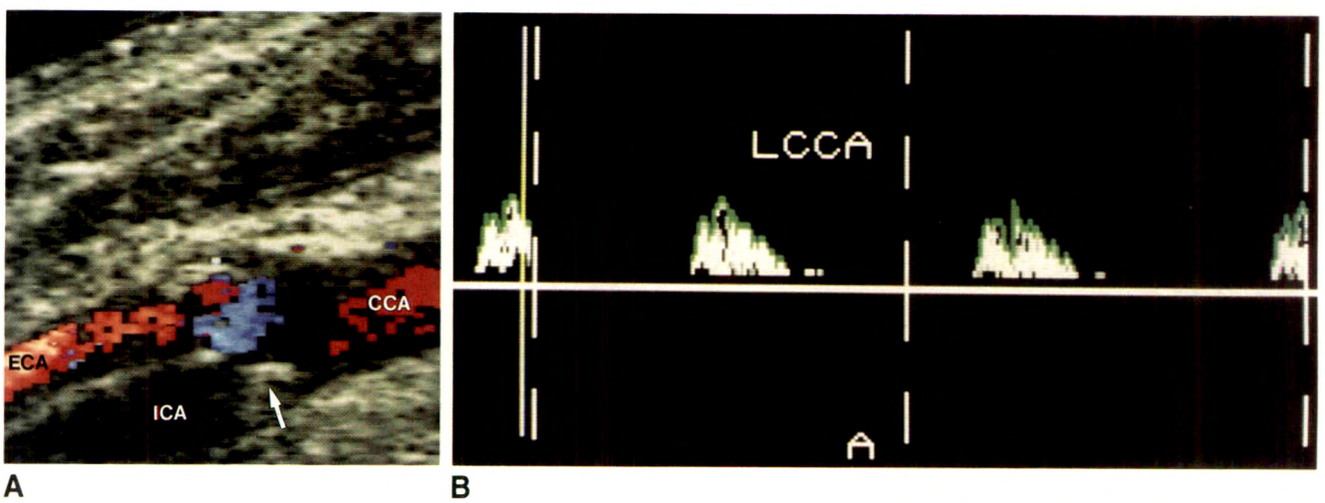

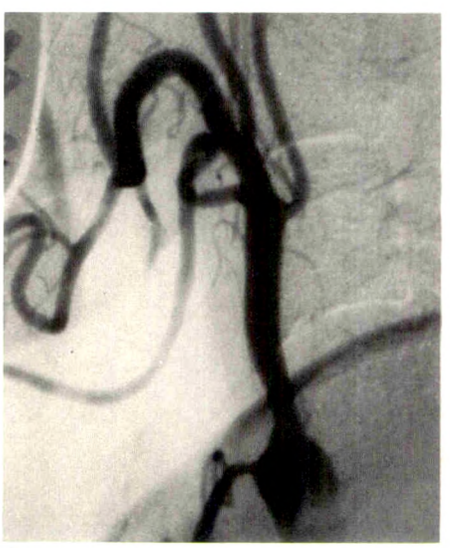

Fig. 11.—Complete obstruction of internal carotid artery.

A, Longitudinal sonographic image shows plaque (*arrow*) at origin of internal carotid artery (ICA) with lack of demonstrable flow in internal carotid artery beyond level of plaque. ECA = external carotid artery; CCA = common carotid artery.

B, Velocity trace from left common carotid artery (LCCA) shows complete lack of flow in diastole. This is referred to as "externalization" of the common carotid artery and is a confirmatory sign of obstruction of the internal carotid artery.

C, Angiogram confirms complete obstruction of internal carotid artery.

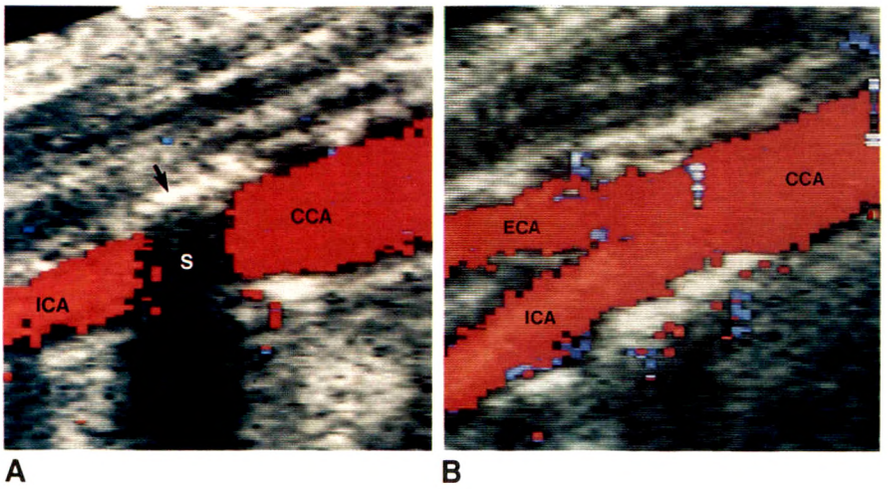

Fig. 12.—Calcified plaque at origin of internal carotid artery.

A, Longitudinal sonographic image from an anterior approach shows a calcified plaque (*arrow*) approximately 5 mm in length at origin of internal carotid artery (ICA). Associated shadow (S) precludes a precise calculation of percentage of stenosis, although lack of any demonstrable flow abnormality distal to plaque argues against significant narrowing. Peak systolic flow velocity was 50 cm/sec, which is within normal limits. CCA = common carotid artery.

B, Longitudinal sonographic view of carotid bifurcation obtained from a posterolateral approach allows for visualization of internal carotid artery (ICA) without associated shadowing from plaque and confirms a lack of significant narrowing. ECA = external carotid artery; CCA = common carotid artery.

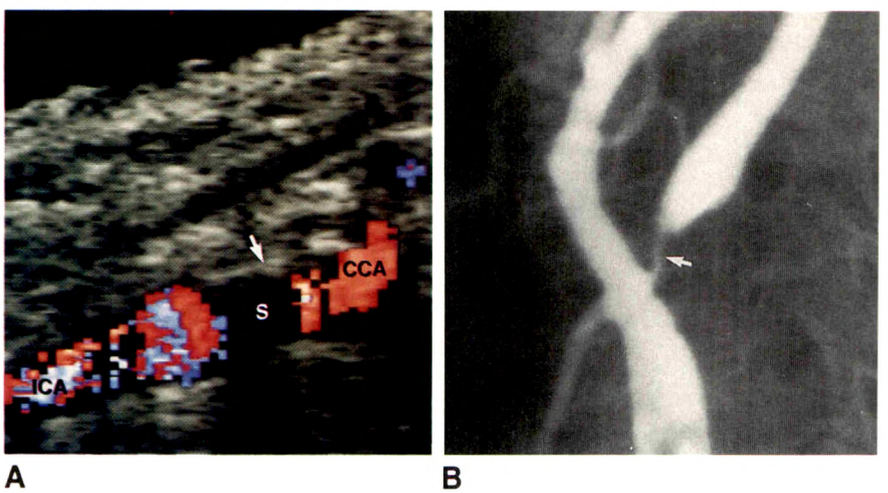

Fig. 13.—Calcified plaque with significant luminal narrowing.

A, Longitudinal sonographic image at origin of internal carotid artery (ICA) shows a calcified plaque (*arrow*) approximately 5 mm in length with associated shadowing (S). Shadowing precludes precise determination of luminal stenosis; however, marked flow abnormality in internal carotid artery suggests high-grade lesion. Peak systolic flow velocity was greater than 250 cm/sec, indicating a stenosis of 75–99%. CCA = common carotid artery.

B, Angiogram confirms high-grade stenosis (*arrow*) at origin of internal carotid artery.

Doppler imaging, color-flow imaging should distinguish more accurately the extremely high-grade lesions with slow distal flow from the lesions causing complete obstruction and absence of flow distally.

Calcified plaques were occasionally encountered; these made it difficult to determine luminal narrowing precisely, as they also do with conventional duplex Doppler imaging. Imaging from different angles was often helpful in estimating whether a high-grade lesion was present (Fig. 12). Analysis of the flow pattern beyond the lesion for the presence or absence of flow disturbances was also helpful (Figs. 12 and 13).

Discussion

Color-flow vascular imaging represents a significant advance in Doppler imaging technology. In addition to conventional Doppler imaging capability, color-flow Doppler imaging provides a dramatic real-time color portrayal of blood flow within the lumen of the vessel. This makes it possible to rapidly identify flow abnormalities and eliminates the need to perform point-spectral analysis from multiple areas in the vessel lumen. In addition, because direction of flow is shown, precise assignment of the Doppler angle can be made. This allows more accurate calculation of flow velocity, particularly in patients with tortuous vessels or nonaxial flow. Therefore, even if used merely as a road map for conventional pulsed Doppler spectral analysis, color-flow imaging should allow a more rapid and accurate examination.

Despite these improvements in velocity determination, many potential pitfalls still exist when flow velocity is the only criterion used. Alterations in cardiac output, cardiac arrhythmias, or high-grade contralateral lesions can lead to both overestimates and underestimates of percentage of stenosis [3, 4]. Because of these limitations in velocity determination, it would be desirable to find a means of directly measuring the percentage of stenosis that is similar to the method used with angiography. Color-flow Doppler imaging can provide this capability since it has the ability to image the vessel wall

in gray scale while simultaneously imaging the flow lumen in color. In fact, since angiography only images the flow lumen and not the vessel wall, color-flow Doppler imaging has the potential to quantitate stenosis even more accurately than angiography can. In addition, since flow patterns are displayed with color-flow Doppler imaging, the local hemodynamic consequences of the lesions can be identified.

Rigorous clinical trials will be necessary to determine the exact impact of this new imaging technique on the diagnosis of carotid vascular disease. However, on the basis of our initial clinical evaluations, we have little doubt that color-flow Doppler imaging will lead to further improvements in the noninvasive evaluation of extracranial neurovascular disease.

REFERENCES

1. Merritt CRB. Doppler color flow imaging of peripheral vessels: initial clinical results. Presented at the annual meeting of the American Institute of Ultrasound in Medicine, Las Vegas, NV, September **1986**
2. Merritt CRB, Bluth EI, Sullivan MA. Doppler color flow mapping of peripheral vessels: comparison of angiodynography with conventional duplex ultrasound. Presented at the annual meeting of the Radiological Society of North America, Chicago, IL, November **1986**
3. Jacobs NM, Grant EG, Schellinger D, Byrd MC, Richardson JD, Cohan SL. Carotid duplex sonography: criteria for stenosis, accuracy, and pitfalls. *Radiology* **1985**;154:385–391
4. Bandyk DF, Levine AW, Pohl L, Towne JB. Classification of carotid bifurcation disease using quantitative Doppler spectrum analysis. *Arch Surg* **1985**;120:306–313

Memorial

Catherine Cole-Beuglet, 1936–1987

Catherine Cole-Beuglet received her bachelor's degree from the University of Western Ontario, London, Ontario, in 1958 and her M.D. from the same institution in 1962. A rotating internship at Harper Hospital, Detroit, MI, was followed by a residency in radiology at Henry Ford Hospital, Detroit, MI, completed in 1966. She widened her circle of friends and admirers by her staff and academic appointments as Staff Radiologist, Henry Ford Hospital, 1966–1967; Teaching Associate, University of Michigan Medical Center, Ann Arbor, 1967–1968; Assistant Professor of Radiology, McGill University and Montreal General Hospital, Montreal, Quebec, 1968–1975; Assistant Professor of Radiology, University of Washington, Seattle, WA 1975–1976; and Assistant Professor of Radiology, University of California, Irvine, Irvine, CA, 1977–1978.

Her next 6 years were spent as Associate Professor of Radiology and Professor of Radiology at Thomas Jefferson University Hospital, Philadelphia, PA. She joined the staff at the University of California, Irvine, as Professor of Radiological Sciences and Chief of the Division of Ultrasound in 1985. She was also active in CT and mammography services until her untimely death on May 16, 1987, from cancer of the colon.

Throughout her career, Cathy was a fine academic radiologist; an excellent investigator; and a warm, pleasant, and helpful teacher and colleague. She had 63 scientific publications to her credit, most of them on sonography and many on sonographic studies of the breast. She frequently served as visiting professor, and she prepared many presentations for international meetings and scientific exhibits. One expression of the high regard in which she was held was that the 5th International Congress on Ultrasonic Examination of the Breast was dedicated to her memory.

Cathy served as a member of the Editorial Board of *Radiology* since 1982; her perceptive and penetrating reviews were of great service to the radiologic literature.

Cathy is survived by her husband and a son. She will be greatly missed in all of her academic activities but most of all as a devoted and giving individual.

William R. Eyler
Detroit, MI 48202

Greenfield Filter: Percutaneous Placement in 50 Patients

Donald F. Denny, Jr.[1]
Gary S. Dorfman[2]
John J. Cronan[2]
Lee H. Greenwood[1]
Steven S. Morse[1]
Moises Yoselevitz[1]

Greenfield filters for prevention of pulmonary emboli may be placed in the inferior vena cava by surgical cutdown or by percutaneous insertion through the femoral or jugular veins. We evaluated the use of the percutaneous techniques 52 times in 50 patients. The right femoral vein was used in 37 of the procedures, the right internal jugular vein in 12, and the left femoral vein in three. Twenty-two patients had altered coagulation factors: 11 were receiving heparin, four were receiving warfarin sodium, six had hepatic cirrhosis, and one had disseminated intravascular coagulation and had been receiving warfarin sodium. Filter placement was successful in 51 of 52 procedures. In the unsuccessful case, placement was attempted via the left femoral vein; the carrier could not be advanced from the common iliac vein to the inferior vena cava. This patient required surgical occlusion of the cava. There was one major complication, a hematoma in the right side of the groin that required transfusion. This occurred in the patient with disseminated intravascular coagulation who had extensive scarring from multiple previous vascular surgical procedures. Two patients required second filters because of severe angulation of the filter found 1 and 4 days after implantation. Clinical thrombosis of the femoral vein after femoral vein access occurred in two (5%) of 40 patients and was proved by venogram in one.

Our experience shows that the percutaneous method is highly successful and suggests that this technique should be the primary method for filter placement in the inferior vena cava.

The most commonly performed procedure for interruption of blood flow in the inferior vena cava is placement of a Greenfield filter (Medi-tech, Watertown, MA) via a cutdown of the jugular or femoral vein. Percutaneous placement of the Greenfield filter by using a 24-French sheath, described by Tadavarthy et al. [1], offers simplicity and speed, and such placement eliminates a surgical scar and the need for an operating room. Our initial experience with the percutaneous technique in 12 patients was highly favorable [2]. While several devices requiring a smaller access tract may be available in the future, only the Greenfield filter is approved at the present time for percutaneous implantation.

We describe the results and complications of percutaneous placement of a Greenfield filter in 50 patients, including the first 12 patients previously reported.

Subjects and Methods

Between May 1984 and October 1986, percutaneous placement of a Greenfield filter was attempted 52 times in 50 patients. The right femoral vein was used in 37 procedures, the right internal jugular vein in 12, and the left femoral vein in three. There were 38 men and 32 women ranging in age from 20 to 88 years (mean, 62 years).

At the time of filter placement, 22 patients had alterations in coagulation function. Eleven patients were heparinized; their partial thromboplastin times varied between 1.5 and 2.5 times control. For these 11, heparin was stopped at the beginning of the procedure; protamine was not administered. Four patients were receiving warfarin sodium and had prothrombin times in the therapeutic range. These patients received one or two units of fresh frozen plasma

Received July 29, 1987; accepted after revision October 7, 1987.

[1] Department of Diagnostic Radiology, Yale University School of Medicine, P.O. Box 3333, New Haven, CT 06510. Address reprint requests to D. F. Denny, Jr.

[2] Department of Diagnostic Radiology, Rhode Island Hospital and Brown University Program in Medicine, 593 Eddy St., Providence, RI 02902.

AJR 150:427–429, February 1988
0361–803X/88/1502–0427
© American Roentgen Ray Society

before the start of the procedure. Six patients had hepatic cirrhosis with mildly elevated prothrombin times despite the administration of vitamin K. One patient had disseminated intravascular coagulation and also was receiving warfarin sodium. Coagulopathy in this patient persisted despite administration of 50 units of fresh frozen plasma.

Placement of the filter was performed by using the technique described by Tadavarthy et al. [1]. For better control of bleeding through the sheath, a 24-French Coons/Amplatz sheath (Medi-tech, Watertown, MA) was used in place of the originally described Amplatz sheath. The Coons/Amplatz sheath has a soft, Silastic cuff at the external end that may be pinched shut, allowing better control of bleeding through the sheath.

When the right internal jugular vein was used for access, the patient's legs were raised on a bolster to minimize the risk of air embolism during inspiration. This maneuver was attempted because a tilt table (our preference) was unavailable. In addition, the patient was asked to perform the Valsalva maneuver when the carrier was being advanced through the sheath. To avoid difficulty in passing the carrier through the right atrium into the inferior vena cava, a straight, 180-cm-long, 0.035-in. (0.89-mm) guidewire was substituted for the 145-cm-long guidewire provided with the carrier, allowing the carrier to be exchanged for the catheter used for venacavography.

After compression of the puncture site, adhesive strips were applied to appose the skin edges. For those patients with deep vein thrombosis of the leg or with pulmonary embolism in whom anticoagulation was not contraindicated, heparin was administered again in 2 hr. Ambulatory patients were kept in bed for 8–24 hr.

Clinical follow-up consisted of examining the puncture site on the day of and on the day after the procedure. For patients undergoing femoral vein procedures, the leg on the side of the puncture was examined for swelling or other indirect evidence of deep venous thrombosis. In addition, the patient's physician was contacted after 1 week and was questioned about symptoms or signs of leg swelling or puncture-site complications.

Results

Filter placement was successful in 49 of 50 patients. The filter was placed above the renal veins in two patients who had infrarenal caval thrombus. The remaining filters were placed in the inferior vena cava below the lowest renal vein seen on cavography. Compression of the puncture site usually required 5–15 min.

The single unsuccessful percutaneous attempt was via the left femoral vein in a patient who had thrombosis of the right femoral and iliac veins on venography and who previously had had surgical ligation of the right internal jugular vein. While left femoral vein dilatation was easily performed, the filter carrier could not be advanced through the common iliac vein into the inferior vena cava, despite the use of a heavy-duty 0.038-in. (0.97-mm) guidewire. Surgical clipping of the inferior vena cava was required.

There was one major puncture site complication, which occurred in a 66-year-old man receiving warfarin sodium who previously had had an aortobifemoral graft and two right femoropopliteal grafts. This patient had disseminated intravascular coagulation and acute gastrointestinal bleeding, with a prothrombin time elevated above the therapeutic range despite administration of 50 units of fresh frozen plasma. Right femoral venipuncture and filter placement were accomplished through the extensively scarred groin. After placement, prolonged bleeding occurred at the puncture site despite local pressure and topical application of Avitene (Alcon, Humacao, Puerto Rico) and Surgicel (Johnson and Johnson, New Brunswick, NJ). Hemorrhage eventually was controlled without surgery, but an extensive hematoma required transfusion of two units of packed red blood cells.

Two patients who had had filters implanted via the right femoral vein were found to have a filter tilt of more than 15° and a caudal migration of 1–2 cm on radiographs obtained for unrelated indications. On a repeat cavogram, the apex of the filter was seen to be lying against the lateral wall of the cava; the filter legs did not appear to have migrated through the opposite wall. Because of concern that the tilt would defeat the filtering function [3, 4], in one patient a second filter was placed through the right jugular vein 1 day after the original implantation; in another patient it was inserted through the right femoral vein 4 days after the original implantation.

Two patients developed swelling of the ipsilateral leg after placement via the femoral vein. The first was the patient in whom placement via the left femoral vein had been unsuccessful. Swelling of the left leg developed 2 days after the procedure, and thrombus was shown by venography 6 days after the procedure. This patient also had pulmonary emboli, hepatic cirrhosis, and variceal hemorrhage. The second patient was admitted with deep venous thrombophlebitis of the left leg and metastatic melanoma. Swelling of the right leg developed 4 days after the right femoral procedure; venography was not performed. No clinical signs or symptoms of new deep venous thrombophlebitis developed in the patients having the remaining 35 femoral vein procedures in the 1-week follow-up period.

Discussion

The initial experiences of Tadavarthy et al. [1] and Denny et al. [2] indicated that the percutaneous method for placement of a Greenfield filter might be preferable to venous access by cutdown. Our present results support this conclusion. Cutdown rarely should be necessary. In the only unsuccessful procedure in our series, direct surgical clipping of the cava was required because of restricted venous access.

The preferred route of access in surgical series is via the right internal jugular vein [3, 5]. Despite the low risk of clinically evident femoral vein thrombosis in our series (two of 40 procedures or 5%), the right femoral vein remains our preferred route of access for percutaneous placement for several reasons. Femoral venipuncture is much more familiar to angiographers than is jugular venipuncture, and it avoids the risks of air embolism, cardiac arrythmia, and inadvertent release of the filter either in the heart or in the renal or hepatic veins. In addition, jugular venipuncture carries the risks of carotid artery puncture, pneumothorax, and hemopericardium [6].

Although we avoided left femoral access because of the reported difficulty in passing the filter carrier through the left iliac veins after cutdown [7], we were successful in two of

three cases using this percutaneous approach.

Just as in surgical series [5], we do not consider anticoagulation therapy a contraindication to the percutaneous route if prothrombin and partial thromboplastin times are within the therapeutic range. In the patients with hepatic cirrhosis, prothrombin times were elevated only mildly, and hemostasis at the puncture site was obtained easily. However, our only major complication was in the patient with a severe, uncorrectable coagulopathy. It is impossible to say which was of more significance in this patient, his disseminated intravascular coagulation or his severe groin scarring from previous surgical procedures. We now avoid a percutaneous approach through extensive scar tissue, but we do not have sufficient experience to say whether severe coagulopathy is a contraindication to percutaneous filter placement.

Our experience in our first 50 patients shows placement of a Greenfield filter by a percutaneous approach to have a high success rate, comparable with that of placement by surgical cutdown. The advantages of the percutaneous approach—ease and speed of placement—may be even more apparent when percutaneous devices requiring an 8- to 14-French tract are available for clinical use.

REFERENCES

1. Tadavarthy SM, Castaneda-Zuniga W, Salomonowitz E, et al. Kimray-Greenfield vena cava filter: percutaneous introduction. *Radiology* **1984**;151:525–526
2. Denny DF, Cronan JJ, Dorfman GS, Esplin C. Percutaneous Kimray-Greenfield filter placement by femoral vein puncture. *AJR* **1985**;145:827–829
3. Gomez GA, Cutler BS, Wheeler HB. Transvenous interruption of the inferior vena cava. *Surgery* **1983**;93:612–619
4. Greenfield LJ, Stewart JR, Crute S. Improved technique for insertion of Greenfield vena caval filter. *Surg Gynecol Obstet* **1983**;156:217–219
5. Greenfield LJ, Peyton R, Crute S, Barnes R. Greenfield vena cava filter experience: late results in 156 patients. *Arch Surg* **1981**;116:1451–1455
6. Carr M, Jagannath A. Hemopericardium resulting from attempted internal jugular vein catheterization: a case report and review of complications of central venous catheterization. *Cardiovasc Intervent Radiol* **1986**;9:214–218
7. Novelline RA. Practical points on transvenous insertion of inferior vena cava filters. *Cardiovasc Intervent Radiol* **1980**;3:319–324

FORTHCOMING ARTICLES

COMMEMORATION OF JUBILEE ANNIVERSARY.

Perspective. Present and future status of MR imaging. *Margulis AR, Crooks LE*

The evolution of mammography. *Bassett LW, Gold RH*

Anniversary reprint from volume 50, 1943. Small intestinal enema. *Schatzki R*

Richard Schatzki, M.D.: a biography. *Schatzki SF*

Commentary. Small intestinal enema. *Carlson HC*

PROGRESS IN RADIOLOGY

Overcoming motion in abdominal MR imaging. *Wood ML, Runge VM, Henkelman RM*

CARDIOPULMONARY RADIOLOGY

Quantification of regional myocardial function by rapid cine MR imaging. *Pflugfelder PW, Sechtem UP, White RD, Higgins CB*

MR imaging of acute myocardial infarction: value of Gd-DTPA. *de Roos A, Doornbos J, van der Wall EE, van Voorthuisen AE*

Aortobronchopulmonary fistula complicating aortic aneurysm: diagnosis in four cases. *Coblentz CL, Sallee DS, Chiles C*

Image intensifier photofluorography and conventional chest radiography: comparison of diagnostic efficacy. *Manninen H, Partanen K, Soimakallio S, Rytkönen H*

Latissimus dorsi cardiomyoplasty: radiographic findings. *Nguyen TH, Hoagn T-A, Dash N, et al.*

Eloesser window thoracostomy for treatment of empyema: radiographic appearance. *Shapiro MP, Gale ME, Daly BDT*

Case report. Balloon dilatation of the left main bronchus in sarcoidosis. *Brown KT, Yeoh CB, Saddekni S*

Case report. Air embolism complicating percutaneous lung biopsy. *Tolly TL, Feldmeier JE, Czarnecki D*

GASTROINTESTINAL RADIOLOGY

MR diagnosis of pancreatic transplant rejection. *Vahey TN, Glazer GM, Francis IR, et al.*

Dual contrast MR imaging of liver cancer in rats. *Weissleder R, Saini S, Stark DD, Wittenberg J, Ferrucci JT*

MR relaxation times and iron content of thalassemic spleens: an in-vitro study. *Gomori JM, Grossman RI, Drott HR*

Gallbladder disease in patients with primary sclerosing cholangitis. *Brandt DJ, MacCarty RL, Charboneau JW, LaRusso NF, Wiesner RH, Ludwig J*

Case report. The effervescent gallbladder: a sonographic sign of emphysematous cholecystitis. *Nemcek AA Jr, Gore RM, Vogelzang RL, Grant M*

Case report. Choledochal varices. *Kim S, Chew FS*

Case report. Small bowel obstruction due to Garren gastric bubble: radiographic diagnosis. *Zeman RK, Benjamin SB, Cunningham MB, et al.*

GENITOURINARY RADIOLOGY

CT of renal cell carcinoma in patients on chronic hemodialysis. *Siegel SC, Sandler MA, Alpern MB, Pearlberg JL*

Arteriovenous malformations of the kidneys: ablation with alcohol. *Takebayashi S, Hosaka M, Ishizuka E, Hirokawa M, Matsui K*

CT diagnosis of circumcaval ureter. *Lautin EM, Haramati N, Frager D, et al.*

Case report. Vaginally induced pneumoperitoneum during pregnancy. *Gensburg RS, Wojcik WG, Mehta SD*

MUSCULOSKELETAL RADIOLOGY

MR imaging of the knee: preliminary results with a 3DFT GRASS pulse sequence. *Spritzer CE, Vogler JB, Martinez S, et al.*

Diagnosis of osteomyelitis by MR imaging. *Unger E, Moldofsky P, Gatenby R, Hartz W, Broder G*

Spinal pseudarthrosis complicating ankylosing spondylitis: comparison of CT and conventional tomography. *Chan F-L, Ho EKW, Chau EMT*

Soft-tissue sarcomas of the extremities: comparison of MR and CT in determining the extent of disease. *Demas BE, Heelan RT, Lane J, Marcove R, Hajdu SI, Brennan MF*

Case report. Avulsion of the innominate artery associated with fracture of the sternum. *Ben-Menachem Y*

VASCULAR RADIOLOGY

The diagnosis of femoropopliteal venous thrombosis: comparison of duplex sonography and plethysmography. *Rosner NH, Doris PE*

Sonography of the radial artery at the wrist. *Gooding GAW*

Case report. The "to-and-fro" sign: duplex Doppler evidence of femoral artery pseudoaneurysm. *Abu-Yousef MM, Wiese JA, Shamma AR*

PEDIATRIC RADIOLOGY

Factors affecting visualization of posterior rib fractures in abused infants. *Kleinman PK, Marks SC, Adams VI, Blackbourne BD*

Balloon dilatation of esophageal stenosis in children. *Sato Y, Frey EE, Smith WL, Pringle K, Soper R, Franken EA Jr*

Acute scrotal abnormalities in children: diagnosis by combined sonography and scintigraphy. *Mueller DL, Amundson GM, Rubin SZ, Wesenberg RL*

Sonographic evaluation of ovarian torsion in childhood and adolescence. *Graif M, Itzchak Y*

NEURORADIOLOGY

Acute intracranial hemorrhage: intensity changes on sequential MR scans at 0.5 T. *Zimmerman RD, Heier LA, Snow RB, Liu DPC, Kelly AB, Beck MDF*

MR imaging of head trauma: the distribution and radiopathologic features of traumatic lesions. *Gentry LR, Godersky JC, Thompson B*

Prospective comparative study of intermediate-field MR and CT in the evaluation of closed head trauma. *Gentry LR, Godersky JC, Thompson B, Dunn VD*

Gradient echo (GRASS) MR imaging in cervical radiculopathy. *Hedberg MC, Drayer BP, Flom RA, Hodak JA, Bird CR*

RADIOLOGIC TECHNOLOGY

Technical note. Radiographic system for use in emergency and intensive care units. *Mirvis SE, Fritz SL, Siegel JH, Ramzy A*

The Collapsed Inferior Vena Cava:
CT Evidence of Hypovolemia

R. Brooke Jeffrey, Jr.[1]
Michael P. Federle

In a review of 100 patients undergoing abdominal CT for blunt abdominal trauma, seven had flattening of the infrahepatic inferior vena cava at multiple levels. In six of these patients, emergency surgery was required to control major hemorrhage. Three patients had hypotension documented during or shortly after abdominal CT. Five patients had major intraabdominal injuries, and one patient had massive hemorrhage from facial lacerations. The severity of the blood loss was not fully appreciated clinically in five of the six patients before CT. The seventh patient had no clinical evidence of significant blood loss; in this case the flattened inferior vena cava probably was related to a normal variant. In a group of 100 patients scanned for nonacute conditions, none had flattening of the infrahepatic inferior vena cava at multiple levels.

Presence of a collapsed inferior vena cava may be CT evidence of significant hypovolemia from major blood loss and should prompt careful hemodynamic and central venous pressure monitoring.

High-resolution CT has contributed significantly to the diagnosis and management of patients with abdominal trauma [1–6]. We recently identified seven patients undergoing CT for abdominal trauma who had a collapsed infrahepatic inferior vena cava (IVC) at multiple levels. Six of these patients experienced major blood loss from traumatic lesions. In five patients, this was not fully appreciated clinically before CT. The presence of a collapsed IVC may be an important CT sign of hypovolemia resulting from major blood loss.

Materials and Methods

The abdominal CT scans and medical records were retrospectively reviewed in 100 consecutive patients with abdominal trauma from January to June 1987. The appearance and configuration of the IVC were evaluated in each case. For the purposes of this study, collapse of the IVC was defined as flattening of the infrahepatic portion of the IVC over at least three sections made at 1-cm intervals.

The medical records were reviewed to determine the hemodynamic status of the patients during the 24-hr period before and after the CT examination. This was to identify patients who had sustained major blood loss and who had clinical evidence of hypotension and/or hypovolemia at the time of the scan.

To determine the frequency of a collapsed IVC in a control group, we noted the appearance of the IVC in 100 patients undergoing CT for nonacute conditions such as diagnosis and staging of intraabdominal malignancies.

All scans were performed with a GE 9800 CT scanner with a 2- to 3-sec scan time. Scans were made during suspended respiration with quiet breathing. Patients were instructed to breath-hold during the scanning without deep inspiration or expiration.

Results

Seven of the 100 patients scanned because of abdominal trauma had flattening of the inferior vena cava over at least three sections made at 1-cm intervals (Figs.

Received September 3, 1987; accepted after revision October 26, 1987.

[1] Both authors: Departments of Radiology, University of California, San Francisco and San Francisco General Hospital, San Francisco, CA 94110. Address reprint requests to R. B. Jeffrey, Jr., Dept. of Radiology 1X55, San Francisco General Hospital, 1001 Potrero Ave., San Francisco, CA 94110.

AJR 150:431–432, February 1988
0361–803X/88/1502–0431
© American Roentgen Ray Society

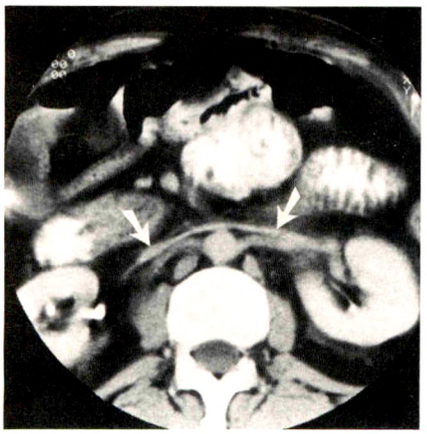

Fig. 1.—CT scan shows collapsed inferior vena cava (IVC) in patient with marked blood loss due to facial lacerations. Renal veins as well as IVC are collapsed (*arrows*). Despite clinical evidence of hypovolemia, renal excretion of contrast material is normal.

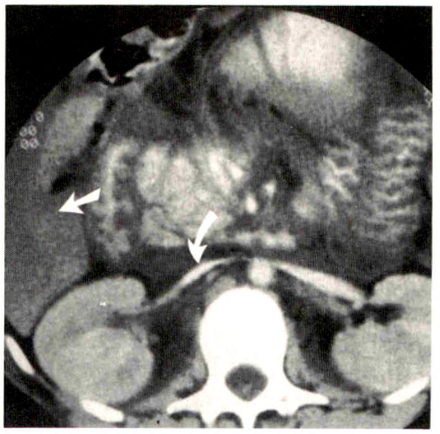

Fig. 2.—CT scan shows collapsed inferior vena cava (*curved arrow*) in patient with hemorrhagic shock due to superior mesenteric artery laceration. Large hemoperitoneum in right paracolic gutter (*straight arrow*) is also evident.

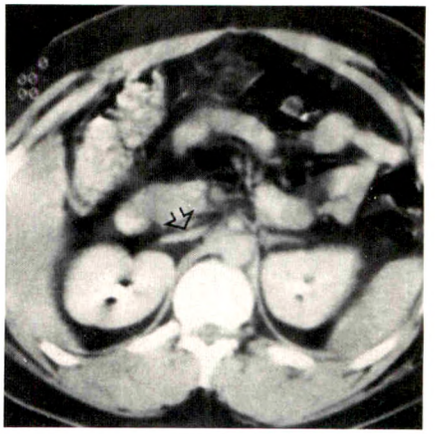

Fig. 3.—CT scan shows flattened inferior vena cava (*arrow*) in patient without hypovolemia. This finding was present at multiple levels and is most likely due to a congenital abnormality of inferior vena cava or deep inspiration during scan acquisition.

1–3). The renal veins were also bilaterally flattened in all seven patients. In six of the seven patients, major blood loss occurred and emergency surgery was necessary. Three patients had hypotension (systolic blood pressure < 100 mm Hg) during or after abdominal CT. In six, hematocrit levels fell to more than 20% of what they had been at the time of admission, and two had abnormally low central venous pressure measurements. The seventh patient had no significant blood loss or hypovolemia. Of the six patients that required emergency surgery, massive blood loss was caused by visceral injuries in five and by extensive facial trauma in one. Three of the patients died, two during surgery from hypovolemic shock and one immediately after surgery because of myocardial infarction associated with hypovolemia that had occurred during surgery.

Review of the medical records of the seven patients with a collapsed IVC on CT showed that only one was recognized clinically as having significant blood loss immediately before the CT scan. This patient had a systolic blood pressure of 80 mm Hg, a pulse of 135/min, and a hematocrit of 19%. Another patient had a limited CT examination because he became hypotensive during the study. This patient underwent emergency laparotomy but died in the operating room from hemorrhagic shock due to a laceration of the right hepatic vein.

None of the remaining 93 patients in whom the IVC was normal had clinical evidence of hemodynamic instability or significant hypovolemia during or shortly after CT. Usually, central venous pressure was not monitored in these cases. Twenty-six of the 48 patients with parenchymal visceral injuries in this group required surgical intervention because of the initial CT findings and/or the presence of a falling hematocrit. None of these patients was shown clinically to have sudden hemodynamic deterioration in the immediate period after the CT scan.

Of the 100 patients scanned because of nonacute indications, the IVC appeared rounded or oval in 98. Two patients had flattening of the IVC seen at a single CT level. Neither of these patients, however, had evidence of a flattened IVC at multiple levels.

Discussion

In patients undergoing CT for abdominal trauma, a collapsed inferior vena cava at multiple levels may be an important sign of hypovolemia resulting from major hemorrhage. Six of the seven patients with this finding had clinical evidence of significant blood loss during or immediately after the scan. Five patients had major intraabdominal injuries, and one patient had massive focal trauma. The extent of the blood loss was not fully appreciated clinically in five of these patients before CT.

The collapse of the IVC in the patients with hypovolemia is most likely due to decreased venous return. In some cases the demonstration of the collapsed IVC preceded the clinical detection of shock. Only two of these six patients with hypovolemia and a collapsed IVC on CT had shock nephrograms. The reason for the flattened IVC in the patient who did not have hypovolemia is unclear. It may represent a rare congenital abnormality of the IVC, or it may be related to a sudden deep inspiration during scan acquisition. A collapsed IVC must be identified *at multiple levels* in order for it to be considered a sign of hypovolemia.

REFERENCES

1. Federle MP, Crass RA, Jeffrey RB, et al. Computed tomography in blunt abdominal trauma. *Arch Surg* **1982**; 117:645–650
2. Jeffrey RB, Laing FC, Federle MP, et al. Computed tomography of splenic trauma. *Radiology* **1981**;141:729–732
3. Toombs BD, Lester RG, Ben Menachem Y, et al. Computed tomography in blunt trauma. *Radiol Clin North Am* **1981**;19:17–35
4. Berger PE, Kuhn JP. CT of blunt abdominal trauma in childhood. *AJR* **1980**;134:263–269
5. Federle, MP. Computed tomography of blunt abdominal trauma. *Radiol Clin North Am* **1983**;21:461–475
6. Doppman JL. Effects of Valsalva maneuver on the inferior vena cava in man. *Invest Radiol* **1967**;2:332–338

Case Report

Splenic Artery Pseudoaneurysms Causing Lower Gastrointestinal Hemorrhage

T. Gregory Walker,[1] Stuart C. Geller, and Arthur C. Waltman

Acute massive lower gastrointestinal hemorrhage is most frequently due to diverticulosis [1]. The diagnostic evaluation generally consists of endoscopy and radionuclide studies. In a small number of patients, however, the source of bleeding remains unknown, despite the use of these techniques. In such patients, angiography may be useful and occasionally may show that the source of bleeding involves the arterial supply to the upper gastrointestinal tract, despite the clinical presentation. We report three patients who presented with massive lower gastrointestinal hemorrhage in whom unsuspected splenic artery pseudoaneurysms were identified by angiography. All had a known history of pancreatitis.

Case Report

A 63-year-old man with lower gastrointestinal bleeding underwent right colectomy at another hospital after an angiographic diagnosis of angiodysplasia. Because of continued lower gastrointestinal bleeding and a history of pancreatitis, a noncontrast CT scan was performed. This showed a pancreatic mass, which was interpreted as a pancreatic pseudocyst. The patient was subsequently referred to our hospital while actively bleeding, where he underwent upper gastrointestinal endoscopy, which was reported as normal. Repeat arteriography showed a splenic artery pseudoaneurysm (Fig. 1) corresponding to the mass that had been incorrectly interpreted as a pancreatic pseudocyst. At surgery, the pseudoaneurysm was found to be in communication with the pancreatic duct. Active pancreatitis was not evident.

Discussion

Splenic artery pseudoaneurysms are a well-recognized yet infrequent cause of gastrointestinal hemorrhage [2]. In patients in whom pseudoaneurysm is unsuspected, the source of hemorrhage may not be clinically apparent. Multiple diagnostic procedures (e.g., endoscopy, radionuclide studies) are often performed before angiography, without detecting the source of the bleeding. These techniques may localize the level at which blood enters the gastrointestinal tract but may fail to further characterize the source of hemorrhage. Angiography may then be the only means by which the conclusive diagnosis is made [3, 4].

Visceral artery pseudoaneurysms that occur in association with inflammatory disease, such as pancreatitis, most commonly involve the splenic artery and its branches [2, 5]. The pathogenesis of pseudoaneurysm formation is the weakening and eventual destruction of the arterial wall by pancreatic enzymes released locally by the inflammatory process. Spread of the inflammatory process also occurs along fascial planes, so that virtually any intraperitoneal or extraperitoneal space may be involved. With progressive expansion of the pseudoaneurysm, eventual rupture into any of the adjacent structures may occur. Alternatively, a pancreatic pseudocyst may erode into a visceral vessel and thus convert the pseudocyst into a large pseudoaneurysm [6, 7].

In the case we describe, a pancreatic pseudocyst was

Received August 10, 1987; accepted after revision September 16, 1987.

[1] All authors: Department of Radiology, Massachusetts General Hospital, Harvard Medical School, Boston, MA 02116. Address reprint requests to T. Gregory Walker, Dept. of Radiology, Massachusetts General Hospital, Boston, MA 02116.

AJR **150:433–434, February 1988** 0361–803X/88/1502–0433 © American Roentgen Ray Society

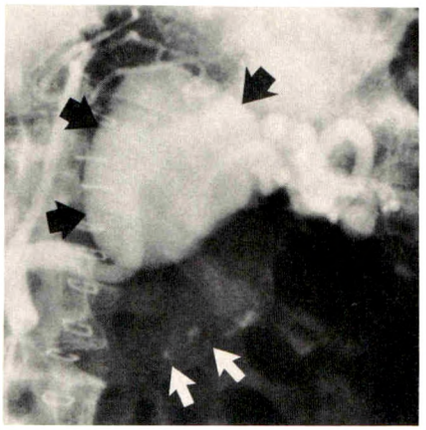

Fig. 1.—Celiac arteriogram reveals pseudoaneurysm (*black arrows*) of splenic artery. Pancreatic calcifications are also visible (*white arrows*).

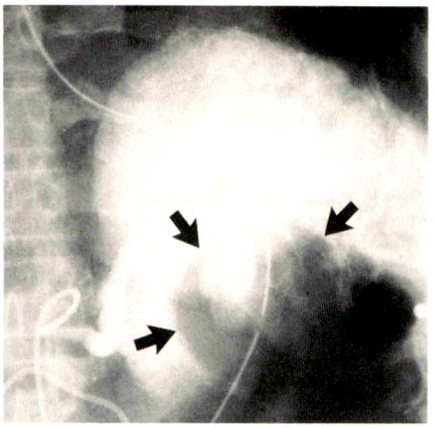

Fig. 2.—Splenic arteriogram obtained in 31-year-old man with history of esophageal varices and upper gastrointestinal hemorrhage who presented with massive lower gastrointestinal hemorrhage. Upper endoscopy failed to reveal a source of bleeding. Arteriogram reveals a splenic artery pseudoaneurysm surrounded by an avascular area of thrombus (*arrows*). Pseudoaneurysm was successfully embolized with a 4-mm detachable balloon, and bleeding stopped.

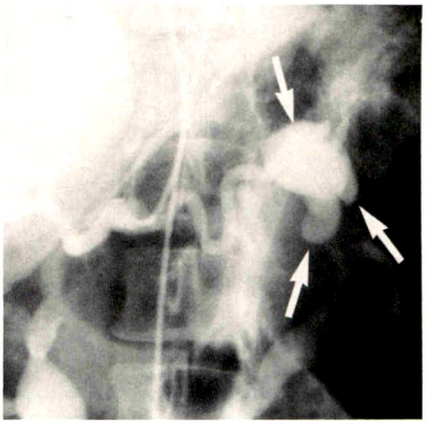

Fig. 3.—Celiac arteriogram obtained in 42-year-old man with known chronic pancreatitis who was admitted with hypotension and massive lower gastrointestinal bleeding. Upper endoscopy was normal; sigmoidoscopy to 20 cm demonstrated bright red blood. Arteriogram shows a splenic artery pseudoaneurysm (*arrows*). At surgery this was found to have eroded into splenic flexure of colon.

incorrectly diagnosed on the noncontrast CT scan. If this examination had been performed with injection of IV contrast material, the splenic artery pseudoaneurysm would most likely have been correctly identified.

We have encountered two additional patients who presented with massive lower gastrointestinal hemorrhage of unknown origin and in whom splenic artery pseudoaneurysm was detected with arteriography (Figs. 2 and 3). These patients also had a known history of pancreatitis but had normal findings on upper gastrointestinal endoscopy. Recognition of the source of hemorrhage in all patients involved a thorough angiographic evaluation, with attention to vascular beds that did not necessarily correspond to the patient's symptomatology. Despite the common pathology of a splenic artery pseudoaneurysm, the site of the bleeding in each patient depended on which visceral structures were in communication with the pseudoaneurysm.

In patients with unexplained lower gastrointestinal bleeding, who are referred for diagnostic arteriography, the vascular evaluation generally includes both the superior and inferior mesenteric arteries. If a source is not readily apparent from the mesenteric arterial supply, the examination should then include celiac and more selective arteriography as indicated, even though the symptoms may not suggest the celiac trunk or its branches as a source for the bleeding. Although this practice is a well-accepted one, the cases we describe further emphasize the importance of examining all potential vascular sources for hemorrhage.

REFERENCES

1. Welch CE, Hedberg S. Gastrointestinal hemorrhage. In: Hardy JD, Zollinger RM, eds. *Advances in surgery*. Chicago: Year Book Publ., **1973**:123
2. Stanley JC, Frey CF, Miller TA, Lindenauer SM, Child CG. Major arterial hemorrhage: a complication of pancreatic pseudocysts and chronic pancreatitis. *Arch Surg* **1976**;111:435–440
3. Koehler PR, Nelson JA, Berenson MM. Massive extra-enteric gastrointestinal bleeding: angiographic diagnosis. *Radiology* **1976**;119:41–44
4. Walter JF, Chuang VP, Bookstein JJ, Reuter SR, Cho KJ, Pulmano CM. Angiography of massive hemorrhage secondary to pancreatic disease. *Radiology* **1977**;124:337–342
5. Stabile BE, Wilson SE, Debas HT. Reduced mortality from bleeding pseudocysts and pseudoaneurysms caused by pancreatitis. *Arch Surg* **1983**;118:45–51
6. Gadacz TR, Trunkey D, Kieffer RF. Visceral vessel erosion associated with pancreatitis. *Arch Surg* **1978**;113:1438–1440
7. Eckhauser FE, Stanley JC, Zelenock GB, Borlaza GS, Freier DT, Lindenauer SM. Gastroduodenal and pancreaticoduodenal artery aneurysms: a complication of pancreatitis causing spontaneous gastrointestinal hemorrhage. *Surgery* **1980**;88:335–344

Pictorial Essay

The Popliteal Artery and Its Branches: Embryologic Basis of Normal and Variant Anatomy

Matthew A. Mauro,[1] Paul F. Jaques,[1] and Melissa Moore[2]

In 1929, Senior [1] first related popliteal artery embryology to adult anatomic variants. Many of the variants can be explained by combinations of persistent primitive arterial segments, abnormal fusions, or segmental hypoplasia or absence. Knowledge of the anatomic variability in this region may have clinical implications regarding vascular grafting, direct surgical repair, transluminal angioplasty, embolectomy, or the diagnosis of arterial injury. In addition, a knowledge of the embryology of the popliteal artery provides a better understanding of the development of atherosclerotic popliteal artery aneurysms and the popliteal artery entrapment syndrome.

Materials and Methods

Between 1984 and 1985, 421 lower extremity arteriograms (421 patients) were performed at the North Carolina Memorial Hospital. We reveiwed these arteriograms retrospectively for the arterial anat-

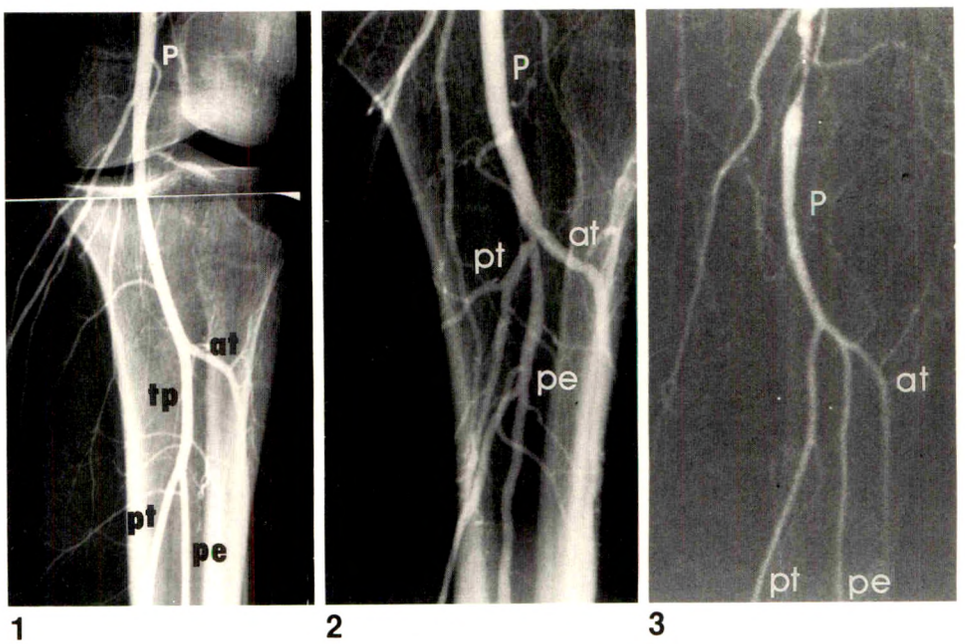

1 2 3

Fig. 1.—Normal popliteal arteriogram. P = popliteal artery, at = anterior tibial artery, pt = posterior tibial artery, pe = peroneal artery, tp = tibioperoneal trunk.

Fig. 2.—Trifurcating popliteal artery (P). at = anterior tibial artery, pt = posterior tibial artery, pe = peroneal artery.

Fig. 3.—Digital subtraction arteriogram of peroneal artery (pe) arising from low anterior tibial artery (at). Knee joint is approximately at level of popliteal artery (P) stenosis. pt = posterior tibial artery.

Received August 3, 1987; accepted after revision September 9, 1987.
Presented as a scientific exhibit at the annual meeting of the American Roentgen Ray Society, Miami Beach, FL, May 1987.
[1] Department of Radiology, University of North Carolina School of Medicine, Chapel Hill, NC 27514. Address reprint requests to M. A. Mauro.
[2] Department of Surgery, University of North Carolina School of Medicine, Chapel Hill, NC 27514.

AJR 150:435–437, February 1988 0361–803X/88/1502–0435 © American Roentgen Ray Society

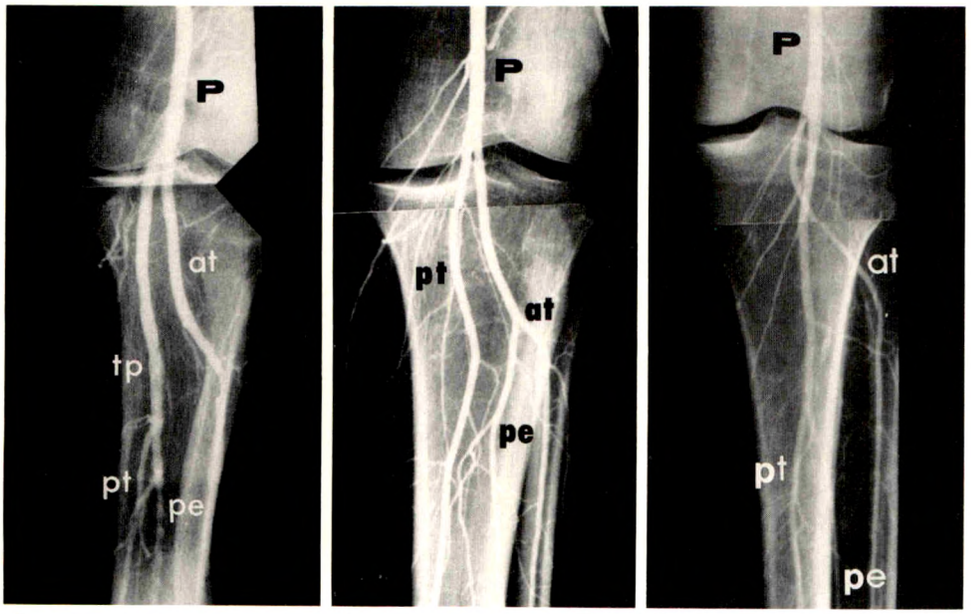

4 5 6

Fig. 4.—High anterior tibial artery (at) origin and peroneal artery (pe) arising from tibioperoneal trunk. P = popliteal artery, tp = tibioperoneal trunk, pt = posterior tibial artery.

Fig. 5.—Peroneal artery (pe) arising from high anterior tibial artery (at). It is uncertain whether anterior tibial artery passes deep or superficially to popliteus muscle. Patient's opposite leg is shown in Fig. 1. P = popliteal artery, pt = posterior tibial artery.

Fig. 6.—Angiographic differentiation between deep and superficial high anterior tibial artery (at) is usually not possible with only an anteroposterior projection. In this case, unusual medial course of anterior tibial artery, apparently crossing the tibioperoneal trunk, indicates a different anatomic plane, deep to the popliteus muscle. P = popliteal artery, pt = posterior tibial artery, pe = peroneal artery.

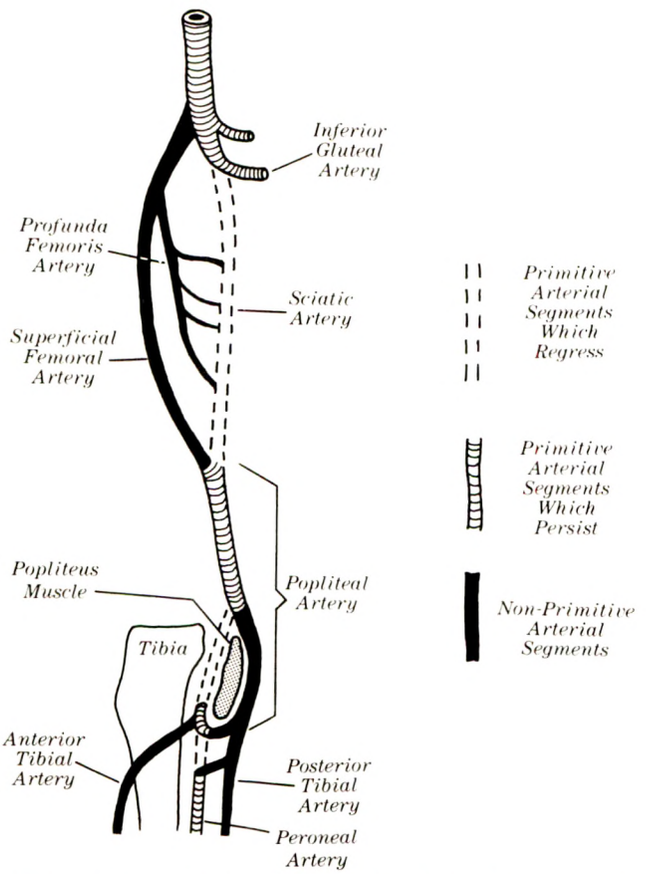

Fig. 7.—Diagram showing embryologic development of arteries to leg. Proximal sciatic artery regresses to be represented by inferior gluteal artery. Anterior tibial artery initially arises as a branch of popliteal artery and passes anteriorly to popliteus muscle; anterior tibial artery is replaced in humans by a superficial popliteal artery that passes posteriorly to popliteus muscle.

omy of the popliteal artery and its branches and for the arterial anatomy at the ankle. Seventy-eight (19%) arteriograms were excluded from the study because the extent of the disease precluded satisfactory classification. Thus, 343 arteriograms were available for analysis.

Results

Of the 343 arteriograms available for adequate classification of limbs, 88% had normal arterial branching (Fig. 1). The popliteal artery courses between the two heads of the gastrocnemius muscle across the lower popliteal fossa and gives rise to the anterior tibial artery at the lower border of the popliteus muscle. The popliteus muscle originates from the lateral femoral condyle and lateral meniscus and inserts on the soleal line of the tibia. The tibioperoneal trunk and the posterior tibial artery are the continuation of the popliteal artery. The peroneal artery arises at a variable position from the posterior tibial artery. The variant patterns identified included: trifurcating popliteal artery, 4.1% (Fig. 2); the peroneal artery arising from a normal anterior tibial artery, 1.2% (Fig. 3); a high origin of the anterior tibial artery at the upper border of the popliteus muscle and passing either superficially or deep to the popliteus muscle, 2.3% (Figs. 4 and 5); a high origin of the anterior tibial artery passing either superficially or deep to the popliteus muscle with the peroneal artery arising from the anterior tibial artery, 0.9% (Fig. 6); and abnormal regression of distal segments where the posterior and/or anterior tibial arteries are hypoplastic or absent, 2.3%.

Discussion

The lower extremity blood supply is detectable in the 9-mm embryo [1]. The sciatic artery, also referred to as the ischiatic or axial artery, is a branch of the internal iliac artery and is the major supplier to the early developing limb bud. By the 14-mm embryo stage, the femoral artery, a branch of the external iliac artery, has anastomosed with the sciatic artery and become the major supply vessel to the lower limb [2]. The more proximal sciatic artery regresses to be represented by the inferior gluteal artery and the artery to the sciatic nerve in the adult. The primitive middle and distal sciatic artery segments persist to form the definitive popliteal and peroneal arteries. The anterior tibial artery arises as a branch of the popliteal artery and initially runs anteriorly (deep) to the popliteus muscle. This is the usual definitive primate anatomy. In

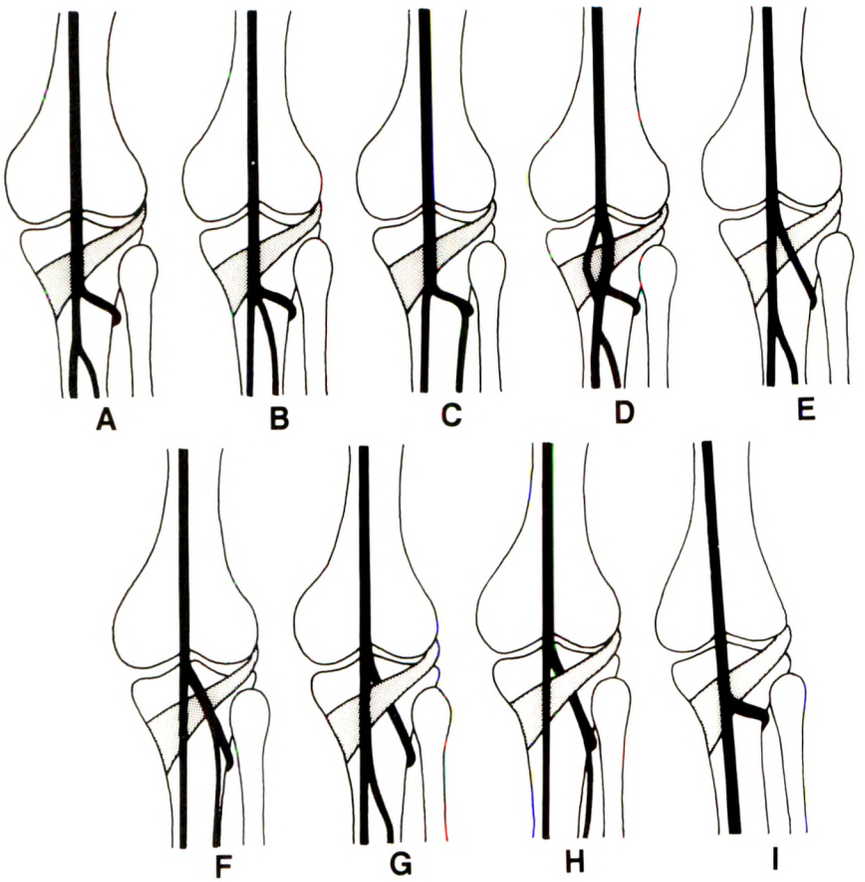

Fig. 8.—Anatomic variations of popliteal artery and its branches. Diagrams represent posterior views of popliteal fossa in which stippled structure represents popliteus muscle.

***A*, Normal.**

***B*, Trifurcating popliteal artery.**

***C*, Peroneal artery arising from low anterior tibial artery.**

***D*, "Island" popliteal artery (very rare); this pattern was not identified in our series.**

***E*, High anterior tibial origin passing superficial to popliteus muscle.**

***F*, Same as *E* with peroneal artery arising from anterior tibial artery.**

***G*, Same as *E* with anterior tibial artery passing deep to popliteus muscle.**

***H*, Same as *F* except anterior tibial artery passes deep to popliteus muscle.**

***I*, Absent posterior tibial artery.**

humans, however, the early anterior tibial artery is replaced by a superficial popliteal artery that passes posteriorly (superficially) to the popliteus muscle, which then gives rise to the definitive anterior tibial artery [3]. The posterior tibial artery is formed by an anastomosis between the early distal femoral artery and the popliteal artery [4] (Fig. 7). The definitive anatomy is completed by 3 months gestation [1].

The embryonic vascular development determines the anatomic variability. Thus, embryonic vessels may either persist or degenerate (degeneration of these vessels is normal), or abnormal fusions may occur [4] (Fig. 8). In their review of arterial variations, Lippert and Pabst [3] illustrate an anomaly not identified in our series: a vessel directly connecting the popliteal artery at the level of the knee joint to the proximal portion of the tibioperoneal trunk, forming what they have called an "island" [3] (Fig. 8D). This is a rare anomaly and thought to represent a persistence with abnormal fusion of the popliteal artery.

The determination of whether a high anterior tibial artery courses superficially or deep to the popliteus muscle is often difficult on an anteroposterior arteriogram. We believe that an initial medial course of the anterior tibial artery (which then travels laterally, apparently crossing the tibioperoneal trunk) indicates that these vessels are in different anatomic planes. In these cases, the tibioperoneal trunk courses superficially and the anterior tibial artery courses deep to the popliteus muscle (Fig. 6). The probability is approximately 10% that any one limb will have an arterial anatomy that significantly differs from the normal. In these cases, there is a 50% chance that the contralateral lower leg will also be "non-normal" or variant [2].

Understanding the embryology and variant anatomy may have significant clinical implications. Vascular grafting and repair is indicated in a variety of disease processes, including atherosclerosis, emboli, and trauma. Anatomic variants will influence the surgical approach and dissection and the choice of suitable arterial graft sites. The trifurcating popliteal artery (Fig. 2) seen in 4.1% of limbs presents a particular technical challenge during angioplasty or embolectomy. Knowledge of an absent posterior or anterior tibial artery may prevent false diagnosis of arterial damage in trauma when the normal ankle pulses are absent or diminished. In the absence of the posterior and anterior tibial arteries, the peroneal artery becomes the sole supplier to the foot (arteria peronea magna) [1, 3].

REFERENCES

1. Senior HD. Abnormal branching of the popliteal artery. *Am J Anat* **1929**;44:111–120
2. Bardsley JL. Variations in branching of the popliteal artery. *Radiology* **1970**;94:581–587
3. Lippert H, Pabst R. *Arterial variations in man: classification and frequency*. Munich: Bergmann Verlag, **1985**:60–64
4. Arey LB. *Developmental anatomy*, 7th ed. Philadelphia: Saunders, **1974**:358–360

American Roentgen Ray Society:
Officers, Committees, and Meeting Information

Officers

President: Raymond A. Gagliardi
President-elect: Lee F. Rogers
1st Vice-president: Gerald D. Dodd
2nd Vice-president: Rosalind H. Troupin
Secretary: Glen W. Hartman
Treasurer: Ronald G. Evens

Executive Council: E. Gedgaudas, J. F. Wiot, L. F. Rogers, R. A. Gagliardi, R. G. Evens, R. N. Berk, F. L. Angell, J. E. Madewell, M. P. Capp, G. W. Hartman, B. G. Brogdon, R. H. Troupin, G. R. Leopold, G. D. Dodd, A. K. Poznanski, A. E. James, Jr., J. T. Ferrucci, Jr., T. C. Beneventano, E. J. Ferris, J. A. Kirkpatrick, Jr., chairman

Committees

Editorial Policy: S. S. Sagel, W. J. Casarella, C. A. Rohrman, Jr., N. C. Whitley, S. V. Hilton, J. M. Taveras, R. N. Berk, M. P. Capp, chairman

Education and Research: C. E. Putman, A. R. Margulis, B. J. Hillman, R. A. McLeod, B. G. Brogdon, chairman

Finance and Budget: B. P. Wood, A. K. Poznanski, L. R. James, A. E. James, Jr., F. L. Angell, chairman

Nominating: A. K. Poznanski, E. Gedgaudas, G. H. Ghahremani

Publications: W. J. Casarella, S. S. Sagel, N. C. Whitley, C. A. Rohrmann, Jr., M. P. Capp, chairman

Membership: E. J. Ferris, G. R., Leopold, A. K. Poznanski, A. E. James, Jr., chairman

Representatives to Other Organizations

American Board of Radiology: E. C. Klatte, L. F. Rogers, T. C. Beneventano

American College of Radiology: L. F. Rogers, G. A. Kling, R. A. Gagliardi, J. M. Dennis, E. J. Ferris, J. E. Madewell

American Medical Association House of Delegates: S. F. Ochsner, K. L. Krabbenhoft, alternate

American National Standards Institute: M. Haskin

National Council on Radiation Protection and Measurements: E. L. Saenger, H. L. Friedell

Meeting Arrangements

Annual Meetings: May 8–13, 1988, Hilton, San Francisco; May 7–13, 1989, Hilton, New Orleans; May 13–18, 1990, Sheraton Washington, Washington, DC

Annual Meeting Committee: H. C. Carlson, G. P. Janetos, E. K. Lang, R. R. Lukin, T. C. Beneventano, chairman

Instruction Courses: R. A. McLeod, associate chairman, J. T. Ferrucci, Jr., chairman

Scientific Program: R. J. Alfidi, A. E. Robinson, J. H. Thrall, M. P. Banner, J. J. Gisvold, T. C. McLoud, E. Buonocore, R. M. Gore, J. J. Kaye, L. F. Rogers, chairman

Scientific Exhibits: K. H. Vydareny, A. V. Proto, S. M. Goldman, J. E. Madewell, chairman

ARRS Membership

An application form is printed in the January 1988 issue of the Journal. For consideration at the 1988 ARRS meeting, send completed forms before February 1, 1988, to Paul Fullagar, administrative director, American Roentgen Ray Society, 1891 Preston White Dr.,Reston, VA 22091. Active members are graduates of an approved medical school or hold an advanced degree in an allied science. They must practice radiology or work in an associated science in the United States or Canada and be certified by the American Board of Radiology or the Royal College of Physicians of Canada or otherwise adequately document training and credentials. Corresponding members are foreign radiologists or scientists who are active in radiology or an allied science. Members-in-training are residents or fellows in radiology or postgraduate students in an allied science. Additional application forms can be obtained from the ARRS offices in Reston, VA.

Business Office

Paul Fullagar, administrative director, American Roentgen Ray Society, 1891 Preston White Dr., Reston, VA 22091; (703) 648-8900

ARRS Meeting Section

Invitation to the 1988 American Roentgen Ray Society Meeting in San Francisco, CA, May 8–13, 1988

I am pleased to extend an invitation to all radiologists to attend the 88th annual meeting of the American Roentgen Ray Society in San Francisco, CA, May 8–13, 1988. In keeping with the ARRS tradition, outstanding scientific and social programs will be provided.

The excitement of a meeting set in the center of San Francisco requires no further description. The opportunity for busy radiologists to attend a major national meeting while enjoying such an environment is ideal.

The scientific program, instructional courses, and categorical course are certain to be interesting and informative (see Table 1 for schedule).

Scientific Program

Two hundred scientific papers have been selected from a record submission of 650 abstracts. Scientific sessions will be devoted to all major body systems, angiography, interventional techniques, sonography, and mammography. Special emphasis has been placed on discussion of newer developments.

The innovative and extremely well-received Friday morning minisymposium is entitled "Chest Imaging Update, 1988." Theresa McLoud and Gordon Gamsu have assembled an outstanding faculty for what I am sure will be a very stimulating program.

Instructional Courses

Joseph Ferrucci, Chairman of the Instructional Course Committee, has put together 60 instructional courses. Faculty members have been drawn from across the entire country, with emphasis on luminaries from the West Coast. A superlative educational experience is anticipated, and advance registration is recommended.

Categorical Course

An extraordinary categorical course on breast imaging has been fashioned by Stephen Feig. The course covers equipment, principles of diagnosis, biopsy techniques, screening, and all the important aspects of breast imaging. This course is certain to be popular, and advance registration is advised.

Scientific Exhibits

The 220 scientific exhibits coordinated by John Madewell will cover the entire breadth of the field of diagnostic radiology. The technical exhibits will be displayed in the same area as the scientific exhibits to enhance the interaction of the attendees with our technical exhibitors.

TABLE 1: Summary of 1988 American Roentgen Ray Society Meeting

Sunday May 8	Monday May 9	Tuesday May 10	Wednesday May 11	Thursday May 12	Friday May 13
	8–9:30 Instructional courses	8–9:30 Instructional courses	8–9:30 Instructional courses	8–9:30 Instructional courses	8–10 Symposium: chest imaging update
9–noon Categorical course: breast imaging	10–10:30 Opening ceremonies				
	10:30–12:30 Scientific programs	10–12:30 Scientific programs	10–12:30 Awards session/ Caldwell lecture	10–12:30 Scientific programs	10:30–12:30 Symposium: chest imaging update
1:30–3 Categorical course: breast imaging	1:30–3:30 Categorical course: breast imaging	1:30–3:30 Scientific programs	1:30–3:30 Scientific programs	1:30–3:30 Scientific programs	
3:30–5:30 Categorical course: Breast imaging	4–5:30 Instructional courses and categorical course: breast imaging	4–5:30 Instructional courses and categorical course: breast imaging	4–5:30 Instructional courses and categorical course: breast imaging	4–5:30 Instructional courses and categorical course: breast imaging	

Caldwell Lecture

Donald L. Resnick of the University of California at San Diego has accepted an invitation to present the Caldwell Lecture for 1988. His lecture, "Common Disorders of Synovial Joints: Pathogenesis, Imaging Abnormalities, and Complications," promises to be a highlight of the meeting.

Social Events

San Francisco offers an unlimited number of diversions, and George Janetos, Chairman of the Local Arrangements Committee, has engaged Tours West to plan a variety of outstanding tours. The annual golf and tennis tournaments for attendees and their companions are scheduled for Monday. The traditional cocktail party given by the Society in the exhibit area for all registrants will be Tuesday evening and will provide a convenient meeting place before an evening on the town.

This promises to be a truly outstanding event in exceptional surroundings. I hope you will be able to accept our invitation. Plan now to attend.

Lee F. Rogers
President-Elect, ARRS

1988 American Roentgen Ray Society Section on Instruction: Courses and Symposium

Joseph T. Ferrucci, director

Fifty-six instructional courses will be presented during the 88th annual meeting of the American Roentgen Ray Society (ARRS) beginning Monday, May 9, and continuing through Thursday, May 12. In addition, there will be a series of courses on breast imaging and a symposium on chest imaging. Each of the courses will be 90 min long; no other activities are scheduled simultaneously.

The Categorical Course in Breast Imaging will have 14.5 hr of instruction and will begin on Sunday, May 8, and conclude on Thursday, May 12. The Symposium on Chest Imaging Update will be on Friday, May 13, from 8 a.m. to 12:15 p.m. All courses carry Category 1 credit on an hour-to-hour basis.

Registration Information

To register for courses, complete the meeting registration form in this section and mail promptly. Tickets will be available at the Instruction Course Registration Desk, San Francisco Hilton and Tower, for courses that have not been sold out. All courses will take place in the headquarter's hotel.

After reviewing the course abstracts, select three for each day. List the course number and name of the first instructor on the registration form.

All who register for the Categorical Course in Breast Imaging (including ARRS members) must pay a fee of $75 and must take the entire series of classes. The categorical course totals 14.5 hr of instruction and includes a syllabus.

Course Schedule

Sunday, May 8, through Thursday, May 12

The Categorical Course in Breast Imaging will have 14.5 hr of instruction over 5 days. Table 1 lists topics and instructors.

Monday, May 9, through Friday, May 13

A total of 56 courses will be offered (Table 2) plus a Symposium on Chest Imaging Update. Course abstracts and a list of faculty follow.

Monday, May 9

101. The analytic approach to the film. Jacobson HG. Diagnostic radiology is an imaging discipline that reflects with considerable accuracy gross pathologic changes that are transmitted through the imaging techniques used by the radiologist. In the "approach to the film," a series of diagnostic parameters are considered in an organized fashion. Such an orderly evaluation generally permits an intelligent perusal of the findings in a given case and often results in a correct diagnosis, even in difficult cases. This approach implies adoption of the concept that the film speaks a basic language and that the radiologist functions as an interpreter of that language. If the language is understood, the interpretation should be accurate. This instructional course is planned to evaluate a number of cases of skeletal abnormalities representative of the different subcategories (e.g., trauma, infection, neoplasm). It is hoped that residents in the group will volunteer to demonstrate the process of applying analytic techniques with the use of the various parameters selected.

102. The radiology of vertebral trauma. Daffner RH. Trauma to the vertebral skeletal column is one of the most common injuries encountered in the daily practice of radiology. The prompt assessment of bone and soft-tissue abnormalities in the "spine-injured patient" is of paramount importance in stabilizing any existing neurologic abnormalities and in preventing additional ones. Furthermore, the inherent stability of the injured vertebral column must be assessed to determine the need for surgical intervention and restoration of normal function. This course will be in four parts. Part I, Technique, discusses plain film, CT, and MR imaging as they apply to the evaluation of the spine-injured patient. Part II, "Fingerprints" of vertebral injuries, revolves around a mechanistic classification of injuries broken into four categories: flexion, extension, shearing, and rotational injuries. The distinct radiographic findings or fingerprints of each type of injury will be discussed. Part III, The ABCs of vertebral trauma, will discuss the overall radiologic approach to these injuries in regard to abnormalities of alignment, bony integrity, cartilage or joint space, and soft tissue. Finally, Part IV, The radiologic assessment of vertebral stability, will define "stable" and "unstable" injuries and discuss the five main parameters that are used to determine the presence of an unstable lesion.

103. Pulmonary emphysema in infants and children. Oh KS, Newman B. A review of the causes and radiographic manifestations of pulmonary emphysema in infants and children will be presented. This will include congenital, acquired, intrinsic, and extrinsic causes and bilateral, unilateral, and focal lesions. The discussion will emphasize an understanding of the pathophysiology of complete and incomplete airway obstruction and the collateral ventilatory pathways. The unique

TABLE 1: Categorical Course in Breast Imaging, May 8–12

Day/Time	Topic/Presenter
Sunday, May 8	
9:00–9:10 a.m.	Welcome from the President (*Gagliardi*)
9:10–9:15 a.m.	Introduction (*Feig*)
9:15–10:00 a.m.	Xeromammography: principles, equipment, technique, quality control (*Sickles*)
10:30–11:30 a.m.	Screen-film mammography: principles, equipment, technique, quality control (*Feig*)
11:30 a.m.–Noon	American College of Radiology Mammography Accreditation Program (*McLelland*)
1:30–2:15 p.m.	Breast masses: differential diagnosis (*Adler*)
2:15–3:00 p.m.	Breast calcifications: differential diagnosis (*Rebner*)
3:30–4:10 p.m.	Mammography of the treated breast (*Paulus*)
4:10–4:50 p.m.	Practical solutions to common mammographic problems (*Sickles*)
4:50–5:30 p.m.	Prebiopsy localization of nonpalpable breast lesions (*Kopans*)
Monday, May 9	
1:30–2:10 p.m.	Mammographic-pathologic correlation (*Troupin*)
2:10–2:50 p.m.	Breast ultrasound: equipment, technique, interpretation, accuracy (*Bassett*)
2:50–3:30 p.m.	Fine needle aspiration biopsy, ductography, pneumocystography (*Logan*)
4:00–4:45 p.m.	Panel: Diagnostic problem cases (Moderator: *Feig*; members: *Bassett, Kopans, Rebner, Troupin*)
4:45–5:30 p.m.	Panel: Subtle signs of carcinoma (Moderator: *Feig*; members: *Adler, Logan, McLelland, Moskowitz, Sickles*)
Tuesday, May 10	
4:00–4:45 p.m.	Issues in breast cancer screening (*Moskowitz*)
4:45–5:15 p.m.	How to establish a low-cost community screening program (*McLelland*)
5:15–5:30 p.m.	Discussion
Wednesday, May 11	
4:00–4:30 p.m.	Wording the mammography report (*Feig*)
4:30–5:15 p.m.	Medicolegal aspects of mammography (*Brenner*)
5:15–5:30 p.m.	Discussion
Thursday, May 12	
4:00–4:30 p.m.	Transillumination lightscanning (*D'Orsi*)
4:30–5:00 p.m.	Breast MR (*Alcorn*)
5:00–5:30 p.m.	Digital mammography (*Merritt*)
5:30–5:35 p.m.	Concluding remarks (*Feig*)

appearance of emphysema in the neonate and the effects of prolonged abnormal ventilation on the growing lung will be presented. An approach for the effective and appropriate use of radiographic imaging in diagnosis will be illustrated.

104. Interventional radiology of the alimentary tract. Ring EJ, McLean GK. (1) Balloon catheters that were developed for angioplasty offer a means of safely accomplishing dilatation of strictures in the gastrointestinal tract. The balloons are inserted and manipulated under fluoroscopic guidance to ensure an intraluminal location. The force of dilatation is perpendicular to the stricture; thus, overdistension and rupture of the thin, dilated segment above the stricture is avoided. Preliminary results have been encouraging. Dawson reported a 90% success rate in a series of 20 patients. McLean reviewed long-term patency and found that 69% of patients were free of symptoms at 2 years. (2) Gastrointestinal intubation has become a routine procedure in the management of a variety of gastrointestinal disorders. Although usually placed for the relief of small-bowel obstruction, tubes increasingly are being used for enteric alimentation. Traditionally, placement of feeding tubes has relied on gravity and on intestinal peristalsis, but catheterization techniques can be used to position tubes rapidly in an appropriate location. This can be accomplished by a transnasal catheterization through a direct percutaneous transgastric approach or through a fistulous tract. (3) Enterocutaneous fistulae pose formidable problems because of fluid loss and associated intraabdominal abscesses. By using fluoroscopic guidance, the effluent from the bowel can be controlled by a large-bore tube placed either through the opening into the lumen of the bowel or immediately adjacent. Abdominal abscesses can be located and drained directly through the fistulous tract or percutaneously. As a mature fibrous tract forms, the tubes eventually can be removed, and the fistula closes much as the tract closes when the T-tube is removed from the biliary tree. (4) Percutaneous puncture of the alimentary tract has been used for enteric hyperalimentation and temporary decompression. The technique of percutaneous gastrostomy and manipulation into the proximal bowel is well established. Recently, additional experience has been gained in directly puncturing and decompressing obstructed afferent loops after gastric surgery and in gaining access to the biliary tree after Roux-en-Y choledochojejunostomies.

105. Practical aspects of MR image interpretation. Bradley WG. This is a practical course aimed at the radiologist who is (or soon will be) reading MR images. What do you *really* need to know to be competent in interpretation of MR images? The following questions are addressed: (1) What determines T1, T2, and proton-density contrast in the traditional spin-echo and inversion-recovery images and in the new fast low-angle shot–type techniques that use gradient echoes and reduced flip angles? (2) How does the protein content of a cystic lesion affect signal intensity through the mechanism of "hydration layer water"? Why does hemorrhage sometimes appear dark and sometimes bright? What is the effect of field strength and type of pulsing sequence (i.e., spin echoes or gradient-echo acquisition)? Why do some paramagnetic substances (e.g., methemoglobin and gadolinium-DTPA) increase signal intensity and others (e.g., deoxyhemoglobin, hemosiderin, and ferritin) decrease signal intensity? (3) Why do flowing blood and CSF sometimes appear dark and sometimes bright? Exactly how do time-of-flight effects, turbulence, odd-echo rephasing, and diastolic pseudogating increase signal? Why do flowing blood and CSF appear bright on the new fast scan (e.g., fast low-angle shot and grade-recalled acquisition in steady state) images? How does one distinguish intraluminal pathology from high-intensity flow effects? How does one use the information in these flow phenomena and turn these "artifacts" to clinical advantage?

TABLE 2: American Roentgen Ray Society Instructional Courses: May 9–May 12, 1988

Topic	Monday	Tuesday	Wednesday	Thursday
		Morning (all sessions begin at 8 a.m.)		
Residents'-masters' tutorial: up close and personal	101. The analytic approach to the film. *Jacobson*	201. How to invent new interventional techniques. *Burhenne*	301. Fun with films (or things your mentor never told you). *Jones*	401. A simplified approach to the radiologic examination of the small bowel. *Margulis*
Miscellaneous	102. The radiology of vertebral trauma. *Daffner*	202. Imaging strategies for gastrointestinal and genitourinary cancer: update 1988. *McClennan, Thompson*	302. How to get your manuscript published without a hassle. *Berk, Hilton, Whalen*	402. SPECT imaging in clinical nuclear medicine. *Handmaker, Bunker*
Pediatric radiology	103. Pulmonary emphysema in infants and children. *Oh, Newman*	203. Pediatric abdominal trauma. *Kushner, Kuhn*	303. MR imaging and sonography of the child's genitourinary tract. *Kangarloo*	403. CT and MR of diseases of childhood. *Brasch, Gooding C*
Vascular/Interventional	104. Interventional radiology of the alimentary tract. *Ring, McLean*	204. Renal hypertension: etiology, imaging, and treatment. *Hillman, Sos*	304. Deep venous thrombosis and pulmonary embolism: diagnosis and intervention. *Dorfman, Cronan*	404. Acquired diseases of the aorta and peripheral vasculature. *Shetty, Haggar*
MR Imaging	105. Practical aspects of MR image interpretation. *Bradley*	205. MR: basic principles (sans mathematics) and practical considerations. *Gray, Morin*	305. MR of the abdomen. *Stark*	405. Technical advances in clinical MR imaging: fast scanning, surface coils, contrast agents. *Edelman, Kneeland, Saini*
Neuroradiology	106. MR imaging: aging, dementia, and movement disorders. *Drayer*	206. Modern imaging evaluation of brain tumors. *Davis DO*	306. Neuroradiology of cerebrovascular disease. *Brant-Zawadzki*	406. Neuroimaging of the sellar regions, including MR. *Davis K*
Skeletal radiology	107. Radiology of the foot and ankle. *Forrester, Kerr*	207. CT of the musculoskeletal system: flying high despite MR. *Sartoris*	307. MR of the musculoskeletal system. *Bassett, Seeger*	407. MR of musculoskeletal trauma and neoplasia. *Berquist, McLeod*
Genitourinary radiology	108. The new contrast media: issues and answers. *McClennan, Rosenquist*	208. MR of the genitourinary system. *Hricak, Fritzsche*	308. Urinary stone disease: update 1988. *LeRoy, Barbaric*	408. Genitourinary imaging strategies—1988. *Davidson, Talner*
Body imaging	109. Liver imaging—1988. *Moss, Shuman*	209. Abdominal imaging in AIDS. *Federle*	309. Pancreatic inflammatory disease: radiologic diagnosis, staging, and management of complications. *Freeny*	409. The modern approach to imaging acute abdominal disorders. *Jeffrey, Baker*
Sonography	110. Deep Doppler sonography. *Taylor, Ralls*	210. Vascular sonography. *Gooding G, Gosink*	310. Sonography of the rotator cuff and of the infant's hip. *Crass, Harcke*	410. Ultrasound image interpretation. Is it real or is it an artifact? *Cooperberg*
		Afternoon (all sessions begin at 4 p.m.)		
Spine imaging	111. MR imaging of the spine. *Norman, Newton*	211. CT of disk disease and spinal stenosis. *Helms*	311. MR of the spine: degenerative disease. *Modic*	411. Osteoporosis: pathogenesis, consequences, and bone-mineral density. *Genant, Rogers*
Gastrointestinal	112. Radiographic pathology of the gastrointestinal mucosa. *Ghahremani, Maklansky*	212. Small bowel radiology: how to do it. *Carlson, Maglinte*	312. Biliary lithotripsy. *Ferrucci, Burhenne*	412. Imaging of inflammatory bowel disease. *Goldberg, Thoeni, Wall*
Cardiopulmonary	113. Advances in cardiac imaging—1988. *Higgins, Lipton*	213. Optimal use of chest CT and MR: when, how, and why. *Feigin*	313. Pulmonary thromboembolism. *Dunnick, Ravin, Sullivan*	413. Interventional radiology in the thorax and pleural space. *Mueller, vanSonnenberg*
Obstetric and Gynecologic Imaging	114. Diagnostic imaging in infertility. *Fleischer, Winfield*	214. Obstetrical sonography. Part I. *Leopold*	314. Obstetrical sonography. Part II. *Filly*	414. Endoluminal sonography: transvaginal and transrectal. *Laing, Rifkin*

106. MR imaging: aging, dementia, and movement disorders. Drayer BP. The imaging of the aging brain using magnetic resonance (MR) requires a thorough understanding of the normal and pathologic alterations that occur in the elderly: (1) *White matter.*—Scattered, small-signal hyperintensities are common in the cerebral white matter (and basal ganglia) in the distribution of noncollateralizing, perforating medullary (and lenticulostriate) arteries. Various potential pathologic changes have been reported, including etat crible, atrophic perivascular demyelination, gliosis, myelin pallor, and infarction. These findings are all compatible with an underlying arteriolopathy (e.g., hypertension) and/or hypoperfusion (e.g., cardiac dysfunction). (2) *Basal ganglia.*—Areas of decreased signal intensity on T2 images normally are seen in adults in the globus pallidus, red nucleus, reticular substantia nigra, and dentate nucleus (sites of maximal brain iron concentration). In the elderly, the putaminal signal hypointensity progressively increases to become almost equal to that in the pallidum. Parkinson disease, particularly Parkinson disease that is poorly responsive to medication (e.g., multiple-system atrophies: striatonigral degeneration, Shy-Drager, olivopontocerebellar atrophy), prematurely present with putaminal hypointensity that may even predominate over the globus pallidus, suggesting accelerated formation of free radicals and accumulation of iron or pigment. (3) *CSF spaces.*—Progressive enlargement of the third and lateral ventricles, cortical sulci, and subarachnoid space may occur with aging. Alzheimer disease presents with dementia and an abnormal widening of the cortical sulci (cerebral atrophy). Abnormal hypointensity may be noted in the parietal cortex in half of patients, suggesting abnormal accumulation of iron.

107. Radiology of the foot and ankle. Forrester DM, Kerr R. The purpose of this course is to provide a systematic approach to the diagnosis of common foot conditions (i.e., arthritis and sports injuries). The differential diagnosis of monarticular arthritis and pain in the big toe will be discussed. Comparison of the presentation of rheumatoid arthritis in the foot with gout and degenerative joint disease will be stressed. The use of CT and MR imaging will be discussed, with emphasis on evaluation of trauma and tumors.

108. The new contrast media: issues and answers. McClennan BL, Rosenquist CJ. The recent introduction of new low-osmolarity, ionic, and nonionic contrast media in the United States has sparked controversy and engendered sharp debate that has focused largely on the current role in radiologic practice of these agents that have been approved by the U.S. Food and Drug Administration. It appears clear to many investigators that these new drugs are associated with better tolerance by patients and better acceptance and safety because fewer physiologic alterations are associated with their use. Decreased morbidity and an apparent decrease in mortality, with equal or slightly improved diagnostic efficacy, have been documented. This refresher course will address and review the scientific evidence for use of low-osmolar ionic and nonionic contrast media in current clinical practice. The indications and categories of patients *at risk* will be outlined. Economic issues, including cost-benefit analysis, cost to a radiology department, the aggregate cost to the health-care system, and appropriate responses of third-party payers will be discussed. The principal legal issues relating to informed consent and standards of care based on usual and customary practice also will be included. Finally, the moral and ethical aspects concerning the patients' and the physicians' roles in the decision-making process and payment choices will be reviewed.

109. Liver imaging—1988. Moss AA, Shuman WP. The liver continues to be a topic of interest and the object of new developments in several imaging techniques. Combining information from CT, MR, and sonography can help narrow differential diagnoses and characterize masses as probably benign or malignant. Some degree of hepatic tissue characterization can be achieved with MR, especially if fat-suppression or chemical-shift imaging are used; frequency-modulation sonography can provide additional assessment of tissue character. Both CT and MR can be used for assessing resectability of liver masses, particularly when CT and MR findings are combined with angiographic information. The issue of which technique is most sensitive and cost-effective for detecting focal masses in the liver continues to evolve, with new claims for sonography and MR. Recent new techniques have been developed for MR, including innovative pulse sequences, contrast agents, and artifact suppression, that improve its usefulness in liver imaging. Questions remain about the best technique for administration of contrast material in dynamic CT, the use of CT and angiography, and new CT contrast agents. Ultrahigh-resolution computed sonography and intraoperative sonography have had a definite impact on the diagnosis and management of liver tumors. A role for positron emission tomography may emerge; image resolution is advancing rapidly, and costs are decreasing. Finally, the value of interventional techniques in the liver is now widely accepted by many referring subspecialists, increasing the impact of the interventional radiologist on the workup of liver disease.

110. Deep Doppler sonography. Taylor KJW, Ralls PW. Recent advances in instrumentation have made abdominal Doppler sonography one of the most exciting areas of investigation in diagnostic sonography. In this session, we will discuss various features of abdominal Doppler sonography, including instrumentation (duplex, continuous wave, and color flow), current clinical applications, and clinical areas under investigation. Normal arterial, portal venous, and systemic venous patterns will be described. Qualitative uses of abdominal Doppler sonography include identification of flow in unsuspected areas, confirmation of flow in vascular structures, identification of vessel type, and differentiation of vascular from nonvascular structures. The use of Doppler techniques in various clinical situations will be discussed. Assessment of patients with portal hypertension will be discussed, including portosystemic shunts. Uses of Doppler techniques in tumors (such as pancreatic carcinoma and hepatocellular carcinoma) will be evaluated. The use of Doppler sonography in organ transplantation, in assessing both vascular complications and suspected rejections, will be discussed. Other areas to be covered include ectopic pregnancy and venocclusive disease. Applications of abdominal color-flow Doppler sonography will be illustrated.

111. MR imaging of the spine. Norman D, Newton TH. MR imaging has altered significantly the approach to diseases of the spinal column and cord. In almost all instances, MR should be selected as the primary imaging technique for intrinsic cord tumors, demyelinating processes, cavitary disease, congenital malformations, and vascular malformations. Pathologic processes such as cryptic malformations and demyelinating processes, heretofore overlooked or suspected on clinical grounds only, now can be imaged. Paramagnetic contrast agents such as gadolinium-DTPA promise to enhance the sensitivity of MR further so that small lesions such as drop metastases and small areas of demyelination will be demonstrable on a routine basis. It is likely that gadolinium-DTPA will be used routinely in any patient who has myelopathy. Additionally, MR is the most appropriate technique for detection of infectious and neoplastic diseases of the spinal column. Its appropriate role in trauma patients is promising but as yet is unresolved. Imaging techniques and interpretation of images will be discussed.

112. Radiographic pathology of the gastrointestinal mucosa. Ghahremani GG, Maklansky D. Alterations in the mucosal pattern of

the gastrointestinal tract usually are well depicted on double-contrast radiographs, but their accurate diagnosis depends on a clear understanding and visual perception of the responsible pathologic process. This course is directed toward practicing radiologists who wish to enhance their knowledge of modern gastrointestinal radiology through correlative radiographic-pathologic studies. The presentation will begin with analysis of normal mucosal patterns that are recognizable in double-contrast views, endoscopy, or gross pathologic observations. A wide spectrum of inflammatory and neoplastic lesions will be illustrated, providing their radiographic features as well as the corresponding morphologic manifestations. Emphasis will be placed on improved diagnostic approach and on practical classification of gastrointestinal mucosal disorders that is based on correlative data derived from radiographic-pathologic studies.

113. Advances in cardiac imaging—1988. Higgins CB, Lipton MJ. MR imaging and ultrafast CT (cine CT) are the newest techniques that have been used for cardiovascular diagnosis. Imaging of the cardiovascular system requires evaluation of both anatomy and function. Both cine CT and MR accomplish this dual purpose and, to some extent, are competitive techniques. However, it is becoming clear that each can have specific indications and can provide advantages over existing techniques, including angiography. This presentation will demonstrate the techniques of ECG-gated spin-echo MR, cine MR (narrow flip angle and gradient-refocused echoes), and cine CT. Anatomic diagnosis by ECG-gated MR has been effective for thoracic aortic disease, pericardial disease, paracardiac masses, and congenital heart disease. Functional evaluation by cine MR has been useful to quantitate ventricular function and the severity of regurgitant valvular lesions. Cine CT also is effective for establishing anatomic abnormalities, but its major asset is to provide true real-time imaging of the heart. It can be used to quantitate function of both ventricles and to estimate cardiac output and regional perfusion. A recent multiinstitutional study has shown a high accuracy for the determination of the patency of coronary artery bypass grafts.

114. Diagnostic imaging in infertility. Fleischer AC, Winfield AC. It is hoped that this course will provide greater understanding of the role of radiologic imaging in the diagnostic evaluation of the infertile couple and will improve the capabilities of the radiologists who participate in the management of this group of patients. (1) The applications of sonography in the management of infertility and complicated pregnancy will be presented. The technique of transvaginal sonography will be emphasized, particularly for follicular monitoring, guided follicular aspiration, and endometrial evaluation. (2) The technique and complications of hysterosalpingography will be presented. The normal configuration of the uterine lumen and its variants will be shown. Abnormalities, such as filling defects of the uterine cavity, synechiae, and effects of maternal exposure to diethylstilbestrol, will be presented as well as more common hysterosalpinographic findings associated with uterine and tubal surgery. (3) The role of diagnostic imaging in male infertility will be reviewed.

Tuesday, May 10

201. How to invent new interventional techniques. Burhenne HJ. This will be an informal and personal presentation on the philosophy and approach underlying the invention of new radiologic techniques, such as dilatation of strictures in the biliary, alimentary, and urinary tracts; extraction of stones; and the radiologic interventional approach to the high-risk patient who has cholelithiasis. How do we convince our clinical colleagues to accept progress in radiology? Catheters and other instruments will be demonstrated, with emphasis on how to develop new technology. The discussion is directed to young, inventive radiologists who want to hear an older radiologist's experience and advice.

202. Imaging strategies and gastrointestinal and genitourinary cancer: update 1988. Sponsored by the Society for Cancer Imaging (SCI). McClennan BL, Thompson WM. The rapid advancement in new imaging technology often has created confusion as the physician attempts to make informed decisions about the application, appropriate sequencing, and cost efficacy of a variety of procedures for the evaluation of the cancer patient. Early diagnosis and therapy continue to have profound effects on prognosis and survival. This course will review and update the state-of-the-art imaging evaluation in patients who have known or suspected cancer of the gastrointestinal and genitourinary systems. The imaging strategies discussed will stress therapeutic efficacy and the patient's outcome. Current concepts in tumor staging and classification will be presented, with further emphasis on detection, definition, and treatment of the various malignancies. Recent advances in the imaging evaluation of cancer of the esophagus, colon, kidney, bladder, and prostate will be highlighted. Controversies and conflicts in imaging and treatment options will be described, and an attempt will be made to develop a flexible and pragmatic approach for both clinicians and radiologists who are faced with daily oncologic imaging and management choices.

203. Pediatric abdominal trauma. Kushner DC, Kuhn G. Appropriate management of children who have suffered abdominal trauma requires careful diagnostic imaging. The most important factors are close communication with the clinical physicians who are caring for the patient, careful planning of the imaging sequence to avoid redundant studies and excessive or unnecessary radiation to the patient or staff, and on-site monitoring by a radiologist who is involved in the diagnostic deliberations. The goals of this session are to provide a knowledge of the pathophysiology of the usual types of trauma in children. In addition, both the unique responses of children that can make accurate diagnosis difficult and the predisposing factors in childhood that can become apparent after trauma will be discussed. Also, the relationship of abused and battered children to the general practice of pediatric trauma diagnosis will be discussed. Discussion will center on the most recent and appropriate techniques of imaging pediatric trauma, with emphasis on CT and standard radiography. A final topic of discussion will be considerations of clinical management (such as sedation, restraint, the involvement of parents, and the use of contrast media) that affect the timing and sequence of imaging studies.

204. Renal hypertension: etiology, imaging, and treatment. Hillman BJ, Sos TA. Renal parenchymal and vascular disease is responsible for an imprecisely known, but important, percentage of hypertension and probably causes a disproportionate amount of hypertension-related morbidity. Advances in imaging and imaging-directed interventional techniques have made it more feasible than before to identify and treat renal hypertension. This course will present the major causes of renal hypertension, discuss pathogenesis, and show images that depict the conditions. Emphasis will be placed on appropriate imaging approaches for depiction of pathology. Experience gained in more than 500 cases of renal angioplasty will be used to discuss the indications, techniques, results, and complications of this procedure.

205. MR: basic principles (sans mathematics) and practical considerations. Gray JE, Morin RL. This nonmathematical refresher

course is an introduction to MR principles and the practical aspects of MR imaging. The course is designed for radiologists who have little or no experience with MR. Basic principles to be covered include definitions, relaxation times, MR pulse sequences, MR imaging system, contrast in MR imaging, and biological effects. Practical aspects of MR imaging include site planning, staffing requirements, problems encountered in bringing an imager on-line, details of a typical MR study, appropriate choice of patients, site security and safety, and problems and pitfalls of MR imaging. The attendee should gain a "big--picture" understanding of MR and an appreciation of some of the practical problems involved in MR imaging.

206. Modern imaging evaluation of brain tumors. Davis DO. The advent of MR scanning has changed irrevocably the strategy for detection of brain tumors. The presence of edema and/or gliosis causes an increase in the proton content, resulting in increased signal on the scans. Mass effect and shift are still reliable indicators of abnormality. The presence of matted signal intensities and bulging of the brain surface seems to correlate with increasing malignancy in supratentorial tumors. Posterior fossa tumors are much better detected with MR because no bone artifacts occur. Although CT still may play a role in the evaluation of supratentorial lesions, it is rarely necessary for lesions that are below the incisura, and in extraaxial lesions CT actually may be misleading. This course will attempt to illustrate the usual MR findings of intra- and extraaxial lesions of the intracranial space, with some CT correlation. The usefulness of gadolinium-DTPA will be discussed. The effect of image quality on detection and evaluation will be emphasized.

207. CT of the musculoskeletal system: flying high despite MR. Sartoris DJ. The purpose of this refresher course will be to review the proved and potential applications and technical considerations of CT in musculoskeletal disorders. Topics of discussion will include degenerative diseases of the spine, characterization of fractures and dislocations, staging of osseous and soft-tissue neoplasms, and evaluation of a variety of congenital abnormalities. For the investigation of articular disorders, the usefulness of computed arthrotomography will be emphasized. Comparative reference to MR imaging will be stressed throughout the presentation when appropriate, as a guide to selection of an optimal cross-sectional imaging strategy in specific situations. The role of CT-guided aspiration and biopsy in musculoskeletal disease will be considered. Technical aspects and established and future applications of multiplanar reformation and three-dimensional imaging/modeling will be discussed in depth. Quantitative implementation of CT for specific musculoskeletal problems will be addressed, with emphasis on noninvasive bone densitometry in the spine and proximal femur. The instructor will encourage active participation by the audience.

208. MR of the genitourinary system. Hricak H, Fritzsche P. Continuing improvements in image quality have increased our confidence in using MR for evaluating the genitourinary tract. (1) *Kidneys and adrenals.*—Short-TR/TE imaging sequences provide detailed anatomic information, whereas long-TR/TE imaging sequences offer excellent characterization of disease processes. Simple cysts can be differentiated from complex cystic and solid lesions. Fast imaging with gradient echoes has provided additional information in the evaluation of acute hemorrhage and vascular patency. The advantages of MR in the staging of renal and adrenal neoplasms include demonstration of tumor origin and local extension, evaluation of vascular integrity, and determination of metastatic lymphadenopathy. (2) *Urinary bladder.*—With the spin-echo technique, images with both short and long TR/TE parameters are essential for complete evaluation of the bladder. The normal or hypertrophied bladder wall can be differentiated from other disease conditions by a low signal intensity on the long-TR/TE image. Infiltrating neoplasms, however, cannot be differentiated from congestion or inflammation. MR imaging is of value in the staging of neoplasms located at the dome or the base of the bladder and in patients who have had bladder surgery, because metallic clips are not detrimental to MR images and postsurgical fibrosis can be differentiated from tumor. (3) *Prostate gland.*—Zonal anatomy of the prostate gland is seen when a spin echo with a long TR/TE is used. Although intraprostate pathologic changes can be shown, MR cannot differentiate benign from malignant disease. The value of MR is in the staging of prostatic carcinoma, including the detection of transcapsular, seminal-vesicle, and bladder-base invasion. Detection of lymph-node metastasis relies on the size of the node, and biopsy remains essential. (4) *Testis.*—The use of MR imaging has been extended for the evaluation of undescended testes and for the evaluation of testicular neoplasms when sonographic studies are inconclusive.

209. Abdominal imaging in AIDS. Federle M. Gastrointestinal disease accounts for the second largest group of diseases seen in patients who have AIDS. These consist of opportunistic infections and neoplasms, some of which are unique to AIDS (and other immunocompromised) patients, whereas others have a distinctly different biological behavior. Some of these disease processes produce radiographic findings that suggest a specific diagnosis. Although patients may have radiographic findings caused by several disease processes, the preponderant radiographic pattern may suggest the particular entity that is most responsible for clinical symptoms. As experience accumulates, additional patterns will become more clearly defined, allowing increasing accuracy in identifying the total extent and etiology of a specific disease. In this presentation, we will review the radiographic features of the most common disorders seen in the alimentary tract, biliary tree, and abdominal viscera of AIDS patients. The role of barium studies, sonography, CT, and cholangiography will be discussed. Indications for radiographic studies based on the presenting symptom complex will be discussed.

210. Vascular sonography. Gooding GAW, Gosink BB. Duplex Doppler technology, including the introduction of color, enables the examiner to find a vessel rapidly, detect flow, and assess the velocity profile and the morphology of the vessel. This discussion will focus on practical applications of these techniques. (1) *Venous disease.*—In the diagnosis of deep venous thrombosis of the lower extremities, a Doppler signal per se does not necessarily exclude the possibility of thrombosis. Ancillary abnormalities that occur with deep venous thrombosis include diminished/absent augmentation of the venous signal, an enlarged vein that fails to expand during the Valsalva maneuver, and lack of venous compressibility. These procedures are best performed on the iliac, common femoral, and superficial and deep femoral veins; and the popliteal and superficial saphenous veins. Venous sonography also can be used to evaluate obstruction of the superior vena cava. In the abdomen, it can be used in the evaluation of portal hypertension and renal vein thrombosis. (2) *Arterial disease.*—The primary use of duplex Doppler studies in arterial evaluation has been in the assessment of the carotid system. This evaluation depends on characterization of visible plaque (homogeneous, inhomogeneous, ulcerated, hemorrhagic) and on Doppler characteristics (wave form, velocities, etc.). This is an extremely accurate technique that is best used as a screening device to select those patients who then may be candidates for angiography. Duplex Doppler evaluation also can be used in evaluating abdominal arteries. The most common application in this area is assessment of renal transplants.

211. CT of disk disease and spinal stenosis. Helms CA. CT examination of the lumbar spine for diagnosis of disk disease and/or spinal stenosis has replaced myelography as the procedure of choice in most institutions. This is appropriate only if high-quality imaging is used along with adherence to sound diagnostic principles. This instructional course will review the appropriate scanning protocols and the diagnostic capabilities and limitations that can be expected with CT scanning of the lumbar spine. Pitfalls in diagnosis of disk disease will be addressed. Spinal stenosis will be discussed in categories of central canal, lateral recess, and neuroforaminal involvement. MR imaging and myelographic enhanced CT will be mentioned as alternatives to plain CT scanning, and the diagnostic accuracy of the techniques will be discussed. Use of CT in evaluating patients for surgery, treatment with chymopapain, and percutaneous nuclectomy will be discussed also.

212. Small bowel radiology: how to do it. Carlson HC, Maglinte DDT. Radiology has retained primary responsibility in the evaluation of the small bowel. The newer imaging methods, such as CT and sonography, have given radiology an added dimension in evaluating the extraluminal aspect of disease of the small intestine, but careful contrast study of the lumen and mucosa is essential in the effective, efficient, and precise detection and identification of almost all disease processes involving this segment of the gut. An update on the various barium imaging techniques will be presented: (1) the fluoroscopic small-bowel examination with oral barium, (2) the upper gastrointestinal series combined with the fluoroscopic small-bowel examination, (3) the gas-enhanced (peroral) double-contrast follow-through, (4) peroral pneumocolon, and (5) the intubation methods (enteroclysis) of small-bowel examination. Meticulously conducted small-bowel examinations are high-yield diagnostic procedures. This "how-to" course will emphasize the fluoroscopic small-bowel examination and demonstrate a simplified method of performing a "humane" enteroclysis.

213. Optimal use of chest CT and MR: when, how, and why. Feigin DS. As CT has proved its usefulness in diagnosis and management of chest abnormalities, its proper role needs to be reassessed and compared with other imaging techniques, especially MR. This course will discuss the major uses and misuses of CT and MR and will include suggestions for optimizing technique that should be tailored to specific clinic needs. CT plays a vital role in analysis of mediastinal abnormalities in view of its advantages over plain-film techniques in both sensitivity and specificity. The proper use of CT for mediastinal masses, infections, inflammations, and metastases will be outlined. Hilar and pulmonary parenchymal abnormalities will then be discussed, with emphasis on the special techniques necessary for adequate diagnosis. The use of CT in pleural abnormalities, including evaluation of empyemas, pleural plaques, and pleural vs. parenchymal abnormalities, represents a particularly difficult area for CT and MR evaluation. Finally, chest wall analysis will be demonstrated. The emerging ability of MR to show chest abnormalities must be judged in terms of advantages over CT and plain films. Analysis of the present status of MR in chest diagnosis will include a summary of the signal production of the major normal and abnormal structures in the chest. Immediate future prospects for MR in vascular and other abnormalities will be considered. Thus, the goal of this course will be to update our abilities to choose and use, most effectively, the newer imaging techniques in the analysis of chest abnormalities.

214. Obstetrical sonography. Part I. Leopold GR. The advent of high-resolution sonography has been the most important diagnostic advance in obstetrics and gynecology in the past 20 years. Today's real-time instruments allow precise outlining of most gynecologic tumors and, more recently, have aided in the diagnosis and treatment of infertility disorders. The noninvasive nature of the technique permits serial evaluation of pregnancy disorders that provides important information about the development of these conditions. Indeed, even the incidence of these disorders is now known to be quite different from that previously suspected. As a result of this knowledge, specific therapeutic approaches to some of these pregnancies is now possible. The addition of Doppler sonography also assists in physiologic evaluation of fetal blood flow and provides increased information about intrauterine growth retardation. An additional benefit of these studies is the ability to define problems unique to fetal life. The hazards of living in a frequently hostile underwater environment are a good example. Even more important is the condition of multiple pregnancy. It is now known that this condition is fraught with difficulties from frequent vascular connections and an increased rate of congenital anomalies. The sonographic evaluation of this condition is complex and requires a detailed knowledge of the physiologic principles involved, many of which are in the process of being reevaluated on the basis of sonographic data.

Wednesday, May 11

301. Fun with films (or things your mentor never told you). Jones MD. Although an increasing number of patients' visits to the modern radiology department lead to the various imaging sections, such as CT, nuclear medicine, sonography, and now MR, the greatest number of procedures are still the routine plain films and examinations. The intelligent use of plain films, with cognitive and intuitive perception and evaluation, is one of the hallmarks of practicing radiology. To this end, certain subtleties easily identified on routine examinations, which are frequently ignored or unrecognized, will provide instructional material. Intellectual challenge and educational reinforcement will be provided by a few case studies for group diagnosis. The setting will be informal and the goal will be to assist the radiologist in amazing the referring physician with the radiologist's astuteness.

302. How to get your manuscript published without a hassle. Berk RN, Hilton SVW, Whalen E. Authors who are unfamiliar with the editorial process often see the disposition of manuscripts in an editorial office as mysterious, capricious, autocratic, and unnecessarily prolonged. This course will explain how manuscripts are handled when they arrive in the editorial office. It will show authors how to reduce their chances of rejection and how to avoid the frustration of many revisions. Understanding the process helps to expedite the flow of manuscripts as they proceed from reviewers, scientific editors, copy editors, and the publisher. The *AJR* editors will discuss the content that is required in papers, describe the logical manner in which the information should be organized, and review the guidelines recommended by both the *AJR* and *Radiology* for preparing manuscripts. Authors who follow these regulations should find that their manuscripts have a better chance of acceptance and, when accepted, are more likely to be published expeditiously.

303. MR imaging and sonography of the child's genitourinary tract. Kangerloo H. Sonography is the procedure of choice in screening suspected diseases of the genitourinary tract in children. MR adds valuable information in the evaluation of renal and juxtarenal neoplasms and in the differentiation of renal from adrenal tumors. Cystic and fluid-filled lesions of the kidneys and location anomalies are evaluated well by sonography. MR is useful to evaluate compli-

cations associated with cystic diseases such as hemorrhage. Evaluation of adrenal glands, particularly adrenal tumors such as neuroblastoma, is best accomplished by using MR. Sonography, however, remains the procedure of choice for screening adrenal disease in children. Sonography also is used for screening the child's pelvis. MR adds valuable information in suspected pelvic neoplasms and in evaluation of pelvic sidewalls. MR allows flexible imaging planes and many different pulse sequences and thus permits the accurate visualization of suspected pathologic changes. MR evaluation of the kidneys and adrenal glands should begin by using a T1-weighted pulse sequence in the coronal plane. Other pulse sequences are added, depending on the initial findings. In evaluation of the pelvis, midline lesions are best imaged sagittally; pelvic sidewall lesions and those of ovaries are best imaged transaxially or coronally. T1-weighted sequences are used first, and T2-weighted sequences are added in selected cases, such as neoplasms.

304. Deep venous thrombosis and pulmonary embolism: diagnosis and intervention. Dorfman GS, Cronan JJ. It has been estimated that 20 million new cases of deep vein thrombosis (DVT) and 600,000 new cases of pulmonary embolism occur in the United States each year. The tests considered the "gold standard" for diagnosis of DVT and pulmonary embolism (contrast venography and pulmonary angiography) are expensive and time-consuming and are associated with significant morbidity and mortality rates. Long-term anticoagulant therapy is associated with morbidity in 5–30% of cases. Newer diagnostic and therapeutic techniques have begun to change the approach to thromboembolic disease. We will review the epidemiology of thromboembolic disease and the radiologic and nonradiologic diagnostic tests currently available. Specific emphasis will be placed on compression/duplex sonography and the role of pulsed Doppler sonography. Sonography rivals the sensitivity and specificity of venography without the disadvantages of injection of contrast material and with the additional capabilities of imaging the vein and surrounding tissues with sequential examinations. The available options for treatment, including thrombolysis and placement of a percutaneous caval filter, will be described in detail. Because of the ease and safety of placement of a percutaneous filter, an expanding number of indications for caval interruption in addition to or instead of anticoagulation are now being espoused. Potential pitfalls, refinements in techniques, and anticipated success rates of percutaneous placement of filters in the inferior vena cava will be discussed. In conclusion, strategies for diagnosis and treatment of thromboembolic disease in a variety of clinical situations will be presented based on the previously discussed material. The presentation will use videotapes and slides of duplex sonographic examinations and placement of caval filters to demonstrate the actual procedures in a "how-to-do-it" format.

305. MR of the abdomen. Stark DD. Clinical applications of MR imaging in the diagnosis of abdominal disorders are now established. Efficacy of MR is determined with respect to the performance and expense of alternative imaging techniques. In this course, both theoretical and practical topics are reviewed: (1) *Pulse-sequence optimization for detecting liver metastases.*—T1- and T2-weighted spin-echo, inversion-recovery, chemical-shift, and fast-scanning techniques will be compared with contrast-enhanced CT. (2) *Reduction of motion artifacts.* (3) *Tissue characterization of liver lesions.*—Characteristic MR features of hepatic hemangiomas and cysts allow differentiation from metastases with 90% accuracy on T2-weighted spin-echo images. (4) *Chemical-shift imaging.*—This technique is applied to identification of diffuse and focal deposition of fat and to improved detection of liver metastases. (5) *Paramagnetic agents*—gadolinium-DTPA and hepatobiliary targeted complexes, such as Fe-HBED, will be compared with superparamagnetic iron oxide (ferrite) particles targeted to reticuloendothelial cells. Contrast agents improve detection of liver lesions by increasing contrast-to-noise per unit time. Rapid patient throughput, improved image quality, and more accurate diagnostic results can be achieved with these new techniques.

306. Neuroradiology of cerebrovascular disease. Brant-Zawadzki M. (1) The diagnosis of acute cerebral infarction on CT studies is difficult, especially within the first 24 hr of such an injury. Early reports stated that CT scanning was unrevealing within the first 48 hr in most cases. After a first "negative" study, follow-up CT scans often are needed to document the site and extent of infarction that is manifest clinically. Newer generations of CT scanners have allowed evaluation of hyperacute changes of cerebral infarction. In our experience, CT can provide evidence of acute infarction within 24 hr in well over 50% of the patients so affected. Noncontrast CT is essential, as injection of contrast material can mask the area of low density produced by the early cytotoxic edema in the brain. Compared with that of CT, the sensitivity of MR to changes in tissue water permits superior detection of cerebral infarction. In more than 20 patients with cerebral infarction of various causes and of different chronicity studied at our institution, MR illustrated this advantage. (2) Digital subtraction angiography (DSA) has all but replaced conventional film-screen technique in our neuroradiologic practice. At first, the IV technique was evaluated for assessment of extracranial cerebral vascular disease, but this technique was inadequate. The role of IV angiography has been relegated to one of screening, somewhere between that of carotid sonography and techniques that require intraarterial injection. On the other hand, the efficiency and high quality of DSA in conjunction with intraarterial injections has allowed us to perform conventional neuroradiologic angiography in much shorter times, with lesser amounts of contrast agent. This results in both an added safety factor for the patient and an economic benefit to the physician and hospital. Outpatient arteriograms are being performed more and more frequently with the addition of DSA image acquisition. Several centers are using selective vessel catheterization for such studies. A retrograde brachial catheterization of the aortic arch with a multisidehole 4-French catheter is used for evaluation of outpatients for cerebrovascular disease.

307. MR of the musculoskeletal system. Bassett LW, Seeger LL. Applications of MR imaging to the musculoskeletal system are increasing. This course presents our experience with MR, with emphasis on the knee, shoulder, and hip. For each region, the presentation includes a review of normal anatomy on MR and the evaluation of musculoskeletal trauma, tumors, and infection. MR evaluation of the knee has replaced arthrography almost completely in our practice. Meniscal tears are well visualized, and injuries of the cruciate and collateral ligaments can be identified. MR is useful in the evaluation of shoulder impingement syndrome and in disease and instability of the rotator cuff. Arthrography may detect smaller tears of the rotator cuff, but bursitis and tendonitis are identified on MR only. Shoulder instability can be evaluated by MR or CT-arthrography, and both methods have merits. MR is more sensitive than radionuclide scanning for the detection of ischemic necrosis; however, MR examinations may result in false-positive findings. Plain films and clinical correlation should be combined with the MR patterns when a diagnosis of ischemic necrosis is made. MR is being used to evaluate the extent of both primary tumors of bone and osseous metastases. We have identified three circumstances in which MR may have a significant effect on the management of patients: (1) patients are symptomatic but the results of conventional studies are negative, (2) abnormalities seen on radiographs or scintigrams are equivocal, and (3)

the extent of a tumor must be determined. MR is a sensitive technique for imaging osteomyelitis. On T1-weighted images, infection will show intermediate to decreased signal. With T2-weighted imaging, the involved area shows increased signal intensity, even higher than that of normal bone marrow.

308. Urinary stone disease: update 1988. LeRoy AJ, Barbaric ZL. Symptomatic renal and urteral calculi continue to be a frequent cause of morbidity, affecting up to 4% of the population in the United States. Diagnosis of these diseases and treatment of these patients is based extensively on the radiologic examination, which traditionally includes plain films of the kidneys, urinary tract, and bladder; tomography; and urography. A more thorough delineation of the extent of disease and of complications, such as renal atrophy, abscess, or perinephric involvement, can be obtained by sonography and CT. Experience with MR imaging in this area is evolving also. The usefulness and application of these various examinations in evaluation of urolithiasis will be reviewed in this course. The therapy of urolithiasis has changed dramatically in the past decade, and current therapeutic techniques and their applications will be discussed. The clinical usefulness of extracorporeal shock-wave lithotripsy (ESWL) for treatment of most stones of the upper tract is widely accepted. However, this will be modified by the progressive technological evolution of the newer lithotriptors and by the long-term evaluation of the complications and success rates of ESWL. Because of the inability of ESWL to treat succesfully all stones of the upper tract, some centers continue to use percutaneous methods to remove stones. Radiologic involvement in all methods continues at several levels, extending from simple percutaneous nephrostomy placement to complex endourologic manipulations, including removal of stones, dilatation of strictures, and stenting procedures. The extensive development of retrograde transurethral ureteroscopy also has modified treatment of kidney stones, introducing laser fragmentation and endoscopic manipulation. A few patients still undergo standard surgical approaches, especially when coexisting anatomic abnormalities require revision. The financial impact of and considerations of patients' tolerance for these therapies will be discussed.

309. Pancreatic inflammatory disease: radiologic diagnosis, staging, and management of complications. Freeny PC. New concepts regarding the radiologic diagnosis and classification of inflammatory disease of the pancreas have been developed over the past several years. In addition, radiology has assumed a critical role in the staging of patients with acute pancreatitis, and various interventional techniques have been applied to the management of many of the associated complications. This course will discuss the radiologic classification of pancreatic inflammatory disease developed at the Cambridge (1983) and Marseille (1984) international meetings. The classification correlates the clinical, pathologic, and functional exocrine status of the pancreas with the morphologic changes shown on sonographic, CT, and endoscopic retrograde cholangiopancreatographic examinations. The critical role of clinical and radiologic staging of patients who have acute pancreatitis also will be discussed. In particular, the role of CT in predicting the clinical outcome of patients who have acute pancreatitis will be emphasized. The central role of radiology in early diagnosis and detection of a variety of complications of pancreatitis also will be presented. In particular, the complications of pancreatic fluid collection and abscess formation, pancreatic phlegmon, pancreatic ascites, biliary tract and gastrointestinal involvement, vascular complications, and pulmonary complications will be discussed. Emphasis will be placed on indications, techniques, and results of interventional procedures for treatment of these complications, particularly percutaneous drainage of pancreatic fluid collections, pseudocysts, and abscesses; angiographic management of vascular complications of pancreatitis; and treatment of biliary complications.

310. Sonography of the rotator cuff and of the infant's hip. Crass JR, Harcke HT. This refresher course will review the recently developed roles of sonography in the evaluation of the rotator cuff and of the infant's hip. (1) Sonography of the rotator cuff is used primarily for the diagnosis of tears of the cuff; it also may play a role in the diagnosis of the subacromial impingement syndrome. The anatomy of the rotator cuff will be reviewed as it relates to scanning technique. Easily learned methods for positioning the patient and methods of scanning that will result in consistently diagnostic images will be demonstrated. The spectrum of sonographic findings in both the normal and the abnormal tendon will be illustrated. An approach to the abnormal but apparently intact tendon will also be presented, including a discussion of the abnormally echogenic tendon. (2) Sonography of infants' hips is used both for detecting congenital dislocation and/or dysplasia and for monitoring the hips during treatment. It is a highly accurate method because structures not visualized on plain films are identified clearly. The dynamic method of evaluation will be reviewed, with emphasis on the three routine views and stress maneuvers. Normal sonograms will be compared with cases of subluxation and dislocation to emphasize the spectrum of abnormalities in congenital dislocation of the hip. Integration of sonography with other imaging techniques will be discussed.

311. MR of the spine: degenerative disease. Modic MT. The role of MR in the evaluation of degenerative diseases of the spine has gone far beyond the original clinical expectations and today has many well-defined applications. The technique is still evolving, and ongoing research and development in coil technology and pulse sequences continue to improve our capability in the evaluation of these diseases. The type of MR examination will be influenced primarily by the anatomic region studied and the suspected disease process. Although the anatomic region usually is defined clearly, the suspected process may include several differential considerations, such as disk herniation, canal stenosis, facet disease, and malalignment abnormalities, that may require specific techniques. MR also may provide us with insight into the changes in signal intensity that are noted within the vertebral bodies in the presence of degenerative disk disease and that can predict the histologic changes. The role of MR in evaluating the spine after surgery also has grown in importance, particularly with the use of gadolinium-DTPA. This presentation will explore technical considerations and pulse sequences in the evaluation of degenerative disease and will correlate MR findings with both surgical and histologic observations. The role of gadolinium-DTPA in both the virgin and postoperative spine will be discussed.

312. Biliary lithotripsy. Ferrucci JT, Burhenne HJ. Extracorporeal lithotripsy of biliary calculi soon may become the standard of care for patients who have symptomatic gallstones, thus replacing cholecystectomy, currently the most common major abdominal operation. Accumulated experience with several different lithotriptor systems in Europe and several hundred patients indicates a high degree of success with low morbidity. Clinical trials are beginning now in some 10–20 centers in the United States and Canada. This course will review the diverse issues raised by this new therapeutic option, including differences between renal and gallstone lithotripsy and differences between fragmentation of gallstones and of common duct stones. Design principles of second-generation shock-wave lithotriptor systems will be discussed, including the lack of an immersion water tank and the use of more efficient spark-gap generators as well as piezoelectric sound-wave generators. Most second-genera-

tion devices will also use ultrasound targeting for both renal and biliary calculi. Adjuvant oral bile-acid therapy for dissolution of cholesterol gallstone fragments also may play an important role. Preliminary clinical results indicate an 80–90% success rate (gallstone-free), with negligible acute complications when primarily IV analgesia only is used. As the volume of potential patients for lithotripsy of renal stones diminishes, gallstone therapy will dominate the lithotripsy marketplace. Because of the critical role of ultrasound targeting, fluoroscopy and digital image manipulation, and the decreasing requirements for analgesia, radiologists should play a much larger role in lithotripsy of gallstones than they were permitted to do in the lithotriptor treatment of urinary calculi.

313. Pulmonary thromboembolism. Dunnick NR, Ravin CE, Sullivan DC. Pulmonary embolism is a common medical problem, yet one that eludes confident clinical diagnosis. Thus, radiographic imaging techniques are essential in helping to make appropriate decisions about treatment. Although nonspecific, the chest radiograph is useful to augment interpretation of the radionuclide ventilation-perfusion (V/Q) scan and to identify other abnormalities that may account for the patient's symptoms. By comparing radionuclide images of pulmonary perfusion and ventilation, regions of mismatch are identified and correlated with the chest radiograph. The number and size of these mismatched regions allow a classification ranging from normal to high probability of pulmonary embolus. Unfortunately, most patients will have a combination of scintigraphic and radiographic findings that fall into the moderate-probability or indeterminate categories. To increase diagnostic certainty in these patients, in patients in whom the results of the V/Q scan are not consistent with the clinical suspicion, or in patients who have a high-probability scan but a contraindication to anticoagulation, pulmonary arteriography may be necessary. This should be performed with selective injections into the region of the highest probability for pulmonary embolus, as judged by the V/Q scan. Careful technique and measurements of pulmonary artery pressure will help to minimize complications from this invasive procedure. Correlation of angiography with V/Q scans and a protocol for examining these patients will be presented.

314. Obstetrical sonography. Part II. Filly RA. **See 214.**

Thursday, May 12

401. A simplified approach to the radiologic examination of the small bowel. Margulis AR. The small bowel can be examined radiologically as part of the upper gastrointestinal examination, by enteroclysis, by peroral pneumocolon, and by retrograde injection via the ileocecal valve (the Roscoe Miller technique). In peroral examinations of the small bowel, the following should be observed: (1) distribution of the small bowel in the peritoneal cavity, (2) width of the small bowel, (3) width of folds, (4) appearance of folds and mesenteric impressions, (5) presence of nodules, (6) dilution, (7) ulcerations, (8) cavitations, and (9) masses. The relationships of these signs singly or in groups will be associated with pathologic changes and disease syndromes. In informal discussion with the participants, the relationships of radiologic signs, clinical history, and laboratory tests will be related to pathologic changes. The Sherlock Holmes approach will be emphasized.

402. SPECT imaging in clinical nuclear medicine. Handmaker H, Bunker SR. The shift toward tomography with the newer morphologic imaging techniques of CT, sonography, and MR imaging is challenging nuclear medicine to optimize the inherently limited spatial resolution of its uniquely physiologic imaging procedures. It is therefore logical that single-photon emission computed tomography (SPECT), with its considerable improvements in contrast resolution, is displacing conventional planar scintigraphic routines so rapidly. This evolution toward tomography has been facilitated by major advances in computerized image-processing technology. It also is not surprising that SPECT is accepted so readily by the medical community; the tomographic image format provides convenient correlation with CT, sonography, and MR. Our experience over the past 4 years indicates that SPECT provides improved sensitivity and specificity to existing procedures. SPECT is the preferred technique for all exercise and dipyridamole stress thallium-201 myocardial perfusion examinations, limited ^{99m}Tc–methylene diphosophonate skeletal evaluations, and ^{99m}Tc–sulfur colloid liver-spleen studies. Additional studies can be performed with SPECT as a function of available camera time and the potential for improved diagnostic yield from tomography. Currently, aproximately 50% of our department's procedures and revenues are generated by SPECT studies. It is our belief that with the development of newer and more specific radiopharmaceuticals and the continued availability of SPECT techniques, this figure may exceed 75% in the future.

403. CT and MR of diseases of childhood. Brasch RC, Gooding CA. (1) The technology of CT has continued to evolve since its introduction into radiology more than a decade ago. Ultrafast computed tomography, also called cine CT, is a relatively new technique that offers an easy, quick, minimally invasive means of acquiring quantitative, dynamic images of infants and children. Ultrafast CT technique, with its data-acquisition time of 0.05–0.1 sec, was developed originally for real-time imaging of the heart, but recently it has been shown to be useful in the evaluation of diseases of the airway, abdomen, and head. The extremely rapid acquisition times of ultrafast CT virtually eliminate the motion artifacts associated with spontaneous respiration and bowel peristalsis that may be observed on conventional CT images. Finally, ultrafast CT in children requires less time to prepare than conventional CT; thus, infants spend less time in the CT suite and thereby the risks associated with hypothermia are decreased. (2) The clearest advantages of MR have been for imaging the CNS, and reports comparing MR and CT for the CNS indicate that MR is superior. In the thorax, MR has been effective in delineating the extent of pulmonary lesions such as cystic fibrosis and mediastinal abnormalities such as lymphoma. MR of congenital heart disease is an exciting application of this new technique. The usefulness of MR as a primary technique for imaging the child's abdomen is less clear than for other anatomic regions, in part because CT and sonography have shown considerable value in the diagnosis of abdominal disease. MR of the skeletal system of children has several unique applications, particularly the diagnosis of acute lymphocytic leukemia, congenital dislocation of the hip, and bone tumors. It is anticipated that improvements in MR technology, such as more rapid image-acquisition sequences, will have a favorable impact on the application of MR in the diagnosis of diseases in children.

404. Acquired diseases of the aorta and peripheral vasculature. Shetty PC, Haggar AM. This presentation will review the use of angiography in patients who present with atherosclerotic or other acquired diseases of the aortic and peripheral vasculature, including aortic dissection and trauma. Emphasis will be placed on the correct application of various techniques such as transfemoral, transaxillary, and translumbar approaches to catheter placement. The role of IV and interarterial digital subtraction angiography will be discussed. In addition, the proper role of correlative imaging techniques, such as

sonography, CT, and MR will be presented: Experience with an outpatient angiography program will be described, including a discussion of the inclusion criteria for patients, postprocedure monitoring, and outcomes based on more than 500 studies.

405. Technical advances in clinical MR imaging: fast scanning, surface coils, contrast agents. Edelman RR, Kneeland JB, Saini S. This course will focus on clinical applications of recent technical developments in MR. (1) *Fast scanning* is becoming increasingly useful as a means of reducing image degradation due to patient motion and maximizing patient throughput. Gradient-echo pulse sequence is one such technique that is widely available and can provide subminute images. Tissue contrast is based on differences in T1 or T2* times and is based on appropriate selection of TR, TE, and flip angle. Clinical applications that will be discussed include rapid MR myelography, fast three-dimensional imaging of the knee, dynamic imaging of the temporomandibular joints, breath-holding imaging of the upper abdomen, identification of hemorrhage, flow imaging, and MR cineangiography. (2) *Surface coils* play an integral role in clinical MR imaging, primarily for improving anatomic resolution. The basic principles of surface-coil operation and practical considerations with regard to their use will be presented. The following topics will be included among others: ultrahigh-resolution coils (<0.3 mm pixel size) for evaluation of bones and joints of the hand and wrist, intracavity coils for the rectum and vagina for prostatic and uterine imaging, and parallel data-acquisition technique that allows simultaneous acquisition of images from two regions of the body. (3) *MR contrast agents* alter tissue signal intensity and have been advocated for improving soft-tissue contrast, characterizing tissue, and showing physiologic processes in vivo. The principles of pharmaceutical manipulation of MR contrast agents and practical considerations for their clinical application will be explored. Gadolinium-DTPA has undergone clinical evaluation, and the dicussion will include its role in imaging diseases of the brain (e.g., differentiating tumor from edema, identifying active foci of multiple sclerosis); spinal cord (detecting metastases); and abdomen (e.g., detecting liver metastases, marking bowel). Investigations with novel magnetopharmaceuticals, such as those with reticuloendothelial specificity (ferrites) and hepatobiliary excretion (Fe-EHPG), that will eventually have a more disease- and organ-specific clinical application will also be presented.

406. Neuroimaging of the sellar region, including MR. Davis KR. Normal anatomy of the sellar region will be reviewed and correlated with images to provide a framework for recognition of abnormal findings. This may be divided into the (1) intra-, (2) para-, (3) supra-, (4) infra-, and (5) retrosellar areas. A variety of common abnormalities encountered in this region will be illustrated with emphasis on (1) MR features and role in evaluation, (2) pattern and sequence of neuroimaging evaluation via MR, and (3) neuroimaging approach if MR is unavailable. Emphasis will be given to the diagnostic strength and importance and to the limitations of each type of neuroimaging procedure.

407. MR of musculoskeletal trauma and neoplasia. Berquist TH, McLeod RA. Musculoskeletal abnormalities represent the most common nonneurologic application of MR imaging. When studies of the CNS are excluded, 85% of our remaining studies are for suspected musculoskeletal disease or injury. Trauma and neoplasm are the two most common conditions leading to the MR examination. Imaging techniques (pulse sequences, coil selection, image planes, field of view, matrix size, and slice thickness) and selection of patients will be reviewed as they apply to MR examination for trauma and neoplasms. Multiple image planes and the ability to clearly define vessels, nerves, tendons, ligaments, and articular and meniscal cartilage make MR an ideal screening technique for soft-tissue and articular injuries. Extraarticular injuries (muscle tears, nerve compression, compartment syndromes, etc.) were difficult to image accurately before MR became available. The value of MR in assessing acute and chronic injuries will be discussed. Comparison with other imaging techniques and the variable appearance of hematoma and hemorrhage (factors largely responsible for MR changes) will be emphasized. MR has several advantages in the evaluation of patients who have musculoskeletal neoplasms. The contribution of MR to the care of these patients will be discussed and illustrated. Emphasis will be placed on tumor detection, diagnosis, staging, and posttreatment evaluation. MR will be compared with other imaging techniques, and recommendations will be given for the proper ordering and sequencing of the various imaging procedures. The common tumor simulators will be discussed and demonstrated.

409. Genitourinary imaging strategies—1988. Davidson AJ, Talner LB. Current approaches to two important uroradiologic problems are presented in this course. The first part focuses on problems in the diagnosis of urinary tract obstruction. Various causes of obstruction and the most direct approaches to their diagnosis are considered. The second part of the course discusses discriminating features and imaging strategies in the diagnosis of renal masses. The use of demographic data, specific imaging characteristics, and the choice of diagnostic techniques are considered in detail.

409. The modern approach to imaging acute abdominal disorders. Jeffrey RB, Baker SR. This course will focus on plain-film radiography, CT, and sonography of clinically important abdominal disorders. The emphasis will be on abnormalities that are difficult to diagnose clinically or are unsuspected before imaging. The plain-film abnormalities will include pneumoperitoneum, intraabdominal abscess, and intestinal obstruction. In addition, selected aspects of bowel ischemia, acute appendicitis, and blunt abdominal trauma will be discussed, especially their CT and sonographic manifestations.

410. Ultrasound image interpretation. Is it real or is it an artifact? Cooperberg PL. Most general sonologists do not need to understand all of the physics involved in the production of sonographic images. However, many types of artifacts that are not related to anatomic structures within the body can appear on sonographic images. It is important to understand the underlying physical principles to appreciate the causes of these artifacts and to be able to differentiate spurious echoes from real pathologic changes. Among the types of artifacts to be described, displayed, and explained are reverberation artifacts, ring-down artifacts, off-axis artifacts, and the various kinds of acoustic shadowing. Although a review of these types of pitfalls in sonographic diagnosis may suggest that diagnoses never can be made, it must be remembered that these difficulties arise only rarely, and most of the time we can make clinically useful diagnoses.

411. Osteoporosis: pathogenesis, consequences, and bone-mineral density. Genant HK, Rogers LF. Osteoporosis and its consequences have emerged as a matter of great public concern. The principal effect of osteoporosis is an increased incidence of fractures, with their attendant morbidity and mortality and cumulative cost of treatment. The radiologist's role in the diagnosis of fractures will be reviewed, particularly the diagnosis of the more obscure injuries and insufficiency fractures peculiar to those affected. Determinations of bone-mineral density have emerged as a potentially important tool in the diagnosis, management, and prevention of osteoporosis. Single-photon and dual-photon absorptiometry (SPA and DPA) and quanti-

tative CT will be discussed and compared. The rationale for current therapeutic regimens will be reviewed.

412. Imaging of inflammatory bowel disease. Goldberg H, Thoeni R, Wall S. In this instructional course, the features of both idiopathic inflammatory disease and inflammation that is the result of known causative agents will be discussed. The major radiographic features of idiopathic ulcerative colitis and Crohn disease will be discussed, indicating that in most cases, when the proper radiographic techniques are used, these two disease processes can be differentiated. Important techniques for the detection and characterization include the double-contrast barium enema, use of the enteroclysis technique for the detection of small bowel lesions, and use of the peroral pneumocolon for the evaluation of the terminal ileum. The use of sonography and CT scanning for the evaluation of inflammatory bowel disease will be demonstrated. In particular, Crohn disease has many features detectable by both sonography and CT, including not only wall thickening, but also mesenteric thickening due to phlegmon, abscess, or simple mesenteric fatty proliferation. In addition, the use of CT for the evaluation of fistulae will be emphasized. Inflammatory processes caused by specific agents have been elucidated more recently. These include the various unusual organisms found in immunosuppressed patients, particularly those who have AIDS, that result in a wide variety of findings from the esophagus to the anus. In addition to diseases such as cryptosporidiosis and infections caused by cytomegalovirus, herpes virus, *Myobacterium avium intercellulare*, and *Candida* that are found in immunosuppressed patients, the gastrointestinal tract can be altered radiographically by giardiasis and by bacterial agents such as *Campylobacter* and *Yersenia*.

413. Interventional radiology in the thorax and pleural space. Mueller PM, vanSonnenberg E. This course will cover all aspects of intervention in the thorax, including biopsy of parenchymal, mediastinal, and pleural lesions; treatment of pneumothoraces; drainage and sclerosis of malignant effusions; and drainage of empyema collections. The course will be divided into several sections, with ample time devoted to discussions in each. The first section will cover guided biopsy of parenchymal, mediastinal, hilar, and pleural lesions. The advantages and disadvantages of fluoroscopy vs CT vs sonography, principles of access, technique, types of needles used, rate of complications, and results will be given. The second portion of the course will be devoted to the various methods used in the treatment of iatrogenically created pneumothoraces, including needle aspiration, catheter insertion, and use of the Heimlich valve. A discussion of the mechanics and appropriate use of Pleur-evacs will be given. The third part of the course will be devoted to the use of sonography and CT for aspiration and drainage of a variety of pleural fluid collections. Methods for sclerosis of benign and malignant effusions will be discussed. Finally, indications for drainage and the management of patients who have empyema collections will be covered.

414. Endoluminal sonography: transvaginal and transrectal. Laing FC, Rifkin MD. Endovaginal pelvic sonography recently has been shown to be of value for evaluating patients who have obstetric complications or gynecologic diseases. Because the transducers used for this examination are placed in close contiguity to the area of interest (when compared to transabdominal transducers), higher frequency probes can be used. The result is improved spatial resolution. Obstetric applications include evaluation of infertility, early complications of pregnancy, ectopic pregnancy, second-trimester placenta previa, and incompetent cervix. Gynecologic applications include evaluation of endometrial pathologic changes; localization of intrauterine devices; evaluation of myometrial texture, pelvic inflammatory disease, and adnexal masses; and assessment of free fluid in the pelvis. Advantages of this technique include (1) improved acceptance by patients (in comparison with abdominal scans) because bladder distension is not required and (2) superior anatomic detail. The primary limitations include orientation difficulties and a limited field of view. Endorectal sonography has been used for evaluation of the prostate for the past 20 years and for evaluation of rectal cancer for the past 3 years. With the improvement in equipment, smaller lesions now can be diagnosed. For prostatic cancer, the technique has major advantages: evaluation of nonpalpable cancer; confirmation of questionable areas of abnormality found on digital rectal examination; and, most importantly, accurate guidance for biopsy. It also is useful in staging of prostatic cancer and in follow-up for the efficacy of treatment. The major benefit of evaluation of rectal cancer is for local staging. Sonography appears to be more accurate than other imaging studies (e.g., barium enema and CT). Although sonography does not detect small cancers as well as the clinical studies do, it more accurately defines extension through the wall of the rectum and involvement of local lymph nodes.

Friday, May 13

Symposium of Chest Imaging Update. See Table 3 for topics and instructors. Register on registration form for this complimentary program.

TABLE 3: Chest Imaging Update

Topic/Time	Presenter
Computed Tomography	Moderator: Stewart Sagel
8:00 a.m.	Overview (*Sagel*)
8:10 a.m.	Focal lung disease (*Zerhouni*)
8:35 a.m.	Diffuse lung disease (*Müller*)
9:00 a.m.	Staging of bronchogenic carcinoma (*Pugatch*)
Interventional Radiography	
9:25 a.m.	Intrathoracic drainage procedures (*Westcott*)
9:45 a.m.	Percutaneous biopsy of central lesions (*Weisbrod*)
Digital Imaging	Moderator: Carl Ravin
10:25 a.m.	Overview (*Ravin*)
10:35 a.m.	Digital angiography (*Barth*)
10:55 a.m.	Digital radiography (*MacMahon*)
Magnetic Resonance Imaging	Moderator: Gordon Gamsu
11:15 a.m.	Overview (*Gamsu*)
11:25 a.m.	Intrathoracic vascular lesions (*Webb*)
11:50 a.m.	Applications of MRI of the thorax (*McLoud*)

Note.—There is no fee for this symposium. However, to facilitate planning, please register on the meeting registration form.

ACR Luncheon Presentations on Socioeconomics of Radiology

A series of luncheon presentations on the socioeconomics of radiology will be arranged by the American College of Radiology (ACR). A box lunch will be provided. The presentations do not conflict with other elements of the program. Advance registration is required. Cost per session is $12.

Date, Topic, Speaker

Monday, May 9: Governmental Issues, Otha W. Linton, associate executive director, ACR

Tuesday May 10: Alphabet Soup: RAPS, RVS, AMA, HFCA, etc., Thomas Meaney, M.D. or Franklin Angell, M.D.

Wednesday, May 11: Marketing of Radiology, Michael Lopiano, M.D.

Thursday, May 12: PPO-RVS Study Progress, James Moorefield, M.D.

Faculty List

Adler, Dorit D., University of Michigan School of Medicine
Alcorn, Franklin S., Rush-Presbyterian–St. Lukes Medical School
Baker, Stephen R., Albert Einstein College of Medicine
Barbaric, Zoran L., University of California, Los Angeles
Bassett, Lawrence W., University of California, Los Angeles
Barth, Klemens H., Georgetown University Hospital
Berk, Robert N., Editor, *American Journal of Roentgenology*
Berquist, Thomas H., Mayo Clinic Foundation
Bradley, William G., Jr., Huntington Medical Research Institute
Brant-Zawadzki, M., University of California, San Francisco
Brasch, Robert C., University of California, San Francisco
Brenner, R. James, Cedars-Sinai Medical Center
Bunker, Stephen R., Children's Hospital of San Francisco
Burhenne, H. Joachim, University of British Columbia
Carlson, Harley C., Mayo Clinic Foundation
Cooperberg, Peter L., University of British Columbia
Crass, Jeffrey R., State University of New York at Stony Brook
Cronan, John J., Rhode Island Hospital
Daffner, Richard H., Allegheny General Hospital
Davidson, Alan J., Armed Forces Institute of Pathology
Davis, David O., George Washington University Medical Center
Davis, Kenneth R., Massachusetts General Hospital
Dorfman, Gary S., Rhode Island Hospital
D'Orsi, Carl J., University of Massachusetts Medical School
Drayer, Burton P., St. Joseph's Hospital and Medical Center
Dunnick, N. Reed, Duke University Medical Center
Edelman, Robert R., Grossmont Hospital
Federle, Michael, University of California, San Francisco
Feig, Stephen A., Jefferson Medical College
Feigin, David S., University of California, San Diego
Ferrucci, Joseph T., Massachusetts General Hospital
Filly, Roy, University of California, San Francisco
Fleischer, Arthur C., Vanderbilt University
Forrester, Deborah M., University of Southern California
Freeny, Patrick C., Virginia Mason Clinic
Fritzsche, Peggy J., Loma Linda University Medical Center
Gamsu, Gordon, University of California, San Francisco
Genant, Harry K., University of California, San Francisco
Ghahremani, Gary G., Evanston Hospital–McGaw Medical Center of Northwestern University
Goldberg, Henry I., University of California, San Francisco
Gooding, Charles A., University of California, San Francisco
Gooding, Gretchen A. W., University of California, San Francisco
Gosink, Barbara B., University of California, San Diego
Gray, Joel E., Mayo Clinic Foundation
Haggar, Allan M., Henry Ford Hospital
Handmaker, Hirsh, Children's Hospital, San Francisco
Harcke, H. Theodore, Alfred I. du-Pont Institute
Helms, Clyde A., University of California, San Francisco
Higgins, Charles B., University of California, San Francisco
Hillman, Bruce J., University of Arizona, Tucson
Hilton, Saskia, associate editor, *American Journal of Roentgenology*
Hricak, Hedvig, University of California, San Francisco
Jacobson, Harold G., Albert Einstein College of Medicine
Jeffrey, Brooke, University of California, San Francisco
Jones, Malcolm D., University of California, Irvine
Kangarloo, Hooshang, University of California, Los Angeles
Kerr, Roger, University of Southern California Medical Center
Kneeland, Bruce, Milwaukee County Hospital
Kopans, Daniel B., Massachusetts General Hospital
Kuhn, Gerald, Buffalo Children's Hospital
Kushner, David C., Massachusetts General Hospital
Laing, Faye C., University of California, San Francisco
Leopold, George R., University of California, San Diego
Leroy, Andrew J., Mayo Clinic Foundation
Lipton, Martin J., University of California, San Francisco
Logan, Wende W., Millard-Fillmore Hospital
MacMahon, Heber, University of Chicago Medical Center
Maglinte, Dean D. T., Methodist Hospital of Indiana
Maklansky, Daniel, Mt. Sinai Medical Center
Margulis, Alexander R., University of California, San Francisco
McClennan, Bruce L., Washington University of St. Louis
McLean, Gordon K., University of Pennsylvania
McLelland, Robert, University of North Carolina School of Medicine
McLeod, Richard A., Mayo Clinic Foundation
McLoud, Theresa C., Masachusetts General Hospital
Merritt, Christopher B., Ochsner Clinic
Modic, Michael T., University Hospitals of Cleveland
Morin, Richard L., Mayo Clinic Foundation
Moskowitz, Myron, University of Cincinnati
Moss, Albert A., University of Washington
Mueller, Peter R., Massachusetts General Hospital
Müller, Nestor, University of British Columbia
Newman, Beverley, University of Pittsburgh
Newton, Hans, University of California, San Francisco
Norman, David, University of California, San Francisco
Oh, Kook S., University of Pittsburgh
Paulus, David D., M.D. Anderson Hospital & Tumor Institute
Pugatch, Robert D., Brigham and Women's Hospital
Ralls, Philip W., University of California, Los Angeles
Ravin, Carl E., Duke University Medical Center
Rebner, Murray, University of Michigan School of Medicine
Rifkin, Matthew D., Thomas Jefferson University Medical Center
Ring, Ernest, University of California, San Francisco

Rogers, Lee F., Northwestern University Medical School
Rosenquist, C. John, University of California, Davis
Sagel, Stuart S., Mallinckrodt Institute of Radiology
Saini, Sanjay, Massachusetts General Hospital
Sartoris, David J., University of California, San Diego
Seeger, Leanne L., University of California, Los Angeles
Shetty, P. C., Henry Ford Hospital
Shuman, William P., University of Washington
Sickles, Edward A., University of California, San Francisco
Sos, Thomas A., New York Hospital–Cornell Medical Center
Stark, David D., Massachusetts General Hospital
Sullivan, Daniel, Duke University Medical Center
Talner, Lee B., University of California, San Diego
Taylor, Kenneth J. W., Yale University School of Medicine
Thoeni, Ruedi, University of California, San Francisco
Thompson, William M., University of Minnesota, Minneapolis
Troupin, Rosalind H., University of Pennsylvania
vanSonnenberg, Eric, University of California, San Diego
Wall, Susan, University of California, San Francisco
Webb, W. Richard, University of California, San Francisco
Weisbrod, Gordon L., Toronto General Hospital
Westcott, Jack, New York Hospital–Cornell Medical Center
Whalen, Elizabeth, *American Journal of Roentgenology*
Winfield, Alan C, Vanderbilt University
Zerhouni, Elias A., The Johns Hopkins Hospital

American Roentgen Ray Society 1988 Scientific Program

The scientific program is divided into parallel sessions so that registrants may choose topics related to their interests. A total of 189 papers will be presented Monday–Thursday, May 8–12. In addition, on Wednesday morning, May 11, a special session will be devoted to award-winning papers and the Caldwell Lecture, to be delivered by Donald Resnick of San Diego. On Friday, May 13, there will be a special 4-hr symposium, Chest Imaging Update.

Monday, May 9, 10:30 a.m.–12:30 p.m.

I. Chest Imaging: I

10:30 1. **Peripheral right upper lobe atelectasis.** Gurney J, Thorsen M, Goodman L

10:42 2. **MRI of superior sulcus tumors.** Pearlberg J, Haggar A

10:54 3. **Role of computed tomography in evaluation of pleural effusions of unknown etiology.** Bourgouin P, McLoud T, Moore E, Shepard J

11:06 4. **Percutaneous catheter drainage of pleural fluid collections.** Merriam M, Dorfman G, Cronan J

11:18 5. **Chest wall venous collaterals: CT indicator of systemic venous hypertension.** Mantello M, White M

11:30 6. **The reliability of mobile-unit radiography for predicting extravascular lung water.** Anderson D, Glazer H, Eisenberg P, Hansbrough J, Schuster D

11:42 7. **Detection of calcification in solitary pulmonary nodules using dual-energy digital radiography.** Sanders C, Sabbagh E, Barnes G, Fraser R

11:54 8. **High-resolution CT in assessment of sarcoid lung disease: correlation with pathology and other staging methods.** Lynch D, Webb W, Golden J, Stulbarg M

12:06 9. **The abnormal secondary pulmonary lobule: high-resolution CT.** Bergin C, Roggli V, Coblentz C, Chiles C

II. Gastrointestinal Imaging: I

10:30 10. **Positive predictive value of a diagnosis of colonic polyp on the single-contrast and double-contrast barium enema.** Scharling E, Ott D, Chen Y, Gelfand D, Wu W

10:42 11. **Large colonic neoplasms missed by endoscopy.** Glick S, Teplick S, Balfe D, Levine M

10:54 12. **The barium enema diagnosis of colon cancer: can the surgeon rely on it?** Frager D, Wagner R, Wolf E, Frager J, Beneventano T

11:06 13. **The accuracy of polyp detection in the presence of diverticulosis.** Simms S, Ackerman L, Feczko P

11:18 14. **Can CT stage esophageal carcinoma after radiation therapy? Comparison of CT with surgical findings.** Halvorsen R Jr, Wolfe W, Foster W Jr, Thompson W

11:30 15. **High-resolution ultrasound in acute appendicitis: the fate of the negative study.** Gaensler E, Jeffrey R

11:42 16. **Vicarious biliary excretion of contrast on computed tomography.** Nemcek A Jr, Urban M, Vogelzang R, Gore R

11:54 17. **Computed tomography of liver metastases: a reappraisal of contrast enhancement methodology.** Zeman R, Brody J, Paushter D, Silverman P, Garra B, Jaffe M

12:06 18. **Periportal tracking of blood: a subtle sign of hepatic trauma.** Macrander S, Lawson T, Foley W, Dodds W, Erickson S, Quiroz F

III. Neuroradiology: I

10:30 19. **MRI and CT in vein of Galen "aneurysm."** Seidenwurm D, Hyman A, Kowalski H, Berenstein A

10:42 20. **New technique for adult transcranial Doppler examination.** Hashimoto B, Hattrick C

10:54 21. **Duplex sonography of the vertebral arteries: measurement of net flow.** Bohm-Velez M, Mendelson E, Pedicelli G, Katanick S, Joseph N, Neiman H

11:06 22. **Color-flow vascular imaging: comparison with point spectral analysis in estimation of carotid artery stenosis.** Erickson S, Foley W, Lawson T, Macrander S, Quiroz F

11:18 23. **Direct visualization of major intracranial vessels of neonates by color-flow Doppler imaging.** Wong W, Tsuruda J, Lieberman R, Vogt J, Gangitano E

11:30 24. **Luxury perfusion in cerebral infarcts: comparison of CT, MRI, and SPECT.** Henkes H, Cordes M, Schörner R, Roland F

11:42 25. **High-resolution MRI of the cervical spinal cord: distinguishing cord anatomy from artifact at high fields.** Carvlin M, Hackney D, Asato R, Muraki A, Rajan S, Mun S

11:54 26. **Total myelographic block from extruded HNP: CT pitfalls.** Teplick J, Haskin M

12:06 27. **MR-gated intracranial liquor dynamics (MR-GILD): evaluation of CSF pulsatile flow.** Njemanze P, Beck J, Lissner J

Tuesday, May 10, 10:00 a.m.–12:30 p.m.

IV. Breast Imaging

10:00 28. **Incidence and long-term follow-up of breast calcification on mammograms.** Wang Y, Feig S, Dick B, Cooperman H

10:12 29. **Breast calcifications in postradiation therapy lumpectomy patients.** Rebner M, Pennes D, Lichter A, Adler D

10:24 30. **Breast carcinomas: the echogenic rim.** Mendelson E, Bhagwanani D, Bohm-Velez M, Rishi U, Neiman H, Joseph N

10:36 31. **Lobular carcinoma of the breast: mammographic-pathologic correlation.** Krecke K, Gisvold J

10:48 32. **Benign breast disease simulating cancer: radiologic-pathologic correlation.** Berkowitz J, Gatewood O, Gayler B

11:00 33. **Breast aspiration biopsy: influence of sample size on sensitivity.** Pennes D, Naylor B

11:12 34. **Radiologic-pathologic correlation of breast localizations with follow-up: 5-year experience.** Archer A, Brody J, Abbondanzo S, Cigtay O

11:24 35. **Sedimented calcium in benign breast cysts: the full spectrum of mammographic presentations.** Linden S, Sickles E

11:36 36. **Comparison of 350 cases of the new black toner xeroradiography with grid film imaging.** Martin J

11:48 37. **Film-screen mammography in females under 30 years old.** Pope T Jr, Loudermilk D

12:00 38. **Development of a quality-assurance program in mammography.** Pavlicek W, Chilcote W, Walmsley J, Kobistek R

12:12 39. **Lucite and/or wax vs BR12 mammography test objects.** Kimme-Smith C, Bassett L, Gold R

V. Genitourinary Imaging: I

10:00 40. **Optimizing use of intravenous urographic contrast in routine abdominal and pelvic CT.** Platt J, Glazer G

10:12 41. **MRI characterization and comparison of hyperfunctioning and nonhyperfunctioning benign adrenal cortical lesions.** Remer E, Weinfeld R, Glazer G, Quint L, Francis I, Gross M, Yeung H

10:24 42. **Determination of optimal contrast within the normal and pathologic uterus via synthetic MR images.** Duberg A, McCarthy S, Lange R

10:36 43. **Fallopian tube recanalization: initial follow-up results.** Thurmond A, Rösch J, Uchida B

10:48 44. **Magnetic resonance imaging of primary bladder carcinoma: radiologic, surgical, and pathologic comparison.** Paling M, Lippert M, Mills S

11:00 45. **Imaging penetrating trauma of the back and flank: the CT enema.** Sclafani S, Phillips T, Scalea T, Teitcher J, Duncan A, Atweh N

11:12 46. **CT of intraperitoneal urinoma.** Raval B, Gutierrez C, Sandler C

11:24 47. **Inferior vena cava tumor thrombus in retroperitoneal malignancies: assessment by MRI.** Raval J, Pritchett T, Colletti P

11:36 48. **Diagnostic workup of patients with renal cell carcinoma suitable for partial nephrectomy: comparison of MR, CT, and angiography.** Fisher M, McVary K, Kozlowski J, Vogelzang R

11:48 49. **The inability to detect kidney disease on the basis of renal echogenicity and anisotropy.** Platt J, Rubin J, Bowerman R, Marn C

12:00 50. **Microradiographic demonstration of human intrarenal microlymphatic pathways.** Cuttino J, Clark R, Jennette J

12:12 51. **Twenty-four–hour delayed benign cortical renal enhancement.** Love L, Lind J, Olson M

VI. Angiography: I

10:00 52. **Total iliac occlusions: introduction of pull-through technique for establishing access for balloon angioplasty.** Thorpe P, Bowles C, Ginsburg R, Wright A, Wexler L

10:12 53. **PTA and endovascular stents for suboptimal arterial graft anastamoses: long-term patency in a canine model.** Brunner M, Alspaugh J, Tuten T, Chuang V, Gianturco C, Casarella W

10:24 54. **Stanford experience with the laser probe and Kensey catheter in superficial femoral artery occlusions.** Thorpe P, Ginsburg R, Jenkins N, Wright A, Wexler L

10:36 55. **Rethrombosis following successful fibrinolytic infusion for lower extremity ischemia.** Sniderman K

10:48 56. **Pseudoaneurysm and arteriovenous fistula. Two major complications of percutaneous transfemoral cardiac catheterization: mechanisms and prevention.** Kim D, Orron D, Porter D, Skillman J, Baim D

11:00 57. **Outpatient angioplasty.** Pollei S, Wolfel D, Lovett B, Gordon R

11:12 58. **Infrapopliteal artery angioplasty.** Bakal C, Sprayregen S, Scheinbaum K, Veith F

11:24 59. **Diagnosis of prosthetic aortic graft infection by magnetic resonance imaging (MRI).** Auffermann W, Olofsson P, Stoney R, Higgins C

11:36 60. **Angiography in penetrating injury in proximity to a major extremity artery.** Reid J, Redman H, Thal E, Weigelt J

11:48 61. **The role of angiography in penetrating neck trauma.** Sclafani S, Cavaliere G, Scalea T, Phillips T, Atweh N, Duncan A, Glanz S

12:00 62. **Color-flow Doppler imaging in hemodialysis access.** Middleton W, Picus D, McCullough C, Melson G, Marx M, Weyman P

12:12 63. **Hemodialysis-associated subclavian vein stenosis: incidence, predisposing factors, and treatment by percutaneous angioplasty.** Saeed M, Cohan R, Schwab S, Perlmutt L, Kadir S

Tuesday, May 10, 1:30–3:30 p.m.

VII. Skeletal Radiology: I

1:30 64. **MRI of wrist disorders.** Feldman F, Singson R, Staron R

1:42 65. **Temporal radiographic changes in the rheumatoid wrist.** Hendrix R, Gutstein L, Rogers L

1:54 66. **MR of osteomyelitis in diabetic foot.** Yuh W, Corson J, Kathol M, Montgomery W, Shamma A, Baraniewski H

2:06 67. **Lymphomatous skeletal involvement: bone and gallium citrate scintigraphic correlation.** Orzel J, Sawaf N, Richardson M

2:18 68. **Skeletal metastases vs radiation necrosis in treated invasive cervical carcinoma: a diagnostic dilemma.** Yousem D, Scott W, Fishman E

2:30 69. **Radiologic features of well-differentiated osteosarcoma.** Siegel C, Ellis J, Martel W, Weatherbee L, Dorfman H, Hudson T

2:42 70. **Evaluation of an X-ray dual-photon absorptiometry bone-mineral scanner.** Smith S, Sorenson J, Collick B, Duke P, Pedersen P

2:54 71. **Quantitative dual-energy digital projection radiography of the lumbar spine: comparison to dual-photon absorptiometry and quantitative computed tomography in patients.** Borders J, Sartoris D, Stein J, Ramos E, Resnick D

3:06 72. **Qualitative CT of the spine: intervertebral body variability.** Thickman D, Nodine C, Iddenden D

3:18 73. **Reproducibility (precision) of QCT: effects of longitudinal slice position, gantry angle, and spine-phantom air gap.** Gillespy T, Davis J

VIII. Interventional Radiology

1:30 74. **Safe transvisceral access using a blunt needle.** Akins E, Hawkins I, Mladinich C, Siragusa R, Tuppler R

1:42 75. **Augmented drainage of viscid fluid collections by percutaneous insertion of large-caliber catheters.** Katz S, Bernstein M, Berman H

1:54 76. **Changing an occluded drainage catheter: some technical options.** Crummy A, McDermott J, Voegeli D, Babel S

2:06 77. **Pain relief via percutaneous CT-guided celiac ganglion block: technique and results.** Mueller P, van Sonnenberg E, Saini S, Casola G, Hahn P, Steiner E

2:18 78. **Techniques and complications of chemoinfusion and chemoembolization of the hypogastric artery for advanced gynecologic malignancies.** Quinn S, Clark R, Kavanagh J, Greenberg H, Cavanagh D, Roberts W, Lapolla J, Hoffman M, Fiorica J

2:30 79. **Results and complications of transcatheter embolization of hemorrhaging pelvic neoplasms.** Lang E

2:42 80. **Minimally invasive modified Sugiura (MIMS) procedure for treatment of variceal bleeding.** Berman H, DelGuercio L, Katz S, Hodgson W, Savino J

2.54 81. **Insertion of subclavian hemodialysis catheters in difficult cases: an interventional radiographic solution.** Selby B, Tegtmeyer C, Amodeo C, Bittner G, Atuk N

3:06 82. **One-stage percutaneous placement of large catheter suprapubic cystostomy: technique and results.** Papanicolaou N, Pfister R, Steiner E

3.18 83. **Povidone-iodine sclerosis for postoperative lymphoceles: a prospective study.** Cohan R, Saeed M, Schwab S, Perlmutt L, Dunnick N

IX. Ultrasonography

1:30 84. **Transvaginal ultrasound in gynecology (excluding infertility).** Bret P, De Stempel J, Atri M, Illescas F, Aldis A

1:42 85. **Endovaginal sonography in the evaluation of pelvic masses.** Leibman A, Kruse B

1:54 86. **Transvaginal sonography in suspected ectopic pregnancy.** Joseph N, Mendelson E, Bohm-Velez M, Neiman H, Pedicelli G, James P, Wiener H

2:06 87. **Transvaginal Doppler assessment of blood flow to the ovaries in infertile patients.** McSweeney M, Baber R, Kossoff G, Gill R

2:18 88. **Inability of sonography to detect imminent ovulation.** Middleton W, Thorsen M, Zandt-Stansny D, Aiman J, Zion A, McAsey M

2:30 89. **Pregnancies associated with congenital uterine anomalies.** Fagan C, Bedi D, Winsett M

2:42 90. **Prenatal sonographic detection of anencephaly.** Goldstein R, Filly R

2:54 91. **Maternal AFP screening: extrafetal findings associated with elevated levels.** Kelly R, Nyberg D, Fitzsimmons J, Mack L, Davis S

3:06 92. **The predictive value of ultrasound to determine retained products of conception following spontaneous miscarriage.** Shlansky-Goldberg R, Kurtz A, Choi H, Needleman L, Pennell R, Baltarowich O, Vilaro M, Mitchell D, Goldberg B

3:18 93. **The spectrum of sonographic findings in endometriomas.** Athey P, Diment D

Wednesday, May 11, 1:30–3:30 p.m.

X. Magnetic Resonance Imaging: I

1:30 94. **Gradient-echo MR screening for liver metastases.** Hahn P, Stark D, Edelman R, Wittenberg J, Ferruci J

1:42 95. **Comparison of gadolinium-DTPA and (Gd-DTPA)-albumin in MR imaging of liver tumors.** Hamm B, Taupitz M, Weinmann H, Bauer H

1:54 96. **Magnetic resonance imaging of atypical cavernous hemangiomas.** King P, Clark R, Quinn S

2:06 97. **Combined CT/MR workup of low-density hepatic lesions at the falciform ligament.** Meyer J, Francis I, Glazer G, Borrello J, Vahey T

2:18 98. **Focal liver lesions in MRI: a new multislice gradient-echo sequence.** Langer M, Bittner R, Laniado M, Sander B

2:30 99. **T2-weighted inversion recovery imaging of liver metastases at high field.** Albert S, Cheung Y, Leeds N

2:42 100. **Early detection of small hepatic tumor using MR/CT experimental and clinical comparison.** Chiu L, Peng T, Butler J, Trezona T, Ong R

2:54 101. **MRI of portal vein thrombosis.** Levy H, Newhouse J

3:06 102. **Hepatic iron overload: diagnosis and quantification by MR imaging.** Chezmar J, Nelson R, Slaker D, Bills E, Malko J, Bernardino M

3:18 103. **Liver imaging with MAST and STIR-MAST techniques.** Bellon E, Pattany P, Benson J, Motta A

XI. Genitourinary Imaging: II

1:30 104. **Age-related changes of the prostate: MRI at 1.5 Tesla.** Allen K, Kressel H, Arger P, Pollack H

1:42 105. **Ultrasound of diffuse prostatic carcinoma: the hypoechoic peripheral zone.** Bree R, Jafri S, Roberts J

1:54 106. **Ultrasonography of whole prostate specimens with morphologic correlation: normal prostate.** Hardt N, Li K, Kaude J, Ros P, Hackett R

2:06 107. **Radiologic treatment for benign prostatic hypertrophy.** Castaneda F, Hulbert J, Reddy P, Letourneau J, Hunter D, Castaneda-Zuniga W, Amplatz K

2:18 108. **Magnetic resonance imaging of patients after balloon dilatation of the prostate.** Johnson S, Castaneda F, Kuni C, Letourneau J, Hunter D, Castaneda-Zuniga W, Amplatz K, Hulbert J, Reddy P

2:30 109. **Maturation of the testis: ultrasound evaluation with histopathologic correlation.** Hamm B, Fobbe F, Dietzel M, Winter S

2:42 110. **Color-flow Doppler imaging of the vascular system in the scrotum.** Thorn D, Middleton W, Melson G

2:54 111. **The practical value of fluoroscopically guided brush biopsy of the upper urinary tract.** Sheline M, Amendola M, Pollack H, Banner M, Morenas A, Wein A

3:06 112. **US-guided percutaneous nephrostomy for urinary obstruction during pregnancy.** vanSonnenberg E, Casola G, Talner L, Varney R, Wittich G, Christensen R

3:18 113. **US-guided transvaginal biopsies in pelvic masses: preliminary experience.** Bret P, Atri M, Illescas F, Seymour R, De Stempel J

XII. Skeletal Radiology: II (Spine)

1:30 114. **The application of MR in management of craniovertebral abnormalities.** Yuh W, Menezes A, Sickels W, Sato Y

1:42 115. **Detection of vertebral destruction with routine lateral radiography: a reevaluation using a controlled study with application of quantitative computed tomography.** Haller J, Resnick D, Andre M, Sartoris D, Mitchell M, Howard B

1:54 116. **MR of vertebral compression fractures.** Zachar C, Yuh W, Barloon T, Sato Y

2:06 117. **MRI STIR of acute vertebral fracture.** Wiener S, Neumann D, Rzeszotarski M

2:18 118. **Radiologic assessment of posttraumatic vertebral stability.** Daffner R, Deeb Z, Goldberg A, Khoury M, Rothfus W

2:30 119. **MRI of ligamentous injuries of the spine.** Gray L, Bennett W, Djang W

2:42 120. **The open-mouth view of the dens revisited: the significance of asymmetry.** Lee C, Woodring J, Jenkins K, Goldstein S

2:54 121. **Plain radiography of unilateral facet lock of the cervical spine: the laminar/facet interspace.** Young J, Rothe A, Resnik C, Mirvis S

3:06 122. **Protocol "driven" radiologic evaluation: an efficacy study for suspected cervical spine injury.** Mirvis S, Joslyn J, Chirico P, Reiner B, Diaconis J

3:18 123. **Cervical spine injury in children: radiologic manifestations.** Ehara S, El-Khoury G, Sata Y

Thursday, May 12, 10:00 a.m.–12:30 p.m.

XIII. Angiography: II

10:00 124. **Incidence of femoral vein thrombosis following percutaneous placement of the Greenfield filter.** Pais S, Tobin K, Austin C, Queral L

10:12 125. **Long-term follow-up of the Günther vena-cava filter.** Fobbe F, Dietzel M, Sörensen R

10:24 126. **Interobserver variability in the interpretation of contrast venography, Tc-99m red blood cell venography and impedance plethysmography (IPG) for the diagnosis of deep vein thrombosis.** Illescas F, LeClerc J, Rosenthall L, Herba M

10:36 127. **Insertion site patency in percutaneous Greenfield placement: technical refinements that positively affect outcome.** Dorfman G, Cronan J, Paolella L, Haas R

10:48 128. **Predictive value of ultrasound diagnosis of lower extremity deep vein thrombosis.** Polak J, O'Leary D, Wade C, Creager M

11:00 129. **High-resolution real-time ultrasonography in the evaluation of lower-extremity deep venous thrombosis.** Meza M, Sadiq S, Miller L, Steele R Jr, Gagliardi R

11:12 130. **A new retrograde basket–antegrade needle impaling technique for vascular and luminal access.** Siragusa R, Feaster S, Hawkins I Jr

11:24 131. **MR angiography.** Lois J, Fisher H, Gomes A

11:36 132. **Abdominal vascular anatomy and patency: clinical utility of two new MRI pulse techniques.** Wozney P, Davis P, Tobben P, White R

11:48 133. **Experience with two new CO_2 injector systems for CO_2 digital subtraction angiography.** Pry R, Hawkins I, Siragusa R, Akins E

12:00 134. **The use of a mechanical power injector for CT contrast enhancement: reflections after 3500 patients.** Zeman R, Clark L, Silverman P, Garra B, Jaffe M, McVay L, Brody J, Jacob W, Choi A

12:12 135. **Radiocontrast-induced acute renal failure in femoral angiography: a comparison of low-osmolar and conventional high-osmolar contrast media.** Lautin E, Freeman N, Schoenfeld A, Bakal C, Sprayregen S, Braha S

XIV. Neuroradiology: II

10:00 136. **Efficiency of MR vs CT in epilepsy.** Heinz E

10:12 137. **High-resolution MR in evaluation of epidural tumor.** Pollei S, Smoker W, Harnsberger H, Osborn A

10:24 138. **Intracranial extraaxial cystic tumors: MRI in 30 proven cases.** Seidenwurm D, Pinto R, Kowalski H, Kricheff I

10:36 139. **Plain and gadolinium-DTPA–enhanced multislice gradient-echo images for evaluation of intracranial tumors.** Kornmesser W, Schoerner W, Sander B, Laniado M, Nakamura T, Felix R

10:48 140. **Intraoperative sonography in low-grade gliomas.** Hatfield M, Rubin J, Gebarski S

11:00 141. **Pseudoenlargement of the optic nerve.** Azar-Kia B, Mafee M, Haag J, Naheedy M, Fine M

11:12 142. **The radiographic evaluation of pulsatile tinnitus.** Remley K, Coit W, Harnsberger H

11:24 143. **Comparison of magnetic resonance imaging with radionuclide scanning for localization of parathyroid adenoma.** Khan A, Attie J, Moskowitz G, Rumancik W, Herman P

11:36 144. **High-resolution computed sonography of the parathyroid glands.** Abu-Yousef M, Fruechte D, Gurll N, Al-Jurf A

11:48 145. **CT of nasopharyngeal carcinoma: significance of widening of the prevertebral soft-tissue space on axial scans.** Hoe J

12:00 146. **Posttreatment CT appearance in advanced neck malignancies.** Radecki P, Mohr R, Friedman A, Johnson M, Caroline D, Lev-Toaff A

12:12 147. **Soft-tissue changes following radiation therapy in patients with head and neck tumors: evaluation by CT.** Bronstein A, Nyberg D, Schwartz A, Shuman W, Griffin B

XV. Gastrointestinal Imaging: II

10:00 148. **Treatment of biliary stones with monooctanoin pre and/or during MTBE chemolysis: a synergistic effect.** Haskin P, Brandon J, Teplick S, Sammon J, Haskin M

10:12 149. **Extracorporeal shock-wave lithotripsy (ESWL) in common bile duct calculi.** Ros P, Li K, King C, Hawkins I

10:24 150. **Extracorporeal lithotripsy in the management of bile duct stones.** Fried L, Lebrun P, Norman R, Fraser D

10:36 151. **Use of a current-generation intravenous cholangiography agent (Iotroxate) for stone targeting during extracorporeal shock-wave lithotripsy: an experimental study.** Becker C, Burhenne H

10:48 152. **Physical characteristics of gallstones removed at cholecystectomy: implications for shock-wave lithotripsy.** Brink J, Ferrucci J, Simeone J, Mueller P

11:00 153. **CT analysis of gallstones: correlation with chemical analysis.** Baron R, Lee S, Teefey S, Shuman W, Rohrmann C Jr

11:12 154. **Percutaneous subhepatic cholecystostomy with removable anchor.** Cope C

11:24 155. **Lasers in biliary obstruction: work in progress.** Dachman A, McGehee J, Beam T, Venbrux A

11:36 156. **Towards painless percutaneous biliary procedures: new strategies and alternatives.** Vogelzang R, Nemcek A Jr

11:48 157. **Percutaneous gastrostomy tube placement for the symptomatic relief of bowel obstruction.** Picus D, Marx M, Weyman P

12:00 158. **The role of interventional radiology for complications of cholecystectomy.** vanSonnenberg E, Casola G, Varney R, Christensen R, Neff C, Withers C, Wittich G, Moossa A

12:12 159. **The occluded biliary endoprosthesis: terminal event or salvageable?** Mueller P, Steiner E, Hahn P, Saini S, Forman B, Silverman S, Ferrucci J

Thursday, May 12, 1:30–3:30 p.m.

XVI. Skeletal Radiology: III

1:30 160. **MRI of the patella and patellofemoral joint.** Stoller D, Genant H

1:42 161. **Pulse-sequence optimization for the knee: 3 DFT-FISP imaging.** Unger E, Cohen M, Brown T

1:54 162. **MRI of popliteal masses of the knee.** Stoller D, Steinback L, Kaplan P, Genant H

2:06 163. **Pseudoliphemarthrosis.** Bohrer S

2:18 164. **High-resolution MR imaging of the tendons of the ankle: normal and pathologic states.** Cheung Y, Jahss M, Noto A, Rosenberg Z

2:30 165. **Limited detection of rotator cuff tears by ultrasound.** Miller C, Karasick D, Kurtz A, Fenlin J

2:42 166. **The Segond fracture: a small avulsion that reflects major ligamentous damage.** Goldman A, Pavlov H, Rubenstein D

2:54 167. **Pylon fractures of the ankle: a distinct clinical and radiological entity.** Mainwaring B, Daffner R, Riemer B

3:06 168. **2D and 3D CT evaluation of acetabular fractures: a systematic approach.** Fishman E, Magid D, Drebin R

3:18 169. **Imaging of osteoporotic sacral fractures.** Martinez S, Vogler J

XVII. Magnetic Resonance Imaging: II

1:30 170. **The economics of MRI in clinical practice, 1988.** Evens R, Evens R Jr

1:42 171. **1.5-Tesla multi-slice STIR imaging: application to body MR.** Shuman W, Baron R, Peters M, Moss A

1:54 172. **Pulse-sequence optimization for STIR inversion recovery sequences.** Unger E, McGlone J, Silver M

2:06 173. **Use of the STIR sequence to differentiate between extracranial fatty and hemorrhagic lesions.** Fisher M

2:18 174. **MR imaging of the abdomen: clinical application of phase imaging.** Levy L, Dwyer A, Begley M, Yang S

2:30 175. **Optimization of GRASS imaging for abdominal MRI.** Weissleder R, Raptopoulos V, Stark D, Waite R, Ferrucci J

2:42 176. **Dual surface coils for MR imaging: capability, advantages, and applications.** Fisher M, Boskamp F, Russell E, Levy J

2:54 177. **Dynamic cardiac MRI to assess viable vs scarred myocardium: comparison with SPECT thallium.** Ziffer J, Pettigrew R

3:06 178. **Review of contrast agent–enhanced fast MRI techniques: dynamic physiologic imaging.** Carvlin M, Arger P, Kundel H, Dougherty L, Kassab E, Moore B

3:18 179. **Image artifacts introduced by MRI gastrointestinal contrast agents: magnitude, cause, and amelioration.** Hahn P, Stark D, Weissleder R, Saini S, Elizondo G, Ferrucci J

XVIII. Chest Imaging: II

1:30 180. **Radiologic evaluation of the subcarinal lymph nodes: a comparative study.** Platt J, Glazer G, Gross B, Quint L, Francis I, Orringer M

1:42 181. **Extrathoracic metastasis without evidence of hilar or mediastinal adenopathy.** Sider L, Horejs D, Cornwell J

1:54 182. **Anatomic observations on lines of the left superior mediastinum: correlative imaging.** Marn C, Glazer G, Gross B, Spizarny D

2:06 183. **Computed tomography of acute mediastinitis.** Wittich G, Schurawitzki H, Karnel F, Kumpan W, Grabenwoeger F

2:18 184. **Three-dimensional CT in central lung tumors.** Quint L, McShan D, Glazer G, Orringer M

2:30 185. **Magnetic resonance imaging of central pulmonary artery anomalies**. Kersting-Sommerhoff B, Sechtem U, Higgins C

2:42 186. **MR imaging of the pericardium: comparison of spin-echo and cine techniques**. Nokes S, Herfkens R, Kisslo J, Spritzer C

2:54 187. **Screening for congenital heart disease with magnetic resonance imaging and two-dimensional echocardiography.** Goldman M, Boxer R, LaCorte M, Gottesman R, Stein H

3:06 188. **Clinical role of MRI for assessment of cardiac mass lesions.** Lund J, Ehman R, Julsrud P, Sinak L, Tajik A

3:18 189. **Noninvasive evaluation of mitral regurgitation by analysis of systolic left atrial signal loss in cine magnetic resonance images.** Auffermann W, Pflugfelder P, Sechtem U, White R, Lipton M, Higgins C

1988 ARRS Meeting: Local Activities and Tennis and Golf Tournaments

The 88th annual meeting of the American Roentgen Ray Society (ARRS) in San Francisco, CA, will feature activities for members, nonmembers, spouses, and friends. G. P. Janetos heads the Local Arrangements Committee. Tours West has planned the local programs. The tennis tournament will be arranged and supervised by G. M. Stevens; the golf tournament will be arranged and supervised by G. P. Janetos. To register for these events, please complete the registration form in this issue.

Golf Tournament

The annual golf tournament will be held at the San Francisco Golf Club, San Francisco, CA, on Monday, May 9. Buses will leave the San Francisco Hilton and Tower at 11 a.m. and will return by 6 p.m. There will be a buffet lunch at 11:30 a.m. and a shotgun start at 12:30 p.m. Participants must bring their own golf clubs and shoes. The Pro Shop and clubhouse will be open, and there will be a no-host bar. The course does not allow golf carts, but good caddies will be available at an extra charge, to be paid at the course. Fee for the golf tournament is $75 and includes transportation, luncheon, greens fee, and prizes.

Men's and Women's Tennis Tournaments

The annual Men's and Women's Tennis Tournaments will be held at the San Francisco Tennis Club, San Francisco, CA, on Monday, May 9, from 1:30–4:30 p.m. Cabs will be arranged for the short ride from the Hilton to the tennis club. Please register early so that arrangements can be made to accommodate all who wish to play. Appropriate dress is required. The fee of $55 includes luncheon, court fees, and balls.

Local Program

Reservations for the social program are limited. To avoid disappointment, send in the reservation form immediately. Reservations will be filled in the order in which they are received. Because guarantees are required for all events, reservations must be received by April 22, 1988. Tickets for all events will be included in the registration packet. Prices for these events include transportation; meal where indicated; escorts and guides; and all entrance fees, taxes, and gratuities. The price does not include any alcoholic beverage with meals. On Sunday, May 8, from 2–5 p.m., and on Monday, May 9, from 8–11 a.m., remaining tickets for events will be sold at the meeting registration desk. These tickets will be sold at a slightly higher cost. Refunds are available if the ARRS office in Reston, VA, receives a written cancellation request by April 23, 1988. No cancellations will be accepted by telephone. Refunds will be issued at the meeting on Sunday and Monday only if the returned tickets can be resold. ARRS reserves the right to cancel any event if registration is insufficient. In that case, refunds will be issued. Children less than 12 years old are not permitted to participate in the social program. Children 12 years or older are welcome at full price for all of the events except the Tuesday wine tour and the Wednesday dinner and cabaret theater.

Sunday, May 8

Chinese Banquet, 7–10 p.m. Your first meal in San Francisco must be an authentic Chinese Banquet. The group will feast on everything from sizzling rice soup and Peking duck to the most exotic fish and vegetables available. This eight-course Oriental feast is served in one of San Francisco's most popular restaurants and will be a memorable gastronomic experience. Fee: $40.

Monday, May 9

Early Bird Shopping, 8–10 a.m. Saks Fifth Avenue has designed a special breakfast fashion seminar. Attendees will have a front row seat to a fashion presentation of a workable and wearable wardrobe—dressing for day and night. Learn how to pack for your next vacation, whether it's for a weekend or for a month. And, most importantly, learn how to copy the designers without copying their price tags. Fee: $25.00.

Deluxe City Tour of San Francisco, 9 a.m.–1 p.m. Ride over the hills of the city right out to the Golden Gate Bridge for a comprehensive city tour. The group will see San Francisco's celebrated sights: Fisherman's Wharf, Golden Gate Park, Haight-Ashbury, Twin Peaks, Chinatown, and the Presidio. Tour members also will visit Nob Hill, Russian Hill, North Beach, and Union Street. The combination of neighborhoods,

parks, bridges, and people is what makes San Francisco such a unique city. There will be several places to stop and take photographs. Fee: $23.

Dinner in Sausalito, 6–10 p.m. Experience San Francisco as the locals do. Depart on a commuter ferry for a ride on the San Francisco Bay. You will get a close-up view of Alcatraz and Angel Island en route to the picturesque village of Sausalito. Enjoy a sumptuous dinner at one of Sausalito's most famous restaurants overlooking the Bay. Return to the hotel via the Golden Gate Bridge aboard a luxury motorcoach. Fee: $48.

Tuesday, May 10

Wine Tour of the Napa Valley, 8:30 a.m.–5 p.m. North of San Francisco lies California's premier wine producing region—the Napa Valley. By far the most popular of the state's wine regions, the Napa Valley is responsible for many of the best known and most respected American wines. After a 90-min drive, the group will enjoy a private tour and tasting at Napa's outstanding champagnerie: Domaine Chandon. Then, it's off for an elegant lunch featuring California cuisine at one of the Valley's newest, most popular restaurants, Tra Vigne. The group will then enjoy a second private tour and tasting before returning to the hotel. Fee: $75.

Wednesday, May 11

The Designers' San Francisco, 9 a.m.–1:30 p.m. Today the group will discover the decorators' San Francisco. Although the wholesale showrooms at Showplace Square are closed to the public, you will be privately guided through the exclusive world of the interior designer. Here you will see the finest furniture, accessories, fabrics, and wall and floor coverings available in today's marketplace. Lunch will be served in one of the complex's most interesting buildings, the Galleria. Buying is restricted to the trade, but arrangements can be made to purchase items through a staff interior designer. Fee: $45.

Dinner and Cabaret Theater 5:30–10:00 p.m. This is the chance to see a truly "only in San Francisco" entertainment phenomenon: Steve Silver's *Beach Blanket Babylon* at the Club Fugazi. This highly acclaimed original cabaret production will provide a great evening for everyone. Both visitors and locals love the musical parodies and imaginative costumes. This is the longest running show in San Francisco theater history. An early dinner at one of North Beach's finest restaurants precedes the show. Fee: $75.

Thursday, May 12

Filoli Mansion and Stanford University, 8:30 a.m.–4:30 p.m. Today the group will travel south for a visit to Filoli, a 43-room mansion built 70 years ago. There's nothing quite like it in the West: 16 acres of groomed gardens around an exquisite home of 36,000 square feet. Used for the filming of "Dynasty" and *Heaven Can Wait*, Filoli is especially beautiful in May. Lunch will be served at the Allied Arts Guild, a showplace of colonial Spanish buildings and gardens housing shops and artisans' studios. After lunch, you will visit Stanford University and enjoy a brief campus tour. Fee: $65.

Champagne, Chocolates, and City Lights, 8–10 p.m. San Francisco comes alive in the evening as your deluxe motorcoach travels through neighborhoods and hills with a thousand twinkling lights. The San Francisco skyline is ablaze with colors as you pass through Fisherman's Wharf, Chinatown, and Nob Hill. The landmarks of this city, the Bay Bridge, the Golden Gate Bridge, and Coit Tower are magical in the evening sunset. Have an early dinner on your own and then join the evening tour for champagne and chocolate desserts. Fee: $32.

Friday, May 13

Treasures of the East, 9:30 a.m.–3:30 p.m. An enthusiasm for the Orient is all that's needed on this trip. You will begin with a visit to the Asian Art Museum, the permanent home of the famous Avery Brundage Oriental Art collection. You will enjoy a privately guided tour of the Museum's highlights before entering the Japanese Tea Gardens, where the beauty and grace of Japan come alive in Golden Gate Park. Lunch is an authentic dim sum selection, another specialty of the Orient. You complete your day with a VIP visit to Gump's, the store that played a major role in introducing Oriental art to the United States. Fee: $45.

May Be Photocopied

Deadline: April 8

Meeting and Local Activities Registration Form: ARRS 88th Annual Meeting May 8–13, 1988, San Francisco, CA

If you plan to attend, please complete this form. Official badges and program booklets will be available at the ARRS Registration Desk, San Francisco Hilton and Tower. **There will be no confirmations before the meeting.** Preregistration by mail will be accepted until April 8. On-site registration will be available.

Make all checks payable to: American Roentgen Ray Society

Mail to: American Roentgen Ray Society
1891 Preston White Drive
Reston, VA 22091

Please type or print:
Registrant

_____
Last Name First Name or Initials

_____
Street

_____
City State ZIP Code

Accompanying Guest

_____
Name (Accompanying person's name to be printed on badge)

_____
Street

_____
City State ZIP Code

Check those desired:	Registration fee:
☐ Member ARRS	None
☐ Nonmember	$250
☐ Physician in training (please fill where indicated below)	$25
☐ Course faculty, scientific paper author, scientific exhibitor	None
☐ ACR luncheon course, Monday, May 9	$12
☐ ACR luncheon course, Tuesday, May 10	$12
☐ ACR luncheon course, Wednesday, May 11	$12
☐ ACR luncheon course, Thursday, May 12	$12
☐ Categorical course on breast imaging. Categorical course registrants may also register for other instructional courses.	$75
☐ Social program (see next page)	____
Total enclosed	____

Section on Instruction

Please register early for Instructional Courses. Attendance is limited. List first, second, and third choices for each day by course number. Ticket orders are filled according to postmark. ARRS members, nonmembers, and those in radiology training may take all courses without charge except the Categorical Course on Breast Imaging. **For the categorical course, all must pay $75. All who wish to attend courses must complete this section. Residents and nonmembers must pay the meeting registration fee.**

Course tickets will be available at the ARRS Registration Desk of the Section on Instruction at the San Francisco Hilton and Tower on and after Saturday, May 7, at 1 p.m.

Complete section at right for courses other than the categorical course. Be sure to fill out second and third choices for each day.

	First Choice	Second Choice	Third Choice
Monday			
Tuesday			
Wednesday			
Thursday			

Friday ____ Check if you wish to attend the Chest Symposium (only course offered this day).

For Physicians in Training:

_____ is in training in my department.

Training Program Director _____

Institution _____ Date _____

(OVER)

Local Activities

No refunds after April 23

Sunday, May 8, 7–10 p.m., Chinese Banquet	_____tickets @ $40	$ _____
Monday, May 9, 8–10 a.m., Early Bird Shopping	_____tickets @ $25	$ _____
Monday, May 9, 9 a.m.–1 p.m., Deluxe City Tour of San Francisco	_____tickets @ $23	$ _____
Monday, May 9, 6–10 p.m., Dinner in Sausalito	_____tickets @ $48	$ _____
Tuesday, May 10, 8:30 a.m.–5 p.m., Wine Tour of the Napa Valley	_____tickets @ $75	$ _____
Wednesday, May 11, 9 a.m–1:30 p.m., The Designers' San Francisco	_____tickets @ $45	$ _____
Wednesday, May 11, 5:30–10 p.m., Dinner and Cabaret Theater	_____tickets @ $75	$ _____
Thursday, May 12, 8:30 a.m.–4:30 p.m., Filoli Mansion and Stanford University	_____tickets @ $65	$ _____
Thursday, May 12, 8–10 p.m., Champagne, Chocolates, and City Lights	_____tickets @ $32	$ _____
Friday, May 13, 9:30–3:30 p.m., Treasures of the East	_____tickets @ $45	$ _____

Preregistration is required.

Annual ARRS Golf Tournament, Monday, May 9

The tournament will be at the San Francisco Golf Club, San Francisco, CA. Transportation, luncheon, greens fee, cart, and prizes are included in the $75 fee. Preregistration is important.

Name: _____ Telephone: _____
Address: _____
Hotel: _____ Handicap (if any) _____
My foursome includes (list handicaps): _____
_____ _____tickets @ $75 $ _____

Men's and Women's Tennis Tournaments, Monday, May 9

The tournaments will be at the San Francisco Tennis Club, San Francisco, CA. Tennis attire is required. Fee of $55 includes transportation, luncheon, court fees, and balls.

Name: _____ Telephone _____
Address: _____

_____tickets @ $55 $ _____

May be photocopied **Deadline: April 8**

Hotel Registration Form: ARRS 88th Annual Meeting May 8–13, 1988, San Francisco Hilton and Tower San Francisco, CA

Mail to:

ARRS Housing Bureau
San Francisco Hilton and Tower
Attention: Reservations Office
333 O'Farrell St.
San Francisco, CA 94102

(PLEASE MAKE CHECKS PAYABLE TO THE SAN FRANCISCO HILTON AND TOWER—*NOT TO THE ARRS*)

Individual guest name _____

Address _____

City & State _____ ZIP _____

Arrival date/time _____ Departure date/time _____

Individual requesting reservation _____

Address _____

City & State _____ ZIP _____

Please forward with your reservation a deposit of one night's room rate to be applied to the last night of your scheduled stay, or provide credit card information to guarantee your reservation. The hotel accepts American Express, Diners Club, Carte Blanche, Visa, Master Card, and Hilton credit cards. The deposit will hold your room until 6 a.m. of the morning following your scheduled arrival date. In the event of an early departure, the deposit is nonrefundable unless the hotel is notified prior to or at the time of check-in. Cancellation notice of 14 days is required for a deposit refund.

Check accommodations desired

Room Category	Rate
Singles	
Standard	_____ $100
Superior	_____ $115
Delux	_____ $130
Doubles	
Standard	_____ $110
Superior	_____ $125
Delux	_____ $140
1-bedroom suite	_____ $275
2-bedroom suite	_____ $375

Deposit amount (1 night's rate) $_____

☐ Check enclosed

☐ Credit card: _____
(Type of card) (Exp. date)

_____
(Card number)

_____
(Signature)

Important Information:

1. Reservations must be received by the San Francisco Hilton and Tower/ARRS Housing Bureau no later than April 8 to be assured of written confirmed accommodation. Reservations after that time are subject to availability. We urge you to make your reservations promptly.
2. Written confirmation of your reservation will be sent to you by the hotel.
3. To change or cancel reservations, please call either Hilton Reservations Service at 1-800-HILTONS or the hotel directly at (415) 771-1400.
4. If you plan to share a room, please send in only one housing form. Be sure to list all names of occupants of rooms. Assignment is delayed until complete information is received.
5. Check-in is after 3 p.m., or earlier if the room is available. Check-out time is 11 a.m.
6. Parking is available at the hotel.

Transportation Discounts

United Airlines is offering special airfares to the 1988 ARRS meeting for travel to and from San Francisco between May 5 and May 16 inclusive. To obtain a 5% discount from any United available/applicable fare (Ultra Savers and first class included) or a 40% discount off standard coach fares (all restrictions waived), follow these steps: (1) telephone toll-free (800) 521-4041 (calls are answered daily between 8 a.m. and 11 p.m. EST), and (2) immediately reference special ARRS account number 8080D. In addition, ARRS attendees who fly on United (as outlined above) will be eligible for a special drawing. The prize is one complimentary round-trip continental U.S. ticket good for travel before December 15, 1988 (holiday periods excluded).

Avis Rent A Car is offering special rental rates for attendees of the 1988 ARRS meeting. These rates range from $37 per day for a compact to $41 per day for a full-sized four-door, based on a 3-day minimum rental. Rates are good for 1 week before and 1 week after the meeting. Make reservations by calling toll-free (800) 331-1600; refer to discount number A/B 746001.

1988 ARRS Meeting Summary, May 8–13, 1988, San Francisco, CA

A comprehensive description of the meeting, including the scientific program, Categorical Course in Breast Imaging, and instructional courses, appears in this issue of the *AJR*. A special loose insert on the meeting also accompanies this issue. Meeting and registration forms will be found in the February and March issues. These may be photocopied.

Accreditation

All courses and scientific sessions carry AMA Category I credit on an hour-for-hour basis.

Meeting Format

Scientific Program. Sessions will be grouped in parallel sessions, Monday–Thursday. A total of 189 scientific papers will be presented. In addition, on Wednesday, May 11, the morning session will feature award papers and the Caldwell Lecture, which will be delivered by Donald Resnick of the University of California, San Diego. On Friday, there will be a special symposium: Chest Imaging Update.

Categorical Course in Breast Imaging. This 14.5-hr course will be Sunday–Thursday.

Luncheon Sessions. Registrants may enroll in special luncheon sessions, Monday–Thursday. A box lunch will be provided.

Exhibits

Scientific and Technical Exhibits and Case of the Day Presentations will be presented in the Grand Ballroom of the San Francisco Hilton and Tower, Monday–Thursday, May 9–12. The Case of the Day will be presented by Lee Sider of Northwestern University, Chicago, IL.

Local Activities

General Reception. Tuesday evening, May 10, for all registrants.

Golf Tournament. Monday, May 9, San Francisco Golf Club, San Francisco, CA. Transportation leaves the hotel at 11 a.m.; shotgun start is at 12:30 p.m.

Men's and Women's Tennis Tournaments. Monday, May 9, at the San Francisco Tennis Club, San Francisco, CA. Transportation by cab will be arranged.

Local Tours. Sunday, May 8, 7–10 p.m., Chinese Banquet; Monday, May 9, 8–10 a.m., Early Bird Shopping; 9 a.m.–1 p.m., Deluxe Tour of San Francisco; 6–10 p.m., Dinner in Sausalito; Tuesday, May 10, 8:30 a.m.–5 p.m., Wine Tour of the Napa Valley; Wednesday, May 11, 9 a.m.–1:30 p.m., The Designers' San Francisco; 5:30–10 p.m., Dinner and Cabaret Theater; Thursday, May 12, 8:30 a.m.–4:30 p.m., Filoli Mansion and Stanford University; 8–10 p.m., Champagne, Chocolates, and City Lights; Friday, May 13, 9:30 a.m.–3:30 p.m., Treasures of the East. No refunds after April 23.

Meeting Registration

Preregistration will be accepted until April 8. There will be on-site registration. Official badges and program books will be available at the registration desk, San Francisco Hilton and Tower. No confirmations will be mailed.

Course Registration

Register early—enrollment is limited. List first, second, and third choices for each period. Also, indicate whether you wish to take the categorical course. Deadline for mail registration is April 8. All ticket orders will be filled by postmark. Course tickets *will not* be mailed. Tickets will be available on and after Saturday, May 7 (after 1 p.m.), at the ARRS registration desk in the San Francisco Hilton and Tower. There will be on-site registration for courses not already filled.

Hotel Registration

Reservations are handled by the ARRS Housing Bureau, San Francisco Hilton and Tower, Attn: Reservations Office, 333 O'Farrell St., San Francisco, CA 94102. These must be received by April 8. Make check payable to San Francisco Hilton and Tower.

Fees

Meeting:	
ARRS members and resident members	No fee
Nonmembers	$250
Nonmember physicians in training (with verification)	25
Categorical course (all who attend)	75
Luncheon sessions/each	12
Golf tournament	75
Tennis tournaments	55
Local tours	23–75

Cancellations and Fee Refunds

Fees will be refunded only if cancellation is received by April 23. Send to American Roentgen Ray Society, 1891 Preston White Drive, Reston, VA 22091.

Transportation Discounts

United Airlines is offering discounts, up to 40%, on airfares. Call (800) 521-4041, and mention ARRS account number 8080D.

Avis Rent A Car is offering special rates on car rentals. Call (800) 331-1600, and mention ARRS discount number A/B 746001.

Letters

Cine CT in Obstructive Sleep Apnea

We read with interest the article by Stein et al., "Cine CT in Obstructive Sleep Apnea" [1], and agree with the authors that cine CT is an important and useful imaging technique for evaluation of the dynamic airway changes that occur in obstructive sleep apnea (OSA). In their article, Stein et al. stated that they found airway obstruction occurring at the midoropharyngeal level in eight of eight patients who had OSA. In addition, they reported that in five of eight patients, obstruction also occurred at the level of the uvula and soft palate and, in six patients, at the level of the low oropharynx. On the basis of these findings, they wondered if they were observing two subgroups of patients: one group who had obstruction at the uvula and soft palate only and a group who had obstruction at the base of the tongue and hypopharynx also. Using cine CT, we now have evaluated the airways of 25 normal volunteers. Five were imaged during isolated nasal and isolated oral breathing. In three volunteers who were breathing via the mouth only, the nasal airway posterior to the uvula and soft palate narrowed or was obliterated completely, whereas, with nasal breathing, it remained widely patent. Although we agree that the primary site of obstruction in OSA appears to occur at the midoropharynx to lower oropharynx, we urge caution in interpreting possible obstructive patterns at the level of the soft palate until further evaluations can be made of the normal physiologic changes that occur in nasal or oral breathing.

William Stanford
Jeffrey Galvin
The University of Iowa
Iowa City, IA 52242

REFERENCE

1. Stein MG, Gamsu G, de Geer G, Golden JA, Crumley RL, Webb WR. Cine CT in obstructive sleep apnea. *AJR* **1987**;148:1069–1074

Reply

Drs. Stanford and Galvin raise an important and interesting point. Little is known about the changes in morphology of the upper airway during changes in breathing patterns, especially during sleep. Our article describes obstruction of the airway during sleep and apnea. After we started this project, we used a thermistor that measured a combination of nasal and oral flow. We therefore can be certain that during the obstructed state, oral breathing was not occurring.

The qualitative and quantitative differences between wakefulness, normal sleep, and sleep apnea, in our study, were clearly evident. Airway obstruction does not appear to be a feature of sleep per se. Further evaluation will be necessary to determine whether persons who, during sleep, convert from nasal breathing to obligatory oral breathing, will show narrowing of the nasopharyngeal and retropalatal airways.

We again thank Drs. Stanford and Galvin for pointing out the complexity and lack of understanding of the morphology of this area during sleep and during apnea.

Mark G. Stein
St. Francis Medical Center
Lynwood, CA 90262
Gordon Gamsu
University of California, San Francisco
San Francisco, CA 94143
Gerard de Geer
University of Geneva
Geneva 4, Switzerland
Jeffrey A. Golden
Roger L. Crumley
W. Rickard Webb
University of California, San Francisco
San Francisco, CA 94143

Comparison Study of the Efficacy of the 22-Gauge Vacu-Cut Needle for Biopsy

Recently, a new biopsy needle was introduced that has the purported advantages of having a built-in chamber that allows adequate suction and precludes the necessity of a syringe. To test this hypothesis, we compared the results of biopsies performed by using our standard needle with the results of those performed by using the new needle.

Tumors in 10 patients were biopsied by using both a 22-gauge Vacu-Cut needle (Angiomed, US Inc., Anaheim, CA) and a 22-gauge Greene needle (Reganes, Inc., Chicago, IL). The Greene needle was used because the cannula has a sharpened circumferential bevel similar to that of the Vacu-Cut needle. The needles were introduced into the tumor in a parallel fashion, with the tips within 2–3 mm of each other. The positions were confirmed by CT. A 20-ml syringe with 5–10 ml of applied suction was used for fine-needle aspiration with the Greene needle. Suction for the Vacu-Cut needle was obtained by withdrawing the stylet three-quarters of the way (Fig. 1). A single pass was made with each needle. The aspirated material from

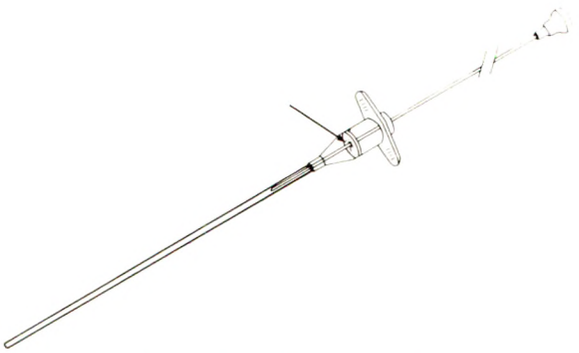

Fig. 1.—Vacu-Cut needle. By withdrawing stylet three-quarters of the way, suction for fine-needle aspiration is created. A sealing membrane within hub of needle (*arrow*) allows creation of a vacuum.

each needle was marked and examined separately by a staff cytopathologist. Both samples were evaluated for amount of material and for the ability to make the diagnosis. The aspirated material was graded as abundant, moderate, scant, or none, depending on the amount obtained. The final interpretation was labeled diagnostic, nondiagnostic, or suspicious.

The lesions ranged from 4 to 10 cm deep and from 2 to 15 cm in size. Six were malignant, and four were benign. The malignant lesions included two hepatocellular carcinomas, two lymphomas, one cervical carcinoma, and one transitional cell carcinoma metastasis to a periaortic lymph node. The four benign lesions were a benign thymoma, a presacral surgical scar, a focal fatty infiltration of the liver associated with a hepatic arterial infarction, and a regenerating hepatic nodule.

The tissue obtained with the Vacu-Cut needle was scant to absent in all six malignant cases. The tissue was sufficient to allow a diagnosis in only one case. In these six cases, the Greene needle provided abundant amounts of material in five and moderate amounts in one. Diagnosis of the malignancy was possible with the specimens obtained by using the Greene needle in the first five cases, and the findings were suggestive in the other one. This last case later was diagnosed as lymphoma on the basis of a specimen obtained by using a Tru-Cut needle.

The amount of tissue obtained with the Vacu-Cut needle in the four benign lesions was moderate in two and scant in two. The material obtained with the Greene needle was moderate in two and scant in two. The material provided by both needles was nondiagnostic in all benign cases.

In this comparative study of the Greene and the Vacu-Cut needles, one characteristic that differed was the mode of suction applied for aspiration. A study by Hueftle and Haaga [1] showed that 10 ml of suction through an 18- or 20-gauge needle would give an optimal yield of tissue. In our preliminary study, the diagnostic results obtained when the 22-gauge Greene needle and a standard method of suctioning were used were better than those obtained when the 22-gauge Vacu-Cut needle was used. The problem with the Vacu-Cut needle may be that it fails to provide effective suctioning. Thus, we think that, at the present, its use is not justified.

David Bodne
Stephen F. Quinn
Santo V. Nicosia
Patricia A. King
Robert A. Clark
H. Lee Moffitt Cancer Center and Research Institute
University of South Florida Medical Center
Tampa, FL 33682-0179

REFERENCE

1. Hueftle MG, Haaga JR. Technical note. Effect of suction on biopsy sample size. *AJR* **1986**;147:1014–1016

Use of the FloSwitch as a Torque Handle for Steerable Guidewires

The recent introduction of the FloSwitch (Medi-tech, Watertown, MA) (Fig. 1) as a disposable high-pressure stopcock was of interest to us because of the capability of closing the FloSwitch to the occluded position while a guidewire is in place through its lumen. This allows hemostasis around a guidewire that is significantly smaller than the lumen of the catheter or sheath into which it is placed and through which a large amount of bleeding ordinarily would occur. Attaching the FloSwitch to a Y-connector or sidearm fitting allows it to function in the same way as a Tuohy-Borst sidearm adapter [1].

Having used the FloSwitch on several occasions for this purpose, we became aware that the FloSwitch in the closed position actually grabs the wire sufficiently well to be a useful torque handle on 0.035- and 0.038-in. (0.09 and 0.10 cm) steerable guidewires. In our experience, the FloSwitch is not effective as a torque handle for the 0.018-in. (0.05 cm) guidewires. Because many of the 0.035- and 0.038-in. steerable guidewires are not supplied with a pin vise or other torque handle, we have adopted use of the FloSwitch, which has an advantage over the standard pin vise: It is more easily and rapidly placed on or removed from the guidewire, and it can be positioned to any location on the wire with a flick of the thumb. This technique also has an advantage, in terms of speed and ease of application, over the commonly used method of looping the wire at the end, especially for those heavy-duty torque wires that tend to be difficult to form into tight loops. Incidentally, after the FloSwitch has been used in this manner, it is often no longer hemostatic.

We hope that mention of this technique will allow greater convenience in the use of steerable guidewires.

Robert F. LeVeen
Hospital of the University of Pennsylvania and Medical Research Service, VA Medical Center
Philadelphia, PA 19104
Lisa M. Fedullo
St. Luke's Hospital
Bethlehem, PA 18017

REFERENCE

1. Gavant ML. Technical note. Improved guidewire immobilization technique for interventional procedures. *AJR* **1987**;149:629–630

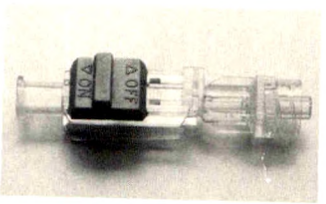

Fig. 1.—FloSwitch (Medi-tech, Watertown, MA), a disposable high-pressure stopcock, can be used as a torque handle for steerable guidewires in interventional radiologic procedures.

Vertical Cassette Alignment in Scoliosis Filming by Using the Gastric Gas Bubble as a Level

One potential pitfall in measuring pelvic tilt on the anteroposterior or posteroanterior upright scoliosis examination is malalignment of the cassette. We have found that occasionally the 91-cm cassettes do not seat firmly in the holder and have a tendency to deviate from a true vertical position. We have devised a simple, safe, fast method of accurately defining the horizontal plane by having the patient drink a glass of water immediately before the examination. This maneuver augments the usual air-fluid level in the stomach, and a perpendicular line can be dropped to determine true vertical.

To test this method, 40 scoliosis films made in the upright position in either the anteroposterior or posteroanterior projection were examined and scored for air-fluid levels by using a grading system of present A/F level or absent A/F level. Twenty were control examinations made via the routine method without the benefit of having the patient drink a glass of water. Eleven (55%) had A/F levels. The remaining 20 patients were given an 8-oz (236.7-ml) glass of water immediately before the examination. Nineteen (95%) had A/F levels. The patient shown in Figure 1A appears to have a pelvic tilt as defined by the position of the ischium oriented with the horizontal margin along the bottom edge of the film. This is depicted in the line drawing (Fig. 1C, see arrowheads). The discrepancy in the length of the left leg is shown to be factitious by Figure 1B. A line parallel to the fluid level is also parallel to the line connecting the most caudal point of each ischium, confirming the fact that the cassette was tilted in the original cassette holder. In fact, the lateral margin of the light-beam collimator was oriented to the true vertical in the illustrated case.

In summary, this method of "in vivo" leveling serves as an internal quality control and eliminates the misdiagnosis of a pelvic tilt that would necessitate the use of heel lifts or other intervention in a patient who has an anatomically level pelvis. A useful air-fluid level was obtained in 95% of patients studied, as compared to 55% in the control population.

Andrew M. Singer
Harvard Medical School and Beth Israel Hospital
Boston, MA 02215
John F. O'Connor
Boston University School of Medicine
Boston, MA 02118

The Need for Prompt, Effective Communication of Mammographic Results

Increasing attention is being given to mammography as a valuable diagnostic tool that can lead to reduction of mortality from breast cancer. Improved equipment and techniques that have reduced radiation dosage to negligible levels and more accurate interpretation that has resulted in earlier detection of breast cancer have increased the visibility and acceptance of mammography by clinicians and patients [1].

Diagnostic radiology is a consultative speciality in which communication between the radiologist, clinician, and patient is vitally important. It is the radiologist's responsibility to provide the most efficient, timely, and precise communication possible. This is particularly important with mammography because of the patient's anxiety, if not fear, frequently associated with this examination and with the possibility of having breast cancer.

Mammographic interpretation is difficult, even for so-called experts. Most clinicians are uncomfortable attempting to interpret the images and depend more on the radiologist's interpretation. Therefore, significant findings must be reported promptly.

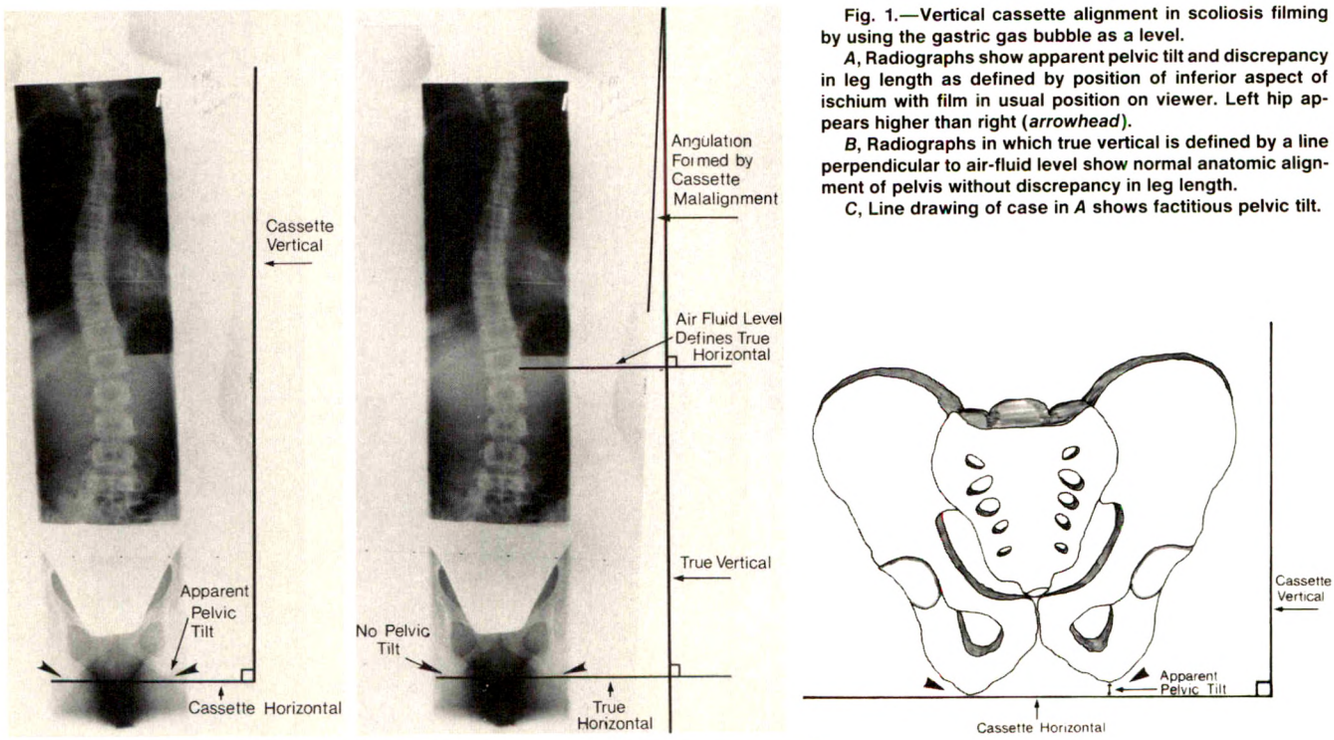

Fig. 1.—Vertical cassette alignment in scoliosis filming by using the gastric gas bubble as a level.

***A*, Radiographs show apparent pelvic tilt and discrepancy in leg length as defined by position of inferior aspect of ischium with film in usual position on viewer. Left hip appears higher than right (*arrowhead*).**

***B*, Radiographs in which true vertical is defined by a line perpendicular to air-fluid level show normal anatomic alignment of pelvis without discrepancy in leg length.**

***C*, Line drawing of case in *A* shows factitious pelvic tilt.**

We have found in the hospital setting that the most efficacious method of communication has been direct, personal contact with the referring physician. This can be done best by a face-to-face meeting, with the images in hand. Clinical concerns and findings can be correlated with mammographic concerns and findings, and confidence levels about suspicious areas can be discussed. The anxiety of the patient and her reliability in returning for follow-up examinations, as known by her physician, can be factors in the decision to aspirate, further study, biopsy, or follow a bothersome or suspicious mammographic finding.

In most clinical situations, especially office practices, personal contact between the radiologist and the referring physician is not possible, and one must rely on the telephone. In all cases that have suspicious findings, we contact the referring physician before the patient leaves the mammography suite. This ensures that the clinician is aware of our findings and concerns, provides an opportunity for discussion, and increases the likelihood of appropriate action and/or follow-up.

This system does not reduce the importance of thorough written reports with succinct conclusions and recommendations. These are generated and disseminated in a timely fashion. When an oral communication has taken place, this is noted in the report. Methods such as these will reduce the menace of litigation [2, 3].

Mammography often brings the radiologist in close contact with an anxious patient who may ask the technologist or radiologist about the results of the examination. When findings are positive or suspicious, discussion with the referring physician before answering the patient is appropriate and can prevent misunderstanding. However this is done, it behooves the radiologist to respond to the patient discreetly and to urge prompt contact with the referring physician. When the results of the examination are negative, the response is easier but should include a comment on the limitations of mammography and the importance of correlation with physical findings. When patients do not inquire about the results of the study, our obligations are (1) to be certain the examination is optimal and complete before the patient leaves so that she will not have to return for additional images and (2) to communicate the results to the referring physician promptly, including a telephone call when findings are positive or suspicious. It is difficult to do this in high-volume, mass-screening mammography centers in which the radiologist often is not on site and interprets the studies in batches later on. Even under those circumstances, a qualified technologist can reduce recalls to a minimum [4].

Effective communication requires more of the radiologist's time at first but will better serve the patient, referring physician, technologist, and radiologist by reducing recalls, anxiety, the number of additional studies and their attendant costs, and mistakes, including unnecessary biopsies.

John T. Cuttino, Jr.
Lahey Clinic Medical Center
Burlington, MA 01805
Robert McLelland
Richard L. Clark
University of North Carolina School of Medicine
Chapel Hill, NC 27514

REFERENCES

1. McLelland R. Mammography 1984: challenge to radiology. *AJR* **1984**;143:1–4
2. Berlin L. Malpractice and radiologists, update 1986: an 11.5-year perspective. *AJR* **1986**;147:1291–1298
3. Smith JP. Opinion. Risk management for the radiologist. *AJR* **1987**;149:641–643
4. Schreiber MH, Winslade WJ. Rights, roles, and relationships in radiology. *Radiology* **1987**;163:269–270

A New, Extra-Long Vascular Sheath

A persistent problem in angiography is manipulation of catheters in tortuous vessels. This problem is especially pronounced when a tortuous iliac artery is involved. Shortly after a catheter has been passed through such an iliac artery, it may become impossible to manipulate or advance the tip to higher positions within the abdomen, chest, or cerebral structures. The cause of this is loss of effective transmission of vector forces along the tortuous course of the catheter. At first, the elastic recoil of the vessel may facilitate transmission of forces to the tip, but as constant pressure is applied by the catheter to the wall of the vessel, both the vessel and the catheter become progressively deformed and absorb these forces. This results in buckling of the artery and "looping" of the catheter within the pelvis.

Currently, two solutions are available: use of a stiffer catheter and/or guidewire or placement of a vascular sheath. Stiffer catheters and guidewires still may buckle, and the currently available vascular sheaths are not always long enough. A recent technical note [1] suggested the use of a 25-cm-long sheath that is available only in Japan. The longest sheaths currently available within the United States are 23 cm long and are designed for use primarily during coronary angioplasty. Frequently, these are too short to extend through the tortuous portions of the pelvic vessels.

We have designed a new 40-cm-long sheath (Fig. 1) that is positioned by using a Van Andel dilator. This Teflon sheath, which is now commercially available (Cook Inc., Bloomington, IN), has a side arm and a hemostatic valve and is designed to accommodate 5- to 7-French catheters. The use of an 80-cm Van Andel–style dilator has facilitated safe placement of the sheath into the vessel and advancement into the lower abdominal aorta [2]. The long Van Andel dilator can easily be advanced the first 40 cm into the patient and then held fixed in place while the sheath is introduced coaxially over it to the sheath's final position without fear of injuring the vessel. Constant perfusion of heparinized saline through the side arm has prevented any complications resulting from clot formation. The sheath, when properly positioned, will straighten the catheter's course through the iliac artery and prevent the catheter from looping or buckling in the pelvic vessels. Working through the long sheath has enabled rapid completion of cerebral, thoracic, and abdominal studies that otherwise would have been exceedingly difficult. In more than a year's experience with this device, we have had no complications resulting from its use. In conclusion, this long sheath with its special long

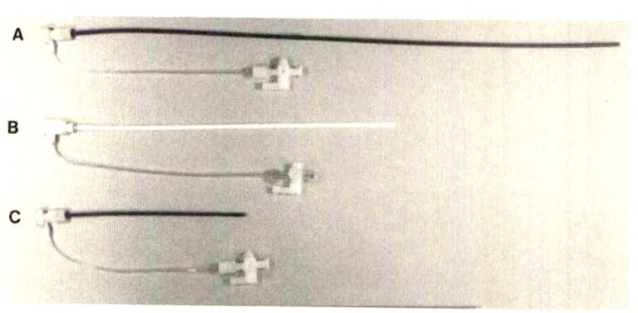

Fig. 1.—Comparison of new, extra-long, 40-cm vascular sheath (*A*) with 23-cm coronary angioplasty sheath (*B*) and standard 15-cm angiography sheath (*C*).

dilator reliably solves a common angiographic problem without risk, difficulty, or excessive cost.

Howard L. Berman
Marc A. Bernstein
Stuart G. Katz
New York Medical College
Valhalla, NY 10595

REFERENCES

1. Nakamura H, Oi H. Newly devised long sheath for transfemoral angiography. *Radiology* **1985**;155:828
2. Berman HL, Martin MB. A simplified method for antegrade sheath introduction into the common femoral artery. *AJR* **1982**;138:973

Hepatocellular Carcinoma: MR Appearance Mimicking Focal Nodular Hyperplasia

I read with great interest the article by Wilbur and Gyi, "Hepatocellular Carcinoma: MR Appearance Mimicking Focal Nodular Hyperplasia," [1] that appeared in the October issue of *AJR*.

It has been my experience that T1-weighted images of the liver are essential before it can be determined if a lesion within the liver is composed of normal hepatocytes. In the case report presented, heavily T1-weighted images were not performed; therefore, the authors really should not have made any statement about whether their findings could have been focal nodular hyperplasia. It is well known that fibrolamellar hepatocellular carcinoma can have a scar. Indeed, since this lesion was biopsied percutaneously only and not excised, its subtype cannot be addressed. On review of two cases from the University of Pennsylvania, I found that the scars of fibrolamellar hepatocellular carcinoma were of low signal intensity on SE 2500/80 images.

Because heavily T1-weighted images were not performed, a statement about normal hepatocytes probably should not be made on the basis of MR criteria. Certainly, the central scar of either focal nodular hyperplasia can be hyperintense on the long-TR/TE images, and the literature remains unclear about whether fibrolamellar hepatocellular carcinomas may also have a hyperintense scar.

M. L. Schiebler
The University of North Carolina
Chapel Hill, NC 27514

REFERENCE

1. Wilbur AC, Gyi B. Case report. Hepatocellular carcinoma: MR appearance mimicking focal nodular hyperplasia. *AJR* **1987**;149:721–722

Reply

Mattison et al. [1] described isointensity or near-isointensity to adjacent liver on long-TR/TE sequences as an essential criterion for an MR imaging diagnosis of focal nodular hyperplasia. When their long-TR/TE sequences were used, all seven hepatocellular carcinomas reported by these authors were hyperintense to liver parenchyma. Our example of hepatocellular carcinoma showed marked peripheral hyperintensity on long-TR/TE images. As this is a reported finding of malignant intrahepatic tumors, but not of focal nodular hyperplasia, we considered it suggestive of cancer and would have considered it such regardless of any similarity to liver on T1-weighted images. Had the tumor shown an intensity close to that of liver on T2-weighted images, a T1-weighted sequence, as suggested by Dr. Schiebler, might have been valuable in that isointensity with hepatic parenchyma on all pulse sequences would have suggested focal nodular hyperplasia or some other abnormal arrangement of otherwise normal hepatocytes.

Our best assessment, based on open surgical biopsy, was that the tumor reported by us did not represent a fibrolamellar variant of hepatocellular carcinoma. Microscopically, the tumor did not show the abundant, lamellated fibrous stroma and prominent eosinophilic cytoplasm characteristic of fibrolamellar hepatomas. The point of subtype is nevertheless moot, as, indeed, it might be even if pathologic examination of the entire tumor had been possible.

Dr. Schiebler shares his interesting observation of long-TR/TE enhancement of the central scar in cases of fibrolamellar hepatocellular carcinoma. This finding further emphasizes the nonspecificity of a bright central scar with T2-weighted MR imaging. Both hepatomas and focal nodular hyperplasia may have this appearance.

Andrew C. Wilbur
University of Illinois Hospital
Chicago, IL 60612

REFERENCE

1. Mattison GR, Glazer GM, Quint LE, Francis IR, Bree RL, Ensminger WD. MR imaging of hepatic focal nodular hyperplasia: characterization and distinction from primary malignant hepatic tumors. *AJR* **1987**;148:711–715

Radiopacity of Glass

In the October issue of *AJR* W. K. Andrew [1] responded to an article by Fornage and Schernberg [2] questioning the radiopacity of glass and attributed this property to its lead content. However, several published studies [3–5], the first in 1932, have shown that all glass is radiopaque. This literature also has shown that most commercial glass does not contain lead and that it is the density of the glass and probably the silicate content that provide its opaque property, not its lead content.

This apparently has been a common misconception, but after careful examination, glass of sufficient size in soft tissues should be visualized.

Edward F. Patz, Jr.
Brigham and Women's Hospital
Harvard Medical School
Boston, MA 02115

REFERENCES

1. Andrew WK. Sonographic diagnosis of foreign bodies of the distal extremities. *AJR* **1987**;149:864
2. Fornage BD, Schernberg FL. Sonographic diagnosis of foreign bodies of the distal extremities. *AJR* **1986**;147:567–569
3. Lewis RW. A roentgenographic study of glass and its visibility as a foreign body. *AJR* **1932**;27:853–857
4. Felman AH, Fisher MS. The radiographic detection of glass in soft tissue. *Radiology* **1969**;92:1529–1531
5. Roberts WE. Radiographic characteristics of glass. *Arch Indust Health* **1958**;18:470–472

Audio Entertainment System in a Radiology Department

The care of children in a radiology department has two important aspects. The first objective is to obtain excellent, quality images as safely as possible. The second, but equally important, objective is to make the entire experience as nontraumatic as possible for the child. This is achieved by having a pleasant physical environment and by having staff trained in and dedicated to the handling of children. In

January 1987, to further improve our care of patients, we installed an audio entertainment system that we think is unique and helps relieve a child's anxiety. The purpose of this letter is to describe the system.

The system provides audio entertainment to the children not only while they are in the waiting areas but also while they are undergoing imaging procedures, including studies such as CT, sonography, nuclear medicine examinations, and fluoroscopy, but not studies such as chest radiographs.

The system provides four channels of music that are listened to through headphones. At each headphone location, each channel can be selected independently, and the volume can be controlled by the headsets. The headsets are located in patients' waiting areas and also in the rooms for CT, special procedures, sonography, and nuclear medicine imaging. In the imaging rooms, the headsets are suspended on a cord hanging from the ceiling just above the head of the imaging table. The children wear the headsets while they are having their imaging studies done. The music for each channel is provided by four Bogan RM 350 audio units (supplied by Custom Sound, Indianapolis, IN). Each unit is capable of AM or FM radio reception and has a commercial-quality tape player with automatic reverse. The tape players can play continuously for an indefinite period. The children are provided with a wide selection of entertainment, including classical, rock, and country music; children's stories; and prerecorded sports highlights. During 8 months of use, the system has been extremely well accepted by children of all ages.

The headphones that we use are heavy-duty and nonstereophonic. The use of the nonstereophonic system and direct wiring of the headphones into the walls in waiting areas have resulted in no thefts during 8 months of operation. The headphone used is a Columbia 600352499, Type C3X (supplied by Custom Sound). In the CT area, a microphone has been wired into the system. At a press of the button, the music is cut out, and the CT technologist can speak directly to the patient through the headphones. The patients can use the system during virtually all imaging studies other than head CT scans.

Mervyn D. Cohen
Riley Hospital for Children, Indiana University Medical Center
Indianapolis, IN 46223
Fred Boyer
General Electric Medical Systems
Indianapolis, IN 46241

Letters are published at the discretion of the Editor and are subject to editing.

Letters to the Editor must not be more than two *doubled-spaced* typewritten pages. One or two figures may be included. See Author Guidelines for letters, page A5.

Letters concerning a paper published in the *AJR* will be sent to the authors of the paper for a reply to be published in the same issue. Opinions expressed in the Letters to the Editor do not necessarily reflect the opinions of the Editor.

Review of Current Literature

Initials and addresses of corresponding authors are provided in parentheses for each article so that the reader can obtain reprints directly. Abstracts are printed verbatim from each journal.

CLINICAL LITERATURE

The New England Journal of Medicine

Prostate-specific antigen as a serum marker for adenocarcinoma of the prostate. Stamey TA, Yang N, Hay AR, McNeal JE, Freiha FS, Redwine E (TAS, Division of Urology (S287), Stanford University School of Medicine, Stanford, CA 94305-5118). *N Engl J Med* 317(15):909–916, Oct. 1987

To compare the clinical usefulness of the serum markers prostate-specific antigen (PSA) and prostatic acid phosphatase (PAP), we measured them by radioimmunoassay in 2200 serum samples from 699 patients, 378 of whom had prostatic cancer.

PSA was elevated in 122 of 127 patients with newly diagnosed, untreated prostatic cancer, including 7 of 12 patients with unsuspected early disease and all of 115 with more advanced disease. The PSA level increased with advancing clinical stage and was proportional to the estimated volume of the tumor. The PAP concentration was elevated in only 57 of the patients with cancer and correlated less closely with tumor volume. PSA was increased in 86 percent and PAP in 14 percent of the patients with benign prostatic hyperplasia.

After radical prostatectomy for cancer, PSA routinely fell to undetectable levels, with a half-life of 2.2 days. If initially elevated, PAP fell to normal levels within 24 hours but always remained detectable. In six patients followed postoperatively by means of repeated measurements, PSA—but not PAP—appeared to be useful in detecting residual and early recurrence of tumor and in monitoring responses to radiation therapy.

Prostate massage increased the levels of both PSA and PAP approximately 1.5 to 2 times. Needle biopsy and transurethral resection increased both considerably.

We conclude that PSA is more sensitive than PAP in the detection of prostatic cancer and will probably be more useful in monitoring responses and recurrence after therapy. However, since both PSA and PAP may be elevated in benign prostatic hyperplasia, neither marker is specific.

Cancer

Primary anorectal lymphoma: a new manifestation of the acquired immune deficiency syndrome (AIDS). Ioachim HL, Weinstein MA, Robbins RD, Sohn N, Lugo PN (HLI, Depts. of Pathology and Surgery, Lenox Hill Hospital, New York, NY). *Cancer* 60:1449–1453, 1987

Non-Hodgkin's lymphomas with particular clinicopathologic features occur with a high incidence in homosexual men affected by AIDS. More frequently than in the general population, these lymphomas have an extranodal location including the gastrointestinal tract. We have recently observed four cases of AIDS-associated lymphomas whose primary location is in the lower rectum and anus. The patients were 27 to 44 years of age, had greatly depressed helper-suppressor T-cell ratios, and antibodies to human immunodeficiency virus (HIV). All four presented with anorectal symptoms and originally had surgery for anorectal fistulas or tumor masses. When staged, three patients had no other organ involvement, the fourth only had lymphoma in an axillary lymph node, and all four had large tumor masses confined within the rectum. In terms of histology, the lymphomas were of undifferentiated or of large cell type and of B-cell phenotype. Lymphomas with primary or major location in the rectum are a rare occurrence in the general population, and until recently, are rare even among the lymphomas associated with the immune deficiency syndrome. At the Lenox Hill Hospital in New York City, no rectal lymphoma among the 58 cases of AIDS-related lymphoma diagnosed during the past 4 years was recorded until 10 months ago. The recognition of the new feature in presentation, a neoplasm associated with AIDS, is obviously important for its early diagnosis and treatment. Its unusual occurrence at the suspected portal of entry of the HIV infection is of interest because it may provide new clues to the association between AIDS and neoplasia.

Reprinted by permission from the American Cancer Society.

Late multifocal gliomas in adolescents previously treated for acute lymphoblastic leukemia. Fontana M, Stanton C, Pompili A, et al. (MF, Division of Neurosurgery, Istituto Regina Elena, V. le Regina Elena 291, 00161, Rome, Italy). *Cancer* 60:1510–1518, 1987

Three of 37 adolescents in long-term remission from childhood acute lymphoblastic leukemia (ALL) developed malignant multifocal gliomas several years after completing treatment that included central nervous system (CNS) prophylaxis with radiation (RT) and intrathecal methotrexate (IT-MTX). No recurrence of the leukemia was evident when the CNS tumors were discovered. Seventeen other similar cases have been recorded. The occurrence of second malignancies is reviewed in the context of this development and of the oncogenic effects of radiation. It is probable that prolonged exposure to IT-MTX may have had a synergistic effect with radiation in contributing to the unusual incidence of glial tumors in these patients.

Reprinted by permission from the American Cancer Society.

Chest

Transthoracic needle biopsy of lung in nonhospitalized patients. Poe RH, Kallay MC (RHP, Highland Hospital, Rochester, NY 14620). *Chest* 92:676–678, 1987

To confirm the safety of transthoracic needle biopsy of the lung (TNB) in the outpatient setting, we reviewed our experience with 106 such procedures over three years. We compared the operating characteristics and morbidity with the 65 similar procedures we were asked to perform on hospitalized patients during the same period. Outpatients did not differ from inpatients in mean age, sex, incidence of clinically apparent COPD, size and location of lesion, or number of needle passes. The operating characteristics of the biopsy were the same for the two groups. Pneumothorax occurred in 29 (27 percent) of 106 outpatient and 26 (40 percent) of 65 inpatient TNBs. Few pneumothoraces not present upon completion of biopsy developed during four hours of observation or later. The requirement for chest tube drainage was similar for both groups, 5.7 and 4.6 percent, respectively. With appropriate caution, TNB can be performed safely on an outpatient basis and the cost of an uncomplicated procedure reduced by 27 percent.

Gastroenterology

Natural history of untreated colonic polyps. Stryker SJ, Wolff BG, Culp CE, Libbe SD, Ilstrup DM, MacCarty RL (BGW, Section of Colon and Rectal Surgery, Mayo Clinic, 200 First St. S. W., Rochester, MN 55905. *Gastroenterology* 93:1009–1013, 1987

The natural history of untreated colonic polyps is uncertain. A retrospective review of Mayo Clinic records from a 6-yr period just before the advent of colonoscopy identified 226 patients with colonic polyps ≥10 mm in diameter in whom periodic radiographic examination of the colon was elected over excisional therapy. In all patients, follow-up of polyps spanned at least 12 mo (mean, 68 mo; range, 12–229 mo) and included at least two barium enema examinations (mean, 5.2; range, 2–17). During the follow-up period, 83 polyps (37%) enlarged. Twenty-one invasive carcinomas were identified at the site of the index polyp at a mean follow-up of 108 mo (range, 24–225 mo). Actuarial analysis revealed that the cumulative risk of diagnosis of cancer at the polyp site at 5, 10, and 20 yr was 2.5%, 8%, and 24%, respectively. In addition, 11 invasive cancers were found at a site remote from the index polyp during the same follow-up period. These data further support the recommendation for excision of all colonic polyps ≥10 mm in diameter. Periodic examination of the entire colon is recommended in this group of patients to identify neoplasms arising at a site remote from the index polyp. Although this study has limitations inherent to any retrospective analysis, comparable prospective data are unlikely to be available in the future because of the current widespread availability of colonoscopy.

Reprinted with permission by the American Gastroenterological Association.

Digestive Diseases and Sciences

Sonographic imaging of the pancreatic duct: new diagnostic possibilities using secretin stimulation. Glaser J. Högemann B, Krummenerl T, et al. (JG, Medical Clinic and Policlinic, University of Münster, Albert-Schweitzer-Str. 33, D-4400 Münster, West Germany). *Dig Dis Sci* 32(10):1075–1081. 1987

The pancreatic duct or at least parts of this structure can be demonstrated today by sonography in 75–85% of all persons examined. In 84 persons we have now measured the caliber of the sonographically visualized pancreatic duct in the region of the proximal body of the pancreas with special attention to dependence on age. The diameter of Wirsung's duct ranged from 1 to 3 mm (mean 1.9 mm) and increased significantly from the fifth decade of life onwards. After intravenous injection of the hormone secretin, healthy persons usually show a distinct duct enlargement, which also depends on age. Nine persons aged 19 through 35 (median 28) years showed a dilatation of the main pancreatic duct by about 110% following secretion injection. Nine further probands, 50–74 (median 58) years old, had a dilatation of about 70%. Eighteen patients with confirmed chronic pancreatitis and a pancreatic duct diameter not exceeding 4 mm generally showed no duct enlargement after secretin stimulation. We believe that periductal fibrosis, which is common in chronic pancreatitis, is the most important reason for these results. The use of the sonographic secretin test in the diagnosis of chronic pancreatitis should be considered.

Changes in colorectal function in patients with chronic colonic pseudoobstruction. Loening-Baucke VA, Anuras S, Mitros FA (VAL, Dept. of Pediatrics, University of Iowa Hospitals and Clinics, Iowa City, IA 52242). *Dig Dis Sci* 32(10):1104–1112, Oct. 1987

Motility studies of the lower bowel, radiology to exclude other gastrointestinal involvement, and rectal biopsies were carried out in 11 patients, age 21–60 years, with isolated chronic colonic pseudoobstruction. Repeated plain abdominal x-rays during symptomatic periods revealed massive gaseous colonic distension in all. Seven patients had the primary form while four patients had an underlying disease which could have been responsible for the chronic colonic pseudoobstruction. Lower bowel motility was decreased in patients with the primary form. Rectal wall elasticity was increased in both the primary and secondary form. Some of the abnormalities measured may suggest myogenic abnormalities of the sigmoid or rectal wall. No specific neural or muscular morphologic defect was identified in colonic transmural sections in eight patients except in the patient with Hirschsprung's disease. Five of seven patients with primary colonic pseudoobstruction achieved symptomatic relief only after subtotal colectomy and ileoproctostomy.

Scandinavian Journal of Gastroenterology

Value of sonography in obstructive jaundice: limitations of bile duct caliber as an index of obstruction. Pedersen OM, Nordgård K, Kvinnsland S (OMP, Dept. of Clinical Physiology, 5016 Haukeland Hospital, University of Bergen, Bergen, Norway). *Scand J Gastroenterol* 22:975–981, 1987

The diagnostic value of sonography was assessed in 176 patients with jaundice who had a final diagnosis on the basis of surgery, autopsy, liver biopsy, endoscopic retrograde cholángiopancreatography, and serum tests positive for hepatitis A and B. Obstructive (n = 113) versus nonobstructive jaundice (n = 63) was diagnosed with a sensitivity of 91% and a specificity of 95%. Nine of the 10 false negatives had choledocholithiasis. Application of stricter criteria for common duct (CD) dilatation than the one used of CD ≥ 8 mm to ≥ 12 mm would have lowered the sensitivity from 91% to 84%. On the basis of these criteria the predicted level of obstruction would have shifted from distal to proximal in 36% of the patients. Choledocholithiasis was more often associated with decreasing bilirubin values than malignancy: 55% versus 9% ($p<0.05$). The present study indicates that intermittent obstruction, usually associated with choledocholithiasis, constitutes the main problem in detection of obstructive jaundice. Diameter criteria used for diagnosing dilatation of the CD may greatly influence sonographic accuracy.

The Journal of Bone and Joint Surgery

Anatomy of the abducter muscles of the hip as studied by computed tomography. Clark JM, Haynor DR (JMC, Dept. of Orthopaedics, RK-10, University of Washington Hospitals and Clinics, Seattle, WA 98195). *J Bone Joint Surg [Am]* 69-A:1021–1031, Sept. 1987

Computed tomography provides a noninvasive method for studying anatomy in live subjects. The abductor muscles of the hip were studied by using computed tomography to describe their position, size, and orientation. The outlines of the muscles were clearly identifiable; patterns that are associated with trauma, arthritis, and so on, differed from normal. The patterns in eighteen normal hips in twelve

adults were mapped in detail. The cross-sectional areas of the abductor muscles were measured and vectors representing the total pull of the abductor muscle in the frontal and sagittal planes were constructed for each hip. The variations in individual and composite muscular anatomy were recorded. The inclination of the axis of the abductor muscle ranged from 17 to 26 degrees (standard deviation, 2.9 degrees) in the frontal plane and from −2 to 14 degrees (standard deviation, 4.2 degrees) in the sagittal plane.

Clinical Orthopaedics and Related Research

Incomplete thickness rotator cuff tears diagnosed by subacromial bursography. Fukuda H, Mikasa M, Yamanaka K (HF, Dept. of Orthopaedic Surgery, Tokai University Oiso Hospital, Oiso, 259-01 Japan). *Clin Orthop* Oct. (223):51–58, 1987

Incomplete thickness rotator cuff tears (ITRCT) adjacent to the bursal sac were diagnosed preoperatively by subacromial bursography and confirmed by surgical exposure. There were five men and one woman with an average age of 41.8 years. The preoperative duration of shoulder pain ranged from four to 36 months (average, 15.8 months). Clinical manifestations included crepitus and a painful arc in five of the six cases. Glenohumeral arthrography was normal in all cases. Subacromial bursography, subsequently performed, revealed pooling of the contrast medium in a torn area of the bursal side of the rotator cuff in all cases. Surgical treatment was recommended after the failure of conservative treatment for three to ten months. The surgical treatment consisted of both anterior acromioplasty and tendon suture. Wedge resection and shoelace suture repair of the tendon produced satisfactory results in all cases followed for ten to 72 months (average, 44.3 months). ITRCT adherent to the bursal sac were noted in 2.4% of a cadaver survey. Subacromial bursography can be a useful diagnostic procedure for this specific entity in subacromial impingement syndrome.

The Journal of Urology

Percutaneous renal calculus removal in an extracorporeal shock wave lithotripsy practice. Leroy AJ, Segura JW, Williams HJ Jr., Patterson DE (AJL, Mayo Clinic, 200 First St., S. W., Rochester, MN 55905). *J Urol* 138:703–706, Oct. 1987

The introduction of extracorporeal shock wave lithotripsy and transurethral ureteroscopy have altered markedly the incidence of standard surgical and percutaneous stone removal procedures. To help define the present role of percutaneous procedures in our practice we evaluated our indications, results and the clinical course of 143 patients who were treated primarily with percutaneous methods during 1 year in which extracorporeal shock wave lithotripsy also was available. The complexity of these residual percutaneous cases necessitated repeat endoscopic or fluoroscopic stone removal procedures in 20 per cent and ancillary extracorporeal shock wave lithotripsy in 22 per cent, and led to a slightly higher complication rate than in our previous percutaneous series. Despite the effectiveness of extracorporeal shock wave lithotripsy, percutaneous methods still are necessary for comprehensive therapy of upper tract urolithiasis.

British Journal of Urology

Renal scarring secondary to vesicoureteric reflux: critical assessment and new grading. Monsour M, Azmy AF, MacKenzie JR (AFA, Dept. of Paediatric Surgery, Royal Hospital for Sick Children, Yorkhill, Glasgow G3 8SJ, United Kingdom). *Br J Urol* 60:320–324, October 1987

One hundred and fifty children with proven urinary tract infection who were assessed by renal ultrasound (U/S), intravenous urography (IVU) and dimercaptosuccinic acid (^{99m}Tc DMSA) scan, were studied to identify the sensitivity of each examination and the pick-up rate of renal scarring secondary to vesicoureteric reflux. Sixty-three of these children who had the examinations carried out within a 6-month period were assessed in detail.

A DMSA scan is the most accurate method of detecting early renal scars in the young age group (0–2 and 2–5 years), followed by ultrasound. The examinations are equally sensitive over the age of 5. A new grading system of the severity of renal scarring is presented.

Pediatrics

Is moderate drinking during pregnancy associated with an increased risk for malformations? Mills JL, Graubard BI (JLM, Epidemiology Branch, Landow/8B06, EBRP, NICHD, NIH, Bethesda, MD 20892). *Pediatrics* 80(3)309–314, Sept. 1987

The relationship between heavy drinking during pregnancy and congenital malformations is well known; however, whether moderate or light drinking is teratogenic is controversial. This prospective birth defects study collected information from 32,870 women about alcohol consumption during the first trimester of pregnancy. Total malformation rates were not significantly higher among offspring of women who had an average of less than one drink per day (77.3/1,000) or one to two drinks per day (83.2/1,000) than among nondrinkers (78.1/1,000). An increased risk as small as 12% in the group averaging less than one drink per day and 45% in those averaging one to two drinks per day would most likely have been detected if it were present. Likewise, major malformations were not increased in these drinking groups. Examining malformations by organ system and individual defect revealed that sex organ malformations and all genitourinary malformations increased significantly ($P < .05$) with increasing alcohol consumption. These findings suggest that alcohol, at the levels usually consumed during pregnancy, is not a significant cause of malformations. Nonetheless, the possibility that there are some malformations for which no safe drinking level exists requires additional investigation.

Reprinted by permission of *PEDIATRICS © 1987.*

Atlantoaxial instability in individuals with Down syndrome: epidemiologic, radiographic, and clinical studies. Pueschel SM, Scola FH (SMP, Child Development Center, 593 Eddy St., Providence, RI 02902). *Pediatrics* 80(4)555–560, Oct. 1987

Atlantoaxial instability is a relatively frequent finding in individuals with Down syndrome. We examined 404 patients with this chromosome disorder and observed their atlanto-dens intervals and spinal canal widths to be significantly different from children without Down syndrome. Significant differences were also noted between boys and girls with Down syndrome in spinal canal widths but not in atlanto-dens interval measurements. When different neck positions were compared, measurements obtained in flexion were significantly greater than in extension or in neutral position. In addition, more patients had ≥5 mm atlanto-dens interval measurements in flexion than in extension or neutral. A total of 59 (14.6%) of 404 patients displayed atlantoaxial instability. Fifty-three (13.1%) patients had asymptomatic atlantoaxial instability, and special precautions will have to be taken with this group of children. Six (1.5%) patients had symptomatic atlantoaxial instability who underwent surgery to prevent further injury to the spinal cord. In our follow-up studies of 95 patients with Down syndrome, we did not find any significant changes during either clinical or radiographic reexaminations.

Reprinted by permission of *PEDIATRICS © 1987.*

The Journal of Pediatrics

Long-term prognosis of giant coronary aneurysm in Kawasaki disease: an angiographic study. Tatara K, Kusakawa S (KT, Dept. of Pediatrics, Tokyo Women's Medical College Daini Hospital, Ni-

shiogu 2-1-10, Arakawa-ku, Tokyo 116, Japan). *J Pediatr* 111:705–710, November 1987

The incidence of coronary obstruction subsequent to giant coronary aneurysm in Kawasaki disease was studied. In 20 cases, aneurysms with a maximal diameter >8 mm were identified by coronary angiography 2 to 120 months (mean 16.9 months) after onset. There were 25 giant aneurysms among these 20 patients, all of whom underwent coronary angiography between 12 and 134 months (mean 31.7 months) after initial examination. Coronary obstruction occurred in six cases (30.0%), all within 4 years of onset of disease. There were five obstructive aneurysms in the right coronary artery (5/12; 41.7%) and two in the left coronary artery (2/13; 15.4%). One of these patients developed symptomatic myocardial infarction. Two had abnormal electrocardiographic findings suggesting myocardial infarction. In five cases, persistent perfusion defects were found by myocardial imaging. On the other hand, in two patients giant aneurysms persisted without obstructive changes for >10 years. In both cases the aneurysm was in the left coronary artery and obstruction of the right coronary artery was found at initial angiography. These results seem to indicate the limited efficacy of antiplatelet therapy for giant coronary aneurysms in Kawasaki disease and that giant aneurysms are likely to progress to become obstructive within a few years even if antiplatelet therapy is given. Other forms of treatment, including surgery, should therefore be considered in such patients.

RADIOLOGY SUBSPECIALTY JOURNALS

The Journal of Nuclear Medicine

Pulmonary embolism and lung scanning: cost-effectiveness and benefit:risk. Specker BL, Saenger EL, Buncher CR, McDevitt RA (ELS, E. L. Saenger Radioisotope Laboratory, Mail Location #577, Dept. of Radiology, University of Cincinnati Hospital, Cincinnati, OH 45267). *J Nucl Med* 28(10):1521–1530, Oct. 1987

The cost-effectiveness of pulmonary imaging (lung scan) on the management of 2,023 patients was studied. Prior and postscan probabilities of pulmonary embolism (PE) were obtained from referring physicians. After the scan, anticoagulant therapy (ACT) was appropriately changed in 20% of the patients and confirmed in 67%. The incremental cost of scanning was $124 per patient when the prior probability was 0.01–9.99%, dropping to $38 when the probability was 10–25%. Hospitalization and ACT cost was reduced when the prior probability was 25.01–99.99%. The greatest benefit in lives saved was when the prior probability was 25–74.99%; 1.5% of this probability group would survive as a result of the change in management attributable to the scan, at a cost of $117 per life saved. The benefit: risk ratio, as measured by lives saved compared to estimates of lives lost due to radiation exposure, was of the order of 6,000:1.

Journal of Thoracic Imaging

Blood supply of pulmonary metastases. Milne ENC, Zerhouni EA (ENCM, Dept. of Radiological Sciences, University of California, Irvine Medical Center, 101 The City Dr., Orange, CA 92668). *J Thorac Imag* 2(4):15–23, 1987

There is a widely held belief that metastases to the lung (like primary lung tumors) are supplied by the bronchial arteries and that pulmonary neovascularization does not occur. In 17 human lungs, we have demonstrated, both in vitro and in vivo, pulmonary circulation to metastases. We have confirmed this in a series of animal studies in which we implanted tumors of various histologies into rats' tails and induced metastases from these tumors into the lungs. Forty-eight percent of these metastases had an *entirely* pulmonary circulation, 36% a primarily pulmonary circulation with a small bronchial component, and only 16% of metastases, located in the central one third of the lung, had an exclusively bronchial circulation. We have now shown that these supplying pulmonary vessels to metastases can be clearly demonstrated on thin-section computed tomography of the lungs. This may prove to be a helpful, noninterventional diagnostic criterion for distinguishing a primary from a metastatic lesion.

Pulmonary tumor embolism: a critical review of clinical, imaging, and hemodynamic features. Chan CK, Hutcheon MA, Hyland RH, Smith GJW, Patterson BJ, Matthay RA (RAM, Pulmonary Section, LCI 105, Dept. of Medicine, Yale University School of Medicine, 333 Cedar St., PO Box 3333, New Haven, CT 06510). *J Thorac Imag* 2(4):4–14, 1987

Pulmonary tumor embolism is a common finding at autopsy but is generally perceived as a difficult diagnosis to make ante mortem. After a retrospective review of 164 reported cases of pulmonary tumor embolism, we identified a typical profile of clinical, laboratory, and imaging features that may permit confident clinical diagnosis in most patients with this condition. The clinical features include a documented or suspected underlying malignancy, acute to subacute onset of dyspnea, and signs of cor pulmonale. Supportive laboratory features are hypoxemia or increased alveolar-arterial oxygen gradient, and invasive or noninvasive evidence of pulmonary artery hypertension. Typical imaging findings are normal chest radiographs; multiple, subsegmental, peripheral perfusion defects on ventilation-perfusion lung scans; and delayed filling with or without subsegmental filling defects but without a thrombus on pulmonary angiogram. Radiolabeled monoclonal antibody imaging and pulmonary microvascular cytology sampling techniques are promising diagnostic tests for early diagnosis of pulmonary tumor embolism.

Pediatric Radiology

The treatment of post-operative and peptic esophageal strictures after esophageal atresia repair. Hoffer FA, Winter HS, Fellows KE, Folkman J (FAH, Dept. of Radiology, The Children's Hospital, Boston, MA). *Pediatr Radiol* 17:454–458, 1987

Nine patients, 6 weeks to 17 years of age with esophageal atresia (EA), developed esophageal strictures and were treated with 26 balloon catheter dilatations over a period of 3 years; 6 are now asymptomatic. Five of the 9 patients had suspected reflux esophagitis, confirmed in 3 by biopsy and treated medically prior to dilatation. Seven of the 9 patients had a primary anastomosis, 1 a gastric tube, and 1 a colonic interposition. Most dilatations in the group of 7 were performed with balloon (B) ≥ the diameter of the distal esophagus (E) (B/E≥ 1). The 3 residually symptomatic patients include an infant dilated conservatively (B/E<1) to facilitate later bouginage, 1 patient with a recurrent stricture after stopping medical therapy and home bouginage, and 1 infant who had a persistent anastomotic stricture, suspected but untreated reflux esophagitis, and a perforation during the second balloon dilatation. Balloon catheter esophageal dilatation, as an alternative to bouginage, is usually a safe and effective procedure when reflux esophagitis is diagnosed and treated prior to dilatation.

Journal of Ultrasound in Medicine

Fetal spine morphology and maturation during the second trimester: sonographic evaluation. Filly RA, Simpson GF, Linkowski G (RAF, Dept. Radiology, L-374, University of California School of Medicine, San Francisco, CA 94143). *J Ultrasound Med* 6(11):631–636, Nov. 1987

We reviewed high-resolution real-time sonographic images (especially selected for a lack of technical artifacts) of the fetal spine of 46

normal fetuses between 18–27 menstrual weeks of development. The degree of visible posterior neural arch ossification was graded and compared with the gestational age. Recognizable early ossification of the laminae was seen in the cervical region of all fetuses studied. Similar ossification followed sequentially in the thoracic, lumbar, and sacral regions; however, sonographically recognizable ossification of the laminae in the lumbar spine was delayed until 22–24 weeks and in the sacral spine until 25 weeks or more. Awareness of these features will help to prevent false-positive diagnoses of dysraphism and, conversely, hopefully augment our ability to detect such lesions.

Reprinted with permission by the American Institute of Ultrasound in Medicine.

Journal of Computer Assisted Tomography

MR imaging of transverse/sigmoid dural sinus and jugular vein thrombosis. McArdle CB, Mirfakhraee M, Amparo EG, Kulkarni MV (EGA, Magnetic Resonance Imaging Division, Dept. of Radiology, G09, University of Texas Medical Branch, Galveston, TX 77550-2780). *J Comput Assist Tomogr* 11(5):831–838, Sept/Oct. 1987

Magnetic resonance (MR) imaging was performed on six patients with thrombosis involving the transverse/sigmoid sinus and jugular bulb/vein. Venographic confirmation was obtained in five cases. Thrombi were characterized by increased intraluminal signal on all planes of section and pulse sequences. The change in signal intensity from first to second echo for thrombi was qualitatively less than that found with slow flow. Partial thrombosis in one case was seen as a ring pattern of central intermediate intensity corresponding to the thrombus, surrounded by a peripheral ring of signal void related to flowing blood. The MR findings closely correlated with venography in predicting thrombosis. Evidence of thrombi was not available from CT. Magnetic resonance is well suited for the diagnosis of occlusive disease of the dural venous sinus and jugular bulb.

Magnetic Resonance Imaging

3D reconstruction of the brain from magnetic resonance images using a connectivity algorithm. Cline HE, Dumoulin CL, Hart HR Jr, Lorensen WE, Ludke S (HEC, General Electric Co., Corporate Research and Development, Schenectady, NY 12301). *Magn Reson Imaging* 5:345–352, 1987

We present high resolution three dimensional (3D) connectivity, surface construction and display algorithms that detect, extract, and display the surface of a brain from contiguous magnetic resonance (MR) images. The algorithms identify the external brain surface and create a 3D image, showing the fissures and surface convolutions of the cerebal hemispheres, cerebellum, and brain stem. Images produced by these algorithms also show the morphology of other soft tissue boundaries such as the cerebral ventricular system and the skin of the patient. For the purposes of 3D reconstruction, our experiments show that T_1 weighted images give better contrast between the surface of the brain and the cerebral spinal fluid than T_2 weighted images. 3D reconstruction of MR data provides a non-invasive procedure for examination of the brain surface and other anatomical features.

News

Bowman Gray Courses in Diagnostic Ultrasound

Bowman Gray School of Medicine, Winston-Salem, NC, is sponsoring courses in diagnostic ultrasound. Physicians and nonphysicians: General, Feb. 1–5; Neurosonology, April 25–29, Nonphysicians only: Physics, April 5–8; Obstetrics, April 11–15 and June 13–17; General, April 18–22 and June 20–24; Arterial and Venous Doppler, May 2–4; Urology, May 5–6; Echocardiology, May 9–13. Category 1 credit: 7 hr per day. Information: Registrar, Ultrasound Center, The Bowman Gray School of Medicine, 300 S. Hawthorne Rd., Winston-Salem, NC 27103; (919) 748-4505.

Annual Advanced Ultrasound Seminar

The Center for Medical Ultrasound, The Bowman Gray School of Medicine, and the Dept. of Radiology, Orlando Regional Medical Center, are sponsoring the 11th annual Advanced Ultrasound Seminar, Obstetrics/Gynecology, Feb. 11–13, at the Buena Vista Palace, Lake Buena Vista, FL. This intense 3-day course will present the latest techniques in obstetric and gynecologic sonography. Program directors: L. D. Greenbaum and F. W. Kremkau. Guest faculty: J. P. Crane, R. A. Filly, E. A. Lyons, L. H. Nelson, R. C. Sanders, and R. L. Teele. Category 1 credit: 14 hr. This course also is approved for 14 cognates, Formal Learning, by the American College of Obstetricians and Gynecologists. Fee: $375. Information: Registrar, Ultrasound Center, The Bowman Gray School of Medicine, 300 S. Hawthorne Rd., Winston-Salem, NC 27103; (919) 748-4505.

Tutorial Seminar on Endovaginal and Endorectal (Prostate) Ultrasound

The International Association for Endosonography Program is sponsoring a tutorial seminar on endovaginal and endorectal (prostate) ultrasound, March 24–26, in Orlando, FL. Program directors: B. Goldberg, M. Resnick, and L. Popp. Category 1 credits will be awarded. Fee: $200 for 1 day; $475 for 3 days. Information: International Association for Endosonography Program, 602 St. Andrews Dr., Media, PA 19063; (215) 565-8175.

Ultrasound 1988

The Dept. of Radiology, Brigham and Women's Hospital, and Harvard Medical School will offer their 13th annual postgraduate course on ultrasound, April 5–8. A special feature will be a Basics of Ultrasound day on April 5. The fee for this portion is $100. Program director: P. M. Doubilet. Category 1 credit: 28 hr. Fee: physicians, $495; residents, fellows, and technologists, $325. Information: Dept. of Continuing Education, Harvard Medical School, 25 Shattuck St., Boston, MA 02115; (617) 732-1525.

Clinical Nuclear Medicine 1988

The 12th annual postgraduate course in clinical nuclear medicine will be offered April 11–14 by the Harvard Medical School and the Joint Program in Nuclear Medicine at the Beth Israel Hospital, the Brigham and Women's Hospital, The Children's Hospital, Dana-Farber Cancer Institute, and the West Roxbury VA Medical Center. Program director: W. D. Kaplan. Category 1 credit: 24 hr. Fee: physicians, $450; residents, fellows, and technologists, $325. Information: Dept. of Continuing Education, Harvard Medical School, 25 Shattuck St., Boston, MA 02115; (617) 732-1525.

INTERFACE '88—Problems in Spinal Disease

SPINECARE—The Children's Spinal Research Foundation is sponsoring INTERFACE '88—Problems in Spinal Disease, April 29–May 1, at the Royal North Shore Hospital, Sydney, Australia. This multidisciplinary conference on spinal imaging, clinical diagnosis, and management will emphasize spinal disease in both children and adults. It will enable a state-of-the-art update, interdisciplinary interchange, and discussion of current problems in spinal disease. Radiologists, orthopedic surgeons, neurosurgeons, neurologists, rheumatologists, and nuclear medicine physicians will participate and contribute. Course directors: T. K. F. Taylor, J. Roche, and W. Sorby. Guest faculty: C. A. Helms and R. B. Winter. Category 1 credit: none applicable. Fee (Australian dollars): full meeting, $250; daily, $125. Information: The Conference Officer, Dept. of Diagnostic Raciology, Royal North Shore Hospital, St. Leonards NSW 2065, Australia; telephone: (02)438-8805 or 438-8505.

Radiology of the Small Intestine

A 1-day course on radiology of the small intestine will take place June 10 at the John Radcliffe Hospital, Oxford, England. The course will feature a review of disorders of the small intestine and will include presentations on plain radiographs, the small bowel enema, angiography, and CT. Fee: £35. Information: Dr. D. J. Nolan, Dept. of

Radiology, John Radcliffe Hospital, Oxford, OX3 9 DU, England; telephone: (865) 817238.

Canadian Association of Radiologists Annual Meeting

The Canadian Association of Radiologists will hold its 51st annual meeting, June 12–16, at the Westin Hotel and Convention Centre, Edmonton, Alberta. In addition to guest lecturers, the program will include symposia, proffered papers, scientific and technical exhibits, and a social program. The Gordon Richards Memorial Lecture will be given by B. C. Lentle; The Royal College Lecture will be presented by D. L. Tyrrell; and The Annual Orator will be Keith Simpkins. Category 1 credit: approximately 30 hr; approval is pending. Information: The Canadian Association of Radiologists, 1440 Ste. Catherine St. W., Suite 506, Montreal, Quebec, Canada H3G 1R8; (514) 866-2035.

Society of Digital Imaging, Management, and Communication

The Society of Digital Imaging, Management, and Communication has been formed. The objectives are to promote computer application in diagnostic imaging, management, and communications in all its aspects and to encourage liaison among radiologists and clinical and allied scientists who are concerned with the application, research, and advancement of the field. The first scientific meeting of the society will be held June 16–18, in Philadelphia, PA. Information about submitting papers for presentation and membership application: S. J. Dwyer III, Ph.D., Dept. of Diagnostic Radiology, The University of Kansas Medical Center, Kansas City, KS 66103 or Yen Wang, M.D., D.Sc., Dept. of Radiology, Thomas Jefferson University Hospital, Philadelphia, PA 19107.

Ultrasound: WFUMB/AIUM 1988 Meeting

The American Institute of Ultrasound in Medicine (AIUM) will host the 5th meeting of the World Federation for Ultrasound in Medicine and Biology (WFUMB), Oct. 17–21, at the Washington DC Convention Center, Washington, DC. The 2nd world congress of Sonographers, planned with the assistance of the Society of Diagnostic Medical Sonographers (SDMS), will convene also. Information: AIUM Convention Dept., 4405 East-West Hwy., Ste. 504, Bethesda, MD 20814.

Update: Society of Cardiovascular & Interventional Radiology Meeting

The Society of Cardiovascular & Interventional Radiology has announced that its 13th annual meeting, March 21–24, will offer 22 hr of category 1 credit. (See November issue of the *AJR* for more information.)

The American Board of Radiology Examinations

Written examinations for the American Board of Radiology (ABR) are scheduled for Oct. 6–7, 1988, and Oct. 5–6, 1989. Oral examinations will be held at the Executive West Hotel in Louisville, KY, on May 23–27, 1988, and June 5–9, 1989. The ABR will accept applications for admission to the examinations after July 1, but not later than Sept. 30 in the year *preceding* the year in which the examination is to be taken. For application forms and further information: Office of the Secretary, The American Board of Radiology, 300 Park, Ste. 440, Birmingham, MI 48009.

Meeting and Course Review

For the reader's convenience, a summary of upcoming meetings and courses is provided. Detailed listings are given in the *AJR* issue given in parentheses.

Visiting Fellowships in MR Imaging, times arranged, San Diego, CA (Aug)
Perceptorships in Imaging and Interventional Radiology, 1987–1988, times arranged, San Diego, CA (Dec)
Delaware Valley Magnetic Resonance Imaging Society Monthly Meetings, continuing through May 1988, Philadelphia (Dec)
Neuroimaging Update, 1988, Jan. 31–Feb. 5, Paradise Island, Bahamas (Nov)
Uroradiology '88, Feb. 1–4, Orlando, FL (Nov)
Breast Imaging 1988, Feb. 1–5, St. Thomas, U.S. Virgin Islands (Sept)
Los Angeles Radiological Society Post Conference Seminar, Feb. 2–6, Kaanapali, Maui, HI (Nov)
International Congress on Interventional Radiology in Cardio-Vascular Diseases, Feb. 3–5, Toulouse, France (Sept)
Thermography in Neuromusculoskeletal Disorders, Feb. 6–7 and April 16–17, New York (Dec)
Intermountain Imaging Conference, Feb. 6–13, Steamboat Springs, CO (Nov)
12th Annual Big Sky Radiology Conference, Feb. 7–12, Great Falls, MT (Sept)
Vascular Imaging and Interventional Radiology at Snowbird, Feb. 7–12, Snowbird, UT (Nov)
Uroradiology Course, Feb. 10–11, Bethesda, MD (Nov)
Practical Aspects of Diagnostic Radiology/Medical Imaging, Feb. 13–19, Snowmass Village, CO (Dec)
Sun Valley Imaging, Feb. 13–20, Sun Valley, ID (Nov)
Diagnostic Radiology and Nuclear Medicine, Feb. 14–21, St. Thomas, U.S. Virgin Islands (Oct)
Palm Beach Magnetic Resonance Imaging Update, Feb. 15–17, West Palm Beach, FL (Sept, Nov)
Winter Imaging Seminar, Feb. 15–19, Cancun, Mexico (Dec)
Computed Body Tomography 1988—The Cutting Edge, Feb. 18–21, Orlando, FL (Nov)
Radiology in Seville, Feb. 20–27, Seville, Spain (Oct)
Neuroradiology Seminar, Feb. 21, Orlando, FL (Jan)
UCSD Imaging and Intervention Conference, Feb. 21–24, San Diego, CA (Jan)
Vail Winter Imaging Seminar IV, Feb. 21–28, Vail, CO (Dec)
Comprehensive Update: Neuroradiology, Body Imaging, and Mammography, Feb. 22–27, Acapulco, Mexico (Nov)
Diagnostic Ultrasound at Thomas Jefferson University Hospital, Feb. 26–27, Philadelphia, PA (Jan)
Aspen Abdominal, Genitourinary, and Interventional Radiology Seminar, Feb. 28–March 2, Aspen, CO (Jan)
Vascular Imaging and Interventional Radiology at Park City, Feb. 28–March 4, Park City, UT (Nov)
Practical Radiology 1988, Feb. 28–March 4, Vancouver, B.C., Canada (Jan)
National Conference on Breast Cancer, Feb. 29–March 4, Los Angeles, CA (Nov)
Annual Skeletal Symposium, Feb. 29–March 4, Sun Valley, ID (Dec)
Annual Course of the Society of Computed Body Tomography, Feb. 29–March 4, Monterey, CA (Dec)

The George Simon Award, deadline for receipt of papers, March 1 (Dec)
Doppler Ultrasound in the Canadian Rockies, March 4, Banff Springs Hotel (Dec)
Masters Diagnostic Radiology Conference, March 6–11, Maui, HI (Oct)
Neuroradiology Update/MR Imaging: Neuroradiology Update, March 7–10; **Magnetic Resonance Imaging,** March 7–11; **MRI for Technologists,** March 8–11, Coronado (San Diego), CA (Jan)
The Lyon Conference: Computer Science and Life, March 10–12, Lyon, France (Nov)
Diagnostic Imaging Down Under, March 12–27, Auckland, New Zealand; Sydney and Melbourne, Australia (Oct)
Imaging Living Brain Chemistry, March 17–18, Baltimore, MD (Dec)
Pediatric Radiology 1988, March 17–19, Philadelphia (Sept)
Skeletal Radiology at the Pointe—1988, March 19–24, Phoenix, AZ (Jan)
Ultrasound at Vail, March 19–25, Vail, CO (Nov)
International Diagnostic Course: Skeletal Radiology, March 19–26, Davos, Switzerland (Dec)
Society of Cardiovascular & Interventional Radiology Meeting, March 21–24, Orlando, FL (Nov)
The Society of Thoracic Radiology—Annual Postgraduate Course, March 27–31, Washington, DC (July)
International London Course in Whole Body Computed Tomography, March 27–31, Perthshire, Scotland (Nov)
Thoracic Imaging '88, March 27–31, Washington, DC (Jan)
Neuroradiology at Vail, March 28–April 1, Vail, CO (Dec)
National Council on Radiation Protection and Measurements Annual Meeting, March 30–31, Washington, DC (Dec)
Spanish Radiology Seminar, April 3–8, Miami Beach, FL (Oct)
Real-Time Ultrasound in Obstetrics and Gynecology, April 18–20, Ann Arbor, MI (Jan)
Southern California Chapter of the American Association of Physicists in Medicine Spring Seminar, April 20–22, Las Vegas, NV (Dec)
International Symposium of the Planning of Radiological Departments, April 20–23, Florence, Italy (Sept)
Practical Interventional Radiology—1988, April 25–28, Boston, MA (Oct)
Imaging the Central Nervous System, April 25–29, Tucson, AZ (Nov)
Oncologic Imaging Update Course, April 29–May 1, Amelia Island, FL (Jan)
Radiology Review Course, May 1–6, Miami, FL (Dec)
CT, MR Imaging, and Radiologic Technologist Program, May 4–6, Ann Arbor, MI (Jan)
Fleischner Society Symposium on Chest Disease, May 16–18, Montreal, Quebec (Dec)
Practical Radiology Review Course, May 16–20, Cincinnati, OH (Jan)
International Workshop for the Study of Vascular Anomalies, June 20–22, Hamburg, Germany (Nov)
European Congress of NMR in Medicine and Biology, June 23–25, Berlin, Germany (Oct)
Bowman Gray Abdominal Radiology Fellowship, begins July 1, Winston-Salem, NC (Nov)
Copenhagen Symposium on Detection of Breast Cancer, Aug. 24–26, Copenhagen, Denmark (Jan)
Conference on Dose, Time, and Fractionation in Radiation Oncology, Sept. 14–17, Madison, WI (Jan)
International Symposium on Magnetic Resonance Imaging, Dec. 14–16, New Dehli, India (Oct)

AJR carries announcements of courses, symposia, and meetings of interest to its readers if received a minimum of 5 months before the event. There is no charge; receipt of items by the *AJR* Editorial Office is not acknowledged. Submit items for publication typed double spaced. Provide title, date, location, brief description, sponsor, course directors, fees, category I credit, and address and telephone number for additional information. Faculty from the host institution will not be listed. Guest faculty names will appear **only** if initials are provided. Mail news items to *AJR* Editorial Office, 2223 Avenida de la Playa, Suite 200, La Jolla, CA 92037-3218.

Classified Advertisements

Positions Available

ISRAEL, DIAGNOSTIC RADIOLOGY. Opportunities for 3–4 week or longer working vacations in a number of Israeli medical centers, on a volunteer basis. Positions varied, arrangements flexible. For information contact: Jonathan H. Fish, M.D., 1844 San Miguel Dr., #302, Walnut Creek, CA 94596; (415) 947-0560. 8xa

SKELETAL RADIOLOGIST—The UCLA School of Medicine has a full-time nontenure faculty position available in the General Diagnostic Division, Dept. of Radiological Sciences. Academic level of appointment to be determined. Must be eligible for California licensure. Provide CV, a statement of background and interests in skeletal radiology, and a listing of 5 references. Reply to Hooshang Kangarloo, M.D., Chair, Dept. of Radiological Sciences, UCLA School of Medicine, Los Angeles, CA 90024. The University of California is an equal opportunity/affirmative action employer and encourages applications from members of minority groups and women. 2a

RADIOLOGY FACULTY POSITION—The Dept. of Radiology of the State University of New York School of Medicine at Stony Brook has an immediate opening for a general radiologist with subspecialty interest in chest and/or genitourinary systems to keep pace with the rapid growth of its University Hospital. Located on the highly desirable North Shore of Long Island, with convenient access to New York City, the medical center provides the benefits of academic practice in a suburban setting. Candidates should be board eligible or board certified, having completed an accredited training program. Fellowship training or practice experience is desirable. Send resume to Morton A. Meyers, M.D., Professor and Chairman, Dept. of Radiology, School of Medicine, Health Sciences Center, SUNY Stony Brook, NY 11794. SUNY Stony Brook is an affirmative action/equal opportunity educator and employer. 2ap

SKELETAL RADIOLOGIST—The Dept. of Radiology at the University of Washington is seeking a board-certified skeletal radiologist. The position involves clinical radiography services, medical instruction for fellows, residents and medical students, and research. Included in the facilities are a PET scanner, several CT and MRI units (including an investigative unit), and dual- and single-photon absorptiometry. Salary is commensurate with rank based on established level at the University of Washington School of Medicine. The University of Washington is an equal opportunity employer. Submit CV to Albert A. Moss, M.D., Professor and Chairman, Dept. of Radiology, SB-05, University of Washington, Seattle, WA 98195. 2a

INTERVENTIONAL RADIOLOGISTS—Position now available with large, well-established group in exciting Las Vegas, NV. Must have additional interventional training. Stimulating academic practice. Excellent standard of living, outstanding recreational opportunities, and superb desert climate. Generous starting salary and benefits leading to full partnership in 4 yr. Practice is associated with University Medical Center of Southern Nevada. Contact Carl A. Recine, M.D., 7:00 a.m. to 5:00 p.m. PST; (702) 383-2241. 2–3a

ACADEMIC INTERVENTIONAL RADIOLOGIST for rank of instructor or assistant professor commensurate with qualification. Responsibilities include all aspects of angiography, venography, lymphography, interventional, therapeutic procedures, teaching, and some administrative duties. Requirements include fellowship training in an acceptable program, board certification in diagnostic radiology, and full medical license in Massachusetts. Contact Victor G. Millan, M.D., Tufts New England Medical Center Hospitals, 750 Washington St., Box 253, Boston, MA 02111; (617) 956-5963. 2–4a

CHIEF, RADIOLOGY SERVICE—The Tuskegee VA Medical Center is seeking board-certified candidates for Chief, Radiology Service in an 831-bed general hospital with a 112-bed nursing home care unit. The medical center is affiliated with the Morehouse School of Medicine. Candidates must qualify for academic appointment and have strong leadership ability. The Tuskegee-Montgomery-Auburn, AL, area offers many opportunities for social and cultural activities. Competitive salary, plus special physician's bonus, and excellent fringe benefits package. Malpractice coverage provided. Applicants should send their CV and names of 3 references to Chief of Staff (11), VA Medical Center, Tuskegee, AL 36083; (205) 727-0550 ext. 3645. 2a

DIAGNOSTIC RADIOLOGIST—Excellent opportunity for a board-eligible or board-certified radiologist to join a 9-member group in New Orleans, LA. The candidate must have training and an interest in all areas of diagnostic radiology. Experience in MRI required. Please submit CV to Harold R. Neitzschman, M.D., 4400 General Meyer Ave., Ste. 211, New Orleans, LA 70131; (504) 368-5074. 2–4a

NUCLEAR MEDICINE, SUBSPECIALTY DIAGNOSTIC RADIOLOGIST to lead section of university-affiliated dept. Rhode Island Hospital is a 715-bed acute care hospital located in beautiful southeastern New England, 1 hr from Boston. Previous administrative experience not necessary. Interest in resident teaching essential and clinical research interests desirable. Competitive salary and excellent work conditions offered. Position available July 1988. Contact John J. Cronan, Dept. of Diagnostic Radiology, Rhode Island Hospital, 593 Eddy St., Providence, RI 02902; (401) 277-5194. 2–5a

DIAGNOSTIC RADIOLOGISTS SOUGHT—In anticipation of a planned clinical expansion with a complete, newly equipped 12-room radiology service, this medical center is actively recruiting staff radiologists. We have openings for board-certified radiologists with experience in CT, ultrasound, MRI, angiography, and DSA. The 327-bed Veterans Administration Medical Center, Radiology Service, is closely affiliated with the University of Iowa College of Medicine, and suitable candidates may be considered for combined University/VAMC appointment at a level and salary commensurate with their training and experience. Send CV to Frank M. Behlke, M.D., Chief, Radiology Service, Veterans Administration Medical Center, Iowa City, IA 52240 or telephone FTS 863-6531, or (319) 338-0581, ext. 531. Equal opportunity/affirmative action employer. 2–3ap

STAFF RADIOLOGISTS—The College of Physicians and Surgeons of Columbia University is searching for junior and senior staff radiologists in our angiography division. Salary and academic rank will be commensurate with experience and qualifications. Responsibilities include patient care, teaching, and supervising residents for junior staff level and research, as well as demonstrated academic ability, for senior staff level. Requirements include board eligibility or certification in diagnostic radiology for junior staff level; board certification and at least 2 yr of cardiovascular and interventional radiology experience for senior staff level. New York state medical license required; narcotics license desirable. Please send resume to David H. Baker, M.D., Dept. of Radiology, 622 West 168th St., New York, NY 10032. Columbia University is an affirmative action/equal opportunity employer. 2a

LARGE, COMMUNITY-BASED RADIOLOGY GROUP seeks part-time board-certified radiologist willing to work 40 hr/wk in 2-3 mo blocks to total 6 mo/yr. Send CV to Victor Gaines, M.D., Radiology Dept., Vassar Bros. Hospital, Poughkeepsie, NY 12601, or call (914) 454-8500, ext. 6681. 2–3ap

NEURORADIOLOGIST to join 9 board-certified radiologists in metropolitan southwestern city. Group consists of an interventional radiologist, 2 neuroradiologists, and 2 radiation therapists. Need due to increased volume. Sophisticated medical community. Excellent modern facilities and equipment. Compensation determined by certification and experience. Reply Box X14, *AJR* (see address this section). 2a

VANCOUVER, CANADA—The University of British Columbia and Vancouver General Hospital fee-for-service group invites applications from radiologists with primary interest in general angiography or abdominal imaging. Send CV and bibliography to H. J. Burhenne, M.D., Professor and Head, Dept. of Radiology, Vancouver General Hospital, 855 West 12th Ave., Vancouver, B.C., Canada, V5Z 1M9. 2a

BC/BE DIAGNOSTIC RADIOLOGIST to join and develop a radiology dept. in a 40-physician multispecialty group. 250,000 service area, near lakes and universities. Send CV to J. Almquist, 1501 S. Madison St., Appleton, WI 54915. 2–7a

RADIOLOGIST, DIAGNOSTIC GENERALIST for McCall Memorial Hospital, located in a resort mountain village in central Idaho. Three days per wk. Board certification preferred. Skills needed include fluoroscopy, special procedures, ultrasonography, and mammography. For further information, please contact Karen Kellie, Administrator, P.O. Box 906, McCall, ID 83638; (208) 634-2221. 2a

BOARD-CERTIFIED DIAGNOSTIC RADIOLOGIST sought with special interest in CT, ultrasound, and angiography, who desires progressive role in residency training in the Veterans Administration setting affiliated with Eastern Virginia School of Medicine. Four radiologists and a nuclear medicine physician assigned. Seeking fifth radiologist. Research activities encouraged. Contact C. B. Mahon, M.D., Chief, Radiology Service, VA Medical Center, Hampton, VA 23667; (804) 722-6661, ext. 363. 2–3a

ULTRASOUND/NUCLEAR MEDICINE—Hospital-based group in Pacific Northwest with private practice limited to ultrasound and nuclear medicine seeks associate with training in these subspecialties. Ultrasound caseload of 9000 studies/yr includes routine and complicated obstetrics, vascular, abdominal, pelvic, and pediatric neurosonography using 3 state-of-the-art Acuson units. Nuclear medicine studies encompass cardiac, bone, hepatobiliary, pulmonary, renal, and SPECT. Send CV to Michael Daly, M.D., Nuclear Medicine/Ultrasound Section, Emanuel Hospital, 2801 N. Gantenbein Ave., Portland, OR 97227. 2–3ap

SPRINGER CLINIC, a 50-physician multispecialty group practice, has openings for 2 board-certified/eligible diagnostic radiologists. Competitive salary leading to full partnership. Generous fringe benefits. No weekends, holidays, or evenings. Experience in CT, ultrasound, and mammography is desirable. Please submit CV with inquiry to Richard A. Callis, Administrator, 6160 South Yale, Tulsa, OK 74136. 2xa

GASTROINTESTINAL RADIOLOGIST—Yale New Haven Medical Center, Yale University School of Medicine is seeking a radiologist with special interest in gastrointestinal radiology for full-time faculty appointment. Academic rank is a level of instructor-associate professor depending on qualifications. A strong interest in patient care, research, and teaching is required. Please send inquiries along with CV to Morton Burrell, M.D., Professor of Radiology, Director of Gastrointestinal Radiology, Yale University School of Medicine, 333 Cedar St., New Haven, CT 06510. Yale University is an equal opportunity employer; applications from women and minority groups are encouraged. 2a

MAMMOGRAPHY, UNIVERSITY OF PENNSYLVANIA—Exceptional opportunity for academic development in a high-volume, rapidly expanding breast imaging section. Ongoing screening and problem-solving mammography, breast ultrasound, and collaborative projects in MRI investigation. Resident and student teaching responsibilities along with flexible participation in bone and chest outpatient radiology. Position available July 1, 1988. Applicant must be ABR-certified and able to obtain license in Pennsylvania. U of P is an affirmative action, equal opportunity employer and specifically encourages applications from women and minorities. Send letter and CV to Rosalind H. Troupin, M.D., Dept. of Radiology, H.U.P., 3400 Spruce St., Philadelphia, PA 19104. 2–5a

BC/BE DIAGNOSTIC RADIOLOGIST to join university-affiliated dept. Experience or fellowship in angiography or neuroradiology desired but will consider other candidates. Dept. includes full range of services including state-of-the-art Doppler duplex sonography, CT, and angiography suite. For information contact Philip D. Gottlieb, M.D., Chief, Radiology Service, Veterans Administration Medical Center, 113 Holland Ave., Albany, NY 12208; (518) 462-3311. 2a

DIAGNOSTIC RADIOLOGIST for July 1988 to join 2 other radiologists in a large, multispecialty group practice serving 4 outpatient health centers in Rochester, NY. New Toshiba fluoroscopy, ATL ultrasound, and LoRad mammography equipment. Ultrasound and mammography experience preferable. 30,000 exams/yr. Please contact Dennis S. Moss, M.D., Wilson Health Center, Radiology Dept., 800 Carter St., Rochester, NY 14621; (716) 338-1400, ext. 4096. EOE/MF. 2–5a

BOARD-CERTIFIED/BOARD-ELIGIBLE DIAGNOSTIC RADIOLOGIST needed for affiliated VA Medical Center with expansive programs in education and research. Academically oriented individual with training in CT and vascular radiology preferred. Equal opportunity employer. Contact J. Kalus, M.D., at (806) 355-9703, ext. 7103. 2–4a

THE UNIVERSITY OF LOUISVILLE, DEPT. OF DIAGNOSTIC RADIOLOGY is seeking applications from BC/BE diagnostic radiologists to fill full-time faculty positions in the following areas in its 400-bed teaching hospital: (1) neuroradiology, (2) cross-sectional body imaging (ultrasound/CT/MRI), (3) general radiology (GI, GU, bone, chest). Candidates must be willing to participate in undergraduate and graduate teaching and in research activities in their respective areas. These are fine opportunities in a growing and busy dept. with excellent equipment. Both tenure and non-tenure track appointments are available and academic rank will be commensurate with training and experience. Compensation negotiable and competitive. Surprisingly, Louisville is currently ranked as one of top ten places to live in America by Rand McNally. Send inquiries with CV and 3 references to Hollis A. Thomas, M.D., Dept. of Diagnostic Radiology, Humana Hospital University, 530 S. Jackson St., Louisville, KY 40202. Equal opportunity/affirmative action employer. 2–3a

BC/PENDING DIAGNOSTIC RADIOLOGIST to establish hospital-based practice in small JCAH-approved hospital located in recreational area of Northern CA. Qualifications include California license and established experience and training in ultrasound, nuclear medicine, CT, and general radiology. Applicants should forward their CV and other pertinent information to Siskiyou General Hospital, Curtis Warrick, 818 S. Main St., Yreka, CA 96097; (916) 842-4121. 2–3a

SEEKING BOARD-CERTIFIED RADIOLOGIST for a 40-bed health-care facility in Haily, ID. Billing service available. Progressive medical community. Located just 10 mi from Sun Valley, ID. For further information contact David Farnes, Administrator, Blaine County Medical Center, P.O. Box 927, Haily, ID 83333; (208) 788-2222. 1–2a

NEURORADIOLOGIST, NEW ENGLAND MEDICAL CENTER—Academic position available in July 1988 at the Assistant Professor level in the Section of Neuroradiology, Dept. of Radiology, New England Medical Center Hospital. The successful candidate would join 2 other staff neuroradiologists. BE/BC required. The candidate must have completed a 2-yr neuroradiology fellowship including training in MRI. Facilities include a 3rd-generation CT scanner, a neuroradiographic suite with biplane capabilities, and a 1-T MRI unit. The hospital is strong in the neurosciences with excellent neurology (adult and pediatric) and neurosurgery depts. The position provides excellent academic opportunities and research is encouraged. Interested candidates should forward their CV to Samuel M. Wolpert, M.D., Neuroradiology Section, New England Medical Center, 750 Washington St., Boston, MA 02111; (617) 956-6333. 2–3a

NEW ENGLAND MEDICAL CENTER-TUFTS UNIVERSITY SCHOOL OF MEDICINE is seeking a radiologist in the General Radiology Section. The candidate should have expertise in bone radiology and a desire to participate in all modalities of bone and joint imaging including contrast arthrography. The candidate should also have an interest in orthopedic radiology. The hospital is a 469-bed (112 pediatric) hospital and the principal teaching affiliate of Tufts University School of Medicine. The candidate should be eligible for a faculty position at the medical school. Please direct inquiries and CV to Robert C. Sarno, M.D., Dept. of Radiology, New England Medical Center Hospitals, 750 Washington St., Boston, MA 02111. 1–2ap

DIRECTOR OF RADIOLOGY—A 200-bed specialty hospital that is affiliated with a prestigious medical school is seeking a board-certified radiologist to direct the activities of our Radiology and Nuclear Medicine Dept. This position requires an individual with strong clinical and teaching skills, as well as demonstrated administrative ability. Compensation includes a base salary commensurate with experience and ability, private practice billing plan, and a comprehensive benefits program. This is an excellent opportunity for a highly qualified radiologist to join the staff of a well-respected, progressive, and innovative institution located on Manhattan's upper East Side. Qualified candidates should reply in confidence to Administration Office, Chairman of The Search Committee, The Hospital for Special Surgery, 535 E. 70th St., New York, NY 10021. 1–2a

NEW YORK CITY SUBURBAN PRACTICE seeks board-certified radiologist, part-time. Hands-on ultrasound skills essential. Solid imaging knowledge. Personality counts. Grow to full-time. CV to Box 18, Meacham Station, Elmont, NY 11003. 1–2a

DIAGNOSTIC RADIOLOGIST—Busy 3-man group covering hospital and multimodality outpatient imaging center is seeking a board-certified radiologist. CT, ultrasound, MRI, nuclear medicine, and angiography skills required. Fellowship training and interest in neuroradiology a plus. Generous salary and liberal benefits leading to early partnership. Send CV to Diagnostic Radiology Consultants, 7703 Picardy Ave., Baton Rouge, LA 70809. 1–3a

THE UNIVERSITY OF SOUTH FLORIDA, DEPT. OF RADIOLOGY, is recruiting additional radiology faculty for the Moffitt Cancer Center and Research Institute. We are seeking general academic radiologists with subspecialty expertise in nuclear, musculoskeletal, chest, abdominal, or interventional radiology. Fellowship or equivalent experience is desirable; subspecialty interest should encompass all imaging modalities including MRI. The positions involve clinical service, teaching, and research. Salary and academic rank based on qualifications. Send CV to Robert Clark, M.D., Dept. of Radiology, Moffitt Cancer Center, P.O. Box 280179, Tampa, FL 33682-0179. 12–2ap

BAYLOR COLLEGE OF MEDICINE, DEPT. OF RADIOLOGY, is seeking a diagnostic radiologist for the position of Director of Radiologic Education. The physician will be responsible for supervising training of 28 residents and 4 postdoctoral fellows in the 8 affiliated hospitals with some 5000 beds. Clinical responsibilities will be tailored to provide sufficient time for teaching and research. Applicants must be certified by the American Board of Radiology and have demonstrated academic leadership. Appointment level will be Associate Professor or Full Professor, according to credentials. Salary is negotiable. Submit CV and 3 references to James E. Harrell, M.D., Professor and Chairman, Dept. of Radiology, Baylor College of Medicine, One Baylor Plaza, Houston, TX 77030. Baylor College of Medicine is an equal opportunity/affirmative action employer. 1–2a

DIAGNOSTIC RADIOLOGIST—Excellent opportunity for a board-eligible or a board-certified radiologist to join a group practice in the New Orleans area. The candidate must have training and interest in all areas of diagnostic radiology. Experience in MRI desired. Please submit CV to Martin A. Belanger, M.D., W. Esplanade Ave., Ste. 206, Kenner, LA 70065; (504) 464-0811. 1–3ap

PEDIATRIC RADIOLOGIST—Children's Hospital Medical Center of Akron has a position available immediately for a pediatric radiologist. Applicant must be board-certified or board-eligible in diagnostic radiology. Additional training in CT, ultrasound, nuclear medicine, and MRI is desirable. Send CV to Lionel W. Young, M.D., Professor and Chairman, Northeastern Ohio Universities, College of Medicine, C/O Children's Hospital Medical Center of Akron, 281 Locust St., Akron, OH 44308. 12–5a

VASCULAR/INTERVENTIONAL OPENING for third vascular and interventional radiologist in subspecialized 22-man private practice in 1200-bed fully-equipped teaching hospital. Must have fellowship training and experience with all aspects of vascular and interventional radiology. Write to A.D. Sears, M.D., Chairman, Dept. of Radiology, Baylor University Medical Center, 3500 Gaston, Dallas, TX 75246. 12–3a

BOARD-CERTIFIED OR -ELIGIBLE DIAGNOSTIC RADIOLOGIST to be part of a 3-person imaging-center staff and outpatient specialty clinic in Tacoma, WA. The radiology staff of this specialty center is associated with the larger radiology dept. in hospitals operated by Group Health Cooperative of Puget Sound in Seattle and Redmond, WA. The practice consists of responsibility in ultrasound, nuclear medicine, GI fluoroscopy, mammography, outpatient CT, and diagnostic X-ray. For further details please contact Director of Medical Staff Personnel, Group Health Cooperative of Puget Sound, 521 Wall St., Seattle, WA 98121; (206) 448-6550. 12–3a

BC/DIAGNOSTIC RADIOLOGIST—Special training in MR and/or ultrasound required. Busy hospital and office practice in Washington D.C. suburbs. Early partnership. Available July 1, 1988. Reply Box B62, *AJR* (see address this section). 12–2a

NEW ENGLAND—Two positions for BC/BE diagnostic radiologists with interest and expertise in ultrasound, CT, and mammography to join current, 4-member, office-practice radiology dept. of large, rapidly expanding, multispecialty, prepaid, and FFS practice. Positions available Jan. 1988 and July 1988. Competitive compensation and benefits. Send CV to Ivan R. Green, M.D., Chairman, Dept. of Radiology, Fallon Clinic, 630 Plantation St., Worcester, MA 01605. 12–2a

BOARD-CERTIFIED RADIOLOGIST needed immediately to work in Ft. Lauderdale area hospital and private office in Boca-Raton. Current practice includes CT, nuclear medicine, ultrasound, interventional mammography, and pediatrics. Competitive starting salary with partnership in 3 yr. Should have Florida license. Contact David Wagner, Administrator; (305) 344-9990. 12–2a

SEEKING A SECOND, FULL-TIME, TENURED-LINE, ACADEMIC NEURORADIOLOGIST with an opportunity to participate in a developing world-class MRI facility at the University of Kentucky. Busy neuroradiology division with 1536 total neuro procedures (596 angiograms and 940 myelograms), 7346 neuro CT scans, and 1172 neuro MRI scans last yr, including 378 head ultrasounds and intraoperative neuro ultrasound. Excellent equipment with 3 fourth-generation CT scanners, new (6-mo-old) neuroangiographic suite with full imaging capability including state-of-the-art DSA, 2 myelographic suites, 0.15-T resistive MRI (second unit, a 1.5-T superconductive MRI, to be installed early spring 1988), and potential for significant participation in MRI spectroscopic unit already in place (4.7-T Bruker unit). A world-class MRI facility will be built in 2–3 yr with excellent opportunity for spectroscopic research. The University is very strong in neurosciences with excellent neurology and neurosurgery departments, and an Aging Research Center with emphasis on Alzheimer research. Exceptional academic opportunities with excellent academic salary. For details write (include CV) or call C. Lee, M.D. (member ASNR), (606) 233-6155; or H.D. Rosenbaum, M.D. (Chairman of Diagnostic Radiology), (606) 233-8088: Dept. of Radiology, University of Kentucky Medical Center, Lexington, KY 40536. 12–3a

DIAGNOSTIC RADIOLOGIST to join expanding private radiology group in Tampa Bay area. All modalities including MRI and SPECT. Board certification or additional training in nuclear medicine desirable. Send CV to Box B74, *AJR* (see address this section). 12–2a

BOARD-CERTIFIED DIAGNOSTIC RADIOLOGIST with subspecialty in cross-sectional imaging (CT/ultrasound) to join established 7-man group at 500-bed, acute-care, medical-school–affiliated hospital in New York City. Well-equipped modern dept. with all imaging modalities (MRI in summer of 1989), plus nearby private office. Minimum of 1-yr fellowship in cross-sectional imaging (CT/ultrasound) required. Postfellowship experience in cross-sectional imaging at a university center would be desirable. Reply Box B85, *AJR* (see address this section). 12xa

GENERAL DIAGNOSTIC RADIOLOGIST WITH INTEREST IN CHEST RADIOLOGY—Diagnostic radiologist with training or experience in MRI. Two positions available on Jan. 1, 1988, to complete staffing for the new VA Medical Center in Minneapolis, MN. Dept. includes MRI, CT, cyclotron with PET scanner, interventional vascular suite, neuroradiology suite, mammography, plus more. Affiliated with the University of Minnesota with non–tenure-tract appointment available at appropriate level. Research and teaching opportunities available. Board certification mandatory for both positions. One-yr fellowship training or equivalent experience in chest radiology and MRI desirable. Send letters of inquiry with CV to Donovan B. Reinke, M.D., Chief of Diagnostic Radiology Service—114, VA Medical Center, 54th St. and 48th Ave. S., Minneapolis, MN 55417. EOE. 12–2a

FORT MORGAN, NORTHEAST COLORADO COMMUNITY serving 25,000, seeks BC radiologist for hospital-based solo practice. Nuclear medicine, ultrasound, mammography, and angiography. Generous practice assistance. Contact PROSEARCH, 305 NE 102nd Ave., Portland, OR 97220; (503) 256-2070. 11–2a

VASCULAR/INTERVENTIONAL RADIOLOGISTS—University hospital offers full-time staff position at assistant to associate professor level for vascular/interventional radiologist. Vascular MRI and research opportunities included. Please contact Klemens H. Barth, M.D., Director, Division of Vascular/Interventional Radiology, Georgetown University Hospital, 3800 Reservoir Rd., N.W., Washington, DC 20007; (202) 625-2891. Affirmative action/equal opportunity employer. 11–2a

GENERAL DIAGNOSTIC RADIOLOGIST AND A BODY CT/ULTRASOUND RADIOLOGIST with an opportunity to participate in a developing world-class MRI facility. The University of Kentucky Medical Center is seeking an additional staff member who will have virtually full-time responsibilities in body cross-sectional radiology. Excellent equipment, including 3 fourth-generation CT scanners. The position also includes a potential for significant participation in the clinical and research activities of a superb, markedly expanded MRI and spectroscopy facility. We are also seeking an additional radiologist with duties in conventional diagnostic procedures. Both positions have exceptional academic opportunities with remuneration far above average for University hospitals. For details call (606) 233-8088 or write (include CV) to H.D. Rosenbaum, M.D., Chairman of Diagnostic Radiology, University of Kentucky Medical Center, Lexington, KY 40536. 11–4a

THOMAS JEFFERSON UNIVERSITY HOSPITAL—Two academically-oriented staff radiologists are sought for positions in a dynamic Dept. of Radiology, now in a rebuilding phase. (1) General diagnostic radiologist. This individual will cover a broad spectrum of diagnostic areas including chest, bone, GI, GU, and breast imaging. One or more of these areas can be emphasized according to individual interests. (2) Ultrasound radiologist. This individual will join one of the largest and most active ultrasound divisions in the world and will participate in the full range of diagnostic and interventional ultrasound studies. Some general diagnostic responsibilities also may be included. Candidates should be board certified or eligible and have interests in clinical radiology, teaching, and research. Please send CV to Robert Steiner, M.D., Co-Director, General Diagnostic Division; Barry Goldberg, M.D., Director, Division of Ultrasound; or David Levin, M.D, Chairman, Dept. of Radiology, Thomas Jefferson University Hospital, Philadelphia, PA 19107. Thomas Jefferson University Hospital is an Equal Opportunity/Affirmative Action Employer. 11–2a

AGGRESSIVE DIAGNOSTIC RADIOLOGY GROUP is in need of new associate approximately January to July 1989. Must be board certified to become partner. Would prefer multitalented background including interventional radiology, nuclear medicine, ultrasound, CT, and MRI experience. Ability to speak Spanish helpful but not required. Our group covers 4 hospitals including regional trauma center and 2 offices. Located in The Sparkling City by the Sea. Kindly send CV to Donald R. Brieger, M.D., or R.P. Chepey, M.D., 2481 Morgan, P.O. Box 5608, Corpus Christi, TX 78405. 11–2a

FULL-TIME, PART-TIME, OR LOCUM TENENS (LEADING TO PERMANENT) office/hospital-based position in south Texas urban community. Board certification, friendly attitude, good training, motivation, and Texas license required. General radiology practice with fluoroscopy, mammography, nuclear medicine, sonography, CT, and limited MRI. Comfortable hours and remuneration with potential to expand. Reply Box W60, *AJR* (see address this section). 11xa

THE UNIVERSITY OF ARIZONA, DEPT. OF RADIOLOGY is recruiting a Section Head of Thoracic Radiology and abdominal imaging radiologist for the University Medical Center and a General Radiologist for the VA Medical Center. Candidates should be trained in appropriate imaging modalities and invasive techniques, and interested in teaching and research. Income and academic rank are negotiable. The University of Arizona is an affirmative action/equal opportunity employer. Contact Bruce J. Hillman, M.D., Vice-Chairman, Dept. of Radiology, University of Arizona Health Sciences Center, Tucson, AZ 85724; (602) 626-7368. 9–2a

RADIOLOGIST—A board-certified/board-eligible radiologist with experience is needed to join the staff of the Alaska Native Medical Center, a 170-bed referral facility for a state-wide system of Indian Health Service hospitals and clinics. Practice stimulating and challenging radiology in a relaxed and casual atmosphere. State-of-the-art in-house CT, sonography, and mammography. Send CV to W. M. Cox, M.D., P.O. Box 10-7741, Anchorage, AK 99510-7741. EOE. 9–2a

Positions Desired

PEDIATRIC RADIOLOGIST, ABR-certified, fellowship trained, with subsequent academic experience seeks full-time pediatric radiology position or combination pediatric radiology and general radiology in private practice. Reply Box C9, *AJR* (see address this section). 2–4b

SEEKING POSITION—Diagnostic radiologist. Licensed in California, Michigan, and Kentucky. Will consider other sites. Reply Box B70, *AJR* (see address this section). 2b

Fellowships and Residencies

CT-MRI FELLOWSHIP—2 GE 9800 CT scanners (Quick Scan). 1 GE 2.0-T Signa MRI, operating at 1.5 T. 560-bed, tertiary care University Hospital with trauma center. Center city Philadelphia. For consideration please send CV to Patricia A. Laffey, M.D., Dept. of Diagnostic Radiology, Hahnemann University Hospital, Broad and Vine Sts., Philadelphia, PA 19102. 2c

INTERVENTIONAL RADIOLOGY FELLOWSHIP—560-bed, tertiary care University Hospital with trauma center. Center city Philadelphia. For consideration please send CV to Steven K. Teplick, M.D., Dept. of Diagnostic Radiology, Hahnemann University Hospital, Broad and Vine Sts., Philadelphia, PA 19102. 2c

NEURORADIOLOGY FELLOWSHIP—2 GE 9800 CT scanners (Quick Scan). 1 GE 2.0-T Signa MRI, operating at 1.5 T. 560-bed, tertiary care University Hospital with trauma center. Center city Philadelphia. For consideration please send CV to Robert G. Peyster, M.D., Dept. of Diagnostic Radiology, Hahnemann University Hospital, Broad and Vine Sts., Philadelphia, PA 19102. 2c

MUSCULOSKELETAL RADIOLOGY FELLOWSHIP—The Dept. of Radiology, Georgetown University Hospital announces a new 1-yr fellowship in musculoskeletal radiology starting July 1, 1988. Equipment includes a 1.5-T Siemens MR; a Varian 4.7-T spectral imager for animal research; 2 GE 9800 Quick CT scanners; and Acuson and ATL ultrasound units. The nuclear medicine equipment includes 4 single-headed SPECT tomographic cameras, the revolutionary Triad tomographic camera, and a dual photon densitometer. Full research and clinical experience opportunities in MRI, CT, MSK tumors, rheumatologic disorders, sports medicine, and trauma are program highlights as well as a strong affiliation with the National Institutes of Health. Send CV to Martha C. Nelson, M.D., Division Director, Musculoskeletal Radiology, Georgetown University Hospital, 3800 Reservoir Rd., N.W., Washington, DC 20007; (202) 784-3415. 2–5c

ULTRASOUND AND INTERVENTIONAL clinical fellowships are provided on a continuing basis for 1–12 wk in diagnostic ultrasound at the University of British Columbia, St. Paul's Hospital, under the direction of Dr. Peter Cooperberg, Professor of Radiology. About 50 cases per day, including abdominal, obstetrical peripheral, and Doppler ultrasound are done. Real-time techniques are emphasized. Hands-on experience is encouraged. Daily reporting rounds and videotape library are also available. For further information contact Jean Center, secretary to Dr. P. Cooperberg, St. Paul's Hospital, Radiology Dept., 1081 Burrard St., Vancouver, B.C. V6Z 1Y6; (604) 682-5026. 2c

VASCULAR/INTERVENTIONAL RADIOLOGY FELLOWSHIP—One-year fellowship beginning July 1, 1988. Must be eligible for a New York state license, have completed an approved residency program, and be BE or BC. Send CV to Glenn Robeson, M.D., Chairman, Radiology, Albany Medical Center, 43 New Scotland Ave., Albany, NY 12208. 2cp

THE NEW YORK HOSPITAL-CORNELL MEDICAL CENTER, DEPT. OF RADIOLOGY has a 1-yr fellowship position available beginning July 1, 1988, in GU radiology. Program will involve participation in clinical aspects of GU imaging including urography, CT, sonography, and MRI. Opportunity for research, particularly that involving MRI, is offered. Applicants should be ABR-certified or eligible. Interested candidates should contact and send CV to Susan Krysiewicz, M.D., Dept. of Radiology, The New York Hospital-Cornell Medical Center, 525 E. 68th St., New York, NY 10021; (212) 472-6136. 2cp

FELLOWSHIP—The College of Physicians and Surgeons of Columbia University is searching for a junior staff radiologist to participate in a 1-yr cardiac imaging program to begin July 1, 1989. Program involves intensive exposure to MRI, echocardiography, nuclear cardiology, and digital imaging, in addition to participation in conventional angiocardiography and coronary arteriography performed in the cardiac catheterization laboratories. Requirements include board eligibility or certification in diagnostic radiology. New York state medical license required; narcotics license desirable. Please send resume to Eric C. Martin, M.D., Dept. of Radiology, Columbia-Presbyterian Medical Center, 622 West 168th St., New York, NY 10032. Columbia University is an affirmative action/equal opportunity employer. 2c

PEDIATRIC RADIOLOGY FELLOWSHIP—One-year position still available beginning July 1, 1988, in an academic teaching children's hospital. Exposure to all current aspects of pediatric diagnostic imaging including CT, ultrasound, nuclear medicine, angiography including DSA, interventional procedures, and MRI. Participation in research and teaching encouraged. Applicants must be board-certified or board-eligible. For further information/application contact Marie A. Capitanio, M.D., Director, Dept. of Radiology, St. Christopher's Hospital for Children, 2600 N. Lawrence St., Philadelphia, PA 19133. 2c

FELLOWSHIP IN BREAST IMAGING—A 1-yr program to start July 1, 1988. Multimodality breast evaluation including xeromammography, film-screen mammography, breast ultrasonography, MRI, physical examination, pathology, medical, surgical, and radiological oncology exposure, and conferences. Clinical research and publication are required. An extensive teaching file available. Located in a 550-bed hospital; 40 mammograms and 2–6 needle localizations are performed daily. Send CV to Olcay S. Cigtay, M.D., Director, Breast Imaging, Dept. of Radiology, Georgetown University Hospital, 3800 Reservoir Rd., N.W., Washington, DC 20007. 2–5c

MUSCULOSKELETAL RADIOLOGY FELLOWSHIP—The Dept. of Radiology, Georgetown University Hospital announces a new 1-yr fellowship starting July 1, 1988, in musculoskeletal radiology. Equipment includes a 1.5-T Siemens MR, a Varian 4.7-T spectral imager for animal research, 2 GE 9800 Quick CT scanners, and Acuson and ATL ultrasound units. Equipment in nuclear medicine includes 4 single-headed SPECT tomographic cameras, the revolutionary Triad tomographic camera, and a dual-photon densitometer. Full research and clinical experience opportunities in MRI, CT, MSK tumors, rheumatologic disorders, sports medicine, and trauma are program highlights, as well as a strong affiliation with the National Institutes of Health. Send CV to Martha C. Nelson, M.D., Division Director, Musculoskeletal Radiology, Georgetown University Hospital, 3800 Reservoir Rd., N.W., Washington, DC 20007. 12–2cp

INTERVENTIONAL/ANGIOGRAPHY/ADVANCED BODY IMAGING FELLOWSHIP IN SAN FRANCISCO AREA—Available July 1, 1988. One-yr fellowship program at 350-bed Stanford University–affiliated hospital and 2 private hospitals. Extensive clinical experience involving all aspects of interventional vascular and nonvascular procedures. Fellow will also participate in MRI scanning and CT scanning including 3-dimensional reconstruction capability. Send inquiries and CV to Ira Fink, M.D., Valley Radiologists Medical Group, Inc., P.O. Box 2F, San Jose, CA 95109. 1–3c

ADVANCED IMAGING FELLOWSHIP—A position is now available for a board-certified or board-eligible radiologist in a University of Rochester teaching-hospital complex. The fellowship emphasizes in-depth exposure to CT, ultrasound, and MRI integrated with invasive procedure exposure. Additional positions will be available in January 1988. Please respond to Steven G. Herbert, M.D., Director, Fellowship Program, Diagnostic Radiology Dept., The Genesee Hospital, 224 Alexander St., Rochester, NY 14607. 1–2c

FELLOWSHIP, DEPT. OF RADIOLOGY—Cedars-Sinai Medical Center, a 1201-bed, acute-care, research, and teaching hospital affiliated with the UCLA School of Medicine, has an opening for a 1-yr fellowship with emphasis on CT, ultrasound, MRI, and mammography available July 1, 1988; 18 radiologists associated in practice in dept. with 135 personnel. There are 104,880 inpatient and 9120 outpatient radiologic exams per yr. Applicant must have completed an approved residency in diagnostic radiology, must be board eligible/certified, and have a California state medical license by July 1, 1988. Send CV to N. Zheutlin, M.D., Dept. of Radiology, Cedars-Sinai Medical Center, 8700 Beverly Blvd., Los Angeles, CA 90048. 12–2cp

INTERVENTIONAL RADIOLOGY FELLOWSHIP—The Rush-Presbyterian–St. Luke's Medical Center is now offering a 1-yr fellowship position beginning July 1, 1988, in interventional radiology. This 750-bed teaching hospital offers extensive experience in all aspects of vascular and nonvascular procedures with a primary emphasis on patient care and clinical research. Send inquiries to Terence Matalon, M.D., Rush-Presbyterian–St. Luke's Medical Center, Dept. of Radiology, 1753 W. Congress Pkwy., Chicago, IL 60612. 11–2c

DEPT. OF RADIOLOGY, UNIVERSITY OF ROCHESTER MEDICAL CENTER—One-year fellowship positions available July 1, 1988, or July 1, 1989. Positions include neuroradiology, cardiovascular/angiography, ultrasound/CT/MRI, and pediatric radiology. Requirements include board eligibility or certification in diagnostic radiology and an accredited radiology residency. Candidates must be licensed or eligible to obtain a license to practice medicine in the state of New York. Apply by Dec. 1 of the year before the fellowship starting date. Contact Beverly P. Wood, M.D., Box 648, University of Rochester Medical Center, Rochester, NY 14642. University of Rochester is an affirmative action, equal opportunity employer. 10–3c

CARDIOVASCULAR-INTERVENTIONAL RADIOLOGY FELLOWSHIP—Available July 1, 1988. One-year fellowship program at a 750-bed teaching hospital. Extensive clinical experience involving all aspects of cardiovascular imaging, interventional vascular and nonvascular procedures, and availability for clinical or animal research. Send CV and inquiries to Oscar H. Gutierrez, M.D., Dept. of Radiology, Box 648, University of Rochester Medical Center, Rochester, NY 14642. EO/AA/M-F employer. 10–3c

Tutorials/Courses

AUSTRALIA-NEW ZEALAND—IMAGING DOWN UNDER, MARCH 12–27, 1988. International faculty. Auckland, New Zealand, March 13–14; Sydney, Australia, March 18–20; and Melbourne, Australia, March 25–26. Information: Medical Seminars, 21915 Roscoe Blvd., Ste. 222, Canoga Park, CA 91304; (818) 719-7380. 9–2d

Other

ALASKA 88—CRUISE THE INLAND PASSAGE—Drs. George Kossoff and Marjorie McSweeney present topics in ultrasound and breast diagnosis. CME I accreditation application made. For registration and information contact 21915 Roscoe Blvd., #222, Canoga Park, CA 91304; (818) 719-7380. 2–6d

AJR Classified Advertisements Information

Box Responses and Address for Ad Placement

Write Box _____, AJR, Suite 200, 2223 Avenida de la Playa, La Jolla, CA 92037; (619) 459-2229.

How to Place an Ad

AJR accepts classified advertising for Positions Available, Positions Desired, Fellowships and Residencies, and Tutorials/Courses. Ads are accepted by mail or telephone. Institutions should supply purchase orders.

Rates: $6.00/line with a $30 minimum charge. Box service is $10 additional for each month the ad appears. There are discounts for multiple insertions: 10% for 2–3 insertions; 20% for 4 or more. To estimate lines, count all words and divide by 5.5.

Billing: Ads may be prepaid or invoices will be sent after the ad appears.

Deadlines. 6 weeks prior to issue date. For specific deadlines telephone the AJR editorial office.

Estimating Ad Charges

Line charge: divide total words by 5.5 and multiply by $6.00 .... $ _____

Multiple insertions? If so, multiply by number ..... × _____

Subtotal ..... $

Box response requested? If so, multiply number of months by $10.00 ..... + _____

Subtotal ..... $

Discount applies to two or more insertions. Subtract 10% if ad appears 2–3 months, 20% if 4 months or more ..... – _____

Approximate advertising charge ..... $

You learn from your experience with

CONTEMPORARY DIAGNOSTIC RADIOLOGY

Editor: **Robert E. Campbell, M.D.**

A Biweekly Review of Clinical Radiologic Practice—26 issues a year!

One of your toughest jobs is keeping up with the many new developments that affect radiology. That's why you want **Contemporary Diagnostic Radiology**... an effective and convenient way to perfect your skills and maintain your professional status.

Contemporary Diagnostic Radiology is designed as a continuing education program that lets you work at your own pace. Every two weeks you'll receive an issue that covers a single topic or procedure in detail. Read the information and study the clearly reproduced radiographs—and then, if you choose, respond to a comprehensive examination in the strictest confidence. You set the pace.
Each biweekly lesson brings you pertinent review of the basics in bone radiology... gastrointestinal radiology... pediatric radiology... genitourinary radiology... MR imaging... and all of the topics you want to know more about.

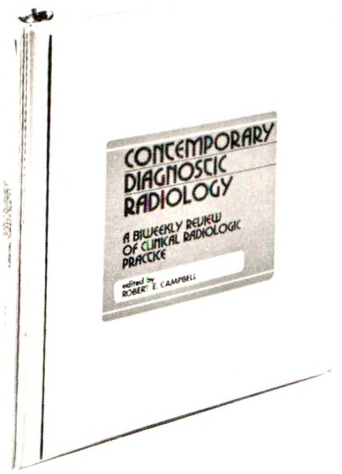

Contemporary Diagnostic Radiology works *two ways*. You may choose to subscribe to the non-scoring version, receiving every issue as an important element of your professional reading. The scoring version, however, supplements your reading and computer-coded examinations with confidential result responses, making you eligible for Continuing Medical Education credits co-sponsored by the University of Pennsylvania School of Medicine.

"As an organization for continuing medical education, the University of Pennsylvania School of Medicine designates this continuing medical education activity as meeting the criteria for 1 credit hour per bi-weekly issue in Category I for Educational Materials for the Physician's Recognition Award of the American Medical Association provided it has been completed according to instructions."

You can begin this ongoing program **today**. **Contemporary Diagnostic Radiology** is a year-round program, so you can join at any time. To begin your lessons, just fill out the enclosed card and return it to us. Or call **FREE** 1-800-638-6423 (except from Alaska). In Maryland call **COLLECT** 528-4105. You'll find that **Contemporary Diagnostic Radiology** is the most efficient and inexpensive way to keep up with your dynamic field.

Williams & Wilkins

P.O. Box 23291
Baltimore, Maryland 21203

266 Fulham Road
London SW10 9EL England

clip & mail

CONTEMPORARY DIAGNOSTIC RADIOLOGY

☐ **Yes!** I want to keep pace in my field! Begin my 26-issue subscription:
☐ Send me the scoring version ($220)
☐ Send me the non-scoring version ($180)
☐ Send me the resident non-scoring version ($160) (add $45 for optional air mail delivery outside the U.S.)
☐ new subscription
☐ renewal

name

address

city/state/zip

payment options
☐ payment enclosed ☐ bill me
☐ American Express ☐ MasterCard ☐ VISA

printed in USA

card # expiration date

signature/P.O. #

Maryland residents add 5% sales tax. Subscriptions outside the U.S. must be prepaid in U.S. dollars only. Rates subject to change without notice. Please allow 8 weeks for delivery of your first issue, up to 16 weeks for surface delivery outside the U.S. Optional airmail rates add $45 per subscription.

Residents are eligible for the special in-training rate for up to three years. When requesting this rate, please include training status and institution.

Don't forget: you can order with a **FREE** phone call at 1-800-638-6423 (except from Alaska). In Maryland, call collect 528-4105.

Williams & Wilkins

P.O. Box 23291
Baltimore, Maryland 21203

266 Fulham Road
London SW10 9EL England

CDRAD 1029 87

MAKE YOUR PRACTICE THRIVE

in today's complex health care environment

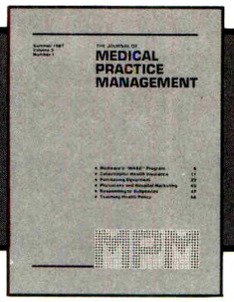

The Journal of MEDICAL PRACTICE MANAGEMENT *Quarterly*

Editor: **Marcel Frenkel, MD, MBA**

■ *Find out what today's issues mean for you and your practice*

Now more than ever, the practice of medicine is changing. You've seen the emergence of HMOs, IPAs, and PPOs...you've felt the impact of DRGs... increased competition...and more. Despite the advent of these alternate delivery systems, most experts firmly believe that private practice is here to stay.

Now there's an intelligent, convenient way to make sure you're getting the important information on trends and issues in health care that will influence your practice of medicine this year... and five years down the road. And for far less than any consultant's hourly fee. With **THE JOURNAL OF MEDICAL PRACTICE MANAGEMENT.**

■ *Timely articles help you make far-sighted decisions*

Featuring articles ranging from the *Financing of Long-Term Care* to *Joint Ventures in Medical Services* to *Medical Practice Where HMOs Dominate*, **THE JOURNAL OF MEDICAL PRACTICE MANAGEMENT** helps you pinpoint what management pitfalls to avoid, what economic forecasts to trust, which markets are targeted for growth, and so much more. In every quarterly issue you'll find departments covering: **health care policy • marketing and organizational structure • taxation, legislation and legal affairs • office management and computerization • manpower and education.**

You'll also find pertinent features like the **Washington Report,** telling you what's brewing in the nation's capital that affects you...**Briefs,** covering statistics, management, hospitals and taxation with timely, concise reports...**Abstracts** of health care management literature...plus **profiles** of for-profit and not-for-profit health care delivery systems.

■ *Founded by a physician for physicians*

Headed by founder and editor Marcel Frenkel, MD, MBA, **THE JOURNAL OF MEDICAL PRACTICE MANAGEMENT** is the only journal of its kind edited by a physician for physicians. Its multidisciplinary editorial board is made up of experts from the fields of public and private management, health care administration, economics, marketing, medical-legal affairs, and others. They are carefully chosen for their extensive knowledge of the management aspects of practicing medicine.

No-risk offer

You've invested a lot of time, money, and hard work to get where you are today. If you'd like to see your practice thrive in today's complex health care environment... give **THE JOURNAL OF MEDICAL PRACTICE MANAGEMENT** a try.

Just return the attached coupon, or call TOLL-FREE 1-800-638-6423, from anywhere in the U.S. except Alaska. In Maryland, call 528-4105 collect. If ever disappointed in your issues of **THE JOURNAL OF MEDICAL PRACTICE MANAGEMENT,** you may cancel your subscription for a full refund on unmailed issues...no questions asked.

☐ **YES!** I want to make the right decisions for my future. Please enter my subscription to THE JOURNAL OF MEDICAL PRACTICE MANAGEMENT *(quarterly)*

☐ Individual $49/year ☐ Institution $65/year
Add $10 outside the U.S.

☐ Check enclosed ☐ Bill me
☐ MasterCard ☐ American Express ☐ VISA

Card # _____ Exp. date _____

Signature/P.O. # _____

Name _____

Address _____

City/State/Zip _____

Maryland residents add 5% sales tax. Subscriptions outside the U.S. must be prepaid. All subscriptions must be paid in U.S. dollars. Please allow 8 weeks for delivery of your first issue, up to 16 weeks for surface delivery outside the U.S. Airmail rates available on request.

Williams & Wilkins
P.O. Box 23291 ☐ Baltimore, Maryland 21203
266 Fulham Road ☐ London SW10 9EL England

MPMAD 50632

Need shelf space?

Williams & Wilkins is your source for back issues of this journal in microform.

Free Up 98% Of
Your Shelf Space With
Microform Conversion

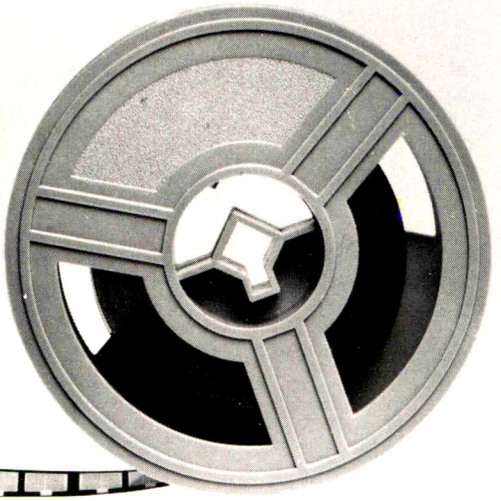

MICROFILM editions are available for this journal direct from the publisher. Many Williams & Wilkins journals as well as those journals distributed by the Publishing Services Division of Waverly Press, Inc. are also available for a single volume year or on a standing order basis.

FOR ORDERING INFORMATION: Write to the address below or call **TOLL-FREE 1-800-638-6423.** In Maryland call **COLLECT** 528-4105.

☐ **Please send me microform back issue ordering information for** _____
Journal Name

Name _____

Title _____

Address _____

City/State/Zip _____

Mail to:

Williams & Wilkins
Microform Sales
Attention: Yvonne Hahn
428 East Preston Street
Baltimore, Maryland 21203

or

266 Fulham Road
London SW10 9EL England

Formats available:
- 16-mm reel
- 35-mm reel
- 16-mm cartridge (3M or Kodak)
- positive or negative film

MICROAD 50567

Get the complete story on the new medical technologies and instrumentation of today...and tomorrow

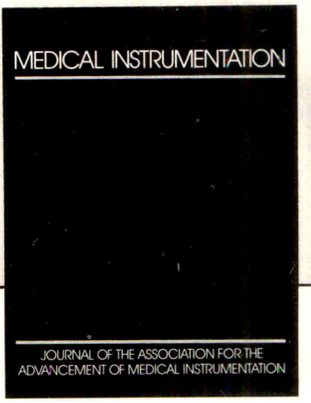

MEDICAL INSTRUMENTATION

The official journal of the Association for the Advancement of Medical Instrumentation

Editor-in-Chief: Charles A. Rawlings, Ph.D., C.C.E.

If you are involved in the design, manufacturing, clinical application, specification, regulation, or administrative facets of medical device technology, make MEDICAL INSTRUMENTATION the first journal you reach for when you want the latest developments, innovations, and advances in this fast-paced field.

Each bimonthly issue alerts you to trends and forecasts in the development, design, regulation, and clinical applications of medical instruments, devices, and systems. Original papers and timely articles help you keep pace with changes in the field that can have great effect on your work...new government standards and codes...new clinical uses...new approaches to enhancing quality, reliability, safety...key technologic breakthroughs ...and more.

Several special issues yearly are carefully planned around a single topic of current interest. Recent and upcoming special issues include —

- Environmental Therapeutic Devices for Infants
- Lasers in Medicine
- Neurologic Instrumentation and Techniques
- Alternative Communication Devices
- Respiratory Equipment

MEDICAL INSTRUMENTATION's coverage spans the disciplines, giving you a well-rounded perspective on trends in many areas — instrumentation for cardiovascular monitoring...clinical engineering...certification...instrumentation in anesthesiology.

Keep pace with technology and subscribe to **MEDICAL INSTRUMENTATION** today! Just clip out the coupon below or call **FREE** 1-800-638-6423 from anywhere in the U.S. (except Alaska), or call **COLLECT** in Maryland at 528-4105.

Williams & Wilkins

GET UP TO 3 YEARS AT THESE LOW RATES!

MEDICAL INSTRUMENTATION

The official journal of the Association for the Advancement of Medical Instrumentation

Keeping pace with the technologies of today... and tomorrow

☐ 3 years ☐ 2 years ☐ 1 year
☐ Individual $60/year
☐ Institution $85/year
☐ In-training $35/year
(Please add $10/year outside U.S.)

☐ Check enclosed ☐ Bill me
☐ VISA ☐ MasterCard ☐ American Express

card # expiration date

signature/PO#

Printed in USA

name

address

city/state/zip

Maryland residents please add 5% sales tax. Subscriptions outside the U.S. must be prepaid, in U.S. dollars only. Please allow up to 8 weeks for delivery of first issue. Surface deliveries outside the U.S. may take up to 16 weeks. Airmail rates available on request.

Mail to:

Williams & Wilkins
P.O. Box 23291
Baltimore, MD 21203

266 Fulham Road
London SW10 9EL England

MIAD 1062 88

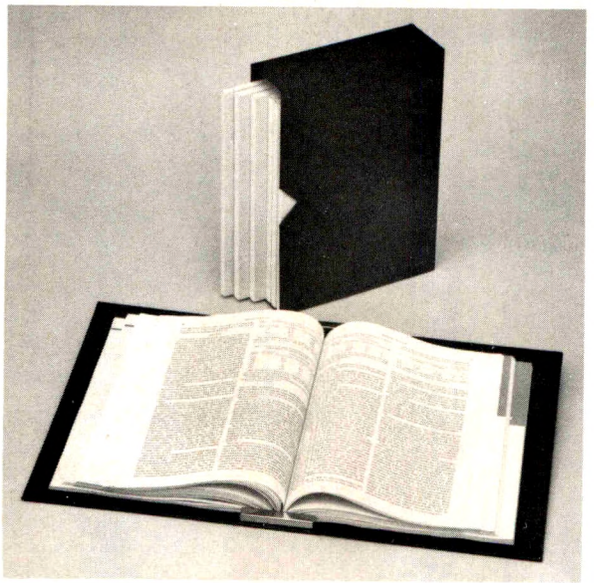

Protect your copies of

AJR: AMERICAN JOURNAL OF ROENTGENOLOGY

with Jesse Jones Binders or Files

Keep your journals clean, orderly, and readily accessible with Jesse Jones Binders or Files. Two Binders or two box style Files are all you need to accommodate a full year's worth of issues. Both Binders and Files are handsomely made with rich black leatherette covers and gold leaf embossed lettering.

Jesse Jones Binders open flat for easy reading and reference and are economically priced at only $9.95 each; 3 for $27.95, or 6 for $52.95 postpaid. The rugged, compact box Files are only $7.95 each; 3 for $21.95, or 6 for $39.95. Add $1.00/unit postage and handling. (Outside the U.S. add $2.50/unit.)

For charge orders call toll free 1-800-972-5858. ($15.00 minimum).

Free gold transfer slips included for indexing volume and year.

Please allow four to five weeks for delivery.

TO: Jesse Jones Industries
499 E. Erie Avenue, DEPT. AJR
Philadelphia, PA 19134

I enclose my check or money order for $_____
(PA residents add 6% sales tax)

Send me ____ ☐ Files ☐ Binders for my journals

Name

Address (will not ship to P.O. Box)

City/State/Zip

Satisfaction guaranteed.

INDEX TO ADVERTISERS

Ackrad Laboratories, Inc. A26

Adria Laboratories A29

AGFA-Gevaert-Rex A16, A17

Berlex Imaging A22, A23

Braintree Laboratories A2

Eastman Kodak A6, A7

Elema Schonander, Inc. A31

E-Z-EM Company . . . . . Cover 2

FUJI . . . . . Cover 3

General Electric A13, A14, A15

Konica Medical Corporation A24, A25

Mallinckrodt, Inc. A9, A10, A11, A12, A33, A34, A35, A36

Nuclear Associates A30

E. R. Squibb & Sons, Inc. . . A18, A19, A20, A21

S & S X-Ray A32

University of Miami A26

Winthrop Laboratories A27, A28, A39, A40

We try to present an accurate index. Occasionally this may not be possible because of a last-minute change or an omission.

In intrathecal imaging:

Because you can't be sure how every patient will react...

Improve the safety profile.

Better patient tolerance, measured subjectively and objectively.[1-5]

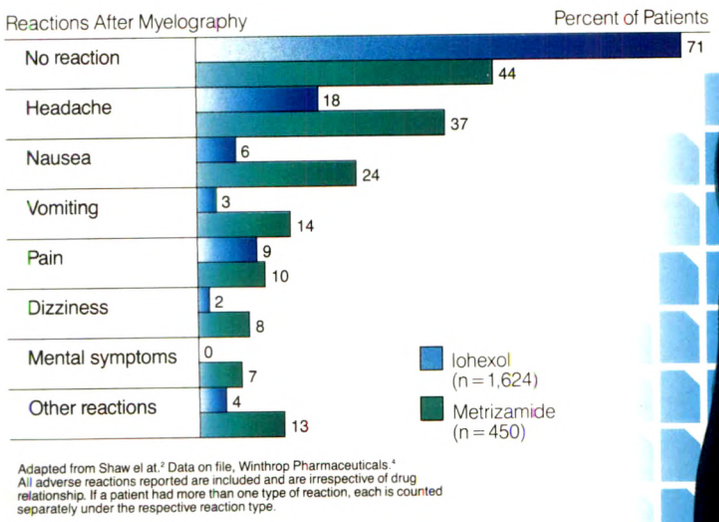

Adapted from Shaw el at.[2] Data on file, Winthrop Pharmaceuticals.[4]
All adverse reactions reported are included and are irrespective of drug relationship. If a patient had more than one type of reaction, each is counted separately under the respective reaction type.

Lower incidence of EEG changes compared with iopamidol or metrizamide.[2,5]

Excellent diagnostic quality.

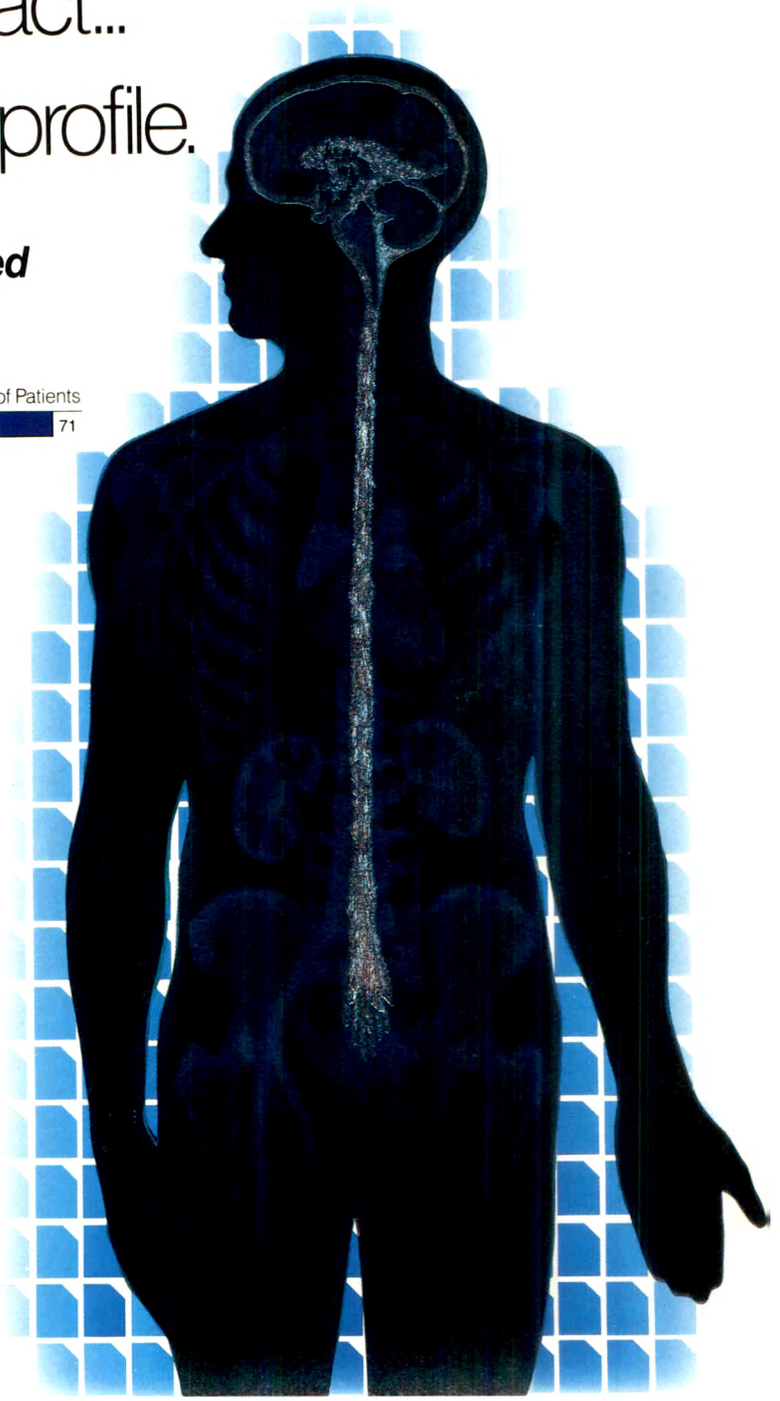

NONIONIC

OMNIPAQUE®

(IOHEXOL)

THE NEW STANDARD IN INTRATHECAL IMAGING.

See next page for important product information concerning contraindications, warnings, adverse reactions, patient selection, and precautionary recommendations.

OMNIPAQUE®
INJECTION (IOHEXOL)
INTRATHECAL

180

240

300

PLEASE CONSULT FULL PRODUCT INFORMATION BEFORE USING. A SUMMARY FOLLOWS:

DESCRIPTION: OMNIPAQUE is a nonionic, water-soluble radiographic contrast medium for intrathecal administration in concentrations of 180, 240, and 300 mgI/mL. Each milliliter of iohexol solution contains 1.21 mg tromethamine and 0.1 mg edetate calcium disodium with the pH adjusted between 6.8 and 7.7 with hydrochloric acid or sodium hydroxide. All solutions are sterilized by autoclaving, are nonpyrogenic, and contain no preservatives, so unused portions should be discarded.

CONTRAINDICATIONS–Intrathecal: OMNIPAQUE should not be administered to patients with a known hypersensitivity to iohexol. Myelography should not be performed in the presence of significant local or systemic infection where bacteremia is likely. Intrathecal administration of corticosteroids with OMNIPAQUE is contraindicated. Because of the possibility of overdosage, immediate repeat myelography in the event of technical failure is contraindicated.

WARNINGS–General: If grossly bloody CSF is encountered, the possible benefits of a myelographic procedure should be considered in terms of the risk to the patient.

Caution is advised in patients with a history of epilepsy, severe cardiovascular disease, chronic alcoholism, or multiple sclerosis.

Elderly patients may present a greater risk following myelography. The need for the procedure in these patients should be evaluated carefully. Special attention must be paid to dose and concentration of the medium used, hydration, and technique used.

Patients who are receiving anticonvulsants should be maintained on this therapy. Should a seizure occur, intravenous diazepam or phenobarbital sodium is recommended. In patients with a history of seizure activity who are not on anticonvulsant therapy, premedication with barbiturates should be considered.

Prophylactic anticonvulsant treatment with barbiturates should be considered in patients with evidence of inadvertent intracranial entry of a large or concentrated bolus of the contrast medium, since there may be an increased risk of seizure in such cases.

Drugs that lower the seizure threshold, especially phenothiazine derivatives, including those used for their antihistamine or antinauseant properties, are not recommended for use with OMNIPAQUE. Others include MAO inhibitors, tricyclic antidepressants, CNS stimulants, and psychoactive drugs described as analeptics, major tranquilizers, or antipsychotic drugs. While the contributory role of these medications has not been established, the use of such drugs should be based on physician evaluation of potential benefits and potential risks. Physicians have discontinued these agents at least 48 hours before and for at least 24 hours postprocedure. Care is required in patient management to prevent inadvertent intracranial entry of a large dose or concentrated bolus of the medium. Also, effort should be directed to avoid rapid dispersion of the medium causing inadvertent rise in intracranial levels (eg, by active patient movement). Direct intracisternal or ventricular administration for standard radiography (not CT) is not recommended.

In most reported cases of major motor seizures with nonionic myelographic media, one or more of the following factors were present. Therefore avoid:

- Deviations from recommended procedure or in myelographic management.
- Use in patients with a history of epilepsy.
- Overdosage.
- Intracranial entry of a bolus or premature diffusion of a high concentration of the medium.
- Medication with neuroleptic drugs or phenothiazine antinauseants.
- Failure to maintain elevation of the head during the procedure, on the stretcher, or in bed.
- Excessive and particularly active patient movement or straining.

PRECAUTIONS–General: Diagnostic procedures that involve the use of radiopaque diagnostic agents should be carried out under the direction of personnel with the prerequisite training and with a thorough knowledge of the particular procedure to be performed. Appropriate facilities should be available for coping with any complication of the procedure, as well as for emergency treatment of reactions to the contrast agent itself. After parenteral administration of a radiopaque agent, competent personnel and emergency facilities should be available, since delayed reactions have been reported (see ADVERSE REACTIONS).

Preparatory dehydration may be dangerous and may contribute to acute renal failure in patients with advanced vascular disease, diabetic patients, and in susceptible nondiabetic patients (often elderly with preexisting renal disease). Dehydration in these patients seems to be enhanced by the osmotic diuretic action of contrast agents. *Patients should be well hydrated prior to and following iohexol administration.*

The possibility of a reaction, including serious, life-threatening, fatal, anaphylactoid, or cardiovascular reactions, should always be considered (see ADVERSE REACTIONS). Therefore, it is of utmost importance that a course of action be carefully planned in advance for the immediate treatment of serious reactions, and that adequate and appropriate facilities and personnel be readily available in case of a severe reaction.

The possibility of an idiosyncratic reaction in susceptible patients should always be considered (see ADVERSE REACTIONS). The susceptible population includes patients with a history of a previous reaction to contrast media, patients with a known sensitivity to iodine per se, and patients with a known clinical hypersensitivity: bronchial asthma, hay fever, and food allergies.

A thorough medical history with emphasis on allergy and hypersensitivity, prior to the injection of any contrast medium, may be more accurate than pretesting in predicting potential adverse reactions.

A positive history of allergy or hypersensitivity does not arbitrarily contraindicate the use of a contrast agent where a diagnostic procedure is thought essential, but caution should be exercised (see ADVERSE REACTIONS). Premedication with antihistamines or corticosteroids, to avoid or minimize possible allergic reactions in such patients, should be considered.

In patients with severe renal insufficiency or failure, compensatory biliary excretion of the drug is anticipated to occur, with a slow clearance into the bile. Patients with hepatorenal insufficiency should not be examined unless the possibility of benefit clearly outweighs the additional risk. Sterile technique must be used with any spinal puncture.

When OMNIPAQUE is to be injected using plastic disposable syringes, the contrast medium should be drawn into the syringe and used immediately. If nondisposable equipment is used, scrupulous care should be taken to prevent residual contamination with traces of cleansing agents. **Parenteral drug products should be inspected and discarded if particulate matter or discoloration is present.**

Repeat Procedures. If in the clinical judgment of the physician sequential or repeat examinations are required, a suitable interval of time between administrations should be observed to allow for normal clearance of the drug from the body.

Information for Patients: When receiving injectable radiopaque diagnostic agents, inform your physician: If you are pregnant; if you are diabetic; if you have multiple myeloma, pheochromocytoma, homozygous sickle cell disease, or known thyroid disorder; if you are allergic to any drugs or food or if you had any reactions to previous injections of dyes used for x-ray procedures; about any other medications you are currently taking, including nonprescription drugs, before you are administered this drug.

Drug Interactions (See WARNINGS–General): In nonelective procedures in patients on the drugs described, consider prophylactic use of anticonvulsants.

Carcinogenesis, Mutagenesis, Impairment of Fertility: No long-term animal studies have been performed to evaluate carcinogenic potential, mutagenesis, or whether OMNIPAQUE can affect fertility in men or women.

Pregnancy Category B: Reproduction studies have been performed in rats and rabbits with up to 100 times the recommended dose. No evidence of impaired fertility or harm to the fetus has been demonstrated due to OMNIPAQUE; there are, however, no studies in pregnant women. Because animal reproduction studies are not always predictive of human response, this drug should be used during pregnancy only if clearly indicated.

Nursing Mothers: It is not known to what extent iohexol is excreted in human milk. However, many injectable contrast agents are excreted unchanged in human milk. Although it has not been established that serious adverse reactions occur in nursing infants, caution should be exercised when intravascular contrast media are administered to nursing women. Bottle feedings may be substituted for breast feedings for 24 hours following administration of OMNIPAQUE.

Pediatric Use: Safety and effectiveness in children have not been established.

ADVERSE REACTIONS–Intrathecal: The most frequently reported adverse reactions with OMNIPAQUE 180, OMNIPAQUE 240, and OMNIPAQUE 300 are headache, mild to moderate pain including backache, neck ache and stiffness, nausea and vomiting. These reactions usually occur 1 to 10 hours after injection, and almost all occur within 24 hours. They are usually mild to moderate in degree, lasting for a few hours and usually disappearing within 24 hours. Rarely, headaches may be severe or persist for days. Headache is often accompanied by nausea and vomiting and tends to be more frequent and persistent in patients not optimally hydrated. Transient alterations in vital signs may occur and their significance must be assessed on an individual basis. Those reactions reported in clinical studies with OMNIPAQUE are listed below in decreasing order of occurrence, based on clinical studies of 1,624 patients.

Headaches: The most frequently occurring adverse reaction following myelography has been headache, with an incidence of approximately 18%. Headaches may be caused either by a direct effect of the contrast medium or by CSF leakage at the dural puncture site. However, in managing the patient, it is considered more important to minimize intracranial entry of contrast medium by postural management than to attempt to control possible CSF leakage (see PATIENT MANAGEMENT).

Pain: Mild to moderate pain including backache, neck ache and stiffness, and neuralgia occurred following injection, with an incidence of about 8%.

Nausea and Vomiting: Nausea was reported with an incidence of about 6%, and vomiting about 3% (see PATIENT MANAGEMENT). Maintaining normal hydration is very important. The use of phenothiazine antinauseants is not recommended (see WARNINGS–General). Reassurance to the patient that the nausea will clear usually is all that is required.

Dizziness: Transient dizziness was reported in about 2% of the patients.

Other Reactions: Other reactions occurring with an individual incidence of less than 0.1% included: feeling of heaviness, hypotension, hypertonia, sensation of heat, sweating, vertigo, loss of appetite, drowsiness, hypertension, photophobia, tinnitus, neuralgia, paresthesia, difficulty in micturition, and neurological changes. All were transient and mild with no clinical sequelae.

General Adverse Reactions to Contrast Media: Physicians should remain alert for the occurrence of adverse effects in addition to those discussed above, particularly the following reactions which have been reported in the literature for other nonionic, water-soluble myelographic media and rarely with iohexol. These have included, but are not limited to, aseptic and bacterial meningitis and CNS and other neurologic disturbances.

An aseptic meningitis syndrome has been reported rarely (less than 0.01%). It was usually preceded by pronounced headaches, nausea, and vomiting. Onset usually occurred about 12 to 18 hours postprocedure. Prominent features were meningismus and fever, sometimes with oculomotor signs and mental confusion. Lumbar puncture revealed a high white cell count and high protein content, often with a low glucose level and absence of organisms. The condition usually started to clear spontaneously about 10 hours after onset, with complete recovery over 2 to 3 days.

Allergy or Idiosyncrasy: Chills, fever, profuse diaphoresis, pruritus, urticaria, nasal congestion, dyspnea, and Guillain-Barré syndrome.

CNS Irritation: Mild and transitory perceptual aberrations, such as hallucinations, depersonalization, amnesia, hostility, amblyopia, diplopia, photophobia, psychosis, insomnia, anxiety, depression, hyperesthesia, visual or auditory or speech disturbances, confusion and disorientation. In addition, malaise, weakness, EEG changes, meningismus, hyperreflexia or areflexia, hypertonia or flaccidity, hemiplegia, paralysis, quadriplegia, restlessness, tremor, echoacousia, echolalia, asterixis, and dysphasia have occurred.

Profound mental disturbances have also rarely been reported: various forms and degrees of aphasia, mental confusion, or disorientation. Onset is usually at 8 to 10 hours and lasts for about 24 hours. Occasionally, they have been manifest as apprehension, agitation, or progressive withdrawal in several instances to the point of somnolence, stupor, and coma. In a few cases, these have been accompanied by transitory hearing loss or other auditory symptoms and visual disturbances (believed subjective or delusional), including unilateral or bilateral loss of vision, which may last for hours. In one case, persistent cortical loss of vision has been reported in association with convulsions. Ventricular block has been reported; amnesia of varying degrees may be present for the reaction event.

Rarely, persistent though transitory weakness in the leg or ocular muscles has been reported. Peripheral neuropathies have been rare and transitory. They include sensory and/or motor or nerve root disturbance, myelitis, persistent leg muscle pain or weakness, 6th nerve palsy, or cauda equina syndrome. Muscle cramps, fasciculation or myoclonia, spinal convulsion, or spasticity are unusual and have responded promptly to a small intravenous dose of diazepam.

In general, the reactions that are known to occur on parenteral administration of iodinated contrast agents are possible with any nonionic agent. Approximately 95% of adverse reactions accompanying the use of water-soluble contrast agents are mild to moderate in degree. However, severe, life-threatening, anaphylactoid, and fatal reactions, mostly of cardiovascular origin, have occurred. Adverse reactions to injectable contrast media fall into two categories: chemotoxic reactions and idiosyncratic reactions.

Chemotoxic reactions result from the physicochemical properties of the contrast medium, the amount of the dose and the speed of injection. All hemodynamic disturbances and injuries to organs or vessels perfused by the contrast medium are included in this category.

Idiosyncratic reactions occur more frequently in patients 20 to 40 years old and may or may not be dependent on the amount of dose injected, the speed of injection, and the radiographic procedure. They are subdivided into minor, intermediate, and severe. The minor reactions are self-limited and of short duration; the severe reactions are life-threatening, and treatment is urgent and mandatory.

The reported incidence of adverse reactions to the contrast medium in patients with a history of allergy is twice that of the general population. Patients with a history of previous reactions to a contrast medium are three times more susceptible than other patients. However, sensitivity to contrast media does not appear to increase with repeated examination.

Most adverse reactions to injectable contrast media appear within 1 to 3 minutes after the start of injection, but delayed reactions may occur.

OVERDOSAGE: Although clinical consequences of overdosage with OMNIPAQUE have not been reported, physicians should be aware that incorrect management of the patient can permit inadvertent early intracranial entry of normal doses of the medium, thereby increasing CNS reactions.

The intracisternal LD_{50} value of OMNIPAQUE (in grams of iodine per kilogram body weight) is greater than 2.0 in mice.

References: 1. Kieffer SA, Binet EF, Davis DO, et al: Lumbar myelography with iohexol and metrizamide: A comparative multicenter prospective study. *Radiology* 1984; 151:665-670. **2.** Shaw DD, Bach-Gansmo T, Dahlstrom K: Iohexol: summary of North American and European clinical trials in adult lumbar, thoracic, and cervical myelography with a new nonionic contrast medium. *Invest Radiol* 1985; 20(suppl 1):44-50. **3.** Latchaw RE, Hirsch WL Jr, Horton JA, et al: Iohexol vs metrizamide: Study of efficacy and morbidity in cervical myelography. *AJNR* 1985; 6:931-933. **4.** Data on file, Winthrop Pharmaceuticals. **5.** Lamb JT: Iohexol vs. iopamidol for myelography. *Invest Radiol* 1985; 20(suppl 1):37-43.

© 1987 WINTHROP PHARMACEUTICALS 71171/3777

Winthrop PHARMACEUTICALS
Winthrop Pharmaceuticals
Division of Sterling Drug Inc.
New York, NY 10016

As a professional, you must be able to depend on the highest quality every time... sheet-to-sheet... box-to-box. Accepting less is a waste of time and effort. It could also result in poor patient care.

Fuji – committed to consistency.

- Fuji has the world's most automated X-ray film factory.
- Fuji's commitment to research has produced exclusive technologies such as non-contact, helical emulsion drying and other developments which have raised the standards for consistent emulsion performance to a new plateau.
- These elements offer the assurance that no manufacturer provides more consistent medical X-ray films than Fuji.

See for yourself the difference between "consistent" and "UNCOMMONLY CONSISTENT." Call your local Fuji representative, or toll free, 1-800-431-1850.

FUJI QUALITY... UNCOMMONLY CONSISTENT.

I&I *Imaging & Information*

FUJI MEDICAL SYSTEMS, U.S.A., INC.
90 Viaduct Road, P.O. Box 4960, Stamford, CT 06907

CIRCLE 7 ON READER SERVICE CARD

COMMEMORATION OF JUBILEE ANNIVERSARY VOLUME

227 ***AJR:* the 50 most frequently cited papers in the past 50 years.** *Chew FS*

235 **Anniversary reprint from volume 50, 1943. Mono-osteitic Paget's disease as a clinical entity: roentgenologic observations in nine cases.** *Groh JA*

249 **Review article. Paget disease of bone: current status and a look back to 1943 and earlier.** *Resnick D*

CONTRAST MATERIAL

257 **Perspective. Pretreatment with corticosteroids to prevent reactions to IV contrast material: overview and implications.** *Lasser EC*

CARDIOPULMONARY RADIOLOGY

261 **Perspective. Lung cancer: update on staging classifications.** *Friedman PJ*

265 **Small-cell bronchogenic carcinoma: CT evaluation.** *Pearlberg JL, Sandler MA, Lewis JW Jr, Beute GH, Alpern MB*

269 **Asbestos-related pleural disease and asbestosis: a comparison of CT and chest radiography.** *Friedman AC, Fiel SB, Fisher MS, Radecki PD, Lev-Toaff AS, Caroline DF*

GASTROINTESTINAL RADIOLOGY

277 **Gastrointestinal inflammation after bone marrow transplantation: graft-versus-host disease or opportunistic infection?** *Jones B, Kramer SS, Saral R, et al.*

283 **MR imaging of portal venous thrombosis: correlation with CT and sonography.** *Zirinsky K, Markisz JA, Rubenstein WA, et al.*

289 **Case report. Hepatic venocclusive disease after bone-marrow transplantation: duplex sonography.** *Kriegshauser JS, Charboneau JW, Letendre L*

291 **Heterotopic gastric mucosa in the duodenum: radiographic findings.** *Agha FP, Ghahremani GG, Tsang T-K, Victor TA*

295 **Chronic intestinal obstruction: value of percutaneous gastrostomy tube placement.** *Picus D, Marx MV, Weyman PJ*

299 **Case report. Infarcted Meckel diverticulum detected by CT.** *Russ PD, Friefeld GD, Nauck CJ, Wilmouth RJ*

301 **Carcinoma of the colon: detection and staging by CT.** *Balthazar EJ, Megibow AJ, Hulnick D, Naidich DP*

GENITOURINARY RADIOLOGY

307 **Extracorporeal shock-wave lithotripsy: prevalence of renal stones 3–21 months after treatment.** *Miles SG, Kaude JV, Newman RC, Thomas WC, Williams CM*

311 **Extracorporeal shock-wave lithotripsy: long-term complications.** *Williams CM, Kaude JV, Newman RC, Peterson JC, Thomas WC*

316 **Commentary. Extracorporeal shock-wave lithotripsy: slam-bang effects, silent side effects?** *Mulley AG Jr, Carlson KJ, Dretler SP*

319 **Renal transplant dysfunction: MR evaluation.** *Winsett MZ, Amparo EG, Fawcett HD, et al*

325 **Case report. Renal embolization for hematuria: coordination with cystoscopy.** *Swartz DA, McLellan GL, Mitchum D, Vines F*

327 **Balloon catheter dilatation of urethral strictures.** *Mohammed SH, Wirima J*

MUSCULOSKELETAL RADIOLOGY

331 **Meniscal and ganglion cysts of the knee: MR evaluation.** *Burk DL Jr, Dalinka MK, Kanal E, et al.*

337 **Knee ligament reconstruction: plain film analysis.** *Manaster BJ, Remley K, Newman AP, Mann FA*

343 **Shoulder impingement syndrome: MR findings in 53 shoulders.** *Seeger LL, Gold RH, Bassett LW, Ellman H*

349 **Case report. MR imaging of hemophilic pseudotumors.** *Wilson DA, Prince JR*

351 **Case report. MR imaging of Mafucci syndrome.** *Unger EC, Kessler HB, Kowalyshyn MJ, Lackman RD, Morea GT*

355 **Case report. Polychondritis affecting the laryngeal cartilages: CT findings.** *Casselman JW, Lemahieu SF, Peene P, Stoffels G*

PEDIATRIC AND FETAL RADIOLOGY

359 **Scoliosis examinations: organ dose and image quality with rare-earth screen-film systems.** *Fearon T, Vucich J, Butler P, et al.*

363 **MR imaging of Ebstein anomaly: results in four cases.** *Link KM, Herrera MA, D'Souza VJ, Formanek AG*

369 **Chest radiography in infant cardiac allotransplantation.** *Toomey FB, Bailey LL, Dang Bui R, et al.*

373 **Case report. Food allergy presenting as obstruction in an infant.** *McIlhenny J, Sutphen JL, Block CA*

377 **Technical note. The use of midazolam for sedation of infants and children.** *Diament MJ, Stanley P*

379 **Case report. Third-trimester fetal sonography: meconium simulating a presacral mass.** *Moreland SI III, Cohen MI, Leopold GR, Gosink BB*

NEURORADIOLOGY

381 **Temporomandibular joint: MR of internal derangements and postoperative changes.** *Schellhas KP, Wilkes CH, Fritts HM, Omlie MR, Heithoff KB, Jahn JA*

391 **Syringomyelia as a consequence of compressive extramedullary lesions: postoperative clinical and radiological manifestations.** *Castillo M, Quencer RM, Green BA, Montalvo BM*

397 **Comparison of MR and CT myelography in imaging the cervical and thoracic spine.** *Karnaze MG, Gado MH, Sartor KJ, Hodges FJ III*

405 **Treatment of vertebral arteriovenous fistulas.** *Halbach VV, Higashida RT, Hieshima GB*

413 **Tolosa-Hunt syndrome revisited: not necessarily a diagnosis of exclusion.** *Kwan ESK, Wolpert SM, Hedges TR III, Laucella M*

VASCULAR RADIOLOGY

419 **Pictorial essay. Color-flow Doppler imaging of carotid artery.** *Middleton WD, Foley WD, Lawson TL*

427 **Greenfield filter: percutaneous placement in 50 patients.** *Denny DF Jr, Dorfman GS, Cronan JJ, Greenwood LH, Morse SS, Yoselevitz M*

431 **The collapsed inferior vena cava: CT evidence of hypovolemia.** *Jeffrey RB Jr, Federle MP*

433 **Case report. Splenic artery pseudoaneurysms causing lower gastrointestinal hemorrhage.** *Walker TG, Geller SC, Waltman AC*

435 **Pictorial essay. The popliteal artery and its branches: embryologic basis of normal and variant anatomy.** *Mauro MA, Jaques PF, Moore M*

ARRS MEETING SECTION

439 **ARRS 1987 meeting invitation**
441 **ARRS section on instruction**
455 **ARRS scientific program**
461 **ARRS local activities**
463 **ARRS registration forms**
466 **ARRS airline discounts**
467 **ARRS meeting summary**

OTHER CONTENT

375 **Errata**
430 **Forthcoming articles**
438 **American Roentgen Ray Society officers**
468 **Letters**
474 **Review of current literature**
479 **News**

Memorials **Edward B. D. Neuhauser** 357
Catherine Cole-Beuglet 426

Book reviews 234, 282, 298, 310, 324, 348, 354, 368, 376, 390, 404

482 **Classified advertisements**
A3 **Guidelines for authors**

JUBILEE VOLUME

Acc.
22.8.88

AJR

American
Journal of
Roentgenology

March 1988

Precise localization of non-palpable lesions ...from E-Z-EM

PercuGuide™

Regardless of your present method of marking non-palpable lesions, PercuGuide™ can improve upon it.

Unlike improvised markers, PercuGuide can't shift with patient movement. It won't disperse over time like a dye. And PercuGuide offers a range of refinements that no other wire guide system can match.

Afterloading of the PercuGuide wire guide eliminates any chance of the barb seating before the needle has been properly positioned. A plastic sheath makes loading easy, and a permanently affixed stiffening cannula protects the wire from being accidentally severed while it acts as a visible guide for the surgeon.

Clearly marked 1 cm gradations on the cannula, and a specially designed gripping hub aid in the precise placement of the needle. And each needle is supplied with an E-Z-MARK® radiopaque marker and a handy ruler.

If you're presently using another system, or if you've never used a wire guide before, PercuGuide can help improve your technique. For more information on PercuGuide, or on any of E-Z-EM's products for interventional medicine, contact your local E-Z-EM representative, or call E-Z-EM Interventional Products Marketing at 1-800-645-3052. In New York call 516-333-8230.

E-Z-EM
More than barium—
much more

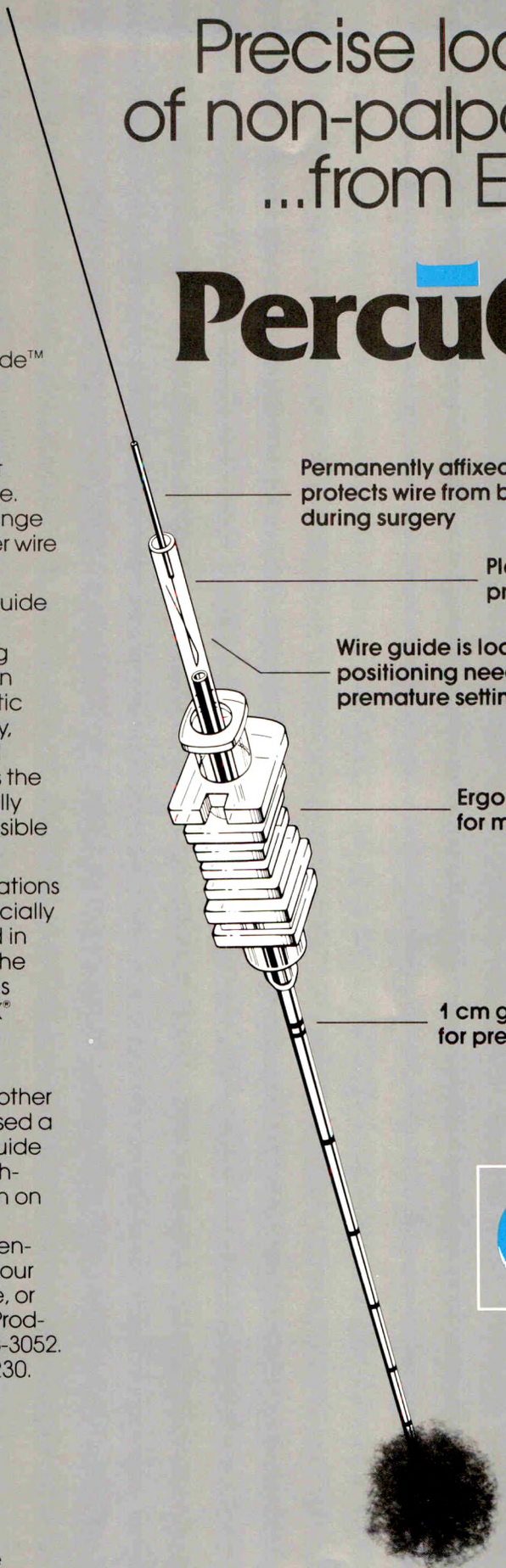

E-Z-MARK® radiopaque marker provided with each PercuGuide needle

E-Z-EM®
E-Z-EM, Inc.,
7 Portland Avenue
Westbury, N.Y. 11590

© 1987 E-Z-EM, Inc.

CIRCLE 5 ON READER SERVICE CARD

Official Journal of the American Roentgen Ray Society

AJR

American Journal of Roentgenology
Diagnostic Imaging and Related Sciences

Editor-In-Chief Robert N. Berk, *San Diego, California*

Editor Emeritus Melvin M. Figley, *Seattle, Washington*

Associate Editor Saskia von Waldenburg Hilton, *San Diego, California*

Consulting Editor Juan M. Taveras, *Boston, Massachusetts*

Statistician Charles C. Berry, *San Diego, California*

Editorial Board

John R. Amberg
William L. Ashburn
Itamar Aviad
Lawrence W. Bassett
Gregory P. Borkowski
William G. Bradley, Jr.
Peter L. Cooperberg
Peter M. Doubilet
N. Reed Dunnick
David K. Edwards
Ronald G. Evens
David S. Feigin
Paul J. Friedman
William R. Hendee
John R. Hesselink
Charles B. Higgins
Melvyn T. Korobkin
Thomas L. Lawson
Bruce L. McClennan
Albert A. Moss
Jeffrey H. Newhouse
Donald L. Resnick
Stewart R. Reuter
Charles R. Rohrmann, Jr.
Peter M. Ronai
Sjef H. J. Ruijs
Stuart S. Sagel
David J. Sartoris
Edward A. Sickles
Barry A. Siegel
David D. Stark
Edward T. Stewart
Eric vanSonnenberg

Editorial Staff: Elizabeth A. Whalen, *publications supervisor*; Linda Wood, Barbara Rose, and Barbara L. Halliburton, *manuscript editors*; Nancy Rydbeck, *office manager*; Elaine Sherman, *administrative assistant*; Geraldine Perillo, *administrative secretary*.

All business correspondence, including display (not classified) advertising, subscriptions, address changes, reprints, and permission requests should be addressed to Williams & Wilkins, 428 East Preston Street, Baltimore, MD 21202. Correspondence regarding editorial matters and classified advertising should be addressed to the editorial office, AJR, 2223 Avenida de la Playa, Suite 200, La Jolla, CA 92037-3218. For manuscript submission, see Guidelines for Authors, next page. Undelivered or damaged copies replaced within 60 days of publication; 90 days for foreign subscribers. Allow 90 days for address changes.
AJR, AMERICAN JOURNAL OF ROENTGENOLOGY (ISSN 0361 803X) is published monthly by American Roentgen Ray Society, 428 E. Preston Street, Baltimore, MD 21202. Annual dues include $50 for journal subscription. Second class postage paid at Baltimore, MD and at additional mailing offices. Postmaster send address changes (Form 3579) to Williams & Wilkins, 428 East Preston St., Baltimore, MD 21202. Subscription rates $100 ($135 foreign); institutions $110 ($145 foreign); in training $25; single copy $16 ($19). Japanese rates include airfreight. Japanese yen price is available from our sole agent USACO Corporation, 13-12, Shimbashi 1-Chome, Minato-Ku, Tokyo 105, Japan, telephone 03-502-6471. Subscriptions in South Korea are available only through our sole agent in Korea: Korea-America Medical Books Co., Ltd. (KAMBOOK) 209 Yun kun-dong, Chongro-ku, Seoul, Korea (telephone: 745-3151; telex: K25211 KAMBC; FAX: 745-3153). All subscriptions to South Korea will be shipped by air freight after January 1, 1988. There is an air freight surcharge of $12.00 over the regular subscription rate for this journal in South Korea to partially compensate for air freight costs. Airmail rates furnished on request. Indexed by *Current Contents* and *Index Medicus*. Copyright © 1987 by American Roentgen Ray Society. 0361-803X/88$2.00

Sets the tract record for BE prep:

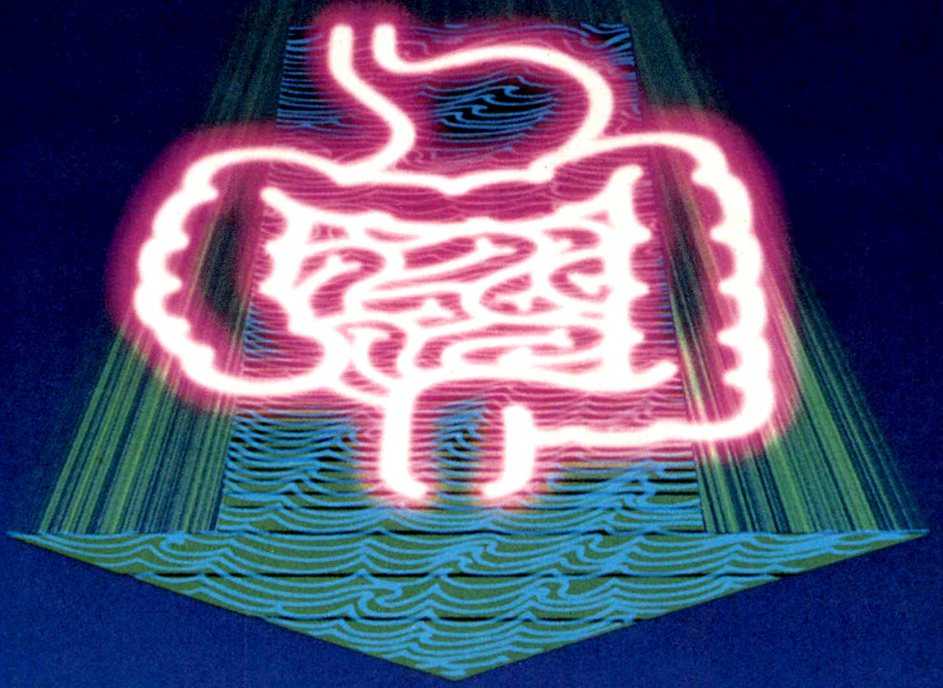

New Lower Price

GoLYTELY®

(PEG Electrolyte for Gastrointestinal Lavage Solution)

Excellent results in 4 hours . . . clinical studies have shown that GoLYTELY is equal in efficacy to a rigorous one- to two-day prep for air-contrast barium studies, particularly if **bisacodyl USP*** is also given to ensure the evacuation of any residual fluid.[1,2]

Patients prefer GoLYTELY because it's a more convenient routine to follow at home and it's usually well tolerated, even by older patients.[3] And since it's premeasured—just make up to volume in its own container with tap water—GoLYTELY guards against incorrect or inadequate usage.

Professionals prefer GoLYTELY because it can keep more patients ambulatory longer. For hospitalized patients, GoLYTELY can reduce length of stay because the prep takes less time.

With a clean bowel, repeat exams are less frequent—a plus under DRGs. Prescribed volumes of GoLYTELY solution can be given without significant change in water or electrolyte balance.

GoLYTELY is generally well tolerated and side effects are transient. Patients with impaired gag reflex who are prone to regurgitation or aspiration should be observed during the administration of GoLYTELY. If obstruction or perforation is suspected, appropriate studies should be performed to rule out these contraindications. GoLYTELY is also contraindicated in patients with gastric retention, toxic colitis, or toxic megacolon.

*Complimentary tablets of bisacodyl, USP, are attached to the patient pamphlet **Bowel Preparation Before Your Barium Enema.** A supply is available to professionals by writing Braintree Laboratories at the address below.

BRIEF SUMMARY: Before prescribing, see package insert or *PDR*.

INDICATIONS AND USAGE: GoLYTELY is indicated for bowel cleansing prior to colonoscopy and barium enema x-ray examination.

CONTRAINDICATIONS: GoLYTELY is contraindicated in patients with gastrointestinal obstruction, gastric retention, bowel perforation, toxic colitis, or toxic megacolon.

WARNINGS: No additional ingredients—eg, flavorings—should be added to the solution. GoLYTELY should be used with caution in patients with severe ulcerative colitis.

PRECAUTIONS: *General:* Patients with impaired gag reflex, unconscious or semiconscious patients, and patients prone to regurgitation or aspiration should be observed during the administration of GoLYTELY, especially if it is administered via nasogastric tube. If a patient experiences severe bloating, distention, or abdominal pain, administration should be slowed or discontinued temporarily until the symptoms abate. If gastrointestinal obstruction or perforation is suspected, appropriate studies should be performed to rule out these conditions before administration of GoLYTELY.

ADVERSE REACTIONS: Nausea, abdominal fullness, and bloating are the most common adverse reactions (occurring in up to 50% of patients) to administration of GoLYTELY. Abdominal cramps, vomiting, and anal irritation occur less frequently. These adverse reactions are transient and subside rapidly. Isolated cases of urticaria, rhinorrhea, and dermatitis —which may represent allergic reactions—have been reported.

CAUTION: Federal law prohibits dispensing without prescription.

STORAGE: Store in sealed container at 59°-86°F. When reconstituted, keep solution refrigerated. Use within 48 hours. Discard unused portion.

(NDC 52268-0100-01). Revised 10/1/86

Made by Lyne Laboratories, Stoughton, MA 02072, for BRAINTREE LABORATORIES, INC., P.O. Box 361, Braintree, MA 02184.

References: 1. Ernstoff JJ, et al: *Gastroenterology* 1983; 84:1512-1516. **2.** Girard CM, et al: AJR 1984; 142:1147-1149. **3.** DiPalma JA, et al: *Am J Gastroenterol* 1986; 81:652-655.

LABORATORIES · INC **Braintree**

CIRCLE 35 ON READER SERVICE CARD

AJR Guidelines for Authors

Address new and revised manuscripts, correspondence, and classified ads to the Editor:

AJR Editorial Office
2223 Avenida de la Playa, Suite 200
La Jolla, CA 92037-3218 Telephone: (619) 459-2229

Inquiries regarding subscriptions, display advertising, reprints, or permission to republish *AJR* material should be addressed to the publisher:

The Williams & Wilkins Co.
428 E. Preston St.
Baltimore, MD 21202 Telephone: (301) 528-4133

The *AJR* publishes original contributions to the advancement of medical diagnosis and treatment. Submitted manuscripts should not contain previously published material and should not be under consideration for publication elsewhere. Papers dealing with neuroradiology should be addressed to: American Journal of Neuroradiology, Dept. of Radiology, Massachusetts General Hospital, Boston, MA 02114. At the discretion of the *AJR* Editor, *AJNR* articles that are of interest to the general reader may be republished in the *AJR*. Neuroradiologic papers sent to the *AJR* will be forwarded to the Editorial Office of the *AJNR*.

Manuscript decisions are based on peer review. Reviewers receive manuscripts without title pages to ensure an unbiased review. All accepted manuscripts are subject to editing. Statements made in the article, including changes made by the Editor or manuscript editor, are the responsibility of the author and not of the *AJR* or its publisher. Authors will be sent the edited manuscript, galley proof, and proofs of illustrations. If the corresponding author will be unavailable to review galleys, arrangements should be made for a coauthor or colleague to read and return the proof.

General Guidelines for Major Papers

Abstract. Clearly state (in 200 words or less) the purpose, methods, results, and conclusions of the study. Include actual data.

Introduction. Briefly describe the purpose of the investigation, including relevant background information.

Methods. Describe the research plan, the materials (or subjects), and the methods used, in that order. Explain in detail how disease was confirmed and how subjectivity in observations was controlled.

Results. Present results in a clear, logical sequence. If tables are used, do not duplicate tabular data in text, but do describe important trends and points.

Discussion. Describe the limitations of the research plan, materials (or subjects), and methods, considering both the purpose and the outcome of the study. When results differ from those of previous investigators, explain the discrepancy.

AUTHOR'S CHECKLIST

For priority handling, complete the following checklist, sign the copyright form on the reverse side of this page, and include both with the manuscript.

_____ Two copies of the manuscript (the original and a photocopy) and two complete sets of figures are submitted. One copy has been retained by the author.

_____ If appropriate, *AJR* Guidelines for case reports, technical notes, pictorial essays, or letters to the Editor have been followed. (See page A5.)

_____ The manuscript, including references, figure legends, and tables, is typed double-spaced on 8½ × 11 in. (21.6 × 27.9 cm) *nonerasable* paper. Right-hand margins are not justified.

_____ All manuscript pages are numbered consecutively beginning with the abstract. Authors' names do not appear on the manuscript pages.

_____ The manuscript is organized as follows: title page, blind title page (title only), abstract, introduction, methods, results, discussion, acknowledgments, references, tables, figure legends, and figures.

_____ Informed consent has been obtained from patients who participated in clinical investigations. If experiments were performed on animals, authors complied with NIH guidelines for use of laboratory animals.

_____ Use of unfamiliar acronyms and abbrevations is kept to a minimum. When abbreviations are used they are defined at first mention, followed by the abbreviation in parentheses.

_____ Metric measurements are used throughout, or the metric equivalent is given in parentheses.

_____ Names and locations (city and state only) of manufacturers are given for equipment and nongeneric drugs.

Title Page

_____ The following information is given: title of article; names and complete addresses (including zip code) of all authors; current addresses of authors who have moved since study; acknowledgment of grant or other assistance. The corresponding author is clearly identified, and a current address and phone number are given.

_____ Two copies of a blind title page are included giving only the title (without the authors' names) for use in the review process.

Abstract

_____ An abstract of approximately 200 words concisely states the purpose, methods, and results of the study in one paragraph. Actual data are included. Conclusions are stated in a second, summary paragraph.

_____ No abbreviations or reference citations are used.

References

_____ References (not to exceed 35) are typed double-spaced starting on a separate page and are **numbered consecutively in the order in which they appear in the text.**

_____ All references are cited in the text and are enclosed in brackets and typed on line with the text (not superscript).

_____ Unpublished data are not cited in the reference list, but are cited parenthetically in the text, for example, (Smith DJ, personal communication), (Smith DJ, unpublished data). This includes papers submitted, but not yet accepted, for publication.

_____ Inclusive page numbers (e.g., 333–335) are given for all references.

_____ Journal names are abbreviated according to *Index Medicus*.

_____ Style and punctuation of references follow the format illustrated in the following examples (all authors are listed when six or less; when seven or more authors, the first three are listed, followed by "et al."):

Journal article

1. Long RS, Roe EW, Wu EU, et al. Membrane oxygenation: radiographic appearance. *AJR* **1986**;146:1257–1260

Book

2. Smith LW, Cohen AR. *Pathology of tumors*, 6th ed. Baltimore: Williams & Wilkins, **1977**:100–109

Chapter in a book

3. Breon AJ. Serum monitors of bone metastasis. In: Clark SA, ed. *Bone metastases*. Baltimore: Williams & Wilkins, **1983**:165–180

Paper presented at a meeting

4. Lau FS, Kirk AN, Beck RA. MR imaging of the spine. Presented at the annual meeting of the American Roentgen Ray Society, Washington, DC, April **1986**

Tables

_____ Each table is typed double-spaced on a separate page without vertical or horizontal rules; each has a short, descriptive title. Tables do not exceed two pages in length and contain at least four lines of data.

_____ Tables are numbered in the order in which they are cited in the text.

_____ Abbreviations are defined in an explanatory note below each table.

_____ Tables are self-explanatory and do not duplicate data given in the text or figures.

_____ All arithmetic (percentages, totals, differences) has been double checked for accuracy, and tabular data agree with data given in the text.

Figures and Legends

_____ Two complete sets of original figures are submitted unmounted in labeled envelopes.

_____ Figures are clean, unscratched, 5 × 7 in. (13 × 18 cm) glossy prints with **white borders.** A separate print is submitted for each figure *part*.

_____ All figure parts relating to one patient are in one figure.

_____ Each figure is labeled on the back with the figure number and an arrow indicating "top." For black-and-white figures, labeling is done on a gummed label, which is then affixed to the back of the print. *Never* use labels on color figures, but write figure number on the back lightly in pencil. *Never* use ink on front or back of any figures.

_____ Author's names are *not* written on the backs of figures.

_____ Only removable (rub-on) arrows and letters are used on the figures. Symbols are uniform in size and style and are not broken or cracked.

_____ Images are uniform in size and magnification.

_____ Line drawings are done in black ink on a white background. They are professional in quality, and all use the same size type. (Only glossy prints are acceptable.)

_____ Written permission has been obtained for use of all previously published illustrations (and copies of permission letters are included), and an appropriate credit line is given in the legends.

_____ Legends are typed double-spaced, and figure numbers correspond with the order in which the figures are cited in the text.

Transfer of Copyright Agreement, Exclusive Publication Statement, and Conflict of Interest Acknowledgment

Complete copyright to the article entitled: _____

_____

is hereby transferred to the American Roentgen Ray Society (for United States government employees to the extent transferable), effective if and when the article is accepted for publication in the *American Journal of Roentgenology*. In the case of the authors who are officers or employees of the United States government, the American Roentgen Ray Society recognizes that works prepared by officers or employees of the United States government as part of their official government duties are in the public domain.

Authors reserve all proprietary rights other than copyright, such as patent rights and the right to use all or part of this article in future works of their own. The authors retain the right of replication, subject only to crediting the original source of publication and receiving written permission from the publisher.

Authors guarantee that this manuscript contains no matter that is libelous or otherwise unlawful, invades individual privacy, or infringes any proprietary rights.

Authors understand that they will receive no royalty or other compensation from the American Roentgen Ray Society or the publisher.

Authors guarantee that the editor has been or will be informed of any proprietary or commercial interest or conflicts of interest the authors may have that relate directly or indirectly to the subject of this article.

Finally, the authors certify that none of the material in this manuscript has been published previously or is currently under consideration for publication elsewhere.

First author/date	Second author	Third author
Fourth author	Fifth author	Sixth author

This agreement must be signed by all authors in order for the manuscript to be published.

Case Reports

A case report is a brief description of a special case that provides a message that transcends the individual patient.

Format. There is no abstract. The introduction should be a short paragraph giving the general background and the specific interest of the case. No more than one case should be described in detail (similar ones can be mentioned briefly in the discussion). Emphasis should be on the radiologic aspects; clinical information must be limited to that necessary to provide a background for the radiology. The discussion should be succinct and should focus on the specific message and relevance of radiologic methods. A review of the literature is not appropriate.

Length. Maximum of five double-spaced, typewritten pages, including the references but not the title page or figure legends.

References. Maximum of eight.

Figures. Maximum of three or four, unless the text is shortened accordingly. Legends must not repeat the text.

Tables and Acknowledgments. Not appropriate in case reports.

Technical Notes

A technical note is a brief description of a specific technique or procedure, modification of a technique, or equipment of interest to radiologists.

Format. No abstract, headings, or subheadings are required. If headings are used, they should be a combination of "Case Report," "Materials and Methods," "Results," and "Discussion." A brief one-paragraph introduction should be included to give the general background. Discussion should be limited to the specific message, including the uses of the technique or equipment. Literature reviews and lengthy case reports are not appropriate.

Length. Maximum of five double-spaced, typewritten pages, including the references but not the title page or figure legends.

References. Maximum of eight.

Figures. Maximum of two, unless the text is shortened accordingly.

Tables and Acknowledgments. Not appropriate in technical notes.

Pictorial Essays

A pictorial essay is an article that conveys its message through illustrations and their legends. Unlike other *AJR* articles, which are based on original research, pictorial essays serve primarily as teaching tools, like exhibits at a scientific meeting. They are not encyclopedic book chapters. No abstract is necessary.

Length. Maximum of four double-spaced, typewritten pages, including the references but not the title page or figure legends.

References. Maximum of four.

Figures. Maximum of 30 figure *parts*. Number should be as few as necessary to convey the message of the paper.

Tables and Acknowledgments. Not appropriate in pictorial essays.

Letters to the Editor and Replies

Letters to the Editor and Replies should offer objective and constructive criticism of published articles. Letters may also discuss matters of general interest to radiologists.

Format. All letters should be typed double-spaced on nonletterhead paper, with no greeting or salutation. Signature and affiliation should appear at the end of the letter. Titles for letters should be short and pertinent. The title for a reply is simply "Reply."

Length. Maximum of two double-spaced, typewritten pages, including references.

References. Maximum of four.

Figures. Maximum of two.

Tables and Acknowledgments. Not appropriate in Letters to the Editor and Replies.

Opinions, Commentaries, and Perspectives

Opinions, commentaries, and perspectives are special articles dealing with controversial topics or issues of special concern to radiologists.

Format. Include a title page but no abstract. Headings may be used to break up the text.

Length. Maximum of five double-spaced, typewritten pages.

References. Maximum of five.

Tables and Figures. Maximum of four.

Computer Page Articles

Articles published on the computer page deal with practical computer applications to radiology.

Format. Include a title page but no abstract.

Length. Maximum of eight double-spaced, typewritten pages.

References. Maximum of five.

Figures and Tables. Maximum of five. Computer printouts are not acceptable. Figures must be submitted as 5 × 7 in. glossy prints.

All submissions to the *AJR* must be accompanied by a completed copy of the Author's Checklist and the signed Copyright Agreement.

WHERE TO FIND RELIABLE PROCESSORS BY KODAK

Kodak processors set the standards for reliability and dependability—and support—in departments of every size in medical facilities everywhere.

Kodak developed the roller transport film processor, and the rest of the world has been playing catch-up ever since. Kodak X-Omat processors are known for reliability, dependability, and consistency. And for support: Kodak representatives and service people stand behind every one. The line now includes the M35A for the smallest operations. Plus the M8 and M6B for the largest, and the M7B for anything in between.

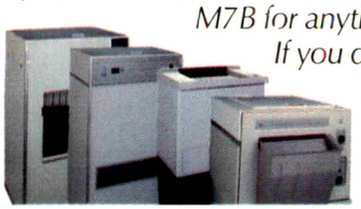

If you don't yet have the speed and consistency of automation, or if you don't have the reliability and backup of Kodak, talk to your Kodak representative.

Kodak
Official Diagnostic Imaging Products Sponsor of the 1988 Olympic Games

The new vision of Kodak

Kodak

tman Kodak Company, 1987

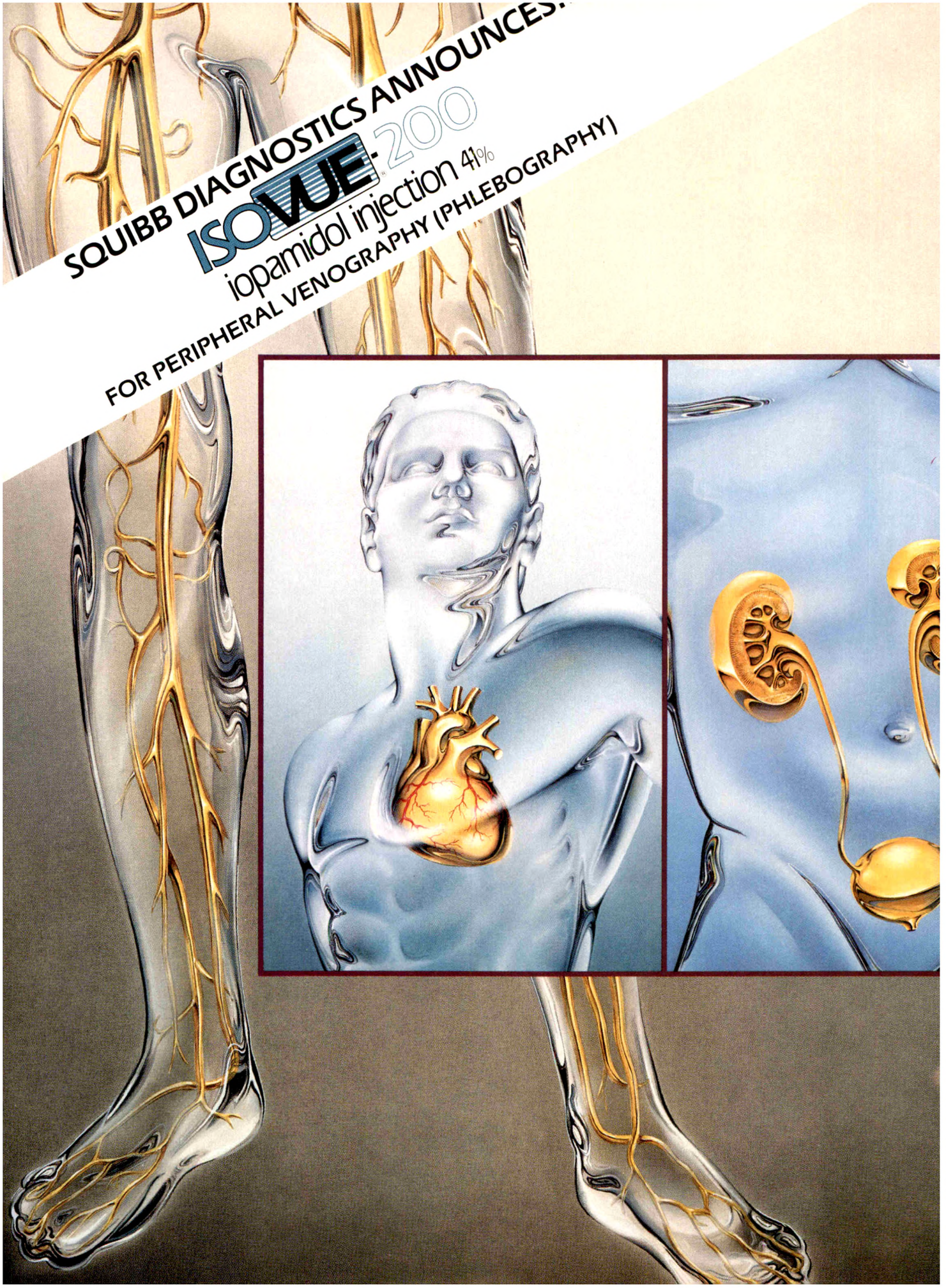
SQUIBB DIAGNOSTICS ANNOUNCES
ISOVUE-200
iopamidol injection 41%
FOR PERIPHERAL VENOGRAPHY (PHLEBOGRAPHY)

In radiologic contrast procedures

ISOVUE® / ISOVUE-M®

iopamidol injection

THE CLEAR CHOICE

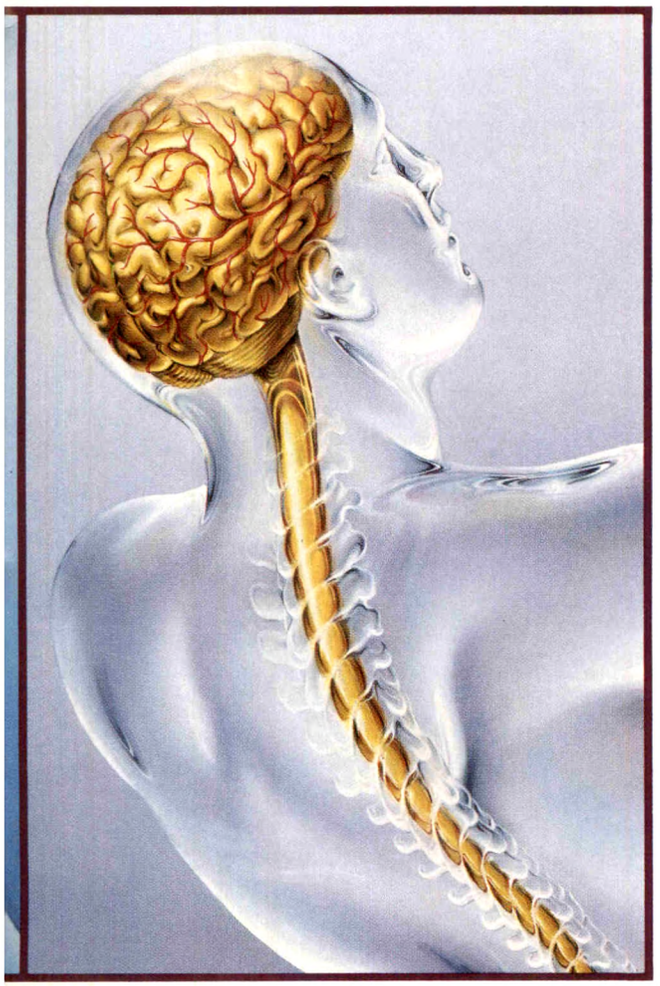

A broad range of indications

Peripheral arteriography
Coronary arteriography and ventriculography
IVP (excretory urography)
Myelography (lumbar, thoracic, cervical, total columnar)
Cerebral arteriography
CT head and body imaging
CT cisternography and ventriculography
Visceral arteriography (selective)
Aortography
IA-DSA
Peripheral venography (phlebography)

The only nonionic contrast agents you need to stock

SQUIBB™ Diagnostics

CIRCLE 14 ON READER SERVICE CARD

Please see brief summary of prescribing information on adjacent pages.

This product is under license from Bracco Industria Chimica, S.p.A. U.S. Patent #4,001,323

© 1988 E.R. Squibb & Sons, Inc., Princeton, NJ

647-508

Issued: January 1988

ISOVUE®-128 (Iopamidol Injection 26%)
ISOVUE®-200 (Iopamidol Injection 41%)
ISOVUE®-300 (Iopamidol Injection 61%)
ISOVUE®-370 (Iopamidol Injection 76%)
ISOVUE-M® 200 (Iopamidol Injection 41%)
ISOVUE-M® 300 (Iopamidol Injection 61%)

INDICATIONS AND USAGE

ISOVUE (Iopamidol Injection) is indicated for intra-arterial digital subtraction angiography (DSA) of the cerebral and abdominal vasculature and for angiography throughout the cardiovascular system, including cerebral and peripheral arteriography, coronary arteriography and ventriculography, selective visceral arteriography and aortography, peripheral venography (phlebography), and intravenous excretory urography and intravenous contrast enhancement of computed tomographic (CECT) head and body imaging.

ISOVUE-M (Iopamidol Injection) is indicated for intrathecal administration in neuroradiology including myelography (lumbar, thoracic, cervical, total columnar), and for contrast enhancement of computed tomographic (CECT) cisternography and ventriculography.

CONTRAINDICATIONS

ISOVUE (Iopamidol Injection)

None.

ISOVUE-M (Iopamidol Injection)

Intrathecal administration of corticosteroids with iopamidol is contraindicated. Because of overdosage considerations, immediate repeat myelography in the event of technical failure is contraindicated (see interval recommendation under DOSAGE AND ADMINISTRATION). Myelography should not be performed in the presence of significant local or systemic infection where bacteremia is likely.

WARNINGS

ISOVUE-M (Iopamidol Injection)

The need for myelographic examination should be carefully evaluated. Iopamidol should be administered with caution in patients with increased intracranial pressure or suspicion of intracranial tumor, abscess or hematoma, those with a history of convulsive disorder, severe cardiovascular disease, chronic alcoholism, or multiple sclerosis, and elderly patients. Particular attention must be given to state of hydration, concentration of medium, dose, and technique used in these patients.

If frankly bloody cerebrospinal fluid is observed, the possible benefits of a myelographic examination should be considered in terms of risk to the patient.

Patients on anticonvulsant medication should be maintained on this therapy.

Direct intracisternal or ventricular administration for standard radiography (without computerized tomographic enhancement) is not recommended. Inadvertent intracranial entry of a large or concentrated bolus of the contrast medium, which increases the risk of neurotoxicity, can be prevented by careful patient management. Also, effort should be directed to avoid rapid dispersion of the medium causing inadvertent rise to intracranial levels (e.g., by active patient movement). If such intracranial entry of the medium occurs, prophylactic anticonvulsant treatment with diazepam or barbiturates orally for 24 to 48 hours should be considered.

Use of medications that may lower the seizure threshold (phenothiazine derivatives, including those used for their antihistaminic properties; tricyclic antidepressants; MAO inhibitors; CNS stimulants; analeptics; antipsychotic agents) should be carefully evaluated. While the contributory role of such medications has not been established, some physicians have discontinued these agents at least 48 hours before and for at least 24 hours following intrathecal use.

Focal and generalized motor seizures have been reported after intrathecal use of water-soluble contrast agents including iopamidol. In several of those cases reported with iopamidol, higher than recommended doses were employed. Therefore *avoid:*

- Deviations from recommended neuroradiologic procedure or patient management.
- Use in patients with a history of epilepsy unless medically justified.
- Overdosage.
- Intracranial entry of a bolus or premature diffusion of a high concentration of the medium.
- Failure to maintain elevation of the head during the procedure, on the stretcher, and in bed.
- Excessive and particularly active patient movement or straining.

ISOVUE (Iopamidol Injection)

Caution must be exercised in patients with severely impaired renal function, those with combined renal and hepatic disease, or anuria particularly when larger doses are administered.

Radiopaque diagnostic contrast agents are potentially hazardous in patients with multiple myeloma or other paraproteinemia, particularly in those with therapeutically resistant anuria. Myeloma occurs most commonly in persons over age 40. Although neither the contrast agent nor dehydration has been proved separately to be the cause of anuria in myelomatous patients, it has been speculated that the combination of both may be causative. The risk in myelomatous patients is not a contraindication; however, special precautions are required.

Contrast media may promote sickling in individuals who are homozygous for sickle cell disease when injected intravenously or intraarterially.

Administration of radiopaque materials to patients known or suspected of having pheochromocytoma should be performed with extreme caution. If, in the opinion of the physician, the possible benefits of such procedures outweigh the considered risks, the procedures may be performed; however, the amount of radiopaque medium injected should be kept to an absolute minimum. The blood pressure should be assessed throughout the procedure and measures for treatment of a hypertensive crisis should be available. These patients should be monitored very closely during contrast-enhanced procedures.

Reports of thyroid storm following the use of iodinated radiopaque diagnostic agents in patients with hyperthyroidism or with an autonomously functioning thyroid nodule suggest that this additional risk be evaluated in such patients before use of any contrast medium.

PRECAUTIONS

General

Diagnostic procedures which involve the use of any radiopaque agent should be carried out under the direction of personnel with the prerequisite training and with a thorough knowledge of the particular procedure to be performed. Appropriate facilities should be available for coping with any complication of the procedure, as well as for emergency treatment of severe reaction to the contrast agent itself. After parenteral administration of a radiopaque agent, competent personnel and emergency facilities should be available for at least 30 to 60 minutes since severe delayed reactions may occur.

Preparatory dehydration is dangerous and may contribute to acute renal failure in patients with advanced vascular disease, diabetic patients, and in susceptible nondiabetic patients (often elderly with preexisting renal disease). *Patients should be well hydrated prior to and following iopamidol administration.*

The possibility of a reaction, including serious, life-threatening, fatal, anaphylactoid or cardiovascular reactions, should always be considered (see ADVERSE REACTIONS). Patients at increased risk include those with a history of a previous reaction to a contrast medium, patients with a known sensitivity to iodine per se, and patients with a known clinical hypersensitivity (bronchial asthma, hay fever, and food allergies). The occurrence of severe idiosyncratic reactions has prompted the use of several pretesting methods. However, pretesting cannot be relied upon to predict severe reactions and may itself be hazardous for the patient. It is suggested that a thorough medical history with emphasis on allergy and hypersensitivity, prior to the injection of any contrast medium, may be more accurate than pretesting in predicting potential adverse reactions. A positive history of allergies or hypersensitivity does not arbitrarily contraindicate the use of a contrast agent where a diagnostic procedure is thought essential, but caution should be exercised. Premedication with antihistamines or corticosteroids to avoid or minimize possible allergic reactions in such patients should be considered (see CONTRAINDICATIONS). Reports indicate that such pretreatment does not prevent serious life-threatening reactions, but may reduce both their incidence and severity.

General anesthesia may be indicated in the performance of some procedures in selected patients; however, a higher incidence of adverse reactions has been reported with radiopaque media in anesthetized patients, which may be attributable to the inability of the patient to identify untoward symptoms, or to the hypotensive effect of anesthesia which can reduce cardiac output and increase the duration of exposure to the contrast agent.

Even though the osmolality of iopamidol is low compared to diatrizoate or iothalamate based ionic agents of comparable iodine concentration, the potential transitory increase in the circulatory osmotic load in patients with congestive heart failure requires caution during injection. These patients should be observed for several hours following the procedure to detect delayed hemodynamic disturbances.

In angiographic procedures, the possibility of dislodging plaques or damaging or perforating the vessel wall should be borne in mind during catheter manipulations and contrast medium injection. Test injections to ensure proper catheter placement are suggested. Following arteriographic procedures, gentle pressure hemostasis is required, followed by observation and immobilization of the limb for several hours to prevent hemorrhage from the site of arterial puncture.

The inhibitory effects of nonionic contrast media on mechanisms of hemostasis have been shown, in vitro, to be less than ionic contrast media at comparable concentrations. For this reason, standard angiographic procedures should always be followed: angiographic catheters should be flushed frequently, and prolonged contact of blood with contrast in syringes and catheters should be avoided.

Selective coronary arteriography should be performed only in selected patients and those in whom the expected benefits outweigh the procedural risk. The inherent risks of angiocardiography in patients with chronic pulmonary emphysema must be weighed against the necessity for performing this procedure. Angiography should be avoided whenever possible in patients with homocystinuria, because of the risk of inducing thrombosis and embolism.

In addition to the general precautions previously described, special care is required when venography is performed in patients with suspected thrombosis, phlebitis, severe ischemic disease, local infection or a totally obstructed venous system.

Extreme caution during injection of contrast media is necessary to avoid extravasation and fluoroscopy is recommended. This is especially important in patients with severe arterial or venous disease.

If nondisposable equipment is used, scrupulous care should be taken to prevent residual contamination with traces of cleansing agents.

Information For Patients

Patients receiving injectable radiopaque diagnostic agents should be instructed to:

1. Inform your physician if you are pregnant.
2. Inform your physician if you are diabetic or if you have multiple myeloma, pheochromocytoma, homozygous sickle cell disease, or known thyroid disorder (see WARNINGS).
3. Inform your physician if you are allergic to any drugs, food, or if you had any reactions to previous injections of substances used for x-ray procedures (see PRECAUTIONS, General).
4. Inform your physician about any other medications you are currently taking, including nonprescription drugs, before you have this procedure.

Drug Interactions

Renal toxicity has been reported in a few patients with liver dysfunction who were given oral cholecystographic agents followed by intravascular contrast agents. Administration of intravascular agents should therefore be postponed in any patient with a known or suspected hepatic or biliary disorder who has recently received a cholecystographic contrast agent.

Other drugs should not be admixed with iopamidol.

Drug/Laboratory Test Interactions

The results of PBI and radioactive iodine uptake studies, which depend on iodine estimations, will not accurately reflect thyroid function for up to 16 days following administration of iodinated contrast media. However, thyroid function tests not depending on iodine estimations, e.g., T3 resin uptake and total or free thyroxine (T4) assays are not affected.

Any test which might be affected by contrast media should be performed prior to administration of the contrast medium.

Laboratory Test Findings

In vitro studies with animal blood showed that many radiopaque contrast agents, including iopamidol, produced a slight depression of plasma coagulation factors including prothrombin time, partial thromboplastin time, and fibrinogen, as well as a slight tendency to cause platelet and/or red blood cell aggregation (see PRECAUTIONS, General).

Transitory changes may occur in red cell and leucocyte counts, serum calcium, serum creatinine, serum glutamic oxalacetic transaminase (SGOT), and uric acid in urine; transient albuminuria may occur.

These findings have not been associated with clinical manifestations.

Carcinogenesis, Mutagenesis, Impairment Of Fertility

In animal reproduction studies performed on rats, intravenously administered iopamidol did not induce adverse effects on fertility or general reproductive performance.

In studies to determine mutagenic activity, iopamidol did not cause any increase in mutation rates.

Pregnancy Category B

No teratogenic effects attributable to iopamidol have been observed in teratology studies performed in animals. There are, however, no adequate and well controlled studies in pregnant women. It is not known whether iopamidol crosses the placental barrier or reaches fetal tissues. However, many injectable contrast agents cross the placental barrier in humans and appear to enter fetal tissues passively. Because animal teratology studies are not always predictive of human response, this drug should be used during pregnancy only if clearly needed.

Radiologic procedures involve a certain risk related to the exposure of the fetus to ionizing radiation.

Labor and Delivery

It is not known whether use of contrast agents during labor or delivery has immediate or delayed adverse effects on the fetus, prolongs the duration of labor or increases the likelihood that forceps delivery or other obstetrical intervention or resuscitation of the newborn will be necessary.

Nursing Mothers

It is not known whether iopamidol is excreted in human milk. However, many injectable contrast agents are excreted unchanged in human milk. Although it has not been established that serious adverse reactions occur in nursing infants, caution should be exercised when intravascular contrast media are administered to nursing women because of potential adverse reactions, and consideration should be given to temporarily discontinuing nursing.

Pediatric Use

Safety and effectiveness in children have not been established.

ADVERSE REACTIONS

ISOVUE (Iopamidol Injection)

Adverse reactions following the use of iopamidol are usually mild to moderate, self-limited, and transient.

In a clinical trial with 100 patients undergoing intra-arterial DSA, adverse reactions possibly attributed to ISOVUE-128 administration were nausea (2%), headache (1%) and vomiting (1%). One patient with preexisting renal impairment and severe bilateral renal vascular disease experienced renal failure, possibly secondary to a subsequent acute episode of congestive heart failure and/or drug administration (see Warnings).

In angiocardiography (597 patients), the adverse reactions with an estimated incidence of one percent or higher are: hot flashes 3.4%; angina pectoris 3.0%; flushing 1.8%; bradycardia 1.3%; hypotension 1.0%; hives 1.0%.

Intravascular injection of contrast media is frequently associated with the sensation of warmth and pain, especially in peripheral arteriography and venography; pain and warmth are less frequent and less severe with ISOVUE (Iopamidol Injection) than with diatrizoate meglumine and diatrizoate sodium injection.

The following table of incidence of reactions is based on clinical studies with ISOVUE in about 1941 patients.

Adverse Reactions

System	Estimated Overall Incidence > 1%	≤ 1%
Cardiovascular	none	tachycardia hypotension hypertension myocardial ischemia circulatory collapse S-T segment depression bigeminy extrasystoles ventricular fibrillation angina pectoris bradycardia transient ischemic attack thrombophlebitis
Nervous	pain (2.8%) burning sensation (1.4%)	vasovagal reaction tingling in arms grimace faintness
Digestive	nausea (1.2%)	vomiting anorexia
Respiratory	none	throat constriction dyspnea pulmonary edema
Skin and Appendages	none	rash urticaria pruritus flushing
Body as a Whole	hot flashes (1.5%)	headache fever chills excessive sweating back spasm
Special Senses	warmth (1.1%)	taste alterations nasal congestion visual disturbances
Urogenital	none	urinary retention

Regardless of the contrast agent employed, the overall estimated incidence of serious adverse reactions is higher with *coronary arteriography* than with other procedures. Cardiac decompensation, serious arrhythmias, or myocardial ischemia or infarction may occur during *coronary arteriography and left ventriculography.* Following coronary and ventricular injections, certain electrocardiographic changes (increased QTc, increased R-R, T-wave amplitude) and certain hemodynamic changes (decreased systolic pressure) occurred less frequently with ISOVUE (Iopamidol Injection) than with diatrizoate meglumine and diatrizoate sodium injection; increased LVEDP occurred less frequently after ventricular iopamidol injections.

In *aortography,* the risks of procedures also include injury to the aorta and neighboring organs, pleural puncture, renal damage including infarction and acute tubular necrosis with oliguria and anuria, accidental selective filling of the right renal artery during the translumbar procedure in the presence of preexisting renal disease, retroperitoneal hemorrhage from the translumbar approach, and spinal cord injury and pathology associated with the syndrome of transverse myelitis.

Adverse effects reported in clinical literature for iopamidol include arrhythmia, arterial spasms, hematuria, periorbital edema, involuntary leg movement, malaise, and triggering of deglutition; some of these may occur as a consequence of the procedure. Other reactions may also occur with the use of any contrast agent as a consequence of the procedural hazard; these include hemorrhage or pseudoaneurysms at the puncture site, brachial plexus palsy following axillary artery injections, chest pain, myocardial infarction, and transient changes in hepatorenal chemistry tests. Arterial thrombosis, displacement of arterial plaques, venous thrombosis, dissection of the coronary vessels and transient sinus arrest are rare complications.

ISOVUE-M (Iopamidol Injection)

The most frequently reported adverse reactions following intrathecal administration of iopamidol are headache, nausea, vomiting and musculoskeletal pain. These reactions usually occur 1 to 10 hours after injection, almost all occurring within 24 hours. They are usually mild to moderate in degree lasting for a few hours and usually disappearing within 24 hours. Rarely, headaches may be severe or persist for days. Headache is often accompanied by nausea and vomiting, and tends to be more frequent and persistent in patients not optimally hydrated.

Backache, neck stiffness, numbness and paresthesias, leg or sciatic-type pain occurred less frequently, often in the form of a transient exacerbation of preexisting symptomatology. Transient alterations in vital signs may occur and their significance must be assessed on an individual basis.

The following table of incidence of reactions is based on clinical studies with ISOVUE-M (Iopamidol Injection) in about 615 patients.

Adverse Reactions

System	Estimated Overall Incidence > 1%	≤ 1%
Body as a Whole	headache (18.1%)	pyrexia muscle weakness hot flashes malaise fatigue weakness
Digestive	nausea (7.3%) vomiting (3.7%)	diarrhea heartburn
Musculoskeletal	back pain (2.3%) leg pain (1.4%) neck pain (1.1%)	leg cramps sciatica cervicobrachial irritation meningeal irritation radicular irritation, lumbosacral other musculoskeletal pain involuntary movement burning sensation
Cardiovascular	hypotension (1.1%)	tachycardia hypertension chest pain
Nervous	none	emotional stress dizziness paresthesia confusion hallucinations lightheadedness syncope numbness cold extremities
Urogenital	none	urinary retention
Respiratory	none	dyspnea
Skin and Appendages	none	rash
Miscellaneous	none	injection site pain

Other adverse effects reported in clinical literature for iopamidol include facial neuralgia, tinnitus, and sweating.

Major motor seizures have been reported in the clinical literature and since market introduction in the United States. Early onset of seizures (less than two hours) is indicative of early substantial intracranial entry. Transitory EEG changes occur and usually take the form of slow wave activity.

While not observed in controlled clinical studies with ISOVUE-M (Iopamidol Injection), or reported in clinical literature, the following adverse reactions may occur because they have been reported with other nonionic contrast agents: cardiovascular (arrhythmias); aseptic meningitis syndrome; allergy or idiosyncrasy (chills, pruritus, nasal congestion, Guillain-Barre syndrome); CNS irritation (psycho-organic syndrome: mild and transitory perceptual aberrations such as depersonalization, anxiety, depression, hyperesthesia, disturbances in speech, sight, or hearing, and disorientation; in addition, hyperreflexia or areflexia, hypertonia or flaccidity, restlessness, tremor, echoacousia, echolalia, asterixis or dysphasia have occurred). Profound mental disturbances have rarely been reported (various forms and degrees of aphasia, mental confusion or disorientation); the onset is usually at 8 to 10 hours and lasts for about 24 hours without aftereffects.

However, occasionally they have been manifest as apprehension, agitation, or progressive withdrawal to the point of stupor in several instances. In a few cases, these have been accompanied by transitory hearing loss or other auditory symptoms and visual disturbances (believed subjective or delusional). Persistent cortical loss of vision in association with convulsions, and ventricular block have been reported. Rarely, persistent though transitory weakness in the leg or ocular muscles has been reported. *Peripheral neuropathies* have been rare and transitory. They include sensory and/or motor or nerve root disturbances, myelitis, persistent leg muscle pain or weakness, or sixth nerve palsy, or cauda equina syndrome. Muscle cramps, fasciculation or myoclonia, spinal convulsion, or spasticity are unusual.

General Adverse Reactions To Contrast Media

Reactions known to occur with parenteral administration of iodinated ionic contrast agents (see the listing below) are possible with any nonionic agent. Approximately 95 percent of adverse reactions accompanying the use of other water-soluble intravascularly administered contrast agents are mild to moderate in degree. However, life-threatening reactions and fatalities, mostly of cardiovascular origin, have occurred.

Reported incidences of death from the administration of other iodinated contrast media range from 6.6 per 1 million (0.00066 percent) to 1 in 10,000 patients (0.01 percent). Most deaths occur during injection or 5 to 10 minutes later, the main feature being cardiac arrest with cardiovascular disease as the main aggravating factor. Isolated reports of hypotensive collapse and shock are found in the literature. The incidence of shock is estimated to be 1 out of 20,000 (0.005 percent) patients.

Adverse reactions to injectable contrast media fall into two categories: chemotoxic reactions and idiosyncratic reactions. Chemotoxic reactions result from the physico-chemical properties of the contrast medium, the dose, and the speed of injection. All hemodynamic disturbances and injuries to organs or vessels perfused by the contrast medium are included in this category. Experience with iopamidol suggests there is much less discomfort (e.g., pain and/or warmth) with peripheral arteriography. Fewer changes are noted in ventricular function after ventriculography and coronary arteriography.

Idiosyncratic reactions include all other reactions. They occur more frequently in patients 20 to 40 years old. Idiosyncratic reactions may or may not be dependent on the amount of drug injected, the speed of injection, the mode of injection, and the radiographic procedure. Idiosyncratic reactions are subdivided into minor, intermediate, and severe. The minor reactions are self-limited and of short duration; the severe reactions are life-threatening and treatment is urgent and mandatory.

The reported incidence of adverse reactions to contrast media in patients with a history of allergy is twice that for the general population. Patients with a history of previous reactions to a contrast medium are three times more susceptible than other patients. However, sensitivity to contrast media does not appear to increase with repeated examinations. Most adverse reactions to intravascular contrast agents appear within one to three minutes after the start of injection, but delayed reactions may occur (see PRECAUTIONS, General).

Because measurable plasma levels are attained following the intrathecal administration of iopamidol, adverse reactions reported with the use of intravascular contrast agents are theoretically possible. In addition to the adverse drug reactions reported for iopamidol, the following additional adverse reactions have been reported with the use of other intravascular contrast agents and are possible with the use of any water-soluble iodinated contrast agent:

Cardiovascular: vasodilation, cerebral hematomas, petechiae, hemodynamic disturbances, sinus bradycardia, transient electrocardiographic abnormalities, ventricular fibrillation.

Digestive: nausea, vomiting, severe unilateral or bilateral swelling of the parotid and submaxillary glands.

Nervous: paresthesia, dizziness, convulsions, paralysis, coma.

Respiratory: increased cough, asthma, laryngeal edema, pulmonary edema, bronchospasm, rhinitis, dyspnea.

Skin and Appendages: injection site pain usually due to extravasation and/or erythematous swelling, skin necrosis.

Urogenital: osmotic nephrosis of proximal tubular cells, renal failure, pain.

Special Senses: bilateral ocular irritation; lacrimation; conjunctival chemosis, infection, and conjunctivitis; itching.

The following reactions may also occur: neutropenia, thrombophlebitis, flushing, pallor, weakness, severe retching and choking, wheezing, cramps, tremors, and sneezing.

HOW SUPPLIED

ISOVUE-128: 10 x 50 mL vials; ISOVUE-200: 10 x 50 mL vials and 10 x 100 mL bottles; ISOVUE-300: 10 x 50 mL vials and 10 x 100 mL bottles and 10 x 150 mL bottles; ISOVUE-370: 10 x 50 mL vials and 10 x 100 mL, 10 x 150 mL and 10 x 200 mL bottles; ISOVUE-M 200: 10 x 20 mL vials; ISOVUE-M 300: 10 x 15 mL vials.

STORAGE

ISOVUE® and ISOVUE-M® (iopamidol injection) should be stored at room temperature not exceeding 86° F. Protect from light.

For full prescribing information consult package insert.

J3-702A/J3-652E/J3-653E.

© 1987 E.R. Squibb & Sons, Inc., Princeton, NJ 647-508 Issued: November 1987

Head, shoulders, spine & body above the rest

Signa... the reference point in MR

Success in MR depends on having a system that can do it all. And from head to toe, the Signa® system delivers.

Excellent image quality. Comprehensive applications. High throughput. And continuing development of advanced software and hardware that keeps Signa sites the community leaders in MR.

A head start

Right from the top, Signa imaging gives you a distinct advantage. Many Signa users report that, on the average, a complete high resolution head study takes only 30 minutes.

Image courtesy of University Diagnostic Institute, Tampa, FL.

Signa enables you to routinely combine single excitation imaging with small FOVs and thin slices to get superb resolution and contrast —quickly. Which is one reason why Signa sites typically build a strong neurological referral base—very quickly.

The backbone of referral strength

Signa MR imaging provides superior visualization of spine anatomy.

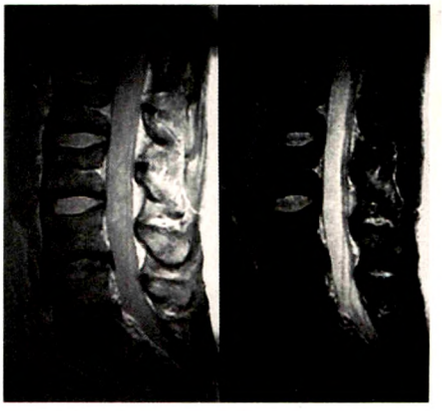

Oblique multi-slice, multi-angle acquisitions mean greater diagnostic sensitivity and efficiency, particularly in the lumbar spine.

Important to
oth lumbar and
ervical spine
udies is the
myelographic
ffect"—easily
chieved with
igna's stan-
ard fast scan
nd flow com-
ensation tech-
iques, and
ith the
eripheral
ating option.

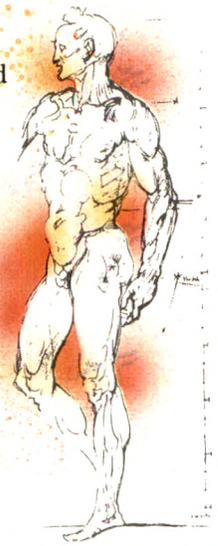

Extraordinary extremities

Orthopedic studies are among
ne fastest growing applications at
igna sites. For good reason. Signa
urface coils can provide submilli-
meter resolution images of the
nee, TMJ or shoulder in less than

age courtesy of Sunrise Diagnostic Center, Las Vegas, NV.

0 minutes. Minute changes in
natomy—rotator cuff and
meniscal tears, TMJ derangements,
nd collateral ligament disease—
an be clearly visualized due to
igna's high sensitivity and ability
o perform small, off-center FOV
naging.

A growing body of work

Excellent body studies have become a clinical reality for Signa users, due to innovative new motion compensation software.

Image courtesy of Diagnostic Imaging, Chattanooga, TN.

This software includes new blood flow compensation pulse sequences that virtually eliminate artifacts caused by pulsatile blood flow—without increasing acquisition time. And EXORCIST pulse sequences that keep respiratory motion artifacts to a minimum.

These advancements enhance Signa's already excellent contrast and spatial resolution for detailed studies of the liver, kidneys, vasculature and genitourinary tract.

A continuum of excellence

Our recent innovations in body imaging are just one example of other Signa applications to come, including MR angiography*, cine cardiac* and routine spectroscopy.*

From head studies that helped establish the diagnostic power of MR to new applications that will determine its future, Signa continues to be the leader in MR.

For more information about the Signa system, please call GE Medical Systems:

(800) 624-5692.

*These Signa system features are currently classified as investigational and limited by federal law to investigational use. As such, they cannot be made commercially available until necessary government approvals are granted.

CIRCLE 3 ON READER SERVICE CARD

GE Medical Systems

CLEAR-Pb® * MOBILE X-RAY BARRIERS
...great performance never looked so good!

A complete family of **CLEAR-Pb** Lead-Plastic Mobile X-Ray Barriers... the most extensive line of its kind ever produced.

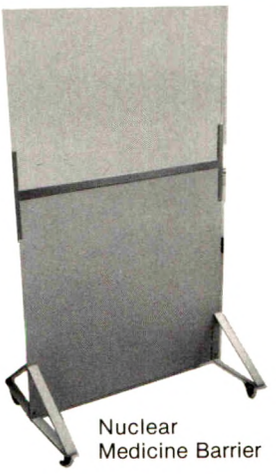

Nuclear Medicine Barrier

CLEAR-Pb Mobile X-Ray Barriers offer you total body protection from secondary radiation in radiology suites, O.R.'s and Special Procedures rooms. You'll also find them in cardiac cath rooms, as well as in mammographic, nuclear medicine and dental suites.

Our lead-impregnated, transparent plastic viewing panels are crystal-clear and shatter-resistant...perfect for mobile unit use. A choice of lead equivalencies and a wide variety of sizes lets you select the correct size to meet the needs of *your* department. Shield one, two or more people the easy way!

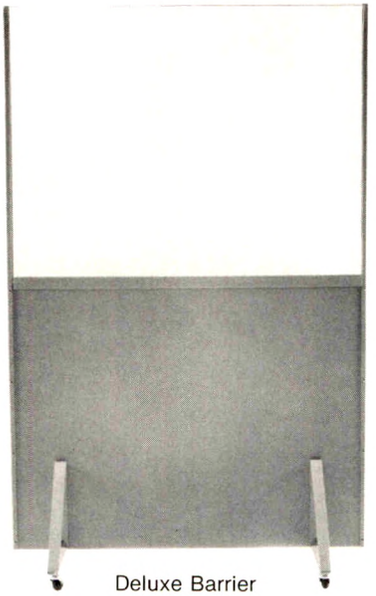

Deluxe Barrier

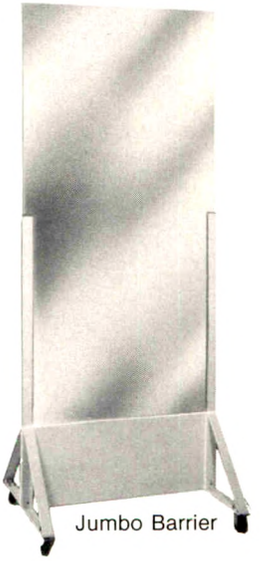

Jumbo Barrier

The Winning Combination: Total-body Shielding and Panoramic Visibility!

The distortion-free clarity and generous size of each CLEAR-Pb viewing panel provides you with exceptional visibility over a wide field of view. Patient and equipment can be seen at a glance, and the large viewing area puts patients at ease, too. No more need to put up with tiny, lead-glass viewing windows. Today's look is attractive, spacious, open, thanks to the versatility of CLEAR-Pb Lead-Plastic.

Need more details?
We have them. Request Bulletin 3225-44

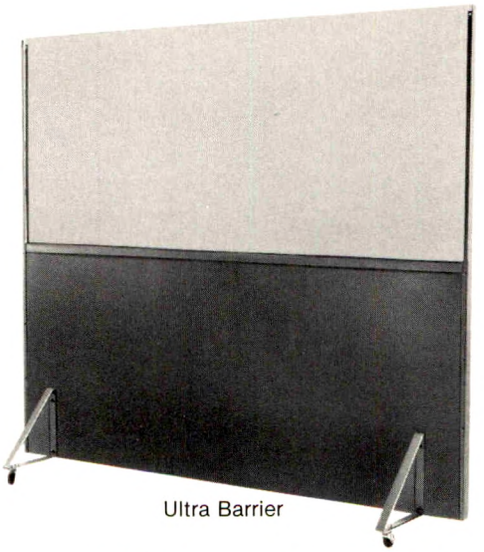

Ultra Barrier

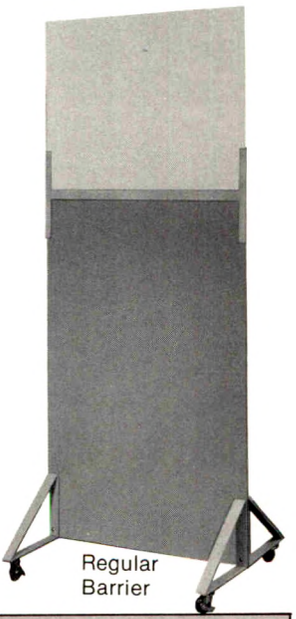

Regular Barrier

NUCLEAR ASSOCIATES

VICTOREEN

A Division of VICTOREEN, INC.
100 VOICE ROAD
CARLE PLACE, NY 11514-1593
(516) 741-6360
A Subsidiary of Sheller-Globe SG

CIRCLE 16 ON READER SERVICE CARD

®VICTOREEN, Inc. *U.S. Patents 4,129,524 and 4,182,821

FOR TOTAL BODY SHIELDING, THE CLEAR CHOICE IS CLEAR-Pb

Evac-Q-Kwik advantages are as clear as the X-ray you get.

Use this checklist to compare other bowel preps:

	EVAC-Q-KWIK	Other Preps
Taste	Pleasant, cherry flavor	
Fluid intake	40 fl oz	
Reconstitution	No	
Enema	No	
Cost	Low	
Adminstration time	6 hours	
Sugar	No	
Alcohol	No	
Sodium content	Low	

Evac-Q-Kwik thoroughly cleans the colon. Patients arrive ready for X-ray. No staff time or extra prepping needed. One take is all—virtually every time. This means better work flow, cost containment and patient comfort.

Everything is in the kit, including easy-to-follow instructions. No mixing, no enemas, no alcohol, no sugar, low sodium… and low cost. Easy to use for better compliance.

Seeing is believing. Give Evac-Q-Kwik a trial.

There's more.

Take advantage of our service materials:
☐ Inservice film for nurses ☐ Multi-language instruction sheets ☐ Radiology work sheets ☐ "What to expect" booklet for patients. Ask your Adria Representative, or drop us a line. Adria Laboratories, Columbus, Ohio 43215.

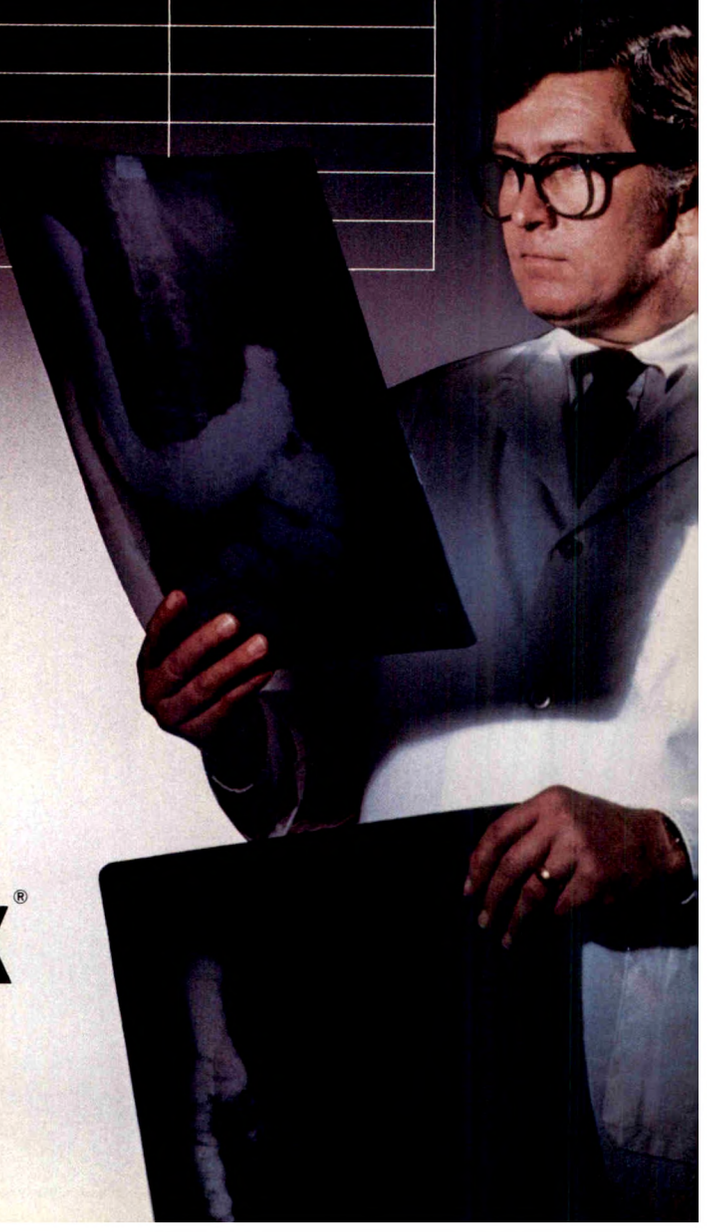

Evac-Q-Kwik®

Clean colon, clear advantages.

Adria®

Adria Laboratories
Columbus, OH 43215

There are reasons
S.&S. X-RAY ACCESSORIES
are preferred...

PROVEN the best in X-Ray Departments throughout the world

UNEQUALLED in design, construction and—quality

REPUTATION unmatched for RELIABILITY and PERFORMANCE

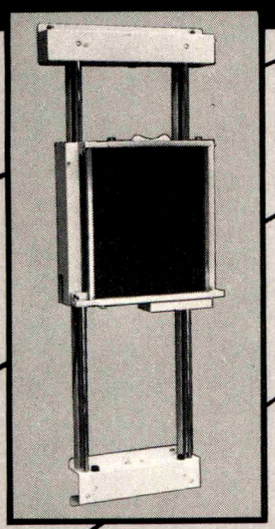

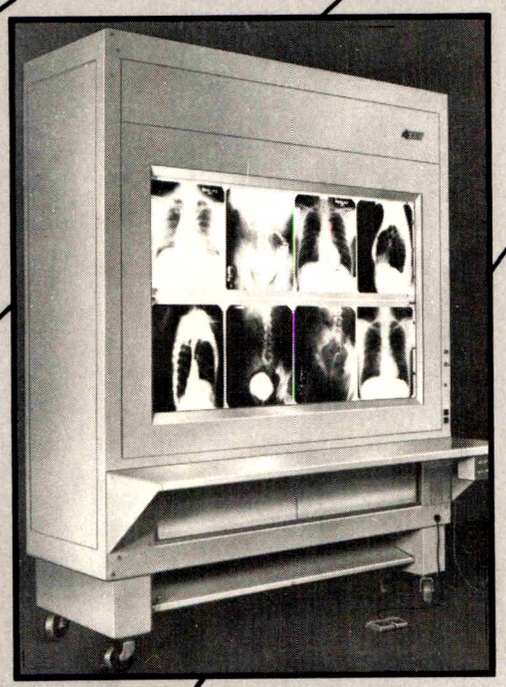

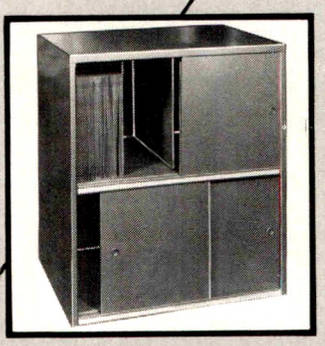

- Motorized Viewers
- Illuminators
- Transfer Cabinets
- File Cabinets
- Protective Panels
- Protective Aprons
- Wall Cassette Holders
- Dryers
- Safelights
- Dark Room Cabinets
- Storage Chests
- Loading Bins
- X-Ray Accessories

For more than 30 years, S. & S. has been meeting Radiologists' needs with a complete line of illuminators and accessories.

Contact S. & S. or your local x-ray dealer for additional information.

MANUFACTURED BY
S. & S. X-RAY PRODUCTS INC.

The Complete Line of X-Ray Accessories
Call Toll Free: 800-221-6634

Telephone: 718-649-8500
1101 LINWOOD STREET, BROOKLYN, NY 11208

CIRCLE 9 ON READER SERVICE CARD

The image of safety.

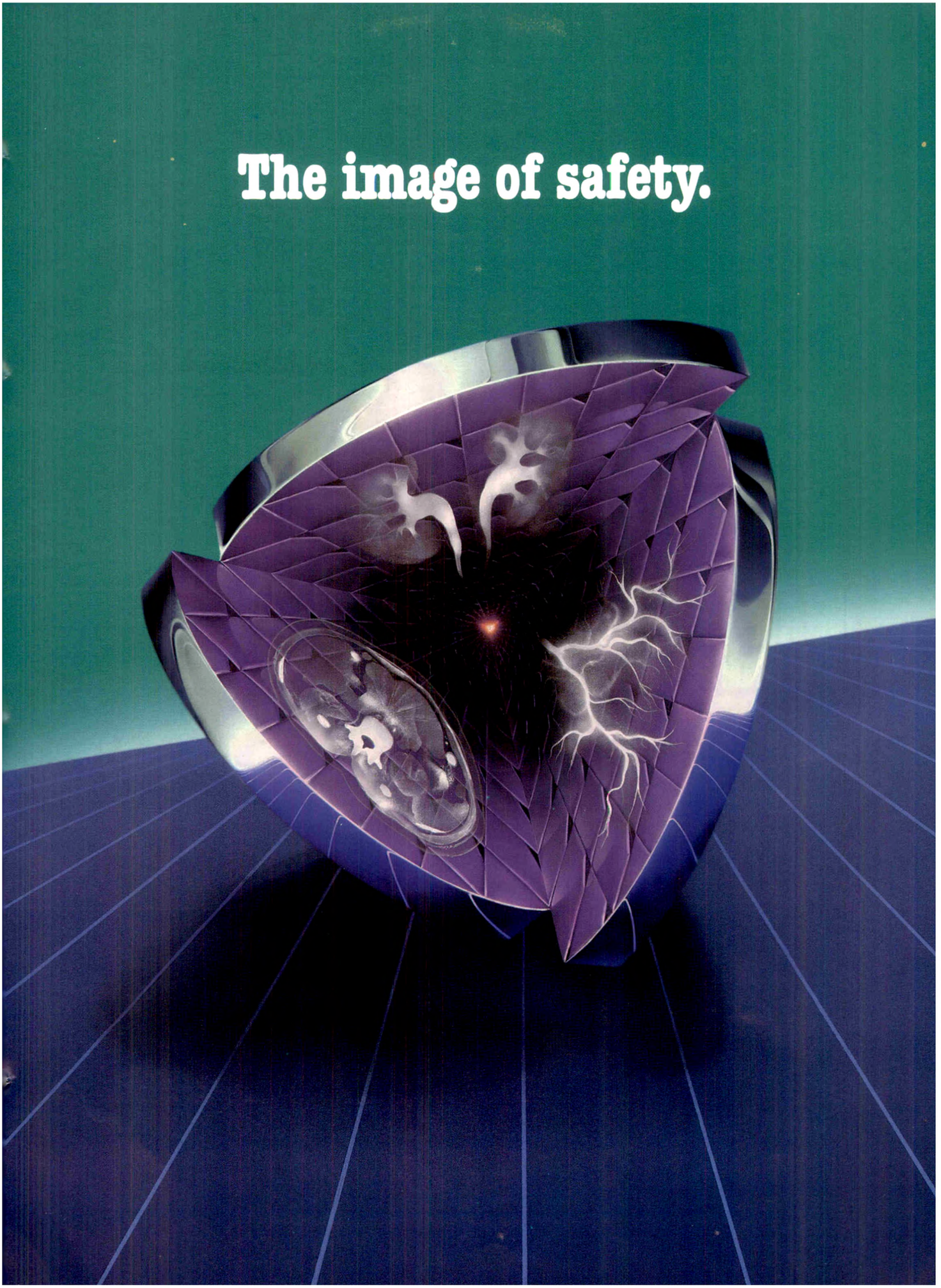

The image of safety in radiographic procedures.

In radiographic contrast procedures, you ask a lot of the contrast agent you use.

Safety.
Imaging performance.
Patient comfort and tolerance.

Experience with OMNIPAQUE in clinical use and trials continues to demonstrate its unique combination of lowest chemotoxicity and low osmolality, providing the best of all three.

CT of lumbar spine with OMNIPAQUE

NONIONIC

OMNIPAQUE®

(IOHEXOL)

An ongoing record of safety in radiographic procedures.

See next page for important product information concerning contraindications, warnings, adverse reactions, patient selection, and prescribing and precautionary recommendations.

OMNIPAQUE® 180 240 300 350

INJECTION (IOHEXOL)
INTRATHECAL/INTRAVASCULAR

PLEASE CONSULT FULL PRODUCT INFORMATION BEFORE USING.
A SUMMARY FOLLOWS:

DESCRIPTION: OMNIPAQUE is a nonionic, water-soluble radiographic contrast medium for intrathecal and intravascular administration and is provided in iodine concentrations of 180, 240, 300, and 350 mgI/mL. Each milliliter of iohexol solution contains 1.21 mg tromethamine and 0.1 mg edetate calcium disodium with the pH adjusted between 6.8 and 7.7 with hydrochloric acid or sodium hydroxide, but it contains no preservatives.

CONTRAINDICATIONS: OMNIPAQUE should not be administered to patients with a known hypersensitivity to iohexol. Myelography should not be performed in the presence of significant local or systemic infection where bacteremia is likely. Intrathecal administration of corticosteroids with OMNIPAQUE is contraindicated. Because of the possibility of overdosage, immediate repeat myelography in the event of technical failure is contraindicated.

WARNINGS—Intrathecal: If grossly bloody CSF is encountered, the possible benefits of a myelographic procedure should be considered in terms of the risk to the patient. Caution is advised in elderly patients and in patients with a history of epilepsy, severe cardiovascular disease, chronic alcoholism, or multiple sclerosis.

Patients who are receiving anticonvulsants should be maintained on this therapy. Should a seizure occur, intravenous diazepam or phenobarbital sodium is recommended. In patients with a history of seizure activity who are not on anticonvulsant therapy, premedication with barbiturates should be considered.

Prophylactic anticonvulsant treatment with barbiturates should be considered in patients with evidence of inadvertent intracranial entry of a large or concentrated bolus of the contrast medium since there may be an increased risk of seizure in such cases.

Drugs which lower the seizure threshold, especially phenothiazine derivatives, including those used for their antihistamine properties, are not recommended for use with OMNIPAQUE. Others include MAO inhibitors, tricyclic antidepressants, CNS stimulants, and psychoactive drugs described as analeptics, major tranquilizers, or anti-psychotic drugs. While the contributory role of these medications has not been established, the use of such drugs should be based on physician evaluation of potential benefits and potential risks. Physicians have discontinued these agents at least 48 hours before and for at least 24 hours postprocedure.

Care is required in patient management to prevent inadvertent intracranial entry of a large dose or concentrated bolus of the medium. Also, effort should be directed to avoid rapid dispersion of the medium causing inadvertent rise to intracranial levels (eg, by active patient movement). Direct intracisternal or ventricular administration for standard radiography (not CT) is not recommended.

In most reported cases of major motor seizures with nonionic myelographic media, one or more of the following factors were present. Therefore avoid: deviations from recommended procedure or in myelographic management; use in patients with a history of epilepsy; overdosage; intracranial entry of a bolus or premature diffusion of a high concentration of the medium; medication with neuroleptic drugs or phenothiazine antinauseants; failure to maintain elevation of the head during the procedure, on the stretcher, or in bed; and excessive and particularly active patient movement or straining.

Intravascular: OMNIPAQUE should be used with extreme care in patients with severe functional disturbances of the liver and kidneys, severe thyrotoxicosis, or myelomatosis. Diabetics with a serum creatinine level above 3 mg/dL should not be examined unless the possible benefits of the examination clearly outweigh the additional risk. OMNIPAQUE is not recommended for use in patients with anuria.

Radiopaque contrast agents are potentially hazardous in patients with multiple myeloma or other paraproteinemia, particularly in those with therapeutically resistant anuria. Although neither the contrast agent nor dehydration has separately proven to be the cause of anuria in myeloma, it has been speculated that the combination of both may be causative factors. The risk in myelomatous patients is not a contraindication; however, special precautions are necessary. Partial dehydration in the preparation of these patients prior to injection is not recommended since this may predispose the patient to precipitation of the myeloma protein in the renal tubules. No form of therapy, including dialysis, has been successful in reversing the effect. Myeloma, which occurs most commonly in persons over age 40, should be considered before instituting intravascular administration of contrast agents.

Ionic contrast media, when injected intravenously or intra-arterially, may promote sickling in individuals who are homozygous for sickle cell disease.

Administration of radiopaque materials to patients known or suspected of having pheochromocytoma should be performed with extreme caution. If, in the opinion of the physician, the possible benefits of such procedures outweigh the considered risks, the procedures may be performed; however, the amount of radiopaque medium injected should be kept to an absolute minimum. The patient's blood pressure should be assessed throughout the procedure and measures for the treatment of hypertensive crisis should be readily available.

Reports of thyroid storm following the use of iodinated, ionic radiopaque contrast media in patients with hyperthyroidism or with an autonomously functioning thyroid nodule suggest that this additional risk be evaluated in such patients before use of any contrast medium.

Urography should be performed with caution in patients with severely impaired renal function and patients with combined renal and hepatic disease.

PRECAUTIONS: Diagnostic procedures that involve the use of radiopaque diagnostic agents should be carried out under the direction of personnel with the prerequisite training and with a thorough knowledge of the particular procedure to be performed. Appropriate facilities should be available for coping with any complication of the procedure, as well as for emergency treatment of severe reactions to the contrast agent itself. Competent personnel and emergency facilities should be available since severe delayed reactions have occurred. The possibility of serious, life-threatening, fatal, anaphylactoid, or cardiovascular reactions should always be considered (see ADVERSE REACTIONS). It is of utmost importance that a course of action be carefully planned in advance for immediate treatment of serious reactions. Preparatory dehydration is dangerous and may contribute to acute renal failure in patients with advanced vascular disease, in diabetic patients, and in susceptible nondiabetic patients (often elderly with preexisting renal disease). *Patients should be well hydrated prior to and following iohexol administration.* Careful consideration to the potential risk of acute renal failure should be given before performing excretory urography in diabetic patients with diabetic nephropathy and in susceptible nondiabetic patients (often elderly with preexisting renal disease). Immediately following surgery, excretory urography should be used with caution in renal transplant recipients. In patients with severe renal insufficiency or failure, compensatory biliary excretion of the drug is anticipated to occur, with a slow clearance into the bile. Patients with hepatorenal insufficiency should not be examined unless the possibility of benefit clearly outweighs the additional risk. The possibility of an idiosyncratic reaction in susceptible patients should always be considered (see ADVERSE REACTIONS). The susceptible population includes patients with a history of a previous reaction to contrast media, patients with a known sensitivity to iodine per se, and patients with a known clinical hypersensitivity: bronchial asthma, hay fever, and food allergies. A thorough medical history with emphasis on allergy and hypersensitivity, prior to the injection of any contrast media, may be more accurate than pretesting in predicting potential adverse reactions.

A positive history of allergies or hypersensitivity does not arbitrarily contraindicate the use of a contrast agent where a diagnostic procedure is thought essential, but caution should be exercised (see ADVERSE REACTIONS). Premedication with antihistamines or corticosteroids to avoid or minimize possible allergic reactions in such patients should be considered and administered using separate syringes. Recent reports indicate that such pretreatment does not prevent serious, life-threatening reactions but may reduce both their incidence and severity.

Even though the osmolality of OMNIPAQUE is low compared to diatrizoate- or iothalamate-based ionic agents of comparable iodine concentration, the potential transitory increase in circulatory osmotic load in patients with congestive heart failure requires caution during injection. These patients should be observed for several hours following the procedure to detect delayed hemodynamic disturbances.

General anesthesia may be indicated in the performance of some procedures in selected adult patients; however, a higher incidence of adverse reactions has been reported in these patients, and may be attributable to the inability of the patient to identify untoward symptoms or to the hypotensive effect of the anesthesia which can reduce cardiac output and increase the duration of exposure to the contrast agent.

Angiography should be avoided whenever possible in patients with homocystinuria, because of the risk of inducing thrombosis and embolism.

In angiographic procedures, the possibility of dislodging plaques or damaging or perforating the vessel wall should be borne in mind during the catheter manipulations and contrast medium injection. Test injections to ensure proper catheter placement are recommended.

Selective coronary arteriography should be performed only in those patients in whom the expected benefits outweigh the potential risk. The inherent risks of angiocardiography in patients with chronic pulmonary emphysema must be weighed against the necessity for performing this procedure.

When OMNIPAQUE is to be injected using plastic disposable syringes, the contrast medium should be drawn into the syringe and used immediately.

The inhibitory effects of nonionic contrast media on mechanisms of hemostasis have been shown, in vitro, to be less than those of ionic contrast media at comparable concentrations. For this reason, standard angiographic procedures should always be followed; angiographic catheters should be flushed frequently, and prolonged contact of blood with contrast media in syringes and catheters should be avoided.

If nondisposable equipment is used, scrupulous care should be taken to prevent residual contamination with traces of cleansing agents.

Parenteral products should be inspected and discarded if particulate matter or discoloration is present.

Drug Interactions: Drugs which lower seizure threshold, especially phenothiazine derivatives including those used for their antihistaminic or antinauseant properties, are not recommended for use with OMNIPAQUE 180, OMNIPAQUE 240, or OMNIPAQUE 300. Others include monoamine oxidase (MAO) inhibitors, tricyclic antidepressants, CNS stimulants, psychoactive drugs described as analeptics, major tranquilizers, or antipsychotic drugs. Such medications should be discontinued at least 48 hours before myelography, should not be used for the control of nausea or vomiting during or after myelography, and should not be resumed for at least 24 hours postprocedure. In nonelective procedures in patients on these drugs, consider prophylactic use of anticonvulsants.

Drug/Laboratory Test Interaction: If iodine-containing isotopes are to be administered for the diagnosis of thyroid disease, the iodine-binding capacity of thyroid tissue may be reduced for up to 2 weeks after contrast medium administration. Thyroid function tests which do not depend on iodine estimation, eg, T_3 resin uptake or direct thyroxine assays, are not affected. Many radiopaque contrast agents are incompatible in vitro with some antihistamines and many other drugs, therefore, no other pharmaceuticals should be admixed with contrast agents.

Carcinogenesis, Mutagenesis, Impairment of Fertility: No long-term animal studies have been performed to evaluate carcinogenic potential, mutagenesis, or whether OMNIPAQUE can affect fertility in men or women.

Pregnancy Category B: Reproduction studies have been performed in rats and rabbits with up to 100 times the recommended human dose. No evidence of impaired fertility or harm to the fetus has been demonstrated due to OMNIPAQUE. There are, however, no studies in pregnant women. Because animal reproduction studies are not always predictive of human response, this drug should be used during pregnancy only if clearly needed.

Nursing Mothers: It is not known to what extent iohexol is excreted in human milk. However, many injectable contrast agents are excreted unchanged in human milk. Although it has not been established that serious adverse reactions occur in nursing infants, caution should be exercised when intravascular contrast media are administered to nursing women. Bottle feedings may be substituted for breast feedings for 24 hours following administration of OMNIPAQUE * injection (iohexol).

Pediatric Use: Safety and effectiveness in children have not been established.

ADVERSE REACTIONS—Intrathecal: The most frequently reported adverse reactions with OMNIPAQUE 180, OMNIPAQUE 240, and OMNIPAQUE 300 are headache, mild to moderate pain including backache, neckache and stiffness, nausea, and vomiting. These reactions usually occur 1 to 10 hours after injection, and almost all occur within 24 hours. They are usually mild to moderate in degree, lasting for a few hours, and usually disappearing within 24 hours. Rarely, headaches may be severe or persist for days. Headache is often accompanied by nausea and vomiting and tends to be more frequent and persistent in patients not optimally hydrated.

Transient alterations in vital signs may occur and their significance must be assessed on an individual basis. Those reactions reported in clinical studies with OMNIPAQUE are listed below in decreasing order of occurrence, based on clinical studies of 1,531 patients.

Headaches: The most frequently occurring adverse reaction following myelography has been headache, with an incidence of approximately 18%. Headache may be caused by either a direct effect of the contrast medium or by CSF leakage at the dural puncture site. However, in managing the patient, it is considered more important to minimize intracranial entry of contrast medium by postural management than attempting to control possible CSF leakage.

Pain: Mild to moderate pain including backache, neckache and stiffness, and neuralgia occurred following injection, with an incidence of about 8%.

Nausea and Vomiting: Nausea was reported with an incidence of about 6%, and vomiting about 3%. Maintaining normal hydration is very important. The use of phenothiazine antinauseants is not recommended. Reassurance to the patient that the nausea will clear usually is all that is required.

Dizziness: Transient dizziness was reported in about 2% of the patients.

Other Reactions: Other reactions occurring with an individual incidence of less than 0.1% included: feeling of heaviness, hypotension, hypertonia, sensation of heat, sweating, vertigo, loss of appetite, drowsiness, hypertension, photophobia, tinnitus, neuralgia, paresthesia, difficulty in micturition, and neurological changes. All were transient and mild with no clinical sequelae.

Intravascular: Adverse reactions following the use of OMNIPAQUE 240, OMNIPAQUE 300, and OMNIPAQUE 350 are usually of mild to moderate severity. However, serious, life-threatening and fatal reactions, mostly of cardiovascular origin, have been associated with the administration of iodine-containing contrast media, including OMNIPAQUE. The injection of contrast media is frequently associated with the sensation of warmth and pain, especially in peripheral angiography; pain and warmth are less frequent and less severe with OMNIPAQUE than with many contrast media.

Cardiovascular System: Arrhythmias including PVCs and PACs (2%), angina/chest pain (1%), and hypotension (0.8%). Others including cardiac failure, asystole, bradycardia, tachycardia and vasovagal reaction were reported with an individual incidence of less than 0.4%. In controlled clinical trials involving 1,213 patients, one fatality occurred. A cause and effect relationship between this death and iohexol has not been established.

Nervous System: Vertigo [including dizziness and lightheadedness] (0.7%), pain (3%), photomas (2%), headache (2%), and taste perversion (1%). Others including anxiety, blurred vision, fever, motor and speech dysfunction, convulsion, paresthesia, somnolence, stiff neck, hemiparesis, and nystagmus were reported, with an individual incidence of less than 0.3%.

Respiratory System: Dyspnea and laryngitis, with an individual incidence of 0.1%.

Gastrointestinal System: Nausea (2%) and vomiting (0.6%). Others including diarrhea, dyspepsia, and dry mouth were reported, with an individual incidence of less than 0.2%.

Skin and Appendages: Urticaria (0.3%) and purpura (0.1%).

General Adverse Reactions to Contrast Media: The following reactions have been reported after administration of other intravascular iodinated contrast media. *Reactions due to technique:* hematomas and ecchymoses. *Hemodynamic reactions:* vein cramp and thrombophlebitis following intravenous injection. *Cardiovascular reactions:* rare cases of cardiac arrhythmias, reflex tachycardia, chest pain, cyanosis, hypertension, hypotension, peripheral vasodilatation, shock, and cardiac arrest. *Renal reactions:* occasionally, transient proteinuria; rarely, oliguria or anuria. *Allergic reactions:* asthmatic attacks, nasal and conjunctival symptoms, dermal reactions such as urticaria with or without pruritus, as well as pleomorphic rashes, sneezing, and lacrimation; rarely, anaphylactic reactions. Rare fatalities have occurred due to these or unknown causes. *Signs and symptoms related to the respiratory system:* pulmonary or laryngeal edema, bronchospasm, dyspnea; or *to the nervous system:* restlessness, tremors, convulsions. *Other reactions:* flushing, pain, warmth, metallic taste, nausea, vomiting, anxiety, headache, confusion, pallor, weakness, sweating, localized areas of edema (especially facial cramps), neutropenia, and dizziness. Rarely, immediate or delayed rigors can occur, sometimes accompanied by hyperpyrexia. Infrequently, "iodism" (salivary gland swelling) from organic iodinated compounds appears 2 days after exposure and subsides by the sixth day.

In general, the reactions that are known to occur upon parenteral administration of iodinated contrast agents are possible with any nonionic agent. Approximately 95% of adverse reactions accompanying the use of water-soluble intravascularly administered contrast agents are mild to moderate in degree. However, severe, life-threatening anaphylactoid reactions, mostly of cardiovascular origin, have occurred. Reported incidences of death range from 6.6 per 1 million (0.00066%) to 1 in 10,000 (0.01%). Most deaths occur during injection or 5 to 10 minutes later, the main feature being cardiac arrest, with cardiovascular disease as the main aggravating factor. Isolated reports of hypotensive collapse and shock are found in the literature. The incidence of shock is estimated to be 1 out of 20,000 (0.005%) patients.

Adverse reactions to injectable contrast media fall into two categories: chemotoxic reactions and idiosyncratic reactions. Chemotoxic reactions result from the physicochemical properties of the contrast media, the amount of dose injected, and the speed of injection. All hemodynamic disturbances and injuries to organs or vessels perfused by the contrast medium are included in this category. Idiosyncratic reactions include all other reactions. They occur more frequently in patients 20 to 40 years old. Idiosyncratic reactions may or may not be dependent on the amount of dose injected, the speed of injection and the radiographic procedure. Idiosyncratic reactions are subdivided into minor, intermediate, and severe. The minor reactions are self-limited and of short duration; the severe reactions are life-threatening and treatment is urgent and mandatory.

The reported incidence of adverse reactions to contrast media in patients with a history of allergy is twice that in the general population. Patients with a history of previous reactions to a contrast medium are three times more susceptible than other patients. However, sensitivity to contrast media does not appear to increase with repeated examinations.

Most adverse reactions to injectable contrast media appear within 1 to 3 minutes after the start of injection, but delayed reactions may occur.

Regardless of the contrast agent employed, the overall estimated incidence of serious adverse reactions is higher with angiocardiography than with other procedures. Cardiac decompensation, serious arrhythmias, angina pectoris, or myocardial ischemia or infarction may occur during angiocardiography and left ventriculography. Electrocardiographic and hemodynamic abnormalities occur less frequently with OMNIPAQUE than with diatrizoate meglumine and diatrizoate sodium injection.

OVERDOSAGE—Intrathecal: Clinical consequences of overdosage with OMNIPAQUE have not been reported. However, based on experience with other nonionic myelographic media, physicians should be alert to a potential increase in frequency and severity of CNS-mediated reactions. Even use of a recommended dose can produce effects tantamount to overdosage if incorrect management of the patient during or immediately following the procedure permits inadvertent early intracranial entry of a large portion of the medium.

The intracisternal LD_{50} value of OMNIPAQUE (in grams of iodine per kilogram body weight) is greater than 2.0 in mice.

Intravascular: Overdosage may occur. The adverse effects of overdosage are life-threatening and affect mainly the pulmonary and cardiovascular systems. The symptoms include cyanosis, bradycardia, acidosis, pulmonary hemorrhage, convulsions, coma, and cardiac arrest. Treatment of an overdosage is directed toward the support of all vital functions and prompt institution of symptomatic therapy.

The intravenous LD_{50} values of OMNIPAQUE (in grams of iodine per kilogram body weight) are 24.2 in mice and 15.0 in rats.

Winthrop PHARMACEUTICALS
Winthrop Pharmaceuticals
Division of Sterling Drug Inc.
New York, NY 10016

© 1988 WINTHROP PHARMACEUTICALS

8038/3815

MAMMOGRAPHIC QA

INSTRUMENTS AND ACCESSORIES

For Evaluating the Overall Imaging Performance of Your Mammographic System

07-492
Mammographic Digital kVp Meter

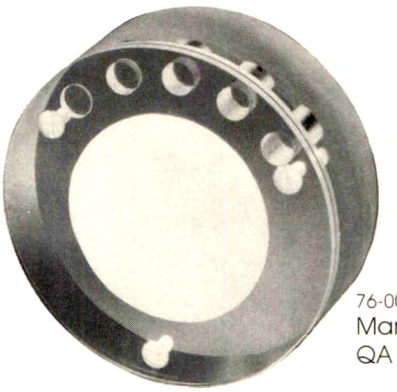

76-001-4
Mammographic QA Phantom

06-526
RAD-CHECK® PLUS X-Ray Exposure Meter

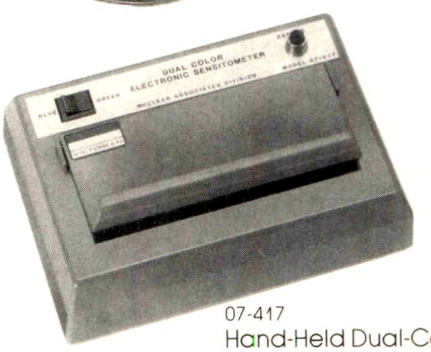

07-417
Hand-Held Dual-Color Sensitometer

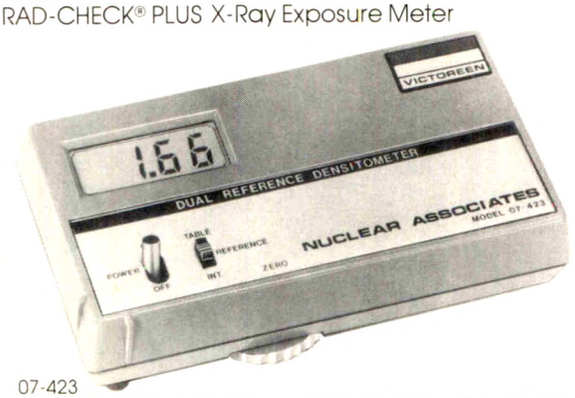

07-423
Hand-Held Dual-Reference Digital Densitometer

07-402
Digital Thermometer

WE CARRY A COMPLETE LINE OF MAMMOGRAPHIC QA PRODUCTS

For more information, request Bulletin 405-44

NUCLEAR ASSOCIATES

VICTOREEN

A Division of VICTOREEN, INC.
100 VOICE ROAD
CARLE PLACE, NY 11514-1593
(516) 741-6360
A Subsidiary of Sheller-Globe SG

CIRCLE 36 ON READER SERVICE CARD

® Victoreen, Inc.

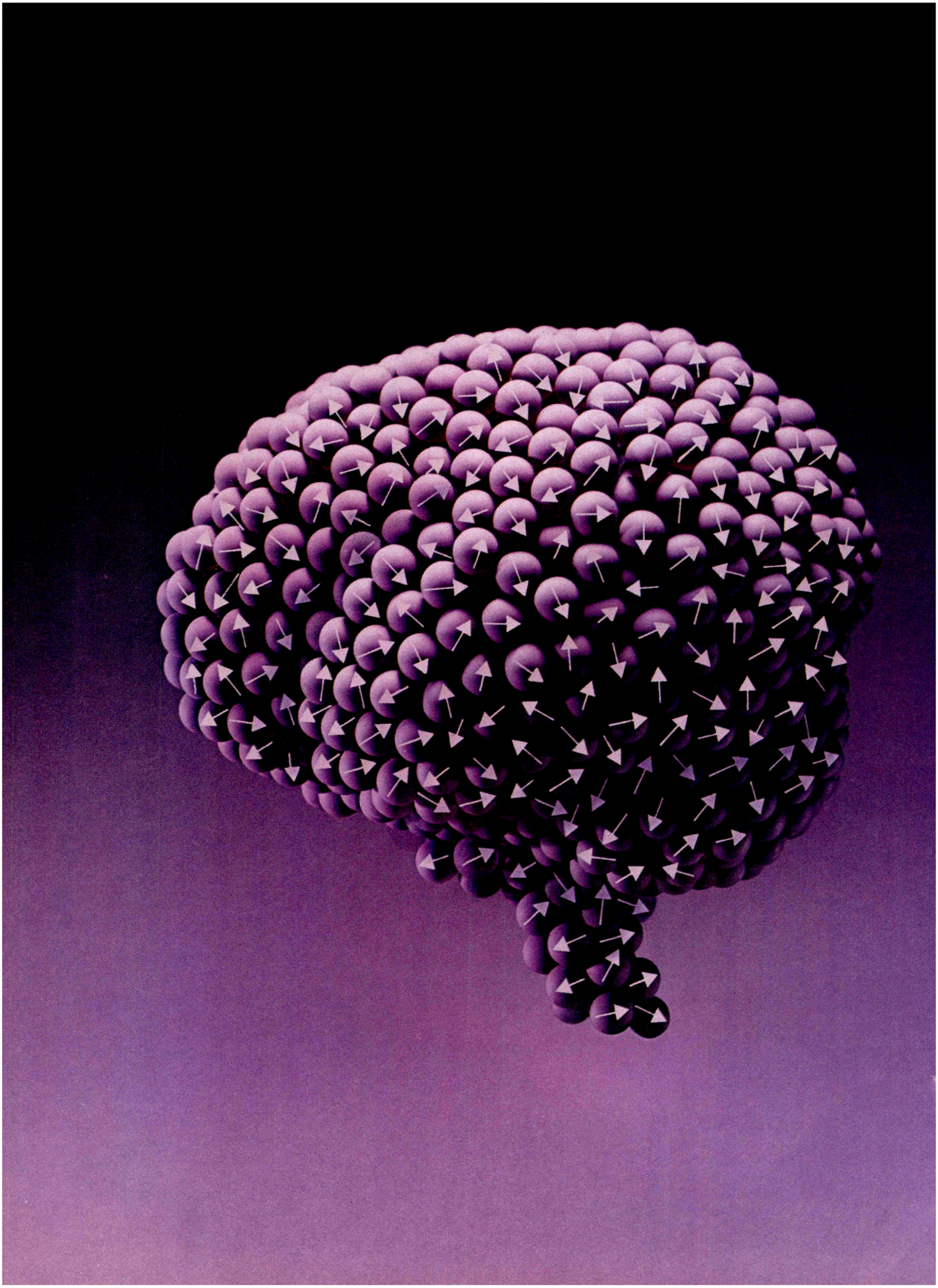

COMING SOONER THAN YOU THINK *MRI*

BEYOND THE IMAGINATION

Imaging that's going to give you the details you've always wanted. Images that help define and differentiate. That's what the researchers at Berlex Imaging have been working on. Our research is dedicated to developing contrast material so you can see as you've never seen before. The results of our research may be here sooner than you think. But it's only the beginning of imaging beyond the imagination from Berlex.

BERLEX IMAGING™

Berlex Imaging
300 Fairfield Road
Wayne, NJ 07470

AJR 3/88

Yes, I want to be one of the first to know about MRI beyond the imagination.

name

address

city state zip

( ) area code telephone no.

specialty (including subspecialty) ID number

CIRCLE 34 ON READER SERVICE CARD

1987, Berlex Laboratories, Inc. All rights reserved.

890-1 890-11 Printed in USA September 1987

DuPont's NEW Mammography Film
reduces radiation by one third

with no loss in diagnostic accuracy

- MICROVISION™ Mammography Film is a single-emulsion, high-contrast, high-speed orthochromatic X-ray film created exclusively for mammography.
- With a relative speed of 150, MICROVISION is 50% faster than the next best single-emulsion mammography film. This can reduce patient radiation exposure by 33% while keeping maximum detail visibility and providing excellent contrast.
- MICROVISION embodies the latest in Du Pont cubic silver halide grain technology. Use it as "drop-in" film with any green-emitting, single-intensifying mammography screen. Ideal for both screening and symptomatic patient imaging, MICROVISION is available in all standard sizes.

For more details, call us at 1-800-527-2601, or ask your Du Pont representative for a free demonstration of MICROVISION Mammography Film on your own equipment.

Depend on us...
because she depends on you.

DU PONT

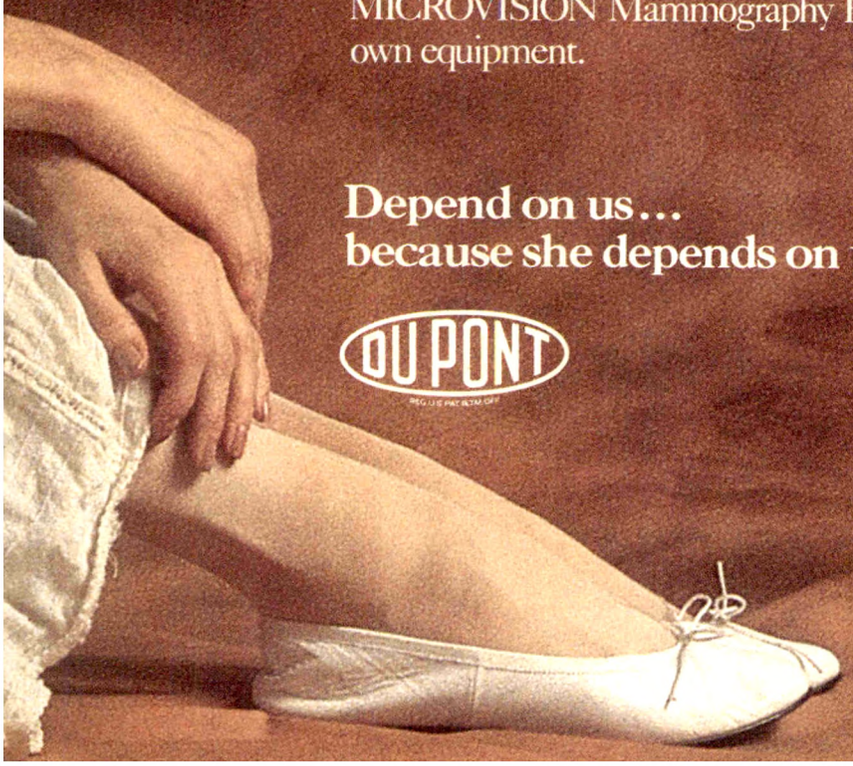

CIRCLE 37 ON READER SERVICE CARD

©1988 DuPont Company

SIEMENS

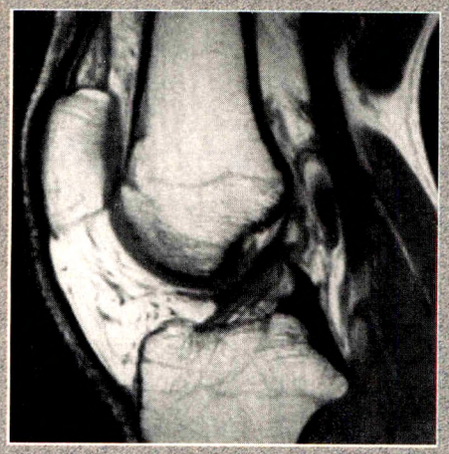

Cruciates
Compare normal anterior and posterior cruciate ligaments (left) to a complete anterior cruciate tear (right).

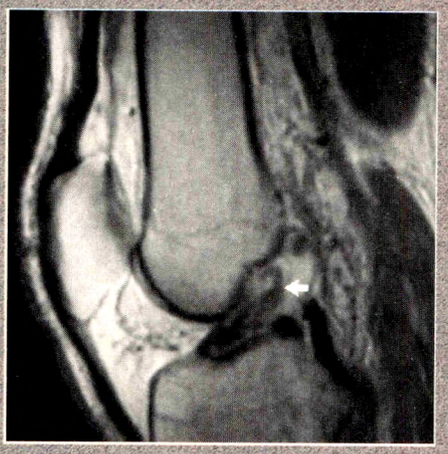

Images courtesy of Georg Bongartz, M.D., University of Muenster and Dr. Keil, Wurzburg

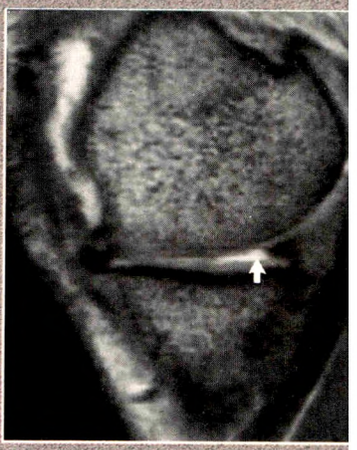

3D Volume
A posterior medical meniscal amput (left) and full thickness focal femora cartilage degeneration and loss (righ be visualized non-invasively. (FISP40 1.7mm, 64 slices in 8 minutes).

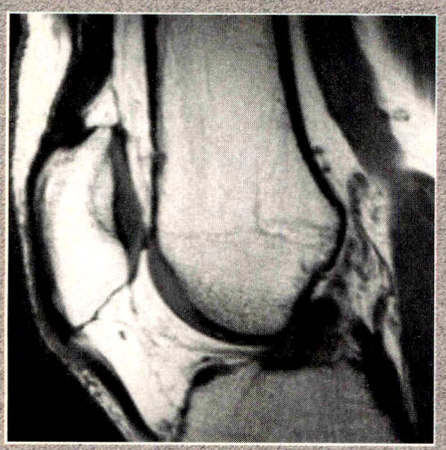

Cartilage
Contrast normal smooth and homogeneous patellar and femoral cartilage (left) to the thinning and loss of patellar cartilage and severe inhomogeneity of femoral cartilage of advanced degenerative changes (right).

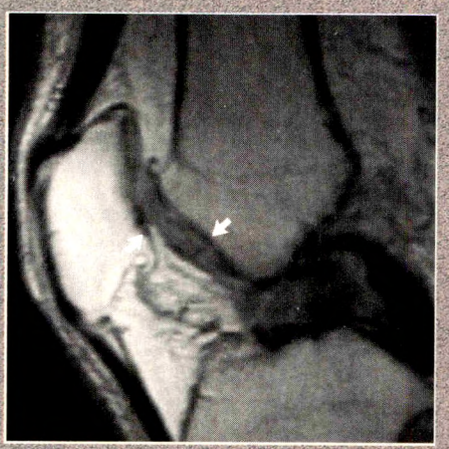

Images courtesy of Rob Tyrrell, M.D., University Hospitals of Cleveland

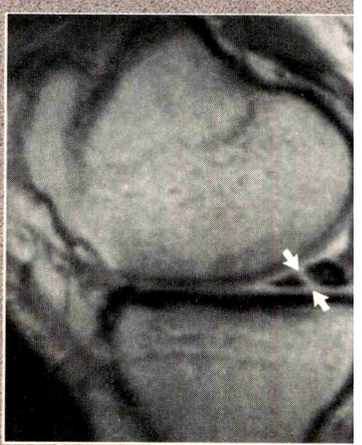

Menisci
A complete tear of the posterior horn medical meniscus is shown in this p density image, which was confirmed surgery.

The Definitive View.

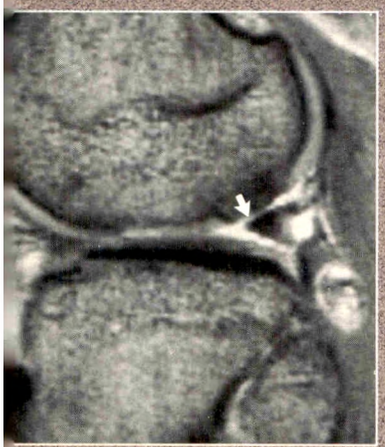

courtesy of Rob Tyrrell, M.D.,
ity Hospitals of Cleveland

courtesy of William O. Thomas,
laging Center of Southwest Virginia

MG/5000-132A WLM 735

Recent enhancements to the MAGNETOM Magnetic Resonance system are expanding the diagnostic range of MR to include imaging of the knee. In many cases, MR can now replace arthrography—a key benefit for your patients.

MR imaging of the knee with the MAGNETOM

Importance of the Signal-to-Noise Ratio (S/N): The MAGNETOM MR system gives physicians the resolving power to confidently grade conditions such as subtle meniscal lesions. It delivers this superior performance through (1) high baseline S/N, and (2) anatomically conformal radio frequency probes, including the MAGNETOM's Helmholtz coil and knee resonator. Together, these features optimize image quality—and keep knee examinations brief.

Rapid Three Dimensional Knee Imaging: 3D imaging of the knee using rapid pulse sequences permits extremely thin, contiguous slices—1.5 mm or less—to be acquired with submillimeter spatial resolution. These very thin sections improve assessment of knee trauma by providing unprecedented visualization of bone marrow, cartilage, meniscal structure and fluid.

MAGNETOM. The Definition of Clinical Value. Through ongoing system enhancements, MAGNETOM users have access to a constantly expanding diagnostic range. Siemens traditional quality and commitment to MR make the MAGNETOM the definition of superior clinical value.

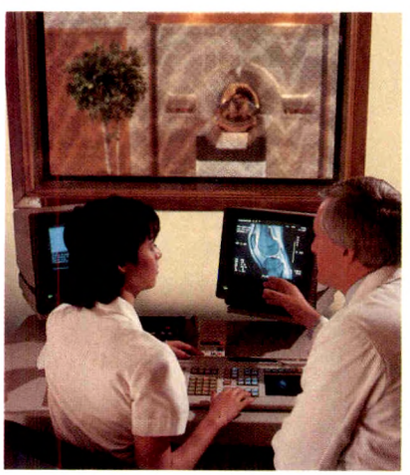

Write for a Poster.
If you'd like an informative poster on MR of the knee, write to:

Siemens Medical Systems, Inc.
MR Product Group
186 Wood Avenue South
Iselin, NJ 08830

The Siemens MAGNETOM has received FDA premarket approval for certain configurations and applications. Those configurations and applications that are currently not approved are only available for investigational use in the U.S.

CIRCLE 8 ON READER SERVICE CARD

Siemens...
technology with integrity.

Announcing... CGR is now GE.

Mammography by CGR

There's never been a better time to be in the market for mammography. With the recent merger of CGR into GE, Senographe® mammography systems are now part of the GE family.

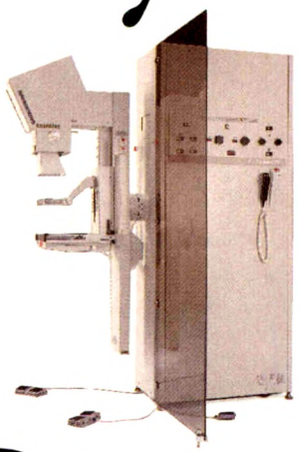

Which gives you the best of both worlds—the finest mammography equipment, backed by the strongest support in the industry.

Take the Senographe 600T, for example. It's everything you should look for in a mammography system. Consistent high quality images. Variable magnification. Excellent reproducibility. Minimal patient exposure. Virtually no retakes.

Peace of mind by GE

And GE support is everything you expect. Prompt, reliable service. Comprehensive training. A wide choice of financing programs. Plus the ongoing R&D that enables your site to keep pace with clinical advances in mammography.

For more information on the complete line of Senographe systems, please call GE Medical Systems:

(800) 624-5692.

CIRCLE 15 ON READER SERVICE CARD

GE Medical Syste

There's never been a better time to choose G

Perspective

Present and Future Status of MR Imaging

Alexander R. Margulis[1] and Lawrence E. Crooks[2]

Although MR imaging was first introduced in 1973 [1], it did not become clinically applicable until 1981 when, almost simultaneously, good, informative images were obtained at both the Royal Postgraduate Medical School, Hammersmith Hospital, London [2] and the University of California, San Francisco [3]. What followed was a veritable explosion of interest in MR, with clinical centers throughout the country and abroad contributing almost daily to advances in this new diagnostic field. The result is that MR imaging is now firmly established in the clinical workup of patients in most larger centers in the United States. The routine use of MR is fast becoming a reality in much of Western Europe and is also expected to become widespread in Japan. The speed with which this medical technology has spread throughout the United States is phenomenal. At the end of 1981, there were only three working clinical imagers in the United States, yet by the beginning of 1987 some 600 units were in use, and by the end of 1987 over 800 will be in clinical operation [4]. Only a few of these units are owned by the federal government or by municipal governments. In fact, most of them are the property of hospitals or groups of physicians, who are enthusiastically acquiring the machines because of the unique type of information they provide.

Clinical Status

After the initial stage of development of clinical MR imaging, a new breed of technically oriented imaging specialists emerged. The MR imaging specialist had to be a general radiologist who also had special technical expertise. Although this was worthwhile for an immature technique for which new approaches were constantly being implemented, advances in MR and its clinical applications are causing MR imaging to return to the province of the organ-oriented subspecialist.

Areas in Which MR Imaging Excels

Today MR is the essential imaging technique in the study of the CNS [5], including the spinal cord (Fig. 1), as well as the face and neck. It is also extremely valuable in studying diseases of the spine and the major joints. Because of its superior soft-tissue contrast resolution, MR is more effective than CT for staging bone tumors. However, MR lags behind CT in providing information about calcification and periosteal bone reaction [6], and newer techniques are continuously adding more information.

MR also provides important information about the male and female genital organs as well as the urinary bladder (Fig. 2) [7]. In addition to its use in staging malignant neoplasms of pelvic organs, MR can also provide information about the hormonal status of the uterus [8]. Moreover, MR imaging is equal to or better than CT in the study of the mediastinum, retroperitoneum, and large vessels [9]. This technique has been shown to be particularly valuable in the study of dissecting aneurysms and in many centers has replaced emergency angiography for the study of these lesions [10]. In the evaluation of the heart, MR imaging excels in the area of ischemic heart disease, congenital heart disease, and abnormalities involving the pericardium [7].

Although MR imaging of the upper abdomen is marred by breathing artifacts, MR imaging of the liver (particularly with the spin-echo technique and a short TR and short TE) has yielded excellent images [11]. Further progress with the use of rapid scanning techniques is expected in the future [12]. MR is already being used to detect metastases in the liver, and investigators report that it is more accurate than other methods, including CT [13]. MR is valuable in the diagnosis of hepatocellular carcinomas and has advantages over CT and sonography in the study of hepatic hemangiomas. These common neoplasms have an unusually long T2. More ad-

Received October 5, 1987; accepted after revision November 17, 1987.
[1] Department of Radiology, University of California, San Francisco, San Francisco, CA 94143-0628. Address reprint requests to A. R. Margulis.
[2] Department of Radiology, University of California, Radiologic Imaging Laboratory, 400 Grandview Dr., South San Francisco, CA 94080.

 0361–803X/88/1503–0487 © American Roentgen Ray Society

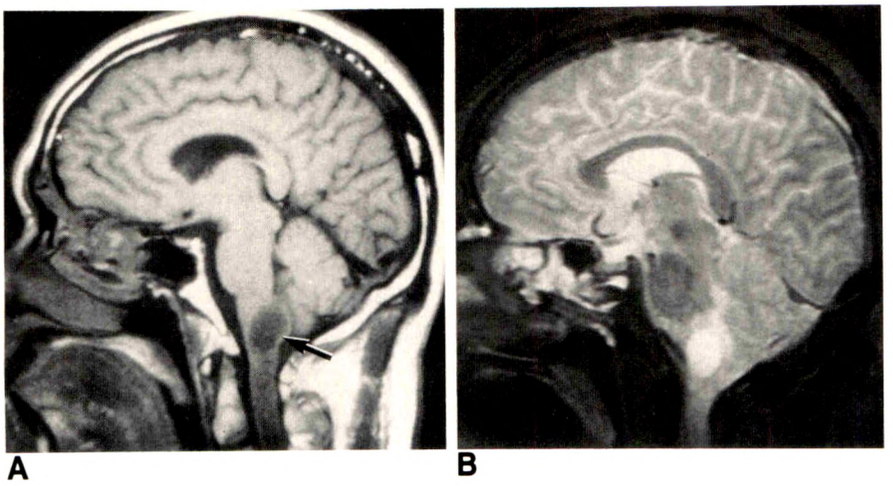

Fig. 1.—Partially cystic astrocytoma of upper cervical cord.

A, Short-TR image showing cystic component and tumor in cord with low signal intensity (*arrow*).

B, Long-TE image shows cystic component with high signal intensity, whereas tumor is isointense with cord.

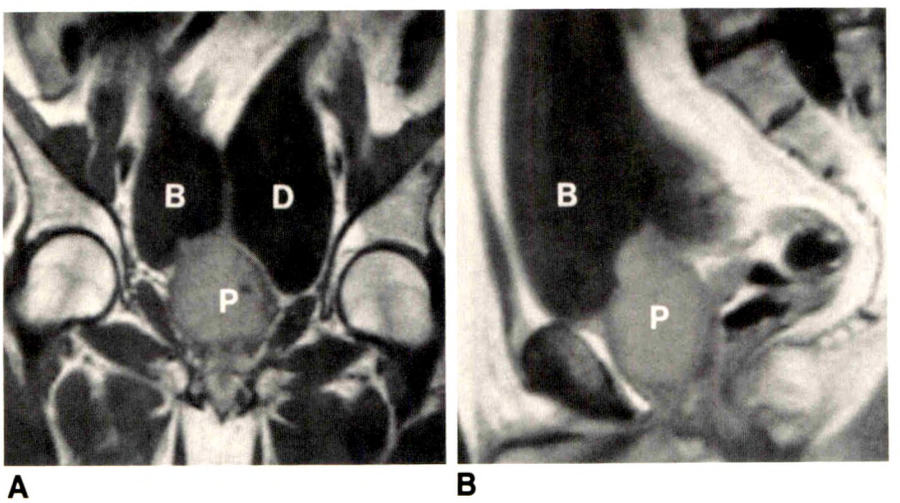

Fig. 2.—Benign prostatic hypertrophy producing bladder obstruction with creation of a large urinary bladder diverticulum. Short-TR images.

A, Coronal section shows large diverticulum (D) of bladder (B) on left with much-enlarged prostate (P).

B, Sagittal section shows protrusion of enlarged prostate (P) into partially obstructed urinary bladder (B).

vances will be necessary before MR totally replaces CT in the study of the liver. At this time, MR examination of the liver is indicated (1) when multiple metallic clips are present in the liver, (2) when hepatic metastases are suspected when the CT findings are negative and other clinical tests suggest that metastases are present, and (3) when lesions located in only one lobe on CT necessitate examination of the whole liver to exclude the presence of additional metastases and to determine resectability.

Areas in Which MR Lags Behind Other Imaging Techniques

The alimentary tube is still best examined with barium. Neoplasms of the alimentary tract are better staged with CT than with MR. New rapid MR imaging sequences and the cessation of bowel motion by giving an intramuscular injection of glucagon will improve the results of MR imaging. Even then, given the present limitations in spatial resolution of the new rapid sequences, it is unlikely that MR imaging will replace barium or CT for the staging of malignant neoplasms, mesenteric disease, or abscesses. This may change with the development of optimized breath-holding sequences and practical intraluminal contrast media for MR.

New MR sequences are being used for the study of the pancreas, but it is too early to know whether MR will prove superior to CT for this purpose [14]. It is likely that the spleen will be studied preferentially with MR. At present, high-resolution CT with a bolus injection of iodinated contrast media is the best imaging approach. MR also lags behind CT in the evaluation of lung parenchyma. Thin-slice CT is particularly effective in the evaluation of diffuse lung disease [15, 16].

Limitations of MR Imaging

The technology of MR imaging is considerably more complex than that of other imaging techniques. MR depends on a multitude of physical parameters such as proton density, T1 and T2 relaxation parameters, proton bulk motion [17], diffusion [18], magnetic susceptibility [19], and chemical shift [20]. In addition, many of the machine parameters are important in determining image quality: magnetic field strength, the design of radiofrequency coils (gradient, emitting, and receiving), the strength of the gradient-power supplies, homogeneity of the field, and so forth [3]. There is also considerable controversy over the optimal magnetic field strength of the devices [21, 22]. This question is still unresolved, since there are advantages and disadvantages associated with each field

strength. Because of concern over this one parameter, additional issues regarding the many other technical characteristics of an imager are often overlooked. High–magnetic-field strength has the advantage of permitting the emission of stronger signals in general and the possibility of a better signal-to-noise ratio (S/N). On the negative side, T1 is longer with high-strength fields and, with present techniques, motion artifacts are emphasized. These artifacts are particularly bothersome when imaging the upper abdomen. Some artifacts are also present in images of the brain and are apparently produced by arterial pulsations [23]. Chemical-shift artifacts are also more pronounced with higher fields [22]. Intermediate and lower fields have lower signal, but for a given chemical-shift artifact, they have a narrower bandwidth and less noise. S/N affects imager slice thickness, with a high S/N allowing thinner slices. Intermediate- and low-field imagers require more care to achieve a high S/N. Low–field-strength machines (0.05–0.07 T) show the promise of fewer artifacts caused by respiratory and other motion. With ECG gating, these machines provide excellent heart images (Fig. 3). The lower the magnetic-field strength, the easier it is to provide a proper site for the imaging devices and the lower the cost of the machine. Low–field-strength units operate with permanent, hybrid, or resistive magnets.

Spatial Resolution

The spatial-resolution limit of present human MR imagers is in the range of 0.5 mm × 0.5 mm × 2.5 mm. Small-animal imagers can now provide voxels that are five times smaller in all dimensions [24]. It appears that under the best of circumstances for typical tissue, in vitro the resolution will be between 3 and 6 μm [25]. Minimizing the effects of diffusion and magnetic susceptibility requires very high gradients. Cryogenic cooling of the specimens and receiver coil will be necessary for noise reduction if finer resolution or shorter imaging times are needed.

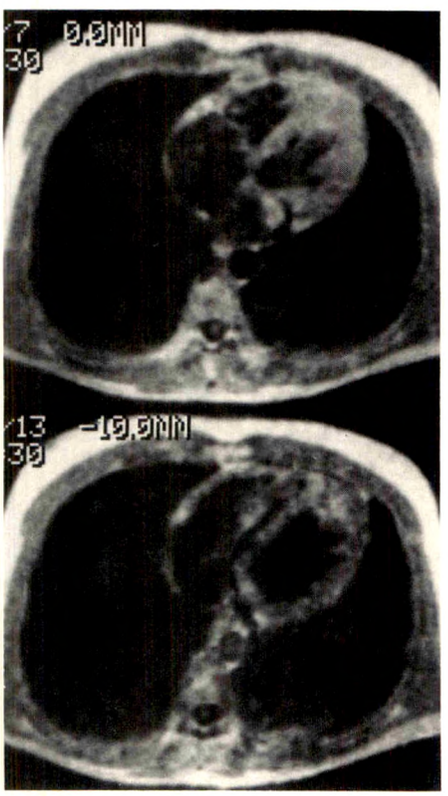

Fig. 3.—Heart images taken at 0.05 T. Gated images use 256 heartbeats. Good definition of chest wall is indicative of immunity to respiratory motion artifacts. Resolution is 2.2 × 2.2 × 10.0 mm.

Imaging Time

Clinical images with voxel volumes of 5 mm^3 and an acceptable S/N are obtained in a few minutes on most present-day imagers. This improvement in performance has occurred only in the past few years. It is due partly to significant improvements in S/N. Echo-planar imaging [26, 27], which collects 64 echoes in 128 msec, has a somewhat poorer resolution but offers real-time imaging (Fig. 4) [28]. So far, the rapid on-and-off switching of the gradient is only applicable in specially designed or small-gradient coils, such as those used for the bodies of children or for heads. The rapid changes of magnetic-field gradients with the associated induced voltages begin to challenge present-day exposure guidelines. New sequences for reducing today's several-minute scanning times are being developed [12], and images obtained with 5- to 10-sec scanning times will become a reality, making accurate abdominal imaging possible.

Hazards

With present-day imagers and techniques, the hazards of MR imaging are well known [29] and, in general, have been circumvented. Patients with cardiac pacemakers are excluded from MR imaging as are metal workers and patients with metallic clips on intracranial aneurysms. The hazard of introducing loose ferrous objects into the magnet has not been a significant threat in clinical situations, since adequate locks, alert supervisory personnel, and the cooperation of patients and referring physicians have prevented mishaps. The radio-frequency heating measured in patients is minor and is considered to be harmless [30]. Heating of prostheses (observed in one phantom study [31]) or movement of metallic clips has not been reported and apparently presents no hazard, and these patients are being routinely studied.

Future Directions for MR

Flow

The sensitivity of MR to flow has been appreciated since the 1950s [32]. The first MR images demonstrated this sensitivity by showing blood as either bright or dark, depending on the imaging technique used. The absence of signal from blood in the heart makes it easier to study wall motion and wall thickening [33]. Spin-echo techniques are also useful for myocardial evaluation—for example, edema associated with infarction. A bright signal from blood can be used to measure the blood's velocity [34, 35] and has the potential for producing velocity or flow images. Currently, the bright signals from blood are used to observe turbulent flow and regurgitant jets in valvular insufficiency [36, 37]. Quantitation of these flows

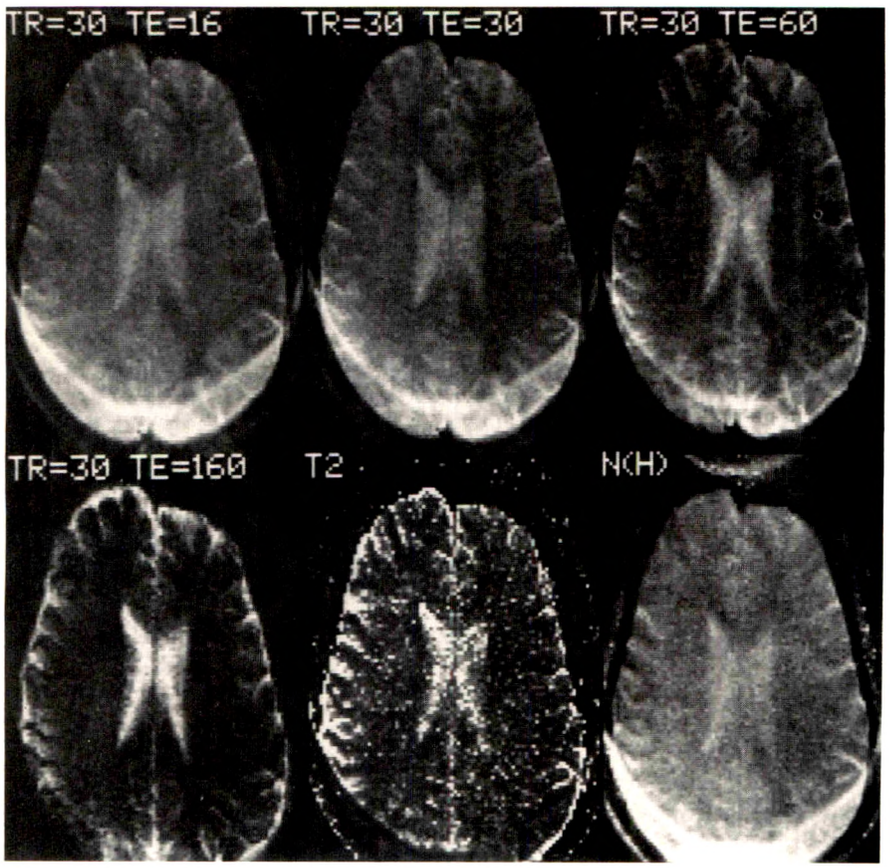

Fig. 4.—Echo-planar images of adult head. Upper row of images were each acquired in 161 msec. They have increasing T2 contrast with longer TE values but no T1 contrast. Lower left image was acquired in 322 msec. It is a late echo giving more T2 contrast. It and the shortest TE image are used to calculate T2 image in middle and hydrogen density image on right. Resolution is 2 × 2 × 10 mm. Note that different chemical shift of subcutaneous fat has moved it up in these images. Shortening imaging time reduces artifacts.

should be possible. Combining cine loops of gated heart images with blood velocity information produces impressive motion pictures [37].

Multinuclear Imaging

Hydrogen is very likely to remain the only practical and useful MR imaging nucleus for a long time. For S/N comparisons between hydrogen and other nuclei, the most effective approach is to consider the case in which all nuclei resonate at the same frequency [38]. The comparison is then independent of the frequency dependency of the receiver coil and complex variables such as tissue conductivity. Phosphorus-31 requires, for instance, 2.7 times the field strength of hydrogen. Carbon-13 has a per gram sensitivity of 1.9% of hydrogen and a relative abundance of 1.1%, giving it a sensitivity of 0.00021 for a gram of carbon as compared with a gram of hydrogen. To image nuclei other than hydrogen, the lower S/N must be accommodated by larger voxels, longer imaging time, or poorer contrast. Nevertheless, imaging of multiple nuclei is possible with hydrogen providing the basic image and nuclei of other elements providing superimposed shading in different colors.

Approaches to Improving the Specificity of MR

Although MR is more sensitive than CT or sonography in most areas of the body, its specificity is only slightly better than that of either of these techniques. Efforts to overcome this drawback are progressing in several directions.

While MR's relative lack of specificity can be addressed by advanced computer programs by using data from its multiple physical parameters, it is still unlikely that significant advances will be made in the field of MR imaging [39]. The depiction of normal tissue using computer-sensitized images based on several parameters (such as proton density, T1, and T2) give encouraging results (Fig. 5), but there is considerable overlap of these parameters for various lesions. It is unlikely that, on the basis of such simple solutions, significantly improved specificity can be attained.

Contrast media of the type that are presently used (e.g., gadolinium DTPA) are helpful in increasing sensitivity, particularly in the region of the spinal cord and brain, but have not improved tissue-specific pathologic diagnoses. It is possible that as the technology of producing monoclonal antibodies improves, such contrast-media–containing chelated paramagnetic metals may be used. Currently, work is proceeding on the development of receptor-based paramagnetic and superparamagnetic agents. Some progress in hepatobiliary, reticuloendothelial, and biochemical-targeted contrast materials is being achieved [40, 41].

Chemical-Shift Imaging

Chemical-shift imaging for water and fat (Fig. 6) [20] is possible even at low–magnetic-field strengths such as 0.02

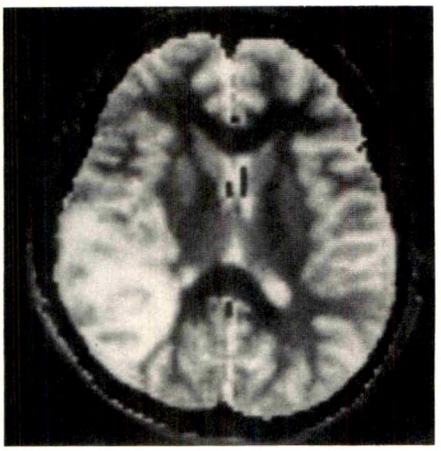

Fig. 5.—Computer-synthesized image using information from T1, T2, and proton density. Long T1, long T2, and high-proton density are imaged with high signal. Lesion in right hemisphere is an infarct. (Courtesy of Douglas Ortendahl. Reproduced with permission.)

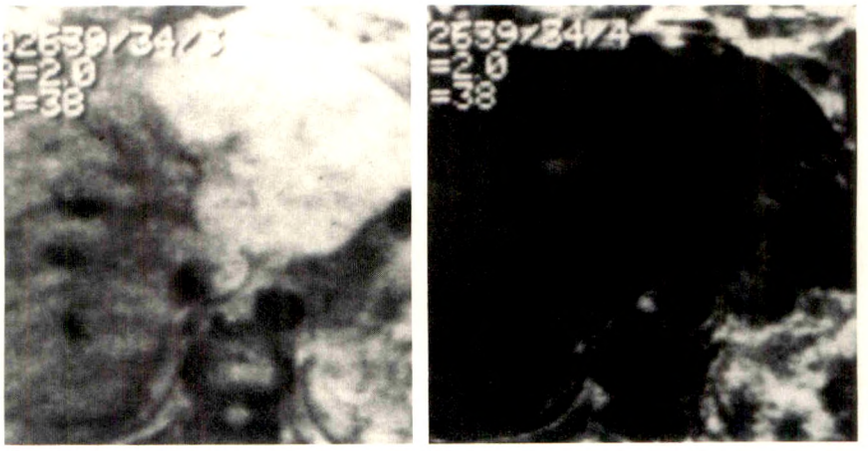

Fig. 6.—Chemical-shift images (Dixon method) [20] of the liver showing a hepatocellular carcinoma.
A, Lesion is richer in water than is liver and therefore has a higher signal.
B, Lesion and liver have practically no fat and therefore liver and lesion are imaged as a dark area.

T [42]. At higher field strengths (e.g., 1.5–4 T), maps of various compounds may be superimposed in various colors, with relatively large pixels, over the map of the proton image. Possible compounds contain phosphorus-31 such as adenosine triphosphate or phosphocreatine, hydrogen such as lactate and aspartate (after suppression of water and fat), and sodium-23 such as sodium chloride.

MR Spectroscopy

MR-localized tissue spectroscopy [43–45] carries with it the highest hope for tissue specificity by obtaining the spectra of various elements like hydrogen (with water and fat suppressed), phosphorus-31 (Fig. 7), sodium-23, and fluorine-19. Specificity could also be enhanced by the introduction of compounds enriched with carbon-13.

The introduction of MR spectroscopy presents difficulties in determining the precise location of a lesion with clinically practicable voxels. A great deal of work will also be necessary to transform MR spectroscopy from a research discipline into a clinical diagnostic technique. If this is successful, there are enormous possibilities for obtaining important biochemical information noninvasively.

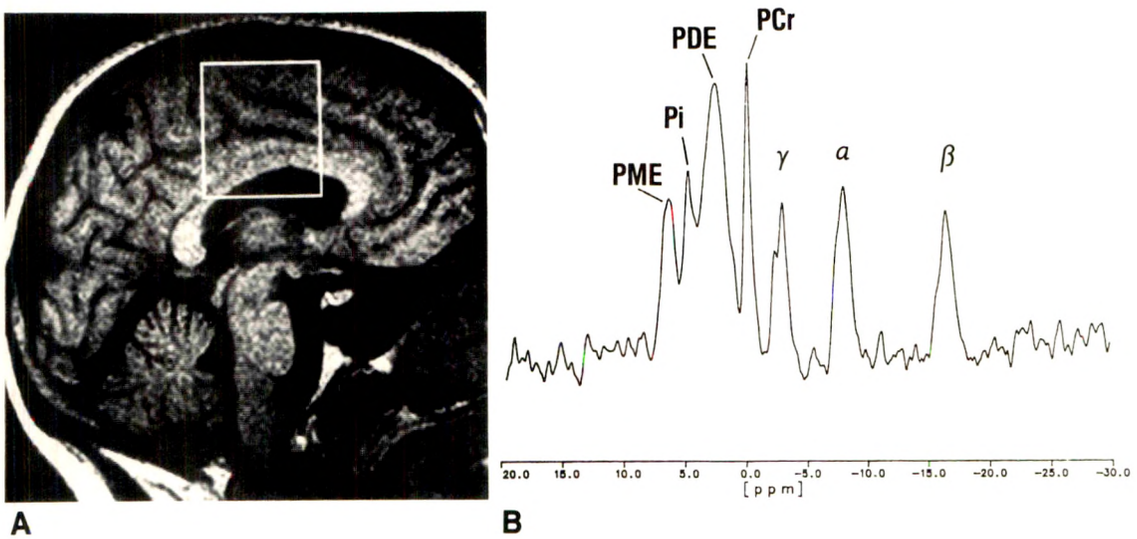

Fig. 7.—Sagittal image and localized phosphorus-31 MR spectrum of a normal human brain.
A, Phosphorus-31 MR spectrum localization from MR image.
B, Phosphorus-31 MR ISIS (image-selected in vivo spectroscopy) spectrum of normal brain. 5 × 5 × 5 cm volume with 20-min acquisition time. PME = phosphomonoester; Pi = inorganic phosphorus; PDE = phosphodiester; PCr = phosphocreatine. Gamma, alpha, and beta indicate adenosine triphosphate peaks; ppm = parts per million. (Hubesch B, Roth K, Matson G, et al., unpublished data.) Note.—ISIS was developed by R. Ordidge, Oxford Instruments, Oxford, UK, and was modified by J. Den Hollander and P. Luyten, Philips, Einthoven, the Netherlands.

Conclusions

MR imaging has become an accepted clinical technique in many areas. It has some inherent limitations, such as resolution (compared with the radiographic technique), speed (compared with sonography), specificity, and poor S/N for nuclei other than hydrogen. Since MR imagers are high-technology machines, the expense of MR studies is high. Cost is being reduced by maturing technology, competition, and the introduction of lower–field-strength machines.

MR techniques and capabilities continue to be moving targets. The potential of MR imaging combined with spectroscopy is immense, and it is anticipated that in the near future MR will become the most important diagnostic technique in medicine.

REFERENCES

1. Lauterbur PC. Image formation by induced local interactions: examples employing nuclear magnetic resonance. *Nature* **1973**;242:190–191
2. Young IR, Burl M, Clarke GJ, et al. Magnetic resonance properties of hydrogen: imaging the posterior fossa. *AJR* **1981**;137:895–901
3. Crooks LE, Arakawa M, Hoenninger JC, et al. Nuclear magnetic resonance whole-body imager operating at 3.5 KGauss. *Radiology* **1982**;143: 169–174
4. *ACR MR site list*. Washington, DC: American College of Radiology, July **1987**
5. Brant-Zawadzki M. *Magnetic resonance imaging of the central nervous system*. New York: Raven, **1987**
6. Pettersson H, Gillepsy T III, Hamlin DJ, et al. Primary musculoskeletal tumors: examination with MR imaging compared with conventional modalities. *Radiology* **1987**;164:237–241
7. Higgins CB, Hricak H. *Magnetic resonance imaging of the body*. New York: Raven, **1987**
8. Demas BE, Hricak H, Jaffe R. Uterine MR imaging: influence of hormonal stimulation. *Radiology* **1986**;159:123–126
9. Webb WR. Magnetic resonance imaging of the hila and mediastinum. *Cardiovasc Intervent Radiol* **1986**;8:306–313
10. Amparo EG, Higgins CB, Hricak H, Sollitto R. Aortic dissection: magnetic resonance imaging. *Radiology* **1985**;155:399–406
11. Stark DD, Witenberg J, Edelmann RR, et al. Detection of hepatic metastases: analysis of pulse sequence performance in MR imaging. *Radiology* **1986**;159:365–370
12. Haase A, Frahm J, Matthaei D, Hanicke W, Merboldt K-D. FLASH Imaging. Rapid NMR imaging using low flip-angle pulses. *J Mag Reson* **1986**;67:258–266
13. Demas BE, Hricak H, Goldberg HI, Margulis AR. Magnetic resonance imaging diagnosis of hepatic metastases in the presence of negative CT studies. *J Clin Gastroenterol* **1985**;7:553–560
14. Tscholakoff D, Hricak H, Thoeni R, Winkler ML, Margulis AR. MR imaging in the diagnosis of pancreatic disease. *AJR* **1987**;148:703–709
15. Moore EH, Webb WR, Muller N, Sollitto R. MRI of pulmonary air space disease: experimental model and preliminary clinical results. *AJR* **1986**;146:1123–1128
16. McFadden RG, Carr TJ, Wood TE. Proton magnetic resonance imaging to stage activity of interstitial lung disease. *Chest* **1987**;92:31–39
17. Crooks LE, Mills CM, Davis PL, et al. Visualization of cerebral abnormalities by NMR imaging: the effects of imaging parameters on contrast. *Radiology* **1982**;144:843–852
18. Wesbey GE, Moseley ME, Ehman RL. Translational molecular self diffusion in magnetic resonance imaging, part II. Measurements of the self-diffusion coefficient. *Invest Radiol* **1984**;19:491–498
19. Ludeke KM, Roschmann P, Tischler R. Susceptibility artefacts in NMR imaging. *Mag Reson Imag* **1985**;3:329–343
20. Dixon T. Simple spectroscopic imaging. *Radiology* **1984**;153:189–194
21. Crooks LE, Arakawa M, Hoenninger JC, McCarten B, Watts JC, Kaufman L. Magnetic resonance imaging: effects of magnetic field strength. *Radiology* **1984**;151:127–133
22. Hoult DI. Field, contrast, and sensitivity in imaging. In: James TL, Margulis AR, eds. *Biomedical magnetic resonance*. San Francisco: Radiology Research and Education Foundation, **1984**:35–45
23. Rubin JB, Enzmann DR, Wright A. CSF—gated MR imaging of the spine: theory and clinical implementation. *Radiology* **1987**;163:784–792
24. Johnson GA, Thompson MB, Gewalt SL, Hayes CE. Nuclear magnetic resonance imaging at microscopic resolution. *J Mag Reson* **1986**;68: 129–137
25. Aguayo JB, Blackband SJ, Schoeniger J, Mattingly MA, Hintermann M. Nuclear magnetic resonance imaging of a single cell. *Nature* **1986**;322:190–191
26. Mansfield P, Pykett IL. Biological and medical imaging by NMR. *J Mag Reson* **1978**;29:355–373
27. Mansfield P, Guilfoyle DN, Ordidge RJ, Coupland RE. Measurement of T1 by echo-planar imaging and the construction of computer-generated images. *Phys Med Biol* **1986**;31:113–124
28. Crooks LE, Arakawa M, Hylton N, et al. Echo planar pediatric imager. *Radiology* (in press)
29. Budinger TF. NMR in vivo studies: known thresholds for health effects. *J Comput Assist Tomogr* **1981**;5:800–811
30. Shellock FG, Crues JV. Temperature, heart rate, and blood pressure changes associated with clinical MR imaging at 1.5 T. *Radiology* **1987**;163:259–262
31. Davis PL, Herfkens R, Margulis AR, et al. Potential hazards in NMR imaging: heating effects of changing magnetic fields and RF fields on small metallic implants. *AJR* **1981**;137:857–860
32. Singer JR. Blood flow rates by nuclear magnetic resonance measurements. *Science* **1959**;130:1652–1653
33. von Schulthess GK, Fisher M, Crooks LE, Higgins CB. Gated MR imaging of the heart: intracardiac signals in patients and healthy subjects. *Radiology* **1985**;156:125–132
34. Singer JR, Crooks LE. Nuclear magnetic resonance blood flow measurements in the human brain. *Science* **1983**;221:654–656
35. Moran PR. Flow zeugmatographic interlace for NMR imaging in humans. *Mag Reson Imag* **1982**;1:197–203
36. Underwood SR, Klipstein RH, Firmin DN, et al. Magnetic resonance assessment of aortic and mitral regurgitation. *Br Heart J* **1986**;5:455–462
37. Pettigrew R, Holt D, Klein L, et al. Comprehensive cardiac MRI: can it replace other noninvasive resting functional studies (abstr). *Proc annual meeting of the Society of Magnetic Resonance in Medicine* **1987**;1:15
38. Crooks LE, Hoenninger JC, Arakawa M, et al. Tomography of hydrogen with NMR and the potential for imaging other body constituents. *Proc Society of Photo-Optical Instrumentation Engineers*, **1979**;206:120–128
39. Ortendahl DA, Hylton NM, Kaufman L, Crooks LE. Automated tissue characterization with NMR imaging. In: Deconinck F, ed. *Information processing in medical imaging*. The Hague: Martinus Nijhoff, **1984**:477–493
40. Runge VM, Claussen C, Felix R, James EA Jr. Contrast agents in magnetic resonance imaging. *Proc International Workshop*, January **1986**, Princeton, NJ
41. Engelstad BL, Wolf GL. Principles of paramagnetic contrast agents. In: Stark DD, Bradley WG, eds. *Magnetic resonance imaging*. St. Louis, MO: Mosby, **1987** (in press)
42. Tanttu JI, Pohjonen JA, Sepponen RE. Chemical shift imaging at 0.02 T (abstr). *Proc annual meeting of the Society of Magnetic Resonance in Medicine* **1987**;1:365
43. Aue WP, Muller S, Cross TA, Seelig J. Volume-selective excitation. A novel approach to topical NMR. *J Mag Reson* **1984**;56:350–354
44. Ordidge RJ, Connelly A, Lohman JAB. Image-selected in vivo spectroscopy (ISIS). A new technique for spatially selective NMR spectroscopy. *J Mag Reson* **1986**;66:283–294
45. Luyten PR, Anderson CM, Den Hollander JA. H1 NMR relaxation measurement of human tissue in situ by spatially resolved spectroscopy. *Mag Reson Med* **1987**;4:431–440

Progress in Radiology

The Evolution of Mammography

Lawrence W. Bassett[1] and Richard H. Gold

It was not until the early 1950s that mammography began to gain recognition as a useful diagnostic procedure. Even then, most radiologists simply considered it a technical ordeal and too specialized to add to their diagnostic procedures. In the 1950s, surgeons and primary-care physicians were only vaguely aware that it was possible to perform a radiographic examination of the breast. This article traces the evolution of mammography through the scientific contributions of those who developed, investigated, and improved it, emphasizing their trenchant articles that appeared in the *American Journal of Roentgenology* (*AJR*) over the last 50 years. This retrospective was undertaken to provide an understanding not only of the origins of state-of-the art mammography, but also of the challenges facing mammography then and now.

Pioneers In Mammography

In 1913, Salomon, a German surgeon, performed radiographs of 3000 excised breasts, correlating radiographic, gross, and microscopic anatomy [1]. Not only did Salomon show how highly infiltrating carcinoma could be radiologically distinguished from circumscribed carcinoma, but he was also the first to recognize nonpalpable breast cancer on a radiograph of a specimen and to report the finding.

In the United States, Stafford Warren pioneered the clinical use of breast radiography when, in 1930, he reported a stereoscopic technique for mammography (Fig. 1). His article [2] described and classified the appearances of normal breasts, identifying fatty and glandular types, as well as illustrating the changes of pregnancy, mastitis, and benign and malignant tumors. Warren also emphasized the importance of comparing images of the right and left breasts by viewing them side by side. In 1933, Lockwood [3] reviewed the then-current diagnostic criteria for mammography, and, in 1938, Gershon-Cohen and Strickler [4] recognized that "a comprehensive knowledge and familiarity of the roentgen appearance of the normal breast under all conditions of growth and physiologic activity must be acquired by the roentgenologist before he can ever hope to make real progress in the development of the roentgen method of diagnosis in breast neoplasia." They, therefore, published a report on variations of the normal mammogram. Otherwise, the literature of the 1930s and 1940s emphasized only the technical difficulties and limitations of mammography; in fact, from 1938 to 1950 the sole mammography article in the *AJR* was a case report of extensive posttrauma calcification [5].

In the 1950s, Leborgne in Uruguay revitalized interest in mammography with the publication of a series of articles reporting plain breast radiography and duct injection. He used nonscreen film and a focus-to-film distance of 60 cm, 20–30 kVp, 5 mAs for each centimeter of compressed breast thickness. Leborgne relied primarily on the cephalocaudal view, which he performed with the patient standing and with "slight pressure with the cone on a small cotton pad placed between the cone and the breast so that the least quantity of breast tissue is interposed" (Fig. 2). A large cone was used for a whole-breast image, and a smaller one was used for a second image of the area of interest [6]. Most importantly, Leborgne reported the occurrence of carcinomatous microcalcifications that, he said, resembled "fine grains of salt"; he detected such microcalcifications in about 30% of breast cancers. This sign provided Leborgne an opportunity for detecting carcinomas

[1] Both authors: Iris Cantor Mammography Screening Clinic, University of California at Los Angeles School of Medicine, UCLA Department of Radiological Sciences, UCLA Medical Center, Room B2-125, 10833 Le Conte Ave., Los Angeles, CA 90024. Address reprint requests to L. W. Bassett.

AJR 150:493–498, March 1988 0361–803X/88/1503–0493 © American Roentgen Ray Society

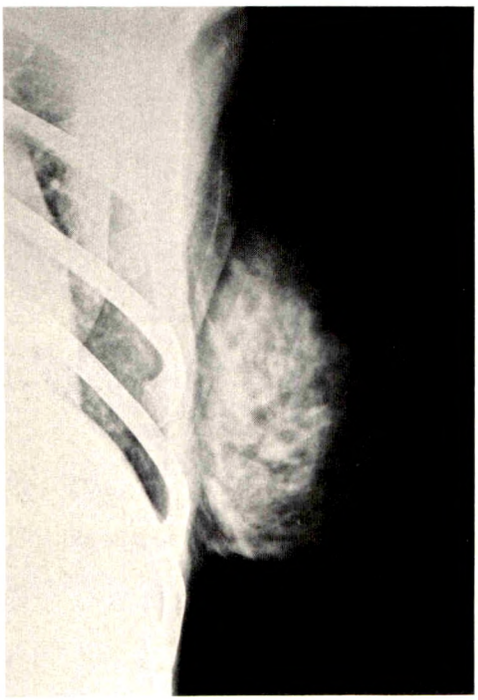

1

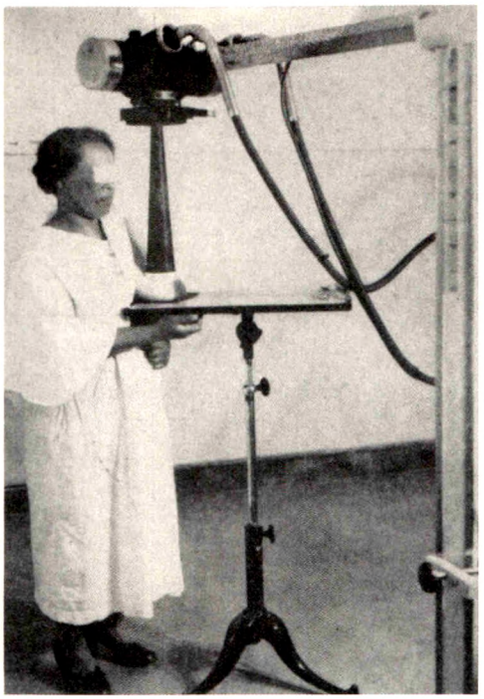

2

Fig. 1.—1939 mammogram by Stafford Warren. Moving grid diminished scattered radiation. Technical factors included 50–60 kVp, 70 mA, 2½-sec exposure, dual par-speed intensifying screens, and lack of compression. Films were viewed stereoscopically. Normal examination. Courtesy of Stafford Warren.

Fig. 2.—Leborgne's positioning for cephalocaudal mammogram. Film lies in opaque paper envelope under breast. From Leborgne [6].

even in the densest breasts. Finally, he performed specimen radiography to localize the calcifications for correlative histopathologic study.

During the 1950s, Gershon-Cohen and his associates published extensively on the malignant and benign abnormalities that they had identified on mammograms [7–9]. Comparison of their mammographic findings with whole-breast histologic sections (1) taught them to recognize the importance of characteristic mammographic findings of benign and malignant disease, some of which had been thought to have no significance, and (2) enabled them to establish reliable diagnostic criteria for carcinoma. Parallel work in Europe, particularly in France by Gros and his coworkers, confirmed and amplified these findings.

By 1960, however, mammography was employed by only a few radiologists, and dissemination of the method was hampered by lack of studies showing reliability and reproducibility. In order to aid radiologists hesitant to attempt mammography, Gershon-Cohen reported on the technical aspects, emphasizing the importance of high-contrast, nonscreen films, collimation, and compression [10]. To overcome the difficulty in obtaining adequate exposure of both the thinner peripheral and thicker juxtathoracic breast tissues, he recommended the "simultaneous exposure of two non-screen films, interposing a thin layer of aluminum 0.5 mm in thickness. The upper film then reveals good contrast of the thicker portions of the breast and the film covered by the aluminum foil reveals good contrast of the anterior portions. . . ."

The widespread adoption of mammography is primarily attributable to the work of Egan and his coworkers. In 1960, Egan described a reproducible, high milliamperage–low kilovoltage technique that used industrial film (Fig. 3B), and he reported excellent results in imaging the breasts of his first 1000 patients [11]. This welcome news overcame the technical barriers to the widespread use of mammography and led to the training of radiologists and technologists across the United States in the performance and interpretation of mammograms (Fig. 3A) [12]. In February 1965, a Standardization Conference on Mammography, sponsored by an Ad Hoc Committee of the American College of Radiology (ACR), produced (1) an agreement on recommended techniques and dosages and (2) a reproducible technique for diagnostic-quality examinations. The ACR took the leading role in mammography training through its establishment of a Mammography Committee chaired by Wendell Scott. With grant support from the Cancer Control Branch of the United States Public Health Service, the committee developed unique teaching aids and established teaching centers throughout the United States, where interested radiologists and technologists could spend 1 week undergoing practical training, with travel and living expenses paid by the government [13].

The evolution of xeromammography provides an excellent example of a successful collaboration between industry and medicine. The basic physical principles of producing electrostatic images were known as early as 1777, when Lichtenberg made charged patterns visible with charged powder [14]. In 1903, Righi made the first radiograph, using powder development of an electrostatic image [15]. Carlson, in 1937, developed the basic principles of xerography that, in 1950, evolved into the commercial production of the Xerox copier for the reproduction of documents [16]. In 1952, a study of the medical potential of xeroradiography was undertaken by Roach and Hilleboe [17]. In 1960, Gould et al. [18] reported on the greater breast image detail that was possible with

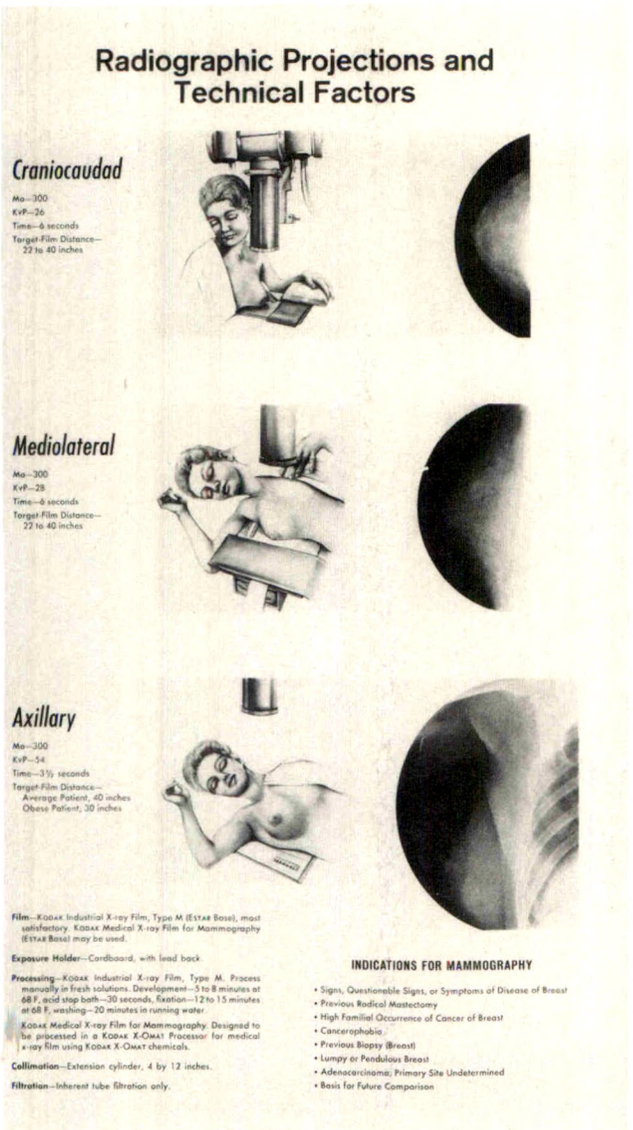

A

B

Fig. 3.—Egan technique.

***A*, Radiographic projections and technical factors for performing mammography were developed by Egan and taught to radiologists throughout the United States during the 1960s. From "Mammography," chart printed by Eastman Kodak Co., Radiography Markets Division, Rochester, NY 14650. Courtesy of Eastman Kodak.**

***B*, Egan mediolateral mammogram showing large cyst. Technical factors included 28 kVp, 300 mA, 6-sec exposure, target-film distance 40 in., nonscreen industrial film. Courtesy of Robert Egan.**

xeroradiography. Wolfe began his investigations of xeromammography in 1966, using a primitive Xerox radiographic unit. Through perseverance and numerous modifications of the equipment, and with the cooperation of the Xerox Company, Wolfe was able to improve image quality and reliability to the point that in 1971, the Xerox System 125 became commercially available. Thus, through advances in both film and xeroradiographic applications, mammography was transformed from an investigative procedure used only in a few large institutions to a valuable clinical diagnostic examination available to all.

Mammography for Cancer Screening

In 1958, Kremens, in reporting his results in 1000 mammograms, included in his list of indications for mammography "a survey project among healthy women for early detection of cancer" [19]. In a 1962 article [20], Egan reported 53 cases of occult carcinoma identified in 2000 consecutive examinations. He defined an occult carcinoma as "one which remains totally unsuspected following examination by the usual methods used to diagnose breast cancer, including an examination of the breast by an experienced and competent physician. To qualify for this definition, no symptoms (vague pain, itching, or heaviness) nor signs (nipple discharge, change in breast contour, or nodules) should be present which would suggest a disease process within the organ." Soon after, Martin et al. [21] confirmed the potential of mammography to detect unsuspected carcinoma in a private-practice setting. Gershon-Cohen et al. [22]; and Levitan et al. [23] were among those who elaborated on the most frequently encountered mammographic sign of nonpalpable breast cancer—microcalcifications. In 1973, Strax et al. [24] reported the 5-year follow-up results of the Health Insurance Plan of Greater New York

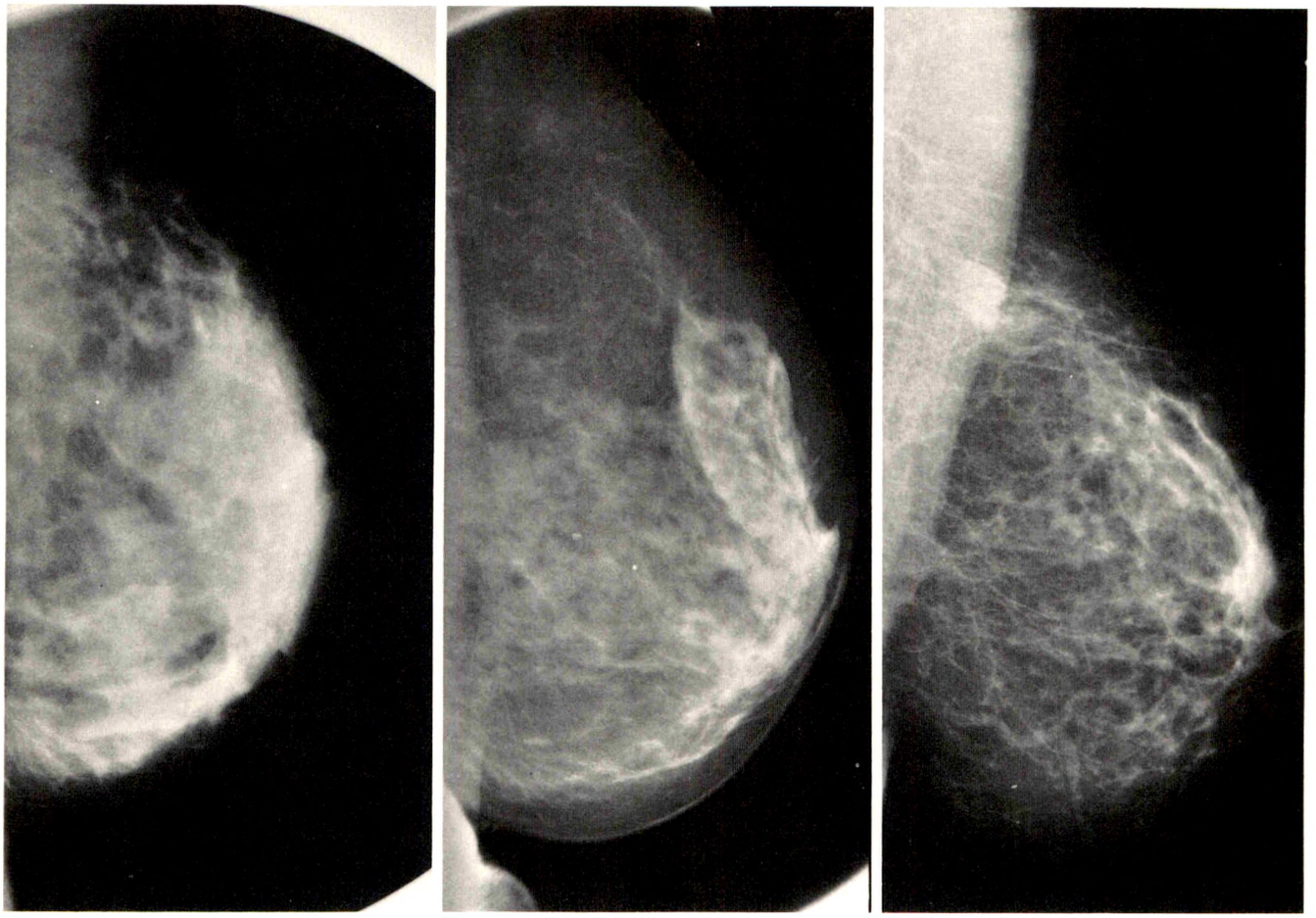

Fig. 4.—Evolution of film mammography with dedicated units.

***A*, 1969 mammogram performed by Dr. Gros with nonscreen, industrial film, 0.7-mm (nominal) focal spot, molybdenum target at 35-cm source-image distance, and technical factors of 28 kVp, 40 mA, 4 sec. Normal examination.**

***B*, 1975 mammogram performed with Du Pont Lo-Dose I single-screen/single-emulsion film combination, 0.7-mm (nominal) focal spot, molybdenum target, 35-cm source-image distance, and technical factors of 28 kVp, 31 mA, 1 sec. Normal examination.**

***C*, 1987 mediolateral oblique mammogram, performed with Kodak MinR rare-earth screen/OM-single-emulsion film combination, 0.3-mm molybdenum target, 60-cm source-to-image distance, moving grid, and technical factors of 28 kVp with automatic exposure control, and extended (3-min) film processing. To ensure that deeper tissues are imaged, portion of pectoral muscle is included down to level of nipple. Carcinoma in axillary tail, near chest wall.**

randomized, controlled, breast cancer screening study. Compared with the mortality rate of the control group, the mortality rate was reduced by one-third for women who were screened by physical examination and mammography.

State of the Art

Advances in technology through the years have ultimately led to a striking improvement in image quality and a dramatic reduction in radiation dose. The first completely dedicated mammography unit was developed by Gros in France in the middle 1960s (Fig. 4A) [25]. A molybdenum target (0.7-mm focal spot) in place of tungsten heightened the contrast between parenchymal, fat, and calcific densities, while a built-in compression device decreased scattered radiation and motion artifacts and separated breast structures. According to Gershon-Cohen et al. [26], these features significantly advanced mammographic imaging. In 1972, the introduction of a high-definition intensifying screen, held by a vacuum in intimate contact with a single-emulsion film, revolutionized film mammography (Fig. 4B) [27]. The new film-screen combination permitted rapid automatic processing, a shorter exposure, a decrease in motion unsharpness, and a greatly reduced dosage. Further advances in dedicated film-screen mammography units included the capability to produce magnified images and the use of grids to reduce scattered radiation (Fig. 4C) [28–30].

Wolfe [31] and Martin [32] popularized xeromammography (Fig. 5A) through their publications and teaching programs. Recently, advances in xeromammography have been directed toward reducing surface exposure through the use of increased aluminum filtration and negative-mode processing (Fig. 5B) [33]. Xerox has just introduced a black-liquid-toner development process that provides improved image resolu-

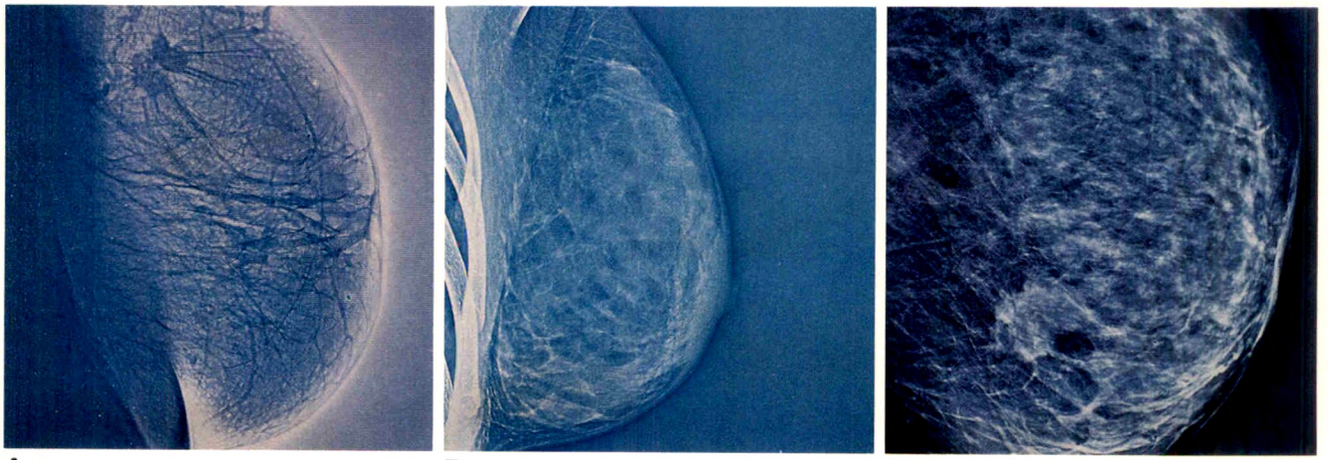

Fig. 5.—Evolution of xeromammography.

Because of space limitations, these images were cropped in the editorial office, significantly decreasing the amount of breast tissue actually depicted in the original images.

A, 1973 positive-mode xeromammogram, Xerox 125 processing system, powder toner, single phase, overhead 1.2-mm tungsten target, 0.5-mm aluminum filtration, 76-cm source-image distance, and technical factors of 40 kVp and 300 mAs. Carcinoma in upper hemisphere.

B, 1978 negative-mode xeromammogram, Xerox 125/6 processing system, powder toner, single phase, overhead 1.2-mm tungsten target, 2.5-mm aluminum filtration, 80-cm source-image distance, and technical factors of 50 kVp and 200 mAs. Normal examination.

C, 1987 negative-mode xeromammogram, Xerox 175 processing system, black liquid toner, Xerox 120 dedicated unit (three phase), 0.3/0.6-mm tungsten target, 2.6-mm aluminum filtration, 80-cm source-image distance, technical factors of 48 kVp and 75 mAs, and enhanced photoreceptor sensitivity. Carcinoma in lower hemisphere. Courtesy of Xerox Corporation.

tion and broad area contrast, with a corresponding reduction in exposure made possible through enhanced photoreceptor sensitivity (Fig. 5C).

Clinical investigations have failed to reveal a significant difference in accuracy between film-screen mammography performed with dedicated equipment and xeromammography [34]. Although film-screen mammography currently requires less radiation than does xeromammography, developments in both techniques have been characterized by significant dose reduction compared with previous radiographic methods [35].

Using state-of-the-art equipment, mammographers have learned to identify subtle, indirect signs of breast cancer in its earliest stage, when there is a high likelihood for cure. In addition to calcifications, these early signs include architectural distortion, a developing neodensity, parenchymal asymmetry between right and left breasts, and a unilateral focus of one or several prominent ducts [36, 37]. Radiologists have also developed guidelines for managing equivocal findings [38].

The detection of more nonpalpable cancers has resulted in a need for better methods to locate these lesions before surgery. In 1966, Berger et al. [39] recommended preoperative localization by means of precise descriptions and carefully prepared diagrams. They also emphasized the importance of specimen radiography to ensure that the suspicious area was removed. Inserting a needle directly into the area of suspicion and leaving it in place to guide the surgeon proved to be a more accurate method for prebiopsy localization [40]. A dye, sometimes mixed with a radiopaque contrast medium, can also be injected through the properly placed needle in or near the nonpalpable lesion [41]. More recently, needle/wire systems have been developed especially for localizing nonpalpable breast lesions [42–45]. Malleable, barbed-tip, self-retaining wires are less likely to be displaced during mammographic compression or at surgery. Special compression devices have been designed to guide needle placement [46], and researchers continue to develop useful variations in localization methods [47–48].

In the late 1970s, the future of breast cancer screening with mammography seemed to be doomed because of public fears of radiation-induced carcinoma. However, recent improvements in the ability of mammography to detect early, curable cancer, in conjunction with markedly lower radiation doses, have enabled radiologists to show that the benefits of mammography far outweigh the theoretical risks [49–50].

Underutilization of Mammography: Responding to the Challenge

In 1955, Gershon-Cohen and Ingleby [51] lamented the underutilization of mammography because "periodic roentgenographic studies of [ostensibly] normal breasts could be is now usually done in patients who accidentally discover the lesions." Since that time, mammography has progressed to used effectively to detect and care for carcinoma earlier than the point where it is now universally endorsed as the most effective method for early breast cancer detection [52].

The challenges that face mammography in the future are both difficult and fascinating. They include working toward the ultimate goal of universal screening for all women, training an adequate number of qualified personnel to perform and interpret the mammograms generated by universal screening, and, finally, further defining the tenuous line that separates mammographically discovered lesions that require biopsy from those that do not.

ACKNOWLEDGMENTS

The authors are grateful for the efforts of Jean Chaintreuil and Dianne R. Lavellee (both of Thomson CGR Medical Corporation, Columbia, MD) and for the help of Ellen M. Proctor and Paul M. Chenderlin (both of Xerox Medical Systems, Pasadena, CA).

REFERENCES

1. Salomon A. Beiträge zur Pathologie und Klinik der Mammakarzinome. *Arch Klin Chir* **1913**;101:573–668
2. Warren SL. A roentgenologic study of the breast. *Am J Roentgenol Radium Ther* **1930**;24:113–124
3. Lockwood IH. Roentgen-ray evaluation of breast symptoms. *Am J Roentgenol Radium Ther* **1933**;29:145–155
4. Gershon-Cohen J, Strickler A. Roentgenologic examination of the normal breast: its evaluation in demonstrating early neoplastic changes. *Am J Roentgenol Radium Ther* **1938**;40:189–201
5. Anthony BW, Pollack HC. Extraordinary calcification in the breast. *Am J Roentgenol Radium Ther* **1943**;49:600–602
6. Leborgne R. Diagnosis of tumors of the breast by simple roentgenography: calcifications in carcinoma. *Am J Roentgenol Radium Ther* **1951**;65:1–11
7. Gershon-Cohen J, Ingleby H. Roentgenography of cancer of the breast: a classified pathological basis for roentgenologic criteria. *Am J Roentgenol Radium Ther Nucl Med* **1952**;68:1–7
8. Gershon-Cohen J, Ingleby H, Hermel MB. Calcification in secretory disease of the breast. *Am J Roentgenol Radium Ther Nucl Med* **1956**;76:132–135
9. Gershon-Cohen J, Ingleby H. The roentgenography of mammary abscess and mammillary fistula. *Am J Roentgenol Radium Ther Nucl Med* **1958**;79:122–128
10. Gershon-Cohen J. Technical improvements in breast roentgenography. *Am J Roentgenol Radium Ther Nucl Med* **1960**;84:224–226
11. Egan RL. Experience with mammography in a tumor institution. Evaluation of 1000 cases. *Radiology* **1960**;75:894–900
12. Egan RL. Reproducibility of mammography: a preliminary report. *Am J Roentgenol Radium Ther Nucl Med* **1963**;90:356–358
13. Scott WG. Mammography and the training program of the American College of Radiology. *Am J Roentgenol Radium Ther Nucl Med* **1967**;99:1002–1008
14. Kossel F. Physical aspects of xeroradiology as a tool in cancer diagnosis and tumor localization. *Prog Clin Cancer* **1967**;3:176–185
15. Righi A. *Die Bewegung der loner fei der Elektrischen Entladung*. Leipzig: Verlag Johan Ambrosius Barth, **1907**
16. Densdale A. Chester F. Carlson: inventor of xerography. *Photogr Sci Eng* **1963**;7:1
17. Roach JF, Hilleboe HE. Xeroradiography. *Am J Roentgenol Radium Ther Nucl Med* **1955**;73:5–9
18. Gould HR, Ruzicka FF, Sanchez-Ubeda R, Perez J. Xeroradiography of the breast. *Am J Roentgenol Radium Ther Nucl Med* **1960**;84:220–223
19. Kremens V. Roentgenography of the breast. *Am J Roentgenol Radium Ther Nucl Med* **1958**;80:1005–1013
20. Egan RL. Fifty-three cases of carcinoma of the breast, occult until mammography. *Am J Roentgenol Radium Ther Nucl Med* **1962**;88:1095–1101
21. Martin JE, Keegan JM, Lemak LL, Yates CW. Clinically unsuspected carcinoma of the breast: a study in private practice. *Am J Roentgenol Radium Ther Nucl Med* **1962**;88:1102–1108
22. Gershon-Cohen J, Yiu LS, Berger SM. The diagnostic importance of calcareous patterns in roengenography of breast cancer. *Am J Roentgenol Ther Radium Nucl Med* **1962**;88:1117–1125
23. Levitan LH, Witten DM, Harrison EG Jr. Calcification in breast disease. Mammographic-pathologic correlation. *Am J Roentgenol Ther Radium Nucl Med* **1964**;92:29–39
24. Strax P, Venet L, Shapiro S. Value of mammography in reduction of mortality from breast cancer in mass screening. *Am J Roentgenol Ther Radium Nucl Med* **1973**;117:686–689
25. Gros CM. Methodologie. *J Radiol Electrol Med Nucl* **1967**;48:638–655
26. Gershon-Cohen J, Hermel MB, Birsner JW. Advances in mammographic technique. *Am J Roentgenol Radium Ther Nucl Med* **1970**;108:424–427
27. Weiss JP, Wayrynen RE. Imaging system for low-dose mammography. *J Appl Photogr Engr* **1976**;2:7–10
28. Muntz EP, Logan WW. Focal spot size and scatter suppression in magnification mammography. *AJR* **1979**;133:453–459
29. Sickles E, Weber WN. High-contrast mammography with a moving grid: assessment of clinical utility. *AJR* **1986**;146:1137–1139
30. Dershaw DD, Malik S. Stationary and moving mammography grids: comparative radiation dose. *AJR* **1986**;147:491–492
31. Wolfe JN. Xerography of the breast. *Radiology* **1968**;91:231–240
32. Martin JE. Xeromammography—an improved diagnostic method: review of 250 biopsied cases. *Am J Roentgenol Radium Ther Nucl Med* **1973**;117:90–96
33. Van de Riet WG, Wolfe JN. Dose reduction in xeroradiography of the breast. *AJR* **1976**;126:1130–1139
34. Pagani JJ, Bassett LW, Gold RH, et al. Efficacy of combined film-screen/xeromammography: preliminary report. *AJR* **1980**;135:141–146
35. Muntz EP, Wilkinson E, George FW. Mammography at reduced doses: present performance and future possibilities. *AJR* **1980**;134:741–747
36. Martin JE, Moskowitz M, Milbrath JR. Breast cancer missed by mammography. *AJR* **1979**;132:737–739
37. Sickles EA. Mammographic features of 300 consecutive nonpalpable breast cancers. *AJR* **1986**;146:661–663
38. Homer MJ. Nonpalpable mammographic abnormalities: timing the follow-up studies. *AJR* **1981**;136:923–926
39. Berger SM, Curcio BM, Gershon-Cohen J, Isard HJ. Mammographic localization of unsuspected breast cancer. *Am J Roentgenol Radium Ther Nucl Med* **1966**;96:1046–1052
40. Threatt B, Appelman H, Dow R, O'Rourke T. Percutaneous needle localization of clustered mammary microcalcifications prior to biopsy. *Am J Roentgenol Radium Ther Nucl Med* **1974**;121:839–842
41. Horns JW, Arndt RD. Percutaneous spot localization of nonpalpable breast lesions. *Am J Roentgenol* **1976**;127:253–256
42. Hall FM, Frank HA. Preoperative localization of nonpalpable breast lesions. *AJR* **1979**;132:101–105
43. Stephenson TF. Chiba needle–barbed wire technique for breast biopsy localization. *AJR* **1980**;135:184–186
44. Kopans DB, Meyer JE. Versatile spring hookwire breast lesion localizer. *AJR* **1982**;138:586–587
45. Parekh NJ, Wolfe JN. Localization device for occult breast lesions: use in 75 patients. *AJR* **1987**;148:699–701
46. Muhlow A. A device for precision needle biopsy of the breast at mammography. *Am J Roentgenol Radium Ther Nucl Med* **1974**;121:843–845
47. Homer MJ. Localization of nonpalpable breast lesions: technical aspects and analysis of 80 cases. *AJR* **1983**;140:807–811
48. Kopans DB, Waitzkin ED, Linetsky L, et al. Localization of breast lesions identified on only one mammographic view. *AJR* **1987**;149:39–41
49. Moskowitz M. Mammography to screen asymptomatic women for breast cancer. *AJR* **1984**;143:457–459
50. Feig SA. Radiation risk from mammography: is it clinically significant? *AJR* **1984**;143:469–475
51. Gershon-Cohen J, Ingleby H. Neglected roentgenography of breast disease. *JAMA* **1955**;157:325–326
52. Feig SA, Shaber GS, Patchefsky A, et al. Analysis of clinically occult and mammographically occult breast tumors. *Am J Roentgenol* **1977**;128:403–408

VOL. 50, NO. 6

SMALL INTESTINAL ENEMA*

By RICHARD SCHATZKI, M.D.
BOSTON, MASSACHUSETTS

THE examination of the small intestine has always been a stepchild of roentgenology. In all other parts of the gastrointestinal tract the examination is performed by observing roentgenoscopically the actual filling of the organ in question and then by studying the partially or completely filled organ. If the usual roentgenological methods are used such an examination of the small intestine is not possible due to the obstacle which the pylorus causes in the continuous outflow of barium.

It seemed likely that a satisfactory examination of the small intestine would become possible if the barium were introduced through a duodenal tube. In this way the filling of the small intestine would become similar to that of the colon through a rectal tube; it would in fact be an enema examination of the small intestine. The initial tests were surprisingly satisfactory.

A review of the literature showed that a similar procedure had been proposed independently in three previous publications. Various authors had used a tube in order to study the duodenum roentgenologically, but Pesquera[3] (1929) was apparently the first to recommend the use of the duodenal tube for a continuous filling of the small intestine in the sense outlined above. He was followed by Ghelow and Mengis[2] (1938) and by Gershon-Cohen and Shay[1] (1939). The last two authors called the method barium enteroclysis. All essential features of the subject are contained in their short but comprehensive article. We have used the tube examination of the small intestine (at first without knowledge of the preceding publications) in approximately 75 cases. The results have been encouraging enough to recommend its use as a routine procedure.

METHOD OF EXAMINATION

Aside from the necessity of an empty stomach, a special preparation is not required. An empty colon is helpful but not obligatory. A soft rubber tube with a metal olive tip (Rehfuss tube) is introduced into the duodenum through the mouth. In sensitive patients it may be advisable to insert the tube without the olive through the nose and attach the olive when the tip of the tube has appeared in the oral pharynx. The patient is ready for the examination as soon as the olive is in the duodenum.

As contrast substance we use a mixture which is thinner than that used for our usual gastrointestinal examination (equal parts of water and barium by volume). For the small intestinal enema two glasses of lukewarm water are added to one glass of the usual barium mixture. This corresponds approximately to 6 parts of barium to 20 parts of water by volume. Some patients complain of uncomfortable sensations in their throats unless the mixture is lukewarm.

Five hundred to 1,000 cc. are necessary to examine the small intestine. In cases with marked reflux of barium into the stomach larger amounts have been used occasionally but have proved to be of no help.

In order to inject the barium mixture, we started by using a syringe. We now find it more advantageous to let the barium run from a small pint container (transfusion flask) which the attendant holds over her head. This guarantees a more continuous flow of the barium, which we believe to be essential for the success of the examination. In most instances the pylorus prevents an appreciable amount of barium from getting into the stomach, but in some cases there is a very disturbing reflux into the stomach.

* From the Department of Radiology, Massachusetts General Hospital, Boston, Massachusetts. Presented at the Forty-third Annual Meeting, American Roentgen Ray Society, Chicago, Ill., Sept. 15–18, 1942.

This paper is reprinted verbatim from *AJR* 1943;50:743–751.

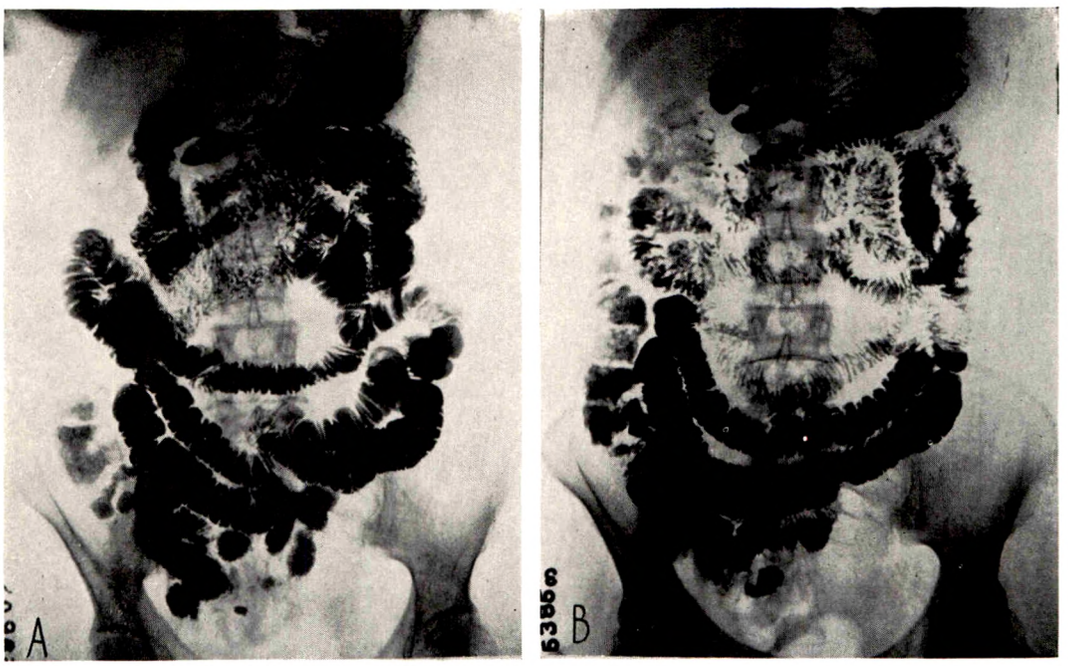

FIG. 1. Normal small intestinal enema. The ileocecal valve was reached at the end of eleven minutes. *A*, roentgenogram taken sixteen minutes after the beginning of the examination. *B*, roentgenogram taken thirty-six minutes after the beginning of the examination.

This reflux is usually not remedied, as might be expected, by lowering the enema can and thereby decreasing the duodenal pressure. For one thing, lowering of the can beyond a certain point is impossible without impeding the progress of the barium column; for another, the reflux is dependent not only on pressure in the duodenum, because it may occur in a patient whose duodenum is incompletely filled.

The filling of the intestine is observed roentgenoscopically. In most normal cases it is possible to follow the head of the barium column; in other cases it is not possible, because the filling of the small intestine is retarded, usually by reflux of barium into the stomach.

In order to avoid overexposure, it is advisable to roentgenoscope with only 2 to 3

FIG. 2. Normal small intestinal enema in a patient with colonic polyposis. (The cecum was reached in eight minutes. This roentgenogram was taken fifteen minutes after the beginning of the examination.)

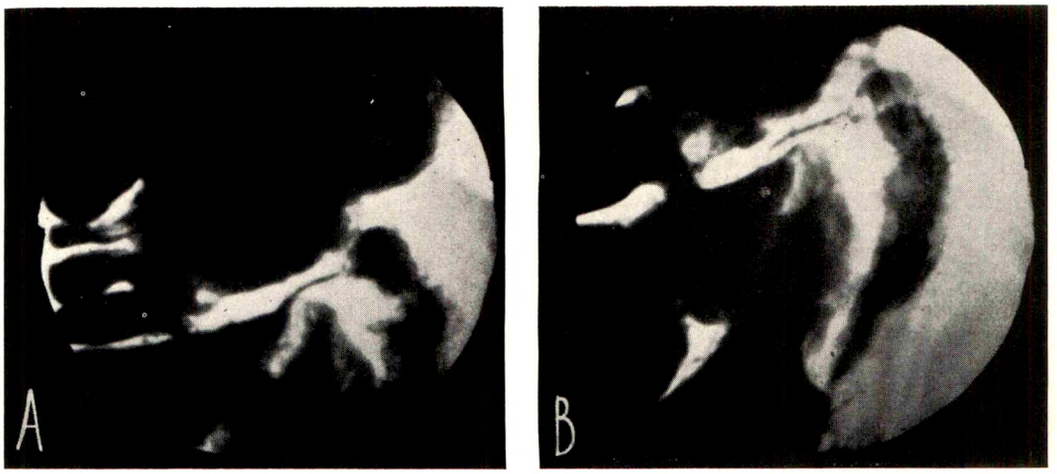

FIG. 3. Normal ileocecal valve demonstrated by small intestinal enema.

ma., which will provide a perfectly satisfactory light for examination of the small intestine. Care should be taken to keep the total time of roentgenoscopy within the zone of safety.

The barium reaches the cecum in a surprisingly short time. In 35 normal cases the

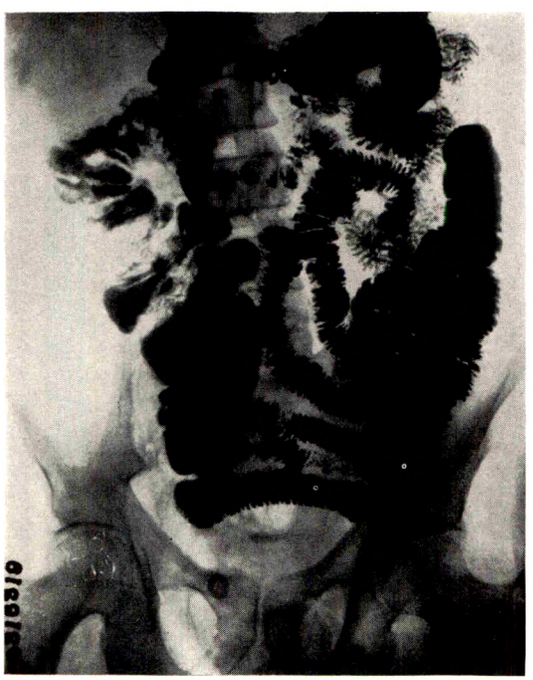

FIG. 4. Clinical diagnosis: actinomycotic abscess in right flank; questionable involvement of cecum and ileum. Small intestinal enema: mass displacing cecum and ileum; no involvement of the intestines. (Cecum was reached in thirteen minutes. This roentgenogram was taken at the end of thirty minutes.)

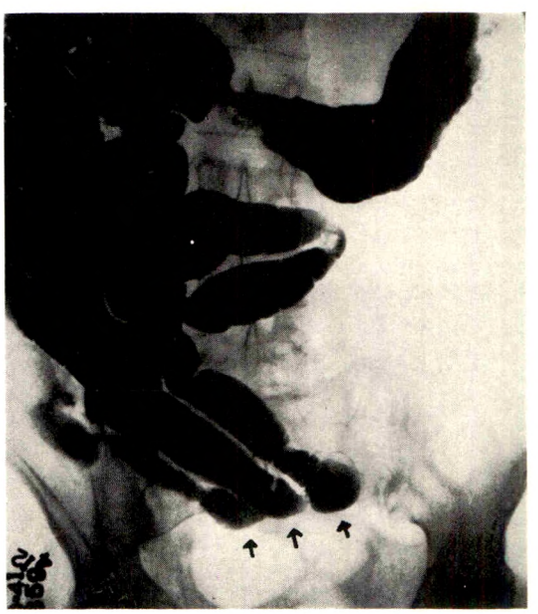

FIG. 5. Clinical diagnosis: treated cancer of cervix; question of intestinal obstruction. Small intestinal enema: three loops of small intestine adherent to pelvic mass (see arrows); no obstruction at present. Congenital absent rotation of small intestine as an accidental finding. (Cecum was reached at the end of thirty-five minutes. This roentgenogram was taken at the end of twenty-seven minutes.)

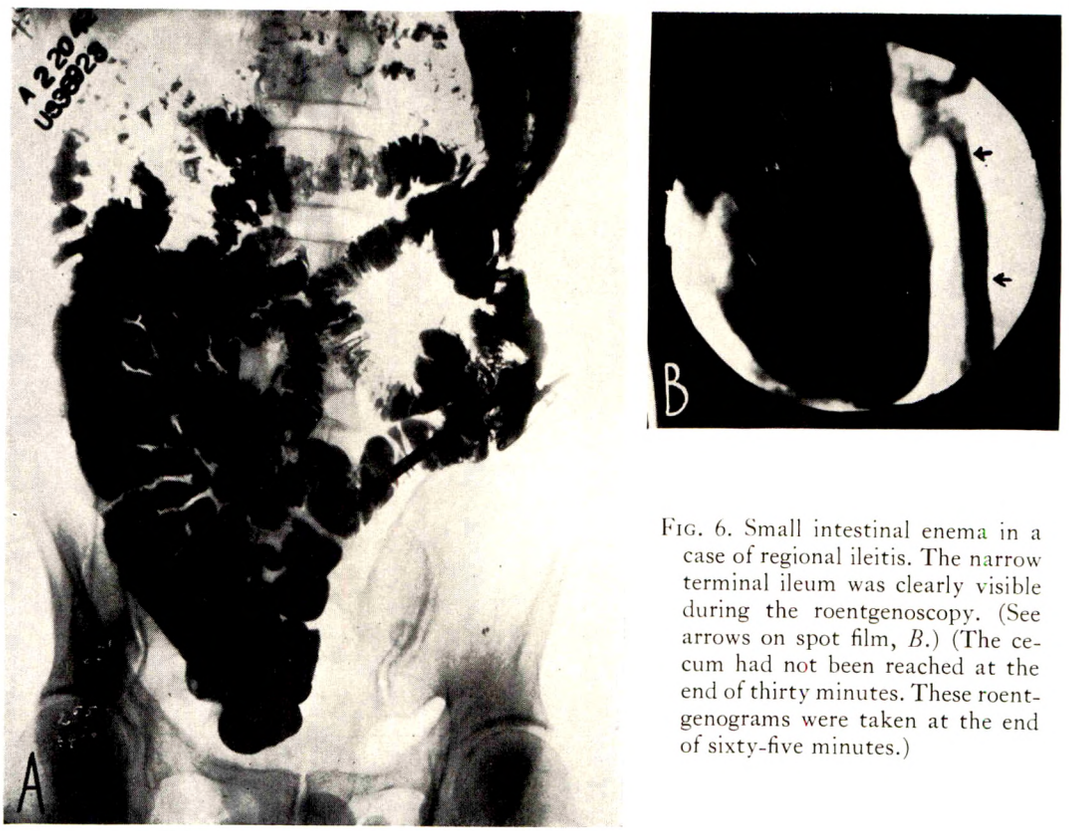

FIG. 6. Small intestinal enema in a case of regional ileitis. The narrow terminal ileum was clearly visible during the roentgenoscopy. (See arrows on spot film, *B*.) (The cecum had not been reached at the end of thirty minutes. These roentgenograms were taken at the end of sixty-five minutes.)

average time was fifteen minutes. The earliest filling of the cecum occurred in five minutes. In 4 normal cases only did the filling require more than twenty minutes (22, 26, 30 and 90 minutes). In all except the first of these cases marked reflux of barium into the stomach caused the delay. In most pathological cases more time was required, the average being thirty-seven minutes in 19 checked cases.

Constant flow of the enema fluid is necessary. Any interruption will delay the examination markedly. The impression is sometimes gained that the filling of the small intestine actually has to start anew after an interruption.

Ghelew and Mengis, as well as Gershon-Cohen and Shay, have used insufflation of

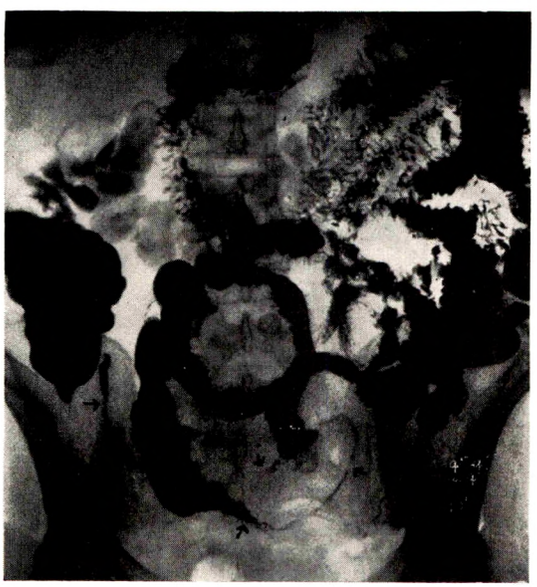

FIG. 7. Extensive regional ileitis (arrows). Small intestinal enema outlines not only the disease but also the approximate length of the uninvolved small intestine. (The cecum was reached at the end of fifteen minutes. This roentgenogram was taken at the end of ninety minutes.)

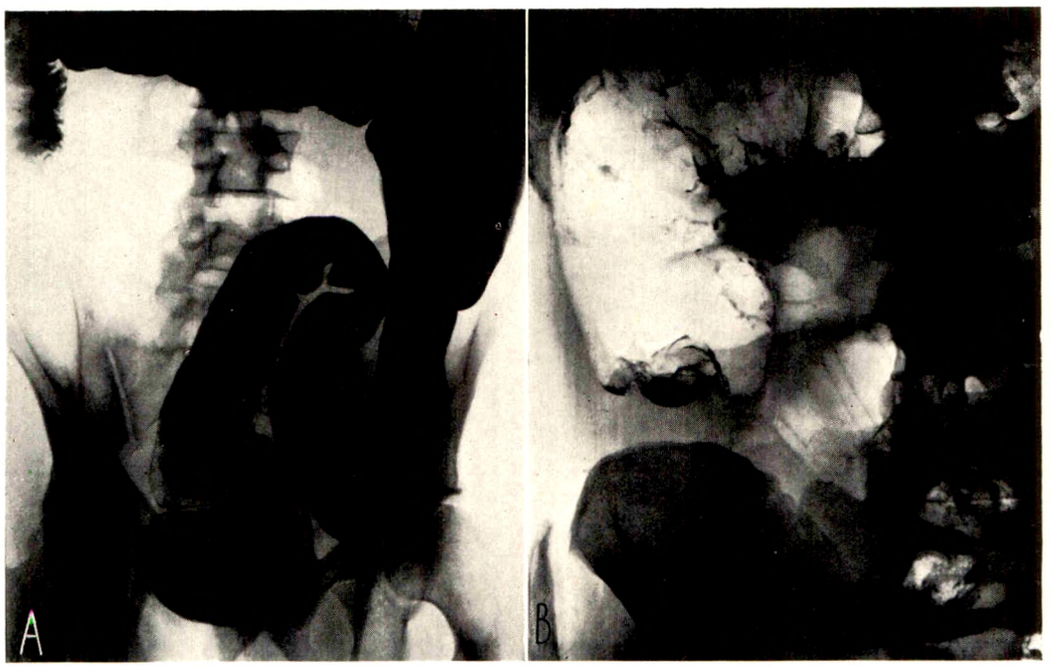

FIG. 8. Ileocecal tuberculosis. Routine barium enema shows obstruction which was erroneously interpreted as a mass in the lower cecum. *A*, before evacuation; *B*, after evacuation and air insufflation. (See also Fig. 9 of the same case.)

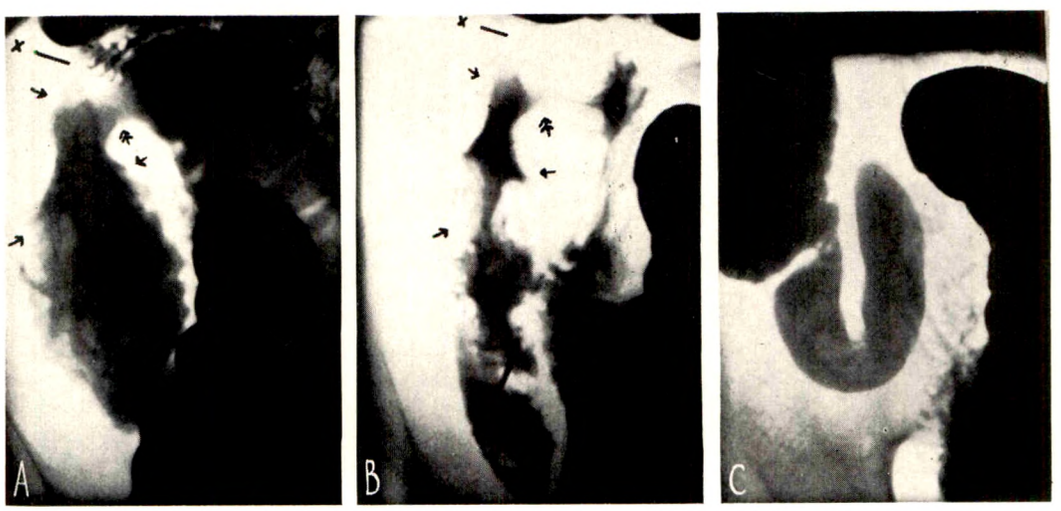

FIG. 9. Same case as in Figure 8. Ileocecal tuberculosis. Small intestinal enema outlines the ulcerated tumor-forming lesion which involves the lower ascending colon and the upper fourth of the cecum (see single arrow). The point of obstruction lies in the ascending colon, and not in the cecum (*X*); the ileocecal valve appears stiff (see double arrow); neither the lower part of the cecum nor the ileum was involved, as is shown by their normal elasticity. Note the distended ileum in *A*, and the distended cecum and appendix in *C*. (The dense shadows on the right side of the figures are produced by the palpating glove.)

air through the duodenal tube for double contrast studies. We have had no experience with this method.

ADVANTAGES OF THE METHOD

1. The small intestine is seen filled in its entirety. The resulting advantages are manifold. Circumscribed lesions can be excluded with more certainty. However, in our series of approximately 75 patients, we have not seen either a small tumor or a Meckel's diverticulum. The position and the relationship of various groups of small intestinal coils can be studied reliably. The presence or absence of small portions of intestine within a hernial sac can be readily visualized. The accurate demonstration of the site of a small intestinal fistula is made possible. In cases of cicatrizing enteritis the length of grossly normal bowel proximal to the diseased area can be estimated with greater accuracy than with the usual method, a fact which may be of decisive importance concerning the operability of a given case (Fig. 7).

2. The actual filling of the small intestinal loops can be observed roentgenoscopically. The ensuing advantages for the discovery and study of pathological conditions are obvious. The extent of a lesion, its relationship to neighboring structures, and the presence or absence of rigidity can be judged with greater accuracy than with the usual methods. In cicatrizing enteritis the barium at times is spurted through the region of maximal narrowing, preventing its demonstration unless the filling is actually seen during the enema examination.

3. Due to the dehydration of the barium mixture the usual peroral examination of the small intestine often results in a lumpy incomplete filling of the ileum. The small intestinal enema transports the barium to the ileum in such short time that notice-

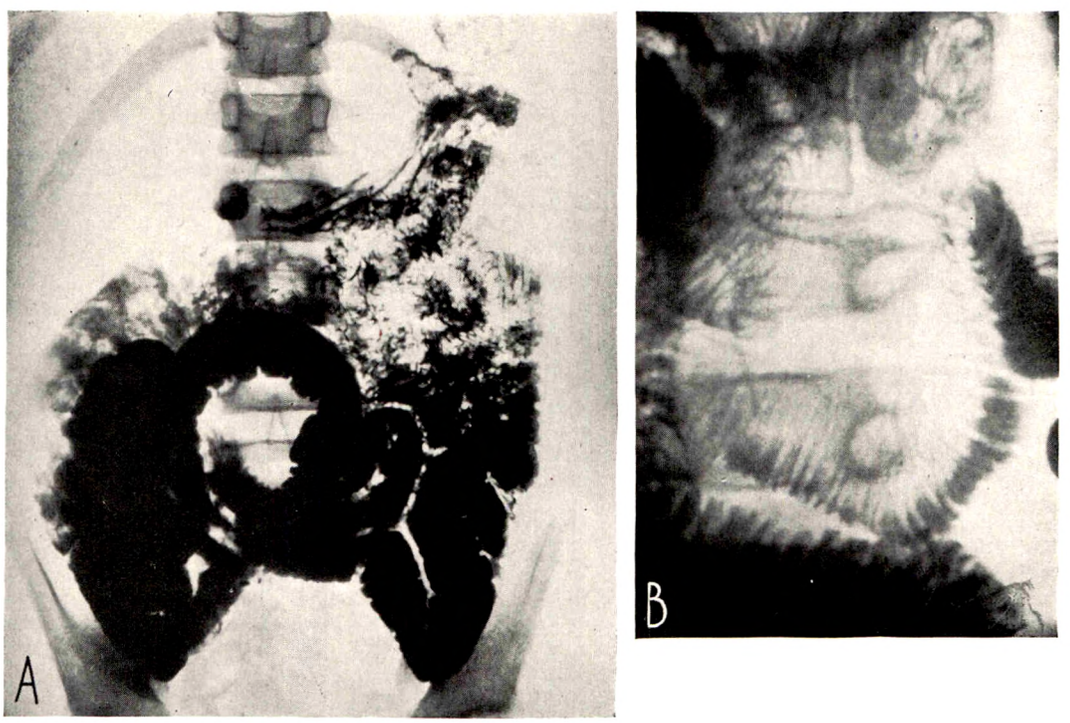

FIG. 10. Extrinsic mass clearly outlined by the small intestinal enema (abdominal lymphoma). The defect was constant during roentgenoscopy as shown by spot film, *B*. Compare with Figure 11. (Lower defect produced by the filled urinary bladder.)

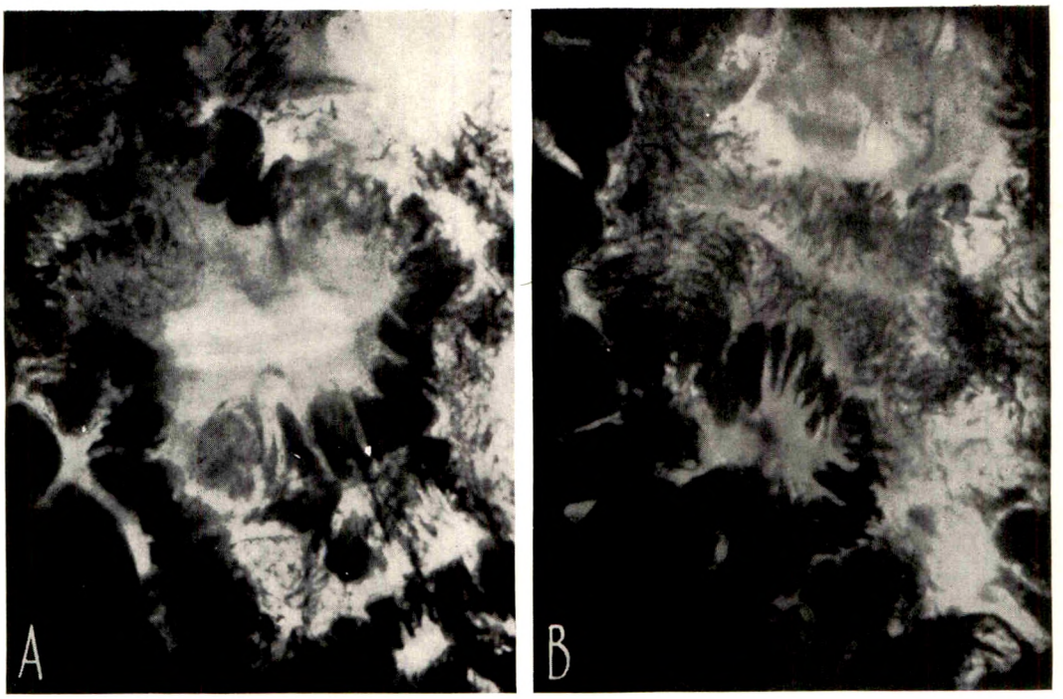

FIG. 11. Pseudo-tumor, commonly seen, produced by interposition of non-filled loops of intestine or by omentum. Note disappearance of pseudo-tumor in expiration in contradistinction to true extrinsic tumor (Fig. 10). *A*, inspiration; *B*, expiration.

able dehydration does not take place.

4. An adequate examination of the ileocecal valve, the cecum, and the ascending colon, with a *fluid* barium mixture, is made possible in all those cases in which an examination by rectal enema is impossible or unsatisfactory (e.g., in anal insufficiency or in spasm of the cecum and ascending colon). (See Fig. 3, 8 and 9.)

5. The time which is required for the actual examination is shortened. The reduction of time is particularly striking in that large group of normal cases in which a pathological condition is to be excluded. In cases with a marked pathological condition the filling time of the small intestine is occasionally no shorter than with the conventional method.

FIG. 12. Small intestinal enema in a patient with tuberculous peritonitis. Rapid filling of the small intestine, the cecum being reached at the end of six minutes; fixed position of the small intestinal loops. The small intestine has risen out of the true pelvis and occupies a smaller space than usual. The peritoneal cavity was found to be obliterated at operation.

DIFFICULTIES CONNECTED WITH THE METHOD

1. The method requires the introduction of a duodenal tube with its usual annoyances and difficulties. With a little experience and patience on the part of the examiner this procedure is not too difficult, and is successful in the great majority of cases. At the beginning of our studies we kept a record of our failures. In only 3 out of 38 attempts did the tube fail to enter the duodenum. The introduction of the duodenal tube is much easier than that of the Miller-Abbott tube, and is, in fact, practical for office procedure.

2. The purpose of the examination is defeated if the filling of the small intestine takes place very slowly, which in normal cases is usually due to reflux of barium from the duodenum into the stomach. Fortunately, cases with marked reflux are the exception, and when they are encountered the progress of the barium can be hastened by having the patient lie partially (or if necessary, completely) on his right side. Attempts to reduce reflux by the addition of an acid buffer to the barium mixture have failed so far to show result, as has decrease in the amount of hydraulic pressure applied, or increase in the amount of barium mixture used.

3. The primary purpose of the method is the demonstration of organic pathology. Functional changes as well as a combination of functional and organic lesions as seen at times in deficiency disease are usually studied better with the conventional type of follow-up examination. The use of *both* methods has been worth while in some conditions.

CONTRAINDICATIONS

Aside from occasional slight cramping pains, which are easily overcome by lowering the enema can, we have not seen any harmful effect from the small intestinal enema. It seems wise, however, to state conditions which are believed to contraindicate the examination:

1. Obviously, the examination should not be performed in any case in which the *routine* examination of the gastrointestinal tract is contraindicated. Therefore, the small intestinal enema is contraindicated in cases with marked mechanical or paralytic ileus. It has been used successfully, however, in several cases of partial obstruction of the small bowel.

2. A small intestinal enema should not be performed in cases with suspected gangrene of the bowel (e.g., mesenteric thrombosis, incarcerated hernia).

3. It seems inadvisable to use the small intestinal enema in patients with an active duodenal ulcer. As a routine procedure it is therefore better to precede the enema by an examination of the stomach and duodenum. The method has been used without difficulty in several cases of old inactive duodenal ulcer.

CONCLUSION

The small intestinal enema represents an improvement in the examination of the small intestine. If successful, it is better than any other available method for the study of morphological changes in the small intestine. The advantages and limitations of the method are discussed.

REFERENCES

1. GERSHON-COHEN, J., and SHAY, H. Barium enteroclysis; method for direct immediate examination of the small intestine by single and double contrast techniques. AM. J. ROENTGENOL. & RAD. THERAPY, 1939, *42*, 456–458.
2. GHELEW, B., and MENGIS, O. Mise en évidence de l'intestin grêle par une nouvelle technique radiologique. *Presse méd.*, 1938, *46*, 444–445.
3. PESQUERA, G. S. Method for direct visualization of lesions in small intestines. AM. J. ROENTGENOL. & RAD. THERAPY, 1929, *22*, 254–257.

DISCUSSION

DR. ROSS GOLDEN, New York City. Although, as Dr. Schatzki said, he did not invent this method, nevertheless he has done us a great service in calling it to our attention and in showing us how useful it can be. I am wondering whether it might not be an advantage to use a tube with a balloon on it, like the Miller-Abbott

tube, which could be inflated when the tip gets into the duodenum and which would promptly be carried around into the jejunum so that barium would be injected into the jejunum and not into the duodenum, thereby avoiding the reflux into the stomach.

The injection of so much water into the small intestine is, of course, not physiological. One function of the intestine is to make isotonic either hypotonic or hypertonic solutions. The question might be raised as to whether it would be of advantage to use normal saline instead of water as the suspending medium to avoid that part of the unphysiological condition. There are obviously certain cases in which this method is particularly indicated. I should like to show a couple of slides to illustrate one such case.

This patient was a colored woman about thirty-seven years old, who was bleeding from the intestine and had developed severe secondary anemia and hypoproteinemia. Her serum protein was about 5.5. A regular small intestine study was done which showed marked segmentation but no cause for the bleeding was demonstrated. A Miller-Abbott tube was then inserted and a specimen was taken at every foot as it went in. At about 6 feet a positive guaiac test was obtained. The patient was explored and a polypoid adenocarcinoma of the lower jejunum about 3 cm. in diameter was removed. It seems as though we should have been able to demonstrate a mass that large in the lumen of the small intestine. However, the disturbance in intestinal physiology resulting from the hypoproteinemia, with very irregular distribution of the barium due to the marked segmentation, made its detection impossible. If we had injected barium as described by Dr. Schatzki, we might have been able to demonstrate that tumor.

On the other hand, we tried this method in another case in which we had been unable to demonstrate a cause for intestinal hemorrhage on five or six attempts with a small intestine study. A small intestinal enema was done and again a lesion was not demonstrated. At operation a patch of gastric mucosa was found in the ileum in which were two ulcers.

This method, I believe, should be accepted as another string to our bow, so to speak. I should not like to substitute it for the routine small intestine study as we are now using it, because the latter has given us information which I do not believe one could get satisfactorily with this method, but I do believe a small intestinal enema will be valuable in selected cases.

DR. SCHATZKI (closing). I thank Dr. Golden very much for his discussion. In regard to the use of saline solution, I was worried for a while about washing out the whole small intestine, in fact cleaning it out with the enema, but actually nothing seemed to happen. The patients felt perfectly all right. The method is certainly unphysiological as are all our routine barium examinations of the gastrointestinal tract. I wonder whether the use of saline solution would make the procedure more physiological.

We first thought that it would be necessary to introduce the tube down to the jejunum. The position of the tube in the jejunum proved, however, to be no definite protection against reflux of barium into the stomach. Although a position of the tube low in the duodenum or in the first loop of jejunum is desirable, a successful examination is possible as long as the tip lies beyond the pylorus.

A few words in regard to those small lesions which escape one or several examinations: I think the small intestine is the most difficult part of the intestinal tract to examine because it has such an extremely thin wall and is so markedly flexible. There may be quite a large lesion occupying one-fourth of the circumference and still the flexibility of the remaining three-fourths makes the intestine appear completely normal.

The reader's attention is directed to the Commentary on this article, which appears on pages 510–511 of this issue.

Richard Schatzki, M.D.: A Biography

Stefan C. Schatzki[1]

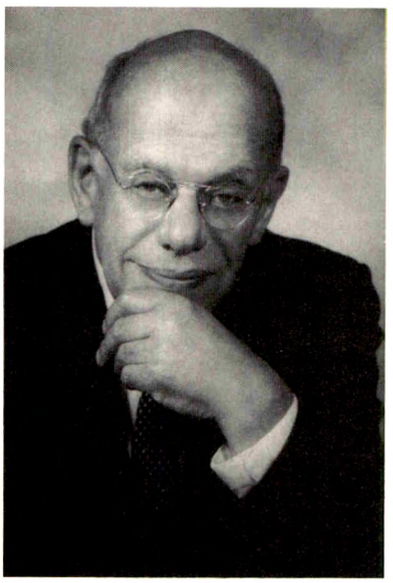

Approaching his 87th birthday, Richard Schatzki continues to have the lively intellect and curiosity that has led to such a large number of fundamental contributions to radiology. While he was reminiscing about his paper on the small intestinal enema, he mused, "It dawned on me how important the pylorus was. Now you could do a small bowel study just like a barium enema."

Richard Schatzki was born on February 22, 1901, in Clafeld, a small suburb of Siegen in Germany. His father was an engineer and died while Richard was a small boy. Richard and his four brothers, all of whom became extremely successful, were nourished by the strength and wisdom of their mother.

After attending local schools, Dr. Schatzki entered medical school when he was 19 years old. As was true for most German medical students of his day, he spent time at a number of medical schools, graduating from the University of Berlin in 1925. He received his M.D. after internships on the medical service at the West End Hospital in Berlin and the surgical service of the University Hospital in Frankfurt am Main. His original thinking was already apparent in the discussion of his M.D. thesis, in which he questioned the relationship between some of the rheumatoid diseases, dermatomyositis, polymyositis, and scleroderma. Unfortunately, his professor crossed out this part of the discussion before publication of the thesis.

Dr. Schatzki spent 1926–1929 on the medical service at the University Hospital in Frankfurt am Main. At first, he was not certain whether to become a surgeon or an internist. Because he believed that some knowledge about radiographic diagnosis would help him in either career, he contacted Dr. Hans Heinrich Berg, an internist who at that time was head of the radiology department of the medical clinic at Frankfurt. Originally Dr. Schatzki planned to spend only 2 months with Dr. Berg, but he stayed for 15 months. However, he did not immediately continue in radiology but worked for 2 additional years on the medical service as head of one of the wards at the University Hospital.

During these 2 years, both he and Greta Stern, another young internist, realized that he was getting less gratification from internal medicine than he wanted. In 1929, following a recommendation by Dr. Berg, Dr. Schatzki accepted an appointment by Professor Paul Morawitz and became chief of the radiology department in the medical clinic at the University Hospital in Leipzig. One year later, he married Greta, thus beginning a close partnership that lasted for more than 50 years.

While in Leipzig, he published the first of numerous articles that were to have such a profound effect on gastrointestinal radiology. In 1931, he presented the first in-depth discussion of esophageal varices and the initial description of gastric varices. The same year he published the first of several articles that were to emphasize the importance of relief studies in the gastrointestinal tract. Two years later, he described the first fluoroscopic demonstration of erosive gastritis, an entity that has been recently rediscovered, and his definitive *Acta* supplement on relief studies of the esophagus, which was to have been his Dozent thesis, was published. As was true in later years, in addition to these papers that presented fundamental advances in gastrointestinal radiology, he published a number of articles in other areas, including one of the first descriptions of the radiographic findings in coarctation of the aorta and calcification of the adrenal gland in tuberculosis.

In 1933, Dr. Schatzki left Germany and arrived, without a position, in Boston. He was met by Dr. Alice Ettinger, another of Berg's students. At Dr. Ettinger's suggestion, he went to Massachusetts General Hospital (MGH), where 1 week later he gave a lecture on relief studies of the esophagus, which he presented in English and, in the German tradition, without notes. Shortly afterward, Dr. George Holmes offered him a position as an assistant in the radiology department, without pay. A small stipend from a committee for displaced scholars allowed Dr. Schatzki to remain in the department until 1935,

[1] Mount Auburn Hospital, 330 Mount Auburn St., Cambridge, MA 02238. Address reprint requests to S. C. Schatzki.

AJR **150:508–509, March 1988** 0361–803X/88/1503–0508 © American Roentgen Ray Society

when a paid position became available. He remained at MGH until he entered the Army in 1943. Between 1933 and 1943, Dr. Schatzki obviously had a profound effect on the trainees in the radiology department, and, as he reminisces about his years at MGH, he believes that he had an equally great influence on the physicians in the department of medicine. He points out that during these years, there was little formal teaching in the radiology department, and that most instruction resulted from the interactions between him and the residents while he interpreted films.

As a native of Germany, Dr. Schatzki did not have to serve during World War II. However, feeling a deep debt to this country, and after a great deal of effort, he was able to persuade the Army to accept him. He served on active duty from June 1943 to April 1946 and reached the rank of lieutenant colonel. Most of this time was spent as chief of radiology services at McGuire Hospital in Richmond, VA.

After World War II, Dr. Schatzki left MGH and became chief of the Radiology Department at the Mount Auburn Hospital in Cambridge, MA. He stayed in that position until 1967 and continued to work until the age of 82. He was largely responsible for changing Mount Auburn from an unsophisticated community hospital into one of the Harvard teaching hospitals. The department grew from two diagnostic rooms in 1947 to a modern 13-room department with its own residency program in diagnostic radiology; in 1984, it was named the Richard Schatzki Department of Radiology. For many years, Dr. Schatzki's elective in radiology was one of the most popular electives for medical students at Harvard. One month of Dr. Schatzki's inspired teaching of radiology had profound effects on several generations of medical students, resulting in several career changes and a number of present-day leaders in radiology.

Starting in 1931, Dr. Schatzki made a large number of seminal contributions to radiology. He believes that the recognition of the lower esophageal ring is perhaps his most important contribution. In a series of articles between 1953 and 1963, together with Dr. John E. Gary, he described and defined this important entity, which is now generally known as the "Schatzki ring." Although the ring is perhaps best known to the general medical public, a critically important concept for radiologists was presented in his 1958 article, again with Dr. Gary, describing the face-on demonstration of ulcers in the stomach. The statement that "the lesser curvature is observed face-on while the barium ebbs and flows like a wave across the beach, leaving holes filled with water" epitomizes the art of fluoroscopy for which Dr. Schatzki was famous. This technique is now called the Schatzki position by many radiologists. In 1942, together with Dr. Lloyd Hawes, he presented the first in-depth discussion and analysis of intramural extramucosal lesions of the gastrointestinal tract and supported that analysis by experimental data. Two years later, after publication of the small intestinal enema paper, he and Dr. Clinton Hale provided the initial description of the entire gastrointestinal spectrum of scleroderma. In addition, his contributions include many articles covering a wide spectrum of gastrointestinal entities, as well as important descriptions of (1) the pulmonary findings after the tragic Coconut Grove fire and (2) the bone changes resulting from frostbite, which were discovered during the Korean War.

Dr. Schatzki's creative initial descriptions and discussions of varices, gastrointestinal relief studies, erosive gastritis, intramural extramucosal lesions, small intestinal enema, face-on demonstration of ulcers, scleroderma, and particularly the lower esophageal ring require no further elaboration. However, he perhaps has had an equal influence in emphasizing the "art" of fluoroscopy to several generations of radiologists. Not only in his direct work with residents but also in many postgraduate courses, he emphasized that proper fluoroscopic technique was essential to successful gastrointestinal fluoroscopy. He thus became revered by many radiologists. In addition, he was the physicians' radiologist. Many problem gastrointestinal cases, not only in Boston but elsewhere in the Northeast, were referred to Dr. Schatzki for definitive interpretations. Some of his philosophy about fluoroscopy was stated in a 1966 editorial discussing the impact of screen intensification. The title of the editorial was "You Still Have to Work For It."

In accordance with his distinguished career, Dr. Schatzki has been honored by his profession. He was an associate clinical professor of Radiology at Harvard Medical School and president of the New England Roentgen Ray Society. In addition to having been a member of most of the national and local radiology societies and a vice president of the American Roentgen Ray Society, he became an honorary member of the radiology societies of Brazil and Colombia. He presented a number of memorial lectures, including those honoring Drs. Caldwell, Holmes, Pancoast, Soule, and Golden. In 1973, the Society of Gastrointestinal Radiologists presented its second Walter B. Cannon Medal to Dr. Schatzki.

Dr. Schatzki has had many outside interests. He is an accomplished pianist. For many years, some radiologists recognized that an effective way to get Richard Schatzki to speak out of town was to arrange an excellent quartet or trio. This interest led to close friendships with other physicians and radiologists who are musicians. In addition, Dr. Schatzki has given benefit concerts in the Boston area. He and Greta enjoyed many cultural activities and traveled extensively worldwide, often in response to requests for to Dr. Schatzki to give papers. The Schatzki household was warm and close, and Richard and Greta proudly followed the careers of their two sons, Stefan, a radiologist, and George, a law school dean.

Richard and Greta Schatzki were inseparable for more than 50 years. In 1981, Greta, Dr. Schatzki's wife, best friend, and major source of support, suddenly passed away. Dr. Schatzki retired in 1983, and since his retirement, he has finally been able to devote adequate time to his continuing interest in music, which has included public performances, as well as his many other interests.

During my recent discussion with him about the "small intestinal enema," the present routine examination of the small bowel, and enteroclysis, he stated simply, "The principles are the same. It's just easier to position the tube." Now almost 87 years old, Richard Schatzki maintains a continual inquiring interest in radiology, which he has so profoundly influenced for half a century.

Commentary

Small Intestine Enema

Harley C. Carlson[1]

A friend who had just retired from active practice once remarked to me that one interesting aspect of maturing is that, as time goes on, less and less is new. Certainly, diagnostic radiology has witnessed many astounding new developments, but, apparently, enteroclysis is not one of them. Richard Schatzki in his 1943 article, "Small Intestinal Enema" [1], displayed his usual plainly stated, factual, and gentlemanly style. He reported that he had used the procedure on several patients, had found it advantageous, and then had searched the literature, only to find that at least three parties already had reported having used the method [2–4]. The earliest article was by Pesquera [2] in 1929, published while he was working in the Department of Roentgenology of the Metropolitan Life Insurance Company Sanitorium. Schatzki gave all three articles credit and went on to recount his own experience.

The advantages (rapid infusion allows controlled distension of the gut, and fluoroscopic observation of the rapidly advancing barium column is possible with very little flocculation of the barium) and the disadvantages (intubation is uncomfortable for the patient and time-consuming for the radiologist) described by Schatzki are those widely agreed upon today. Even the published prepared discussion of his paper (a practice we should consider emulating today) was prophetic. Ross Golden suggested using a balloon-tipped tube to promote passage into the jejunum and prevent reflux into the stomach.

Another question raised by Golden was whether opaque material given via an enema tube would impair the assessment of the physiology of the small intestine. After all, the early use of X-ray imaging of the gut by Walter Canon [5] was for the purpose of studying the gut's movements and the effect of those movements on its contents. Schatzki seemed convinced, however, that the purpose of the examination was the demonstration of organic pathologic change, and this view prevails even today, with a few special exceptions.

The story of the small-bowel enema parallels to some extent that of the double-contrast barium enema of the colon, which was first reported shortly after World War I, used sporadically, largely abandoned, and then rejuvenated and extolled by enthusiastic advocates up to the present time. Today, many believe that the double-contrast barium enema is the preferred method for almost all circumstances.

Comparisons of the oral small-bowel examination and enteroclysis usually have shown that the enema takes less total time but more fluoroscopic and room time to perform and results in considerably more discomfort for the patient, chiefly because of the intubation required. Sensitivity has been found to be similar by some, but most reports conclude that the small-bowel enema is decidedly better than the so-called routine small-bowel follow-through [6–11]. Some advocates find it superior for the detection of all types of pathologic processes, and others regard it as especially useful in the demonstration of Meckel diverticulum and partial obstruction due to adhesions. In one report [12], the authors found that the small-bowel follow-through had missed about 60% of ultimately "proved" cases of regional enteritis, whereas the small-bowel enema missed only 5%. This article so piqued my interest that I undertook my own study [13]. Seventy-four new cases with a final clinical diagnosis of regional enteritis were studied over a period of about 6 months. The large-volume per-oral small-bowel examination with frequent fluo-

This article is a commentary on the preceding anniversary reprint by Schatzki, pages 499–507 of this issue.

[1] Department of Diagnostic Radiology, Mayo Clinic, Rochester, MN 55905. Address reprint requests to H. C. Carlson.

AJR 150:510–511, March 1988 0361–803X/88/1503–0510 © American Roentgen Ray Society

roscopy and vigorous manual compression was used in the examination of these patients. The findings were highly accurate for the assessment of regional enteritis, agreeing with the clinical diagnosis or surgical findings in about 95% of cases.

Why the difference in the results of these two studies of regional enteritis? I am convinced that the difference is in the use of fluoroscopy as the primary means of visual data gathering together with aggressive manual compression and manipulation in a variety of positions, carried out frequently and with a large volume of barium. Administering barium by tube directly into the jejunum often allows almost continuous progressive opacification of most of the small bowel, a very satisfying sequence, especially if fluoroscopy and manual compression are done. However, opacification also can be controlled fairly effectively by having the patient drink a large volume of barium over a short period of time. The stomach empties exponentially, a certain fraction of the content leaving each unit of time. If a large volume of fluid is put in, a large volume leaves per unit time. When such a large volume of standard commercial barium suspension is used, about half of our patients finish in 30 min after two fluoroscopic examinations, and about 80% finish in 45 min after three fluoroscopic examinations. Fluoroscopy must be used as the actual means of producing diagnostic information and not simply as a guide to positioning the patient for the production of films. The decisive observation of the fluoroscopic image, as outlined, produces much more diagnostic information than do the production and interpretation of films.

Of course, if films are relied on for virtually all of the diagnostic information, enteroclysis probably has the capability of producing a much more complete film record, especially if the double-contrast methylcellulose method is used. Like the double-contrast barium enema of the colon, the procedure and the production of films can be learned in a short period of time. Interpretation of the films is a much more complex matter. Primary diagnostic fluoroscopy also requires a more prolonged on-line learning experience under the guidance of an experienced teacher.

During the past year, we have tried to encourage gastroenterologists to order enteroclysis by telling them of possible advantages of the method and by making it as easy to order as the oral examination. This has given us some experience, but we have been disappointed with the rate of use. Conversations with the referring physicians indicate that they are (1) generally satisfied with the sensitivity of the oral-fluoroscopic examination and (2) reluctant to subject patients to the discomfort of intubation unless the possible gain in diagnostic information is substantial or unique. My experience with use of the small-bowel enema allows me to make a few tentative observations: (1) Examination of the small intestine is still a difficult procedure whether the barium is administered orally or via an enema. (2) In both methods, overlapping loops in the pelvis are capable of obscuring substantial pathologic processes. (3) The greatest bonus in diagnostic information obtained during the procedure comes from the fluoroscopy of the advancing barium column. If manual compression and frequent repositioning of the patient are added, the bonus is multiplied. (4) Occasionally, the examination can be tailored to address a particular diagnostic question, but the systematic, objective demonstration of the anatomy of the entire small intestine must be the aim of every examination.

The wisdom of Golden in his discussion of Schatzki's paper can be embraced by many: "This method, I believe, should be accepted as another string to our bow, so to speak. I should not like to substitute it for the routine small intestine study as we are now using it. . ." [1]

I called Dr. Schatzki on the telephone to chat with him about this paper. His memories about enteroclysis were a bit hazy, but he remembered using the procedure with some regularity. His son, Stefan Schatzki, who practiced radiology with him at Mount Auburn Hospital in Cambridge for a number of years, recalled that the small intestine enema was used quite sparingly, usually after the results of an oral study were negative and in the face of high clinical suspicion of small bowel disease. Also, in patients intubated for the treatment of clinical small bowel obstruction, the procedure was used to show the site, degree, and nature of the obstructing process. The elder Dr. Schatzki is keeping himself busy and alert. When I called, he was with his piano teacher, preparing for a performance. He remarked that he was still not too old to have a teacher.

REFERENCES

1. Schatzki R. Small intestinal enema. *Am J Roentgenol Radium Ther* **1943**;50:743–751
2. Pesquera GS. A method for the direct visualization of lesions in the small intestines. *Am J Roentgenol Radium Ther* **1929**;22:254–257
3. Ghelew B, Mengis O. Mise en évidence de l'intestin grele par une nouvelle technique radiologique. *Presse Med* **1938**;46:444–445
4. Gershon-Cohen J, Shay H. Barium enteroclysis: a method for the direct immediate examination of the small intestine by single and double contrast techniques. *Am J Roentgenol Radium Ther* **1939**;42:456–458
5. Cannon WB. The influence of emotional states on the functions of the alimentary canal. *Am J Med Sci* **1909**;137:480–487
6. Maglinte DDT, Burney BT, Miller RE. Lesions missed on small-bowel follow-through: analysis and recommendations. *Radiology* **1982**;144:737–739
7. Diner WC, Hoskins EO, Navab F. Radiologic examination of the small intestine: review of 402 cases and discussion of indications and methods. *South Med J* **1984**;77:68–74
8. Caroline DF, Herlinger H, Laufer I, Kressel HY, Levine MS. Small-bowel enema in the diagnosis of adhesive obstructions. *AJR* **1984**;142:1133–1139
9. Ott DJ, Chen YM, Gelfand DW, Van Swearingen F, Munitz HA. Detailed per-oral small bowel examination vs. enteroclysis. Part I: Expenditures and radiation exposure. Part II: Radiographic accuracy. *Radiology* **1985**;155:29–34
10. Taverne PP, van der Jagt EJ. Small-bowel radiography: a prospective comparative study of three techniques in 200 patients. *ROFO* **1985**;143:293–297
11. Maglinte DDT, Lappas JC, Kelvin FM, Rex D, Chernish SM. Small bowel radiography: how, when, and why? *Radiology* **1987**;163:297–305
12. Gurian L, Jendrzejewski J, Katon R, Bilbao M, Cope R, Melnyk C. Small-bowel enema: an underutilized method of small-bowel examination. *Dig Dis Sci* **1982**;27:1101–1108
13. Carlson HC. Perspective: the small bowel examination in the diagnosis of Crohn's disease. *AJR* **1986**;147:63–65

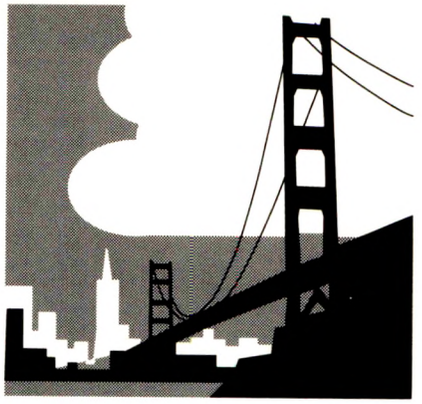

Come to the American Roentgen Ray Society 88th ANNUAL MEETING

San Francisco Hilton
May 8–13, 1988

Scientific Program (200 papers)
Instructional Courses (60 hours)
Categorical Course on Breast Imaging
The Caldwell Lecture
Award Papers
Scientific Exhibits
Social, Golf, and Tennis Programs
Guest Programs

Progress In Radiology

Overcoming Motion in Abdominal MR Imaging

Michael L. Wood,[1] Val M. Runge,[2] and R. Mark Henkelman[3]

Periodic motion not only blurs MR images but also causes a unique image artifact [1–3], consisting of ghostlike replicas of moving anatomic structures. These ghosts can obscure abnormalities when they become superimposed on other structures. The abdominal motion that is part of respiration certainly is not the only source of motion artifact, but it is the single factor most detrimental to MR imaging of the body. Abdominal viscera such as the liver can be displaced as much as 75 mm superiorly to inferiorly during deep breathing [4], and the average displacement is about 14 mm [5]. Usually fat has high image intensity, and consequently its movement creates the most conspicuous ghosts. In fact, the anteroposterior displacement of fat on the abdominal wall can be as much as 15 mm, which typically corresponds to 10 pixels in an MR image. Clearly there is much individual variability in the amplitude, period, and pattern of respiratory motion, with some diseases of the heart or lungs producing exaggerated breathing.

Numerous methods have been advanced for diminishing motion artifacts. It is the purpose of this article to explain the characteristics and causes of motion artifacts and then to review the various methods designed to suppress them. Table 1 lists the most common respiratory motion artifact suppression methods and provides some common acronyms or a brief explanation. The methods have been classified according to whether the motion of the patient needs monitoring, and this is the order in which each method is explained in a subsequent section. Since no method is completely efficacious on its own, we begin with a description of the ways in which motion artifacts arise.

Characteristics of Motion Artifacts

The ghosts that arise from moving anatomic structures are unique to the Fourier imaging technique [6]. Two-dimensional Fourier MR images have a frequency-encoding direction and a phase-encoding direction, which arise after separate Fourier transforms to the rows and columns of measured data, respectively. This separation of frequency and phase encoding is inherently responsible for the propagation of ghosts into the phase-encoding direction of MR images.

Frequency encoding is achieved much more quickly than phase encoding. In about 10 msec, all of the spatial information in the frequency-encoding direction is encoded by the readout gradient into differences in frequency. In contrast, 128 or 256 separate acquisitions are required to encode spatial information in the phase-encoding direction. With TR times greater than 1 sec, phase encoding requires several minutes. Respiratory motion introduces a modulation into the phase-encoded data, which appears as periodically displaced ghosts in the phase-encoding direction of the resulting MR image. Figure 1 shows that the choice of phase-encoding direction affects the overlap of ghosts with other structures. Note the high-intensity ghost from pulsatile flow in the aorta, which falls on top of the right lobe of the liver in the lower image. The preferred orientation for phase encoding depends on the anatomic site, slice orientation, and diagnostic task.

Before motion-artifact formation was well understood, it was hoped that the predominantly anteroposterior abdominal motion would not create ghosts when the phase-encoding direction was mediolateral instead of anteroposterior. How-

Received October 23, 1987; accepted after revision December 3, 1987.

[1]Department of Radiation Oncology, New England Medical Center and Tufts University School of Medicine, Boston, MA 02111. Address reprint requests to M. L. Wood, Medical Physics Division, New England Medical Center, Box 246, 750 Washington St., Boston, MA 02111.

[2]Department of Radiology, New England Medical Center and Tufts University School of Medicine, Boston, MA 02111.

[3] Ontario Cancer Institute and Department of Medical Biophysics, University of Toronto, Toronto, Ontario M4X 1K9, Canada.

AJR **150:513–522, March 1988** 0361–803X/88/1503–0513 © American Roentgen Ray Society

TABLE 1: Methods for Suppressing Abdominal Motion Artifacts

Monitoring required:
☐ Respiratory gating
☐ Reordering of phase encoding (ROPE, COPE, Exorcist)
No monitoring required:
☐ Physical restraining
☐ Breath-holding
☐ Restricting the field of view
☐ STIR[a]
☐ Averaging of data
☐ Pseudogating (synchronization of imaging with respiration)
☐ Gradient moment nulling (correction for motion between excitation and readout, gradient moment reduction, MAST[b])

Note.—ROPE, COPE, and Exorcist are all patented methods used for the reordering of phase encoding. (See text for explanation.)

[a] Short-tau inversion recovery.

[b] Motion artifact suppression technique.

ever, it was shown that motion in any direction causes ghosts in MR images [3, 7, 8]. Periodic motion of a drop of oil in all three orthogonal directions generated ghosts in the phase-encoding direction of Figure 2, showing that no direction of motion is immune to ghosting.

Separation of Ghosts

Neither the direction nor the amplitude of motion affects the separation of ghosts. The number of pixels Y_G between two consecutive ghosts depends on the total imaging time divided by the period of motion, as given below.

$$Y_G = \frac{Y_{tot} \times n_{av} \times TR}{T} \quad (1)$$

Here Y_{tot} is the total number of pixels across the field of view, n_{av} is the number of acquisitions averaged before each new phase-encoding step, TR is the repetition time, and T is the period of motion. The influence of the factors on the right-hand side of equation 1 is shown in Figure 3. In fact, the validity of this equation can be tested by plugging the values given in the Figure 3 legend into equation 1.

Ghosts that would have appeared beyond a boundary of the images in Figure 3 were wrapped around to the opposite side. This is due to a phenomenon called aliasing, which is regularly encountered in MR imaging [9]. Aliasing occasionally places two different ghosts in close proximity, as seen in Figure 3. Substitution of common imaging parameters in equation 1 reveals that aliasing of ghosts is common. As will be shown later, it is even exploited deliberately in the method called pseudogating.

Intensity of Ghosts

The intensity of ghosts depends on the amplitude of motion and the intensity of the moving structure [10]. Higher-order ghosts, which belong farther from their source structure, are less intense [10]. The physical displacement measured in terms of the number of pixels traversed, rather than the displacement in centimeters, is the appropriate parameter determining ghost intensity. Motion across more pixels not only increases the intensity of ghosts that were already conspicuous, but also raises the intensity of ghosts that were previously inconspicuous.

The intensity of a ghost is also proportional to the intensity of the moving anatomic structure that created the ghost. Both the imaging technique and characteristics of the MR system are important here. In fact, greater image intensity relative to noise makes ghosts more conspicuous in high-field images [10]. The practice of averaging fewer acquisitions of data and using narrower pixels at high-field strengths also contribute. Because of the high MR image intensity of fat in most imaging techniques, the most conspicuous ghosts usually arise from the anterior abdominal wall. However, other moving structures generate ghosts, too.

Ghosts add to or subtract from the image intensity of underlying tissues. Addition results in a bright artifact, which mimics certain diseases on T2-weighted images. Conversely, subtraction leads to a darker region, which can mimic disease on T1-weighted images. Motion not only degrades the image

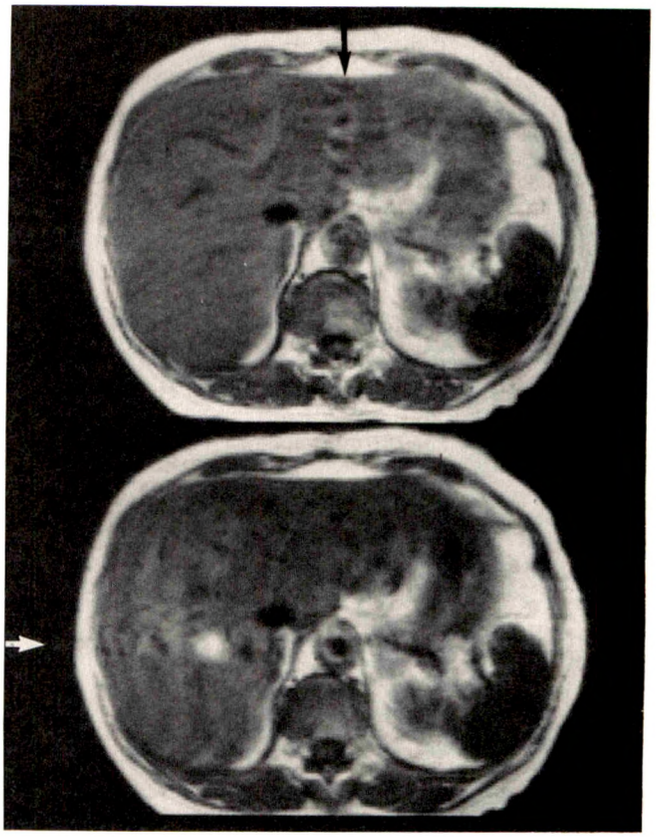

Fig. 1.—Two 1.0-T transverse images exhibiting ghosts from periodic movement of fat on anterior abdominal wall and pulsatile flow of blood in aorta and vena cava. Details of imaging technique include spin-echo (600/17, averaging of two acquisitions of data, 10.0-mm slice thickness, and 256 × 256 pixels across a 417-mm field of view. Each *arrow* points to a column of ghosts in phase-encoding direction, which was anteroposterior for upper image and mediolateral for lower image.

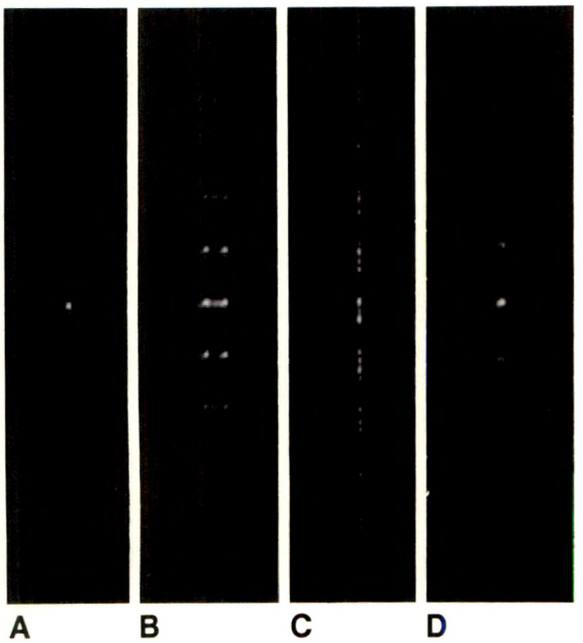

Fig. 2.—Four separate MR images of a drop of oil illustrating that periodic motion in any direction generates ghosts in the phase-encoding direction. Blurring of drop itself identifies direction of motion. For clarity, only a central slab of each image has been displayed. Drop was stationary in *A*, but it moved periodically in frequency-encoding, phase-encoding, and slice-selection directions for *B*, *C*, and *D*, respectively. (Reprinted with permission [1].)

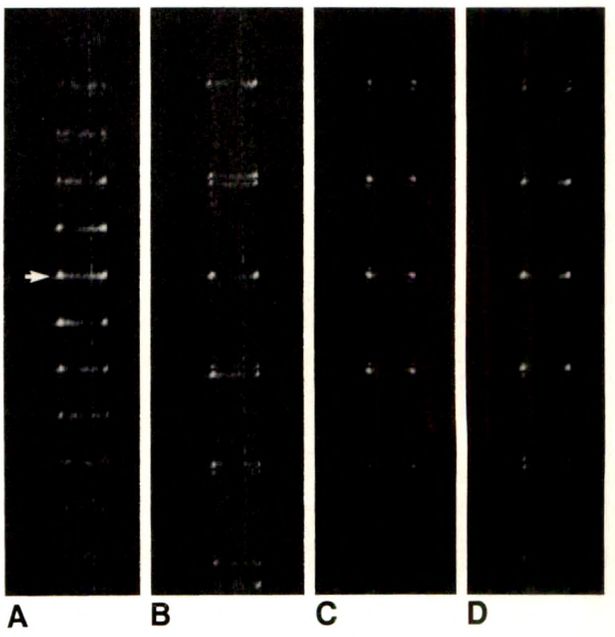

Fig. 3.—Factors that affect separation of ghosts are shown in these four images of an oil drop that moved periodically across 18 pixels in frequency-encoding direction. Pertinent conditions for reference image *A* included n_{av} = 4, TR = 0.2 sec and period T = 10.0 sec. Separation Y_G between ghosts was 20 pixels, where Y_{tot} = 256. *Arrow* in *A* points to the true location of the blurred oil drop. Conditions for other three images were similar, except for *B*, period T = 5.0 sec; for *C*, TR = 0.4 sec; and for *D*, n_{av} = 8. There were 40 pixels between each ghost in these last three images. (Reprinted with permission [1].)

contrast of stationary structures through the interference of ghosts, but the ghosts extract image intensity from the moving structure, which makes it appear less intense than if it had remained stationary.

Motion Artifact Suppression Methods

Methods for suppressing motion artifacts can reduce either (1) the motion, (2) the image intensity of moving structures, or (3) phase-encoding errors induced by motion. Some methods impose constraints on the selection of pulse sequences and timing parameters or limit the field of view. The most convenient methods do not require monitoring of patient motion and are compatible with the various imaging techniques in clinical use. Less convenient methods require monitoring of motion, which inevitably prolongs the time for patient preparation and imaging.

The monitoring of respiratory motion involves several stages: a transducer, electronic hardware to process the transducer signal, and software to control the acquisition of data for the MR image. The most commonly used transducers are sensitive to physical displacement [11, 12]. Respiratory motion has no convenient physiologic trigger analogous to the R wave of the ECG, and it is also less regular. Not surprisingly, respiratory monitoring can be difficult to implement successfully. Nevertheless, respiratory gating and reordering of phase encoding are two well-known methods that make use of information provided by a respiratory monitor.

Respiratory Gating

Respiratory gating [11–13] allows the acquisition of data only when the position of the abdomen, as indicated by a respiratory monitor, falls within a predetermined "window." Whenever this condition fails, the data for a particular phase-encoding step is rejected even though the RF excitations are performed. Consequently, the data are acceptable only during part of the respiratory cycle, often during end expiration, because that is usually the longest portion of the cycle. Such was the case illustrated in Figure 4B. Compared with the normal technique, which created Figure 4A, gating reduced both the ghosts and the blurring.

An inescapable consequence of rejecting data is the prolongation of image acquisition. There are at least two ways to prevent the imaging time from becoming too long. One is to apply gating for only part of the data. It has been shown theoretically [14] that the improvement in image quality is proportional to the fraction of data over which gating occurs. For example, if gating occurred for one-half of the measured data, it would be about one-half as effective as if it had occurred for all the data. The second way resembles the operation of cardiac gating and consists of triggering the acquisition of data as soon as the position of the abdomen returns inside the window [11, 12]. However, the irregularity of respiratory motion and the lack of a well-defined physiologic trigger introduce much variability in TR. Image artifacts similar to the ghosts from motion are the unfortunate consequence of variable TR [8,14]. Although these two adaptations reduce

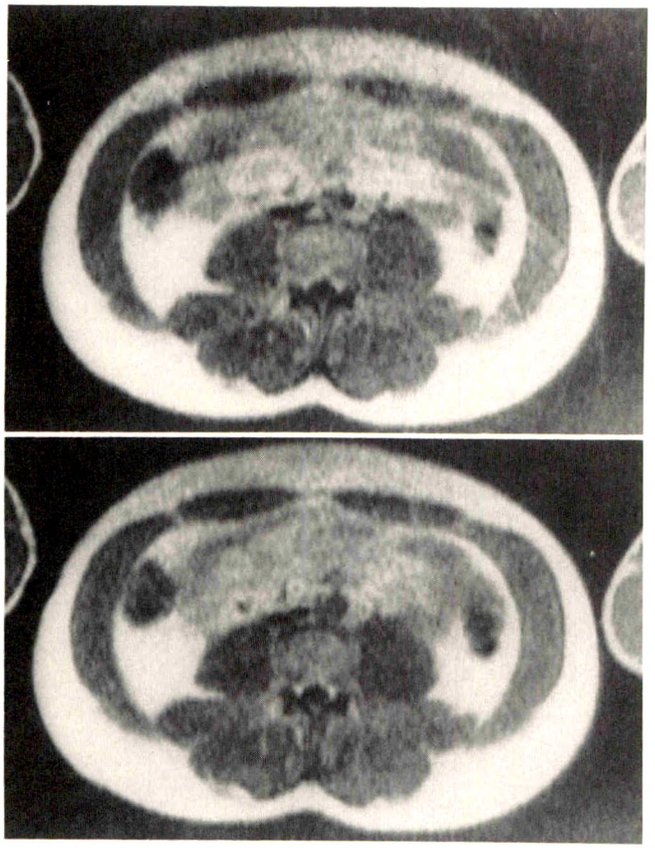

Fig. 4.—Two similar 0.15-T spin-echo 500/32 MR images. Respiratory gating was used for *lower image* but not for *upper image*. Other imaging parameters included a 15-mm slice thickness, no averaging of data, and 128 phase-encoding steps. (Reprinted with permission, courtesy of D. Drost and F. Proto.)

the extra imaging time, they also reduce the effectiveness of respiratory gating.

Reordering of Phase Encoding

Artifacts, as explained in an earlier section, arise when the data corresponding to different phase-encoding steps exhibit a modulation caused by movement of the patient. When this modulation occurs periodically through the data, regularly spaced ghosts appear in the MR image. Aside from altering the motion of the patient, the modulation of data can be smoothed by reordering the sequence in which the phase-encoding steps of data are acquired [8, 15]. In particular, when data are to be acquired during periodic motion, the order of acquisition can be changed to make the apparent motion much slower. In Figure 5, reordering made it appear as if the patient had simply inhaled once during imaging, even though he really completed almost five periods of respiratory motion. Most important of all, unlike respiratory gating, reordering does not interrupt the steps of imaging, so the imaging time need not be prolonged. Reordering of phase encoding is a general concept, which is fundamental to the specific methods designated respiratory ordering of phase encoding (ROPE) [15], centrally ordered phase encoding (COPE) [8], and Exorcist (General Electric Medical Systems, Milwaukee, WI).

The effectiveness of reordering can be assessed by comparing the two images in Figure 6. Reordering reduced the ghosts, most noticeably those over the back muscles. The image remains blurred, however. Theoretical studies [14] have concluded that reordering can eliminate ghosts, while producing images with slightly more than the usual blurring. Clinical experience with these reordering methods is limited because of difficulties in implementation.

Physical Restraining

Movement of the abdomen can be restrained through the use of an inflexible band. The band need not be wrapped uncomfortably tight for it to be effective. Figure 7 compares an image made by using a band to restrain abdominal motion with one made without such a band. Greater motion occurred without the band, as suggested by the more extensive blurring. The intensity of ghosts was estimated through the

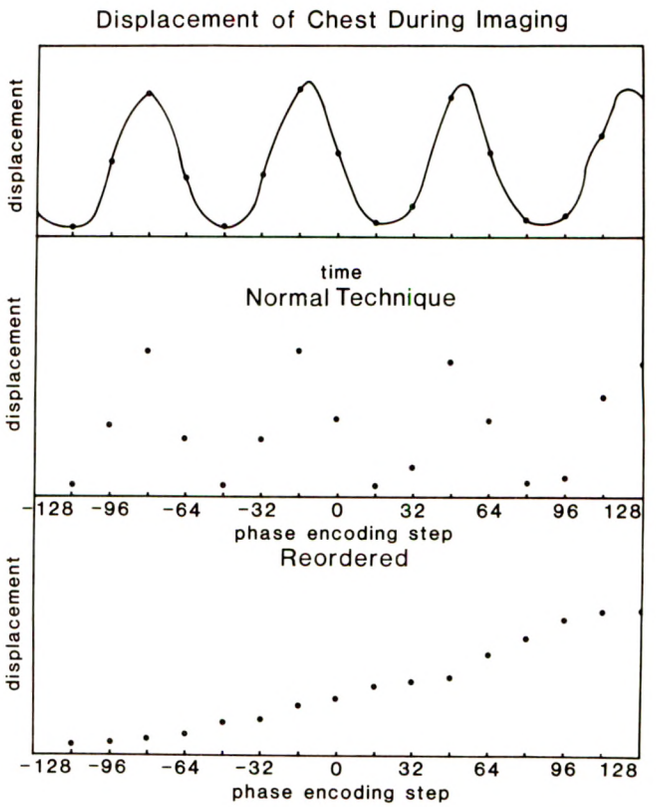

Fig. 5.—Anteroposterior displacement of lower chest in a patient measured for 40 sec. Peaks represent full inspiration and, conversely, troughs indicate full expiration. Displacement at every sixteenth phase-encoding step is superimposed on *top curve*. *Middle* and *bottom curves* show same displacements plotted against corresponding phase-encoding step in a normal MR imaging technique (*middle*) and one for which the steps have been reordered to make the displacement change more slowly (*bottom*). (Reprinted with permission [1].)

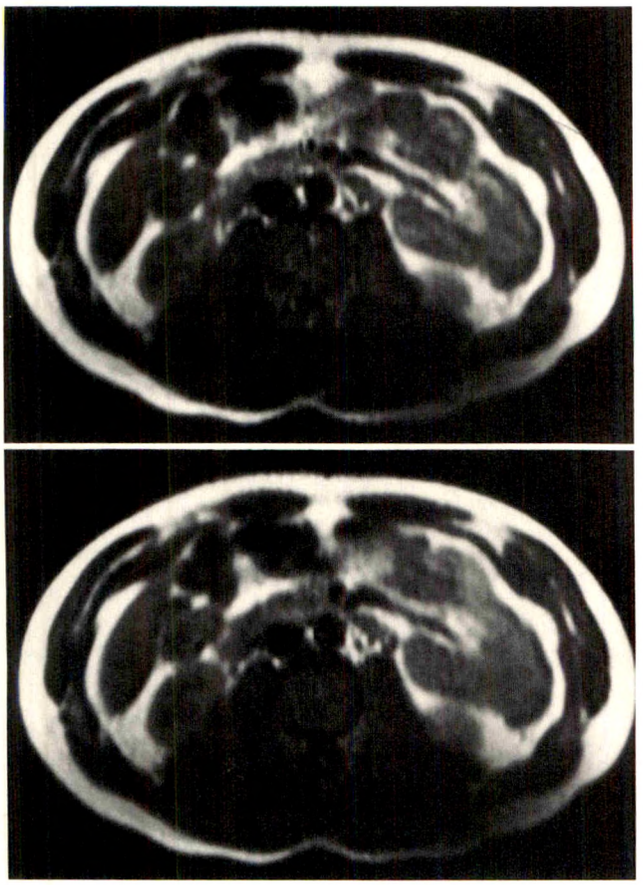

Fig. 6.—Comparison of two 1.5-T spin-echo 1000/25 MR images acquired normally (*upper image*) and by reordering the sequence of phase encoding (*lower image*). Other imaging parameters included a 10-mm slice thickness, a 480-mm field of view, averaging of two acquisitions of data, and 128 phase-encoding steps.

standard deviation of image intensity measured within a background region containing ghosts. This measurement was approximately 35% greater in the image without the band.

Physical restraint is one of the few practical methods that can decrease the amount of blurring in addition to the ghosting. However, restraining the patient only reduces artifacts resulting from respiratory motion and leaves ghosts from the pulsatile flow of blood and peristaltic bowel motion.

Breath-Holding

The simplest method for suppressing respiratory motion artifacts requires the patient to refrain from breathing during imaging [16]. Such a restriction is possible with techniques for fast MR imaging, of which there are many. Despite subtle differences, most fast imaging techniques are capable of freezing respiratory motion to a similar extent. However, ghosts from the pulsatile flow of blood can actually be more conspicuous. These ghosts can be reduced either by the gradient moment nulling method that will be described later or through RF pulses that saturate tissue outside of the slice [17]. As Figure 8 illustrates, the absence of ghosts and the sharpness of anatomic structures make breath-holding an attractive method.

Restricting the Field of View

Intense moving structures can be excluded from the field of view by using either surface coils or specialized techniques for imaging a "strip" rather than the whole plane [18]. The spatial presaturation methods [17] mentioned above can also reduce the intensity of moving structures. Surface coils are generally most sensitive near the coil itself. When the sensitivity is poorest near a moving anatomic structure, it can actually be beneficial. For example, the lower image in Figure 9 was acquired using a surface coil, which made the intensity of fat on the anterior abdominal wall only a small fraction of that on the posterior wall close to the coil. Ghosts from movement of the anterior abdominal wall and also the heart were correspondingly less intense.

STIR

Short-tau-inversion-recovery [19] (STIR) uses an inversion recovery (IR) technique to make fat have little or no image intensity. This, in turn, eliminates any ghosts from the move-

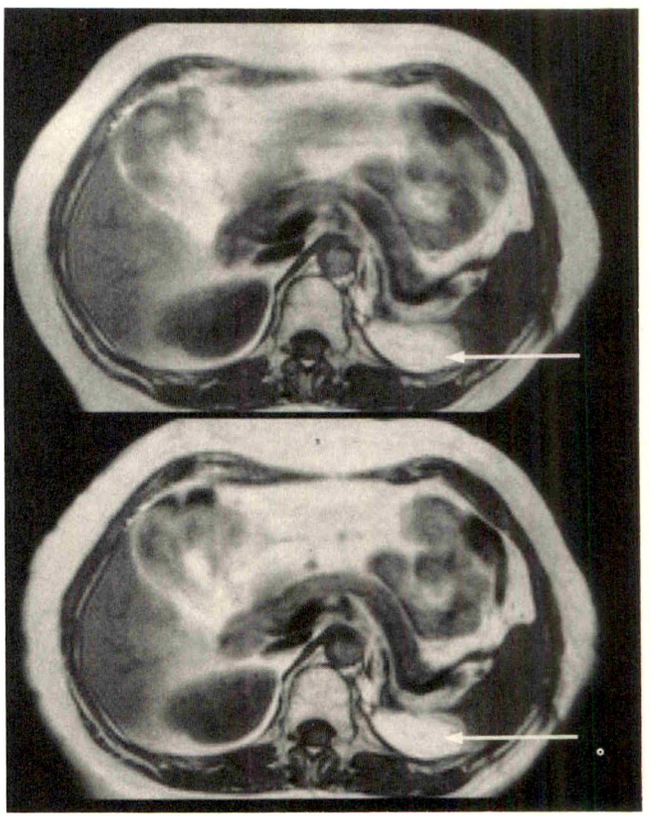

Fig. 7.—Improvement in image quality realized by restraining abdominal movement with an inflexible band. A band was used for *lower image* only. The two images were made with the same imaging technique as those in Fig. 1. *Arrows* indicate a recurrent liposarcoma in a patient who underwent a nephrectomy.

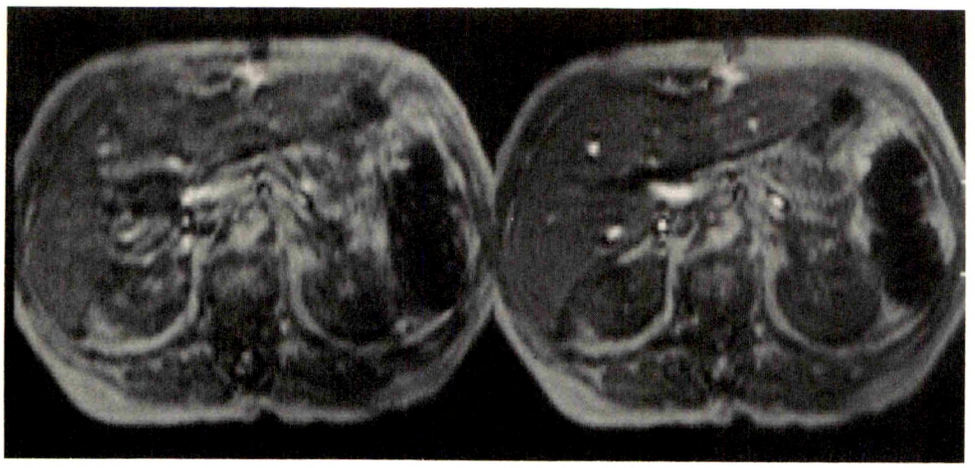

Fig. 8.—Two 1.0-T gradient-echo 25/9 images each acquired in 6 sec. Patient breathed normally for *image on left*, but held his breath for *image on right*. Additional details of the imaging technique include a 10-mm slice thickness, averaging of two acquisitions of data, a 500-mm field of view, and 128 phase-encoding steps.

ment of fat. The ghost that obscures both kidneys in the upper image of Figure 10 is not evident in the lower image, which was made with STIR. It is the short T1 of fat that allows STIR to nullify the image intensity of fat and still achieve contrast between other tissues. The low contrast in the STIR image in Figure 10 is a serious limitation, however.

Averaging

Averaging is the common practice of repeating each phase-encoding step more than once. The usual motivation for averaging is to reduce the random noise in the image. As Figure 11 illustrates, averaging also reduces the systematic noise arising from ghosts, provided that the position is different during each acquisition. If we consider the pattern of ghosts that would have arisen from independent reconstruction of each set of phase-encoding steps, the patterns would appear similar, except for the phases of the individual ghosts. The effect of averaging these sets of data together is that ghosts interfere destructively and sometimes even cancel completely [14]. Since it is difficult to construe the precise situation for cancellation, averaging that is implemented without specific reference to the motion still attenuates numerous ghosts partially [7]. Although averaging reduces ghost intensity, it does not reduce blurring [14].

Greater attenuation of ghosts occurs when more acquisitions are averaged. Theoretical analysis of simulated MR images of a moving object [14, 22] has shown the intensity of ghosts to be approximately inversely proportional to the number of averages (Fig. 12). The exact behavior depends on the particular motion and imaging conditions, but a similar trend nevertheless is observed. These theoretical predictions are in general agreement with experimental measurements on clinical images [20, 21].

Averaging has approximately similar effects on random noise, and the systematic noise of ghosts in that subsequent improvement becomes progressively more time-consuming. Averaging can be used with every imaging protocol, but because it prolongs the imaging time, it is more practical when the TR is short [16, 20, 21]. Averaging reduces the noise, thereby compensating for the lower image intensity due to the shorter TR. The use of a short TE provides better signal-to-noise-ratios, unless the echo-sampling time becomes too short. The use of a short TE has also been found to reduce the intensity of ghosts [20]. The short TR is most compatible with strongly T1-weighted images. Averaging is not as practical for T2-weighted images, for which TR can be as long as 3 sec.

Pseudogating

The objective of pseudogating [7, 14, 22] is to separate the ghosts so far that aliasing folds them back on top of each other. The factors that affect the separation appear in equation 1. A previous estimate of the period of motion is needed first. Then, typically, n_{av} and TR are selected to make $(n_{av} \times TR)/T = 0.5$. The movements are expected to repeat at every second phase-encoding step. Then, every second ghost falls back on the moving anatomic structure, and the others are superimposed one-half field of view away. Other possibilities for $(n_{av} \times TR)/T$ include multiples of 0.5 or 1.0, but these sequences take longer.

The two images in Figure 13 illustrate that pseudogating can shift the position of ghosts so that they no longer interfere with other anatomy, but blurring is not diminished. Pseudogating is most useful when n_{av} and TR are not required to be too different than they would have been otherwise. Unfortunately, for abdominal motion n_{av} and TR are often quite different than usual. However, pseudogating is more useful for controlling the ghosts from more rapid cardiovascular motion, which requires a smaller $n_{av}TR$.

Gradient Moment Nulling

Motion along a magnetic field gradient alters the phase of the magnetization. This is true for both gradient echoes and spin echoes. Because the motion usually changes, the amount of dephasing is different in the echoes of each phase-encoding step, causing an artifact in the phase-encoding direction. The dephasing attributed to motion can be mini-

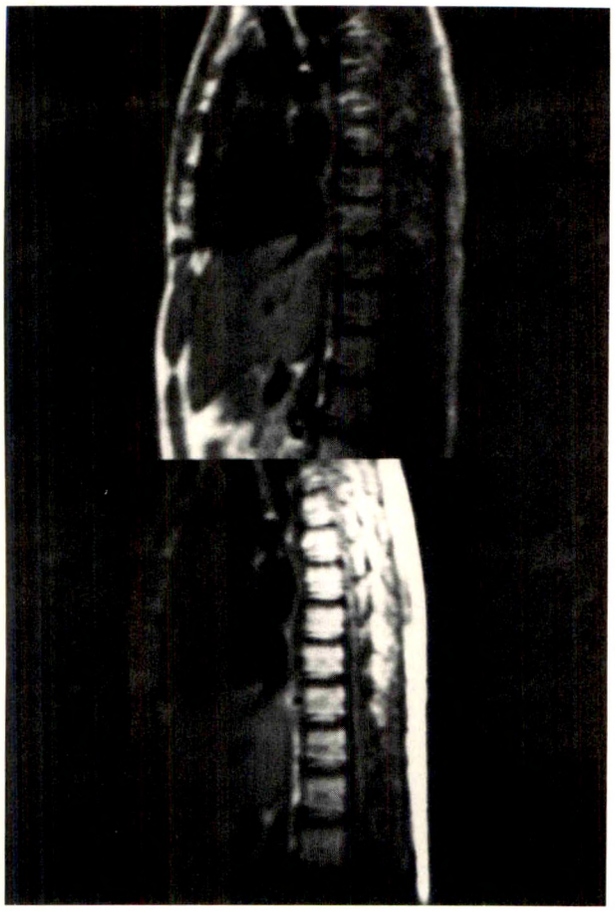

Fig. 9.—Two 1.5-T sagittal spin-echo 1000/25 images of same patient. A surface coil with low sensitivity to anterior structures was used for *lower image*. Imaging technique was similar to that used in Fig. 7.

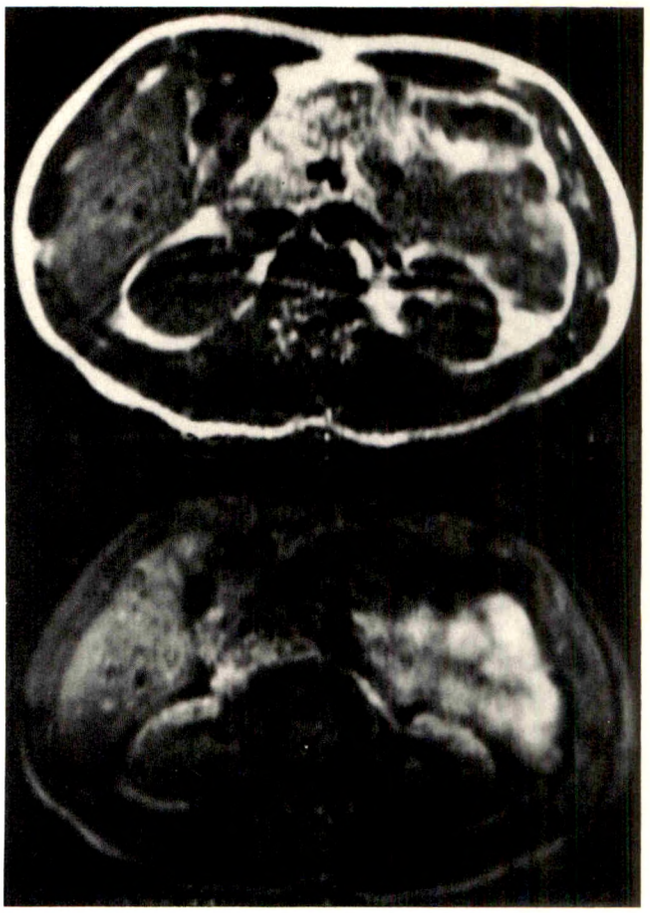

Fig. 10.—Two 1.5-T inversion recovery 1000/25 images of same patient. For *upper* and *lower images*, TI was 400 and 150 msec, respectively. Slice thickness was 10 mm, field of view was 480 mm, two acquisitions of data were averaged, and there were 128 phase-encoding steps.

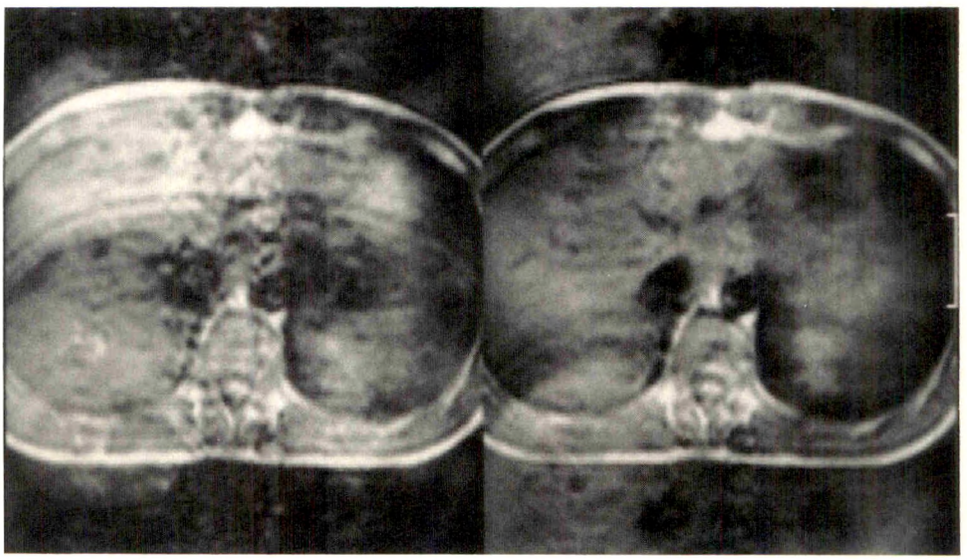

Fig. 11.—Two 1.0-T spin-echo 600/17 images of same patient. No averaging occurred for *left-hand image*, but two acquisitions of data were averaged for the *right-hand image*. Other details include a 500-mm field of view, 10-mm slice thickness, and 128 phase-encoding steps.

mized through special design of the magnetic field gradients in the imaging technique [23–25]. There are many other names for this method, including motion artifact suppression technique (MAST®) [23], gradient moment reduction, and bipolar gradients.

Additional gradient pulses are introduced to rephase the MR signal produced by moving tissue in much the same way that the MR signal is rephased in stationary tissue. The concept is similar to "even-echo rephasing" [26], which describes a recovery of image intensity for moving fluids in even-numbered echoes. One additional gradient pulse (or many more) can be included to compensate for the additional dephasing of moving tissue. The associated benefits often justify the additional complexity of the imaging technique, as Figure 14 shows. The two images in Figure 14 were produced under similar conditions, except that the technique that created the right-hand image compensated for motion along the frequency-encoding and slice-selection directions. Measurements of ghost intensity in the background of the right-hand image were one-quarter of that in the left-hand image. Furthermore, the intensity that was extracted from the ghosts was restored to the associated anatomic structures.

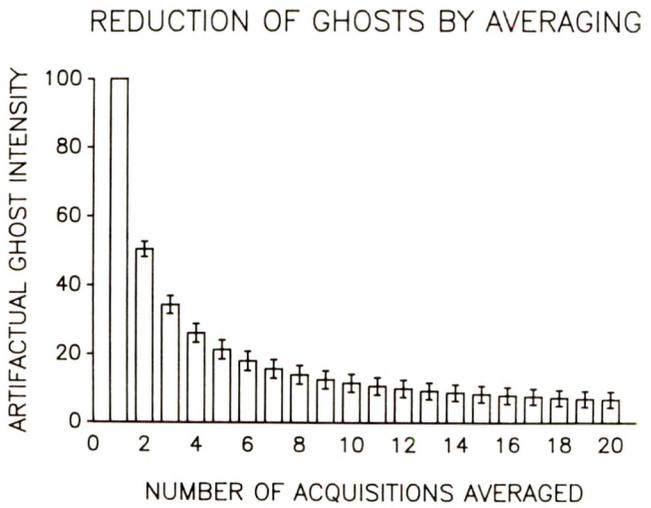

Fig. 12.—Intensity of ghosts is plotted against number of acquisitions averaged. Images of a point object moving periodically across five pixels were simulated mathematically and cumulative intensity of ghosts was measured. Error bars represent standard deviation in this measurement for different motion.

The method applies separately for motion along each of the three axes. The phase-encoding direction is the least critical, because the phase-encoding gradient is usually activated only once and briefly during each phase-encoding step. Any type of motion in the body can be broken down into components, the first two of which are constant velocity and acceleration. One additional gradient pulse can allow for complete rephasing from constant velocity motion, but many more are needed for more complex motion. In practice, the decision about the number of additional gradient pulses depends primarily on the shortest TE that is required. Gradient moment nulling can be employed in almost any imaging technique, and it can reduce artifacts from several moving structures simultaneously.

Summary

Anatomic structures that move periodically during the acquisition of data for an MR image become multiple ghosts in the phase-encoding direction. There is a constant spacing in pixels between consecutive ghosts, which is equal to the number of cycles of motion that occurred during the acquisition of data. The intensity of ghosts depends on the intensity of the moving structure and the number of pixels over which the motion occurred.

No single method is completely satisfactory at suppressing motion artifacts. The major attributes and limitations of each method are summarized in Table 2, with plus (+) signs denoting merit. Theoretically, some methods perform better in reducing the intensity of ghosts and restoring the image intensity to its proper place. This certainly is not the final

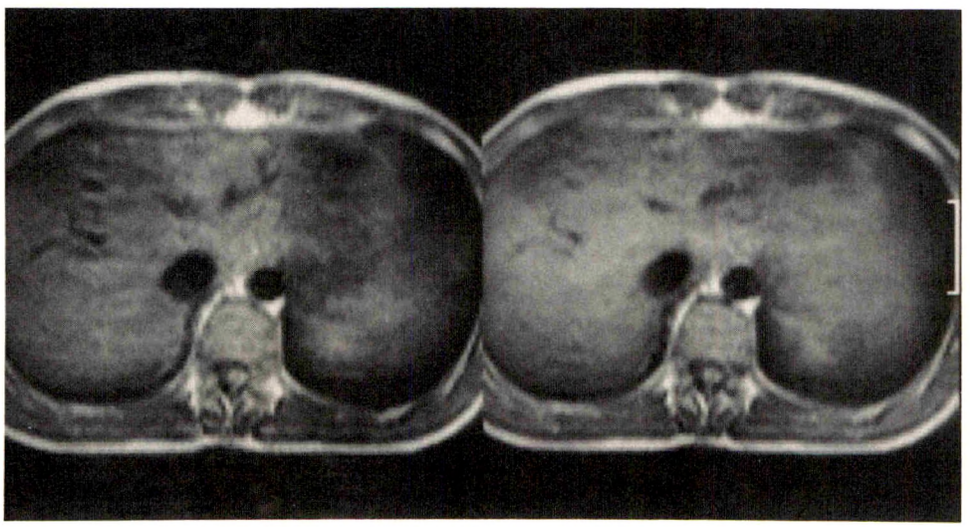

Fig. 13.—Two 1.0-T spin-echo 600/17 images of same patient that illustrate pseudogating. Conditions were similar to those in Fig. 11, except that four and eight acquisitions of data were averaged for the *left-hand* and *right-hand images*, respectively. This made the separation between ghosts either one-half (*left*) or one whole (*right*) field of view.

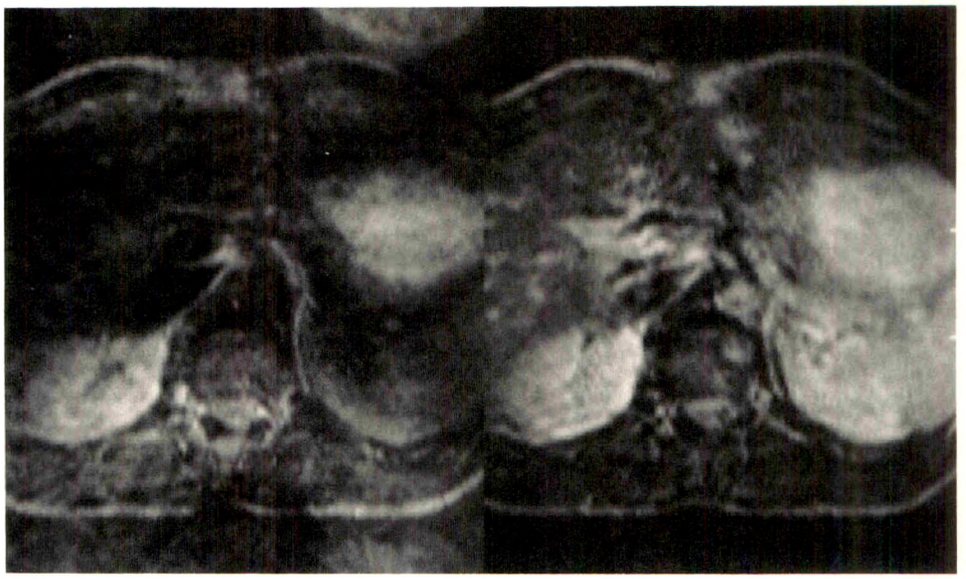

Fig. 14.—Two 1.0-T spin-echo 2000/50 images showing gradient moment nulling. The only difference was imaging technique, which used magnetic-field gradients that partially rephased the MR signal from structures moving along the frequency-encoding and slice-selection directions. Slice width was 10 mm, and field of view was 417 mm. There were 128 phase-encoding steps and no data were averaged.

TABLE 2: Overall Rating of Respiratory Motion Artifact Suppression Methods

Method	Theoretical Performance	Attributes		Deficiencies	Overall Rating
		Less Blurring	Other Motion		
Gating	+++	Yes	No	Time, cooperation	+
Reordering	+++	No	No	Cooperation	+++
Restraining	++	Yes	No	Less comfortable	++
Breath-holding	+++	Yes	No	Limited time, cooperation	++
Restricting FOV	+	No	No	Limited FOV	++
STIR	+	No	No	Limited contrast	+
Averaging	++	No	Yes	Long time	+++
Pseudogating	++	No	No	Time, cooperation	+
Gradient moment nulling	+++	No	Yes	Longer minimum TE	++++

Note: ++++ = excellent, +++ = very good, ++ = good, + = fair. STIR = short-tau inversion recovery; FOV = field of view.

criterion, however. Some methods reduce the blurring in addition to suppressing the ghosts, or they suppress ghosts without prolonging the time for imaging. Certain methods also reduce ghosts from other kinds of motion. It is very appealing for a method to function without monitoring. The success of monitoring often depends too much on the cooperation of both the patient and technologist. The theoretical performance, attributes, and deficiencies of the various methods have been combined into a subjective overall rating in the last column of Table 2.

All of the methods can be effective under the appropriate circumstances. Moreover, the methods are not mutually exclusive. It is advantageous, therefore, to combine methods to achieve even greater suppression. For example, physical restraint can be used for all but the most uncooperative patients. Most imaging techniques can be designed with gradients that rephase the signals from moving structures. Then other methods, such as averaging or reordering, can be applied as necessary.

Fortunately, there are effective motion artifact suppression methods, even though not all are widely available yet on commercial equipment. Consistent suppression of motion artifacts will enhance the quality of MR images. Elimination of motion artifacts will improve the capability of MR to detect lesions and will provide a higher standard of performance for MR in the body.

REFERENCES

1. Wood ML. Abdominal motion artifacts. In: Stark DD, Bradley W, eds. *Magnetic resonance imaging: a comprehensive text*. St. Louis: Mosby, **1988**:792–803
2. Schultz CL, Alfidi RJ, Nelson AD, Kopiwoda SY, Clampitt ME. Effect of motion on two-dimensional Fourier transformation magnetic resonance images. *Radiology* **1984**;152:117–121
3. Wood ML, Henkelman RM. MR image artifacts from periodic motion. *Med Phys* **1985**;12(2):143–151
4. Weiss PH, Baker JM, Patchen EJ. Assessment of hepatic respiratory excursion. *J Nucl Med* **1972**;13:758–759
5. Harauz G, Bronskill MJ. Comparison of the liver's respiratory motion in the supine and upright positions: concise communication. *J Nucl Med*

1979;20(7):733–735
6. Kumar A, Welti D, Ernst RR. NMR Fourier zeugmatography. *J Magn Reson* **1975**;18:69–83
7. Axel L, Summers RM, Kressel HY, Charles C. Respiratory effects in two-dimensional Fourier transform MR imaging. *Radiology* **1986**;161:795–801
8. Haacke EM, Patrick JL. Reducing motion artifacts in two-dimensional Fourier transform imaging. *Magn Reson Imaging* **1986**;4:359–376
9. Henkelman RM, Bronskill MJ. Artifacts in magnetic resonance imaging. *Rev Magn Reson Med* **1987**;2(1):1–126
10. Wood ML, Henkelman RM. The magnetic field dependence of the breathing artifact. *Magn Reson Imaging* **1986**;4:387–392
11. Ehman RL, McNamara MT, Pallack M, Hricak H, Higgins CB. Magnetic resonance imaging with gating: techniques and advantages. *AJR* **1985**;143:1175–1182
12. Lewis CE, Prato FS, Drost DJ, Nicholson RL. Comparison of respiratory triggering and gating techniques for the removal of respiratory artifacts in MR imaging. *Radiology* **1986**;160:803–810
13. Runge VM, Clanton JA, Partain CL, James AE. Respiratory gating in magnetic resonance imaging at 0.5 Tesla. *Radiology* **1984**;151:521–523
14. Wood ML, Henkelman RM. Suppression of respiratory motion artifacts in magnetic resonance imaging. *Med Phys* **1986**;13(6):794–805
15. Bailes DR, Gilderdale DJ, Bydder GM, Collins AG, Fermin DN. Respiratory ordering of phase encoding (ROPE): a method for reducing respiratory motion artifacts in MR imaging. *J Comput Assist Tomogr* **1985**;9(4):835–838
16. Edelman RR, Hahn PF, Buxton R, et al. Rapid MR imaging with suspended respiration: clinical application in the liver. *Radiology* **1986**;161:125–131
17. Felmlee JP, Ehman RL. Spatial presaturation: a method for suppressing flow artifacts and improving depiction of vascular anatomy in MR imaging. *Radiology* **1987**;164:559–564
18. Schajor W, Oppelt A. 3D-MR-proton imaging of selected regions. Presented at the annual meeting of the Society of Magnetic Resonance in Medicine, New York, NY, August **1984**
19. Bydder GM, Young IR. MR imaging: clinical use of the inversion recovery sequence. *J Comput Assist Tomogr* **1985**;9(4):659–675
20. Stark DD, Hendrick RE, Hahn PF, Ferrucci JT. Motion artifact reduction by fast spin echo imaging. *Radiology* **1987**;164:183–191
21. Stark DD, Wittenburg J, Edelman RR, et al. Detection of hepatic metastases; analysis of pulse sequence performance in MR imaging. *Radiology* **1986**;159:365–370
22. Haacke EM, Lenz GW, Nelson AD. Pseudo-gating: elimination of periodic motion artifacts in magnetic resonance imaging without gating. *Magn Reson Med* **1987**;4:162–174
23. Pattany PM, Phillips J, Chiu LC, et al. Motion artifact suppression technique (MAST) for MR imaging. *J Comput Assist Tomogr* **1987**;11(4):369–377
24. Haacke EM, Lenz GW. Improving image quality in the presence of motion by using rephasing gradients. *AJR* **1987**;148:1251–1258
25. Xiang QS, Nalcioglu O. A formalism for generating multiparametric encoding gradients in NMR tomography. *IEEE Transactions on Medical Imaging* **1987**;MI-6(1):14–20
26. Waluch V, Bradley WG. NMR even echo rephasing in slow laminar flow. *J Comput Assist Tomogr* **1984**;8(4):594–598

Quantification of Regional Myocardial Function by Rapid Cine MR Imaging

Peter W. Pflugfelder[1]
Udo P. Sechtem[1,2]
Richard D. White[1,3]
Charles B. Higgins[1]

The capability of rapid (cine) MR imaging to quantitate left ventricular function was assessed in 13 normal subjects and in 15 patients with ischemic heart disease and regional wall-motion abnormalities proved by echocardiography and/or by contrast ventriculography. Fifteen to 20 MR images/cardiac cycle were acquired by using partial flip angles, short repetition times, and gradient-refocused echoes. Regional wall motion was assessed qualitatively in the equatorial left ventricular section by using the cine display and quantitatively by measuring myocardial thickness at end-diastole and at end-systole in six left ventricular segments in this plane. In normal volunteers, wall motion was normal in all segments. Heterogeneity of systolic wall thickening was observed in normal subjects, ranging from 33% ± 17% in the posteroseptal segment to 66% ± 29% in the posterior segment. Overall systolic wall thickening was 48% ± 28%. From the cinematic display of MR images, abnormal wall motion was observed in 40 of 90 segments in patients with ischemic heart disease, which correlated well with results of echocardiography or contrast ventriculography. Twenty-one segments were hypokinetic, 15 were akinetic, and four were dyskinetic. In patients with ischemic heart disease, percentage systolic wall thickening was 43% ± 31% in the segments with normal wall motion, 6% ± 18% in hypokinetic segments, −4% ± 24% in akinetic segments, and −13% ± 25% in dyskinetic zones. Absolute systolic wall thickening was less than 2 mm in 31 of 40 abnormal segments and was greater than 2 mm in only three.

Rapid acquisition, improved temporal resolution, and the capacity for cine display make this new MR technique potentially useful not only for qualitative assessment of cardiac wall motion, but also for quantification of regional myocardial function.

Contrast angiography, echocardiography, radionuclide angiography, and MR imaging all provide useful and complementary information about cardiac structure and function. In the evaluation of ischemic heart disease, diminished or absent left ventricular systolic wall thickening (which may be a more sensitive indicator of regional myocardial function than abnormal wall motion [1, 2]) can be measured by echocardiography [3–5], cine CT [6], and conventional ECG-gated, spin-echo MR imaging [7].

Compared with conventional cardiac MR techniques, a newly developed method using limited flip angles, gradient-refocused echoes, and very short repetition times [8] has the advantages of improved temporal resolution through the cardiac cycle and shorter imaging times. Using a clinical MR scanner, we assessed this new cardiac imaging technique for its ability to (1) detect regional wall-motion abnormalities and (2) quantitate left ventricular dysfunction by measurement of systolic wall thickening.

Accordingly, we studied 13 normal subjects and 15 patients with ischemic heart disease to document and quantitate regional left ventricular wall-motion abnormalities.

Methods

Study Subjects

Thirteen normal subjects underwent MR imaging of the heart; in all 13 the cine technique was used. The mean age was 31 years (range, 21–37 years). None had evidence of

U. P. Sechtem is a research fellow in magnetic resonance imaging and is supported by grant SE 441-2 from the Deutsche Forschungsgemeinschaft, Bonn, West Germany.

[1] Department of Radiology, C-309, University of California, San Francisco, San Francisco, CA 94143. Address reprint requests to C. B. Higgins.

[2] Present address: Department of Cardiology, University of Köln, Köln, West Germany.

[3] Present address: Department of Radiology, Georgetown University Hospital, 3800 Reservoir Rd., N.W., Washington, DC 20007.

***AJR* 150:523–529, March 1988**
0361–803X/88/1503-0523
© American Roentgen Ray Society

cardiovascular disease on clinical examination. Fifteen patients with ischemic heart disease and left ventricular wall-motion abnormalities were studied. Fourteen patients had a documented history of myocardial infarction, and one had wall-motion abnormalities with no definite history of myocardial infarction (Table 1). Regional left ventricular dysfunction was documented by two-dimensional echocardiography in eight patients, by contrast angiography in two, and by both techniques in five. Documentation of wall-motion abnormalities was obtained within 4 weeks of the MR study.

MR Imaging

Study subjects underwent MR imaging performed on a 1.5-T superconducting clinical imager (Signa, General Electric Medical Division, Milwaukee, WI). An initial spin-echo, multilevel, gated sequence was obtained in the coronal plane to determine the inferior and superior extent of the heart as a reference for imaging in the transverse plane.

Transverse cine images of the entire heart were acquired by using the recently developed technique of gradient-recalled acquisition in the steady state (GRASS), which, in this study, consisted of flip angles of 30°, a pulse repetition time of 21 msec, and an echo time by gradient reversal of 12 msec. Pulse repetition was independent of the ECG signal, which was simultaneously recorded and stored on a microcomputer that in turn controlled advancement of the phase-encoding gradient with every second R wave (two averages per data point). The number of time frames (images) per cardiac cycle corresponded to the number of pulse sequences (21 msec in duration) that could be delivered per R to R interval. Thus, in a subject with a heart rate of 60 beats/min, 48 (1000 msec/21 msec) time frames would fall within the R to R interval. If more than one anatomic level was acquired simultaneously, the excitations alternated between levels. This would result in 24 images/cardiac cycle and temporal resolution of 42 msec/frame in the case of a two-level acquisition or 16 images/cardiac cycle and temporal resolution of 63 msec/frame for a three-level acquisition. So, the effective TR was 42 msec for a two-level acquisition and 63 msec for a three-level acquisition. Imaging time was therefore dependent on the total number of slices acquired and the subject's heart rate (imaging time = 128 phase-encoding steps × two excitations × number of series × 60/heart rate). Typically, simultaneous two- or three-level acquisitions were performed and required an average of 4 min. Twelve levels were usually obtained per study. Image reconstruction time was 5–8 min/acquisition.

Variability in the R to R interval resulted in a slight difference in the number of pulses for each cardiac cycle during the imaging period.

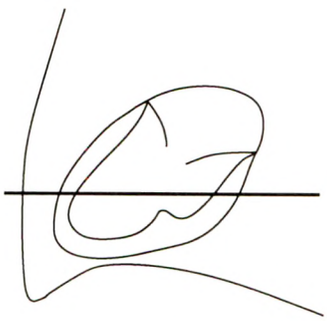

Fig. 1.—Schematic representation of heart in sagittal plane illustrating level in transverse plane (*thick line*) used for analysis of wall motion and wall thickening.

TABLE 1: Characteristics of Patients and Correlative Studies

Patient No.	Age (years)	History of MI	ECG Results	Wall Motion by 2D or Angio	Wall Motion by Cine MR
1	45	8 mo	A MI	Hypo PS; Ak A, AS; Dys AP	Hypo P; Ak A, AS
2	54	5 mo	I MI	Ak PL, D, PB	Hypo P; Ak PL
3	59	3 mo	Lat MI, LVH	Hypo IL, PS	Hypo PL, P, PS
4	64	12 mo	I MI	Ak P, PS	Hypo PL, P, PS
5	58	6 yr, 1 mo	AS MI	Hypo global; Dys	Hypo global; Dys A
6	57	10 mo	AS MI	Hypo AS, A; Dys AP	Hypo P; Ak A, AS
7	61	2 mo	AS MI	Hypo PS, Ak A, AS; Dys AP	Ak AL, AS; Dys A
8	66	2 mo	I MI	Ak D, PL, PB	Hypo PL, P, PS
9	64	2 wk	A + I MI	Hypo AS, Dys AP	Ak AS; Dys A
10	66	2 wk	A MI, LVH	Dys AP	Ak A
11	55	15 yr	I MI	Ak I, AP	Hypo A, P, PS
12	60	1 mo	NS A ST	Ak A, AP	Hypo As, Ak A
13	71	4 yr	I MI	Hypo AP, AL, I, IS	Hypo P, PS, AS; Ak AS, PS
14	70	15 yr	I MI, NS A ST	Hypo AP, AL; Ak I	Hypo A
15	73	Not known	P MI, LVH	Hypo I	Hypo PL

Note.—A = anterior, Ak = akinetic, AL = anterolateral, Angio = angiography, AP = apex, AS = anteroseptal, D = diaphragmatic, Dys = dyskinetic, Hypo = hypokinetic, I = inferior, IL = inferolateral, IS = inferoseptal, Lat = lateral, LVH = left ventricular hypertrophy, MI = myocardial infarction, mo = month, NS = nonspecific , P = posterior, PB = posterobasal, PL = posterolateral, PS = posteroseptal, ST = segment changes, 2D = 2-dimensional echocardiography, wk = week, yr = year.

To provide a constant number of time frames per R to R interval for image reconstruction, the image data were subjected to linear interpolation. The image plane was 10 mm thick. The acquisition matrix was 128 × 256 interpolated to 256 × 256 for display.

Image Analysis

From the acquired series of images, the left ventricle was usually confined to five or six levels. From these, the mid-ventricular slice (Fig. 1) was selected for analysis. Images within that slice were displayed in the cinematic mode, and six segments were analyzed independently by two observers experienced in interpretation of MR studies. Wall motion was assessed qualitatively and wall thickening was assessed quantitatively. Wall motion was scored as normal (0 points), hypokinetic (1 point), akinetic (2 points), dyskinetic (3 points), or uninterpretable; scores were given for six myocardial segments identified as anterior, anterolateral, posterolateral, posterior, posteroseptal, and anteroseptal (Fig. 2). When observers disagreed in their interpretations, the study was reviewed jointly and a consensus was reached.

Measurements of left ventricular myocardial thickness were made using manufacturer-supplied software programs. The accuracy of the measurements was confirmed with a phantom of known dimensions. To standardize signal intensity and to minimize observer variability, the pixel intensity level was set to the mean of signal intensities of the blood pool and of myocardium. The width of the window was arbitrarily set to 50–75% of the level value. The region of the heart was displayed at 1.5× magnification for measurements. The end-diastolic and end-systolic frames for each study were identified visually as those with the largest and smallest cross-sectional areas of blood pool, respectively. The visual impression was confirmed by measuring the cross-sectional area of blood pool in that frame and in the frames that preceded and followed.

For measurement of left ventricular wall thickness, a grid consisting of radians at 60° intervals was imprinted on a plastic transparency (Fig. 2). The 0°/180° axis was placed parallel to the septum through the most anterior extent of the left ventricle. The intersection of the six radians was positioned at the midpoint of the long axis of the left ventricle. The same procedure was performed on both the end-diastolic and end-systolic images. Measurements were made by using a manufacturer-supplied computer caliper program after visual determination of the endocardial and epicardial surfaces by the operator. Wall thickness was measured perpendicular to the endocardium from the intersection of each of the six radians and the endocardial border (Fig. 2). Measurements were rounded to the nearest millimeter. If papillary muscle was encountered, that segment was excluded from analysis. Absolute and percentage wall thickening (absolute thickening/end-diastolic wall thickness × 100) were calculated for each segment. Wall-thickness measurements were performed in the 13 normal subjects by two observers independently and were repeated after 4 weeks by the first observer to establish inter and intraobserver variability.

Statistical Analysis

The mean data are presented ±1 standard deviation. In normal subjects, the variability of wall thickness and percentage wall thickening among the six segments were assessed by single-factor analysis of variance. Segmental means were compared by Scheffé's [9] test. Pooled wall-thickness data from all normal segments were compared with those segments in patients with ischemic heart disease designated as normal, hypokinetic, akinetic, or dyskinetic by single-factor analysis of variance. Scheffé's test [9] was used to assess individual means. Inter- and intraobserver variability was assessed by linear regression analysis and by determination of the mean percentage difference between measurements:

$$100 \times \frac{\text{observer 1} - \text{observer 2}}{\text{mean of observer 1} + \text{observer 2}}$$

Nonparametric testing was done by chi-square analysis with contingency correction. A p value less than .05 was considered significant.

Results

Normal Subjects

Table 2 gives data on wall thickening in normal subjects. In contrast to conventional MR images, the blood pool in GRASS images has higher signal intensity than myocardium (Fig. 3). Wall motion, by analysis of the cine display, was normal in all normal volunteers. Diastolic wall thickness ranged from 8.5 ± 1.1 mm (mean ± SD) in the posterior segment to 11.4 ± 1.9 mm in the posterolateral segment ($p < .05$). In systole, thickness ranged from 13.2 ± 2.2 mm in the posteroseptal segment to 15.9 ± 2.1 mm in the anterolateral segment (not significantly different). Heterogeneity of absolute systolic wall thickening was noted among the different myocardial segments, although the differences did not reach statistical significance. Values ranged from 0 to 10 mm (Fig. 4). Values of absolute wall thickening less than 2 mm occurred in only three of the entire 78 segments in the 13 normal volunteers. Heterogeneity of percentage wall thickening was also seen be-

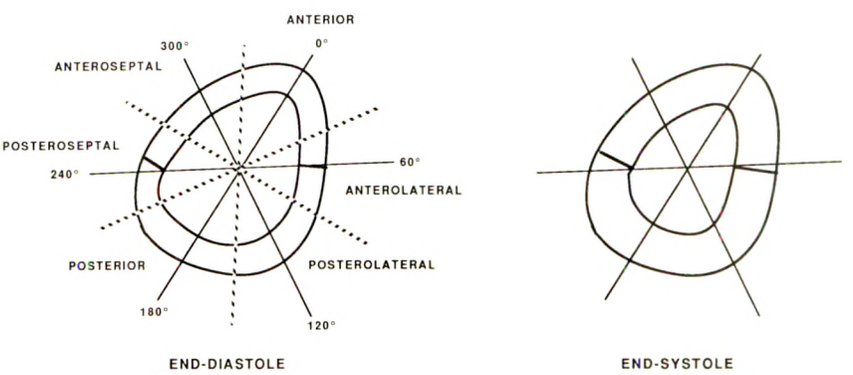

Fig. 2.—Illustration of myocardial segments (*between hatched lines*) graded for wall-motion abnormalities and radial grid (*solid lines*) used to locate sites for measurement of wall thickness. Measurements were made perpendicular to endocardium, as illustrated.

TABLE 2: Wall Thickening in Normal Subjects

Measurement	Segments					
	Anterior	Anterolateral	Posterolateral	Posterior	Posteroseptal	Anteroseptal
Thickness diastole (mm)	9.8 ± 1.6	11.3 ± 1.1	11.4 ± 1.9	8.5 ± 1.1[a]	9.9 ± 1.1	9.6 ± 1.8
Thickness systole (mm)	15.3 ± 2.2	15.9 ± 2.1	15.8 ± 2.4	14.0 ± 2.4	13.2 ± 2.2	14.1 ± 2.3
Absolute thickening (mm)	5.4 ± 2.3	4.6 ± 2.3	4.5 ± 2.6	5.5 ± 2.6	3.2 ± 1.7	4.5 ± 1.9
% thickening	59 ± 31	42 ± 25	42 ± 30	66 ± 29	33 ± 17	49 ± 23

[a] $p < .05$ vs anterolateral and posterolateral; numbers are means ± 1 SD.

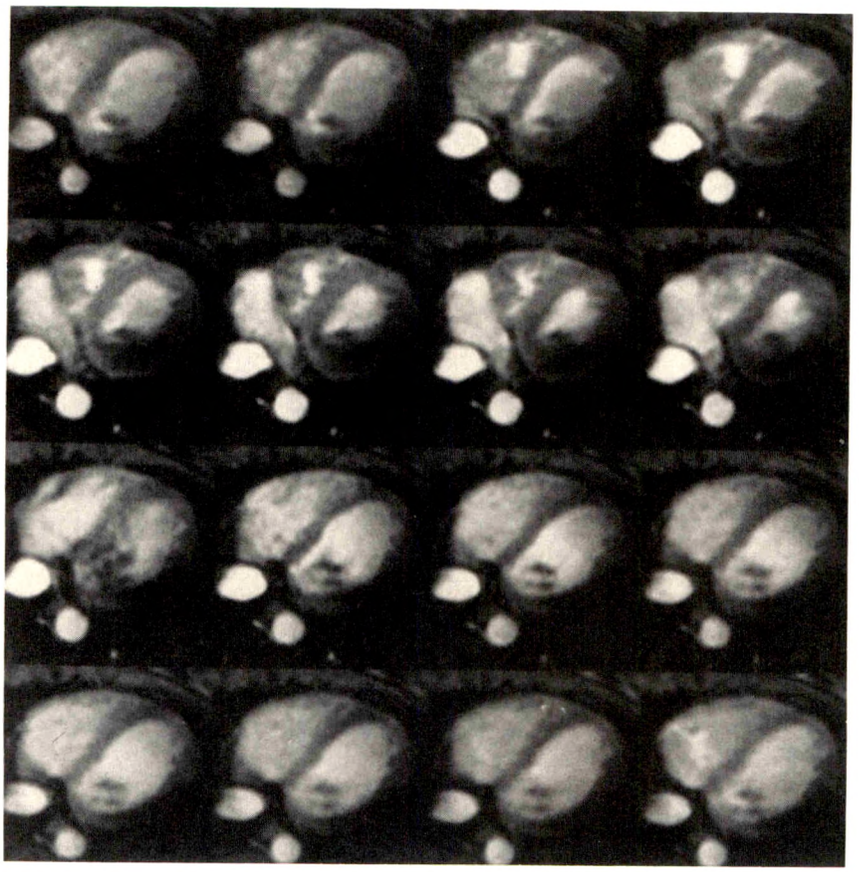

Fig. 3.—Images of a normal volunteer throughout cardiac cycle at mid-ventricular level show normal myocardial thickening.

tween segments, although again, the differences were not statistically significant. Overall percentage systolic wall thickening in all normal segments was 48% ± 28%. Thickness measurements could not be obtained for eight of the 78 segments—in six segments because of papillary muscle within the segment and in two posterior segments because of partial volume averaging with the left atrium in systole.

Ischemic Heart Disease

On analysis of the cine display, 45 segments in patients with ischemic heart disease exhibited normal wall motion (Fig. 5). Of the remaining segments, 21 were hypokinetic, 15 were akinetic, and four were dyskinetic. In one instance, an inferior wall-motion abnormality shown by angiography was not seen in the cine MR study. In the remaining segments, location of wall-motion abnormalities corresponded to comparable regions in the documentary studies (Table 1).

Mean diastolic wall thickness of normal segments in patients with ischemic heart disease was higher than mean wall thickness in normal subjects ($p < .05$). Diastolic thickness alone (i.e., wall thinning) did not distinguish hypokinetic and akinetic segments from normal segments in patients with ischemic heart disease because considerable overlap was present (Table 3). Only dyskinetic segments were significantly thinner ($p < .05$) than in normal volunteers at end-diastole. Systolic thickness was greater for normal segments in patients compared with normal segments in normal volunteers ($p < .05$). Abnormal segments in patients with ischemic heart disease were significantly thinner at end-systole than were normal segments in these patients ($p < .05$) and in normal volunteers ($p < .05$), although some overlap with normal segments existed.

Absolute systolic wall thickening was similar for normal segments in patients with ischemic heart disease and in normal subjects. Absolute thickening of abnormal segments

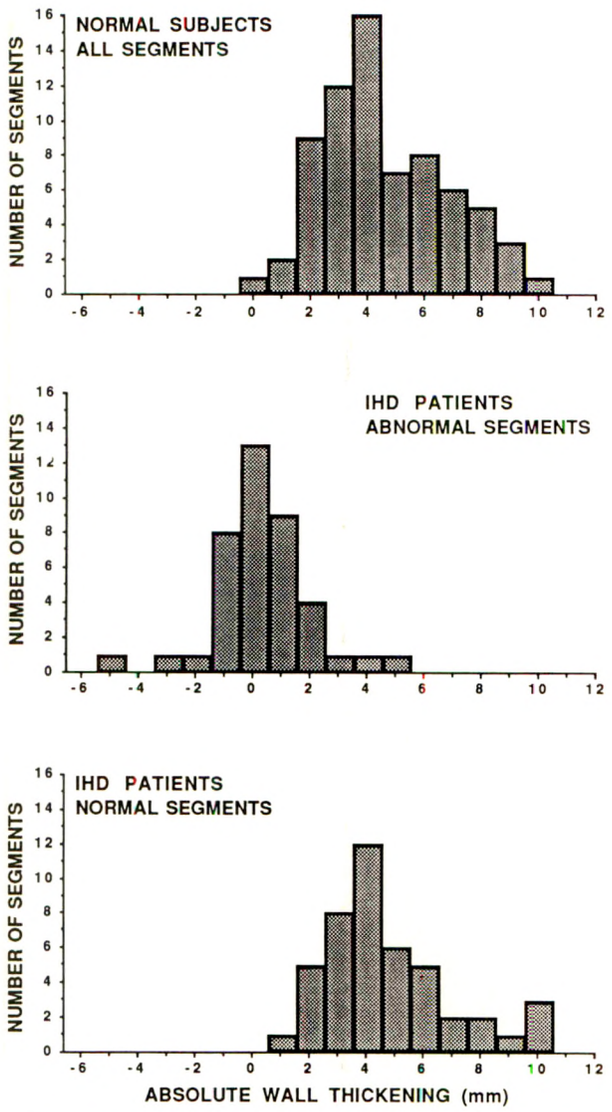

Fig. 4.—Frequency distribution of absolute wall thickening (mm) in normal and abnormal myocardial segments. IHD = ischemic heart disease.

in patients was 0.3 ± 1.7 mm overall, which was significantly less than for both normal segments in this group and normal volunteers ($p < .001$). Absolute wall thickening was less than 2 mm in 31 of 40 abnormal segments and greater than 2 mm in only three segments. Very little overlap of values for wall thickening was observed between normal and abnormal segments (Fig. 4). Percentage systolic wall thickening was similar in segments of normal subjects (48% ± 28%) and normal segments in patients with ischemic heart disease (43% ± 31%). Overall percentage wall thickening in abnormal segments was 0% ± 22% (Table 3).

In the patient group, five of 90 segments could not be analyzed, in four because of papillary muscle within the segment and in one because of partial-volume averaging with the left atrium in systole.

Inter- and Intraobserver Variability

From the subjective analysis of the cinematic displays, the two observers disagreed on the assessment of wall motion in 10 segments; this occurred most often in the distinction between hypokinetic and akinetic wall motion. Disagreement was never by more than one grading point. Correlation between observers for diastolic and systolic wall thickness measurements was 0.85 ($p < .0001$). The mean difference in measurements was 10.8% ± 9.2%. Intraobserver correlation for measurements was 0.90 ($p < .0001$). The mean difference for intraobserver measurements was of 9.4% ± 8.5%.

Discussion

In this study, the capabilities of a new MR technique for assessing left ventricular function were examined. Rapid MR imaging not only provides the spatial resolution customary in conventional MR studies but can also, because of shallow flip angles and short repetition times, acquire a large number of images per cardiac cycle. The latter innovation allows processing of multiple images into a closed-loop cinematic display for analysis of cardiac function. The inherent contrast between

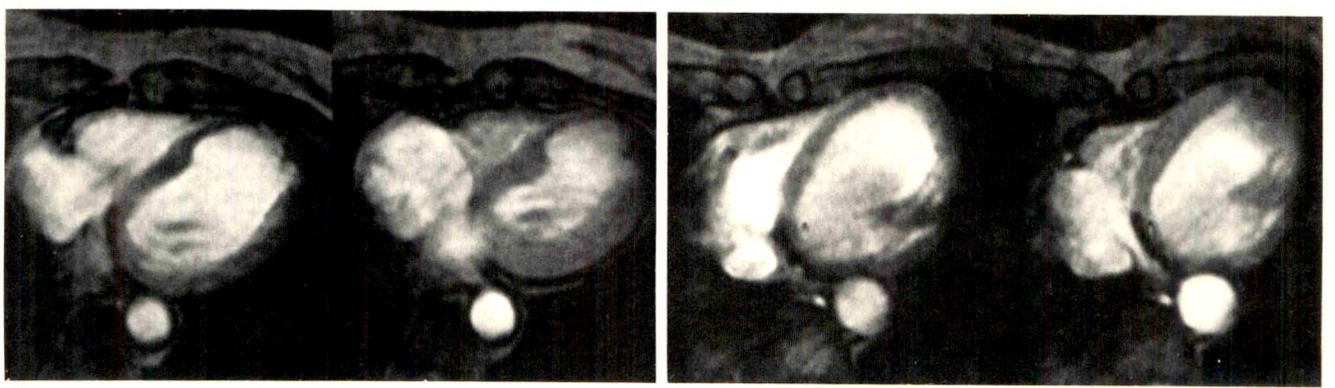

Fig. 5.—*A*, Anterior myocardial infarction (diastole at left, systole at right). Absence of thickening in the anterior and anteroseptal segments. Wall thickening is normal in other segments.

***B*, Inferior myocardial infarction (diastole at left, systole at right). Wall thickening is absent in extensive area in the posterolateral, posterior, and posteroseptal segments.**

TABLE 3: Wall Thickening in Patients with Ischemic Heart Disease

Measurement	Segments				
	Normal (n = 70)	Normal IHD (n = 45)	Hypokinetic (n = 21)	Akinetic (n = 15)	Dyskinetic (n = 4)
Thickness diastole (mm)	10.1 ± 1.7	12.2 ± 3.5[a]	9.1 ± 4.7[b]	8.5 ± 2.9[b]	5.0 ± 3.4[c]
Thickness systole (mm)	14.7 ± 2.4	17.0 ± 3.8[a]	9.8 ± 5.6[c]	8.4 ± 4.1[c]	4.8 ± 3.8[c]
Absolute thickening (mm)	4.6 ± 2.2	4.7 ± 2.3	0.7 ± 1.7[c]	−0.1 ± 2.0[c]	−0.3 ± 0.5[c]
% thickening	48 ± 28	43 ± 31	6 ± 19[c]	−4 ± 24[c]	−13 ± 25[c]

Note.—IHD = ischemic heart disease; means presented ± 1 SD.
[a] $p < .05$ normal vs normal IHD.
[b] $p < .05$ vs normal IHD.
[c] $p < .05$ vs normal and normal IHD.

blood pool, lung, and myocardium further allows determination of myocardial wall thickness, from which an index of regional ventricular function can be derived when measured at end-diastole and end-systole.

Analysis of the cinematic display of MR images within the plane of study was accurate in locating wall-motion abnormalities documented by other techniques, despite the fact that the image plane in this study was not ideal for visualizing the apex of the heart, the inferior wall, or the anterobasal segment. In many cases, the degree of the wall-motion abnormality was the same, although the exact degree and extent of abnormality could not be correlated accurately because the field of view of the heart and the imaging planes were not strictly comparable between the three imaging techniques. An equatorial transverse plane of section obtained by two-dimensional echocardiography has recently been described by Sharkey et al. [10]. The authors point out that the advantage of such a view is for detection or confirmation of posterior wall-motion abnormalities.

Although cross-sectional echocardiography can reliably detect jeopardized myocardium during acute myocardial infarction by wall-motion analysis [11–13], diminished or absent systolic wall thickening may be a more sensitive indicator of the extent of regional myocardial ischemia and infarction than abnormal wall motion. From an intricate study of 48-hr-old myocardial infarction in a dog model, Lieberman et al. [3] concluded that endocardial motion assessed by echocardiography was less sensitive in discriminating infarcted from noninfarcted myocardium than measurement of systolic wall thickening, resulting in overestimation of true infarct size. Buda et al. [14] noted similar results when studying the extent of myocardial injury and myocardium at risk in a canine model of acute coronary occlusion. In humans with myocardial infarction examined at autopsy, Weiss et al. [15] found that analysis of wall motion by two-dimensional echocardiography was accurate in locating myocardial infarction, but overestimated the extent of the abnormality.

In the current study, substantial variability of wall thickening was seen both among subjects and among myocardial segments in any one individual in the group of normal volunteers, an observation previously noted in both animal and human studies. LeWinter et al. [16] noted that, in dogs, the percentage shortening of myocardial fibers was less in the midventricle than at the apex. In humans, Pandian et al. [4] found considerable heterogeneity in wall thickening determined by echocardiography using analytical methods similar to those used in the current study. In 12 normal young men, segmental wall thickening ranged from 0% to 150%, although differences between myocardial segments were not found to be significant. Haendchen et al. [5] arrived at similar results in a study of both canine and human hearts studied at various planes from apex to base.

Cross-sectional echocardiography [4], cine CT scanning [6], and conventional MR [7] have all previously been reported as useful for determining myocardial systolic wall thickening. Each of these techniques, however, has inherent limitations. Echocardiography is reliant on ideal acoustic conditions for image acquisition, which in turn determine the ability to accurately detect endocardial and epicardial borders. Pandian et al. [4] found that intraobserver variability for wall-thickening measurements exceeded 25%. Cine CT scanning, which provides high-resolution tomographic images similar to those of cine MR, requires IV injection of iodinated contrast media and exposure to ionizing radiation. Conventional MR has excellent spatial resolution but has limited temporal resolution and requires relatively long imaging times, and images cannot easily be viewed in a cinematic format.

Cine MR is noninvasive and does not require contrast agents to define the blood pool. Although in this study, by design, only a limited region of the heart was analyzed in detail, it is apparent that the three-dimensional capability and the ability to image in any plane make MR imaging and in particular cine MR imaging ideally suited for assessment of global cardiac function.

Limitations of the Study

As noted above, wall-motion abnormalities determined from cine MR were not strictly comparable with the documentary studies because of different fields of view and differences in nomenclature. However, the imaging plane selected for analysis is truly representative of the three major (anterior descend-

ing, right, and circumflex) cardiac vascular territories. Therefore, significant ventricular dysfunction in any of those regions would be discernible by imaging in the equatorial plane. Wall-motion abnormalities confined exclusively to the inferior or diaphragmatic segment or to the apical or anterobasal portion of the heart are difficult to detect in the transverse plane. Further studies need to be performed to evaluate the usefulness of imaging in other planes for detection of abnormalities in these regions.

Cross-sectional imaging techniques, including echocardiography, result in a certain degree of obliquity of section when imaging the heart. The equatorial plane minimizes oblique sectioning of the anterior wall and septum, although the difference in diastolic thickness between the posterior and anterolateral and posterolateral segments may be a reflection of slightly more obliquity of the plane of section through the lateral left ventricular myocardium. As the ability to image in planes oriented to the long and short axes of the heart becomes more widely applied [17], this problem may be minimized. However, no existing data indicate that MR in nonorthogonal (short- or long-axis) planes results in less heterogeneity of wall thickening compared with MR in the transverse plane.

Conclusions

The new technique of cine MR adds the important dimension of motion to cardiac MR studies. In addition to detailed anatomic information, useful functional information, both qualitative and quantitative, can now be derived from MR studies of the heart. The ability to image the entire heart in multiple planes may offer a means of more accurately assessing and following the extent of ischemic myocardial damage.

REFERENCES

1. Vatner SF. Correlations between acute reductions in coronary blood flow and function in conscious dogs. *Circ Res* **1980**;47:201–210
2. Falsetti HL, Marcus ML, Kerber RE, Skorton DJ. Quantification of myocardial ischemia by left ventricular imaging. *Circulation* **1981**;63:747–751
3. Lieberman AN, Weiss JL, Jugdutt BI, et al. Two-dimensional echocardiography and infarct size: relationship of regional wall motion and thickening to the extent of myocardial infarction in the dog. *Circulation* **1981**;63:739–746
4. Pandian NG, Skorton DJ, Collins SM, Falsetti HL, Burke ER, Kerber RE. Heterogeneity of left ventricular segmental wall thickening and excursion in 2-dimensional echocardiograms of normal human subjects. *Am J Cardiol* **1983**;51:1667–1673
5. Haendchen RV, Wyatt HL, Maurer G, et al. Quantitation of regional cardiac function by two-dimensional echocardiography. 1. Patterns of contraction of the normal left ventricle. *Circulation* **1983**;67:1234–1245
6. Lanzer P, Garrett J, Lipton MJ et al. Quantitation of regional function by cine computed tomography: pharmacologic changes in wall thickness. *J Am Coll Cardiol* **1986**;8(3):682–692
7. Sechtem UP, Sommerhof BA, Markiewicz W, White RD, Cheitlin MD, Higgins CB. Assessment of regional left ventricular wall thickening by magnetic resonance imaging: evaluation in normal persons and patients with global and regional dysfunction. *Am J Cardiol* **1987**;59:145–151
8. Haase A, Matthei D, Hänicke W, et al. Rapid NMR imaging using low flip-angle pulses. *J Magn Reson* **1986**;67:258–266
9. Scheffé H. A method for judging all contrasts in the analysis of variance. *Biometrika* **1953**;40:87–104
10. Sharkey SW, Asinger RW, Elsperger KJ, Siegel J. Two-dimensional echocardiographic detection of left ventricular posterior wall motion abnormalities using an inferior angulation view. *Am J Cardiol* **1986**;58:704–709
11. Heger JJ, Weyman AE, Wann LS, Rogers EW, Dillon JC, Feigenbaum H. Cross-sectional echocardiographic analysis of the extent of left ventricular asynergy in acute myocardial infarction. *Circulation* **1980**;61:1113–1118
12. Visser CE, Lie KI, Kan G, Meltzer R, Durrer D. Detection and quantification of acute, isolated myocardial infarction by two dimensional echocardiography. *Am J Cardiol* **1985**;47:1020–1025
13. Horowitz RS, Morganroth J. Immediate detection of early high-risk patients with acute myocardial infarction using two-dimensional echocardiographic evaluation of left ventricular regional wall motion abnormalities. *Am Heart J* **1982**;103:814–822
14. Buda AJ, Zotz RJ, Pace DP, Krause LC. Comparison of two-dimensional echocardiographic wall motion and wall thickening abnormalities in relation to the myocardium at risk. *Am Heart J* **1986**;111:587–592
15. Weiss JL, Bulkley BH, Hutchins GM, Mason SJ. Two-dimensional echocardiographic recognition of myocardial injury in man: comparison with postmortem studies. *Circulation* **1981**;63:401–408
16. LeWinter MM, Kent RS, Kroener JM, Carew TE, Covel JW. Regional differences in myocardial performance in the left ventricle of the dog. *Circ Res* **1975**;31:191–199
17. Dinsmore RE, Wismer GL, Miller SW, et al. MRI of the heart using planes oriented to cardiac axes: experience in 100 cases. *AJR* **1985**;145:1177–1183

Book Review

Diagnosis of Diseases of the Chest, 3rd ed., vol. 1. By Robert G. Fraser, J. A. Peter Paré, P. D. Paré, Richard S. Fraser, and George P. Genereux. Philadelphia: Saunders, 764 pp., 1987. $65

This is the first of a projected four-volume revision of the major reference work on radiology of the chest, Fraser and Paré's second edition. The authors, a radiologist and a chest physician, have enlisted the collaboration of their sons, who are experts in chest pathology and physiology, and another chest radiologist to help with the enormous job of updating this most comprehensive text. This edition attempts a broader approach to chest disease. Although it features radiologic findings, it presents more physiology than previous editions did. The amount of work entailed in editing and revising such a large work justifies the separate publication of each volume, but some users may wish to wait until the volumes on chest disease begin to appear before buying this introductory volume.

The book begins with a glossary, taken with minor changes from that published in this Journal by the Fleischner Society Nomenclature Committee, which is headed by Dr. Fraser. It is a thoughtful addition to a textbook meant for new as well as experienced chest physicians and radiologists. The section on normal anatomy has been supplemented by a larger section on physiology, and even includes a clear summary of findings and issues in radiologic perception. Methods of examination are covered thoroughly, from slit-scanned digital imaging to pulmonary function tests; an extensive list of bacteriologic findings is included. Illustrations are sparse in this section, and presumably the volumes on disease will have illustrations of pathologic conditions. The final chapter, more than 200 pages, is a compendium of basic radiologic signs, those that increase or decrease film density, and findings of pleural disease. This is a textbook in itself, of patterns, radiologic-pathologic correlation, and differential diagnosis.

How good a job have the authors done? First, there is nothing with which to compare this book. It has breadth and detail beyond any other past or contemplated textbook of chest diagnosis. It continues the tradition of providing a superb and current bibliography. Illustrations, both diagrams and radiographs, are profuse. CT scans appear in substantial number in this edition, including many of Dr. Genereux's extensive collection of sagittal and coronal reconstructions. MR imaging is introduced thoroughly, but few illustrations appear yet; subsequent volumes undoubtedly will have more.

The quality of the illustrations is surprisingly uneven. Many of the illustrations of radiographs are first class, not exceeded in the textbook literature by any except the magnificent positive images of the Schinz opus. However, others are too light, too dark, or too flat. The CT scans are mostly good, including the somewhat jagged reconstructions, but I do not care for the light lung windows used in some cases. I hope the next volumes will have some high-resolution CT scans to illustrate specific diseases. On the whole, I do not know of any textbooks that consistently have better pictures, but this one has some that are disappointing.

The editing has been good. I found few errors; one in particular was a substitution of "humeral" for "humoral" twice in half a dozen pages. In looking carefully at some areas of personal interest, I was disappointed to see the term "apical pleural thickening" used for the parenchymal density seen at the apex in many cases. The book has little on pleural fat, mentioning only a "companion shadow" at the apex and omitting several other common sites that should be distinguished from pleural abnormalities. The classification of mediastinal lymph nodes proposed by the American Thoracic Society is listed clearly, but the description and illustrations of nodes use a different proprietary scheme. The authors' use of "end stage lung" for interstitial fibrosis is also regrettable because fibrosis is but one of several possible end stages (consider also bronchiectasis and emphysema). The basic material on lobar collapse is not supplemented by much on segmental disease, but that might take another textbook.

In summary, the third edition of *Diagnosis of Diseases of the Chest* is in a class by itself. It is not perfect, but it is very good. If you do not have the second edition on your shelves already, it is time to buy this one.

Paul J. Friedman
University of California, San Diego
La Jolla, CA 92093

MR Imaging of Acute Myocardial Infarction: Value of Gd-DTPA

Albert de Roos[1]
Joost Doornbos[1]
Ernst E. van der Wall[2]
Ad E. van Voorthuisen[1]

The potential of gadolinium (Gd)-DTPA to improve the detection of acute myocardial infarction by MR has been shown in experimental canine studies. To determine its value in humans, we studied five patients 2–17 days after myocardial infarction by using ECG-gated MR before and after administration of 0.1 mmol/kg Gd-DTPA. One patient had a rupture of the interventricular septum, complicating an acute inferior-wall infarction. Spin-echo images were obtained before and immediately after injection of Gd-DTPA and were repeated every 10 min for up to 40 min. In four patients, intensity-vs-time curves revealed increasing signal intensity in the infarcted area in the first 20 min after injection of gadolinium. Contrast between normal and infarcted myocardium was greatest 20–30 min after Gd-DTPA injection. In one patient, increasing signal intensity of the infarcted myocardium was observed up to 40 min after Gd-DTPA injection. The precontrast intensity ratio between infarcted and normal myocardium was 1.1 at echo time (TE) = 30 msec and was 1.4 at TE = 60 msec ($p < .05$). The postcontrast intensity ratio was 1.6, which was not statistically different from the ratio at TE = 60 msec but which was significantly higher than the ratio at TE = 30 msec ($p < .01$). Infarct definition was substantially improved on postcontrast images. The septal rupture was clearly seen, and the infarcted myocardium surrounding the septal rupture showed enhancement on postcontrast images.

These results suggest that Gd-DTPA can improve MR visualization and detection of acute myocardial infarction.

MR imaging of the heart can identify and quantitate acute myocardial infarction noninvasively, as shown by experimental canine studies [1]. In humans, MR can be used to detect and localize acute myocardial infarction by showing local wall thinning, increased signal intensity in the infarcted area, and increased flow signal in the ventricular cavity [2–5].

Prolongation of T1 and T2 relaxation times in the edematous infarcted zone occurs consistently. T2 prolongation appears to predominate and therefore an increased myocardial signal is best appreciated on spin-echo images with long echo times [4]. Sometimes, however, no contrast between infarcted and normal myocardium is observed. Furthermore, subendocardial increased signal intensity can be difficult to differentiate from flow-related enhancement. Other problems in diagnosing myocardial infarction by MR are the occurrence of an increased myocardial signal, an increased flow-related signal, and myocardial wall thinning in asymptomatic volunteers [3].

Gd-DTPA is a clinically useful paramagnetic contrast agent for MR [6]. In humans, it has been used primarily for the examination of brain tumors. Because of its favorable pharmacokinetic properties and lack of adverse reactions, Gd-DTPA is safe for use in humans [6]. Gd-DTPA produces significant shortening of T1 relaxation time of irreversibly damaged canine myocardium, resulting in increased signal intensity of the infarct relative to normal myocardium [7, 8]. In this study, we evaluated the use of Gd-DTPA for detection of acute myocardial infarction in five patients.

Received September 10, 1987; accepted after revision November 2, 1987.

[1] Department of Diagnostic Radiology, University Hospital Leiden, Rijnsburgerweg 10, 2333 AA Leiden, the Netherlands. Address reprint requests to A. de Roos.

[2] Department of Cardiology, University Hospital Leiden, 2333 AA Leiden, the Netherlands.

AJR 150:531–534, March 1988
0361–803X/88/1503–0531
© American Roentgen Ray Society

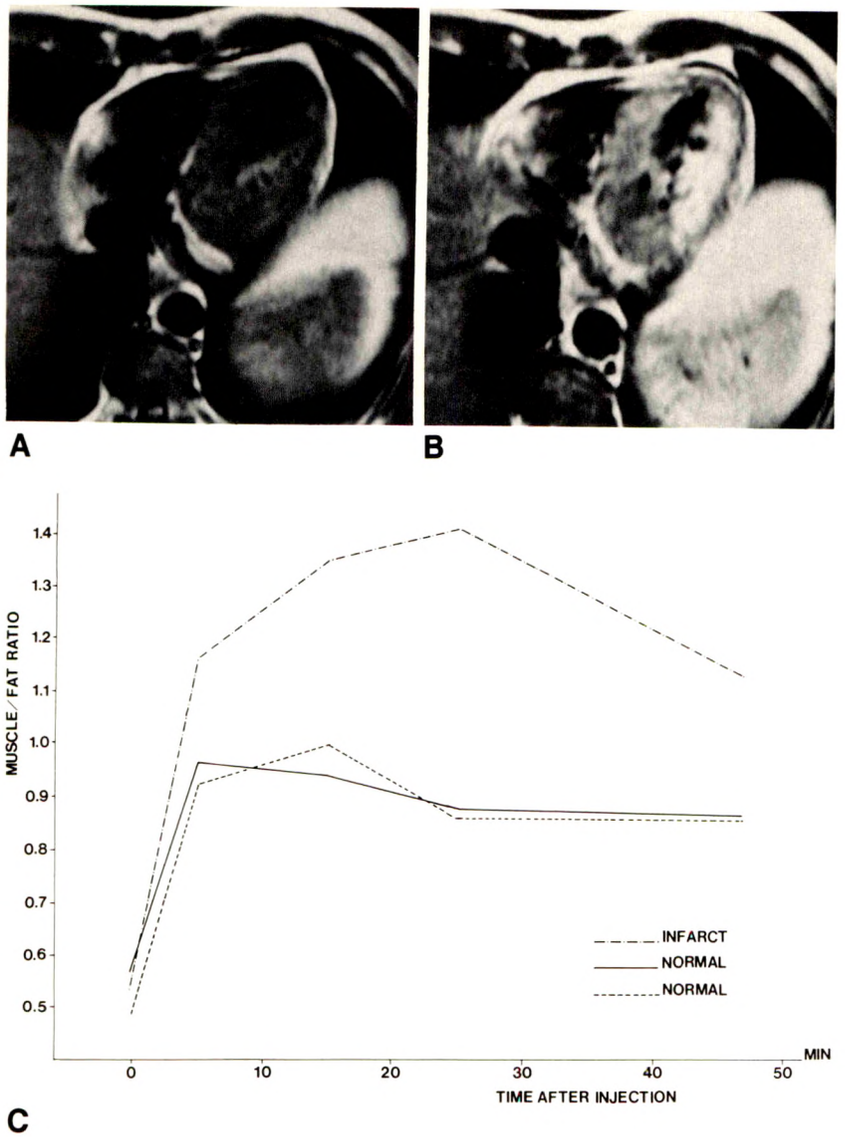

Fig. 1.—*A*, Precontrast transaxial MR image through left ventricle in 49-year-old man suffering from a 7-day-old myocardial infarction. Acute posterolateral myocardial infarction cannot be identified.

***B*, Postcontrast image at same level made 20 min after Gd-DTPA injection. Enhancement of infarcted area improves detection of infarct.**

***C*, Intensity-vs-time curves in same patient show maximal contrast between infarction and two areas of normal myocardium 20–30 min after administration of Gd-DTPA.**

Subjects and Methods

Four men (38–60 years old) with acute myocardial infarction were studied by ECG-gated MR within 1 week after the acute event. A fifth patient (a 61-year-old man) who had a ventricular septal rupture complicating an acute inferior-wall infarction was studied 17 days after the acute event. Diagnosis of acute myocardial infarction was based on history, ECG changes, and typical evolution of plasma creatine kinase levels. The location of the infarct was confirmed by both ECG and coronary angiography, which showed an occluded or stenotic infarct-related artery. In the first four patients, peak plasma creatine kinase levels varied between 235 and 740 U/l (mean, 490 U/l). The fifth patient (with septal rupture) was first admitted 2 weeks after the acute event; therefore, maximal creatine kinase level was not available. Informed consent was obtained. Spin-echo images were made in axial planes before and after IV administration of 0.1 mmol Gd-DTPA/kg. Images were obtained immediately after bolus injection of Gd-DTPA, and repeat examinations were performed every 10 min for up to 40 min thereafter. This 40-min period was chosen on the basis of experimental data [7] and because of time restrictions. In the patient with acute inferior-wall infarction complicated by septal ruptures, short-axis images were obtained with single electronic angulation starting from the transverse images.

MR examinations were performed with a Philips 0.5-T Gyroscan unit. The repetition time was determined by the heartbeat interval by ECG triggering at every heartbeat. The trigger delay was 200 msec after the R wave of the ECG. Six 10-mm-thick slices with 1-mm gaps were obtained in transaxial planes with an echo-time (TE) of 30 msec and four measurements. In addition, a single-slice, four-echo image (TE = 30, 60, 90, and 120 msec) was obtained through the largest diameter of the left ventricle. A matrix size of 256 × 128 was used for acquisition; the images were displayed with a 256 × 256 matrix.

All images were assessed visually for the presence of signs indicative of myocardial infarction. Signal intensities were calculated by region-of-interest analysis after visual inspection. The operator-defined regions of interest were 1 cm^2. In order to account for instrumental variations, the myocardial regions of interest were normalized to the intensity of subcutaneous axillary fat. Mean values of the

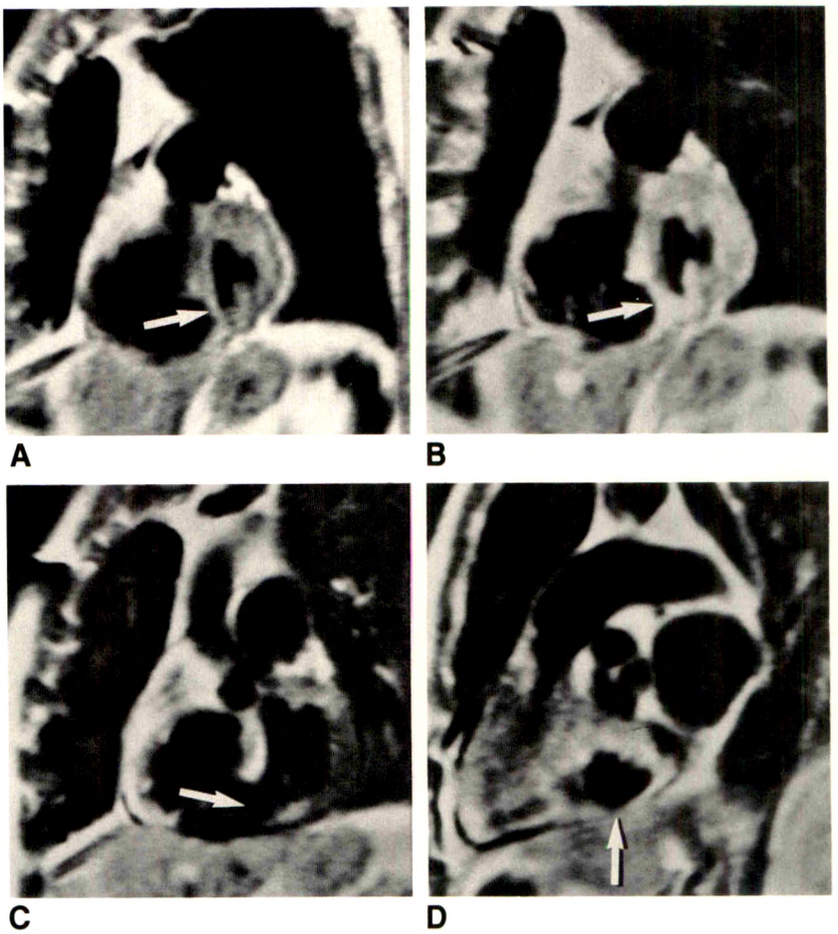

Fig. 2.—*A*, Precontrast short-axis view through left ventricle in 61-year-old man with 17-day-old inferior-wall infarction complicated by septal rupture. Image was obtained adjacent to ruptured septum. Note local wall thinning in septal region (*arrow*).

***B*, Postcontrast image at same level. Note enhancement of infarcted myocardium in inferior wall and septum (*arrow*). Small enhancing liver lesion (high signal intensity compatible with hemangioma was seen at long-TR/TE images) is also visible.**

***C*, Postcontrast short-axis view perpendicular to interventricular septum obtained by using single electronic angulation. Septal rupture is clearly seen (*arrow*).**

***D*, Postcontrast long-axis view parallel to interventricular septum. Note enhancement of infarcted myocardium surrounding septal rupture (*arrow*).**

measurements obtained by two independent observers were determined both for precontrast images, (TE = 30 and 60 msec) and for postcontrast images. The ratio of the myocardial intensity of the apparently infarcted myocardium to that of normal myocardium in the same image was measured. This intensity ratio is a measurement of the contrast between infarcted and normal tissue. Intensity-vs-time curves were constructed for infarcted and normal myocardium.

Differences between signal intensity values were analyzed with the Wilcoxon rank test. A p value of less than .05 was considered significant.

Results

Short-TE precontrast images showed local wall thinning consistent with myocardial infarction in one patient. Multiecho images showed an increased wall signal compatible with infarction in four patients. Delineation of the infarcted area was poor when a multiecho technique was used because the signal-to-noise ratio was less than optimal. After Gd-DTPA injection, the infarcted areas were more visible in all five patients, improving infarct definition as compared with definition on precontrast images (Fig. 1). The average precontrast intensity ratio was 1.1 with a TE of 30 msec and 1.4 with a TE of 60 msec ($p < .05$). The average intensity ratio 20–30 min after Gd-DTPA administration was 1.6; this was a significant increase over the precontrast ratios with a TE of 30 msec ($p < .01$). The difference between the intensity ratio with a TE of 60 msec and the postcontrast ratio did not reach statistical significance. In four patients, intensity-vs-time curves showed greatest contrast between normal and infarcted myocardium at 20–30 min after Gd-DTPA administration (Fig. 1). In one patient, the contrast was still increasing 40 min after Gd-DTPA injection. MR clearly showed the septal rupture as well as enhancement of the infarcted myocardium surrounding the defect (Fig. 2).

In the first 20–30 min after gadolinium injection, an average enhancement of 40% (range, 15–80%) for normal myocardium was observed; the infarcted myocardium showed an average enhancement of 90% (range, 50–160%). Improved infarct definition after Gd-DTPA administration was assessed by visual inspection and by measuring significantly higher contrast ratios between normal and infarcted myocardium in all five patients.

Discussion

The present study demonstrates the potential of Gd-DTPA to improve detection and definition of acute myocardial infarction in humans. A bolus injection of 0.1 mmol/kg Gd-DTPA

induced a marked shortening of T1 relaxation time in the infarcted area, thereby enhancing the signal intensity of the infarcted myocardium. Both visual inspection and measurement of the signal intensity of the infarcted myocardium relative to normal myocardium showed improved infarct definition on postcontrast images. These results are in accordance with a recent study comparing Gd-DTPA enhancement in different stages of myocardial infarction [9].

Maximal contrast between normal and infarcted myocardium was seen 20–30 min after Gd-DTPA administration in four patients, probably because of delayed washout of the contrast agent from the infarcted zone as compared with normal myocardium.

Our study also shows an average enhancement of 40% for normal myocardium. Enhancement of normal myocardium is related to myocardial blood flow and offers the potential to detect hypoperfusion distal to severe stenotic coronary arteries as demonstrated in experimental studies [10].

Although MR without the use of contrast agents can detect and localize myocardial infarction, there are still notable limitations. When no contrast agent is used, spin-echo images with long echo times (multiecho images) usually are acquired for improved definition of the infarct. However, these images have a less-than-optimal signal-to-noise ratio as compared with images that have short echo times. Another advantage of the multislice, single-echo technique is the potential capability of obtaining images of the entire left ventricle with high signal-to-noise ratio. However, the signal-to-noise ratio of second-echo, multislice cardiac images is poor because of cardiac movement. Flow artifacts are also more pronounced when the multiecho technique is used.

The effect of Gd-DTPA administration is observed to best advantage on images with short echo times. Therefore, the application of Gd-DTPA obviates the use of multiecho techniques and thereby eliminates some potential pitfalls. Furthermore, Gd-DTPA probably can discriminate between the areas of increased wall signal caused by infarction and the areas of increased myocardial signal observed on the T2-weighted images of asymptomatic volunteers. Areas of increased wall signal in asymptomatic persons can occur in up to 83% of the population and are not well understood [3]. Probably respiratory motion or cardiac wall motion can account for this increased-wall-signal artifact [5]. Another potential application of Gd-DTPA is the differentiation between reversible and irreversible myocardial injury [11].

In conclusion, Gd-DTPA–enhanced MR using spin-echo images with short echo times improves the detection and definition of acute myocardial infarction in humans and eliminates some confounding factors that are related to multiecho techniques.

ACKNOWLEDGMENT

We thank Schering AG (Berlin, W. Germany) for providing Gd-DTPA/dimeglumine and Ineke Lek for her secretarial assistance.

REFERENCES

1. Caputo GR, Sechtem U, Tscholakoff D, Higgins CB. Measurement of myocardial infarct size at early and late time intervals using MR imaging: an experimental study in dogs. *AJR* **1987**;149:237–243
2. McNamara MT, Higgins CB, Schechtmann N, et al. Detection and characterization of acute myocardial infarction in man with use of gated magnetic resonance. *Circulation* **1985**;71(4):717–724
3. Filipchuk NG, Peshock RM, Malloy CR, et al. Detection and localization of recent myocardial infarction by magnetic resonance imaging. *Am J Cardiol* **1986**;58:214–219
4. Johnston DL, Thompson RC, Liu P, et al. Magnetic resonance imaging during acute myocardial infarction. *Am J Cardiol* **1986**;57:1059–1065
5. Fisher MR, McNamara MT, Higgins CB. Acute myocardial infarction: MR evaluation in 29 patients. *AJR* **1987**;148:247–251
6. Carr FH, Brown J, Bydder GM, et al. Clinical use of intravenous gadolinium-DTPA as a contrast agent in NMR imaging of cerebral tumours. *Lancet* **1984**;2:484–486
7. Rehr RB, Peshock RM, Malloy CR, et al. Improved in vivo magnetic resonance imaging of acute myocardial infarction after intravenous paramagnetic contrast agent administration. *Am J Cardiol* **1986**;57:864–868
8. Tscholakoff D, Higgins CB, Sechtem U, McNamara MT. Occlusive and reperfused myocardial infarcts: effect of Gd-DTPA on ECG-gated MR imaging. *Radiology* **1986**;160:515–519
9. Eichstaedt HW, Felix R, Dougherty FC, Langer M, Rutsch W, Schmutzler H. Magnetic resonance imaging in different stages of myocardial infarction using the contrast agent gadolinium-DTPA. *Clin Cardiol* **1986**;9:527–535
10. Johnston DL, Liu P, Lauffer RB, et al. Use of gadolinium-DTPA as a myocardial perfusion agent: potential applications and limitation for magnetic resonance imaging. *J Nucl Med* **1987**;28:871–877
11. McNamara MT, Tscholakoff D, Revel D, et al. Differentiation of reversible and irreversible myocardial injury by MR imaging with and without gadolinium-DTPA. *Radiology* **1986**;158:765–769

Aortobronchopulmonary Fistula Complicating Aortic Aneurysm: Diagnosis in Four Cases

Craig L. Coblentz[1]
D. Skip Sallee
Caroline Chiles

Aortobronchopulmonary fistula, a fistulous connection between the aorta and lung, is uniformly fatal in untreated cases. However, with early recognition and surgery, the survival rate exceeds 80%. We have had four patients with aortobronchopulmonary fistula, all of which resulted from thoracic aortic aneurysms (two after grafting of thoracic aortic aneurysms, one mycotic, one atherosclerotic). All four patients presented with hemoptysis. All four had a chest radiograph, which in two showed the aneurysm and in three showed airspace disease adjacent to the aorta. The aneurysm was shown by CT in one of two patients and by aortography in two of three patients. Neither CT nor aortography showed the fistula. Aortobronchopulmonary fistula was proved by surgery in two of the patients and by autopsy in the other two.

A high index of suspicion is necessary to make the diagnosis of aortobronchopulmonary fistula. The diagnosis should be considered in patients who have minor or major hemoptysis, with either coexisting thoracic aortic aneurysms or history of thoracic aneurysm repair.

An aortobronchopulmonary fistula is a fistulous connection between the aorta and lung, most commonly occurring in patients with thoracic aortic aneurysms [1]. If undiagnosed, this entity is uniformly fatal. However, with surgery, the survival rate exceeds 80%. Unfortunately, premortem diagnosis is made in less than 50% of cases [1, 2]. We describe our experience in four patients.

Case Reports

Case 1

A 58-year-old man was admitted for investigation of chest pain and hemoptysis of 1-week duration. He had a history of long-standing, chronic obstructive lung disease and congestive heart failure. A chest radiograph 1 year earlier showed aneurysmal dilatation of the thoracic aorta (Fig. 1A). An admission chest radiograph showed left upper lobe airspace disease that obscured the lateral margin of the aortic arch (Fig. 1B). Shortly after admission, the patient became hypotensive, developed ventricular tachycardia, and died despite attempts at cardiac resuscitation.

Autopsy revealed both new and old myocardial infarcts. In addition, a 4 × 3 cm saccular atherosclerotic aneurysm was found at the junction of the transverse arch and descending aorta that had eroded into the adjacent left upper lobe bronchus (Fig. 1C).

Case 2

A 54-year-old man presented with recurrent hemoptysis and chest pain. Five months earlier at another hospital, a left upper lobectomy was performed for hemoptysis thought to be caused by an aspergilloma within a tuberculous cavity. An admission chest radiograph revealed volume loss of the left hemithorax from previous surgery and a new aneurysm of the aortic arch (Fig. 2A). Aortography showed a large saccular aneurysm. The patient was not considered a good surgical candidate and was discharged from the hospital. He returned

Received September 17, 1987; accepted after revision November 10, 1987.

[1] All authors: Department of Radiology, Box 3808, Duke University Medical Center Durham, Durham, NC 27710. Address reprint requests to C. L. Coblentz.

AJR 150:535–538, March 1988
0361–803X/88/1503–0535
© American Roentgen Ray Society

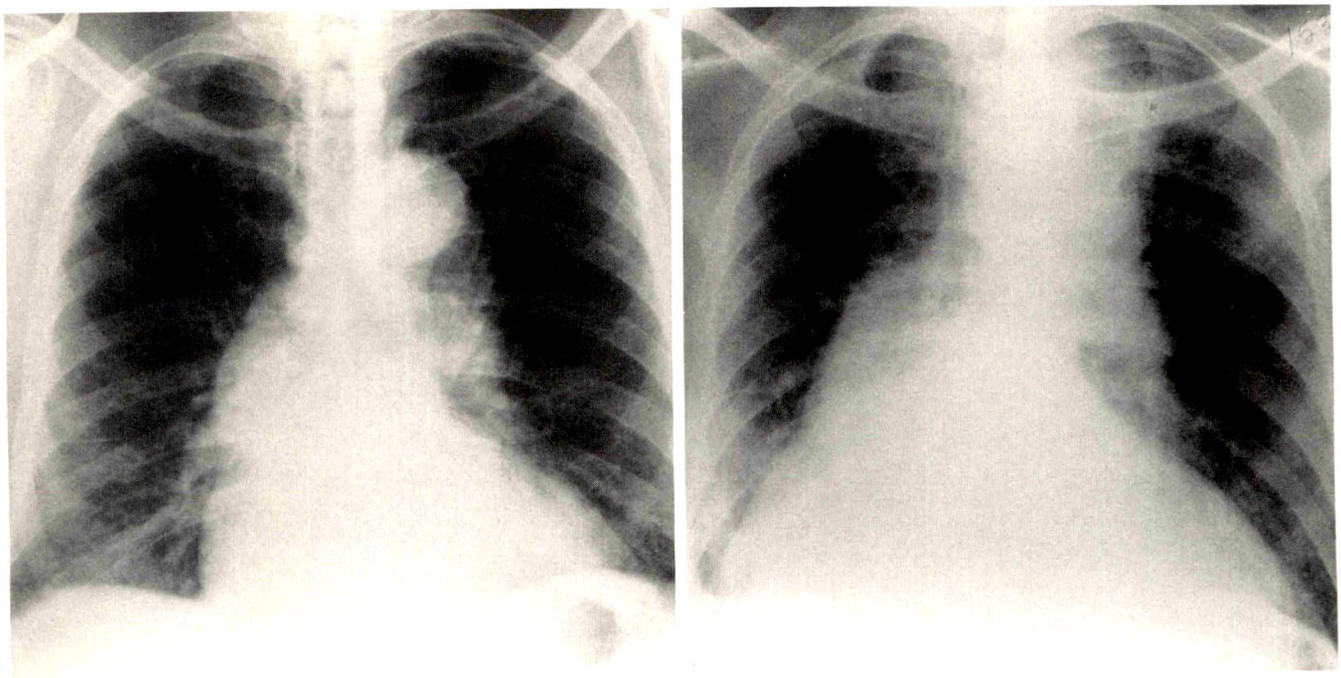

A B

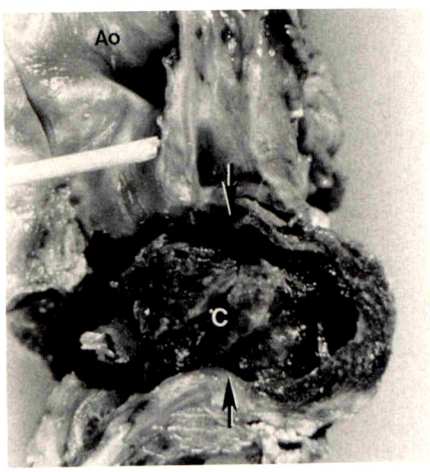

C

Fig. 1.—Aortobronchopulmonary fistula caused by atherosclerotic aortic aneurysm.

A, Posteroanterior chest radiograph taken 1 year before admission shows cardiomegaly and dilatation of thoracic aorta.

B, Anteroposterior chest radiograph on admission shows left upper lobe airspace disease with obliteration of aortic arch outline.

C, Autopsy specimen of aorta (Ao). Fistula (*arrows*) that contains clot (C) has formed from erosion of aneurysm into left upper lobe.

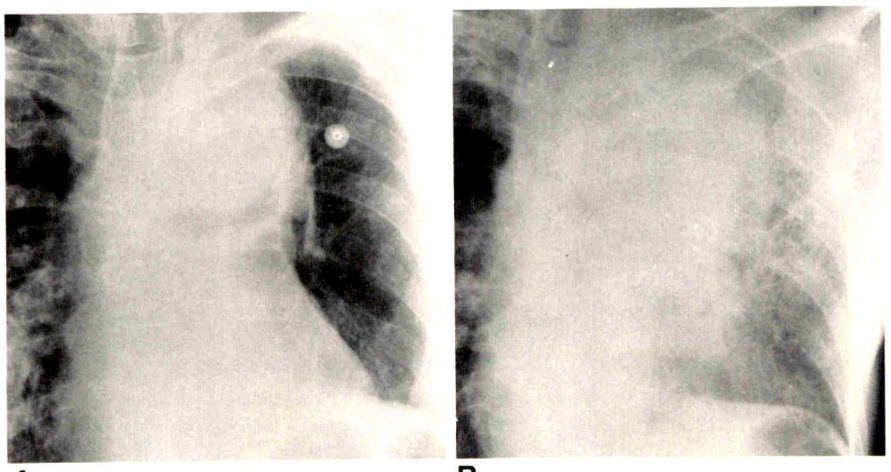

A B

Fig. 2.—Aortobronchopulmonary fistula caused by invasion by *Aspergillus*.

A, Posteroanterior chest radiograph shows aneurysm of aortic arch.

B, Posteroanterior chest radiograph made 5 days after *A*, when patient developed hemoptysis, shows airspace disease about aortic arch.

5 days later with massive hemoptysis. A chest radiograph revealed left upper lobe consolidation (Fig. 2B). Two days after admission, the patient had a respiratory arrest and died.

At autopsy, a 10 × 6 cm aneurysm of the proximal descending thoracic aorta was found adherent to the posteromedial pleural surface of the left lung. Invasion of the aortic wall by *Aspergillus* had caused a perforation connecting the aneurysm to a diffusely hemorrhagic left lung.

Case 3

A 42-year-old man with Marfan syndrome presented at another hospital with recurrent hemoptysis. Ten years earlier, a descending thoracic aortic aneurysm had been repaired with a synthetic graft. A chest radiograph showed left lower lobe consolidation adjacent to the aortic graft. Bronchoscopy revealed bright red blood coming from the left lower lobe bronchus. CT showed a 5 × 7 cm aneurysm of the descending thoracic aorta with adjacent airspace disease (Fig. 3A). The patient was referred to our hospital with a presumed diagnosis of aortobronchopulmonary fistula. Aortography showed a synthetic graft arising distal to the left subclavian artery and terminating 4 cm above the diaphragm (Fig. 3B). A large saccular aneurysm arose just below the distal anastomosis.

At thoracotomy, the aneurysm was found adherent to the posterior basal segment of the left lower lobe. An aortobronchopulmonary fistula had developed from a failed suture line at the distal anastomosis (Fig. 3C). Wedge resection of the posterior basal segment and aneurysm repair with a woven Dacron graft were performed. Subsequent cultures of the resected aneurysm and graft were sterile. The patient had an uneventful recovery.

Case 4

Three years after receiving an aortic graft for an atherosclerotic aneurysm of the descending thoracic aorta, a 71-year-old man presented with persistent hemoptysis. Frontal and lateral chest radiographs on admission showed an unfolded aorta and a graft of the descending thoracic aorta. The lungs were normal. Bronchoscopy showed blood coming from the left main bronchus. CT and aortography showed no evidence of recurrent aneurysm, dissection, or fistula. The hemoptysis stopped after 2 days, and the patient was discharged from the hospital. After 5 days, he returned with recurrent hemoptysis and underwent thoracotomy for a presumed aortobronchopulmonary fistula.

The surgeons found a tear in the native aorta, adjacent to the proximal anastomosis with adherence of the left lung to the descending aorta. Repair of the fistula was complicated by cardiac arrest, and the patient died during surgery.

Discussion

First reported in 1934 [3], an aortobronchopulmonary fistula is a fistulous connection between the thoracic aorta and lung. Most fistulas result from thoracic aortic aneurysms; this was the case in 23 of 25 patients reviewed by Demeter and Cordasco [1]. In their series, the cause of the aneurysm could be determined in 19 and was atherosclerotic in eight (42%), postsurgical in four (21%), mycotic in six (32%), and traumatic in one (5%). However, not all aortobronchopulmonary fistulas arise from aneurysms; spontaneous fistulas without aneurysm or dissection may occur [4]. Also reported are fistulas in association with congenital heart disease such as aortic coarctation or patent ductus arteriosus [5, 6]. Before 1970, mycotic aneurysms caused by tuberculosis and syphilis were the leading cause of aortobronchopulmonary fistulas [2]. Now the most common causes are postsurgical and atherosclerotic aneurysms. Although mycotic aortobronchopulmonary fistulas still occur, they are more likely to occur as a postoperative complication after aortic repair.

Postoperative aortobronchopulmonary fistulas result not only from infection, but also from recurrence of the aneurysm [7, 8] and from erosion of the aorta by an adjacent chest tube, spinal fixation device, or other hard foreign body [9]. Garrett et al. [10] believe that the risk of a postoperative aortobronchopulmonary fistula is reduced by subadventitial resection of the aneurysm. This prevents adherence of lung to a vascular suture line by providing a fibrous covering of the sutures and graft. Others [8] argue that postsurgical aorto-

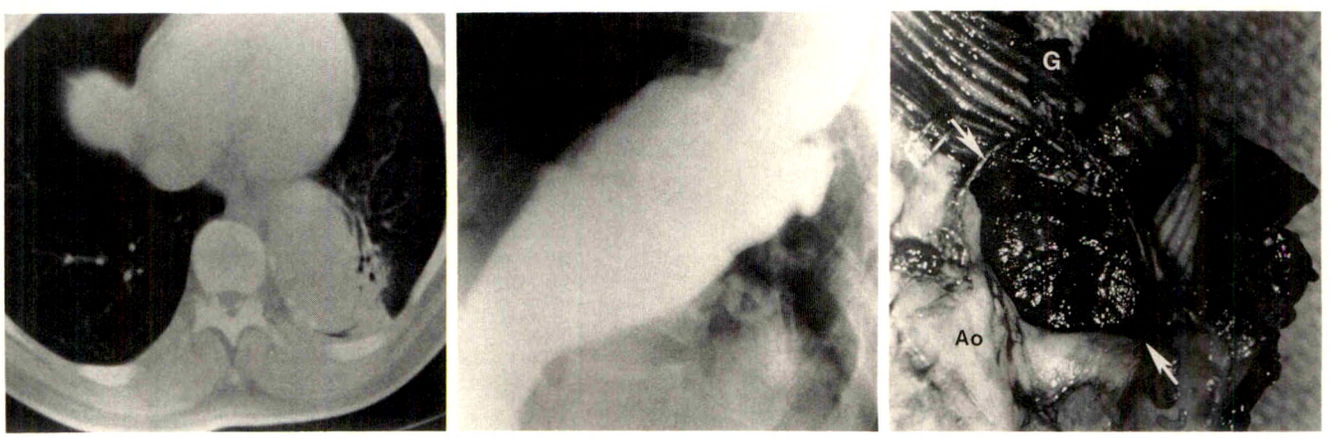

Fig. 3.—Aortobronchopulmonary fistula after aneurysm repair.
***A*, CT shows aortic aneurysm with associated left lower lobe airspace disease.**
***B*, Aortography shows large saccular aneurysm arising just below graft's distal anastomosis.**
***C*, Resected aneurysm shows fistula (*arrows*) arising at anastomosis of graft (G) and native aorta (Ao).**

bronchopulmonary fistulas are caused by a degenerative process independent of the type of resection or anastomosis performed.

Aortobronchopulmonary fistulas have been described after a variety of surgical repairs, including external wall reinforcement with Dacron [11], preserved homografts [12], and Ivalon grafts [7]. Fistulas may occur years after surgery, with reported examples occurring 10 or more years postoperatively [13] and one 15 years after homograft repair of a congenital aortic coarctation [12]. Our postsurgical patients presented 3 and 10 years after surgery, respectively.

Symptoms of aortobronchopulmonary fistula include chest pain, cough, dyspnea, and hemoptysis [1]. Hemoptysis is the most common presenting symptom and occurs in over 95% of cases [1]. The hemoptysis is usually massive, but occasionally it is minor and intermittent.

The aneurysm erodes into the lung by either pressure necrosis or a low-grade inflammatory process. The hemoptysis may diminish or even cease as thrombus forms within the fistula. Subsequent lysis or dislodgment of the clot may cause the process to repeat itself, giving rise to intermittent hemoptysis. Without intervention, the fistula may enlarge and lead to fatal exsanguination [13]. Therefore, minor hemoptysis may be the clue to the diagnosis and precede a fatal hemorrhage anywhere from 2 days to 1 year; this allows sufficient time for diagnosis and definitive treatment [2, 13].

Unfortunately, hemoptysis is a nonspecific symptom. With minor and intermittent hemoptysis, the diagnosis may go unrecognized. This may end in death [1, 3, 12], as in our case 4 when (as in other reports) the minor and intermittent hemoptysis led to the mistaken diagnosis of bronchitis [10, 13]. A history of hemoptysis in a patient with either radiographic evidence of a thoracic aortic aneurysm or previous surgical repair of a thoracic aortic aneurysm should suggest the diagnosis of aortobronchopulmonary fistula.

Lung consolidation, resulting from hemorrhage into lung through the fistula, is the most common radiographic finding in aortobronchopulmonary fistula. A more specific finding is the demonstration of a thoracic aortic aneurysm, which can be seen on the chest radiograph in 46% of cases [1]. If the aneurysm is small or if the outline is obscured by adjacent airspace disease, aortography or CT may show the aneurysm. Although aortography may show the fistula, this is unusual because the fistula is usually filled with clot [13].

Bronchoscopy is considered the best means to identify the source of hemoptysis regardless of its cause. In aortobronchopulmonary fistula, bronchoscopy may allow visualization of the fistulous opening into the tracheobronchial tree. However, bronchoscopy should be performed with caution because bronchoscopic manipulation could dislodge clot within the fistula [13] or perforate the aneurysm that is adherent to the lung. This could result in life-threatening hemorrhage.

Aortobronchopulmonary fistula was universally fatal until 1959, when DeProphetis et al. [14] described the first successful repair. Surgery remains the treatment of choice [1, 13].

Aortobronchopulmonary fistula is an uncommon but uniformly fatal condition if left untreated. The diagnosis should be suspected in patients who have both hemoptysis (usually massive, but also minor and intermittent) and a thoracic aortic aneurysm. Aortobronchopulmonary fistula must be excluded in any patient with hemoptysis and a graft of the thoracic aorta.

ACKNOWLEDGMENTS

We wish to thank Vera Mills for her secretarial assistance and William Foster and William Djang for their help in the preparation of this manuscript.

REFERENCES

1. Demeter SL, Cordasco EM. Aortobronchial fistula: keys to successful management. *Angiology* **1980**;31:431–435
2. Bryant LR, Bowlin J, Malette W, Danielson GK. Thoracic aneurysms with aorto-bronchial fistula. *Ann Surg* **1968**;168:79–84
3. Keefer CS, Mallory K. The pulmonary and pleural complications of aortic aneurysm. *Am Heart J* **1934**;10:208–220
4. Rodriguez HF, Rivera E. Spontaneous rupture of the thoracic aorta through an atheromatous plaque. *Ann Intern Med* **1961**;54:307–313
5. Wood AE, Stevenson HM, Cleland J. Aortobronchial fistula: a late complication of division of the persistent ductus arteriosus. *Ann Thorac Surg* **1984**;38:402–405
6. Kakos GS, Kataria YP, Vasko JS. Occult hemoptysis: iatrogenic aortobronchial fistula (letter). *Arch Surg* **1975**;110:352
7. Davey MG. Aorto-pulmonary fistula due to failure of an Ivalon graft for coarctation of the aorta. *Thorax* **1962**;17:363–365
8. Neville WE, Correll NO Jr, Maben H. Resection of aortic-bronchial fistula occurring ten years after graft replacement of the descending aorta. *Ann Thorac Surg* **1966**;2:82–86
9. Symbas PN, Hunter RM, Vlasis SE, Ansley JD. Infected descending aortic fistula. *Ann Thorac Surg* **1986**;41:647–651
10. Garrett HE, Ricks RK, Lewis JM, Howell JF, DeBakey ME. Hemoptysis secondary to aortopulmonary fistula. A report of two cases of successful treatment by operation. *J Thorac Cardiovasc Surg* **1963**;49:588–593
11. Dhillon JS, Randhawa GK, Straehley CJ, McNamara JJ. Late rupture after Dacron wrapping of aortic aneurysms. *Circulation* **1986**;74[suppl I]:I11–I14
12. Oldham KT, Johnsen K, Winterscheid L, Larson EB. Remembrance of things past: aortobronchial fistula 15 years after thoracic aortic homograft. *West J Med* **1983**;139:225–228
13. Graeber GM, Farrell BG Jr, Neville JF Jr, Parker FB. Successful diagnosis and management of fistulas between the aorta and the tracheobronchial tree. *Ann Thorac Surg* **1980**;29:555–561
14. DeProphetis N, Armitage HV, Triboletti ED. Rupture of tuberculous aortic aneurysm into lung. *Ann Surg* **1959**;150:1046–1051

Image-Intensifier Photofluorography and Conventional Chest Radiography: Comparison of Diagnostic Efficacy

Hannu Manninen[1]
Kaarina Partanen
Seppo Soimakallio
Hannu Rytkönen

Photofluorography with a large image intensifier, which provides an image field of 40 × 40 cm, reduces both the radiation dose and the imaging costs in chest radiography as compared with the film-screen technique. The two techniques were evaluated in a clinical study of 135 patients with suspected chest abnormalities. Photofluorographs and film-screen chest radiographs were interpreted independently by three radiologists. The diagnoses were confirmed by CT, follow-up radiographs, and clinical records. Among the 135 patients, 75 had primary lung cancer, 39 had pulmonary nodules, 52 had hilar or mediastinal abnormalities, 17 had pleural fluid, and 45 had pneumonic or atelectatic changes. Twenty-three normal subjects were included. Differences in diagnostic accuracy, measured by sensitivity and specificity, were not statistically significant. A larger number of true-positive cases (65%) with peripheral lung nodules were found by photofluorography than by film-screen radiography (54%) ($p < .05$).

The results suggest that the diagnostic accuracy of chest images made by photofluorography is sufficient to warrant using it instead of the film-screen technique in routine chest radiography, especially to detect lung tumors and metastases.

The introduction of an image intensifier with an input screen large enough for chest examination (Optilux 57, Siemens, Erlangen, West Germany) has resulted in the adaptation of image-intensifier photofluorography to clinical chest radiography. The technique offers several important advantages, including a small radiation dose as well as financial savings. Previous studies on this imaging technique have reported good visualization of most anatomic details of the chest [1, 2]. Investigations have shown it to have a detection rate for peripheral nodules and hilar or pleural diseases that is comparable with that of conventional film-screen chest radiography [1].

We compared the diagnostic efficacy of image-intensifier photofluorography with that of conventional film-screen chest radiography in the diagnosis of lung tumors, metastases, and associated findings in a group of patients admitted for CT evaluation of suspected pulmonary malignancy.

Materials and Methods

The study group consisted of 150 consecutive patients who were admitted to the Kuopio University Central Hospital for CT examination of the chest because of suspected primary lung tumor or pulmonary metastases. After the CT scans, posteroanterior and lateral chest radiographs were obtained by both conventional full-size film-screen radiography and image-intensifier photofluorography (Table 1). The same parameters were used for both techniques: 125 kVp, 2-m focus-to-film/image-intensifier distance, stationary grid, and automatic exposure-timing control. For conventional chest radiography, a three-phase, six-pulse generator (Valmet BR 2002, Tampere, Finland) with a Comet 22/52-150 tube (Bern, Switzerland) was used. Photofluorograms were obtained with a Siemens Optilux 57 image intensifier coupled to a 100-mm magazine camera (Sircam 100L, Siemens, Erlangen, West Germany). In image-intensifier photofluorography, the image from the output screen of the image intensifier is

Received August 31, 1987; accepted after revision November 10, 1987.

This work was supported in part by a grant from Instrumentarium Ltd. Science Foundation.

[1] All authors: Department of Diagnostic Radiology, University Central Hospital of Kuopio, SF-70210 Kuopio, Finland. Address reprint requests to H. Manninen.

AJR 150:539–544, March 1988
0361–803X/88/1503–0539
© American Roentgen Ray Society

TABLE 1: Radiographic Techniques

System	Film	Screen	Grid	Relative Radiation Dose[a]
Conventional film-screen technique	Dupont Cronex 4	Agfa Gevaert Curix Special	Stationary 10:1, 40 lines/cm	3.9
Image-intensifier photofluorography[b]	Agfa Gevaert Scopix RP1	Not used	Stationary 12:1, 40 lines/cm	1.0

[a] Relative radiation dose is expressed as a ratio of doses of the two procedures (conventional film screen/photofluorography).
[b] The equipment used was a Siemens Optilux 57 (Erlangen, West Germany).

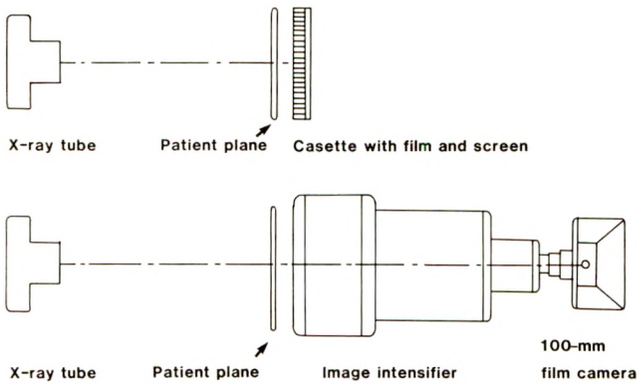

Fig. 1.—Schematic representation of image-intensifier photofluorography (*bottom*) and film-screen radiography (*top*).

recorded on 100 × 100 mm photospot film (Fig. 1). The maximum image format of the device, providing a 40 × 40 cm rectangular image field, was used.

After a follow-up period of 6 months–1.5 years, the radiographic results and clinical data for each patient were assembled. CT was the principal radiographic reference for the findings. All previous and subsequent plain chest radiographs as well as other CT scans and, in some cases, conventional tomograms were available. Bronchoscopy was performed in 130 cases, mediastinoscopy was performed in five cases, and thoracoscopy was performed in one case. Histopathologic diagnosis was also available. After CT examination, a diagnosis of enlarged hilar or mediastinal nodes was made if individual nodes 2 cm or more in diameter were found or if several nodes that were at least 1 cm in diameter were found. Tumor invasion of pulmonary hilum, mediastinum, or pleura was diagnosed if direct contact between a tumor and these structures was observed by CT.

Chest abnormalities were unequivocally confirmed in 138 (92%) of the 150 patients, three of whom were excluded from the study because their chest radiographs or photofluorograms were inadequate (e.g., because the phase of inspiration was inappropriate or the patient was positioned incorrectly). Thus, 135 patients (102 men and 33 women) with a mean age of 64 years (range, 28–85 years) were included in the chest-film comparison. The selection of the test radiographs and the registration of the confirmed diagnoses were done by a supervising radiologist who did not participate in the interpretation of the test films.

The radiographs were assigned code numbers and were interpreted independently by three radiologists. All the interpreters had had previous experience with photofluorographic chest examinations, which make up about 15% of all the chest radiographs in our department. Photofluorograms and conventional radiographs were interpreted at separate sessions with at least a 2-week interval between the viewing of radiographs in the same patient. The conventional films were interpreted on a conventional view box, and the photofluorograms were interpreted on an illuminator with an attached magnifying glass. In each case, extra light was carefully blended from the film by masking the view box and spot-film illuminator to the film size. Room illumination was dim and constant. The time reserved for film interpretation was unlimited, but to avoid reader fatigue, the maximal number of films per reading session was 30. The radiologists were asked to record the following pattern of findings and to locate each finding on diagrams of frontal and lateral chest radiographs: (1) primary lung tumor and its possible invasion of pulmonary hilum, mediastinum, or pleura; (2) pulmonary nodules; (3) hilar and/or mediastinal disease; (4) pleural fluid; (5) pneumonic and/or atelectatic changes. Neither the proportion of abnormal cases nor any information concerning previous radiologic findings or clinical history was provided. Before test-film interpretation, each observer was trained in diagnostic criteria under the guidance of the supervising radiologist; 10 chest films that had been excluded from the series were used. The record forms were graded by two of the authors after the entire study had been completed.

In 135 patients, there were 75 primary lung cancers, 11 of which were resectable (no invasion of hilar region, mediastinum, or pleura). In 52 cases, hilar or mediastinal abnormalities were present, and there were 39 pulmonary nodules (34 were metastases and five were benign tumors). Most nodules were less than 3 cm in diameter; clearly calcified lesions were not included in the nodule category. Pleural fluid was found in 17 cases, and 45 patients had pneumonic/atelectatic changes, usually caused by a primary lung tumor. Chest radiographs in 23 patients were normal with respect to these registered findings and showed only insignificant abnormalities such as pleural plaques, postinflammatory changes, or mediastinal lipomatosis. In 53 patients, however, two or more findings were seen. In the nodule category, all nodules were registered as individual findings: five patients had two peripheral nodules, three patients had three, and one patient had five. The total number of observations for all categories (except pulmonary nodules) was 405 (three radiologists interpreted 135 chest radiographs); the total number of observations for pulmonary nodules was 450.

For the statistical analysis of the differences in sensitivity and specificity values between image-intensifier photofluorography and film-screen radiography, the McNemar chi-square test was applied, and 95% confidence intervals for the differences were calculated.

Results

Sensitivity and specificity of the image-intensifier photofluorography and conventional chest radiography averaged over all observers are given in Tables 2 and 3. Diagnostic efficacy of the two imaging techniques was almost identical with respect to the detection of primary lung tumors and medias-

TABLE 2: Sensitivity of the Imaging Techniques for Each Finding[a]

Finding	Sensitivity		Difference in Sensitivities of the Two Techniques ± 95% Confidence Interval
	Conventional Chest Radiography	Image-Intensifier Photofluorography	
Primary lung tumor	0.84 (189/225)	0.82 (185/225)	0.02 ± 0.05
Pulmonary nodules	0.54 (63/117)	0.65 (76/117)[b]	−0.11 ± 0.09
Mediastinal/hilar disease	0.61 (95/156)	0.64 (100/156)	−0.03 ± 0.07
Pleural fluid	0.49 (25/51)	0.61 (31/51)	−0.12 ± 0.16
Pneumonia/atelectasis	0.72 (97/135)	0.79 (106/135)	−0.07 ± 0.08
Total findings	0.69 (469/684)	0.73 (498/684)[c]	−0.04 ± 0.04

Note.—Sensitivity number = number of correctly diagnosed positive cases ÷ number of all positive cases.

[a] Absolute frequencies of observartions are in parentheses.

[b] $\chi^2 = 5.83$, $p = .025$

[c] $\chi^2 = 6.22$, $p = .025$

TABLE 3: Specificity of the Imaging Techniques for Each Type of Finding[a]

Finding	Specificity		Difference in Specificities of the Two Techniques ± 95% Confidence Interval
	Conventional Chest Radiography	Image-Intensifier Photofluorography	
Primary lung tumor	0.94 (170/180)	0.94 (169/180)	0.00 ± 0.02
Pulmonary nodules	0.96 (320/333)	0.94 (313/333)	0.02 ± 0.01
Mediastinal/hilar disease	0.92 (229/249)	0.91 (226/249)	0.01 ± 0.02
Pleural fluid	0.95 (336/354)	0.96 (339/354)	−0.01 ± 0.01
Pneumonia/atelectasis	0.97 (261/270)	0.97 (261/270)	0.00 ± 0.01
Total findings	0.95 (1316/1386)	0.94 (1308/1386)	0.01 ± 0.01

Note.—Specificity = number of correctly diagnosed negative cases ÷ number of all negative cases.

[a] Absolute frequencies of observations are in parentheses.

tinal/hilar disease. No statistically significant difference was found between the two methods in detecting hilar, mediastinal, and pleural invasion of the tumor, with sensitivity values of 0.90 and 0.92 and specificity values of 0.73 and 0.60 for image-intensifier photofluorography and conventional radiography, respectively. The greater number of true-positive findings with image-intensifier photofluorography regarding pleural fluid and pneumonic/atelectatic changes was not statistically significant. A larger number of true-positive cases (65%) with pulmonary nodules were found by image-intensifier photofluorography than by film-screen radiography (54%) ($p < .05$). Photofluorography also proved to be better in terms of the frequency with which a pulmonary nodule was missed by one imaging technique but was detected by the other. On conventional film, a lung nodule remained undetected in 21 cases in which it was correctly detected on the photofluorogram, whereas a pulmonary nodule detected on full-size film was missed only eight times on photofluorography. When all findings are considered, image-intensifier photofluorography resulted in fewer false-negative results (27% vs 31%) ($p < .05$). The good overall performance of this new imaging technique is illustrated by the fact that the false-positive rate of image-intensifier photofluorography was not significantly higher than that of conventional chest radiography, (6% vs 5%, respectively).

Diagnostic accuracy obtained by the individual radiologists varied considerably (Table 4). Differences in sensitivity and specificity between the techniques for any of the findings did not reach statistical significance for any of the interpreters. Table 4 also indicates that the overall accuracy of the imaging techniques was almost equal.

In this series, some of the findings were so obvious that no error was made by any of the observers. Although such cases are not useful for discriminating between the imaging techniques, they were included because they are representative of a typical radiologic search for pulmonary malignancy. To test whether these obvious cases influenced the results, those findings in which all three radiologists had recorded a true-positive or a true-negative diagnosis by both techniques (472/690 or 67%) were excluded. Twenty-eight of the 135 patients had obvious findings with respect to all findings. Figure 2 shows the diagnostic performance of the imaging techniques when cases in which there were no diagnostic errors with either imaging technique have been excluded.

TABLE 4: Diagnostic Performance of Image-Intensifier Photofluorographs and Conventional Chest Radiographs by Individual Radiologists. Totals for All Findings.

Radiologist Number	Sensitivity		Specificity		Overall Accuracy	
	Conventional Radiography	Image Intensifier Photofluorography	Conventional Radiography	Image Intensifier Photofluorography	Conventional Radiography	Image Intensifier Photofluorography
1	0.73	0.82	0.94	0.95	0.87	0.90
2	0.72	0.77	0.95	0.93	0.88	0.87
3	0.60	0.60	0.95	0.95	0.84	0.83
Mean	0.69	0.73	0.95	0.94	0.86	0.87

Note.—Overall accuracy = (correctly diagnosed positive cases + correctly diagnosed negative cases) ÷ total number of cases. Sensitivity and specificity calculated as noted in Tables 2 and 3.

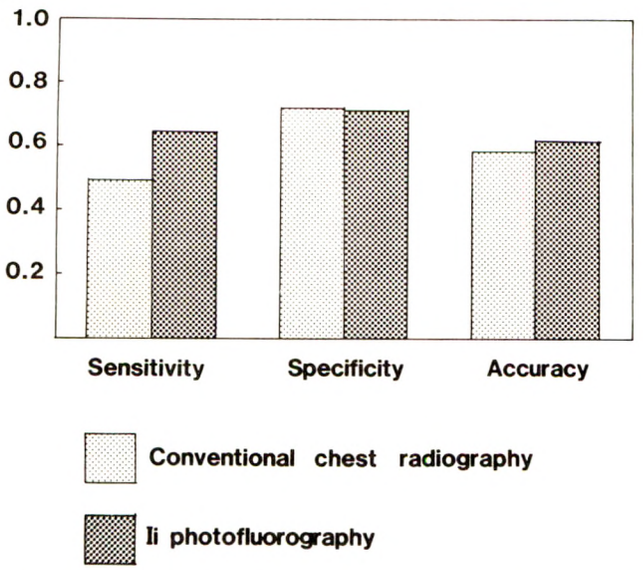

Fig. 2.—Diagnostic performance of image-intensifier (Ii) photofluorographs and conventional chest radiographs for all findings averaged for all observers (678 determinations); cases in which there were no diagnostic errors with either imaging technique have been excluded.

Regarding the individual findings, the order of superiority between the techniques did not change nor did the statistical significance of the differences.

Finally, consistency of agreement among the radiologists on the correct interpretation was tested for both imaging techniques. The radiologists all agreed on the correct response in 75% (1557/2070) of the findings on conventional radiographs and in 76% (1572/2070) of the findings on photospot films. The result further confirms that the overall diagnostic accuracy of the two imaging techniques is similar. Figure 3 shows two pairs of chest radiographs obtained by using the two imaging techniques; all four radiographs are of the same patient.

Discussion

A few reports have been published concerning experiences with large-screen image-intensifier photofluorography in clinical chest radiography [1–4]. Although the spatial resolution of the technique is only 70–90% of that of most film-screen combinations used in conventional radiography, and despite the moderate electron-optical distortion in the peripheral field, image-intensifier photofluorography has been promising in these preliminary studies. However, a thorough clinical evaluation (using an independent reference method for confirmation) of the diagnostic efficacy of this new imaging technique in comparison with conventional chest radiography has not been published previously. Because the search for and the staging of lung tumors and metastases is of major importance in chest radiology, we wanted to determine the diagnostic performance of the new technique in this difficult area.

The anatomic regions situated in the central part of the imaging field are well visualized with image-intensifier photofluorography [1, 2]. Thus, the good performance of image-intensifier photofluorography in hilar and mediastinal disease as well as in primary lung tumors is not surprising. The short exposure time (about one-third that of the conventional technique) certainly has a favorable effect on the visualization of the hilum, since lack of sharpness due to motion may blur anatomic details in these regions [5]. Disease detection is, however, not only a matter of visualization but also of pattern recognition. Our experience with image-intensifier photofluorography in routine clinical work is that some familiarity with the photospot films was required before a consistent degree of diagnostic accuracy could be achieved. The fact that consistency of agreement among the radiologists on the correct response was almost identical with both imaging techniques indicates that the participating radiologists had adequate experience in the interpretation of the photospot films.

The good sensitivity of image-intensifier photofluorographs in the diagnosis of pleural fluid (Table 2) is in agreement with the finding of Neufang et al. [1] regarding the fine visualization of costopleural angles with this imaging technique. The reason that the detection of pneumonia or atelectasis is slightly more accurate on photospot films is not obvious, since subtle interstitial changes, especially in the lung periphery, have been reported to be poorly visualized [1]. The false-negative interpretation of inflammatory changes in our study probably is a problem of pattern recognition. Further analysis revealed that most of the false-negative cases were classified by the interpreters as chronic parenchymal changes.

Image-intensifier photofluorography showed somewhat better sensitivity for detecting pulmonary nodules than did conventional chest radiography (Table 2). A decrease in the number of false-negative results (31 vs 44 of 117 observations) was achieved at the expense of a smaller increase in false-positive results (20 vs 13 of 333 observations). Thus, theoretically, 13 new nodules were detected at the expense of seven additional cases of false-positive findings. Because of the relatively small number of pulmonary nodules in the present series, this result should be verified by further studies.

Detection of small peripheral nodules of threshold contrast in a complex background requires careful visual scanning. Radiologists may have studied photofluorograms more thoroughly than they did conventional chest radiographs. The time spent searching for pulmonary nodules was not analyzed, but the time required for the total interpretation procedure for all findings did not differ markedly between the imaging techniques. A more likely explanation for the good diagnostic performance of photospot films may be found in some aspects of the perception of pulmonary nodules. Spatial resolution is not critical for the detection of solitary pulmonary nodules [6, 7]. An important factor for nodule detection is probably the image size. Tuddenham [8] was the first to show that the visibility of structures with ill-defined margins is significantly improved by image reduction. The 3.5× magnifying spot-film viewer has not been useful in the detection of pulmonary structures [2]. In clinical practice, we prefer a conventional spot-film illuminator with either an attached magnifying glass or Mattson's viewer (Siemens-Elema, Stockholm, Sweden).

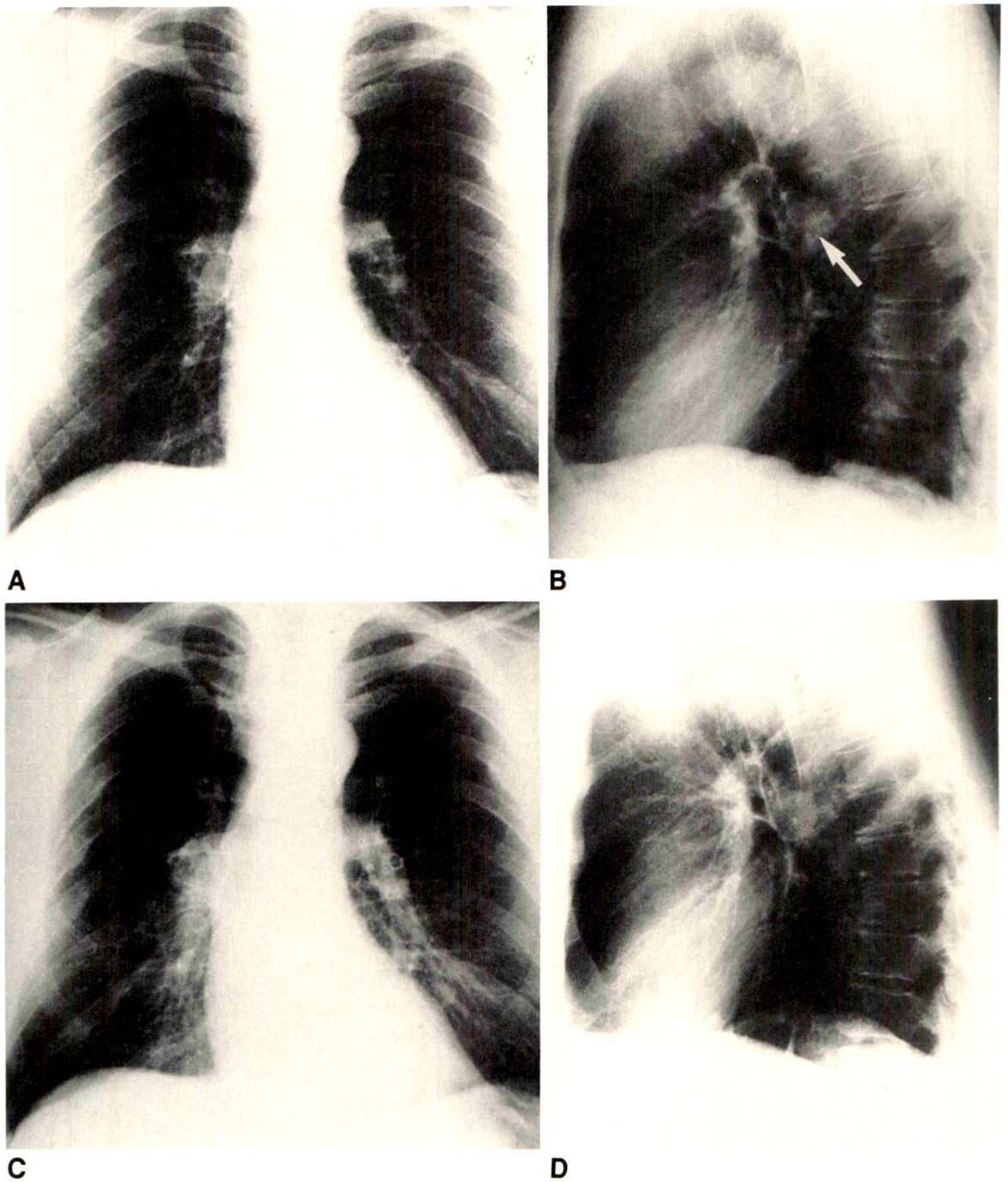

Fig. 3.—Frontal (*A*) and lateral (*B*) chest radiographs obtained with image-intensifier photofluorography. Frontal (*C*) and lateral (*D*) radiographs obtained by using film-screen technique. Patient has a centrally situated hamartoma (*arrow* on *B*) behind right pulmonary hilum.

The present results indicate that photofluorography with a large-screen image intensifier is applicable to radiographic diagnosis of pulmonary malignancies. The technique offers significant reduction of the radiation dose in comparison with most film-screen combinations used in the full-size technique. Although the cost of large-screen image-intensifier equipment is somewhat higher than that of conventional chest radiographic equipment, a savings of about 80% in the film and processing chemical costs, as well as the decisively smaller filing space it requires, makes the technique highly competitive financially. Because of the small size of the photospot film, some practical problems remain with viewing the photofluorograms. Care must also be taken to block extra light from around the photospot film. A conventional autoalternator or view box is thus not suitable for film viewing, unless additional masks are used.

REFERENCES

1. Neufang KFR, Friedman G, Peters PE, Fischer PG, Kronholz HL. Erste klinische Erfahrungen mit einem neuen Grossbildverstärker in der Thoraxdiagnostik. *ROFO* **1982**;137:535–539
2. Manninen H, Rytkönen H, Soimakallio S, Terho EO, Hentunen J. Large-screen image intensifier photofluorography compared with full-size screen-film technique in chest radiography. *Acta Radiol [Diagn]* (*Stockh*) **1985**;26:525–533
3. Manninen H. *Physical image parameters and diagnostic quality of roentgenographs. Investigations on chest imaging chains* (academic dissertation). Kuopio, Finland: Publications of the University of Kuopio, Medicine, Series Original Reports 1/**1985**
4. Heuck FHW, Hofmann FW. Bedeutung eines neuen Gross-format-Bildverstärkers für die Reihenuntersuchung der Thoraxorgane. *Radiologe* **1984**;24:139–143
5. Manninen H, Terho EO, Wiljasalo M, Wiljasalo S, Soimakallio S. An evaluation of different imaging chains in clinical chest radiography. *Br J Radiol* **1984**;57:991–995
6. Seeley GW, Roehrig H, Nudelman S, Frost MM, Capp MP. Psychophysical evaluation of videosystems compared to film. *Appl Photogr Eng* **1978**;4:160–165
7. Lams PM, Cocklin ML. Spatial resolution requirements for digital chest radiographs: an ROC study by observer performance in selected cases. *Radiology* **1986**;158:11–19
8. Tuddenham WJ. Problems of perception in chest roentgenology: facts and fallacies. *Radiol Clin North Am* **1963**;1:277–289

Latissimus Dorsi Cardiomyoplasty: Radiographic Findings

Thong H. Nguyen[1]
Thu-Anh Hoang[1]
Nilima Dash[1]
Ignacio Christlieb[2]
Anthony R. Lupetin[1]
Irwin Beckman[1]
Rolf L. Schapiro[1]
George J. Magovern[3]

Left latissimus dorsi muscle cardiomyoplasty is a surgical procedure in which the muscle is mobilized as a pedicled flap, moved into the left pleural and mediastinal cavities, and used for surgical repair and/or mechanical augmentation of a failing left ventricle. Chest radiographs in four patients who had undergone this procedure were evaluated. In all four patients, there was bandlike or diffuse increase in density in the left midhemithorax with loss of the left heart border. These findings, which could be misinterpreted as lung disease, represent the transposed muscle flap. CT showed the exact anatomic position of the flap in relation to the intrathoracic structures.

Familiarity with the postoperative radiographic appearance of this type of myoplasty is important to avoid misinterpretation.

Dynamic cardiomyoplasty is a recently developed surgical technique that uses electrostimulated autogenous skeletal muscle for long-term mechanical cardiac assistance, myocardial replacement, and myocardial revascularization. It is used in patients with irreversible pump failure refractory to other forms of therapy [1, 2]. It avoids the problems of allograft tissue rejection, immunosuppressive therapy, and donor supply inherent in cardiac transplantation, and overcomes the problems of dependence on external power sources, thromboembolism, and frequent infection common to artificial heart replacement. Three successful cases have been reported in the literature [3, 4].

The left latissimus dorsi muscle (LLDM) is ideal for this purpose because of its proximity to the heart, its large contractile mass, the lack of appreciable morbidity caused by its displacement to the thorax, and the technical simplicity in transposing it to the heart [5]. The radiographic findings created by the transposed LLDM flap in four patients who underwent this procedure are the subject of this report.

Materials and Methods

Between September 1985 and February 1987, four patients underwent LLDM flap cardiomyoplasty at Allegheny General Hospital. The patients included two men and two women ranging in age from 45 to 65 years. In three cases, the LLDM was used to repair large ventricular aneurysms, which had significantly compromised the cardiac function. The fourth patient has a right coronary artery bypass graft at the time of cardiomyoplasty, which was performed with the intention of using the LLDM flap primarily for left ventricular augmentation.

Chest radiographs of the four patients were taken throughout their postoperative course, which ranged from 33 to 65 days. The radiographs were reviewed and correlated with CT findings and clinical data. The preoperative chest radiographs were available in all patients for comparison. Three of the four patients who are surviving had follow-up chest radiographs at 3½–21 months after surgery. Early postoperative radiographs were obtained with the portable technique, with the patient in the semierect or erect position. Later in the postoperative course, whenever the patient's condition permitted, standard posteroanterior and lateral films were obtained. Lateral decubitus views were also obtained when indicated.

CT scans were obtained in all four patients at 17 days, 42 days, 15 months, and 21

Received August 26, 1987; accepted after revision December 3, 1987.

[1] Department of Diagnostic Radiology, Allegheny General Hospital, 320 E. North Ave., Pittsburgh, PA 15212-9986. Address reprint requests to N. Dash.

[2] Department of Thoracic Surgery Research, Allegheny General Hospital, Pittsburgh, PA 15212-9986.

[3] Department of Surgery, Allegheny General Hospital, Pittsburgh, PA 15212-9986.

AJR 150:545–547, March 1988
0361–803X/88/1503–0545
© American Roentgen Ray Society

months, respectively, after LLDM cardiomyoplasty on a Picker International, Inc., (Highland Heights, OH) 1200 SX scanner, with scanning techniques of 2 sec, 130 kVp, 332 mAs, 10-mm collimation, and 10-mm intervals. One patient was studied without and with IV administration of water-soluble contrast medium, one patient with contrast enhancement only, and two patients without contrast enhancement.

The surgical procedure is as follows [3, 4]. The left latissimus dorsi muscle is dissected free and brought into the chest, with its preserved neurovascular bundle, through a window created by partially resecting a left upper rib. Through a midline sternotomy, the muscle is brought across the surface of the heart and attached to the left ventricle and to a portion of the right ventricle for myocardial wall reinforcement and functional augmentation. A permanent dual-chamber pacemaker is implanted to stimulate the LLDM flap to contract synchronously with the ventricular systole. Myocardial electrodes are implanted on the right heart for sensing, and two pacing electrodes are affixed onto the LLDM, one proximally and one distally over the muscle flap (Fig. 1). The pulse generator is implanted subcutaneously just below the costal margin.

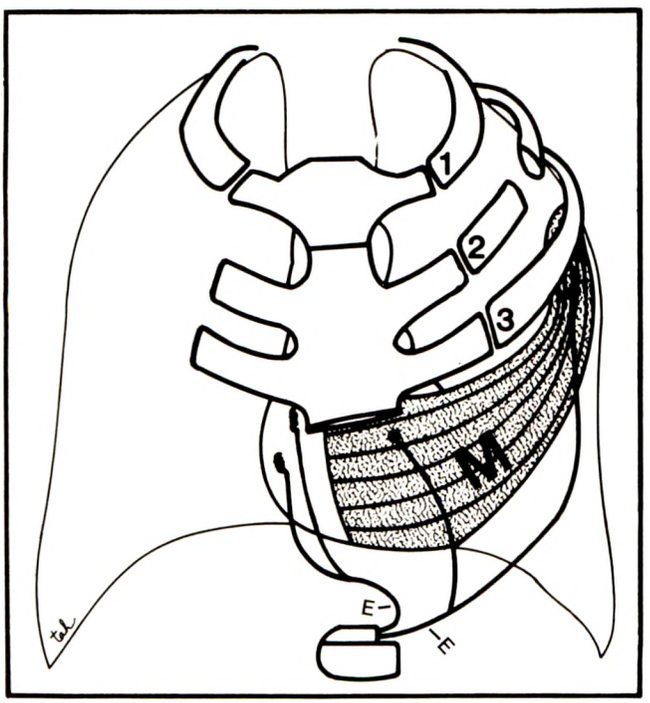

Fig. 1.—Diagram shows transposed left latissimus dorsi muscle flap (M) descending from third left rib to join and wrap around ventricular surface of heart. Note defect in left second rib created surgically to bring muscle flap into left hemithorax. Also note relative position of pacemaker electrodes (E).

Results

The chest radiographs in all patients showed bandlike or diffuse density in the left midhemithorax, causing total or partial loss of the left heart border from the apex to as high as the level of the main pulmonary segment (Figs. 2 and 3A). This density is difficult to recognize on early postoperative portable chest radiographs because of postoperative left lower lobe atelectasis and/or pleural effusion. It becomes more apparent on later radiographs. In the lateral view, the muscle is seen in an anterior and extrapleural location (Fig. 3B).

Pacemaker wires indicate the expected position of the proximal end of the flap near the neurovascular bundle and the distal end of the flap over the left ventricle. The position of the sensing electrodes varies.

CT scans localized the transposed LLDM flap and delineated its anatomy and course within the left hemithorax. A common finding was the presence of a well-circumscribed,

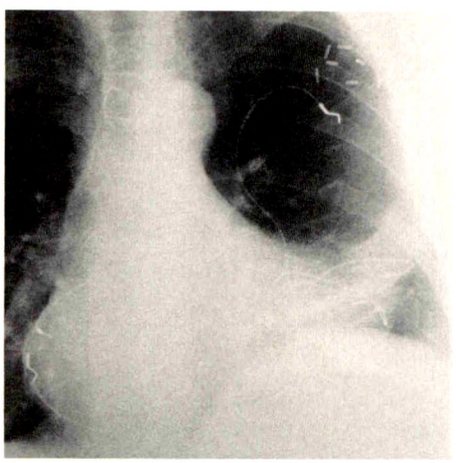

Fig. 2.—Chest radiograph after left latissimus dorsi cardiomyoplasty shows bandlike density with partial loss of left heart border, which mimics the appearance of lingular lobe atelectasis or consolidation. Elevation of left hemidiaphragm is evident.

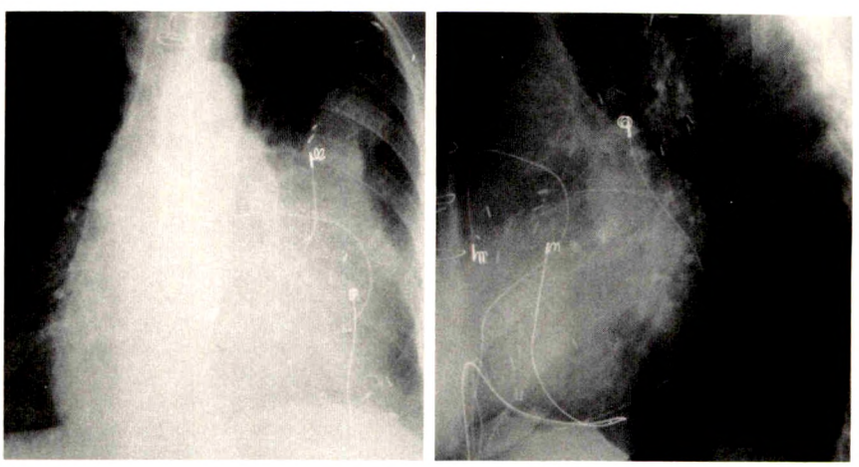

A **B**

Fig. 3.—*A*, Chest radiograph shows diffuse increase in density of left midhemithorax with total loss of left heart border. Note extracardiac location of pacemaker electrodes in left upper chest and surgical defect of left second rib.

***B*, Lateral chest radiograph shows anterior, extrapleural location and nonsegmental, nonlobar distribution of density seen on posteroanterior film.**

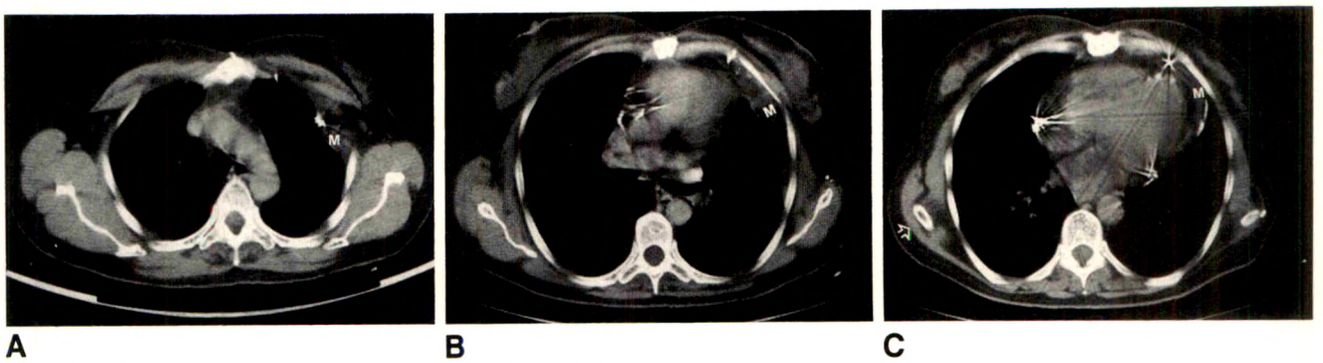

Fig. 4.—CT scans after left latissimus dorsi muscle cardiomyoplasty.
***A*, Superior intrathoracic portion of left latissimus dorsi flap (M) just immediate to its entry into thoracic cavity at level of aortic arch.**
***B*, Midintrathoracic portion of flap (M) abutting anterolateral aspect of left chest cavity as it descends medially toward heart.**
***C*, Cardiac portion of flap (M) as it wraps around anterior, apical, and apicoposterior aspects of heart. Note difference between flap and myocardium in terms of attenuation, homogeneity, and enhancement. Also note linear density of fat attenuation around heart, distinguishing it from flap. Absence of surgically removed latissimus dorsi muscle is evident on left side, as distinguished from its normal position on right side (*arrow*).**

nonhomogeneous soft-tissue mass, pleural in character, abutting the left anterolateral chest cavity from the level of the aortic arch and descending inferomedially to join the ventricular surfaces of the heart (Fig. 4). Variations in the inferior aspect of the soft-tissue flap as it coursed toward the heart were observed in all patients.

Discussion

Chest radiographs in four patients undergoing LLDM cardiomyoplasty revealed a bandlike or diffuse density in the left midhemithorax, which obscured the left heart border. This density represented the muscle flap, which descended anterolaterally from one of the upper ribs to join and wrap around the heart, particularly the left ventricle.

CT provides a cross-sectional view of the muscle flap and its relation to other intrathoracic structures. CT can identify and separate the flap from lung parenchyma or pleural effusion when chest radiographs are ambiguous [6, 7], and is thus an important tool in the detection of pulmonary infection. Potential pitfalls caused by the shadow of the flap on the heart—namely, lingula/left upper lobe disease or anterior loculated effusion—may be clarified by CT.

CT is useful for evaluating the cardiac size and cardiothoracic ratio, which cannot be done by routine chest radiographs owing to the loss of the left heart border.

The distinction between muscle flap and myocardium by CT can be suggested in most cases by differences in attenuation, homogeneity, and especially contrast enhancement [8]. The last gives the best result for evaluating the muscle flap–myocardium relationship.

ACKNOWLEDGMENT

We thank Maggie Cauley for her secretarial assistance in preparing the manuscript.

REFERENCES

1. Walsh G, Chiu RCJ. Skeletal muscle for cardiac repair and assist: a historical overview. In: Chiu RCJ, ed. *Biomedical cardiac assist: cardiomyoplasty and muscle-powered devices*. Mount Kisko, NY: Futura, **1986**:1–18
2. Dewar ML, Drinkwater DC, Wittnich C, Chiu RCJ. Synchronously stimulated skeletal muscle graft for myocardial repair. An experimental study. *J Thorac Cardiovasc Surg* **1984**;87:325–331
3. Carpentier A, Chachques JC. The use of stimulated skeletal muscle to replace diseased human heart muscle. In: Chiu RCJ, ed. *Biomedical cardiac assist*. Mount Kisko, NY: Futura, **1986**:85–102
4. Magovern GJ, Heckler FR, Park SB, et al. Paced latissimus dorsi used for dynamic cardiomyoplasty of left ventricular aneurysms. *Ann Thorac Surg* **1987**;44:379–388
5. Chachques JC, Mitz V, Hero M, et al. Experimental cardiomyoplasty using the latissimus dorsi flap. *J Cardiovasc Surg* **1985**;26:457–462
6. Benjamin JJ, Cascade PN, Rubenfire M, Wajszczuk W, Kerin NZ. Left lower lobe atelectasis and consolidation following cardiac surgery: the effect of topical cooling on the phrenic nerve. *Radiology* **1982**;142:11–14
7. Goodman LR. Postoperative chest radiograph. II. Alterations after major intrathoracic surgery. *AJR* **1980**;134:803–813
8. Lipton MJ, Herfkens RJ, Gamsu G. Computed tomography of the heart and pericardium. In: Moss AA, Gamsu G, Genmant HK. *Computed tomography of the body*. Philadelphia: Saunders, **1983**:401–425

Chest Imaging Update

American Roentgen Ray Society Annual Meeting Friday Symposium

May 13, 1988, San Francisco Hilton and Tower, San Francisco, CA

Computed Tomography	Moderator: Stewart Sagel
8:00 a.m.	Overview (*Sagel*)
8:10 a.m.	Focal lung disease (*Zerhouni*)
8:35 a.m.	Diffuse lung disease (*Müller*)
9:00 a.m.	Staging of bronchogenic carcinoma (*Pugatch*)
Interventional Radiography	
9:25 a.m.	Intrathoracic drainage procedures (*Westcott*)
9:45 a.m.	Percutaneous biopsy of central lesions (*Weisbrod*)
10:05 a.m.	Coffee break
Digital Imaging	Moderator: Carl Ravin
10:25 a.m.	Overview (*Ravin*)
10:35 a.m.	Digital angiography (*Barth*)
10:55 a.m.	Digital radiography (*MacMahon*)
Magnetic Resonance Imaging	Moderator: Gordon Gamsu
11:15 a.m.	Overview (*Gamsu*)
11:25 a.m.	Intrathoracic vascular lesions (*Webb*)
11:50 a.m.	Applications of MRI of the thorax (*McLoud*)

Eloesser Window Thoracostomy for Treatment of Empyema:
Radiographic Appearance

Matthew P. Shapiro[1]
M. Elon Gale[1]
Benedict D. T. Daly[2]

The modified Eloesser procedure or open-window thoracostomy is a surgical treatment for chronic pleural empyema in which a relatively permanent drainage opening is created in the chest wall. The chest radiographs and CT scans of 13 patients who underwent a modified Eloesser window procedure were studied. On chest films, the Eloesser window characteristically appeared en face as an elliptical or crescent-shaped radiolucency with sharp superior and ill-defined inferior margins. It appeared in profile as a downward-sloping chest-wall defect with round superior and straight inferior margins. The first radiographs made after surgery often showed potentially confusing densities caused by the iodinated gauze used to pack the drained empyema cavity. On sequential chest films, the defect in the chest wall was always detectable, while the pleural cavity diminished in size and usually disappeared within 6 months.

This analysis shows that the postoperative chest radiographs and CT scans in patients having the Eloesser window thoracostomy have features that are characteristic of the procedure.

Pleural empyema is a commonly encountered disease. Generally, primary treatment is closed thoracostomy drainage with either one or more chest tubes. However, in rare instances initial open surgical management may be indicated [1]. There are several techniques for either primary or delayed surgical intervention. One method of surgical treatment, known as an Eloesser flap or window after the surgeon who devised the procedure, has had a resurgence of use [2]. It involves the creation of a small, relatively permanent opening in the chest wall, allowing for long-term drainage of the empyema without need for indwelling tubes. The appearance of chest radiographs obtained after Eloesser window surgery has not been well documented.

The surgical procedure involves making a U-shaped incision through the skin, subcutaneous tissue, and muscle down to the ribs, creating a soft-tissue flap. Five-centimeter-long segments of the exposed two or three adjacent ribs are resected to prevent closure of the drainage channel. The resultant opening usually measures approximately 5 × 7 cm. The empyema is then entered and drained as completely as possible. The superiorly attached skin flap is folded inward underneath the chest wall and sutured to the parietal pleura and empyema peel. At the end of the procedure, the empyema cavity is usually packed with iodinated gauze.

Materials and Methods

During the years 1979–1986, 17 patients at our institution underwent a modified Eloesser window procedure for treatment of chronic nontuberculous empyema. Of these 17 patients, serial postoperative radiographs were available for retrospective review in 13 (76%). In addition to standard chest radiographs, six of these patients also had postoperative CT scans. The follow-up ranged from 1 to 60 months (mean, 12; median, 2.5). There were seven right-sided and six left-sided empyemas in the study group. Three patients had had a previous pneumonectomy, and 10 had not. The preponderant causes for these empyemas were

Received September 17, 1987; accepted after revision November 23, 1987.

[1] Department of Radiology, Boston Veterans Administration Medical Center, Boston, MA 02130, and Tufts University School of Medicine, Boston, MA 02111. Address reprint requests to M. P. Shapiro, Dept. of Radiology, Boston V. A. Medical Center, 150 S. Huntington Ave., Boston, MA 02130.

[2] Department of Thoracic Surgery, Boston Veterans Administration Medical Center, Boston, MA 02130, and Tufts University School of Medicine, Boston, MA 02111.

AJR 150:549–552, March 1988
0361–803X/88/1503–0549
© American Roentgen Ray Society

pneumonia (seven patients) and surgical complications (five patients). In the group that had empyemas caused by surgical complications, three occurred after pneumonectomy, one developed after combined right-middle and right-lower lobe lobectomies, and one was due to an anastomotic leak after esophagectomy and gastric interposition. In one patient, a Boerhaave-type tear of the esophagus with esophagopleural fistula was the cause of empyema. Patients ranged in age from 49 to 70 years (average, 59 years); all were men.

Results

The appearance of the Eloesser window itself was similar in all cases. However, the radiographs of the 13 patients were divided into two groups, since the postoperative appearance of the pleural space differed in those patients who had had a pneumonectomy ($n = 3$) and those who had not ($n = 10$).

Patients Who Had Not Undergone Pneumonectomy

Initial postoperative radiographs revealed localized elliptical or round pleural cavities ranging in size from 7 × 1.5 cm to 11 × 8 cm in the region of the evacuated empyema. Commonly, partial or complete filling of the space with radiopaque iodinated gauze mimicked pulmonary consolidation (Figs. 1A–1C). The window was located on the lateral chest wall in five patients and on the posterior chest wall in five patients. When seen en face, the thoracostomy window itself was sometimes visible as an ellipse or crescent of increased lucency superimposed on the larger lucency caused by air in the evacuated cavity (Fig. 1B). The Eloesser window always had a sharply defined superior margin and usually had an ill-defined inferior margin (Fig. 2). When viewed in profile, the chest-wall defect had a round superior border and a straight downward-sloping inferior contour (Fig. 3).

In instances in which sequential radiographs were available, the cavity size always appeared to be decreased or unchanged, but never increased, on successive studies (Fig. 4). In five patients, the cavity eventually disappeared at 1 month, 2 months, 4 months, 6 months, and 14 months, respectively. One patient had a small pleural cavity still present 2.5 years after surgery. No long-term follow-up radiographs were available in the remaining four patients.

CT scans from the postoperative period were also available in six of the 10 cases. Only one of the three patients who had scans performed within the first postoperative month had residual pleural fluid, and that had resolved completely at 6

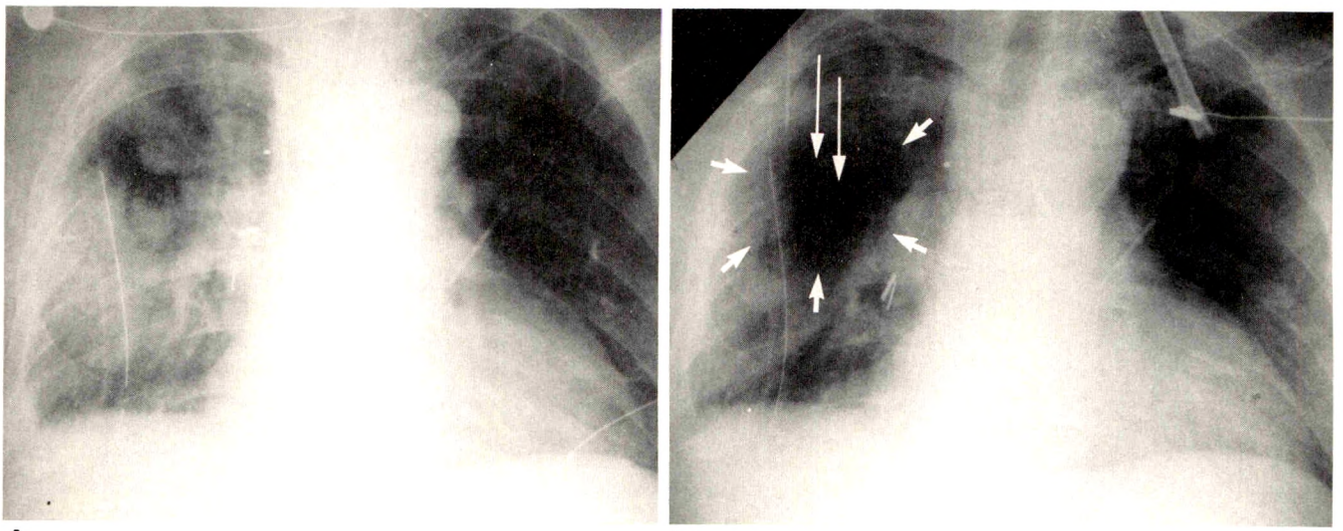

Fig. 1.—56-year-old man who developed an empyema after esophagogastrectomy.

***A*, Mobile postoperative radiograph shows areas of density and radiolucency in right mid chest due to a combination of iodinated sponge packing and Eloesser window. Density caused by the sponge could easily be mistaken for postoperative pneumonitis.**

***B*, Radiograph made after iodinated packing was removed the next day shows an irregular radiolucency (*short arrows*). Radiolucency is greatest in the center because of rib resection, chest-wall defect, and loculated air-filled empyema cavity. Superior margin of Eloesser window is irregular but relatively sharply defined (*long arrows*).**

***C*, CT scan 1 week later shows surgical sponge extending through Eloesser window into evacuated empyema cavity. There is no evidence of residual fluid within cavity, but pleura is clearly thickened. A chest tube is present anteriorly, and postoperative changes of an esophagogastrectomy are present in the posterior mediastinum.**

Fig. 2.—68-year-old man 1 year after Eloesser procedure. Posteroanterior radiograph shows resected ribs, and a round radiolucency is seen at level of left atrium caused by posterior Eloesser window.

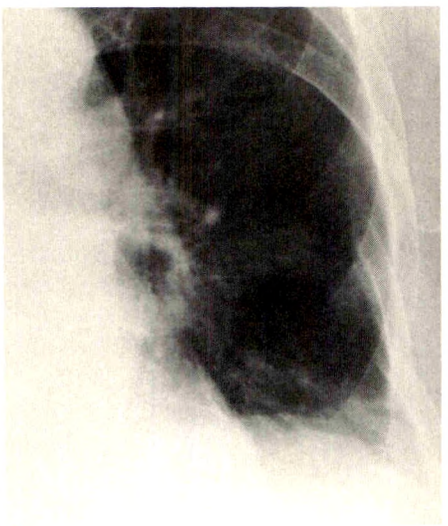

Fig. 3.—49-year-old man 4 months after Eloesser procedure for empyema associated with necrotizing aspiration pneumonia. Superior margin (*arrow*) of window is sharp, but inferior edge (*arrowheads*) is poorly defined.

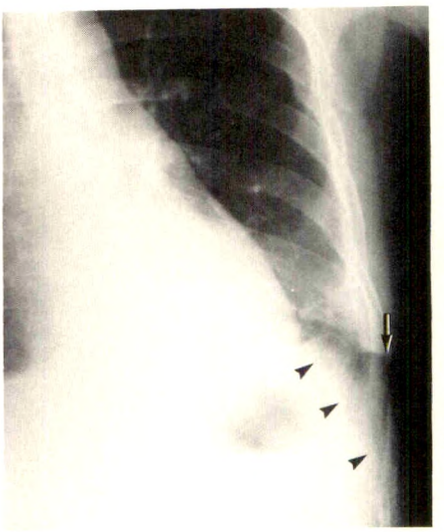

2 3

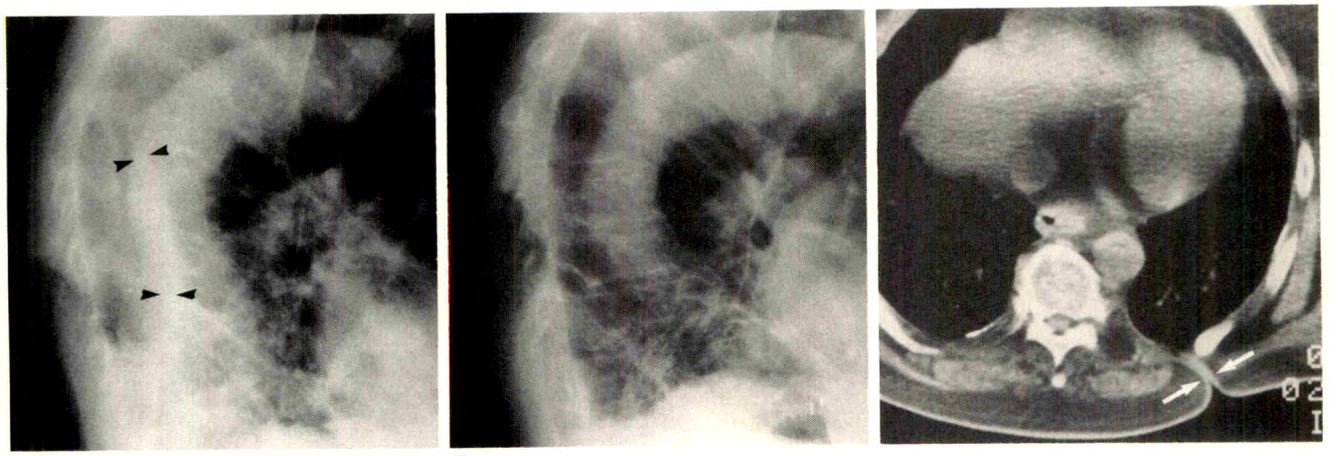

A B

Fig. 4.—70-year-old man with chronic right empyema and bronchopleural fistula complicating necrotizing pneumonia.

A, Lateral chest radiograph made 23 days after surgery shows posterior chest-wall window defect. Air in empyema cavity outlines visceral pleural peel (*arrowheads*).

B, 3 months later, pleural cavity is completely obliterated and Eloesser window itself is more clearly seen.

Fig. 5.—56-year-old man who had had an Eloesser window procedure 4 years earlier. CT scan shows narrow tract (*arrows*) at site of Eloesser window.

months. The other two scans obtained within 1 month showed only minimal pleural thickening or scarring around the perimeter of the air-filled cavity with no evidence of residual fluid.

In the three other patients, a total of five CT scans were performed between 1 and 4 years after surgery. These scans showed persistent but narrowed thoracostomy windows at the last follow-up examinations at 1, 2, and 4 years, respectively (Fig. 5). Clinically, each of these patients had a minimal amount of chronic drainage. However, no residual or recurrent pleural empyema fluid was shown on the CT scans during this long-term follow-up period; rather, only minimal localized pleural fibrosis was observed.

Patients After Pneumonectomy

Postoperative radiographs in all postpneumonectomy patients showed complete disappearance of the infected pleural fluid seen preoperatively. Unlike the 10 nonpneumonectomy cases, the empyema cavity represented the entire postpneumonectomy space. On the anteroposterior chest films of all three patients, the chest-wall defect was seen in profile to have a smooth, round superior contour and a straight and laterally sloping lower margin, similar to that seen in the nonpneumonectomy patients with lateral windows. However, since the empyema had filled the whole postpneumonectomy space, a zone of intermediate radiolucency surrounding the Eloesser window (as was seen in nonpneumonectomy cases) was never present when the window was imaged en face on lateral radiographs. In one patient, an unusual appearance was created by the surgical packing that filled virtually the entire postpneumonectomy space (Fig. 6). Follow-up radiographic examinations in this group were limited to 1 month, and none showed any recurrence of empyema during this period.

Discussion

In 1935, Leo Eloesser [3], the surgeon who devised the procedure now associated with his name, reported its use as an alternative to existing methods of treatment for acute tuberculous empyema that were associated with a high mortality from secondary infection and sepsis. In his original description of the operation, he stressed the importance of constructing the window with a flap so that it functioned as a one-way valve, allowing egress of freely mobile fluid while preventing air from entering the pleural space and causing lung collapse.

The subsequent development of antibiotics and antituberculous drugs made the operation obsolete for its originally intended purpose. However, variations in the operation can be useful in the present-day management of intractable nontuberculous empyema [4–7]. The original operation has been modified by substituting a comparatively wide open-window thoracostomy for the slit-like one-way valve opening described by Eloesser [2]. The valve mechanism is not necessary in cases of chronic pyogenic empyema because the visceral and parietal pleura are fused at the margins of the empyema. This fusion isolates the empyema cavity from the rest of the pleural space, preventing lung collapse despite the presence of the large pleurocutaneous communication.

As illustrated by the present cases, the time at which the air-filled pleural cavity is obliterated varies over a substantial range. In those patients for whom long-term follow-up was available, obliteration occurred in four of five cases within 6 months. This is similar to the experience of Weissberg [4] who observed complete obliteration of the empyema cavity in 10 of 12 patients within 6 months of surgery. However, unlike Weissberg's cases, our series did not show a good correlation between the size of the empyema cavity and the amount of time required for cavity closure. The largest cavity closed within 1 month, whereas the smallest required 6 months. Although none of the postpneumonectomy cases in this series had long-term follow-up, the pleural cavity in these patients should never be completely obliterated. This is likely because no lung is available to fill the void, and much of the exudative fluid that normally fills a postpneumonectomy space drains through the patent Eloesser window.

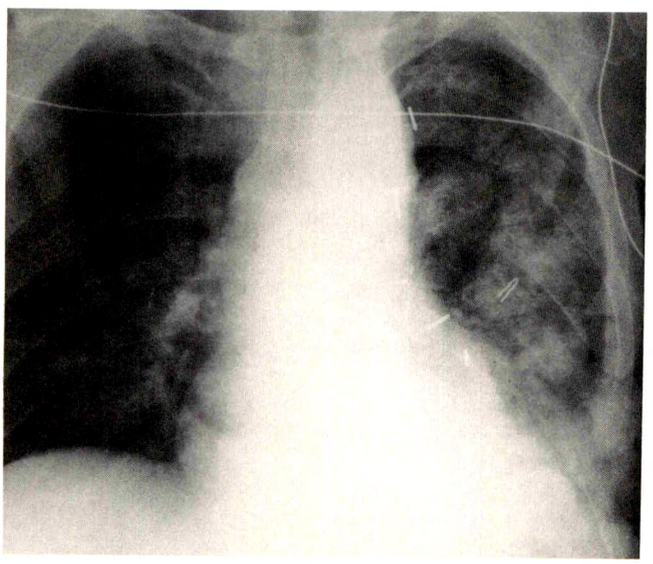

Fig. 6.—53-year-old man 1 day after Eloesser procedure for postpneumonectomy empyema. Entire left chest appears dense because of presence of a large amount of gauze packing, simulating a diffuse unilateral pneumonia or unilateral pulmonary edema.

Although the chest-wall window in nonpneumonectomy patients should eventually close over by granulation tissue after the pleural cavity obliterates, a persistent stoma with chronic minimal drainage may remain. A tract persisted in three of our patients and in five of eight cases reported by Adebo and Osinowa [5]. In our patients this may have resulted from secondary colonization of the residual pleural cavity, since there were no clinical signs of local or systemic infection and no evidence of residual empyema identified on chest radiographs or CT scans. In nearly all cases, the last available radiograph or CT scan only showed residual pleural thickening or fibrosis, an area in which a tiny focus of undetectable superinfection might reside.

The chest radiograph remains abnormal years after the window has closed and the pleural cavity has been obliterated. This results from the depression in the chest wall where the skin is in close proximity to the pleura, separated only by the intervening granulation tissue. The resultant radiolucency where the soft tissues are absent may mimic a lung cavity or bullae when only one radiographic projection of the chest is obtained. However, the elliptical or crescent shape of the radiolucency related to the original U-shaped surgical incision and the associated segmental rib resections are distinguishing features.

The size of the window may appear to be different on chest radiography and CT. This discrepancy arises when a patient with a posterior window is scanned while in a supine position. In this position, the edges of the flap may be artifactually compressed together or spread apart by the patient's own weight and shifting position on the scanning table. Therefore, the appearance and size of the window on physical examination probably correlate more closely with findings of chest radiography than with findings of CT.

In summary, the postoperative chest radiographic and chest CT findings in patients with Eloesser windows are characteristic. These include changes due to the limited chest wall resection and the presence of iodinated packing. As the underlying empyema resolves, the radiographic appearance should change in a sequence that is predictable but over a period of time that is variable.

REFERENCES

1. Mayo P. Early thoracotomy and decortication for nontuberculous empyema in adults with and without underlying disease. *Am Surg* **1985**;51:230–236
2. Hurvitz RJ, Tucker BL. The Eloesser flap: past and present. *J Thorac Cardiovasc Surg* **1986**;92:958–964
3. Eloesser L. An operation for tuberculous empyema. *Surg Gynecol Obstet* **1935**;60:1096–1097
4. Weissberg D. Empyema and bronchopleural fistula. Chest **1982**;82:447–450
5. Adebo OA, Osinowa O. Management of empyema and bronchopleural fistula, experience with Eloesser window. *Trop Doct* **1987**;17:26–29
6. Symbas PN, Nugent JT, Abott OA, Logan WD, Hatcher CR. Nontuberculous pleural empyema in adults, role of a modified Eloesser procedure in its management. *Ann Thorac Surg* **1971**;12:69–78
7. Shamjii FM, Ginsberg RJ, Cooper JD, et al. Open window thoracostomy in the management of postpneumonectomy empyema with or without bronchopleural fistula. *J Thorac Cardiovasc Surg* **1983**;86:818–822

Case Report

Balloon Dilatation of the Left Main Bronchus in Sarcoidosis

Karen T. Brown,[1] Chin Bor Yeoh,[2] Souheil Saddekni[3]

Congenital and acquired narrowings of the tracheobronchial tree are difficult clinical problems that often require complicated surgical management. Percutaneous balloon dilatation has found widespread clinical applications in the vascular, gastrointestinal, and genitourinary systems. Its use also has been reported in the tracheobronchial tree, and postsurgical and postintubation strictures in both adults and neonates have been successfully dilated [1–4]. We report a case of balloon dilatation of the left main bronchus in an adult with sarcoidosis and mediastinal fibrosis. This is the first report to our knowledge in which balloon dilatation has been used in an adult with disease extrinsic to the bronchus.

Case Report

A 35-year-old black woman was in excellent health until 1984 when she developed pericarditis. Over the last 3 years she noticed increasing dyspnea on exertion and had frequent episodes of bilateral pneumonia. Conventional tomography in early 1987 showed segmental narrowing of the left main bronchus. Her dyspnea on exertion had progressed, and she became essentially homebound. She was referred to our institution.

The chest radiograph showed increased interstitial markings and cardiomegaly. Echocardiography revealed that the sizes of the left and right ventricles were at the upper limits of normal and that concentric left ventricular hypertrophy was present. The ECG showed Wenckebach heart block to be present. Repeat conventional tomography (Fig. 1A) confirmed the previous findings of narrowing of the left main bronchus extending over a 3-cm segment with a luminal diameter of 3.5 mm. In addition, a 5-mm polypoid mass was noted along the right lateral wall of the distal trachea just proximal to the origin of the right main bronchus. A CT scan of the chest performed with and without contrast material showed a diffuse hazy increase in the density of the mediastinum, consistent with fibrosing mediastinitis, and narrowing of the left main bronchus. None of the major vessels within the mediastinum was involved. Room-air arterial blood gases showed a pH of 7.42, a partial pressure of carbon dioxide of 37 mm Hg, and a partial pressure of oxygen of 69 mm Hg; all other laboratory data were normal. The pulmonary function tests showed a combined obstructive and restrictive ventilatory pattern. The forced expiratory volume in 1 sec was 1.25 l with a forced vital capacity of 2.16 l. On the flow-volume loop, the peak expiratory flow rate was 3.14 l/sec, and the maximal midexpiratory flow rate was 0.74 l/sec.

On the seventh hospital day, the patient underwent mediastinoscopy and rigid bronchoscopy. Surgical and pathologic findings confirmed the diagnoses of sarcoidosis and fibrosing mediastinitis. At that time the narrowed left main bronchus was visualized and, under direct vision, a straight Newton B guidewire was advanced into the lower lobe division. We chose a soft guidewire to avoid trauma to the more distal respiratory tree. The bronchoscope was removed, and the patient was intubated. The distal segment of the left main bronchus that appeared most normal was 10 mm in diameter; consequently, a 10-mm balloon was chosen for the procedure. A 7-French angioplasty catheter with a 10-mm high-pressure balloon extending over a 4-cm segment (Medi-Tech, Watertown, MA) was then advanced alongside the endotracheal tube and positioned under fluoroscopic guidance.

The narrowed left main bronchus was dilated by using three inflations of the balloon; each inflation was maintained by hand for 15 sec (Figs. 1B and 1C). By the third inflation, no "waist" was visible. The balloon catheter then was removed, and bronchoscopy was performed again after adequate ventilation. Repeat bronchoscopy showed wide patency of the left main bronchus, with a minimal amount of blood in the tracheobronchial tree. The polypoid mass that had been visualized along the right lateral tracheal wall on initial bronchoscopy was no longer present. We believe that this was an

Received September 14, 1987; accepted after revision October 29, 1987.
[1] Department of Radiology, St. Luke's/Roosevelt Hospital, 428 W. 59th St., New York, NY 10019. Address reprint requests to K. T. Brown.
[2] Department of Surgery, St. Luke's/Roosevelt Hospital, 428 W. 59th St., New York, NY 10019.
[3] Department of Radiology, St. Luke's/Roosevelt Hospital, Amsterdam Ave. and 114th St., New York, NY 10025.

AJR **150:553–554, March 1988** 0361–803X/88/1503–0553 © American Roentgen Ray Society

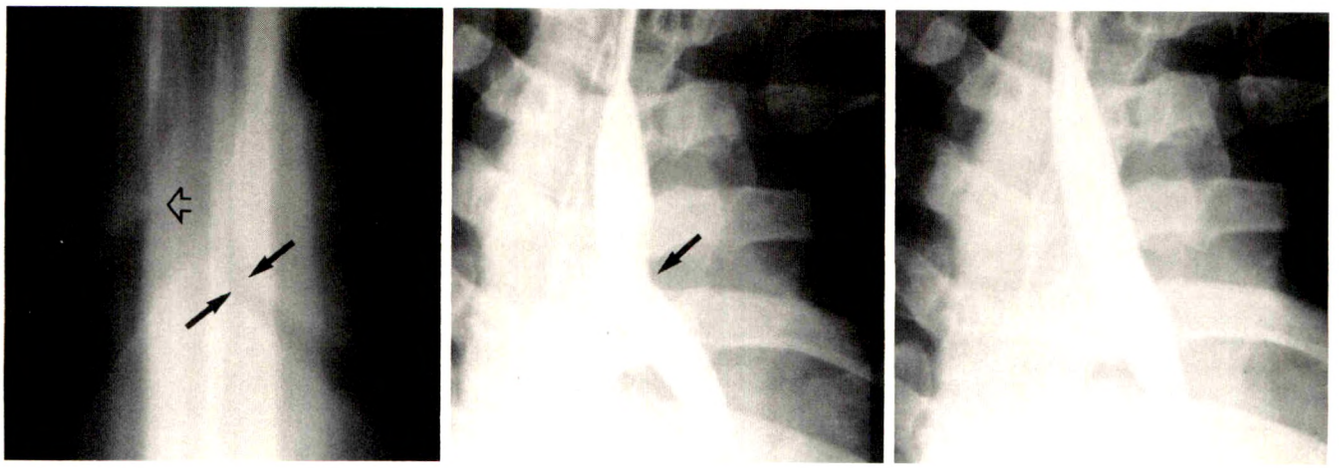

Fig. 1.—*A*, Conventional tomogram shows severely narrowed left main bronchus (*solid arrows*) and polypoid mass in distal trachea (*open arrow*) just above carina.

***B* and *C*, Radiographs obtained during surgery show balloon dilatation of left main bronchus. Note "waist" at narrowed segment (*arrow* in *B*). Balloon is fully inflated in *C*.**

inflammatory polyp that was flattened or otherwise disrupted by the balloon. The patient tolerated the procedure well, no complications occurred, and she recovered uneventfully.

Conventional tomography was repeated 2 days after surgery and showed the diameter of the left main bronchus to be 8 mm. The pulmonary function tests were repeated at the same time and showed improvement in the obstructive ventilatory pattern. The forced expiratory flow in 1 sec was 1.6 l, and the forced vital capacity was unchanged at 2.16 l. On the flow-volume loop, the peak expiratory flow had increased to 4.08 l/sec and the maximal midexpiratory flow had increased to 1.61 l/sec. The patient was discharged 3 days after surgery and has continued to do well. Conventional tomography performed 3.5 months after the dilatation showed no change; the left main bronchus was still 8 mm in diameter. The patient currently walks several miles with no shortness of breath.

Discussion

Fixed narrowings of the tracheobronchial tree may occur after prolonged mechanical ventilation or as a complication of sleeve resection for bronchial lesions. The most common cause of fixed airway narrowing is neoplastic disease, which may be either intrinsic or extrinsic. Idiopathic mediastinal fibrosis may result in compromise of the airway, as was the case in our patient. These narrowed segments also may be seen de novo on a congenital basis or as a result of intrinsic disease (e.g., submucosal infiltrative processes, bronchial neoplasms, relapsing polychondritis, and tracheobronchopathia osteochondroplastica). Present surgical techniques for the treatment of these conditions include surgical resection, photoresection, and cryotherapy. Balloon dilatation has been reported as a treatment in infants with congenital and acquired bronchial stenoses [1–3] and in an adult [4] with an anastomotic stricture after a sleeve resection for an endobronchial carcinoma.

The nature of disease extrinsic to the airways suggests that such lesions may not respond to intraluminal balloon dilatation alone and may require surgical therapy or an expandable stent [5] after balloon dilatation. Unfortunately, these stents are not yet available for clinical use. Given the complexity of surgical treatment and the relative ease with which peroral balloon dilatation can be performed, we chose to attempt balloon dilatation as the primary treatment in this case. The advantages of this method of treatment include the ease with which it can be performed and the fact that it can be repeated, should the lesion recur, possibly without bronchoscopy. No significant morbidity has been associated with the few cases reported thus far. Although the length of follow-up in all cases reported is limited, the preliminary results are encouraging. Ultimately, bronchial balloon dilatation could be performed on an outpatient basis.

REFERENCES

1. Cohen MD, Weber TR, Rao CC. Balloon dilatation of tracheal and bronchial stenosis. *AJR* **1984**;142:477–478
2. Groff DB, Allen JK. Gruentzig balloon catheter dilatation for acquired bronchial stenosis in an infant. *Ann Thorac Surg* **1985**;39:379–381
3. Brown SB, Hedlund GL, Glasier CM, Williams KD, Greenwood LH, Gilliland JD. Tracheobronchial stenosis in infants: successful balloon dilatation therapy. *Radiology* **1987**;164:475–478
4. Fowler CL, Aaland MO, Harris FL. Brief communications: dilatation of bronchial stenosis with Greuntzig balloon. *J Thorac Cardiovasc Surg* **1987**;93:308
5. Wallace MJ, Charnsangavej CC, Ogawa K, et al. Tracheobronchial tree: expandable metallic stents used in experimental and clinical applications. *Radiology* **1986**;158:309–312

Case Report

Air Embolism Complicating Percutaneous Lung Biopsy

Thomas L. Tolly,[1] John E. Feldmeier, and David Czarnecki

Thin-needle biopsy is a common diagnostic procedure in diseases of the chest. Inherent risks of the procedure most commonly include pneumothorax and hemorrhage. Air embolism is a rare and often disastrous complication with the diagnosis frequently presumptive and most often based on the patient's rapid neurologic deterioration [1]. We report a CT-documented case of air embolism complicating biopsy of a lung lesion.

Case Report

A 32-year-old man had his right arm amputated to treat synovial sarcoma; subsequently he had a resection for bilateral pulmonary metastases. When a mass was discovered in the right lower lobe, the patient underwent a CT-guided, thin-needle aspiration biopsy of the lesion.

With the patient lying in the prone position, the lesion was located by CT imaging. A 22-gauge spinal needle was inserted approximately 4–5 cm into the lung parenchyma with the patient in end-inspiration. CT imaging showed the needle to be directed medially (Fig. 1A), but it was subsequently repositioned. Immediately after CT imaging was performed to verify the new position of the needle, the patient coughed, became agitated, and obtunded. The biopsy needle was removed, and the patient was turned supine. At this time he was diaphoretic and had a pulse of 40 and a nonobtainable blood pressure. Supportive measures were instituted. The patient remained obtunded for 1–2 min with his pupils dilated and his eyes deviated to the left. After elevating the patient's feet, his heart rate increased to 70 and his blood pressure returned to normal. The patient became alert, but he was aphasic with a persistent leftward gaze and right leg hemiple-

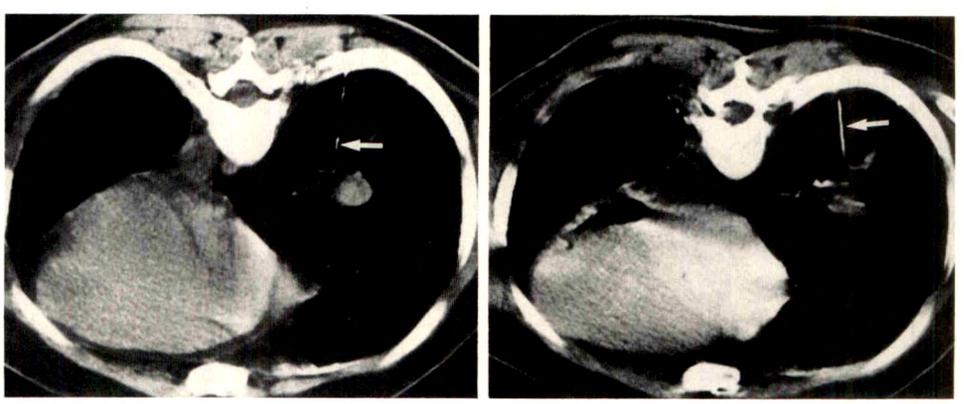

Fig. 1.—*A*, Initial CT scan with patient in prone position shows needle adjacent to mass (*arrow*) and no air in left atrium.

***B*, Subsequent CT scan with needle in position (*arrow*) shows air-fluid level in left atrium indicating air embolism.**

Received August 11, 1987; accepted after revision October 13, 1987.

[1] All authors: Department of Radiology, St. Luke's Hospital, 2900 W. Oklahoma Ave., Milwaukee, WI 53215. Address reprint requests to T. L. Tolly.

AJR 150:555–556, March 1988 0361–803X/88/1503–0555 © American Roentgen Ray Society

gia. Fundoscopic examination was unremarkable. Within 15 min after the onset of symptoms, the patient's neurologic status had returned to normal. Chest radiographs showed no pneumothorax, and a head CT scan showed no air embolism. The patient remained well and subsequently had a right thoracotomy for excision of a pathologically proved metastatic sarcoma.

In retrospect, the CT image obtained immediately after needle repositioning showed an air-fluid level in the left atrium that was not present on the original CT images (Fig. 1B).

Discussion

Percutaneous thin-needle biopsy of the lung is a widely accepted diagnostic procedure [2]. Pneumothorax is the most frequent complication occurring in 27%, followed by local bleeding occurring in 11% and hemoptysis in 7% [1]. Fortunately, more serious sequelae such as air embolism are rare. Sinner [1] reported two suspected cases of air embolism in 2726 needle biopsies of the chest. The diagnosis of air embolism is largely dependent on clinical manifestations of rapid deterioration of neurologic status and/or cardiac arrhythmias. Westcott [3] reported a case of cerebral artery air embolism that was radiographically documented with postmortem skull radiographs after percutaneous lung biopsy.

The mechanism of air embolism may be a communication between a bronchus or cannula and a pulmonary vein. Factors that increase the risk of this complication include sudden elevation of airway pressure due to a cough, the Valsalva maneuver or positive pressure ventilation, use of larger-bore needles, or delay in attaching the syringe to the needle after removing the obturator [4].

The immediate treatment includes administration of 100% oxygen, placing the patient in the left lateral decubitus position with the head dependent, and routine supportive measures [5]. When the complication is suspected, hyperbaric oxygen therapy should be considered. This treatment reportedly reduces the size of air bubbles, helping to restore circulation and oxygenation [6].

REFERENCES

1. Sinner WN. Complications of percutaneous transthoracic needle aspiration biopsy. *Acta Radiol [Diagn]* (Stockh) **1976**;17:813–828
2. Berquist TH, Bailey PB, Cortese DA, Miller WE. Transthoracic needle biopsy: accuracy and complications in relation to location and type of lesion. *Mayo Clin Proc* **1980**;55:475–481
3. Westcott JL. Air embolism complicating percutaneous needle biopsy of the lung. *Chest* **1973**;63:108–110
4. Lalli AF, McCormack LJ, Zelch M, Reich NE, Belovich D. Aspiration biopsies of chest lesions. *Radiology* **1978**;127:35–40
5. Thomas AN, Roe BB. Air embolism following penetrating lung injuries. *J Thorac Cardiovasc Surg* **1973**;66:533–539
6. Murphy BP, Harford FJ, Cramer FS. Cerebral air embolism resulting from invasive medical procedures: treatment with hyperbaric oxygen. *Ann Surg* **1985**;201:242–245

MR Diagnosis of Pancreatic Transplant Rejection

Thomas N. Vahey[1, 2]
Gary M. Glazer[1]
Isaac R. Francis[1]
King Li[1, 3]
Donald C. Dafoe[4, 5]
Alex M. Aisen[1]
David M. Smid[6]

To determine the role of MR imaging in the assessment of pancreatic transplant rejection, we prospectively obtained 13 MR scans in nine transplant patients. The presence of rejection was verified pathologically by pancreatic transplant biopsies in five patients. In two additional patients, rejection was proved by concordant renal transplant biopsy as well as by compatible clinical and laboratory data. In the remaining two patients, in whom no biopsy was done, clinical and laboratory data showed no evidence of rejection. The mean T2 of the seven pancreata undergoing rejection was significantly elevated (86 msec) compared with the mean T2 of the two transplants not undergoing rejection (59 msec) ($p < .002$).

These preliminary results suggest that MR may be useful in the noninvasive diagnosis of pancreatic rejection.

Pancreatic transplantation is used in the treatment of diabetes mellitus in an effort to establish normal glucose metabolism and to prevent or retard the progression of neurovascular complications associated with the disease [1–5]. As the number of pancreatic transplantations increases, there is a correspondingly greater need to develop an accurate means of detecting rejection noninvasively. We studied the use of MR imaging for this purpose.

Materials and Methods

Over an 18-month period we performed 13 MR examinations in nine patients who had undergone pancreatic transplantation. Six examinations were performed during the initial hospitalization, an average of 3 weeks (range, 1–6.5 weeks) after transplantation. Five examinations were performed at the time of a routine follow-up visit, an average of 30 weeks (range, 18–44 weeks) after transplantation. Two MR scans were performed during readmission for suspected rejection, 8 and 46 weeks after transplantation.

The surgical technique used for the transplantation was the intraperitoneal placement of a whole-organ allograft with anastomosis of vessels to the iliac vessels. The pancreatic duct was drained via a periampullary patch of donor duodenum anastomosed to the recipient urinary bladder. All but one patient had had a renal transplant at the time of pancreatic transplantation. In three patients, an irradiated spleen was transplanted en bloc with the pancreas.

Spin-echo MR studies were performed on a Diasonics MTS system operating at 0.35 T. The minimum study consisted of contiguous, 1-cm-thick, axial, spin-echo images through the pelvis, with relatively T1-weighted (repetition time [TR] = 0.5 sec, echo time [TE] = 30 msec) and T2-weighted (TR = 2 sec, TE = 30, 60 msec or TR = 2 sec, TE = 50, 100, 150 msec) sequences. These images were occasionally supplemented with coronal scans. No respiratory or ECG gating was employed.

The transplanted pancreas was localized by correlating surgical records and CT examinations with the MR images. MR intensity measurements of the transplant were made by using an electronic cursor to define regions of interest. The region of interest was drawn within the body and tail of the pancreatic transplant to ensure that the transplanted duodenal segment was not included, and to avoid volume averaging with the bladder. The mean T2 was

Received March 17, 1987; accepted after revision October 28, 1987.

This work was supported in part by a grant from the University of Michigan Biomedical Research Council.

[1] Department of Radiology, University of Michigan Medical Center, Ann Arbor, MI 48109. Address reprint requests to G. M. Glazer, Dept. of Radiology, Box 0030, University of Michigan Hospitals, University Hospital, B1D429/0030, 1500 E. Medical Center Dr., Ann Arbor, MI 48109-0030.

[2] Present address: Department of Radiology, Methodist Hospital, Indianapolis, IN 46202.

[3] Present address: Department of Radiology, University of Florida College of Medicine, Gainesville, FL 32611.

[4] Department of Surgery, University of Michigan Medical Center, Ann Arbor, MI 48109.

[5] Present address: Department of Surgery, University of Pennsylvania, Philadelphia, PA 19104.

[6] Department of Pathology, University of Michigan Medical Center, Ann Arbor, MI 48109.

AJR 150:557–560, March 1988
0361–803X/88/1503–0557
© American Roentgen Ray Society

calculated by using intensity data collected from three separate regions of interest. The direct calculation of T1 was not possible because our imaging sequences used different echo times.

In five patients, pancreatic tissue was available for pathologic documentation of the presence of rejection. Mononuclear cell infiltration of vessel walls (vasculitis) was regarded as evidence of acute rejection [6]. Rejection was graded as mild, moderate, or severe depending on the intensity of the vasculitis and the associated mononuclear cell infiltrate in the pancreatic acini. In the remaining four patients, a variety of parameters, including the status of synchronous renal transplant, urinary amylase, serum glucose, and subsequent clinical course, were used to determine the presence of rejection. When several MR examinations were performed, the status of the pancreas was established by using all available clinical data for each separate examination. The status of the pancreas was assigned to one of three categories: (1) nonrejecting, (2) rejecting, and (3) indeterminate. The mean T2 values of rejecting and nonrejecting glands were compared by using the unpaired Student t test.

Results

The nine patients were divided into three groups: (1) those in whom there was biopsy proof of transplant rejection, (2) those in whom there was clinical and laboratory evidence of rejection, and (3) those in whom there was no evidence of rejection.

In five patients, pancreatic rejection was confirmed by histologic evaluation after open surgical biopsy. In four of the five cases, the T2 values were equal to or greater than 70 msec at the time of rejection. Two of these patients had several MR examinations. In one patient with mild rejection proved by pancreatic biopsy, the initial T2 value 2 weeks after transplantation was 72 msec, but this value had increased to 90 msec by 6 weeks after transplantation (Fig. 1). In the other patient, T2 was 57 msec initially and laboratory data supported a nonrejecting status. However, 7 days later there was an episode of histologically proved rejection. Because the rejection episode occurred so soon after the MR examination, the initial transplant status was placed in the indeterminate category.

Two patients were thought to be undergoing rejection on the basis of clinical data. In both, rejection was proved because renal transplant biopsy indicated renal rejection, and laboratory and clinical data supported the diagnosis. At the time of rejection of the pancreatic transplant, T2 values in these patients were 110 and 75 msec, respectively. In both patients, the rejection episode was successfully treated. Scans obtained after serum glucose and renal function had returned to normal showed pancreatic transplant T2 values of 60 and 54 msec, respectively (Fig. 2).

Two patients with normal fasting blood-sugar levels and stable renal function were not thought to be undergoing rejection. Pancreatic transplant T2 times were 56 and 67 msec, respectively.

The mean T2 value of pancreatic transplants undergoing rejection was 86 msec (n = 8, SD = 15 msec), compared with a mean value of 59 msec (n = 4, SD = 6 msec) for nonrejected glands. This difference is statistically significant ($p < .002$) (Fig. 3).

Discussion

Unlike renal transplants, for which Doppler sonography can provide some information about rejection status [7] and for which biopsy is relatively straightforward, there is no reliable, noninvasive means of detecting pancreatic rejection. The presence of hyperglycemia is nonspecific, and islet cell destruction is often extensive and irreversible by the time the serum glucose rises [8]. Pancreatic rejection can be inferred by the diagnosis of synchronous renal rejection in cases of simultaneous renal/pancreatic transplantation [2, 3, 9]. Although this relation is valuable, it is not always the case since the renal transplant is more susceptible to rejection. However, in such patients, no isolated cases of pancreatic rejection have been documented [9].

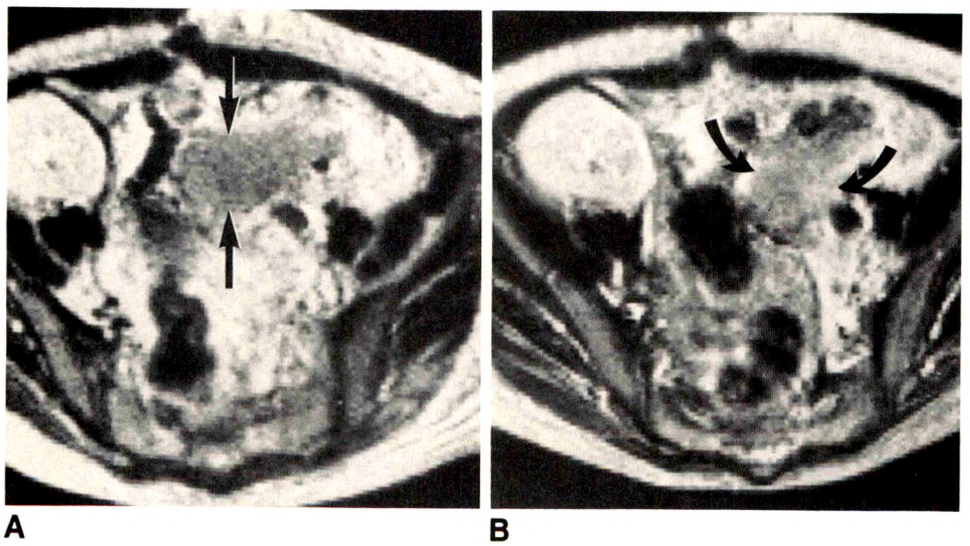

Fig. 1.—Increase in T2 with progression of rejection in 34-year-old woman.
***A*, Initial MR scan obtained during episode of biopsy-proved rejection. Axial T2-weighted MR image (SE 2000/150 msec) of transplanted pancreas (*arrows*). T2 was calculated to be 72 msec.**
***B*, Follow-up MR scan (SE 2000/150 msec) 6 weeks later, when clinical parameters strongly suggested worsening of rejection, showed an increase in T2 to 90 msec and increased signal intensity of the transplant (*arrows*).**

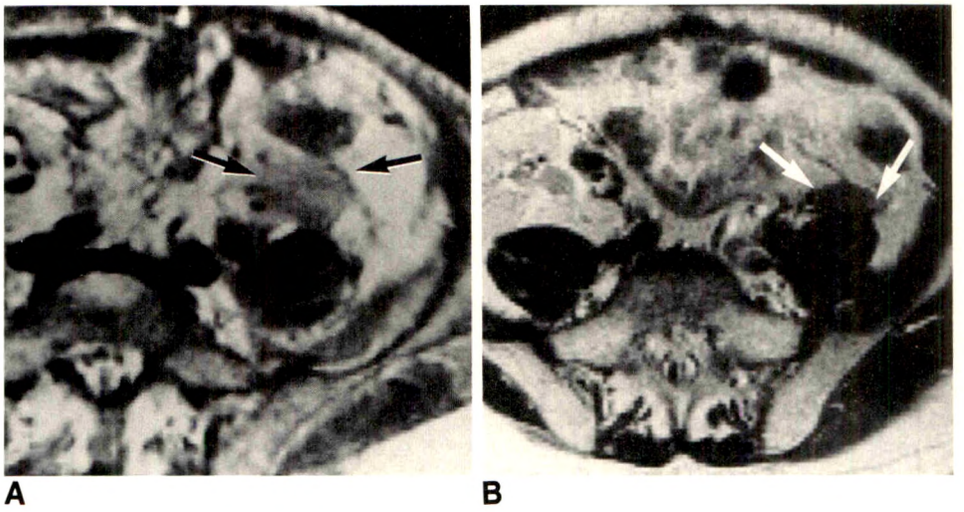

Fig. 2.—Decrease in T2 with resolution of rejection in 30-year-old man.

***A*, Moderately T2-weighted MR scan was obtained during episode of clinically diagnosed rejection (SE 2000/50 msec). T2 of transplant (*arrows*) was 110 msec.**

***B*, Follow-up MR scan (SE 2000/60) 23 weeks later, after resolution of clinical signs of rejection, shows a decrease in transplant T2 to 60 msec, interval diminution in size, and decreased signal intensity compared with *A*. Renal transplant is present in right iliac fossa.**

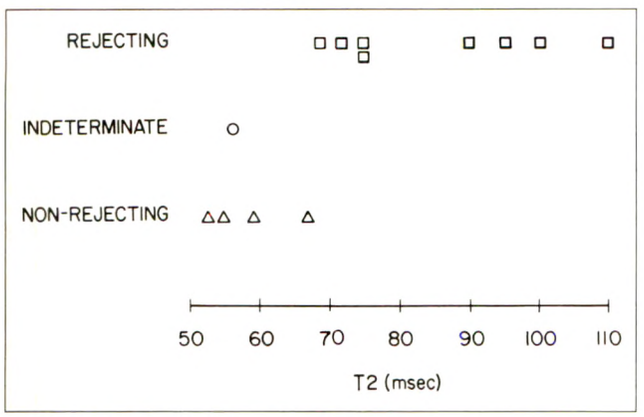

Fig. 3.—Histogram of T2 times of pancreatic transplants.

A sensitive and specific noninvasive measure of pancreatic rejection is needed because pancreatic biopsy requires general anesthesia and open laparotomy. Percutaneous fine-needle biopsy cannot determine whether rejection is occurring, and large-gauge core biopsy needles cannot be used because of the proximity of the transplant to the splenic artery and vein and because of possible pseudocyst formation.

In vivo measurement of T1 and T2 is difficult, and determinations made under different circumstances (e.g., with different pulse sequences or field strengths) or on different equipment are likely to show substantial discrepancies [10]. Nonetheless, when a single imaging device is used, reasonable reproducibility can be achieved [11, 12]. The position of the transplanted pancreas in the pelvis minimizes respiratory motion that otherwise would severely degrade relaxation-time measurements. Experiments performed on our scanner with a phantom have confirmed that a reproducible measurement of T2 can be made in the range of 20–100 msec by using the pulse sequences employed in the current studies [13].

T2 prolongation has not proved to be reliable in assessing renal transplant rejection [14]. The T2 value, calculated at 0.35 T, for the normal pancreas (48 ± 11.6 msec) is, however, significantly shorter than the T2 of renal cortex (75.9 ± 26.6 msec) and medulla (81.4 ± 24.5 msec) [15]. Thus MR assessment of rejection may be more sensitive in the pancreas than it is in the kidney. This is supported by the demonstration that T2 lengthening is a valid indicator of cardiac rejection in the heart [16], which has a normal T2 (43.9 msec) roughly equivalent to that of normal pancreas [17].

A consideration in the evaluation of the rejecting pancreas is the differentiation between acute and chronic rejection. As seen in all of the rejecting glands in our study, acute rejection is histologically characterized by mononuclear cell infiltration of blood vessel walls. The vasculitis is typically associated with a mononuclear cell infiltrate in surrounding acini and interstitial edema. This edema may have resulted in the observed elevation of T2 with pancreatic rejection. Chronic rejection can manifest as fibrosis and atrophy of the transplanted pancreas, which would not be expected to elevate the T2. This may, however, result in a decrease in gland size, which is an additional variable that could be followed with MR imaging.

A limitation of this study was the inability to control the time interval between transplantation and the MR examinations. All but one of the MR scans were performed within 6.5 weeks of transplantation. Although it is uncertain whether postoperative changes in the transplant (such as pancreatitis) can simulate rejection, significant elevation of T2 values of the gland in one patient during pathologically documented rejection suggests that rejection independent of postoperative edema can result in elevated T2 values. This limitation can be overcome by serial studies of the transplanted pancreas.

Although further investigation is required, our preliminary results suggest that MR may be important in the evaluation of pancreatic transplant rejection. The mean T2 value of the rejecting glands (86 msec) was significantly higher than the

mean T2 of the nonrejecting glands (59 msec). No rejecting pancreas had a T2 of less than 70 msec, and no normal transplant had a T2 of more than 70 msec.

REFERENCES

1. Groth CG. Clinical pancreatic transplantation. *Transplant Proc* **1985**;17:302–306
2. Tydén G, Wilczek H, Lundgren G, et al. Experience with 21 intraperitoneal segmental pancreatic transplants with enteric or gastric exocrine diversion in humans. *Transplant Proc* **1985**;17:331–335
3. Corry RJ, Nghiem DD, Schulak J, et al. Surgical treatment of diabetic neuropathy with simultaneous pancreatic duodenal and renal transplantation. *Surg Gynecol Obstet* **1986**;162:547–555
4. Land W, Landgraf R, Illnen WD, et al. Improved results in combined segmental pancreatic and renal transplantation in diabetic patients under cyclosporine therapy. *Transplant Proc* **1985**;17:317–324
5. Starzl TE, Iwatsuke S, Shaw BW, et al. Pancreaticoduodenal transplantation in humans. *Surg Gynecol Obstet* **1984**;159:265–272
6. More AR. The kidneys and urinary tract. In: Anderson R, ed. *Muir's textbook of pathology*, 12th ed. London: Edward Arnold, **1985**:22.1–22.69
7. Rifkin MD, Needleman L, Pasto ME, et al. Evaluation of renal transplant rejection by duplex Doppler examination: value of the resistive index. *AJR* **1987**;148:759–762
8. Schulak JA, Drevyanko TF. Experimental pancreas allograft rejection: correlation between histologic and functional rejection and the efficacy of anti-rejection therapy. *Surgery* **1985**;98:330–336
9. Dubernard JM, Traeger J, Touraine JL, et al. Patterns of renal and pancreatic rejection in double-grafted patients. *Transplant Proc* **1981**;13:305–307
10. Bottomley PA, Foster TH, Argersinger RE, Pfeifer LM. A review of normal tissue hydrogen NMR relaxation times and relaxation mechanisms from 1–100 MH_z: dependence on tissue type, NMR frequency, temperature, species, excision and age. *Med Phys* **1984**;11(4):425–447
11. Breger RK, Wehrli FW, Charles HC, MacFall JR, Haughton VM. Reproducibility of relaxation and spin-density parameters in phantoms and the human brain measured by MR imaging at 1.5 T. *Mag Reson Med* **1986**;3:649–662
12. Kjos BO, Ehran RL, Brant-Zawadski M, et al. Reproducibility of relaxation times and spin density calculated from routine MR imaging sequences: clinical study of the CNS. *AJNR* **1985**;6:271–276
13. Borrello JA, Chenevert TL, Aisen AM, Glazer GM. Comparison of MR imaging relaxation times obtained using an in vitro unit and whole body imager. Presented at the annual meeting of the Radiological Society of North America, Chicago, IL, December **1986**
14. Hricak H, Terrier F, Demas B. Renal allografts: evaluation by MR imaging. *Radiology* **1986**;159:435–441
15. Ehman RL, Kjos BO, Hricak H, et al. Relative intensity of abdominal organs in MR images. *J Comput Assist Tomogr* **1985**;9(2):315–319
16. Aherne T, Tscholakoff D, Finkbeiner W, et al. Magnetic resonance imaging of cardiac transplants. *Circulation* **1986**;74(1):145–156
17. Fisher MR, McNamara MT, Higgins CB. Acute myocardial infarction: MR evaluation in 29 patients. *AJR* **1987**;148:247–251

Dual-Contrast MR Imaging of Liver Cancer in Rats

Ralph Weissleder[1]
Sanjay Saini
David D. Stark
Jack Wittenberg
Joseph T. Ferrucci

MR contrast agents increase hepatic tumor conspicuity, as measured in terms of contrast-to-noise (C/N) ratios. With an animal model of hepatic metastases from breast cancer, IV administration of Gd-DTPA (0.2 mmol/kg) shows a biphasic time response, transiently increasing the signal intensity of liver relative to tumor, with C/N ratio magnitudes increasing from −5.7 to −16.3 (SE 250/20); after a delay, the signal intensity of tumor increases relative to liver with a reversal of the C/N sign from negative to positive and an increase in the C/N magnitude to +25.0. IV administration of ferrite particles (0.05 mmol Fe/kg) shows a monophasic time response, increasing signal intensity of tumor relative to liver from +1.5 to +49.5 (SE 500/30). When both contrast agents were administered together (dual-contrast technique), the tumor-liver C/N magnitude reached a maximum of +67.8 (SE 500/30) 12 min after drug infusion. Analysis of individual contrast and noise factors contributing to this technique revealed a strong correlation between the signal intensity of liver and the signal intensity of ghost artifacts, which increase after administration of Gd-DTPA (r = .89) and decrease after administration of ferrite (r = 1.0).

Dual-contrast imaging shows a synergistic addition of contrast and suppression of noise from ghost artifacts, maximizing the C/N and increasing the conspicuity of focal liver lesions.

Abdominal MR imaging is becoming an important diagnostic tool in the detection [1–3] and differential diagnosis [4–7] of focal liver lesions. MR contrast agents have been used to increase tumor-liver contrast and enhance lesion conspicuity [8–11]. Chelated transition cations are paramagnetic, predominantly shorten T1 relaxation times of perfused tissue [12, 13], and are best imaged with T1-weighted pulse sequences [14]. Unfortunately, gadolinium-DTPA (Gd-DTPA) nonspecifically enhances the signal intensity of both liver and tumor in a time-dependent fashion and may obscure liver metastases, as commonly used iodinated contrast agents do [8, 12].

Ferrite particles are superparamagnetic and predominantly shorten T2 relaxation times [15, 16]. Therefore, T2-weighted pulse sequences with longer TRs and TEs (T2-weighted) are best suited to ferrite-enhanced MR [16]. Ferrite particles are cleared from the blood by macrophages of the reticuloendothelial system (RES). RES-containing tissues such as liver, spleen, and bone marrow show a profound signal loss after administration of ferrite, whereas tumor signal intensity is not affected.

We sought to determine whether the complementary pharmacologic and magnetic properties of these two contrast agents would be synergistic to enhance detection of focal liver lesions.

Materials and Methods

Animal Model

A rat model of liver cancer resembling human breast cancer metastatic to the liver was used in this investigation [17]. Rat mammary adenocarcinoma (R 3230 AC, EG&G Mason

Received August 10, 1987; accepted after revision November 6, 1987.

R. Weissleder is supported by the Deutscher Akademischer Austauschdienst, Bonn, W. Germany; S. Saini by the Radiological Society of North America Educational and Research Fund; and D. D. Stark by American Cancer Society Junior Faculty Research Award #163 and PDT–326.

[1]All authors: Department of Radiology, Massachusetts General Hospital and Harvard Medical School, Boston, MA 02114. Address reprint requests to J. T. Ferrucci.

AJR 150:561–566, March 1988
0361–803X/88/1503–0561
© American Roentgen Ray Society

Research Institute, Worcester, MA) was subcutaneously implanted into two female Fischer 344 rats. At 2 weeks, a 2- by 3-cm tumor was minced into fragments (approximately 1 mm^3). These fragments were implanted in the liver by trocar inoculation into 19 200- to 250-g Fischer rats at laparatomy. Three animals died and were excluded from the study. The hepatic puncture site was sutured with 6–0 catgut and sealed with collagen hemostat (Avitene, Alcon, Inc., Humacao, PR) to minimize bleeding. The abdominal wall was closed with 2–0 silk sutures in two continuous layers. Two weeks after implantation, 1.0-cm intrahepatic solid tumor nodules were found [17].

MR Imaging

MR imaging was performed by using a 0.6-T (25.1-MHz) Technicare imager. Images were acquired in the transverse plane, slice thickness was 4 mm, and nine contiguous slices were obtained simultaneously. The field of view was set at 21 cm, and the 192 × 256 image matrix yielded an inplane spatial resolution of 1.1 × 0.8 mm. Strongly T1-weighted images were obtained by using an SE 250/20 (spin echo TR/TE) sequence. Images with mixed T1 and T2 contrast dependencies were obtained by using an SE 500/30 sequence. T2-weighted images were acquired with SE 1500/60. Averaging two acquisitions and obtaining 192 phase-encoding steps, the scanning time was 1.6 min for the SE 250/20 pulse sequence, 3.2 min for the SE 500/30, and 9.6 min for the SE 1500/60.

Contrast Agents

Anesthetsized animals were restrained with adhesive tape. Before the imaging procedure was started, a heparin-flushed IV line was placed in the tail vein. Gd-DTPA (Berlex, Cedar Knolls, NJ) and polymer-coated ferrite particles with an average size of 100 nm (Advanced Magnetics Inc., Cambridge, MA) were injected via the tail vein without removing the animal from the imager. All 16 animals were imaged with T1- and T2-weighted pulse sequences before administration of contrast agents. Gd-DTPA was administered to seven animals at a concentration of 0.2 mmol/kg and ferrite was administered to nine other animals at a concentration of 0.05 mmol Fe/kg. In five of seven animals receiving Gd-DTPA and six of nine animals receiving ferrite, serial SE 250/20 imaging was performed for up to 20 min after drug administration. At 12–20 min after drug administration, SE 500/30 and SE 1500/60 images were obtained.

The dual-contrast technique of simultaneous administration of Gd-DTPA and ferrite was achieved by first administering Gd-DTPA. Ferrite (0.05 mmol Fe/kg) was injected into the seven animals 15 min after administration of Gd-DTPA, and additional images (SE 250/20, SE 500/30, and SE 1500/60) were obtained (Gd-Fe dual-contrast technique). Alternatively, Gd-DTPA (0.2 mmol/kg) was injected into the four animals 12 min after administration of ferrite, and additional images (SE 250/20, SE 500/30, and SE 1500/60) were obtained (Fe-Gd dual-contrast technique).

To determine whether magnetic field strength would significantly alter the effects of Gd-DTPA and ferrite, we scanned three additional animals with the Fe-Gd dual-contrast technique at 1.4 T (Technicare prototype, 8-cm bore) [8]. Pulse-sequence timing parameters were identical to those used at 0.6 T.

Image Analysis

Operator-defined regions of interest (ROIs) were used to measure the signal intensity (SI) of liver, tumor, muscle, and fat. Total background image noise (N_{tot}) was measured by using an ROI that was displaced ventral to the animal in the phase-encoding direction [1]. Statistical noise (N_{stat}) was measured with an ROI that was placed lateral to the animal, avoiding ghost artifacts [18]. Both measurements of image noise were recorded as the standard deviation of pixel signal intensities. Systematic noise (N_{sys}) was mathematically derived from measured values of N_{tot} and N_{stat} by quadrature subtraction [1]:

$$N_{sys} = [(N_{tot})^2 - (N_{stat})^2]^{0.5} \quad (1)$$

Contrast between the tumor and liver, expressed as the C/N ratio, was calculated as the tumor-liver signal difference normalized to the standard deviation of background noise [1]:

$$\text{C/N ratio} = (SI_{tumor} - SI_{liver}/N_{tot} \quad (2)$$

The C/N ratio is an effective parameter for quantitating MR pulse sequence performance, as the absolute magnitude of C/N, designated as $|\pm\text{C/N ratio}|$, correlates with lesion detectability [19]. It follows from equation 2 that negative C/N values indicate relatively hypointense (dark) pathology and positive C/N values indicate relatively hyperintense (bright) pathology. Values near zero denote isointensity and poor lesion conspicuity.

For comparison of different pulse sequences and contrast-enhancement techniques, measured C/N ratios were normalized to reflect a standard scanning time of 3.2 min, except for the 1.6-min fast scans obtained in five animals immediately after injection of Gd-DTPA [9]. Timing normalization was performed to objectively compare C/N values, which have a well-known relationship to the number of acquisitions averaged, and scanning times. Fast scans by definition could not be extended to 3.2 min under any circumstance, and therefore time normalization was not appropriate for this subset of data. Normalization of scans obtained by using conventional techniques was performed with the formula [18]:

$$\text{C/N ratio}_{3.2\ min} = \text{C/N ratio}_{measured} \times (3.2\ \text{min/scanning time})^{0.5} \quad (3)$$

Results

Precontrast Images

Native (non–contrast-enhanced) tissue characteristics of our animal model were evaluated with pulse sequences in routine clinical use. The SE 250/20 pulse sequence showed the tumor as hypointense relative to liver with a mean C/N value of −5.7 ± 8.3 (Table 1). With the SE 500/30 pulse sequence the tumor appeared isointense relative to liver, and the average C/N ratio was +1.5 ± 2.3. The SE 1500/60 pulse sequence showed the tumor hyperintense relative to liver, reaching a C/N ratio of +6.2 ± 3.2. Similar C/N values have been reported for human adenocarcinoma metastatic to the liver [1], providing validation of this model for subsequent experiments.

Precontrast noise levels were recorded to allow determination of the influence of contrast-agent–induced changes in tissue signal intensity on statistical (N_{stat}) and systematic (N_{sys}) image noise. Statistical noise was similar with the T1-weighted (20.0 ± 2.1), T2-weighted (19.2 ± 4.3), and SE 500/30 (18.4 ± 3.2) pulse sequences (Table 2). Systematic noise was lowest on T1-weighted images (28.6 ± 6.9) and highest on T2-weighted images (52.6 ± 7.3). These animal data are

TABLE 1: Contrast-to-Noise Ratios for Pulse Sequences and Contrast Agents Used in Studying Rats with Liver Cancer

Contrast Agent	Contrast-to-Noise Ratio		
	SE 250/20	SE 500/30	SE 1500/60
Precontrast	−5.7 ± 8.3	+1.5 ± 2.3	+6.2 ± 3.2
Gd-DTPA:			
Fast scan	−16.3 ± 11.9	–	–
Delayed scan	+25.0 ± 9.7	+18.0 ± 4.1	–
Ferrite	+35.8 ± 5.9	+49.5 ± 6.8	+39.9 + 3.5
Gd-DTPA + Ferrite	+54.9 ± 17.7	+67.8 ± 14.8	+41.6 ± 14.6

Note.—All values are time-normalized for a 3.2-min standard scanning time, except for the fast scans immediately after administration of Gd-DTPA. Averaging two acquisitions, Gd-DTPA fast scans were obtained within the first 2 min (SE 250/20/2, scanning time = 1.6 min) and as delayed scans (SE 250/20/2, scanning time = 1.6 min; SE 500/30/2, scanning time = 3.2 min) 10–15 min after administration of Gd-DTPA.

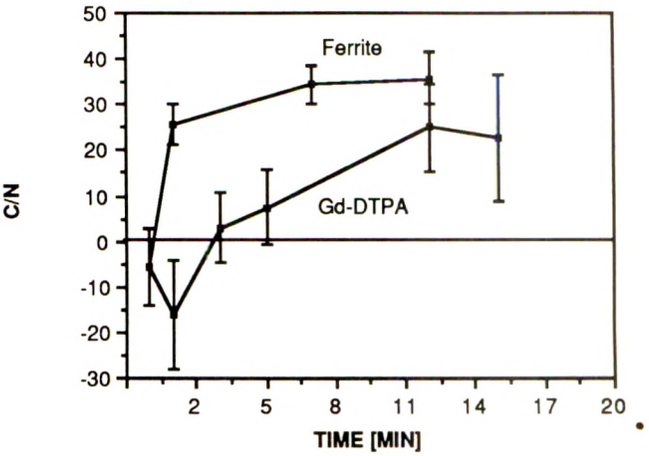

Fig. 1.—Tumor-liver contrast after administration of MR contrast agents. Serial imaging (SE 250/20/2, 1.6-min scanning time) of liver tumors after administration of Gd-DTPA (n = 5) and ferrite (n = 6). After administration of Gd-DTPA there is an early peak of negative contrast-to-noise ratio (C/N) followed by reversal in tumor-liver C/N. After administration of ferrite there is a constant increase in C/N.

consistent with the previous clinical experience that T2-weighted images are most sensitive to motion-artifact degradation [18].

Gd-DTPA

Sequential scanning was performed with the SE 250/20 pulse sequence averaging two acquisitions (scanning time, 1.6 min). Two minutes after administration of Gd-DTPA, the signal intensity of liver increased 73% while the signal intensity of tumor was unchanged. As a result, the liver became hyperintense relative to tumor, increasing the C/N ratio from −5.7 ± 8.3 to −16.3 ± 11.9 (Table 1). Delayed scans obtained at 3 and 5 min after injection showed the tumor to be isointense relative to liver (Fig. 1). Later, 7–20 min after injection, the signal intensity of tumor increased over the signal intensity of liver, resulting in a maximum C/N ratio of +25.0 ± 9.7. The time-dependent behavior of the C/N ratio is caused by the complex pharmacokinetics and biodistribution of Gd-DTPA described previously [8]. Two time points exist for Gd-DTPA–enhanced detection of hepatic lesions: (1) immediately after administration of Gd-DTPA (tumor hypointense relative to liver, -C/N ratio maximized) and (2) after 7–10 min (tumor hyperintense relative to liver, +C/N ratio maximized). Scanning between these time points may obscure lesion detectability, because the tumor may appear isointense relative to liver.

Image noise increased after the administration of Gd-DTPA. This increase was from an increase in N_{sys} from 28.6 ± 6.9 to 57.0 ± 14.6; N_{stat} did not change (Table 2). N_{sys} was directly proportional to liver signal intensity (r = .85) and showed a parallel time dependence (Fig. 2). For example, 15 min after administration of Gd-DTPA, liver signal intensity was increased 36% relative to that in control animals and N_{sys} was increased by 20%. Despite the increase in image noise, the increases in liver signal intensity and tumor-liver contrast were

TABLE 2: Noise Measurements for Various Pulse Sequences and Contrast Agents Used in Studying Rats with Liver Cancer

Contrast Agent: Pulse Sequence	Noise Measurement		
	N_{tot}	N_{stat}	N_{sys}
Precontrast:			
SE 250/20	34.9 ± 6.9	20.0 ± 2.1	28.6 ± 6.9
SE 500/30	43.8 ± 6.3	18.4 ± 3.2	39.7 ± 5.4
SE 1500/60	56.0 ± 8.8	19.2 ± 4.3	52.6 ± 7.3
Gd-DTPA:			
SE 250/20, early scan	61.0 ± 14.4	21.8 ± 1.8	57.0 ± 14.6
SE 250/20, delayed scan	40.0 ± 6.6	20.4 ± 2.3	34.4 ± 6.3
Ferrite:			
SE 500/30	20.6 ± 2.4	19.8 ± 1.9	5.8 ± 1.9

Note.—Averaging two acquisitions, the scanning time was 1.6 min for the SE 250/20/2, 3.2 min for the SE 500/30/2, and 9.6 min for the SE 1500/60/2 pulse sequences. Statistical image noise (N_{stat}), due to microscopic (brownian) motion, is similar with a variety of pulse sequences and contrast agents. Systematic noise (N_{sys}) increases with increasing TR and TE and after administration of Gd-DTPA, and decreases after administration of ferrite. Total image noise (N_{tot}) consists of statistical and systematic noise.

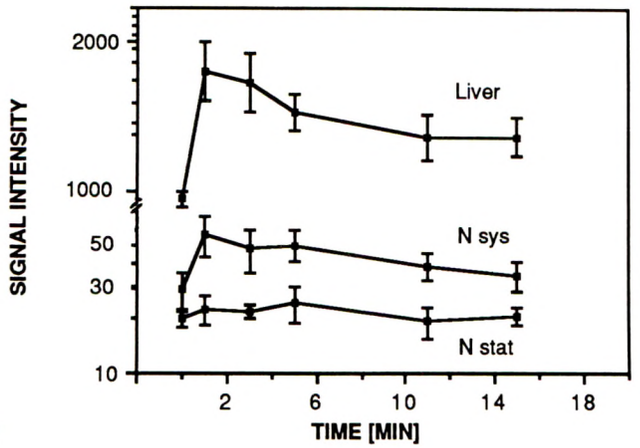

Fig. 2.—Effect of Gd-DTPA on image noise. Gd-DTPA produces an increase in liver signal intensity and systematic image noise (N sys). Statistical noise (N stat) does not change significantly.

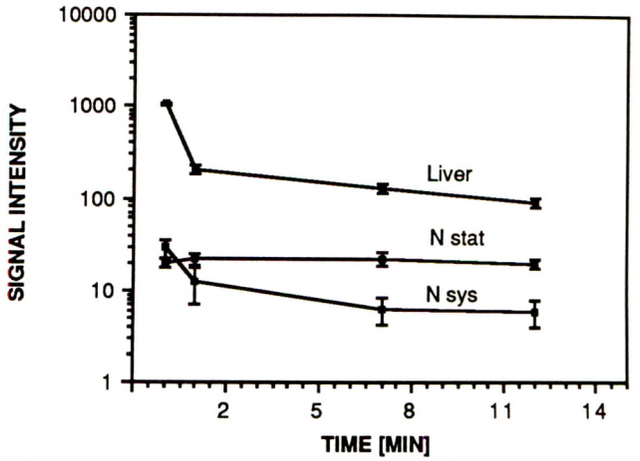

Fig. 3.—Effect of ferrite on image noise. Administration of ferrite decreases liver signal intensity and systematic noise (N sys). Statistical noise (N stat) does not change significantly.

greater; therefore, the C/N ratio increased after administration of Gd-DTPA.

Ferrite

Sequential scanning with the T1-weighted SE 250/20 pulse sequence showed that ferrite decreased hepatic signal intensity within 2 min, with little variation thereafter (Fig. 3). Tumor signal intensity did not change after administration of ferrite, and the maximum tumor-liver C/N ratio (+35.8 ± 5.9) was achieved 12 min after infusion of ferrite (Fig. 1, Table 1).

Image noise decreased after administration of ferrite. This decrease was due to a decrease in N_{sys} from 28.6 ± 6.9 to 5.8 ± 1.9; N_{stat} did not change (Table 2). N_{sys} was directly proportional to liver signal intensity ($r = 1.0$) and showed a parallel time dependence (Fig. 3). For example, 12 min after administration of ferrite, liver signal intensity decreased 91% and N_{sys} decreased 80%.

To determine the influence of pulse-sequence timing parameters on ferrite-enhanced tumor-liver C/N, we performed additional imaging studies within 60 min of drug administration. For equal scanning time, the SE 500/30 sequence permitted fewer acquisitions for averaging, and therefore N_{sys} was greater than for the SE 250/20 sequence (Table 2). However, tumor-liver contrast increased and, as a result, the C/N ratio was increased for the SE 500/30 sequence (Table 1). Further increases in TR and TE increased contrast; however, the gain was offset by increased ghost artifacts, resulting in a net decrease of C/N for the SE 1500/60 sequence.

Dual-Contrast Technique

Administration of ferrite particles 15 min after Gd-DTPA injection (Gd-Fe technique) resulted in a rapid and profound signal loss of liver signal intensity surrounding the tumor. With the SE 250/20 sequence, the tumor-liver C/N ratio further increased from +25.0 ± 9.7, the maximum value after administration of Gd-DTPA alone, to +54.9 ± 17.7 (Figs. 4 and 5). Administration of Gd-DTPA 12 min after ferrite injection (Fe-Gd technique) also resulted in an increase of the tumor-liver C/N ratio from +35.8 ± 5.9, the maximum value after administration of ferrite alone, to +53.4 ± 16.8 (SE 250/20) (Figs. 6 and 7). The difference between the maximum values of the C/N ratios for the Gd-Fe and Fe-Gd techniques was not statistically significant.

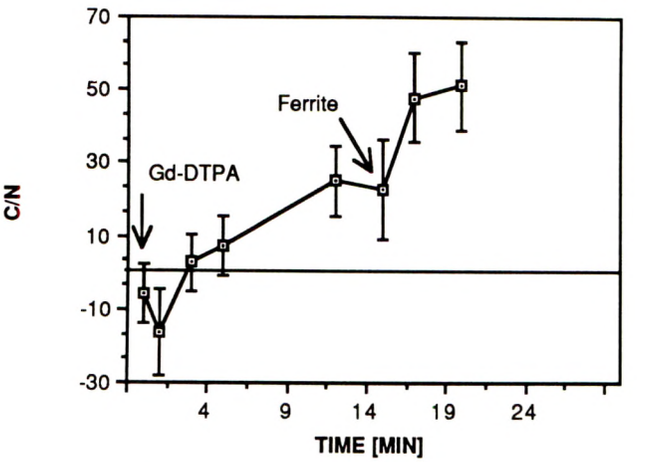

Fig. 4.—Gd-Fe dual-contrast technique (SE 250/20/2). Administration of ferrite after administration of Gd-DTPA causes a profound signal loss from hepatic tissue despite the presence of Gd-DTPA. Tumor signal intensity is increased by Gd-DTPA and unaffected by ferrite. As a result, tumor-liver contrast-to-noise ratio (C/N) increases to greater C/N values than with either contrast agent used alone.

To determine the influence of pulse-sequence timing parameters on the magnitude of tumor-liver C/N, we performed additional imaging studies (Table 1). The SE 500/30 sequence (C/N ratio = +67.8 ± 14.8) outperformed both the SE 250/20 (C/N ratio = +54.9 ± 17.7) and the SE 1500/60 (C/N ratio = +41.6 ± 14.6) sequences for dual-contrast MR imaging.

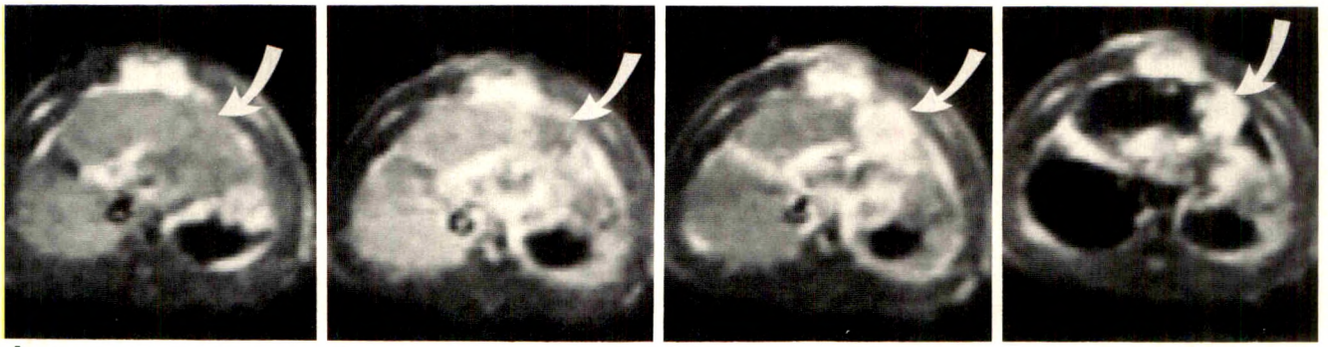

Fig. 5.—Gd-Fe dual-contrast technique (SE 250/20/2).
***A*, Precontrast image. *Arrow* shows tumor.**
***B*, Immediately after injection of Gd-DTPA, liver signal intensity increases, whereas that of tumor (*arrow*) is unaffected.**
***C*, Delayed image shows hyperintense tumor (*arrow*).**
***D*, After ferrite is administered, there is profound signal loss from hepatic tissue despite presence of gadolinium in liver. Tumor-liver contrast-to-noise ratio increases maximally, resulting in tumor signal (*arrow*) that is very hyperintense in contrast to surrounding hypointense liver.**

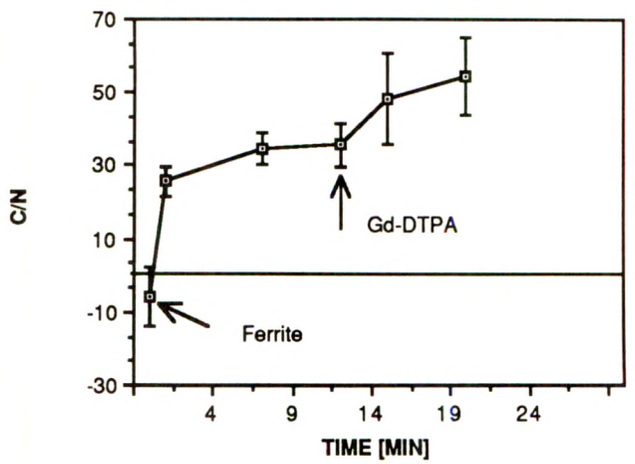

Fig. 6.—Fe-Gd dual-contrast technique (SE 250/20/2). Ferrite enhances tumor-liver contrast-to-noise ratio (C/N) by depleting signal from only normal hepatic tissue. If gadolinium is then administered also, tumor-liver C/N is further enhanced owing to increase in signal intensity of tumor.

The C/N ratio was lower on the SE 250/20 sequence owing to loss of T2-dependent contrast. The SE 1500/60 sequence was more sensitive to noise from ghost artifacts, resulting in a net decrease of C/N. The three additional animals imaged with the dual-contrast technique at a field strength of 1.4 T showed enhancement patterns and mean C/N values that were similar to those observed at 0.6 T (Fig. 7).

Discussion

Native T1 and T2 contrast between tumor and liver limits the image C/N ratio achievable by pulse-sequence manipulation, and therefore some lesions may not be detected by MR imaging [20]. Contrast agents alter the relaxation times of liver and/or tumor and potentially increase image C/N, increasing lesion conspicuity and diagnostic accuracy. Unfortunately, existing contrast agents place constraints on imaging time and pulse sequence selection, and they may even adversely affect achievable C/N ratios [8].

Gd-DTPA is rapidly distributed to liver tissue and is initially excluded by some (hypovascular) tumors, thereby increasing tumor-liver C/N ratios. Unfortunately, this biodistribution is time-dependent and reverses within 5 min owing to washout of Gd-DTPA from normal liver and retention in tumor. Hypervascular tumors can enhance to the same degree as or more than normal liver and be obscured during the initial phase. Therefore, T1-decreasing perfusion agents require rapid scanning and achieve variable results. Our data indicate that gains in signal intensity and contrast are partially offset by increased noise artifacts.

Ferrite is an RES-specific intracellular superparamagnetic contrast agent with a biodistribution similar to that of sulfur colloid used in scintigraphy and ethiodol oil emulsion (EOE-13) experimentally used in CT [21]. Particles are selectively phagocytosed by hepatic Kupffer cells, decreasing signal intensity of normal liver but not tumor. After administration of ferrite, pharmacokinetics are monotonic and stable. Widely available mildly "T1-weighted" pulse sequences such as SE 500/30 have sufficient T2 contrast dependence to create a T2-weighted ferrite-enhanced image, and can be signal averaged, resulting in high contrast and low image noise. The C/N ratio is further increased by eliminating the source of a significant fraction of N_{sys} (ghost noise), namely, the liver itself.

Liver imaging with coordinated administration of Gd-DTPA and ferrite exploits the pharmacokinetic advantages of both agents. Ten min after administration of both contrast agents, tumor signal intensity is increased by Gd-DTPA (predominant T1 shortening) and liver signal intensity is decreased by ferrite (predominant T2 shortening). Resultant C/N values are greater than with either contrast agent alone; as C/N has been shown to correlate with lesion detectability, it is expected that the dual-contrast technique will help improve diagnostic accuracy and decrease the threshold size for lesion detection.

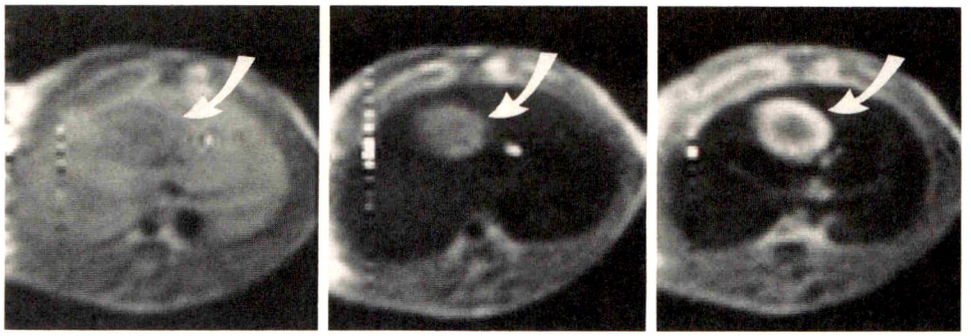

Fig. 7.—Fe-Gd dual-contrast technique (SE 250/20).

***A*, Precontrast image of 6- by 8-mm tumor (*arrow*).**

***B*, Ferrite decreases signal intensity from normal hepatic tissue; tumor signal (*arrow*) remains about the same.**

***C*, When gadolinium is administered also, signal intensity of tumor (*arrow*) increases.**

Toxicity is a major concern and must be balanced against the incremental diagnostic gain of any technique in clinical use. Gd-DTPA and ferrite each appear to be substantially less toxic than iodinated contrast agents, with the safety factor (ratio of LD_{50} to the effective dose) being used as a criterion for comparison [22, 23]. Gd-DTPA and ferrite have no known interaction in vitro or in vivo, and adverse reactions should not be increased by coordinated use of the drugs together. The simultaneous use of both contrast agents may, in fact, allow reduction in the total dose of contrast media, while improving diagnostic performance.

REFERENCES

1. Stark DD, Wittenberg J, Edelman R, et al. Detection of liver metastasis by MR: analysis of pulse sequence performance. *Radiology* **1986**;159: 365–370
2. Reinig JW, Dwyer AJ, Miller, et al. Liver metastasis detection: comparative sensitivities of MR imaging and CT scanning. *Radiology* **1987**;162:43–47
3. Stark DD, Wittenberg J, Butch RJ, Ferrucci JT. MR detection of hepatic metastases: a randomized, controlled comparison with CT. *Radiology* **1987**;165:399–406
4. Glazer GM, Aisen AM, Francis IR, Gyves JW, Lande I, Adler DD. Hepatic cavernous hemangioma: magnetic resonance imaging. *Radiology* **1985**;155:417–420
5. Itai T, Ohtomo K, Furui S, et al. MR imaging of hepatocellular carcinoma. *J Comput Assist Tomogr* **1986**;10:963–968
6. Butch RB, Stark DD, Malt R. Magnetic resonance imaging of hepatic focal nodular hyperplasia. *J Comput Assist Tomogr* **1986**;10:874–877
7. Stark DD, Felder R, Wittenberg J, et al. Magnetic resonance imaging of cavernous hemangioma of the liver: tissue-specific characterization. *AJR* **1985**;145:213–220
8. Saini S, Stark DD, Brady TJ, et al. Dynamic spin-echo MRI of liver cancer using gadolinium-DTPA. *AJR* **1986**;147:357–362
9. Saini S, Stark DD, Hahn PF, et al. Ferrite particles: a superparamagnetic MR contrast agent for enhanced detection of liver cancer. *Radiology* **1987**;162:217–222
10. Ohtomo K, Itai Y, Yoshikawa K, et al. Hepatic tumors: dynamic MR imaging. *Radiology* **1987**;163:27–31
11. Mano I, Yoshida H, Nakabayashi K, et al. Fast spin echo imaging with suspended respiration: gadolinium-enhanced MR imaging of liver tumors. *J Comput Assist Tomogr* **1987**;11:73–80
12. Weinmann JC, Brasch RC, Press WR, Wesby GE. Characterization of gadolinium-DTPA complex: a potential MR contrast agent. *AJR* **1984**;142:619–624
13. Wolf GL, Joseph PM, Goldstein EJ. Optimal pulse sequences for MR contrast agents. *AJR* **1986**;147:367–372
14. Greif WL, Bunton RB, Lauffer RB, et al. Pulse sequence optimization for MR imaging using a paramagnetic hepatobiliary contrast agent. *Radiology* **1985**;157:461–466
15. Mendoca-Diaz MH, Lauterbur P. Ferromagnetic particles as contrast agents for magnetic resonance imaging of the liver and spleen. *Mag Reson Med* **1986**;3:328–330
16. Saini S, Stark DD, Hahn PF, et al. Ferrite particles: a superparamagnetic MR contrast agent for the reticuloendothelial system. *Radiology* **1987**;162:211–216
17. Saini S, Stark DD, Wittenberg J, et al. A rat model of liver cancer for imaging research. *Invest Radiol* **1987**;22:149–152
18. Stark DD, Hendrick RE, Hahn PF, et al. Motion artifact reduction by fast spin echo imaging. *Radiology* **1987**;164:183–192
19. Henkelman RM, Hardy P, Poon PY, Bronskill MJ. Optimal pulse sequence for imaging hepatic metastases. *Radiology* **1986**;161:727–734
20. Tsang YM, Stark DD, Chen M, Weissleder R, Wittenberg J, Ferrucci JT. Ferrite enhanced MR detection of hepatic micrometastases: animal investigation. *Radiology* (in press)
21. Thomas JL, Bernardino ME, Vermess M, et al. EOE-13 in the detection of hepatosplenic lymphoma. *Radiology* **1982**;145:629–634
22. Bacon BR, Stark DD, Park CH, et al. Ferrite particles: a new MRI contrast agent. Lack of acute or chronic hepatotoxicity following intravenous administration. *J Lab Clin Med* **1987**;110:164–171
23. Bousquet JC, Saini S, Stark DD, et al. Gadolinium-DOTA: characterization of a new paramagnetic complex. *Radiology* (in press)

MR Relaxation Times and Iron Content of Thalassemic Spleens: An In Vitro Study

John M. Gomori[1]
Robert I. Grossman[2]
Henry R. Drott[3]

To determine the relationship between MR relaxation times and the iron content of the spleens in patients with thalassemia, we measured these parameters at 0.19 and 1.18 T in 19 thalassemic spleen specimens in vitro. The correlation was best between iron content and the dependence between the interecho interval and the 1/T2 (T2 relaxation rate) at 1.18 T($r = .9361$, $p < .001$). No statistically significant correlation was found between T1 and iron content at either field strength.

The variation of the 1/T2 with interecho interval may be useful for measuring iron content in vivo. It supports the theory that the T2 relaxation of iron deposits occurs via cellular field gradients produced by intralysosomal granules of hemosiderin.

Hemosiderin deposits are hypointense on spin-echo MR imaging at field strengths higher than 0.04 T [1–9]. This hypointensity originally was ascribed to a proton-electron dipole-dipole proton relaxation enhancement (PRE) caused by Fe^{3+} (ferric iron) in ferritin, hemosiderin, or other, less abundant, iron-containing moieties (1–4, 7]. However, in vivo and in vitro evidence indicates that a selective T2 PRE is a result of the dephasing of proton spins in water molecules that are diffusing through cellular field gradients caused by the intralysosomal granules of hemosiderin [6, 10].

This study was conducted to test the validity of this theory when clinical samples were imaged and to assess the potential of using spin-echo MR imaging for in vivo measurement of tissue concentrations of iron.

Materials and Methods

Splenic samples were obtained from 19 patients undergoing splenectomy for thalassemia minor or major, with or without other hematologic disorders such as sickle cell disease. The tissue samples were frozen immediately with liquid nitrogen and acetone and were stored on dry ice. They were thawed at room temperature before analysis. Iron content was measured by flame atomic absorption spectrophotometry of tissue lysates obtained by heating the samples with aqua regia (concentrated 1:1 solution of HCl and HNO_3). MR relaxation experiments were performed at room temperature at 0.19 and 1.18 T on a variable-field, pulsed spectroscopy unit (homemade unit built for Mildred Cohen at the University of Pennsylvania). T1s were obtained by determining the null point of the inversion recovery sequence. T2s were obtained by fitting an exponential decay rate to spin-echo trains by using interecho intervals ($2\tau_{cpmg}$) of 2 and 8 msec. Each T1 was measured twice and averaged, and each T2 was measured once. Statistical analysis was performed by using a standard commercial program (SPSS/PC+, Chicago, IL).

Results

Table 1 shows the results for the 19 samples. Excluded are the measurements for cases 13 and 18 at 0.19 T and $2\tau_{cpmg} = 8$ msec. At 0.19 T all the T2 relaxation times were the same for $2\tau_{cpmg} = 2$ and 8 msec, except for case 13 (115.5 and 99.9 msec) and case 18 (40.6 and 25.6 msec).

Received June 22, 1987; accepted after revision November 10, 1987.

[1] Department of Radiology, Hadassah University Hospital, Jerusalem, Israel 91120.

[2] Department of Radiology, Hospital of the University of Pennsylvania, 3400 Spruce St., Philadelphia, PA 19104. Address reprint requests to R. I. Grossman.

[3] Department of Clinical Chemistry, Children's Hospital of Philadelphia, Philadelphia, PA 19104.

AJR 150:567–569, March 1988
0361–803X/88/1503-0567
© American Roentgen Ray Society

TABLE 1: Relaxation Times and Iron Content of Thalassemic Spleen Samples

Spleen Sample	T1 (msec)		T2 (msec)			Iron Content (mg/g)
	0.19 T	1.18 T	0.19 T[a]	1.18 T[b]	1.18 T[c]	
1	230	554	80.6	60.5	53.9	0.130
2	216	497	80.9	3.9	53.8	0.220
3	120	187	36.1	23.1	13.9	3.886
4	75	202	33.8	16.1	9.9	9.491
5	130	259	39.0	19.9	13.4	4.437
6	68	158	28.8	14.1	10.2	2.950
7	130	302	41.6	18.8	12.6	2.432
8	151	295	75.2	12.3	10.4	1.937
9	72	245	53.4	22.4	17.9	1.511
10	180	418	88.0	53.2	49.3	0.432
11	158	353	52.7	31.6	24.7	1.380
12	151	274	46.7	27.1	17.5	2.429
13	216	504	115.5	70.5	70.5	0.101
14	180	425	61.0	20.7	16.5	1.726
15	107	137	78.1	57.3	50.0	0.554
16	216	307	25.4	9.0	6.0	10.629
17	230	439	50.2	29.9	22.2	1.088
18	101	202	40.6	17.8	11.5	4.256
19	194	439	56.2	32.8	25.6	1.486

Note.—The T2 at 0.19 T was the same for both interecho intervals.
[a] Interecho intervals = 2 and 8 msec.
[b] Interecho interval = 2 msec.
[c] Interecho interval = 8 msec.

TABLE 2: Correlation of Relaxation Times and Rates with Iron Content of Thalassemic Spleen Samples

Relaxation Time/Rate	Field Strength (T)	Interecho Interval (msec)	Correlation Coefficient
T1	0.19	NA	−.2759
T1	1.18	NA	−.4654
T2	0.19	2 and 8	−.7005[a]
T2	1.18	2	−.6458[b]
T2	1.18	8	−.6343[b]
1/T1	0.19	NA	.2953
1/T1	1.18	NA	.3034
1/T2	0.19	2 and 8	.8317[a]
(A)	1.18	2	.7799[a]
(B)	1.18	8	.8663[a]
(A) − (B)	NA	NA	.9361[a]

Note.—NA = not applicable. (A) and (B) = the T2 relaxation rates (1/T2) at 1.18 T with interecho intervals of 2 and 8 msec, respectively. Their difference is (A) − (B).
[a] $p < .001$, by one-tailed significance test.
[b] $p < .01$, by one-tailed significance test.

Table 2 shows the correlations of the relaxation times and rates with iron content. Multiple regression analysis for the relaxation times and rates with iron content yielded maximal correlation for the difference in T2 relaxation rates (1/T2) at 1.18 T between interecho intervals of 2 and 8 msec. When this difference was used as a single variable, it had a correlation coefficient of r = .9361 ($p < .001$) with iron content.

Discussion

Both ferritin and hemosiderin have about 2000 Fe^{3+} ions per molecule and each ion has five unpaired electrons (i.e., each molecule has about 10,000 unpaired electrons). Because ferritin and hemosiderin are superparamagnetic, all the electrons of each particle (domain) are parallel to each other. However, their common direction fluctuates extremely rapidly, and only the average magnetization is observed. Thus, each ferritin or hemosiderin macromolecule has its own superparamagnetic susceptibility (orders of magnitude larger than that of an equivalent solution of Fe^{3+}), resulting in very large field gradients near these macromolecules [10]. Diffusion or exchange of water across these field gradients results in a T2 PRE. However, it is insufficient to account for the T2 PRE observed in hemosiderotic deposits [7, 10]. Coarser cellular field gradients, caused by the lysosomal distribution of hemosiderin, account for most of the T2 PRE observed on clinical MR imaging [10]. Both these T2 PREs increase as the square of the magnetic field strength for spin-echo sequences, but only the T2 PRE that is due to the lysosomal distribution of hemosiderin increases with increasing interecho intervals greater than 2 msec [10].

The lack of significant correlation of the T1s and the 1/T1s with iron content of the spleen confirms the absence of significant proton-electron dipole-dipole PRE in hemosiderotic deposits. Therefore, the correlation of iron content with the T2s, and even more so with the 1/T2s, is consistent with a selective T2 PRE that is due to dephasing by diffusion across field gradients. The existence of a significant difference in 1/T2s measured with interecho intervals of 2 and 8 msec at 1.18 T confirms the dominance of field gradients of cellular, rather than intermacromolecular, dimensions [10]. This difference was correlated most significantly with iron content because only the 1/T2 due to field gradients that are on the order of gradients of cellular dimension will vary with $2\tau_{cpmg}$ in this time range (i.e., all other contributions to the tissue 1/T2 are canceled by the subtraction). The lack of a significant difference in 1/T2s at 0.19 T measured with interecho intervals of 2 and 8 msec is consistent with the quadratic behavior with field strength for this difference. The interecho intervals used in clinical MR imaging are longer than 8 msec, and the system noise is different than in our spectrometer. Therefore, the optimal pulse sequence and field strength for clinical measurement of iron content only can be suggested by these results. The lower the concentration of iron is, the higher the optimal field strength and the bigger the difference in $2\tau_{cpmg}$ should be.

Gradient-echo imaging [11] is sensitive to T2* (the time it takes the free induction signal to decay to 37% of its initial value). Although these images are noisier, they are more sensitive to field inhomogeneities than spin-echo images are. They may be useful for measuring iron concentration at low field strengths or for measuring extremely low iron concentrations at higher field strengths. Another method for measuring iron content by MR is by measurement of magnetic susceptibility. A recent report [12] indicated that this method may be inferior to T2 assessment on spin-echo MR. The same techniques that are sensitive to tissue deposits of iron should be equally sensitive to the particulate iron found in contrast agents for the reticuloendothelial system [10, 13–16].

The dependence of 1/T2 on $2\tau_{cpmg}$ at higher field strength and its correlation with iron content confirms the importance of the heterogeneous distribution of hemosiderin (intralysosomal) to the MR appearance of iron deposits and suggests a method that can be used to measure iron content in vivo.

ACKNOWLEDGMENTS

The authors are grateful to Eli Schwartz for the thalassemic spleen samples.

REFERENCES

1. Stark DD, Bass NM, Moss AA, et al. Nuclear magnetic resonance imaging of experimentally induced liver disease. *Radiology* **1983**;148:743–751
2. Runge VM, Clanton JA, Smith FW, et al. Nuclear magnetic resonance of iron and copper disease states. *AJR* **1983**;141:943–948
3. Leung A W-L, Steiner RE, Young IR. NMR imaging of the liver in two cases of iron overload. *J Comput Assist Tomogr* **1984**;8:446–449
4. Brasch RC, Wesbey GE, Gooding CA, Koerper MA. Magnetic resonance imaging of transfusional hemosiderosis complicating thalassemia major. *Radiology* **1984**;150:767–771
5. Gomori JM, Grossman RI, Bilaniuk LT, Zimmerman RA, Goldberg HI. High-field MR imaging of superficial siderosis of the central nervous system. *J Comput Assist Tomogr* **1985**;9:972–975
6. Gomori JM, Grossman RI, Goldberg HI, Zimmerman RA, Bilaniuk LT. Intracranial hematomas: imaging by high-field MR. *Radiology* **1985**: 157:87–93
7. Stark DD, Moseley ME, Bacon BR, et al. Magnetic resonance imaging and spectroscopy of hepatic iron overload. *Radiology* **1985**:154:137–142
8. Gomori JM, Grossman RI, Goldberg HI, Hackney DP, Zimmerman RA, Bilaniuk LT. High field MR of occult cerebral vascular malformations. *Radiology* **1986**;158:707–713
9. Drayer B, Burger P, Darwin R, Riederer S, Herfkens R, Johnson GA. Magnetic resonance imaging of brain iron. *AJNR* **1986**;7:373–380
10. Gomori JM, Grossman RI. Variable-field NMR spectroscopy of ferritin and other paramagnetic compounds: a comparative study and analysis of relaxation enhancement mechanisms relevant to hemosiderotic deposits (abstr). *Proc annual meeting Soc Mag Reson Med*, Montreal, August **1986**:61–62
11. Edelman RR, Johnson K, Buxton R, et al. MR of hemorrhage: a new approach. *AJNR* **1986**;7:751–756
12. Bachus R, Margosian P, Schalk KP, Kaltwasser JP. Clinical tests of magnetic susceptibility imaging (abstr). *Radiology* **1986**;161(P):72
13. Wolf GL, Burrett KR, Goldstein EJ, Joseph PM. Contrast agents for magnetic resonance imaging. In: Kressel H, ed. *Magnetic resonance annual*. New York: Raven, **1985:**231–265
14. Renshaw PF, Owen CS, McLaughlin AC, Frey TG, Leigh JS. Ferromagnetic contrast agents: a new approach. *Mag Reson Med* **1986**;3:217–225
15. Saini S, Stark DD, Hahn PF, Wittenberg J, Brady TJ, Ferrucci JT. Ferrite particles: a superparamagnetic MR contrast agent for the reticuloendothelial system. *Radiology* **1987**;162:211–216
16. Widder DJ, Greif WL, Widder KJ, Edelman RR, Brady TJ. Magnetite albumin microspheres: a new MR contrast material. *AJR* **1987**;148: 399–404

Categorical Course in Breast Imaging

American Roentgen Ray Society 88th Annual Meeting

• ***May 8–12, 1988, San Francisco Hilton and Tower, San Francisco, CA***

Program Chairman: *Stephen A. Feig*, *Philadelphia*, *PA*; (215) 928-7253

Sunday, May 8	
9:00–9:10 a.m.	Welcome from the President (*Gagliardi*)
9:10–9:15 a.m.	Introduction (*Feig*)
9:15–10:00 a.m.	Xeromammography: principles, equipment, technique, quality control (*Sickles*)
10:30–11:30 a.m.	Screen-film mammography: principles, equipment, technique, quality control (*Feig*)
11:30 a.m.–Noon	American College of Radiology Mammography Accreditation Program (*McLelland*)
Break	
1:30–2:15 p.m.	Breast masses: differential diagnosis (*Adler*)
2:15–3:00 p.m.	Breast calcifications: differential diagnosis (*Rebner*)
Break	
3:30–4:10 p.m.	Mammography of the treated breast (*Paulus*)
4:10–4:50 p.m.	Practical solutions to common mammographic problems (*Sickles*)
4:50–5:30 p.m.	Prebiopsy localization of nonpalpable breast lesions (*Kopans*)
Monday, May 9	
1:30–2:10 p.m.	Mammographic-pathologic correlation (*Troupin*)
2:10–2:50 p.m.	Breast ultrasound: equipment, technique, interpretation, accuracy (*Bassett*)
2:50–3:30 p.m.	Fine needle aspiration biopsy, ductography, pneumocystography (*Logan*)
Break	
4:00–4:45 p.m.	Panel: Diagnostic problem cases (Moderator: *Feig*; members: *Bassett*, *Kopans*, *Rebner*, *Troupin*)
4:45–5:30 p.m.	Panel: Subtle signs of carcinoma (Moderator: *Feig*; members: *Adler*, *Logan*, *McLelland*, *Moskowitz*, *Sickles*)
Tuesday, May 10	
4:00–4:45 p.m.	Issues in breast cancer screening (*Moskowitz*)
4:45–5:15 p.m.	How to establish a low-cost community screening program (*McLelland*)
5:15–5:30 p.m.	Discussion
Wednesday, May 11	
4:00–4:30 p.m.	Wording the mammography report (*Feig*)
4:30–5:15 p.m.	Medicolegal aspects of mammography (*Brenner*)
5:15–5:30 p.m.	Discussion
Thursday, May 12	
4:00–4:30 p.m.	Transillumination lightscanning (*D'Orsi*)
4:30–5:00 p.m.	Breast MR (*Alcorn*)
5:00–5:30 p.m.	Digital mammography (*Merritt*)
5:30–5:35 p.m.	Concluding remarks (*Feig*)

Gallbladder Disease in Patients with Primary Sclerosing Cholangitis

David J. Brandt[1]
Robert L. MacCarty[1]
J. William Charboneau[1]
Nicholas F. LaRusso[2]
Russell H. Wiesner[2]
Jurgen Ludwig[3]

We evaluated the gallbladders of 121 patients who had well-documented primary sclerosing cholangitis. Sonograms, cholangiograms, and CT scans were reviewed, and the findings were correlated with surgical or autopsy findings, when available. Pathologic examination of the gallbladder was available in 55 (45%) of the 121 patients; of these, 49 (89%) had abnormal gallbladders. Ninety-three of the 121 patients had one or more radiologic examinations of the gallbladder: 77 had sonograms, 80 had cholangiograms, and 18 had CT scans. Seventy-five (62%) of the 121 patients had abnormal gallbladders on histologic examination or had positive findings on one or more imaging study. By excluding 25 patients who had histologic changes of borderline significance and/or patients who had thick-walled gallbladders attributable to end-stage liver disease, we concluded that 50 (41%) of the 121 patients had intrinsic abnormalities of the gallbladder. Thirty-two (26%) had gallstones, 18 (15%) had probable primary sclerosing cholangitis involving the gallbladder, and five (4%) had benign or malignant neoplasms.

Our study indicates that gallbladder abnormalities are common among patients with primary sclerosing cholangitis, and sonography is the most useful technique for evaluating these conditions.

Primary sclerosing cholangitis is a chronic cholestatic syndrome of undetermined cause. It is characterized by diffuse fibrosing inflammation of the intrahepatic and extrahepatic bile ducts, resulting in bile duct obliteration, biliary cirrhosis, and hepatic failure [1–7]. Primary sclerosing cholangitis and ulcerative colitis are frequently associated [1, 7, 8]. The occurrence of gallbladder abnormalities in primary sclerosing cholangitis has been mentioned occasionally in the literature [1, 4, 5, 7, 9, 10], but to our knowledge, no systematic study of the gallbladder in a large population of patients with primary sclerosing cholangitis has been published to date.

The aims of our study were to determine (1) how often gallbladder abnormalities occur in patients with primary sclerosing cholangitis, (2) what pathologic changes occur in these patients, and (3) what radiologic findings are associated with gallbladder abnormalities.

Received September 8, 1987; accepted after revision November 9, 1987.

[1] Department of Diagnostic Radiology, Mayo Clinic and Mayo Foundation, Rochester, MN 55905. Address reprint requests to R. L. MacCarty.

[2] Division of Gastroenterology and Internal Medicine, Mayo Clinic and Mayo Foundation, Rochester, MN 55905.

[3] Section of Medical Pathology, Mayo Clinic and Mayo Foundation, Rochester, MN 55905.

AJR 150:571–574, March 1988
0361–803X/88/1503–0571
© American Roentgen Ray Society

Subjects and Methods

We reviewed the records of 121 consecutive patients with well-documented primary sclerosing cholangitis. There were 77 men (64%) and 44 women (36%) in our study group. The patients ranged in age from 21 to 70 years (mean, 43.3 years). Ninety-two patients (76%) had inflammatory bowel disease (almost all had ulcerative colitis). The diagnosis was based on clinical, biochemical, cholangiographic, and histologic criteria [1–3]. The results of sonograms, cholangiograms, and CT scans were correlated with those of other imaging techniques as well as with surgical or autopsy findings, when available. Pathologic confirmation was available in 55 patients.

We defined a thickened gallbladder wall on sonography as a wall thickness of 2 mm or more when the lumen was distended to at least 2 cm in transverse diameter. When histologic

confirmation was not available, gallbladder wall thickening that was asymmetric or that occurred in the absence of hypoalbuminemia, portal hypertension, or other known extrinsic causes was considered to be indicative of intrinsic gallbladder disease and to be due to primary sclerosing cholangitis.

Of the 121 patients, 93 underwent one or more radiologic investigations of the gallbladder: 77 had sonograms, 80 had cholangiograms, and 18 had CT scans.

Results

Pathologic Results

Gallbladder abnormalities were classified into four categories: gallstones, probable primary sclerosing cholangitis, neoplasms, and cholesterolosis. In some instances, gallbladders had features that allowed them to be classified into two or more categories.

Gallstones were found in 32 patients. In 16 of these, the gallstones were confirmed at surgery or autopsy; in eight of the 16, the stones were described as bilirubinate (black) stones. In this subgroup of patients in whom pathologic proof was available, two patients had positive sonograms and one had a positive cholangiogram. Sonograms showed stones in an additional 15 patients in whom there was no pathologic proof, and cholangiograms showed stones in six of these 15. In one case, gallstones were detected by cholangiography alone.

Thirty-nine gallbladders without stones were examined histologically. Eleven showed evidence of fibrosis and inflammation, consistent with primary sclerosing cholangitis involving the gallbladder, and 28 were normal or had changes that were of questionable pathologic significance. Malignant or benign (or both) neoplasms were found in five patients: three with adenocarcinoma, one with adenomyoma, and two with adenoma. Cholesterolosis was detected in three patients.

Imaging Results

Thirty-eight (49%) of 77 patients had abnormal results on sonography: 17 (22%) had stones, 20 (26%) had thick gallbladder walls without stones, and one had an adenoma.

Of the 20 patients with thick gallbladder walls but no stones, 14 had hypoalbuminemia (albumin <2.5 g/dl), portal venous hypertension (clinical evidence of esophageal varices or ascites), or both. Either hypoalbuminemia or portal venous hypertension can produce thickening of the gallbladder wall without intrinsic gallbladder disease. In remaining six patients with thick walls, there was no evidence of hypoalbuminemia, portal venous hypertension, or other causes for this finding; these patients were considered to have primary sclerosing cholangitis with involvement of the gallbladder (Fig. 1A).

Five patients had asymmetric wall thickening; in one of these, there was no evidence of hypoalbuminemia or portal venous hypertension. In the remaining four, there was a proved adenomyoma (Fig. 1B). Even though the remaining three patients had end-stage liver disease, the asymmetric distribution of the wall thickening was suggestive of intrinsic gallbladder disease, consistent with primary sclerosing cholangitis involvement (Fig. 1C). Overall, therefore, nine of these 20 patients had unexplained symmetric or asymmetric wall thickening attributable to primary sclerosing cholangitis (two had histologic confirmation).

Among the 80 patients who had not had previous cholecystectomies and whose cholangiograms were of sufficient quality to evaluate the gallbladder, abnormalities were present in 14%. Stones were seen in eight patients, gallbladder adenoma in one, and an extrinsic mass in one. Nonfilling of the gallbladder occurred in one case in which adenocarcinoma was later confirmed. In three instances, small stones seen on sonograms were missed at cholangiography. A limitation of cholangiography is its inability to evaluate the thickness of the gallbladder wall; in 16 cases in which cholangiograms were negative, wall thickening was seen on sonograms. Among the 16 CT examinations, gallbladder thickening was seen in three. In one patient, stones were found by sonography but were missed by CT.

Overall, in 75 (62%) of the 121 patients, gallbladder abnormalities were confirmed by histologic examination or by one or more imaging techniques. Excluding those patients with end-stage liver disease who had questionable acalculous cholecystitis on pathologic studies and/or symmetric gallbladder wall thickening on sonography, 50 (41%) had abnormal gallbladders. Twenty-six percent had gallstones, 15% had probable primary sclerosing cholangitis involving the gallbladder, and 4% had malignant or benign neoplasms of the gallbladder. (Percentages add to more than 41% because some patients had more than one abnormality.)

Discussion

No specific histologic changes in the gallbladder or on liver biopsy specimens are pathognomonic for primary sclerosing cholangitis, and the diagnosis is usually based on a combination of clinical, biochemical, histologic, and radiologic abnormalities. The term "primary sclerosing cholangitis" is applied, regardless of associated conditions such as ulcerative colitis, when congenital biliary tract disease and known causes of biliary sclerosis such as choledocholithiasis, previous surgical trauma, and malignancy can be ruled out [1–4].

Tobias et al. [7] found gallstones in three patients with primary sclerosing cholangitis. They pointed out that some authors consider the presence of gallstones to invalidate the diagnosis of primary sclerosing cholangitis because bile-duct changes may be caused by subsequent choledocholithiasis. However, they concluded that many cases of bona fide primary sclerosing cholangitis will be excluded if this criterion is applied indiscriminately. The incidental finding of gallstones does not exclude an otherwise firm diagnosis of primary sclerosing cholangitis.

The frequency of gallstones in our series (26%) was higher than expected for this group of predominantly young men, which strongly suggests that the gallstones are causally related to the primary sclerosing cholangitis. Several possible mechanisms may explain the increased occurrence of gallstones in primary sclerosing cholangitis [11]. The high frequency of pigment stones (eight of 16) in this series suggests

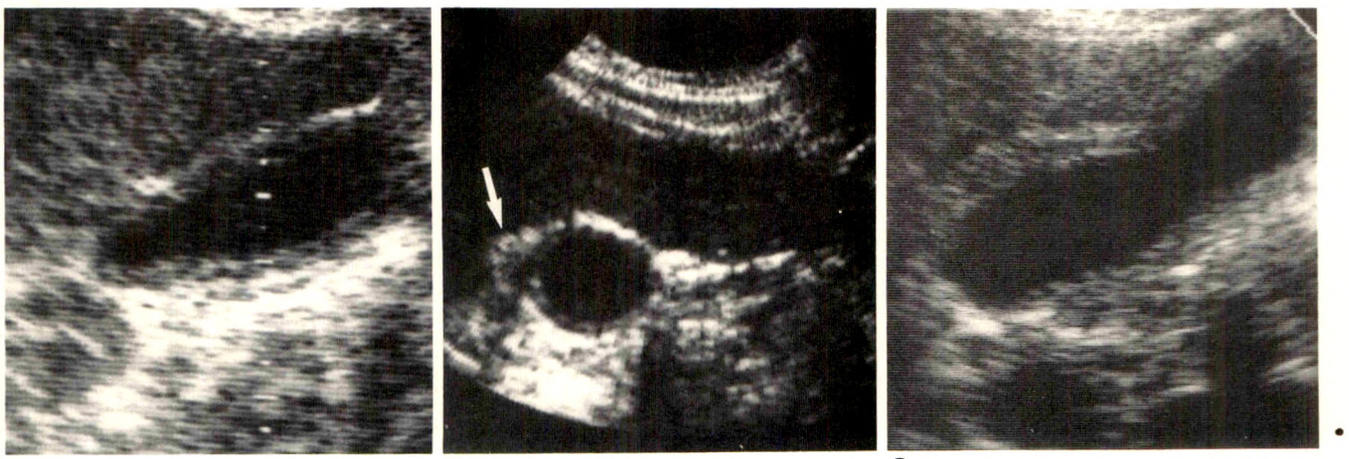

Fig. 1.—Sonograms in three patients with primary sclerosing cholangitis show gallbladder abnormalities.
***A*, Note symmetric thickening of gallbladder wall, thought to be due to primary sclerosing cholangitis. Patient had a normal serum albumin level, no evidence of cirrhosis on liver biopsy specimen, and no clinical evidence of portal venous hypertension.**
***B*, Focal asymmetric thickening of gallbladder wall is due to adenomyoma (*arrow*).**
***C*, Diffuse, pronounced, asymmetric thickening of gallbladder wall. Histologically, fibrous thickening and lymphocytic infiltrates were present and were attributed to primary sclerosing cholangitis involving the gallbladder.**

that the underlying duct disease and underlying cholestasis are etiologically important.

Previous authors have suggested that primary sclerosing cholangitis can directly involve the gallbladder itself [4, 5, 9, 10], and cholangiographic abnormalities of the cystic duct region also have been reported [4]. One study [5] described a patient in whom the gallbladder wall was greatly thickened, primarily because of the extension of fibrosis into the serosa.

In our series, a range of histologic features was seen with various patterns of inflammation, degree and location of fibrosis, smooth muscle hyperplasia, and other features, including those described by one study [5]. Pathognomonic histologic features were not seen. Hence, these cases were classified as probable rather than definite primary sclerosing cholangitis involving the gallbladder.

The significance of the sonographic appearance of gallbladder wall thickening has been a matter of long-standing controversy. Clearly, it is a nonspecific sign and can occur in many conditions [5, 12–14]. Primary sclerosing cholangitis may lead to end-stage liver disease, along with hypoalbuminemia or portal venous hypertension (or both). Therefore, when a thickened gallbladder wall without stones is seen in a patient with primary sclerosing cholangitis, the first hypothesis should be that it is probably due to end-stage liver disease. Generally, this thickening is diffuse and symmetric. However, when asymmetric thickening is observed, or when gallbladder wall thickening occurs in the absence of portal hypertension or hypoalbuminemia, the presence of primary intrinsic gallbladder disease, such as a mass or inflammatory process, should be presumed.

A precise estimate of the frequency of involvement of the gallbladder by primary sclerosing cholangitis is impossible to determine from our study. First, no pathognomonic histologic findings have been identified. Second, we eliminated from our series 20 gallbladders that had borderline histologic changes, some of which could have been due to early or minimal primary sclerosing cholangitis. Third, some of the gallbladders containing stones could have had underlying primary sclerosing cholangitis, which was masked by the chronic cholecystitis of cholelithiasis. Also, some of the inflammatory changes in the gallbladders without stones, which we attributed to primary sclerosing cholangitis, could have been caused by stones that had passed. However, given the significant involvement of the common duct by inflammation and stricture formation in most patients with primary sclerosing cholangitis, a significant number of patients probably would not pass gallstones successfully. Therefore, we consider our findings (15% of the patients in our series had primary sclerosing cholangitis involving the gallbladder) to be conservative.

Papillary adenomas of the gallbladder, considered to be rare lesions [15, 16], were found in two of our 121 patients with primary sclerosing cholangitis. Adenocarcinomas of the gallbladder are also uncommon malignant lesions, particularly in the absence of gallstones. Three of our patients had gallbladder carcinomas, and one of these had no concurrent cholelithiasis. A definite association between primary sclerosing cholangitis and cholangiocarcinoma has been shown [17, 18], and this may be analogous to the increased frequency of adenocarcinomas of the colon in patients with long-standing ulcerative colitis. Therefore, the occurrence rate of both benign and malignant neoplasms of the gallbladder is most likely greater in patients with primary sclerosing cholangitis than in the general population.

The sensitivity of sonography for detecting gallstones in patients with primary sclerosing cholangitis is much higher than that of either CT or cholangiography. Cholangiography does not evaluate abnormalities of the gallbladder wall as well as sonography does. In this series, sonograms were the most useful in evaluating all of the abnormalities found in the gallbladders of patients with primary sclerosing cholangitis.

REFERENCES

1. Wiesner RH, Ludwig J, LaRusso NF, MacCarty RL. Diagnosis and treatment of primary sclerosing cholangitis. *Semin Liver Dis* **1985**;5:241–253
2. Wiesner RH, LaRusso NF. Clinicopathologic features of the syndrome of primary sclerosing cholangitis. *Gastroenterology* **1980**;79:200–206
3. LaRusso NF, Wiesner RH, Ludwig J, MacCarty RL. Primary sclerosing cholangitis. *N Engl J Med* **1984**;310:899–903
4. MacCarty RL, LaRusso NF, Wiesner RH, Ludwig J. Primary sclerosing cholangitis: findings on cholangiography and pancreatography. *Radiology* **1983**;149:39–44
5. Case records of the Massachusetts General Hospital (Case 6-1982). *N Engl J Med* **1982**;306:349–358
6. Doyle TCA, Roberts-Thomson IC. Radiological features of sclerosing cholangitis. *Australas Radiol* **1983**;27:163–166
7. Tobias R, Wright JP, Kottler RE, et al. Primary sclerosing cholangitis associated with inflammatory bowel disease in Cape Town, 1975–1981. *S Afr Med J* **1983**;63:229–235
8. Rohrmann CA Jr, Ansel HJ, Freeny PC, et al. Cholangiographic abnormalities in patients with inflammatory bowel disease. *Radiology* **1978**;127:635–641
9. Rahn NH III, Koehler RE, Weyman PJ, Truss CD, Sagel SS, Stanley RJ. CT appearance of sclerosing cholangitis. *AJR* **1983**;141:549–552
10. Carroll BA, Oppenheimer DA. Sclerosing cholangitis: sonographic demonstration of bile duct wall thickening. *AJR* **1982**;139:1016–1018
11. LaRusso NF. Sclerosing cholangitis and gallstones. *Contemp Issues Gastroenterol* **1985**;4:231–236
12. Shlaer WJ, Leopold GR, Scheible FW. Sonography of the thickened gallbladder wall: a nonspecific finding. *AJR* **1981**;136:337–339
13. Tsujimoto F, Miyamoto Y, Tada S. Differentiation of benign from malignant ascites by sonographic evaluation of gallbladder wall. *Radiology* **1985**;157:503–504
14. Fiske CE, Laing FC, Brown TW. Ultrasonographic evidence of gallbladder wall thickening in association with hypoalbuminemia. *Radiology* **1980**;135:713–716
15. Berk RN, van der Vegt JH, Lichtenstein JE. The hyperplastic cholecystoses: cholesterolosis and adenomyomatosis. *Radiology* **1983**;146:593–601
16. Ochsner SF. Solitary polypoid lesions of the gallbladder. *Radiol Clin North Am* **1966**;4:501–510
17. MacCarty RL, LaRusso NF, May GR, et al. Cholangiocarcinoma complicating primary sclerosing cholangitis: cholangiographic appearances. *Radiology* **1985**;156:43–46
18. Wee A, Ludwig J, Coffey RJ Jr, LaRusso NF, Wiesner RH. Hepatobiliary carcinoma associated with primary sclerosing cholangitis and chronic ulcerative colitis. *Hum Pathol* **1985**;16:719–726

Case Report

The Effervescent Gallbladder: A Sonographic Sign of Emphysematous Cholecystitis

Albert A. Nemcek, Jr.,[1] Richard M. Gore, Robert L. Vogelzang, and Mysti Grant

Emphysematous cholecystitis is an uncommon form of acute inflammation of the gallbladder. In this disorder, gas typically accumulates within the gallbladder wall or lumen but occasionally may be found in the bile ducts or pericholecystic area [1]. The sonographic features of emphysematous cholecystitis have been well described: highly echogenic collections with shadowing and reverberation emanating from the gallbladder wall or lumen [2–7]. We report a case of emphysematous cholecystitis in which tiny echogenic foci (gas bubbles) were observed rising from the dependent portion of the gallbladder, reminiscent of rising champagne bubbles. This striking and previously undescribed appearance on real-time sonography led to the correct diagnosis.

Case Report

A 60-year-old man with a history of insulin-dependent diabetes mellitus presented with right upper quadrant pain, temperature of 100.8°F (38.2°C), and a 3-day history of decreased appetite. Palpation of the right upper quadrant revealed mild tenderness, which according to the patient, had diminished significantly since the onset of his symptoms. Laboratory tests showed elevation of the white count (24,000 cells/μl), aspartate serum transferase (34 IU/l), lactate dehydrogenase (238 IU/l), and alkaline phosphatase (161 IU/l). The total bilirubin was normal (0.7 mg/dl).

Sonography of the right upper quadrant disclosed multiple shadowing gallstones, thickening of the gallbladder wall, and slight distension of the gallbladder (Fig. 1A). Additionally, multiple tiny echogenic foci were noted within the gallbladder lumen. They arose from the dependent part of the gallbladder and were observed "floating" to the nondependent wall (Figs. 1A–1C). The effect was reminiscent of bubbles rising in a glass of champagne. Further changes in the patient's position revealed a small area of hyperreflectivity in the most nondependent part of the gallbladder; a shadow with multiple reverberations emanated from this area (Fig. 1D). Also, a short linear focus of increased echogenicity without recognizable shadowing was seen in the region of the gallbladder neck (Fig. 1D). Although vague right upper quadrant tenderness was present, no clear sonographic Murphy sign was noted.

On the basis of the sonographic examination, emphysematous cholecystitis was suspected. Plain films of the abdomen revealed a small amount of gas in the right upper quadrant that could not be localized with certainty to the gallbladder. Abdominal CT (Fig. 1E) showed a small collection of gas within the lumen of the gallbladder as well as within the wall of the gallbladder neck. Mural thickening of the gallbladder was again shown, as well as extensive pericholecystic soft-tissue edema and thickening of the wall of the adjacent duodenum.

At surgery, the gallbladder was found to be surrounded by purulent material and appeared extremely inflamed and edematous. Adjacent bowel was also edematous but otherwise normal, with no evidence of perforation or fistula formation. On gross examination, both the external and mucosal surfaces of the gallbladder were markedly hemorrhagic with focal areas of purulent material. The wall was 5 mm thick, except in one small portion where it measured only 1 mm. Multiple, predominantly pigment calculi were present within the gallbladder.

Cultures of the gallbladder obtained at surgery grew *Escherichia coli*. The patient was treated postoperatively with gentamicin and clindamycin. His recovery was uneventful, and he was discharged from the hospital on the ninth day after surgery.

Received August 11, 1987; accepted after revision October 19, 1987.

[1] All authors: Department of Radiology, Northwestern University Medical School, Chicago, IL 60611. Address reprint requests to A. A. Nemcek, Jr., Department of Radiology, Northwestern Memorial Hospital, 710 N. Fairbanks Ct., Chicago, IL 60611.

AJR 150:575–577, March 1988 0361–803X/88/1503-0575 © American Roentgen Ray Society

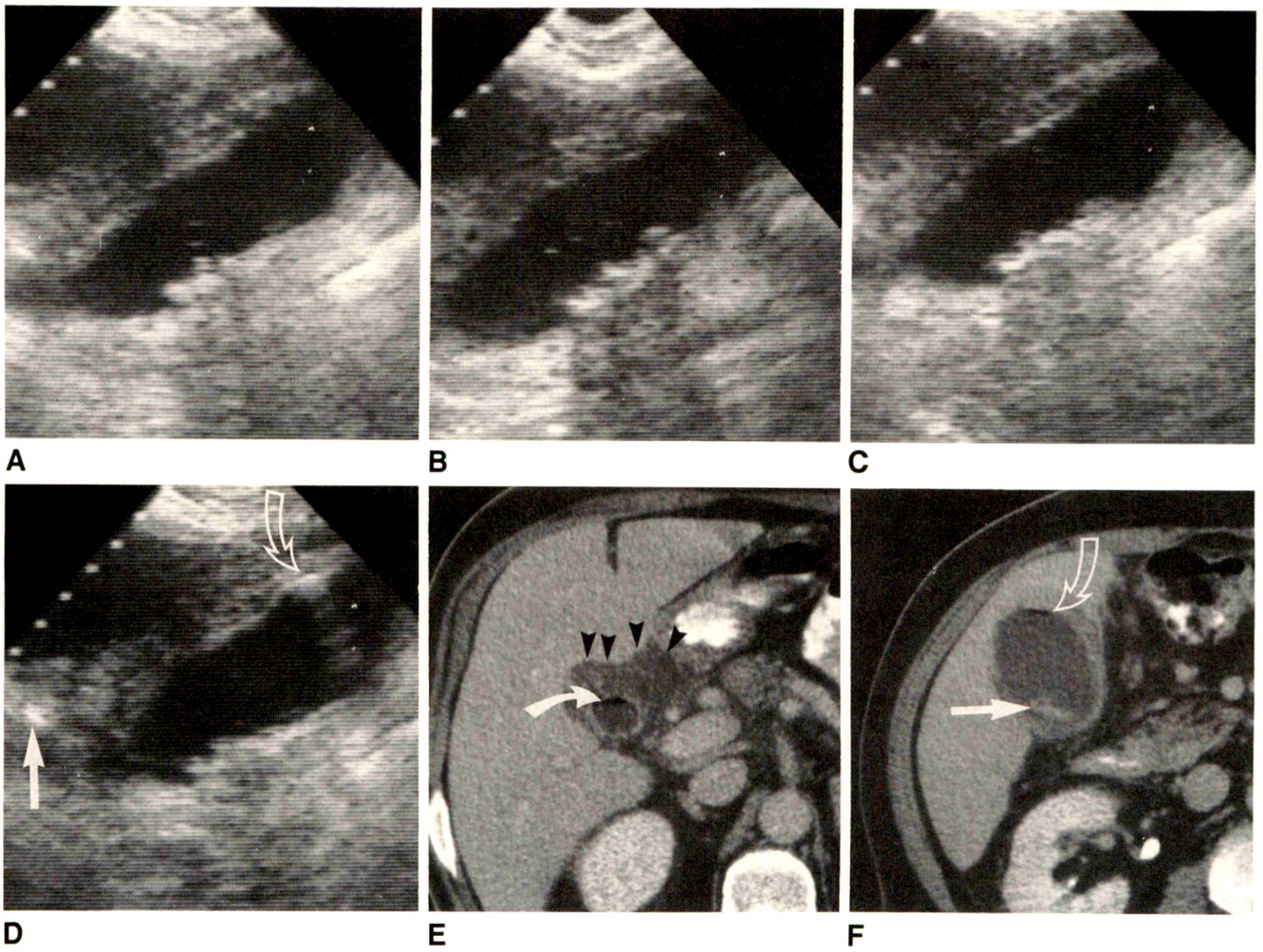

Fig. 1.—*A–C*, Sonograms of gallbladder all obtained in the span of a few minutes. Echogenic foci could be followed as they rose vertically. Shadowing gallstones are also seen.

D, Reverberation shadow arises from nondependent wall of the gallbladder (*open arrow*). Persistent hyperreflective focus is present in gallbladder neck region (*solid arrow*).

E, CT scan shows gas collections within gallbladder lumen and wall (*curved arrow*), and there is a soft-tissue density in pericholecystic area (*arrowheads*).

F, Dilated gallbladder with mural thickening, gas within gallbladder lumen (*open arrow*), and gallstones (*solid arrow*).

Discussion

Emphysematous cholecystitis is a distinct clinical entity; several major features distinguish it from acute cholecystitis [1]. Emphysematous cholecystitis occurs more commonly in men, whereas acute cholecystitis is more common in women. Diabetics appear particularly susceptible to emphysematous cholecystitis. The morbidity and mortality rates for emphysematous cholecystitis are much higher than those for acute cholecystitis, a difference that is especially pronounced in patients younger than 60 years. Despite the potentially more lethal nature of this disorder, patients with emphysematous cholecystitis often have deceptively mild clinical findings. A sonographic Murphy sign could not be elicited from our patient. For this reason, imaging studies play a critical role in the prompt identification of this serious disorder.

The diagnosis of emphysematous cholecystitis can be made sonographically by identifying gas within the wall or the lumen of the gallbladder that produces a highly echogenic collection corresponding to the shape and location of the gallbladder [2–6]. Typically, a shadow with multiple reverberations is seen trailing from the gas collection. The gas and its resultant echoes may shift in response to gravity as the patient changes position [6]. These sonographic findings should be confirmed by plain abdominal radiographs [5], because a large, heavily calcified gallstone or a porcelain gallbladder may produce similar sonographic findings. In our case, these features were present but subtle because of the

small amount of coalescent gas. Our search for these findings was prompted by the identification of tiny echogenic foci rising within the gallbladder lumen. Although there is no way to prove that the foci themselves represented gas bubbles seeping from the infected gallbladder wall, their appearance, behavior, and proved association with a gas collection within the gallbladder lumen allow no other reasonable explanation. As would be expected for tiny air bubbles, these foci were echogenic [7], showed no acoustic shadowing [8], and rose to the nondependent surface of the fluid-filled gallbladder lumen.

Because of the low prevalence of emphysematous cholecystitis, the frequency of the findings we have described has not been established. We hope that our report will spur other investigators to look for this finding in patients with suspected gallbladder disease.

REFERENCES

1. Mentzer RM Jr, Golden GT, Chandler JG, Horsley JS. A comparative appraisal of emphysematous cholecystitis. *Am J Surg* **1975**;29:10–15
2. Hunter ND, Macintosh PK. Acute emphysematous cholecystitis: an ultrasonic diagnosis. *AJR* **1980**;134:592–593
3. Kutchner R, Rosenblatt R, Weissman H. Sonographic appearance of emphysematous cholecystitis. *NY State J Med* **1981**;81:1192–1194
4. Blaquiere RM, Dewbury KC. The ultrasound diagnosis of emphysematous cholecystitis. *Br J Radiol* **1982**;55:114–116
5. Paruleker SG. Sonographic findings in acute emphysematous cholecystitis. *Radiology* **1982**;145:117–119
6. Bloom RA, Fisher A, Pode D, Asaf Y. Shifting intramural gas: a new ultrasound sign of emphysematous cholecystitis. *JCU* **1984**;12:40–42
7. Yeh HC, Wolf BS. Ultrasonic contrast study to identify stomach tap-water microbubbles. *JCU* **1977**;5:170–174
8. Conrad MR, Bregman R, Kilman WJ. Ultrasonic recognition of parenchymal gas. *AJR* **1979**;132:395–399

Case Report

Choledochal Varices

Seukky Kim[1] and Felix S. Chew

To our knowledge, only four cases of choledochal varices with cholangiographic demonstration have been reported in the English-language literature [1–3]. We present two additional anatomically proved cases. Each has unique and potentially confusing radiographic findings.

Case Reports

Case 1

A 77-year-old white man with alcoholic hepatic cirrhosis was admitted with jaundice and weight loss of recent onset. Physical examination revealed stigmata of alcoholic cirrhosis. The hematocrit was 32.0%, alkaline phosphatase was 566 IU/1, total bilirubin was 7.0 mg/dl, and SGOT was 256 IU/l. Multiple space-occupying masses in the liver were shown by sonography and liver-spleen scintigraphy; hepatocellular carcinoma and advanced cirrhosis were found on biopsy. Percutaneous transhepatic cholangiography showed a nodular intraluminal filling defect at the proximal common hepatic duct (Fig. 1A). An oblique view revealed this to be an elongated intraluminal defect extending the entire length of the common hepatic duct (Fig. 1B). This defect was thought to represent intraluminal metastases from the liver. Two nodular extrinsic defects were also noted at the midportion of the common duct (Figs. 1A and 1B); these were thought to be metastatic lymphadenopathy along the bile duct. The patient became progressively worse and died. An autopsy confirmed the presence of extensive hepatocellular carcinoma and advanced cirrhosis, but no extrahepatic metastases were found. Massive collateral veins at the porta hepatis were present and were found to be compressing the common bile duct (Fig. 1C).

Case 2

A 37-year-old white woman with congenital hepatic fibrosis and portacaval shunt at the age of 18 years was admitted with acute right upper quadrant pain, fever, and chills. Antibiotic therapy for what was assumed to be acute cholecystitis resulted in rapid clinical improvement. Angiography showed occlusion of the portacaval shunt and massive collateral veins at the porta hepatis. During surgery for mesocaval shunt and cholecystectomy, subacute cholecystitis and massive varices along the common bile duct were found. There were many fine, tortuous veins along the surface of the common bile duct. A cholangiogram obtained during surgery showed spiral extrinsic defects along the common duct at the cystic duct level due to large encircling varices (Fig. 2A). The wall of the common bile duct and part of the common hepatic duct showed a fine irregularity resulting from varices of the choledochal venous plexus. The surgical findings are illustrated in Figure 2B.

Discussion

Extrahepatic obstruction of the portal vein with resulting portal hypertension may cause extensive collateral venous circulation at the porta hepatis. These collateral veins may compress and narrow the common bile duct, sometimes causing obstructive jaundice [4, 5]. There are two venous systems along the extrahepatic bile ducts, the paracholedochal veins of Petren [6] (Fig. 3A) and the epicholedochal venous plexus of Saint [7] (Fig. 3B). The paracholedochal veins course parallel to the common duct and are connected

Received August 31, 1987; accepted after revision October 26, 1987.

[1] Both authors: Department of Radiology, State University of New York, Health Science Center at Syracuse, 750 E. Adams St., Syracuse, NY 13210. Address reprint requests to S. Kim.

AJR 150:578–580, March 1988 0361–803X/88/1503–0578 © American Roentgen Ray Society

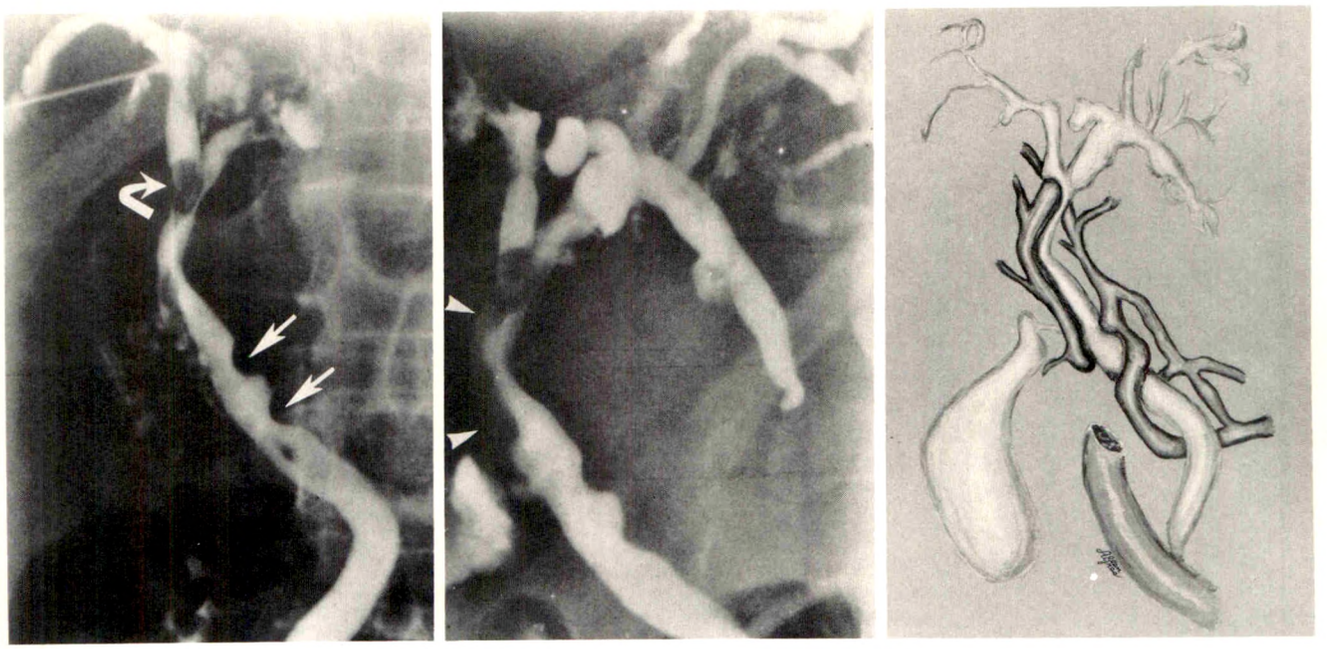

Fig. 1.—Case 1: Varices of paracholedochal veins.
A, Percutaneous transhepatic cholangiogram shows intraluminal nodular defect at proximal common hepatic duct (*curved arrow*) and two nodular extrinsic defects at middle of common duct (*straight arrows*).
B, Oblique projection shows intraluminal nodular defect extending distally along lateral aspect of common hepatic duct (*arrowheads*).
C, Artist's rendering of autopsy findings shows paracholedochal veins indenting common duct. A long varix protrudes into common hepatic duct, causing an intramural filling defect.

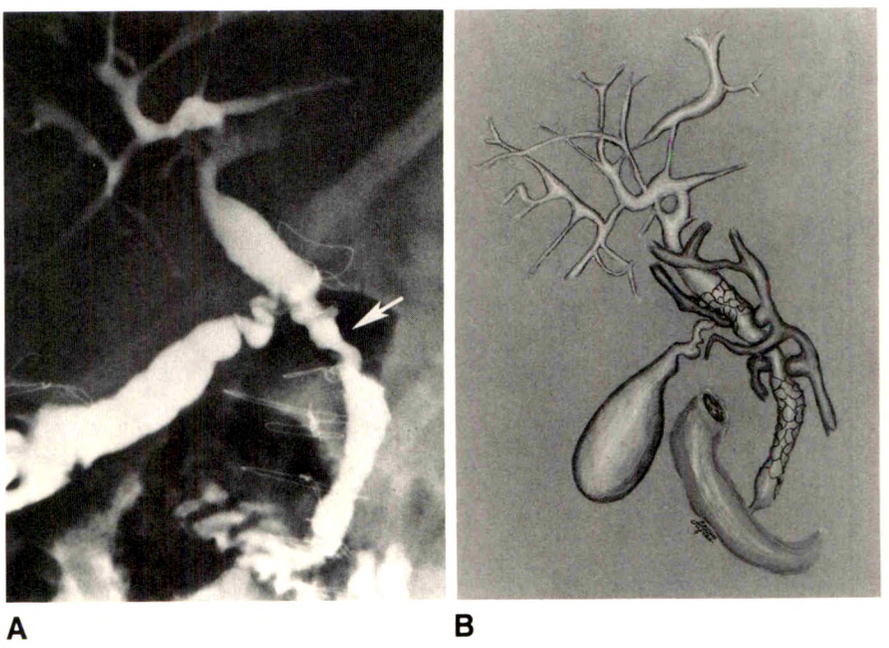

Fig. 2.—Case 2: Varices of paracholedochal veins and of epicholedochal venous plexus.
A, Cholangiogram obtained during surgery shows spiral extrinsic filling defect of common bile duct with slight narrowing (*arrow*). Walls of common duct are finely irregular. Hepatic biliary radicals are deformed.
B, Artist's rendering of surgical findings shows paracholedochal varices encircling common duct and extensive varices of epicholedochal venous plexus.

to the gastric vein, the pancreaticoduodenal vein, the portal vein, and to the liver directly [6]. The paracholedochal veins are separate structures from the bile ducts, and their varices cause extrinsic impressions (Figs. 1 and 2). The appearance is similar to that of the more familiar ureteral notching resulting from paraureteral collaterals that is sometimes seen on IV urograms. The epicholedochal venous plexus is a fine reticular mural structure in intimate contact with the outer surface of

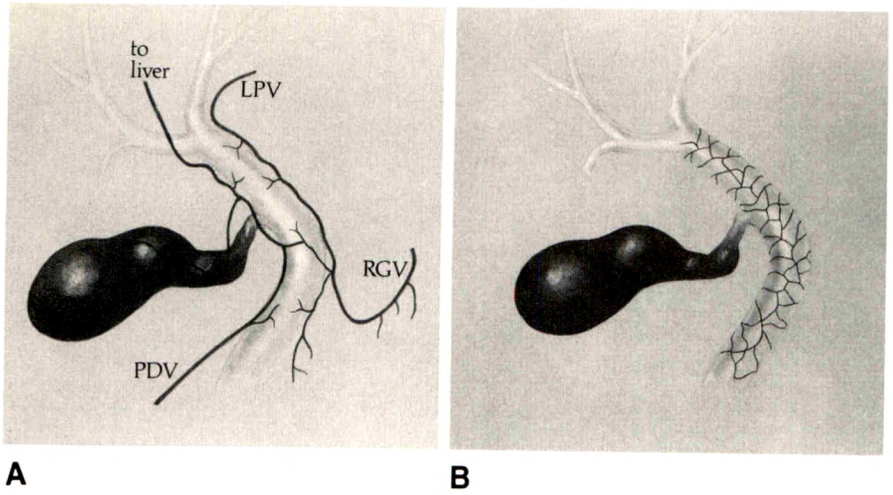

Fig. 3.—Normal anatomy of choledochal veins.

***A*, Paracholedochal venous plexus of Petren. Veins course parallel to common duct, communicating with each other and eventually draining to larger veins. LPV = left portal vein, PDV = pancreaticoduodenal vein, RGV = right gastric vein.**

***B*, Epicholedochal venous plexus of Saint. A fine reticular venous plexus covers outer surface of common hepatic and common bile ducts.**

the common duct (Fig. 3B). Saint [7] observed the plexus at surgery and confirmed its structure and anatomy with injection studies of cadaver specimens. The veins of the plexus vary in size, but normally are no larger than 1 mm. Varices of the plexus alter the normally smooth intraluminal surface of the common duct and produce fine, irregular mural changes (Fig. 2).

The cholangiographic demonstration of choledochal varices was first described by Williams et al. [1] in 1982; since then, three additional cases have been reported [2, 3], two with anatomic correlation. The apparent intraluminal filling defect along the common hepatic duct in the first case presented (Fig. 1) has not been described previously. The thinness and pliability of the bile duct wall may have allowed protrusion of the varicose paracholedochal vein into the lumen, resulting in an appearance resembling that of esophageal varices. Recognition of this unique manifestation of choledochal varices as well as the more usual smooth extrinsic nodular, spiral, or stenotic impressions will prevent errors in diagnosis. Forewarning the clinician of their presence may prevent surgical accident as a varicose vessel may be mistaken for the common duct [2, 3]. Differential diagnostic considerations include metastases, cholangiocarcinoma, lymphoma, a submucosal lesion such as one of the rare intramural benign tumors of mesenchymal origin, lymph nodes, crossing vessels, adherent stones, or parasites [2, 3]. One of the two cases of choledochal varices described in Spira et al. [3] probably included varices of the epicholedochal venous plexus. These have not been described without accompanying varices of the paracholedochal veins, and Saint's anatomic studies [6] suggest that dilatation of the paracholedochal veins will occur first in portal hypertension. Although the mural irregularity that results from varices of the epicholedochal venous plexus may mimic cholangitis, in the clinical setting of long-standing portal hypertension and in the presence of paracholedochal varices, diagnostic confusion should not occur.

REFERENCES

1. Williams SM, Burnett DA, Mazer MJ. Radiographic demonstration of common bile duct varices. *Gastrointest Radiol* **1982**;7:69–70
2. Dan SJ, Train JS, Cohen BA, Mitty MA. Common bile duct varices: cholangiographic demonstration of a hazardous portosystemic communication. *Am J Gastroenterol* **1983**;78:42–43
3. Spira R, Widrich WC, Keush KD, Jackson BT, Katzman HE, Coello AA. Bile duct varices. *Arch Surg* **1985**;120:1194–1196
4. Hunt AH. Compression of the common bile-duct by an enlarging collateral vein in a case of portal hypertension. *Br J Surg* **1965**;52:636–637
5. Meredith HC, Vujic I, Schabel SI, O'Brien PH. Obstructive jaundice caused by cavernous transformation of the portal vein. *Br J Radiol* **1978**;51:1011–1012
6. Saint JA. The epicholedochal venous plexus and its importance as a means of identifying the common duct during operations on the extrahepatic biliary tract. *Br J Surg* **1961**;48:489–498
7. Petren T. Die extrahepatischen Gallenwegsvenen und ihre pathologisch-anatomische Bedeutung [The veins of the extrahepatic biliary system and their pathologic-anatomic significance]. *Verh Anat Ges* **1932**;41:139–143

Case Report

Small Bowel Obstruction Due to Garren Gastric Bubble: Radiographic Diagnosis

Robert K. Zeman,[1] Stanley B. Benjamin,[2] Michael B. Cunningham,[1] Russell J. Nauta,[3] David F. Fleischer,[2] James H. Lewis,[2] Martin J. Collen,[2] Edward L. Cattau, Jr.,[2] and Mark H. Jaffe[1]

The Garren (Garren-Edwards) gastric bubble (American Edwards, Irvine, CA) has been used in more than 20,000 patients for the treatment of morbid obesity [1, 2]. The efficacy of this device as an adjunct to weight loss has been questioned [3, 4], yet it remains widely used along with a variety of similar devices being evaluated by the U.S. Food and Drug Administration. The most significant complication associated with use of the Garren bubble is bowel obstruction due to spontaneous deflation with passage of the bubble into the small bowel [5–7]. Although small bowel obstruction due to the Garren-Edwards balloon has been previously described, the characteristic plain film findings have not been described [5, 6]. The plain radiographs of two patients with small bowel obstruction resulting from deflated Garren gastric bubbles are reported. In vitro studies were also performed to clarify the radiographic appearance of the deflated bubble.

Case Reports

Case 1

A 39-year-old woman who had a Garren gastric bubble in place for 5 months presented with a 3-day history of nausea, vomiting, and abdominal cramps. An abdominal radiograph showed mild dilatation of the small bowel with numerous air-fluid levels. The patient's gastric bubble was not evident in the stomach. On a second radiograph obtained after placement of a nasogastric tube, the deflated Garren gastric bubble was seen in a small bowel loop (Fig. 1A). Barium examination confirmed the presence of partial small bowel obstruction due to the deflated bubble in the mid-ileum (Fig. 1B). An enterotomy with removal of the device was performed.

Case 2

A 47-year-old woman who had a Garren gastric bubble for 4 months presented with abdominal pain, bloating, and distension. Dilatation of the small bowel with air-fluid levels was present on abdominal radiographs. The patient improved clinically, and a second plain abdominal radiograph made 24 hr later showed less small bowel distension. A collapsed Garren balloon was evident in the distal transverse colon (Fig. 2A). Small bowel barium examination confirmed the colonic location (Fig. 2B). The patient subsequently passed the balloon per rectum and became asymptomatic.

In Vitro Investigation

The Garren gastric bubble was radiographed fully deflated and partially deflated with the balloon in air or in a water bath. Kilovoltage used was 65 kVp. A 0.5-mm lead filter was used to simulate X-ray beam attenuation by body structures. In the water bath, intersecting radiolucent areas of residual air within the partially deflated balloon were present. The borders of the balloon were obscured by the surrounding fluid [8]. When the balloon was radiographed in air, the walls of the balloon were seen as intersecting soft-tissue densities. These in vitro studies prove that the radiographic appearance of the deflated Garren gastric bubble is dependent on the medium that surrounds it. Within a fluid-filled bowel loop, the balloon is identified by residual air within its lumen. When the balloon is surrounded by air, its walls are evident.

Received July 23, 1987; accepted after revision October 26, 1987.

[1] Department of Radiology, Body Imaging Division, Georgetown University Hospital, 3800 Reservoir Rd., NW, Washington, DC 20007. Address reprint requests to R. K. Zeman.

[2] Department of Medicine, Division of Gastroenterology, Georgetown University Hospital, Washington, DC 20007.

[3] Department of Surgery, Georgetown University Hospital, Washington, DC 20007.

AJR 150:581–582, March 1988 0361–803X/88/1503–0581 © American Roentgen Ray Society

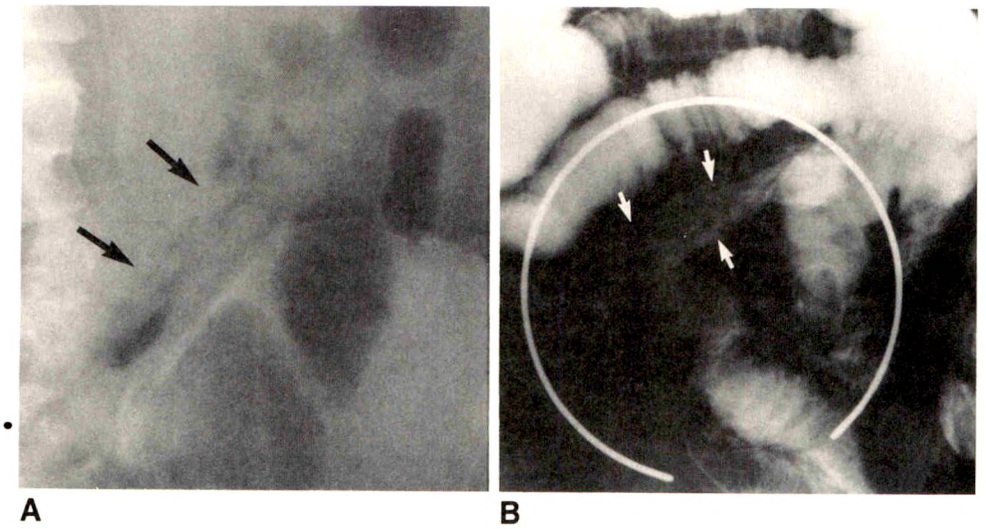

Fig. 1.—Small bowel obstruction due to balloon impaction in mid-ileum.
***A*, Plain abdominal radiograph shows deflated Garren balloon lodged in mid-ileum (*arrows*). It appears as linear air-density shadows.**
***B*, Small bowel examination confirms presence of collapsed balloon in small bowel (*arrows*).**

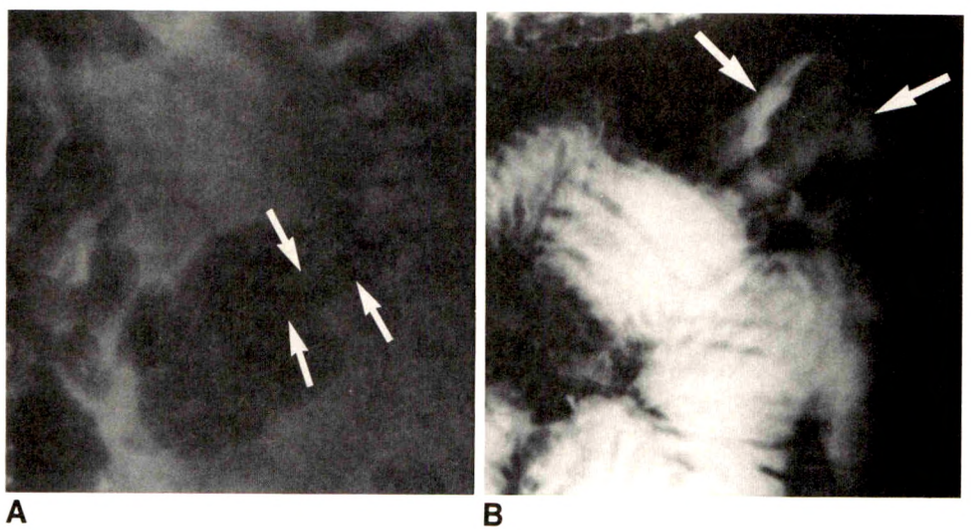

Fig. 2.—Spontaneous resolution of small bowel obstruction due to deflated balloon.
***A*, Plain abdominal radiograph shows the deflated Garren balloon in distal transverse colon (*arrows*).**
***B*, Small bowel examination confirms intracolonic location of deflated balloon (*arrows*).**

Discussion

Deflation of the Garren gastric bubble poses a significant clinical problem and may give rise to partial or intermittent obstruction of the small bowel. Eighty-three cases of small bowel obstruction have been reported to the manufacturer of the Garren bubble [7]. Of these patients, 79% had had the balloon in place for longer than 3 months, suggesting that long-term balloon placement increases the risk of deflation and subsequent bowel obstruction.

After balloon deflation, patients often are not certain whether the balloon has passed with their bowel movements. When the inflated gastric bubble is not radiographically identified in the stomach, deflation has occurred [2] and a search for the bubble must be carried out.

When the partially deflated balloon is surrounded by air, its walls appear as linear soft-tissue densities on radiographs. However, when the balloon is surrounded by fluid, residual air within the balloon appears as intersecting, linear radiolucent areas. The balloon wall itself is silhouetted. If abdominal radiographs do not show the location of the deflated balloon clearly, barium examination will locate the device.

REFERENCES

1. Garren M, Garren LR, Giordance F. The Garren gastric bubble: a treatment for the morbidly obese. *Endosc Rev* **1984**;2:57–60
2. Edell SL, Wills JS, Garren LR, Garren MC. Radiographic evaluation of the Garren gastric bubble. *AJR* **1985**;145:49–50
3. Stoltenberg PH, Piziak VK, Dietscher JE. Intragastric balloon therapy of obesity: a randomized double blind trail. *Gastroenterology* **1987**;92:1655
4. Benjamin SB, Maher K, Ciarleglio C, et al. A double-blind cross-over study of the Garren-Edwards anti-obesity bubble (abstr). *Gastrointest Endosc* **1987**:33:168
5. Boyle TM, Agus SG, Bauer JJ. Small intestinal obstruction secondary to obturation by a Garren gastric bubble. *Am J Gastroenterol* **1987**;82:51–53
6. Kirby DF, Mills PR, Kellum JM, Messmer JM, Sugerman HJ. Incomplete small bowel obstruction by the Garren-Edwards gastric bubble necessitating surgical intervention. *Am J Gastroenterol* **1987**;82:251–253
7. Benjamin SB. Small bowel obstruction and the Garren-Edwards bubble: lessons to be learned? *Gastrointest Endosc* **1987**;33:183
8. Felson B, Felson H. Localization of intrathoracic lesions by means of the postero-anterior roentgenogram: the silhouette sign. *Radiology* **1950**;55:363–374

CT of Renal Cell Carcinoma in Patients on Chronic Hemodialysis

Sharon C. Siegel[1,2]
Michael A. Sandler[1]
Michael B. Alpern[1]
Jay L. Pearlberg[1]

The occurrence rate of renal cell carcinoma is significantly higher in the native kidneys of patients undergoing chronic hemodialysis than in kidneys of normal subjects. These carcinomas may be difficult to detect because these kidneys tend to be small and distorted owing to acquired cystic disease. Four cases of renal cell carcinoma detected by CT are presented (three in patients undergoing chronic hemodialysis, and one in a patient with a functioning transplant who had history of dialysis). All kidneys had extensive acquired cystic disease. In two cases, contrast-enhanced scans showed a solid lesion of lower density than the kidney. In another case, in which IV contrast material could not be given, the mass was of higher density than the kidney and retroperitoneal lymphadenopathy was present. In the fourth case, no distinct solid mass could be identified. The only sign of malignancy in this case was extensive lymphadenopathy.

Whenever CT examination of the abdomen is performed in a patient undergoing chronic hemodialysis, the kidneys must be evaluated carefully because of the increased frequency of renal cell carcinoma. In a few cases, a distinct solid lesion may not be apparent or may be subtle owing to distortion of renal anatomy by acquired cystic disease.

Compared with normal subjects, patients with end-stage renal disease undergoing chronic hemodialysis have an increased frequency of both acquired cystic disease and solid renal tumors, including renal cell carcinoma [1–5]. The use of CT to detect and stage suspected renal cell carcinoma is well established. However, there have been only a few reports of the CT appearance of renal cell carcinoma in the native kidneys of these patients [3, 5–7].

We present three patients on chronic hemodialysis and one patient with a functioning renal transplant who had a history of hemodialysis. In all four patients, renal cell carcinoma was detected by CT. The CT appearance of the tumors is the basis of this report.

Materials and Methods

Four men with end-stage renal disease caused by hypertension had CT examinations of the abdomen. Three were receiving long-term hemodialysis, and one with a functioning renal transplant had received long-term hemodialysis (range, 3.5–11 years in duration). The patients' ages ranged from 45 to 67 years (average, 58). All CT scans were performed because of abdominal and/or flank pain, and all four patients had renal cell carcinomas confirmed by surgery. The patient with the transplanted kidney had a right nephrectomy because of pyelonephritis. Clinical findings in this patient have been described elsewhere [8].

CT scans were performed on either a General Electric 9800 scanner or a Picker 1200 scanner. Contiguous scans (10 mm thick) were obtained from xyphoid process to pubic symphysis. Oral contrast material was administered to all patients. Three of the patients received bolus injections of 100–150 ml of IV contrast material. In one case, IV contrast material could not be given.

Received July 31, 1987; accepted after revision November 9, 1987.

[1] Department of Diagnostic Radiology, Henry Ford Hospital, 2799 W. Grand Blvd., Detroit, MI 48202. Address reprint requests to M. A. Sandler.

[2] Present address: Department of Radiology, Sinai Hospital of Detroit, Detroit, MI 48235.

AJR 150:583–585, March 1988
0361–803X/88/1503–0583
© American Roentgen Ray Society

Results

CT showed multiple small renal cysts in all patients, including the one with a functioning renal transplant. Contrast-enhanced CT scans in two patients showed solid renal masses, 4 and 6 cm in diameter, respectively. Both tumors had lower density than did the renal parenchyma (Figs. 1 and 2). Tumor extension into the left renal vein was evident on CT in one case. In the case in which IV contrast material could not be given, unenhanced CT scans showed a 4-cm renal mass that had higher density than did the renal parenchyma (Fig. 3). Extensive pericaval and periaortic lymphadenopathy was also present. In the fourth patient, the solitary left kidney had numerous cysts, but no solid mass could be detected (Fig. 4). Periaortic and pericaval lymphadenopathy, extending from the level of the renal hila to the aortic bifurcation, was present. All of the patients had renal cell carcinomas confirmed at surgery. None of the lesions extended into the perinephric space. The enlarged lymph nodes were due to metastatic disease.

Discussion

Renal cell carcinoma occurs in approximately 5.8% of patients with acquired cystic disease, a rate seven times greater than the general population [4]. The cause of this is uncertain; it has been proposed that atypical cysts, lined by hyperplastic epithelium, may give rise to the tumors [2].

A few previous reports have described the CT appearance of renal cell carcinoma in the native kidneys of patients on chronic hemodialysis. Ishikawa et al. [3] mentions three tumors detected by CT and illustrates two of them. Scanlon and Karasic [5] reported a case in which CT showed a solid mass. Griffin and Williams [7] mention one case detected by CT without any further description. None of these patients had lymphadenopathy. In the two reported cases of renal

A

B

Fig. 1.—CT scans of 59-year-old man on hemodialysis.
A, Contrast-enhanced CT scan at level of renal hila shows numerous cysts in left kidney.
B, Contrast-enhanced CT scan shows solid carcinoma (*arrow*) arising from lower pole of left kidney.

Fig. 2.—Contrast-enhanced CT scan of 67-year-old man on hemodialysis shows solid carcinoma (*arrow*) arising from left kidney.

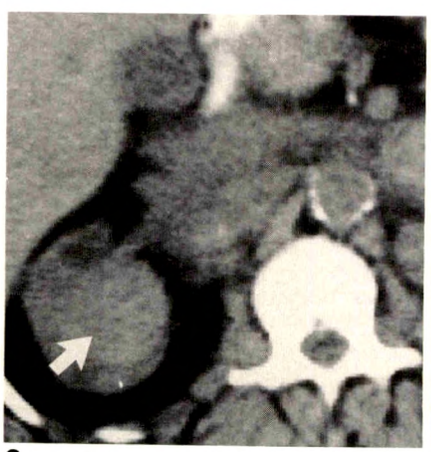

3

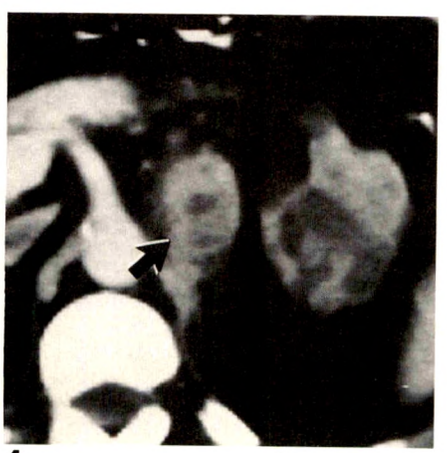

4

Fig. 3.—Unenhanced CT scan of 60-year-old man on hemodialysis shows hyperdense carcinoma in right kidney (*arrow*) and numerous enlarged lymph nodes.

Fig. 4.—Contrast-enhanced CT scan of 45-year-old man with history of hemodialysis shows cystic changes in left kidney but no definite solid mass. Enlarged lymph nodes (*arrow*) were only indication of renal cancer of left kidney, which was identified at surgery.

carcinoma occurring in patients on renal dialysis [6], one patient had a typical solid mass. In the other patient, who had an 8-cm carcinoma, only retrocaval lymphadenopathy was detected by CT. This finding was similar to the CT findings in one of our patients. In another one of our cases, extensive lymphadenopathy was present, although a mass of higher density than the unenhanced kidney could be identified.

Because of the distorted architecture and numerous cysts seen in patients on chronic hemodialysis with acquired cystic disease, a small to moderately large renal cell carcinoma may not be visualized on CT as a distinct mass. All of our patients had multiple cysts. Therefore, the presence of retroperitoneal lymphadenopathy in a patient with acquired cystic disease should raise strong suspicion of renal cell carcinoma, although lymphoma could also present with this appearance. In some cases, other secondary signs (including renal vein invasion, inferior vena cava invasion, and liver metastasis) may be the only findings suggestive of carcinoma.

REFERENCES

1. Grantham JP, Levine E. Acquired cystic disease: replacing one kidney disease with another. *Kidney Int* **1985**;28:99–105
2. Hughson MD, Hennigar GR, McManus JFA. Atypical cysts, acquired renal cystic disease and renal cell tumors in end stage dialysis kidneys. *Lab Invest* **1980**;42:475–480
3. Ishikawa I, Sato Y, Onouchi Z, et al. Development of acquired cystic disease and adenocarcinoma in the kidney in glomerulonephritic chronic hemodialysis patients. *Clin Nephrol* **1980**;14:1–6.
4. Hughson MD, Buchwald D, Fox M. Renal neoplasia and acquired cystic kidney disease in patients receiving long term dialysis. *Arch Pathol Lab Med* **1986**;110:592–601
5. Scanlon MH, Karasic SR. Acquired renal cystic disease and neoplasia: complications of chronic hemodialysis. *Radiology* **1983**;147:837–838
6. Cho C, Freedland GW, Swenson RS. Acquired renal cystic disease and renal neoplasms in hemodialysis patients. *Urol Radiol* **1984**;6:153–157
7. Griffin SC, Williams G. Metastatic hypernephroma from a native kidney after cadaver renal transplantation (letter). *Postgrad Med J* **1985**;61:471
8. Faber M, Kupin W. Renal cell carcinoma and acquired kidney cystic disease after renal transplantation (letter). *Lancet* **1987**;1(8540):1030–1031

Book Review

The Use of Transrectal Ultrasound in the Diagnosis and Management of Prostate Cancer. Edited by Fred Lee and Richard D. McLeary. New York: Alan R. Liss, 223 pp., 1987. $38

Prostatic carcinoma, the single most prevalent cancer in American men, is diagnosed annually more than all other urinary tract neoplasms combined. Statistics from the National Cancer Institute suggest that prostatic carcinoma was diagnosed in 96,000 men and that 27,000 men died of it in 1987. A well-founded understanding by physicians dealing with this common malignancy is warranted.

Approximately 30% of men more than 50 years old who are dying have latent prostatic carcinoma; however, the annual death rate in the United States is only 79 per 100,000 males. Put another way, for every patient who will die of the neoplasm, and for every three whose prostatic cancer will be diagnosed, about 375 men have latent prostatic cancer.

What, then, is the role for transrectal ultrasound (TRUS) in the detection and management of prostatic cancer? Will we simply mostly be detecting cancers that never would have mattered in the first place? Will we be using medical resources that should be used more efficiently for diseases for which an impact is more likely? Although at times uneven in style and content, this inexpensive monograph tries to bring these questions into focus. The book is the proceedings of a conference held in Detroit in September 1986, and it is a helpful starting point for radiologists and urologists who perform prostatic TRUS. The contributors (nine radiologists, six urologists, two sonographers, two pathologists, and one internist) present the recent history of TRUS in the detection and management of prostatic cancer, pertinent sonographic physics, prostatic anatomy and pathology, and other important issues of prostatic sonography. Pictures and figures are generally clear, with understandable labels and pathologic correlation. However, the widely accepted McNeal model of the gland in which CG = central gland, TZ = transitional zone, and PZ = peripheral zone is used for many of the figures without reference to this in the legends. Practical techniques for performing the examination, sonographically guided fine-needle aspiration, and TRUS for transperineal ^{125}I seed implantation are well described. Pathologic correlation of sonographic findings is emphasized. The experience of investigators in the United States, the United Kingdom, Germany, and Japan is presented.

Although sensitivity has been high, the low specificity of prostatic TRUS limits its value at present in screening for early cancers. How to deal with the serendipitously discovered cancers is an important question worthy of further discussion. It is perhaps too early to identify anything but theoretical benefits of early detection of prostatic carcinoma by TRUS. Although carcinomas as small as 3 mm can be recognized, tumors less than 10 mm in diameter are low grade and rarely metastasize. Size criteria could serve to stratify patients in whom suspicious lesions are identified. The potential social costs of monitoring asymptomatic prostatic carcinomas, moreover, must be weighed and, indeed, could be staggering. The costs of this technology were not addressed and might be an important addition to future symposia.

Ultimately, the not-so-high-tech and inexpensive digital rectal examination (DRE), although less sensitive, continues to rival the best imaging technologies and must be the gold standard with which TRUS and other techniques are compared. Peeling and colleagues from the University of Wales reviewed their data for unconfined, invasive (T3/T4; stage C) prostatic carcinomas. The accuracies of both DRE and TRUS were 96%. Others have shown a degree of superiority for sonography. For clinically confined cancers (T1/T2; stage B), the accuracy of DRE dropped to 50%, whereas the accuracy of TRUS was 93%.

The purpose of this monograph was to bring together contributions from multiple specialties dealing with detection and management of prostatic carcinoma. The text of the proceedings will interest anyone who wishes to have a better understanding of TRUS and prostatic cancer.

David B. Spring
Kaiser Permanente Medical Center
Oakland, CA 94611

Arteriovenous Malformations of the Kidneys: Ablation with Alcohol

Shigeo Takebayashi[1]
Masahiko Hosaka[2]
Eiichi Ishizuka[3]
Makoto Hirokawa[4]
Kengo Matsui[1]

Ablation of renal arteriovenous malformations with absolute alcohol was performed in seven patients with massive hematuria. In three patients, total occlusion of the malformations was accomplished by ablation of two arterial branches. In the remaining four patients, the malformations were partially occluded by ablation of one or two arterial branches. In addition to ablation with alcohol, two of the four patients underwent subselective embolization with Gelfoam (absorbable gelatin sponge) under epinephrine pharmacoangiography, which resulted in the disappearance of the remaining malformations. None of the patients had serious complications from ablation with alcohol, although dyspnea and headache occurred in one patient with marked arteriovenous shunting. During long-term follow-ups, hematuria disappeared in six patients. In the remaining patient hematuria recurred but did not require treatment.

These data suggest that alcohol ablation is useful and safe in the treatment of renal arteriovenous malformations.

Renal arteriovenous fistulas caused by vascular malformations are relatively rare, with a reported prevalence of less than 0.04% [1]. Most of these arteriovenous malformations (AVMs) are of little clinical importance; however, AVMs causing persistent massive hematuria provide a clear indication for therapeutic intervention. Transcatheter intraarterial infusion of absolute alcohol has been used successfully in the renal artery in the treatment of renal cell carcinoma [2], angiomyolipoma [3], and uncontrolled systemic hypertension [4]. The risks of alcohol infusion include major injury to the kidney by direct cellular toxicity [5] and bowel infarction by reflux out of the renal artery [6]. However, alcohol is readily available, inexpensive, and easy to handle, and it causes permanent occlusion of the artery [2]. We describe our experience with alcohol ablation in the treatment of seven patients with renal AVMs causing massive hematuria and evaluate the efficacy and safety of this technique.

Received September 29, 1987; accepted after revision November 10, 1987.

[1] Department of Radiology, Yokohama City University School of Medicine, 3–46 Urafune-cho, Minami-ku, Yokohama 232, Japan. Address reprint requests to S. Takebayashi.

[2] Department of Urology, Yokohama City University School of Medicine, Yokohama 232, Japan.

[3] Department of Urology, Yokohama Red Cross Hospital, 2–85, Negishi-cho, Naka-ku, Yokohama 231, Japan.

[4] Department of Urology, Fujisawa City Hospital, 2–6–1, Fujisawa, Fujisawa 251, Japan.

AJR 150:587–590, March 1988
0361–803X/88/1503–0587
© American Roentgen Ray Society

Materials and Methods

Between April 1984 and September 1986, seven patients with renal AVMs underwent treatment with intraarterial infusion of absolute alcohol. All patients were 28- to 64-year-old women, and all had massive hematuria. The malformations involved the right kidney in four patients and the left kidney in three. The lesions were 3–6 cm in diameter, as measured on angiograms. All AVMs were cirsoid and had more than one arterial feeder. In two patients, the AVM recanalized after previous embolization with Gelfoam (absorbable gelatin sponge, Upjohn, Kalamazoo, MI).

By using the Seldinger technique, a 6.5-French polyethylene catheter was first placed in the main renal artery to obtain a localizing angiogram. The catheter was than advanced into the arterial branch supplying the AVM. If possible, it was wedged into the branch to prevent reflux of the alcohol. Before absolute alcohol was slowly injected by hand at a rate of approximately 0.1–0.2 ml/sec, a test injection at the same rate was performed with contrast material to confirm the absence of reflux. Injections were 2 ml of alcohol in an interlobular

branch and 3 ml in a segmental branch. Each injection was followed by infusion of 1 ml of saline at the same rate. After 10 min, the catheter was slowly withdrawn and aspirated to remove possible residual alcohol and debris. Angiography was repeated to evaluate the success of ablation. If the AVM was patent, the alcohol was injected a second time by using the same technique. If the catheter could be introduced into other arterial branches supplying the AVM, the branches were also occluded with the same technique. However, alcohol was not infused if there were a risk of ablation causing impairment of renal function.

Of the patients in whom AVMs remained unablated after this technique, two underwent subselective embolization with Gelfoam to completely ablate the AVM: The catheter was placed in a segmental artery that supplied branches of the AVM. A test injection was performed with contrast material after intraarterial infusion of 3 μg of epinephrine. Then, 10 to 20 pieces of approximately 2- by 3-mm Gelfoam were infused. Finally, the catheter was placed in the main renal artery for postembolization angiography.

The patients were followed for 12–40 months to determine the presence of gross hematuria or delayed complications.

Results

Ablation of the branch supplying the AVM was easily accomplished by one or two infusions of alcohol in all patients. Total occlusion of the AVM by alcohol was accomplished in three patients: Two patients underwent alcohol ablation of one interlobular branch and one segmental branch, and one patient underwent ablation of two interlobular branches. Partial occlusion of the AVM by alcohol was accomplished in the other four patients: Three patients underwent ablation of two interlobular branches and one patient underwent ablation of one interlobular branch. In these patients, other branches supplying the AVM could not be ablated with alcohol because of the risk of impairing renal function. In two of the four, no further treatment was attempted because one patient had severe atrial fibrillation and the other was elderly. In the remaining two patients, ablation of the remaining AVM was achieved by subselective embolization with Gelfoam under epinephrine pharmacoangiography (Fig. 1).

No serious complications occurred in ablation of the AVM with alcohol. However, in one patient who had marked arteriovenous shunting (Fig. 2), dyspnea followed by headache occurred immediately after infusion of 2 ml of alcohol into an interlobular arterial branch. The symptoms were severe and lasted for 3 min. The patient did well and no abnormality was revealed on either a lung perfusion scintigram or CT scan of the head. In another case, the function of the kidney was

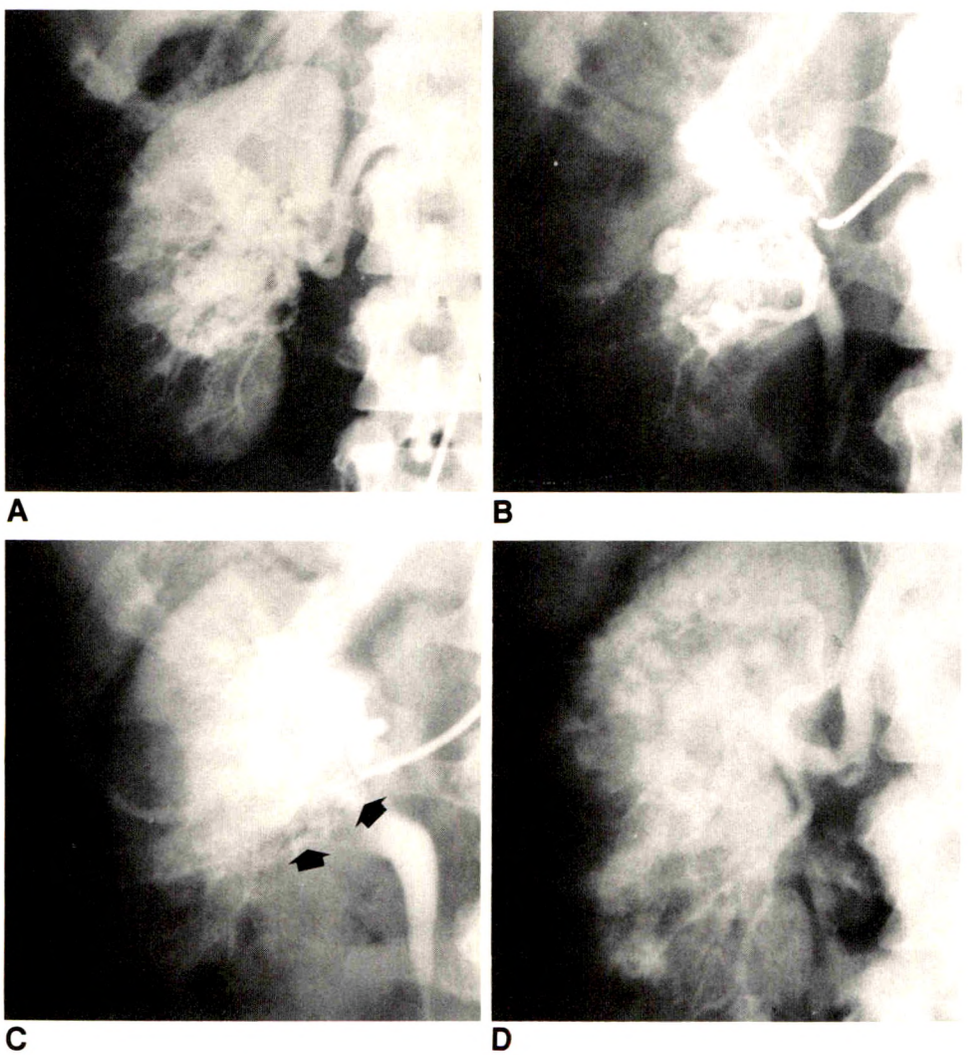

Fig. 1.—40-year-old woman with massive gross hematuria.

***A*, Right renal arteriogram shows large, cirsoid arteriovenous malformation (AVM) extending to upper and lower poles.**

***B*, Selective angiogram through catheter in segmental artery shows several vessels feeding AVM. Single injection of 3 ml of alcohol ablated the branch.**

***C*, Selective arteriogram through catheter placed in another segmental artery shows other AVMs (*arrows*). Because ablation of this branch with alcohol may have led to impaired renal function, subselective embolization with Gelfoam was carried out under epinephrine pharmacoangiography.**

***D*, Postembolization angiogram. Remaining AVMs have disappeared, and hematuria has resolved. Gross hematuria recurred 2 years later, but was mild and required no treatment.**

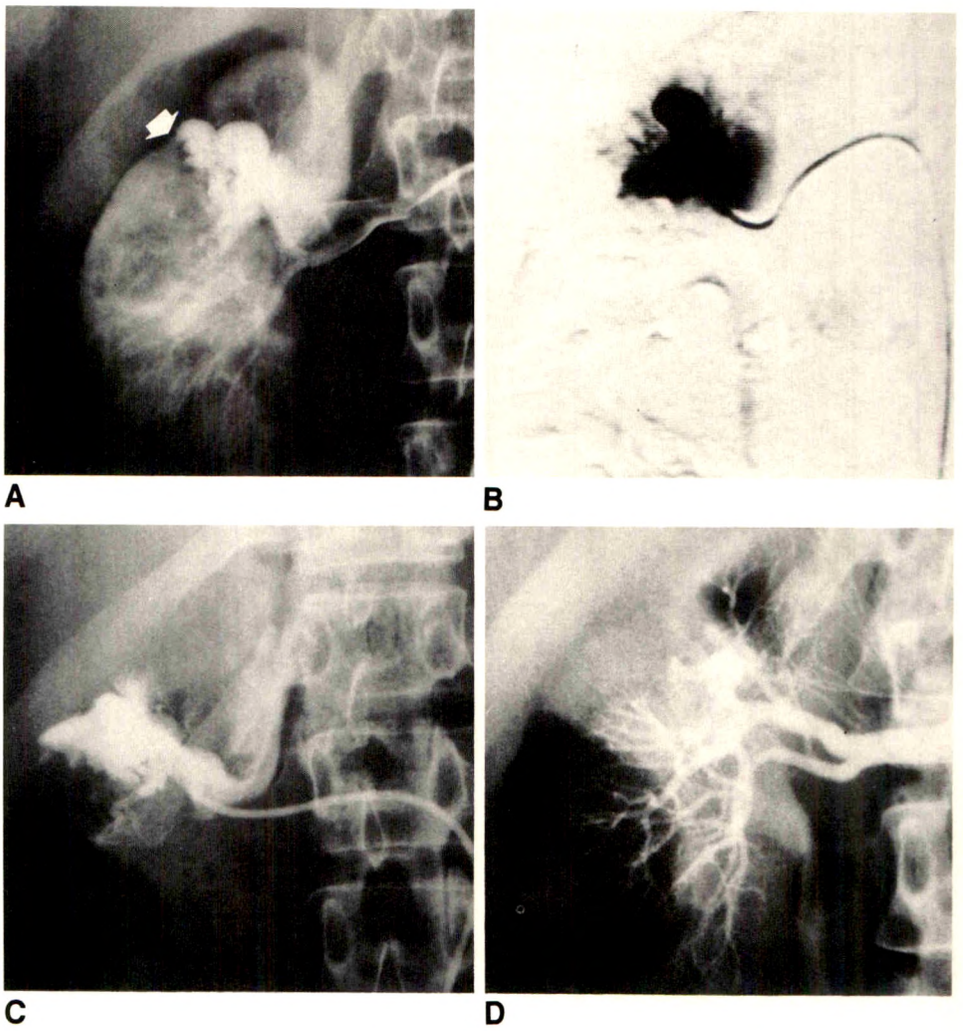

Fig. 2.—28-year-old woman with massive gross hematuria from recanalized arteriovenous malformation (AVM) 1 year after embolization with Gelfoam.

***A*, Right renal arteriogram shows two AVM masses in upper pole. Scar is from previous embolization (*arrow*).**

***B*, Digital subtraction angiogram through catheter placed in interlobular arterial branch shows opacification of medial AVM. No reflux of injected contrast material was observed. Single injection of 2 ml of alcohol ablated the branch.**

***C*, Selective angiogram through catheter placed in another interlobular feeding vessel shows laterally located AVM with marked arteriovenous shunting. After single, slow injection of 2 ml of alcohol, severe dyspnea occurred, followed by headache.**

***D*, Postembolization arteriogram shows complete ablation of AVM.**

markedly impaired by ablation of the proximal segmental arteries from reflux of Gelfoam.

Gross hematuria disappeared in all patients after treatment. In follow-up periods of 12–40 months, the hematuria resolved in six patients. In the other patient, the hematuria recurred 2 years later but did not require treatment. Delayed complications, such as hypertension, were not observed.

Discussion

Renal AVMs with multiple feeding vessels have been treated successfully by subselective embolization with Gelfoam [7]. Gelfoam is almost selectively transported to the AVM by a siphoning effect [8], and the injection of Gelfoam under epinephrine pharmacoangiography is more effective [9]. However, ablation with a permanent occlusive agent is desirable because the AVM occluded with Gelfoam is usually recanalized with recurrent massive hematuria.

Either steel coils or detachable balloons are effective for closure of traumatic renal arteriovenous fistulas [10]. In treating an AVM, the core of the lesion itself must be obliterated. However, these agents alone are not suitable for occlusion of an AVM because they lodge proximally. Proximal occlusion of the feeding arteries accomplishes little, because collateral vessels develop and continue to feed the lesion [11].

The use of alcohol for ablation of renal AVMs has several advantages over other embolic agents. It is inexpensive and easy to handle, and it causes complete and permanent ablation [2]. Furthermore, alcohol, a liquid material, can alone obliterate the core of the AVM [11]. Selective infusion of alcohol into an AVM with marked arteriovenous shunting may cause dyspnea and headache, because less-diluted alcohol reaches the lungs and the brain. However, the small dose of alcohol that we used for ablation causes little tissue damage, because dilution of alcohol below 50% eliminates its toxicity [4]. In order to avoid this reaction, the alcohol should be injected slowly, at a rate of less than 0.2 ml/sec while the catheter is being placed selectively in the feeding vessel.

When alcohol is injected slowly at a rate of 0.1 ml/sec, vessel occlusion is produced by clumps of damaged erythrocytes and denatured protein that become trapped in small arteries [2]. This slow-injection technique is preferred in the treatment of benign conditions, such as AVMs, because it causes less damage to the glomeruli [5].

The balloon occlusion technique has been recommended in renal ablation with alcohol to prevent reflux of alcohol. Earthman et al. [3] found that a 5-French Swan-Ganz catheter is useful in subselective infusion of alcohol to ablate renal angiomyolipomas. However, selective catheterization of small renal arterial branches with the Swan-Ganz catheter is technically difficult because the catheter lacks torque control. We used a 6.5-French torque catheter without a balloon for selective infusion of alcohol, because it was easily controlled and large enough to be wedged into a renal arterial branch to prevent reflux of alcohol. In our series, there was no reflux of alcohol when a dose of 2–3 ml of alcohol was slowly injected through the catheter into the small branches. However, if available, a polyethylene balloon catheter, which can be shaped and has torque control, is even better for prevention of reflux.

When treating AVMs, which are benign, preserving normal renal parenchyma and minimizing complications are essential. Since it is not feasible technically for the catheter to be placed selectively in every branch, alcohol ablation cannot accomplish total occlusion of the lesion. Because of this, subselective embolization with Gelfoam is useful to completely occlude the remaining AVM. However, it is difficult to judge the dose of Gelfoam needed for this technique, and infusion of excess Gelfoam causes unintended ablation of the branch with resulting impairment of function of the kidney. Moreover, the lesions ablated with Gelfoam are usually recanalized. Even partial occlusion of the AVM with alcohol successfully prevents hematuria, which requires long-term treatment. Therefore, alcohol ablation alone is sufficient for the initial treatment of AVMs.

REFERENCES

1. Cho KJ, Stanley JC. Non-neoplastic congenital and acquired renal arteriovenous malformations and fistulas. *Radiology* **1978**;129:333–343
2. Ellman BA, Parkhill BJ, Curry TS, Marcus PB, Peter PC. Ablation of renal tumors with absolute ethanol: a new technique. *Radiology* **1981**;141:619–626
3. Earthman WJ, Mazer MJ, Winfield AC. Angiomyolipomas in tuberosis: subselective embolotherapy with alcohol, with long-term follow-up study. *Radiology* **1986**;160:437–441
4. Nanni GS, Hawkins IF Jr, Orak JK. Control of hypertension by ethanol renal ablation. *Radiology* **1983**;148:51–54
5. Buchta K, Sands J, Rosenkrantz H, Roche WD. Early mechanism of action of arterially infused alcohol U.S.P. in renal devitalization. *Radiology* **1982**;145:45–48
6. Cox GC, Lee KR, Price HI, Gunter K, Nobel MJ, Mebust WK. Colonic infarction following ethanol embolization of renal-cell carcinoma. *Radiology* **1982**;145:343–345
7. Nakamura H, Uchida H, Kuroda C, et al. Renal arteriovenous malformations: transcatheter embolization and follow-up. *AJR* **1981**;137:113–116
8. Lang EK. Current and future applications of angiography in the abdomen. *Radiol Clin North Am* **1979**;17:55–76
9. Narimatsu Y, Kodera K, Okuno T, et al. Renal arterial embolization with epinephrine enhanced technique. *Rinsho Hoshasen* **1984**;29:15–21
10. Eckstein MR, Waltman AC, Athanasoulis CA. Interventional angiography of the renal fossa. *Radiol Clin North Am* **1984**;22:381–392
11. Athanasoulis CA. Transcatheter arterial occlusion for arteriovenous fistulas and malformations of the trunk, pelvis and extremities. In: Athanasoulis CA, Pfister RC, Greene RE, Roberson GH, eds. *Interventional radiology*. Philadelphia: Saunders, **1982**:203–222

CT Diagnosis of Circumcaval Ureter

Everett Marc Lautin[1]
Nogah Haramati[1]
David Frager[1]
Arnold C. Friedman[2]
Kenneth Gold[1]
Alan Kurtz[3]
Jerry Self[4]

Variability in the normal course of the ureter makes it difficult to differentiate a normal variant from a congenital anomaly or deviation caused by a mass. CT can be useful in making this distinction. We present five cases of circumcaval ureter in which contrast-enhanced CT, by showing the ureter passing posterior and medial to the inferior vena cava (IVC), provided the definitive diagnosis. In addition, we studied the position of the inferior vena cava in the midlumbar region in 100 consecutive contrast-enhanced CT scans and compared the results with the position of the IVC in our five cases of circumcaval ureter plus one case of circumcaval ureter taken from the literature. Whereas only 6% of the normal patients had an IVC lateral to the right pedicle of the third lumbar vertebra, all of the patients with a circumcaval ureter and the one case in the literature had the IVC lateral to the pedicle. Therefore, the finding of a laterally placed IVC on CT is suggestive but not pathognomonic of circumcaval ureter.

Contrast-enhanced CT can be used to prove the diagnosis of circumcaval ureter, and lateral placement of the IVC on non–contrast-enhanced CT suggests the diagnosis.

A circumcaval ureter results from anomalous development of the inferior vena cava (IVC) and not from anomalous development of the ureter [1–4]. In circumcaval ureter, the ureter crosses posterior to the IVC and then travels around the medial border anteriorly to partially encircle the IVC.

The abnormal position of the ureter results from the anomalous development of the infrarenal IVC from the right posterior cardinal vein that is embryologically more laterally placed instead of from the supracardinal vein that is embryologically more medial. We hypothesize that the IVC might still be lateral in position in adults with circumcaval ureters.

Because contrast-enhanced CT shows the ureter and the IVC simultaneously, it can be used to make a definitive diagnosis of circumcaval ureter. CT is also useful in evaluating the possibility of persistent lateral placement of the IVC in circumcaval ureter.

Materials and Methods

Five patients who were being evaluated for various urologic complaints had an IV urogram that showed a medial position of the right ureter suggestive of circumcaval ureter; a contrast-enhanced CT scan was then performed in each case. In one case, CT scans were performed before and after administration of contrast material. Figures 1–4 illustrate four of the cases; the fifth case is not shown.

In addition, 100 consecutive contrast-enhanced CT scans of the abdomen were reviewed, and the positions of the right ureter, the IVC, and their relationships to each other and to the L3 vertebral body were noted. The IVC was considered to be lateral to the L3 vertebral body if more than 50% of the volume of the IVC was lateral to the lateral margin of the right pedicle.

Received July 30, 1987; accepted after revision November 12, 1987.

[1] Department of Radiology, Montefiore Medical Center, 111 E. 210 St., Bronx, NY 10467. Address reprint requests to E. M. Lautin.

[2] Department of Radiology, Temple University Hospital, 3401 N. Broad St., Philadelphia, PA 19140.

[3] Department of Radiology, Thomas Jefferson University Hospital, 11th and Walnut Sts., Philadelphia, PA 19107.

[4] 512 E. Charlotte Rd., Rutherford, NC 28139.

AJR 150:591–594, March 1988
0361–803X/88/1503–0591
© American Roentgen Ray Society

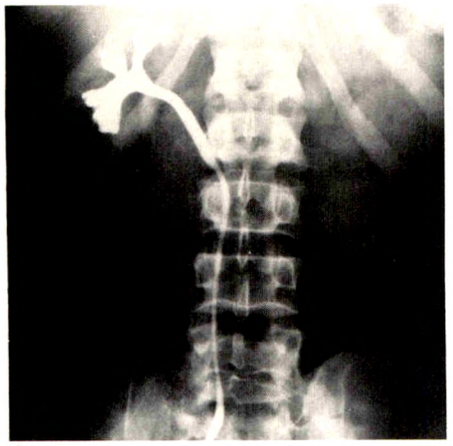

A

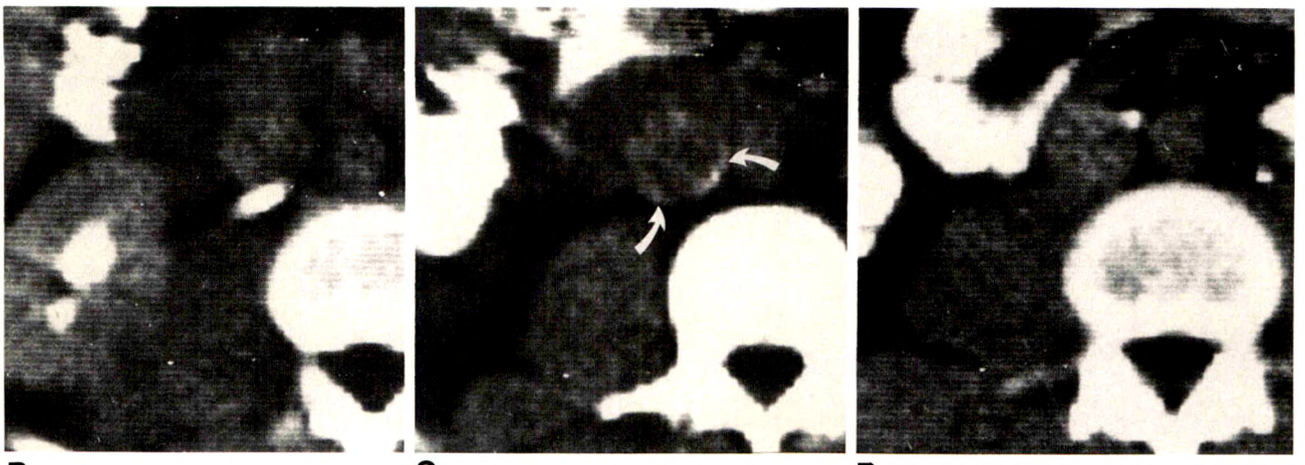

B C D

Fig. 1.—36-year-old man with intermittent gross and microscopic hematuria.

A, Retrograde pyelogram shows right ureter crossing medial to pedicle of L3 and descending medial to pedicles of L4 and L5 with minimal hydronephrosis. In the absence of a mass, diagnosis of circumcaval ureter is likely.

B–D, Contrast-enhanced CT scans show right ureter crossing posterior to inferior vena cava (*B*), circumscribing posterior medial aspect of inferior vena cava (*arrows*) (*C*), and crossing medial anterior to inferior vena cava at L3 (*D*).

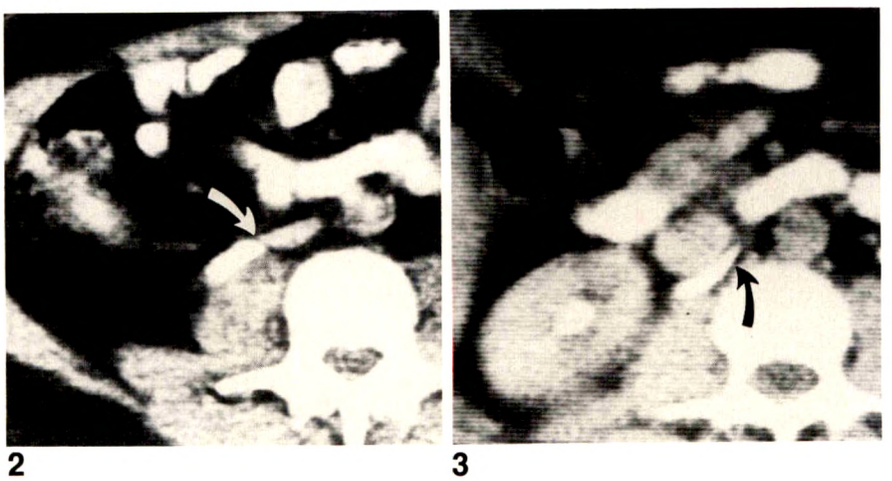

2 3

Fig. 2.—58-year-old man with right flank pain. CT scan at level of obstruction shows that dilated ureter has a tapered narrowing as it passes between right psoas muscle and inferior vena cava (*arrow*). An IV urogram revealed that moderate right hydronephrosis with a dilated right ureter that crossed the pedicle at L3 and was not seen distal to obstruction.

Fig. 3.—CT scan at level of L3 shows right ureter passing posterior and medial to inferior vena cava (*arrow*). CT cuts at a lower level showed ureter to have a normal course in pelvis. An IV urogram revealed a ureter with a medial course suggesting circumcaval ureter.

Results

The ureter passed posterior and medial to the IVC in four of our five cases and in the one previously published case [5]. In one of the cases, the ureter entered the notch between the IVC and the right psoas muscle, but because of obstruction at that level it was not seen more distally (Fig. 2). In none of the 100 consecutive CT scans did the right ureter go medial to the IVC or to the medial aspect of the right pedicle of the third lumbar vertebra. The right ureter, at this level, did approximate the notch between the IVC and the right psoas muscle in 18% of cases.

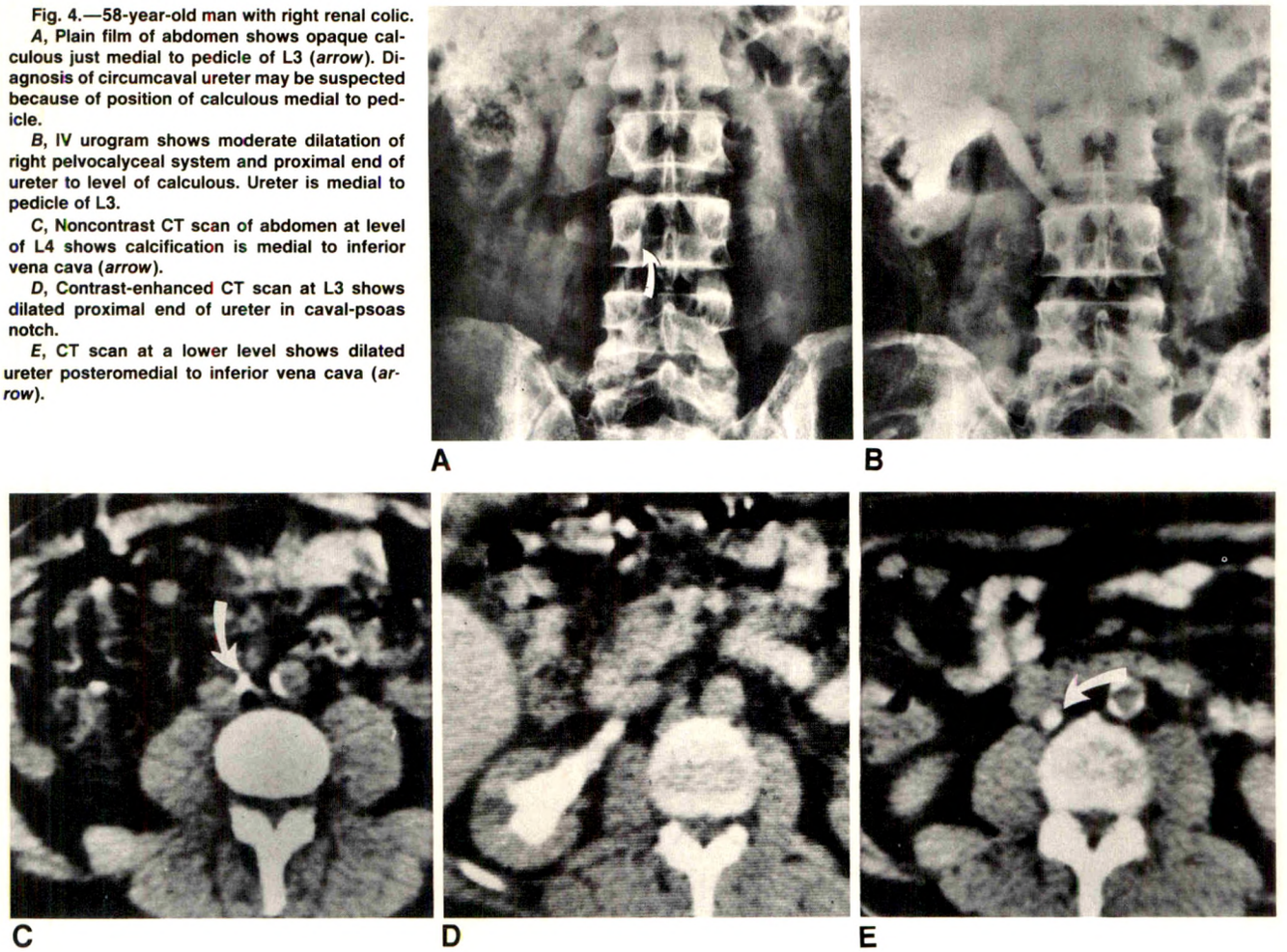

Fig. 4.—58-year-old man with right renal colic.
A, Plain film of abdomen shows opaque calculous just medial to pedicle of L3 (*arrow*). Diagnosis of circumcaval ureter may be suspected because of position of calculous medial to pedicle.
B, IV urogram shows moderate dilatation of right pelvocalyceal system and proximal end of ureter to level of calculous. Ureter is medial to pedicle of L3.
C, Noncontrast CT scan of abdomen at level of L4 shows calcification is medial to inferior vena cava (*arrow*).
D, Contrast-enhanced CT scan at L3 shows dilated proximal end of ureter in caval-psoas notch.
E, CT scan at a lower level shows dilated ureter posteromedial to inferior vena cava (*arrow*).

The IVC was placed lateral to the right pedicle of the third lumbar vertebra in all five patients with circumcaval ureter and in the one patient described in the literature [5]. In the 100 consecutive CT scans at the level of the third lumbar vertebra, the IVC is usually located between the center of the vertebral body and the lateral aspect of the right pedicle. In 6% of the patients, the IVC was lateral to the right pedicle.

Discussion

Circumcaval ureter has a reported autopsy prevalence of about 0.9 in 1000 (one in 1100) with a 2.8:1 male-to-female ratio [6]. Symptoms, when present, are related to ureteral obstruction, which is a frequent but not inevitable complication of circumcaval ureter [7, 8]. In circumcaval ureter, the ureter crosses posterior to the IVC and then travels medially and anteriorly to partially circumscribe the IVC [9].

The findings at IV urography, while suggestive of circumcaval ureter, are not diagnostic [9]. Medial deviation of the ureter in the lumbar region may be caused by retroperitoneal fibrosis, a retroperitoneal mass, or previous surgery, as well as by circumcaval ureter. A more definitive test is needed. A retrograde pyelogram or IV urogram when done in conjunction with an inferior venacavogram has been advocated in the past for making the diagnosis. Because the ureter and the IVC often are shown simultaneously on contrast-enhanced CT, this procedure can also be diagnostic while avoiding the possible complications and expense of an invasive procedure.

If the right ureter partially encircles the IVC on CT, the diagnosis of circumcaval ureter is proved, because this is the definition of circumcaval ureter. If the ureter is posterior to the IVC, this finding is diagnostic of retrocaval ureter and suggestive of circumcaval ureter. The right ureter often is obstructed in circumcaval ureter, frequently lateral to the IVC, and therefore the distal portion of the ureter may not be seen [9]. In addition, the distal portion fortuitously may not be filled with contrast material, owing to peristalsis on the appropriate CT sections, in nonobstructive circumcaval ureter.

The anomalous development of the IVC leading to circumcaval ureter may explain the lateral position of the IVC in these cases. The IVC develops from the posterior cardinal, subcardinal, and supracardinal veins, which undergo sequential development, anastomosis, and regression to become the inferior vena cava and azygos venous system. Normally, the right subcardinal vein forms the prerenal IVC, the subcardinal-supracardinal anastomosis forms the renal segment, and the right supracardinal vein forms the postrenal IVC. The circumcaval ureter most likely results when the posterior cardinal vein fails to regress and instead forms the postrenal segment

of the IVC [1–4]. Some authors and some current textbooks state that the circumcaval ureter results when the supracardinal vein fails to regress [10–13]. The right posterior cardinal vein is lateral to both the right subcardinal vein and the supracardinal vein [2, 14]. The posterior cardinal vein forms the postrenal portion of the IVC in cases of circumcaval ureter, so this probably explains the lateral position of the IVC in circumcaval ureter.

Lateral placement of the IVC occurred in 100% (6/6) of the cases of circumcaval ureter and in only 6% of the cases without circumcaval ureter. Because of the rarity of circumcaval ureter (one in 1100), in any individual case in which there is lateral placement of the IVC, the likelihood that circumcaval ureter is present is increased to approximately one in 60. Scoliosis can cause an apparent lateral displacement of the IVC *without* the presence of circumcaval ureter.

Contrast-enhanced CT that shows the ureter circumscribing a course posterior and medial to the IVC is diagnostic of circumcaval ureter. The finding of lateral placement of the IVC is not pathognomonic of circumcaval ureter, but it should suggest the possible diagnosis of circumcaval ureter.

REFERENCES

1. Mayo J, Gray R, Louis E, Grossman H, McLoughlin M, Wise D. Anomalies of the inferior vena cava. *AJR* **1985**;140:339–345
2. Chaung VP, Mena CE, Hoskins PA. Congenital anomalies of the inferior vena cava. Review of embryogenesis and presentation of a simplified classification. *Br J Radiol* **1974**;47:206–213
3. Ferris FJ, Florencio HA, Paul KC, Phillips E, Shapiro JH. *Venography of the inferior vena cava and its branches*. Baltimore: Williams & Wilkins, **1967**:10
4. Bolooki H, Margulis M, Yermakov VM, Gliedman ML. Portal hypertension with anomalies of inferior vena cava and hepatic veins. *Arch Surg* **1967**;94:267
5. Gefter WB, Arger PH, Mulhern CB, Pollack HM, Wein AJ. Computed tomography of circumcaval ureter. *AJR* **1978**;131:1086–1087
6. Johansson NT, Nilsson SV, Scherston T, Schvarz W, Weiland PO. Retrocaval ureter: a report of a case and a short review of the literature. *Scand J Nephrol* **1969**;3:53–58
7. Shown TE, Moore CA. Retrocaval ureter: four cases. *J Urol* **1971**;105: 497–501
8. Crosse JEW, Soderdahl DW, Teplick SK, Clark RE. Nonobstructive circumcaval (retrocaval) ureter. *Radiology* **1975**;116:69–71
9. Bateson EM, Atkinson D. Circumcaval ureter: a new classification. *Clin Radiol* **1969**;20:173–177
10. Emmett JL. Anomalies of the genitourinary tract. In: Witten DM, Myers GH, Utz DC, eds. *Emmett's clinical urography*. Philadelphia: Saunders, **1977**:677–678
11. Elkin M. *Radiology of the urinary system*. Boston: Little, Brown, **1980**: 120–122
12. Ney C, Friedenberg RM. *Radiographic atlas of the genitourinary system*. Philadelphia: Lippincott, **1981**:1136
13. Gruenwald P. Die Entwicklung der Vana Cava caudalis beim Menschen. *Z Mikrosk Anat Forsch* **1938**;43:275–331
14. McClure CFW, Butler EG. The development of the vena cava inferior in man. *Am J Anat* **1925**;35:331–383

Case Report

Vaginally Induced Pneumoperitoneum During Pregnancy

Ronald S. Gensburg,[1] W. Gregory Wojcik, and Snehal D. Mehta

The female genital tract is a known conduit for introduction of air into the peritoneal cavity during a variety of sexual and athletic activities. However, occurrence of such pneumoperitoneum during pregnancy has not been reported previously. We report a case of spontaneous pneumoperitoneum that developed during a second-trimester pregnancy after the patient's participation in a water sport.

Case Report

A 22-year-old gravida 4, para 1, 0-2-1 (16-week menstrual age by dates) woman presented to an outlying emergency department after right shoulder and chest pain had started suddenly while she was doing housework. A chest radiograph showed pneumoperitoneum (Fig. 1A). The patient had been in excellent health throughout her life and had no history of peptic ulcer disease or surgery. The pregnancy was remarkable for at least two episodes of vaginal bleeding caused by small placental abruptions that had been documented by a previous sonographic examination. Because of the suspicion of perforated viscus, the patient was transferred to our institution.

On arrival, the patient was in no acute distress. Vital signs showed pulse rate of 72/min, blood pressure of 132/70 mm Hg, unlabored respirations at 16/min, and a temperature of 37.3°C. Physical examination revealed a soft, minimally tender abdomen, without guarding or rebound tenderness. The bowel sounds were normal in pitch and slightly hypoactive. Initial laboratory studies showed a WBC count of 10,300/mm^3 and a hemoglobin of 11.2 g/dl. Other laboratory examinations, including serum amylase, were unremarkable.

Because the patient appeared in no distress, she was specifically questioned regarding possible benign causes of pneumoperitoneum. She stated that 2 days earlier she had been pulled behind a speedboat in an inflated inner tube. She also recalled being thrown off in the water without apparent injury.

The patient was admitted to the surgical intensive care unit for observation and administration of prophylactic antibiotics. The WBC count peaked at 21,700/mm^3 but rapidly decreased to 10,700/mm^3 over serial studies covering 36 hr. Exploratory laparotomy was avoided. On the second hospital day, the patient reported feeling completely well. An obstetric sonogram showed a single viable fetus estimated at 17 weeks menstrual age. Multiple small echogenic foci, representing small air bubbles, were seen around the placenta and further proved the origin of the patient's pneumoperitoneum (Figs. 1B and 1C). The patient was released without symptoms on the third hospital day.

Discussion

Spontaneous pneumoperitoneum, the nontraumatic, noniatrogenic presence of intraperitoneal gas, is usually (>90% of cases) an ominous radiographic sign indicating an acute condition requiring surgery [1]. The most common etiology is visceral perforation caused by peptic ulcer disease [2]. Many "benign" causes of pneumoperitoneum have been identified, such as pneumatosis intestinalis, intrathoracic processes [3], and even dental extraction [4]. Felson and Wiot called this "spontaneous pneumoperitoneum without peritonitis" [5].

The female genital tract may act as a pathway for gas to reach the peritoneal cavity. This is the basis for demonstrating

Received September 1, 1987; accepted after revision October 20, 1987.

[1] All authors: Medical School, Department of Radiology, University of Texas Health Science Center at Houston, 6431 Fannin, Rm. 2.132 MSMB, Houston, TX 77030. Address reprint requests to S. D. Mehta.

 0361–803X/88/1503–0595 © American Roentgen Ray Society

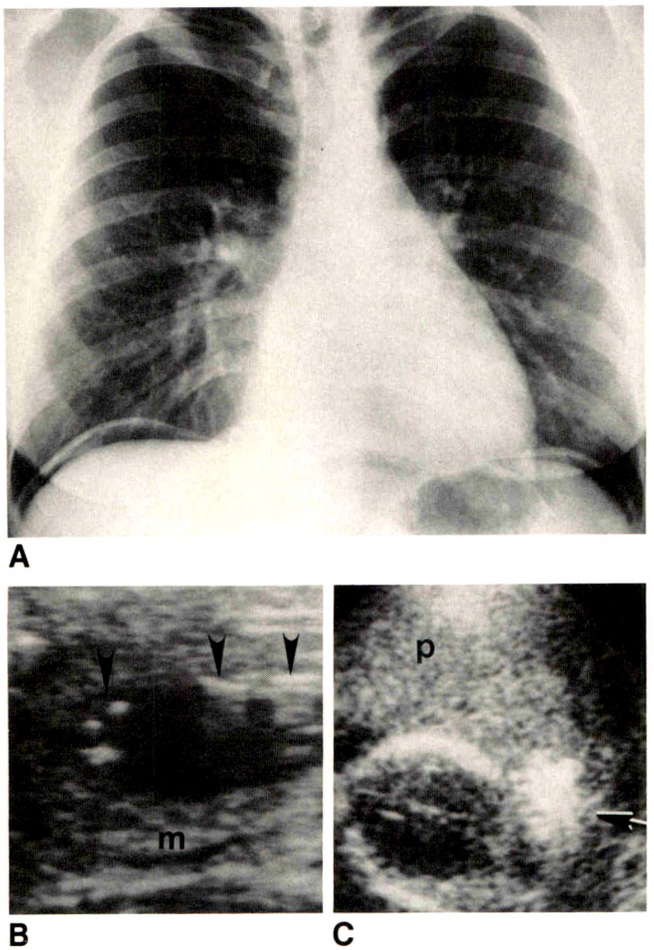

Fig. 1.—*A*, Initial upright posteroanterior chest radiograph showing pneumoperitoneum.

***B* and *C*, Sonographic examination. *B*, Magnified left parasagittal image of uterus showing multiple small echogenic foci (*arrowheads*) with shadowing representing gas collections; m = myometrium. *C*, Transverse image showing fetal head with large gas collection (*arrow*) at edge of placenta (p).**

tubal patency in Rubin's test. This mechanism for development of pneumoperitoneum has been described as occurring after intercourse, oral-genital insufflation, douching, and athletic activities (e.g., waterskiing, horseback riding), and in the postpartum period [6]. Our case is unique in that the benign pneumoperitoneum occurred during pregnancy.

It might be expected that the cervical mucus plug and gestational products would effectively act as a barrier to the passage of air during a viable pregnancy. Recent bleeding in our patient may explain the patency of the cervix. According to Hamilton and Mossman [7], obliteration of the uterine cavity occurs at about 4½ months gestation, when the chorion laeve fuses with the decidua parietalis. This disrupts the communication between the vagina and the peritoneal cavity. During the second trimester, the decidua capsularis is undergoing atrophy and replacement by chorion laeve, which then comes in contact (and eventually fuses) with the decidua parietalis. By 16 weeks, at which time this patient presented, this fusion is incomplete and thus may allow passage of air from the vagina to the peritoneal cavity.

Our case reiterates that pneumoperitoneum in an otherwise healthy individual without peritoneal signs warrants a careful search for benign causes, so that unnecessary laparotomy can be avoided. Furthermore, pregnancy (at least up to 16 weeks) does not exclude the benign causes of pneumoperitoneum specific to females in which air enters via the genital tract. Sonography, together with physical findings, was helpful in verifying the benign etiology in this patient.

REFERENCES

1. McGlone FB, Vinion CG, Meir L. Spontaneous pneumoperitoneum. *Gastroenterology* **1966**;51:393–398
2. Rice RP, Thompson WM, Gedgaudas RK. The diagnosis and significance of extraluminal gas in the abdomen. *Radiol Clin North Am* **1982**;20(4):819–837
3. Macklin MT, Macklin CC. Malignant interstitial emphysema of the lungs and mediastinum as an important occult complication in many respiratory diseases and other conditions. An interpretation of the clinical literature in the light of laboratory experiment. *Medicine* **1944**;23:281–358
4. Sandler CM, Libshitz HI, Marks G. Pneumoperitoneum, pneumomediastinum, and pneumopericardium following dental extraction. *Radiology* **1975**;115:539–540
5. Felson B, Wiot JF. Another look at pneumoperitoneum. *Semin Roentgenol* **1973**;8:437–443
6. Lozman H, Newman AJ. Spontaneous pneumoperitoneum occurring during postpartum exercises in the knee-chest position. *Am J Obstet Gynecol* **1956**;72:903–905
7. Hamilton WJ, Mossman HW. *Human embryology*. Baltimore: Williams & Wilkins, **1972**:110–112

MR Imaging of the Knee: Preliminary Results with a 3DFT GRASS Pulse Sequence

Charles E. Spritzer[1]
James B. Vogler[1]
Salutario Martinez[1]
William E. Garrett, Jr.[2]
G. Allan Johnson[1]
M. J. McNamara[2]
John Lohnes[2]
Robert J. Herfkens[1]

The knees of 17 patients (18 extremities) with possible meniscal, cruciate ligament, and articular cartilage abnormalities were examined with a three-dimensional Fourier transform (3DFT), gradient-refocused acquisition in a steady state (GRASS) pulse sequence. Arthroscopic confirmation was available in all cases and was the standard for comparison. Thirteen of these extremities were also examined by using a two-dimensional Fourier transform spin-echo pulse sequence with a 2000-msec repetition time and 20- and 80-msec echo time. In these 13 cases, both pulse sequences correctly identified seven of eight meniscal abnormalities. However, interpretation of the 3DFT GRASS images resulted in fewer false-positive meniscal tears (three vs six). Cruciate ligament tears were detected more readily on the 3DFT GRASS images (six vs three with two possible tears on the spin-echo images).

These preliminary findings suggest that the overall accuracy of MR imaging of the knee could be improved by including 3DFT gradient-refocused pulse sequences.

MR imaging has been shown to be useful in evaluating the knee. Meniscal abnormalities, cruciate and collateral ligamentous injuries, and osteonecrosis of the femoral condyles have been detected routinely [1–9]. Harms and Muschler [10] reported that three-dimensional Fourier transform (3DFT) data acquisitions provided several advantages when compared with conventional two-dimensional Fourier transform (2DFT) spin-echo pulse sequences for imaging the knee. Advantages included (1) improved signal-to-noise ratio for a given slice thickness and spatial resolution, (2) truly contiguous slices, and (3) the ability to obtain isotropic voxels enabling the reformation of data in nonorthogonal planes. The major disadvantage of 3DFT spin-echo data acquisitions is the prolonged scanning time, ranging up to 50 min depending on the imaging parameters chosen.

Recently, several limited-flip-angle, gradient-refocused pulse sequences known by acronyms such as FLASH (fast low-angle shot) and GRASS (gradient refocused acquisition in a steady state) have been introduced [11, 12]. These pulse sequences typically tilt the net magnetic moment vector at at angle of less than 90°. This allows the protons to recover more quickly, making possible the use of short repetition times. This in turn allows high-resolution images to be generated in as little as 3 sec. A 3DFT version of this type of pulse sequence has been available for clinical trials at our institution for the past several months.

The purpose of this study was twofold: (1) to determine if 3DFT limited-flip-angle gradient-refocused imaging is accurate in diagnosing abnormalities of the knee when compared with arthroscopy and (2) to determine if this pulse sequence provides advantages when compared with 2DFT spin-echo pulse sequences in detecting these abnormalities.

Subjects and Methods

Seventeen patients (18 extremities), 12 men and five women ranging in age from 16 to 61 years old (mean age, 31 years), who were clinically suspected as having possible internal

Received August 28, 1987; accepted after revision October 28, 1987.

[1] Department of Radiology, Box 3808, Duke University Medical Center, Durham, NC 27710. Address reprint requests to C. E. Spritzer.

[2] Department of Orthopaedic Surgery, Duke University Medical Center, Durham, NC 27710.

AJR 150:597–603, March 1988
0361–803X/88/1503–0597
© American Roentgen Ray Society

derangements of the knee, were studied with gradient-refocused MR imaging. Arthroscopic confirmation was available in each case. In nine cases, the two studies were performed within 24 hr of each other, while in the remaining eight cases, the two studies were separated by 1–8 days.

MR imaging was performed on a General Electric Signa system (Milwaukee, WI) operating at 1.5 T. A transmit-and-receive extremity coil was used in each case. The patients were scanned in the supine position with the knees extended and in neutral position.

GRASS is the version of the limited-flip-angle, gradient-refocused pulse sequence available on our imager. By using a 3DFT technique, sagittal GRASS images were obtained with the following parameters: repetition time (TR) = 60 msec, echo delay (TE) = 16 msec, nominal flip angle = 30°. Sixty-four contiguous, 1.2-mm-thick slices were acquired by using a 256 × 256 matrix and one excitation. Inplane resolution was 0.5 × 0.5 to 0.8 × 0.8 mm, depending on the field of view. The actual scanning time was 16.25 min.

Sagittal 2DFT spin-echo images were also acquired in 13 patients (13 extremities) by using the following parameters: TR = 2000 msec, TE = 20 and 80 msec. The slices were 5 mm thick with 2.5-mm interslice gaps and two excitations. A 128 × 256 matrix was selected with inplane resolution of 0.5 × 0.75 to 0.8 × 1.2 mm. The scanning time was approximately 9 min. Four patients (five extremities) who underwent 3DFT GRASS MR imaging of the knee did not undergo 2DFT spin-echo imaging owing to time constraints and/or patient fatigue.

The 3DFT GRASS and 2DFT spin-echo images for each extremity were reviewed by three of the authors at separate sessions without knowledge of the arthroscopic results. A retrospective approach was necessary since diagnostic criteria for evaluating the GRASS images were developed as the study progressed. The menisci, cruciate ligaments, and articular cartilage were assessed in every case in accordance with results published by Reicher et al. [7] and Stoller et al. [13]. Menisci were considered torn if a linear area of slightly increased signal was seen within the meniscus extending to the surface. Horizontal areas of slightly increased signal not communicating with the surface were considered a sign of degenerative change and, while noted, were not interpreted as a tear [6, 7, 13]. The cruciate ligaments were considered torn or partially torn if (1) they were not identified, (2) they were in an abnormal position, or (3) if they contained areas of abnormally increased signal. Miscellaneous abnormalities including loose bodies, joint effusions, and osteonecrosis were also noted. Final interpretations were determined by a consensus of the three reviewing authors.

Results

Normal Anatomy

The appearance of the knee on GRASS images with the parameters outlined above was similar to that of a spin-echo pulse sequence with TR = 2000 msec and TE = 20 msec (Figs. 1 and 2). Normal menisci are composed of fibrocartilage and appeared as uniform, triangular structures of decreased signal. Similarly, the cruciate ligaments were identified as structures of decreased signal within the intercondylar notch. With the knee extended, the posterior cruciate ligament had the appearance of a dark cord, while the anterior cruciate ligament had slightly higher signal intensity and assumed more of a fanlike configuration. The hyaline articular cartilage was seen as a uniform band of intermediate signal adjacent to the low signal of the cortical bone. Fat had the brightest signal, while marrow was isointense to hypointense relative to fat depending on the absence or presence of hemopoietic elements.

3DFT GRASS vs 2DFT Spin-Echo Imaging

The results are summarized in Table 1. In the 13 extremities in which both 2DFT spin-echo and 3DFT GRASS images were obtained, both pulse sequences correctly identified five of six torn menisci and two partial medial meniscectomies. However, fewer false-positive tears were identified on the 3DFT GRASS pulse sequence than on the 2DFT spin-echo images (three vs six) (Fig. 3).

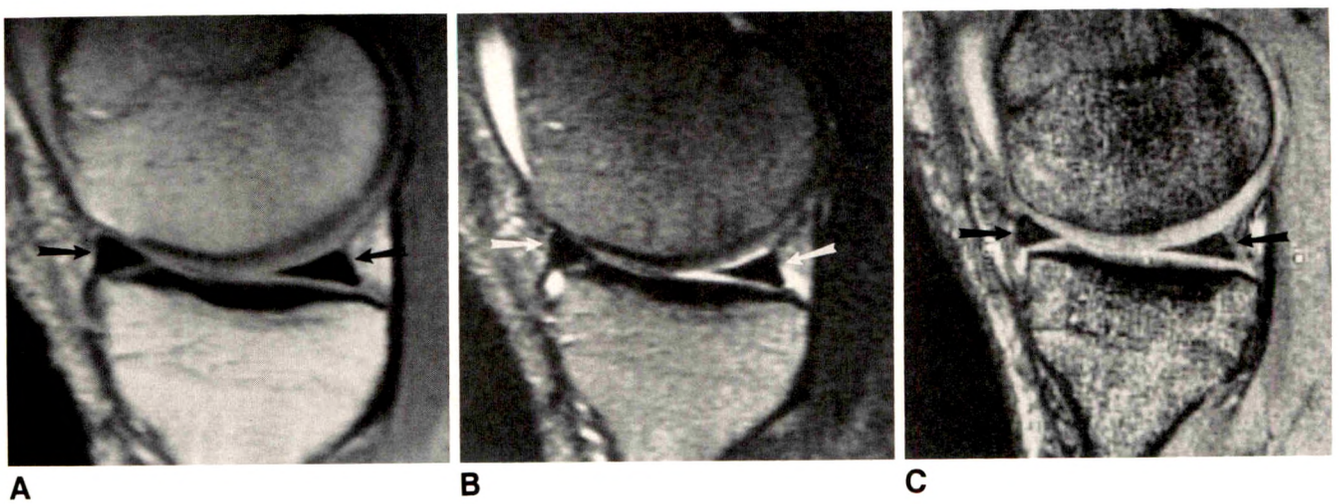

Fig. 1.—Normal medial meniscus and articular cartilage.

***A* and *B*, 2DFT spin-echo images (TR = 2000 msec, TE = 20 [*A*] and 80 [*B*] msec, 5 mm thick, two excitations, 16-cm field of view). Anterior and posterior horns (*arrows*) of medial meniscus appear as homogeneous triangles of decreased signal. Articular cartilage is of uniform thickness and appears brighter than fibrocartilage of menisci.**

***C*, 3DFT GRASS image (TR = 60 msec, TE = 16 msec, 30° flip angle, 1.2 mm thick, 16-cm field of view) displays similar findings. Anterior and posterior horns of medial meniscus appear as homogeneous triangles of low signal (*arrows*). Articular cartilage is brighter than meniscus in adjacent bone marrow.**

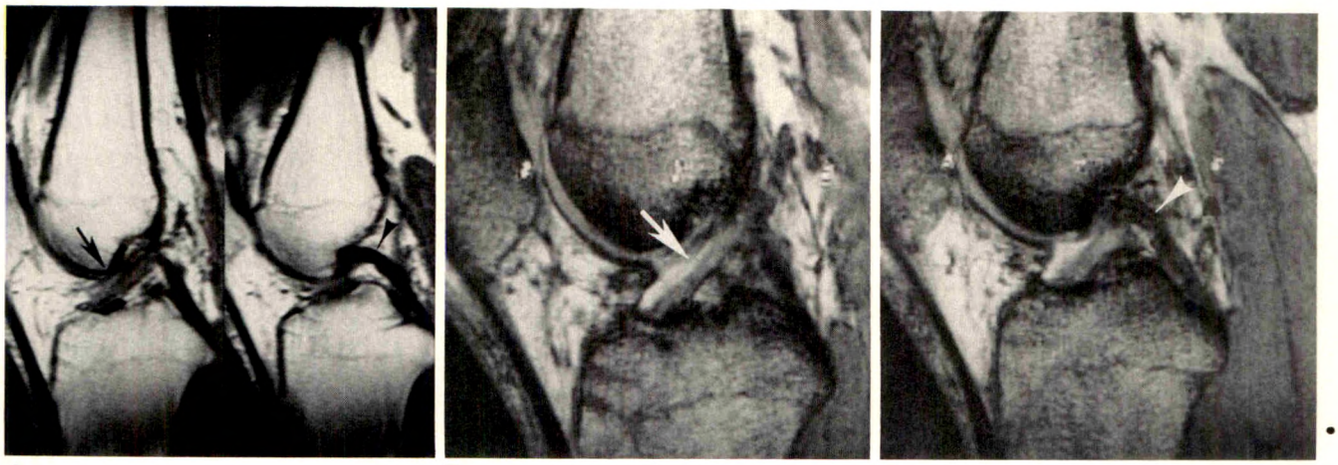

Fig. 2.—Normal cruciate ligaments.
***A*, 2DFT spin-echo image (TR = 2000 msec, TE = 20 msec, 5 mm thick, two excitations, 16-cm field of view).**
***B* and *C*, 3DFT GRASS images (TR = 60 msec, TE = 16 msec, 30° flip angle, 1.2 mm thick, 16-cm field of view).**
In both sequences, anterior cruciate ligament (*arrows*) is of slightly increased signal relative to posterior cruciate ligament (*arrowheads*).

TABLE 1: 3DFT GRASS and 2DFT Spin-Echo Imaging vs Arthroscopy of the Knee

Location: MR Sequence	No. of Cases (n = 13)			
	Arthroscopy Negative		Arthroscopy Positive	
	True Negative	False Positive	True Positive	False Negative
Medial meniscus:				
3DFT GRASS	5	2[a]	6[b]	0[c]
2DFT spin echo	4	3[a]	6[b]	0[c]
Lateral meniscus:				
3DFT GRASS	10	1	1	1[c]
2DFT spin echo	8	3	1	1[c]
Anterior cruciate ligament:				
3DFT GRASS	8	0	5	0
2DFT spin echo	6	2	4[d]	1
Posterior cruciate ligament:				
3DFT GRASS	11[e]	1[f]	1	0
2DFT spin echo	11	1[f]	1	0

Note.—3DFT = three-dimensional Fourier transform; GRASS = gradient refocused acquisition in the steady state; 2DFT = two-dimensional Fourier transform.

[a] Two tears seen by MR were in the posterior horn and could have been missed arthroscopically.

[b] Includes two partial meniscectomies.

[c] Anterior horn tear.

[d] Two were possible tears.

[e] Two were probably intact.

[f] One case had history of old trauma.

Cruciate ligament tears were detected more readily by 3DFT GRASS than by 2DFT spin-echo imaging (six vs three with two possible tears on spin-echo imaging). Also, there were fewer incorrect interpretations by 3DFT GRASS imaging (one vs three false positives and zero vs one false negative) (Fig. 4). One false-positive finding by both pulse sequences was attributed to old trauma.

Cartilaginous abnormalities were detected arthroscopically in three of 13 extremities. Only one cartilaginous abnormality was detected on GRASS imaging, while all three cases were thought to be normal on spin-echo images.

In the four cases (five extremities) in which only GRASS images were obtained, one additional medial meniscal tear, one anterior cruciate ligament tear, and three cartilaginous abnormalities were identified correctly. The cartilaginous defects were seen as focal areas of decreased signal when compared with the adjacent normal articular cartilage (Fig. 5). A medial meniscus was incorrectly considered torn.

For the 17 patients (18 extremities) studied in this series, GRASS imaging correctly identified six meniscal tears and two medial meniscectomies, with four false-positive findings and one false-negative interpretation. Cruciate ligament tears were correctly identified in six cases, with one false-positive finding. Of six cases with arthroscopically proved cartilaginous abnormalities, defects were correctly identified on GRASS images in four studies.

The one case of osteonecrosis in our series was correctly identified on all pulse sequences (Fig. 5). Loose bodies were questioned in three cases on GRASS images, only one of which was confirmed arthroscopically.

Discussion

While MR imaging has been shown to be valuable in the assessment of internal derangements of the knee, the best scanning sequences are still evolving [1–10]. Recent technical advances (that is, 3DFT gradient-refocused pulse sequences) have resulted in the ability to produce thin, truly contiguous magnetic images. Conceivably this could improve the accuracy of MR studies by reducing errors associated with volume averaging created by thick slices and large interslice gaps.

In our preliminary series, 3DFT GRASS imaging was as sensitive as 2DFT spin-echo imaging in detecting meniscal abnormalities, with both pulse sequences correctly identifying

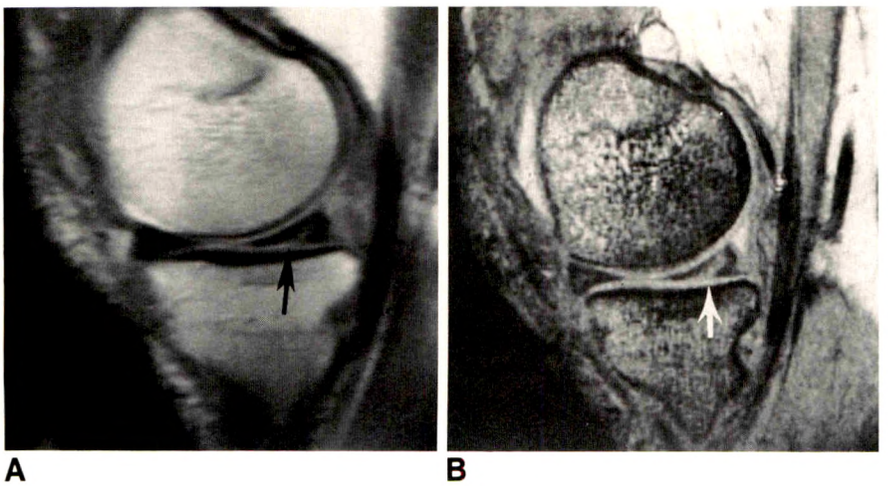

Fig. 3.—MR images of knee of 61-year-old man with arthroscopically confirmed tear in posterior horn of medial meniscus. Both 2DFT spin-echo (TR = 2000 msec, TE = 20 msec) (*A*) and 3DFT GRASS (*B*) images show disruption of posterior horn of medial meniscus (*arrows*).

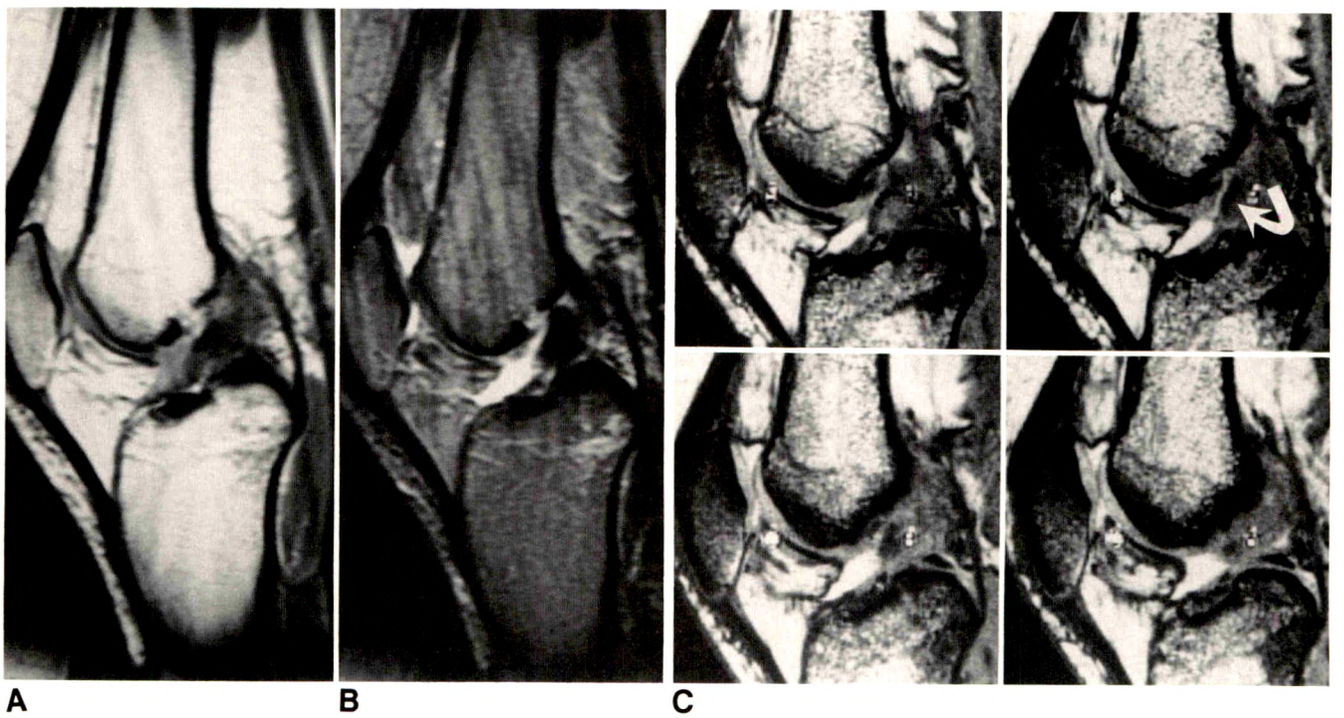

Fig. 4.—MR images of knee of 49-year-old woman with torn anterior cruciate ligament.

A and *B*, 2DFT spin-echo images (TR = 2000 msec, TE = 20 [*A*] and 80 msec [*B*], 5 mm thick, two excitations, 16-cm field of view) show soft tissue in expected region of anterior cruciate ligament. On these images, anterior cruciate ligament was interpreted as being probably intact, although partial tear could not be excluded.

C, 3DFT GRASS images (TR = 60 msec, TE = 16 msec, 30° flip angle, 1.2 mm thick, 16-cm field of view) show residual ligamentous tissue of anterior cruciate (*arrow*), but no attachment to femur.

Complete tear of anterior cruciate ligament was confirmed arthroscopically.

five of six torn menisci and two meniscectomies. The one false negative in both series was a small tear located in the anterior horn of the lateral meniscus. This was clearly seen at arthroscopy. Even in retrospect, this lesion could not be identified by MR imaging.

Six meniscal tears were false positive on spin-echo pulse sequences, and three were false positive with GRASS imaging when compared with arthroscopy. Two of the three possible tears detected on the 3DFT GRASS pulse sequences were located in the posterior horn of the medial meniscus and were also incorrectly identified as tears on the 2DFT spin-echo images. Other studies comparing MR imaging and arthroscopy have reported similar findings [6, 7, 14]. Reicher et al. [7] reported identifying 32 tears of the posterior horn of the medial meniscus in 130 patients, five of which were considered false positive when compared with arthroscopy. Citing other studies [15–18], which reported the accuracy of arthroscopy in detecting posterior horn medial meniscal tears to range from 39 to 95%, Reicher et al. questioned whether at least three of the five false-positive studies in fact represented arthroscopic misses. On review of the MR images in our study, the arthroscopist conceded that meniscal tears

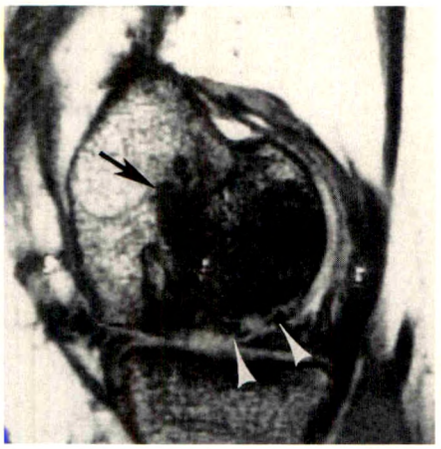

Fig. 5.—MR image of knee of 33-year-old woman with ulcerative colitis on steroids. Osteonecrosis and osteochondritis dessicans of right medial femoral condyle were diagnosed on plain films. Sagittal 3DFT GRASS image (TR = 60 msec, TE = 16 msec, 30° flip angle, 1.2 mm thick, 16-cm field of view) shows abnormally decreased signal in marrow of medial condyle (*arrow*) (compare with Fig. 1). Normal homogeneous appearance of articular cartilage is disrupted by focal areas of decreased signal, suggesting disruption of cartilage (*arrowheads*). At arthroscopy, numerous chondral and osteochondral fragments were identified.

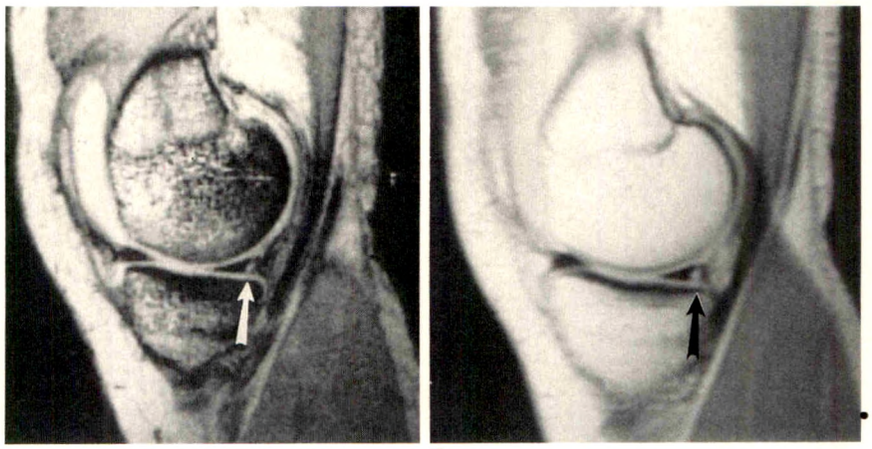

A B

Fig. 6.—MR images of knee of 16-year-old girl with left knee pain and negative arthroscopy. 3DFT GRASS (*A*) and 2DFT spin-echo (TR = 2000 msec, TE = 20 msec) (*B*) images both suggest tear (*arrows*) of posterior horn of medial meniscus. After reviewing MR findings, arthroscopist believed tear could have been missed during arthroscopy.

could have been missed in the two studies in which both the 3DFT GRASS and 2DFT spin-echo images identified tears located posteriorly in the medial meniscus (Fig. 6).

Three of the four remaining false-positive meniscal tears seen on the spin-echo images were located in the lateral meniscus and were interpreted as not representing tears on the GRASS pulse sequence. While the three false-positive meniscal tears detected only on the 2DFT spin-echo images could represent true-positive findings not seen arthroscopically or on the GRASS images, they are more likely the result of misinterpreting degenerative changes as meniscal tears. The thinner 3DFT GRASS slice thickness (1.2 vs 5 mm) may have facilitated the distinction between degenerative changes and true meniscal tears, in accordance with the criteria established by Reicher et al. [7] and Stoller et al. [13] (Fig. 7).

A meniscal tear was incorrectly diagnosed in the posterior horn of the medial meniscus in one of the three cases in which only GRASS images were obtained. In this instance, the arthroscopist believed that he would not have missed a tear of the size suggested by MR. Beltran et al. [19] noted that the decreased signal of the joint capsule was separated from the dorsal aspect of the menisci by a band of higher signal and that this could be confused with a pathologic meniscal separation. In retrospect, what was thought to be a separated meniscal fragment on 3DFT GRASS imaging most likely represented a prominent joint capsule. A similar although not as pronounced appearance was noted on the contralateral side in the same patient.

All six cruciate ligament tears were detected on the GRASS sequences vs three definite cruciate ligament tears and another two possible tears on the corresponding spin-echo images. In addition, three false-positive tears were seen with spin-echo imaging compared with one false-positive tear on the GRASS sequence. The one false-positive finding in both series was attributed to old trauma.

Turner et al. [5] reported that six of nine torn cruciate ligaments and 38 of 39 normal cruciate ligaments were correctly identified by MR. The somewhat poorer accuracy in our spin-echo series may be attributed to several technical factors. We elected to examine patients with their legs extended in a neutral position. This position was chosen so that the patient's leg would more easily remain immobile during the 17-min 3DFT data acquisition. However, externally rotating the knee 20–30° and/or flexing at the knee joint have been shown to visualize the anterior cruciate ligament better [2–4]. The final factor that may have resulted in the poorer accuracy on spin-echo images is partial-volume averaging. Because of the 5-mm slice thickness and 2.5-cm interslice gap used on the 2DFT spin-echo images, the anterior cruciate ligament is often not seen in its entirety, making it difficult to exclude a tear. The contiguous thin slices available with 3DFT imaging, however, allow identification of the entire anterior cruciate, facilitating detection of even partial tears. Partial-volume averaging on spin-echo images could have resulted in both false-positive and false-negative cruciate ligament tears (Fig. 4). The posterior cruciate ligament was often better seen on spin-echo than on GRASS images, although in no instance did this result in an incorrect interpretation on the GRASS pulse sequences.

An insufficient number of cases with documented cartilaginous abnormalities were examined in our series to draw any conclusions about the overall accuracy of 3DFT GRASS

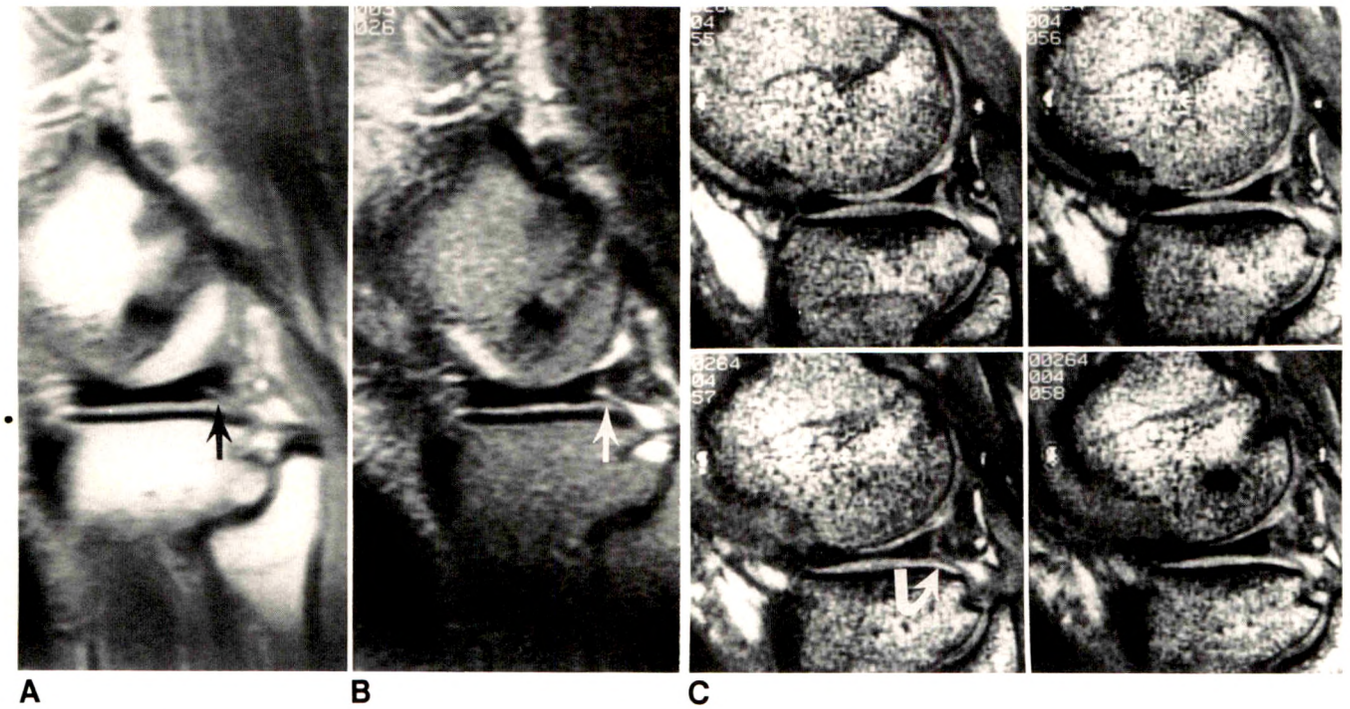

Fig. 7.—*A* and *B*, 2DFT spin-echo images (TR = 2000 msec, TE = 20 [*A*] and 80 [*B*] msec, 5 mm thick, 2.5-mm interslice gap, two excitations 16-cm field of view raise possibility of tear in extreme lateral aspect of lateral meniscus posteriorly (*arrows*).

***C*, 3DFT GRASS images (TR = 60 msec, TE = 16 msec, 1.2 mm thick, 30° flip angle, 16-cm field of view) reveal no abnormality. Possible "tear" caused by partial-volume averaging on spin-echo images is shown to be meniscocapsular ligament (*arrow*). No tear was seen arthroscopically.**

imaging and how it would compare with spin-echo imaging in detecting cartilaginous lesions. Nonetheless, four of six cartilaginous abnormalities were correctly identified by GRASS imaging. The two false-negative cases both had chondromalacia patellae arthroscopically. If the axial plane had been directly imaged or if the 3DFT sagittal data had been reformatted axially, these abnormalities might have been detected. Also contributing to the false-negative problem is the lack of clearly defined MR standards for the diagnosis of chondromalacia patellae. Buckwalter et al. [20] reported correctly identifying 13 of 16 cartilaginous abnormalities by using contiguous, 5-mm-thick, sagittal and coronal spin-echo images. We can reasonably assume that 1.2-mm-thick 3DFT GRASS images would have at least comparable accuracy.

In only one of three cases in which GRASS imaging suggested loose bodies was there arthroscopic confirmation. In the other two cases, the possible loose bodies were located either in the suprapatellar bursa or laterally near the popliteal tendon. Both of these areas can be difficult to see arthroscopically, so it is uncertain whether these cases represent true- or false-positive findings. Geniculate vessels, osteophytes, and occasionally fascial planes surrounded by fat may produce an appearance similar to that of loose bodies on GRASS images unless care is taken in examining adjacent images.

The 3DFT data acquisition has several advantages over its 2DFT counterparts: (1) Because 3DFT pulse sequences excite an entire volume of tissue, truly contiguous slices are obtained, unlike 2DFT pulse sequences, in which cross-talk from adjacent slices may occur [21]. (2) Although signal-to-noise ratio is dependent on a number of instrumental factors including TR, TE, theta, and the number of slices acquired, for the 3DFT data acquisition used in our series, the signal-to-noise ratio was greater than that expected for a 2DFT GRASS image of comparable thickness [22]. The increased signal to noise may be used to obtain thinner slices and/or better in-plane resolution. (3) Practical limitations on band width and gradient output currently limit slice thickness with 2DFT imaging (but not with 3DFT imaging) to approximately 3 mm [23, 24].

Because of the small voxel size, image reformation in multiple orthogonal and oblique planes is possible without additional scanning time or repositioning of the patient. This would be expected to allow better visualization of the cruciate ligaments and possibly better detection of cartilaginous abnormalities.

The primary disadvantage of 3DFT spin-echo imaging has been the long data-acquisition time. However, gradient-refocused imaging with its short repetition enables the scan to be completed within 17 min, making it both a time-saving and cost-effective pulse sequence.

The TR, TE, and flip angle used in this study produce an image with T1, T2*, and proton-density information [11]. However, by varying the parameters, an image can be obtained with either more proton-density or more T2* information. This could replicate the "arthrogram" effect seen by converting synovial fluid to high signal on T2-weighted spin-echo images. Future studies will determine if this will increase

the detectability of meniscal tears and cartilaginous abnormalities.

In conclusion, 3DFT limited-flip-angle gradient-refocused imaging appears to be an accurate, time-effective means of evaluating the knee. In this series, it compares favorably with conventional 2DFT spin-echo imaging in detecting meniscal, cruciate, and cartilaginous abnormalities. These preliminary findings suggest that the overall accuracy of MR imaging of the knee could be improved with the addition of 3DFT gradient-refocused pulse sequences. With the advent of image reformatting and possible adjustment of the imaging parameters, it may well become the pulse sequence of choice for evaluating the knee.

REFERENCES

1. Kean B, Preston B, McKin-Thomas H, Hawkes R. Nuclear magnetic resonance imaging of the knee: examples of normal anatomy and pathology. *Br J Radiol* **1983**;56:355–364
2. Li KC, Henkelman RM, Poon PY, Rubenstein J. MR imaging of the normal knee. *J Comput Assist Tomogr* **1984**;8(6):1147–1154
3. Reicher MA, Rauschning W, Gold RH, Bassett LW, Lufkin RB, Glen W. High-resolution magnetic resonance imaging of the knee joint: normal anatomy. *AJR* **1985**;145:895–902
4. Reicher MA, Bassett LW, Gold RH. High-resolution magnetic resonance imaging of the knee joint: pathologic correlations. *AJR* **1985**;145:903–909
5. Turner DA, Prodromos CC, Petasnick JP, Clark JW. Acute injury of the ligaments of the knee: magnetic resonance evaluation. *Radiology* **1985**;154:717–722
6. Burk DL, Kanal E, Brunberg JA, Johnstone GF, Swensen HE, Wolf GL. 1.5-T surface-coil MRI of the knee. *AJR* **1986**;147:293–300
7. Reicher MA, Hartzman S, Duckwiler GR, Bassett LW, Anderson LJ, Gold RH. Meniscal injuries: detection using MR imaging. *Radiology* **1986**;159:753–757
8. Pollack MS, Dalinka MK, Kressell HY, Lotke PA, Spritzer CE. Magnetic resonance imaging in the evaluation of suspected osteonecrosis of the knee. *Skeletal Radiol* **1987**;16:121–127
9. Hartzman S, Reicher MA, Bassett LW, Duckwiler GR, Mandelbaum B, Gold RH. MR imaging of the knee: Part II. Chronic disorders. *Radiology* **1987**;162:553–557
10. Harms SE, Muschler G. Three-dimensional MR imaging of the knee using surface coils. *J Comput Assist Tomogr* **1986**;10(5):773–777
11. Wehril FW. *Introduction to fast-scan magnetic resonance*, publ. no. 7299. Milwaukee, WI: General Electric Medical Systems, **1986**:1–12
12. Haase A, Frahm J, Matthael D, Hanicke W, Merboldt KD. FLASH imaging. Rapid NMR imaging using low flip-angle pulses. *J Mag Reson* **1986**;67:258–266
13. Stoller DW, Martin C, Crues JV III, Kaplan L, Mink JH. Meniscal tears: pathologic correlation with MR imaging. *Radiology* **1987**;163:731–735
14. Manco LG, Lozman J, Coleman ND, Kavanaugh JH, Bilfield BS, Dougherty J. Noninvasive evaluation of knee meniscal tears: preliminary comparison of MR imaging and CT. *Radiology* **1987**;163:727–730
15. Levinsohn EM, Baker BE. Prearthrotomy diagnostic evaluation of the knee: review of 100 cases diagnosed by arthrography and arthroscopy. *AJR* **1980**;134:107–111
16. Ireland J, Trickey EL, Stoker DJ. Arthroscopy and arthrography of the knee: a critical review. *J Bone Joint Surg [Br]* **1980**;62-B:3–6
17. Thijn CJP. Accuracy of double-contrast arthrography and arthroscopy of the knee joint. *Skeletal Radiol* **1982**;8:187–192
18. Selesnick FH, Nopble HB, Bachman DC, Steinberg FL. Internal derangement of the knee: diagnosis of arthrography, arthroscopy, and arthrotomy. *Clin Orthop* **1985**;198:26–30
19. Beltran J, Noto AM, Mosure JC, Weiss KL, Zuelzer W, Chrostoforidis AJ. The knee: surface-coil MR imaging at 1.5T. *Radiology* **1986**;159:747–751
20. Buckwalter KA, Braunstein EM, Wilson MR, Wojtys EM, Martel W. Evaluation of hyaline cartilage of the knee with MR imaging. *Radiology* **1986**;161(P):239
21. Kneeland JB, Shimakawa A, Wehrli FW. Effect of intersection spacing on MR image contrast and study time. *Radiology* **1986**;158:819–822
22. Brunner P, Ernst RR. Sensitivity and performance time in NMR imaging. *J Mag Reson* **1979**;33:83–106
23. Bureau of Radiological Health. *Guidelines for evaluating electromagnetic exposure risk for trials of clinical NMR systems*. Washington, DC: Department of Health and Human Services, US Public Health Service, Food and Drug Administration, **1982**
24. National Radiological Protection Board. Revised guidance on acceptable limits of exposure during nuclear magnetic resonance clinical imaging. *Br J Radiol* **1983**;56:974

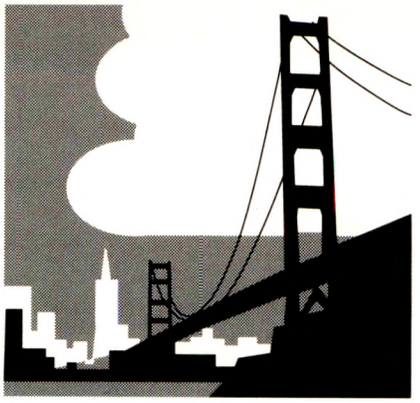

Come to the American Roentgen Ray Society 88th ANNUAL MEETING

San Francisco Hilton
May 8–13, 1988

Scientific Program (200 papers)
Instructional Courses (60 hours)
Categorical Course on Breast Imaging
The Caldwell Lecture
Award Papers
Scientific Exhibits
Social, Golf, and Tennis Programs
Guest Programs

Diagnosis of Osteomyelitis by MR Imaging

Evan Unger[1]
Philip Moldofsky
Robert Gatenby
William Hartz
George Broder

Bone scans are highly sensitive for the diagnosis of acute osteomyelitis, but the difficulty of separating bone-marrow processes from soft-tissue disease limits the specificity and accuracy. A diagnostic technique capable of distinguishing bone-marrow processes from soft-tissue disease would improve the diagnostic accuracy of osteomyelitis. To evaluate the use of MR in the diagnosis of osteomyelitis, MR examinations were performed in 35 patients with suspected acute osteomyelitis. Twelve of these were proved to have osteomyelitis either by surgery (nine patients) or by clinical follow-up (three patients). In the other 23, osteomyelitis was excluded by surgery (12 patients) or by the clinical course (11 patients). Evidence of osteomyelitis on MR consisted of abnormalities of the bone marrow with decreased signal intensity on the T1-weighted images and increased signal intensity on the T2-weighted or short-TI inversion recovery (STIR) images. MR and bone scintigraphy were interpreted by two radiologists who were given no clinical information other than to rule out osteomyelitis. The sensitivities of MR and static bone scan were 100% for bone-marrow abnormality. Because bone-marrow abnormality in osteomyelitis associated with healing fractures was incorrectly diagnosed by MR (one case) and bone scintigraphy (two cases), the sensitivities of MR and scintigraphy for the diagnosis of osteomyelitis were 92% and 82%, respectively. The specificities of MR and scintigraphy were 96% and 65%, respectively ($p < .05$). The overall accuracy for the diagnosis of osteomyelitis was 94% for MR and 71% for bone scan ($p < .05$).

Because of its ability to separate soft-tissue disease from underlying bone marrow, MR may be used to evaluate patients with positive bone scintigraphy to improve the specificity and accuracy of diagnosis for osteomyelitis.

Distinguishing osteomyelitis from soft-tissue infection adjacent to bone is of paramount clinical importance. The latter may be treated with local care, a short course of antibiotics, and minor surgery. Osteomyelitis is more refractory to treatment, and prolonged IV antibiotics and, in some cases, bony debridement are required.

This distinction is made with difficulty by bone scintigraphy. Radionuclide uptake associated with cellulitis may simulate uptake in osteomyelitis. Because of poor spatial resolution, nuclear medicine techniques may confuse conditions such as healing fractures or arthritis with osteomyelitis. Because of its sensitivity to changes in fat and water, MR is able to detect bone-marrow processes such as infection and should be able to differentiate isolated soft-tissue abnormality from underlying marrow involvement. To evaluate MR in the diagnosis of osteomyelitis, we performed MR scans on 35 consecutive patients who were clinically suspected to have acute osteomyelitis and compared the results with those of bone scintigraphy.

Materials and Methods

Thirty-eight MR examinations were performed in 35 consecutive patients who were clinically suspected to have acute osteomyelitis. There were 20 males and 15 females ranging in age

Received September 11, 1987; accepted after revision November 20, 1987.

[1] All authors: Fox Chase Cancer Center and the Jeanes Hospital, Philadelphia, PA 19111. Address reprint requests to E. Unger, Division of Nuclear Magnetic Resonance, Fox Chase Cancer Center, 7701 Burholme Ave., Philadelphia, PA 19111.

AJR 150:605–610, March 1988
0361–803X/88/1503–0605
© American Roentgen Ray Society

from 1 to 84 years (mean, 52 years). Fourteen (40%) of the patients had diabetes.

The parts examined were the feet (nine patients), ankles (seven patients), tibia (two patients), knees (two patients), pelvis (three patients), hips (five patients), spine (two patients), hands (two patients), elbows (two patients), and skull (one patient).

All MR examinations were performed on a Siemens 1.5-T Magnetom. The spin-echo technique was used. Helmholtz surface coils (17 cm) were used to examine feet, ankles, knees, hands, and elbows; in two examinations of the forefoot, the orbit coil was used. The legs and skull were examined with a 30-cm head coil. An elliptical surface coil was used for spine examinations, and the hip and pelvis were examined with the body coil. T1-weighted images were obtained with 400–450/16 (TR/TE). T2-weighted spin-echo images were obtained with 2500/28 in 35 examinations and 3500/70 in three examinations . To evaluate the use of different pulse sequences, triggered gradient-echo fast low-angle shot (FLASH) images were made with a flip angle of 30° in two spine examinations. In 11 examinations, STIR (short inversion time recovery) with inversion time (TI) = 100–110 and TR/TE 2500/16–28 was performed in addition to spin-echo images. Slice thickness ranged from 8 mm in large bones to 3 mm in small bones.

Thirty-three (94%) of the 35 patients having MR studies also had scintigraphy. The scintigrams were performed within several hours of MR (16 cases), within 1 day (five cases), within 2 days (six cases), and within 4 days (four cases).

Delayed single-phase bone scintigraphy was performed using 20 mCi (540 MBq) ^{99m}Tc methylene diphosphonate given intravenously. Images were obtained with a gamma camera.

Criteria for osteomyelitis on MR were focal abnormal signal intensity in bone marrow on either T1-weighted (decreased signal intensity) or T2-weighted (increased signal intensity) images. Normal uninvolved marrow was used as a reference standard. Criteria on bone scintigraphy was focal osseous radionuclide activity not typical of arthritis.

MR studies and scintigrams were interpreted prospectively by two observers in a blinded fashion without knowledge of the results of the other study and with no clinical information other than an instruction to rule out osteomyelitis. The examinations were evaluated again by four observers after the diagnoses were established, and the interpretations were compared. The images were studied to compare the extent of soft-tissue and bone-marrow abnormality.

The diagnosis of acute osteomyelitis was confirmed in 12 of the 35 patients (34%). In nine of these, the diagnoses were established by surgery. In the other three, the diagnoses were confirmed clinically. In 12 of the other 23 cases, the absence of osteomyelitis was confirmed by surgery. In the other 11, the absence of infection was proved clinically. Follow-up in these patients was for a minimum of 3 months.

The sensitivity, specificity, and accuracy of MR and bone scintigraphy for diagnosis of acute osteomyelitis was calculated for the patients having either MR or bone scintigraphy. For statistical analysis of the relative accuracy of MR and bone scintigraphy, only those cases with both MR and bone scintigraphy (performed within 4 days of MR) were compared using the Fischer exact test (two-tailed).

Results

Patients with osteomyelitis (12 cases) had decreased signal intensity in the bone marrow on T1-weighted images that was generally equal to that of adjacent muscle; they also had increased signal intensity on T2-weighted images, ranging from slightly greater to much brighter than that of bone marrow and approaching the signal intensity of water (Figs. 1 and 2). STIR, performed in five cases that were positive for osteomyelitis, showed a dramatic increase in the signal intensity of bone marrow corresponding to the region of infection. Except for the case of *Staphylococcus aureus* discitis, shown in Figure 2, all other cases of osteomyelitis had high signal intensity in the soft tissue adjacent to the area of osseous infection.

In all acute cases of osteomyelitis, both MR and bone scans showed at least some area of bone-marrow abnormality. In cases associated with healing fractures, MR findings were negative for osteomyelitis in one case and bone scintigraphy findings were negative for osteomyelitis in two cases.

In seven cases, bone scintigraphy was falsely positive for osteomyelitis. In five of these cases, overlying soft-tissue activity could not be separated from underlying bone marrow. In two additional cases (one of healing fracture and the other of erosive enthesitis), diagnoses of osteomyelitis were also incorrect. Except for the case of enthesitis, MR showed normal bone marrow. Bone scintigraphy performed in diabetics had a particularly high false-positive rate. Five (36%) of the fourteen patients with diabetes had bone scintigraphy findings that were false positive for osteomyelitis. MR showed normal bone marrow with soft-tissue disease or fracture in these cases and was correctly interpreted as negative for osteomyelitis. Follow-up studies confirmed the absence of osteomyelitis in these patients.

Cellulitis (10 patients without osteomyelitis) and soft-tissue disease associated with osteomyelitis had increased signal intensity on the T2-weighted image (approaching the intensity of water), infiltrating fat and in some cases muscle. On the T1-weighted image in those cases with soft-tissue infection involving fat, there was decreased signal intensity in fat. Even when cellulitis extended to the periosteal tissue, the bone marrow showed normal signal intensity in the absence of osteomyelitis (Fig. 3).

Soft-tissue abscesses (four patients) were seen as focal, well-defined fluid collections within soft tissue with high signal intensity similar to that of water on T2-weighted or STIR images. On T1-weighted images, abscesses had signal intensity ranging from slightly less to slightly greater than that of muscle.

Septic arthritis (four patients) was shown as fluid collections within joint spaces with signal intensity similar to that of water on the T2-weighted image and less than to slightly greater than that of muscle on the T1-weighted image. Unless involved by osteomyelitis, bone marrow showed normal signal intensity (Fig. 4).

Healed osteomyelitis was examined as a follow-up study in one patient after successful treatment of acute osteomyelitis and in three other patients who had old healed osteomyelitis but who were clinically suspected of having new acute osteomyelitis. Follow-up studies confirmed the absence of osteomyelitis in these patients. MR showed increased signal intensity on the T1-weighted image and normal signal intensity on the T2-weighted image or slightly decreased signal intensity on the gradient-echo image (Fig. 2) corresponding to the region of healed bone marrow.

STIR examinations performed in 11 cases provided high contrast between normal and diseased bone marrow and soft

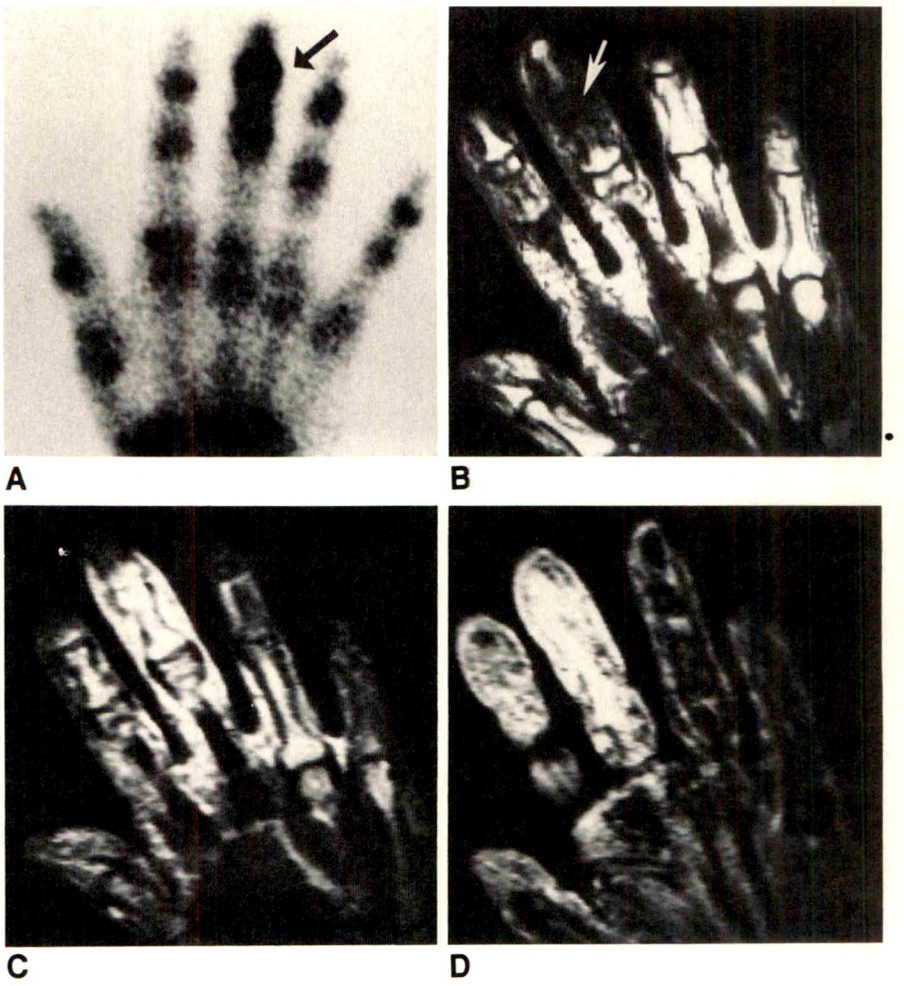

Fig. 1.—77-year-old woman who developed osteomyelitis after steroid injection into a cyst in third finger of right hand.

***A*, Bone scan shows increased activity in third finger of right hand (*arrow*) centered about distal interphalangeal joint.**

***B*, T1-weighted image (300/16). 3-mm slice shows decreased signal intensity (*arrow*) of bone marrow in distal and proximal portion of middle and distal phalanges, respectively, of third finger. Fusiform soft-tissue swelling with decreased signal intensity is seen.**

***C*, T2-weighted image (2500/70). 3-mm slice at a similar level shows fusiform high-signal-intensity soft-tissue swelling. There is generalized increased signal intensity of middle phalanx and proximal third of distal phalanx of third finger.**

***D*, STIR (short-TI inversion recovery) image (2500/110/16). 3-mm slice shows high signal intensity affecting soft tissues and entire middle and distal phalanges of third finger.**

tissue. On STIR with an inversion time of 100–110 msec set at the crossover time of fat (approximately two-thirds the T1 of fat), fatty bone marrow and subcutaneous fat appeared dark and hematopoietic bone marrow appeared somewhat brighter. Muscle also appeared dark but was brighter than subcutaneous tissue. Fluid-filled structures (e.g., bladder or spinal fluid) appeared very bright. Osteomyelitis and cellulitis were depicted as areas of markedly increased signal intensity involving bone marrow and soft tissue, respectively. The contrast on STIR images between abnormal bone marrow or soft-tissue disease and adjacent tissue generally appeared greater on STIR images than on spin-echo images.

The sensitivity, specificity, and accuracy of MR and scintigraphy for the diagnosis of osteomyelitis are shown in Table 1. The sensitivity of MR and bone scans were comparable, but the specificity and accuracy of MR were greater than those of scintigraphy ($p < .05$).

Discussion

Osteomyelitis can be difficult to diagnose clinically. Although nuclear medicine techniques are helpful, their specificity may be decreased by the difficulty of differentiating between bone-marrow processes and soft-tissue disease [1]. A previous investigation compared the prospective accuracy of MR with combined bone/gallium studies in the evaluation of spinal osteomyelitis and found MR and nuclear medicine comparable [2]. The difference between our results and those of MR imaging of spinal osteomyelitis most likely reflects differences in the patient population and the different degree of associated or coexisting soft-tissue disease in the two groups. In spinal osteomyelitis, most infections are probably blood borne and soft-tissue disease will not usually antecede infection [3]. In the extremities where soft-tissue infection adjacent to bone marrow is more prevalent, this is more apt to decrease the specificity of bone scintigraphy in excluding osteomyelitis [4].

Many of the bone scans that were falsely positive for osteomyelitis were performed in diabetics with cellulitis and chronic skin ulcers. Periostitis probably coexisted with soft-tissue disease in these patients. Still, MR showed normal signal intensity of the bone marrow except when osteomyelitis was actually present or in other cases of bone marrow disease (e.g., metastasis or bony erosion caused by enthesitis).

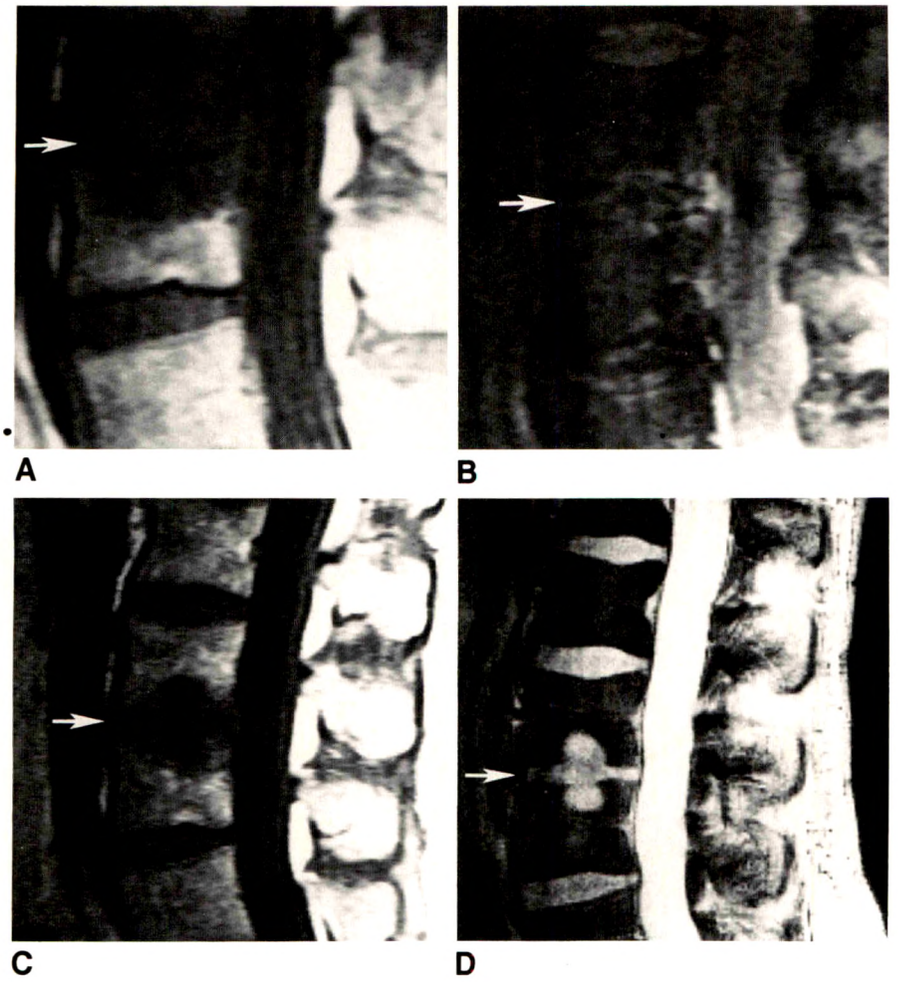

Fig. 2.—39-year-old man with back pain, fever, *Staphylococcus aureus* sepsis, and discitis at L3–L4.

***A*, T1-weighted image (450/16) shows decreased signal intensity of bone marrow adjacent to L3–L4 disk space (*arrow*).**

***B*, T2-weighted image (2500/70) shows near isointense bone marrow with subtle speckled areas of increased signal intensity adjacent to L3–L4 disk (*arrow*).**

***C*, Follow-up examination performed 3 months after therapy with clinical response. T1-weighted image (450/16) shows increased signal intensity adjacent to L3–L4 disk as compared with that in pretreatment study (*arrow*), which most likely represents increased or regeneration of fat in healing areas of bone marrow. There is loss of disk height and irregularity of vertebral end plates.**

***D*, Gradient-echo fast low-angle shot (FLASH) image with 30° tip angle (TR = approximately 1 sec, gated to heart rate/TE 13). Slight decreased signal intensity in vertebral end plates is seen. There is loss of disk height (*arrow*) with protrusion of high-signal-intensity material into adjacent central vertebral end plates.**

The results of this study in some respects are similar to those recently reported by Beltran et al. [4]. In Beltran's experience, and in ours, it does appear that MR can be used to separate soft-tissue disease from bone-marrow disease and that osteomyelitis and soft-tissue infections appear on T2-weighted images as areas of increased signal intensity. Our results differ, however, in the relative sensitivity of T1- and T2-weighted sequences for the detection of diseased bone marrow. In our experience, osteomyelitis involving fatty bone marrow is better shown on T1-weighted images. Beltran used a less T1-weighted technique (longer TR and TE) than we did, and this may explain some of the differences in our results. Additionally, in our four cases of abscesses, we did not see a halo of decreased signal intensity.

The findings in osteomyelitis of decreased signal intensity in the bone marrow on the T1-weighted image and increased signal intensity on the T2-weighted image most likely reflect a decrease in the fat of the bone marrow and probably an increase in water content within the bone marrow suggested by the T2-weighted image. The STIR sequence that suppresses signal from fat showed increased signal in osteomyelitis, indicating an increase in water fraction within the bone marrow. Increased water fraction may correspond to hyperemia or edema.

In 11 of 12 cases, osteomyelitis was associated with signal changes in the adjacent soft tissue. Soft-tissue signal intensity changes may be helpful in differentiating osteomyelitis from conditions such as metastasis in which soft-tissue involvement may be minimal.

An interesting finding in this study was the signal-intensity change observed in four cases of healed osteomyelitis. The T1-weighted images showed increased signal intensity within the bone marrow. The increase in signal intensity on the T1-weighted image most likely reflects an increase in fat within a portion of the bone marrow and a decrease in the hematopoietic element.

As evidenced by the healing fracture that was false negative for infection on MR and by the findings of other investigators [5], it may be difficult to diagnose osteomyelitis with MR in patients who have had a previous fracture or surgery [5]. Also, the presence of pins or plates in the bone will result in artifacts that may make interpretation difficult on MR [6]. These artifacts are more severe at higher field strengths, and on our 1.5-T system, hip prostheses, pins, screws, and other metallic devices result in marked artifacts that often preclude evaluation of the adjacent bone marrow.

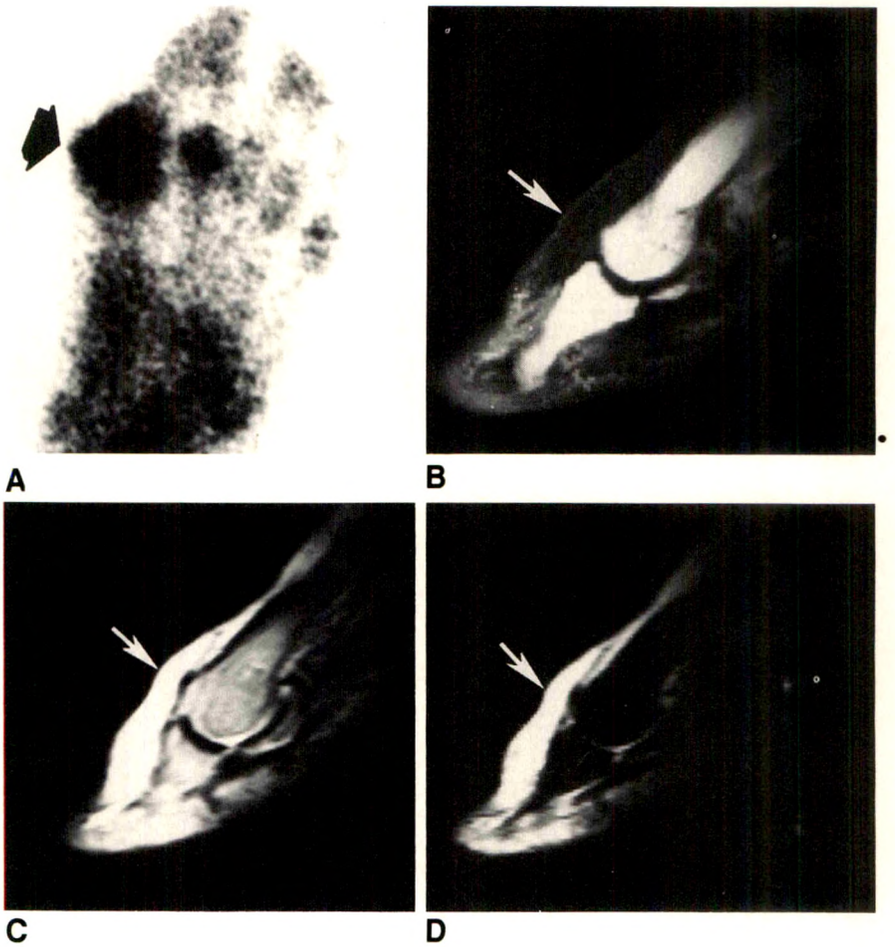

Fig. 3.—86-year-old diabetic woman with cellulitis of left great toe.

A, Bone scan (plantar view) shows increased activity in left great toe at first metatarsal phalangeal joint (*arrow*).

B, T1-weighted image (450/16) of left great toe shows normal high–signal-intensity fatty bone marrow with low-signal swelling of subcutaneous tissue anterior to first metatarsal phalangeal joint (*arrow*).

C, T2-weighted image (2500/70) shows normal–signal-intensity bone marrow with high–signal-intensity swelling of subcutaneous tissue (*arrow*).

D, STIR image (2500/100/30) shows normal appearance of low–signal-intensity bone marrow with high signal intensity in swollen subcutaneous tissue (*arrow*).

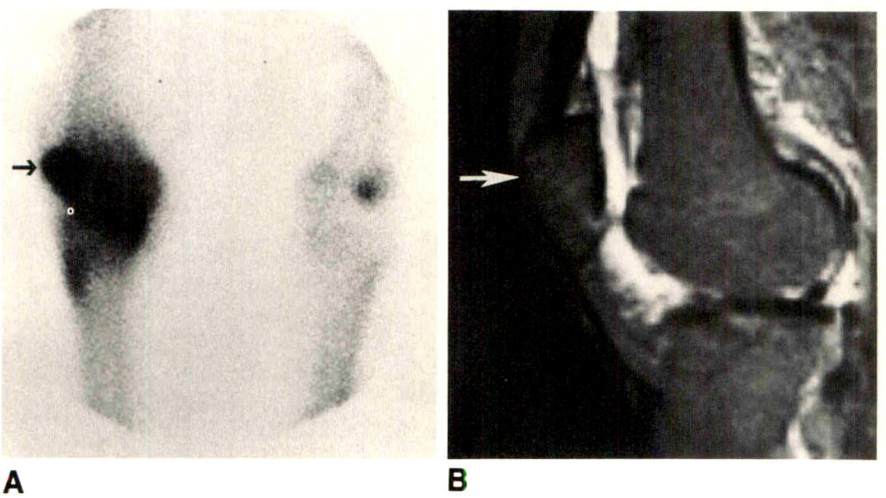

Fig. 4.—84-year-old woman with *Escherichia coli* septic arthritis of right knee.

A, Bone scan shows generalized increased activity around right knee joint and focal intense activity in patella (*arrow*), prospectively interpreted on bone scan as possible patellar osteomyelitis.

B, T2-weighted image (sagittal view) shows loculated high–signal-intensity effusion in right knee joint. Normal intermediate signal intensity is seen in bone marrow of patella (*arrow*), femur, and tibia.

The results of this study indicate that MR is helpful for evaluating osteomyelitis and increases the specificity of diagnosis. An important finding was the ability of MR to differentiate soft-tissue infection from bone-marrow involvement, particularly in diabetic patients. In this study, diabetics with chronic skin ulcers and cellulitis had normal–signal-intensity bone marrow on MR in the absence of bone-marrow infection.

In our experience, both T1- and T2-weighted spin-echo sequences are usually necessary for evaluating soft-tissue infection and osteomyelitis with MR. Generally, soft-tissue

TABLE 1: Comparison of MR and Bone Scintigraphy in the Diagnosis of Osteomyelitis

Findings	MR[a]	Bone scan[b]
True positive	11/12	9/11
True negative	22/23	13/20
False positive	1/23	7/20
False negative	1/10	2/10
Sensitivity	92%	82%
Specificity	96%	65%
Accuracy	94%	71%

Note.—The difference between the specificity of MR and the specificity of bone scan was statistically significant ($p < .05$), as was the accuracy of MR vs that of bone scan ($p < .05$).

[a] $n = 35$.

[b] $n = 31$.

disease is much better seen with the T2-weighted technique. Fatty bone marrow is better evaluated with the T1-weighted technique. STIR may be particularly useful for evaluating osteomyelitis and soft-tissue infection because STIR provides high contrast for both bone marrow and soft tissue. Indeed, since in STIR, T1- and T2-weighted contrast are additive, it could be possible to perform STIR sequences alone and have the sensitivity of a T1-weighted sequence for the fatty bone marrow and that of a T2-weighted sequence for the soft tissues. This would significantly decrease scan time and thus warrants further evaluation.

It should be cautioned that the bone-marrow findings of acute osteomyelitis on MR are nonspecific. Noninfectious inflammatory conditions of bone and healing fractures and metastases may have signal intensity changes that are similar to those seen in osteomyelitis [7, 8]. However, MR findings of decreased signal intensity in the bone marrow on the T1-weighted image with increased signal intensity on the T2-weighted image, in combination with the appropriate clinical setting, should be highly accurate for the diagnosis of osteomyelitis.

Because of the relatively limited experience thus far, MR should not be considered the initial test for osteomyelitis. Rather, we recommend that bone scintigraphy be performed because, if scintigraphy is negative, then osteomyelitis can be excluded with reasonable accuracy. If bone scintigraphy is positive and there is clinical evidence of soft-tissue disease, then MR demonstration of abnormal bone marrow will confirm the diagnosis of osteomyelitis. Conversely, if MR shows normal bone marrow and coexisting soft-tissue disease, then osteomyelitis should be excluded.

ACKNOWLEDGMENTS

The authors thank Jeanette Hengy for manuscript preparation, Sue Higman, Phyllis Hendy, and Tammy Willard for imaging, and Samuel Litwin for statistical analysis.

REFERENCES

1. Freeman LM. *Freeman and Johnson's clinical radionuclide imaging*. 3rd ed., vol. 2. New York: Grune & Stratton, **1984**:1333–1339
2. Modic MT, Feiglin DH, Piraino DW, et al. Vertebral osteomyelitis: assessment using MR. *Radiology* **1985**;157:157–166
3. Kahn DS, Pritzker KPH. The pathophysiology of bone infection. *Clin Orthop* **1973**;96:12–19
4. Beltran J, Noto AM, McGhee RB, et al. Infections of the musculoskeletal system: high-field-strength MR imaging. *Radiology* **1987**;164:449–454
5. Berquist TH, Brown M, Fitzgerald R, May G. Magnetic resonance imaging: application in musculoskeletal infection. *Mag Reson Imag* **1985**;3:219–23
6. Modic MT, Pflanze W, Feiglin DH, Belhobek G. Magnetic resonance imaging of musculoskeletal infections. *Radiol Clin North Am* **1986**;24:247–258
7. Porter BA, Shields AF, Olson DO. Magnetic resonance imaging of bone marrow disorders. *Radiol Clin North Am* **1986**;24:269–274
8. Daffner RH, Lupetin AR, Dash N, et al. MR in the detection of malignant infiltration of bone marrow. *AJR* **1986**;146:353–358

Spinal Pseudarthrosis Complicating Ankylosing Spondylitis: Comparison of CT and Conventional Tomography

Fu-Luk Chan[1]
Eric K. W. Ho[2]
Edward M. T. Chau[1]

Pseudarthrosis, a functional false joint, is an important mechanical complication of advanced ankylosing spondylitis. For correct determination of prognosis and therapy, the presence and extent of the abnormality must be assessed accurately. CT findings in 18 patients with 22 pseudarthroses were compared with the results of conventional tomography. The condition was confirmed by surgery in nine patients (50%). CT scans clearly characterized the pseudarthrosis, providing data not provided by conventional tomography in 17 (77%) of the 22 lesions. CT showed irregular diskovertebral osteolysis with reactive sclerosis and more frequently detected the vacuum phenomenon and paraspinal swellings. In all cases, CT showed either a fracture or mobile facet joints in the posterior elements and allowed clear differentiation between the two. In four cases, such differentiation was impossible on conventional tomograms. Associated spinal stenosis was suspected on conventional tomograms in three lesions, but it was shown clearly by CT in 10 lesions.

Our results suggest that CT offers considerable advantages over conventional tomography in the investigation of spinal pseudarthrosis complicating ankylosing spondylitis.

One of the most important complications of ankylosing spondylitis is spinal pseudarthrosis caused by chronic progressive diskovertebral osteolysis and replacement by fibrous tissue. Pseudarthrosis is a state of mobile nonunion that functions as a false joint. Evaluation of the abnormality is necessary to establish the diagnosis and to assess the extent and severity of the condition. It has been studied by conventional radiography [1, 2], scintigraphy [3], and specimen radiography [4]. We obtained CT scans in 18 patients with this abnormality and compared the findings with the results of conventional tomography.

Subjects and Methods

Eighteen patients (16 men and two women ranging in age from 24 to 70 years; mean age, 38) who had a total of 22 spinal pseudarthroses associated with long-standing ankylosing spondylitis were selected for study. All patients had complete rigidity of the thoracolumbar spine, localized back pain, and tenderness on palpation over the pseudarthrosis. In all cases, the abnormality was evaluated before surgery by plain films, tomography, and CT. Two patients had pseudarthroses at two levels. The most commonly affected segments were T11–T12 (n = 4), T12–L1 (n = 7), and L1–L2 (n = 5). In nine patients, pseudarthrosis was confirmed by subsequent surgery and pathologic findings. The diagnosis was established in the other patients by a combination of clinical and radiographic findings. A postoperative CT evaluation was performed in two patients because of a recurrence of back pain 1 year after anterior spinal fusion; both patients were found to have developed a new pseudarthrosis.

CT was performed on a General Electric 9800 system (Milwaukee, WI) in 17 patients and on a General Electric 8800 system in one patient. In seven patients, two CT studies were performed. Most patients were examined in the supine position, with tilting of the gantry when necessary. Patients with significant kyphosis were scanned in the lateral decubitus position. Sequential, unenhanced 3-mm-thick axial CT slices were obtained at 3-mm intervals

Received August 11, 1987; accepted after revision November 5, 1987.

[1] Institute of Radiology & Oncology, Department of Diagnostic Radiology, Queen Mary Hospital, Pokfulam Rd., Hong Kong. Address reprint requests to F.-L. Chan.

[2] Department of Orthopedic Surgery, University of Hong Kong, Queen Mary Hospital, Hong Kong.

AJR 150:611–614, March 1988
0361–803X/88/1503–0611
© American Roentgen Ray Society

at the level of the affected interspace and the two adjacent vertebrae. The scans were obtained by using a bone algorithm, with a 13-cm field of view. Selected scans had additional retrospective reconstruction in a standard or soft-tissue algorithm. Reformations were acquired in the sagittal, coronal, and oblique planes in all cases.

Localized anteroposterior and lateral plain radiographs of the affected portion of the spine were obtained at presentation and at annual follow-ups. Sagittal and coronal conventional tomograms were obtained in the helical mode at 5-mm intervals.

The CT scans were analyzed by two radiologists independently. In all patients the findings were compared with the information obtained from plain films and tomograms. Follow-up CT scans, obtained in five patients preoperatively and in two patients postoperatively, were correlated with previous studies.

• Results

CT, plain radiography, and conventional tomography showed irregular osteolysis of the end plates and adjacent vertebral bodies on each side of the affected disk. Such changes were detected equally well by the three techniques, although axial CT scans showed the cross-sectional display of the osteolysis in detail (Figs. 1 and 2). The sagittal reformatted images were more useful than the axial scans in delineating the axial extent of the osteolysis and the axial relations of the vertebrae at the level of the pseudarthrosis. Various degrees of sclerosis adjacent to the osteolysis were observed equally well by the three techniques.

CT scans identified the vacuum phenomenon in the intervertebral space in seven cases, only two of which were evident on plain radiographs or tomograms. In three cases, CT scans showed mild paravertebral soft-tissue swelling that had not been observed on plain films or tomograms.

Associated features were detected in the posterior spinal elements of the affected segment with evidence of a mechanical defect. Either a transverse fracture in the posterior elements (n = 15) or a nonankylosed facet joint (n = 5) was shown, and the two were easily differentiated on CT scans (Fig. 3). Plain films and conventional tomograms failed to detect the posterior element defect in one case and incorrectly diagnosed the nature of the posterior defect in four cases. These cases were clarified by the CT studies. On axial CT scans, a transverse fracture appeared as an irregular, linear hairline radiolucency, measuring up to a few millimeters wide, usually running in a horizontal direction across the ankylosed posterior spinal elements without predilection for any particular anatomic structures (Fig. 1). In four cases, the bones bordering the transverse fracture were fragmented. Depending on the angle of the CT section relative to the plane of the transverse fracture, such fractures were difficult to diagnose on axial scans alone in five lesions. In these cases, the transverse fracture was evident on oblique coronal reformatted images (Fig. 4). Hypertrophy and sclerosis were present in the related posterior bony elements to various degrees in 10 lesions. CT also detected the vacuum phenomenon in the nonankylosed joints in two cases, while conventional tomography did not.

Assessment of the spinal canal by the cross-sectional display of CT was superior to that by either plain films or tomograms. Encroachment on the spinal canal at the pseudarthrotic segment was suspected on conventional tomograms in three cases, but it was diagnosed by CT in 10 cases. The axial CT scans together with the reformatted images clearly assessed the presence, nature, and severity of the spinal stenosis. They delineated the causes of the spinal stenosis, which included severe acute kyphos (n = 1), posterior osteophytosis (n = 2), osseous overgrowths at the anterior aspect of the transverse fracture of the posterior spinal elements (n = 4) (Figs. 5 and 6), free bone fragments (n = 2) (Fig. 7A), and ossified ligamentum flavum (n = 1). Subarticular canal stenosis from hypertrophic changes of the transverse fracture involving the pars interarticularis was observed in one case.

In five patients who had preoperative follow-up CT scans at intervals of 1.5–3 years after the initial study, the diskovertebral osteolysis was not progressive in three, although a vacuum phenomenon of the intervertebral disk became evident in one. One patient with pseudarthroses at T11–T12

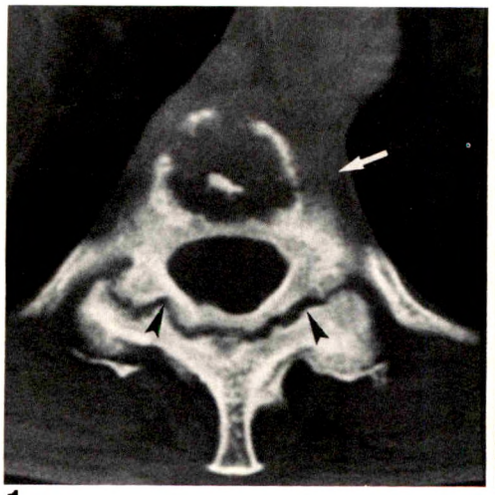

1

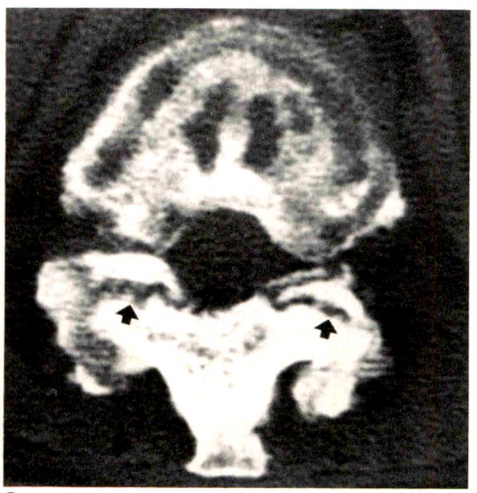

2

Fig. 1.—CT scan of 34-year-old man with pseudarthrosis at T10–T11 segment shows nearly complete osteolysis of vertebral body. Well-defined irregular transverse fracture (*arrowheads*) of laminae and articular process is evident. Slight paravertebral swelling (*arrow*).

Fig. 2.—CT scan of T11–T12 segment of a 24-year-old man shows patchy, circumscribed areas of osteolysis in vertebral body. Irregular transverse fracture (*arrows*) is present across ankylosed facet joints, associated with marked osteosclerosis of articular processes and laminae.

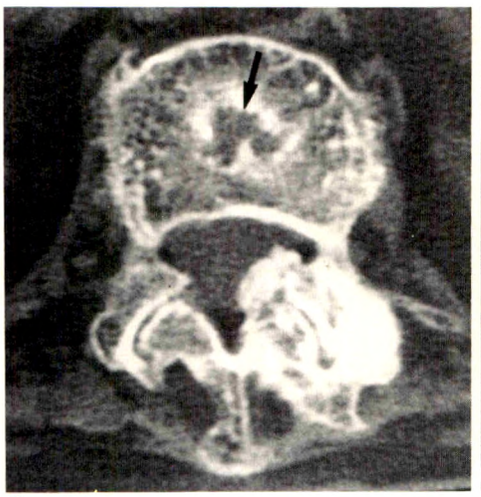

Fig. 3.—CT scan of 70-year-old woman with nonankylosed facet joints at L1–L2 level shows marked hypertrophic changes around left facet joint, leading to narrowing of left posterior portion of spinal canal. Slight osteolysis is noticed in vertebral body (*arrow*).

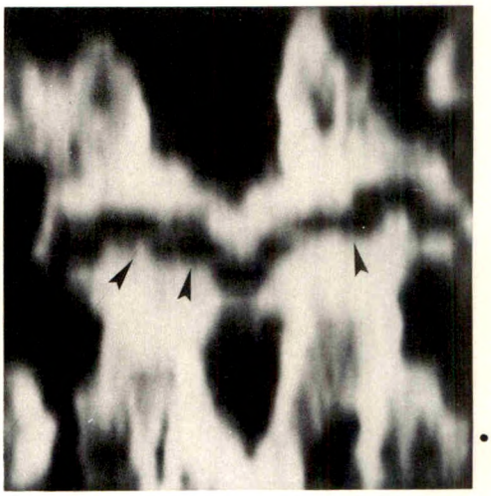

Fig. 4.—Coronal reformation of ankylosed posterior spinal elements of T11–T12 segment of a man with spinal pseudarthrosis clearly delineates complete transverse fracture (*arrowheads*) seen poorly on transaxial scans.

3 4

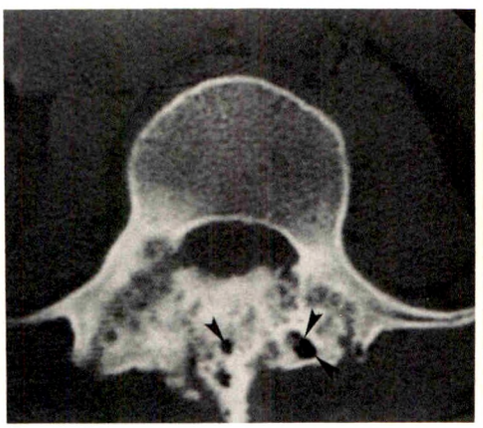

Fig. 5.—CT scan of pseudarthrosis at L2–L3 segment shows diffuse narrowing of spinal canal caused by thickening of bones around transverse fracture. Vacuum phenomenon in the form of areas of gas density (*arrowheads*) is present on fragmented parts of transverse fracture, suggesting mechanical instability.

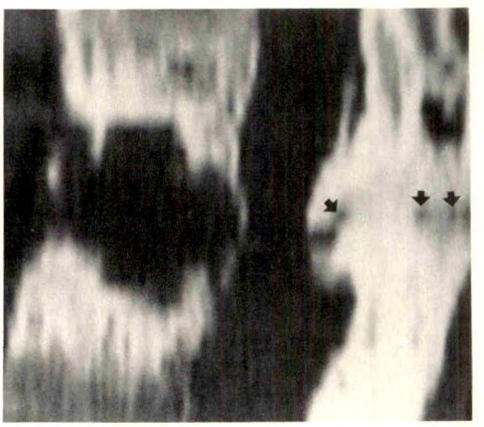

Fig. 6.—Sagittal reformation of spinal pseudarthrosis at T11–T12 level shows extent and axial relations of vertebral body osteolysis and posterior transverse fracture (*arrows*). Osteophytes on anterior aspect of transverse fracture are causing focal spinal stenosis.

5 6

and L3–L4 had spontaneous ankylosis at the lower lesion, whereas the upper one showed progressive deterioration owing to diskovertebral osteolysis. Follow-up in another patient showed widening of the transverse fracture of the posterior elements and progressive diskovertebral osteolysis. In two cases, the osseous overgrowths at the anterior aspect of the transverse fracture of the posterior elements became larger.

Postoperative CT studies in two patients in whom symptoms recurred after an initial good response to anterior spinal fusion showed ankylosis at the operated segments, whereas new pseudarthroses appeared at one or two segments caudal to the initial lesions. In one patient, only a transverse fracture of the posterior elements was detected at the new lesion before the development of diskovertebral osteolysis (Fig. 7B).

Discussion

CT has been used to evaluate various components of ankylosing spondylitis including sacroiliitis [5], apophyseal changes [6], associated muscle atrophy [7], spinal fractures [8], cauda equina syndrome with dural ectasia and subarachnoid diverticuli [9], ossification of the posterior longitudinal ligament [10], and spinal stenosis [11]. To the best of our knowledge, no other report discusses CT findings in a relatively large group of patients with pseudarthrosis complicating this disease.

Among the different types of erosive diskovertebral lesions that occur in long-standing ankylosing spondylitis, pseudarthrosis is the most important biomechanical complication. It is painful and progressive, sometimes is associated with neurologic sequelae, and often requires surgery. In patients with spinal pseudarthrosis, the essential radiographic feature is diskovertebral osteolysis, and its evaluation by plain radiography has been described fully in the literature [1, 2]. In addition, an area of mechanical weakness is present in the posterior spinal elements in the form of a transverse fracture or nonankylosed facet joints. The differentiation between them is important because patients with nonankylosed joints frequently have a milder clinical course and better prognosis. The mechanical weakness of the posterior elements has also been shown to initiate and contribute toward the development

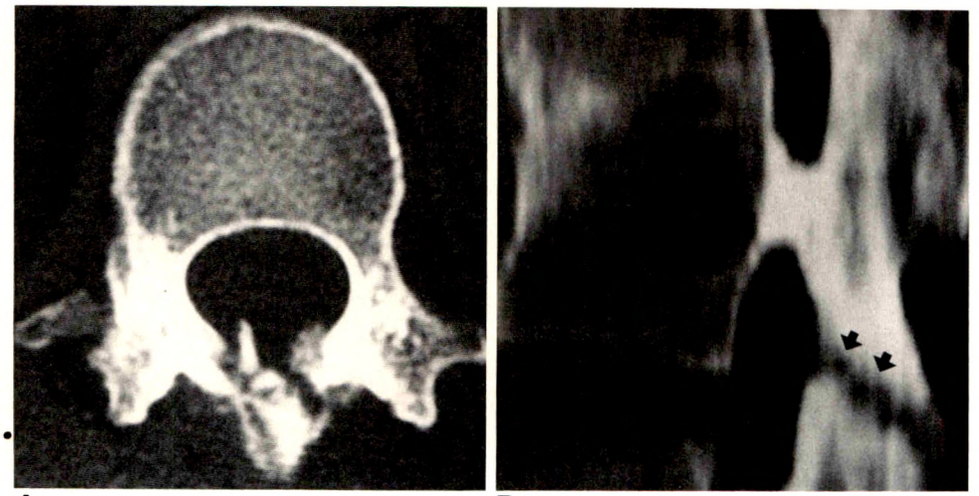

Fig. 7.—CT scans of 33-year-old man with pseudarthrosis at L1–L2 segment.

***A*, Preoperative CT scan shows fragmentation in posterior fracture of L1, with free bone fragment protruding into spinal canal.**

***B*, 2 years after anterior spinal fusion of L1–L2 segment. Sagittal reformation of postoperative CT study shows stable union at operative site. A new transverse fracture is observed at inferior articular facets of L2 (*arrows*). Vertebral bodies of L2 and L3 are still preserved.**

of the diskovertebral osteolysis [12]. Changes in the posterior elements are difficult to interpret on plain films or tomograms because of the abnormal spinal curvature with superimposition and the heavily ossified spinal ligaments. These difficulties are overcome by CT because of its cross-sectional nature.

In pseudarthrosis, CT scans clearly locate the diskovertebral osteolysis in the transverse plane. CT readily diagnoses mild paravertebral soft-tissue swelling, which may be reactive to the biomechanical derangement. Conversely, plain radiography establishes the spinal-curvature alteration easily, and flexion/extension lateral films yield a dynamic estimation of the mobility at the abnormal segment. Changes in the posterior spinal elements are characterized more distinctly on CT scans. CT also is more sensitive than conventional radiography in the demonstration of vacuum phenomenon, the emergence of which may signify mechanical instability [13].

The transverse display of the spinal canal that is possible with CT also helps determine the presence, location, severity, and nature of spinal stenosis. Central-canal stenosis at the pseudarthrotic segment may arise from osteophytes, hypertrophic changes, fragmented bony overgrowths, ossified ligaments, vertebral displacement, or severe kyphos deformity. Hypertrophic changes at transverse fractures traversing the pars interarticularis also may cause stenosis of the subarticular canals, simulating spondylolysis [14]. Fibrous tissue overgrowths or granulation associated with pseudarthrosis are not seen on CT scans. CT evidence of canal encroachment warrants closer clinical observation for neurologic complications and possibly earlier surgery.

The greater sensitivity of CT in the detection of minor changes facilitates follow-up in symptomatic patients to monitor regression or progression of the pathologic changes. Earlier surgical immobilization may be required for documented progressive or unstable osteolysis.

We propose that plain films be used in the initial and short-interval follow-up imaging of pseudarthrosis. For further characterization of the disease, CT should replace conventional tomography, because CT offers higher diagnostic yield and lower radiation dose. CT may be used at longer intervals for evaluating the progress of the disease. It may also be applied in the postoperative assessment of the outcome of surgical intervention and identification of recurrent pseudarthrosis.

ACKNOWLEDGMENTS

We thank Y. Y. Chan and other radiographic staff members for technologic support and Kitty Kwok for secretarial assistance.

REFERENCES

1. Cawley MID, Chalmers TM, Kellgren JH, Ball J. Destructive lesions of vertebral bodies in ankylosing spondylitis. *Ann Rheum Dis* **1972**;31: 345–358
2. Dihlmann W, Delling G. Disco-vertebral destructive lesions (so-called Andersson lesions) associated with ankylosing spondylitis. *Skeletal Radiol* **1978**;3:10–16
3. Park WM, Spencer DG, McCall TW, Ward DJ, Buchanan WW, Stephens WH. The detection of spinal pseudarthrosis in ankylosing spondylitis. *Br J Radiol* **1981**;54:467–472
4. Pastershank SP, Resnick D. Pseudarthrosis in ankylosing spondylitis. *J Can Assoc Radiol* **1980**;31:234–235
5. Carrera GF, Foley WD, Kozin F, Ryan L, Lawson TL. CT of sacroiliitis. *AJR* **1981**;136:41–46
6. Russel AS, Jackson F. Computer assisted tomography of the apophyseal changes in patients with ankylosing spondylitis. *J Rheumatol* **1986**;13:581–585
7. Sage MR, Gordon TP. Muscle atrophy in ankylosing spondylitis: CT demonstration. *Radiology* **1983**;149:780
8. Weinstein PR, Karpman RP, Gall EP, Pitt M. Spinal cord injury, spinal fracture and spinal stenosis in ankylosing spondylitis. *J Neurosurg* **1982**;57:609–616
9. Grosman H, Gray R, St. Louis EL. CT of long-standing ankylosing spondylitis with cauda equina syndrome. *AJNR* **1983**;4:1077–1080
10. Ho EKW, Leong JCY. Traumatic tetraparesis: a rare neurological complication in ankylosing spondylitis with ossification of posterior longitudinal ligament of the cervical spine. *Spine* **1987**;12:403–405
11. Luken MG III, Patel DV, Ellman MH. Symptomatic spinal stenosis associated with ankylosing spondylitis. *Neurosurgery* **1982**;11:703–705
12. Chan FL, Ho EKW, Fang D, Hsu LCS, Leong JCY, Ngan H. Spinal pseudarthrosis in ankylosing spondylitis. *Acta Radiol [Diagn]* (Stockh) **1987**;28:383–388
13. Lardé D, Mathieu D, Frija J, Gaston A, Vasile N. Spinal vacuum phenomenon: CT diagnosis and significance. *J Comput Assist Tomogr* **1982**;6: 671–676
14. Newman PH. Stenosis of the lumbar spine in spondylolisthesis. *Clin Orthop* **1976**;115:116–121

Soft-Tissue Sarcomas of the Extremities: Comparison of MR and CT in Determining the Extent of Disease

Barbara E. Demas[1]
Robert T. Heelan[1]
Joseph Lane[2]
Ralph Marcove[2]
Steven Hajdu[3]
Murray F. Brennan[2]

A prospective comparison of the accuracy of MR and CT in determining the anatomic extent of disease was carried out in 40 patients who had histologically proved soft-tissue sarcomas of the extremities. Tumor resection, performed by using either en bloc excision or amputation in all patients, allowed detailed pathologic verification of imaging findings. Image analysis included measurement of maximum tumor dimensions, notation of tumor position in relation to deep fascia, recording of anatomic compartment and individual muscle involvement, and documentation of the spatial relationships between tumor, neurovascular structures, underlying bones, and joints. MR and CT were equally accurate in measurement of maximal tumor diameter, detection of tumor depth, and delineation of tumor, neurovascular, osseous, and articular relationships. Evaluation of anatomic compartment and individual muscle involvement was more accurately accomplished with MR imaging; nine (23%) of 40 MR studies showed tumor involvement of one or more individual muscles that appeared normal in CT scans.

These results suggest that MR imaging may be the staging procedure of choice in patients with soft-tissue sarcomas of the extremities.

The radiographic evaluation of primary soft-tissue tumors of the extremities has progressed with the development of cross-sectional imaging techniques. Although conventional radiography, scintigraphy, and arteriography were at one time standard, the introduction of CT allows direct visualization of the tumor and simplifies staging [1–6]. For these reasons, CT has become routine in this clinical setting. The recognition of the striking soft-tissue contrast resolution offered by MR imaging has prompted investigators to reexamine the imaging characteristics of benign and malignant tumors of soft-tissue origin and to compare the quality of tumor delineation by MR and CT [7–9]. Most of these studies have included heterogeneous populations of benign and malignant tumors. In many cases, it has not been possible to correlate imaging findings with the results of pathologic examinations.

We conducted a prospective evaluation of MR imaging and CT in 40 patients with primary soft-tissue sarcomas of the extremities, focusing not on comparative image quality or subjective evaluation of lesion conspicuity but on the accuracy of determining the extent of local disease as verified at the time of tumor resection.

Subjects and Methods

During the period from February 1986 to June 1987, 134 patients with primary soft-tissue sarcoma of an extremity were admitted to our institution for surgical management. Of these patients, a subset of 40 was evaluated with both MR and CT before surgical treatment. This group included 16 men and 24 women, ranging in age from 3 to 87 years. Tumors arose in the thigh in 28 patients, in the leg in eight, in the upper arm in three, and in the forearm in one. Thirty-four patients were evaluated at the time of initial clinical presentation; six were imaged at the time of a postsurgical tumor recurrence. Twenty-seven patients were imaged before biopsy and 13 after incisional biopsy. Tissue diagnoses included liposarcoma (14), malignant fibrous histiocytoma (six), tenosynovial sarcoma (four), fibrosarcoma (five), rhab-

Received July 30, 1987; accepted after revision November 11, 1987.

[1] Department of Medical Imaging, Memorial Sloan-Kettering Cancer Center, 1275 York Ave., New York, NY 10021. Address reprint requests to B. E. Demas, University of California, San Francisco, San Francisco, CA 94143.

[2] Department of Surgery, Memorial Sloan-Kettering Cancer Center, New York, NY 10021.

[3] Department of Pathology, Memorial Sloan-Kettering Cancer Center, New York, NY 10021.

AJR 150:615–620, March 1988
0361–803X/88/1503–0615
© American Roentgen Ray Society

domyosarcoma (three), neurofibrosarcoma (three), leiomyosarcoma (two), unclassified spindle-cell sarcoma (one), hemangiopericytoma (one), and extraosseous osteosarcoma (one). No specific criteria were used to determine which patients admitted with a suspected diagnosis of soft-tissue sarcoma would undergo both types of imaging studies. The demands of clinical scheduling in the radiology department and the operating rooms frequently dictated whether both examinations were completed before surgery. MR and CT examinations for each patient were completed within 14 days of each other.

Data acquisition and analysis were prospective; only patients with histologically confirmed and subsequently resected soft-tissue sarcomas were included. It was our intention to determine the relative value of MR and CT in preoperative staging of extremity soft-tissue sarcomas, not to evaluate the ability of either method to distinguish soft-tissue sarcomas from other diseases.

MR scans were obtained with a 1.5-T superconducting magnet system (General Electric, Milwaukee, WI). T1- and T2-weighted images were obtained in all patients by using spin-echo pulse sequences with TR/TE combinations of 800–1000/20–25 and 1500–2000/35–40, 70–80 (first echo, second echo). All patients were imaged in the transaxial plane; 15 patients were also evaluated with coronal plane images and six with sagittal plane images. Coronal and sagittal plane images were obtained most frequently in patients whose tumors arose from tissue near a joint. A whole-body coil was used for 34 patients; specialized extremity surface coils were used for the remaining six patients. Section thicknesses varied from 5 to 10 mm, with interslice gaps of 1–5 mm; thicker slices and wider intervals generally were used for patients with very large tumors. Fields of view varied with the size of the patient and the body part and with the specific receiving coils selected. An image matrix of 256 × 256 was used in all cases. Two signal acquisitions were standard.

Twenty-four CT studies were performed by using a General Electric 9800 CT/T unit. These studies were generated by using rapid-sequence scanning with sequential table movement during the IV injection of 80–120 ml of 60% iodinated contrast material at a rate of 1 ml/sec. Five- to 10-mm transaxial sections, contiguous or with 2- to 5-mm interslice gaps, were selected. Images were photographed by using soft-tissue and bone windows. Sixteen patients underwent CT scanning elsewhere, and the technical factors were predictably varied. All scans were of good-to-excellent technical quality.

Each MR and CT study was monitored by one of two radiologists. Image analysis was performed by one radiologist. MR and CT scans were interpreted separately, and an interval of at least 3 days was allowed to elapse between review of MR and CT scans in any single patient. Image analysis was performed without knowledge of subsequent surgical findings. However, the requirement that each clinical examination be monitored by a qualified radiologist precluded totally blind comparison of MR and CT findings.

The following information was recorded from MR and CT studies: (1) maximum tumor dimension, (2) position of tumor in relation to deep fascia, (3) anatomic compartment(s) involved, (4) specific muscles invaded, (5) relationship of tumor to regional neurovascular structures, and (6) relationship of tumor to skeletal and articular structures.

Drawing on the reported experience of other authors [7–12] who have described the characteristic MR appearance of primary musculoskeletal sarcomas, we identified tumors in T1-weighted MR images as masses with a signal intensity similar to that of skeletal muscle (Fig. 1A). Tumors were identified in T2-weighted images as masses with a signal intensity greater than that of either skeletal muscle or subcutaneous fat (Fig. 1B). Tumor involvement of a specific muscle was suspected when an area of heterogeneous high signal intensity was identified within muscle substance with or without deformity of normal muscle contour. Homogeneous linear streaks of high signal intensity were thought to represent adjacent edema and were not interpreted as representing tumor infiltration. On CT images, the presence of intramuscular tumor was reported when a mass of heterogeneous density similar to (but often slightly less than) that of skeletal muscle altered the attenuation characteristics and/or the contour of a muscle (Fig. 1C). Assessment of the spatial relationship of tumor to regional neurovascular structures included classification of each mass as lying separate from, in contact with and displacing, or completely encasing major vessels and associated nerves. Evaluation of the relation of each tumor to underlying osseous and articular structures included a similar classification; tumors were described as being separate from, in contact with, or clearly invading bone or joint. In MR images, tumors were said to invade adjacent cortical bone when irregularity in contour or clear interruption of the cortical signal void was noted in both T1- and T2-weighted images (Fig. 2A). Tumor invasion of the medullary cavity was identified when low-to-medium signal-intensity material replaced normal marrow fat in T1-weighted images (Fig. 2A). In CT images, bone invasion was reported when lytic cortical destruction or increased medullary attenuation was present (Fig. 2B). Joint invasion was described when a soft-tissue mass projected into the expected confines of a joint capsule or when tumor immediately adjacent to a joint was seen to involve a ligament or tendon that ran in an intraarticular location in any part of its course.

All 40 patients underwent surgical excision of their soft-tissue sarcomas after imaging. Thirty-five were treated with wide excisions and limb preservation; five were treated with limb amputations. Imaging findings were confirmed at the time of surgery and gross dissection. Surgeons reported the spatial relationships of tumors to regional vessels and nerves and to appropriate skeletal structures and recorded the details and extent of muscular resection in one or more anatomic compartments. Gross pathologic examination with recording of tumor dimensions and macroscopic assessment of resection boundaries was performed by several different pathologists. Histologic diagnoses were made, and detailed microscopic reviews of tumor boundaries were performed by a single attending pathologist, who was aware of imaging findings in some, but not all, cases. Correlation between surgical, pathologic, and imaging findings was discussed in detail at a weekly multispecialty clinical conference.

Results

MR images revealed soft-tissue masses in all 40 cases. CT scans showed gross tumor in 37 of 40 patients and showed no visible soft-tissue mass in three of 40 cases. At surgical exploration, gross tumor was identified in all 40 patients.

Maximum tumor dimensions as measured in MR images ranged from 2 to 28 cm (mean, 10.9 ± 7.4). Maximum tumor dimensions in CT scans varied from 2 to 30 cm (mean, 11.1 ± 8.2). Maximum tumor dimensions as recorded at examination by a surgical pathologist ranged from 3 to 27 cm (mean, 10.2 ± 6.8). The differences between CT and pathologic measurements for individual tumors ranged from 0 to 9 cm (mean, 2.9 ± 2.9). The differences between MR and pathologic measurements for individual tumors varied from 0 to 8.5 cm (mean, 2.2 ± 2.3). Of the four cases in which MR and CT estimates of maximum tumor dimensions varied from the diameters recorded at dissection by more than 5 cm, three tumors were resected in fragments, and pathology measurements were expressed as sums of several diameters. Correlation with imaging appearances was inexact. In one of these four patients, postbiopsy edema and hematoma obscured lesion boundaries in both MR and CT images. In the

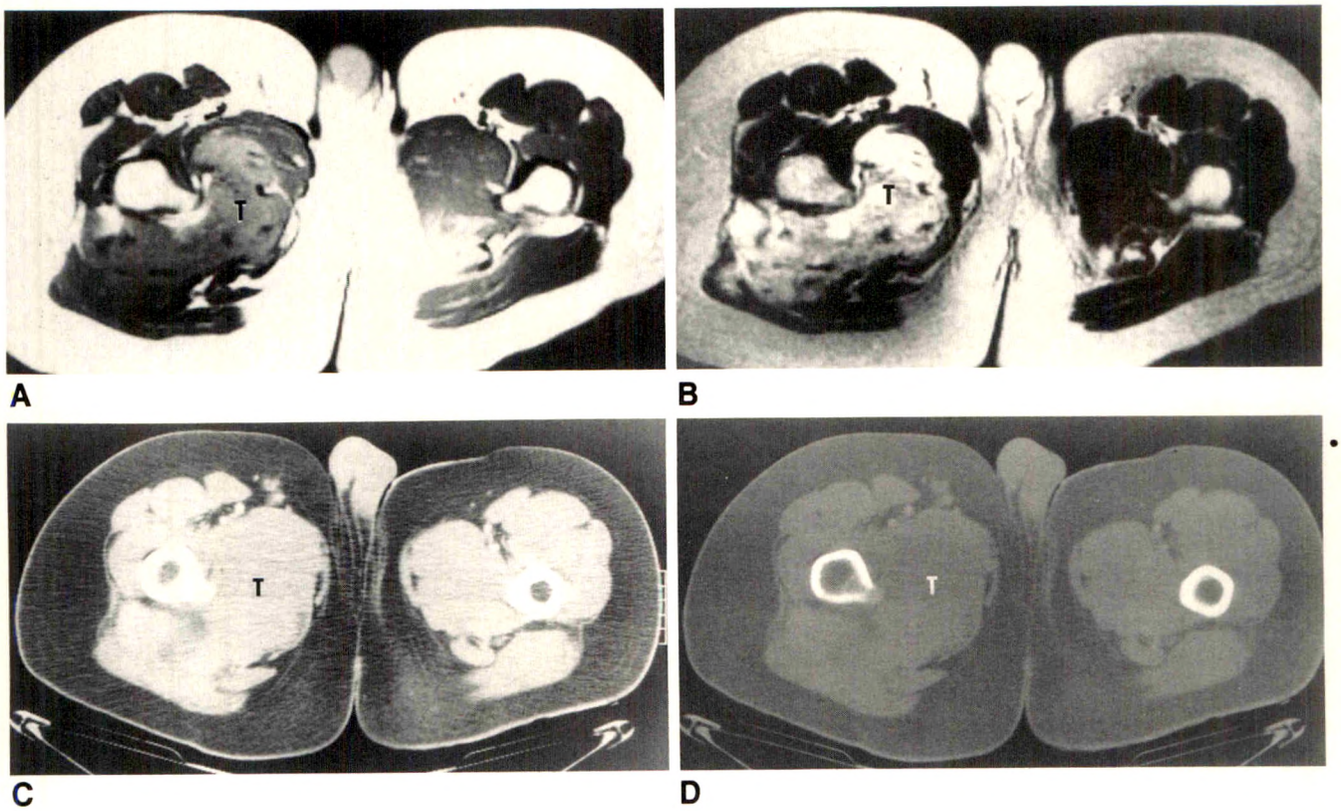

Fig. 1.—*A*, Transaxial MR image (SE 800/25) of a deeply situated fibrosarcoma (T) in right thigh. Tumor lies in posteromedial compartment of thigh. Although tumor is immediately adjacent to femoral cortex, there is no sign of cortical destruction or medullary invasion. Mass extended over a distance of 30 cm in posterior thigh and involved sciatic nerve.

B, Transaxial MR image (SE 2000/80) shows striking contrast between high-signal-intensity tumor (T) and low signal intensity of skeletal muscle. Tumor involves thigh adductors and extends into gluteus maximus muscle.

C, Contrast-enhanced CT scan shows contour abnormality in thigh adductors and gluteal region caused by intramuscular tumor (T).

D, CT scan photographed at a bone window reveals no femoral destruction by tumor (T).

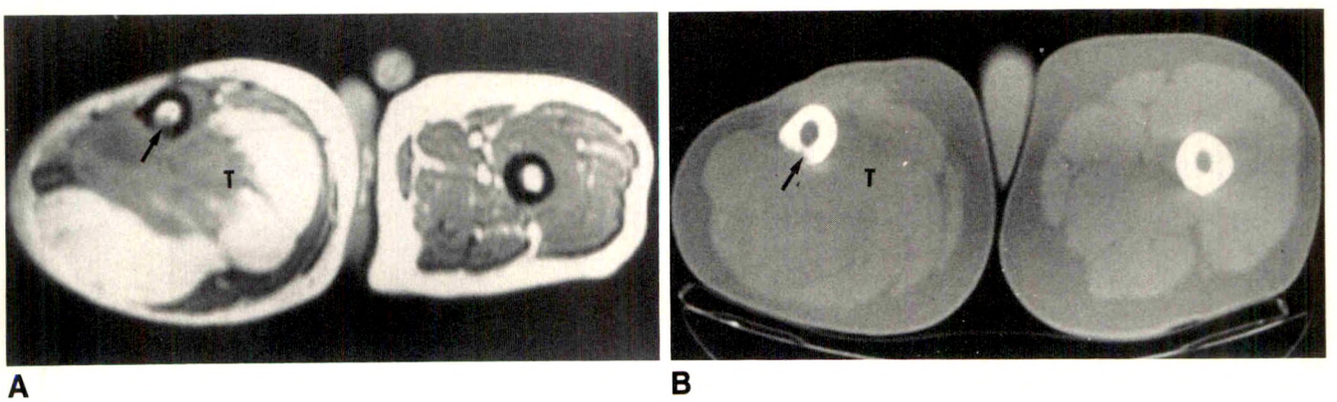

Fig. 2.—*A*, Transaxial MR image (SE 800/20) of a recurrent leiomyosarcoma (T) of posteromedial compartment of right thigh. Muscles of anterior compartment have been resected previously. Signal intensity of tumor is heterogeneous with areas of intense signal, representing hemorrhage and necrosis. Tumor invades femoral cortex and medullary space (*arrow*).

B, CT scan of recurrent leiomyosarcoma (T) photographed at a bone window shows femoral invasion by adjacent tumor (*arrow*).

remaining patients, both MR and CT estimates of maximal tumor diameter were within 3 cm of pathologic measurements. Approximately 40% of the imaging measurements were smaller than those obtained at gross dissection, whereas 60% equaled or exceeded dimensions recorded by an examining pathologist. No statistically significant difference was detected in the accuracy of MR and CT measurements of maximal tumor dimensions.

Both MR and CT correctly assessed the positions of tumors in relation to the deep fascia in every patient. Six tumors lay external to deep fascia, and 34 masses lay within deep fascial planes.

More detailed anatomic comparison was carried out in the 37 patients who were seen to have gross tumor on both MR and CT scans. MR images of these patients revealed that disease was confined to the anterior compartment of the thigh in 10 patients, was restricted to the posterior of the thigh in eight, and involved both the anterior and the posterior compartments in 10. CT scans indicated anterior thigh compartment masses alone in 10 cases, posterior compartment masses alone in nine, and bicompartmental disease in nine. Surgical findings confirmed MR assessment of compartmental involvement within the thigh in all 28 patients; CT assessment was incorrect in one patient.

MR and CT images showed tumor involving the anterior compartment of the leg in one patient, the posterior compartment of the leg in six, and both the anterior and lateral compartments of the leg in one. Surgical findings verified the accuracy of compartmental evaluation by both MR and CT scans in these eight cases.

MR and CT scans both revealed periscapular disease in one patient. However, MR images also showed tumor within the lateral chest wall musculature, whereas CT images showed tumor in the infraspinatus region only. Surgical exploration verified the presence of the more extensive disease as noted in the MR scans.

Of the 34 deeply situated tumors, three involved only one muscle as judged by both MR and CT. The remainder invaded from two to nine individual muscles. In nine patients, MR images revealed the presence of tumor in one or more muscles that were normal in contour and density in the CT images (Figs. 3A and 3B). These patients included three with totally negative CT scans and six with CT scans showing involvement of fewer specific muscles than were abnormal in MR images. In two patients, this finding altered the imaging assessment of single or multiple anatomic compartment disease. Examination of resected specimens confirmed MR findings. MR images therefore more accurately reflected the detailed extent of intramuscular disease in nine (23%) of 40 patients. In no case did CT evaluation suggest involvement of a muscle that appeared normal in MR.

The relationships of the soft-tissue sarcomas to regional neurovascular structures are summarized in Table 1. MR assessment of this relationship was correct in all cases. CT assessment was correct for all but the three patients whose small isodense tumors caused no skeletal muscle deformity and therefore were undetected.

The relationships of the soft-tissue tumors to the bones of the affected extremities are summarized in Table 2. Bone invasion was detected in five patients by both MR and CT and was documented at surgery in six cases. The single patient whose MR and CT scans were falsely negative for

TABLE 1: Relationship of Tumor to Neurovascular Structures

Finding	No. of Cases		
	MR	CT	Pathology
Separated by normal tissue	24	22	24
Tumor contacts NVB[a]	1	1	1
Tumor displaces NVB	6	6	6
Tumor encases NVB	9	8	9
No macroscopic tumor visible	0	3	0

[a] NVB = neurovascular bundle.

TABLE 2: Relationship of Tumor to Bone

Finding	No. of Cases		
	MR	CT	Pathology
Separated by normal tissue	15	12	15
Tumor contacts bone	20	20	19
Tumor invades bone	5	5	6
No macroscopic tumor visible	0	3	0

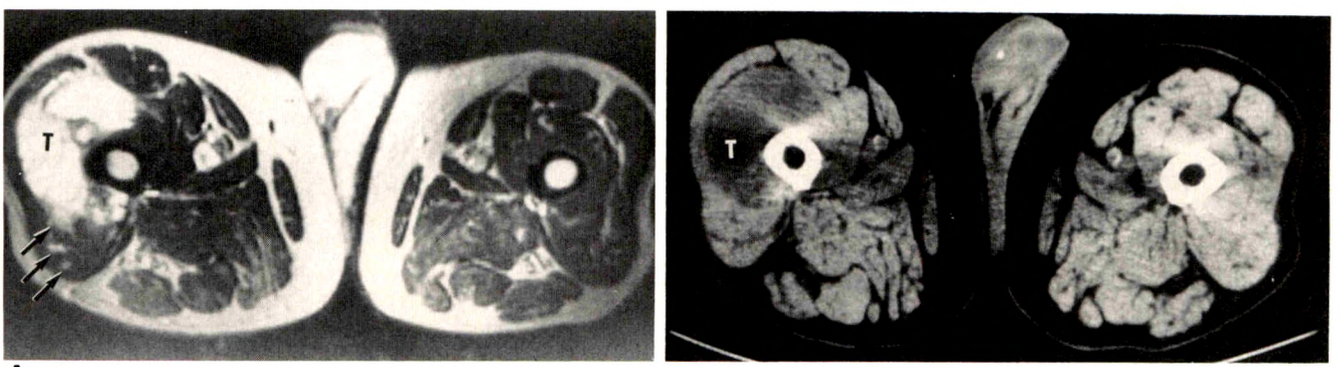

A B

Fig. 3.—*A*, Transaxial MR image (SE 2000/80) of extraosseous osteosarcoma (T) of right thigh. Tumor involves vastus medialis and intermedius muscles, and satellite nodules are present in vastus lateralis muscle (*arrows*). Superficial femoral vessels are separated from tumor by normal tissue. Femoral cortex immediately abuts tumor, but there is no bone invasion.

***B*, CT scan shows involvement of vastus medialis and intermedius muscles with tumor (T). However, vastus lateralis muscle appears normal in contour and density. CT findings underestimated local extent of disease.**

bone invasion was found at pathologic evaluation to have microscopic infiltration of the scapular medullary cavity.

The relationships of tumors to joints are summarized in Table 3. MR images correctly assessed the presence or absence of joint invasion in all patients with macroscopic disease (Fig. 4). CT correctly assessed the presence or absence of joint involvement in all but the three previously mentioned patients whose macroscopic tumors produced no anatomic abnormalities in CT images.

Discussion

The population described in this report includes only patients with histologically documented and subsequently resected soft-tissue sarcomas. Within the past 2 years, several authors have published studies comparing MR and CT in the evaluation of primary musculoskeletal tumors [1–12]. Most of these studies have involved heterogeneous populations, including patients with inflammatory, posttraumatic, and primary and metastatic neoplastic lesions, and have not provided detailed pathologic correlation [7–9]. Petasnick et al. [7] compared the MR and CT appearances of soft-tissue masses of the musculoskeletal system in a group of 35 patients, nine of whom had diagnoses of primary extremity soft-tissue sarcomas. Although the local extent of disease was thought to be concordant in MR and CT studies for all patients, Petasnick et al. [7] concluded that MR was superior to CT in showing tumor, neurovascular, and skeletal relationships. This study did not include gross pathologic correlation and did not allow assessment of the accuracy of either MR or CT in delineation of the anatomic extent of disease. Totty et al. [8] reported a similar study in which three independent reviewers evaluated the MR delineation of soft-tissue masses in 33 patients, 23 of whom also had CT scans. MR and CT scans were compared qualitatively for their clarity of anatomic display in five areas: (1) visualization of the mass, (2) contrast with surrounding tissue, (3) tumor margination, (4) local tumor extent, and (5) tumor calcification. Concluding that MR was at least as good as and possibly better than CT in the delineation of soft-tissue masses, these authors remarked that the striking soft-tissue contrast resolution of MR facilitated image interpretation and emphasized the value of using both T1- and T2-weighted scans. Of the 33 masses evaluated, only 10 were explored surgically. Detailed verification of the accuracy of the imaging findings could not be assessed. Pettersson et al. [9] reported comparison of MR with other techniques in a group of 176 patients, 48 of whom had soft-tissue sarcomas. Although MR was considered to be excellent in determining the extent of soft-tissue tumor, no pathologic verification of image interpretation was described.

TABLE 3: Relationship of Tumor to Joint

Finding	No. of Cases		
	MR	CT	Pathology
Separated by normal tissue	33	30	33
Tumor contacts joint	4	4	4
Tumor invades joint	3	3	3
No macroscopic tumor visible	0	3	0

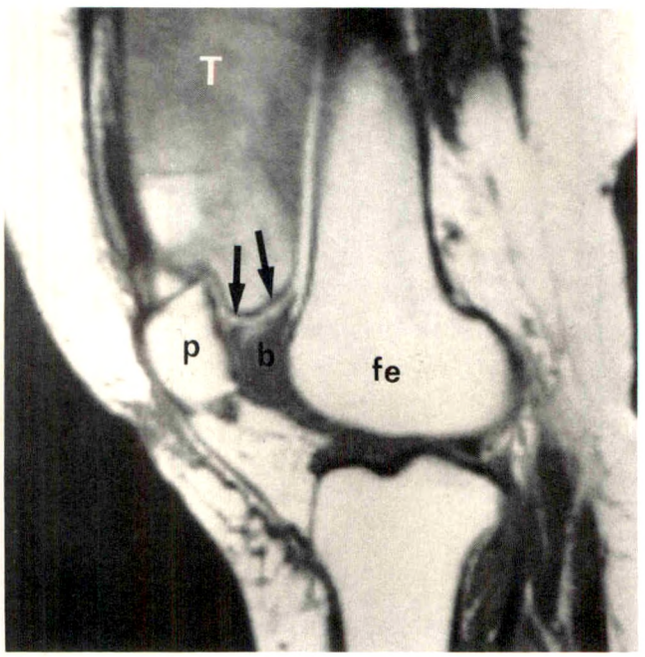

Fig. 4.—Sagittal MR image (SE 800/20) of primary soft-tissue sarcoma (T) involving anterior muscular compartment of thigh reveals a fat plane (*arrows*) between tumor pseudocapsule and suprapatellar bursa (b). Femur (fe), patella (p), and knee joint compartment have not been invaded by large adjacent tumor.

At present, MR imaging is generally more time-consuming and often twice as costly as CT scanning. The dangers of CT scanning include the relatively insignificant exposure to ionizing radiation and the possibility of adverse reactions to IV contrast agents. Determination which technique—MR or CT—best facilitates treatment planning requires verification of the accuracy of imaging results by correlation with surgical and gross pathologic examinations.

Preoperative evaluation of our patients involved prediction of the feasibility of wide excision with limb salvage or the necessity for amputation. En bloc excision of a soft-tissue sarcoma was performed in most patients. Surgical goals were to minimize the probability of local tumor recurrence and to preserve limb function. Collin et al. [13] have defined the criteria used at our institution for assessment of the adequacy of local tumor resection. Resection margins are considered adequate when all gross tumor and a cuff of surrounding normal tissue are removed and specimen boundaries are microscopically negative. Resection is marginal when all gross tumor is removed but microscopic foci of tumor are within millimeters of the specimen boundary. Surgical margins are considered inadequate when gross tumor remains in place or when tumor is visualized or entered during surgery.

A muscle invaded by tumor is best resected from its point of origin to its point of insertion [14]. Although resection of

an entire muscular compartment may be performed with a surprisingly modest compromise of limb function, preservation of uninvolved muscles within a specific anatomic compartment is desirable. These principles emphasize the importance of accurate documentation of individual muscle involvement preoperatively. The subsequent surgical procedure may be planned to optimize resection boundaries, and the effect of complete tumor resection on limb function may be predicted. The value of correct preoperative assessment of neurovascular, osseous, and articular integrity is clear.

Quantitative assessment of MR and CT in evaluation of local extent of disease is not simple. The use of maximal tumor dimension as a parameter for MR, CT, and pathologic comparison is convenient if somewhat crude. Edema and hematoma after biopsy may obscure true tumor margins in MR and CT images. Differences in the locations of MR and CT scan planes and in tumor orientation during imaging and pathologic examination may exaggerate disparities. In our patients, surgical specimens were tagged with identifying sutures to alert the examining pathologist to the location of the superior, inferior, and deep margins of resection. However, irregular lobulated tumor contours may have been altered when resected specimens were no longer confined within fascial planes, and tumor shrinkage may have occurred when desiccation accompanied delays in gross pathologic dissection. In our experience, MR and CT were equivalent in their ability to predict a single maximal tumor diameter.

MR and CT were equally accurate in the assessment of tumor relationships with neurovascular structures. Neither study could be used to predict tumor adherence to neurovascular structures, except in those cases in which complete encasement by tumor was identified.

Both MR and CT correctly assessed tumor relationships to bone in all but one case, and both were falsely negative for scapular invasion in one instance. Neither could predict periosteal invasion in the absence of gross bony destruction. In the five cases in which bone invasion was detected, plain radiographs were also abnormal. Both MR and CT were equally and highly accurate in the assessment of articular involvement; sagittal and coronal images assisted in joint evaluation as observed by other investigators [7–9], but transaxial images alone generally allowed adequate periarticular anatomic display.

All these factors being equal, does MR in fact possess any important advantage over CT in presurgical imaging of patients with primary extremity soft-tissue sarcomas? The fact that MR images revealed tumor involvement of one or more individual muscles that appeared normal on CT scans in 23% of our patients constitutes a point of superiority for MR. We acknowledge that this impression has been offered in other published studies, but the strength of support given to our conclusions by the availability of pathologic verification in all cases is important.

We do not advocate MR as a screening or primary diagnostic study, but we do believe it is an ideal staging procedure when surgical therapy is mandated. In addition to providing a road map for primary surgery, MR may be helpful in predicting a need for development of myocutaneous flaps for wound coverage and may assist in planning adjuvant radiation therapy.

MR generally can be expected to be equal to and often will be superior to CT in the evaluation of soft-tissue sarcomas, both in terms of subjective factors such as image quality, ease of tumor detection, and clarity of lesion boundaries and in terms of real accuracy in reflecting the anatomic extent of disease. When a treatment plan includes en bloc wide excision with preservation of limb function, we believe MR is the most valuable imaging technique for preoperative anatomic staging.

REFERENCES

1. Totty WG. Radiographic evaluation of soft tissue sarcomas. *Orthop Rev* **1985**;14:27–39
2. Golding SJ, Husband JE. Radiology of soft tissue sarcoma: discussion paper. *J R Soc Med* **1982**;75:729–735
3. Ekelund L, Herrlin K, Rydholm A. Comparison of computed tomography and angiography in the evaluation of soft tissue tumors of the extremities. *Acta Radiol [Diagn]* (Stockh) **1982**;23:15–28
4. Paushter DM, Borkowski GP, Buonocore E, Belhobek GH, Marks KE. Digital subtraction angiography for preoperative evaluation of extremity tumors. *AJR* **1983**;141:129–133
5. Neifeld JP, Walsh JW, Lawrence W. Computed tomography in the management of soft tissue tumors. *Surg Gynecol Obstet* **1982**;155:535–540
6. Weekes RG, McLeod RA, Reiman HM, Pritchard DJ. CT of soft-tissue neoplasms. *AJR* **1985**;144:355–360
7. Petasnick JP, Turner DA, Charters JR, Gitelis S, Zacharias CE. Soft-tissue masses of the locomotor system: comparison of MR imaging with CT. *Radiology* **1986**;160:125–133
8. Totty WG, Murphy WA, Lee JKT. Soft-tissue tumors: MR imaging. *Radiology* **1986**;160:135–141
9. Pettersson H, Gillespy T III, Hamlin DJ, et al. Primary musculoskeletal tumors: examination with MR imaging compared with conventional modalities. *Radiology* **1987**;164:237–241
10. Moon KL Jr, Genant HK, Helms CA, Chafetz NI, Crooks LE, Kaufman L. Musculoskeletal applications of nuclear magnetic resonance. *Radiology* **1983**;147:161–171
11. Aisen AM, Martel W, Braunstein EM, McMillin KI, Philips WA, Kling TF. MRI and CT evaluation of primary bone and soft-tissue tumors. *AJR* **1986**;146:749–756
12. Daffner RH, Lupetin AR, Dash N, Deeb ZL, Sefczek RJ, Schapiro RL. MRI in the detection of malignant infiltration of bone marrow. *AJR* **1986**;146:353–358
13. Collin C, Hajdu SI, Goldbold J, Shiu MH, Hilaris BI, Brennan MF. Localized, operable soft tissue sarcoma of the lower extremity. *Arch Surg* **1986**;121:1425–1433
14. Karakousis CP, Emrich LJ, Rao U, Krishnamsetty RM. Feasibility of limb salvage and survival in soft tissue sarcomas. *Cancer* **1986**;57:484–491

Case Report

Avulsion of the Innominate Artery Associated with Fracture of the Sternum

Yoram Ben-Menachem[1,2]

The simultaneous occurrence of sternal fractures and injuries to the innominate artery is usually regarded as coincidental [1–3]; however, it is sometimes acknowledged that injuries to the ascending aorta and aortic arch are most likely to be produced by fractures and dislocations of the anterior chest wall, rather than by deceleration [4]. My own experience with blunt injuries of the innominate artery indicates that avulsion of the innominate artery from the aortic arch might result from contact wounding by a transverse fracture of the sternum. The purpose of this report is to call attention to the possible association between the two injuries and to discuss a proposed mechanism of injury, since recent evidence suggests that the frequency of sternal fractures in seat belt users is relatively high [5, 6].

Subjects and Methods

Three patients were injured in head-on automobile collisions, in which the patients had not worn seat belts and the vehicles were traveling at moderate speeds. All three sustained steering-wheel impact and were admitted with transverse sternal fractures and innominate artery avulsions. Two of these patients were described previously [1, 2], but the possible causal association between the sternal and innominate injuries was not realized at the time. The possibility that the fractured sternum may directly injure the innominate artery was brought up subsequently and was given further support with the admission of the third patient.

Case Report

A 17-year-old male driver of a sedan was involved in a head-on automobile collision. He was not wearing a seat belt and was driving at moderate speed. He was admitted in stable condition with blunt trauma to the chest. A portable chest film in the emergency room revealed a large superior mediastinal hematoma and left hemothorax. A lateral chest radiograph was not obtained. The patient was taken directly to the angiographic suite, where thoracic aortography revealed partial avulsion of the innominate artery from the aortic arch (Fig. 1). Because of the nature of the vascular injury and the accident environment, the patient also was presumed to have suffered a transverse fracture of the sternum, and the surgeon was so advised. A transverse fracture of the sternum was found at thoracotomy. The innominate artery was found to have been partially avulsed from the aortic arch and was repaired. The patient recovered without incident.

Discussion

Injuries of the innominate artery account for about 9% of all major blunt intrathoracic arterial injuries [2, 4].

Fractures of the sternum are seen in 8–10% of patients with violent blunt trauma to the chest, primarily those who are victims of automobile accidents [3, 7]. The frequency of sternal fractures in seat belt users is much higher than that in those who are unrestrained [5, 6]. Most fractures occur within 2 cm of the manubriosternal joint. Patients usually have a benign clinical course and recover without incident [7].

Received September 9, 1987; accepted after revision October 20, 1987.

[1] Department of Radiology, Baylor College of Medicine, Ben Taub General Hospital, Houston, TX 77030, and the Veterans Administration Medical Center, Houston, TX 77211.

[2] Present address: Department of Radiology, University of Washington, Harborview Medical Center, 325 Ninth Ave., Seattle, WA 98104. Address reprint requests to Y. Ben-Menachem.

AJR 150:621–622, March 1988 0361–803X/88/1503–0621 © American Roentgen Ray Society

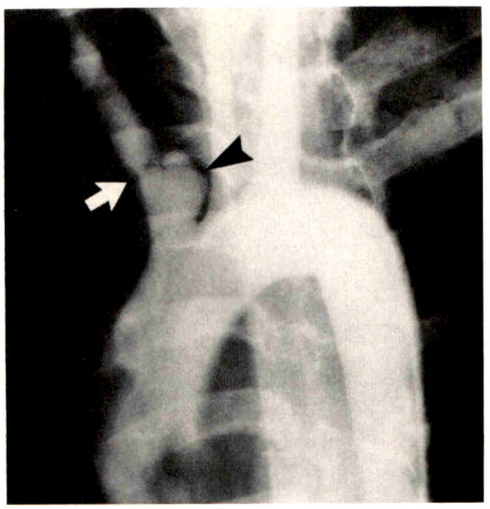

Fig. 1.—Arch aortogram shows partial avulsion of innominate artery from aorta. There is a false aneurysm at site of injury (*arrowhead*). Disruption of intima and media, of which only distal boundary is seen on aortogram (*arrow*), was shown at surgery to have begun at aortoinnominate junction.

However, in a few instances the fractured sternum may injure the heart and/or aorta [4].

The type of injury associated with a sternal fracture is partial avulsion of the innominate artery from the aortic arch [1, 2, 7]. In survivors of this injury, only the intima and media are disrupted, but there may also be a small adventitial defect at any point in the circumference of the artery. The angiographic presentation is of a false aneurysm originating in the innominate artery and sometimes involving the aortic arch as well [2, 8]. There may also be a dissection of the innominate artery, with occlusion either by the dissertion or by a second laceration [2, 9].

The presumed wounding mechanism includes a transverse fracture of the sternum in a frontal collision, probably but not necessarily resulting from the impact of the steering wheel [5], with buckling of the fragments inwards at the fracture line.

The fractured sternum usually buckles outward [10], in which case it does not produce cardiovascular injury. However, if it buckles inward, its upper fragment (hinged on the sternoclavicular joints) would move inward and upward and would peel the innominate artery from the aorta. The anatomic vicinity of the innominate artery and sternum [11] not only makes this mechanism highly feasible but also allows for the probability of avulsion of the innominate artery from the arch by a dislocated manubriosternal joint. Indeed, it is quite possible that this mechanism was responsible for innominate artery avulsions in published cases in which sternal fractures were not described in the reports [12].

The diagnosis of sternal fracture usually can be made on the lateral chest film [1, 2]. However, sternocostal disruption and fractures with minimal or no displacement at all are often missed, and CT is required for their diagnosis [11]. Lateral chest radiographs or CT scans of severely injured patients with violent blunt trauma to the chest usually are not obtained in the emergency room. Therefore, the diagnosis of a sternal fracture often is delayed, and the fracture may be discovered only during thoracotomy [13]. In the case presented here, the angiographic findings led to a presurgical diagnosis of fractured sternum.

We are concerned with the association between sternal fractures and innominate artery trauma in view of the evidence that sternal fractures are more common in seat belt users [5, 6]. Therefore, the combination of mandatory seat belt use and higher speed limits is anticipated to produce higher numbers of sternal fractures and, with them, a greater number of innominate avulsions. Even when a fractured sternum is not present, a certain number of innominate artery lacerations may be caused directly by seat belts.

Although most patients with aortoinnominate injuries have significant mediastinal hematomas on admission chest films, in some a hematoma will be absent initially [1, 2, 9]. Therefore, a high index of suspicion and liberal use of aortography are essential in all cases of violent blunt trauma to the chest.

REFERENCES

1. Ben-Menachem Y. *Angiography in trauma: a work atlas*. Philadelphia: Saunders, **1981**:115–117
2. Fisher RG, Hadlock F, Ben-Menachem Y. Laceration of the thoracic aorta and brachiocephalic arteries by blunt trauma. Report of 54 cases and review of the literature. *Radiol Clin North Am* **1981**;19:91–110
3. Kemmerer WT, Eckert WG, Gathright JB, Reemstma K, Creech O Jr. Patterns of thoracic injuries in fatal traffic accidents. *J Trauma* **1961**;1: 595–599
4. Keen G. Closed injuries of the thoracic aorta. *Ann R Coll Surg Engl* **1972**;51:137–156
5. Newman RJ, Jones IS. A prospective study of 413 consecutive car occupants with chest injuries. *J Trauma* **1984**;24:129–135
6. Muwanga CL, Cole RP, Sloan JP, Bruce E, Dove AF, Dave SH. Cardiac contusion in patients wearing seat belts. *Injury* **1986**;17:37–39
7. Harley DP, Mena I. Cardiac and vascular sequelae of sternal fractures. *J Trauma* **1986**;26:553–555
8. Lundell CJ, Quinn MF, Finck EJ. Traumatic laceration of the ascending aorta: angiographic assessment. *AJR* **1985**;145:715–719
9. Magilligan DJ Jr, Davila JC. Innominate artery disruption due to blunt trauma. *Arch Surg* **1979**;114:307–309
10. Sevitt S. Fatal road accidents. Injuries, complications, and causes of death in 250 subjects. *Br J Surg* **1968**;55:481–505
11. Stark P, Jaramillo D. CT of the sternum. *AJR* **1986**;142:72–77
12. Faro RS, Monson DO, Weinberg M, Javid H. Disruption of aortic arch branches due to nonpenetrating chest trauma. *Arch Surg* **1983**;118:1333–1336
13. Thieman KC, Grooters RK. Double disruption of an innominate artery secondary to blunt trauma. *Ann Thorac Surg* **1982**;33:285–289

Diagnosis of Femoropopliteal Venous Thrombosis: Comparison of Duplex Sonography and Plethysmography

Neal H. Rosner[1]
Peter E. Doris[1, 2]

Duplex sonography and impedance plethysmography were correlated with contrast venography to compare the sensitivity, specificity, and accuracy of the two noninvasive techniques for the diagnosis of femoropopliteal venous thrombosis. Sensitivity, specificity, and accuracy of duplex sonography were 90%, 100%, and 97%, respectively, when compared with venography in 32 patients. Sensitivity, specificity, and accuracy of plethysmography were 100%, 63%, and 72%, respectively, when compared with venography in 25 patients. In 21 patients, plethysmography was either nondiagnostic or could not be done because of clinical difficulties. Eighteen of these patients had diagnostic duplex examinations.

Duplex sonography exhibits similar sensitivity but higher specificity than plethysmography. Duplex sonography also permits diagnostic examinations in patients in whom diagnostic plethysmography cannot be performed.

The clinical diagnosis of lower extremity deep venous thrombosis is difficult. Physical examination for the evaluation of deep venous thrombosis has been shown to be unreliable [1–3]. Contrast venography has remained the standard diagnostic method. However, venography is both expensive and invasive. In addition, risks are associated with the use of contrast material, including allergy, renal dysfunction, and venous thrombosis [4, 5]. Various noninvasive techniques for the evaluation of femoropopliteal venous thrombosis have been developed. Impedance plethysmography (IPG), one of the most well-established techniques, has been widely accepted as a sensitive and cost-effective screening technique [6–10]. Other reports, however, have noted serious limitations in the accuracy of IPG [11–13].

Recently, real-time sonography has been used to evaluate femoropopliteal venous thrombosis. These studies have shown high accuracy rates in evaluation of femoropopliteal deep venous thrombosis [14–17].

We determined the relative sensitivity and specificity of real-time duplex sonography and IPG in the evaluation of femoropopliteal deep venous thrombosis.

Subjects and Methods

The study group consisted of patients seen during a 13-month period who were referred to the Vascular Laboratory with clinically suspected femoropopliteal venous thrombosis. Duplex sonography was performed in 166 patients. One hundred twenty-three of these patients had both IPG and duplex sonography. IPG was not performed in 43 patients because of technical or clinical difficulties (21 patients) or because the patients were examined after hours when vascular technologists were unavailable (22 patients). Correlative contrast venography was performed in 32 patients. Twenty-five patients were examined by using all three techniques: duplex sonography, IPG, and venography. Correlative venographic studies were unsolicited and were obtained only when requested by attending or consulting physicians. Venography was performed within 48 hr of the noninvasive studies. Venography and noninvasive studies were interpreted independently by staff radiologists. Fifty-seven men and

Received August 31, 1987; accepted after revision November 9, 1987.

[1] Vascular Laboratory Division, Department of Radiology, St. James Hospital Medical Center, 1423 Chicago Rd., Chicago Heights, IL 60411. Address reprint requests to N. H. Rosner.

[2] Departments of Radiology and Emergency Medicine, University of Chicago Hospitals, Chicago, IL 60637.

AJR 150:623–627, March 1988
0361–803X/88/1503–0623
© American Roentgen Ray Society

109 women (age range, 20–91 years; mean, 59) were examined. Forty-one patients were outpatients, and 125 were inpatients.

Duplex sonography was performed by using a commercially available scanner (Diasonics Small Parts, Milpitas, CA) with a 7.5-MHz arc-sector imaging transducer and a 3.0-MHz pulsed Doppler. Imaging of the common femoral and proximal superficial femoral veins was performed with the patient in the supine position with the head elevated approximately 30°–35°. Imaging of the popliteal region was performed with the patient in the prone position, or in the decubitus position when patients could not assume a prone position. Veins were assessed for the presence or absence of visible intraluminal thrombi and compressibility. Duplex study also permitted Doppler tracings of the common femoral and popliteal veins. A normal study showed the absence of intraluminal thrombi, normal compressibility, normal spontaneous phasic common femoral venous signals, and appropriate augmentation of the Doppler signal in response to distal compression of the calf or thigh. An abnormal examination showed echogenic intraluminal thrombi, lack of compressibility, and absent Doppler signals.

The Valsalva maneuver was not performed because of variability in the patients' compliance. Abdominal compression was used to assess common femoral reflux. Sonographic evaluation of distal thrombosis was not attempted because of poor visualization of the calf veins.

Plethysmography was performed by using a commercially available unit (IPG 710, Interscience Corp., Brea, CA). Examinations were performed by using the occlusion-cuff technique described by Wheeler et al. [18]. Patients were examined while they were lying supine with their legs elevated 15°–30°. A pneumatic cuff was applied to the mid thigh and inflated to occlude venous return; it was then deflated. Changes in blood volume produced changes in impedance, which were recorded on a strip. The rise in blood volume and the changes in impedance after cuff occlusion were plotted against the fall in blood volume during the first 3 min after deflation. The ratio of the rise over the fall, called the venous function index, was plotted on a graph with a discriminant line. Patients whose venous function index values fall above the discriminant line are called normal; those whose values fall below the discriminant line are called abnormal. If an abnormal result is obtained, up to four repeat examinations are performed. If, on repeat examination, the venous function index value falls into the normal range, the examination is interpreted as normal. If the venous function index value remains in the abnormal range at the end of four repeat examinations, this final result then is interpreted as abnormal.

Venography was performed by using a modification of the technique described by Rabinov and Paulin [19]. The patient was placed in a semiupright position. A 19- or 21-gauge butterfly needle was introduced into one of the dorsal pedal veins, and 150 ml of 40% water-soluble contrast medium was injected. Multiple views of the calf and thigh were obtained and the patient was returned to a supine position. The examined leg was elevated then, and the femoral vein was compressed manually. A radiograph of the groin and pelvic area was obtained immediately after release of femoral vein compression.

Results

Duplex Sonography and Venography

Real-time duplex sonography was compared with contrast venography in 32 patients for the evaluation of femoropopliteal (proximal) deep venous thrombosis. Proximal deep venous thrombosis was identified on 10 venograms. One venogram identified a small distal thrombus within a branch of the gastrocnemius vein.

Real-time duplex sonography resulted in nine true-positive and one false-negative examinations. The single false-negative result occurred in a patient with an anatomic variation: a proximal division of the popliteal vein into three separate veins above the knee and a small nonoccluding thrombus in one of the three veins.

Duplex sonography resulted in 22 true-negative examinations. There were no false-positive examinations. Sensitivity of duplex sonography for femoropopliteal deep venous thrombosis was 90% with a 95% confidence interval (73%, 100%); specificity was 100% (87%, 100%); predictive value for negative study was 96% (81%, 100%); and accuracy was 97% (82%, 100%).

Impedance Plethysmography and Venography

IPG was compared with contrast venography in 25 patients. Venography showed femoropopliteal deep venous thrombosis in six of these patients. There were no false-negative examinations. There were seven false-positive and six true-positive examinations. Sensitivity of IPG for proximal deep venous thrombosis was 100% with a 95% confidence interval (84%, 100%); specificity was 63% (48%, 81%); and accuracy was 72% (50%, 87%).

Impedance Plethysmography and Duplex Sonography

In 123 patients, both duplex sonography and IPG were performed. There were 16 cases in which both examinations were positive, 34 in which IPG was positive and sonography was negative, one in which IPG was negative and sonography was positive, and 72 in which both were negative. From these data, it is apparent that when the two examinations disagree, it is more likely that IPG will produce a positive result and sonography will produce a negative result.

Clinical Limitations of IPG

IPG was attempted in 21 patients but either was nondiagnostic or could not be performed because of technical or clinical difficulties. Reasons for not obtaining a diagnostic IPG tracing included late pregnancy (one patient), the patient's inability to lie flat because of severe congestive heart failure/chronic obstructive pulmonary disease (six patients), interfering bandages and metal sutures from recent surgery (seven patients), involuntary muscle contractions (six patients), and flexion contractures (one patient). Eighteen of these 21 patients had diagnostic real-time duplex venous examinations.

Duplex Doppler Findings

In 103 of the 106 patients with a normal duplex sonographic examination, normal spontaneous phasic venous signals were shown in the common femoral vein (Fig. 1). These patients also had normal augmentation responses to calf and thigh compression. Doppler examinations could not be performed in three patients because of the depth of the vein.

Spontaneous popliteal signals were seen in only seven of

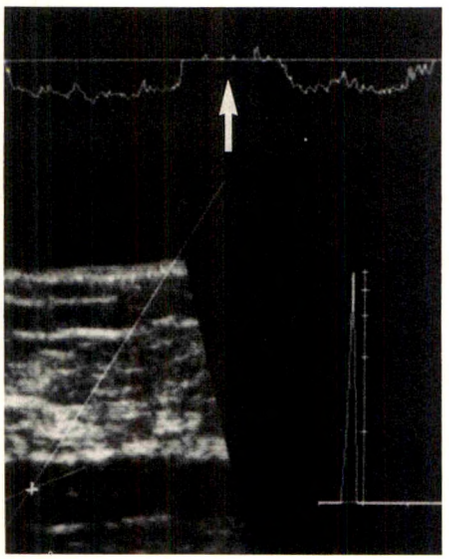

Fig. 1.—63-year-old woman with congestive heart failure and a 2-month history of bilateral leg edema. Duplex sonogram of common femoral vein shows normal Doppler tracing. A normal venous signal is phasic with respiration. This refers to a decrease in venous return and therefore to a decreased signal (*arrow*) on inspiration, when intraabdominal pressure is increased, and an increased signal on expiration, when intraabdominal pressure is decreased.

the 106 patients with a normal sonographic examination. Four of these patients had clinical evidence of cellulitis; in all of these patients, popliteal and common femoral signals were more pronounced in the affected leg than in the normal leg.

Eleven patients had both common femoral and popliteal thrombi. In all of these patients, a normal Doppler signal was absent, and no augmentation response was seen.

Five patients had popliteal thrombi only. In three out of the five, normal augmentation was absent. Two patients, however, showed a normal popliteal augmentation signal above the leading edge of the thrombus (Fig. 2).

Duplex Doppler sonography showed deep venous incompetence (reflux) in five patients. Two of these five patients had a history of previous deep venous thrombosis at least 6 months before the current examination and had no sonographic evidence of acute intraluminal thrombi. Saphenous, femoral, or popliteal deep venous reflux was observed in three patients who did not have a well-documented history of previous deep venous thrombosis but who did have varicose veins and dermal changes of chronic venous stasis. Venous reflux was shown by an abnormal reversed flow in popliteal, saphenous, or common femoral veins in response to thigh or abdominal compression (Fig. 3).

Discussion

Impedance plethysmography has been widely accepted in the evaluation of lower extremity deep venous thrombosis. Sensitivities and specificities as high as 95% have been reported in the evaluation of femoropopliteal (proximal) deep venous thrombosis [6–9]. In this study, the accuracy of IPG was significantly lower. Although the sensitivity of IPG was similar to that in these other studies, specificity was significantly lower relative to venography (63%).

Since IPG is an indirect physiologic test that depends on

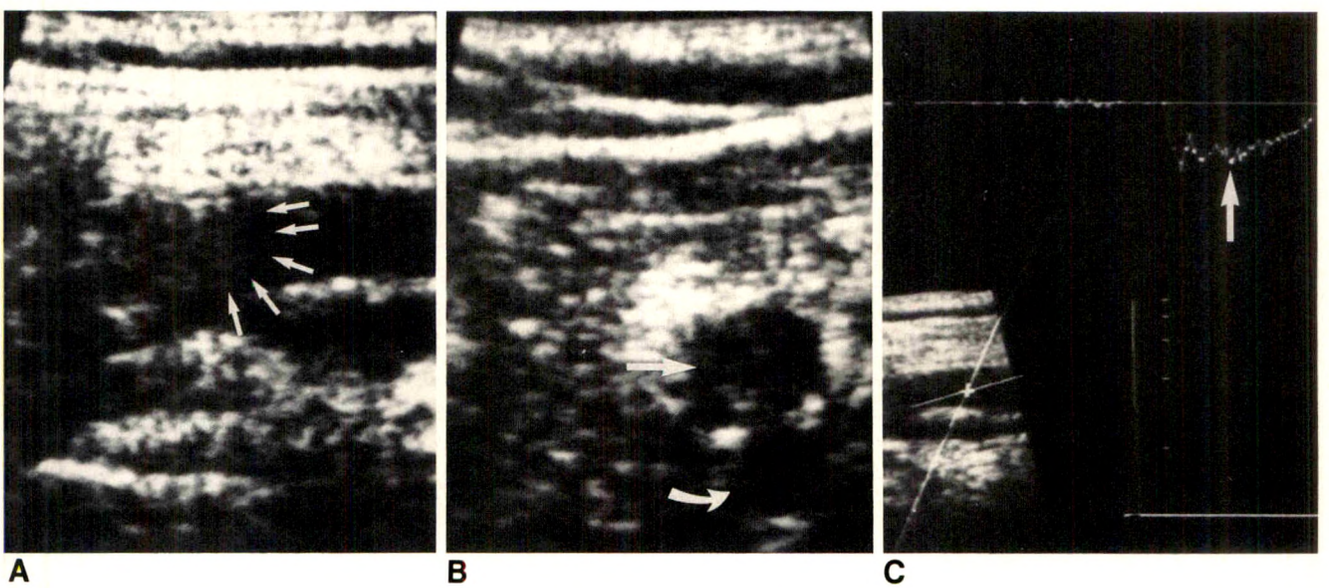

Fig. 2.—42-year-old man with a 3-day history of right calf pain and swelling.

A, Longitudinal sonogram shows leading edge of a noncompressible thrombus (*arrows*) in distal popliteal vein.

B, Transverse section shows noncompressible thrombus (*straight arrow*) within popliteal vein. This thrombus was confirmed on contrast venography. Normal popliteal artery (*curved arrow*) is immediately adjacent to vein.

C, Duplex examination of popliteal vein. Calf compression in a normal Doppler examination results in increased flow through popliteal vein and therefore an increased (augmented) Doppler signal. Cursor is in popliteal vein above thrombus. There is a normal Doppler augmentation signal (*arrow*) in response to calf compression. This is misleading and suggests a normal examination, despite the presence of visible thrombus.

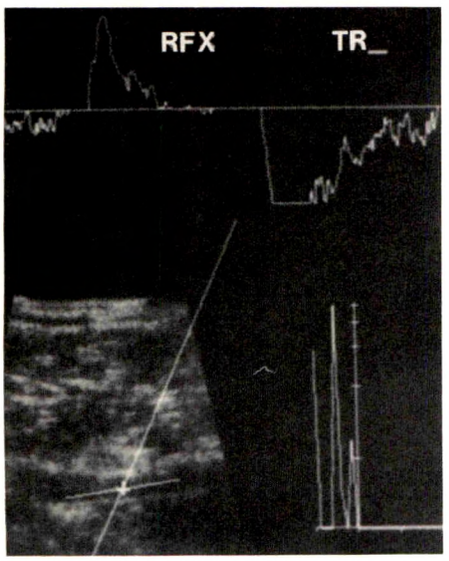

Fig. 3.—Longitudinal duplex sonogram of popliteal vein in 56-year-old man with venographically documented popliteal thrombosis 2 years previously. Deep venous reflux is shown by reverse flow (RFX) above baseline in response to thigh compression. In a normal patient, competent valves prevent reversal of flow. Reversal of flow in this patient implies that these valves are incompetent, a sequela of previous deep venous thrombosis. Normal forward flow below baseline (TR) is noted in response to release of thigh compression.

abnormalities in venous outflow to detect thrombosis, any abnormality that alters venous outflow may produce false-positive IPG examinations. Such abnormalities include pelvic masses, pregnancy, congestive heart failure, chronic obstructive pulmonary disease, Baker cysts, massive edema, and previous deep venous thrombosis [20].

Differences between our results and those of Hull et al. [9] may be due to differences in the two populations of patients. Seventy-five percent of our patients were inpatients, whereas in the study by Hull et al. [9], 75% were outpatients. Of the 34 patients in this study who had positive IPG and negative sonographic examinations, 19 (56%) had underlying clinical conditions that may have produced a false-positive result. Pelvic masses were observed in three of these patients; two had cellulitis and marked edema, and six had previous deep venous thrombosis and stasis changes. Baker cysts were noted in two patients. Five patients had severe congestive heart failure, and one had severe chronic obstructive pulmonary disease. Patients in our referral group therefore were more likely to have underlying clinical conditions that would make interpretation of IPG results difficult.

Real-time duplex sonography, by comparison, is a direct imaging technique. Therefore, it is less dependent on physiologic alterations that may contribute to a false-positive IPG examination.

One limitation of this study is the relatively small number of correlative venograms (32 patients). Despite this limitation, the sensitivity and specificity of duplex sonography relative to venography is similar to the sensitivity and specificity reported in other recent studies [14–17].

Sensitivity appears to be comparable for IPG and sonography, whereas specificity seems higher for sonography (100% [87%, 100%]) than for IPG (63% [48%, 81%]).

In evaluating the larger group of patients (n = 123) examined by sonography and IPG, it would be expected therefore that discrepancies between the findings of IPG and sonography would more likely be cases in which IPG was positive and sonography was negative (as was observed).

Duplex sonographic examinations depend primarily on established real-time criteria for the diagnosis of deep venous thrombosis, that is, visualization of echogenic, noncompressible thrombi [14–17]. In two patients with popliteal thrombi, Doppler augmentation signals were normal. Evaluation of these two patients by Doppler criteria alone without real-time imaging would have resulted in two additional false-negative examinations.

The Doppler component of the duplex examination was useful in identifying increased flow in patients with cellulitis and reflux in patients with a history of venous thrombosis and varicose veins.

Our inability to obtain spontaneous popliteal Doppler signals is due to the limitations of our present equipment. Early experience with newer commercially available units (Diasonics, SPA 1000, Milpitas, CA) showed spontaneous popliteal Doppler signals in three normal volunteers.

A broader spectrum of patients can be examined by duplex sonography than by IPG. In 18 of 21 patients who could not undergo IPG or who had an uninterpretable IPG examination, diagnostic duplex sonographic studies were performed. A duplex sonographic examination does not require that the patient be lying flat as IPG does; therefore, patients with severe congestive heart failure or chronic obstructive pulmonary disease can be examined more easily and without significant discomfort. Motion by the patient is less problematic with duplex sonography than with IPG. Examination by duplex sonography also takes less time (10–15 min) per examination than IPG does (up to 40 min when multiple repetitions are required).

Neither IPG nor duplex sonography is accurate in the diagnosis of calf vein thrombi. The risk of developing pulmonary emboli from isolated distal calf vein thrombi is minimal [21]. Calf vein thrombi are clinically important because they may extend proximally into the popliteal vein or above.

Huisman et al. [10] advocate serial IPG examinations for the evaluation of deep venous thrombosis. Similarly, repeat real-time duplex sonography in high-risk patients whose initial examinations are normal may be useful in assessing the development of proximal extension of any distal, nonvisualized calf vein thrombi into the popliteal vein.

In summary, real-time duplex sonographic examination is a superior technique for evaluating femoropopliteal deep venous thrombosis. Compared with IPG, duplex sonography has a much higher specificity and similar sensitivity. Duplex sonography takes less time and can be performed in those patients in whom IPG cannot be performed. Duplex sonography is a direct imaging technique and therefore is less

affected by movement by the patient or physiologic alterations. Duplex sonography also may show hemodynamic changes, such as increased flow from cellulitis and deep venous reflux.

ACKNOWLEDGMENTS

The authors thank Janet Maginot and Charlotte Williams for their assistance and Dave Suddick for his statistical assistance.

REFERENCES

1. Salzman EW. Venous thrombosis made easy. *N Engl J Med* **1987**;314:847–848
2. Sigel B, Felix R Jr, Popky GL, et al. Diagnosis of lower limb venous thrombosis by Doppler ultrasonic technique. *Arch Surg* **1972**;104: 174–179
3. Nicalaides AN, Kakkar VV, Field ES, et al. The origin of venous thrombosis: a venographic study. *Br J Radiol* **1971**;44:653–663
4. Bettman MA, Paulin S. Leg phlebography: the incidence, nature and modification of undesirable side effects. *Radiology* **1972**;122:101–104
5. Albrechtsson U, Olson C-G. Thrombotic side effects of lower limb phlebography. *Lancet* **1976**;1:723–724
6. Hull R, Hirsch J, Sackett DL, Powers P, Turpie ACG, Walker I. Combined use of leg scanning and impedance plethysmography in suspected venous thrombosis: an alternative to venography. *N Engl J Med* **1977**;296:1497–1500
7. Hull R, Hirsch J, Sackett DL, Stoddart G. Cost effectiveness of clinical diagnosis, venography and non-invasive testing in patients with symptomatic deep vein thrombosis.
8. Hull R, Van Aken WG, Hirsch J. Impedance plethysmography using the occlusive cuff technique in the diagnosis of venous thrombosis. *Circulation* **1976**;53:696–700
9. Hull R, Hirsch J, Sackett DL. Replacement of venography in suspected venous thrombosis by impedance plethysmography and 125 I-fibrinogen leg scanning—a less invasive approach. *Ann Intern Med* **1981**;94:12–15
10. Huisman MV, Buller HR, Tencate JW, Ureeken J. Serial impedance plethysmography for suspected deep venous thrombosis in outpatients. *N Engl J Med* **1986**;314:823–828
11. Sandler DA, Duncan JS, Ward P, et al. Diagnosis of deep vein thrombosis: comparison of clinical evaluation, ultrasound, plethysmography and venoscan with x-ray venogram. *Lancet* **1984**;2:712–719
12. Ramchandani P, Soulen R, Fedullo L, Gains V. Deep venous thrombosis: significant limitations of non-invasive tests. *Radiology* **1985**;156:47–49
13. Holden RW, Klatte EC, Park HM, et al. Efficacy of noninvasive modalities for diagnosis of thrombophlebitis. *Radiology* **1981**;141:63–66
14. Ragjavendra BN, Horvi SC, Hilton S, Subramamyam BR, Rosen RJ, Lam S. Deep venous thrombosis: detection by probe compression of veins. *J Ultrasound Med* **1986**;5:89–95
15. Cronan JJ, Dorfman GS, Scola FH, Schepps B, Alexander J. Deep venous thrombosis: US assessment using vein compression. *Radiology* **1987**;162:191–194
16. Appelman AT, DeJons TE, Lampmen LE. Deep venous thrombosis of the leg: US findings. *Radiology* **1987**;163:743–746
17. Vogel P, Laing FC, Jeffrey RB, Wing VW. Deep venous thrombosis of the lower extremity: US evaluation. *Radiology* **1987**;163:747–751
18. Wheeler HB, Pearson D, O'Connell D, Mullick SC. Impedance plethysmography. *Arch Surg* **1972**;104:164–169
19. Rabinov K, Paulin S. Roentgen diagnosis of venous thrombosis in the leg. *Arch Surg* **1972**;104:143–144
20. Wheeler HB, Anderson FA. Impedance plethysmography: the diagnosis of venous thrombosis by occlusive impedance plethysmography. In: Bernstein EF, ed. *Noninvasive diagnostic techniques in vascular disease*, 2nd ed. St. Louis: Mosby, **1982**:482–496
21. Moser KM, LeMoine JR. Is embolic risk conditioned by location of deep venous thrombosis? Part I. *Ann Intern Med* **1981**;94:439–444

Videotape Review

RSNA Today, Vol. 1, No. 1. Oak Brook, IL: The Radiological Society of North America, 1987. $75; by subscription, 4 issues annually at $225 for RSNA members and $275 for nonmembers

The Radiological Society of North American (RSNA) recently announced the expansion of its educational efforts with the production of a new videotape digest series entitled *RSNA Today*. The RSNA has marketed videotapes of refresher courses for several years, and it is expected that sales of *RSNA Today* will soon exceed those of their older slide-tape sets. With this new series, the RSNA will further tap the teaching potential of video by producing tapes that are both entertaining and educational.

The tapes will not go into subjects in detail but will use multiple, short features to emphasize concepts and techniques at the cutting edge of radiology. As part of each tape, the American College of Radiology will have a short section on contemporary subjects of social, economic, or political interest. The first tape, lasting about 55 min, consists of segments dealing with extracorporeal shock-wave lithotripsy (ESWL), breast cancer screening from the scientific as well as a political point of view, percutaneous drainage of abscesses, MR imaging in relation to examination of the neonate, and a commentary on nuclear accidents. Plans are to release four issues per year, at a price of $225 for RSNA members.

The format resembles that of a typical evening news program with professional male and female moderators introducing program segments that last from about 4 to 12 min. The method of presentation varies from the more customary didactic discussion to interviews of participants; the cast ranges from well-known radiologists to elected politicians who want to ensure that screening mammography is a reimbursable examination.

The brevity of the segments limits in-depth treatment, but much educational material still is transmitted. The quality of the production is outstanding. One disconcerting feature, however, is the insertion between some of the segments of short commercials from several well-known radiologic equipment and supply companies.

I showed the tape to a mixed audience of practicing radiologists, students, and residents and solicited their comments. Not surprisingly, they expressed a variety of opinions: "It looks like a video-magazine and is too glitzy." "Too abbreviated." "Entertaining." "Educational and stimulating." Personally, I found the tape quite enjoyable. Although it did not contain much new material, it was interesting to hear, for example, about the effect of ESWL on radiologic practice at the University of Pennsylvania, to gain insight into Dr. Gerzoff's approach to abscess drainage, and to have Myron Moskowitz share his thoughts about proper indications for mammographic screening.

The RSNA should be praised for extending its already extensive educational activities. Whether this style of presentation, a synoptic, video digest, magazine approach to selected topics in radiology, will be successful depends on the audience's preference. Without a shadow of doubt, the Neilsen ratings of *RSNA Today* will reveal all.

M. L. Janower
St. Vincent Hospital
Worcester, MA 01604

Sonography of the Radial Artery at the Wrist

Gretchen A. W. Gooding[1]

The radial artery as a superficial structure at the wrist is susceptible both to direct penetrating injury and to blunt trauma, with the potential development of both false and true aneurysms. This report summarizes the sonographic features of seven consecutive patients who were referred for evaluation of the radial artery. The diagnoses include two cases of radial artery aneurysm, one tortuous nonaneurysmal artery, two cases of arteriovenous fistulae (one surrounded by fluid and one aneurysmal), a ganglion, and an inflammatory mass of the wrist.

Although radial aneurysms are unusual and angiography may be required to define the nature and extent of distal embolization to the hand, the nature of a palpable aneurysm in this region, vascular vs avascular, is easily and quickly assessed with high-resolution sonography.

At the wrist, the radial artery is a palpable, superficial vessel susceptible to both blunt and penetrating injury [1, 2]. True aneurysms are associated with blunt trauma from injury to the media [3, 4], whereas false aneurysms are associated with penetrating injuries of the arterial wall, which with enlargement, result in secondary trophic changes and symptoms related to nerve compression. The aneurysms are distinctly uncommon. The literature suggests that wrist angiography is the technique of choice for detecting the presence of thrombosis or distal embolization and for determining the location and morphology of aneurysms [1]. Alternatively, soft-tissue masses in the area need to be distinguished from radial artery abnormalities, and sonography is highly regarded in the examination of such superficial structures [5, 6].

This report summarizes the sonographic features of seven consecutive patients referred for evaluation of the radial artery (Fig. 1). Two patients had false aneurysms, two had iatrogenic arteriovenous fistulas, one had radial artery tortuosity, and two had extravascular lesions.

Subjects and Methods

Seven men, ranging in age from 40 to 70 years, had palpable abnormalities of the wrist; the abnormality pulsated in five, had a transmitted pulse in one, and had no pulsations in another. Each patient had high-resolution 10-MHz real-time sonography of the wrist in both longitudinal and transverse planes. The transducer (a mechanical, linear scanner) had a water-bath interface (Picker, Microview, Cleveland, OH). Acoustic gel was the coupling agent.

Results

Sonography showed a number of abnormalities. In two patients, there were pulsatile false radial-artery aneurysms that were subsequently confirmed by angiography (Figs. 2 and 3). In one, there was a tortuous nonaneurysmal radial artery, also confirmed by angiography (Fig. 4). In two patients on hemodialysis, there was

Received September 14, 1987; accepted after revision November 13, 1987.

[1] Department of Radiology, University of California, San Francisco, San Francisco, CA 94143 and Veterans Administration Medical Center, San Francisco, CA 94121. Address reprint requests to G. A. W. Gooding, Dept. of Radiology, VA Medical Center, 4150 Clement St., San Francisco, CA 94121.

AJR 150:629–631, March 1988
0361–803X/88/1503–0629
© American Roentgen Ray Society

Fig. 1.—Longitudinal sonogram shows normal radial artery.

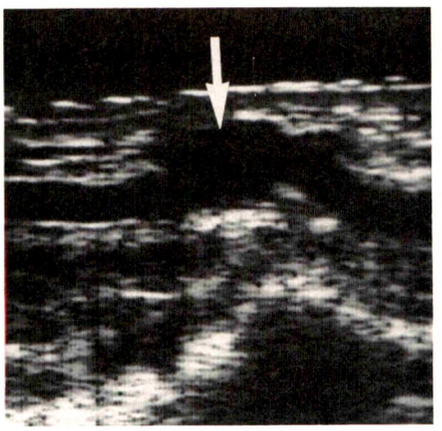

Fig. 2.—Longitudinal sonogram shows small fusiform aneurysm of radial artery (*arrow*).

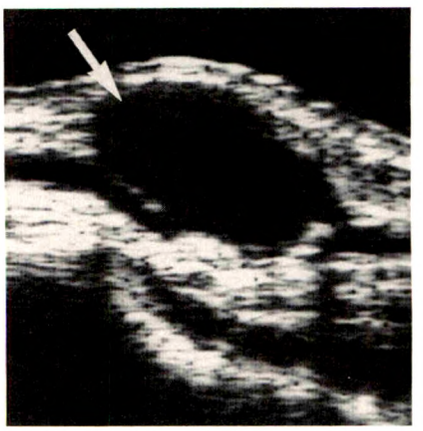

Fig. 3.—Longitudinal sonogram shows saccular radial artery aneurysm (*arrow*).

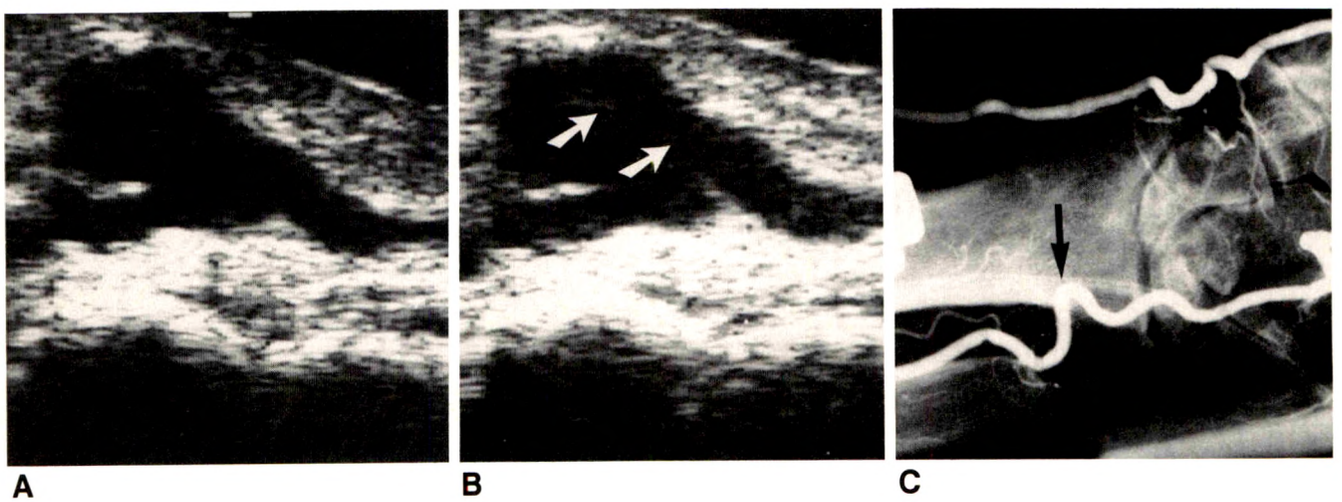

Fig. 4.—*A* and *B*, Longitudinal sonograms define what appears in *A* to be a radial artery aneurysm. More meticulous evaluation (*B*) defines tortuosity rather than aneurysm (*arrows* along tortuous wall of radial artery).
C, Angiogram shows tortuous radial artery (*arrow*).

one instance of fluid around an iatrogenic arteriovenous fistula (Fig. 5) that was subsequently proved to be infected. There was also a case of radial aneurysmal dilatation of another iatrogenic fistula.

One of the two patients with a radial artery aneurysm had a distinct dilatation of the right radial artery in a fusiform configuration (Fig. 2). The other patient had a distinct saccular aneurysm emanating from the wall of the radial artery (Fig. 3). These false aneurysms were well discriminated from the proximal normal radial artery (Fig. 1) and had distinct pulsations on real-time sonography without any perivascular component. Both of these patients had had previous arterial line placement in the area. One of them had developed a periarterial abscess and, subsequent to that, a septic arthritis; the other had developed a radial artery aneurysm that produced showers of septic emboli to the fingers.

A third patient who had had a penetrating injury of the radial artery had what at first glance appeared to be a radial artery aneurysm sonographically, but closer inspection revealed a markedly tortuous bend of the radial artery; this was subsequently confirmed by angiography (Fig. 4).

Another patient had a palpable mass with a faint pulsation clinically at the radial wrist, which on sonography appeared to be a tiny ganglion of the flexor tendon sheath next to the normal radial artery (Fig. 6) [5].

A seventh patient with a nonpulsatile mass in the same area was subsequently proved to have coccidioidomycosis, a disease process emanating from an adjacent septic arthritis and not affecting the radial artery (Fig. 7). These last two patients were the only ones who did not have a confirmatory angiogram.

Discussion

On sonography, the normal radial artery appears as a smooth wall tube with a distinct pulsation. An aneurysm of

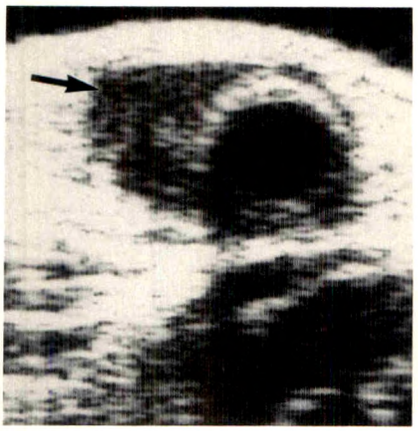

Fig. 5.—Transverse sonogram shows fluid (*arrow*) around an arteriovenous shunt at wrist.

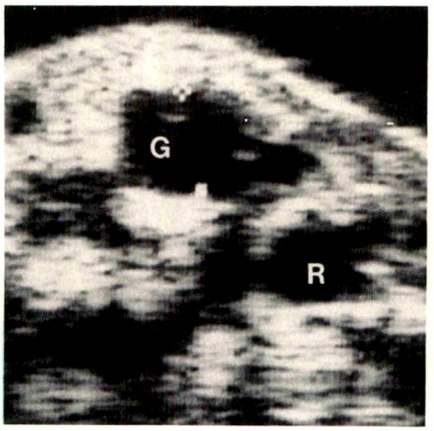

Fig. 6.—Transverse sonogram shows ganglion (G) adjacent to radial artery (R).

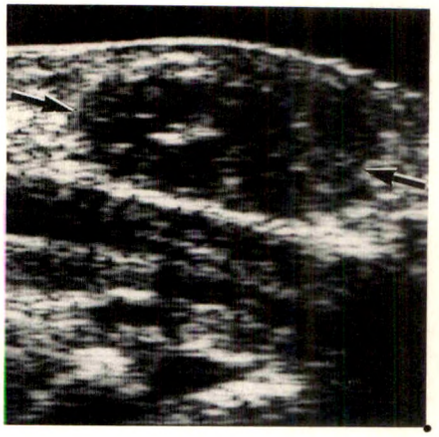

Fig. 7.—Longitudinal sonogram shows discrete inflammatory mass of coccidioidomycosis (*arrows*), at wrist separate from radial artery (which is not seen in image).

the radial artery produces a focal expansion, either fusiform or saccular, that may or may not contain visible thrombus.

Arteriography is an expensive, invasive, but appropriate method of determining the nature and extent of the involvement of the radial artery. Angiography is required to define the nature and extent of distal embolization to the hand and can pinpoint the radial artery as a possible source.

However, high-resolution real-time sonography, which does not require contrast material, is a quick and effective method of diagnosing radial abnormalities. High-resolution sonography allows a rapid diagnosis—that is, an aneurysm or tortuosity vs a mass adjacent to the radial artery—with a transmitted pulse.

The value of sonography of the radial artery is that not only can a normal vessel be distinguished from an aneurysm, but the characteristics of the wall can be defined and pulsation appreciated. In addition, the nature of the tissue beyond the wall can be assessed, and adjacent solid masses or fluid collections that would not be shown by angiography may be identifiable. Either solid or cystic extravascular lesions around the wrist, such as the ganglion and the inflammatory mass, can be distinguished from the radial artery [5].

REFERENCES

1. Eugenidis N, Fink F, Anabitarte M. False traumatic aneurysms of the radial and palmar arteries. *Radiology* **1976**;121:331–332
2. Duchateau J, Moermans J-P. False aneurysms for the radial artery. *J Hand Surg [Am]* **1985**;10-A(1):140–141
3. Ho PK, Dellon AL, Wilgis EFS. True aneurysms of the hand resulting from athletic injury: report of two cases. *Am J Sports Med* **1985**;13(2):136–138
4. Leitner DW, Ross JS, Neary JR. Granulomatous radial arteritis with bilateral, nontraumatic, true arterial aneurysms within the anatomic snuffbox. *J Hand Surg [Am]* **1985**;10-A(1):131–135
5. De Flaviis L, Nessi R, Del Bo P, Calori G, Balconi G. High-resolution ultrasonography of wrist ganglia. *JCU* **1987**;15:17–22
6. Gooding GAW. Tenosynovitis of the wrist: a sonographic demonstration. *J Ultrasound Med* (in press)

Case Report

The "To-and-Fro" Sign: Duplex Doppler Evidence of Femoral Artery Pseudoaneurysm

Monzer M. Abu-Yousef,[1] James A. Wiese,[1] and Asad R. Shamma[2]

Hematoma formation is a common complication of femoral artery catheterization. In a small percentage of cases, there may be persistent communication between the artery and the hematoma [1]. A clot forms in the periphery of the collection, and there is eventually fibrous encapsulation. It may not be possible to distinguish these pseudoaneurysms from noncommunicating hematomas on clinical grounds. However, definitive diagnosis is essential because these false aneurysms either may rupture or may be complicated by distal embolization, infection, or local pressure effects. Diagnosis by real-time sonography depends on the demonstration of expansile pulsations in the collection. Arteriography is often necessary to show the presence and site of communication between the collection and the artery. The introduction of Doppler sonography makes possible confirmation of the diagnosis of pseudoaneurysm by the demonstration of arterial flow in the fluid collection. We present a Doppler sign of pseudoaneurysm seen in four cases referred for evaluation of a fluid collection in the groin after femoral artery catheterization.

Case Report

An 83-year-old man was referred for sonographic evaluation of a 3-cm pulsatile groin swelling that developed after right femoral artery puncture for cardiac catheterization with an 8-French catheter. The mass became painful and continued to increase in size during a 6-day period. Bruit was heard on physical examination.

Real-time sonographic evaluation using a high-resolution, phased-linear-array transducer (Acuson, Mountain View, CA) showed an anechoic mass with expansile pulsation communicating with the superficial femoral artery (Fig. 1A). Duplex Doppler examination showed femoral arterial-like flow signals within the collection (Fig. 1B). Doppler sampling was directed to the neck of the fluid collection at the junction of the bifurcation of the common femoral artery. This was identified by a "to-and-fro" flow signal (i.e., blood flowing into the collection during systole and in the opposite direction during diastole) (Fig. 1C). During surgery, a 3 × 4 cm well-encapsulated pseudoaneurysm of the right common femoral artery was resected, and the hole in the artery was repaired.

Discussion

False aneurysm formation is a well-known complication of vascular injury. Real-time sonography provides a simple, reliable, and inexpensive assessment. The sonographic signs consist of expansile pulsations in the pseudoaneurysm and a point of communication with the artery. Pulsed duplex Doppler sonography improves the specificity of diagnosis by allowing demonstration of arterial-like and sometimes turbulent flow within the lumen of the false aneurysm.

The duplex Doppler examination has been used in the diagnosis of pseudoaneurysms of the splenic artery [2], hepatic artery [3], renal artery [4], ascending aorta [5], and left ventricle [6]. In each of these reports, the presence of turbulent or pulsatile flow within the pseudoaneurysm has been shown. In addition, the reports of Wendel et al. [5] and Chou et al. [4] include demonstrations of Doppler tracings at the

Received August 11, 1987; accepted after revision November 3, 1987.
[1] Department of Radiology, The University of Iowa Hospitals and Clinics, Iowa City, IA 52242. Address reprint requests to M. M. Abu-Yousef.
[2] Department of Surgery, The University of Iowa Hospitals and Clinics, Iowa City, IA 52242.

AJR 150:632–634, March 1988 0361–803X/88/1503-0632 © American Roentgen Ray Society

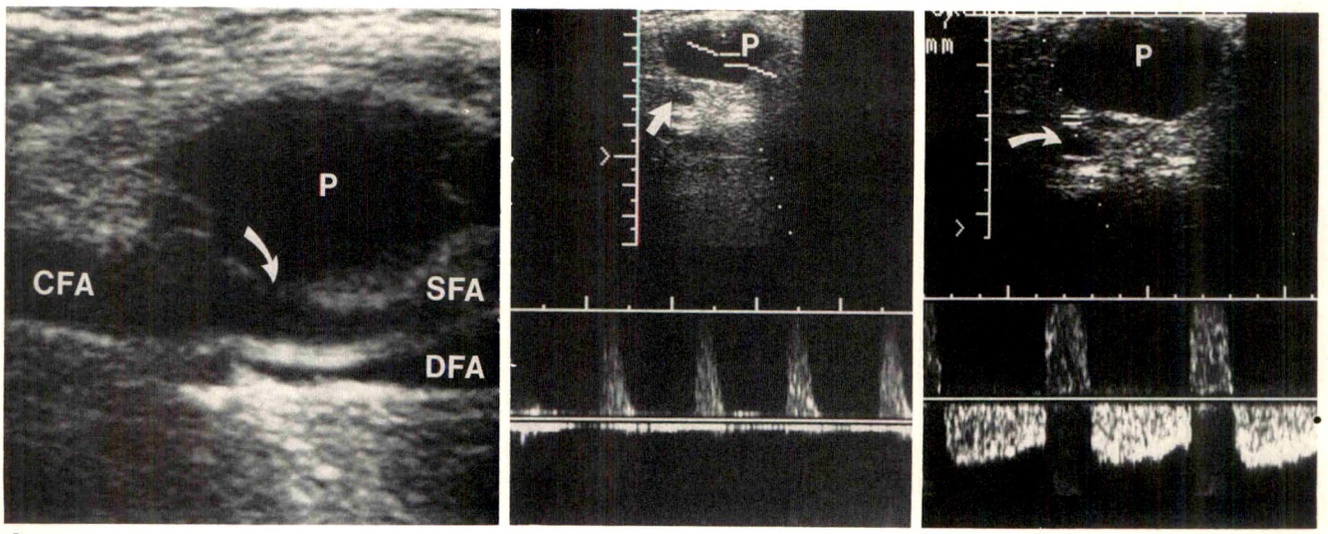

Fig. 1.—*A*, Longitudinal view shows large pseudoaneurysm (P) anterior to superficial femoral artery (SFA). Neck of pseudoaneurysm (*arrow*) is well seen. DFA = deep femoral artery, CFA = common femoral artery.

***B*, Simultaneous Doppler and real-time scan shows pseudoaneurysm (P) superficial to femoral artery (*arrow*) in this transverse view of groin. Arterial-like Doppler wave form is shown, with sample volume positioned in center of false aneurysm.**

***C*, Transverse duplex scan of groin shows fluid collection (P) anterior to femoral artery (*arrow*). Sample volume is positioned between pseudoaneurysm and artery, at communicating channel. Typical "to-and-fro" Doppler wave form is depicted in lower half of scan. Note reversal of flow during diastole. Communicating channel itself is not well seen.**

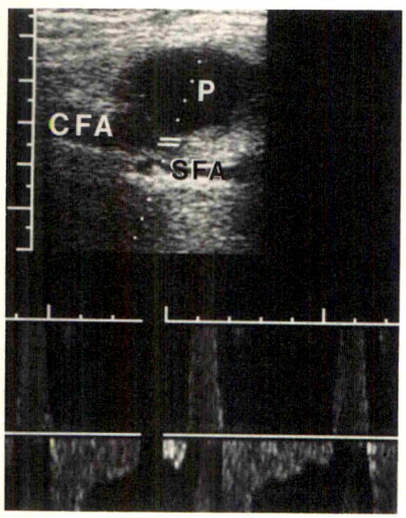

2

Fig. 2.—Duplex scan shows pseudoaneurysm (P) in longitudinal plane superficial to superficial femoral artery (SFA). Sample volume is positioned at relatively echolucent neck, which is faintly visualized. Flow at this location is directed anteriorly into pseudoaneurysm during systole and away from transducer and pseudoaneurysm in diastole. An aliasing artifact seen during systole and diastole results from high-flow velocity in narrow channel between pseudoaneurysm and artery. CFA = common femoral artery.

mouth of pseudoaneurysms of the left ventricle and ascending aorta showing systolic flow into the pseudoaneurysm and diastolic flow out of the pseudoaneurysm. The "to-and-fro" sign has not been previously described in association with femoral artery pseudoaneurysms. Indeed, this finding should be present in every pseudoaneurysm that has a narrow neck, regardless of the artery of origin.

This feature of pseudoaneurysms has been graphically shown by angiography in the past [1]. However, no report has emphasized the importance of this significant finding in the duplex evaluation of these lesions. We observed the "to-and-fro" duplex Doppler sign in three other cases, one of which was proved surgically. The flow velocity was either partially uniform during diastole (Fig. 1C) or was very high immediately after systole, then became slow during the latter half of diastole (Fig. 2). This Doppler sign can be explained by the fact that during systole the pressure is higher in the artery than in the pseudoaneurysm, leading to influx of blood into the pseudoaneurysm. During diastole, the pressure and flow in the artery, especially in extremity arteries, drop down to zero, and there may even be reversal of flow due to high resistance in the peripheral circulation. Blood then flows back through the pseudoaneurysm neck as a result of the pressure gradient between the overdistended, high-pressure pseudoaneurysm and the low-pressure artery.

This Doppler sign observed at the neck of the pseudoaneurysm together with the "turbulent or arterial-like flow" sign seen within its lumen helps to confirm the real-time sonographic diagnosis and obviate angiography. The "to-and-fro" sign is also helpful in identifying the exact point of communication between the pseudoaneurysm and either the superficial or common femoral artery, which is helpful in preoperative planning. When a pseudoaneurysm is considered in the differential diagnosis of a fluid collection in the groin, especially

Factors Affecting Visualization of Posterior Rib Fractures in Abused Infants

Paul K. Kleinman[1]
Sandy C. Marks[2]
Vernard I. Adams[3]
Brian D. Blackbourne[3]

Rib fractures frequently are encountered in abused infants and commonly occur in the posterior rib arcs. Fractures occurring near the costovertebral articulations are rarely identified radiographically in the acute phase, and callus formation usually is the first indication of injury. To assess the factors influencing the visibility of fractures near the costovertebral articulations in abused infants, 103 posterior rib fractures occurring in 16 abused infants were studied radiologically. The plain radiologic studies were correlated with the pathologic findings in 15 ribs from four patients. The limited visibility of fractures relates to (1) the frequent superimposition of the transverse process over the rib fracture site, (2) a fracture line that crosses at an obliquity to the radiographic beam, and (3) nondisplacement of rib fragments due to preservation of the posterior periosteum. Fresh fractures invisible on a frontal projection are clearly defined when the rib is viewed axially with postmortem radiography. These findings explain the reported superior sensitivity of radionuclide bone scans vs radiography in the identification of fresh posterior rib fractures. A knowledge of the factors influencing the visibility of these important injuries is useful in planning an appropriate diagnostic evaluation in cases of suspected infant abuse.

Fractures of the posterior rib arcs carry a high specificity for infant abuse [1, 2], but unfortunately fractures near the costovertebral articulations are often difficult to identify radiographically, even in the healing phase. Although radionuclide scintigraphy may be more sensitive in identifying these fractures, the success of the technique depends on the technical quality of the studies as well as on interpreter expertise [3–8]. Recent studies have elucidated the morbid anatomy of fractures near the costovertebral articulations in abused infants [9]. Using the insights gained from this work, we undertook the present study to provide an understanding of the factors influencing the visibility of posterior rib fractures in abused infants.

Methods and Materials

The skeletal surveys and clinical data in 16 consecutively studied abused infants less than 1 year old with documented posterior rib fractures were reviewed. Diagnosis was based on the presence of associated skeletal abnormalities considered indicative of abuse, including metaphyseal "bucket-handle" and "corner" fractures of the extremities, scapular fractures, spinous process fractures, and characteristic traumatic central nervous system injury. The ribs were radiographed in all patients in at least one projection, and on occasion oblique views were obtained. Of 15 rib fractures noted at gross examination in four patients, pathologic material from nine ribs was made available for microscopic analysis. Rib specimens were radiographed with high-detail film-screen systems or direct exposure. Pathologic material was fixed in formalin, decalcified, sectioned in an axial plane, and stained with hematoxylin and eosin. A correlation of the histologic material with the pre- and postmortem radiologic studies was carried out.

Each rib articulates with the vertebral column at two points (Fig. 1). The head of the rib articulates with the costal facet of the vertebra anteriorly, and the tubercle articulates with the transverse process posteriorly. The rib head and tubercle as well as much of the vertebral

Received March 2, 1987; accepted after revision November 10, 1987.

This work was supported in part by the University of Massachusetts Public Service Endowment Grant 1-61516.

[1] Department of Radiology, University of Massachusetts Medical Center, 55 Lake Ave. N., Worcester, MA 01655. Address reprint requests to P. K. Kleinman.

[2] Department of Anatomy, University of Massachusetts Medical Center, Worcester, MA 01655.

[3] Department of Pathology and the Office of the Medical Examiner, University of Massachusetts Medical Center, Worcester, MA 01655.

AJR 150:635–638, March 1988
0361–803X/88/1503–0635
© American Roentgen Ray Society

body have substantial cartilaginous components in infancy, a factor that influences radiographic appearances [10].

Results

One hundred three fractures involving the posterior arc of the ribs were documented radiographically and/or pathologically. The number of rib fractures per patient ranged from two to 24.

Location of Fractures

For analysis, the posterior arcs of the ribs were divided into medial and lateral halves (Fig. 1). Ninety-one fractures (88%) involved the medial half of the posterior arcs, and 12 (12%) involved the lateral half. The medial arcs were further divided into a portion occurring at or medial to the costotransverse process articulation and a portion lateral to the costotransverse process articulation. The number of fractures occurring in these regions was 66 (64%) and 25 (24%), respectively. Thus, a substantial majority of posterior rib fractures occurred at or medial to the costotransverse process articulation.

Chronicity of Fractures

With the exception of a single fracture involving the lateral half of the posterior rib arc, no acute rib fractures were identified on conventional radiographs in infants surviving assaults (Table 1). Of 15 posterior rib fractures identified at autopsy, eight were acute. None of these acute fractures could be identified on conventional radiography. In an infant with two acute fractures, postmortem specimen radiography in the frontal projection failed to show the fractures, and only when viewed in an axial projection could they be identified (Fig. 2). Evidence of healing manifested by callus formation was essential for reliable diagnosis of fractures near the costovertebral articulations (Fig. 3).

Orientation of Fracture Lines

The radiolucency produced by an acute fracture will be viewed only if the radiographic projection is parallel to the plane of the fracture. Fracture lines oriented at an obliquity to the plane of projection will be invisible (Fig. 2B) but will be identified easily in an axial projection (Fig. 2C).

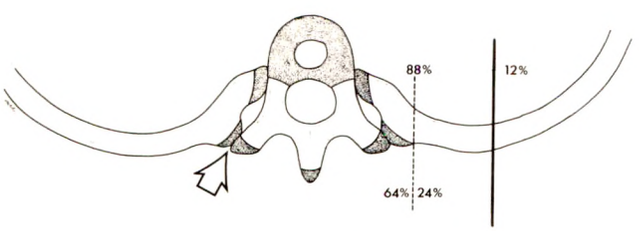

Fig. 1.—Distribution of 103 fractures in 16 abused infants is indicated. 64% of fractures occurred at or medial to costotransverse process articulations (*arrow*).

TABLE 1: Chronicity of Posterior Rib Fractures

Patient Group	Acute	Old	Total
Infants with radiographic assessment only ($n = 12$)	1	87	88
Autopsied infants ($n = 4$)			
Radiographically identified	0	7	7
Pathologically (gross) identified	8	7	15

Position and Alignment of Fragments

In most cases, there is little displacement or angulation of posterior rib fractures. Only eight displaced fractures could be identified with certainty on frontal radiographs. These were generally identified in massively traumatized infants who apparently had received severe blows to the trunk. Maintenance of the posterior periosteal attachment in all fractures examined histologically most likely explains the tendency for most posterior rib fractures to be undisplaced (Figs 2A and 3B).

Discussion

Rib fractures are reported to account for between 5% and 27% of all fractures occurring in abused children [11–13]. In this study, radiography failed to identify fractures near the costovertebral articulation present at postmortem in more than half the cases. Furthermore, radiography failed to identify any of the eight acute fractures noted at postmortem. These findings are supported by data suggesting that radionuclide scintigraphy will identify greater numbers of rib fractures than radiography [3–6]. Although most authorities agree on the high sensitivity of scintigraphy as a screening examination for skeletal injury, a variety of factors have militated against its use in cases of abuse [7, 8, 14].

The importance of rib fractures in the diagnosis of child abuse has been appreciated for nearly four decades [3, 15–18]. The specificity of fractures near the costovertebral articulation for the diagnosis of infant abuse is comparable with that of the classic metaphyseal "bucket-handle" and "corner" fractures. We have suggested that most infant rib fractures near the costovertebral articulations occur during episodes of violent shaking with thoracic compression in the anterior/posterior plane [9]. Presumably, the ribs are excessively levered over a fulcrum of the transverse process, resulting in disruption of the ventral periosteum and cortex of the rib, usually leaving the dorsal periosteum intact. This mechanism of injury is in keeping with the severe accelerational and decelerational forces producing metaphyseal, scapular, and CNS injuries in infants who have been shaken [9].

What steps can be taken to enhance identification of posterior rib fractures? In centers employing the radiographic skeletal survey, strict attention to technique is essential. The standard radiograph of the chest is inadequate because of the higher kilovoltage and the posteroanterior technique that usually are employed. A standard anteroposterior projection of the rib cage with lower kilovoltage appropriately chosen to visualize the osseous structures is essential as a screening

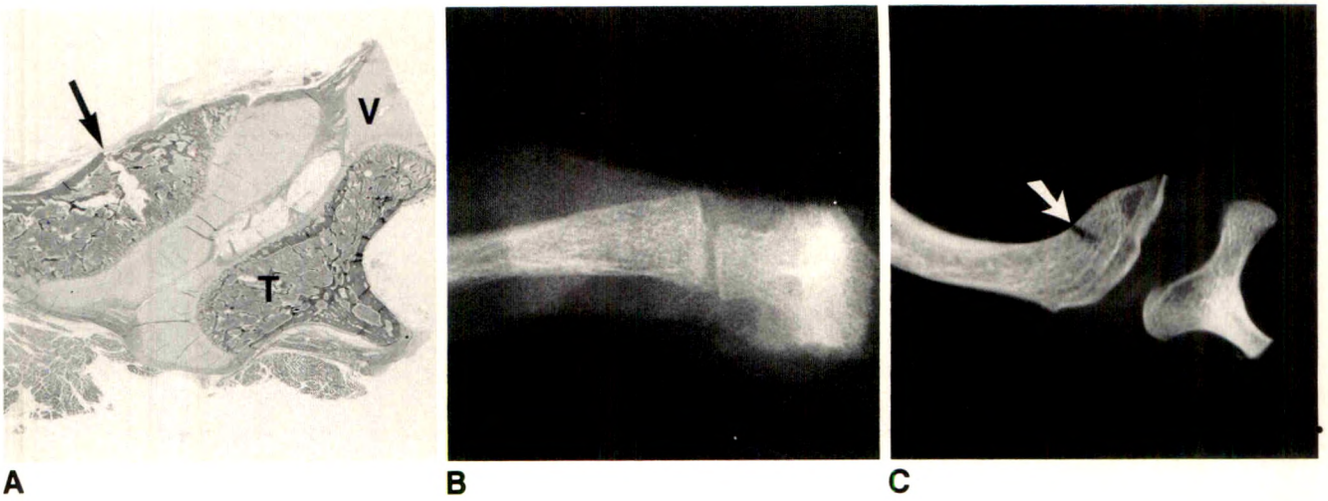

Fig. 2.—*A*, Axial histologic section through costovertebral junction in 2-month-old abused infant with acute rib fracture found at autopsy. A fracture is seen (*arrow*) opposite costotransverse process articulation. Fracture disrupts ventral periosteum, extends through thin ventral cortex and medullary space, but does not reach cartilage of rib tubercle. V = vertebral body; T = transverse process.

***B*, Radiograph of same rib in frontal projection shows no abnormality.**

***C*, A second radiograph obtained by rotating rib 90° into axial plane shows fracture (*arrow*), which correlates precisely with fracture noted in *A*.**

Fig. 3.—*A*, Views of costovertebral junctions in 3-month-old abused infant. Fractures at costovertebral junction of fifth through seventh ribs are evident with callus formation (*arrows*).

***B*, Histologic section of fifth rib shows a healing fracture (*solid arrow*) just lateral to rib head. Periosteal reaction (*open arrows*) is noted only along ventral surface of rib extending laterally to level of rib tubercle. Dorsal cortex and periosteum are preserved.**

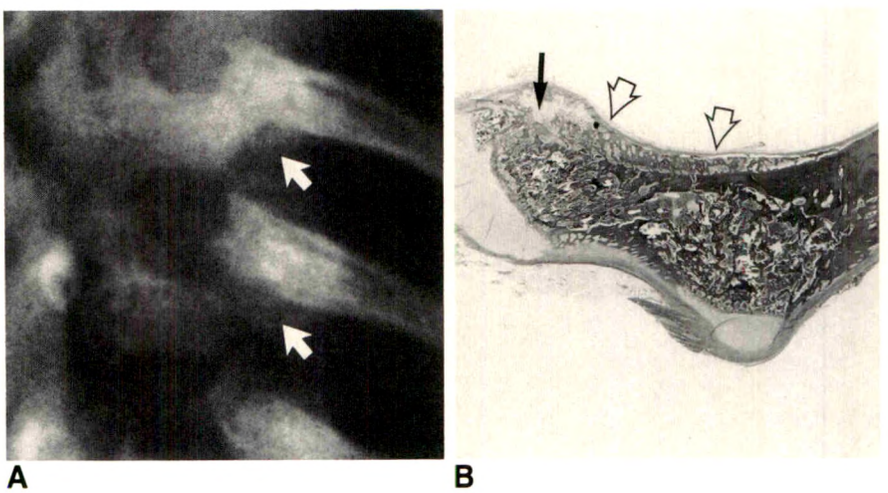

examination. Coned-down and oblique views of the ribs probably are not justified on a routine basis, but when there is strong suspicion of abuse on clinical grounds, or when equivocal findings are present on standard projections, oblique and coned-down views may be useful [2]. In departments that use skeletal scintigraphy as the primary imaging technique, all questionable findings should be studied radiographically. In centers that use radiography as a screening examination, scintigraphy should supplement an equivocal skeletal survey. Whichever approach is used, a knowledge of the factors influencing the visibility of posterior rib fractures is important in planning an appropriate diagnostic evaluation in cases of suspected infant abuse.

REFERENCES

1. Thomas PS. Rib fractures in infancy. *Ann Radiol (Paris)* **1977**;20:115–122
2. Cameron JM, Rae L. The radiological diagnosis. In: *Atlas of the battered child syndrome*. London: Churchill Livingstone, **1975**:20–50
3. Smith FW, Gilday DL, Ash JM, Green MD. Unsuspected costo-vertebral fractures demonstrated by bone scanning in the child abuse syndrome. *Pediatr Radiol* **1980**;10:103–106
4. Jaudes PK. Comparison of radiography and radionuclide bone scanning in the detection of child abuse. *Pediatrics* **1984**;73:166–168
5. Sty JR, Starshak RJ. The role of bone scintigraphy in the evaluation of the suspected abused child. *Radiology* **1983**;146:369–375
6. Haase GM, Ortiz VN, Stakianakis GN, Morse TS. The value of radionuclide bone scanning in the early recognition of deliberate child abuse. *J Trauma* **1980**;20:873–875

7. Berdon WE. Should the radionuclide skeletal survey be used as a screening procedure in suspected child abuse victims? (letter). *Radiology* **1983**;148:576
8. Diament MJ. Should the radionuclide skeletal survey be used as a screening procedure in suspected child abuse victims? (letter). *Radiology* **1983**;148:573
9. Kleinman PK. Bony thoracic trauma. In: *Diagnostic imaging of child abuse*. Baltimore: Williams & Wilkins, **1987**:67–89
10. Warwick R, Williams PL, eds. Arthrology. In: *Gray's Anatomy*, 35th Br. ed. Philadelphia: Saunders, **1973**:388–471
11. Herndon WA. Child abuse in a military population. *J Pediatr Orthop* **1983**;3:73–76
12. Akbarnia B, Torg JS, Kirkpatrick J, Sussman S. Manifestations of the battered-child syndrome. *J Bone Joint Surg* [*Am*] **1974**;56-A:1159–1166
13. Barrett IR, Kozlowski K. The battered child syndrome. *Australas Radiol* **1979**;23:72–82
14. Berdon WD. Editorial. Battered children: how valuable are bone scans in diagnosis? *Appl Radiol* **1981**;10:12, 124
15. Lis EF, Frauenberger GS. Multiple fractures associated with subdural hematoma in infancy. *Pediatrics* **1950**;6:890–892
16. Woolley PV Jr, Evans WA Jr. Significance of skeletal lesions in infants resembling those of traumatic origin. *JAMA* **1955**;158:539–543
17. Marie J, Apostolides P, Salet J, Eliachar L, Lyon G. Hematome sous-dural du nourrisson associe a des fractures des membres. *Ann Pediatr* (*Paris*) **1954**;30:1757–1763
18. Silverman FN. The roentgen manifestations of unrecognized skeletal trauma in infants. *Am J Roentgenol Radium Ther Nucl Med* **1953**;69:413–427

Now Available
(Limited Quantities)

1987 American Roentgen Ray Society Categorical Course Syllabus
Gastrointestinal Radiology
Editor: Gary G. Ghahremani, M.D.

Contains 161 pages of textbook-quality information and illustrations reviewing recent advances and current concepts in gastrointestinal radiology. Written by leading authorities in the field.

Send $25 per copy, along with name and address, to:

American College of Radiology
Publications Division
P.O. Box 2348
Merrifield, VA 22116–2348

(Price includes shipping/handling charges at book rate. Indicate if first-class delivery requested and add $5 per copy.)

Balloon Dilatation of Esophageal Stenosis in Children

Yutaka Sato[1]
Edward E. Frey[1]
Wilbur L. Smith[1]
Kevin C. Pringle[2]
Robert T. Soper[2]
Edmund A. Franken, Jr.[1]

Balloon dilatation of benign esophageal strictures is an accepted mode of therapy in adults. This report describes balloon dilatation in 20 consecutive infants and children. The lesions treated include 11 strictures at surgical anastomotic sites, seven restrictive Nissen fundoplications, and three nonanastomotic esophageal strictures. One patient had two lesions. Most dilatations were performed on an outpatient basis without anesthesia. All strictures responded immediately to dilatation. In most cases, long-term resolution occurred after three or fewer procedures. A subgroup of patients was identified in which a prolonged course of treatment was needed. These included patients with long strictures due to esophageal atresia, patients with chronic severe esophagitis, and patients with strictures at the site of esophageal perforation. No significant complications were encountered.

Balloon dilatation of esophageal stenosis in children is effective and safe and should be considered before other methods of treatment are used.

Dilatation of esophageal stenosis by means of an inflatable balloon catheter under fluoroscopic control has been an established mode of therapy in adults [1–5], and use of this approach in children has been described [6–8]. We report our experience with 20 consecutive infants and children who received 68 dilatations for 21 esophageal stenotic lesions.

Subjects and Methods

Between October 1984 and January 1987, 20 infants and children with symptomatic esophageal stenosis were referred for balloon dilatation. In total, 68 dilatations were performed for 21 lesions using polyethylene Grüntzig balloon dilating catheters (Medi-tech, Watertown, MA). Summaries of the clinical courses of these patients are presented in Table 1.

Eleven of the strictures occurred at the site of a surgical anastomosis for the repair of esophageal atresia. In four instances, diagnosis and subsequent balloon dilatations of anastomotic strictures were precipitated by episodes of obstructive esophageal foreign body when the patients were 1–4.5 years old. In three cases, esophageal strictures were caused by esophagitis of various causes. Seven patients had restrictive Nissen fundoplications. Four patients had previous endoscopic bougienage.

Patients injested nothing orally for at least 4 hr before the procedure. All balloon dilatations were performed in the radiology suite under fluoroscopic control and were continuously monitored by ECG; frequent suction also was used. General anesthesia was used on one occasion in the early phase of the study; otherwise, no sedatives were used.

A red rubber catheter was introduced through the mouth or nose and was positioned at the proximal aspect of the stricture. An angiographic guidewire with a soft tip was then passed through the catheter and across the stricture. The tip of the guidewire was left in the stomach until the dilatation was completed. The red rubber catheter was replaced by a Grüntzig balloon dilating catheter, which was passed over the guidewire. The size of the initial dilating balloon was chosen on the basis of the estimated caliber of the esophagus, which was determined by the initial barium swallow.

In neonates, the first dilatation usually was made with a balloon that was 6–8 mm in

Received August 3, 1987; accepted after revision October 27, 1987.

Presented at the annual meeting of the American Roentgen Ray Society, Miami Beach, FL, April 1987.

[1] Department of Radiology, The University of Iowa Hospitals and Clinics, Iowa City, IA 52242. Address reprint requests to Y. Sato.

[2] Department of Surgery, The University of Iowa Hospitals and Clinics, Iowa City, IA 52242.

AJR 150:639–642, March 1988
0361–803X/88/1503–0639
© American Roentgen Ray Society

TABLE 1: Balloon Dilatations in Children

Patient No.	Age[a]	Gender	Abnormalities		Balloon Catheter Dilatation				Result (follow-up period)
			Primary	Associated	Postop. Interval	Number of BCD	Maximum Diameter (mm)	Maximum Pressure (atm)	
1	1 mo	F	EA/distal TEF	None	3 wk	2	8	4	Resolved (21 mo)
2	1 mo	M	EA/double fistulae	None	3 wk	4	10	6	Resolved (12 mo)
3	2 mo	M	EA/double fistulae	Anastomotic leak	7 wk	5	12	8.5	Resolved (13 mo)
4	3 mo	F	EA	GER	2 wk	12[b]	10	10	Reanastomosed in 18 mo
5[c]	6 mo	F	EA/distal TEF	GER (Nissen)	6 mo	5	15	5	BCD at 2- to 3-mo intervals
	1.5 yr		Nissen	EA/distal TEF and GER	9 mo	1	15	3	Resolved (6 mo)
6	3 yr	M	EA	GER	9 mo	5[b]	18	5	BCD at 2- to 3-mo intervals
7	11 yr	M	EA/distal TEF	Colonic interposition	10 yr	7[b]	15		Reanastomosed in 2 yr
8	1 yr	M	EA/distal TEF	Foreign body	1 yr	1	12	4	Resolved (8 mo)
9	1 yr	F	EA/distal TEF	Foreign body	1 yr	2	18	5	Resolved (27 mo)
10	2 yr	M	EA/distal TEF	Foreign body	2 yr	3	12	3.5	Resolved (20 mo)
11	4.5 yr	M	EA/distal TEF	Foreign body	4.5 yr	1	12	3.5	Resolved (5 mo)
12	2 yr	F	Caustic esophagitis	None	1 yr	1	10	3	Endoscopic dilatation
13	5 yr	M	Radiation esophagitis	None	3 yr	7	18	3.5	Died of unrelated cause
14	7 yr	F	*Candida* esophagitis	None	5 yr	1[b]	15	3	BCD at 6-wk intervals
15	1.5 yr	M	Nissen	None	11 mo	3	15	6	Nissen removed
16	1.5 yr	M	Nissen	None	8 mo	3	12	4	Resolved (15 mo)
17	2 yr	M	Nissen	None	7 mo	1	15	3	Resolved (8 mo)
18	2.5 yr	F	Nissen	None	2 wk	1	10	3	Resolved (8 mo)
19	1.5 yr	F	Nissen	None	3 wk	1	12	9.5	Resolved (15 mo)
20	2 yr	M	Nissen	None	17 mo	1	10	3	Resolved (21 mo)

Note.—BCD = balloon catheter dilatation; atm = atmospheric pressure; EA = esophageal atresia; TEF = tracheoesophageal fistula; GER = gastroesophageal reflux; Nissen = restrictive Nissen fundoplication; wk = week; mo = month; yr = year.

[a] Age at time of the first balloon catheter dilatation.

[b] History of endoscopic dilatation.

[c] This patient had two lesions. She developed an obstruction at the site of the Nissen fundoplication, which was performed for gastroesophageal reflux.

diameter; in infants, the balloon diameter was 10–12 mm. The size of the balloon was increased in increments of 2 mm for each subsequent dilatation. With the balloon portion of the catheter at the stricture, the balloon was slowly inflated with dilute contrast material to specified pressures for each balloon; a pressure gauge was used to monitor the pressures. Balloon displacement was obviated by using a 4-cm-long balloon. The inflation was maintained for 60 sec and then repeated three times during each dilatation. After removal of the catheter and wire, the integrity of the esophageal lumen was confirmed by esophagram.

In patients with a gastrostomy who required repeated balloon dilatation, a thin Silastic catheter was retrieved through the gastrostomy by the guidewire and the ends of the line were tied for future access. The entire process was accomplished within 30 min. The patients were allowed to drink after the procedure was completed.

Results

Among 11 patients who had had anastomotic stricture after esophageal atresia repair and who had completed a course of three or fewer dilatations, seven were free of symptoms 5–27 months after the procedures. Two patients continued to need intermittent dilatation, and two required further surgical correction.

Those patients who failed to achieve long-term relief after the third balloon dilatation were readily identified as having complex abnormalities, including a missed proximal tracheoesophageal fistula (one), a proximal fistula and postoperative anastomotic leakage (one), severe gastroesophageal reflux (three), isolated esophageal atresia with a long gap (two) (Fig. 1), and a colonic interposition complicated by postoperative leakage (one).

Patients with tracheoesophageal fistula who presented with an esophageal foreign body in late infancy but who had no immediate postoperative symptoms (four) responded well to balloon dilatation (Fig. 2).

All but one of the seven patients who underwent balloon dilatation for restrictive Nissen fundoplication were free of symptoms after three or fewer balloon dilatations (Fig. 3). Two developed small, asymptomatic para-Nissen herniae after balloon dilatation. Patient 15 underwent three balloon dilatations without relief of obstructive symptoms, and the Nissen fundoplication was surgically removed.

Among three patients with chronic esophagitis from various causes, two had temporary palliation after balloon dilatation. One patient who had proximal esophageal stenosis caused by caustic ingestion could not tolerate the procedure because of the development of upper-airway obstruction. One patient who had chronic esophageal stricture from previous radiation therapy for a malignant spinal teratoma died of an unrelated cause after eight balloon dilatation procedures over a period

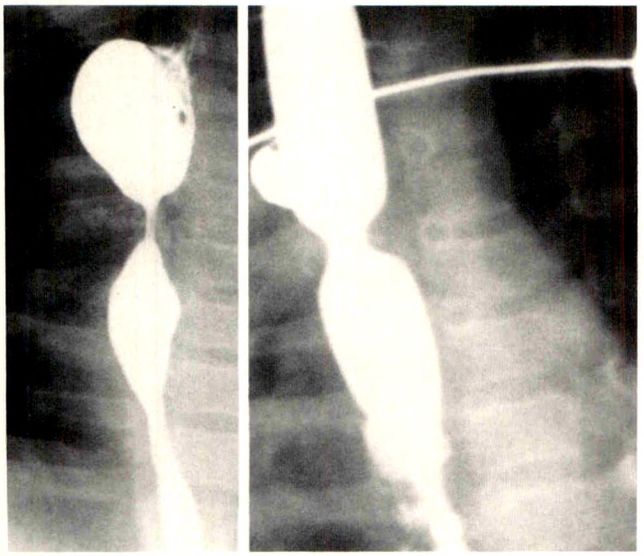

Fig. 1.—Case 4: 3-month-old girl with isolated esophageal atresia without fistula.

A, Barium study performed 1 month after delayed anastomosis showed severe stenosis at site of anastomosis. Despite multiple balloon catheter dilatations with temporary symptomatic relief, patient required another anastomosis at age 18 months.

B, 10-mm balloon inflated to 3 atm of pressure shows persistent "waist" at stenosis.

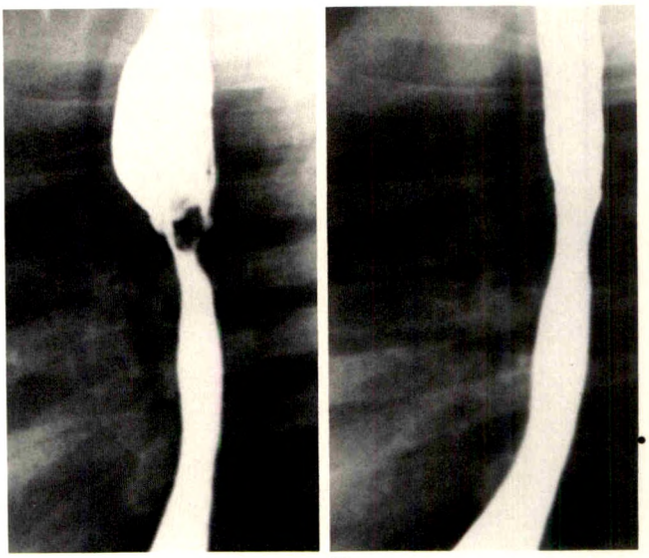

Fig. 2.—Case 8: 12-month-old boy who was surgically treated during neonatal period for esophageal atresia with distal tracheoesophageal fistula shows acute symptoms of esophageal obstruction (*A*).

A, Lateral esophagram showed foreign body at anastomotic site. A piece of carrot was extracted using a Foley balloon catheter.

B, Postdilatation lateral esophagram. A satisfactory long-term result was obtained.

of 15 months. At the time of his death, this patient's esophageal symptoms had decreased, and it had been 3 months since his last balloon dilatation.

In infants less than 3 months old, adequate dilatation was accomplished by using a Grüntzig catheter with a diameter of 8–10 mm. The older children required a balloon diameter of 10–15 mm. All strictures dilated with a 6-mm balloon required subsequent, larger balloon dilatation.

In summary, of the 21 lesions treated, 13 were resolved; three patients required intermittent balloon dilatation at 1.5- to 3-month intervals, three required additional surgery, one could not tolerate balloon dilatation, and one patient died from an unrelated cause. In three patients who continued to require intermittent balloon dilatation and in two who underwent additional surgery, the persistent waist on the balloon at the site of the stricture was noted even at maximal inflation of the balloon (Fig. 1).

No balloon was ruptured during inflation. However, bradycardia was observed in small infants during maximal inflation of the balloon. This resolved spontaneously on deflation of the balloon, and the procedure could be completed.

Discussion

Other reports [1–5] have described the successful use of balloon dilatation to treat esophageal stenosis in adults; however, our experience shows that this mode of treatment is also useful in infants and children. In our series, there were no major complications, and no hospitalization was required for the procedure. Balloon dilatation was successful in achieving a cure or palliation in a number of infants and children with esophageal stenosis.

Wesdorp et al. [9] reported an 8% perforation rate in 100 adult patients with benign esophageal stricture who underwent bougienage. Starck et al. [1] experienced approximately the same rate of perforation among their patients who underwent bougienage. On the other hand, there are only two reported cases of esophageal perforation caused by balloon dilatation, one in a 35-month-old infant with esophageal stricture caused by ingestion of lye [6] and the other in an adult with lung carcinoma that had invaded the distal esophagus [10].

Fluoroscopically controlled passage of the guidewire, aided by a red rubber catheter, and subsequent introduction of the balloon catheter across the stenosis (which is outlined by contrast material) is a simple procedure. Only radially directed forces are transmitted to the most narrowed esophageal segment without additional longitudinal and shearing forces of bougienage; therefore, trauma to the esophageal wall is reduced and the risk of esophageal rupture is much lower. Many strictures that are treated with bougienage recur, so it is not surprising that balloon-dilated strictures also recur. In those cases, our experience parallels that of Starck et al. [1] who, in the study comparing mean relapse-free time between bougienage and balloon dilatation, reported prolonged symptom-free intervals after balloon dilatation. They attributed this result to decreased trauma to the esophagus and to the larger luminal width available with balloon dilatation.

Most patients with complicated esophageal atresia repair and those with stricture caused by long-standing esophagitis

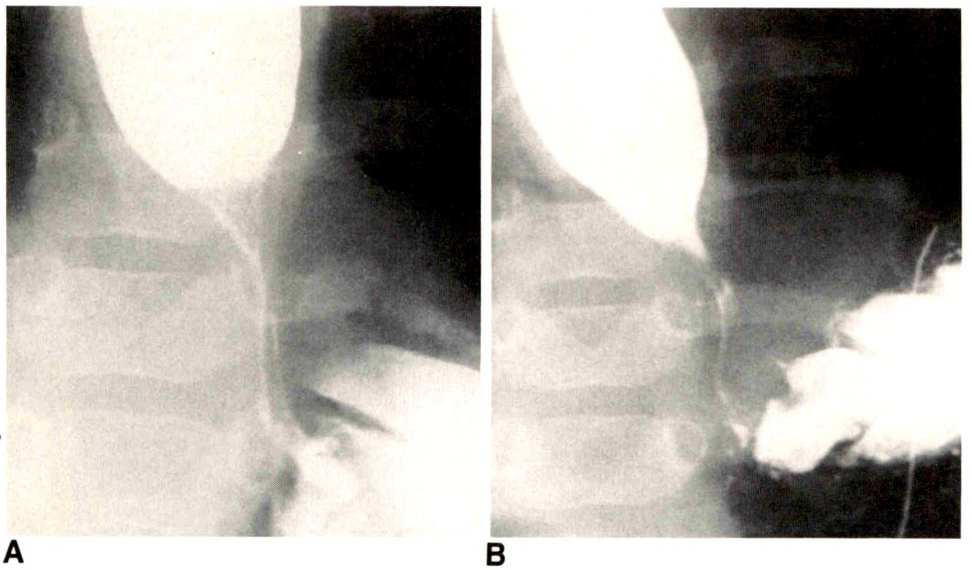

Fig. 3.—Case 19: 18-month-old girl with symptoms of progressive esophageal obstruction after Nissen fundoplication.

***A*, Anteroposterior esophagram shows narrowing of distal esophagus with proximal dilatation.**

***B*, Despite symptomatic relief, postdilatation esophagram shows little change.**

achieved good palliation with balloon dilatations, with steadily increasing intervals between dilatations. We postulate that the effect of dilatation was limited because of dense and extensive fibrosis of the stenotic area and alterations to the intrinsic blood supply to the area.

Persistence of the waist on the balloon at the site of the stricture indicates a limited response to balloon dilatation. In these cases, balloons that tolerate greater pressure may be required.

Patients with restrictive Nissen fundoplication responded well to the balloon dilatation. In these patients, immediate postdilatation esophagrams may show no change, despite significant symptomatic relief. In two patients whose condition had improved, para-Nissen hernias were induced by balloon dilatations, probably because of fractures of the suture lines. Neither of these patients had symptoms related to this complication.

Balloon dilatation in infants and children appears to be a rapid, safe, and lasting alternative to standard treatments for esophageal stenosis caused by postoperative stricture, restrictive Nissen fundoplication, and esophagitis; balloon dilatation should be considered before other modes of treatment.

REFERENCES

1. Starck E, Paolucci V, Herzer M, Crummy AB. Esophageal stenosis: treatment with balloon catheters. *Radiology* **1984**;153:637–640
2. London RL, Trotman BW, DiMarino AJ Jr, et al. Dilatation of severe esophageal strictures by an inflatable balloon catheter. *Gastroenterology* **1981**;80:173–175
3. Kollath J, Starck E, Vittorio P [*sic*]. Dilation of esophageal stenosis by balloon catheter. *Cardiovasc Intervent Radiol* **1984**;7:35–39
4. Owman T, Lunderquist A. Balloon catheter dilatation of esophageal stricture—a preliminary report. *Gastrointest Radiol* **1982**;7:301–305
5. Blundell GE, Burhenne HJ. Balloon catheter dilatation of malignant esophageal stricture. *J Can Assoc Radiol* **1984**;35:180–182
6. Ball WS, Strife JL, Rosenkrantz J, Towbin RB, Noseworthy J. Esophageal strictures in children. Treatment by balloon dilatation. *Radiology* **1984**;150:263–264
7. Goldthorn JF, Ball WS Jr, Wilkinson LG, Seigel RS, Kosloske AM. Esophageal strictures in children: treatment by serial balloon catheter dilatation. *Radiology* **1984**;153:655–658
8. Johnsen A, Jensen LI, Mauritzen K. Balloon-dilatation of esophageal strictures in children. *Pediatr Radiol* **1986**;16:388–391
9. Wesdorp ICE, Bartelsman JFWM, den Hartog Jager FCA, Huibregtse K, Tytgat GN. Results of conservative treatment of benign esophageal strictures: a follow-up study in 100 patients. *Gastroenterology* **1982**;82:487–493
10. LaBerge JM, Kerlan RK Jr, Pogany AC, Ring EJ. Esophageal rupture: complication of balloon dilatation. *Radiology* **1985**;157:56

Acute Scrotal Abnormalities in Children: Diagnosis by Combined Sonography and Scintigraphy

Dagmar L. Mueller[1]
Gary M. Amundson[1]
Steven Z. Rubin[2, 3]
Richard L. Wesenberg[1]

Both scintigraphy and real-time sonography have been used to assess acute symptoms involving the scrotum. However, because of its high sensitivity and ability to document physiologic abnormalities, scintigraphy has been the procedure of choice. Scintigraphy, however, lacks specificity; its value lies mainly in serving to distinguish torsion from nontorsion. The purpose of this study was to supplement scrotal scintigraphy with sonography to determine if the combination improves diagnosis and management compared with scintigraphy alone. Forty-three scrotal scintigrams and sonograms were performed on 40 consecutive patients with acute scrotal symptoms. The interpretation of the scintigram was altered by sonography in six (14%) of the combined scans, directly affecting clinical management. In three patients with acute hydroceles diagnosed by sonography, exploratory surgery was avoided despite scintigraphic findings suggesting testicular torsion. Scintigraphy was normal in two patients with spontaneous testicular detorsion, whereas sonography showed recent spermatic-cord torsion that required subsequent orchiopexy. In a patient with epididymitis and orchitis, sonography showed a complicating scrotal abscess, which was not apparent on scintigraphy and which required antibiotic treatment.

The addition of sonography to the scintigraphic evaluations of children with acute scrotal abnormalities changed the diagnosis and clinical management in 14% of the patients studied.

The child presenting with an acutely painful and/or swollen scrotum constitutes an emergency requiring immediate diagnosis and treatment [1]. The causes include epididymitis and/or orchitis, spermatic-cord "testicular" torsion (torsion of the spermatic cord and testis), torsion of a testicular appendage (most commonly appendix testis or appendix epididymidis), acute hydrocele, strangulated hernia, idiopathic scrotal edema, hemorrhage in a testicular tumor or associated with trauma, Henoch-Schönlein purpura, and scrotal fat necrosis [2]. Of these epididymitis (and/or orchitis) and torsion occur most frequently and pose the greatest diagnostic dilemma. Clinical differentiation of these two entities cannot be made with absolute certainty, and the distinction may not be possible in up to 50% of patients [3]. Furthermore, diagnosing torsion is particularly difficult when it is intermittent.

The physician must differentiate those conditions that can be adequately treated medically (epididymitis and/or orchitis) from those requiring prompt surgery (spermatic-cord torsion, testicular rupture). Scintigraphy and high-resolution real-time sonography have each been used for this purpose with various results [4]. The purpose of this study was to evaluate prospectively the usefulness of combined sonography and scintigraphy in children with acute scrotal symptoms.

Subjects and Methods

From 1983 to 1986, 43 scrotal sonograms and scintigrams were performed on 40 patients ranging in age from 1 day to 15 years (mean, 8 years) and presenting with acute scrotal pain

Received August 13, 1987; accepted after revision November 17, 1987.

Presented in part at the International Congress of Radiology, Honolulu, HI, July 1985.

[1] Department of Radiology, Alberta Children's Hospital, 1820 Richmond Rd. S.W., Calgary, Alberta, T2T 5C7, Canada. Address reprint requests to D. L. Mueller.

[2] Department of Surgery, Alberta Children's Hospital, Calgary, Alberta T2T 5C7, Canada.

[3] Present address: Department of Surgery, Children's Hospital of Eastern Ontario, 401 Smyth, Ottawa, Ontario K1H 8L1, Canada.

AJR 150:643–646, March 1988
0361–803X/88/1503–0643
© American Roentgen Ray Society

(left side in 24, right side in 19). The duration of pain before clinical presentation varied from 2 hr to 3 days. In three of the patients, two series of studies were performed for separate episodes of acute scrotal symptoms.

Scintigraphy was performed with a Siemens ZLC 37, dual-headed emission, computerized axial tomographic scanner. The anterior camera was used; the patients were scanned supine with the legs abducted (frog-legged in infants), and the penis was taped cephalad on the abdomen. A bolus of ^{99m}Tc–sodium pertechnetate (1.0–15.0 mCi [37–555 MBq], depending on body weight) was injected intravenously. Nine first-pass, angiographic scintigraphic images were obtained at 2- to 4-sec intervals by using a converging low-energy collimator. An immediate blood-pool image (2.5 million counts) was then obtained (magnified 2.75 times). At 5–8 min, a static magnified image (1 million counts) was obtained by use of high-resolution, low-energy, parallel-hole collimators. On the final image, the symptomatic testicle was demarcated, and the median raphe was identified with radionuclide markers. Thyroid uptake was blocked by the oral administration of potassium perchlorate (10 mg/kg).

Sonography was performed with either a Diasonics DRF-400 (10-MHz) or an ATL MK-600 (7.5-MHz) real-time scanner. With the patient supine, transverse, longitudinal, and coronal scans of each testis were obtained with direct transducer contact on the scrotum by using a large amount of E-Z gel (E-Z-EM Canada Ltd., Whitby, Ontario) as the coupling agent. The complete sonographic examination was obtained within 15 min of scintigraphy. The final diagnosis was established surgically in 13 patients: (spermatic cord torsions (seven patients), torsion of testicular appendages (three patients), epididymitis and orchitis (two patients), and traumatic hemorrhage with hematocele (one patient). In the remaining 27 patients, the diagnosis was established by subsequent clinical course.

Results

Of the various scrotal abnormalities encountered in this study, epididymitis and/or orchitis was the most common, occurring in 16 (37%) of 43; spermatic-cord torsion was found in seven (16%), hydrocele in four (9%), traumatic hemorrhage in four (9%), and torsion of a testicular appendage in four (9%). Eight patients were normal.

Five patients with symptoms lasting from 10 hr to 2 days had characteristic sonographic and scintigraphic abnormalities that were caused by surgically confirmed spermatic-cord torsion (Fig. 1). However, two patients had spermatic-cord torsion that, at the time of the imaging studies, had undergone spontaneous detorsion. Scintigraphy showed normal testicular perfusion on the flow study without evidence of a central "cold" defect on the blood-pool static images; sonography depicted testicular enlargement and hyperechogenicity, findings consistent with torsion. At surgery, these testicles were enlarged, discolored, and congested, but the spermatic cord was no longer twisted. In one of these patients, sonography confirmed that the symptomatic testicle was maldescended.

In three of the four patients with torsion of a testicular appendage, focal hyperemia superolateral to the testicle was seen on scintigraphy. The sonograms of two of these patients were normal; in the third, sonography showed a small hydrocele with minimal enlargement of the testis and epididymis. In the fourth patient, both radionuclide scintigraphy and sonography were normal. In these four patients, duration of symptoms ranged from 10 hr to 3 days. Surgery was performed on three of these patients for persistent pain.

In all patients with epididymitis and/or orchitis (mean duration of scrotal pain, 25 hr), scintigraphy showed increased perfusion and increased radiotracer deposition in the symptomatic hemiscrotum; sonography showed enlargement and altered echogenicity of the epididymis and/or testis in all but one patient. In six of the 16 patients, sonography yielded additional diagnostic information by showing either a hydrocele (small- to moderate-sized) or an abscess (one patient) (Fig. 2).

In three patients, scintigraphy showed normal or decreased perfusion and central "cold" defects in the symptomatic scrotum, suggesting acute spermatic-cord torsion; these defects were caused by large uncomplicated hydroceles, that were easily identified by sonography, and no underlying abnormalities of the testicle or epididymis were present (Fig. 3). In a fourth patient, with an acute hydrocele detected by sonography, scintigraphy was normal. Mean duration of the patients' symptoms in these four children was 16 hr.

In the four patients with testicular trauma, three were evaluated because the degree of trauma seemed insufficient to explain the clinical signs. These patients had generalized hyperemia on scintigraphy with focal alteration of testicular echogenicity on sonography that corresponded to areas of contusion. In two of these patients, sonography identified a hematocele. In the fourth patient, scintigraphy was normal yet sonography detected focal areas of testicular contusion. The symptoms in these patients had lasted from 2 to 12 hr.

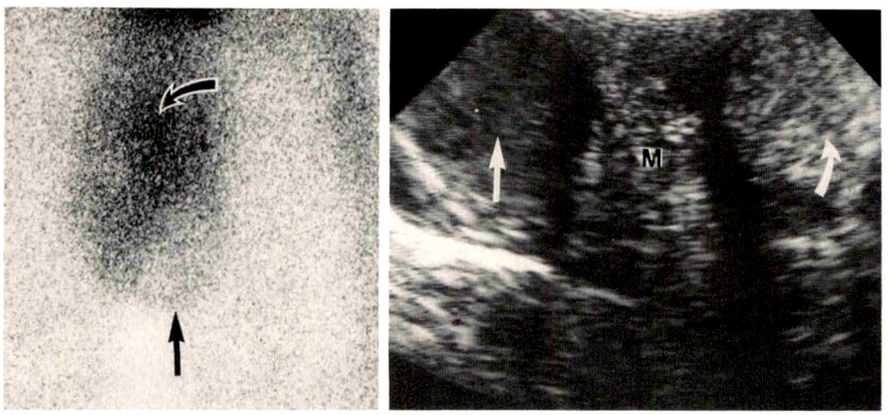

A B

Fig. 1.—12-year-old boy with scrotal pain for 24 hr. Surgically confirmed spermatic-cord torsion.

***A*, Scintigraphic static image shows a rounded "cold" area in expected location of left testicle (*straight arrow*). *Curved arrow* shows base of penis.**

***B*, Transverse sonogram shows area of increased echogenicity due to hemorrhage (*curved arrow*) in enlarged left testicle. *Straight arrow* shows normal right testis. M = median raphe.**

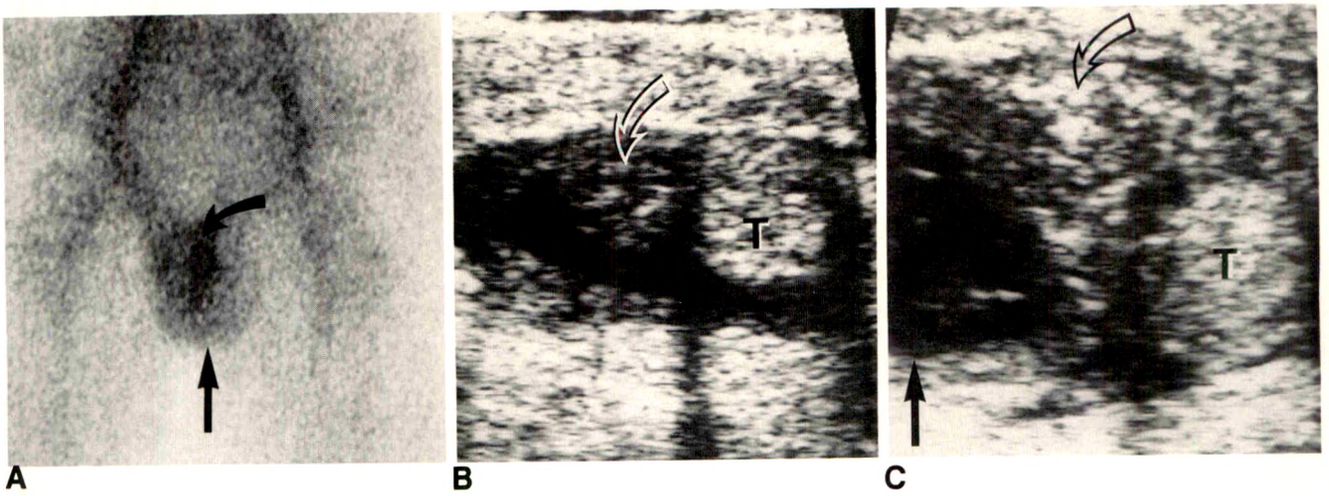

Fig. 2.—6-year-old boy with right epididymitis and abscess, surgically confirmed.

A, Scintigraphic static image shows diffuse increased intake in the right hemiscrotum caused by epididymitis. Scintigraphic angiogram (not shown) shows increased perfusion. *Straight arrow* shows median raphe; *curved arrow* shows base of penis.

B, Sagittal sonogram shows enlarged, hypoechoic head of epididymis (*open arrow*) surrounded by small hydrocele. T = testicle.

C, Sagittal sonogram shows ill-defined, inhomogeneous abscess (*open arrow*) surrounding right testicle (T). *Closed arrow* = unusually enlarged spermatic cord.

Fig. 3.—3-year-old boy with right hydrocele presenting with scrotal pain for 12 hr.

A, Scintigraphic static image shows central "cold" area in right hemiscrotum suggestive of spermatic-cord torsion (*closed arrow*). *Open arrow* shows normal left testicle. Radionuclide angiogram (not shown) showed decreased flow to right hemiscrotum.

B, Sagittal sonogram shows large hydrocele surrounding normal testicle (*straight arrow*) and epididymis (*curved arrow*).

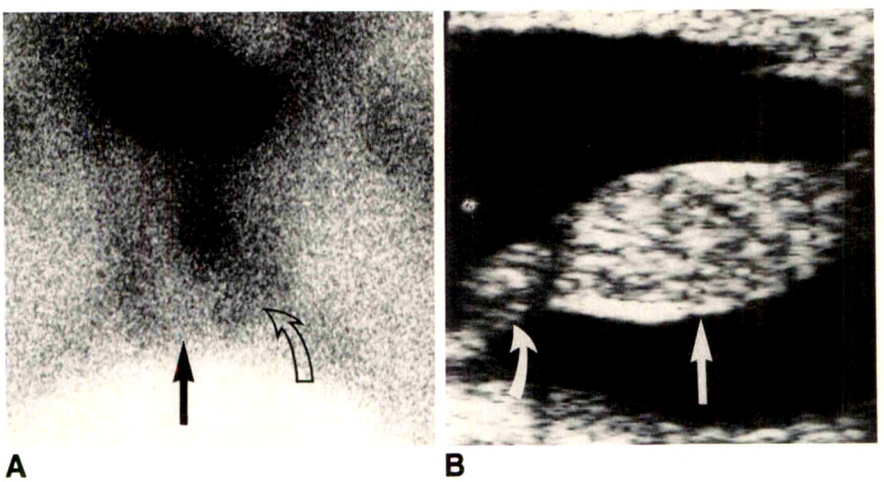

In eight patients (mean duration of scrotal pain, 25 hr), both scintigraphy and sonography were normal, and symptoms abated shortly after evaluation. No evidence of subsequent testicular atrophy was found by sonography and clinical examination. The causes of the symptoms in these patients remain undetermined.

Discussion

The necessity to distinguish spermatic-cord torsion from epididymitis and/or orchitis ultimately is related to testicular salvage rates, which is determined by the duration and degree of torsion. The testicular salvage rate is 80–100% if surgery is performed within 5–6 hr of the onset of pain, 70% if surgery is undertaken within 6–12 hr, but only 20% if surgery is delayed for more than 12 hr [1]. Orchiopexy is indicated in all patients with spermatic-cord torsion to salvage the afflicted side and to prevent this complication in the nonaffected side.

In patients with unilateral spermatic-cord torsion in whom the affected necrotic testis has not been surgically removed, histologic damage may occur in the contralateral testis. This degeneration, consisting of aspermatogenesis and seminiferous tubule atrophy, is mediated by the immune system and ultimately results in decreased fertility [5]. The extent of histologic damage is also dependent on the duration of torsion. For preservation of the integrity of the contralateral testis, the damaged testis must be removed in instances of prolonged testicular torsion [5]. Since the clinical history, physical examination, and laboratory data are usually not specific in differentiating spermatic-cord torsion from other acute scrotal abnormalities [6], improvement in testicular salvage rates has relied on immediate surgery [7]. However, spermatic-cord torsion occurs in only 35–60% of patients who undergo exploratory surgery for acute scrotal pain and swelling [8]. Therefore, if those patients with scrotal abnormalities other than spermatic-cord torsion can be identified, surgery may be avoided in 40–65% of these cases.

The diagnostic techniques currently used to evaluate the acutely painful scrotum include scintigraphy [8, 9], sonography [10], and Doppler sonography [11]. Although these methods of investigation have been useful, they do not have 100% reliability, which is the desired goal [2, 4, 7, 12]. Doppler

sonography has a reported accuracy of 79–88% [7, 13], and the accuracy of scintigraphy is about 95% [7, 14].

Scintigraphy relies on decreased perfusion to the symptomatic testicle (flow studies) and identification of a central "cold" defect (static images) to diagnose spermatic-cord torsion. Because scintigraphy provides physiologic data, it is widely considered the most accurate method currently available [7], and, as such, is the procedure of choice [2]. Despite meticulous technique, however, adequate perfusion may be difficult to detect, particularly in small infants. Furthermore, both false-negative and false-positive results have been reported [7, 15]. Any large fluid collection (hydrocele, hematocele) or hernia overlying the testis will attenuate photons, thereby suggesting an incorrect diagnosis of spermatic-cord torsion.

Sonography relies on altered testicular echogenicity, enlargement of the testis and/or epididymis, and the identification of small hydroceles to diagnose spermatic-cord torsion [4, 10, 16].

The aim in testicular diagnostic imaging is to detect all patients with spermatic-cord torsion and reduce the number of exploratory operations performed for diagnosis. Thirteen (33%) of 40 children in this series had surgery. Three additional patients would have had surgery on the basis of the scintigraphic findings alone (diminished perfusion and "cold" defect in the symptomatic scrotum—findings suggestive of spermatic-cord torsion) if large hydroceles had not been identified on sonography. This represents a 19% (3/16) decrease in surgical intervention. The two cases in which surgery was done for epididymitis and/or orchitis occurred early in the study, before the reliability of the combined studies had been established. On the basis of our current knowledge, these two additional patients would not have undergone surgery. Therefore, our results show a potential 31% (5/16) reduction in surgical intervention. Furthermore, in two patients with spontaneous testicular detorsion, the recent torsions were detected on sonography, and the patients subsequently underwent orchiopexies. Consequently, the number of surgical explorations can be decreased by the combined imaging approach if surgery is reserved primarily for spermatic-cord "testicular" torsion.

Supplementing scintigraphy with sonography in evaluation of acute scrotal pain has the following advantages: (1) Findings on sonography will decrease the impact of scintigraphic false-positive scans caused by spuriously decreased perfusion on the flow study (maldescended testes, hernia) or the photopenic defects (hydrocele, hematocele) on static scans. (2) Sonography will identify abnormalities or substantiate normalcy when scintigraphic perfusion patterns are indeterminate. (3) Sonographic abnormalities consistent with testicular torsion [10] combined with normal scintigraphy can probably be considered diagnostic of spontaneous detorsion. This additional diagnostic information will directly affect the decision to operate.

Sonography has further advantages in that it is a useful technique in (1) establishing the presence of testicular atrophy after spermatic-cord torsion, (2) confirming the position of maldescended testes detected clinically, and (3) doing follow-up on patients with epididymitis and/or orchitis or trauma to identify complications (abscess, testicular rupture, hematoma, hematocele). Furthermore, in cases of nontorsion, sonography adds confidence to the clinical decision to defer surgery. Sonography yielded information that was not apparent by scintigraphy and that resulted in a specific diagnosis in 10 (25%) of 40 patients in this series. This, however, does not imply that sonography was not beneficial in the remaining 75% of patients examined. Sonography is useful even when findings are normal. For example, if scintigraphy shows increased perfusion and radiotracer deposition in the symptomatic scrotum, a normal sonogram eliminates the diagnoses of traumatic hemorrhage and epididymitis and/or orchitis and therefore makes torsion of a testicular appendage the most likely explanation for the scintigraphic findings.

Based on results of this study, our policy is to evaluate all children presenting with acute symptoms in the scrotum with both sonography and scintigraphy. Both types of imaging studies are available on an emergency basis (within 1 hr) to rapidly and accurately evaluate these patients. Thereby, we believe that the number of exploratory operations for diagnosis will decrease, but those patients needing prompt surgical intervention will be identified.

ACKNOWLEDGMENTS

We thank Erna Schultz, Anne Wilson, Carmen Mancini, and Kathy Bray for their technical expertise in providing high-quality sonograms and scintigrams and Clara McChesney and Joyce Hutchings for manuscript preparation.

REFERENCES

1. Donohue RE, Utley WLF. Torsion of spermatic cord. *Urology* **1978**;11: 33–36
2. Holder LE, Melloul M, Chen D. Current status of radionuclide scrotal imaging. *Semin Nucl Med* **1981**;11(4):232–248
3. Bunce PL. Scrotal abnormalities. In: Glenn JF, ed. *Urologic Surgery*. Hagerstown, MD: Harper & Row, **1975**:232–249
4. Hricak H, Jeffrey RB. Sonography of acute scrotal abnormalities. *Radiol Clin North Am* **1983**;21(3):595–603
5. Nagler HM, White R. The effect of testicular torsion on the contralateral testis. *J Urol* **1982**;128:1343–1348
6. Holder LE, Martire JR, Holmes ER III, Wagner HN Jr. Testicular radionuclide angiography and static imaging: anatomy, scintigraphic interpretation and clinical indications. *Radiology* **1977**;125:739–752
7. Haynes BE, Bessen HA, Haynes VE. The diagnosis of testicular torsion. *JAMA* **1983**;249:2522–2527
8. Kogan SJ, Lutzker LG, Perez LA, et al. The value of the negative radionuclide scrotal scan in the management of the acutely inflamed scrotum in children. *J Urol* **1978**:122:223–225
9. Lutzker LG. The fine points of scrotal scintigraphy. *Semin Nucl Med* **1982**;12:387–393
10. Bird K, Rosenfield AT, Taylor KJW. Ultrasonography in testicular torsion. *Radiology* **1983**;147:527–534
11. Perri AJ, Slachta GA, Feldman AE, Kendall AR, Karafin L. The Doppler stethoscope and the diagnosis of the acute scrotum. *J Urol* **1976**;116: 598–600
12. Brereton RJ. Limitations of the Doppler flow meter in the diagnosis of the "acute scrotum" in boys. *Br J Urol* **1981**;53:380–383
13. Rodriguez DD, Rodriguez WC, Rivera JJ, Rodriguez S, Otero AA. Doppler ultrasound versus testicular scanning in the evaluation of the acute scrotum. *J Urol* **1981**;125:343–346
14. Mendel JB, Taylor GA, Treves S, Cheng TH, Retik A, Bauer S. Testicular torsion in children: scintigraphic assessment. *Pediatr Radiol* **1985**;15: 110–115
15. Abu-Sleiman R, Ho JE, Gregory JG. Scrotal scanning: present value and limits of interpretation. *Urology* **1979**;13:326–330
16. Krone KD, Carroll BA. Scrotal ultrasound. *Radiol Clin North Am* **1985**;23(1):121–139

Sonographic Evaluation of Ovarian Torsion in Childhood and Adolescence

M. Graif[1]
Y. Itzchak

Emergency sonographic examination of the pelvis was performed in 41 girls (mean age, 13 years old) with clinical suspicion of ovarian torsion. Sonographic features consistent with diffuse swelling of the ovarian parenchyma and follicular enlargement in the cortical zone were detected in eight patients and were considered highly suggestive for torsion of the ovary. Surgery revealed ovarian torsion in seven of these cases and hemorrhagic ovarian cyst in one case. A cystic or complex ovarian mass was detected by sonography in five additional cases, and ovarian torsion was included in the differential diagnosis. Surgery revealed ovarian torsion in four of these cases and hemorrhagic ovarian cyst in one. A 100% sonographic sensitivity for space-occupying disease of the ovary was obtained with a positive predictive value of 88% for the diagnosis of ovarian torsion. The specificity of the method was 93%.

Sonography appears to be an excellent method to evaluate patients with suspected torsion of the ovary.

Torsion of the ovary may be the cause of an acute abdomen in girls and women. Prompt diagnosis and surgical restoration of blood flow may avoid irreversible ovarian damage [1]. Correct clinical diagnosis is difficult in girls in whom a vaginal examination is not feasible. Our study evaluates the accuracy of sonography in the preoperative diagnosis of ovarian torsion in 41 girls.

Subjects and Methods

From June 1981 to December 1986, 41 girls with suspected torsion of the ovary were referred for sonographic evaluation on an emergency basis. Torsion of the ovary was clinically suspected when sudden onset of lower quadrant abdominal pain accompanied by local tenderness was present, regardless of the presence or absence of a palpable mass.

The sonographic examinations were performed with commercially available dynamic-sector and linear scanners with 3- to 5-MHz transducers.

Transverse and longitudinal sonograms of the pelvis were obtained in all patients. The technique required distension of the urinary bladder by either the oral or IV route. The ovarian volume was calculated by using a simplified formula for an ellipsoid (length × height × width × one-half).

Ovarian volume was considered normal when it measured 0.46 cm^3 up to 2 years old and 1 cm^3 up to 12 years old. The average volume of a normal ovarium in the postpuberal girl is 3 cm^3 with the longest axis measuring up to 5 cm [2, 3]. The normal ovary is almond-shaped and moderately echogenic.

Results

The patients were 3–19 years old (mean ± SD, 13 ± 4.5 years; median 12 years). Symptoms included pelvic pain with a mean duration of 4.6 days, located on the right side in 23 cases, on the left side in nine, and diffuse in the pelvis in nine; leukocytosis in four; vomiting in three; and paralytic ileus in one.

Received July 24, 1987; accepted after revision October 23, 1987.

Presented at the meeting of the International Pediatric Radiology Society, Toronto, Ontario, Canada, June 1987.

[1] Both authors: Division of Diagnostic Ultrasound, The Chaim Sheba Medical Centre and Sackler School of Medicine, Tel Aviv University, Tel Hashomer 52621 Israel. Address reprint requests to M. Graif, at The Chaim Sheba Medical Centre.

AJR **150:647–649, March 1988**
0361–803X/88/1503–0647
© American Roentgen Ray Society

On sonography, 28 of the patients had normal-sized ovaries and 13 had enlarged ovaries. The volume of the enlarged ovaries ranged from 34 to 365 cm^3 (mean, 130 ± 99 cm^3). All 13 enlarged ovaries were oval or globular in shape. Eight of these showed a solid pattern with multiple enlarged follicles (8–15 mm in diameter) at the periphery of the ovarium (Fig. 1). The other five enlarged ovaries showed a mixed appearance either with distinct solid and fluid components (Fig. 2) or with an amorphous pattern (Fig. 3).

Another sonographic finding (present in three cases) was a semisolid mass in the right lower quadrant extending into the pelvis (Fig. 4). These masses were clearly separated from the ovaries, which appeared normal. The main sonographic diagnosis was periappendiceal abscess. In the other cases (normal ovaries), small amounts of fluid were detected in the Douglas pouch as an isolated finding.

In 17 patients, surgical exploration of the pelvis was performed within 48 hr of sonography; the other 24 were hospitalized until symptoms resolved. All of these patients remained asymptomatic for follow-up periods of 6–63 months.

Surgical exploration revealed torsion in 11 patients, hemorrhagic ovarian cyst in two, periappendiceal abscess in three, and acute appendicitis in one. Ovarian torsion occurred in seven previously normal ovaries, three ovaries with a cyst, and one ovary with tumor (fibroteratoma). The surgical procedure consisted of detorsion in six of 11 cases. In three of these there was an associated cyst, which was aspirated in two instances and resected in one. Oophorectomy was needed in the remaining five cases.

Ovarian enlargement was detected by sonography in all 11 patients with torsion and in both patients with hemorrhagic ovarian cysts. The diagnosis of ovarian torsion was correctly established in seven cases and wrongly suggested in one case of hemorrhagic ovarian cyst, yielding a positive predictive value of 87.5% for this particular diagnosis. The possibility of torsion, with less emphasis on this specific condition, was mentioned by the sonologist in the remaining four cases of torsion and one case of hemorrhagic cyst. Sonography excluded torsion of the ovary in 28 cases suspected clinically of this condition, yielding a specificity of 93.3%. In addition, sonography suggested correctly the presence of three periappendicular abscesses.

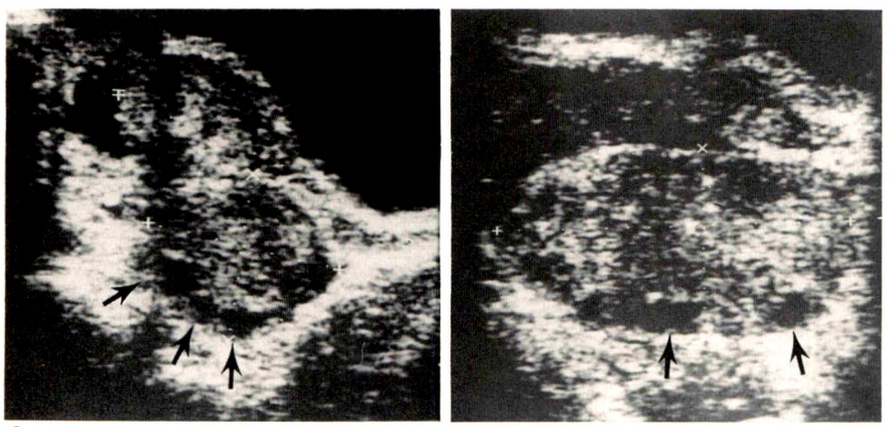

Fig. 1.—Transverse (*A*) and longitudinal (*B*) sonograms of ovarian torsion in 7-year-old girl show left ovarian enlargement (5.7 × 3.2 × 2.9 cm). Enlarged follicles (*arrows*) at periphery.

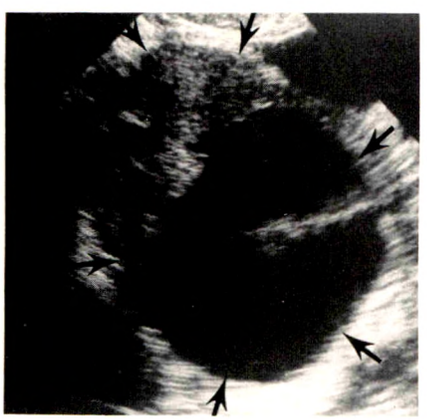

Fig. 2.—Oblique sonogram of right pelvis shows enlarged right ovary (*arrows*) in torsion. Note mixed components.

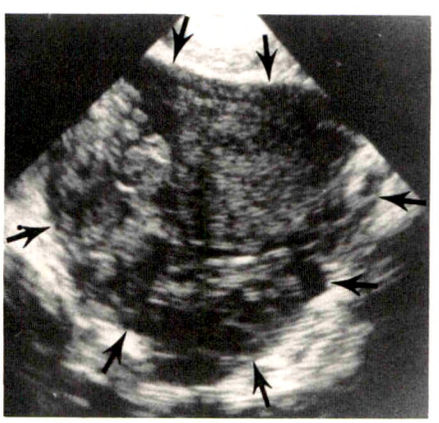

Fig. 3.—Transverse sonogram of pelvis shows large, irregular mixed-type mass (*arrows*). Laparoscopy revealed hemorrhagic cyst.

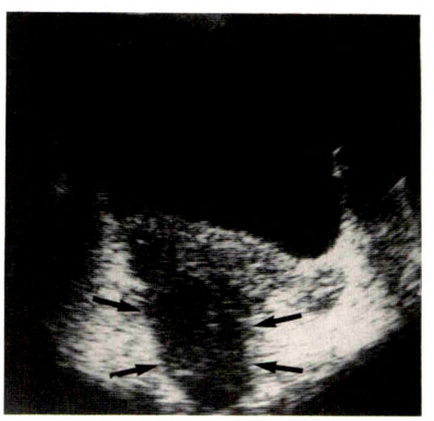

Fig. 4.—Transverse sonogram of pelvis in girl with periappendicular abscess shows both normal ovaries and semisolid mass (*arrows*) posteriorly.

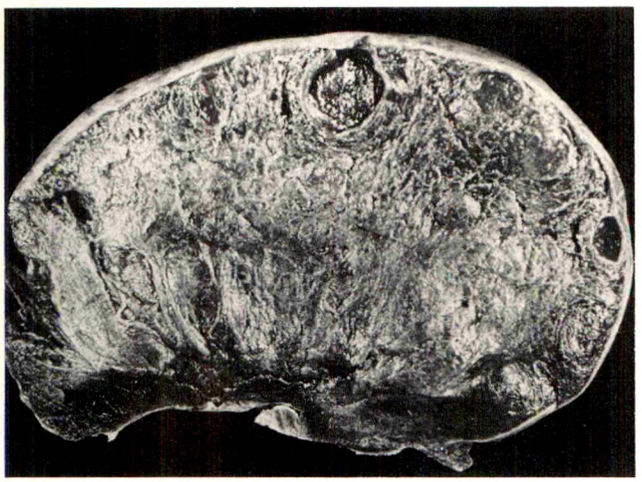

Fig. 5.—Section of gross specimen of 4-year-old girl's ovarium in torsion. Note swollen stroma and enlarged follicles.

Discussion

Torsion of the ovary is caused by partial or complete rotation of the ovarian pedicle on its axis. Arterial, venous and lymphatic supply and drainage are compromised, causing massive congestion of the ovarian parenchyma and eventual hemorrhagic infarction. Torsion may occur in normal ovaries, but is more common in ovarian cysts or tumors. These masses may act as a fulcrum to potentiate torsion of the ovary and fallopian tube [4, 5]. Schultz et al. [6] theorized that normal adnexa in girls may be especially mobile, allowing torsion at the mesosalpinx with changes in intraabdominal pressure or body position. The overall clinical picture is one of lower abdominal pain that subsides only to recur again within a few days or weeks. Anorexia, nausea, vomiting, constipation, diarrhea, and leukocytosis may be present [5, 7]. A palpable mass is commonly present in the adult patient but is appreciated in only 50% of children [6], since a vaginal examination usually is not feasible. The differential diagnosis of ovarian torsion may include other surgical conditions such as appendicitis, Meckel diverticulum, and obturator hernia, as well as medical conditions such as regional ileitis, acute gastroenteritis, salpingitis, urinary colic or infection, and acute bursitis of the hip joint. Surgical intervention in these last conditions is unwarranted and often harmful [8, 9].

Sonographic findings including solid, cystic, and complex pelvic masses with and without fluid collection in the Douglas pouch were described as adnexal torsion. Although these findings are not specific, their presence in a child or a young woman with lower abdominal pain should raise the possibility of adnexal torsion [10–12]. The only specific sonographic sign of torsion is demonstration of multiple follicles (8–12 mm in size) in the cortical portion of a unilaterally enlarged ovarium (Fig. 5). This multifollicular enlargement was attributed to transudation of fluid into the follicles as part of the congestion of the ovary from circulatory impairment. This feature has been detected by careful examination in up to 74% of torsion cases [12].

Ovarian enlargement is easy to determine: It is at least 34 times larger than the average normal prepubertal ovarium and 15 times larger than the adult ovarium.

Diffuse swelling of the ovarian parenchyma with multiple enlarged follicles at the periphery was the sonographic appearance in 64% of the cases of torsion in our series. This category of sonographic findings yielded a positive predictive value of 87.5% for the diagnosis of torsion, with a specificity of 93.3%. An ovarian mass of a mixed nature characterized the sonographic appearance of torsion in 46% of our cases of torsion. In these cases the diagnosis was less specific, and the possibility of torsion was considered in the differential diagnosis with simple cyst, hemorrhagic cyst, and dermoid cyst.

Sonography is a useful technique to exclude the diagnosis of ovarian torsion and will facilitate prompt surgical intervention and salvage of the ovary.

REFERENCES

1. Berger RL, Robbins G. Torsion of the normal ovary. *Am J Surg* **1961**;102:716–719
2. Kurtz AB, Rifkin MD. Normal anatomy of the female pelvis: ultrasound with computed tomography correlation. In: Saunders RC, James EA, eds. *Ultrasonography in obstetrics and gynecology*, 3rd ed. East Norwalk, CT: Appleton-Century-Crofts, **1985**:117–118
3. Gates GF. *Atlas of abdominal ultrasonography in children*. New York City: Churchill Livingstone, **1978**:159–160
4. Jones GS, Jones HW. *Novack's textbook of gynecology*, 10th ed. Baltimore: Williams & Wilkins, **1979**:471, 564–565
5. James DF, Barber HR, Gorber EA. Torsion of normal uterine adnexa in children: report of three cases. *Obstet Gynecol* **1970**;35:226–230
6. Schultz LR, Newton WA, Clatworthy HW. Torsion of previously normal tube and ovary in children. *N Engl J Med* **1963**;268:343–346
7. Grosfeld JL. Torsion of normal ovaries in the first two years of life. *Am J Surg* **1969**;117:726–727
8. Steinheber FU. Medical conditions mimicking the acute surgical abdomen. *Med Clin North Am* **1973**;57(6):1559–1567
9. Dunphy JE. Acute abdomen. In: Way LW, ed. *Current surgical diagnosis and treatment*. Los Altos, CA: Large Medical Publications, **1983**:420
10. Farrell TP, Boal DK, Teele RL, Ballantine TV. Acute torsion of normal uterine adnexa in children: sonographic demonstration. *AJR* **1982**;139:1223–1225
11. Warner MA, Fleischer AC, Edell SL, et al. Uterine adnexal torsion: sonographic findings. *Radiology* **1985**;154:773–775
12. Graif M, Shalev J, Strauss S, Engelberg S, Mashiach S, Itzchak Y. Torsion of the ovary: sonographic features. *AJR* **1984**;143:1331–1334

Memorial

Marcus J. Smith, 1918–1986

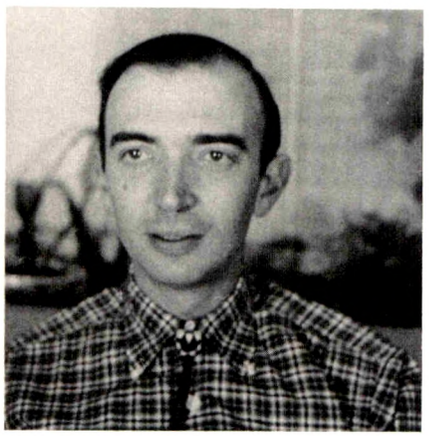

Dr. Marcus J. Smith died May 25, 1986, after many months of courageous struggle against a slow but progressive form of Alzheimer disease. Marc was born in New York City on December 14, 1918, where he received his primary education. He was awarded a Bachelor's degree from New York University, College of Arts and Science, and a medical degree from Long Island College of Medicine (SUNY). His internship was taken at King's County Hospital in Brooklyn and his radiology residency was completed at the University of Minnesota, under the direction of Leo Rigler. Marc was always proud to have been "one of Leo's boys."

Dr. Smith served with distinction during World War II and was with the first U. S. Army unit to liberate the concentration camp at Dachau, an event that was to have a profound influence on the remainder of his life. After many years of research, Marc wrote a heartrending account of Dachau, *The Harrowing of Hell, Dachau,* that was published by The University of New Mexico Press in 1972.

After his discharge from military service and completion of residency training, Dr. Smith settled in Santa Fe, NM, where he practiced radiology, served as president of the St. Vincent Hospital Medical Staff and as president of the Santa Fe County Medical Society, and was a New Mexico editor of the *Rocky Mountain Medical Journal* for 20 years. When the *Rocky Mountain Medical Journal* merged with the *Western Journal of Medicine*, Marc continued as a staff member with the *Western Journal of Medicine*. Dr. Smith was a fellow of the American College of Radiology and a member of the American Roentgen Ray Society and the Radiological Society of North America.

In 1967, Charles C Thomas, Publisher, published Dr. Smith's milestone study, *Error and Variation in Diagnostic Radiology*, and in 1977, Marc received a grant from the National Endowment for the Humanities to write a monograph of the history of medicine during New Mexico's territorial period. Additionally, Marc was a coauthor of a book on the lengthy history of St. Vincent Hospital in Santa Fe.

Marc was a respected and much admired member of both the medical and lay communities in Santa Fe, and in addition to his love of medicine, he had a deep and lifelong love affair with music. He spent much of his spare time performing with or assisting the Santa Fe Chorus, First Presbyterian Church Choir, Santa Fe Concert Association, and the Santa Fe Opera. In 1985, he and his wife, Dr. Carol Smith, a Santa Fe pediatrician, were proclaimed by Santa Fe as living treasures for their many contributions to medicine and the arts in Santa Fe.

Dr. Smith is missed by all of us who had the good fortune to practice with him here in Santa Fe. Marc is survived by his wife, Carol; four children: Patricia, Frederick, Peter, and Andrew; and a sister, Sylvia Rabinof. Our memory of Marc is well served by the legacy he left behind.

Raphiel J. Benjamin
Santa Fe, NM 87501

Acute Intracranial Hemorrhage: Intensity Changes on Sequential MR Scans at 0.5 T

Robert D. Zimmerman[1]
Linda A. Heier[1]
Robert B. Snow[2]
David P. C. Liu[1]
Anna B. Kelly[1]
Michael D. F. Deck[1]

Thirty-seven patients underwent MR imaging at 0.5 T within 7 days of a CT-documented intracranial hemorrhage. A total of 57 hematomas were evaluated. Twelve patients underwent serial scanning and 12 patients had multiple hemorrhages into different intracranial compartments. The appearances of the hematomas on spin-echo (SE) images with a short repetition time (TR) of 500 msec and short echo time (TE) of 32 msec (SE 500/32), long TR/intermediate TE (SE 2000/60), and long TR/long TE (SE 2000/120) were carefully evaluated with specific attention to the precise time after ictus. Hematomas showed heterogeneous, complex, rapidly changing intensities. There was a significant amount of variation among patients, especially between the third and seventh days. Hematomas studied between 12 and 24 hr after hemorrhage were mildly hyperintense on short TR scans and markedly hyperintense on long TR (intermediate and long TE) scans (stage I). These findings in acute hemorrhage have received little prior attention. Over the next 1–2 days, hematomas became iso- to mildly hypointense on short TR scans and markedly hypointense on long TR scans (stage II). Hypointensity on long TR scans has previously been described at high field strengths; our communication demonstrates that this phenomenon is seen routinely at intermediate field strengths as well. Hematomas became markedly hyperintense on short TR scans beginning on approximately the fourth day postictus and redeveloped hyperintensity on long TR scans approximately 5–6 days after ictus (stage III). By the end of the first week they were hyperintense on all pulse sequences (stage IV).

MR findings on the first day after intracranial hemorrhage (in particular, subtle hyperintensity on short TR scans) probably allow for a specific diagnosis, while the variable, heterogeneous, and rapidly changing intensities noted between days 2 and 7 are often less specific.

This article appears in the January/February 1988 issue of *AJNR* and the March 1988 issue of *AJR*

Received March 13, 1987; accepted after revision August 12, 1987.

Presented at the annual meeting of the American Society of Neuroradiology, San Diego, January 1986, and presented in part at the Symposium Neuroradiologicum, Stockholm, June 1986.

[1] Department of Radiology, New York Hospital–Cornell University Medical Center, 525 E. 68th St., New York, NY 10021. Address reprint requests to R. D. Zimmerman.

[2] Department of Neurosurgery, New York Hospital–Cornell University Medical Center, New York, NY 10021.

***AJR* 150:651–661, March 1988**
0361–803X/88/1503–0651
© American Roentgen Ray Society

The MR appearance of intracranial hemorrhage has been the subject of many communications. Findings in acute hemorrhage, particularly within 48 hr of ictus, remain controversial and incompletely delineated [1–9]. The intensity of hematomas is known to be dependent on multiple factors including time from ictus and pulse sequence employed [1, 6, 7]. Recently, it has been suggested that the field strength of the MR imager may also affect intensity such that "acute" (under 7 days) hemorrhage may be detected more easily at ultralow (0.02 T) [4] or high (1.5 T) field strengths [5] than at intermediate field strengths (0.1–0.6 T). Unfortunately, all prior studies of acute hemorrhage are limited by the small number of patients evaluated in each series. Extrapolations from these limited data have led to confusing and often contradictory conclusions. To clarify the findings in acute hemorrhage on MR, we studied 37 patients within 1 week of an acute hemorrhagic ictus with specific attention to the precise relationship between the intensity of the lesion and the time from ictus. The implications of these findings on previously presented theories of hematoma intensity will be discussed, as will the efficacy of MR and CT in the clinical evaluation of patients with suspected acute intracranial hemorrhage (AIH).

TABLE 1: Relationship Between Time After Ictus and Cause and Location of Hemorrhage

Cause/Location	No. by Day							Total
	1	2	3	4	5	6	7	
Cause:								
Trauma	0	2	3	6	2	3	5	21
Hypertension	1	2	2	1	1	0	0	7
Vascular[a]	1	1	0	0	0	2	1	5
Neoplasm	0	1	0	1	0	0	0	2
Idiopathic/miscellaneous[b]	0	1	0	1	1	1	4	8
Location of hematoma:								
Epidural	0	0	1	1	0	2	0	4
Subdural	1	1	1	5	2	1	5	16
Parenchymal	2	6	3	5	2	4	6	28
Subarachnoid	0	2	0	1	0	1	1	5
Intraventricular	1	2	1	0	0	0	0	4
Total	4	11	6	12	4	8	12	57

[a] Includes aneurysms, arteriovenous malformations, and venous angiomas.
[b] Includes hemorrhage without known cause, venous thrombosis, and amyloid angiopathy.

Subjects and Methods

Thirty-seven patients were included in this study. In each case, a CT-documented hemorrhage had occurred within 1 week of the initial MR. The time from clinical ictus to MR imaging was identified as precisely as possible, as were the cause and location of the hemorrhage (Table 1). All patients were evaluated on a 0.5-T MR imaging device.* When hematomas in multiple compartments (12 cases) were present, these were evaluated separately, since they often had different intensities (see Results). Serial studies (12 cases) were also evaluated individually and included within the overall tabulation. Thus, the total number of hematomas evaluated (57) exceeded the number of patients (37). T1-weighted spin-echo (SE) images with a short repetition time (TR) of 500 msec and short echo time (TE) of 32 msec (SE 500/32) were obtained in all cases. Moderately T2-weighted long TR/intermediate TE (SE 1500/90) single-echo images were obtained in the initial six patients, while the remaining 31 patients had multiecho scans with a TR of 2000 msec and two echoes (TE = 60–120 msec) or four echoes (TE = 30–120 msec). These scans were subdivided into long TR/intermediate TE images (for example, SE 2000/60), in which spinal fluid was gray, and long TR/long TE images (for example, SE 2000/120), in which spinal fluid was white. The intensity of the hemorrhages was qualitatively compared with that of white matter on all images. More precise quantitative measurements were not attempted, because hematomas showed quite heterogeneous intensities. The MR findings on each pulse sequence were compared with each other and with CT findings to determine the relative clinical efficacy of each pulse sequence and of MR, in general, when compared with CT in the evaluation of AIH.

Results

Hematomas undergo rapid, reversible changes in intensity that vary with the pulse sequences used. Therefore, relationships between time and intensity for each pulse sequence have been tabulated and are presented in graphic form (Fig. 1). The effects of two additional factors, recurrent hemorrhage and site of hemorrhage, were also evaluated.

* Technicare.

Short TR/Short TE Images

Hematomas evaluated 12–24 hr after an acute ictus (Fig. 2) were subtly and uniformly hyperintense relative to white matter in three examples of AIH (Figs. 2C and 2D) and isointense in one case. The average intensity of AIH diminished over the next 2 days (Fig. 1). Appropriately timed serial studies were not performed in any of these patients and, therefore, the diminishing intensity could not be demonstrated directly. Lesions studied at 24–48 hr had variable intensity, ranging from mild hypo- to mild hyperintensity (Fig. 3). The two hematomas that were hyperintense were evaluated early on the second day (30 and 32 hr, respectively). Hematomas studied on the third to fourth postictal day (Figs. 3–5) demonstrated the greatest variation; mild hyperintensity was the most commonly encountered pattern (Figs. 4C and 5B). Features were similar to those seen on day 1, except that small foci of more marked hyperintensity were often seen within these older hematomas (Fig. 3G). Thereafter, there was a dramatic and progressive increase in intensity (Fig. 6B), which was most prominent near the periphery of the hematoma. This phenomenon was directly observed in five patients studied serially within the first week of ictus (Figs. 4E and 5E) and in another four patients in whom follow-up examinations were performed after 1 week (10–28 days).

Long TR/Intermediate to Long TE Images

Hematomas evaluated within 24 hr of ictus were typically hyperintense (Figs. 2E–2H); hypointensity was present in only one case studied at 24 hr. Thereafter, there was a dramatic decrease in intensity. Hypointensity was present in seven of 11 hemorrhages evaluated during the second postictal day (Fig. 1). The four hematomas without hypointensity were in two patients with multiple hemorrhages evaluated before 36 hr. On the third postictal day, hypointensity was seen in five of six hematomas, and the hypointense components were larger and/or darker than those seen on day 2 (Fig. 4D). The

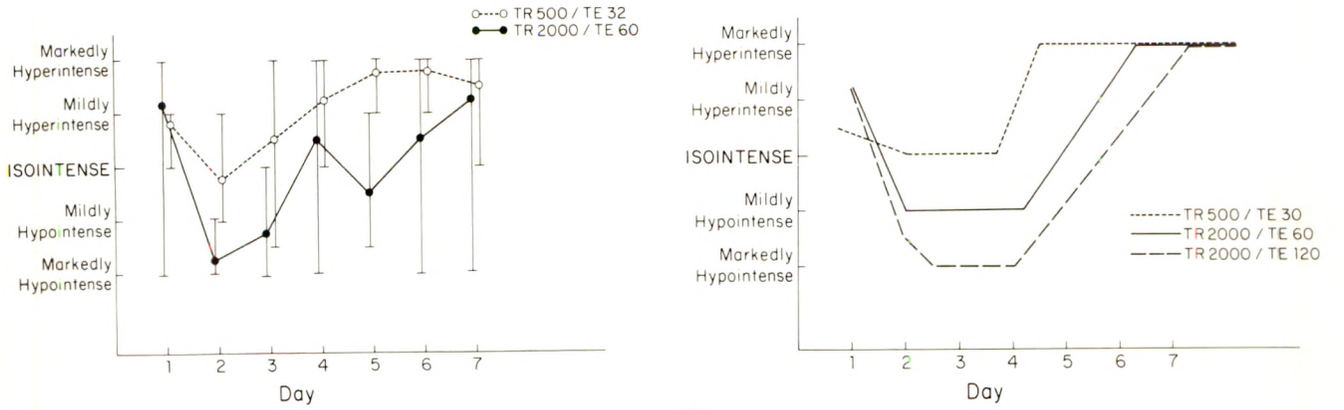

Fig. 1.—Time/intensity curves for acute intracranial hemorrhage.

***A*, All hematomas are plotted. Intensity on each day is given relative to white matter. Range of intensities is shown by vertical bars and mean intensities for all hematomas on each day are *open circles* (TR = 500 msec, TE = 32 msec) or *solid circles* (TR = 2000 msec, TE = 60 msec).**

***B*, Mean intensities only are plotted for SE 500/32 and SE 2000/60–120 scans. Cases in which multiple episodes of hemorrhage were present have been eliminated to simplify curves.**

development of hypointensity from days 1 to 3 was observed directly in four hematomas studied serially during this period (Figs. 3E and 3H). From days 4–7, there was a trend toward increasing intensity, but AIHs studied during this period showed the greatest variation in intensity on long TR images (Figs. 4 and 6).

Comparison of Pulse Sequences

There was poor correspondence between short and long TR scans. The intensities encountered within individual hematomas were different, as was the degree of heterogeneity (Fig. 4). The timing and rate of change of intensity reversals were also different (note the differences in the slopes of the time/intensity curves in Fig. 1B). By contrast, hematomas had similar appearances on long TR/intermediate TE and long TR/long TE scans; the only discernible difference was accentuation of hypointensity on the long TE sequence (Figs. 5C and 5D).

Additional Factors That Affect AIH Intensity

The AIHs in 12 patients with CT and/or clinical evidence of multiple episodes of hemorrhages were more heterogeneous in appearance and more likely to vary from "typical" intensities than those encountered in patients with single hemorrhagic events (Fig. 4). The effect of hematoma location was analyzed by evaluating the patients with hemorrhages into multiple intracranial compartments. In nine of 12 cases, intensity differences were observed. The greatest differences occurred in patients in whom extraaxial or parenchymal hematomas were combined with hemorrhages into spinal fluid compartments (Fig. 3). In patients with simultaneous extraaxial and parenchymal hematomas, the intensities tended to be similar (Fig. 2).

Discussion

The MR features of AIH are complex, fascinating, and incompletely understood. Different investigators have reported a variety of findings and have come to often contradictory conclusions about the physical basis of these phenomena and their clinical implications [1–9]. In our judgment, this confusion and contradiction arise from attempts to extrapolate general principles from very limited clinical and/or experimental data. This type of analysis worked well with CT, in which the densities of hematomas are relatively uniform and change slowly [10, 11]. However, the intensity patterns and shifts that occur with MR are much more complex. Hematoma intensity is typically heterogeneous, and changes rapidly and continuously during the first postictal week. Findings in our series indicate that these shifts are bidirectional (AIH decreasing and then increasing in intensity) and subject to significant variation among patients. Thus, general conclusions drawn from limited clinical experience have proved to be incorrect or, at least, incomplete. Previous attempts to reconcile contradictory findings have centered on the effects of extrinsic, equipment-dependent factors, such as variations in pulse sequences and, more recently, the field strength of the MR imager [4, 5]. Although these factors are undoubtedly important, their true contributions remain unclear. Data from our series indicate that at least some of the apparent discrepancies disappear when a large number of cases are analyzed with careful attention to both the precise time after ictus and the exact intensities encountered. These data also make it possible to gain a firmer understanding of the underlying biochemical changes that produce these alterations in intensity and to delineate four stages in AIH evolution, each with a typical pattern of intensity on multiple pulse sequences.

On short TR/short TE scans, AIH is hyperintense relative to brain when studied between 15 and 24 hr (Fig. 2). The initial mild hyperintensity is unexpected, since most authors report that hematomas are iso- to hypointense relative to

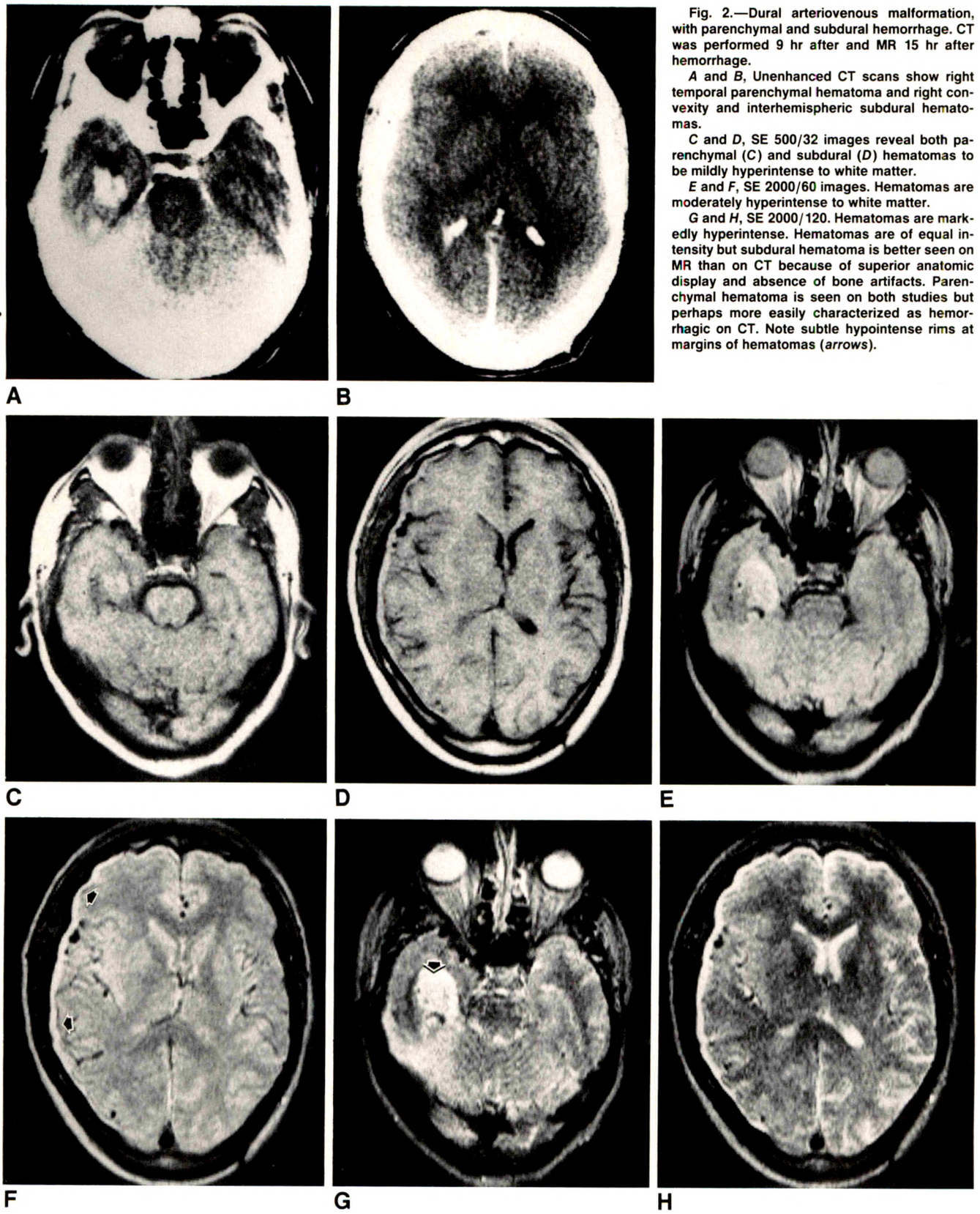

Fig. 2.—Dural arteriovenous malformation, with parenchymal and subdural hemorrhage. CT was performed 9 hr after and MR 15 hr after hemorrhage.

A and *B*, Unenhanced CT scans show right temporal parenchymal hematoma and right convexity and interhemispheric subdural hematomas.

C and *D*, SE 500/32 images reveal both parenchymal (*C*) and subdural (*D*) hematomas to be mildly hyperintense to white matter.

E and *F*, SE 2000/60 images. Hematomas are moderately hyperintense to white matter.

G and *H*, SE 2000/120. Hematomas are markedly hyperintense. Hematomas are of equal intensity but subdural hematoma is better seen on MR than on CT because of superior anatomic display and absence of bone artifacts. Parenchymal hematoma is seen on both studies but perhaps more easily characterized as hemorrhagic on CT. Note subtle hypointense rims at margins of hematomas (*arrows*).

Fig. 3.—Traumatic epidural and subarachnoid hematomas.

A and *B*, CT scans at 21 hr after trauma show hyperdense frontal epidural hematoma and focal left suprasellar subarachnoid hematoma (*A*).

C, SE 500/32 scan at 36 hr. Epidural hematoma is isointense to brain but easily detected; subarachnoid hematoma cannot be seen (nor was it seen on long TR images at this time).

D and *E*, SE 2000/30 (proton-density) (*D*) and SE 2000/90 (heavily T2-weighted) (*E*) scans at 36 hr. Epidural hematoma is hyperintense to brain. Nodules of hypointensity are seen within epidural and subgaleal hematomas.

F and *G*, SE 500/32 scans at 72 hr. Subarachnoid hematoma is now hyperintense to white matter (*F*); epidural hematoma (*G*) is now mildly hypointense to white matter; medial hypointense rim (*G*) represents displaced dura (*arrow*). Epidural hematoma is well seen despite lack of contrast due to improved anatomic display.

H, SE 2000/60 scan at 72 hr. Epidural and subgaleal hematomas have become markedly hypointense to white matter (compare with *E*).

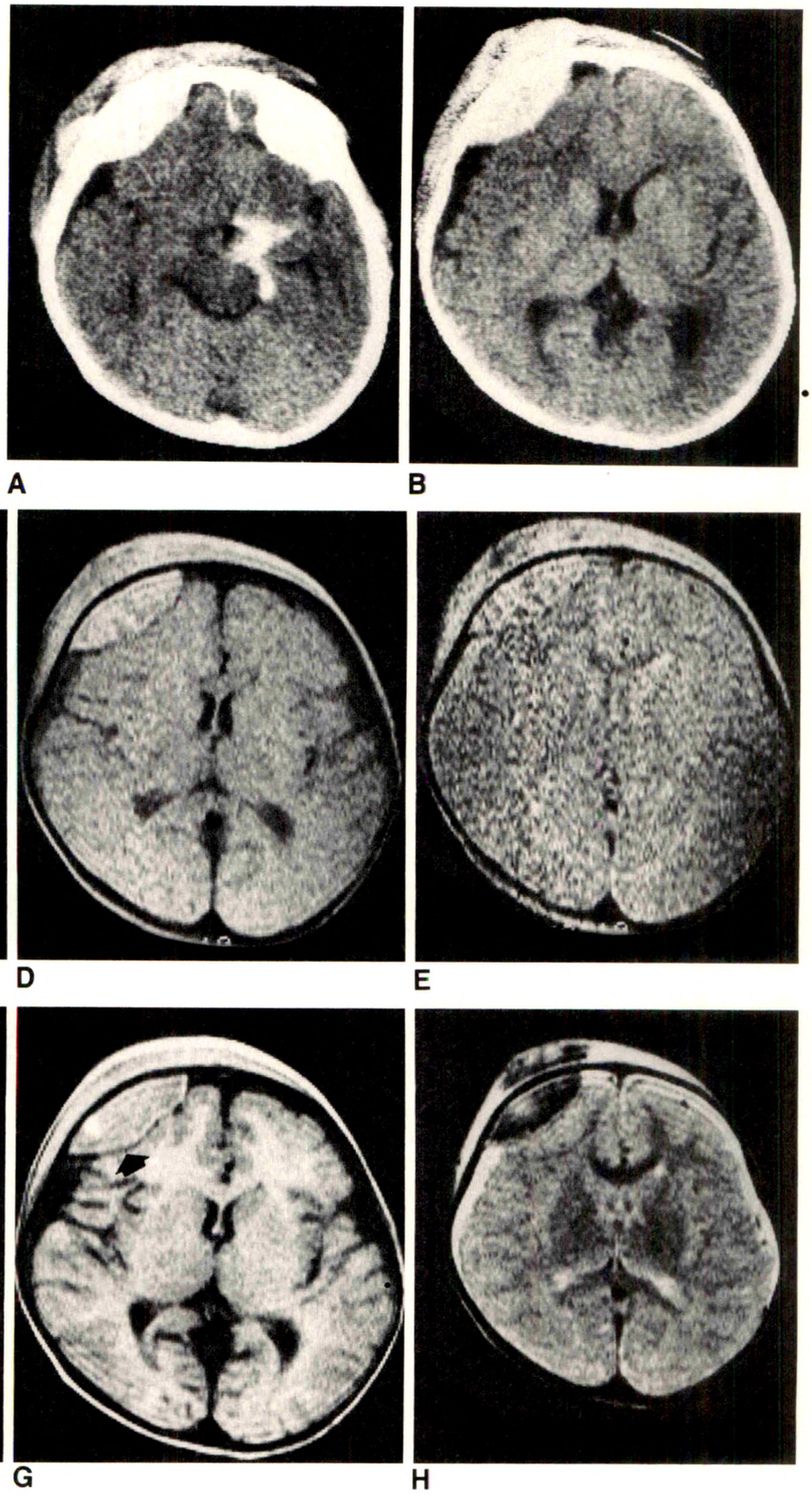

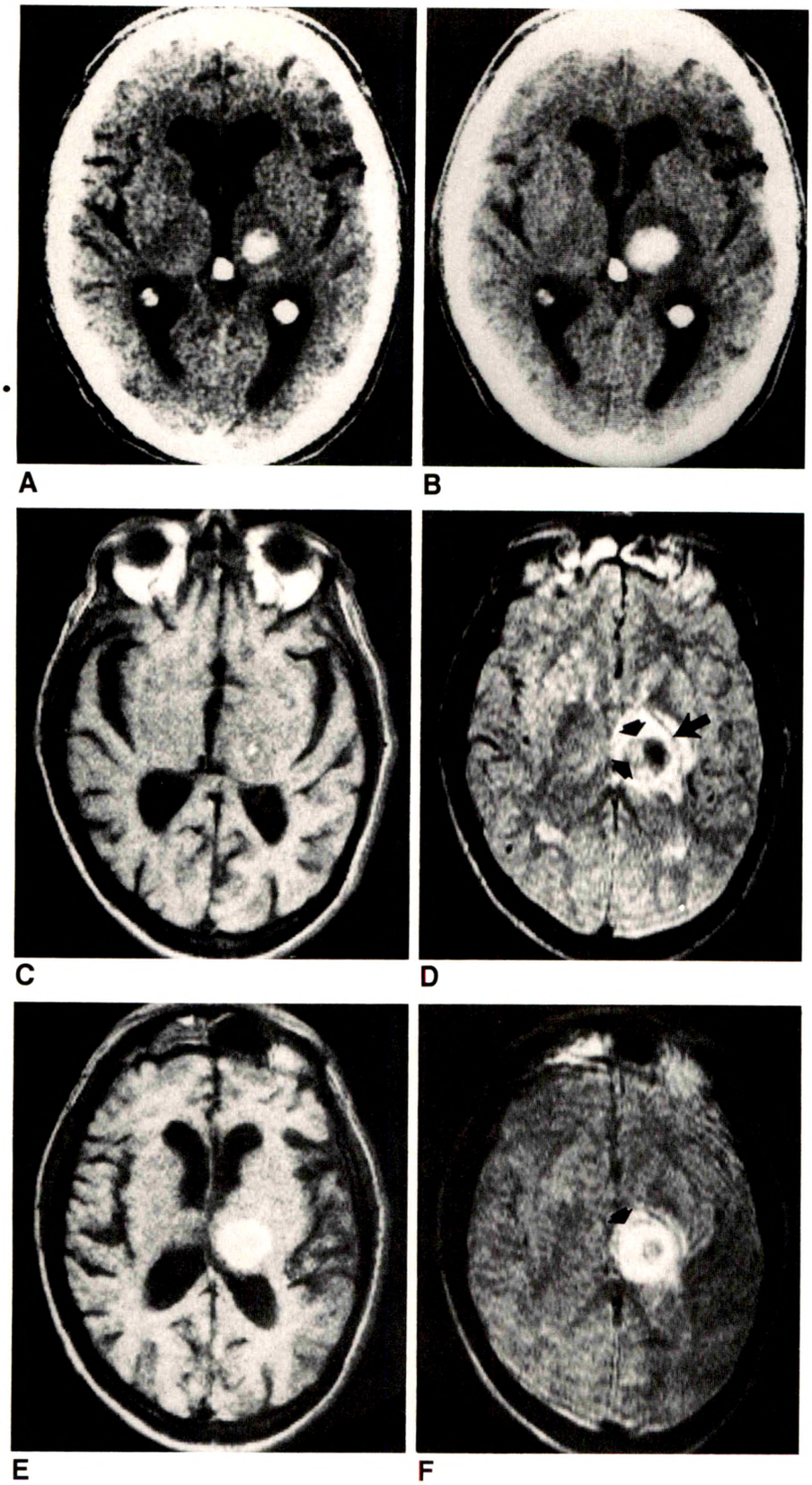

Fig. 4.—Recurrent hypertensive thalamic hemorrhage.

A, Initial CT scan 24 hr after initial ictus shows left thalamic hematoma.

B, Follow-up study 1 day later because of increasing drowsiness shows recurrent hemorrhage with enlargement of hematoma.

C, SE 500/32 scan 72 hr after initial hemorrhage. Lesion is predominantly hypointense with small central focus of hyperintensity.

D, SE 2000/60 scan at the same time. Eccentric hypointense focus is noted in lateral aspect of hematoma. Curvilinear hypointensity is also noted within and at margin of hematoma (*short arrows*). More laterally placed linear hypointensity corresponds to internal capsule (*long arrow*).

E, SE 500/32 scan at 6 days. Hematoma is diffusely hyperintense.

F, SE 2000/60 scan at 6 days. Lesion is predominantly hyperintense with small focus of hypointensity near center of hematoma. Hypointense rim marks edge of hematoma (*arrow*).

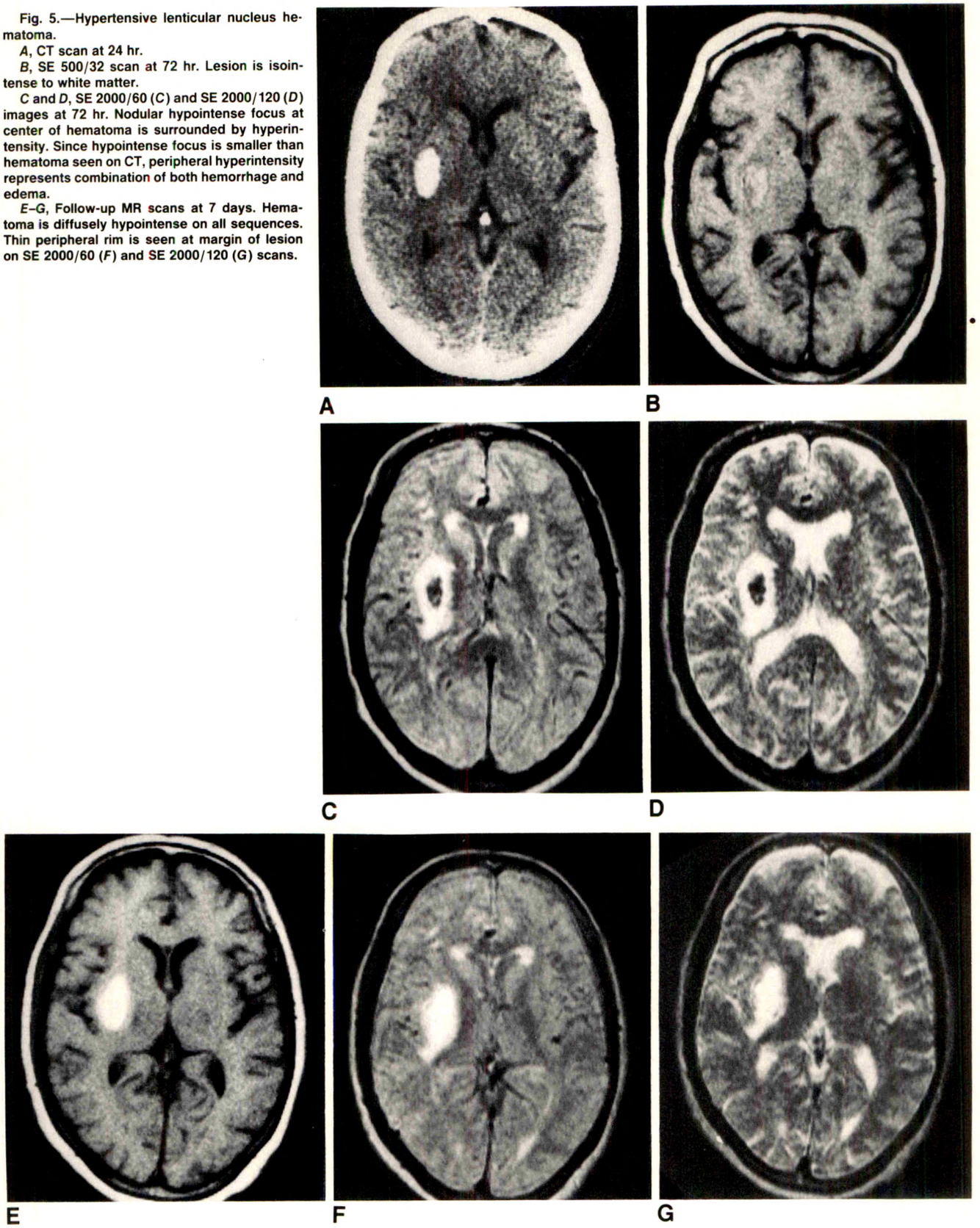

Fig. 5.—Hypertensive lenticular nucleus hematoma.

***A*, CT scan at 24 hr.**

***B*, SE 500/32 scan at 72 hr. Lesion is isointense to white matter.**

***C* and *D*, SE 2000/60 (*C*) and SE 2000/120 (*D*) images at 72 hr. Nodular hypointense focus at center of hematoma is surrounded by hyperintensity. Since hypointense focus is smaller than hematoma seen on CT, peripheral hyperintensity represents combination of both hemorrhage and edema.**

***E–G*, Follow-up MR scans at 7 days. Hematoma is diffusely hypointense on all sequences. Thin peripheral rim is seen at margin of lesion on SE 2000/60 (*F*) and SE 2000/120 (*G*) scans.**

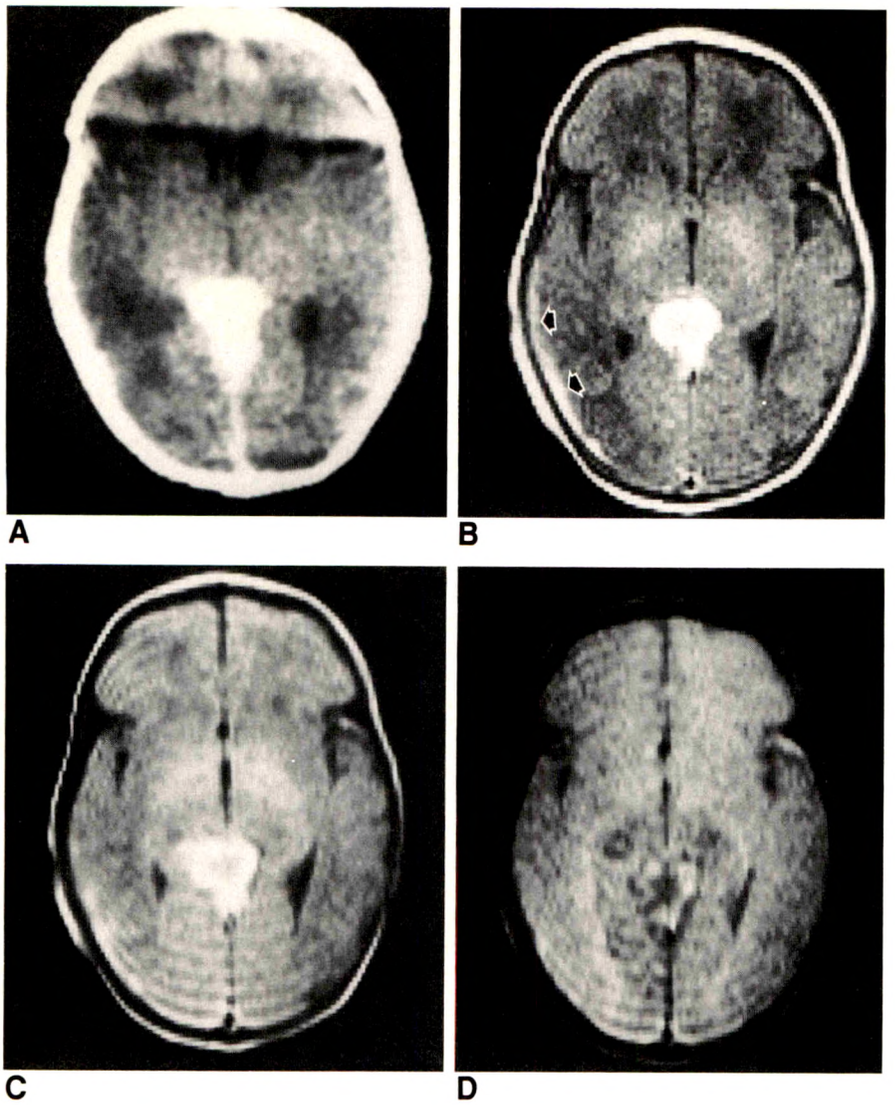

Fig. 6.—Birth trauma with retro-third ventricular subarachnoid and subdural hematoma.

***A*, CT scan 3 days after birth. Subarachnoid hematoma is noted behind third ventricle.**

***B*, SE 500/32 image 6 days after birth. Retro-third ventricular hematoma is hyperintense. Small-convexity hematoma (*arrows*) could not be seen on CT.**

***C* and *D*, SE 2000/60 (*C*) and SE 2000/120 (*D*) images 6 days after birth. Hematoma becomes progressively less intense and mimics intensity of subcutaneous and intraorbital fat. Thus, retroventricular lesion could be confused with congenital midline fat-containing lesion.**

brain throughout this period [2, 5–7]. Careful review of published images, however, reveals subtle diffuse or focal hyperintensity within hematomas that are generally characterized as isointense (see Fig. 1B of Dooms et al. [7]). The underlying basis of this finding is unclear. Hyperintensity on short TR/short TE scans usually results from T1 shortening (relative to adjacent brain), and yet in vivo [1, 7, 12] and in vitro [12, 13] calculations indicate that T1 is initially prolonged relative to white matter. It seems likely, therefore, that the subtle hyperintensity initially encountered on short TR/short TE scans is related to changes in other MR parameters. Since T2 prolongation does not generally produce hyperintensity on short TR/short TE scans [14, 15], high proton density must be considered the probable cause of this phenomenon. Hyperintensity caused by high proton density may be directly observed on an SE 2000/30 ("proton-density") scan (Fig. 3D). The high proton density of acute extravasated blood is probably a reflection of the high water content of liquid blood before clot formation and retraction.

Over the next day, the mean intensity diminishes, and by the end of the second day, hematomas are iso- to hypointense relative to brain (Fig. 3). This decrease in intensity (compare Figs. 2 and 3) may be from T1 prolongation. An alternate explanation, however, is that the T2 shortening that occurs during this period (see below) may be of sufficient magnitude to diminish intensity on these so-called T1-weighted short TR scans in which the TE is 32 msec.

Between the third and fifth days after hemorrhage, the intensity on short TR/short TE scans dramatically and abruptly increases so that hematomas become markedly hyperintense (more prominently at the periphery than at the center of the AIH) in as little as 24 hr (Figs. 4–6). This phenomenon has been demonstrated in previous reports [1–8] and is believed to be secondary to a paramagnetic effect of the oxidative breakdown product methemoglobin, which begins to appear on about the third posthemorrhage day [16, 17]. By the end of the first week, all hematomas show marked hyperintensity on short TR/short TE scans.

On long TR scans, hematomas are more heterogeneous and show greater variation in intensity than on short TR scans. The lesions are generally hyperintense relative to brain when evaluated 12–24 hr after ictus (Fig. 2). Small nodules of hypointensity may be identified within the AIH, and a peripheral rim of hypointensity is commonly seen (Fig. 2). More generalized hypointensity, of variable degree and occupying a variable amount of the hematoma (as identified by CT), develops late in the first or early in the second postictal day and becomes most marked by the third to fourth postictal day (Figs. 3–5).

The inital hyperintensity and early conversion to hypointensity were seen directly in serial studies in two of our patients (Fig. 3) and in one published example [18]. These serial changes were documented in an experimental hematoma studied by Di Chiro et al. at 0.6 T [12]. The early hyperintensity on long TR scans is indicative of T2 prolongation relative to normal brain. Whether this is a property of normal, nonflowing blood or represents some early postextravasation biochemical change is not known, but it is probably related to the fact that, as a fluid, blood has a higher water content and thus a longer T2 than normal brain tissue does. The subsequent development of hypointensity is indicative of T2 shortening. This phenomenon was initially described by Gomori et al. [5], who postulated that it was a paramagnetic effect of the deoxyhemoglobin within intact hypoxic RBCs. Paramagnetic T1 shortening does not occur with deoxyhemoglobin despite the presence of four unpaired electrons, because its molecular structure does not allow the proximity (3 Å) of unpaired electrons necessary to produce T1 shortening [19]. Before cell lysis, however, the deoxyhemoglobin may produce T2 shortening because of its effect on magnetic susceptibility (the ratio between external applied magnetic field and the internal field generated by the sample). The intracellular deoxyhemoglobin produces stronger magnetic fields than those generated in the deoxyhemoglobin-free extracellular space. This heterogeneity of magnetic field strength within the sample leads to the presence of local magnetic gradients between the intra- and extracellular spaces, resulting in rapid dephasing (short T2) of protons that freely diffuse across the cell membrane [5, 20–22].

This hypothesis receives strong support from two independent sources. First, it has recently been demonstrated that the hypointensity within hematomas is seen more commonly and extensively with gradient-echo pulse sequences than with long TR/long TE SE pulse sequences [21]. Gradient-echo scans are more sensitive to magnetic susceptibility effects because they are more dependent on T2* than on T2. Second, magnetic susceptibility effects of deoxyhemoglobin have been demonstrated in vitro with MR spectroscopy, even before the development of MR imaging [16, 20].

With MR spectroscopy, the degree of T2 shortening is proportional to the square of both the hemoglobin concentration and the magnetic field strength [20, 22]. The in vitro data help to explain some of the phenomena encountered in our clinical cases, but in other important ways are at variance with clinical experience. The dependence of intensity on the square of the deoxyhemoglobin concentration is probably the cause of the variability of intensity (both within an individual hematoma and between hematomas) as well as the rapid changes in intensity that occur over time. Unfortunately, the intensity patterns encountered at 0.5 T do not match those predicted by in vitro data. Hypoxic, intact RBCs are located at the center of hematomas, and thus central hypointensity should be the commonly encountered pattern [5]. In our experience, however, hypointense foci are often located eccentrically (Fig. 4), and, as previously stated, a thin rim of hypointensity is seen at the margin of many clots (Figs. 2, 4, and 5). The eccentric location of the hypointense focus may reflect areas of recurrent hemorrhage (Fig. 4); one of the striking features in our series was the evidence of clinically silent rehemorrhage (as documented by serial CT and/or MR studies demonstrating increase in hematoma size) in six cases. Given the apparent sensitivity of clot intensity to deoxyhemoglobin concentration, even minimal rehemorrhage might significantly alter the intensity of the hematoma.

The hypointense peripheral rim is more puzzling. This phenomenon has been described in chronic hemorrhage, where it is said to reflect a magnetic susceptibility effect of hemosiderin within macrophages in the capsule of aging hematomas [5]. The hypointense rim in acute hematomas is less prominent but otherwise similar in appearance. At this stage of hematoma evolution, hemosiderin-laden macrophages are not present [23–25]; thus, another explanation for this phenomenon must be sought. Edelman et al. [21] noted this hypointense rim and suggested that it might represent a border-zone phase-shift phenomenon. In our experience, similar rims have also been seen at the margin of all abscesses and some metastatic foci [26, 27]. Pathologic studies in these cases have demonstrated the presence of macrophages, but without hemosiderin. We believe that this represents a paramagnetic effect of free radicals produced by macrophages during active phagocytosis [27] and believe it may account for the rim hypointensity encountered in acute hematomas as well.

A far more striking and troubling discrepancy between predictions based on in vitro MR spectroscopy and clinical data is the dependence of magnetic susceptibility on the square of the field strength of the MR unit [20, 22]. This led Gomori et al. [5] to state that hypointensity would be seen only at high field strengths (1.5 T). This is clearly not the case in clinical practice. Hypointensity is routinely seen on intermediate-field-strength systems (0.35–0.6 T), as demonstrated by us (Figs. 3–5) and in other publications [8, 12, 18, 21], even though magnetic susceptibility is theoretically one-ninth that seen at 1.5 T. More surprisingly, acute hematomas studied at 0.15 T (magnetic susceptibility 1/100 that seen at 1.5 T) and even at 0.02 T (magnetic susceptibility 1/5625 that seen at 1.5 T) also demonstrate mild hypointensity (see Fig. 2E of Sipponen et al. [1], Fig. 2C of DeLaPaz et al. [3], and Figs. 1B and 6C of Sipponen et al. [4]). Based on a comparison of published images, it appears that the degree of hypointensity does indeed vary with field strength, but to a lesser extent than that predicted by in vitro studies. The discrepancy between experimental prediction and clinical observation should not come as a complete surprise, given the complexity of hemorrhagic brain lesions. Reactive changes within and/or adjacent to hematomas could modify the intensities encountered on clinical images. Additional factors, un-

affected by field strength, could thus contribute to the development of hypointensity at low fields or militate against full expression of hypointensity at high field strengths, lessening the dependence of intensity on field strength.

The next major change in hematoma intensity on long TR scans is the redevelopment of hyperintensity (Figs. 4 and 5), which begins on approximately the fourth postictal day. (This reversal of intensity may occur quickly; that is, in 24–48 hr.) Thus, hematomas pass through a second isointense phase (Fig. 6) to become hyperintense relative to brain by the end of the first week. The redevelopment of hyperintensity is a result of RBC lysis. The overall deoxyhemoglobin concentration decreases and deoxyhemoglobin becomes homogeneously distributed in the extracellular space. This eliminates the heterogeneous magnetic field, and thus local magnetic gradients within the sample disappear. The increased intensity, therefore, results from a simple subtraction of the T2 shortening effect of the intracellular deoxyhemoglobin; the intrinsically prolonged T2 of blood is unmasked and the intensity returns to its initial high level. Additional prolongation of T2 during this period may result from an increase in water within the hematoma as cells lyse and the clots age [23, 24]. It is important to remember that the increase in intensity that occurs on long TR scans during this period is not caused by the presence of methemoglobin, which produces the nearly simultaneous increase in intensity seen on short TR scans. The paramagnetic effect of methemoglobin produces marked T1 and, to a lesser extent, T2 shortening. On long TR scans, all intracranial soft tissues have undergone complete interpulse recovery; thus, a decrease in T1 does not increase the intensity of the hemorrhage relative to brain. The T2 shortening effect of methemoglobin should actually cause diminished signal intensity, but this effect is obviously overcome by more powerful determinants of T2. High proton density may also contribute to the increased intensity encountered on long TR scans at this stage, especially when used in conjunction with a short or intermediate TE.

In addition to these already complex phenomena, two additional factors significantly affect hematoma intensity. The first factor is recurrent hemorrhage, which is extremely difficult to diagnose in any individual case because rapid intensity changes occur with (Fig. 4) or without (Fig. 5) rehemorrhage. In general, rehemorrhage appears to be a major source of the heterogeneity and variability of hematoma intensity. The admixture of extravasated blood of various ages probably accounts for the almost random pattern of heterogeneous intensity encountered within recurrent hemorrhages (Fig. 4). The presence of unsuspected preexisting hemorrhage and the development of postictal rehemorrhage explain, at least in part, the overall variations in intensity encountered among different patients. For instance, MR performed in an elderly patient 60 hr after the onset of mild hemiparesis and obtundation demonstrated a large subdural hematoma that was "prematurely" hyperintense on short TR/short TE scans. It is most likely, given the patient's clinical and CT findings, that this was a rehemorrhage into a clinically silent chronic subdural hematoma. Postictal rehemorrhage may account for the persistence of hypointensity on long TR scans into the sixth and seventh days in five of the examples of rehemorrhage evaluated in our series (Fig. 4F).

The other source of intensity variation is the location of the hematoma. When time/intensity relationships for AIH in different intracranial compartments were studied, no clear trends were discerned, but, when scans demonstrating hemorrhage into multiple compartments were evaluated, it was noted that the intensities were different in nine of 12 cases. This difference was most marked when hemorrhage into a spinal fluid compartment (intraventricular or subarachnoid) was seen in conjunction with either a parenchymal or extraaxial hematoma (Fig. 3). Subarachnoid hemorrhage was particularly difficult to detect on MR. Acute (under 3 days) and/or diffuse subarachnoid hemorrhage could not be detected (Fig. 3C). This poor visualization of diffuse subarachnoid hemorrhage has already been noted [3, 13]. Some investigators have ascribed it to the higher oxygen tension of CSF when compared with brain, which leads to a low deoxyhemoglobin concentration [28, 29]. In the absence of deoxyhemoglobin, T2 shortening and hypointensity do not develop during the acute posthemorrhage period. Another factor that may contribute to the poor visualization of diffuse subarachnoid hemorrhage is the effect of spinal fluid pulsation on observed intensity. Recent studies indicate phase-shift effects of spinal fluid pulsation may contribute significantly to the observed intensity within spinal fluid spaces [30]; therefore, it is possible that the effects of hemorrhage on spinal fluid intensity might be masked.

In summary, the complexity of the intensities encountered in AIH is a true reflection of the complex biochemical changes that occur during the first posthemorrhagic week. These changes are clearly interdependent, but the extent to which each occurs, the timing of the occurrence, and the location within an individual hematoma vary. The overall intensity and/or specific intensity pattern encountered within any individual hematoma will, therefore, reflect the nearly unique interplay of these factors at one particular moment. Under these circumstances, the variable, heterogeneous, and somewhat unpredictable appearance of these lesions is to be expected.

Since a wide range of intensities are encountered in AIH, it is obvious that no single sequence and no single intensity can characterize acute hemorrhage. It is, however, possible to define characteristic (although not necessarily specific) combinations of intensities on multiple-pulse sequences at four different stages of AIH evolution:

Stage I (under 24 hr)—subtle hyperintensity on short TR/short TE scans and moderate to marked hyperintensity on long TR/intermediate TE and long TR/long TE scans, respectively (Fig. 2). This combination is relatively specific (especially when a thin, hypointense rim is also present), since most lesions hyperintense on long TR scans are hypo- to isointense on short TR scans.

Stage II (1–3 days)—iso- to mild hypointensity on short TR/short TE scans and marked hypointensity on long TR/intermediate to long TE scans (Figs. 3–5). Although characteristic, this pattern is not as specific as previously suggested [5]. Marked hypointensity may also be encountered in densely calcified lesions [31] and noncalcified nonhemorrhagic granulomatous masses [26, 32, 33].

Stage III (4–6 days)—hyperintensity on short TR/short TE images and markedly variable intensity on long TR/interme-

diate to long TE scans. When marked hypo- or hyperintensity are present on long TR scans, hemorrhage may be diagnosed with confidence; however, if scans are obtained just as intensity is beginning to increase on long TR scans, findings may be indistinguishable from those seen in fat-containing lesions (Fig. 6).

Stage IV (more than 6–7 days)—hyperintensity on short TR/short TE and long TR/intermediate-to-long TE scans. This combination is considered specific, but it may be encountered rarely in intracranial dermoids [34].

The ability to detect and characterize hematomas is dependent on anatomy as well as intensity; therefore, the degree to which a lesion distorts normal anatomy also has a significant effect on hematoma detection. Subarachnoid hemorrhage is difficult to visualize on MR, not only because it fails to alter intensity, but also because it fails to produce anatomic distortion (Fig. 3). Parenchymal hematomas (Fig. 2) are always detected on MR, but they may be difficult to specifically characterize as hemorrhagic lesions; conversely, extraaxial hematomas (subdural and epidural, Figs. 2 and 3) have characteristic and relatively specific anatomic configurations that make the diagnosis of hematoma possible regardless of intensity. In fact, because of the absence of bone artifacts and the excellent contrast between brain and adjacent spinal fluid, small, extraaxial hematomas are detected much more easily on MR than on CT (Fig. 2) [6, 35].

In conclusion, the complex nature of the intensity changes encountered in acute intracranial hemorrhage and the difficulty in distinguishing some of these changes from those seen in other lesions suggest that CT will remain the procedure of choice as the screening test in the evaluation of any patient suspected of acute intracranial hemorrhage. Once the hemorrhagic nature of the lesion is identified on CT, MR can be used to increase diagnostic information by more accurately demonstrating the extent of the abnormality, assessing the time from hemorrhage, and detecting the presence of underlying lesions.

REFERENCES

1. Sipponen JT, Sepponen RE, Sivula A. Nuclear magnetic resonance (NMR) imaging of intracerebral hemorrhage in the acute and resolving phases. *J Comput Assist Tomogr* **1983**;7:954–959
2. Han JS, Kaufman B, Alfidi RJ, et al. Head trauma evaluated by magnetic resonance and computed tomography: a comparison. *Radiology* **1984**; 150:71–77
3. DeLaPaz RL, New PF, Buonanno J, et al. NMR imaging of intracranial hemorrhage. *J Comput Assist Tomogr* **1984**;8:599–607
4. Sipponen JT, Sepponen RE, Tanttu JI, Sivula A. Intracranial hematomas studied by MR imaging at 0.17 and 0.02T. *J Comput Assist Tomogr* **1985**;9:698–704
5. Gomori JM, Grossman RI, Goldberg HI, Zimmerman RA, Bilaniuk LT. Intracranial hematomas: imaging by high field MR. *Radiology* **1985**; 157:87–93
6. Snow RB, Zimmerman RD, Gandy SE, Deck MDF. Comparison of magnetic resonance imaging and computed tomography in the evaluation of head injury. *Neurosurgery* **1986**;18:45–52
7. Dooms GC, Uske A, Brant-Zawadzki M, et al. Spin echo MR imaging of intracranial hemorrhage. *Neuroradiology* **1986**;28:132–138
8. Zimmerman RD, Deck MDF. Intracranial hematomas: imaging by high field MR. *Radiology* **1986**;159:565
9. Zimmerman RA, Bilaniuk LT, Grossman RI, et al. Resistive NMR of intracranial hematomas. *Neuroradiology* **1985**;27:16–20
10. New PF, Aronow S. Attenuation measurements of whole blood and blood fractions in computed tomography. *Radiology* **1976**;121:635–640
11. Scotti G, Terbrugge K, Melancon D, et al. Evaluation of the age of subdural hematomas by computerized tomography. *J Neurosurg* **1977**;47:311–315
12. Di Chiro G, Brooks RA, Girton ME, et al. Sequential MR studies of intracerebral hematomas in monkeys. *AJNR* **1986**;7:193–199
13. Chakeres DW, Bryan RN. Acute subarachnoid hemorrhage: in vitro comparison of magnetic resonance and computed tomography. *AJNR* **1986**;7:223–228
14. Bydder GM, Magnetic resonance imaging of the brain. *Radiol Clin North Am* **1984**;22:779–794
15. Wehrli FW, MacFall JR, Shutts P, Breger R, Herfkens RJ. Mechanisms of contrast and NMR imaging. *J Comput Assist Tomogr* **1984**;8:369–380
16. Brooks RA, Battocletti JH, Sances A, et al. Nuclear magnetic relaxation in blood. *IEEE Trans Biomed Eng* **1975**;22:12–18
17. Bradley WG, Schmidt PG. Effect of methemoglobin formation on the MR appearance of subarachnoid hemorrhage. *Radiology* **1985**;156:99–103
18. Harms SE, Siemers PT, Hildenbrand T, Plum G. Multiple spin echo magnetic resonance imaging of the brain. *Radiographics* **1986**;6:117–134
19. Wolf GL, Burnett KR, Goldstein EJ, Joseph PM. Contrast agents for magnetic resonance imaging. In: Kressel HY, ed. *Magnetic resonance annual 1985*. New York: Raven, **1985**:231–266
20. Brittenham GM, Farrell DE, Harris JW, et al. Magnetic susceptibility measurements of human iron stores. *N Engl J Med* **1982**;307:1671–1675
21. Edelman RR, Johnson K, Buxton R, et al. MR of hemorrhage: a new approach. *AJNR* **1986**;7:751–756
22. Thulborn KR, Waterton JC, Matthews PM, Radda GK. Oxygenation dependance of the transverse relaxation time of water protons in whole blood at high fields. *Biochim Biophys Acta* **1982**;174:265–270
23. Stehbens WE. Intracerebral and intraventricular hemorrhage. In: *Pathology of cerebral blood vessel*. Saint Louis: Mosby, **1972**:284–350
24. Adams RD, Sidman RL. *Introduction of neuropathology*. New York: McGraw Hill, **1968**:177–178
25. Lindenberg R. Pathology of craniocerebral injuries. In: Newton TH, Potts DE, eds. *Radiology of the skull and brain, vol 3. Anatomy and pathology*. Saint Louis: Mosby, **1977**:3049–3087
26. Zimmerman RD, Becker RD, Devinsky O, et al. MRI features of cerebral abscesses and other intracranial inflammatory lesions (excluding AIDS patients). Presented at the Symposium Neuroradiologicum, Stockholm, June **1986**
27. Fleming CA, Zimmerman RD, Becker RD, Deck MDF. The diagnostic significance of rim intensity and edema patterns in the differentiation of intracranial mass lesions on MRI. Presented at the annual meeting of the American Society of Neuroradiology, New York City, May **1987**
28. Kemp SS, Grossman RI, Ip CY, et al. The importance of oxygenation in the appearance of acute subarachnoid hemorrhage on high field magnetic resonance imaging. Presented at Symposium Neuroradiologicum, Stockholm, June **1986**
29. Gomori JM, Grossman RI. Mechanisms responsible for the MR appearance and evolution of intracranial hemorrhage. *Radiology* **1986**;161(P):364
30. Rubin JB, Enzmann DR. Imaging spinal CSF pulsation by 2DFT magnetic resonance: significance during clinical imaging. Harmonic modulation of proton MR precessional phase by pulsatile motion: origin of spinal CSF flow phenomenon. Presented at the annual meeting of the American Society of Neuroradiology, San Diego, January **1986**
31. Oot RF, New PF, Pile-Spellman J, et al. Detection of intracranial calcifications by MR. *AJNR* **1986**;7:801–810
32. Becker RD, Zimmerman RD, Sze G, Haimes AB, Deck MDF. MR of subdural empyema and other extra-axial inflammatory lesions. Presented at the annual meeting of the American Society of Neuroradiology, New York City, May **1987**
33. Sherman JL, Hayes WS, Stern BJ, Citrin CM, Pulaski PD. MR evaluation of intracranial sarcoidosis: comparison with CT. Presented at the annual meeting of the American Society of Neuroradiology, New York City, May **1987**
34. Newton DR, Larson TC, Dillon WP, Newton TH. Magnetic resonance characteristics of cranial epidermoid, dermoid and teratomatous tumors. Presented at the annual meeting of the American Society of Neuroradiology, New York City, May **1987**
35. Zimmerman RD, Snow RB, Gandy SE, et al. Comparison of MRI and CT in the evaluation of head trauma: review of initial 100 cases. Presented at the Symposium Neuroradiologicum, Stockholm, June **1986**

FORTHCOMING ARTICLES

COMMEMORATION OF JUBILEE ANNIVERSARY

Anniversary reprint from volume 1, 1914. The direct method of diagnosis of duodenal ulcer by means of the Roentgen ray. *George AW, Gerber I*

Commentary. Gastrointestinal radiology: a short history and predictions for the future. *Gelfand DW*

SPECIAL ARTICLE

X-ray Gogs: preliminary evaluation of a "new" imaging modality. *Edwards DK III*

REVIEW ARTICLES

Magnetism: a primer and review. *Saini S, Frankel RB, Stark DD, Ferrucci JT Jr*

Statistical techniques for medical decision making: applications to diagnostic radiology. *Doubilet PM*

The role of radiology in fatality investigations. *Lichtenstein JE, Fitzpatrick JJ, Madewell JE*

PULMONARY RADIOLOGY

Determining the cause of pulmonary atelectasis: a comparison of plain radiography and CT. *Woodring JH*

Chest radiography with a shaped filter at 140 kVp: diagnostic accuracy compared with standard radiographs. *Guilbeau JC, Mazoyer BM, Pruvost P, Verrey B, Grenier P*

CT appearance of acute radiation-induced injury in the lung. *Ikezoe J, Takashima S, Morimoto S, et al.*

The number and size of normal mediastinal lymph nodes: a postmortem study. *Kiyono K, Sone S, Sakai F, et al.*

Case report. Tracheobronchomegaly (Mounier-Kuhn syndrome): CT diagnosis. *Shin MS, Jackson RM, Ho K-J*

ENDOCRINE RADIOLOGY

Color-flow Doppler sonography in Graves disease: "thyroid inferno." *Ralls PW, Mayekawa DS, Lee KP, et al.*

BREAST RADIOLOGY

Opinion. Observations on mammographic screening and false-positive mammograms. *Kopans DB, Swann CA*

Case report. Migration of breast biopsy localization wire. *Davis PS, Wechsler RJ, Feig SA, March DE*

Case report. Milk of calcium in breast microcysts: manifestation as a solitary focal disease. *Homer MJ, Cooper AG, Pile-Spellman ER*

Technical note. Innovations for mammographic compression. *Eklund GW*

VASCULAR RADIOLOGY

Traumatic aortic rupture: false-positive aortographic diagnosis due to atypical ductus diverticulum. *Morse SS, Glickman MG, Greenwood LH, et al.*

Case report. Late venous rupture after angioplasty of an arteriovenous dialysis fistula. *Bourne EE*

Technical note. Simpson catheter for percutaneous transluminal removal of atheromata. *Schwarten DE, Katzen BT, Simpson JB, Cutcliff WB*

Technical note. Technical advances in penile arteriography. *Delcour C, Vandenbosch G, Delatte P, Wespes E, Struyven J*

GASTROINTESTINAL RADIOLOGY

Percutaneous aspiration and drainage of abdominal fluid collections after pancreatic transplantation. *Letourneau JG, Hunter DW, Crass JR, Thompson WM, Sutherland DE*

Radionuclide surveillance of the allografted pancreas. *George EA,*

MR imaging of the gastrointestinal tract: value of Gd-DTPA. *Laniado M, Kornmesser W, Hamm B, Clauss W, Weinmann H-J, Felix R*

MR imaging of focal splenic tumors. *Hahn PF, Weissleder R, Stark DD, Saini S, Elizondo G, Ferrucci JT*

GENITOURINARY RADIOLOGY

CT prior to second-look operation in ovarian cancer. *Silverman PM, Osborne M, Dunnick NR, Bandy LC*

Perspective. Imaging of renal transplants. *Letourneau JG, Day DL, Ascher NL, Castaneda-Zuniga WR*

Azotemia caused by renal artery stenosis: treatment by percutaneous angioplasty. *Martin LG, Casarella WJ, Gaylord GM, Chuang VP, Alspaugh JP*

MUSCULOSKELETAL RADIOLOGY

Pictorial essay. Soft-tissue abnormalities of the foot and ankle: CT diagnosis. *Keyser CK, Gilula LA, Hardy DC, Adler S, Vannier M*

Bone stress lesions in ballet dancers: scintigraphic assessment. *Nussbaum AR, Treves ST, Micheli L*

The accessory sacroiliac joint: a common anatomic variant. *Ehara S, El-Khoury GY, Bergman RA*

Spinal chordoma: radiologic features in 14 cases. *de Bruine FT, Kroon HM*

Technical note. Distal radioulnar joint arthrography. *Gilula LA, Hardy DC, Totty WG*

Case report. Langerhans cell histiocytosis with the radiographic findings of Erdheim-Chester disease. *Waite RJ, Doherty PW, Liepman M, Woda B*

Case report. Migrating mouse: a sign of dissecting popliteal cyst. *Wilson AJ, Ford LT, Gilula LA*

PEDIATRIC AND FETAL RADIOLOGY

Pictorial essay. MR imaging in juvenile rheumatoid arthritis. *Senac MO Jr, Deutsch D, Bernstein BH, et al.*

Elevated alpha-fetoprotein and a normal fetal sonogram: association with placental abnormalities. *Fleischer AC, Kurtz AB, Wapner RJ, et al.*

Ventilator-induced pulmonary pseudocysts in preterm infants. *Williams DW, Merten DF, Effmann EL, Scatliff JH*

MR evaluation of early myelination patterns in normal and developmentally delayed infants. *Dietrich RB, Bradley WG, Zaragoza EJ IV, et al.*

Sonography of cerebral infarction in infancy. *Hernanz-Schulman M, Cohen W, Genieser NB*

NEURORADIOLOGY

MR imaging of pseudotumor cerebri. *Moser FG, Hilal SK, Abrams G, Bello JA, Schipper H, Silver AJ*

Gadolinium-DTPA in the evaluation of intradural extramedullary spinal disease. *Sze G, Abramson A, Krol G, et al.*

Epidural fibrosis and recurrent disk herniation in the lumbar spine: MR imaging assessment. *Bundschuh CV, Modic MT, Ross JS, Masaryk TJ, Bohlman H*

ARRS ANNUAL MEETING CASE OF THE DAY

Introduction. *Sider L*

Chest case of the day. *Sider L, Horton ES*

Abdominal case of the day. *Gore RM, Vogelzang RL, Fisher MR, Nemcek AA Jr*

Musculoskeletal case of the day. *Hendrix RW, Spies WG, Houk RW, Fisher MR, Poznanski AK*

Neuroradiology case of the day. *Russell EJ, Fagan SJ, Goldblatt D,*

MR Imaging of Head Trauma: Review of the Distribution and Radiopathologic Features of Traumatic Lesions

Lindell R. Gentry[1,2]
John C. Godersky[3]
Brad Thompson[1]

The distribution and extent of traumatic lesions were prospectively evaluated with MR imaging in 40 patients with closed head injuries. Primary intraaxial lesions were classified according to their distinctive topographical distribution within the brain and were of four main types: (1) diffuse axonal injury (48.2%), (2) cortical contusion (43.7%), (3) subcortical gray-matter injury (4.5%), and (4) primary brainstem injury (3.6%). Diffuse axonal injury most commonly involved the white matter of the frontal and temporal lobes, the body and splenium of the corpus callosum, and the corona radiata. Cortical contusions most frequently involved the inferior, lateral, and anterior aspects of the frontal and temporal lobes. Primary brainstem lesions were most commonly seen in the dorsolateral aspects of the rostral brainstem. The pattern and distribution of primary lesions seen by MR were compared with those expected from previous pathologic studies and found to be quite similar. Our data and review of the literature would also indicate that MR detects a more complete spectrum of traumatic lesions than does CT. Secondary forms of injury (territorial arterial infarction, pressure necrosis from increased intracranial pressure, cerebral herniation, secondary brainstem injury) were also visible by MR in some cases. The level of consciousness was most impaired in patients with primary brainstem injury, followed by those with widespread diffuse axonal injury and subcortical gray-matter injury. The best MR imaging planes, pulse sequences, and imaging strategies for evaluating and classifying traumatic lesions were evaluated, and the mechanisms by which traumatic stresses result in injury were reviewed.

MR was found to be superior to CT and to be very effective in the detection of traumatic head lesions and some secondary forms of injury. While T2-weighted images were most useful for lesion detection, T1-weighted images proved to be most useful for anatomic localization and classification.

This article appears in the January/February 1988 issue of *AJNR* and the March 1988 issue of *AJR*.

Received February 18, 1987; accepted after revision July 23, 1987.

Presented at the Symposium Neuroradiologicum, Stockholm, June 1986.

[1] Department of Radiology, University of Iowa Hospitals and Clinics, Iowa City, IA 52242.

[2] Present address: Department of Radiology, University of Wisconsin Hospital and Clinics, 600 Highland Dr., Madison, WI 53792. Address reprint requests to L. R. Gentry.

[3] Department of Surgery, Division of Neurosurgery, University of Iowa Hospital and Clinics, Iowa City, IA 52242.

***AJR* 150:663–672, March 1988**
0361–803X/88/1503–0663
© American Roentgen Ray Society

In the last decade CT has played a critical role in the diagnostic evaluation of patients with closed head trauma, providing an accurate means of diagnosing potentially reversible intracranial hematomas [1–10]. Despite fulfilling this important role, CT has been less helpful in the detection and characterization of many types of traumatic lesions. It is apparent from pathologic studies that CT underestimates the severity of many forms of cerebral injury such as primary brainstem injury, nonhemorrhagic cortical contusion, and diffuse axonal injury [3, 5, 10–18]. Although autopsy studies have been helpful in characterizing the distribution and morphology of these lesions, they only reflect the nature of the disease in the most severely injured patients.

Since CT cannot accurately assess the full spectrum of lesions in patients, it has not been possible to develop clinically useful CT imaging criteria for classifying and staging the severity of cranial trauma [10, 13, 16–18]. MR, however, has been shown to be highly sensitive in detecting both hemorrhagic and nonhemorrhagic lesions [16]. With this new method, it should now be possible to accurately identify all types of traumatic lesions, classify them, and stage their extent in the living patient.

The purpose of this study was to determine the ability of MR to prospectively

identify and characterize the traumatic intraaxial lesions found in 40 patients with closed head trauma by using a simple anatomic and topographic method of classification. The location, frequency, and distribution of all visualized lesions were compared with that expected from postmortem and animal studies. The best imaging planes and pulse sequences for evaluating each category of traumatic lesion were assessed. We also reviewed the mechanisms by which traumatic stresses result in cerebral injury.

Subjects and Methods

A prospective MR study of 40 patients with acute closed head trauma was initiated after approval of the protocol by our hospitals' institutional review board. A more complete description of the study methodology is provided in the first article in this two-part report [16]. The ages of the patients ranged from 1 month to 82 years (mean, 26.6 years). The severity of injury, as measured by the admission Glascow Coma Scale (GCS), varied from 3 to 14 (mean, 9.8). MR scans were obtained as soon as possible after injury, unless the patients were medically or neurologically unstable. Twelve patients were examined with MR while being mechanically ventilated with a nonferromagnetic fluidic ventilator, as described by Dunn et al. [19].

Contiguous nonenhanced 8-mm CT scans were obtained in all patients within the first 24 hr of admission with a fourth-generation scanner.* MR scans were obtained with a 0.5-T system.† Contiguous 10-mm scans were obtained by using an interleaved multislice technique with two-dimensional Fourier reconstruction. Both T1- and T2-weighted pulse sequences were used in most patients. T2-weighted images were obtained by using a spin-echo sequence with a repetition time (TR) of 2300–2900 msec and echo time (TE) of 80–120 msec. T1-weighted images were obtained with either an inversion-recovery sequence with TR = 2000–2300 msec and inversion time (TI) of 500–600 msec or a spin-echo sequence with TR = 400–1000 msec, TE = 25–40 msec. Thirty-four patients were examined with two or more imaging planes, while six were studied with only one plane of imaging. Thirty-nine patients were studied in the transverse plane, while 31 and five patients, respectively, were studied in the coronal and sagittal planes.

An attempt was made to differentiate *primary* lesions (resulting from the initial traumatic force) from *secondary* ones (caused by diffuse brain swelling and edema, brain displacement and herniation, delayed hemorrhage, cerebral infarction, diffuse hypoxic injury) (Table 1) [11–13]. In many cases distinction between primary and secondary lesions was difficult. For purposes of statistical analysis, however, all focal abnormalities that were not obviously secondary in nature were classified as primary lesions. Primary intracranial lesions were classified according to the method outlined in Table 1. Primary intraaxial lesions were further subclassified by their location: (1) diffuse axonal injury (white-matter "shear" injury) (Figs. 1 and 2), (2) cortical contusion (Figs. 1–4), (3) subcortical gray-matter injury (Fig. 4), and (4) primary brainstem injury (Fig. 5) [16].

For statistical purposes, two MR criteria were used to classify a lesion as hemorrhagic. On T1-weighted scans, the shortening of the T1 relaxation time by methemoglobin within the hematoma had to be of sufficient degree that the hematoma was at least partially hyperintense relative to white matter. On T2-weighted images, we required evidence of central hypointensity (relative to brain parenchyma) within the hematoma. As described by Gomori et al. [20], the central hypointensity appears to be secondary to preferential T2 proton relaxation enhancement caused by either deoxyhemoglobin or methemoglobin within intact RBCs.

The MR and CT examinations were initially analyzed separately and then compared to determine the relative sensitivities of the imaging studies. These data constitute the substance of an accompanying report [16]. The frequency, anatomic distribution, and extent of all the major types of primary traumatic lesions were assessed on the MR images and compared with that expected from postmortem and animal studies [3, 11–15, 17, 21–30] to determine their conformity with previously hypothesized mechanopathologic theories of injury. The best MR imaging planes, pulse sequences and imaging strategies were determined from analysis of the data.

TABLE 1: Classification of Traumatic Intracranial Lesions

Types and Locations of Lesions
Primary lesions:
Intraaxial:
Diffuse axonal injury
Cortical contusion
Subcortical gray-matter injury
Primary brainstem injury
Extraaxial hematomas:
Subdural
Epidural
Diffuse hemorrhage:
Subarachnoid
Intraventricular
Secondary lesions:
Pressure necrosis (secondary to brain displacement and herniation)
Territorial arterial infarction
Diffuse hypoxic injury
Diffuse brain swelling
Boundary and terminal zone infarction
Other (e.g., fatty embolism, secondary hemorrhage, infection)

Classification, Characterization, and Localization of Primary Traumatic Lesions

Diffuse Axonal Injury

The most common type of primary lesion identified in this series was diffuse axonal injury [11, 14–17, 21–28]. Lesions classified in this category had to spare the overlying cortex and be localized to the white matter or gray/white-matter interface (corticomedullary junction). Diffuse axonal injury typically was characterized by diffuse, small, focal abnormalities limited to white-matter tracts. These lesions constituted 48.2% of all traumatic lesions in this series (Table 2) (Figs. 1 and 2). When present they tended to be multiple, with 50.3% of lesions found in the 15 patients with the most severe initial impairment of consciousness. Although most of the lesions were nonhemorrhagic, 18.8% did contain small central foci of blood. Hemorrhage within diffuse axonal lesions occurred more often in those portions of the white matter with the greatest vascularity. While 25.0% of capsular and 19.7% of lobar white-matter lesions were hemorrhagic, only 10.7% of the diffuse axonal lesions in the less vascular corona radiata contained blood. The size of diffuse axonal lesions ranged from 5 to 15 mm and varied with location. Peripheral lesions tended to be smaller than central ones. The shape of the lesions was usually ovoid to elliptical with the long axis parallel to the direction of the fiber bundles (Figs. 1 and 2). They were typically found near the corticomedullary interface of the lobar

* Picker 600 and 1200 scanners, Picker International, Highland Heights, OH.
† Picker International, Highland Heights, OH.

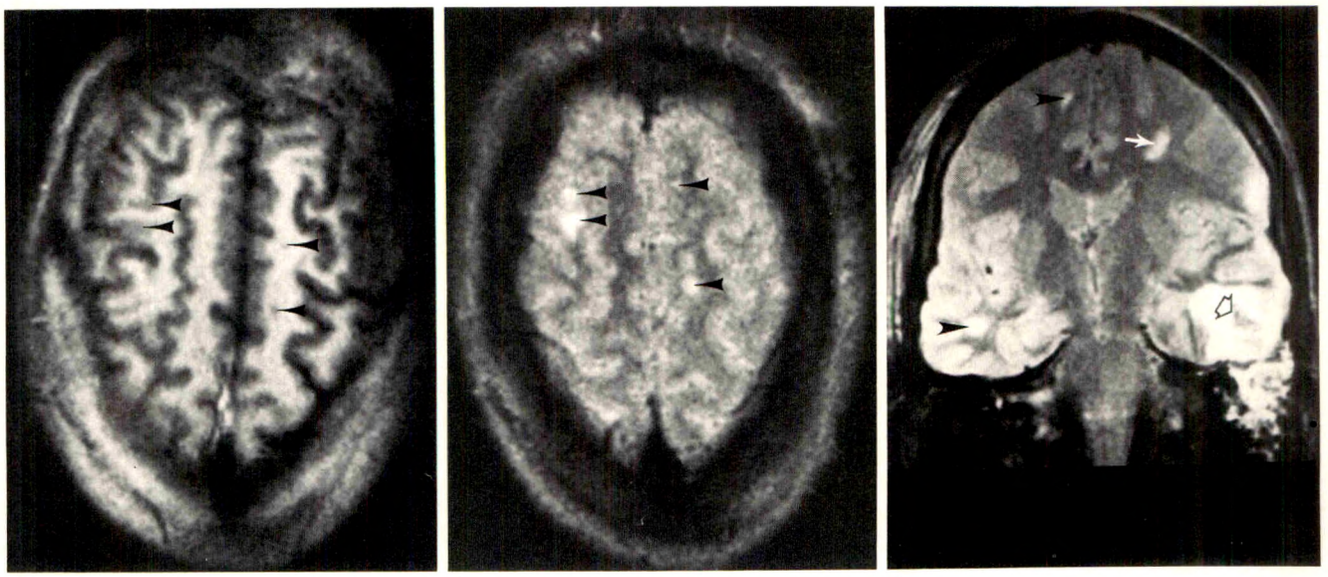

Fig. 1.—25-year-old man 4 days after trauma. Axial T1-weighted inversion-recovery (TR = 2100 msec, TI = 600 msec) MR image (*A*) and axial (*B*) and coronal (*C*) T2-weighted spin-echo (TR = 2300 msec, TE = 80 msec) MR images. Multiple bilateral diffuse axonal lesions are at corticomedullary interface of frontal, parietal, and temporal lobes (*arrowheads*).

***C*, Coronal T2-weighted MR image aids in lesion classification by helping to confirm that diffuse axonal lesions are within white matter, rather than at depths of cortical sulci. Note sparing of overlying cortex. Larger ovoid diffuse axonal lesion (*solid arrow*) is present in corona radiata, oriented parallel to direction of fiber tracts. Typical cortical contusion is present in inferolateral aspect of temporal lobe (*open arrow*). Note.—Contusion is cortically based and displaces uninvolved white matter. Peripheral zone of nonhemorrhagic injury is around central hypointensity of hematoma (*open arrow*). Hypointensity of acute hematoma at 0.5 T is always less pronounced than at higher field strengths.**

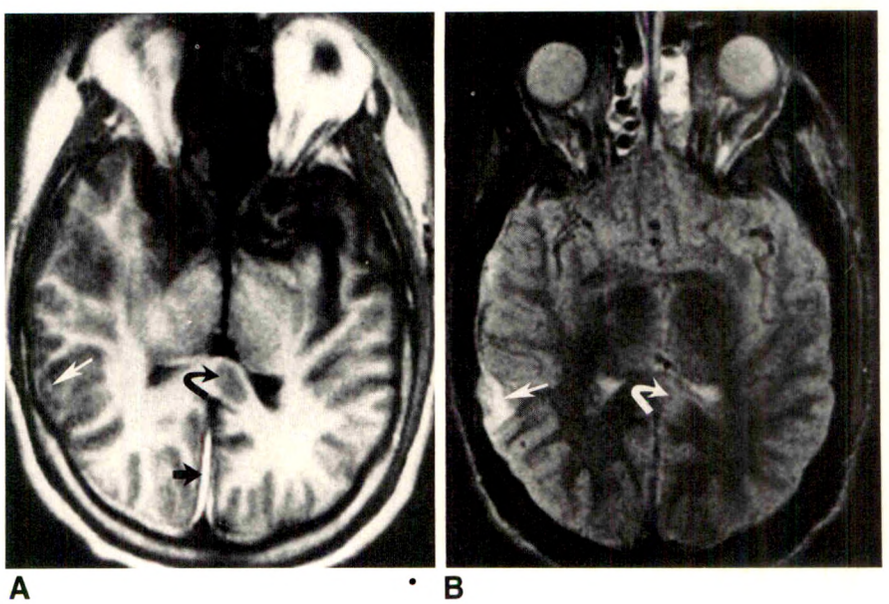

Fig. 2.—35-year-old man 4 days after trauma. Axial T1-weighted inversion-recovery (TR = 2100 msec, TI = 600 msec) MR image (*A*) and axial T2-weighted spin-echo (TR = 2300 msec, TE = 80 msec) MR image (*B*) show large ovoid diffuse axonal lesion in splenium of corpus callosum (*curved arrows*). Callosal diffuse axonal lesions were most common in this location. Also noted is small temporal lobe cortical contusion (*straight arrows*) that is difficult to identify on T1-weighted image (*A*). Four-day-old interhemispheric subdural lesion (*black arrow* in *A*) is more clearly seen at this age on T1-weighted scan.

white matter or in the large white-matter fiber bundles (corona radiata, corpus callosum, internal capsule).

The majority of the diffuse axonal lesions (50.3%) were located adjacent to the gray matter in the lobar white matter. The frontal and temporal lobes were involved most commonly, with 48.0% and 30.7% of lesions, respectively, located in these regions (Table 2). The parietal lobes, occipital lobes, and cerebellum were involved less often. The lesions of the frontal white matter were distributed equally along the superior, inferior, and lateral aspects of this lobe. White-matter lesions in the temporal lobe tended to lie adjacent to the temporal horn of the lateral ventricle (Fig. 1).

The corpus callosum was the second most common area involved in diffuse axonal injury (21.5% of lesions). The vast majority (71.9%) of callosal lesions were found in the splenium (Fig. 2). Although the splenial lesions were usually unilateral and slightly eccentric to the midline, in several instances involvement was bilateral. These lesions were most clearly imaged on highly T1-weighted (inversion-recovery or spin-echo) axial scans. There was a very strong association be-

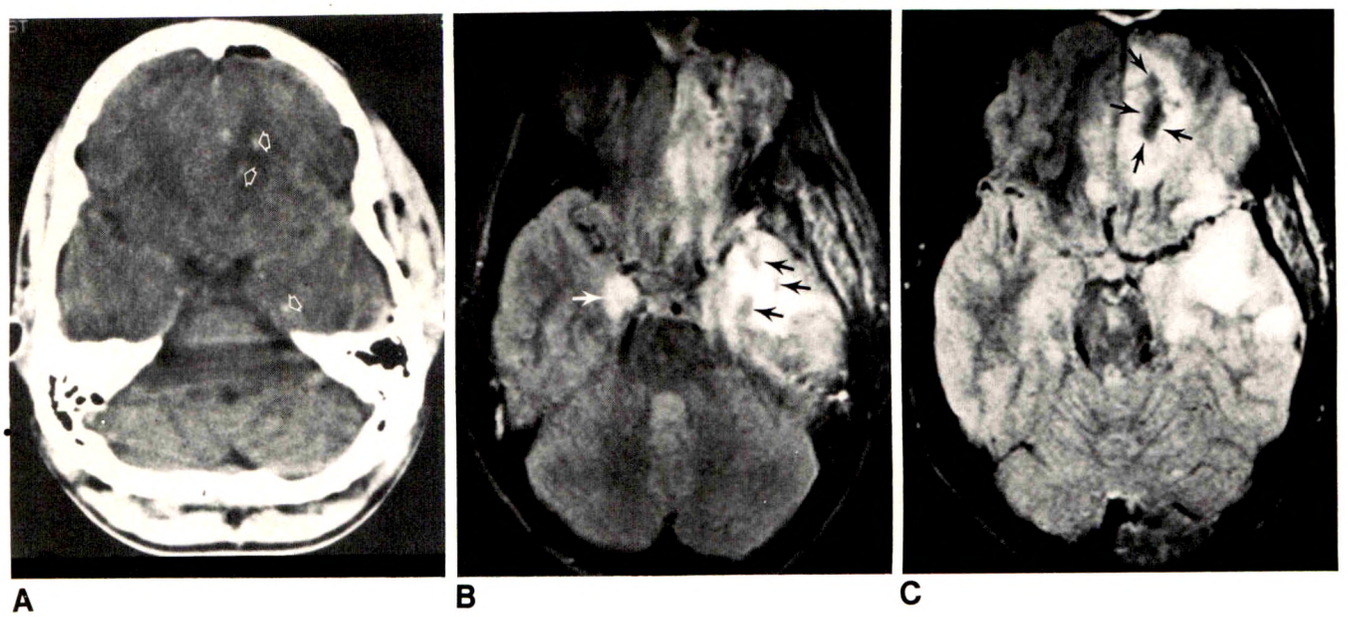

Fig. 3.—18-year-old man.

A, Axial CT scan the day of trauma appears essentially normal except for small petechial hemorrhages (*arrows*) in medial temporal and inferior frontal lobes. Note slight medial displacement of uncus of left temporal lobe.

B and *C*, Axial T2-weighted spin-echo scans (TR = 2300 msec, TE = 80 msec) 5 days after trauma. Areas of abnormality (hemorrhagic contusions) are much more extensive on MR. Hemorrhagic areas (*black arrows*) are surrounded by much larger regions of nonhemorrhagic injury. Lesion in right temporal uncus (*white arrow*) could either represent primary cortical contusion or be secondary to pressure necrosis from transtentorial herniation.

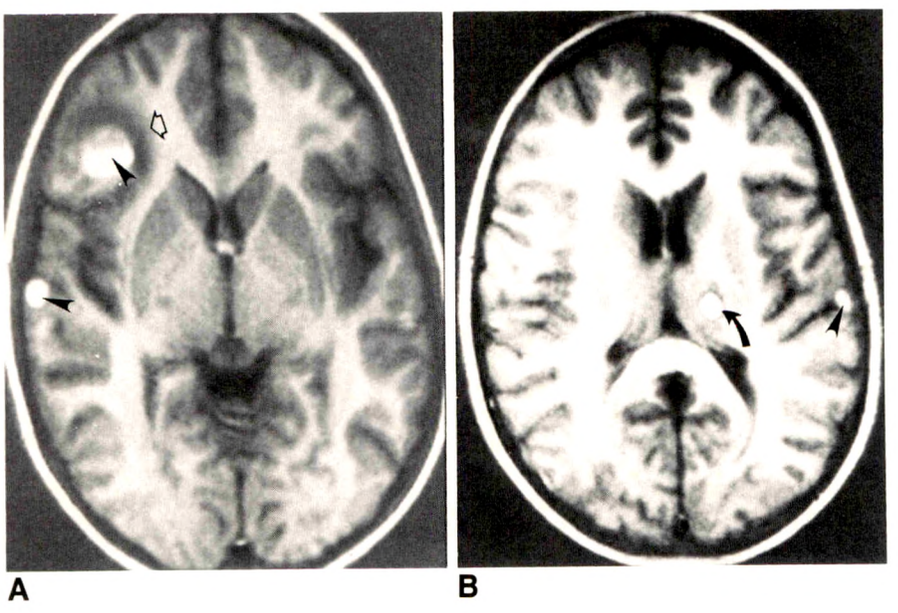

Fig. 4.—15-year-old girl. Axial T1-weighted inversion-recovery (TR = 2100 msec, TI = 600 msec) MR images 6 days after trauma show multiple hemorrhagic cortical contusions along inferolateral aspects of frontal and temporal lobes (*arrowheads*). Hemorrhagic nature of contusions is evident by short T1 of methemoglobin within hematomas. Peripheral nonhemorrhagic zone of injury and edema (*open arrow*) is hypointense because of its long T1. Note hemorrhagic subcortical gray-matter lesion in thalamus (*curved arrow*). This type of lesion may result from shear-strain disruption of perforating blood vessels.

tween the presence of corpus callosum lesions and intraventricular hemorrhage (IVH). While only 8.7% of the 23 patients without callosal lesions had IVH, 52.9% of the 17 patients with callosal lesions demonstrated IVH. The sizes of diffuse axonal lesions in the corpus callosum were usually larger than those in other locations.

Of the diffuse axonal lesions, 18.8% were located in the corona radiata, with slightly more than half in its posterior portion. These were usually slightly larger than those located more superficially in the lobar white matter. Only 8.1% of diffuse axonal lesions were in the capsular region, with most of these involving the posterior limb of the internal capsule. Most internal capsule lesions were found at its junction with the cerebral peduncle.

Cortical Contusions

The second most common type of traumatic lesion was the cortical contusion [13, 16, 17, 24–30]. To be placed in this category, the lesion had to (1) primarily involve the superficial cortex; (2) show relative sparing of the underlying white matter; (3) have a dural or osseous base; and (4) have a

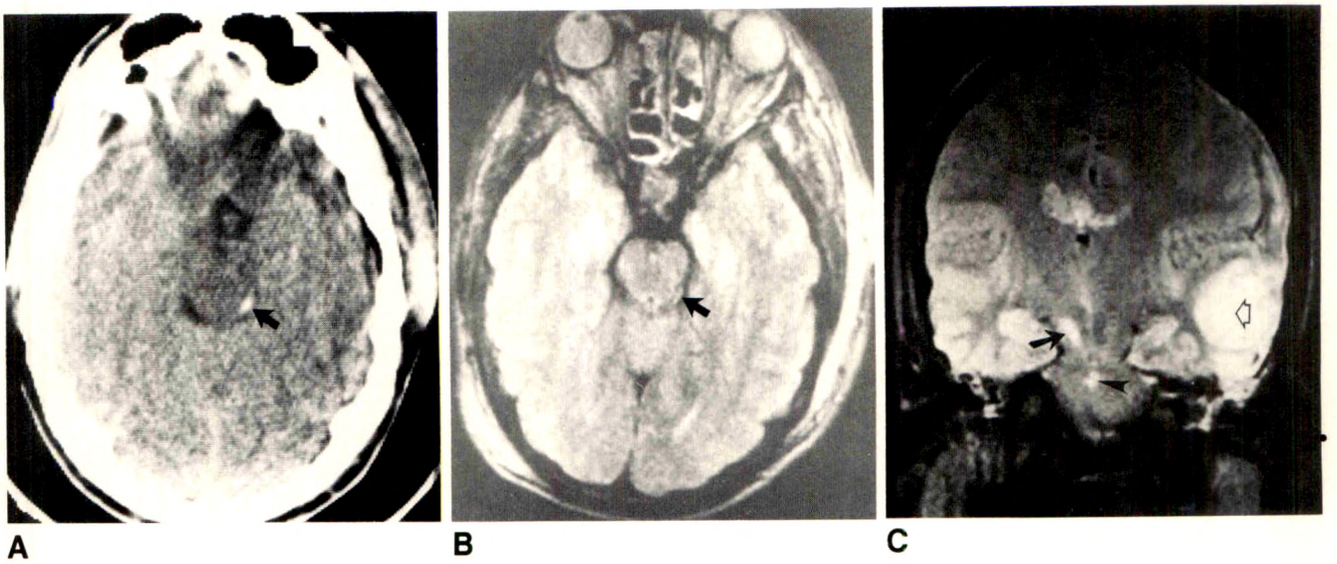

Fig. 5.—Primary brainstem injury.

***A* and *B*, Axial CT scan the day of trauma (*A*) and T1-weighted spin-echo MR image (TR = 1000 msec, TE = 40 msec) 2 days after trauma (*B*) in 21-year-old man. Lesion in dorsolateral aspect of midbrain (*arrows*) is typical in location for primary brainstem injury. Although lesion is clearly seen on CT scan it was seen on MR only retrospectively.**

***C*, Coronal T2-weighted MR image (TR = 2300 msec, TE = 80 msec) 5 days after trauma reveals central area of abnormality in pons (*arrowhead*) and large traumatic lesion in right cerebral peduncle (*solid arrow*). Also noted is large cortical contusion in lateral aspect of temporal lobe (*open arrow*).**

TABLE 2: Diffuse Axonal Injury—Frequency and Distribution of Lesions

Location	No. of Lesions		
	Hemorrhagic	Nonhemorrhagic	Total
Corona radiata (n = 28):			
Anterior	1	11	12
Posterior	2	14	16
Corpus callosum (n = 32):			
Genu	0	3	3
Body	4	2	6
Splenium	2	21	23
Capsule (n = 12):			
Internal	2	7	9
External	1	2	3
Lobar white matter (n = 71):			
Frontal	8	28	36
Temporal	4	19	23
Parietal	2	5	7
Occipital	0	5	5
Cerebellum (n = 4)	1	3	4
Other (n = 2)	1	1	2
Total	28	121	149

shape, character, and anatomic distribution not compatible with an infarct. Cortical contusions represented 43.7% of all primary lesions (Table 3) (Figs. 1–5). Cortical contusions also tended to be multiple, with 54.8% of lesions found in 20% of the study patients. Unlike diffuse axonal injury, cortical contusions were less likely to be associated with severe initial impairment of consciousness, as measured by the admission GCS scores. A much higher percentage of cortical contusions (51.9%) were hemorrhagic than were diffuse axonal injury lesions (18.8%). This may reflect the greater vascularity of gray matter. The hemorrhagic foci tended to be multiple, irregular, often confluent regions found within larger nonhemorrhagic zones of injury (Figs. 1, 3, and 4). Hemorrhagic lesions were more often distributed along the inferolateral surfaces of the frontal and temporal lobes (Table 3).

The temporal lobe was the most common site of cortical contusions (45.9% of lesions). Although the lateral aspect of the temporal lobe was the region most often injured, a significant percentage of lesions was also found along the medial surface and anterior pole. In this series, only 9.7% of temporal-lobe contusions primarily involved the inferior surface. The frontal lobe was the second most common site for contusions (31.1% of lesions). The vast majority of these lesions were found along the lateral aspect of this lobe or in a subfrontal location just above the lesser sphenoid wing and planum sphenoidale. The frontal pole was seldom involved.

The parietooccipital lobes and cerebellum were the sites of 13.3% and 9.6% of cortical contusions, respectively. Those in the parietooccipital region were most prevalent along the lateral convexity. Cerebellar lesions typically involved the superior vermis, tonsils, and inferior aspects of the hemispheres.

Subcortical Gray-Matter Lesions

Fourteen traumatic lesions were localized to the subcortical gray matter, representing only 4.5% of all primary lesions (Fig. 4). A higher percentage of these lesions (57.1%) were hemorrhagic as compared with any other type of lesion. This is most likely due to the high vascularity of this portion of the brain, supplied by a rich network of perforating vessels. The majority of these lesions were confined to the thalamus (Table 4). The severity of neurologic impairment for the eight patients with this type of injury was greater (mean GCS = 7.6) than that for all patients in this series (mean GCS = 9.8). The mechanism for production of this type of lesion may be the same as that for a similar category of lesions described by

TABLE 3: Cortical Contusion—Frequency and Distribution of Lesions

Location	No. of Lesions		
	Hemorrhagic	Nonhemorrhagic	Total
Frontal lobe (n = 42):			
Inferior	14	6	20
Superior	3	0	3
Medial	1	2	3
Lateral	10	3	13
Pole	1	2	3
Temporal lobe (n = 62):			
Inferior	5	1	6
Medial	5	13	18
Lateral	10	13	23
Pole	6	9	15
Parietooccipital (n = 18):			
Medial	3	1	4
Lateral	6	5	11
Superior	2	1	3
Cerebellum (n = 13):			
Hemisphere	3	5	8
Vermis	1	4	5
Total	70	65	135

TABLE 4: Subcortical Gray-Matter Lesions—Frequency and Distribution

Location	No. of Patients		
	Hemorrhagic	Nonhemorrhagic	Total
Thalamus	6	3	9
Caudate nucleus	0	0	0
Lentiform nucleus:			
Globus pallidus	2	0	2
Putamen	0	3	3
Subtotal	2	3	5
Total	8	6	14

TABLE 5: Brainstem Lesions—Frequency and Distribution of Lesions

Location	No. of Patients		
	Hemorrhagic	Nonhemorrhagic	Total
Midbrain:			
Tectum	0	1	1
Lateral tegmentum	1	1	2
Ventral tegmentum	0	1	1
Cerebral peduncle	0	1	1
Subtotal	1	4	5
Pons	1	3	4
Medulla	0	2	2
Total	2	9	11

Adams et al. [11, 27, 28]. They described a diffuse type of injury characterized by multiple petechial hemorrhages primarily located in the ventral brainstem, basal ganglia, and frontotemporal white matter. These lesions are most often seen in severely injured patients who die shortly after head injury. It was postulated by Adams et al., and consistent with the predictions of Holbourn [24, 25], that this form of injury may be secondary to disruption of multiple small perforating blood vessels (Fig. 4B).

Primary Brainstem Lesions

Ten patients (11 lesions) were thought to have lesions of the brainstem (Table 5) (Fig. 5) that were believed to have been caused by the initial traumatic force [12, 26–28, 31–33]. This group of patients generally had multiple other lesions, most of which were typical of diffuse axonal injury. Only two (18.2%) of the brainstem lesions were hemorrhagic. The severity of initial impairment of consciousness in this group of patients was greater than that for any other group. The mean initial GCS for these patients was 7.0. Five patients had focal neurologic findings that were anatomically compatible with the lesion imaged by MR. The other five patients had altered levels of consciousness but no focal neurologic findings. The majority of primary brainstem lesions (six of 11) were localized to the dorsal and lateral aspects of the rostral brainstem (midbrain and rostral pons) (Table 5). These lesions are most likely from diffuse axonal injury of the brainstem secondary to rotationally induced shear strains [26–28].

Classification, Characterization, and Localization of Secondary Brain Injury

Although the thrust of this article is concerned with primary forms of injury, we did observe several instances of secondary forms of injury that must be differentiated from primary lesions (Table 1). A number of excellent pathologic reports have dealt with the differentiation of primary and secondary forms of injury [11, 13, 17, 26–33]. Pressure necrosis, commonly associated with increased intracranial pressure and brain herniation syndromes, typically results when neural structures are compressed against rigid osseous and dural margins. This most commonly involved the cingulate (n = 5) and parahippocampal (n = 7) gyri in our series. It was often difficult to separate pressure necrosis from primary lesions (Fig. 3). The presence of significant mass effect, cisternal compression, and midline displacement often suggested pressure necrosis. Territorial arterial infarction was encountered in only one patient (Fig. 6). Diffuse hemispheric brain swelling and edema were not apparent in any patient as an isolated process, but were always associated with an underlying injury to the brain (cortical contusion, diffuse axonal injury, extraaxial hematoma, territorial infarction).

MR Imaging Plane and Pulse Sequences

The visibility of a lesion on a particular pulse sequence was influenced by a number of factors (presence of hemorrhage, interval of time since injury, size and anatomic location of the lesion). The overall relationships between lesion detectability and the presence of hemorrhage for various MR pulse sequences were examined in part 1 of this report [16]. The most important factor that affected lesion visibility was the MR imaging pulse sequence used. T2-weighted images were the

most sensitive over the whole course of injury (acute and subacute phases) and were similarly sensitive for hemorrhagic and nonhemorrhagic forms of injury. T1-weighted images were highly sensitive for hemorrhagic lesions, especially if the study was performed at least 3 days after injury. T1-weighted scans were less sensitive for nonhemorrhagic lesions and for very small (<1.0 cm) hemorrhagic lesions in the first 2 days after injury. T1-weighted images were slightly superior to T2-weighted images for the evaluation of the brainstem. This was primarily because small brainstem lesions were more often obscured on the T2-weighted scans by phase-shift artifacts arising from vascular and CSF pulsation. T2-weighted images were usually superior when these artifacts were absent.

The MR imaging plane was less important than the pulse sequence in lesion detectability (Table 6). The axial and coronal planes showed similar sensitivities for detecting all types of lesions. This was true for both T1- and T2-weighted pulse sequences. For specific lesions, however, one plane of imaging was often superior. The superficial lesions were seen best when the imaging plane was perpendicular to the cortical base of the lesion. Deep subcortical lesions were seen equally well with all imaging planes. The best plane for visibility of callosal lesions depended on the portion involved. Axial scans were superior for visualizing lesions in the genu and splenium (Fig. 2), while coronal scans were better for those within the body. Since brainstem lesions were usually small, multiple imaging planes were frequently helpful in detecting them.

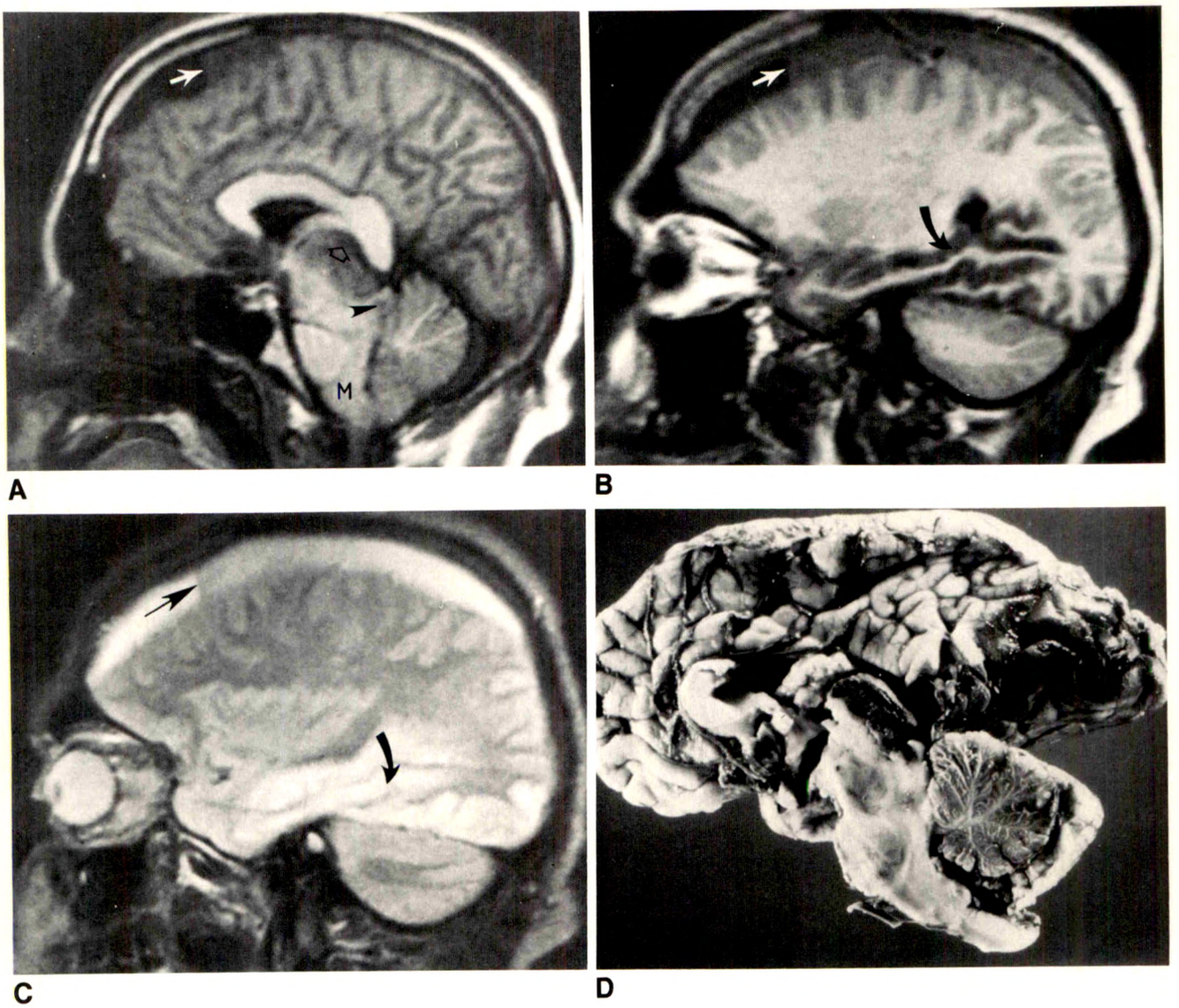

Fig. 6.—34-year-old comatose man who had several episodes of head trauma 1–3 weeks earlier.

***A–C*, Sagittal T1-weighted inversion-recovery (TR = 2350 msec, TE = 600 msec) MR images (*A* and *B*) and T2-weighted spin-echo (TR = 2300 msec, TE = 80 msec) MR image (*C*) show subdural hematoma with sedimentation level (*straight solid arrows*). There are areas of infarction in inferomedial temporal lobe (*curved arrows*) and thalamus (*open arrow*), respectively, in distributions of posterior cerebral and thalamoperforating arteries. There is evidence of transtentorial and tonsillar herniation. Note marked compression of midbrain (*arrowhead*), fourth ventricle, and interpeduncular cistern as well as kinking of medulla (M).**

***D*, Autopsy specimen. Lateral view of left half of brain after midsagittal section confirms MR findings.**

Multiple imaging planes were also helpful for classifying the type of traumatic lesion. For example, it was often difficult, with only one plane of imaging, to determine whether a small lesion close to the cortical surface was from diffuse axonal injury or cortical contusion. Only when the imaging plane was perpendicular to the adjacent calvarium was this reliably established (Fig. 1).

Discussion

Mechanisms of Cerebral Injury

Holbourn [24, 25] was the first to systematically analyze the mechanisms by which traumatic stresses produce cerebral injury. His experimental work, which used a gelatin model of the brain, has served as a fundamental basis for understanding the mechanisms of cerebral injury. He analyzed the mechanics of injury from a physicist's point of view and emphasized that injury to the brain could only occur through two types of structural deformations. *Compression-rarefaction strain* is characterized by a change in volume without a change of shape and is of minimal importance in the production of cerebral injury. *Shear-strain* deformation, however, is characterized by a change in shape without a change in volume and is responsible for the vast majority of mechanically induced lesions. The brain is relatively resistant to injury by compression-rarefaction strain because of its incompressibility. Brain tissue is quite susceptible, however, to shear-strain injury, since this depends on rigidity to prevent deformation. The brain, unlike the highly rigid skull, has a low index of rigidity and is ineffective in preventing this type of deformation [24, 25].

Holbourn also described two major types of forces responsible for brain deformation and injury. The first type of force is localized to the site of impact and is from skull distortion (contact phenomenon). These injuries are produced by localized inbending and fracture of the skull and are mediated through shear-strain distortions localized to the superficial regions of the brain. Compression-rarefaction strain waves do emanate from the site of impact but, according to Holbourn, they play little or no role in injury. The second group of forces includes those that arise irrespective of skull deformation (linear acceleration, rotational acceleration, centrifugal force, Coriolis force). Of the four forces in this group, rotational acceleration plays the predominant role in the production of intraaxial cerebral lesions [14, 24, 25]. Rotational forces produce traumatic lesions by deformation of brain tissue mediated through shear strains. The other three forces are much less important in the production of structural damage, either because the magnitude of the deforming force is small or because the force primarily exerts itself through deformations of the compression-rarefaction variety [13, 24–26].

Injuries from the shear-strains generated by rotational forces, as would be expected, are more diffuse in location than those from skull deformation. The expected anatomic distribution of traumatic lesions induced by nonimpact rotational acceleration was experimentally mapped by Holbourn [24, 25] with a gelatin brain model. Despite the limitation of this model, the location and distribution of traumatic lesions in fatal head injuries [11, 13–15, 17, 22, 23, 28] and animal trauma models [13, 26, 27] have generally followed Holbourn's theoretical predictions (Fig. 7). Injuries from rotational forces are expected to correspond closely in location to the sites of maximum shear-strain. Shear-strain will be greatest at the junction of tissues of different rigidity (gray/white-matter interface, brain/CSF interface, skull/brain interface, dura matter/brain interface) [24, 25]. The location of rotationally induced shear-strain lesions is primarily dependent on the plane of rotation (Fig. 7) and is independent of the direction of rotation within a given plane. The location of maximum shear-strain is also independent of the distance from the center of rotation, the arc of rotation, and the intensity of the force. The magnitude of shear-strain, however, is dependent on these factors as well as on the duration of the rotational force. Figure 7 illustrates the location of maximum shear-strain for all three orthogonal planes of rotation [24, 25]. Holbourn [24, 25] also emphasized that rotationally induced shear-strain deformations also act on nonneuronal tissue (penetrating blood vessels, bridging veins).

For a number of years Holbourn's classic work went ignored. Strich [22, 23] was the first to recognize the significance of Holbourn's observations with the publication of a pathologic description of shear injuries of the white matter. Since that time, most of Holbourn's observations have been largely supported by postmortem observations [11, 13–15, 17, 27, 28]. It was not until Gennarelli et al. [13, 21, 26, 27] developed an animal model of cranial trauma, however, that Holbourn's observations were confirmed experimentally. In an important series of experiments with a primate model of cranial trauma, these authors have confirmed that all of the major types of traumatic lesions can be reproduced by nonimpact inertial loading of the head in an appropriate manner. The exact nature of the resulting injury will depend on the type (angular, linear), rate, duration, and plane of head acceleration.

TABLE 6: Sensitivities of MR Imaging Planes in Detecting Primary Lesions

Type of Lesion	No. of Lesions Imaged/Total = % Sensitivity			
	Axial Plane		Coronal Plane	
	T1-Weighted	T2-Weighted	T1-Weighted	T2-Weighted
Diffuse axonal injury	71/90 = 78.9	140/149 = 94.0	40/58 = 69.0	59/67 = 88.1
Cortical contusions	60/81 = 74.1	127/135 = 94.1	38/51 = 74.5	65/70 = 92.9
Subcortical gray-matter lesions	9/10 = 90.0	13/14 = 92.9	3/5 = 60.0	8/8 = 100
Brainstem	7/9 = 77.8	7/11 = 63.6	2/3 = 66.8	4/7 = 57.1
Total	147/190 = 77.4	287/309 = 92.9	83/117 = 70.9	136/152 = 89.5

Classification and Distribution of Primary Traumatic Lesions

It is apparent from the studies of Holbourn [24, 25] that most intraaxial traumatic brain lesions result from either (1) skull deformation or fracture (contact phenomenon) or (2) nonimpact stresses related to rotational acceleration. Furthermore, these two types of mechanisms are primarily mediated through the same type of deformation (shear-strain). Since all traumatic lesions are produced by the same type of deformation and differ primarily by their location, it seems most valid to base their classification on the latter point. We believe the primary traumatic intraaxial lesions found in this study clearly fit into four anatomically well-defined categories: (1) diffuse axonal injury, (2) cortical contusion, (3) subcortical gray-matter injury, and (4) brainstem injury (Tables 2–5). This proposed classification scheme, based on the topographic and anatomic location of lesions, closely resembles that used by other authors [11, 13–17, 26–28, 32, 33]. We think that this simple method of classification is practical and applicable to both radiologic imaging and pathologic analysis. It also avoids imprecise nomenclature that may falsely imply mechanistic processes (for example, coup/contracoup/intermediary coup, contusion laceration, stretching contusion, gliding contusion) [11].

Previously, there has not been a satisfactory means for anatomically staging and classifying lesions in the living patient. The GCS has provided a clinical means for judging the severity of injury, making decisions about the need for intracranial pressure monitoring, determining the prognosis for recovery, and comparing responses to treatment. Accurate anatomic classification of traumatic lesions would also be potentially useful for similar reasons. It might also prove helpful for further clarifying the mechanisms of cerebral injury. Despite these potential benefits, CT has not been particularly useful for classifying and staging injury. Its low sensitivity for nonhemorrhagic lesions and the difficulty of obtaining multiplanar images have severely limited its usefulness [13, 16–18].

MR offers distinct advantages over other imaging methods for classifying traumatic cerebral lesions. The ability of MR to image in multiple planes is particularly beneficial since this makes lesion localization much easier (Fig. 1). Unless two planes of imaging are used, it is often difficult to differentiate a diffuse axonal injury lesion involving the gray/white-matter interface from a small cortical contusion. In addition, more lesions can be classified with MR than with CT because MR has a much higher sensitivity for nonhemorrhagic lesions (Fig. 3) [16].

We believe there is little difficulty, with this classification scheme, in separating the various types of primary lesions, since the anatomic location of each type of lesion is distinctive. We did experience some difficulty in distinguishing primary and secondary lesions, since both types are often found in the same locations (Fig. 3). This problem, however, is not unique to MR, as it may also be difficult to make this distinction at autopsy or on a histologic basis [11–15, 27–33]. Despite these problems, we believe that in most cases a distinction can be made with MR on the basis of the size, shape, distribution, and location of the lesions. It is possible, however, that a number of lesions that we believed to be primary were actually secondary. Much experience is needed in closely correlating the MR and histologic appearances of lesions in various stages of evolution to accomplish this goal. Sequential MR scanning, beginning shortly after trauma, may be helpful.

An important limitation of the value of this prospective study is the lack of pathologic confirmation in the majority of our cases. Autopsy confirmation of the exact nature of the lesions was possible in only one patient, since 39 of 40 patients survived their injuries. Despite this limitation, we believe that, for the first time in the living patient, it is possible to detect and classify most types of traumatic injuries with MR. A comparison of the anatomic distribution of the lesions in our group of patients with that from pathologic [13–15, 17, 22, 23, 28] and animal studies [13, 26, 27] reveals an identical overall pattern. The pattern of lesions seen in our patients (Tables 2–5) is also remarkably similar to the theoretical predictions of Holbourn [24, 25] (Fig. 1). The similarity in the patterns would suggest that MR does detect the full spectrum of lesions.

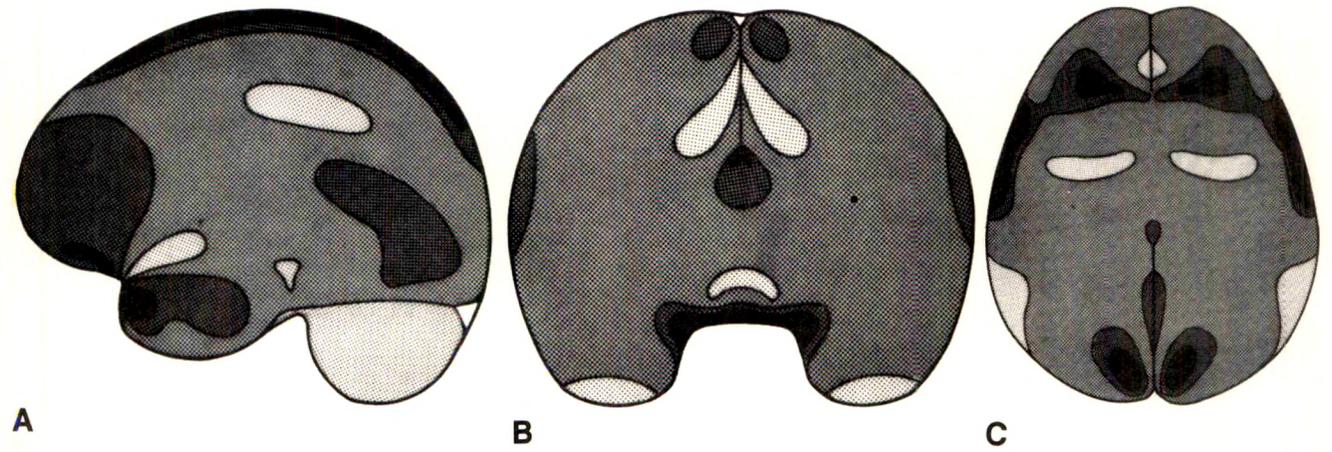

Fig. 7.—Areas of maximum shear-strain and predicted distribution of traumatic intraaxial lesions for three orthogonal planes of rotational acceleration. Expected location of traumatic lesions for rotation in sagittal (*A*), coronal (*B*), and axial (*C*) planes. Greater frequency of lesions is to be anticipated in more darkly shaded regions, which represent areas of maximum shear-strain. (Adapted from [24].)

MR Imaging Plane and Pulse Sequences

We believe that is is essential to obtain images that emphasize both T1 and T2 contrast differences in at least two different imaging planes to accurately detect, characterize, and classify traumatic lesions [16]. Generally speaking, T2-weighted images are most useful for lesion detection, both types of images are necessary for accurate detection and temporal staging of hemorrhagic lesions [20], and T1-weighted images are most useful for anatomically localizing the lesions for purposes of classification. The protocol that we find most practical for our particular scanner is as follows: (1) Sagittal T1-weighted images (short TR, short TE spin-echo scans) are initially obtained, the images of which are used to plan the imaging planes for the other pulse sequences; (2) an axial T2-weighted (long TR, long TE spin-echo) study is then performed. If no abnormalities are seen on the first two sequences the examination is stopped. If traumatic lesions are visualized, then the study also includes (3) coronal T1-weighted images with either an inversion-recovery or short TR, short TE spin-echo sequence through regions of pathology.

REFERENCES

1. Zimmerman RD, Danziger A. Extracerebral trauma. *Radiol Clin North Am* **1982**;20:105–121
2. Hryshko FG, Deeb ZL. Computed tomography in acute head injuries. *J Comput Tomogr* **1983**;7:331–334
3. Zimmerman RA, Bilaniuk LT, Gennarelli T. Computed tomography of shearing injuries of the cerebral white matter. *Radiology* **1978**;127:393–396
4. Zimmerman RA, Bilaniuk LT, Bruce D, Dolinskas C, Obrist W, Kuhl D. Computed tomography of pediatric head trauma: acute general cerebral swelling. *Radiology* **1978**;126:403–408
5. French BN, Dublin AB. The value of computerized tomography in the management of 1000 consecutive head injuries. *Surg Neurol* **1977**;7:171–183
6. Moseley IF, Zilkha E. The role of computerized axial tomography (EMI-scanning) in the diagnosis and management of craniocerebral trauma. *J Neuroradiol* **1976**;3:277–296
7. Bricolo A, Pasut MI. Extradural hematoma toward zero mortality. A prospective study. *Neurosurgery* **1984**;14:8–12
8. Seelig JM, Becker DP, Miller JD, Greenberg RP, Ward JD, Choi SC. Traumatic acute subdural hematoma. Major mortality reduction in comatose patients treated within four hours. *N Engl J Med* **1981**;304:1511–1518
9. Lanksch W, Grumme T, Kazner E. Correlations between clinical symptoms and computerized tomography findings in closed head injuries. In: Frowein RS, Wilcke D, Karimi-Nejad A, Brock M, Klinger M, eds. *Advances in neurosurgery*, vol 5. *Head injuries—tumors of the cerebellar region*. Berlin: Springer-Verlag, **1978**:27–29
10. Snoek J, Jennett B, Adams JH, Graham DI, Doyle D. Computerized tomography after recent severe head injury in patients without acute intracranial hematoma. *J Neurol Neurosurg Psychiatry* **1979**;42:215–225
11. Adams JH, Graham DI, Scott G, Parker LS, Doyle D. Brain damage in fatal non-missile head injury. *J Clin Pathol* **1980**;33:1132–1145
12. Cooper PR, Maravilla K, Kirkpatrick J, et al. Traumatically induced brainstem hemorrhage and the computerized tomographic scan: clinical, pathological and experimental observations. *Neurosurgery* **1979**;4:115–124
13. Adams JH, Gennarelli TA, Graham DI. Brain damage in non-missile head injury: observations in man and subhuman primates. In: Smith WT, Cavanagh JB, eds. *Recent advances in neuropathology*, vol 2. Edinburgh: Churchill Livingston, **1982**:165–190
14. Adams JH, Graham DI, Murray LS, Scott G. Diffuse axonal injury due to non-missile head injury in humans: an analysis of 45 cases. *Ann Neurol* **1982**;12:557–563
15. Adams JH, Mitchell DE, Graham DI, Doyle D. Diffuse brain damage of immediate impact type: its relationship to primary brainstem damage in head injury. *Brain* **1977**;100:489–502
16. Gentry LR, Godersky JC, Thompson B, Dunn VD. Prospective comparative study of intermediate-field MR and CT in the evaluation of closed head trauma. *AJNR* **1988**;9:91–100
17. Hardman JM. The pathology of traumatic brain injuries. *Adv Neurol* **1979**;22:15–50
18. Perini S, Beltramello A, Pasut ML, Benati A, Bricolo A. CNS trauma: head injuries. *Neurol Clin* **1984**;2:719–743
19. Dunn VD, Ely-Coffman C, McGowan JE, Ehrhardt JC. Mechanical ventilation during magnetic resonance imaging. *Magnetic Resonance Imag* **1985**;3:169–172
20. Gomori JM, Grossman RI, Goldberg HI, Zimmerman RA, Bilaniuk LT. Intracranial hematomas: imaging by high field MR. *Radiology* **1985**;157:87–93
21. Gennarelli TA, Spielman GM, Langfitt TW, et al. Influence of the type of intracranial lesion on outcome from severe head injury. *J Neurosurg* **1982**;56:26–32
22. Strich SJ. Diffuse degeneration of the cerebral white matter in severe dementia following head injury. *J Neurol Neurosurg Psychiatry* **1956**;19:163–185
23. Strich SJ. Shearing of nerve fibers as a cause of brain damage due to head injury, a pathological study of twenty cases. *Lancet* **1961**;2:443–448
24. Holbourn AHS. Mechanics of head injuries. *Lancet* **1943**;2:438–441
25. Holbourn AHS. The mechanics of brain injuries. *Br Med Bull* **1945**;3:147–149
26. Gennarelli TA, Thibault LE, Adams JH, Graham DI, Thompson CJ, Marcincin RP. Diffuse axonal injury and traumatic coma in the primate. In: Dacey RG Jr, Winn HR, Rimel RW, Jane JA, eds. *Trauma of the central nervous system*. New York: Raven, **1985**:169–193
27. Adams JH, Graham DI, Gennarelli TA. Contemporary neuropathological considerations regarding brain damage in head injury. In: Becker DP, Polishock J, eds. *Central nervous system trauma status report*. Bethesda, MD: National Institute Neurological and Communicative Disorders and Stroke, National Institute of Health. **1985**:65–77
28. Adams JH. Head injury. In: Adams JH, Corsellis JAN, Duchen LW, eds. *Greenfield's neuropathology*, 4th ed. New York: Wiley, **1984**:85–124
29. Lindenberg R, Freytag E. The mechanism of cerebral contusions: a pathologic-anatomic study. *Arch Pathol Lab Med* **1960**;69:440–469
30. Lindenberg R, Fisher RS, Durlacher SH, Lovitt WV Jr, Freytag E. Lesions of the corpus callosum following blunt mechanical trauma to the head. *Am J Pathol* **1955**;31:297–317
31. Rosenblum WI, Greenberg RP, Seelig JM, Becker DP. Midbrain lesions: frequent and significant prognostic feature in closed head injury. *Neurosurgery* **1981**;9:613–620
32. Tomlinson BE. Brainstem lesions after head injury. *J Clin Pathol [Suppl]* (R Coll Pathol) **1970**;4:154–165
33. Tsai FY, Teal JS, Quinn MF, et al. CT of brainstem injury. *AJNR* **1980**;1:23–29, *AJR* **1980**;134:717–723

Prospective Comparative Study of Intermediate-Field MR and CT in the Evaluation of Closed Head Trauma

Lindell R. Gentry[1,2]
John C. Godersky[3]
Brad Thompson[1]
Val D. Dunn[1,4]

Forty patients with closed head trauma were evaluated prospectively with CT and intermediate-field-strength MR imaging to compare the diagnostic efficacies of the two techniques. Traumatic lesions were detected in 38 patients. The severity of injury, as determined by the Glascow Coma Scale, ranged from 3 to 14. The sensitivities of CT and MR were calculated for all subgroups of lesions: (1) hemorrhagic and nonhemorrhagic intraaxial lesions (diffuse axonal injury, cortical contusion, subcortical gray-matter injury, primary brainstem injury); (2) extraaxial hematomas (subdural, epidural); and (3) diffuse hemorrhage (subarachnoid, intraventricular).

CT and MR (T1- and T2-weighted) studies were both highly and comparably sensitive in the detection of hemorrhagic intraaxial lesions. MR scans, however, were much more sensitive in detecting nonhemorrhagic lesions. Cortical contusions and diffuse axonal injury constituted 91.9% of all intraaxial lesions. The sensitivities of the imaging techniques for this combined group of lesions were (1) nonhemorrhagic lesions (CT = 17.7%, T1-weighted MR = 67.6%, T2-weighted MR = 93.3%); (2) hemorrhagic lesions (CT = 89.8%, T1-weighted MR = 87.1%, T2-weighted MR = 92.5%). MR was also significantly better in detecting brainstem lesions (CT = 9.1%, T1-weighted MR = 81.8%, T2-weighted MR = 72.7%). The sensitivities of the diagnostic studies in the detection of extraaxial hematomas were CT = 73.2%, T1-weighted MR = 97.6%, T2-weighted MR = 90.5%). Intraventricular hemorrhage was consistently seen with all three imaging studies, but subarachnoid hemorrhage was detected much more frequently with CT.

In summary, MR has clear advantages over CT in evaluating closed head trauma. Although its sensitivity in detecting hemorrhagic lesions is similar to that of CT, it is much better than CT in detecting nonhemorrhagic lesions, which are more prevalent. MR is more useful than CT in classifying primary and secondary forms of injury and directing treatment. CT's one advantage over MR is its ability to more rapidly assess unstable patients who may need surgery.

This article appears in the January/February 1988 issue of *AJNR* and the March 1988 issue of *AJR*.

Received February 18, 1987; accepted after revision August 19, 1987.

Presented at the annual meeting of the American Society of Neuroradiology, San Diego, January 1986.

[1] Department of Radiology, University of Iowa Hospitals and Clinics, Iowa City, IA 52242.

[2] Present address: Department of Radiology, University of Wisconsin Hospital and Clinics, 600 Highland Dr., Madison, WI 53792. Address reprint requests to L. R. Gentry.

[3] Department of Surgery, Division of Neurosurgery, University of Iowa Hospital and Clinics, Iowa City, IA 52242.

[4] Present address: Department of Radiology, American Fork Hospital, American Fork, UT 84003.

***AJR* 150:673–682, March 1988**
0361–803X/88/1503–0673
© American Roentgen Ray Society

During the past decade, CT has contributed significantly to the management of patients with closed head trauma [1–9]. CT has improved the survival and reduced the morbidity of patients with closed head trauma, primarily through the early recognition and treatment of extracerebral hemorrhage [1, 2, 5–9]. CT has been less beneficial, however, in the recognition and management of other types of cerebral injury [3–5, 9–14]. In the acute phase, CT findings often do not correlate with neurologic impairment or the level of consciousness as measured by the admission Glascow Coma Scale (GCS) [9–15]. Although certain CT findings are associated with a poor outcome [3, 16–22], the extent of posttraumatic recovery of neurologic and cognitive function is generally not reliably predicted from the pattern of injury on the initial CT scan [5, 9–13]. The lack of correlation of CT findings with the acute and chronic sequelae of closed head trauma is due, in part, to the insensitivity of CT to many types of cerebral injuries [3, 9–11, 19]. Although MR imaging has been shown to be more sensitive than CT in detecting many diseases involving the CNS, it has not been extensively used for the evaluation of acute closed head trauma. A few reports deal only with subacute or chronic posttraumatic extracerebral hematomas [23–26]. A number of investigators have

studied the MR appearance of hemorrhagic lesions, but many of these lesions were not posttraumatic in nature [27–33]. A few series of patients with closed head trauma have also been studied by MR [34–39]. But one of these series was very small [35], and others included patients in the subacute/chronic phase of injury [37–39]. A large prospective comparative study of CT and intermediate-field-strength MR has not been reported. In this study, we prospectively evaluated 40 patients with acute closed head trauma to determine (1) the feasibility of MR for evaluating these patients and (2) the relative sensitivities of CT and MR for detecting various types of cerebral injuries.

Subjects and Methods

A prospective comparative study of the usefulness of CT and MR for the evaluation of 40 patients with acute closed head trauma was initiated after approval of the protocol by our hospital's institutional review board. Inclusion in the study required a thorough neurologic evaluation and determination of the level of consciousness (GCS) [40] by an experienced neurosurgeon or neurologist within 6 hr of admission to the hospital. Patients who experienced transient loss of consciousness without focal neurologic deficits and who had complete recovery of consciousness within the first 12 hr were excluded from the study. Also excluded were patients who died shortly after hospitalization, those with contraindications to MR scanning, and those with multisystem trauma who were medically unstable. The age of the patients ranged from 1 month to 82 years (mean, 26.6 years). Eight female and 32 male patients constituted the study group. The severity of injury, as measured by the admission GCS, ranged from 3 to 14 (mean, 9.8).

The MR scans were obtained as soon as possible after injury but only after the patients were considered stable. The interval from injury to MR evaluation was 2–19 days (mean, 7.6; median, 5–6). The intervals between CT and MR studies for the study population are summarized in Table 1. Those patients with the most severe injuries were usually evaluated after the intracranial pressure had stabilized. Twelve patients were examined with MR while being mechanically ventilated with a fluidic ventilator, as recently described by Dunn et al. [41]. This was accomplished by modification of a Monaghan 225 SIMV Volume Ventilator* to eliminate ferromagnetic material from the supporting stand.

Nonenhanced CT scans were obtained in all patients within the first 24 hr after trauma by using a fourth-generation scanner.† A slice thickness of 8 mm was used in all instances. MR was performed with a 0.5-T cryogenic system.‡ Thirty-nine patients were examined with both T1- and T2-weighted pulse sequences while one patient was studied only with a T2-weighted sequence. Scans were obtained with a contiguous interleaved multislice technique with a slice thickness of 10 mm. The T2-weighted scans were obtained with a spin-echo sequence with a repetition time (TR) of 2300–2900 msec and echo time (TE) of 80–120 msec. T1-weighted scans were obtained in 37 patients with an inversion-recovery sequence with a TR of 2000–2300 msec and inversion time (TI) of 500–600 msec and in 12 patients with a spin-echo sequence (TR = 400–1000 msec, TE = 25–40 msec). Two or more imaging planes were used in 34 of 40 patients. Images were obtained in the axial plane in 39 patients, while the coronal and sagittal planes were used in 31 and 5 patients, respectively.

* Monaghan Medical Corp., Plattsburg, NY.
† Picker 600/1200 scanner (Picker International, Highland Heights, OH).
‡ Picker International, Highland Heights, OH.

TABLE 1: Time Interval Between Head Trauma and CT and MR Scans

No. of Days	No. of Patients		
	Injury–MR Scan	First CT–MR Scan	Closest CT–MR Scan[a]
0	0	1	4
1	0	6	9
2–5	21	20	21
6–8	11	8	4
9–12	4	4	1
13–19	4	1	1

[a] The CT scan closest to the time of the MR scan.

TABLE 2: Classification and Frequency of Primary Traumatic Brain Lesions in 40 Patients

Type: Location	No. of Patients[a]	Total No. of Lesions
Intraaxial lesions:		
Diffuse axonal	34	149
Cortical contusion	31	135
Subcortical gray matter	8	14
Primary brainstem	10	11
Total	38	309
Extraaxial hematoma:		
Subdural	26	39
Epidural	3	3
Total	27	42
Diffuse hemorrhage:		
Subarachnoid	20	20
Intraventricular	11	11
Total	25	31

[a] Some of the 40 patients had more than one type of lesion.

The MR and CT scans were analyzed independently, and all visualized abnormalities were classified [42]. An attempt was made to differentiate between injuries resulting from the initial traumatic force (primary) and those arising from delayed posttraumatic (secondary) causes such as diffuse brain swelling, brain displacement and herniation, delayed hemorrhage, cerebral infarction, and diffuse hypoxic injury [42]. In many instances it was difficult to separate primary and secondary damage. For purposes of statistical analysis, however, all focal abnormalities that were not obviously secondary in nature were classified as primary lesions (Table 2). Primary intracranial lesions were classified as (1) intraaxial lesions; (2) extraaxial hematomas (subdural, epidural); and (3) diffuse hemorrhage (intraventricular, subarachnoid). Intraaxial lesions were subclassified as diffuse axonal injury (white-matter "shear" injury), cortical contusion, subcortical gray-matter injury, or primary brainstem injury. All intraaxial lesions were further separated into hemorrhagic and nonhemorrhagic subsets.

We used the following criteria to classify a lesion as hemorrhagic on MR. On T1-weighted images we required that the shortening of T1 by the paramagnetic properties of methemoglobin be of sufficient degree that the hematoma was at least partially hyperintense relative to white matter (Fig. 1). On T2-weighted images we required the

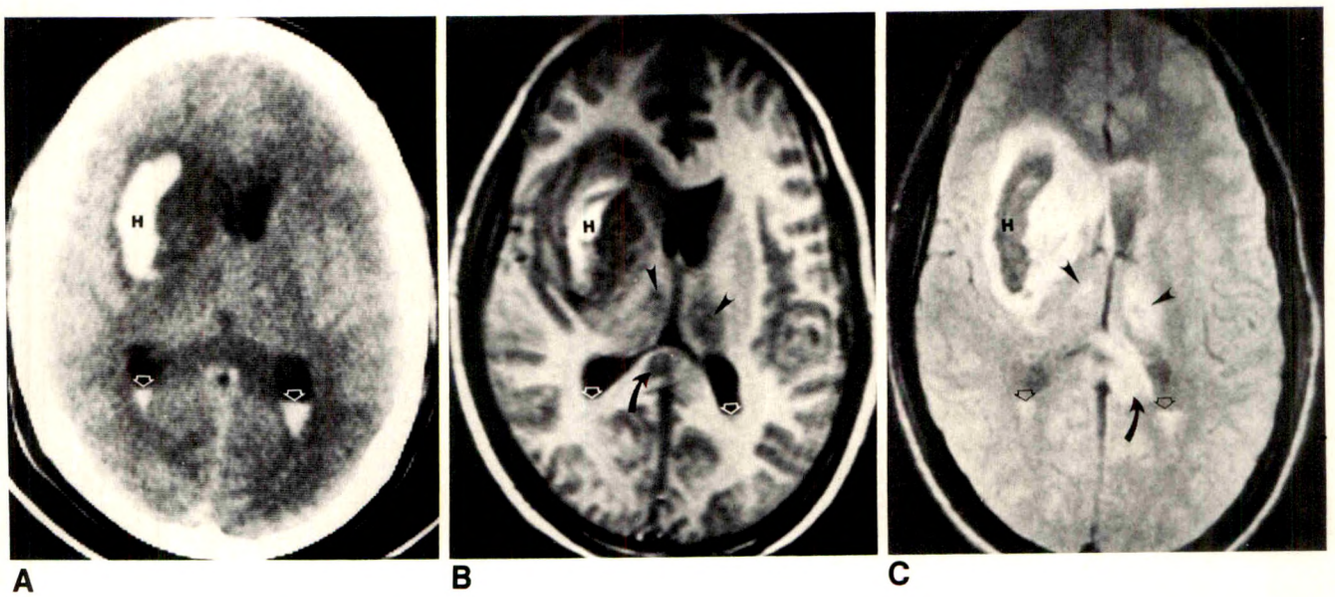

Fig. 1.—19-year-old man 2 days after head trauma.
***A*, Axial CT scan shows large basal ganglia intracerebral hematoma (H) with surrounding edema as well as intraventricular hemorrhage (*arrows*).**
***B*, and *C*, T1-weighted inversion-recovery (TR = 2100 msec, TI = 600 msec) (*B*) and T2-weighted spin-echo (TR = 2300 msec, TE = 80 msec) (*C*) scans confirm hematoma and intraventricular hemorrhage (*open arrows*). Large nonhemorrhagic diffuse axonal lesion is in splenium of corpus callosum (*curved arrows*), and bilateral subcortical gray matter lesions (*arrowheads*) are seen. Note.—Acute hematoma is hyperintense relative to brain parenchyma on T1-weighted image and hypointense on T2-weighted image. Intraventricular hemorrhage is hyperintense relative to CSF on T1- and T2-weighted scans and isointense relative to white matter on T1-weighted scan.**

presence of central hypointensity within the hematoma. As recently described by Gomori et al. [30], central hypointensity in acute hematomas appears to be secondary to preferential T2 proton relaxation enhancement caused by methemoglobin or deoxyhemoglobin within intact RBCs (Figs. 1 and 2).

After initial individual analysis, the CT and MR scans were compared and the total number of lesions in each category determined. Since autopsy confirmation of the lesions was only possible in one patient, we required that a lesion be seen on more than one study (CT, T1-weighted MR, T2-weighted MR) or imaging plane (axial, sagittal, coronal) to be regarded as a true traumatic lesion. Equivocal abnormalities seen on only one study or imaging plane were omitted from further analysis. The sensitivities of CT and MR were determined from the tabulated data. Separate calculations were made for each MR pulse sequence, imaging plane, and category of intraaxial and extraaxial lesion. The influence of hemorrhage on lesion detectability was also assessed.

Results

Intraaxial Lesions

The most common type of traumatic lesion identified in this series was diffuse axonal injury [21, 42–46]. These lesions have also been called shear lesions [3, 45] or diffuse damage to the white matter of the immediate-impact type [10, 13, 46]. These lesions typically were less than 1 cm in greatest dimension, spared the adjacent cortical surface of the brain, and were located entirely within white matter or at the gray-/white-matter interface. The vast majority (81.2%) of these lesions were nonhemorrhagic (Table 3). In the nonhemorrhagic subset there was a marked difference in the sensitivities of the three imaging studies. T2-weighted MR was most sensitive, detecting 92.4% of lesions. CT was very insensitive, detecting only 19% of lesions. Diffuse axonal lesions were typically seen by CT only if larger than 1.5 cm or located in the corona radiata or internal capsule. Small nonhemorrhagic lesions in other locations were rarely seen by CT (Figs. 2 and 3). T1-weighted MR was also more sensitive (72.3%) than CT (19.0%) but less sensitive than T2-weighted MR. For the hemorrhagic subset, the sensitivities of all three imaging methods were quite high and very similar (T2-weighted MR, 91.3%; T1-weighted MR, 86.2%; CT, 85.7%) (Table 3).

The second most common type of traumatic lesion seen in our series was that involving the cortical surface of the brain (cortical contusion) [13, 43]. These lesions were usually much larger than diffuse axonal lesions, often being 2–4 cm in greatest dimension (Figs. 4–6). By definition, they were primarily localized to the cortical surface of the brain with relative sparing of the underlying white matter. There was a great tendency for confluence of the lesions and associated hemorrhage. Hemorrhage was detected in 51.8% of cortical contusions in this series (Table 3). All three imaging methods were very sensitive in the detection of hemorrhagic cortical contusions (T2-weighted MR, 92.4%; T1-weighted MR, 87.5%; CT, 91.4%). The true size of the lesion (hemorrhagic and nonhemorrhagic components), however, was usually underestimated by both CT and T1-weighted MR (Figs. 4–6).

T2-weighted MR was significantly more sensitive (95.0%) in the detection of nonhemorrhagic cortical contusions than was T1-weighted MR (58.3%) or CT (15.4%) (Figs. 4–6). In some instances a lesion could be indirectly suspected on CT

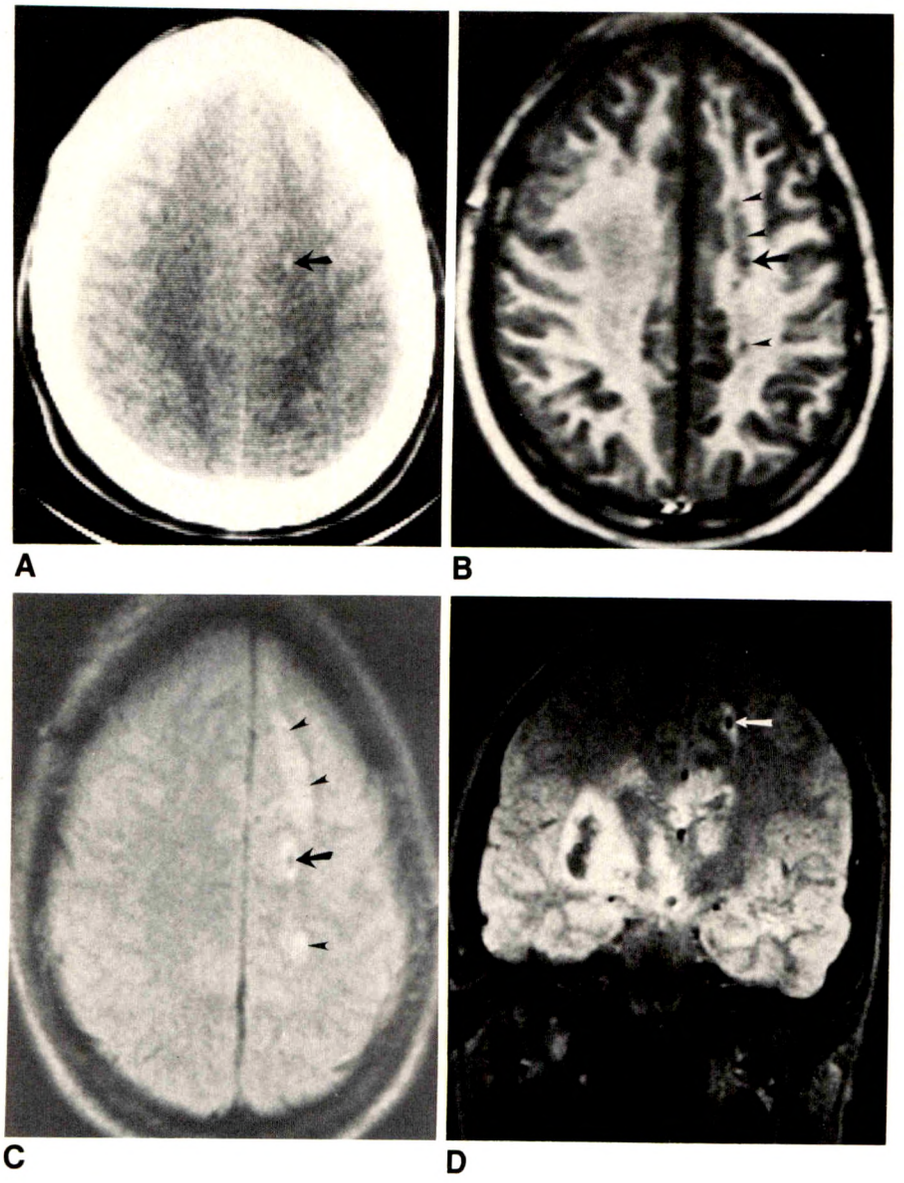

Fig. 2.—19-year-old man.

***A*, Axial CT scan 1 day after head trauma shows very subtle 0.5-cm hemorrhagic lesion (*arrow*) consistent with diffuse axonal injury in deep white matter.**

***B–D*, Axial T1-weighted inversion-recovery MR image (TR = 2100 msec, TI = 600 msec) (*B*), axial T2-weighted spin-echo MR image (TR = 2300 msec, TE = 80 msec) (*C*), and coronal T2-weighted spin-echo MR image (TR = 2300 msec, TE = 80 msec) (*D*) 2 days after head trauma confirm hemorrhagic diffuse axonal lesion (*arrows*) as well as multiple other nonhemorrhagic diffuse axonal lesions (*arrowheads*).**

The presence of acute hemorrhage is indicated on T2-weighted images (*C* and *D*) by central hypointensity (*arrows*). Note that the small hemorrhage is not hyperintense 2 days after trauma on T1-weighted image, as methemoglobin has not yet formed (*D*). Also present are multiple other hemorrhagic and nonhemorrhagic lesions.

scans by local mass effect (ventricular or sulcal effacement), but the lesion itself was often not apparent. This was because the contrast between the normal and injured cortex was typically very low on CT scans. The relative insensitivity of T1-weighted MR was from very low contrast differences between normal cortex; surrounding CSF; and edematous, contused cortex (Fig. 5). The T1-weighted spin-echo images were slightly more sensitive than inversion-recovery images in lesion detection, although the latter were superior for anatomic delineation.

Only 14 lesions were confined entirely to the subcortical gray matter. These involved the thalamus and lentiform nucleus (Fig. 1) and were similarly distributed between the hemorrhagic and nonhemorrhagic subsets (Table 4). The pattern of sensitivities for this small but clinically important [13, 44] number of lesions was similar to that for diffuse axonal injury and cortical contusion. Hemorrhagic lesions were detected accurately by all three examinations, while nonhemorrhagic lesions were poorly visualized with CT.

Eleven brainstem lesions, thought to be primary lesions, were identified in 10 patients. All but one of the lesions were initially detected with MR. The lesion that was not seen initially by MR was identified retrospectively. T1- and T2-weighted images were similarly sensitive, detecting nine and eight lesions, respectively (Table 4). CT identified only one (hemorrhagic) brainstem lesion.

Extraaxial Hematomas

Thirty-nine subdural hematomas were identified in 26 patients. Thirty were supratentorial and located along the convexity, eight were interhemispheric or along the tentorium,

TABLE 3: Sensitivities of CT and MR in the Detection of Cortical Contusions and Diffuse Axonal Injury

Lesion: Study	True Positive/Total = % Sensitivity		
	Diffuse Axonal Injury (n = 149)	Cortical Contusion (n = 135)	Total (n = 284)
Nonhemorrhagic	n = 121	n = 65	n = 186
CT	23/121 = 19	10/65 = 15.4	33/186 = 17.7
T1-weighted MR:			
Axial	53/68 = 77.9	21/38 = 55.3	75/106 = 69.8
Coronal	33/51 = 64.7	14/22 = 63.6	47/73 = 64.4
Both views	86/119 = 72.3	35/60 = 58.3	121/179 = 67.6
T2-weighted MR:			
Axial	114/121 = 94.2	62/65 = 95.4	176/186 = 94.6
Coronal	43/49 = 87.8	33/35 = 94.3	76/84 = 90.5
Both views	157/170 = 92.4	95/100 = 95	252/270 = 93.3
Hemorrhagic:	n = 28	n = 70	n = 98
CT	24/28 = 85.7	64/70 = 91.4	88/98 = 89.8
T1-weighted MR:			
Axial	18/22 = 81.8	39/43 = 90.7	57/65 = 87.7
Coronal	7/7 = 100	24/29 = 82.8	31/36 = 86.1
Both views	25/29 = 86.2	63/72 = 87.5	88/101 = 87.1
T2-weighted MR:			
Axial	26/28 = 92.9	65/70 = 92.9	91/98 = 92.9
Coronal	16/18 = 88.9	32/35 = 91.4	48/53 = 90.6
Both views	42/46 = 91.3	97/105 = 92.4	139/151 = 92.5

Note.—Some totals are greater than the number of lesions because more than one scan plane was used for some T1- and T2-weighted pulse sequences.

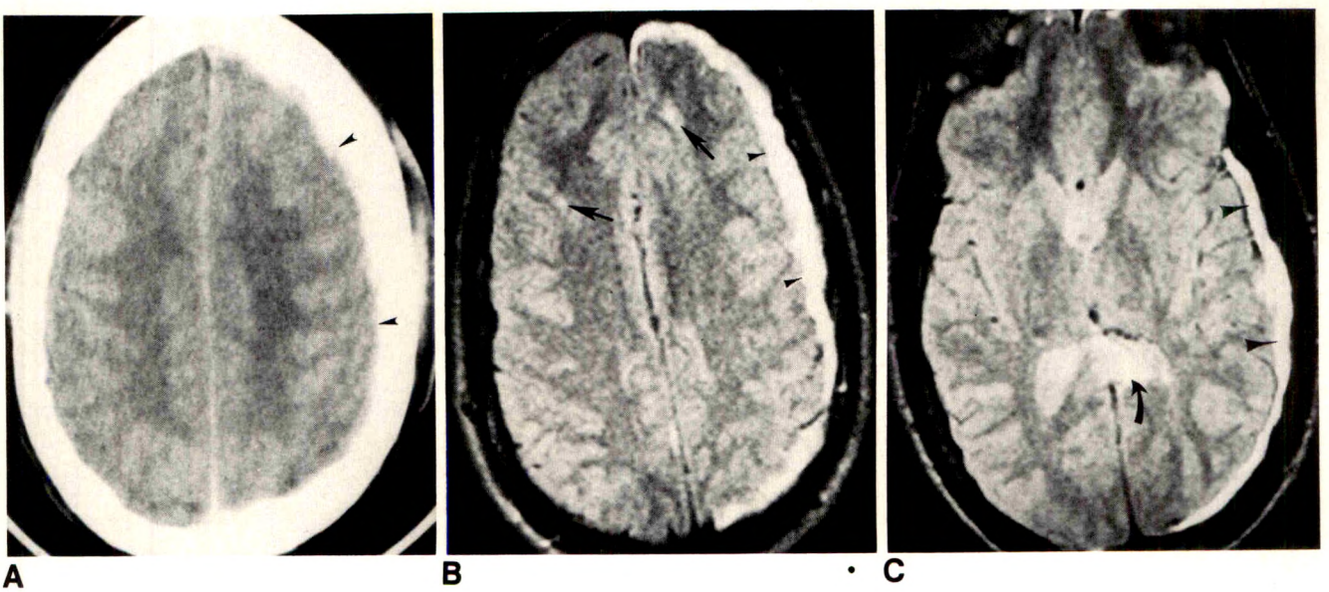

Fig. 3.—18-year-old man.
***A*, Axial CT scan 1 day after cranial trauma appears normal except for very subtle subdural hematoma (*arrowheads*).**
***B* and *C*, T2-weighted spin-echo MR images (TR = 2300 msec, TE = 80 msec) 9 days after trauma. Subdural hematoma (*arrowheads*) is more easily appreciated on MR. Also present are focal nonhemorrhagic diffuse axonal lesions at gray-/white-matter interface (*straight arrows*) of frontal lobe and in splenium of corpus collasum (*curved arrow*), not apparent on CT.**

and one was infratentorial. T1-weighted MR identified all but one (97.4%) 2-mm interhemispheric lesion that was isointense relative to adjacent brain parenchyma. T2-weighted MR identified 89.7% of the subdural lesions, missing four isointense lesions that were less than 3 mm thick. All lesions missed by T2-weighted MR, however, were hyperintense on T1-weighted MR and easily visible.

Only 27 (71.1%) of 38 subdural hematomas were detected

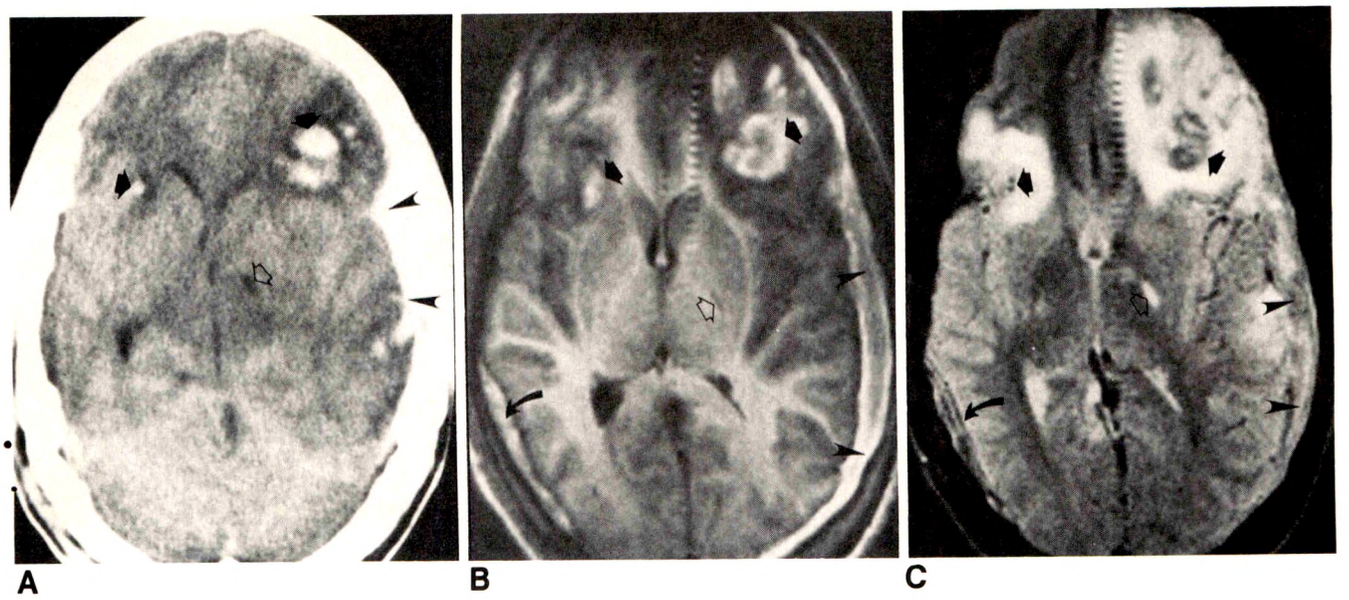

Fig. 4.—17-year-old man.

A, Axial CT scan 1 day after cranial trauma reveals left subdural hematoma (*arrowheads*), bilateral hemorrhagic cortical contusions of inferior aspects of frontal lobes (*solid arrows*), and nonhemorrhagic diffuse axonal lesion of internal capsule (*open arrow*).

B and *C*, T1-weighted inversion-recovery MR image (TR = 2100 msec, TI = 600 msec) (*B*) and T2-weighted spin-echo MR image (TR = 2300 msec, TE = 80 msec) (*C*) 5 days after trauma confirm left subdural (*arrowheads*) and small right subdural (*curved arrows*) hematomas. Bifrontal hemorrhagic cortical contusions (*straight solid arrows*) and nonhemorrhagic diffuse axonal internal capsule lesion (*open arrows*) are also seen. Extent of contusions is seen more clearly on T2-weighted scan. Also note hyperintensity of acute subdural hematoma on T1-weighted image but relative isointensity on T2-weighted image.

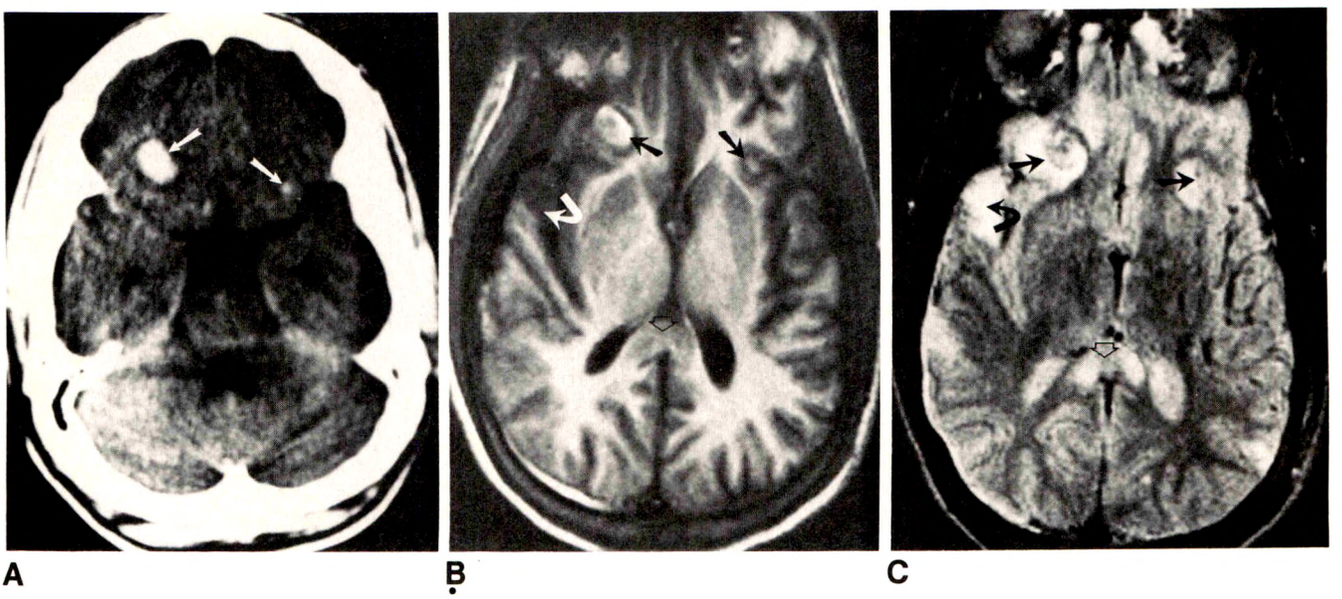

Fig. 5.—25-year-old man.

A, Axial CT scan 1 day after cranial trauma reveals bifrontal hemorrhagic contusions (*arrows*).

B and *C*, T1-weighted inversion-recovery MR image (TR = 2100 msec, TI = 600 msec) (*B*) and T2-weighted spin-echo MR image (TR = 2300 msec, TE = 80 msec) (*C*) 5 days after trauma confirm bifrontal hemorrhagic contusions (*straight solid arrows*). There is also a nonhemorrhagic contusion of temporal lobe (*curved arrows*) and nonhemorrhagic diffuse axonal lesion in corpus callosum (*open arrows*). On T1-weighted image, note low level of contrast between edematous and normal temporal lobe cortex (*curved arrow*).

on the initial CT scan. All of the 11 subdural hematomas that were missed by CT were considered clinically insignificant. Only one of 11 missed subdural hematomas was more than 5 mm thick; most were 1–3 mm. Five of these 11 subdural hematomas were visualized retrospectively when CT scans were compared with MR scans. One large hematoma (14 mm) had obviously developed between the initial CT and MR examinations and was excluded from statistical consideration.

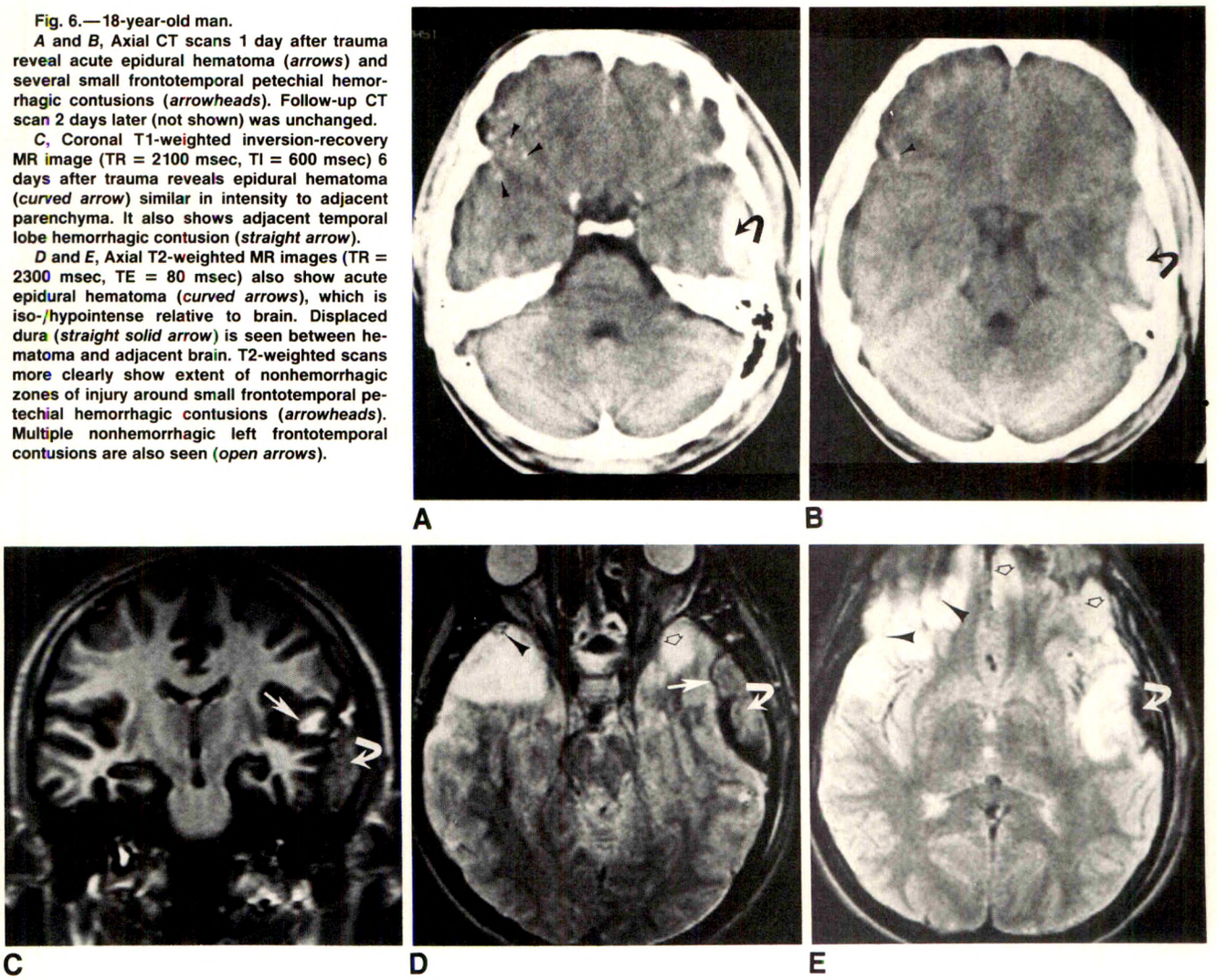

Fig. 6.—18-year-old man.

***A* and *B*, Axial CT scans 1 day after trauma reveal acute epidural hematoma (*arrows*) and several small frontotemporal petechial hemorrhagic contusions (*arrowheads*). Follow-up CT scan 2 days later (not shown) was unchanged.**

***C*, Coronal T1-weighted inversion-recovery MR image (TR = 2100 msec, TI = 600 msec) 6 days after trauma reveals epidural hematoma (*curved arrow*) similar in intensity to adjacent parenchyma. It also shows adjacent temporal lobe hemorrhagic contusion (*straight arrow*).**

***D* and *E*, Axial T2-weighted MR images (TR = 2300 msec, TE = 80 msec) also show acute epidural hematoma (*curved arrows*), which is iso-/hypointense relative to brain. Displaced dura (*straight solid arrow*) is seen between hematoma and adjacent brain. T2-weighted scans more clearly show extent of nonhemorrhagic zones of injury around small frontotemporal petechial hemorrhagic contusions (*arrowheads*). Multiple nonhemorrhagic left frontotemporal contusions are also seen (*open arrows*).**

TABLE 4: Relative Sensitivities of CT and MR in the Detection of Primary Brainstem and Subcortical Gray-Matter Lesions

Type of Lesion	No.	True Positive/Total = % Sensitivity		
		CT	T1-Weighted MR	T2-Weighted MR
Primary brainstem	11	1/11 = 9.1	9/11 = 81.8	8/11 = 72.7
Subcortical gray	14	8/14 = 57.1	10/14 = 71.4	14/14 = 100.0

All three epidural hematomas identified in this series were larger than 5 mm in thickness and were readily seen by CT and T1- and T2-weighted MR (Fig. 6).

Diffuse Hemorrhage

In 20 patients there was enough subarachnoid blood after trauma to be recognizable on CT. In seven instances only a small amount of blood was present adjacent to a hemorrhagic cortical contusion. The blood was diffuse in 10 cases, localized to the sylvian fissure in two instances, and confined to the interpeduncular cistern in one patient. T2-weighted MR detected only those three focal clots within the sylvian and interpeduncular cisterns. We did not identify any subarachnoid clots with T1-weighted MR scans in this series.

Eleven of 40 patients had evidence of intraventricular hemorrhage. The majority of the patients had only a trace of blood and it was limited to the occipital horns, although in one case blood was also present in the third ventricle. Intraventricular hemorrhage was seen with T2-weighted MR in all 11 instances, with CT in nine cases, and with T1-weighted MR in five of seven patients whose scans included the region in which the blood was localized. In four patients, coronal T1-weighted scans were not obtained through the occipital horns. Intraventricular hemorrhage was always visualized on T2-weighted spin-echo scans (TR = 2300 msec, TE = 80 msec)

as an area of hyperintensity within the dependent portion of the occipital horns (Fig. 1). On T1-weighted inversion-recovery scans (TR = 2100 msec, TI = 600 msec), the blood was always hyperintense relative to CSF and, depending on its age, either iso- or hyperintense relative to white matter.

Discussion

The best diagnostic imaging test for the evaluation of traumatic brain injury should possess a number of characteristics. It should be highly sensitive and specific, provide useful anatomic information for guiding therapeutic intervention, allow classification of the type of injury, offer accurate prognostic information, and be easily and safely performed in severely injured patients. In the last decade CT revolutionized the care of patients with closed head trauma because it represented a significant improvement over previous diagnostic methods [1–9]. Despite its significant contribution to the management of closed head trauma, CT suffers from a number of diagnostic limitations. Numerous authors have noted a marked discrepancy between the clinical severity of injury and the CT findings in the acute setting [9–15, 34]. CT findings often correlate poorly with focal neurologic deficits, as well as with more global indicators of cerebral injury such as intracranial pressure and level of consciousness. Autopsy and histopathologic studies confirm the relative insensitivity of CT to many forms of neural injury [13, 16, 43, 44, 46]. The primary deficiency of CT is its insensitivity to small nonhemorrhagic lesions (Table 3). These lesions are difficult to discern because the difference in X-ray attenuation between normal and injured brain is small, resulting in a low level of contrast between these tissues (Figs. 1, 2, and 6). Since many nonhemorrhagic lesions are not detected, therapeutic decisions must be made without complete delineation of the extent of injury. Previously, CT has been used mainly to diagnose "surgical" lesions. Choosing proper "medical" therapy and judging the prognosis of recovery has been primarily based on the clinical manifestations of injury (GCS, intracranial pressure, neurologic examination) [34, 37].

Early experience with MR suggested that it might be more sensitive than CT in detecting some types of traumatic lesions [23–39]. Our prospective study has confirmed that MR is more sensitive than CT for detecting all types of traumatic lesions, with the exception of subarachnoid hemorrhage. Although the difference in sensitivity was minimal for the hemorrhagic lesions, there was a great discrepancy for nonhemorrhagic intraaxial lesions. An increased sensitivity might be expected with MR, since differentiation of normal and injured tissues with this technique depends on several imaging parameters. Lesion contrast is influenced by relative differences in the T1 and T2 relaxation times of the tissues as well as the proton density [23–25, 29–35]. The superior sensitivity of MR for nonhemorrhagic lesions is most likely from its greater ability to detect local alterations of water in injured tissues. Neural injury, like most pathologic processes, is invariably accompanied by changes in the local water environment [43]. Intracellular edema may accompany trauma-induced alterations of cellular metabolism from hypoxia or hypoxemia. Extracellular edema may be produced by disruption of the blood-brain barrier or as a result of direct injury to the axons (axoplasmic leakage) [43].

MR was also superior in the detection of extraaxial hematomas, although the difference was less striking. The only lesions typically missed by CT were very small, clinically silent subdural hematomas usually less than 3 mm in thickness. These small, high-density lesions were very hard to distinguish from adjacent bone on CT scans obtained at standard window settings (Figs. 3 and 4). They were easily seen, however, with either T1- or T2-weighted MR scans as high-intensity lesions adjacent to the signal void of cortical bone. Since both the CT and MR scans were analyzed without the benefit of optimizing the image contrast on the monitor, this factor does not bias against CT. Rather, the wider latitude of contrast differences between the hematoma and adjacent structures was responsible for MR's greater sensitivity. The sensitivities of CT and MR were similar for intraventricular hemorrhage. We concur with others, however, that CT has a significant advantage over MR in the detection of acute/subacute subarachnoid blood [32, 37]. Visualization of subarachnoid hemorrhage with MR was difficult in the acute phase unless it was a large, localized clot.

There are a number of methodologic observations concerning this study that should be emphasized when comparing the relative sensitivities of MR and CT. Owing to medical and logistic reasons, the CT and MR scans could not usually be obtained on the same day. CT was usually performed first, so that therapeutic decisions could be made on the basis of a proven diagnostic method. MR was performed only after the patient was considered stable, usually resulting in a delay between CT and MR of zero to 10 days. For this reason it is possible that some traumatic lesions became more apparent over time, thus improving the sensitivity of MR. Although this factor may have been operative, it cannot be the sole explanation for the vast differences in the sensitivities of the two methods. To test the importance of this factor, we also compared the sensitivities of initial or follow-up MR or CT scans obtained within 1 day of each other (Table 5). The sensitivities in the 13 patients in this subgroup were (1) nonhemorrhagic parenchymal lesions (CT, 26.8%; T1-weighted MR, 61.1%; T2-weighted MR, 100%) and (2) hemorrhagic parenchymal lesions (CT, 84.8%; T1-weighted MR, 80.6%; T2-weighted MR, 90.9%). Although a few more nonhemorrhagic lesions were detected on the follow-up CT scans, more small hemorrhagic lesions were missed.

Because the MR scans were usually obtained after the CT scans, the possibility also exists that the MR examinations were "tailored," thus improving the MR sensitivity. This is not apparent to us from looking at our data, since a "routine" MR examination consisted of both a T1- and T2-weighted study, usually in at least two planes. In no instance was the slice thickness for the MR scans smaller than that for CT. The CT scans generally were not available to the MR examiner before the MR study.

It is also possible that the additional lesions seen with MR resulted from interval development of new (secondary) lesions. Previous authors have shown that, in up to 19% of patients whose clinical condition deteriorates after trauma, delayed hematomas will be evident [22]. In those patients in our series, however, who were restudied with CT for intervening neurologic deterioration, no delayed intraaxial hematomas were detected. It is apparent also that the discrepancy in sensitivity was in the nonhemorrhagic subset of lesions rather than the hemorrhagic lesions. It is possible that other intervening nonhemorrhagic secondary forms of injury (infarction, hypoxia, pressure necrosis, etc.) could explain the ad-

TABLE 5: Sensitivities of CT and MR in 13 Patients in Whom the Studies Were Performed 1 Day Apart

Type of Lesion	True Positive/Total = % Sensitivity		
	CT	T1-Weighted MR	T2-Weighted MR
Subdural/epidural	14/16 = 87.5	16/16 = 100.0	16/16 = 100.0
Parenchymal			
Nonhemorrhagic	11/41 = 26.8	22/36 = 61.1	41/41 = 100.0
Hemorrhagic	28/33 = 84.8	25/31 = 80.6	30/33 = 90.9
Total	39/74 = 52.7	47/67 = 70.1	71/74 = 95.9

Note.—Interval from injury to MR examination: mean = 6.6 days, range = 2–19 days.

ditional lesions seen by MR [43]. This seems unlikely in view of the data in Table 5 and because the clinical course of the patients was one of improvement rather than deterioration. Thus, it seems clear to us and in agreement with others [34, 37, 39] that MR is truly much more sensitive than CT in detecting traumatic lesions.

Early reports suggested that low- and intermediate-field-strength MR systems would be less sensitive for detecting acute hemorrhage [30]. The low signal intensity within acute hematomas on T2-weighted MR scans is thought to be from a heterogeneity of magnetic susceptibility caused by intracellular deoxyhemoglobin or methemoglobin. It is directly proportional to the square of the main magnetic field [30]. The difference in the magnetic susceptibility effects between a 0.5- and 1.5-T system should differ by approximately one magnitude. It is expected, therefore, that the hypointensity of acute hematomas at 0.5 T would be significantly less than at 1.5 T. We found this to be true, although the effect was still adequate enough at 0.5 T to detect acute hematomas as accurately as CT did in the first 4 days after trauma (Table 3). The intraparenchymal hematomas were always surrounded by peripheral halos of edema. This always aided in contrasting the central hypointensity of the hematomas with adjacent normal brain parenchyma. Although there are distinct theoretical advantages of higher magnetic fields for detection of acute hemorrhage, we believe that this is of lesser practical significance in the clinical imaging of patients. We believe that our data support the fact that acute hematomas can be accurately imaged in the first 4 days after trauma with an intermediate-field-strength system with strongly T2-weighted spin-echo pulse sequences (TR = 2300 msec, TE = 80–120 msec). Others have also reported visualization of central hypointensity in acute hematomas with intermediate-field-strength MR systems [32, 33, 47]. Recently, Edelman et al. [33] have also shown that it is possible to maximize the differences in magnetic susceptibility at intermediate and low field strengths. By using small radiofrequency pulse angles and gradient-recalled echoes, they have shown that acute hematomas can be detected easily at these field strengths.

The specificity of MR (and CT) in lesion characterization is difficult to determine from our study since surgical and pathologic confirmation of the lesions was not possible in the vast majority of patients. Two large intracerebral hematomas were surgically confirmed in two patients. Four extraaxial hematomas were surgically confirmed in four patients, and bilateral subdural hematomas were confirmed at autopsy in one patient. The other lesions in this series remain pathologically unsubstantiated but closely resemble the primary traumatic lesions described in many autopsy series in their location, size, distribution, and character [10, 13, 42–46]. The possibility should be considered that a few of the lesions that were detected by MR and CT were preexisting nontraumatic lesions (demyelinating disease, subcortical arteriosclerotic encephalopathy, infarcts, etc.) It is doubtful, however, that preexisting disease could explain the vast majority of lesions seen in this series. The clinical histories did not reveal any patients with prior neurologic symptoms compatible with demyelinating disease or stroke. The mean age of the study population was only 26.6 years, and only 12.5% of patients were more than 40 years old, making it unlikely that vascular disease could account for any significant percentage of the lesions. Only one of the five patients older than 40 had a history of hypertension and vascular disease. Five subcortical lesions were found in this patient, and they were considered to be of indeterminate cause, compatible with either diffuse axonal injury or lacunar infarcts. These lesions were therefore excluded from statistical analysis. One of the five patients older than 40 had a normal MR scan, and in the three remaining patients the lesions were not suggestive of vascular disease.

MR also appears to be greatly superior to CT in its ability to precisely localize a lesion for purposes of classification. As Gennarelli [14] and others [20, 37, 43, 44, 46] have pointed out, it is important to accurately classify the various traumatic lesions since the prognosis, frequency of secondary complications, mechanism of injury, and therapeutic management may be quite different. MR is advantageous because direct multiplanar images allow a more precise localization of the lesion. Multiplanar images also provide a better three-dimensional view of the lesion, helping to separate primary from secondary forms of injury [42].

Our report indicates that MR is not only useful in patients with closed head trauma but that it is also quite feasible. Evaluation of respirator-dependent patients is more problematic with MR than with CT. A ventilatory system should be used that does not contain ferromagnetic materials, and close monitoring of patient's ventilation is required [41]. Monitoring of other vital systems is also more difficult than with CT scanning, but is also feasible [41]. Imaging mechanically ventilated patients was often advantageous, however, since agitated or combative patients could be pharmacologically paralyzed to eliminate motion artifacts.

Our study agrees with those of others who suggest that MR is valuable for detecting and characterizing traumatic lesions [23–37]. Most of these reports, however, were retrospective studies of patients with minimal intracranial injuries, subdural hematomas without intraparenchymal lesions, or studies of patients with a mixture of acute and chronic head injuries. Our study constitutes the first large prospective study comparing CT with intermediate-field-strength MR for detecting traumatic lesions in patients with moderate to severe acute closed head trauma. When using a 0.5-T system, our

conclusions are similar to those of Zimmerman et al. [34] in their retrospective study with a 1.5-T system. We agree that MR is significantly more sensitive than CT in the detection of acute and subacute nonhemorrhagic parenchymal lesions, small acute subdural lesions, subacute subdural lesions, subacute hemorrhagic lesions, brainstem injuries, and infarcts.

In summary, MR has significant advantages over CT in evaluating patients with closed head trauma. MR is similar in sensitivity to CT for detecting hemorrhagic lesions but vastly superior to CT in detecting the much more prevalent nonhemorrhagic lesions. MR is also more useful than CT for characterizing and classifying primary and secondary forms of injury [42]. More accurate detection and delineation of traumatic lesions with MR should permit more accurate prediction of neurologic and cognitive recovery and assist in optimizing "medical" forms of treatment. Because a more rapid assessment of "surgical" lesions can be made with CT, it is still of prime importance for the initial evaluation of unstable patients with head injuries.

REFERENCES

1. Zimmerman RD, Danziger A. Extracerebral trauma. *Radiol Clin North Am* **1982**;20:105–121
2. Hryshko FG, Deeb ZL. Computed tomography in acute head injuries. *J Comput Tomogr* **1983**;7:331–334
3. Zimmerman RA, Bilaniuk LT, Gennarelli T. Computed tomography of shearing injuries of the cerebral white matter. *Radiology* **1978**;127:393–396
4. Zimmerman RA, Bilaniuk LT, Bruce D, Dolinskas C, Obrist W, Kuhl D. Computed tomography of pediatric head trauma: acute general cerebral swelling. *Radiology* **1978**;126:403–408
5. French BN, Dublin AB. The value of computerized tomography in the management of 1000 consecutive head injuries. *Surg Neurol* **1977**;7:171–183
6. Moseley IF, Zilkha E. The role of computerized axial tomography (EMI-scanning) in the diagnosis and management of craniocerebral trauma. *J Neuroradiol* **1976**;3:277–296
7. Bricolo A, Pasut ML. Extradural hematoma toward zero mortality. A prospective study. *Neurosurgery* **1984**;14:8–12
8. Seelig JM, Becker DP, Miller JD, Greenberg RP, Ward JD, Choi SC. Traumatic acute subdural hematoma. Major mortality reduction in comatose patients treated within four hours. *N Engl J Med* **1981**;304:1511–1518
9. Lanksch W, Grumme T, Kazner E. Correlations between clinical symptoms and computerized tomography findings in closed head injuries. In: Frowein RS, Wilcke D, Karimi-Nejad A, Brock M, Klinger M, eds. *Advances in neurosurgery. Vol 5: Head injuries. Tumors of the cerebellar region*. Berlin: Springer-Verlag, **1978**:27–29
10. Snoek J, Jennett B, Adams JH, Graham DI, Doyle D. Computerized tomography after recent severe head injury in patients without acute intracranial hematoma. *J Neurol Neurosurg Psychiatry* **1979**;42:215–225
11. Perrone P, Porazzi D, Ricotta E, Secchi P, Rovetta P. Brain contusion in minor cranial trauma. *Ital J Neurol Sci* **1985**;6:43–45
12. Bruce DA, Schut L, Bruno LA, Wood J, Sutton LN. Outcome following severe head injuries in children. *J Neurosurg* **1978**;48:679–688
13. Adams JH, Graham DI, Scott G, Parker L, Doyle D. Brain damage in fatal non-missile head injury. *J Clin Pathol* **1980**;33:1132–1145
14. Gennarelli TA, Spielman GM, Langfitt TW, et al. Influence of the type of intracranial lesion on outcome from severe head injury. *J Neurosurg* **1982**;56:26–32
15. Bruce DA, Alavi A, Bilaniuk L, Dolinskas C, Obrist W, Uzzell B. Diffuse cerebral swelling following head injuries in children: the syndrome of "malignant brain edema." *J Neurosurg* **1981**;54:170–178
16. Cooper PR, Maravilla K, Kirkpatrick J, et al. Traumatically induced brainstem hemorrhage and the computerized tomographic scan: clinical, pathological and experimental observations. *Neurosurgery* **1979**;4:115–124
17. Sweet RC, Miller JD, Lipper M, Kishore PRS, Becker DP. Significance of bilateral abnormalities on the CT scan in patients with severe head injury. *Neurosurgery* **1978**;3:16–21
18. Tsai FY, Huprich JE, Gardner FC, Segar HD, Teal JS. Diagnostic and prognostic implications of computed tomography of head trauma. *J Comput Assist Tomogr* **1978**;2:323–331
19. Tsai FY, Teal JS, Quinn MF, et al: CT of brainstem injury. *AJNR* **1980**;1:23–29, *AJR* **1980**;134:717–723
20. Lipper MH, Kishore PRS, Enas GG, Domingues da Silva AA, Choi SC, Becker DP. Computed tomography in the prediction of outcome in head injury. *AJNR* **1985**;6:7–10, *AJR* **1985**;144:483–486
21. Lobato RD, Cordobes F, Rivas JJ, et al. Outcome from severe head injury related to the type of intracranial lesion: a computerized tomography study. *J Neurosurg* **1983**;59:762–774
22. Clifton GL, Grossman RG, Makela ME, Miner ME, Handel S, Sadhu V. Neurological course and correlated computerized tomography findings after severe closed head injury. *J Neurosurg* **1980**;52:611–624
23. Young IR, Bydder GM, Hall AS, et al. Extracerebral collections: recognition by NMR imaging. *AJNR* **1983**;4:833–834
24. Sipponen JT, Sepponen RE, Sivula A. Chronic subdural hematoma: demonstration by magnetic resonance. *Radiology* **1984**;150:79–85
25. Moon Jr KL, Brant-Zawadzki M, Pitts LH, Mills CM. Nuclear magnetic resonance imaging of CT-isodense subdural hematomas. *AJNR* **1984**;5:319–322
26. Levin HS, Handel SF, Goldman AM, Eisenberg HM, Guinto FC. Magnetic resonance imaging after "diffuse" nonmissile head injury. *Arch Neurol* **1985**;42:963–968
27. Zimmerman RA, Bilaniuk LT, Grossman RI, et al: Resistive NMR of intracranial hematomas. *Neuroradiology* **1985**;27:16–20
28. Sipponen JT, Sepponen RE, Tanttu JI, Sivula A. Intracranial hematomas studied by MR imaging at 0.17 and 0.02 T. *J Comput Asisst Tomogr* **1985**;9:698–704
29. Sipponen JT, Sepponen RE, Sivula A. Nuclear magnetic resonance (NMR) imaging of intracerebral hemorrhage in the acute and resolving phases. *J Comput Assist Tomogr* **1983**;7:954–959
30. Gomori JM, Grossman RI, Goldberg HI, Zimmerman RA, Bilaniuk LT. Intracranial hematomas: imaging by high-field MR. *Radiology* **1985**;157:87–93
31. Dooms GC, Uske A, Brant-Zawadzki M, et al. Spin-echo MR imaging of intracranial hemorrhage. *Neuroradiology* **1986**;28:132–138
32. DeLaPaz RL, New PFJ, Buonanno FS, et al. NMR imaging of intracranial hemorrhage. *J Comput Assist Tomogr* **1984**;8:599–607
33. Edelman RR, Johnson K, Buxon R, Shoukimas G, et al. MR of hemorrhage: a new approach. *AJNR* **1986**;7:751–756
34. Zimmerman RA, Bilaniuk LT, Hackney DB, Goldberg HI, Grossman RI. Head injury: early results comparing CT and high-field MR. *ANJR* **1986**;7:757–764, *AJR* **1986**;147:1215–1222
35. Langfitt TW, Obrist WD, Alavi A, et al. Computerized tomography, magnetic resonance imaging, and positron emission tomography in the study of brain trauma. Preliminary observations. *J Neurosurg* **1986**;64:760–767
36. Gandy SE, Snow RB, Zimmerman RD, Deck MDF. Cranial nuclear magnetic resonance imaging in head trauma. *Ann Neurol* **1984**;16:254–257
37. Snow RB, Zimmerman RD, Gandy SE, Deck MDF. Comparison of magnetic resonance imaging and computed tomography in the elvaluation of head injury. *Neurosurgery* **1986**;18:45–52
38. Hans JS, Kaufman B, Alfidi RJ. Head trauma evaluated by magnetic resonance and computed tomography: a comparison. *Radiology* **1984**;150:71–77
39. Jenkins A, Teasdale, G, Hadley MDM, MacPherson P, Rowan JO. Brain lesions detected by magnetic resonance in mild and severe head injuries. *Lancet* **1986**;2(8504):445–446
40. Teasdale G, Jennett B. Assessment of coma and impaired consciousness. A practical scale. *Lancet* **1974**;2:81–84
41. Dunn VD, Ely-Coffman C, McGowan JE, Ehrhardt JC. Mechanical ventilation during magnetic resonance imaging. *Magnetic Resonance Imag* **1985**;3:169–172
42. Gentry LR, Godersky JC, Thompson B. MR imaging of head trauma: review of the distribution and radiopathologic features of traumatic lesions. *AJNR* **1988**;9:101–110
43. Adams JH, Gennarelli TA, Graham DI. Brain damage in non-missile head injury: observations in man and subhuman primates. In: Smith WT, Cavanagh JB, eds. *Recent advances in neuropathology,* vol 2. Edinburgh: Churchill Livingston, **1982**:165–190
44. Adams JH, Graham DI, Murray LS, Scott G. Diffuse axonal injury due to non-missile head injury in humans: an analysis of 45 cases. *Ann Neurol* **1982**;12:557–563
45. Strich SJ, Shearing of nerve fibers as a cause of brain damage due to head injury: a pathological study of twenty cases. *Lancet* **1961**;2:443–448
46. Adams JH, Mitchell DE, Graham DI, Doyle D. Diffuse brain damage of immediate impact type: its relationship to primary brainstem damage in head injury. *Brain* **1977**;100:489–502
47. Zimmerman RD, Deck MDF. Intracranial hematomas imaged by high-field MR (letter). *Radiology* **1986**;159:565

Gradient Echo (GRASS) MR Imaging in Cervical Radiculopathy

Mary C. Hedberg[1]
Burton P. Drayer
Richard A. Flom
John A. Hodak
C. Roger Bird

Limited flip angle (LFA), gradient echo imaging was performed in 130 patients for evaluation of cervical radicular complaints. The LFA study was compared with myelography, CT myelography, and surgical results. Image quality was considered good or excellent for 128 patients. The use of a 10° flip angle with a TR of 75 msec and TE of 12.3 msec consistently provided good contrast and signal-to-noise ratio, giving a CT myelographic effect. The use of both axial and sagittal LFA images was important for optimal detection of extradural defects and for distinction of herniated disk versus osteophyte. There was excellent correlation between the MR and surgical findings.

Our results suggest that MR imaging is the initial procedure of choice for the evaluation of suspected cervical radiculopathy.

Myelography and CT have been the standard methods for demonstrating degenerative spondylosis and herniated disks. The complications and patient discomfort inherent in intrathecal injection of contrast medium and subsequent imaging are well established [1–7]. MR imaging of the cervical spine is being used with increasing frequency to study these patients [8–11]. In most patients with clinically significant findings, however, myelography and CT are often performed after MR imaging and before surgery. New limited flip angle (LFA) MR imaging techniques in such patients may obviate the need for myelography and CT in making a diagnosis and meticulously delineating anatomy preoperatively [12–14]. High-resolution imaging of the cervical spine in the axial and sagittal planes with clear distinction of bony and disk margins, neural foramina, nerve roots, CSF, and spinal cord can be achieved with recently developed gradient recalled acquisition in the steady state (GRASS) techniques [12]. Another advantage of LFA imaging is rapid data acquisition, which improves the clinical efficiency of the examination and minimizes patient discomfort and motion.

Subjects and Methods

One hundred and thirty consecutive patients with known or suspected cervical radiculopathy were studied with MR LFA techniques between August 1986 and December 1986 with a 1.5-T GE Signa MR system. Imaging parameters included 5-mm-thick sections, contiguous imaging, 128 × 256 acquisition matrix, 24-cm field of view, four excitations (two averages), flip angle of 10° or 20°, TR = 75 msec, and TE = 12.3 msec. It generally required 16 sequential single axial sections to include the C3–T1 levels. LFA images were performed in the axial (n = 130) and sagittal (n = 75) planes. A flow compensation regimen (gradient moment nulling) was used with the GRASS sequences [12]. Image quality of the LFA studies was rated as poor, good, or excellent. T1-weighted (spin echo TR = 600, TE = 20 msec) and T2-weighted (spin echo TR = 2500, TE = 30 and 60 msec) sagittal images were also acquired. Myelography was done in 20 patients after intrathecal instillation of iopamidol (Isovue M-200 or 300).* CT myelography was performed after the cervical myelogram in 16 individuals. MR, CT, and conventional myelographic studies were divided into four groups depending on the dominant findings: (1) normal; (2) ventral extradural ridging, central; (3)

* Squibb, New Brunswick, NJ.

This article appears in the January/February 1988 issue of *AJNR* and the March 1988 issue of *AJR*.

Received June 29, 1987; accepted after revision September 2, 1987.

Presented at the annual meeting of the American Society of Neuroradiology, New York, May 1987.

[1] All authors: Department of Radiology and the Barrow Neurological Institute of St. Joseph's Hospital and Medical Center, 350 W. Thomas Rd., Phoenix, AZ 85013. Address reprint requests to B. P. Drayer.

***AJR* 150:683–689, March 1988**
0361–803X/88/1503–0683
© American Roentgen Ray Society

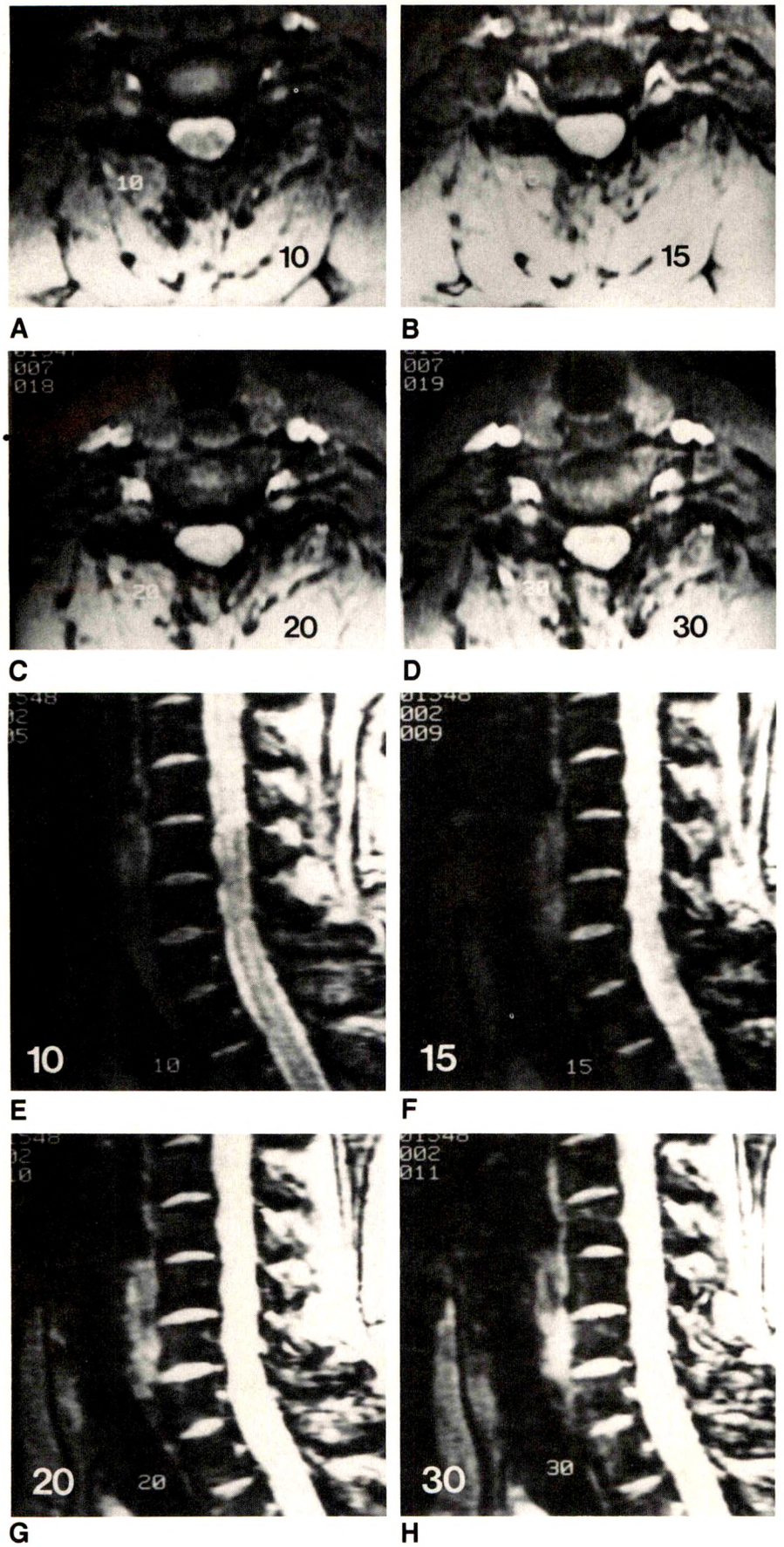

Fig. 1.—Optimizing flip angle for gradient echo imaging.

A–D, Axial MR images (TR = 75 msec, TE = 12.3 msec). TR and TE are held constant while flip angle is varied (10°, 15°, 20°, and 30°). Although signal-to-noise ratio is best at 30°, the contrast between spinal cord and surrounding CSF is best at 10°, and signal-to-noise is sufficient.

E–H, Sagittal MR images (TR = 75 msec, TE = 12.3 msec). Signal-to-noise ratio is again best at 30° but cord vs CSF contrast is best at 10° flip angle.

ventrolateral extradural, degenerative spurring; and (4) ventrolateral extradural, herniated disk. Pathologic confirmation of the diagnosis at surgery was obtained in 13 patients.

Results

Image quality, evaluated from the LFA images, was judged as excellent (n = 95), good (n = 33), or poor (n = 2). A 10° or 15° flip angle provided better image contrast of the spinal cord versus surrounding subarachnoid space than a 30° flip angle when using TR = 75 msec and TE = 12.3 msec (Fig. 1). The signal intensity of the CSF was greater than the spinal cord, similar in appearance to that seen with intrathecally enhanced CT scanning (Fig. 2). There was no significant CSF pulsation artifact. The central portion of the spinal cord was of higher signal intensity than the periphery on axial images, suggesting a distinction of central gray from surrounding white matter and/or truncation artifact because the shape does not precisely coincide with the anterior and posterior horns (Fig. 3). A thin central ribbon of high signal intensity was seen on the sagittal 128 × 256 matrix images of the spinal cord and was absent on 256 × 256 matrix images, consistent with truncation artifact [15]. The upper cervical cord and cervicomedullary junction were also visualized on the cervical studies. The neural foramina were routinely evident on axial studies and contained linear, lower signal intensity nerve roots (Fig. 3). The cervical vertebral bodies were of lower signal intensity than the intervening disks.

Thirty-one studies were judged normal. Neither surgery nor conventional or CT myelography was performed on these patients.

Extradural defects were apparent in 99 of 130 MR studies. Both conventional and CT myelography were performed in 20 patients, and five patients had nonenhanced CT with confirmation of the MR findings in all cases. The extradural defects, whether central or lateral, were clearly delineated due to compression of the neural foramina, nerve roots, and adjacent subarachnoid space. The distinction of osteophyte versus herniated disk material was apparent in the majority of cases (Table 1). Degenerative bony ridging was of lower signal intensity than disk material (Fig. 4). The herniated disk (Fig. 5) often created a smooth, lateralized compression of the subarachnoid space on the sagittal MR studies that resembled a double density on a lateral conventional myelographic study. Larger extradural defects resulted in spinal cord compression and often posterior displacement. The vertical band of increased signal intensity in the central spinal cord was focally lost with milder cord effacement from either bony ridge or herniated disk. The MR study always provided equivalent and, at times, additional information, compared

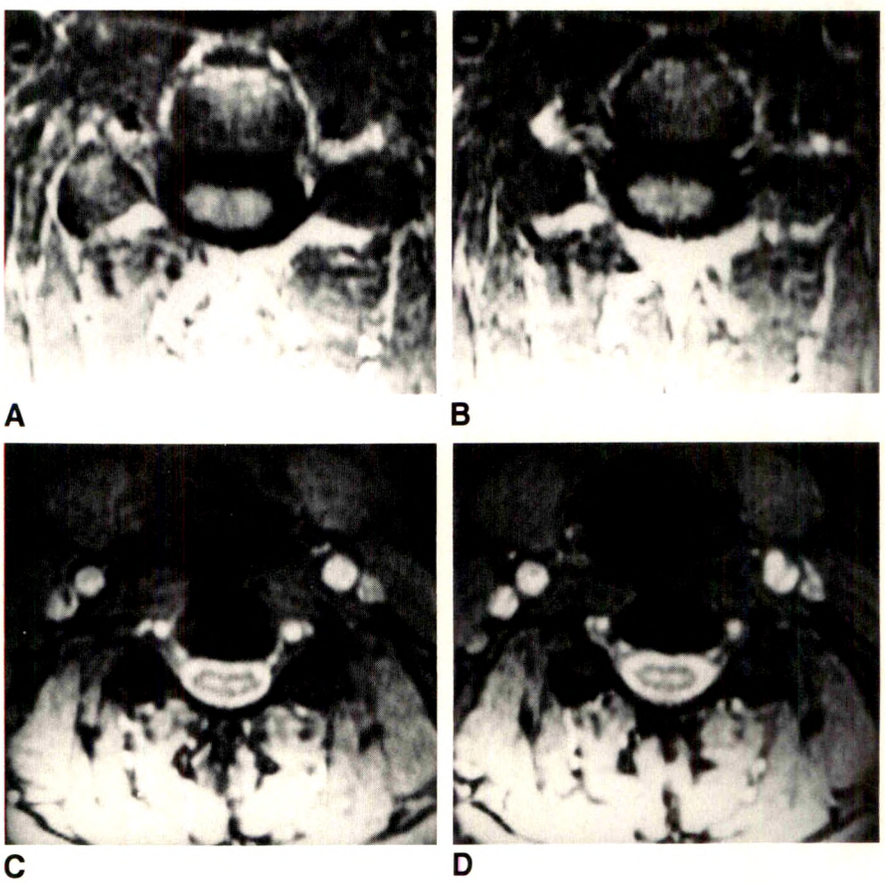

Fig. 2.—Spin echo vs GRASS images of cervical spine.

***A* and *B*, T1-weighted spin echo images (TR = 600 msec, TE = 20 msec) at C5–C6 level depict spinal cord excellently. Surrounding CSF is also well defined but extradural defects are difficult to visualize (e. g., both CSF and bony degenerative abnormalities are low signal intensity).**

***C* and *D*, Gradient echo (GRASS) images (TR = 75 msec, TE = 12.3 msec, flip angle at 10°) at same C5–C6 level clearly define spinal cord, surrounding CSF, neural foramina, and exiting C6 nerve roots. CT myelographic appearance improves the ability to readily differentiate normal from abnormal studies.**

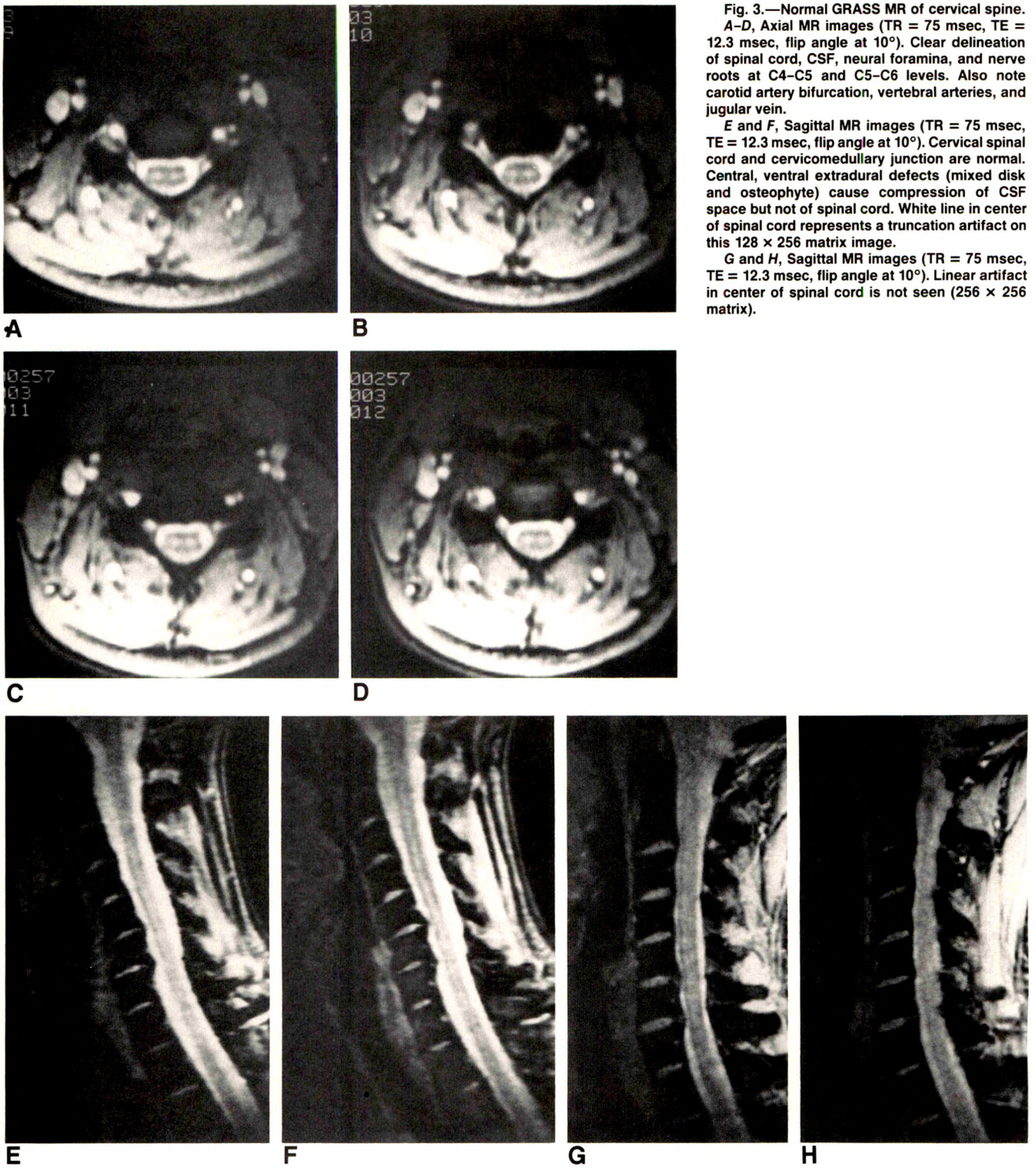

Fig. 3.—Normal GRASS MR of cervical spine.

***A–D*, Axial MR images (TR = 75 msec, TE = 12.3 msec, flip angle at 10°). Clear delineation of spinal cord, CSF, neural foramina, and nerve roots at C4–C5 and C5–C6 levels. Also note carotid artery bifurcation, vertebral arteries, and jugular vein.**

***E* and *F*, Sagittal MR images (TR = 75 msec, TE = 12.3 msec, flip angle at 10°). Cervical spinal cord and cervicomedullary junction are normal. Central, ventral extradural defects (mixed disk and osteophyte) cause compression of CSF space but not of spinal cord. White line in center of spinal cord represents a truncation artifact on this 128 × 256 matrix image.**

***G* and *H*, Sagittal MR images (TR = 75 msec, TE = 12.3 msec, flip angle at 10°). Linear artifact in center of spinal cord is not seen (256 × 256 matrix).**

with myelography and CT. A subtle, but definite sign of an extradural defect on the axial images was loss of the increased signal intensity CSF anterior to the spinal cord. The anterior CSF space and the space posterior to the spinal cord should be similar in size, creating an oblong shape of equal thickness (Figs. 2 and 3). The correlation of surgical pathology and the GRASS MR findings was excellent (Table 2). There was lack of correlation only at the level where the bony

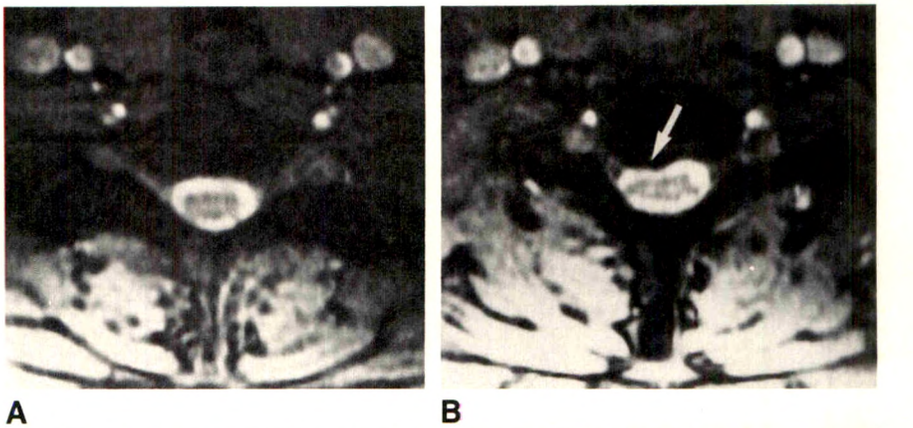

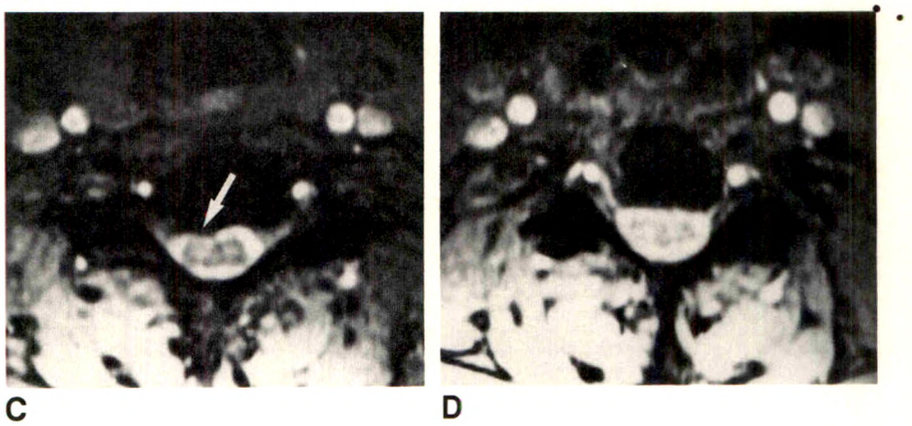

Fig. 4.—Ventrolateral extradural defect, C7 radiculopathy. GRASS images (TR = 75 msec, TE = 12.3 msec, flip angle at 10°) at C7–T1 (*A*), C6–C7 (*B* and *C*), and C5–C6 levels (*D*). Prominent ventrolateral extradural defect (*arrow*) on right at C6–C7 level causes compression of subarachnoid space, neural foramen, and C7 nerve root. Extradural defect is of mixed low and intermediate signal intensity, consistent with hard and soft disk material, respectively. Characterization of degenerative bony versus herniated disk material often requires sagittal image information due to partial volume averaging effects.

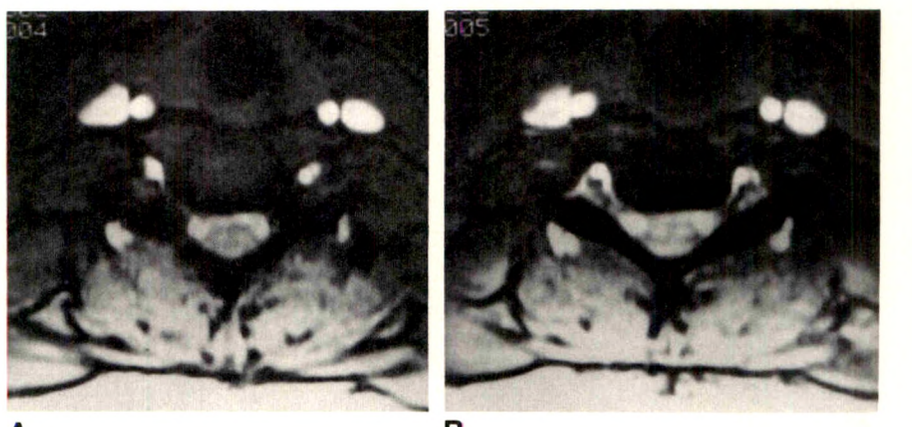

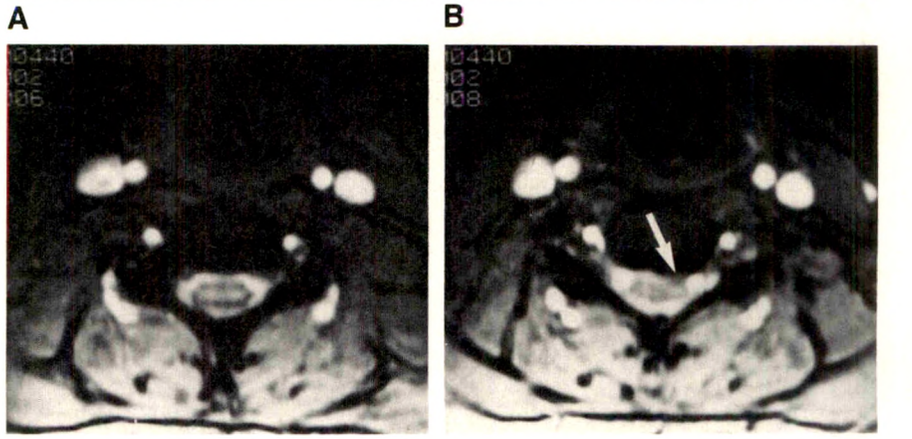

Fig. 5.—Herniated cervical disk. GRASS images (TR = 75 msec, TE = 12.3 msec, flip angle at 10°) at C6–C7 levels (*A* and *B*) and at C5–C6 levels (*C* and *D*). A small herniated disk (*arrow*) is present on the left at C5–C6 level, causing compression of subarachnoid space but not of the neural foramen. The intermediate signal intensity distinguishes this soft disk from uncovertebral spurring.

TABLE 1: GRASS MR Imaging in Cervical Radiculopathy

A. Diagnosis
Normal (n = 31)
Extradural defects (n = 99)
Central, ventral (52)
Ventrolateral
Degenerative (osteophyte) (26)
Herniated disk (4)
Degenerative/herniated (17)
B. Imaging quality
Excellent (95)
Good (33)
Poor (2)
C. GRASS correlation
CT/myelography (25/25)
Surgical (13/13)

TABLE 2: GRASS/Surgical Pathology Correlation[a]

	Surgical Pathology	GRASS Correlation
Ventral extradural		
Degenerative	15	15
Herniated disk	1	1
Ventrolateral extradural		
Degenerative	12	11
Herniated disk	2	2

[a] Results are from 13 patients in whom 30 locations were surgically explored.

degenerative abnormality on the MR study was more prominent on the right, while surgery was performed on the left (the side of milder MR abnormality) due to clinical symptomatology.

Conclusions

Conventional spin echo imaging paradigms have provided excellent delineation of the spinal cord for the evaluation of myelopathy but have proved somewhat disappointing when used to detect the source of radiculopathy [9]. The emergence of variable flip angle, gradient echo pulse sequences greatly enhances the ability to obtain diagnostic images for the clinical evaluation of cervical radiculopathy. The major advantage of the variable flip angle, gradient echo method (compared with spin echo sequences) becomes most apparent when imaging the cervical spine in the axial plane. There is sharp delineation of bone and disk margins, excellent contrast between the spinal cord and surrounding subarachnoid space, and clear visualization of the neural foramina and exiting nerve roots. The visual effect of these noninvasive MR images is similar to that of intrathecally enhanced CT (CT myelographic effect). The gradient echo technique has the additional advantage of providing good signal-to-noise ratio with a short acquisition time [12].

Central and ventrolateral extradural defects were readily delineated using variable flip angle MR imaging. There was clear distinction of nerve roots, neural foramina, and spinal cord impingement. Surgical correlation with the gradient echo images was excellent. The MR studies gave equal or more detailed information compared with myelography/CT in all cases in which both were performed.

Degenerative bony ridging was of lower signal intensity than herniated disk material. This distinction was often difficult using axial, 5-mm sections, and it is thus critical to analyze carefully both axial and sagittal images to make this differentiation. In 17 cases we were unable to definitely differentiate osteophytes and disk material, generally due to the extradural defect containing a mixture of both. Larger extradural defects compressed not only the subarachnoid space and nerve roots but also displaced the spinal cord. Subtle cord effacement resulted in loss of the central cord region high signal intensity. This high signal intensity is related to a truncation artifact [15] that is seen with a 128 × 256 acquisition matrix, but not with a 256 × 256 matrix. It is also important to recognize that even mild to moderate effacement of the anterior subarachnoid space on axial images is diagnostic of an extradural defect.

The limited flip angle MR images were obtained with a GRASS pulse sequence and gradient moment nulling (flow compensation) to eliminate signal loss from motion-induced temporal and spatial phase shift [12]. Pulse flip angles of less than 90° produce a greater signal than the traditional 90° pulse used for spin echo imaging, particularly when used with a short TR. The shorter flip angle is followed by a negative gradient in the readout direction causing dephasing of spins and then a positive gradient causing rephasing [12]. By obtaining a series of images with a TR of 75 msec and TE of 12.3 msec, we empirically determined that even though the signal-to-noise ratio was greatest with a 30° flip angle the contrast between the spinal cord and surrounding subarachnoid space was greatest at a 10° flip angle. We chose a TR of 75 msec for a better signal and because a shorter TR (e.g., TR-25 msec) sequence was extremely uncomfortable (loud gradient knocking) for the patient. Imaging contrast and relative relaxation time weighting in GRASS imaging are thus related not only to the operator-selected TR and TE, as with spin echo imaging, but also to pulse flip angle.

The use of limited flip angle GRASS imaging greatly facilitates the clinical evaluation of cervical radiculopathy. A routine cervical study can now be performed in 21 min, 53 sec using the following pulse sequences: (1) sagittal multislice spin echo, TR = 600 msec, TE = 20 msec, 256 × 256 matrix, two excitations; (2) sagittal GRASS, TR = 75 msec, TE = 12.3 msec, flip angle 10°, 256 × 256 matrix, four excitations, 5 slices; and (3) axial GRASS, TR = 75 msec, TE = 12.3 msec, flip angle 10°, 128 × 256 matrix, four excitations, 24-cm field of view, and approximately 16 slices (C3–T1). All images are flow compensated, and contiguous 5-mm-thick (0 skip) sections are used. The major limitation of the GRASS images is that they provide suboptimal visualization of spinal cord disease. In patients presenting with myelopathy an additional sagittal multislice, multiecho, flow compensated spin echo pulse sequence (TR = 2000 msec, TE = 35/70 msec, 128 ×

256 matrix, two excitations) is performed. This study suggests that MR imaging may obviate the need for the more invasive myelography and CT scanning in individuals with suspected cervical radiculopathy.

ACKNOWLEDGMENTS

We appreciate the superb technical assistance of MR technologists James Winters, Kevin King, Linnea Tyman, and Laura Castillo.

REFERENCES

1. Drayer BP, Rosenbaum AE. Metrizamide brain penetrance. *Acta Radiol [Suppl] (Stockh)* **1977**;355:280–293
2. Sykes RHD, Wasenaar W, Clark P. Incidence of adverse effects following metrizamide myelography in nonambulatory and ambulatory patients. *Radiology* **1981**;138:625–627
3. Hauge O, Falkenberg H. Neuropsychological reactions and other side effects after metrizamide myelography. *AJR* **1982**;139:357–360
4. Davis CE Jr, Smith C, Harris R. Persistent movement disorder following metrizamide myelography. *Radiology* **1982**;144:A975
5. Killebrew K, Whaley RA, Hayward JN, Scatliff JH. Complications of metrizamide myelography. *Radiology* **1983**;149:A343
6. Meador K, Hamilton WJ, El Gammal TAM, Demetropoulos KC, Nichols FT. Irreversible neurologic complications of metrizamide myelography. *Radiology* **1985**;154:A564
7. Drayer BP, Vassallo C, Sudilovsky A, et al. A double-blind clinical trial of iopamidol versus metrizamide for lumbosacral myelography. *J Neurosurg* **1983**;58:531–537
8. Modic MT, Weinstein MA, Pavlicek W, Boumphrey F, Starnes D, Duchesneau PM. Magnetic resonance imaging of the cervical spine: technical and clinical observations. *AJR* **1983**;141:1129–1136, *AJNR* **1984**;5:15–22
9. Modic MT, Masaryk TJ, Mulopulos GP, Bundschun CV, Han JS, Bohlman H. Cervical radiculopathy; prospective evaluation with surface coil MR imaging; CT with metrizamide and metrizamide myelography. *Radiology* **1986**;161:753–759
10. Daniels DL, Hyde JS, Kneeland JB, et al. The cervical nerves and foramina: local-coil MR imaging. *AJNR* **1986**;7:129–133
11. Modic MT, Masaryk TJ, Ross JS, Mulopulos GP, Bundschun CV, Bohlman H. Cervical radiculopathy: value of oblique MR imaging. *Radiology* **1987**;163:227–231
12. Wehrli FW, Shimakawa A, Gullberg GT, MacFall JR. Time-of-flight MR flow imaging: selective saturation recovery with gradient refocusing. *Radiology* **1986**;160:781–785
13. Perkins TG, Wehrli FW. CSF signal enhancement in short TR gradient echo images. *Magn Reson Imaging* **1986**;4:465–467
14. Enzmann DR, Rubin JB, Wright A. Cervical spine MR imaging: Generating high signal CSF in sagittal and axial images. *Radiology* **1987**;163:233–238
15. Wood ML, Henkelman RM. Truncation artifacts in magnetic resonance imaging. *Mag Reson Med* **1985**;2(6):517–526

Come to the American Roentgen Ray Society 88th ANNUAL MEETING

San Francisco Hilton
May 8–13, 1988

Scientific Program (200 papers)
Instructional Courses (60 hours)
Categorical Course on Breast Imaging
The Caldwell Lecture
Award Papers
Scientific Exhibits
Social, Golf, and Tennis Programs
Guest Programs

We did it.

Fuji Presents Today's Alternative

Easy to use control panel features digital temperature display, ready and replenishment lights and one-touch power.

The **FPM4200** 90 second, cold-water, X-ray film processor.

Fuji has applied today's technology to *reduce cost, improve performance,* and manufacture the "*next generation*" of 90 second, high capacity processors. The first alternative was the Fuji FPM4000. A hard act to follow right? Wrong. Fuji has put all of the reliability and performance you have come to expect from Fuji into the FPM4200, **TODAY'S ALTERNATIVE.**

We haven't cut corners, we just did what we do best when it comes to the radiological environment—we turn our best ideas into the best products.

- 90 second, cold-water processing
- High capacity, 280 sheets of 14x17 per hour
- Film activated, automatic standby
- Waist-high film delivery
- Digital temperature display
- Extremely quiet operation
- Superior water efficiency

Get the full details about the FPM4200 from your Fuji sales representative, or call toll free 1-(800)-431-1850 In CT (203) 353-0300.

CIRCLE 7 ON READER SERVICE CARD

FUJI I&I *Imaging & Information*

FUJI MEDICAL SYSTEMS U.S.A., INC.
90 Viaduct Road, Stamford, CT 06907

COMMEMORATION OF JUBILEE ANNIVERSARY

487 **Perspective. Present and future status of MR imaging.** *Margulis AR, Crooks LE*

493 **Progress in radiology. The evolution of mammography.** *Bassett LW, Gold RH*

499 **Anniversary reprint from volume 50, 1943. Small intestinal enema.** *Schatzki R*

508 **Richard Schatzki, M.D.: a biography.** *Schatzki SC*

510 **Commentary. Small intestine enema.** *Carlson HC*

PROGRESS IN RADIOLOGY

513 **Overcoming motion in abdominal MR imaging.** *Wood ML, Runge VM, Henkelman RM*

CARDIOPULMONARY RADIOLOGY

523 **Quantification of regional myocardial function by rapid cine MR imaging.** *Pflugfelder PW, Sechtem UP, White RD, Higgins CB*

531 **MR imaging of acute myocardial infarction: value of Gd-DTPA.** *de Roos A, Doornbos J, van der Wall EE, von Voorthuisen AE*

535 **Aortobronchopulmonary fistula complicating aortic aneurysm: diagnosis in four cases.** *Coblentz CL, Sallee DS, Chiles C*

539 **Image-intensifier photofluorography and conventional chest radiography: comparison of diagnostic efficacy.** *Manninen H, Partanen K, Soimakallio S, Rytkönen H*

545 **Latissimus dorsi cardiomyoplasty: radiographic findings.** *Nguyen TH, Hoang T-A, Dash N, et al.*

549 **Eloesser window thoracostomy for treatment of empyema: radiographic appearance.** *Shapiro MP, Gale ME, Daly BDT*

553 **Case report. Balloon dilatation of the left main bronchus in sarcoidosis.** *Brown KT, Yeoh CB, Saddekni S*

555 **Case report. Air embolism complicating percutaneous lung biopsy.** *Tolly TL, Feldmeier JE, Czarnecki D*

GASTROINTESTINAL RADIOLOGY

557 **MR diagnosis of pancreatic transplant rejection.** *Vahey TN, Glazer GM, Francis IR, et al.*

561 **Dual-contrast MR imaging of liver cancer in rats.** *Weissleder R, Saini S, Stark DD, Wittenberg J, Ferrucci JT*

567 **MR relaxation times and iron content of thalassemic spleens: an in vitro study.** *Gomori JM, Grossman RI, Drott HR*

571 **Gallbladder disease in patients with primary sclerosing cholangitis.** *Brandt DJ, MacCarty RL, Charboneau JW, LaRusso NF, Wiesner RH, Ludwig J*

575 **Case report. The effervescent gallbladder: a sonographic sign of emphysematous cholecystitis.** *Nemcek AA Jr, Gore RM, Vogelzang RL, Grant M*

578 **Case report. Choledochal varices.** *Kim S, Chew FS*

581 **Case report. Small bowel obstruction due to Garren gastric bubble: radiographic diagnosis.** *Zeman RK, Benjamin SB, Cunningham MB, et al.*

GENITOURINARY RADIOLOGY

583 **CT of renal cell carcinoma in patients on chronic hemodialysis.** *Siegel SC, Sandler MA, Alpern MB, Pearlberg JL*

587 **Arteriovenous malformations of the kidneys: ablation with alcohol.** *Takebayashi S, Hosaka M, Ishizuka E, Hirokawa M, Matsui K*

591 **CT diagnosis of circumcaval ureter.** *Lautin EM, Haramati N, Frager D, et al.*

595 **Case report. Vaginally induced pneumoperitoneum during pregnancy.** *Gensburg RS, Wojcik WG, Mehta SD*

MUSCULOSKELETAL RADIOLOGY

597 **MR imaging of the knee: preliminary results with a 3DFT GRASS pulse sequence.** *Spritzer CE, Vogler JB, Martinez S, et al.*

605 **Diagnosis of osteomyelitis by MR imaging.** *Unger E, Moldofsky P, Gatenby R, Hartz W, Broder G*

611 **Spinal pseudarthrosis complicating ankylosing spondylitis: comparison of CT and conventional tomography.** *Chan FL, Ho EKW, Chau EMT*

615 **Soft-tissue sarcomas of the extremities: comparison of MR and CT in determining the extent of disease.** *Demas BE, Heelan RT, Lane J, Marcove R, Hajdu SI, Brennan MF*

621 **Case report. Avulsion of the innominate artery associated with fracture of the sternum.** *Ben-Menachem Y*

VASCULAR RADIOLOGY

623 **The diagnosis of femoropopliteal venous thrombosis: comparison of duplex sonography and plethysmography.** *Rosner NH, Doris PE*

629 **Sonography of the radial artery at the wrist.** *Gooding GAW*

632 **Case report. The "to-and-fro" sign: duplex Doppler evidence of femoral artery pseudoaneurysm.** *Abu-Yousef MM, Wiese JA, Shamma AR*

PEDIATRIC RADIOLOGY

635 **Factors affecting visualization of posterior rib fractures in abused infants.** *Kleinman PK, Marks SC, Adams VI, Blackbourne BD*

639 **Balloon dilatation of esophageal stenosis in children.** *Sato Y, Frey EE, Smith WL, Pringle KC, Soper RT, Franken EA Jr*

643 **Acute scrotal abnormalities in children: diagnosis by combined sonography and scintigraphy.** *Mueller DL, Amundson GM, Rubin SZ, Wesenberg RL*

647 **Sonographic evaluation of ovarian torsion in childhood and adolescence.** *Graif M, Itzchak Y*

NEURORADIOLOGY

651 **Acute intracranial hemorrhage: intensity changes on sequential MR scans at 0.5 T.** *Zimmerman RD, Heier LA, Snow RB, Liu DPC, Kelly AB, Deck MDF*

663 **MR imaging of head trauma: review of the distribution and radiopathologic features of traumatic lesions.** *Gentry LR, Godersky JC, Thompson B*

673 **Prospective comparative study of intermediate-field MR and CT in the evaluation of closed head trauma.** *Gentry LR, Godersky JC, Thompson B, Dunn VD*

683 **Gradient echo (GRASS) MR imaging in cervical radiculopathy.** *Hedberg MC, Drayer BP, Flom RA, Hodak JA, Bird CR*

RADIOLOGIC TECHNOLOGY

691 **Technical note. Radiographic system for use in emergency and intensive care units.** *Mirvis SE, Fritz SL, Siegel JH, Ramzy A*

OTHER CONTENT

662 **Forthcoming articles**

693 **Letters**

700 **Review of current literature**

705 **News**

709 **ARRS 1988 meeting summary**

711 **ARRS 1988 meeting registration forms**

715 **American Roentgen Ray Society information**

650 **Memorial: Marcus J. Smith**

716 **Classified advertisements**

Book reviews 530, 586

Videotape review 628

A3 **Guidelines for authors**